ISB 2015 GLASGOW

XXV CONGRESS OF THE INTERNATIONAL SOCIETY OF BIOMECHANICS

XXV Congress of the International Society of Biomechanics

Abstract Book

Scottish Exhibition and Conference Centre (SECC),
Glasgow, UK
12th – 16th July 2015

ISB

www.isbglasgow.com

Get involved on Twitter!
@ISB_Glasgow

Contents and Search

To Search this Digital Document

Click the search button below.

Open Search

Enter your term in the search box. You can enter full or partial text for a speaker's name, abstract number, category or topic. Clicking the search button will then list all successful matches for the search term, and clicking on any of the results in the list will take you immediately to the appropriate page.

The search window can be shown at any time by selecting "Edit > Search" or "Edit > Advanced Search" (depending on your software version) from the top file menu, or using the following shortcut keys:

"Shift - Control - F" on a Windows operating system

"Shift - Command - F" on an Apple operating system
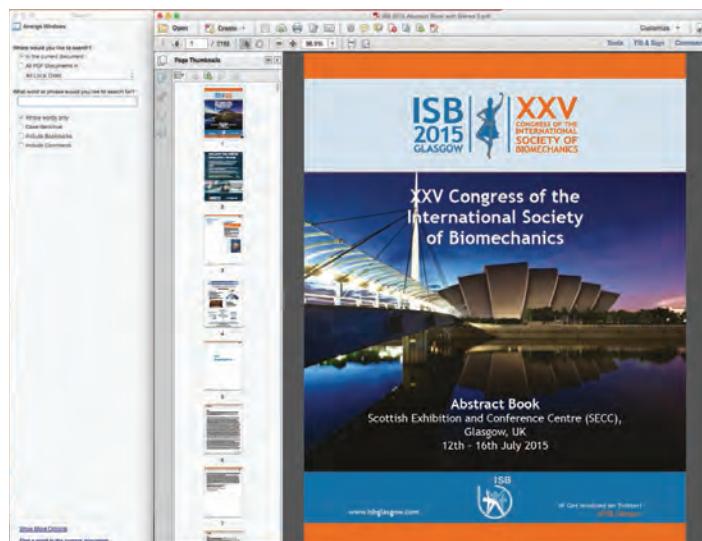
International Society of Biomechanics

Join the largest network of biomechanists in the world!

https://isbweb.org/

Membership Benefits

- Reduced registration fees for ISB Congresses
- Reduced journal subscription fees
- International travel grants
- Awards for excellence in research
- International network of specialists
- Student support and awards
- Support for biomechanics in economically developing countries

XXIII ISB Congress – Brussels, Belgium

Technical Groups

- Computer Simulation
- Footwear Biomechanics
- 3D Analysis of Human Movement
- International Shoulder Group

ISB Sponsors

DELSYS®

NIKE

VICON

QUALISYS
Motion Capture Systems

MotionAnalysis

KISTLER
measure. analyze. innovate.

NDI
Northern Digital Inc.
RESEARCH-GRADE MOTION CAPTURE

ELSEVIER

AMTI
FORCE AND MOTION

The International Society of Biomechanics promotes and supports international contacts amongst scientists, the dissemination of knowledge, and the activities of national organizations in the field of biomechanics.

Join Now! See website for details!

Oral Presentations

Sport

AS-0001

THE EFFECTS OF SQUATTING FOOTWEAR ON THREE-DIMENSIONAL LOWER LIMB AND SPINE KINETICS.

Shane Petersen [1,*]Daniel Southwell [1]Tyson Beach [2]Ryan Graham [1]

[1]School of Physical and Health Education, Nipissing University, North Bay, [2]Faculty of Kinesiology and Physical Education, University of Toronto, Toronto, Canada

Introduction and Objectives: The barbell back squat is widely accepted and prescribed as an effective exercise for increasing muscular strength in the lower extremities. There has been some debate as to the best footwear for squatting. Benefits of weightlifting shoes may include providing a firmer base and the maintenance of a more upright posture to reduce external shear forces on the spine [1]. Conversely, benefits of squatting barefoot may include improved proprioception, balance, and training of the intrinsic musculature of the foot and ankle [2]. While various studies have attempted to assess the overall effectiveness and safety of the various shoe types (i.e. barefoot, shod, weightlifting shoe) during the back squat [e.g. 1-2], they have been limited to 2-D analyses. To address this, a recent paper assessed the influence of the three footwear types on 3-D kinematics and muscle activation during a 70% 1-RM back squat in males [3]. The authors found that compared to barefoot the running shoe was associated with increased squat depth, knee flexion, and rectus femoris activation [3]. However, to better understand the effects of these shoe types on the human body, kinetic analyses of joint loading are also required. Thus, the purpose of this study was to examine 3-D lower limb and spine kinetics to comprehensively evaluate the benefits and limitations of each type of squatting footwear.

Methods: 24 experienced weightlifters (12M, 12F) performed one trial per footwear condition (barefoot, shod, weightlifting) in a randomized order. Each trial required participants to perform three repetitions of 80% 1RM barbell back squats at a self-selected speed, depth, and body positioning (average mass lifted = 97±38.3kg). During all trials, 3-D kinematic data were collected from body segments at 200 Hz (Oqus 400+, Qualisys, Sweden). Participants placed one foot on each of two force plates (FP6090, Bertec, USA), which recorded the 3-D ground reaction forces and moments at 2000Hz. Using Visual-3D (C-Motion Inc., USA) an inverse dynamical linked-segment model was developed to calculate lower extremity and lumbar spine moments. Furthermore, lumbosacral joint compression and shear forces were calculated in Visual-3D by combining the estimated force from a single-muscle equivalent with the reaction forces resulting from the inverse dynamics analyses [4]. Ensemble averages across the repetitions were taken, and minimum and maximum values were extracted for each shoe condition and compared using repeated-measures ANOVAs with post-hoc tests in SPSS 22 (IBM Corporation, USA). The critical p-value was adjusted to 0.01 using the false discovery rate technique.

Results: There was no effect of footwear on ankle moments in any body-fixed movement plane. For the knee there was a significant main effect of shoe type on the knee extension moment (p= 0.001), where post-hoc testing revealed that the running and weightlifting shoes produced significantly larger moments than the barefoot condition. There was also a main effect of shoe type on internal knee rotation moments (p= 0.002), where the weightlifting shoe produced significantly larger moments than both other conditions. Conversely, for the hip there was also a main effect of shoe type on the extension moment (p= 0.004), where the barefoot condition produced significantly larger moments than either the shod or weightlifting shoe condition. Lastly, there was also a significant main effect of shoe type on both internal (p=0.005) and

external (p=0.003) hip rotation moments, where the barefoot condition produced greater external rotation and less internal rotation than either shoe type condition. There were no differences in lumbar spine moments (p>0.01) or lumbosacral compression (p= 0.18) or shear (p= 0.954) forces between conditions.

Conclusion: The results from this novel 3-D kinetic analysis indicate that altering footwear conditions appears to redistribute the internal biomechanical loading amongst the lower extremity joints during the back squat exercise and would perhaps alter the musculoskeletal adaptations elicited. Thus, trainers and coaches may be able to modify both squat difficulty (i.e. joint targeting) as well as musculoskeletal injury risk (i.e. joint unloading) via footwear modifications. However, between-condition differences in joint kinetics were relatively small in magnitude (~3-20 Nm) and therefore future research should incorporate more sophisticated modelling approaches to discern the practical significance of these findings, and how they may fluctuate across individuals (i.e. experience) and squat variations (i.e, frequency, intensity, time, and type).

References: [1] Sato et al., J. Strength. Cond. Res., 26: 28-33, 2012.

[2] Sato et al., Int. J. Sports. Sci. Coach., 8: 571-578, 2013.

[3] Sinclair et al., Eur. J. Sports. Sci., In Press, 2014.

[4] Howarth et al., Theor. Iss. Ergonom. Sci., 11: 474-488, 2010.

Disclosure of Interest: None Declared

Sport

AS-0002

THE EFFECT OF AUGMENTED FEEDBACK ON IMPULSE GENERATION DURING A QUICK FIRST STEP

Christopher D. Ramos [1,*] Ben Sidaway [2] Jill McNitt-Gray [3]

[1]Biomedical Engineering, University of Southern California, Los Angeles, [2]Physical Therapy, Husson University, Bangor, [3]Biological Sciences, University of Southern California, Los Angeles, United States

Introduction and Objectives: A quick first step is advantageous when navigating through challenging environments. Individuals often need to read and react to an unexpected event and then quickly configure their body so that they can quickly redirect the center of mass (CM) trajectory by generating impulse in a desired direction. Initiating a quick first step out of a relatively stationary position involves adopting postures in which the lead leg center of pressure is behind the CM prior to initiation of rapid joint extension [1,2]. Central to development of a quick first step, we hypothesized that performance could be enhanced by providing individuals with augmented feedback regarding horizontal-reaction forces generated during foot contact [3]. To facilitate skill acquisition and visualize the reaction forces causing the observed movement, augmented feedback was generated in the form of video replay of the individuals movements with the lead and lag leg reaction force-time curves overlaid onto the video. To determine the influence of this augmented feedback on performance, differences in horizontal reaction force-time characteristics during quick first steps performed before, after, and two days following practice with augmented feedback were compared. Comparisons were also made to players who practiced quick first steps without access to this feedback. Improvements in horizontal impulse generation were expected to involve greater lead leg average force during impulse generation, quicker time to peak force associated with rapid joint extension, and shorter times between peak forces generated by the lag and lead legs (P2P)[4].

Methods: Female volleyball players (n=13, 10 with feedback, 3 no feedback) competing on top-10 collegiate varsity teams volunteered to participate in accordance with the institutional review board. Players faced a ball-launching machine in their self-selected 'ready position' and were instructed to move as quickly as possible toward a ball launched in an unexpected direction, either to their left (4 times) or in front (2 times). Force plates (Kistler, 1200 Hz) recorded ground reaction forces for each foot while frontal plane kinematics were recorded using high-speed video (Casio, 300 Hz). RF-time curves for both lead and lag legs were overlaid onto frontal plane video (Panasonic, 30 Hz) and later shown to the players as augmented feedback between performance rounds (6 trials each). Baseline performance was determined by having players complete 2 blocks of 6 performance trials without any feedback. Ten players then practiced 3 blocks of 6 trials with augmented feedback provided after each block of 6 trials. Three players practiced in a similar manner but without feedback. Ten minutes after practice was completed, all players performed a retention test consisting of 2 blocks of trials without feedback to determine if any benefit derived from the feedback was maintained. A similar retention test was completed 2 days after the practice session to assess whether there were any long-term benefits of practicing with the feedback. Feedback was directed primarily toward quick horizontal impulse generation (area under the curve) by increasing the force magnitude (vertical axis) over time (horizontal axis). Lead leg average force during horizontal impulse generation (normalized by body mass), time to lead leg peak force, and P2P time were then computed and compared within-player between sessions using medians.

Results: Ten minutes following completion of practice, eight of the ten players receiving feedback showed improvement in parameters associated with quick horizontal impulse generation in a quick first step. In contrast, only one player in the no-feedback control group improved. Improvement in horizontal impulse generation was manifested by an increase in normalized average force (associated with greater horizontal force generation during foot contact), reduction in P2P time (associated with an initial placement of the lead leg foot more posterior to the CM), and a reduction in time to lead-leg peak force (associated with a greater rate of lead leg joint extension). These movement initiation related parameters showed a significant decline from the 10-minute to the 2-day retention test but were nevertheless still improved over baseline measures.

Figure:

Improvement for Each Player from Baseline to Same-Day Retention
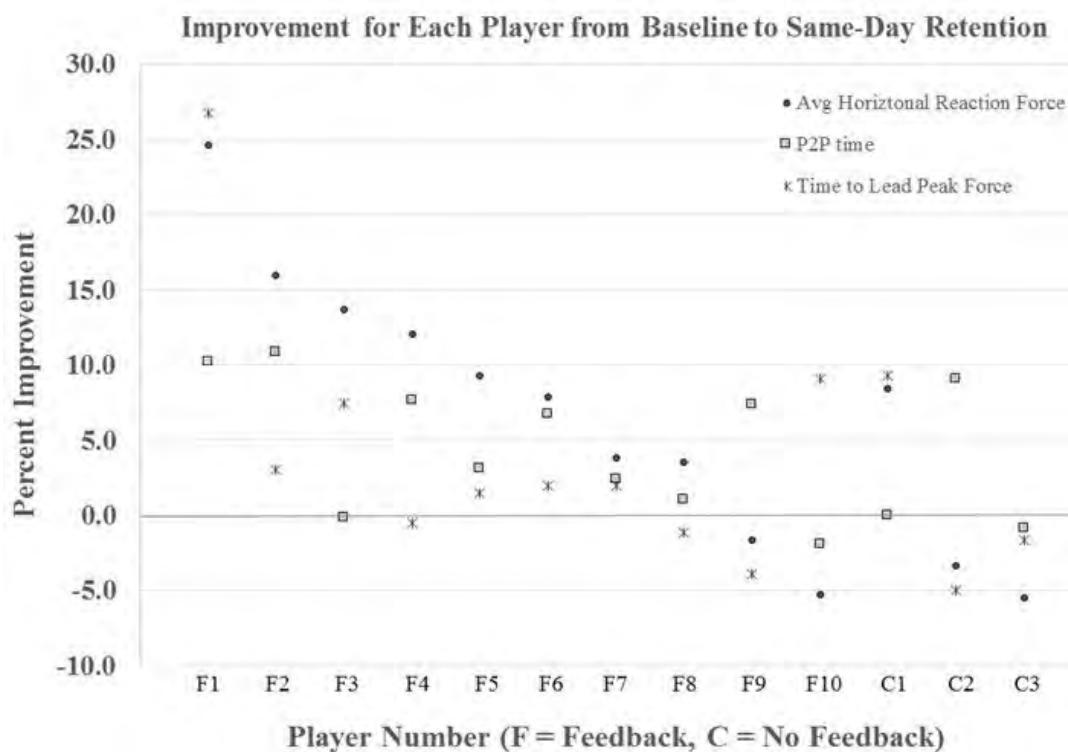
Conclusion: The findings from this initial study are promising given that augmented feedback, in the form of video replay of the individuals movements with the lead and lag leg reaction force-time curves overlaid onto the video improved a number of movement initiation related parameters after only 18 performance trials. It remains to be seen if more practice trials with this feedback is able to establish lasting improvements in the performance of a quick first step.

References: [1]Mathiyakom W, et al. *J Appl Biomech* **23**, 149-161, 2007.

[2]McNitt-Gray JL, et al. *J Biomech* **34**, 1471-1482, 2001.

[3]Wulf G, et al. *J Motor Behavior* **34**, 171-182, 2002.

[4]McNitt-Gray JL et al. *Sports Eng & Tech* (in press)

Disclosure of Interest: None Declared

Sport

AN INTEGRATED MULTISCALE ANALYSIS OF INJURY MECHANISMS IN SPORT IMPACTS: AN APPLICATION TO CERVICAL SPINE BIOMECHANICS IN RUGBY UNION SCRUMMAGING

Ezio Preatoni [1,*] Dario Cazzola [1] Tim P Holsgrove [2] Sabina Gheduzzi [2] Anthony W Miles [2] Keith Stokes [1] Richie HS Gill [2] Grant Trewartha [1]

[1] Department for Health, [2] Department of Mechanical Engineering, University of Bath, Bath, United Kingdom

Introduction and Objectives: By generating repetitive high-energy impacts (during the engagement phase) and intense sustained loads (during the sustained push phase) under unstable conditions [1], the Rugby Union scrum has been indicated as a possible risk factor for degenerative spinal injuries for forward players, and has been associated with ~40% of all catastrophic injuries in rugby [2]. However, little is known about how these external loading conditions translate into internal stresses on the spinal structures. The aim of this study was to investigate the biomechanics of cervical spine injury during rugby activities using an integrative approach: in-vivo and in-vitro experiments combined with musculoskeletal modelling.

Methods: Three levels of analysis (Levels 1-3) were integrated. Level 1 was a biomechanical study of scrummaging (N=9 experienced rugby forwards) including motion capture (Oqus, Qualisys, Sweden), force measurement (force plates: Kistler 92876BA, Switzerland; and instrumented scrum machine, [1]), and EMG of neck and trunk muscles (Delsys Trigno, Delsys Inc, USA), carried out to assess the external kinematic and kinetic conditions acting on front row players. The subsequent phases of scrummaging, initial engagament (impact and shock absorption) and sustained push, were observed. Level 2 developed a bespoke musculoskeletal model (Rugby Model, [3]), consisting of 27 anatomical segments, 26 joints, 78 cervical muscles, and 11 torque actuators, in OpenSim (OpenSim 3.2, SimTK, USA). The Rugby Model was driven by the experimental data from Level 1 and was used to estimate joint dynamics, with a specific interest in cervical joint motions and moments. Level 3 performed an in-vitro laboratory experiment to study the injury mechanisms of porcine cervical spines subjected to impact loading conditions similar to those during scrummaging. Load (2 load cells: SLC41/005000, RDP Electronics Ltd, UK) and deformations caused by impacts (mass of 12.86 kg dropped from a height of 250 mm to give an impact velocity of ~2.2 m/s) were measured in a custom made impact rig, and high-speed videos (2 Fastcam SA3, Photron Europe Ltd, UK) were used to investigate the mechanisms of injury through digital image correlation (Vic-3D 2009.1.0, Correlated Solutions Inc, USA).

Results: Results from the biomechanical analysis confirmed that the load acting on the players, especially during the initial engagement, was of a considerable magnitude (~2.8 kN compression force in single-player machine scrummaging). Muscle activation patterns were affected by scrummaging conditions (e.g. machine vs. contested scrummaging; 'Crouch-touch-set' vs. 'Crouch-bind-set' sequence) and phases of the scrum (e.g. pre-engagement vs. engagement vs. sustaned push). For example, the activity of the *erector spinae* was significantly lower (in excess of 65%) in machine scrummaging than in contested scrummaging, and the activation of *sternocleidomastoid* and *upper trapezius* through pre-engagement and engagement were higher in the current 'Crouch-bind-set' technique than in the past 'Crouch-touch-set' one. The computational musculoskeletal model highlighted an antiphase change in movement and loading patterns between the

upper and lower cervical levels (i.e. flexion load on the lower vertebrae and extension on the upper vertebrae), and resulted in a "flattening" of the lordotic cervical curve during the impact phase. The present findings do not provide direct evidence for injury mechanisms but seem in line with the patterns of injury that previous authors have described in relation with scrum-related neck traumas [2]. The patterns of strain, load and resulting damages on the cervical structures of the impacted porcine specimens were also similar to those clinically observed in injured players, with the caudal vertebrae (C4-C6) more prone to damages (6 out of 8 specimens) as a consequence of the impact. Fractures resulted from tension in the vertebral bodies due to first order buckling of the cervical spine in extension. The mean maximum load in the cranial and caudal load cells was 5.8±2.0 kN and 6.0±2.1 kN and was reached at a time of 5.1±1.0 ms and 5.6±1.1 ms after impact, respectively.

Figure:

Conclusion: The proposed integrative approch provided novel and more thorough insight into how external loading conditions, muscular activity and body posture affect the internal stresses acting on the cervical spine structures. This understanding will help in elucidating injury factors related to scrummaging and represents a promising framework for future research in the area of impact-related injuries in sports. It will be further developed by including forward dynamics simulations and finite element analysis.

References: [1] Preatoni et al., BJSM, 10.1136/bjsports-2013-092938, 2014.

[2] Trewartha et al., BJSM, 10.1136/bjsports-2013-092972, 2014

[3] Cazzola et al., Proceedings of the 7th World Conference of Biomechanics (Boston, USA), 2014

Disclosure of Interest: None Declared

Sport

AS-0004

EFFECTS OF PEDALLING CADENCE ON VASTUS LATERALIS FASCICLES BEHAVIOUR

Julio Cézar Lima Da Silva [1,*]Rodrigo Rico Bini [2]Fábio Juner Lanferdini [3]Tiago Canal Jacques [3]Anton Arndt [1]Marco Aurélio Vaz [3]

[1]The Swedish School of Sport and Health Sciences, Stockholm, Sweden, [2]School of Physical Education of the Army, Rio de Janeiro, [3]Federal University of Rio Grande do Sul, Porto Alegre, Brazil

Introduction and Objectives: Pedalling cadence is important in cycling power production because of its influence on muscle fibers shortening velocities and cycling performance [1]. Previous studies evaluated muscle architecture parameters during cycling to assess the behaviour of active muscle components. One study reported that changes in pedalling cadence (50 vs. 80 rpm) did not affect vastus lateralis (VL) fascicle length [2]. However, this study was limited to non-cyclists, which may not reflect training adaptations. Therefore, the purpose of this study was to compare the effects of two pedalling cadences (70 and 90 rpm) on VL muscle architecture of cyclists.

Methods: Nineteen competitive cyclists performed an incremental cycling test to exhaustion to determine their maximal power output, oxygen uptake and the workload of their second ventilatory threshold. They warmed up at 150 W for 10-min using their own bicycles on a stationary cycling trainer (Computrainer, Racermate, USA). The test started at 100 W with increments of 25 W/min until exhaustion while cadence was controlled at 90±2 rpm. After 48 hours they cycled for 1-min at their maximal workload measured during the first session at 90 rpm. After 1-min of rest, cyclists cycled for 2-min at the workload of their second ventilatory threshold at 90 and 70 rpm, in random order, separated by 1-min of rest. The cycling trainer was configured at constant workload mode. Muscle architecture parameters for their right VL were acquired using a linear probe (60 mm, 7.5 MHz) connected to an ultrasound system (ALOKA, SSD 4000, Tokyo, Japan). Video files with ultrasound images were stored at 30 Hz. Frames were digitized by two technicians using a motion analysis software (Skill Spector, Video4Coach, Denmark). Fascicle length, muscle thickness and pennation angle were defined as shown in Figure 1. Variables were averaged for the propulsion phase (45° to 135°) of the crank cycle for each cyclist [3]. Student's t-tests were employed for statistical comparison between the 70 and 90 rpm trials and significant differences were assumed when $p < 0.05$.

Results: The VL fascicle length increased by 12% at the higher cadence ($p = 0.01$). A decrease of 19% in pennation angle ($p < 0.01$) without changes in muscle thickness were observed ($p = 0.14$) (Table 1).

In this study, longer fascicle lengths and smaller pennation angles for VL were seen at 90 rpm. Austin et al.[2] assessed non-cyclists pedalling at workloads of ~250 W, which differed from the present study (324±37 W). Differences to Austin's study may be due to greater fascicle strain and due to the larger contribution from muscle passive elements in our study. Therefore, further research is warranted to assess if cyclists and non-athletes would differ in terms of VL muscle architecture behaviour during pedalling. Less skilled subjects may have greater co-contraction [4], which could affect VL muscle force and change muscle architecture for cycling at similar workloads.

Figure:
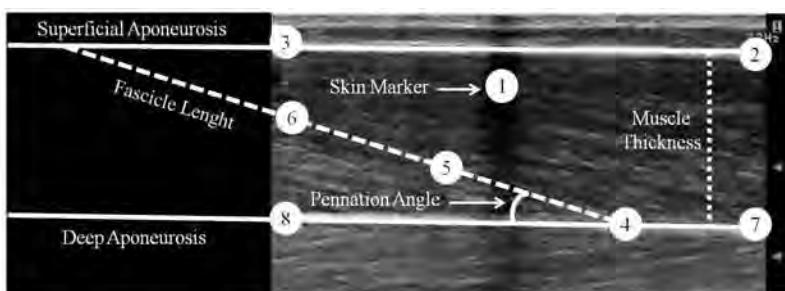
Figure 1. Illustration of vastus lateralis architecture. Markers (numbers) digitized for each video frame taken from ultrasound: (1) skin marker; (2-3) superficial aponeurosis; (4) fascicle insertion at the deep aponeurosis; (5-6) fascicle; and (7-8) deep aponeurosis. Fascicle length defined as the distance between fascicle insertion at the deep and at the superficial aponeuroses. Pennation angle defined as the angle between the deep aponeurosis and the fascicle. Muscle thickness defined as the perpendicular distance between superficial and the deep aponeurosis.

Conclusion: In conclusion, changing pedalling cadence from 70 to 90 rpm at constant workload increases VL fascicle length and decreases pennation angle.

Table: Table 1. Vastus lateralis fascicle length, pennation angle and muscle thickness at 70 and 90 rpm.

(%POmax trial)	70 rpm	90 rpm
Fascicle length	#74±33%	#86±35%
Pennation angle	#115±45%	#96±34%
Muscle thickness	101±5%	99±6%

# indicates significant difference between pedalling cadences (p≤0.05).

References: [1] Ansley L, et al. Determinants of "optimal" cadence during cycling. Eur. J. Sport Sci. 9: 61-85, 2009.

[2] Austin N, et al. In vivo operational fascicle lengths of vastus lateralis during sub-maximal and maximal cycling. J. Biomech. 43: 2394-9, 2010.

[3] Dorel S, et al. Changes of pedaling technique and muscle coordination during an exhaustive exercise. Med. Sci. Sports Exerc. 41: 1277, 2009.

[4] Chapman AR, et al. Patterns of leg muscle recruitment vary between novice and highly trained cyclists. J Electromyogr Kinesiol. 18: 359-71, 2008.

Disclosure of Interest: None Declared

AS-0005

FORCE PRODUCTION AND WEIGHT SHIFTING DURING OLYMPIC LIFTS UNDER DIFFERENT ATTENTIONAL FOCUS CONDITIONS

James Becker [1] Natalie Maltz [1,*] Anthony Vidal [1] Will Wu [1]

[1] Kinesiology, California State University, Long Beach, Long Beach, United States

Introduction and Objectives: When providing coaching cues for snatch lift (SL), coaches may manipulate verbal instructions to elicit different attentional focus (AF) strategies from the athlete. Altering the AF directly affects the performance outcome[1], with instructions which direct the AF of the performer externally yielding greater improvements in performance than instructions which direct the participant's AF internally [1-4]. While some mechanisms behind these effects have been examined, how AF affects the forces generated by a lifter during a SL has not been examined.   Therefore, the purpose of this study was to examine the force production and weight shift during first pull (1P), transition (T), and second pull(2P) of the SL and whether different AFs change the pattern of weight shift and ground reaction forces. It was hypothesized that the lifters would produce greater impulses with instructions which focused their attention externally compared instructions which focused their attention internally.

Methods: Nine experienced lifters (age: 24.5±3.02 years, experience lifting: 3.1±1.90 years). Participants performed snatch lifts at 80% of their 1-repetition maximum under three different attentional focus conditions: baseline (B), internal focus of attention (IF), and external focus of attention (EF). For the IF condition participants were instructed to "raise their elbow up rapidly" while in the EF condition they were instructed to "lift the bar up as fast as possible." The F-Scan (Tekscan Inc., Boston MA) in shoe plantar pressure system was used to measure normal forces under the foot, sampling at 500 Hz. A custom LabView (National Instruments, Austin TX) program was used to trim each lift from immediately before the lift began to just before the feet contacted the ground at the end of the second pull.   Vertical impulse and peak vertical force were then extracted for analysis. Additionally, the forces under the whole foot, heel region, and metatarsal region were evaluated at the local peak force maximum during the 1P, T, and 2P phases of the lift.   Differences in peak force and vertical impulse between conditions were evaluated using a one-way repeated measure ANOVA.   Differences in forces under each region and between the three attentional focus conditions were evaluated using a 2-way repeated measure ANOVA.

Results: Peak force through the entire lift was not different between conditions (B: 2241.8 N ±559.8; IF: 2316.8±491.0 N; EF: 2345.7±475.8 N; $p = 0.575$). Propulsive impulse throughout the entire lift was lower in the EF condition than in the B condition (EF: 611.2±66.7 N*s; B: 667.1±67.2 N*s; $p = 009$), but there were no differences in propulsive impulse between EF and IF condition (IF: 624.9±71.9 N*s; $p = .395$).

There was no focus by phase interaction effect for force under the heel ($F_{1,1} = 4.8$, $p = 0.2$) or force under the metatarsals ($F_{1,1} = 1.2$, $p = 0.06$). Similarly, there was no main effect of attentional focus for force under the heel ($F_{1,17} = 1.7$, $p = 0.2$) or force under the metatarsals ($F_{1,17} = 1.5$, $p = 0.2$). There was no main effect for force under the heel at any phase of the lift ($F_{2,17} = 1.9$, $p = 0.2$). There was a significant difference between the forces under the metatarsals for the three phases, with force under the metatarsals being significantly higher in the 1P and 2P phases than during the T phase (T:

168.6±20.8 N, p=0.0). Finally, forces under the metatarsals were higher in the 2P than then 1P (1P: 373.2 ± 32.2 N, 2P: 513.3± 39.2 N, p=0.002).

Conclusion: The results of this study suggest focus of attention cues affect the impulses but not peak forces generated during the SL. The hypothesis was not supported by the results in that the external focus cue would be associated with a larger propulsive impulse. This seemingly contradictory finding may be partially explained by the constrained action hypothesis which suggests an external focus of attention results in a more efficient neuromuscular system. That peak vertical force was not affected by the application of different attentional focus cues agrees with previous results[1].   However, despite a difference in force production, improved performance outcomes were observed. Previous research on performance of the SL has suggested the rearward shifting of weight during the transition phase was a key element for a successful lift. While the results of this study do not fully support this hypothesis, there was a significant decrease in force under the metatarsals during the transition phase. Future research is required to examine if the magnitude of this weight shift is related to successful completion of the lift.

References: 1. Wu, W. *J. Strength Cond. Res.* **26,** 1226-1231, 201.

2. NcNevis, N. et al. *Psychol. Res. 67,* 22-29, 2003.

3. Wulf, G. *Int. Rev. Sport. Exerc. Psychol.* **6,** 77-104, 2013.

4. Garhammer, J. et al. *Int. Maxachievment Institutes*, 1973.

Disclosure of Interest: None Declared

Sport

AS-0006

3D MOTION ANALYSIS OF WRIST ENGAGEMENT AND MALLET TRAJECTORY IN CROQUET

Jenny C. Clarke [1,*]Gavin Blackwell [1]

[1]School of Sport and Physical Education, University of Canterbury, Christchurch, New Zealand

Introduction and Objectives: A croquet swing is generated by holding the mallet with one hand gripping the mallet shaft above the other, and swinging so that the head of the mallet moves between the ankles backwards then forwards to strike a croquet ball. The swing is generated primarily from movement at the shoulders, though some body movement and flexion of the elbows and wrists can be involved.

The aim of this study was to investigate the dynamics of the swing of a croquet mallet with specific attention to the wrist flexion of the lower hand and lateral deviation of the mallet head during the swing. Excessive wrist flexion has been associated with discomfort, particularly among older croquet players who dominate the sport's demographic. Lateral deviation of the mallet, a twisting of the mallet about its shaft, leads to a swing in which the mallet head does not follow a desirable straight trajectory, requiring the player to accurately correct the trajectory of the mallet at the moment of impact for a straight hit. This research sought to determine if there was a correlation between excessive wrist flexion and lateral rotation of the mallet head.

Methods: Twenty-six association croquet players (17 male, 9 female) with ages ranging from 21 to 85 yeas old participated in the croquet swing study. All respondents use the 'standard' croquet grip with the knuckles of the top hand facing forward, the palm of the lower hand facing forward, and both hands either very close together or slightly overlapping. A BTS 3D imaging system was used which utilizes 4 infra-red cameras to track reflective markers placed on the arms, hands, feet of the participants. Additional tracked markers were placed at the front and back of the head of the mallet and at the top of the shaft of the mallet. Dynamic position information was recorded with an accuracy of 0.5mm. In addition, high definition and high-speed (300 frames per second) cameras were used to capture visual footage of the strokes.

Each participant had 2-3 practise strokes in the lab before taking 10 shots hitting a croquet ball with their own mallet in their usual stance and style at a stationary croquet ball which was 4.5m from the striker's ball. The flexion of the wrist from the starting point of the swing to the peak of the backswing was measured for each stroke, as well as the angle of lateral rotation of the mallet at the peak of the backswing compared to the neutral position at the starting position of the swing. A Pearson correlation was used to test if there was a relationship between wrist flexion and rotation of the mallet about the shaft (lateral deviation) at the peak of the backswing. The peak of the backswing is the point at which the swing is most crooked.

Results: A significant correlation was found between the flexion of the wrist on the lower hand gripping the mallet and the rotation of the mallet head about the shaft of the mallet. This provides evidence that an undesirable twisting motion in the croquet swing is caused, at least in part, by excessive engagement of the wrist.

Figure:
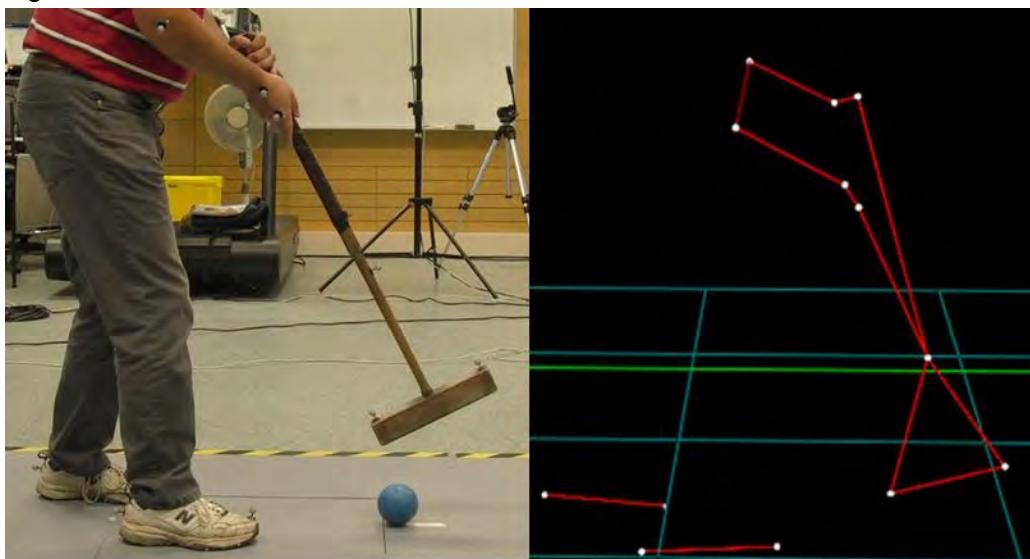
Caption: Placement of markers for 3D motion capture analysis of croquet swing and marker tracking using BTS Smart Tracker. The lower hand markers clearly indicate the wrist angle of interest.

Conclusion: The study sought to determine if there is a relationship between flexion of the lower wrist of a standard grip croquet player between the start of the backswing and at the peak of the backswing.

A straight backward and forward swing produces a longer period of path of the swing during which contact between the mallet and ball will result in a straight and accurate shot. While a crooked swing can still be straight at the time of impact, numerous anecdotal evidence suggests that extended periods of inaccurate shooting can affect players with crooked swings, and that these "bad spells" can be harder to correct or recover from. Additionally,

A significant relationship was found between the lateral deviation at peak backswing and flexion of the lower wrist from the start of the swing to the peak of the backswing. This provides strong evidence that a significant mechanism generating the crooked backswing is lower wrist flexion.

This study has found both an anatomical mechanism for an undesirable swing characteristic in the mallet sport of croquet, and suggests an 8-week intervention using psychological and physical training in the form of visualisation and non-striking swinging practice to reduce this characteristic and affect an improvement in shooting performance of croquet players.

Future work involves testing the intervention in-season on a group of croquet players, while monitoring swing accuracy and physical comfort. The next stage involves developing and implementing a more detailed/methodological intervention for croquet coaches to disseminate to club and higher level players. Finally, this analysis can be immediately applied to putting in golf.

References: [1] David R. Appleton, Journal of the Royal Society of Medicine, 90(4), 218-220, 1997.

Disclosure of Interest: None Declared

AS-0007

MODELLING AND SIMULATION OF OSTEOCHONDRAL AUTOGRAFT TRANSFER: QUANTIFYING THE EFFECTS OF CARTILAGE THICKNESS MISMATCH BY FINITE ELEMENT ANALYSIS

Yuxing Wang [1,*]Richard A. Black [2]Yubo Fan [1]

[1]School of Biological Science and Medical Engineering, Beihang University, Beijing, China, [2]Department of Biomedical Engineering, University of Strathclyde, Glasgow, United Kingdom

Introduction and Objectives: Injuries sustained by articular cartilage are relatively common and lesions persist as cartilage is avascular and has a relatively poor capacity for healing. Acute injuries and degeneration of the joints affect not only the elderly but younger, physically active people also. Without treatment, these lesions can easily aggregate and progress to osteoarthritis so it is important that patients are treated at an early stage. Surgical approaches such as Osteochondral Autograft Transfer (OATS), autologous chondrocyte transplantation or articular resurfacing may be considered in such cases. OATS involves harvesting 'plugs' of cartilage and underlying bone from healthy regions to restore damaged areas, but the biomechanical basis for this procedure is unclear. While the size, mechanical properties, and shape of such grafts have been the subject of previous studies, little attention has been paid to the differential properties of the tissues involved: grafts are harvested from non-load bearing sites on the periphery and transplanted to the damaged area, which is usually located more centrally (see Figure). Consequently, there is likely to be a mismatch of cartilage thickness between the implant and surrounding tissue. The aim of this study, therefore, was to quantify the impact of this mismatch on the stress distribution and contact pressures generated within the cartilage of the apposing surfaces, and within the graft itself, under loading conditions representative of the human knee joint.

Methods: A parametric analysis was carried out to investigate the influence of cartilage thickness mismatch using a finite element model of the human knee joint [1]. The 3D model was developed in MIMICS, and was based on magnetic resonance images of a healthy knee, including bony parts, cartilages, menisci and major ligaments. The individual components were meshed with hexahedral elements within Abaqus, and assigned mechanical properties determined from the literature. A cylindrical defect was created at the medial condyle of the femur; likewise, a cylindrical osteochondral 'graft' was added to simulate the transplantation. The cartilage thickness of the graft was varied from one third up to twice the original thickness to simulate the thickness mismatch, as shown in the Figure. A static compressive load of 1000N was applied during each simulation. Forces originating from the surrounding musculature were also represented, and assigned values reported in the literature – quadriceps (215N), biceps femoris (31N), and semimembranosus muscles (54N).

Results: The results of the simulations are tabulated in terms of Von Mises stresses and contact pressures that develop within the cartilage compartments in each case. Here, the mismatch in cartilage thickness is expressed as a ratio of autograft to intact thickness. The results indicate that a mismatch in cartilage thickness where the cartilage of the autograft is thinner than the surrounding cartilage gives rise to greater contact pressures and stresses, and that these stresses return to the levels seen in the intact tissue as the thickness of the cartilage increases. It follows that a graft having a greater cartilage thickness is to be preferred in cases where a perfect match is difficult to achieve.

Figure:
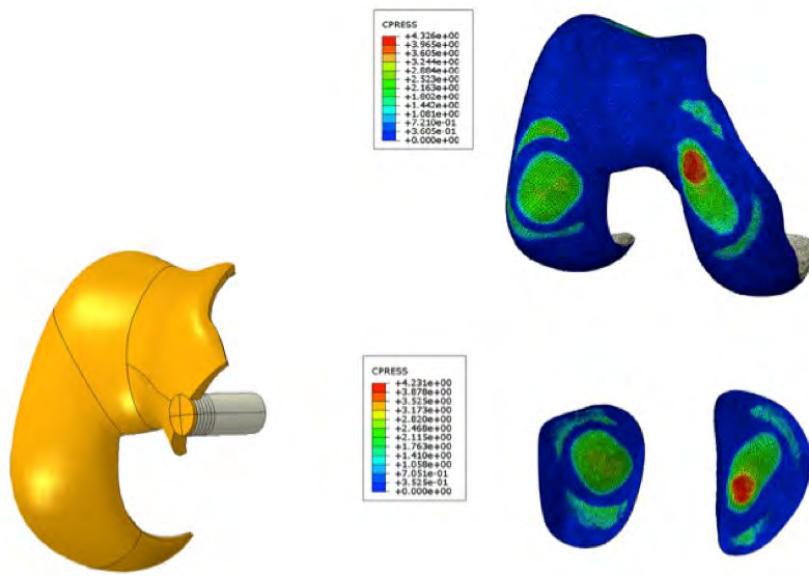
Caption: Contact pressures (MPa) following osteochondral autograft transfer (OATs) procedure. The knee model is based on that developed by Wang et al., 2014 [1].

Conclusion: The finite element model of the intact knee was originally developed to determine the stresses developed in knee cartilage during kneeling and standing [1]. Here, the model has been modified to determine the contact pressures and stress distribution in human knee cartilage following osteochondral autograft transfer. The results of the present study suggest that better matching of graft dimensions may improve the quality of engraftment, but it remains to be shown whether improvements in fixation will lead to better outcomes in the longer term. With further refinement, however, we believe that modelling approaches of this kind will improve our understanding of the role of tissue properties and biomechanical factors in the fixation of osteochondral grafts during surgery, and their subsequent remodelling post operatively.

Table:

	Femoral Surface		Tibial Surface	
Autograft/Intact Cartilage Ratios	Peak von-Mises Stress (MPa)	Peak Contact Pressure (MPa)	Peak von-Mises Stress (MPa)	Peak Contact Pressure (MPa)
Intact Cartilage	1.62	3.27	1.49	3.27
Void (autograft absent)	3.15	3.95	1.72	3.89
1/3	1.71	3.70	2.14	4.23
2/3	1.62	3.21	1.76	3.67
Full thickness autograft	1.72	3.06	1.50	3.27
4/3	1.91	3.03	1.48	3.05
5/3	1.95	3.02	1.46	3.00
6/3	1.97	3.00	1.45	2.99

Caption: Peak von-Mises stresses and contact pressures as a function of autograft cartilage thickness relative to intact cartilage.

References: [1] Wang et al., Medical Engineering & Physics, 36(4): 439-447, 2014.

Disclosure of Interest: None Declared

Computer Simulation

AS-0008

BOTTOM-UP MECHANO-STRUCTURAL MODELING OF THE CARTILAGE MATRIX

Ying-Chun Chen [1,*]Minsi Chen [2]Andrew Price [1]Cameron Brown [1]

[1]Nuffield Department of Orthopaedics, Rheumatology and Musculoskeletal Sciences, University of Oxford, Oxford,

[2]Department of Computing and Mathematics, University of Derby, Derby, United Kingdom

Introduction and Objectives: To understand early interventions for diseases such as osteoarthritis, we need to understand what constitutes functionally viable tissue, and the 'tipping point' at which damage becomes irreversible. As one of the major structural components and determinants of function in the cartilage matrix, collagen plays a central role in the disease process.[1] Collagen meshwork disruption is rarely repaired,[2] and reconfiguration in early stages of disease has been observed before histological changes become apparent.[3]

Modeling can be used to explore mechano-structural changes in both disease and repair. Cartilage modeling has been extensively pursued using continuum approaches, with a number of recent approaches considering collagen organisation.[e.g. 4] Simulating local restructuring or damage progression on a relevant scale for early disease is challenging. The aim of this study is to develop a structure-based computational model to explore ultrastructural responses to the load with time accumulation and local damage feedbacks. We take a 'bottom-up' approach to set the arrangement, orientation and properties of each constituent part at the nano- to micro-scale, and assemble them into a tissue structure. Here, we report our development of a collagen-fluid interaction model.

Methods: Our current model comprises of the interstitial fluids (e.g. collagen, proteoglycan) and the extracelluar collagen matrix. The incompressible interstitial fluids are modeled using the Navier-Stokes equation over a regular Eulerian grid. We use an FFT based solver for the incompressible fluids. The collagen matrix consists of a collection of masses interconnected by non-linear springs. The configuration of the matrix including the mass connectivity is taken directly from previous experiments.[3] With this approach, the mechanical properties of the collagen fibril [5] are embedded in the non-linear spring force connecting the masses. Our current implementation is written in C++ which utilises the GPU for fluids related computation and the host CPU for simulating the collagen structure.

The resolution of matrix-fluid interaction is divided into two phases similar to the immersed boundary methods. Firstly, masses on the collagen matrix are advected over the fluid grid. Following the advection, each matrix mass exerts a force to the fluid based on the strain in connecting springs. We tested different levels of abstraction/simplification on a single-fibril system under a far-field constant fluid velocity. The interaction was calculated and applied at the nearest fluid-grid node to the mass-spring node, at ±3 and ±5 fluid-grid nodes, and at the fluid-grid nodes along the fiber. Impulse-based collision calculations were also tested. Once interactions were established in the single fibril configuration, they were applied to a regular grid.

Results: Under a constant far-field fluid velocity applied perpendicular to the single fibre, the fibril deformed and settled in the configuration shown in Figure 1a. Solid node reactions of the single fibril, accelerating against the direction of fluid flow, are given in Figure 1b. Upon resetting the fluid velocity field to zero, the spring returns to its original position over a period of 3.5 minutes. Altering the interaction implementation had little effect on the global response of the fluid and solid,

however the local fluid field was adversely affected for the single fluid-grid node and ±3 node setups (Figure 1c). This effect was limited at low fluid velocities.

Using a regular grid configuration and locally applied fluid velocity fields or collagen meshwork deformations (Figure 1d), the constraints added by adjacent solid nodes further limited the adverse effects of simplified interactions. Again, the system deformed under the applied load and returned to its original configuration when the fluid velocity field was reset. Enabling damage feedbacks in the solid caused irrecoverable deformation.

Figure:
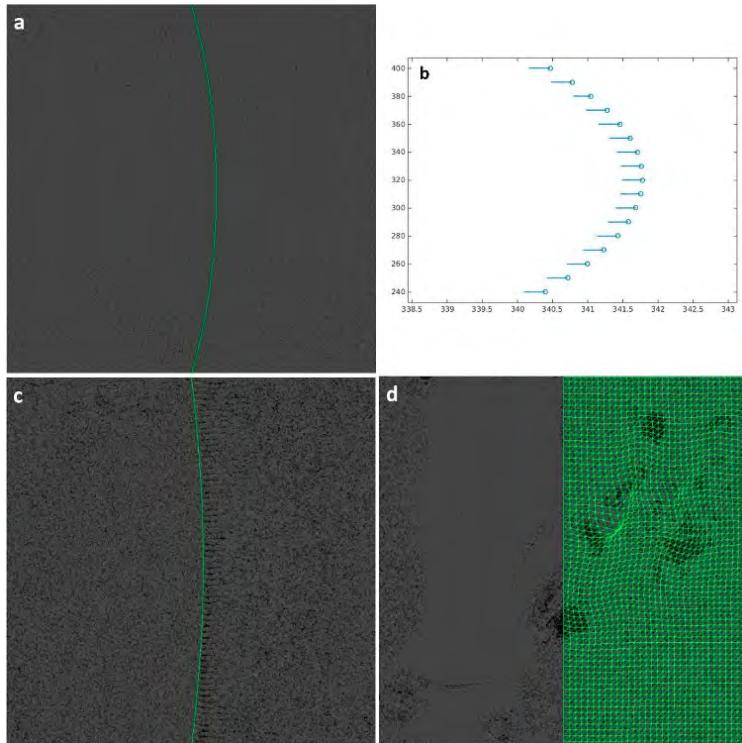
Caption: Collagen-fluid interaction results: (a) Typical single fibril deformation under fluid flow; (b) reaction of solid nodes opposing fluid flow; (c) nearest-neighbour interaction showing local fluid field inhomogeneity to right of fibril; (d) deformation and fluid field patterns in regular grid configuration.

Conclusion: The current implementation of the 'bottom-up' spring-mass-fluid model can simulate the interaction between fluid and the collagen meshwork on a scale relevant for early damage. Using this structure-centred approach, physical and biological feedbacks can be used to simulate degradation and repair processes. Further work will be required to include aggrecan behaviour and interactions, and to link structural damage with diagnostic parameters.

References: [1]   Broom et al., Arthritis Rheum., 25: 1209-1216, 1982.

[2]   Hunziker et al., Osteoarth. Cartilage, 10: 432-463, 2002.

[3]   Brown et al., Biomed.l Opt. Exp., 5, 2014.

[4]   Ateshian et al., J Biomech. Eng., 131: 061003, 2009.

[5]   van der Rijt et al., Macromol. Biosci., 6: 697-702, 2006.

Disclosure of Interest: None Declared

COMPARISON BETWEEN ELASTIC AND POROELASTIC MODEL TO SIMULATE CARTILAGE-MENISCUS-CARTILAGE INTERACTIONS

Bernardo Innocenti [1,*] Cristiano Vitanza [2] Leonardo Ruggiero [3] Alberto Audenino [2] Thierry Massart [4] Walter Pascale [5] Silvia Pianigiani [5]

[1] BEAMS Department, Université Libre de Bruxelles, Bruxelles, Belgium, [2] Politecnico di Torino, Torino, Italy, [3] Department of Mechanics of Materials and Constructions, Vrije Universiteit Brussel, [4] Building, Architecture & Town Planning, Université Libre de Bruxelles, Bruxelles, Belgium, [5] IRCCS, Istituto Ortopedico Galeazzi, Milano, Italy

Introduction and Objectives: Articular cartilage and menisci are two soft tissues playing an important role in the knee joint biomechanics. In fact, they act as load bearing structures and shock absorbers. However, in the literature, there is not agreement in describing these two soft tissues mechanical behaviour. Usually, they are mainly modeled with elestic or poroelestic in order to develop close-to-real native knee finite element models, but discordant approaches can be found. For these reasons, the aim of this work is to develop and compare different models to simulate the femoral cartilage-meniscus-tibial cartilage (CMC) interaction by means of finite element analysis (FEA).

Methods: Both cartilages and meniscus were modelled as simplified geometries. Similar rectangles in a frictionless contact where considered for 2D-axisymmetric simulations in which both the cartilage and the meniscus material were modelled as poroelastic or elastic only. The values to characterize the properties for the two selected models were based on literature studies.

The same mesh element was chosen for both material models. The addiction of the bilinear pore pressure characteristic was considered for the poroelastic model.

Developing a model with poroelastic properties, boundary conditions (BCs) must differentiate in mechanical and fluid BCs. Particularly, in a poroelastic numerical model, the contact between two or more structures has a fundamental role. A literature study analysed the contact with sealed and contact dependent surfaces, and they obtained that surfaces have the same behaviour for the first two seconds of a simulation. According with these results, the cartilage surfaces contacting were assumed sealed and the interaction between the two structures frictionless. Based on these findings, the CMC model was set to simulate a soil analysis and Nlgeom, parameter to consider finite deformation. As presented in experimental studies, a homogeneous pressure of 12 kPa was axially applied on the top of the rectangular representing the femur cartilage.

Contact pressures, stresses and displacements are analysed under these conditions.

Results: A significant difference, particularly in terms of contact pressure and displacements, is shown by the obtained outputs comparing the poroelastic and elastic model. The contact pressure (Figure 1a) of the elastic model decreases up to 38% for the poroelastic configuration with respect the elastic one. Analysing the displacements, in both the radial (Figure 1b) and in the axial direction (Figure 1c), the poroelastic model presents higher values than the elastic (up to 2-3%). The mechanical response in term of Von Mises stresses (Figure 1d) shows no differences between the two modelling approaches and also a similar qualitative distribution can be observed.

Figure:
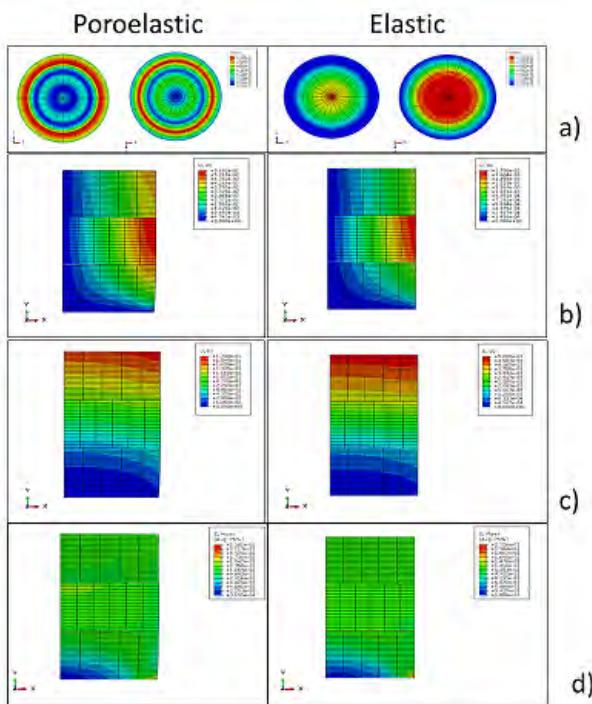
Figure 1: a) contact pressure; b) radial displacement;
c) axial displacement; d) qualitative stress distribution

Conclusion: The aim of this study was to develop a methodology to compare different models to simulate the CMC interactions by means of FEA. For this reasons, the CMC interaction has been modeled using elastic and poroelastic material characteristics under boundary conditions replicating experimental tests.

The results show that the elastic model is more rigid than the poroelastic one, above all comparing the contact pressure and displacements, nevertheless the same mechanical response in terms of stress was obtained. One limitation of this study is the use of 2D-axisymmetric model with simplified geometries to simulate real CMC in a knee joint. Moreover, permeability depends on the deformation state of the soft tissue, but in the present study was assumed to be constant. However, this assumption does not reply in the analysis of other outputs, as contact pressure and displacements, which requires the development of a poroelastic model. In addition, these simplifications allow reducing the computational time for the solutions of both models, in particular of the poroelestic one.

For these reasons, we can conclude that our findings are important in order to simulate close-to-real native knee FEA models and different approaches in material definition can be followed dependently on the investigation type. Our model can be improved considering real geometries of the analysed soft-tissue structures, but it can deliver a first important advice for the modelling and the understanding of these structures behaviour under different loading conditions. The use of the outcomes of this work are useful in providing replies for question related to cartilage and meniscus behaviour derived from clinical practice and to provide useful information for the development of new material replicating these structures.

Disclosure of Interest: None Declared

Computer Simulation

AS-0011

POROELASTIC FINITE ELEMENT MODEL OF OSTEOGENESIS WITHIN A TITANIUM SCAFFOLD COUPLING BIOLOGY AND MECHANICS

Mary Schmitt [1,*] Rachele Allena [1] philippe Rouch [1]

[1] LBM / Institut de Biomécanique Humaine Georges Charpak, Arts et MétiersParisTech, Paris, France

Introduction and Objectives: Bone is a living tissue able to restore itself when it is injured. However, when a defect exceeds a critical size a structural support such as a scaffold is required in order to enhance osteogenesis. Recently, several experimental [1] and numerical works [2,3] have been developed to better understand the complex process of osteogenesis within scaffolds.

Following a preliminary study [4], we propose here a more exhaustive three-dimensional poroelastic finite element model, which couples mechanics and biology and simulates bone ingrowth within a titanium scaffold implanted into ewes' mandibles during twelve weeks. The main goal of the present work is to evaluate the effects of the mechanics on the cellular activity (*i.e.* the mechano-transduction phenomenon).

Methods: Our model is based on an experimental study, which aims to evaluate the osteogenesis within a titanium scaffold implanted on the non-toothed part of ewes' mandible during 12 weeks. We use a simplified 3D beam to represent the titanium scaffold (18mm long and 12mm width, Figure 1a). The left boundary of the scaffold is clamped, while the right boundary is submitted to a cyclic load describing the ewe's mastication with a period of 1s.

For the sake of computation time, an algorithm has been developed.

First, since the interstitial fluid may have a real impact on cells activity [5], the scaffold is considered as a poro-elastic material and the poroelasticity equations are solved during one mastication cycle. More specifically, the total stress is related to the effective stress in the solid phase and to the interstitial pressure in the fluid phase. Furthermore, the variation of the pressure satisfies a partial differential equation depending on the porosity, on the permeability of the scaffold, on the compressibility and the viscosity of the interstitial fluid as well as on the global displacement of the structure. We assume that the external boundaries of the system are free draining.

At the end of the mastication cycle, the average fluid velocity, which will be involved in the differentiation pathway of the mesenchymal stem cells (MSCs), is stored.

Second, the reaction-diffusion equations which describe the complex cellular activity within the scaffold are solved for 1 week. This complex cellular activity occurs in 4 successive steps and involves different type of cells: i) the migration and the proliferation of the MSCs ii) the differentiation of the MSCs into either osteoblasts, chondrocytes or fibroblasts iii) the proliferations of the osteoblasts, chondrocytes and the fibroblasts and iv) the formation of the extracellular matrix (bone, cartilage and fibrous tissues respectively). Thus, the evolution of the different cells concentrations in the scaffold are regulated by three processes: migration, proliferation and differentiation. The migration term allows coupling the cells concentrations with the principal stress and directions of the structure. The proliferation term allows simulating the cell division (mitosis) until the maximum total cells concentration is not reached. Finally, the differentiation term allows the MSCs differentiation into either osteoblasts, chondrocytes or fibroblasts and starts after a maturation time of 14 days.

Moreover, since cells differentiation may be affected by the mechanical environment, the differentiation pathway is regulated by two biophysical stimuli: the shear strain and the interstitial fluid velocity [2].

After 1 week, the cells distribution and the mechanical properties of the scaffold are updated and stored. Then, steps one and two are recomputed to cover a time interval of 12 weeks.

Results: In Figure 1b, the evolution with respect to time of MSCs and osteoblasts concentrations is represented. We can observe that the cellular colonization of the MSCs takes place from the exterior towards the interior of the scaffold as it has been experimentally observed. Moreover, since the differentiation process starts after 14 days of maturation, we observe that after 4 weeks, there are few osteoblasts.

Currently, micro-computed tomography scanners of the 12 weeks explanted hemi-mandibles are being performed in order to validate our mechano-biological approach.

Figure:
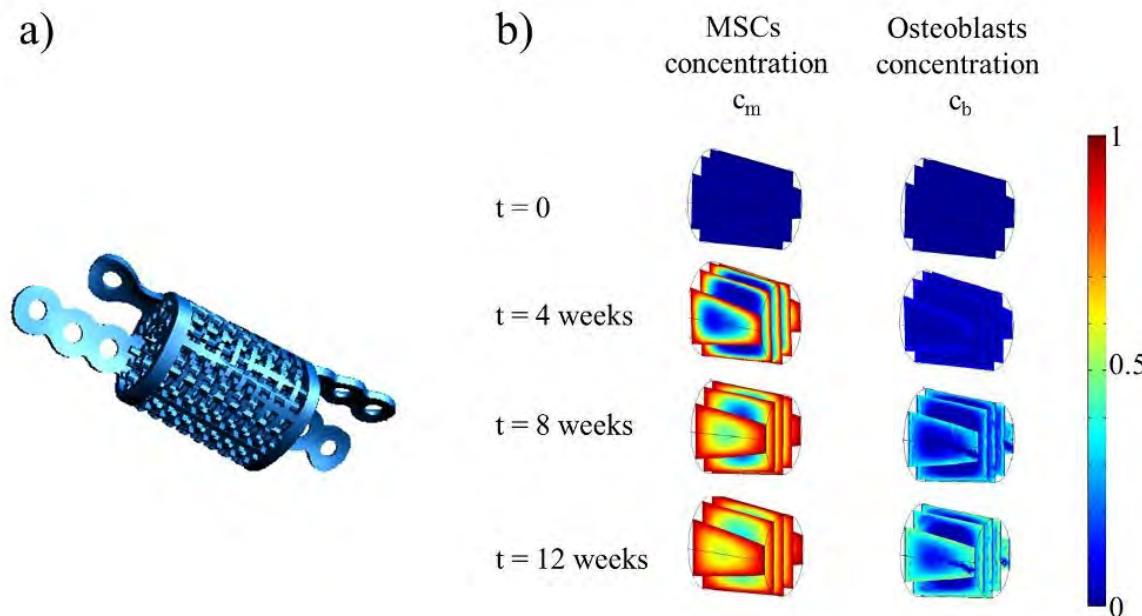
Caption: (a) Titanium scaffold (b) MSCs and osteoblasts concentration cm and cob respectively at 0, 4, 8 and 12 weeks.

Conclusion: In conclusion, we propose a 3D poroelastic finite element model of osteogenesis able to predict bone ingrowth during 12 weeks within a titanium scaffold submitted to a cyclic load while keeping a reasonable computation time.

References: [1] Karageorgiou et al., Biomaterials, 26:5474–5491, 2005.

[2] Prendergast et al., J. Biomech., 30:539–548, 1997.

[3] Checa et al., J Biomech., 43:961–968, 2010.

[4] Schmitt et al., Comput. Method. Biomech., 16 (sup1), 266 267, 2013.

[5] Cowin et al., J. Biomech. Eng., 113 (2), 191 197, 1991.

Disclosure of Interest: None Declared

Modelling

AS-0012

A NEW STRAIN ENERGY FUNCTION FOR THE HYPERELASTIC MODELLING OF LIGAMENTS AND TENDONS BASED ON FASCICLE MICROSTRUCTURE

Tom Shearer [1,*]

[1]School of Mathematics, University of Manchester, Manchester, United Kingdom

Introduction and Objectives: Ligaments and tendons are fundamental structures in the musculoskeletal systems of vertebrates. Ligaments connect bone to bone to provide stability and allow joints to function correctly, whereas tendons connect bone to muscle to allow the transfer of forces generated by muscles to the skeleton. The wide variety of roles played by different ligaments and tendons requires them to have considerably different mechanical responses to applied forces, and their differing stress-strain behaviours have been well documented.

Ligaments and tendons consist of collagenous fibres organised in a hierarchical structure. Their main subunit is the fascicle which consists of fibrils arranged in a crimped pattern. In this talk I will derive a new strain energy function for the hyperelastic modelling of ligaments and tendons based on the geometrical arrangement of their fibrils, and will compare the ability of the new model to match experimental data with that of the commonly-used Holzapfel-Gasser-Ogden (HGO) model [1]. There have been many attempts to mathematically model the behaviour of ligaments and tendons within a non-linear elastic framework; however, the vast majority of these (including the HGO model) are phenomenological. A micro-structurally based model will allow us to understand *how* the mechanical reponse of ligaments and tendons results from the arrangement of their constituent subunits.

Methods: Kastelic et al. [2] derived the stress-strain response of a fascicle under uniaxial tension as a function of the microstructural arrangement of its fibrils. Unfortunately, however, an error in the implementation of Hooke's law in that paper led to the derived stress-strain relationship being incorrect. In this talk, I correct the mistake in [2] and use a new functional form for the radial crimp angle distribution in order to derive an analytical expression for the stress-strain response of a single fascicle and use this expression to derive the new strain energy function.

Results: The new model is compared with the HGO model and it is shown that the new model gives a better match to exisiting stress-strain data for human patellar tendon [3] than the HGO model, with the average relative error when using the new model being 0.053 (compared with 0.57 when using the HGO model), and the average absolute error when using the new model being 0.12MPa (compared with 0.31MPa when using the HGO model). In the figure, the experimental and theoretical stresses are plotted as a function of the longitudinal strain; the red dots are the experimental data taken from [3], the solid black line is the new model, and the dashed blue line is the HGO model.

Figure:
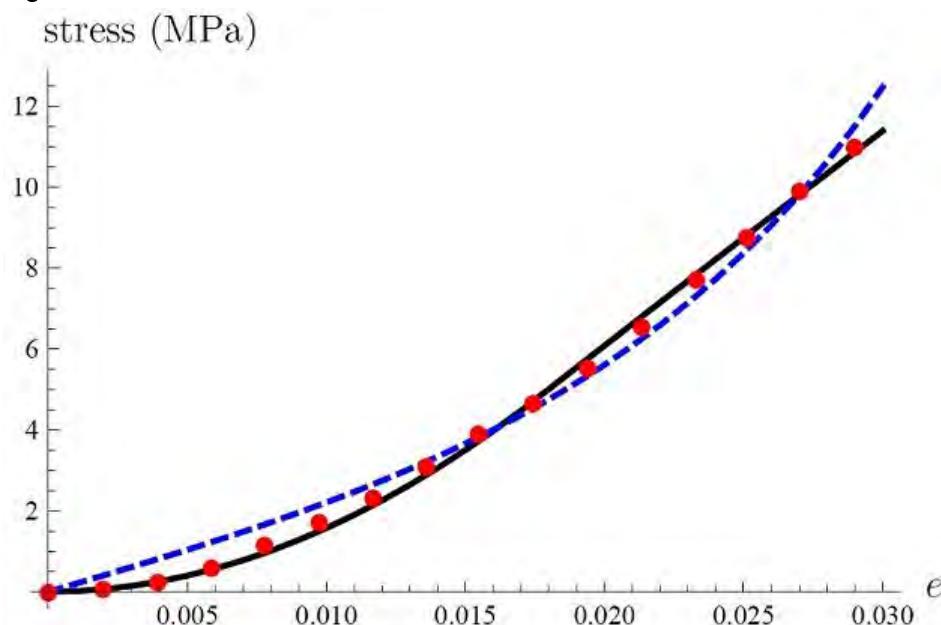
Conclusion: The new model shows excellent agreement with experimental data and also has the advantage of only containing parameters that can be *directly measured via experiments*. Since the model is expressed in terms of a strain energy function, it can easily be implemented into finite element software in order to decribe complex mechanical deformations. In the future, it will hopefully be possible to extend this model to incorporate viscoelasticity in order to understand phenomena such as hysteresis and stress-relaxtion, which have been observed experimentally in ligaments and tendons.

References:

[1] Holzapfel et al., J. Elasticity, 61: 1-48, 2000.

[2] Kastelic et al., J. Biomech., 13: 887-893, 1980.

[3] Johnson et al., J. Orthopaed. Res., 12: 796-803, 1994.

Disclosure of Interest: None Declared

Motion Analysis

AS-0013

KINETIC COMPARISON OF WALKING ON AN INSTRUMENTED TREADMILL VERSUS OVER GROUND IN CHILDREN WITH AND WITHOUT CEREBRAL PALSY

Marjolein M. Van Der Krogt [1,*] Lizeth Sloot [1] Jaap Harlaar [1]

[1]Rehabilitation Medicine, VU University Medical Center, Amsterdam, Netherlands

Introduction and Objectives: Instrumented treadmills are increasingly used in clinical gait analysis and gait (re)training, since they allow for measurement of many consecutive steps and facilitate use of feedback and perturbations. Previous studies found consistent but small differences between overground (OG) and treadmill (TM) walking for healthy adults [1,2]. These include slower walking speed, shorter and wider steps, and small differences in kinematics, kinetics and EMG.

Recently it has been shown that kinematics are generally similar between OG and TM for typically developing children and children with cerebral palsy (CP) [3]. However, kinetics have not yet been compared for children nor for individuals with CP.

The aim of this study was to compare kinetic outcomes (ground reaction forces (GRF), center of pressure (CoP), joint moments and joint powers) between OG and TM walking in a virtual environment, for typically developing (TD) children and children with spastic CP.

Methods: 20 children were included: 9 children with spastic CP (4 male, 5 female; age 11.6 ± 2.1 years, range 8-14; height 1.49 ± 0.13 m; weight 40.9 ± 10.3 kg) and 11 TD children (7 male, 4 female; age 10.6 ± 2.2 years, range 8-15; height 1.52 ± 0.15 m; weight 38.2 ± 10.5 kg).

In one session, subjects walked in random order 1) OG in a conventional gait lab with two embedded force plates (AMTI); and 2) on a dual-belt instrumented TM (R-Mill, Forcelink), placed in a speed-matched virtual environment (GRAIL system, Motek Medical BV). The speed of the belt was real-time adjusted to match the subject's time-varying walking speed, by means of a self-paced speed algorithm [4]. 3D motion capture data were collected using identical systems in both labs (Optotrak, Northern Digital Inc.).

Joint moments and powers were calculated using ISB definitions [5]. As outcome measures, key peak values were calculated for GRF, CoP (relative to heel marker), hip, knee, and ankle moments and powers, as well as the total amount of positive and negative work done by hip, knee and ankle. Walking speed was analyzed as a potential confounding factor. All data was averaged over five strides per subject for each lab. Condition (OG/TM), group (TD/CP) and interaction effects were determined using an ANOVA for repeated measurements.

Results: Peaks of vertical and anterior-posterior GRF were identical between OG and TM, but mediolateral GRF was on average 96% larger in TM ($p < 0.001$). CoP was 10% of foot length more posterior in TD and 13% more anterior in CP (interaction $p < 0.001$). Furthermore, CoP was more medial in TD (20% of foot width, $p = 0.004$), but similar in CP children. Peak hip extension moment and hip and knee abduction moments were increased in TM by 35% and 36% respectively ($p < 0.01$; Fig. 1). Peak ankle extension moments were decreased by 7% in TD but increased by 9% in CP (interaction

p=0.039). Total positive hip work increased by 15% in TM (p=0.014), while total positive ankle work decreased by 25% (p=0.002). Peak ankle power tended to be lower (p=0.09). Walking speed did not differ significantly.

Figure:
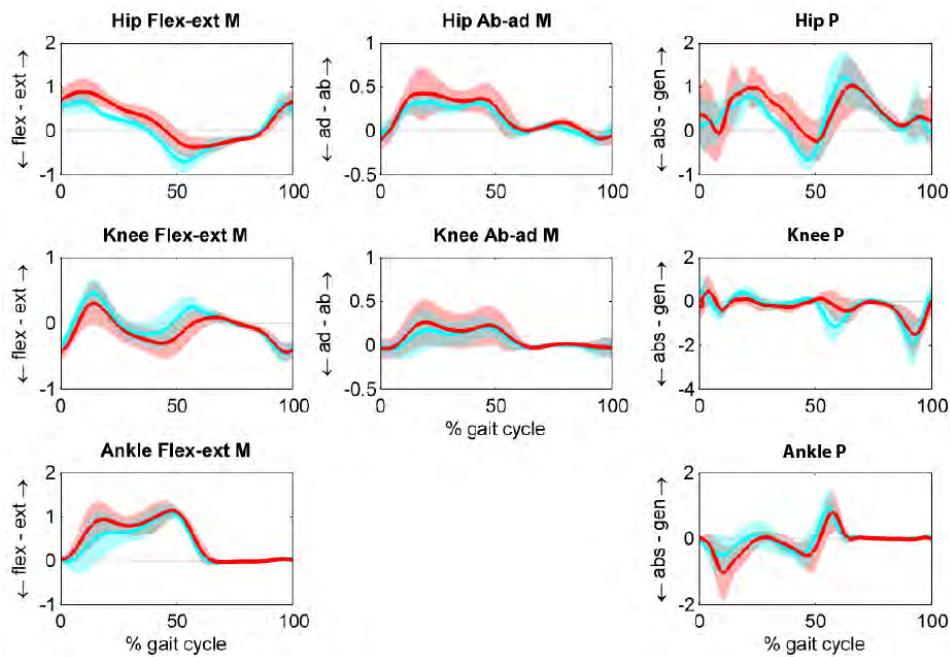
Caption: Figure 1. Hip, knee, and ankle moments (M) and powers (P) averaged over all children with CP for OG (cyan) and TM (red).

Conclusion: Kinetics differed considerably between TM and OG walking. Mediolateral GRF and joint moments were larger in TM than OG, which could be explained by a 3-4 cm larger stride width in TM for these subjects [3]. A shift was observed from ankle to hip work, indicating that subjects relied more heavily on a hip strategy in TM. Despite similar vertical and anterior-posterior GRF, no consistent shift in CoP, and very similar kinematics [3], hip extension moments were considerably larger in TM. This could be explained by 4° more forward lean of the trunk on the TM, possibly due to looking more downward. This resulted in a more backward positioning of the hip relative to the CoP (too subtle to be visible in individual joint angles) and hence a larger hip moment. The increased ankle moment (Fig.1) and anterior shift of the CoP in early stance in CP are consistent with increased ankle dorsiflexion angle found for these subjects in this same phase [3]. Differences were larger than previously found for healthy adults [1,2].

This study indicates that CP and TD children show differences in joint moments and powers on a TM, and hence kinetic data collected on a TM cannot be readily compared with OG data. For clinical applications, it must be considered that both OG and TM conditions constitute highly controlled experimental settings. Therefore the key clinical question - which controlled situation is most relevant for clinical treatment decision and evaluation to improve walking performance - remains open.

References: [1] Riley PO et al. Gait Posture;26(1):17-24, 2007.
[2] Lee SJ & Hidler J. J Appl Physiol;104(3):747-55, 2008.
[3] van der Krogt MM et al. Gait Posture;40(4):587-93, 2014.
[4] Sloot LH et al. Gait Posture;39(1):478-84, 2014.

[5] Cappozzo A et al. Clin Biomech;10(4):171-8, 1995.

AS-0014

IMPROVED CALIBRATION OF INSTRUMENTED TREADMILLS USING AN INSTRUMENTED STICK

Lizeth Sloot [1,*]Han Houdijk [2]Marjolein van der Krogt [1]Jaap Harlaar [1]

[1]Rehabilitation Medicine, VU University Medical Center, [2]Faculty of Movement Sciences, VU University, Amsterdam, Netherlands

Introduction and Objectives: Accurate measurement of ground reaction forces and centre of pressure (COP) is essential for calculation of joint moments in gait analysis. Since instrumented treadmills are more prone to measurement error compared to traditional force plates, because of their large and compliant structure, it is important to improve their accuracy by means of precise calibration.

Until now, only one protocol has been published to calibrate treadmill-embedded force plates over all axes [1], by manually exerting a range of known forces at different spots on the belt. While this method increased the COP accuracy considerably [1], the optimal number of spots or duration of trials is not known, possible non-homogeneity in COP error across the belt surface is not corrected for, and the calibration is not performed under experimental conditions. This study examined if the calibration could be improved by 1) variation of the measurement time per spot and the number of spots; 2) correction of non-homogeneous distribution of COP error; and 3) by performing the calibration on an operative belt, i.e. dynamic calibration.

Methods: An instrumented stick, equipped with 3 optical markers for motion tracking and a 1DOF axial load cell, was used to manually apply a range of forces over all axes, starting by maximal vertical force application followed by a circular movement, on a dual-belt instrumented treadmill (R-Mill, ForceLink). To construct different calibration matrices, 85 calibration trials of 5s each were performed at different spots equally spread over the area of each belt. A validation dataset consisting of 11 trials per belt was captured to determine the mean accuracy of the different calibration matrices. For dynamic calibration, 12 calibration and 3 validation trials were measured per belt at 1 km/h, exerting force with the stick while walking aside the treadmill.

First, a reference calibration matrix was constructed using 20 datasets of 5s, similar to Collins [1,]by minimizing the mean-square error between reference (stick) and offset-corrected treadmill outputs. To examine the effect of measurement time and number of spots, new calibration matrices were constructed using from 0.5 to 5 seconds of the included trials and from 4 up to 85 spots using a selective bootstrapping procedure of 50 repetitions. The 'optimal' duration and number of spots was defined as less reduction in error than 0.1%. For correction of non-homogeneity in COP error, 2 correction algorithms were fitted to the COP errors calculated from the 85 trials per belt [2,3] and applied to the validation data. To evaluate the effect of dynamic calibration, both the reference static matrix and a constructed dynamic calibration (using the dynamic calibration data) matrix were evaluated with the dynamic validation trials.

Results: The reference calibration resulted in mean COP error of 6.5 mm. The accuracy of COP increased with increasing measurement time (up to 5 seconds) and number of spots (up to 31), reducing the error to 5.4 mm (figure 1A). Vertical force accuracy was most optimal when using only the first 2 seconds of each trial, during which the highest vertical forces were applied.

One correction algorithm [3] resulted in reduced non-homogeneity in the COP error compared to the reference calibration (figure 1B), with an average error of 6.1 mm, in contrast to the 6.5 mm of the other [2].

Under dynamic conditions, the COP error of the static calibration increased up to 4 times. The dynamic calibration resulted in 24% lower COP errors than the static calibration under these conditions.

Figure:
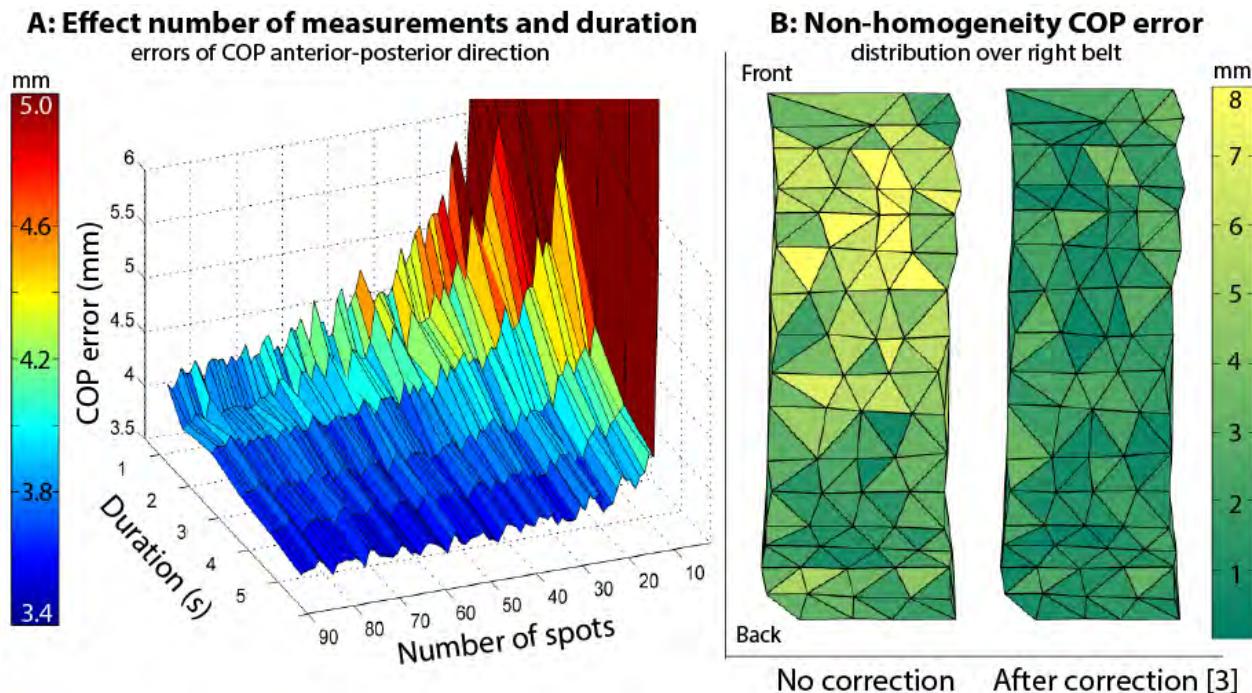
Caption: Figure 1 A) Effect of the number of spots and duration on the COP error of the left belt; B) distribution of the average COP error over the right belt, before and after correction

Conclusion: We found that the result of calibration of instrumented treadmills depends on the measurement duration and number of spots, with capturing 31 points for 5 seconds proving best results. However, the relation between accuracy and exerted force during the stick movement found for the vertical force, suggests that the movement could be further optimized.

Correction of the presented non-homogeneity also reduced the COP error. Such a correction is specifically important for measurements where subjects use the entire belt, eg. during self-paced walking, and might be further optimized by creating a correction algorithm for the treadmills' specific distortions.

Most calibrations are performed under static conditions, however, the accuracy considerably decreases when examined under experimental conditions, even at the slow speed we measured. This, together with the finding that dynamic calibration provided better accuracy, underlines the need for further development of dynamic calibration methods.

References: [1]   Collins S.H. et al. 2009. Gait Posture 29:59-64

[2]   Schmiedmayer H.B. et al. 1998. 16th ISBS.

[3]   Verkerke G.J. et al. 2005. J Biomech 38:1881-1885

Disclosure of Interest: None Declared

Motion Analysis

AS-0015

FUNCTIONAL ESTIMATION OF THE METACARPOPHALANGEAL JOINT AXES OF ROTATION

Pierre Devos [1,*]Clint Hansen [1]Khalil Ben Mansour [1]Frédéric Marin [1]

[1]Laboratoire de biomécanique et bioingénierie - CNRS UMR 7338, Université de Technologie de Compiègne, Compiègne, France

Introduction and Objectives: In order to prevent injuries of the hand and to improve therapies, it is essential to understand the hand kinematics (Vignais et al, 2013). Kinematic description of the hand requires the estimation of the joint axes of rotation (AoR). The aim of this paper is to compare two functional methods to estimate the metacarpophalangeal (MCP) joint AoR of fingers.

Methods: Ten healthy volunteers aged from 19 to 54 years participated in the experiment. Subjects were asked to do three repetitions in flexion-extension (F-E) and abduction-adduction (Abd-Add) of the MCP joints from the index finger to the little finger.

Three 1.5 mm diameter markers were fixed on each proximal phalanx, and six 6 mm diameter markers were fixed on metacarpals (figure). Data were collected using a motion capture system (17 cameras T160, Vicon, Oxford Metrics Ltd, Oxford, UK). The data analyses were performed using MATLAB 7.6 (Mathworks, Inc.; Natick, MA).

Two functional methods were used to estimate the joint AoR. In the Plane-Fitting (PF) method, movements of the distal segment are assumed to be planar and circular. Least squares planes and least squares circles are calculated from the markers trajectories. The orientation and the location of the joint AoR are obtained from the normal vector of the least squares plane and the center of the least squares circle, respectively. In the Sphere-Fitting (SP) method, marker trajectories of the distal segment are assumed to belong to a sphere. Least squares spheres are calculated from these trajectories. The AoR is estimated by computing the square line from the centers of the spheres.

RMS of the least squares planes and circles in the PF method were compared to the RMS of the least squares spheres in order to find the most appropriate method of estimation of the MCP joint AoR in F-E and in Abd-Add.

Results: In Abd-Add and F-E, the RMS computed from the least squares planes are much smaller than the ones computed from the least squares circles and spheres (table). Moreover, the RMS computed from the least squares circles are substantially greater than the least squares spheres in Abd-Add. Thus, the results show that the SF method is more appropriate for the AoR estimation of MCP joints in Abd-Add. However, the difference between the RMS computed from the circles least squares and the spheres least squares in F-E are not as large as the one in Abd-Add. Thus, it is difficult to find which between the PF method and the SF method is more appropriated in F-E.

Figure:
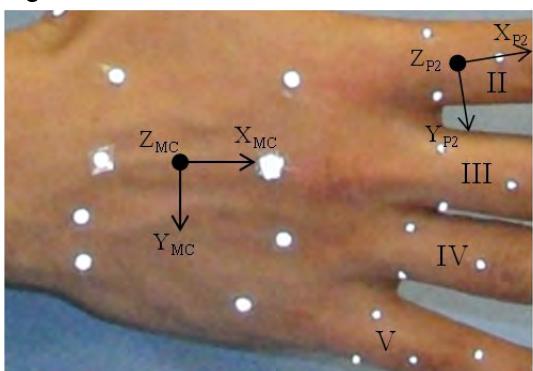
Caption: Location of skin-fixed markers on the proximal phalanxes and the dorsal face of the hand.

Conclusion: RMS results from Plane-Fitting and Sphere-Fitting methods were presented in order to find the most appropriate method for the AoR estimation of the MCP joints in abduction-adduction. No results were presented for the MCP3 joints because no movement was observed during the natural motion of fingers in Abd-Add.

RMS tend to increase from the index finger to the little finger. This tendency may be due to the skin movement artefacts, which add errors in the measurement data (Chèze et al, 1995). Markers were carefully fixed distant from the joints in order to minimize errors due to skin movement. However, the length of proximal phalanges decreases from the index finger to the little finger; thus, the impact of skin movements on marker trajectories is more important. (Devos et al 2014).

Results of the RMS show that movement in F-E of the MCP joints is planar. However, the assumption about the circular movement was not proved. One possible explanation may be that the MCP joints should not be considered as a spherical joint but rather as an ellipsoidal joint based on the geometry of this joint (Kapandji et al., 2002). Computations of a least-square ellipsoid should be considered rather than a circle in order to improve the fit of marker trajectories and have a better estimation of the MCP joints AoR.

In conclusion, the aim of this study was to present two functional methods for the estimation of the AoR of the MCP joints and find the most appropriate one in F-E and Abd-Add. SF is the most appropriate method in Abd-Add but ellipsoidal joint assumption should be considered.

Table:

	Method	RMS (mm)	MCP2	MCP4	MCP5
F-E	PF	Plane	0,038 ± 0,021	0,038 ± 0,022	0,044 ± 0,015
		Circle	0,258 ± 0,093	0,326 ± 0,063	0,629 ± 0,199
	SF	Sphere	0,251 ± 0,113	0,274 ± 0,087	0,541 ± 0,251
Abd-Add	PF	Plane	0,015 ± 0,01	0,015 ± 0,007	0,022 ± 0,008

| 36 | | Circle | 1,253 ± 0,68 | 1,051 ± 0,277 | 1,455 ± 0,92 |
| | SF | Sphere | 0,142 ± 0,039 | 0,253 ± 0,168 | 0,36 ± 0,35 |

Caption: RMS and residuals (mm) of the least squares planes and circles in the Plane-Fitting method, and RMS of the least-square sphere in the Sphere-Fitting method.

References: Chèze et al., J. Biomech. 28: 879-884, 1995.

Devos et al., Comput. Methods Biomech. Biomed. Engin. 1:96-97, 2014.

Kapandj (5th Ed.). The Physiologie of the Joints: Upper Limb, Volume 1. Churchill Livingstone. 1983.

Vignais et al., Appl. Ergon. 44: 566-574, 2013.

Disclosure of Interest: None Declared

AS-0016

JOINT KINEMATIC CALCULATIONS BASED ON STANDARD CLINICAL DIRECT KINEMATIC VERSUS CONTEMPORARY INVERSE KINEMATIC APPROACHES: HOW LARGE IS THE DIFFERENCE?

Hans Kainz [1] [2],[*]Luca Modenese [1]Lee Barber [3]John Walsh [2]Roslyn N Boyd [3]David G Lloyd [1]Christopher P Carty [1] [2]

[1]Centre for Musculoskeletal Research, Griffith University, Gold Coast, [2]Queensland Children's Gait Laboratory, Children's Health Queensland, [3]Queensland Cerebral Palsy and Rehabilitation Research Centre, Brisbane, Australia

Introduction and Objectives: Clinical gait analyses typically use Direct Kinematics (DK) to estimate segment and joint kinematics directly from markers that are attached to the skin by assuming rigid connection between bone and markers. In contrast, Inverse Kinematics (IK), now preferably used for research, estimates joint kinematics by moving a musculoskeletal model to best match the motion of skin based markers without violating predefined anatomical constraints, and additionally enables musculoskeletal analyses (e.g. muscle tendon length analysis). Direct comparison between DK and IK is difficult due in part to different definitions of joint coordinate frames and errors due to scaling and marker placement. The aim of the current study was to create subject-specific kinematic models from magnetic resonance imaging (MRI) to directly evaluate the difference in joint kinematic estimates between DK and IK.

Methods: MRI and 3D motion capture data were collected from four children with cerebral palsy with a mean (SD) age of 11.3 (3.2)years, height 1.46 (0.18)m, weight 37.6 (13.5)kg, and BMI 17.2 (3.1). The conventional Vicon Plug-in-Gait DK (PiG-DK) [1] model and the standard 2392 OpenSim IK (OS-IK) model [2] were used to obtain standard DK and IK lower limb joint kinematics. For the MRI based models the pelvis and bones of the lower limbs were manually segmented using Mimics (Materialise, Belgium) and used to derive subject-specific joint centres and coordinate frames using pre-defined anatomical landmarks (Figure 1). NMSbuilder (NMSPhysiome) was used to create a DK and IK based subject-specific OpenSim model for each participant (similar to [3]). Joint kinematic waveforms derived from standard DK (PiG-DK) and IK models (OS-IK), as well as between both MRI based models (MRI-DK and MRI-IK) were compared using a modified coefficient of multiple correlation (CMC) [4]. Since CMC is a dimensionless measure, the following nine clinically relevant kinematic variables derived from each model were also compared: average hip rotation in stance, knee flexion at initial contact, range of pelvis tilt, average pelvis rotation, range of pelvis rotation, peak knee flexion during swing, peak dorsiflexion during swing, peak dorsiflexion in stance and minimum hip flexion.

Results: Joint kinematics from PiG-DK and OS-IK models had a mean (SD) CMC of 0.79 (0.18), whereas the MRI based DK and IK models showed better agreements with a CMC of 0.94 (0.06). The mean (SD) difference in discrete variable between the PiG-DK and OS-IK models was 5.6 (4.9)degrees, whereas difference of the MRI models was 1.0 (0.7)degrees (Table 1).

Figure:
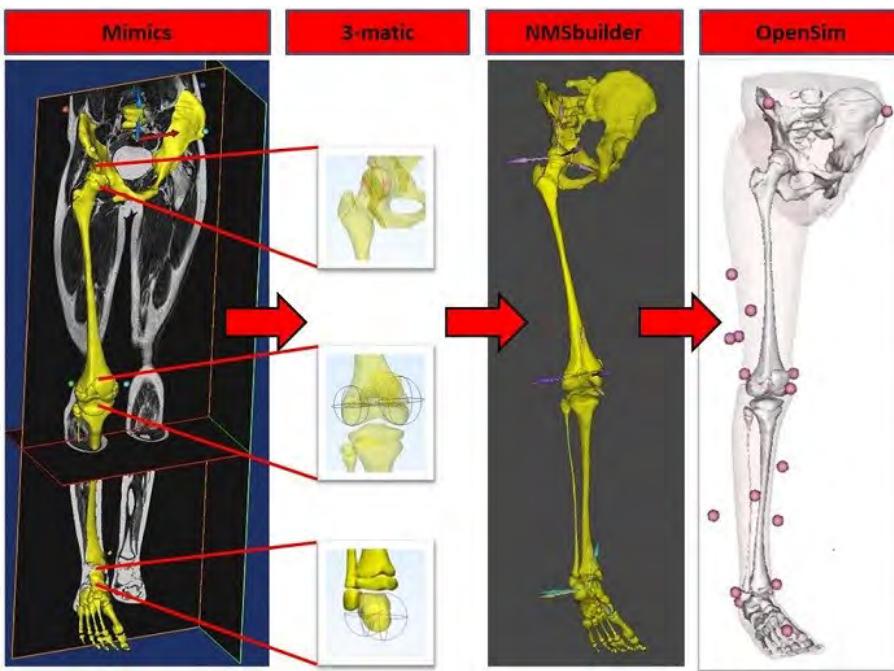
Caption: Workflow for creating patient-specific kinematic models: (1) Mimics was used for segmenting lower limb bones and the external skin shell. (2) Joint centres and axes were defined by fitting geometrical shapes to the bone structures using 3-matic. (3) NMSbuilder was used to create patient-specific DK and IK OpenSim models. (4) Joint kinematics were calculated in OpenSim.

Conclusion: We found moderate-to-good CMC values, with discrete variables differences of up to 16.4 degrees, between the standard clinical PiG-DK and OS-IK models. In comparison the medical imaging DK and IK models produce very similar joint kinematic outputs, with excellent CMC values with discrete variables differences below 3.2 degrees). However, the MRI-DK model did permit unacceptable non-physiological joint displacements (e.g. hip joint displacements up to 24mm). Therefore, we recommend using IK to calculate joint kinematics in clinical gait analyses if a reliable anatomical model is available as this ensures anatomically viable joint movement. IK also enables additional musculoskeletal analysis that may improve clinical decision-making. Future research should evaluate the sensitivity of joint angles to potential errors introduced with the anatomical model, establish more reliable and accurate methods to scale generic models, and estimate joint centers and axes as these factors have substantial impacts on joint kinematics.

Table:

Variables Analyzed	**PiG-DK and OS-IK** model differences	**MRI-DK and MRI-IK** model differences
Average Hip Rotation Stance	6.5 (5.3)	1.6 (0.5)
Knee Flexion Initial Contact	3.4 (2.6)	0.8 (0.6)
Average Pelvis Tilt	15.6 (0.8)	0.7 (0.5)

Average Pelvis Rotation	1.2 (0.8)	0.3 (0.1)
Range of Pelvis Rotation	2.1 (2.2)	0.7 (0.4)
Peak Knee Flexion Swing	5.0 (2.1)	0.8 (0.4)
Peak DorsiFlexion Swing	3.3 (1.6)	2.5 (1.2)
Peak DorsiFlexion Stance	5.3 (1.8)	0.4 (0.3)
Minimum Hip Flexion	13.0 (2.9)	1.5 (1.2)

Caption: Differences mean (SD) between DK and IK models in clinical relevant kinematic variables in degrees.

References:

[1] Kadaba et al., J. Orthopaedic Research, 7(6): 849-60, 1989.

[2] Delp et al., IEEE Transactions on Biomedical Engineering, 54(11): 1940-50, 2007.

[3] Valente et al., PLoS ONE, 9(11):e112625, 2014.

[4] Ferrari et al., Gait & Posture, 31: 540-42, 2010.

Disclosure of Interest: None Declared

Motion Analysis

AS-0017

GAIT INITIATION IN PATTELAR CHONDROMALACIA SUBJECTS

Georgia Cristina Lehnen [1]Matias Noll [1,*]Thales Baliero Takáo [1]Fernanda Nora [1]Marcus Fraga Vieira [1]

[1]Bioengineering and Biomechanics Laboratory, Universidade Federal de Goiás, Goiânia, Brazil

Introduction and Objectives: Gait initiation is the transition from a standing position to the gait cyclic movement [1]. The transition phase from a static to a dynamic condition involves contradictory postural stabilization functions: to prepare to an action and to recover from the perturbation [2]. Thus, the analysis of gait initiation by means of biomechanical parameters allows a better understanding of the central and peripheral control mechanisms involved in transient tasks [3]. The comparison of these parameters between different groups provides clues as to how certain musculoskeletal restrictions interfere in these control mechanisms. Thus, this study aimed to compare the gait initiation between healthy subjects and subjects with patellar chondromalacia, from kinetic and kinematic parameters, in order to analyze the adjustments due to this pathology to this task.

Methods: Twenty one subjects of both sexes, aged 18-35 years, enrolled in this study. They were divided into healthy group (HG, n = 10) without patellar chondromalacia, and patellar chondromalacia group (CG; n = 11), whose pathological condition was confirmed by magnetic resonance imaging. Data were collected in a laboratory equipped with four AMTI force platforms and ten Bonita Vicon cameras, at a frequency of 100 Hz, using Vicon Nexus 2.0 software with Vicon Plug-in Gait with 35 reflective markers. Kinematic data were processed using the Vicon Polygon software and kinetic data were processed using a custom Matlab code. Both groups performed five trials from a static standing position with one foot on each force platform. Two other force platforms recorded the first and second steps. The participants stood still until a sound command to start the gait with the right limb, walking six meters on a horizontal surface. Data acquisition started two seconds prior the sound command. Kinematic (knee maximum flexion angle) and kinetic parameters (center of pressure - COP) were evaluated. For evaluation of the COP, the gait initiation was divided into three phases [4]: 1) Anticipatory adjustments phase; 2) Swing foot unloading phase and 3) Support foot unloading phase (Figure 1). At each phase, the following COP descriptors were calculated: the anterior-posterior and medial-lateral displacement, calculated as the distance between the maximum and minimum position of the COP in the anterior-posterior and medial-lateral directions, and anterior-posterior and medial-lateral velocity, calculated dividing the COP displacements by the duration of each phase. For statistical analysis, we used the Shapiro-Wilk normality test and the paired T-test for intragroup comparisons and independent T-test for between group comparison ($\alpha = 0.05$).

Results: Only the CG showed significant differences for the maximum knee flexion angle during swing phase of gait, being higher ($p = 0.005$) on the affected knee (51.08 ± 6.11 °) compared to healthy knee (46.38 ± 3.14 °). There was no significant difference for knee angle between the groups. The CG presented significant higher values than the HG for the COP descriptors, particularly in phases 1 and 3 (Table 1).

Figure:
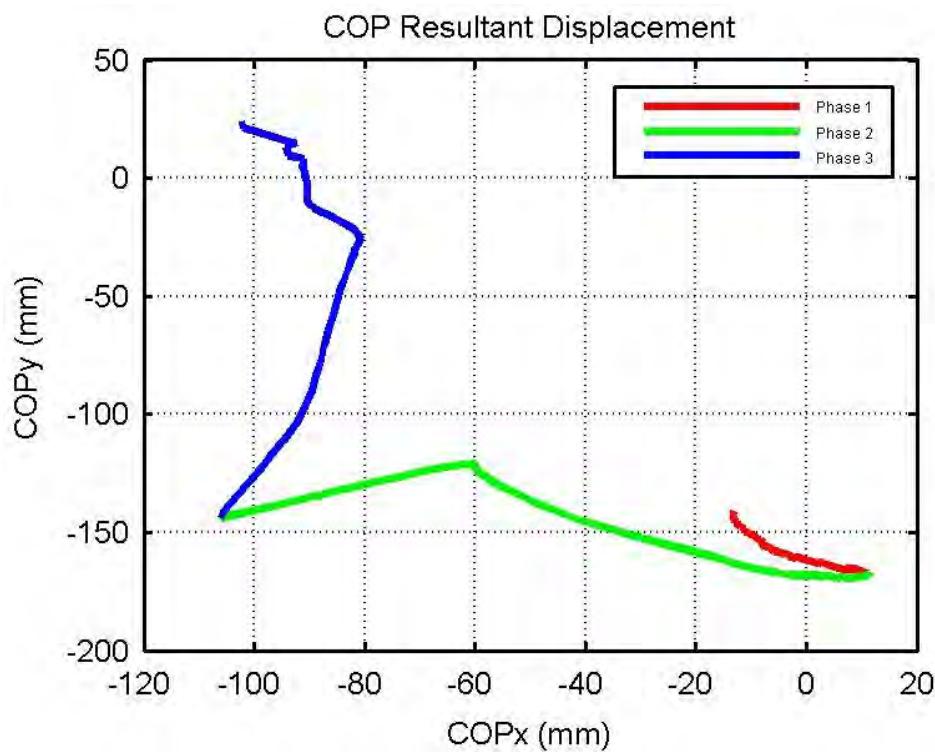
Caption: Figure 1. COP displacement during gait initiation.

Conclusion: In this study, the CG executed the gait initiation faster than HC. Higher values of anterior-posterior COP displacement, especially in the anticipatory phase (phase 1), imply higher steady-state gait velocities [5]. Anticipatory adjustments create the propulsive forces necessary to reach steady-state gait [1]. Besides, higher velocities during gait, within certain limits, are associated with greater stability [6]. Thus, these results suggest that individuals with patellar chondromalacia execute the gait initiation faster in order to ensure greater stability, possibly an adaptation to the studied pathological condition.

Table:

Kinetic parameters	Phase	HG	CG	p
Displacement (mm)	AP: 1	29,42±7,87	40,44±12,70	0,029 *
	AP: 2	55,91±25,18	51,89±21,84	0,700
	AP: 3	155,60±19,97	199,34±42,86	0,008 *
	ML: 1	30,71±11,39	41,13±14,34	0,083
	ML: 2	132,33±43,42	147,70±28,89	0,347
	ML: 3	44,73±13,17	74,04±35,38	0,023 *
Velocity (mm/s)	AP: 1	84,13±21,40	118,39±34,44	0,014 *
	AP: 2	154,19±70,61	180,98±65,72	0,379
	AP: 3	267,55±34,95	354,20±70,62	0,002 *
	ML: 1	91,14±37,32	123,54±52,47	0,123
	ML: 2	366,70±110,49	551,53±157,91	0,006 *

	ML: 3	76,51±20,83	132,28±64,07	0,017 *
Kinematic parameters				
Knee maximum flexion angle (°)		49,51±9,19	48,73±5,31	0,733

AP: anterior-posterior direction, ML: medial-lateral direction, HG: healthy group (n=10), CG: patellar chondromalacia group (n=11).

* p < 0,05

Caption: Kinetic and kinematic results.

References: [1] Isais et al., PloS ONE, 9(4):e92736.

[2] Bouisset and Do, Clin Neurophysiol, 38:345-362, 2008.

[3] Xu et al., J Mot Behav, 36:316-326, 2004.

[4] Hass et al., Clin Biomech, 23:743-753, 2008.

[5] Ledebt et al., Exp Brain Res, 120:9-17, 1998.

[6] Kang and Dingwell, Gait Posture, 27:572-577, 2008.

Disclosure of Interest: None Declared

AS-0018

COMPARISON OF BIOMECHANICAL PARAMETERS OF HEALTHY ADULT GAIT USING THREE MARKER BASED MODELS

Manunchaya Samala [1,*]Craig Childs [1]Anthony McGarry [1]Philip Rowe [1]

[1]Biomedical Engineering, University of Strathclyde, Glasgow, United Kingdom

Introduction and Objectives: Biomechanical gait analysis is a systematic measurement, which is becoming an important tool used to assess, plan, and treat individuals with conditions affecting their ability to walk. Gait analysis requires specialized hardware and software for collecting, processing, analyzing biomedical parameters for human locomotion. The common tool, which is one of hardware for tracking and describing the kinematics of the human gait in three dimensions, is marker-based motion capture (Kent & Franklyn-Miller 2011; Pitkin 2006). The most commonly utilized marker model used in clinical environments for gait analysis is Vicon's plug-in gait (PiG; Vicon Motion Systems, Oxford, UK), which is known for its ease of use and fast implementation. However, this conventional marker set provides less repeatable results than cluster based marker set and also takes a lot of preparation time of the subjects. In additional, the thigh and calf markers positions are critical for correct alignment of the knee joint axis in PIG but less so in cluster systems.(Ceseracciu et al. 2014; Duffell et al. 2014; Papi et al. 2014). Different protocols are known to yield different results, specifically for out-of-sagittal plane rotations(Duffell et al. 2014).

The study's aim was to evaluate the inter-protocol variability of kinetics, kinematics and temporal-spatial parameters output of three protocols, using a Strathclyde cluster model(Papi et al. 2014), the Human Body Model(van den Bogert et al. 2013) and Plug-in-Gait model (Vicon).

Methods: Ten healthy adult subjects age between eighteen and fifty year old were analyzed using the a 12 camera Vicon bonita Motion capture system. Each subject wore a single comprehensive set of markers which merged the required markers for the Strathclyde cluster model, the Human Body Model and Plug-in-Gait model to allow a simultaneous data capture for all three models. During the experiment, subjects walked on a treadmill which is part of the CAREN system (Motekforce Link VB, Amsterdam,The Netherland) and include two, 2 metre long force plates one for each leg under two split belts of the treadmill. They walked at up to seven different speeds (very slow 0.3 m/s, slow 0.8 m/s, moderate 1.3 m/s, fast 1.8 m/s, very fast 2.3 m/s, self – paced variable speed and self-selected fixed speed) .

Results: The 3-D marker trajectories and the force data were captured synchronously and joint angles/moments etc were calculated using the three marker models and approriate software. One left and one right gait cycle wiere extracted for each of the three trials.The raw marker trajectory data and ground reaction force data were processed and calculated separately on each data set according to the gait analysis software package for each marker model. All data wee imported to excel and time normalized to the gait cycle. Inter- and intra-model Coefficient of Multiple Correlation (CMC) were calculated for joint kinematics and joint kinetics data and this was achieved by comparing exactly the same gait acquisition from each subject, condition and marker set. Intra-subject variability was also analysed using 3 gait trials for each subject and, inter-subject variability was assessed by comparison of the averages of the 3 walking trials among the 10 participants. The results showed differences between analyses from the 3 models and these will be presented.

Conclusion: The results of study enabled us to select the model which is the easiest, most accurate, and most repeatable to analyses walking performance in below knee amputees. The research will continue by using the selected marker set to analyse the gait of below knee amputees undergoing limb dynamic alignment. In this new procedure the prosthist will remotely control and automatically adjusting lower leg pylon as the subject walks on the treadmill. The selected cluster system will be used to record their gait and visualise it in real time with suitable calculated gait parameters on a screen in real time. The prosthetist will be able to remotely adjust the alignment of the prosthetic leg and hence tune the prosthesis. In this way the system will allow the prosthetist to quickly and effeciently optimise the set up of the below knee prosthetic alignment and maximise patient walking function.

References: 1) Van den Bogert, A.J. et al., 2013. *Med & bio eng & com*, 51(10), pp.1069–77.

2) Ceseracciu, E., Sawacha, Z. & Cobelli, C., 2014. *PloS one*, 9(3)

3) Duffell, L.D., Hope, N. & McGregor, A.H., 2014. . *Proc IMECHE. Part H, J of eng in med*, 228(2), pp.206–10.

4) Kent, J. & Franklyn-Miller, A., 2011. P&OI. 35(2), pp.124–39.

5) Papi, E., 2012. University of Strathclyde. PhD Thesis

6) Papi, E. et al., 2014. . *Gait & Posture*, 39(2014), pp.S9–S10.

7) Pitkin, M.R., 2006. *Biomechanics of Lower limb prosthetics*

8) Vicon Motion Systems., 2008. Plug-in gait product guide – foundation notes.

Disclosure of Interest: None Declared

Musculoskeletal

AS-0019

COLLAGEN CROSSLINKING DOES NOT DICTATE STIFFNESS IN A TRANSGENIC MODEL OF SKELETAL MUSCLE FIBROSIS

Mark A. Chapman [1,*] Rajeswari Pichika [2] Richard Lieber [3]

[1]Bioengineering, [2]Orthopaedic Surgery, University of California - San Diego, La Jolla, [3]Rehabilitation Institute of Chicago, Chicago, United States

Introduction and Objectives: Fibrosis results when skeletal muscle is damaged and the regenerative process fails to recapitulate normal development. Skeletal muscle fibrosis is the abnormal accumulation of ECM between myofibers, specifically expressed as increased collagen content [1]. Apart from biochemical changes, biomechanical changes are also observed in skeletal muscle, cardiac and liver fibrosis [2, 3, 1]. While collagen content and tissue stiffness both increase with fibrosis, there is not a strong correlation between these two values [4, 5]. Interestingly, a recent cardiac study showed that collagen crosslinks, not collagen abundance, dictated tissue stiffness [6] which suggests that collagen crosslinks may also explain increased tissue stiffness in muscle fibrosis. Therefore, the goal of this study was to correlate tissue stiffness with lysyl-pyridinoline (LP), hydroxylysyl-pyridinoline (HP), and pentosidine (PE) collagen crosslinks. In this study, we used our recently described nesprin-desmin double knockout mouse (DKO) model of skeletal muscle fibrosis [4].

Methods: Passive mechanical testing of skeletal muscle bundles from wild-type (WT) [n=10], nesprin-1 knockout (nesprin$^{-/-}$) [n=8], desmin knockout (desmin$^{-/-}$) [n=10] and DKO [n=13] mice was conducted as previously described (7). Briefly, muscle bundles were secured to a force transducer one side and a fixed titanium pin connected to a rotational bearing on the other. A stress-relaxation protocol was implemented by increasing sarcomere length by 0.25 µm/stretch and stress-relaxing for 3 minutes. From these data, tangent stiffness was determined by calculating the slope of the stress-sarcomere length plot at a sarcomere length of 3.2 µm.

HP, LP and PE concentrations of muscle samples were determined as previously described [8]. These samples were derived from adjacent portions of the same muscle samples used for mechanical testing. Samples were prepared for HPLC and injected into the HPLC column. Elution of crosslinks was achieved at 40°C at a flow rate of 1.0 mL/min in two steps. Hydroxyproline content was determined using an HPLC column.

Stepwise regression analysis was performed using IBM SPSS Statistics (Armonk, NY) to determine which parameters (collagen content, HP, LP, and/or PE if any) could predict muscle tissue stiffness.

Results: When tissue stiffness was plotted against collagen, HP or PE values, there was a significant correlation between stiffness and collagen and crosslink content (collagen:$p<0.05$, $r^2=0.62$; HP:$p<0.05$, $r^2=0.73$; PE:$p<0.05$, $r^2=0.52$; Figs. 1A,B & D). However, when examining each genotype separately, this relationship disappeared. Thus, the correlation was caused by differences between genotypes and created only a pseudocorrelation [9]. LP crosslink content also had no correlation with tissue stiffness (Fig. 1C). These conclusions were further validated using stepwise regression. In the stepwise regression model, the only variable that entered the linear model was HP content ($r^2=0.73$), suggesting a good relationship. However, it should be noted that when data from any single genotype were run through stepwise regression,

no variables were included in the model. Finally, no relationship was found between tissue stiffness and normalized collagen crosslinks.

Figure:
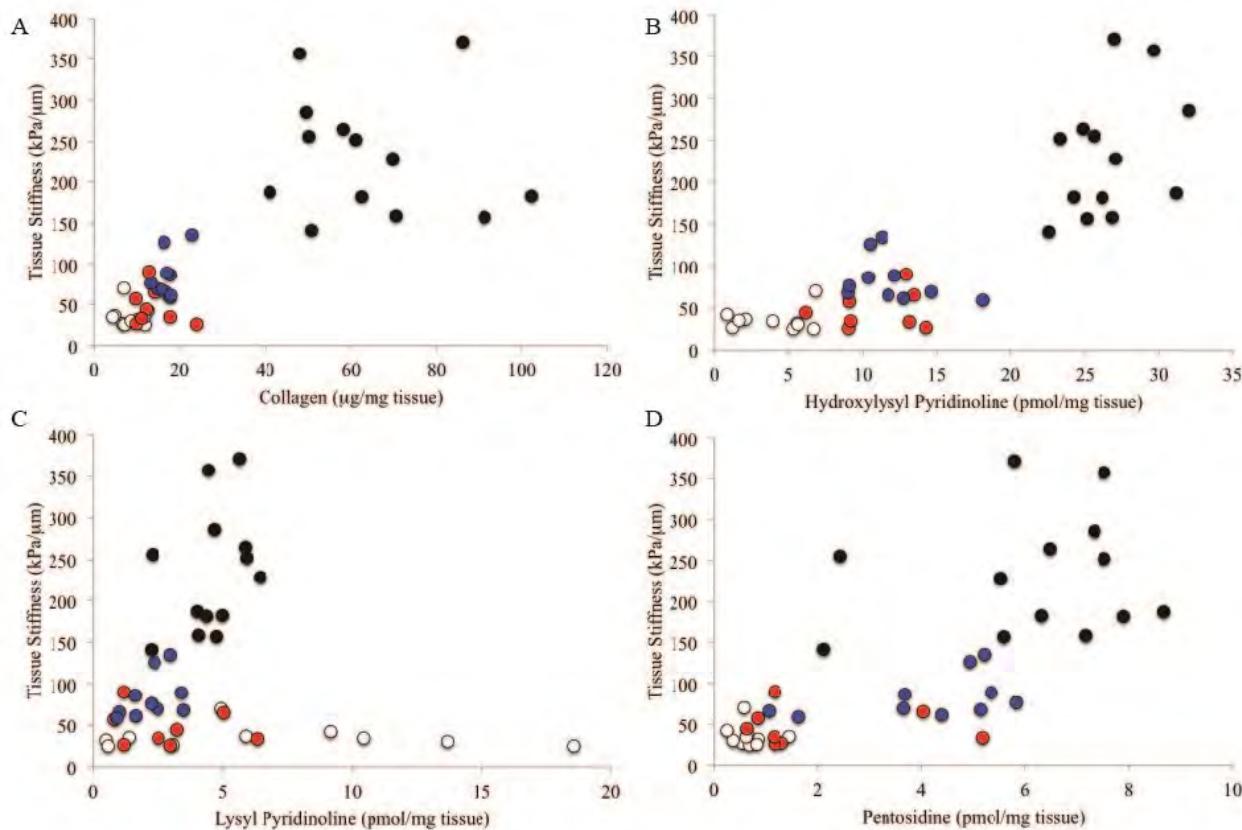
Conclusion: In spite of the current findings, it remains unclear which parameters in skeletal muscle ECM are responsible for dictating tissue stiffness. Although neither collagen content nor collagen crosslinks are highly correlated with tissue stiffness, collagen organization within the ECM remains a potential contributer to tissue stiffness. None of the methods used account in any way for the gross arrangement of collagen bundles which are rich in the perimysial space [10]. Recently, a serial block face scanning electron microscopy method was used to reconstruct skeletal muscle ECM over hundreds of microns [11]. This technology holds great potential for determining collagen/ECM ultrastructure, and could answer questions about whether tissue stiffness is related to ECM organization. Other factors such as proteoglycans may also affect stiffness, as it has been shown that decorin and biglycan are also increased in muscle fibrosis models [12].

Caption: Figure 1: Muscle bundle stiffness versus collagen content and collagen crosslink concentrations.

References: [1] Lieber and Ward, *Am. J. Physiol. Cell Physiol.*, 305: C241–52, 2013.

[2] Carrión et al., *Hepatology*, 51: 23–34, 2010.

[3] Jalil et al., *Circ. Res.*, 64: 1041–50, 1989

[4] Chapman et al., *Hum. Mol. Gen.*, 23: 5879–92, 2014.

[5] Smith and Barton, *Am. J. Physiol. Cell Physiol.*, 306: C889–98, 2014.

[6] López el al, *Hypertension*, 60: 677–83, 2012.

[7] Fridén and Lieber, *Muscle Nerve*, 26: 157–64, 2003.

[8] Bank et al., *J. Chromatogr. B*, 703: 37–44, 1997.

[9] Draper and Smith, John Wiley & Sons, Inc., New York, 1981.

[10] Gillies and Lieber, *Muscle & Nerve*, 44: 318–31, 2011.

[11] Gillies et al., *Microsc Microanal*, [Epub ahead of print], 2014.

[12] Fadic et al., *J. Cell. Mol. Med.*, 10: 758-69, 2006.

Disclosure of Interest: None Declared

Musculoskeletal

AS-0020

LONG-TERM STIMULATION RESULTS IN SARCOMERE LENGTH NON-UNIFORMITY

Maria Engel [1,*] Tim Leonard [1] Walter Herzog [1]

[1] Human Performance Laboratory, University of Calgary, Calgary, Canada

Introduction and Objectives: Muscle spasticity is a condition found in many patients, for example in children with Cerebral Palsy (CP), and it is characterized by muscles that are tight and stiff. Spasticity decreases the range of motion about joints, making every day functions, such as walking or holding a glass of water, very difficult to do. Patients with muscle spasticity have velocity-dependent, hyper-active stretch reflexes, producing increased and undesired muscle activation compared to normal patients without spasticity.

It has been shown that the muscles of CP patients have decreased fascicle lengths and increased sarcomere lengths[1,2]. Intuitively, this implies that spastic muscles have decreased serial sarcomere numbers. Long-term muscle stimulation has been shown to decrease the serial sarcomere number within a muscle in guinea pig and rat models[3,4]. These results been replicated in our laboratory[5] in New Zealand White rabbits and in the medial gastrocnemius (MG), plantaris (PL), and the soleus (SOL) muscles. Ten hours of stimulation of these muscles also resulted in a 25% decrease in serial sarcomere numbers. Within analysis of these experiments, laser diffraction was used to measure the average sarcomere length.

In muscles that have been stimulated for 10 hours, it has been observed that laser diffraction produces a thick band at the first order of diffraction rather than a thin line. This implies that multiple sarcomere lengths are present within the muscle fascicle. Therefore, the purpose of this study was to quantify sarcomere length non-uniformity and qualitatively examine any extent of muscle damage.

Methods: Triceps surae muscles of New Zealand White rabbits (n=3) were stimulated with a nerve cuff at 20 Hz (3x alpha motor neuron threshold) for 10 hours continually. The leg was unrestrained. Muscles examined included the MG, PL, and the SOL. The contralateral limb served as the non-stimulated control. After the stimulation period, muscles were harvested, fixed with 10% formalin, and then digested in 30% nitric acid. Individual fascicles were mounted on slides for analysis. Using a light microscope, images at 64x magnification were taken at 9 sections of the fascicle; 3 at each end, and 3 in the middle. The images were then imported into Matrox Inspector. The average of 4 sarcomere lengths in series was measured. This was repeated in series along the muscle 10 times in each image for a total of 90 data points for each fascicle. To quantify the extent of sarcomere non-uniformity, standard deviations about the mean sarcomere lengths were calculated and reported. The coefficient of variation using means and standard deviations were calculated for the stimulated and non-stimulated muscles. Muscle injury was qualitatively observed by examining the captured images.

Results: The coefficient of variation of sarcomere lengths were consistently larger in the stimulated muscles compared to the non-stimulated contralateral control, implying long-term stimulation results in sarcomere length non-uniformity. For example, in the PL, coefficient of variation in the stimulated muscle was 7.0%, while the non-stimulated muscle resulted in 0.9%. In all three muscles, sarcomere lengths were significantly shorter in stimulated muscles compared to the control (p<0.05). Images acquired showed signs of muscle injury including disorganization of A-bands, sarcomere streaming, and areas with completely disorganized protein structure (figure 1).

Figure:
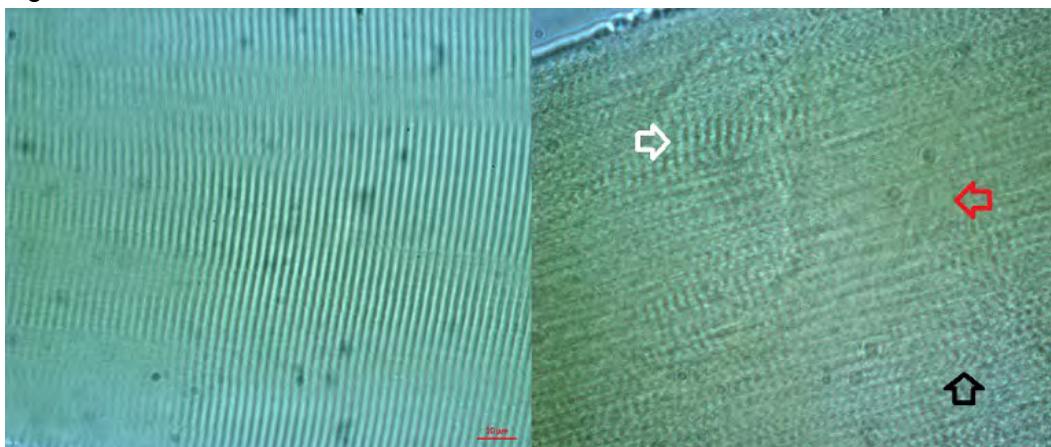
Caption: Figure 1: An example of a non-stimulated contralateral control muscle (left) and a 10 hour stimulated muscle (right). Arrows indicate signs of muscle injury; white indicates A-band disorganization, black indicates streaming of sarcomeres, and red indicates complete disorganization.

Conclusion: Sarcomere length non-uniformity and structural disorganization appears to result from long-term muscle stimulation. Examination of injury sights may give clues as to how sarcomeres are being removed in response to increased stimulation. Due to the force-length relationship of sarcomeres, the muscle may remove sarcomeres to allow remaining sarcomeres to be maintained at their optimal force-producing length[6]. Removal of sarcomeres may occur throughout the muscle fibres, as muscle injury appears along the entire fibre after long-term stimulation.

Patients with muscle spasticity, such as in CP, may be experiencing muscle injury due to chronic increased muscle activity. This could lead to muscle adaptation such as sarcomere loss, resulting in functional mechanical changes to the muscle.

References: [1] Smith et al., *J Physiol*, 589:2625–39, 2011.

[2] Matthiasdottir et al., *Clin Biomech*, 29:458–62, 2014.

[3] Tabary et al., *Muscle Nerve*, 4:198–203, 1981.

[4] Jakubiec-Puka et al., *Sarc Non-sarc Muscles Basic Appl Res Prospect 90's*, 385–390, 1988.

[5] Yamamoto et al., *JURA*, 1, 2011.

[6] Tabary et al., *J Physiol*, 224:231–244, 1972.

Disclosure of Interest: None Declared

Musculoskeletal

AS-0021

RISK OF FALLS IN WOMEN WITH FIBROMYALGIA

Suelen M. M. Goes [1 2,*] Andre L. F. Rodacki [2] Joice M. F. Stefanello [2] Angelica Lodovico [2] Diogo Homann [2] Neiva Leite [2] Cheryl Hubley-Kozey [1]

[1]Faculty of Health Professions, Dalhousie University, Halifax, Canada, [2]Physical Education, Federal University of Parana, Curitiba, Brazil

Introduction and Objectives: Fibromyalgia (FM) is a chronic pain condition (Henriksen et al., 2009) associated with reduced muscle strength, which can lead to functional incapacity and higher risk of falls (Goes et al., 2012). The mechanisms for muscle strength reduction may be related to either muscle activation impairment (antagonist co-activation and voluntary activation failure) (Valkeinen et al., 2008; Graven-Nielsen et al., 2002) or metabolic changes (insulin resistance and high glucose levels) (Loevinger et al., 2007) due to FM symptoms. However, how these factors interact is not clear. The purpose of this study was to compare torque production, antagonist co-activation, voluntary activation failure, metabolic changes (glucose levels and insulin resistance), and falls risk between women with and without FM. Additionally, the relationship between FM symptoms, metabolic factors, torque production and falls in women with FM were determined.

Methods: Fifty-nine middle-aged women (29 with FM and 30 as control group) were recruited. Pain intensity and threshold, anthropometric measurements, and fall history (last six months) were assessed. In addition, plasma glucose, glycosylated hemoglobin (HbA1c), and insulin resistance (IR) were determined at the same time. Participants were encourage to perform ankle dorsiflexion and plantar flexion maximum isometric voluntary contractions (MIVC), from which peak torque and rate of torque development (RTD) were calculated, as well as, anterior tibialis and gastrocnemius lateral head (GL) electromyography (EMG), and central activation ratio (CAR) in the anterior tibialis muscle were evaluated. In order to calculate the GL co-activation during dorsiflexion, the integrated EMG (iEMG) was used. The full voluntary muscle activation was evaluated by burst superimposition with supramaximal electrical train stimuli during dorsiflexion MIVC. The CAR was calculated as the maximum voluntary torque produced prior to delivery of the train divided by the maximum torque produced during the superimposition of the train.

Results: Women with FM had lower pain threshold, higher pain intensity, and reported greater number of falls compared to control group (CG) ($p < 0.05$). In addition, participants with FM exhibited higher IR (FM: 2.0±1.1; CG: 1.8±0.9; $p < 0.05$), although there were no differences in glucose and HbA1c levels between groups. The FM group showed reduced plantar flexors RTD and dorsiflexors RTD compared to CG ($p < 0.05$). Additionally, subjects with FM showed lower plantar flexors peak torque, had more antagonist co-activation during dorsiflexion (Figure 1), and decreased CAR (FM: 89.5±12.4%; CG: 97.8±4.3%; $p < 0.05$) than the CG. The lower CAR was explained by HbA1c level (R^2adj=0.21; $p < 0.05$). Reduced plantar flexors and dorsiflexors peak torque explained, together, 80% of falls variance; also, high antagonist co-activation (OR=1.6; $p < 0.05$) and high IR (OR=1.8; $p < 0.05$) increased the chance of falls in the FM group (Table 1).

Figure:
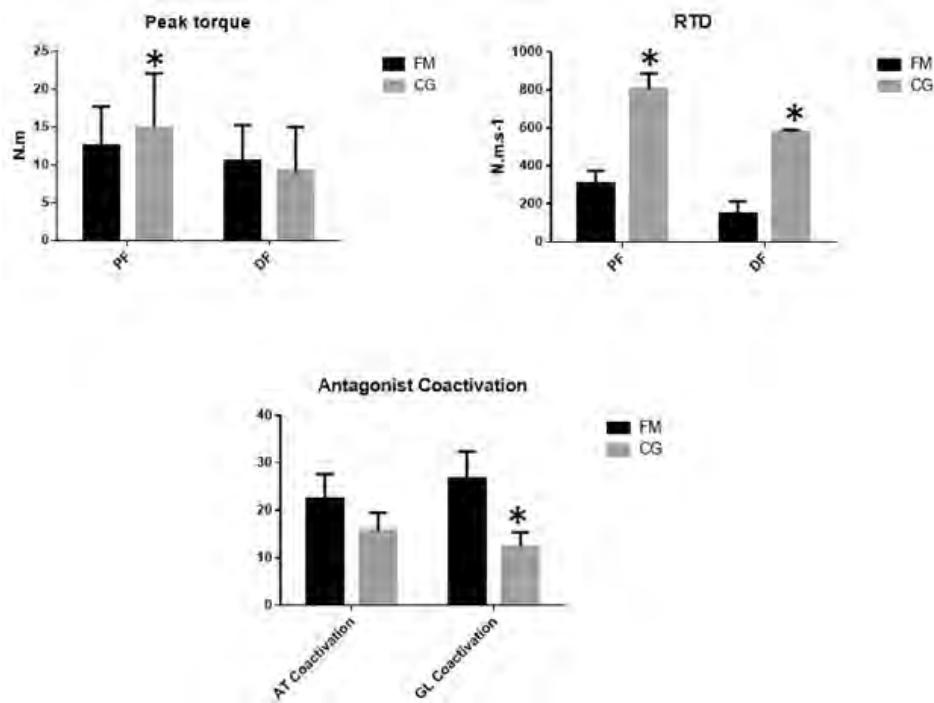
Caption: Figure 1 – Torque production in the ankle in both groups. Note: FM: Fibromyalgia group; CG: Control group; PF: Plantar flexors; DF: Dorsiflexors; RTD: Rate of Torque Development; AT: Anterior Tibialis; GL: Gastrocnemius lateral head.

Conclusion: Women with FM showed reduced plantar flexors and dorsiflexors torque production, high IR and high number of falls. A combination of factors in FM, such as IR and torque production impairment in the ankle joint increase the odds of having a fall. Ankle musculature function is important to produce stabilizing moments during balance and other functional tasks. Thus, a multi-pronged approach to treatment focusing on decreasing glucose level and IR, as well as, ankle exercises directed at increasing muscle strength may increase the effectiveness of clinical and community interventions designed for improving balance and reducing falls in women with FM.

Table:

		B	SE	*OR*	*p*	CI - 95%
Falls						
	Model 1:					
	IR	23.6	12.1	1.8	0.05	0.8	3.755
	(Constant)	66.2	48.4	5.6	0.171		
	Model 2:					

PF Peak Torque	-17.2	7.5	0.3	0.021	0	0.075
DF Peak Torque	-0.5	0.2	0.9	0.024	1.1	2.751
GL Coactivation	0.1	0	1.6	0.031	0.9	0.993
(Constant)	17.6	8.2	45.01	0.031		

Logistic Regression Analysis with the FM group. Variables insert on Model 1: Body Mass Index; Waist Circumference, Insulin, Insulin Resistance, HbA1c. Variables inset on Model 2: PF peak torque, DF peak torque, PF RTD; DF RTD; AT coactivation; GL coactivation; CAR. Note: B: Beta value; SE: Standard Error; OR: Odds Ratio; IR Insulin Resistance; PF: Plantar flexors; DF: Dorsiflexors; GL: Gastrocnemius Lateral head; RTD: Ratio of Torque Development; AT: Anterior Tibialis; CAR: Central Activation Ratio.

Caption: TABLE 1 – Fall predictors in the FM group.

References: [1] Henriksen et al., Arthrit Care Res, 61(6):732-739, 2009.

[2] Goes et al., Clin Biomech (Bristol, Avon),27(6):578-583,2012.

[3] Valkeinen et al., Int J Sports Med, 29(5):408-413, 2008.

[4] Graven-Nielsen et al., Muscle & Nerve, 26(5):708-712, 2002

[5] Loevinger et al., Metabolism,56(1):87-93,2007.

Disclosure of Interest: None Declared

Musculoskeletal

AS-0022

ACUTE EFFECTS OF CONTRACT-RELAX STRETCHING, STATIC STRETCHING AND ISOMETRIC CONTRACTIONS ON MUSCLE-TENDON MECHANICS

Anthony Kay [1,*] Jade Husbands-Beasley [1] Anthony Blazevich [2]

[1] Sport, Exercise & Life Sciences, The University of Northampton, Northampton, United Kingdom, [2] Centre for Exercise & Sport Science Research, Edith Cowan University, Joondalup, Australia

Introduction and Objectives: Maximum joint range of motion (ROM) and resistance to joint rotation within that range (i.e. resistance to stretch) are important physical characteristics that influence the capacity to perform activities of daily living and athletic tasks [1], and are affected considerably by aging and disease [2]. The loading characteristics of different muscle stretching techniques likely influence the specific mechanisms responsible for acute increases in range of motion (ROM). Identifying mechanisms allows the determination *a priori* as to whether these interventions might be useful in different clinical populations, why such stretch interventions elicit different responses in different individuals, and to optimize/improve the methodology of, and response to, the stretch technique. Therefore, the effects of contract-relax proprioceptive neuromuscular facilitation (CR) stretching, static stretching (SS) and maximal isometric contraction (Iso) interventions were studied in 17 healthy human volunteers.

Methods: Passive ankle moment was recorded on an isokinetic dynamometer with electromyographic (EMG) recording from the triceps surae, simultaneous real-time motion analysis, and ultrasound imaging recorded gastrocnemius medialis muscle and Achilles tendon elongation. The subjects then performed each intervention randomly on separate days before reassessment. The SS condition included 4 x 15 s plantar flexor stretches with 15 s rest between stretches, the CR condition included 10 s stretches followed immediately by a 5-s ramped maximal isometric plantar flexor contraction in a fully stretched position, repeated four times giving a total duration of 60 s; identical to the SS condition. The Iso condition included 4 x 5 s ramped maximal isometric plantar flexor contractions performed in the anatomical position, with 15 s rest between contractions.

Results: Significant increases in dorsiflexion ROM (2.5-5.3°; $P < 0.01$) and reductions in whole muscle-tendon stiffness (10.1-21.0%; $P < 0.01$) occurred in all conditions, with significantly greater changes detected following CR ($P < 0.05$). Significant reductions in tendon stiffness (see Figure 1, A) were observed after CR and Iso (17.7-22.1%; $P < 0.01$) but not after SS ($P > 0.05$), while significant reductions in muscle stiffness (see Figure 1, B) occurred after CR and SS (16.0-20.5%; $P < 0.01$) but not after Iso ($P > 0.05$). Increases in peak passive moment (stretch tolerance) occurred after Iso (6.8%; $P < 0.05$), CR (10.6%; $P = 0.08$) and SS (5.2%; $P = 0.08$); no difference in the changes between conditions was found ($P > 0.05$). Significant correlations ($r_s = 0.69$-0.82; $P < 0.01$) were observed between the changes in peak passive moment and maximum ROM in all conditions.

Figure:
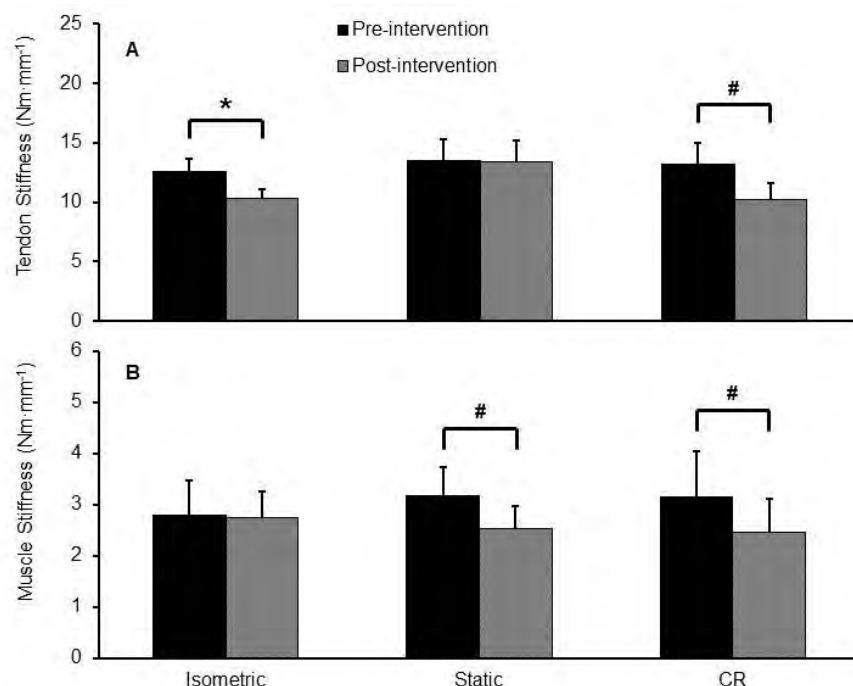
Caption: Figure 1. Achilles tendon stiffness [A] and gastrocnemius medialis (GM) muscle stiffness [B] pre- and post-intervention.

Conclusion: While similar ROM increases occurred after isometric contractions and static stretching, changes in muscle and tendon stiffness were distinct. The concomitant reductions in muscle and tendon stiffness after contract-relax stretching suggest a broader adaptive mechanical response that likely explains its superior efficacy to acutely increase ROM. These are the first data to confirm that acute changes in tendon stiffness may contribute to PNF stretching's superior efficacy to increase ROM, above other stretching modes. However, while mechanical changes appear tissue-specific between interventions, significant correlations between the change in peak passive moment and the change in ROM were observed in all conditions, indicative of a neurological adaptation (i.e. increased stretch tolerance) also being important for the acute increases in ROM. The reduction in tendon stiffness and increase in ROM detected following the Iso condition have important methodological implications as these data indicate that the performance of contractions 'on stretch' during PNF stretching may not be needed. Modifying PNF stretching to perform the contraction phase in the anatomical, rather than highly stretched position, removes the need for partner assistance, decreases the likelihood of inducing pain, tissue damage and muscle strain injury during the technique, which may enhance PNF's suitability and practicality for athletic and clinical populations.

References: [1] Mulholland & Wyss. Int J Rehabil Res, 24: 191-198, 2001.

[2] Duffin et al., Diabet Med, 16: 125-130, 1999.

Disclosure of Interest: None Declared

Musculoskeletal

AS-0023

EXPLORING THE RELATIONSHIP BETWEEN LOCAL AND GLOBAL SPINE STABILITIES DURING REPETITIVE LIFTING TASKS.

Matthew Mavor [1,*]Ryan Graham [1]

[1]School of Physical and Health Education, Nipissing University, North Bay, Canada

Introduction and Objectives: Lifting is a major occupational risk factor for low back injury. Lifters experience small continual perturbations, because moving a load provides a disturbance to the lifter's balance and equilibrium [1]. In healthy individuals, these perturbations are offset in order to maintain a stable trunk and spine during movement. However, lifters also experience larger perturbations due to a variety of factors such as loads shifting in boxes or unstable/slippery floors, which can cause slipping and/or tripping. With enough internal (local) stability the lifter can offset such an external (global) perturbation and return to their desired movement trajectory without injury to the spine system (i.e. passive tissues, muscles, nervous system) [2]. The goal of the present study was to examine the relationship between local and global spine stabilities during perturbations introduced at the foot-floor interface. It was hypothesized that there would be good agreement between both stability metrics, and that both local and global stabilities would be progressively increased as the lifted load in the hands was increased [3].

Methods: 12 healthy males were recruited to participate in this study. Mean age, height, and mass were 23.2 years (SD = 4.0), 178.2 cm (SD = 6.9), and 73.5 kg (SD = 10.7), respectively. Participants completed a freestyle lifting protocol on a perturbation treadmill, while wearing a harness that was secured to the ceiling (V-Gait, Motek Medical, Holland) (Figure 1). Participants lifted a box from knee to shoulder height under three load conditions (0, 4, and 8kg in a randomized order), at a rate of 6 cycles per minute to the beat of a metronome. Under each load condition participants performed a total of 40 lifts; the first 20 lifts were without any perturbations. Then, in the following 20 lift cycles (in blocks of 5), participants were randomly given perturbations by the treadmill in each of the four direction combinations (forward or backward tilt of 4° and left or right displacement of 5cm). Perturbations were programmed to not occur back to back, and were initiated when the box eclipsed 50% of the participant's height on the way up. During all trials, 3-D kinematic data were collected from the pelvis and spine at 100Hz (Oqus 400+, Qualisys, Sweden). 6-D state spaces (x,y,z linear and angular velocities of the trunk relative to pelvis) were created using data recorded from the first 20 unperturbed lift cycles (attractor), and local dynamic spine stability was quantified using the local divergence exponent, λ_{max} [4,5]. In addition, we analyzed the distance traveled from the unperturbed lifting pattern (B), the time to max distance (Tau), the relaxation distance (A), and the rate of return toward the normal lifting pattern (Beta) following each external perturbation [4,5]. Each global perturbation metric was then averaged across the four perturbations, and both local and global stability values were compared using repeated-measures ANOVAs in SPSS 22 (IBM Corporation, USA).

Results: An increase in load lifted lead to significantly increased local spine stability (decreased λ_{max}) during the unperturbed lifts (p = 0.046) (Table 1). Post-hoc testing revealed that the 8kg condition was significantly more stable than the 0kg condition (p= 0.011). Higher load also lead to decreased distance (B) traveled away from the unperturbed

trajectory (p = 0.023). Post-hoc testing revealed that both the 4 and 8kg conditions were more stable than the 0kg condition (p= 0.007 and 0.018).

Figure:
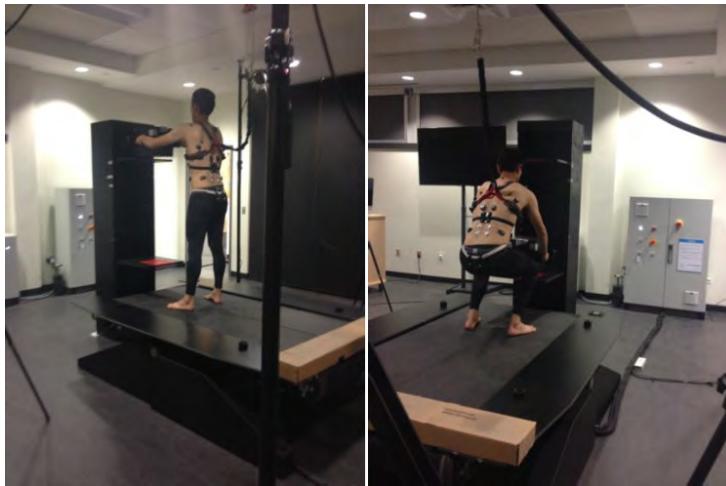
Caption: Figure 1. Experimental set-up. Under each load condition participants were required to repetitively lift between the targets placed at shoulder and knee height.

Conclusion: Results agree with our previous research that increasing the load lifted significantly improves local spine stability during non-perturbed lifting due to higher muscle activation that translates into greater lumbar spine rotational stiffness [3]. Here we have shown that these changes also translate into a greater ability to resist external global perturbations, which may reduce injury risk and should be explored in the future. The exact relationships between local and global stabilities are currently being analyzed in each individual subject using linear mixed modelling (repeated-measures regressions).

Table:

Stability Values		0 kg	4 kg	8 kg	Repeated-Measures ANOVA Results
		Mean (SD)	Mean (SD)	Mean (SD)	p-value
Local	λmax	1.09 (0.25)	0.99 (0.17)	0.96 (0.14)	**0.046**
Global	A	3.14 (0.77)	3.14 (0.97)	2.96 (0.54)	0.652
	B	38.6 (16.7)	31.0 (13.2)	27.7 (10.0)	**0.023**
	Tau	57.4 (21.3)	58.7 (21.6)	56.8 (19.3)	0.966
	Beta	0.17 (0.09)	0.24 (0.09)	0.22 (0.11)	0.105

Caption: Table 1. Stability mean (standard deviation) and ANOVA results. Bolded values indicate significance at p<0.05.

References: [1] Graham et al., Gait Posture, 34: 561-563, 2011.

[2] Panjabi, M., J. Spinal Disord., 5: 383-389, 1992.

[3] Graham et al., J. Biomech., 45: 1593-1600, 2012.

[4] Bruijn et al., J. Exp. Biol., 213: 3945-3952, 2010.

[5] Toebes et al., Gait Posture., 40: 215-219, 2014.

Disclosure of Interest: None Declared

AS-0025

IN SEARCH OF THE UNDERLYING MECHANISMS RESPONSIBLE FOR IMPAIRED GAIT-RELATED POSTURAL CONTROL IN PEOPLE WITH PARKINSON'S DISEASE

Brook Galna [1,*] Chris Buckley [2] Aodhán Hickey [1] Silvia Del Din [1] Alan Godfrey [1] Claudia Mazzá [2] Lynn Rochester [1]

[1]Institute of Neuroscience / Newcastle University Institute for Ageing, Newcastle University, Newcastle upon Tyne, [2]MRC-Arthritis Research UK Centre for Integrated Research into Musculoskeletal ageing (CIMA) / Insigneo Institute for in silico medicine, Department of Mechanical Engineering, The University of Sheffield, Sheffield, United Kingdom

Introduction and Objectives: The ability to make small yet precise adaptations to step width is crucial for the coupling of postural control and gait. People with incident Parkinson's disease (PD) walk with a less variable step width, suggesting early changes in gait-related postural control [1]. Impaired postural control during gait puts people with PD at a high risk of falls. A better understanding of the underlying mechanisms responsible for reduced step width variability in PD may help facilitate earlier and better targeted interventions to prevent future falls. Previous analysis suggests reduced trunk accelerations during gait contribute to a less variable step width in PD [2]. Rigidity is one of the cardinal symptoms of PD and may affect trunk accelerations by resisting the counter rotation between the pelvis and trunk; hence we hypothesise that increased trunk rigidity indirectly influences step width variability in PD. However, there are important technical and clinical challenges in addressing this hypothesis. First, we do not know whether upper body trunk accelerations can be used as a proxy measure of trunk rigidity during gait in PD. Second, the relationship between trunk accelerations, rigidity and step width variability may vary between different PD phenotypes (subtypes). Therefore, the aims of this analysis were to: i) investigate the relationship between clinical measures of rigidity and trunk accelerations during gait; ii) examine whether step width variability correlates with rigidity and trunk accelerations; and iii) test whether these relationships are similar across different PD phenotypes.

Methods: Step width variability (within-person SD of step width) of 84 people with early PD (Mean (SD) Age:69 (9.6) years; 35 females; Unified Parkinson's disease rating scale (UPDRS) III:28(11), 18-22 months since diagnosis, tested at peak dose of their medication) was measured over 4 x 10m walks using an instrumented walkway (GAITRite). For sub-group analysis, participants were classified into postural instability and gait difficulty (PIGD, n = 31), indeterminate (n = 17, excluded from sub-group analysis) and tremor dominant (n = 36) phenotypes using established methods [3]. Anterior-posterior (AP) and mediolateral ML trunk accelerations were measured during gait using 3D accelerometers (100Hz, ±8g, 4th order Butterworth 20Hz low-pass filter) taped onto the chest (mid way between the xiphoid process and clavicular notch) and lumbar spine (L5). The following variables were calculated: root mean square acceleration (RMS), harmonic ratio (HR) and attenuation of acceleration from the L5 to Chest sensor derived from RMS accelerations [4]. Rigidity was assessed using the average response from 5 rigidity items incorporated into the UPDRS III (each item scored from 0 no rigidity to 4 severe). Partial correlations were used to assess the relationship between trunk accelerations, rigidity and step width variability correcting for age, sex, gait speed and step duration. A $p \leq .05$ was used to guide interpretation.

Results: There were no significant correlations between trunk accelerations and rigidity. Reduced step width variability was correlated with reduced ML RMS$_{Chest}$ (r =.237, p=.028), with no other significant correlations being observed. This

correlation was stronger in the PIGD sub-group (r=.420, p=.021) whereas no correlations between trunk accelerations and step width variability were found in the tremor dominant sub-group.

Conclusion: Our findings suggest that impaired trunk motion is associated with reduced step width variability in people with early PD, especially in people with a PIGD phenotype. However, we found no support for the use of upper body trunk accelerations as a proxy measure of rigidity in people with PD, hampering our ability to test the hypothesis that trunk rigidity is associated with step width variability. The lack of correlation between trunk motion and rigidity may be due to: i) the lack of sensitivity of the UPDRS subscale to rigidity in our relatively mild PD group; and ii) the UPDRS III items focus primarily on peripheral and not axial rigidity features and may not be as sensitive as direct mechanical assessment [5]. Although our findings suggest altered trunk accelerations are related to reduced step width variability, more appropriate methodology is needed to assess trunk rigidity during gait to assess its contribution to the coupling of postural control and gait in early PD.

References: [1] Rochester et al. Neurosci, 18(265), 2014.

[2] Galna et al. ISPGR conference proceedings, P1-0-84, 2014.

[3] Stebbins et al. Mov Disord, 28(5), 2013.

[4] Mazzà C et al. J Neuroeng Rehabil, 5(30), 2008.

[5] Wright et al. Exp Neurol, 208(1), 2007.

Disclosure of Interest: None Declared

Neurological and Motor Control

AS-0026

INDIVIDUALS WITH CHRONIC ANKLE INSTABILITY USE DIFFERENT PATTERNS OF MUSCULAR ACTIVATION TO MAINTAIN BALANCE WHILE KICKING A BALL IN SINGLE-LEG STANCE

Jaqueline Lourdes Rios [1 2,*] Josilene S Conceição [3] Ana Luiza Gorges [3] Felipe Gustavo S de Araújo [3] Marcio Jose dos Santos [4 5]

[1] Faculty of Knesiology, University of Calgary, Calgary, Canada, [2] Center of Sports and Health Sciences, [3] Physical Therapy, [4] Physical Therapy and Center of Sports and Health Sciences, Santa Catarina State University, Florianopolis, Brazil, [5] Physical Therapy and Rehabilitation Sciences, University of Kansas Medical Center, Kansas, United States

Introduction and Objectives: Kicking a ball is a task commonly used at athletic clubs and rehabilitation sites to train and rehabilitate individuals with chronic ankle instability (CAI), especially with athletes and soccer players [1]. Recent studies showed that, during this task, subjects with CAI exhibited reduced magnitude of electromyographic (EMG) activity at the ankle muscles in the supporting leg. However, it is still unknown which muscles around the ankle are driving the postural equilibrium of these individuals during this task. The aim of this study was to investigate the muscle activity patterns of the ankle joint during the kicking a ball task in individuals with CAI.

Methods: We used the principal component analysis (PCA) to identify differences in patterns of muscle activation between 60 individuals with CAI and 21 healthy controls while they performed the kicking a ball task standing in a single-leg stance. We registered the EMG activities of the ankle muscles of the supporting leg: soleus (SOL), medial and lateral heads of the gastrocnemius (GasM and GasL), tibialis anterior (TA) and peroneus longus (PL) as well as of the adductor (AD) muscle of the kicking leg. We calculated the magnitudes of the EMG activities (integrals: ∫EMG) during the time intervals of anticipatory (APA) and compensatory (CPA1, CPA2 and CPA3) postural adjustments according to the AD activity onset. We performed the PCA analysis on the ∫EMGs across these 4 time intervals.

Results: The first three principal components covered about 80% (41%, 23%, and 15%) of the spread of the data in the CAI group and 84% (46%, 19% and 18%) in the control group. The muscles seen significantly loaded (with the absolute value over 0.5 [2]) for the CAI group were: *PC1*: TA and PL; *PC2*: GasL and GasM; *PC3*: SOL while for the control group were: *PC1*: GasL and GasM; *PC2*: TA; *PC3*: SOL and PL (Table 1). The magnitudes of the SOL and TA ∫EMG were smaller in the CAI than in the control group during the APA time interval. The PL ∫EMG was smaller in the APA and CPA1 phases. **Discussion:** The dominant principal components differed between the control and CAI groups. For the CAI group, PC1 clustered the TA and PL muscles; while for the control group, this component included GasL and GasM. These results suggest that individuals with CAI primarily control the inversion/eversion muscles to maintain their balance during the kicking task. In contrast, the healthy control used predominantly the GasL and GasM, which is expected since kicking a ball involves an anteroposterior perturbation. It is possible that CAI factors such as ligament laxity, weakness, reduction in nerve conduction velocity [3] and decreased muscular activity (observed in this study) lead to increased instability in the frontal plane. This will make individuals with CAI employ a pattern of muscle activity with amplified control of mediolateral ankle stability during the kicking task.

Figure:
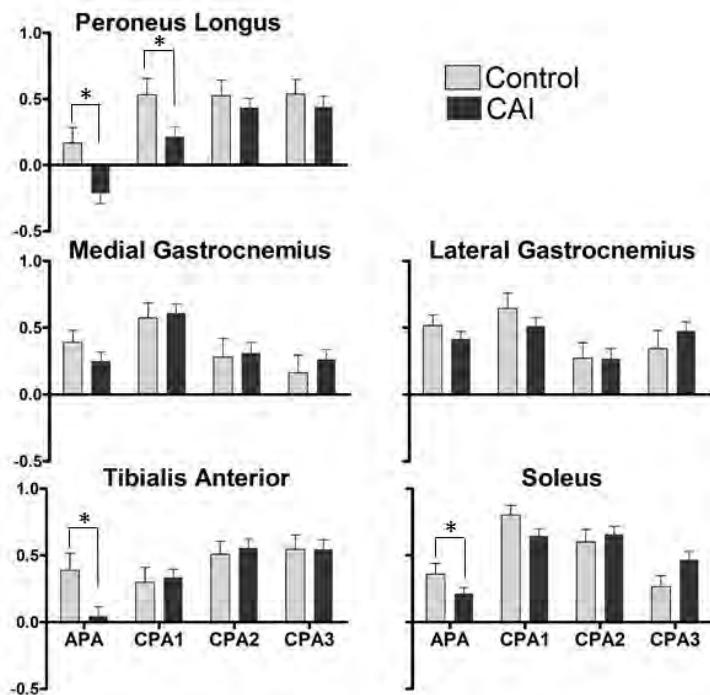
Caption: Fig 1. Mean normalized of the ∫EMG (arbitrary units) of muscles around the ankle for individuals with (CAI) and without (Control) chronic ankle instability, during the anticipatory (APA) and compensatory postural adjustments (CPA1, 2 and 3). * Indicate significant differences between groups at p<0.05.

Conclusion: CAI may alter the muscle control strategy during kicking to better stabilize the ankle mediolaterally. Further research is needed to determine whether rehabilitation interventions based on this or other balance perturbation trainings enhance this functional adaptation or reverse it to normal patterns of those without CAI.

Table:

	CAI			Control		
Muscles	PC1	PC2	PC3	PC1	PC2	PC3
SOL	.076	-.041	.953	.421	.322	.637
TA	.836	.119	.116	-.117	.977	-.024
GasL	.141	-.881	-.136	.910	.059	-.047
GasM	-.117	-.850	.199	.986	-.163	.000
PL	.827	-	-	.354	.286	-

		.147	.050			.710

Caption: Table 1. Results of PCA for all muscles of both groups during the kicking task; loadings over 0.5 are shown in bold. Soleus (SOL), medial head of the gastrocnemius (GasM), lateral head of the gastrocnemius (GasL), tibialis anterior (TA), and peroneus longus (PL).

References: [1] Hale et al., J Orthop Sports Phys Ther, 37(6):303-311, 2007.

[2] Krishnamoorthy et al., Biol Cybern, 89(2):152-161, 2003.

[3] Santos et al., J Orthop Sports Phys Ther, 38(3):150-157, 2008.

Disclosure of Interest: None Declared

Neurological and Motor Control

AS-0027

INDIVIDUALS WITH KNEE OSTEOARTHRITIS USE DIFFERENT MUSCLE ACTIVATION PATTERNS THAN HEALTHY SUBJECTS DURING MAXIMAL ISOMETRIC KNEE EXTENSIONS

Jaqueline Lourdes Rios [1] [2],[*]Conrad Tang [1]Walter Herzog [1]

[1]Faculty of Kinesiology, University of Calgary, Calgary, Canada, [2]Coordenadoria de Aperfeiçoamento de Pessoal de Nível Superior (CAPES), Brasília, Brazil

Introduction and Objectives: Patients with knee osteoarthritis (KOA) have demonstrated impaired postural balance, decreased medial knee compartment loading, increased stance times during walking, and muscle weakness. Furthermore, strength training has not been effective in reducing the progression of KOA, and muscle activation patterns in KOA have not been well defined under controlled conditions. Specifically, electromechanical delay (EMD), a key indicator of proper muscle function, has not been evaluated in patients with early KOA. Abnormal EMD might provide important insight into the loss of control of the knee extensor muscles which are crucial for optimal knee loading. Therefore, the aim of this study was to analyze EMD in KOA patients and age-matched controls during maximal isometric contractions.

Methods: Fifty-six patients with KOA (KOA group) and ten healthy individuals (control group), matched by age, performed three isometric knee extensor contractions at 60° of knee flexion. For the KOA group, the knee with the more severe OA symptoms was studied. For the control group, both knees were used for testing (20 knees). The vastus medialis, vastus lateralis and rectus femoris muscle activation onset (MO) and torque onset were identified. EMD was then calculated as the difference in time between MO and torque onset [1]. MO was defined as the instant when the EMG amplitude exceeded ± 2SD of baseline values and lasted for more than 50ms [2]. This assessment of MO was defined as method 1. Qualitative analysis of the EMG signals revealed a burst of EMG activity lasting less than 50ms that often preceded the regular EMG in KOA patients. Therefore, MO was also defined as the first burst of EMG activity independent of its duration (method 2). Differences between groups were analyzed using a one-way ANOVA ($\alpha=0.05$).

Results: Using method 1, KOA patients had a significantly shorter EMD (40ms on average) than the healthy control subjects. However, using method 2, there was no difference between groups (Fig.1-D). 86% of the muscles from the control group subjects presented a MO pattern that is considered standard in the literature, that is EMG onset is clearly defined by a long burst of activity (Fig.1-C). For these trials, analysis method 1 and 2 gave the same result. However, for the KOA group subjects, 86% displayed a non-standard activation pattern in which a continuous burst of EMG activity was preceded by a short (about 25ms) burst that was followed by a distinct (46ms) silent period or a period of low activation not exceeding ±2SD of the resting EMG. For these trials, analysis methods 1 and 2 give distinctly different EMD values. 35% of muscles of KOA group subjects had this low activation (Fig.1-B), and 51% showed a silent period between the initial burst and the standard MO (Fig.1-A). This last pattern was responsible for most of the differences observed between KOA and control group subjects, since the mean difference in EMD was 71ms for the two analysis methods. These altered muscle recruitment pattern in the KOA patients could be associated with pain experienced by the KOA patients [3]. When recruiting the knee extensor muscles, knee pain may have triggered muscle inhibition that was

subsequently overcome by voluntary activation on order to fulfill the required knee extensor task. In addition, the low activation following the initial burst in some KOA patients could be an avoidance strategy adopted by KOA patients to dealing with the chronic pain. Since the first component of pain acceptance is a willingness to experience pain, and the second is the pursuit of goals and activities despite having pain, the current results might be explained within this framework [4].

Figure:
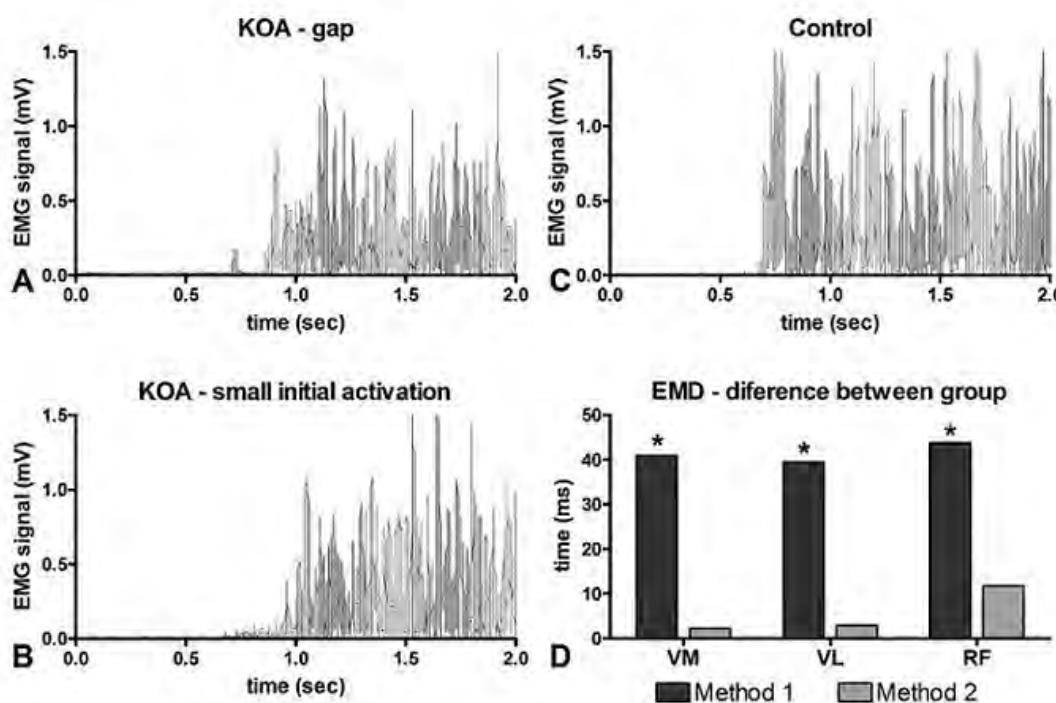
Caption: Fig.1.(A) Raw data from an exemplar trial for a subject with KOA, showing a gap between the first burst and the standard MO, and (B) decreased initial activation. (C) Healthy subject presenting typical MO. (D) Difference between EMD of subjects with KOA and healthy using method 1 and 2.

Conclusion: Individuals with KOA presented with distinctly different EMG activation patterns in the knee extensor muscles during an isometric task which resulted in a decreased EMD compared to control subjects. KOA patients also frequently had a distinct short initial burst of activation not seen in control subjects. Therefore, we conclude that knee extensor activation patterns in KOA subjects are impaired and result in shorter EMD. The mechanism underlying these altered activation strategies in KOA patients are not known. Therefore, these results set up potential investigations to examine the detailed activation mechanisms in patients with KOA.

References: [1]Nordez et al., J Appl Physiol, 106:1970-1975, 2009.

[2]Santos et al., J Electromyogr Kinesiol, 20:388-397, 2010.

[3]Urwin et al., Ann Rheum Dis, 57:649-655, 1998.

[4]McCracken et al., Pain, 109:4–7, 2004.

Disclosure of Interest: None Declared

MUSCLE SYNERGIES IN LEVEL AND INCLINED WALKING

Lars Janshen [1,*]Alessandro Santuz [1]Antonis Ekizos [1]Adamantios Arampatzis [1]

[1]Training and Movement Science, Humboldt-Universität zu Berlin, Berlin, Germany

Introduction and Objectives: Neuromuscular coordination in human walking can be described by general patterns referred to as motor modules or muscle synergies [1]. There is evidence that muscle synergies are neurophysiological entities whose combination constructs a large set of movement [2]. The number of synergies and their structure resulting from the amplitude time courses of the contributing muscles are mainly consistent across individuals and different conditions in level walking, e.g. walking speed [3]. During inclined walking the characteristic of joint torques is different compared to level walking [4] and this may result in a different modular organization of the neuromuscular system. However, there is no knowledge about potential changes in the modular organization in non-level walking. The aim of this study was to compare the muscle synergies of level and inclined walking, hypothesising differences in neuromuscular organization between both conditions as a result of changes in the dynamic demands during inclined walking.

Methods: Surface EMG activity of 24 muscles [5] of the right body side of ten males and ten female participants was recorded over 50 cycles during level and inclined walking performed in a randomized order on a treadmill instrumented with a pressure plate. All participants performed each of two trials of level and inclined walking on the same day as well as in a second measurement at least 48 h (122±84 h) later. Walking speed was self-selected for level walking (1,4±0,2 m/s) and was 85% of this speed during walking at 10° incline. Gait cycles were determined from pressure plate data. EMG signals were band-pass filtered at cut off frequencies of 5 Hz and 400 Hz respectively by the recording system. The signals were high pass filtered, fully rectified and low pass filtered at 50 Hz and 20 Hz respectively using IRR 2nd order zero-lag Butterworth filters. EMG envelopes were time normalized to 200 data points per gait cycle [6] and amplitude normalized to one. To be comparable to the existing literature, muscle synergy extraction was performed using a customized Gaussian non-negative matrix factorization (NMF) algorithm [7]. A sufficient number of synergies was reached, when additional synergies did not increase the total explained variance represented by the rate of changes in the R^2 curve of reconstructed to original signal. To analyse the differences between level and non-level walking an ANOVA for repeated measures was used.

Results: No significant differences in gender as well as for both, the intraday and the inter-day measurements for each participant were observed. Level and inclined walking tasks could be reconstructed by 5±1 synergy with an R^2 of 0.92 and 0.90 respectively. The respective synergies majorly represented the muscular activity of (1) the hip and knee joint extensors attributed to foot strike, (2) the upper body muscles in the late stance phase, (3) the ankle joint extensors during push off, (4) the knee flexor and upper body muscles during late swing in preparation of the next stance phase and (5) the upper body muscles during stance and swing phase. However, during inclined walking in 32 % of all trials a sixth synergy shape for the upper body muscles during stance was observed. In 44 % this led to a total number of six synergies. Within five synergies, this resulted in a merge of synergy three and four or one and five. The flexor and extensor muscles of the

hip and ankle joint demonstrated higher weights for the respective synergies during inclined compared to level walking. These differences were predominantly significant (p<0.05).

Figure:
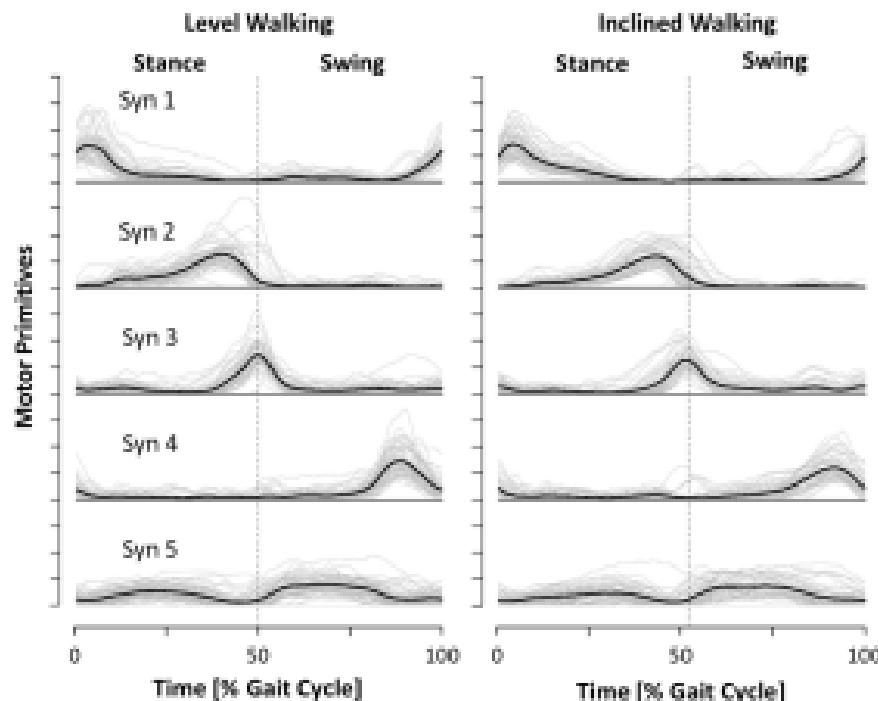
Caption: Motor primitives in level (left) und inclined walking (right).

Conclusion: The applied data acquisition methods seem to be robust against measurement artefacts occurring at multiple measurements even when repositioning the EMG electrodes. The congruence of synergies in the majority of the investigated trials (i.e. 5 synergies) during level and incline walking indicate a similar modular organisation of the neuromuscular system in both conditions. The observed higher weights of the flexor and extensor muscles of the hip and ankle joint could probably be attributed to the increased demands on the mechanical output of these muscles during inclined compared to level walking. However, the redistributions in muscle synergies in some cases may indicate changes in the neuromuscular control in inclined compared to level walking.

References: [1] E. Bizzi et al., Brain Res. Rev. 2008, 57, 125.

[2] E. Bizzi & V. C. K. Cheung, Neurosci. 2013, 7, 51.

[3] Y. P. Ivanenko et al. J. Physiol. 2004, 556, 267.

[4] P. DeVita et al. J. Biomech. 2008, 41, 3354.

[5] K. M. Steele et al. Front. Comput. Neurosci. 2013, 7, 105.

[6] V. C. K. Cheung et al., J. Neurophysiol. 2009, 101, 1235.

[7] D. D. Lee et al., Nature 1999, 401, 788.

**Disclosure of Interest**: None Declared

AS-0029

THE EFFECTS OF FATIGUE ARE INFLUENCED BY MUSCLE ACTION (ECCENTRIC VS CONCENTRIC) AND FORCE DEMANDS (SUBMAXIMAL VS MAXIMAL)

Chad A. Sutherland [1,2,*] Nicholas La Delfa [1] Jim Potvin [1]

[1]Kinesiology, McMaster Univeristy, Hamilton, [2]Kinesiology, University of Windsor, Windsor, Canada

Introduction and Objectives: It is generally accepted that muscle fibers can generate more force during eccentric efforts, compared to both concentric and isometric efforts, under isotonic conditions. However, it appears that individuals are limited in their ability to produce maximal muscle activation during voluntary eccentric efforts. LaDelfa et al. (2014) termed this a "neural tension-limiting mechanism" (NTLM) and showed that processing the raw sEMG signal with alternative methods, such as extreme high pass filtering or whitening, allows for novel insights into the different neurophysiological control strategies used during fatiguing efforts. The purpose of the current study was to investigate the effects of fatigue on the agonists during the concentric and eccentric phases of repetitive knee extensor efforts that were either submaximal or maximal.

Methods: Sixteen male participants performed continuous maximal knee extension efforts on a Biodex dynamometer, concentrically (CON) at a velocity of 30°/s and eccentrically (ECC) at -30°/s, between 50-110° of knee flexion, until exhaustion. After a week of rest, fourteen participants repeated the protocol at a submaximal effort level of 33% MVC. We recorded the net knee extensor moment and raw sEMG signals from vastus medialis, vastus lateralis and rectus femoris. The sEMG signals were Butterworth filtered with a 6th order, extreme high pass cutoff of 140 Hz (see Potvin & Brown, 2004). A weighted average EMG value (EMG_{WA}) was calculated based on the PCSA of each of three quadriceps muscles, relative to their total PCSA. We then used a regression analysis to estimate the EMG_{WA}-to-Moment ratio at the start (rested) and end (fatigued) of each session, and then a ratio of fatigued/rested for the CON and ECC directions.

Results: Participants completed an average of 12.1±2.6 and 25.5±7.8 cycles, for the maximal and submaximal protocols, respectively. During both protocols, the increase in EMG_{WA}-to-Moment ratio was much more pronounced during the CON vs ECC efforts (Figure 1). These findings are in agreement with Gonzalez-Izal et al. (2014), who showed that fatiguing protocols cause a greater loss of force in CON efforts, compared to ECC efforts. Furthermore, we observed a larger effect of fatigue, on increasing the EMG_{WA}-to-Moment ratio, for submaximal vs maximal efforts. Consequently: 1) during the submaximal protocol, fatigue had the greatest effect on the CON efforts as it was associated with a 93% increase in activation, relative to the constant, submaximal moment (Figure 1), and 2) during the maximal protocol, fatigue had the least affect on the ECC efforts, as only a 26% decrease in activation was associated with a 56% decrease in the maximal extensor moment.

Figure:

Concentric / Eccentric axis with Maximal and Submaximal series. Y-axis: EMG-to-Moment Ratio (Fatigued vs Rested). Values: Submaximal Concentric 1.93, Eccentric 1.25; Maximal Concentric 1.04, Eccentric 0.74.
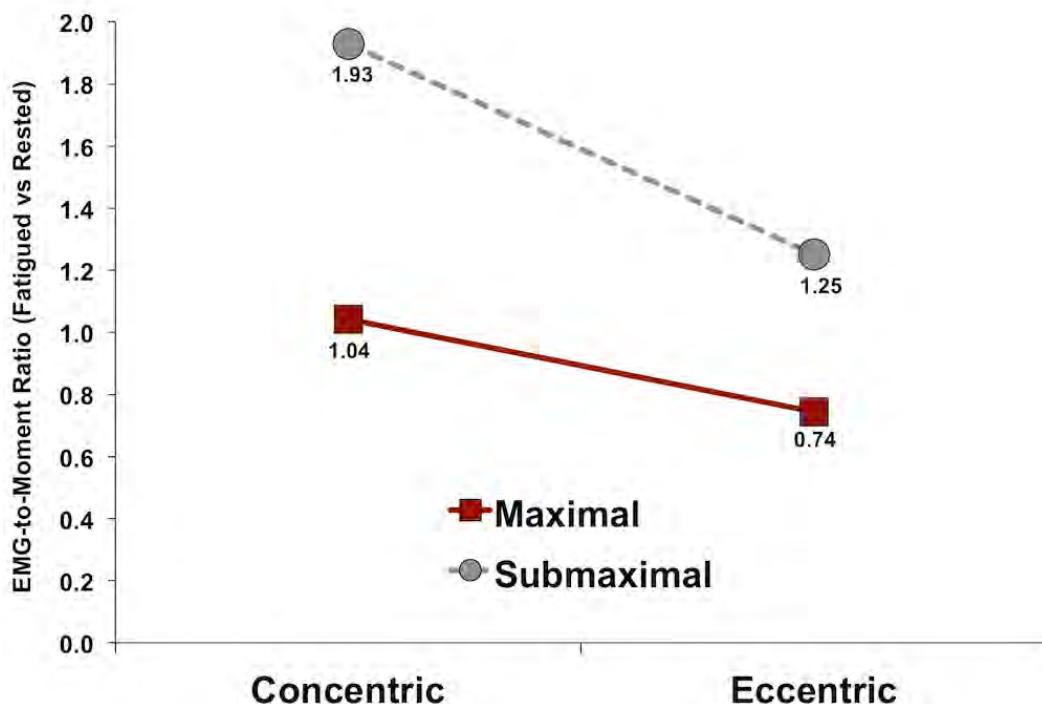
Caption: Figure 1. The EMGWA-to-Moment ratio was calculated at the start and end of the fatiguing trial during both the CON and ECC efforts. This figure shows fatigued ratios relative to the rested ratios. The ECC values are much lower than CON, particularly with the submaximal effort.

Conclusion: During repeated, maximal and submaximal, dynamic knee extension efforts to exhaustion: 1) ECC efforts were less affected by fatigue than CON efforts and, 2) maximal efforts were less affected by fatigue, than submaximal efforts. Lastly, the use of alternative sEMG processing methods, specifically extreme high pass filtering, has enhanced our ability to interpret how the neuromuscular system modifies the NTLM in the presence of fatigue.

References: [1] La Delfa et al., Muscle & Nerve, 50: 384-392, 2014.

[2] Potvin & Brown, J Electromyogr Kinesiol, 14:389–399, 2004.

[3] Gonzalez-Izal et al., Muscle & Nerve, 49: 389-397, 2014.

Disclosure of Interest: None Declared

Neurological and Motor Control

AS-0030

EXISTENCE OF MUSCLE SYNERGIES INCREASE LEARNING SPEED: SIMULATION STUDY BASED ON NEURAL NETWORK MODEL

Shota Hagio [1,*] Motoki Kouzaki [1]

[1]Graduate School of Human and Environmental Studies, Kyoto University, Kyoto, Japan

Introduction and Objectives: The concept of muscle synergies has been proposed to simplify redundant motor control by low-dimensionally organizing functionally similar muscles [1, 2]. Reduction of neuronal redundancy due to muscle synergies will contribute to upgrading learning performance as acquiring complicated movements. However, the functional roles of muscle synergies during motor learning remain unknown. The simulation analysis using neural network model makes it possible to specify the functional roles by evaluating leaning performance, such as learning speed, in the presence and absence of muscle synergies. The purpose of this study was to clarify the functional roles of muscle synergies during motor learning based on neural network simulation.

Methods: The descending neural network model including 3 intermediate layers (synergy model) was constructed based on the previously used model [3]. The neural network performed isometric force-generation around right wrist on a horizontal plane (elbow and shoulder joint flexion angles: 90° and 30°, respectively). The first intermediate layer contained 1000 neurons in primary motor cortex (M1). Each neuron received a desired shoulder flexion and/or elbow flexion torque vectors from the input layer with a synaptic weight (W_{neu}). These M1 neurons were connected to the second intermediate layer that indicated the muscle synergies as spinal interneurons [4, 5, 6, 7] with a uniformly distributed constant innervation. The number of muscle synergies was varied across continuous leaning. The muscle synergies controlled 26 muscles spanning elbow and shoulder joints with a synaptic weight (W_{syn}) in the third intermediate layer. The muscle mechanical pulling vector was determined by physiological parameter of each muscle. These muscles were then grouped into 8 muscle groups. W_{neu} and W_{syn} were modified using an error back-propagation algorithm [8] to minimize the error between output torque generated from muscles and randomly presenting desired 12 input torques, which were uniformly distributed on the two joint torque plane with the same intensity. The experiment was additionally conducted, which required the same task as above. We then extracted muscle synergies by measured muscle activities using non-negative matrix factorization [9]. Leaning performance in the presence and absence of muscle synergies was evaluated by comparing the synergy model with the previously constructed model, which didn't include the layer of muscle synergies (non-synergy model) [3]. When the state of the neural network was constant after leaning, we exposed the neural network to a force field: the output torque was rotated. During the adaptation period to the force field, W_{neu} was only modified [10].

Results: Four muscle synergies were required to appropriately produce the desired torques and to decrease motor redundancy. The synaptic weights (W_{syn}) between synergy and muscle layers after learning (Figure; left) were similar to the muscle weightings of the extracted synergies in the experiment. The simulated muscle synergies had specific preferred directions, which indicated the highest activations (Figure; right top). The synergy model increased learning speed and decreased the final error between the desired and output torques as compared with non-synergy model (Figure; right bottom). After adaptation to the force field, the preferred directions of muscle synergies were rotated to the

direction of the force field. In this case, the synergy model also increased learning speed, suggesting that the acquired neural basis as muscle synergies contributes to increasing adaptation speed against the changes of external environment.

Figure:
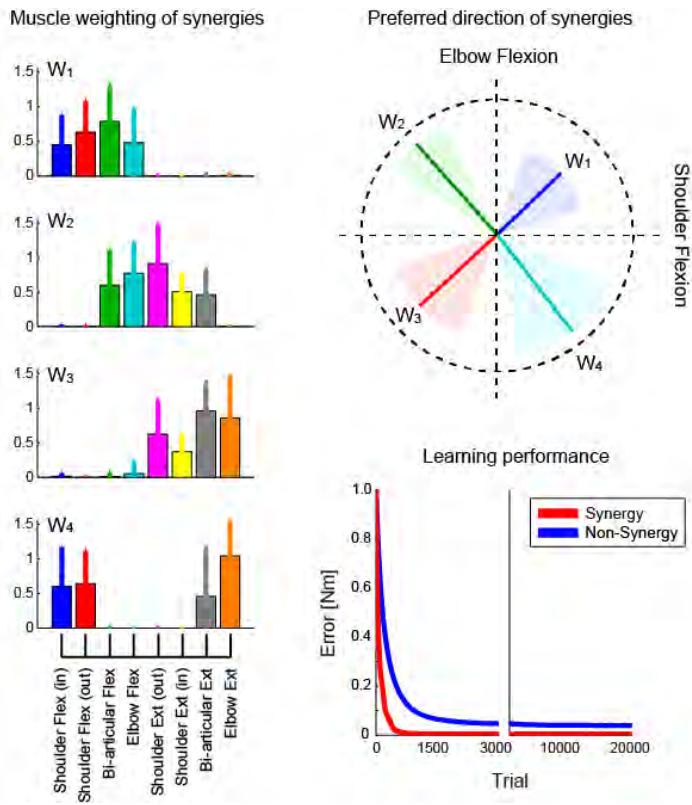
Caption: Simulated muscle synergies and leaning performance.

Conclusion: The neural network model including muscle synergies increased learning speed as compared with non-synergy model. These results suggest that one of the functional roles of muscle synergies is to increase speed of motor learning.

References: [1] Hagio et al., J Neurophysiol, 112(2): 316-327, 2014.

[2] Tresch et al., Nat Neurosci, 2(2): 162-167, 1999.

[3] Hirashima et al., PLoS Comput Biol, 8(6): e1002590, 2012.

[4] Hart et al., J Neurosci, 30(4): 1322-1336, 2010.

[5] Overduin et al., Neuron, 76(6): 1071-1077, 2012.

[6] Overduin et al., Front Comput Neurosci, 8: 20, 2014.

[7] Takei et al., J Neurosci, 20(50): 17041-17050, 2010.

[8] Rumelhart et al., Nature 323: 533–536, 1986.

[9] Lee et al., Nature, 401(6755): 788-791, 1999.

[10] Kadota et al., J Neurosci, 34(37), 12415-12424, 2014.

Disclosure of Interest: None Declared

MALPOSITIONING OF THE PATIENT DURING X-RAY ACQUISITION CAN AFFECT THE ASSESSMENT OF SAGITTAL PELVIC PARAMETERS: EVALUATION IN ADULTS AND CHILDREN

Ayman Assi [1,*]Ziad Bakouny [1]Elie Saghbini [1]Nour Khalil [1]Lydia Chelala [1]Elias Naoum [1]Christophe Sauret [2]Wafa Skalli [2]Ismat Ghanem [1]

[1]Laboratory of Biomechanics and Medical Imaging, School of Medicine, University of Saint-Joseph, Beirut, Lebanon, [2]Laboratoire de Biomécanique, Arts et Métiers ParisTech, Paris, France

Introduction and Objectives: In order to assess sagittal balance, clinical parameters are measured on lateral X-rays of the pelvis [1,2]. These radiographs require standard positioning of the patient during acquisition. To our knowledge, there are no studies that have investigated the effect of pelvic axial rotation on sagittal clinical parameters. The aim of this study was to estimate the effect of erroneous positioning of patients, during pelvis lateral X-ray acquisition, on the reliability and validity of sagittal pelvic parameters.

Methods: Helical pelvis CT-Scans (slice thickness: 0.6mm) of 8 children (3 F and 5 M, age: mean 12 - SD 2.2) and 9 adults (5 F and 4 M, age: mean 51 - SD 26) were considered. Lateral Digitally Reconstructed Radiographs (LDRRs) were reconstructed from CT-Scans using a homemade software. Then, for each patient, axial rotation of the pelvis was simulated and the corresponding LDRRs were reconstructed at 5°, 10°, 15° and 20° of axial rotation. Clinical parameters were measured digitally on each radiograph using the SterEOS® 2D toolbox: sacral slope (SS), pelvic incidence (PI), pelvic tilt (PT), pelvic inclination (PIL), sagittal pelvic thickness (SPT), bifemoral distance (BFD) and pelvic depth (PD). Three trained operators repeated the measurements 3 times each, in each axial rotation position and for each radiograph (Figure 1). The Intraclass Correlation Coefficient (ICC) was evaluated for inter-observer agreement. The 95% confidence interval (95%CI) was calculated as 2SD of inter-observer reliability. The bias of each clinical parameter, in each axial rotation position, was calculated as the absolute mean difference relatively to the 0° position.

Results: Inter-observer agreement was shown to be very high (ICC>0.88) for all parameters and in all axial rotation positions. In the absence of axial rotation of the pelvises (0°), the 95% CI of the SS and the PI were lower than 4°, lower than 2° for PT and PIL and lower than 1 cm for both SPT and BFD. The 95% CI increased with pelvic axial rotation; at 20° of rotation it exceeded 7° for SS and PI, 7° and 4° for PIL and PT respectively, and remained constant for SPT and BFD. All the parameters showed an increase in the bias during axial rotation of the pelvis, where PI showed the greatest bias by reaching 6° at 20° position. Only SPT and PD exhibited a bias which was minimal and constant (< 0.5cm) for all axial rotation positions. Even though insignificant (p>0.05), the bias on PI and SS was shown to be higher in children than in adults.

Figure:
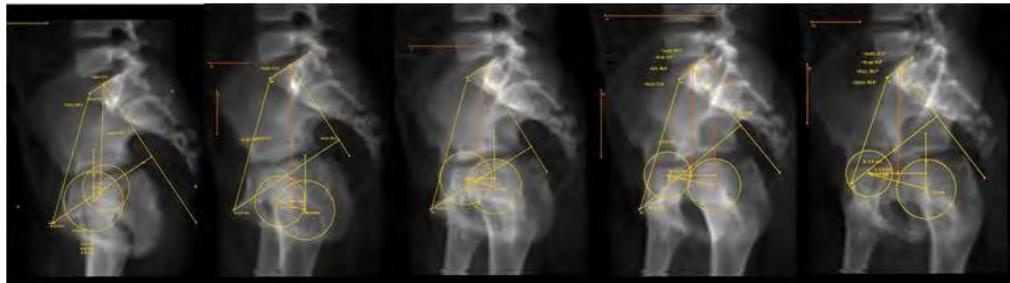
Caption: Figure 1- Lateral radiographs of the pelvis at 0°, 5°, 10°, 15°, 20° of axial rotation with pelvic parameters measurements

Conclusion: Clinical parameters measured on lateral radiographs were shown to be less accurate and less reliable when pelvic axial rotation increased. The bias exceeded 10% of the normative values of each clinical parameter when the AR exceeded 10°. This bias could significantly affect orthopedic decision-making in patients with sagittal malalignment.

References: [1] Roussouly et al., Eur Spine J, 20 : 578-585,2011

[2] Vrotvec et al., Spine J, 12 : 433-446, 2012

Disclosure of Interest: None Declared

AS-0032

THE POSTPARTUM DIASTASIS RECTIS ABDOMINIS AND THE ABILITY OF THE ABDOMINAL MUSCLES TO STABILIZE THE PELVIS DURING THE DOUBLE-LEG LOWERING EXERCISE

Augusto G. Pascoal [1,*]Cristiana Vaz [1]Patricia Mota [1]Filipa João [1]António Veloso [1]

[1]University of Lisbon, Faculty of Human Kinetics, CIPER, LBMF, Lisbon, Portugal

Introduction and Objectives: Postpartum distasis rectis abdominis (DRA) refers to the separation of both recti abdominis (RA) muscles starting in the last trimester of pregnancy and extends up to 8-16 weeks postpartum. DRA is quantified by the inter-recti distance (IRD) measured around the umbilicus. Postpartum IRD vary between 20-50mm which may change the line of action of both RA muscles [1] compromising their ability to produce torque on thorax and/or on pelvis. Mostly postnatal women are encouraged to resume abdominal exercises, such as curl-ups and double-leg lowering (DLL) exercises, to restore their abdominal figure. The DLL involves the subject lying supine and starts with both lower extremities placed in a vertical position. Then both legs are lowered to the horizontal while knees are kept straight and low back flat [2]. Abdominal muscles contraction maintains the pelvis in a posterior-tilted position counteracting the anterior-tilted action produced by the hip flexors muscles [3]. A negative correlation was found between postpartum IRD and the abdominal muscles ability to perform a curl-up exercise [4, 5]. However no information is available about the implication of the postpartum DRA on the ability of the abdominal muscles to stabilize the pelvis in a posterior-tilted position against a resistance. The main purpose of this study was to investigate the relationship between the width of the IRD and the abdominal muscle function to stabilize pelvis against resistance during the DLL exercise. Additionally, the effect of pregnancy on IRD and pelvic tilt angle was also analyzed.

Methods: A convenience sample of 11 postpartum (age:32.9±3.5 years; postpartum weeks: 10.7±3.3) and 11 nulliparous (age:29.8±4.9 years) women was tested on 2 static positions of the DLL exercise: 1) starting flexion position (FPos), at 90º hip flexion and 2) final extended position (EPos) at 10º hip flexion. On each DLL position, the pelvis tilt angle was recorded by means of a motion capture system (13 Qualisys cameras;FR:50Hz). Pelvis position was tracked by means of 4 reflective markers (on both anterior-superior iliac spines and iliac crests) and a set of 10 reflective markers (on both acromion, lateral projections of the xiphoid, iliac crests, anterior superior iliac spines and lateral and medial femoral condyles) and two marker clusters (one at the thigh segment and other at the sternum region) was used to build and track the thorax and thigh segments position. The Visual 3D (Basic RT) software was used for segment 3D reconstruction and calculation of Euler angles describing pelvis and thigh position in global, pelvis and thorax coordinate systems. Simultaneously an ultrasound image was collected (GE Logic-e; 4-12 MHz,39mm) by placing the transducer transversely along the midline of the abdomen (2 cm below the umbilicus) allowing the measurement of DIR. A two-way repeated measure ANOVA was performed to determine whether any change in each dependent variables (pelvic tilt angle and IRD) was the result of the interaction between women's group (nulliparous and postpartum) and DLL positions (FPos and EPos).The relationship between IRD and pelvic tilt angles was examined using the Person product-moment correlation coefficients.

Results: A positive correlation was found between mean IRD values and the pelvic tilt angle, both in FPos (r=0.70;p=0.02) and in EPos (r=0.65; p=0.03) position. This relationship was in such a way that women with highest IRD were those that tended to place pelvis in a more anterior tilt angle. This finding suggests that in postpartum women the incomplete recovery of the abdominal wall integrity, revealed by the width of IRD, may lead to a certain mechanical deficit, resulting in a reduction in the ability of the abdominal muscles to stabilize the pelvis in a posterior-tilted position. However, no differences were found between groups with respect to the pelvic tilt angle on both DLL positions, despite the postpartum women exhibited a significantly greater IRD [$F(1,19)$=12,p<0.05]. Thus, the postpartum group had a significantly greater IRD (17,0±1,6mm;IC95:13,7-20,3mm) comparing to the control group (9,4±1,5mm;IC95:6,3-12,6 mm) with a difference of 7,6±2,2mm (IC95:3,0-12,2mm). These results are in accordance with previous studies [6, 7].

Conclusion: In postpartum women a negative relationship was found between IRD and the ability of abdominal muscles to keep the pelvis in a posterior tilt position on two positions of the DLL exercise. However, on both DLL position no differences were found on pelvic tilt angle between postpartum and nulliparous women.

References: [1] Mota P, et al. Manual Therapy.18:294-8 2013.

[2] Zannotti CM, et al. J Orthop Sports Phys Ther.32:432-6 2002.

[3] Krause DA, et al. Arch Phys Med Rehabil.86:1345-8 2005.

[4] Liaw LJ, et al. J Orthop Sports Phys Ther.41:435-43 2011.

[5] Gilleard WL, et al. Phys Ther.76:750-62 1996.

[6] Pascoal AG, et al. Physiotherapy 2014.

[7] Mota PG, et al. Man Ther 2014.

Disclosure of Interest: None Declared

Spine

AS-0033

A GOAL PROGRAMMING MODEL FOR ASSESSING SAGITTAL SPINAL CURVATURE UNDER BACKPACK CARRIAGE

Daniel H. Chow [1,*]Simon Li [1]

[1]Department of Health & Physical Education, The Hong Kong Institute of Education, Hong Kong, Hong Kong

Introduction and Objectives: Previous research established that load carriage would induce immediate changes in spinal curvature which was associated with spine disorders [1]. Neutral upright standing has been proposed as the healthy posture for minimizing spine loading [2]. It was hypothesized that the maximum load should be one that induced minimum changes to the spine curvature in neutral upright stance. In this study, a multi-objective optimization goal programming (GP) model [3] was developed and applied to determine the optimal limit of backpack load for upright standing.

Methods: This was a single factor randomized repeated measure design. Spinal curvatures [in terms of the angles of cervical lordosis (CVL), upper thoracic kyphosis (UTK), lower thoracic kyphosis (LTK) and lumbar lordosis (LBL)] were measured non-invasively using five sensors affixed to the middle of the back of head, C7, T7, T12 and pelvis [4, 5]. All subjects were instructed to maintain a standardized and relaxed barefoot erect stance without load and with a backpack loaded at 5, 10, 15 and 20% of their body weights. The four curvature angles among the five sensors were measured by a motion analysis system. The sequence of experimental trials was randomized. Three trials for each unloaded and loaded conditions were recorded. Regression equations predicting the four loaded curvatures were obtained. The deviations of loaded from unloaded curvatures and the target levels of the predicted mean loaded curvatures were formulated as the cost and constraint functions of the GP model respectively. The sequence of optimization process of the GP was prioritized with respect to the magnitude of the mean loaded curvature deviations. The optimal mean loading condition was determined by solving the sequential optimization problems.

Results: Ten young male adults (age between 20 and 29) were evaluated. The baselines of mean curvatures of CVL, UTK, LTK and LBL were 32.1^o, 32.9^o, 10.3^o, and 17.2^o respectively. The respective mean deviations under loaded conditions were -0.6^o, -5.0^o, 1.6^o, and -2.1^o. The r^2 of the 2nd order regressions were 0.97, 0.99, 0.91, and 0.91 respectively. The sequence of optimization process was UTKàLBLàLTKàCVL. On average, significant flattening of the CVL, UTK and LBL as well as significant increased curvature in LTK were observed ($p<0.05$). The mean allowable load limit was found to be 7.4% of body weight. The predicted mean curvatures of CVL, UTK, LTK and LBL were 29.6^o, 26.8^o, 13.1^o, and 14.8^o respectively.

Conclusion: A symmetric backpack load at 7.4% of body weight was recommended, in order to achieve an optimal standing posture with minimal spinal curvature deviations from the unloaded condition.

References: [1] Orloff et al. Spine, 29: 1325-1329, 2004.

[2] Mac-Thiong et al. Eur Spine J 20: 586-590, 2011.

[3] Oddoye et al. Eur J Operational Res 193: 250-261, 2009.

[4] Roussouly et al. Spine 30: 346-53, 2005.

[5] Bruno et al. J Bone Mineral Res 27: 2144-2151, 2012.

Disclosure of Interest: None Declared

Spine

AS-0034

INTERVERTEBRAL DISC STRESS IN STANDING AND SITTING; MAGNETIC RESONANCE IMAGING BASED FINITE ELEMENT STUDY

Sahand Zanjanipour [1,*] Christopher Smith [2] C Peter Winlove [1] Jude Meakin [1]

[1]Physics, [2]Engineering, University of Exeter, Exeter, United Kingdom

Introduction and Objectives: The cause of disc degeneration can be attributed to mechanical loading, which varies in different postures. The effect of different daily postures such as standing and sitting for instance has previously been investigated by measuring the pressure within the discs (which is invasive) or by computational models (based on generic anatomical data which largely ignore differences between individuals).

 The aim of this project was to non-invasively investigate the stress distribution in standing and sitting postures by incorporating magnetic resonance (MR) imaging data in subject-specific finite element (FE) models. Objectives were defined as:

- Create a FE model for each subject based on MR images;
- Determine boundary conditions of the standing and sitting postures with respect to reference posture (supine);
- Compare the stress distribution in standing and sitting postures.

Methods: Two-dimensional FE models of the lumbar spine (L1 to S1) were created for nine healthy individuals. The initial geometry of each model was based on MR images of the individual in the supine posture. Two types of FE model were investigated: a time-dependent model and a simple elastic model. In the time-dependent model, material properties of the disc were defined as poroelastic.

 The disc was modelled with an annulus (Young's modulus, E=2.5 MPa, Poisson's ratio, v=0.4) and a nucleus (E=1 MPa, v=0.45). In the time-dependent model poroelastic properties were assigned to the annulus (Permeability, $K=1.83E-12$ ms^{-1}, void ratio, e=3.54), nucleus ($K=2.06E-12$ ms^{-1}, e=4.88) and the vertebral bodies ($K=1E-23$ ms^{-1}, e=0.02).

 Boundary conditions were determined by considering the vertebrae as rigid bodies and applying the translation and rotation of each vertebral body in either the sitting or standing posture, with respect to the supine posture. In the poroelastic model, a fluid boundary condition was set to allow fluid movement across the interface between the vertebrae and discs.

 The resulting stresses in a central region of the L4/L5 disc were averaged and used to determine the normal disc stress (i.e. the stress acting perpendicular to the mid-plane of the disc). For the time-dependant model the results were taken at the time-point corresponding to the duration of the MR scan and comprised two components: the effective stress normal to the disc and the pore pressure.

Results: Figure 1 shows the normal disc stresses and the pore pressure on the L4/L5 disc in standing and sitting for each individual. In both the elastic and poroelastic models, the sitting posture created more normal disc stress than standing in all subjects except one. For the poroelastic model, the pore pressure was also more in sitting than standing except two subjects. These results are consistent with experimental measurements of disc pressure reported in the literature where sitting tends to produce a higher intradiscal pressure than standing. The absolute values of the disc stress are lower than

we would expect from experimental measurements, this is due to assumptions in the modelling (i.e. the two-dimensional modelling and the material properties assigned to the discs).

Further visual analysis of the models showed that in some individuals the highest disc stress occurred within other intervertebral discs along the lumbar spine.

Figure:
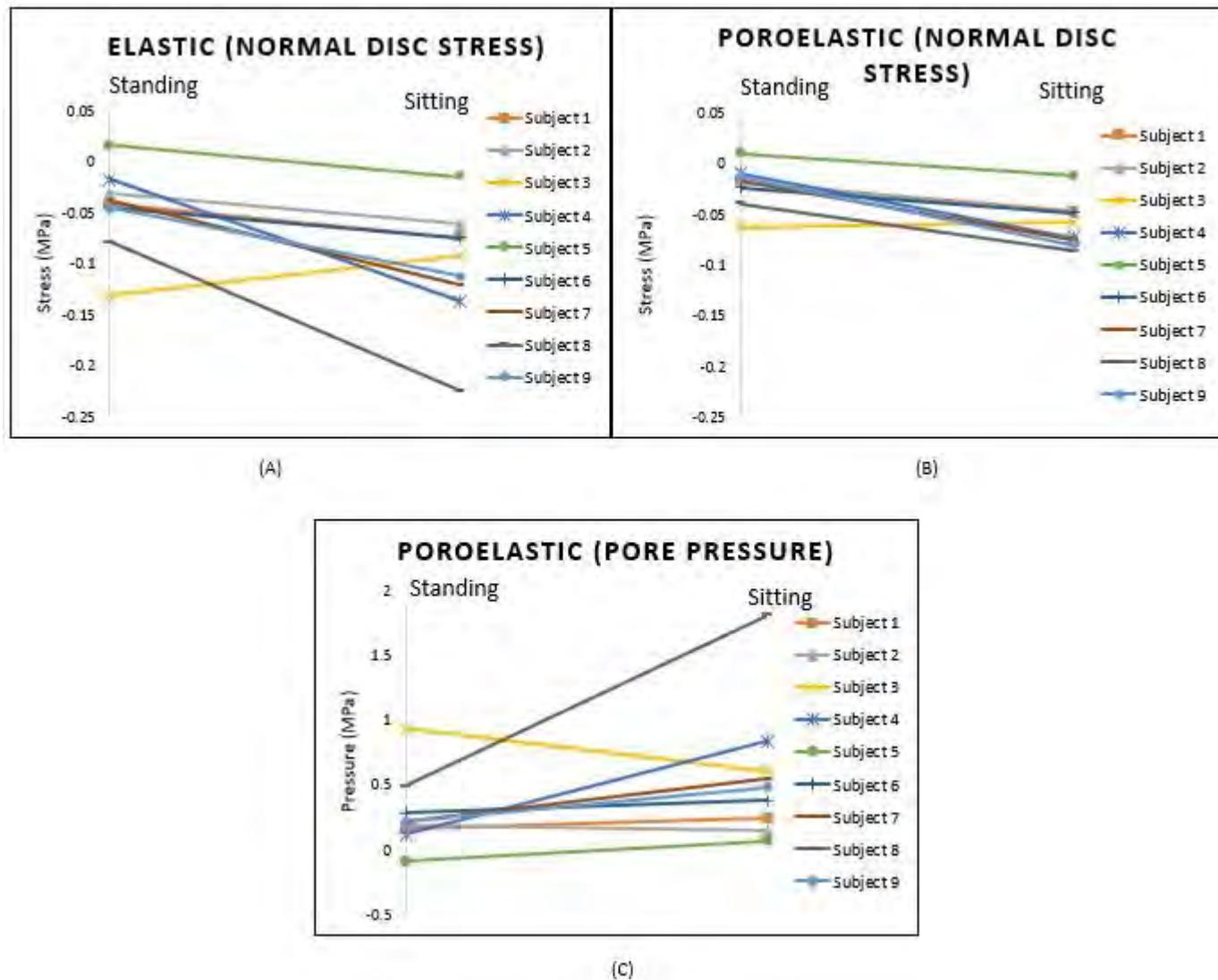
Caption: Figure 1: The normal disc (L4/L5) stress in standing and sitting for (A) elastic model and (B) poroelastic model. (C) Pore pressure within the disc in the poroelstic model.

Conclusion: Incorporating information from MR images in a displacement based FE model offers a non-invasive way of determining the relative intervertebral disc stresses induced by postural change. The results of elastic and time-dependent models are consistent with each other. This method may be useful in investigating other more extreme postures such as those experienced when lifting loads.

Disclosure of Interest: None Declared

Spine

AS-0035

IS THERE A CHANGE IN THE ABILITY TO REACT TO A PERTURBATION FOLLOWING A BOUT OF PROLONGED SITTING?

Tara Diesbourg [1,*]Peter Sheahan [1]Geneviève Dumas [2]Steven Fischer [1]

[1]School of Kinesiology and Health Studies, [2]Department of Mechanical and Materials Engineering, Queen's University, Kingston, Canada

Introduction and Objectives: Standing rest-breaks are often recommended during seated work in order to mitigate the ill-effects of prolonged sitting on spine health [1]. These ill-effects include changes in the passive stiffness of the trunk, thought to be a result of the creep response of the trunk's passive tissues, and are hypothesized to decrease the body's ability to respond to a perturbation, which may increase an individual's risk for injury [2]. While evidence indicates that passive stiffness is affected by prolonged sitting, it is currently unknown whether the response to a perturbation (represented by the active trunk stiffness) is also affected. Therefore, the purpose of the current study was to examine changes in the active stiffness of the trunk following a 1-hour sitting task.

Methods: Twenty healthy subjects (10 male, 10 female: mean height – 174cm, mean weight – 72kg) were recruited from a university population. Trunk stiffness was estimated using a quick-release method described by Hodges and colleagues [3]. Subjects were asked to adopt a semi-seated position with their arms crossed over their chest. Using electromagnets on cables affixed to the anterior and posterior aspects of a chest harness, weights (15% body weight) were suspended from the subject. At a random time (0-5s) and in random order, either the front or the back weight was dropped (10 repetitions each), perturbing the subject in the opposite direction. A uniaxial load cell between the subject and the attached load was used to measure force. Acceleration was obtained from the force and was double-integrated to obtain displacement. It is assumed that the displacement of the load represents the linear displacement of the trunk. The maximum displacement (D) and the time required to achieve this maximum displacement (TMD) were used to determine the ability of the subject to respond to the perturbation. Increased TMD and increased D were assumed to represent a decreased ability of the subject to respond to a perturbation.

 Trunk stiffness was estimated using a least-squares optimization algorithm which used time-varying force, acceleration, velocity, and displacement traces to estimate the system's effective mass, damping, and stiffness (TK) coefficients [3]. In the current study, only the TMD, D, and TK were examined.

 This protocol was completed prior to and immediately following a seated 60 minute typing task. At 10 minute intervals, the subject was asked to complete a Visual Analog Scale (VAS) according to their level of low back discomfort. Subjects who showed an increase in VAS score of 10 or more units were classified as being Pain Developers (PD), those that did not were classified as Non-Pain Developers (NPD) [4].

 The data from the first front and first back perturbations for each subject were collapsed and Repeated Measures (RM) ANOVAs were conducted to identify whether a main effect of time (pre vs post sitting task) existed. Additionally, interactions between time (pre vs. post sitting task) and PD/NPD were tested for all variables (TMD, D, and TK).

Results:

Due to malfunction within the load cells, the trials for 7 of the subjects were discarded from the analysis.

The mean (SD) for each variable is presented in Table 1. No main effect was identified for any of the variables of interest ($0.522 < p < 0.953$). There was no interaction of PD/NPD on any of the variables ($0.691 < p < 0.938$).

Conclusion:

The current study sought to identify if subjects altered their response to perturbations following a prolonged seated task. Previous research has shown a decrease in passive stiffness following prolonged sitting, where it was suggested that perturbation response may also be compromised [2]. The results of the current study suggest that 60 minutes of prolonged sitting does not affect the active stiffness of the trunk. While changes in passive stiffness have been attributed to a creep response of passive tissues [2], participants were able to maintain active stiffness despite potentially altered passive stiffness. This may be accomplished by increasing baseline muscle activity, as described by Brown and McGill [5]. In order to determine whether this effect is present, an analysis of the muscle activity throughout the perturbation is necessary.

Table: Mean (SD) for the variables of interest. TMD = Time to maximum displacement (ms), D = maximum displacement (mm), TK = Active Trunk Stiffness (N/m).

	Forward Perturbation		Backward Perturbation		Collapsed	
	Pre	Post	Pre	Post	Pre	Post
TMD (ms)	408 (67)	382 (61)	379 (98)	381 (97)	393 (17)	382 (16)
D (mm)	47 (12)	51 (9)	33 (10)	29 (8)	40 (3)	40 (3)
TK (N/m)	3997 (1455)	4913 (1977)	3748 (1143)	3748 (1143)	4188 (1520)	4330 (1690)

References:

[1] Davis & Kotowski, *Hum Factors*. 56(7): 1249-1261, 2014.

[2] Beach et al. *Spine J.* 5: 145-154, 2005.

[3] Hodges et al. *J Biomech*. 42: 61-66, 2009.

[4] Nelson-Wong. *PhD Dissert*, 2009.

[5] Brown & McGill. *Clin Biomech*. 23(1): 15-22, 2008.

Disclosure of Interest: None Declared

AS-0036

INTRA-TRUNK COORDINATION EXHIBITED DURING TREADMILL RUNNING BY INDIVIDUALS WITH SPINAL FUSION FOR ADOLESCENT IDIOPATHIC SCOLIOSIS

Yumeng Li [1],*Rumit Kakar [2]Yang-Chieh Fu [3]Timothy Oswald [4]Cathleen Brown [1]Kathy Simpson [1]

[1]University of Georgia, Athens, [2]Ithaca college, Ithaca, [3]University of Mississippi, Oxford, [4]Pediatric orthopedic associates, Atlanta, United States

Introduction and Objectives: Spinal fusion for adolescent idiopathic scoliosis (SF-AIS) largely corrects abnormal spinal curvature but limits motions among the fused vertebrae, decreases sensitivity of spinal proprioception[1]. Reduced spinal motions and proprioception may alter intra-trunk coordination during high-effort running; however, this has not been previously investigated. Therefore, the purpose of the present study was to compare intra-trunk coordination of axial-rotation between SF-AIS and healthy control individuals (CON) during high-effort treadmill running.

Methods: 11 SF-AIS (>1 yr postop, mid-thoracic to minimum of 1 lumbar intervertebral joint fused) and 11 CON (matched for mass, height, age, gender and physical activity level) ran on a treadmill with CON running at the SF-AIS matched speed (range: 2.2-3.8m/s, perceived-effort >14 on Borg scale). Locations of 24 reflective markers placed on the trunk, spine and pelvis were captured by a 7-camera Vicon system (240 Hz) for 10 strides. Axial segmental angles for the trunk segments (upper [UP]: C7 to T8; middle [MID]: T9 to T12; lower trunk [LOW]: L1 to L5), and pelvis (PEL) were used in cross-correlation analyses between adjacent segments to determine phase lag and in the generation of the coupling angle (CPA) using the vector coding method[2]. Each CPA was classified into a phase-coordination pattern[2]: in-phase, anti-phase, superior-segment dominant phase or inferior-segment dominant phase (Fig. 1). Phase lag and time spent in each phase-coordination pattern were scaled to % stride. A two-way, mixed model ANOVA with within-subjects effect of adjacent segments (UP-MID, MID-LOW and LOW-PEL) and between-subjects effect of group (SF-AIS and CON) was used to test phase lag (p<0.05). Independent t-tests were used to compare time spent in each phase-coordination pattern between the two groups (p<0.05).

Results: The main effect of group was significant $F(1, 20)$=11.6, p<0.01, indicating that the phase lag was significantly lower for SF-AIS (M=2.2, SE=0.6) compared to CON (M=5.0, SE=0.6). The main effect of trunk segment was significant $F(2, 40)$=21.2, p<0.01. Post-hoc analyses indicated that the intra-trunk phase lag was significantly increased from superior to inferior adjacent segments (Table 1). The interaction effect was non-significant $F(2, 40)$=1.1, p=0.36. Typically, the superior trunk segment led the inferior segment, although there were individual participant variations. For phase-coordination time, SF-AIS spent longer time in-phase and shorter time in anti-phase and superior-segment phase for LOW-PEL (Fig. 1). No other significant differences were observed.
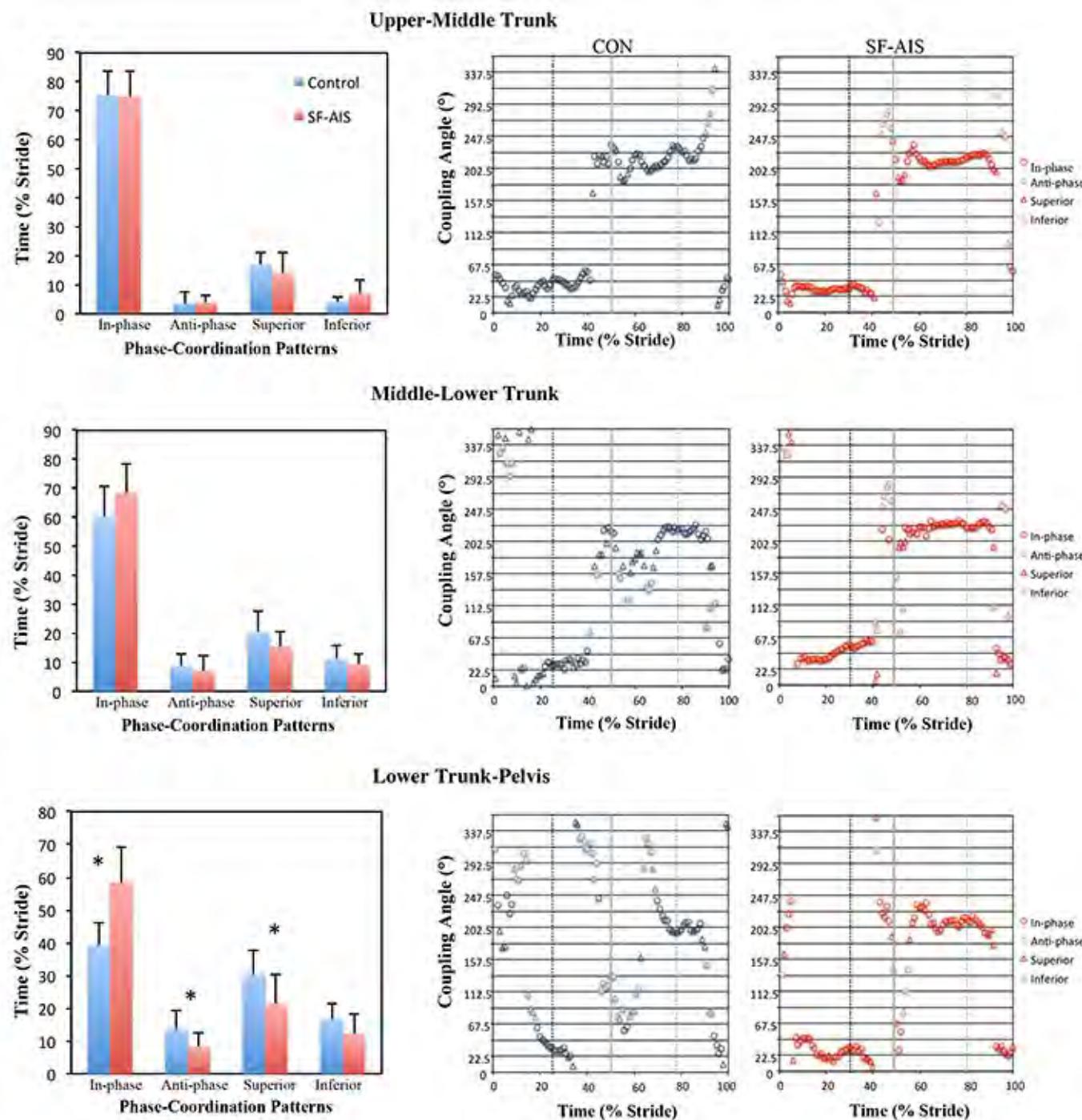
Caption: Figure 1. Intra-trunk coordination outcomes between adjacent segment pairs. Scatter plots: coupling angles of a representative CON and SF-AIS participant exhibited during each % of the stride (0% = rt foot touchdown) are displayed by phase-coordination pattern. Vertical lines: black = right foot, gray = left foot; solid = touchdown, dotted = toeoff. Bar graphs: total time spent in phase-coordination patterns; * indicates significant difference (p < .05) between groups.

Conclusion: Spinal fusion did allow some normalcy of typical phase-coordination patterns, as both groups displayed a pattern of increased phase lag and decreased in-phase coordination time at more caudal segment locations. However, the SF-AIS did not decouple their trunk motions to the same degree as healthy spines likely due to the intervertebral fusion. Group differences became significant between the most caudal adjacent segments, i.e., the LOW-PEL, whereby SF-AIS had lower phase lag and greater in-phase coordination time. Conversely, the phase lag and timing values between the most cephalic segments (UP-MID) of SF-AIS were more similar to CON. Previously, we reported that the maximum axial LOW-PEL displacements of SF-AIS were comparable to CON for running[3]. Hence, whether these more coupled LOW-PEL vertebral motions of SF-AIS influence running performance or affect lumbar mechanics is not known at present. In conclusion, the SF-AIS trunk displays similar patterns of phase lag and coordination as CON for axial rotation during treadmill running, but the spinal fusion hinders decoupling of intra-trunk motions, particularly between the lower back- pelvis motions.

Table:

	UP-MID		MID-LOW		LOW-PEL	
	CON	SF-AIS	CON	SF-AIS	CON	SF-AIS
Mean	1.8	0.1	4.6	2.1	8.7	4.5
SD	2.2	2.1	2.4	1.6	5.5	2.8
Min.	-0.6	-2.3	0.7	-0.6	2.9	0.6
Max.	6.5	5.3	9.1	4.8	19.5	10.2
Median	1.7	-0.5	4.7	2.7	7.1	4.1
No. of people displayed:						
Lag > 2%	4	1	10	6	11	9
Lag < |2%|	7	8	1	5	0	2
Negative lag	2	6	0	1	0	0
95% CI	0.5, 3.2	-1.3, 1.4	3.3, 5.9	0.9, 3.4	6.0, 11.5	1.8, 7.3

Caption: Table 1. Phase lag (% stride) between adjacent trunk segments and between-group comparisons. Positive and negative phase lag: superior segment leads and lags the inferior segment, respectively.

References: [1] Pao et al. J Phys Ther Sci *26*(8): 1165-1171, 2014.

[2] Chang et al. *41*(14): 3101-3105, 2008.

[3] Kakar et al. *ASSICON. Kolkata, India,* 2014.

Disclosure of Interest: None Declared

Fluid Mechanics

AS-0037

THE EFFECT OF BREATHING ON ACTIVE DRAG WHILE SWIMMING

Pendar Hazrati [1,*] Peter Sinclair [2] Bruce Mason [1]

[1]Australian Institute of Sport, Canberra, [2]University of Sydney, Sydney, Australia

Introduction and Objectives: In competition, a swimmer must supply adequate oxygen to the muscles for continuing movement. For this to occur, the swimmer should perform the breathing phase while their body has adequate rotation which should be integrated into the stroke cycle without increasing resistive forces. Di Prampero et al. (1974) found that the breathing phase may increase the hydrodynamic drag of the body. It was also reported that the efficiency of stroke mechanics might be impeded by the breathing frequency (Stager et al. 1989). Town and Vanness (1990) reported that restricted breathing patterns (one breath every stroke, two, three or four strokes) may impede the efficiency of the stroke mechanics. Two main forces have a major effect on performance. The first is the propulsive force produced by the swimmer to propel their body through the water. The second is the drag force which is exerted by the water on the swimmer. Hence, it is essential for swimmers and coaches to understand the effect of breathing on each of these forces. The aim of this research is to determine the effect of breathing on active drag using resisted method, and how the breathing phase influences the swimmer's technique.

Methods: Nine international male swimmers completed all testing protocols each day over two alternate days. Two maximum effort free swim trials were performed over a 25 m distance (one without and one with breathing), with the mean velocity computed over six full strokes. Then, two trials were performed using a resistive dynamometer to achieve a velocity which was 5% to 8% slower than the mean maximum swim velocity over six full strokes (one without and one with breathing). The swimmers had five minute rest between each trial to eliminate fatigue on their performance. Using velocities from free swimming and tethered trials, together with the belt force that was slowing the swimmers, active drag was calculated using the formula developed by Kolmogorov and Duplischeva (1992). Active drag was calculated separately for breathing trials and non-breathing trials.

Results: Slower swim velocities were obtained for breathing trials than non-breathing trials (p=0.022), however no change was observed in active drag (p=0.258)(Table). No difference was observed between days of testing.

Conclusion: The mean active drag values of breathing and non-breathing found in this study were similar to those previously reported by Kolmogorov & Duplischeva (1992) (97.1±42.3 N at 1.83 m/s). Although, no statistically significant difference was found between the active drag values of breathing and non-breathing, there was inconsistency in the results of individual swimmers. Some swimmers who had a slower speed during the breathing trials than the non-breathing trials had a correspondingly greater active drag value for the breathing trials. The slower mean velocity during breathing trials was likely caused by a greater resistive force exerted on the swimmers due to the breathing technique. Extra rotation of head and trunk could have been increasing their active drag. Swimmers having extra rotation of the head and trunk would encounter a greater surface area. Also, the head rotation could affect form drag as well, because; a cavity is created behind the head during the breath.

Some swimmers had similar active drag values in both breathing and non-breathing trials. It is likely that these swimmers performed their breathing in a more efficient manner and therefore spent less energy to overcome active drag moving through the water. Hence, as performing breathing is more important for mid to long distance swimmers, practice is required to perform with greater efficiency while spending less energy.

Table:

	Day one		Day two	
	No breathing	Breathing	No breathing	Breathing
Active drag (N)	109.4±23.1	100.3±25.7	101.8±31.8	93.7±22.1
Swim velocity (m/s)	1.83±0.08	1.82±0.07	1.84±0.08	1.82±0.08

Caption: The mean active drag values and mean speed for both days

References: Di Prampero et al., J.Applied Physiology, 37(1), 1–5, 1974.

Kolmogorov, S.V. et al., J. Biomechanics, 25(3), 311–318, 1992.

Stager, J.M. et al., J. Swimming Research, 5(1), 5–10, 1989.

Town, G.P. et al., J. Medicine & Science in Sports & Exercise, 22(1), 112–116, 1990.

Disclosure of Interest: None Declared

Fluid Mechanics

AS-0038

UTILITY OF VOLUMETRIC FLOW ULTRASOUND INDICES IN PREDICTING INTRAUTERINE GROWTH RESTRICTION FETUSES

Shier Nee Saw [1] Dawn Chia [2] Citra Nurfarah Zaini Mattar [3] Arijit Biswas [3] Choon Hwai Yap [1,*]

[1]Biomedical Engineering, National University of Singapore, [2]Fetal Care Centre, National University Hospital, [3]Department of Obstetrics and Gynaecology, National University of Singapore, Singapore, Singapore

Introduction and Objectives: Intrauterine Growth Restriction (IUGR) is a disease where the placenta experiences vasculopathy and high vascular resistance to blood flow, preventing the fetus from receiving enough nutrients and oxygen to meet growth potential. Its prevalence is approximately 3% in developed countries [1] and up to 10-15% in developing countries [2]. There is current no treatment or prevention for IUGR, but with detection, early delivery can be induced to reduce *in-utero* malnutrition and hypoxia to improve outcome [3]. It is thus important to evaluate and improve IUGR detection techniques. Currently, IUGR is detected using umbilical ultrasound Doppler indices such as Resistance Index (RI) and Pulsatility Index (PI), which were shown to correlate with increase vascular resistance of blood flow in the placenta [4]. However, mathematically, these indices measures flow pulsatility instead of resistance, and experimentally, it has been shown that RI describes compliance better than resistance [5], leading to our question of their theoretical applicability to high-resistance detection, and motivating our current study. In this study, we performed numerical modelling of umbilical-placental circulation and analysed clinical human fetal ultrasound scans to review the reliability of various Doppler indices as surrogate for placental vascular resistance, and to propose indices and quantification techniques for improved accuracy.

Methods: Lumped-parameter numerical modelling (Figure 1(a))) was performed to study flow in the umbilical-placenta circulation. Various umbilical Doppler indices were evaluated for their reliability in detecting high placenta vascular resistance. Clinical Doppler ultrasound scans of 537 normal and 13 IUGR human fetuses from GUSTO study [6] were investigated for their capabilities for distinguishing IUGR from normal fetuses.

To improve the quantification accuracy of indices involving umbilical vascular cross-sectional areas, we employed 3D reconstruction of vessels in the quantification and examined the improvement in accuracy.

Results: Numerical results showed that the RI and PI showed significant dependence on both placenta vascular resistance and compliance, and could not be unique representations of vascular resistance and of placenta insufficiency. Mean forward flow through the umbilical arteries, on the other hand, is independent of compliance, and dependent only on resistance, indicating improved ability to represent placenta insufficiency. Clinical data showed that mean flow parameters such as UATAV and UVVF may be more useful in distinguishing IUGR fetus compared to pulsatility indices (RI and PI), having lower p-value and higher area under receiver operating characteristic curve (Table 1).

QMean flow parameters, however, require the measurement of vascular cross-sectional area on top of velocity. Our results showed that 3D method can quantify cross-sectional areas better than 2D methods can, allowing arterial inflow to match vcenous outflow with a higher correlation coefficient. 3D methods of vascular size quantification can thus aid in more accurate quantification of mean umbilical vascular flow rates.

Figure:
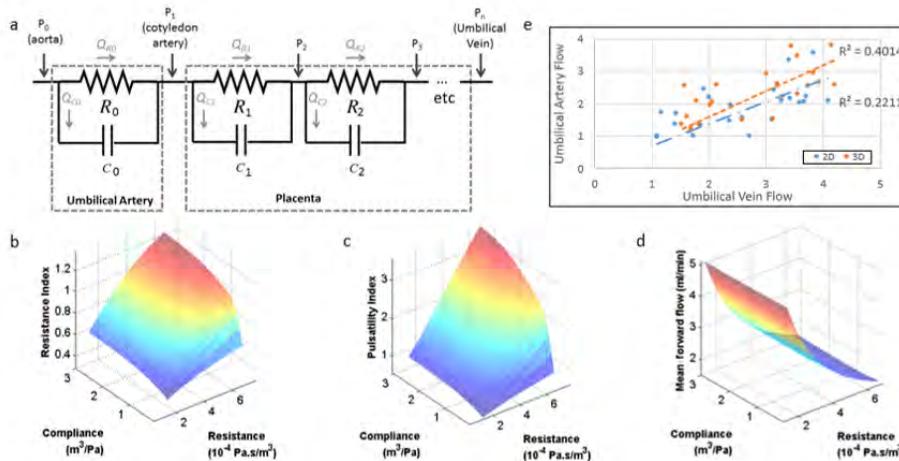
Caption: Figure 1. (a) Schematic of the lumped-parameter model. The umbilical-placenta circulation is modeled as electrical circuits equivalents. Ri – ith resistance; Ci – ith compliance; Pi – pressure at i; QRi – Flow through the ith resistance; QCi – rate of fluid going into compliance storage. (b-c) Results of modeling the dependence of RI, PI and mean forward flow on vascular resistance and compliance. (e) Comparison of 2D and 3D methods in quantifying umbilical vascular flows.

Conclusion: Our computational work suggests that mean forward flow is a better parameter in gauging IUGR and clinical results corroborate this notion. 3D quantification of blood flow is more accurate compared to conventional 2D quantification method.

Table:

Doppler Indices	Area Under ROC Curve	P-value
Umbilical Artery Time-Averaged Velocity (UATAV)	0.617	0.012
Pulsatility Index (PI)	0.616	0.025
Resistance Index (RI)	0.612	0.059
Umbilical Vein Area (UVA)	0.600	0.024
Umbilical Vein Velocity (UVV)	0.582	0.175
Umbilical Vein Volumetric Flow (UVVF)	0.582	0.049

Caption: Table 1 Area under ROC curve for prediction of IUGR fetuses using different umbilical Doppler indices and P-value indicates statistical test for difference between normally-grown and IUGR fetuses.

References: [1] Barut, F. et al., Diagn Pathol, 5: 24, 2010.

[2] Gardosi, J., Clin Perinatol, 38: 21-31, 2011.

[3] Lindqvist, P.G., et al., Ultrasound Obstet Gynecol, 2005. 25: 258-264, 2005

[4] Lausman, A., et al., J Obstet Gynaecol Can, 34: 17-28, 2012.

[5] Bude, R.O., et al., Radiology, 211: 411-417, 1999.

[6] Soh S.E., et al., Int J Epidemiol, 43:1401-1409, 2014.

Disclosure of Interest: None Declared

Cardiovascular

AS-0039

EFFECT OF PULSATILITY RATE ON THE HEMODYNAMICS OF BILEAFLET MECHANICAL PROSTHETIC HEART VALVES (ST. JUDE MODEL) FOR THE AORTIC POSITION IN THE OPENING PHASE; A COMPUTATIONAL STUDY

Mehdi Jahandardoost [1,*]Guy Fradet [2]Hadi Mohammadi [1]

[1]Biomedical Engineering, [2]Department of Surgery, University of British Columbia, Kelowna, Canada

Introduction and Objectives: Bileaflet mechanical heart valves (MHVs) designs are known for providing a uniform flow profile and a lower incidence of structural complications. However, thrombus formation on the hinges, valve failure and leaflet escapement have been reported in certain designs. To date, to the best of the authors' knowledge, almost in all of the studies performed around the hemodynamics of the bileaflet MHVs, a pulsatility rate (PR) or a heart rate (HR) of 70-72 beats per minute (bpm) has been considered. In fact, the HR of ~72 bpm does not represent the entire normal spectrum of physiological conditions under which the native or prosthetic aortic valves function. The HRs of 60 bpm or 120 bpm may lead to hemodynamic complications such as plaque formation and/or thromboembolism in patients. The objective of this study is to assess the hemodynamic performance of the bileaflet MHVs in a wide range of normal and physiological HRs, i.e., 60-150 bpm in the forward flow phase.

Methods: We applied an idealistic computational platform in this study which was recently developed in our laboratory [1]. Also, a similar model was developed for benchmarking of our results in which the SJM bileaflet mechanical valve was replaced by a native aortic valve. The flow around the bileaflet MHV (SJM model) is considered pulsatile and encompasses the three regimes of laminar, transient, and turbulent. To predict the salient features of flow around the bileaflet MHV, the shear stress transport (SST) low-Re two-equation turbulence models were applied.

Results: The hemodynamic performance of the SJM valve such as the regions of high shear stress, recirculation zones, vortex shedding and velocity profiles were assessed. Results suggest that the peak values of the velocity profile downstream of the valve increase as the HR increases but the location of the maximum velocity changes with HR. Results also indicate that the maximum values of shear stress and the wall sheer stresses (WSS) downstream of the valve are proportional to the HR values. Interestingly, the increase rate of WSS in the model with the SJM valve is remarkably higher than that in model with the native valve. More importantly in the model with the SJM valve, when the range of the HR is 90 bpm and higher, the threshold of the platelet activation is met in multiple locations of the aortic root which in turn may lead to thrombogenic complications.

Conclusion: Lack of adequate studies in the hemodynamic assessment of the MHVs at a variety of normal and physiological HRs was the motivation for the present study. Our results suggest a high risk of thrombogenicity associated with the hemodynamic performance of MHVs when the HR is high (90-150 bpm). The high value of shear stress in the areas around the valve housing and leaflet leading edges and wakes meets the threshold for platelet activation. These findings may be of importance in the hemodynamic performance of bileaflet MHVs and may play an important role in the design improvement of conventional prosthetic heart valves and the design of the next generation of prosthetic valves.

References: [1] Jahandardoost M. et a. IMECH J Eng in Med, Under Review

Disclosure of Interest: None Declared

Respiratory

AS-0040

MODELLING EXPIRATION USING VISCOELASTIC PRESSURE DEPENDANT RECRUITMENT MODELS – IS IT THE SAME AS INSPIRATION

Daniel Redmond [1,*] Jörn Kretschmer [2] Yeong Shiong Chiew [1] Christopher Pretty [1] Knut Möller [2] J Geoffrey Chase [1]

[1] Department of Mechanical Engineering, University of Canterbury, Christchurch, New Zealand, [2] Institute for Technical Medicine, Hochschule Furtwangen University, Villingen-Schwenningen, Germany

Introduction and Objectives: Viscoelastic Pressure Dependent Recruitment Model (VEPRM) models recruitment, over-distension and viscoelastic effects under various ventilation manoeuvres [1]. This model improves understanding of respiratory pathophysiology in complex lung diseases such as Acute Respiratory Distress Syndrome (ARDS) and allows accurate model predictions of patient response to differing ventilator settings which can be used in a clinical setting to improve patient care.

Methods: VEPRM [1] is based on the pressure recruitment model which uses the alveolar recruitment mechanism proposed by Hickling [2], where viscoelastic effects are assigned to each layer of the recruitment model. This results in pressure dependant compliance and resistance. Passive expiration can be modelled by the analysis of the VEPRM with a reverse in the direction of the flow, and the addition of an expiratory resistance, which represents the resistance to expiration due to the ventilator tubing. Expiratory resistance can be estimated by simple linear regression of the airway pressure and flow [3].

During expiration, to determine the recruitment status of a layer of lung units, threshold closing pressure (TCP) is required in addition to threshold opening pressure (TOP) used in inspiration as stated by Hickling [4]. During expiration, an opened lung unit remains open if the alveolar pressure is greater than the sum of superimposed pressures and TCP. Thus, if the VEPRM is successfully fitted to inspiration, the only free parameter required for fitting the model to the expiration is TCP. This identification is performed by a simplex search, using TOP as an initial estimate of TCP.

Airway pressure and flow data, sampled at 125Hz were measured from 12 mechanically ventilated ARDS patients. The study was approved by the local ethics committees of participating hospitals. The expiration data used comes from dynamic slice manoeuvres. The dynamic slice is an inspiration of 600mL/s for 2 seconds followed by free expiration. Data from low flow and static compliance automated single step manoeuvres are used for identification of inspiratory parameters, as explained in [1]. See [5] for a detailed description of the experimental setup. A hierarchical individualisation process is used to identify the VEPRM model parameters for inspiration. In this process, the simpler models are identified first, and then used as initial guesses for the more complex models [1,6].

Results: When fitting to the dynamic slice data, there was a very good fit on inspiration for 12 patients, coefficient of determination CD > 0.9. 4 patients had their inspiration parameters fitted well (CD > 0.9) to the expiration data with median [Interquartile range (IQR)] CD of 0.912[0.905-0.919]. 8 remaining patients had poor model fits with median [IQR] CD of 0.711[0.654-0.770].

In 6 patients, the identified TCP is greater than TOP which is not physiologically plausible and does not follow the recruitment model assumptions [4,7] where TOP is always higher than TCP. An identified TCP greater than TOP is an artefact of the numerical method for model fitting or a sign of mismatch between the model and the dynamics of reality. While some patients have poor model fits, it is of particular importance that there is systematic error, with pressure being underestimated at the beginning of expiration, and overestimated at the end of expiration as shown in Figure 1. This poor fitting suggests that some parameters that have been assumed constant for inspiration and expiration are actually different. It is likely that the resistance parameters used are not the same during inspiration and expiration. This difference is due to the flow having different geometry during inspiration, where the airways are bifurcating, from expiration, where airways are joining [8].

Figure:
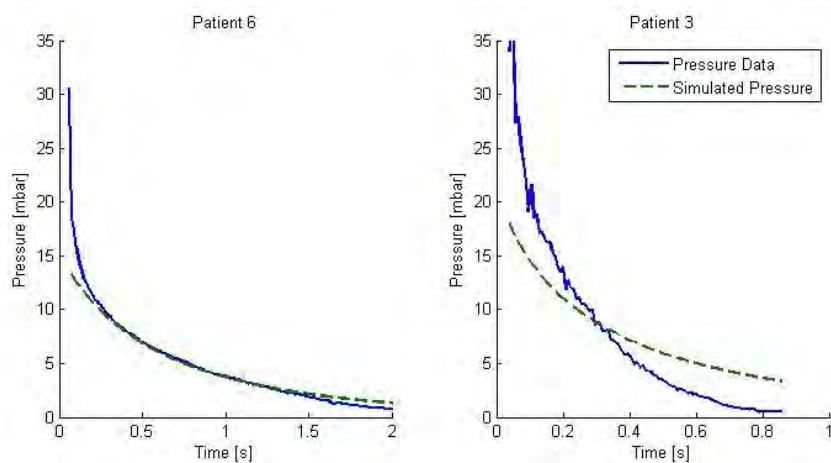
Caption: The VEPRM model fitted to expiration for two different patients. The expiration of Patient 6 fits well to the model, whereas the model does not capture the behaviour exhibited by Patient 3.

Conclusion: The viscoelastic pressure dependent recruitment model can only be used to model expiration in 4 of 12 patients. In most patients, the parameters identified from inspiration no longer describe the pressure response of the lung during expiration. In order to use expiration data for respiratory mechanics models and to better understand respiratory processes, further studies are required to investigate which model parameters are the same in inspiration and expiration, and which are different.

Caption:

References: [1] C. Schranz et al., Proc. IEEE EMBS, 5220–5223, 2013

[2] K. Hickling, Am. J. Respir. Crit. Care Med., 158: 194–202 1998

[3] J. Bates, Lung mechanics. Cambridge University Press, 2009.

[4] K. G. Hickling Am. J. Respir. Crit. Care Med., 163: 69–78, 2001.

[5] C. A. Stahl et al., Crit. Care Med., 34: 2090–8, 2006.

[6] C. Schranz et al., IEEE Trans. Biomed. Eng., 58: 3234–41, 2011.

[7] S. Crotti et al., Am. J. Respir. Crit. Care Med., 164: 131–140, 2001.

[8] W. Ulmer et al. J. Physiol. Pharmacol., 55: 149–153, 2004.

Disclosure of Interest: None Declared

Cardiovascular

AS-0041

A COUPLED HUMAN LEFT VENTRICLE AND SYSTEMIC ARTERIES MODEL

Weiwei Chen [1,*]Hao Gao [1]Xiaoyu Luo [1]NA Hill [1]

[1]Mathematics & Statistics, University of Glasgow, Glasgow, United Kingdom

Introduction and Objectives: Cardiovascular disease leads to over 17 million deaths worldwide per year, which makes it the single greatest cause (48%) of motality. Understanding how the disease develops and relationships between each part in the cardiovascular system are very important for reducing motality and morbidity. Computational simulation is effective in studying the cardiovascular system, but modelling a detailed three-dimensional description of a left ventricle (LV) combined with a dynamic systemic arterial circulation remains a major challenge.

Methods: Two advanced independent mathematical and computation models for the LV and the systemic arteries are coupled to study the interactions in the systemic arterial circulation. The coupled model consists of a dynamic three-dimensional finite-strain structure-based LV, and a one-dimensional dynamic physiologically-based model for the systemic arteries. The fluid-structure interaction (FSI) is described by an Immersed Boundary (IB) approach, in which an incompressible solid is immersed in a viscous incompressible fluid, and solved by a Lagrangian Finite Element (FE) method. The passive and active material parameters in the LV model are determined by fitting the end-diastolic and end-systolic volumes to measurements of the left ventricular volume. The systemic circulation model consists of two groups of arteries, large arteries and small arteries (vascular beds). The large arteries model uses a Lax-Wendroff scheme to compute the cross-sectional area-averaged flow and pressure based on physiological parameters of the arterial tree, such as length, radius and compliance, which are measured and using MRI. The small arteries are modelled as asymmetric structured trees to give outflow boundary conditions at the end of each large arteries. The coupling is achieved by matching the pressure and flow rate at the aortic root, i.e. the circulation model feeds back the pressure as a boundary condition to the LV model, and the flow rate from the LV is used as the input for the circulation model. An explicit method is used. Among the four phases during one cardiac cycle in the LV, the coupling only happens during systole; two models are separate during all the other phases, i. e. diastolic filling, iso-volumetric contraction and relaxation. The coupling starts when the pressure in the LV is higher than the end-of-diastolic pressure in the ascending aorta, and it ends when backflow occurs at the interface.

Results: The results of this coupled model (normal case) show good agreement compared with measured data (less than 5% in peak flow rate). Three disease-related cases are studied in the coupled model, i. e. stiffening of arterial wall, changing end-of-diastolic pressure and simulating functional rarefaction. Results of the disease-related cases are compared with the normal case.

Increasing the stiffness of the large arteries by 50% and 100% result in increased pulse pressure (3.8% and 8.0%) and decreased trough pressure (4.1% and 8.0%) in the ascending aorta, while increasing the stiffness of small arteries has less effect on the pressure or the flow rate during systole. Increasing the degree of vascular rarefaction (5.8%, 13% and 20%) increases both peak and mean pressure in the aorta (2.6%, 8.6% and 17.6% for peak pressure), but the peak flow rate barely changed. Increasing the EDP from 8 mmHg to 10 mmHg leads to an 4.1% increase of the end-of-diastolic

volume and 9.76% increase of the cardiac output as well as a 5.9% increase of the peak LV pressure, while decreasing the EDP has the opposite effects on these characteristics.

Figure:
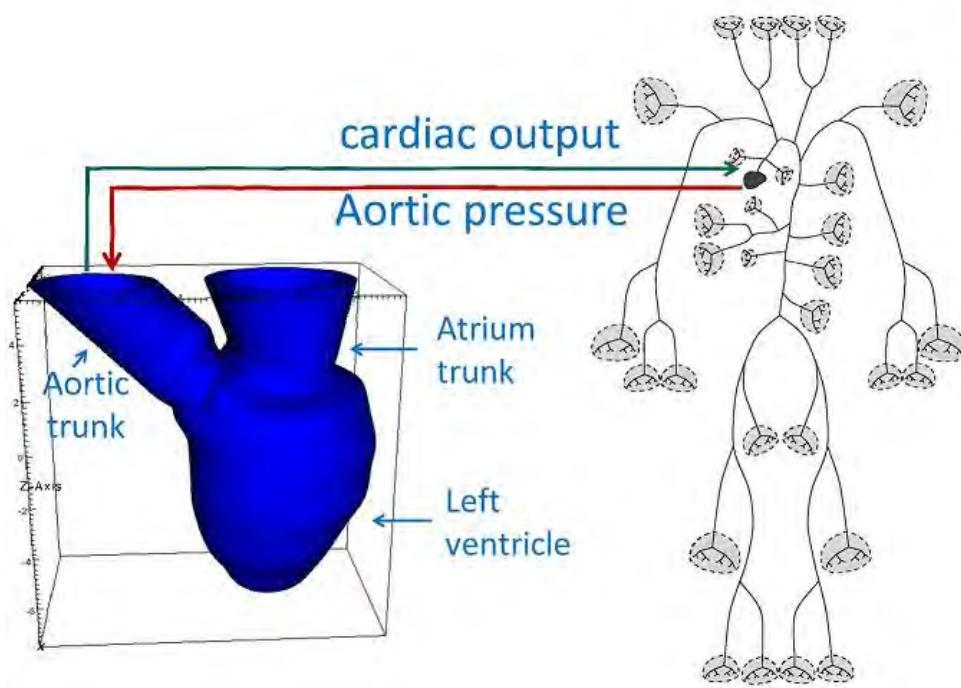
Caption: Coupling the 3-D LV model and the 1-D systemic circulation model

Conclusion: We have developed a dynamic left ventricle and circulation model, which contains a dynamic FE/IB LV model and a cross-sectional area-averaged systemic circulation model. The model provides insight into the roles of the physiological parameters, as well as predictions of blood flow and pressure at any position in the systemic arteries. The coupled model can be used to analysis the interactions of the LV and the systemic arteries during systole as well as to explore the causes and development of cardiovascular diseases.

References: [1] Gao H et al., Dynamic finite-strain modelling of the human left ventricle in health and disease using an immersed boundary-finite element method, IMA Journal of Applied Mathematics, 79:978-1010, 2014.

[2] Gao H, et al., Initial experience with a dynamic imaging-derived immersed boundary model of human left ventricle, Functional Imaging and Modeling of the Heart: 7th International Conference, 7945-11-18, 2013.

[3] Olufsen MS et al., Numerical Simulation and Experimental Validation of Blood Flow in Arteries with Structured-Tree Outflow Conditions, Annals of biomedical engineering, 28:1281-1299, 2000.

[4]. Olufsen MS et al, Rarefaction and blood pressure in systemic and pulmonary arteries, J Fluid Mech, 705:280-305, 2012

Disclosure of Interest: None Declared

Fluid Mechanics

AS-0042

NUMERICAL INVESTIGATION OF DESIGN PARAMETER EFFECTS ON HEMODYNAMICS IN A NOVEL SPIRAL-INDUCING BYPASS GRAFT

Andres Ruiz-Soler [1,*] Amir Keshmiri [1 2]

[1]School of Engineering, Manchester Metropolitan University, [2]School of Mechanical, Aerospace and Civil Engineering (MACE), The University of Manchester, Manchester, United Kingdom

Introduction and Objectives: In the present work, a numerical investigation has been conducted to analyse the blood flow in an End-To-Side (ETS) distal graft anastomosis. The aim is to evaluate the hemodynamic effects of different geometrical parameters involved in the design of a novel spiral-inducing prosthetic graft [1], the performance of which is based on the identification of the blood motion as a swirling flow in the whole arterial system [2]. The relevance of spiral and helical configurations of prosthetic graft lies in the physiological benefits of the swirling flow as a natural phenomenon for the stabilisation of the blood flow with the inhibition of stagnation and flow separation points [3]. It is known that the hemodynamic parameters play an important role in the development of stenosis at the junction due to thrombosis, atherosclerosis and intimal hyperplasia, which are the main causes of graft failure [4].

Methods: Computational Fluid Dynamics (CFD) has been used to simulate the blood flow through a peripheral bypass graft anastomosis that engenders a spiral flow by means of a helical ridge in the internal wall of the graft. The effects of different design parameters have carefully been studied including the ridge cross-sectional area, position and number of ridges. All the three-dimensional simulations were conducted for different Reynolds numbers (570, 1140 and 1700) and the blood flow was assumed as laminar, incompressible and Newtonian fluid. The walls were considered as rigid with no-slip condition.

Results: The results show that changing the orientation of the trailing edge as well as increasing the height of the elliptical ridge and the cross-sectional area of the circular ridge have significant influence on producing secondary flow in the lumen. Furthermore, the effects of such design parameters are observed in the distribution of Wall Shear Stress (WSS) that represents a fundamental hemodynamic factor in the enhancement of bypass graft patency rates. By contrast, changing the width of the elliptical ridge was found to have marginal effects.

Figure:
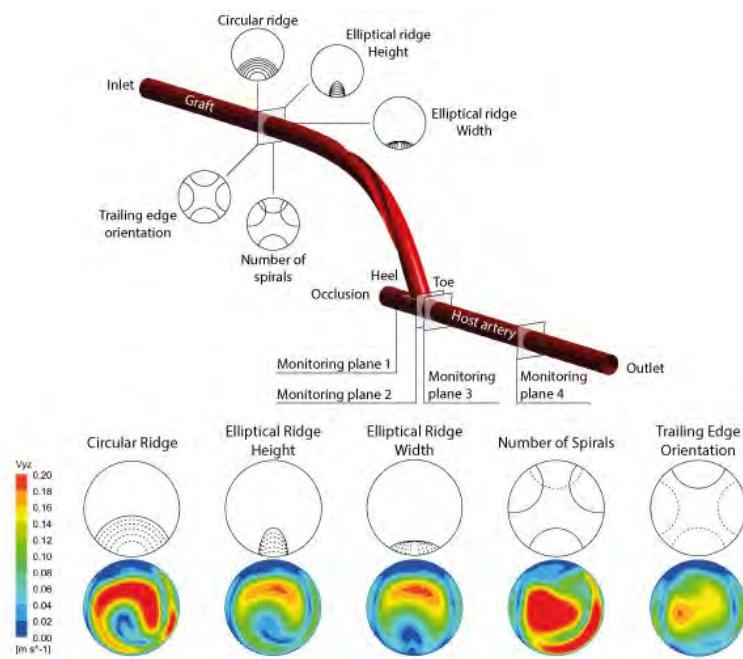
Caption: Top: Schematic of the computational model. Bottom: Secondary velocity magnitude contours at the monitoring plane 2 for different geometrical parameters. The results correspond to the schematics of ridges with solid lines.

Conclusion:

In this work, the physiological importance of secondary flow motion produced by spiral ridges on peripheral bypass graft anastomosis has been studied using CFD in order to determine the qualitative influence of different design parameters. In addition, the effects of pulsatile inlet flow and the non-Newtonian behaviour of the blood will also be analysed using different haemodynamic metrics (e.g. Oscillatory Shear Index and Relative Residence Time) to present a more physiologically-accurate prediction.

References:

[1] Kokkalis et al., Ultrasound Med. Biol., 39: 2295–2307, 2013.

[2] Stonebridge et al., Lancet, 338:1360–1361, 1991.

[3] Liu et al., Ann. Biomed. Eng., 1-13, 2014.

[4] Ghista et al., Biomed. Eng. Online, 12:129, 2013.

Disclosure of Interest: None Declared

Wheelchair

AS-0043

OPPORTUNITIES FOR MEASURING WHEELCHAIR KINEMATICS IN MATCH SETTINGS; RELIABILITY OF A THREE INERTIAL SENSOR CONFIGURATION

rienk V. D. slikke [1,2,*] monique berger [1] daan bregman [2] dirk jan veeger [2]

[1]Faculty of Health, Nutricion and Sports, The Hague University of Applied Sciences, The Hague, [2]3ME, Delft University of Technology, Delft, Netherlands

Introduction and Objectives: *:* Increased professionalism in wheelchair basketball has raised the need for scientific input into optimizing performance. Knowledge of wheelchair kinematics during a match is prerequisite for this performance improvement [1]. Unfortunately, no measurement system providing key kinematic outcomes has proven reliable in competition. A method for measurement of wheelchair kinematics in match play would allow for applied research into athlete-wheelchair interaction by determining the relation between wheelchair settings, kinematics and performance. That knowledge could provide basis for more precise and faster optimization of individual wheelchair settings and thereby support existing experience-based expertise. In this study, the reliability of acquiring wheelchair kinematics based on a three inertial measurement unit (IMU) configuration was assessed in match-like basketball conditions.

Methods: Twenty participants performed a series of tests reflecting different motion aspects of wheelchair basketball, such as a straight 5m sprint; a slalom; a U-turn; moving back and forth while rotating; collide and spin (see Figure 1). During these tests wheelchair kinematics were simultaneously measured using IMU's on wheels and frame, and a 24-camera optical motion analysis system serving as gold standard. Calculated outcomes of wheelchair kinematics based on IMU and gold standard were compared to test the reliability of the IMU sensor configuration.

Results: Results show only small deviations of the IMU method compared to the gold standard. As expected, kinematics derived from wheel rotation showed increased errors in wheel skidding conditions. Therefore newly skid correction algorithms were developed, using multiple sensor information. Once these algorithms were applied, calculated Root Mean Square Errors (RMSE) showed good estimates for frame displacement (RMSE$\leq$ 0.05m) and speed (RMSE$\leq$ 0.1m/s), except for three truly vigorous tests (during collisions and an evoked skidding stop). Estimates of frame rotation in the horizontal plane (RMSE<3°) and rotational speed (RMSE<7°/s) were very accurate in all tests. Differences in calculated instantaneous rotation centres (IRC) were small, but somewhat larger in tests performed at high speed. At normal speed the error in calculated distance between IRC and frame centre stayed below an RMSE of 0.1m, but at high performance speeds it reached up to an RMSE of 0.19m. For linear speed (ICC's > 0.90), rotational speed (ICC>0.99) and IRC (ICC> 0.90) average outcomes showed high correlations between IMU data and gold standard. So, even estimates with higher RMSE values, showed small errors once averaged per test.

Figure:
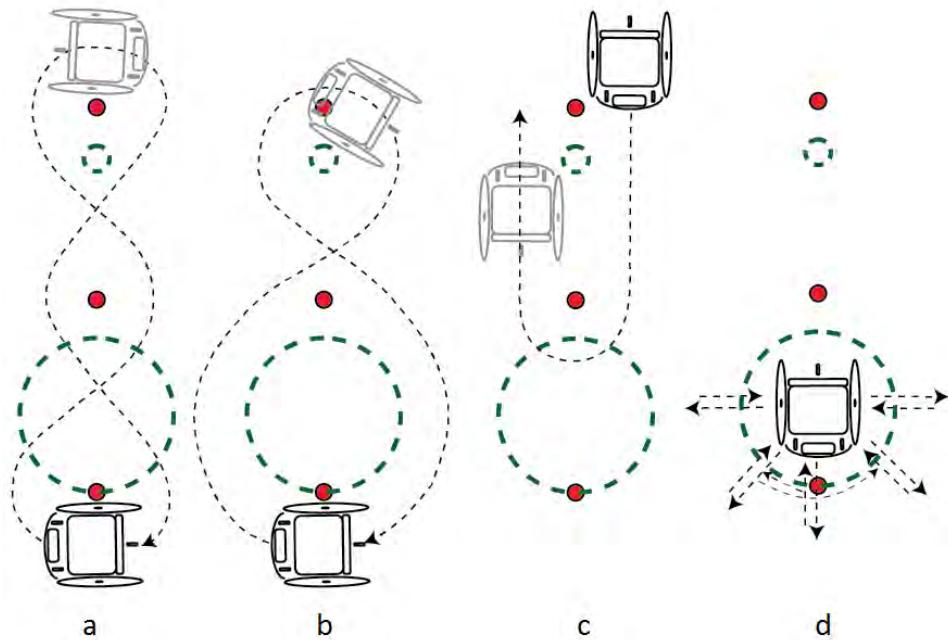
Caption: Test track lay-out and example tests: a) Slalom test; b) Figure eight test; c) U-turn (left & right); d) Star twist (moving back and forth, combined with rotation)

Conclusion: The developed method provides a valuable tool for wheelchair athletes, coaches and researchers to perform ambulant measurements and applied research in the field of wheelchair sports. Wheelchairs can easily be equipped with cheap lightweight IMU sensors, providing reliable wheelchair kinematics if wheel diameter and track width are known. In future research, the use of this method might allow for a more detailed profile of wheelchair kinematics during a match. Combined with measurement of additional quantities, such as exerted force or observed game performance information, this allows for composition of an athlete specific performance profile. Such a profile could be used to determine the effect of sport specific training or wheelchair setting adjustment.

Table:

Test		Displ.(m)	Speed (m/s)		Rotation (°)	Rot. speed (°/s)		IRC dist. (m)	
	Speed	RMSE	RMSE	ICC	RMSE	RMSE	ICC	RMSE	ICC
Straight	Normal	0.02	0.03	0.998					
	High	0.02	0.09	0.997					
Slalom	Normal	0.03	0.02	1.000	1.9	4.48	0.999	0.08	0.988
	High	0.03	0.05	1.00	1.8	5.6	0.99	0.	0.95

					0		2	8	13	8
Figure 8	Normal	0.02	0.02	0.999	1.2	4.12	0.998	0.10	0.983
	High	0.04	0.05	0.999	1.3	5.33	0.998	0.14	0.945
U-Turn	Normal	0.02	0.02	0.999	1.1	3.11	0.997	0.08	0.988
	High	0.03	0.07	0.998	1.2	4.26	0.997	0.19	0.973
Turn on spot	Normal	0.03	0.03	0.989	1.5	4.67	0.999	0.05	0.917
	High	0.02	0.06	0.987	2.6	6.80	0.998	0.03	0.974
Star Twist	High	0.03	0.04	0.997	1.7	5.79	1.000	0.08	0.979
Star Move	High	0.10	0.08	0.993	1.4	3.97	1.000	0.10	0.986
Collision	High	0.07	0.27	0.936					
Straight Skid	High	0.04	0.21	0.971					

Caption: The RMSE values and ICC for test means are calculated for the difference between the IMU method and Optitrack gold standard. Calculated average parameters are: displacement (displ.), speed, rotation, rotational speed (Rot. speed) and IRC during typical tests performed at normal and high speed.

References: [1] Mason, B. S. et al. (2013). *Sports Medicine, 43*(1), 23-38.

Disclosure of Interest: None Declared

Wheelchair

AS-0044

MODIFICATIONS OF PROPULSION MECHANICS WITH INCREASES IN SPEED ALTERS DISTRIBUTION OF MECHANICAL DEMAND IMPOSED ON THE UPPER EXTREMITY

Ian M. Russell [1,*]Philip S. Requejo [1]Sara Mulroy [2]Carmen Muller-Karger [3]Mary M. Rodgers [4]Jill L. McNitt-Gray [1]

[1]Biomedical Engineering, University of Southern California, Los Angeles, [2]Rehabilitation Engineering, Rancho Los Amigos National Rehabilitation Cen, Downey, United States, [3]Department of Mechanical Engineering, Simon Bolivar University, Caracas, Venezuela, Bolivarian Republic Of, [4]Physical Therapy & Rehabilitation Science, University of Maryland School of Medicine, Baltimore, United States

Introduction and Objectives: Preservation of shoulder function is important for manual wheelchair (WC) users with spinal cord injury (SCI). Manual WC propulsion is an effective form of low-cost wheeled mobility as it preserves upper body strength, cardiovascular conditioning as part of daily activities, and community participation. Repetitive mechanical loading of the upper extremity often leads to physical impairment (e.g. shoulder pain) that affects activities of daily living.[1,2] Current experimental research and clinical guidelines promote improved interaction between the individual and the WC as a means to mitigate detrimental mechanical loading of the shoulders.[3]

Manual WC propulsion requires generation of a reaction force (RF) at the handrim with a component tangential to the wheel. The mechanical demand (Net Joint Force (NJF), Net Joint Moment (NJM)) imposed across the upper extremities, however, is affected by orientation of the resultant RF relative to the body segments.[4,5] Model simulation results indicate a 2-fold increase in RF magnitude can result in minimal changes in shoulder NJM magnitude without decrements in performance if the orientation of the RF relative to the upper extremity segments is modified.[4] The aim of this study was to determine if individuals with SCI modify mechanical load distribution imposed on the upper extremity by reorienting the RF relative to the forearm and upper arm when manually propelling their WC under free as compared to self-selected fast conditions.

Methods: Forty-one experienced manual WC users (8 Females, 33 Males) with paraplegia (8 ± 6 yrs post SCI) from the Rancho Los Amigos National Rehabilitation Center volunteered to participate in accordance with the Institutional Review Board. Individuals were excluded from participation if they reported a history of shoulder pain that altered performance of daily activities. Kinematics (VICON, 50Hz) and pushrim RFs (SmartWheel, 240Hz) were collected during manual WC propulsion on a stationary ergometer at self-selected free and fast conditions. Joint kinetics (NJM, NJF, Visual 3D) and mechanical load distribution represented as a percent of the total NJM (e.g. NJM elbow/(|NJMshoulder| + |NJMelbow|)) were used to characterize within subject differences in propulsion mechanics during the push phase at self-selected free and fast conditions.

Results: Within-subject analyses revealed that over a third of the participants in this study modified the mechanical load distribution imposed on the upper extremity during the push phase by more than +/-10% when manually propelling their WC under free as compared to self-selected fast conditions. The median mechanical load distribution imposed on the shoulder was 77% for both free and fast conditions. Participants with a load distribution exceeding the median under the free condition demonstrated increased elbow and reduced shoulder contributions to NJM during the fast condition. In

contrast, participants with a load distribution less than the median under the free condition exhibited mixed results. In this group, redistribution of mechanical load was achieved by redirecting the reaction force, modifying forearm and upper arm orientation, or some combination of both. Figure 1 illustrates how two exemplar participants, with similar increases in RF magnitude with speed, modified the orientation of their RF relative to the upper extremities and, as a result, redistributed the mechanical demand. Exemplar Subject1 increased the mechanical demand imposed on the elbow by 28% when shifting from free to fast conditions, resulting in a decrease in rotational demand imposed on the shoulder. Note however that more vertically oriented reaction forces associated with reduced contribution of the shoulder NJM are likely to add to the upward component of the shoulder NJF. In contrast, exemplar Subject 2 generated similar increases in RF at the faster speed, yet the RF force acted posterior to the forearm thereby changing the elbow NJM from an extensor to a flexor moment and thereby increasing the demand imposed on the shoulder.

Figure:

Upper Extremity NJM Distribution for Free and Fast Propulsion Conditions
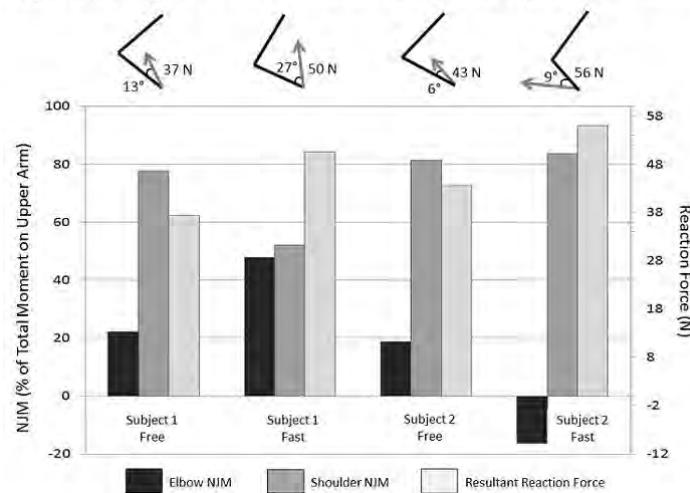
Caption: Fig 1 NJM distributions for 2 participants with comparable increases in RF during push between free and fast propulsion conditions.

Conclusion: Knowledge of how experienced manual WC users regulate increases in mechanical demand imposed on the shoulder joint in response to increased speed requirements provides an important step in identifying effective propulsion strategies for individuals to maintain and improve performance while mitigating the repetitive loading associated with the development of shoulder pain.

Funded in part by the Southern California Clinical and Translational Science Institute

References: [1]Dalyan et al. *Spinal Cord*.1999;37(3):191-195.

[2]Bayley et al. *J Bone Joint Surg Am*. 1987;69(5):676-678.

[3]Consortium for Spinal Cord Medicine *Paralyzed Veterans of America*, 2013

[4]Munaretto et al. Clin Biomech (Bristol, Avon).2012;27(3):255-262.

[5]Raina et al. J Spinal Cord Med.2012;35(3):148-155.

Disclosure of Interest: None Declared

Wheelchair

AS-0045

EVALUATION OF A WHEELCHAIR TRICYCLE ATTACHMENT FOR PERSONS WITH DISABILITIES IN DEVELOPING COUNTRIES

Rodrick Shangali [1,*] Harold Shangali [2]

[1]Engineering Department, [2]TATCOT, TATCOT, Moshi, Tanzania, United Republic of

Introduction and Objectives: The design was done in reference to need, opportunity identification, brainstorming within groups, visiting search field, making observation and interviews to identify the existing needs and evaluation to select design opportunities. The use of the attachment will allow the user (disabled persons) to access the daily socio-economic activities for personal development and income generation. The attachment can provide large distance coverage as compared to the manual wheelchair which is mostly for indoor activities.

The main objective of this project was to develop a wheelchair tricycle attachment for easier accessibility and increased performance to the wheelchair users in Dar es Salaam and Kilimanjaro regions (Tanzania).

Methods: The design was done in reference to need, opportunity identification, brainstorming within groups, visiting search field, making observation and interviews to identify the existing needs and evaluation to select design opportunities. Each wheelchair user will have his/her unique set of needs which the wheelchair should cater for. The wheelchair should take into account the wheelchair users as: Home environment, Disability, Lifestyle and Economic situation. This was done by investigating the existing driving systems for both wheelchairs and tricycles. Literature review, survey, information analysis, observations, manufacturing, design testing, evaluation and interviews was carried out. Conceptual design was done followed by embodiment design and detail design The evaluation was done by looking through the following criteria; i.e. easy to manufacture, low production cost, reasonable product price, easy to operate, simple design, efficiency, ergonomics, aesthetics and weight.

Detail and assembly drawings of various components and manufacturing were carried out at Tanzania Training Centre for Orthopaedic Technologist (TATCOT). Thirty disabled people were interviewed. Finally we were able to manufacture five units. From these units we were able to test on 5 wheelchair users tested as shown as one of them in (Figure.1) with the consideration of Operating efficiency, Conformance to standards, Torque transmitted, Power transmitted and Conformance to ergonomics requirements.

From the evaluation point of view, we began by identifying the static loads on the wheelchair and attachment when the attachment is in use. We made the conservative estimate that the center of gravity of the user will be at the center of the seat. Using equations from summing moments about the rear wheel axle and summing the vertical forces in the device. The reaction forces at both wheels could be obtained for a predetermined human load. In order to make a simple calculation of the moment on the device at the place the attachment connects to the wheelchair.

The Clip-on Tricycle Attachment is a quick release clip-on, clip-off attachment which can be fitted to the Motivation Rough Terrain wheelchair. It converts the wheelchair into a tricycle allowing the user to travel greater distances more effectively. After attaching to the main frame of wheelchair, need to lock it so as to avoid twisting and dismantle of the front attachment. The mounting / junction part to the main beam of the wheelchair need to be clamped so as the castor wheel

to inclined at an angle. For longer distance accessibility, the user can use the attachment by altering/changing gear depending with topographic of the land. For indoor activities such as office, home, hospital and other places, user will remove the attachment easily and park lock on the security area.

Results: The results of the majority of the wheelchair users interviewed became disabled early in life with a birth defect or polio, of which most had to resort to crawling as a means of mobility before obtaining a wheelchair or tricycle. Most of the interviewed needed to travel multiple kilometers per day. For long distance a tricycle required less much power than a wheelchair. One major problem observed during the assessment was the inability of many people to purchase their own mobility aid. As a result, the tricycles attachment was observed to be a proper solution for wheelchair users and also for environmental concerns (Indoor & Outdoor).

Figure:

Conclusion: The attachment during attaching/detaching on the wheelchair was agreed to be a better solution for wheelchair users.

Table:

TESTING CRITERIA	WHEELCHAIR USER RESPONDS(N=5)
Operating efficiency	80%
Conformance to standards	85%
Power transmitted	90%
Conformance to ergonomics requirements	88%
Aesthetics	90%

Caption: Table 1: Testing criterias for the wheelchair users (n=5)

References:

Pugh, S. 1991. Integrated Methods for Successful Product Engineering, Addison-Wesley Publishing Company. pg 32-50.

1. Winter, G. 2005. Assessment of Wheelchair Technology in Tanzania, Cambridge.pg 10-30

2. Cornick, P. 2002.Wheelchair Technology Manual, UK, Motivation. pg 10-15

Disclosure of Interest: R. Shangali Conflict with: Travel, allowance and accommodation, H. Shangali: None Declared

Wheelchair

AS-0046

INFLUENCE OF THE MANUAL WHEELCHAIR SETTINGS WHEN ROLLING ON A CROSS-SLOPE : A THEORETICAL STUDY

Joseph Bascou [1,*] Christophe Sauret [2] Fanni Li [1] Coralie Villa [1] Francois Lavaste [2] Hélène Pillet [2]

[1] Institution Nationale des Invalides / CERAH, Créteil, [2] Institut de Biomécanique Humaine Georges Charpak, Paris, France

Introduction and Objectives: The manual wheelchair (MWC) allows disabled people to retrieve both mobility and autonomy. However, it can induce overload on the upper body [1], which can be amplified by some daily situations, such as cross slopes. This specific situation requires additional efforts to counterbalance the MWC tendency to roll the hill down [2], [3], [4].

This additional load could be limited by appropriate adjustments of the MWC. Unfortunately, MWC has a large panel of geometrical and material settings, making the selection of the best combination for propelling on a cross-slope difficult. If the effect of the fore-aft location of the user's center of mass was rapidly identified [4], the effects of other settings such as tire type, swiveling resistances, etc, are not yet defined.

So, the aim of this study was to evaluate, by means of a theoretical model, the effects of a large panel of MWC settings on the counterbalancing braking moment required to maintain the straightforward displacement on cross slopes.

Methods: : A static mechanical model of a subject and the wheelchair on cross-slope was defined with a three wheeled MWC, to fulfill iso-static conditions (Figure 1). This model allowed linking the braking moment $M_{s\to w}$ applied by the subject at the center of rear wheel axle on the wheelchair, to 10 geometrical and mechanical parameters of the MWC, the cross slope and the subject, leading to the following expression:

$$M_{s\to w} = (n_s * P_s + n_w * P_w) * \sin\theta \quad - \quad C * d/d_1$$
$$- f_{rf} * \cos\theta * (n_s * P_s + n_w * P_w) * (1/d + 1/d_1)$$
$$- f_{rr} * \cos\theta * (P_s * (d-n_s)/d + P_w * (d-n_w)/d) \qquad \text{(equation 1)}$$

Ranges of variation of each parameter were defined according to the literature as follows : n_s / n_w are the distances between the subject (s) / the wheelchair (w) centers of mass and the rear wheel axle, both ranging from 0.05 m to 0.3m; m_s / m_w are the subject / wheelchair masses, ranging from 50kg to 90kg for the subject and from 7 kg to 20 kg for the wheelchair ; C is the fork pivot resistance, ranging from 0.02 Nm to 0.1 Nm; d is the wheelbase, ranging from 0.3 m to 0.45m, d_1 is the horizontal length of the fork, ranging from 0.03m to 0.06m; f_{rr} / f_{rf} are the front / rear wheel swiveling resistance parameters, both ranging from 0.001m to 0.002m. In this study, the inclination of the cross slope (θ) was chosen equal to 6°.

A 2-level *in-silico* experimental plan was designed to cover every possible wheelchair parameter sets, each parameter taking the minimal or the maximal value of its variation range, resulting in 1024 parameter sets. For each set, the resulting braking moment was calculated according to equation 1.

Results: Relatively to the averaged braking moment $M_{s\to w}$ of 7.4 Nm, the variations – named "effects" – due to a change between medium and maximal value of the tested parameters were expressed in table 1.

With respect to the range of their individual variations, parameters with the greatest effects were the fore-aft distance of the subject's center of mass (ns), but also the horizontal length of the fork and the swiveling resistance of the front wheel, for instance.

Figure:
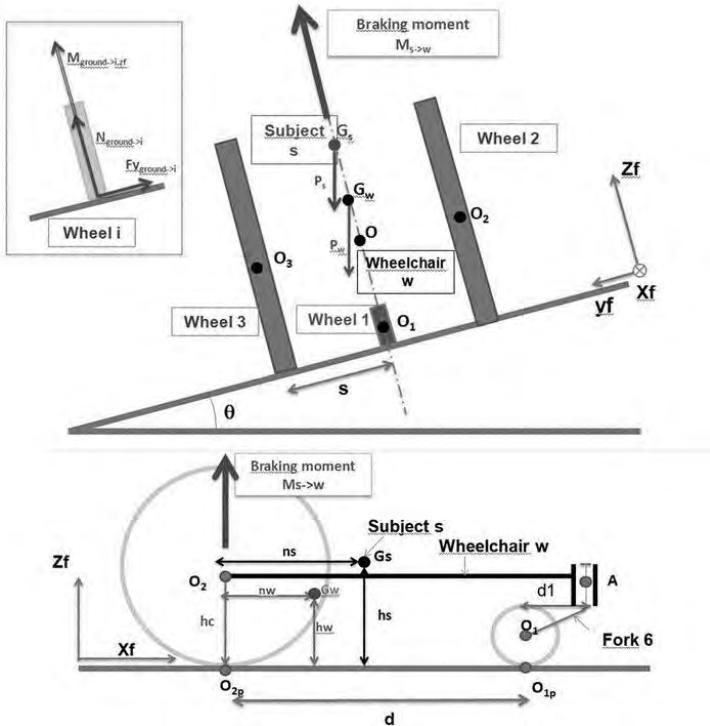
Caption: Figure 1: free body diagram of the static wheelchair on a cross slope

Conclusion: This study allowed quantifying the effects of manual wheelchair parameters on the counterbalancing braking moment required during propulsion on cross slopes. As found in the literature, the fore-aft distance between the subject center of mass and the rear wheel axle is the major lever to limit load on upper limbs during cross slope propulsion [2]: placing the total center of mass above the rear wheel axle should cancel the effect of the cross slope. Unfortunately, this setting would increase the MWC backward tilting risk. However, this study demonstrates that reducing the length of the fork or increasing the swiveling resistance of the front wheel, for instance, could also help in limiting the users' efforts. Further experimentations need to be conducted to confirm the results of this theoretical study.

Table:

Effect / Interaction	Label	Effect (Nm)
n_s	Distance subject center of mass / rear axle [m]	5,77
fr_f	Front wheel swiveling resistance parameter [m]	-1,98
d_1	Horizontal length of the fork [m]	1,97
m_s	Subject mass [kg]	1,86
n_w	Distance wheelchair center of mass / rear axle [m]	1,40

m_w	Wheelchair mass [kg]	0,70
C	Fork pivot resistance [Nm]	-0,38
fr_r	Rear wheel swiveling resistance parameter [m]	-0,35
d	Wheelbase [m]	-0,19

Caption: Table 1: Effects of the parameter variation from medium to maximal value on braking moment for a 6° cross slopes.

References: [1]   Van-der-Woude et al., Medical Engineering & Physics, vol. 23, n° 110, pp. 713-733, dec 2001.

[2]   Brubaker et al., J Rehabil Res Dev, vol. 23, n° 12, pp. 55-58, Apr 1986.

 [3]   Sauret et al., CMBBE, , 16 Suppl 1, 124-125, 2013.

[4]   Tomlinson et al., Phys Ther, vol. 74, n° 14, pp. 349-355, Apr 1994.

Disclosure of Interest: None Declared

Wheelchair

AS-0047

SPINAL POSTURE AND BALANCE IN INDIVIDUALS WITH SPINAL CORD INJURY IN RESPONSE TO WHEELCHAIR SEAT CHANGES

Beth A. Cloud [1,*]Kristin D. Zhao [2]Kai-Nan An [3]

[1]Mayo Graduate School, Center for Clinical and Translational Science, [2]Rehabilitation Medicine Research Center, Department of Physical Medicine and Rehabilitation, [3]Biomechanics Laboratory, Division of Orthopedic Research, Mayo Clinic, Rochester, United States

Introduction and Objectives: Seating parameters have been shown to affect how one functions from a manual wheelchair (MWC) base. This includes effects on upper extremity kinematics during propulsion in response to axel position [1] as well as effects on vertical reach distance and possible influences on postural parameters in response to seat angle changes [2]. Positioning in one's MWC is a means by which to optimize function. This is imperative considering the amount of time individuals spend in their MWC and the high prevalence of upper extremity pain and pathology in this population [3]. The purpose of this study was to investigate the effects of a seat dump angle change on postural and functional parameters, including sagittal plane spinal curvature and balance, in MWC users with spinal cord injury. We hypothesize that increased seat dump angle (created by increasing the height of the front of the seat relative to the back) will increase lordosis in the thoracolumbar region of the spine and increase balance as measured by a seated reach test.

Methods: Chronic MWC users (>1 year from onset of MWC use) with spinal cord injury (SCI) or disease were recruited. Each participant's MWC was modified with custom wedges to create 0° and 14° seat dump angles (relative to horizontal) with a vertical backrest. Spinal posture was measured with a fiber optic system overlying spinous processes from the first sacral to seventh cervical vertebral level. Spinal curvature was defined as regions of kyphosis and lordosis quantified as the angles created from the normal to the curve at the endpoints of each region [4]. Posture was captured with participants looking straight ahead, hands in their lap. Balance was assessed with the modified functional reach test (MFRT), previously validated for use with individuals with SCI [5]. Electromagnetic sensors were used to track thorax and humerus segments. The excursion of the sternal notch in the global coordinate system was used to determine forward reach distance while the dominant arm was held parallel to the ground. Five trials were completed in each seat condition. The minimum and maximum distances were excluded and the mean of the remaining three were used to determine MFRT values. Lordosis, kyphosis, and MFRT values were compared between each condition using a Wilcoxon signed-rank test. All data was combined, to plot a correlation between MFRT and curvature (lordosis or kyphosis) values.

Results: Six participants (3 male; age: 34-52 years; duration MWC use: 2.83-19.25 years; SCI level C6/7-T10) participated in the study to date. Changes in seat dump angle did not have a consistent, statistically significant effect on lordosis, kyphosis or MFRT values. Kyphosis value did not have an association with MFRT. Lordosis, when present, was correlated with MFRT values (R^2= 0.66, $p < 0.01$).

Figure:
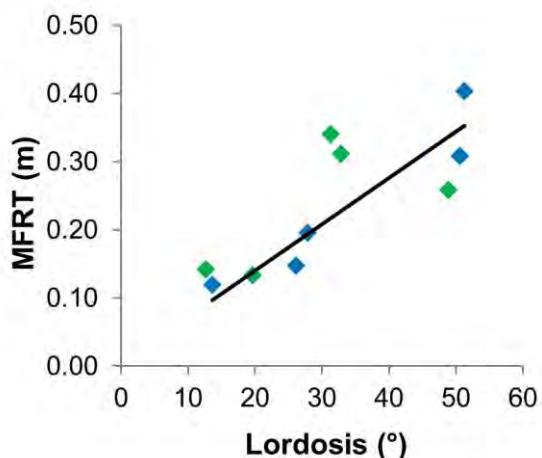
Caption: Figure 1: Correlation between lordosis values for all participants with detectable lordosis, data from both seat positions combined (R^2= 0.66, $p < 0.01$). Black line indicates fit; blue diamonds indicate values in 0° seat dump angle condition; green diamonds indicate values in 14° condition.

Conclusion: The seat dump angle changes evaluated in this study had different effects on amount of lordosis in MWC users with SCI. These differences may be due to SCI level as individuals with higher level injuries (T4 and above) tended to experience an increase in lordosis (when present) with increased seat dump angle. Those with lower level injuries had less lordosis in the larger seat dump angle condition. Larger values of lordosis, regardless of seat dump angle, were associated with increased reach distance. The relationships observed will continue to be assessed as additional participants are recruited. Seat dump angle did not have a consistent effect on participant posture in this study. However, increased spinal lordosis may be associated with enhanced balance and function from a MWC base.

References: [1] Boninger et al, Arch Phys Med Rehabil, 81: 608-13, 2000.

[2] Hastings et al, Arch Phys Med Rehabil, 84: 528-34, 2003.

[3] Dyson-Hudson et al, J Spinal Cord Med, 27: 4-17, 2004.

[4] Cloud et al, Gait Posture, 40: 369-74, 2014.

[5] Lynch et al, Phys Ther, 78: 128-33, 1998.

Disclosure of Interest: None Declared

AS-0048

ESTIMATED ATHLETE'S BASKETBALL MATCH PERFORMANCE BASED ON MEASUREMENT OF WHEELCHAIR KINEMATICS USING INERTIAL SENSORS.

R.M.A van der Slikke, M.A.M. Berger, D.J.J. Bregman, H.E.J. Veeger

Introduction & Objectives: Since wheelchair basketball events have become more and more competitive, there is a need to optimize all factors contributing to team performance. One of these factors is individual kinematic performance of the athletes, yet to date limited kinematic match information is available. Knowledge of wheelchair kinematics during a match is prerequisite for further performance improvement [1]. In this study wheelchair kinematics profiles of athletes on different competition levels are measured during a match, using a newly developed inertial sensor based measurement method [2]. Measurement outcomes provide an impression of typical match characteristics and show which characteristics seem sensitive to discriminate between performances based on classification and competition level.

Methods: Twenty nine participants were measured in their own wheelchair during basketball competition matches at top national as well as international level, with twelve male first division players (National), nine female internationals (NL & UK) and eight male internationals (NL, ISR & AUS). Field positions (guard, forward and center), as well as athletes' classification points were evenly distributed over the different groups (Table 1).

Each wheelchair was equipped with three inertial sensors, one on each wheel axis and one on the rear frame bar, providing key aspects of wheelchair kinematics: displacement, speed, acceleration, rotation, rotational speed and rotational acceleration. Additionally, the time to reach a certain displacement (2, 4 or 6m) or rotation (90° or 135°) was calculated. Data were compared at competition level and at the level of athletes' classifications, with one group class 2.5 or less and one group class 2.5 over.

Results: For all 29 measurements a kinematic profile could be made, although in seven measurements partial data loss occurred due to vast collisions. During movement time (frame center speed>0.05 m/s) an average speed of 1.22 m/s and rotational speed of 47.3 °/s was measured, with minor (not significant) differences between competition level groups and classification groups. The average time to reach a certain distance or rotation, was based on sprints as well as on movements where no maximal performance was required, such as wheeling to a free throw. Therefore, the average of the 10 fastest sprints and rotations are displayed in the graph (Figure 1). Analysis of competition level revealed only significant ($p<.05$) differences for the time to a rotation (90° and 135°), between the national players and both international male and female players. When grouped by classification, the differences in time to a certain distance or rotation showed all significant ($p<.05$).

Figure: Average time (± stdev.) from standstill to a certain distance (2, 4 or 6 meter) or rotation (90° or 135°), grouped by competition level (left chart) and classification (right chart).
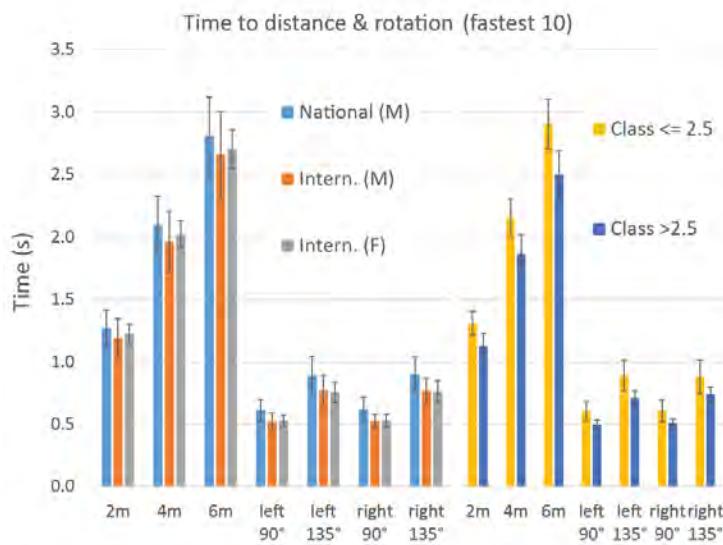

Table: Wheelchair athlete (n=29) data, grouped by classification and by competition level.

Group		Min	Max	Mean	SD	N	Level	Freq.	%
Class <= 2.5	Class	1.0	2.5	1.7	0.6		National (M)	7	41%
	Age	15	42	28.6	7.4	17	Intern. (M)	5	29%
							Intern. (F)	5	29%
Class >2.5	Class	3.0	4.5	4.0	0.6		National (M)	5	42%
	Age	14	46	28.6	9.4	12	Intern. (M)	3	25%
							Intern. (F)	4	33%
National (M)	Class	1.0	4.5	2.5	1.4	12			
	Age	14	46	27.9	9.4				
Intern. (M)	Class	1.0	4.5	2.8	1.1	8			
	Age	22	42	30.0	6.0				
Intern. (F)	Class	1.0	4.5	2.8	1.3	9			
	Age	15	39	28.3	8.8				

Conclusion: Average speeds, accelerations, rotational speeds and rotational accelerations, do not discriminate between groups based on either competition level or classification. To determine best match performance only the ten fastest forward movements and rotations are included in the analysis, discriminating well between different classification groups. Competition level based comparison only showed significant differences between national and international players for the time to rotation. Although the average time to a certain distance also shows noticeable differences between national and international level, these differences were not statistically significant due to the large standard deviation. Future enlargement of the measurement population would allow for classification based division *within* competition level groups, most likely reducing performance outcomes standard deviations.

Further data analysis and additional research is needed to identify the most sensitive performance measures as well as its stability over consecutive matches. Once established, this method provides a valuable tool for wheelchair athletes,

coaches and researchers to perform ambulant measurements and applied research in wheelchair sports. Combined with measurement of additional quantities, such as exerted force or observed game performance, this allows for composition of an athlete specific performance profile. Such a profile could be used to determine the effect of sport specific training or wheelchair setting adjustment.

References

[1] Mason et al. *Sports Medicine, 43*(1), 23-38, 2013.

[2] van der Slikke et al. *Submitted 2014*

AS-0049

SOFT TISSUE ARTIFACT DESCRIPTION USING TRIANGULAR COSSERAT POINT ELEMENTS

Dana Solav [1,*]MB Rubin [1]Andrea Cereatti [2]Valentina Camomilla [3]Alon Wolf [1]

[1]Mechanical Engineering, Technion, Haifa, Israel, [2]POLCOMING department, Information Engineering Unit, University of Sassari, Sassari, [3]Department of Movement, Human and Health Sciences, University of Rome, Rome, Italy

Introduction and Objectives: Accurate estimation of the position and orientation (pose) of a bone from the motion of skin markers is limited mostly by the relative motion between the markers and the bone, which is known as the Soft Tissue Artifact (STA). Various methods have been proposed that employ clusters composed of a redundant number of skin markers (>3) to minimize the effect of the STA on the bone pose estimation, but no satisfactory solution yet exists. The objective of this paper is to propose a method for the description of the non-rigid kinematics of marker clusters within a theoretical framework of continuum mechanics. The method entails the definition of time-variant parameters for the description of the marker cluster strain and the relative rotation and translation between clusters due to the presence of STA. The latter exercise may provide new insights for the development of novel methods aimed at compensating for the STA effects.

Methods: The cluster of markers on the skin of the analysed bone is characterized by Triangular Cosserat Point Elements (TCPEs) defined by all combinations of three markers. The kinematics of each TCPE is evaluated in terms of its translation vector and deformation gradient tensor [1]. Subsequently, three instantaneous scalar TCPE parameters $\{E, \Phi, T\}$ are defined, to characterize the magnitude of strain in each TCPE, and the relative rotation and relative translation between pairs of TCPEs, respectively. The proposed method was evaluated using previously collected *ex-vivo* data [2] on the motion of the lower limbs of three cadavers measured simultaneously from skin markers and bone pins, as shown in Fig. 1. The cluster of twelve skin markers was used to construct 220 TCPEs. The instantaneous femur position error $\Delta\theta$ and orientation error Δt, and the parameters $\{E, \Phi, T\}$ were obtained for each TCPE. The bone pose errors were also calculated by applying the Procrustes Superimposition (PS) approach on the entire cluster of markers, for comparison.

Results: Statistics of the values of the parameters $\{E, \Phi, T\}$ and the pose errors $\{\Delta\theta, \Delta t\}$ for all the TCPEs are shown in Table 1. The maximum values of $\Delta\theta$ and Δt obtained by a single TCPE were 36 degrees and 95mm, respectively. When selecting the TCPE with the smallest error at each time step, the maximum values were reduced to 5.2 degrees and 7.5 mm, respectively. In particular, it is noted that a number of TCPEs exhibited errors smaller than those estimated by the PS approach applied on the entire cluster of markers (on average, 31% of the TCPEs had smaller orientation errors and 21% had smaller position errors). This suggests that the pose errors could be reduced if selection of quality TCPEs, which best represent the underlying bone pose, is feasible. To examine the ability of the parameters $\{E, \Phi, T\}$ to predict the quality of the TCPEs' pose estimation, Spearman's rank correlation coefficients (R_s) between the errors $\{\Delta\theta, \Delta t\}$ of the TCPEs and each of the parameters $\{E, \Phi, T\}$ were calculated at each time step. Statistics of the values of R_s are also shown in Table 1. The results revealed mostly poor to moderate correlations between E and the errors, suggesting that the strain magnitude may not be a good parameter for selection of quality TCPEs to estimate bone pose. The strongest correlations were found

between Φ and $\Delta\theta$ and between T and Δt. This suggests that TCPEs with smaller Φ should more accurately represent bone orientation and TCPEs with smaller T should more accurately represent bone position.

Figure:
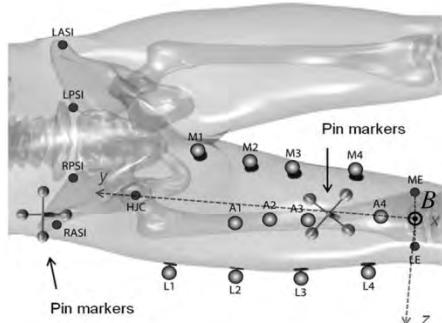
Caption: Fig. 1. Pin and skin markers configuration

Conclusion: The TCPE method proposes a number of physical parameters that can be used to describe the deformation of the body segment under analysis. It has been shown that some of these parameters correlate well with femur pose errors measured *ex-vivo*, which suggests that they can be used to select, at each instant, subset groups of TCPEs which are more likely to accurately estimate the underlying bone pose. It has been proved that, if an effective method for the selection of optimal subset groups of TCPEs is devised, the bone pose accuracy can be highly improved. It is expected that the operational framework provided by the TCPE method can be used to describe the body segment deformation and to lay the foundation for the compensation of the STA in *in-vivo* measurements of different populations, motor tasks and body segments when a high number of observation points are recorded.

Table:

	Min	Max	Median	IQR
E (%)	0	61.3	5.9	8.5
Φ (deg)	0	6.8	40.9	6.2
T (mm)	0	87	15	14
$\Delta\theta$ (deg)	0	36.2	5.2	6.6
Δt (mm)	0	95.8	9.7	14.4
R_s (E, $\Delta\theta$)	-0.49	0.79	0.40	0.26
R_s (Φ, $\Delta\theta$)	-0.19	1.00	0.70	0.31
R_s (T, $\Delta\theta$)	-0.44	0.90	0.56	0.20
R_s (E, Δt)	-0.24	0.85	0.50	0.22
R_s (Φ, Δt)	-0.11	0.89	0.57	0.21
R_s (T, Δt)	-0.05	1.00	0.78	0.19

Caption: Table 1. Statistical values of the TCPE parameters, pose errors, and Spearman correlation coefficients.

References: [1] Solav et al., Int J Eng Sci,85:1-9, 2014.

[2] Cereatti et al., J. Biomech, 42: 818-823, 2009.

Disclosure of Interest: None Declared

Motion Analysis

AS-0050

HUMAN PERFORMANCE IN SIMULATED REDUCED GRAVITY ENVIRONMENTS

Matt Cowley [1,*] Lauren Harvill [1] Sudhakar Rajulu [2]

[1]Human Health and Performance, NASA / Lockheed Martin, [2]Human Health and Performance, NASA, Houston, United States

Introduction and Objectives: NASA is currently designing a new space suit capable of working on the moon and Mars. Designing a suit is very difficult and often requires trade-offs between optimal human performance, cost, mass, and system complexity. To design the suit for optimal human performance, we need to first understand human performance in a non-earth planetary environment.

Our current understanding of human performance in reduced gravity environments (the moon or Mars) is limited to lunar observations, aided by studies from the Apollo program and other reduced gravity analogs [1-3] and from recent studies conducted at JSC using state-of-the-art reduced gravity simulators. This study will look at ambulation in our most recent reduced gravity simulator, the Active Response Gravity Offload System (ARGOS), compared to both the C-9 reduced gravity plane (gold standard) and ambulation in Earth gravity.

Methods: Subjects ambulated in reduced gravity analogs to obtain a baseline for human performance. Subjects were tested in lunar gravity (1.6 m/s^2) and Earth gravity (9.8 m/s^2) in minimal clothing. Subjects ambulated over ground at prescribed speeds on the ARGOS, but ambulated at a self-selected speed on the C-9 due to time limitations of the flight parabolas. Subjects on both systems were given time to acclimate to the gravity environment before data was collected. Nine subjects were tested in the ARGOS (6 males, 3 females, 79.5 ± 15.7 kg), while six subjects were tested on the C-9 (6 males, 78.8 ± 11.2 kg).

Data was collected with an optical motion capture system (Vicon, Oxford, UK) and custom and commercial force-platforms (AMTI, Watertown, MA, USA) and was analyzed using customized analysis scripts in BodyBuilder (Vicon, Oxford, UK) and MATLAB (MathWorks, Natick, MA, USA).

Results: In both reduced gravity environments, variation between subjects and within subjects increased compared to Earth gravity. Kinematics in the ARGOS at lunar gravity resembled earth gravity ambulation more closely than in the C-9 (see fig 1). Toe-off occurred 10% earlier in both reduced gravity environments compared to earth gravity, shortening the stance phase. Likewise, ankle, knee, and hip angles remained consistently flexed and had reduced peaks compared to earth gravity, especially on the C-9. Peak ground reaction force in lunar gravity were 0.4 ± 0.2 (mean ± SD, normalized to Earth body weight) on the ARGOS, but only 0.2 ± 0.1 on the C-9 plane.

Figure:
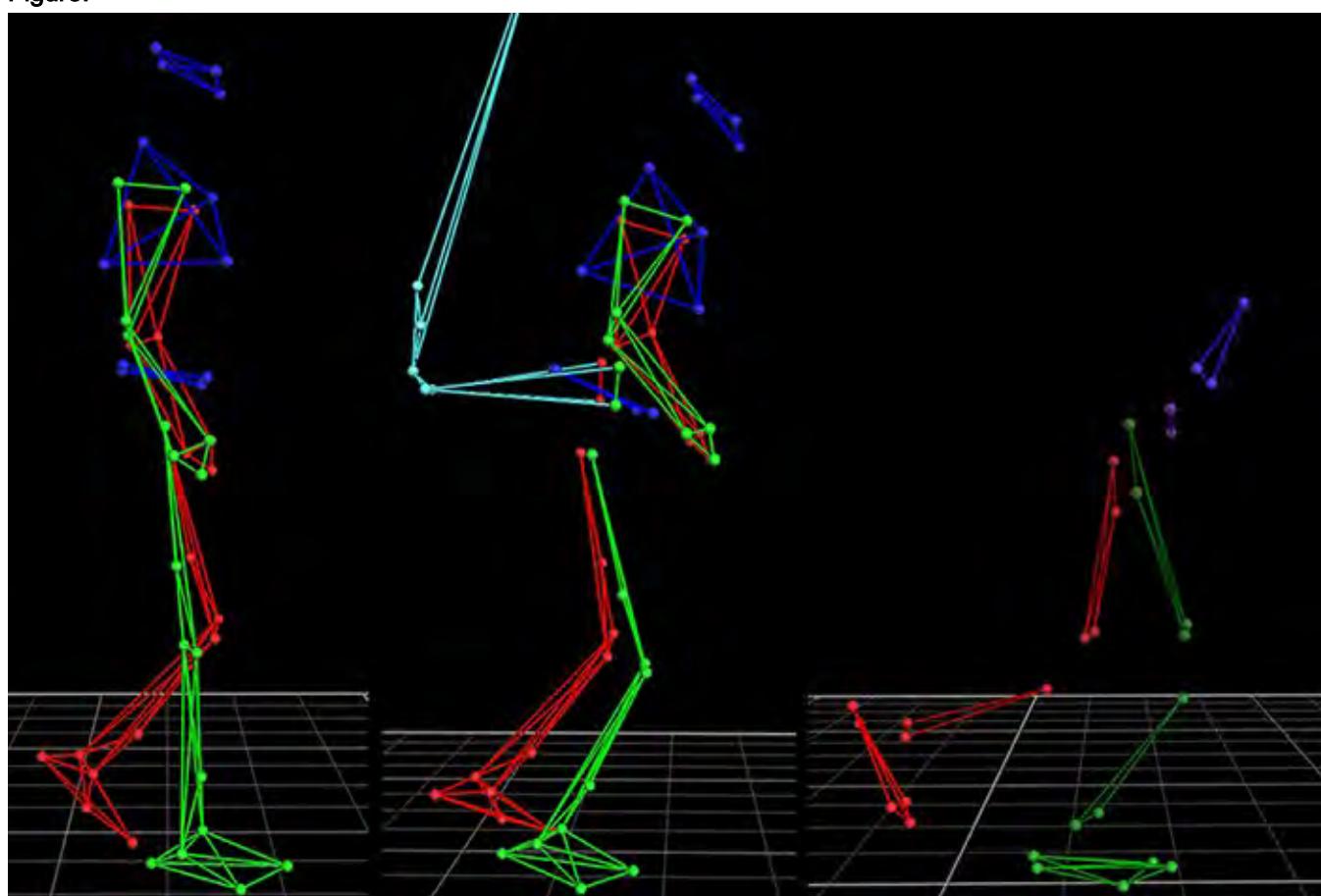
Caption: Figure 1. Over-ground ambulation shown in mid-stance for Earth gravity (left), lunar gravity (ARGOS), and lunar gravity (C-9 plane).

Conclusion: Kinematic and kinetic analysis demonstrated noteworthy differences between the tested reduced gravity environments and Earth gravity, as would be expected. Although most of the subjects chose a somewhat unique gait style as a result of learning to ambulate in a new gravity environment, all but two subjects in the ARGOS were consistent with keeping an Earth-like gait. The analysis showed a trend to change the ambulation style in an offloaded environment to a rolling-loping walk (resembling cross-country skiing) with increased swing time. The general uniformity of the modified ambulation styles would indicate that the subjects are using similar optimization strategies to maintain gait efficiencies. Benchmarking the differences between the ARGOS (and other offloading systems) and the C-9 reduced gravity plane are imperative to all future reduced gravity studies for NASA and will allow NASA to continue to use less expensive earth-bound reduced gravity simulators while maintaining the integrity of the study results and conclusions.

References: [1] Bartley et al., NASA CR-66120, Vol. IV, 1965.

[2] Griffin et al. J Appl Physiol, 86:383-390, 1999.

[3] Ivanenko et al., J Neurophysiol, 87:3070-3089, 2002.

Disclosure of Interest: None Declared

Motion Analysis

AS-0051

PREGNANCY-RELATED CHANGES IN CENTRE OF PRESSURE DURING GAIT

Jeanne Bertuit [1,*]Clara Leyh [2]Véronique Feipel [1]Marcel Rooze [1]

[1]Laboratory of Functional Anatomy, [2]Laboratory of Anatomy, Biomechanics and Organogenesis , Université Libre de Bruxelles, Brussels, Belgium

Introduction and Objectives: During pregnancy, physical and hormonal modifications occur. These changes can lead to an increase in postural instability and to a higher risk of falls during gait [5, 7]. To evaluate gait and balance of subjects, the centre of pressure (COP) is commonly used. The aim of this study was to describe the evolution and variability of COP parameters during the four last months of pregnancy and in post-partum. A comparison with nulliparous women was conducted in order to assess the changes during pregnancy.

Methods: We used an electronic walkway (GAITRite system). Fifty-eight pregnant women (four last months of pregnancy), 9 post-partum women and 23 healthy non-pregnant women participated in this study. Women performed three gait trials at each of three different speeds (preferred, slow and fast) following standardised instructions. The order of speeds was randomized. COP path was extracted for each stance phase. Excursion, velocity and length of COP path were computed and averaged. COP parameter variability was computed for each subject as the standard deviation over all sampled stance phases. Gait speed and stance phase duration (stance time) were also computed. COP characteristics for pregnant and non-pregnant participants were compared using ANOVA.

Results: Pregnancy was marked by a significantly slower gait speed (-20%) and increased stance time (+12%). During the four last months of gestation, COP parameters did not change significantly.

COP excursion decreased by 5% (p=0,003) for all speeds as compared to control group.

COP velocity differed significantly from that of the control group (p<0,001) with a decrease by 16% and from that of the post-partum group (p=0,022) by 3% along the postero-anterior (PA) axis.

For the medio-lateral (ML) axis pregnant women differed from the control group (p<0,001), with a decrease of 20%%, and from the post-partum group (p=0,030) of 9%.

COP inter-individual variability was different between pregnant women and the control group: variability was greater for the control group.

Conclusion: The COP parameters appear slightly influenced by pregnancy, which suggests that pregnant women establish very specific and individual strategies:

COP velocity along PA and ML axes was slower. A longer stance time indicates some difficulty in balance during gait [8]. The changes observed here are consistent with this statement and may aim at increasing the stability of pregnant women. During pregnancy foot length and width were reported to remain unchanged [1, 3]. This can explain the observation that AP COP displacements were not found to evolve during pregnancy in our study. Medio-lateral COP displacement also remained unchanged. Pregnant women compensate with an increase in step width to maintain or increase during gait [2]. We may think that pregnant women develop very specific strategies such as step widening, alteration of spine posture, and centre of gravity to maintain stable COP displacements during gait as compared to nulliparous women. These types

of strategies provide a stable and safe gait. The variability was in general larger for frontal plane COP parameters, confirming previous observations [6]. This suggests that pregnant women establish specific control strategies along the ML axis, such as an increase step width. Nevertheless, low variability in gait parameters, as found here, were previously shown to be correlated with greater stability and a lower risk of fall [4].

Table: Mean (SD) COP parameters at all speeds (slow, S; preferred, P; fast, F) during pregnancy, Post Partum (PP) and for Control Group (CG).

	Speed	Pregnancy	PP	CG	P value Groups	P value Velocity	P value Months
Excursion XY (m)	S	0.20 (0.02)	0.21 (0.01)	0.21 (0.02)	0.009	0.003	0.76
	P	0.19 (0.01)	0.20 (0.01)	0.20 (0.01)			
	F	0.19 (0.01)	0.20 (0.01)	0.20 (0.02)			
Velocity XY(m/s)	S	0.23 (0.03)	0.26 (0.04)	0.26 (0.03)	<0.001	<0.001	0.40
	P	0.28 (0.03)	0.29 (0.03)	0.33 (0.04)			
	F	0.34 (0.05)	0.38 (0.04)	0.40 (0.05)			
Length COP X (m)	S	0.16 (0.01)	0.17 (0.01)	0.16 (0.01)	0.15	<0.001	0.91
	P	0.16 (0.01)	0.17 (0.01)	0.16 (0.01)			
	F	0.19 (0.01)	0.18 (0.01)	0.17 (0.01)			
Width COP Y (m)	S	0.03 (0.01)	0.03 (0.00)	0.03 (0.00)	0.48	<0.001	0.44
	P	0.03 (0.01)	0.03 (0.00)	0.03 (0.00)			
	F	0.02 (0.01)	0.03 (0.00)	0.03 (0.01)			
Stance time (s)	S	0.90 (0.15)	0.81 (0.11)	0.84 (0.12)	<0.001	<0.001	0.64
	P	0.72 (0.10)	0.69 (0.06)	0.63 (0.06)			
	F	0.58 (0.07)	0.54 (0.05)	0.51 (0.05)			

Caption: Mean (SD) COP parameters at all speeds (slow, S; preferred, P; fast, F) during pregnancy, Post Partum (PP) and for Control Group (CG).

References: [1] Alvarez et al., J Bone Joint Surg Am, 70: 271–274, 1988.

[2] Bertuit et al., Acta Bioeng Biomech, in press, 2014.

[3] Bird et al., J Am Podiatr Med Assoc, 89: 405–409, 1999.

[4] Dingwell et al., J Biomech, 39: 444–452, 2006.

[5] Dumas et al., Clin Biomech, 10: 98-103, 1995.

[6] Lymbery et al., J Am Podiatr Med Assoc, 95: 247–253, 2005.

[7] McCrory et al., J Biomech, 43: 2434–2439, 2010.

[8] Nyska et al., Isr. J. Med. Sci, 33: 139–146, 1997.

Disclosure of Interest: None Declared

Motion Analysis

AS-0052

QUANTIFYING VARUS AND VALGUS THRUST IN INDIVIDUALS WITH SEVERE KNEE OSTEOARTHRITIS

Lauren Sosdian [1,*] Rana Hinman [1] Tim Wrigley [1] Kade Paterson [1] Peter Choong [2] Michelle Dowsey [2] Kim Bennell [1]

[1] Department of Physiotherapy, The University of Melbourne, [2] St. Vincent's Hospital, Melbourne, Australia

Introduction and Objectives: Varus and valgus thrust are of interest in knee osteoarthritis (OA) as they indicate dynamic instability and varus thrust has been associated with an increased risk of OA progression (1). They have been previously defined as the visualized dynamic bowing-out/bowing in of the knee (1, 2), or the abrupt worsening of existing varus/valgus during the weight bearing phase of walking. While varus thrust has generally been assessed using visual observation, only one study has attempted to quantify varus thrust using 3-dimensional gait analysis and measured the change between the varus angle at heelstrike to the peak varus angle (3). However, this measurement did not examine valgus thrust, or any movements that might occur before the peak knee varus angle. Another study has related visual varus thrust to peak knee varus angle and peak knee angular velocity (4), but did not quantify thrust or consider valgus thrust. Other measurement parameters that quantify thrust need to be investigated.

The aims of this study using 3-D gait analysis were to 1) determine the prevalence of varus and valgus thrust in a severe knee OA population compared to a healthy, asymptomatic control group and 2) quantify varus and valgus thrust and compare frontal plane dynamic movement quantitative parameters between the OA and control groups.

Methods: 35 patients with severe knee OA (46% M 54% F, mean (SD), age = 69.9 (7.7) years, BMI = 30.7 (4.0) kg/m2) awaiting total knee joint replacement and 31 healthy control participants (35% M 65% F, mean (SD), age = 59.7 (6.0) years, BMI = 24.9 (2.5) kg/m2) were recruited and underwent 3-dimensional gait analysis. Kinematic data (120 Hz) were acquired using a Vicon motion capture system (Vicon, Oxford, UK) and Nexus software with 12 MX cameras. A custom seven-segment, marker-triad-based lower limb direct kinematics model written in BodyBuilder (Vicon, Oxford, UK) was used (5). Knee frontal plane dynamic motion variables of interest included: overall, early, and mid-stance peak knee varus Cardan angles, maximum and minimum knee angular velocities, and maximum thrust (varus and valgus thrusts were labelled as positive and negative, respectively) and absolute value of the maximum thrust during stance loading phase. Thrust was extracted as the maximum angular excursion of the first three frontal plane knee movements within stance phase in the varus and valgus directions (Figure 1). These varus or valgus movements were classified as thrusts if the maximum or minimum knee angular velocities occurred at the same time. Prevalence of thrust between groups was compared using Chi square tests while student t-tests and Kruskal-Wallis tests were used to compare normally and non-normally distributed frontal plane parameters between groups. OA and control participants were then divided into varus and valgus groups for further analysis based on the direction of their maximum thrust.

Results: There was no difference in the prevalence of varus and valgus thrust between groups with 21 (70%) and 13 (30%) of the OA groups having a maximum thrust in the varus and valgus direction respectively compared with 16 (52%) and 15 (48%) of the control group (p>0.05).The minimum knee angular velocity and the absolute value of the maximum thrust were both significantly higher in controls when compared to the OA group. The same differences remained when comparing the varus thrust OA group to the varus thrust control group. The OA varus thrust group also had a higher varus

angle in early and mid-stance. No significant differences were found between groups when comparing the valgus thrust OA and valgus thrust control groups.

Figure:
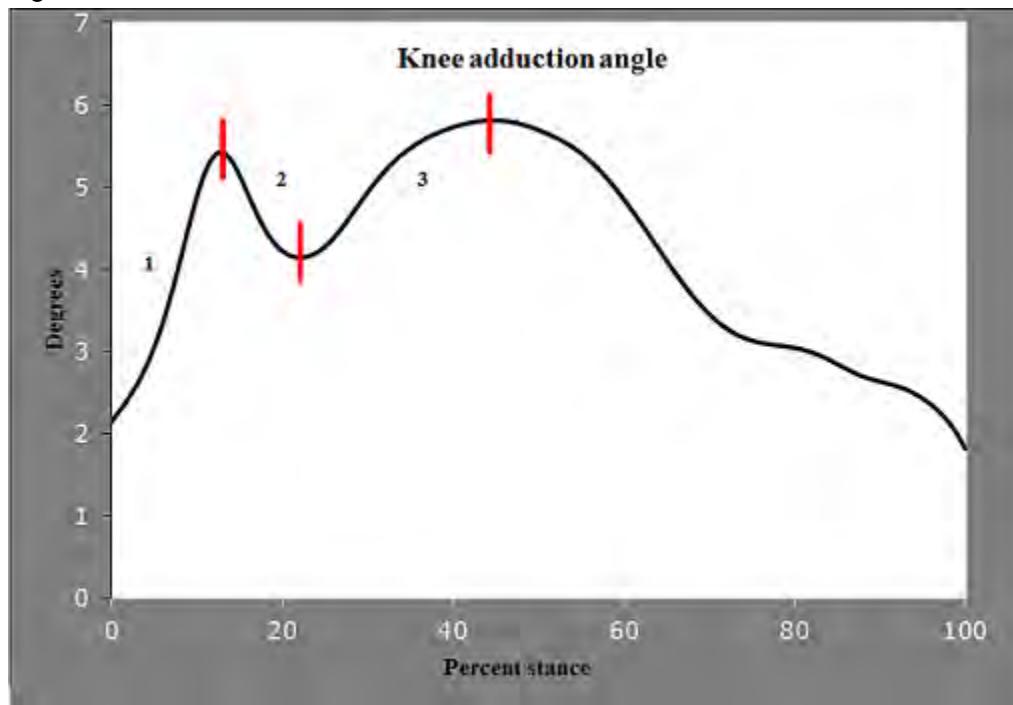
Caption: Example of first three thrusts

Conclusion: This study introduces a new method that quantifies both varus and valgus thrust. It is the first to compare differences in thrust and frontal plane dynamic motion variables in individuals with severe OA and healthy controls. Although no difference was found in the prevalence of varus and/or valgus thrust between OA and control groups, the control group demonstrated a larger thrust magnitude, likely due to a faster walking speed. The OA varus thrust group walked with a higher varus knee angle in early and mid-stance than the controls with a varus thrust. No significant differences were found between OA and control valgus thrust groups, indicating that valgus thrust may not have as much effect on frontal plane dynamic motion variables. Future work in this cohort includes investigation of the effect of a total knee replacement on these variables.

References: [1] Chang A, et al. 2004;50(12):3897-903.

[2] Chang A, et al. Arthritis and Rheumatism. 2010;62(5):1403-11.

[3] Kuroyanagi Y, et al. The Knee. 2012;19(2):130-4.

[4] Chang AH, et al. Osteoarthritis and Cartilage / OARS, Osteoarthritis Research Society. 2013;21(11):1668-73.

[5] Besier TF, et al. Journal of Biomechanics. 2003;36(8):1159-68.

Disclosure of Interest: None Declared

KINEMATIC AND MUSCULAR CHANGES IN THE GAIT PATTERN DURING CROSS-SLOPE WALKING WITH MINIMAL SHOES AND BAREFOOT

Lea Nösberger [1,2,*] Anna Estermann [1,2] Lukas Stammler [2] Beat Göpfert [3,4]

[1]Health Division, Bern University of Applied Sciences, Bern, [2]BZG, Bildungszentrum Gesundheit Basel-Stadt, Münchenstein, [3]Center of Biomechanics, University of Basel, [4]Laboratory for Movement Analysis Basel, Children's University Hospital Basel (UKBB) Basel, Basel, Switzerland

Introduction and Objectives: Walking on cross-sloped surfaces occurs often in our daily activity. Very little is known about the changes in the movement and muscular activation pattern wearing different shoes. The goal of this study was to analyse the changes in the kinematics and the wavelet-transformed surface-electromyogram (WT-EMG) while overground walking on flat and cross-sloped surface within 2 footwear conditions: barefoot and minimal shoes (Aapa, Feelmax, Finland).

Methods: A whole body 3D-gait-analysis (Vicon, 12 Cameras T20, 240Hz) with a synchronous EMG (Myon, 2400Hz) of the following right leg muscles was done: Tibialis anterior (TA), Peroneus longus (PL), Gastrocnemius medialis (GM) and lateralis (GL), Vastus medialis (VM) and lateralis (VL), Rectus femoris (RF), Semitendinosus (ST), Biceps femoris (BF). 10 subjects (f, 22-25y) walked at a self-selected speed on flat and on a cross-sloped surface (6°). 10 trials of each condition and surface were measured: flat (F), cross-slope up-side-leg (US), cross-slope down-side-leg (DS). The time was normalised over a gait-cycle, the averaged kinematic data and the normalized WT-EMG-Total-Intensity (I_{tot}) was analyzed within a gait-cycle for each subject and overall subjects while walking under different conditions.

Results: Around 26 gait-cycles were collected per subject and footwear condition.

The average knee flexion is significantly 3° to 4° higher for the minimal shoes compared to barefoot. Furthermore, the up-side-leg showed the highest flexion in the ankle, knee and hip joint while the down-side-leg had the lowest flexion in general. During the stance phase no significant changes occurred in the flexion angles barefoot vs. with shoes, but variations were seen between the surface conditions. Additionally, the down-side-foot had in the terminal stance and swing phase a significant lower internal rotation than up-side-foot independent of the footwear condition. In the frontal plane occurred a significant higher lateral pelvis tilt barefoot vs. with shoes on the cross-slope, but not in the thorax.

The averaged I_{totMAX} overall subjects showed for all muscles a time shift during the stance phase between the three surface conditions within the same footwear condition and a more pronounced time shift between the footwear conditions. Additionally the shape of I_{totMAX} changed for e.g. VL in the loading response phase from barefoot flat and down-side-leg with a double-peak to single-peak with shoes (A, Fig.1a) or the TA in the early swing phase from a sharper to more rounded peak (B, Fig.1b).

Figure:

Fig. 1a) and Fig. 1b): I_tot [mV²] plotted against Gait cycle [%]. Legend: TA right barefoot, flat; TA right barefoot, US; TA right barefoot, DS; TA right minimal shoe, flat; TA right minimal shoe, US; TA right minimal shoe, DS.
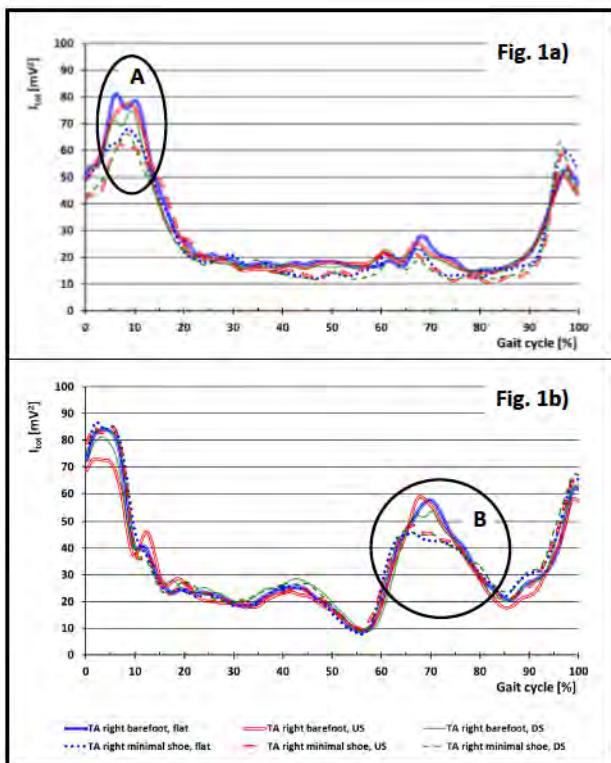
Conclusion: The results show a kind of parallel shift in the kinematic movement pattern between the different conditions with an increased range of motion with the minimal-shoe. The changes in the angular values are small but are reliable, because the measurements for all conditions were taken in one session. Only the markers on the foot had to be new placed between the two footwear conditions. The increased range of motion with the minimal shoes might be related to a slightly bigger size and different shape of the foot. Therefore it can be expected that the shape and design of the shoe has to be considered as a substantial factor in changing the loading conditions. They may alter the "preferred movement path" [1].The I_{tot}-patterns of the different muscles show often a two-dimensional shift between the different conditions, once in time and another shift in the intensity. The overall intensity changes are more depending on the footwear as on the surface conditions. The effect of the surface is more seen in anatomical function of the muscles. Like muscles located on the lateral side of the loading axis have a higher activity in the up-side-leg condition while the medial ones are more active in the down-side-leg. The temporal variation might also be linked to slightly different foot size and shape within the different setups. These temporal adaptions may be needed to balance and adjust the small variation in the different loading conditions and may follow the preferred movement pattern [1].

Our results show that cross-slope walking influences the movement pattern in all joint axes and has a detectable effect on muscular balancing and interplay especially in the frontal plane. Therefore it would be interesting to measure the effect of cross-slope walking in subjects with a total joint replacement. In such a setup muscular adaptions are more difficult due to the changed proprioception in the joint.

References: 1: Nigg BM. Biomechanics of sport shoes. Topline Printing; 2010.

Disclosure of Interest: None Declared

Motion Analysis

AS-0054

THE INFLUENCE OF WALKING ON A SLOPED INCLINE AND DECLINE SURFACE ON LUMBAR-PELVIC COORDINATION: A DYNAMICAL SYSTEMS APPROACH

Robert Needham [1,*]Nachiappan Chockalingam [1]

[1]Sport & Exercise, Staffordshire University, Stoke-on-Trent, United Kingdom

Introduction and Objectives: Optoelectronic motion capture is widely used in the study of human gait. Normal activities of daily life regularly require individuals to walk on slopes at varying gradients, yet the investigation of gait has primarily focused on the analysis of walking over-ground on a level surface.

Recently, Gallagher et al. [1] investigated the effect of prolonged standing on a sloped surface on an individual's perception of LBP. Altered spinal posture from standing on a sloped surface was associated with a reduction in the perception of LBP. Therefore, an understanding of changes in spinal posture and to the coordinated interaction between the pelvis and lumbar spine during sloped waking could provide support for gait re-training and rehabilitation programs. Nevertheless, one study to date has provided 3D motion analysis of the lumbar region during incline slope walking [2]. Also, the influence of decline slope walking on lumbar motion is restricted to the sagittal plane [3].

Vector coding (VC) is a non-linear technique employed by dynamical systems theorists to quantify coordination and variability. Although non-linear techniques have been used for the purpose of understanding the differences in pelvis-trunk coordination in healthy individuals to those with LBP [4,5], information on lumbar-pelvic coordination during gait is limited to a single study [6].

Therefore, this study aimed to investigate pelvis and lumbar spine kinematics during incline and decline walking at various gradients by applying a modified VC technique to quantify lumbar-pelvic coordination.

Methods: Eight male participants with no history of musculoskeletal impairments participated in the study. Ethical Approval was sought and received from the University Research Ethics Committee. An eight camera motion capture system (VICON, UK) was used to collect pelvis and lumbar spine kinematic data [6] over five trials for each walking condition; level over-ground, incline (6° and 13°) and decline (6° and 13°). Data was processed using a low-pass Butterworth filter with a cut-off frequency of 6Hz and normalized for time to 100% of the gait cycle (GC). Angle–angle diagrams were created with the proximal oscillator (lumbar) on the horizontal axis and the distal oscillator (pelvis) on the vertical axis. A VC technique was applied to quantify lumbar-pelvic coordination and circular statistics calculated the mean coupling angle (CA) between trials and across all participants. The CA is the outcome measure of the VC technique and represents the vector orientation between two adjacent time points on an angle-angle diagram relative to the right horizontal [6]. Mean coupling angles were classified into one of four coordination patterns; in-phase pelvis, in-phase lumbar, anti-phase pelvis, anti-phase lumbar.

Results: Figure 1 represents the mean CA across all eight participants for level ground (LG), incline (6° and 13°) and decline (6° and 13°) walking and corresponds to frontal plane movement of the pelvis and lumbar spine. Between 0-5% of the GC, an anti-phase pelvis coordination pattern between all walking conditions is noted. The decline walking (DW) conditions follow a similar coordination pattern to LG walking up to 10% of the GC. Between 10 and 30% of the GC which

represents mid-stance for LG walking, there is an in-phase coordination between the two segments with the pelvis being the dominant segment. The same coordination pattern is shown for the incline walking (IW) conditions but unlike LG walking this in-phase pelvis phase extended until approximately 50% of the GC. Between 30-45% of the GC the CA orientation was approximately 270° which suggests pelvis dominancy with little contribution of the lumbar spine to relative movement. During the latter stages of the swing phase an in-phase coordination pattern is highlighted for the IW conditions, yet during walking on an incline of 6° the lumbar spine was the dominant segment in comparison to walking at an incline of 13° where pelvis dominancy was noted. During the swing phase, the DW walking conditions revealed an anti-phase coordination pattern similar to LG walking.

Figure:
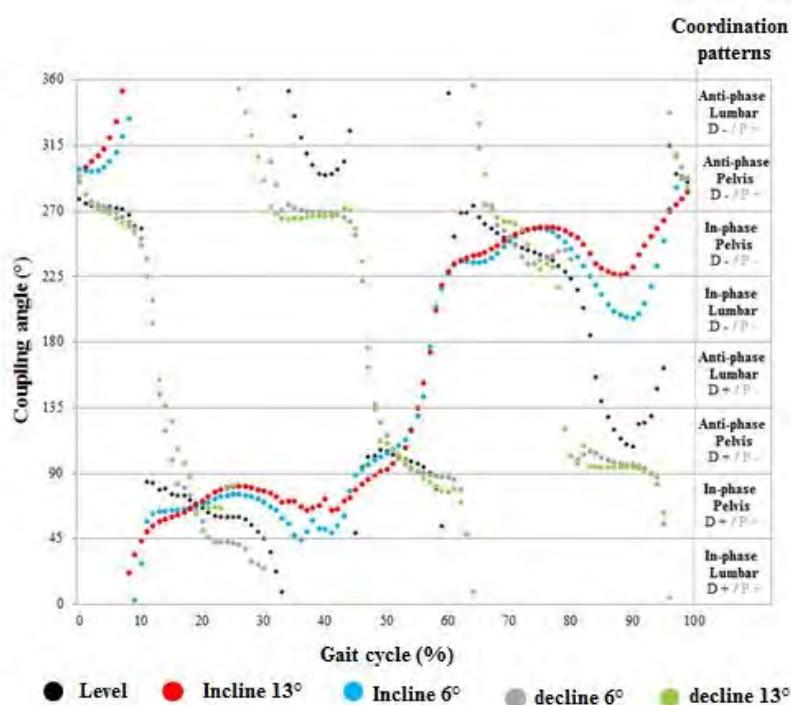
Caption: Mean coupling angle for all eight participants

Conclusion: The coordination patterns for LG walking corresponded to a previous investigation [6]. Although there is currently no research to compare the results regarding the incline and decline walking conditions, this abstracts presents novel data on pelvis and lumbar coordination in healthy young males during slope walking. This baseline information could be useful for future studies involving patients with lumbar–pelvic pathologies and other related clinical conditions.

References: 1.   Gallagher et al., *Gait Posture*, **3**;37(3):313–8, 2013.
2.   Vogt et al., *Gait Posture*, **9**(1):18–23, 1999.
3.   Levine et al., *J Athl Train*. **42**(1):29–34, 2007.
4.   Seay et al., *Spine*, **15**;36(16):E1070–9, 2013.
5.   Selles et al., *Clin Biomech*, **16**(3):175–81, 2001.
6.   Needham et al., *J Biomech*, **47**(5):1020–6, 2014.

Disclosure of Interest: None Declared

ASSESSMENT OF LIMPING DURING GAIT BY ACCELEROMETERS

Ligia C. S. Fonseca [1,*] Kathrin Koch [1] Jorge Gooding [1] Thomas Claus [2] Catherine Disselhorst-Klug [1]

[1]Department of Rehabilitation & Prevention Engineering, Institute of Applied Medical Engineering, Aachen, [2]Dr. Becker Rhein-Sieg-Klinik, Nümbrecht, Germany

Introduction and Objectives: Knee osteoarthrosis (OA) is a common chronic joint disease with cartilage loss that results to increased stiffness and joint deformity leading to pain and loss of physical function, subsequent in significant limitation in daily life activities and reduction in quality of life. The conventional therapy includes information, exercise, and weight loss and when necessary even a prescription of pain-reducing pharmacologic agents. It can be positive for many young patients, but with increasing age, cartilage repair becomes more complex and the outcome is less predictable, been necessary an arthroplasty and intensive rehabilitation after the surgery to minimize pain and postoperative limping severity. Although patients are able to walk in a normal pattern after this intensive rehabilitation, they fall back into their limping patterns unintentionally. Limping may be caused by general fatigue or pain. However, walking in a pathological movement pattern means additional stress to the already damaged tissues. The goal of this study is to present a portable, wearable assistance system which can be used autonomously and provides a direct feedback about the quality of the gait and occurrence of limping to the patient.

Methods: Triaxial-accelerometer based sensor unit was integrated into commercially patellar tendon straps and used in the limping leg of the patient. The unit measured the acceleration of the knee and transmitted the digital data wireless through an integrated ANT sender module. On the receiver's end, an iOS device equipped with an ANT dongle receives and processes the data for being able to evaluate the quality of the gait. To calculate the gait events, the signals of the three channels of the sensor were used. The gait is divided into two different phases: swing and stance. To detect that gait phases, the extraction of the characteristics events toe off, heel strike and toe strike is necessary. These events were represented by extrema in the acceleration signals and could be extracted. The acceleration in the sagittal plane provides the information about the toe off by the minimum values of the signal and about the heel strike by the maximum values of the signal (see Figure 1). In order to describe the quality of the gait several parameters (see Table 1) were calculated for each step from the measured signals. For this stage 15 healthy subjects were evaluated for the development of the Norm collective. Ten parameters were extracted and used for the development of a scale within 0-10 points used to classify the gait in four different categories: normal gait (NG≤2), light limping (LL= 3 to 5), strong limping (SL= 6 to 8) and very strong limping (VSL≥9). From each parameter the patient can have a score from 0 to 1 and in the end a simple addition was made to give a final result (see the example in Table 1). However, in order to minimize the effect of single outliers, as may be the case with a sudden change of direction while walking, the features of single steps were averaged every five seconds during gait.

Results: A sample of 10 patients aged 41 to 75 years (mean 59.8 ± 10.0) in rehabilitation after knee or hip replacement surgery were recruited for the measurements. They were asked to walk over a straight, 10 m-long path, four times, in a comfortable speed. The patients were evaluated by the portable system and by a physical therapist. The system classified

the patients using the parameters and the professionals should classify the gate from a visual analogue scale from 0 to 10 based in their own expertise. The system classified eight patients in the same category as a physical therapist evaluation. The professionals classified the two other patients as a normal gait but the system could detect a light limping. The mean score of the patients was 5,2 ± 0,78 points at the system and 4,6 ± 1.5 points evaluated by the physical therapist.

Figure:
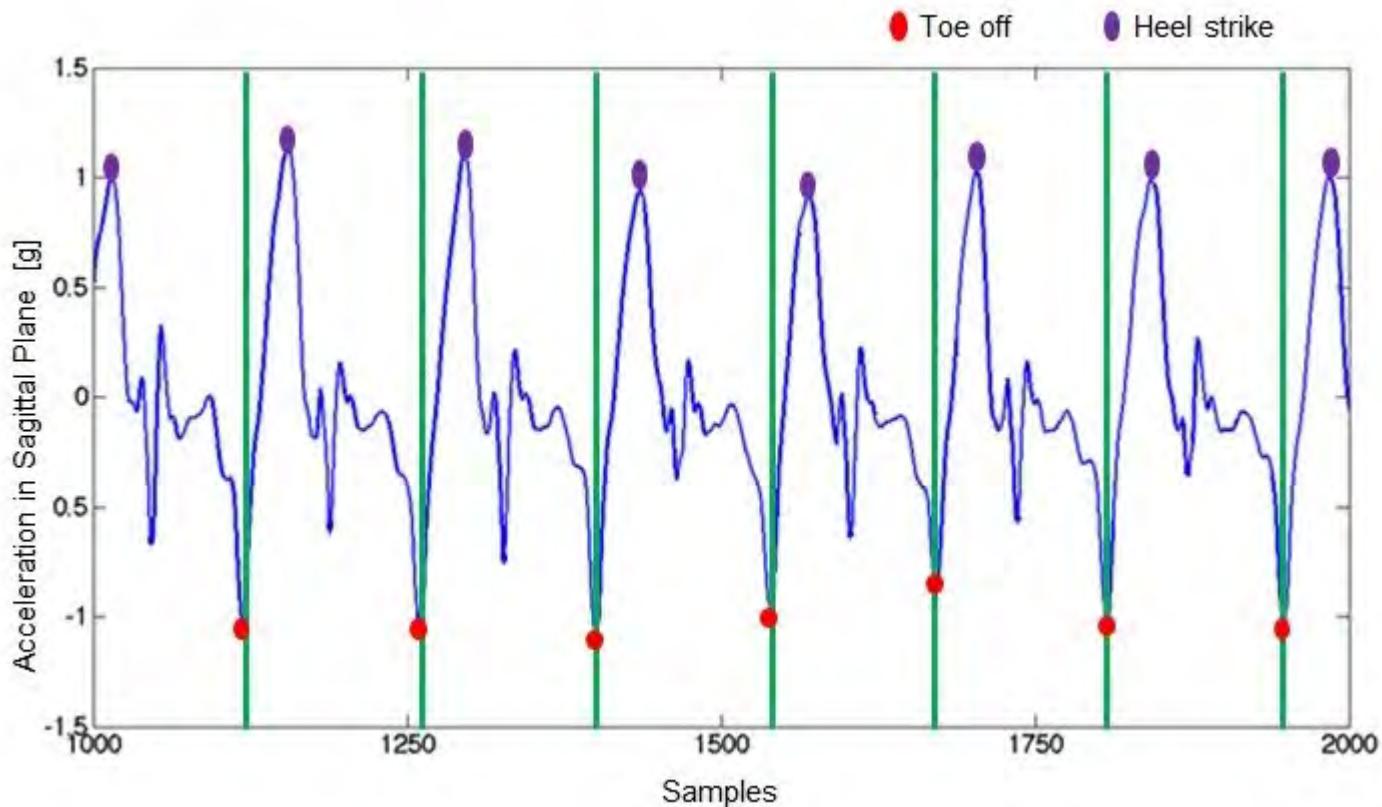
Caption: Figure 1: Detection of toe off and heel strike

Conclusion: The developed system demonstrated ability to quantify the quality of gait providing a valuable, easy to use tool for the objective assessment of gait during the rehabilitation. Additional tests series are being carried out to later quantify more precisely the gait quality, allowing not only the detection of pathological gait, but also providing valuable information regarding the severity of the abnormality, which should give insights into the effect of the rehabilitation phase in the clinic, as well in the residential setting, where the system can be used to provide a direct feedback to the patient regarding the quality of the gait in daily living situations.

Table:

Parameters	Example
Mean of slope	0
Negative values of slope	0
Positive area of swing phase	1
Ratio toe-off/toe-strike	0

Ratio toe-off/heel-strike	0
Ratio heel-strike/maximum	1
Ratio swing phase/stance phase	0
Cross correlation to Norm collective	0
Time outside the standard deviation	0
Area outside the standard deviation	1
	∑ 3

Caption: Table 1: Parameters for limping detection

Disclosure of Interest: None Declared

MUSCLE AND JOINT CONTACT LOADING DURING ASSISTED UPPER-EXTREMITY MOVEMENTS PERFORMED WITH A ROBOTIC EXOSKELETON

Wen Wu [1] Justin Fong [1] Denny Oetomo [1] David Lloyd [2] Thor Besier [3] Mark Halaki [4] Karen Ginn [5] Peter Lee [1] David Ackland [1,*]

[1] Mechanical Engineering, University of Melbourne, Parkville, [2] School of Allied Health Sciences, Griffith University, Gold Coast, Australia, [3] Auckland Bioengineering Institute, Auckland University, Auckland, New Zealand, [4] Faculty of Health Sciences, [5] Biomedical Sciences, School of Medical Sciences, University of Sydney, Sydney, Australia

Introduction and Objectives: Assistive technologies for stroke patients, including exoskeletons and robotic-assistive devices, are receiving increasing attention in neurorehabilitation as these strategies may complement physiotherapy, resulting in more efficient motor relearning and mobility both at home and in the clinic. Developing a strategy to evaluate neuromuscular control of upper limb movement will improve our ability to diagnose neuromuscular impairments, and aid in development of robot-assistive rehabilitation strategies. Since no non-invasive muscle force measurement strategies are available, computational simulations are widely used to infer muscle and joint function. The objective of this study was to use musculoskeletal modelling to quantify muscle and joint-contact loading during upper limb movement, and evaluate the influence of an assistive robotic exoskeleton on muscle and joint behaviour during simulated weightless motion.

Methods: Two healthy male adults, P1 (age 35 yrs, weight 82 kg) and P2 (age 24 yrs, weight 77kg), were recruited. Subjects were seated and asked to perform an upper-limb reaching task from an initial neutral position (30º shoulder abduction, 0º elbow flexion) to an extended reach position (90º shoulder flexion, 0º elbow flexion). Reaching tasks were performed at each subject's self-selected speed. Six repetitions of the tasks were performed synchronised to a metronome, while three-dimensional shoulder and elbow kinematics were recorded with a magnetic motion tracking system (G4TM, Polhemus, USA). The reaching task was then repeated while the subject was interfaced with a 6 degree-of-freedom robotic upper-limb exoskeleton (ArmeoPower, Hocoma, Switzerland) (Fig. 1A). The anatomical joint coordinate systems for the upper limb were aligned with those of the robotic exoskeleton. The reaching task was performed under two conditions: (1) 100% weightlessness, i.e., with the robotic exoskeleton compensating for entire mass of the upper extremity and its own weight and inertia; and (2) 0% weightlessness, i.e., with the robotic exoskeleton only compensating for its own weight and inertia. A musculoskeletal model describing 9 degrees of freedom of motion at the clavicle, scapula, humerus, radius and ulna was developed (Fig. 1B) (OpenSim, SimTK). The model was actuated by 35 Hill-type muscle-tendon units representing the major upper-limb muscle groups. Muscle-tendon parameters and muscle moment arms were taken from the literature [1, 2]. Anatomical shoulder and elbow joint torques were calculated using inverse dynamics. Torques applied by the robotic exoskeleton to the upper limb joints during weightless motion were obtained by subtracting the measured exoskeleton torques at 0% weightlessness from those at 100% weightlessness. The resultant net internal anatomical joint torques were then obtained by subtracting the torques applied to the subject's shoulder and elbow joints by the robotic exoskeleton from the anatomical torques calculated using inverse dynamics. Muscle and joint-contact forces were then calculated for the assisted and unassisted upper limb motions using static optimisation.

Results: There were no substantive differences in shoulder and elbow joint kinematics between the unassisted reaching task and the robotic-assisted reaching task. Robotic-assisted upper limb motion under simulated weightless conditions substantially affected each subject's muscle recruitment patterns. The middle deltoid muscle force was an average 81% smaller under simulated weightless conditions (Table 1). The infraspinatus and subscapularis muscle force was an average 47% and 55% smaller, respectively. The magnitude of the glenohumeral joint reaction force decreased by 42% under the robotic-assisted upper limb motions.

Figure:
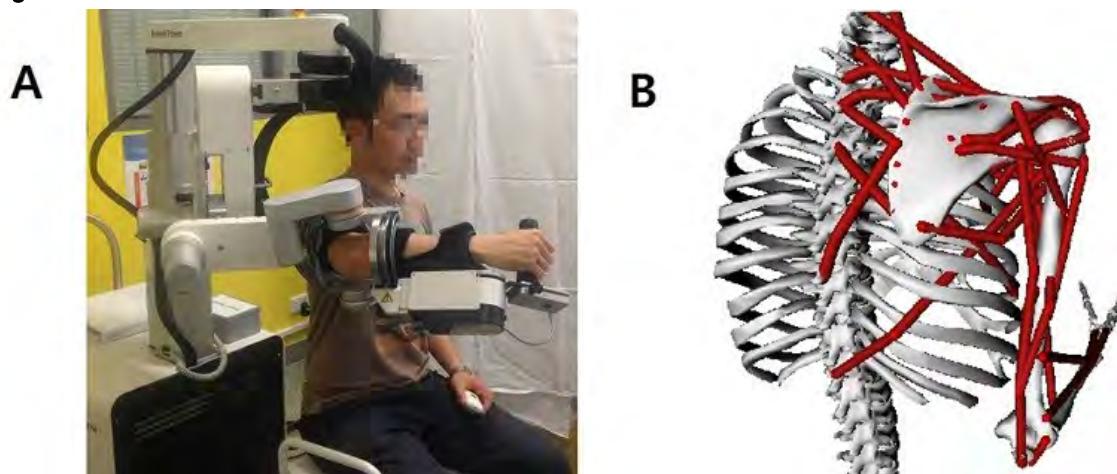
Caption: The ArmeoPower robotic-assistive rehabilitation device (A), and posterior view of the musculoskeletal upper extremity model (B)

Conclusion: The results of the present study demonstrate that a robotic-assistive upper extremity exoskeleton has the potential to significantly influence muscle and joint-contact load patterns at the shoulder. During weightless motion, finite deltoid muscle activity was still observed in the upper limb, most likely due to arm resistance against the robotic exoskeleton. The quantitative modelling framework in this study may be useful for targeted intervention in stroke patients using robotic assistive rehabilitation technology. Future studies will employ parameter-optimization approaches to evaluate muscle-tendon parameters, and electromyography-informed methods to derive muscle excitations.

Table:

	Subject P1		Subject P2	
	Unassisted	Assisted	Unassisted	Assisted
Deltoid	0.14	0.00	0.17	0.06
GHJF	0.40	0.27	0.33	0.15

Caption: Middle deltoid and glenohumeral joint force magnitude (GHJF) during unassisted motion and robotic assisted 'weightless' motion (units are Body Weight)

References: [1] Holzbaur KR, Murray WM, Delp SL, Annal Biomed Eng, 2005. 33(6) 829-840

[2] Ackland DC and Pandy MG, J Anat, 2008. 213(4) 383-390.

Disclosure of Interest: None Declared

ANALYSIS AND SIMULATION OF VARIOUS STEWART PLATFORM CONFIGURATIONS FOR LOWER LIMB REHABILITATION

Alireza Rastegarpanah [1,*] Mozafar Saadat [2] Hamid Rakhodaei [2]

[1]School of Mechanical Engineering, Doctoral researcher - University of Birmingham, [2]School of Mechanical Engineering, University of Birmingham, Birmingham, United Kingdom

Introduction and Objectives: The aim of physiotherapy by robots is to move paralyzed and disabled organs because of diseases such as cerebral apoplexy. Using the mobile platform under the patient's foot in order to create movement is a mechanism which is used in the rehabilitation of the ankle. In this mechanism, by programming the movement of the mobile platform, the entire foot or some parts of the foot are impelled to move. Parallel robots are closed loop mechanisms that have high mobility and accuracy [1].

With respect to different arrangements of the joints on platforms and the shape of the platforms, there are different structures with varying levels of stability. In this study three platforms of different structures were investigated; one of them is the PSRH structure (a platform with semi-regular hexagons); all of its base joints and all its mobile joints are coplanar and the distance between the actuators is so much greater than in other structures. Another structure is that of the TSSM (Triangular simplified symmetric manipulator); the mobile platform in this structure is triangular and the joints of the upper platform are close to each other. The last configuration, called the MSSM (Minimal simplified symmetric manipulator), combines the TSSM with a 3-3 platform, and its mobile and fixed platforms have a similar triangular shape [2].

According to the performed gait analysis in the West Midland rehabilitation centre, the foot trajectories of healthy volunteers were analysed during a gait cycle and this trajectory was used as a desired motion for movement of Stewart platform. To choose the most suitably structured Stewart platform for rehabilitation applications, one must consider the anatomy of the ankle and the stability of the three different Stewart platform structures, as analyzed by Solidworks software. Next, the kinematic of the Stewart platform for all configurations was considered and on this basis the maximum workspace of the selected robot was examined.

Methods: To define an accurate path motion for rehabilitation of ankle, gait analysis was performed in West Midland Rehabilitation Centre (WMRC), UK. Twenty able-bodied participated in this experiment with age (year) of 24.34±4.83, weight (kg) of 73.41±5.2, height (cm) of 172.74±4.2. Laboratory was equipped by 16 Vicon cameras, two digital cameras and a Kistler force plate. After anthropometric measurements, reflective markers were attached to the lower limbs based on Oxford foot model. Barefoot participants were asked to walk along the walkway in self-speed and for each participant 6 trials were recorded. All three structures were designed and analyzed statically in the home position, while the maximum ground reaction force was measured and applied to the end-effector. Finally, length of actuators and workspace of robot during trajectory were calculated based on kinematics of hexapod.

Results: Based on gait analysis, the mean value maximum ground reaction force Maximum force of 603.4 N was exerted on the end effector and the maximum displacement and maximum stress for each structure were measured. By exerting a force of 603.4 N, the PSRHs structure had the maximum displacement of 6.628× mm and maximum stress of 21 (Mpa).

The primary stress analysis shows that the maximum displacement for MSSM and TSSM were 5.84× mm and 2.21× mm. PSRH had the highest factor of safety (1.31) and stiffness 26619 (N/mm) of all structures and these results lead to the choice the PSRH structure as the most stable one for manufacturing application.

Figure:
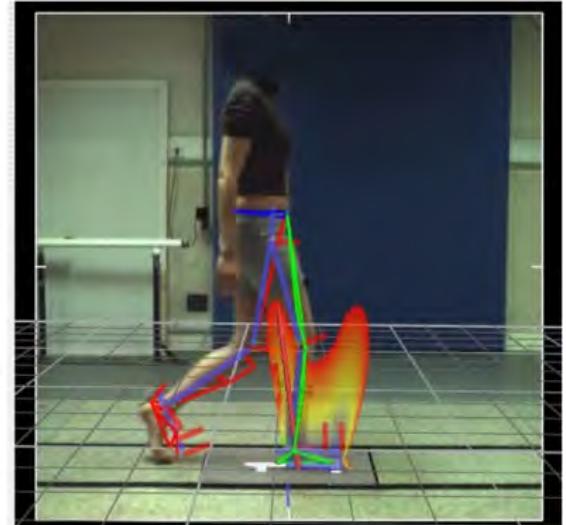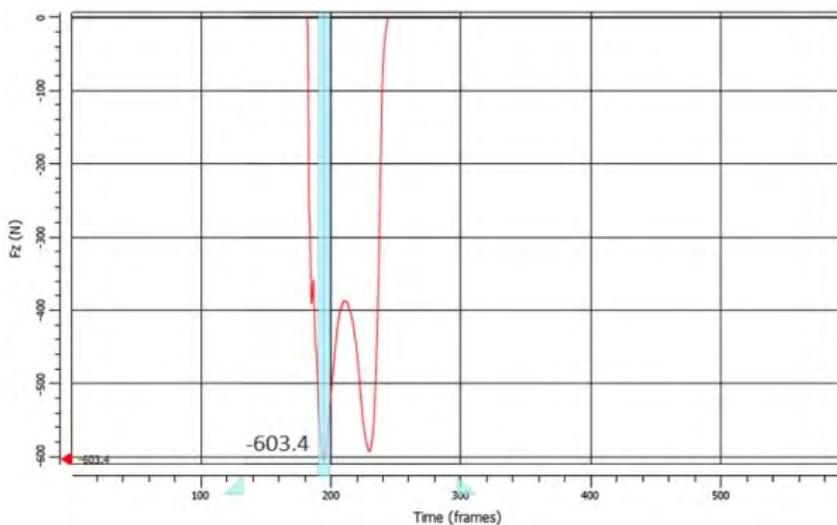
Caption: The profile of ground reaction force

Conclusion: Different configurations of parallel robot have been modelled and with respect to FEA analysis, their stability compared with each other. Platform of semi regular hexagons showed more stability in compare with other structures and it was found that the stability of different structures completely depends on the position of the joints and actuators and the shape of the platforms. With respect to kinematic analysis and gait analysis, the motion of ankle during a gait cycle was defined as a rehabilitation exercise and based on kinematic analysis and defined path motion, the workspace of robot was calculated. With respect to FEA analysis, Kinematic analysis and range of motion of lower limb`s joints, it was found that PSRH structure is a suitable choice for rehabilitation purposes.

References: [1]Speich. J. E and Rosen. J, Medical robotics, Marcel Dekker: New York, 983–993,2004.

[2]Rakhodaei. H, Saadat. M, Rastegarpanah. A, Motion Simulation of a Hybrid Parallel Robot for Ankle Rehabilitation, Proceedings of the ASME 12th Conference on Engineering System and Analysis, Jun 25-27, 2014, Copenhagen, Denmark.

Disclosure of Interest: None Declared

Assistive Technology

AS-0058

REHABILITATION ROBOT PATH PLANNING AND TRACKING USING KINECT

Alireza Rastegarpanah [1,*]Mozafar Saadat [2]Jack Foxcroft [2]Guanqi Zhang [2]

[1]School of Mechanical Engineering, Doctoral researcher - University of Birmingham, [2]School of Mechanical Engineering, University of Birmingham, Birmingham, United Kingdom

Introduction and Objectives: The accuracy position of a leg rehabilitation robot needs to be detected by independent measurement system to help reduce possible errors of controller and optimize the tracking of robot. Due to cheap price and high accuracy of kinect camera as a depth camera device, it uses in different applications such as robotics, gait assessment, gesture tracking and Image data capturing [1]. In this study, ability of utilizing of 6 degree of freedom Hexapod, consisting of a moving platform supported by six actuators, was investigated during a rehabilitation exercise

Methods: Based on Gait analysis, the path motion of walking for 30 healthy subjects have been analysed and extracted .Then, a Hexapod with universal joints at both ends was used in this experiment and three different colour markers were attached on moving platform and skeleton model of leg. As it shows in figure1, Kinect camera was placed on sagittal plane of Hexapod to detect the movements of end-effector and skeleton model during a gait cycle of skeleton model based on obtained trajectory of right leg during a gait cycle. Based on control system of Hexapod, mentioned movement performed and position error of Kinect camera was calculated. The principle of detection of pixel position and distinguishing different color markers have been addressed clearly and Clustering algorithm method was utilized to calculate the center position of target color. Primary colors; green, red and blue were detected by kinect camera at each pixel and they were translated into binary numbers. To find the minimum diameter of markers which can be detected by Kinect, different marker diameters have been tested ranging from 8mm-30mm .

Results: The minimum diameter of 12mm marker was detected by the camera and based on obtained results, the minimum diameter of 12mm detected by Kinect and the position error of 1.65mm, 1.63mm and 1.16 mm were observed, during movement of end-effector in X, Y and Z axis respectively.

Figure:
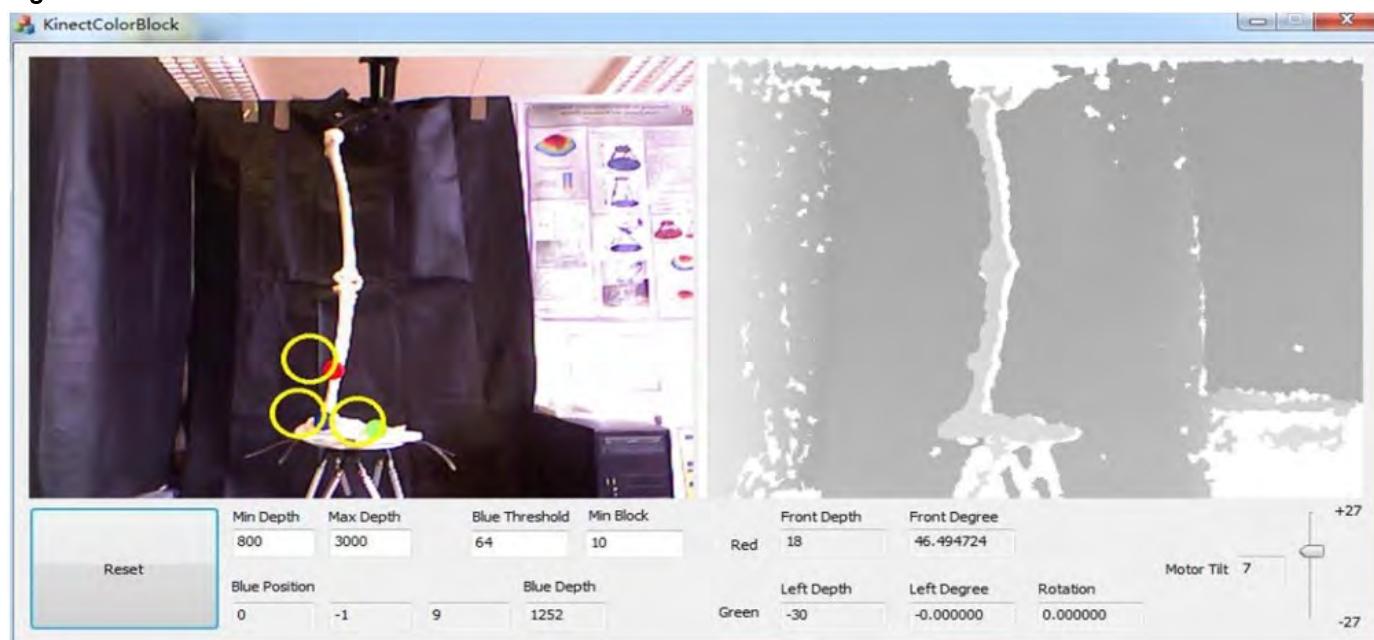
Caption: Kinect camera in sagittal plane

Conclusion: Kinect measurement system detected the robot plate's positions with an average error around 2mm for every 100ms. The advantages of this system are the low price, simple installation. In particularly, it can be used for detect under 6 freedoms machine's position, the output data of this system, as a feedback value, can be used to check the condition of this machine to reduce the position error. According to accuracy, cheap price and easy installation of Kinect, it can be used for path tracking and position detection of robots in different applications.

References: [1] R. Henselmans, L.A. Cacace, G.F.Y. Kramer, P.C.J.N. Rosielle, M. Steinbuch, The NANOMEFOS non-contact measurement machine for freeform optics. Precision Engineering. 1 (35), p607– 624,2011.

Disclosure of Interest: None Declared

Assistive Technology

AS-0059

EVALUATION OF INDIVIDUAL MOVEMENT PERFORMANCE BASED ON MOVEMENT ANALYSIS USING INERTIAL SENSORS

Catheriene Disselhorst-Klug [1,*]Michael Hennes [1]

[1]Rehabilitation and Prevention Engineering, Applied Medical Engineering, RWTH Aachen University, Aachen, Germany

Introduction and Objectives: Due to the growing number of patients with musculoskeletal and neurological disorders, individualized physiotherapeutic rehabilitation becomes increasingly relevant. The challenges involved can only be solved, if the patients will do their exercises autonomously. Different assistive systems have been developed during the last years encouraging the patients to do self-motivated training. However, most of them permit compensation movements if the patients have problems in executing the movement tasks. Consequently, patients' movements have to be monitored during the exercise to detect harmful compensation movements and to give individual feedback. Conventional movement analysis systems are suitable but in general too complex to be used autonomously by the patient and available more elementary systems, like e.g. the Microsoft Kinect, are frequently not applicable in pathological movements.

The aim of this paper is to introduce a method based on inertial sensors, which allows the detection as well as a patient-tailored evaluation of the executed movements.

Methods: Since in some disorders additional masses put on the patients' body influence the individual movement performance, very small (2x2x0.5 mm) and lightweight (5 g) inertial measurement units (IMU) have been developed. Each IMU consists of a 3D accelerometer, a 3D magnetomer and a 3D gyroscope (figure 1). One IMU is mounted on every segment of the joint chain (e.g. scapula, upper arm, forearm and hand) to detect the movement of the patient.

Since noise is a general problem when using IMUs, the orientation of each body segment in the lab-coordinate system has been estimated by an unscented Kalman filter and initially represented in quaternions. Afterwards the quaternions have been transformed to Euler angles representing the orientation of each body segment. The variations of these Euler angles with time are used for the following evaluation of the performed movement.

To evaluate the exercise performed autonomously by the patient a reference movement has been detected during a so called teaching phase, which respects the needs and potentials of each individual patient. Therefore, the physiotherapist guides the patient to perform the desired movement while the IMUs record the Euler angles as a function of time.

The time course of the Euler angles of the teaching phase and the time course of the Euler angles of each repetition of the exercise are compared to each other by using a set of features describing the difference between nominal (teaching) and actual (exercise) values. Fuzzy logic which represents the individual movement performance by a number between 0 (bad movement performance) and 10 (perfect movement performance) has been used to evaluate the performed exercise on the basis of the features.

Results: To demonstrate the feasibility of the approach, five healthy subjects and one subject suffering from a hemiparesis after stroke were asked to repetitively perform a "hand from knee to mouth" movement. Movement performance during each repetition has been evaluated by the introduced method. Figure 1 shows exemplarily the movement behavior of the patient. Decreasing movement performance can be found after 7 repetition associated with compensation movements.

Figure:
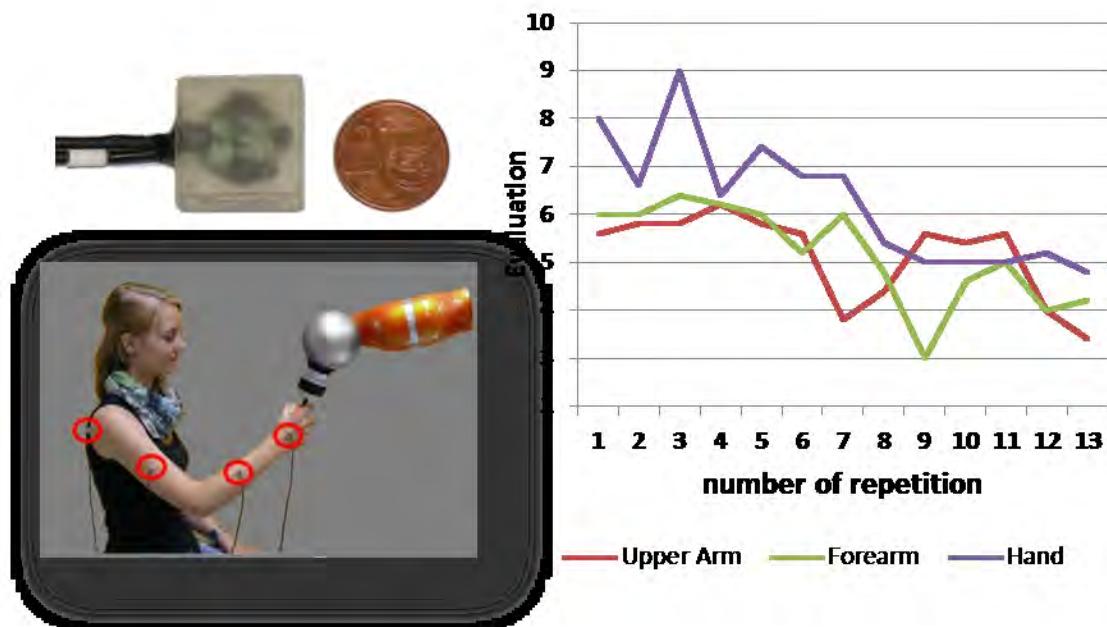
Conclusion: Inertial sensors are suitable to evaluate the performance of an exercise executed autonomously by the patient. Using an unscented Kalman filter the orientation of the body segments can be expressed in Euler angles. Based on these Euler angles an evaluation of movement performance becomes possible when using fuzzy logic. This information can be used to detect compensational movements and to give feedback to the patients during self-motivated training.

Disclosure of Interest: None Declared

Assistive Technology

AS-0060

FALL RISK MONITORING: FROM LABORATORY TO PORTABLE DEVICE, INFLUENCE OF SAMPLING FREQUENCY.

Paola Tamburini [1,*]Rita Stagni [1]

[1]DEI - Department of Electrical, Electronic and Information Engineering, University of Bologna, Bologna, Italy

Introduction and Objectives: Falls represent a major community and public health problem, with large clinical and economic consequences. The understanding of locomotors stability is a critical issue in clinical assessment procedures. Clinicians use clinical rating scales for fall risk assessment; but this approach highly relies on the clinician's subjective judgment [1].

Several variability and stability measures were proposed in the literature for the subject specific assessment of fall risk. Although promising, the assessment of fall risk without any indication of the subject specific factors leading to it, can not provide indication for the design of any effective clinical intervention for its effective reduction. Recent work [2,3] demonstrated that clustering appropriate selected indexes can provide indication regarding the specific subject alterations increasing fall risk. The effective exploitation of this approach is meant in its implementation on a portable device for the continuous monitoring of subjects at risk, either pathological (e.g. stroke subjects) or elderly subjects. The ideal device to maximise the exploitation, and subject acceptance is a mobile phone. Although the IMUs mounted on standard smart phones have nothing to envy to other commercially available devices, but sampling frequency at 100 or 200 Hz is not compatible with the computational characteristics. The influence of reduced sampling frequency on the assessment of variability and stability indexes used for the monitoring must be assessed, and this is the aim of the present work. This is an essential step for bringing the method from the laboratory to real practice without loosing the performance.

Methods: Ten healthy young subjects, 7 males and 3 females (28+-3 years, 174+-11 cm, 67+-13 kg), participated to the study. They performed a straight walking at self selected speed on 250 m long dead-end road wearing 2 tri-axial accelerometers, one located at the level of the fifth lumbar vertebra and one on the right ankle.

Right heel strike instants were obtained from the angular velocity measured by the sensor on the ankle with wavelet analysis based method [4] and stride time was calculated accordingly.

The first and last three strides were removed in order to exclude gait initiation-termination phase.

Acceleration and angular velocity in vertical (V), medio-lateral (ML) and antero-posterior (AP) were acquired with sample frequency of 128 Hz. Eleven gait variability and stability measures (Standard Deviation (SD), Coefficient of Variation (CV), Nonstationary index (NI), Inconsistency of Variance (IV), Poincaré Plots (PSD1/PSD2), Maximum Floquet Multipliers (maxFM), short/long-term Lyapunov exponents (sLE/lLE), Harmonic Ratio (HR), Index of Harmonicity (IH), Multiscale Entropy (MSE) and Recurrence Quantification Analysis (RQA)) were calculated on stride time and trunk acceleration data during gait. The two latter measures produce 6 and 5 sub-measures respectively, based on the time scale in MSE or based on the feature of the recurrence plot that was analysed in RQA (recurrence rate (rr), determinism (det), average length of diagonal lines (avg), maximum length of diagonal lines (max), divergence (div)).

Each measure was calculated for the acquired signal (at 128 Hz) and for other two signals obtained from the original one by under-sampling at 64 and 32 Hz and also for anterior-posterior (AP), medio-lateral (ML) and vertical (V) acceleration

directions. The obtained measures were testing with gaussianity test (Kolmogorov-Smirnov test) in such way was possible performed the right statistical analysis: ANOVA test with a p-value of 5%.

The statistical analysis compares the obtained measures by original signal (the reference) with the measures obtained by under-sampling from the original one.

Results: CV, PSD2, HR, IH, ILE, maxFM, rr and MSE for the time shifting 5 and 6 didn't show significantly differences varying the sampling frequency.

SD, sLE, det, avg, max, div and MSE for time shifting varying between 1 and 4 shown significantly differences varying the sampling frequency.

NI, IV and PSD1 shown significantly differences only for the sampling frequency at 32 Hz.

Conclusion: The results show that the measures calculated in the frequency domain (HR and IH) and those that describe the system as a whole (maxFM and lLE) were not affected by the reduction of sampling frequency, supporting the maintenance of the performance of the method when implemented on a portable device.

MSE can be affected by reduction of sampling frequency, depending on the amplitude of selected time shift: the higher the time shift the least the measure is sensitive to frequency changes.

References: [1] Hamacher D et al., J R Soc Interface 8(65), 1682-1698, 2011.

[2] Riva et al., conference proceeding SIAMOC-ESMAC 36, 2014.

[3] Riva et al., conference proceeding SIAMOC-ESMAC 146, 2014.

[4] Aminian et al., J. Biomech 35:689-699, 2001.

Disclosure of Interest: None Declared

Sport

AS-0061

BIOMECHANICS ANALYSIS OF BASEBALL PITCHING: COMPARISON AMONG STANDARD, WEIGHTER AND LIGHTER BALLS

Simone Ciacci [1] Valerio Trentini [2] Andrea Giovanardi [2] Silvia Fantozzi [3,*]

[1]Biomedical and Neuromotor Sciences, [2]School of Pharmacy, Biotechnology and Sport Science, [3]Electric, Electronic and Information Engineering, University of Bologna, Bologna, Italy

Introduction and Objectives: The fundamental issues for an efficient throw are: the precision, the effect and the velocity of release of the ball (1,2). The latter can be improved, without modifying the precision, by both refining the technique of the motor task and increasing the production of power (1). Throwing balls of different weight with respect to the standard one is a typically used special training mode. Previous studies suggested that this type of training contributes to increase the throwing velocity, but no indication has been provided about the optimal ball weight to be used (3) and about the influence of this type of training on the kinematic variables of the throwing arm (2). The aim of the present study was to investigate the effect of using of weighter and lighter balls on kinematic variables of the throwing arm, ball velocity release and precision in 6 pitchers throwing 5oz, 6oz, 7oz and 4oz balls.

Methods: *Athletes and task description*. Six baseball right-handed pitchers (age 21.7 ± 3.1 years, mass 78.2 ± 7.5 kg, height 182.8 ± 7.9 cm) were analyzed. At the time of acquisition the players were in the final phase of the regular season (Italian Championship League A). After a general and sport specific warm-up, each pitcher performed at least 16 throws at maximum intensity with balls of different weights with the following sequence: 5 oz, 6 oz, 7 oz, 4 oz. A strike zone (40 cm) was placed at 18.44 m from the mound.

Kinematic analysis. The upper limb was modeled as an open kinematic chain constituted by 3 rigid segments: thorax, shoulder girdle, upper-arm, and forearm, with 7 degrees of freedom (protraction-retraction and elevation-depression of the shoulder girdle, flexion-extension, abduction-adduction, and internal-external rotation of the gleno-humeral, flexion-extension and pronation-supination of the elbow joint) (4). The 3D biomechanical analysis was performed by means of stereophotogrammetry (BTS Smart-DX 7000, 10 TVC, 250Hz, BTS Engineering Spa, Milano). 5 markers were placed on the thorax, pelvis and hand anatomical landmarks, 5 on the humerus, and 4 on the forearm to form technical clusters. Anatomical calibrations were then performed. The following phases, reflecting meaningful temporal or kinematic characteristics of the throw, were identified: cocking, arm acceleration and arm deceleration. The statistical analysis was performed using SPSS software (SPSS inc. Chicago, Illinois, USA).

Results: No differences in kinematic parameters were found between the standard and the other balls. Throwing kinematics when using the 7oz and the 4oz ball is shown in the table. The higher velocity of the ball when using the 4oz ball is associated with a lower precision of the throw (25% and 74% for the 4oz and 7oz, respectively), and with higher maximum shoulder internal rotation velocity, and maximum elbow extension velocity (table).

Conclusion: Throwing training with weighter and lighter balls in baseball may be a useful tool to improve the maximum ball velocity (1,3). The sequence of the different weighted balls used in the present study led to an improvement of the ball

velocity, but to a lower precision of the throw. These findings suggest to use balls with 1oz weight difference to get a positive effect on ball speed without altering the precision and overloading the arm throwing joints.

Table:

Pitching phases and variables	5 oz ball	6 oz ball	7 oz ball	4 oz ball
Arm Acceleration				
Max Shoulder Internal Rotation Velocity (°/s)	5102 ± 504	4749 ± 615	4786 ± 414*	5247 ± 548*
Maximum Elbow Extension Velocity (°/s)	2198 ± 395	2160 ± 421	2167 ± 453*	2260 ± 422*
Istant Ball Release				
Ball Relase velocity (m/s)	31.9 ± 1.9	30.5 ± 2.6	29.9 ± 1.7*	32.6 ± 2.3*
Arm Deceleration				
Max Ball Velocity (m/s)	35.3 ± 2.8	35.9 ± 2.8	32.9 ± 0.7*	37.0 ± 1.9*

Caption: Kinematic variables (* $p<0.05$)

References: [1] Fleisig et al., Sports Biomechanics, 8:10-21, 2009.

[2] Fortenbaugh et al., Athletic training, 314-320,2009.

[3] Escamilla et al., Sports Med, 29:259-272, 2000.

[4] Garofalo et al., Med Biol Eng Comput, 47:475-486,2009.

Disclosure of Interest: None Declared

Sport

AS-0062

ELITE ATHLETES EXHIBIT INCREASED VERTICAL FORCES DURING RUNNING AT DIFFERENT SPEEDS

Stephen J. Preece [1,*]Duncan Mason [1]Christopher Bramah [1]

[1]Health Sciences, University of Salford, Manchester, United Kingdom

Introduction and Objectives: There has been comparatively little research carried out investigating the biomechanical characteristics of high-performing endurance elite athletes. As this group are able to maintain relatively high running speeds for long periods of time, it is likely that they have developed a running gait which is highly economical. However, there is disagreement in the literature between studies which have investigated the link between biomechanical variables and running economy. Specifically, some research has found that excessive changes in vertical momentum increase metabolic cost [1] whereas others have shown that greater vertical oscillation of the centre of mass is linked to a decrease in metabolic cost [2]. Interestingly Hiese et al [1] performed their experiments on recreational runners (10Km race times between 38-45 minutes), whereas Targuga et al [2] investigated higher level runners (10Km race times between 30-36 minutes). The different findings of these studies suggest that elite runners employ a running style which is distinctly different from that of recreational athletes. The aim of this study was therefore to compare the biomechanical characteristics between elite and recreational runners at a range of different speeds.

Methods: Fourteen elite endurance runners (8 male, mean(SD) BMI 20.6(1.9)) were matched with fourteen recreations runners (8 male, mean(SD) BMI 20.2(1.2)). To be included in the elite group, participants had to have achieved 10Km race time of less than 32 minutes (males) or less than 36 minutes (females) over the preceding 12 months. Runners in the recreational group were required to have a corresponding race time no better than 38 minutes (males) and 42 minutes (females). Both force data and kinematic data from the pelvis, lower limbs and feet were collected at four different speeds (3.2, 3.8, 4.8 and 5.5ms-1) as each participant ran along a 35m track. For each speed an ensemble average vertical force profile, normalised by body weight, was created from at least 5 separate running trials for each runner. Similarly, ensemble average kinematic profiles were calculated for the hip, knee and ankle and spatiotemporal parameters for each participant derived at each of the four speeds. Two-way ANOVA testing was then used to investigate the effect of both speed and also participant group (elite vs recreational) on a number of biomechanical parameters

Results: There were no differences in stride length between the two groups, however the elite athletes had consistently shorter stance times (P<0.03) across the different speeds. Visual inspection of the vertical ground reaction force (GRF) profile showed clear differences between the two groups which were evident at each of the four running speeds (Figure 1). The primary difference was the magnitude of the vertical GRF which lead to a net vertical impulse which was consistently higher in the elite group (p<0.01), indicating a greater range of motion of the centre of mass. The pattern of hip and ankle motion was very similar between the elite and recreational runners; however the pattern of movement at the knee showed a distinct difference at initial contact (Figure 1b). Specifically, at all speeds the athletes contacted the ground with a more flexed knee (p<0.02).

Figure:
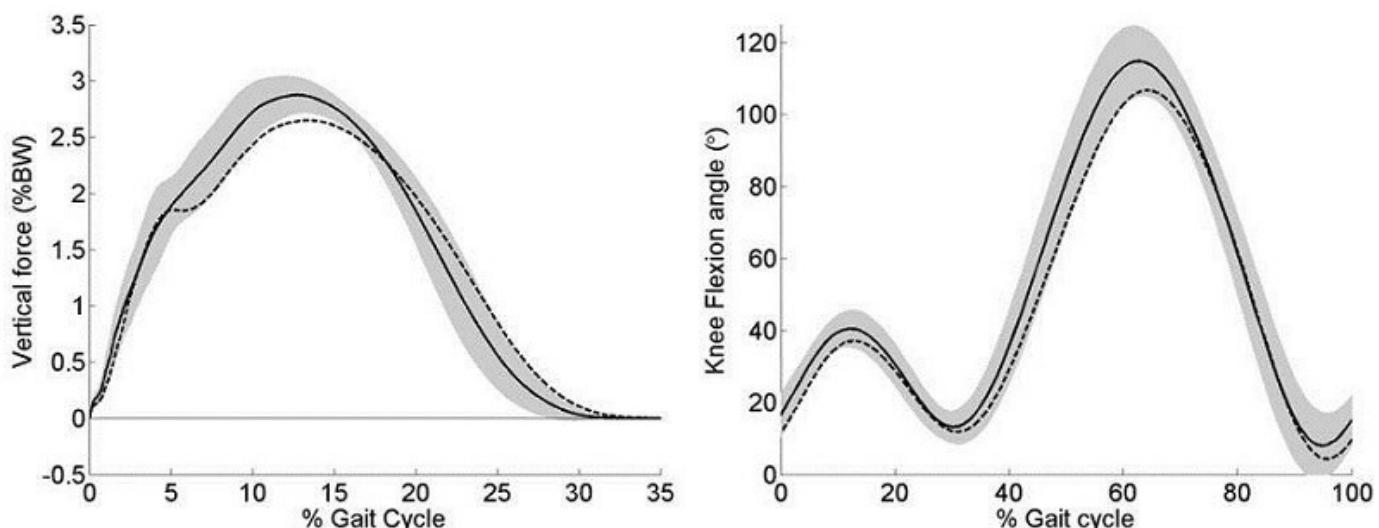
Caption: Figure 1: (a) vertical ground reaction force and (b) knee flexion angle at 3.8 ms-1 (speed 2) for elite athletes (solid line with SD) and recreational runners (dashed line)

Conclusion: Our data supports the idea that elite athletes employ a running style which differs from recreational runners. This style is characterised by an increased net vertical impulse and therefore an increased vertical movement of the centre of mass. During the float phase of running, the centre of mass follows a ballistic trajectory and therefore increased vertical movement has the potential to increase stride length. However, stride length was not different between the two groups and this may have been the result of a more flexed knee configuration at contact in the elite group. Previous researchers have suggested that large changes in momentum during stance phase may lead to metabolically wasteful movement patterns [3]. However, it is possible that elite athletes are able to store energy from vertical momentum changes as elastic energy in the Achilles Tendon and to return this energy during later phases of the gait cycle. It is possible that optimal storage and return of this energy may be facilitated with a flexed knee configuration at initial contact.

References: [1] Hiese et al., Eur. J. Appl. Physiol., 84:438-42, 2001. [2] Tartaruga et al., Res. Quart. Exerc. & Sport., 83:367-75, 2012. [3] Williams et el., J. Appl Physiol., 63:1236-35, 1987.

Disclosure of Interest: None Declared

AS-0064

COMPARISON OF SUBJECT-SPECIFIC TORQUE PROFILES OF ATHLETES BASED ON ISOKINETIC DYNAMOMETER DATA

Frederik Heinen [1,*]Mark King [2]Carsten Møller Mølgaard [3]John Rasmussen [4]Mark de Zee [1]

[1]Health Science and Technology, Aalborg University, Aalborg East, Denmark, [2]School of Sport , Exercise and Health Sciences, Loughborough University, Loughborough, United Kingdom, [3]Orthopaedic surgery, Aalborg University Hospital, Aalborg, [4]Department of Mechanical and Manufacturing Engineering, Aalborg University, Aalborg East, Denmark

Introduction and Objectives: Isovelocity dynamometers are widely used to quantify strength properties of athletes, because the device allows collection of torque data for a joint at different angles, contraction types and velocities in a standardized manner [1]. The experimentally obtained joint torque data have been widely applied throughout literature, especially combined with torque-driven models, to generate subject-specific torque profiles and predict performance of an individual [2]. However, variation of the torque profiles amongst athletes that perform different types of lower extremity sport activities has not been well investigated. The aim of this study is to compare subject-specific torque profiles from runners and cyclists based on experimental torque data.

Methods: The experiment was conducted at two testing facilities on two different isovelocity dynamometers (Contrex multi-joint, CMV AG, Swizerland and Biodex System 4 Pro, Biodex Medical Systems, United States of America). Ten male athletes were included in this experiment. Four runners and six cyclists (body mass: 79.3kg ± 13.3, height: 1.79m ± 0.08). Isometric (five evenly spaced angles) and isokinetic (four-eight evenly spaced velocities) measurements were performed for the ankle, knee and hip flexors and extensors for the dominant leg. A similar dynamometer setup as proposed by Lewis et al. 2011 was adopted. All subjects attended a familiarization session and a testing session. Alignment of joint and dynamometer axes of rotation was performed carefully during submaximal loading. All dynamometer data was low pass filtered at 12 Hz by a fourth-order zero-lag Butterworth filter. Maximal isometric torque and corresponding joint angle were located. Isokinetic torques and angles were identified at isovelocity. Gravity correction was performed as recommended by the manufacturer's prior measuring. An optimization procedure (Simulated Annealing, [3]) was adopted to fit a nine parameter mathematical torque-angle-velocity profile to the subject-specific dynamometer data [4]. Bounds for the nine parameters were set based on literature. The objective function minimized the unbiased weighted root mean square difference between the calculated and measured isometric and isokinetic torque data as proposed by Lewis et al. 2011. The weighting encouraged the function to give a better fit with the larger torque measurements. As it was assumed more likely that the subject performed submaximal rather than supramaximal during the measurements.

Results: Only the plantar flexors optimization results are presented in the abstract. No clear difference was observed for maximal isometric torque and optimal joint angle between the two groups. However, differences in maximal contraction velocity between the cyclists and runners were observed. Large inter and intra group variability was likewise observed for the ankle plantar flexors as presented in figure 1 and table 1. Similar results were observed for the knee and hip flexors and extensors. Whether the results are influenced by usage of two different dynamometers could be argued. However, the same testing procedure was used as well as both dynamometers were calibrated as recommended by the

manufacturer prior to measurements thereby minimizing the effect. All measurements were included in optimization of the torque function approximation, including some submaximal measurements. It could be argued whether these measurements should have been excluded from the optimization. However, an objective exclusion criterion would be required to this end.

Figure:

Plantar flexor torque-velocity profile
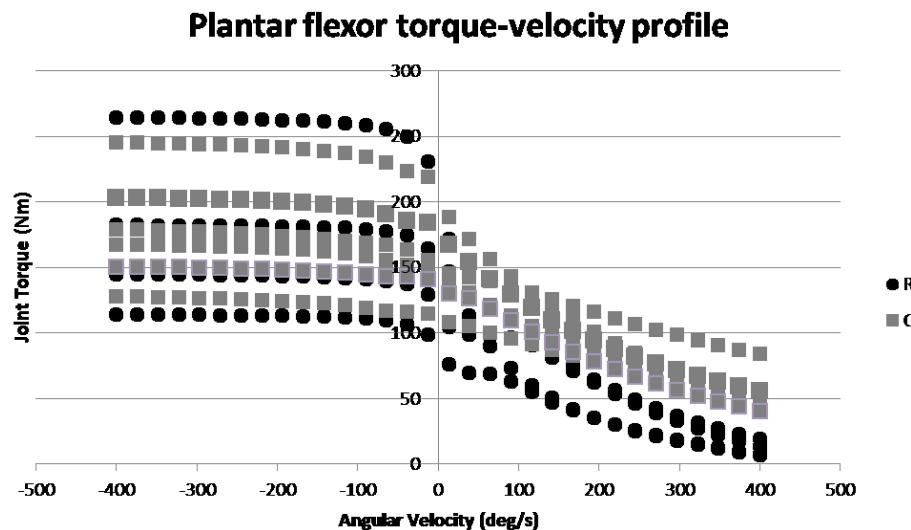
Caption: Optimized torque-velocity profiles of all subjects at their maximal isometric joint torque angles for the ankle plantar flexor for (R) runners and (C) cyclists.

Conclusion: Differences between the optimal joint angle and maximal contraction velocity for runners and cyclists were observed. However, due to the limited number of participants in this study further investigation is needed in order to establish whether the difference is generic between athletes of different sports.

Table:

	Optimization runners (mean ± std)	Optimization cyclists (mean ± std)
Joint angle corresponding to Maximal isometric torque	32.4° ± 9.3°	33.6° ± 7.2°
Maximal isometric torque	189.9Nm ± 35.9Nm	172,0Nm ± 25,4Nm
Maximal contraction velocity	530.1°/s ± 40.6°/s	1280.4°/s ± 372.0°/s

Caption: Comparing plantar flexor data from optimized joint-torque profiles between runners and cyclists. A positive joint angle describing a more dorsi flexed ankle.

References: [1] Parkin S, et al. *J. Sports Sci.* **19**:7,521-526,2001

[2] King MA, et al. *J Appl Biomech.* **22**:264-274,2006.

[3] Goffe WL. *J Stud Econ Econometrics.* **1**:169-176,1996

[4] Lewis MGC. Et al. *J Appl Biomech.* **28**:520-529,2012

Disclosure of Interest: None Declared

Sport

AS-0065

CAN COMPRESSION AID IN MAINTAINING JUMP PERFORMANCE OVER A FATIGUING PROTOCOL?

John W. Wannop [1,*]Marie Wolter [1]Nicole Schrier [1]Ryan Madden [1]Jay Worobets [1]Darren Stefanyshyn [1]

[1]Kinesiology, University of Calgary, Calgary, Canada

Introduction and Objectives: Recently, compression apparel has shown it can improve maximal effort, short duration performance [1,2]. While compression can improve short duration performance, it is unclear how compression influences longer duration performance. Therefore, the purpose of this study was to determine whether compression apparel could aid in maintaining jump height performance over a fatiguing protocol.

Methods: Twenty athletes participated in the study with Phase I determining each athlete's optimal compression using a previously established maximal effort jump test [2]. Phase II divided the athletes randomly into two groups, with one group performing in their optimal compression and the other in loose fitting shorts. During phase II, both groups performed maximal effort counter-movement squat jumps every twenty seconds until fatigue. An athlete was classified as fatigued if they could no longer maintain 88% of their maximum vertical-jump height. Kinematic (240Hz) and kinetic data (2400Hz) were collected during both phases with a motion capture system and a Vertec measuring jump height.

For phase I, the athletes jump height in their optimal compression was compared to the control using a paired t-test ($\alpha=0.05$). For phase II, an independent t-test was used to compare the total number of jumps during the fatiguing protocol between groups ($\alpha=0.05$). For kinematic and kinetic data analysis, the duration of each athlete's jumping protocol was divided into 5 sections, with each section representing 20% of the fatiguing protocol (Figure 1a). The initial 20% was used as the baseline and the difference in each variable relative to the baseline of the jumping protocol was compared for the subsequent sections between groups using a paired t-test with a Holm-Bonferroni sequential correction. If no differences were found between the two groups, additional analysis was performed by treating all athletes as a single sample. Comparisons were made using a paired t-test with a Holm-Bonferroni correction, on adjacent 20% sections of the jump decay curve.

Results: During phase I, optimal compression significantly increased the athletes maximum jump height (a mean 2cm increase, $p<0.001$). No difference in performance was seen during phase II between the 10 athletes who wore compression and the 10 athletes who wore the control (Figure 1b). No significant differences were observed for any of the variables for any joint when comparing the two groups.

Combining all athletes into a single group, a significant reduction in hip peak power and angular velocity at peak power occurred during 61-80% of the fatigue protocol ($p=0.0041$ and $p=0.0040$). A significant increase in the knee moment at peak power occurred during the 21-40% region ($p<0.001$) and a significant reduction of the ankle joint peak power ($p=0.0099$) and angular velocity at peak power ($p=0.003$) occurred during the fatigued state (last three jumps).

Figure:
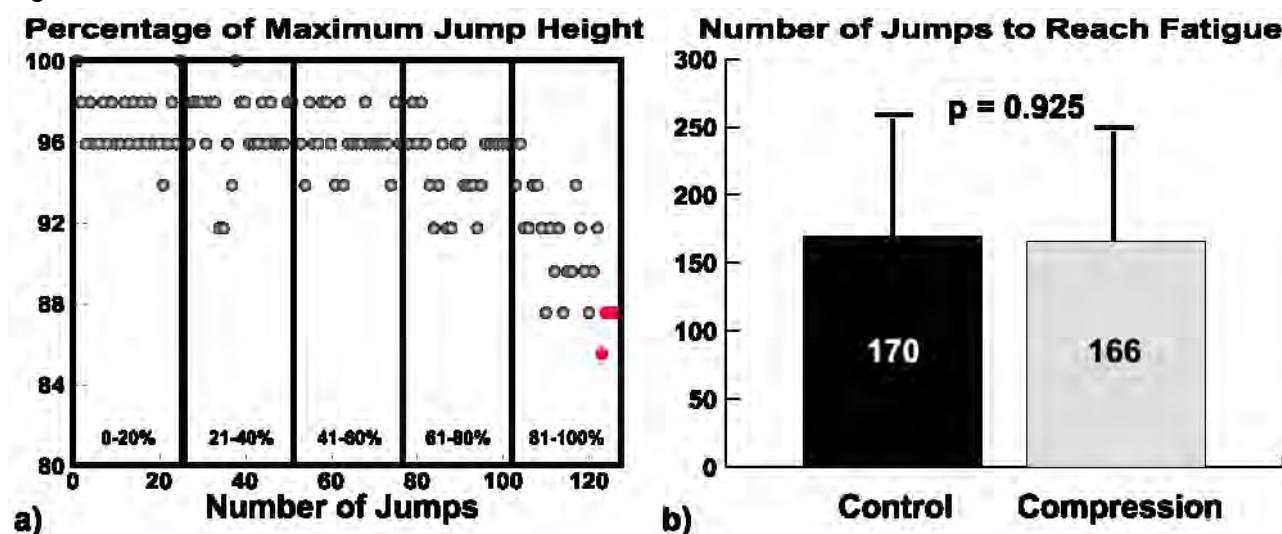
Caption: a) Jump height decay curve of a representative athlete with the last points indicating fatigue b) the number of jumps of the Control and Compression groups before they reached fatigue.

Conclusion: The study indicated that compression does not increase long term jumping performance compared to a control. It should be noted that there were no negative effects of compression.

Both the hip and ankle joint limit athlete performance as fatigue progresses. When fatigued, athletes reduce their angular velocity at both joints, thereby reducing their power production and joint energy generated. The hip joint was affected earlier, and the athletes attempted to increase their knee joint moment and knee joint power to compensate. During the late stages of fatigue, the hip joint angular velocity continues to decrease, while the ankle joint angular velocity and peak power dramatically decrease, leading to the inability of the athlete to maintain performance.

In summary, compression increased initial maximum jump height and athletes maintained performance to a similar extent to loose fitting shorts during a fatiguing protocol, suggesting that compression is beneficial for athletes. With respect to fatigue, the hip joint angular velocity and power is affected first, while the ankle joint has a significant influence during the later stages of fatigue.

Table:

Joint		0-20%	21-40%	41-60%	61-80%	81-100%	Fatigue
Hip	Angular Velocity at Peak Power [°/s]	378	391	387	**362**	343	341
	Moment at Peak Power [Nm]	166	162	167	165	163	161
	Peak Power [W]	1121	1090	1092	**1054**	993	978
Knee	Angular Velocity at Peak Power [°/s]	583	577	579	575	571	563
	Moment at Peak Power [Nm]	93	**99**	98	100	102	103
	Peak Power [W]	986	1023	1027	1039	1037	1036
Ankl	Angular Velocity at Peak Power [°/s]	739	745	746	745	731	**707**

e	Moment at Peak Power [Nm]	94	93	95	94	94	95
	Peak Power [W]	1320	1330	1350	1336	1302	**1266**

Caption: Hip, knee and ankle joint kinematic and kinetic mean data of all athletes when treated as a single group. Bold values represent a significant differences from the preceding adjacent region.

References: [1] Worobets et al. Proc ISB Congress XXII, 2009.

[2] Wannop et al. Proc ISB Congress XXIV, 2013.

Disclosure of Interest: J. Wannop Conflict with: adidas, M. Wolter: None Declared, N. Schrier: None Declared, R. Madden Conflict with: adidas, J. Worobets: None Declared, D. Stefanyshyn Conflict with: adidas

Lower Limb

AS-0067

CAN PATELLOFEMORAL JOINT (PFJ) ALIGNMENT BE ASSESSED CLINICALLY USING A CUSTOM MADE CALLIPER?

Kevin D. Campbell-Karn [1,*] Thomas Korff [2] Ian McDermott [2]

[1]Faculty of Life Science and Computing, London Metropolitan University, London, [2]College of Health and Life Sciences, Brunel University, Uxbridge, United Kingdom

Introduction and Objectives: Knee problems are a common complaint among the general population with a high proportion of physical injuries being knee-related. Up to one in six knee related conditions have been coded as a 'patellofemoral condition' which includes anterior knee pain. However, anterior knee pain can have several causes. One common cause is mal-alignment of the patellofemoral joint (PFJ) and is considered as an abnormal static position of the patella within the trochlear groove during knee extension and flexion. This can cause undue stress to the joint and surrounding structures, with resultant damage and potential pathology. Mal-alignment of the PFJ causes patellar kinematic abnormalities predominantly in the last 20° of knee extension mainly due to the decreased congruency as the patella rises out of the trochlear groove in this range. Clinicians currently assess the alignment of the patella via measurement of the Q-angle, functional testing and the so-called McConnell technique. The latter was developed by McConnell and has been broadly adopted by the physiotherapy community when assessing and treating alignment of the patellofemoral joint. The goal of this method is to determine the centre of the patella in relation to the femoral epicondyles and is reliant on accurate localisation of the medial and lateral borders and the femoral epicondyles. Whilst the McConnell technique may be useful within a clinical context, this subjective measurement is reported to have limited reliabilityIt is clear therefore that there is a need for the position of the patella in relation to the femur to be determined more objectively and reliably. Therefore the purpose of this study was to assess the suitability and reliability of a custom-made 'patellofemoral tracking calliper' to assess the patellar position with resepct to the femur.

Methods: A calliper, which measures the medial-lateral offset of the middle of the patella with respect to the mid-point of the femoral epicondyles (Patellofemoral Tracking Calliper [PFTC]) was developed (Figure 1) and assessed for accuracy and reliability. To assess accuracy, 39 right knees were measured with the calliper and compared to the equivalent measures obtained from MRI images. For this purpose, the knee was placed in an MRI scanner with the tibiofemoral joint positioned in 30° of flexion and the rotation of the leg orientated by using a spirit level along the medial side of the foot. The knee was supported with wedges and strapped to the MRI table in this position to prevent any deviation from the desired orientation. This position was replicated for measurements with the PFTC. During MRI analysis, the midpoint of the femoral epicondyles was defined as the half distance between the widest epicondyle points and the mid-point of the patella was defined as the half distance between the widest medial and lateral borders of the patella. This followed the same measurement methods as the PFTC, however this device used these landmarks via physical contact from the calliper arms.

Thus, both the PFTC and the MRI equivalent provided information about the superficial position for the patella with respect to the femur. To assess agreement between both methods, the Pearson product moment correlation coefficient was determined, and the Bland and Altman limits of agreement test was used to assess bias and limits of agreement. Each calliper measure was taken three times, and the reliability of the PFTC was assessed using intra-class correlation coefficients (ICC).

Results: The patellofemoral tracking calliper was highly reliable (ICC=0.990-0.991). The limits of agreement with regards to the MRI equivalent method were ±8 mm. The Bland and Altman plot highlighted a systematic bias of 2 mm. The calliper measures correlated significantly with the MRI equivalent method (r = 0.675, p = 0.001).

Figure:

Caption: Figure 1. Application of the Patellofemoral Tracking Calliper

Conclusion: The patellofemoral tracking calliper is a useful tool, where the reliable assessment of patella position with respect to the femur is needed. The superficial landmarks of the patella and femur require further investigation into their accuracy in providing true alignment outcome measures of the patellofemoral joint. The McConnell method for assessing alignment may have questionable methods when the anatomical shape and interaction of the joint surfaces is considered alongside the data presented here.

Disclosure of Interest: None Declared

FEASIBILITY AND RELIABILITY OF THREE-DIMENSIONAL ULTRASOUND FOR MEASURING HUMAN TIBIALIS ANTERIOR MUSCLE DEFORMATION DURING ISOMETRIC CONTRACTIONS

Brent Raiteri [1,*] Andrew Cresswell [1] Glen Lichtwark [1]

[1]School of Human Movement and Nutrition Sciences, The University of Queensland, Brisbane, Australia

Introduction and Objectives: The deformation of muscle during contraction can potentially influence the length changes of the contractile and connective tissues. In pennate muscle, biaxial strain of the aponeurosis has been suggested to be an important parameter influencing muscle force production [1]. However, due to the difficulty in measuring deformation in muscle during contractions, these effects have not been measured in human muscles. Freehand three-dimensional ultrasound (3DUS) is a reliable and valid technique for the *in vivo* measurement of human gastrocnemius muscle belly length and volume [2] and could potentially be used to examine biaxial aponeurosis strains in humans during contractions. This study aims to determine the feasibility and reliability of 3DUS for examining *in vivo* tibialis anterior (TA) muscle deformation during voluntary isometric contractions (VIC) at varying intensities.

Methods: Subjects (n = 6) were seated in a reclined position with the plantar aspect of their left foot flush against a custom-built rigid footplate. The left ankle was at 90° (foot sole relative to the shank) and the left knee fully extended. After pre-conditioning contractions, subjects performed two ~40-s isometric dorsiflexion contractions at 5, 10, 25 and 50% maximal VIC in a randomised order. 3DUS scans of TA were performed at each contraction intensity and also at rest. The 3DUS scan involved synchronous B-mode ultrasound imaging and motion capture of the position and orientation of the transducer, while successive cross-sectional slices of the muscle were made whilst sweeping the transducer from the proximal to distal end of the muscle. Freely available software (Stradwin, Cambridge University) was used to collect and analyse all data. Muscle cross-sectional area was segmented from sequential transverse images of the scan at ~15 mm intervals along the length of TA. Muscle volume was calculated using 3D rendering algorithms and muscle and central aponeurosis lengths were calculated as the straight-line distance between the most proximal and distal locations in 3D space. The principal muscle axes (x, y and z) were determined using a weighted principal component analysis. The muscle cross-sectional area and perimeter in the transverse plane (x-axis) was calculated at 5% increments of the muscle belly length from the muscle centroid. All measures were averaged across two scans from the same contraction condition and the intra-class coefficient (ICC) and coefficient of multiple correlation (CMC) was used to assess intra-session repeatability of the measurements.

Results: The intra-session ICCs for muscle volume and muscle and central aponeurosis lengths were greater than 0.99. Muscle cross-sectional area and perimeter along the transverse plane was highly repeatable, with overall CMC values of greater than 0.99.The TA remained iso-volumetric across the contraction conditions and the muscle was found to shorten and the central aponeurosis shown to lengthen as contraction intensity increased. Muscle and central aponeurosis strain peaked at -2.9 ± 0.1% and 3.1 ± 0.4% respectively (mean ± standard error) in the 50% maximal VIC condition. The TA cross-sectional area in the transverse plane progressively increased around the muscle belly centre with increased contraction intensity, peaking at 99 ± 22 mm^2 (9.8% increase), in the 50% maximal VIC condition. The transverse muscle

perimeter also increased with contraction intensity, peaking at 5.2 ± 1.2 mm (5.6% increase), although this peaked distal to the muscle belly centre (Figure 1).

Figure:
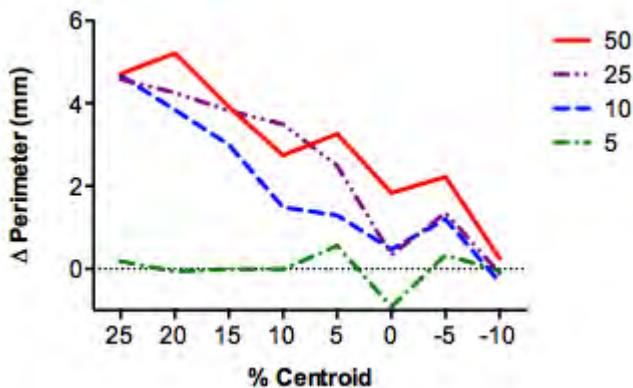
Caption: Figure 1: Mean tibialis anterior (TA) perimeter changes from rest along the transverse plane at 5, 10, 25 and 50% of maximal voluntary isometric contraction (VIC). Negative percentages are proximal to the muscle centroid.

Conclusion: This study is the first to implement 3DUS to characterize *in vivo* muscle deformation in the human TA muscle. The TA muscle bulged centrally, orthogonal to the line of action of the muscle as contraction intensity increased. This occurred presumably because of the transverse strain present in the muscle fibres as they shortened and were constrained to maintain a constant volume. These shape changes are likely to represent variable aponeurosis strains in the transverse plane with regional differences in aponeurosis compliance.

3DUS of the TA is a feasible and reliable technique for measuring muscle volume, muscle and central aponeurosis lengths and muscle cross-sectional area and perimeter along the transverse plane during contractions. We have demonstrated that as fibres develop force, the central aponeurosis of the muscle acts like a serially arranged elastic spring and the transverse muscle perimeter increases most in the distal muscle belly. How these deformations influence storage and return of energy in the aponeurosis (which constrains the shape changes of muscles) requires further investigation.

References: [1] Azizi et al., J. Physiol, 587: 4309-4318, 2009.

[2] Barber et al., J. Biomech, 42: 1313-1319, 2009.

Disclosure of Interest: None Declared

Lower Limb

AS-0069

INFLUENCE OF STRIKE PATTERN ON BIOMECHANICS ASSOCIATED WITH TIBIAL STRESS FRACTURE IN FEMALE RUNNERS

Clare E. Milner [1,*]Richard A Brindle [1]

[1]Physical Therapy and Rehabilitation Sciences, Drexel University, Philadelphia, PA, United States

Introduction and Objectives: Tibial stress fracture is a common overuse injury in female runners and requires an extended recovery time for the bone to heal [1]. Previous work has identified biomechanics associated with tibial stress fracture in female runners with a rearfoot strike pattern [2]. Large peaks in rearfoot eversion angle, hip adduction angle, and absolute free moment were predictive of previous tibial stress fracture [2]. While a rearfoot striking is the most common pattern in distance runners, recent interest has focused on non-rearfoot strike patterns. In particular, it has been suggested that non-rearfoot strike patterns may reduce the risk of overuse injury in runners [3]. The effect of strike pattern on the biomechanical variables associated with tibial stress fracture is unknown. Thus, the purpose of this study was to determine whether the magnitude of these variables differ between healthy female runners who are habitual rearfoot and non-rearfoot strikers. We hypothesized that peak rearfoot eversion angle, peak hip adduction angle, and absolute peak free moment would be smaller in non-rearfoot strikiers compared to rearfoot strikers.

Methods: As part of an ongoing study, female runners between 18 and 45 years of age running at least 10 miles per week for a year or more were recruited. All participants provided written informed consent prior to participation and all procedures were approved by the institutional review board. Fourteen participants were recruited, 7 rearfoot strikers (26 ± 5 y; 55.2 ± 7.1 kg; 1.64 ± 0.08 m; 24 ± 11 miles per week) and 7 non-rearfoot strikers (28 ± 6 y; 59.7 ± 15.4 kg; 1.67 ± 0.07 m; 23 ± 14 miles per week). Participants wore standard laboratory footwear and retroreflective markers were attached to the pelvis and right lower limb. Three-dimensional gait analysis was conducted while participants ran over ground in the laboratory at 3.7 m/s ± 5 %. Segment position and ground reaction force data were recorded synchronously for five trials. Kinematic data were filtered at 8 Hz and processed using rigid body analysis and joint coordinate systems, following standard procedures [4]. Ground reaction force data were filtered at 50Hz for the determination of free moment. Foot strike pattern was determined from strike index, with values of ≤ 0.33 indicating rearfoot strikers and larger values indicating non-rearfoot strikers. Variables of interest were extracted from each trial and averaged per participant, then within each strike pattern group. Independent t-tests were used to identify any differences between groups, with $p < 0.05$ considered significant.

Results: Both peak rearfoot eversion angle ($P < 0.001$) and peak hip adduction angle ($p = 0.003$) were significantly smaller in the non-rearfoot strikers compared to the rearfoot strikers (Table 1). However, absolute peak free moment ($p = 0.664$) was not different between groups.

Conclusion: The two kinematic variables of interest, peak rearfoot eversion angle and peak hip adduction angle, were both smaller in the non-rearfoot strikers. Our finding of smaller peak rearfoot eversion angle in non-rearfoot striking runners compared to rearfoot strikers is in agreement with previous work [5]. Peak hip adduction angle and absolute peak free moment differences between these groups have not been reported previously. These kinematic differences provide

initial evidence to support adoption of a non-rearfoot strike pattern by rearfoot striking female runners at risk of tibial stress fracture. In particular, female rearfoot strikers with large rearfoot eversion and hip adduction angles may benefit from switching to a non-rearfoot strike pattern. However, it should be noted this study was cross-sectional and identified group differences in kinematics associated with tibial stress fracture in currently healthy runners. Future work should explore gait retraining protocols to assist rearfoot striking runners with aberrant kinematics in transitioning to a non-rearfoot strike pattern, and monitor injury incidence. In summary, non-rearfoot striking female runners have smaller peak rearfoot eversion and peak hip adduction angles, but similar absolute peak free moment compared to rearfoot striking female runners.

Table: Table 1: Mean (standard deviation) for variables of interest in each foot strike pattern group

	Peak rearfoot eversion angle (degrees)	Peak hip adduction angle (degrees)	Absolute peak free moment ($x10^{-3}$)
Rearfoot strikers	7.8 (1.7)	16.9 (2.7)	5.4 (2.9)
Non-rearfoot strikers	3.0 (1.6)	11.2 (3.0)	6.1 (2.4)

References: [1] Arendt et al., Am. J. Sports Med., 31: 959-968, 2003.

[2] Pohl et al., J. Biomech., 41: 1160-1165, 2008.

[3] Daoud et al., Med. Sci. Sports Exerc., 44: 1325-1334, 2012.

[4] Cole et al., Trans. ASME, 115: 344-349, 1993.

[5] Stackhouse et al., Clin. Biomech., 19, 64-70, 2004.

Disclosure of Interest: None Declared

Lower Limb

AS-0070

DIFERENCES IN GLOBAL GAIT ASYMMETRY BETWEEN KNEE OSTEOARTHRITIS PATIENTS AND HEALTHY ADULTS

Silvia Cabral [1,*] W. Scott Selbie [2] Rita Fernandes [1] [3] Flávia Yázigi [1] Vera Moniz-Pereira [1] Paulo A. Armada-da-Silva [1] Margarida Espanha [1] António P. Veloso [1]

[1] Laboratório de Biomecânica e Morfologia Funcional, U Lisboa, Faculdade de Motricidade Humana, CIPER, P-1499-002 Lisboa, Portugal, [2] HAS-Motion, Inc., Kingston, ON, Canada, [3] Departamento de Fisioterapia, Escola Superior de Saúde, Instituto Politécnico de Setúbal, Setúbal, Portugal

Introduction and Objectives: Research suggests that the gait alterations associated with knee osteoarthritis (KOA) possibly lead to between-limb asymmetries [1]. Consequently, the load is distributed unequally between the weight bearing joints, which in turn may increase the risk of developing multi-articular lower limb osteoarthritis [1-2].

Between-limb asymmetries have been reported in KOA patients. However, the asymmetry is often measured using discrete and local parameters. By using discrete parameters, the temporal information of the gait waveform is neglected, which means that potentially important asymmetries that are due to time shifts or that occur outside the chosen time frame could be missed [3-4]. Additionally, the extraction of discrete parameters is subjective and potentially difficult in atypical waveforms such as those of KOA patients [3]. Using local parameters, several values are needed to capture the global aspect of gait asymmetry and to assess the influence of specific interventions, which may lead to results that are difficult to interpret [5]. Conversely, the strength of global symmetry measures composed of continuous variables is their ability to reduce all the information from various local parameters throughout the gait waveform in one score.

The aim of this study was to determine if the global gait asymmetry score of a group of KOA patients was different from that of a healthy control group. Our hypothesis was that patients with KOA are more asymmetric than the healthy participants.

Methods: Subjects were divided in 2 groups: 14 were healthy controls (4 male, age 38.1 ± 11 years, height 1.54 ± 0.44 m, body mass 64.6 ± 10.8 Kg), who were free from any musculoskeletal pathology, and 14 were diagnosed with clinical plus radiographic KOA (3 male, age 58.2 ± 6.1 years, height 1.57 ± 0.07 m, body mass 86.6 ± 15.3 Kg).

Participants walked along an 8 m walkway at their self-selected comfortable speed. Passive markers were placed on the participants' skin, according to the calibrated anatomical system technique [6]. The 3D coordinates of these markers were collected at 200 Hz using a system with 8 high speed infrared cameras (Oqus 300, Qualisys AB, Gothenburg, Sweden), were low-pass filtered using a 4th order Butterworth filter with a cut off frequency of 10Hz and were used to create a model with 7 segments (feet, shanks, thighs and pelvis), each with 6 degrees of freedom. Joint angles were computed into the joint coordinate system [7]. The 3D joint angles of the hip, knee and ankle and the 3D absolute pelvis angle were normalized in time to the gait cycle. The global gait asymmetry (GGA) score was calculated for each cycle, by integrating the squared differences between the right and left time normalized signals, taking the square root, and adding them across all 12 variables. Thus, higher scores represent greater asymmetry levels. All data processing and model building were done in Visual3D (Version 5.01.18, C-Motion, Inc, Rockville, USA).

The GGA scores (average of 3 cycles) of the control and KOA groups were compared using an independent T-test (IBM SPSS Statistics 21, Inc. Chicago, Illinois, USA) with an alpha of 0.05. This analysis was complemented with an effect size and power analysis (G*Power 3.1.7 [8]). Data were checked for normality and presence of outliers prior to analysis.

Results: The statistical analysis shows that the KOA group had significantly higher GGA scores than the control group [mean (± SD): KOA 604 (±101°), Control 511 (±65°)].

Figure:
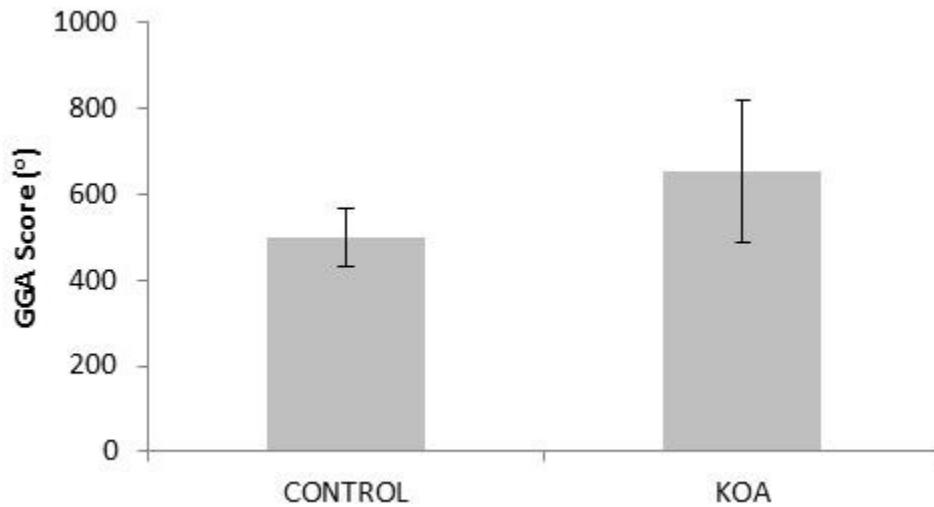
Caption: Global Gait Asymmetry (GGA) score of Control and Knee OA (KOA) groups

Conclusion: As hypothesized, the overall level of asymmetry of a group of KOA patients was significantly higher than that of a group of healthy controls. Due to the different nature of the groups, further studies are needed to analyze if the asymmetry score is influenced by group characteristics other than the presence of KOA. Moreover, the variables that compose the GGA score could be selected and normalized according to their relevant contribution to the final score, so that it is better tuned to analyze gait asymmetry in KOA.

References: [1]   Mills et al., Arch. Phys. Med. Rehabil., 94: 2241–7 2013

[2]   White et al., Arch. Phys. Med. Rehabil., 86: 1958–63 2005

[3]   Deluzio et al., Gait Posture, 25: 86–93 2007

[4]   Nigg et al., Gait Posture, 38: 115–119 2013

[5]   Hoerzer et al., Am. Soc. Biomech. 36th Annu. Meet., 2–3 2012

[6]   Cappozzo et al., Clin. Biomech., 10: 171–178 1995

[7]   Grood et al., J. Biomec., 105: 136–144 1983

[8]   Faul et al., Behav. Res. Methods, 39: 175–91 2007

Disclosure of Interest: None Declared

Lower Limb

AS-0071

STATIC ANKLE RANGE OF MOTION IS ASSOCIATED WITH DYNAMIC ANKLE MOTION DURING A SURF-LIKE SIMULATED AERIAL TASK

James R. Forsyth [1,*] Diane L. Riddiford-Harland [1] Lina Lundgren [2] John W. Whitting [3] Jeremy M. Sheppard [2] Julie R. Steele [1]

[1]Biomechanics Research Laboratory, University of Wollongong, Wollongong, [2]School of Exercise & Health Science, Edith Cowan University, Joondalup, [3]School of Health & Human Sciences, Southern Cross University, Lismore, Australia

Introduction and Objectives: During surfing competitions, a judging panel scores surfers according to how they perform manoeuvres on a wave. Points are awarded for speed, power and flow, as well as innovation and risk-taking. Consequently, surfers who include dynamic, innovative and risky manoeuvres such as aerials, where surfers project themselves into the air before landing on the water, receive higher scores, on average, than those who only perform turns [1]. Aerial manoeuvres, however, have been associated with increased lower limb injury [2]. In land-based sports, utilising a greater ankle range of motion (ROM) over which to distribute the impact forces generated during landing is thought to reduce the risk of lower limb injury at foot-ground contact [3]. However, whether surfers use a large ankle ROM when landing aerials is unknown. Therefore, the purpose of this study was to: (i) identify the dynamic ankle motion used during landing a simulated aerial task, and (ii) evaluate the association between static ankle ROM and dynamic ankle motion.

Methods: A twin-axis electronic goniometer (Model SG110; Biometrics Ltd, UK) was used to measure dynamic sagittal and frontal plane ankle motion during repeated trials of a simulated aerial task for the trail limb of 21 consenting skilled surfers (age = 19.7 ± 4.4 years, height = 179.0 ± 7.6 cm, mass = 70.3 ± 10.2 kg, surfing experience = 12.4 ± 4.6 years). The simulated aerial task required each participant to run at a self-selected pace parallel to a thick padded landing mat (305 x 1740 x 3650 mm), jump onto a mini trampoline, and project themselves up into the air. Once airborne the participants rotated 90 degrees while positioning a soft-top surfboard (with the fins removed) under their feet, before landing on the board (and the padded landing mat), and then held a stabilised landing position for 3 seconds. Static flexed-knee ankle joint ROM was characterised using the knee-to-wall test [4]. Pearson product moment correlations were used to determine the strength of the associations between the participant's static ankle joint ROM and a dynamic ankle motion quantified during landing the simulated aerial task ($p \leq 0.05$).

Results: At initial board-mat contact, participants displayed slight plantar flexion (2.6 ± 9.7°) combined with an inverted foot position (4.0 ± 4.2°). By the Stabilisation phase of landing, the participants displayed a dorsiflexed ankle (22.1 ± 7.1°) with a neutral foot posture in the frontal plane (0.7 ± 5.8°). The greatest ankle joint range of motion was displayed during the Absorption phase (29.3 ± 7.0°; a phase during which the participants were flexing their lower limb joints to absorb the forces generated following initial board-mat contact), relative to both Pre-Landing and Stabilisation. The greatest peak dorsiflexion angle, however, was displayed during the Stabilisation phase of landing (20.6 ± 6.4°). Static flexed-knee ankle ROM was significantly correlated with peak dorsiflexion during Stabilisation ($r = 0.70$, $p < 0.001$; see Figure 1) and total sagittal ankle displacement during Absorption ($r = 0.60$, $p = 0.004$).

Figure:
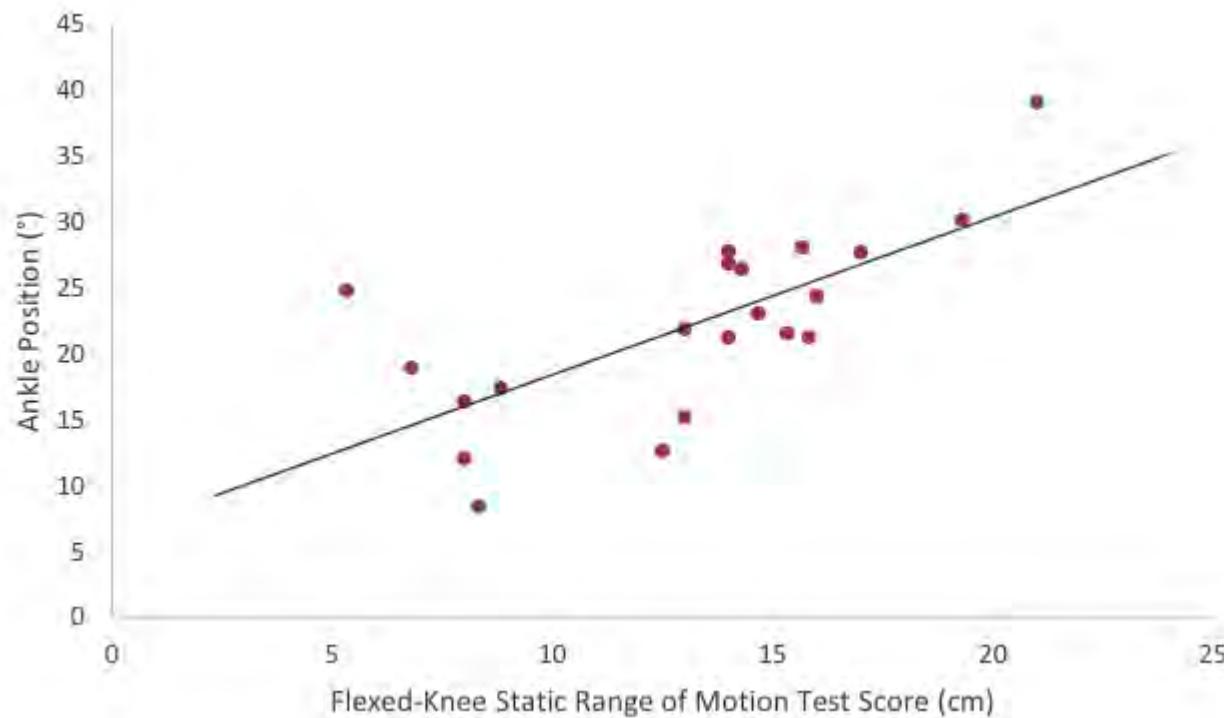
Caption: Figure 1. Correlation between static flexed-knee ankle ROM test score (cm) of the trail limb and the ankle position at Stabilisation (°) during the simulated aerial task

Conclusion: Compared to previous data published on fixed-ground landing tasks [5], the participants' ankle plantar flexion was somewhat restricted by the surfboard prior to initial board-mat contact. Furthermore, those participants who had a limited static ankle ROM displayed a stiffer landing style. It is postulated that this stiffer landing technique is likely to increase ankle and knee joint loading when landing a simulated aerial task. It is therefore important that surfing athletes incorporate lower limb flexibility training, particularly soleus muscle extensibility activities to increase their static ankle ROM and, in turn, improve their dynamic ankle ROM when landing.

References: [1] Lundgren L et al., *Int J Sport Sci Coach*, 9: 663-670, 2014

[2] Furness J et al., *Australian Physiotherapy Conference*, 58-59, 2013

[3] Whitting J et al., *Aviat Space Environ Med*, 78: 1135-1142, 2007

[4] Techovanich W et al., *Aust J Physiother*, 44: 175-80, 1998.

[5] Kernozek TW et al., *Med Sci Sports Exerc*, 37: 1003-1012, 2005

Disclosure of Interest: None Declared

Lower Limb

AS-0072

IMPACT OF RELIABILITY ON REPEAT KNEE EXTENSOR STRENGTH TESTING

Jamie E Hibbert [1,*] Patrick M Rider [1] Zachary J Domire [1]

[1] Kinesiology, East Carolina University, Greenville, United States

Introduction and Objectives: Maximal strength testing is a commonly used method in both biomechanics research and clinical assessments of muscle and joint function [4]. The reliability and validity of different types of dynamometers have been shown to be acceptable in previous studies [1,2,5]. However, when testing human participants there are other factors that may cause variability in strength measurements, such as sincerity of effort and familiarization with both the equipment and environment. It is common for researchers to bring participants in for a familiarization session prior to beginning true data collection for their study [3]. The purpose of this study was to determine the effect of repeat testing on peak torque, mean torque and variability between trials. We hypothesized that peak torque and mean torque would be higher and less variable the second and third test days than on the first test day.

Methods: Twenty-five healthy, young (age 21.3±3) participants (13 males, 12 females) reported to the biomechanics lab for maximal isometric strength testing three times. Each participant completed all three visits within 7 days of beginning the protocol. Prior to each testing session, participants completed a 5-minute warm-up on a cycle ergometer. Participants then completed 3 maximal isometric voluntary contractions (MVICs) of the right knee extensors with the knee in 90° of flexion using a HUMAC isokinetic dynamometer (HUMAC NORM Testing & Rehabilitation System, CSMI Medical Solutions, Stoughton, MA). Participants were given two trial repetitions prior to the test each day for familiarization purposes. Consistent verbal encouragement by the researcher was provided during each testing session. The data collected were analyzed for peak torque produced by each subject on each day as well as the mean torque produced over the three maximal trials. The standard deviation was also calculated to determine variance between trials. Paired two tailed t-tests were used to evaluate the statistical differences in the data. A p-value of 0.05 was set as the cut off for significance. All procedures were approved by the Institutional Review Board and written informed consent was obtained from each participant prior to the start of testing.

Results: The values for the average peak torque, average mean torque, and average standard deviation were compared between the different days of testing using a 2-tailed paired t-test. It was found that there was a statistically significant decrease in the average mean torque between day 1 and day 3 (p<0.05) and the difference in the average peak torque (p=0.078) and average standard deviation (p=0.060) trended in the same direction. The differences in the values from day 1 to day 2 were not statistically significant. The statistical values for average mean torque, average peak torque and average standard deviation were p=0.430, p=0.524 and p=0.501, respectively. The differences in the values from day 2 to day 3 were also not statistically significant. The statistical values for average mean torque, average peak torque and average standard deviation were p=0.354, p=0.180 and p=0.163, respectively.

Figure:
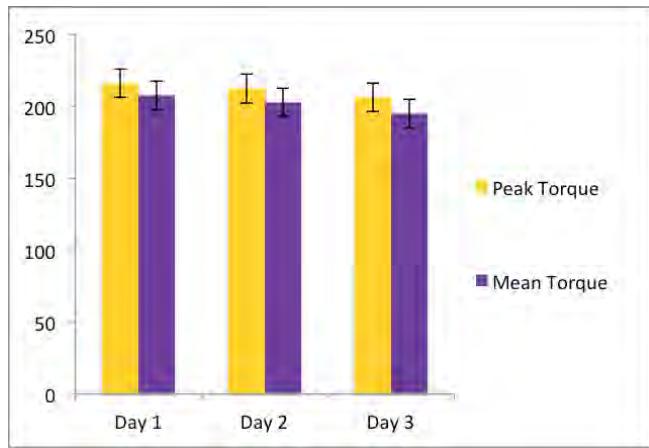
Conclusion: Based on the data collected, healthy, young adults are able to produce peak knee extensor torques on the first day of MVIC testing that is not different from those produced on the second day of testing and are greater than those produced on day 3. These results are the opposite of the hypothesized results. It is possible that the decreased MVIC torque output from day 1 to day 3 could be a result of lingering fatigue from the previous sessions, however this seems unlikely due to the small number of repetitions performed. The increase in variability observed on day 3 may indicate that maximal effort was not being expended. It is possible that some participants were too comfortable with the protocol by the third day and this may have decreased their desire to perform at their true maximum effort. These results indicate that when young, healthy participants are involved in a study it may not be necessary to have a familiarization day prior to beginning testing or if the researcher does bring participants in prior to beginning the study it may be beneficial to have the participant engage in sub-maximal training trials. These results highlight the need to develop a method to control for participation motivation and sincerity of effort. One such method could involve superimposition of electrical stimulation during MVIC.

Table:

	Average Peak Torque (Nm)	Average Mean Torque (Nm)	Average Standard Deviation (Nm)
Day 1	216.32	207.59	8.79
Day 2	212.40	203.04	9.63
Day 3	206.56	194.92	11.47

References: [1] Drouin et al., Eur J Appl Physiol, 91:22-29, 2004.

[2] Madsen. Eur J Appl Physiol Occup Physiol, 74:206-210, 1996.

[3] Mayhew et al., J Appl Physiol, 107:1655-1662, 2009.

[4] Rantanen et al., J Am Geriatr Soc, 45:1439-1445, 1997.

[5] Shechtman et al., J Hand Ther, 18:339-347, 2005.

Disclosure of Interest: None Declared

Modelling

AS-0073

THE EFFECT OF PROPHYLACTIC KNEE BRACING ON LOWER-LIMB MUSCLE FORCES DURING DOUBLE-LEG DROP LANDING

Katie Ewing [1,*]Rezaul Begg [2]Peter Lee [1]

[1]Mechanical Engineering, University of Melbourne, [2]Institute of Sport, Exercise and Active Living, Victoria University, Melbourne, Australia

Introduction and Objectives: Anterior cruciate ligament (ACL) injuries, which account for the majority of sports-related injuries, are painful, costly, and debilitating to the injured athlete. Non-contact ACL injuries often occur during landing, which is frequently performed in sporting activities. Some athletes wear prophylactic knee braces to help prevent knee injury, but the evidence support or discouraging knee bracing is conflicting [1]. Previous studies have found differences in kinematics [2] and electromyography (EMG) muscle activity [3] between braced and non-braced athletes, suggesting that bracing alters neuromuscular control. Computer-based musculoskeletal models provide a means to quantify muscle contributions to complex movements in more detail compared to EMG alone. During impact loading, muscle forces could explain the resulting tension on the ACL that can lead to rupture [4], thus providing critical information for improved injury prevention methods. To further quantify changes in muscle function due to knee bracing, the purpose of this study is to calculate and compare lower-limb muscle forces in braced and unbraced recreational athletes during a double-leg drop landing task.

Methods: Four participants who regularly participate in a landing sport have undergone testing in the Gait Analysis Laboratory at Victoria University (Melbourne, Australia). A motion analysis system consisting of ten optical infra-red cameras (500 Hz; VICON Mx, Oxford Metrics, UK) collected the three-dimensional kinematic data from 54 retro-reflective markers, while two synchronized force plates (1000 Hz, AMTI, USA) simultaneously recorded ground reaction forces. Each participant was instructed to step off a 60 cm platform with his or her dominant leg and land barefoot onto the force plate using both legs. The landing phase was defined as the duration from foot strike to maximum knee flexion angle. Subject-specific musculoskeletal models (31 degrees-of-freedom, 92 musculoskeletal tendon units) were developed in OpenSim, an open-source 3D musculoskeletal modeling software [5]. Inverse kinematics calculated the joint angles that best matched the experimental marker trajectories. A unique solution of individual muscle forces was solved via static optimization by minimizing the sum of the squares of muscle activations. It was assumed that the effect of bracing was expressed in the experimental data and thus knee brace forces and elements were not included in the simulations. The average of three trials for each condition was used for analysis. Forces were normalized to body weight (B.W.).

Results: Prophylactic knee bracing did not alter the peak vertical ground reaction force (GRF) (2.16±0.40 B.W. with brace vs. 2.15±0.32 B.W. without brace). The time of peak GRF during the landing phase was slightly increased with bracing (18.89±5.06% with brace vs. 16.16±3.51% without brace). There was also a small change in the maximum knee flexion angle (97.60±11.86 degrees with brace vs. 99.32±13.12 degrees without brace). Table 1 presents the peak force of the major muscle groups with and without bracing. Generally, slight increases in peak forces of the quadriceps, gastrocenemii, and soleus muscles were observed with bracing. The medial hamstrings were the only muscle group that

demonstrated a decrease in peak force with bracing. These results suggest that knee bracing may have a negative consequence on the knee joint during landing since the quadriceps, which produce much greater force than the hamstrings, can increase stresses in the ACL, while the hamstrings provide a protective effect. However, the large forces produced by the soleus muscle could help to protect the ACL by generating a posterior tibial force [6].

Conclusion: The usefulness of prophylactic knee braces during sporting activities remains under debate. This study provides a more quantitative assessment of the effectiveness and mechanism of knee bracing by examining changes in muscle forces during landing. To further investigate the significance of bracing on muscle function, a total of twenty participants will be tested, followed by rigid body modeling and statistical analyses.

Table:

	Medial Hamstrings	*Lateral Hamstrings*	*Rectus Femoris*	*Vastus Medialis*	*Vastus Intermedius*	*Vastus Lateralis*	*Medial Gastroc*	*Lateral Gastroc*	*Soleus*
No Brace	0.89 ±0.34	1.59±0.19	1.54±0.08	1.62±0.30	1.63±0.23	3.11±0.52	1.15±0.08	0.25±0.02	4.66±0.76
Brace	0.83±0.21	1.70±0.14	1.66±0.66	1.78±0.30	1.76±0.25	3.41±0.55	1.27±0.16	0.28±0.04	4.71±1.10

Caption: Table 1. Mean ± standard deviation of peak muscle forces (normalized to B.W.) with and without a prophylactic knee brace.

References: [1] Rishiraj N et al. *Sports Med,* **11**:937-960, 2009.

[2] Yu B0 et al. *Am J Sport Med,* **32**:1136-43, 2004.

[3] Osternig L et al. *Am J Sport Med,* **21**:733-737, 1993.

[4] Pflum MA et al. *Med Sci Sport Exer,* **36**: 1949-58, 2004.

[5] Delp SL et al. *IEEE T Biomed Eng,* **54**:1940-50, 2007.

[6] Mokhtarzadeh H et al. *J Biomech*, **46**, 1913-20, 2013.

Disclosure of Interest: None Declared

Modelling

AS-0074

ACCURACY OF THE KNEE JOINT AXIS ORIENTATION AGAINST FREEHAND 3D ULTRASOUND

Elyse Passmore [1 2 3,*] Marcus Pandy [2] H Kerr Graham [3 4 5] Morgan Sangeux [1 2 3]

[1]The Hugh Williamson Gait Analysis Laboratory, The Royal Children's Hospital, [2]Mechanical Engineering, The University of Melbourne, [3]Gait Lab and Orthopaedics, The Murdoch Childrens Research Institute, [4]Orthopaedics, The Royal Children's Hospital, [5]Paediatrics, The University of Melbourne, Melbourne, Australia

Introduction and Objectives: Inaccurate identification of the knee joint axis leads to cross-talk and influences the hip rotation profile. The influence on hip rotation is particularly important when utilised to assess patients for de-rotation osteotomies. No gold standard exists for defining the knee axis making it difficult to evaluate previous methods. Initially the knee axis was assumed to be coincident with the trans-epicondylar axis. However, 3D imaging techniques suggest the axis is aligned with the posterior aspect of the condyles [1]. Conventional methods rely upon manual palpation or visual alignment. Another approach is functional methods which rely upon joint range of motion movements to determine the axis. Ultrasound imaging of musculoskeletal structures coupled with motion capture [2] has previously been used for identification of the hip joint centre [3]. In this study 3D ultrasound has been used to locate the most posterior aspect of the femoral condyles as the anatomical knee axis. The aim was to quantify the accuracy of conventional and functional methods to locate the knee axis.

Methods: Ten healthy adults (5♂, 5♀) with no history of gait pathology gave written informed consent to participate in this study. Approval was granted by the ethics committee of the local institute. Reflective markers were attached to the subject according to the Plug-in-Gait marker set ([4], Vicon Motion Systems). Subjects walked up and down a walkway at a self-selected speed. A 10-camera motion-capture system (Vicon Motion Systems) and 5 force platforms (ATMI, Advanced Mechanical Technology, Inc) were used to measure the subjects' kinematics and kinetics.

The knee axis was determined using a conventional, marker based method through manual palpation of the epicondyles and three functional methods; the axis transformation technique (ATT or SARA) [5], the geometrical method [6] and a method closely related to the dynamic KAD (DynaKAD) [7,8]. For the ATT and geometric methods only frames where knee flexion was between 20°-90° were used to determine the axis. The functional methods were applied to various activities; three open chain active knee flexion-extensions, three bilateral squats and three walking strides.

The reference method was the condylar axis obtained from 3D ultrasound imaging. The accuracy of the other methods was expressed as the angular difference of the various knee axes in the transverse plane.

Results: The conventional axis was predominantly external compared to the ultrasound condylar axis, 7.5° on average. The ATT and Geometrical functional methods resulted in an axis mostly external with the flexion activity presenting the least amount of variability (SD: ATT 7.4°, Geometrical 8.4°). The DynaKAD method most closely aligned with the condylar axis for all activities, with the most accurate results obtained for walking (mean: 3.1°, SD: 6.1°).

Figure:
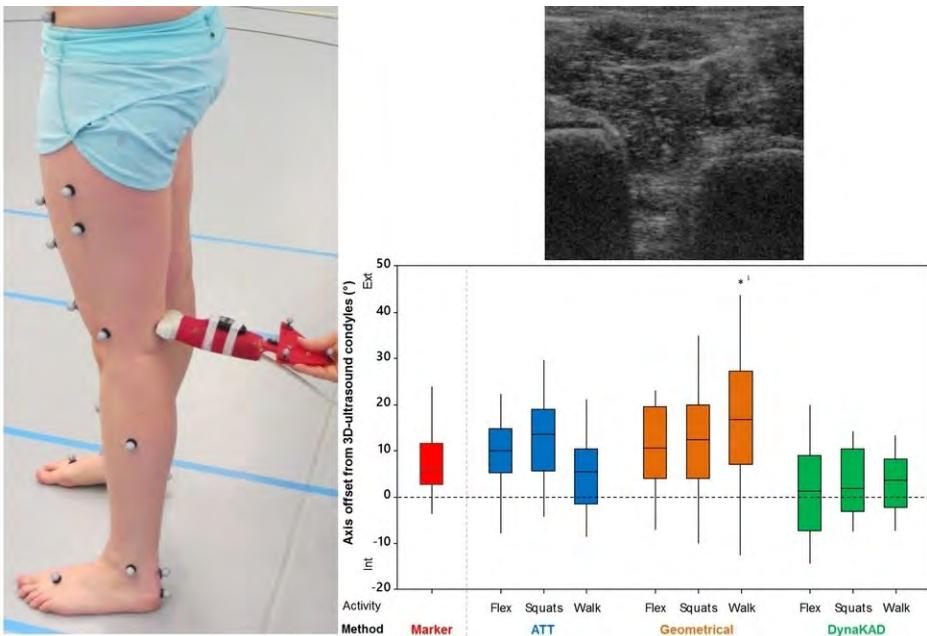
Caption: Left: subject with marker set undergoing 3D-ultrasound imaging of the posterior aspect of the femoral condyles. Right: top, ultrasound image of femoral condyles. Bottom, boxplot of angular difference of knee axes from the 3D-ultrasound condylar axis in the transverse plane (* represents outlying data points). 1 Outlying data point actual location beyond graph range.

Conclusion: We described a method to locate the knee axis in-vivo using 3D ultrasound imaging. The DynaKAD method applied to the walking activity provided the axis closest aligned to our condylar 3D ultrasound reference. This study only assessed healthy adults and our results need to be confirmed on those with pathology.

References:

[1]   Eckhoff DG et al. J Bone Joint Surg Am. 87 Suppl 2:71–80, 2005.

[2]   Gee A et al. Br J Radiol.77:S186–93, 2004.

[3]   Peters A et al. Gait Posture. 31:530–2, 2010.

[4]   Davis Ret al. Hum Mov Sci. 10:575–87, 1991.

[5]   Ehrig RM et al. J Biomech. 40:2150–7, 2007.

[6]   Chang LY et al. J Biomech. 40:2707–15, 2007.

[7]   Baker R et al. Hum Mov Sci. 18:655–67, 1999.

[8]   Schache AG et al. Gait Posture. 24:100–9, 2006.

Disclosure of Interest: None Declared

Computer Simulation

AS-0075

TESTING MODEL-BASED CONCLUSIONS ON THE OPTIMAL CONTROL OF HUMAN MOVEMENT USING FORMAL STATISTICAL ANALYSES

Ross H. Miller [1,*] Farzad Ehtemam [1]

[1]Department of Kinesiology, University of Maryland, College Park, United States

Introduction and Objectives: Optimal control theory (OCT) has made many elegant and reasonably accurate predictions of human motor behavior. However, the traditional implementation of OCT in biomechanics [1] is extremely computationally demanding for large-scale musculoskeletal models. Consequently, most model-based OCT studies on locomotion have used a single generic model. With data from only one "subject" that does not reflect the biological variance present in even the healthy human population, the generalizability of such results is unclear.

Recent simulation methods can rapidly generate many OCT simulations in practical amounts of time [2], opening the possibility of performing "virtual" experiments with multi-subject datasets that can undergo formal statistical analysis as is standard for laboratory-based experiments, adding an important new element of validity to simulation of human movement. Our objective was to test the hypothesis that conclusions on locomotor control from OCT are robust to healthy variation in anthropometric and muscular properties.

Methods: We used implicit direct collocation [2] to generate predictive simulations of human walking with models representing 10 subjects drawn from standard normal parameter distributions (Table 1). The basic structure of the model was the same for all 10 subjects: 12 degrees of freedom, 24 Hill-based muscles, and a model of muscle energy expenditure [3].

For each subject, walking was simulated on a temporal grid of 101 nodes/step. We first performed a data-tracking simulation that optimized the musculoskeletal states, muscle excitations, and step duration to track mean human experimental data [4] with minimum metabolic cost. The data-tracking result was used as the initial guess for predictive simulations with two different cost functions:

"Minimum Fatigue": minimize the largest muscle activation.

"Minimum Effort": minimize sum of muscle activations, each weighted by muscle mass.

Equality constraints enforced dynamic consistency, periodicity and bilateral symmetry, and Froude number 0.14. The average deviation of the knee angle from mean human experimental data in the first half of stance [4] was expressed in multiples of the experimental standard deviation (SD). Metabolic cost and average knee angle deviation was compared between cost functions using matched-pair Student's t-tests (critical $p = 0.05$).

Results: A single simulation required ~ 20 minutes in MATLAB on an iMac. The models tracked the mean human gait data to an average deviation of 0.60±0.03 SD with a metabolic cost of 3.41±0.16 J/m/kg.

The gross metabolic cost was lower for the Minimum Effort simulation (2.10±0.11 J/m/kg vs. 3.00±0.19 J/m/kg, $p < 0.00001$). The range in differences was 0.77-1.12 J/m/kg (Fig. 1).

The average knee angle deviation was greater for the Minimum Effort simulation (2.16±0.25 SD vs. 1.53±0.55 SD, p = 0.00084). The range in differences was 0.07-1.14 SD. Minimum Effort tended to predict a straight knee in stance, while Minimum Fatigue predicted stance phase knee flexion (Fig. 1).

Figure:

Caption: Metabolic cost (left) and knee angle accuracy (right) when using the "Minimum Fatigue" and "Minimum Effort" cost functions. Dashed lines are simulations with the different models, solid lines are means over all 10 models. The inset figures in the left panel show the average knee angle waveforms predicted by each cost function, compared to the experimental data.

Conclusion:

The qualitative consistency of predicted gaits between subjects suggests it may have been safe to draw conclusions from one subject. However, the difference in the average knee angle deviation was over 1.0 SD for three subjects and under 0.2 SD for three others. These data may suggest different conclusions if considered in isolation. Simulations with multiple model parameter sets were needed to discover the average behavior and the consistency between subjects. Simulation studies have often made modeling decisions for computational speed rather than physiological fidelity, or excluded particular analyses due to computational time rather than relevance. With rapid advances in computing power and simulation methods, the validity of these limitations is diminishing. We suggest that simulation studies whenever possible should be held to the same standards of statistical rigor applied to laboratory-based studies.

Table:

Model	Height (m)	Mass (kg)	Muscle (kg)	Speed (m/s)
1	1.66	61.0	20.9	1.10
2	1.64	57.9	19.4	1.09
3	1.72	54.6	19.4	1.12
4	1.55	55.1	17.9	1.03
5	1.70	69.7	23.6	1.12

6	1.63	53.5	17.9	1.12
7	1.68	59.5	21.0	1.12
8	1.65	63.0	22.5	1.11
9	1.66	53.8	17.7	1.12
10	1.67	64.0	23.0	1.09
Mean	**1.66**	**59.2**	**20.3**	**1.10**
SD	**0.05**	**5.3**	**2.2**	**0.03**

Caption: Height, body mass, muscle mass, and walking speed of the 10 musculoskeletal models.

References: [1] Pandy et al., *J. Biomech. Engr.,* **114**: 450-460, 1992.

[2] Van den Bogert et al., *Proc. IUTAM,* **2**: 297-316, 2011.

[3] Minetti & Alexander, *J. Theor. Biol.,* **186**: 467-476, 1997.

[4] Miller et al., *Med. Sci. Sports Exerc.,* **46**: 572-579, 2014.

Disclosure of Interest: None Declared

AS-0076

NON-NEUROPATHIC DIABETIC INDIVIDUALS SHOW REDUCED ESTIMATED MUSCLE FORCES AT THE GAIT PUSH-OFF PHASE

Aline A. Gomes [1,*] Guilherme Bighetti [1] Maria Orselli [2] Marko Ackermann [3] Isabel Sacco [1]

[1] Physical Therapy, Speech, Occupational Therapy Department, University of Sao Paulo, [2] Biomedical Engineering Department, Centro Universitário Franciscano, [3] Department of Mechanical Engineering, Centro Universitário da FEI, Sao Paulo, Brazil

Introduction and Objectives: Investigation of lower limb muscles force still suffers experimental limitations and computational simulations add relevant information to the knowledge already acquired by direct EMG measurements (Sawacha et al., 2012), providing, for instance, estimations of muscle forces, important to a deeper understanding of the human gait. The aim of this study is to investigate the coordination of proximal (*iliopsoas- PS* and *biceps femoris- BF*) and distal muscles (*gastrocnemius medialis – GM, lateralis – GL, soleus- SO* and *tibialis anterior- TA)* of diabetic individuals during gait using an OpenSim model and static optimization tool to estimate muscle forces.

Methods: Data from ground reaction force (GRF) and hip, knee and ankle kinematics of 7 diabetic (DG – 56.0±9.4 yrs old, 70.0± 13.6 kg, 1.7±0.1 m, 4.5 yrs of diabetes, median of 4.5 MNSI-questionnaire score) and 18 healthy individuals (CG – 53.3 ± 8.5 yrs old, 69.0±6.8 kg, 1.7±0.04 m) were used as input variables for the computational gait model gait2392 in the OpenSim software. 3D kinematic data was recorded by an 8-camera *Optitrack®* (Natural Point, EUA) at a rate of 100 Hz. An AMTI OR61000 (Watertown, EUA) platform was used to acquire GRF at 1000 Hz. The force time series of proximal and distal muscles were calculated using the static optimization tool in OpenSim. The maximum muscle force and its time occurrence were calculated during some sub phases of the gait cycle and were compared between groups by t-tests (p<0.05).

Results: DG individuals showed lower maximum force of IL and GM at the push-off phase, compared to CG (table 1/ fig. 1). These muscles are important for this phase, and their insufficient strength may compromise the propulsion during walking. This fact could be responsible for some alterations in spatial–temporal patterns of diabetic walking (lower velocity, step length and stride length). Mueller et al. (1994) discussed that hip flexor muscles can drive the limb forward at the offset of stance phase to compensate the impaired function of gastrocnemius (hip gait strategy) in diabetic neuropathic individuals. However, ours results revealed lower distal and proximal forces of DG during push-off, and the iliopsoas didn´t compensate the impaired function of distal muscles. At the initial stance, DG exhibited higher muscle force of GM, GL and SO, DG also presented lower TA maximum force in the push-off phase compared to CG (table 1/ fig. 1). Furthermore, DG showed a late time occurrence of GL and SO maximum force at the initial stance, and an anticipated time occurrence of TA maximum force at the initial and terminal stance, compared to CG. These important muscle force deviations already present in diabetic subjects may not be solely attributed to nerve impairment but also to skeletal muscle dysfunction and degeneration prior to neuropathic complications (Andreassen et al., 2009; Krause et al., 2011).

Figure:
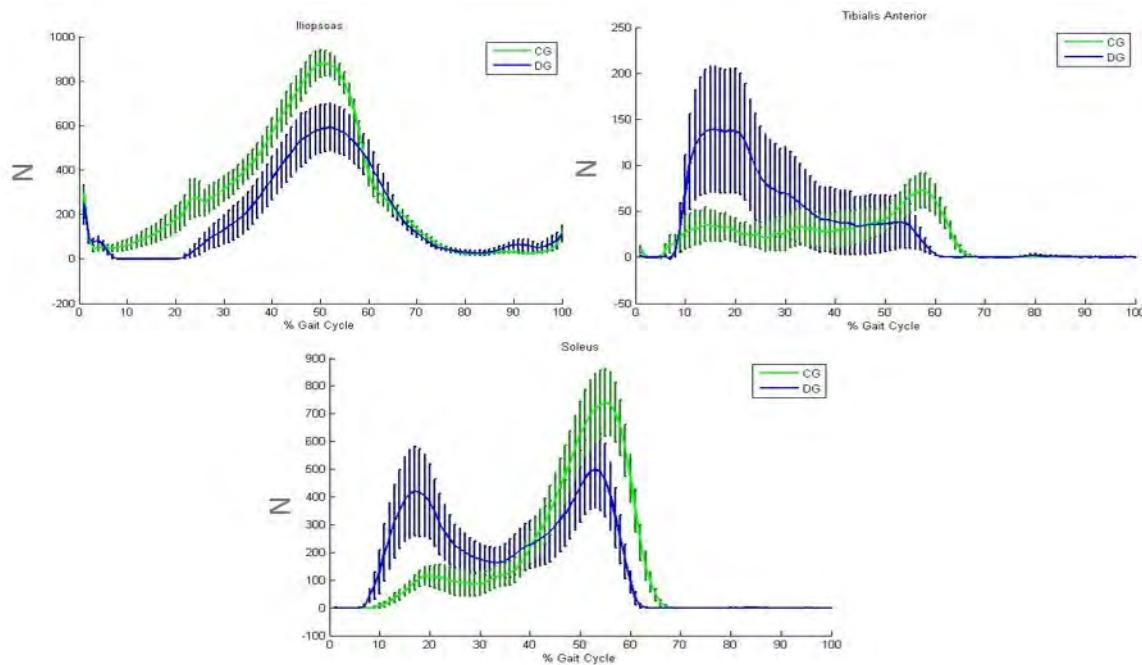
Caption: Figure 1. Time series of iliopsoas, tibialis anterior and soleus muscles force of Control Group (CG – n=18) and Diabetic Group (DG – n=7) during the gait cycle.

Conclusion: DG and CG showed distinct muscle force patterns of the distal muscles. DG individuals showed a higher maximum force and late time occurrence of maximum force of GL and SO at the initial stance. The lower maximum force of IL and GM in the transition of stance to swing phase in DG could compromise the propulsion during gait.

Table:

Muscles	Maximum Force (N)		*p-value	Occurrence of Maximum Force (% gait cycle)		*p-value
	CG (n=18)	DG (n=7)		CG (n=18)	DG (n=7)	
Biceps Femoris (0 – 15%)	229.3 ± 65.7	274.1 ± 60.7	0.139	3.7 ± 0.6	3.6 ± 1.1	0.867
Iliopsoas (30 – 70%)	923.1 ± 268.5	515.7 ± 81.0	<0.001	46.6 ± 4.5	44.2 ± 6.4	0.310
Gastroc. Medialis (0 – 10%)	437.7 ± 212.7	707.7 ± 170.8	0.006	3.9 ± 1.2	4.5 ± 1.5	0.306
Gastroc. Medialis (30– 50%)	898.3 ± 274.9	578.2 ± 224.5	0.011	36.9 ± 6.4	37.1 ± 7.6	0.945
Gastroc. Lateralis (0 – 10%)	55.0 ± 50.5	126.2 ± 65.7	0.007	3.5 ± 0.7	4.6 ± 1.5	0.016
Gastroc. Lateralis (30 – 50%)	172.6 ± 64.8	117.8 ± 42.1	0.051	38.9 ± 5.8	37.1 ± 7.6	0.530
Soleus (0 – 20%)	148.7 ±	440.9 ±	0.002	9.7 ± 8.5	17.2 ± 2.8	0.034

	176.7	233.1				
Soleus (30 – 60%)	864.9 ± 452.7	716.9 ± 126.6	0.408	50.4 ± 3.5	44.9 ± 10.1	0.053
Tibialis Anterior (0 – 20%)	213.7 ± 94.8	281.7 ± 75.9	0.076	5.2 ± 1.6	3.6 ± 0.3	**0.024**
Tibialis Anterior (40 – 70%)	80.6 ± 17.2	67.1 ± 13.5	**0.047**	58.6 ± 7.6	50.9 ± 9.2	**0.046**

*Independent t-test/ **Bold**: p<0.05

Caption: Table 1. Mean (± 1 standard deviation) of maximum force and time ocurrence of maximum force of proximal (psoas and biceps femoris) and distal muscles (gastrocnemius medialis and lateralis, soleus and tibialis anterior) of Control Group (GC) and Diabetic Group (DG).

References: [1] Sawacha et al., Gait Posture, 35(1):101-5, 2012.

[2] Mueller et al., Physical Therapy, 74:229-308, 1994.

[3] Andreassen et al., Diabetologia, 52:1182–91, 2009.

[4] Krause MP, Riddell MC, Hawke TJ. Pediatr Diabetes, 12:345–64, 2011.

Disclosure of Interest: None Declared

Modelling

AS-0077

MUSCLE CO-CONTRACTIONS – A NEUROLOGICAL PROBLEM?

Christian Wyss [1]Sebastian Krapf [1,*]Marie Freslier [1]Katrin Schweizer [1]

[1]Laboratory of Movement Analysis, Childrens University Hospital Basel, University of Basel, Basel, Switzerland

Introduction and Objectives: Co-contractions are often regarded as a sign of poor coordination and muscle control. There is the concept that an agonist activation should switch off the antagonist in a physiological situation and that the reason for a co-contraction is considered a failure of reciprocal inhibition [1]. A Simultaneous agonist and antagonist activity is considered abnormal, especially in patients with spastic neurological disorders such as cerebral palsy. Another putative reason for co-contractions lies in gaining stability by locking the joints spanned by the antagonistic muscles [2]. The hypotheses of this paper are first, that a co-contraction of an antagonist can be produced in an inverse dynamic model solely by changing the mechanical behavior of the agonist. This can be achieved in the absence of any neurological disorders. Second, we hypothesize that co-contractions not necessarily improve joint stability.

Methods: An instrumented gait analysis was performed in a healthy, normally developed 29 year old woman (53.6 kg, 1.62 m). The representative trial from 12 trials was determined using the SMaRT method [3]. Muscle modeling was done with the AnyBody Lower Extremity Model (AnyBody Version 6.0.3). The PlugInGait marker setup was supplemented by one marker below the lateral malleolus and one marker on the 1st and 5th metatarsal head to improve modeling of the subtalar joint. Kinematics were optimized using an algorithm introduced by Andersen [4]. For scaling a length mass fat scaling method [5] was applied. In a first step (norm model) an inverse dynamic analysis using force dependent kinematics [6] was performed. The model calculates the translation between talus and tibia in anterior-posterior and distal-proximal direction in the local coordinate system of the ankle joint. In the second step (stiff model) co-contractions were evoked by changing muscle stiffness only. This was achieved using the AnyMuscleActivityBound class of the AnyScript language by setting the upper bound of the muscle activity proportional to the muscle's shortening velocity, which we derived as a result from the first step (normal model). Thereby, the gastrocnemii muscles depend more on their stretch velocity which increases stiffness with faster muscle contraction.

Results: During the whole stance phase there is a slight co-contraction of the tibialis anterior muscle even though the examined subject was healthy and showed no spasticity (Fig 1, blue).

Increasing stiffness enlarged the force of the gastrocnemii muscles in early stance and in late swing phase. This change resulted in a contemporary increase of the tibialis anterior muscle force (Fig 1, red).

The second parameter of interest was the shift at the ankle joint. In the normal situation there is a translation in posterior direction with a peak of 1.6 mm at 20% of the gait cycle. Increased muscle stiffness leads to an unstable situation at 10% gait cycle shown by oscillation of the translational movement. In contrast to the "norm model", the "stiff model" showed a massive translation of the talus in posterior direction at the moment of co-contraction of the tibialis anterior muscle (between

40 - 60% and between 70 - 90% of the gait cycle).

Figure:

M. Tibialis anterior
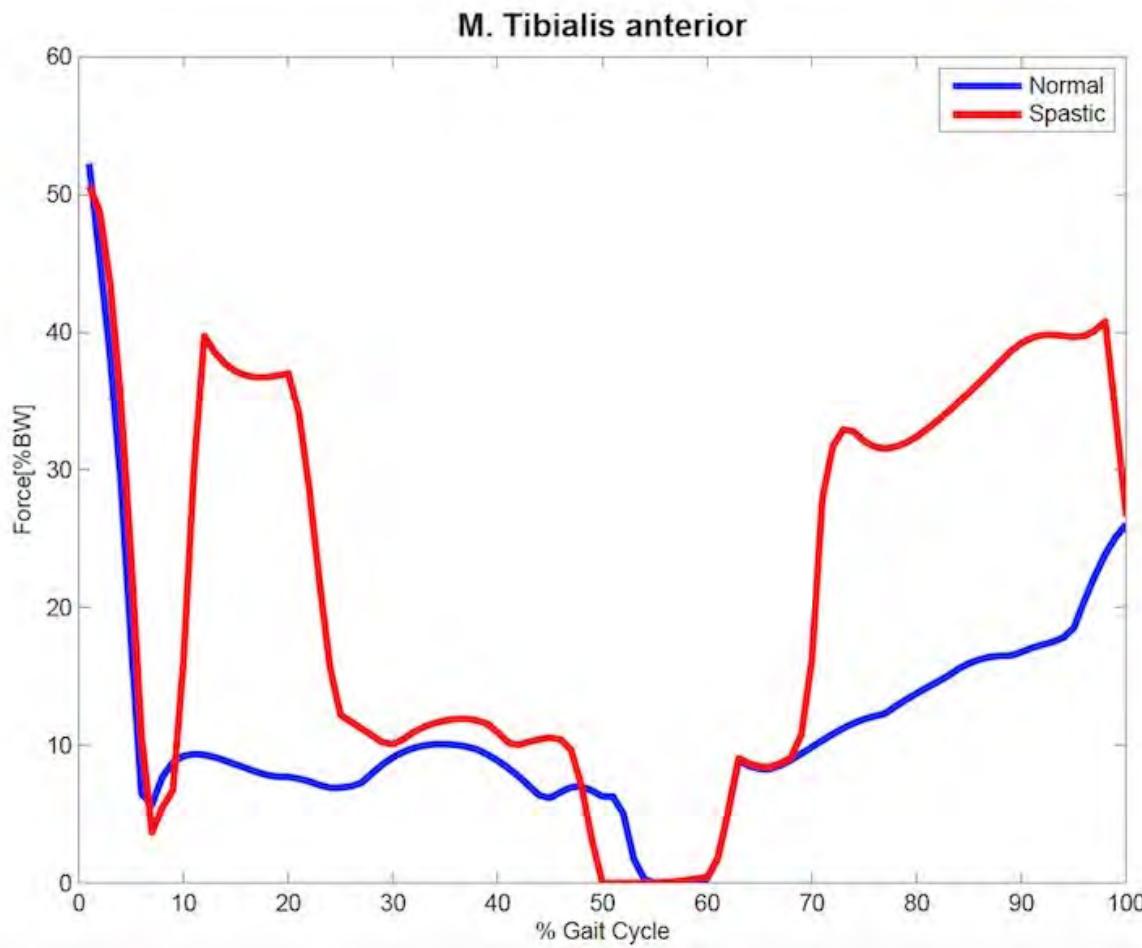
Caption: Figure 1

Conclusion: We conclude that increased activity of a biarticular muscle due to a stiffer material behavior may lead to a co-contraction of its antagonists without the presence of any neurological disease. Consequently, it is not conclusive that co-contractions are a sign of a neurological disease as many clinicians still assume. Moreover these co-contractions result in an increased translational shift which indicates a potential joint instability.

References:

[1] Gelber et al., Human Press, 1–397, 2002

[2] Besier et al., Journal of Biomechanics, 42(7), 898–905, 2009

[3] Schweizer et al., Journal of Biomechanics, 45(13), 2306–2309, 2012

[4] Andersen et al., Computer Methods in Biomechanics and Biomedical Engineering, 13(2), 171–183, 2010

[5] Rasmussen et al., International Symposium on Computer Simulation in Biomechanics, 2005

[6] Andersen et al., 13th Biennial International Symposium on Computer Simulation in Biomechanics, 2011

Disclosure of Interest: None Declared

Prosthetics

AS-0078

IS KINETIC ASYMMETRY IN BELOW-KNEE AMPUTEE GAIT INEVITABLE? -- A PREDICTIVE SIMULATION STUDY

Anne Koelewijn [1,*]Antonie van den Bogert [1]

[1]Department of Mechanical Engineering, Cleveland State University, Cleveland, OH, United States

Introduction and Objectives: An important goal for amputee walking is to regain a symmetric walking pattern. Below-knee amputees are often able to regain close to normal joint kinematics in the hip and knee when using a prosthetic foot [1], but the joint moments are asymmetric and different from joint moments in able bodied gait [1], which may contribute to a higher occurrence rate of osteoarthritis in amputees [2].

We hypothesize that amputees choose to have asymmetry in joint moments to minimize the effort of walking. To test this hypothesis, we used a musculoskeletal model to predict amputee gait with and without a symmetry constraint on the hip and knee moment. The results were compared in terms of effort of walking.

Methods: Predictive simulations of gait were performed with a sagittal plane model having nine degrees of freedom and 16 muscles. An open loop optimal control problem was formulated to find a gait cycle that minimizes deviation from normal gait kinematics and a weighted sum of muscular effort, which was defined as the mean of the cubed muscle activations. The model and solution method were identical to [3], but a full gait cycle was simulated.

The optimal control problem was solved for an able-bodied system and a below-knee amputee system. For the latter case, three muscles in the lower leg were removed and replaced by a passive rotational spring in the ankle that applies a moment to the ankle given the angle and angular velocity. The stiffness and damping of the spring were chosen to be equal to 600 [Nm/rad] and 15 [Nms/rad].

The optimal control problem for the below-knee amputee system was first solved without symmetry constraint (baseline), then with a symmetry constraint on the hip moment, with a symmetry constraint on the knee moment and with a symmetry constraint on the hip and knee moment. The symmetry constraint was defined such that the joint moment in the left and right leg should be the same with a phase shift of 50% of the gait cycle.

Results: Table 1 gives an overview of the results that were found for the predictive simulations. The mean muscle activation decreased by 1.4% with a symmetry constraint applied to the hip moment. An increase of 0.76% and 4.3% was seen when a symmetry constraint was placed on the knee moment and the knee and hip moment, respectively. The symmetry constraint on the knee moment also improved the symmetry in the hip moment. However, the opposite was true when a constraint is placed on the hip moment.

Figure 1 shows joint angles and joint moments when a symmetry constraint was applied to the knee and hip moment (black line), compared to the baseline (red line). One can see that the symmetry constraint yields a decrease in peak extension knee moment of the intact leg (dashed line), but an increase in peak extension hip moment in the residual leg (solid line).

Figure:
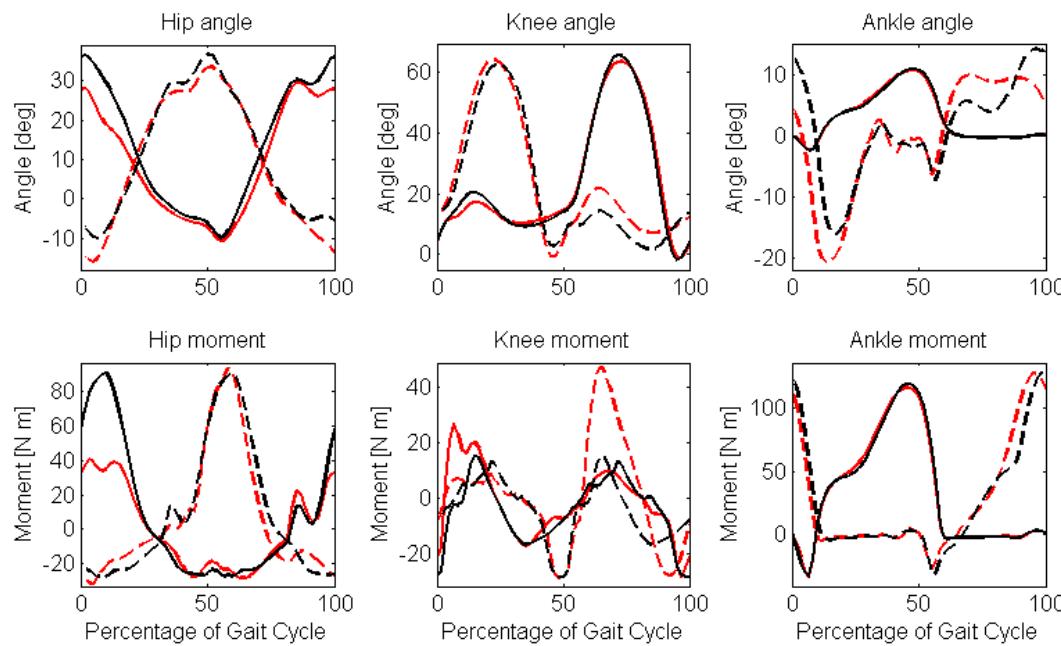
Conclusion: The amputee model was able to walk with perfectly symmetric joint moments, but the hypothesized increase in effort did not occur. The effort even decreased when a symmetric hip moment was imposed on the model. The kinematic tracking error increased slightly in all cases where joint moment symmetry was required. This indicates that there is a trade-off in below-knee amputee gait between walking with symmetric joint moments and walking with normal kinematics. When the amputee model walked with symmetric joint moments, the knee and hip moments, while symmetrical, were very different from a normal able-bodied joint moments. Especially, the peak hip extension moment in the both legs became excessively high, suggesting that it is not advantageous for below-knee amputees to walk with symmetric joint moments, since this might yield an increased chance of developing osteoarthritis in both legs. Therefore, our results show that it is desirable to have a kinetic asymmetry in below-knee amputee gait.

Table:

System	Mean Muscle Activation	RMS tracking error [deg]			Peak Knee Extension Moment		Peak Hip Extension Moment	
	x1e-2	Hip	Knee	Ankle	Residual	Intact	Residual	Intact
Able-Bodied	7.88	3.7	1.5	1.7	41.6	41.6	43.5	43.5
BKA, no constraint	8.56	5.3	2.3	2.5	26.9	47.5	40.6	93.8
BKA, hip constraint	8.44	5.6	3.2	5.4	15.2	58.6	66.7	66.7

BKA, knee constraint	8.63	5.8	3.0	5.2	26.2	26.2	53.7	87.7
BKA, both constraints	8.93	7.6	4.3	5.8	15.3	15.3	91.0	91.0

Caption: Table 1 - Overview of the results of the predictive simulations

References: [1] Ventura, J. D., G. K. Klute, and R. R. Neptune. "The effects of prosthetic ankle dorsiflexion and energy return on below-knee amputee leg loading." *Clinical Biomechanics* 26.3 (2011): 298-303.

[2] Lemaire, E. D., and Fisher F. R. "Osteoarthritis and elderly gait." *Arch Phys Med Rehabil* 75 (1994): 1094-1099.

[3] Van den Bogert, A. J., et al. "Predictive musculoskeletal simulation using optimal control: effects of added limb mass on energy cost and kinematics of walking and running." *Proc Inst Mech Eng, P: J of Sports Eng Technol* (2012).

Disclosure of Interest: None Declared

Musculoskeletal

AS-0079

DOES ACHILLES TENDON CONTRIBUTE TO THE FORCE POTENTIATION INDUCED BY STRETCH-SHORTENING CYCLE?

Atsuki Fukutani [1 2 3,*]Andrew Sawatsky [1]Timothy Leonard [1]Walter Herzog [1]

[1]Kinesiology, University of Calgary, Alberta, Canada, [2]Research Organization of Science and Technology, Ritsumeikan University, Shiga, [3]Research Fellowship for Young Scientists, Japan Society for the Promotion of Science, Tokyo, Japan

Introduction and Objectives: Tendon elongation is considered to be the primary reason for the force potentiation by stretch-shortening cycle (SSC effect) because tendons can store elastic energy during the eccentric phase and release it during the subsequent concentric phase [1]. In addition, tendon elongation can optimize muscle length changes [2]. However, direct examination of the influence of tendon elongation on the SSC effect has not been conducted. Therefore, the purpose of this study was to examine directly whether tendon elongation contributes to the SSC effect by comparing the amount of SSC effect obtained for the following two conditions; (1) SSC with the tendon fully intact, and (2) SSC with the free tendon removed.

Methods: The soleus muscle of rats was dissected free of surrounding connective tissue with the blood supply left intact. In the "intact tendon" condition, the calcaneus was held rigidly by attaching it to a load cell. For the "removed tendon" condition, the muscle-tendon junction was identified and held rigidly using a specifically designed tendon clamp, thereby eliminating the free tendon from contributing to the mechanics of the soleus under these conditions. In both conditions, three types of contraction were evoked to calculate the amount of the SSC effect. First, a concentric contraction without prior activation (Pure CON) was performed. Second, a concentric contraction following an isometric contraction was performed (Pre ISO).Finally, a concentric contraction immediately following an eccentric contraction was performed (Pre ECC). Muscle lengthening and shortening was 3 mm, and the lengthening and shortening velocities were 6 mm/s and 20 mm/s, respectively. Work done during the concentric phase was quantified as the determinant for the SSC effect. The SSC effect was expressed as the relative value of work obtained in Pre ISO and Pre ECC with respect to Pure CON.

Results: For the intact and removed tendon conditions, work done during the concentric phase was largest for the Pre ECC (intact: 3.34 ± 0.20 J·10^{-3}; removed: 3.22 ± 0.03 J·10^{-3}), followed by the Pre ISO (intact: 2.46 ± 0.11 J·10^{-3}; removed: 2.38 ± 0.26 J·10^{-3}), and finally the Pure CON (intact: 1.45 ± 0.06 J·10^{-3}; removed: 1.44 ± 0.16 J·10^{-3}). The SSC effect was significantly greater for the Pre ECC (intact: $230.8 \pm 22.7\%$, removed: $226.0 \pm 27.6\%$) than the Pre ISO (intact: $169.3 \pm 0.7\%$, removed: $165.5 \pm 0.5\%$) independent of the tendon condition. For all corresponding concentric contractions, the work done was similar for the intact and removed tendon conditions. However, peak forces at the onset of the concentric phase were higher in intact than in removed tendon condition.

Figure:

Intact tendon · Removed tendon

● Onset of concentric contraction

Force (N)

Muscle length from optimal length (mm)
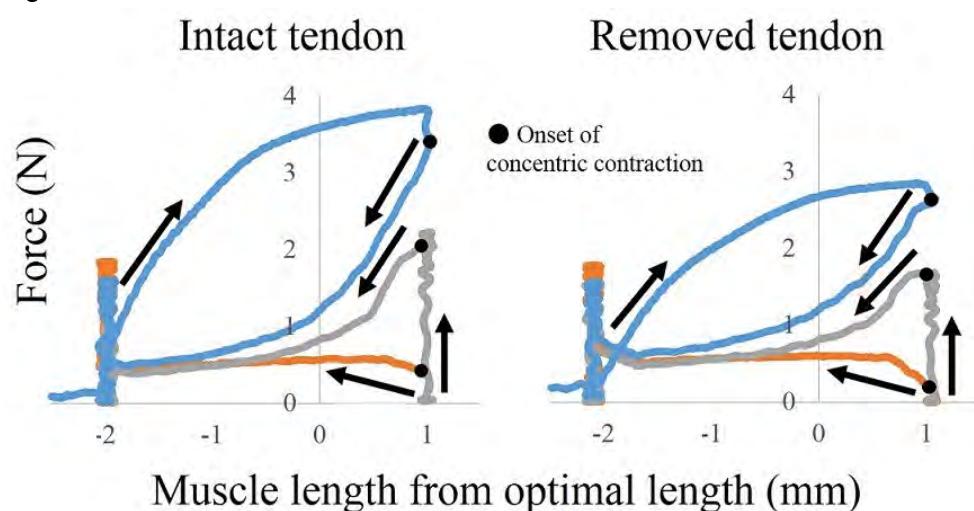
Caption: Force-length loop obtained during SSC with the tendon intact (left) and the tendon removed (right). Orange, gray, and blue lines show force-length data obtained for the Pure CON, Pre ISO, and the Pre ECC conditions, respectively. Work done during the concentric phase was calculated as the area under the force-length curve obtained during concentric contraction.

Conclusion: Although many studies have suggested that tendon elongation is the primary factor for the SSC effect, no difference in the SSC effect was found between the intact and removed tendon conditions. This result may be attributable to a negligible tendon elongation. The fact that we observed a substantial SSC effect even with the tendon removed indicates that tendon elongation is not the primary factor for SSC effect. Other factors contributing to the SSC effect could be the stretch reflex response, pre-activation, and residual force enhancement. Because a fully-tetanic electrical stimulation was used in this study, the influence of any stretch reflex response can be discarded. We confirmed that the SSC effect was found in Pre ISO, where no active lengthening was present, thus pre-activation likely contributes substantially to the SSC effect. Considering that the SSC effect was larger in the Pre ECC than the Pre ISO, active lengthening-induced force potentiation (residual force enhancement) likely also contribute to the SSC effect. Peak force at the onset of the concentric contraction was different, although work done was similar between the intact and removed tendon conditions. Since work performed was similar, we exclude the possibility of muscle fatigue or damage as the cause for the reduced peak forces in the tendon removed conditions. This surprising result will need to be considered in detail in the future. In conclusion, tendon elongation does not contribute to the SSC effect in the rat Achilles tendon, and large SSC effects are possible without a free tendon. This result may be applied to the human Achilles tendon which is thought to be relatively stiff as well. More compliant and/or longer tendons, such as in kangaroo hind limbs, which are known to store and release elastic energy, may behave differently than observed here in the rat soleus.

References: [1] Alexander, Nature, 265: 114-117, 1977.

[2] Fukunaga et al., Proc. Biol. Sci., 268: 229-233, 2001.

Disclosure of Interest: None Declared

Musculoskeletal

AS-0080

A BETTER UNDERSTANDING OF CEREBRAL PALSY PATHOLOGY USING 3D SUBJECT-SPECIFIC MUSCULOSKELETAL MODELING

Ayman Assi [1,*]Abir Massaad [1] [2]Ziad Bakouny [1]Nour Khalil [1]Christophe Sauret [3]Wafa Skalli [3]Ismat Ghanem [1]

[1]Laboratory of Biomechanics and Medical Imaging, School of Medicine, University of Saint-Joseph, [2]Gait lab, SESOBEL, Beirut, Lebanon, [3]Laboratoire de Biomécanique, Arts et Métiers ParisTech, Paris, France

Introduction and Objectives: Spasticity in children with cerebral palsy (CP) affects muscle function and geometry and is related to the development of skeletal malalignments during growth, which can both cause gait alterations [1,2]. Assessment of the pathology is usually based on the evaluation of muscle function, the medical imaging of skeletal lower limbs and gait analysis. Generic models are widely used in the literature in order to understand CP pathology. The aim of this study is to use 3D subject-specific data obtained from musculoskeletal modeling along with gait analysis in order to better understand motor dysfunctions in CP and to compare these to normal locomotion in typically developing (TD) children.

Methods: Twenty-two spastic CP children (mean age: 11±3; diplegia N=16, hemiplegia N=6; GMFCS I N= 14, GMFCS II N=6, GMFCS III N=2), with neither medical nor surgical histories, had undergone 3D gait analysis. Joint kinematics of the lower limbs were calculated in the frontal, sagittal and horizontal planes. An EOS® biplanar X-ray exam was performed in order to calculate the 3D skeletal parameters of the pelvises and the lower limbs: femoral anteversion, tibial torsion, neck shaft angle, acetabular parameters and pelvic parameters [3]. This was performed on 44 lower limbs of CP children. Axial MRI acquisitions were performed on 28 lower limbs of the CP group, in order to obtain 3D subject-specific reconstructions of 18 muscles in each limb [4] (Figure 1). Based on these reconstructions, each muscle's length and volume were calculated and then normalized to lower limb length and body mass respectively. All kinematic and musculoskeletal parameters were age-matched to 22 lower limbs of TD children. Statistical differences were investigated between the CP and TD populations for all parameters (T-test and Wilcoxon). Correlations between the parameters were evaluated using the Pearson and Spearman tests.

Results: Femoral anteversion, pelvic incidence and sacral slope were significantly increased in CP when compared to TD children (p<0.001). Anova test showed a significant difference for the femoral anteversion between TD children and CP children with GMFCS level II. The normalized lengths of the gracilis, vastus intermedius, soleus, adductor brevis and longus were significantly smaller in CP children with GMFCS level II compared to TD children (p<0.001). The normalized muscle volumes of the CP children were smaller for the femoral biceps longus, rectus femoris, gastrocnemius medius, vastus intermedius, adductor brevis and longus in CP children with GMFCS II when compared to TD children (p<0.001). Fifteen lower limbs of children with CP presented excessive internal hip rotation during gait when compared to normative values. For these 15 lower limbs, femoral anteversion was significantly increased in children with CP (p<0.001), when compared to TD children, and was correlated to mean hip rotation during stance phase (R=0.54). 3D acetabular anteversion and abduction were correlated to hip rotation at initial contact (R=0.64) and peak hip rotation during stance phase (R=-0.5) respectively.

Figure:

Caption: Figure 1- Example of subject-specific 3D reconstruction of musculoskeletal lower limbs in children with cerebral palsy

Conclusion: For the first time, musculoskeletal 3D subject-specific parameters in CP could be compared to those of TD children. In these preliminary results, femoral anteversion, pelvic parameters and hip adductors, among other muscles, were only shown to be significantly altered when GMFCS was higher than I. These results showed that 3D femoral anteversion might contribute to internal hip rotation during gait, which is not in concordance with previous studies based on generic models [5,6]. Moreover, 3D acetabular parameters, studied for the first time in CP, were shown to be related to internal hip rotation during gait. Larger groups of subjects will allow us to better understand the evolution of the musculoskeletal deformities that occur during the growth of spastic CP children, when compared to the growth of TD children.

References: [1] Shortland A., Dev Med Child Neuro, 2002. [2] Mohagheghi AA., Clinical Biomechanics, 2007. [3] Assi A, Eur J Radiology, 2013. [4] Jolivet E, CMBBE, 2008. [5] Aktas S., JPO, 2000. [6] Carriero A., JPO, 2009.

Disclosure of Interest: None Declared

AS-0081

WALKING VS. NORDIC WALKING EXERCISE: DIFFERENCES IN TRUNK MUSCLE ACTIVITY AND IMPACT ACCELERATION

Luca Zoffoli [1]Francesco Lucertini [1]Ario Federici [1]Massimiliano Ditroilo [2,*]

[1]Department of Biomolecular Sciences - Division of Exercise and Health Sciences, University of Urbino 'Carlo Bo', Urbino, Italy, [2]Department of Sport Health and Exercise Science, University of Hull, Hull, United Kingdom

Introduction and Objectives: According to the International Nordic Walking Association, Nordic Walking (NW) is "… *a form of physical activity, where regular, natural walking is enhanced by the addition of the active use of a pair of specially-designed Nordic Walking poles*". When compared to walking (W), previous research has shown that NW can enhance several physiological parameters, including the energy expenditure [1]. Notably, NW has been successfully used with the elderly, in obesity management, in chronic low-back pain, etc [2].

Despite the increasing popularity of the NW as an exercise intervention there is a paucity of biomechanical research to explain the effectiveness of this type of exercise and its benefits over W.

The role of the trunk muscles during walking, for example, is of great interest because altering their function can lead to pathologies such as chronic low-back pain [3]. Likewise, information on the strain experienced by the lumbar spine, as measured by accelerometry, may be relevant [4]. Accordingly, this study aimed to concurrently measure the activity of 5 trunk muscles and the impact accelerations at the sacrum whilst performing W and NW at different velocities and slopes.

Methods: Twenty-one healthy participants (10 males and 11 females) aged 31.2 ± 8.3 years old have been recruited for this study, which required two visits to the lab on separate days. The first visit was used to familiarise the participants with the procedures and to determine the Preferred Transition Speed (PTS, the greatest speed at which the participant can comfortably walk before starting running). During the second visit EMG electrodes were placed on the following muscles: upper (RAp) and lower (RAd) portion of the Rectus Abdominis, medial portion of the External Oblique (EO), Erector Spinae (ES) and Multifidus (MF) on the arm-dominant side. Further, two 3D accelerometers were placed over the tibia and sacrum. Following 5 minutes of warm-up, walking (either W or NW) was performed at different slopes (0% or 7%) and different speeds (60%, 80% and 100% of the PTS). Each trial was performed for 1 minute, separated by at least 1 minute rest, in random order.

All signals were sampled at 1500Hz at 16bit-resolution. Appropriate filtering and processing were carried out to obtain a linear envelope for EMG and a smoothed acceleration signal. They were then time-normalised to 101 points and the 30 central valid steps for each tested condition were averaged point by point. For each muscle the mean EMG amplitude was calculated and then normalized to the W-0% slope-100% PTS condition. Vertical and resultant sacrum acceleration peaks were determined whereas vertical peaks of the tibia were only used as a reference to calculate steps length and frequency.

Generalized Estimating Equations were used to determine whether statistical differences in the dependent variables occurred across type of walking, slope and speed conditions.

Results: The key results presented here focus on the effects of type of walking and slope on the nine dependent variables and on the interaction of type of walking, slope and speed on the MF muscle. Step length, step frequency and EO mean amplitude show a significant difference between W and NW. Specifically NW induced an increase in step length (1.63±0.21 vs. 1.54±0.21 m, p<0.001) and a reduction in step frequency (0.93±0.12 vs. 0.98±0.11 Hz, p<0.001) whilst the activity of the EO muscle is increased in NW when compared to W (1.15±0.83 vs. 0.72±0.34, p<0.05). Slope reduced step frequency (0.93±0.12 vs. 0.98±0.11 Hz, p<0.001) and increased the activity of the EO muscle (0.98±0.66 vs. 0.89±0.68, p<0.01). The activity of the MF muscle is significantly augmented when walking uphill (figure 1). Interestingly, at lower speed the MF exhibited greater amplitude during NW whereas at higher speed the trend is reversed (figure 1).

Figure:
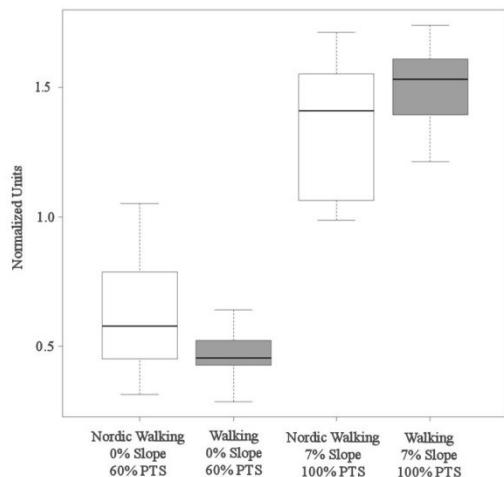
Caption: The effect of type of walking, slope and speed on the Multifidus muscle. The thick line represents the mean values. Min, Max, first and third quartile are also reported.

Conclusion: The results suggest that the poles used during NW altered the lower limb walking kinematics producing effects similar to those related to uphill walking and this makes it generally suitable for healthy individuals. NW yielded a greater activity of the EO muscle arguably because of the higher trunk torsion due to longer steps. Further, whilst it did not influence the impacts at the sacrum level, it did alter the recruitment pattern of the lower back muscles (MF) suggesting the effectiveness of NW at specific conditions. Based on the latter result, this particular muscle would be stressed to a lesser extent in patients suffering from low-back pain if they undertook NW uphill and W on a flat surface.

References: 1.   H. Figard-Fabre, et al., Eur J Appl Physiol, 108 (6): 1141-1151, 2010.

2.   B. Fritz, et al., Gait posture, 34 (2): 234-238, 2011.

3.   S. P. Silfies, et al., Clin Biomech, 20 (5): 465-473, 2005.

4.   J. J. Kavanagh, et al., Gait posture, 28 (1): 1-15, 2008.

Disclosure of Interest: None Declared

Musculoskeletal

AS-0082

LOWER AGONIST ACTIVATION MAY EXPLAIN WHY LENGTHENING THE RECTUS FEMORIS MUSCLE DOES NOT INCREASE KNEE EXTENSION TORQUE

Theodoros Bampouras [1 2,*]Neil Reeves [2]Bill Baltzopoulos [3]Constantinos Maganaris [4]

[1]Medical and Sport Sciences, University of Cumbria, Lancaster, [2]School of Healthcare Science, Manchester Metropolitan University, Manchester, [3]Centre for Sports Medicine and Human Performance, Brunel University, Uxbridge, [4]Research Institute for Sport and Exercise Sciences, Liverpool John Moores University, Liverpool, United Kingdom

Introduction and Objectives: Knee extensor muscle torque has been shown to change with different hip joint angles. The change in position can affect the biarticular rectus femoris muscle, which contributes approximately 17% to quadriceps torque output. Consequently, the position change will affect the overall torque generated by the knee extensors. Indeed, musculoskeletal modelling studies predict higher quadriceps torque with the rectus femoris muscle in a lengthened position (e.g. supine) compared to a shortened one (e.g. seated). However, this has not been confirmed by results from experimental studies. As experimental studies typically utilise voluntary contractions of the quadriceps, the reasons for this contradiction could be due to differences in agonistic muscle activation capacity or differences in antagonistic muscle co-activation, in one position compared to the other. The aim of the present study was to establish whether this discrepancy is attributed to differences in muscle activation capacity and / or differences in antagonistic muscle co-activation.

Methods: Following Institutional Ethics approval, nine healthy, active males (age 30.2 ± 7.7 years, stature 1.78 ± 0.09 m, body mass 81.7 ± 11.2 kg), free from any musculoskeletal injuries, were tested in seated (hip joint angle = 90˚), and supine (hip joint angle 160˚) (full hip joint extension = 180˚) positions, with the knee and ankle joint angles at 90˚ for both conditions. Subjects were fixed in a custom-made dynamometer, specifically developed for assessing isometric contractions and had very limited compliance of the lever arm and the bed. In addition, firm fixation was ensured with straps over the pelvis and tested thigh. The lower leg was securely strapped to the force transducer. For the supine position, additional constraints were placed on the shoulders preventing extraneous movement. Subjects performed seated and supine maximum voluntary isometric contractions (MVC) and torque from the quadriceps was recorded. Antagonistic torque was estimated from bicep femoris EMG during isometric maximal and submaximal knee flexion contractions. Corrected MVC torque for both positions was also calculated, as the sum of the recorded torque during the respective MVC and the antagonistic torque elicited by co-contraction. Finally, supramaximal electrical stimulation intensity was examined in both positions to confirm that the same level of stimulation intensity can activate the muscles to similar levels with the rectus femoris lengthened and shortened. Subsequently, quadriceps submaximal tetanic stimulation (with the same stimulation intensity) was also performed in both positions and torque was recorded (STIM). Differences between the two positions for all variables were examined using a dependent Student's t-test and effect size (ES) was calculated for significantly different comparisons.

Results: MVC was not significantly different between supine (245 ± 71.8 Nm) and seated (241 ± 69.8 Nm) positions. Similarly, corrected MVC was not significantly different in supine (257 ± 77.7 Nm) compared to seated (267 ± 87.0 Nm)

positions. Supramaximal stimulation intensity did not differ between positions, however STIM was significantly higher (p=0.001, ES = 1.0) in supine (111 ± 31.9 Nm) than seated (99 ± 27.5 Nm) positions.

Conclusion: The higher STIM torque in the supine compared to the seated position agrees with predictions from musculoskeletal model studies. However, when the contractions were voluntary (and, thus, neural input involved), neither MVC nor corrected MVC were different. The combination of these results suggest that the discrepancy in quadriceps torque between musculoskeletal modelling and experimental studies is not because of antagonistic co-activation but due to reduced rectus femoris activation capacity in the lengthened (supine) position. This reduced activation is likely attributed to a) inadequate fixation of the pelvis during the supine assessment position, and b) reduced vestibular feedback in the supine position, resulting in reduced muscle activity. These findings should allow closer monitoring of the true torque and standardisation of muscle function assessment procedures. Additionally, they should assist the development of more realistic muscle models which will account for the change in activation capacity in different muscle lengths.

Disclosure of Interest: None Declared

AS-0083

LONG-TERM BIOMECHANICAL ADAPTATION IN A BIOLOGICALLY-RECONSTRUCTED FEMUR AFTER EWING SARCOMA

Giordano Valente [1,*] Lorenzo Pitto [1] Sabina Piroddi [1] Enrico Schileo [2] Andrea Roncari [1] Alberto Leardini [3] Marco Manfrini [4] Fulvia Taddei [1]

[1] Medical Technology Laboratory, [2] Computational Bioengineering Laboratory, [3] Movement Analysis Laboratory, [4] Musculoskeletal Oncology, Rizzoli Orthopaedic Institute, Bologna, Italy

Introduction and Objectives: Biological reconstruction of the femur using massive bone allograft (MBA) is a worldwide solution for limb-salvage surgery after bone sarcoma. Because of the risk of MBA mechanical failure and size limitations of vascularised fibula autografts (VFA), a combination of VFA placed inside a MBA represents an original solution [1]. However, the remodelling and long-term survival of the reconstruction are not consistent [2], and there is limited knowledge about functional outcomes after surgery based on quantitative data.

Our aim is to study the long-term biomechanical adaptation in a paediatric oncology case of biologically reconstructed femur, by analyzing: (i) musculoskeletal forces and muscle compensation strategies in different motor tasks through image-based musculoskeletal modeling; (ii) mechanical stress in the reconstruction during the motor tasks through finite element analysis, also including potential revision surgery scenarios.

Methods: The patient (male, 8 years old) underwent a biological reconstruction of the proximal right femur, and was then continuously disease free. CT scans of the lower limbs were acquired post-operatively and during follow-ups at every 6 months for routine controls. The evolution of bone morphology and density was quantitatively evaluated. After 7 years, the patient underwent gait analysis (walking, chair rise/sit, stair ascent/descent, squat) and CT scanning after being instrumented with the same reflective marker setup [3]. A 9-body segment, 12 degree-of-freedom articulated 3D linkage actuated by 85 musculotendon actuators was created from these images (Figure) using a previously developed framework [4], and a typical inverse dynamics and static optimization approach was then applied to calculate muscle and joint contact forces during each motor task. Subject-specific finite element models of both femurs were built using a validated procedure [5]. The subject-specific muscle and joint contact forces were applied as loading conditions onto the corresponding nodes, and physiologically-oriented constraints were used [6]. Plate and screws safety was tested in terms of von Mises stresses against fatigue limit. Bone principal strains and strain energy density were computed to assess risk of fracture [5] and remodeling stimulus [7], respectively. In the operated femur, the finite element analyses were repeated simulating different screw-removal configurations to reduce the expected stress-shielding.

Results: Overall, joint contact forces were larger in the contralateral limb during all motor tasks, except for walking. Knee and ankle loads were markedly higher (up to 3 body-weight difference), particularly in double-support tasks (chair rise/sit and squat). Muscle compensation strategies showed large forces of the vasti and gastrocnemius muscles of the contralateral limb, while gluteii and biarticular hip muscle forces of the operated leg were marked.

Plate and screws stresses were below critical values for titanium alloy fatigue in all motor tasks. While maximum strains were not critical in both femurs (safety factor of 3 or above) in the non-demanding motor tasks, the average strains in the

operated femur were lower than in the intact contralateral. A marked regional variation in strains and strain energy density was observed within the allograft: normal levels in medial compartment, extremely low values in anterior and posterior compartments. Despite the allograft thinning already observed during follow-up, the mechanical condition in the anterior and posterior compartments appears compatible with a further bone resorption. When simulating different patterns of proximal screws removal, we found that their complete removal would be needed to restore a more physiological bone strain configuration.

Figure:
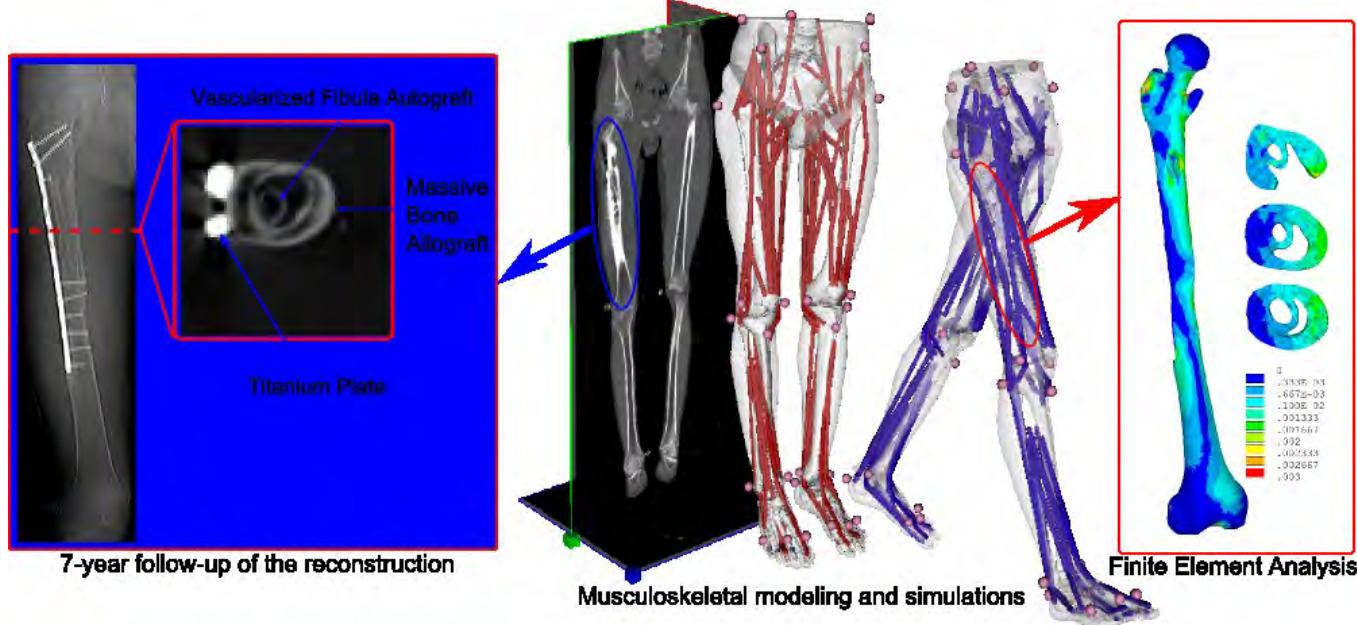
Caption: Workflow of subject-specific musculoskeletal modeling and simulations of the motor tasks and finite element analysis of the femurs

Conclusion: This study presents a successful integration of subject-specific musculoskeletal modeling and finite element organ level analysis of a long-term biomechanical reconstruction after Ewing sarcoma. The predicted musculoskeletal forces and muscle compensation strategies can provide advice for rehabilitation therapy in specific clinical scenarios. The results from finite element analysis allow interpretation of the complex bone remodeling mechanism, and seems not to imply a high risk for the remaining screws and plate, nor for bone in the medial compartment, but suggests caution in the post-operative phase due to reduced bone thickness and density in the lateral compartment.

References: [1] Manfrini et al., AJR A. J. Roengenol, 182: 963-70, 2004.

[2] Ogilvie et al., Clin Orthop Relat Res, 467: 2685-90, 2009.

[3] Leardini et al., Gait Posture, 26: 560–571, 2007.

[4] Valente et al., PLoS ONE, 9: e112625, 2014.

[5] Schileo et al., J Biomech, 47: 3531-8, 2014.

[6] Speirs et al., J Biomech, 40: 2318-23, 2007.

[7] Huiskes et al., Clin Orthop Relat Res, 274: 124-34, 1992.

Disclosure of Interest: None Declared

Musculoskeletal

AS-0084

A SIMPLE, MRI-BASED METHOD FOR MEASURING 3D MOMENT ARMS OF HUMAN MUSCLES UNDER DYNAMIC CONDITIONS

Elizabeth Clarke [1,*] Joshua Martin [1] Agnes d'Entremont [2] Marcus Pandy [3] David Wilson [2] Robert Herbert [4]

[1] Kolling Institute, Sydney Medical School, University of Sydney, Sydney, Australia, [2] Mechanical Engineering and Department of Orthopaedics, University of British Columbia, Vancouver, Canada, [3] Mechanical Engineering, University of Melbourne, Melbourne, [4] Neuroscience Research Australia, University of New South Wales, Sydney, Australia

Introduction and Objectives: Muscle moment arms are widely used in biomechanics. Applications include measuring muscle length changes with joint angle and determining muscle force from joint torque and subject-specific musculoskeletal models. Some applications require subject-specific muscle moment arms to be measured non-invasively in living human subjects. Many researchers capture joint and tendon images in a single anatomical plane (2D) but this may overestimate the 3D muscle moment arm [1]. Other methods capture tendon and joint images at one or a few static joint positions, but it may be interesting to know how the moment arm changes throughout the joint's range, and moment arms may differ under static and dynamic conditions [2]. A 3D dynamic MRI method has been developed [3] but it uses cyclic rotation of the joint and MRI-gating. We aimed to develop and validate a simple method for non-invasively and dynamically measuring 3D muscle moment arms in vivo from a single joint rotation cycle in humans.

Methods: The Achilles tendon moment arm was measured in 5 men and 5 women aged 22-48 years. Participants lay supine in a 3T scanner (Philips Achieva) and the relaxed ankle was slowly rotated through range. Two sets of scans were obtained: a high resolution 3D MRI scan of the stationary joint (3D T1-weighted FSE, 4.7 minutes, flip angle 90º, matrix 320×320, FOV 160×160mm, TR/TE = 355.76/16.68ms, slice thickness 1mm; approx. 4 minutes) and a series of ultra-fast MRI scans of the slowly moving joint (ultrafast (turbo) gradient echo, flip angle 10º, matrix 320×320, FOV 320×320mm, TR/TE = 2.731/1.34ms, slice thickness 4mm, slice gap 0.4-3.0mm depending on joint size, 40 dynamics (phases), 8 slices, 104 seconds,). Bone and tendon geometries were manually segmented [4] from the high-resolution images to create 3D models. The high-resolution bone models were registered with the dynamic scans to reconstruct the bone motion, using custom Matlab code [4]. Tibio-talar helical axes were calculated for consecutive joint angles and the mid-line of the tendon was calculated for each joint angle. The muscle moment arm was determined at each joint angle as the length of the mutual perpendicular between the joint axis and the tendon line-of-action. A validation was conducted by rotating a dissected sheep tibia about a fixed gelatin-filled axis of rotation, using a gelatine-filled latex tube as a tendon surrogate. These components had known trajectories and physical measurements. The moment arm (from the tendon surrogate to the gelatine-filled axis of rotation) was measured using the MRI method (at 14 angles) and directly from the apparatus at the same rotation angles. The image processing was repeated 3 times. The mean RMS error between the MRI measurements and the corresponding physical measurements was calculated to assess the accuracy of the MRI method.

Results: The mean Achilles tendon moment arms across the ankle range of motion for the 10 subjects in this study were similar in scale to other studies (see Figure 1), despite differences in the methods, subjects, loading (relaxed versus active

muscle contraction) and definitions (centre of rotation, ankle angle and tendon line-of-action). Three trials of MRI validation data from 14 apparatus positions yielded a mean RMS error of 3.2 mm. The 95% confidence interval for the mean absolute error between MRI and physical measurement was 2.3-3.5 mm. The mean Achilles tendon moment arms for individual subjects in the current study ranged from 39.6 mm to 64.1 mm, therefore the upper 95% confidence limit of the error equates to an error of 5-9%.

Figure:
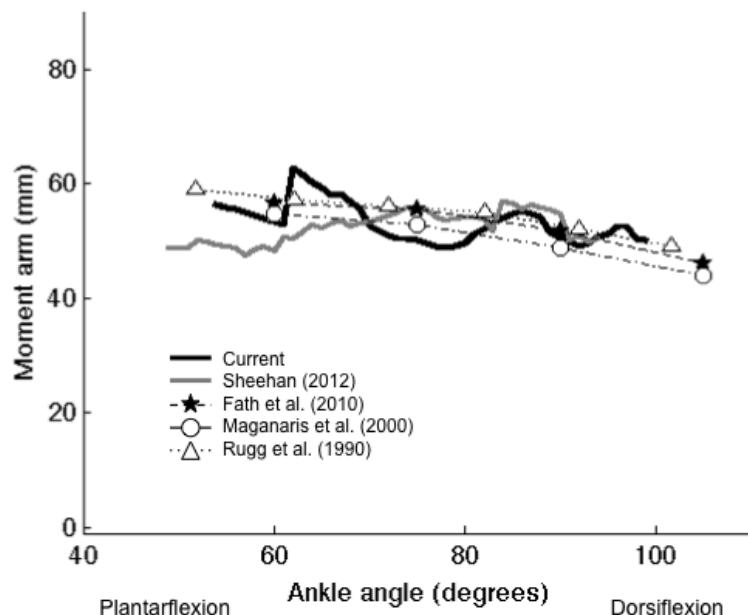
Caption: Figure 1. Comparison with data from literature

Conclusion: We have developed a simple method for measuring moment arms of human muscles under dynamic conditions. The method was validated against physical measurements from a surrogate apparatus. Potentially the method could be applied under active muscle conditions and to different joints. The method is capable of measurements from a single cycle of joint rotation, which could be particularly advantageous for clinical populations or under conditions of high muscular effort.

References: [1] Hashizume et al., J Biomech, 45: 409-13, 2012.

[2] d'Entremont et al., Mag Res Med, 69: 1634-44, 2012.

[3] Sheehan, J Biomech, 45: 225-30, 2012.

[4] We share code at: http://code.google.com/p/mkrtk

Disclosure of Interest: None Declared

Neurological and Motor Control

AS-0086

CONTROL OF MUSCULOSKELETAL ARM MODEL USING MUSCLE SYNERGY

Reza Sharif Razavian [1,*] Borna Ghannadi [1] John McPhee [1]

[1] Systems Design Engineering, University of Waterloo, Waterloo, Canada

Introduction and Objectives: Muscle synergy has been considered as a possible mechanism employed by the human nervous system to control movements [1]. This theory suggests that the nervous system may contain sets of muscle activity patterns, i.e. certain muscles are activated together via fixed patterns. Many researchers have studied the synergies by looking at the measured muscle activity signals, but few have used synergies to generate a desired action using the muscle synergy framework. In this project, we have used muscle synergies to control the motion of a musculoskeletal arm model.

Methods: A planar 2 degree of freedom musculoskeletal arm model is studied in this project. The arm muscles (Hill-type muscle model) are lumped into six muscle groups, including mono- and bi-articular flexors and extensors (see Fig. A). We have used muscle synergies to produce arbitrary hand acceleration, efficiently and in real-time. This two-stage process is described below.

1. Identifying the synergies

The measurable muscle activities during an action is the summation of multiple synergies. Non-negative matrix factorization (NNMF) is widely used to extract the underlying synergies from the measurable muscle activities [2], and has been used here to obtain the synergies.

First, we used a standard optimization routine to find the muscle activation levels that would result in a certain hand acceleration. This optimization problem was solved for a variety of joint angle configurations, and different directions of hand acceleration. Next, this large data set is used to obtain the muscle synergies. In each joint angle configuration, matrix $A_{6 \times 24}$ containing the six muscle activities for 24 acceleration directions is formed. With NNMF, matrix A can be approximated as $A_{6 \times 24} \approx S_{6 \times m} C_{m \times 24}$, where m is the number of synergies, and S and C are the synergy and coefficient matrices, respectively.

For this project, it is assumed that the synergies are posture-dependent [3]; i.e. the synergy matrix S is a function of the two joint angles. Although the synergies are calculated at a limited number of joint angle configurations, it is possible to obtain the synergies at an intermediate posture by interpolating the synergy matrix data.

### 2. Using the synergies to produce arbitrary hand accelerations

The activation of each synergy results in hand acceleration in a certain direction. The acceleration vectors resulting from all m synergies can be considered as a basis set for the two-dimensional vector space. In other words, any arbitrary hand acceleration vector can be written as a linear combination of the synergy-produced acceleration vectors. Since the synergies can only be activated in one direction (muscles can only pull), the linear combination is meaningful only if the coefficients are positive, which leads to a positive decomposition problem.

Mathematically, in an n-dimensional space, $n+1$ basis vectors are necessary for positive decomposition of any arbitrary vector. With three synergies, our 2D decomposition problem will have a unique solution. The uniqueness of the answer is

one fundamental aspect that is missing in many muscle synergy studies. In general, if the muscle synergies are obtained so that the generalized forces generated by the synergies span the operational space, there will be a unique solution to the synergy-sharing problem, and consequently a unique solution for the muscle force-sharing problem.

Additionally, since the relation between the muscle activations and the resulting acceleration is linear in this approach, the same coefficients of the vector decomposition can be used to make linear combinations of the synergies, which will result in the desired hand acceleration.

Results: Fig. B shows the activity of the six muscles versus the direction of the hand acceleration. The synergy-based control is compared against the optimal solutions. As can be seen, the activity patterns are similar, but not identical. The small difference is unavoidable with the dimension reduction of muscle synergies. The time to calculate the solution, however, is substantially lower in the proposed synergy method (20 times faster than the optimization).

Figure:
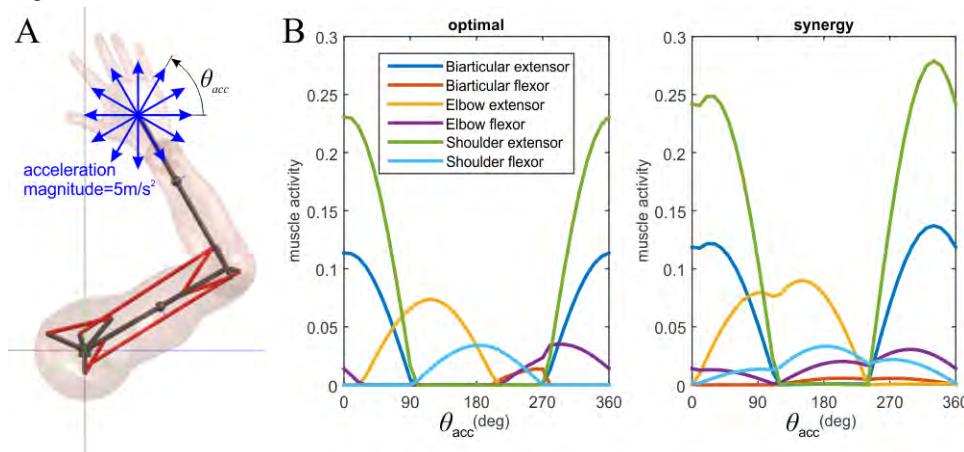
Caption: A. The 2D arm model. B. Comparison of the muscle activities: muscle synergy versus optimization.

Conclusion: We showed that muscle synergies can be used to control a musculoskeletal arm in real-time. Using this muscle synergy approach, the indeterminate force-sharing problem reduces such that the solution is unique. Our results showed that the dimension reduction allows for the fast solution of the force-sharing problem in musculoskeletal systems, while resulting in close to optimal muscle activities. Our method can be enhanced by introducing closed-loop control logic that may include predictive and learning properties of the human motor control system.

References: [1] Bizzi et al., Brain Res Rev, 57 (1), p. 125-133, 2008.

[2] Moghadam et al., Comput Method Biomec, 16 (3), p. 291-301, 2013.

[3] de Rugy et al., Front Comput Neurosc, 7 (Mar), p. 1-13, 2013.

Disclosure of Interest: None Declared

AS-0087

DEDUCING MUSCLE SYNERGIES FROM EXPERIMENTAL JOINT MOMENTS

Anantharaman Gopalakrishnan [1 2,]*Luca Modenese [3]Andrew Phillips [1 2]

[1]The Royal British Legion Centre for Blast Injury Studies at Imperial College London, [2]Structural Biomechanics, Civil and Environmental Engineering, Imperial College London, London, United Kingdom, [3]Griffith Health Institute, Centre for Musculoskeletal Research, Griffith University, Gold Coast, Australia

Introduction and Objectives: Prior experimental research has supported the existence of muscle groupings or 'synergies' which can be co-activated by a common control signal to actuate a family of limb movements in vertebrates. Muscle synergies could simplify the control of redundant musculature (more muscles in comparison to degrees of freedom (DOFs)), by reducing the dimensionality of the control problem. Each synergy's 'structure' can be quantified by a set of scalar muscle weightings (representing the extent of membership of each muscle to a synergy) and a synergy control signal which excites each muscle in proportion its weighting value. Excitations reaching each muscle would be an algebraic sum of the contributions from each synergy. This study adopted the hypothesis [1] that an invariant set of muscle weightings along with movement-specific synergy controls is capable of actuating a family of movements. Traditionally, the statistical factorization of experimental EMG during a family of functionally similar movement tasks has been used to deduce muscle synergy structure. This approach is limited by the inability to record EMG from all muscles and the expertise needed to avoid issues such as cross-talk. In this study, we present an alternative computational technique – synergy constrained torque decomposition (SCTD) [2] – for deducing muscle synergy structure from experimental joint moments. We applied this technique to deduce muscle synergies for a family of healthy walking movements and compared the results to EMG-derived synergies (termed 'experimental synergies') from a study by Clark et al. [3]

Methods: A single healthy subject walked on an instrumented treadmill at speeds of 0.7 and 1.7 m/s while marker-based motion capture and force plates respectively recorded the kinematics and kinetics (ground reaction forces) of gait. Three consecutive gait cycles at each speed were taken to collectively represent a family of walking. An OpenSim [4] musculoskeletal model of the right leg (5 DOFs, 24 muscles) was then scaled to match the subject's anthropometry followed by inverse kinematics which computed the joint angle trajectories from marker data. OpenSim's inverse dynamics tool was used to compute joint moments for the family of walking movements using joint angle trajectories and kinetics.

SCTD was formulated as an optimal control problem (OCP) whose unknowns were the muscle weightings and speed-specific synergy control signals. When excitations formed by the synergies were input to models of muscle dynamics, they resulted in 'simulated', muscle-generated moments at the 5 DOFs of the musculoskeletal model. The OCP's cost function sought to minimize the differences between simulated and experimental joint moments. The OCP was solved using the method of direct collocation, to solve for muscle weightings and synergy controls at each speed. The experimental synergies from Clark et al. (2010) were compared to their simulated counterparts by computing similarity indices – dot product of the normalized muscle weighting vectors from two synergies; an index of 1 would indicate exactly similar

muscle groupings – and correlation coefficients – between control signals from two synergies – between correspondent synergies from each dataset.

Results: Four muscle synergies were deemed sufficient for simulating the joint moments for the walking tasks, which was equal to the number of synergies determined by Clark et al. (2010). The mean similarity index computed between correspondent synergies from the experimental and simulated datasets (see Figure A) was 0.76 +- 0.14 (averaged over four synergies), which was taken to indicate similar muscle groupings in the two datasets. The mean correlation coefficients between synergy controls from the two datasets (Figure B) was 0.53 (p < 0.01) which was taken to indicate moderate similarities between experimental and simulated synergy controls.

Figure:

(A)   (B)
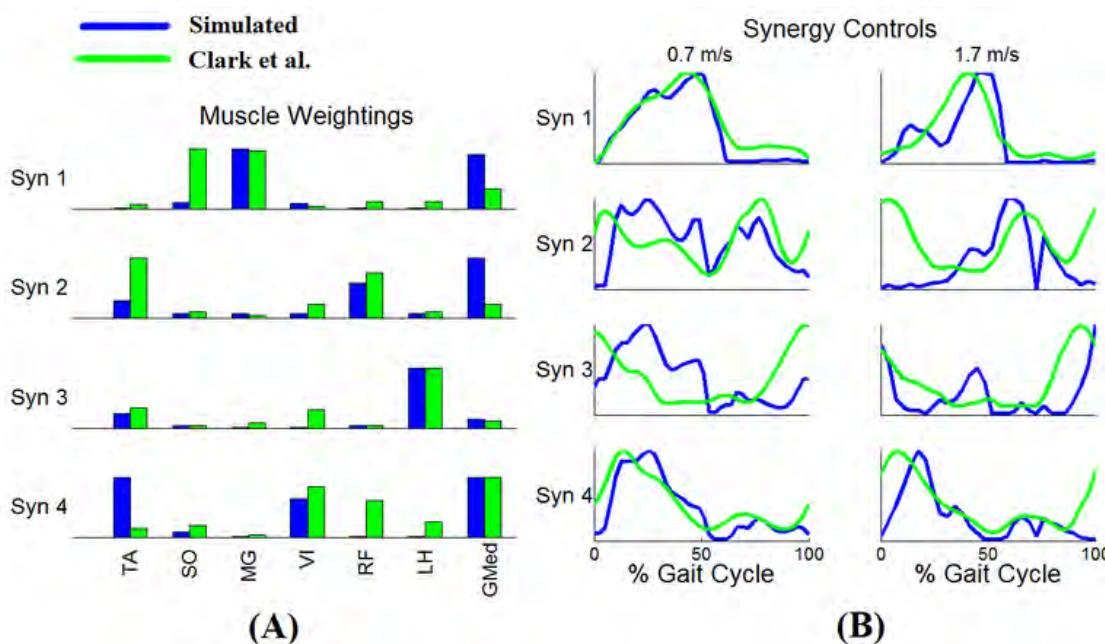
Conclusion: SCTD succeeded in identifying muscle synergies from a family of walking joint moments which bore several resemblances to their EMG-derived counterparts. This suggests that the examination of variations in EMG as well as joint moments across a family of movements, points toward the presence of similar, underlying synergy based control structures for walking. SCTD could assign muscle groupings to all the muscles in the model, which overcomes a limitation of EMG-derived synergies. However, SCTD results were still susceptible to errors arising from factors such as noisy motion capture data and generalized musculoskeletal model parameters. The ability of SCTD to account for dynamic muscle behaviour permits models of muscle spindles and Golgi tendon organs to be included in future studies, to see how afferent feedback would affect synergy structure.

References: [1] Ting and J. Macpherson, J Neurophysiol, 93:609-13, 2005.

[2] Gopalakrishnan et al., Front in Comp Neuroscience, vol 8, 2014.

[3] Clark et al. J Neurophysiol, 103: 844-57, 2010.

[4] Delp et al., IEEE Trans Biomed Engg, 54:940-1950, 2007.

Disclosure of Interest: None Declared

Neurological and Motor Control

AS-0088

DECLINE OF CONDUCTION TIME MAY LEAD TO CENTRAL NERVOUS SYSTEM ADAPTIONS THAT ARE IMPORTANT FOR POSTURAL CONTROL AND GAIT

Shuqi Zhang [1,*] Li Li [1]

[1]Health & Kinesiology, Georgia Southern University, Statesboro, United States

Introduction and Objectives: Slowed time course of the efferent / afferent pathway and slow processing time at the central level have been considered as the main causation of decreased postural control in aging population. However, there is no report of the correlation between the time course of pathway and measures of postural control. Therefore, this study is aimed at examining the correlation between different time courses of neuro-pathway (lower extremity sensory / motor nerve conduction velocity, and conduction time of H-reflex) and signal processing (characterizes of H-reflex) as well as the measures of postural control in aging population.

Methods: Six participants (one male, five female) were recruited. The proximal sural nerve conduction nerve conduction velocity (SCV) test, tibia nerve conduction velocity (MCV) test, plantar pressure sensitivity (PPS) tests, and H-reflex test at soleus muscles, were conducted. Based on the results of the H-reflex tests, we have also calculated the peak magnitude of H-wave (H), the peak magnitude of M-wave (M), H / M ration (H/M) and H-index. H-index was calculated using the equation of H_{index} = the square of (the height of the participants in cm / H-M latency in ms) X 2. For physical performance, the participants performed quite standing trials with their eyes open and closed, as well as a 6-minute walking (6MW) test and a timed-up and go test (TUG). Pearson correlations were used to examine the correlations among the measures of nerve function test as well as the correlations between the measures of nerve function tests and the outcomes of the physical tests.

Results: Age (70.5 ± 7.4 years old), body mass (82.4 ± 25.3kg), and height (162.7 ± 7.5 cm) of participants were recorded. The nerve function tests were conducted while the skin temperature was above 31°C. PPS (4.5 ± 0.84) among the participants were close to 5 points and indicates minimal loss of foot sole sensation. Therefore the following results were not under the influence of foot sole numbness as often the case for many elderly. The observed MCV (29.3 ± 2.2, range from 26.2 to 31.5 m/s) and SCV (22.7 ± 3.5, range from 17.2 to 25.7 m/s) are lower than the 40 m/s, the recognized healthy lower threshold for healthy elderly reported in the literature. The observed average conduction velocities were lower for sensory than that of the motor nerves. The observed range for sensory (~37%) was wider than that of the motor (~18%) conduction velocities. The observed H_{index} (75.6 ± 16.8, ranging from 53.0 to 97.3) has the largest variation (58.6%) among the three conduction time related measures. The other H-reflex related values were: H (1.00 ± 0.74 mv), M (4.57 ± 1.99mv), and H/M (0.25 ± 0.23). For the physical performance tests, participants exhibited greater 95% sway areas ($A_{95\%}$) during eyes closed conditions (205 ± 246 mm*mm) comparing to the eyes opened conditions (177± 115 mm*mm). But average sway velocities (V_{AVG}) were comparable for eyes closed (317 ± 72 mm/s) and eyes opened (O: 321 ± 76 mm/s) conditions. On average, participants walked (523 ± 116 m) in 6 minutes, and spend (7.07 ± 1.44ms) during TUG tests. Those values indicate normal locomotion capacities among participants. The correlation results are very revealing. SCV was positively correlated with H_{index} (r =0.811, $P < .05$), where correlation between MVC and H-index

were not significant ($P > .05$), suggesting H-index value were mainly influence by sensory nerve among this population. Further, SCV was negatively correlated with H/M (r = -0.972, $P < .001$) and H (r = -0.951, $P < .001$), but positively correlated with M (r = 0.805, $P < .05$). These observations, slower sensory conduction velocity accompanied by greater H-wave, could mean that sensory nerve impairments lead to increase spinal facilitation of H-reflex, as a compensatory mechanism. Along the same line, H_{-index} was negatively correlated with H/M (r = -0.749, $P < .05$), but positively correlated with M (r = 0.823, $P < .05$). Although we have failed to observe significant correlation between H_{-index} and any physical performance, but H/M was positively correlated with V_{AVG} (eyes open: r = 0.808, $P < .05$; eyes closed: r = 0.786, $P < .05$). The observations indirectly links the greater sway velocity with slower H_{-index} since them both (V_{AVG} and H_{-index}) correlated with greater H/M value.

Conclusion: Slowed sensory nerve conduction velocity with increased conduction time of H-reflex were accompanied by increase the magnitudes of H and H/M, may indicates central nervous system adaptation to peripheral impairments during aging. These changes in the tested nervous system were not directly related to postural control and locomotion tests without observable foot sole numbness. The lack of correlation here may suggest H-reflex related pathway is not the primary reflexive mechanism for postural control and locomotion when cutaneous sensation is intact.

Disclosure of Interest: None Declared

THE EFFECT OF SLOPE ON THE ACTIVITY AND VARIABILITY OF SEVEN PROXIMAL LOWER LIMB MUSCLES DURING WALKING

Annette Pantall [1,*] Jade Sharrer [2]

[1]College of Osteopathic Medicine, [2]Department of Kinesiology, Michigan State University, East Lansing, United States

Introduction and Objectives: Slope walking is associated with increased instability and greater risk of falling [1].The purpose of this study was to investigate lower limb muscle activity patterns during walking on level and sloped surfaces with an incline of 4.8°, the angle the American with Disabilities Act specifies for handicapped access ramps.Most previous studies have investigated walking on slopes with inclines of 8.5° and greater [2,3].We anticipated altered motor activity patterns for slope walking compared to level walking due to different mechanical demands.Specifically, we hypothesized that the adductor magnus (AM) and tensor fasciae latae (TFL) would exhibit increased activity during slope walking to improve mediolateral stability. Additionally, we expected the inter-stride variability for all muscles to be greater for slope walking compared to level walking.

Methods: Four healthy females participated in the study. Electromyographic (EMG) signals were recorded from vastus medialis (VM), vastus lateralis (VL), rectus femoris (RF), AM, semimembranosus (SM), biceps femoris (BF) and TFL of the right lower limb at a sampling rate of 1000 Hz.Bipolar surface electrodes were attached over the muscle bellies and an accelerometer was attached to the posterior calcaneus (Biometrics Ltd; Gwent, United Kingdom).The participants walked on a straight level surface at their comfortable self-selected speed for 200 m and then 10 times up and down a 4.2 m ramp with an incline of 4.8°.All data processing was performed in the MATLAB environment (v R2013a, The Mathworks, Natick, MA, USA). The EMG data were band pass filtered, rectified and smoothed at 10 Hz and divided into stride cycles, using heel contact times determined from filtered accelerometer data. EMG stride data were then time normalized and amplitude normalized to the maximum recorded during upslope walking.Repeatability was assessed through calculation of the coefficient of multiple correlation (CMC), a value of 1 indicating maximum repeatability and 0 minimum repeatability [4].The effect of slope on EMG amplitude was determined for each muscle with the significance set at $p < 0.05$.

Results: In total, 81 steps were analyzed for downslope (mean stride duration 1041ms ±23), 513 steps for level (mean stride duration 1030ms ±22) and 69 steps for upslope (mean stride duration 1127ms ±39).All muscles changed significantly from level to slope walking. VM, VL and RF increased during early stance for upslope and throughout stance for downslope walking.AM increased during late swing and early stance for downslope and upslope. SM and BF increased during late swing and throughout stance.BF for downslope walking displayed an additional burst of activity during late stance.TFL increased during early stance for slope walking and there was a further increased bout of activity for upslope during midstance. Averaged across participants, the CMC for AM was below 0.90 for all 3 conditions and the average CMC across all muscles was lowest at 0.89 for downslope.

Figure:
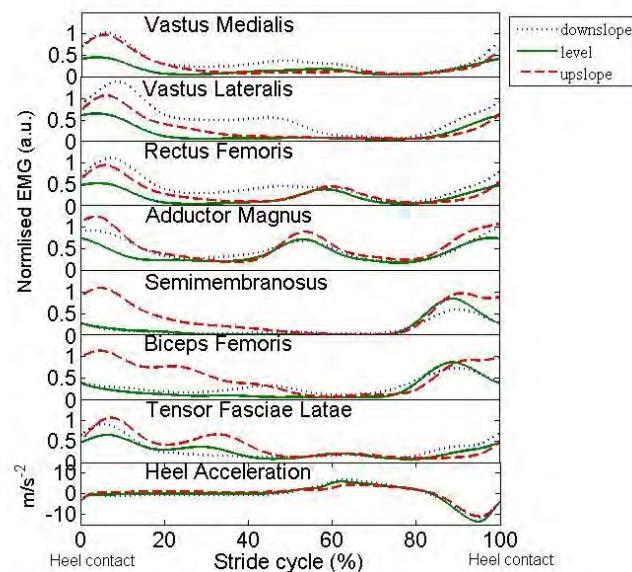
Caption: Mean stride cycle EMG amplitude for 7 proximal lower limb muscles and mean heel acceleration averaged across 4 participants for downslope, level and upslope walking.

Conclusion: Results for VM, RF, SM and BF were similar to previously reported findings recorded from steeper slopes.VL showed a similar increase to VM during slope walking with a greater increase for downslope walking due possibly to the increased step width during downslope walking with altered patellofemoral mechanics [1]. The adductor AM and abductor TFL displayed increased activity during early stance, increasing mediolateral stability. The lower repeatability of AM suggests that neural control of this muscle may be a major factor in mediolateral instability for all walking conditions. The lower repeatability for downslope walking across all muscles suggests that motor control is less stable for this walking condition. In conclusion, even at gentle inclines, different motor control strategies are employed by all muscles. Clinically, an understanding of neural control strategies in healthy subjects will help understand problems in clinical populations during slope walking, for example, in individuals with transfemoral amputation [5].

Table:

	DOWNSLOPE	LEVEL	UPSLOPE
Heel Acceleration	0.993	0.994	0.991
Vastus Medialis	0.919	0.841	0.942
Vastus Lateralis	0.847	0.964	0.949
Rectus Femoris	0.919	0.930	0.930
Adductor Magnus	0.845	0.892	0.872
Semimembranosus	0.894	0.952	0.934
Biceps Femoris	0.863	0.941	0.884
Tensor Fasciae Latae	0.943	0.879	0.922
Mean EMG CMC	**0.890**	**0.914**	**0.919**

Caption: Coefficient of Multiple Correlation(CMC) for heel acceleration and 7 proximal lower limb muscles during level and slope walking.

References: [1] Sheehan et al., Appl. Erg., 43:473-478,2012.

[2] Lay et al., J.Biomech., 40:1276-1285,2007.

[3] Gottschall et al., Phil.Trans.R.Soc., 366:1565:1579,2011.

[4] Kadaba et al.,J.Orthop.Res., 7:849-860,1989.

[5] Pantall et al. JRRD., 50(4):499-514,2013.

Disclosure of Interest: None Declared

Neurological and Motor Control

AS-0090

GAIT CHARACTERISTICS OF OBSTACLE CROSSING IN OLDER ADULT FALLERS WITH AND WITHOUT PARKINSON'S DISEASE: INFLUENCE OF OBSTACLE TYPE AND DUAL TASK

Lisa Alcock [1,*]Brook Galna [1]Jeffrey Hausdorff [2]Sue Lord [1]Lynn Rochester [1]

[1]Institute of Neuroscience, Newcastle University Institute of Ageing, Newcastle University, Newcastle upon Tyne, United Kingdom, [2]Department of Neurology, Tel Aviv Sourasky Medical Center, Tel Aviv, Israel

Introduction and Objectives: The prevalence of falls is high in older adults and people with Parkinson's disease (PD) [1,2] with up to 50% falls resulting from a trip on an obstacle [3]. Safe obstacle negotiation requires accurate modulation of gait during the approach and crossing phases. Gait must also be adaptive to overcome environmental hazards of varying dimensions, including those that are small (i.e. clearing a carpet edge), long (i.e. avoiding a broken tile) or high (i.e. negotiating a pavement increment). In addition, successful obstacle negotiation can be compromised when performing a concurrent cognitive task [4]. Although previous studies have identified obstacle crossing impairments in people with PD and older adults [5], little is known about how the interaction of increased cognitive and motor demands may compromise safety during obstacle negotiation. The aim of this study was to understand the temporal-spatial characteristics of obstacle negotiation as a function of obstacle type and explore this relationship with respect to dual task in older adult fallers with and without PD.

Methods: Gait was measured in 9 people with PD (Mean age[SD]68.9[7.1]y, Hoehn & Yahr II-III) and 10 older adults (76.6[7.9]y) with a history of recurrent falls whilst negotiating three different sized obstacles (H/W/D): small (2/60/2cm), long (2/60/15cm) and high (15/60/2cm). Spatiotemporal gait characteristics (walking speed, step length, duration and width) were measured using an instrumented walkway (GAITRite). All obstacle conditions were completed under single and dual task (maximal digit span recall). A general linear model was used to evaluate the effects of obstacle type (small, long, high) and obstacle step (penultimate (A2) and final (A1) approach steps, and the lead (Ld) and trail (Tr) crossing steps) on gait characteristics under both single and dual task in PD and older adult fallers.

Results: There was a main effect of step for all gait outcomes (p<.029) and of obstacle type for speed, width and duration (p<.001) such that the crossing steps were completed more slowly with a wider step for the high obstacle. As expected, there was a main effect of cognition whereby all conditions were completed at a slower speed during dual task (p=.039). Interaction effects were observed for speed (ObstacleType*step p<.001 and ObstacleType*step*group p=.037), length (ObstacleType*step p=.029 and Cognition*step p=.003), width (ObstacleType*step p=.008) and duration (ObstacleType*step p<.001 and Cognition*step*group p=.041). Interaction effects revealed that lead and trail crossing steps were slower than approach steps for both groups; PD fallers slowed down earlier in the approach phase compared with older adult fallers (A1; Figure 1a). In addition, dual task had a significant effect on step duration such that the approach steps were of longer duration and the trail limb step was shorter in length for PD fallers compared to that observed during single task (Figure 1b). Although not significant, it is of interest to note that there was a tendency for people with PD to widen their step considerably when crossing the small (26% increase) and high (28% increase) obstacles but not the long obstacle (1% increase) when performing the dual task.
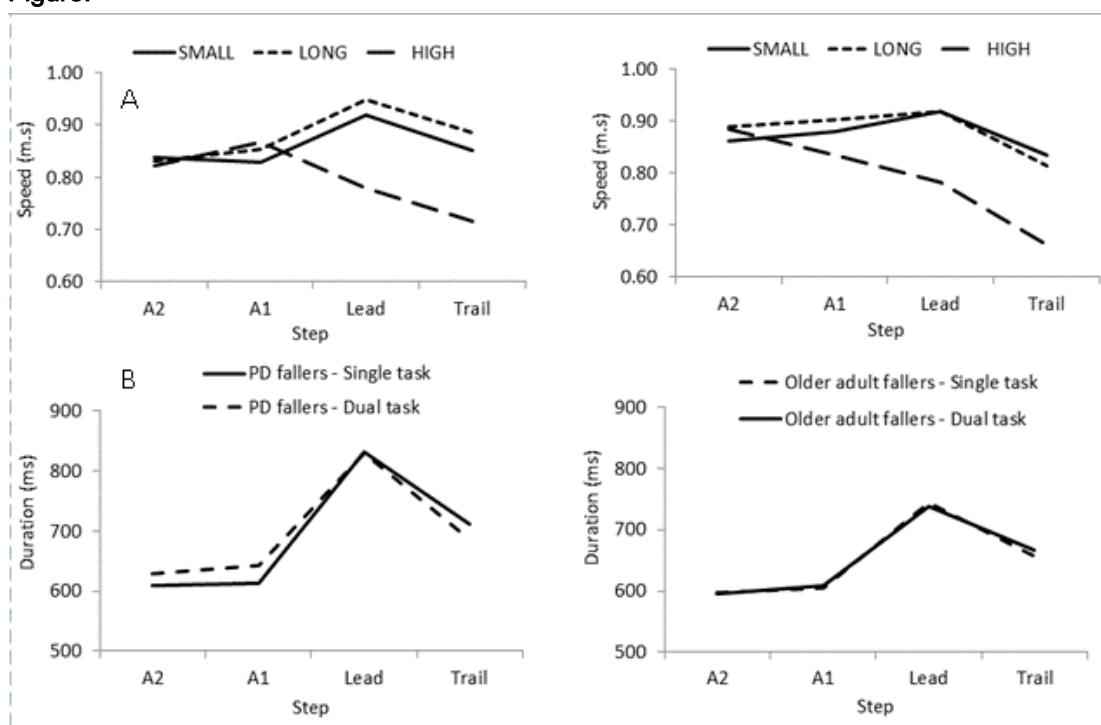
Caption: Figure 1 – Interaction effects of dual task on speed (A) and step duration (B) for PD and elderly fallers

Conclusion: Our findings suggest a complex interaction between the mechanical and cognitive demands of obstacle negotiation in PD and older adult fallers. Both groups modulated their gait in response to obstacles of varying sizes, with the greatest changes observed when crossing the high obstacle which presented greatest mechanical challenge. Performing a dual task resulted in slower obstacle negotiation, with the greatest effect seen during the trail crossing step. PD fallers were slower during their approach and this prolonged the motor planning phase, suggesting greater cognitive interference during the approach. PD fallers also took longer to complete both crossing steps irrespective of obstacle type or cognitive load resulting in a longer time spent in single limb support, when maintaining postural control is most difficult. Increasing step width when crossing small and high obstacles may be a compensation to help widen their base of support and maintain postural control. A lack of step width adaptation when negotiating long obstacles may be a result of needing to lengthen their step and thus hinder the ability to widen steps, putting people at a greater risk of falling sideways. These results highlight the need for further work to understand the physical and cognitive demands of obstacle negotiation.

References: [1] Perell *et al., J Gerontology: Series A: Bio Sci and Med Sci,* M761-M766, 2001.

[2] Allen *et al., Parkinson's disease,* 2013-2016, 2013.

[3] Lord *et al., Age & Ageing,* ii55-ii59, 2006.

[4] Harley *et al., Gait & Posture,* 428-432, 2009.

[5] Galna *et al., Hum Mov Sci,* 843-852, 2010.

**Disclosure of Interest**: None Declared

Mechanics

AS-0092

EFFECT OF WRIST POSTURE AND RATE OF FORCE DEVELOPMENT ON FINGER INDEPENDENCE

Steve May [1] Peter Keir [1,*]

[1] Kinesiology, McMaster University, Hamilton, Canada

Introduction and Objectives: When asked to move or apply a force with an individual finger, movements and/or forces tend to occur in the other fingers to varying degrees [1]. This involuntary "enslaving effect" (EE) is attributed to both mechanical and neural factors. While posture affects muscle length and thus muscle force, the effect of wrist posture on EE has yet to be examined. Wrist posture alters muscle length, which modulates both active and passive muscle force and likely alters the stress in interconnections between tendons. Rate of motion has been shown to affect enslaving [2], as has changing force levels in isometric contractions [3]. The purpose of this investigation was to evaluate the effect of wrist posture on enslaving effect during isometric finger exertions with constant force, as well as increasing, and decreasing forces at different rates.

Methods: Twelve male participants performed submaximal isometric finger flexion and extension exertions of the index and ring fingers with all fingers secured to force transducers via adjustable rings (MLP50, Transducer Techniques, Temecula, CA, USA). Trials were performed at 3 wrist angles: (i) 30° flexion, (ii) 0° (straight), and (iii) 30° extension (Figure 1). Each trial consisted of the task finger (index or ring) performing a 5 second isotonic contraction at 25% maximum voluntary contraction (MVC) and two ramp contractions. Ramp contractions increased to 50% MVC and returned to zero with a 0.5 s hold at 50%. They were performed at 25% MVC/s and 10% MVC/s. Each condition was repeated 3 times for a total of 108 trials. Surface EMG (Biometrics Ltd., Gwent, UK) was recorded from each compartment of extensor digitorum (ED 2-5) and flexor digitorum superficialis (FDS 2-5). Force in the non-task (slave) fingers were normalized to MVC to yield enslaved force (EE). Enslaved forces and EMG were analyzed at 25% MVC for the isotonic, ascending and descending contractions. Multiple rANOVAs were followed up with Tukey's HSD where necessary (IBM Statistics 20.0, SPSS Inc. Chicago, IL, USA).

Results: There was a significant posture x direction x slave finger interaction seen by greater EE of the fingers adjacent to the task finger in extension exertions with the wrist extended (all $F_{4, 44} > 2.6$, $p < 0.05$). Thus, for extension exertions, enslaving was higher at shorter muscle lengths (Table 1). There was a significant posture x compartment interaction in muscle activity for extension exertions (both $F_{14, 154} > 15.512$, $p < 0.0001$), and ring finger flexion exertions ($F_{14, 154} = 3.918$, $p < 0.0001$) where muscle activity of non-task fingers was significantly greater at shorter muscle lengths (extended or flexed wrist, respectively). In ramp exertions, rate and phase significantly affected EE for both index and ring finger exertions (all $p < 0.001$). In fingers adjacent to the task finger, EE was higher with the slower force rate in the descending phase. Despite the EE being higher with a slower force rate and in the descending phase, muscle activity was not significantly increased in these exertions ($p < 0.05$).

Figure:
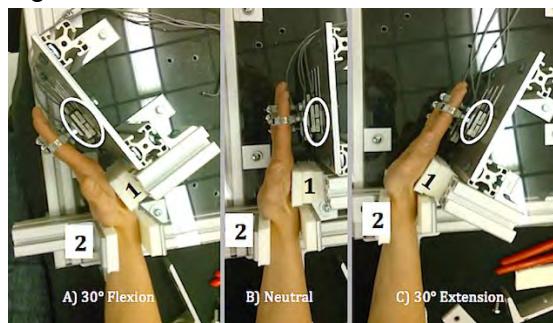
Caption: Figure 1. Top view of the apparatus securing the hand into: (A) 30° wrist flexion, (B) 0°, and (C) 30° wrist extension. Force transducers (circled) were attached to padded rings . "1" = adjustable dorsal hand support, and "2" = adjustable wrist support.

Conclusion: We found that wrist posture significantly affected enslaving, most notably in fingers adjacent to the task finger in extension exertions at a shorter muscle length. When the extensors were active and shortened there was an increase in muscle activity across all compartments, suggesting the extensors may be controlled to some extent by a common drive. Additionally, the rate of force production and type of contraction (isotonic, increasing or decreasing force) both had a significant effect on enslaving, without increasing muscle activity.

Table:

Index						
	Flexion Force			Extension Force		
	Flexed	Neutral	Extended	Flexed	Neutral	Extended
Index	25	25	25	25	25	25
Middle	3.8 ± 0.8	3.2 ± 0.8	4.1 ± 1.3	3.6 ± 1.0	3.7 ± 0.8	6.4 ± 1.0*
Ring	-3.1 ± 1.4	-4.8 ± 1.0	-1.8 ± 1.2	1.9 ± 0.5	2.3 ± 1.0	1.9 ± 0.9
Little	-1.4 ± 1.0	-1.2 ± 1.0	-1.9 ± 1.2	1.0 ± 0.7	0.4 ± 1.0	1.5 ± 0.9

Ring						
	Flexion Force			Extension Force		
	Flexed	Neutral	Extended	Flexed	Neutral	Extended
Index	-2.1 ± 1.0	-3.2 ± 1.0	-1.9 ± 1.2	2.2 ± 0.7	2.6 ± 0.6	5.4 ± 1.3*
Middle	7.1 ± 1.2	6.7 ± 1.3	6.1 ± 1.0	8.8 ± 1.6	8.8 ± 1.3	11.4 ± 2.1
Ring	25	25	25	25	25	25
Little	1.2 ± 1.3	-0.4 ± 1.9	-1.4 ± 2.2	6.6 ± 1.8	8.1 ± 2.0	13.9 ± 2.1*

Caption: Table 1. Force for each finger for index (top) and ring (bottom) exertions at wrist angles of 30° flexion, 0°, and 30° extension. Task finger (index or ring) is shown as a nominal 25% force, while the enslaved forces are shown for the "slave" fingers in %MVC ± SEM. Negative values indicate forces opposing the task finger direction. *Significantly greater than flexed wrist posture.

References: [1] Zatsiorsky et al., *Exp Brain Res,* 131(2): 187-95, 2000.

[2] Kim et al., *Hum Movement Sci,* 27: 408-422, 2008

[3] Sanei & Keir, *Hum Movement Sci,* 32(3): 457-471, 2013.

Disclosure of Interest: None Declared

AS-0093

EFFECT OF FATIGUE ON HIGH SCHOOL UNDERHAND FEMALE PITCHERS

Andrew Kraszewski [1,*]Mandi Gibbons [1]Howard Hillstrom [1]Andreas F. S. Kontaxis [1]

[1]Leon Root Motion Analysis Laboratory, Hospital for Special Surgery, New York, United States

Introduction and Objectives: The repetitive stress that occurs with pitching alters both structural as well as functional mechanics of the shoulder complex. [1] In addition to structural adaptations, functional factors, such as abnormal scapular motion, has been noted in previous pitching studies [2] and may contribute to the development of shoulder pain. Most of our current knowledge related to the mechanics of pitching is derived from simplified kinematic measurements of the humerus relative to the trunk. No data exists outlining the three-dimensional motions of the humerus relative to the scapula during an underhand softball pitch, although these motions have been identified in clinical studies as key contributors to the development of shoulder pain

The purpose of this investigational team is to develop a protocol to objectively determine normative pitching kinematics (scapula and humeral thoracic) for the high school female underhand pitcher and identify potential kinematics adaption due to fatigue

Methods: Eight female high school athletes between the ages of 15 and 18 years were recruited for this study. Only softball pitchers in their sophmore or junior years were included that had no history of previous shoulder injury. The kinematic recordings were performed in a motion analysis laboratory using a 12 camera 3D motion capture system recording at 200Hz. A set of reflective markers were used to define technical and anatomical frames for the hand, forearm, humerus, scapula and trunk (Figure). The marker placement and the anatomical calibration of bony landmarks followed the recommendations of ISB [3]. For the dynamic tracking of the scapula, a special device was designed based on the recommendations of Karduna et al [4]. In order to mimic a game-like situation, a pitching mound was set up at regulation distance (43') from home plate where a pitching target with a designated strike zone was located. All athletes completed 105 pitches in sets of 15 with a rest of 5 minutes between intervals. Speed and accuracy were measured for all throws; accuracy was defined as a ball or strike from a single observer and speed throw was recorded with a radar gun placed close to the home plate. Voluntary maximal isometric strength of the internal and external rotators was evaluated before and after pitching using a Biodex dynamometer (Biodex Medical Systems, Shirley, New York) in three positions (45° IR, 0° neutral, and 45° ER) with the arm abducted in 45 deg. A paired t-test (2-tail) was used to compare pre- and post-pitching strength.

Results: Results showed a large glenohumeral (GH) motion during pitching, but with a very consistent pattern for all 3 DoF (Table). Statistically significant differences were noticed on glenohumeral flexion and rotation ROM as well as scapula protraction ROM, but all differences were small. Measures of ball speed also showed consistency within subjects with the ball velocity values being constant between first and last pitch. Pre and post-pitching strength measurements also showed no significant changes, indicating no fatigue among the players. Accuracy data (ball or strikes) were variable with no specific pattern across the 105 pitches.

Figure:

(a)

Softball Pitching Speed across Sets

(b)
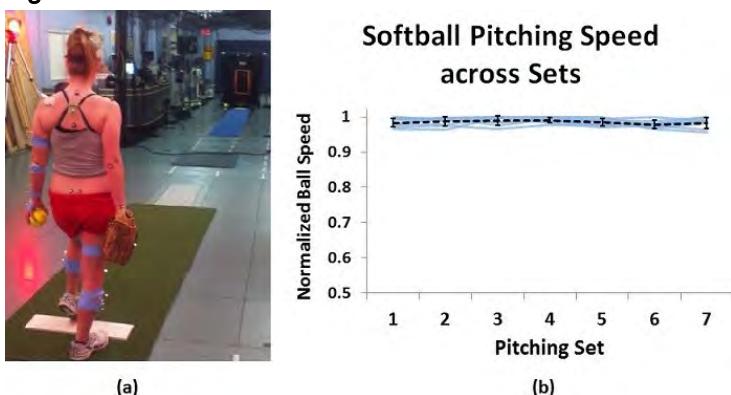
Caption: (a) Indoor pitching set-up. Athletes pitched from a mount to a a designated strike zone at regulation distance. (b) Ball speed data showed that athletes were able to maintain pitch velocity during all 7 sets (105 pitches)

Conclusion: The study has demonstrated a protocol for the study of underhand softball pitching. To our knowledge, this is one of the first studies to analyze humeral thoracic as well as scapula thoracic kinematics during softball pitching. The results do not indicate any GH kinematics changes during the throwing protocol which may suggest that the subjects are not fatiguing during the 105 throws. This is also supported by the constant strength and speed ball values that did not drop during the 105 pitches.

Table:

Shoulder Joint Parameters		
	Set 1	Set 7
GH Flexion ROM (°)	125.8 ± 13.1	129.4 ± 13.2*
GH Abduction (°)	130.7 ± 12.3	141.4 ± 12.1
GH Rotation (°)	133.0 ±14.0	135.9 ± 22.1*
ST Tilt (°)	26.2 ± 3.0	28.5 ± 3.1
ST Protraction (°)	41.4 ± 6.0	43.4 ± 8.1*
ST Sup/Inf Rot (°)	49.7 ± 5.5	52.5 ± 5.8
Scapulohumeral Coupling	0.30	0.31

Caption: Comparison of shoulder joint ROM (mean ± SD) between the first and last set of pitching (* indicates significant difference between first and last set; α = 0.05)

References: [1]   Bigliani LU et al., (1997), Am J Sports Med., v25, pp.609-613.

[2]   Burkhart SS et al., (2003) , Arthroscopy, v19, pp. 641-661

[3]   Wu, G. et al., (2005), J.Biomech. v 38, pp 981-992

[4]   Karduna, A. R. et al., (2001). J.Biomech.Eng, v 123, pp 184-190

Disclosure of Interest: None Declared

Upper Limb

AS-0094

INTEGRATED ANATOMICAL DATABASE FOR THE CREATION OF A COMPLETE MUSCULOSKELETAL MODEL OF THE HUMAN HAND

Faes Kerkhof [1,*]Evie Vereecke [1]

[1]Development and Regeneration @ Kulak, Leuven University, Kortrijk, Belgium

Introduction and Objectives: By combining arthrokinematics with soft-tissue anatomy and known external forces, a musculoskeletal model (MSM) can be created. These models make calculations of muscle and joint forces possible and are a valuable tool to explore the functioning of healthy and pathological joints.

Gathering the data needed to create a MSM can be challenging. 3D osteological data can easily be acquired through CT and MR imaging. Physiological data (muscle length, cross-sectional area, pennation angle, etc.) from arm and hand muscles exist as well. However, precise information of muscle pathways and moment arms are hard to obtain. Previous studies often used specimens with altered tissue properties due to embalming, or described muscle pathways without using a bone reference frame making it impossible to determine precise pathways and moment arms. To date, there is no integrated data set in which osteological and soft-tissue data have been collected together, which might also explain why a complete MSM of the hand has not yet been developed. Therefore, the goal of the present study is to create an integrated and open anatomical database of the human hand that can be used for musculoskeletal modelling.

Methods: A fresh-frozen cadaveric arm was mounted in a frame with a polycarbonate rod for stabilization. Four polycarbonate bone pins where used to create a fixed anatomical reference frame of the forearm. The Philips screw indent of the bone pins were used to assure repeatable, precise tip placement of the 3D digitizer stylus (Polhemus Fastrak). To obtain the bone geometry and the precise localisation of the bone pins in relation to the bone, a CT scan of the entire rig-mounted specimen was made. The cartilage and soft tissue geometry was visualised with a 3T MRI scanner using contrast fluid. For each muscle-tendon unit (MTU), origin, insertion and via points were digitized using a 3D digitization system with sub-millimeter accuracy (+/- 0.5 mm). Muscle attachment points >5 mm were digitized as a single point. All other attachment points where digitized along the edges of the muscle 'footprint'. In total, 19 intrinsic and 20 extrinsic muscles were digitized. In addition, origin and insertion of the major ligaments were also digitized using the same protocol. After digitization, the MTU was prelevated from the specimen and muscle mass, MTU length, muscle belly length, fascicle length, pennation angle, muscle volume, external and internal tendon length were measured. Subsequently, the physiological cross-sectional area was calculated for each muscle. Distances were measured with a digital caliper and muscle mass was determined using a digital scale (+/-0.01 g). The pennation angle was measured at three places within the muscle belly. Muscle volume was determined by the volume of water displaced in a measuring glass by submersion of the muscle belly. For the smallest intrinsic muscles (< 1 ml), volume was calculated by multiplying the mass with the average muscle density of the larger hand muscles.

Results: The results of this study provide important information which can be used to build more complete and more accurate musculoskeletal models of the human hand. Importantly, this study combines osteological and soft-tissue data from the same specimen, data which is fully digitized and quantified.

The decision to collect data from only one specimen was a conscious decision. Previous investigations have shown that there is a high variation in anatomical properties between individuals as well as a wide variety of motor control strategies to perform a single task. Hence, creation of an "average" forearm would contribute little to our understanding of joint functioning. Ideally, a subject-specific model of the hand should be created based on morphological parameters from the patient (using MRI, EMG and ultrasound), but this will be a topic for future investigation. First, we want to create an accurate and validated MSM of the hand.

Conclusion: By creating an open access and digitized anatomical database of the human forearm and hand, information is available to create a more accurate and more complex MSM. Furthermore, by the open nature of this study, everyone who wants to make a model of the hand, can create one and/or the data can be complemented with additional functional data (e.g. force data, other kinematics, EMG). In addition, the fact that it considers an integrated dataset makes that combining different datasets is no longer necessary.

Disclosure of Interest: None Declared

Upper Limb

AS-0095

USE OF SCAPULOHUMERAL RHYTHM, SYMMETRY AND KINEMATICS TO IDENTIFY ABNORMAL MOVEMENTS OF THE SHOULDER

Aliah F. Shaheen [1,*]Alexander van Heesewijk [1]Alexander van Heesewijk [1]

[1]Mechanical Engineering Sciences, University of Surrey, Guildford, United Kingdom

Introduction and Objectives: Abnormal shoulder movement and biomechanics have been associated with a number of shoulder pathologies [1]. However, previous studies investigating the nature of abnormal movement present in different pathological populations have reached different conclusions regarding both the direction and degree of movement deviation. Instrumented movement analysis techniques have been used for decades to analyse gait; these methods are commonly used to quantify deviations from normal movement in pathological populations. However, the use of these techniques has not been extended to benefit clinical applications in upper-limb pathology. This is because of a number of technical issues in measuring and quantifying upper-limb movement, such as the presence of sot-tissue artefact and its large range of movement. In addition, the large variability in upper-limb movement has been reported to hinder the use of traditional techniques in detecting the presence of abnormal movement. Although some studies have reported statistical differences between pathological and healthy populations [1], the parameters describing a normal shoulder movement are not fully defined meaning that it is difficult to identify the type of abnormal movement present in a single symptomatic subject. Understanding the abnormal movement present in the symptomatic shoulder could provide important insight into the mechanisms responsible for developing pathology or injury and it could be used to direct rehabilitation. Scapulohumeral rhythm refers to the ratio of scapulothoracic and glenohumeral movement during elevation in the scapular plane, it is one of the most basic measures of coordination and it has been suggested as an indicator for the presence of abnormal deviation. Shoulder symmetry and scapular resting position and movement have similarly been suggested as possible indicators for pathological deviation.

The aim of this study was to investigate the use of scapulohumeral rhythm, symmetry and shoulder kinematics to identify the presence of abnormal shoulder movement in symptomatic shoulders compared to normative values obtained from healthy individuals.

Methods: Measurements from 8 healthy shoulders and 3 symptomatic shoulders were collected, participants were asked to fill-out DASH forms [2] to assess their physical function. Asymptomatic participants did not have history of upper-limb pathology or pain, symptomatic participants had a mean DASH score of 86 ±10, but they were not classified according to their underlying pathological condition. A motion analysis system with 11-cameras (Qualysis) running at 200 Hz was used to capture the data of reflective markers attached to the participants' upper-limb and pelvis. Measurements were obtained of both dominant and non-dominant side to assess symmetry. Participants performed flexion and scaption as well as three tasks simulating activities of daily living (ADLs); combing the hear, washing the back and putting on a seatbelt.

Data obtained from the healthy shoulders were used to compute mean rotations and normative bands (± 1 standard deviation). Rotations obtained from the pathological subjects were then overlaid and examined for obvious deviations.

Coordinate frames were defined for the thorax, scapula, humerus and pelvis and Euler angle rotations were used to compute the scapulothoracic, glenohumeral and thoracic rotations according to the ISB recommendations.

Results: The variability of the joint angular rotations were high in healthy shoulders, this meant that none of the pathological subjects consistently fell out of the normal range. In addition, the joint ranges of motion of the pathological subjects were comparable to those of the healthy subjects. However, the scapular internal rotation seemed to show the greatest difference between the pathological subjects and the healthy population in some of the performed tasks; for example hair combing is illustrated in the figure.

Interestingly, shoulder symmetry was not a good indicator of the presence of abnormal movement with healthy and pathological shoulders showing similar degrees of asymmetry between their dominant and non-dominant side. Only one of the pathological subjects had a scapulohumeral rhythm which was significantly higher than the normative range.

Figure:
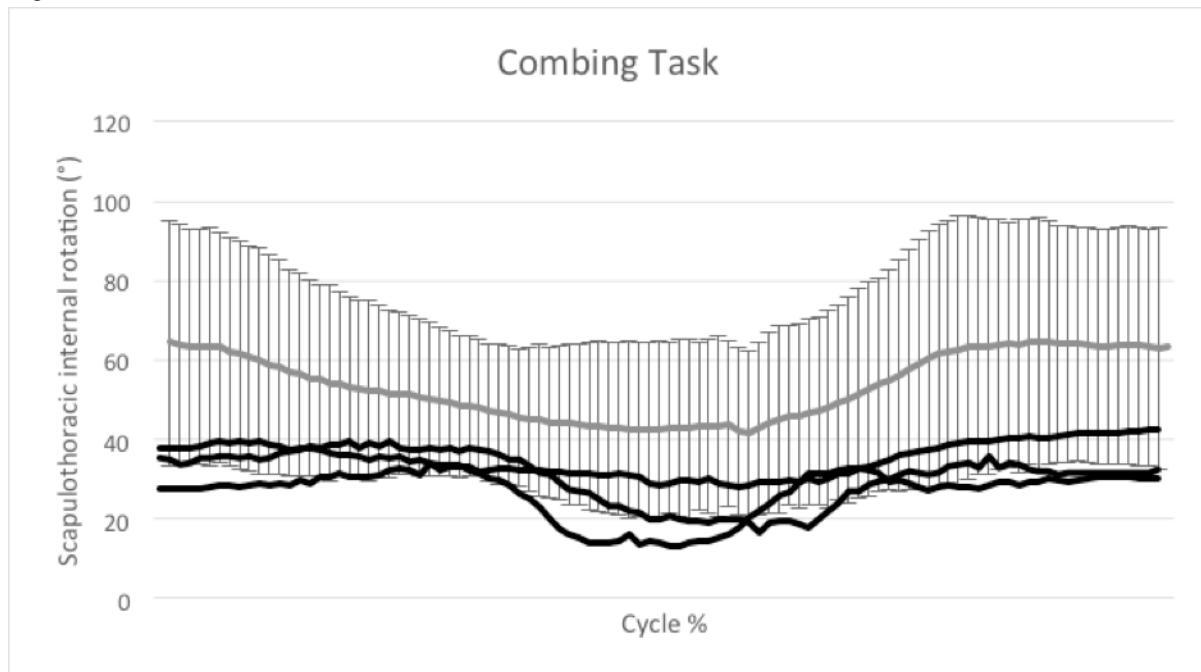
Caption: Mean and standard deviations of scapular internal rotation in healthy shoulders (grey) and the rotations of the three pathological subjects (black)

Conclusion: The high variability present in the normal shoulder means that it is difficult to identify the presence of abnormal movement in pathological populations. Joint kinematics remain to be better at identifying pathological deviations than other measures such as scapulohumeral rhythm and symmetry. However, a combination of these measures may be a superior alternative in detecting abnormal movements in symptomatic shoulders.

References: [1] Ludewig, P.M. and J.F. Reynolds. *J Orthop Sports Phys Ther*, 2009. **39**(2): p. 90-104.
[2] Hudak, PL. et al (1996). *Am J Ind Med.* 29 (6) pp. 602 - 8.

Disclosure of Interest: None Declared

Upper Limb

AS-0096

INTRAMUSCULAR EMG AND KINEMATIC ANALYSIS OF HAND POSTURES THAT CORRESPOND WITH GRASPING AND POINTING TASKS

Marije De Bruin [1] [2],*Sarah Wohlman [1] [3]Wendy Murray [1] [2] [3] [4]

[1]Sensory Motor Performance Program, Rehabilitation Institute of Chicago, [2]Physical Medicine and Rehabilitation, Northwestern University, Chicago, [3]Department of Biomedical Engineering, Northwestern University, Evanston, [4]Edward Hines Jr. VA Hospital, Hines IL, United States

Introduction and Objectives: In our daily life, we constantly and almost unconsciously use our hands during what seem to be uncomplicated tasks: making a sandwich, tying our shoelaces, or shaking someone's hand. However, the hand is astoundingly complex, both from a mechanics and control point of view: over 20 degrees of freedom are controlled through nearly 40 muscles.

The muscles that control the hand can be divided into intrinsic and extrinsic muscles. The intrinsic muscles originate and insert within the hand, whereas extrinsic muscles originate in the forearm and cross the wrist before inserting on the fingers and thumb. Persons that lose their hand through amputation also lose the intrinsic muscles. As a result, any prosthetic hand controller that relies on EMG activity of muscles as input signals (e.g. i-Limb, Bionic arm) only has access to the extrinsic muscles of the hand.

Creating a controller for a multi degree-of-freedom prosthetic hand that allows the artificial hand to behave like the intact hand requires a broader understanding of how hand muscles produce complex hand motions. Previously, studies involving complex movements have focused on EMG only (e.g. [1]) or used surface EMG sleeves that are not able to attribute activity to a specific muscle (e.g. [2]). Our objective was to characterize how people perform movements that resemble pointing and grasping. To reach this objective, we simultaneously collected both hand kinematics and muscle activations of thumb and index finger during American Sign Language (ASL) gestures. The gestures were selected so that they resemble pointing or grasping.

Methods: Fourteen subjects were included after having given informed consent, the human subjects protocol was approved by the IRB of Northwestern University. Intramuscular EMG data were recorded using bipolar, fine-wire electrodes. The electrodes were inserted into each muscle, using a 27-gauge hypodermic needle. EMG signals were collected at 2000 Hz using a Delsys Bagnoli-16 system (Delsys Inc., Boston MA) and filtered 4th order Butterworth band-pass 10-500 Hz, notch 59.5-60.5 Hz, and low-pass 8 Hz). The highest peak activity per muscle was selected after applying a Gaussian smoothing algorithm with a 100ms window.

Subjects were instrumented with a Cyberglove II (Cyberglove Systems LLC, San Jose CA) to measure kinematics of the thumb. A custom calibration protocol was used to convert voltages of the Cyberglove sensors to joint angles [3]. Joint angles were collected at 100 Hz and interpolated to 2000 Hz to enable comparison with EMG.

Subjects were instructed to closely follow a video of a hand gesturing an "L", "D" or "O" in ASL (Fig. 1A). The video included the same initial position for each trial (Fig. 1A, screen 1&5). Subjects then moved to the posture intended to signal starting and ending of the ASL movement (extended fingers, Fig. 1A, screen 2&4). Joint angles of the middle finger

were then used in a customized algorithm [4] to automatically and objectively determine start- and endpoints of the trials and normalize them to time.

Results: We have developed an experimental protocol that enables subjects to perform complex hand gestures in a standardized and repeatable manner. This approach, combined with a data processing algorithm implemented to objectively define the start and endpoints of the complex gesture, result in a well-defined, time-normalized gesture (Fig. 1A-C). This methodology enables us to directly compare the motion and EMG data across trials and subjects, similar to comparison of several gait cycles in gait analysis. In an example subject, the standard deviation of MCP flexion-extension of the thumb is less than 10 degrees across three trials when the hand is in the target posture (cf., 40-65% of trial, Fig. 1D). However, the muscle activation strategies this subject used to achieve the posture sometimes varied considerably across trials (cf., standard deviations of muscle activation during L, Fig. 1D).

Figure:
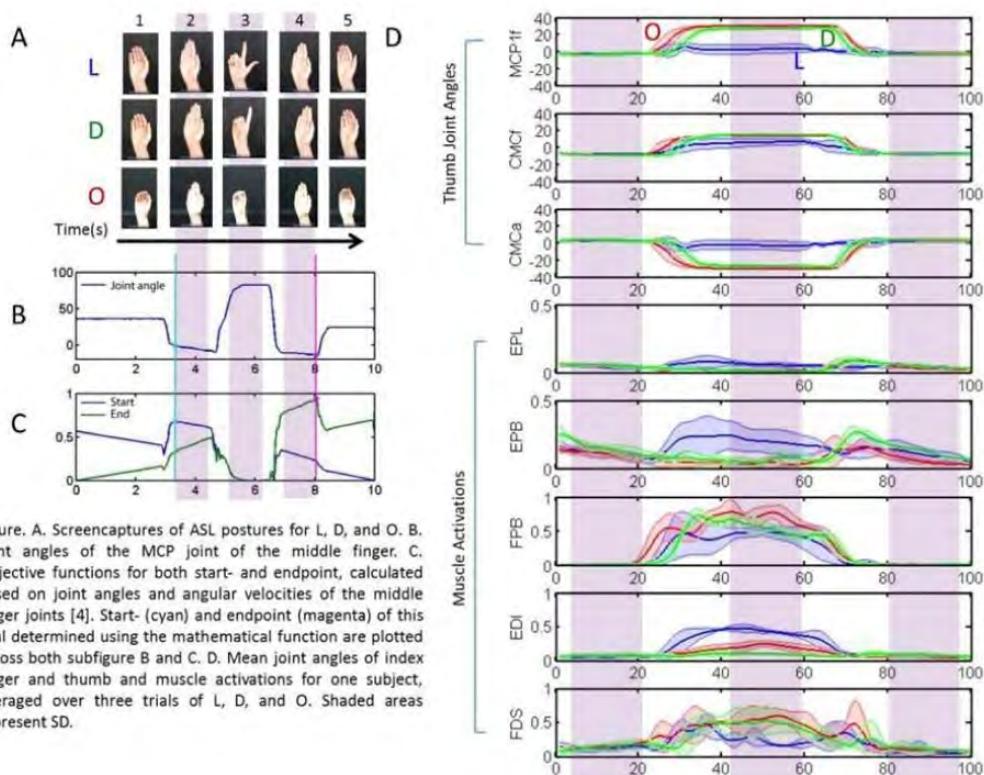
Figure. A. Screencaptures of ASL postures for L, D, and O. B. Joint angles of the MCP joint of the middle finger. C. Objective functions for both start- and endpoint, calculated based on joint angles and angular velocities of the middle finger joints [4]. Start- (cyan) and endpoint (magenta) of this trial determined using the mathematical function are plotted across both subfigure B and C. D. Mean joint angles of index finger and thumb and muscle activations for one subject, averaged over three trials of L, D, and O. Shaded areas represent SD.

Conclusion: We have collected a substantial dataset, describing how subjects both move their hand and activate the muscles of thumb and index finger during the performance of different ASL letters. Our long-term goal is to use the EMG-data from this study to drive feed-forward simulation of a musculoskeletal system of the upper extremity and compare the kinematic outcomes of the simulations to the experimentally measured joint angles. The chosen letters approximate functional movements, like pointing, grasping, or pinching, without actually exerting external forces on the system, which simplifies modeling these movements. Using this model will not only advance our knowledge about the control of the intact hand, but will also enable us to study situations in which sets of muscles are lost to injury or disease.

References: [1] Birdwell et al., IEEE Trans Biomed Eng, epub, 2014.

[2] Gazzoni et al., PLoS One, 9(10), 2014.

[3] Buffi et al., J Biomech Eng, 1;136(12), 2014.

[4] De Bruin et al., Hand Brain and Technology, p77, 2014.

Disclosure of Interest: None Declared

Sport

AS-0097

ANALYSIS OF MUSCLE ACTIVITIES OF THE BOWLING ARM IN CRICKET DURING DELIVERY PHASE

Rucha Kashalkar [1]Vikram Mhaskar [1]Graham Arnold [1]Rami Abboud [1]Weijie Wang [1,*]

[1]University of Dundee, Dundee, United Kingdom

Introduction and Objectives: Cricket is a popular sport world-widely, especially in commonwealth countries. Upper limb injuries remain to be of concern in cricket fast bowlers. Shoulder injuries are more common in these bowlers. Efficient muscle action combined with a co-ordinated movement of the bowling arm will help sportsmen to generate higher ball speed and reduce injuries. So far, the muscle activities of the bowling arm during delivery phase have not been fully investigated. The aim of this study was to study the electromyography (EMG) in the upper limbs during delivery phase in cricket.

Methods: Twenty right handed male fast to medium bowlers were recruited for this study. The data collection was carried out in an indoor pitch with artificial grass simulating field bowling action. The EMGs and joint movements of the bowling arm were collected using Delsys® and Vicon® systems, respectively. A nine reflective marker of model was used to calculate the joint ranges of motion (RoM) in the shoulder and elbow. EMG was collected by surface electrodes connected through a wireless recording system for the Biceps, Anterior deltoid, Lateral deltoid, Pectoralis major, Trapezius, Latissimus dorsi and Triceps. The EMG from 80 individual bowling deliveries was processed in terms of maximum voluntary contraction (MVC). Root mean square (RMS) of muscle activity, onset and termination positions, maximum muscle activity, and position of maximum activity in the delivery phase were calculated. The bowlers were compared in 2 groups, professional (N=36 deliveries) and amateur (N=44 deliveries) for selected variables.

Results: The Pectoralis major was found to be the most active and important muscle (RMS= 63% of MVC). Maximum muscle activity surpassed its MVC value for Pectoralis major were 195% of MVC, for the Anterior deltoid 151% of MVC and for Latissimus dorsi 102% of MVC. The peak muscle activities for all muscles were found to occur within 40-60% of the delivery phase. Muscle activation sequence was also analysed. The comparison between the two groups for RMS and maximum muscle activity revealed significantly different results for Anterior deltoid ($p<0.01$) and Latissimus dorsi ($p<0.01$). Joint ROMs were also found to be statistically different between the two groups. The elbow angles were found to be varying above the legal limit in amateur bowlers.

Conclusion: The Pectoralis major and Latissimus dorsi are important contributors to speed in cricket bowling. Professional bowlers use these two muscles along with co-ordinated movement of the trunk and the bowling arm to produce higher ball speeds. Amateur bowlers tend to use Anterior deltoid instead of Latissimus dorsi which may predispose them to overuse injuries. This study provides a helpful guide for coaching and rehabilitation purpose for cricket bowling.

Disclosure of Interest: None Declared

Sport

AS-0098

THE TIME-COURSE CHANGE OF PITCHING BIOMECHANICS IN A SIMULATED BASEBALL NINE INNINGS

Ryosuke Akaguma [1,*]Shoma Kudo [1]Akinori Nagano [2]

[1]Department of Sport and Health Science, [2]Faculty of Sport and Health Science, Ritsumeikan University, Shiga, Japan

Introduction and Objectives: In Japanese amateur baseball scenes, we often see one player pitch in two or three successive games over 100 pitches per game under the hot summer sun. Decreasing ball speed and / or control in the latter stage is a major determinant of victory or defeat. The purpose of this study was to reveal the mechanism and effect of pitching fatigue in the latter stage.

Calabrese (2013)[1] divided pitching motion into six stages: Wind-up, Stride (Early Cocking), Late Cocking, Acceleration, Deceleration, and Follow Through. They studied the behavior of kinetic chain to seek the factor of fatigue. Their study analyzed one pitching motion when the pitcher had already been fatigued. We examined the time-course change of kinetic chain when pitchers do pitching over 100 pitches in this current study.

Escamilla et al. (2007)[2] studied pitching motion through approximately 100 pitches with an optical motion capture system. The study focused on joint angle and torque. We performed detailed analysis using the kinetic data from force plate. Using force plate, we can obtain information about the change of postural perturbation at the time of standing, and postural shifting at the time of landing.

Methods: College baseball players were recruited as subjects (age 21±0.5). (1) The subjects threw 15 pitches per inning for 9 innings. Pitching interval was 5 seconds. This protocol simulated a baseball game in the laboratory. Inning intervals were 5 minutes. (2) We measured back muscle strength, grip strength, CMJ (counter movement jump height), and heartbeat in inning intervals. (3) The subjects threw only fastball at full speed. The measure of control was divided into 3 categories: (a) strike zone (b) a ball zone away from the strike zone by two balls (c) others. We obtained kinematic and kinetic data of pitching motions with an optical motion capture system (MAC3D) and force plate (TF-4060-B). The data were further analyzed using a musculoskeletal model (nMotion musculous, nac).

Results: (1) Maximum height of the elbow at the time of a throw decreased in the 9th inning compared to in the 1st inning. The value decreased approximately 3cm~5cm. For subject A the change was from 128.3cm to 125.0cm. For subject B the change was from 141.6cm to 137.8cm. For subject C the change was from 112.7cm to 107.0cm (height above the ground).

(2) In subject C, the maximum height of left heel at the time of standing gradually decreased (max=67.4cm in 9th inning, min=30.3cm in 3rd inning). Subject A and B did not exhibit this decrease (subject A, 69.3cm±3cm. subject B, 69.0cm±2cm).

(3) Ball speed did not change significantly. The ball speed of subject A changed from 108 km/h to 109 km/h. The ball speed of subject B changed from 98 km/h to 105. The ball speed of Subject C changed from 117km/h to 112 km/h (average of 1st inning and 9th inning).

(4) There were no change in the values of: back muscle strength, grip strength, CMJ and heartbeat.

(5) Wrist speed did not decrease. The wrist speed of subject B and C hardly changed from 1st to 9th inning. The wrist speed of subject A decreased until 6th inning, but the value improved after 7th inning.

(6) The time from the instant when the front leg contacts the ground to the instant when the elbow height gets maximum decreased in subject A and B. Subject C did not exhibit this tendency. Whether the subject bent the knee or not is thought to be a reason.

Figure:
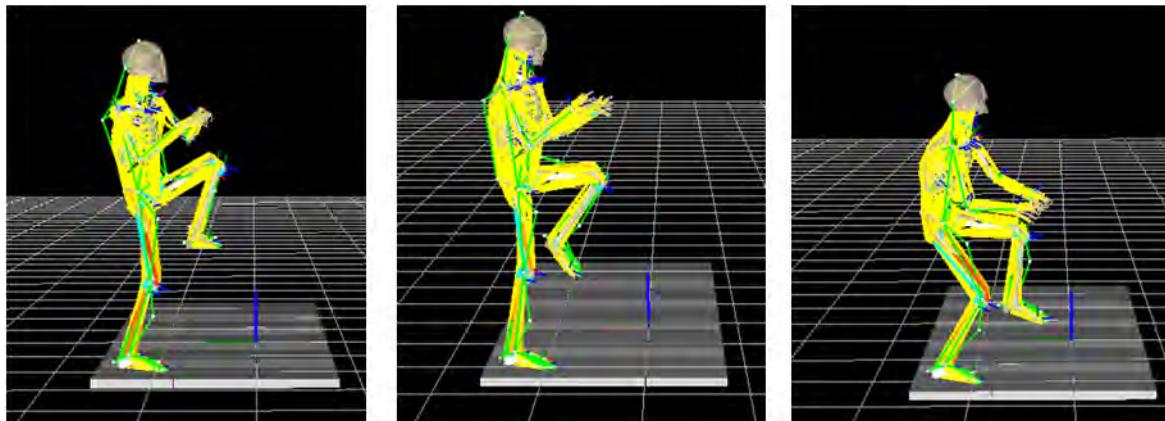
Caption: Snapshot of pitching kinematics for subject A, B and C

Conclusion: All subjects decreased the height of the elbow at the time of throwing.

There were no significant change of values in back muscle strength, grip strength, CMJ, and heartbeat.

The change pattern of pitching form was subject specific.

References: [1] Calabrese. The International Journal of Sports Physical Therapy, 8: 652, 2013.

[2] Escamilla et al., The American Journal of Sports Medicine, 35: 23-33, 2007

Disclosure of Interest: None Declared

Sport

AS-0099

THE MECHANICAL POWER OUTPUT – VELOCITY CURVES FOR VELOTRON ERGOMETER CYCLING AND TRACK CYCLING, AND THE RELEVANCE FOR CYCLING PERFORMANCE AND PACING RESEARCH.

Florentina J. Hettinga [1,]*Patrick Schoenmakers [1]Albert Smit [2]

[1]School of Biological Sciences, Centre of Sport and Exercise Science, University of Essex, Colchester, United Kingdom, [2]Netherlands Olympic Committee*Netherlands Sports Confederation, Papendal, Netherlands

Introduction and Objectives: Interaction with a realistic environment is an important aspect determining pacing behaviour in athletes[1]. To understand cycling performance, it is important to evaluate this performance in a well-controlled laboratory setting, while simulating competition. Besides reliability of the testing equipment, ecological validity is an important aspect. The computer-controlled, electronically-braked Velotron Racermate cycle ergometer has been introduced to closely resemble competitive situations. On screen opponents can be offered, it allows gearing and wind and hilly conditions can be imposed. Another important aspect is that in contrast to most other ergometers, the Velotron claims to incorporate the non-linear relation between mechanical power output and velocity. Due to the effects of air-frictional forces, which are non-linearly related to velocity, it will cost an athlete more energy to accelerate above his/her mean power output than it will save him/her effort to equally decelerate below mean power output in a competitive race. Any variations in velocity over the race thus lead to larger energy costs throughout the race. This biomechanical aspect is essential in determining successful pacing behaviour in competition[2,3] and is of influence on the decisions that athletes make during the race regarding their energy expenditure. Therefore, the modelling of this non-linear relation between mechanical power output and velocity in a well-controlled valid laboratory setting is essential in studying pacing behaviour. The aim of the present study is therefore to determine the relation between mechanical power output and velocity in Velotron cycling compared to track cycling.

Methods: The relation between mechanical power output and velocity in incremental cycling for a cyclist of 75kg on the Velotron Racermate Dynafit (6Hz sampling rate) was determined with a recommended Velotron drag factor setting of 100%, which should be comparable to neutral (no wind) conditions. The Velotron was propelled using a dynamic calibration rig to simulate a continuous pedalling cadence of 90 RPM. The rig was attached to the crank of the Velotron via a counterbalanced double universal joint. The axle was centred at the bottom bracket of the Velotron cycle and attached to the crank at the position of the left pedal. By upshifting gears (18 different gears with 18-33 for the lowest velocity and 56-12 for the highest) while keeping the cadence on 90 rpm, a range of velocities and accompanying power outputs could be evaluated. The calibration rig was powered by a 3 Ph – AC electro motor with a maximum power output of 2.2 kW. Power output and speed were collected over 30s of steady state cycling per stage, resulting in the power-velocity curve. The relation between mechanical power output and velocity was also determined on a cycling track. Data of an elite track cyclist (bodymass + bike: 89.9 kg) were obtained while riding in a standard position with hands on the handlebars on a 250m indoor velodrome in Apeldoorn, The Netherlands. The track bike was equipped with a SRM 7 track system (Schoberer Rad Meßtechnik, Jülich, Germany). Sample rate was set at 2 Hz and actual measured values for wheel circumference were set. 2 Laps at six different speeds were cycled, starting at 30 km/h, with an increase of 5 km/h

to 55 km/h. For Velotron cycling as well as track cycling, trendlines were added based on least-squares fits, and coefficients of determination were obtained.

Results: Best fits were obtained using power fit trendlines, evidencing the non-linear character of the power-velocity curves (Velotron: $r^2 = 0,9971$; Track: $r^2 = 0,9962$). In Velotron cycling as well as in track cycling, a linear model resulted in a lower coefficient of determination (Velotron: $r^2 = 0,9252$; Track: $r^2 = 0,9835$). The required power output to obtain a certain velocity was ~18 % higher in Velotron cycling compared to equal velocities in track cycling. See figure 1.

Figure:

## Power velocity curves of Velotron and track cycling.
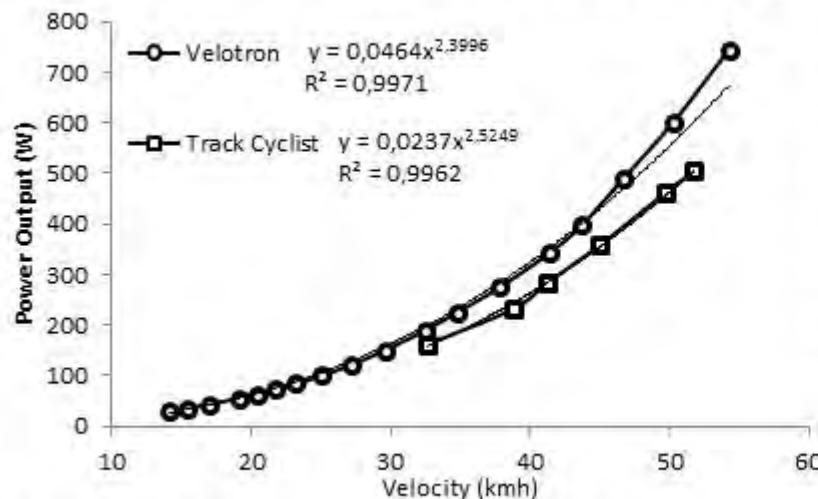
Figure 1a. Best fit Velotron and Track cycling data
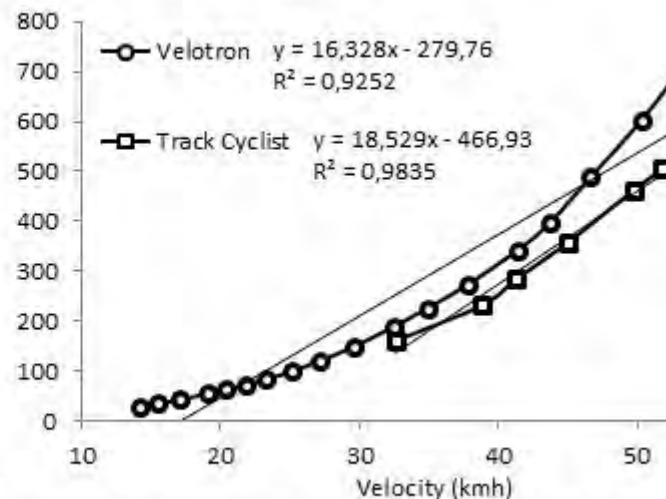
Figure 1b. Linear fit Velotron and Track cycling data

Caption: Mechanical power output-velocity curves of Velotron ergometer cycling and track cycling, with best fit power (1a) and linear (1b) trendlines added.

Conclusion: It seems that the Velotron provides a realistic and valid setting to study pacing behaviour with respect to the non-linear power-velocity relation that has been shown to be relevant for choosing effective pacing strategies[2,3]. The large range of velocities tested on the Velotron clearly showed a non-linear curvature, comparable to track cycling evaluated over a smaller range of velocities (within the domain of human capabilities). However, Velotron cycling seemed to underestimate track cycling performance: Lower velocities were reached at similar power outputs in Velotron cycling compared to track cycling. Future research should aim to study if a draft setting of <100% could more closely mimic track cycling performance.

References: [1]Smits et al.,Sports Med.,44(6):763-775,2014
[2]de Koning et al.,J. Sci. Med. Sport,2(3):266-277,1999
[3]Hettinga et al.,Br.J.Sports Med.,46(1):30-35,2012

Disclosure of Interest: None Declared

Sport

AS-0100

MOVEMENT SCREENS: MEASURING MOVEMENT DYSFUNCTION OR MOVEMENT SKILL?

James Becker [1]Anthony Vidal [1,*]Mimi Nakajima [1]Will Wu [1]

[1]Kinesiology, California State University, Long Beach, Long Beach, United States

Introduction and Objectives: Movement screens are becoming an increasingly popular form of assessing athletic readiness.   Currently popular screens are designed to place individuals in extreme positions where weakness and imbalances become noticeable if appropriate stability and mobility is not utilized by the athlete. It has been suggested that tests assessing multiple domains of function (e.g., balance, strength, and range of motion) can possibly help with early identification of athletes at risk for injury[1]. Using fundamental movement patterns, coaches and practitioners are able to evaluate athletes' dynamic and functional capabilities to quickly identify deficits in mobility and stability.

To date, designers of movement screens fail to understand the difference between skill and mobility. Therefore, one might ask whether "movement dysfunctions", commonly observed on these screens, are more reflective of a lack of skill that can be easily fixed with properly designed test instructions. An abundance of studies within the motor control and learning literature demonstrate the importance of providing proper verbal instructions and demonstration/ observational learning to performers [2]. The purpose of this study was to evaluate performance on the overhead squat (OHS), a common test used in movement screens, when performed with three different sets of instructions.

Methods: Twenty participants performed the OHS under three instructional conditions. For the baseline condition (B) each participant was first instructed to perform three consecutive repetitions of the OHS with no further instructions. Participants then performed the OHS under one of two sets of instructions: instruction demonstration and practice (IDP), or the instructions used by the Functional Movement Screen (FMS)[3]. For the IDP condition each participant was given verbal instructions on how to perform the OHS consistent with motor control and learning principles of instruction. After the verbal instructions where given each participant viewed a demonstrator performed the correct OHS. Next, they performed three non-consecutive practice OHS to allow for any corrections needed in the squat form. Upon completion of the demonstration and practice, the participant performed three consecutive OHS which were recorded for analysis. For the FMS condition each participant performed three OHS squats after receiving the exact instructions from the FMS testing protocol[3]. To account for the three practice squats in the IDP condition, participants were instructed to perform three 'washout' squats prior to the FMS instructions keeping the total number of squats consistent between compared conditions. The order in which participants performed the IDP or FMS conditions was randomized.

A 12-camera motion capture system (Qualisys, Gothenburg, Sweden) was used to record three-dimensional marker trajectories. A thirty one reflective marker set was used to create a thirteen segment model to calculate the center or mass (COM). Custom LabVIEW (National Instruments, Austin TX) programing was used to calculate the following dependent variables. Peak ankle dorsiflexion of each repetition, body COM vertical displacement; horizontal distance from body's COM to the dowel's COM and, forward trunk lean were calculated at the point of the body's COM lowest vertical point (representing the bottom of the squat position) for each OHS. Averages of the three repetitions were

calculated and used in analysis. One-way ANOVAs were used to examine differences in variables between B, FMS, and IDP conditions.

Results: COM displacement was greater in IDP (0.45±0.10 m.) than FMS condition (0.32±0.20m.; p = 0.003), but not different than baseline (0.39±0.12m.; p = 0.047). Forward trunk lean was also greater in IDP (0.33±0.65m.) than FMS condition (0.29±.096m.; p =0.013) but not different than baseline (0.30±0.07m., p = 0.048). Ankle dorsiflexion was greater in IDP (21.33°±5.22) than FMS condition (17.62°±6.26; p = 0.01) but not different than baseline (20.94°±4.7; p = 0.035). Bar to body distance was not different between any conditions.

Conclusion: The results of this study show that OHS performance can be immediately altered by the use of properly designed instructions, demonstrations, and practice. Considerations of these results are critical when conducting movement screen assessments and evaluating mobility, as practioners must be able to dissociate skill and function. If conducted properly, movement screens can provide valuable information that provides detail on restrictions of mobility and range of motion. However, if conducted poorly, any conclusions regarding functional limitations may simply reflect a lack of movement skill.

References: 1. Minick, K. et al. *J. Strength & Condit. Res.* **24**, 479-486, 2010.
       2. Magill, D. *Motor Learning and Control: Concepts and Applications.* McGraw-Hill, 2013.
       3. Gook, G. *Movement: Functional Movement Systems*. On Target Publications, 2011.

Disclosure of Interest: None Declared

Sport

AS-0101

RELATIONSHIP BETWEEN PELVIS-TORSO COORDINATION AND STRIDE CHARACTERISTIC VARIABILITY

James Becker [1]Renae Jackson [1,*]Will Wu [1]Mimi Nakajima [1]

[1]Kinesiology, California State University, Long Beach, Long Beach, United States

Introduction and Objectives: In a given year, approximately half of all runners will sustain an overuse related musculoskeletal injury [1]. Previous studies have shown higher levels of bilateral asymmetry in runners who have sustained stress fracture injuries [2], however, kinematic factors responsible for the observed kinetic asymmetry have not been clarified. For example, asymmetry in the distance the foot contacts the body in front of the center of mass (foot contact distance, FCD) would result in asymmetric braking forces and loading rates. A separate series of studies have reported low levels of coordination variability are associated with chronic overuse injuries in runners [3]. In regards to FCD in particular, the coordinated movement between the transverse plane rotation of the pelvis and torso may be important since altered coupling of pelvis-torso movement affects pelvis rotation, which in turn affects FCD. However, to date, links between torso motion and stride characteristics such as FCD have been minimally examined. Therefore, the purpose of this study is to examine the relationship between variability in transverse plane pelvis-torso coordination and variability in FCD and secondly, to determine if asymmetric pelvis-torso coordination is associated with asymmetric FCD's.

Methods: Whole body kinematics were recorded on 20 runners (sex: 10 male, 10 female; age: 25.7 ± 7.8 years; weekly mileage: 48.5 ± 16.9 miles) using a 12 camera motion capture system (Qualisys, Gothenburg, Sweden) while participants ran on a treadmill, at self selected speeds approximating their easy training pace. Marker trajectories were exported to Visual 3D (C-Motion, Inc., Rockville MD) where pelvis and torso segment angles were determined relative to the laboratory system. A vector coding technique was used to quantify coordination of movement between the pelvis and torso segments in the transverse plane. Coordination variability was determined by calculating the standard deviation of coupling angles across the gait cycle. FCD was defined as the distance between the foot center of mass and the whole body center of mass at the moment of foot contact. Timing of foot contact and toe off were determined using the methods suggested Fellin et al [4]. The coefficient of variation was used to quantify variability in FCD. A symmetry index was calculated from mean coupling angles during the left and right strides, and FCD on left and right strides, respectively. The symmetry index was then used to evaluate asymmetries in pelvis-torso coordination and FCD, with a higher value indicating a higher level of asymmetry. The relationships between coordination variability and FCD variability and coordination asymmetry and FCD asymmetry were evaluated using simple linear regression.

Results: There was a significant relationship between variability in pelvis-torso coordination and variability in foot contact distance for both the left strides (R^2 = 0.214, p = 0.039) and right strides (R^2 = 0.214, p = 0.039). There was no significant relationship between asymmetries in pelvis-torso coordination and FCD asymmetries (R^2 = 0.009, p = 0.679).

Conclusion: The results of this study suggest there is a relationship between the coordinated movements of the torso and pelvis, which may affect stride parameters such as FCD. Previous studies have suggested there is a link between reduced variability and repetitive joint loading. Although the functional consequences of these relationships need to be examined further, increased FCD variability may be a mechanism whereby runners avoid loading the lower extremity in

exactly the same location and manner on each stride. Both coordination variability and movement asymmetry have been suggested as possible factors in overuse injuries. However, the lack of any relationship between asymmetry in pelvis-torso coordination and asymmetry in FCD suggests that movement variability and movement asymmetry may be involved injury etiology through different mechanisms, however this requires further clarification.   Additional research examining how the movement and coordination of the upper body affects lower extremity movements, especially as it relates to running injuries is required.

References: 1. Ferber, et al. *Sports Health* **1**, 242-245, 2009.

2. Zifchock, et al. *J of Biomechanics* **39**, 2792-2797, 2006.

3. Heidersheit, Hamill, et al. *Human Kinetics* **18**, 110-121, 2002.

4. Fellin, et al. *J. of Science and Medicine in Sport* **13**, 646-650, 2010.

Disclosure of Interest: None Declared

Sport

AS-0102

THE RELATIONSHIP OF SEPARATION FACTORS ON THROW DISTANCE OF FEMALE HAMMER THROWERS

Suzanne Konz [1,*]

[1]Kinesiology, Marshall University, Huntington, WV, United States

Introduction and Objectives: Athletes utilizing their entire kinetic chain to throw need to separate the hips and shoulders, typically, to provide a rigid block over which they accelerate the implement being thrown. The hammer is unique in that it provides 3 different separation factors that allow the athlete the opportunity to accelerate the hammer. The separation factors occur between the feet and hips, the hips and shoulders, and the shoulders and the ball. No literature statistically has investigated the relationship of these separation factors and throwing technique of female hammer throwers. The aim of this study was to determine relationship of the separation factors on the final throw distance for female hammer throwers.

Methods: The best performances of the top 10 female throwers at the 2014 USA Track and Field Nationals and 2014 USATF CV OTC meet were examined. Video was captured using two 60 Hz cameras. The best throw of each athlete was digitized and analyzed using the Contemplas Motus 10.0.1 motion analysis system.

Results: : Correlation analysis of separation factors within a throw revealed the separation between the feet and hips at take-off of Turn 1 (p=.000 r= .824), the separation between the feet and hips at take-off of Turn 4 (p=.03 r=. 866), the separation between the shoulders and hammer at take-off of Turn 4 (p=.01 r= -.919), the separation between the shoulders and hammer at touch-down of Turn 4 (p=.01 r= -.934) correlate with throw distance. A stepwise linear regression of separation factors indicated that the separation of feet and hip at release (β= .050), the separation of hips and shoulders at touch-down at Turn 1(β= -.058), and the separation of hips and shoulders at touch-down at Turn 2 impact throw distance (β= .007). A stepwise linear regression of all hammer throw factors (p<.000 r=.1.00) indicates that the separation of the feet and hips at release and the vertical position of the hammer at the take-off during Turn 4 are predictors of throw distance.

Conclusion: The interesting item with the analysis is that there still is no clear path to understanding which components impact throw distance. The fact there is no agreement between the correlation and stepwise linear regression is interesting. A second interesting component is the negative impact that too great of a separation can negatively impact at throw as in the correlation results of Turn 4 take-off and Turn 4 touch-down. It is at this point the ball should be moving at its highest velocities prior to release. By opening the separation factors at these points, the athlete may actually lose control of the system. Athletes use different separation factors during their throw to maintain cable tension, momentum, and speed. No clear cut method to predict hammer throw distance can be developed due to athlete variability within this group.

Disclosure of Interest: None Declared

Mechanics

AS-0103

A COMPARISON OF OVERGROUND AND TREADMILL GROUND REACTION FORCES DURING LOAD CARRIAGE

Angela Boynton [1,*]

[1]Human Research and Engineering Directorate, US Army Research Laboratory, Aberdeen Proving Ground, MD, United States

Introduction and Objectives: Force-sensing treadmills (TMs) provide a convenient means to study the effects of military load carriage on gait dynamics, particularly over long durations. During overground (OG) walking, stance time and peak ground reaction forces (GRFs) increase with carried load [1, 2]. While generally considered equivalent, minor biomechanical differences have been reported between OG and TM walking. In particular, reductions in stance time and peak GRFs are associated with unloaded walking on a TM compared to OG [3, 4]. Differences between OG and TM gait dynamics can limit our ability to generalize the results of TM-based studies to outcomes in a real-world environment, but the impact of load carriage on the magnitude of those differences is currently unknown. Therefore, the objective of this study was to quantify differences in GRFs between walking OG and on a TM with a militarily relevant load.

Methods: An instrumented TM (AMTI Corp.) embedded in the laboratory floor was used to collect GRF data (1200 Hz) for 12 subjects (8M/2F, 1.80±0.07 m, 86.6±12.6 kg) with recent military load carriage experience. Subjects walked at a self-selected pace OG across the surface of the TM and then at a matched pace on the TM, unloaded (NL) and while carrying a 33kg rucksack (LR). A minimum of 5 strides per combination of walking mode and load condition were analyzed for each subject. For each load condition, mean differences in stance time and peak GRFs (Vmax1, Vmin, Vmax2, APmin, APmax, MLmin, MLmax in Figure 1) were calculated between walking modes, and their statistical significance was determined using paired t-tests (α=0.05). Differences between walking modes were additionally compared to the mean inter-stride variability during OG walking (OGvar) for each variable and any difference found to be greater than the calculated OGvar was considered meaningful.

Results: Mean differences in stance time were negligible (<0.01 s) during both unloaded and loaded walking. Mean stance phase GRF curves for each walking mode and load condition combination are shown in Figure 1, and calculated differences between peak values are summarized in Table 1. A statistically significant but non-meaningful increase in the loading peak GRF (Vmax1) occured with TM walking during the NL condition. Statistically significant differences in peak GRFs were also found in the anterio-posterior direction. Peak braking (APmin) and propulsive (APmax) forces were significantly less during TM than OG walking for both load conditions, however, only the LR condition differences exceeded the OGvar values. These reductions in peak braking and propulsive forces may be related to fluctuations in the TM belt speed following heel contact and just prior to toe-off. The subsequent deceleration and acceleration of the TM belt at those time points could serve to dampen the reaction force, and this effect might be magnified as the applied forces increase with carried load.

Figure:
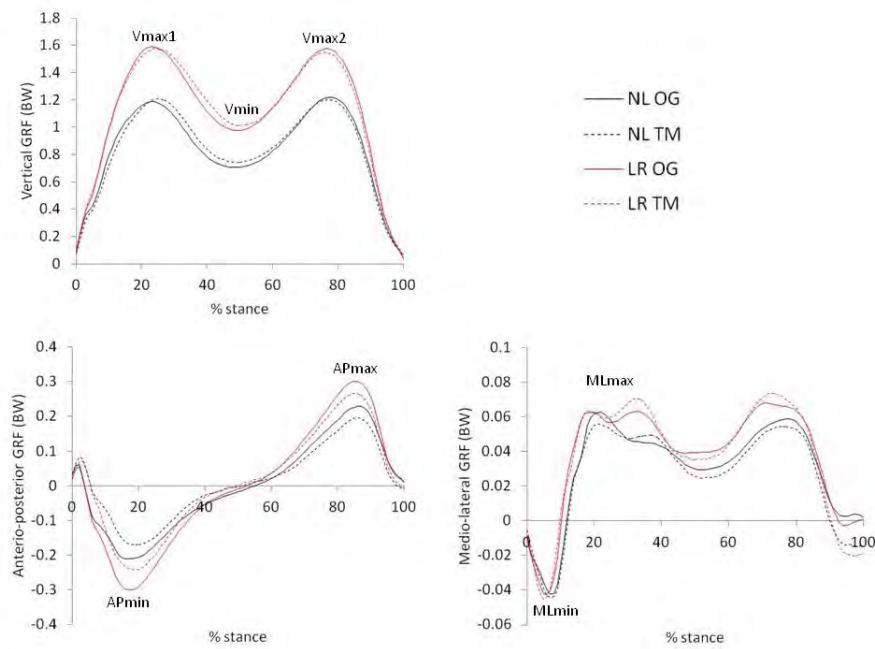
Caption: Figure 1. Stance phase GRFs during OG and TM walking with and without a loaded rucksack.

Conclusion: While peak vertical and medio-lateral GRFs appear to be comparable between OG and TM walking, peak anterio-posterior forces are significantly reduced during TM walking, and these differences exceed OG inter-stride variability when a heavy military load is carried. Changes in joint moments and muscle activity related to this difference between OG and TM walking kinetics could limit the utility of instrumented treadmills for assessing the effects of load carriage in studies where fatigue is of interest or one desires to generalize the results to OG walking. Further study is needed to determine the impact of the observed GRF differences on those variables.

Table:

GRF peak (%BW)	NL			LR		
	difference	t-test	OG var	difference	t-test	OG var
Vmax1	2.5	**0.02**	3.5	0.2	0.73	7.6
Vmin	1.5	0.11	4.7	2.2	0.32	4.6
Vmax2	0.5	0.58	3.8	-2.2	0.35	4.1
APmin	-2.8	**0.00**	4.0	-5.6	**0.00**	**2.9**
APmax	-2.3	**0.00**	2.9	-3.1	**0.00**	**1.8**
MLmin	0.7	0.05	1.7	0.4	0.22	1.7
MLmax	-0.1	0.12	4.2	-0.5	0.38	3.0

Caption: Table 1. Peak GRF differences between OG and TM walking with and without a loaded rucksack. Negative differences indicate TM value less than OG value.

References: [1] Harman et al., USARIEM Technical Report, T00-17, 2000.

[2] Kinoshita, Ergonomics, 28: 1347-1362, 1985.

[3] Lee & Hidler, J Appl Physiol, 104: 747-755, 2008.

[4] Riley et al., Gait & Posture, 26: 17-24, 2007.

Disclosure of Interest: None Declared

Musculoskeletal

AS-0104

EFFECT OF SUBJECT-SPECIFIC MUSCULOSKELETAL GEOMETRY ON MODEL PREDICTIONS

Vincenzo Carbone [1]Marjolein van der Krogt [1] [2]Sjoerd Kolk [3]Jan Schepers [4]Bart Koopman [1,*]Nico Verdonschot [1] [5]

[1]Laboratory of Biomechanical Engineering, University of Twente, Enschede, [2]Department of Rehabilitation Medicine, VU University Medical Center, Amsterdam, [3]Department of Rehabilitation , Radboud University Medical Centre, Nijmegen, Netherlands, [4]Materialise, Leuven, Belgium, [5]Orthopaedic Research Laboratory, Radboud University Medical Centre, Nijmegen, Netherlands

Introduction and Objectives: When exploring complex biomechanical problems, such as in orthopedic surgery to simulate the effects of joint replacements and tendon transfers, or in sport to optimize athletes' performances and prevent injuries, subject-specific musculoskeletal models are essential to achieve reliable predictions. Therefore, it is crucial to develop efficient methods that allow collecting personalized information in a fast and accurate way, without intensive manual intervention.

In this study, we reconstructed the subject-specific musculoskeletal geometry of the lower extremity of ten healthy subjects from MRI scans, using the TLEM*safe* modeling workflow [1], and we assessed the effect of personalization on the model predictions.

Methods: Ten healthy subjects (5 males, age 40.1±15.7 years, height 174.9±11.1 cm, weight 74.8±11.9 kg) were analyzed. For each subject, MRI scan of the lower extremity was obtained (3T, T1-weighted, voxel size of 1.0*1.0*3.0 mm for pelvis, knee and ankle region, and 1.0*1.0*8.0 mm for the remaining upper and lower leg). Then, several gait trials at comfortable, slow and fast speed were measured using 3D motion capture and force-plate data.

Using Mimics® 17.0 and 3-matic® 10.0 (Materialise N.V., Leuven, Belgium), bone surfaces of pelvis, femur, tibia and fibula were segmented from MRI scans, then joint geometry was estimated: hip joint center based on the best fitting sphere to the acetabulum and femur head, knee joint center and direction based on the best fitting cylinder to the femoral condyles. Ankle and subtalar joint were linearly scaled, based on the position of the medial and lateral malleoli. Finally, automatic morphing was applied to the segmented bone surfaces, under the assumption that muscles attachments sites follow the non-linear morphing transformation [2].

Ten subject-specific models were created combining the MRI-based personalized information with the recent Twente Lower Extremity Model 2.0 [3] implemented in the AnyBody Modeling System™ ver. 6.0.3 (AnyBody Technology A/S, Aalborg, Denmark). Inverse kinematics and inverse dynamics were used to calculate joint kinematics and joint net moment when reproducing the measured gait trials, then subject-specific model predictions were compared with linearly scaled models.

Results: Subject specific models allowed a sensible improvement of the accuracy of the musculoskeletal geometry information. Linear model presented errors larger than 10 mm in the estimated segment size, larger than 20 mm in the estimated position of hip and knee joint center, and larger than 10° in the estimated knee joint direction. Moreover, linear models presented errors larger than 10 mm in the estimated position of muscle attachment sites, in particular errors larger than 20mm for some of the most sensitive muscle, such as glutei, piriformis and biceps femoris [4].

Although reproducing the same gait trials, linear and subject-specific and models presented significant differences in the predicted joint kinematics (Fig. 1A), in particular for knee flexion and subtalar eversion (larger than 20°) and for hip flexion and hip external rotation (larger than 10°). Finally, subject-specific models predicted a reduction of joint net moment compared to linear models (Fig. 1B), in particular for subtalar eversion (larger than 10%), and for hip flexion and ankle plantarflexion (larger than 5%).

Figure:
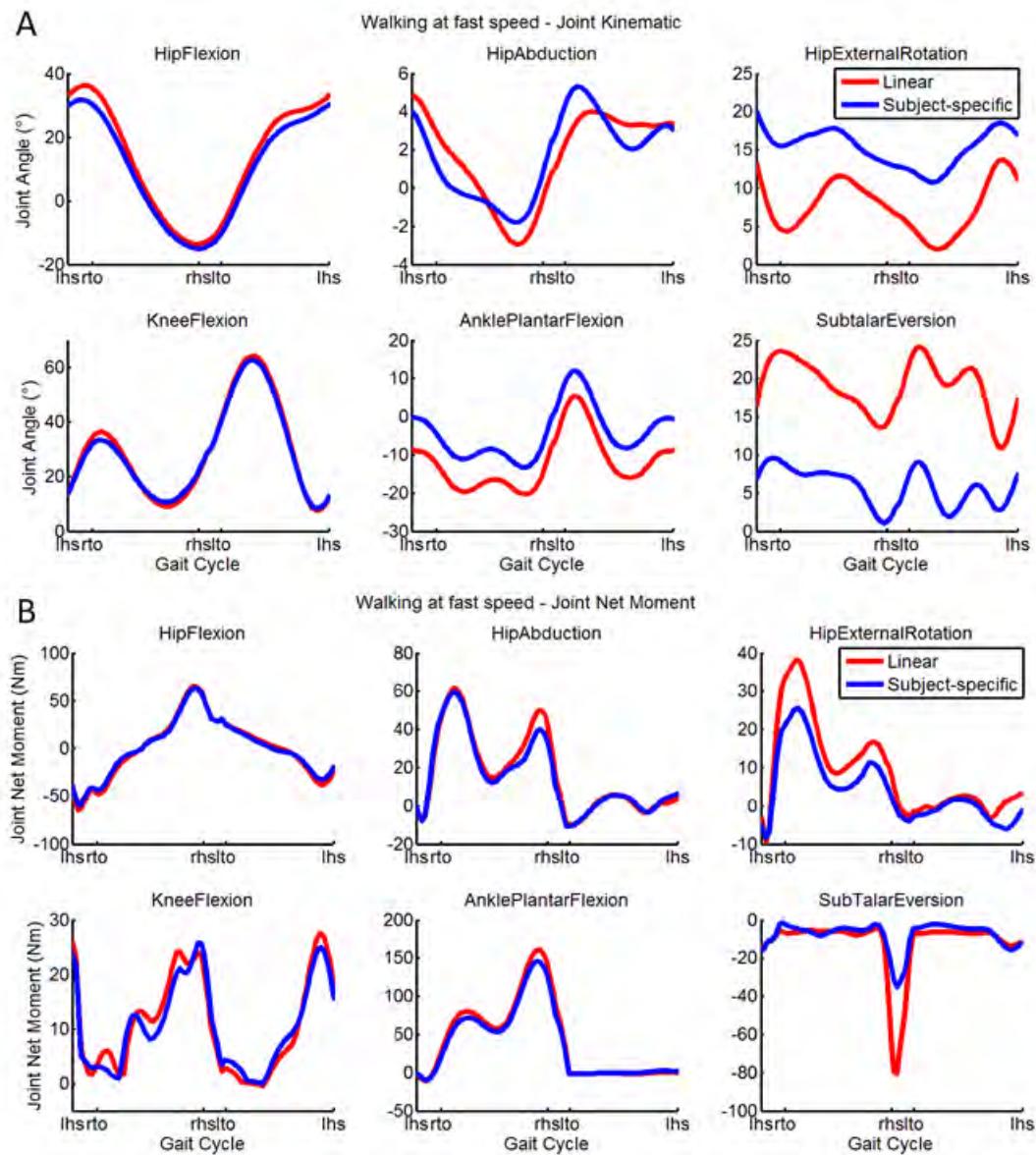
Caption: Predicted joint kinematics (A) and joint net moment (B) during walking at fast speed, using linear and subject-specific model - Example showing one of the ten healthy subjects measured.

Conclusion: Subject-specific models, based on individual bone surfaces extracted from MRI, showed a sensible improvement of the accuracy of musculoskeletal geometry information (bone segment size, joints center and direction, position of muscle attachment sites) when compared to linearly scaled models. These improvements led to large

differences in the predicted joint kinematics, which eventually resulted in a reduction of the predicted joint net moment, indicating that subject-specific models are more efficient than linearly scaled models when reproducing the same task.

The subject-specific models analyzed in this study were obtained semi-automatically using the TLEM*safe* modelling workflow [1]. Application on a large scale of this workflow would permit to reduce errors in musculoskeletal geometry information and model predictions, achieving the validity and reliability necessary in specific applications such as clinical decision making.

References: [1] Carbone et al., Proceedings of WCB 2014, Boston, USA.

[2] Pellikaan et al., J. Biomech., 47, 5: 1144-1150, 2014

[3] Carbone and Fluit et al., accepted by J. Biomech.

[4] Carbone et al., J. Biomech, 45, 14:2476-2480, 2012.

Disclosure of Interest: None Declared

Musculoskeletal

AS-0105

FRONTAL PLANE ACHILLES TENDON MOMENT ARM CHANGES WITH FRONTAL PLANE MOVEMENT OF THE FOOT

Susann Wolfram [1,*]Emma Hodson-Tole [2]Islay McEwan [1]Christopher Morse [1]Keith Winwood [1]

[1]Department of Exercise and Sport Science, Manchester Metropolitan University, Crewe, [2]School of Healthcare Science, Manchester Metropolitan University, Manchester, United Kingdom

Introduction and Objectives: Achilles tendon (AT) moment arms are frequently determined in order to estimate tendon forces in musculoskeletal models. Previously, AT moment arms have been determined in the sagittal plane using the centre-of-rotation method (COR) to estimate tendon forces during plantarflexion. However, the triceps surae muscle group and the associated Achilles tendon have also been found to contribute to both inversion and eversion movements. To date, little is known about the magnitude of Achilles tendon moment arms in the frontal plane and differences in AT moment arms in different frontal plane foot positions. The purpose of this study was to investigate the use of the COR method to determine AT moment arm in the frontal plane and to determine differences in AT moment arm in different frontal plane foot positions.

Methods: MR images of the left ankle were obtained from ten, supine, participants (five female, five male, age 26.3 ± 4.71 years), using a 0.2 T MRI scanner (TE/TR/flip angle of 16 ms/580 ms/75°). The field of view was 83.5 mm and contained 15 slices with a slice thickness of 5 mm and a gap between slices of 0.5 mm. A total of five scans were conducted with the foot positioned at 20° eversion, 10° eversion, 0°, 10° inversion or 20° inversion using a styrofoam wedge. In the obtained images, representative reference points were chosen on the lateral and medial side of the calcaneus at its posterior articulation with the talus. The COR method was then applied to find the centre of rotation, where the talus was assumed to be stationary and where the calcaneus rotates around the subtalar joint axis. The frontal plane AT moment arm was defined as the perpendicular distance from the bisection of the AT to the identified centre of rotation. Moment arms were obtained for the foot in 10° eversion, 0° neutral and 10° inversion. The angle of the AT bisection and the vertical was also measured to account for changes in moment arm. Differences in AT moment arm and the AT angle between the three foot positions were tested with a One-Way ANOVA. The level of significance was set to 0.05.

Results: The AT showed an eversion moment in all three positions. The moment arm in the neutral position was 3.5 ± 4.3 mm which was significantly smaller than the moment arm in eversion (10.6 ± 3.9 mm, p = 0.005) and inversion (12.3 ± 5.4 mm, p = 0.001) The difference in moment arms between eversion and inversion was not significantly different (Figure 1). AT angle was 85.3° ± 2.5°, 85.7° ± 2.1° and 86.0° ± 2.1° in eversion, neutral and inversion, respectively. Differences in AT angle were not significant.

Figure:
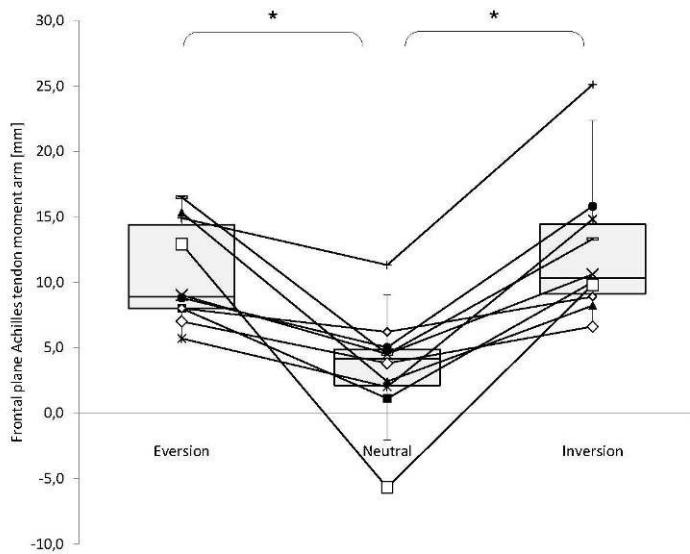
Caption: Figure 1. Box-and-whisker plots for the entire data set with each box plot representing the data distribution for one foot position (eversion, neutral, inversion). The line graphs show moment arm values for each individual subject in each of the three conditions with one line corresponding to one subject. *Significant difference between neutral and eversion, neutral and inversion.

Conclusion: This study showed that the COR method can be applied to determine frontal plane AT moment arms. One previous study reported frontal plane AT moment arms determined using the tendon excursion method [1]. Moment arm values obtained in the present study were considerably larger due to the fact that tendon displacement is generally underestimated with the TE method. Furthermore, the subtalar joint axis is not located perpendicular to the frontal plane but deviates from it. Therefore, the identified centre of rotation is also deviated, which results in a considerable overestimation of the AT moment arm. However, the present study does demonstrate that the AT moment arm varies considerably depending on foot position. This change cannot be attributed to a displacement of the AT as the AT angle was unchanged in all three positions. Therefore, changes in the magnitude of the AT moment arm in the frontal plane can be attributed to subtalar joint configuration. This information could be useful for examining musculoskeletal models of the lower leg and foot when estimating moment arms in more than one plane. Further investigation is necessary to determine frontal AT moment arms more accurately.

References: [1] Lee and Piazza, J.Biomech, 41: 3366-3370, 2008.

Disclosure of Interest: None Declared

Musculoskeletal

AS-0106

TRANSVERSE EXPANSION OF MUSCLE FIBRES DURING CONTRACTION

James Wakeling [1,*]Hadi Rahemi [1]Avleen Randhawa [1]Nilima Nigam [2]

[1]Biomedical Physiology and Kinesiology, [2]Mathematics, Simon Fraser University, Burnaby, Canada

Introduction and Objectives: Muscles come in a range of shapes and sizes, with different fibre lengths, cross-sectional areas and pennation angles, and the muscle size and structure is an important determinate of muscle function. During contraction the muscle fibres can shorten and rotate to greater pennation leading to changes in the length and cross-sectional area of the muscle belly. Due to the ability of the fibres to rotate, their shortening velocity can become uncoupled from the velocity of the muscle belly in a process known as belly gearing. Gearing can change in response to the contractile conditions and may be important in shaping the force, power output and function of the muscle during contraction.

The extent to which the muscle bellies bulge and the fibres rotate is different between the medial and lateral gastrocnemii, despite them being anatomically and functionally similar. It has been suggested that the way in which the fibres increase in girth during contraction may be different and this may lead to the differences in the shape changes in the muscle bellies during contraction [1]. However, until recently we have been without the experimental or conceptual framework to test such predictions. The purpose of this study was to test whether there are asymmetries in the transverse expansion of muscle fibres during contraction, and to investigate the mechanisms for and consequences of such an effect.

Methods: In order to quantify the transverse expansion of muscle fascicles during contraction we developed new image processing techniques to extract the fascicle width from B-mode ulrasound images of muscle contraction [2]. Ultrasound images of contracting medial and lateral gastrocnemii were collected for 6 subjects. The muscle belly region was segmented and pre-processed with multiscale vessel-enhancement filtering. 2D Discrete Fourier Transforms of these images revealed the spatial frequencies within the image in the x and y directions, and these were converted into wavelengths and resolved into the component transverse to the longitudinal axis of the fascicles within the mid-longitudinal plane of the muscle.

In order to test mechanisms that cause the asymmetries in the transverse expansion of the muscle fascicles, we developed a 3D finite element model of the muscle belly based on the continuum theory for fibre-reinforced composite biomaterials [3]. The material properties of the base-material were isotropic and the fibre properties only acted along the longitudinal axes of the muscle fascicles. The model was used to simulate contractions in the gastrocnemii (a unipennate geometry with superficial and deep aponeuroses), and was tested for aponeuroses of different stiffnesses.

Results: During muscle fascicle shortening the fascicle width increased but to a lesser extent than had been expected, giving a Poisson's ratio of 0.09 [2]. These results indicated that a greater fascicle expansion likely occurred in the transverse direction that was orthogonal to the mid-longitudinal plane than in the scanning plane that was parallel to the mid-longitudinal plane. This was confirmed on a further 10 subjects by simultaneously imaging the muscle from two orthogonal directions.

Despite the radial symmetries in the material properties of the muscle fascicles in the finite element model [3], an asymmetry occurred in the transverse expansion of the fascicles during contraction. The Poisson's ratio in the mid-longitudinal plane was 0.089 and matched the experimental findings, and the transverse expansion was greater in a direction orthogonal to this plane. The transverse expansion of the muscle fascicles depended on the stiffness of the aponeurosis and affected their rotations to higher pennation as the contractions progressed.

Conclusion: The abilities of the muscle fibres to shorten and change pennation depend on their transverse expansion and their interaction with the aponeuroses. Pennation of the muscle fibres results in an asymmetry to the structure of the muscle belly that in turn causes anisotropy in the transverse fibre expansion, despite their material properties being transversely isotropic. The structural properties of the muscle tissue combined with the stiffness of the connective tissues thus affect the differences in the transverse fibre expansion during contraction. This in turn affects fibre shortening, force development and thus muscle function.

References: [1] Randhawa et al., Eur. J. Appl. Physiol. 113: 437-447, 2013.

[2] Wakeling et al., Int. J. Biomed. Imaging. 4: 1-9, 2014.

[3] Rahemiet al., Front. Physiol. (Int. Physiol.) 5: 298, 2014.

Disclosure of Interest: None Declared

Musculoskeletal

AS-0107

COMPLETE OPENSIM SUBJECT-SPECIFIC LOWER LIMB JOINT-SKELETAL MRI-BASED MODEL

Simao Brito Da Luz [1,*]David Saxby [1]Luca Modenese [1]Peter Mills [1]Belinda Beck [1]Thor Besier [2]David Lloyd [1]

[1]Center for Musculoskeletal Research, Griffith University, Gold Coast, Australia, [2]ABI, University of Auckland, Auckland, New Zealand

Introduction and Objectives: OpenSim [1] is commonly used for musculoskeletal simulation, representing bones and joints while enabling inverse kinematics (IK) and dynamics (ID) solutions to movement. OpenSim can be employed for clinical purposes e.g. simulate the effects of joint replacement [2] or understand the aetiology of osteoarthritis [3].

OpenSim uses pre-defined joint-skeletal models. Tibiofemoral (TFJ) and patellofemoral (PFJ) kinematics are 2D sagittal planar joints, talocrural (TAJ) and subtalar (STJ) are hinge joints, while the hip joint (HJ) is a ball-and-socket. However not all joints degrees of freedom (DOFs) are defined e.g. no tibia Int-External (IE) or Abd-Adduction (AA) rotations. These models were obtained from a limited set of cadaveric data. For each subject joints kinematics and bones are generically scaled from motion capture (MOCAP) external markers. Joint-skeletal system might not be accurately represented, possibly leading to overestimation of measured TFJ contact forces. In contrast other studies showed improved results when using subject-specific 1) TFJ and PFJ models [4] or 2) hip geometry and hip joint center (HJC) [5]. Therefore, methods are needed to readily create such subject-specific models.

Different models have been used to represent subject-specific joints: 1) TFJ, PFJ and TAJ kinematics are well predicted using 3D parallel mechanisms [6,7]. These models are constrained by the bones, ligaments and tendon geometries, 2) STJ hinge axis can be defined by spheres fitted to the talus [8] and 3) HJC approximated by center of sphere fitted to femoral head.

We aimed to use MRI images of *in vivo* joint tissues to generate subject-specific HJ, TFJ, PFJ, TAJ and STJ models to be used in OpenSim. For the same subject we compared the TFJ and PFJ model results, HJC location and STJ hinge axis orientation with those from generic scaled OpenSim.

Methods: MOCAP data and MRIs were acquired from 14 participants. Each subject's MOCAP marker 3D positions were used to scale the generic OpenSim model's 1) HJC location, 2) STJ hinge axis location and orientation, and 3) TFJ and PFJ locations and kinematics. Alternatively, subject-specific models were created using the geometries from their MRIs. The TFJ, PFJ and TAJ locations and kinematics were estimated using 3D parallel mechanisms [6,7,9]. The STJ axis location and orientation were created from the centers of two spheres fitted to the calcaneal and sustentaculum talus facets, while the HJC was the center of a sphere fitted to the femoral head (Fig.1).

Subject-specific TFJ and PFJ kinematics were compared to those from scaled OpenSim using Pearson's correlation and root mean square differences (RMSD). Both models estimated TFJ Ant-Posterior (AP) and Prox-Distal (PD) translations while PFJ models estimated also FE rotations and Med-Lateral (ML) translations. The differences between the HJC location and STJ axis orientation estimated using each model were also calculated.

Results: Differences in HJC location between the two models were 36.7, 0.033 and 7.7 mm at X, Y, Z respectively with 37.4 mm total difference. STJ axis orientation differences were 0, 0.1 and 0.25 at X, Y, Z. High correlation values (Table 1) and similar STJ axis orientation suggests that for common DOFs the two models estimated similar kinematic patterns.

Figure:
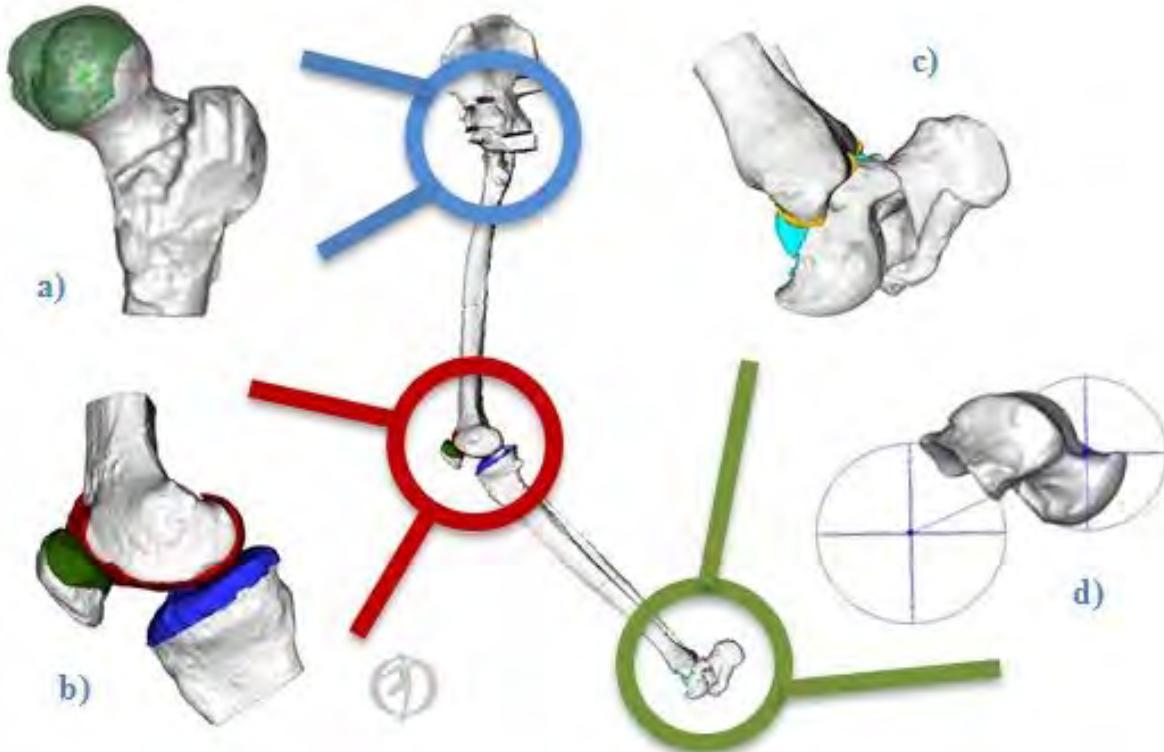
Caption: Figure 1- Subject-specific models a) HJC from femoral head sphere, b) TFJ and PFJ, c) TAJ, d) STJ axis from talus spheres.

Conclusion: Complete OpenSim subject-specific lower limb joint-skeletal models can be created using 3D mechanisms and parameters from MRI. We suggest that OpenSim model scaling can be improved, indicated by the large differences in the HJC location and large RMSD for TFJ and PFJ particularly PD. However generic OpenSim models do not include all DOFs and therefore a complete comparison is not possible. Our ongoing IK and ID analyses using each type of model suggest subject-specific models may be more repeatable.

Table:

	Correlation / RMSD			
	FE	AP	PD	ML
TFJ	-	0.85 / 1.7	0.98 / 62.5	-
PFJ	-0.55 / 7.4	0.99 / 4.4	0.88 / 21.3	0 / 10.2

Caption: Table 1: Correlation and RMSD (n=1) between TFJ and PFJ subject-specific and generic scaled OpenSim models (RMSD in mm except FE in degrees)

References: [1] Delp et al., IEEE Trans Biomed Eng, 54:p. 1940-1950, 2007.

[2] Lundberg et al., J Biomech, 45: p. 990-996, 2012.

[3] Winby et al., J Biomech, 42: p. 2294-2300, 2009.

[4] Gerus et al., J Biomech, 46: p. 2778-2786, 2013.

[5] Lenaerts et al., J Biomech, 42: p. 1246-1251, 2009.

[6] Sancisi et al., J Mech Robot, 3:041003-1-041003-7, 2011.

[7] Franci et al., J Biomech, 42: p. 1403-1408, 2009.

[8] Parr et al., J Biomech, 45: p. 1103-1107, 2012.

[9] Brito da Luz et al., ISB Abstract, 2015.

Disclosure of Interest: None Declared

Musculoskeletal

AS-0108

PASSIVE AND ACTIVE SOLEUS MUSCLE FORCES IN CHRONIC HEART FAILURE

Fausto Antonio Panizzolo [1,*]Andrew J. Maiorana [2]Louise H. Naylor [1]Lawrence Dembo [3]David G. Lloyd [4]Daniel J. Green [5]Jonas Rubenson [1]

[1]School of Sport Science, Exercise and Health, University of Western Australia, CRAWLEY, [2]Advanced Heart Failure and Cardiac Transplant Service, Royal Perth Hospital, [3]Advanced Heart Failure and Cardiac Transplant Service, Royal Perth Hospital, Perth, [4]Centre for Musculoskeletal Research, Griffith University, Gold Coast, Australia, [5]Research Institute for Sport and Exercise Science, Liverpool John Moores University, Liverpool, United Kingdom

Introduction and Objectives: Reduced skeletal muscle strength has been linked to the compromised exercise capacity characterizing chronic heart failure (CHF) (1). However, it is not clear if the reduction in peak voluntary strength in CHF is associated primarily with reduced muscle size. This shortcoming might stem from the reliance on net joint moment-based measurements that reflect activity in all synergist and antagonist muscles crossing a joint. Therefore, the aim of this study was to investigate the size-specific active voluntary force (force per muscle physiological cross sectional area, PCSA) and passive force in a single muscle, the soleus (SOL), of CHF patients and age- and physical activity-matched control participants. The SOL was selected as it is a key muscle for postural control and locomotion (2), and its muscle architecture is severely affected by CHF (3).

Methods: Twelve patients with CHF (63.5±10.9 yo, 168.2±9.6 cm, 67.9±14.8 kg) in the class II-IV of the New York Heart Association and 12 age- and physical activity-matched control participants (62.7±5.6 yo, 173.3±6.1 cm, 69.7±8.5kg) who were free from musculoskeletal disorders and lower limb musculoskeletal injuries were recruited for this study. Voluntary active and passive SOL forces and PCSA were obtained by means of a novel approach combining experimental data (dynamometry, electromyography, muscle imaging) with a musculoskeletal model (4).

Results: We found reduced absolute peak voluntary SOL forces (~25%) as well as reduced passive forces (~30%) (at equivalent levels of muscle stretch) in CHF *vs.* healthy individuals. These differences were eliminated when force was normalized by PCSA, indicating that reduced peak voluntary force and passive force may be strongly associated with muscle size. Fascicle lengths at which the peak active forces were generated () as well as the passive fascicle lengths were shorter in CHF *vs.* controls.

Conclusion: Our results showed that a main determinant of muscle strength in CHF is muscle size. These findings, which might be in contrast with previous investigations on different muscle groups (5), reinforce the specificity of the SOL muscle in the CHF syndrome and further suggests its possible use as a predictor of the disease (3).

The differences reported in length at, as well as the passive fascicle lengths, might also offer additional insight into the altered gait mechanics of CHF patients (6). A combination of the shorter SOL muscle fascicles in CHF patients and their greater dorsiflexion during mid-stance of gait (6) may cause significantly greater SOL strain. This might place the muscle on to the descending limb of the force-length curve where large passive forces develop (4). In this scenario CHF patients would rely more on their passive forces to support the plantarflexion moment during walking, which has the benefit of

reducing metabolically expensive active force development. This may help explain why CHF patients rely proportionately more on their ankle for powering walking as speed and metabolic demand increases (6).

These findings raise the importance of exercise rehabilitation targeting an increase in muscle hypertrophy, and for the calf muscles, exercise that promotes muscle lengthening.

References:

[1] Harrington et al., J Am Coll Cardiol, 30: 1758-64, 1997.

[2] Mc Gowan et al, J Biomech, 42: 850-6, 2009.

[3] Panizzolo et al., Med Sci Sports Exerc, 2014, In press.

[4] Rubenson et al., J Exp Biol, 215: 3539-51, 2012.

[5] Toth et al., Int J Cardiol, 143: 276-82, 2010.

[6] Panizzolo et al., J Biomech, 2014, In press.

Disclosure of Interest: None Declared

AS-0109

HIP POWER ANALYSIS IN INDIVIDUALS WITH TRANSFEMORAL AMPUTATION: A DIFFERENT STRATEGY FROM STABILISATION DURING GAIT STANCE

Raphael Dumas [1 2 3,*] Laurent Frossard [4 5] Catheryne Robert-Leblanc [6] Pierre-Marc Beaulieu [6] Rickard Branemark [7 8]

[1]Université de Lyon, Lyon, [2]Université Claude Bernard Lyon 1, Villeurbanne, [3]Laboratoire de Biomécanique et Mécanique des Chocs , IFSTTAR, Bron, France, [4]Queensland University of Technology, Brisbane, [5]University of the Sunshine Coast, Maroochydore, Australia, [6]University of Quebec In Montreal, Montreal, Canada, [7]Department of Orthopaedics, University of Gothenburg, [8]Centre of Orthopaedic Osseointegration, Sahlgrenska University Hospital, Gothenburg, Sweden

Introduction and Objectives: Joint moments and joint powers during gait are widely used to determine the effects of rehabilitation programs as well as prosthetic fitting. Following the definition of power (dot product of joint moment and joint angular velocity) it has been previously proposed to analyse the 3D angle between both vectors, α_{Mw} [1].

Basically, joint power is maximised when both vectors are parallel and cancelled when both vectors are orthogonal. In other words, $\alpha_{Mw} < 60°$ reveals a propulsion configuration (more than 50% of the moment contribute to positive power) while $\alpha_{Mw} > 120°$ reveals a resistance configuration (more than 50% of the moment contribute to negative power). A stabilisation configuration (less than 50% of the moment contribute to power) corresponds to $60° < \alpha_{Mw} < 120°$.

Previous studies demonstrated that hip joints of able-bodied adults (AB) are mainly in a stabilisation configuration (α_{Mw} about 90°) during the stance phase of gait [1, 2]. Individuals with transfemoral amputation (TFA) need to maximise joint power at the hip while controlling the prosthetic knee during stance.

Therefore, we tested the hypothesis that TFAs should adopt a strategy that is different from a continuous stabilisation. The objective of this study was to compute joint power and α_{Mw} for TFA and to compare them with AB.

Methods: Three trials of walking at self-selected speed were analysed for 8 TFAs (7 males and 1 female, 46±10 years old, 1.78±0.08 m 82±13 kg) and 8 ABs (males, 25±3 years old, 1.75±0.04, m 67±6 kg). The joint moments are computed from a motion analysis system (Qualisys, Goteborg, Sweden) and a multi-axial transducer (JR3, Woodland, USA) mounted above the prosthetic knee [3, 4] for TFAs and from a motion analysis system (Motion Analysis, Santa Rosa, USA) and force plates (Bertec, Columbus, USA) for ABs. The TFAs were fitted with an OPRA (Integrum, AB, Gothengurg, Sweden) osseointegrated implant system and their prosthetic designs include pneumatic, hydraulic and microprocessor knees. Previous studies showed that the inverse dynamics computed from the multi-axial transducer is the proper method considering the absorption at the foot and resistance at the knee [4].

Results: The peak of positive power at loading response (H1) was earlier and lower for TFA compared to AB. Although the joint power is lower, the 3D angle between joint moment and joint angular velocity, α_{Mw}, reveals an obvious propulsion configuration (mean α_{Mw} about 20°) for TFA compared to a stabilisation configuration (mean α_{Mw} about 70°) for AB.

The peaks of negative power at midstance (H2) and of positive power at preswing / initial swing (H3) occurred later, lower and longer for TFA compared to AB. Again, the joint powers are lower for TFA but, in this case, α_{Mw} is almost comparable (with a time lag), demonstrating a stabilisation (almost a resistance for TFA, mean α_{Mw} about 120°) and a propulsion configuration, respectively. The swing phase is not analysed in the present study.

Figure:
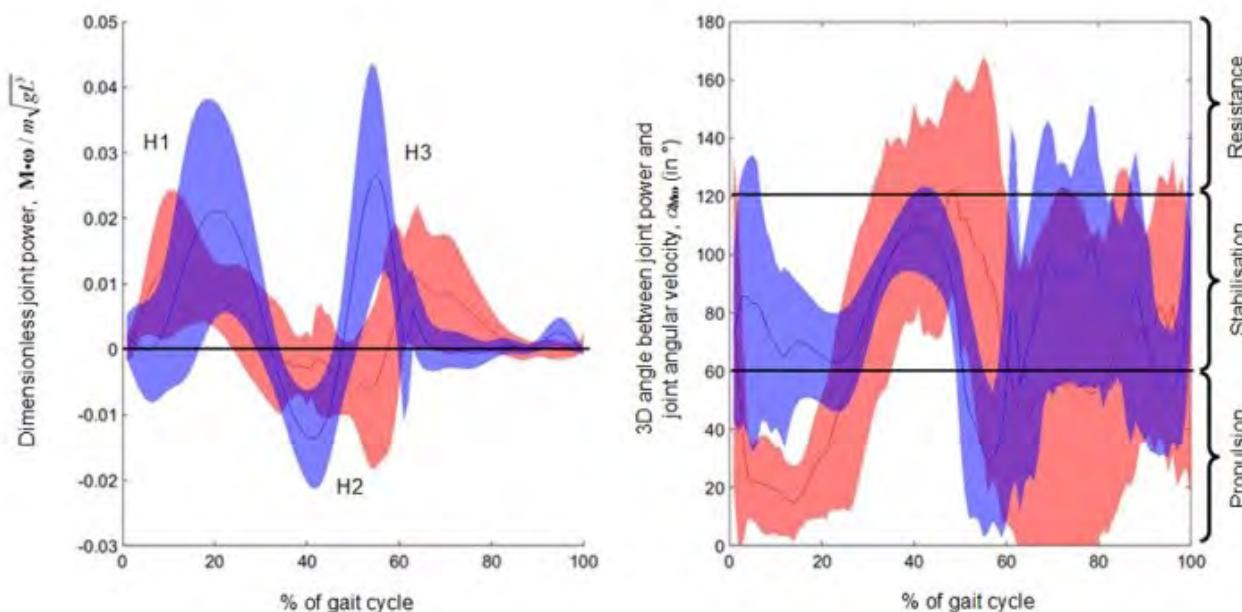
Caption: Dimensionless hip joint power (m is the body mass, g is 9.81 m/s2 and L is length length) and 3D angle between joint moment and joint angular velocity: Red and blue lines and areas are means · standard deviations for individuals with transfemoral amputation (TFA) and able-bodied adults (AB), respectively.

Conclusion: The analysis of hip joint power may indicate that TFAs demonstrated less propulsion and resistance than ABs during the stance phase of gait. This is true from a quantitative point of view. On the contrary, the 3D angle between joint moment and joint angular velocity, α_{Mw}, reveals that TFAs have a remarkable propulsion strategy at loading response and almost a resistance strategy at midstance while ABs adopted a stabilisation strategy.

The propulsion configuration, with α_{Mw} close to 0°, seems to aim at maximising the positive joint power. The configuration close to resistance, with α_{Mw} far from 180°, might aim at unlocking the prosthetic knee before swing while minimising the negative power.

This analysis of both joint power and 3D angle between the joint moment and the joint angular velocity provides complementary insights into the gait strategies of TFA that can be used to support evidence-based rehabilitation and fitting of prosthetic components.

References: [1] Dumas and Cheze, Gait Posture 28: 243–250, 2008

[2] Samson et al., J Biomech 42: 2447–2453, 2009

[3] Lee et al., Med Eng Phys 30:825-33, 2008.

[4] Dumas et al., Gait Posture 30: 560–562, 2009

Disclosure of Interest: R. Dumas: None Declared, L. Frossard: None Declared, C. Robert-Leblanc: None Declared, P.-M. Beaulieu: None Declared, R. Branemark Conflict with: stock in Integrum. The authors believe that this not of nature to influence their interpretation of the results.

Motion Analysis

AS-0110

IS THE RESULTANT MOMENT A MORE SENSITIVE METRIC OF STRUCTURAL OSTEOARTHRITIS PROGRESSION THAN INDIVIDUAL MOMENTS?

Kerry E. Costello [1,*]Cheryl L. Hubley-Kozey [1 2 3]Janie L. Astephen Wilson [1]

[1]School of Biomedical Engineering, [2]School of Physiotherapy, [3]School of Health and Human Performance, Dalhousie University, Halifax, Canada

Introduction and Objectives: Measuring joint loads directly or implementing modeling techniques may provide better estimates of joint contact forces in the context of knee osteoarthritis (OA) progression, but these techniques are often not feasible. Developing better estimates of loading exposure from gait data might be more practical. Research on medial compartment knee OA progression has focused on the knee adduction moment (KAM) as it is considered a surrogate of medial:lateral compartment loading ratio. Recent studies have also linked non-frontal plane loading metrics (knee flexion and rotation moments, KFM & KRM) with OA progression [1-2]. Total loading exposure depends on all three dimensions, thus resultant moments that combine the various dimensions into a single measure may provide a more sensitive OA progression metric. The purpose of this study was to compare the ability of single plane moments versus resultant moments to distinguish between individuals with medial compartment knee OA who will progress structurally and those who will not.

Methods: Three dimensional motion (100 Hz) and ground reaction forces (2000 Hz) were recorded for self-selected speed walking in 46 individuals with moderate medial knee OA (high function, non-surgical candidates). Standard anterior-posterior radiographs taken at baseline and 5-10 years later were scored for medial joint space narrowing (JSN) [3] by a single orthopedic surgeon. Progression (P) and no progression (NP) groups were defined based on whether or not the JSN grade increased in 5-10 years. Knee angles (joint coordinate system) and external moments (normalized to body mass, Nm/kg) were calculated from inverse dynamics and time-normalized to a single gait cycle. A two-dimensional resultant moment (2D) was calculated as the vector sum of KAM and KFM, and a three-dimensional resultant moment (3D) was calculated using all three planes. A non-frontal plane resultant moment (2DNFP) was calculated from KFM and KRM. Five separate analyses were performed. A 2-way mixed model ANOVA was run using scores calculated from principal component analysis (PCA) [4] of the set of KAM (1D), 2D, and 3D waveforms with model (1D, 2D, 3D) as a within subjects factor and group (P, NP) as a between subjects factor. PCA allows each participant's waveforms to be scored (PCscores) for shape and magnitude features (PCs) extracted from the set of waveforms. A separate PCA was run for each of the following: 2DNFP waveforms, KAM waveforms, KFM waveforms, and KRM waveforms. Student's t-tests were used to identify between-group PCscores differences (Mann Whitney U tests used in cases of non-normal PCscores distributions)(α=0.05).

Results: There were no between-group baseline differences in age, body mass index (BMI), speed, Western Ontario and McMaster Universities Osteoarthritis Index (WOMAC), or strength ($p > 0.05$, Table 1). The two-way ANOVA showed main effects of model (1D, 2D, or 3D) but no main effect of group for any PC ($p > 0.05$). A PC capturing the difference between mid and late stance moment had a significant interaction effect ($p = 0.044$). Post-hoc tests showed 1D was different from

2D (p=0.045) and 3D (p=0.043), but no group differences. In contrast, 2DNFP had one between-group difference with P having higher 2DNFP in late stance compared to early (p=0.018). Additionally, when investigating the individual moments (KAM, KFM, & KRM), two between-group, non-frontal plane differences were found: P had greater extension and internal rotation moments throughout stance than NP (p=0.044 and p=0.017, respectively). No between-group differences were identified for KAM.

Figure:
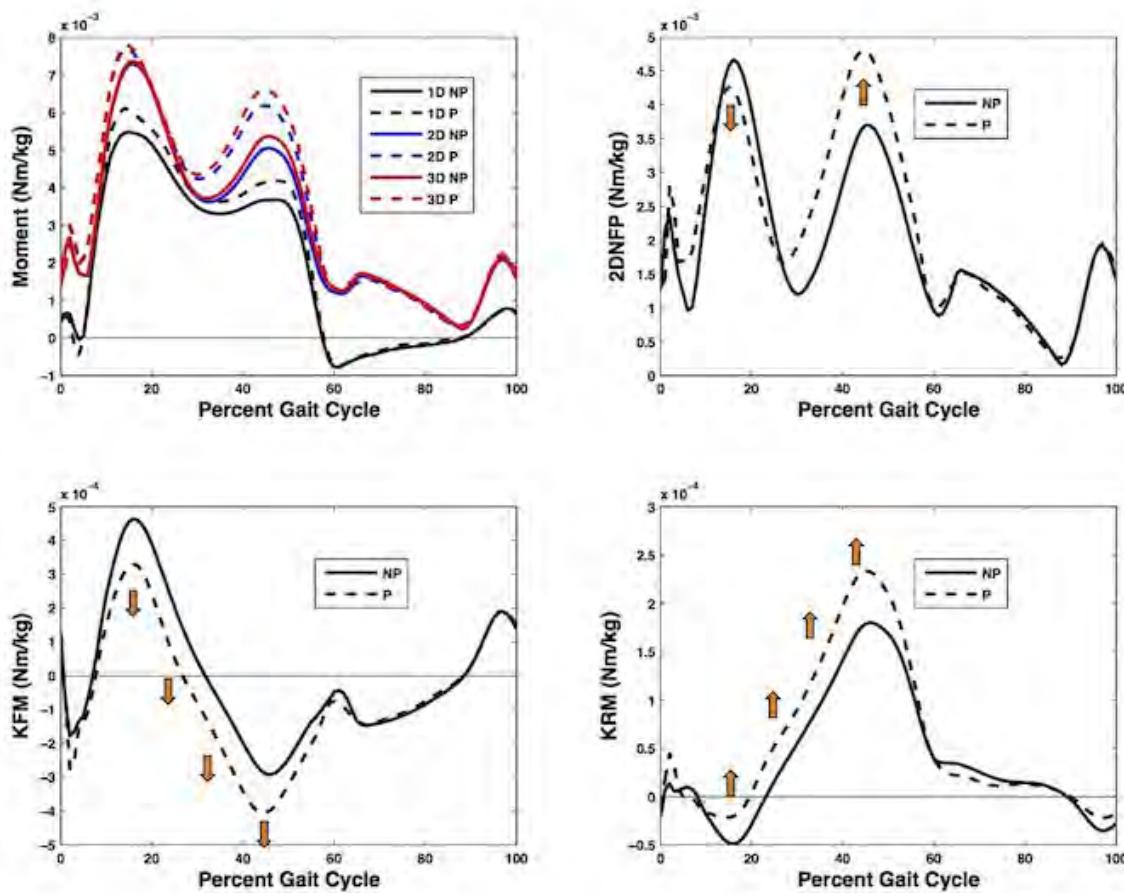
Caption: Mean moment waveforms (1D (KAM), 2D, 3D, 2DNFP, KFM, and KRM) with JSN Progression (P) and No JSN Progression (NP) group differences indicated with arrows (p<0.05)

Conclusion: KAM moments alone or resultant moments incorporating KAM did not discriminate between baseline data from individuals with OA who progressed structurally versus those who did not. A non-frontal plane resultant moment and individual non-frontal plane moments did discriminate between groups. While KAM was not significantly different between groups, it tended to dominate the resultant moment, masking differences between groups in the non-frontal planes. Care should be taken when combining different planes into a resultant moment that includes KAM, as group differences in individual planes can be lost in the process.

Table:

	NP	P
N	20	26
JSN Baseline (0:1:2:3)	0:5:15:0	2:13:11:0
Male:Female	14:6	17:9
Age	57±10	57±6
BMI (kg/m^2)	31±5	31±6
Speed (m/s)	1.2±0.2	1.3±0.2
WOMAC	35±19	29±17
Knee Flexion Strength (Nm)	55±13	62±20
Knee Extension Strength (Nm)	115±39	120±43
Plantar Flexion Strength (Nm)	93±36	86±30

Caption: Clinical, demographic, and strength characteristics of the JSN Progression (P) and No JSN Progression (NP) groups

References: [1] Chehab et al., OA&C, 22:1833-1839, 2014.

[2] Costello et al., World Congress on Biomechanics, 2014.

[3] Scott et al., Invest Radiol, 28:497-501, 1993.

[4] Landry et al., J Biomech, 40:1754-1761, 2007.

Disclosure of Interest: None Declared

Motion Analysis

AS-0111

A COMPARISON OF HUMAN WALKING USING A CONVENTIONAL GAIT LABORATORY AND THE MOTEK MEDICALA COMPUTER ASSISTED REHABILITATION ENVIRONMENT WITH VARYING LEVELS OF "IMMERSIVNESS"

Andre Attard [1,*]Andrew J. Murphy [1]

[1]Biomedical Engineering, University of Strathclyde, Glasgow, United Kingdom

Introduction and Objectives: Treadmills provide a convenient and controlled environment which promotes ease of motion analysis data due to the lesser spatial volume used, however such configurations lack visual feedback from the surrounding environment which has a detrimental effect on the users' gait (Sloot *et al.*).Virtually realistic optic flow during treadmill based rehabilitation has been recently introduced as a novel alternative to conventional over ground laboratories. Sloot *et al.* stated that imposing an immersive virtual reality environment during a fixed speed treadmill modality will elicit walking that is closer to that which is obtained during over ground walking (Sloot *et al.*). The primary objective of this project was to add to the growing body of literature which quantifies differences between over ground walking, and walking conducted in a virtual reality based environment with varying levels of complexity in the so called "optic-flow".

Methods: Motion capture was carried out using a 12 camera Vicon T-series for over ground walking and a 12 camera Vicon Bonita10 system which was installed within a Computer Assisted Rehabilitation ENvironment (CAREN) extended suite (Motekforce Link, Amsterdam). Following ethical approval, 7 healthy participants volunteered (age = 27.6 ± 3.8). A repeated measures design was followed for four walking conditions, over ground (WC1), treadmill (WC2), treadmill with a virtually generated grass pathway (WC3), and treadmill with a grass pathway and a simplified avatar (WC4, Figure 1). Participants walking speed was individualised inter participant but not inter walking condition.

Primary outcome measures which were assessed for the four walking conditions were walking speed (m/s), cadence (steps/min), stride length (m), maximum hip flexion angle (°), maximum knee flexion angle (°) and maximum ankle dorsiflexion angle (°). Data was exported to IBM SPSS, where it was checked for normality. A non-parametric approach was implemented to compare for inter walking condition effects using the Wilcoxon Signed Ranked Test, with a Bonferroni Correction.

Results: Refer to Table 1.

Figure:
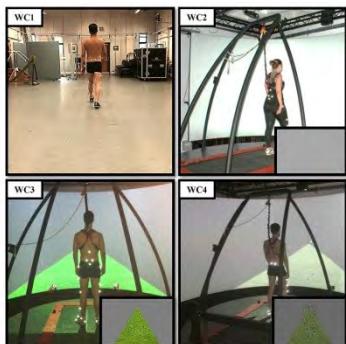
Caption: The four walking conditions. In the bottom right corner of WC2 to WC4, the VRE rendered for each condition is shown.

Conclusion: The fixed speed modality used during the treadmill ambulation reflected on the measured results. This modality affected the participants' temporal spatial parameters (TSPs) across the different virtual reality (VR) scenario. This provided evidence that with increasing immersiveness of the VR during treadmill walking (WC2 - WC4), the TSPs converge to those measured during WC1. The relatively high immersiveness of the VR used during WC4 increased the participants' confidence which led to a faster walking speed, but due to the fixed treadmill speed modality the participants unconsciously altered their cadence and stride lengths. This occurs as a result of the TSPs' intra-dependency which states that when walking speed is decreased, cadence is decreased while the stride length is increased.

The statistical study reported statistical differences between over ground walking and treadmill walking conditions, within five out of six of the outcome measures. This shows that these outcome measures are affected by the walking speed. Statistical differences between the different treadmill walking conditions were noted, within five out of six of the outcome measures investigated. This shows that the optic flow has an impact on these parameters, mainly the maximum knee and ankle flexion angles.

Conclusion: Although the gait parameters investigated in this study showed statistically different values amongst a number of cases, the differences were within the range of repeatability of the gait parameters' variability, hence considered clinically insignificant. Thus, treadmill walking for motion analysis purposes in conjunction with virtually realistic optic flow systems is deemed acceptable to utilise instead of over ground walking as long as a high quality VR environment is used and the motion analyst is aware of the variability that occurs within the parameters.

Table:

	WC1	WC2	WC3	WC4
Walking Speed (m/s)	1.44 ± 0.14 (¤)(†)(‡)	1.07 ± 0.1 (*)	1.07 ± 0.1 (*)	1.07 ± 0.1 (*)
Cadence (steps/min)	115.99 ± 5.99 (¤)(†)(‡)	108.91 ± 2.58 (*)(‡)	109.01 ± 2.35 (*)	107.57 ± 2.77 (*)(¤)
Stride Length (m)	1.49 ± 0.14 (¤)(†)(‡)	1.24 ± 0.1 (*)(‡)	1.25 ± 0.1 (*)	1.25 ± 0.1 (*)(¤)
Maximum Hip Flexion Angle (°)	36.26 ± 4.63 (¤)(†)(‡)	33.93 ± 6.4 (*)(†)	33.38 ± 6.18 (*)(¤)	33.68 ± 6.36 (*)
Maximum Knee Flexion Angle (°)	63.42 ± 5.88	63.79 ± 4.81 (†)(‡)	64.27 ± 4.65 (¤)	64.24 ± 475 (¤)
Maximum Ankle Dorsiflexion Angle (°)	21.18 ± 7.25 (¤)(†)(‡)	14.95 ± 2.53 (*)(†)(‡)	15.63 ± 2.48 (*)(¤)	15.66 ± 2.16 (*)(¤)

Caption: A summary of the results. Indications of statistically significant differences between walking conditions are shown: different to WC1 (*), WC2 (¤), WC3 (†) and WC4 (‡).

References: Sloot et al. The biomechanical effect of a virtual reality depends on treadmill mode. *Gait & Posture*, [online] 39(1), pp.S49-S50, 2014

Disclosure of Interest: None Declared

Motion Analysis

AS-0112

HIP JOINT CENTRE MODELS IN FAI POPULATION

Giulia Mantovani [1,*] K.C. Geoffrey Ng [2] E. Paul Beaulé [3] Mario Lamontagne [1 2]

[1]School of Human Kinetics, [2]Department of Mechanical Engineering, [3]Division of Orthopaedic Surgery, University of Ottawa, Ottawa, Canada

Introduction and Objectives: An accurate location of the hip joint center (HJC) is crucial for motion analysis and musculoskeletal modelling. HJC misplacement of just 3cm can cause up to a 22%>difference in hip flexion-extension moment, and can considerably affect muscle moment arms [1]. When imaging data are not available, the HJC can be estimated using regression equations that incorporate anthropometric measurements [2,3], with recent studies suggesting that Harrington's regression equations provide higher accuracy than Davis model [4]. No study has investigated the accuracy of these regression equations applied to special populations such as cam-type femoroacetabular impingement (FAI) patients. Cam FAI is the result of a femoral head deformity characterized by an elevated alpha angle and the alteration of other pelvic anatomical parameters [5]. Because of this, it cannot be assumed *a priori* that the same regression equations can properly locate HJCs in individuals with FAI. Therefore, the objective of this study was to evaluate the accuracy and reliability of Harrington and Davis HJC regression models for FAI and non-FAI populations.

Methods: Sixty-six participants took part in the study: 18 control participants (CON), 25 with an asymptomatic femoroacetabular deformity (aFAD), and 23 with symptomatic FAI (sFAI) (Table 1). Bilateral anterior and posterior iliac spines were identified from each participant's blinded CT data, using ITK-SNAP 2.4 (PICSL, USA), to define the pelvic local reference system and estimate HJC from the regression models. The hip geometric centers were also located on CT images and considered as the actual HJC. The measurements were completed by three readers, each performing three readings, with near-perfect inter- and intra-observer reliability (ICC>0.90).

The errors between the estimated and the actual HJC were calculated in the three orthogonal directions (D_x, D_y D_z) together with the Euclidean distance (D_L). HJCs from each regression model were directly compared to the actual HJC, using Bland-Altman test [6]. A one-way ANOVA was used to identify significant differences among the participant groups. A paired t-test compared the average error between the two models.

Results: No differences were found among the three groups and between sides (symmetry between hips), therefore, participants and sides were pooled together for a total of 122 samples per regression method. Paired t-tests showed a significantly lower error for Harrington's equations (D_L = 16.9±7.6mm) than Davis's (D_L = 31.3±9.3mm, p<0.001). The Bland-Altman limits of agreements (LOA) were corrected to adjust the linear relationship between average and difference. Less than 5% of the samples fell outside the LOA (Figure 1).

Figure:
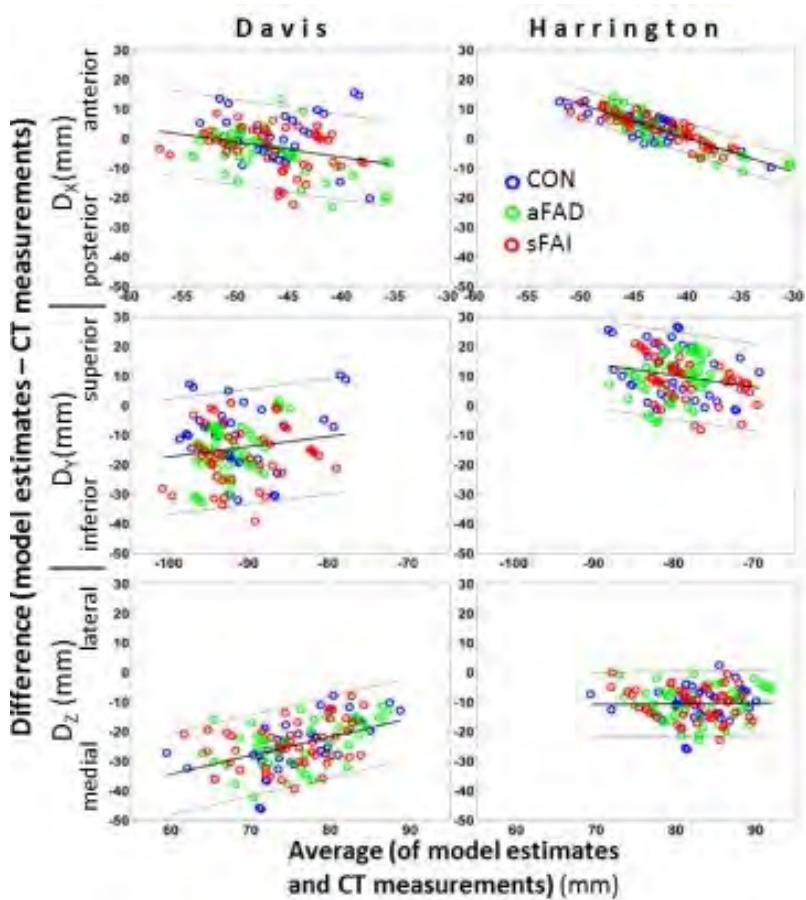
Caption: Bland-Altman scatter plots for estimated vs. actual HJC coordinates. Black lines represent the regression line and corrected limits of agreements (b0 + b1•avg ±1.96 residual std)

Conclusion: The anatomical differences in the FAI population do not significantly alter HJC location, with respect to a healthy population. Interestingly, the marginal differences between groups were non-significant and beyond the accuracy of the prediction methods. Therefore, motion analyses on FAI populations (asymptomatic and symptomatic) can use the same HJC regression equations, used for the healthy population.

Since less than 5% of the samples fell outside the LOA in both regression models (Figure 1), the HJC model estimates were in statistical agreement with the actual CT HJC. However, Bland-Altman tests showed a linear relationship between errors and coordinate magnitudes, such as for Harrington's D_X, where the best estimation (i.e. smallest error) was achieved when HJC_x coordinate was near -40mm, but was increased when deviating from this range. A clear bias was seen in D_Z, where the average error was larger than 20mm for Davis and 10mm for Harrington throughout the whole range. While the linear dependency is harder to correct, the bias could be added to the regression equations to reduce the estimation error.

The average errors in HJC estimations were consistent with previous studies [2, 3]. Davis model produced double the error respect to Harrington model, thus confirming the superiority of Harrington's equations in predicting accurate HJC. The reduced error can improve inverse kinematics and dynamics calculations and muscle force estimation.

Table:

	N (male/female)	Age (years)	Height (cm)
CON	18 (15/3)	34±6	174±9
aFAD	25 (22/3)	31±6	178±8
sFAI	23 (20/3)	37±8	175±6

Caption: Population demographics

References: [1] Stagni, R., et al., J Biomech, 33: 1479-1487, 2000.

[2] Davis III, R.B., et al., Hum Movement Sci, 10: 575-587, 1991.

[3] Harrington, M.E., et al., J Biomech, 40: 595-602, 2007.

[4] Sangeux, M., et al., Gait Posture, 2014.

[5] Ng, K.G., et al., Clin Orthop Relat Res, 2014.

[6] Bland, J.M. et al., Lancet, 327: 307-310, 1986.

Disclosure of Interest: None Declared

Motion Analysis

AS-0113

A COMPARISON BETWEEN FOUR FOOT MODEL PROTOCOLS: THE EFFECT OF WALKING ON A TREADMILL

Roberto Di Marco [1 2,*] Stefano Rossi [3] Vitomir Racic [4] Paolo Cappa [1 5] Claudia Mazzà [2 6]

[1]Department of Mechanical and Aerospace Engineering, 'Sapienza' University of Rome, Rome, Italy, [2]Department of Mechanical Engineering, The University of Sheffield, Sheffield, United Kingdom, [3]Department of Economics and Management, Industrial Engineering, University of Tuscia, Viterbo, Italy, [4]Department of Civil Engineering, The University of Sheffield, Sheffield, United Kingdom, [5]Laboratory of Movement Analysis and Robotics (MARlab), Children hospital 'Bambino Gesù', Fiumicino, Italy, [6]INSIGNEO Institute for in silico medicine, The University of Sheffield, Sheffield, United Kingdom

Introduction and Objectives: The interest on the foot ankle complex modelling is increasing in the last years. In gait analysis, the most widespread models are those proposed by Stebbins *et al.* [1], Leardini *et al.* [2], Sawacha *et al.* [3], and Saraswat *et al.* [4], which segment the foot-complex in three bodies, coherently with the anatomy. To the Authors' knowledge, a comparative exam of the performances inherent with the previously indicated models is not available. The main goal of the research project is the comparison of the foot models described in [1–4] by applying the four marker sets simultaneously on the subject.

Considering the significant number of markers to be applied (i.e. 27) and to facilitate marker tracking and labelling, the trials were conducted on a treadmill. However, kinematic and kinetic variables obtained in treadmill or overground walking might show different values [5]. Thus, as a prior study toward a comparison of the model outputs on a larger sample of individuals, this work investigated the comparability of treadmill and overground walking conditions in terms of main joint kinematics variables obtained for the four examined foot models.

Methods: The right lower limb and pelvis of four healthy adults with no ankle impairments were simultaneously equipped with the four marker sets [1-4] (4 mm hemispherical markers), Figure 1. The data collection was performed using a Vicon system (T 10-camera-workstation, Nexus 1.8.5 software, 100 Hz, Vicon Motion Systems, Oxford - UK).

A static trial was collected to define the local coordinate systems (CS), and five strides were then collected on a treadmill and overground. The treadmill speed was set at 3 m/s, whereas in the overground condition subjects were asked to walk at a self-selected speed.

Each model was analysed by properly selecting the relative marker set to obtain the kinematic angles. Joint kinematic angles were first expressed as a percentage of the gait cycle and then the sagittal range of motion (ROM) and the maximum plantar flexion and dorsiflexion for all the joints defined in the models were extracted using MATLAB (MathWorks, Natick - USA). The mean values were calculated along the five strides. The output of each model was tested with a repeated measure ANOVA ($p=0.05$) to investigate the differences between the two walking conditions (IBM SPSS Statistics v21, IBM Corporation, Armonk - USA).

Results: As a qualitative result, we can report the difficulty in tracking the marker trajectories when walking overground, while the tracking was simple enough in the case of using the treadmill. The statistical analysis shows that none of the joint kinematic variables significantly changed between the two conditions ($p>0.05$). We found the lowest *p*-values for the

plantar/dorsiflexion ROM of the forefoot relative to calcaneus in the Saraswat's model (p=0.16) and for the maximum dorsiflexion of the mid-foot relative to calcaneus in the Sawacha's model (p=0.23). The largest value (p=0.99) has been obtained for the plantar/dorsiflexion ROM of the forefoot relative to tibia in the Stebbins model, for the foot relative to tibia both in the Leardini and Sawacha models, and for the maximum plantar flexion of the forefoot relative to tibia in the Saraswat model.

Figure:

Caption: Figure 1 – The full marker set obtained by fusing the four foot protocols: 13 markers for the Stebbins' model [1], 14 markers for the Leardini's model [2], 13 markers for the Sawacha's model [3] and 16 markers plus the triad on the hallux for the Saraswat's model [4].

Conclusion: Since that to the Authors' knowledge there are no articles on the described comparison considering a segmented foot model as the ones proposed in [1–4], in the present study we achieved an evaluation of the kinematic variables defined on the sagittal plane from four subjects equipped with the four foot models. The same variables were extracted both from a walking trial collected asking the subjects to walk on a treadmill and to walk overground.

While Riley *et al.* [5] asserted the differences on the hip, knee and ankle angles on the sagittal plane considering the two walking conditions, the 21 variables here examined indicate that no significant differences were observed between the two walking conditions (p always ≥0.16).

This finding allows the Authors to develop a methodology in the on-going phase of the research project for quantifying the goodness of the models in terms of repeatability, reproducibility and reliability that include the use of the treadmill for the walking trials.

However, it has to be noticed that the number of subjects involved in the study might have affected the results.

References: [1] Stebbins et al., Gait Posture, 23: 401-410, 2006.

[2] Leardini et al., Gait Posture, 25: 453-462, 2007.

[3] Sawacha et al., J. Neuroeng Rehabil, 6: 37, 2009.

[4] Saraswat et al., Gait Posture, 37: 121-125, 2012.

[5] Riley et al., Gait Posture, 26: 17-24, 2007.

Disclosure of Interest: None Declared

Motion Analysis

AS-0114

ESTIMATION OF FORCE, STIFFNESS AND ELASTIC ENERGY BASED ON KINEMATIC DATA WHILE RUNNING

Didier Staudenmann [1,*]Jacques Robadey [1]Silvio Lorenzetti [2]Wolfgang Taube [1]

[1]Movement and Sport Science, Department of Medicine, University of Fribourg, Fribourg, [2]Institute for Biomechanics, Department of Health Sciences and Technology, Swiss Federal Institute of Technology , Zurich, Switzerland

Introduction and Objectives: Recording of ground reaction forces (GRF) provides crucial information to evaluate the running pattern. Furthermore, in combination with kinematic data, GRF can be used to determine the leg stiffness [1] and its elastic energy (Ee). However, although the assessment of these parameters is important, force recordings during running require complex laboratory settings with multiple imbedded force plates or instrumented treadmills. Consequently, this kind of approach is limited in its applicability. The aim of this study was to investigate the accuracy of estimating force, stiffness and Ee based on kinematic data of the COM, in comparing these values against GRF data.

Methods: In 13 subjects we measured full body kinematics and GRF of two steps (two force plates) during running (v=3.0±0.3m/s). From the kinematics we assessed the COM in sagittal plane, which was low-pass filtered (Savitzky-Golay) and differentiated to obtain acceleration and – after taking into account the respective body mass – force F. During the stance phase we estimated the "leg length" as the distance between COM and the center of pressure and considered its length change (Δl) in sagittal plane during foot strike and maximally flexed leg [cf. 1]. During the same interval we considered the change in sagittal force (ΔF), which allowed quantifying leg stiffness during stance as $k=\Delta F/\Delta l$. Based on force and stiffness we estimated the elastic energy in sagittal plane as $Ee=1/2\cdot(F_1^2/k_1 + F_2^2/k_2)$ for leg1 and leg2. The accuracy of F, ΔF, k, and Ee was estimated by comparing kinematic-based to GRF-based data using correlation coefficients.

Results: The kinematic approach estimated vertical force better (r=0.98±0.01) than the horizontal force (r=0.71±0.08, see Figure). The change in "leg length" Δl was 6.8±1.1 cm. The kinematic-based ΔF was significantly lower (9%) than the measured GRF (1.4±0.3kN vs. 1.6±0.3kN, p<0.01) and the kinematic-based leg stiffness-k was also significantly lower (10%) than the GRF-based data (22±5kN/m vs. 24±6kN/m, p<0.01). The kinematic-based Ee showed a considerable congruence with the vertical GRF-based values (r=0.97±0.02; see Figure).

Figure:
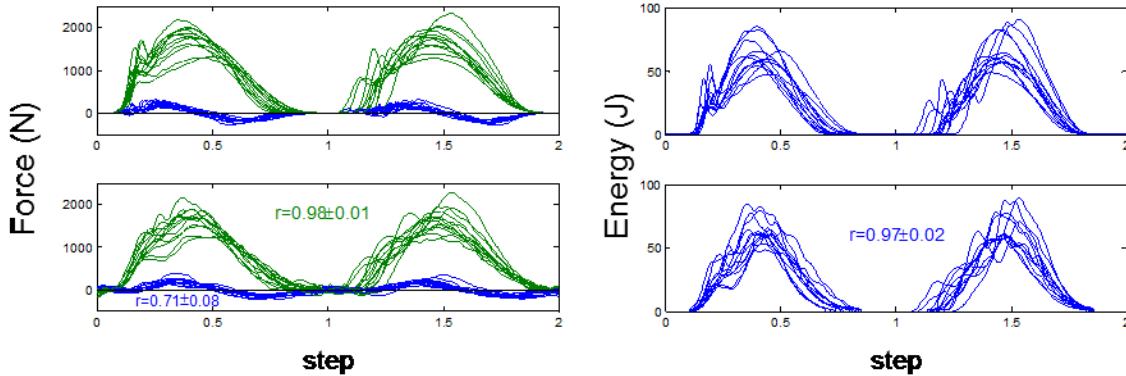
Caption: Result of force (left) and elastic energy (right) for two steps of 13 subjects. Upper panels show GRF-based outcomes and lower panels show kinematic-based outcomes. The correlation coefficients between the kinematic-based and the GRF-based values provide information about the accuracy of this approach.

Conclusion: Force, stiffness and elastic energy represent important parameters to evaluate running. The present study shows that these parameters can be estimated based on kinematic data. When considering the accuracy of this force estimation, the horizontal force was more difficult to estimate than the vertical force and strongly depended on the filter settings. However, as the vertical force is considerably larger than the horizontal force it will have a stronger effect on the further outcomes (k, ΔF, Ee). In this sense, Ee showed indeed a comparable accuracy than the vertical force (see Figure). It can be concluded that force, leg stiffness, and elastic energy can be estimated with kinematic data but the accuracy of this estimation depends strongly on the filter settings that are applied to the COM kinematics.

References: [1] Blickhan et al., J Biomech, 22: 1217-1227, 1989

Disclosure of Interest: None Declared

CORTICAL MODULATION OF ABERRANT LOWER LIMB MUSCLE SYNERGIES FOLLOWING STROKE

Andrew Q. Tan [1,*]Yasin Dhaher [2]

[1]Neuroscience, [2]Biomedical Engineering, Northwestern University, Chicago, United States

Introduction and Objectives: Growing evidence demonstrates unique synergetic signatures in the lower limb(LL) post-stroke, with a specific across-plane and across-joint representations. Observations of such neural constraints include coupled cross planar kinetic outflow[1] and altered muscle synergy structure[2]. Recent findings from our lab illustrated that additional activation of the lesioned hemisphere (L-H) upregulates the expression of these aberrant muscle synergies in the LL [3]. While the inhibitory role of the ipsilateral hemisphere in the upper limb has been widely reported, examination of the role of the contralesional hemisphere (CON-H) in modulating these synergies in the LL following stroke is lacking. Accordingly, we test the hypothesis that stimulation of L-H and CON-H motor cortices will have differential effects on the motor evoked potential (MEP) patterns of the paretic LL. We proposed a novel TMS paradigm to identify patterns of MEPs across multiple LL muscles during a task where synergistic actions have been reported.

Methods: 10 control and 12 chronic stroke participants with single hemispheric stroke were recruited. Motor evoked potentials (MEP) were elicited in 8 LL muscles using single pulse TMS. Surface electromyography (EMG) were recorded from: vastus medialis (VM), vastus lateralis (VL), rectus femoris, adductor longus (ADD), tibialis anterior (TA), medial gastrocnemius, and biceps femoris. Single pulse TMS was delivered using a Magstim 200 stimulator via a 110 mm diameter double-cone coil. The coil position was incrementally adjusted to locate the ADD hotspot over L-H motor cortex contralateral to the test limb (stroke paretic limb). Optimal coil position and intensity was mapped as the lowest stimulation intensity required to evoke ADD MEPs of 50 µV in peak-to-peak amplitude in 3 of 5 consecutive trials. The hotspot for the test limb ADD was similarly mapped for stroke contralesional hemisphere (CON-H) or control ipsilateral hemisphere to test limb. Stimulator output for the CON-H was increased in order to match contralateral (cMEP) and ipsilateral (iMEP) ADD amplitudes.

Participants were isometrically locked in the toeoff gait posture in an instrumented exoskeleton with 3 6-DOF load cells used to measure the interaction forces and moments. Participants matched isometric hip adduction torques at 40% of their maximum while receiving instantaneous visual feedback in the form of moving a circular cursor. A successful trial was considered if the participant matched the target torque within ±5% of the torque magnitude and direction and hold for a minimum of 200ms.

For each trial the TMS coil was placed over the hotspot location for either hemisphere. When the participants successfully matched the target adduction torque, the TMS device was triggered by software. Matched ADD MEPs together with nontargeted muscles were simultaneously recorded. 10-30 trials were performed for each hemisphere. An 80 ms window following the TMS pulse was searched for the MEP onset when 5 consecutive points in the EMG trace were above 3 standard deviations of the mean pre-TMS EMG activity. MEP amplitudes were measured peak-to-peak and calculated as the difference between the background activation and the average of a 20 ms window centered at the peak MEP rectified pulse. The ratio of the mean iMEP amplitude over the mean cMEP amplitude was quantified for each muscle. A statistical

value less than one indicate a reduction in iMEP amplitude relative to the cMEP amplitude following TMS of the ipsilateral hemisphere.

Results: By quantifying the CON-H / L-H MEP ratio across muscles, we characterized a significant inhibition of aberrant MEP coupling between ADD and VM (p=0.0078) and VL (p=0.047) following CON-H stimulation exclusive to the stroke group (ANOVA,p=0.028), an inhibition that was muscle dependent (ANOVA, p= 0.039). We find a significant reduction of TA MEPs in both groups following ipsilateral hemisphere stimulation (p=0.0014 stroke; p=0.015).

Figure:

Conclusion: Our results indicate that stimulation of CON-H reduced the expression of abnormal synergistic activations in individuals with stroke. Our observations seem incongruent with the notion of maladaptive motor output from CON-H post stroke suggested in the UL. Furthermore, a majority of the interhemispheric MEP onset latency differences occur below 3ms, consistent with the interpretation of ipsilateral corticospinal projections to the LL despite equivocal findings of their functionality the UL. Combined with the systemic inhibition of TA across groups, we argue that the ipsilaterally mediated MEP signature provides indirect evidence of inhibitory intracortical connectivity between abnormally synergistic muscles. This study takes an important step in exploring the relation between CON-H cortical reorganization and the modulation of abnormal LL muscle synergies post stroke.

References: [1]Tan et al., J Biomech, 2014.

[2]Cruz et al., IEEE Eng Med Bio Soc, 3956-9, 2009.

[3]Krishnan et al., Exp Neuro, 233:400-7, 2012.

Disclosure of Interest: None Declared

Neurological and Motor Control

AS-0116

DYNAMIC MOTOR CONTROL DURING WALKING PREDICTS TREATMENT OUTCOMES IN CEREBRAL PALSY

Michael Schwartz [1 2,*] Adam Rozumalski [2 3] Katherine M. Steele [4]

[1]Biomedical Engineering, University of Minnesota, Minneapolis, -, [2]James R. Gage Center for Gait & Motion Analysis, Gillette Children's Specialty Healthcare, St Paul, [3]Biomedical Engineering, University of Minnesota, Minneapolis, [4]Mechanical Engineering, University of Washington, Seattle, United States

Introduction and Objectives: Cerebral palsy (CP) impacts roughly 3 out of every 1000 individuals, impairing movement and coordination after an injury to the brain near the time of birth [1]. There are many treatment options to improve movement for individuals with CP; however, treatment outcomes are unpredictable, and not always satisfactory [2]. Since every brain injury is unique, each individual with CP has unique impairments, creating a challenge for clinicians to determine optimal treatment. Further, many treatments, such as orthopaedic surgery, focus primarily on musculoskeletal deformities and do not address underlying neural control. A long-held clinical belief is that part of the variability in outcomes after treatment is due to differences in neural control between individuals [3]. An individual with near-normal motor control may have greater improvements after orthopaedic surgery compared to an individual with more severely impaired motor control who, even after significant musculoskeletal correction, does not have the neurological capacity for unimpaired walking. In this study we sought to test this hypothesis by using EMG synergy analysis to quantify changes in dynamic motor control during walking and evaluate the effect of dynamic motor control on treatment outcomes.

Methods: We retrospectively identified individuals with a diagnosis of diplegic CP, age < 21 years, who had previously received gait analysis including surface electromyography (EMG – rectus femoris, medial gastrocnemius, anterior tibialis, medial hamstrings) and a follow-up gait analysis 9-36 months later. For each individual, EMG data was processed using nonnegative matrix factorization [4] to identify weighted groups of muscles that are consistently activated together (synergies). The variance accounted for by one synergy was scaled to a z-score relative to a database of EMG from 84 typically-developing children to define the dynamic motor control index during walking (walk-DMC). Thus, a walk-DMC value of 100 equals the average variance accounted for by one synergy of typically-developing children and each 10 point increment represents one standard deviation. Values less than 100 indicate a more simplified control strategy in which a single synergy can describe greater variance in muscle activity than unimpaired individuals.

A stepwise linear regression model was computed predicting the change in gait kinematics (Gait Deviation Index, GDI, [5]) from initial to follow-up gait analysis. A constant model was initially assumed, with $p < 0.05$ for variable entry, and $p > 0.10$ for variable removal. Possible predictors included walk-DMC and measures previously shown to be associated with outcomes: initial GDI, age, prior surgery (yes/no), and treatment group.

Results: The analysis included 518 individuals with CP who met all inclusion criteria. Dynamic motor control was reduced in this population compared to typically-developing children with an average walk-DMC of 85.6 +/- 7.5 The final regression model to predict changes in gait kinematics included initial GDI, walk-DMC, treatment group, and an interaction term between initial GDI and treatment group ($r^2 = 0.31$, Fig. 1). The effect size for initial GDI and walk-DMC were similar in magnitude, but had opposite signs, such that individuals with dynamic motor control more similar to typically-developing

children (walk-DMC closer to 100) had better outcomes. More aggressive treatments (multi-level orthopaedic surgery and rhizotomy) resulted in larger positive GDI changes, but the magnitude of the treatment effect was significantly smaller than the magnitude of GDI and walk-DMC effects.

Figure:
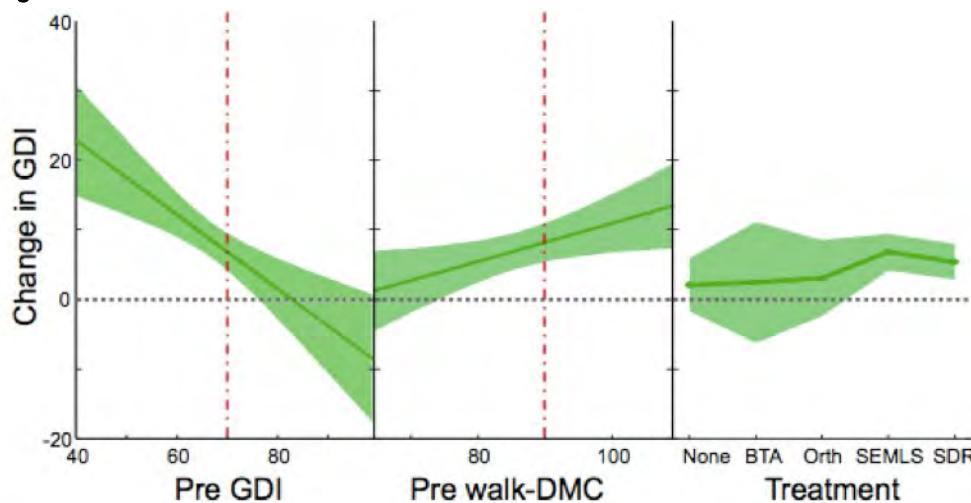
Conclusion: Dynamic motor control was significantly associated with treatment outcomes, even after controlling for differences in gait pattern. For example, among individuals undergoing single-event multi-level orthopaedic surgery, those with the highest walk DMC improved nearly 12 GDI points more than those with the lowest walk-DMC. These results suggest that dynamic motor control plays a significant role in predicting gait outcomes after treatment and may provide a useful measure for treatment planning that can be calculated from currently available clinical gait analysis data.

Caption: Final regression model of change in gait deviation index (GDI). Regression lines show a slice through the regression surface at the average initial GDI and walk-DMC values (dotted red lines). Shaded area show 95% confidence interval for regression lines. Treatment groups included botulinum toxin/casting (BTA), single orthopaedic surgery (Orth), single-event multi-level orthopaedic surgery (SEMLS), and selective dorsal rhizotomy (SDR).

References: [1] Yeargin-Allsopp et al., Pediatrics, 121(3):547-54, 2008.

[2] Rutz et al., Gait Posture, 38:455-60, 2013.

[3] Phelps, JBJS, 39:53, 1957.

[4] Tresch et al., J Neurophys, 95:2199-2212, 2006.

[5] Schwartz et al., Gait Posture, 28:351-7, 2008.

Disclosure of Interest: None Declared

MODELING OF DYNAMIC RESPONSE OF CALF MUSCLES TO FUNCTIONAL ELECTRICAL STIMULATION

Hossein Rouhani [1 2,*]Michael Same [1 2]Ya Qi Li [1 2]Kei Masani [1 2]Milos R Popovic [1 2]

[1]Institute of Biomaterials and Biomidecal Engineering, University of Toronto, [2]Rehabilitation Engineering Laboratory, Lyndhurst Centre, Toronto Rehabilitation Institute - University Health Network, Toronto, Canada

Introduction and Objectives: Functional electrical stimulation (FES) is referred to applying electrical pulses to intact motor neurons of paralyzed muscles to artificially induce muscle contractions and to restore functional motor tasks in individuals with spinal cord injury, traumatic brain injury, stroke or other neuromuscular impairments. FES can be utilized as neuroprosthesis for the purpose of permanently substituting lost motor function such as grasping, walking or standing [1,2]. The dynamic response of muscles to FES (as a transfer function) is an integral component of the closed-loop system controlling neuroprostheses, which is task-dependent and should be modeled before designing such neuroprostheses. Here we investigated the dynamic response of ankle muscles to FES in a standing posture, which can be implemented into closed-loop controlled FES system for standing balance. We applied FES pulse trains within a frequency range, and measured the dynamic response of the ankle dorsiflexors and plantarflexors to FES.

Methods: Eleven subjects (5 female, 25±4 years old, 172±9 cm, 68±9 kg) participated in the experiment. The subject stood on a standing frame with his/her extended knee and hip mechanically locked. The subject's feet, positioned horizontally, were fixed firmly to the foot-plates that were also locked. A programmable functional electrical stimulator (Compex Motion II, Compex SA, CH) was utilized to bilaterally stimulate the plantarflexors and dorsiflexors through surface electrodes. The stimulus waveform was rectangular, balanced, biphasic and asymmetric, applied at frequency of 20 Hz with pulse duration set to 0.3 msec. The pulse amplitude was modulated on sinusoids between 20 mA and 60 mA at frequencies of 0.07, 0.15, 0.3, 0.75, and 1.2 Hz. The plantarflexors and dorsiflexors were separately stimulated and the exerted isometric ankle torque was recorded using a torque transducer (TS11-200, Durham Instruments, DE) connected to the foot-plates. After discarding the first second of each trial, we fitted the generated ankle torque curves to at least two complete periods of sinusoids. The sinusoid of FES pulse amplitude and the fitted torque curve were considered as input and output, respectively. The amplitude gain, and phase lag between input and output were calculated on each frequency. We plotted a Bode diagram using amplitude gains and phase lags for all measured frequencies. We fitted a first-order linear model to the diagrams. Then, the parameters of the first-order linear model, i.e., gain (K) and time constant (T), were estimated for each subject (Figure 1).

Results: The gain (K) of the first-order model with FES amplitude as an input and ankle torque as an output was estimated to be 3.82±0.84 and 0.78±0.42 for plantarflexors and dorsiflexors, respectively (the mean ± standard deviation for the group of 11 subjects). Large inter-subject variability (coefficient of variation: 22% and 54% for plantarflexors dorsiflexors, respectively) in the estimated gains were observed. However, the estimated gain can be a function of muscle strength, electrode placement and skin-electrode contact conditions, and thus large variability among subjects was expected. The time constant of the first-order model with FES amplitude as an input and ankle torque as an output was estimated to be 0.31±0.05 and 0.27±0.05 for plantarflexors and dorsiflexors, respectively. Inter-subject variability of the estimated time

constant (coefficient of variation: 17% and 19% for plantarflexsors and dorsiflexors, respectively) was smaller compared to the estimated gain. This indicated similar muscle dynamics among subjects. Therefore, the identified cut-off frequency ($f_c=1/(2.\pi.T)$) of the first-order filters, that modeled muscle dynamics, were 0.53±0.09 Hz and 0.60±0.12 Hz for plantarflexsors and dorsiflexors, respectively.

Figure:
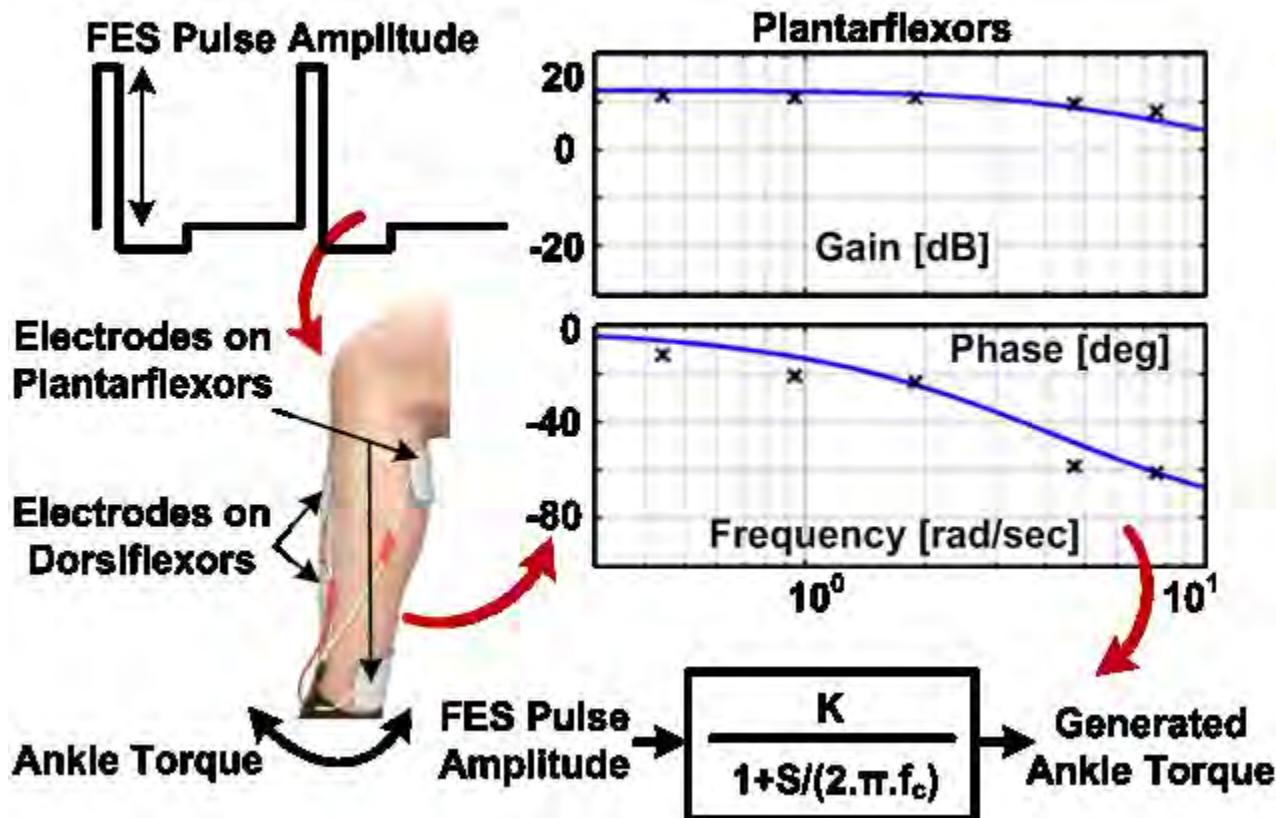
Caption: Figure 1. Modeling dynamic response of ankle plantarflexors and dorsiflexors to functional electrical stimulation as a first-order model.

Conclusion: We identified the dynamic response of ankle muscles to FES in a standing posture. We successfully modeled the dynamic response of planterflexors and dorsiflexors using a first-order filter with FES as an input and the exerted isometric ankle torque as an output. However, higher order models and nonlinear components can also be investigated. Finally, this finding should be considered in the design of closed-loop controlled neuroprostheses when immediate torque generation is expected. The physiological interpretation of this modeling should be further studied.

References: [1] Vette et al., *IEEE Tr. on Neural Systems & Rehabilitation Engineering*, 15: 235-243, 2007.
[2] Same et al., *J. Automatic Control,* 21: 31-36, 2013.

Disclosure of Interest: None Declared

Neurological and Motor Control

AS-0118

BRAIN ACTIVATION DURING RHYTHMIC LOCOMOTOR TASKS IS COORDINATED WITH THE MECHANICAL DEMANDS OF THE MOVEMENT CYCLE

Hendrik Enders [1,*]Filomeno Cortese [2]Benno Nigg [1]

[1]Human Performance Lab, [2]Seaman Family MR Research Centre, University of Calgary, Calgary, Canada

Introduction and Objectives: Coordinated movement is a complex process required for daily living, work and personal enjoyment. For individuals suffering from neuromuscular disorders, coordinated movement can be difficult if not impossible. Prosthetics and neuro-rehabilitation devices have been developed in order to improve movement for those with disability. Most studies have largely focused on the mechanics with less emphasis on the neuromechanical coordination between brain, the musculoskeletal system and the environment. This motor control problem, however, needs to be addressed in order to make rehabilitation devices and programs more efficient. Efficient rehabilitation for patient populations, however, requires a sound understanding of the underlying mechanisms in healthy humans first. Therefore, as a first step toward this goal, it is critical to understand healthy brain function during locomotor tasks in order to develop efficient devices that can mimic healthy human movement. The shortcoming in this area thus far is that real-time brain function and activity during unconstrained movement has rarely been assessed due to the difficulty of collecting noise-free data during dynamic tasks. Recent advances in hardware and software now allow researchers to image the brain in real time during dynamic situations [1]. Therefore, the purpose of this study was to investigate the time-frequency patterns of electrical brain activity during rhythmic movements in healthy individuals.

Methods: Ten healthy individuals were cycling at a constant intensity that was normalized to their maximum power output while real-time cortical activity was recorded using a 64-channel electroencephalography (EEG) and 7 muscles were collected using surface electromyography electrodes. Cycling serves as an excellent model for rhythmic locomotor type tasks in humans and has minimal head movement that interferes with the EEG recordings. This abstract will focus on the results obtained by the EEG analysis. Adaptive Mixture Independent component analysis (AMICA) was used to remove eye artifacts and non-cortical noise components [2]. The cleaned EEG signal was resolved into spatially independent components represented as two dimensional topographic maps. An anatomical head model consisting of the average of 152 MRI scans was used to perform source analysis in order to locate the origin of neural activity in brain space [3]. A k-means clustering algorithm was used to group the identified sources of neural activity across subjects. Time-frequency patterns of cortical activity were visualized as event-related spectral perturbations (ERSP) in order to quantify the oscillatory behavior of neural sources located in three dimensional brain space. Cluster-based permutation statistics were used to test if the ERSP data showed significant spectral perturbations from baseline ($P < 0.05$).

Results: Neural sources were spatially localized to Brodmann area (BA) 9 (left and right frontal cortex), BA 4 (primary motor cortex), BA 6 (Premotor cortex) and BA 31 (posterior cingulate cortex) (Figure 1). The ERSP showed significant changes in spectral power across the pedaling cycle with the strongest activity being present in the premotor cortex cluster, followed by activity in the frontal lobe and the primary motor cortex. We were able to show neural excitation in

primary and secondary motor areas prior to the down stroke of the pedaling cycle which corresponds to the phase where the musculoskeletal system needs to produce the majority of the mechanical power output.

Figure:
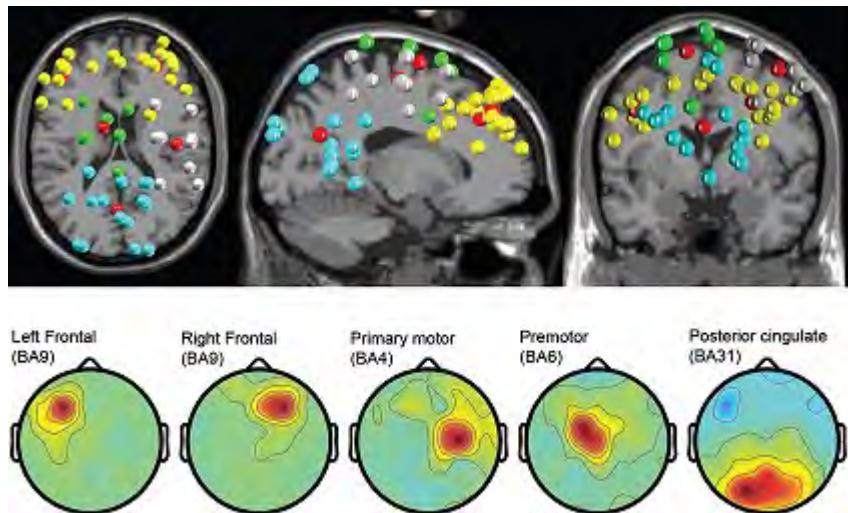
Conclusion: To the best of our knowledge this is the first study reporting intra-trial fluctuations of brain activity localized to specific cortical areas during cycling. Based on our results we suggest a cortical network model of cycling that includes executive brain centers (frontal cortex), the premotor area for movement planning and the primary motor area for descending motor commands and integration of sensory afferent feedback. Our results suggest that the temporal pattern of neural activity in the motor areas of the brain corresponds well to the time frame of mechanical power production by the lower limb muscles during the pedaling cycle.

References: [1] Gramann K, et al., *Rev Neurosci.* 22: 593-608, 2011.

[2] Jung TP, et al., *Psychophysiology.* 37: 163-178, 2000.

[3] Gwin J, et al., *Neuroimage* 54: 1289-1296, 2011.

Disclosure of Interest: None Declared

EMG

AS-0119

USING SURFACE ELECTROMYOGRAPHY (SEMG) TO NON-INVASIVELY MONITORING THE ACTIVATION OF DEEP AND SUPERFICIAL EXTRINSIC FOOT MUSCLES

Cara Swanepoel [1,*] Yumna Albertus-Kajee [2] Lester John [1]

[1] MRC/UCT Medical Imaging Research Unit, Division of Biomedical Engineering, Department of Human Biology,
[2] UCT/MRC Research Unit for Exercise Science and Sports Medicine, Department of Human Biology, University of Cape Town, Cape Town, South Africa

Introduction and Objectives: Using current methods of Electromyography (EMG) to measure the activity of both deep and superficial muscles would require a combination of surface and invasive intra-muscular electrodes, as present-day surface EMG (sEMG) is unable to distinguish between deep and superficial muscle activation. A novel technique utilising monopolar sEMG in conjunction with a separation algorithm (for example Independent Component Analysis) and muscle specific activation protocol[1] has previously been implemented to detect the activation of the deep Brachialis[2] and Tibialis Posterior[3] muscles. The technique was adapted and utilised to detect the activation of deep (Tibialis Posterior [TP], Flexor Digitorum Longus [FD], Flexor Hallucis Longus [FH], Extensor Hallucis Longus [EH]) and superficial (Triceps Surae [TS] (Gastrocnemius and Soleus), Tibialis Anterior [TA], Peroneus Longus [PL], Extensor Digitorum Longus [ED]) extrinsic foot muscles during a platform-guided isometric contraction sequence.

Methods: Four concentric rings, each consisting of 10 non-commercial application-specific electrodes, were placed around the lower segment of the right lower limb of 17 healthy male participants. The rings were arranged in 2 pairs, spaced 20mm apart and placed at 1/3 and 2/3 of the distance from the medial malleolus to the tip of the fibula. Monoploar EMG signals were recorded while the participants performed a specifically designed, platform-guided isometric contraction protocol, repeated 10 times with both the knee flexed at 90° and fully extended. The muscles within the capture area of the EMG electrodes were selectively activated by contractions of Toe Flexion (TFlex), Toe Extension (TExt), Plantar Flexion (PFlex), Dorsi Flexion (DFlex), Inversion (Inv) and Eversion (Evn), (40%of Maximum Voluntary Contraction- confirmed by strain gauges), randomised and interspersed with rest periods. ICA (fastICA) was applied to the sEMG signals to separate-out source activations, known as the Independent Components (ICs) which were Root Mead Square (RMS) smoothed (moving window of 250s) and normalised. A contraction sequence specific, anatomically defined[4], expected EMG activation patterns (with timing informed by strain gauges) for each muscle under investigation is compared to the ICs using Pearson's Correlation Coefficient. The ICs are ranked according to correlation coefficients (ρ) and the highest ranking IC for each muscle was considered to represent the EMG activity. (Typical example in Figure 1).

Results: The mean correlation between the expected EMG patterns and the detected Independent Components, for each muscle over the 10 repetitions for all 17 participants, were calculated for both the knee flexed at 90 degrees and fully extended. Good correlation values indicate that the ICs detected are highly likely to represent the EMG activity of the muscles under investigation. Lower correlation values could be due to poor adherence to the contraction protocol by participants or possibly co-contractions. In surface muscles these could be confirmed by extracting standard bi-polar

sEMG measurements from the measured signals. Limitations of the fastICA algorithm could account for incomplete separation of the ICs which could indicate activity when no activity was present.

Figure:

Gastrocnemius (IC23) — CC =0.68448
Soleus (IC9) — CC =0.71455
Tibialis Anterior (IC7) — CC =0.8212
Peroneus Longus (IC11) — CC =0.81948
Tibialis Posterior (IC18) — CC =0.78495
Flex Digi Longus (IC15) — CC =0.75275
Ext Digi Longus (IC19) — CC =0.65134
Flex Hallucis Longus (IC6) — CC =0.86771
Ext Hallucis Longus (IC22) — CC =0.78118

Normalised Amplitude

Invert   Evert   Dorsi   TFlex   TExt   Plant
Isometric Contraction Sequence

Caption: Typical expected EMG activation patterns (dark) and top ranked ICs (light) for each muscle from a single experimental run for 1 participant. Vertical divisions indicate transitions between contractions and rest periods.

Conclusion: The detection of EMG activity from deep and superficial extrinsic foot muscles using sEMG was possible as the ρ values indicate a correlation between measured activity and the expected activation patterns generated. Further verification of the technique and results is on-going.

References: [1] John, L.R., PCT/IB2010/001876, priority date: July 30 2009

[2] Moroaswi S. et al., MScMed thesis (unpublished), Dept. Human Biology, Univ. Cape Town, 2010.

[3] Sayed, A. et al., presented at Int. Soc. Electromyogr. Kinesiol. Conf., Rome, 2014

[4] Gilroy, A.M. et al., Atlas of Anatomy, Theime Medical Publishers, 2008

Disclosure of Interest: C. Swanepoel: None Declared, Y. Albertus-Kajee: None Declared, L. John Conflict with: the noninvasive deep muscle electromyography method and device is patented (inventor: co-author L.R. John; assignee: University of Cape Town and the South African Medical Research Council) in China (201080030787.6) and South Africa (2011/09253), and patent-pending in the USA (13/387,897), Europe (10803972.8), Japan (J2012-522271), India (2823/MUMNP/2011)

EMG

AS-0120

DIAGNOSIS OF PATELLOFEMORAL PAIN SYNDROME IS POSSIBLE USING SURFACE ELECTROMYOGRAPHY

Deisi Ferrari [1,*]Fábio Azevedo [2]Nathalie Faria [2]Danilo Silva [2]Marcella Pazzinatto [2]Ronaldo Briani [2]Neri Alves [1]

[1]Bioengineering Postgraduate Program , University of São Paulo, São Carlos, [2]University of Sao Paulo State, Presidente Prudente, Brazil

Introduction and Objectives: Despite the high incidence and physical limitations caused by patellofemoral pain syndrome (PFPS), there is no consensus on diagnosis and etiologic factors. One hypothesis explains PFPS as alterations in the muscle activation or muscle inhibition of the vastus medialis (VM) and vastus lateralis (VM)[1], which can be visualized by changes in the spectral properties of the electromyogram [2]. In this context, the association between EMG and clinical findings might be a new method for the diagnosis of PFPS. The purpose of this study was to assess the diagnostic accuracy of surface EMG parameters associated with anterior knee pain for diagnosing PFPS.

Methods: To perform a study on diagnostic accuracy it is necessary to compare the index test, i.e., the test under evaluation, with the standard reference which is defined as the best-available method to determine the absence or presence of the condition of interest. 29 pain free subjects and 22 subjects with PFPS were recruited according to the standard reference and, posteriorly submitted to assessment using the index test. The index test in this case was the association between 2 clinical criteria and an electromyography parameter. The electromyography parameter should be reliable, precise and able to differentiate the groups. The clinical criteria were an anterior knee pain level of at least 2 cm on a visual analog scale in the preceding month and anterior knee pain whilst performing at least 2 functional activities (squatting, kneeling, running and stair climbing). The EMG signal was collected for the VM and VL muscle during the functional movement of stair climbing. The staircase used had seven steps, and coupled to the fourth step was a force plate to detect the exact moment that the individual touched the ground. The tests were run on two days, each test consisted of ten stair climbing trials. The EMG signals were processed in Matlab®. The Discrete Fourier Transform was used to calculate the median frequency (MF) and the normalized power spectrum was divided into three bands denominated low (15 to 45Hz), medium (45 to 96Hz) and high frequency (96 to 400Hz). The $ICC_{2,k}$ (intraclass correlation coefficient), SEM (standard error of measurement) and independent t test were calculated. Sensitivity, specificity, negative and positive likelihood ratios (LR- and LR+),and negative and positive predictive values (NPV and PPV) were calculated for diagnostic accuracy. To determine the cutoff of the EMG signal for diagnosis, several confidence intervals of the control group were considered. The confidence interval selected was the one that showed the best sensitivity and specificity.

Results: Table 1 presents the descriptive and relyabilty data of the EMG parameters. The outcomes of the diagnostic accuracy of the index test refer to the medium-frequency band (B2) because this parameter was reliable, precise and able to differentiate the groups for both muscles. The cutoff value determined corresponds to a 95% confidence interval. The interval was between 26.72 and 31.26 for the VM muscle and 24.75 and 29.01 for the VL muscle. The participants who reported values within these ranges were considered pain-free, and the participants with values outside these ranges

were considered as having PFPS. Diagnostic accuracy results were: sensitivity = 0.70, specificity = 0.87, PPV = 0.86, NPV = 0.72, LR- = 5.63 and LR+ = 5.63.

Conclusion: Our results showed that the medium-frequency band (B2) parameter was reliable, precise, and able to differentiate participants with and without PFPS. This study provides evidence for the use of the EMG signal for the diagnosis of PFPS.

Table:

	VM		VL	
	GPFPS	GC	GPFPS	GC
Fmed (Hz)				
Day 1 (M±SD)	57.44 ± 12.42	52.71 ± 8.0	56.77 ± 12.95	53.77 ± 11.87
Day 2 (M±SD)	55.89 ± 8.14	51.37 ± 7.44	56.12 ± 10.51	55.57 ± 12.43
ICC (IC - 95%)	0.82 (0.57 – 0.92)	0.83 (0.65 – 0.92)	0.89 (0.74 – 0.95)	0.85 (0.68 – 0.93)
SEM (%)	5.8 (10.23%)	4.05 (7.78%)	5.25 (9.30%)	6.16 (11.26%)
MDD (%)	0.16	0.11	0.14	0.17
B1(u.n.)				
Day 1 (M±SD)	47.84 ± 12.13	55.68±10.56	48.18 ± 11.18	54.96 ± 12.98
Day 2 (M±SD)	49.89 ± 11.47	56.0±8.52	49.25 ± 11.42	52.68 ± 12.64
ICC (IC - 95%)	0.85 (0.66 – 0.94)	0.87 (0.74 – 0.94)	0.73 (0.34 – 0.88)	0.84 (0.67 – 0.92)
SEM (%)	5.83 (11.93%)	4.53 (8.11%)	7.43 (15.25%)	6.58 (12.22%)
MDD (%)	0.16	0.12	0.20	0.18
B2(u.n.)				
Day 1 (M±SD)	32.90 ± 8.42*	28.21±5.0*	31.90 ± 7.28*	25.88 ± 4.93*
Day 2 (M±SD)	32.84 ± 8.03	27.74±4.67	31.40 ± 7.99	26.29 ± 4.75
ICC (IC - 95%)	0.90 (0.76 – 0.96)	0.81 (0.61 – 0.91)	0.85 (0.65 – 0.94)	0.80 (0.57 – 0.90)
SEM (%)	3.52 (10.70%)	2.71 (9.68%)	3.87 (12.22%)	2.81 (10.77%)
MDD (%)	0.09	0.07	0.10	0.07
B3(u.n.)				
Day 1 (M±SD)	1.76 ± 1.26	1.47±0.78	1.81 ± 1.34	1.86 ± 1.14
Day 2 (M±SD)	1.59 ± 0.87	1.43±0.61	1.81 ± 1.07	2.06 ± 1.16
ICC (IC - 95%)	0.63 (0.12 – 0.85)	0.91 (0.81 – 0.96)	0.88 (0.73 – 0.95)	0.91 (0.81 – 0.95)
SEM (%)	0.79 (47.30%)	0.28 (19.31%)	0.54 (29.83%)	0.45 (22.95%)
MDD (%)	0.02	0.007	0.01	0.01

References: 1.Rathleff et al.,Med Sci Sports Exerc,45:1730–9,2013.

2.Tscharner et al.,J Electromyogr Kinesiol,20:676–83,2010.

Disclosure of Interest: None Declared

Rehabilitation

AS-0121

DOES THE ABDOMINAL DRAWING-IN MANEUVER CHANGE THE LOCAL DYNAMIC STABILITY OF REPETITIVE SPINE MOVEMENTS IN A HEALTHY POPULATION?

Daniel Southwell [1,*]Nicole Hills [2]Linda McLean [2][3]Ryan Graham [1][4]

[1]School of Physical and Health Education, Nipissing University, North Bay, [2]School of Rehabilitation Therapy, Queen's University, Kingston, [3]School of Rehabilitation Sciences, University of Ottawa, Ottawa, [4]School of Kinesiology and Health Studies, Queen's University, Kingston, Canada

Introduction and Objectives: Selective activation of the transversus abdominis (TrA) through the abdominal drawing-in maneuver (ADIM), has been adopted as common clinical practice in the prevention and rehabilitation of low back pain (LBP) [1]. However, there is still a debate in regards to the role the ADIM has in maintaining a stable spine [2-3]. There is also limited evidence to support the use of the ADIM during dynamic movement tasks to enhance spine stability and currently no literature that shows spinal control is less optimal when activation of the TrA is changed [3]. Spinal control cannot be accurately tested in many current biomechanical models as few include contributions of intra-abdominal pressure and fascial tension [3]. One way to assess control and take into account all aspects of spine stability is to look directly at the outcome kinematics during repetitive movement using non-linear dynamic systems analyses [4]. Thus, the purpose of this study was to (i) examine whether TrA activation could be increased during dynamic movements following five minutes of training, and (ii) assess whether changes in TrA activation could alter dynamic spine control and stability.

Methods: Thirteen healthy participants (7M, 6F) performed two sets of 35 cycles of repetitive unloaded spine flexion with a constrained pelvis to the beat of a metronome at a rate of 15 cycles/min [4] (Figure 1). Between sets, participants were instructed by a Registered Physiotherapist on how to perform the ADIM in standing. Ultrasound (US) imaging (Voluson i, GE Health Care, UK) was used as biofeedback to ensure successful contraction of TrA. Surface EMG was recorded at 2000Hz from four muscles bilaterally: thoracic and lumbar erector spinae (TES and LES), and internal and external oblique (IO and EO) (Trigno, Delsys Inc., USA). Indwelling EMG was recorded synchronously from three muscles unilaterally (right side): IO, TrA, and multifidus (MF). Indwelling electrodes were inserted under US guidance to ensure correct positioning in each muscle (Figure 1). During all trials, 3-D kinematic data were collected at 50 Hz (Oqus 400+, Qualisys, Sweden), and Visual-3D was used to calculate 3-D spine kinematics (C-Motion Inc., USA). EMG data were processed and local dynamic spine stability was calculated using published methods [4]. The average peak EMG across all cycles and the local dynamic stability values were then compared between the baseline and trained trials using repeated-measures ANOVA's in SPSS 22 (IBM Corporation, USA).

Results: Average peak EMG and local dynamic stability results can be found in Table 1. Results indicate that following ADIM training, there were significantly greater ($p<0.05$) levels of activation in all of the tested abdominal muscles during movement. Conversely, there were no significant increases in activation of any of the back muscles tested. Moreover, no significant change in the local dynamic stability of spine movements was observed following training ($p=0.855$).

Figure:
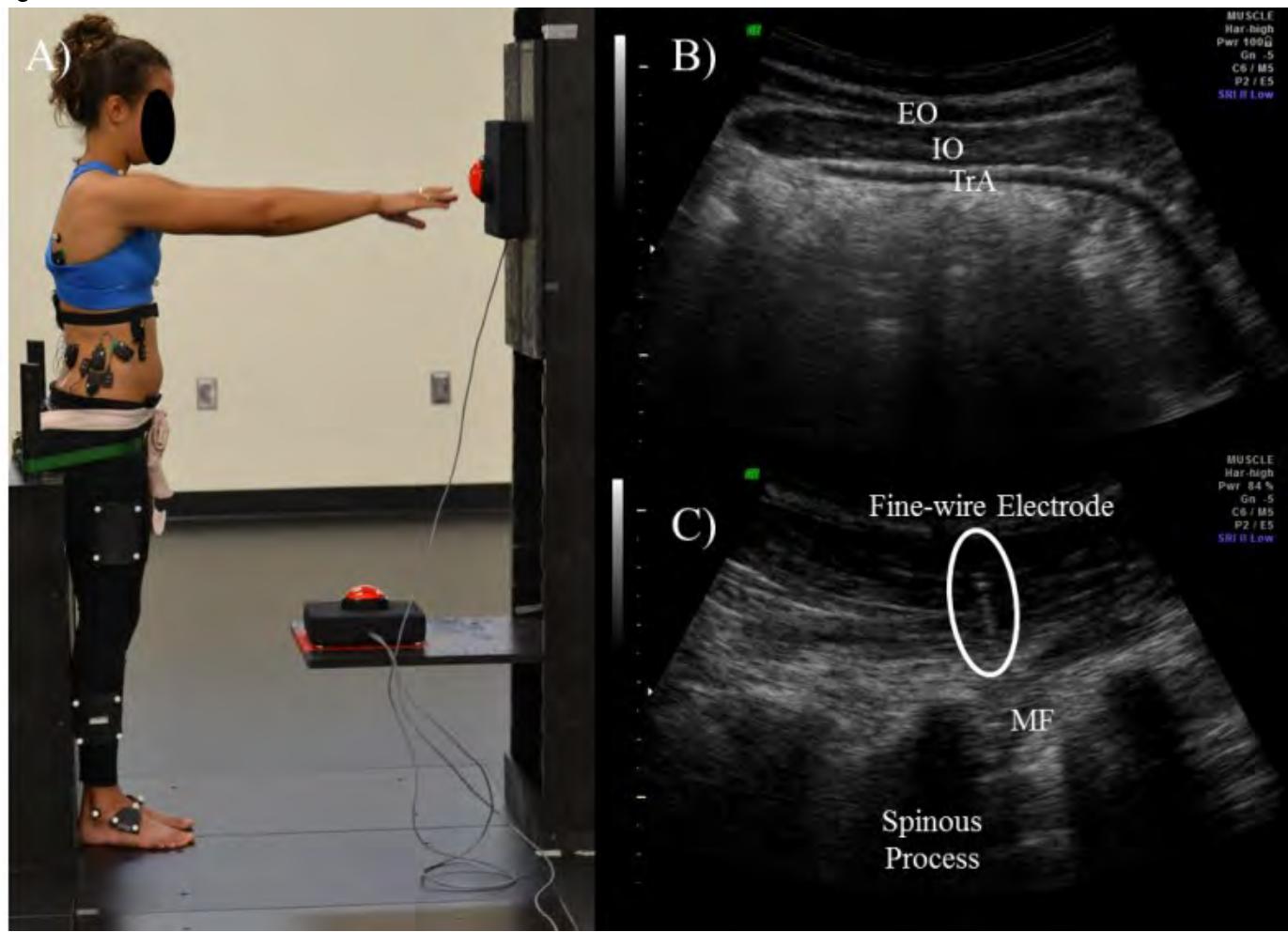
Caption: Figure 1. A) Experimental set-up. B and C) Representative abdominal and lumbar spine ultrasound images.

Conclusion: The results indicate that in a healthy population, increasing activation of the TrA does not increase dynamic spinal control or stability. While this finding agrees with previous research [2], it may also be partly explained by participants' non-familiarity with activating their TrA during movement (although not reported, abdominal muscle activation variability was significantly greater during the trained trial). Previous literature has shown that focusing internally on the activation of a muscle rather than externally on the task at hand, can impair neuromuscular coordination and movement outcomes [5]. To assess such a motor learning effect, we are currently analyzing data from a second day of testing after participants performed a home exercise program of TrA activation and stabilization exercises for one week. Our future work will also investigate the effects of the ADIM on the dynamic stability of spine movements and TrA timing in LBP patients, since TrA training may be effective in reducing symptoms in such populations [3].

Table:

			Baseline		Trained		ANOVA
			Mean	SD	Mean	SD	p-value
Average Peak EMG (%MVC)	Indwelling	IO	9.8	(8.1)	18.4	(10.9)	**0.000**
		TrA	18.2	(15.7)	31.4	(18.9)	**0.001**
		MF	33.7	(21.9)	32.5	(31.4)	0.753
	Surface	R IO	12.9	(7.4)	34.3	(29.5)	**0.009**
		L IO	13.0	(7.9)	35.6	(20.6)	**0.000**
		R EO	4.5	(3.2)	12.9	(8.7)	**0.001**
		L EO	3.6	(2.0)	8.9	(5.8)	**0.002**
		R LES	31.5	(15.2)	31.0	(13.3)	0.705
		L LES	33.8	(13.5)	33.9	(14.0)	0.970
		R TES	20.6	(8.6)	21.1	(12.1)	0.794
		L TES	20.9	(8.8)	21.0	(10.5)	0.941
Dynamic Stability (λ_{max})			2.12	(0.19)	2.11	(0.19)	0.855

Caption: Table 1. EMG and dynamic stability mean (standard deviation) and ANOVA results. Bolded values indicate significance at $p < 0.05$.

References: [1]   Richardson et al., Spine., 27: 399-405, 2002.

[2]   Grenier et al., Arch. Phys. Med. Rehabil., 88: 54-62, 2007.

[3]   Hodges. P., Br. J. Sports Med., 42: 941-944, 2008.

[4]   Graham et al., J. Biomech., 47: 1459-1464, 2014.

[5]   Lohse et al., Acta Psychol., 140: 236-245, 2012.

Disclosure of Interest: None Declared

Rehabilitation

AS-0122

GAIT IMPROVEMENT INDUCED BY REAL-TIME FEEDBACK BASED ON DYNAMIC FOOT PRESSURE INDEX FOR DYNAMIC EQUINUS IN CHILDREN WITH CEREBRAL PALSY

Weiyan Ren [1 2,*]Fang Pu [1 2]Wei Chen [1 2]Deyu Li [1 2]Feng Zhao [1 2]Yubo Fan [1 2]

[1]School of Biological Science and Medical Engineering, [2]Key Laboratory of Rehabilitation Technical Aids of Ministry of Civil Affair, Beihang University, Beijing, China

Introduction and Objectives: Cerebral palsy (CP) children with dynamic equinus often walk on their toes, which can be treated with gait rehabilitation. Real-time feedback is considered to be helpful in improving gait training efficiency, but previous toe-walking gait monitoring systems had the problem of inaccurate feedback and insufficient analysis for patient ambulation. Dynamic foot pressure index (DFPI)[1] is an useful parameter to quantify the degree of toe-walking gait in children with CP. This study is to explore the impact of real-time feedback based DFPI on gait improvement during rehabilitation gait training for CP children with dynamic equinus.

Methods: Real-time feedback cue for toe-walking gait was generated by a wearable device based on DFPI. Ten CP children with dynamic equinus were tested their daily gait and training gait under real-time feedback by wearing the device with sound off and sound on respectively. The mean values of DFPI in normal gait (NORG) and in toe-walking gait (TOEG) were selected as parameters to evaluate walking performance in the two experimental stages for each subject.

Results: Compared with the walking performance of patient daily gait，testing results of training gait under real-time feedback have significant improvement in both NORG (P = 0.011) and TOEG (P = 0.030).

Conclusion: Real-time feedback training method based on DFPI can effectively correct toe-walking gait, which can contribute to improve walking abilities in CP children with dynamic equinus.

References: [1] Bennett et al., J. J Pediatr Orthoped, 27: 288-294, 2007.

Disclosure of Interest: None Declared

Rehabilitation

AS-0123

FORCE MANTAINANCE OF THE PELVIC FLOOR MUSCLES ARE INFLUENCED BY THE COMBINED ACTION OF HIP ABDUCTOR MUSCLES IN HEALTHY WOMEN

Amanda C. Amorim [1,*]Licia Cacciari [1]Anice Passaro [1]Simone Brandao [2]Isabel Sacco [1]

[1]Physical Therapy, Fonoaudiology and Occupational Therapy, [2]University Hospital, University of Sao Paulo, Sao Paulo, Brazil

Introduction and Objectives: The strength and coordination of the pelvic floor (PF) muscles are related to the severity of urinary incontinence and sexual satisfaction (1). Clinicians intending to facilitate the PF treatment commonly associate classical PF strengthening exercises with hip adduction/abduction activity, but to this date the benefits of this combination and the anatomical/ biomechanical rationale to adopt those associations in exercise treatments, are still unknown. The levator ani muscle inserts into the obturatorius internus muscle internal fascia (2), then if its tension increases by hip external rotation and/or abduction, one may improve the quality of PF contraction, contributing with its treatment. Here our aim was to investigate the effect of the association of hip adduction and abduction in the force production and maintenance of PF muscles.

Methods: Twenty continent and nulliparous young woman (28.5±5.3 years old, 56.0 ±10.1 kg, 1.61±0.10 cm) were assessed in supine with knees flexed (figure), with 2 dynamometers (figure) (into the vaginal cavity and around the tights to measure the hip add/abduction force) in 3 different conditions: (a) isolated PF contraction for 10 seconds; (b) associated with hip adduction (30% maximal voluntary contraction) for 10 seconds; and (c) associated with hip abduction (30% maximal voluntary contraction) for 10 seconds. The strain gauge data were sampled at 100Hz, filtered with a low-pass of 8Hz and subtracted from the passive force (assessed after one-minute accommodation period following the vaginal probe insertion). From the temporal series, we calculated the maximal force (N), endurance (N.s) (area under the curve – 8 seconds window) and force maintenance (N.s) (area of an 8s projected interval where the value is constant and equal to the first peak minus the force curve integral). Repeated measures ANOVAs followed by Newman-keuls post hoc tests were used to compare the conditions ($p < 0.05$).

Results: The results showed a significantly reduced maximal force and endurance for the condition with hip adduction. This result means that this association do not improve the magnitude or maintenance of PF strength capacity and that the adductors muscles may not contribute with the PF muscles contraction. The force-time integral (endurance variable) was significantly greater for the isolated contraction, what means that this condition led to a greater magnitude of PF strength capacity. It is possible that in both dual-task conditions, the attention was shifted for the hip action goal (30% of maximum voluntary contraction), competing with the PF muscles contraction. Interestingly the condition with hip abduction showed significant positive strength maintenance when compared to the other two conditions. This result suggests that, during the hip abduction, the subjects were able to recover (or restore) their PF strength, in the time period evaluated (8 seconds). According to our hypothesis, it could mean there was a tension transmission through obturatorius internus muscle internal fascia optimizing the PF muscle function.

Figure:

Caption: Figure. Vaginal Dynamometer and tight dynamometers

Conclusion: The association of PF muscles contraction and hip abduction action have improved the force maintenance in young woman and could be used during sustained contraction practices and daily function.

Table:

	Isolated PF contraction (1)	Associated with hip ADDUCTION (2)	Associated with hip ABDUCTION (3)	EFFECT SIZE
Maximal Force (N)	10.74 (±3.75)	9.23 (±3.95)*	10.32 (±3.16)	(1) x (2) 0.4 medium effect (1) x (3) 0.13 negligible effect (2) x (3) 0.31 small effect
Endurance (N.s)	70.25 (±26.26)*	52.79 (±25.00)*	60.86 (±26.41)*	(1) x (2) 0.7 medium effect (1) x (3) 0.37 small effect (2) x (3) 0.32 small effect
Force maintenance (N.s)	-10.43 (±5.98)*	-0.39 (±6.42)*	4.83 (±10.46)*	(1) x (2) 1.66 huge effect (1) x (3) 1.84 huge effect (2) x (3) 0.62 medium effect

Caption: Table: Means (± standard variation) of Maximal Force (N), Endurance (N.s), Force maintenance (N.s) calculated in three conditions (Isolated PF contraction, associated with hip adduction, associated with hip abduction) and the effect size of each comparison. *Represent significant different conditions.

References: [1] Fernandez-Fraga, Gastroenterology,123:1441-1450,2002.

[2] Ashton-Miller and DeLancey, Reproductive Biomechanics, 1101:266-296, 2007.

Disclosure of Interest: None Declared

Rehabilitation

AS-0124

EFFECTS OF HIP EXTENSOR MUSCLES STRENGTHENING ASSOCIATED WITH LANDING STRATEGY MODIFICATION IN AN ATHLETE WITH PATELLAR TENDINOPATHY: A CASE REPORT

Rodrigo Scattone Silva [1,*]Ana Luisa Granado Ferreira [1]Theresa Nakagawa [1]Lucas Aoki [1]José Mourão dos Santos [2]Fábio Serrão [1]

[1]Department of Physiotherapy, [2]Department of Medicine, Federal University of São Carlos (UFSCar), São Carlos-SP, Brazil

Introduction and Objectives: Patellar tendinopathy is one of the most common causes of anterior knee pain in the athletic population. Although eccentric exercises have been considered a cornerstone of patellar tendinopathy rehabilitation, the outcomes with this intervention are sometimes less than ideal. Bahr *et al.* [1] found that only 55% of elite athletes treated with eccentric exercises had a satisfactory return to sports practice 1-year after the intervention. Therefore, the effectiveness of other treatment options for treating this dysfunction should be investigated. A recent study has shown that athletes with patellar tendinopathy have diminished hip extensor torque when compared to asymptomatic controls [2]. Previous research has also shown that athletes with patellar tendon abnormalities have altered jump-landing mechanics in comparison to controls without such abnormalities [3]. Therefore, an intervention aiming to address these aspects might be effective for the rehabilitation of athletes with patellar tendinopathy. The purpose of this case-report was to verify the effects of an intervention involving hip muscles strengthening and jump-landing strategy modification on pain and lower limb biomechanics of an athlete with patellar tendinopathy.

Methods: The patient was a 21-years-old male volleyball athlete who presented with pain in the patellar tendon during tendon-loading tasks for 9 months and patellar tendon ultrasound abnormalities, being diagnosed with patellar tendinopathy. The subject's worst pain in the previous week was assessed using a 10cm visual analogue scale (VAS) and the severity of his symptoms was quantified with the Victorian Institute of Sport Assessment-Patella questionnaire (VISA-P). A handheld dynamometer (Lafayette Instruments, IN, USA) was used to measure hip extension strength during isometric maximal contractions. A force plate (Bertec Corporation, OH, USA) and the Qualisys Motion Capture system (Qualisys Medical, AB, SWE) were used to evaluate kinetics and kinematics while the subject performed a drop vertical jump task from a 31-cm box. After the baseline evaluations, the subject was submitted to an intervention of 8-weeks. In phase 1 (weeks 1–4), the subject performed open kinetic chain hip extension exercises (**Figure 1A–1B**) and a training aiming to increase trunk flexion during drop jumps (**Figure 1C**). In phase 2 (weeks 5–8) more demanding hip extensor strengthening exercises were performed (**Figure 1D–1E**) and the jump-landing training involved drop vertical jumps with emphasis on trunk flexion in both landings (**Figure 1F**). The subject was allowed to continue his sports participation during the intervention period. After 8 weeks, all baseline evaluations were repeated. The Visual3D (C-Motion, MD, USA) software was used for data analysis. Joint moments were calculated using inverse dynamics and the patellar tendon forces were calculated [4]. The primary outcomes of the jump-landing evaluations were the peak knee and hip flexion angles, internal knee and hip extensor moments and patellar tendon forces during the landing phase of the drop vertical jump task.

Results: A substantial decrease in the patient's symptoms occurred after the intervention, with important changes observed in the VAS (baseline=6.0; after intervention=0.0) and in the VISA-P scores (baseline=61; after intervention=95). The subject reported being completely asymptomatic during sports practice after the intervention. The subject's isometric hip extensor strength had a 77% increase in 8 weeks. In the drop vertical jump the subject presented a 31% increase in peak hip flexion during landing, with little difference on peak knee flexion, after intervention (**Table 1**). Also, a 21% decrease in the knee extensor moment, a 50% increase in the hip extensor moment, and a 26% decrease in the patellar tendon force were observed during landing after the intervention (**Table 1**).

Figure:

Caption: Figure 1 – A. Hip extension in prone-lying; B. Hip extension in quadruped position; C. Drop jump landing training; D. Bird Dog exercise; E. Single-leg deadlift; F. Drop vertical jump landing training

Conclusion: The results of this case-report indicate that an intervention involving hip muscles strengthening and jump-landing modifications can substantially diminish pain and improve lower limb biomechanics during jump-landings in an athlete with patellar tendinopathy.

Table:

	Baseline	After Intervention	% Change
Hip Flexion (deg)	70.45	92.14	+30.79
Knee Flexion (deg)	104.50	100.52	-3.81
Hip Extensor Moment (N.m/kg)	2.09	3.13	+49.76
Knee Extensor Moment (N.m/kg)	2.19	1.73	-21.00
Patellar Tendon Force (BW)	5.04	3.75	-25.59

Caption: Table 1: Kinematic and kinetic variables during the landing phase of the drop vertical jump task at baseline and after intervention

References:

[1] Bahr et al., J Bone J Surg Am, 88: 1689-1698, 2006.

[2] Scattone Silva et al., Br J Sports Med, 48: A60, 2014.

[3] Edwards et al., Med Sci Sports Exerc, 42: 2072-2080, 2010.

[4] Nisell et al., Scand J Rehabil Med, 17: 63-74, 1985.

Disclosure of Interest: None Declared

AS-0125

DEVELOPMENT OF A BESPOKE MOTION CAPTURE SYSTEM ALLOWING REAL-TIME BIOFEEDBACK OF MOVEMENT FOR USE IN THE CLINICAL ENVIRONMENT.

Lindsay Clarke [1,*] Andrew J Murphy [1] Phil Rowe [1]

[1] Biomedical Engineering, University of Strathclyde, Glasgow, United Kingdom

Introduction and Objectives: The feedback of information to patients in the clinical environment is a key aspect to achieving a desirable outcome following a treatment intervention[1]. Biofeedback may be provided in many different ways. It has been suggested that providing patients with augmented visual feedback may have a positive effect on functional outcomes[2]. One of the easiest ways to provide this type of feedback is through motion capture technology. However, a high level of technical expertise is often required to operate motion capture systems and distil useful information from the results. Further, feedback to patients is limited by the technical nature of such systems and the data that they provide. This has limited their widespread use in the clinical environment to date[3,4]. The current study aims to develop a motion capture system which overcomes these issues and is capable of providing biofeedback to patients and clinicians in a clear and accessible manner.

Methods: A bespoke pelvis and lower limb cluster marker set combined with strategically placed anatomical markers was designed and implemented. Marker trajectory data was captured and labelled using Vicon hardware and acquisition software (Vicon Motion Systems, Oxford, UK). This data was streamed in real-time to an object-orientated application development package, D-Flow (Motek Medical, Netherlands). Bespoke scripting modules written in Lua programming code were used to create an avatar from tracked markers and calculated joint centres. The method described by Grood and Suntay[5] was used to calculate inter-segmental kinematics (figure 1). A colour coded joint system was developed to allow real-time feedback regarding hypermobility and pathological movements (figure 1).

Results: A biomechanical model was developed which removes an aspect of the technical inaccessibility of current commercially available motion capture systems. The model allows output of kinematics and visual feedback of movement to the patient and clinician. Currently, flexion/extension, internal/external rotation and ab/adduction angles can be displayed for all joints. Shank/thigh to vertical angle and pelvic, tilt, obliquity and rotation can also be displayed.

Figure 1. Biofeedback during walking. **a.** Avatar and knee flexion angle **b.** Hyperextension of the knee causes joint to turn red.
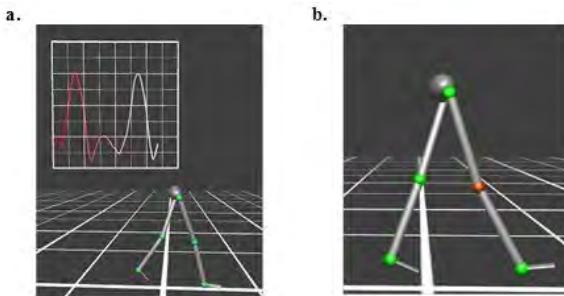
Conclusion: The need for technical expertise in motion capture is greatly reduced with the use of this model. Cluster markers reduce the need for accurate marker placement and visualisation and data feedback can be given in real-time. The use of real-time biofeedback will hopefully lead to increased patient understanding and an improved clinician-patient dialogue.

References: [1] Rosewilliam *et al.* Clin Rehabil, 25:501-514, 2011.

[2] Loudon*et al.* Health Informatics, 3:171-180, 2012

[3] Coutts F. Manual Therapy, 4, 2-10, 1999

[4] Toro *et al.* Arch Phys Med Rehabil, 12:1878-1884, 2003.

[5]Grood *et al.* J Biomech Eng, 2:136-144, 1983.

Disclosure of Interest: None Declared

AS-0126

DETECTING CONTROL PRIORITIES WHEN REGULATING ANGULAR IMPULSE GENERATION IN WELL-PRACTICED GOAL-DIRECTED TASKS

Travis Peterson [1,*]Phillip Requejo [1 2] [3]Henryk Flashner [4]Jill McNitt-Gray [1 2]

[1]Biomedical Engineering, [2]Biological Sciences, University of Southern California, Los Angeles, [3]Rehabilitation Engineering, Rancho Los Amigos National Rehabilitation Center, Downey, [4]Aerospace and Mechanical Engineering, University of Southern California, Los Angeles, United States

Introduction and Objectives: Populations with balance-related impairments (older populations, persons with lower limb amputations, etc.) often have limitations in their ability to generate linear and angular impulse required in activities of daily living (ADL) such as fall recovery [1], stair descent [2], and gait termination [3]. For example, the inability to reliably regulate reaction forces (RF) generated with the prosthetic limb appears to affect the role of each leg in regulating the linear and angular impulse needed in a variety of weight bearing tasks [1–3]. The balance regulation strategies involved in effective performance of ADLs are also common to the golf swing. Participation in golf could improve an individual's capacity for coordinating impulse generation between legs and as a result, serve as an effective and engaging community-based intervention to assist in overcoming balance-related impairments.

During the course of play, players can use golf clubs of different length and club face angles to regulate the trajectory of the ball during flight. Previous research indicates that skilled players using a 6-iron modify shot distance by regulating the magnitude of the target and/or rear leg resultant horizontal reaction forces (RFh), with minimal changes in RFh orientation relative to the target [4]. These results suggest that angular impulse about the center of mass (CM) during the swing can be affected in a comparable way by regulating RFh magnitude and CM trajectory in relation to the point of wrench application (PWA). We tested this hypothesis by comparing the angular impulse generated about the CM when individual players hit a golf ball with a driver as compared to a 6-iron.

Methods: Skilled players (n = 11, handicap < 5) volunteered to participate in accordance with the institutional review board. Each player performed four shots towards a target with a 6-iron (6I) and a driver (D, Taylor Made adidas golf). Shots were initiated using their preferred address position with each foot fully supported by a force plate (Kistler, 1200 Hz). The magnitude and direction of the peak resultant horizontal reaction forces at the artificial turf/plate interface and PWA were computed for each leg [5]. Moments about the CM were calculated by the cross-product of the RFhs and distance between the CM and PWA for each leg. Angular impulse (AI) normalized by body mass was calculated as the area under the moment curves for each leg during the period of net positive AI beginning near transition and ending near ball contact. Statistical analysis estimated the probability that factors contributing to AI were less in trials with the 6-iron than with the driver [6].

Results: The net AI for swings with the driver were found to be greater than net AI for swings with the 6-iron for all players (**Figure 1**). Nine of eleven players increased target leg AI by more than 0.01 Nms/kg (up to 0.07). Eight of 11 increased rear leg AI by a comparable amount (up to 0.09).

All players increasing target leg AI increased the RFh (2.68-7.67% BW) while 4 of 11 experienced reductions in moment arm length (>0.01m). Less than half of the players increasing rear leg AI (5 of 11) increased RFh (1.03-3.51%BW), while 10 of 11 experienced increases in moment arm (0.03-0.19m).

However, player 11 chose to decrease target leg AI while increasing rear AI. As the target leg moment arm decreased at peak RFh, rear leg moment arm increased dramatically at peak RFh to achieve the increase of rear leg AI (**Figure 1**).

Figure:
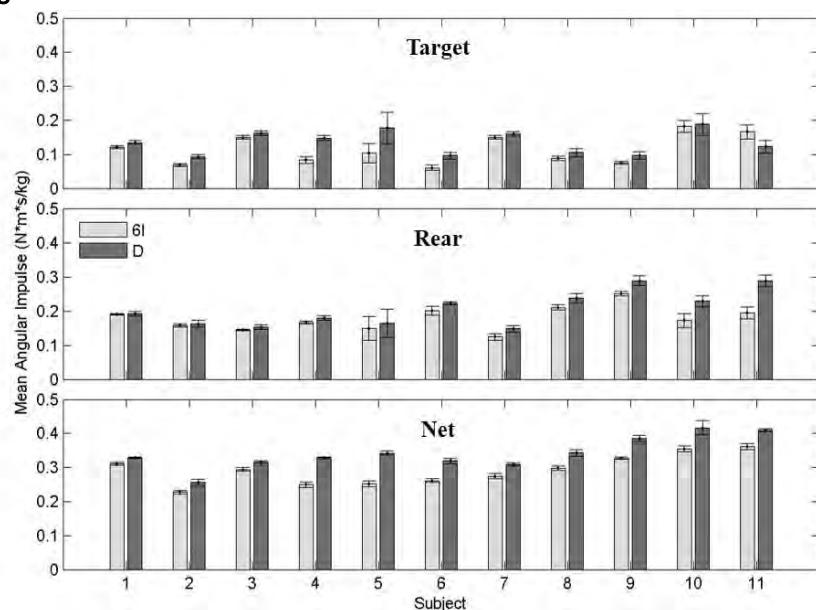
Caption: Figure 1: Angular impulse of target and rear legs towards net AI for 6-iron and driver.

Conclusion: All players generated more angular impulse when using a driver as compared to a 6-iron. Target leg AI was increased primarily by increasing the RFh magnitude, whereas rear leg AI was increased primarily by increases in the moment arm. Some players increased rear leg peak RFh as a strategy to increase rear leg AI. Almost all players increased rear leg moment arm to increase AI to compensate for the lack of increased rear leg RFh.

These findings indicate that performance of a golf swing provides a unique opportunity to practice regulation of linear and angular momentum and promotes improvement in function at the whole body level. Regardless of technique, completing the golf swing allows for balance regulation skills to be practiced and honed by populations with balance impairments. Participation in golf related activities may prove to be an engaging rehabilitation intervention that can be effectively delivered in a community setting as part of the continuum of care where movement is medicine [7].

References: [1] Mathiyakom et al., Exp. Brain Res., **169**(3), 377-88, 2006.

[2] Bosse I., et al., Hum. Mov. Sci., **31**(6), 1560-70, 2012.

[3] Vrieling et al., Gait Posture, **27**(1), 82-90, 2008.

[4] McNitt-Gray et al., Sport Biomech., **12**(2), 121-131, 2013.

[5] Williams et al., Med Sci. Sport., **15**(3), 247-255, 1983.

[6] Wilcox, Mod. Stat., CRC Press Taylor & Francis Group, 2012.

[7] World Health Organization, World Report on Disability, 2011.

Disclosure of Interest: None Declared

Mechanics

AS-0127

ADAPTATION OF CHONDROCYTES TO MECHANICAL COMPRESSION: ARE MEMBRANE RUFFLES UNFOLDED FOR CELL PROTECTION?

Eng Kuan Moo [1,*]Svetlana Kuznetsova [1]Walter Herzog [1]

[1]Human Performance Laboratory, University of Calgary, Calgary, Canada

Introduction and Objectives: Impact/fast loading results in chondrocyte deaths [1]. Cell membranes can only sustain very small strains (3-4%) [2], but are thought to use membrane ruffles, also known as membrane reservoirs, to buffer tensile strains [3, 4]. We found that tensile strain rates in chondrocyte membranes may be crucial in deciding impact-induced cell deaths [5]. However, this hypothesis is based on the premise that cells can access their membrane reservoir effectively in their native environment at slow but not at high strain rates. Geometrically, it has been shown that isolated cells respond to hypotonic osmotic loading by unfolding their surface ruffles [6], and such unfolding events have also been documented in compressed agarose-seeded cells [7]. However, little is known about cell membrane behavior in an intact extracellular matrix. Therefore, the purpose of this study was to investigate changes in membrane topology of in situ cells during slow physiological cartilage compression. We hypothesized that cells unfold their membrane ruffles when loaded mechanically to protect the membrane from stretch.

Methods: Bovine cartilage-bone explants were loaded at 5μm/s to nominal strains ranging from 0-50%. After holding the final strains for ~60 min to allow tissues to approach a steady compressed state, the loaded cartilage was pre-fixed using Ruthenium Hexamine Trichloride fixative solution. The cartilage layer was then post-processed and stained with 0.5% Uranyl Acetate for visualization of cell ultrastructure using transmission electron microscopy (TEM, Hitachi H7650). The changes in surface topology in superficial zone cells by mechanical loading (strains of 0%, n=14; 10%, n=5; 30%, n=5; 50%, n=6) were quantified from the planar TEM image in two ways: (i) using the waviness of the surface ruffles, by measuring the difference in cell circumference between the manually-tracked cell boundary (represents cells with surface ruffles) and the boundary of the ellipse obtained by a best-fit to the manually-tracked cell area (represents cells without surface ruffles) [8], and (ii) using the complexity of the surface ruffles, by measuring the increase in box-counting fractal dimension (Image J, FracLac) of the manually-tracked cell boundary compared to the smoothened cell boundary. Cell shape is quantified by the aspect ratio (AR, defined as the ratio of major axis length to minor axis length) of the ellipse that best-fits individual cell.

Results: Compression of cartilage tissue resulted in corresponding deformation of the residing cells, as reflected in a load-dependent increase in cell aspect ratio (strains of 0%, AR=2.6 ± 1.2; 10%, AR=2.1 ± 1.0; 30%, AR=5.2 ± 2.4; 50%, AR=10.8 ± 3.3). Qualitatively, the cell surface ruffles that existed prior to loading (Figure 1a) disappeared when cartilage was loaded at 50% nominal strain (Figure 1b). Quantitatively, the waviness and the complexity of cell membranes decreased with increasing load magnitudes (Figure 1c), suggesting a load-dependent use of membrane reservoirs.

Figure:
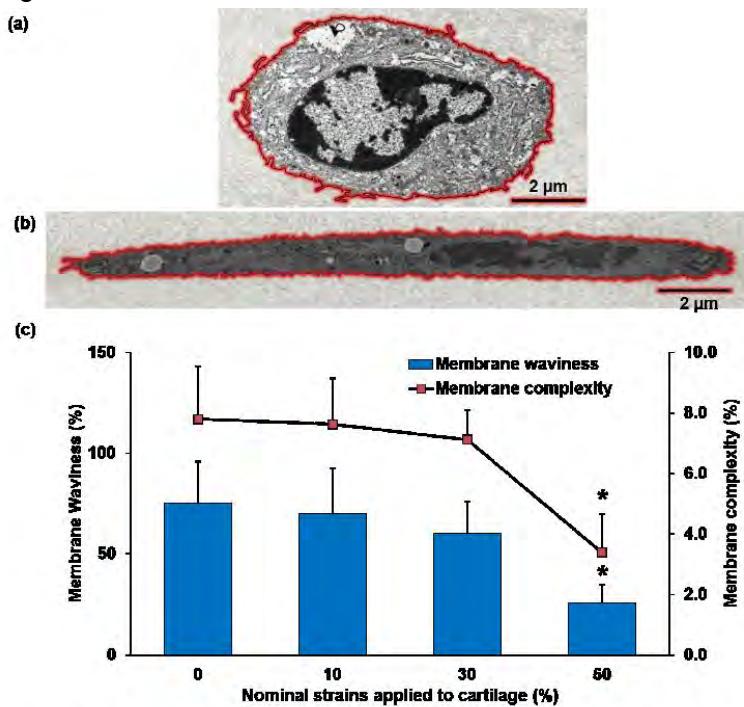
Caption: Figure 1. Ultrastructure of chondrocytes in (a) unloaded cartilage, and (b) 50% nominally-loaded cartilage. (c) Membrane waviness (primary y-axis) and membrane complexity (secondary y-axis) as a function of nominal tissue strain.

Conclusion: During mechanical compression, pictorial observation of disappearance of membrane folds is confirmed by a decrease in waviness and complexity in cell membranes. We conclude from the results of this study that chondrocyte membranes unfold in a load-dependent manner when cartilage is loaded mechanically. This membrane unfolding is likely associated with no stretch of the cell membranes under physiologically meaningful conditions and suggests a protective mechanism used by chondrocytes during physiological mechanical loading via the membrane reservoir. This result can have influence on the pharmaceutical strategy used for cell injury prevention and treatment. Future tests will need to determine if the membrane unfolding is rate-dependent.

References:

[1] Milentijevic et al. J Biomech, 38: 493-502, 2005.

[2] Nichol et al. J Physiol, 493:187-198, 1996.

[3] Raucher et al. Biophys J, 77:1992-2002, 1999.

[4] Moo et al. Biophys J, 105:1590-1600, 2013.

[5] Moo et al. Biomech Modeling in Mechanobiol, 11: 983-993, 2012.

[6] Guilak et al. Biophys J, 82: 720-727, 2002.

[7] Lee et al. J Biomech, 33: 81-95, 2000.

[8] Mulchrone et al. J Struct Geol, 26: 143-153, 2004.

Disclosure of Interest: None Declared

Soft Tissue

AS-0128

TRANSMISSION OF A MECHANICAL WAVE THROUGH THE LOWER LIMB DURING A DROP LANDING

Laura-Anne M. Furlong [1,*] Pui Wah Kong [2] Matthew T. Pain [1]

[1]School of Sport, Exercise and Health Sciences, Loughborough University, Loughborough, United Kingdom, [2]Nanyang Technological University, Nanyang, Singapore

Introduction and Objectives: During a drop landing, large ground reaction forces are observed which are subsequently transmitted through the body via mechanical waves. These waves have been observed using high speed footage, showing large amounts of soft tissue movement relative to the underlying rigid bone. Recent work suggests this movement may help dissipate force and energy (Zelik and Kuo, 2010). The characteristics of the wave can be quantified using markers on the surface of the segment, with changes indicative of the mechanical properties of the underlying soft tissues. In comparison with the skin the muscle-tendon complex has high stiffness, therefore the deformation wave due to an impulsive loading will not be due to skin motion as much as it is due to the motion of the underlying muscle because of the low stiffness of the skin at low strains not propagating forces well. The aim of this study was to investigate the characteristics of mechanical waves propagating through the shank during drop landings.

Methods: Following university ethical committee approval, six healthy, recreationally active males (age: 23 $\pm$ 3 years, height: 1.81 $\pm$ 0.08 m, mass: 81 $\pm$ 5 kg) provided written informed consent to participate in this study. All were familiar with the performance of a drop jump task. A total of 48 spherical retro-reflective markers, 7.9 mm in diameter, were attached around the shank in a 6x8 array using standard double-sided adhesive tape. A ten-camera motion analysis system (700 Hz, 612 series, 1.3 megapixel cameras, Oxford Metrics Group PLC., Oxford, UK) recorded the position of a 48 marker array on the shank (5-65% of shank length). A series of drop landings from box, where landing was heavily favoured onto the test leg, were performed from four different heights (0.3, 0.5, 0.7 and 0.9 m) onto a force plate sampling at 1200 Hz (Kistler 9281B-11, Amherst, NY, USA). All data pre-processing was completed using Vicon Nexus 1.4.116 with any incomplete marker trajectories reconstructed using the quintic spline gap filling procedure.

Marker data were subsequently analysed in Matlab (MathWorks, Natick, MA., USA)., to calculate the motion of the 48 markers, and the 40 sectors defined by the 48 markers, around the shank for data filtered at 50 Hz (with a second order, zero lag Butterworth filter). This gave eight columns with six markers in them, and eight columns with 5 sectors in them. The sector area was calculated from the three-dimensional co-ordinates to account for movement of the soft tissue in all three planes. The time delays between minima in local motion between markers and areas moving from the most distal to most proximal regions were calculated. This was repeated independently for the first maxima as well. This gives the speed at which the wave motion travels up the calf. The linear amplitude of the marker motion whilst undergoing a wavelike motion and the change in area of the sectors were also determined along with the frequency of the wave motion.

Results: Wave velocity was higher in the active compared to passive conditions. Average velocity for wave minima in the active condition was 8.7 m.s^{-1} compared to 4.7 m.s^{-1} in the passive. Similar average wave amplitudes were observed in the active (0.008 m) and passive (0.008 m) conditions. The dominant frequency of the wave was low-frequency (<5 Hz). Average change in the area of marker sectors was larger in the active (18.3%) compared to passive conditions (12.6%).

Conclusion: The results support the presence of wave motion in the soft tissues of the shank during a drop landing, the characteristics of which vary dependent on muscle activation conditions. Higher wave velocities were observed in the active contraction condition. Increased muscle activation increases the stiffness of the underlying muscle-tendon unit, with increased stiffness associated with increased speed of wave transmission. Wave amplitudes were similar in both contraction conditions, but it is possible that the amplitude of the wave is limited by the soft tissue itself.

The marker movement is dependent on the behaviour of the underlying soft tissues, which move with muscle contraction. Previous work has suggested increased muscle activation is associated with decreased soft tissue movement, to minimise the stress on the body (Wakeling et al., 2003). The results of this analysis show the opposite with increased tissue movement with increased activation, but results may be confounded by the greater impact forces exerted on the body during the active condition. Further work is required to determine the relationship between activation and area changes, and to further investigate the characteristics of the wave-like motion of the soft tissue during landing, to provide us with insight into the body's response to impact and potential injury risk.

References: WAKELING, J. M., LIPHARDT, A.-M. & NIGG, B. M. 2003. *Journal of Biomechanics,* 36**,** 1761-1769.
ZELIK, K. E. & KUO, A. D. 2010. *Journal of Experimental Biology,* 213**,** 4257-4264.

Disclosure of Interest: None Declared

Soft Tissue

AS-0129

REPRODUCIBILITY OF A NOVEL IN-SHOE ULTRASOUND METHOD FOR ASSESSING SOFT TISSUE BEHAVIOUR OF THE FOREFOOT DURING WALKING

Beverley O'Neill [1,*]

[1]School of Health and Life Sciences, Glasgow Caledonian University, Glasgow, United Kingdom

Introduction and Objectives: Diabetes is a major public health concern worldwide, and significantly contributes to risk of foot ulceration [1]. In healthy individuals, the plantar soft-tissues (PST) provide protection to bone, superficial connective tissue and skin. Changes in PST behaviour in people with diabetes may be a key factor in causal pathways for diabetic foot ulceration [2]. In vivo, monitoring the dynamic behaviour of PST during weight-bearing activities is difficult and existing techniques tend to be limited to unloaded indentation tests or single step methods. We have recently demonstrated the feasibility of using a shoe-embedded ultrasound (US) transducer to measure dynamic heel pad behaviour [3]. The aim of this study was to develop and assess the reproducibility of a novel protocol to measure forefoot PST behaviour during gait.

Methods: A modified shoe incorporating an US probe within a 3D printed insert was developed to enable US images of PST to be obtained from healthy participants. Data were collected at 2 sites (2nd, 5th metatarsal heads, MTHs) on either foot (n=19/21 feet per site) during 25s treadmill walking trials. Maximum (unloaded) and minimum (loaded) PST thickness was subsequently measured from US cineloop files using Kinovea (version 0.8.15) open access software. Number of steps required to achieve the desired level of validity was evaluated by calculating coefficient of variation (CoV) for each incremental number of steps (2-10 steps). CoV of 2% was used as the threshold for acceptable within-trial variation. Measurements collected from participants by the same tester at two time points were used to evaluate between-session reproducibility. Intraclass correlation coefficients (ICCs), Bland Altman plots, and indices of changes in the mean and measurement variability (see Table 1 for description of statistics) were calculated for each PST variable.

Results: Six steps were found to yield acceptable within-trial variation (CoVs <2%) for all variables. Between-session ICC values were fair to good [4] for minimum (0.642) and maximum (0.559) PST thickness at the 5th MTH, and excellent for minimum (0.906) and maximum (0.888) thickness at the 2nd MTH. Bland Altman plots (Fig. 1) indicated no systematic errors between sessions. Outliers (Fig.1, circled data points) corresponded to unusually large between-session differences in PST thickness measures that were most likely due to tester inconsistencies (e.g. method and/or interpretation errors). Summary statistics are presented in Table 1. The mean absolute difference (d) between sessions ranged from 0.05-0.12cm for analysed variables, with measurements for minimum PST thickness tending to show smaller differences at both sites. CV% ranged from 4.69–12.25%, being larger at the 5th compared to 2nd MTH. For example, a mean minimum PST thickness of 0.95cm at the 2nd MTH, with CV%=5.36, would produce a typical between-session variation of 0.05cm, thus a greater change would be required to indicate a clinically significant difference in this population.

Figure:
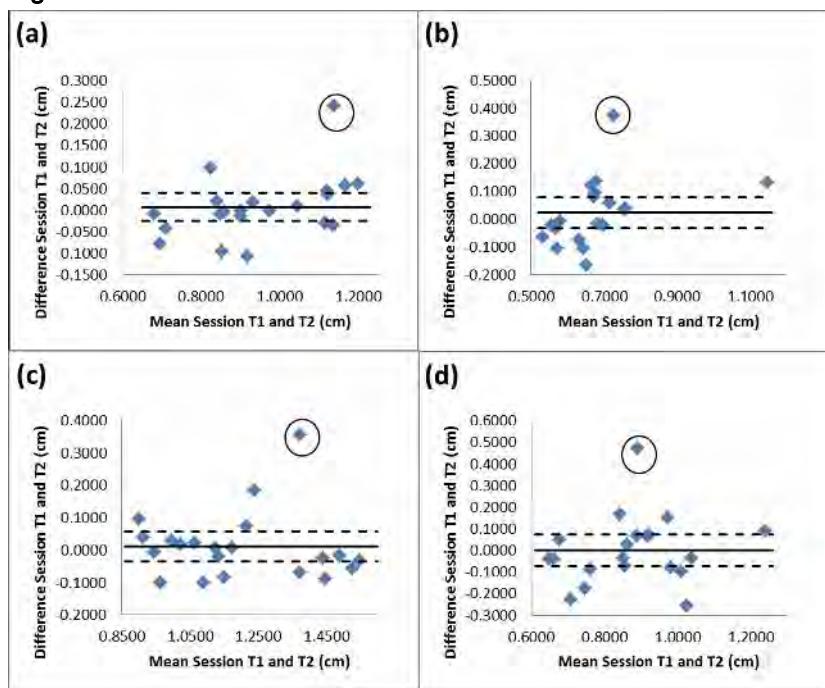
Caption: Figure 1 Bland Altman plots indicating 95% confidence interval (dashed lines) of the mean difference between two sessions (solid line) for (a) minimum PST thickness at 2nd MTH, (b) minimum PST thickness at 5th MTH, (c) maximum PST thickness at 2nd MTH and (d) maximum PST thickness at 5th MTH. Outliers are circled.

Conclusion: This novel method appears to enable good between-session reproducibility with acceptable levels of random error and measurement variability for PST measures at both 2nd and 5th MTH sites in a healthy population. As such, further evaluation of the use of this method in disease populations would be appropriate. Measurement of PST behaviours in people with diabetes may provide insight into causal pathways for diabetic foot ulceration.

Table:

	Change in Mean				Measurement Variability			
PST Variable/Site	d	SD$_{diff}$	SE	95% CI	ME	SEM	CV%	SEM%
Min PST, 2MTH	0.05	0.06	0.01	0.02-0.07	0.04	0.05	5.36	5.88
Min PST, 5MTH	0.08	0.08	0.02	0.05-0.12	0.06	0.08	12.25	14.33
Max PST, 2MTH	0.07	0.08	0.02	0.03-0.10	0.06	0.07	4.69	6.11
Max PST, 5MTH	0.12	0.11	0.02	0.07-0.16	0.08	0.11	8.66	12.82

Caption: Table 1 Summary statistics for between-session reproducibility for minimum and maximum PST thickness measures at two sites (2nd and 5th MTH).   Indices of changes in the mean (mean absolute difference between two test sessions, đ⁻ ; standard deviation of differences between two test sessions, SDdiff; standard error of đ⁻, SE; and 95% confidence interval of đ⁻, 95% CI), and measurement variability (method error, ME; average standard error of measurement between two test sessions, SEM; between-session coefficient of variation, CV%; percentage SEM, SEM%).

References: [1] Diabetes UK. Diabetes in the UK 2012*, 2013*

[2] Abouaesha et al., J. Am. Pod.Med. Assoc., 94: 39-42, 2004.

[3] Telfer et al., Gait Posture, 39:328-332, 2014.

[4] Fleiss. Design and Analysis of Clinical Experiments, John Wiley & Sons, 1986.

Disclosure of Interest: None Declared

Soft Tissue

AS-0130

INFLUENCE OF CAPSULAR PLICATION ON TRANSLATION IN A SIMULATED MDI SHOULDER

Andrew Kraszewski [1,*]Stephanie Mayer [2]Andreas Kontaxis [1]Russel Warren [2]

[1]Rehabilitation, [2]Orthopaedic Surgery, Hospital for Special Surgery, New York, United States

Introduction and Objectives: The glenoumeral capsule is a complicated shoulder structure that passively checks joint translation, but is susceptible to injury espcially in rigorous overhead activities. Symtopmatic glenonumeral laxity is common among young athletes, and when conservative management is often insufficient treatment typically regresses to orthopaedic intervention in the form of capsulorrhaphy, i.e. plication. In general, surgeons lack objectively-based clinical tools to judge the efficacy and performance of surgical interventions especially during surgery.
Our objective was to understand the effect of sequential regional plication on glenohumeral translation within and across multiple rounds of plication.

Methods: A cadaveric CT scan was taken and checked for significant degenerative pathology by an orthopaedic surgeon. At the time of thaw the specimen included a full scapula and humerus. All musculature was removed leaving only the glenohumeral capsule. Passive marker tracking clusters were fixed to each segment with two parallel trans-cortical rods per segment (see Figure 1A). Anatomical coordinate frames [1] were constructed from palpation and a functional joint method [2] and then rigidly embedded in the cluster tracking frames. The scapula and humerus were separately potted and fixed to a frame that allowed fixed glenohumeral orientation and full floating 3D translation. A 6DOF loadcell (MA1000, AMTI) was attached in series with the humerus to record external loads. Six optical motion cameras (Motion Analysis Corp) at 30 frames per second captured marker motion along with loadcell data at 300 frames per second. Model building and post-processing was done in Visual3D (C-Motion, Inc).
The capsule was preconditioned to reduce the effects of viscoelastic behavior. MDI laxity was simulated by stretching the capsule by internally and externally rotating the humerus based on a previous study [3]. The capsule was plicated over three rounds; within each round the capsule was plicated in a consistent order: first anteriorly (3:00), then posteriorly (9:00) and lastly inferiorly (6:00). Plication magnitude was larger each successive round: Round1 - 0.5cm, Round2 - 1.0cm, Round3 - 1.5cm. Glenohumeral orientation was fixed in neutral rotation and flexion with abduction at 60 degrees. External manual traction was applied to the scapula in the anterior, posterior and inferior directions, chosen randomly. Outcome measurements of interest were anterior, posterior and inferior glenohumeral translation at 20 Newtons of load. Descriptive statistics are reported.

Results: Outcomes are reported in Figure 1B and Table 1. On average anterior translation decreased per plication round, indicating increased capsule tightness as plication magnitude increased. The largest within-round changes occurred between anterior and posterior plications, whereas changes between posterior and inferior plication were much smaller. In Figure 3B, Round3 posterior translation is very low with repsect to both anterior and inferior directions, which was unexpected. This anomaly is believed to reflect negative pressure that was occasionally generated due to a temporary suction mechanism from the interaction of the joint cartilage and highly conforming joint geometry.

Figure:

Figure 1A

Figure 1B
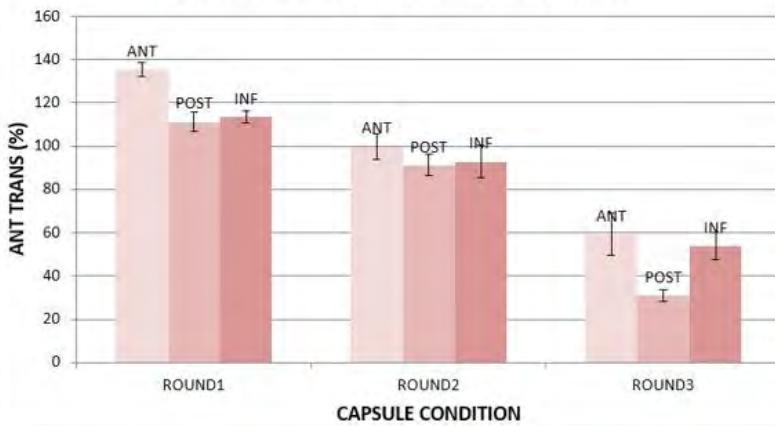
Caption: Figure 1. A - Picture of potted and inverted humeral and scapula with tracking clusters; posterior plication sutures circled. B - Graph indicating changes in anterior translation within and across plication rounds.

Conclusion: The study is ongoing with one specimen collected to date. Lack of statistical power precludes inferential conclusions. However our results show, expectedly, that as plication magnitude increases translation decreases. More interestingly the data suggest that inferior plication may not influence anterior translation. Clinically, this may dissuade surgeons from plicating inferiorly in certain cases, as it may be unncessary.

References: [1] Wu et al., J. Biomechanics, 38: 981-992, 2005.

[2] Schwartz & Rozumalski, J. Biomechanics, 38: 107-116, 2005.

[3] Shafer et al., J Bone Joint Surg, 90: 136-144, 2008.

Disclosure of Interest: None Declared

CORNEA BIO-INSPIRED CONSTRUCTS BASED ON ORIENTED LONG COLLAGEN FIBERS BIO-COMPOSITES

Mirit Sharabi [1] [2],*David Varssano [3] [4]Dafna Benayahu [2]Yehuda Benayahu [5]Rami Haj- Ali [1]

[1]School of Mechanical Engineering, The Fleischman Faculty of Engineering, [2]Department of Cell And Developmental Biology, Sackler School of Medicine, [3]Sackler School of Medicine, Tel Aviv University, [4]Department of Ophthalmology, Tel Aviv Sourasky Medical Center, [5]Department of Zoology, George S. Wise Faculty of Life Sciences, Tel Aviv University, Tel Aviv, Israel

Introduction and Objectives: The cornea contains highly organized collagen fiber laminates, providing strong and durable structure that withstands inner and outer pressures. Here we present a biocomposite inspired for bio-mimetics of the construct based on structure-function needs towards engineering of cornea.

A novel bio-inspired constuct based on long collagen fibers bio-composite embbeded and crosslinked in polyacrylamide/alginate hydrogel (PAAm-Alginate) is made to mimic the human cornea. The research is focused on the fabrication of the biocomposite complexed structure and its non-linear mechanical behavior which is typical for the native cornea.

Methods: A novel fiber reinforced bio-composite was designed and fabricated based on our previous work [1], [2]. The construct included collagen fibers [3] aligned in varied directions (i.e. every 30 °) with clear center of 4.5mm diameter. The aligned fiber structure was embedded and cross-linked to hybrid gel double network of PAAm-Alginate) [4]. This composite was subjected to cyclic indentation, where the spherical indenter was pushed into the construct to simulate the physiological loading modes. In addition, three dimentional and hyperelastic finite element (FE model) was built for solving the inverse problem of calculating stress-strain values from the load-deflection experimental results using the measured material properties.

Results: A novel composite construct was fabricated from aligned collagen fibers embedded in PAAm-Alginate matrix. The anisotropic construct presented hyperelastic behavior with large deformations of about 20% strain. Effective hyperelastic stress-strain behavior of the indentation was calculated using the FE model and found to provide good fitting to the corneal tissue. The cornea's working range (10-20mmHg) was found in the initial part of the stress-strain curve of the bio-composite, allowing durabilty of the costruct in extreme cases of loading as injury or fall.

Figure:
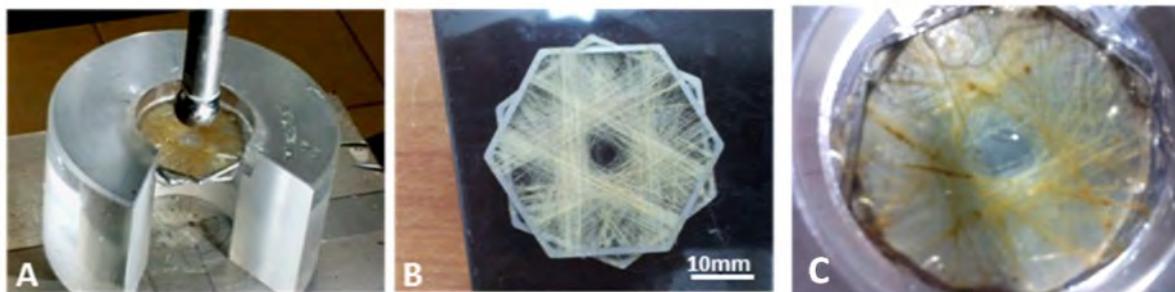
Caption: Cornea bio-inspired construct. (a) Mechanical indentation of bio-composite. (b) Collagen fibers alignment. (c) Final cornea bio-mimetic construct.

Conclusion: Bio-inspired cornea construct can properly mimic the native cornea function providing hyperelastic behavior and mechanical durability, based on the novel collagen fiber–reinforced composite structure. FE modeling allows better understanding of the composite structure and thus to design custome-made bio-inspired cornea constructs, these *in silico* experiments enable saving time and resources in the engineering process.

References: [1]   Sharabi et al. *J. Mech. Behav. Biomed. Mater.*,36:71–81, 2014.

[2]   Haj-Ali et al. Patent application: WO 2013118125 A1 2013.

[3]   Benayahu et al. Patent application:US20110038914A1, 2011.

[4]   Sun et al. *Nature*, 489,:133–6, 2012.

Disclosure of Interest: None Declared

Soft Tissue

AS-0132

MINIMUM INDENTATION DEPTH FOR CHARACTERIZATION OF 2ND SUB-METATARSAL HEAD AND HEEL PAD TISSUE PROPERTIES

Taeyong Lee [1] Jee Chin Teoh [2,*] Ying Bena Lim [2] Jaeyoung Park [3]

[1]Department of Medical Biotechnology, Dongguk University, Seoul, Korea, Republic Of, [2]Department of Biomedical Engineering, National University of Singapore, Singapore, Singapore, [3]Department of Leisure Sports, Dongeui University, Pusan, Korea, Republic Of

Introduction and Objectives: At present, there are several existing in-vivo indentation systems developed for the characterization of plantar soft tissue properties. Through using these devices, several studies have been conducted to investigate and quantify the relationship between plantar soft tissue properties and conditions that cause plantar soft tissue stiffening such as aging and diabetes(Chao, Zheng et al. 2010, Kwan, Zheng et al. 2010, Mickle, Munro et al. 2011).

The variable mechanical properties of plantar soft tissue depend on the extent of tissue deformation (Chao, Zheng et al. 2010) as well as the configuration of the metatarsophalangeal joint (MTPJ) (Garcia, Hoffman et al. 2008), specifically for the forefoot region. Thus, measurements of tissue stiffness should only be performed under a controlled environment with an appropriate degree of tissue deformation to obtain meaningful results.

Most in-vivo indentation techniques are limited by the lack of adequate indentation into the plantar soft tissue. Moreover, there is a lack of consensus on the appropriate indentation depth, resulting in the inability to make unambiguous remarks from literature. Consequently, the purpose of this study is to investigate and determine the minimum indentation depth required to effectively characterize the biomechanical properties of plantar soft tissue under weight-bearing conditions.

Methods: Twenty young subjects (20-25 years) participated in this study. The test was conducted with equal weight borne on each of the participants' feet to mimic the static stance of the gait cycle. During the experiment, the indenter probed the 2nd sub-metatarsal head (MTH) and heel pad tissue at a constant rate of 12.3mm/s. The maximum tissue deformation induced was varied from 1.2mm to 6.0mm, in steps of 1.2mm. The tissue stiffness obtained from the tissue response curves was compared and fitted to the proposed viscoelastic model(Garcia, Hoffman et al. 2008) as shown in Fig. 1A.

Results: The viscoelastic model used in this is shown in Fig. 1A. K_1 and K_2 capture the elastic response of plantar soft tissue at the initial and subsequent phases of indentation. C characterizes the viscous behavior of tissue which is only prominent at the latter stage of indentation. X_s is the minimum indentation depth beyond which the tissue exhibits nonlinear viscoelastic behavior. The model suggests that there is a need to indent the tissue beyond X_s in order to assess both K_1 and K_2. This differs from the paper by Garcia et. al. (2010), where there is no mention of the reference value of X_s.

As the probe tip indents deeper into the plantar soft tissue beyond a threshold depth (i.e. X_s), the force gradient increases notably (Fig. 1B and 1C). As shown in Table 1, the absolute value of X_s was approximately 2.23mm and 2.14mm at the heel and 2nd sub-MTH respectively. Indentation depths which were less than this threshold depth might not be representative of the nature of plantar soft tissue nor reflect the critical deformation it experiences during physical activities that expose the tissue to risk of ulceration.

Figure:
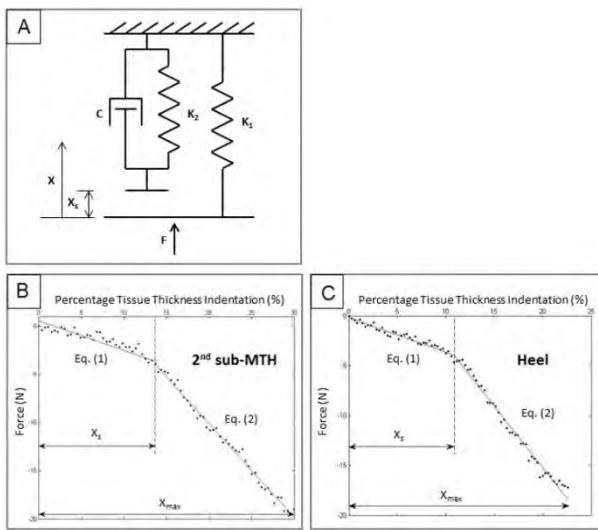
Caption: Figure 1. (A) The viscoelastic model proposed by Garcia et al. (2010). Detailed tissue response of (B) 2nd sub-MTH and (C) heel pad.

Conclusion: The results of this study demonstrate the existence and significance of a minimum indentation depth (X_s) required for investigating plantar soft tissue properties. Adoption of an inappropriate indentation parameter may result in erroneous tissue stiffness measurements. Hence, a proper quantifiable reference helps provide valuable insights into plantar soft tissue behavior, which can be used for computational modeling to better understand complex foot mechanisms and pathologies. Furthermore, the tissue properties elicited provide valuable information and possible indication of disease (Jahss, Michelson et al. 1992). Hence, a rigorous description of plantar soft tissue behavior is crucial and has good potential for application in the diagnosis of foot abnormalities related to diseases such as diabetes.

Table:

	2nd sub-MTH	Heel	p-value
Average Tissue Thickness (mm)	13.80 ± 1.76	18.04 ± 2.42	< 0.01*
Stiffness coefficient, K_1 (N/% tissue thickness)	0.230 ± 0.122	0.492 ± 0.151	< 0.01*
Stiffness coefficient, K_2(N/% tissue thickness)	0.477 ± 0.168	1.015 ± 0.406	< 0.01*
X_s(% tissue thickness)	16.177 ± 1.909	11.845 ± 1.284	< 0.01*
Damping coefficient, C(N/% change in tissue thickness per second)	0.767 ± 0.667	1.803 ± 0.651	0.03*

Caption: Plantar soft tissue properties of 2nd sub-MTH and heel pad

References: [1] Chao et al., Clin Biomech, 25(6): 594-600, 2010

[2] Garcia et al., Foot, 18(2): 61-67, 2008

[3] Jahss et al., Foot and Ankle, 13(5): 233-242, 1992

[4] Kwan et al., Clin Biomech, 25(6): 601-605, 2010

[5] Mickle et al., J Orthop Res, 29(7): 1042-1046, 2011

Computer Simulation

AS-0133

SINERGY-BASED TWO-LEVEL OPTIMIZATION FOR PREDICTING KNEE CONTACT FORCES DURING WALKING

Gil Serrancolí [1,*] Allison L. Kinney [2] Benjamin J. Fregly [3] Josep M. Font-Llagunes [1]

[1]Department of Mechanical Engineering, Universitat Politècnica de Catalunya, Barcelona, Spain, [2]Department of Mechanical and Aerospace Engineering, University of Dayton, Dayton, [3]Department of Mechanical and Aerospace Engineering, University of Florida, Gainesville, United States

Introduction and Objectives: Musculoskeletal models and optimization methods are combined to calculate muscle forces. Some model parameters cannot be experimentally measured due to the invasiveness, such as the muscle moment arms or the muscle and tendon lengths. Moreover, other parameters used in the optimization, such as the muscle synergy components, can be also unknown. The estimation of all these parameters needs to be validated to obtain physiologically consistent results. In this study, a two-step optimization problem was formulated to predict both muscle and knee contact forces of a subject wearing an instrumented knee prosthesis. In the outer level, muscle parameters were calibrated, whereas in the inner level, muscle activations were predicted. Two approaches are presented. In Approach A, contact forces were used when calibrating the parameters, whereas in Approach B, no contact force information was used as input. The optimization formulation is validated comparing the model and the experimental knee contact forces. The goal was to evaluate whether we can predict the contact forces when in-vivo contact forces are not available.

Methods: The experimental data used in this study came from the 4th Grand Challenge Competition to Predict In Vivo Knee Loads [1]. The subject wore an instrumented knee implant in his right leg. An inverse dynamic analysis of six gait trials was carried out in OpenSim [2]. Muscle activations were obtained applying the muscle activation dynamics to the available EMG measurements for all six trials. A muscle synergy analysis was carried out to obtain Synergy Vectors (SV_{exp}) and Neural Commands (NCs) from experimental activations. A unique set of SVs was obtained for all six trials and one NC for each trial represents the time-activation pattern. Three gait trials were used to calibrate the model. A two-step optimization formulation was developed to calibrate the muscle parameters in the outer level, and to calculate activations at the inner level. In the outer level, SVs of the muscles without experimental data (SV_{model}), scale factors for the SV_{exp}, moment arm deviations, scale factors for the muscle optimal length and the tendon slack length were calibrated. The outer cost function had terms to minimize the passive force and the residual activations and, only in Approach A, it had terms to track the knee medial and lateral contact forces. It also had bound terms to constrain SVs, moment arm deviations, the optimal muscle lengths and the tendon slack lengths. In the inner level, muscle activations were calculated by means of the resolution of a quadratic programming problem. Muscle activations were minimized while inverse dynamics muscle contributions were matched with the calculated ones. Three different gait trials were used to predict the knee contact forces. In this case, muscle parameters previously calibrated in the outer level were used to run the inner level.

Results: Table 1 shows the R^2 values (and RMSE in parenthesis) of the match between experimental and model knee contact forces (medial, lateral and total, respectively) when calibrating the model and when predicting the contact forces, using knee contact forces to calibrate the model (Approach A) and without using them (Approach B). Figure 1 shows the

knee contact force prediction in two trials (Approach A and B). The mean RMSE difference of the muscle parameters between Approach A and B for time varying quantities were computed: muscle activations 0.08, muscle forces 65.62, normalized length of the muscles 0.11. The mean absolute difference for muscle parameter values was 0.009 for optimal length of the muscles, 0.010 for slack length of the tendons and 0.290 for scale factors of the experimental activations.

Figure:
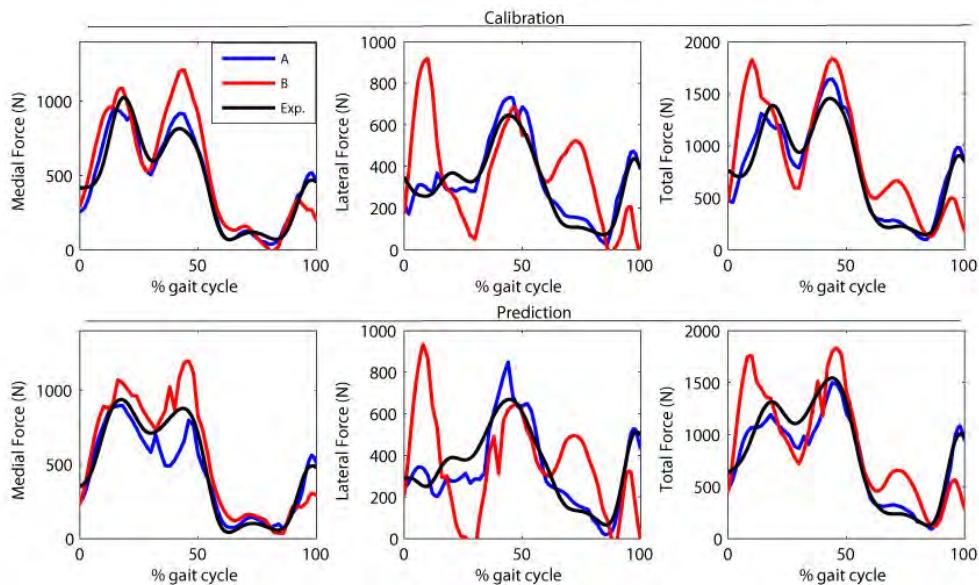
Caption: Fig. 1. Contact forces in one calibration and one prediction trial for both approaches and their experimental values

Conclusion: Medial contact forces were better predicted than lateral forces in both approaches, what is in agreement with other studies [3]. Overall, all muscle parameters are similar except some of them that would explain the differences in the contact force predictions. For instance, tensor fasciae latae, a muscle which crosses the knee, had a different activation in both approaches due to the lack of the knee contact force constrains in approach B. In Approach A, the contact force prediction were quite better predicted than in B, what means that for this subject the use of neural commands alone was not sufficient to calibrate the model such that predicted good contact forces.

Table:

	Approach A	Appoach B
Calibration	0.97 (56.97), 0.84 (64.18), 0.95 (110.39)	0.69 (194.64) / -2.07 (284.33) / 0.44 (363.88)
Prediction	0.91 (96.38), 0.76 (85.36), 0.91 (145.13)	0.68 (185.01) / -1.75 (288.64) / 0.44 (353.04)

Caption: Table 1. Mean R2 values of the knee contact force match (medial, lateral and total, respectively).

References: [1] Fregly BJ et al. *J Orthop Res* **30**: 503:513, 2012.

[2] Delp SL et al. *IEEE T Bio-Med Eng* **54**: 1940-50, 2007.

[3] Kinney AL et al. J Biomech Eng **135**: 021012, 2013.

Disclosure of Interest: None Declared

FORWARD-DYNAMICS TRACKING WITH REACTION FORCE TARGETS

Benedikt Sagl [1,*]Ian Stavness [1]Rudolf Slavicek [2]

[1]Department of Computer Science, University of Saskatchewan, Saskatoon, Canada, [2]A.E.R.S Dental Medicine Organisations, Vienna, Austria

Introduction and Objectives: Forward-dynamics assisted tracking has become a widely-used tool for analyzing muscle contributions to dynamic human movements. This type of analysis has been developed in a number of simulators, notably as Computer Muscle Control (CMC) in OpenSim [1]. Tracking simulations use optimization to predict a trajectory of muscle forces that will drive a 3D dynamic musculoskeletal model to closely follow a target action. CMC simulations use kinematics as the target variable to track and require that external reaction forces between the model and the external world be prescribed. For example, in gait simulations, ground-to-foot reaction forces measured by force plates in the floor or treadmill are "played back" and applied to the model's feet during the gait simulation. Many human actions, however, involve reaction forces with the external world that are difficult to measure or infer. Examples include the force applied by one's hand to a tool or the forces that arise between opposing teeth during chewing. In these cases the standard CMC analysis is inappropriate. To solve this problem, our objective is to create a tracking simulation that includes reaction forces as a dynamic target, rather than as a fully prescribed quantity.

Methods: We have extended the well-known forward-dynamics assisted tracking algorithm to include reaction-force targets in addition to kinematics targets. This allows tracking simulations to predict muscle forces that cause a model to simultaneously slide (or roll) along a surface while applying a force normal to that surface. Our approach relies on a standard formulation of musculoskeletal dynamics that includes rigid bilateral constraints to enforce reactions between the model and the external world or between two internal contact surfaces within the model. In this formulation, the addition of reaction-force targets to a tracking simulation with kinematics targets results in negligible additional computational cost because the model's velocities and reaction force magnitudes (Lagrange multipliers) are already computed simultaneously. We have implemented our reaction-force target tracking method within the open source ArtiSynth biomechanics simulation platform (www.artisynth.org).

We have demonstrated our reaction-force tracking simulation in the context of teeth grinding. It is difficult to accurately measure contact forces between the teeth during clenching and grinding actions because the introduction of any material between the teeth, even a very small or thin force transducer, will alter a patient's biting action and trigger a reflex response to reduce bite force. Therefore, the standard CMC algorithm is not appropriate for simulating teeth grinding because the tooth-to-tooth reaction force cannot be prescribed from experimental measurements. Without a reaction-force target, we expect that a tracking simulation will activate a set of muscles that fulfills the kinematics target using a minimal level of muscle forces and will barely create any closing force. We expect that the inclusion of a reaction-force target will elicit larger muscle forces and consequently a larger force between tooth facets during the grinding action.

We simulated a 2.5 mm inward grinding movement with a dynamic multibody jaw model [2] and a tooth-to-tooth frictional force that opposed sliding movements. The simulation started with the jaw in a 2.5 mm left lateral position and moved the

jaw inward toward a neutral jaw position. This movement simulates a left chewing-like power stroke that is typical of tooth grinding. We performed two simulations: (1) without a reaction-force target and (2) with a reaction-force target of 350 N.

Results: For the simulation with no reaction-force target, the kinematics target was fulfilled with very low muscle activations (Figure, left panel). Consequently, virtually no force was applied between the opposing teeth during the sliding movement. The inclusion of a target tooth-to-tooth reaction force of 350 N resulted in much higher activation of the jaw closing muscles (Figure, right panel), and the simulation was able to track both the sliding kinematics simultaneously with a 350 N force between the teeth.

Figure:
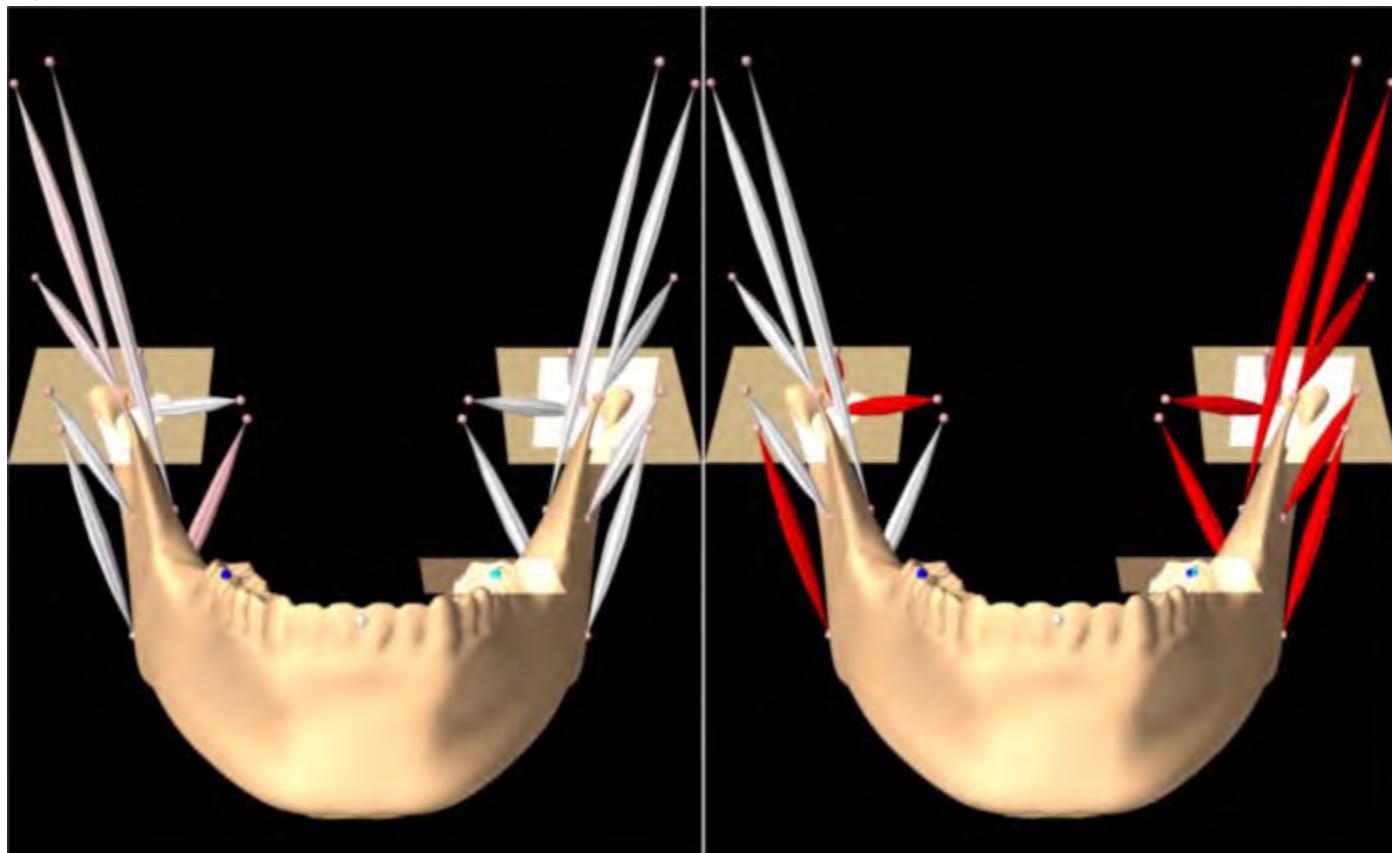
Caption: Two tracking simulations of tooth grinding with a dynamic multibody jaw model: one with no reaction-force target (left) and the other with a 350 N reaction-force target between opposing teeth (right). Muscle color denotes activation level from 0% activation (white) to 100% activation (red).

Conclusion: At ISB we will report our results on muscle contributions to teeth grinding and demonstrate that the reaction force-tracking approach is a useful augmentation to the standard CMC-style analysis tool for musculoskeletal research.

References: [1] Seth et al., Procedia IUTAM, 2: 212-232, 2011.

[2] Hannam et al., J Biomech, 41: 1069-1076, 2008.

Disclosure of Interest: None Declared

COMPARISON OF GEOMETRIC APPROXIMATION AND ANATOMICALLY SEGMENTED MODELS OF THE AORTA USING FINITE ELEMENT METHOD

Francisco Carrasco-Hernandez [1,*] Alan Parish [1] Richard Brooks [1] David Richens [2] Donal McNally [1]

[1] University of Nottingham, [2] The Trent Cardiac Centre, Nottingham, United Kingdom

Introduction and Objectives: Simulation utilizing Finite Element Method (FEM) of organic tissues has become important in the design of medical devices. To design a specimen for FEM the simplest way is to approximate the geometry of it is using a Computational Assisted Design Software (CAD), or by segmenting out the specimen form medical data [1]. The advantages of using an approximated geometry specimen, includes the simplicity of its creation and also the increased speed in FEM due to its symmetry and uniformity. The segmentation of 3D medical images, can be used to generate an anatomically precise model of a specific human anatomy (SM), this more accurately shaped specimen, requires significantly more computational power for FEM than the approximated geometric specimen (GM). This study tests the hypothesis that a numerical simulation with a geometric approximation is less accurate than using a segmented model.

Methods: In order to find how advantageous the use of this methodology is in cardiovascular biomechanics, this paper presents the comparison of these two models. The anatomical model was created by segmenting the blood within the aorta from a 3D dataset using Mimics V17.0 (Materalise) and then wrapping the blood with three aorta layers using 3-Matic V9.0 (Materalise), while the simple geometric model was created in PTC CREO Parametric 2.0. Both model a 10mm long segment of human aorta, with three tissue layers, with hyper-elastic rubber-like mechanical properties taken from published literature, and confirming in a bubble bi-axial inflation test. These models were subjected to a variable internal pressure in FEM (LS-Dyna), to simulate the reaction of this tissue to the beating of the heart. Using two different pressure curves, first a High pressure of 0 – 2025mmHg (0 – 270KPa) [Pearson] representing rupture and secondly a normal physiological pressure values of 0 – 170 mmHg (0 – 23KPa) [2].

Results: The results can be observed in separate values for stress, strain and resultant displacement, obtaining errors between the two models, highlighting the first value of the high pressure curve, i.e. 225mmHg (30KPa), which is where an error of 18.3% in stress values is presented, and then drooping meanwhile the pressure is increasing.

With this reaction on the models, the normal physiological pressure is introduced, highlighting the sixth step (140mmHg – isolated systolic hypertension), where the SM changes shape into a circle, approaching to the GM as the strain error of 1.6% and displacement error of 36.2% represents

Figure:
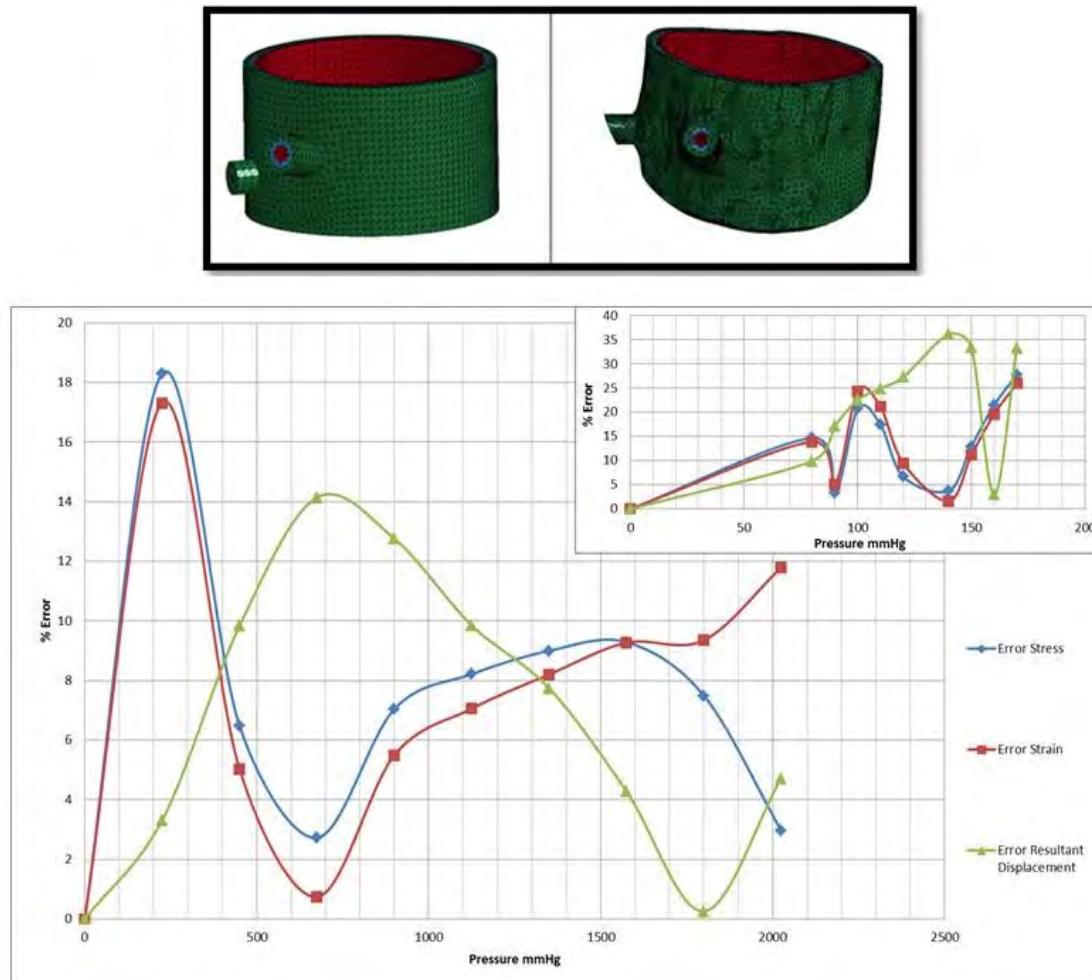
Caption: Figure 1. Error between Geometric Approximation V.S. Segmented Model in High and normal physiological pressure

Conclusion: It is important to verify the feasibility of first create a geometric approximation of a biological tissue in order to give an idea of the mechanical reaction of the tissue using a FEM simulation. But more importantly to stablish the methodology to follow, as the GM specimen is less time consuming than the SM specimen. After stablishing a methodology for the simulation, the generated SM sample can be used to validate results.

Table:

Pressure (mmHg)	Error Stress	Error Strain	Error Resultant Displacement
90	3.27%	5.02%	17.19%
140	3.76%	1.59%	36.20%
170	27.77%	25.96%	33.38%
225	18.30%	17.31%	3.31%
675	2.72%	0.74%	14.14%
2025	2.97%	11.79%	4.71%

Caption: Table 1. Maximum and Minimum Error Values for Stress Strain and Resultant Displacement

References: [1]   V. Spitzer, et al, *J. Am. Med. Informatics Assoc.*, 3:2, 118–130, 1996.

[2]   A. V Chobanian, et al, *Hypertension*, 42:6, 1206–52, 2003.

Disclosure of Interest: None Declared

A COMPUTATIONAL STUDY OF STENT DEPLOYMENT INSIDE A DISEASED ARTERY WITH VARIABLE DEGREES OF STENOSIS, ASYMMETRY AND CURVATURE

Alessandro Schiavone [1,*]Liguo Zhao [1]

[1]Wolfson School of Mechanical and Manufacturing Engineering, Loughborough University, Loughborough, United Kingdom

Introduction and Objectives: Angioplasty and stenting are commonly used to treat cardiovascular diseases such as atheroscleroris. So far, research on stents is largely focused on the development of new materials and designs for better scaffolding, drug delivery and bioabsobability [1]. However, stent deployment and performance are also strongly affected by the thickness and asymmetric nature of plaque layers as well as the curvature of arteries, which has not been well studied yet. With this work, we aimed to understand how these biological factors influence the stent deployment and also to identify their possible connections with arterial damage [2, 3] and chest pain [4] caused by stenting.

Methods: Abaqus/Explicit has been used for finite element simulation of stent deployment. A model of Xience stent with 6mm in length and a crimped diameter of 1.5mm was meshed into 111380 incompatible brick elements. The folded balloon consisted of 7791 4-node shell elements. The artery (with separate intima, media and adventitia layers) had a length of 40mm, an inner diameter of 4mm and a thickness of 1mm. It was meshed into 72576 brick elements with reduced integration. Both straight and curved arteries (bended by 30° and 60°) were modelled.

The stenotic plaque had a length of 6mm, and its thickness was chosen to be 1.6mm (40% stenosis), 2.0mm (50% stenosis) and 2.5mm (60% stenosis), respectively. For asymmetric plaque layer, the ratio between the maximum and the minimum thickness was chosen to be 7:3 and 9:1, respectively. The plaque layer was meshed into around 25000 brick elements with reduced integration.

Elastic-plastic material properties were assigned for the stent material Co-Cr alloy L605. The balloon was modelled as a linear elastic material. The arterial layers and the stenotic plaque were all simulated using the Ogden hyperelastic model. The ends of the artery and the balloon were fully constrained to remove rigid body motion. The pressure applied on the inner surface of the balloon was linearly increased (up to 1.4MPa) during inflation and decreased to zero during deflation. Hard contacts were defined between the artery, the stent and the balloon.

Results: Results showed that it was more difficult to open arteries with severe stenosis via the expansion of stent. The diameter achieved at the maximum expansion for arteries with 40%, 50% and 60% stenosis was 4.2mm, 4.1mm and 3.7mm, respectively. Also, both the recoiling and dogboning effects increased with the increased level of stenosis. Almost twice higher stress was obtained on the stenotic plaque when the stenosis was increased from 40% to 60%, indicating a potential for plaque rupture.

The asymmetry of plaque did not affect the overall stent expansion and recoiling effect, but the stresses in the plaque-artery system increased for asymmetric plaque. For the plaque, the maximum stress was 2.27Mpa in the symmetric case and 2.58MPa in the asymmetric case (ratio 9:1) (Figure 1a and b). For the artery, the stress was 0.08MPa in the case of

symmetric plaque and 2.26MPa when the plaque layer had an asymmetric ratio of 9:1 (Figure 1c and d) localised in the regions with relatively thin layer of plaque as a result of overstretch.

For curved arteries, stent expansion became non-uniform in the circumferential direction, which was also the case for development of dogboning. For a curved artery, the diameter change against pressure did not have a sustained period of expansion as that for straight arteries. However, results confirmed that the levels of stress developed in the plaque and arterial layers were comparable for stent deployment in curved and straight arteries.

Figure:
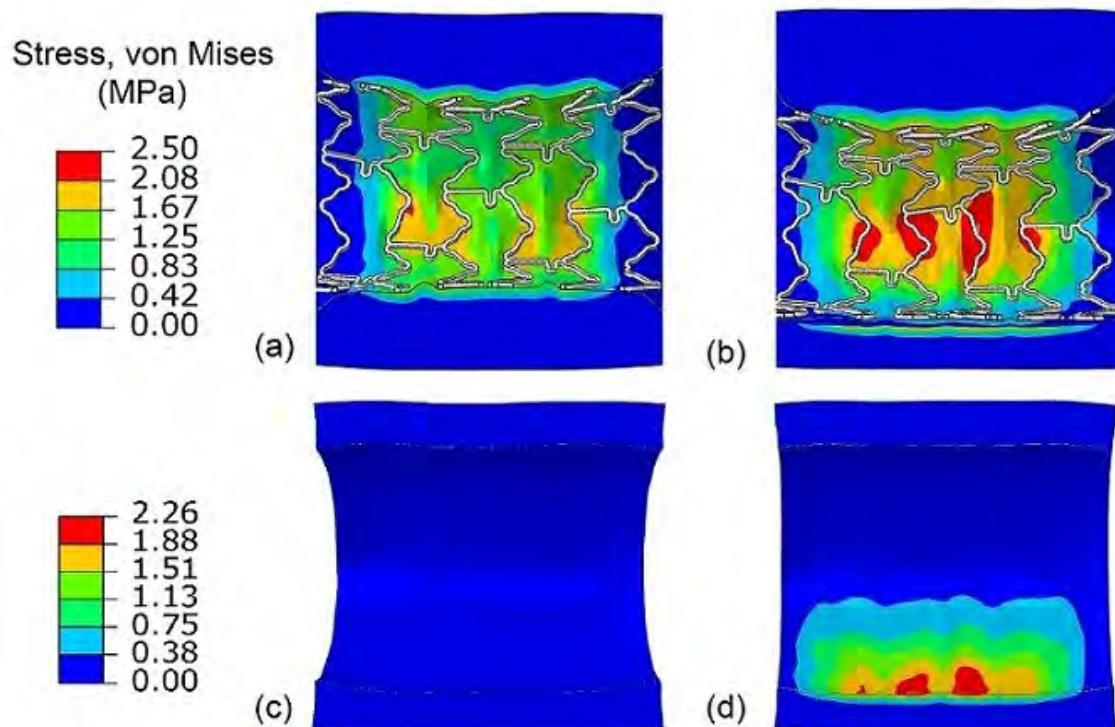
Caption: Figure 1. Contour plot of stress on (a) symmetric stenotic plaque, (b) asymmetric (ratio 9:1) plaque, (c) arterial wall with symmetric plaque and (d) arterial wall with asymmetric plaque (ratio 9:1).

Conclusion: This study suggests that future stent designs may need to be patient specific with expansion that can be tuned circumferentially according to the thickness of plaque layer. This will help protect the arterial layers from being overstretched and damaged by stenting, which is potentially associated with chest pain.

References: [1] Ormiston et al., Circ Cardiovasc Imaging 2: 255-260, 2009.

[2] Javaid et al., 2006, Am J Cardiol 98: 911-914, 2006.

[3] Yıldız et al., Health 5: 1-5, 2013.

[4] Johnston et al., J Vasc Surg 2: 70-73, 2014.

Disclosure of Interest: None Declared

AS-0137

FREEWARE IS A VIABLE ALTERNATIVE TO COMMERCIAL SOFTWARE WHEN CREATING SUBJECT-SPECIFIC FE MODEL GEOMETRY

Jennifer L. Boyd [1,*]Cameron Brown [1]Andrew Price [1]

[1]Nuffield Department of Orthopaedics, Rheumatology and Musculoskeletal Sciences, University of Oxford, Oxford, United Kingdom

Introduction and Objectives: Subject-specific finite element (FE) models are gaining popularity within personalized medicine. These models represent a specific individual and situation, and offer the possibility of simulating variations of treatments before selecting the optimal procedure for the individual. Subject-specific geometry is crucial to subject-specific models; using idealized geometries overestimates contact areas and underestimates stresses [1].

Subject-specific geometry is derived from medical scans. Geometry structures are segmented based on voxel grayscale values. Then any gaps or spikes in segmented surfaces are smoothed. Finally, structures are assembled into the FE model geometry. Commercial software provides efficient yet costly purpose-specific segmentation and smoothing workflows. Multiple freeware alternatives are also available. The objective of this study was to create subject-specific geometry using both commercial and free software. We then compared the volumes of the commercial and freeware segmented geometries and of the commercial and freeware smoothed geometries.

Methods: A 3T MRI scan (T1-weighted, sagittal-sliced, resolution=0.230mm^3) was taken of a healthy male's knee (47yrs, 108kg). Nine structures [bones (femur, tibia, patella), cartilage (femoral, medial tibial, lateral tibial, patellar), and menisci (medial and lateral)] were segmented using both commercial software (Mimics 14.01, Materalise, Leuven, Belgium) and freeware (ITK-SNAP 2.4.0, Cognitica Corporation and National Library of Medicine, USA). The 2D slice segmentations were combined to create 3D surfaces. Each structure's volume (including voxels internal to the surface) was calculated. The nine commercial and nine freeware segmentation volumes were compared.

Each structure was then smoothed. Commercial segmentations were smoothed using commercial software (Geomagic Studio 11, Geomagic, Inc., Research Triangle Park, NC, USA); freeware segmentations were smoothed using freeware (Blender 2.68a, Stichting Blender Foundation, Amsterdam, The Netherlands). The volume of each smoothed structure was calculated. The nine commercial and nine freeware smoothed volumes were compared.

The smoothed structures were then assembled into the FE model geometries (SolidWorks 2010, Dassault Systèmes SolidWorks Corp., Concord, MA, USA; Academic License cost $150/£100). Structures were automatically imported based on the original MRI scan coordinates. Therefore, structure orientations and positions matched those in the MRI scan. The knee assemblies created using commercial and free software were visually compared.

Results: Volumes of the nine structures segmented using commercial and freeware differed by 3.0% ± 3.7%. Commercial and freeware smoothed volumes differed by 7.1% ± 10.3%. Both segmented and smoothed structures tended to have slightly larger volumes when created using commercial software. This trend was at least partially explained by different segmentation and smoothing strategies used in the commercial and free software.

During segmentation, the user identifies pixels which represent a specific structure; the pixels are then used to define the structure boundaries. Therefore, structure boundaries will not be smooth, but stepped, due to the pixels. The commercial software used in this study artificially added material to avoid excessively-stepped surfaces, whereas the freeware used in this study did not add material. The material added by the commercial software led to larger volumes.

The larger commercial volumes persisted after smoothing. The commercial software automatically smoothed the structures, only removing volume in areas with geometric spikes. The freeware did not automatically remove spikes; the entire surface of each structure had to be smoothed to remove any potential spikes. Therefore, areas without spikes were also smoothed, resulting in smaller freeware volumes.

Visually comparing the knee assemblies showed that the gross morphologies of the commercial and freeware geometries were similar, with the details of the freeware geometry appearing smoother. There were some differences between the two assemblies: patellar cartilage (yellow) extended further distally and the anterior medial meniscus (red) was thinner when freeware was used. These differences were user-dependent and reflect the subjective nature of segmentation/smoothing, rather than systematic differences in software choice.

Figure:
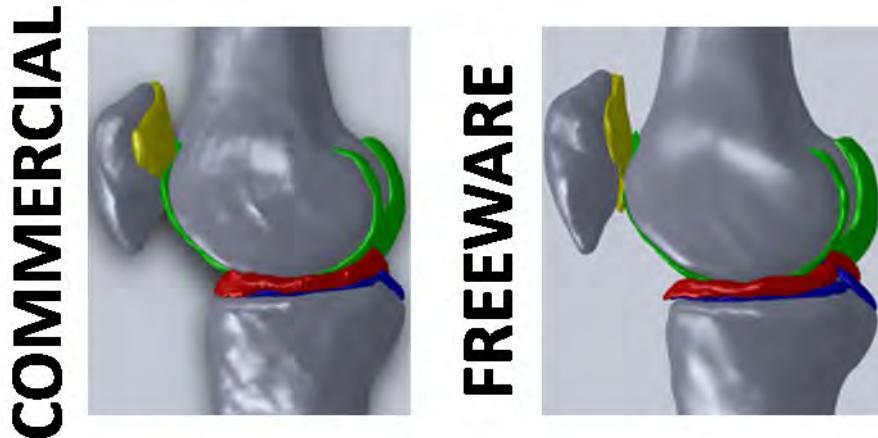
Caption: Geometry created using (left) commercial and (right) free software.

Conclusion: Both commercial and free software were capable of creating morphologically similar subject-specific geometry. Therefore, we conclude that freeware provides a viable alternative to commercial software. We do not think one is "better" than the other. Users should understand the trends associated with using either commercial or free software. Freeware structures tended to be smoother with less volume; users must be careful to avoid over-smoothing surfaces.

References: [1] Anderson et al., J. Biomech., 43: 1351-57, 2010.

Disclosure of Interest: None Declared

Feet and Footwear

AS-0139

THE RELATION BETWEEN CLINICAL DIAGNOSED MECHANICALLY INDUCED METATARSALGIA, INCREASED PLANTAR PRESSURE, AND REACTION FORCES AT THE FOREFOOT.

Katrin Schweizer [1,*]Sebastian Krapf [1]Jacqueline Romkes [1]Marie Freslier [1]Christian Wyss [1]

[1]Laboratory of Movement Analysis, University Children's Hospital, Basel, Switzerland

Introduction and Objectives: Metatarsalgia is defined as forefoot pain beneath the second, third, and fourth metatarsal heads [1]. Diseases, such as rheumatoid arthritis or neuralgia, but also altered forefoot biomechanics can cause metatarsalgia [2]. *Mechanically induced metatarsalgia* is a common medical diagnosis based on a clinical examination. The logical treatment approach is to reduce the mechanical forefoot load, either with orthotic devices or by surgery. However, these treatments can be expensive and often do not successfully relieve the pain [3]. The unsatisfactory treatment outcomes of patients with metatarsalgia lead to our research question: Can clinical examination diagnose a biomechanical overload beneath the forefoot?

A mechanical forefoot correction is only appropriate if there actually exists a biomechanical overload of the forefoot. Therefore, the main research objective was to evaluate the sensitivity and specificity of the clinical examination to diagnose mechanically induced metatarsalgia beneath the second metatarsal head. This was done by comparing the clinical diagnosis to the peak plantar pressure and the estimated reaction forces beneath the second metatarsal head.

Methods: Plantar pressure data of 340 subjects diagnosed with mechanically induced metatarsalgia beneath the second metatarsal head and 207 subjects without metatarsalgia were retrospectively compared. All subjects were examined by one experienced clinician. Plantar pressure of the second step was measured when walking over a pressure platform (EMED SF, Novel, Munich) at floor level. Five trials per subject were averaged and analysed.

The peak pressure beneath the second metatarsal head was calculated for each step using MATLAB. The estimated reaction forces at the second metatarsal head were calculated for each foot with the modified [4] inverse dynamics model of Jacob et al. [5]. Thresholds for normal pressure and reaction force values were derived by confidence interval of the subjects without metatarsalgia.

To compare the clinical examination with the peak pressure and the reaction forces, the sensitivity, specificity, positive and negative likelihood ratios together with the associated 95% confidence intervals (CI) were calculated from contingency Tables 1a and 1b.

Results: The sensitivity (true positive rate), meaning that metatarsalgia was diagnosed and the pressure is increased, was 65.5 % (CI: 58.5 % - 72.0 %). The specificity (true negative rate); hence, the probability that no metatarsalgia was diagnosed when the pressure is normal was 39.8 % (CI: 34.6 % - 45.2 %). The positive likelihood ratio was 1.09 (CI: 0.95-1.24), the negative likelihood ratio 0.87 (CI: 0.69-1.09).

Compared to the reaction force at the second metatarsal head the sensitivity of the clinical examination was 67.3 % (CI: 60.7 % - 73.3 %). The specificity reached 41.4 % (CI: 36.0 % - 47.0 %). The positive likelihood ratio was 1.15 (CI: 1.01 - 1.31) and the negative likelihood ratio 0.79 (CI: 0.63 - 0.99).

Figure:

A		Peak plantar pressure		
		+ increased	**-** normal	**N**
Clinical diagnosis	**+** Metatarsalgia	133	207	340
	- No metatarsalgia	70	137	207

B		Reaction force		
		+ increased	**-** normal	**N**
Clinical diagnosis	**+** Metatarsalgia	152	188	340
	- No metatarsalgia	74	133	207

Caption: Table 1: Contingency tables of diagnosis: (a) peak plantar pressure at second metatarsal head vs. clinical diagnosis and (b) reaction forces vs. clinical diagnosis.

Conclusion: Our sensitivity values indicate that clinicians diagnose a mechanically induced metatarsalgia beneath the second metatarsal head in less than 68 % correctly. Even worse, in less than 42 % (specificity) they can correctly declare a subject for healthy considering the forefoot loading. The positive likelihood ratios were below 2 where above 10 is considered a good value [6]. Our negative likelihood ratios of above 0.75 were too high, as values below 0.1 are considered as good [6]. Consequently, it is hardly possible to correctly diagnose a mechanically induced metatarsalgia by clinical examination. We conclude that biomechanical measurements, such as plantar pressure or estimated reaction forces at the forefoot can reduce the number of wrongly treated patients, especially when a metatarsalgia is accompanied by a missing mechanical overload. In this sense the benefit of the biomechanical measurements is the false-positive detection because these patients are unlikely to benefit from any orthotic or surgical treatment to unload the forefoot.

References: [1] Schuh et al., Foot & Ankle Clinics, 16: 583-595, 2011.

[2] Feibel et al., Foot & Ankle Clinics, 6: 473–789, 2001.

[3] Goodman, Southern Medical J, 97: 867-870, 2004.

[4] Wyss, Clinical Biomechanics, 20: S41–S42, 2005.

[5] Jacob et al., Clinical Biomechanics, 16: 783-792, 2001.

[6] Fargan, N Engl J Med, 293: 257-261, 1975.

Disclosure of Interest: None Declared

Feet and Footwear

AS-0140

DO STATIC FOOT MEASURES PREDICT MEDIAL LONGITUDINAL ARCH MOTION DURING RUNNING?

Ben Langley [1,*]Mary Cramp [2]Stewart Morrison [1]

[1]School of Health, Sport and Bioscience, University of East London, London, [2]Centre of Health and Clinical Research, University of the West of England, Bristol, United Kingdom

Introduction and Objectives: Static assessment of the structural alignment and/or characteristics of the foot are commonly advocated by running shoe manufacturers and retailers to classify the foot, with a view to recommending the appropriate type of running shoe. Despite this, the extent to which static measures predict dynamic foot motion during running is unsubstantiated, with findings from previous research producing conflicting results [1, 2, 3]. The purpose of this work was to determine whether static foot assessment could predict medial longitudinal arch (MLA) motion during running.

Methods: Fifteen physically active males (27 ± 5 years, 1.77 ± 0.04m, 80 ± 10kg) participated in the study. Foot Posture Index (FPI-6), MLA and rearfoot angles were measured in a relaxed standing position. Static MLA and rearfoot angles, and dynamic MLA motion were calculated from the position of retro-reflective markers tracked by a VICON motion analysis system. Markers were attached to the medial malleolus, navicular tuberosity and the first metatarsal head in order to calculate the MLA angle and to the base of the calcaneus, the Achilles tendon attachment, the centre of the Achilles tendon at the height of the medial malleoli and the centre of the posterior aspect of the shank to calculate the rearfoot angle. Participants ran barefoot on a treadmill at a self-selected pace (2.8 ± 0.5m.s^{-1}) during dynamic trials. Bivariate linear regression was used to determine whether the static foot classification measures predicted MLA range of motion (ROM) and MLA angles at initial contact (IC), midsupport (MS) and toe off (TO).

Results: All three foot classification measures were significant predictors of MLA angle at IC, MS and TO ($p < .05$) explaining 40-91% of the variance (Table 1). None of the static foot classification measures were significant predictors of the range of MLA motion during the stance phase of running (Table 1).

Conclusion: The findings of this study revealed that all selected static classification measures were significant predictors of MLA angles at discrete time points within the running gait cycle. Static MLA angle explained the greatest amount of variance in dynamic MLA angles at discrete time points within the running gait cycle, accounting for 91%, 87% and 84% of the difference in MLA angles at IC, MS and TO respectively. However, the importance of being able to predict MLA angles at discrete time points is questionable, as angles at discrete time points provide only limited information as to the dynamic functioning of the foot. In contrast, MLA ROM during the stance phase of running gait gives an indication as to the dynamic flexibility and function of the foot, which have theoretical links to the development running related injuries [4, 5]. The absence of a significant relationship ($p > .05$) between the foot classification measures and MLA ROM during running has implications for both clinicians and the running community, specifically running shoe retailers, who commonly use static foot classification measures to recommend running shoes.

The findings from this work suggest that static foot classification measures do not predict MLA motion during running. This finding lends support to the view that static foot assessment may not be an appropriate approach to classify the foot with a view to recommending footwear interventions designed to reduce injury risk.

Table:

| | Dynamic MLA motion | | | |
	ROM	IC	Midsupport	TO
FPI-6	-.03	-.68*	-.76**	-.73**
MLA angle	.07	.95***	.93***	.92***
Rearfoot angle	-.46	.68*	.76**	.64*

* *p* < .05   ** *p* < .005   *** *p* < .001

Caption: Table 1. Coefficient of determination (r) for static foot classification measures and aspects of dynamic MLA motion throughout the stance phase of the running gait cycle

References: [1] Nachbauer et al,. Med Sci Sports Exerc. 24: 1264-9 1992.

[2] McPoil et al., J Am Podiatr Med Assoc. 97: 102-7, 2007.

[3] Lee et al., J Athl Train.47: 83-90, 2012.

[4] Williams et al., Clin Biomech. 16: 341-7, 2001.

[5] Asplund et al., The Phys Sportsmed. 33: 17-24, 2005.

AS-0141

INTRA-ARTICULAR PRESSURE DISTRIBUTION IN THE NATIVE AND PROSTHETIC ANKLE JOINT

Tassos Natsakis [1,*] Josefien Burg [2] Greta Dereymaeker [1] Jos Vander Sloten [1] Ilse Jonkers [2]

[1]Biomechanics section, [2]Faculty of Kinesiology and Rehabilitation Science, KU Leuven, Leuven, Belgium

Introduction and Objectives: Ankle osteoarthritis (OA) is a joint degenerative disease with high impact on quality of life. As ankle OA is often of post-traumatic nature, its onset has been linked to aberrant joint loading. When reaching end-stage (i.e. considerable lack of joint mobility, pain), the treatment options for ankle OA are limited to surgical interventions, such as Total Ankle Arthroplasty (TAA), which restores the mobility of the joint. However, TAA is associated with high failure rates, often related with bone resorption and cyst formation in the bone-implant interface or mechanical failure of one of the prosthetic components. To further investigate the link between joint loading and the development of OA, as well as the success of TAA, we quantified the topology joint loading conditions in the native ankle and TAA joint during gait.

Methods: Gait simulations were performed on 8 cadaveric foot specimens, amputated mid-tibially, by imposing tibial kinematics and applying muscle forces on nine tendons [1,2]. Intra-articular pressure distribution was measured with a Tekscan #5033 sensor (Tekscan Inc, Boston, MA) at 100 Hz in the ankle joint of the specimens before and after implantation of a Hintegra three component TAA (New Deal, Lyon, France). The peak pressure was calculated for five intervals of stance phase and six regions of the ankle joint. We tested for statistical significant differences between the native ankle and TAA joint with a non-parametric rank sum test (Wilcoxon) for each interval and region. The test was performed both for each specimen separately and for all the specimens grouped to differentiate individual and group response. Statistical significance was reported for $p \leq 0.05$

Results: For the native ankle, the highest peak pressures were measured in the anterior and medial regions of the joint. The maximum observed median pressure was 1.1 MPa and it occurred between 21%>40% of stance phase. For the TAA joint, the highest peak pressures were measured in the central and medial regions with the maximum observed median pressure being 5.11 MPa between 81%>100%. For most regions and stance phase intervals, significant increase in peak pressure was detected in five out of eight specimens, with only one specimen in most cases showing a significant decrease. No significant increase was detected for the grouped comparison in any interval or region, except for the anterior and medial region between 41%>60% (1.99 MPa increase, p=0.038) and posterior and lateral region between 41%>60% (0.29 MPa increase, p=0.05) and 61%>80% (0.31 MPa increase, p=0.05).

Figure:
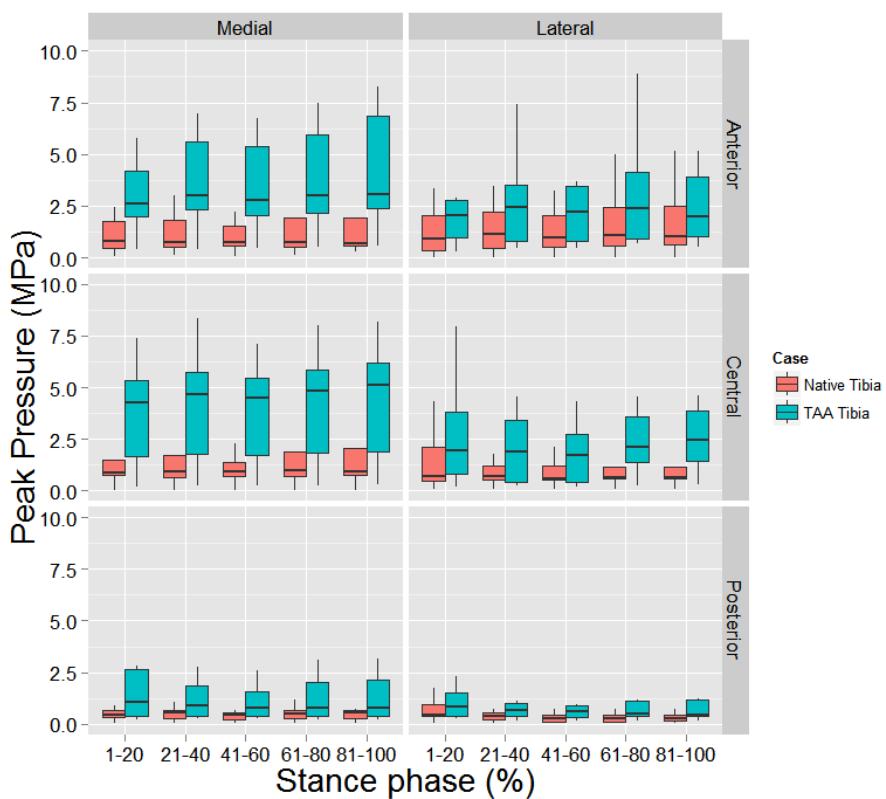
Caption: Peak pressure distribution on the tibial articular surface before (red) and after (blue) TAA implantation. The peak pressure for six areas of the tibial articular surface is visible for five intervals of stance phase.

Conclusion: The regions that are more loaded in the ankle joint are coinciding with the regions that are often reported in literature with higher incidence of ankle OA [3]. This further supports the hypothesis that high joint loading and OA onset may be linked. Furthermore, a non-physiologic increase in joint loading is present in the joint after implantation of TAA, which might have a negative impact on the mechanobiology and bone growth of the distal tibia. This increase is significant in five out of eight specimens, however not significant for the group average; this indicates that even though the increase is significant in individual specimens, the amount of increase is not consistent.

References: [1] Peeters et al. J. Eng. Med. 9; 955-967,2013

[2] Natsakis et al. J. Biomech., 2014 (in print)

[3] Koepp et al. J. Orthop. Sci., 4, 407-412, 1999

Disclosure of Interest: None Declared

Feet and Footwear

AS-0142

CHANGES IN FOOT TEMPERATURE AS A FUNCTION OF WALKING SPEED

Prabhav Nadipi Reddy [1,*]Rhoda Sulaimon [2]Glen Cooper [1]Andrew Weightman [3]Emma Hodson-Tole [2]Neil Reeves [2]

[1]Engineering, [2]Healthcare Science, Manchester Metropolitan University, [3]School of Mechanical, Aerospace and Civil Engineering, University of Manchester, Manchester, United Kingdom

Introduction and Objectives: Foot ulcers are a major concern for diabetic people. It has been shown that a difference of 2^0C or more between the same locations on the contralateral feet indicate a risk of ulceration in the foot with the higher temperature[1]. The mechanisms of this temperature rise are unknown. The first step to evaluating the role of temperature in ulceration is to understand the fundamental physiology of foot temperature changes with loading and walking. To this end, we studied the temperature of the feet of healthy human participants as they walked on a motorised treadmill at three different speeds.

Methods: 14 participants (21-40 years;13 male), without diabetes, foot problems or loss of sensation were recruited for the study. To record temperatures of the feet as participants walked we made insoles embedded with temperature sensors TMP35 (Analog Devices) at four locations: hallux, between the first two metatarsal heads, the lateral side of the foot, and the heel. The insoles were placed in standard 'Darco' shoes with the wiring from each sensor located under the insole to the lateral side of the foot. Temperature data were stored on a USB memory stick using the analog input channels of two myRIOs (National Instruments) – a reconfigurable input-output device – which digitised (12 bit resolution) and stored the data. We also recorded acceleration from an on-board (the myRIO) 3-axis accelerometer. All data were synchronously recorded at a sample rate of 100 Hz. During the experiment, the participants removed their shoes and rested with legs stretched out for 10 minutes, to ensure that the feet returned to their resting state. After the rest, temperature sensors were put on the feet and the subjects were asked to sit for 5 minutes followed by 10 minutes of standing. The subjects then walked on the treadmill at a fixed speed for 40 minutes. After walking, there was 15 minutes sitting while the temperature recording continued. It was intended that each participant walked on the treadmill three times at different speeds: 0.8 m/s, 1.2 m/s and 1.6 m/s. The order in which the participants walked at different speeds were randomized. For logistical reasons, not all participants walked all the speeds. Five participants walked all the three speeds. In total, the temperatures were recorded on 27 occasions.

Results: Fig. 1 shows the mean (over all participants) temperature rise profiles of the right foot while walking. The mean temperature rise over the duration of the walk are given in Table 1. We performed a factorial 3x4x2 ANOVA with speed, location of the foot and the two feet -right and left. It showed a significant main effect of speed on the temperature rise with walking, $F_{(2,190)}=3.75$, $p=0.025$. There is a mild effect of location, $F_{(3,1279)}=1.69$,$p=0.169$ and no effect of the foot, $F_{(1,1279)}=0.937$,$p=0.749$. The interaction between location and speed was not significant, $F_{(6,1279)}=0.35$,$p=0.912$. The temperatures of the foot were lowest for the medium speed and highest for the maximum speed (Min-Med: $p=0.04$,CI–[0.04,1.38]; Min-Max: $p=0.02$,CI–[-2.16,0.15]; Max-Med: $p=0.002$,CI–[0.8,3.17]). We found that the temperature of the metatarsal head was significantly higher than the other locations (Met head-Hallux: $p=0.0002$,CI–[0.61, 1.0]; Met Head-Lateral Side: $p<0.0001$,CI–[0.66, 1.4]; Met Head-Heel: $p=0.0016$,CI–[0.38, 1.52]).

Figure:
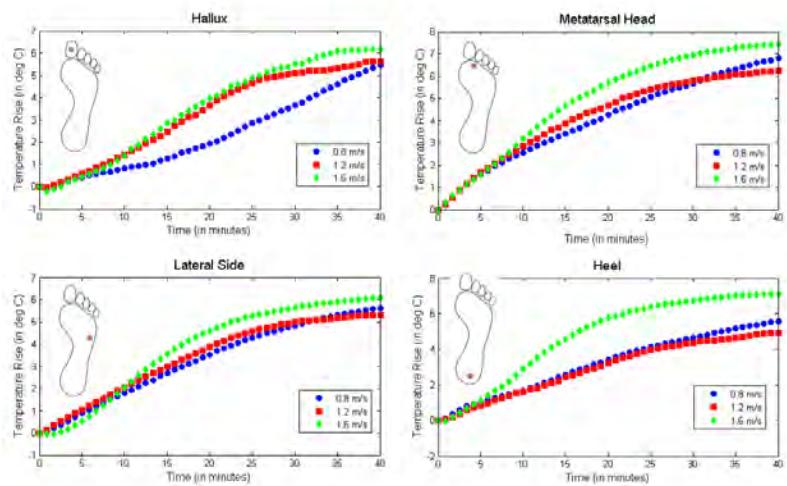
Caption: Mean temperature rise curves during walking for different speeds and locations of the foot.

Conclusion: It is clear from our data that foot temperature increases as people walk. The temperature rise increases with increasing speed. The deviations from this trend may be due to the variations in the pressure-time integrals at different speeds. Temperature change also depended on the location of the foot, and likely reflects differences in loading at the locations. We are currently doing experiments to investigate these phenomena.

Since we sampled temperature from four different sites on the foot, we were able to identify some issues with two of the sensor sites that could be addressed by future changes to the measurement approach. Specifically, we found that the sensor under the hallux was not always touching the plantar tissue due to variations in foot size between participants. In addition, we found that in some cases the foot lifted off the sensors during walking.

Our study gives baseline data that we can use to inform our fundamental understanding of the mechanism(s) behind the rise in foot temperature as we move towards measurements in diabetics. We hope that this will help us to better understand the onset of diabetic foot ulceration.

Table:

	Hallux	Metatarsal Head	Lateral Side	Heel
0.8 m/s	2.01 ± 1.51	3.55 ± 1.36	3.16 ± 0.99	3.01 ± 0.89
1.2 m/s	2.80 ± 2.02	3.74 ± 1.43	3.14 ± 0.97	2.69 ± 1.29
1.6 m/s	3.12 ± 2.16	4.55 ± 1.39	3.70 ± 1.19	4.23 ± 2.50

Caption: Temperature rise (in 0C) while walking (mean ± standard deviation; N=18 for each value)

References: [1] Houghton et al., J Foot Ankle Res, 6:1-13, 2013.

Disclosure of Interest: None Declared

Feet and Footwear

AS-0143

TEST AND RE-TEST RELIABILITY OF ANKLE AND KNEE KINEMATIC VARIABLES DURING RUNNING

Andrea N. Onodera [1] [2],*Ana Paula Ribeiro [3]Licia Cacciari [1]Maria Isabel Roveri [1]Isabel C N Sacco [1]

[1]Physical Therapy, Speech and Occupational Therapy Dept. School of Medicine, University of São Paulo, São Paulo, [2]Dass Nordeste Calçados e Artigos Esportivos Inc, Ivoti, [3]Universidade de Santo Amaro, Universidade de Santo Amaro - Campus I, São Paulo, Brazil

Introduction and Objectives: The Brazilian National Standards Organization[1] establishes 20 steps for determining the footwear pronation rate during walking and running.The data acquisition of 20 trials could imply discomfort for runners and more expenses for employees performing the biomechanical tests, especially for footwear studies in which two or more shoe models are compared in the same experiment.In addition, the number of analyzed trials has been considered of great importance for the reliability of locomotion measurements [2]. Some studies report 5 trials to assure good reliability of knee and ankle kinematics during running [3, 4, 5], however Ferber et al [3] and Diss [4] only analyzed Intraclass Correlation Coefficients (ICC) for 5 trials and Sinclair et al [5] analyzed the ICC and Standard Error of Measurements (SEM) for 5 trials.The ICC can provide the consistency between trials, while SEM quantifies the precision of scores in the test to define the ideal number of trials for the experiment.Therefore, the purpose of this study is to quantify the reliability of 12 kinematic variables using ICC and SEM across 18 trials, intending to optimize the biomechanical test protocols, yet assuring high confidence levels.

Methods: Ten healthy runners (39.0±9.3 yrs old, 70.0±6.1 kg, 170±6 cm) with rearfoot strike pattern ran over a 25 meters walkway in constant and natural velocity (2.64 to 2.92 m/s). All runners used the same commercially available sport shoe construction for the test. Eighteen valid trials were collected and the kinematics measured by 6 IR cameras at 300 Hz (VICON T-40, Oxford, UK). Sixteen reflexive markers (14 mm Ø) were attached according to Plug'n Gait marker set (Nexus, VICON) and sagittal knee and ankle angles and frontal ankle angles were analyzed. The right leg data was filtered at 12Hz using a Butterworth 4th order zero-lag filter. Reliability tests were performed, after confirming that the data was normally distributed (Kolmogorov-smirnov), for 2 to 18 trials by intraclass correlation coefficients (ICC(1,1) = (MSb-MSw)/(MSb + (k-1)MSw)) and Standard Error of Measurements (SEM = SD$\sqrt{1-ICC}$). The means and standard deviations between subjects for all trials.

Results: For the knee kinematics in the sagittal plane, 3 to 4 trials are enough to get the best reliability and low SEM. For ankle kinematics in the frontal and sagittal planes, 6 trials result in a good reliability for ICC score and low SEMs. The only exception was the ankle extension during the toe-off, which did not achieve the acceptable classification even in the best ICC score. The ICC score should be carefully interpreted since the variability between subjects can interfere in the results. The ICC is very sensible to between-subjects variability [6]. That is why the SEM is also analyzed in these cases. The interpretation of SEM centers on the assessment of reliability within individual subjects and it is in the same units as the measurements of interest. The ankle extension during the toe-off had poor ICC score and also a high SEM probably because the take off can be performed with more or less ankle extension and is extremely variable among subjects. Our study shows that for all kinematic variables analyzed, more than 10 trials resulted in lower ICC and higher SEM. The

number of trials used for other authors [3,4,5] are better than the recommended by the Brazilian National Standards Organization, however, 6 trials for ankle kinematics and 4 trials for knee sagittal kinematics seems better than 5. The data acquisition of 20 trials would be a waste of experiment time and also would reduce the data consistency, probably explained by the increased chance of error.

Figure:
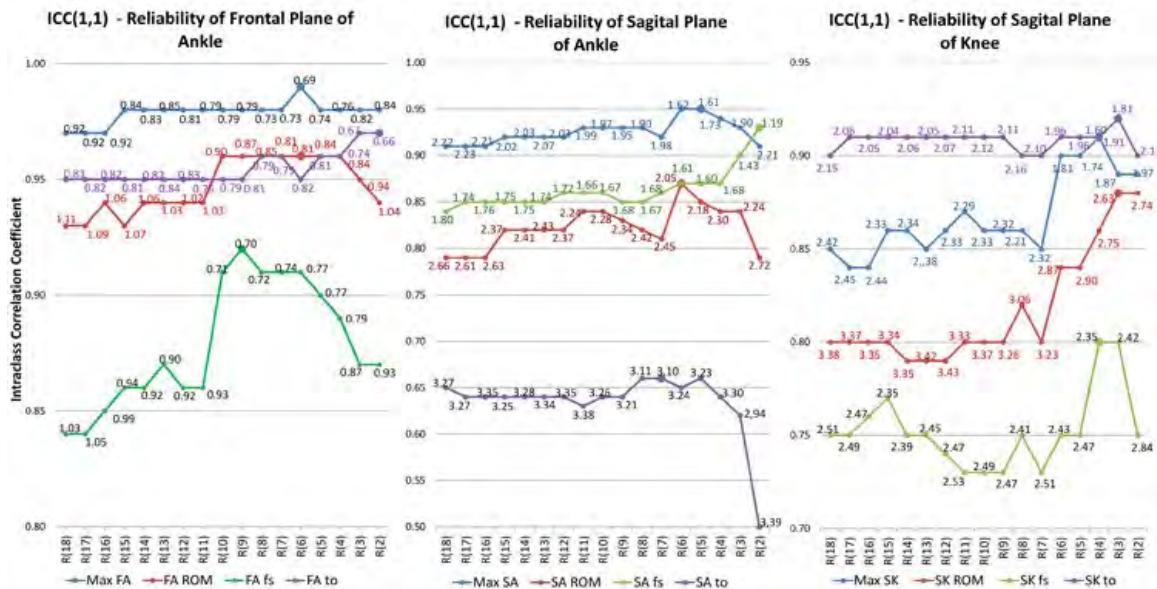
Caption: Ilustration of Intraclass correlation coefficient (lines) and Standard Error of Measurement (numbers above or under each mark) of ankle and knee kinematic parameters during 2 to 18 trials.

Conclusion: Six trials guarantee good reliability for almost all variables when analyzing ankle sagittal and frontal plane kinematics during running. For the sagittal plane of knee, four trials are necessary for a good reliability.

Table:

Variables	Mean	SD
Maximum Knee Flexion (º) – Max SK	49.9	6.0
Sagital Knee ROM (º) – SK ROM	31.6	7.1
Knee Flexion @ Footstrike (º) – SK fs	18.2	4.5
Knee Flexion @ Toe-off (º) – SK to	16.9	6.7

Maximum Ankle Flexion (º) – Max SA	36.4	7.4
Sagital Ankle ROM (º) – SA ROM	19.1	5.3
Ankle Flexion @ Footstrike (º) – SA fs	17.3	4.4
Ankle Flexion @ Toe-off (º) – SA to	0.6	4.6
Maximum Ankle Eversion (º) – Max FA	9.5	5.9
Frontal Ankle ROM (º) – FA ROM	9.1	4.3
Ankle Inversion @ Footstrike (º) – FA fs	-0.3	2.5
Ankle Inversion @ Toe-off (º) – FA to	-0.6	3.7

Caption: Means and standard deviations of all variables for 18 trials.

References:

[1] ABNT, NBR14839, 2011.

[2] McGinley JL et al., Gait Posture 29: 360-9, 2009.

[3] Ferber R et al., J Orthop Res 20: 1139-45, 2002.

[4] Diss CE, Gait Posture 14: 98-103, 2001.

[5] Sinclair J et al., Gait Posture 40: 707-11, 2014.

[6] Wier JP, J Strength Cond Res 19(1): 231-40, 2005.

Disclosure of Interest: None Declared

AS-0144

USING FINITE ELEMENT ANALYSIS TO IMPROVE THE DESIGN OF SOCCER SHOES OUTSOLES

Michel Behr [1,*]Sylvain Blanchard [1]Maxime Llari [1]Yves Godio-Raboutet [1]Lionel Thollon [1]Jerome Palestri [2]Jean-Luc Guer [2]

[1]Laboratoire de Biomécanique Appliquée, IFSTTAR/Aix-Marseille Université, [2]Wizwedge SARL, Marseille, France

Introduction and Objectives: Soccer is the most popular sport in the world, and also one of those with a particularly high injury rate per hours of play [1]. The shoe itself is suspected to be often involved and sometimes even responsible for this high injury risk exposure [2]. Among the various possibilities, custom-made shoes was identified as one promising way to improve players protection [3]. The current study aims at using numerical simulation to improve shoe design procedures in order to reduce players exposure to the most frequent pathologies occuring in soccer, and explore the possible benefits of the custom-made shoes approach.

Methods: An parametric finite element model of the lower limb, derived form the LLMS model [4] was widely validated under quasi-static and dynamic loading conditions and afterwards coupled to a soccer shoe model. Particular attention was put on foot to shoe interactions and initial constraints. The shoe model includes an original outsole architecture offering the possibility to customize heel and footarch support geometry and materials according to each player characteristics.

A database of mechanical properties of 40 podiatric foams has also been build, by performing compression tests at 3 different energy levels and inverse analysis. Anti-vibration, shock-absorbing and propulsive properties of each tested foam were quantified by simulating hign energy impacts, in order to rate and classify each of these materials.

Finally, volunteer tests were performed on european first football leagues players in order to record plantar pressures and corresponding body kinematics in typical soccer movements such as jump landings or shootings. Recorded data would then define boundary conditions of these typical soccer movements, used as inputs for shoe structure and materials optimization. Optimization objectives were based on biomechanical criteria such as reduced vibrations and stress peaks at the major joints (see Figure 1).

Results: The characterization of foams revealed a great variety of visco-elastic behaviors. A classification of these foams into three groups (ie anti-shock, propelling and anti-vibration) could be proposed, with the most efficient materials identified in each of these groups. Optimization made it possible to achieve a combination of materials and define each layer thickness to reduce by up to 80 % vibrations transmitted to the bones and by 40 % the recorded peak stresses at joints.

Figure:
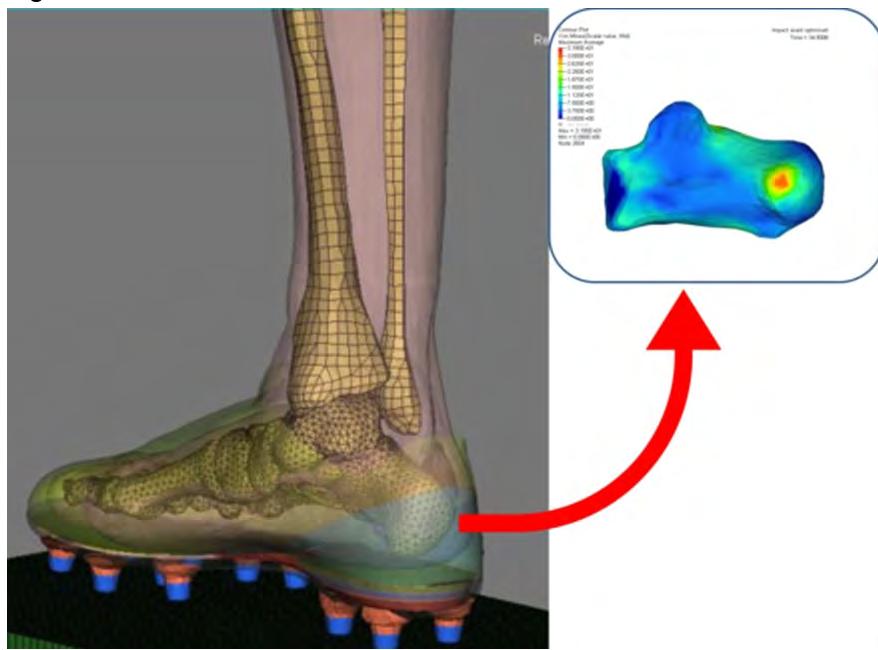
Caption: Figure 1. Example of jump landing simulation, and corresponding stress peak recorded on the calcaneus bone.

Conclusion: A modification of the outsole structure and materials significantly acts on the biomechanical response of lower limbs (and by extension on the entire human body). A significative improvement of lower limbs exposure to risk of injury can be considered from this type of approach.

References: [1] Olsen et al., Br J Sports Med. 38(1):89-94, 2004.

[2] Kinchington, ASPETAR sports medecine journal, 1:360-368, 2013.

[3] O'Connor et al. Foot Ankle Clin, 18 (2), 369-380, 2013.

[4] Behr et al., J Biomech Eng., 128(2):223-231, 2006.

Disclosure of Interest: None Declared

Motion Analysis

AS-0145

CROSS CUT BIOMECHANICS ARE AFFECTED TO A GREATER EXTENT WHEN PERFORMED IN AN UNANTICIPATED CONDITION COMPARED TO A FATIGUED CONDITION

Enda Whyte [1,*]Kieran Moran [1] [2]Chris Richter [1] [2] [3]

[1]School of Health and Human Performance, DCU, [2]Insight:Centre for Data Analytics, [3]Sports Medicine, Sports Surgery Clinic, Dublin, Ireland

Introduction and Objectives: Anterior cruciate ligament (ACL) are common in sports during landing, deceleration and cutting activities[1] particularly during the later stages of sporting activities[2]. This suggests that fatigue has a negative effect on lower limb biomechanics predisposing an athlete to injury. Further, many field sports produce relatively unanticipateable events, requiring participants to react with appropriate neuromuscular strategies[3]. This requires the integration of visual scanning and decision making with implementation of the appropriate neuromuscular strategy[4]. Non–contact ACL injuries tend to occur during sub-maximal activities in response to a sporting stimulus[1], suggesting that a chosen strategy may result in pathological loading.

Cutting activities are divided into side cutting where the participant plants one foot and cuts to the opposite side; and the cross cut where the participant plants one foot and cuts to the same side[5]. To the authors' knowledge, no studies have analysed the combined effect of fatigue and decision making on the biomechanics of the cross cut. Therefore, this study aims to examine the effects of fatigue and anticipation on the biomechanics of a cross cut.

Methods: Kinematic and kinetic data were recorded for 30 healthy, male intervarsity athletes during a cross cut in anticipated (ANT) and unanticipated (UNANT) conditions, before (PRE) and after (POST) an exercise protocol[6]. Participants jumped forward 70% of their maximum jump, landed on their dominant leg and performed a cross cut at 45º. This was employed to limit the variable effect of a 'free run' approach. In the ANT condition, a light indicated the direction of the cut five seconds prior to the task. For the UNANT, the light was triggered by breaking an infra-red light during the jump (approx. 139ms before ground contact).

The deceleration phase of the cross cut was analysed (initial contact to the first propulsive forces). Analysis of Characterising Phases detected differences between the conditions by generating scores from key phases (phases of variance) identified using principal components that captured >99% of the variance in the data[7]. A Repeated Measures ANOVA was performed and Cohen's D (d) was calculated to measure the effect of statistical differences (α = .05). Only significant findings of waveforms with a medium (d >.5) or large effect size (d >.8) are reported.

Results: PRE vs. POST analysis revealed multiple statistical differences without reaching a medium effect size. For the ANT vs. UNANT condition, key phases in knee and hip moments, and pelvic and thoracic angles were found to be significantly different (table 1) with the minimum of a medium effect size (d>0.5). A full list of examined key phases is illustrated in figure 1. Multiple significant effects of fatigue (ground reaction force, ankle moments, knee and hip angles and moments, and pelvic and thoracic angles) were observed, supporting previous studies examining the effects of fatigue during cutting movements[8]. However, none of these factors reached a medium effect size suggesting that fatigue has a relatively low effect on the biomechanics of a cross cut.

ANT vs. UNANT findings supported previous studies examining the effect of anticipation on biomechanics during cutting[8,9]. However, within the present study these had a small effect size (knee flexion, abduction and rotation angle, hip flexion and rotation angles). Anticipation had the greatest effect on proximal biomechanics with medium effect sizes at the knee and hip moments and pelvic angles and large effects sizes at the thoracic abduction angle supporting the association between trunk kinematics and ACL injury risk[10]. This has important implications for future studies on unanticipated cutting and ACL injury prevention programmes.

Figure:
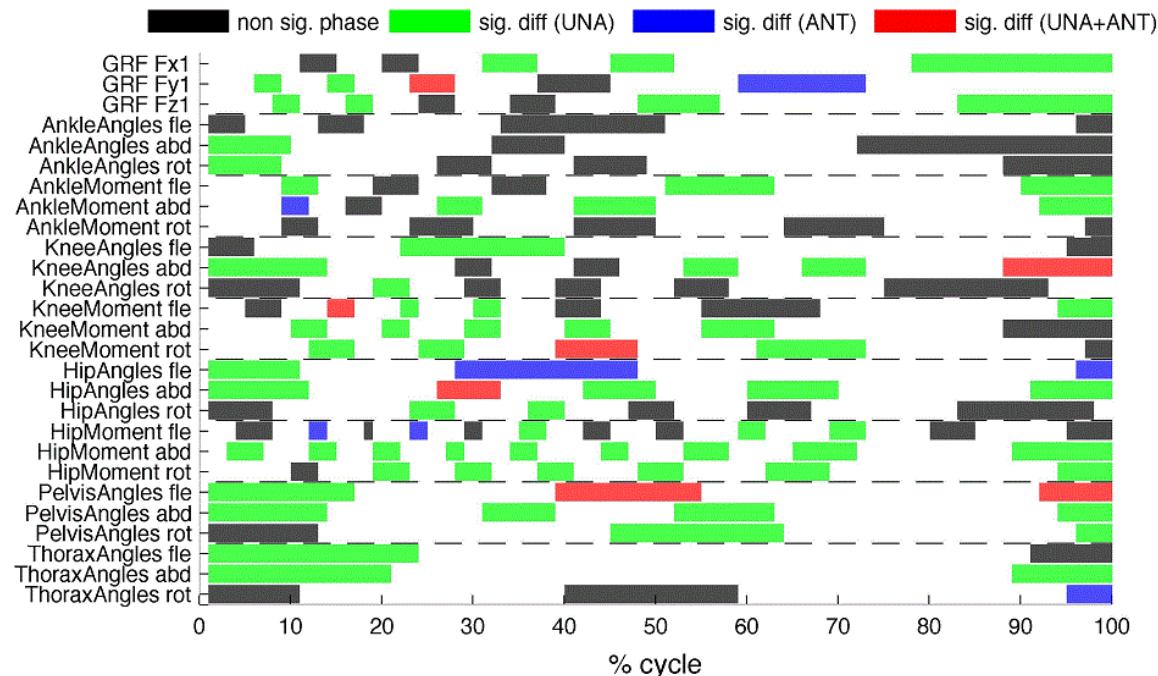
Caption: Figure 1: Key phases examined.

Conclusion: The current study demonstrate that fatigue and anticipation alter the biomechanics of a cross cut. The effects of anticipation have a much greater influence on proximal biomechanics in particular.

Table:

Variable	Key Phase	P value	Cohens D
Knee Abduction Moment	20-23 & 29-33	<.001	-.57-.55
Hip Abduction Moment	12-15, 19-22, 27-29, 44-47 & 53-58	<.001	-.52, -.83, -.63, -.74 & -.58
Hip Flexion Moment	35-38	<.001	.6

Hip Rotation Moment	19-23, 28-32, 37-41, 48-53 & 62-69	<.001	.54, .54, ,53, .6 & .54
Pelvis Flexion Angles	39-55	<.001	.55
Thorax Abduction Angles	1-21 & 89-100	<.001	-.96 & -.99

Caption: Table 1: Statistical significant differences

References: 1.Boden et al. *Am J Sports Med*. 2009;37(2):252-259

2.Gabbett TJ. *J Sports Sci*. 2004;22(5):409-417

3.Borotikar BS et al. *Clin Biomech*. 2008;23(1):81-92

4.Cortes N et al. *J Athl Train*. 2013;48(3):306-313

5.McLean SG et al. *Med Sci Sports Exerc*. 2009;41(8):1661-1672

6.Sheppard JM, Young WB. *J Sports Sci*. 2006;24(9):919-932

7.Kim JH et al. *Am J Sports Med*. 2014;42(8):1985-1992

8.Whyte EF et al. *J Sport Rehabil*. 2014. doi: 2014-020

9.Richter C et al.*J Biomech*. 2014;47(12):3012-3017

 10.Hewett TE et al. *Br J Sports Med*. 2009;43(6):417-422

Disclosure of Interest: None Declared

BIPEDAL LOCOMOTION OF THE JAPANESE MACAQUE: INTERACTIONS BETWEEN TRUNK, LEGS AND SELF-STABILITY.

Emanuel Andrada [1,*] Yefta Sutedja [2] Eishi Hirasaki [3] Reinhardt Blickhan [2] Naomichi Ogihara [4]

[1] Institute of Systematic Zoology and Evolutionary Biology, [2] Science of Motion, Friedrich-Schiller-University, Jena, Germany, [3] PRI, Kyoto University, Inuyama, [4] Department of Mechanical Engineering, Keio University, Yokohama, Japan

Introduction and Objectives: The adoption of bipedalism as preferred mode of terrestrial locomotion is a fundamental step in evolution of many species. Bipedalism evolved first about 230 million years ago in archosaurs, a group that includes both crocodilians and dinosaurs, being the most recent ancestors of modern bird species. A second evolution towards bipedalism occurred ca. 7 millon years ago in Africa, and marked the start of the divergence of the human lineage from that of other African apes. Interestingly, while the lineage of Theropoda leading to modern birds kept the pronograde (almost horizontal) body posture inherited from quadruped ancestors, early and actual humans adopted an erected trunk posture during bipedal locomotion. Despite trunk orientation, bipedal locomotion needs hip moments to balance the trunk. Controlling hip torque in a way that the ground reaction force points towards a point above the center of mass (CoM) termed Virtual Pivot Point (VPP) can help to stabilize the trunk [1-3]. Our recent investigations show that the balance of the trunk at a certain orientation influences the function of the effective leg (segment hip-foot contact; [3]). In small birds the effective leg, which works asymmetric like a parallel spring –damper, has an effect on balancing the trunk at one hand and stabilizes pronograde locomotion on the other hand. Interestingly, for pronograde posture the majority of the self-stable solutions are grounded running (a running gait without aerial phases, [3]). In the present study, we investigated the dynamics of the interaction between trunk and legs during the bipedal locomotion of a non-human quadrupedal primate, Japanese macaques (*Macaca fuscata*), as their facultative bipedalism may represent an intermediate state between the bird and human bipedal locomotion [4].

Methods: Two adult trained macaques locomoted bipedally on an instrumented walking track at self-chosen speed. The gait-lab setup in the Primate Research Institute at Inuyama (Japan) consisted of a 3D-forceplate (strain gage based; Kyowa Dengyo, EFP-S-1.5KNSA2), a wooden track to match floor height, and two video cameras (Canon, iVIS HF S21; res. 1920 X 1080 pxls, 60 half-frames/s; shutter: 1/200 s). The videos were stored as half frame .avi's and digitized manually using Winanalyse (Mikromac, Germany). The resulting data were further processed using custom Matlab® software. We computed VPP height, axial leg function, leg stiffness (k), leg damping (c), leg length at TD (l_0), and % of Congruity as shown in [3]. We simulated macaque locomotion with the bio-inspired Pronograde VPP model [3]. Model parameters were obtained from the experimental results and literature [5].

Results: Macaques locomoted bipedally with an erected trunk at speed ranging from 0.7 m/s to 1.1 m/s without aerial phases. They exhibited a left-skewed ground reaction force (GRF) profile, which is similar to those observed in bird grounded running. Accordingly, the values of the % of congruity were higher than 50, indicating bouncing-like mechanics (grounded running) during macaque locomotion. Intersections of GRF in a VPP point were not always as clear as observed for humans and birds. The calculated VPP height was in mean 0.28 m above the CoM. Similar to birds, the

effective leg function was asymmetric (leg length is longer than at touch-down than at toe-off, and protraction angle at TD was larger than retraction angle at TO). Thus a parallel spring-damper leg model was used to fit leg force. The results of the non-linear fit yielded to following mean values: leg stiffness k= 600 Nm^{-1}; leg damping c=20 Nsm^{-1}. When computing only leg stiffness from maximal force and mean leg contraction, the value was k_{sym}= 1500 Nm^{-1}.

In simulations, the PVPP model did not find stable solutions for trunk inclinations ranging from 5° to 50°. Still the model is able to balance the trunk and to locomote for more than 100 steps, but locomotion speed continuously increased even for larger damping values. Interestingly, with vertical trunk and spring-like legs, we found stable walking at speeds ranging from 0.7 to 0.8 ms^{-1}.

Figure:

Caption: Bipedal locomotion of the japaneese macaque and the PVPP model

Conclusion: Contrary to the results obtained for pronograde locomotion, grounded running is not self-stable for vertical or close to vertical trunk orientation. We conclude that rather than the upright locomotion per se, the important locomotion innovation characterizing the human lineage is likely to be the development of a less 'compliant' and more symmetric effective leg function, which enabled the exploration of self-stable walking domains.

References: [1] Maus et al., *Nature communications* 1, 70, 2010.

[2] Andrada et al., *J Exp Biol* 216, 3906-3916, 2013.

[3] Andrada et al., *Proc R Soc B* 281(1797), 2014.

[4] Ogihara et al., *J Exp Biol* 217(Pt 22):3968-73, 2014.

[5] Ogihara et al., *J Hum Evol* 58(3):252-61, 2010.

Disclosure of Interest: None Declared

Motion Analysis

AS-0147

WHEN ESTIMATING BONE POSE USING PROCRUSTES SUPERIMPOSITION, ONLY THE RIGID COMPONENT OF THE SOFT TISSUE ARTIFACT IMPACTS ON END RESULTS

Tecla Bonci [1 2 3 4 5,*]Valentina Camomilla [4 5]Raphaël Dumas [1 2 3 5]Laurence Chèze [1 2 3 5]Aurelio Cappozzo [4 5]

[1]Université Lyon 1, Lyon, [2]Université Claude Bernard Lyon 1, Villeurbanne, [3]LBMC UMR_T9406, Laboratoire de Biomécanique et Mécanique des Chocs, IFSTTAR, Bron, France, [4]Department of Movement, Human and Health Sciences, [5]Interuniversity Centre of Bioengineering of the Human Neuromusculoskeletal System, Università degli Studi di Roma ''Foro Italico'', Rome, Italy

Introduction and Objectives: To reconstruct the pose of a bone in the 3D space, stereophotogrammetry and a skin-marker cluster are used. The movement between skin-markers and the underlying bone is regarded as an artefact (soft tissue artefact, STA) having devastating effects on end results. This STA can be described at marker-cluster level by a series of geometrical transformations, such as rotations and translations (cluster rigid motion: CRM), homotheties and stretches (cluster non-rigid motion: CNRM). Recent studies quantified these STA components [1]–[4], showing that CRM is normally predominant with respect to CNRM. Based on this observation, it is concluded, either explicitly or implicitly, that CNRM has a limited impact on bone pose estimation (BPE) and that STA compensation should concentrate on CRM. This study disputes the message carried by this statement and demonstrates that CNRM does not have a limited effect on BPE accuracy, but, rather, it has no effect whatsoever and that this is the case independently from its magnitude relative to CRM. For this reason, the only STA component to be compensated for is CRM.

Methods: The data obtained in [5] and relative to the trajectories of both skin and pin thigh markers recorded during 5 trials of each of 3 running subjects (S1, S2, S3) were used. For each trial and subject, a bone anatomical frame (AF) was defined, based on the pin markers, and the movement of four skin-markers reconstructed in the AF. Relevant displacement vectors were represented, in each k-th sample, as an STA vector field $V(k)$, ($k=1{:}n$) [6]. This field was decomposed into modes, by projecting it onto an orthogonal base of unit vectors chosen so that the first six modes represent rotations and translations (CRM), and the further six homotheties and stretches (CNRM) [6]: $V(k)=\Sigma_{l=1\ldots12}\, a^l(k)\Phi^l$. The energies associated with CRM and CNRM were calculated as $E_{CRM}=\Sigma_{l=1\ldots6}(1/n\,\Sigma_{k=1\ldots n}\,(a^l(k))^2)$ and $E_{CNRM}=\Sigma_{l=7\ldots12}(1/n\,\Sigma_{k=1\ldots n}\,(a^l(k))^2)$, respectively. The ratio between the former and the latter energy (R) was determined.

To assess the impact that CNRM has on BPE, a Monte Carlo Simulation was used to generate a set of one thousand STA fields that have the same CRM and amplified CNRMs: $V_S(k)=\Sigma_{l=1\ldots6}\, a^l(k)\Phi^l + r\Sigma_{l=7\ldots12}\, a^l(k)\Phi^l$. The amplification factor r was randomly generated in the range from 1 to $2(R)^{\frac{1}{2}}$ so that the mean CNRM energy of this set was equal the CRM counterpart. Then, the CRM components were removed from both the measured and the amplified STA fields, generating STA fields affected only by the real, $V_N(k)=V(k)-\Sigma_{l=1\ldots6}\, a^l(k)\Phi^l$, and simulated CNRM, $V_{SN}(k)=V_S(k)-\Sigma_{l=1\ldots6}\, a^l(k)\Phi^l$. Skin-marker trajectories were generated from the reference AF pose and the STA fields available ($V(k)$, $V_S(k)$, $V_N(k)$, $V_{SN}(k)$) and used to estimate the artefact-affected pose of the AF in the global reference frame with a Procrustes Superimposition (PS) approach. The root mean square difference between the artefact-affected and reference AF pose

was calculated and considered as an error (rmse$_\theta$ for orientation (attitude angle) and rmse$_{px}$, rmse$_{py}$, rmse$_{pz}$, for position components).

Results: The median (inter-quartile range) values of the R factors were 7(1), 18(4), and 14(15), for S1, S2 and S3, respectively. Obviously, the CNRM amplification caused an increase in the energy percentage of this component with respect to the total energy: mean (±standard deviation) values went from 8±3% ($V(k)$) to 52±22% ($V_S(k)$) (Fig. a). Before and after the amplification of CNRM, errors in pose estimation were exactly the same (although the total STA energy increased) (Fig. b). In all cases, after removing CRM, not altered throughout the simulation, the error was null.

Figure:
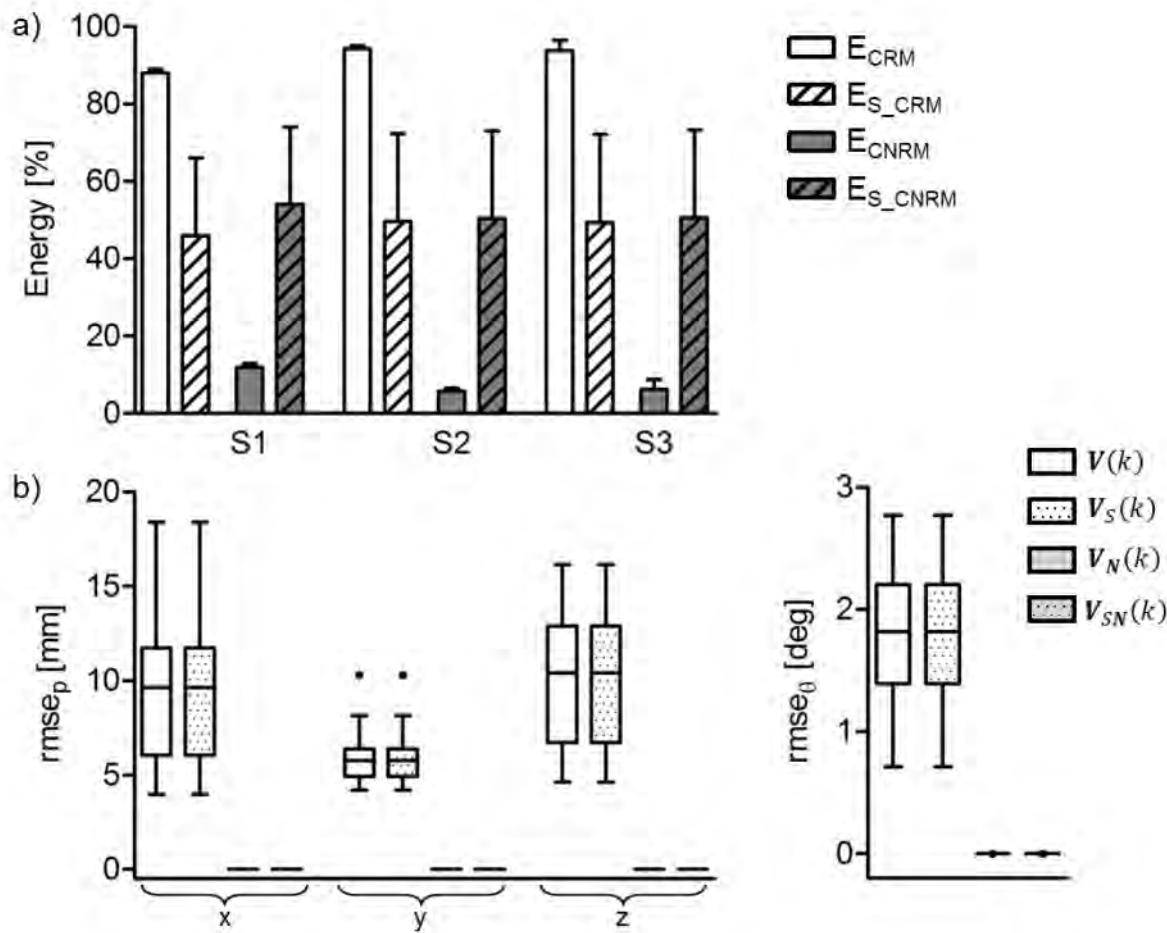
Caption: a) Mean values of the CRM and CNRM energy in percentage of the total energy, for the measured (ECRM and ECNRM) and simulated STA (ES_CRM and ES_CNRM). Statistics performed over all trials and subjects (S1, S2, S3). b) Box-plots (minimum, lower quartile, median, upper quartile, and maximum) of the BPE errors, for position and orientation, relative to all the STA fields available.

Conclusion: The results empirically showed that, using a PS approach, only CRM has an impact on the accuracy of the BPE, independently of the amplitude of CNRM. Moreover, after removing CRM, the real BPE was obtained. It must be acknowledged that a reference pose obtained with pin markers was used to compute the modes and to remove CRM from skin-marker trajectories. In the present context, this choice does not constitute a limitation, but does simply show that the

CNRM has no effect on BPE. Results suggest that, in a STA compensation perspective, future work should be focused on modelling and removing only CRM.

References: [1] Andersen et al, *Gait Posture*, 35:606–11,2012.

[2] Barré et al, IEEE *T Bio-Med Eng*, 60:3131–3140,2013.

[3] de Rosario et al, *Med Biol Eng Comput*, 50:1173–1181,2012.

[4] Grimpampi et al, IEEE *T Bio-Med Eng*, 61:362–367,2014.

[5] Reinschmidt et al, *J Biomech*, 30:729–732,1997.

[6] Dumas et al, *J Biomech*, 47:476–481,2014.

Disclosure of Interest: None Declared

Motion Analysis

AS-0148

ACETABULAR STRESS IN PERSONS WITH AND WITHOUT CAM FEMOROACETABULAR IMPINGEMENT: THE INFLUENCE OF HIP KINEMATICS AND BONY MORPHOLOGY DURING A MAXIMUM DEPTH SQUAT

Jennifer Bagwell [1,*]Christopher Powers [1]

[1]Biokinesiology and Physical Therapy, University of Southern California, Los Angeles, United States

Introduction and Objectives: Cam femoroacetabular impingement (FAI) has been reported to be a cause of hip chondral damage, acetabular labral tears, and osteoarthritis [1]. Cam FAI is defined by abnormal bony morphology (decreased offset at the femoral head-neck junction). Previous finite element modeling studies have demonstrated that as severity of this bony deformity increases, the bony contact shifts from the acetabular cup with the femoral head to the anterosuperior acetabular rim with the femoral head-neck junction [2]. This "impingement" results in a significant increase in acetabular cartilage stress. To date, little is known about the kinematic contributions to cam FAI. More specifically, it is not clear if cam FAI is more a result of abnormal hip kinematics (ie. increased hip internal rotation) or altered bony morphology. The purpose of the current study was to compare kinematics between persons with and without cam FAI during a maximum depth squat task. We also evaluated the contact location and magnitude of acetabular cartilage stress using finite element (FE) models that incorporated respective group kinematics and bony morphological profiles.

Methods: Fifteen persons with cam FAI (9 female, 6 male) and 15 age and gender matched controls participated. 3D kinematics were obtained during maximum depth squatting using a motion capture system (Qualisys, Inc., Gothenburg, Sweden). To create the FE models, 3T magnetic resonance imaging (GE scanner, General Electric Healthcare, Milwaukee, WI) was performed using a 3D high resolution, fat-suppressed, fast spoiled gradient recall echo sequence on one asymptomatic person who did not have FAI morphology or hip dysplasia. Images were manually segmented in Sliceomatic (Tomovision, Montreal, Quebec) and the femur and hemipelvis meshes were created in Hypermesh (Altair Engineering Inc., Troy, MI). The femur was modeled as a rigid body and the acetabulum was modeled using homogenous, isotropic, tetrahedral elements with an elastic modulus of 17.0 MPa and a Poisson ratio of 0.30. Nodes were manually added to the model at the femoral head neck junction (1:30 position) and the mesh was recreated. This resulted in one model without FAI morphology (control) and one model with moderate cam morphology (alpha angle 66°). The mean kinematics at the time of peak hip flexion during the maximum depth squat task were compared between groups using independent t-tests ($\alpha=0.05$). Additionally, the control group kinematics were utilized in the control group FE model and the cam group kinematics were utilized in the cam FE model. Simulations were run in Abaqus (SIMULIA, Providence, RI) using a hard contact algorithm, with a surface-to-surface, small sliding contact with a surface coefficient of friction of 0.02. The forces used for both models were identical and were derived from peak hip forces from a previous instrumented hip prosthesis study [3]. The modeling variables of interest were location of contact and the peak acetabular von Misses stres.s.

Results: Peak hip flexion was greater in the control group compared to the cam group ($113.0 \pm 6.7°$ vs. $105.8 \pm 14.7°$, respectively; p=0.048). Peak hip internal rotation also was greater in the control group than in the cam group ($105.8 \pm$

14.7° vs. 9.5 $\pm$ 8.0°; p=0.043). There was no statistically significant difference in peak hip abduction between groups (12.0 $\pm$ 6.8° vs. 11.6 $\pm$ 6.0°; p=0.864).

The contact location in the control FE model was within the acetabular cup, whereas the contact location in the cam FE model was at the anterosuperior acetabular rim (Figure 1). The corresponding acetabular peak stresses for the control and cam group FE models were 289 MPa and 673 MPa, respectively.
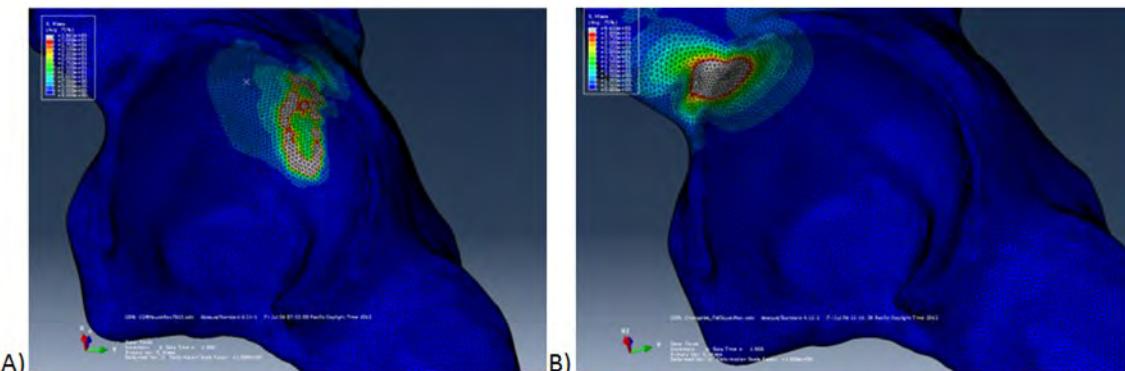
Figure:

Caption: Figure 1. Acetabular stress profiles with the femur removed for A) the control group kinematics applied to control FE model and B) the cam group kinematics applied to cam FE model.

Conclusion: Despite lower mean hip flexion and internal rotation angles during a maximum depth squat task in the cam FAI group, the cam FE model demonstrated contact locations corresponding to impingement (abutment of the femoral head-neck junction with the anterosuperior acetabular rim). In contrast, the control FE model resulted in a normal contact location (femoral head with the acetabular cup). These results indicate that bony morphology is likely a more important contributing factor in cam FAI during this task.

References: [1] Beck et al., J Bone Joint Surg Br, 87(7):1012-8, 2005.

[2] Chegini et al., J Orthop Res, 27(2):195-201, 2009.

[3] Bergmann et al., J Biomech, 34(7):859-71, 2001.

Disclosure of Interest: None Declared

Motion Analysis

AS-0149

A RELIABLE PROTOCOL FOR THE ASSESSMENT OF STEP COUNT ACCURACY OF PHYSICAL ACTIVITY MONITORS IN MULTIPLE SCLEROSIS

Fabio A. Storm [1 2,*] Sivaraman Nair [3] Alison Clarke [4] Jill Van der Meulen [4] Shanmuganathan Periyasamy [5] Claudia Mazzà [1 2]

[1]Department of Mechanical Engineering, [2]INSIGNEO Institute for in Silico Medicine, The University of Sheffield, [3]Department of Neurology, [4]The Gait Laboratory, Sheffield Teaching Hospitals NHS Foundation Trust, [5]Sheffield Institute of Translational Neuroscience, Sheffield, United Kingdom

Introduction and Objectives: Physical activity intervention and monitoring are becoming prominent in a number of patient populations and accelerometry is currently the most exploited technology in this context [1]. One of the essential features in activity monitoring is step counting, the accuracy of which is typically limited by the fact that signals are recorded from patients with altered walking patterns and reduced walking speed. Only little evidence is available on the validity and reliability of step counts, and the effect of these errors on the estimation of the final physical activity is unclear.

The aim of this study is to propose a method for the reliable assessment of patient-specific inaccuracies when using a physical activity monitor (PAM) for step detection in patients with multiple sclerosis. The relationship between step count accuracy and walking speed will also be investigated as an indicator of the suitability of a given monitor for those patients with highly restricted walking ability.

Methods: Seventeen participants (8 males, age range 39-75) with diagnosis of multiple sclerosis were recruited for the study. Written informed consent and ethical approval were obtained. The participants were asked to walk four times along a predefined straight walkway while two light-gates recorded their walking speed (WS). Then, they were asked to freely walk for 1 minute in a 100 m^2 empty space. The number of walked steps (N_{PAM}) was recorded during both experiments using a PAM (DynaPort Movemonitor^{TM}, Mc Roberts). Two inertial sensors (N_{REF}, OPAL^{TM}, ADPM Inc.) placed on the shanks of the participants were used as reference [2]. The same protocol was repeated after seven days to assess its reliability. Between the two lab sessions, the PAM was given to the participants for continuous physical activity recording for one week. Differences between sessions and walking conditions (straight versus free walking) were assessed for N_{PAM} and N_{REF} using repeated measures ANOVA. Bland-Altman plots were used to assess the agreement between N_{PAM} and N_{REF} and the mean absolute percentage error (MPE) between them was also calculated. The reliability of the error estimate was assessed using the Intraclass Correlation Coefficient (ICC(3,1)) [3]. Since walking speed is a commonly used primary outcome measure in clinical studies on physical activity, the relationship between WS and MPE was also investigated using power regression analysis.

Results: Five out of seventeen participants reached the low-active lifestyle threshold of 5000 steps per day.

The difference between N_{PAM} and N_{REF} was not statistically significant (p=0.065). No statistically significant differences between visits or walking conditions were found for step count (p=0.60 and p=0.98) and for MPE (p=0.42 and p=0.27). The mean (±SD) underestimation in the PAM was equal to 16±20 steps for straight walking and 14±28 steps for free walking.

The power regression trendline used to best fit the data showed a Pearson's r=0.74 for straight walking and r=0.61 for free walking. Two groups of patients where clearly identifiable from the MPE-WS plots (Figure 1), the first one having a high error in step detection (MPE>40%) and a slow walking speed (MWS<0.5 m/s), the second having a lower error (MPE<20%) and a higher WS. Test-retest relative reliability for MPE was high for both straight walking (ICC=0.80) and free walking (ICC=0.89).

Conclusion: The method presented in this study allowed to reliably assess step detection error (MPE) in indoor straight and free walking in a group of patients with multiple sclerosis. When using the same PAM adopted in the study or an equivalently performing one, a walking speed of 0.5 m/s or higher is needed to ensure an error in step detection lower than 20%. The consequences of inaccurate step count from a PAM can be estimated by projecting the error calculated in the lab over the seven days period of observation: the average number of potentially not detected steps per day was 513 (±712), equal to 10% of the low-active daily lifestyle threshold. This method could be used to assess any available PAM and the reference step calculation might be obtained with any alternative system. Reported results suggest that extreme care should be used when interpreting physical activity monitors data obtained in patients walking at significantly reduced speed.

References: [1] Chen et al., Med. Sci. Sports, 44:S13–23, 2012.

[2] Aminian et al., J. Biomech., 35:689–699, 2002.

[3] Rankin et al., Clin. Rehabil., 12:187–199, 1998.

Disclosure of Interest: None Declared

Motion Analysis

AS-0150

BALLET DANCERS OF DIFFERENT BACKGROUNDS PERFORM SAUTÉ JUMPS WITH DIFFERENT HIP ROTATION

Debora Cantergi [1,*]Andreja Picon [2]Carolina Rodes [2]Jefferson Loss [1]Isabel Sacco [2]

[1]Federal University of Rio Grande do Sul, Porto Alegre, [2]University of São Paulo, São Paulo, Brazil

Introduction and Objectives: The sauté is one of the first jumps a child learns in ballet class and the basis for other jumps in ballet. The sauté jump takes off and lands on both feet, and may be performed in all five ballet positions [1], which require the dancer to laterally rotate the lower limbs (turnout) [2]. While this is common in all ballet methods, the methodology used for teaching the sauté depends on the teachers' background [3]. Most ballet methods are empirical. At least one method, the Royal Academy of Dance (RAD), has developed a pedagogical progression in the study of ballet. This study aimed to evaluate the 3D kinematic characteristics of the ankle, knee and hip joints during the performance of sauté movement in first position by ballet dancers trained in empirical and RAD methods.

Methods: Eighteen elite ballerinas (9 from RAD and 9 from empirical method) performed 2 series of 8 sauté movements with classical music and the 6 central movements were analyzed. 3D kinematic data of hip, knee and ankle joint of the left lower limb were acquired by 6 IR cameras (OptiTrack FLEX: V100, Natural Point). An AMTI force plate was used to identify the contact and aerial phases of sauté. Kinematic trajectories were processed by low-pass 4th order Butterworth filter, cut-off frequency of 6 Hz (Visual 3D, CMotion). A sauté starts when the dancer leaves the force plate until the end of the next aerial phase (aerial phase + landing + full bending of the knees + push off until take off). Maximum and minimum joint angles and the range of motion (ROM) of all joints in 3 planes of motion were compared between groups using t-tests (p<0.05).

Results: Difference was found between hip ROM on the transversal plane (rotation), where the RAD group presented a greater ROM than the empirical group. No differences were found between RAD and empirical methods in ROM and maximum and minimum joint angles in all other planes (table 1, figure 1). Shippen showed that the lateral rotation of each joint is not constant while maintaining the same summed turnout in the whole lower limb during the performance of the demi-plié [4]. In a qualitative analysis of the time series of our results, we observed a similar kinematic pattern in the transverse plane during both contact (demi-plié) and aerial phases of the sauté. This qualitative analysis in addition to the observed difference between the methods in the hip ROM in the transverse plane, suggests that the perceived change in the lateral rotation happens in both movement phases in sauté. When the dancer is in contact with the floor, she can use the contact forces to manage her turnout, but in the aerial phase, it was expected that only the hip would perform lateral rotation, what did not happened. The RAD group had a significantly higher ROM than the empirical group, mainly when the dancers were in contact with the floor. It is possible that the RAD dancers had used the contact forces in order to enhance their natural lateral rotation.

Figure:
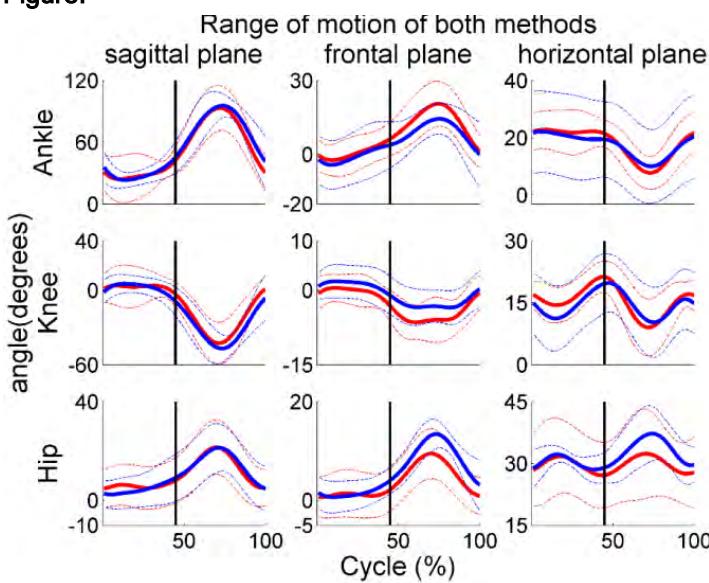
Caption: Mean range of motion of all dancers in empirical (red) and RAD (blue) groups. Positive values represent ankle and hip flexion, knee extension, ankle, knee and hip abduction and ankle, knee and hip lateral rotation. The contact phase goes from 45 to 100%.

Conclusion: Dancers trained in the RAD method perform the sauté with higher hip ROM in the transverse plane compared to dancers trained in empiric methods, suggesting that the use of a pedagogical method for teaching ballet may influence the turnout position when performing the sauté movement.

Table:

	Sagittal plane			Frontal plane			Horizontal plane		
	Empirical	RAD	p	Empirical	RAD	p	Empirical	RAD	p
	Mean±SD	Mean±SD		Mean±SD	Mean±SD		Mean±SD	Mean±SD	
A max	103.0±5.8	102.2±6.4	0.74	20.9±9.1	16.6±13.2	0.31	24.1±6.5	24.2±13.4	0.98
A min	19.8±6.0	20.4±5.3	0.79	-4.8±4.3	-7.6±12.2	0.42	5.2±4.1	4.7±15.5	0.91
A ROM	83.0±7.7	81.6±4.4	0.55	25.6±6.9	24.0±8.3	0.57	19.1±7.5	19.5±7.4	0.90
K max	7.3±7.6	4.9±6.7	0.36	1.5±2.2	5.4±7.6	0.06	22.0±3.3	22.4±6.4	0.84
K min	-51.4±5.9	-52.6±8.3	0.65	-8.7±3.9	-6.1±4.5	0.10	7.3±4.9	7.2±7.7	0.98
K ROM	58.4±6.3	57.7±6.6	0.78	10.1±3.6	11.5±6.4	0.49	14.8±3.4	15.6±2.4	0.45
H max	23.2±9.6	27.0±7.4	0.22	12.6±2.8	13.1±5.9	0.78	35.8±8.8	39.6±10.1	0.28
H min	0.4±9.0	3.6±7.0	0.27	0.4±3.2	0.4±3.7	0.99	26.2±8.3	26.8±9.2	0.84
H ROM	22.8±4.2	23.2±3.7	0.76	12.2±2.7	12.9±4.4	0.60	9.8±2.2	12.6±3.7	**0.02**

Caption: Mean and standard deviation of maximum (max), minimum (min) and ROM (degrees) of each joint in all 3 planes of movement in ankle (A), knee (K) and hip (H), of each group of ballet dancer and the p-values of comparisons between groups.

References: [1] Ryman, RS. Dictionary of classical ballet terminology. Royal Academy of Dancing, 1996.

[2] Hamilton, D. Br J Sport Med. 40(4):299-303, 2006. [3] Wilmerding, M, et al. J Dance Med Sci 5(3):69-74, 2001.

[4] Shippen, J. Arts Biomechanics 1(1):33-43, 2011.

Disclosure of Interest: None Declared

Lower Limb

AS-0151

LOWER LIMB MUSCLE FASCICLE FUNCTION DURING GAIT IN CHILDREN WITH CEREBRAL PALSY

Lee Barber [1,*]Chris Carty [2] [3]Luca Modenese [3]John Walsh [2]Roslyn Boyd [1]Glen Lichtwark [4]

[1]Queensland Cerebral Palsy and Rehabilitation Research Centre, School of Medicine, The University of Queensland, [2]Queensland Children's Gait Laboratory, Queensland Health, Brisbane, [3]Centre for Musculoskeletal Research, Griffith Health Institute, Griffith University, Gold Coast, [4]Centre for Sensorimotor Neuroscience, School of Human Movement Studies, The University of Queensland, Brisbane, Australia

Introduction and Objectives: During gait in typically developed (TD) individuals, the muscles of the calf contract at levels that maintain a relatively constant muscle fibre length while the more compliant Achilles tendon acts like a spring to absorb and return energy during each step[1]. However the calf muscles of individuals with Cerebral Palsy (CP) adapt in response to spasticity to become smaller, weaker, more resistant to stretch, have increased antagonist co-contraction and the Achilles tendon becomes longer[2,3]. These neuromuscular adaptations of the calf in CP could reduce muscular force generation capacity and contribute to altered gait kinematics, however it is difficult to know what impact these spasticity driven adaptations will have on fascicle or tendon behaviour. The primary aim of this study was to investigate the function of medial gastrocnemius and soleus muscle-tendon unit (MG_{mtu}, SOL_{mtu}) and fascicles (MG_{fas}, SOL_{fas}) in children with CP compared to TD children.

Methods: 14 children with CP, age 9 years 10 months (2 years 9 months), 9 males, 5 female, 8 hemiplegia, 6 diplegia, GMFCS I=10, GMFCS II=4, and 10 TD, age 9 years 11 months (2 years 3 months), 6 males, 4 females, participated in the study. Participants performed 10 walking trials at a self-selected speed, barefoot, over a level walkway approximately 10m in length with force platforms embedded in the centre of the walkway. Trajectories of reflective markers attached to the trunk, pelvis, and upper and lower limbs were recorded and 3D gait kinematics and kinetics were computed. The vertical ground reaction force data was used to determine the step and stride times. During walking B-mode ultrasound images of the MG_{fas} and SOL_{fas} were also acquired. Fascicle lengths were analysed using a semi-automated tracking algorithm and MG_{mtu} and SOL_{mtu} were determined using OpenSim. Primary outcome measures were changes in MG_{mtu} and MG_{fas} length during mid- and terminal-phase of stance. An independent t-test ($p<0.05$) was used to compare differences between groups.

Results: In mid-stance the MG_{mtu} increased length similarly in both groups (CP = 5.5(3.8)mm; TD = 5.6(3.9)mm, p=0.96), however fascicles underwent significantly different lengthening between groups (p=0.02) with CP = 1.6(1.9)mm and TD = 0.1(0.8)mm. During late-stance the MG_{mtu} and SOL_{mtu} shortened similarly in both groups (CP = 21.0(6.8)mm, 7.7(2.4)mm; TD = 19.9(6.9)mm,7.4(4.9)), while the MG_{fas} shortened less (p=0.04) in the CP group (CP = 1.9(1.4)mm; TD = 3.4(1.9)mm). The SOL_{fas} underwent significantly different length changes between groups (p=0.04) with CP SOL_{fas} lengthening 0.6(1.7)mm and TD shortening by 0.7(0.8)mm.

Figure:
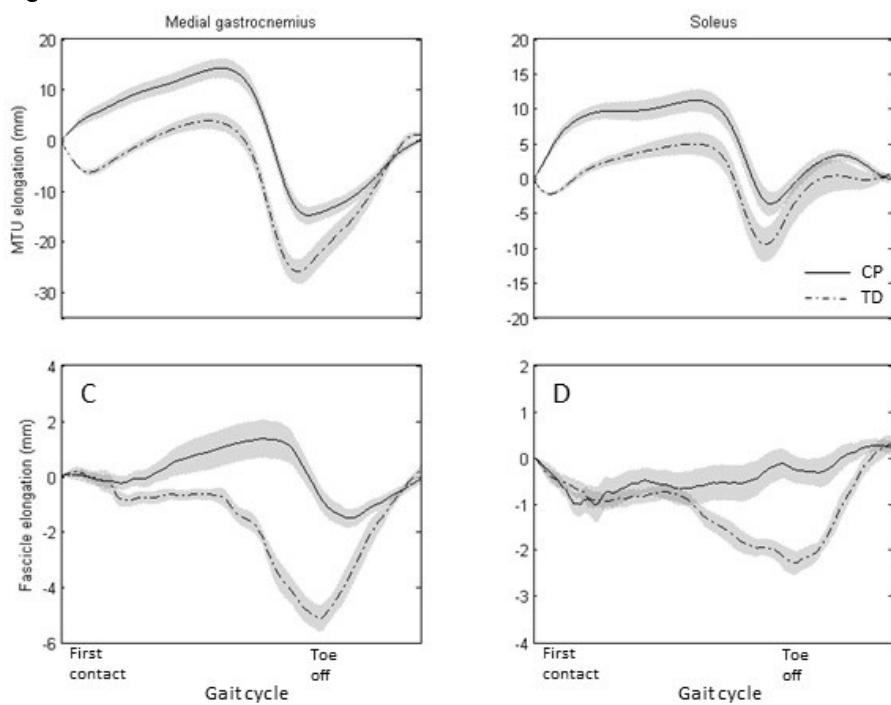
Caption: Medial gastrocnemius and soleus muscle tendon unit (MTU) and fascicle length change during one gait cycle in CP and TD. Data are mean ± SEM.

Conclusion: During walking, while the MG_{mtu} lengthens comparably between the groups, the MG_{fas} in the CP group lengthens through mid-stance while they remain relatively isometric in TD individuals. The eccentric action of the CP muscle fascicles during walking is consistent with the greater passive stiffness and perhaps greater reliance on passive rather than active muscle force. During the "push-off" phase the CP group had less MG_{fas} and SOL_{fas} shortening indicating that active muscle contraction contributed less to forward propulsion during walking. The altered behaviour is thought to result from structural and functional neuromuscular adaptations, however, conclusions about the contribution of the lengthening fascicles to passive force generation within the MTU cannot yet be established without further investigation. This is the first description of altered in vivo lower limb muscle fascicle and MTU behaviour during walking in children with CP. These novel findings raise clinical questions about the effects of repeated eccentric contractions on muscle function and recovery as eccentric contractions cause muscle damage, muscle soreness and delayed recovery in TD muscles. Furthermore, investigations of the impact of walking speed and gradient, and most importantly, treatments on fascicle, tendon and MTU behaviour are required to inform therapists, paediatric specialists and orthopaedic surgeons and guide conservative, pharmacological and surgical management.

References: [1] Lichtwark et al., J. Biomech. 40: 157-164, 2007.

[2] Barber et al., J. Biomech. 44: 2496-2500, 2011.

[3] Barber et al., J. Biomech. 45: 2526-2530, 2012.

Disclosure of Interest: None Declared

Lower Limb

AS-0152

PARTIAL DIRECTED COHERENCE APPLIED IN LOWER LIMB KINEMATIC DATA DURING RUNNING

Theresa H. Nakagawa [1,*] Ana F. Santos [1] Giovana Y. Nakashima [2] Fábio V. Serrão [1] Carlos D. Maciel [3]

[1] Physical Therapy Department, Federal University of São Carlos, São Carlos, [2] Federal Institute of Education, Science and Technology of São Paulo, Salto, [3] Eletrical Engineering Department, University of São Paulo, São Carlos, Brazil

Introduction and Objectives: Despite the increasing number of runners and the health benefits related to running, this sport presents a potential risk to musculoskeletal injuries. Knee injuries are highly prevalent in runners. Although there is evidence supporting the dynamic coupling between lower limb joints, the causal interaction and the direction of this coupling is inconclusive [1]. In this sense, the *Partial Directed Coherence* (PDC), an approach of Granger causal inference analysis, has the potential to fill this gap of knowledge [2] clarifying if the hip, knee and ankle interjoint couplings occur in the distal to proximal or in the proximal to distal direction. Therefore, the purpose of this study was to analyze the causal directed interaction pattern of the hip, knee and ankle kinematics during running in healthy runners.

Methods: Thirty-one recreational runners (age: 27.7 ± 5.4 years; mass: 72.1 ± 13.6 kg; height: 23.7 ± 2.9 m; average running distance: 35.7 ± 18.3 km/wk; running experience: 4.1 ± 4.0 years) participated in this study. The participants were between 18 and 35 years of age and met the following criteria: they were rearfoot strikers (RFS), familiar with treadmill running and ran a minimum of 20 km/wk at least 3 months prior to study enrollment. After a 5-minute warm-up, the three-dimensional (3D) hip, knee and ankle kinematic data of the dominant lower limb (5 left, 26 right) were recorded at 240 Hz during treadmill running with a six-camera Qualisys motion analysis system (Qualisys Inc., Gothenburg, Sweden). The running trial was performed for 1-minute and 30-s samplings of data were collected. The Cardan angles were calculated using the Visual 3D software (C-Motion Inc, Rockville, MD). To compute PDC, the best Bayesian Information Criterion (BIC) order was used to estimate auto-regressive model. Taken in pairs, all channels PDC values were calculated and the average of their highest value was used in the results. All routines were developed in Python 2.7.4 (Python Software Foundation, USA). Paired samples t-tests were used to compare the distal-proximal or proximal-distal causal influence of the ankle-knee and hip-knee kinematics. The alpha level was set at .05.

Results: For the ankle-knee pair, the PDC value in the proximal-distal direction was significantly higher compared with the distal-proximal direction in the sagittal, frontal and tranverse plane (Table 1 and Figure 1). The PDC was also higher in the proximal-distal direction for the knee-hip pair in the frontal plane. There were no differences in the sagittal and transverse plane for the knee-hip kinematic pair. Granger causality concept has been used to determine causal influences among multivariate time series [3]. Its formulation is based on a simple idea: a causal interaction from a process Y to a process X is suggested if there is a reduction of prediction error of X when including the past of Y. PDC is a different approach of Granger causality applied in frequency-domain [1]. To the best of the author's knowledge, this was the first study to apply PDC analysis in the kinematic data in healthy runners. The causal influence of the ankle-knee and hip-knee pairs showed a predominant proximal-distal influence, meaning that the movement of the proximal joints of the lower limb have greater influence on the movements generate in the distal joints.

Figure:

1. SAGITTAL ANKLE
2. FRONTAL ANKLE
3. TRANSVERSE ANKLE
4. SAGITTAL KNEE
5. FRONTAL KNEE
6. TRANSVERSE KNEE
7. SAGITTAL HIP
8. FRONTAL HIP
9. TRANSVERSE HIP
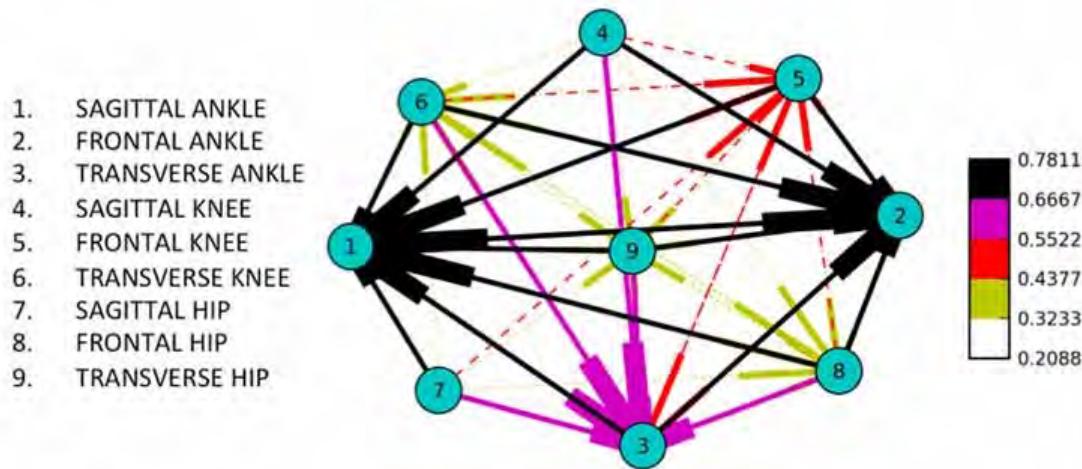
Caption: Causal influence in kinematic data during running. Nodes 1 to 9 are the 3D kinematic joints, labeled at left. Each edge represents the maximum PDC computed between the joints, where thicker stubs represent "arrows". Right label shows the ranges of maximum PDC values with different colors, where the first one is black (higher) and the last one is white (lower, invisible due to the white background).

Conclusion: The causal directed influence of the hip, knee and ankle movements during running occurred predominantly in the proximal-distal direction. The understanding of the pattern of causal directed influence may enhance the knowledge about the human movement, allowing a better diagnostic of the movement disturbances and improving the prevention and treatment programs for musculoskeletal injuries related to running.

Table: Mean (SD) of the joint pairs PDC values.

Joint Pairs	PDC value			
Sagittal Plane	Distal-proximal	Proximal-distal	*P-value*	Direction Result
Ankle-Knee	0.24 (0.14)	0.71 (0.13)	0.000*	Proximal-distal
Knee-Hip	0.24 (0.12)	0.26 (0.13)	0.51	~
Frontal Plane				
Ankle-Knee	0.45 (0.17)	0.75 (0.15)	0.000*	Proximal-distal
Knee-Hip	0.35 (0.11)	0.48 (0.18)	0.002*	Proximal-distal
Transverse Plane				
Ankle-Knee	0.41 (0.13)	0.58 (0.15)	0.001*	Proximal-distal
Knee-Hip	0.36 (0.14)	0.41 (0.13)	0.11	~

Caption: *$P < .05$

References: [1] Chuter & Jonge, Gait Posture, 36(1): 7-15, 2012.

[2] Baccalá & Sameshima, Biol Cybern, 84(6): 463-74, 2001.

[3] Chicharro, Biol Cybern, 105(5-6): 331–47, 2011.

Disclosure of Interest: None Declared

Lower Limb

AS-0153

ACHILLES TENDON SHEAR WAVE SPEEDS SHOW NON-UNIFORM AGING EFFECTS

Laura C. Slane [1,*] Jack Martin [2] Ryan DeWall [1] Darryl Thelen [3] Ken Lee [1]

[1]Radiology, [2]Materials Science Program, [3]Mechanical Engineering, University of Wisconsin-Madison, Madison, United States

Introduction and Objectives: Tendon injuries and disease increase in incidence during aging. This susceptibility may result from age-related changes in tendon tissue properties, including reduced compliance of the interfascicular matrix [1] and an increase in collagen cross-linking [2]. However, it remains unclear how these microstructural changes affect macro-scale tendon compliance. Further, recent reports suggest that tendons are mechanically heterogeneous, with significant variations in material properties both within regions of the same tendon [3], and between different types of tendons [4]. Thus, it is also important to consider whether age-related changes progress uniformly throughout the tendon structure. Shear Wave Elastography is an ultrasound-based approach capable of noninvasively measuring localized shear wave speed (SWS) in soft tissues [5]. In transversely isotropic materials, such as tendon, SWS is believed to primarily depend on the shear elastic modulus [6], thus reflecting an important tissue mechanical characteristic. We have recently shown that SWS varies spatially throughout the Achilles tendon and increases with passive stretch [3], with middle-aged adults showing evidence of increased compliance in the proximal Achilles tendon (i.e. the gastrocnemius aponeurosis) [7]. The purpose of this study was to test the hypothesis that older adults would exhibit even greater declines in proximal Achilles SWS, and that evidence of the reduced compliance would extend into the more distal aspects of the Achilles tendon.

Methods: Thirty-five healthy adults (aged 21-71, mean: 46±19 yrs) were recruited for this study. Subjects provided written consent and were positioned prone on an exam table with their leg extended. SWS data were collected from the Achilles free tendon, the soleus aponeurosis and the medial gastrocnemius aponeurosis of the right limb. Data were collected from three different ankle postures in a random order: resting (R), dorsiflexed (R-15 deg) and plantarflexed (R+15 deg). SWS data were evaluated post-hoc at regions of interest defined within tendon boundaries. Regression analyses of SWS and age were performed for each tendon region and ankle posture, with significance evaluated at $p < 0.05$.

Results: SWS varied significantly with age in all tendon regions. Similar to aging effects observed previously in middle-aged adults [7], we found SWS in the dorsiflexed gastrocnemius aponeurosis to correlate negatively with age ($p<0.001$). With the inclusion of older adults (aged 61+) in this study, we also saw evidence of increased compliance in the soleus aponeurosis when the tendon was in a stretched position ($p<0.001$). This result suggests that not only does an age-related change in tendon compliance progress in severity with increased age, but that the location of these aging effects also progresses from the proximal region of the Achilles (i.e. the gastrocnemius aponeurosis) to more distal regions (i.e. the soleus aponeurosis). To our knowledge, only a few studies have evaluated non-uniform progression of aging effects in tendon, but of these, a similar progression was observed in a study of mouse tibialis anterior tendon stiffness [8].

In contrast to the other regions of the tendon, in the Achilles free tendon we found a significant aging effect only when the ankle was plantarflexed, and in this posture we found aging to correlate with increased SWS ($p=0.005$). In this posture, the Achilles tendon is close to its slack length [9], and is almost entirely unstretched. Thus, we hypothesize that this

decrease in compliance arises from age-related changes in tendon composition that have previously been observed (e.g. reduced compliance of the interfascicular matrix [1]).

Figure:
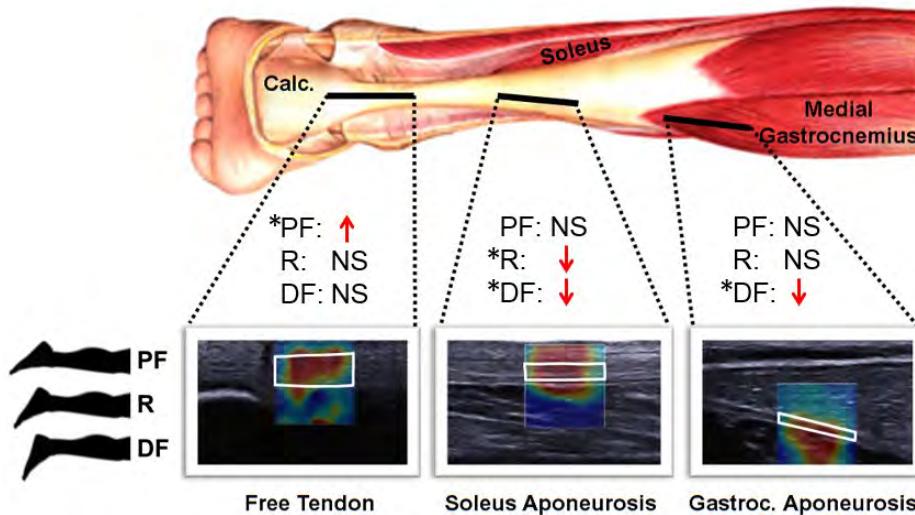
Caption: SWS data were collected from the Achilles tendon in plantarflexed (PF), resting (R) and dorsiflexed (DF) postures. Regions of interest (represented in white) were defined within the tendon boundaries. Significant SWS trends with aging are shown in red. *p<0.05, NS: Not significant, Calc: Calcaneus

Conclusion: Achilles tendon SWS is highly dependent on age, tendon stretch (i.e. ankle posture), and tendon region. These results suggest that aging-related changes in tendon progress non-uniformly with age, with different regions of the tendon showing contrasting effects of aging on compliance. Future studies will consider how spatially varying material properties affect localized tendon tissue strains, which is important for understanding the increased susceptibility for tendon tissue damage seen with aging.

References: 1. Thorpe CT et al., Eur Cells Mater 25: 48-60, 2013.

2. Couppe C et al., J Appl Physiol (1985) 107: 880-886, 2009.

3. DeWall RJ et al., J Biomech 47: 2685-2692, 2014.

4. Thorpe CT et al., J R Soc Interface 9: 3108-3117: 2012.

5. Bercoff J et al., IEEE Trans Ultrason Ferroelectr Freq Control 51: 396-409, 2004.

6. Royer D et al., J Acoust Soc Am 129: 2757-2760, 2011.

7. Slane LC et al., J Appl Physiol, in review, 2014.

8. Wood LK et al., J Appl Physiol 111: 999-1006, 2011.

9. Hug F et al., J Biomech 46: 2534-2538, 2013.

Disclosure of Interest: None Declared

Lower Limb

AS-0154

IMPACT OF COMPETITION ON STRIDE RATE IN DISTANCE RUNNING

Michelle Norris [1,*] Ross Anderson [1] Ian Kenny [1]

[1] Physical Education and Sport Sciences, University of Limerick, Limerick, Ireland

Introduction and Objectives: Stride rate (SR) has been identified as a major contributing factor to running economy and run completion time (Hunter and Smith 2007). However, much of the research investigating stride rate has focused around elite athletes. Whilst recent research surrounding recreational runners has investigated step width alterations (Brindle *et al.* 2014) there is no data pertaining to stride rate over a longitudinal period within this population. Objectives were to investigate how the stride rate of recreational runners during training compared to their stride rate during a competitive distance running event and its relationship with event outcome i.e. time.

Methods: To investigate stride rate changes accelerometer data from four recreational runners training for, and completing, a half marathon was collected. Participants were required to attach a tri-axial accelerometer (SHIMMER, Dublin, Ireland) to their anterio-medial distal tibia bi-laterally for each training run and the half marathon event. Data were sampled at 204.8 Hz (range = ±6 g, sensitivity = 200 mV/g). Participants' half-marathon race data were analysed as a competitive race (114 ± 13 minutes), whilst their longest recorded training run was analysed as a non-competitive comparison (106.5 ± 23 minutes). Data processing was performed using a custom built LabView™ programme (National Instruments, Berkshire, UK) with subsequent analysis in Excel. Running stride time data was extracted with any stride above 1s eliminated as this was designated to be a walking step (Rowe *et al.* 2011). Run time was then broken into 1% epochs and stride rate (strides per minute) was calculated for each epoch. Predicted half marathon time was calculated via the McMillan Running Calculator (McMillan 2014).

Results: Modal stride rate for the 1% epochs illustrated that competitive stride rate varied compared to non-competitive. Participant 1 chose a lower stride rate during the competitive run compared to their non- competitive run (83 vs 86 strides per minute). In contrast participant 4 ran at a higher stride rate than ran in their non-competitive run (90 vs 87 strides per minute). When investigating half marathon completion time participants 1 and 3 completed in less time than predicted (-10 and -2.5 minutes), whereas participants 2 and 4 completed in greater time than predicted (+5 and +6 minutes) (Table 1). Participant 1 and participant 4's data (Figure 1) are comparable to their modal stride rate. Participant 1 ran at a lower stride rate in all but 6 of the 1% epochs, while participant 4 ran at a higher stride rate in all but 5 of the 1% epochs. In contrast participant 2's stride rates indicate that for the majority of the competitive run they ran at a higher stride rate than the non-competitive run, whilst their modal stride rates were the same. Participant 3's data also illustrates variation to both to a higher and lower stride rate, with clear differences for the beginning and end of the runs. Both participant 2 and participant 4 completed the half marathon outside of their predicted completion time whilst also running at a higher stride rate for the majority of the run than in their non-competitive run.

Figure:
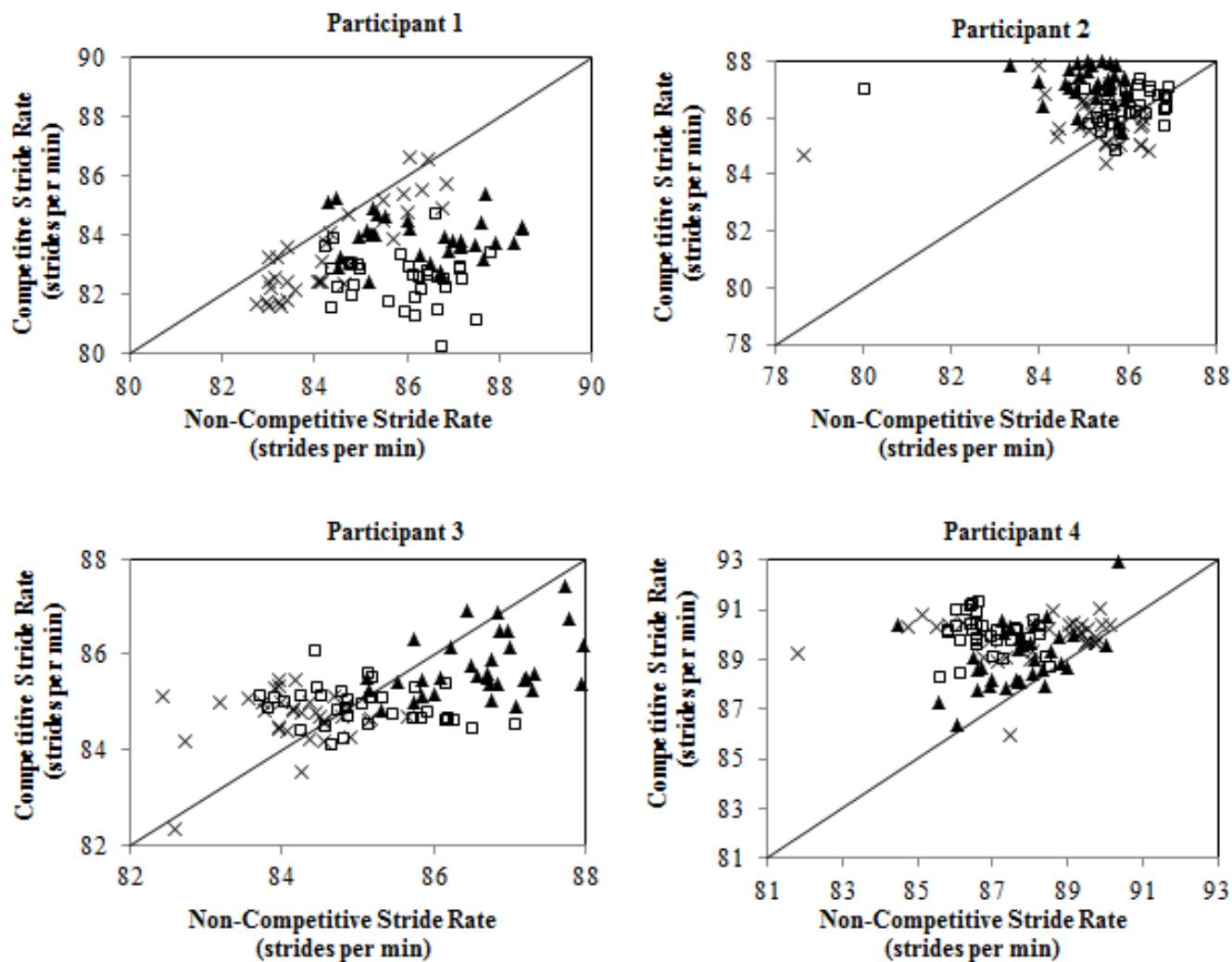
Caption: Figure 1. Comparison of 1% epoch stride rates for competitive and non-competitive runs. Diagonal line inserted representing no change in stride rate between competitive and non-competitive runs at that % epoch

Conclusion: Recreational runners' stride rates are variable both within a competitive running event and when compared to non-competitive runs. Results here indicate that variable and lower stride rate than previously utilised may be a better strategy to completing a running event. Participants who ran at higher stride rates then had previously been performed (participants 2 and 4) resulted in a decline in predicted performance outcome. Whilst participant 3 and participant 4 saw identical increases (0.07 m/s) in speed from non-competitive to competitive runs participant 3 may have adopted more efficient stride rates throughout the race resulting in a preferred race outcome. As increased stride rate is associated with numerous biomechanical alterations linked to injury and efficiency, such as impact shock and decreased centre of mass vertical excursion (Schubert *et al.* 2014), perhaps more emphasis should be placed upon stride rate than previously thought.

Table:

	Participant 1	Participant 2	Participant 3	Participant 4
Non-Competitive Average Speed (m/s)	2.96	2.47	3.48	3.04
Competitive Average Speed (m/s)	3.06	2.71	3.55	3.11
Non-Competitive Modal Stride Frequency (strides per minute)	86	86	85	87
Competitive Modal Stride Frequency (strides per minute)	83	86	85	90
Predicted Marathon Time (minutes)	125	125	102.5	107
Half Marathon Completion Time (minutes)	115	130	99	113

Caption: Table 1. Non-competitive and competitive speed and time parameters.

References: Brindle et al., Gait Posture, 39: 124-128, 2014.

Hunter et al., Eur J Appl Physiol, 100: 653-661, 2007.

Rowe et al., Med Sci, 43: 312-318, 2011.

Schubert et al., Sports Health, 6: 210-217, 2014.

Disclosure of Interest: None Declared

AS-0155

LEG LENGTH DISCREPANCY AFFECTS THE SAGITTAL PLANE BIOMECHANICS OF THE LOWER LIMBS DURING THE STANCE PHASE OF WALKING

Renan Alves Resende [1,*]Kevin Deluzio [2]Renata Noce Kirkwood [3]Renato Guilherme Trede Filho [1]Carolina Carvalho Martins [1]Sérgio Teixeira Fonseca [4]

[1]Physical Therapy, Universidade Federal dos Vales do Jequitinhonha e Mucuri, Diamantina, Brazil, [2]Mechanical and Materials Engineering, Queen's University , Kingston, [3]Kinesiology and Physical Education, Wilfrid Laurier University, Waterloo, Canada, [4]Physical Therapy, Universidade Federal de Minas Gerais, Belo Horizonte, Brazil

Introduction and Objectives: Leg length discrepancy (LLD) occurs in up to 70% of the population[1]. LLD has been related to the occurrence of different lower limb injuries, such as trochanteric bursitis[2], patello-femoral pain[3] and posterior tibial tendon dysfunction[4]. Although it has already been demonstrated that LLD greater than 2 cm affects the biomechanics of lower limbs during gait, there is no consensus regarding the effects of having LLD smaller than 2 cm. Therefore, the purpose of the present study was to investigate the effects of small LLD on the angular displacement and moments of force of the ankle, knee and hip in the sagittal plane during the stance phase of gait. These findings may improve understanding of the relationship between LLD and the occurrence of lower limb injuries, since most people have LLD smaller than 2 cm.

Methods: Kinematic and kinetic data of 19 participants were collected while they walked wearing flat thick and flat thin sandals (1.45 cm of thickness difference between sandals). Individuals with true or functional LLD were excluded. Two conditions were investigated: (1) control condition - the participant walked wearing flat thick sandals; (2) short limb condition – thin flat sandal on the right foot and thick flat sandal on the left foot. The right lower limb biomechanics were analyzed for both conditions. Ankle, knee and hip angular displacement and internal moments of force during the stance phase were measured with a motion capture system and force platforms. Principal component analysis was used to compare differences between conditions[5]. The scores of the principal components retained for analysis were compared between conditions using Student's t-test.

Results: Table 1 presents the results of this study. Gait waveforms represented by high (+ 1 standard deviation) and low (- 1 standard deviation) principal component scores for each significant principal component are shown in Figure 1.

Figure:

— Control
···· Short

High and low single PC reconstructions

a. DORSIFLEXION / PLANTARFLEXION — Ankle angle (deg) vs % Stance phase
b. DORSIFLEXION / PLANTARFLEXION — Ankle moment (Nm/kg) vs % Stance phase

High and low single PC reconstructions

c. FLEXION / EXTENSION — Knee kinematic (deg) vs % Stance phase
d. FLEXION / EXTENSION — Knee moment (Nm/kg) vs % Stance phase

High and low single PC reconstructions

e. FLEXION / EXTENSION — Hip kinematic (deg) vs % Stance phase
f. FLEXION / EXTENSION — Hip moment (Nm/kg) vs % Stance phase
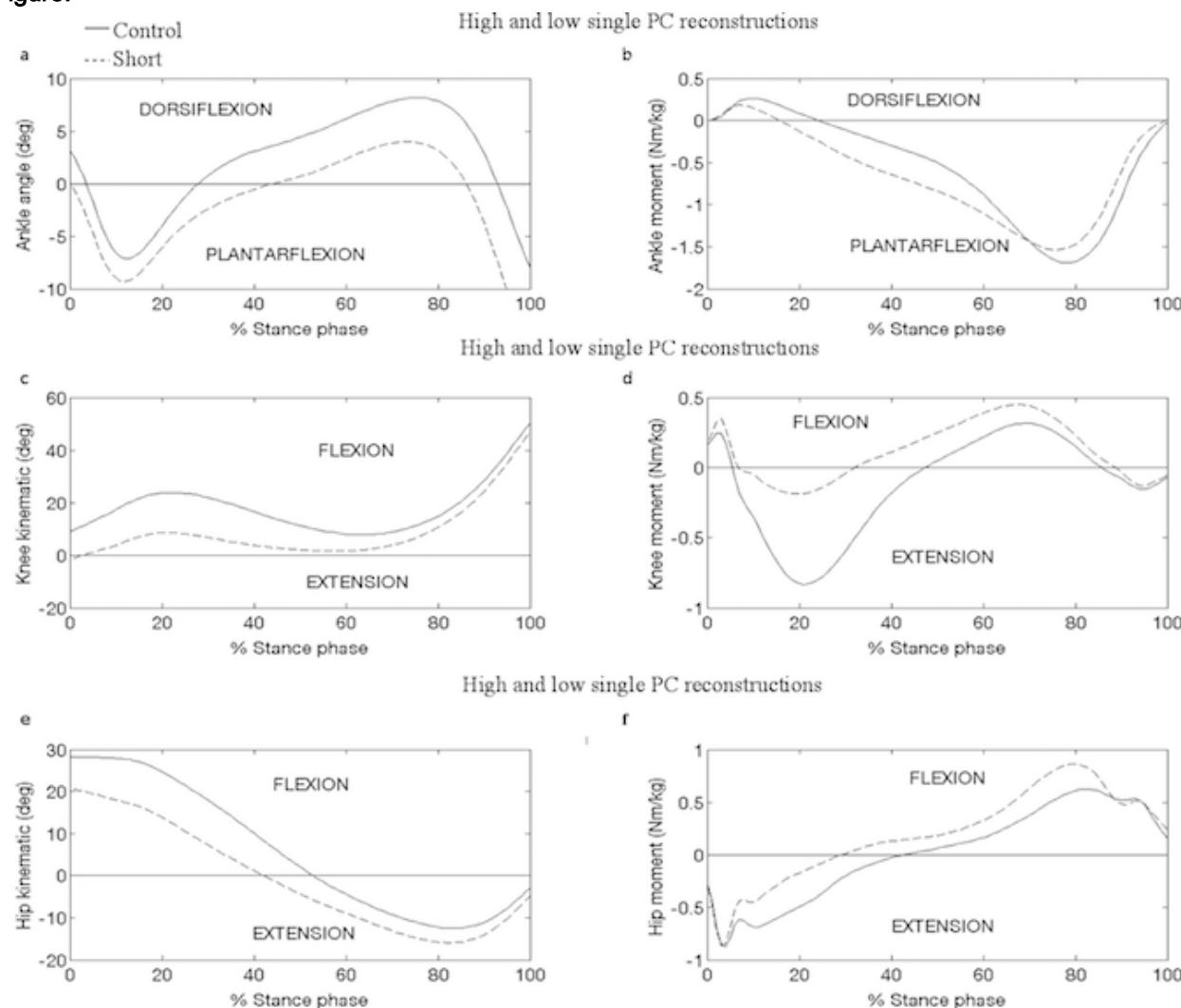
Caption: Control and short limb condition differences demonstrated by the Student's t-test. Shown in the figures are the waveforms that represent high and low principal component (PC) scores for the indicated measure and PC. In all cases, the waveform that represents the PC score (i.e. high or low PC score) that characterizes the short limb condition is shown as a dashed line; the solid line is the waveform that represents the control condition PC score. The ankle dorsiflexion angle PC1 (a); ankle dorsiflexion moment PC1 (b); knee flexion angle PC1 (c); knee flexion moment PC1 (d); hip flexion angle PC1 (e); hip flexion moment PC1 (f).

Conclusion: The increased ankle plantarflexion and knee extension and reduced hip flexion angles may be the strategies implemented by the participants in order to increase functional lower limb length during the short limb condition. The increased ankle plantarflexion moment may help to explain the relationship between LLD and the posterior tibial tendon dysfunction[4]. In addition, the increased knee extension angle and reduced knee extension moment during early stance may indicate reduced quadriceps action on the short lower limb, which may help to explain the association between patella-femoral pain and LLD[3]. Therefore, the results of this study suggest that LLD smaller than 2 cm should not be overlooked in clinical settings.

Table:

Measure	PC	Variance explained (%)	*p-value*	Effect size	Interpretation based on the effects of the short limb condition
Ankle dorsiflexion angle	1	53.7	<0.001	0.85	Had greater ankle plantarflexion throughout stance.
Ankle dorsiflexion moment	1	60.3	<0.001	0.92	Had greater ankle plantarflexion moment in early stance and smaller plantarflexion moment in late stance.
Knee flexion angle	1	73.2	0.018	0.52	Had greater knee extension in early stance.
Knee flexion moment	1	76.2	0.002	0.64	Had smaller knee extension moment in early stance.
Hip flexion angle	1	78.8	<0.001	0.90	Had smaller hip flexion during the first half of the stance phase.
Hip flexion moment	1	50.4	<0.001	0.84	Had smaller hip extension moment in early stance and greater hip flexion moment in late stance.

Caption: Principal components (PCs) that demonstrated differences between short limb and control conditions. Percentage of variance explained and an interpretation of each PC are also provided.

References: [1] Woerman et al., Leg length discrepancy assessment: accuracv and precision in five clinical methods of evaluation. J. Orthop. Sports Phys. Ther. 5: 230-9, 1984.

[2] Rothenberg. Rheumatic disease aspects of leg length inequality. Semin. Arthritis Rheum 17: 196-205, 1988.

[3] Carlson et al., Are differences in leg length predictive of lateral patello-femoral pain? Physiother. Res. Int, 12: 29-38, 2007.

[4] Sanhudo et al., Association between leg length discrepancy and posterior tibial tendon dysfunction. Foot Ankle Spec. 7: 119-26, 2014.

[5] Kirkwood et al., Application of principal component analysis on gait kinematics in elderly women with knee osteoarthritis. Rev Bras Fisioter. 15: 52–8, 2011.

Disclosure of Interest: None Declared

Lower Limb

AS-0156

THE MECHANICAL FUNCTION OF THE TIBIALIS POSTERIOR MUSCLE AND ITS TENDON DURING WALKING

Jayishni Maharaj [1,*]Andrew Cresswell [1]Glen Lichtwark [1]

[1]School of Human Movement and Nutrition Sciences, The University of Queensland, Brisbane, Australia

Introduction and Objectives: During walking, the tibialis posterior (TP) muscle is active during initial contact, to resist subtalar joint (STJ) pronation and presumably to absorb mechanical energy. The TP muscle is also active during mid- to late-stance to enable STJ supination and generate mechanical energy in the frontal plane. The ability of a muscle to store and release energy is highly dependent on the interaction of its muscle fascicles and series elastic element (SEE), consisting of the tendon and aponeurosis. Compliant tissues are able to decouple the length changes of muscle fibres from the whole muscle-tendon unit (MTU) during cyclic activities such as gait [1]. Therefore, distinguishing the roles of the contractile and SEE is fundamental in understanding the mechanics and energetics of the whole MTU during locomotion. Based on the architectural properties of the TP, which has short fibres and a long SEE, we hypothesised the TP tendon might be sufficiently compliant to store and release energy during walking, particularly to buffer stretch in early stance. We speculated a lengthening in the TP MTU during early stance with little or no stretching of its muscle fascicles.

Methods: We directly measured TP length and activation in healthy subjects (n=8, 6 male, age 19-35yrs, height 1.60-1.87m, mass 54-100kg) at a preferred speed. Muscle electrical activity was recorded using bipolar fine-wire electrodes inserted in the TP under ultrasound guidance. MTU strain and joint moments were modelled in Opensim [2] in a custom, scaled model driven through an inverse kinematics and dynamics approach. Muscle fascicles were imaged in the sagittal plane using dynamic ultrasound imaging (80 Hz) and fascicle length changes were tracked with a semi-automated optic flow algorithm [3]. Length changes of the MTU and fascicles were calculated relative to mean fascicle length at foot contact for each participant and mean values were calculated for complete stride cycles across all subject.

Results: As illustrated in Figure 1A, TP fascicles followed a different strain pattern than that of the MTU over the stride cycle. At contact, the MTU rapidly lengthened, indicated by a peak positive velocity during early stance, whilst its activation increased (Figure 1B). The TP muscle was actively generating a supinatory moment during this time to decelerate the rapid STJ pronation. Active MTU lengthening with isometric fascicles (Figure 1A) indicates stretch and absorption of energy in the SEE. Muscle fascicles did lengthen after the MTU ceased stretching, indicating some absorption of energy by the fascicles, however the magnitude of the fascicle lengthening velocity was significantly less than the MTU ($P \leq 0.05$). During late stance, most of the shortening observed in the muscles fascicles occurred during muscle deactivation (Figure 1B) when the elastic tissues were also rapidly recoiling. Energy stored in the SEE was likely released during late stance to power supination of the STJ.

Figure:
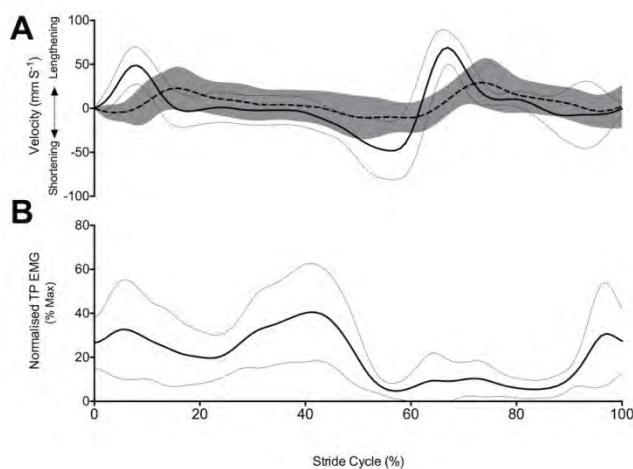
Caption: Figure 1: Group mean and standard deviation of (A) velocity of tibialis posterior (TP) muscle fascicles (dotted line) and MTU (solid line) and (B) TP muscle activity (rectified and filtered) during a stride cycle at preferred walking speed. Initial contact occurs at 0% of the stride cycle.

Conclusion: The results of this study illustrate two important findings. First, decoupling of muscle fascicle strain from MTU strain was enabled by the compliant SEE of TP. This finding is consistent with results from other distal lower limb muscles (e.g. medial gastrocnemius) during gait [4], however this is the first demonstration in a lower limb muscle that acts predominately in the frontal plane.

Second, we showed that immediately following contact, TP fascicles remained relatively isometric whilst its MTU lengthened, suggesting stretch of the SEE. Energy absorbed in the SEE during this period was a result of a rapid supinatory moment at the STJ with excessive STJ pronation (negative STJ power) in the braking phase of walking. It is apparent that TP tendon compliance can mechanically buffer excessive strain and high velocities in the muscle fascicles, potentially protecting its fascicles from eccentric muscle damage. The role of the SEE in dissipating energy has mainly been illustrated in the distal tendons of wild turkeys and cats [5], [6]. This study, presents a similar role for the human TP muscle during walking. Excessive strain of the SEE during early stance may, however, predispose some individuals to overuse tendon pathologies. Further investigations into how extrinsic factors and foot dynamics influence TP tendon strain is required.

References: [1] Fukunaga et al., *Proc. R. Soc*, 268:229–233, 2001.

[2] Delp et al., *IEEE Trans. Biomed. Eng.*, 54:1940–1950, 2007.

[3] Croni et al., *J.* Applied Physiology, 111:1491–1496, 2011.

[4] Lichtwark et al., *J. Experimental Biology*, 209:4379–4388, 2006.

[5] Konow et al., *Proc. R. Soc*, 270:1108-1113, 2011.

[6] Griffiths, *J. Physiology*, 436:219–236, 1991.

Disclosure of Interest: None Declared

Sport

AS-0157

THE EFFECT OF A RIGID ANKLE BRACE ON JOINT KINETICS DURING MAXIMAL CYCLING

Paul R. Barratt [1,*]Thomas Korff [1]

[1]Centre for Sports Medicine and Human Performance, Brunel University, Uxbridge, United Kingdom

Introduction and Objectives: Maximal cycling power is predominantly produced by hip extensor, knee extensor, knee flexor and plantarflexor power. Hip extensor power is absorbed by the plantarflexors and transferred to the crank [1,2]. For this mechanism to work effectively, the plantarflexors need to contract quasi-isometrically to stiffen the ankle joint, which requires strong plantarflexor muscles.

It has previously been demonstrated that the plantarflexors are maximally recruited during maximal cycling [3], and that ankle extension strength differentiates between more and less powerful sprint cyclists [4]. Interestingly, it has also been reported that the hip extensors are not maximally recruited during maximal cycling [3] , and that hip extension strength does not differ between more and less powerful sprint cyclists [4]. Taken together, these findings suggest that the amount of usable hip extension power may be limited by the plantarflexor's ability to stiffen the ankle joint sufficiently. If this was the case, a stiffer ankle joint could allow the hip extensors to operate closer to its maximal capacity, which would in turn result in higher overall maximum power.

In this study, we used an ankle brace to probe this mechanism. We hypothesized that the increased joint stiffness imposed by a rigid brace that fixed the ankle in place would allow the hip extensors to generate more power during maximal cycling.

Methods: Eight male cyclists (31 ± 5 years old, 79.2 ± 6.1 kg), performed a short (4 s) isokinetic maximal cycling bout at 90 rpm with braces that held the ankle joints in a fixed-position. For the control condition, the participants performed the same protocol with weights of equivalent mass to the braces (1.16 kg per leg) attached to each leg. Joint powers were determined by means of sagittal plane inverse dynamics. Kinetic data were acquired by instrumented force cranks, and kinematic data were acquired by means of high speed motion analysis. A paired t-test was used to test the hypothesis that mean hip extension power would be greater when using the ankle braces compared to the ankle weights.

Results: In conformity with our hypothesis, cyclists produced greater hip extension power when cycling with the rigid ankle braces compared to the ankle weights (Braces; 567 ± 112 W vs. Weights; 501 ± 74 W, p = 0.028). The magnitude of this effect was moderate (effect size; 0.73). Figure 1 illustrates that the ankle brace (red) and ankle weights (blue) hip power curves tend to diverge at the point of peak power production during the pedal cycle (approximately 135 degrees).

Figure:
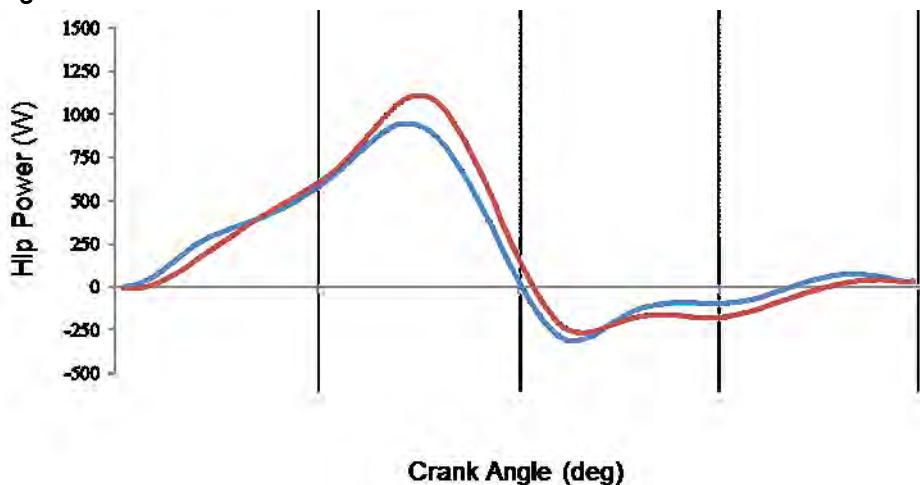
Caption: Figure 1. Hip power during maximal sprint cycling when using ankle braces (red) and ankle weights (blue).

Conclusion: These results demonstrate that the ability to stiffen the ankle joint limits hip extension power during maximal cycling. They thereby explain previous findings as to why the hip extensors are not maximally activated during maximal cycling.

Confirmation of this mechanism gives significant insights into the mechanisms underlying power production during maximal multi-joint movements. In particular, these results highlight the importance of all power producing muscle groups during maximal cycling. Previous research focussed predominantly on the dominant power producing actions of knee extension and hip extension during maximal cycling. Our results add to this body of knowledge that the plantarflexors are an important muscle group to consider not only for their power producing capability but also for their ability to enable muscular power to be transferred from the proximal muscles to the pedal.

From an applied perspective, these findings give insights into the potential benefits of training interventions targeting ankle joint strength for sprint cycling performance. They suggest that strengthening the plantarflexors could result in improved sprint cycling performance.

References: [1] Fregly BJ et al., J. Biomech, 29(1): 81-90, 1996

[2] Raasch CC et al., J. Biomech, 30(6): 595-602, 1997

[3] Dorel S et al., Med Sci Sport Exec, 44(11): 2154-2164, 2012

[4] Barratt PR, Ph.D Dissertation, Brunel University 2014

Disclosure of Interest: None Declared

Sport

AS-0158

BIOMECHANICAL ANALYSIS OF THE UPPER BODY IN THE PEN-HOLD GRIP AND THE HAND-SHAKE GRIP IN TABLE TENNIS

Tianjiao Dai [1]Graham Arnold [1]Walter Williamson [1]Rami Abboud [1]Weijie Wang [1,*]

[1]University of Dundee, Dundee, United Kingdom

Introduction and Objectives: There are two ways of griping the table tennis bat, pen-hold grip and hand-shake grip. Argument about which grip is better is endless where one group belief suggests that the pen-hold grip provides a faster speed but may more easily result in wrist injury; whereas others think that the hand-shake grip can get a larger range of motion. Although there were some previous studies comparing the two grips, their research methods were limited to video observation or literature review. The aim of this study was to investigate the movements and muscle activities in the upper limbs, back, and waist during the hitting ball in both pen-hold grip and hand-shake grip and to compare the differences between these two hand grips biomechanically.

Methods: Seventeen male subjects aged from 21 to 31 were recruited in this study. They were required to play the hitting ball using four ways, pen-hold forehand, pen-hold backhand, hand-shake forehand, and hand-shake backhand. A set of markers on their body were collected using Vicon® motion capture system, and the electromyography (EMG) in the brachioradialis, pronator teres, biceps brachii, triceps brachii, deltoid, trapezius and erector spinae were synchronically measured using wireless Delsys® system. An in-house made model was deigned to calculate the joint movements in the shoulder, elbow and wrist.

Results: Significant differences were found in the shoulder, elbow and wrist joint angles and seven muscles EMGs between the pen-hold and hand-shake grips. Four ways of holding bat produce different ranges of motion in the shoulder, e.g. in Table 1. In general, the pen-hold backhand needs the largest movement of the three joints, followed by the hand-shake forehand, the pen-hold forehand and the hand-shake backhand as the least. As whole, the pen-hold grip requires larger movements in joints than hand-shake grip in a swing motion. Regarding to EMG, it is readily identified that the pen-hold grip relies on the forearm, back and waist muscles much more than the hand-shake grip. Although the hand-shake grip employs more upper arm muscles than the pen-hold one, the assessing scores from both grips are very similar. Therefore, the pen-hold grip needs to active more muscles to achieve a swing motion than the hand-shake one.

Conclusion: Evidence of this study suggests the hand-shake grip is appropriately recommended for the table tennis beginners, recreational players and amateurs, while the pen-hold grip is more suitable for the more skilful players. The pen-hold grip generally needs a larger range of motion, especially in the elbow flexion, and involves more muscle activities, especially in the forearm, back, and waist than the hand-shake grip. This may result in a higher risk in the injury of wrist, elbow, and waist for using the pen-hold grip.

Table:

Hand-grips	Mean (Degree)	Std. Error	p
Pen-hold Forehand	90.15	1.18	-
Pen-hold Backhand	85.88	1.07	0.008
Hand-shank Forehand	84.82	1.15	0.001
Hand-shank Backhand	84.70	1.22	0.001

Caption: Table 1. Range of motions in the shoulder flexion and extension from 4 holding ways (p values against the pen-hold forehand)

Disclosure of Interest: None Declared

Sport

AS-0159

SPRINT ACCELERATION MECHANICS: THE ROLE OF HAMSTRING MUSCLES IN HORIZONTAL GROUND REACTION FORCE PRODUCTION

Jean-Benoit Morin [1,*]Pascal Edouard [2]Philippe Gimenez [3]Pierrick Arnal [2]Pedro Jimenez-Reyes [4]Pierre Samozino [5]Jurdan Mendiguchia [6]Matt Brughelli [7]

[1]University of Nice Sophia Antipolis, Nice, [2]University of Saint-Etienne, Saint-Etienne, France, [3]University of Montreal, Montreal, Canada, [4]Catholic University of San Antonio, Murcia, Spain, [5]University of Savoy, Chambéry, France, [6]Zentrum Rehab and Performance Center, Barañain, Spain, [7]Auckland University of Technology, Auckland, New Zealand

Introduction and Objectives: Recent literature has clearly shown the importance of horizontal ground reaction force (GRF) production in sprint acceleration performance, with direct applications in numerous sports such as soccer, rugby or athletics [1,2]. Furthermore, an increasing number of modeling and clinical studies have shown that hip extensors, hamstring muscles in particular, are (i) very likely contributors of sprint acceleration performance [3] and (ii) some of the most frequently injured and re-injured muscles in all sports that involve sprinting [4,5]. However, no study has approached the problem using synchronous experimental measurements of GRF and muscle activity during accelerated (i.e. non-constant speed) runs. In this context, the ability to develop high amounts of horizontal GRF during sprint acceleration, notably at high velocity and/or in an upright body posture, could be related to a higher contribution of hip extensors. Our aim was therefore to experimentally test the role of the main hip extensor muscles (hamstring and gluteus) in producing horizontal GRF during short, maximal sprints.

Methods: The torque capability of knee and hip extensors and flexors were tested concentrically and eccentrically with an isokinetic dynamometer in 14 males familiar with sprint running (team sports and athletics). Then, subjects performed 6-s sprints from a crouched still start on a motorized instrumented sprint treadmill. EMG activity of Vastus Lateralis, Rectus Femoris, Biceps Femoris and Gluteus Maximus muscles of the right leg was synchronized (1000 Hz) with horizontal and vertical GRF measurements. For each muscle, EMG activity was expressed relative to the activity measured during a maximal voluntary isometric contraction in a standardized position. EMG and GRF data were averaged for all the steps from the second step to the end of the 6-s. EMG data were also averaged over the first half of stance, entire stance, entire swing and end-of-swing phases.

Results: None of the isokinetic variables were significantly correlated with horizontal GRF. Only a tendency ($P = 0.074$) was found between EMG activity of the BF at the end of the swing and horizontal GRF. However, multiple linear regression analysis showed a significant relationship ($P = 0.024$) between horizontal GRF and the combination of both BF EMG during the end of the swing and peak torque during eccentric knee flexion. Finally, gluteus force and EMG activity were not related to horizontal GRF production. We found similar results when sub-dividing the analysis into an early acceleration phase (first 3 seconds), and a late acceleration phase (last 3 seconds).

Figure:
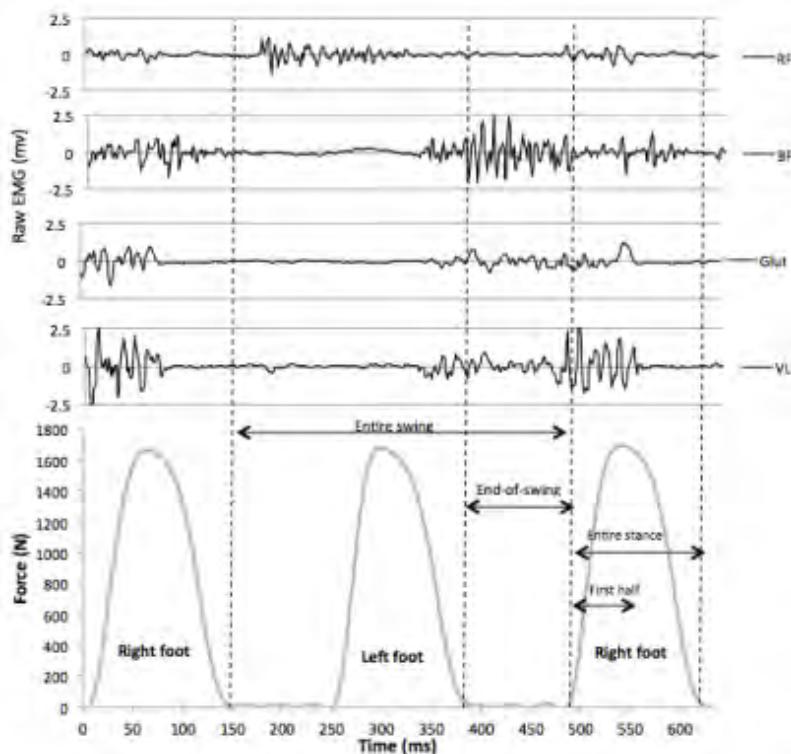
Caption: Synchronized raw EMG data and vertical GRF signals during a typical sprint stride (7th stride of a maximal 6-s acceleration). The following phases for EMG analysis were determined from vertical GRF data (30 N threshold): entire swing, end-of-swing, entire stance and first half of the stance.

Conclusion: The greatest amount of horizontal GRF production during sprint acceleration was found in subjects who were both able to highly activate their hamstring muscles just before ground contact and had the greatest capacity to produce eccentric hamstring torque. In other words, hamstring EMG activity during the swing and end-of-the-swing phases and eccentric knee flexor peak torque is related to the amount of horizontal GRF produced during sprinting, likely because of the backward "pawing" action of the leg just before contact. This relationship, observed here experimentally for the first time, makes even more sense when accounting for the electromechanical delay between EMG activity and force production by the muscles.

References:

[1] Morin, et al., Med Sci Sports Exerc, 43(9):1680-8, 2011

[2] Rabita, et al., Scand J Med Sci Sports, In Press, 2014.

[3] Dorn, et al., J Exp Biol, 215(11):1944-56, 2012.

[4] Schache, et al., Gait Posture, 32(1):136-40, 2010.

[5] Opar, et al., Sports Med, 42(3):209-26, 2012.

Disclosure of Interest: None Declared

UNEXPECTED CHANGES IN FRICTION ON CLAY COURT SURFACES ARE ASSOCIATED WITH ANKLE INVERSION INJURY RISKS IN TENNIS PLAYERS

Chelsea Starbuck [1,*]Victoria Stiles [2]Daniel Ura [3]Matt Carre [3]Sharon Dixon [2]

[1]Sport and Health Sciences, University of St Mark and St John, Plymouth, [2]Sport and Health Sciences, University of Exeter, Exeter, [3]Sports Engineering Research Group, The University of Sheffield, Sheffield, United Kingdom

Introduction and Objectives: Ankle inversion injuries are the most commonly reported injuries in tennis [1]. Although lower friction clay surfaces have been associated with reduced injury risks [2, 3], lower limb injuries are still reported on clay [4]. During match play friction properties across the surface may change due to player interaction with the court. Therefore there may be areas of expected and unexpected friction levels to which players must respond and attempt to maintain balance in order to successfully execute a tennis stroke. The current study aims to examine players' response to expected and unexpected changes in friction and the implications biomechanical factors associated with injury risk.

Methods: Sixteen university tennis players (19.93 ± 0.96 years, 1.74 ± 0.10 m and 66.75 ± 10.36 kg) volunteered for the current study approved by the Institutional Ethics Committee. On a synthetic clay surface participants performed an 180° turning movement (running approach speed 3.9 ± 0.20 m.s^{-1}). To adjust friction levels the volume of sand above the force plate was altered (kg per m^2 surface area). Five testing conditions consisted of a baseline condition (12 kg/m^2), two expected conditions (16 kg/m^2 and 20 kg/m^2) and two unexpected conditions (16 kg/m^2 and 20 kg/m^2). The order of the five testing conditions were randomly assigned. Ten trials of each condition were collected with any unsuccessful trials omitted and repeated. Participants were told which condition (12/ 16/ 20 kg/m^2) they would receive for the expected trials. However, for the unexpected trials the were told they would experience the baseline condition. Prior to each test trial participants performed a baseline condition to allow them to make comparisons with the baseline condition. Ankle kinematics (Peak Performance Technologies, 120 Hz), in-shoe pressure data (Pedar, 100 Hz) and onset time of tibialis anterior muscle activity (Delsy trigo wireless system, 4000 Hz) were collected. Ankle frontal plane moments were calculated using inverse dynamics from synchronised force (AMTI, 960 Hz) and kinematic data. A mixed model ANOVA was conducted to examine the influence of expectation and friction level on players' biomechanical response.

Results: The expected friction conditions resulted in lower ankle inversion angles at ground contact (-.33 ± 3.82°) compared to the unexpected conditions (-7.73 ± 3.24°; ES = .595, P =.001). For the lowest friction condition, the tibialis anterior activated earlier during the expected conditions (.031 ± .014 s) compared to the unexpected changes in friction (.016 ± .021 s; ES = .343, P =.013). Significantly (P <.05) greater pressures were produced in the medial regions of the foot (forefoot, midfoot and heel) for the expected conditions compared to the unexpected conditions. The expected 16 kg/m^2 condition resulted in greater everter moments (-158.43 ± 99.39 N.m) compared to the unexpected 16 kg/m^2 condition (-150.56 ± 95.04 N.m; ES = .330, P =.04). However, no differences in everter moments were observed between the expected and unexpected conditions with 20 kg/m^2 of infill.

Conclusion: Results indicated differences in biomechanical measurements associated with greater risk of ankle inversion injuries during unexpected conditions on a clay court surface. Later onset of muscle activity of the tibialis anterior, which

eccentrically controls ankle inversion during ground contact, is consistent with greater initial inversion angles during the unexpected conditions. Previous reports have suggested larger initial inversion angles to increase risk of the occurrence of an ankle inversion injury [5]. Thus, when clay court friction is unexpectedly reduced players are at greater risk of sustaining an ankle inversion injury. During the expected conditions players increased their control of sliding through greater pressures in the medial regions of the foot. Additionally, players had greater everter moments during the expected conditions and therefore were able to control the subtalar joint during sliding. Greater control of sliding and of the subtalar joint suggest reduced player risk of ankle inversion injuries during the expected conditions when compared to the unexpected conditions. Unexpected changes in clay court friction may occur during match play as a result of players' interaction with the surface, which could have implications on biomechanical aspects related to injury. Therefore maintenance of the clay court surfaces during match play in addition to appropriate conditioning training of the lower limb musculature controlling the subtalar joint is important in preventing ankle inversion injuries on clay court surfaces.

References: [1] Abrams et al., Br. J. Sports Med., 46: 492-498, 2012.

[2] Nigg et al., Sports Med., 5: 375-385, 1988.

[3] Bastholt. Med. and Sci. Tennis, 5: 2000.

[4] Hjelm et al., Scand. J. Med. Sci. Sports, 22: 40-48, 2012.

[5] Kristianslund et al., J. Biomech, 44: 2576-2578, 2011.

Disclosure of Interest: None Declared

SPATIOTEMPORAL VARIABLES OF ABLE-BODIED AND AMPUTEE SPRINTERS IN MEN'S 200-M SPRINT

Hiroaki Hobara [1,*] Yoko Sano [1] Yoshiyuki Kobayashi [1] Thijs Heldoorn [1] Masaaki Mochimaru [1]

[1] Digital Human Research Center, National Institute of Advanced Industrial Science and Technology, Tokyo, Japan

Introduction and Objectives: Time difference of world records between able-bodied sprinters and amputee sprinters using running-specific prostheses (RSPs) in the men's 200-m sprint is still about 1.5 seconds (as of 12 December 2014). Theoretically, forward velocity in a 200-m sprint is the product of step frequency and step length. According to a previous study, the differences in 100-m sprint performance between able-bodied (ABS) and amputee sprinters (bilateral and unilateral transtibial amputees using RSPs) groups would be due to a shorter step length rather than lower step frequency [1]. However, it remains unclear if the step length deterioration in amputee sprinters exists or changes at other sprint events. Therefore, the goal of this study was to examine the hypothesis that the difference in the 200-m sprint performance of ABS and amputee sprinters is due to a shorter step length rather than a lower step frequency.

Methods: 16 ABS, 13 sprinters in the T44 class (defined as any athlete with lower limb impairment/s that meets the minimum disability criteria for lower limb deficiency, impaired lower limb passive range of motion, impaired lower limb muscle power, or leg length difference) and 5 sprinters in the T43 class (defined as double below-knee amputees and other athletes with impairments that are comparable to a double below-knee amputation) competing in men's 200-m races were analyzed from publicly available internet broadcasts. These races included several Olympics and Paralympics (2008 and 2012) competitions, the International Association of Athletics Federations (IAAF) World Championships in athletics (2009, 2011, and 2013), the International Paralympic Committee (IPC) Athletics World Championships (2011 and 2013), and the IPC Athletics European Championship (2014).

Data were collected only from the finals in each competition. In the present study, individual races were excluded from the analysis if the athlete did not complete the race or the athlete's body was not visible throughout the entire race. In the case of the T44 and T42 athletes, sprinters who did not use RSPs were also excluded from the analysis.

According to a previous study [1], we determined the mean forward velocity in the 200-m sprint (V_{200}) of each individual by dividing the race distance (200 m) by the official race times, which were obtained from each competition's official website. In the present study, we calculated the average step frequency (f_{step}) by dividing the number of steps by the official race time. Finally, average step frequency (L_{step}) was computed by dividing race distance (200-m) by the number of steps. One-way analyses of variance (ANOVA) were performed for V_{200}, f_{step}, and L_{step} to determine whether there were significant differences among the four groups (ABS, T44 and T43). Bonferroni post-hoc multiple comparison tests were performed if a significant main effect was observed. Statistical significance was set to be $p < .05$.

Results: As shown in Figure 1-A, we found that the V_{200} of ABS was faster than that of the T44, T43 and T42 groups. Furthermore, although there were no significant differences in f_{step} among the three groups, the L_{step} of the ABS was significantly longer than in the T44 and T43 groups (Figure 2-B and C). The results of the present study suggest that the differences in 200-m sprint performance between ABS and amputee sprinters can indeed be attributed to a shorter L_{step} rather than a lower f_{step}. A shorter L_{step} in amputee sprinters may be the result of lower force generation in their RSPs

compared with the legs of ABS [2-5]. Additionally, in 200-m sprint events, races are performed in a counterclockwise direction, beginning on the curve and ending on the home straight. Amputee sprinters have to compensate for higher rotational forces by using remaining joints when running in the bend track, leading to a relatively shorter step length.

Figure:
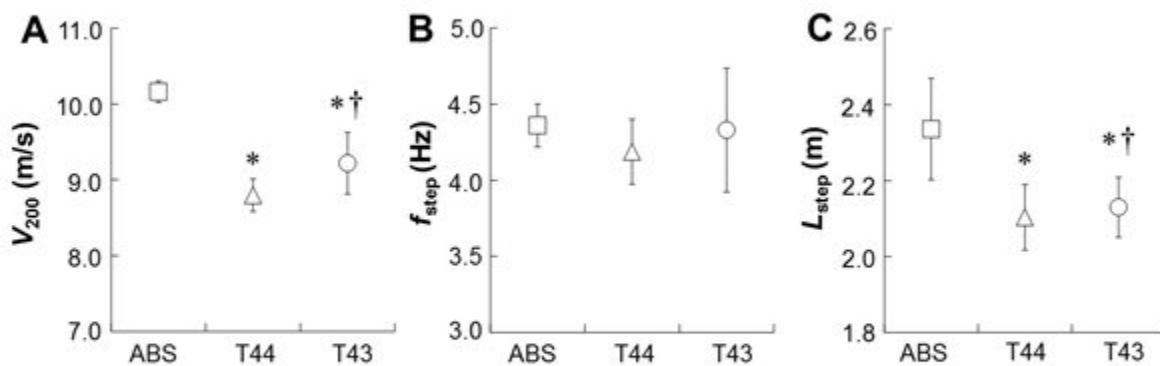
*Significant differences from ABS at $p < 0.01$.
†Significant differences from T44 at $p < 0.01$.

Caption: Comparison of average forward velocity (A), step frequency (B), and step length (C) for the four groups.

Conclusion: In conclusion, the results of the present study support our initial hypothesis that the difference in the 200-m sprint performance of ABS and amputee sprinters is due to a shorter step length rather than a lower step frequency. A shorter step length in amputee sprinters may be the result of lower force generation in their RSPs compared with the legs of ABS, or compensatory strategies for running on a curved track.

References: [1] Hobara et al., Int J Sports Med, in press.
[2] Brüggemann et al., Sports Tech, 1: 220-227, 2009.
[3] Grabowski et al., Biol Lett, 6: 201-204, 2010.
[4] Hobara et al., J Biomech, 46: 2483-2489, 2013.
[5] Weyand et al., J Appl Physiol, 107: 903–911, 2009.

Disclosure of Interest: None Declared

Sport

AS-0162

FATIGUE LEADS TO MORE CHANGES IN TRUNK AND HIP KINEMATICS IN NOVICE VERSUS COMPETITIVE RUNNERS

Ellen Maas [1,*]Jorien de Bie [1]Riet Vanfleteren [1]Wouter Hoogkamer [1]Benedicte Vanwanseele [1]

[1]department of kinesiology, KU Leuven, Leuven, Belgium

Introduction and Objectives: The development of overuse injuries has been associated with kinematic variables of all lower limb joints such as increased hip internal rotation[1,2], hip adduction[3,4], knee adduction, knee internal rotation[3,4] and ankle pronation[5]. Some of these variables have been found to be influenced by fatigue, developed over the course of a run. Fatigue, and subsequently altered kinematics, can magnify risk factors for developing overuse injury. The influence of fatigue on kinematics is likely to be related to training status, since well-trained runners are more resistant to muscular fatigue and are trained to maintain their running technique and posture even when fatigued. Therefore, the aim of the present study was to compare kinematic changes during a run to exhaustion in novice versus competitive runners.

Methods: 15 novice (training distance <10 km/week) and 15 competitive long distance runners (training distance >50 km/week for females and >70 km/week for males) performed a treadmill run till voluntary exhaustion at their average 3200m time-trial pace. Joint angles of the lower limb, as well as absolute trunk and pelvis angles were recorded before and after the fatiguing run using a 3D motion analysis system (Vicon, Oxford, UK) on an instrumented treadmill (Forcelink, Culemborg, the Netherlands).

Results: Some significant differences in peak joint angle between both groups in the non-fatigued state were found in the trunk, hip and knee. Interaction effects of group and fatigue, indicating a different adaptation to fatigue between groups, were the main findings of interest from this study. At the level of the trunk, significant interaction effects were found for peak global trunk flexion at both LS and HS, peak global trunk extension at both LS and HS and lateroflexion ROM at LS (figure 1). All these effects indicated more trunk flexion and more lateroflexion in the novice group as a result of fatigue. At the level of the pelvis, a larger change in obliquity ROM at LS with fatigue was found in the novice group. At the hip level, a significant interaction effect was found at LS for peak hip flexion, occurring at the end of the swing phase, which increased in the novice group and decreased in the competive group. Peak hip abduction (during swing phase) increased more due to fatigue in the novice group. Finally, peak knee flexion during swing phase at HS increased in the competitive group and decreased in the novice group.

Figure:
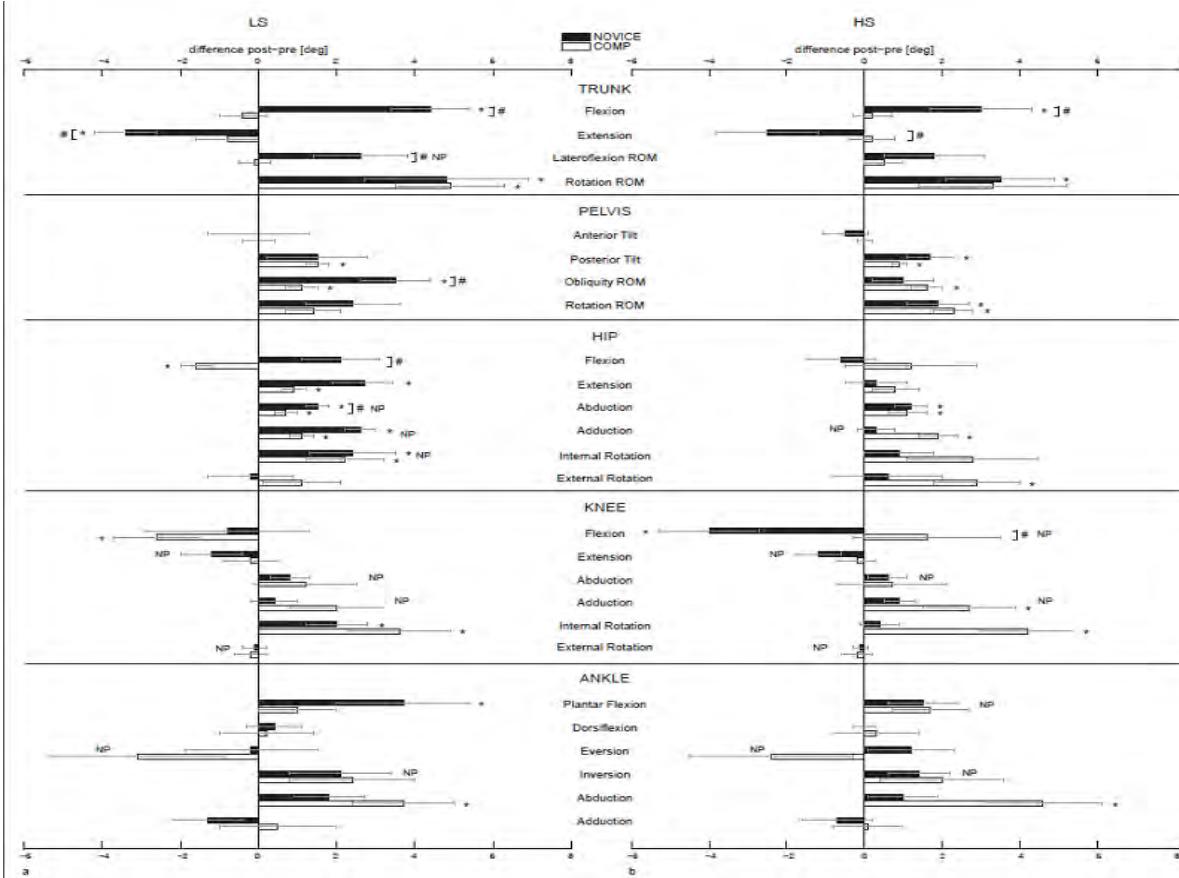
Caption: Figure 1a: differences in joint angles between pre and post fatigue for both groups for low speed (LS). Black bars represent data for novice runners (NOVICE), white bars represent data for competitive runners (COMP). Error bars indicate standard deviation. Figure 1b: differences in joint angles between pre and post fatigue for both groups for high speed (HS).

Conclusion: Fatigue had an effect on the kinematics of the lower limb and trunk in both novice and competitive runners. These effects were largest at the level of the trunk and hip. Kinematic changes were more pronounced in the novice runners, indicating that less experienced runners alter their running style more when fatigued. This may increase injury risk in novice runners. The difference in kinematic changes between both groups can be explained by better trunk and hip muscle strength and endurance in the competitive group. Upon post-hoc questioning, the competitive runners indeed spent more time training core and hip strength. This could indicate a negative relationship between core strength training and kinematic changes with fatigue during running, demonstrating the importance of core strength training for injury prevention.

References: [1] Boling MC et al., Am J Sports Med, 37: 2108-16, 2009.

[2] Ferber R et al., Sports Health,1: 242-6, 2009.

[3] Ferber R et al., J Orthop Sport Phys Ther, 40: 52-58, 2010.

[4] Noehren B et al., Clin Biomech, 22: 951-6, 2007.

[5] Willems TM et al. Med Sci Sports Exerc, 39: 330-9, 2007.

Disclosure of Interest: None Declared

Musculoskeletal

AS-0163

ACCURACY OF ULTRASOUND MEASUREMENTS OF HUMAN MEDIAL GASTROCNEMIUS MUSCLE ARCHITECTURE

Bart Bolsterlee [1,*]DirkJan (HEJ) Veeger [2] [3]Frans CT van der Helm [2]Simon C Gandevia [1]Robert D Herbert [1]

[1]Neuroscience Research Australia, Sydney, Australia, [2]Dept. of Biomechatronics & Biorobotics, Delft University of Technology, Delft, [3]Research Institute MOVE, Vrije Universiteit Amsterdam, Amsterdam, Netherlands

Introduction and Objectives: When muscle architecture is measured from ultrasound (US) images, as is frequently done, it is assumed that fascicles are oriented in the image plane and that the image plane is perpendicular to the aponeurosis at the intersection of fascicle and aponeurosis. This study presents an *in vivo* validation of those assumptions by comparing US image plane orientation to 3D reconstructions of muscle fascicles and aponeuroses obtained with diffusion tensor imaging (DTI) and anatomical MRI scans of the human medial gastrocnemius (MG). The consequences for fascicle length and pennation angles measurements are also reported.

Methods: All measurements were conducted under static, passive conditions with the subjects lying supine, the knee slightly flexed and the ankle in a dorsiflexed position. Fascicle orientations, fascicle lengths and pennation angles were obtained at 16 locations in the left MG on a group of 8 healthy subjects by two methods, one based on US and the other based on DTI and MRI data. Two linear-array US transducers (Esaote MyLab 25) casted into a single unit (image size: 111×40mm with an 18mm gap) were positioned over each of the 16 sites in the MG while recording the 3D orientation of the transducers and leg with a motion capture system. For each of the images, both of the intersections of a clearly visible fascicle and its proximal and distal aponeuroses were identified. The distance between these intersections is the US fascicle length and the mean of the angles between fascicle and aponeuroses at their respective intersections is the US pennation angle. From each subject, 75 axial MRI and DTI images of the left lower leg were obtained with a 3 Tesla MRI scanner. The DTI scans were obtained twice. Muscle boundaries of the MG were outlined on the anatomical scans and a 3D surface mesh was created. DTI data were denoised, and the diffusion tensor was calculated for each voxel. MRI and US coordinate systems were aligned by using MRI-visible markers whose locations could also be identified in US coordinates. DSI studio was used to obtain 100 tracts which passed through a seed region of 9 voxels near the midpoint of an US fascicle, as well as through the deep and superficial aponeuroses (Figure 1). After trimming the ends of tracts that intersected the surface mesh, a line connecting the median location of the endpoints was extended until the muscle surface was intersected. The distance between the intersections of the fascicle with the proximal and distal aponeuroses is the DTI fascicle length and the mean of the two angles between the tangent plane to the surface mesh at the points of intersection and the line connecting the two endpoints is the DTI pennation angle.

To quantify US measurement errors, the angle ϕ between the DTI fascicle and the US image plane was calculated, as were the differences between US and DTI fascicle lengths and between US and DTI pennation angles.

Results: On average, fascicles reconstructed with DTI made an angle ϕ of 1.1 ± 6.7° with the US image plane. This small mean value indicates there was little or no systematic error in the alignment of the US transducers. The mean *absolute* angle, $|\phi|$, which quantifies the average misalignment of the US transducer in individual measurements was 5.5 ± 4.1°

(90th percentile 10.8°). Fascicles reconstructed with US were slightly longer (mean length 54.6mm) than those reconstructed with DTI (52.8mm and 51.5mm). Although *mean* measurements of fascicle length made using US and DTI differed only slightly (1.2 and 2.9mm), the individual pairs of US and DTI measurements differed on average by about 10mm. Pennation angles measured with US were significantly smaller than pennation angles measured from the DTI scans (-5.4° and -6.0°).

Figure:
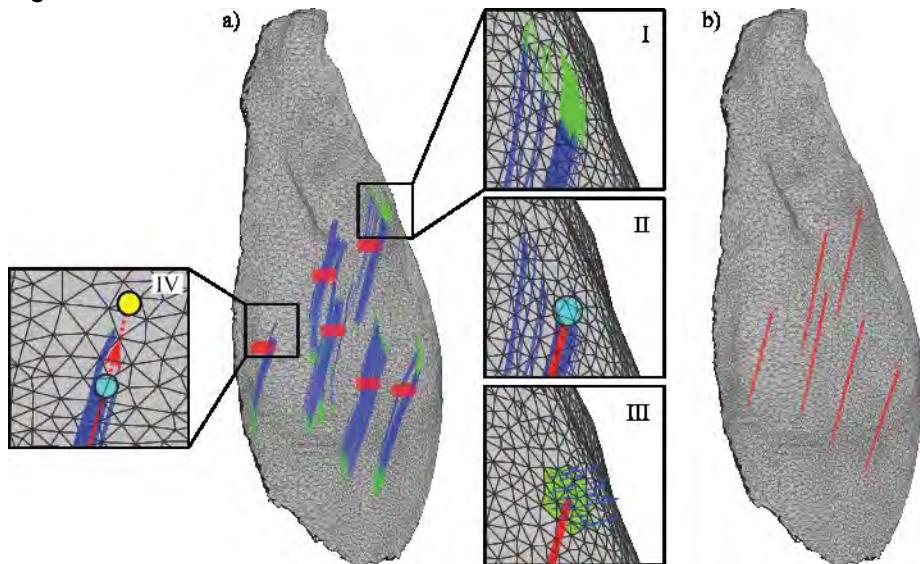
Caption: Fig. 1 a) To reconstruct a muscle fascicle, DTI fibre tracts (blue lines) were trimmed to the muscle surface (I), the median endpoint location (II) was extended to the surface (IV) and the pennation angle was calculated (III). b) Example of 6 fascicles (red lines).

Conclusion: On average, DTI measured muscle fascicles lay very close to the US image plane, but for individual measurements there was substantial misalignment of DTI muscle fascicles with the plane of the US image. On average, US yielded similar measurements of fascicle lengths to DTI (mean difference <3mm), suggesting that the measurements were unbiased. However the mean absolute difference in length between any pair of measurements made with US and DTI was substantial (10mm or 20% of the mean), indicating US measurements were imprecise. The significantly smaller pennation angle measured with US (mean difference 6°) was apparent only at the superficial insertion of the muscle fascicles, and was probably due to pressure on the skin applied by the US probes. It is concluded that US measurements of deep pennation angles and fascicle lengths in the medial gastrocnemius are unbiased but have a low precision and that superficial pennation angles are underestimated by approximately 10°.

Disclosure of Interest: None Declared

Musculoskeletal

AS-0164

ACTIVE MUSCLE FORCE IS INFLUENCED BY MUSCLE COMPRESSION

Tobias Siebert [1,*]Norman Stutzig [1]Olaf Till [2]Reinhard Blickhan [2]

[1]Sport and Motion Science, University of Stuttgart, Stuttgart, [2]Motion Science, Friedrich-Schiller University, Jena, Germany

Introduction and Objectives: External forces compress skeletal muscles during daily activities such as sitting, carrying loads or wearing orthoses. Surrounding muscles, connective tissue, and bones also transfer external forces that compress the muscle. In a recent study [1] we transversally applied external forces to the line of pull in the middle of the muscle belly. Corresponding to the mean pressure at the body-seat interface during sitting, a transversal muscle load of 1.3 N/cm^2 revealed a reduction in maximum force (F_{im}) and rate of force development of approximately 5 and 25 %, respectively. Comparatively higher muscle compressions are, however, expected for e.g. car drivers during accidents or athletes involved in contact sports (e.g. boxing and wrestling). Thus, the aim of the present study was to examine the influence of increasing transversal muscle loading on contraction dynamics.

Methods: We performed isometric experiments on isolated rat *M. gastrocnemius medialis* (n=9) without and with five different transversal loads corresponding to increasing pressures of 1.3 N/cm^2, 2.3 N/cm^2, 3.3 N/cm^2, 4.3 N/cm^2 and 5.3 N/cm^2 at the contact area between muscle and load. Muscle loading was induced by a custom-made plunger which was able to move in transversal direction. During supramaximal muscle stimulation, the isometric force was measured at the distal tendon and the movement of the plunger was captured with a high-speed camera.

Results: Increasing transversal muscle loading (1.3 till 5.3 N/cm^2) resulted in an almost linear decrease in muscle force from 4.8 ± 1.8 % to 12.8 ± 2 % F_{im}. Compared to an unloaded isometric contraction, rate of force development decreased from 20.2 ± 4.0 % at 1.3 N/cm^2 muscle loading to 33.9 ± 4.4 % at 4.3 N/cm^2. Further increase of compression up to 5.3 N/cm^2 had no significant impact on the rate of force development. Lifting height of the plunger decreased from 1.69 ± 0.24 mm at the lowest transversal load to 0.61 ± 0.18 mm at the maximum load applied. Lifting work performed to lift the load increases significantly from 1.06 ± 0.14 Nmm at 65 g muscle loading to 1.50 ± 0.19 Nmm at 115 g. Further increase of transversal loads did not result in significant differences in lifting work.

Conclusion: Transversal muscle loading influences contraction dynamics and should be considered in musculo-skeletal models simulating the interaction of muscles with transversal forces, e.g. in impact biomechanics. Experimental observation of the impact of transversal muscle loading on contraction dynamics may help to better understand muscle tissue properties and to describe more precisely compression of the human body in rehabilitation studies. Moreover, applying transversal loads to muscles opens a window to analyse three-dimensional muscle force generation. Data presented in this study may be important to develop and validate muscle models which enable simulation of muscle contractions under compression and enlighten the mechanisms behind.

References: [1] Siebert et al., Comput. Methods Biomech. Biomed. Engin., 17: 217-229, 2014.

Disclosure of Interest: None Declared

AS-0165

ESTIMATION OF ELASTIC AND DYNAMIC PROPERTIES OF A FINGER ATTRIBUTED TO MUSCLE-TENDON COMPLEX BY MEASURING JOINT ANGLES

Satoshi Makita [1,*]Momoko Maeda [2]Yuki Kawafuchi [3]Ryota Nawata [4]

[1]Control Engineering, [2]Advanced Course of Information Technology, Sasebo College, National Institute of Technology, Sasebo, [3]Yaskawa Electric Corporation, Kitakyushu, [4]General Education, Sasebo College, National Institute of Technology, Sasebo, Japan

Introduction and Objectives: The objective of the paper is to estimate elastic and dynamic properties of a finger easily by measuring joint angles. We show some measurement results of the properties: the relationship along joint angles, resultant fingertip forces and angular velocities of the finger.

 Muscle-tendon complex (MTC) exerts tension and accumulates elastic energy during stretching, and converts the energy into kinetic energy to move bones with high velocity during shortening. As to ball games such as volleyball, the actions of hands are key issue to perform dynamic and flexible contacts with a ball.

 Two typical methods to analyze viscoelastic property of MTC are measuring isolated MTC mechanically [1] and observing MTC by using a ultrasonography [2]. These methods are, however, difficult to observe the behavior of MTC in sports activities including quick movements of upper limbs because of its lack of portability.

 Another approach to analyze human-body movement is to use motion capture, which is generally expensive to introduce. It is, however, difficult to track both fingers and whole body in same time.

 Our proposed method is to measure joint angles of fingers, which can be easily measured by data gloves. It aims to estimate elasticity of fingers attributed to the MTC immediately for evaluation of performances in sports.

Methods: We introduce a hypothesis that MTC of a finger composed of flexor digitorum muscle and its tendon can stretch during dorsiflexion by pushing the fingertip with external forces. The MTC stretches and exerts resultant force according to increasing the angle of MP joint, and then we can estimate fingertip force by measuring the angle of the joint.

 Moreover we can also estimate the resultant angular velocity of the joint after the applied external force is removed because the movement of finger is induced by the MTC shortening with energy transduction.

 For the above estimations, we before have to obtain the relationship between them. First, we fix a hand of a subject person on the measurement equipment. Since MTC is few stretched by its own tension of muscle, the subject can lift up his/fer index finger at a certain angle. We define the angle as "initial angle". Next, we push his/her fingertip to lift it up. Then the MP joint angle and the applied force can be measured by a goniometer and a force sensing resister respectively. When the limitation angle that the finger cannot move no longer occurs, the measurement is suspended. This process from the initial to the limitation angle is called as "loading". After the limitation angle, we bring the finger down and similarly measure the two parameters until the initial angle. The downward process is "unloading".

 As to measuring angular velocity, we use the same equipment to load and unload an external force to a fingertip. We lift the finger up to a certain angle, and remove the load supporting it instantly to release it. The angular velocity can be

estimated from several images captured by a high-speed camera. In unloading process, we lift the finger up to the limitation angle once and bring it down to a certain angle, and release it.

Results: The relationship between angles of MP joint and the applied external forces, which are equal to the resultant forces exerted by the fingertip, in a loading process can be approximated by an exponential function. This trend is similar to a relationship between tension and length of an isolated tendon reported in previous works [1, 3]. The relationship in a unloading process has, however, larger hysteresis with sudden reduction of exerted force than that of the isolated tendon. The loss of the force may be caused by any loss of muscular strength, although the factor has not yet been proved.

 On the other hand, the relationship between the angle of MP and the angular velocity of the finger can be expressed by an approximation derived from the energy transduction. Note that it also has large hysteresis in its trend, which is probably caused by the loss of elastic energy mentioned above.

Figure:
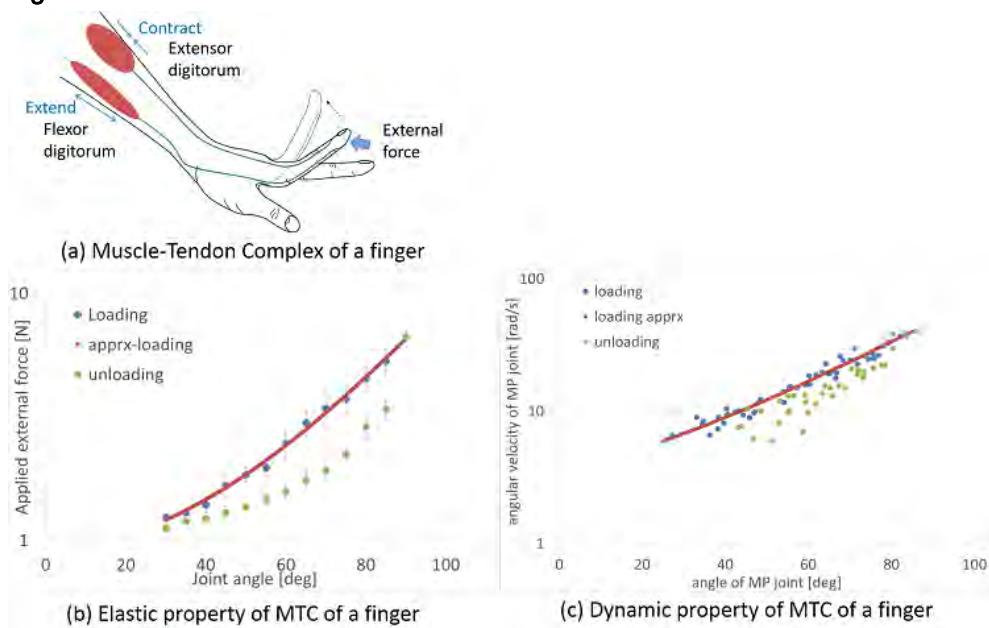
Caption: Estimating elastic property of muscle-tendon complex of a finger

Conclusion: This paper presented a method of estimating elastic and dynamic properties of muscle-tendon complex of a finger easily by measuring joint angles. Based on the hypothesis that the MTC can stretch during dorsiflexion with pushing the fingertip with an external force, we obtained the relationship between the joint angle and the exerted force as an approximation of relationship between tension and length of MTC. The obtained relationship derived an expression of estimating angular velocity of the finger induced by removing the applied force, from formulas of energy transduction. Consequently, the measured angular velocities can fit to the approximation.

References: [1] R. F. Ker, J. of Exp. Biol., 93: 283-302, 1981.

[2] S. Kurosawa et al., J. of Appl. Physiol., 90: 1349-1358, 2001.

[3] M. Nordin and V. H. Frankel, Basic Biomechanics of the Musculoskeletal System, Lippincott Williams and Wilkins, 2001.

Disclosure of Interest: None Declared

AS-0166

A PATIENT-SPECIFIC MUSCULOSKELETAL MODELLING PIPELINE APPLIED TO PHALANGEAL LOADING CONDITIONS IN GAIT.

Joe A. I. Prinold [1] [2]Claudia Mazzà [1] [2,*]Stefan Wesarg [3]Roberto Di Marco [4]Pieter van Dijkhuizen [5]Laura Tanturri De Horatio [6]Clara Malattia [5]Marco Viceconti [1] [2] and MD-PAEDIGREE Consortium

[1]Mechanical Engineering, [2]Insigneo Institute for in silico medicine, The University of Sheffield, Sheffield, United Kingdom, [3]Visual Healthcare Technologies, Fraunhofer IGD, Darmstadt, Germany, [4]Department of Mechanical and Aerospace Engineering, Sapienza University of Rome, Rome, [5]UOC Pediatria II - Reumatologia, Istituto Giannina Gaslini, Genova, [6]Ricerca Sanitaria, Ospedale Pediatrico Bambino Gesù, Rome, Italy

Introduction and Objectives: Juvenile Idiopathic Arthritis (JIA) is the leading cause of childhood disability from a musculoskeletal disorder (affects 0.16-4 in 1000; [1]). Distal joints, like the ankle, are often affected first [1]. JIA is an auto-immune disease of unknown aetiology. It is hypothesized that altered joint loading (JRF), due to pain and inflammatory processes, influences disease progression. Musculoskeletal modelling predicts patients' JRF. Standard modelling practice involves scaling a generic model to a patient [2]. However, JRF is sensitive to muscle moment arms [3] and patient-specific moment arms can differ significantly from a scaled generic model [4] – particularly in a pathological juvenile population.

Musculoskeletal models usually idealise the foot as one, two or three segments [2,5]. However, the importance of these assumptions to ankle joint loading is unclear. The aim is to develop a pipeline for construction of a lower-limb model with a patient-specific foot. The resulting model simulations will analyse sensitivity of ankle JRF to foot segment idealisations.

Methods: An MRI scan of the foot and the distal shank was segmented to give a patient-specific foot geometry. Landmarks were virtually palpated and used to register the hindfoot (10 landmarks), metatarsal (15), and toe (17) segments of two generic models [2,5] onto the virtually palpated landmarks on the patient-specific foot geometry. The muscle attachments and via points were transformed according to the same registration. The registered muscle points were then adjusted to fit the muscles seen in the patient's MRI data. The joint coordinate systems and joint centres were defined from the patient-specific foot geometry [2] and the modified Oxford Foot Model [6]. A cylinder fitted to the talus defined the ankle joint centre. This gave a three segment, 7 degree of freedom foot model. 3 proximal segments of the generic model were scaled homogeneously (femur, shank and patella) and 1 non-homogeneously (pelvis). These segments were fitted to the patient-specific distal tibia via a rigid registration. The resulting model was exported as an OpenSim model. This processing was completed with the open-source NMS Builder software. Gait analysis markers [6] were included in the MRI scan of the foot. These markers were fixed to the relevant segments of the musculoskeletal model. Thus, gait analysis markers drove the model's motion via OpenSim's Inverse Kinematics routine. Static Optimization (minimising the sum of the squared muscle activations) and Joint Reaction Analysis was then used to compute the ankle joint forces. In the Static Optimisation the fore/hindfoot rotations and the int/external hindfoot rotation were locked, and thus not required to reach static equilibrium.

Two models of JIA patients (ages: 12 & 15 years) were simulated, according to the described pipeline (five trials per patient). Sensitivity to segment idealisation was tested by analysing two cases of possible ground reaction force (GRF) application. In the one segment assumption (1SEG) the GRF was applied to the hindfoot segment throughout the trial, thus underestimating the toe loading. In the two segment assumption (2SEG) the GRF was applied to the hindfoot segment until the centre of pressure crossed the metatarsophalangeal joint's flexion/extension axis. At this point the GRF was applied to the toe segment, thus overestimating the toe loading (the metatarsal heads share some of the load).

Results: A large effect of the 1SEG and 2SEG assumptions on the toe flexor muscles is observed (Figure 1). The mean difference between the segment assumptions (|1SEG – 2SEG|) is 2% body weight (BW): 1.3% higher ankle JRF in the 2SEG assumption than in the 1SEG assumption. So, even with the large differences in muscle activations, there is a negligible effect on the magnitude of the ankle JRF.

Figure:
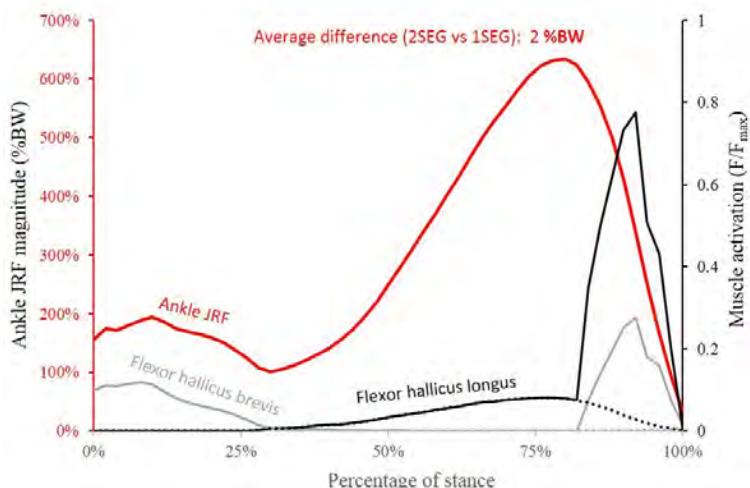
Caption: Figure 1: Mean ankle joint reaction force (thicker red line, left axis) and mean flexor muscle activations (black and grey lines, right axis) during the stance phase of gait, with the 1SEG (dashed lines) and 2SEG (solid lines) assumptions. The black lines represent the flexor hallucis longus and the grey lines the flexor hallucis brevis. Abbreviations: JRF (joint reaction force), %BW (percentage of body weight), Fmax (maximum isometric muscle force).

Conclusion: A novel pipeline for the construction of a lower-limb model with a patient specific foot has been presented. This modelling process has been applied to predict the ankle JRF in JIA patients during gait. Finally, the effect of a one or two segment foot has been shown to be small through a comparison of two GRF applications that underestimate (1SEG) and overestimate (2SEG) the toe loading.

References: [1] Ravelli et al., Lancet, 369: 767-78, 2003.

[2] Arnold, et al., Ann Biomed Eng, 38: 269-79, 2010.

[3] Ackland, et al., J Biomech, 45: 1463-71, 2012.

[4] Gatti, et al., Clin Biomech, 22: 639-44, 2007.

[5] Saraswat, et al., J Biomech, 43: 1645-52, 2010.

[6] Stebbins, et al., Gait & Posture, 23: 401-10, 2006.

Disclosure of Interest: None Declared

Musculoskeletal

AS-0167

MUSCULAR ARCHITECTURE DIFFERENCES BETWEEN MALE AND FEMALE AMATEUR SOCCER PLAYERS

Maher A. Hamzeh [1,*] Marit Undheim [1] Adam Taylor [1]

[1] Life Sciences, University of Roehampton, London, United Kingdom

Introduction and Objectives: It has been well documented that adult males have significantly greater absolute strength compared to adult females. The mechanisms resulting in sex differences in muscle performance are not well understood (Chow et al., 2000)[1]. When considering what affects muscle performance, muscle architecture has shown to greatly affect the muscle's force-production capacity. Muscle architecture changes during contraction and data measured when the muscle is relaxed might not represent the accurate sex differences in muscle architecture. Therefore, the purpose of the study was to investigate the sex differences in muscle thickness of the rectus femoris (RF) and pennation angles of the vastus lateralis (VL) when the knee extensor muscles were at rest and while performing isometric knee extensions at 25%, 50%, 75%, and 100% maximal voluntary contraction (MVC).

Methods: Fifteen male amateur soccer players (age 22.6 ±2.3 years; body mass 78.1± 9.2 kg; height 1.81 ±0.07 m; mean ±s) and 15 female amateur soccer players (age 27.2±2 years; body mass 65.7 ±12.6 kg; height 1.68 ±0.08 m) volunteered to participate in the present study. Participants performed a 5 minute warm- up. Prior to testing, the sites at which the ultrasound measurements were taken were located on the participants' dominant legs. Participants were then seated in the isokinetic dynamometer (Cybex, Norm, USA) in an upright position with their hips at 85^0 of flexion and their dominant knee at 70^0 of flexion. The muscle thickness and pennation angles were recorded twice when the muscles were at rest and at 100%, 75%, 50% and 25% of their MVC using a real-time ultrasound scanner (Sonosite, M-Turbo, USA). Independent t-test was run for each measurement and the significant value was set at $P<0.05$.

Results: The results in Table 1 show that males had statistically significantly ($p<0.05$) greater muscle thickness in the RF compared to females at rest, 50% MVC, 75% MVC and 100% MVC, but not at 25%. There was no statistical significant difference ($P>0.05$) between males and females in pennation angle of the VL muscle (Table 1). Significant differences ($P<0.05$ were found in the muscular strength between male and female participants.

The results of muscle thickness are similar to those found by Chow et al. (2000)[1] and Kubo et al. (2003)[2] who reported that young males had significantly greater muscle thickness and pennation angles compared with young females for three different muscles (VL, medial gastrocnemius and long head triceps brachii). However, the present study did not find any significant differences in pennation angle between males and females. Ichinose et al. (1998)[3] reported that male soccer players had significantly greater muscle thickness of the triceps branchii compared to female soccer players, but not for pennation angles which confirmed the findings of the present study.

Conclusion: The results suggest that muscle thickness contributes more towards sex differences in muscle performance compared to pennation angle. However, further research needs to be done on various muscle groups and at various measurement locations.

Table:

Contraction	Muscle thickness (mm)		Pennation angle (^{0})	
	Males	Females	Males	Females
100% MVC	35.09±3.90	31.52*±3.58	16.77±1.68	17.75±3.05
75% MVC	34.69±3.60	31.79*±3.77	16.37±1.79	17.52±2.46
50% MVC	34.73±3.50	31.87*±3.29	15.50±1.83	16.79±2.34
25% MVC	33.96±3.99	32.13±2.87	14.31±1.74	15.85±2.50
0% MVC	29.99±3.36	27.45*±2.75	13.57±1.49	14.82±2.04

*Significant lower ($P<0.05$) than male participants

Caption: Table 1 Average muscle thickness of RF and penation angle of VL of males and females at various isometric contraction conditions (mean ± s)

References:

[1] Chow et al., Eur J Appl Physiol., 82, 236-244, 2000

[2] Kubo et al., Int J Sports Med., 24, 125-130, 2003

[3] Ichinose et al., Eur J Appl Physiol., 78, 109-114,

Disclosure of Interest: None Declared

AS-0168

CHANGES IN PEAK VERTICAL FORCE AND LOADING RATES AT THE BEGINNING AND END OF LOADED WALKING

Jennifer Neugebauer [1],[*]Angela Boynton [1]

[1]Dismounted Warrior Branch, U.S. Army Research Laboratory, Aberdeen Proving Ground, United States

Introduction and Objectives: As military loads carried by Soldiers increase, walking kinetics increase as well, specifically vertical ground reaction forces (Fz) and loading rates (LRz) [1,3]. To date, little is known about the effect of distance walked on the differences in peak Fz and LRz at the beginning and end of a loaded walk. Increased Fz and/or LRz over the course of a loaded walk may result in decrements in Soldier performance or injury [2]. The objective of this study was to determine if peak Fz and LRz during the stance phase of gait differ between the first and last minute of walking for a light, short walk (1.45 km with 27.6 kg) and for a heavy, long walk (5.63 km with 38.5 kg).

Methods: For the light, short walk, 12 active duty Soldiers (86.9 ± 10.9 kg, 1.77 ± 0.07 m) carried a 27.6 kg military load (weighted rucksack, body armor, dummy weapon) for a 1.45 km walk (20 minutes on a treadmill at 1.25 m/s). For the heavy, long walk, 12 active duty Soldiers (78.0 ± 14.6 kg, 1.72 ± 0.06 m) carried a 38.5 kg military load (weighted rucksack, body armor, dummy weapon, helmet) for a 5.63 km walk (5 minutes on a treadmill at 1.25 m/s before and after a 4.83 km walk outdoors through uneven terrain). Ground reaction forces (GRFs) were collected using a force plate instrumented treadmill. Data were collected for 20 seconds during first and last minute of walking. Peak Fz (N) and LRz (N/sec) were determined during the stance phase of gait for the left leg while walking. Fz and LRz were normalized to both body weight (BW) and loaded BW (LBW), defined here as BW plus carried load weight. The first and last minute of walking were compared within each load using paired t-test (p < 0.05). If no differences were found, average peak Fz and LRz were compared between the two walking conditions using a t-test (p < 0.05).

Results: Peak Fz was significantly greater during the last minute compared to the first minute of the long, heavy walk. LRz did not differ (p > 0.17) between the first and last minute of walking for either the short, light walk or the heavy, long walk (Table 1). Additionally, when normalized to LBW, peak Fz at each time point did not differ between load conditions (p> 0.10) while when normalized to BW, peak Fz was greater in the long, heavy load compared to the short, light load (short, light: first minute 1.50 ± 0.09 BW, last minute 1.49 ± 0.11 BW; long, heavy: first minute 1.66 ± 0.14 BW, last minute 1.68 ± 0.15 BW). LRz was greater for the long, heavy walk compared to the light, short walk at both the first and last minute of walking regardless of the normalization method used.

Conclusion: Over the course of a long, heavy load walk, peak Fz increased while LRz did not differ. During a short, light load walk, no differences in peak Fz or LRz at the beginning and end of the walk were observed. Generally, higher forces suggest greater loads on the body and may be indicative of muscle fatigue which may affect Soldier performance. Further investigations are needed to determine if the load or the distance resulted in increased Fz at the end of the long, heavy walk. When normalized to LBW even though peak Fz did not differ between load conditions LRz was greater for the heavy load. Increased loading rates are considered unfavorable [2,4] and may lead to injury after prolonged exposure. It should be noted that the two conditions compared involved treadmill walking and treadmill walking combined with outdoor

walking. Although all data were collected while the subjects walked on the treadmill, walking on different terrain may have affected the findings. Future studies should vary the loads and distance walked on similar terrain (either all outdoors or all treadmill walking). Additionally, further comparisons of medial-lateral and/or braking-propulsive GRFs may illustrate kinetic changes with increasing carried loads for longer distances.

Table: Walking kinetics for the short, light walk and the long, heavy walk normalized to LBW. Peak Fz was greater in the last minute compared to the first (*). LRz was greater in the long, heavy load compared to the short, light load (#) at each time. Average ± standard deviation is presented for data collected during the final 20 seconds of the first and last minute of walking.

Condition	Distance (km)	Load Carried (kg)	Peak Vertical Force (LBW)		Vertical Loading Rate (LBW)	
			First minute	Last minute	First minute	Last minute
Short, light	1.45	27.6	1.13 ± 0.05	1.12 ± 0.06	6.12 ± 0.57	6.05 ± 0.61
Long, heavy	5.63	38.5	1.10 ± 0.05	1.11 ± 0.06*	8.41 ± 0.99#	8.36 ± 0.92#

References: [1] Birrell et al., Gait Posture, 26: 611-614, 2007.

[2] Crowell et al., J Ortho Sports Phys Ther, 40: 206-214, 2010.

[3] Harman et al., USARIEM Technical Report T00-17, 2000.

[4] Wang et al., Mil Med, 177: 152-156, 2012.

Disclosure of Interest: None Declared

EMG

AS-0169

FLEXIBLE FOOT LONGITUDINAL ARCHES ARE LOWERED MORE IN PASSIVE LOADING AND LIFTED MORE DURING SINGLE-LEG STANCE COMPARED TO RIGID ARCHES ALTHOUGH MUSCLE ACTIVATIONS ARE SIMILAR

K. Michael Rowley [1,*] Toshiyuki Kurihara [2] Stephen Reischl [1] Lucinda Baker [1] Kornelia Kulig [1]

[1] Biokinesiology and Physical Therapy, University of Southern California, Los Angeles, United States, [2] Graduate School of Sport and Health Science, Ritsumeikan University, Shiga, Japan

Introduction and Objectives: Passive loading of the lower leg has been used to investigate behavior of the longitudinal arch of the foot and the muscles controlling it. From recent research into the function of intrinsic foot musculature, it has been suggested that intrinsic muscles can produce enough force to aid in postural stabilization by shifting center of pressure location [1], support for the concept of the foot core [2]. It is known that arch flexibility varies greatly in an asymptomatic population, but it is largely unknown how intrinsic and extrinsic foot muscle activity differs with flexibility and whether all feet respond similarly to loads applied passively or actively. The objective of the current study was to investigate the change in height and muscle activity of the longitudinal arch of the foot in response to passive loading and single-leg stance (SLS) conditions in feet with rigid and flexible arches.

Methods: Healthy young adults were screened for inclusion in the study. The foot contralateral to the preferred kicking foot was examined to include participants with a range of foot arch flexibility. Arch deformation, measured by percent change in navicular height, comparing the unloaded arch and the arch loaded at 100% of body weight ranged from 2.4% to 32.4%. Cutoffs of < 11% and > 15% deformation were chosen to define rigid and flexible arches, respectively. Eight participants had rigid arches (4 male) and seven participants had flexible arches (all female). Fine-wire intramuscular electrodes were inserted into the abductor hallucis (AH), flexor hallucis longus (FL), flexor hallucis brevis (FB), and tibialis posterior (TP) muscles in the supporting foot of each participant. Surface electromyography (EMG) was collected from peroneus longus (PL) and tibialis anterior (TA). Three-dimensional kinematic data were obtained using an 11-camera motion capture system. Ground reaction force (GRF) data were collected using a force plate.

Each participant was tested in two conditions. Incremental loads up to 100% of body weight measured by vertical GRF under the instrumented foot were applied to the distal aspect of thigh using a custom built rig. The participant was asked to refrain from any voluntarily elevation of the knee or foot, hold arms across chest, and sit up straight. Each participant then stood in SLS for 5s. This was repeated three times and results were averaged. Data were analyzed using paired t-tests to compare within-subjects between conditions and using independent sample t-tests to compare means between arch flexibility groups. Significance levels were set at α=.05.

Results: In both rigid and flexible arch groups, muscle activation amplitudes of all muscles instrumented were significantly greater during SLS than during passive loading even though both loads were 100% body weight (p<.05) (Table 1). During passive loading, a trend was observed showing greater activation in all muscles in flexible arches. This difference was greatest in the intrinsic foot muscles, but only reached significance in the AH (p=.003). There were no significant differences in activation amplitude between groups during SLS. Arch deformation during passive loading of body weight deformed rigid arches by 7.5 ± 3.5% and was significantly less than deformation of flexible arches by 22.4 ± 6.7%

(p<.001) (Figure 1). During SLS most subjects lifted the arch where the average lift in the rigid arch group was 0.19 ± 11.3% and was significantly less than the average lift in the flexible arch group, 15.6 ± 15.7% (p=.046).

Figure:
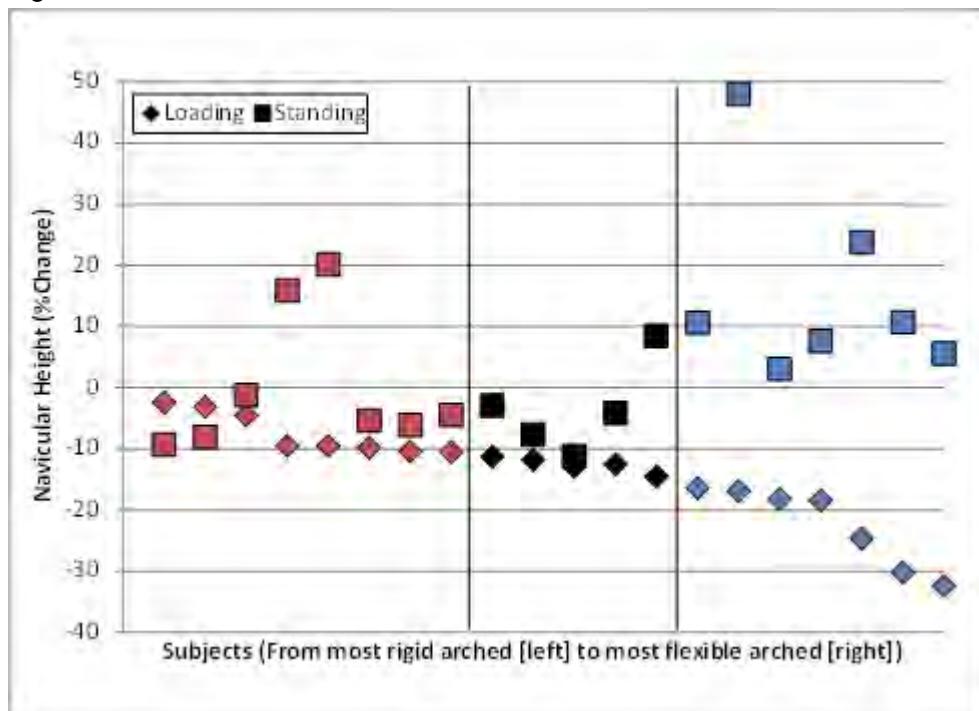
Caption: Navicular height change during passive loading and single-leg stance.

Conclusion: For all arch types, both intrinsic and extrinsic foot muscles controlling the longitudinal arch were more active during SLS compared to passive loading of 100% body weight. Flexible arches were both lowered more in passive loading and lifted more during SLS, even though muscle activation was not different between groups. Passive loading was not sufficient to elicit muscle activations and arch lift seen during SLS indicating that muscle activation plays a role in postural stabilization and is not merely a response to loading. Control of arch stiffness may be necessary to use the foot as a lever to aid in balance. Despite the fact that all subjects tested were asymptomatic and free of injury or pathology, there are clear differences in behavior and control of the longitudinal arch. This wide range of asymptomatic arch behavior calls into question the homogeneity of healthy control groups used in foot and lower extremity research.

Table:

	TP	FL	FB	AH	TA	PL
	Rigid N=8					
Load	4.0*	3.2*	3.0*	2.7*†	7.1*	3.1*
Stance	67.7*	21.5*	65.4*	70.0*	28.2*	40.5*
	Flexible N=7					
Load	8.7*	3.6	13.0*	20.2*†	7.7*	4.0*

Stance	63.3*	30.8	66.5*	75.8*	34.2*	50.6*

Caption: Mean muscle activation amplitudes as a % maximum voluntary isometric contraction. *Difference between loading and stance (p<.05). †Difference between flexible and rigid (p<.05).

References: [1] Kelly et al., J R Soc Interface, 11, 2014.

[2] McKeon et al., Br J Sports Med, 2014.

Disclosure of Interest: None Declared

THE AMPLITUDE OF H-REFLEX AS AN OUTCOME FOR TO INVESTIGATE MUSCLE INHIBITION IN PEOPLE WITH PATELLOFEMORAL PAIN SYNDROME

Nathalie C. S. Faria [1,*]Fernando Magalhães [2]Deisi Ferrari [3]Danilo Silva [1]Marcella Pazzinatto [1]Neri Alves [3]Fábio Azevedo [1]

[1]Physiotherapy, Universidade Estadual Paulista- UNESP, Presidente Prudente, [2]Universidade de São Paulo-USP, São Paulo, [3]Universidade de São Paulo-USP, São Carlos, Brazil

Introduction and Objectives: The Patellofemoral Pain Syndrome (PFPS) is characterized by presence of anterior knee pain on retropatellar region[1] and it is a common found in actives adults[2].The pain commonly appears during some functional or physical activities [3], demonstrating intermittent characteristic. Although the PFPS has a high incidence until this moment its etiology is unclear [4,5]. The traditional therapeutic exercise many times demonstrate not very good prognostic with little increase at the strength and little decrease of pain level. [6,7]. The disinhibitory interventions are suggested for to improve clinical outcomes by changing the neuromuscular function [6,7]. Since the presence of muscle inhibition has been suggested to prevent the total recuperation of function of the person after injury [6]. The H-reflex is a confident measure for analyzes the inhibition and activation muscle [8]. We hypothesize that many times people with PFPS can be free of the pain but the muscle inhibition process continues installed and this favors the recurrence of pain and the characterization of the PFPS with intermittent pain. Our objective is to compare the amplitude of the vastus medialis H-reflex in asymptomatic and PFPS women and to investigate if this measure can be an outcome for to examine the muscle inhibition before and after treatments.

Methods: Twenty women participated of this study (10 asymptomatic and 10 with PFPS) with average age 23.05(3.53) years, the peak to peak maximum H-reflex amplitude (Hmax) and the peak to peak maximum M-wave magnitude (Mmax) of vastus medialis were assessed of all participants. The Mmax was used as a normalization factor. For to record the Hmax and Mmax the participants were at supine position, the femoral nerve was stimulated in the inguinal region and the electromyography signal was captured at the vastus medialis. The femoral nerve was stimulated using 1 ms pulses until the H wave reaches its maximum and thus the same was done to Mmax. Ten signals of each wave were recorded.

Results: The test T for independent sample was performed at the SPSS Statistical Package. The mean and standard deviation of normalized Hmax for the group with PFPS and asymptomatic were 0.09(0.06) and 0.19(0.10) respectively. We found statistical differences at the normalized Hmax between the groups with a p-value of 0.023 and a F-value of 1.25 at the Levene's test. Our results showed that the women with PFPS have smaller amplitude than asymptomatic. This achieved support that the presence of intermittent pain is accompanied by muscle inhibition. This inhibition is an important alteration that needs to be broken [7]to obtain good results after treatments.

Conclusion: The amplitude of Hmax is smaller in women with PFPS than asymptomatic women and the measure of the H-reflex is a confident diagnostic for the muscle inhibition. Therefore the measure of H-reflex can be a technic useful for to investigate the changes in the neuromuscular function after treatments.

References: [1]   Ribeiro DC, Loos JF, Caneiro JPT. Electromyographical analysis of the quadriceps during knee extension 2005;13:189–93.

[2]   Ng GYF, Zhang a Q, Li CK. Biofeedback exercise improved the EMG activity ratio of the medial and lateral vasti muscles in subjects with patellofemoral pain syndrome. J Electromyogr Kinesiol 2008;18:128–33. doi:10.1016/j.jelekin.2006.08.010.

[3]   Lack S, Barton C, Woledge R, Laupheimer M, Morrissey D. The immediate effects of foot orthoses on hip and knee kinematics and muscle activity during a functional step-up task in individuals with patellofemoral pain. Clin Biomech 2014;29:1056–62. doi:10.1016/j.clinbiomech.2014.08.005.

[4]   Lin F, Wilson N a, Makhsous M, Press JM, Koh JL, Nuber GW, et al. In vivo patellar tracking induced by individual quadriceps components in individuals with patellofemoral pain. J Biomech 2010;43:235–41. doi:10.1016/j.jbiomech.2009.08.043.

[5]   Nunes GS, Stapait EL, Kirsten MH, de Noronha M, Santos GM. Clinical test for diagnosis of patellofemoral pain syndrome: Systematic review with meta-analysis. Phys Ther Sport 2013;14:54–9. doi:10.1016/j.ptsp.2012.11.003.

[6]   Pietrosimone BG, Saliba S a, Hart JM, Hertel J, Kerrigan DC, Ingersoll CD. Effects of transcutaneous electrical nerve stimulation and therapeutic exercise on quadriceps activation in people with tibiofemoral osteoarthritis. J Orthop Sports Phys Ther 2011;41:4–12. doi:10.2519/jospt.2011.3447.

[7]   Harkey MS, Gribble P a, Pietrosimone BG. Disinhibitory interventions and voluntary quadriceps activation: a systematic review. J Athl Train 2014;49:411–21. doi:10.4085/1062-6050-49.1.04.

[8]   Alrowayeh HN, Sabbahi MA. Vastus medialis H-reflex reliability during standing. J Clin Neurophysiol 2006;23:79–84. doi:10.1097/01.wnp.0000193632.75002.d3.

Disclosure of Interest: None Declared

EMG

AS-0171

IMPROVING EMG DATA CLASSIFICATION ACCURACY BY SUPPORT VECTOR MACHINE SPACES

Stefan Hoerzer [1,*] Vinzenz von Tscharner [1] Erica Buckeridge [1] Benno Nigg [1]

[1] Human Performance Lab, University of Calgary, Calgary, Canada

Introduction and Objectives: The classification and interpretation of EMG signals is important in sports research for a functional understanding of group differences caused by, for example, different skillsets or sports-equipment [1,2]. EMG data classification has also significant clinical applications, such as assessing neuromuscular diseases [3] or providing input information for robotic prostheses [4]. Especially in such clinical settings, high data classification accuracy is crucial. EMG signals can demonstrate high inter-subject variability and the signal-to-noise ratio is often unfavourable. Thus, EMG data classification accuracy might be often low, especially when the EMG signals were recorded during highly dynamic movements (e.g. running; ice skating) or when the expected group differences are small (e.g. at the onset of a disease; when comparing sports-equipment). Recently, Support Vector Machines (SVM) were used to extract all the discriminating information between groups in a given data set and isolate them in a new data/vector space (SVM space) [5]. It is hypothesized that classifying EMG data in a SVM space would enhance classification accuracy. Thus, the study objective was to investigate if EMG data classification accuracy could be improved by the utilization of a SVM space.

Methods: Sixteen healthy male subjects (31.4±6.8yrs) performed 15 maximum effort forward skating trials. Using this setup, the following groups were established: *skater caliber* (low vs. high skillset) and *skate design* (low vs. high quality sports-equipment). During each trial muscle activation was measured using bipolar surface EMG electrodes on the vastus lateralis, tibialis anterior and medial gastrocnemius. The ice contact phases of two specific skating strides (i.e. accelerative and steady state stride) were used for the analysis. EMG data were processed with a non-linear wavelet transform. The resulting time-frequency patterns of each muscle and trial were used as input data for the data classification task. This task included classifying skater caliber and skate design. To this purpose, three frequently used data classification algorithms were utilized: SVM-Linear kernel (SVM-LN), SVM-Gaussian Radial Basis Function kernel (SVM-RBF), and k-Nearest Neighbor classification (kNN). First, all algorithms were used in the original data space. The classification accuracy was determined by calculating classification rates (CR) using a leave-one-out cross validation approach. Second, the original data space was decomposed by an iterative application of the SVM-LN into 20 orthogonal discriminants. Afterwards, 20 SVM spaces were created spanned by 1 to 20 discriminants. All classification algorithms were then applied to each of the 20 SVM spaces and the corresponding CRs were obtained. A binominal test ($\alpha=0.05$) was used to determine if the calculated classification rates were significant and indicated statistically significant group differences.

Results: When classifying skater caliber, the SVM space allowed maximally improving the CR by 20.0% (SVM-LN), 15.7% (SVM-RBF), or 13.0% (kNN) (Fig. 1a). Considering only the maximum CR showed that each algorithm achieved a significant classification in the SVM space. Classifying skate design revealed that the SVM spaces maximally improved

the CR by 19.1% (SVM-LN), 11.5% (SVM-RBF), or 13.7% (kNN) (Fig. 1b). None of the CRs obtained in the original space were significant. However, the SVM space allowed each algorithm to reach a significant classification.

Figure:
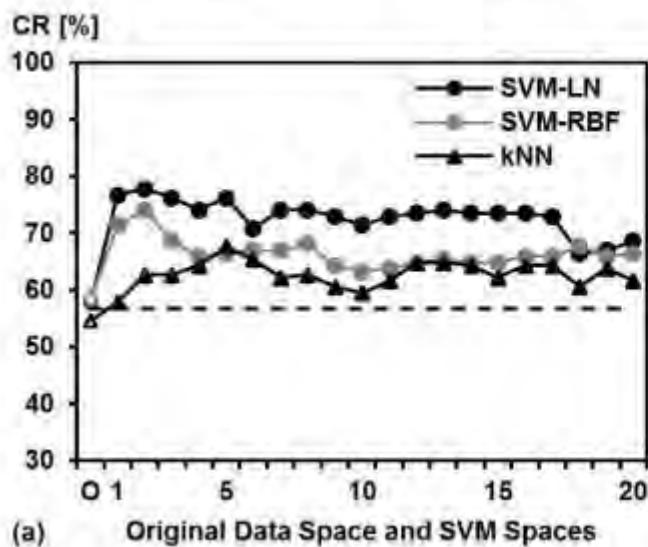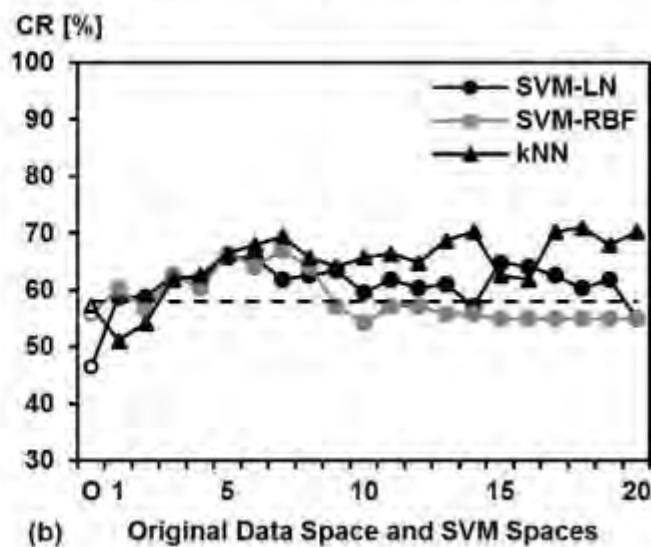
Caption: Classification rates (CR) between ice skater calibers and skate designs. The first hollow data point of each data series represents the CR in the original data space (O) and the following points indicate CRs based on SVM spaces formed by 1-20 discriminants. Three classification algorithms were used: SVM-Linear kernel (SVM-LN), SVM-Gaussian Radial Basis Function kernel (SVM-RBF), k-Nearest Neighbor classification (kNN). The dotted black horizontal line indicates the lowest statistically significant CR.

Conclusion: Classifying different skillsets and sports-equipment based on surface EMG signals provided a low accuracy. Using SVM spaces to filter out non-discriminating information provided a significant improvement in classification accuracy, independent of the algorithm used. In some cases statistically significant and, therefore, meaningful differences could only be detected in the SVM space. Thus, it is expected that the SVM space classification will lead to higher EMG data classification accuracy in both clinical and sports-related applications. In the future, reconstructing data in the SVM space will allow to visually assess the group differences, therefore, providing potential for functional interpretations.

References: [1] Chapman et al., J. Sci. Med. Sport, 11: 519-26, 2008.

[2] von Tscharner et al., J. Biomech., 36: 1169-76, 2003.

[3] Subasi, Comput. Biol. Med., 43: 576-86, 2013.

[4] Shenoy et al., IEEE Trans. Biomed. Eng., 55: 1128-35, 2008.

[5] von Tscharner et al., PLoS One, 8: 1-7, 2013.

Disclosure of Interest: None Declared

AS-0172

SHAPE AND MAGNITUDE OF LOWER EXTREMITY KINETICS CHANGED STEPS BEFORE GAIT TRANSITION DURING INCREASING SPEED INDUCED WALK-TO-RUN TRANSITION

Jiahao Pan [1,*]Li Li [1]

[1]Kinesiology, Shanghai University of Sport, Shanghai, China

Introduction and Objectives: Walking and running represents two different steady states in human locomotion. Study walk-to-run gait transition helps us to understand how human movement changes from one steady state to another. The purpose of this study was to investigate lower extremity joint moments and power patterns during gait transitions with continuously increased walking speeds.

Methods: Walk-to-run gait transitions were tested with thirteen college aged participants. The gait transitions were induced by increase treadmill speed. Full body reflective markers were captured using eight digital cameras while the participants walked on a force plate embedded treadmill. Inverse dynamics was employed to estimate sagittal plane ankle, knee, and hip joint moments / power for the last five steps before walk to run gait transition.

Results: Ensemble curves of joint moments data presented in Figure 1. Horizontal axes represent 100% of a gait cycle. Vertical dotted lines indicate the end of stance phase and the beginning of swing phase. We have used horizontal (or slightly slopped) dotted lines to represent changes of a particular parameter across the five steps before walk-to-run gait transition. Ankle joint moments can be seen at the upper panel of Figure 1, where plantarflesor moments are presented as positive. The most observable changes occurred at the last step before walk-to-run gait transition, where 1) the peak plantarflexor moment increased and happened earlier during the stance phase, along with 2). the disappearance of the dorsal flexor moments which commonly happens at the beginning of the stance phase. There are three knee joint moment peaks can be observed during the stance in the middle panel: extensor peaks at the beginning and end of the stance phase, as well as the flexor peak between the two. The first extensor peak increased slightly during the first four steps displayed here where the other two remain largely unchanged. The first peak in creased to almost twice as observed in the previous steps, with the other two almost disappeared during last step before gait transition. Hip joint moments (lower panel in Figure 1) remained steady for the first four steps presented here. But hip joint flexor moments reduced significantly during the last step before changed to run. Joint power data will not be presented here with the limited spaces allow for this abstract but they do support the same trends observed with the joint moments.

Figure:
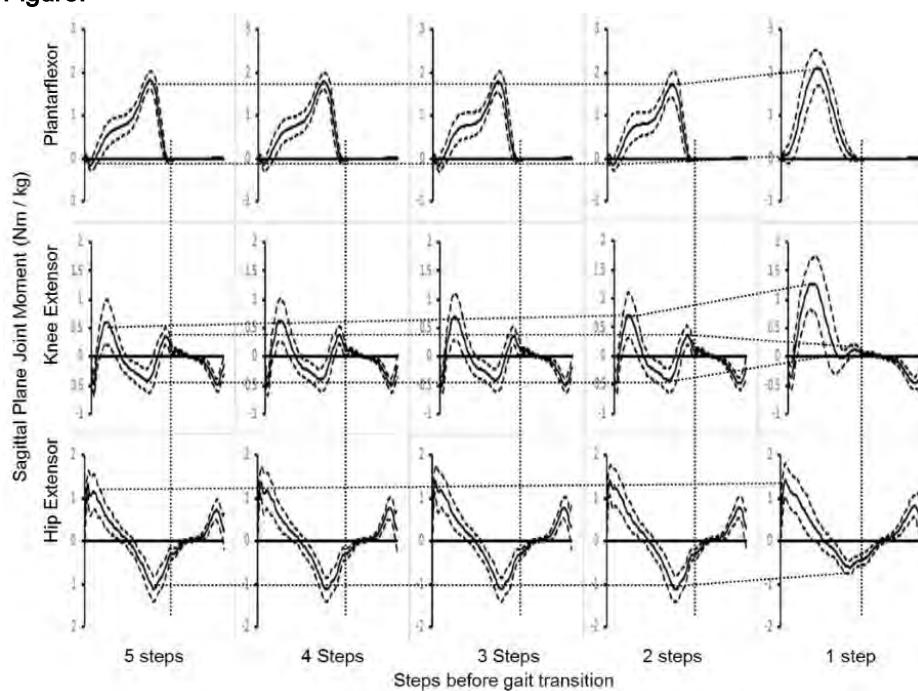
Caption: Figure 1. Sagittal plane ankle (upper), knee (middle) and hip (lower) joint moments ensemble curves five steps before walk to run gait transition (see text for details of the figure).

Conclusion: We have observed transition specific non-linear joint kinetic behavior in this study. Sagittal plane lower extremity joint moments and joint power changed in shape and magnitudes during the five steps approach walk to run transition, especially the last step before transition. These results indicated that, in preparation for transition, joint kinetic changes steps before gait transition along with increased walking speed.

Disclosure of Interest: None Declared

AS-0173

A COMPARATIVE STUDY OF THE MUSCLE SYNERGY PATTERNS IN HEALTHY AND ACL-DEFICIENT SUBJECTS

Gil Serrancolí [1,*] Joan C Monllau [2 3 4] Josep M Font-Llagunes [5]

[1]Department of Mechanical Engineering and Biomedical Engineering Research Centre, Universitat Politècnica de Catalunya, [2]Department of Orthopaedic Surgery, Hospital del Mar, [3]ICATME, Hospital Universitari Quirón-Dexeus, [4]Universitat Autònoma de Barcelona, [5]Department of Mechanical Engineering, Universitat Politècnica de Catalunya, Barcelona, Spain

Introduction and Objectives: It is believed that human gait is controlled by a muscle synergistic pattern [1]. This can be represented by signal factorization of muscle activations or electromyography (EMG) in Neural Commands (NCs) and Synergy Vectors (SVs). NCs are time dependent signals, and SVs represent the weight factors of each muscle to the NCs. As far as the authors know, no muscle synergy analysis has been applied for the study of ACL-deficient subjects. The goal of this study is to investigate whether there are observable differences in NCs and SVs between healthy and ACL-deficient subjects.

Methods: Ten healthy subjects, five men and five women (age 31.5 ± 12.9 years), and eighteen ACL-deficient subjects, twelve men and six women (age 32.3 ± 10.99 years), volunteered as participants in this study. All injured subjects were classified as adapters [2]. They were asked to walk some gait trials over ground. EMG signals of 16 muscles (8 from each leg) were measured (Biometrics, Newport, United Kingdom). The 8 muscles are the main contributors to the human gait (Extensor Digitorus Longus, Tibialis Anterior, Soleus, Gastrocnemius Lateralis, Vastus Lateralis, Rectus Femoris, Semitendinosus and Gluteus Maximus). Ground Reaction Forces (AMTI, Watertown, MA) and trajectories of 2 foot markers (NaturalPoint, Corvallis, OR) were also measured to identify the gait cycle.

EMG data were filtered and normalized to maximum values obtained after doing certain MVC exercises. The processed EMG signals were factorized by means of a Non-Negative Matrix Factorization (NNMF) algorithm based on a non-linear least squares algorithm that minimizes the error between the reconstructed and the experimental EMG signals [3]. NCs and SVs were calculated when factorizing data with 1 to 6 modules. For each set of data, VAF (variance accounted for) was calculated for each muscle to evaluate the dimensionality.

The subjects were divided in three groups: Control (healthy subjects), Ipsilateral (injured subjects' injured legs) and Contralateral (injured subjects' non-injured legs). SVs and NCs were compared between groups.

Results: The analysis of dimensionality showed that 5 modules can account for ≥ 90% of the variability for each individual EMG signal. There were no significant differences regarding the dimensionality among groups, therefore, muscle synergy components of all three groups were compared using 5 modules.

The correlations among NCs and SVs from two modules of different groups were calculated (Table 1). The obtained patterns showed similar tendencies (Figure 1), but some differences were observed. The most representative ones are that the Ipsilateral NC of module 2 has two peaks, whereas the same NC of the Control group shows only one peak; and that modules 3 and 4 have higher Ipsilateral's NC values compared with the ones obtained for the Control group.
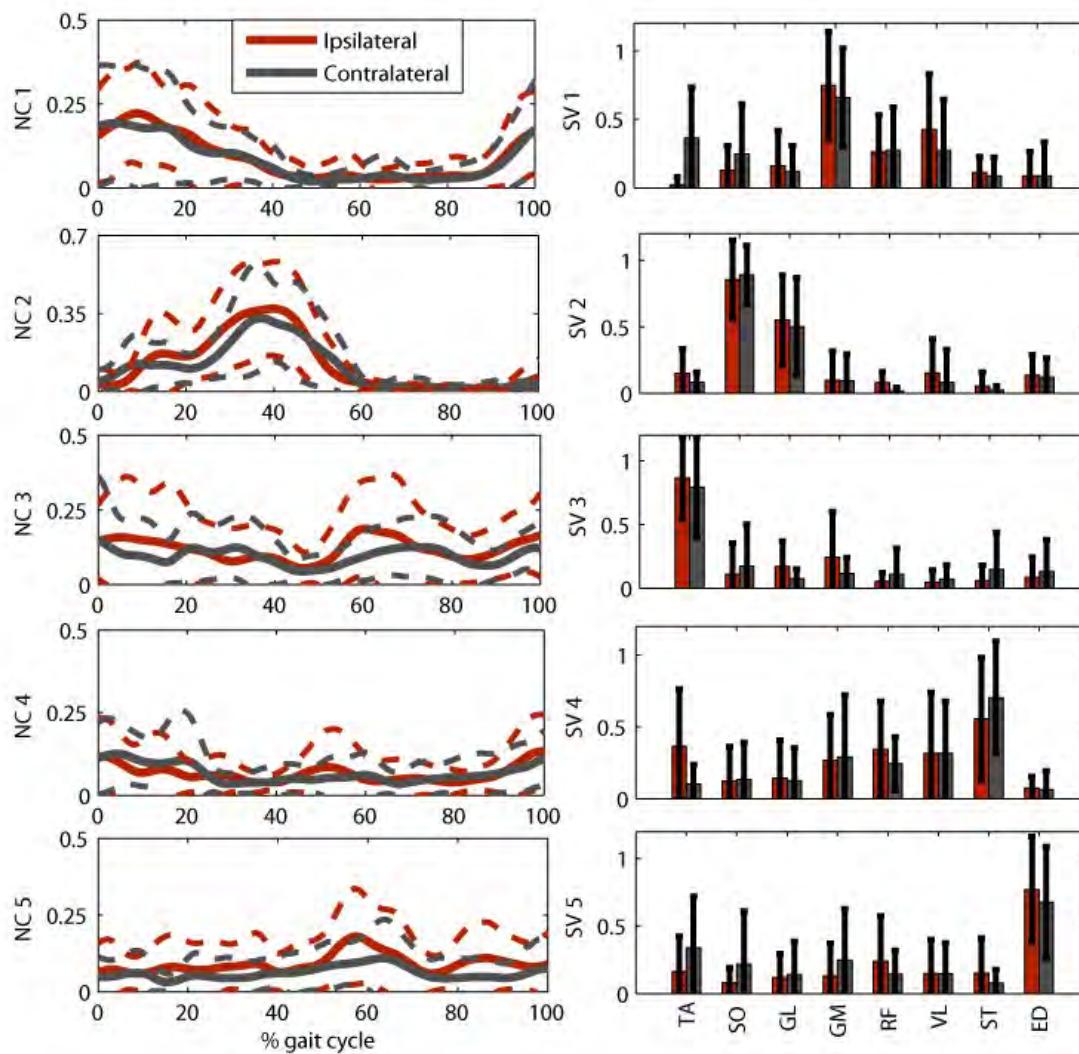
Figure:

Caption: Figure 1. NCs (left) and SVs (right) of Control and Ipsilateral groups. Both cases show the mean value (solid line and bar) and the standard deviations (dashed line and error bar).

Conclusion:

NCs and SVs were in general comparable with other published studies [4-5]. The fact that there were no significant differences in the dimensionality of the signal factorization means that the pattern of all groups has the same complexity.

The observed differences in NCs and SVs among groups can be associated with the changes in the strategy that the Central Nervous System uses to activate the muscles in ACL-Deficient subjects. The higher values of NCs that contain basically activations of ankle plantar flexors and dorsiflexors (modules 2 and 3) during the stance phase, suggest that there is a transfer of the leg control away from the injured knee joint.

This study on muscle synergy analysis can be useful at two levels. In a clinical field, to evaluate the progress during the rehabilitation treatment of ACL-deficient subjects; and, in a computational dynamic analysis, to reduce the indeterminacy in the muscle force calculation of ACL-deficient subjects.

Table:

Groups	SV	NC
Controls vs. Ipsi.	0.70/0.99/0.96/0.80/0.96	0.86/0.94/0.69/0.77/0.81
Controls vs. Contra.	0.91/0.99/0.95/0.93/0.96	0.84/0.92/0.43/0.79/0.73
Ipsi. vs. Contra.	0.82/0.99/0.96/0.77/0.87	0.69/0.96/0.49/0.98/0.72

Caption: Table 1. Correlation values among the 5 modules of different groups (Control, Ipsilateral and Contralateral).

References: [1] Ting et al., Int. J. Numer. Meth. Biomed. Eng., 28:1003-1014, 2012.

[2] Button et al., Br. J. Sports Med., 40:853-859, 2006.

[3] Walter et al., J. Biomech. Eng., 136:021031, 2014.

[4] Clark et al., J. Neurophysiol., 103:844-857, 2010.

[5] Neptune et al., J. Biomech., 42:1282-1287, 2009.

Disclosure of Interest: None Declared

EMG

AS-0174

DOES A HIGH FREQUENT ROTATION IN INDUSTRIAL TASKS POSITIVELY AFFECTS MUSCLE FATIGUE AND PERCEIVED DISCOMFORT?

Tessy Luger [1 2 3,]*Marco Hoozemans [1]Tim Bosch [2 3]Dirkjan Veeger [1]Michiel de Looze [2 3]

[1]MOVE Research Institute, Faculty of Human Movement Sciences - VU University Amstserdam, [2]Body @ Work, Research Centre of Physical Activity, Work and Health, Amsterdam, [3]TNO, Leiden, Netherlands

Introduction and Objectives: Upper extremity musculoskeletal disorders are a major problem in occupational work. Task rotation can be used to counteract musculoskeletal disorders because it may attenuate effects of important risk factors including high repetitiveness and monotony. However, a clear evidence based advice as to the effectiveness of task rotation in industry is not available. The aim of this study was to determine the influence of low and high task rotation frequency on muscle fatigue and perceived discomfort during a one-hour simulated industrial work setting including a pick-and-place and box-lifting task.

Methods: 10 healthy subjects performed a pick-and-place and a box-lifting task in 2 one-hour conditions: (1) a low rotation frequency condition, 1 rotation (LRF): 30 minutes pick-and-place work followed by 30 minutes box-lifting work; (2) a high rotation frequency condition, 9 rotations (HRF): 6 minutes pick-and-place work and 6 minutes box-lifting work interchanged 9 times. We recorded muscle activity in the Transversal and Descending part of the M. Trapezius with multichannel surface electromyography; from the recordings we calculated the amplitude and median frequency. Furthermore, subjects rated their locally perceived shoulder discomfort with the CR10 Borg scale. Measurements were recorded at the start and at the end of each condition. The sequence of the conditions was systematically varied between subjects.

Results: At 60 minutes, the amplitude and median frequency of both the Transversal (see Figures) and Descending part of the M. Trapezius did not significantly differ between the two rotation conditions. Furthermore, the discomfort rating at 60 minutes did not show differences between the low and high rotation frequency conditions either.

Figure:
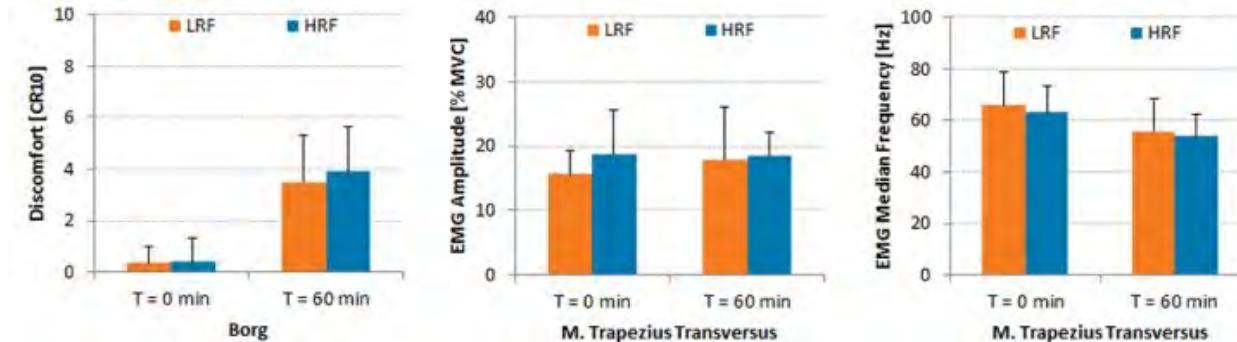
Conclusion: We expected that a high task rotation frequency between the pick-and-place and the box-lifting task would result in (more) opportunities for recovery, and thus less manifestations of muscle fatigue and perceived discomfort at the shoulder, compared to a situation in which both tasks are switched only once. Since the differences we found between the

low and high rotation frequency were relatively small and not significant, the effectiveness of a higher task rotation frequency in the attenuation of musculoskeletal symptoms in the upper extremity can still be debated.

Both muscle fatigue and perceived discomfort at the shoulder are minimally influenced by high rotation frequency of pick-and-place and box-lifting tasks in a simulated industrial work setting.

Disclosure of Interest: None Declared

Computer Simulation

AS-0175

MODELING AND COMPUTATIONAL COMPARISON OF FOOT ORTHOSES FOR PLANTAR PRESSURE RELIEF

Óscar Libardo Rodríguez-Montaño [1,*] Carlos Julio Cortés-Rodríguez [1][2] Octavio Silva-Caicedo [1][3]

[1]Biomechanics Research Group, [2]Department of Mechanical Engineering and Mechatronics, [3]Faculty of Medicine, Universidad Nacional de Colombia, Bogotá, Colombia

Introduction and Objectives: The high-pressure areas in the plantar foot region are related to the pain and development of injuries, due to mechanical stresses on regions that support the forces owed to both body weight and dynamics of the movement during walking. Pathological conditions such as diabetic foot could increase complication risks of foot injuries produced by high pressures. These injuries could trigger ulcers that eventually can lead to partial or total foot amputation. Such conditions demand the use of prevention strategies like plantar pressure relief with therapeutic orthoses (also called insoles). Besides orthosis material, its effectivity depends on the upper surface topography and specially on the effective contact area provided by this surface. The design and manufacturing of foot orthoses is generally high-dependent on the clinical specialist expertise, who usually employs prefabricated orthotic inserts. This is due to the lack of clear guidelines to design the upper topography or the surface contact between the foot and the orthosis. This work shows the development and implementation of algorithms for the generation of insoles based in geometric and load criteria, and their respective effects on plantar pressure distributions, which were assessed using a dynamic simplified non-linear finite element model of foot during the stance phase.

Methods: Computed tomography (CT) information from a subject with diabetic foot condition was used to obtain 3D foot geometry. The soft tissue was defined by a hyperelastic constitutive model [1]. Bones, tendons and joints were defined as isotropic elastic materials. Muscle and body weight forces were set in their respective application regions. The pressure distributions produced by three upper-orthoses topographies were compared: a plantar shape-based topography; a topography obtained by an own proposed method which implements an algorithm that uses the dynamic average pressure maps (DAPM) in the gait cycle providing by in-shoe plantar pressure analysis system F-Scan® (Tekscan, USA); and a clinical-prescribed custom orthosis topography that was digitized with a 3D laser scanner. The material of foot orthoses was defined as EVA (Ethylene vinyl acetate), which is a foam that was employed to model all orthoses, due to the fact that it is a material commonly used in therapeutic footwear [2]. The EVA's behaviour was described by Ogden's hyperfoam material model. Additional to the gait normal phases in barefoot and custom orthosis employment effects (Figure 1a.), the contact effects on the upper surface of an EVA rectangular block were compared. This scenario allows to assess the response of EVA in plantar pressure relief without the influence of a custom topography. In order to assess the validity of the model, the comparison of center of pressure (COP) trajectories, values and distributions of pressures and force vs. time curves of the model with experimental data obtained from both F-Scan® and force plates in a gait laboratory (BTS-GAITLAB, BTS Bioengineering, Italy), was performed. Other scenarios with higher rate loads than the normal step case were also simulated, in order to observe the plantar pressure relief effects provided by the orthosis in each case (Figure 1b.).

Results: Regardless of the simplifications that were made in the model, the maximum pressure values and COP trajectories for the barefoot simulation are consistent with the experimental data.The contact pressures were notably reduced in all evaluated cases on the simulations, if they are compared with barefoot pressures (Table 1).

The insole model that shows the best results is generally the dynamic DAPM-based topography, followed by the shaped-based form.

Figure:
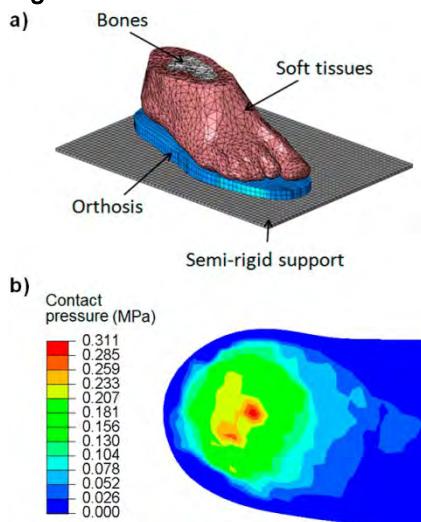
Caption: Figure 1: a) Mid Stance simulation with clinical-prescribed custom orthosis, b) Contact Pressure distribution on heel provided by plantar shape-based topography during an instant of heel strike.

Conclusion: The obtained results show that the implementation of computational techniques, based on quantitative criteria such as dynamic gait-process pressure maps, could be a useful tool to validate clinical-prescribed insoles and therapeutic footwear, giving the possibility to know the behaviour in dynamic conditions with more certainty in the results than those obtained by employing standard devices or experience-based designs. This is crucial especially in cases where the value of plantar pressures is critical, such as in diabetic subjects.

Table:

Scenario	Support Topography Type			
	EVA Flat Surface	Plantar Shape-Based	DAPM-Based	Clinical-prescribed custom
Heel Strike	50%	67%	67%	43%
Mid-Stance	8%	45%	60%	21%
Initial Push-off	40%	41%	52%	35%
Final Push-off	62%	55%	46%	37%

Caption: Table 1: Reduction percentages in maximum contact pressure, compared to barefoot model.

References: [1] Cheung, J. T. M., Zhang, M., Finite element modeling of the human foot and footwear. ABAQUS Users' Conference. 2006.

[2] VERDEJO, R., MILLS, N. J., Heel–shoe interactions and the durability of EVA foam running-shoe midsoles. Journal of biomechanics, 37-9: 1379-1386, 2004.

Disclosure of Interest: None Declared

AS-0176

STRETCHING YOUR ENERGETIC BUDGET: THE EFFECT OF TENDON COMPLIANCE ON THE METABOLIC COST OF RUNNING

Thomas Uchida [1,*] Jennifer Hicks [1] Christopher Dembia [2] Scott Delp [1 2]

[1]Bioengineering, [2]Mechanical Engineering, Stanford University, Stanford, California, United States

Introduction and Objectives: Humans naturally conserve energy, selecting running stride lengths that are most energetically economical [1], for example. The drive to maximize locomotion efficiency is also evident in the physiology of our musculoskeletal system. The triceps surae muscle group has evolved to allow storage and release of elastic strain energy in the calcaneal tendon [2]. Several studies have investigated the sensitivity of triceps surae efficiency to calcaneal tendon compliance and running speed. Lichtwark and Wilson [3] used a simplified, isolated model of the medial gastrocnemius (MG) musculotendon actuator during running at 2.8 m/s, and found that the simulated calcaneal tendon was most efficient at its physiological compliance. In this work, we investigate the effect of tendon compliance on the metabolic cost of running using a full-body musculoskeletal model with a detailed model of muscle energetics. We perform simulations of running at several speeds and tendon compliances, and predict the resulting whole-body and per-muscle metabolic costs. We explore two hypotheses: (1) whole-body metabolic cost is minimal when tendon compliance is physiological, and (2) the muscles crossing the ankle experience a greater increase in metabolic cost than those crossing the knee or hip as tendon compliance increases.

Methods: Simulations are generated for 10 subjects running at 2, 3, 4, and 5 m/s using the Computed Muscle Control (CMC) tool in OpenSim [4]. We use a 3D musculoskeletal model with 86 lower extremity muscles [5]. The CMC simulation results are used as inputs to a modified version of the muscle energetics model proposed by Umberger et al. [6]. We first simulate several running cycles for each subject at each speed, using the methods reported by Hamner and Delp [5], for physiological tendon compliances. We then repeat each simulation with a range of tendon force–strain curves that produce between 1% strain at maximum isometric force (Fmax) and 10% strain at Fmax. Averages of energy consumed by each muscle are obtained for each subject at each running speed; averages are then computed across the entire cohort.

Results: Our simulations correctly predict that the average power expended by muscle increases as running speed increases when tendon compliance is physiological (see figure). We also find that whole-body metabolic cost is minimal when tendon strain is 2–4% at Fmax, which falls just below the physiological range [7]. Further, muscles crossing the hip are most sensitive to tendon compliance at high running speeds, while muscles crossing the ankle experience a substantial increase in metabolic cost with increasing tendon compliance when running at low speed. These results coincide with the known shift in power generation from the ankle to the hip as running speed increases. The MG musculotendon actuator is the largest contributor to the increase in metabolic cost at the ankle when running at 2 m/s with very compliant tendons. When the tendon is compliant, the MG fiber is operating far from its optimal length during the stance phase, thereby requiring a greater activation signal to generate the necessary plantarflexion moment and

increasing the activation heat rate in the metabolic model. The MG fiber shortening velocity is also greater when the tendon is compliant, which increases the shortening and lengthening heat rate.

Figure:
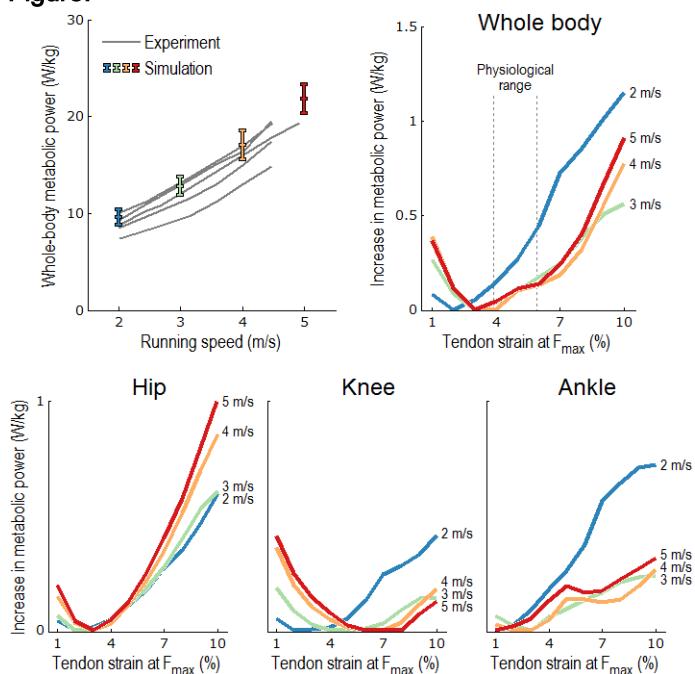
Caption: Comparison between whole-body metabolic power measured experimentally [8] and predicted by our simulations using physiological tendon force–strain curves (top-left); increase in average metabolic power from the lowest metabolic power at each speed, observed in all lower extremity muscles (top-right) and in muscles crossing each of the lower extremity joints (bottom row) as tendon compliance varies. Averages over 10 subjects are shown. At the hip and knee, less compliant tendons are favored at low running speeds, while more compliant tendons are favored at high speeds. At the ankle, very compliant tendons are particularly detrimental when running at low speed.

Conclusion: Our simulations predict that whole-body metabolic cost is minimal when tendon strain is 2–4% at Fmax, which falls near the physiological range and confirms our first hypothesis. Our second hypothesis—that the muscles crossing the ankle experience a greater increase in metabolic cost than those crossing the knee or hip as tendon compliance increases—is true in our simulations only when running at 2 m/s; at higher running speeds, it is the muscles crossing the hip that are most sensitive to variations in tendon compliance.

References: [1] Alexander, Am. J. Hum. Biol., 14: 641–648, 2002.

[2] Ishikawa et al., Gait Posture, 25: 380–384, 2007.

[3] Lichtwark et al., J. Biomech., 40: 1768–1775, 2007.

[4] Thelen et al., J. Biomech., 36: 321–328, 2003.

[5] Hamner et al., J. Biomech., 46: 780–787, 2013.

[6] Umberger et al., Comput. Methods Biomech. Biomed. Eng., 6: 99–111, 2003.

[7] Maganaris et al., J. Biomech., 35: 1639–1646, 2002.

[8] Steudel-Numbers et al., J. Hum. Evol., 56: 355–360, 2009.

Computer Simulation

AS-0177

RAPID QUANTIFICATION OF BONE ANATOMY FROM MRI

Saikat Pal [1,*] Marc Safran [2] Gary Beaupre [3] Garry Gold [4] Scott Delp [5]

[1]Biomedical Engineering, California Polytechnic State University, San Luis Obispo, [2]Orthopaedic Surgery, Stanford University, Stanford, [3]Veterans Affairs, Palo Alto, [4]Radiology, [5]Bioengineering, Stanford University, Stanford, United States

Introduction and Objectives: Computed tomography (CT) scanning provides large contrast between bone and surrounding soft-tissue structures, enabling rapid segmentation and reconstruction of bone geometry. These 3D reconstructions are routinely used in clinics for diagnosis and treatment of bone geometry abnormalities, such as femoroacetabular impingement (FAI). CT scanning exposes patients to radiation and its side-effects, including cancer [1]. FAI is prevalent in young adults, and subjecting the pelvic region of young adults to multiple CT scans is particularly alarming because their reproductive organs are exposed to radiation. Magnetic resonance imaging (MRI) provides an alternative to CT scanning for evaluation of bone geometry abnormalities in patients with FAI. There is no exposure to radiation from MRI. However, clinical use of MRI scanning remains qualitative, with radiologists relying on visual detection of bone abnormalities. A major limitation in quantitative use of MRI for clinical evaluation of bone abnormalities is the time-intensive process of manual segmentation of bones. The objectives of this study were – 1) to develop a computational method to segment rapidly bone geometry from MRI of patients diagnosed with FAI, and 2) to quantify the errors in bone geometries from our MRI-based method compared to a standard CT-based method.

Methods: We acquired MRI and CT data from four patients (3 males, 1 female; 29.3±3.7 years) with FAI. The images were collected as part of standard clinical practice. The MRI scans were obtained from a GE 3T scanner: coronal IDEAL SPGR, in-plane resolution 0.8 mm, slice thickness 1.5 mm, TR 7.2 ms, TE 3.0 ms, flip angle 45º, ~12 minutes. The CT scans were obtained from a Siemens scanner: axial in-plane resolution 0.8 mm, slice thickness 1 mm, 120 kVp, exposure time 500 ms, and tube current 317 mA. We developed an interactive graphical user interface (GUI) in Matlab (Mathworks Inc., MA) to segment bone geometry from fat- and water-saturated MRI (Figure 1A,B). We used a k-nearest-neighbors algorithm [2] to cluster pixels associated with cancellous and cortical bone, with the remaining pixels binned with background pixels. We used a user-guided iterative bridge-breaker algorithm [3] to break spurious connections between the cancellous bone and background pixels. We used a logical OR operator to combine the cancellous and cortical bone pixels, and repeated the iterative bridge-breaker algorithm until we were left with only the desired bone pixels. We extracted the boundaries of the bone pixels and smoothed the boundaries using a locally weighted smoothing algorithm. The bone boundaries from all slices of an MRI dataset were output as a 3D point cloud. We converted the point cloud data to a 3D surface using Geomagic (3D Systems, NC) [4]. We used a standard threshold-based algorithm to segment the bone geometries from CT data. The bone boundaries from all slices of a CT dataset were output as a 3D point cloud and converted to a 3D surface. We registered the MRI and CT geometries spatially, and quantified the differences in surface morphology by measuring the shortest distance from a point on the CT-based geometry to any point on the MR-based geometry.

Results: We developed an interactive GUI to segment rapidly bone geometry from MRI. It took ~2 minutes and ~15 mouse clicks to create a 3D point cloud of a proximal femur bone using our GUI. In contrast, it takes ~30 minutes and several hundred mouse clicks to create a 3D point cloud of a proximal femur bone using manual segmentation.

For the proximal femur, average difference in surface morphology between the MRI and CT-based methods was 1.0 mm from the four FAI patients (Figure 1C, Table 1). The average difference was 0.7 mm in the femoral head and neck regions, which are the regions of interest in FAI.

Figure:
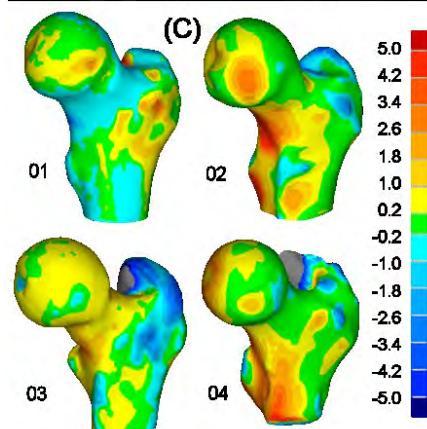
Caption: Multi-contrast MRI images with (A) fat-saturated and (B) water-saturated sequences. (C) Comparison of proximal femur surface morphologies from MRI and CT from four FAI patients. The contour maps represent the shortest distance between the surfaces in millimeters.

Conclusion: The results of this study demonstrate that our MRI-based method produces bone geometries that closely match geometries obtained from CT imaging, and at a fraction of the time compared to manual segmentation. The average differences in morphology between the MRI and CT-based methods were similar to the in-plane resolution of the images (0.8 mm). Our study has the following clinical applications in diagnosis and treatment of FAI – 1) eliminate the need for CT scanning for surgical planning, 2) minimize radiation dose in young adults, and 3) reduce health care costs.

Table:

Patient	Proximal femur (mm)	Femoral head & neck (mm)
01	0.8	0.7
02	1.0	0.7
03	0.8	0.6
04	1.3	0.9

Caption: Average difference in surface morphology between the MRI and CT-based methods from four FAI patients.

References: 1. Brenner DJ et al., N Engl J Med 2007

2. Warfield S, Pat. Recog. Let., 1996.

3. Cline HE et al., SPIE, 2003.

4. Besier et al., Med Sci Sports Exerc, 2005.

Disclosure of Interest: None Declared

Modelling

AS-0178

PREDICTION OF THE SUBJECT-SPECIFIC KNEE PASSIVE MOTION FROM NON-INVASIVE MEASUREMENTS

Nicola Sancisi [1,*]Michele Conconi [1]Vincenzo Parenti-Castelli [1]

[1]DIN - Department of Industrial Engineering, University of Bologna, Bologna, Italy

Introduction and Objectives: The passive motion of the knee is the natural motion of the joint in unloaded conditions. It is the joint starting condition when loads are applied, thus affecting the joint behaviour also in loaded conditions. For this reason, the knowledge of this motion is useful in all applications which aim at replicating or restoring the natural behaviour of the knee, such as lower-limb modelling, surgical planning, prosthetic design. Several studies measured the passive motion of the joint and the mean results can be used as a reference [1-3]. However, there is an increasing request of subject-specific results that would allow personalization of model parameters or of prosthesis geometry on a patient. In these cases, the subject motion would be required. An accurate estimation of the joint motion is difficult to obtain in vivo: non-invasive techniques can be inaccurate (skin-markers) or too complicated (fluoroscopy) for standard practice, while more invasive techniques (bone-pins) are not acceptable in several applications. Thus, new techniques are needed to predict the natural joint motion with a good accuracy, starting from non-invasive measurements. Two techniques were proposed for the knee passive motion modelling. Both methods start from the consideration, supported by relevant experimental analyses [2,3], that in passive conditions the knee behaves as a single degree-of-freedom (1DOF) system guided by the passive structures of the joint. The first technique (T1) predicts the passive motion by maximizing the joint congruence at all flexion angles [4]: it only requires the 3D model of articular surfaces with menisci, that can be obtained by MRI. T1 was developed for the ankle joint. At this stage, its application to the knee revealed a good accuracy, but the errors increased at high flexion angles, particularly for some motion components. The second technique (T2) models the knee as a 1DOF spatial mechanism, featuring the two articular contacts and the three isometric fibres of the anterior cruciate, posterior cruciate and medial collateral ligaments [3,5]. T2 was very accurate to replicate the passive motion of specimens over the full flexion arc, but a reference motion is needed to adjust the model parameters and the specimen motion was previously used [3]. The limitations of T1 and T2 are overcome in this paper by combining the two methods. An estimate of the joint motion is obtained by T1. This estimate is used as an input for T2 by which a new motion prediction is defined. The idea is that ligament constraints of T2, starting from the estimate provided by T1, can improve the overall motion prediction over the full flexion arc. The technique is here presented and applied on a specimen.

Methods: Geometrical data were obtained from a knee specimen, free from anatomical defects [3]. Anatomical landmarks, articular surfaces and ligament attachment areas were digitized by a stereo-photogrammetric device. For validation purposes only, several full passive flexion-extension cycles were performed and the same device recorded the tibia-femur relative motion by bone pins. Anatomical reference frames were defined and the relative motion was represented as 6 motion components (i.e., 3 displacements and 3 rotations) [3]. The digitized surfaces were used to apply T1. Flexion angle was imposed and the other 5 motion components were obtained by maximizing joint congruence; the procedure was repeated over the full flexion arc [4]. This T1 motion estimate was used as an input for T2: preliminary mechanism

parameters were obtained from the surface and ligament data, and were then adjusted (maximum difference of 2mm for all parameters) to best-fit the T1 motion [3]. The specimen motion was never used, except for result analysis.

Results: The passive motion was well predicted by T1 if flexion angle was not too high (Fig. 1): T1 began to diverge from the specimen motion at 100° and 80° respectively for ab/adduction and in/external rotation, and at 60° and 90° respectively for ant/posterior and lateral/medial displacements. The mechanism defined by applying T2 after T1 improved the motion estimate (Fig. 1): except for proximal/distal displacement beyond 90°, errors were lower and curve trend was more similar to the specimen motion over the full flexion arc.

Figure:
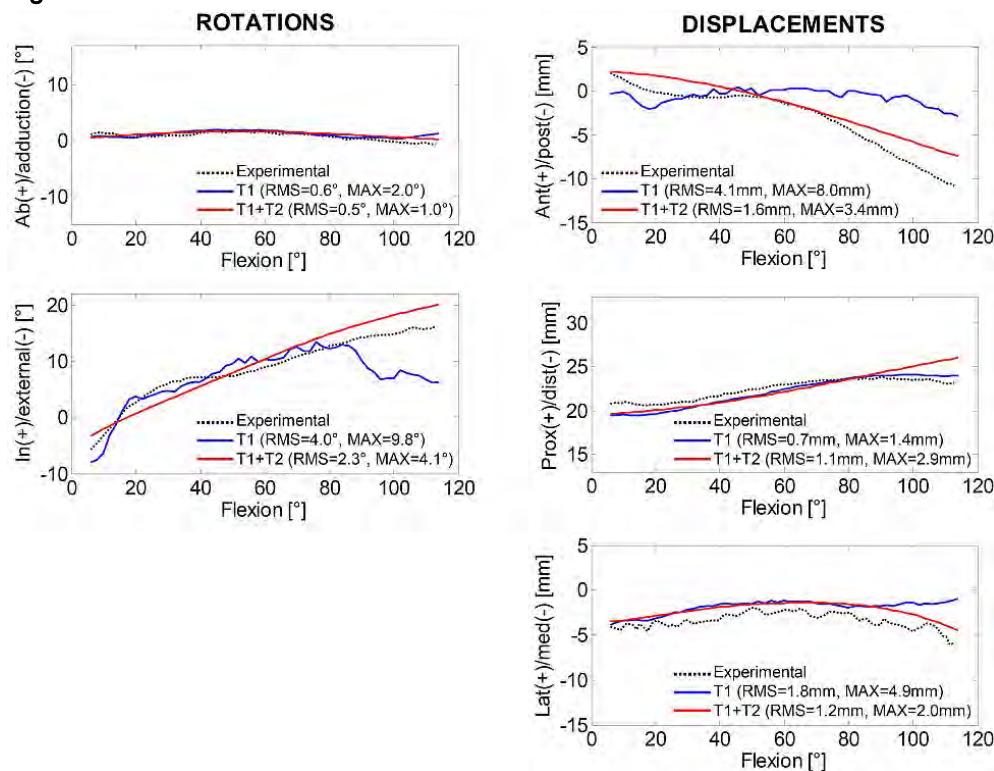
Caption: Experimental motion components, together with T1 and T1+T2 predictions. RMS and maximum errors are also reported.

Conclusion: The combination of joint congruence maximisation and of equivalent spatial mechanisms allows prediction of the natural subject-specific passive motion of the knee with a good accuracy. The proposed technique does not require invasive measurements and the motion can be obtained by standard MRI.

References: [1] Blankevoort et al., J Biomech, 21: 705-720, 1988.

[2] Wilson et al., J Biomech, 33: 465-473, 2000.

[3] Ottoboni et al., P I Mech Eng H, 224: 1121-1132, 2010.

[4] Conconi et al., *IDETC/CIE 2013*, Portland, USA, 2013.

[5] Parenti-Castelli et al., Advances in Robot Kinematics, Springer, 2000.

Disclosure of Interest: None Declared

Modelling

AS-0179

CORRESPONDENCELESS GROUPWISE REGISTRATION OF ANATOMICAL OBJECTS USING SPHERICAL EXTENT FUNCTIONS

Anton Semechko [1] Anne Agur [2] Jeremy Mogk [3,*]

[1]Institute of Medical Science, [2]Department of Surgery, Division of Anatomy, University of Toronto, [3]Autodesk Research, Autodesk Canada, Co., Toronto, Canada

Introduction and Objectives: Aligning anatomical objects to a common frame of reference is a key pre-processing step for many biomedical applications, including analyses of joint kinematics and bone morphology. How to reliably align multiple samples (N≥2) of the same bone remains an open research problem. Common solutions, such as iterative closest point (ICP) algorithms, minimize the distances between corresponding points on multiple surfaces; however, suboptimal correspondences can result, thus reducing the quality of the registration. When N>2, the reference sample selected can bias alignment solutions [1]. We describe a new and robust technique that aligns multiple samples of a bone type to an unbiased frame of reference, without needing to determine surface correspondence. Further, we compare our new method to three other registration techniques using sample bone data.

Methods: Bone data originated from an electronic database containing triangular surface meshes for the 8 carpal bone types (60 wrists) [2]. Prior to aligning each bone type set, we aligned all samples of a common bone type by their centroids, and divided the surface coordinates of each bone sample by the cube-root of its volume to normalize scale. Using the normalized surface meshes, we applied each of four registration techniques to align the 60 samples of each bone type. For our new registration method, we first computed the spherical extent function (SEF) for each bone surface (Fig. 1a). Next, we randomly searched for three SEFs, $\{SEF_A, SEF_B, SEF_C\}$, for which the rotations that optimally aligned them met the following condition: $R_{AB}R_{BC} \approx R_{AC}$, where R_{jk} is the rotation that best aligned the j-th and k-th surfaces by minimizing the total absolute difference between SEFs. After rotating SEF_A and SEF_B to align with SEF_C, these three SEFs were averaged to create a reference SEF, to which we registered the SEFs of the remaining 57 bones. The mean of the registered SEFs became the new reference SEF, and the SEFs of all 60 bones were registered to that new reference. This registration-update cycle ended once the reference SEF changed by <1% (2 to 4 iterations). We parameterized rotations using three Euler angles (ZYZ convention) and optimized using gradient descent, initialized by grid-search (9x9x9 grid). We compared our new registration method to three other techniques. The first involved aligning the principal axes of inertia (PAI) across bone samples. The second used a symmetric ICP algorithm to minimize the sum of squared differences between the bone surfaces. The third, considered state-of-the-art, registered multiple surfaces using rotations that minimized the description length (DL) for each bone set [3]. We evaluated registration quality using V_{ovr}/V_{ave} as our alignment metric, where V_{ovr} is the volume of the overlap region (Ω_{ovr}) enclosed by the registered surfaces (Fig. 1b), and V_{ave} is the average volume of the registered bones. Division by V_{ave} made the metric invariant to global scaling.

Results: Based on registration quality, the SEF approach aligned bone surfaces as closely as the DL method, and greatly improved alignment over ICP and PAI (Table). Specifically, the SEF method aligned bone surfaces to within 3% of the DL

technique (across bone types), and performed 40-50x faster than DL. In comparison to ICP and PAI methods, our SEF registration improved the alignment of bone surfaces by an average of 35% and 53%, respectively.

Figure:
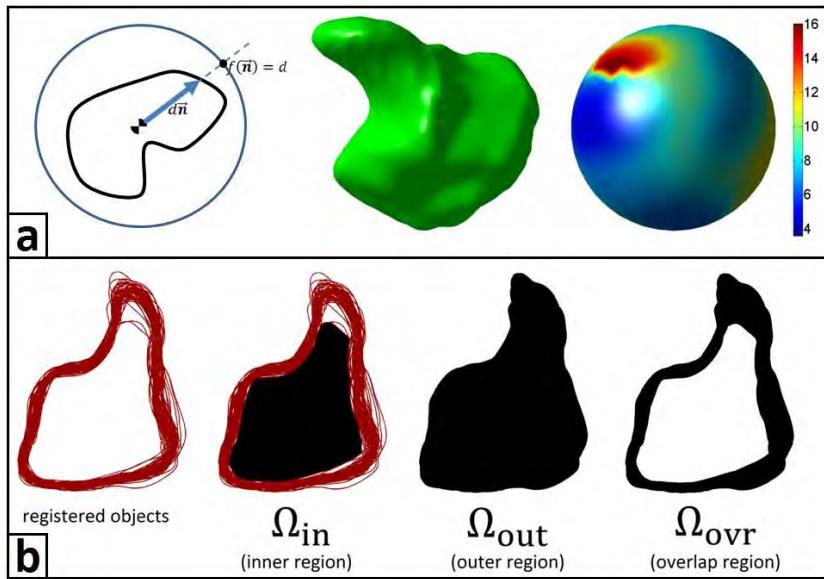
Caption: Process to compute a) the SEF for a sample hamate bone, and b) the metric used to evaluate registration quality. a) The maximal distances from the centroid to the surface are computed in uniformly distributed sample directions and projected onto the enclosing sphere. b) Better aligned surfaces (i.e., higher quality registration) show less difference between the outer (Ωout) and inner (Ωin) regions enclosed by the registered surfaces, and thus have smaller volumetric overlap (Ωovr).

Conclusion: Bone alignment using our new SEF approach closely matched that of the state-of-the-art DL method, and reduced registration time by removing the need to compute surface correspondences. Compared to working with the original surfaces, SEFs create representations that are simpler to work with, yet rich enough to encode the underlying morphology. Thus, the registered SEFs could be used to evaluate morphological differences between populations (e.g., normal vs. diseased, female vs. male) and identify where on the bone variations occur.

Table:

Registration Method	Bone type							
	sca	lun	trq	pis	tpd	tpm	cap	ham
DL	0.903	0.740	0.782	0.827	0.889	0.783	0.829	0.995
SEF	0.933	0.756	0.801	0.860	0.924	0.799	0.858	1.020
ICP	1.742	0.973	1.079	1.144	1.530	1.282	1.622	1.650
PAI	2.745	1.912	1.565	1.626	1.666	1.455	2.038	2.160

Caption: Quality metric values used to quantify groupwise alignment of the 8 carpal bone types, for each of the 4 registration methods. Lower values indicate better alignment.

References: [1] Crum et al., *Br J Radiol*, 77: S140-153, 2004.

[2] Moore et al., *J Biomech*, 40: 2537-42, 2007.

[3] Davies et al. (Eds.). *Statistical Models of Shape*, Springer, 2008.

Disclosure of Interest: None Declared

AS-0180

CALCULATION OF STUMP-SOCKET PRESSURE IN TRANSTIBIAL PROSTHESES DURING DYNAMIC GAIT SIMULATIONS.

Wouter Aerts [1]Friedl De Groote [2,*]Luiza Muraru [1] [3]Louis Peeraer [3] [4]Ilse Jonkers [5]Jos Vander Sloten [1]

[1]Mechanical Engineering, Biomechanics Section, [2]Mechanical Engineering, PMA, KU Leuven, Leuven, [3]MOBILAB, Thomas More, Geel, [4]Department of Kinesiology, Musculoskeletal Rehabilitation, [5]Department of Kinesiology, Human Movement Biomechanics, KU Leuven, Leuven, Belgium

Introduction and Objectives: One of the major concerns in transtibial amputees is the avoidance of pressure sores. Resulting gait compensations often result in an asymmetrical gait pattern [1]. Identifying the relation between gait pattern and pressure sore formation is of high clinical interest, since it would allow optimizing the socket design and foot-prosthesis alignment.

This cause-effect relationship is currently most often calculated using finite elements for describing the contact in static or quasi-static situations. Nevertheless these fail to incorporate important dynamic effects during gait. . In this study, we introduce a numerical efficient contact model that allows us to calculate the interface pressure between stump and socket during dynamic gait simulations based on 3D Mocap data. The simulated pressures are evaluated through comparison against measured pressures.

Methods: The gait pattern of one transtibial amputee is simulated using open-source software OpenSim [2] based on integrated 3D motion capture data. This data is collected in the gait laboratory of the research center Mobilab, Belgium, using a four cameras stereophotogrammetric system (Codamotion, Charnwood Dynamics Ltd, UK, 200 Hz) and two force plates (AMTI, Watertown (MA, USA), 200Hz). Simultaneously the pressure between socket and stump is measured with 20 M-flex pressure sensors (Maasbree, the Netherlands, 100 Hz) uniformly distributed over the stump.

A forward simulation is performed based on a dedicated musculoskeletal model representative for a transtibial amputee that integrates a patient-specific description of the contact between socket and stump (figure 1).The socket-stump contact is described using an elastic foundation model [3], which calculates the interaction via spring-damper systems scattered over the stump and inside of the prosthesis socket. Patient-specific contact geometries are obtained from a 3D surface scan of the stump, and from a CT-scan of the inner surface of the socket. The spring-damper systems are placed at each triangle of the triangle mesh representing these contact geometries. Stiffness and damping are estimated based on values for the Young's modulus found in literature [4].

The root mean square errors (RMSE) between the simulated pressures and the corresponding measured pressures for the 22 pressure sensors are calculated.

Results: The range and the median of the RMSE of the 20 sensors are shown in table 1. The median RMSE for all sensors has a low value of 25kPa, with a range of 29kPa, which is low compared to the maximum measured pressure of 184kPa. When grouping the sensors according to their location on the stump, the results show a smaller error for the lateral, anterior and medial aspect compared to the posterior aspect of the stump.

Figure:
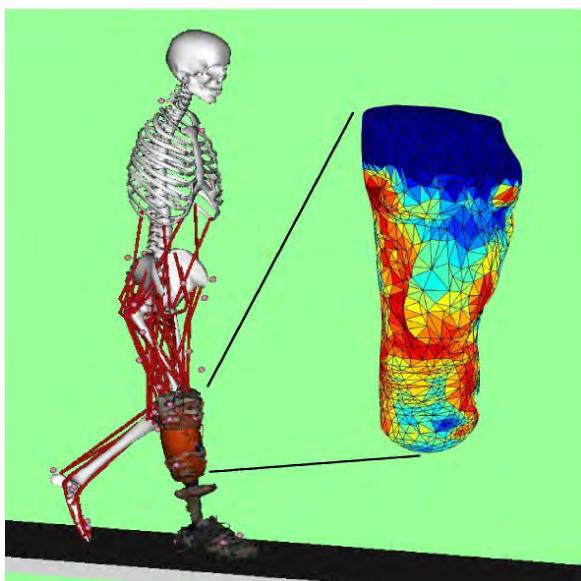
Caption: Musculoskeletal model used in the dynamic gait simulation with a zoom out of the simulated pressure on the stump

Conclusion: The stump-socket interaction can be calculated accurately during dynamic gait simulations. This allows us to further investigate the effect of the gait pattern, stump and socket geometries, and prosthesis alignment on contact pressure. Future work aims at further reducing the RMSE by using non-uniform contact model parameters that are related to the local stiffness of the stump.

Table:

Median and range of RMSE of simulated pressure						
	Total		Posterior	Lateral	Anterior	Medial
Median RMSE (kPa)	25.16		38.06	22.22	24.95	22.86
Range RMSE (kPa)	29.09		7.10	14.16	20.26	18.28

Caption: Median and range of RMSE between simulated and measured pressure for 20 pressure sensors

References: [1] Gailey et al., J Rehabil Res Dev, 45:15-30, 2008.

[2] Delp et al., IEEE I Bio-Med Eng, 55: 1940-1950, 2007.

[3] Sherman et al., Procedia IUTAM, 2:241-261, 2011.

[4] Portnoy et al., Ann Biomed Eng, 37: 2583–2605, 2009.

Disclosure of Interest: None Declared

Elderly

AS-0181

OLDER ADULTS SHOW LESS TRICEPS SURAE MUSCLE FASCICLE SHORTENING IN WALKING COMPARED TO YOUNG ADULTS

Lauri Stenroth [1,*] Patricio Pincheira [1] Sarianna Sipilä [2] Neil Cronin [1] Taija Finni [1]

[1]Department of Biology of Physical Activity, [2]Department of Health Sciences, University of Jyväskylä, Jyväskylä, Finland

Introduction and Objectives: Aging is associated with alterations in Achilles tendon mechanical properties [1]. This could lead to alterations in triceps surae muscle function in walking, even if walking kinematics are preserved with aging. Altered triceps surae muscle function with aging could partly explain the pronounced deficit in ankle joint power production observed in older compared to younger adults [2]. The aim of this study was to compare medial gastrocnemius (MG) and soleus muscle fascicle behavior in healthy young and older adults in walking.

Methods: 10 young adults (18-30 years old) and 11 older adults (70-80 years old) participated in the study. Subjects walked over a 10 meter force platform at their preferred speed while MG and soleus fascicles were scanned with ultrasonography at 80 Hz. In addition to the preferred speed, older adults walked at a speed that was matched to the mean walking speed (1.4 m/s) of young adults. Average walking speed was determined using photocells at the start and end of the force platform. Muscle fascicle length was tracked from the ultrasonography videos using an automatic tracking algorithm [3]. Gait cycles were separated based on ground reaction force data and normalized to 100 data points. Fascicle length was normalized to the length at heel strike and averaged across gait cycles. Fascicle length (relative to heel-strike) at toe-off and amount of fascicle shortening (peak-to-peak amplitude of fascicle length) during ground contact were calculated for each subject. Differences between young and older adults were compared with independent samples t-test and differences between preferred and matched speed within older adults were compared with paired samples t-test. Level of statistical significance was set at $\alpha < 0.05$.

Results: The preferred walking speed was significantly faster in young compared to older adults (1.4±0.1 vs. 1.1±0.1 m/s, p<0.001) but the matched walking speed was similar between the groups (1.4±0.1 vs. 1.4±0.0 m/s, p=0.443).

Both in young and older adults, MG fascicles showed first shortening and then lengthening from heel strike to mid-stance. From mid-stance to toe-off the fascicles shortened consistently (figure 1). In older adults, soleus fascicles first elongated during mid-stance and then shortened during push-off. At mid-stance, soleus fascicles in young adults showed near isometric muscle function. Despite 20 % increase in walking speed from preferred speed to matched speed in older adults, fascicle length changes were only minimally altered. Neither fascicle length at toe-off nor fascicle shortening during ground contact significantly changed in either muscle between the speeds. Fascicle length at toe-off was significantly shorter in young compared to older adults at preferred speed for both muscles (MG p=0.027, soleus p=0.002) but at matched speed only for soleus (p=0.005). MG shortened significantly more during ground contact in young compared to older adults at preferred speed (p=0.021) but not at matched speed (p=0.063). No significant differences between the groups were observed in peak-to-peak amplitude of soleus fascicle length during ground contact at either speed.

Figure:
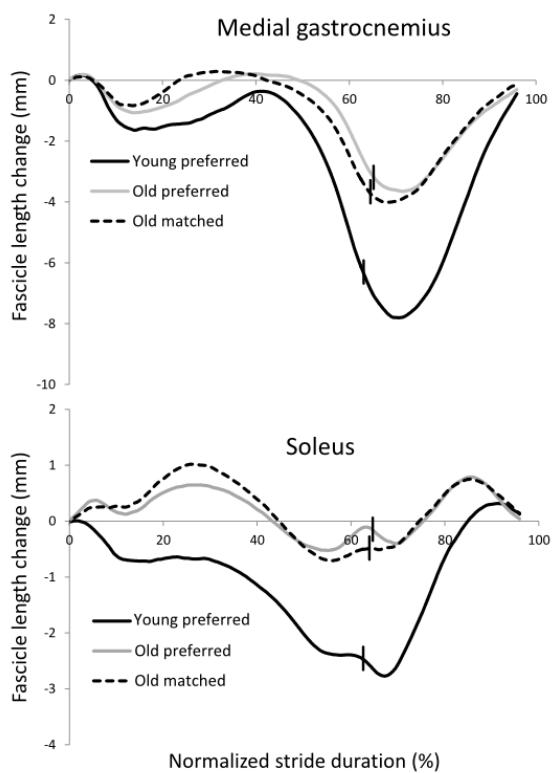
Caption: Figure 1. Average fascicle length changes in young and older adults across the mean stride (heel contact to heel contact). Fascicle length is normalized to length at heel contact. Short vertical line crossing the fascicle length data indicates instant of toe-off.

Conclusion: The main result of the study was that older adults showed less length changes in MG fascicles in walking at preferred speed compared to young adults. In addition fascicle length relative to heel strike was shorter at toe-off in young adults compared to older at preferred speed in both muscles and in soleus at matched gait speed.

In general older compared to young adults showed less shortening in triceps surae muscle fascicles during ground contact in walking. The observed difference may reflect decreased functional capacity of triceps surae muscles in older adults and consequential compensation by other muscle groups such as hip extensors [2, 4]. Triceps surae muscles should be taken into account when designing interventions for improving or maintaining mobility in old age.

References: [1] Stenroth et al., J Appl Physiol, 113: 1537-1544, 2012.

[2] Kulmala et al., J R Soc Interface 11: 20140858, 2014.

[3] Cronin et al., J Appl Physiol 111: 1491-1496, 2011.

[4] DeVita et al., J Appl Physiol 88: 1804-1811, 2000.

Disclosure of Interest: None Declared

Rehabilitation

AS-0182

REVEALING QUADRICEPS INHIBITION IN MALES AND FEMALES WITH KNEE OSTEOARTHRITIS USING A SIMPLE MUSCULOSKELETAL MODEL

Daniel L. Benoit [1 2,*] Heather J. Bigham [1] Mohammad S. Shourijeh [1]

[1]Faculty of health Sciences, [2]Faculty of Engineering, University of Ottawa, Ottawa, Canada

Introduction and Objectives: Quadriceps weakness and increased muscle activation is commonly reported in healthy, older females and those with knee osteoarthritis (OA), [1]. Loss of muscle mass and arthrogenous muscle inhibition contribute to a decrease in muscle strength, and in response it has been suggested that normalised muscle activation increases to compensate. Musculoskeletal models are commonly used to predict muscle forces and provide more in-depth information on joint mechanics in various populations, including this vital information of voluntary activation deficits will result in more reliable predictions. As quadriceps play an important role in providing general stability to the knee joint, it is vital to understand the level of activation deficit in various populations. Therefore, we propose the use of a subject-specific model to determine the quadriceps and knee flexor level of voluntary activation deficit in older males and females with and without OA.

Methods: Peak knee extension and knee flexion torque (MVIT) data were collected on a *Biodex* dynamometer from twelve females with OA (64(6) years; 27.0(3.2) kg/m^2), sixteen healthy females (60(5) years; 23.1(2.7) kg/m^2), fourteen males with OA (69(7) years; 25.2(3.8) kg/m^2), and sixteen healthy males (64(8) years; 25.4(2.7) kg/m^2), along with EMG of eight muscles crossing the knee joint.

The OpenSim Gait2354 model was used to extract moment arms of these muscles with the hip (30° flexion), knee (30° flexion), and ankle (10° plantar flexion) positions corresponding to the MVIT tests. Within a mathematical framework [2] using optimization, maximum isometric force parameter F_0^{max} of the muscles was tuned to minimize the error between the simulation and the MVIT with initial values set so that F_0^{max} corresponded to those of [3]. A strength ratio representing the level of voluntary activation was defined as: $a_s = T^B/T^I$, where T^B is the *Experimental* peak torque (MVIT) and T^I is the *Ideal* peak torque calculated for each participant, to determine quadriceps and knee flexor strength deficiencies (lower value represents greater level of activation deficiency). The *Ideal* peak torque had all agonist muscles set at 100% of their potential force with no antagonist force production.

Results: Based on the optimal model-derived force production capability of the subjects, the mean level of voluntary activation of the quadriceps was significantly lower in OA participants and healthy females compared to healthy males (p<0.03) (Fig. 1A), representing quadriceps strength deficiencies in these groups. Mean±SD quadriceps muscle contribution ratios were not different between groups (p>0.05); however, standard deviations were high in all groups, suggesting this variable is subject-specific.

Ratios of mean±SD knee flexion voluntary activation were not different between groups (p>0.05; Fig. 1B). The lower activation ratios may be due to a lack of semimembranosus in the model and the gastrocnemius muscles never achieving 100% during the knee MVIT experimental tests and conclude the these values are not representative of hamstrings

activation deficits. However, the similarity between groups indicates that hamstring voluntary activation level is similar in older adults irrespective of sex and the presence of OA.

Figure:
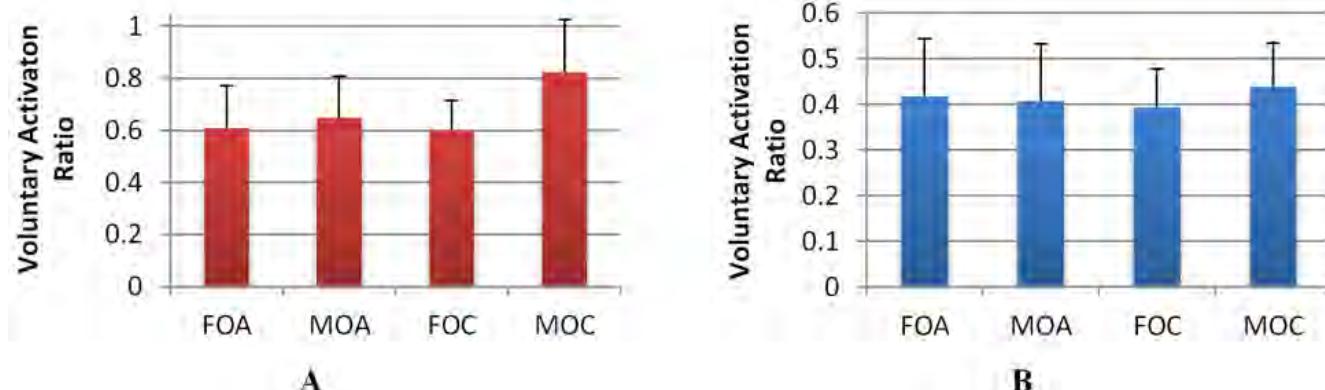
Caption: 1A: Mean voluntary activation ratios (VAR) of the quadriceps in females and males with OA (FOA, MOA) and healthy controls (FOC, MOC); 1B: Mean VAR of the knee flexors in of FOA, MOA, FOC and MOC groups. Error bars represent standard deviation.

Conclusion: This study presents a novel method for estimating strength deficiencies during maximum effort at the knee and produced subject-specific estimations of voluntary activation deficits similar to those determined with supramaximal stimulation techniques in OA males [4], allowing us to quantify quadriceps inhibition as the deficit in level of voluntary activation achieved compared to the quadriceps' capacity to produce maximum knee extensor torque. Healthy females had similar levels of quadriceps inhibition than those with OA suggesting this may be an etiological factor that increases their risk of OA development. As our results support the notion that quadriceps inhibition is present in older males and females with and without OA. We suggest generic musculoskeletal models should make necessary adjustments of this variable to improve the validity of their model output predictions for these populations.

References:

[1] Rudolph et al., *Phys. Ther.*, 87: 1422-1432, 2007.

[2] Shourijeh et al., Hybrid Forward Inverse Dynamics Framework for Human Musculoskeletal Simulations, submitted, *ISB*, 2015.

[3] Delp et al., *IEEE Trans. Biomed. Eng.*, 37: 757-767, 1990.

[4] Becker et al., *Ortho. Res.*, 22: 768-773, 2004.

Disclosure of Interest: None Declared

Rehabilitation

AS-0183

MULTI-CHANNELS FUNCTIONAL ELECTRICAL STIMULATION WALKING SYSTEM INSPIRED BY PURE REFLEXIVE CONTROLLER

Lin Meng [1,*] Bernd Porr [1] Henrik Gollee [1]

[1] Biomedical Engineering, University of Glasgow, Glasogw, United Kingdom

**Introduction and Objectives:**

Most commercialized functional electrical stimulation (FES) walking systems are designed based on open-loop control [1] due to the issues of sophisticated closed-loop controllers including high computational power request, difficulties in implementing the control strategy on a human model[2]. However, an automatic FES system has a large potential market if it is able to free the subject's hands and manage to generate an adaptive gait pattern. A bio-inspired approach provides a way to exploit simple but efficient, robust control methods by abstracting the control principles from animals [3]. The Runbot is the first biped robot with pure reflexive controllers [4]. It is driven by local reflexes without zero moment control algorithms or central pattern generators. We created an abstract robot controller based on actual human walking in [6] by exploring the causal relationship between the foot contact information and the muscle activation (EMG). In this paper, we will present a multi-channels reflexive FES controller derived from the robotic model for use to gait rehabilitation.

Methods: A reflexive neural controller is utilized to generate locomotion of a robot [4], and is built based on reflexive mechanisms in humans [7]. The controller has a hierarchical structure where the sensor neurons contact the motor neurons directly (Fig.1 A). Foot contact information is the main feedback modulating the stepping, while the hip anterior extreme angle (AEA) triggers the ipsilateral knee extensor in swing. The EMG estabilishes the relationship to the biomechanical movement as it correlates with the muscle tensions [8]. It can be related to the joint movement in a ballistic locomotion which indicates the possibility to transfer the robotic controller to FES of muscles[6]. Four muscles were selected due to their functional roles in human walking (Tibialis Anterior (TA), Lateral Gastrocnemius (LG), Biceps Femoris (BF) and Rectus Femoris (RF)). Based on the previous work [6], we determine the timing for each muscle during one gait cycle (Table.1). Five gait phases are used in our model – heel strike (HS), foot flat (FF), heel off (HO), Toe off (TO), late swing (LS) when the hip reaches its AEA. For the detection of gait phases, the system replies on the combination of two types of sensors. The force sensitive resistors (FSRs) (Interlink Electronics, Camarillo, CA, USA) are embedded in standard shoe insoles, and will indicate when the foot contacts the ground and when not. The motion sensors (MPU9150, InvenSense) measure the hip angle in the sagittal plane. The whole system structure is shown in Fig.1 B. The detected gait phases are transmitted via the reflexive control model which sends the updated stimulation parameters to the programmable electrical stimulator (RehaStim, HASOMED, Germany). Filter transfer functions are used to generate the reflex responses. An user-friendly GUI window allows to control all parameters in real-time.

Results: The purpose of the experiment was to test the feasibility of the FES system with reflexive controller. In particular, we were interested in determining if the timing of the stimulation is appropriate for various walking speeds. One subject was asked to walk with different speeds (slow 1 km/h, fast 3.0 km/h) on the treadmill. The system worked successfully

and provide the stimulation sequences at correct timing in all conditions (as seen Fig.1C). A video demonstrates this proof of concept can be accessed at https://www.youtube.com/watch?v=-_AjptV9wcw

Figure:
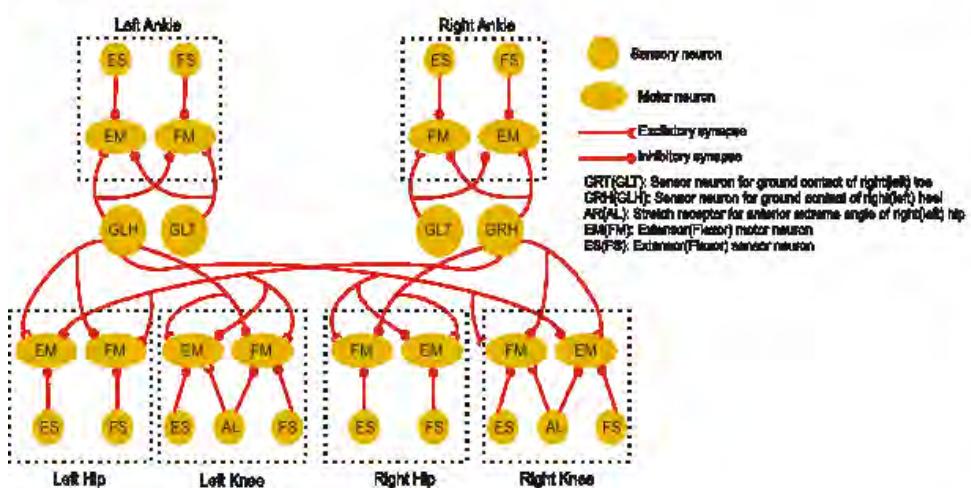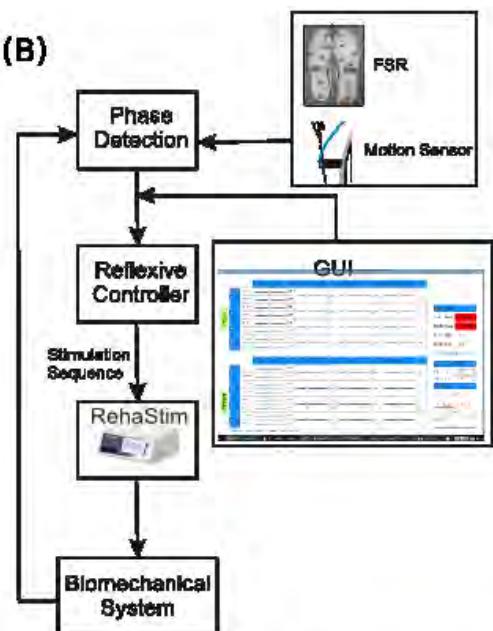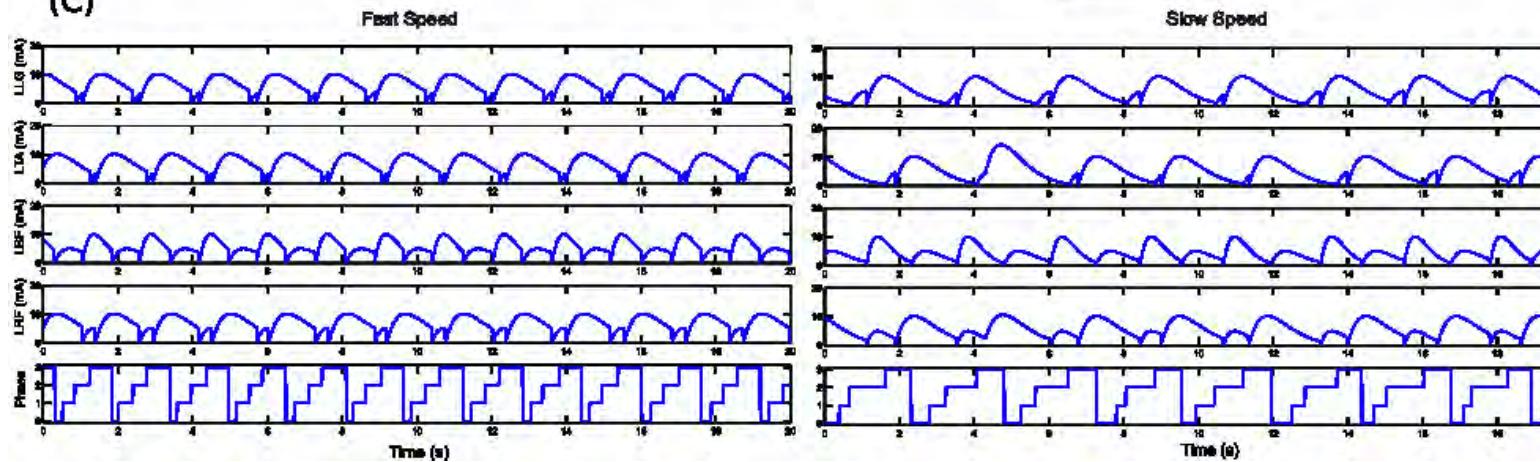
Caption: (A) The reflexive controller of Runbot. (B) The structure of FES reflex walking system. (C) The stimulation sequences generated by gait phases

Conclusion:

We successfully adapted the simple reflex control model employed in the Runbot into a FES controller for gait rehabilitation. The automatic electrical stimulation system is simple, but effective, efficient and robust. The gait phases detected by FSRs in shoe insoles and motion sensors give the correct time for triggering specific muscles during walking. The GUI allows to individualize the stimulation patterns for different subjects and control stimulation parameters in real-time. In future, we will study the benefit of this reflex FES system for the walking of incomplete SCI patients.

Table:

Gait Phases	Stimulated Muscles
Ipsilateral HS	BF
Ipsilateral HO	LG
Ipsilateral TO	TA
Ipsilateral LS	RF, TA
Contralateral HS	BF,LG,RF

Caption: Trigger Timing for Muscles

References:

[1] G. M. Lyons et al. IEEE Trans Neural Syst Rehabil Eng, 10:260–279, 2002.

[2] G. P. Braz et al. Neuromodulation: Technology at the Neural Interface, 12:180–190, 2009.

[3] R. D. Beer et al. COMMUN ACM, 40:pp. 30–38, 1997.

[4] T. Geng et al. Neural Comput., 18:1156–1196, 2006.

[5] J. B. Nielsen et al. Sensorimotor Control of Movement and Posture, Springer, 2002.

[6] C. A. Macleod et al. PloS one, 9: e109959, 2014.

[7] B. M. Van Wezel et al. J. Neurosci., 17:3804–3814, 1997.

[8] D. Winter et al. Electroencephalogr. Clin. Neurophysiol., 67:402–411, 1987.

Disclosure of Interest: None Declared

Rehabilitation

AS-0184

IDENTIFICATION OF KINEMATIC AND CLINICAL FEATURES THAT PREDICT EXERCISE INTERVENTION OUTCOMES FOR TREATMENT OF PATELLOFEMORAL PAIN.

Ricky Watari [1,*]Dylan Kobsar [1]Angkoon Phinyomark [1] [2]Blayne Hettinga [1] [2]Reed Ferber [1]

[1]Kinesiology, University of Calgary, [2]Running Injury Clinic, Calgary, Canada

Introduction and Objectives: Exercise interventions are widely used for treatment of patellofemoral pain syndrome (PFPS) [1]. However, controversy remains on the effects of exercise therapy in pain reduction. It has been postulated that the inconsistent responses to an exercise therapy may be due to different gait profiles and kinematic patterns within this PFPS group. The aim of the current study was to retrospectively select parameters from sagittal and frontal plane gait kinematics, and self-reported pain and function measures, to predict the response of runners with PFPS to an exercise intervention protocol.

Methods: Data from 49 recreational runners with PFPS were collected prior to and following a 6-week muscle strengthening exercise protocol. The data collection included lower limb 3-D kinematics while running on an instrumented treadmill, knee function from the Anterior Knee Pain Scale (AKPS), and pain from a Visual Analogic Scale (VAS). Subjects were classified into Responders and Non-Responders based on their improvement on AKPS and VAS [1]. Pre-intervention gait and clinical data underwent three steps: (i) data reduction, using Principal Component Analysis (PCA); (ii) feature selection, based on effect size of the Principal Components (PCs) between Responders and Non-Responders, and (iii) supervised classification, with linear discriminant analysis (LDA), from which the combination of PCs with the highest classification accuracy were selected using a leave-one-out cross-validation method.

Results: The best classification model between Responders and Non-Responders when comparing the baseline data used 4 predictors; 2 clinical PCs (Clinical PC1 and PC2) and 2 gait PCs (Gait PC3 and PC24) to achieve 87.8% classification accuracy and explain 72% of variance of the treatment outcome. Clinical PC1 represented the amplitude of VAS and AKPS, while Clinical PC2 was a difference feature, with low scores indicating a worse VAS compared to AKPS. Gait PC3 was generally related to ankle and hip frontal plane angles in late swing and initial contact, and hip extension angles in mid-stance and early swing phases, while Gait PC24 was related to ankle dorsiflexion angle prior to initial contact. Compared to Non-Responders, Responders had higher Clinical PCs and Gait PC24 scores while Gait PC3 scores were lower. Overall, Responders were characterized as having a significantly higher pain VAS at baseline (p = 0.001), but no significant differences in functional measure of AKPS (p = 0.732). In contrast with our results, past studies on treatment response prediction have found higher pain scores at baseline to be predictive of poor treatment outcome [2]. Regardless, factors chosen by a prediction model are highly specific to the adopted interventions and sample population. Furthermore, Gait PCs indicated that, compared to Non-Responders at baseline, Responders exhibited greater ankle inversion angles in late swing, more abducted hip angles in late swing and initial contact, greater hip extension angles in mid-stance and early swing phases, and reduced ankle dorsiflexion angles prior to initial contact. In the current study, hip and ankle frontal plane kinematics during swing are represented by Gait PC3, confirming the importance of these features. Inconsistencies in literature may be due to heterogeneity among PFPS subjects,

considering the existing differences in response to treatment. For example, Responders had greater ankle inversion and hip abduction as compared to Non-Responders. Also, as Gait PC24 had a large influence in the LDA model, this finding supports previous research indicating that discrimination of running kinematics is a complex classification problem, reflecting relationships among many kinematic variables [3].

Figure:
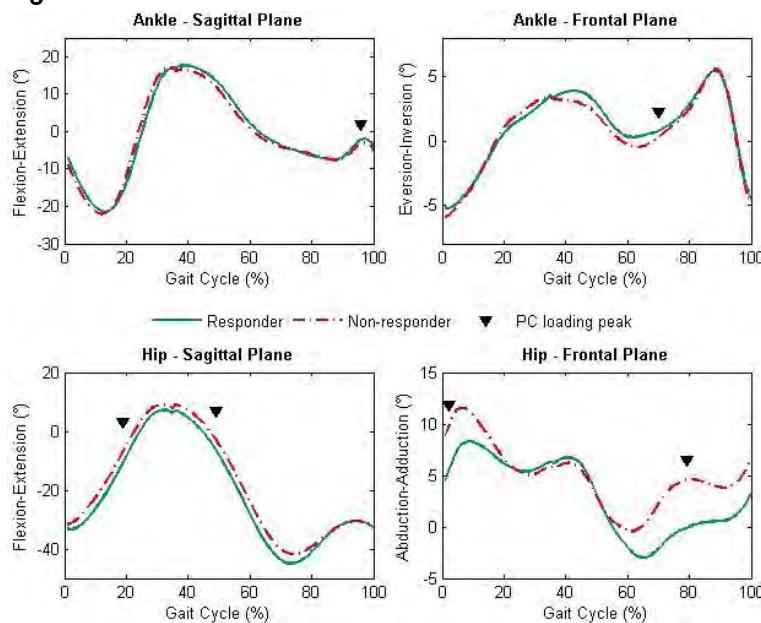
Conclusion: Principal components that represent self-reported baseline pain and function, along with hip and ankle kinematics were able to predict the outcome of exercise intervention for PFPS treatment with 87.8% accuracy.

Table:

	Discrete variable	Responder (n=17)	Non-Responder (n=32)
Clinical PCs	VAS (cm)	5.9 (1.1)	3.7 (2.2)
	AKPS (score)	75.8 (8.4)	73.5 (10.3)
Gait PC3	Ankle inversion at 70% gait cycle (°)	0.79 (2.97)	0.24 (3.72)
	Hip adduction at 1% gait cycle (°)	4.49 (4.33)	8.83 (6.91)
	Hip adduction at 80% gait cycle (°)	0.07 (5.88)	4.53 (8.03)
	Hip extension at 20% gait cycle (°)	10.57 (6.34)	6.73 (7.64)
	Hip extension at 50% gait cycle (°)	6.60 (5.94)	3.01 (7.25)
Gait PC 24	Ankle dorsiflexion at 95% gait cycle (°)	2.17 (2.60)	3.21 (3.36)

Caption: Mean (SD) of discrete variables that represent the Principal Components (PC) used in the Linear Discrimination Analysis. Joint angles were extracted from the instant in gait cycle when the PC had a peak in loading coefficient.

References: [1] Crossley et al., Arch Phys Med Rehabil, **85(5)**:815–22, 2004.

[2] Collins et al., Br J Sports Med, **47**:227-33, 2013.

[3] Phinyomark et al., PLoS ONE, **9(8)**:e105246, 2014.

Disclosure of Interest: None Declared

Rehabilitation

AS-0185

EVALUATION OF HIP POSITION IN THE DEVELOPMENT OF STRENGTH AND ELECTROMYOGRAPHY RESPONSE OF THE RECTUS FEMORAL MUSCLE. SUMMARY TITLE : EVALUATION OF FORCE AND ELECTROMYOGRAPHIC RESPONSE IN RELATION TO THE HIP POSITION .

Paulo Veiga [1,*]

[1]University of Pernambuco, Recife, Brazil

Introduction and Objectives: The rectus femoral muscle is known as a bi -articular muscle. Its efficiency is significantly influenced by the position of the two joints, in accordance with the principles governing the relations of length - muscle tension. To understand the function of the rectus femoral muscle in relation to the hip position .

Methods: The sample consisted of 30 volunteers of both sexes, aged 18 and 25, which underwent strength testing and electromyographic evaluation of the rectus femoris muscle in three positions: (seated with the hip at 90 ° and knees flexed to 90°, seated with the hip and knee flexed 45 ° to 90 °, lying with the hip and knee flexed 0 ° to 90°). Movement of knee extension , with maximum power for 10 seconds at each position, with a time of 2 minutes of rest between them was asked. The data were stored in individual records for further inferential statistical analysis. Considered the level of significance where p-value ≤ 0.05.

Results: It was observed in the study, no statistical significance of strength and electromyographic response of the rectus femoris muscle in relation to the hip position.

Conclusion: Comparing the analysis of force and electromyographic response of the rectus femoris muscle in relation to the position of the hip assessed in the respective angles 90 ° , 45 ° and 0 ° , there was no statistical significance. However, they showed up differences between genders. Given this, the authors emphasize the need for more studies on the subject .

References: Reference 1

Alencar TAM,Bini RR, Matias KFS, Diefenthaeler F, Carpes FP. (1010) Influência do comprimento do pedivela no desempenho de ciclistas. Brazilian J Biomotricity., 4:32-47.

Reference 2

Aquino CF, Fonseca ST, Gonçalves GGP, Silva PLP, Ocarino JM, Mancini MC. (2010) Stretching versus strength training in lengthened position in subjects with tight hamstring muscles: a randomized controlled trial. Manual Therapy., 15:26-31.

Reference 3

Tassi NF, Gonçalves JG, Vitti M, Krool M. (1990) Electromyographic evaluation of the rectus femoris muscle during exercises performed on the leg press. Electromyogr Clin Neurophysiol., 38:223-9.

Disclosure of Interest: None Declared

Biofeedback

AS-0186

EFFICACY OF PHARMACOLOGICAL AND NON-PHARMACOLOGICAL STRATEGIES TOWARDS CEREBRAL PALSY INDUCED SPASTICITY

Dinesh Bhatia [1,*]Bablu Lal Rajak [1]Protima Nomo Sudro [1]

[1]Biomedical Engineering, North-Eastern Hill University, Shillong, India

Introduction and Objectives: Pharmacological and non-pharmacological (repetitive Transcranial Magnetic Simulation (rTMS), Transcranial direct current stimulation) strategies are being widely used in therapeutic and investigative studies. Both these strategies have been extensively used in patients suffering with multiple sclerosis, stroke, spinal cord injuries and cerebral palsy (CP). Various studies have examined both these strategies and yielded effective results like medicines for relaxing muscle spasms, control pain, seizures and improvement in range of movement. Due to the velocity-dependent increase in muscle tone, various issues like tendon jerks, clonus, spasms and hyper-excitability resulting from stretch reflex were observed in patients with muscle spasticity. Based upon the number of affected joints and muscles leading to the impairment of activity limitation, spasticity is categorised as focal spasticity and multi-focal spasticity. The paradigm of treatment for them also varies according to the impairments around a specific joint or multiple joints. The aim of this study is to comprehensively review both the pharmacological and non-pharmacological approaches towards cerebral palsy induced spasticity patients and study the effects of different techniques (long term potentiation, long term depression, activity dependent metaplasticity, shift in excitability and so on) employed on remedial treatment till date for neuro-rehabilitation. The group is presently working on sponsored projects from the government to study effects of r-TMS on muscle spasticity in CP kids. This review/study would be beneficial in working towards this objective.

Methods: This review reports the medication techniques of many identified studies involving excitation, inhibition, motor evoked potential (MEV) size, stimulation parameters like low and high frequency, time, angle of stimulation, region of stimulation (target area) and stimulation responses. Innumerable novel stimulation paradigms have been developed consisting of significant potential for altering respective cortical excitability thereby minimizing spasticity in CP patients. However, further research as per literature reviewed till 2013 shows that different innovative paradigms such as Botulinum neurotoxin, posterior rhizotomy, neuromuscular electric stimulation and dynamic bracing are being carried out to attain optimum stimulation techniques in order to overcome central nervous system (CNS) disorder causing balance and movement problems. This would help in people suffering from the above mentioned diseases.

Results: Of all pharmacological and non-pharmacological medications, rTMS being a non-invasive technique utilizing the principle of non-invasive brain stimulation by exploiting electromagnetic induction was found to be very effective for the treatment of muscle spasticity in CP kids (Gunduz A, et al. 2013). Abdelkader. A.A. et al. 2013, specified that rTMS has the potential to contribute improvement in spasticity which ultimately improves the quality of patients life. Terreaux L, et al. 2013 exhilarates the effects of rTMS in reducing reflex excitability and stiffness of ankle-plantarflexors in patients affected from muscle spasticity. Valle A.C. et al. 2007 found that high frequency rTMS is beneficial in reducing spasticity in children with CP and it was later on proved by many clinical trials on these subjects. Cabre et al. 2005 provide the juncture influencing spinal excitability and modify descending corticospinal influences in controlled manner by using rTMS

Conclusion: From these results, it can be concluded that r-TMS would be beneficial in treating spasticity in above population group thereby improving their quality of life and enabling them to perform activities of daily ADL tasks in an effective manner.

Keywords: Pharmacological and non- pharmacological strategy, spasticity, cerebral palsy and rTMS.

Disclosure of Interest: None Declared

Upper Limb

AS-0187

COMPARISON OF TWO DIRECT KINEMATIC MODELLING APPROACHES FOR SPORT-SPECIFIC UPPER LIMB MODELLING

Denny Wells [1,*]Cyril Donnelly [1]Bruce Elliott [1]Jacqueline Alderson [1]

[1]The School of Sport Science, Exercise and Health, The University of Western Australia, Perth, Australia

Introduction and Objectives: Since the publication of the Calibrated Anatomical Systems Technique (CAST)[1], modelling approaches, generally speaking, can be segregated into those that use this approach (*complex*), and those that do not (*simple*). There is however, a paucity of research that has directly compared the kinematic estimates of both models. In a sport such as cricket, where strict limitations are placed on elbow extension range (EER) during the bowling delivery, the modelling approach used could inadvertently influence the rulings on a bowler's legality. The aim of this research is to compare the upper limb kinematic estimates and ruling of cricket bowling legality between one *simple* and one *complex* modelling approach.

Methods: Two marker sets were simultaneously applied to nine bowlers who each bowled 24 trials together with two static/neutral trials. The *complex* approach stored joint centre (JC) estimates relative to technical co-ordinate systems (triads of markers). The shoulder JC was calculated as per Campbell[2,3], and stored in the proximal upper arm and acromion triads; elbow JC as the midpoint of the medial and lateral epicondyles, stored in distal upper arm triad[4]; wrist JC as the midpoint of two markers on either side of the wrist during the static trial, stored in distal forearm triad. The *simple* modelling approach calculated the JC as the midpoint of two markers placed on either side of each joint. Kinematic variables were calculated from upper arm horizontal (UAH) to ball release (BR) (delivery phase): 1) segment (forearm and upper arm) lengths and 2) elbow flexion/extension (FE) angles. Elbow FE angles were further analysed by a) a traditional zero dimension (0D) statistic - ANOVA - investigating specific elbow FE events (UAH, maximum flexion, minimum flexion, BR, EER), and b) across time with one dimensional statistical parametric mapping paired t-test (SPM1D)[5].

Results: The 0D analysis of *simple* and *complex* dynamic bowling trials found no difference (and high correlation) in elbow FE events at the beginning of the delivery phase (UAH), then significant differences at each event for the rest of the delivery: Maximum Flexion (*simple*: 34.8°; *complex*: 39.9°; p < 0.001), Minimum Flexion (*simple*: 7.3°; *complex*: 14.0°; p < 0.001) and BR (*simple*: 8.9°; *complex*: 15.7°; p < 0.001). Importantly, there was no significant differences (and high correlation) to EER between *simple* and *complex* modelling approaches. The International Cricket Council enforced 15° EER[7] limit was applied to each of the deliveries within the dataset to find what the recommendation of bowling legality would be made. Four of 216 (2%) deliveries did have different results with the application of the 15° elbow extension rule. In each case the *simple* approach returned illegal (>15° EER); the *complex* approach legal (<15° EER). Three separate participants were affected and had conflicting legality rulings (1/3 total participants). The SPM1D analysis shows the *simple* and *complex* elbow FE modelling approaches produce different elbow FE results for the whole delivery phase. The smallest difference is at UAH (where 0D analysis shows no difference), greatest difference at approximately 90%. The accelerations and large range of motion experienced by the shoulder during this phase result in STA, which is supported by the presence of fluctuating segment lengths[6]. Upper arm and forearm segments for both modelling approaches

changed length throughout the dynamic trials (average 2.34%). The combination of large scapula movement during the overhead movement and STA present in the second half of the delivery phase (specifically 60-100%) coincides with the greatest differences found by the SPM1D analysis. Cricket bowlers are subject to EER limits and can be banned for exceeding EER limits. It is recommended future research looks to improve the dynamic modelling of the shoulder JC and investigate the use of inverse kinematics for modelling the upper limb during cricket bowling.

Figure:
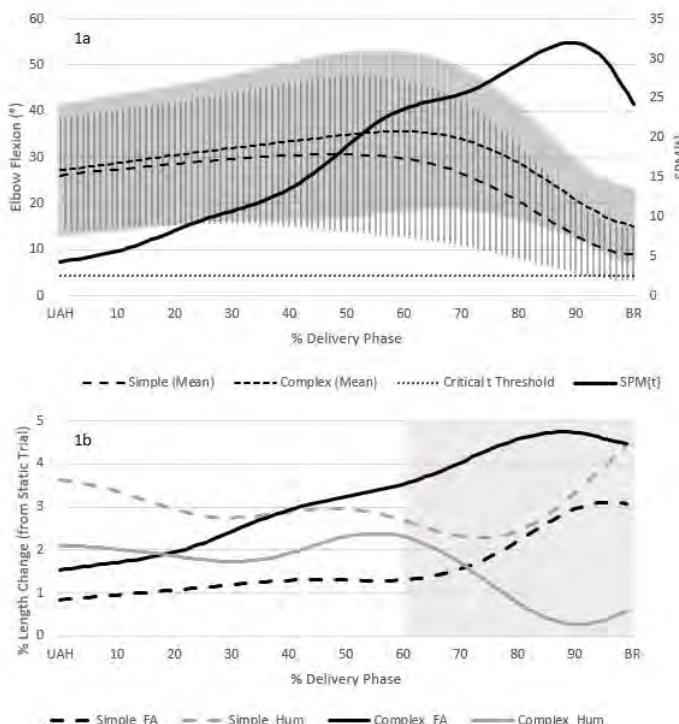
Caption: Figure 1a: Mean and SD plotted on left axis, SMP1D analysis on the right.

Conclusion: *Simple* and *complex* modelling approaches produce different estimates of elbow FE during cricket bowling. This is due to STA and the relatively simplistic model of the shoulder during dynamic sporting tasks like cricket bowling. When the modelling approaches produced conflicting legality recommendations the *simple* always returned illegal EER whilst the *complex* returned legal EER.

Acknowledgements: Mark King, Wayne Spratford and Elissa Phillips

References: [1] Cappozzo, A, et al., Clinical Biomechanics, 10:171-178, 1995.

[2] Campbell, A, et al., Med & Biol Eng & Computing, 47:543-550, 2009.

[3] Campbell, A, et al., J. Biomechanics, 41: Supplement 1, S165, 2008.

[4] Eftaxiopoulou, T, et al., J. Sports Sciences, 31:1722-30, 2013.

[5] Pataky, T, J. Biomechanics, 46:2394-401, 2013.

[6] Wells, D, et al., ISBS, Melbourne, Australia, 2012.

[7] ICC 2013. ICC Regulations for the Review of Bowlers Reported with Suspected Illegal Bowling Actions. Annexure 1.6.

Disclosure of Interest: None Declared

Upper Limb

AS-0188

ACCURACY OF GLENOID PLACEMENT IN REVERSE SHOULDER ARTHOPLASTY. CAN SURGEONS CORRECT THE PRE-OPERATIVE GLENOID DEFORMITIES IN OSTEOARTHRITIC SHOULDERS?

Julien Berhouet [1]Lawrence Gulotta [1]Xiang Chen [2]Andreas F. S. Kontaxis [3,*]

[1]Sports Medicine devision, [2]Biomechanics, [3]Leon Root Motion Analysis Laboratory, Hospital for Special Surgery, New York, United States

Introduction and Objectives: Reverse shoulder arthroplasty (RSA) is a popular option for treating patients suffering from cuff tear arthropathy, complex humerus fractures and failure of primary shoulder prostheses (2). Clinical and biomechanical studies have shown the benefits of RSA (2,3). RSA procedure remains technically challenging for the surgeon. The management of pathologic glenoid with bone deformities and defects makes it difficult to identify reliable anatomical landmarks, and consequently accurately position the glenoid component with a good primary bony fixation. Glenoid component placement during RSA on an arthritic eroded glenoid remains challenging for orthopaedic surgeons. Clinical results have shown that glenoid version and tilt should be corrected to anatomical values after the joint replacement. The objective of this study was to investigate whether surgeons can achieve glenoid version and tilt correction during RSA when they cannot visually assess the scapula orientation

Methods: This study included CT data from 24 pre-operative pathologic shoulders with highly eroded glenoids. All 3D-CT scapula reconstruction were created using Mimics®, Materialize. Glenoid version and tilt was defined by a single operator according to the recommendations of Friedman et al.,(2). RSA virtual surgery was performed in all shoulders using a virtual 3D model of the Biomet Comprehensive® Reverse Total Shoulder prosthesis. The focus of this study was the placement of the glenoid baseplate which was performed by two surgeons with experience in RTSA with two different techniques/methods:

i) In the first method the 3D geometry of the scapula was fully visible and the surgeons could interactively choose the placement of the baseplate in 3D and in 2D CT planes (named 'interactive method'.

ii) In the second method the surgeons placed the glenoid baseplate while only the glenoid, acromion and coracoid were exposed (named 'blind method').

In both methods the surgeon's objective was to position the glenoid baseplate as inferiorly as possible but to also correct the version and tilt of the eroded glenoid to anatomical values. The accuracy in glenoid component alignment was determined by the correction of the pre-operative glenoid version and tilt. Repeated measures ANOVA with post hoc analysis was used to determine the differences on glenoid correction (version and tilt) between pre and post-operative methods (interactive vs blind).

Results: The average pre-operative glenoid version and tilt were 8.4° (SD: 7.7°) and 9.8° (SD: 9.5°), respectively. The average version and tilt after the surgery with the 'interactive method' were 0.5° (SD: 0.7°) and 0.4° (SD: 0.4°), which means that it corrected the glenoid version of the highly eroded glenoids. When the surgeons used the 'blind method' (they could not see the orientation of the scapula) they placed the baseplate in 6.1° (SD: 6.0°) version and 12.4° (SD: 7.8°) tilt. Results showed that the two surgeons were not different (p>0.05) from each other and did not significantly

correct the pre-operative glenoid version and tilt (p>0.05). In 11 out of the 24 scapulae the baseplate placement resulted in glenoid volt violation by the peg of the baseplate.

The positioning of the glenoid plate showed that in average the two surgeons (that used the 'blind method') chosen almost the same inferior position as the operator of the 'interactive' method (Figure 2). That was probably because this study did not simulate the soft tissue that surrounds the glenoid or the narrow window that surgeons usually operate during shoulder replacement.

Figure:
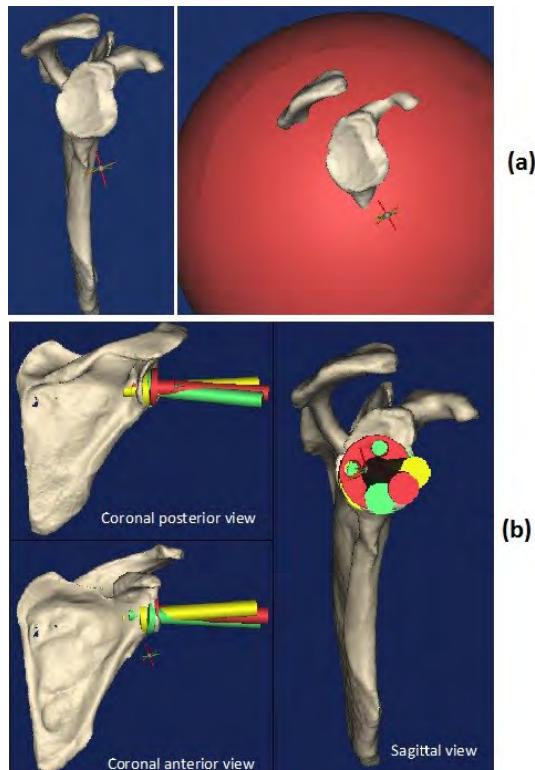
Caption: (a) Two surgeons placed the glenoid baseplate with two methods: i)with scapula fully visible 'interactive method' (right picture), ii) with the body of the scapula hidden 'blind method' (middle picture). (b) The results showed different placement for the two methods

Conclusion: The results of this study suggest that when surgeons operate on highly eroded glenoids, where they cannot assess accurately the position of the scapula in space, they risk not correcting the post-operative glenoid alignment. Misalignment of glenoid fixation in total shoulder arthroplasty can affect load transfer and result in loosening. As a general conclusion, the study suggests that pre-operative planning with surgical navigation or specific tools/guides should be used to help the surgeons achieve accurate glenoid placement.

References: [1] Boileau P, et al., 2006, J Shoulder Elbow Surg. 2006 Sep-Oct;15(5):527-40

[2] Friedman RJ, et al., J Bone Joint Surg Am. 1992 Aug;74(7):1032-7

[3] Kontaxis A, et al., Clin Biomech (Bristol, Avon). 2009 Mar;24(3):254-60

Disclosure of Interest: None Declared

SHOULDER ROTATIONAL RANGE OF MOTION PATTERN IN ELITE VOLLEYBALL AND HANDBALL PLAYERS

Augusto G. Pascoal [1,*] Andrea Ribeiro [2] Sofia Neves [1]

[1]University of Lisbon, Faculty of Human Kinetics, CIPER, LBMF, Lisbon, [2]Fernando Pessoa University, Faculty of Health Sciences, Porto, Portugal

Introduction and Objectives: Shoulder adaptive morphological and functional changes have been described on overhead-throwing athletes [1]. The throwing shoulder, when compared to the non-throwing shoulder, exhibits a significantly increased humeral external rotation (external rotation gain) and a significantly decreased humeral internal rotation (glenohumeral internal rotation deficit) while the total range of motion (external rotation + internal rotation) is kept the same. Although the extensive research about kinetics and kinematics of overhand throwing motion, most of the published studies have focused on baseball, while few studies focused specially on handball or volleyball. Thus, the purpose of this study was to compare humeral rotational changes among groups of overhead athletes who participate in two different sports (handball and volleyball) and non-overhead athletes.

Methods: Ninety healthy subjects participated in this study, divided into three groups (N=30): handball group (20.7±1.4 years;76.8±4.1kg;184±4cm); volleyball group (20.7±1.0years;65.7±8.25 kg;177.7±6.1cm); and the control group, with non-overhead athletes (19.5±1.9years;64.3±4.3kg;174.8±3.4cm). An electromagnetic tracking device was used to record 3D shoulder kinematics (100Hz) with a set-up of 3 sensors: thorax-sensor attached to the skin over T1; arm-sensor fitted on a cuff and firmly adjusted to the subject's lateral arm and scapular-sensor, attached to the superior flat surface of the acromion process. A fourth sensor mounted on a hand-held stylus (±65cm) was used for bony landmarks digitalization to link sensors to local anatomical coordinate systems (LCS) and subsequently calculate segments and joint rotations according to the shoulder ISB standardization protocol [2]. In a seated position and the dominant arm at 90º of humeral elevation at scapular plane, subjects were asked to actively reach maximal internal and external shoulder rotation, keeping the scapula stable. The end-range value of internal and external arm rotation with respect to the thorax and the scapula was used to calculate the internal, external and total rotation arcs in the LCS of the thorax (IRth, ERth and TAth) and scapula (IRgh, ERgh and TAgh). Internal and external arcs were defined as the absolute angular difference between the rotational end-range and the neutral rotation. The total arc corresponds to the sum of both internal and external arcs. The neutral rotation corresponds to the point when both humeral epicondyles had the same orientation as the Y-axis of the thorax or the scapula LCSs. A one-way ANOVA with post hoc testing (alpha=0.05) was applied to compare dependent variables between groups.

Results: Volleyball group had significantly ($p<.05$) greater ERgh (volleyball=81.3º±12.8º; handball=71.0º±8.8º; control=55.4º±9.9º) and significantly less IRth (volleyball=33.1º±9.3º; handball=41.5º±16.8º; control=43.2º±2.5º) compared to handball and control. The volleyball group showed also had a significantly greater ERth (volleyball=67.1º±11.1º;handball=63.4º±11.2º;control=51.3º±9.5º) and less IRth compared to control. The handball group had significantly greater ERgh and ERth compared to control ($p<.05$). Volleyball group had significantly greater TAgh (volleyball=114.4º±15.6º;handball=112.5º±10.5º;control=98.5º±10.5º) and handball group a significantly greater TAth

(volleyball=96.2º±14.7º;handball=105.6º±9.8º;control=89.8º±11.9º), compared to the control. Taken the control group as reference, the external arc of rotation (glenohumeral and thoracohumeral) represents 55% (range:49-61%) of the total active arc of motion. This percentage were significantly greater on volleyball (71%) compared to handball (60%) and control (55%) groups.

Conclusion: The glenohumeral external rotation gain observed on throwers in comparison with control agrees with previous reports [e.g 3]. However the glenohumeral internal deficit was observed in volleyball players but not in handball players. Results showed a sport-related effect that must be considered on the assessment and/or rehabilitation of throwers athletes. Further studies about kinetic and kinematics sport pattern of motion are required in order to full understanding the adaptive changes on the throwing shoulder. In conclusion, the handball and volleyball groups showed humeral rotational changes with respect to control. Those changes identified an increased active glenohumeral and thoracohumeral external rotation motion. The glenohumeral and thoracohumeral internal rotation deficit was only observed in volleyball group. A glenohumeral external rotation shift and a thoracohumeral internal rotation deficit were observed on volleyball in comparison to handball group.

References: [1] Zheng N, et al. Int J Sports Med.33:463-8 2012.
[2] Wu G, et al. J Biomech.38:981-92 2005.
[3] Myers JB, et al. Am J Sports Med.34:385-91 2006.
[4] McCully SP, et al.J Shoulder Elbow Surg.14:602-10 2005.
[5] Borsa PA, et al. Med Sci Sports Exerc.38:21-6 2006.

Disclosure of Interest: None Declared

Upper Limb

AS-0190

ACCURACY OF PRE-OPERATIVE PLANNING IN REVERSE SHOULDER ARTHROPLASTY

Andreas F. S. Kontaxis [1,*] Julien Berhout [2] Daniel Choi [3] Chen Xiang [3] Lawrence Gulotta [2]

[1] Leon Root Motion Analisys Laboratory, [2] Sports Medicine Devision, [3] Biomechanics, Hospital for Special Surgery, New York, United States

Introduction and Objectives: Reverse total shoulder arthroplasty (RTSA) is a popular option for treating patients suffering from cuff tear arthropathy (1) or other challenging arthropathies (4). Clinical and biomechanical studies have shown the benefits of RTSA (1,2) in pain relief and functional recovery, but concerns still remain regarding impingement and the presence of scapular notching on the scapular inferior border(3).

Recent studies have highlighted the importance of accurate glenoid prosthesis placement (3) and reported the use of patient-specific guides in aim to improve accuracy in glenoid positioning for RTSA. However there are no direct comparisons of how glenoid placement of a standard RTSA surgery compares to a guided RTSA surgery in cadavers and whether it results in better functional outcomes. The objective of this study was to investigate whether using a musculoskeltal model (for pre-operative plan) and a guided surgery can achieve larger impingement free range of motion (ROM) compared to a standard RTSA surgery.

Methods: This study performed RTSA surgery in 20 cadaveric specimens with two methodologies i) traditional procedure where glenoid baseplate placement is determined with the help of standard surgical instrumentation ii) a subject specific-guide where aids the surgeon in glenoid placement according to a pre-operative plan.

Surgeries were performed from a single surgeon with experience in RTSA. The Biomet Comprehensive RTSA (Biomet, Warsaw, Indiana) was used in the study (size: 28mm glenoid baseplate; 36mm diameter standard glenosphere; 44mm diameter standard onlay humeral tray)

For the standard procedure the standard instrumentation set was used to place the steinman pin on the glenoid. For the guided surgeries, a pre-operative position was defined using an interactive shoulder model, the Newcastle Shoulder Model (NSM) (2). The NSM was customized to describe a virtual RTSA surgery and the placement of the glenoid sphere was modified to maximize impingement free range of motion. Specific guides were manufactured by a 3D printer. The objective of the guide was to place the Steinman pin into the desired glenoid position based on the anatomical landmarks of the anterior glenoid border and coracoid foot.

Pre and post-operative CTs were used to assess the glenoid version and tilt after the surgery as well as the position of the baseplate. The impingement free ROM was evaluated with a motion analysis system post-operatively for i) scapula plane elevation and ii) internal external rotation in 30 degrees of glenohumeral abduction.

Results: The average age and BMI of the specimens in the 'standard procedure' were 31.4 (SD) and 71.0 yo (SD 8.0) respectively and for the 'guided procedure' were 31.0 (SD 7.2) and 71.4 yo (7.0). The results of the glenoid alignment showed that in average both standard and guided RSA surgeries changed the post-operative glenoid version and tilt, but none of the changes were statistically significant (p>0.05).

In contrast, the guided surgery had a significant impact on the placement of the glenoid baseplate (Figure 2). Results showed that the guided surgeries placed the baseplate in average 4.2 mm (SD 4.0) more inferiorly compared to the standard procedure (p<0.05).

This difference in baseplate placement had also an effect on the impingement results. The average inferior impingement was recorded at 10.4° (SD 4.3) and superior impingement averaged at 67.9° (SD 4.3) for the guide surgery specimens. Even if the results were different from the pre-operative plan (the virtual surgery with the model showed no inferior impingement), it was better than the cadavers that received surgery with the standard instrumentation tools (average inferior impingement: 29.6 deg, SD 13.7, average superior impingement 59.3 deg SD 1.54, p<0.05). Rotation range of motion was 113 deg (SD 15.0) for the specific guide group and 63.3 deg (SD 27.4) for the standard guide group (p<0.05)

Figure:
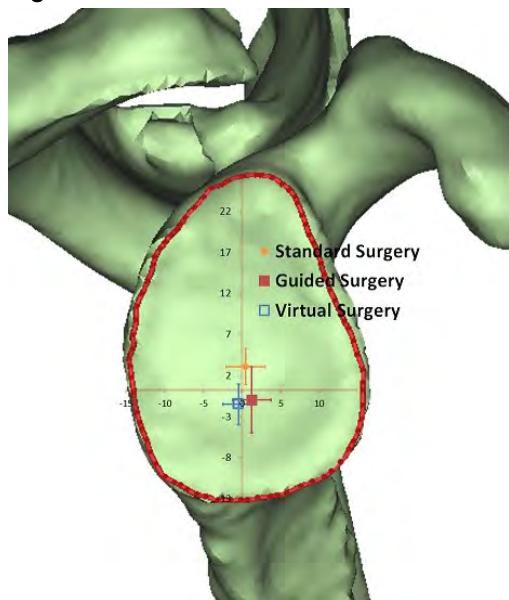
Caption: Results of the glenoid placement for the different procedures. Glenoid placement with subject specific guides resulted in more inferior glenoid baseplate placement (red 'Guided Surgery' vs orange 'Standard Surgery'). The specific guides placed the glenoid close the pre-operative plan – model's virtual surgery (blue 'Virtual Surgery')

Conclusion: The guided surgeries provided a glenoid placement that was close to the pre-operative plan that was designed with the model. The specimens that received the guided surgery achieved a more inferior glenoid placement compared to the specimens that had the standard surgery. The latter translated in a better functional outcome with a larger free impingement range of motion.

Musculoskeletal models and custom surgical guides can be used to create pre-operative plans and help surgeons maximizing functional outcomes in RTSA.

References: [1] Boileau P, et al., JSES 2006 Oct;15(5):527-40

[2] Kontaxis A, et al., Clin Biomech 2009 Mar;24(3):254-60

[3] Simovitch RW, et al., JBJS Am. 2007 Mar;89(3):588-600

[5] Wall B, et al., JBJS 2007 Jul 1;89(7):1476–1485

Disclosure of Interest: None Declared

AS-0191

A COMPARISON OF ARTIFICIAL NEURAL NETWORK AND REGRESSION MODELS FOR PREDICTING MANUAL ARM STRENGTH BASED ON HAND LOCATION

Nicholas L. La Delfa [1,*] Jim Potvin [1]

[1]Kinesiology, McMaster University, Hamilton, Canada

Introduction and Objectives: The accurate estimation of manual arm strength (MAS) is an important component of ergonomic task evaluation. Strength prediction has typically been accomplished using complex linked segment biomechanical models, and estimates of strength about each axis of the wrist, elbow and shoulder joints. However, it has recently been shown that multiple regression approaches, using the simple task-relevant inputs of hand location and force direction, may be a better method for predicting MAS [1]. Alternatively, the use of artificial neural networks (ANNs) has seldom been used to predict strength, despite being shown to be a valuable data-fitting tool for small and noisy data sets [2]. Therefore, the main objective of this study was to perform a direct comparison between ANN and regression models, by evaluating their ability to predict identical sets of development and validation MAS data.

Methods: The MAS data from 71 female participants, with an age-range representative of the working population, were compiled from previous studies in our lab (see [1] for further details). These data consisted of MAS measurements in the six primary force directions (i.e. up, down, anterior, posterior, medial, lateral – termed '1D' forces) in 28 hand locations within the reach envelope. In addition to the 1D data, 42 of the participants also performed maximum force exertions in combinations of two (2D, eg. up & anterior) and three (3D, eg. up, anterior & lateral) of the six primary force directions. These additional measurements were obtained from 8 of the hand locations (Table 1). ANN & regression models were developed using: 1) all of the MAS data (Universal models), and 2) only the 1D data (1D models). Both the Universal and 1D models were developed using a random, but identical, sample of 85% of the Universal and 1D datasets, respectively. The remaining 15% of the data were used to validate each of the four models, by determining how the models would predict MAS values not included in their development. The ANN models were developed in Matlab (v2014b) using a double-layer feed-forward network, trained using the Bayesian Regularization algorithm. The multiple regression equations were developed in SPSS (v21) using a stepwise approach. The coordinates of the hand (relative to the shoulder) and the direction cosines of the manual force vector, were used to create 20 input variables for developing and evaluating each model. Model performance was evaluated using Pearson's correlation analysis and evaluation of root mean square errors (RMSE).

Results: Overall, the ANN models explained more variance, and had lower errors, compared to the regression models (Figure 1). Both ANN models had a mean RMSE of 5.7 N, compared to a mean RMSE of 16.4 N for the regression models. The 1D ANN model had a higher explained variance compared to the Universal ANN model (1.000 vs. 0.957, respectively), but the Universal ANN model had a lower RMSE. In the validation test, both Universal models (regression & ANN) predicted MAS better than the 1D models, with the Universal ANN model producing a 30.7% lower RMSE, and a higher correlation, compared to the Universal regression model.

Figure:
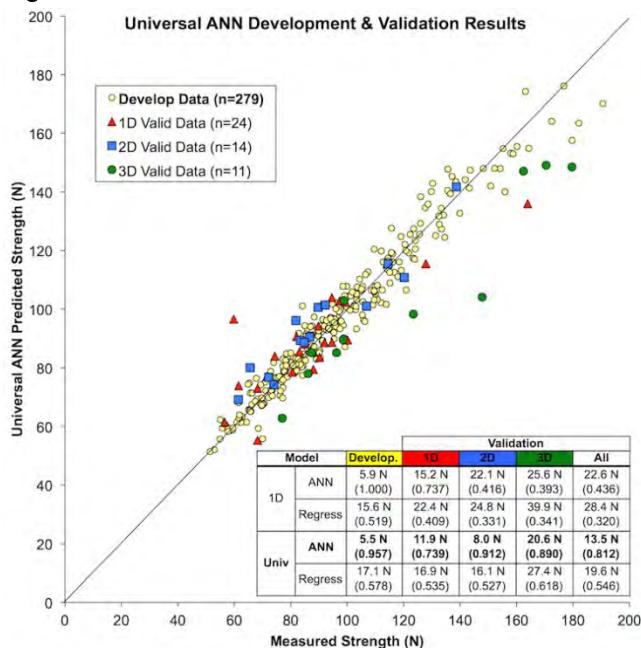
Caption: Figure 1: Scatter plot of the Universal ANN model, which was the best performing model of the four that were developed (RMSE = 5.5 N, r-squared = 0.957). The model's prediction of 1D, 2D and 3D validation data are also shown on the scatterplot. The inset table shows the RMSE & r-squared values (in parentheses) of all development models, and their validation results. Cells that are bolded indicate the model that exhibited the lowest RMSEs for each column.

Conclusion: ANNs provided a viable method for accurately predicting MAS, and this will be particularly beneficial for ergonomics analyses. Though regression approaches have shown promise for predicting MAS, particularly for one exertion direction, it appears that ANNs may be a more universal approach when exertion direction is included as a predictor variable. This will allow future MAS models to predict average strength capability for a force vector oriented in any possible direction, rather than being limited to the six primary force directions. Furthermore, all models were more robust in the validation test when they were developed using Universal data (i.e. 1D, 2D & 3D data). Therefore, these models can likely be further improved by including more universal strength data from more hand locations within the reach envelope.

Table:

Type of Data	# of Subjects	# of Hand Locations	# of Exertion Directions	Total # of Conditions
1D	71	28	6	168
2D	42	8	12	96
3D	42	8	8	64
			Total:	328

Caption: Table 1: Details of the MAS used in the development and validation of the regression and ANN models.

References: [1] La Delfa et al., Ergonomics, 57: 254-261, 2014.

[2] Eksioglu et al., Int. J. Ind. Ergo, 18: 431-441, 1996

Disclosure of Interest: None Declared

Upper Limb

AS-0192

AGE, GENDER, TRAINING AND ARM DOMINANCE – IMPLICATIONS FOR KINAESTHESIA AND MOVEMENT PERFORMANCE IN THE UPPER EXTREMITIES

Sybele Williams [1,*]

[1]Department of Physics, The University of the West Indies, St. Augustine, Trinidad and Tobago

Introduction and Objectives: The use of the upper extremities in the efficient performance of the activities of daily living is highly dependent on the joints' functionality and associated kinaesthesia for the goal-directed movements of the limbs, movement correction and locating limbs without visual control. One aspect of kinesthesia is proprioception or joint position sense (JPS). The bony structure of the glenohumeral joint facilitates a large range of motion however it often comes at a price since the joint is predisposed to pain and sensory disturbance due to overuse or injury. This leads to dysfunctional proprioceptive ability and JPS which can compromise an individual's safety and negatively affect the sense of security and quality of life when carrying out the activities of daily living (ADL) [1]. As such when investigating the functional capacity of a joint it is important to understand that characteristics of the subject collective e.g. JPS may be uniquely influenced by age, gender, training and arm dominance.

Methods: In this study, 6 male patients (mean age: 60.6 ± 13.0 yrs.) and 9 female patients (mean age: 62.8 ± 6.9 yrs.) with diagnosed SAIS were screened to determine the degree to which the dysfunction in the glenohumeral joint affects the functional capacity of the joint. The patient group was compared with three groups: healthy counterparts in the same age group (40 – 79 years), healthy younger groups and healthy trained athletes (handball players) in the age group 18 – 39 years. The group of healthy counterparts consisted of 14 males (mean age: 42.8 ± 2.5 yrs) and 12 female subjects (mean age: 46.4 ± 6.2 yrs). The group of healthy, untrained, young subjects was composed of 2 males (mean age: 29.0 ± 5.7 yrs.) and 7 females (mean age: 27.4 ± 5.1 yrs.) while the group of handball players consisted of 8 males (mean age: 26.3 ± 3.6 yrs.). For the investigation of the functional capacity of the joint a three-dimensional motion analysis system was used. For the assessment of the JPS of the glenohumeral joint each subject actively reproduced 6 standardised joint positions: abduction 50°, 65° and 80° as well as anteversion 50°, 65° and 80° under standardised conditions [2]. Two modalities were investigated, firstly all joint angle reproductions were tested with visual control (WVC) then the subjects were blindfolded i.e. no visual control (NVC) and the joint position sense was re-tested for each of the joint positions. The difference from the target joint angle was averaged over the three repetitions for each joint position reproduced. Multi-factorial unrelated analysis of variance (ANOVA) was used to determine group differences.

Results: Considering the dominant arm of male subjects it was found that the proprioceptive ability assessed according to the WVC modality was best for the athletes and worst for the patients. However healthy, untrained male subjects aged 18 – 39 years demonstrated proprioceptive abilities which were similar to patients under the same test. Additionally, it was found that performance worsened for the anteversion test angles set. Female subjects tested under the same modality showed no significant differences for any of the tests. With respect to the proprioceptive tests performed according to the NVC modality athletes once again demonstrated the best proprioceptive ability while patients displayed impaired joint position sense. However healthy, untrained male subjects aged 18 - 39 yeas and healthy, untrained males aged 40 – 79

years exhibited similar proprioceptive ability. Under the same modality the joint position sense of females was worse than that for males. An increasing inability to correctly re-position the arm was also displayed over the six test movements and their associated angles with a peak occurring at anteversion 65°.

Conclusion: The early identification and management of chronic joint disorders e.g. subacromial impingement syndrome (SAIS) in the glenohumeral joint are extremely important in managing the joint health of the affected person. This can be attained through the objective and quantitative assessment of individual movement patterns [3]. However the performance of daily movements is dependent on the kinaesthetic senses of the subject. In the case of complex, multi-joint daily movements a fuller understanding of the factors which may affect the biomechanical and coordinative strategies of healthy subjects and patients is important with respect to successful intervention approaches and rehabilitative therapies.

References: [1] Myers et al., Manual Therapy,11:197-201, 2006

[2] Jerosch et al., Archives of Orthopaedic and Trauma Surgery, 123:151-157, 2003

[3] Li et al., Clinial Interventions in Aging, 9:1123-1131, 2014

Disclosure of Interest: None Declared

Upper Limb

AS-0193

FATIGUE AND RECOVERY IN THE SHOULDER COMPLEX WHILE PERFORMING SIMULATED REPETITIVE WORK

Alison McDonald [1,*]Calvin Tse [1]Peter Keir [1]

[1]Kinesiology, McMaster University, Hamilton, Canada

Introduction and Objectives: Low load, repetitive work is common in modern workplaces and these demands can contribute to the development of musculoskeletal disorders[1]. The anatomy and mobility of the shoulder complex allows kinematic and muscular adaptations to maintain performance despite fatigue-reduced capacity. Multi-joint compensations in the upper extremity have been employed to maintain performance during repetitive tasks[2]. How people utilize opportunities for kinematic and muscular variability and adapt during fatiguing work could change their physical exposure and risk for injury at work. The purpose of this study was to examine kinematic and muscular adaptations during continued performance of submaximal, repetitive work following a fatiguing protocol.

Methods: Twelve male participants completed a sequence of three protocols: (1) 20 pre-fatigue work cycles, (2) anterior deltoid fatigue protocol, (3) 60 post-fatigue work cycles. Each work cycle was 60 seconds and consisted of 4 tasks: (1) power grip handle pull (10 x 2 kg), (2) knob turn (5 rotations), (3) anterior drill press (10 s, 50% max), (4) power grip handle push (10 x 2 kg). The fatigue protocol was completed after 20 work cycles. The protocol was designed to fatigue the anterior deltoid muscle using static and dynamic exertions. Fatigue was quantified through changes in strength, ratings of perceived exertion (RPE), decreased EMG frequency and increased EMG amplitude during submaximal, static, reference exertions. Activity of 14 muscles of the upper extremity, back and chest were collected with surface electrodes at 2000 Hz (Delsys Inc., Boston, MA, USA). Kinematics were tracked with a passive motion capture at 100 Hz (Motion Analysis Corporation, Santa Rosa, CA) using 26 reflective markers and a custom scapular tracker[3]. For the data analysis, the work cycles were decomposed into the 4 tasks and the handle pull and push tasks were further divided into loading and return phases. Multiple repeated measures ANOVAs and preplanned Tukey HSD tests were used for the statistical analysis (SPSS Statistics 20.0, IBM, NY, USA).

Results: Immediately following the fatigue protocol, there were significant signs of muscle fatigue and reduced physical capacity (Table 1). These changes were accompanied by significant muscular and kinematic adaptations in the work tasks during the post-fatigue work cycles (PF1-8) ($p<0.05$). Although the handle push and handle pull tasks were quite constrained, there were several kinematic and muscle activity changes in both the loaded and the return phases of the tasks. Scapular changes, including increased superior rotation and decreased internal rotation were seen during the performance of different tasks throughout the recovery process. Amongst other changes following fatigue, reduced glenohumeral flexion was seen during the drill task ($p<0.05$). Concurrent with this was an increase in middle and posterior deltoid activity and a trend of increased glenohumeral abduction (Figure 1). At the end of the 60 post-fatigue work cycles, indicators of fatigue developed in the middle deltoid, however participant ratings of perceived exertion returned to pre-fatigue levels.

Figure:
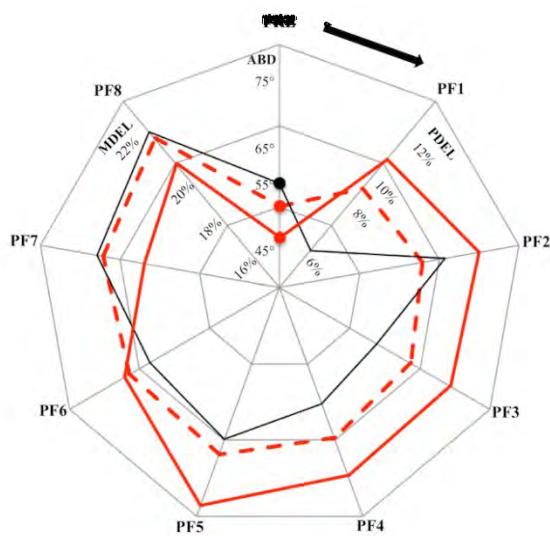
Caption: Glenohumeral abduction (ABD - black line) increased along with middle (MDEL- solid red line) and posterior (PDEL - dashed red line) deltoid muscle activity (%MVE) during the drill task in the post-fatigue work cycles (clockwise pre-fatigue (PRE) to post-fatigue 8 (PF1-PF8)). By the end of the post-fatigue work-cycles the middle deltoid exhibited significant signs of muscle fatigue ($p < .05$).

Conclusion: We found that participants used kinematic and muscle recruitment adaptations following the fatigue protocol to maintain task performance for 60 post-fatigue work cycles. Although these adaptations allowed for recovery in some muscles, fatigue persisted and developed in other muscles by the end of the post-fatigue work cycles, despite subjective ratings of perceived exertions returning to pre-fatigue levels. If people are unable to perceive negative behavioural changes during repetitive work, they may be at greater risk of developing workplace injuries.

Table:

Measure	Baseline	Pre-Fatigue	Post-Fatigue	Post-60 Cycles
RPE	0.17 (0.32)*	2.41 (1.22)	5.88 (2.13)*	2.17 (1.56)
Strength (kg)	14.9 (2.6)	12.9 (2.2)	9.2 (3.0)*	13.8 (2.9)
Fatigued Muscles	N/A	N/A	Anterior deltoid, Posterior deltoid, Latissimus dorsi, Serratus anterior	Anterior deltoid, Middle deltoid, Serratus anterior

Caption: Fatigue was quantified by changes in RPE, strength and muscle fatigue (significant increase in EMG amplitude and decrease in median power frequency). Pre-planned comparisons were made between the pre-fatigue values and the other time points. * denotes statistically significant difference from "Pre-fatigue".

References: [1] Nordander C et al, 2009. *Ergonomics* 52(10), 1226-1239.

[2] Fuller JR et al, 2009. *J Electromyogr Kines* 19, 1043-1052.

[3] Karduna AR et al, 2001. *J Biomech Eng-T ASME* 123, 184-190.

Disclosure of Interest: None Declared

AS-0194

THE VACUUM PHENOMENON WITHIN A TOTAL SHOULDER REPLACEMENT CAUSING GLENOID COMPONENT DISSOCIATION – A NOVEL OBSERVATION

György Kocsis [1,*]Donal McNally [2]Angus Wallace [3]

[1]Shoulder and Elbow Unit, [2]Engineering, University of Nottingham, [3]Shoulder and Elbow Unit, Nottingham University Hospitals, Nottingham, United Kingdom

Introduction and Objectives: The Nottingham Total Shoulder Replacement (TSR) System is an anatomical shoulder prosthesis design, primarily intended for use with a metal glenoid baseplate. It is made up of the following components. A metal glenoid baseplate is inserted onto the bony glenoid after bone preparation. There is a humeral stem, onto which an artificial humeral head is assembled. Between the two metal components is a liner or bearing that is made of Ultra High Molecular Weight Polyethylene. The Nottingham TSR socket was designed to be fully congruent with the artificial humeral head. The design of the baseplate and liner was intended to ensure that the liner is clipped solidly and irreversibly onto the metal glenoid baseplate.

With the Nottingham TSA system glenoid liner disassembly from the metal glenoid baseplate became a relatively frequent complication. In our unit 32 dissociations were recorded in 464 primary and revision arthroplasty cases (6.89%), with the glenoid implant dissociation ranging from 2 months to over 7 years postop. We have explored the hypothesis that these dissociations are a consequence of the vacuum forces between the glenoid liner and the artificial humeral head. A model to measure the vacuum forces was developed, and fatigue tests were also carried out to assess the strength of the clip-on mechanism between the metal glenoid baseplate and the glenoid liner.

Methods: The measurement of the vacuum forces - A new Nottingham metal glenoid baseplate, polyethylene glenoid liner and a humeral head was mounted on an Instron 3367 tensile test machine. The artificial joint components were surrounded by a commercially available latex condom to simulate the joint capsule. Within the restraint, bovine synovial fluid was introduced. The space between the artificial joint components was free of air bubbles. The radius of curvature of the glenoid liner was the same as that of the humeral head prosthesis. The head component and the glenoid components were initially compressed with approximately 10N, then quickly moved away from each other along an axis perpendicular to the plane of the baseplate, and the forces were measured. Control measurements were completed using the same setup but using air instead of the synovial fluid.

The fatigue tests - A new Nottingham metal glenoid baseplate was mounted on an Instron 3367 machine. The plastic liner was clipped on, and using rods, the plastic liner was repeatedly pushed out of the baseplate along an axis perpendicular to the metal baseplate. The endpoint of the test was the complete disassembly of the liner from the baseplate. The tests were carried out using 40, 60 and 80N forces.

Results: The vacuum tests showed a peak force of 50.44N (SD 3.844) from which an average of 10.2N (SD 0.0145) was attributed to the resistance of the experimental system at the peak force. This proves that in our experiment about 40N of vacuum force was present.

The plastic liner disengaged from the metal glenoid baseplate after 25000 cycles using 40N of push out force in the fatigue tests. Using 60N of force the dissociation happened after 11000 cycles, using 80N force resulted in the disengagement of the plastic liner after 187 cycles.

Conclusion: Although the existence of vacuum forces is a generally accepted factor in the stability of a native shoulder joint, vacuum forces were not considered to be important during the design of the Nottingham prosthesis. Publications on failures of other designs of shoulder prosthesis do not mention this potential mechanism.

A very obvious explanation for the glenoid component disassembly would be surgical error, improper assembly of the components. In our experience surgical error leads to early disassembly of the glenoid components, within days after surgery. The temporal distribution of our disassembly cases does not support surgical error being the cause in the majority of cases.

Our in vitro tests verified two important conclusions. In our experimental setting vacuum forces of up to about 40N could be observed. This means that vacuum forces could also be important in vitro, and that these forces would need to be taken into account during artificial joint design. The other conclusion is that the clipping mechanism between the plastic glenoid liner and the metal glenoid baseplate of the Nottingham TSR System is a poor design, as dissociation can happen with a force as little as 40N after only 25000 cycles.

A weakness of our study is that the in vivo conditions might be significantly different from our experimental setup, however, our results are a viable explanation for the dissociations which have occurred in our clinical practice.

References: [1] Rosenberg N et al., In: *BMC Musculoskelet Disord.* Vol. 8. England, 2007:76.

[2] Scarlat MM et al., *Journal of Arthroplasty* 2001;16-6:795-801.

[3] Bergmann G et al., 2007;40-10:2139-49.

[4] Swieszkowski W et al., Journal of engineering in medicine. 217-1:49-57.

[5] McKellop HA. *Biomaterials* 2007;28-34:5049-57.

Disclosure of Interest: None Declared

Upper Limb

AS-0195

HUMERAL HEAD REPLACEMENT- DOES IT WORK?
A KINEMATIC STUDY OF SHOULDER MOTION FOLLOWING COPELAND® SHOULDER RESURFACING ARTHROPLASTY

Arpit Jariwala [1]Iain Hyndman [2,*]Linda Johnston [1]Weijie Wang [1]Graham Arnold [1]Carlos Wigderowitz [1]Rami Abboud [1]

[1]Department of Orthopaedic and Trauma Surgery, Tayside Orthopaedic and Rehabilitation Technology (TORT) Centre, Ninewells Hospital and Medical School, [2]School of Medicine, Ninewells Hospital and Medical School, University of Dundee, Dundee, United Kingdom

Introduction and Objectives: Copeland® shoulder resurfacing arthroplasty (CSRA) proponents suggest that it replicates the normal joint anatomy by providing restoration of the humeral head structure in terms of offset, version, angulation and shape. Most studies note the clinical improvement after CSRA but lack objective kinematic assessment. The aim of this study was to investigate the changes in motion analysis in patients following CSRA for range of motion (ROM) tasks namely; flexion, abduction, external and internal rotation. In addition, all patients were kinematically assessed on their ability to perform three activity of daily living (ADL) tasks namely; reaching behind the head, reaching for the contralateral shoulder and reaching behind the back.

Methods: Twenty-three shoulders (19 patients) with glenohumeral osteoarthritis agreed to participate in the study. Pre-operatively, patients underwent a clinical assessment, pain scoring (VAS 0-10) and shoulder scoring with Constant-Murley (CS) and Oxford Shoulder Score (OSS) by an independent nurse practitioner. Subsequently, patients underwent motion analysis, which involved placement of reflective markers on their upper torso that accurately recorded specific parameters of shoulder movement using eight high-tech three-dimensional (3D) Vicon cameras. The markers were placed according to the International Society of Biomechanics (ISB) guidelines. The same set of assessments was postoperatively recorded at 4 and 12 months for both ROM and ADL tasks.

Results: Nineteen shoulders (15 patients) completed the study. There were 15 female and 4 male shoulders. Two patients were unwell to return for analysis and one patient moved away. The mean age of the patients was 72 years (range 52-84). The VAS pain score improved significantly post-operatively ($p<0.001$). Both CS and OSS improved significantly following surgery at both follow-up periods ($p<0.001$).

Clinically both flexion and abduction improved significantly post-operatively ($p<0.001$). However, the motion analysis data showed that only abduction improved significantly post-operatively ($p<0.001$). Flexion improved significantly ($p<0.007$) by 4 months post-operatively but thereafter a loss of flexion was noted at the 12 month mark. Both external and internal rotation significantly improved post-operatively ($p<0.05$) when comparing the pre-operative value to the two post-operative assessments both clinically and kinematically.When analysing the three ADL tasks kinematically significant improvements in movement (both flexion-extension and abduction-adduction planes) were noted post-operatively ($p<0.05$) when compared to the pre-operative value for the reaching behind the head and behind the back tasks. The contralateral shoulder tasks did not show a significant improvement when comparing pre-operative measurements to either of the two post-operative assessments (4 and 12 months) in any plane.

Conclusion: This present study is the first research to utilise objective biomechanical tools in addition to clinical measurements and outcome scores to assess overall CSRA outcomes. In addition, the present study also investigated the effect the CRSA procedure had on the ability of patients to undertake ADL. It confirmed substantial improvements in shoulder motion by state of the art kinematic analysis methods, which compliments the enhanced clinical scores in patients undergoing CSRA. We have shown in the present prospective study that CSRA provided significant improvement in pain, range of motion, functional tasks and outcomes scores making it a viable alternative to conventional stemmed shoulder arthroplasty in a select group of patients. The finding that the scores and function following CSRA continue to improve with time up to one year is important to know as this will help clinicians and therapists to plan the future management of post-operative patients and allow them to investigate those patients who do not follow the trend.

This study fully supports the use of 3D motion analysis as a useful tool for assessing and monitoring treatments and surgical procedures providing independent, objective, standardised and sensitive analysis of outcomes. The results from the study also complement those reported elsewhere in the literature. The ability to pick up loss of flexion with time exclusively by the kinematic method as noted in the present study is an important finding. It highlights the ability of the kinematic methods to pick up small but significant changes in shoulder motion which may have important clinical implications. Its strength to analyse complex motion of joints especially in upper limb will encourage its use as a vital tool in future orthopaedic assessment practice.

Disclosure of Interest: None Declared

EMG

AS-0196

NORMAL SHOULDER BIOMECHANICS: AN EMG STUDY

David Hawkes [1,*]Omid Alizadehkhaiyat [2]Anthony Howard [1]Simon Frostick [1]

[1]Musculoskeletal Science Research Group , University of Liverpool, [2]Sport and Exercise Science, Liverpool Hope University, Liverpool, United Kingdom

Introduction and Objectives: The shoulder is a multi-axial ball and socket synovial joint. Due to its limited bony constraint, the humeral head can translate on the glenoid fossa when the powerful shoulder girdle muscles contract. Therefore, precisely modulated muscle activity is required to achieve and maintain a stable fulcrum for arm movement. The aim of this study was to define, using EMG, normal muscle activation patterns during arm elevation throughout the globe of shoulder movement

Methods: Twenty healthy participants with a normal clinical examination and no history of musculoskeletal problems were studied. Bipolar surface electrodes were used to record EMG from 10 shoulder girdle muscles (anterior, middle and posterior Deltoid, upper, middle and lower Trapezius, Serratus Anterior, Teres Major, Latissimus Dorsi and Pectoralis Major). The activity of the Supraspinatus, Infraspinatus, Subscapularis and Rhomboid Major was recorded using indwelling fine wire electrodes. Participants completed 10 cycles of shoulder elevation in 4 different planes: Flexion, Scapular Plane Elevation, Abduction and Extension. Mean EMG amplitude was compared for each muscle between movements using a repeated measures ANOVA.

Results: Table 1 presents the mean amplitude for all muscles. There were significant differences between movements for the middle and posterior Deltoid, middle Trapezius and Pectoralis Major (Figure 1). Mean amplitude (± standard error of the mean) was 52±2%, 72±5%, 78±5%, 98±8% for the middle Deltoid in Flexion, Scapular Plane Elevation, Abduction and Extension, respectively. Significant differences were seen between all movements (p=0.02 - <0.001). Similarly, significant differences in mean amplitude were seen for the Posterior Deltoid: 51±2%, 68±5%, 81±7%, 153±19% between the above movements respectively (p=<0.01-0.02). The activity in the Middle Trapezius significantly increased as subjects progressed from Flexion to Extension: Flexion 55±3%, Scapula Plane Elevation 63±4%, Abduction 82±13% and Extension 104±10% (p=<0.01-0.02). Significantly higher activity was seen in the Pectoralis Major during Flexion (54±3%) as compared to Scapula Plane Elevation (39±5%), Abduction (37±4%) and Extension (29±3%) (p=<0.01-0.01).

Figure:
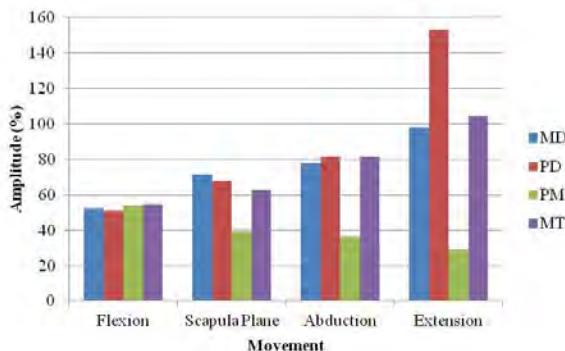
Caption: Mean muscle amplitude during the different planes of shoulder elevation

Conclusion: The normal shoulder girdle muscle activation patterns during shoulder elevation through the globe of shoulder movement have been comprehensively defined. Significant differences between movements were found for the middle and posterior Deltoid, middle Trapezius and Pectoralis Major. Higher activity in the posterior Deltoid during Extension was expected given its line of action. Similarly, higher activity in middle Trapezius reflects scapula retraction during shoulder Extension. Significantly higher activity was seen in the Pectoralis Major during Flexion which was anticipated given its accepted role as a flexor of the shoulder joint. The results provide a comprehensive basis for better understanding of the muscle activation alterations associated with shoulder pathologies.

Table:

	Mean Amplitude (%)			
Muscle	Flexion	Scapula Plane	Abduction	Extension
Anterior Deltoid	59±2	69±4	71±5	69±6
Middle Deltoid	52±2	72±5	78±5	98±8
Posterior Deltoid	51±2	68±5	81±7	153±19
Upper Trapezius	62±2	75±6	74±5	98±12
Middle Trapezius	55±3	63±4	82±13	104±10
Lower Trapezius	59±4	57±4	68±10	78±12
Serratus Anterior	58±2	60±3	57±3	52±5
Pectoralis Major	54±3	39±5	37±4	29±3
Teres Major	61±2	64±4	62±3	69±4
Latissimus Dorsi	58±2	67±3	63±4	72±8
Supraspinatus	57±4	78±11	88±14	90±19
Infraspinatus	57±3	64±13	74±15	72±12
Subscapularis	58±2	56±5	59±5	57±9
Rhomboid Major	63±7	77±18	90±23	124±41

Caption: Mean muscle amplitude during the shoulder elevation

Disclosure of Interest: None Declared

AS-0197

SHOULDER INSTABILITY TESTS AS EFFECT MEASURES AFTER SHOULDER INTERVENTIONS – AN INTER-EXAMINER RELIABILITY OF THE CLINICAL TESTS

Henrik Eshoj [1,*]Camilla Marie Larsen [1]Kim Gordon Ingwersen [1]Birgit Juul-Kristensen [1 2]

[1]Institute of Sports Science and Clinical Biomechanics, Faculty of Health Sciences, University of Southern Denmark, Odense M, Denmark, [2]Department of Health Sciences, Institute of Occupational Therapy, Physiotherapy and Radiography, Bergen University College, Bergen, Norway

Introduction and Objectives: Shoulder instability is a common problem due to the large range of motion, which in general compromises the stability. Consequently highly active people in their second and third decades are often experiencing shoulder problems related to instability. In order to decide the optimal intervention precise diagnosis of shoulder instability is fundamental and mostly performed. To obtain an accurate diagnosis clinical tests need to be reliable. Hence, the objective was to investigate the inter-examiner reliability of six specific selected and standardized clinical shoulder instability tests.

Methods: A standardized protocol for carrying out reliability studies was used, containing a training, an overall agreement and a study phase. Male and females between 18-60 years of age were eligible for this study. Participants with an instable shoulder were included if they had at least one positive clinical instability test out of six, besides answering yes to either having a sense of shoulder instability and/or a prior shoulder injury. Shoulder healthy participants with no prior shoulder injury and no actual shoulder pain were included as shoulder healthy participants. Two examiners with six-months clinical experience performed the clinical tests and were blinded to both their independent test results and the status of the involved subjects. The clinical tests for shoulder instability were load and shift, apprehension, relocation, surprise, Gagey and the sulcus sign. Cohens kappa and Prevalence-and-bias-adjusted-kappa (PABAK) values, corresponding to adjustments for not reaching 50% of the index condition, were used in the analysis and interpreted according to Landis and Koch: 0.0-0.40 (poor); 0.40-0.75 (fair to good); and 0.75-1.00 (good to excellent).

Results: 40 participants (11 males, yrs 27±8), 13 with shoulder instability and 27 with unimpaired shoulders were included in the final study phase. Overall, kappa values varied from 0.39 to 0.77, corresponding to poor to excellent reliability. Gagey was the only test with good to excellent reliability (kappa 0.77). The load and shift, apprehension and surprise tests had fair to good reliability (kappa 0.50, 0.66, 0.66) whereas the relocation and sulcus sign tests had poor reliability (both with kappa 0.39). However, calculation of PABAK, improved the overall kappa-values to range 0.74-0.94. Hence, Gagey were joined by load and shift, apprehension and surprise in the group with good to excellent reliability and relocation and sulcus sign improved to the group with fair to good reliability.

Conclusion: When using PABAK kappa values increased to good to excellent. This means that with a standardized protocol for reliability studies, including a training, an overall agreement and a study phase the current clinical tests for assessing shoulder instability are reliable.

Disclosure of Interest: None Declared

Rehabilitation

AS-0198

MUSCLE CO-CONTRACTION AT THE SHOULDER DURING THE DYNAMIC RELOCATION TEST: A CROSS-SECTIONAL STUDY WITH ASYMPTOMATIC INDIVIDUALS

Daniel C. Ribeiro [1,*] Jonathan Shemmell [2] Carrie Falling [1] Gisela Sole [1]

[1]School of Physiotherapy, [2]School of Physical Education, Sport and Exercise Sciences, University of Otago, Dunedin, New Zealand

Introduction and Objectives: The dynamic relocation test (DRT) was designed to test the patient's ability to recruit the rotator cuff muscles, and can be used as an exercise to enhance the control of such muscles [1]. The test consists of applying a gentle longitudinal traction to the humerus, while asking the patient to counterbalance this traction by retracting the humerus [1]. Patients may present with reduction in symptoms after 10 accurate executions of the DRT within the same session. The patient is deemed to have good control of the rotator cuff if no contraction of superficial muscles such as pectoralis major (PM) is observed. The clinician manually monitors activity, and verbally discourage contraction of PM. Nevertheless, muscle co-contraction may still occur. Due to motor redundancy, the central nervous system has an infinite number of possible motor strategies for performing a specific task. At early stages of motor learning, co-contraction is commonly observed, and it is expected to decline as learning occurs [2]. The DRT is a novel and unusual task for most individuals. It is reasonable to expect a reduction on co-contraction levels between infraspinatus and PM muscles.

The aims of the study were to: (i) quantify the co-contraction between infraspinatus and PM during successful executions of the dynamic relocation test over ten trials; and (ii) compare co-contraction levels between the 1st and 10th execution of the DRT. We hypothesized that co-contraction levels would reduce after ten trials.

Methods: A cross-sectional study design with sample of convenience was used. Asymptomatic individuals from a university community were recruited for the study, approved by the University of Otago Human Ethics Committee. Participants performed maximal isometric voluntary contraction (MIVC) for each monitored muscle. Then they were requested to perform the DRT, sustaining it for 10 seconds, with an interval of 5 seconds. To enhance external validity, only successful trials (n=10) were recorded. For a trial to be considered successful, participants had to sustain an isometric contraction with minimal recruitment of superficial muscles (e.g. PM). As per clinical practice, successful trials were defined as those in which the clinical researcher could not manually identify contraction of the PM.

Surface electromyography (SEMG) was used to measure activity of infraspinatus and PM, following SENIAM guidelines [3]. Myoelectric signals recorded using a 16 channel wireless Noraxon TeleMyo 2400T G2, at a 1500 Hz sampling frequency with a gain of 500. The analog bandpass filter was set for 10-500 Hz, and the common mode of rejection ratio was set at 100dB. SEMG data was processed using MyoResearch XP, Master Edition. SEMG recordings were reduced to eliminate ECG artifact spikes, root mean square smoothed using a 50-millisecond average window. The SEMG recordings were then normalized by the MVIC.

The primary outcome measure was the co-contraction index (CCI), which was calculated as:

$$CCI = 2 \times I_{PM}/I_{total} \times 100\%$$

Where I_{PM} is the integral of total activity of PM, and I_{total} is the integral of the sum of PM and infraspinatus during each DRT execution. The CCI was calculated using MATLAB 7.12.

Statistical analyses were performed using R software. Paired t-test was used for assessing differences in CCI between the 1st and 10th DRT execution, with data bootstrapped 2000 times.

Results: A total of 30 participants (12 male/18 female) took part in the study. The mean age was 23±4 years, and mean BMI of 23.8±2.7 kg/m². Mean (standard deviation) CCI values over the ten trials are presented in Figure 1. No significant differences were found for CCI between the 1st and 10th DRT execution (mean difference = 0.18, 95% confidence interval: -1.23 to 1.61).

Figure:
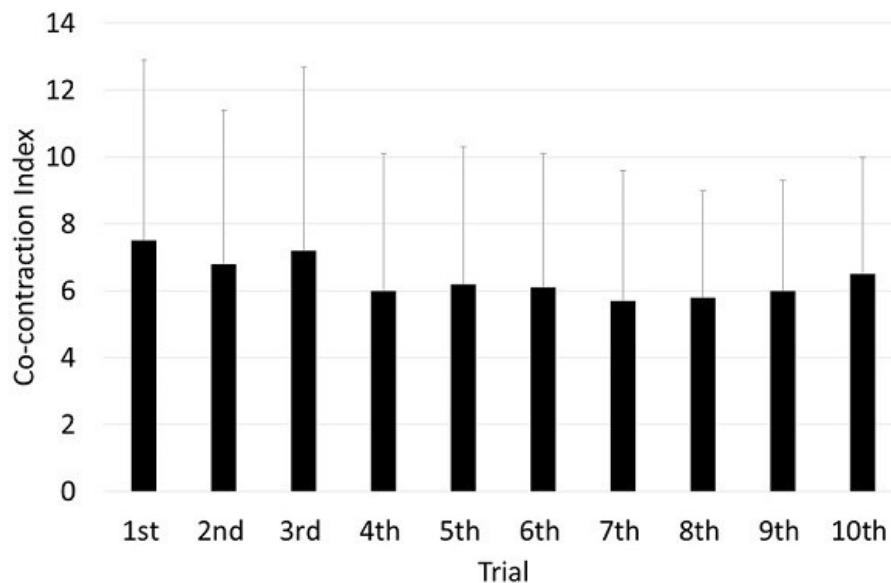
Caption: Figure 1. Co-contraction index mean and standard deviation for 1st and 10th trials..

Conclusion: Co-contraction between infraspinatus and PM is present during successful DRT trials, and that does not change over ten trials. These findings suggests that 10 repetitions is potentially insufficient for motor learning to occur. Contraction of PM may be small and difficult to manually identify. It is possible that the net result of shoulder muscle synergy will help increasing glenohumeral joint stability. Co-contraction may be required for fine-tuning of torque production or shoulder moment balancing [4].

References: 1. Magarey, M.E. and M.A. Jones, Dynamic evaluation and early management of altered motor control around the shoulder complex. Man Ther, 8(4), 195-206, 2003.

2. Valero-Cuevas et al., Structured variability of muscle activations supports the minimal intervention principle of motor control. J Neurophysiol, 102(1), 59-68, 2009.

3. Hermens, et al., Development of recommendations for SEMG sensors and sensor placement procedures. J Electromyogr Kinesiol, 10(5), 361-74, 2000.

4. Darainy, M. and D.J. Ostry, Muscle cocontraction following dynamics learning. Exp Brain Res, 190(2), 153-63, 2008.

Disclosure of Interest: None Declared

Sport

AS-0199

QUALITATIVE AND QUANTITATIVE CRITERIA FOR ASSESSING THE TEMPORAL STRUCTURE OF INDOOR ROWING TECHNIQUES

John S. Fothergill [1,*]

[1]Computer Laboratory, University of Cambridge, Cambridge, United Kingdom

Introduction and Objectives: Bridging the gap between objective performance metrics and coaches' qualitative assessments of motor-skill techniques, promotes a deeper understanding of sporting performances, leading to more efficient and safer training [1]. Coaches' descriptions of athletes' performances come from developing their selective attention and mental models of technique. Six experienced rowing coaches described the technique in 26 videos of indoor rowing. Aspects of technique they referred to were identified through inductive content analysis of their natural-language comments [2]. A temporal structure to the aspects emerged (Fig. 1): Multiple aspects start and end at different times during a rowing stroke; the duration of aspects ranged from momentary, to the complete stroke.

We choose objective performance metrics that measure the temporal structure: This study thresholds the times between intra-stroke events to distinguish between strokes from new and experienced rowers. Metrics indicative of rower experience are used to focus and elaborate on the qualitative assessment criteria. Rowers of different abilities have been classified from stroke kinetics [3]. No work compares correlations of intra-events times with rowers' experience or unites quantitative and qualitative assessment.

Methods: Sensors were fixed to a Concept 2 ergometer; signals were time-stamped using the same clock; each stroke was segmented at the finish. The 3D positions of the handle and seat, aligned to the anatomical coordination system, were recorded at 100Hz to between 2×10^{-3}m and approximately 1×10^{-2}m, using a bespoke tracking system [4]. The dimension of handle motion with largest variance (hande_m) was used to compute metrics. The force applied to the handle (handle_f) was also used, measured using a Concept 2 monitor at 20Hz, as was the force applied through the balls of the left (l_foot) and right (r_foot) feet, recorded at 200Hz using thin FSRs attached to the foot stretcher [5]. Participants (18-35, 75% male) were 8 new rowers, providing 224 strokes after basic instruction and 8 experienced rowers, providing 202 strokes from regular training. Ergometers usefully simulate on-water rowing but don't record oar angle or rower movement on the recovery [6]; we focus on the drive. Intra-stroke events were the onset, offset and peaks of sensor signals. Times between events are normalised by stroke duration. The mean percentages of strokes classified as the correct rower-class were calculated over the rowers left out of a 16-fold cross-validation, with optimal thresholds exhaustively determined for the N-1 rowers (Table 1). Signals were resampled to the same rate and classification repeated at 200, 100, 10, 5, 2 and 1Hz.

Results: The variance in accuracy over rowers was high. Two-tailed, paired Student-t tests with a Bonferroni correction (a=0.12), over the left-out rowers, showed only the time between the peak handle force and catch (threshold: new rowers > 21%) to be significantly more accurate than any other metric. The ratio of drive to recovery time had a similar overall accuracy of 80%. These accuracies were consistent above 5Hz.

Figure:
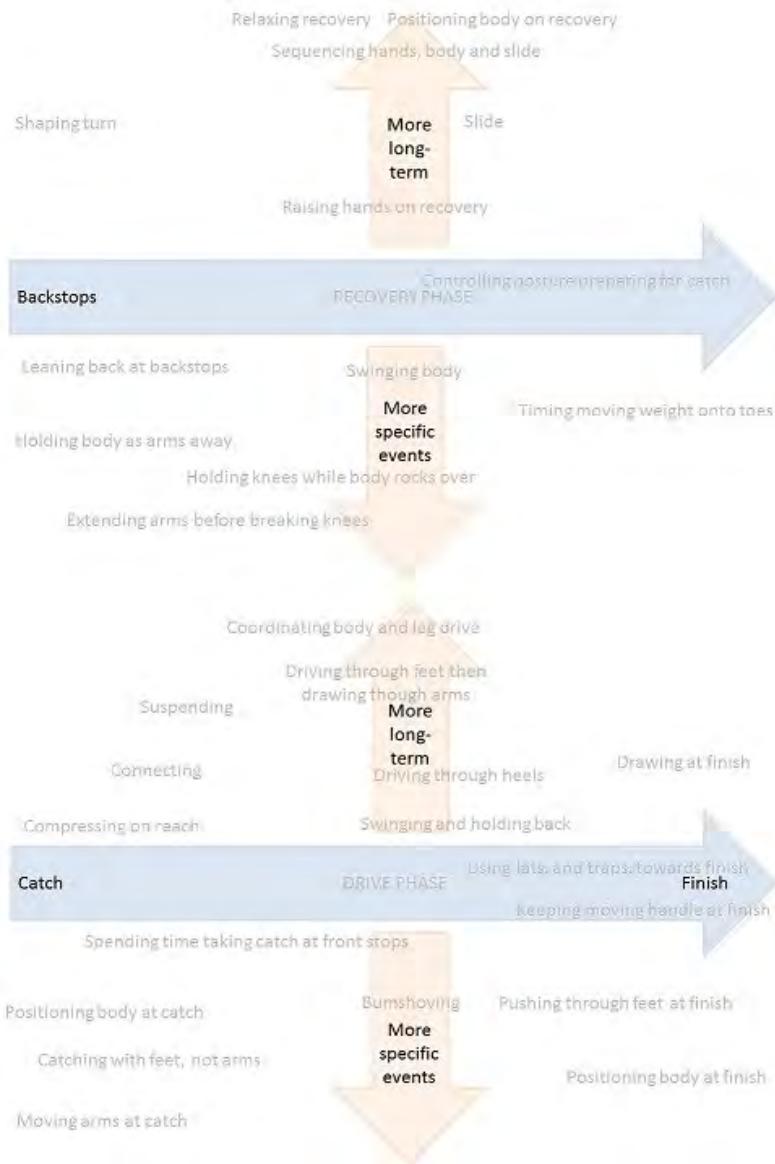
Caption: The temporal hierarchy of aspects coaches use to qualitatively assess rowing strokes.

Conclusion: Designing performance metrics that reflected humans' assessment criteria gave key indicators of rowers' experience that can objectively track progress during training with 80% accuracy. Such summaries may not overwhelm athletes under pressure. Binary assessment of ability is useful to screen athletes. The metrics can be automatically provided when coaches are unavailable using our system. Aspects used by coaches refer to the period between the catch and peak handle force more than any other section of a stroke, suggesting their attention is appropriately focused. That the objective analysis encourages early application of force, clarifies the purpose of the aspects that begin the drive, such as "Connecting" and "Catching with feet, not arms". A deeper understanding of rowing performance and technique has been possible from uniting qualitative and quantitative analytical approaches, finding key biomechanical metrics and considering how they relate to practical coaching.

Table:

Metric	Accuracy (%)
Handle_f, handle_m peaks	80.0
Handle_f, l_foot peaks	60.4
Handle_f, r_foot peaks	51.0
Handle_f peak, r_foot release	35.5
Handle_f peak, r_foot onset	49.1
SeatOnset	68.7
Handle_f peak	60.5
Handle_m peak	77.1
StrokeDuration	70.2

Caption: Average percentage of athletes' strokes correctly classified over 16-fold cross validation

References:

[1] Irwin et al., J. Sports Sciences, 23:1089-1099, 2005.

[2] Fothergill. The Coaching-Machine Learning Interface : Indoor Rowing, University of Cambridge, 2013.

[3] Smith et al., J Sports Sciences, 20:783-791, 1995.

[4] Hay et. al., Itnl. Sym. Mixed and Augmented Reality, 159-160, 2008.

[5] Kuntze et al, Itnl. Asc. Computer Science in Sport, 71-75, 2009.

[6] Ritchie, Sports Tech., 1:110-116, 2008.

Disclosure of Interest: None Declared

Sport

AS-0200

COORDINATION ANALYSIS BETWEEN OPPONENT TENNIS PLAYERS USING VECTOR CODING TECHNIQUE.

Tiago Pereira [1] Felipe A. Moura [1,*]

[1]Sports Sciences Department, State University of Londrina, Londrina, Brazil

Introduction and Objectives: A very important step studying tennis as a dynamical system is to identify the collective variables that reflect the invariance and the change in players' comportment during the match. A simple analysis of tennis match can gives us some clues of how to understand tennis in a dynamical perspective. During a tennis match, the players are constantly moving away to hit a ball and returning to the middle of the court waiting for the next one, resulting in constant to-and-fro displacements from that home position that renders the players as oscillators. A fundamental property of oscillators is the phase synchronization. One only study investigated tennis from a dynamical approach [1], using Hilbert transform, and found that there are just two patterns of synchronization between the lateral displacement between opponent players: in-phase and anti-phase. However, time-series relative phase analysis using continuous relative phase (CRP) or other techniques such as Hilbert transform may not allow interpreting which oscillator is leading the time series and which is lagging relative to the other oscillator. At this point vector coding technique [2] may offer additional information about tennis' dynamics. Therefore the purpose of this study was to investigate the coordination between opponent tennis players during official matches. Specially, we were interested in to determine which player leads the behaviour of the other one (the serving player or the returning one) and if there are differences of behaviour between different proficiency levels.

Methods: We analyzed two matches, one during a professional single tournament organized by the association of professional tennis players (ATP) and the other during a junior world circuit organized by the International Tennis Federation (ITF). The matches were filmed by two digital cameras. Player positions as a function of time were obtained with an automatic tracking method. Vector coding analysis was computed for players lateral displacement, to identify the coordination patterns during 103 and 60 rallies of the junior and professional matches. The coupling angles were divided in four coordination patterns: anti-phase, in-phase, serving player phase and returning player phase. Data normality was tested using Lilliefors test. Two-way analysis of variance was used to compare the percentage of time spent in each condition according two factors: phase (with four factor levels) and level (professional and junior). Data are expressed in terms of mean and standard deviation.

Results: Table 1 presents the percentage o time in each phase condition during rallies of the professional and junior matches. The statistical analysis presented no effect between levels ($F_{(1, 644)} = 0.67$; $p = 0.2$) and for the interaction between levels and phase ($F_{(3,644)} = 0.24$; $p = 0.8$), and there was not a significant difference among the phases ($F_{(3,644)} = 1.08$; $p = 0.3$). The results showed no coordination differences between players of different levels which suggests that tennis' dynamics is the same, independently of level of proficiency. Although no significant differences were found among coordination patterns, it seems that there is a tendency of the returning players in to lead the time series in relation to the serving players. This behaviour may be related to the advantage of the serving player has in relation to returning one. The serving player has the possibility of starting point command, performing more powerful and well

426

directed serves, making the returning player move firstly to return the serve. For this reason the displacements performed by the returning player may be happening in response to the strokes performed by the serving player. Thus probably the time series is led by returning player because the serving player is being more offensive and is constantly shifting his opponent.

Conclusion: Vector coding technique allowed identifying additional coordination patterns between players' lateral displacement, providing further information about players' interaction during rallies. Although no differences were found between levels and among coordination patterns, results indicated that, generally, the lateral displacement coordination between players is leaded by the returning player. Further studies may investigate if the success during rallies is determined by different coordination patterns than the ones of the present study.

Table:

Coordination Pattern	Professional	Junior
Anti-phase	22.2 (17.4)	22.1 (18.4)
In-phase	23.3 (19.0)	21.3 (16.3)
Serving player phase	14.3 (15.3)	14.8 (15.1)
Returning player phase	40.0 (22.1)	41.7 (22.5)

Caption: Percentage of time spent in each coordination pattern during the rallies.

References: [1] Palut et al., Y. A dynamical analysis of tennis: concepts and data. J Sports Sci. 2005 Oct;23(10):1021-32. [2] Sparrow et al. W. A. Using relative motion plots to measure changes in intra-limb and inter-limb coordination. J Mot Behav. 1987 Mar;19(1):115-29.

Disclosure of Interest: None Declared

OPTIMUM TECHNIQUE FOR MAXIMISING ROTATION IN A ROCHE VAULT

Fred Yeadon [1,*]MIchael Hiley [1]

[1]Sport, Exercise and Health Sciences, Loughborough University, Loughborough, United Kingdom

Introduction and Objectives: In the handspring group of vaults the gymnast rotates forwards onto the vaulting table in the pre-flight phase and continues this forwards rotation during the contact and post-flight phases. In the handspring double somersault vault (Roche) the gymnast performs two and a half somersaults during the post-flight phase (Figure 1). The aims of this study were to optimise touchdown orientation and configuration together with contact technique in order to maximise rotation potential in forward rotating vaults and to identify realistic limiting vaults.

Methods: In order to investigate the effects of initial conditions and table contact technique on vaulting performance a torque-driven computer simulation model was used. The model simulated the interaction between a seven-segment gymnast and a single-segment vaulting table during the table contact phase of the vault. An evaluation of the model was conducted by assessing how accurately simulations matched the recorded performances of three recorded vaults. Three optimisations were carried out in order to maximise the rotation potential (RP) in post-flight under different conditions. RP was calculated as the product of the angular momentum about the mass centre at take-off and the post-flight time, normalised to give the number of straight somersaults (ss) possible in the post-flight phase. In the first optimisation the table touchdown configuration and orientation were varied whilst torque activations from the matched simulation were maintained. The second optimisation used the touchdown configuration and orientation from the recorded performance and the torque generator activation parameters were varied in order to determine the potential improvement arising from contact phase technique changes. In the third optimisation the configuration, orientation, and torque generator activation parameters were allowed to vary in order to maximise RP. The model was constrained to stay on the parabola defined by the gymnast's horizontal and vertical velocity at springboard take-off in all optimisations.

In order to investigate limiting vaults estimates of maximal horizontal pre-flight velocity in handspring double front vaults were obtained from Takei et al. (2003) and the vaults re-optimised.

Results: The post-flight RP of the recorded vault was 1.16 ss. When the configuration and orientation at touchdown were varied (optimisation 1) the post-flight RP increased to 1.33 ss. When just the torque generator activation parameters were varied (optimisation 2), the post-flight RP increased to 1.48 ss. In the third optimisation where the touchdown configuration, orientation and table contact activations were allowed to vary (optimisation 3) the post-flight RP increased to 1.60 ss (Table 1).

When the pre-flight horizontal velocity was increased by 0.25 m/s and then 0.5 m/s, the optimised RP increased from 1.60 ss to 1.65 ss and 1.70 ss, respectively, allowing more complex vaults to be simulated.

Figure:
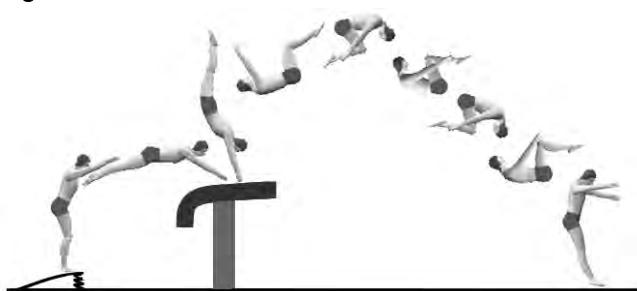
Caption: Figure 1. The handspring double somersault vault (Roche).

Conclusion: When the initial configuration and orientation of the model were allowed to vary along with the table contact technique (optimisation 3), there was a considerable increase in post-flight RP from 1.16 to 1.60 ss. Both table contact technique touchdown configuration and orientation made substantial contributions to this increase. In optimisation 3 the initial configuration and orientation changed from those adopted by the gymnast (Table 1). Yeadon et al. (2014) demonstrated that having an angle at the shoulder and the hip hyper-extended at touchdown was optimal for generating post-flight height since more work could be done during table contact. From the present study, however, it appears that having the arm in line with the trunk and the hip flexed at touchdown is optimal for generating maximum RP.

Table:

Simulation	Gymnast	Opt1	Opt2	Opt3
Touchdown angles				
torso [°]	-3°	1°	-3°	38°
shoulder [°]	128°	137°	128°	180°
hip [°]	181°	192°	181°	162°
Post-flight				
peak height [m]	3.00	2.95	2.81	2.76
rot. potential [ss]	1.16	1.33	1.48	1.60
time [s]	1.04	1.02	0.95	0.98

Caption: Table 1. Table touchdown and take-off variables from the recorded and optimised

References: [1} Takei, Y., 2007. J Appl Biomech 23, 1-11.

[2] Yeadon et al., 2014. J Biomech 47, 3143–3148.

Disclosure of Interest: None Declared

Sport

AS-0202

THE EFFECTS OF ALTERED FOREFOOT BENDING AND TORSIONAL STIFFNESS ON THE BIOMECHANICS OF CURVED RUNNING

Ryan Madden [1,*] Nicole Schrier [1] Doug Kondro [1] Rosemary Grover [1] John Wannop [1] Darren Stefanyshyn [1]

[1] Kinesiology, University of Calgary, Calgary, Canada

Introduction and Objectives: Many competitive running events incorporate curves on the racecourse. Despite this, the main focus of previous running research has been straight-line movements. Shoe characteristics such as bending and torsional stiffness can alter running biomechanics, however, no studies have attempted to clarify the influence of shoe bending and torsional stiffness on curved sprinting. Therefore, the purpose of this study was to investigate the effects of bending and torsional stiffness on maximal effort curved running.

Methods: Six varsity track athletes performed maximal-effort curved sprinting (r=36.5 m, ~9 m/s) in three shoes: (i) low bending stiffness and low torsional stiffness (L_bL_t), (ii) low bending stiffness and high torsional stiffness (L_bH_t), and (iii) high bending stiffness and high torsional stiffness (H_bH_t, Table 1). Kinetics and kinematics of the feet and shanks of both the inside and outside leg were collected. Two successful trials were obtained for each shoe/foot (inside/outside) combination. Data were analyzed for the stance phase of running in each condition. All comparisons were made using paired t-tests with a Holm-Bonferroni sequential correction to account for multiple comparisons (α_1=0.0167, α_2=0.025, α_3=0.05).

Results: Increasing the bending stiffness acting on the inside foot resulted in reduced dorsiflexion at touchdown and greater plantarflexion at takeoff (p<0.001 H_bH_t vs. L_bL_t, p=0.068 H_bH_t vs. L_bH_t). Limited forefoot bending combined with the changes in ankle kinematics would shift the ground reaction force (GRF) anteriorly, increase the moment arm about the ankle joint and possibly improve sprint performance [1,2]. High bending stiffness also tended to increase peak medial GRF during the first 10% of stance for the inside foot (p=0.023 H_bH_t vs. L_bL_t, p=0.091 H_bH_t vs. L_bH_t). Increasing medial GRF on the inside foot would direct the athletes away from the intended direction of travel and may therefore be detrimental. Interestingly, the only observed effect of increasing the forefoot bending stiffness of the outside shoe during curved running was a decrease in peak MTP extension angle (p=0.004 H_bH_t vs. L_bH_t, p=0.017 H_bH_t vs. L_bL_t). There was a trend towards an increasing medial GRF with increasing bending stiffness of the outside shoe (p=0.087 H_bH_t vs. L_bH_t, p=0.091 H_bH_t vs. L_bL_t). The increased outside foot medial GRF may be beneficial to performance by guiding the athlete around the curve. For the inside foot, high torsional stiffness resulted in decreased forefoot inversion (p=0.004 H_bH_t vs. L_bL_t, p=0.013 L_bH_t vs. L_bL_t), increased ankle joint eversion (p<0.001 H_bH_t vs. L_bL_t, p=0.058 L_bH_t vs. L_bL_t), and an increased transverse plane ankle joint moment (p=0.001 L_bH_t vs. L_bL_t, p=0.002 H_bH_t vs. L_bL_t). As increased eversion may limit plantarflexor force production and increased transverse plane ankle moments may increase athlete injury risk [3], high torsional stiffness may have a negative impact on the biomechanics of the inside foot. The response of the outside foot to alterations in torsional stiffness was markedly different. As torsional stiffness increased, there was a trend of decreasing ankle eversion at touchdown (p=0.001 H_bH_t vs. L_bL_t, p=0.051 L_bH_t vs. L_bL_t) and takeoff (p=0.038 H_bH_t vs. L_bL_t, p=0.002 L_bH_t vs. L_bL_t). Although not observed here, decreased ankle eversion may benefit performance by improving plantarflexor moment generation [4].

Figure:

(A) Effects of Increased Bending Stiffness

Inside Leg
↓ ankle plantarflexion angle
↑ medial GRF (during first 10% of stance)

Outside Leg
↓ Metatarsalphalangeal bending
↑ medial ground reaction force (trend)

(B) Effects of Increased Torsional Stiffness

Inside Leg
↓ peak forefoot inversion
↑ peak ankle eversion
↑ ankle internal rotation moment

Outside Leg
↓ ankle eversion at TD and TO
↓ ankle external rotation moment
↑ medial ground reaction force

Caption: Illustrated summary of main findings

Conclusion: Alterations in the torsional and bending stiffness of footwear influence curved running biomechanics in a side-dependent manner. The inside foot benefits most from a low torsional stiffness shoe, which improves ankle joint alignment and reduces transverse plane ankle joint loading. Conversely, outside foot ankle alignment is improved with a high torsional stiffness shoe that, along with high bending stiffness, also increases the medial GRF. Both the inside and outside feet may benefit from high bending stiffness shoes to maximize straight-line sprint, although further work is required to determine the appropriate level of bending stiffness for an inside foot shoe such that the positive effects are maintained while the increased initial medial GRF is minimized.

Table:

Footwear Condition		Bending Stiffness [N/mm]	Torsional Stiffness [Nm]
Low Bending Stiffness Low Torsional Stiffness	(L_bL_t)	18.1	1.75
Low Bending Stiffness High Torsional Stiffness	(L_bH_t)	14.3	3.51
High Bending Stiffness High Torsional Stiffness	(H_bH_t)	33.6	3.91

Caption: Mechanical data of the footwear used in this study

References: [1] Stefanyshyn et al., Sports Biomech, 3: 55-66, 2004.

[2] Willwacher et al., Gait Posture, 40: 386-390, 2014.

[3] Colville et al., Am J Sport Med, 18: 196-200, 1990.

[4] Luo et al., J Biomech, 45: 2763-8, 2012.

Disclosure of Interest: R. Madden Conflict with: adidas, N. Schrier Conflict with: adidas, D. Kondro Conflict with: adidas, R. Grover Conflict with: adidas, J. Wannop Conflict with: adidas, D. Stefanyshyn Conflict with: adidas

Sport

AS-0203

CONCEPT2 ROWING PERFORMANCE CAN BE IMPROVED WITH GREATER ROWING FREQUENCY AND LESS ROWING RESISTANCE

Xie Wu [1,*] Li Li [1] Matthew Holmes [2]

[1]Kinesiology, Shanghai University of Sport, Shanghai, China, [2]Health & Kinesiology, Georgia Southern, Statesboro, United States

Introduction and Objectives: Concept2 land rowing competition has become a worldwide sport. Commonly used rowing frequencies are ranged between 30 to 40 strokes per minute with a resistance level set at level 4 on the machine. The purpose of the study was to investigate the effect of increase rowing frequency and reduce rowing resistance on rowing performance. We have hypothesized that a higher frequency and lower resistance rowing pattern can increase rowing power output and improve rowing performance.

Methods: With the approval of local IRB committee we have recruited 14 male college students, 20 ± 3 years old, 178 ± 7 cm tall, with body mass of 71 ± 6 kg. There were a total of nine rowing trials. Three rowing frequencies (40, 50, and 60 strokes per minute) were tested at each of the three different resistances at levels 2, 3, and 4. The order of the nine testing trials was randomized. The rowing tests were conducted on a Concept2 rowing machine (Concept2, Inc., Morrisville, VT, USA). Following the ticktack of the metronome, the participants were instructed to pull the handle as forceful as possible at every tick. The range of the pull was adjusted based on metronome to achieve the best possible synchronization with the targeted rowing frequency. Each rowing condition was tested for 20 seconds with a 5 minutes rest period in between. The effects of frequency and resistance on each of the outcome variables (distance, estimated 500 m time, energy expenditure and mean power output) were examined using two-factor (resistance X frequency) multivariate analysis of variance (MANOVA) with repeated measures. Post-Hoc analysis (pairwise comparison and trend analysis) used if necessary. Alpha level was set at .05.

Results: The observed rowing frequencies were $41.4\pm.2$, $50.3\pm.3$, $60.0\pm.4$ when targeting at 40, 50, and 60 strokes per minute, those rates were significantly different from each other ($F_{2,13}=0.426$, $p =.66$). Rowing frequencies were not affected by resistances ($F_{2,13}=0.426$, $p =.66$). For rowing distance within 20 seconds, there was no significant resistance X frequency interaction observed. However, distance was significantly influenced by both resistance ($F_{2,13}=6.64$, $p < .007$) and frequency ($F_{(2,13)}=7.22$, $p < .009$). Further, the linear by linear contrast of resistance * frequency ($F_{1,13} = 4.777$, $p = 0.048$) was significant. Here are the results for rowing distance (mean ± standard error of the mean) at three different levels of resistance: 85.3 ± 1.1, 86.1 ± 1.5 and 88.2 ± 1.2 m for levels 2, 3, and 4, respectively. Rowing distance for resistance level 4 was significantly greater that of level 2. The rowing distances at three different frequencies were: 83.7 ± 1.7, 86.8 ± 1.4 and 89.1 ± 1.3 m for 40, 50, and 60 strokes per minute, respectively. Greatest rowing distance was observed at the highest stroke rate (60), which was significantly longer than that of the lowest rate (40). The combination of highest frequency (60) with lowest resistance (level 2) resulted with the greatest distance (89.6 ± 1.6 m), where the combination of lowest frequency (40) with lowest resistance (level 2) resulted with the least distance (81.3 ± 1.4). The Estimated 500m Time exhibited the same results as the rowing distance, where the no significant interaction observed but

significant resistance ($F_{2,13}$=4.47, $p < .05$) and frequency ($F_{2,13}$=7.04, $p < .004$) influences observed. The estimated time for resistance levels 2, 3, and 4 were 118±1, 117±2 and 114±2, respectively. The estimated time for frequencies at 40, 50 and 60 strokes per minute were 120.3±2.6, 116.0±1.8, and 112.6±1.6 sec, respectively. The effects of the rowing frequency and resistance could be explained, partially, by the energy expenditure during the tests. Both energy expenditure and mean power output were increase with both frequency (Energy: $F_{2,13}$=6.67, $p < .005$; Power: $F_{2,13}$=6.64, $p < .005$) and resistance (Energy: $F_{2,13}$=7.79, $p < .002$; Power: $F_{2,13}$=7.92, $p < .002$). The linear by linear contrast of resistance*frequency for both energy and power were significant (Energy: $F_{1,13}$= 5.009, $p = .042$; Power: $F_{1,13}$=5.146, $p = 0.041$). The greatest energy expenditure (power output) occurred with the combination of highest frequency (60) with lowest resistance (level 2) at 1176±48 J (255±14W), where least energy expenditure (power output) occurred with the combination of lowest frequency (40) with lowest resistance (level 2) at 951±34 J (189±10W).

Conclusion: During 20 seconds all out rowing tests with Concept2 rowing machine higher rowing stroke per minute, combined with lower resistance, produced faster performance. This result is supported by greater power output observed with this condition.

Disclosure of Interest: None Declared

Sport

AS-0204

EFFECT OF RUNNING SPEED ON INTRA-TRUNK ANGULAR DISPLACEMENTS EXHIBITED DURING TREADMILL RUNNING

Kathy J. Simpson [1,*] Yumeng Li [2] Marika Walker [1] Rumit Singh Kakar [3]

[1]Kinesiology, [2]University of Georgia, Athens, [3]Department of Physical Therapy, Ithaca College, Ithaca, United States

Introduction and Objectives: Our limited understanding of the trunk's role in producing running locomotion[1,2] is partly due to lack of knowledge of the intra-trunk motions and how these motions change with running speed. We expected increased intra-trunk motions at faster running speeds, particularly for segments with lower anatomical constraints[3]. Thus, the purpose of the study was to determine if intra-trunk displacements increase with greater running speed.

Methods: Participants (n = 20, age = 22.4 ± 3 yr; mass = 67.4 ± 12.9 kg, height = 1.7 ± 0.1 m, moderate to vigorous physical activity = 6 ± 3 hr/wk) ran on a treadmill at self-selected speeds of natural (range: 2.2 – 4.2 m/s), 110% above natural (2.5 – 4.7 m/s) and maximal (range: 2.9 – 5.4 m/s). Locations of 24 reflective markers placed on the trunk and pelvis were captured by a 7-camera Vicon system (120 Hz) for 10 strides. For all speeds and motion planes, relative angles between adjacent trunk segments (upper [UP]: C7 to T8; middle [MID]: T9 to T12; lower [LOW]: L1 to L5) and pelvis (PEL) were calculated; maximum angular displacements were averaged across 10 strides. Displacements were compared across speeds using one-way repeated-measures ANOVA, Tukey's HSD posthoc test ($p < 0.05$), and 95% confidence intervals (CI).

Results: Increased speed was observed from ANOVA for all maximum displacements except for UP-MID flex/extension. Posthoc tests (Fig 1) indicated that all other speed comparisons were significant (Fig 1); although for LOW-PEL ext/flexion, only natural and maximal speed displacements varied. For significant comparisons, CI ranges were 0.1° to 2.9° (LB) and 1.7° to 7.8° (UB).

Figure:
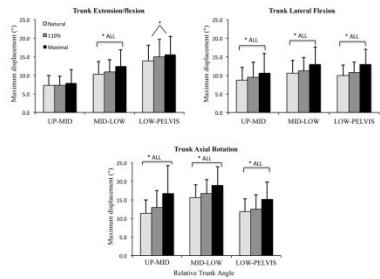
Caption: Fig 1. Means and SD of the relative angles between upper (UP), (MID) and lower (LOW) trunk and pelvis (PEL) by speed. Significant speed comparisons for given movement and relative angle (p < .05): * ALL: all comparisons are significant; *: natural and maximum speed are signficantly different..

Conclusion: Displacements increased at greater speeds, especially for non-sagittal plane motions. Previous investigators have suggested that, at faster locomotor speeds, greater trunk movement may help to produce increased trunk momenta to help cancel some of the greater total body angular momenta[1,4]; move the pelvis into positions that allow increased leg

rotations and longer step lengths[5]; transfer or generate mechanical energy to/from extremities[6]; and/or minimize nonessential COM motion via compensatory shifting of intra-trunk mass[7]. However, the magnitudes of the difference means were relatively modest (range: 0.6° to 5.3°; median difference between natural and maximum= 2.7°), suggesting that only low changes to intra-trunk rotations are utilized. As all of the displacement magnitudes at maximum speed were well within reported flexibility values of these segments[3,7], it is unlikely that increases of intra-trunk displacement were limited by structural-functional constraints of the spine and other trunk tissues. However, the modest increases may also be due to some individuals' low running speed ranges, running technique or skill; running on a treadmill; and/or our methodology.

In conclusion: At these self-selected treadmill running speeds, intra-trunk displacements increase at faster speeds, but only low changes to intra-trunk rotations may be desired or needed.

References: [1] Hinrichs. Int J Sport Biomech., 3: 242-263, 1987.

[2] Ford, et al. Med Sci Sports Exerc., 45: 1125-1130, 2013.

[3] Parke et al. Rothman-Simeone The spine, Saunders & Elsevier, 2006.

[4] Bennett et al. Hum. Movem. Sci., 29:114-124, 2010.

[5] Saunders et al..Clin Biomech., 20:784-793, 2005.

[6] Gracovetsky. Spine in sports, CV Mosby, 1990.

[7] Fisicaro, et al. Spine: Core knowledge in orthopaedics, Elsevier & Mosby, 2010.

Disclosure of Interest: None Declared

AS-0205

THE INTERFASCICULAR MATRIX ENABLES FASCICLE SLIDING AND RECOIL IN TENDON, AND BEHAVES MORE ELASTICALLY IN ENERGY STORING TENDONS

Chavaunne T. Thorpe [1,*]Marta Godinho [1]Graham Riley [2]Helen Birch [3]Peter Clegg [4]Hazel Screen [1]

[1]School of Engineering and Materials Science, Queen Mary University of London, London, [2]University of East Anglia, Norwich, [3]UCL, Stanmore, [4]University of Liverpool, Neston, United Kingdom

Introduction and Objectives: Our previous work shows that the interfascicular matrix (IFM) is critical for tendon function, facilitating sliding between fascicles to allow tendons to stretch [1]. We have shown that this is particularly important in energy storing tendons such as the human Achilles tendon and equine superficial digital flexor tendon (SDFT), which experience strains as high as 16% during exercise [2], and therefore require the capacity for considerable inter-fascicular sliding. This capacity is not required in positional tendons such as the equine common digital extensor tendon (CDET). Further, we have shown that the IFM in the energy storing SDFT becomes stiffer with age, which may explain why aged tendons are more prone to injury [3]. While the failure properties of the IFM have been studied previously [1], it has not been established if the IFM is able to recoil and recover from loading. The aim of this study was therefore to assess the recoil capacity and failure properties of the IFM in the SDFT and CDET from young and old horses. We hypothesised that the IFM has the ability to recoil, and that elasticity is greater in the energy storing SDFT than in the positional CDET. Further, we hypothesised that the recoil capacity of the IFM decreases with ageing and the stiffness of the IFM increases, specifically in the SDFT.

Methods: Groups of 2 intact fascicles (bound together by IFM) were dissected from the SDFT and CDET from young (aged 3-7 years) and old (aged 17-20 years) horses. Using a polarised light microscope and a dissection rig, the opposing end of each fascicle was cut transversely, leaving a 10 mm length of intact IFM. Samples were preconditioned from 0-0.5mm for 10 cycles (Fig.1a), and then pulled apart to failure. Hysteresis and stress relaxation were calculated during preconditioning. A force-extension curve was derived from the failure test data, and IFM extension was calculated from 10-80% failure load (Fig.1b&c). Statistical significance was tested using an ANOVA.

Results: The IFM was able to recoil in both tendon types (Fig.1a). Hysteresis and stress relaxation were significantly greater in CDET than in SDFT IFM samples (p<0.01). IFM failure load and failure extension did not differ between tendon types. At and below 40% of failure force, there was significantly greater extension within the SDFT IFM than the CDET IFM (p<0.01, Fig.1b&c). Hysteresis did not change with age, but stress relaxation increased with ageing in both tendon types. Ageing resulted in decreased extension at the interface in SDFT samples (p<0.05, Fig.1d).

Figure:
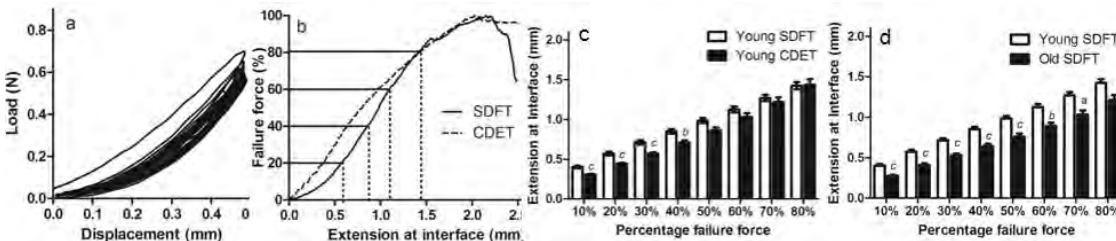
Caption: Fig.1. Response of IFM to cyclic loading (a) and test to failure (b). IFM extension was calculated at different percentages of failure load (b). Extension at interface differed with tendon type (c) and with age (d).

Conclusion: The results support the hypothesis, showing that the IFM exhibits reversible deformation behaviour. Further, the IFM in the SDFT has a greater ability to recoil, with less hysteresis and stress relaxation than in the CDET, providing further evidence that the IFM is crucial for efficient function of energy storing tendons. The results also indicate that the IFM is less able to resist repetitive loading as it ages, becoming stiffer with age in the SDFT. Future work will characterise the fatigue behaviour of the IFM and determine how this influences whole tendon fatigue properties. Full understanding of IFM specialisation in energy storing tendons and the age-related changes that result in loss of function is important for the development of effective preventative measures and treatments for age-related tendon injury.

References: [1] Thorpe et al J R Soc Interface 9:3108-17 2012.

[2] Stephens et al Am J Vet Res 50:1089-95 1989.

[3] Thorpe et al Eur Cell Mater 8:48-60 2013.

Disclosure of Interest: None Declared

Musculoskeletal

AS-0206

SHEAR WAVES ELASTOGRAPHY FOR BIOMECHANICAL ASSESSMENT OF ACHILLES TENDON

Thomas-Xavier Haen [1 2,*]Anthony Roux [2]Marc Soubeyrand [3]Charlotte Labruyere [2]Phillipe Rouch [2]Sébastien Laporte [2]

[1]Service de Chirurgie Orthopédique, Hopital Raymond Poincaré, Garches, [2]Arts et Metiers ParisTech, Institut de Biomécanique Humaine Georges Charpak, Paris, [3]Service de Chirurgie Orthopédique, Hopital de Bicêtre, Le Kremlin-Bicetre, France

**Introduction and Objectives:** Achilles tendon (AT) represents the main site of tendon rupture in terms of frequency[1]. Treatment of AT rupture remains controversial. This controversy is due to certain extend to the lack of tools available for a clinical assessment of the healing tendon's mechanical properties. Shear Wave Elastography (SWE) is a new mode of ultrasound imaging which allows real-time and in-vivo assessment of the Young modulus within the soft tissues[2]. It has been previously proposed as a tool to assess biomechanical properties of the AT. Until now, no study has correlated SWE findings in human with biomechanical conventional testing. The aim of the present study was to (1) set up a reproducible and « bedside like » SWE protocol of the AT and (2) to correlate the findings of SWE with conventional tensile testing.

Methods: We used eight lower limbs of fresh frozen human cadavers (Age = 84 ± 5 years, mean ± SD). First, the AT was assessed with SWE (Aixplorer®, Supersonic Imagine, Aix-en-Provence, France) through a custom « bedside like » protocol. The latter consisted in assessing the AT with longitudinal and axial slices performed at three successive levels (0, 3 and 6 cm from the calcaneal insertion) and in three ankle positions (25° plantar flexion, rest and maximal dorsal flexion). Each assessment was performed blindly by three operators in order to determine repeatability and reproducibility. Then the triceps with the AT was isolated, where their femoral, tibial and calcaneal insertions were kept intact. The anatomic preparation was subjected to tensile tests (at 0.5, 1 and 2 mm/s, until 20 mm of elongation) during which a continuous SWE examination was performed. Tendon's displacement was recorded with an ultra-fast HD camcorder. At the end, a break strength testing (at 2 mm/s) was done.

Results: Our custom « bedside like » protocol had a high intra and inter-observer reliability for longitudinal slices, in the cadaveric model. Moreover, the stiffness increased with tensile load, in SWE measurements (figure1-a) and material testings (figure1-b). The correlation between the two modes was significant (p<0.001) and the regression coefficient was R^2=0.99 (figure1-c). During break strength test, no tendon rupture was observed, but a tear (4 ± 0.5 % strain, mean ± SD) in the muscle. Having maintained every bone insertions, our protocol was very close to the physiologic functioning (figure1-d).

To our knowledge, only manual elastography was described, in human cadaveric tendon, without biomechanical correlation [3]. In animal studies, one study showed increased shear waves speed with increasing strain, in porcine tendon [4], and one study showed good correlation between SWE and material testing, during tensile tests, in porcine muscle [5].

Figure:
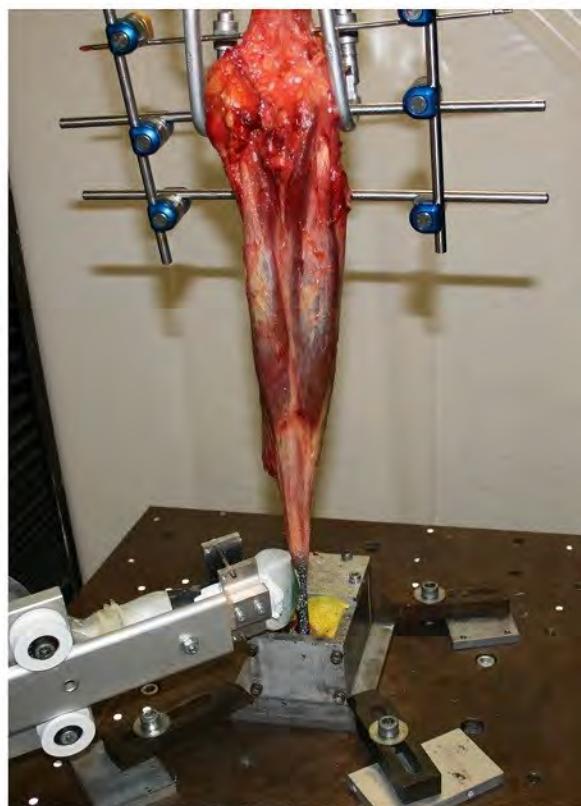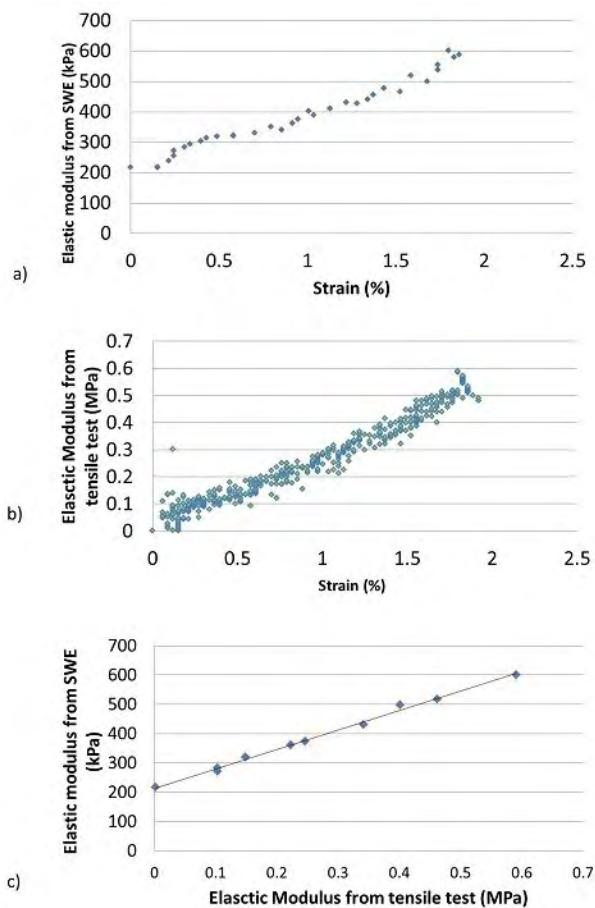
Caption: Tensile test's data from a representative specimen: a) Elastic modulus from SWE vs. Strain b) Elastic modulus from tensile test vs. Strain c) Correlation between Elastic modulus from SWE and Elastic modulus from tensile test d) Experimental set-up (Ultrasoud transducer aligned with long axis of the Achilles' Tendon)

Conclusion: SWE used with our protocol allows to determine biomechanical properties of intact AT of fresh frozen cadavers and to link SWE to tensile tests' results.

References: [1]   B. M. Józsa et al., Am J Sport. Med., vol. 17, no. 3, 1989

[2]   J.-L. Gennisson et al., Diagn. Interv. Imaging, vol. 94, no. 5, pp. 487–95, 2013

[3]   A. S. Klauser et al., Radiology, vol. 267, pp. 837–842, 2013

[4]   R. J. Dewall et al., Ultrasound Med. Biol., vol. 40, no. 1, pp. 158–67, 2014

[5]   S. F. Eby et al., J. Biomech., vol. 46, no. 14, pp. 2381–7, 2013.

Disclosure of Interest: None Declared

AS-0207

THE INFLUENCES OF DEVELOPMENT AND PATHOLOGY ON THREE DIMENSIONAL HUMERAL SHAPE MORPHOLOGY THROUGHOUT THE PEDIATRIC AGE SPECTRUM

Frances Sheehan [1,*] Jesi Kim [1] Michael Pearl [2] Katharine Alter [1]

[1]Rehabiliation Medicine, National Institutes of Health, Bethesda, [2]Orthopaedic Surgery, Kaiser Permante, Los Angeles, United States

Introduction and Objectives: To understand the relationship between humeral morphology and pathology, developmental shape changes must be understood. Little data exist in regards how pathology and development influence 3D humeral shape. A pediatric cadaver study did establish humeral anterversion with age[1], but the lack of an ossified head in younger children (~ <5 years) prevented direct measures of humeral head orientation. Closing this knowledge gap is crucial for treating pathologies such as Obstetrical Brachial Plexus Palsy (OBPP), where the current trend supports earlier intervention (physical therapy, botulinum toxin injections, surgery) to rebalance muscle forces, prevent osseous deformities, and maintain function. The purpose of this study is to quantify the 3D humeral morphology in children across the pediatric age span (6 months-18 years old) with unilateral OBPP and documented internal rotation contractures in order to test the following hypotheses: 1) development alters 3D humeral for the unaffected arm; 2) the impaired arm has significant multi-planar shape deformities, relative to the unimpaired arm, which increase with age.

Methods: In total 29 bilateral 3D axial MR images of children/adolescents with unilateral OBPP were included in this study. The first set (n=17, age=1.5±1.2 years) was acquired as part of a pre-surgical evaluation protocol (author MLP). The second set of 12 subjects (age=11.8±3.3 years), was taken from a previously published study[2]. Both centers had IRB approval. The humeral head and shaft/elbow were segmented by manually outlining the outer cartilage and cortical bone surface, respectively[2]. The resulting point cloud was fitted with a 3D mesh and aligned to its principle axes. The epicondylar axis and the lesser tuberosity (LT) were identified on the 3D model (Fig 1).

The model was then converted back to a point cloud and imported into a customized Matlab program. This program determined the best-fit ellipsoid and cylinder to the humeral head and central shaft, respectively. From these data the inclination angle and two retroversion angles, **V1** and **V2** were calculated (Fig 1). Paired t-tests were used to identify significant ($p<0.05$) differences between sides. Pearson's correlations were run to determine the relationship of specific variables to age.

Results: The humeral head was significantly less retroverted (D**V1**= -10.3° and D**V2**= -16.9°, $p<0.008$), more elliptical ($p<0.001$), and smaller in all 3-dimensions ($p<0.001$) for the unimpaired arm. The decreased retroversion disagreed with the past 2D study in younger children[3], whereas all other results are supported by past 2D work[4]. Although **V1** was strongly correlated to **V2** (r=0.83, $p<0.001$), the variation in D**V1** and D**V2** and the more elliptical humeral head on the impaired side demonstrates that retroversion is associated with both the orientation of the humeral head realtive to the elbow and the shape of the humeral head itself. The level of pathology increased with age (r=0.507, p=0.012), which may explain the discrepancy in retroverstion when comparing to past work[3]. A longitudinal study is needed to identify how shape changes with age in individual subjects, yet the results indicate that intervening early may help prevent larger

musculoskeletal pathologies later in life. Although the inclination angle was not significantly different between sides, the results were noteworthy when analyzing patient specific changes. Six and five subjects showed declination and inclination, respectively, greater than one standard deviation away from the control average. This discrepancy suggests that patient-specific, 3D morphometric analyses will support optimal treatment. There was a significant correlation between humeral morphology and age for the control side (**V1**: r= -0.57; **V2**: r= -0.711; and inclination: r= -0.477, p<0.05). Numerous factors such as increases in the variety of tasks performed and changes to the external forces on the arm (e.g., the initiation of crawling) may influence the relationship between shape and age on the control side. These natural developmental changes must be taken into account when assessing pathology. In addition, these changes in shape influence the musculotendon moment arms[5], confirming the concept that musculoskeletal models must be tailored to the pediatric population and not be derived by simply scaling adult models.

Figure:
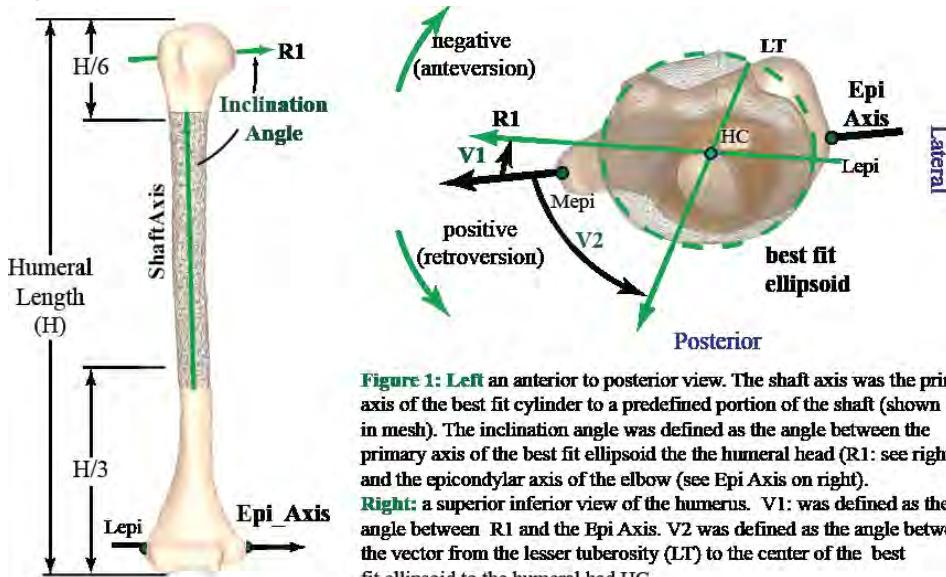
Figure 1: Left an anterior to posterior view. The shaft axis was the primary axis of the best fit cylinder to a predefined portion of the shaft (shown in mesh). The inclination angle was defined as the angle between the primary axis of the best fit ellipsoid the the humeral head (R1: see right) and the epicondylar axis of the elbow (see Epi Axis on right).
Right: a superior inferior view of the humerus. V1: was defined as the angle between R1 and the Epi Axis. V2 was defined as the angle between the vector from the lesser tuberosity (LT) to the center of the best fit ellipsoid to the humeral had HC.

Conclusion: This study is the first to evaluate 3D humeral shape changes in OBPP across the full pediatric age span. It provides novel findings in terms of inclination. The increased understanding of 3D morphologic changes in both the control and impaired arms of children with OBPP can lead to improvements in determining the unique and optimal treatment options for an individual based on subject-specific 3D morphological analyses.

References: 1 Edelson (2000) J Should & Elb Surg
2 Sheehan et al (2014) J Should & Elb Surg
3 van der Sluijs et al (2002) JBJS
4 Pearl et al (2014) J Should & Elb Surg
5 Voight el al (2011) J Ortho Trauma
Disclosure of Interest: None Declared

Musculoskeletal

AS-0208

RELATIONSHIP BETWEEN MUSCLE FASCICLES BEHAVIOR DURING MAXIMAL ECCENTRIC EXERCISE AND SUBSEQUENT MUSCLE DAMAGE

Gaël Guilhem [1,*]Valentin Doguet [2]Lilian Lacourpaille [1]Hugo Hauraix [2]Marc Jubeau [2]Arnaud Guével [2]François Hug [3]Antoine Nordez [2]Sylvain Dorel [2]

[1]Research Department, French National Institute of Sport (INSEP), Paris, [2]Laboratory Motricité, Interactions, Performance - EA 4334, University of Nantes, Nantes, France, [3]NHMRC Centre of Clinical Research Excellence in Spinal Pain, Injury and Health, University of Queensland, Brisbane, Austria

Introduction and Objectives: While current knowledge of the muscle dynamics during eccentric contractions has been mainly inferred from animal and in vitro studies [1], the advent of non-invasive techniques (i.e. ultrasonography) allows to explore human muscle mechanics that lead to exercise-induced muscle damage in vivo. Recent data obtained from the gastrocnemius medialis (GM) did not evidence a direct relation between muscle fascicle lengthening (18% of optimal fascicle length) during a submaximal eccentric exercise (i.e. backward walking) and the subsequent decrease in electrically-induced isometric torque [2]. The present study aimed to determine the potential relationship between changes in muscle fascicle length during maximal isokinetic eccentric contractions and the extent of muscle damage. We hypothesized that GM fascicle lengthening during maximal eccentric contractions would be higher than during backward walking and correlated to the decrease in maximal isometric torque.

Methods: Seventeen healthy subjects performed an initial test session two days before they performed a maximal isokinetic eccentric exercise of the plantar flexor muscles at $45°.s^{-1}$ on a Con-Trex isokinetic dynamometer over 60° until maximal dorsiflexion angle (0°=foot perpendicular to the tibia). The same test session was repeated 5 min and 48h after the exercise. During the exercise, torque and joint angle were collected from the dynamometer. Surface EMG activity of the gastrocnemius lateralis (GL), and GM fascicle length and pennation angle were continuously measured using ultrafast ultrasonography (100 Hz). During each test session, maximal voluntary isometric (MVC) torque, delayed onset muscular soreness (DOMS) and Achilles tendon active stiffness were measured. Separate one-way ANOVAs (time effect) with repeated measures and Newman-Keuls post-hoc procedures were applied to determine the effect of eccentric exercise on MVC torque and DOMS. Multivariate linear correlations were performed between muscle mechanics variables and the decrease in MVC torque at 48h. The significance level was set at $P<0.05$.

Results: Eccentric torque ranged from 11±5 N.m at 12° to 100±35 N.m at -28° during the exercise (Fig. 1a), with a significant 31±18% decrease in average torque from set 1 to set 10. EMG activity of GL muscle did not significantly changed from set 1 to set 10 (Fig. 1b). Overall, GM muscle fascicle lengthened from 35 ± 8 mm to 58±11 mm (i.e. 36±21% of optimal fascicle length) during the eccentric contractions (Fig. 1c). GM fascicle length increased from set 1 to set 10 (+12±5%). MVC torque significantly decreased immediately after maximal isokinetic eccentric exercise (-43±15%), and at 48h (-24±22%). DOMS significantly increased to 4.4 ± 2.8 at 48h. Multivariate correlations showed a significant relationship between maximal fascicle lengthening and MVC torque decrease at 48h (R=0.68, P<0.5; Fig. 1d). In addition, we observed a tendency for MVC torque to decrease as tendon active stiffness increased (R=0.48; P=0.08).

Figure:
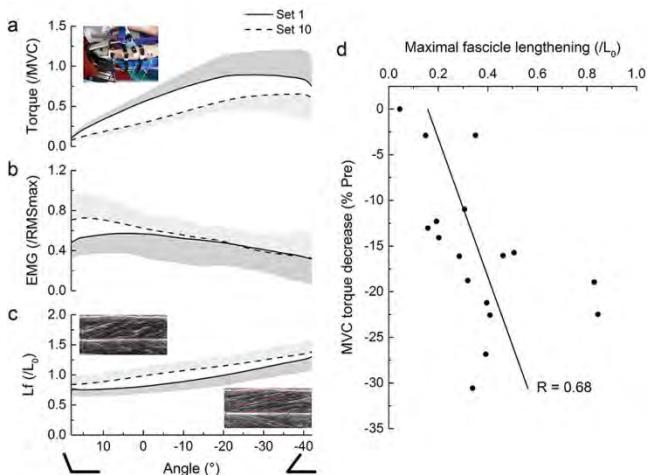
Caption: Plantar flexor torque (a), EMG activity of gastrocnemius lateralis normalized to the maximal root mean square (RMSmax) value obtained during MVC (b) and gastrocnemius medialis fascicle length (c) during maximal isokinetic eccentric contractions performed over 60° until maximal dorsiflexion angle. Values are mean ± SD. The decrease in MVC torque was significantly correlated to the maximal fascicle lengthening (d).

Conclusion: Maximal isokinetic eccentric contractions of the pantar flexors elicited a fascicle lengthening twice superior to the one observed during backward walking (36% vs. 18% of optimal fascicle length). Our findings also evidenced progressive adjustments in muscle dynamics as illustrated by the significant decrease in torque and the increase in fascicle length throughout the exercise. This increase in fascicle length could be reflective of a reduction in active cross-bridges or contraction level due to fatigue occurrence, and/or a consequence of cytoskeletal alterations caused by eccentric contractions [3]. Such muscle mechanics resulted in muscle damage as shown by the 24% drop in maximal force-generating capacities at 48h post-exercise. Interestingly, the decrease in MVC torque was significantly correlated to maximal fascicle lengthening, which slightly differs from results obtained during backward walking [2]. This may indicate that active lengthening on the descending limb of the torque-length curve and the strain amplitude may influence the level of muscle damage, confirming previous data from in vitro studies that used higher fiber stretches. The correlation tendency between Achilles tendon stiffness and the extent of muscle damage confirms that elastic properties of tendinous tissue contribute to mitigate muscle strain during lengthening contractions in humans.

References: [1] Butterfield, Exerc Sport Sci Rev, 38: 51-60, 2010.

[2] Hoffman et al., J Appl Physiol, 116: 1455-1462, 2014.

[3] Proske & Morgan, J Physiol, 537: 533-545, 2001.

Disclosure of Interest: None Declared

Musculoskeletal

AS-0209

COMPARISON OF HIP MUSCLE FORCES OBTAINED USING A CALIBRATED EMG-INFORMED MODEL AND STATIC OPTIMIZATION IN A HIP OSTEOARTHRITIC POPULATION

Hoa X. Hoang [1,*]Claudio Pizzolato [1]Luca Modenese [1]Peter Mills [1]David Lloyd [1]

[1]Centre for Musculoskeletal Research, Griffith University, Gold Coast, Australia

Introduction and Objectives: Hip osteoarthritis (OA) is a progressive and debilitating disease for which there is no cure and is the main reason for total hip replacements. Mechanical wear of the hip joint may be an key factor in the development of hip OA [1];however, hip joint disease is relatively under-studied and mechanical factors for the progression of hip OA are still poorly understood.Neuro-musculoskeletal (NMS) models can estimate muscle forces used to calculate internal joint contact forces (JCFs). However,these models have estimated muscle forces using static optimization (SO) that uses objective functions that are not physigiologialy based.We investigated the effect of using a Hybrid Calibrated EMG-Informed NMS (CEINMS-Hybrid) versus a SO approaches [2] to estimate muscle forces during walking in a hip OA and age-matched healthy populations.

Methods: We recruited and tested 26 individuals (> 45 years) with unilateral radiographic hip OA that has Kellgren-Lawrence (KL) score of 2 or 3 and 26 age-matched healthy participants used for controls. Participants were fitted with a full-body retro-reflective marker set and 16 surface EMG electrodes were placed on the affected leg of the hip OA participants while the side was randomly selected for the healthy participants. The system and data included: 10MX-camera Vicon system (200Hz), 2 AMTI force platforms (1,000Hz), and a 16-channel wireless EMG Cometa system. Participants performed a set of static trial and 10 walking trials. Hip joint centers were estimated using the Harrington regression equation while the knee and angle joint center were estimated using the midpoint of markers. Markers and ground reaction forces were filtered using a low-pass 4th-order Butterworth filter (6Hz). EMGs were processed by first a band-pass filtered with 4th-order Butterworth filter (30-300Hz), then full-wave rectified, and low-passed filtered using a 4th-order Butterworth filter (6Hz). The resulting linear envelopes were normalized to the maximum processed EMG values recorded from the entire set of trials. A full-body generic NMS model [2] was scaled in OpenSim to match each subject's anthropometry using the static trials. The model had 12 segments consisting of 19 DOFs across the lower extremities, pelvis, and trunk. The model included 34 muscle-tendon units (MTUs). In OpenSim, inverse kinematics (IK) was used to calculate joint angles for each walking trial while inverse dynamics (ID) was used to determine the net forces and torques at each joint. The musculotendon moment arms and fibre lengths for each MTU were calculated in OpenSim. The 16 experimental EMG signals were allocated to the 34 MTUs. Model parameters (musculotendon activation filtering coefficients, non-linear EMG to force relationship shape factor, tendon slack length, optimal muscle fibre length, muscle strength coefficient) were calibrated using the first 6 walking trials. Calibration was done by minimizing the predicted moments in CEINMS with the ID moments for the following degrees of freedom: hip flexion-extension, hip adduction-abduction, knee flexion-extension, and ankle plantar-dorsiflexion.Muscle forces were estimated from the remaining 4 walking trials with the CEINMS-hybrid approach using the recorded EMGs as inputs to drive the calibrated model [3]. The psoas major and iliacus did not have EMG recording as they were too deep for surface recordings; therefore, SO was

used to generate the excitations in the CEINMS-hybrid approach.Similarly,standard SO was also used to estimate muscle forces using an objective function to minimize sum of the activation squared.Muscle forces were normalized to each subject's body mass (N/kg).

Results: So far we have been processed data from 5 healthy female (61.3kg ± 6.6; 61.7y ± 11.9) and 5 hip OA female (69.9kg ± 9.9; 63.8y ±8.2) participants were processed during the stance phase of gait. The mean walking speed of the healthy and hip OA participants were 1.33m/s ± 0.13 and 1.13 m/s ±0.17, respectively. The CEINMS-hybrid approach estimated lower MTU forces muscles compared to SO (Fig.1).The average normalized hip MTU forces were generally higher in hip OA versus controls subjects.

Figure:
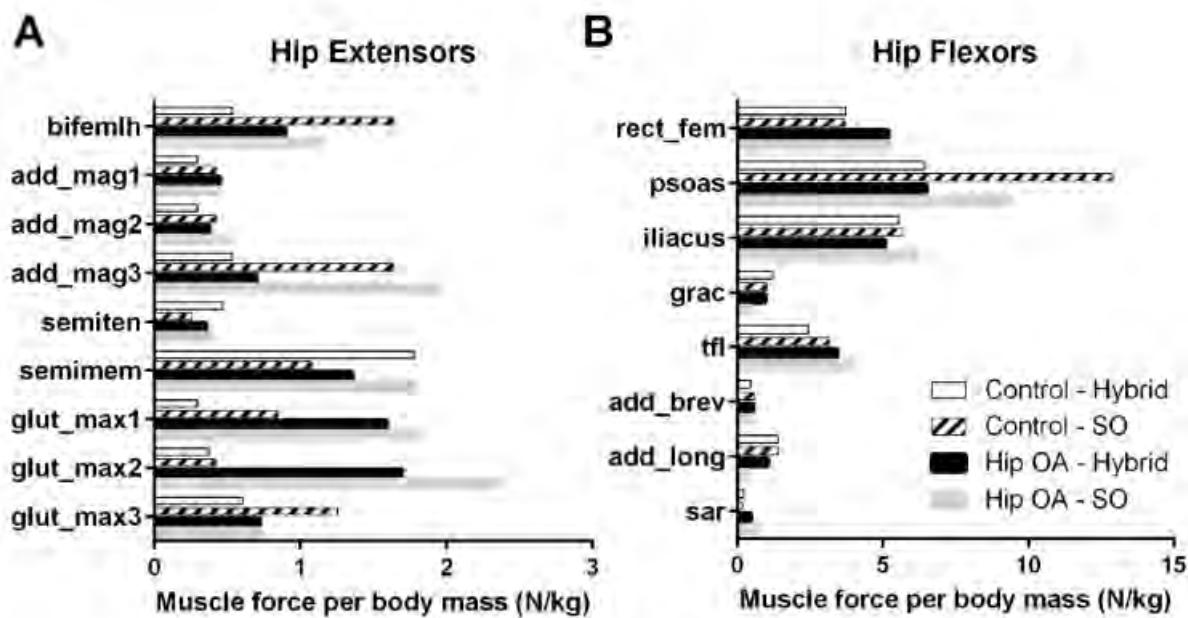
Caption: Muscle force normalized to body mass for the (A) hip extensor muscles, and the (B) hip flexor muscles

Conclusion: MTU forces estimated from SO were higher than the CEINMS-hybrid model for both groups. This suggests neurophysiologically based EMG-informed NMS modeling may be a promising alternative to SO in estimating muscle and joint contact forces, as SO over estimates hip joint contact forces.Lower estimated internal joint contact forces are expected using CEINMS-hybrid and is the focus of our current analyses.The hip MTUs of the hip OA group tended to be higher values than the healthy group,possibly to compensate for pain associated with OA.This also suggests that hip joint over loading may be a possible cause for rapid hip OA progression.

References: [1] Radin EL et al. Lancet. 1972 [2] Sartori M et al. J Biomech. 2014[3] Hamner S et al. J Biomech. 2010

Disclosure of Interest: None Declared

Musculoskeletal

AS-0210

SHEAR WAVE SPEED IN PLANTARFLEXORS OF INDIVIDUALS WITH CEREBRAL PALSY

Sabrina Lee [1 2,*]Li-Qun Zhang [2]Deborah Gaebler [2]William Rymer [2]Katherine M. Steele [3]

[1]Physical Therapy and Human Movement Sciences, Northwestern University, [2]Rehabilitation Institute of Chicago, Chicago, [3]Mechanical Engineering, University of Washington, Seattle, United States

Introduction and Objectives: Individuals with cerebral palsy (CP) tend to have altered muscle properties such as changes in fiber architecture and fiber composition[1], but little is known about the changes in muscle material properties, specifically stiffness that evolve as the individual matures. Quantification of muscle material properties has been limited to invasive methods such as biopsies. Shear wave (SW) ultrasound elastography allows SW speed, which is related to stiffness, to be measured *in vivo* in individual muscles[2]. Earlier studies have measured SW speed in both healthy muscles[3] and muscles of individuals with neuromuscular dysfunction[4]. Building upon these results, the goal of this study was to evaluate SW speed of the medial gastrocnemius (MG) and tibialis anterior (TA) in children with unilateral and bilateral CP over a range of ankle positions and torques.

Methods: Nine individuals (6 males, 3 females; age, 10.3±3.6 yrs.; height,1.36±0.16 m, mass, 33.9± 12.0 kg; 2 diplegic, 6 hemiplegic, and 1 quadriplegic, GMFC scores: 1-3) participated in the study.

Subjects were seated in a device (Intelligent Stretcher, Rehabtek) with their knee in full extension and foot strapped to a foot-plate, which rotated the ankle. B-mode and SW elastography ultrasound measurements (Aixplorer, Supersonic Imagine) of the tibialis anterior (TA) and medial gastrocnemius (MG) muscles, as well as joint angle and torque measurements, were made with the ankle set at different angles (neutral, maximum dorsiflexion (DF), maximum plantarflexion (PF), and two other intermediary angles) while the muscle was passive. Mean SW speed was calculated from a 12mm by 12mm region of the ultrasound images.

Results: Our key findings were that we recorded greater SW speed in the MG of the more-affected limb of individuals with unilateral CP by 11% (more-affected: 9.09±2.45m/s; less-affected: 8.21±1.95m/s, p=0.043, Fig. 1), especially when the muscle was set at its longest length. SW speed in MG and TA increased with increasing ankle angle and joint torque (linear fit of SW speed versus torque for the MG with r^2=0.48 (p<0.001) and a quadratic fit of SW speed versus angle for MG and TA with r^2=0.59 (p<0.001) and r^2=0.30 (p<0.001), respectively). There was a significant correlation between SW speed of the MG and ankle range of motion as indicated by the maximum DF angle (r^2=0.35, p=0.01). There was no significant correlation between SW speed and functional impairment as indicated by the GMFCS levels.

Figure:
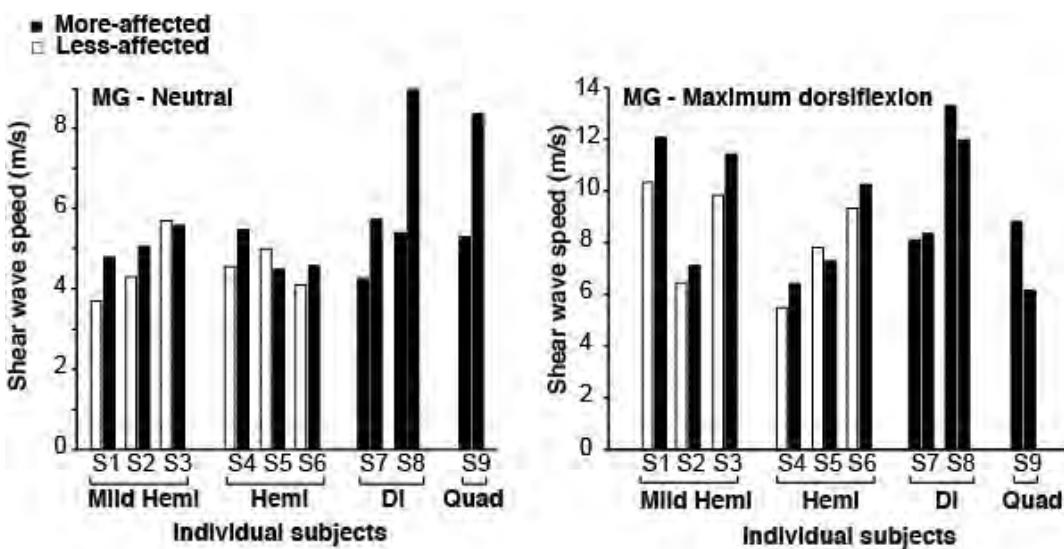
Caption: Figure 1. Mean shear wave speed of the less-affected (grey bars) and more-affected (black bars) medial gastrocnemius for individual subjects at neutral ankle angle and maximum dorsiflexion. Subjects are categorized as mild-hemiplegic (Mild Hemi), hemiplegic (Hemi), diplegic (Di), and quadriplegic (Quad) as diagnosed by the physician and GMFCS level. Both bars for the diplegic and quadriplegic are denoted in black as both limbs are affected.

Conclusion: We demonstrated that SWs travel faster in the MG of the more-affected than the less-affected side of individuals with CP, suggesting that the affected muscles have altered material properties, specifically greater stiffness. Significantly increased SW speed was observed in MG but not in TA, likely due to the more severe impairment in plantar flexor function, as compared to dorsiflexor function in this group of individuals. Possible sources of increased passive stiffness include increased collagen content in the extracellular matrix and other connective tissue, which has been shown to be correlated with clinical measurements of muscle spasticity[5]. Our result of increased SW speed with longer muscle lengths further suggests that increased passive tension is largely responsible for the changes in SW speed rather than muscle activity or hypertonicity. Moreover, greater SW speed was correlated with reduced ankle range of motion, indicating that increased stiffness of the MG was limiting DF range of motion for some individuals.

Use of SW elastography in the clinic may provide an additional means to quantify muscle material properties that are patient-specific, non-invasive, and occur in real-time. This is important for elucidating the complex nature of altered muscle properties that contribute to decreases in range of motion and force generation in individuals with CP. Being able to characterize altered muscle material properties is important for understanding the causes of abnormal muscle function, aiding diagnosis, and guiding treatment planning.

References: : [1] Lieber et al., Muscle & nerve, 29:615-627, 2004.

[2] Bercoff et al., IEEE Trans. Ultrason., Ferroelectr.,, and Freq. Control., 51:396-409, 2004.

[3] Lacourpaille et al., Physiological measurement, 33:N19-28, 2012.

[4] Kwon et al., Radiology, 263:794-801, 2012.

[5] Smith et al., Journal Physiol., 589:2625-2639, 2011.

Disclosure of Interest: S. Lee: None Declared, L.-Q. Zhang Conflict with: Equity position in Rehabtek, D. Gaebler: None Declared, W. Rymer: None Declared, K. M. Steele: None Declared

AS-0211

PREDICTING TIMING OF FOOT STRIKE FOR TREADMILL WALKING AND RUNNING WITH A PRINCIPAL COMPONENT MODEL OF GAIT.

Sean Osis [1,2,*] Blayne Hettinga [1,2] Reed Ferber [1,2]

[1]University of Calgary, [2]Running Injury Clinic, Calgary, Canada

Introduction and Objectives: The accurate detection of events during gait, such as foot strike, can be challenging without force measurements. Consequently, there are many disparate methods used to detect foot strike in walking and running by means of specialized marker sets [1,2,3,4]. Recently, a novel approach to this problem was developed based on the use of feature selection using principal component analysis (PCA), and when applied to running, demonstrated improved predictions of timing, irrespective of varying striking techniques [5]. Therefore, the purpose of this study was to evaluate the use of this previously developed method in predicting the timing of foot strike during treadmill walking.

Methods: Kinematics were collected using eight high-speed (200 Hz) video cameras (Vicon, Oxford, UK), and retro-reflective markers. Kinetics were obtained from an instrumented treadmill (Bertec, Columbus, OH). Markers were placed over anatomical landmarks and a standing neutral trial was collected. Segment kinematics during walking were collected using clusters of markers strapped to the pelvis, thighs, shanks and feet.

Marker and kinetic data for n = 127 subjects (71 females; 38.3 +/- 10.1 years; 1.73 +/- 0.09 m; 70.1 +/- 12.4 kg; 1.12 +/- 0.01 m/s) were extracted from a database of walking biomechanics for analysis. Joint angles were calculated using a singular value decomposition approach, and a joint coordinate system. Gold-standard identification of foot strikes was based on a 10 N threshold of vertical force.

A previously developed PCA model [5] was applied to the current data by projecting sagittal plane joint accelerations into an existing principal component space. The resulting scores from the first PC were used to predict timing of foot strike according to the previously trained regression model [5]. The timing of predicted frames were then compared with the gold standard timing from kinetics.

Results: A bias of 7 frames in the distribution of errors was found after initial implementation, and was subsequently removed by subtracting 7 frames from the predicted frame of foot strike for each step. The resulting distribution of errors demonstrated good agreement with foot strike as determined by kinetics, with 90% of subjects having a median error less than +/- 3 frames, or 15 ms (Figure 1).

Figure:
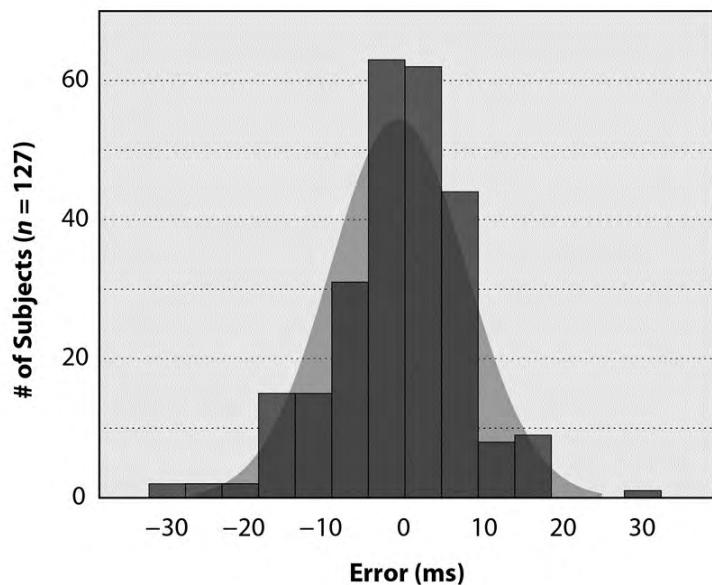
Conclusion: The errors found in the current study are comparable to, or slightly more than, recent approaches in the literature ([3] 94% of errors within 17 ms; [4] 95% of errors within 7 ms). However, the current method has the advantage of not being reliant on specific marker sets for the prediction of gait events.

Interestingly, although the method was trained using data from running, it seems to apply equally well to walking. This result suggests that the underlying PCA model accounts for both gait type (walking vs running) and the previously reported striking technique (forefoot vs rearfoot) [5]. Therefore, this PCA method is a convenient and unified means of using joint kinematics to predict timing of foot strike during treadmill gait.

Caption: Figure 1 – Histogram of median error for each subject in the prediction of foot strike using the PCA regression model, as compared with detections of foot strike by kinetics.

References: [1] Fellin et al., J Sci Med Sport, 13:646-50, 2010.

[2] Leitch et al., Gait Posture, 33:130-2, 2011.

[3] Zeni Jr. et al., Gait Posture, 27:710-4, 2008.

[4] Kiss, Med Eng Phys, 32:662-7, 2010.

[5] Osis et al., J Biomech, 47:2786-9, 2014.

Disclosure of Interest: None Declared

Motion Analysis

AS-0212

OBJECTIVELY-MEASURED DAILY PHYSICAL ACTIVITY PATTERNS AND THEIR ASSOCIATIONS WITH BMI IN OLDER WOMEN

Emma Fortune [1,*]Shreyasee Amin [2]Kenton Kaufman [1]

[1]Orthopedic Surgery, [2]Rheumatology, Mayo Clinic, Rochester, United States

Introduction and Objectives: Regular physical activity (PA) with aging is critical for health and function [1]. It is recommended that 75-150 minutes/week of moderate-vigorous PA (MVPA) are performed to sustain a healthy weight [2]. As PA declines with age, accurate PA measurement in older community-dwelling adults is crucial when assessing health status, but challenging. Increasing evidence suggests that too much sedentary time and too little light intensity PA (LPA) can impose huge health implications for weight and cardiovascular health, independent of reaching current MVPA recommendations [3]. Recent reports also suggest that distributing PA throughout the day may be more beneficial to weight and cardiovascular health than meeting MVPA recommendations in concentrated periods of time [4]. However, current objective PA and sedentary time measures are simplified, considering only daily total PA or sedentary time, and use methods of limited accuracy [5]. An objective portable method for measuring PA patterns in the free-living environment is necessary to fully determine associations with obesity and its related diseases. Therefore, this study's objectives were to (1) examine both the daily amount and the variations of active time, step counts, and the number of times that sedentary time was broken up (sedentary break number; SBN) of 11 older women using custom-built activity monitors (AMs) in the free-living environment and (2) investigate the associations of these parameters with BMI to determine the importance of PA variations during the day for BMI management in older women.

Methods: Eleven older women (age 77±9 yrs; BMI 26±5 kg/m^2) wore AMs, each containing a tri-axial accelerometer (±16g, 100 Hz), on the waist and ankle for lab-based walking trials (for validation by comparison to video data simultaneously recorded at 60 Hz) and 4 days in the free-living environment. The protocol was approved by the IRB and written informed consent was obtained. Step counts, active time (classified as MVPA for cadence>92 steps/min [6]) and SBN (number of activity segments ≥30 s) were estimated from acceleration data using a previously validated algorithm [7]. Sensitivity and positive predictive value (PPV) were used to assess the algorithm's ability to accurately detect active time in seconds and steps and the Bland-Altman method was used to assess cadence as determined by the AM algorithm and video observation for the lab-based trials. The associations of the PA parameters' total daily values and the coefficient of variations (CoVs) of their hourly values (to quantify activity variation throughout the day) with BMI were assessed using linear regression with Pearson correlation analysis. The data were also analyzed after adjusting for age.

Results: Median sensitivity and PPV of active time and step detection were >98% for lab trials. Mean cadence error was <1%. The median (IQR) daily step count, cadence, and active time measured in the free-living environment were 7689 (5406) steps, 73 (16) steps/min, and 109 (81) min. Median step counts were higher than expected for older adults [2]. However, most subjects were self-reportedly very active and many algorithms cannot accurately detect steps at gait velocities <0.8m/s [7]. BMI was inversely associated with active time, MVPA time, step counts, and SBN (Fig. 1) consistent with associations of greater activity with healthier weight [2]. The higher association of active time compared to

MVPA time with BMI is consistent with suggestions that LPA should be considered in addition to MVPA [3]. BMI was positively associated with active time/hour CoV (r^2=.50, p<.001), step number/hour (Fig. 1D), and SBN/hour (Fig. 1F), with slightly higher r^2 values compared to these parameters daily totals, suggesting that activity variation may be important to consider in future studies with larger sample sizes. Both the SBN and the CoV of SBN/hour had the highest associations with BMI, agreeing with previous reports that abdominal obesity, which can be predicted from BMI, is affected by sedentary time [6]. Age was not significantly associated with any investigated variable (p_{age}>.17) other than the CoV of SBN/hour (adjusted r^2=.91, p_{age}=.03), with the association of SBN/hour CoV with BMI slightly decreasing as age increased.

Figure:
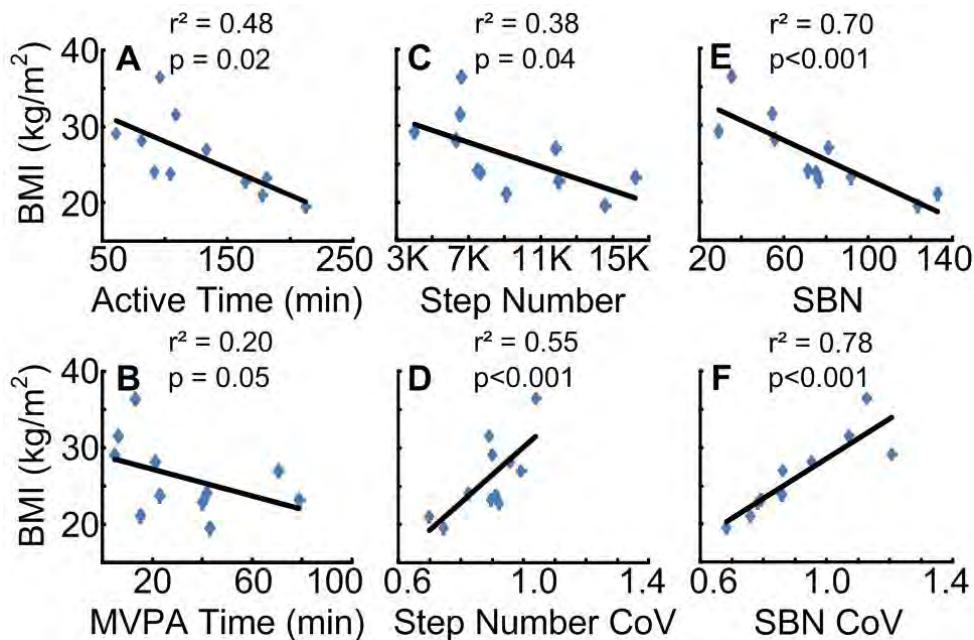
Caption: Figure 1. Associations of BMI with mean daily A active minutes, B MVPA minutes, C step number, D step number/hour CoV, E sedentary break number (SBN), and F SBN/hour CoV.

Conclusion: These data support suggestions to break up sedentary time with both LPA and MVPA and distribute PA throughout the day to sustain a healthy BMI.

References: [1] Arnardottir et al., Age Ageing, 42: 222-229, 2013.

[2] Tudor-Locke et al., Sports Med, 34: 1-8, 2004.

[3] Bankoski et al., Diabetes Care, 34: 497-503, 2011.

[4] Duvivier et al., PLoS One, 8: e55542, 2013.

[5] Chastin et al., Gait Posture, 31: 82-86, 2010.

[6] Chastin et al., Age Ageing, 41: 111-114, 2012.

[7] Fortune et al., Med Eng Phys, 36: 659-669, 2014.

Disclosure of Interest: None Declared

EFFECTS OF FATIGUE AND ANTICIPATION ON THE KINEMATICS AND KINETICS DURING A SIDE CUT

Chris Richter [1] [2] [3],*Kieran Moran [1] [2]Enda Whyte [2]

[1]Insight:Centre for Data Analytics, [2]School of Health and Human Performance, Dublin City University, [3]Sports Medicine, Sports Surgery Clinic, Dublin, Ireland

Introduction and Objectives: Uni-lateral multi-directional movements (e.g. cutting) are common in most sports and deficiencies in neuromuscular control have been identified as risk factors for injuries, e.g. ACL injuries[1]. Two factors that may decrease neuromuscular control are fatigue and anticipation. Previous research has shown that fatigue can neg. effect biomechanical variables that are associated with injury[2] and that injuries tend to occur when a person is fatigued, e.g. towards the end of a game[3]. Regarding anticipation, athletes have to respond instantaneously to external stimuli by selecting movement strategies. Hence, anticipation can influence the execution of a movement (e.g. the time between choosing a strategy and its execution may be too small in some instances), forcing the athlete to execute a non-optimal movement. To date, few studies have examined the effects of fatigue and anticipation of cutting tasks. Therefore, the aim of this study was to examine the effects of fatigue and anticipation on the biomechanics during a side cut.

Methods: Trunk and lower limb kinematics and kinetics were recorded for 30 healthy male during a side cut. Data was recorded for an anticipated (ANT) and unanticipated (UNA) condition before (PRE) and after (POST) exposure to an high-intensity exercise protocol[4]. A side cut was performed, with participants jumping horizontally (70% of their max. jump distance), landing on their dominant leg and performing a side cut at 45 degrees. In the ANT condition, a flashlight indicated the movement direction five seconds before the task was performed. In the UNA condition, the participant triggered this light by breaking an infrared beam during the jump. Kinematic and kinetic variables were recorded, over the full cycle of contact with a force plate, and examined for differences between the conditions using Analysis of Characterizing Phases (ACP), which generated subject scores from key phases (phases of variance) that were identified using principal components that captured >99% of the variance in the data[5]. Only the deceleration phase was examined, which was defined as the phase from initial contact to the first occurrence of propulsion forces. To identify statistical differences, a Repeated Measures ANOVA was performed. To measure the effect size of the statistical differences Cohen's D (d) was calculated. The alpha level was set to 0.05. Only significant findings for waveforms that had at least one key phase with a medium ($.5>d>.8$) or large effect ($d>.8$) are reported.

Results: Findings showed multiple significant effects of fatigue (ankle flexion angle, knee flexion angle and moment, hip and pelvis flexion angles as well as thorax rotation), supporting previous studies that examined the effect of fatigue during cutting movements[2,6]. However, none of these factors reached a medium effect, indicating a low effect of fatigue on biomechanical measures. When comparing ANT vs. UNA, findings matched previous studies that examined the effect of anticipation on cutting tasks[2] have been proposed to be risk factors for ACL injuries. However, most of these factors had a small effect (anterior GRF, ankle flexion and abduction angles and moments, knee flexion angles and moments, knee abduction moments, hip abduction angles, hip flexion rotation moments, pelvis angle flexion and rotation, thorax flexion and rotation angles). Interestingly, the identified factors with medium or large effects have not been examined/reported

previously (pelvis & thorax abduction angles, as well as non peak knee flexion moments). Factors with large effect sizes were only identified in this study due to the use of a continuous data analysis approach, which considers the whole waveform rather than selected discrete points, and has been shown previously to be more effective than the traditional analysis method of analyzing discrete data points (e.g. peak angle)[5]. Effect sizes indicated a medium to strong effect of anticipation on biomechanical measures.

Figure:
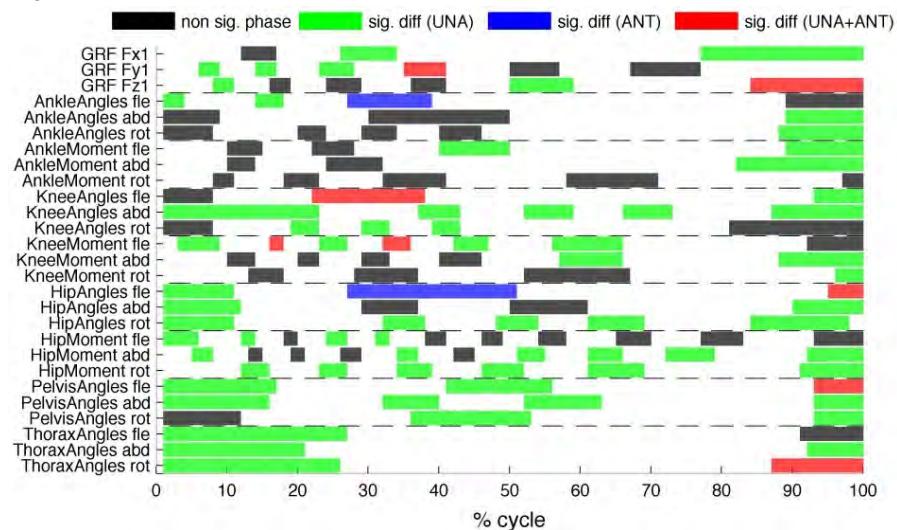
Caption: Key phases examined

Conclusion: Findings indicate both fatigue and anticipation can alter the biomechanics of a side cut, while the effects of anticipation have a much greater influence.

Table:

variable	key phase	p value	Cohens D
GRF-ant.	35-41 & 84-100	<.001	-.51 & -.53
Ankle Moment-fle	89-100	<.001	.62
Knee Angle-fle	22-38 & 93-100	<.001	-.59 & -.57
Knee Moment-fle	3-9; 16-18, 23-24, 32-36 & 42-47	<.001	-.70, -.75, -.76, -.70 & .67
Hip Angle-abd	1-12	<.001	.59
Hip Moment-fle	31-33	<.001	.52
Hip Moment -rot	46-52, 61-69 & 91-100	<.001	-.52, -.59 & -.60
Pelvis Angle-fle	1-17 & 41-56	<.001	.63 & .51
Pelvis Angle-abd	1-16, 32-40, 52-63 & 93-100	<.001	.98, .93, 1.11 & 1.12
Pelvis Angle-rot	93-100	<.001	.63
Thorax Angle-abd	1-21 & 92-100	<.001	.82 & .74

Caption: Significant differences (effect>medium)

References: 1-Shultz et al. 2010,*J Athl Train,45*(5):499

2-Borotikar et al. 2008,Clin Biomech,23(1):81-92

3-Gabbett 2004,J Sports Sci,22(5):409-417

4-Whyte et al. 2014,J Sport Rehabil,doi:2014-0201

5-Richter et al. 2014,J Biomech,*47*(12):3012-3017

6-Quammen et al. 2012,J Athl Train,47(1):32-41

Disclosure of Interest: None Declared

AS-0214

SENSITIVITY OF A DISTRIBUTIVE TACTILE SENSING DEVICE FOR THE ASSESSMENT OF ARM FUNCTION AFTER STROKE

Amir A. Mohagheghi [1,*]

[1]Department of Life Sciences, Brunel University, London, United Kingdom

Introduction and Objectives: In contrast to healthy individuals, stroke survivors flex their trunk to reach to targets located within the reach of the arm (near targets). For targets placed beyond the reach of the arm (far targets), both healthy and stroke individuals, flex their trunk to reach to the targets, and the magnitude of trunk flexion increases with increasing target distance. Contribution of trunk to reaching has been shown to be correlated to the level of motor impairments in stroke survivors. Moreover, a clinical threshold may exist at which trunk contribution to reaching alters as a result of changes in the severity of motor impairment [1]. Therefore, determination of trunk contribution to the reaching tasks might have a prognostic value in the rehabilitation after stroke. We have developed a Distributive Tactile Sensing (DTS) device which can provide a low cost (both analytically and financially) alternative to the traditional real-time optoelectronic motion analysis systems. The device works by detecting deformation responses of flexible surfaces (e.g. thin steal or plastic plates), when subjected to variable force stimuli provoked by the human body movement. Surface deformations are recorded by a small number of low-cost infrared displacement sensing elements (typically 3-5) placed under the surface at strategic points where the deflections are likely to be more pronounced. Different combinations of the sensors outputs (transients) can be used to detect the exact location of the force applied to the surface. In the same way, temporal profile of the applied force can provide information on the pattern of force application to the surface. The development proposed in the current study involved modification of a standard office chair integrated with a simple sensing system. In healthy and stroke participants, we assessed presence and magnitude of trunk contribution to a reaching task toward near and far targets, and compared the DTS device sensing transients and movement kinematics recorded using motion analysis. The aim was to assess the sensitivity of the DTS device as a clinical tool for the assessment of selective arm function after stroke.

Methods: A convenient sample of ten Healthy (H) adults and five chronic stroke survivors (S) whose upper limb (UL) were mildly to severely impaired took part in the study. Participants were instructed to sit upright in an instrumented chair and reach out to targets placed in front of them using their dominant (H) or paretic UL (S). Targets were placed at distances determined using different percentages of the length of the individual's arm. Specific features of the sensing transients from the DTS device were extracted, and associated with the UL segments and trunk kinematics using motion analysis. Movement was performed at a self-selected speed after a verbal cue. Wilcoxon signed-rank test was used to analyse data.

Results: For the H group, DTS transients showed minimal change compared to the baseline with movement of the UL segment in reaching toward near targets. For far targets, DTS transients showed specific characteristics (Figure) representing recruitment and level of involvement of the trunk. Peak-to-peak (p-p) amplitude of the transients ($z=2.803$; $p=0.005$) and trunk flexion angles ($z=2.803$; $p=0.005$) increased with increasing target distance. Importantly, DTS

transients characteristic started before the onset of trunk movement (mean range: 119-140 ms). For the S group, the characteristic DTS transients (and trunk movement) were present during reaching tasks for all near and far targets. Similar to the H group, p-p amplitude (z=2.023; p=0.043) increased with increasing target distance, and showed a similar trend for trunk flexion (z=1.826; p=0.068). Mean delay between onset of DTS transients characteristic and trunk movement was 195-288 ms.

Figure:
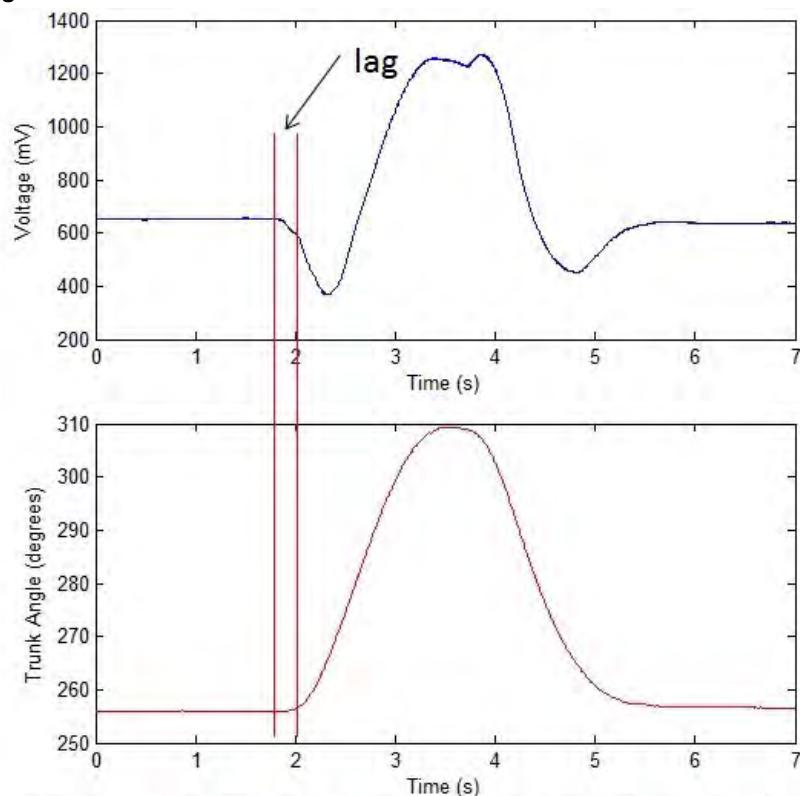
Figure – illustrates the lag between onset of downward drift in DTS transient (top) and trunk flexion (bottom).

Caption: Figure – illustrates the lag between onset of downward drift in DTS transient (top) and trunk flexion (bottom).

Conclusion: Conclusion: DTS device showed sensitivity to the presence and magnitude of trunk flexion. Presence and magnitude of trunk movement during reaching tasks to near targets is associated with the severity of motor impairment after stroke. Therefore, DTS device can be used for the objective assessment of arm function after stroke. The characteristic DTS transients started several milliseconds prior to trunk flexion in both groups. This lag may represent backward movements of the centre-of-mass and/or lower limb muscles activity providing stability before the onset of trunk flexion. It is likely that alteration of the lag is associated with alteration in the level of motor disability.

References: [1] Cirstea, MC and Levin, MF. (2000). Compensatory strategies for reaching in stroke. *Brain*. May;123 (Pt 5): 940-53.

Disclosure of Interest: None Declared

Motion Analysis

AS-0215

IS THE DYNAMIC COEFFICIENT OF FRICTION INDEPENDENT OF VELOCITY IN HUMAN GAIT?

Ilaria Pacifici [1,*] Ana F.R. Kleiner [1][2] Manuela Galli [3][4] Ricardo M.R. Barros [2]

[1]Luigi Divieti" Posture and Movemengt Analysis Laboratory, Department of Electronics, Information and Bioengineering, Politecnico di Milano, Milano, Italy, [2]Laboratory of Instrumentation for Biomechanics, Faculty of Physical Education, University of Campinas, Campinas, Brazil, [3]"Luigi Divieti" Posture and Movemengt Analysis Laboratory, Department of Electronics, Information and Bioengineering, Politecnico di Milano, Milano, [4]Gait Analysis Lab, IRCCS San Raffaele, Rome, Italy

Introduction and Objectives: Friction plays an important and necessary role in the activity of walking. Without friction we could not move from one place to another. To accomplish desired motion, the tangential forces associated with the accelerations of the body must be resisted by ground reaction forces. The study of friction is documented since the end of XIV century in the manuscripts written by Leonardo da Vinci, who discovered that the friction force is proportional to the load (normal force) and is independent of the area of contact. In 1875, Charles A. Coulomb affirmed that kinetic friction between two rigid bodies is independent of the sliding speed; it was referred as the third law of friction.

In the human locomotion, the required Coefficient of Friction (RCOF) is a parameter able to evidence a floor surface kinetic requirement, to support walking [1]. This coefficient is usually applied to analyze the happening of falls related to slips and it is determined by the resultant of the ground reaction forces generated during the gait, with the use of 3 axial force plates.

Considering the relevance of the COF for the human gait, it is important to verify if the COF is dependent on the walking speed. The purpose of this study was to examine the dependence of the dynamic coefficient of friction by the gait velocity.

Methods: Seventeen healthy volunteers were recruited in this study (8 males and 9 females; 24.64 ± 1.27 years old; 64.29 ± 15.40kg; 172.17 ± 11.67cm). The participant was oriented to walk barefoot at three selected cadences (72bpm, 96bpm, 120bpm) according to a metronome, along the pathway and over two force platforms (Kistler 9286BA), embedded in the data collection room floor. The force plate's ground reaction force (GRF) components (F_x, F_y, F_z) were normalized by the subject body weight and expressed in function of the percent of support phase of the gait cycle. Kinetic raw data were filtered using a 2nd order low-pass digital Butterworth filter, with a cut-off frequency of 10 Hz. An algorithm developed in Matlab was used to filter raw data and to calculate dependent variables. The COF curve was calculated as the ratio of the shear to normal GRF during stance [1, 2] - Equation 1.

$$COF = (F_Y^2 + F_X^2)^{1/2} / F_Z \qquad (1)$$

F_Y is the anterior-posterior GRF, F_X is the lateral GRF and F_Z is the vertical GRF. Then, as illustrated in Figure 1a, the following parameters of the COF curves were calculated: the COF in the loading response (LR), mid stance (MS) and terminal stance (TS) phases. The nonparametric data was analyzed by Friedman test and the Bonferroni post-hoc test ($\alpha < 0.05$). The software SPSS (version 19) was used to perform all statistical analysis.

Results: The Figure 1 presents the differences among the walking speeds (72 bpm, 96 bpm and 120 bpm) for the RCOF in the LR (F_2=32.760; p=0.0001), MS (F_2=41.880; p=0.0001) and TS (F_2 = 219.893; p=0.0001) phases. In all three phases, the higher is the walking speed the higher was the RCOF value.

Figure:
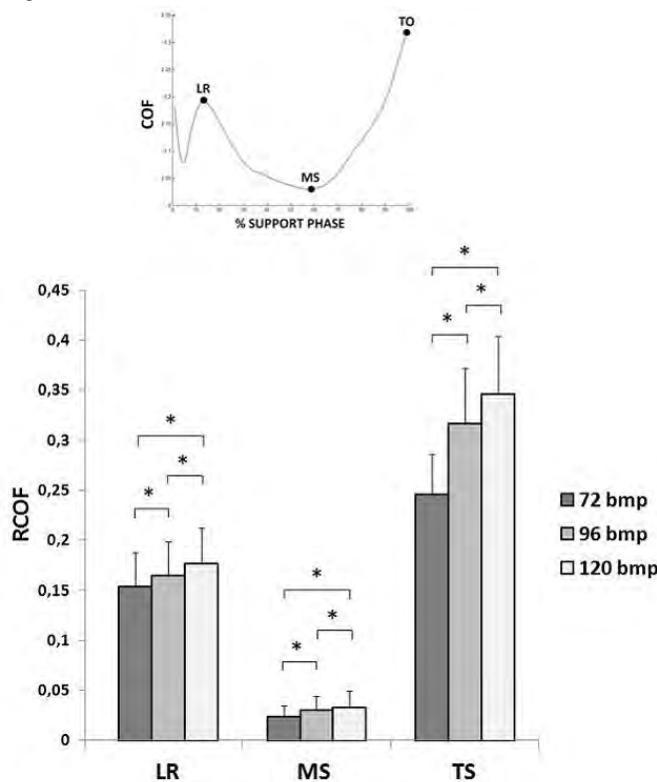
Caption: Figure 1: (a) Illustration of COF curve variables ; (b)differences among velocities for loading response, mid stance and terminal stance

Conclusion: In this study the dynamic COF was observed with respect to adaptations to the walking velocity. The Coulomb's third law of friction, that assumes that the friction is independent by the velocity, is applicable for friction between two rigid bodies, but it does not explain the pedestrian friction. The foot-floor interface during the human gait requires a more complex viscoelastic model of friction in which the mechanisms of adhesion and rolling friction between surfaces should be better explained. Thus, these results show that the dependence of the COF by the walking speed have to be considered when the COF is applicable to study the gait features of normal and/or pathological subjects.

References: [1] F.P. Bowden et al., Oxford University Press, 1964

[2] Chang WR et al., Ergonomics, 55(3):308-315, 2012

[3] Redfern, M.S. et al., Ergonomics, 44(13), 1138-1166, 2001

[4] Mills PM et al., Hum. Move. Sci.2001:427–446.

[5] Perkins PJ et al., Ergonomics, 26(1):73–82, 1983

Disclosure of Interest: None Declared

Motion Analysis

AS-0216

EFFECTS OF TWO FATIGUE PROTOCOLS ON LOWER EXTREMITY KINEMATICS AND IMPACT FORCES IN DROP LANDING TASKS

Rui Xia [1,*]Weijie Fu [1]Xi Wang [1]Xini Zhang [1]

[1]Key Laboratory of Exercise and Health Sciences of Ministry of Education, Shanghai University of Sport, Shanghai, China

Introduction and Objectives: Numerous studies have shown that prolonged and high-intensity exercise would induce neuromuscular fatigue of the human body. Altered neuromuscular control strategies during fatigue potentially contribute to the increased risk of sports injury [1]. No scientific consensus, however, has been reached yet to suggest which type of fatigue protocol results in greater biomechanical changes in the lower extremity during landing movement [2]. Therefore, the purpose of this study was to determine the changes in the lower extremity kinematics and ground reaction forces between two fatigue protocols when performing a landing task.

Methods: Eight trained male athletes (age: 21±1.1 years, height: 176.4±4.7 cm, mass: 70.8±6.3 kg) volunteered to participate in the study. Two fatigue protocols, i.e., long-term running fatigue protocol and functional short-term fatigue protocol, were used to induce fatigue randomly. Specifically, the long-term running fatigue protocol requested participants to run at 4.0 m/s on a treadmill until exhaustion. The functional short-term fatigue protocol requested participants to first perform five consecutive countermovement jumps within a height above 70% of their maximal vertical jump height. They subsequently completed the short-term fatigue protocol consisting a group of shuttle running (6×10 m) with their maximal effort. Participants needed to repeat the above process until the average height of five consecutive countermovement jumps was below 70% of their maximal vertical jump height. Before and after fatigue protocols, each participant was required to execute five successful trials of drop landings from a 60-cm platform. 3D kinematics (Vicon, 240 Hz) of the dominant leg and ground reaction force (Kistler, 1200 Hz) were measured simultaneously. The main variables included 1) the sagittal joint kinematics of the hip, knee, and ankle; 2) the peak vertical ground reaction force and peak loading rate (determined by the maximum slope of adjacent points of vertical GRF) during the impact phase of landings. Paired-tests were used to determine the influence of independent variable (fatigue) on each of the dependent variables (joint angle and GRF) in the two separated fatigue protocols using SPSS 13.0 (SPSS Inc., Chicago, IL, U.S.A.). The significance level was set at a = 0.05.

Results: For the kinematics, post-tests using functional fatigue protocol showed a significant decrease in the minimum angle of the hip ($p = 0.008$) and knee ($p = 0.028$) joints, and an increase in the range of motion of these two joint (hip: $p = 0.004$; knee: $p = 0.002$) compared to pre-tests. However, there were no significant differences in the lower extremity kinematics (pre- vs. post-test) using the long-term running fatigue protocol. Meanwhile, no changes were found in the peak vertical ground reaction force and peak loading rate between pre- and post-test for both fatigue protocols.

Conclusion: In this pilot study, we found the functional short-term fatigue protocol would induce an increase in hip and knee flexion, but not in ankle, resulting in a more flexed landing posture. In contrast, no significant effect of long-term running fatigue protocol was showed on sagittal kinematic changes in the lower extremity. These results will provide a preliminary reference for the selection of fatigue protocols in laboratory tests.

Table:

Joint	Kinematic variables	Long-term running fatigue protocol		Functional short-term fatigue protocol	
		Pre-test	Post-test	Pre-test	Post-test
Ankle	Maximum angle	125.9±8.4	123.9±12.3	123.8±10.5	123.8±9.1
	Minimum angle	80.2±5.2	80.6±5.9	82.8±4.9	82.4±9.3
	Range of motion	45.6±6.6	43.3±10.1	41.0±10.5	41.4±10.4
Knee	Maximum angle	164.0±5.9	160.8±10.4	158.8±6.7	160.6±7.1
	Minimum angle	94.9±19.5	88.6±26.1	87.9±18.4	75.6±20.4*
	Range of motion	69.2±15.1	72.2±17.5	70.9±14.8	85.1±14.4**
Hip	Maximum angle	147.0±10.4	142.5±16.1	143.4±9.3	144.0±13.3
	Minimum angle	103.9±29.1	94.3±35.2	93.6±22.0	80.8±22.2**
	Range of motion	43.1±19.7	48.2±19.7	49.8±15.8	62.3±15.4**

* Significantly different between pre- and post-tests in the same fatigue protocol with $p < 0.05$.

Caption: Descriptive statistics for kinematic variables (mean ± SD) at ankle, knee, and hip joints in two fatigue protocols (pre-test vs. post-test).

References: [1] Enoka, R. M., J Biomech, 45: 427-433, 2012.
[2] Quammen et al., J Athletic Training, 47(1): 32-41, 2012.

Disclosure of Interest: None Declared

Computer Simulation

AS-0217

TIBIAL FRACTURE AFTER UNICOMPARTMENTAL KNEE REPLACEMENT: THE IMPORTANCE OF SURGICAL CUT ACCURACY

Elise C Pegg [1,*]Hemant G Pandit [1]Harinderjit S Gill [2]David W Murray [1]

[1]Nuffield Department of Orthopaedics, Rheumatology and Musculoskeletal Sciences, Univeristy of Oxford, Oxford,

[2]Department of Mechanical Engineering, University of Bath, Bath, United Kingdom

Introduction and Objectives: Tibial fracture is a possible complication after unicompartmental knee replacement (UKR) which can have severe consequences for patient recovery and outcome [1]. It appears that the issue is not product specific, as peri-prosthetic fractures have been reported in numerous designs, both mobile and fixed. However, it has been suggested that cementless components might be at greater risk than cemented [2]. The exact causes of tibial fracture are unknown, although surgical factors are most commonly proposed in the literature [1,3].

The objectives of the study were to; (1) determine the range of positions and depths of the surgical cuts required to prepare the tibial plateau for a UKR, (2) use the measured parameters to create a representative range of finite element models, (3) statistically assess the influence of each surgical parameter on the risk of fracture.

Methods: Tibial plastic Sawbones (n=23) were prepared for mobile UKR during an instructional course. The parameters measured from the sawbones were: (a) the resection depth, (b) the angle between the horizontal and vertical cuts, (c) the distance between the vertical wall and the keel slot, how excessively deep the vertical cut and horizontal cuts were anteriorly (d and e, respectively), and posteriorly (f and g, respectively), and (h) the depth of the pin hole (Figure 1).

A parametric finite element model was created in ABAQUS software (v6.12, Dassault Systèmes) with an automated python script to create the surgical cuts. One hundred models were created, where the surgical cut parameters were varied within the distributions measured from the Sawbones. A mesh element size of 2.4 mm was used, selected as a result of a mesh convergence study. The tibia was modelled as a heterogeneous linear elastic material, with a Poisson's ratio of 0.3. The modulus of each element was assigned based upon the corresponding position of that element in the CT scan of the tibia. The equations used for this have been previously defined and the tibial model validated [4]. Muscle and joint loading of a tibia at 15% of the gait cycle was applied, corresponding to maximal medial contact force, and the distal portion of the tibial constrained in all degrees of freedom. The risk of fracture was quantified based upon the Maximum Principal Stress criterion equations defined by Schileo et al. [5].

The influence of each surgical parameter on the risk of fracture was assessed using linear regression with R (r-project).

Results: In the tibial Sawbone measurements, the greatest surgical variation was observed in the depth of the posterior vertical cut and the pin hole, which had standard deviations of 3.9 and 6.8 mm respectively (Table 1).

The only surgical cut parameters which were found to significantly affect the risk of fracture were the resection depth, and the posterior depth of the vertical cut (p=0.009, and p=0.000001, respectively).

Some finite element models demonstrated a noticeable region at high risk of fracture, which extended diagonally from the vertical saw cut, past the base of the keel slot to the tibial cortex. This matched well with typical fracture paths observed clinically [1].

Figure:
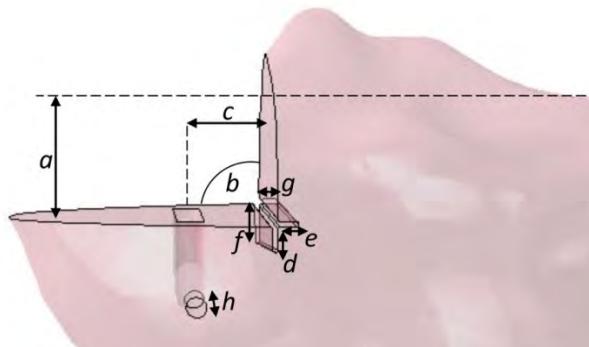
Caption: Figure 1. The surgical cut parameters made on a right Sawbone tibia which were recorded were: the resection depth (a), the angle between the horizontal and vertical cuts (b), the wall to keel distance (c), how excessive the vertical and horizontal cuts were anterior (d, e) and posterior (f, g), and the depth of the pin hole for fixing the cutting guide (h).

Conclusion: This study has shown accuracy in the depth of the vertical cut made to prepare the tibial plateau for UKR, has the greatest clinical variation and has the greatest influence on the risk of fracture out of all the parameters assessed in this study. It is therefore important that instrumentation be designed to improve surgical accuracy for this part of the operative technique.

Table:

Parameter	Mean	Standard Deviation
A: Resection Depth (mm)	8.8	1.7
B: Angle between cuts (deg)	90.6	1.4
C: Wall to keel distance (mm)	8.5	0.7
D: Anterior depth vertical cut (mm)	0.5	1.0
E: Anterior depth horizontal cut (mm)	0.7	0.9
F: Posterior depth vertical cut (mm)	4.2	3.9
G: Posterior depth horizontal cut (mm)	1.3	2.1
H: Depth of pin hole (mm)	28.6	6.8

Caption: Table 1. Summary of the measured surgical cut parameters from Sawbones prepared during an instructional course

References: [1] Pandit, H., et al., Orthopedics, 30: 28-31, 2007.

[2] Seeger, J.B., et al., Knee Surg Sports Traumatol Arthrosc, 20: 1087-1091, 2012.

[3] Clarius, M., et al., The Knee 16: 314-316, 2009.

[4] Gray, H.A., et al., J Biomech Eng, 130: 031016, 2008.

[5] Schileo, E., et al., J Biomech, 41: 356-367, 2008.

Disclosure of Interest: E. C. Pegg Conflict with: Biomet, H. G. Pandit Conflict with: Biomet, H. S. Gill Conflict with: Biomet; Smith & Nephew; Stryker, Conflict with: Smith & Nephew, D. W. Murray Conflict with: Bluebelt Technologies, Conflict with: Biomet; Stryker; Zimmer, Conflict with: Biomet

Modelling

AS-0218

BIOMECHANICAL ANALYSIS OF THE UNIVERSAL 2 IMPLANT IN TOTAL WRIST ARTHROPLASTY: A FINITE ELEMENT STUDY.

Magnús K. Gíslason [1,*]Euan Foster [2]Marc Bransby-Zachary [3]David Nash [2]

[1]Institute of Biomedical and Neural Engineering, Reykjavik University, Reykjavik, Iceland, [2]Department of Mechanical and Aerospace Engineering, University of Strathclyde, [3]Department of Orthopaedic Surgery, Southern General Hospital, Glasgow, United Kingdom

Introduction and Objectives: Load mechanics of the implanted wrist are poorly understood. To date most surgeons would prefer to carry out partial or total wrist arthrodesis to treat the painful and unstable wrist joint opposed to using a total wrist prosthesis. The success rates of the wrist implants have been poor compared to the hip and knee implants. It has been demonstrated that partially fusing the wrist will alter the load mechanics and can potentially have detrimental effect on the untreated joints within the wrist [1]. Few wrist implant models exist [2] due to complex interaction between the carpal bones and the prosthesis. The presented study looks at the mechanical response of the Universal 2 wrist implant under loading. The Universal 2 wrist implant is the most commonly used implant in the UK.

Methods: The three dimensional geometrical model was created from a 7T MRI scan of a healthy human cadaveric model. The in plane resolution of the scan was 0.250mm and the slice thickness 1mm. The scans ranged from the proximal third of the metacarpals to the distal end of the radius and ulna. The segmentation of the scans were carried out using Mimics (Materialise). Three dimensional objects of the carpal bones were created and meshed using tetrahedral elements. An STL file of the Universal 2 implant was virtually implanted into the wrist and Boolean operators used to create the boundaries between the implant and the bones. The finite element model was assembled and solved using Abaqus (Simulia). The implant comprised of three components: a proximal stem attaching in the radius made from a CoCr alloy, distal carpal component attaching to the capitate made from a titanium alloy and a polyethylene spacer between the two components made from UHMWPE. The implant and bone material properties can be seen in Table 1. Additionally two screws on the radial and the ulnar side were modelled. Cartilage was manually created at each articulation within the wrist and surface to surface contact established between the bones. The implant components were modelled as being fully bonded to the bones. An illustration of the finite element model can be seen in Figure 1. Compressive loads were applied to the metacarpals and the proximal ends of the radius and ulna were kept fixed.

Results: The model was solved using the explicit solver. The results demonstrated that the majority of the load was transmitted through the proximal component of the radius. Little load was transmitted through the ulna as the procedure compromises the biomechanical stability of the ulnocarpal joint.

Figure:

Caption: Finite element model of the implanted wrist

Conclusion: The results demonstrated how finite element models can be used to simulate the in-vivo loading through the implanted wrist. The understanding of the load transfer mechanics can be fed back into the design process of the next generation of wrist implants in order to improve the design.

Table:

Material	Young's modulus [GPa]
CoCr	207
Titanium	114
Cortical bone	18
Cancellous bone	0.1

Caption: Material properties

References: 1. Skie M, Hand, 2:194-198, 2007

2. Bajuri MN et al. Med. Biol. Eng. Comput., 51(1):175-186, 2013

Disclosure of Interest: None Declared

Computer Simulation

AS-0219

TOWARDS AN AUTONOMOUS REACTIVE FINITE ELEMENT MODEL OF THE HUMAN ARM

Dorian Salin [1][2],*Pierre-Jean Arnoux [2]Kambiz Kayvantash [1]Michel Behr [2]

[1]CADLM, Massy, [2]LBA, IFSTTAR, Marseille, France

Introduction and Objectives: In biomechanics, Finite Element (FE) models have been wide spread in various domains like medicine and traumatology. However in the category of musculo-skeletal models a recurrent issue is the missing of muscle bracing. Some authors used experimental data to add muscle forces, but these models are not sensitive to boundary conditions modifications during the simulation. Thus, in this study we developed a reactive FE model of the upper limb integrating sensory motor loops. This model is then used to study the effects of various properties of these loops in the reaction process during well-known reflexive actions.

Methods: At first we developed a FE biomechanical model of the arm with realistic geometry of bones, muscles, and tendons in the LS-DYNA environment. The model illustrated in figure 1 is composed of 187491 elements (solids, shells and discrete) and 83768 nodes. Joints of the upper limb are simplified and allow only the extension-flexion of the elbow. The muscles contain contractile components allowing flexion and extension movements of the elbow. We then added to this model two types of proprioceptive sensors, i.e. muscle spindles and Golgi tendon organs.

The myotatic and inverse myotatic reflexes resulting from these sensors are also integrated with the help of an external software which allows to generate and manage data flows from various software platforms. We then studied sensitivity of the model reaction after the impact of a hammer on the biceps brachial tendon (stretch reflex). The parameters of this sensitivity analysis are listed in table 1.

The reflex delay, i.e. time between sensory information to muscular activation, is ranged from 5 to 40ms. The inverse myotatic reflex is alternatively switched On and Off to study the effect of Golgi Tendon Organs in the late phase of the stretch reflex. The agonist/antagonist coupling is the situation where the effects of a reflex (either excitation or inhibition) are applied to the relative muscle itself and to its agonists, and the opposite effect is applied to its antagonist. This coupling is alternatively switched On and Off to study its effects on the model reaction.

Results: The typical reaction of the model with a delay of 40ms, the inverse myotatic reflex and the agonist/antagonist reflex is: a first activation of the flexor muscles from 45ms to 60ms after the hammer impact, at high level (peak of 45% of maximal force), followed by a second activation from 60ms to 90ms at a lower activation level (peak of 15% of maximal force). These activations generate a flexion of the elbow of 5.5°. After this flexion the extensor muscle is activated at a low level from 90ms to 140ms (peak of 10% of maximal force) which bring back the elbow to a flexion of 3°.

The sensitivity analysis on the proposed sensory and motor loop model properties was realized and showed promising results. First of all a short reflex delay is not necessarily good for the stability of the arm, it can even induce instability for a delay as short as 5ms Because of the short delay, the vibration induced by the impactor is amplified by the muscular contractions and the arm results to be unstable. The inverse myotatic reflex provides an earlier return to the initial position and the agonist/antagonist coupling amplifies the reaction in the case of this stretch reflex test.

Figure:

Caption: Biomechanical model with sensors (muscle spindles in black, Golgi tendon organs in blue)

Conclusion: We developed a realistic FE model with autonomous reactive behaviour with human-based sensory and motor loops. The two main sensors intervening in human proprioception were integrated and the effects of various properties of the sensory and motor loops response were studied. This showed promising results and offers a good opportunity to jointly study neurosciences and biomechanics over the range of daily tasks and rather to unfamiliar and/or traumatic cases. The application domains of this model are automotive safety, sports, or medicine.

Table:

Sensory and motor loop properties	Variations
Reflex delay	Range from 5 to 40 ms
Inverse myotatic reflex	On/Off
Agonist/antagonist coupling	On/Off

Caption: properties and their variations

Disclosure of Interest: None Declared

Modelling

AS-0220

A COMBINED EMG-CONSTRAINED AND ENTROPY-ASSISTED STATIC OPTIMIZATION MODEL OF THE INDEX FINGER

Alex Macintosh [1] Peter Keir [1,*]

[1]Kinesiology, McMaster University, Hamilton, Canada

Introduction and Objectives: Determining tendon tension in the finger is essential to understanding forces that may be detrimental to hand function and accurate measurement of intrinsic muscle activity is particularly difficult. Modelling solutions are needed to account for intrinsic muscle contributions. The objective of this work was to improve muscle activity predictions during static pressing of the index finger by applying a novel combined EMG-constrained and entropy-assisted static optimization solution method.

Methods: A custom model of the index finger was built in OpenSim for this analysis. The model includes all extrinsic and intrinsic muscles controlling the index finger. The muscles are represented as multiple paths which extend to the central and terminal slips of the finger. To predict muscle activity, the OpenSim static optimization analysis tool was expanded in two ways. First, EMG constraints were programmatically incorporated. Predicted muscle activity was constrained to match the experimental activity ± 15% maximum voluntary exertion. Second, an entropy-assisted objective function (Jiang and Mirka, 2007) was compared with the default sum of squared activation objective function available through OpenSim. Ten right-hand dominant volunteers (five female, five male; 25.3 ± 3.1 years) performed a series of static finger pressing tasks. During static pressing tasks, participants pressed directly down into the force sensor from the pulp of the distal phalanx. Force was applied at three levels: 5, 15, and 30 N, and in three postures: all-flexed, PIP-flexed, and extended. In the all-flexed posture both the DIP and PIP joints are flexed, while in the PIP-flexed posture the DIP remained extended. Kinematics, contact forces, and extrinsic muscle EMG were collected. Muscle activity predicted from the two EMG-constrained objective functions (sum of squared activation and entropy-assisted) were separately compared to recorded muscle activity. Two dependent variables were used to assess fit between predicted and recorded activity: (i) coefficient of determination (r^2) as an index of shape similarity, and (ii) normalized root mean square deviation (NRMSD) to reflect differences in magnitude. Additionally, tendon tensions were calculated based on predicted activity, moment arm, and maximum isometric force of each muscle.

Results: Recorded muscle activity during static finger pressing ranged from 10.2 ± 3.6% in the EDC during 5 N straight finger pressing to 51.3 ± 18.1% in the FDP during 30 N bent finger pressing. Using the EMG-constrained entropy-assisted optimization, three of four muscles (FDS, FDP and EDC) gave lower NRMSD than the EMG-constrained solution alone (F = 28.285, p = 0.046). There was an interesting relationship between NRMSD and r^2. A decrease in NRMSD was accompanied by a decrease in the r^2 between predicted and experimental activity. The EMG-constrained sum of squared activation method averaged a higher NRMSD (7.0 ± 2.1) and r^2 (0.4 ± 0.15), while the combined EMG-constrained entropy-assisted method averaged a lower NRMSD (6.6 ± 2.1) and r^2 (0.3 ± 0.13). Predicted muscle activations were used to calculate normalized tendon tension for each index finger muscle during static pressing and compared to literature estimates (Figure 1).

Figure:
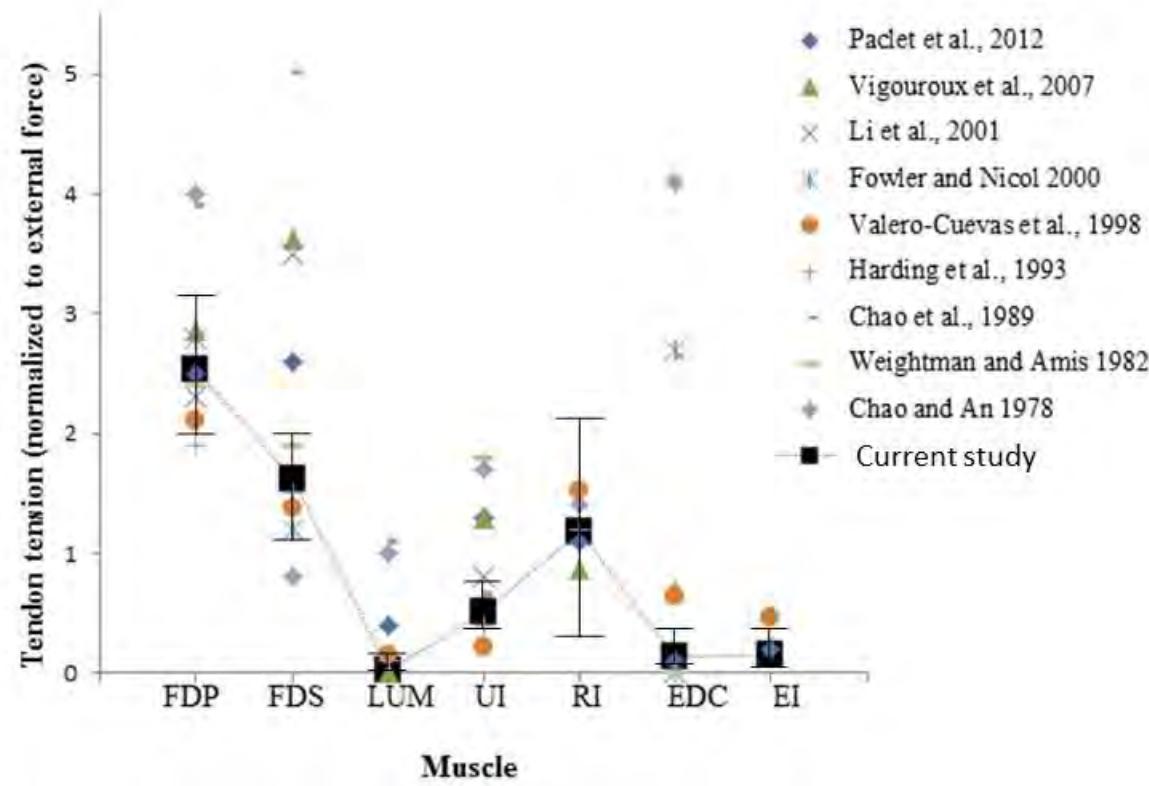
Caption: Tendon tension estimates for each muscle controlling the index finger. Current study estimates and standard deviations are averaged across trials and compared with previous literature.

Conclusion: The unique combination of EMG-constrained and entropy assisted optimization has improved muscle force distribution in the finger by more closely matching recorded extrinsic muscle activity while predicting intrinsic muscle activity. These findings support an increase in antagonist activity, known to be important for proper coordination during palmarly directed pressing (Valero-Cuevas et al., 1998). By further exploring the allowable deviations and weightings in the objective function further improvement may be possible. In this study, tendon loading estimates made across multiple pressing postures and forces correlated well with previous investigations. The combined approach developed here is useful for modelling a variety of manual tasks. Analysis methods that are robust enough to derive meaningful results from a variety of tasks are critical to developing rehabilitation strategies that enhance the functional ability of affected individuals.

References: [1] Jiang et al., J.PHFE, 2007.

[2] Valero-Cuevas et al., J. Biomechanics, 31(8), 693-703, 1998.

Disclosure of Interest: None Declared

Modelling

AS-0221

MODELING COORDINATED JOINT RANGE OF MOTION OF THE HUMAN HAND -- CHARACTERISTICS OF COORDINATION AND GRASPING IN RELATION TO THE ROM BOUNDARY --

Natsuki Miyata [1,*]Satoshi Hagiwara [2]Yusuke Maeda [2]

[1]Digital Human Research Center, National Institute of Advanced Industrial Science and Technology, Tokyo, [2]Yokohama National University, yokohama, Japan

Introduction and Objectives: For deeper understanding of the human hand function, joint range of motion (ROM) should be measured and described precisely. Traditionally, ROM of the hand was defined by independently bounding each joint angle from observation of extreme posture. However, it is difficult to express actual human's complex ROM with such simple boundaries because human hand has multiple joints that move in coordination. Therefore, we have developed a new method to model ROM of the hand by defining outer boundary of collected various posture data through motion capturing.

Objective of this study is to find characteristics of the coordinated motion of the human hand by measuring and comparing several subjects ROM. In addition, grasping postures are analyzed in terms of location in ROM, which can be utilized to plan rehabilitation with quantitative goal.

Methods: The human hand is a multidimensional system that consists of many joints and its posture is expressed with multiple variables. It is difficult to directly deal with all the couplings among the joints at the same time. We therefore proposed a model of the range of motion of the whole hand as a set of all the relationships between two of the posture variables[1]. Each relationship between two of the joint angles was presented as a united area in which all the projected measured postures on the plane were minimally bounded using the alpha-shape algorithm. We call this smallest unit a coupled ROM. As can be seen in the examples in the Figure, each derived boundary occupies smaller area than a rectangle corresponding to the traditional ROM.

On motion measurement, we gave subjects the same set of 21 exercises selected to include various joint postures both in the middle and on the boundary. This was because our precedent observation showed the difficulty for the subjects to move widely across their ROM when instructed to "move arbitrarily." Furthermore, it was necessary to evenly spread the variety of motions among the subjects as much as possible for proper comparison.

These exercises to model ROM are all unloaded motion. Such ROM can be called "active" ROM. The ROM would be slightly expanded when an external force is applied as in grasping. To analyze such grasping posture with our active ROM, we additionally collected 801 grasping postures. We determined grasping postures by adding variations to grasp taxonomy proposed by Feix [2] which considers contact regions when grasping.

Results: Measurement and modeling experiments on four subjects were conducted to analyze characteristics of the coordinated motion. To study the coordination of the joints of the hand, we ranked the coulpled ROMs for each subject by the index "Coord" defined in [1], which can be calculated considering the area reduction rate compared with traditional rectangle ROM and coefficient of determination. The comparison showed that strong coordination were observed similarly

for all the subjects in (1) the adjacent metacarpophalangeal (MP) joints and (2)proximal and distal phalangeal joints of the same fingers.

As for the grasping postures, some of the postures were located outside the active ROM as expected. In addition, our results showed that MP joints were largely extended when grasping (in the left graph of Figure).

Figure:
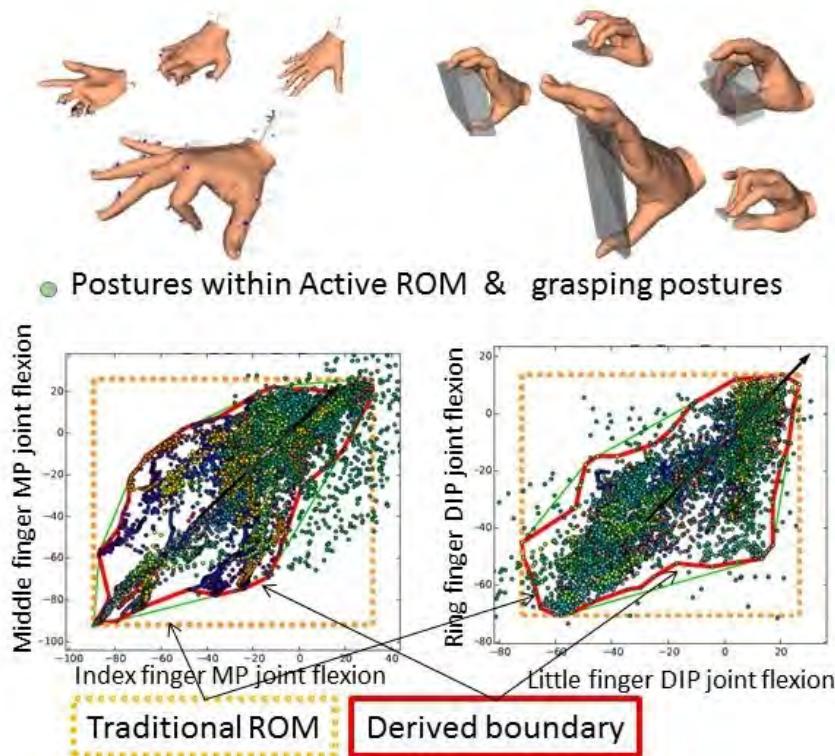
Caption: Two examples of the modeled active ROM with grasping postures. Some of the grasping postures were observed to lie outside the active ROM boundary.

Conclusion: This study analyzed the coordinated human hand motion by comparing active range of motion that modeled by appropriately deriving boundary from a variety of measured postures. Comparison based on the coordination index showed that the coordination categories were similar among subjects. Plotting of the grasping postures with the active ROM clearly showed the deviation of passive ROM difference from active one.

References: [1]N. Miyata, et al., "A Measuring and Analysis Method of Coupled Range of Motion of the Human Hands", Proceedings of the 2013 IEEE Int. Conf. on Systems, Man, and Cybernetics, pp.2623--2628, 2013.

[2] T. Feix, et al. "A comprehensive grasp taxonomy," in Robotics, Science and Systems Conference: Workshop on Understand the Human Hand for advanced Robotic Manipulation, 2009.

Disclosure of Interest: None Declared

Computer Simulation

AS-0222

PREDICTION OF IN-VIVO KNEE KINEMATICS: DEVELOPMENT OF A PATIENT-SPECIFIC MUSCULOSKELETAL MODEL OF THE KNEE FOR CLINICAL APPLICATION

Malte Asseln [1,*] Ghaith Al Hares [1] Joerg Eschweiler [2] Klaus Radermacher [1]

[1]Chair of Medical Engineering, Helmholtz-Institute for Biomedical Engineering, RWTH Aachen University, [2]Department of Orthopaedics, Aachen University Clinic, RWTH Aachen University, Aachen, Germany

Introduction and Objectives: For a proper functional restoration of the knee following knee arthroplasty, a comprehensive understanding of bony and soft tissue structures and their effects on biomechanics of the individual patient is essential. Conventional intraoperative ligament balancing only considers passive knee kinematics, ignoring the fact that the majority of load and active kinematics in the knee are due to muscular forces. Musculoskeletal models have the potential, however, to predict dynamic interactions of the knee joint and provide insights into knee biomechanics [1]. Musculoskeletal models of the knee have been developed and used to simulate orthopedic procedures, such as osteotomies, tendon transfers and total joint replacements [2]. Although previous model-based studies helped to understand the complex biomechanics of the knee and have provided clinically useful insights, major hurdles for their broad clinical application remain. These include e.g. average data on function and morphology, idealized joint kinematics, modelling parameters obtained from cadaveric measurements, limitations in modelling of anatomical complexity and lack of clinical workflow integration for the patient-specific therapy.

Our goal in this study was to develop a generic musculoskeletal model of the knee which is easily adaptable to subject-specific situations and to evaluate the model on the basis of in-vivo kinematic measurements using Upright-MRI image data [3] (Fig 1 A).

Methods: The simulation model has been developed and adapted to a total number of 9 subject-specific cases in the multi-body simulation software AnyBody based on the StandingModel from the AnyBody Repository. The standard hinge joint was replaced with a new complex knee joint with 6DoF. The 3D bone geometries were obtained from an optimized MRI scan using expert's manual segmentation [3] and were then post-processed by mesh reduction and smoothing filters available in the mesh processing software MeshLab.

In this study, the anatomical locations of ligaments (ACL, PCL, MCL and LCL) and muscle attachments were determined based on literature data, since the model adaptation process was aimed to be valid for CT-data where no soft tissue information are available. For the same reason cartilage was approximated by a homogenous dilation of 3 mm for each bone and menisci were neglected.

For the subject-specific adaptation a general scaling, taking segment length, mass and fat into account, was used. The scaling was further modified to allow a detailed adaption of the subject-specific knee morphology including ligament and muscle attachments in the reference model.

The boundary conditions were solely described by analytical methods and ground reaction forces have been predicted by adding muscle forces between the foot and environment. A single leg deep knee bend was simulated by kinematic

constraints, such as that the center of mass is positioned above the ankle joint. The contact forces in the knee joint were computed using the force dependent kinematic algorithm presented by Andersen et al. [2].

The simulation model was adapted to the 9 subjects, single leg deep knee bends were simulated and subject-specific kinematics were recorded according to the definition of Grood et al. [4]. The simulated kinematic results were then compared to their corresponding subject-specific in-vivo kinematic measurements data obtained by Upright-MRI under the same full-weight bearing condition in 5 static postures.

Results: We were able to simulate the whole group of subjects over the complete range of motion. The tibiofemoral kinematics of all 9 subjects could be simulated showing the overall trend correctly, whereas absolute values partially differ (Fig 1 B). Particularly, translations show a good agreement, e.g. the RMSE for medial/lateral translation was 0.49 for S05, whereas the rotations seem to be more sensitive to the model parameters, e.g. the RMSE for internal/external rotation was 7.19 for S06. The overall adaptation process takes about 15-30 min. per subject from the segmented data to the full personalized biomechanical model.

Figure:
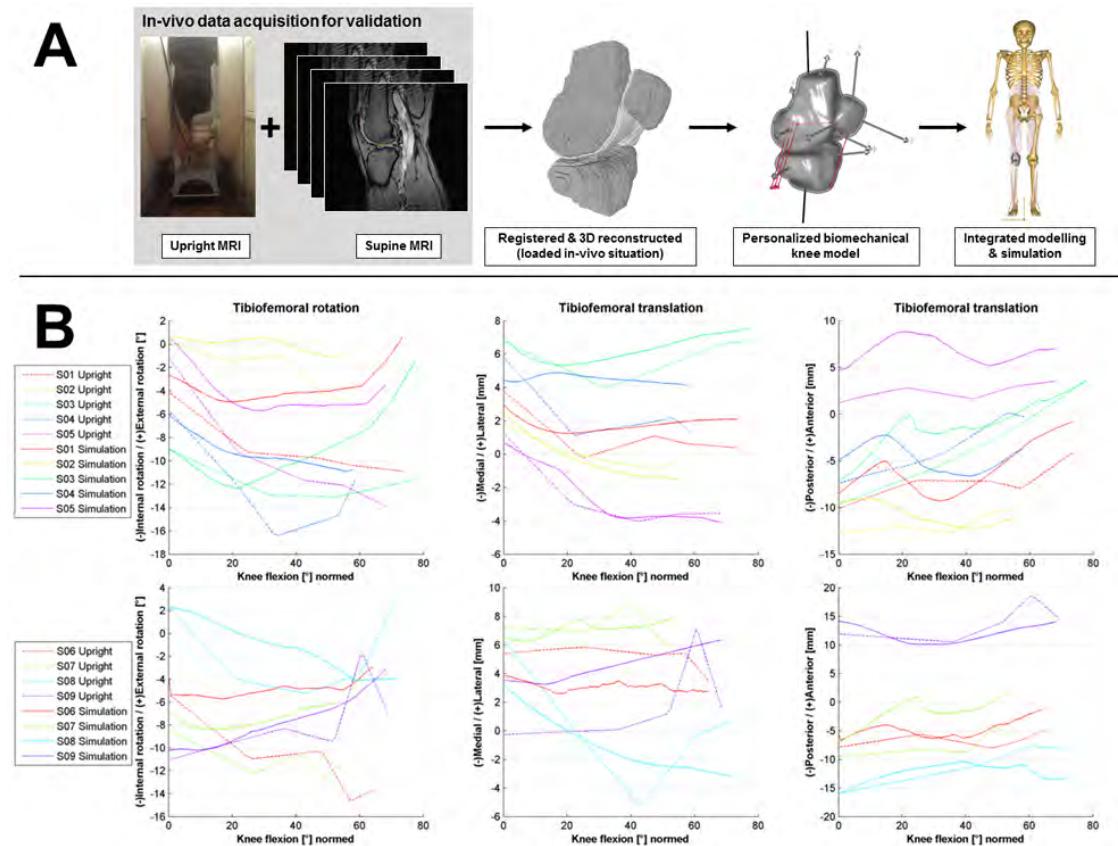
Caption: A Experimental workflow for validation, B Predicted in-vivo kinematics vs. measured kinematics for 9 subjects

Conclusion: The presented simulation model is adaptable to an individual situation and seems to be suitable to predict, or at least approximate, subject-specific knee kinematics for e.g. investigation of the extensor mechanism, morphological analyses and optimization of the articulating geometries and surgical interventions. Principally, the trend of the kinematics

is captured, although absolute values partially differ. However, model optimization, sensitivity analyses of selected parameters and a semi-automation of the workflow are parts of our ongoing work.

References: [1] Heller et al., Der Orthopäde, 36, 188-194, 2007

[2] Andersen et al., Proceedings of the ISB Conference, 2011

[3] Al Hares et al., Proceedings of the CAOS Conference, 197-199, 2013

[4] Grood et al., J. Biomech., 105, 136–144, 1983

Disclosure of Interest: None Declared

Elderly

AS-0223

EFFECT OF EXERCISE-INDUCED CHANGES OF THE INTRINSIC TRICEPS SURAE MUSCLE-TENDON UNIT PROPERTIES ON MAXIMAL WALKING VELOCITY IN THE ELDERLY

Gaspar Epro [1 2,*] Andreas Mierau [3] Gert-Peter Brüggemann [1] Kiros Karamanidis [2]

[1]Institute of Biomechanics and Orthopaedics, [2]Institute of Movement and Sport Gerontology, [3]Institute of Movement and Neurosciences, German Sport University Cologne, Cologne, Germany

Introduction and Objectives: It has previously been reported that deterioration in contractile strength and tendon stiffness in the elderly is associated with altered motor task execution and reduced performance while walking [1,2], and that resistance training improves muscle function, resulting in more effective and safer gait characteristics in the older population [3]. In particular, triceps surae (TS) muscle-tendon unit (MTU) properties seem to be an important determinant for walk-to-run transition speed [4], emphasizing the relevant role intrinsic MTU properties play in gait performance. The objective of this empirical study was to examine the hypothesis that maximal walking velocity is related to TS MTU mechanical and morphological properties and their enhanced capacities would improve gait velocity in the elderly.

Methods: Thirty four older female adults (66±7 yrs.) took part in the study. Nineteen of them were recruited for the experimental group, who underwent a 14-week TS MTU physical exercise intervention which has been previously established to increase muscle strength and tendon stiffness [5]. The remaining 15 subjects formed the control group (no physical exercise intervention). The experimental group performed three times per week five sets of four repetitive (3·s loading, 3·s relaxation) isometric plantar flexion contractions in order to induce high cyclic strain magnitudes on the TS tendon and aponeurosis. Maximal walking velocity, defined as walking with a double support phase, was determined by using two force plates (60 x 40 cm, 1080 Hz; Kistler, Winterthur, CH) and a motion capture system (Vicon Motion Systems, Oxford, UK) with 12 infrared cameras operating at a frequency of 120 Hz. TS MTU properties were assessed using simultaneous dynamometry and ultrasonography (Esaote MyLab Five; Esaote Biomedica, Genoa, IT).

Results: A significant correlation was found between the TS MTU mechanical and morphological properties and maximal gait velocity ($0.40 < r < 0.64$; $P < 0.05$; $n = 34$). The experimental group showed higher TS contractile strength, tendon stiffness, and higher gastrocnemius medialis muscle thickness post- compared to pre-intervention ($P < 0.05$). However, calculated maximal gait velocity did not differ between pre and post-intervention measurements (2.39 ± 0.41 vs. 2.44 ± 0.45 m·s^{-1}). Control subjects showed no statistically significant differences in maximal gait velocity or TS MTU mechanical and morphological properties.

Conclusion: This empirical study confirms previous forward simulation models [4] proposing that intrinsic TS MTU properties are significant determinants of gait performance. However, older adults may not be capable of fully utilizing improvements of the MTU capacities while walking at maximal velocities following a 14 week physical exercise intervention. Therefore, the benefits of a long term physical exercise intervention (1.5 years) will be discussed.

References: [1] Beijersbergen et al., Ageing Res Rev, 12: 618-627, 2013.

[2] Reeves et al., J Electromyogr Kinesiol, 19(2): 57-68, 2009.

[3] Karamanidis et al., PLoS One, 9(6): e99330, 2014.

[4] Neptune et al., J Exp Biol, 208: 799-808, 2005.

[5] Arampatzis et al., J Exp Biol, 210(15): 2743-53, 2007.

Disclosure of Interest: None Declared

AS-0224

ROLE OF EACH LEG TOWARDS ANGULAR IMPULSE GENERATION DURING TURNING-WHILE-WALKING PERFORMED AT DIFFERENT SPEEDS BY OLDER ADULT FALLERS

Antonia Zaferiou [1,*] Laura Held [2] Witaya Mathiyakom [3]

[1]Biomedical Engineering, University of Southern California, [2]U.S. Department of Veterans Affairs, Los Angeles, [3]Department of Physical Therapy, California State University, Northridge, Northridge, United States

Introduction and Objectives: Turning-while-walking (TWW) is an essential functional activity [1]. During TWW, the horizontal trajectory of the total body center of mass (CM) is controlled relative to the base of support via resultant horizontal ground reaction forces (RFh) generated during foot contact [2]. The RFh generated by the lower extremity must be coordinated during preparation, redirection, and termination foot contacts such that the linear impulse and angular impulse (AI) requirements of the task are satisfied while maintaining balance of the CM over the base of support. Achieving these mechanical objectives during TWW can be challenging to older adult fallers, as indicated by the high incidence of falls and serious injuries sustained during TWW [3-5]. As turn speed increases, the mechanical demands required to generate both linear and angular impulse increases, which increases task difficulty, particularly for older adult fallers. An understanding of how older adult fallers generate angular impulse is currently limited, but necessary in order to improve performance of TWW in this population. The goal of this study was to identify how AI was generated during TWW. Specifically, we aimed to investigate the role of the lower extremity during preparation and redirection foot contacts in generating AI during TWW at normal and faster than normal speed. We expected that as the CM horizontal speed increased, AI generated during preparation and redirection ground contacts would increase and the redirection ground contact would generate more AI than will the preparation contact.

Methods: Six older adult fallers (ages: 65-80) participated in this study. These older adults were classified as transitionally frail [6] and had at least two falls over the period of 12 months prior to the study. At the time of data collection, they did not have any acute medical, musculoskeletal, and neurological conditions, including vestibulopathy, which would have affected TWW performance. These older adult fallers were asked to perform a series of experimental tasks of 90 degree redirections using self-selected ("normal") and "faster than normal" ("fast") speeds. Five successful trials of each task were collected. During the experimental tasks, ground reaction force (AMTI, 1200Hz) and kinematic data (Vicon, 120Hz) were captured simultaneously during preparation and redirection ground contacts. The moments applied about the CM were calculated, and used to determine angular impulse generated during each step. Between-task differences in mean angular impulse generated under each turn condition by each leg were compared using paired t-test.

Results: As expected, the majority of the AI was generated during the redirection step of TWW tasks performed at both normal and fast speed. When comparing between speeds, there was no significant difference in AI generated during the preparation step. However, during the redirection ground contact, AI was significantly greater during the fast trials compared to the normal speed (P=0.04). As a result, the horizontal CM velocity in the turn direction at the end of redirection ground contact was also greater for the fast TWW tasks compared to normal speed TWW. Additionally,

subject-specific mechanisms (e.g., RFh magnitude, direction, and/or moment arm modulation) were used to increase the peak moment applied by the redirection ground contact during fast trials.

Figure:
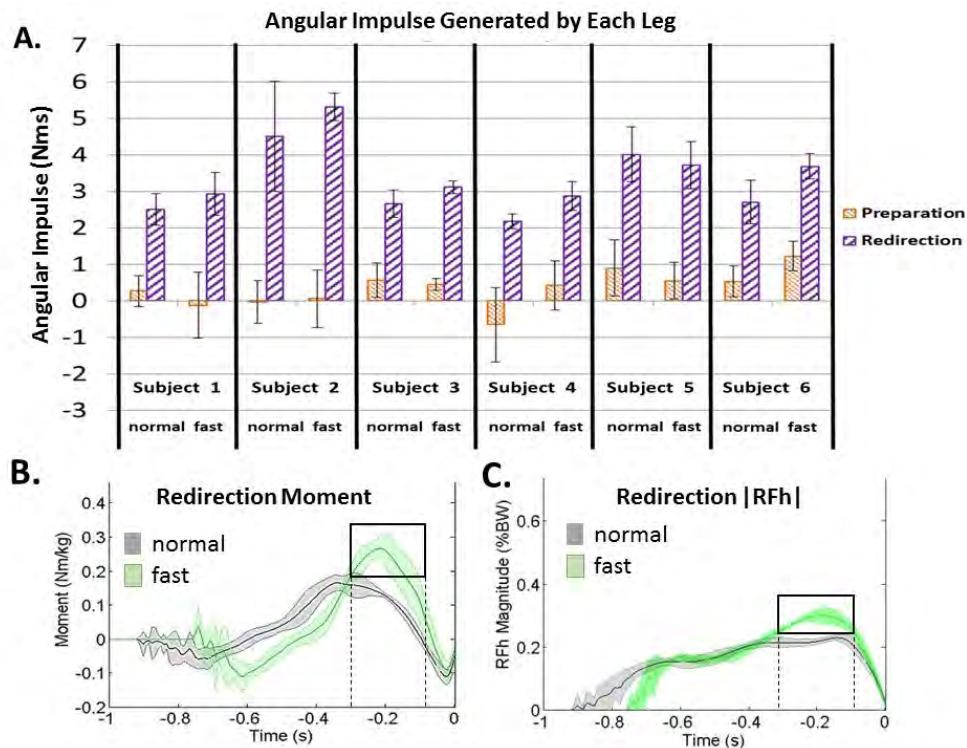
Caption: (A) Mean (SD) angular impulse generated by each subject during preparation and redirection ground contacts in each turn condition (normal vs. fast). (B) Mean (SD) moment applied by redirection ground contact for exemplar Subject 1 for each turn condition (normal vs. fast). (C) Mean (SD) redirection ground contact RFh magnitude for exemplar Subject 1 for each turn condition (normal vs. fast). The increase in mean peak moment during redirection ground contact of fast trials performed by Subject 1 (B) was mainly due to an increase of RFh magnitude (C).

Conclusion: The results of this study suggest differences in the role of each leg to generate angular impulse required for TWW performed by older adult fallers. The preparation leg contributed minimally to the AI required for the turn, while the redirection leg contributed significantly to the AI. These results also suggest that the termination ground contact must generate AI in opposition to that generated by the redirection ground contact in order to maintain the desired CM trajectory. However, further research is needed to prove this contention.

References: [1] Glaister BC et al., Gait Posture, 25(2):289-94, 2007.

[2] Patla AE, Adkin A, Ballard T., Exp Brain Res, 129(4):629-34, 1999.

[3] Stack E, Ashburn A., Physiother Res Int, 4(3):190-200, 1999.

[4] Nevitt MC, Cummings SR., J Am Geriatr Soc, 41(11):1226-34, 1993.

[5] Stevens JA, Corso PS, Finkelstein EA, Miller TR., Inj Prev,12:290–5, 2006.

[6] Speechley M, Tinetti M., J Am Geriatr Soc, 39(1):46-52, 1991.

Disclosure of Interest: None Declared

Elderly

AS-0225

EFFECTS OF STRENGTHENING AND STRETCHING EXERCISES ON RUNNING BIOMECHANICS IN OLDER ADULTS: A RANDOMIZED CONTROLLED TRIAL.

Reginaldo Fukuchi [1,*]Darren Stefanyshyn [2]Lisa Stirling [2]Reed Ferber [2]

[1]Biomedical Engineering, Federal University of ABC, Santo André, Brazil, [2]Kinesiology, University of Calgary, Calgary, Canada

Introduction and Objectives: Increases in running participation have been followed by an increased injury rate among older adults[1]. Muscle weakness and loss of flexibility have been associated with age-related changes in gait[2]. Despite the fact that flexibility and strengthening exercises to address these decrements may mitigate the effects of ageing and prevent running-related injuries[3], few studies have investigated the inter-relationship between increases in flexibility and strength and concomitant changes in gait biomechanics. Therefore, the purpose of this study was to investigate the effects of an 8-week strengthening or flexibility protocols on gait mechanics in older runners.

Methods: For this randomized controlled trial, 105 older subjects (55-75yrs) were randomly assigned to one of the three groups: strengthening (STG), flexibility (FXG) or a control group (CTG). Subjects were assessed before and after an 8-week exercise protocol. Written informed consent was obtained from each participant prior to the initial data collection. Maximal isometric voluntary contraction (MIVC) measures were obtained, using a hand-held dynamometer (HHD), for the hip abductors, external rotators, and extensors; knee extensors, and ankle plantar-flexors. Flexibility (FLX) measures were obtained by assessing the joint range of motion (ROM), using a goniometer, of the following movements: hip adduction, hip internal and external rotation and ankle dorsiflexion. Gait kinematic and kinetic measures (BIO) were obtained using a motion analysis system while the subjects ran at 2.7m/s on an instrumented treadmill[4]. The effects of exercise on the dependent variables were evaluated by a general linear mixed model (GLMM; $\alpha=0.05$) across group (STG, FXG, CTG) and time (pre-post).

Results: 93 subjects returned for their 8-week follow-up (retention rate of 88.7%). There was a significant time-effect for the majority of clinical variables, indicating that increased flexibility and muscle strength occurred following intervention. No group effect was observed for the gait or clinical variables (Table 1 and Fig.1). Few studies have investigated the effect of strength or flexibility training in older runners despite the fact that these exercises have been widely recommended to improve function and to prevent running-related injuries[5]. We speculate that the room for improvement in both flexibility and strength was limited since the older runners in the present study were already physically active. Additionally, the exercise program adopted in this study (volume, intensity, frequency, etc.) may not be sufficient to improve function in older active individuals. An increased ankle DF-PF excursion angle, Tho/Pel IR-ER excursion angle and knee ER impulse were observed following intervention but, similar to the clinical variables, these changes were irrespective of the type of exercises (Table 1 and Fig.1). We speculate that gait-related changes may be related to factors such as familiarization with testing procedures or other extraneous effects.

Figure:
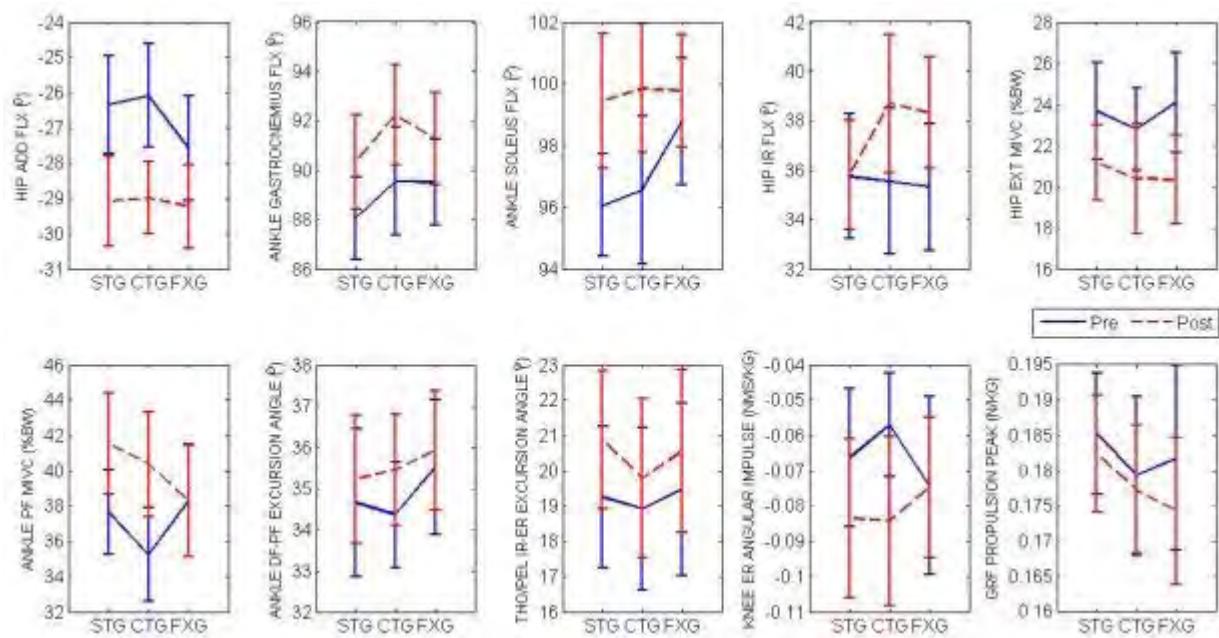
Caption: Interaction plots showing mean and 95% confidence intervals for the variables before and after intervention.

Conclusion: The results of the present study suggests that an 8-week strengthening or flexibility training protocol results in clinical improvements for these measures but did not have an influence on discrete gait biomechanical variables.

Table:

Variables	STG	FXG	CTG	Group		Time		Interaction	
				x^2	p	x^2	p	x^2	p
Hip ADD (FLX) (°)	-2.75	-1.66	-2.90	0.476	0.788	7.678	**0.006**	1.361	0.506
Ankle DF (FLX) (°)	3.36	1.00	3.30	2.512	0.285	9.766	**0.002**	1.915	0.384
Hip ER (FLX) (°)	-1.76	-0.35	-1.30	1.043	0.594	2.352	0.125	0.651	0.722
Hip IR (FLX) (°)	0.06	3.00	3.15	1.314	0.518	3.895	**0.048**	2.150	0.341
Hip ABD (MIVC) (%BW)	-0.12	-1.66	0.21	2.075	0.354	0.462	0.497	1.024	0.599
Hip EXT (MIVC) (%BW)	-2.50	-3.74	-2.41	0.588	0.745	10.379	**0.001**	0.477	0.788
Ankle PF (MIVC) (%BW)	3.88	-0.02	5.13	1.725	0.422	6.410	**0.011**	3.646	0.162
Hip ADD-ABD angle (BIO) (°)	-0.16	0.11	-0.23	0.592	0.744	0.263	0.608	0.663	0.718

Ankle DF-PF angle (BIO) (°)	0.58	0.40	1.09	0.810	0.667	8.431	**0.004**	1.624	0.444
Knee ABD impulse (BIO) (Nms/kg)	-0.03	0.03	-0.01	2.676	0.262	0.071	0.790	2.345	0.310
Knee ER impulse (BIO) (Nms/kg)	-0.02	0.00	-0.03	0.127	0.939	6.245	**0.013**	3.697	0.158
Ankle INV impulse (BIO) (Nms/kg)	0.00	0.02	0.01	0.042	0.979	1.135	0.287	0.879	0.644
Ankle ABD impulse (BIO) (Nms/kg)	-0.03	0.02	-0.04	0.970	0.616	2.107	0.147	4.248	0.120
Knee positive work (BIO) (J/kg)	0.08	0.01	0.02	0.855	0.652	1.819	0.177	1.245	0.537
Ankle positive work (BIO) (J/kg)	-0.03	-0.10	0.01	0.521	0.771	2.120	0.145	2.349	0.309
GRF propulsion peak (BIO) (N/kg)	0.00	-0.01	0.00	1.036	0.596	4.118	**0.042**	1.361	0.506
GRF vertical active peak (BIO) (N/kg)	-0.01	-0.02	-0.01	0.209	0.901	2.568	0.109	0.868	0.648
GRF max. loading rate (BIO) (BW/s)	0.33	-1.17	-1.05	0.868	0.648	2.711	0.100	3.957	0.138

Caption: Mean change (post-pre) values and GLMM statistical results ($x2$ and p).

References: [1] Fields, Curr. Sports Med. Rep., 10: 299-303, 2011.

[2] McGibbon, Exerc Sport Sci Rev, 31: 102-8, 2003.

[3] Johnston et al., Can Fam Physician, 49: 1101-9, 2003.

[4] Fukuchi et al., Clin Biomech, 29: 304-10, 2014.

Disclosure of Interest: None Declared

AS-0226

REDUCED CYCLING SPEED ALONE DOESN'T EXPLAIN DIFFERENCES IN CYCLING KINEMATICS BETWEEN OLDER AND YOUNG CYCLISTS

Rosemary Dubbeldam [1,*]Chris Baten [1][2]Jaap Buurke [1][2]Hans Rietman [1][3]

[1]Roessingh Research and Development, [2]Faculty of Electrical Engineering, Mathematics and Computer Science , Department of Biomedical Signals and Systems, [3]Faculty of Engineering Technology,   Department of Biomechanical Engineering, University of Twente, Enschede, Netherlands

Introduction and Objectives: The Dutch are a cycling nation: they get on their bikes as often as they get into their cars. Not only the young but also elderly make frequent use of their bicycles, among others for short trips to shops or friends and for longer recreational or sport trips. While cycling contributes to health and the quality of life, older cyclists have a high risk of sustaining a fall with their bicycle and sustaining a serious injury. About three-quarters of these falls are single-bicycle-accidents, accidents where no other road user is directly involved. In an ageing population where the daily kilometres cycled per elderly are increasing, it is expected that by 2020 the number of seriously injured elderly in single-accident bicycle crashes will increase to 1700 per year. Therefore, prevention of single-bicycle accidents is needed.

Multiple studies have analysed older cyclist single-accident situations and causes and have defined accident prototypes and confounding personal, infra-structural and other environmental factors. Among others, as we all know from daily observations, older cyclists cycle at low velocities and tend to sway across the roads. However, little is known about the effect of age on cycling kinematics and even less about the underlying personal accident mechanisms of older cyclists, which may play an important role in explaining the higher accident risk with increasing age. A better understanding of elderly cycling behaviour (kinematics) and accident mechanisms may in future lead to the development of safer bicycles and fall risk evaluation tools for clinicians. As a first step, this study aimed to analyse straight-forward cycling behaviour (kinematics) of older and younger adults in an ambulant setting and relate their cycling behaviour to their corresponding cognitive and physical abilities.

Methods: Fifteen young (18-40 years) and 33 elderly (65-82 years) cyclists, with and without a bicycle fall-history, participated in this study. Physical and cognitive assessments were performed and included: knee proprioception, Berg Balance Scale, handgrip strength, short-term memory and reaction time. Bicycle motion was recorded outdoors with two Inertial Measurement Units, one attached to the steer and one attached to the bicycle frame (Fig. 1). The cyclists were asked to mount the test bicycle, cycle straight for about 200 m and dismount. These tasks were performed during normal cycling, slow cycling and cycling while performing a dual-task. FUSION 3D Tools software was used to assess cycling variability by means of the standard deviation (SD) of the steer, roll and sway angle and angular velocity. The cycling velocity was calculated by integrating the longitudinal acceleration from the IMU accelerometer signal on the bicycle frame. First, differences in physical, cognitive and kinematic parameters between the groups of young and elderly cyclists were identified. Second, a multi-linear regression model was used to study the relationship between clinical and kinematic parameters (significance set at $p < 0.05$).

Results: As expected, the older cyclists demonstrated lower scores on the short-term memory tests, Berg-balance score, handgrip strength, dual task performance and Go/No-go reaction time compared to the young cyclists ($p<0.05$). For the older participants, the mean cycling velocity (9 vs. 14 km/h) was lower and the SD of the sway (1.8 vs. 1.4 deg) and roll angle (0.88 vs. 0.72 deg) were higher compared to the younger cyclists.

The linear regression model included cycling velocity and the physical and cognitive factors that were significantly different between age groups. The predictive strength of this linear regression model varied for the studied kinematic parameters: R squared values were assessed for SD of steer angle (0.141), SD roll angle (0.318) and SD sway angle (0.295). Higher variation (SD) of the steer and sway angle were significantly related to lower cycling velocities but not to physical and cognitive abilities. On the contrary, higher variation (SD) of the roll angle was significantly related to worse performance on dual task performance, handgrip strength and short-term memory tests but not to cycling velocity.

Figure:

Caption: Figure 1. Cyclist on test bicycle with inertial measurement units attached

Conclusion: The results of this study suggest that reduced cycling velocity alone does not explain observed differences between young and older cyclist bicycle kinematics. Personal cyclist abilities such as handgrip strength, short-term memory and dual-task performance influence cycling kinematics and may be predicting factors in the fall-risk of elderly cyclists.

Disclosure of Interest: None Declared

AS-0227

ARE THERE DIFFERENCES IN ELDERLY BETWEEN OBSTACLE CROSSING WITH THE PREFERRED AND WITH THE NON-PREFERRED LEG LEADING?

Eliane C. Guadagnin [1,*]Emmanuel S da Rocha [2]Maarten Bobbert [3]Jacques Duysens [4]Marco A Vaz [1]Felipe P Carpes [5]

[1]Federal University of Rio Grande do Sul, Porto Alegre, [2]Federal University of Santa Maria, Santa Maria, Brazil, [3]VU University Amsterdam, Amsterdam, Netherlands, [4]KU Leuven, Leuven, Belgium, [5]Federal University of Pampa, Uruguaiana, Brazil

Introduction and Objectives: Falls in the elderly are frequently associated with obstacle contacts during walking. Whether a person will cross an obstacle first with the preferred leg or with the non-preferred leg will vary in daily life, depending on the motor activity being developed and, in the case of crossing obstacles, depending on factors such as approach distance and space available. It might be more difficult for a person to cross an obstacle first with the non-preferred leg, and perhaps fallers will tend to fall because of obstacle contacts occurring when the non-preferred leg is leading. Only few studies have studied asymmetries in obstacle crossing (TOMAR; GUPTA, 2012; ROCHA et al., 2013). Here we compared performance of obstacle crossing in elderly with the preferred leg leading and with the non-preferred leg leading. As in daily life most people will typically be thinking of other things while walking, we had our participants performing simultaneously a cognitive task.

Methods: Volunteers participating in this study were elderly (n=20) aged 66 ± 4.4 years, body mass of 67.9 ± 14.2 kg and height of 1.54 ± 0.06 m, all able to walk independently. Participants walked barefoot at self-selected speed along an 8 m walkway and crossed a polystyrene obstacle (20 cm wide and with height defined as 20% of each subject's leg length), which was placed in the middle of the walkway, and it was always visible to the subjects. Bilateral kinematics was sampled at 200 Hz using Plugin Gait markers (Vicon Motion Systems, Oxford, UK). Kinematic data were low-pass filtered with a 4th order Butterworth filter at a cut-off frequency of 8 Hz.

The following cognitive task was used: when experimenter said "red" or "blue", the participant had to reply "no" and "yes", respectively. When the experimenter mentioned any other color name, the participant had to simply repeat the color name. Trials were recorded until 10 trials were obtained for each leg. Crossings with different leading legs were elicited by having subjects initiate walking from a standing position with either the left or the right leg. Participants did not receive any instruction concerning which leg should cross the obstacle first. Leg preference was verified using the revised Waterloo footedness questionnaire (ELIAS et al., 1998).

Leading limb toe clearance, trailing limb toe clearance, leading limb heel clearance, trailing limb pre-obstacle distance, leading limb post-obstacle distance and gait speed were determined. Data normality was verified using the Shapiro-Wilk test. The legs were compared with paired t-test at a 0.05 significance level.

Results: Leading limb post-obstacle distance was statistically larger in the preferred than the non-preferred leg (Table 1). No differences were observed between preferred and non-preferred legs for leading limb toe clearance, trailing limb toe clearance, leading limb heel clearance, trailing limb pre-obstacle distance, and gait speed.

Asymmetry in the leading limb post-obstacle distance was found in elderly performing obstacle crossing during walking at preferred gait speed and while performing a dual task. A shorter post-obstacle distance has been reported as a possible cause for tripping (the heel coming down too close to the obstacle before landing (HEIJNEN et al., 2012)). Nevertheless, most of the other kinematic variables were not different between the legs, indicating that the obstacle used can be considered as a minor factor for the risk of falling increase. To test this potential increase it would be valuable to compare elderly with and without a falling history.

Conclusion: It is concluded that the use of the non-preferred leg as the leading limb for obstacle crossing during dual task performance on a walkway mildly increases the risk of falling.

Table:

	Preferred	Non-preferred
Leading limb toe clearance (cm)	12.2±2.4	12.1±2.4
Trailing limb toe clearance (cm)	11.3±4.1	11.6±4.1
Leading limb heel clearance (cm)	10.7±2.4	9.9±2.2
Trailing limb pre-obstacle distance (cm)	11.6±1.9	11.6±2.3
Leading limb post-obstacle distance (cm)	12.4±3.9	11.0±2.9*
Gait speed (m/s)	0.9±0.1	0.9±0.1

References:

1. Elias et al., Neuropsychologia, 36(1):37-43, 1998.

2. Heijnen et al., Exp Brain Res, 223(2):219-31, 2012.

3. Rocha et al., Human Movement, 14(2):138-143, 2013.

4. Tomar; Gupta. J Neurosci Rural Pract, 3(3):324-327, 2012.

Disclosure of Interest: None Declared

Elderly

WALKING WITH A PLANTAR FLEXION ASSISTING ANKLE-FOOT EXOSKELETON IN AN OLDER POPULATION

Samuel Galle [1,*]Philippe Malcolm [1]Dirk De Clercq [1]

[1]Movement and Sport Sciences, Ghent University, Gent, Belgium

Introduction and Objectives: Walking is the most frequent way of locomotion in humans and the ability to walk has a strong influence on quality of life. With the contribution of biomechanists and physiologists in the field of robotics, assistive robotic legs (exoskeletons) that can be attached to the legs are developed to restore walking ability for subjects with reduced walking capacity. Walking capacity diminishes while getting older and when walking becomes difficult, people are dependent on walking frames, wheelchairs or mobility scooters. These devices are often unpractical and dissociate us from our natural way of interacting with our environment. Reduced walking speed in the elderly is related to reduced ankle power and therefore an ankle-foot exoskeletons that adds ankle power to the biological ankle joint seems a practical solution to improve their walking capacity. For such mobility assistance, reduction in human energy cost is the benchmark. On the other hand, the assisted walking has to remain a stable gait pattern. Previous research in 3 subjects [1] suggested that the elderly could walk with plantarflexion assistance which resulted in a reduction in metabolic cost but the number of subjects was insufficient to draw conclusions.

The objective of this study was to test if a healthy older population (age 65 or more) could walk after a short habituation with a simple pneumatically actuated ankle-foot exoskeleton with plantarflexion assistance [2], if this results in a reduced metabolic cost for powered exoskeleton walking compared to walking with normal shoes and if walking stability is influenced. This study must be seen as a necessary step towards the assistance of an older population with walking impairments.

Methods: Eight healthy subjects with no specific walking impairments and no experience with treadmill nor exoskeleton walking participated in the experiment. One subject was not able to walk with the device comfortably because of deviating walking kinematics, which resulted in reduced exoskeleton function. The seven remaining subjects (6 male and 1 female; age 69.3±3.5 years; body mass 73.1±6.9 kg; stature 170.4±6.2 cm; European shoe size 42.1±1.8) performed a 30 min habituation protocol on a first day. On a second day, subjects performed four 5-min walking intervals at 1.11 m·s^{-1} (normal shoes, unpowered exoskeleton and 2 times powered exoskeleton: Powered 1 and Powered 2). O_2 consumption and CO_2 production, subjects' perception and exoskeleton kinetics were measured for every condition on this second day.

Results: Subjects did not perceive walking on the treadmill with their own shoes significantly more difficult than overground walking and perceived exoskeleton walking during the second powered condition less difficult compared to unpowered exoskeleton walking. The net metabolic cost during walking with the powered exoskeleton was significantly reduced with 9.4±6.1% for the first powered condition and 12.0±6.9% in the second powered condition compared to unpowered walking (Fig.). This indicates that also an older population can benefit from plantarflexion assistance. However, no significant differences in net metabolic cost could be found between powered exoskeleton walking and walking with normal shoes, which is mainly due to the 9.8±8.0% increase in metabolic cost in the powered condition due to the weight and the hindrance of the unpowered exoskeleton. Recent improvements in exoskeleton design and function

have shown that this penalty could be reduced to 0 to 5%, which would result in a reduction in net metabolic cost for powered walking versus walking with normal shoes, also in an older population.

Figure:

Net metabolic power of the 4-min walking conditions
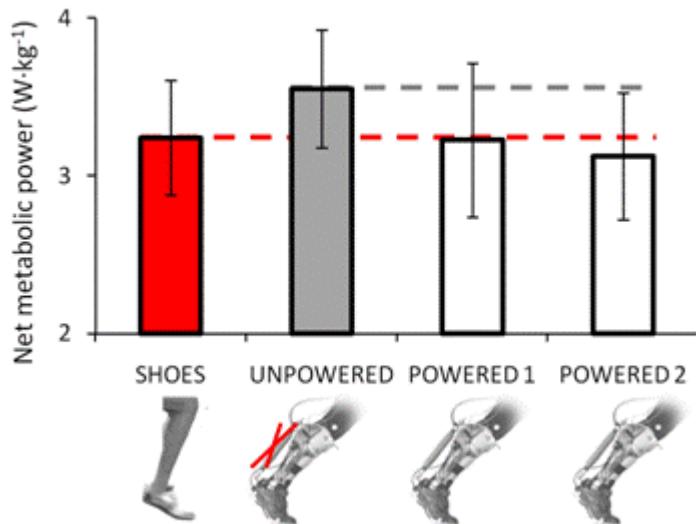
Caption: Net metabolic power for walking with normal shoes (SHOES), walking with the exoskeleton without actuation of the pneumatic muscles (UNPOWERED), a first condition (POWERED 1) and a second condition with assistance of the pneumatic muscles (POWERED 2).

Conclusion: Our findings support the introduction of (ankle-foot) exoskeletons in the elderly as we found a reduction of more than 12% for powered exoskeleton walking versus unpowered exoskeleton walking. However, not all subjects were able to walk with our standard exoskeleton with a fixed assistance algorithm and further data analysis needs to learn us how walking stability is influenced. Also, regardless of the prior habituation session there seemed to be a habituation effect during the data collection as both the reduction in metabolic cost and the perceived difficulty further reduced from the first to the second powered condition. This suggests that a more individual approach for actuation optimization and a longer habituation, together with improved exoskeleton design and hardware, could lead to reductions in metabolic cost for powered exoskeleton walking versus normal walking in the elderly and could ultimately lead to exoskeletons that can assist elderly (with walking impairments) during daily life.

References: [1] Malcolm et al., PloS One 8: e56137, 2013

[2] Norris et al. Gait Posture 25: 620-627, 2007

Disclosure of Interest: None Declared

AS-0229

ARE THE FEET AS LOCALLY STABLE AS THE CENTER OF MASS DURING WALKING?

Claude Pothrat [1,*]Marvin Dufrenne [1]Elke Viehweger [2]Eric Berton [1]Guillaume Rao [1]

[1]Institute of Movement Sciences, Aix Marseille Université, MARSEILLE cedex 09, [2]Pediatric orthopedic department, APHM, La Timone Hospital, 13005 Marseille, France

Introduction and Objectives: The goal of any locomotion task is to move the center of mass from one point to another in space. An important shortcoming of traditional gait analyses methods is that they do not consider the cyclical nature of gait. Bipedal walking is known to be naturally unstable due to micro-perturbations such as internal neuro-muscular noise, or external changes of the environment. Characterizing gait dynamic stability is essential for a functional approach including the comprehension of motor control adjustments that avoid falling. Non-linear time series analyses have been widely used to quantify local and orbital dynamic stability of locomotor tasks[1]. Studies have been conducted on the influence of various parameters on stability such as speed, footwear, type of support, pathologies, that affect the Center of Mass (CoM) stability. It is however unclear how the limbs stability is controlled relatively to the CoM stability. Look et al's result suggest during running that the lower local dynamic stability of the knee is compensated in order to maintain a better stability at the CoM. The present study aimed at investigating on the dynamic stability of gait, both at the foot and at the CoM levels. We hypothesized that, as the foot segment is the only contact with the ground, the local dynamic stability will be low compared to the CoM .

Methods: 6 men and 6 women (aged 27±3.5, height: 174±7 cm, weight: 68±10 Kg) participated in the study. Participants were asked to walk on a treadmill during 3 minutes. Walking speed was normalized using the Froude number. Participants were equipped with retro-reflective markers on both feet following Graf's protocole. The finite helical angle has been calculated for both feet between the rear- and front-foot segments, in order to get the intrinsic foot kinematics[2]. A 3D accelerometer was placed on the sacrum. 60 gait cycles were extracted from the recording, and the dynamical responses to perturbations were investigated in terms of short- and long-term Lyapunov exponents. State spaces were constructed using the delay coordinate embedding method, for each time series. The number of dimensions was calculated using a global false nearest neighbor analysis and the time delay was estimated with the first minimum of the average mutual information function. Short term (λ_{ST}) and long term (λ_{LT}) maximum Lyapunov exponent were calculated and compared between for time series data (foot Helical angle (HA) and 3D sacrum acceleration). Repeated measures ANOVA have been performed to compare foot and sacrum short- and long-term stabilities, and a Newman-Keuls post hoc test was used whenever necessary ($p < 0.05$).

Results: Increasing coefficients meant a loss of dynamic stability. λ_{ST} of the HA was 4.33±0.25 on average for right and left feet. The coefficients for the acceleration of the sacrum reached 1.1±0.09 for anteroposterior, 1.3±0.15 for the mediolateral and 1.3±0.14 for the vertical directions. No significant difference was observed between the time series for the long-term coefficient except for the mediolateral acceleration of the sacrum, lower than all the other ones (Fig 2.b).

Figure:

2.a Short term Lyapunov exponents
Local dynamic stability

2.b Long term Lyapunov exponents
Orbital dynamic stability
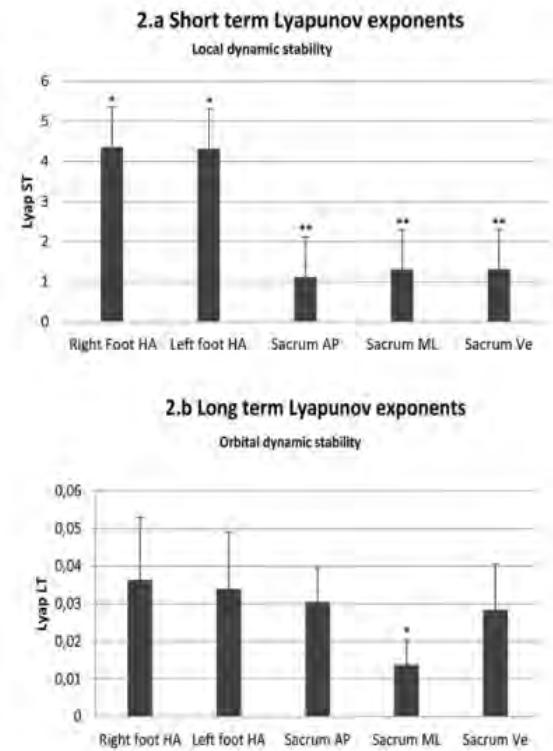
Caption: 2.a Short term Lyapunov coefficients. HA stands for helical angle, AP (AnteroPosterior), ML(MedioLateral), Ve (Vertical). 2.b shows the long term lyapunov coefficients for the same time series data. Different numbers of * means results are significantly different.

Conclusion: No difference emerged in λ_{ST} and λ_{LT} between the two feet for all the time series. λ_{ST} on the time series data of the feet were significantly higher than for the sacrum, revealing a lower stability for this segment relative to the CoM. On the contrary, no difference emerged on the long-term coefficient, with feet as stable as the sacrum. If the feet obviously handle a lot of stress during walking, the motor control system seems to be able to dissipate the short-term perturbation to remain stable over the long term. Moreover adaptations seem to be established along the kinematic chain to keep the CoM much more stable than the feet segments.

Results on the sacrum long term stability showed a significantly smaller lyapuvov coefficient for mediolateral acceleration. Considering the redundancy of the human body kinematic chain, and the number of degrees of freedom to control, the motor control system is likely to stiffen some movement in order to allow the performance of walking task. In our case, the mediolateral displacement of the CoM seems to be more controlled in terms of orbital stability. In order to keep the dynamic stability as elevated as possible at the CoM level, the motor control system seems to make limbs handle most of the short term perturbations while the system remains orbitally stable at both the CoM and limbs levels.

References: [1] Dingwell JB et al. J Biomech eng, 123(1):27-32,2001

[2] Graf ES et al., Comput Math Methods Med, 2012:368050, 2012.

Disclosure of Interest: None Declared

Feet and Footwear

AS-0231

CHANGES IN COMFORT AND HEEL CUSHIONING PERFORMANCE OF BASKETBALL SHOES WITH INCREASING SHOE USAGE TIME

Wing Kai Lam [1,*] Guoqing Wu [1][2] Hui Liu [2] Jason Tak-Man Cheung [1]

[1]Li Ning Sports Science Research Center, Li Ning (China) Sports Goods Company, [2]Department of Kinesiology, Beijing Sport University, Beijing, China

Introduction and Objectives: Basketball is one of the most popular sports in the world. Players perform an average of 70 jumps and experience up to nine times of vertical impact forces of one's body weight [1]. Impact attenuation is one of the most key functions of the basketball shoes. Previous studies demonstrated that running shoe degradation was associated with reduced cushioning performance [2,3], such information on basketball functionality (cushioning and perception) is unavailable. This study aimed to investigate the cushioning and perception performance of basketball shoes across different controlled wearing time.

Methods: Fifteen male university basketball players (age: 20.9±1.2 yrs, height: 178±3.0 cm, weight: 73.4±7.6 kg) performed five trials of drop jump landing and layup maneuvers in each of the three identical test shoes (Hard, Medium, Soft) at 0 and 18, 36, 54, and 72 hours of court training wearing time. The shoes only differed in midsole hardness at the heel region. Mechanical impact performance (peak acceleration) was measured with an impact tester (Exeter Research V2.6, USA) at each time condition (Table 1). The shoe usage condition was standardized by asking three standard shoe wearers, who were similar in age, size, weight, and playing position, to use the shoes in the same typical training sessions that included footwork, fast break, and competitive game training at the university. All shoes were randomly presented in each of the time sessions across participants.

A wooden top 900x900 force plate (AMTI, USA) was used to measure the ground reaction forces (GRF) during landing impacts for each of the two maneuvers. Perception of heel cushioning was assessed immediately after execution of movements using a Visual Analog Scale (VAS) from 0 to150 mm. The second impact peak of drop jump and the first impact peak of layup were selected to evaluate heel cushioning performance (peak vertical GRF and the maximum loading rate of vertical GRF) [4]. All variables were analyzed using a Shoe x Time (3 x 5) ANOVA with repeated measures. The significant level was set at $p < .05$.

Results: In drop jump landing, Shoe and Time effects were found for peak GRF, maximum loading rate, and heel cushioning perception. Higher peak vertical GRF and maximum loading rate with poorer perception were found for Hard shoe compared to softer shoes ($p < .05$). Meanwhile, greater peak GRF and loading rate were found for latter time conditions than the initial time condition. Players perceived better heel cushioning at 36h than 0h, 54h, and 72h conditions ($p <.05$).

For the first step of layup, Shoe and Time effects were found for peak vertical GRF and maximum loading rate while only Time effect was found for perception rating. Smaller peak vertical GRF and loading rate were found for Medium shoe compared to Hard and Soft shoe conditions ($p < .05$); Greater peak impact forces were found at 54h and 72h ($p < .05$). Better heel cushioning perception rating was found for 36h compared to 0h and 72h conditions ($p <.05$).

Figure:
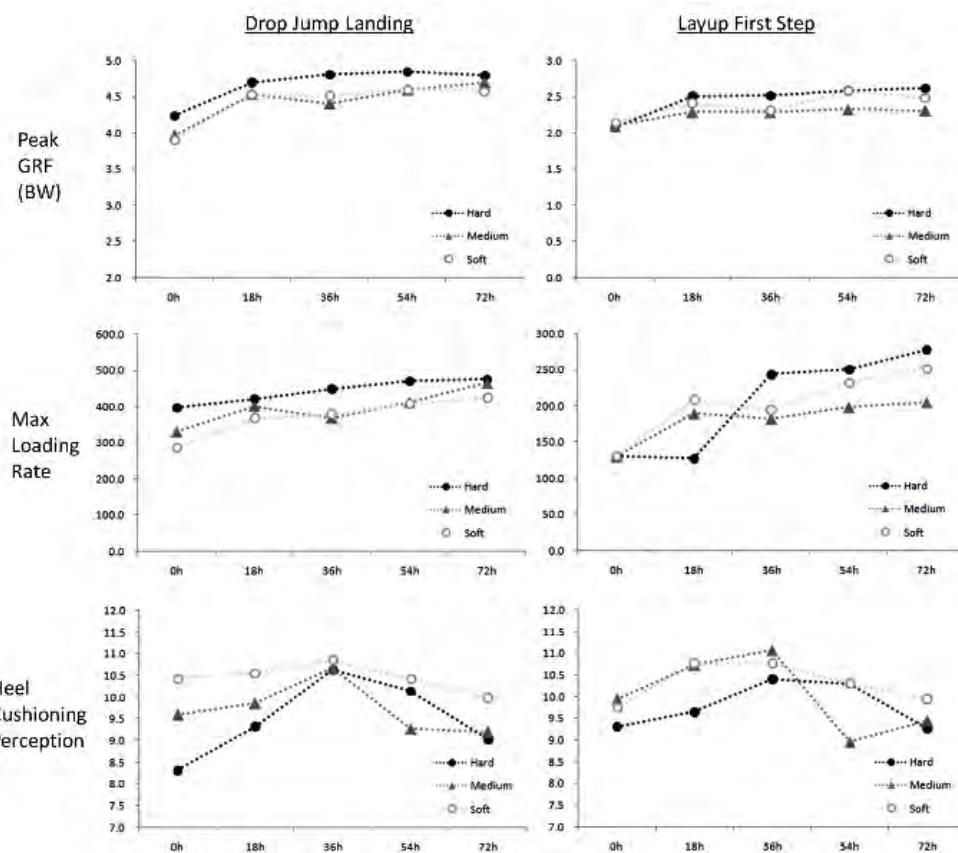
Caption: Figure 1. Peak vertical GRF, maximum loading rate of peak vertical GRF, and heel cushioning perception scores for drop jump landing and layup first step landing.

Conclusion: Increased shoe usage time would play a role in shoe comfort and cushioning performance. Hard shoe demonstrated inferior perceived and biomechanical cushioning performance than Medium and Soft shoes. Interestingly, superior shoe perception was found for the 36h condition in both tested maneuvers, suggesting that the shoe that worn after 36 hours might enable an optimal break in period for better perceived shoe fit and comfort for players. Due to the possible changes in mechanical properties and perceived comfort of footwear with varying usage time, a standard shoe accommodation period and footwear properties evaluation protocols should be implemented in footwear research especially for large scale and longitudinal studies, in which shoe usage time variation can be significant.

Table:

	0h	18h	36h	54h	72h
Hard (Asker 62C)	10.89	11.04	11.93	11.83	12.00
Medium (Asker 52C)	10.02	10.44	10.57	11.20	11.17
Soft (Asker 47C)	9.24	10.86	10.32	10.42	11.19

Caption: Table 1. Mechanical impact performance (Peak acceleration, g) across different wearing time of the three test shoes (without insole).

References: [1] McClay et al., J. Appl. Biomech., 10: 205-221, 1994.

[2] Kong et al., Br. J. Sports Med., 43: 745-749, 2009

[3] Wang et al., Footwear Science, 2: 141-147, 2010

[4] Nin et al., 5th Conference of Asia Society of Sports Biomechanics, 2014

Disclosure of Interest: None Declared

Feet and Footwear

AS-0232

BAREFOOT VS. SHOD: A COMPARISON OF LOWER LIMB MOTION DURING RUNNING

Ben Langley [1,*]Mary Cramp [2]Stewart Morrison [1]

[1]School of Health, Sport and Bioscience, University of East London, London, [2]Centre of Health and Clinical Research, University of the West of England, Bristol, United Kingdom

Introduction and Objectives: There is controversy regarding the association between running footwear and footwear-related injury [1]. In response to this, assessment of barefoot running patterns has emerged as a trend within the biomechanics literature and fuelled the debate around the impact of footwear on running biomechanics. Recent studies [1,2] have revealed significant differences between shod and barefoot running in sagittal plane hip, knee and ankle joint motion at discrete time points within the gait cycle. However, analysis of discrete events offers limited insight into the kinematic differences between barefoot and shod running patterns and relies upon the subjective selection of key variables within the waveform. Therefore, the aim of this study was to further examine differences in barefoot and shod lower limb kinematics during running using trend symmetry (TS) analysis.

Methods: Fifteen males (27 ± 5years, 1.77 ± 0.04m, 80 ± 10kg) ran at a self-selected pace (2.8 ± 0.5m.s-1) on a treadmill in barefoot and shod conditions (standardized ASICS running shoes). Kinematic data were collected using an eight camera VICON MX motion analysis system, sampling at 200Hz. Hip, knee and ankle angles were calculated using the Plug in Gait model [3]. TS analysis [4] was used to compare kinematic curves between the two conditions. TS values were calculated for each subject and averaged across all subjects. Within the TS analysis, the range offset (RO) and range amplitude ratio (RAR) were calculated. Additionally, joint angles upon initial contact (IC) and stance phase range of motion (ROM) were compared between conditions using paired t-tests and Wilcoxon matched pairs analysis.

Results: TS, RO and RAR values are reported for each joint in Table 1. TS analysis revealed highly symmetrical (TS > 0.95) kinematic patterns between barefoot and shod conditions at the hip, knee and ankle in the sagittal plane, hip and ankle in the frontal plane and the knee and ankle in the transverse plane. Knee joint motion in the frontal plane was the least symmetrical (TS = 0.87). The RO revealed small mean differences between conditions (RO < 4°). RAR scores highlight greater ranges of motion in the shod condition for all joints, apart from sagittal plane ankle joint movement. Significant (p < 0.05) differences between conditions upon IC were recorded at the ankle in all three planes. Sagittal plane knee, and transverse plane hip, knee and ankle joint motion were significantly (p < 0.05) greater in the shod condition. Sagittal plane ankle joint motion was significantly (p < 0.05) greater in the barefoot condition.

Conclusion: The aim of this study was to further examine differences in barefoot and shod lower limb kinematics during running using TS analysis. When compared over the entire kinematic waveform, barefoot and shod running patterns are generally highly symmetrical, with small mean differences (RO) between conditions. The highly symmetrical motion patterns between conditions may suggest that kinematic adaptations to barefoot running have less of an influence upon running patterns than previously suggested based upon analysis of discrete variables. Despite highly symmetrical movement patterns, the key adaptation to running barefoot appears to be an increase in ankle joint plantar flexion upon IC, which demonstrates a move towards mid- to fore-foot striking patterns within this condition. It is speculated that the

differences in joint ROM between conditions reported in this study are a direct result of the change in foot striking patterns. Previous research [5] has suggested that the changes in joint ROM between foot striking patterns, as reported between conditions within the current study, maybe indicative of changes in the shock attenuation mechanisms as a result of different loading patterns.

Table:

		TS (unitless)	RO (°)	RAR (unitless)
Hip	Sagittal	1.00 (0.00)	-1.00 (3.40)	0.98 (0.08)
	Frontal	0.98 (0.02)	-0.24 (1.79)	0.89 (0.24)
	Transverse	0.89 (0.11)	-0.74 (8.33)	0.85 (0.24)
Knee	Sagittal	0.98 (0.02)	-0.34 (3.81)	0.88 (0.14)
	Frontal	0.87 (0.14)	-0.41 (4.66)	0.75 (0.42)
	Transverse	0.98 (0.02)	2.29 (7.63)	0.83 (0.22)
Ankle	Sagittal	0.98 (0.02)	0.08 (4.80)	1.09 (0.17)
	Frontal	0.98 (0.02)	0.56 (0.94)	0.91 (0.17)
	Transverse	0.98 (0.02)	-3.29 (7.25)	0.88 (0.19)

NOTE: Positive range offset and range amplitude ratios above 1 denote greater motion in the barefoot condition

Caption: Table 1. Trend symmetry (TS), range offset (RO) and range amplitude ratio (RAR) values for the comparison of barefoot and shod foot and lower limb motion patterns, averaged over 15 participants

References: [1] Liebermann et al., Nature, 463: 531-535, 2010.

[2] Sinclair et al., Footwear Sci, 5: 45-53, 2013.

[3] Davis et al., Hum Mov Sci, 10: 575-587, 1991.

[4] Crenshaw et al., Gait Posture, 24: 515-521, 2006.

[5] Gruber et al., JSHS, 3: 113-121, 2014.

AS-0233

NORM DATA FOR BENDING AND TORSIONAL LOADS OF THE FOOT IN SHOES INCLUDING THE EFFECT OF GENDER

Annette Kerkhoff [1,*]Klaus Peikenkamp [1]

[1]Laboratory of Biomechanics, Physical Engineering, University of Applied Sciences, Münster, Germany

Introduction and Objectives: The measurement and estimation of foot loading is of great interest, especially in case of diabetes mellitus. The weight bearing of the foot has been widely measured in several studies with the help of pressure distribution systems [1]. One problem of pressure measurement is that it only measures the vertical component of the force acting on the foot. In daily life, the foot is protected and supported by shoes. Insole-Systems are used to receive information about the interaction between foot and shoe. A new system: betois (bending torsional insole system) which measures three dimensional deformations was developed. It measures bending and torsional moments between foot and shoe proximal to the Metatarsophalangeal Joint (MTP) I and V and distal to the processus calcaneus (H) with a coefficient of determination of $R^2 > 0.99$ and a linearity near 1. These moments seem to be important variables in the detection of stresses acting on the foot. Before pathological moments can be determined, data from healthy subjects must be available and the effect of gender has to be investigated.

Methods: Betois measures bending (Mb) and torsional (Mt) moments using strain gauges proximal to the caput metatarsal I and V and distal to the processus calcaneus. 53 healthy subjects (38,7y ± 11,7y) participated in this study walking at self-selected speed with the same shoe (Saucony Hattori LC) on a treadmill. After a familiarization period, data were collected with a sampling frequency of 125 Hz over one minute of walk. For data analysis, data were low-pass filtered (Butterworth, 10Hz, 2. order). Heel strike was determined using the sensor beneath the heel. Afterwards, gait cycle curves were normalized to 100 % of gait cycle (gc) (101 data points) and the mean of 30 steps computed. Mean curves and 95 % confidence bands were calculated using the bootstrap-method. Positive values represent dorsalextension and negative plantarflexion moments. In case of torsional moments positive values describe eversion and negative inversion moments. To examine the difference between the gender groups the confidence bands for the difference of the mean (CBDM) were established [2].

Results: For MTP I and V alternating bending moments were measured. At the beginning of gc a slight plantarflexion moment occurs with its maximum of -21Nmm at 21 % of gc for MTP I and –27Nmm at 28% of gc at MTP V. At terminal stance the moments act in direction of dorsalextension. MTP I reaches its maximum at 63% gc with 243Nmm. Simultaneously, MTP V reaches its maximum with 174Nmm (figure a).

The torsional moments are smaller than bending moments. At loading response a slight eversion moment occurs until 50% of gc at MTP I. Afterwards an inversion moment occurs with its maximum of 82Nmm at 62% gc. At MTP V an inversion moment is measured with its maximum of 58Nmm at 56% gc (figure b).

For the heel a sharp rising dorsalextension moment occurs with its maximum of 166Nmm at 14% gc. Then it flattens slowly until zero crossing at 61 % gc (figure a). The mean of the torsional moment is near zero with a wide confidence band (figure b).

Comparing gender groups, bending moments at MTP I and V were significantly different at mid stance with a maximum difference of 38Nmm (43% gc) at MTP I and 48Nmm (38% gc) at MTP V (figure c). There is also a slight difference for torsional moments at MTP V during loading response. Looking at the gender difference for the bending moment at the heel, significant differences occur from 17 % until 32 % gc, with men tend to have higher bending moments (max. 80Nmm, figure c). For the torsional moments significant differences can be measured from 8 % until 39 % gc (max. 83Nmm). Men tend to have higher eversion moments.

Figure:
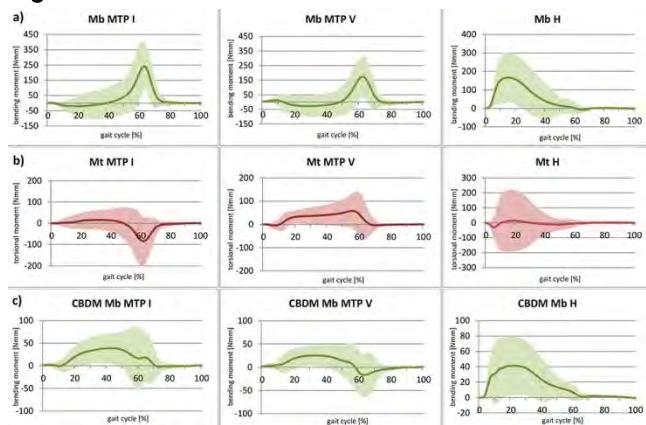
Conclusion: In this study norm data for bending and torsional loads were collected. Due to the large number of subjects and the large age range, the norm data created are representative of the loads on healthy feet. An alternating bending moment could be measured at MTP I and V. This alternating moment can be related to the deceleration before the mid-stance and push-off after mid-stance. The data show clearly a higher variability for torsional stresses compared to bending, and further investigation is needed to detect the reason for this variability. The norm curves can be used for comparing different groups of subjects, such as Diabetics with neuropathy. The examination of gender has shown that it has to be considered when comparing data. This result confirms the findings of other studies [3]. The significantly different bending moments in the middle and late stance phase indicate a gender-specific performance of the stance phase. Furthermore, the influence of other factors like age, walking speed, bodyweight or step length has to be determined.

References: [1] Owings et al.,Diabet.Med.,26:1141–1146,2009.

[2] Duhamel et al.,Gait & Posture,20:204-212,2004.

[3] Roislien et al.,Gait & Posture,30:441-445,2009.

Disclosure of Interest: None Declared

Feet and Footwear

AS-0234

LOWER LIMB BIOMECHANICS DURING THE FORWARD LUNGE: THE INFLUENCE OF A SHOE WITH IRREGULAR DEFORMATIONS OF THE MIDSOLE

Charlotte Apps [1,*] Thorsten Sterzing [2] Thomas O'Brien [1] [3] Jason Cheung [2] Mark Lake [1]

[1]School of Sport and Exercise Sciences, Liverpool John Moores University, LIVERPOOL, United Kingdom, [2]Sports Science Research Center, Li Ning (China) Sports Goods Co Ltd, Beijing, China, [3]School of Sport, Health and Exercise Sciences, Bangor University, Bangor, United Kingdom

Introduction and Objectives: The concept of motor variability has established the importance of having many motion pathways to adapt to different constraints. Constraints used as training devices to enhance variability tend to have the same dimension, and risk becoming predictable by causing similar perturbations [1]. Unstable footwear, for example, cause initial increases in movement variability that reduces with further use [2, 3]. The creation of a randomly perturbing shoe sole can be likened to moving across uneven ground, where continuous unanticipated perturbations are likely to provide an improved training stimulus [4]. Consequently, a training shoe was developed to enhance variability by causing irregular and unpredictable midsole deformations. The purpose of this study was to examine the acute effects of this shoe on the variability of lower limb biomechanics during a typical gym movement task, the forward lunge.

Methods: Seventeen young, female gym class participants completed two sets of ten right leg forward lunges in a shoe with a stable midsole (SM) and with an irregular midsole (IM). Lunge frequency (20 bpm) was controlled by a drum beat. The IM was created by attaching independent highly flexible rubber bags (sidewalls 1.5 mm) to the shoe upper at the rearfoot, midfoot and forefoot. Small ball bearings (Ø:12 mm) and cube shapes (Ø:15mm, hardness: 85A Shore, TPU material) were placed inside the bags and allowed to move independently. SM was cut to the same medio-lateral shape as the IM bags and weights were attached to match the IM sole weight with the same shoe upper.

Right lower limb joint and segment angles and velocities at touchdown and maximum values (300 Hz, Vicon Peak, United Kingdom) as well as ground reaction forces (GRF) (900Hz, AMTI, United States) were synchronized and measured. Perception of overall lunge movement variability and shoe stability were assessed (9-point Likert Scale). A paired t-test revealed no differences between the first and second set of lunges in the same midsole condition, so both sets were collapsed together. Variables were compared between IM and SM by paired t-tests ($p<.05$).

Results: Participants perceived lunges in IM as more unstable and variable. In IM, sagittal plane kinematics revealed participants adopted a flatter shoe-surface touchdown angle, less ankle dorsiflexion at touchdown and higher maximum ankle dorsiflexion (Figure 1), and reduced maximum foot-slap and knee joint flexion velocities during loading. In the frontal plane, there was a more lateral foot shoe-surface angle, more ankle inversion at touchdown, a smaller maximum ankle eversion angle and a larger frontal ankle range of motion in IM. Variability was generally higher in IM and particularly in the frontal plane of the foot (51%) and ankle (55%) maximum angles and ankle range of motion (41%) (Figure 1). Resultant landing foot velocities were similar, but the trajectory of the foot was modified such that the vertical speed was 13% greater and anterio-posterior (AP) speed reduced 30% in IM. GRF results showed 13% larger and 46% more variable vertical loading rates and a 13% reduced AP GRF integral in IM.

Figure:
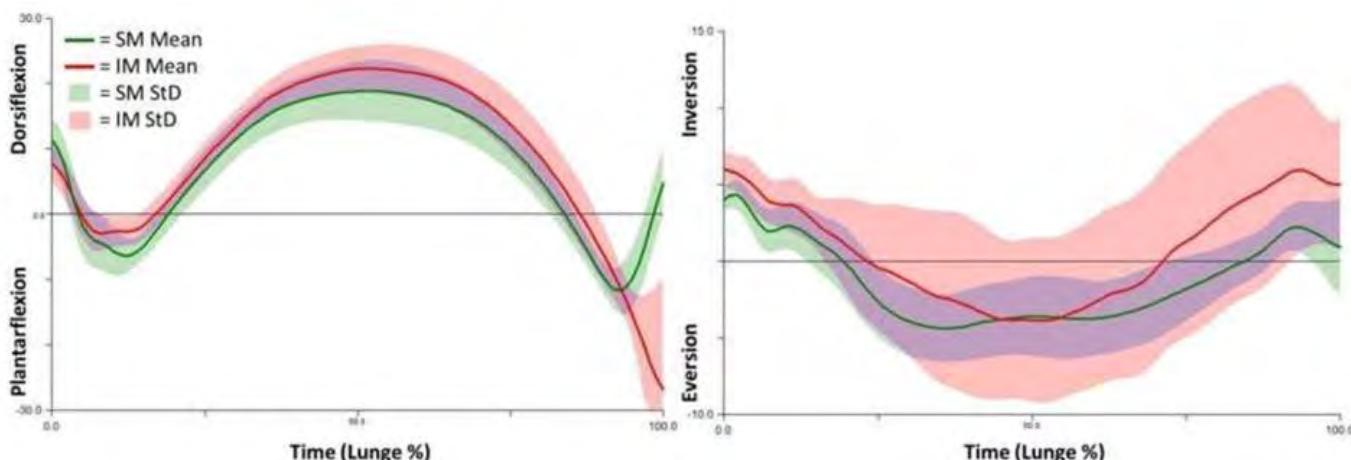
Caption: Figure 1: Mean and standard deviation (StD) of sagittal (left) and frontal (right) ankle angles during 2 sets of forward lunges in SM (green) and IM (red) of a typical subject. Time is normalised from touchdown until toe-off.

Conclusion: The irregular shoe midsole was a clear constraint to participants when performing forward lunges causing acute biomechanical and variability alterations. Foot velocities and sagittal joint angles at touchdown, and joint velocities during stance indicated a more cautious approach with IM shoe to reduce the AP GRF integral. Increased variability of initial vertical impact loading, and frontal shoe-surface and ankle angles indicates participants were unable to control these parameters. Therefore, the irregularly deforming midsole succeeded in causing increased variability of frontal plane foot and ankle movements, revealing potential to induce increased and sustained movement variability. Future work should confirm whether IM is able to maintain movement variability in the long term, through unpredictability, and explore potential lower limb training effects.

References: [1] McAndrew et al., J. Biomechanics, 43: 1470-1475, 2010.

[2] Stöggl et al., Clin Biomech, 25: 816-822, 2010.

[3] Blair et al., Footwear Sci, 5(Suppl.1): 139-141, 2013.

[4] Kim and Ashton-Miller., J. Biomechanics, 45: 1850-1853, 2010.

Disclosure of Interest: None Declared

AS-0235

PROTECTIVE CAPACITIES OF ICE HOCKEY HELMETS FOR DIFFERENT MECHANISMS OF HEAD INJURY

J. Michio M. Clark [1,*] Andrew Post [1] T. Blaine Hoshizaki [1] Michael D. Gilchrist [2]

[1]Human Kinetics, University of Ottawa, Ottawa, Canada, [2]Mechanical and Materials Engineering, University College Dublin, Dublin, Ireland

Introduction and Objectives: Mild traumatic brain injury (mTBI) is common in ice hockey and can lead to long term disability. The use of helmets has reduced the incidence of traumatic brain injuries (TBI), however the incidence of concussion has remained unaffected.[1] Current ice hockey helmet certification standards were primarily designed to mitigate the risk of TBIs. The ice hockey helmet standard employs a monorail drop device to simulate a fall to the ice. However, in ice hockey, the risk of mTBI is primarily associated with collisions and not with falls.[2] The impact characteristics of a collision are different than those of a fall. As a result, the protective characteristics of current ice hockey helmets may not adequately protect against the conditions of impact that commonly lead to mTBI. The purpose of this study is to measure the protective capacity of ice hockey helmets for different mechanisms of mTBI in ice hockey

Methods: A helmeted (ice hockey helmet) and unhelmeted 50% instrumented Hybrid III headform were impacted at two sites (Table 1) and three velocities of 3, 5 and 7m/s under conditions that represented three common mechanisms of injury in ice hockey. Falls to the ice were simulated using a monorail drop rig with a MEP anvil to represent ice. Collisions were simulated using a pneumatic linear impactor with two different strikers. A vinyl nitrile (VN) striker was used to represent a collision with a stiff elbow, and a more compliant shoulder pad striker was used to simulate shoulder-to-head impacts.[3] The impact mass was 13.1kg.[3] Three trials were conducted for each condition with the resulting accelerations used as input for the University College Dublin Brain Trauma Model (UCDBTM). Peak resultant linear and rotational acceleration of the headform was measured and maximum principle strain (MPS) in the cerebrum was calculated using the UCDBTM.

Results: The protective capacities of ice hockey helmets to reduce MPS for different mechanisms of head injury are presented in Figure 1. Comparison between mechanism of injury for linear and rotational acceleration and MPS revealed significant differences for all conditions ($p<0.05$), except for MPS when comparing falls and elbow collisions at site 1 when impacted at 3 m/s. Comparison of helmeted and unhelmeted impacts showed significant differences in linear and rotational acceleration for all conditions ($p<0.05$) with the exception of rotational acceleration and MPS of shoulder impacts at site 2 at all velocities.

Overall, the ice hockey helmet was successful in reducing the risk of brain injury from TBI magnitudes to where mTBI would be a likely result, except for velocities of impact at 7m/s.[3,4] At 7m/s the fall and elbow condition both resulted in magnitudes of response where there was a high risk of TBI. When examining the mechanisms of injury in reference to the literature,[3,4] helmets were effective at reducing the risk for both mTBI and TBI when determined by acceleration measures for falls and elbow collisions, but not for shoulder collisions. When MPS was used to determine risk, all mechanisms of injury represented a significant risk of mTBI for all velocity conditions, except for the shoulder at 3 m/s.

Figure:
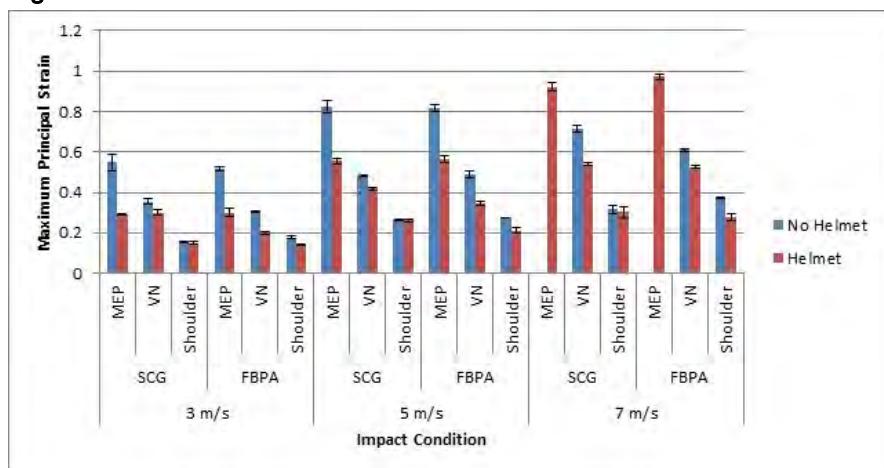
Caption: Figure 1. The protective capacity of an ice hockey for three mechanisms of head injury on maximum principle strain.

Conclusion: This study examined the protective capacities of ice hockey helmets for different mechanisms of head injury. This result demonstrates the limitations of protective capacity of ice hockey helmets across mechanisms of injury commonly occurring in ice hockey. These results suggest that to influence the incidence of mTBI in ice hockey, helmet designs and current ice hockey helmet standards need to be improved to better reflect the nature of risk within the sport.

Table:

	Location on headfrom	Impact angle
Site 1	Right intersection of the coronal and absolute	No vertical or horizontal rotation was
Site 2	Midpoint between the ant mid-sagittal and right coronal planes in absolute transverse plane	45° rotation in the transverse plane

Caption: Table 1. Impact locations and angles on the ice hockey helmet

References: [1] Wennberg & Tator, Can J Neurol Sci, *30*.206–209, 2003.

[2] Hutchison et al., Br J Sports Med, 00:1-5, 2013

[3] Rousseau P. PhD Thesis, University of Ottawa, Canada, 2014.

[4] Zhang et al., J Biomech Eng, 126:226-236, 2004.

Disclosure of Interest: None Declared

AS-0236

THE RELATIONSHIP BETWEEN HEAD ACCELERATION AND BRAIN TISSUE RESPONSE VARIABLES FOR THREE COMMON IMPACTS IN AMERICAN FOOTBALL

R. Anna Oeur [1,*]Katrina Zanetti [1]Blaine Hoshizaki [1]Michael Gilchrist [1] [2]

[1]Human Kinetics, University of Ottawa, Ottawa, Canada, [2]Mechanical and Materials Engineering, University College Dublin, Dublin, Ireland

Introduction and Objectives: Head impacts are the main cause of concussion for American football players for all levels of play [1]. The most common types of head impacts include head collisions, forearm strikes, and falls to the ground [2]. Head injury risk is measured using linear and angular head acceleration, however, resultant brain stresses and strains from finite element analysis have been proposed to be more appropriate in quantifying injury to the tissue [3]. Epidemiological research demonstrates that the nature of the accident event influences the type of concussive deficits observed in patients. A higher percentage suffered deficits from falling objects and assaults, as compared to sport impacts and motor vehicle accidents [4]. How an impact accelerates the head and injures the brain has been shown to influence the outcome type and severity [5]. The degree to which head acceleration is related to brain tissue response variables has yet to be understood for different conditions occurring in American football. An understanding of these relationships will provide information as to how concussion risk occurs. The objective of this study was to determine the correlation between peak resultant linear and angular accelerations with maximum principal strain (MPS), von Mises stress (VMS), and strain rate for three impacts in American football.

Methods: Head to head impacts were conducted at 11 m/s using a linear impactor, falls to the ground at 6 m/s using a monorail drop rig, and forearm strikes to the head at 5.5 m/s by a pendulum system. Impacts were performed at centric and non-centric sites with head dynamic response collected using a helmeted Hybrid III headform [6]. Accelerations were input into the University College Dublin Brain Trauma Model to obtain peak values of MPS, VMS, and strain rate in the cerebrum [7]. Pearson product-moment correlation coefficients (r) were calculated for each peak resultant linear and angular acceleration with peak MPS, VMS, and strain rate.

Results: Table 1 presents correlations between peak head acceleration and brain tissue results. Forearm strikes resulted in only angular acceleration having moderately high relationships with MPS and VMS. Falls showed moderately low correlations between both types of head acceleration for VMS and strain rate. All correlations for head to head impacts were found to be significant, with VMS having the strongest relationships with linear and angular acceleration. Figure 1 is an example of a chart depicting the relationship between VMS and angular acceleration. By breaking down the relationships by centric and non-centric sites, the correlation between VMS and linear (r=0.928) and angular (r=0.869) was improved for head to head impacts (p=<0.001). Similarly, angular acceleration and MPS had a stronger relationship for head to head impacts when only examining non-centric sites (r=0.910, p=0.001).

Figure:
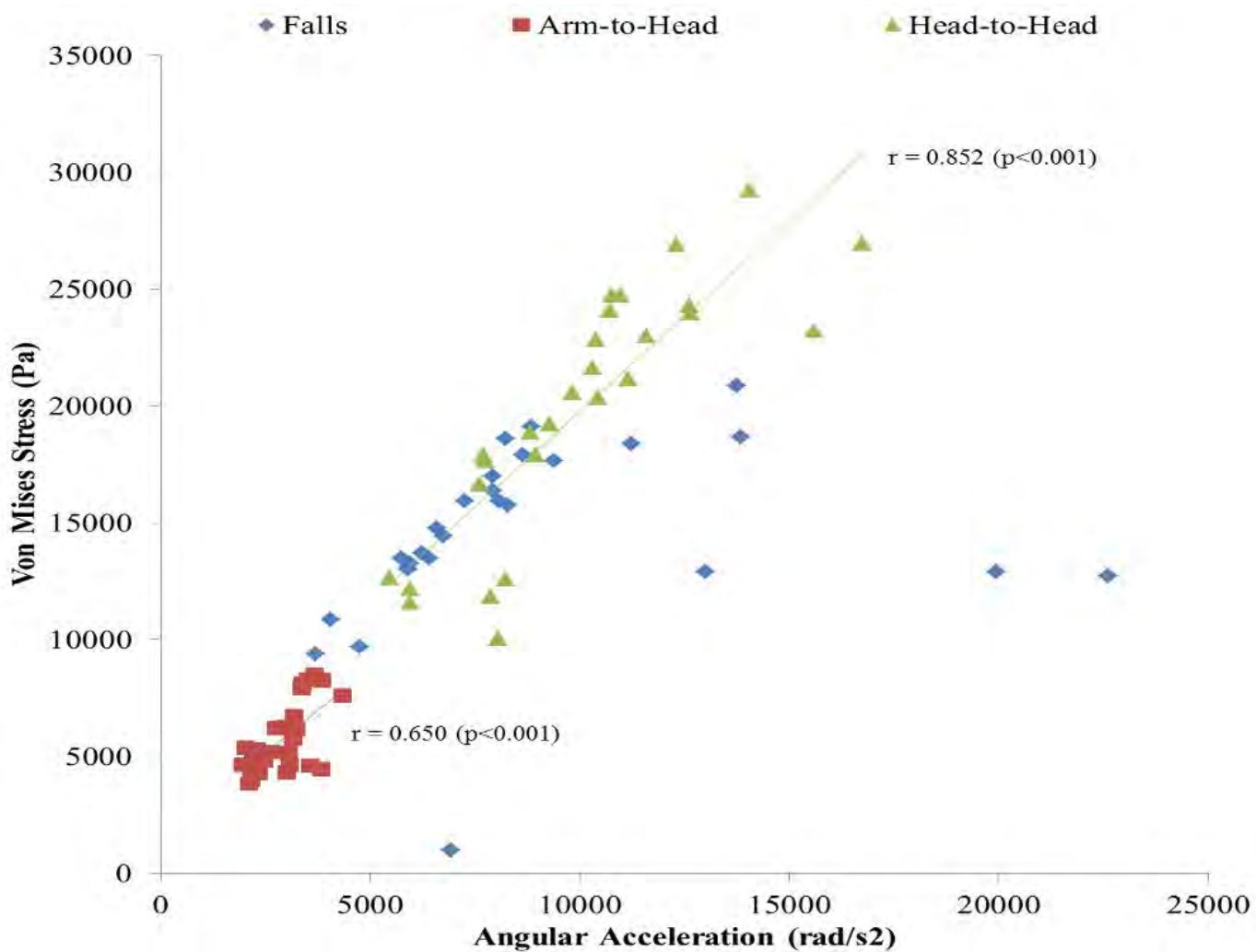
Caption: Example data chart depicting the relationship between VMS and angular acceleration

Conclusion: Strength of correlations between head acceleration and brain response is specific to impact type. Head collisions had the strongest relationships, whereas forearm strikes and falls had generally weaker and more variable correlations. The high velocity nature of head to head impacts likely caused a coupling of the head and brain responses resulting in a spread of data that was more strongly and linearly related (Figure 1). Despite falls resulting in a near complete transfer of energy to the head and brain, where one would expect coupling, there was more variability in the data for these types of impacts, which lead to weaker relationships. Arm strikes were the least severe impacts, where the responses tend to cluster. These findings support the notion that injury risk is related to how impact occurs and demonstrates the limitation of using head acceleration to characterize concussion risk across all types of impacts occurring in American football.

Table:

Head Dynamic Response	Brain Tissue Variable	Falls	Forarm-To-Head	Head-To-Head
Linear Acceleration (g)	MPS			r = 0.477
				p = 0.012
	VMS	r = 0.420		**r = 0.858**
		p = 0.029		**p = <0.001**
	Strain Rate	r = 0.495		r = 0.425
		p = 0.009		*p = 0.027*
Angular Acceleration (rad/s^2)	MPS		r = 0.705	r = 0.690
			p = <0.001	*p = <0.001*
	VMS		r = 0.650	**r = 0.852**
			p = <0.001	**p = <0.001**
	Strain Rate	r = 0.667		r = 0.647
		p = <0.001		*p = <0.001*

Caption: Pearson Correlation Results

References: [1] Daneshvar et al., *Clinics in Sports Medicine, 30*(1); 1-17, 2011.

[2] Pellman et al., Neurosurgery, 53(4); 799-814, 2003.

[3] King et al., Proceedings of IRCOBI Conference, Lisbon, Portugal, 2003.

[4] Hanlon et al., *Brain Injury*, 13(11); 873-887, 1999.

[5] Gennarelli, T.A., Acta Neurochirurgica, Suppl., 31; 1-13, 1983.

[6] Post et al., Computer Methods in Biomechanics and Biomedical Engineering, doi: 10.1080/10255842.2013.766724, 2014

[7] Horgan et al., International Journal of Crashworthiness, doi: 10.1533/ijcr.2004.0299, 2004

Disclosure of Interest: None Declared

Impact

AS-0237

UNDERSTANDING HIGH FORCE TRANSMISSION ON TRAUMA IN THE GLENOHUMERAL JOINT

David J. Hughes [1,*] Farhad Nabhani [1]

[1]School of Science and Engineering, Teesside University, Middlesbrough, United Kingdom

Introduction and Objectives: Understanding the transmission of forces through joints is crucial to all aspects to fracture prevention and repair. Until recently however, the accurate measurement of transmitted forces in the Glenohumeral joint has been difficult to calculate and define. Now, forces and moments are measured in-vivo using telemeterised shoulder implants. This method however, limits testing during high forces leading to trauma or fracture repair failure. For this reason ex-vivo testing which maintains the in-vivo loading conditions is needed to understand the non-linear dynamics of high force transmission into joints.

Methods: The Teesside Shoulder Rig is used to generate in-vivo loadings in 6 degrees of freedom simulating the supraspinatus, subscapularis, infraspinatus/teres minor, long head biceps and anterior, middle, and posterior deltoid muscles. Transferred forces and translational movement of the Proximal Humeral head are measured during a series of multi component, high impact load cases.

Results: The study shows the value of simulating and tracking force transfer through the Glenohumeral joint. During automotive rear impact loading simulations two clear forces are seen through the head, a shearing force through the coronal plane showing maximum forces of 970.5N and a compressive force into the Glenoid Fossa. Translation to the point of joint dislocation is achieved and individual muscular reaction forces measured. The joint is laterally impacted with up to 200% body weight forces showing clear force transfer into the Glenoid fossa but identifying the damping effect of the Glenoid capsule and force transfer into the coronal and sagittal planes. Stresses are calculated through the humeral head showing maximum transferred stresses of $345.4KN/m^2$ when laterally loaded.

Conclusion: The testing provides accurate and measurable results for high impact loadings in the Glenohumeral joint. Clear patterns are observed which illustrate the body's remarkable ability to distribute forces and reduce stress generation in joints through muscular management. A greater understanding of the complex force transfer patterns of the Glenohumeral joint will enable improved high impact simulation, injury prevention and protective design approaches.

Disclosure of Interest: None Declared

AS-0238

HOW DO GROUND REACTION IMPACT FORCES RESPOND TO CHANGES IN SUBMAXIMAL GAIT SPEED?

Emmanuel S. Da Rocha [1,*] Ana de David [2] Darren Stefanyshyn [3] Felipe Carpes [4]

[1]Applied Neuromechanics Research Group, Federal University of Santa Maria, Santa Maria, [2]University of Brasília, Brasília, Brazil, [3]Human Performance Lab, University of Calgary, Calgary, Canada, [4]Applied Neuromechanics Research Group, Federal University of Pampa, Uruguaiana, Brazil

Introduction and Objectives: Ground reaction force (GRF) magnitude, especially the vertical component, is widely described as proportional to locomotion speed. Although this general affirmation is true when high running speeds are considered, GRF patterns during submaximal speeds are not clearly described in the literature. As walking, fast walking and submaximal running speeds are often observed among recreational runners, in which high levels of lower extremity injuries are also described as related to impact, we wanted to know what happens with the GRF peak at heel strike when subjects are walking or running at different sub-maximal speeds. Therefore, the aim of this study was to compare the impact peak during comfortable walking, self-selected fast walking, slow running and running in male recreational runners.

Methods: Eleven recreational male runners (age 21.2 ± 1.8 years; height 1.77 ± 0.60 m; body mass 74.8 ± 5.6 kg) participated in this study. They were all rearfoot strikers, which was determined by visual inspection of their gait kinematics, training regularly without recent history of lower extremity injuries, and signed an informed consent form approved by the local ethics committee before the start of testing. All participants had recreational running experience (at least three times per week) in the last six months before the experiments.

Participants were evaluated while walking and running overground at different speeds using control running shoes (Adizero Tempo 5 M, Adidas Int.) in a single session in the laboratory. The trials started after measurement of body mass and height. Kinetic data were acquired at four different conditions as follows: (a) comfortable walking at self-selected pacing (1.61±0.11 m/s), (b) fast walking at the maximal possible walking speed (2.09±0.14 m/s), (c) slow running at a speed corresponding to 30% slower than running (2.90±0.09 m/s) and (d) running at 4.07±0.12 m/s.

The speed was measured using photoelectric cells 2 m apart (Banner Engineering Corp., Minneapolis, MN, USA) and placed just before and after the force plate. Ground reaction forces were sampled at 1200 Hz using a 3D force platform (Kistler 135 AG, Winterthur, Switzerland) in a 30-m walkway with data being acquired in the middle of the trial.

Data were filtered using a forth-order Butterworth low-pass filter (50 Hz cut-off). All walking and running waveforms were normalized to 100% stance phase. Kinetic data were normalized by body mass of each subject. Data were grouped and means and standard deviations were calculated. The peak forces at foot strike were identified for each subject.

Data normality was verified using a Shapiro-Wilk's test. An one-way analysis of variance with Tukey post-hoc when suitable was performed to determine the effect of speed on GRF. All tests were performed with SPSS 20.0 considering a significance level of 0.05.

Results: An effect of speed for the peak impact GRF was observed (F=11.65; p<0.001). Post-hoc analysis showed that the vertical GRF impact measured during running was higher than comfortable walking (P<0.01), fast walking (P<0.01) and slow running (P<0.01). Peak magnitudes of horizontal GRF were lower than observed for the vertical component.

However, effects of speed were also observed for both anteroposterior (F=34.51; p<0.001) and mediolateral (F=3.18; p=0.034) components. Anteroposterior GRF was higher during fast walking (P<0.01). For the mediolateral component, we observed differences between walking and running (P<0.01). Figure 1 shows the mean peaks for each GRF component and the average waveform for each component during stance phase. Horizontal forces did not follow a similar pattern and showed very low magnitudes when compared to the vertical component.

Figure:
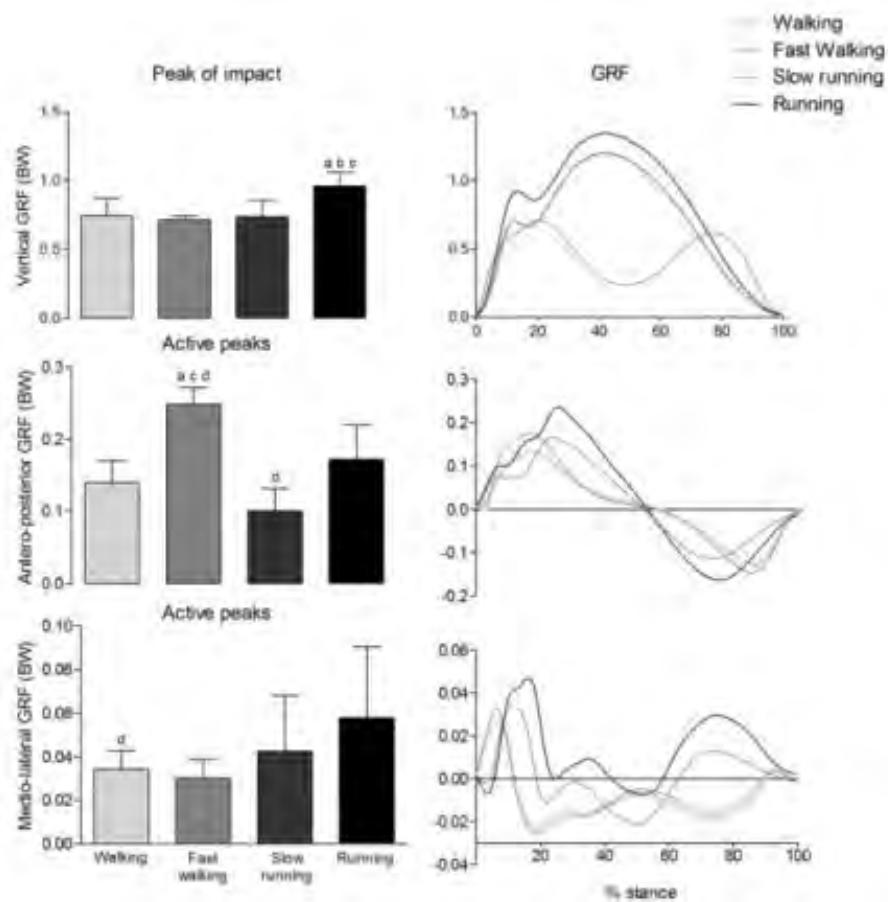
Caption: Figure 1. In the left column the average peak values for impact force, normalized to body weight, for each ground reaction force component. In the right column, waveforms representing the average pattern for each force component and each speed. Note: a – different from comfortable walking (P<0.01); b – different from fast walking (P<0.01); c – different from slow running (P<0.01); d –different from running (P<0.01). BW: body weight.

Conclusion: Walking or running at speeds lower than 4.07±0.12 m/s elicited similar peak impact forces among recreational runners evaluated in our study. Horizontal forces did not follow a consistent pattern in response to changes in gait speed.

Disclosure of Interest: None Declared

AS-0239

EVALUATING THE PROTECTIVE CAPACITY OF BASEBALL HELMETS TO CONCUSSIVE IMPACTS

Clara Karton [1,*] Andrew Post [1] T Blaine Hoshizaki [1] Micheal Gilchrist [2] Julian Bailes [3]

[1]University of Ottawa, Ottawa, Canada, [2]University College Dublin, Dublin, Ireland, [3]University of Chicago, Evanston, United States

Introduction and Objectives: Baseball is a widely participated sport, particularly in the United States in which approximately 19 million people of all ages engage each year[1]. The most prevalent and severe head injury mechanism in baseball is ball to head impacts, typically involving the batter hit by a pitch[2]. Although helmets worn by the batter protect the athlete against catastrophic injury, concussions are still being reported. The purpose of this study was to examine the protective capacity of baseball helmets from ball impacts and develop a methodology that could be used to evaluate their performance against a common cause of concussion.

Methods: The impacts were performed using a pneumatic ball launcher and an instrumented Hybrid III headform outfitted with a baseball batter helmet. The ball was launched at 35.7m/s (80mph) which was measured with a laser timegate. A video review of ball to head impacts resulting in concussion within Major League Baseball was conducted and four impact sites were chosen as commonly impacted sites. An additional three impact sites were chosen based on current standard methods, for a total of seven projectile impact sites. Four helmet models were evaluated in this research, with a new helmet used for each of three impact trials per site. The results of each impact were recorded in linear and rotational acceleration. These acceleration loading curves were then used as input for the University College Brain Trauma Model to determine the peak maximum principal strain in the brain for each impact. This variable was used as it has been found in the past to have the highest correlation with risk of concussive injury.

Results: Results for head dynamic response and brain tissue strain for the four common concussion impact sites for helmet models A-D are presented (Table 1). Statistical analyses found significant main effects between both impact site and helmet model. Impact site comparison showed significant differences, but not between all sites, which is likely a result of the high standard deviations caused by collapsing all helmet results. Helmet model analysis revealed that rotational acceleration had more significant differences than any other metric.

The magnitudes found for all sites would be in ranges that would suggest a high likelihood of concussion[3]. This could be explained by the fact that there was little difference between helmet energy absorbing liners. Interestingly helmet D, which had a very hard composite shell, produced the lowest magnitudes for 5 of the 7 impacts (sites 1- 5). Suggesting that for this type of projectile impact, having a hard shell to help distribute the forces would be desirable. This hard shell led to a lengthening the duration of the impact which engaged more foam and reduce the magnitudes of the impact, reducing risk of injury (figure 1).

Figure:
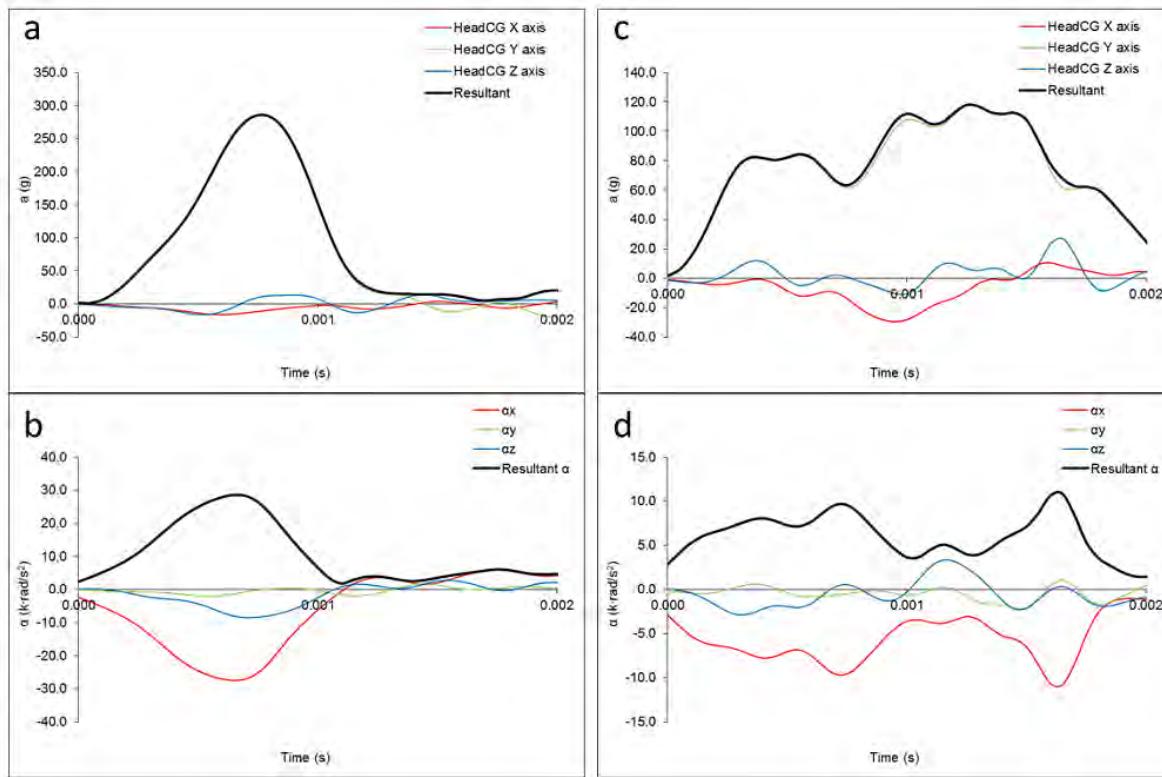
Caption: Figure 1. Comparison of the acceleration loading curves for helmet C (a and b) and D (c and d).

Conclusion: The methodology proposed used a series of impact sites that were successful in distinguishing differences in design characteristics between helmet models in dynamic and brain tissue response. In addition, at 80 mph, these sites showed a consistent high level of risk regardless of the helmet worn, indicating limited protection by these helmets for concussive impacts. The mechanism of concussion shown by this research are baseball impacts that result in very brief (2ms or less) acceleration loading curves. These curves are distinct from other sports, suggesting the understanding of concussion and development of protective helmet technologies must be specific to baseball.

Table:

		Peak acceleration			Maximum principal strain
Impact site	Helmet model	Linear (g)	Rotational (krad/s^2)		Cerebrum
4	A	192.0 (35.3)	22.9 (3.2)		0.336 (0.03)
	B	157.8 (5.8)	19.2 (0.7)		0.351 (0.01)
	C	210.5 (6.8)	23.8 (0.2)		0.328 (0.06)
	D	151.8 (18.3)	13.8 (1.7)		0.274 (0.05)
5	A	140.4 (23.4)	14.6 (3.8)		0.285 (0.008)
	B	99.7 (11.0)	8.3 (1.4)		0.244 (0.007)
	C	133.9 (15.8)	13.7 (0.9)		0.251 (0.03)

	D	94.8 (23.0)	10.4 (2.0)		0.261 (0.01)
6	A	50.3 (3.4)	5.1 (0.2)		0.192 (0.04)
	B	81.7 (13.9)	6.4 (1.0)		0.193 (0.02)
	C	67.8 (4.7)	6.3 (0.6)		0.228 (0.006)
	D	92.5 (11.4)	10.0 (1.3)		0.233 (0.01)
7	A	191.2 (24.4)	11.3 (3.7)		0.242 (0.05)
	B	96.5 (12.9)	4.8 (0.2)		0.186 (0.01)
	C	86.8 (5.0)	6.5 (1.3)		0.213 (0.04)
	D	109.4 (8.3)	6.4 (0.3)		0.197 (0.009)

Caption: Table 1. Dynamic response and brain strains for impact sites 4–7. (SD in brackets)

References: [1]   Nicholls RL et al., Sports Med, 34(1): 17-25, 2004.

[2]   Gessel LM et al., J Athletic Train, 42(4): 495-503, 2007.

[3]   Zhang L et al., J Biomech Eng, 126: 226-236, 2004.

Disclosure of Interest: None Declared

Impact

AS-0240

A COMPARISON OF STRESS DISTRIBUTION IN THE HEALTHY AND OSTEOARTHRITIS-AFFECTED EQUINE THIRD METACARPAL UNDER IMPACT LOADING USING FINITE ELEMENT ANALYSIS

Cristin Mccarty [1,*] Jeffrey J. Thomason [1] Karen Gordon [2] Timothy A. Burkhart [3] David W. Holdsworth [4] Jaques S. Milner [5]

[1] Biomedical Science, [2] Biomedical Engineering, University of Guelph, Guelph, [3] Mechanical and Materials Engineering, [4] Surgery and Robarts Research Institute, [5] Robarts Research Institute, Western University, London, Canada

Introduction and Objectives: The metacarpophalangeal (MCP) joint of horses is a valuable, large-animal model for studying bone disease of mechanical origin. Osteoarthritis (OA) in the MCP joint is common among racehorses [1] and is associated with a change in the micro-architecture of the subchondral bone and overall joint geometry [2]. Exercise-induced bone remodeling in the distal articular condyle of the third metacarpal (MC3) can cause subchondral bone sclerosis and damage to the articular cartilage. This damage weakens the joint integrity and can lead to catastrophic condylar failure that ultimately results in early retirement or euthanasia of young horses [1]. The underlying bone structure within the MCP joint is representative of the mechanical loading history (dependent on magnitude, rate and repetitiveness) sustained during high-speed racing and training [3]. Contact stress during midstance (i.e., at full joint extension) has been shown to be associated with site-specific changes within the distal end of MC3 [3]. Force magnitudes are considerably lower at impact (~2-10% of the peak at midstance), but it is known that repetitive impact can be involved in the etiology of osteoarthritis [4]. Accelerations of high magnitude and high frequency have also been shown to elicit bone changes and contribute to damage within a joint [4]. Repetitive loading under high-speed locomotion occurs 100-150 times per minute during racing and training, and imposes large stresses on the MCP joint. Characterization of stresses associated with the loading conditions at all stages of the stance is essential in understanding the biomechanical causes associated with the changes in bone tissue. Given the complexities that are associated with measuring the joint forces and contact areas *in vivo*, computational models, specifically finite element models, are practical alternatives. Finite element modeling (FEM) provides a non-destructive method for predicting the stresses and strains in structures that have complex geometries, specific material properties and that are subjected to complex loading patterns. Finite element modelling has been used within equine research to examine the stress distribution at midstance in the hoof [5], proximal phalanx [6], third metacarpal [6] and entire distal forelimb [7]. While these studies have provided valuable data including the stress distribution within the MCP joint under quasi-static loading associated with midstance, there is no equine FEM that examines the effect of impact loading. Therefore, the purpose of this study was to create two subject-specific, three-dimensional, finite-element models of the equine MCP joint (one with advanced OA and one healthy) and compare the stress distribution patterns under impact loading in each model.

Methods: Two right MCP joints (third metacarpal and proximal phalanx) were scanned using micro-computed tomography (μCT). Images were segmented, and meshed using modified 10-node quadratic tetrahedral elements. Bone material properties were assigned based on the bone density. An impact velocity of 3.55 m/s was applied to each model and contact pressures and stress distribution were calculated for each. In a separate iteration, the third metacarpal was loaded statically. A sampling grid of 160 equidistant points was superimposed over selected slices, and average peak

stresses were calculated for 6 anatomical regions. Within-region maximal peak and average von Mises stresses were compared between healthy and OA bones in both midstance and impact loading.

Results: Average impact stresses across all regions, in both locations (palmar and dorsal) were greater in the OA model (Figure 1). Highest impact stresses were located in the dorsal medial condyle in the healthy (12.8 MPa) and OA (14.1MPa) models, and were lowest in the palmar medial and lateral parasagittal grooves in the healthy (5.94 MPa) and OA (7.07 MPa) models. The healthy static model had higher peak (up to 49.7% greater) and average (up to 38.6% greater) stresses in both locations and across all regions compared to the OA static model.

Figure:
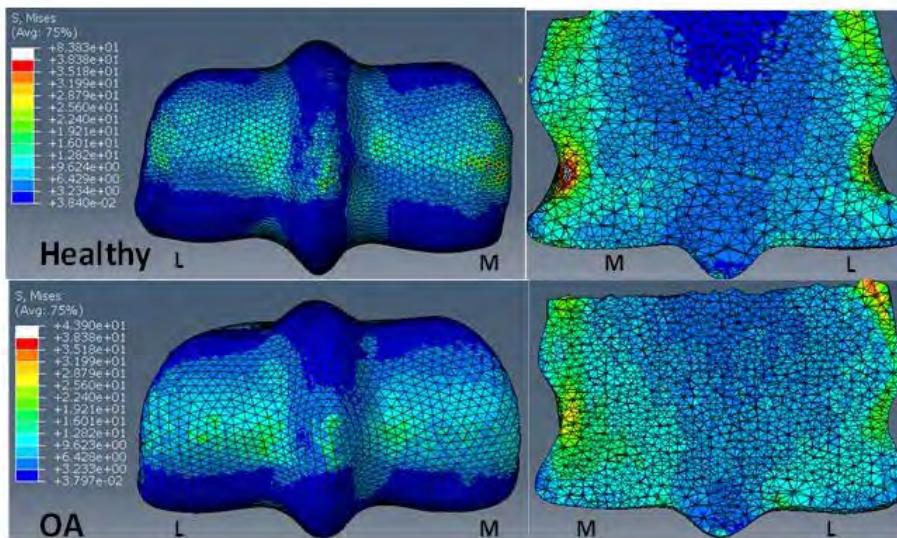
Caption: Figure 1: Comparison of von Mises (MPa) surface stress (left) and a lateromedial slice of von Mises stress (right) between healthy and OA models under impact loading. M: Medial, L: Lateral

Conclusion: Impact loading creates stresses similar to those found during midstance and both loading conditions are likely to contribute to the repetitive stress that overtime lead to OA within the MCP joint. Both impact and static loading should be considered for future studies involving joint mechanics in the context of injury causation.

References: 1. Parkin TDH, et al., Vet J.171(1):157-65, 2004.

2. Easton, KL., PhD Thesis, Colorado State University, 2012.

3. Young BD, et al., Am J Vet Res 68: 841-849, 2007.

4. Radin EL, Paul IL., Arthritis Rheum 14: 356-362, 1971.

5. Hinterhofer C, S., et al. Equine Vet J 33: 58-62, 2001.

6. Harrison SM, et al., J Biomech 47: 65-73, 2014.

7. Collins S, M., et al. Equine Vet J 41: 219-224, 2009.

Disclosure of Interest: None Declared

Neurological and Motor Control

AS-0241

FACILITATED SOLEUS H-REFLEX AND NORMAL GAIT VARIABILITY DURING WALKING IN PEOPLE WITH KNEE OSTEOARTHRITIS

Tine Alkjaer [1,*]Helle Dalsgaard [1]Peter C. Raffalt [1]Erik B. Simonsen [1]Nicolas C. Petersen [2]Henning Bliddal [3]Marius Henriksen [3]

[1]Department of Neuroscience and Pharmacology, [2]Department of Neuroscience and Pharmacology & Department of Nutrition and Exercise, University of Copenhagen, Copenhagen N, [3]Clinical Motor Function Laboratory, The Parker Institute, Department of Rheumatology, Copenhagen University Hospitals, Frederiksberg, Denmark

Introduction and Objectives: Osteoarthritis (OA) of the knee is very common [1] and associated with significant pain and mobility limitations. Walking is a fundamental movement, which enables humans to ambulate independently and walking disability has been independently associated with higher all-cause mortality in people with knee OA [2]. Adequate function of the knee joint is critical for normal walking performance and may be impaired by knee OA. Numerous studies have compared neuromuscular and biomechanical aspects of walking in people with knee OA with those of healthy controls suggesting different muscle activation, kinematic and/or kinetic patterns. These differences in neuromuscular and biomechanical aspects of walking could link to differences in basic movement control strategies that can be determined from basic neuromechanical assessments, such as the soleus (SO) Hoffmann (H)-reflex [3] and altered gait pattern variability [4]. Thus, in the present study we assessed the SO H-reflex modulation during walking and gait variability in patients with knee OA and in healthy controls. The purpose was to test the hypothesis that the excitability of the SO H-reflex would be facilitated and that the gait pattern regularity would be increased in patients with knee OA compared with healthy age-matched subjects.

Methods: We included patients with a clinical diagnosis of knee OA (radiographically verified) from the OA outpatient clinic at Copenhagen University Hospital Bispebjerg and Frederiksberg. Healthy age-matched volunteers were recruited among colleagues and relatives of employees at the University of Copenhagen. The experiment consisted of two parts: 1) Assessment of soleus (SO) H-reflex modulation during walking and 2) assessment of the temporal structure of kinematic gait pattern (i.e. regularity) and muscle activities during walking. The SO Hoffmann (H)-reflex modulation was assessed during treadmill walking due to the method described in [3]. In separate trials the kinematic gait variability was assessed from goniometry of the ankle and knee joints. The regularity of the kinematic gait pattern was assessed by sample entropy. In addition, muscle activities of ankle and knee joint muscles were recorded. The subjects were asked to walk continuously for 6 min on the treadmill at 3.5 km/h, while the muscle activity and goniometer signals were recorded. The sampling was triggered by a footswitch placed under the heel.

Results: Fifteen OA patients (females) met the inclusion criteria and were invited to participate in the study. Eleven OA patients accepted the invitation while four patients were unable to participate for logistical reasons. Eleven healthy age-matched female subjects were recruited as controls. The SO H-reflex excitability was significantly increased in the knee OA group around heel strike when compared with the controls (Fig. 1). The mean group difference in the H-reflex in the

initial part of the stance phase (control – knee OA) was -6.6 %Mmax (95% CI: -10.4 to -2.7, p=0.041). No statistically significant mean group differences were observed in the kinematic gait pattern regularity or muscle activity.

Figure:
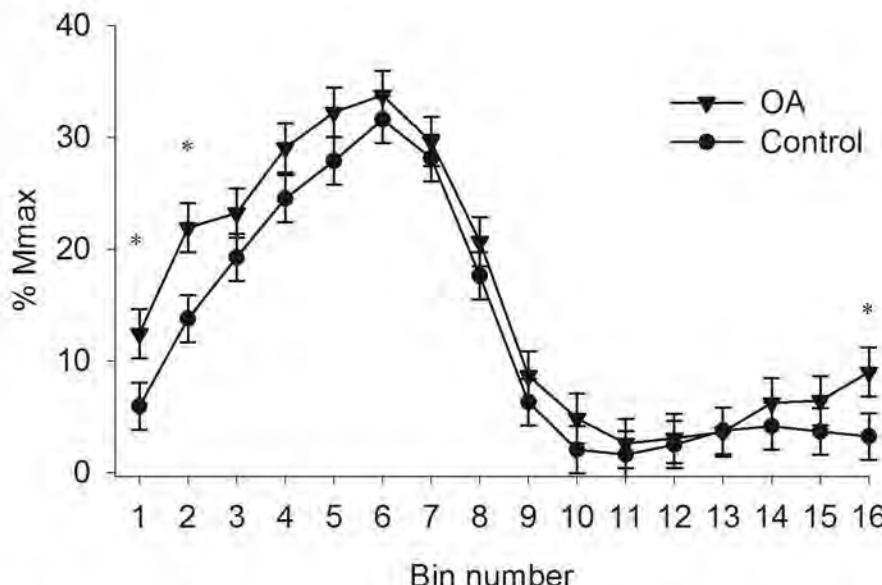
Fig. 1 The SO H-reflex modulation over the gait cycle averaged in 16 bins (stance phase bin 1-10 and swing phase bin 11-16) of the OA (filled triangles) and control groups (filled circles). Error bars are ±SE. Asterisks indicate statistical significant differences between the groups at p<0.05.

Conclusion: We suggest that these results reflect that the OA group walked according to a neural strategy favoring protection against loading induced pain in the loading acceptance phase of the gait cycle. This indicates that the OA group increased the excitability of the plantarflexor stretch reflex as a preparatory mechanism to avoid sudden pain induced quadriceps inhibition during walking that may result in episodes of "giving way" of the knee joint which are common in knee OA.

References: [1] Lawrence et al., Arthritis and Rheumatism 58: 26-35, 2008.

[2] Hawker et al., PloS one 9: e91286, 2014.

[3] Simonsen et al., J Phys 515 (Pt 3): 929-939, 1999.

[4] Stergiou et al., Hum Mov Sci 30: 869-888, 2011.

Disclosure of Interest: None Declared

EMG

AS-0243

SUBJECT-SPECIFIC INTRINSIC AND EXTRINSIC THUMB MUSCLE ACTIVITY DURING FUNCTIONAL TASKS OF DAILY LIFE

Faes Kerkhof [1,*] Gertjan Deleu [1] Priscilla D'Agostino [1] Evie Vereecke [1]

[1] Development and Regeneration @ Kulak, Leuven University, Kortrijk, Belgium

Introduction and Objectives: The trapeziometacarpal (TMC) joint is subjected to severe compressive forces during manual tasks which are for a large part due to muscle contraction. Furthermore, muscles surrounding the TMC joint are important stabilizers of this highly mobile, and intrinsically unstable, joint. On the other hand, joint instability and high compressive forces have been linked to the onset of osteoarthritis (OA), suggesting that the muscles surrounding the TMC joint play an important role in the development of TMC OA. The aim of this study is to explore if specific muscle activation patterns can be found during a lateral key pinch, power grasp and jar twist task to eventually relate those to joint loading.

Methods: Isometric forces and fine-wire electromyographic (fEMG) activity produced by 4 intrinsic thumb muscles (m. abductor pollicis brevis, m. adductor pollicis, m. flexor pollicis brevis, m. opponens pollicis) and 4 extrinsic thumb muscles (m. extensor pollicis brevis, m. extensor pollicis longus, m. abductor pollicis longus, m. flexor pollicis longus) were measured in 11 healthy female volunteers. Muscle activity was captured using an 8 channel Delsys wireless system. Pairs of disposable hooked wire electrodes were inserted by a certified hand surgeon using an ultrasound guided technique.

Isometric force data were collected using a load cell embedded in a custom-made polycarbonate jig. The participants performed isometric contractions for 5 seconds during a key pinch, a power grasp and a jar twist task. They were instructed to perform two maximal isometric contractions and one contraction at 80% of their maximal force per task. The tasks were executed with and without EMG recording to verify if electrode placement influenced force production.

The raw EMG signals were filtered (10 Hz, high pass 2nd order Butterworth) and the full wave was rectified using EMGworks 4.0 analysis software. Normalization was achieved by using the highest EMG amplitude per muscle and per subject.

A Wilcoxon signed-rank test was used to statistically test the difference between the normalized intrinsic and extrinsic muscle activity. A paired t-test was applied to compare the generated force pre- versus post-electrode insertion.

Results: A high interindividual variability in muscle activity was seen in all three tasks. In both the maximum effort as well as the 80% effort, no significant differences in activation between intrinsic and extrinsic muscles were found in the pinch or grasp task ($p \geq 0.05$). However, the maximal effort jar twist task resulted in a significantly higher activation of the intrinsic compared to the extrinsic muscles ($p = 0.003$).

Insertion of the fEMG electrodes appeared to significantly decrease the external force production in all tasks during both maximum and 80% effort contractions (table 1).

Conclusion: The thumb muscles display a high interindividual variability in muscle activity during functional tasks of daily life, such as pinch, grasp and jar twist. The results of this study suggest that to produce a substantial amount of force, a well-integrated, but subject-specific, co-contraction between the intrinsic and extrinsic thumb muscles is necessary. Despite the variability, these findings can be used as input for an EMG-driven musculoskeletal model. Further research

will focus on how differences in muscle activation patterns influence joint loading and if this could contribute to the onset of trapeziometacarpal joint osteoarthritis.

Table:

Effort	Task	Force Before (N)	Force After (N)	p-value
Maximum	Grasp	119.04±26.38	97.13±23.67	p<0.001[1]
	Pinch	100.96±27.45	75.85±17.34	p<0.001[1]
	Jar twist	148.97±45.14	112.24±43.65	p<0.05[1]
80%	Grasp	82.95±20.24	73.04+18.29	p<0.05[1]
	Pinch	72.30±18.87	58.58±14.53	p<0.05[1]
	Jar twist	100.69±27.98	82.24±31.50	p<0.05[1]

Caption: Table 1. Exerted force during maximum and 80% effort for each task, before and after insertion of the fEMG electrodes (values are mean ± SD). 1 Significant difference in produced force before and after electrode insertion at P<0.05

Disclosure of Interest: None Declared

Neurological and Motor Control

AS-0244

MOVEMENT CONTROL DURING ACTIVE SPINAL RANGE OF MOTION IS ACHIEVED BY A DIFFERENTIAL USE OF ECCENTRIC AND CONCENTRIC MUSCLE ACTIVITY

Stephanie Valentin [1,*] Theresia Licka [1]

[1]Movement Science Group, Equine Clinic, University of Veterinary Medicine Vienna, Vienna, Austria

Introduction and Objectives: Neuromuscular control of the rectus abdominis (RA), obliquus internus (OI), obliquus externus (OE), and erector spinae (ES) muscles has been widely investigated during a range of conditions such as perturbations [1], stability exercises [2], gait [3] and other functional exercises [4] using electromyography (EMG). However, little attention has been paid to activity of these muscles during spinal range of motion exercises, in particular in a 4-point kneeling posture (4P), even though this posture is often adopted for low back pain exercises. The aim of this study was to investigate the concentric and eccentric activity of trunk muscles during active spinal range of motion exercises in young and mature healthy adults in two postures.

Methods: Twenty-four healthy participants (12 young, aged 18-25 years; 12 mature, aged 45-60 years) were included. Reflective markers were attached over the spinous process of the 11th thoracic vertebra (T11), the head, the left and right styloid processes, and lateral femoral condyles. Three-dimensional kinematic data were collected using 10 high speed cameras (Eagle Digital Real Time System, Motion Analysis Corp., 120Hz). Surface EMG electrodes (Delsys Trigno, 1200Hz) were attached over the left and right ES, RA, OE, and OI after skin preparation. Data were collected during three repetitions of 10s of flexion and extension movements in U and 4P. Participants were instructed to perform each movement to their end range and return to the starting posture in one fluent movement. Raw EMG data were resampled, rectified, zero-mean offset, and a 4th order low pass Butterworth filter applied. Processed EMG data from 0.5s before movement onset and 0.5s after movement cessation (both based on vertical T11 movement) were included for analysis. EMG data were normalised to the maximally observed muscle activity from any trial and movement for each muscle, and the maximum and 1st, 2nd, and 3rd quartiles (Q1, Q2, Q3) calculated for the concentric and eccentric phase of muscle activity. Due to non-normally distributed data, differences between concentric and eccentric activity were compared for Q1, Q2 and Q3 in the young and mature groups separately using a Wilcoxon Rank test.

Results: Significant differences were found for every muscle and quartile, although this was dependant on age group, posture adopted and movement direction. Where significant differences occurred in 4P, concentric activity was greater than eccentric activity for flexion and extension in both the young group (flexion: RA left Q1, all abdominal muscles Q2 and Q3; extension: ES Q2 and Q3, RA and OE left Q1 and Q2, OI all quartiles; all $p<0.05$) and mature group (flexion: ES left all quartiles, ES right Q1, all abdominals Q3, RA right and OI left Q2, extension: ES Q2 and Q3, OI and OE Q1 and Q2, OI right Q3; all $p<0.05$). However, for both age groups in U during flexion, concentric activity was significantly greater than eccentric activity for ES in all quartiles, but eccentric activity was significantly greater than concentric activity in the abdominal muscles (young group: OE left Q1, OI right all quartiles; mature group: OE left Q1 and Q2, OE right Q2 and Q3, OI left all quartiles; all $p<0.05$). The opposite was found for extension, where eccentric activity was significantly greater than concentric activity for ES but only in the young group (all quartiles; $p<0.05$), and concentric activity was

significantly greater than eccentric activity in the abdominal muscles (young group: OE left Q3, OI Q1 and Q3; mature group: RA Q3, OE and OI left Q1, OE right and OI Q3; all p<0.05).

Conclusion: Muscle activity is generally larger during concentric than during eccentric muscle use [5]. However, the overall findings from this study would indicate that antagonist muscle activity is usually greater during the concentric phase and agonist muscle activity is greater during the eccentric phase during active range of motion exercises in U. This is in contrast with 4P, where concentric muscle activity was greater than eccentric activity in both agonists and antagonists. These findings were identified in both age groups. Probably the effect of gravity in U reduces the need for concentric activity during active range of motion exercises and the eccentric activity, which provides control and deceleration during approach of the neutral posture, plays a more important role. The results of this study may be of relevance when selecting range of motion exercises in a low back pain rehabilitation setting.

References:

[1] Kanekar et al., Exp Brain Res, 232: 1127-36, 2014.

[2] Ekstrom et al., J Orthop Sports Phys Ther, 37: 754-62, 2007.

[3] Hu et al., Hum Mov Sci, 31: 880-96, 2012.

[4] Lee et al., Ann Rehabil Med 37: 804-13, 2013.

[5] Qi et al., J Electromyogr Kinesiol 21: 1056-1063, 2011.

Disclosure of Interest: None Declared

EMG

AS-0245

THE ASSESSMENT OF BRACHIALIS MUSCLE ACTIVATION WITH SURFACE ELECTROMYOGRAPHY

Didier Staudenmann [1,*]Wolfgang Taube [1]

[1]Movement and Sport Science, Department of Medicine, University of Fribourg, Fribourg, Switzerland

Introduction and Objectives: The brachialis muscle (BR) represents an important elbow flexor and its activity has so far mainly been measured with intramuscular electromyography (EMG). In contrast to the biceps brachii (BB) that inserts into the radius (biceps tubercle) and is thus active during elbow flexion and forearm supination, the BR inserts into the ulna and therefore exclusively contributes to flexion force. Consequently, pure elbow flexion should result in activity in both BB and BR whereas elbow flexion with superimposed forearm supination (flexion+supination) should preferentially activate the BB – provided that recordings in BR are not contaminated by the neighboring BB muscle. Thus, the aim of this study was to examine whether the activity of the BR can be assessed with surface EMG without interference from the BB.

Methods: With eight subjects we measured surface EMG of the arm flexor synergists BR, BB, and brachioradialis (BRR) during two isometric voluntary contraction types (see Figure): 1) pure elbow flexion and 2) flexion+supination. The correlation coefficients between EMG amplitudes and flexion force (supination torque) were determined.

Results: During pure flexion the activities of all synergists were similarly correlated with the flexion force (r=0.96±0.02; p=0.075, see Figure). During flexion+supination the activity of the BR was significantly distinct from the activity of the BB (p<0.01), with a 14% higher correlation for the BR with the flexion force and a 40–64% lower correlation with the supination torque. The BB predicted supination torque substantially better than the BR and BRR (r=0.93±0.02; p<0.01).

Figure:
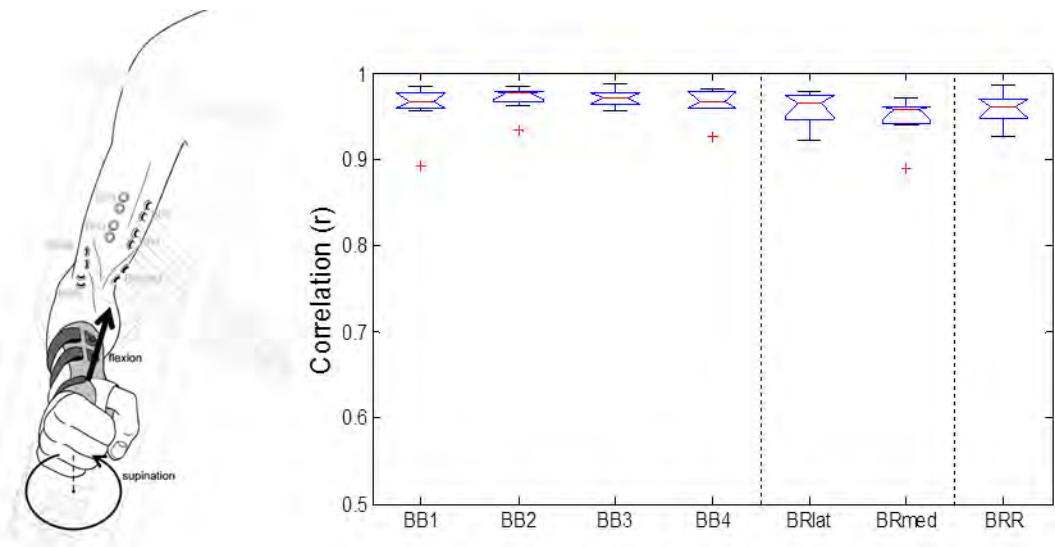
Conclusion: The muscles generating an elbow flexion are the BB, BR and BRR, with a major contribution from the BR. However, it was not clear so far, whether it is possible to record activity of the BB with surface EMG without interference from BR. The current results indicate a clear distinction between BB and BR as activity in these synergistic muscles was similarly well correlated to flexion force in the first contraction type (pure flexion) but different for the second contraction

type (flexion+supination). It can therefore be concluded that the activity of the BR can be assessed with surface EMG without substantial interference from the BB.

Caption: Figure: Left: Position of the right arm during isometric elbow flexion (forearm supination) with electrode over biceps brachii (BB), brachialis (BR) and brachioradialis (BRR). Right: correlation between EMG amplitude and elbow flexion for the different muscle sites.

References: [1] Staudenmann et al., J. Electromyogr. Kinesiol, submitted.

Disclosure of Interest: None Declared

Neurological and Motor Control

AS-0246

THE EFFECT OF FEAR OF FALLING AND VESTIBULAR SENSORY FEEDBACK ON POSTURAL CONTROL KINEMATICS

Jonathan de Melker Worms [1,*]John Stins [2]Peter Beek [2]Ian Loram [1]

[1]Faculty of Science and Engineering, School of Healthcare Science, Manchester Metropolitan University, Manchester, United Kingdom, [2]MOVE Research Institute Amsterdam, Faculty of Human Movement Sciences, VU University Amsterdam, Amsterdam, Netherlands

Introduction and Objectives: In the elderly, fear of falling is associated with an increased risk of falling. In this study we focus on direct effects of fear of falling and vestibular sensory feedback on full body postural control. Using galvanic vestibular stimulation (GVS) sensory information from the vestibular nerve is modified, causing increased body sway [1]. The literature shows inconsistent effects of fear of falling and vestibular sensory feedback on postural control. Using kinematic data Osler et al. [1] inferred that induced body sway within 800 ms after GVS onset is unaffected by fear of falling, by comparing subjects standing at height and at ground level. Conversely, using a continuous stochastic GVS signal (SVS) and recording ground reaction force (GRF) data, Horslen et al. [2] found increased SVS-GRF coupling at height compared to ground at 2 time points in the early time domain. The time points were termed short latency peak (SLP) at ~150 ms and medium latency peak (MLP) at ~ 300 ms of delay. We aimed to investigate the kinematic mechanism of the SLP and MLP processes identified in the SVS-GRF coupling. Using full body kinematics we investigated the effect of fear of falling on the timing of the GVS response of the whole kinematic chain.

Methods: For 16 young healthy adults (10 men and 6 women, age: 25.9 ± 5.1 years, height: 1.74 ± 0.1 m, weight: 69.5 ± 13.5 kg, BMI: 22.9 ± 3.5) vestibular-evoked balance responses were studied while standing on a narrow walkway at ground level and at a height of 3.85 m to induce fear of falling (Fig. 1A). In the height condition some participants appeared to have difficulty to leave the safety of the first floor mezzanine and step onto the exposed walkway. Full-body kinematics was collected (Vicon Motion Systems Ltd., Oxford, UK) and skin conductance was recorded during all trials as a measure of physiological arousal. GVS was delivered using carbon rubber electrodes (46 by 37 mm) placed in a binaural bipolar configuration similar to the method of Osler et al. [1]. Each subject was tested in the high and ground walkway conditions in counter-balanced order. Subjects' feet were placed together, directed along the antero-posterior axis of the walkway. They stood with eyes closed and head facing directly forwards. In each condition 30 GVS impulses of 2 seconds (15 anode-left, 15 anode-right, randomly ordered) were applied at intervals of 20 seconds.

Results: Between 1-1.5 s after GVS onset the maximum mediolateral displacement of the COM was higher at ground level (t=3.45, df=15, p=0.004) than at height (Fig 1B, lines are averages and shaded areas are 95% confidence intervals). When the mediolateral COM acceleration time series at ground and height are compared, three peaks can be distinguished (Fig. 1C). We refer to these peaks as short latency peak (SLP: minimum 0.05-0.3s), medium latency peak (MLP: maximum 0.2-0.8s) and late latency peak (LLP: minimum 0.5-1.5s). In the height condition SLP amplitude was increased (t = -2.15, df = 15, p = 0.049) and MLP and SLP occurred earlier compared to ground, (MLP: t = 5.21, df = 15, p < 0.001; LLP: t = 3.39, df = 15, p = 0.004). Figure 1D shows the mediolateral anode sided knee acceleration. SLP

amplitude of the mediolateral sway acceleration of the knees was increased at height (Anode sided knee: t = -2.27, df = 15, p = 0.039; Cathode sided knee: t = -2.74, df = 15, p = 0.015). No height effect was found on neck and lower back joint angle acceleration GVS responses in the frontal plane.

Figure:
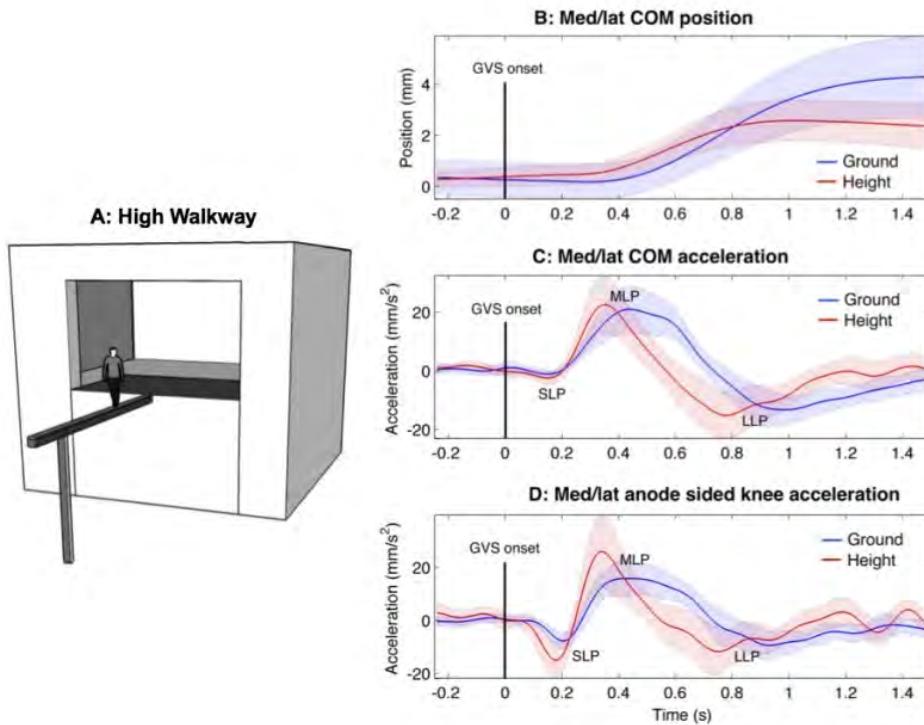
Conclusion: The time domains and directions of our SLP and MLP COM acceleration data was congruent with SVS-GRF coupling data from Horslen et al. [2]. We interpret the SLP and MLP to be part of a reflexive response that initiates increased body sway, whereas LLP is mediated by higher order sensory integration of proprioceptive and vestibular information that terminates the body sway caused by GVS. The increase of early (SLP and MLP) body segment acceleration at height was only present in the lower extremities. This effect was strongest in the acceleration of the knee joint centres and it is in line with a more excited early motor response to vestibular stimuli. This might also provide the mechanism of the early effect of postural threat on the SVS response identified by Horslen et al. [2]. Our results are in accordance with Forbes et al. [3] who found early GVS neck muscle responses to be task independent as opposed to appendicular muscle responses that were attenuated when they were less relevant for balance control. In conclusion, fear of falling changes the effect of vestibular sensory feedback on lower extremity kinematics during standing and these postural effects are present within a short time delay of 0.1 s. This indicates modification of appendicular vestibular fast reflexive pathways caused by fear of falling.

References: [1] Osler et al., Eur J Neurosci, 38(8), 3239-3247, 2013.

[2] Horslen et al. J Physiol, 592, 3671-3685, 2014.

[3] Forbes et al., J Physiol, in press, 2014.

Disclosure of Interest: None Declared

Motion Analysis

AS-0247

ARE MANDIBULAR KINEMATIC MEASUREMENTS RELIABLE DURING MAXIMUM MOUTH OPENING IN HEALTHY SUBJECTS?

Letícia B. Calixtre [1,*] Theresa Helissa Nakagawa [1] Lianna Rosa [1] Bruno Leonardo Grüninger [1] Francisco Alburquerque-Sendín [2] Ana Beatriz Oliveira [1]

[1] Physical Therapy, Federal University of São Carlos, São Carlos, Brazil, [2] Physical Therapy, Salamanca University, Salamanca, Spain

Introduction and Objectives: The knowledge about reliability of kinematic measurement during maximum mouth opening (MMO) can provide information regarding the consistency of motor patterns. This measurement is often compromised among patients with temporomandibular dysfunctions (TMD), affecting their functionality.

Fixing markers on the skin can cause movement artifacts due to the skin stretching and the palpation of anatomical structures that can vary according to the evaluator skill and anthropometric characteristics of the subjects.

Therefore, the purpose of this study was to analyze test-retest reliability and standard error of measurement (SEM) of mandibular movements during MMO recorded with a motion capture system and a vernier caliper.

Methods: Twenty-one healthy subjects (8 males and 13 females; 23.95±2.47 years; 23.61±2.73kg/m^2) with no current history of mandibular or neck trauma and absence of signs and symptoms of TMD, like: pain on temporomandibular joint (TMJ), difficulty to perform mandibular movements, muscular pain or fatigue during chewing, clicking during mandibular function, and parafunctional habits. They achieved at least 3.5mm of MMO.

Two evaluations were performed in the same day (E1 and E2), and a third one was performed 5-7 days later (E3). MMO was measured three times with a caliper (Somet, 150mm, Inox, Czechoslovakia) while the subject was seated (E1). Markers were positioned and kinematics recordings were performed (E1). After 10 min, the same rater replaced the markers and kinematics was recorded again (E2) for intra-session reliability analysis. The same procedure (E1) was repeated in E3 to evaluate inter-session reliability. All kinematic data was recorded at 120 Hz with a six-camera motion capture system (Qualisys Inc., Gothenburg, Sweden). The subject performed two series of five MMO at free velocity, starting from mandibular intercuspal position. Tridimensional movements of head, mandibulla, and trunk were tracked through passive markers (Figure 1) by the Qualisys Track Manager (Qualisys AB Packhusgatan, Gothenburg, Sweden). An equilateral triangular stainless steel extraoral antenna (side 40 mm; weight 2 g), fixed on the mandibular anterior gingiva using surgical adhesive, and markers on the TMJs, provided a mandibular reference system. On the static take, a marker was located on the midline incisal edge to identify a dental landmark, relative to the antenna system. Three-dimensional reconstruction was performed using Visual 3D software. Incisor displacement (mm), MMO on sagittal plane (deg), condylar translation during mouth opening and closing (mm) were analysed by a custom made Matlab software (version 7.0.1, MathWorks Inc., Natick, USA) [1]. Intra and inter-session reliability was evaluated through the Intraclass Correlation Coefficient (ICC) using SPSS software (v19, SPSS, Chicago, IL). SEM was calculated using Excel (SEM = SD×√1−ICC). ICC's upper to 0.61 and 0.81 were considered as good and very good, respectively [2].

Results: All kinematic data are presented in Table 1. The MMO measurements with caliper from the first session (E1) presented mean±standard deviation of 48.8±6.9, 48.95±6.8 and 49.3±6.4, while on the second session (E2) of 49.23±7.1, 49.23±6.5 and 49.6±7.1. The intra-session ICCs were very good (0.987 and 0.972) with low SEMs (0.75 and 1.14) and as well as the inter-session ICC (0.91) and SEM (2.01).

Figure:
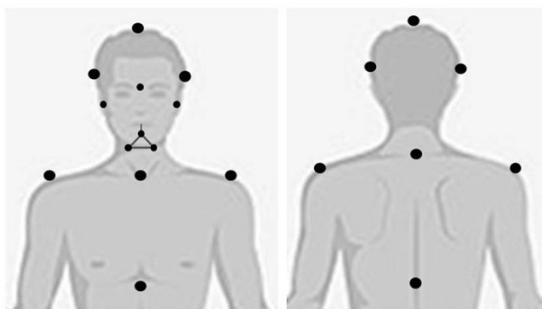
Caption: Figure1. Position of the passive markers.

Conclusion: Incisor displacement as well as MMO measured with the caliper presented very good intra-session and inter-session reliability, both with low SEM. The other kinematic variables had good intra-session reliability and low SEM, while inter-session reliability was low and SEM was high. These results support the use of 3D kinematic video analysis and caliper rule to measure mandibular movements during MMO. However, caution must be taken when interpreting MMO on sagittal plane, and condylar translation movements over time due to the low inter-session reliability and high SEM.

Table:

Variable	E	Mean (SD)	ICC		SEM	
			INTRA	INTER	INTRA	INTER
Incisor displacement (mm)	1	40.34 (7.7)	0.871	0.827	2.48	2.88
	2	40.14 (6.2)				
	3	40.96 (7.7)				
MMO on sagittal angle (deg)	1	-27.90 (4.2)	0.86	0.37	1.59	7.64
	2	-27.02 (4.4)				
	3	-27.95 (13)				
Condylar translation - mouth opening (mm)	1	14.02 (4.9)	0.699	0.204	2.51	5.25
	2	12.35 (4.2)				

		3	17.18 (6.4)				
Condylar translation - mouth closing (mm)		1	14.93 (4.9)	0.671	0.192	2.71	5.51
		2	13.57 (4.6)				
		3	18.06 (6.7)				

Caption: Table 1. Mean, standard deviation (SD) of kinematic measurements recorded in the three evaluations (E). ICC and SEM are presented for both intra (INTRA) and inter-session (INTER) comparisons.

References: [1] Mapelli et al., Clin Anat. 2009 Apr;22(3):311–8.

[2] Altman et al., Ann Intern Med. 2001;134:663-694.

Disclosure of Interest: None Declared

Motion Analysis

AS-0248

GAIT ANALYSIS OF TKA PATIENTS AT 2 WEEKS AND 4 WEEKS AFTER SURGERY USING WEARABLE SENSORS

Ryo Takeda [1,*]Tadashi Fujisawa [1]Giulia Lisco [2]Laura Gastaldi [2]Stefano Pastorelli [2]Harukazu Tohyama [3]Shigeru Tadano [1]

[1]Engineering, Hokkaido University, Sapporo, Japan, [2]Mechanical and Aerospace Engineering, Politecnico di Torino, Torino, Italy, [3]Health Science, Hokkaido University, Sapporo, Japan

Introduction and Objectives: This work investigates the changes in kinematic and spatio-temporal gait parameters of patients with total knee arthroplasty (TKA) after 2 and 4 weeks of surgery using wearable sensors. The objective of this work was to compare the gait parameters of TKA patients between 2 and 4 weeks after surgery and verify the rehabilitation training effects within those time periods. All the materials of this work was conducted with wearable sensors attached to the lower limbs.

Methods: The wearable gait analysis system H-Gait (Development Code, Laboratory of Biomechanical Design, Hokkaido University, Sapporo, Japan) was used in this work. Seven sensors units containing tri-axial acceleration and tri-axial gyro sensors were attached to seven locations of the lower limb (pelvis, both thighs, both shanks and both feet). The acceleration and angular velocity data of each sensor unit of each body segment of the patient could be collected by a computer in real-time by Bluetooth wireless transmission.

Five patients with TKA surgery (3 right TKA, 2 left TKA) to only one knee participated in the measurements. All patients gave their consent for the measurements. Seven sensors units (WAA-006, Wireless Technologies, Inc.) were fixed by straps to the lower limb segments of the patient. The acceleration and angular velocity data of each sensor unit were measured at a sampling rate of 100Hz during level walking (7 to 10m) at 2 weeks and 4 weeks after surgery. In between the measurements patients were went through rehabilitation training at the Hokkaido University Hospital (Sapporo, Japan). For safety purposes the walking speed for each measurement was at the discretion of the patient. These measured data were sent to a computer via Bluetooth and then converted to three dimensional segment orientation data using a developed quaternion based algorithm [1]. The developed algorithm contained countermeasures to reduce the effect of signal drift errors such as, an infinite impulse response (IIR) digital 4th order Butterworth filter, mode value offset extraction, double derivative and integration (DDI) and two posture sensor attachment calibration [2]. In addition the lower limb segment length of the patients was measured using reflective maker attached to anatomic characteristic points. Lower limb gait joint kinematic parameters such as: flexion-extension angle (hip and knee), dorsi/plantar flexion angle (ankle), adduction-abduction angle (hip, knee and ankle), internal-external rotation angle (hip, knee and ankle) , sagittal joint center trajectory (hip, knee and ankle) and horizontal joint center trajectories (knee and ankle) were calculated. Furthermore, spatio-temporal gait parameters such as: gait cycle, cadence, step length, step width, stride length, walking speed, limp index, stand ratio, swing ratio and heel contact timing and toe off timing of the foot were calculated.

Results: As a result, the following was found by comparing the gait data of all patients between 2 and 4 weeks after surgery. The range of motion of the TKA side's knee increased by 40%, the range of motion of the TKA side's hip by 26%, the range of motion of the not TKA side hip by 27%, the stride length by 40%, the cadence by 25%, the walking speed by 72%, the step length of TKA side by 51% and the step length of the not TKA side by 32% and the ratio of stance phase in

TKA side decreased 5.7% and the ratio of stance phase in not TKA side decrease 7.1% on average. And the difference of each side's step length has decreased from 4.3cm to 0.4cm. This means that the patients at 4weeks after surgery were able to walk more symmetric than at 2 weeks. The increase of knee extension angle at heel contact timing by 4.7deg and the increase of hip flexion angle at heel contact timing by 2.7deg result in developed stride and step length increase.

Conclusion: From the result presented above, it was verified that a wearable sensor system can evaluate a patient's rehabilitation progress by providing quantitative kinematic and spatio-temporal gait parameters in clinical situations.

Table:

Parameter	Side	2 weeks	4weeks	p-value
Walking speed [m/min]	-	28.89	46.37	0.01
Step length [cm]	TKA	32.14	48.65	0.00
	NOT TKA	36.42	47.96	0.00
ROM of Hip [deg]	TKA	29.75	37.43	0.00
	NOT TKA	28.51	36.14	0.00
ROM of Knee [deg]	TKA	22.84	33.37	0.00
	NOT TKA	41.08	44.25	0.25
ROM of Ankle [deg]	TKA	20.95	20.42	0.36
	NOT TKA	16.18	17.04	0.26
Hip flexion angle at HC [deg]	TKA	15.72	18.41	0.15
	NOT TKA	18.77	19.91	0.35
Knee flexion angle at HC [deg]	TKA	9.84	5.11	0.01
	NOT TKA	10.78	9.04	0.28
Ankle dorsiflexion angle at HC [deg]	TKA	-11.18	-14.35	0.05
	NOT TKA	-10.62	-9.83	0.38

Caption: Comparison of the gait parameters of the patients between 2 and 4 weeks after surgery.

References: [1] Tadano, Takeda, Miyagawa. Sensors. 13(7):9321-9343, 2013.

[2] Takeda, Lisco, Fujisawa, Gastaldi, Tohyama, Tadano. Sensors. 14(12):23230-23247, 2014.

Disclosure of Interest: None Declared

AS-0249

VALIDATION OF A NEW ALGORITHM FOR THE DETECTION OF STEP DURATIONS IN SHORT EPISODES OF GAIT USING A SINGLE ACCELEROMETER DEVICE ON THE LOWER BACK.

María E. Micó Amigo [1,*]Idsart Kingma [1]Erik Ainsworth [2]Stefan Walgaard [2]Martijn Niessen [2]Rob van Lummel [2]Jaap H. van Dieen [1]

[1]MOVE Research Institute Amsterdam, Faculty of Human Movement, VU Amsterdam University, Amsterdam, [2]McRoberts B.V., McRoberts B.V., The Hague, Netherlands

Introduction and Objectives: To assess the validity of a new algorithm for the detection of step durations in healthy elderly subjects from accelerometry signals measured on the lower back during short episodes of gait.

Short episodes of gait are common in daily-life activity of the elderly [1], who select gait strategies with different spatio-temporal parameters for different distances. Thus, the assessment of short episodes of gait may provide clinical information that differs from information based on the assessment of long episodes of gait [2]. Subjects who cannot participate in long gait protocols due to their limited mobility might be able to perform short gait episodes instead, which are relevant for their independency at home. Moreover, short gait protocols are well suited to studying the initiation of gait and are easily implemented in clinical practice, given limited space and time requirements [3,4] However, only a few studies have analysed short episodes of gait with the use of body-fixed-sensors (BFS) to date. The location of the sensor on the lower back is near to the centre of mass, and it is well accepted by older adults. Furthermore, this location permits to assess postures and transitions in daily-life activity, and it may predict risk of falling [5].

Methods: 22 healthy elderly subjects (74.3±8.4 years old) walked a distance of 5 meters twice, wearing a BFS (DynaPort McRoberts) on the lower back, and a BFS (DynaPort MiniMod McRoberts) on the outside of each heel. Data were recorded at a sampling rate of 1 sample/10 ms. For step duration detection we developed a novel algorithm, which defines a template based on the autocorrelation of the raw acceleration signal in the anterior-posterior direction (AP).Subsequently, it calculates a signal (Diff), which is the difference in amplitude between the template and the raw AP signal. Then, the SD of the Diff signal is normalized to the SD of the template, giving a new signal (SD_Diff). The cross correlation signal between SD_Diff and the raw AP signal contains pronounced peaks, which remark periodic events being detected close in time to heel-strike events. The intervals between these events define the step durations. Step durations from the lower back acceleration signals were validated by comparison with step durations calculated from the combination of the right and left heel acceleration signals. Absolute differences between both methods for each interval were averaged within and over trials and subjects.

Results: 4 trials were excluded from the results due to the loss of a heel accelerometer during gait. The average difference for the other 40 trials was 28.6±14.6 ms (5.02 % of the average step duration).

Conclusion: A novel method for the detection of step durations in short episodes of gait based on a single accelerometer placed on the lower back is described and appears to provide valid estimates. The extraction of temporal parameters from short episodes of gait might provide relevant clinical information, starting from the detection of each step duration.

References: [1] *Van Schooten et al., J Aging Phy Act, PMID: 24306934 Dec 4, 2013.*

[2] *Najafi et al., Gait Posture, 29: 261-6,2009.*

[3] *Zijlstra et al., Eur J Ageing, 4: 3-12,2007.*

[4] *Aminian et al., Computer Animation and Virtual Worlds, 15: 79-94,2004.*

[5] *Rispens et al.,Neurorehabil Neural Repair , 29: 54-61, 2014.*

Disclosure of Interest: None Declared

AS-0250

3D BODY CENTRE OF MASS TRAJECTORY IN LOCOMOTION: COMPARISON BETWEEN DIFFERENT MEASUREMENTS METHODS

Gaspare Pavei [1]Elena Seminati [1 2,*]Dario Cazzola [2]Alberto Enrico Minetti [1]

[1]Dept of Pathophysiology and Transplantation - Human Physiology Section, Università degli Studi di Milano, Milano, Italy, [2]Department for Health, University of Bath, Bath, North East Somerset, United Kingdom

Introduction and Objectives: Body centre of mass (BCoM) trajectory is largely used to describe human and animal locomotion with the final aim to estimate the mechanical work performed by muscles. The BCoM can be calculated through 2 different methods: i) by double integration of ground reaction forces (GRF) and ii) by the weighted mean of the local centres of mass of the body anatomical segments, which are collected through an optoelectronic system. Although both methods are currently exploited, the use of the GRF is considered the gold standard as it provides a (relative) BCoM trajectory as caused by both hard and soft tissue motion. However, it allows capturing only a limited number of strides and repeated trials are requested for reliable results. Kinematic measurements, conversely, can be carried out while moving on a treadmill, so that an adequate strides number and speed could be collected. Several biomechanical models are available to analyse the kinetics of human body and the use of different anthropometric tables could bring discrepancies in the BCoM computation. In addition, markers placement, skin motion and the rigid segment assumption could lead to systematic errors. Previous studies compared these methods, but only few locomotion paradigms were investigated, mainly analysing only BCoM vertical motion. Aim of this study was to compare the 3D BCoM trajectory and the associated mechanical work (W_{EXT}) concurrently calculated by means of GRF and kinematic in 5 gaits and a wide range of speeds. Kinematic results were compared across 5 different sets of markers in order to verify their reliability.

Methods: One participant (1.78m, 63kg), performed different gaits on treadmill at incremental speeds: walking from 0.28 to 1.94m/s (increment 0.28m/s); running from 2.22 to 5.56m/s (increment 0.28m/s); race walking from 2.22 to 4.17m/s (increment 0.28m/s), mono- and bi-lateral skipping from 0.83 to 3.06m/s (increment 0.56m/s). An 8-camera Vicon system (Oxford Metrics, UK) sampled kinematics data at 300Hz for 1 minute at each velocity. Simultaneously a Mercury LT med treadmill (HP Cosmos, Germany), equipped with 4 3D strain-gauge force traducers, recorded GRF at 900Hz.

5 markers set were compared at the same time: 1) a single marker placed on the 7th cervical vertebra (C7); 2) the mean of anterior and posterior superior iliac spines (Spinae); 3) a 11-segments body model based on Dempster tables (18mkr); 4) a 14-segments body model based on De Leva tables (DeLeva); 5) a 14-segments body model based on the Vicon Plug-in-Gait model (PIG). In addition BCoM was obtained by double integration of the filtered GRF (low pass filter 4th order Butterworth with 30Hz cut off frequency). BCoM trajectory of each stride (local coordinates on treadmill) was isolated and the loop forced to close, according to Minetti's method [1]. A point-by-point 3D root mean square (3D RMS) was computed between the (reference) trajectory evaluated with GRF method and the one calculated with each of the 5 kinematic models. W_{EXT}, i.e. the positive work done to accelerate and raise BCoM, was calculated for each trajectory by summing the increment of total energy time course.

Results: The 3D RMS between the trajectories calculated with GRF method and kinematic methods indicated that the marker set exploiting C7 and Spinae showed the greatest discrepancy from GRF, whereas 18mkr and DeLeva models well matched all gaits and PIG was in accordance to GRF method only in running (see Fig.). Although the BCoM trajectory in race walking showed a small discrepancy in terms of RMS, its 3D contour was very different when compared to the one computed from GRF. W_{EXT} obtained from kinematic showed the slightest discrepancies when adopting PIG, 18mkr and DeLeva models (see Tab.).

Figure:
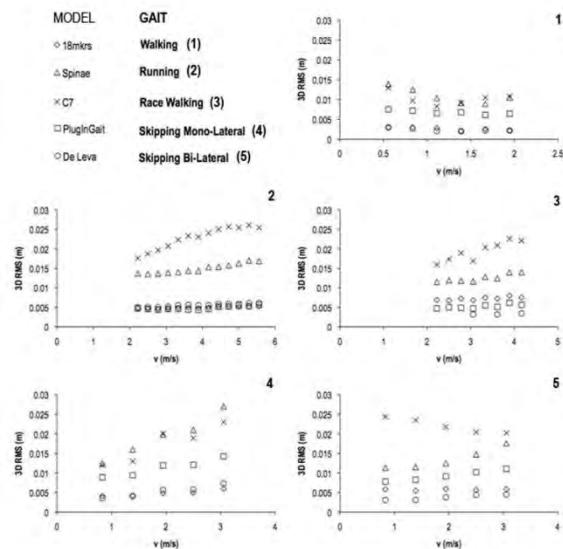
Caption: 3D RMS (in meters) between the trajectories calculated with GRF and kinematic methods.

Conclusion: The choice of the method (GRF or Kinematics) and of the biomechanical model has to be considered carefully, to obtain a reliable characterization of the BCoM. Commonly used whole-body biomechanical models (18mkr and DeLeva), lead to BCoM trajectories and W_{EXT} in walking, running and skipping very close to the one calculated through the gold standard. In contrast the use of a single marker placed on the trunk or the mean position from the pelvis landmarks is not a reliable estimation of the 'true' BCoM position, and negatively affects W_{EXT} calculation.

Kinematic measurements can be exploited to describe the BCoM in locomotion, but the result could be completely different from the real one when the gait differs from standard locomotion paradigms. In race-walking for example, although the pattern of the BCoM travels within an acceptable 3D volume, its shape completely differs from the 'reference' one (GRF).

Table:

	Walking	Running	Race Walking	Skipping
C7	+16%	-18%	-24%	+4%
Spinae	+35%	+106%	+78%	+30%
18mkr	+13%	+22%	+10%	+15%
DeLeva	+13%	+10%	+17%	+3%
PlugInGait	+6%	+12%	-13%	+15%

Caption: WEXT discrepancies (=(kinematic model – GRF)/GFR, %).

References: [1] Minetti et al., J Biomech. 44:1471-77,2011.

Motion Analysis

AS-0251

DEVELOPMENT OF A BESPOKE BIOMECHANICAL MODEL FOR REAL-TIME CALCULATION OF LOWER LIMB KINEMATICS.

Lindsay Clarke [1,*] Andrew J Murphy [1] Phil Rowe [1]

[1]Biomedical Engineering, University of Strathclyde, Glasgow, United Kingdom

Introduction and Objectives: Human movement analysis may be considered an essential tool in clinical and research biomechanics[1,2]. A number of commercially available systems allow the accurate and quantitative description of a participant's gait[3]. However, the use of these systems generally limits the user to predefined models or requires users to have significant technical expertise for creating bespoke models. Further, while it is possible to manipulate certain aspects of the established motion analysis process, current platforms do not allow complete customisation. The aim of this investigation was to build a customisable, bespoke biomechanical model (LJC) using an object-oriented application development package with integrated Lua based programmatic scriting modules; D-flow (Motek Medical, The Netherlands). The components of the model include a marker set, a method of calibrating a participant and calculation of kinematics.

Methods: A bespoke cluster marker set with strategically placed anatomical markers was implemented. Marker trajectory data was captured, labelled and streamed into D-Flow using Vicon hardware and acquisition software (Vicon Motion Systems, Oxford, UK). A static calibration method was devised whereby the offsets of the calibration markers from the clusters are calculated for each segment. The Winter method[4] was used to reconstruct calibration markers during dynamic trials and the Grood and Suntay[5] method was used to calculate kinematics. This was implemented in D-Flow using bespoke scripting modules written in Lua programming code. Pilot testing against Plug in Gait (PIG; Vicon Motion Systems, Oxford, UK) was completed with one typically developing adult participant.

Results: Flexion angles of the hip, knee and ankle were examined during normal treadmill walking (figure 1). Results demonstrated similarities in trace and range of motion (ROM), however, for all joint angles there was a consistent offset of absolute angle. When the mean difference between datasets was added to PIG data, there was much stronger agreement.

Figure 1. Black - PIG; grey - LJC; dashed - PIG plus mean difference. **a.** Hip **b.** Knee **c.** Ankle.
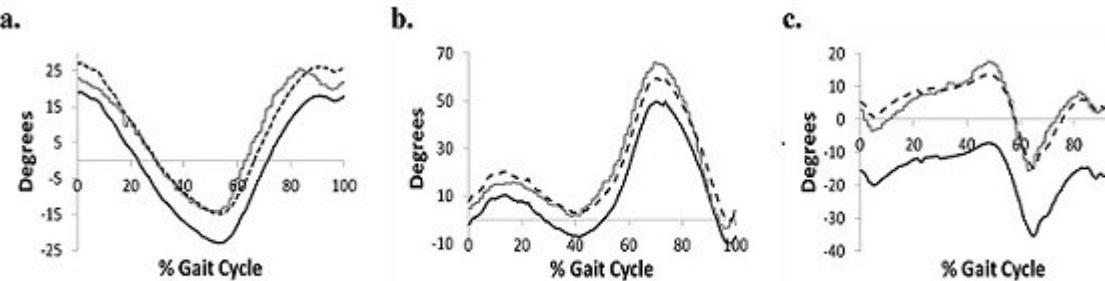
Conclusion: Initially, results do not indicate good agreement between PIG and LJC. However, the offset between data sets appears to be consistent across all joints. It may be that inaccurate PIG marker placement contributed to errors in PIG data. Tibial and femoral wands were not used which could contribute to inaccuracies. Further, PIG ankle data suggests that no dorsiflexion occurs throughout the cycle. This is highly unlikely for a typical adult which suggests that there may be some error in PIG data. Work is ongoing to determine the source of the errors.

The development of a bespoke biomechanical model allows complete customisation. The model can be altered to allow a choice of marker set or calibration methods. The possibility also exists to build specific functionalities for specific users, providing an advantage over commercially available models.

References: [1] Gage JR. Clin Orthop Relat Res, 288:126–34, 1993.

[2] Cook RE *et al.* J Pediatr Orthoped, 23:292-295, 2003.

[3] Ehara *et al.* Gait & Posture, 3:166-169, 1995.

[4] Winter (3rd ed). Bioemchanics and Motor Control of Human Movement. Wiley 2004.

[5] Grood *et al.* J Biomech Eng, 2:136-144, 1983.

Disclosure of Interest: None Declared

AS-0252

EFFECT OF WEARABLE TRUNK SUPPORT FOR WORKING IN SUSTAINED STOOPED POSTURE ON LOW BACK NET EXTENSION MOMENTS

Chris T.M. T. Baten [1,*] Remon van der Aa [1] Annechien Verkuyl [2]

[1]Ambulatory 3D Analysis of Movement, Roessingh Research and Development, Enschede, [2]Intespring, Delft, Netherlands

Introduction and Objectives: Recently a unique method has been further developed by Baten et al. [1] for direct estimation of low back load exposure to low back structures during actual work in terms of the net moment around the intervertebral body at level L5/S1. This paper applies this method to evaluate a concept version for a novel wearable trunk support for working in sustained stooped posture [Laevo, Intespring]. This is a comfortably wearable trunk support device that claims to assist the low back structures in generating the extension net moments required to cope with the load exposure of working in repetitive static stooped posture. This paper discusses the experimental evaluation of this claim in simulated real life working conditions.

Methods: Three series of experimental sessions were done (each around 30 trials); one series under laboratory conditions to test hardware and software, one session in a hospital setting with five nurses as subjects and one session in an industrial environment with four metal workers as subjects. For each subject a series of recordings was done comprising calibration movements, a series of simulated tasks with the Laevo prototype not active, plus a series of the same simulated tasks with the prototype actively supporting the trunk of the subject. For each subject 3D kinematics of all body segments were recorded using 3D Inertial Magnetic Motion tracking Units (Xsens MTw) and surface EMG recordings (2 x TMSI, Moby) from the main back extensor and flexor muscles. In the first session and also in two of the subjects of the second session also 6-DOF ground reaction forces were recorded with instrumented shoes (own development). All data was recorded synchronously together with 2 wireless video streams and analyzed with the custom developed FusionTools ambulatory monitoring software suite. Net moment generated by the back structures are estimated by an artificial neural network (ANN) from surface EMG and kinematics data, that was trained with target net moment estimates from kinematics and force shoes alone (supervised, known load handling). For these sessions the net moment estimates for training and testing of the ANN method were calculated using a linked segment model from the ground up (LSM-BU) validated against those calculated top-down (LSM-TD), applying standard solid body equations. ANN estimates were trained with, and validated against, both LSM methods. Comparisons were made visually and numerically (peak net moments differences estimates and coefficient of determination (R^2).The differences in net moment generated by the trunk structures with and without active support of the Leavo prototype were assessed in a variety of tasks by comparing the net extension moments curves estimated with the ANN method for all corresponding trials.

Results: Net sagittal extension moments estimated from kinematics assessments from the upper body (LSM-TD) versus those estimated from kinematics assessments of the lower body (LSM-BU) appear to be similar within ca. 10% of the maximum in both all stooped tasks in the sagittal plane and also in all stooped tasks somewhat to the side. Also all ANN estimates were within 10% of corresponding LSM-TD and LSM –BU estimates. When comparing net back extension moments for all trials in which the same task was performed with and without active support of the Laevo prototype, a

clear effect of the Laevo prototype was found. Smoothed Rectified EMG data (SRE) of some of the main trunk supporting muscles dropped to zero whenever the Laevo prototype was actively supporting in stooped posture and simultaneously the net extension moments generated by the low back structures dropped to 10% of the value without Laevo support.

Figure:
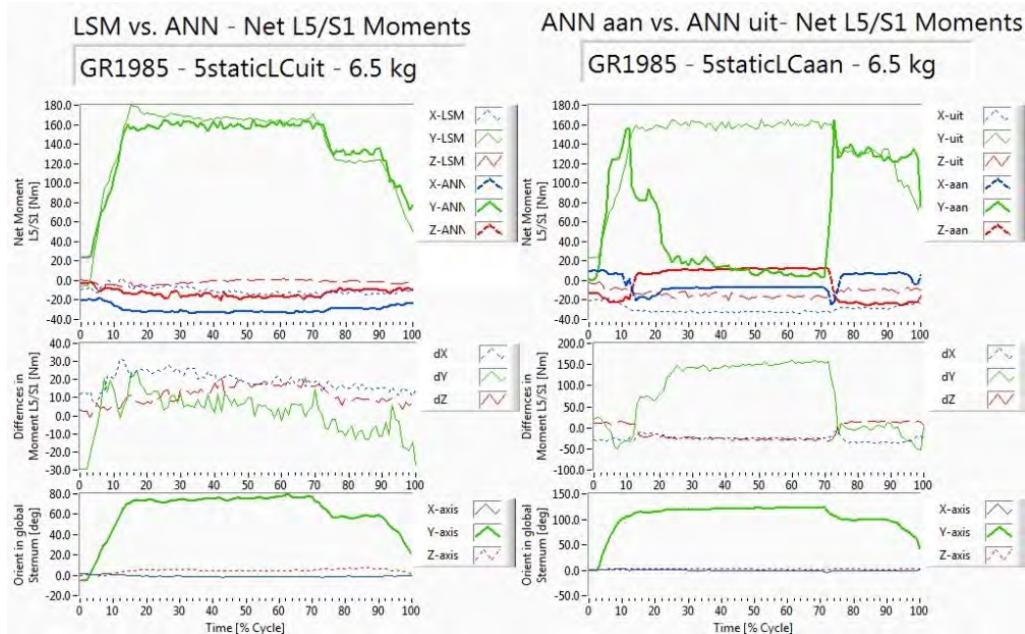
Caption: Figure 1: L5/S1 joint net moment estimation comparison LSM-TD, representing the total net moment of Laevo plus back structures, against TD-trained ANN, representing only net moment generated by low back structures. Left: with Laevo prototype inactive; right: with Laevo prototype active. Top row: Data from a straight "static" lifting task of a box 6.5 kg. 2nd row: Absolute differences between the methods, representing effect of the Laevo prototype. 3rd row: The orientation of the sternum in the global frame.

Conclusion: The data suggests that extension net moments normally generated by the low back structures are taken over by this version/configuration of the Laevo prototype trunk support for about 90% from a certain stoop angle. Still some freedom of movement can be enjoyed in this Laevo prototype, because it is constructed in such a way that when the subject first flexes the knees the Laevo prototype trunk support is deactivated.This study implies that the ANN method for net trunk extension moment estimation can be a valuable tool in evaluating the actually support percentage function achieved in test and final versions.

References: [2] Baten, CTM, Advancements in sensor-based ambulatory 3D motion analysis Journal of Biomechanics, 40, pS422-S422, Jan 2007.

Disclosure of Interest: C. T. Baten: None Declared, R. van der Aa: None Declared, A. Verkuyl Conflict with: Intespring

AS-0253

THE RELATIONSHIP OF ENERGY COST TO BIOMECHANICS AND MUSCULAR RESPONSES DURING PROLONGED LOAD CARRIAGE

John W. Ramsay [1][2],*Tyler Brown [1]Meghan O'Donovan [1]Kari Loverro [1][2]Carolyn Bensel [1][2]Leif Hasselquist [1]

[1]Natick Soldier Research, Development and Engineering Center, Natick, MA, [2]Oak Ridge Institute for Science and Education (ORISE), Belcamp, MD, United States

Introduction and Objectives: During military operations, soldiers often march with heavy body-borne loads (i.e. ≥40 kg) for an extended period of time covering large distances over varied topography. During marches, energy cost reportedly increases with greater loads and steeper grades. However, there is a dearth of information on the relationship of load and grade to biomechanical and muscular responses during a prolonged march. Modified joint kinematics and altered muscular responses may contribute to decreased mechanical efficiency and changes in energy cost over time. These adaptations may also increase risk of injury and decrease physical performance, which will ultimately change a soldiers' ability to perform military functions effectively. Therefore, the objective of this study was to determine the physiological, kinematic and muscular responses that occur during prolonged load carriage over different levels of exertion.

Methods: Joint kinematics, energy expenditure and muscular activity were collected on 11 males (age 23 ± 3 yrs; wt. 83.1 ± 19.8 kg; ht. 178.6 ± 6.5 cm; mean $VO_{2,max}$ 49.1 ± 4.3 ml/kg/min) during prolonged treadmill walking with three levels of exertion (I: 0% grade, ~2-kg; II: 0% grade, 40-kg; III: 4% grade, 40-kg). Each exertion level lasted 120 min and data were recorded at 5 time intervals (0, 30, 60, 90, 120 min) for 20 seconds. Joint kinematics were recorded using an 8-camera motion analysis system as each subject walked on a split-belt instrumented treadmill. Kinematic variables included sagittal range of motion (ROM) for the ankle, knee, hip and trunk. Energy expenditure was measured using a metabolic measurement system and determined by oxygen consumption (VO_2). Raw EMG from the tibialis anterior (TA), medial gastrocnemius (MG), vastus medialis (VM), vastus lateralis (VL), medial hamstrings (MH) and lateral hamstrings (LH) were collected at 1200 Hz, filtered using a band pass filter (20-500 Hz), rectified, and a linear envelope was obtained by using a 10 Hz low pass filter. The root mean square (RMS) was determined for the middle 16 sec of each condition and each muscle signal was normalized to the RMS calculated from a prior baseline walking condition. Due to incomplete data sets for three subjects, only 8 subjects were included in the EMG analysis. Two-way (Level x Time), repeated measures ANOVA ($p<0.05$) were performed to assess the effects of the three exertion levels at five time intervals on VO_2 (ml/kg/min), joint ROM (degrees) and EMG RMS (% of baseline). If the ANOVA yielded a significant main effect, Bonferroni post-hoc analyses were performed ($p<0.05$).

Results: The level of exertion significantly increased VO_2 ($p < 0.001$) and across time VO_2 increased at a greater rate as level increased ($p < 0.001$). Steady state energy expenditure was not achieved for levels II and III, and responses were significantly different as time progressed ($p < 0.001$). Soldier kinematics were significantly altered by exertion level and there was an interaction found between exertion level and time. Joint ROM for III, when compared to I and II differed significantly with increasing ankle ($p < 0.001$), decreasing knee ($p = 0.002$), and increasing hip ROM ($p = 0.027$). As time progressed, maximum trunk and hip angles reflected a significantly increased flexed posture for II and III ($p = 0.016$).

EMG RMS increased during II and III for the medial gastrocnemius (p < 0.001), vastus lateralis (p =0.006) and medial (p = 0.004, p = 0.015) and lateral hamstrings (p = 0.007). For III, when compared to I and II, we saw additional significant increases in medial gastrocnemius EMG RMS (Table 1).

Conclusion: During prolonged load carriage, soldiers increase energy cost with higher levels of exertion, but may not achieve steady state when walking with load and/or up a grade. The observed biomechanical changes indicate a greater flexed posture with extended periods of increased exertion. These changes may decrease the soldier's metabolic efficiency and increase energy requirements over time. Patterns of muscular response to load indicate an increase in overall muscular activity of the ankle plantar flexors, knee flexors and knee extensors. The findings indicate an additional increase in gastrocnemius activity due to the increase in grade. Further investigation is required to determine whether any changes occur in the underlying EMG signals components (i.e. frequency shift) that may contribute to increases in energy cost over time.

Table:

Condition	Mean EMG RMS Normalized to Percent of Baseline Walking (%)					
	TA	MG	VM	VL	MH	LH
I (NL0%)	97.5_A	93.2_A	92.0_A	94.2_A	89.2_A	95.9_A
II (AL0%)	102.1_A	121.4_B	130.8_B	135.6_B	112.4_B	109.3_{AB}
III (AL4%)	107.9_A	154.6_C	117.9_{AB}	125.8_{AB}	131.4_B	130.0_B

Condition	Global VO$_2$ Mean	Time Progression (min) of VO$_2$ (ml/kg/min)				
		0	30	60	90	120
I (NL0%)	13.1_A	13.0_A	13.1_A	13.1_A	13.1_A	13.1_A
II (AL0%)	17.4_B	13.1_A	16.7_{AB}	16.8_{AB}	17.5_B	18.3_C
III (AL4%)	23.9_C	22.8_A	23.4_A	23.9_B	24.4_B	24.8_B

Caption: Exertion Level Means for Muscle Response and Energy Cost. Means that do not share the same subscript differed significantly in post-hoc tests (p<.05)

Disclosure of Interest: None Declared

OLDER ADULTS AND RECOVERED LOW BACK INJURED PARTICIPANTS HAVE UNIQUE TRUNK MUSCLE MOTOR ADAPTATIONS TO A DYNAMIC LEG LOADING TASK

David A. Quirk [1,*]Cheryl Hubley-Kozey [1]

[1]Biomedical Engineering, Dalhousie University, Halifax, Canada

Introduction and Objectives: Relative to young healthy adults, older healthy adults and recovered low back injured (rLBI) participants have been shown to use altered neuromuscular control patterns to perform dynamic tasks [1,2]. Findings from spatial-temporal analysis of trunk electromyograms (EMG) suggest that rLBI and older adults have similar recruitment including sustained agonist activity and increased antagonist co-activity [1,2]. These patterns are thought to increase active spinal stiffness compensating for changes in osteoligementous, muscular, and neural components of the spine associated with both aging and spinal pathology. Whether neuromuscular adaptations are general or unique responses in these populations is not clear. However, trunk muscle synergies found in older adults [2] suggest these populations have unique motor adaptations. The objective of this study was to test the hypothesis that rLBI and older adults would have similar neuromuscular adaptations in response to a controlled dynamic leg loading task, but would differ from a young healthy control group.

Methods: Twelve older adults (65+ yrs) were sex, height, and mass matched to a younger cohort (20-45 yrs) of rLBI (n=15) (4-12 weeks post injury with minimal pain and disability) and no-LBI controls (n=21). Starting in supine, participants performed 3 trials of a leg loading task timed to a 4 second count while instructed to minimize pelvic motion (Figure). Surface EMG were collected from 24 trunk muscle sites (12 abdominal and 12 back extensors) at 1000Hz synchronized with 3D angular motion data collected from magnetic sensors placed on the iliac crest. Root mean square (RMS) EMG amplitudes were calculated and normalized to maximum voluntary contractions. To examine temporal patterns, EMG data were full-wave rectified, low-pass filtered (6 Hz), time normalized to 100% and amplitude normalized to average task amplitude. Motion data were low-pass filtered (1Hz) and maximum displacements were calculated for the entire task for 3D angles. EMG ensemble-average profiles were calculated from the waveforms for three trials for each muscle site and subject. Temporal features were captured using principal component (PC) analysis models constructed separately for the abdominal and back sites. Mixed model ANOVA (group, muscle) were conducted on RMS amplitude and PC scores. One way ANOVA (group) compared angular displacement and movement time ($\alpha=0.05$). Tukey HSD post-hoc analyses were performed.

Results: Participants completed the task in 3.7±0.3 seconds with no group differences. Pelvic motion was less than 5.5° in all directions, with between group differences (p<0.05). rLBI had less flexion/extension motion than older adults and controls, and older adults had more axial rotation than rLBI and controls.

Mean abdominal RMS amplitudes over the entire exercise were not different between groups (p>0.05). All three abdominal PC scores had group*muscle interactions (p<0.001) as illustrated by the unique temporal patterns for each group (Figure). PC1 captured early onset activity for rLBI relative to older adults and controls (Figure). PC2 captured differences between older adults and rLBI for all sites. Older adults had a pattern of lower activity whereas rLBI had

sustained activity during right leg lower (Figure). PC3 scores were different between older adults and rLBI for all sites. Older adults had sustained mid-task activity while rLBI supressed activity (Figure). PC2-3 differences were found between controls and both rLBI and older adults. These differences were not consistent across all muscle sites, with controls having an intermediate temporal response between both groups (Figure). rLBI group had no PC score differences among abdominal muscle fibres indicative of temporal synergies, whereas older adults and controls had differences among abdominal muscle sites indicative of differential responses. Back muscle sites RMS amplitudes had a group*muscle interaction ($p<0.05$). All 12 rLBI and 4/12 older adult back sites had higher antagonist co-activation than controls.

Figure:
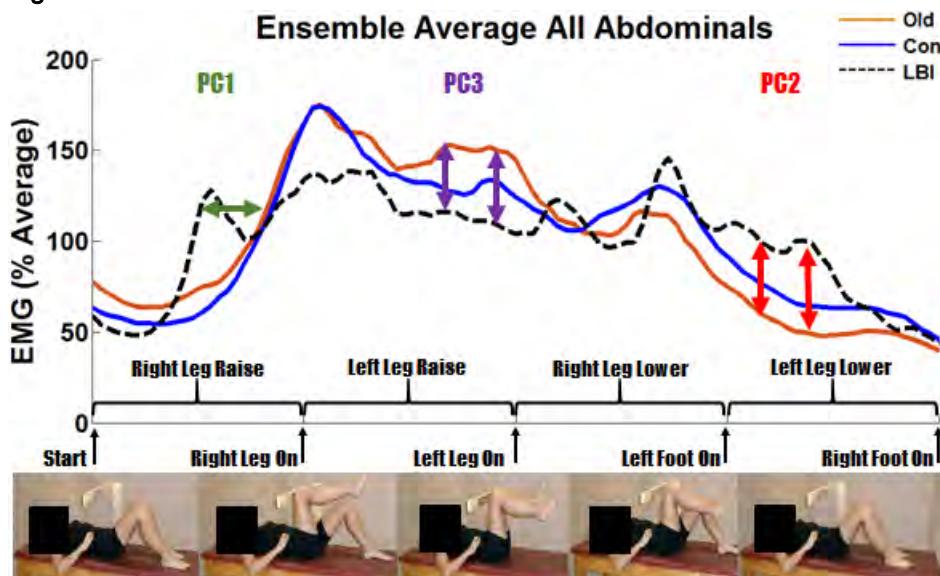
Caption: Ensemble average waveform response to dynamic task.

Conclusion: Consistent with previous findings, both rLBI and older adults differ from controls having sustained abdominal activation and higher antagonist co-activation [1,2]. However, rLBI and older adult groups had different temporal patterns to one another, including differences in temporal synergies. While sustained/higher activation can increase spinal stiffness, less spinal motion was only found in rLBI participants. Altered oblique muscle synergies used by older adults (PC2) may explain their higher transverse plane motion. In conclusion, these data reject our hypothesis showing that both older and rLBI groups had unique motor adaptations compared to controls, and to each other, providing evidence that adaptations are not general, but are sensitive to changes in specific spinal components.

References: [1] Hubley-Kozey et al., Work, 47; 87-100, 2014

[2] Quirk et al., Hum Movement Sci, 38; 262-280, 2014

Disclosure of Interest: None Declared

EMG

AS-0255

NON-NEGATIVE MATRIX FACTORIZATION FOR MUSCLE SYNERGY ANALYSIS: ROBUSTNESS ASSESSMENT AND IMPROVEMENT

Mohammad S. Shourijeh [1,*]Teresa E. Flaxman [1]Daniel L. Benoit [1][2]

[1]Faculty of Health Sciences, [2]Faculty of Engineering, University of Ottawa, Ottawa, Canada

Introduction and Objectives: Muscle synergies have been extracted by means of non-negative matrix factorization (NMF) in recent studies during static and dynamic tasks. NMF is a linear decomposition technique that outputs the optimized basis (synergy) vectors and corresponding weight (coefficient) vectors through minimizing the error between the original signal and the reconstructed data. NMF has been used by a number of studies for simplifying the representation of muscle activities using EMG values obtained during both static and dynamic tasks. By extracting muscle synergies, the number of variables required for describing neuromuscular control may be reduced. However, NMF might have many local minima caused by (1) scaling optimal coefficients and synergies by an invertible matrix so that the error still remains the same, (2) swapping of the coefficient/synergy indices, and (3) not convergence of the optimization problem, thus leading to repeatability issues. In order to address this, Frère and Hug [1] proposed using paired comparisons for each extracted synergy and generating a number of random permutations of the coefficients. This resulted in 3600 Pearson coefficients. Mean r-values of the paired comparisons were >0.71 and were not considered statistically different. Although these results suggest the outputs of NMF are repeatable for each subject and robust between subjects, the overall outputs may not be deemed consistent across runs since the variability is split between coefficients and synergies. Another issue arises when trying to use the NMF to evaluate the similarity between subjects in a given group. Again, Frère and Hug [1] used paired comparisons for each of their 9 subjects, resulting in 9*8 cases. In each paired comparison, the first subject was set as the reference subject, and then fixed the synergy of the second subject equal to that of the first subject, and computed the coefficient matrix. This was repeated but rather the coefficient matrix was fixed in order to compute the synergy matrix. Aside from the tedious process required to evaluate many paired cases, the differences are split between those considered pairs, and also between two variables of coefficients and synergies. Thus, interpretation of the similarity of the NMF outputs may not be valid. Due to the local minima issue, NMF outputs require a functional sorting method when comparing different sets of data. Studies have tried to reorganize the indices by finding the maximum correlation between the repeated runs or between subjects. Regardless of what measure is used for order reorganization, it might not be conclusive as the synergy order switch has occurred along with a numerical local minimum effect, in which case the sorting might be done by a poor correlation.

Methods: In order to minimize the aforementioned issues, we propose using a concatenated non-negative matrix factorization (CNMF) approach. A concatenated matrix will be formed that consists of the EMG signals of all subjects; there will be a corresponding concatenated coefficient matrix that includes the coefficient array of all subjects. An unknown synergy will be kept fixed between all subjects (and/or trials--if any), which will be determined within the CNMF. This will facilitate to assess consistency between subjects, as we will be left with only coefficients to be compared. For this

approach, we will not use paired comparisons; we believe that we should compare all subjects together simultaneously, by running intra-class correlation between the output coefficients of the CNMF.

Results: NMF and CNMF were both used to extract knee joint muscle synergies from the EMG data (taken from [2]) using the framework shown in Figure 1. Acceptable number of synergies must provide a VAF (Variance accounted for) of greater than 95%. Repeatability and between subject similarity were evaluated for each method using intra-class correlation coefficients (ICCs). High repeatability was found for CNMF compared to NMF: ICCs of >0.99 for the CNMF versus >0.26 in the NMF. Reasonable consistency across subjects was improved using the CNMF over the NMF approach.

Figure:
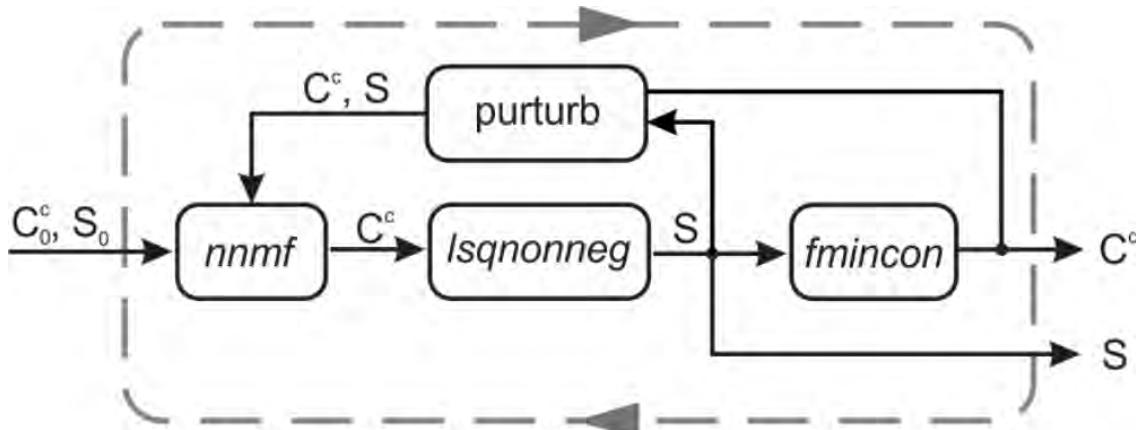
Caption: Framework schematic used for synergy identification: C is the coefficient matrix and S is the muscle synergy array; subscript 0 refers to random initial array, and superscript c designates concatenated matrix. nnmf, lsqnonneg, and fmincon are MATLAB routines.

Conclusion: This study evaluated NMF and introduced concatenated NMF (CNMF) to analyze and robustly extract muscle synergies. CNMF is proposed to be a more reliable approach than NMF and suitable for between subject comparison of muscle synergies. As applications of muscle synergies are growing in rehabilitation and motor control research every day, the CNMF approach will be helpful for deductions on muscle synergies and EMGs from different subjects and populations in different movements.

References:

[1] Frère et al., *Front. in Comp. Neurosci.,* 6: 1-13, article 99, 2012.

[2] Flaxman et al., *J. Biomech.*, 45: 2570-2576, 2012.

Disclosure of Interest: None Declared

AS-0256

NEURO-MECHANICAL CONTROL OF THE PRECISION JUMP. EFFECTS OF AMPLITUDE AND PRECISION CONSTRAINTS IN A FITTS' LIKE TASK.

David Pagnon [1,*]Olivier Martin [1]

[1]Saiga, Gipsa-Lab, Grenoble, France

Introduction and Objectives: A precision jump (PJ) consists in a standing jump toward a thin landing area, requiring a stabilization of the posture at landing without additional step. It requires both preparatory and on-line complex neuro-mechanical controls of the whole body balance. Currently, one single study has questioned the control processes associated to jump amplitude and precision altogether, and it focused on short amplitudes and low index of difficulty (ID)[1].

The purpose of this study was to analyze how the neuro-mechanical control system deals with the distance D to jump and the width W of the reception area. First we determined the phases affected the most by each constraint, then we focused on the differences in the management of both constraints, and lastly we compared the PJ with a Fitts task[2].

Methods: 7 male subjects participated in the experiment, all experts in Parkour (6.7±3.2 years of practice) which involves such abilities. They performed PJs from one force plate, toward another one on which was fastened a reception area. For each subject, 3 D conditions were set at 40, 60 and 80% of their maximal jump distance (Dmax) performed during pre-tests. 3 W conditions were set at 264, 132 and 44mm which made ID = log2(2D/W) range from 9.5 to 13.4. Each PJ condition (3Dx3W) was repeated 10 times. Resting period and jump start were at the subjects' decision.

Integrated surface electromyography (iEMG) of lower limb muscles (Tibialis anterior Ta, Gastrocnemius Ga and Quadriceps Qc) was recorded, as well as dynamics of the ground forces (antero-posterior forces FAp and their derivative dF/dt) on impulsion and reception plates.

Data were processed and analyzed all along the 6 phases composing a PJ: preparation PR, counter-movement CM, push-off PO, flight FL, reception RE, and stabilization ST. ST was defined as the phase going from 1 to 2 seconds after RE. A trial was considered successful if FAp during ST never went under 70% of the bodyweight.

A 3Dx3W factorial ANOVA design was conducted for each phase of successful trials, from all subject's means of times, iEMGs, force data and success rate to estimate the effects of D and W on neuro-mechanical strategies. Correlations were additionally sought among times of PR and FL and ID.

Results: The overall success rate was 85%. D played a lesser role than W in the success rate reduction (-9% vs. -17%). More precisely, the chronological phase's analysis showed that at **PR**, time increased more with D than with W (see Table for significances). At **CM**, forces and iEMGs of Ta increased with D, whereas they decreased with W. At **PO**, an increase of D implied a decrease of time, whereas force and iEMG activities of Ga and Qc increased. W had no significant effect. At **FL**, time increased with D and iEMG of Ta increased both with D and W. At **RE**, FAp, dF/dt and iEMG of Ta and Qc increased with D, whereas dF/dt and iEMG of Ta decreased with W. At **ST**, iEMG of Ta and Qc increased with W. D had no significant effect.

The analysis of ID effect showed that PR time was not correlated with ID, contrary to time of FL (T=0.36+0.041xID, r=0.36, p<0.05).

Figure:

Jump phases	PR	CM	PO	FL	RE	ST
Distance effect (80% vs. 40% of Dmax)	T : +54%***	F Ap: +48%*** iEMG Ta: +63%**	T : -17%* F Ap: +10%*** iEMG Ga:+37%** iEMG Qc: +72%***	T : +31%*** iEMG Ta: +74%**	F Ap: +93%*** dF/dt: +626%*** iEMG Ta: +37%*** iEMG Qc: +58%**	Success : -9%*
Precision effect (44mm vs. 264mm)	T : +19%*	F Ap: -11%* iEMG TA: -27%*	No effect	iEMG Ta: +14%**	dF/dt: -16%* iEMG Ta: +19%**	Success : -17%*** iEMG Ta: +56%*** iEMG Qc: +41%**

Caption: Table: Effects of D and W on time (T), antero-posterior forces (FAp) and lower limb muscle activities (iEMG) along each jump phases. *p<0.05, **p<0.01, ***p<0.001

Conclusion: Our results show that both distance and precision of the jump involve adjustments of forces and lower limb iEMGs, but not at the same time nor in the same way. Both D and W constraints increase time of PR. Then the key phases for D are PO and RE, whereas for W it is ST. PO and RE reflect the early need of a greater impulse to reach the reception area, and ST reflects the subsequent need of a greater sensori-motor control to stabilize the balance on a thin area. Thus the neuro-mechanical system allows a prioritization of the constraints, and anticipates first both D and W in parallel in a feedforward mode, and then it deals with D then W in a series in feedback mode.

The effects of D and W are opposed during CM and RE. Whereas both constraints affect the same variables, they are processed differently. This is due to the fact that an increase of D requires an global amplification of the jump parameters, whereas W constraint involves rather modulation and fine control. While with a wide reception area an over-estimation of the impulse needed let some latitude to adapt the PJ on line, this over-estimation becomes deleterious in case of a majored W constraint: means of forces and iEMGs are consequently reduced.

Fitts' law is followed during FL but not during PR, which doesn't corroborate the common hypothesis that the law reflects preparation of movement (feedforward) rather than on-line adjustments (feedback). Time of FL can be adjusted by jumping higher or by extending the legs later. That might be emphasized by the expertise of the subjects, who are able to make on-line adjustments quick and accurate enough not to involve a long PR.

References: [1]Juras et al, J Mot Behav,41(6):525-528,2009

[2]Fitts,J Exp Psychol,47(6):381-391,1954

Disclosure of Interest: None Declared

Neurological and Motor Control

AS-0257

MUSCLE ACTIVATION PATTERNS DIFFERENCES IN RUNNING TECHNIQUES

Victor H. Munoz-Martel [1,*]

[1]Kinesiology, Universidad SEK, Santiago, Chile

Introduction and Objectives: Running biomechanics is highly related with competition performance and lower limb injuries. Three different techniques has been described[1], differentiated by foot strike pattern. These techniques behave very different on biomechanics elements [2] and natural technique selection by a subject is associated with evolutionary and socio-cultural elements[3].

Global limbs movement pattern are achieved by stimulation of neural pools within the spine[4], reinforcing the idea that neural organizations at the spine are responsible for cycling activities, this organization are known as central pattern generators (CPG) which are believe to be task specific[5].

EMG patterns from individual muscles during locomotion show high variability within steps. Nevertheless, if several cycles are considered, a stable pattern representative for inter-subjects muscle activity during the cycle is possible to obtain[6]. This pattern is associated with task specificity for each muscle contribution within the cycle and, therefore, task related muscle synergies might be studied[7].

Principal component analysis (PCA) is a high order statistical tool that permits to determine common characteristics within a data set in order to reduce the dimensions of the data array and represent the signal by a few new set of patterns. For EMG signals PCA reduces the number of signals to a fewer number of patterns that account for EMG activity of individual muscles. It has been suggested that principal components might represent the activity of a few oscillator controlling complex EMG activity within a cycle[8]. Since foot positioning is a relevant task for load response during locomotion is possible to theorize a synergy for it and, therefore it might have a control component associated.

It has been reported that five basic component accounts for over 90% of EMG activity during walking and running, however running techniques has not been considerate. The present study proposes that since there is more than one running techniques is possible to theorize more than one control strategy for each technique, which would be associated to a specific central command.

Objectives.

The aim of this study is to determine if there is different spinal control mechanism for each running techniques expressed as different synergies observed by principal component analysis.

Therefore, objectives are:

- Determine muscular activation patterns as control elements for the two most common techniques in habitual runners

- Describe muscular synergies differences between running techniques by principal components analysis

Methods: All trials were performed in the Human Performance Laboratory of the Universidad de Chile's Kinesiology School.

Four habitual runners run on a treadmill at 12 Km/h per 5 minutes. Wireless electromyography surface signals (BTS EMG capture, Milano Italy) were obtained from 16 lower limb and trunk ipsilateral muscles during 3 minutes. Cycles were determined by a foot switch that generated an electric pulse to the capture module whith pressure threshold of 5 mm/hg, foot switch was attached to running shoes and had two sensors, one on the calcaneus area and one on the metatarsal-phalanges region.

EMG signals from individual muscles were trimmed according to each cycle's duration and averaged to obtain a signal pattern representative to muscle activity during a stride.

Each muscle stride pattern was concatenated to obtain a matrix containing all 16 muscles cycle activity. Activation patterns and muscular sequences were obtained by principal component analysis. Principal components weight were obtained. Components representing over 95% of EMG activity were selected for further analysis and techniques comparison.

Principal component were rotated by a varymax rotation. Components were analyzed to obtain time to peak activity from initial contact. Componentes were then organized in ascending order based on to time to peak from initial contact. Each principal component weight was calculated and a morphological analysis was performed in order to match principal components to a task according to Ivanenko's previous work[9]. Muscle synergie contribution was clasiffied by svm.

Component's time to peak, weigth, statics and muscle contribution were compared between techniques.

Results: Differences were observed in components composition and weigth.

Conclusion: Recognizing activations patterns as neural control elements may contribute to understand how running techniques are organized by CNS.

Differences in activation patterns were observed between running techniques suggesting different task oriented oscillators activity within the spine.

Considering the relationship between mechanical element with running techniques, understanding neuromuscular variables associated with running may contribute to orientate to a neuromuscular vision of distance running performance training, injury prevention and treatment.

Disclosure of Interest: None Declared

Neurological and Motor Control

AS-0258

EFFECTS OF ADDITIONAL CONSTANT AND IMPROMPTU COGNITIVE LOADINGS ON LOWER EXTREMITY GAIT PERFORMANCE

C.K. Chan [1,*] J.C. Teoh [1] Luis C. Hernandez-Barraza [1] Desmond Y.R. Chong [1] C.H. Yeow [1]

[1] BIOMEDICAL ENGINEERING, NATIONAL UNIVERSITY OF SINGAPORE, SINGAPORE, Singapore

Introduction and Objectives: Recent research has delineated that simultaneous dual-task texting and walking affect the sensorimotor balance control and locomotion. This may lead to accidents due to navigational complications among pedestrians. Although past studies have examined both upper and lower extremities biomechanical analysis during dual-task scenarios [1-2], little attention is given to the effects of constant and impromptu cognitive loading on the gait performance of the pedestrian. This study, thence, aimed to investigate how additional constant and/or impromptu cognitive loading may be prioritized and affect the gait parameters, which comprise of sagittal-plane kinematics, kinetics and energetics analysis. Constant and impromptu cognitive loadings, introduced in this study, were texting and attending auditory cue respectively.

Methods: Twelve young voluntary participants (six male and six female) were recruited. Trials were conducted in gait laboratory, comprised eight infrared cameras and two force-plates. Four walking modalities were designed: (a) normal walking; (b) walking while texting on cellphone; (c) walking while attending auditory cue; and (d) walking and cellphone texting whilst attending to auditory cue. The cue was given to the subject to step onto designated colour regions placed on the force-plate. The force-plate was equally separated into two different colour regions. Failing to step onto the required region, the respective trial was repeated with different colour combination. As for texting on cellphones, sentences were instructed to the participants. Accuracy of the sentences was evaluated, which the trial shall be repeated if the accuracy was less than 50%. Data extracted from Vicon Nexus. Two-way ANOVA analysis and Tukey post-hoc testing was performed.

Results: Our findings indicated a reduction in ankle joint power in the late stance. The plausible reason for the reduction is the deviation of the prioritization [2] during texting-walking while attending auditory cue, resulting in reluctance to propel forward. This factor further elicited lower gait velocity and smaller step length during texting-walking as reported in [3]. Moreover, the percentage of texting success for the subjects in following the auditory cue was reduced in the case where the subjects performed texting while walking as compared to normal walking. Due to additional cognitive loading, the alertness of the subjects was attenuated in order to divert their attention partially to the phone. Furthermore, human locomotion depends on the optic flow in steering the motion direction [4]. Reduction in the sagittal knee moment and knee power suggests that both optic flow and cognitive loading may contribute to deviation in prioritization [2] and cascade consequences in both kinetics and energetics.

Figure:
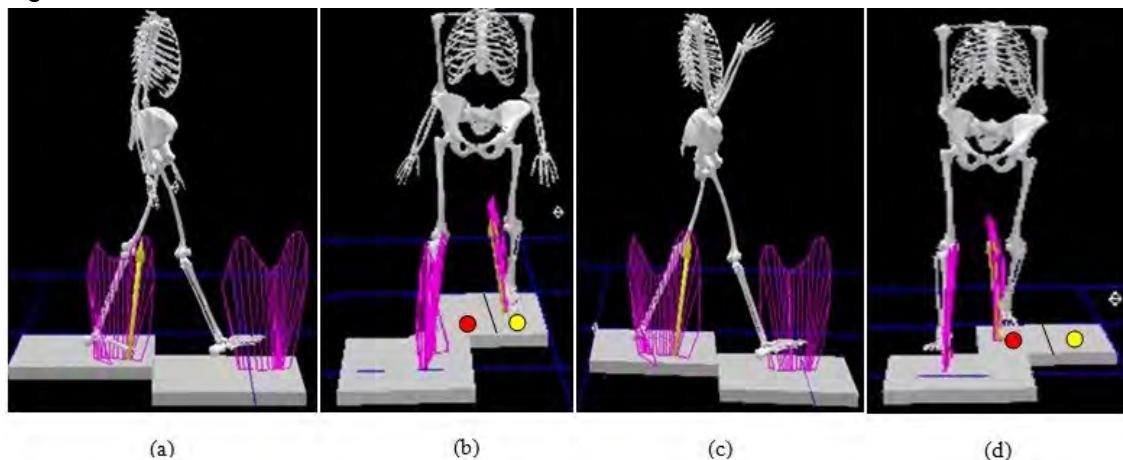
Caption: Figure 1: (a) Normal walking; (b) Walking while attending to auditory cue in stepping onto the yellow region of the force-plate; (c) Texting while walking; and (d) Walking and texting while attending to auditory cue in stepping onto the red region of the force-plate.

Conclusion: Two key factors that contributed to the walking control strategy were cognitive loading and optic flow adjustment. Furthermore, prioritization in cognitive loading may alter the balance and stability in maintaining walking trajectory. Hence, simultaneous adjustment of additional cognitive loading and interrupted optic flow in attending sudden obstacles besides texting while walking will further disturb the prioritization strategy. Consequently, this may affect the stability and cause unforeseen mishaps. This research is essential in conveying that pedestrians, who perform texting while walking, are prone to accidents as they may not be aware of their surroundings and are unable to react promptly if there is an additional impromptu cognitive loading.

Table:

Maximum Ankle Power			
Factor B	Factor A		P-value
	Walking without texting	Walking with texting	
With auditory cue	3.30 (0.90)	4.05 (0.35)	0.0413*
Without auditory cue	3.50 (0.92)	4.01 (1.00)	0.338
Minimum Knee Power			
Factor B	Factor A		P-value
	Walking without texting	Walking with texting	
With auditory cue	-0.49 (0.30)	-0.05 (0.45)	0.287
Without auditory cue	-0.76 (0.59)	-0.48 (0.14)	<0.001*
Maximum Knee Flexion Moment during Swing Phase			
Factor A	Factor B		P-value
	With auditory cue	Without auditory cue	
Walking with texting	0.17 (0.11)	0.23 (0.14)	0.031*
Walking without texting	0.31 (0.24)	0.38 (0.30)	0.208

*Values are means (standard deviation). * denotes significant difference, P<0.05.*

Caption: Table 1: Significant Differences in Biomechanical Parameters

References: [1] Springer et al., D. M.D., 21: 950-957, 2006.

[2] Plummer et al., T. G&P,2014.

[3] Kannape et al., C. PO, 9,2014.

[4] Hidler, B.JoAP, 104:747-755,2007.

Disclosure of Interest: None Declared

Sport

AS-0259

IDENTIFYING TREADMILL RUNNING FATIGUE USING TRUNK ACCELEROMETRY BASED MEASURES

Kurt H. Schutte [1 2 3,*] Ellen Maas [2] Rachel Venter [1] Vasileios Exadaktylos [3] Daniel Berckmans [3] Benedicte Vanwanseele [2]

[1] Dept of Sport Science, Stellenbosch University, Stellenbosch, South Africa, [2] Dept of Kinesiology, [3] Dept of Biosystems, KU Leuven, Leuven, Belgium

Introduction and Objectives: The ability to identify and correct deterioration in a runner's technique due to fatigue is of value to enhancing athletic performance and might have potential to prevent injuries [1]. In the context to running, fatigue may play a role in the complexity of the neuromuscular control system output, whereby movement errors become more apparent and necessitate frequent movement corrections [2]. Controlling centre of mass (CoM) movement while running has been considered as a plausible safety mechanism for pain avoidance, self-preservation of musculoskeletal structures [3], and conserving and maintaining efficiency [4]. This suggests that CoM control during running could play an important role in the prevention of running injuries.

In contrast to traditional 3D motion capture, wireless body-worn tri-axial accelerometers offer a novel approach to movement analysis that eliminates the need for timely set-up of gait analysis equipment, and facilitates easier data collection over a diverse array of indoor or outdoor settings. To the best of the authors' knowledge, no previous study has applied accelerometry methods to analyse dynamic gait stability of the CoM during running until exhaustion. The aim of this study was therefore to investigate dynamic CoM stability in relation to running-induced fatigue in both novice and competitive runners using tri-axial lower-back accelerometry based measures. We hypothesized that tri-axial lower-back accelerometry would be able to detect 1) higher step irregularity 2) higher complexity (unpredictability), and 3) greater horizontal plane (mediolateral and anteroposterior axes) contribution to the resultant acceleration with running fatigue in both competitive and novice runners.

Methods: Twenty-two age-matched (18-33 years) runners (10 novice; 12 competitive) were recruited to participate in this repeated measures study. Ten seconds of raw, tilt corrected tri-axial (vertical, mediolateral, and anteroposterior) accelerations extracted from a lower-back mounted accelerometer at the start and end (volitional exhaustion) of a treadmill running fatigue protocol. Step and stride regularity, sample entropy, and each independent axis root mean square (RMS) contribution to the resultant RMS were used to quantify both linear and non-linear dynamic CoM stability of running. Accelerometry measures were collected in two speed conditions, namely a standardized low speed (1.94 m·s^{-1}), and self-selected high speed ranging $2.11 - 3.33 \text{ m·s}^{-1}$.

Results: After treadmill running to exhaustion, fatigue runners experienced a significant decrease in step regularity in the anteroposterior (22 % low speed; 26 % high speed) direction, an increase in sample entropy in the vertical (25% low speed; 23 % high speed) and anteroposterior (12 % low speed; 8 % high speed) directions, and an increase in horizontal plane contribution to the RMS ratio for the mediolateral (17 % low speed; 12 % high speed) and anteroposterior (17 % low speed; 9 % high speed) directions.

Figure:
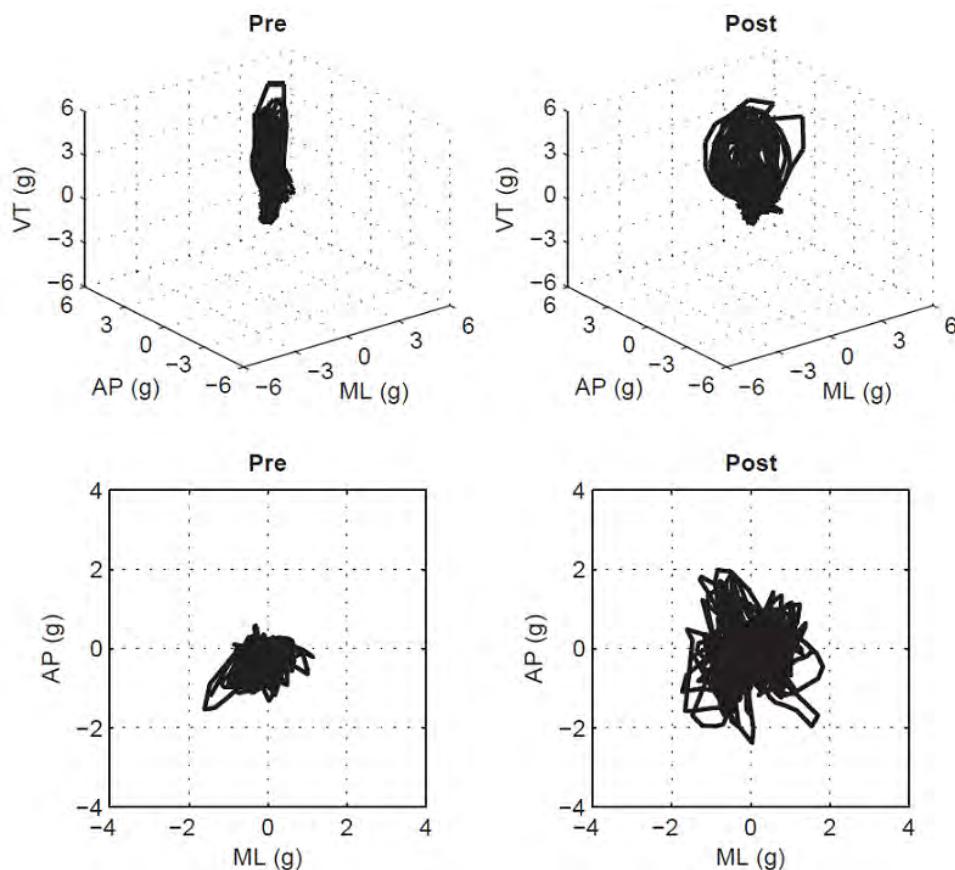
Caption: Stabilograms from 10 seconds of extracted accelerometry signals for an exemplary novice runner, represented as 3D resultant acceleration vector (above) and 2D horizontal accelerations (below) at Pre and Post fatigue. Observed increases in horizontal accelerations with fatigue consisted of increases from the mediolateral (ML) and anteroposterior (AP) acceleration components.

Conclusion: Running fatigue influenced both novice and competitive runners to alter dynamic accelerometry measures of CoM control in the form of more irregular steps, higher complexity (more unpredictability), and increased contribution of horizontal plane accelerations to the resultant, demonstrating that a single lower back-mounted accelerometer can provide useful information about the process of treadmill running fatigue. Our results support the concept that accelerometry signals during running are not confined only to discrete measurements but are also well suited for measuring raw continuous time-varying measures from independent axes. Applying different accelerometry based measures serves to broaden our understanding as to how runners control their CoM in response to fatigue.

References: [1]   Elliott et al., *Res. Q. Exerc. Sport,* 52: 160–166, 1981.

[2]   Meardon et al., *Gait & Posture*, 33, 36–40, 2011.

[3]   Morin et al., *Med. Sci. Sports Exerc.*, 43, 829–36, 2011.

[4]   Novacheck, *Gait & Posture*, 7, 77–95, 1998.

Disclosure of Interest: None Declared

HOW PLAYERS CONTROL TENNIS RACKET VIBRATION TRANSFERRED TO THEIR FOREARM?

Delphine Chadefaux [1,*]Guillaume Rao [1]Philippe Androuet [2]Eric Berton [1]Laurent Vigouroux [1]

[1]Institute of Movement Sciences, UMR CNRS 7287, Aix-Marseille University, Marseille, [2]Department of Movement Sciences, Oxylane Research, Villeneuve d'Ascq, France

Introduction and Objectives: The ball impact on the tennis racket stringing leads to vibration waves propagating into the handle and the player's forearm through his hand. The characteristics of these vibrations may influence the pathology risks and contribute to the player's comfort and feeling. In spite of a well-extended knowledge of tennis racket physics leading to accurate racket models, little is known about the player's ability to control stroke-induced vibrations. The hand/racket interaction is however crucial in the vibration waves propagation. This study contributes to get insight into such a control mechanism by analyzing stroke-induced vibration at the racket and the forearm levels for various stroke intensities and spectral contents.

Methods: 14 right-handed male participants with no pathology were involved in the experiments. They were tennis experts (ITN > 3.5), 21 ± 3 years old, 182 ± 8 cm tall, and weighted 73 ± 8 kg. After an unlimited warm-up period with their own racket, they were asked to hit forehands toward a target in 15 conditions. To investigate stroke-induced vibration signals in a wide range of intensities and spectral contents, 5 rackets with various mechanical characteristics as well as 3 stroke intensities (weak, medium and hard) were tested. A one dimensional accelerometer (Dytran ; ± 500 g ; [1.6 – 10000] Hz) was disposed on the racket handle at 15 cm of the butt cap and two three-axis accelerometers (Endevco ; ± 50 g ; [20 – 6000] Hz) were fixed on participant's wrist and elbow (see Figure). Note that motion reproducibility was controlled through a high-resolution motion-capture system (Vicon, Oxford UK, 8 infrared cameras, 200 Hz). Besides, a grip force index was computed according to electromyographic signals (extensor digitorum communis, extensor carpi radialis longus, flexor digitorum profondus and superficialis, and flexor carpi ulnaris) recorded with a wireless Delsys system combined with a preliminary calibration task. These databases were gathered at 12000 Hz.

Results: Regarding first the intensity, results indicated that the vibration energy at the wrist and the elbow increases with the stroke intensity. A linear relationship, specific to each participant, occurred between wrist and elbow energies. The participants' action thus could lead to a constant ratio of energy transferred to the forearm, dependent on the participant but not on the stroke intensity. Additionally, the grip force increased with the stroke intensity which obviously modified the mechanical linkage between the hand and the handle. These grip adaptations can be seen from two points of view. First, it could be assumed that grip force adjustments participate in keeping the former energetic ratio constant. A second hypothesis is that participants stabilized the hand/racket interaction by increasing the grip force. Indeed, when increasing the grip force, a minimization of the vibration energy transmitted in the plane perpendicular to the racket was shown while the vibration energy transmitted in the longitudinal plane grows.

Although most of the spectral content of a tennis racket was lower than 1500 Hz, only the first bending mode at about 140 Hz appeared in the accelerometer' signals measured at the wrist. Moreover, the modal parameters were modified by the grip when assessing frequency and damping values through classical modal analysis in free boundary condition.

Indeed, the modal damping raided from less than 1 % to about 10 %.Meanwhile depending on the participant and the racket, the modal frequency decreased of 1 Hz to 20 Hz. By controlling the grip position and the force intensity, players can thus finely tune vibration waves transferred to the forearm such as an adaptive filter. Due to these modifications, two different rackets held by a given participant showed closer modal parameters than the same racket held by two participants. Interestingly, it results that the participant effect is at least as significant as the racket physical features on the spectral properties of the vibration waves propagating from the racket to the participant's forearm.

Figure:
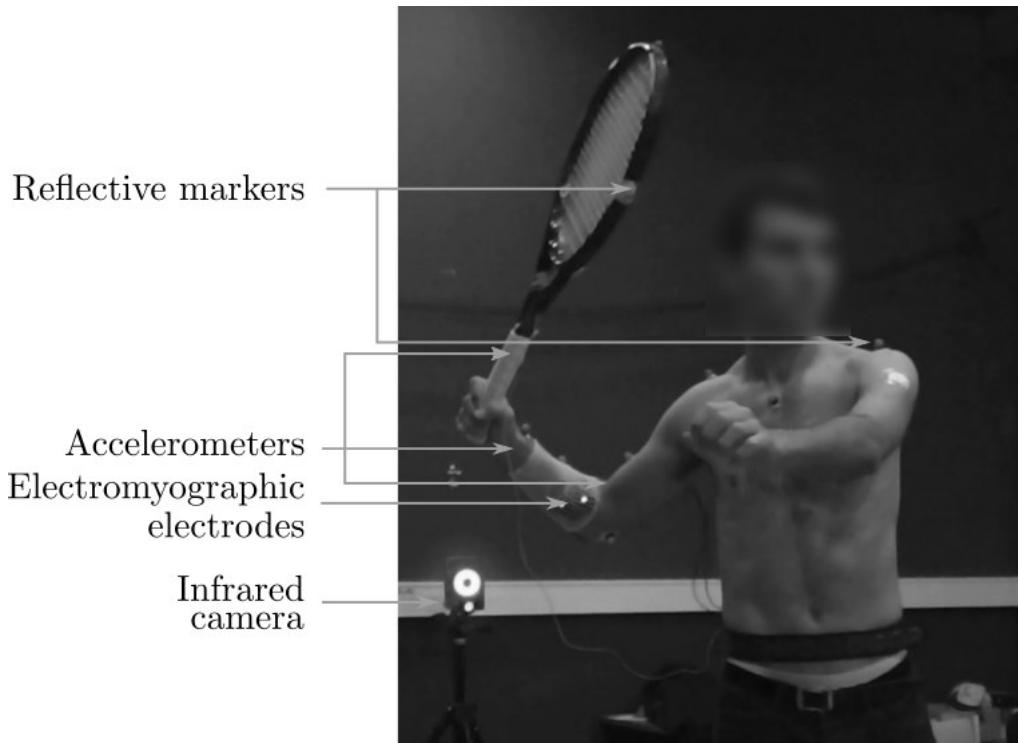
Caption: Experimental setup. Forehand strokes were performed by participants with 5 rackets and 3 intensities. Classical biomechanical signals were gathered (EMG, kinematics and vibration waves) on the racket as well as on the participant

Conclusion: The main results of this study pointed out that the vibration characteristics are highly dependent on the player's grip. The players seemed to adopt strategy by modifying the grip of the racket. The individual grip strategy seemed to determine both the intensity and the orientation of the vibration transferred to the forearm. These results enforce consideration of the hand-grip as an adaptive filter, whose characteristics are more dependent on the player than on the racket itself. Assuming this non-negligible effect of the player's grip on vibration waves, a renewal of equipment designs could emerge by considering the deep interaction between the player and the racket.

Disclosure of Interest: None Declared

RELATIONSHIP BETWEEN PRE-STRETCH AUGMENTATION OF JUMP PERFORMANCE, ANKLE DORSIFLEXION RANGE OF MOTION AND ANKLE STIFFNESS DURING THE SUPPORT PHASE OF DROP JUMP IN WUSHU ATHLETES

Léo Benouaich [1,*] Philippe Rouch [1] Françoise Natta [2] Patricia Thoreux [1][3]

[1] LBM/Institut de Biomecanique Humaine Georges Charpak, Arts et Metiers ParisTech, [2] Institut National du Sport, de l'Expertise et de la Performance, [3] Hôpital Avicenne, APHP, Université Paris 13, Sorbonne Paris Cité, Paris, France

Introduction and Objectives: Research in sports biomechanics enables better understanding of performance mechanisms, leading to improved performance and reduced risk of injury. Wushu, better known as kungfu, is the sportive and modern form of Chinese martial arts, and consists in performing a routine of martial movements associated with acrobatic jumps. Athletes must have both an important ankle range of motion in dorsal flexion to perform low stances with heels on the ground, and a high vertical jump for acrobatics. As in many sports, jumps are performed with a running up followed by a support phase with eccentric and concentric phases. One challenge for athletes is to be able to benefit from initial velocity to jump higher than they would do without any prior eccentric phase [1]. In this ability, ankle function can be studied threw ankle stiffness [2]. The aim of this study was to analyze if there are links between the benefic use of initial velocity, ankle stiffness during the concentric phase and maximal dorsiflexion angle in wushu athletes.

Methods: After a standardized warm-up and maximal ankle dorsiflexion angle measures, 12 athletes of the French wushu team performed 3 repetitions of 2 maximal jumps: squat jump (SJ) and drop jump (DJ). 42 reflective markers were placed over skeletal landmarks. Kinematics were registered at 300 Hz with a 13 cameras Vicon system and ground reaction forces with 2 AMTI force plates at 900 Hz. Marker positions were filtered with an adaptive Butterworth filter [3] and body segment inertial parameters were personalized [4]. Flexion moments, calculated using inverse dynamics, and flexion angles of both ankles were expressed between 0 and 100% of the support phase.

Performance was defined as the maximum height of the Center of Mass (CoM) during the flight phase minus the CoM height in static position. Pre-stretch augmentation (PSA) is defined as the ratio between the maximal performance in DJ and the maximal performance in SJ, minus 1 [5]. Ankle flexion moments were plotted versus ankle flexion angles, and two linear regressions were performed for the two halves of the concentric phase. The two regression slopes were defined as the ankle dorsiflexion stiffness in the first half of the concentric phase (k_1) and the ankle dorsiflexion stiffness in the second half of the concentric phase (k_2).

Athletes were separated into three groups with respect to their PSA during DJ: Low (LPSA), Medium (MPSA) and High PSA (HPSA). Data of the best performance for each subject and each jump condition were kept for analysis. Wilcoxon tests were performed for k_1, k_2 and maximal dorsiflexion angle for LPSA and MPSA, with HPSA as reference.

Results: PSA was different between groups whereas performance, anthropometric data and training experience were similar. In LPSA and MPSA, k_1 was lower than in HPSA ($p<0.05$). Maximal dorsiflexion angle was lower in LPSA than in HPSA ($p<0.05$), 0° corresponding to the dorsiflexion angle in static standing position. Results are presented in the table.

Typical flexion moment vs. flexion angle curves of HPSA and LPSA, and their respective k_1 and k_2 are presented in the figure.

Figure:
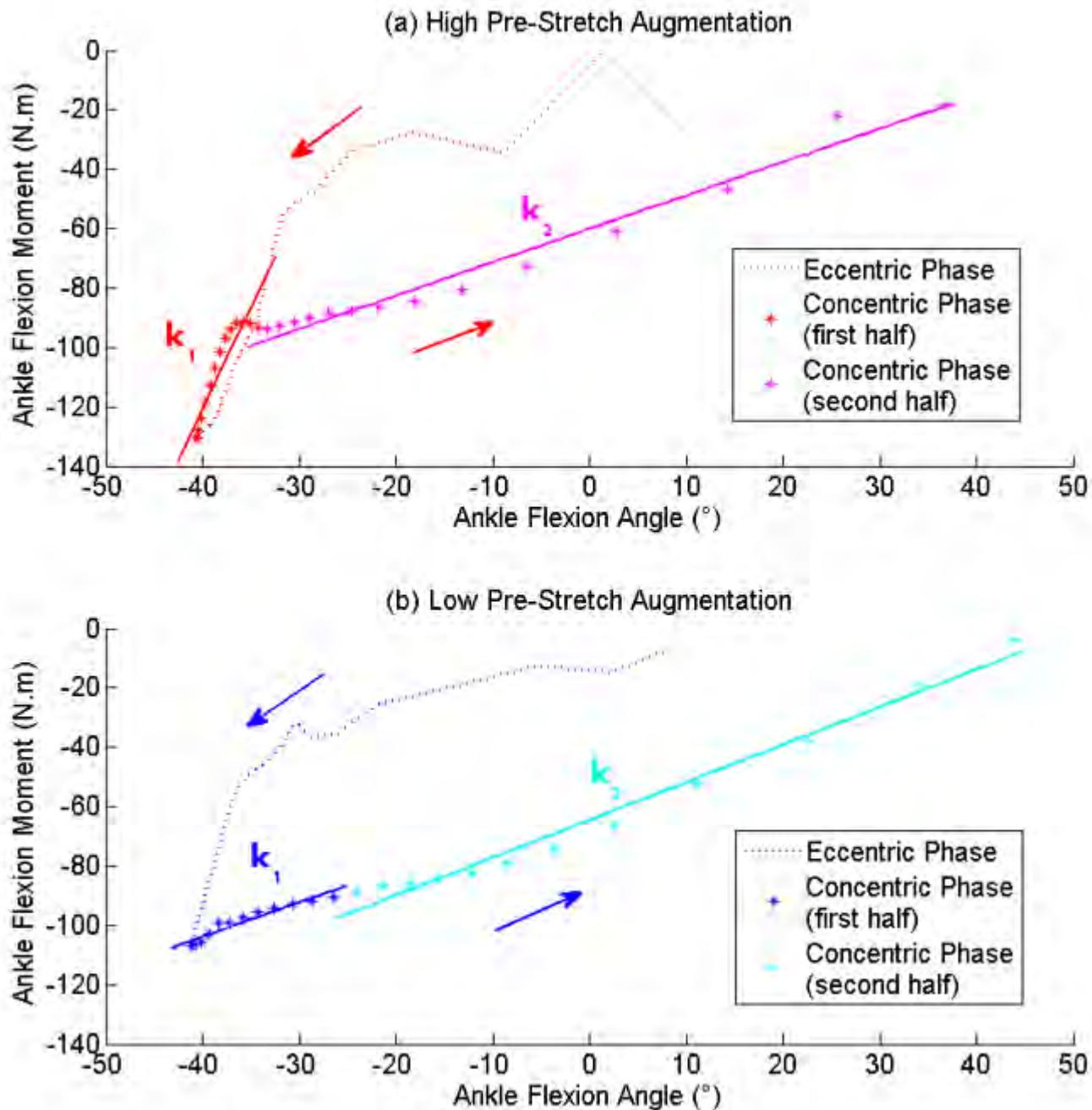
Caption: Typical ankle flexion moment vs. ankle flexion angle curves during the support phase in HPSA (a) and LPSA groups (b)

Conclusion: The ankle stiffness bilinear evolution in HPSA can be interpreted as two different mechanisms predominating consecutively during the concentric phase. The first and higher slope could be mainly explained by the passive shortening of previously stretched tissues, whereas the second and lower slope could be the effect of the active shortening of the triceps surae muscle fibers. In LPSA, the second mechanism appears to be predominant. The higher dorsiflexion RoM observed in LPSA could explain the difficulty for this group to store and recoil elastic energy, and their choice of a predominant 'active strategy' during the stance phase, in opposition to the 'combined active-passive strategy' used by HPSA.

As PSA in drop jump does not only depend on the ankle joint, athletes of the MPSA group used both strategies at the ankle level, explaining the absence of characteristic ankle strategy for this group.

Those two different strategies involving two different dynamic behaviors of the ankle joint, it would be interesting to take them into account for personalized training optimization, injury prevention and the return to training after injury.

Table:

	PSA (%)	DJ Performance (cm)	k_1 (Nm/°)	k_2 (Nm/°)	Maximal Dorsiflexion Angle (°)
HPSA	19 ± 3	54 ± 7	5.5 ± 2.6	1.5 ± 0.3	- 34 ± 4
MPSA	12 ± 2	46 ± 5	3.0 ± 2.3 *	1.5 ± 0.6	- 41 ± 8
LPSA	7 ± 2	54 ± 6	2.9 ± 1.2 *	1.9 ± 0.4	- 42 ± 6 *

Caption: PSA, Drop Jump performance, k1, k2 and Maximal Dorsiflexion Angle for the 3 groups, HPSA, MPSA and LPSA. * correspond to p-values lower than 0.05.

References: [1] Cavagna et al., J Appl Physiol, 24: 21-32, 1968.

[2] Kubo et al., Eur J Appl Physiol, 99: 235-243, 2007.

[3] Erer, J Biomech, 40: 2934-2943, 2007.

[4] Pillet et al., Gait Posture, 31: 147-152, 2010.

[5] Walshe et al., Eur J Appl Physiol, 73: 332-339, 1996.

Disclosure of Interest: None Declared

Sport

AS-0262

DIFFERENCES IN ANKLE AND KNEE JOINT KINEMATICS AND KINETICS DURING THE FIRST STANCE PHASE OF THE ACCELERATION PHASE DIFFERENTIATE BETWEEN YOUNG AND ADULT HIGH LEVEL SPRINTERS

Jeroen Aeles [1,*] Ilse Jonkers [1] Sofie Debaere [1] Christophe Delecluse [1] Benedicte Vanwanseele [1]

[1] Department of Kinesiology, KU Leuven, Leuven, Belgium

Introduction and Objectives: Sprint running can be divided in several distinct phases including the sprint start, acceleration phase and maximum velocity phase [1]. In the acceleration phase, the first stance phase is a unique element, in which power is transferred from the block phase to the rest of the acceleration phase. To better understand the difference in sprinting performance between adult and youth sprinters, joint power, joint stiffness and individual muscle-tendon complex maximal stretching and shortening velocities at the ankle and knee joint of the stance leg were determined during the first stance phase following a block clearance.

Methods: Eleven adult athletes (6 male and 5 female) and thirteen young athletes (5 male and 8 female) performed an explosive sprint start action. Twelve MX3 cameras (250Hz) and a Kistler force plate (1000 Hz) were used to collect 3D marker coordinates and the ground reaction force (Nexus, Vicon). A musculoskeletal model [2] was scaled to each subject's individual anthropometry using OpenSim 1.9. An inverse kinematics procedure was conducted to obtain joint angles and to derive joint angular velocity and individual muscle-tendon complex lengths of ankle plantar flexor and knee extensor muscles. An inverse dynamics procedure was conducted to calculate the net joint moments and joint power at the ankle, knee and hip. Joint stiffness was defined as the slope of the linear regression line on the moment-angle curve. For each joint this curve was split in two at the maximal moment, joint stiffness was thus calculated for the ascending limb and the descending limb of both the ankle and knee joint. Muscle-tendon complex length changes were normalised to the muscle-tendon complex lengths in a neutral standing position (ankle, knee and hip joint angles were set to 0 deg. for each individually scaled model). Afterwards the derivative of these curves, showing the muscle-tendon complex length changes were calculated for maximal stretching and shortening velocities of 7 individual muscle-tendon complexes. All parameters were first tested for skewness, after which a one-way ANOVA was used to determine significant ($p < 0.05$) differences between groups for the non-skew parameters. All data presented in the results section were normally distributed.

Results: Joint power contribution to total power generation (sum of ankle, knee and hip joint power) was significantly different between the youth and adult sprinters. The contribution of the ankle joint was larger ($p = 0.024$) in the youth sprinters (32 ± 10%) compared to the adult sprinters (21 ± 12%). The adult sprinters, on the other hand, had a larger ($p < 0.001$) contribution from the knee joint (34 ± 12%) to total power generation compared to the youth sprinters (12 ± 5%). Knee joint stiffness on the descending limb of the moment-angle curve was larger ($p = 0.005$) in the adult (5.56 Nm/deg. ± 2.18 Nm/deg.) compared to the youth sprinters (3.38 ± 1.18 Nm/deg.). Although maximal stretching velocities were not different between groups, the maximal shortening velocities were larger ($p < 0.045$) in the adult (0.94 ± 0.12 mm/ms; 0.87 ± 0.11 mm/ms; 0.89 ± 0.11 mm/ms for the) compared to the youth sprinters (0.79 ± 0.20 mm/ms; 0.71 ± 0.20 mm/ms; 0.73 ± 0.21 mm/ms) for the m. soleus, m. gastrocnemius medialis and m. gastrocnemius lateralis respectively.

Conclusion: Joint power and joint stiffness results suggest that the faster adult sprinters rely more on the knee joint than on the ankle joint, as opposed to the youth athletes. Although youth sprinters have a larger power generation in the ankle joint, their plantar flexor muscles are shortening at a lower maximal velocity compared to the adult sprinters. Since the knee but not the ankle joint stiffness was different between our groups and increasing running velocity has been linked with an increased stiffness in the knee and not in the ankle joint [3], it appears that sprint running performance may be more dependent on knee rather than ankle joint stiffness.

References: [1] Charalambous et al., *J Sports Sci.*, 30:1–9. 2012

[2] Hamner et al., *J Biomech.*, 43:2709–2716. 2010

[3] Kuitunen et al., Med Sci Sports Exerc., 34:166–173. 2002

Disclosure of Interest: None Declared

AS-0263

THE ROLE OF TORSIONAL ROTATION OF TRUNK IN SPRINT RUNNING

Natsuki Sado [1,*]Senshi Fukashiro [1]

[1]The University of Tokyo, Tokyo, Japan

Introduction and Objectives: In various dynamic movements of sports, the trunk muscle activities exert an influence on the performances. From this view point, many studies have reported on the kinematics of the pelvis and trunk during running (Novacheck 1998; Schache et al. 2002). However, the kinetics of the trunk are not yet fully examined. The purpose of the present study was to investigate the role of trunk in sprint running, based on the kinetics of the trunk.

Methods: Ten healthy, male sprinters (age: 20.8 ± 1.3 years, height: 1.75 ± 0.03 m, and body mass: 64.7 ± 3.3 kg) participated in this study. All subjects preformed 40 m sprint running with maximal effort. The motion capture system (mac 3D system, USA/nac, Japan, 200 Hz) with a synchronized force platform (Force Plate 9281E, Kistler, Switzerland, 200 Hz) was used to collect kinematics and ground reaction force data. An inverse dynamics approach was used to calculate forces and torques at the ankle, knee, hip, and lumbosacral joints. Mechanical powers induced by forces and torques at the joints were calculated. The kinetics of all participants were divided by their respective body masses. The anatomical components of the hip and lumbosacral joint torques were projected onto the z_{pel} axis (superior-inferior axis of the local coordinate system defined at the pelvis). The contribution to pelvic moment around the z_{pel} axis from each of the anatomical components of the hip and lumbosacral joint torques was determined. A two-tailed paired t-test was used to determine the differences between the contributions of the anatomical components of the hip and lumbosacral joint torque. The significance was accepted at $p < 0.05$.

Results: Fig.1a showed an example of mechanical power induced by x_{pel}, y_{pel} and z_{pel} axes components of force at the hip joint of the support leg. Although the x_{pel} (right-left axis of the local coordinate system defined at the pelvis) and z_{pel} axes components exerted little power, the y_{pel} (anterior-posterior axis of the local coordinate system defined at the pelvis) axis component exerted a large negative power during the late swing phase and a large positive power during the early swing phase. Fig.1b showed an example of the contribution of the anatomical components of hip and lumbosacral joint torques to the pelvic moment around the z_{pel} axis. The rotational torque exerted by the lumbosacral joint had a large negative contribution (toward the support leg side) during the late swing phase and a large positive contribution (toward the free leg side) during the contact and early swing phase. During the late and early swing phases, there were significant differences between the mean contributions of the rotational torque exerted by the lumbosacral joint and the mean contributions of all anatomical components of the hip joint torque ($p < 0.001$). The moment of the pelvis toward the free leg side applies an anterior force to the support leg. Conversely, the moment of pelvis toward the support leg side applied a posterior force to the support leg. These results suggested that the rotational torque exerted by the lumbosacral joint mainly generate the force at the hip joint, generating great mechanical power.

Figure:
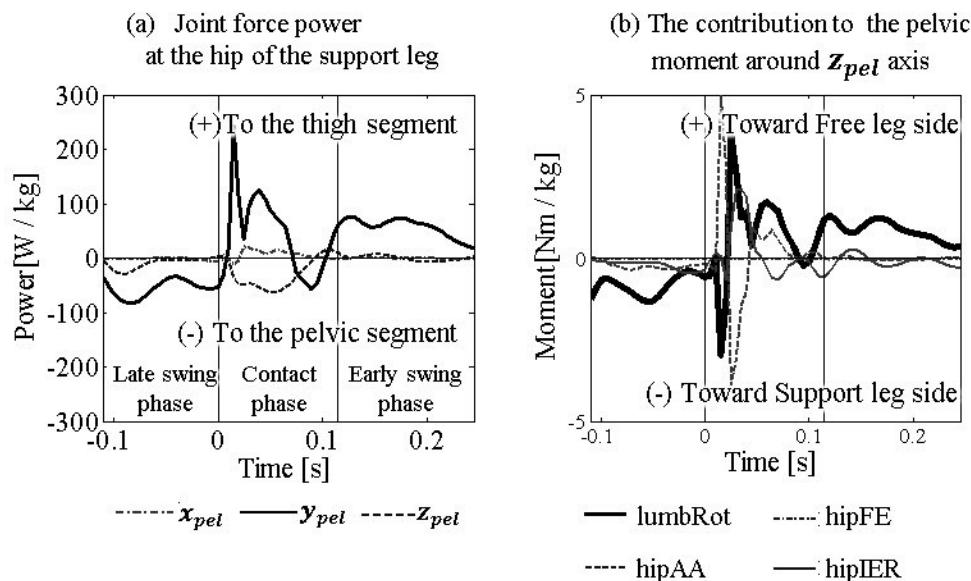
Fig.1 An example of mechanical power induced by x_{pel}, y_{pel} and z_{pel} axes components of force at the hip joint of the support leg (a), and the contribution of the anatomical components of hip and lumbosacral joint torques to the pelvic moment around the z_{pel} axis (b).
lumb: the lumbosacral joint, Rot: Rotation, FE: Flexion / Extension, AA: Abduction / Adduction, IER: Internal / External Rotation

Conclusion: The rotational torque exerted by the lumbosacral joint contributed the largest to the pelvic moment around the z_{pel} axis. By applying the anterior force to the backward leg and the posterior force to the forward leg, the rotational muscles generated negative mechanical power to the forward leg and positive mechanical power to the backward leg.

References: [1] Novacheck, Gait and Posture, 7(1), 77-95, 1998

[2] Schache et al. Human Movement Science, 21(2), 273-293, 2002

Disclosure of Interest: None Declared

Sport

AS-0264

PUSHOFF FORCES AND POSTURE ANALYSIS OF TACKLE IN ELITE RUGBY PLAYERS: A PILOT STUDY

Davide Pavan [1] Fabiola Spolaor [2] Annamaria Guiotto [2] Claudio Cobelli [2] Giorgio Sbrocco [1] [3] Zimi Sawacha [2,*]

[1]Department of Biomedical Science, [2]Department of Information Engineering, University of Padova, [3]Italian Rugby Federation (FIR), Padova, Italy

Introduction and Objectives: Increased professionalism in rugby has elicited rapid changes in the techniques for evaluating the performance of elite players [1]. Commonly state of art concentrate on the physiological assessment of rugby players through protocols including vertical jump, weight lifting tests, timed short sprints and the isokinetic machine tests [1,2]. However, these measuring techniques represent an indirect measure of the ability of the players and can't be applied to directly assess their performance in the real game. Furthermore there is a paucity of research dedicated to investigating the biomechanics of tackling [2]. There is the need for significant refinement of investigations on task-specific testing procedures, in particular with respect to the assessment of tackling performance in rugby players. The aim of this work is to study the differences in the maximum individual pushing force produced by tackling in two different body postures (2 body heights) with a self-developed tracking of motion software [3] and a plantar pressure (PP) insoles system.

Methods: 10 subjects participated in the study (mean ± standard deviation (SD) BMI: 27.3±1.6, age: 21.4 ± 3.1 years) however in the present contribution only the results concerning a single athlete will be presented. All the athletes belong to the University Team of Padova (CUS Padova) that plays in the National Championship. Subjects were asked to perform 6 repeating tackles (see Figure 1) at two different heights: between the knee and the hip (KH) and between the hip and the pelvis (HP). Plantar pressure (PP) distribution was recorded (see Figure 1) by means of Novel Pedar system (novel GmbH, Germany) and 4 synchronized cameras (Logitech, C525) were used for capturing the subjects' motion. Trunk, hip, knee and ankle joints kinematics were determined by tracking specific features bilaterally (acromions, C7, anterior iliac spines, lateral femoral epicondyles, lateral malleoli, a point on the shoes approximately corresponding to the 5th metatarsal head, elbows, wrists) directly on the motion sequences with a self developed software [3]. Joints angles, peak PP (PPP) and peak vertical force (PV) were determined in Matlab (Matlab R 2013) codes [4] and their position with respect to 4 different events estimated: side step (SS), contact (C), landing, standing and ball catching.

Results: The current protocol enabled highlighting differences in the lower limb joints angles excursion between the tackle performed in the two different conditions (see Figure 1 Top right). With this respect the maximum flexion was reached at the ankle joint (130°) between 60 and 80% of the SS-C phase in HP condition, and the maximum extension was reached at the knee joint at 30% of the SS-C phase. Results concerning the PPP and PV values registered in the 2 best tackles in each condition were reported in Figure 1. It can be noticed that the subject displayed the highest PV value in correspondence of the tackle performed in HP condition at SS with a PV of 3535.8 N (left foot in contact with the ground).

Figure:
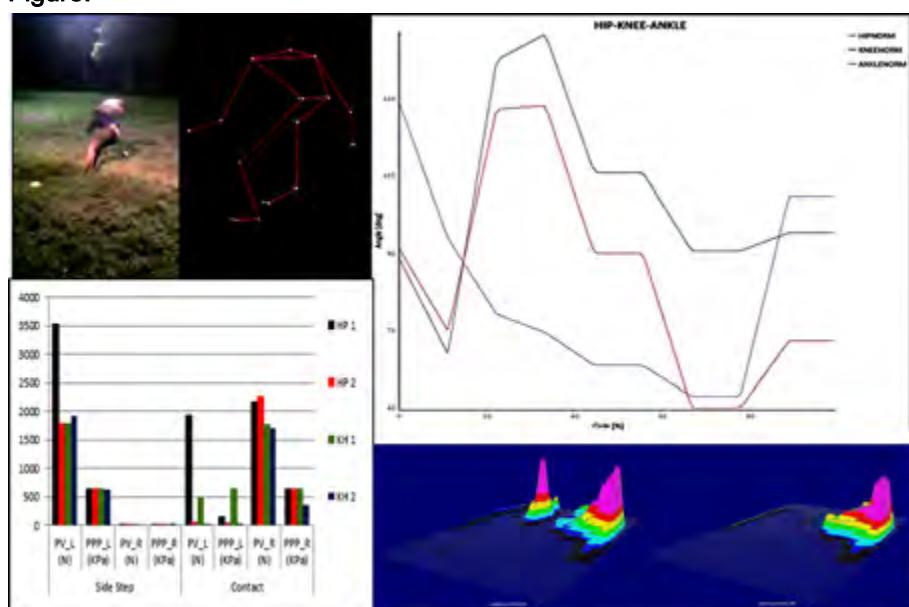
Caption: Figure 1. Top left figure: an athlete while performing a tackle in condition HP and his video sequence's 3d reconstruction. Top right figure: hip (blue)-knee (black)-ankle (red) joints flexion (-) and extension (+) angles of the best tackle in HP condition from SS (0% cycle) to C (100% cycle). Lower left figure: comparison between PPP and PV of the best 2 tackles respectively in condition KH and HP. PPP and PV are reported with respect to their values in the 4 different events. Lower right figure: comparison between 2 tackles' PP distribution in the two conditions KH (KH1) and HP (HP2) respectively (from left to right) during the contact.

Conclusion: Preliminary results showed that the present protocol allowed highlighting differences in the two tackle conditions either in the ground reaction forces or the joint angles. Furthermore differences in PV and PPP were observed with respect to significant events that characterized the tackle task. In particular a better performance of the athlete in term of PV was registered in HP condition. Future development will include completing the data analysis over the complete sample subjects and investigating the relationship between peak of forces and joints' angles.

References: [1] Jenkins, D., and P. Reaburn. Australian Sports Commission and C.J. Core, eds. Champaign, IL: Human Kinetics (2000) 327–333.

[2] Milburn, P.D. The Biomechanics of Rugby Scrummaging. University Of Wollongong, 1990.

[3] Meghales, F., et al. Journal of sports science & medicine 11/2013; 12(4):660-667.

[4] Sawacha, Z., et al. JNER, 2012, 9:63.

Disclosure of Interest: None Declared

Musculoskeletal

AS-0265

DOES CARDIAC MUSCLE EXHIBIT HISTORY-DEPENDENT PROPERTIES?

Kevin Boldt [1,*] Venus Joumaa [1] Walter Herzog [1]

[1] Kinesiology, University of Calgary, Calgary, Canada

Introduction and Objectives: Force enhancement is a property of muscle which occurs during and following the stretch of an activated muscle, or an eccentric contraction1. Specifically, residual force enhancement (RFE) occurs when an activated muscle is stretched from a short length to a long length, which results in a greater steady-state isometric force than that produced in a purely isometric contraction at the long length2. Conversely, passive force enhancement (PFE) is defined as the increase in passive force following deactivation of an actively stretched, compared to a passively stretched muscle3. These history-dependent properties have been well identified across skeletal muscle hierarchy including whole muscle, fascicles, fibres, and myofibrils1, 4, 5. However, RFE and PFE have not been investigated in cardiac muscle. Cardiac muscle has a distinctly different structure, particularly with regards to its passive components. Importantly in this context, the structural protein titin, which is thought to be a crucial molecule in contributing to RFE and PFE, is much shorter in cardiac compared to skeletal muscle6, and is deficient in the so-called N2A region7 which has been implicated as a crucial regulator of RFE and PFE. Therefore, the purpose of this study was to determine if RFE and PFE were also present in isolated cardiac myofibrils.

Methods: Hearts were dissected from New Zealand White Rabbits and strips of tissue from the left ventricle were skinned overnight using a 1% Triton skinning solution and stored at -20°C. On the day of experiments, the strips of tissue were blended and a myofibril with a good striation pattern was identified and suspended between a glass needle and a nanolever allowing for length changes and force measurement, respectively. Myofibrils were set at an average sarcomere length (SL) of 2.4µm and activated isometrically to establish a reference contraction before being deactivated and passively stretched to a SL of 3.2µm to establish resting passive forces. After a rest period, myofibrils were activated at a SL of 2.4µm, actively stretched to a SL of 3.2µm, held for one minute and then deactivated. RFE was calculated as the difference between the steady-state force obtained after active stretch and the corresponding isometric force at 3.2µm which could be calculated based on the isometric reference force at optimal SL. PFE was calculated as the difference between the passive force following deactivation of the actively stretched myofibril and the corresponding passive force following passive stretching of the myofibril to an average SL of 3.2µm.

Results: All myofibrils (n=5) produced more force when stretched actively compared to the calculated reference isometric force, indicating the presence of RFE in cardiac myofibrils (Figure 1). The average RFE was 55±15%. Similarly, all myofibrils (n=5) had a greater passive force following active compared to passive stretching (Table 1). The average PFE was 55±11%.

Conclusion: The presence of RFE and PFE in cardiac myofibrils supports that these properties are universal across striated muscle. However, RFE was substantially smaller than the more than 200% observed in skeletal muscle myofibrils4. Rabbit cardiac muscles contain titin isoforms that are substantially smaller than those found in skeletal muscle, and they lack the N2A region of skeletal muscle titin, a region that is thought to be crucial for binding titin to actin, thereby

causing a large part of the RFE (LeWinter et al., 2006). Therefore, the much smaller RFE in cardiac compared to skeletal muscle myofibrils might be explained with the different titin isoforms and the lack of the N2A region in cardiac muscle. In future work, we will evaluate cardiac fibres and fascicles to see if the properties observed on the myofibrillar level are maintained, or altered across different structural levels of cardiac muscle. Investigation using cardiac muscle may shed new light and provide new avenues for investigating the mechanisms underlying force enhancement and its properties, particularly the role of titin in residual and passive force enhancement.

Table:

	Passive Force Enhancement (%)	Residual Force Enhancement (%)
Myofibril 1	70	107
Myofibril 2	94	42
Myofibril 3	50	80
Myofibril 4	30	14
Myofibril 5	32	31
Mean	55	55
SEM	11	15

Caption: Passive and residual force enhancement following active stretch in cardiac myofibrils.

References: [1] Abbott et al., Journal of Physiology,117(1): 77-86, 1952.

[2] Herzog et al., Journal of Physiology, 574: 635-642, 2006.

[3] Joumaaet al., Am. J. Phyiol. Cell Physiol., 294(1): 74-78, 2008.

[4] Joumaa et al., Proceedings of the Royal Society, 275: 1411-1419, 2008.

[5] Seiberlet al., Journal of Applied Biomechanics, 26: 256-264, 2010.

[6] Granzier et al., Biophysical Journal, 68: 1027-1044, 1995.

[7] LeWinteret al., Clinica Chimica Acta, 375: 1-9, 2006.

Disclosure of Interest: None Declared

Musculoskeletal

AS-0266

IN VIVO EFFECTS OF EPIMUSCULAR MYOFASCIAL FORCE TRANSMISSION ON SARCOMERE LENGTH OF MUSCLES IN THE RAT HINDLIMB

Chris Tijs [1,*] Jaap H. van Dieën [1] Huub Maas [1]

[1] MOVE Research Institute Amsterdam, Faculty of Human Movement Sciences, VU University Amsterdam, Amsterdam, Netherlands

Introduction and Objectives: Finite element models predict that, for active muscle conditions, epimuscular myofascial force transmission may cause non-uniformities in sarcomere length in-series within muscle fibers [1]. Imaging studies have reported inhomogeneous strains in soleus (SO) muscle [2] and shortening of SO muscle fibers [3] due to passive knee extension (i.e. proximally lengthening of the two-joint gastrocnemius (GA) and plantaris (PL) muscles). While these studies did not actually measure sarcomere length, they do suggest regional effects of epimuscular myofascial force transmission on sarcomere length. The purpose of the present study was to assess effects of epimuscular myofascial force transmission on i) mean sarcomere length and on ii) the distribution of sarcomere lengths within passive fibers of one-joint muscles within the anterior (tibialis anterior, TA) and posterior (SO) compartments of the rat hindlimb.

Methods: After anaesthesia and euthanasia, left and right rat hindlimbs (n=24) were shaved, positioned in predefined knee (55^0, 90^0, 125^0, 160^0) and ankle angles (90^0, 125^0), and fixed in a 3.7% formalin solution. Note that knee flexion results in shortening of GA and PL and lengthening of EDL, while the muscle-tendon unit length of TA and SO remains constant. The applied combinations of joint angles were used to assess if length changes of synergistic muscles affect the length of sarcomeres within TA and SO for two different ankle angles. Whole fibers (2-4) were taken from multiple regions within the lateral half of SO and TA muscles. Photographs of small fiber sections (~280 µm) were made using a microscope and mean sarcomere length of each section was calculated. Each fiber was divided into three regions (proximal/intermediate/distal) and mean sarcomere lengths of the proximal and distal regions individually as well as for the entire muscle fiber were assessed.

Results: <u>Soleus</u>: fiber mean SO sarcomere length was not affected by knee angle (mean: 2.43±0.03µm; p=0.727 and mean: 2.19±0.05µm; p=0.403 for ankle angles of 90^0 and 125^0, respectively). Sarcomere lengths in the proximal and distal region were also not affected differently by knee angle (p=0.432 and p=0.997 for ankle angles of 90^0 and 125^0, respectively).

<u>Tibialis anterior</u>: fiber mean TA sarcomere length was not affected by knee angle (mean: 2.33±0.05µm; p=0.957 and mean: 2.51±0.07µm; p=0.888 for ankle angle of 90^0 (Fig. 1A) and 125^0, respectively). However, non-uniform length changes were found for both ankle angles. A significant interaction between knee angle and fiber region was found (p=0.002) at 90^0 ankle angle (Fig. 1B), with sarcomeres proximally within TA muscle fibers lengthening (p=0.013) and sarcomeres in the distal region shortening (p=0.014) when the knee was flexed from 160^0 to 55^0. At 125^0 ankle angle, also a significant interaction between knee angle and fiber region was found (p=0.031), but there were no main effects of knee angle on the sarcomere length in the proximal and distal regions (p=0.589 and p=0.222, respectively).

Figure:
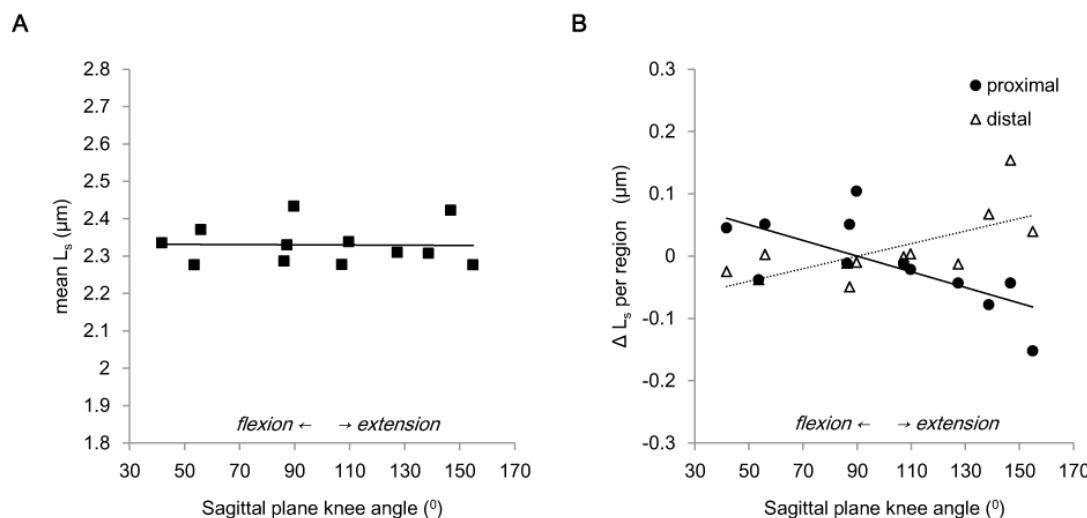
Fig 1. Effects of knee angle on the sarcomere length (L_s) within muscle fibers of tibialis anterior muscle with the ankle set to 90^0 (n=12). (A) Absolute sarcomere lengths for the entire fiber (■). (B) Changes in sarcomere length (relative to 90^0) for the proximal (●) and distal (Δ) region of the same fibers.

Conclusion: We found no effects of knee flexion on SO sarcomere length, indicating that SO muscle is not affected by surrounding structures. This is in agreement with a previous study in cats [4], which found no effect of knee angle on active ankle moment exerted by SO. Our results showed that knee flexion and, hence, proximally lengthening of EDL increased the sarcomere length in the proximal region and decreased the sarcomere length in the distal region of TA muscle fibers. In contrast, finite element modelling studies predicted proximal shortening and distal lengthening of TA sarcomeres when EDL was lengthened proximally [1]. This discrepancy may be explained by i) the state of the muscle (active in finite element models vs. passive in our study) and by ii) the non-specific geometry of muscles within the model. Therefore, a general finite element model that does not take into account muscle specific geometry (e.g. pennation angle) may not be able to explain effects of myofascial force transmission accurately.

Our study shows that the relative position of synergistic muscles does not affect the mean sarcomere length of SO and TA muscle fibers, but that it does result in non-uniform length changes of in-series sarcomeres within TA muscle fibers. Therefore, we conclude that, while SO acts independent from its surroundings, epimuscular myofascial force transmission is present between TA and neighbouring structures in vivo.

References: [1] Yucesoy et al., J Biomech 36: 1797–1811, 2003.

[2] Huijing et al., Surg Radiol Anat 33: 869–879, 2011.

[3] Tian et al., J Appl Physiol 113: 517–523, 2012.

[4] Maas et al., J Appl Physiol 104: 1557–1567, 2008.

Disclosure of Interest: None Declared

Musculoskeletal

AS-0267

A NEW METHOD FOR ESTIMATING MUSCLE-TENDON PARAMETERS FOR SUBJECT SPECIFIC MUSCULOSKELETAL MODELS OF THE LOWER LIMB

Luca Modenese [1,*] Elena Ceseracciu [2] Monica Reggiani [2] David Lloyd [1]

[1] Centre for Musculoskeletal Research, Griffith University, Southport, Australia, [2] Department of Management and Engineering, University of Padua, Vicenza, Italy

Introduction and Objectives: Tools and methodologies are currently available to create subject specific anatomical musculoskeletal models from medical images. However, due to difficulties in estimating personalized muscle-tendon parameters these models have not been used in muscle actuated simulations that can be applied clinically. The aim of this work was two-fold: 1) present a methodology that allows estimation of optimal fibre length (Lopt) and tendon slack length (Lts) for Hill-type muscle actuators representing muscles of the lower limb from a subject specific model, and 2) to demonstrate a practical case of application.

Methods: A subject specific musculoskeletal model of the hip joint was created using bone and muscle meshes available through the publicly available LHDL dataset (www.physiomespace.com). The medical images were from a female donor (81 years old, 1,67 m, 63 kg) and 27 muscle-tendon lines were created with pathways travelling within the 19 muscle volumes spanning the hip joint (see Figure). NMSBuilder [1] was used to generate a model usable in OpenSim 3.2 [2]. The muscle-tendon parameters were estimated for each muscle-tendon unit by: 1) uniformly sampling the spanned joints' ranges of motion using 10 points per generalized coordinate in the reference model [3], thus generating a set of model poses, and 2) mapping the reference model's normalized fibre lengths, obtained by "equilibrating" muscle-tendon, in each pose into the corresponding pose of the subject specific model. Equilibrating was achieved ensuring that for the given values of Lopt and Lts the tendon force equalled the muscle contractile element force, multiplied by the cosine of pennation angle, with the muscle fully activated. This mapping operation was implemented as an optimization procedure with Lopt and Lts being the design variables that were adjusted to minimised the difference in the normalized fibre lengths between reference and subject specific model. We included constraints to prevent solutions causing infeasible muscle-tendon states and pennation angle was set equal to the reference model.

The results were evaluated in terms of root mean squared error (RMSE) and mean tracking error (absolute value) between the reference and subject specific normalized fibre lengths in all model poses. The obtained results were also compared against a recent dataset of muscle parameters [4].

Results: Using the described methodology, the normalized operative fibre lengths of 27 muscle actuators of the reference model were mapped into the MRI-based model with a mean RMSE of 0.0799, standard deviation (SD) 0.0571, and mean mapping error calculated across all muscles of 13% (SD: 17.4). Average variation of muscle parameters was 18% (SD: 26) for Lopt and -22% (SD: 45) for Lts.

The comparison of the muscle parameters obtained through our mapping procedure against the reference model and [4] yielded values within two SD of the measured Lopt, except some bundles of the gluteus maximus and adductor maximus (Figure).

Figure:
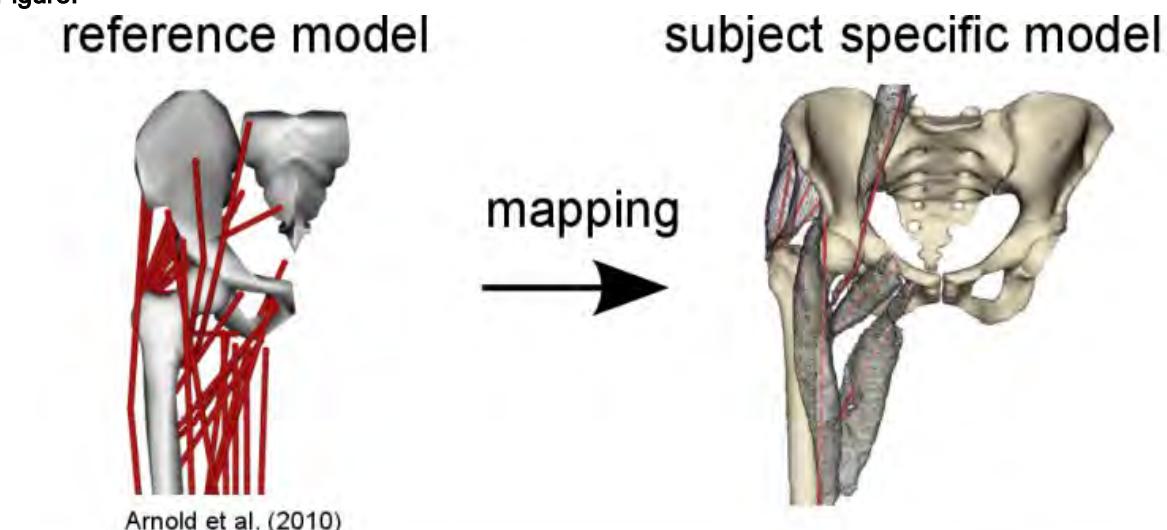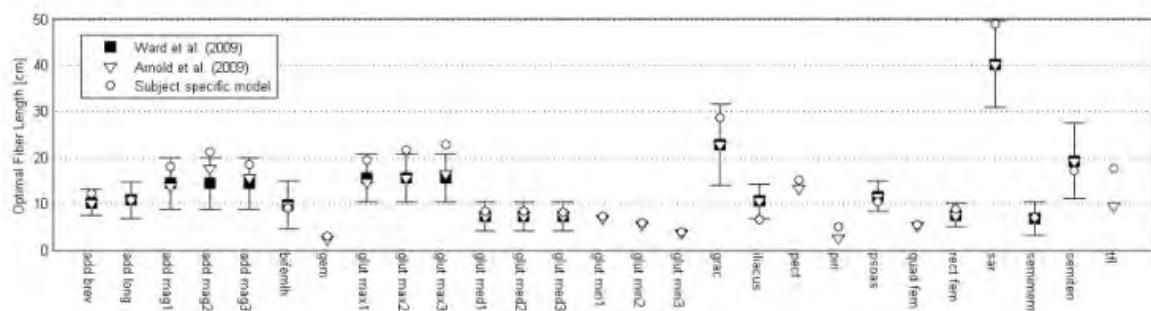
Caption: The reference and subject specific model are in top row and the comparison between the muscle parameters obtained by optimization, included in the reference model [3] and measured in 21 cadaveric specimen [4] is in the bottom row.

Conclusion: This method generated acceptable muscle parameters without using experimental data, and can serve as starting point for further optimization or to integrate existing muscle datasets [5]. Being the reference model mostly based on [4], it is interesting to note that muscles for which parameters were not measured in that study but included from older datasets, eg gemellis, yielded the larger mapping errors.

Remarkably, the method was implemented as an OpenSim plugin and already used in other practical cases such as optimizing the muscle parameters of linearly scaled musculoskeletal models and estimating tendon slack lengths in a model with measured optimal fibre lengths.

References: [1] Valente et al., PLoS ONE, 9:p. e112625, 2014.

[2] Delp et al., IEEE Trans. Biom. Eng. 54:1940-50, 2007.

[3] Arnold et al., Ann Biom Eng, 38: p. 269-279, 2010.

[4] Ward et al., Clin Orthop Rel Res, 467:1074-1082, 2009.

[5] Klein Horsman et al., Clin Biomech, 22:239-47, 2007.

Disclosure of Interest: None Declared

Musculoskeletal

RESIDUAL FORCE ENHANCEMENT CONTRIBUTES TO INCREASED PERFORMANCE IN FAST STRETCH-SHORTENING CYCLES OF HUMAN SKELETAL MUSCLES

Wolfgang Seiberl [1,*]Geoffrey A. Power [2]Walter Herzog [2]Daniel Hahn [3]

[1]Biomechanics in Sports, Technische Universität München, Munich, Germany, [2]Human Performance Laboratory, University of Calgary, Calgary, Canada, [3]Human Movement Science, Ruhr-University Bochum, Bochum, Germany

Introduction and Objectives: Combinations of lengthening and shortening muscle actions, so called stretch-shortening cycles (SSC) [1], lead to a performance enhancement during the shortening phase of the SSC. Early explanations this enhancement of work/force incorporated the idea that mechanisms responsible for residual force enhancement (RFE) may play a significant role [2], since RFE is known to generate increased isometric steady-state forces after active stretch compared to isometric reference forces at identical muscle length and activation. However, direct evidence is missing and the primary mechanisms associated with performance enhancement during SSCs are (i) the activation dynamics, (ii) the contribution of stretch reflexes, and (iii) the storage and release of elastic energy. If RFE indeed also contributes to force increase in the shortening phase of SSCs, persistent enhanced forces should be measureable beyond shortening during an isometric phase following the SSCs This prediction has never been tested, and the aim of this study is to test if there is remnant RFE following SSCs.

Methods: The adductor pollicis of 14 healthy male subjects was electrically stimulated over the ulnar nerve Digitimer, UK; 50Hz; square-wave pulses; 100µs pulse-width). Thumb adduction forces were measured using a strain-gauge based, custom-designed dynamometer (sample rate 2kHz). Testing consisted of three blocks using a pseudo-randomized design. First block: Three pure shortening contractions beginning at a thumb angle of 30° and shortening amplitudes of 10°, 20° and 30° (thumb angles increase with abduction, ranging from 0-30°). Second block: Three SSCs and the corresponding isometric reference contractions. SSCs started with 30° lengthening, followed by 10°, 20° or 30° shortening. Third block: A pure lengthening contraction from 0° to 30°, and the corresponding isometric reference contraction. All dynamic contractions were performed using an angular acceleration of 500°/s². Force data were low-pass filtered (10Hz), and peak force, minimum force (end of shortening), concentric work during shortening, and force during a 500ms time period (2.5-3s after shortening) were used for statistical analysis (repeated measures ANOVA and Bonferroni-Holm post-hoc comparisons; $\alpha < 0.05$). All experimental procedures were approved by the Conjoint Ethics Committee of the University of Calgary.

Results: Mean electrically evoked isometric forces reached 50% of the maximum voluntary contractions. Pure shortening contractions resulted in significantly ($p < .01$) depressed forces reaching approximately 90% of the corresponding isometric reference forces (Fig. 1). Pure lengthening contractions resulted in enhanced forces reaching 116% of the corresponding isometric reference forces. Forces after the stretch-shortening contractions with shortening amplitudes of 20° and 30° did not differ from the corresponding isometric reference contractions. Forces after SSCs with 10° shortening showed enhanced forces averaging 111% compared to the corresponding isometric reference contractions (Fig. 1).

Concentric work for pure shortening contractions averaged 60% of the corresponding work produced during shortening in SSCs.

Figure:
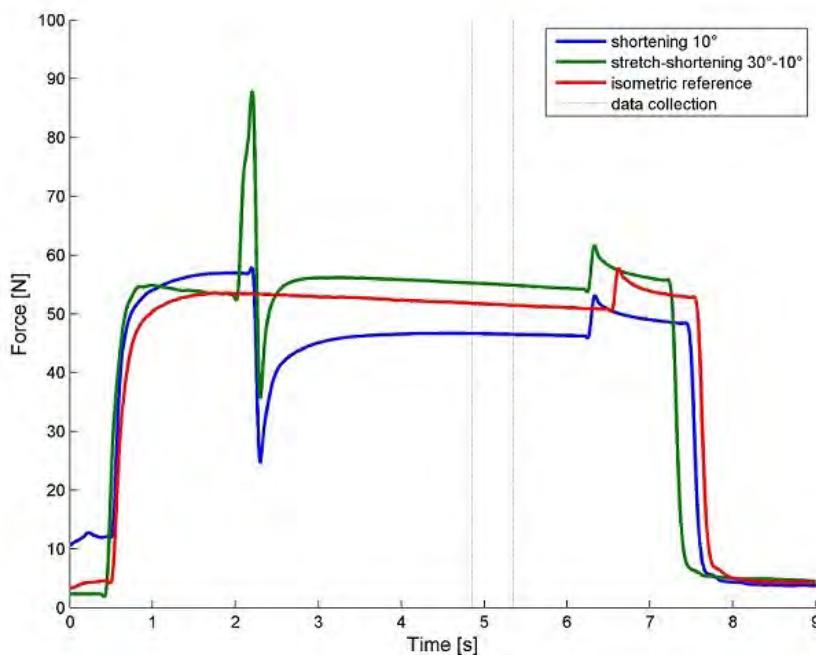
Caption: Force-time histories of exemplar contractions ending at the same thumb angle position. Note, at interval of data collection, there is residual force enhancement (green over red) or force depression (red over blue) after stretch-shortening or pure shortening, respectively.

Conclusion: Active lengthening of the adductor pollicis muscle reduced the amount of force depression observed if shortening was not preceded by stretch. Furthermore, for SSCs in which shortening was only 1/3 of the stretch amplitude, there was a remnant RFE averaging 11%. Conventional explanations for the increase in positive mechanical work in SSCs, such as the storage and release of elastic energy, cannot explain the enhanced steady-state force after SSCs. Therefore, it appears that the stretch-induced RFE is not immediately abolished during shortening, but contributes to the increased force and work during the shortening phase of SSCs. This novel finding indicates that the mechanisms underlying residual force enhancement likely contribute to the increased amount of work performed during active shortening compared to situations where shortening is not preceded by stretch. The increased mechanical work in SSCs compared to pure shortening contractions was caused by the increased forces at the beginning of shortening and the persistent force enhancement throughout the shortening phase. Since the speed of shortening is inversely related to force depression, but the speed of stretching does not affect RFE, the results obtained here might have been favored by the high speeds of shortening, and might not have been as obvious had we chosen a relatively slow speed of shortening.

References: [1] Komi, P. V. 2000. J. Biomech., 33, 1197-206.

[2] Cavagna, G. A., Dusman, B. & Margaria, R. 1968. J Appl Physiol, 24, 21-32.

Disclosure of Interest: None Declared

Musculoskeletal

AS-0269

METABOLIC AND MUSCLE CONTRIBUTORS TO DIABETIC FOREFOOT DEFORMITY

Victor Cheuy [1,*] Mary Hastings [1] Michael Mueller [1]

[1] Physical Therapy, Washington University in St. Louis, St. Louis, United States

Introduction and Objectives: Identifying the mechanisms that contribute to the development of diabetic foot deformity is imperative to reducing the incidence of neuropathic ulceration and lower extremity amputation. Metatarsophalangeal joint (MTPJ) hyperextension is a forefoot deformity (i.e., hammer or claw toe) associated with excessive peak plantar pressures under the metatarsal heads, and is a known risk factor for skin breakdown and amputation.[1] A hyperglycemic environment and advanced glycation end-product (AGE) accumulation are thought to contribute to three potential risk factors of deformity: neuropathy, intrinsic foot muscle deterioration, and limited joint mobility at the ankle.[2] Weakened intrinsic foot muscles from neuropathy and adipose infiltration can no longer stabilize the MTPJ, and AGE accumulation increases random collagen cross-linking, resulting in limited joint mobility. Decreased ankle dorsiflexion range of motion may contribute to extrinsic toe extensor compensation, resulting in muscle shortening and MTPJ hyperextension. The objectives of this study were 1) to determine the relationships between intrinsic foot muscle deterioration, joint deformity, and active joint motion, and 2) to determine the relationships between AGEs, severity of neuropathy, and limited joint mobility.

Methods: 19 participants (59±9 years) with diabetic neuropathy were studied. To measure MTPJ and ankle joint angles, CT scans were taken at three foot positions: resting MTPJ neutral, max active MTPJ flexion, and max ankle dorsiflexion. A custom MatLab program was used to measure the percent adipose tissue of the intrinsic foot muscle compartment from coronal MR images taken from the talonavicular joint through the midpoint of the second metatarsal.[3] Severity of neuropathy was assessed using the Michigan Neuropathy Screening Instrument (MNSI), involving a foot inspection, and reflex and sensory testing. Skin intrinsic fluorescence was measured using the SCOUT DS device (Veralight, NM, USA) as an indicator of AGE accumulation in the dermal collagen and oxidative stress levels in the epidermis. One-tailed Pearson correlation coefficients were calculated between the variables of interest.

Results: Intrinsic foot muscle deterioration was significantly correlated with MTPJ deformity (r = -0.47, p < 0.03, Figure 1A) and max active MTPJ flexion (r = -0.56, p < 0.01, Figure 1B). Skin intrinsic fluorescence was significantly correlated with the MNSI score (r = 0.62, p < 0.01, Figure 1C) and intrinsic foot muscle deterioration (r = 0.41, p < 0.05, Figure 1D), but not with max ankle dorsiflexion (r = -0.05).

Figure:
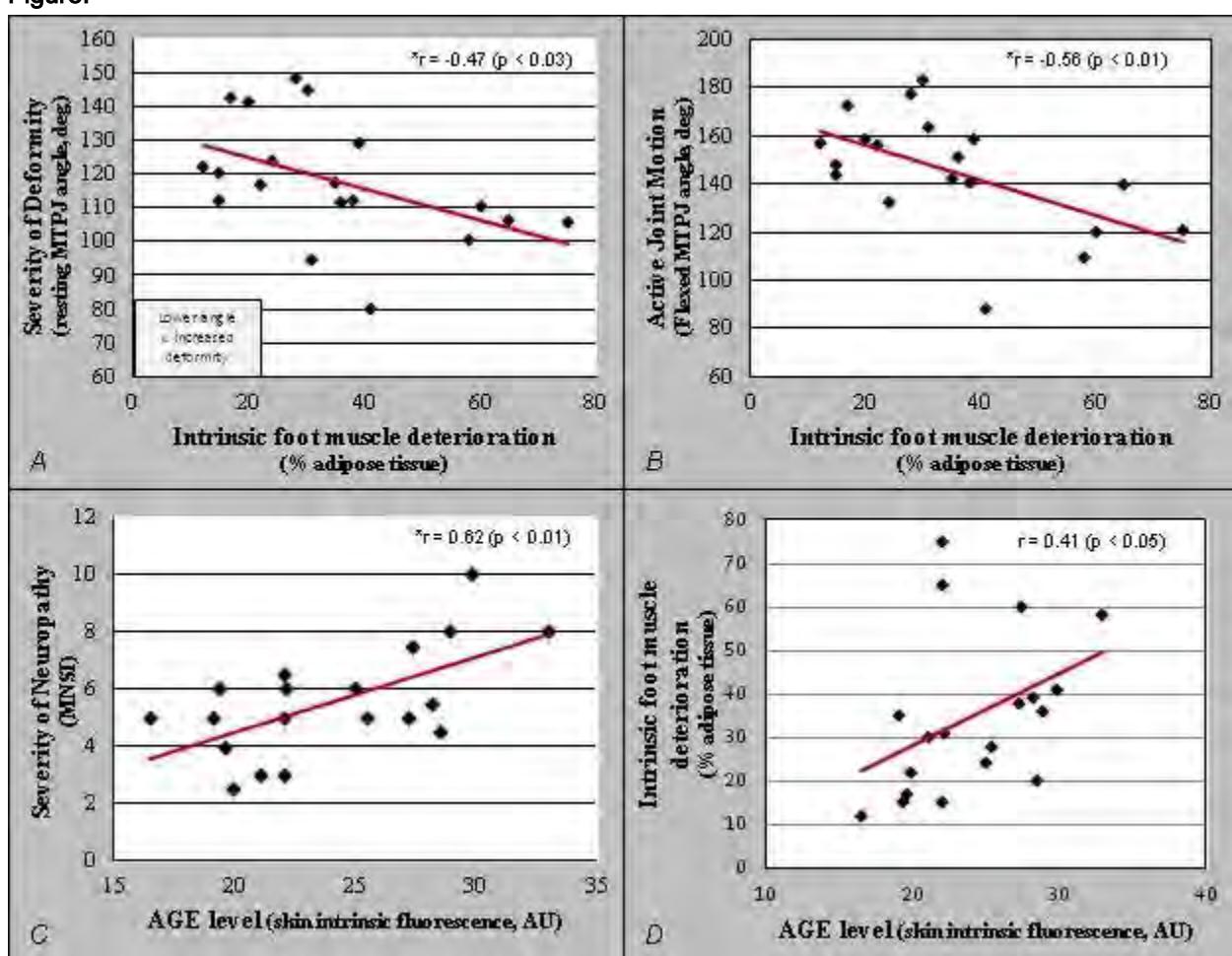
Conclusion: The results of this study show that intrinsic foot muscle deterioration and AGE levels are important indicators of disease progression. Increasing intrinsic foot muscle deterioration was associated with more severe MTPJ hyperextension, and reduced max active MTPJ flexion. Increasing skin intrinsic fluorescence, an indicator of larger AGE accumulation, was associated with more severe neuropathy. These findings are preliminary, and further work is necessary to define these relationships prospectively. Identifying deterioration of the intrinsic foot muscles as a risk factor for MTPJ deformity supports the need for targeted interventions early in the disease process that preserve these muscles, perhaps through strengthening exercises.

References: [1] Mueller et al., J Biomech, 36: 1009-17, 2003.

[2] Meerwaldt et al., Diabetologia, 48: 1637-44, 2005.

[3] Cheuy et al., JMRI, 38: 1083-93, 2013.

Disclosure of Interest: None Declared

AS-0270

MECHANICAL INTERACTIONS BETWEEN HUMAN LOWER LEG MUSCLES IN VIVO SHOWN USING ELASTOGRAPHY

Filiz Ates [1] [2],*Ricardo Andrade [2] [3]Sandro Freitas [3]Lilian Lacourpaille [2]Can A. Yucesoy [1]Antoine Nordez [2]

[1]Biomedical Engineering Institute, Bogazici University, Istanbul, Turkey, [2]Faculty of Sports Science, University of Nantes, Nantes, France, [3]Faculdade de Motricidade Humana, Universidade de Lisboa, Lisboa, Portugal

Introduction and Objectives: Lateral transmission of muscle force mediated by the epimysium (i.e. via collagenous linkages between muscles and common connective tissues) is referred to as epimuscular myofascial force transmission (EMFT). EMFT is characterized by the interplay of stiffness of intramuscular and epimuscular tissues as determined by relative positions of muscles and non-muscular structures [1, 2]. Shear elastic modulus measured using supersonic shear imaging (SSI) provides accurate estimates of changes in muscle tissue stiffness [3]. In addition, it is well correlated to localized passive muscle tension developed during stretching imposed in relaxed state [4, 5]. Thus, it can be a useful tool to assess the in vivo local EMFT effects. We hypothesized that lateral gastrocnemius (GL) length change due to externally imposed knee angle positioning would alter the stiffness of mono-articular soleus (SOL), peroneus longus (PERL), and tibialis anterior (TA) muscles. The aim of this study was to test this hypothesis and hence to analyze intermuscular interactions in human lower leg by using SSI technique.

Methods: Two experiments were performed on healthy adults. The participants lied (prone for Exp I, n=8; supine for Exp II, n=10) in an isokinetic dynamometer system with the right foot fastened to a footplate. The knee and hip were fixed. An Aixplorer ultrasound scanner was coupled with a linear transducer array in SSI mode. From 40° plantarflexion to -20° dorsiflexion (at 2º/s), shear wave elastography recordings were done for tested muscles during passive ankle motion: Exp I, GL and SOL proximally and SOL distally. Exp II, GL, PERL, and TA proximally. Each measurement was repeated 3 times. Assessments were performed with the knee flexed (90°) and fully extended (0°) in a randomized order. SSI recordings were exported in "mp4" format, sequenced into images ("jpeg" compression) and were processed using MATLAB. An average value of the colored map converted into shear elastic modulus was calculated for each image. Stiffness values were synchronized with the ankle angle and torque values.

Two-way ANOVAs for repeated measures (factors: ankle and knee angles) subsequently Bonferroni post-hoc procedure were used to analyze the effects of knee angle change on stiffness of each muscle. P values < 0.05 were considered as significant.

Results: *Exp I:* Significant main effects and interaction showed increased stiffness for the GL (maximally by 26.9±1.8%) in dorsiflexed positions (starting from 4° plantar flexion) due to altered knee angle. The imposed length change on the GL caused quite complex effects on the SOL located in the same compartment: Proximally, significant main effects and interaction showed a decrease in stiffness (maximally by 65.4±4.1%) only in dorsiflexed ankle positions from 6° plantar flexion. Distally, significant main effects but no significant interaction demonstrated increase in stiffness (43.8±9.5% in average) independently from ankle position.

Exp II: Significant main effects and interaction showed that the GL stiffness increased (maximally by 55.9±8.5%) in dorsiflexed positions (starting from 2° plantar flexion) due to altered knee angle. Significant main effects but no significant interactions were found for the PERL stiffness (mean increase of 10.4±3.8%) and for TA muscle (mean increase of 12.3±4.4%) due to altered knee angle.

These findings show occurrence of mechanical interactions between lower leg muscles leading to local muscle stiffness changes. Differently changing stiffness of the SOL proximally and distally is remarkable and in concert with EMFT phenomenon previously reported [2]. Overall, the knee angle change imposes relative position changes affecting muscle stretch and length of epimuscular connections. Ankle movement leads to varying stretches of lower leg musculature and their epimuscular connections. For some muscles a balance of these effects causes a net stiffness increase.

Figure:
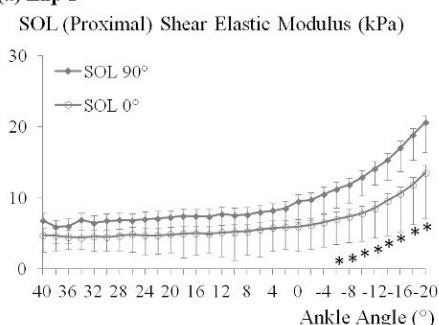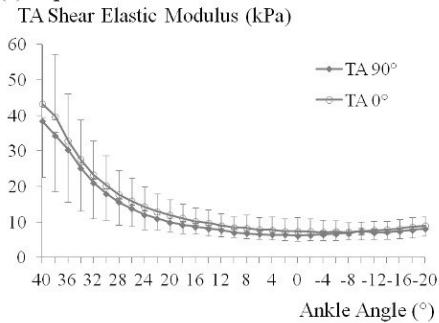
Caption: Shear elastic modulus of (a) SOL (proximal) and (b) TA muscles with respect to ankle angle. * indicates that modulus values measured at 90° and 0° of knee angle are significantly different for SOL (proximal).

Conclusion: Our results show that altered knee angle imposes changes in shear elastic modulus for not only the GL but also the SOL, PERL and TA muscles. These findings confirm our hypothesis and show the strength of SSI technique in assessing effects of intermuscular mechanical interactions in terms of muscle stiffness.

References: [1] Huijing PA, et al., J Biomech. 42: 9-21, 2009.

[2] Yucesoy CA, Exerc Sport Sci Rev, 38: 128-34, 2010.

[3] Eby SF, et al., J Biomech, 46: 2381-7, 2013.

[4] Maissetti O, et al., J Biomech, 45: 978-84, 2012.

[5] Koo TK, et al., J Biomech, 46: 2053-59, 2013

Disclosure of Interest: None Declared

TOWARDS AN UNDERSTANDING OF THE MECHANISMS UNDERLYING FORCE ENHANCEMENT

Krysta L. Powers[* 1], Kiisa Nishkawa[2], Walter Herzog[1]

[1]Faculty of Kinesiology, University of Calgary, Calgary, Canada, [2]Department of Biological Sciences, Northern Arizona University, Flagstaff, AZ, United States

Introduction and Objectives: Since the early 1950's, a single theory has governed our basic understanding of muscle force production, which predicts force by sarcomere length, or number of attached cross-bridges (CBs) [1]. Under this theory, the predictions of force following active lengthening are vastly underestimated [2]. The state of enhanced force following active lengthening above that predicted by the CB theory is referred to as residual force enhancement. Residual force enhancement has been demonstrated in vivo and down to the level of the sarcomere [3], prompting the development of alternative mechanisms to explain the history-dependence of muscle force. Experiments from our laboratory suggest that titin, a dynamic spring protein in the sarcomere, is the primary source of sarcomere force enhancement. Titin stiffness increases up to 400% in actively stretched sarcomeres, partly by a Ca2+-based increased in its spring stiffness, but predominantly by an unknown mechanism [4]. We speculate that titin becomes stiffer and contributes to residual force enhancement when it binds to the thin filament, becoming shorter and stiffer during active sarcomere stretch [3], thus for a given amount of stretch, more force can be produced. This idea has been conceptually validated using a mathematical model to predict the force of actively stretched sarcomeres with titin bound to the thin filament [4]. Therefore, the aim of this study was to experimentally investigate this mechanism of titin binding by examining the mechanical properties of sarcomeres in a titin-mutation model [5], in which the region of the titin protein predicted to bind to the thin filament is deleted.

Methods: Mechanical testing of intact sarcomeres was achieved using isolated psoas myofibrils from normal wild type mice and mice with a deletion in the distal N2A-PEVK region of titin (mutant) [5]. Myofibrils were mounted between a motor for controlled length changes, and cantilever of known stiffness for force calculations, at 100X magnification. Myofibrils were then slowly stretched at a speed of 0.1 um per sarcomere per second passively and at maximal Ca2+-activation from optimal filament overlap (2.2-2.5 um) to sarcomere lengths well beyond filament overlap (6.0 um) for direct observation of titin based force enhancement in the absence of CB force.

Results: The passive mechanical properties of normal and mutant myofibrils did not differ suggesting that in the absence of Ca2+-activation the stiffness of the mutant sarcomere is not altered by the deletion in the titin protein. However, when activated and stretched, the mechanical properties of mutant sarcomeres were distinctly different from wild type controls (Fig 1). Force was lower at all sarcomere lengths and titin-based force enhancement was deficient in actively stretched mutant sarcomeres compared with the wild type controls (Fig.1).

Figure:
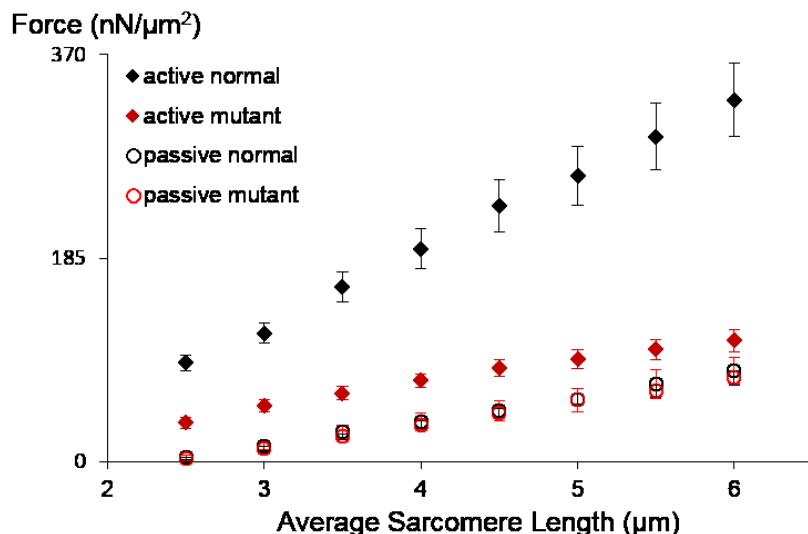
Fig. 1. Force sarcomere length relationships of actively (diamonds) and passively (circles) stretched myofibrils from normal (black) and mutant mice with a deletion in the titin protein (red). Mutant sarcomeres generate less force than normal myofibrils at all sarcomere lengths during active stretch.

Conclusion: This study demonstrates that a deletion in the titin protein can directly influence active force production. In actively stretched mutant sarcomeres the total force and titin based force enhancement were severely disrupted. These findings suggest that the region of titin that modulates its spring stiffness is contained within the deleted region of the mutant protein and that titin force modulation likely plays a role in muscle contraction as well as residual force enhancement. We remain in support of the idea that titin binds to the thin filament during active stretch; effectively shortening it's mechanical spring. As the force of actively stretched mutant sarcomeres was vastly reduced at all sarcomere lengths, we suggest that titin thin filament binding is relevant within the muscles working sarcomere lengths and provides additional structural support by strongly resisting extension of contracting sarcomeres. This is an important mechanism for predicting muscle force during dynamic locomotion and for the prevention of stretch-induced muscle injury. While there are many possible mechanisms by which titin based force enhancement occurs, we believe titin provides the sarcomere with additional force during active stretch by binding to the thin filament, which offers a viable explanation of how skeletal muscles achieve enhanced force following active lengthening. Future studies will aim to validate the results of this study in a skinned fiber preparation and further elucidate the mechanism.

References: 1.Huxley & Simmons (1971). Nature 2. Abbott & Aubert (1952). J. Physiol. 3. Leonard et al., (2010). Am. J. Physiol. Cell Physiol.

Disclosure of Interest: None Declared

AS-0271

THE EFFECTS OF A DUAL-TASK ON OVERGROUND MINIMUM TOE CLEARANCE AND GAIT PARAMETERS DURING WALKING IN OLDER ADULTS

Kim R. Duffy [1,*]Matthew Taylor [1]Jo Jackson [2]

[1]Centre of Sports and Exercise Science, Biological Science, [2]Health and Human Science, University of Essex, Colchester, United Kingdom

Introduction and Objectives: Falls in older adults are common, with the majority occurring due to tripping whilst walking. Although falls are multifactorial, tripping while walking accounts for 53% of all falls [1]. Alterations in gait patterns such as reduced minimum toe clearance (MTC), walking speed and stride length occur in ageing [2]. Insufficient MTC has been found to cause tripping whilst walking and also during dual-tasks [3, 4]. There is a paucity of research looking at MTC during manual dual-tasks (walking whilst holding an object) in older adults. Therefore the aim of this study was to examine MTC and spatial-temporal parameters during normal and dual-task walking in community-dwelling older adults.

Methods: Fifteen healthy older adults (8 males, 7 females; 62.7±1.5yrs) participated. Each performed two tasks on a 10m level walkway, 1: normal walking, and 2: walking whilst holding a cup of water (manual dual-task). A 7 camera Vicon (Oxford, UK) motion analysis system was used. MTC was calculated using the vertical displacement of the shoe-mounted marker on the heads of the 2nd metatarsals. This coincided with maximum horizontal toe velocity in swing (Fig 1). Spatial-temporal parameters were also calculated. Five trials for both tasks were averaged and analysed. A paired t-test was executed for parameters except for toe-off (%) which was analysed using a Wilcoxon test.

Results: There were no significant differences between MTC (15.79±6.67 vs. 15.15±6.95mm) or maximum horizontal velocity (4.55±0.36 vs. 4.60±0.46m.s-1) for older adults performing normal and dual-task walking. Significant differences for the spatial-temporal parameters revealed older adults altered their gait pattern by increasing their stride length and walking speed during dual-task walking when compared to normal walking (1.46±0.17 vs. 1.44±0.16m; 1.44±0.19 vs. 1.39±0.15m.s-1 respectively), with no significant difference for cadence (118±6 vs. 116±6), toe-off (61.0s IQR = 2.4 vs. 62.7s IQR = 3.8) or stride time (1.02±0.06 vs. 1.04±0.05s) (Table 1, Fig 1).

Figure:
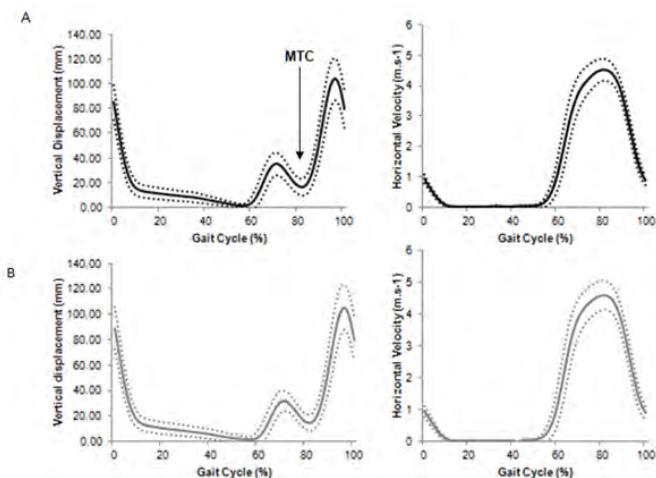
Caption: Figure 1 Averaged (±SD) toe vertical displacement and horizontal velocity over one gait cycle for 15 participants during normal walking (A) and dual-task walking (B). Note: initial contact was at 0% and 100% and toe-off approximately at 60%.

Conclusion: MTC for older adults aged 62-64 years did not alter when performing a dual-task whilst walking when compared to normal walking. Previous research found similar findings for MTC during manual dual-task walking (10.3±0.3mm) when compared to normal walking (9.8±0.5mm) [4]. However, stride length and walking speed did increase during dual-task walking and this is potentially due to motor task prioritisation. Previous research [5, 6] comparing dual-task walking to normal walking have found older adults have shown to prioritise their motor performance in dual-task situations by altering their gait to an increased stride length and walking speed. Research comparing young adults found during dual-task walking their gait pattern is consistent to normal walking [5] or it alters to shorter stride length and slower walking speed, whereas older adults increase their stride length and walking speed [6]. This prioritisation of motor performance during dual-task walking has been associated with fall prevention in older adults [5]. Therefore, similar to previous research older adults in this study may have increased their stride length and walking speed to prioritise the motor performance over the dual-task to potentially minimise the risk of falling. Future research is underway involving 107 community-dwelling older adults in three age groups (55-64, 65-74 and 75+ yrs) performing four functional tasks (normal walking; manual dual-task walking; stepping onto and down off a step; obstacle negotiation), to determine the MTC, horizontal velocity and spatial-temporal parameters for all tasks

Table:

Gait parameter	Dual-task walking	Normal walking	P Values
Vertical displacement of the toe (MTC) (mm)	15.15 ± 6.95	15.79 ± 6.67	t_{14} = -0.507, P < 0.05
Maximum horizontal velocity of the toe (m.s^{-1})	4.60 ± 0.46	4.55 ± 0.36	t_{14} = 1.262, P < 0.05
Cadence (steps/min)	118 ± 6	116 ± 6	t_{14} = 0.847, P < 0.05
Toe-off (%)*	61.0 IQR = 2.4	62.7 IQR = 3.8	t = 77.00, P < 0.05
Stride length (m)	**1.46 ± 0.17**	**1.44 ± 0.16**	t_{14} = -1.956, P < 0.05
Stride time (s)	1.02 ± 0.06	1.04 ± 0.05	t14 = 2.679, P > 0.05
Walking speed (m.s^{-1})	**1.44 ± 0.19**	**1.39 ± 0.15**	t14 = 2.784, P > 0.05

Note: * signified median values for the parameter which was not normally distributed. **Bold** values represent significant differences.

Caption: Table 1 Gait parameters

References: [1] Winter et al., Phys Therapy, 70, 340-347, 1990.

[2] van Dieën et al., Safety Sci, 43, 437-453, 2005.

[3] Winter., Phys Therapy, 72, 45-53, 1992.

[4] Schulz et al., Gait & Posture, 32, 18-22, 2010.

[5] Schaefer et al., Exp Brain Res, 17, 2014.

[6] Yogev-Seligmann et al., Phys Therapy, 90, 177-186, 2010.

Disclosure of Interest: None Declared

Elderly

AS-0272

IS THE DIFFERENCE BETWEEN PREFERRED AND NON-PREFERRED LEADING LEG OBSTACLE CROSSING LARGER IN ELDERLY FALLERS THAN IN NON-FALLERS?

Emmanuel S. da Rocha [1,*]Eliane C Guadagnin [2]Maarten Bobbert [3]Jacques Duysens [4]Felipe Carpes [5]

[1]Federal University of Santa Maria, Santa Maria, [2]Federal University of Rio Grande do Sul, Porto Alegre, Brazil, [3]VU University Amsterdam, Amsterdam, Netherlands, [4]KU Leuven, Leuven, Belgium, [5]Applied Neuromechanics Research Group, Federal University of Pampa, Uruguaiana, Brazil

Introduction and Objectives: Falls in the elderly are frequently associated with obstacle contacts during walking. Recently, we have shown that obstacle crossings with the preferred leg leading are different from those with the non-preferred leg leading. In the present study, we set out to determine asymmetries in obstacle crossings and investigate whether they are larger in elderly fallers than in non-fallers. As in daily life most people will typically be thinking of other things while walking, we had our participants perform a secondary task during the obstacle crossings.

Methods: Elderly fallers (n=10) aged 66 ± 5 years old, body mass of 63.5 ± 13.4 kg and height of 1.52 ± 0.04 m, and non-fallers (n=10) aged 66 ± 4 years old, body mass 72.3 ± 1.5 kg and height 1.47± 0.06 m, all able to walk independently, volunteered for participation in this study. Participants walked barefoot at self-selected speed along an 8 m walkway and crossed a polystyrene obstacle 20 cm wide and with height defined as 20% of leg length, which was placed in the middle of the walkway. Bilateral kinematics was sampled at 200 Hz using Plugin Gait markers (Vicon Motion Systems, Oxford, UK). Kinematic data were low-pass filtered with a 4th order Butterworth filter at a cut-off frequency of 8 Hz.

The following cognitive task was used: when experimenter said "red" or "blue", the participant had to reply "no" and "yes", respectively. When the experimenter mentioned any other color name, the participant had to simply repeat the color name. Crossings with different leading legs were elicited by having subjects initiate walking from a standing position with either the left or the right leg. Participants did not receive any instruction concerning which leg should cross the obstacle first. Trials were recorded until we had 10 trials for each leg. Leg preference was determined using the Waterloo inventory. Leading limb toe clearance, trailing limb toe clearance, leading limb heel clearance, trailing limb pre-obstacle distance and leading limb post-obstacle distance were determined. Data normality was verified using the Shapiro-Wilk test. An analysis of variance for repeated measures was performed to verify effects for group (fallers *vs* non-fallers) and limb (preferred *vs* non-preferred), followed by post hoc pairwise tests when suitable. All tests were performed with SPSS 20.0 at a significance level of 0.05.

Results: Table 1 presents results from elderly fallers and non-fallers. Comparison between preferred and non-preferred leg yielded a statistically significant asymmetry in lead limb post-obstacle distance in both groups (Table 1), with an asymmetry index (AI) defined as: [AI= Preferred/(Non-preferred+Preferred)]. Lead limb post-obstacle distance AI was 0.52±0.58 among fallers and 0.53±0.55 among non-fallers. No significant asymmetry was observed for the other kinematic variables, in which AI ranged from 0.49 to 0.53 (Table 1).

We studied obstacle crossing with the preferred and non-preferred leg in elderly fallers and non-fallers, while performing a dual task. Both groups showed a difference between preferred and non-preferred leg for lead-limb post-obstacle distance

but the 2 groups did not differ. This indicates that this parameter is not sufficiently sensitive to discriminate between fallers and non-fallers. The absence of differences for other parameters such as toe clearance is in line with data from the literature on obstacle avoidance without dual tasking. In the review of Barrett et al. (2010) it was concluded that toe clearance did not systematically differ between older fallers and non-fallers. However, variability in this parameter did differ. Hence in future studies it is suggested to take variability into account as well. The present data do not support the contention that this type of dual tasking profoundly affects performance in obstacle avoidance.

Conclusion: No asymmetries were found in obstacle clearance between elderly fallers and non-fallers. We did find an asymmetry in post-obstacle distance, but this asymmetry was not larger in elderly fallers than in non-fallers and hence does not seem to pose an elevated fall risk in fallers

Table:

	Fallers (n=10)			Non-fallers (n=10)		
	P	NP	AI	P	NP	AI
Lead limb toe clearance (cm)	12.2 ±1.3	12.1 ±3.0	0.50 ±0.30	12.2 ±1.3	12.2 ±1.8	0.50 ±0.42
Trail limb toe clearance (cm)	12.5 ±4.7	12.4 ±5.6	0.50 ±0.46	10.1 ±3.9	10.6 ±1.5	0.49 ±0.72
Lead limb heel clearance (cm)	10.6 ±2.0	10.4 ±2.5	0.50 ±0.44	10.6 ±2.9	9.4 ±1.9	0.53 ±0.60
Trail limb pre-obstacle distance (cm)	12.1 ±2.1	11.6 ±1.9	0.51 ±0.53	11.1 ±1.6	11.5 ±2.8	0.49 ±0.36
Lead limb post-obstacle distance (cm)	10.9 ±2.9	9.9 ±2.4 *	0.52 ±0.55	13.9 ±4.2	12.1 ±3.0 *	0.53 ±0.58
Gait speed (m/s)	0.9 ±0.1	0.8 ±0.1	0.53 ±0.50	0.9 ±0.1	0.9 ±0.1	0.50 ±0.50

Caption: Results for gait variables with the preferred leg (P) and with the non preferred leg (NP) leading; * indicates difference between legs (p<0.05). No difference was observed between the groups. AI: asymmetry index (see text).

References: [1] Barret, R.S. et al. **Gait Posture**, 32 (4):429-35, 2010.

Disclosure of Interest: None Declared

AS-0273

EFFECTS OF TAI CHI EXERCISE ON LOWER EXTREMITY IN ELDERS DURING WALKING

Po-Chieh Chen [1,*]Chen-Fu Huang [1]Bo-Jen Ko [1]Chung-Lin Wu [1]

[1]Physical Education, National Taiwan Normal University, Taipei, Taiwan, Republic of China

Introduction and Objectives: Elders were found to have slower walking speed and lower ankle plantarflexor power during gait due to the gait-muscle weakness [1]. The compensation mechanism of lower extremity, therefore, has become very important for elders. Tai Chi exercise has been demonstrated to improve muscle strength and postural stability [2], and thus might enhance the knee and hip ability for reductions of ankle plantarflexor power. The purpose of this study was to investigate the effects of Tai Chi exercise on lower extremity in elders during walking.

Methods: The self-selected speed walking motions and ground reaction forces of thirty elders (Tai Chi group, TCG: N=15, 4 females and 11 males, Experience of Tai-Chi: 8.05±3.67 yrs, Age: 74.27±6.20 yrs, Height: 1.62±0.08 m, Weight: 60.42±6.03 kg; Control group, CG: N=15, 7 females and 8 males, Age: 73.20±6.66 yrs, Height: 1.62±0.09 m, Weight: 62.65±10.63 kg) were collected by a 10-camera Vicon motion capture system (250 Hz) and a Kistler force plate (1,000 Hz) respectively. Inverse dynamic was used to calculate the joint moment and power during support phase of gait. Raw data were filtered using a Butterworth 4th-order low-pass filter with a cut-off frequency of 6 Hz. Kinetic variables were normalized to a percentage of subject's body weight (B.W.) and transferred to 100% of the right foot contact time on the force plate. A t-test was used to compare group differences (α= .05).

Results: The results revealed that walking speed in TCG was faster than CG (TCG: 1.17±0.18 m/s; CG: 1.06±0.13 m/s, $p <$ .05). The knee extensor moment and the maximum positive power of hip showed significantly greater in TCG during braking phase (TCG-knee: 0.4±0.12 Nm/kg, hip: 1.31±0.42 watts/kg; CG-knee: 0.27±0.16 Nm/kg, hip: 0.97±0.2 watts/kg, $p <$ .05). The minimum negative power of knee showed significantly greater in TCG during propulsive phase (TCG: 0.32±0.02 watts/kg; CG: 0.69±0.13 watts/kg, $p <$ .05).

Figure:
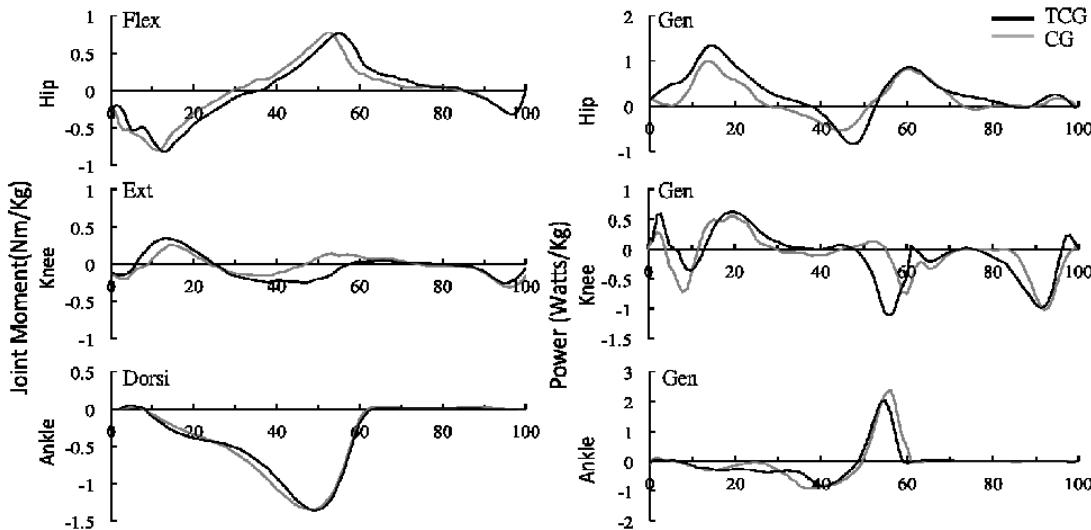
Caption: Joint moments and powers of lower extremity in Taichi and control group during stance phase.

Conclusion: The reduction of power in hip and knee was found to be relative to the slower walking speed due to the muscle weakness [1] and the increased knee extensor joint moment could enhance the stability of the knee [3]. Therefore, the results in TCG demonstrated that Tai Chi exercise might be able to enhance muscle strength about knee and hip and had more stable knee movement. This might be due to the continuing lower body center of mass and semi-squat position emphasized in Tai Chi exercise. It suggested that Tai Chi exercise might have the potential of maintaining the walking ability, and lessening the muscular weakness caused by aging.

References: [1] DeVita et al., J. Appl Phys, 88(5):1804-11, 2000.

[2] Qin et al., J. Bone Miner Metab, 23(2): 186-90,2005

[3] Schipplein et al., J. Orthop Res, 9(1): 113-9, 1991

Disclosure of Interest: None Declared

AS-0274

ANKLE POWER PEAK AND DYNAMIC JOINT STIFFNESS OF THE ANKLE IN RHEUMATOID ARTHRITIS POSTMENOPAUSAL WOMEN WITH AND WITHOUT FALLS HISTORY

Pedro Aleixo [1,*] Ivo Roupa [1] Paulo Coelho [2] José Vaz Patto [2] João Abrantes [1]

[1]Biomechanics, MovLab/Universidade Lusófona de Humanidades e Tecnologias, [2]Rheumatology, Instituto Português de Reumatologia, Lisbon, Portugal

Introduction and Objectives: The lack of lower limb joint stability could be a reason for the increased fall risk in rheumatoid arthritis (RA) patients[1] and in postmenopausal women[2], well as a reason for the lower functional capacity in RA patients[3]. Proprioception and stiffness play an important role in joint stability[4]. For optimal joint stability is needed some level of stiffness, however too much or too little stiffness it is not advisable[5]. To study the lower limb joint stiffness has been developed the concept of dynamic joint stiffness (DJS)[6]. DJS is defined as the stiffness of muscles and other joints structures during intersegmental displacement as a reaction to the external moment[6,7]. The slope of the joint moment plotted as a function of the joint angle is an approach to the DJS measure and has been used as quantitative reference[6,7]. During the stance phase of walking, the ankle joint supports and propels the body through three distinctive phases of nearly constant stiffness: the controlled plantar flexion, the controlled dorsiflexion and the powered plantar flexion[8]. Moreover, were found lower values of ankle power peak (APP) in elders with low functional capacity[9], and accordingly with literature, APP is an essential component of functional mobility in older women with functional limitations[10]. So, the objective of this study was to compare APP and DJS of the ankle during gait in RA postmenopausal women with and without falls history.

Methods: The 19 RA postmenopausal women selected for this retrospective study (without lower limbs prostheses), answered the question: "how many times did you fall last year?". A tridimensional analysis was used to assess the biomechanical parameters. The Vicon® Motion Capture system recorded kinematics data (9 MX1.3 cameras, 200Hz) synchronized with a force plate (AMTI BP400600-200, 1000Hz). Data analyzed by Vicon® Nexus software (1.7.1) based on an integrated model of 41 reflective markers relocation and subject anthropometric data, developing mechanical segments and joints centers. Subjects performed 14 valid trials (7 left and 7 right foot-step on force plate). Ankle "moment of force-angle" plot was divided in 3 phases and computed the matching DJS: controlled plantar flexion, controlled dorsiflexion and powered plantar flexion. T test was used.

Results: Eleven subjects had at least one fall in the previous year. The DJS of the subjects ankles with falls history did not show differences relatively to the subjects ankles without falls history (K values in figure 1). The R-squared mean of the subjects linear models were higher than 0.85 in all phases for both groups (figure 1). APP was lower in the subjects ankles with falls history (1.97 ± 1.03 W *vs* 2.73 ± 0.90 W, p=0.021).

Figure:
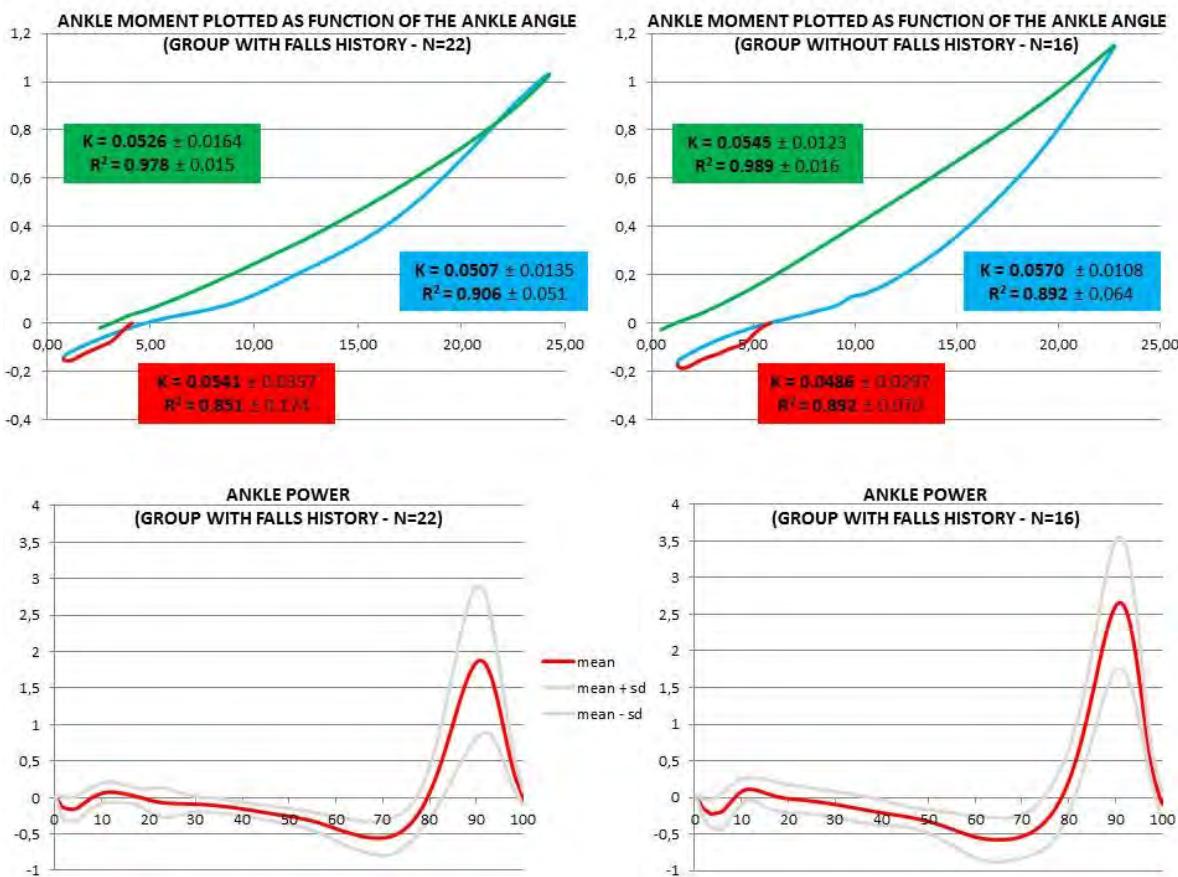
Caption: Figure 1. Ankle moment plotted as function of the ankle angle and ankle power, during foot contact with force plate (groups of subjects with and without falls history).

Conclusion: The R-squared results showed that the three phases of the stance period can be translated into a linear moment-angle relationship in RA postmenopausal women. The DJS results of the second and third phase were consistent with the results of other studies in healthy people[6–8], however the results of these studies in the first phase were much lower than the results observed in our study for both groups. Despite the small sample size, the lack of differences between the subjects ankles with and without falls history seems indicate that DJS of the ankle shall not be a parameter associated with the occurrence of falls. In contrast with DJS, the APP seems to be a gait biomechanical parameter that is associated with falls in RA postmenopausal women. Interventions for enhance this parameter could be advisable and exercise programs appear as a possibility.

References: [1] Hayashibara et al., Osteoporos. Int., 21(11):1825-1833, 2010.

[2] Cangussu et al., BMC Musculoskelet. Disord. 13:2, 2012.

[3] Aydoğ et al., Clin. Rheumatol., 25(4):462-467, 2006.

[4] Docherty et al., Electromyogr. Kinesiol., 14:317-324, 2004.

[5] Butler et al., Clin. Biomech., 18(6):511-517, 2003.

[6] Davis et al., Gait Posture, 4:224-231, 1996.

[7] Gabriel et al., Phys. Ther. Sport, 9:16-24, 2008.

[8] Safaeepour et al., Biomed. Eng. Online, 13:19, 2014.

[9] Graf et al., Arch. Phys. Med. Rehabil., 86(11):2177-2183, 2005.

[10] Suzuki et al., J. Am. Geriatr. Soc., 49:1161-1167, 2001.

Disclosure of Interest: None Declared

AS-0275

THE INFLUENCE OF FUNCTIONAL FITNESS LEVEL ON THE STRATEGIES ADOPTED BY THE ELDERLY TO ACCELERATE THE BODY UPWARDS DURING STAIR ASCENT

Vera Moniz-Pereira [1,*] Thomas M. Kepple [2] Silvia Cabral [1] Filipa João [1] António P. Veloso [1]

[1]Laboratório de Biomecânica e Morfologia Funcional, CIPER, Faculdade de Motricidade Humana - U Lisboa, P-1499-002 Lisboa, Portugal, [2]C-Motion, Inc, Germantown, MD, United States

Introduction and Objectives: The age decline in functional fitness, particularly in muscle strength, leads to problems in mobility and difficulties in performing daily activities[1], especially locomotor activities involving stairs[2]. As a consequence, studies show that older adults re-distribute their joint moments while ascending stairs in order to be able to meet the task demands[3-4]. However, these studies do not directly quantify the consequences of this re-distribution to the body upward acceleration, one of the main goals of stair ascent.

The aims of this study were: to quantify, using induced acceleration analysis (IAA), joint moments and gravity contributions to the vertical acceleration of the center of mass during stair ascent in the elderly and, to verify the influence of the subjects' functional fitness level in those contributions.

Methods: The sample included 6 community-dwelling older adults over 65 years (72.5±5.1y), without any condition that would affect their gait. The subjects were divided in 2 groups according to their functional fitness level (LFFL – low functional fitness level; HFFL – high functional fitness level), established through a score (max: 24 points) composed by the results of 6 field tests: the 8 foot Up&Go and the Chair Stand test from Senior Fitness Test battery[5]; and items 4 – step up and over, 5 – tandem walk, 6 – stand on one leg and 7 – stand on foam eyes closed, from Fullerton Advanced Balance Scale[6].

Kinematic and kinetic data were collected using 8 infrared cameras (Qualisys Oqus 300) working at a frequency of 200Hz and synchronized with 2 Kistler force plates (9281B, 9283U014), one in front of the stairs and the other embedded below the first step. Participants walked at their comfortable pace.

Three trials were analyzed. A 10 Hz 4th order Butterworth filter was applied to both kinematic and kinetic data. The CAST marker set[7] was used and a 7 segments model (feet, shanks, thighs and pelvis) was built and optimized through global optimization[8]. Joint moments were determined through inverse dynamics and expressed relatively to the proximal segment. IAA was processed based on[9], during two phases of the cycle, when the ground reaction forces sum was above (pull up) and below (forward continuance) the body weight. Further, the foot was fixed to the floor when it was flat on the floor and allowed to rotate about the center of pressure for the rest of the time. All data processing was performed in Visual 3D software (Professional Version v5.01.18, C-Motion, Inc).

Results: The groups differed in terms of functional fitness level (HFFL: 24±0 LFFL: 19±1 points) and stride velocity (HFFL: 0.62±0.1 LFFL: 0.50±0.1 lower limb length/s), but were similar regarding age (HFFL: 72±3.6 LFFL: 73±7.2 y) and body mass index (HFFL: 26±5.1 LFFL: 27±2.6 Kg/m²).

Agreeing with the joint moment results, the IAA showed that the plantaflexor moment, together with the knee and hip extensor moments, were the primary contributors to accelerate the body upwards during both the pull up and the forward

continuance phases and added that gravity also plays an important role, especially during the latter phase (Fig 1). All the other contributions were below 5% of the total acceleration and therefore are not presented.

The mentioned contributions varied with the subjects' functional fitness level. In the pull up phase, both groups pushed the body upwards mainly using the plantarflexor and knee extensor moments. However the contribution from the plantarflexors in the LFFL group was relatively lower, which may explain their lower stride velocity. During the forward continuance phase, the HFFL group supported the body more actively through the plantarflexor and the knee extensor joint moments, whereas the LFFL group were more passive, i.e., relied less on muscle activity, which is shown by the higher gravity contribution (Fig 1).

Figure:
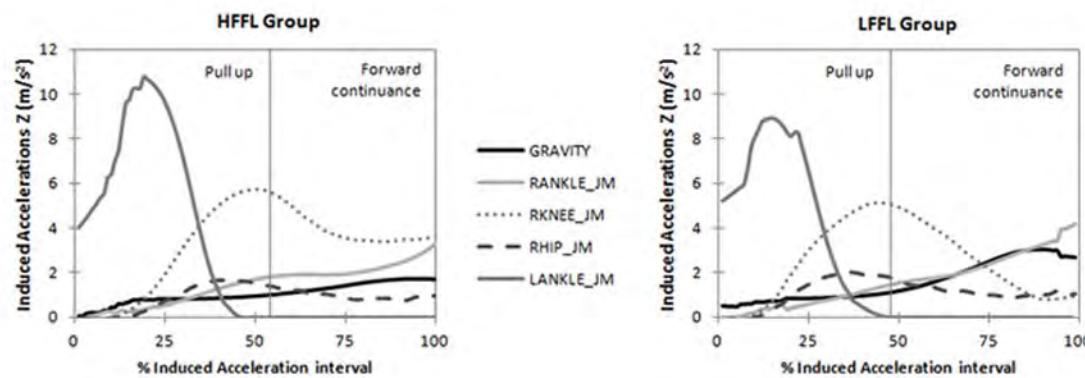
Caption: Vertical induced accelerations generated by sagittal plane lower limb joint moments and gravity.

Conclusion: This study shows that the strategy adopted by older adults to accelerate the body upwards during stair ascent depends on their functional fitness level. Due their lack of strength, older adults with a lower functional fitness showed to have a smaller contribution from the plantarflexor moment during the pull up phase and to support the body more passively during the forward continuance phase, relying less on their knee extensor moment.

Acknowledgements

Table:

References: [1] Vandervoort, *Muscle Nerve*, **25**: 17–25, 2002

[2] Startzell et al., *J. Am. Geriatr. Soc.*, **49**: 567–80, 2000

[3] Reeves et al., *J. Electromyogr. Kinesiol.*, **19**: 57–68, 2009

[4] Novak et al., *Gait Posture*, **33**: 54–60, 2011

[5] Rikli et al., *J. Aging Phys. Act.*, **7**: 129–161, 1999

[6] Rose et al., *Arch. Phys. Med. Rehabil.*, **87**: 1478–85, 2006

[7] Cappozzo et al., *Clin. Biomech.*, **10**: 171–178, 1995

[8] Lu et al., *J. Biomech.*, **32**: 129–34, 1999

[9] Kepple et al., *Gait Posture*, **6**: 1–8, 1997

Disclosure of Interest: None Declared

AS-0276

JOINT TORQUES DIFFER IN OLD AND YOUNG DURING MAXIMUM STEPPING TASK

Kathleen Bieryla [1,*]Christine Buffinton [2]

[1]Biomedical Engineering, [2]Mechanical Engineering, Bucknell University, Lewisburg, United States

Introduction and Objectives: Following a balance perturbation, a stepping response is commonly used to regain support. The maximum step length test, where a person steps out and back with one leg as far as possible, has been used as a clinical assessment of balance. Because this out and back movement does not occur when recovering from a fall, the focus on completing a forward step was examined. The purpose of this study was to examine age-related differences in joint kinetics at maximum step distance.

Methods: Twenty young (mean(SD): 20.0(1.8) years) and twenty old (75.6(4.9) years) adults were recruited for the study. The study was approved by the University's Institutional Review Board and written consent was obtained prior to participation. Participants completed a step starting from double support, with one leg in front of the other, at an initial distance equal to the individual's average step length. The distance was increased by 10% body height until the participant could not successfully complete the step. Whole body kinematics and ground reaction forces were recorded. Lower extremity sagittal plane joint torques were estimated. A one-way repeated measures ANOVA was used to determine the effects of age on joint kinetics during maximum step distance trial.

Results: One young female subject was removed from all analyses due to equipment failure during data collection. Maximum step length was significantly higher in young adults, 1.23(0.138) m compared to old adults, 0.961(0.150) m ($P<0.001$). Young adults were able to safely complete an average maximum step distance of 70.8% height compared to old adults who completed an average maximum step distance of 57.8% height. During maximum stepping trials, old adults had larger peak maximum plantarflexion ankle torques for the stepping leg ($P<0.001$) (Table 1). There was no significant difference in peak plantarflexion ankle torques for the stance leg ($P=0.558$). During maximum stepping trials, young adults had larger peak knee extension torques for both the stepping ($P<0.001$) and stance ($P=0.002$) leg, larger peak knee extension torques for the stance leg ($P<0.001$) and larger peak hip flexion torques for the stepping leg ($P<0.001$).

Conclusion: Young adults completed a significantly longer step distance than old adults. During the maximum step distance trial, in general, kinetic measures were greater in the young than in the old. This test is easy to administer and may be more challenging than the maximum step length test. Future work should be completed to determine the feasibility of this test to discriminate between fallers and non-fallers.

Table:

	Young	Old	P value
Peak Ankle Plantarflexion, Stepping	0.186(0.099)	0.368(0.107)	<0.001
Peak Ankle Plantarflexion, Stance	0.275(0.153)	0.254(0.153)	0.558
Peak Knee Extension,	1.384(0.313)	0.878(0.327)	<0.001

Stepping			
Peak Knee Extension, Stance	0.840(0.197)	0.626(0.254)	0.002
Peak Hip Flexion, Stepping	2.120(0.462)	1.521(0.602)	<0.001
Peak Hip Extension, Stance	1.325(0.368)	0.788(0.243)	<0.001

Caption: Table 1: Mean(SD) peak joint torques (Nm/m*kg) for maximum step distance, young and old adults, right leg as the stepping leg.

Disclosure of Interest: None Declared

Orthopaedic Implants

AS-0277

SMART KNEE PROSTHESIS FOR ORTHOPEDIC SURGERY: THE IMPLANTABLE AND WEARABLE MEASUREMENT SYSTEM

Kamiar Aminian [1,*] Arash Arami [1] David Forchelet [2] Philippe Renaud [2]

[1]Laboratory of Movement Analyisis and Measurement, [2]Microsystems Laboratory 4, EPFL, Lausanne, Switzerland

Introduction and Objectives: Recent advances in remote powering and telemetry permitted the use of sensors inside body. A few studies have been already done on smart knee prostheses, but all focused on monitoring the in-vivo contact forces and moments [1-4]. A smart design, compatible with mechanical structure of commercially-available knee prostheses, that provides force and accurate 3D kinematics feedback was suggested with all electronics housed in the polyethylene insert (PE) [6]. The current work addresses the designed kinematics and force measurement system of that smart implant and its validation in a robotic knee simulator.

Methods: *Kinematics measurement*- Two inertial measurement units (IMUs), each consists of a 3D accelerometer and 3D gyroscope, were considered to be fixed on stretch belts and placed around the thigh and shank (Fig.a). Three anisotropic magnetoresistive (AMR) sensors (S1, S2, S3) were configured in PE, based on a sensitivity analysis. A magnet (M) was capsulated in the prosthesis femoral part to convert its movement to changes of magnetic field (Fig. b). Three angle estimators were deigned. First, a linear regression using only the implantable AMR sensors. Second estimator solely used IMUs' measurements using the strapdown integration of angular velocities [6] combined by a linear model for drift removal. Third estimator was based on a fusion of IMUs and low-frequency (10Hz) sampled AMRs in order to reduce power consumption of the implanted part. This estimator used strapdown integration of the angular velocities with a locally linear model, using the difference estimate (IMU-AMR) for drift removal.

Force measurement-Two biocompatible force sensing gauges fabricated and configured in the medial and lateral sides of PE, above two devised cavities in a sealed capsule (Fig.c). The sensors measure the forces applied on each condyle through the stretch of the layer on top of cavities. The sensors are placed into separate Wheatstone bridges where all elements were structured into the sensors for temperature compensation. The capsule was glued in between PE sections, and cured for 16 hours at 45ºC under the pressure. A linear model for each sensor was used for calibration.

Knee simulator- A robotic knee simulator was used to validate the force and kinematics measurements. It held the smart knee prosthesis with embedded sensors. The IMUs were attached to the simulator segments to provide wearable measurements. Data collected from subjects during treadmill walking using X-ray fluoroscopy, optical motion capture systems and an implanted instrumented prosthesis [7-8] were used to replicate 4 gait patterns in the simulator. A motion capture system (Vicon, UK) and reflective markers attached to the simulator segments, was used as the kinematic reference. A force sensor (ATI, USA) was integrated below the prosthesis tibial part in the robotic knee as the force reference.

Results: The obtained performances of AMR-based, IMU-based and IMU-AMR based flexion angle estimators over four gait patterns are shown in Table. IMU-based estimates were not very precise, but the use of AMR sensors either alone or in the fusion framework drastically improved the results, RMS error<1.2º. The raw measurements of the force sensors

showed high corelation with the reference total forces, $R^2>0.98$. The obtained RMS errors for lateral and medial sensors on train data were 20.0N and 5.9N respectively

Figure:
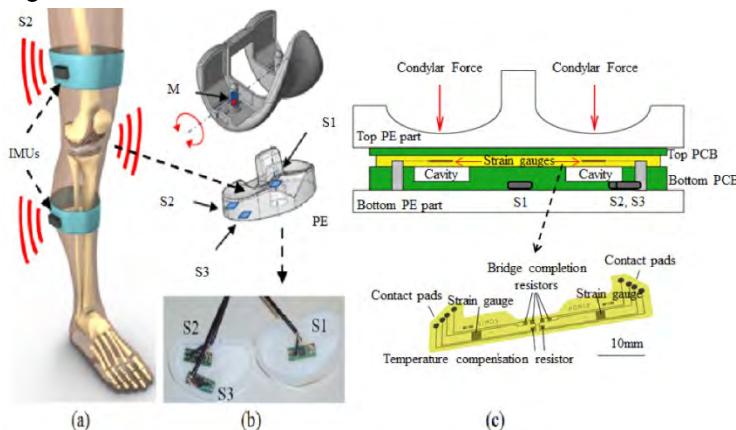
Caption: (a) Wearable IMUs, (b) implanted AMR sensors (S1-3), (c) the capsule with designed strain gauges

Conclusion: Using implanted (AMR sensors and biocompatible embedded strain gauges) and wearable technology (IMU) a mixed measurement system was proposed able to estimate simultaneously the kinematics and force with a smart knee implant. Angle and force estimators were evaluated with realistic walking patterns replicated in a robotic knee simulator. The best kinematics estimation was obtained from fusion of IMUs and AMR sensors which is also optimum for reducing power consumption. The force sensors behaved linearly in fixed flexion angles, with no measurement drift. They can estimate the M-shape pattern of total force during gait, but showed different sensitivities to the applied forces in different angles. Fusion of estimated angles and force can enhance the force estimations.

Table:

Estimators	E(error)	SD(error)	RMS(error)	R^2
AMR	0.46±0.09	1.09±0.30	1.19±0.28	0.99+0.00
IMU	1.65±1.45	1.70±1.11	2.43±1.70	0.97±0.03
IMU-AMR	0.47±0.10	1.08±0.25	1.18±0.25	0.99±0.00

Caption: Performance of different angle estimators

References: [1] Damm et al., *Clin. Biomech.*28(5), 2013.

[2] D'Lima et al., *J. Arthrop.* 21(2), 2006.

[3] Heinlein et al., *J. Biomech.* 40, 2007.

[4] Kirking et al., *J. Biomech.* 39(9), 2006.

[5] Arami et al, IEEE Trans Auto Scie Eng. 10(3), 2013.

[6] Favre et al., *J. Biomech.* 42(14), 2009.

[7] Barré et al., *IEEE Trans. Biomed. Eng.* 60(11), 2013.

[8] Fregly et al., *J. Orthop. Res.* 30(4), 2012.

Disclosure of Interest: None Declared

Orthopaedic Implants

AS-0278

TASK DEPENDENCY OF KNEE IMPLANT KINEMATICS BY MEANS OF VIDEOFLUOROSCOPY

Pascal Schütz [1,*]Barbara Postolka [1]Hans Gerber [1]Marco Hitz [1]Stephen Ferguson [1]William R. Taylor [1]Renate List [1]

[1]Institute for Biomechanics, ETH Zurich, Zürich, Switzerland

Introduction and Objectives:

In order to better understand the mechanisms leading to unsatisfactory outcome in total knee arthroplasty (TKA), the assessment of kinematic and kinetic data during functional activities in vivo is crucial.

To overcome the limitations of a static image intensifier and motion capture of the knee without the influence of soft tissue artefact [1], an automated moving fluoroscope has been developed [2, 3] that allows tracking of the knee joint throughout complete cycles of level walking and stair descent. The aim of this study was to analyse task dependency of the kinematic behavior, especially anterio-posterior (A-P) translation of a cruciate retaining TKA, during activities of daily living.

Methods: One female and five male subjects (72.8±8.5y, >1 year postop, painfree), who had each received a unilateral PFC Sigma Curved CR fixed-bearing (DePuySynthes) TKA, were assessed during free level gait, stair descending (3-step-staircase), pivot turn (swing phase followed by a 90° pivot turn), rising from a chair and sitting down by means of a moving fluoroscope (25Hz, 1ms shutter) [2, 3].

The 2D/3D registration of the 2D fluoroscopic images was performed using CAD models of the implant components. Registration errors, assessed for a similar TKA, were <1degree for all rotations, <1mm for in-plane and <3mm for out-of-plane translations [2]. The relative rotations between the femoral and tibial components were determined using the joint coordinate system by Grood et al. [4] based on the femoral and the tibial implant coordinate systems. A-P translations of the femoral flexion axis relative to the tibial component were described using a medial and a lateral point on the femoral flexion axis. For statistical analysis a linear mixed model (α=0.05) was used.

Results: Stair descent showed a significantly higher A-P translation with no differences in flexion/extension range of motion (ROM) in comparison to sit-to-stand and stand-to-sit. Only the pivot turn showed significant differences to other tasks for internal/external rotation and adduction/abduction.

No significant differences in ROM were found for either medial or lateral femoral A-P translation between level gait and stair descent (Table 1). For stair descent, the A-P translation was significantly larger during the unloaded swing phase than during the loaded stance phase.

At a specific flexion angle the A-P translation showed a clear task dependency and the differences in A-P translations were even more prominent when comparing loaded stance to unloaded swing phases (Fig.1). The two walking as well as sitting tasks showed a similar characteristic of A-P translation-flexion-coupling whereas the pivot turn showed a distinctive pattern. Except pivot turn, maximal A-P translation occured in the range of 36-42° flexion.

Figure:
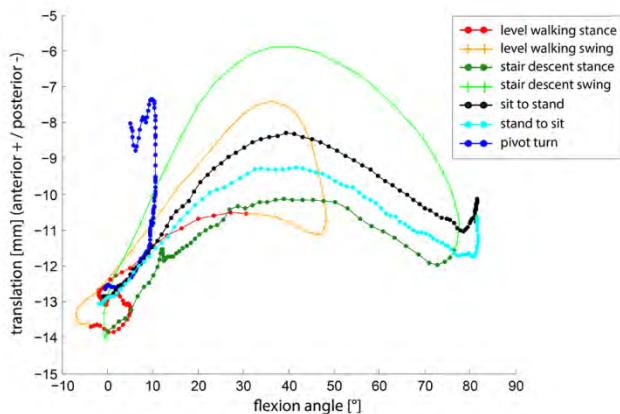
Caption: Translation–flexion–coupling. Flexion angles and the corresponding A-P translation of the medial condyle point. Mean values are shown for 6 subjects.

Conclusion:

The pivot turn showed the highest ROM in A-P translation and a completely different translation-flexion-coupling pattern from the other activities. However the 90° turn transfers the direction of A-P translation from an in plane to an out of plane direction and the latter is affected by a limited registration accuracy [2].

Although the translation-flexion-coupling patterns lead to the assumption of a movement direction dependency, the ROM of A-P translation did not differ significantly between sit-to-stand and stand-to-sit.

Banks et al. [5] found a slightly higher flexion of 47° and 56° for the maximal A-P translation of the medial contact point in a step up exercise. This can be explained by different definitions of points to describe A-P translation, TKA designs and tasks.

The differences of the tibiofemoral kinematics between the different tasks and the different loading conditions indicate the importance of analyzing whole gait cycles and a variety of functional tasks. For a better understanding of the underlying mechanisms, the loading conditions should be taken into account.

Table:

	flexion/ extension [°]	abduction/ adduction [°]	internal/external rotation [°]	medial ap translation [mm]	lateral ap translation [mm]
level gait	58.5±4.1	3.1±0.9	8.3±1.5	7.8±1.6	7.9±1.8
level gait stance	36.7±3.6	2.2±0.5	6.1±1.2	4.7±1.1	5.5±1.2
level gait swing	57.7±3.6	2.8±0.9	6.8±1.5	7.5±1.6	7.3±1.3
stair descent	83.5±6.1	3.4±0.7	9.3±2.0	10.2±2.5	9.2±1.2
stair descent stance	77.4±6.4	2.9±0.3	6.3±1.8	5.1±1.5	5.3±1.4
stair descent swing	82.9±5.9	2.5±0.8	8.5±2.4	9.8±2.7	9.1±1.3
pivot turn	16.0±4.2	1.6±0.3	5.3±0.9	10.9±1.1	12.3±1.8
sit to stand	83.4±5.6	2.4±1.1	8.9±1.7	6.0±1.6	6.4±0.6
stand to sit	84.9±5.0	2.3±0.7	7.8±1.9	5.1±1.0	6.2±0.8

Caption: ROM for rotations and A-P translations. Mean and standard deviation are presented for 6 subjects.

References:

[1] Cappozzo et al., Gait Posture, 21(2): 186-196, 2005.

[2] Foresti, PhD Thesis ETH Zurich, Nr: 18368, 2009.

[3] Zihlmann et al., Gait Posture, 24(4): 475-81, 2006.

[4] Grood et al., J Biomech Eng, 105(2): 136-44., 1983.

[5] Banks et al., J Arthroplasty, 12(3): 297-304, 1997.

Disclosure of Interest: None Declared

Prosthetics

AS-0280

J-CURVE AND SINGLE-RADIUS FEMORAL DESIGNS DURING DAILY ACTIVITIES. ARE THERE ANY BIOMECHANICAL DIFFERENCES?

Bernardo Innocenti [1,*] Héctor Robledo Yague [1] Raquel Alario Bernabé [1] Walter Pascale [2] Silvia Pianigiani [2]

[1] BEAMS Department, Université Libre de Bruxelles, Bruxelles, Belgium, [2] IRCCS, Istituto Ortopedico Galeazzi, Milano, Italy

Introduction and Objectives: The lack of awareness of the exact number of instantaneous centers of knee flexion/extension rotation leads to the presence in the market of Total Knee Arthroplasty (TKA) femoral components designed under different hypotheses. Single radius (SR) designs are thought to replicate the physiological anatomy in a more realistic way than J-curve (JC) thanks to the constant radius during flexion that should provide a constant lever arm for the patella and isometry of the collateral ligaments. Although these theoretical advantages, surgery experts are usually more confident with the guaranteed performance of multiple radii components like the JC design. Any literature study compares in depth these two solutions for TKAs.

For these reasons, the aim of this study is to compare a SR to JC solution for the same posterior stabilized (PS) TKA design under daily activities conditions. Both kinematic and kinetics outputs have been analyzed. The study has been performed by means of finite element analysis.

Methods: For the two analyzed solutions, the same tibial component has been used. A standard gait cycle and the downward movement of a squatting activity up to 120° were simulated for both situations. The tibiofemoral kinetics and kinematics have been investigated comparing the contact area between components, the internal-external rotation, the position and magnitude of the contact forces and the Von Misses stresses on the polyethylene.

Results: The results show that the two solutions did not present significant differences for any of the analyzed outputs for the low demanding task daily activity (up to 60°) (Figure 1a). On the other hand, significant differences in the behavior are highlighted during the squatting motion especially after 80° of knee flexion. From this point, the contact area and forces, especially for the post-cam interaction, change and also the kinematics is altered presenting an anomalous drop for the SR design both in antero-posterior translation and internal-external rotation. Moreover, the stress on the polyethylene insert presents higher values on the posterior part of the insert (Figure 1b).

Figure:
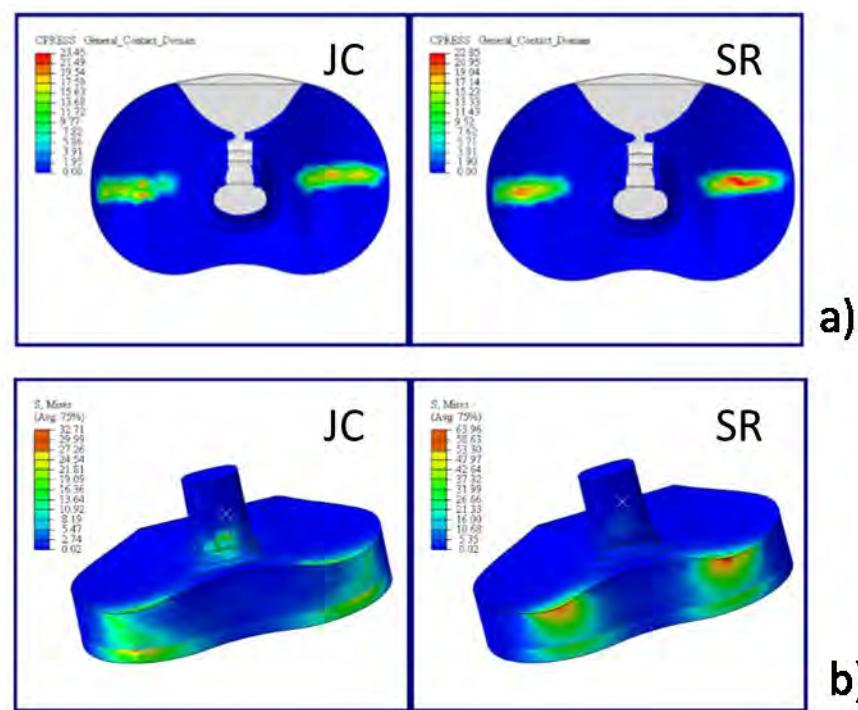
Figure 1: a) Qualitative stress distribution for the maximum flexion reached for the low demanding task; b) qualitative stress distribution for the maximum flexion reached for the high demanding task

Conclusion: The aim of this study was to make a consistent analysis to compare the same PS TKA design for a JC or a SR solution. To be able to perform this analysis in a reproducible manner, a finite element model has been developed to analyzed the solution behavior under walking and squatting conditions.

The results show that the two solutions are comparable for low demanding task like walking obtaining similar kinetics and kinematics outputs, but could diverge for higher knee flexion like during squatting. Even if this numerical model present some limitations, some of the obtained results are in agreement with the literature.

The diferrences in performances can be critical for a possible early wear of the SR prosthesis leading to an early failure of the TKA.

The authors have nothing to disclose.

Disclosure of Interest: None Declared

Orthopaedic Implants

AS-0281

INVESTIGATION OF THE LOAD CONTRIBUTIONS OF THE ANTERIOR CRUCIATE LIGAMENT BUNDLES AGAINST DEGREE OF FREEDOM RELEASE

Ryo Takeda [1,*]Keisuke Okuzumi [1]Katsuhiko Sasaki [1]

[1]Engineering, Hokkaido University, Sapporo, Japan

Introduction and Objectives: About 40% of knee joint injuries cases are related to ligament damage. Of these cases, the anterior cruciate ligament (ACL) is the most commonly ruptured, and the reconstruction of this ligament has been the attention of study. Single and double bundle reconstruction techniques are the most common methods of treatment but there are controversies on which is more effective in restoring the load capabilities. The difference of the two treatment methods depends on consideration of load capabilities of the anteromedial (AM) and posterolateral (PL) bundles of the ACL. Therefore in this study, the load capabilities of the AM and PL bundles of the ACL will be investigated along its relationship to the release of certain degrees of freedom (DoF) of the knee joint.

Methods: In this report we measured loads induced during anterior-posterior (AP) translation (drawer) tests of the cruciate ligament bundles. Although works in the past have investigated the force versus displacement behaviour, there has been little data on how releasing or constraining DoFs affects the load measurements[1][2].

For this study, a knee joint biomechanical testing platform was designed and developed. The platform consisted of a 6 axis force/torque sensor (WEF-6A1000-30-RC5, Wacoh-Tech Inc.) attached to a single axis material testing machine (Ezgraph, Shimadzu Corp.) and a bespoke DoF passive fixture. The passive fixture was capable of releasing or constraining 2 translational DoFs (medial-lateral (ML) and proximal-distal (PD)) and 3 rotational DoFs (internal-external (IE), varus-valgus (VV) and flexion-extension (FE) rotation) by means of bearings and locking screws. Ex-vivo knee joint specimens are placed in the testing platform by attaching the femoral bone to the axis force/torque sensor and the tibial bone to the passive fixture. Once attached, AP translational drawer motion can be induced by the material testing machine and the load was recorded by the force/torque sensor. For this report, the knee joint specimens were fixed in the testing platform at 60 deg flexion angle and a ±5 mm AP displacement was induced.

In this work, porcine stifle joints were used as knee joint specimens. The specimens were subject to three different ligament conditions: ACL intact (Intact), AM bundle cut (AM cut) and AM+PL cut (ACL cut). In addition, six DoF release conditions were considered: No DoF release (the passive fixture is totally constrained), ML release, ML+PD release, ML+PD+IE release, ML+PD+IE+VV release and ML+PD+IE+VV+FE release.

Results: The results load capabilities of the ligament in the AP direction are shown in Fig. 1. The results showed that releasing a combination of DoFs lowered the AP directional load when compared to releasing a single DoF or none at all. When comparing the AP load between the No DoF and the ML+PD+IE+VV+FE release state the load decreased down to 14%, 19% and 26% for the intact, AM cut and ACL cut states respectively. Furthermore, the AM bundle contributed to about 25% while the PM bundle about 19% for the AP directional load contributions during a No DoF state. However hardly any differences in load contribution were measured for the ML+PD+IE+VV+FE release state. This means that both the AM and PL bundle load capacities are dependant.

Figure:
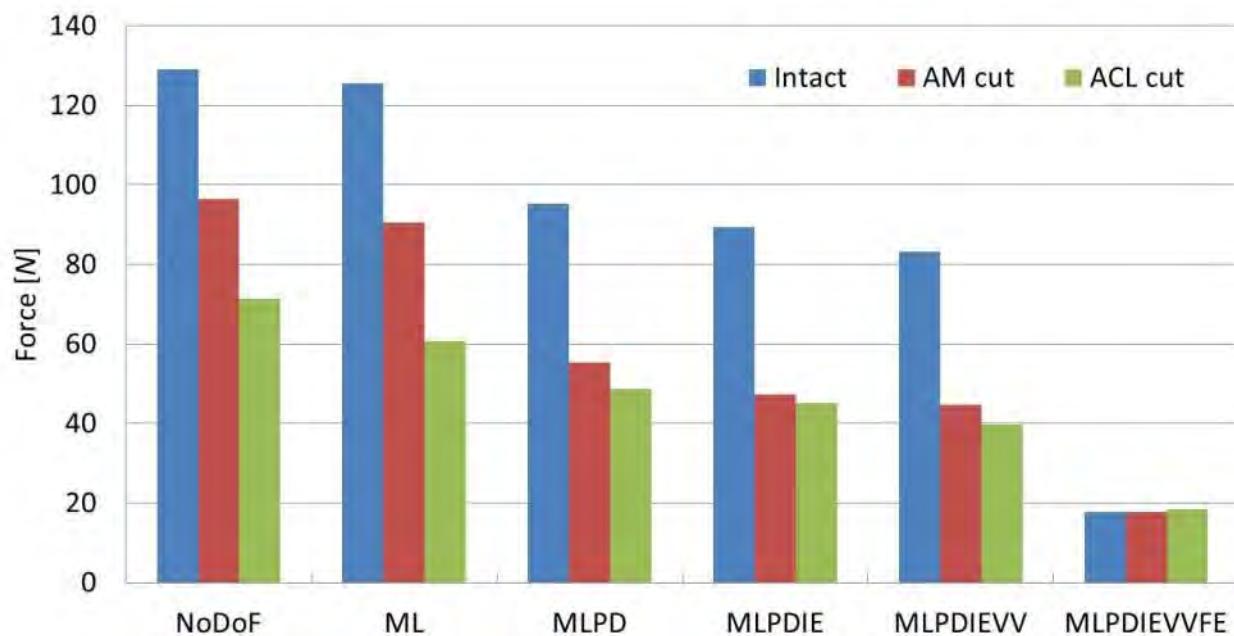
Caption: Fig. 1. AP directional load vs. DoFs release conditions vs. ligament conditions

Conclusion: This work inverstigated and measured the load condributions of the AM and PL bundles of the ACL. It was found that the load capacities of both bundles behave differently according to the DoFs release conditions.

References: [1]   Fujie, Mabuchi, Woo, Livesay, Arai, Tsukamoto. J. Biomechanical Engineering, 115, 211-217, 1993.
[2]   Race, Amis. J. Biomechanics, 29, 873-879, 1996.

Disclosure of Interest: None Declared
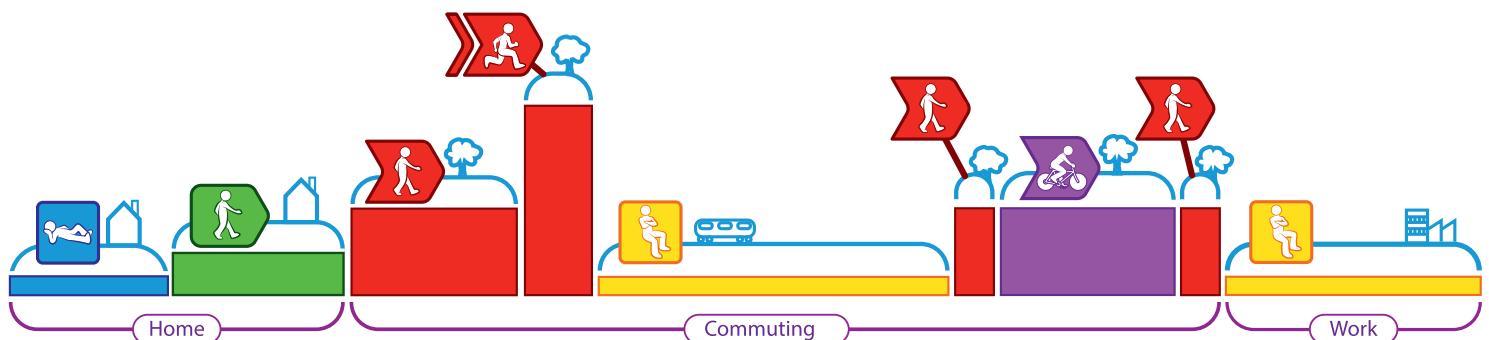
*activ*PAL™ - sensor to solution
The researcher's preferred choice for quantifying physical behaviours

Home Commuting Work

Lying

Sitting

Standing

Stepping
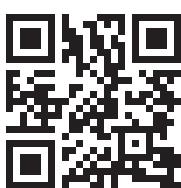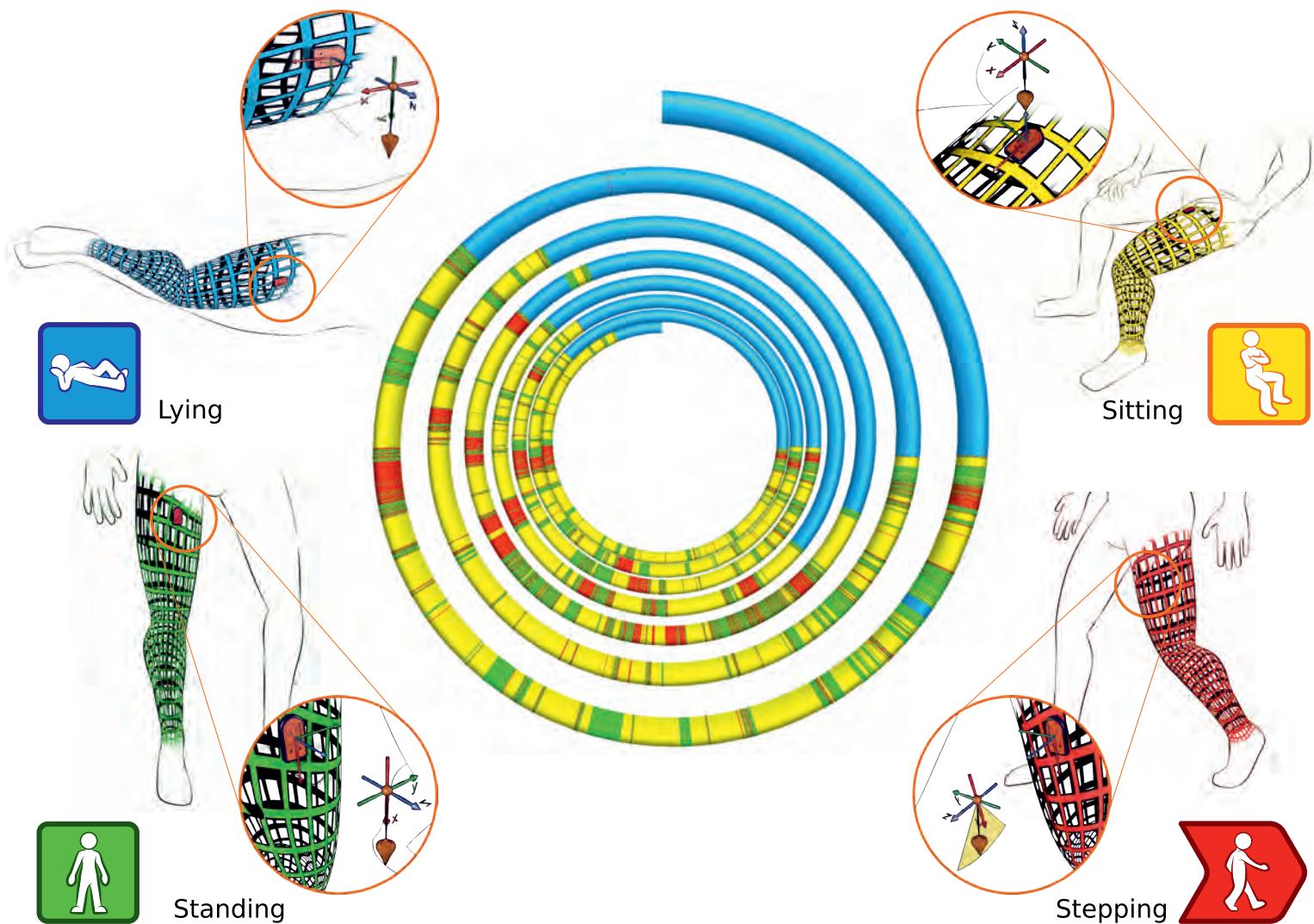
www.paltechnologies.com
Rising to the challenge of objectively quantifying
physical behaviours including sedentary
activities, active commuting
and car travel

PALtechnologies
Limited
PROVIDING THE EVIDENCE

Orthopaedic Implants

AS-0282

THE RELATIONSHIP BETWEEN ALIGNMENT, FUNCTION AND LOADING IN TOTAL KNEE REPLACEMENT: IN-VIVO ANALYSIS OF A UNIQUE PATIENT POPULATION

David Williams [1,*] Andrew Metcalfe [1] June Madete [1] Gemma Whatling [1] Ishaak Saleem [1] Alexis Roux [1] Peter Kempshall [2] Kathleen Lyons [2] Mark Forster [2] Cathy Holt [1]

[1] Arthritis Research UK Biomechanics and Bioengineering Centre, Cardiff University, [2] University Hospital of Wales, Cardiff, United Kingdom

Introduction and Objectives: One of the main surgical goals when performing a total knee replacement (TKR) is to ensure the implants are properly aligned and correctly sized; however the effect of alignment on the biomechanics of the knee during functional activities is not well understood. Cardiff University has a unique access to a group of patients within the local region who have a relatively high frequency of poor alignment, and early failure [1]. Despite the obvious disappointment, it provides a rare insight into how mal-alignment of TKR's can affect patients from a clinical and biomechanical point of view to determine how to best align a TKR. The aim of this study was to perform an in-vivo analysis investigating the relationship between alignment and biomechanical function to assist surgeons by determining the optimum alignment for patients. For this particular study we focused on comparing patients with neutral alignment (-2° to 2°) to patients with varus alignment (>2°).

Methods: Fifteen patients with 18 Kinemax (Stryker) TKR's were recruited, 10 with neutral alignment and 8 with varus alignment. Ethical approval was obtained. Single plane video fluoroscopy of the knee was taken for each subject during a step-up and step-down task. Joint Track image registration software (University of Florida, USA) was used to match CAD models of the TKR components to each fluoroscopy image. This technique is known to have high accuracy in measuring TKR kinematics [2]. Further processing using JointView software (University of Florida, USA) calculated 3D joint kinematics and the tibio-femoral contact points. Bespoke code developed within MATLAB (The Mathworks Inc, USA) was utilised to calculate the centre of rotation (CoR) using the contact point data and was normalised to the length and width of the tibial component. The data was separated into three phases of the activity: step-up, step down and transition between the two with CoR calculated for each section. Long-leg radiographs were used to define limb alignment. Hip-Knee-Ankle (HKA) angle was measured from the radiographs to determine long leg alignment in the frontal plane with lateral distal-femoral angle (LDFA), medial proximal tibial angle (MPTA) and tibial slope calculated as secondary measures. CT scans were used to calculate both femoral and tibial component rotational alignment and inter-component rotation.

Results: The mean age of the patient group was 74 (range 60-89). Mean HKA measurement for the varus group was 5.9° and for the neutrally aligned group 0.7°. The mean CoR medial-lateral position for step up and down was found to be 2.83% (Lateral(-) /Medial(+)) for the neutral group and -4.65% for the varus group . Mean tibial slope for varus group was 3.33° and neutral group 5.96°. CoR calculations showed that 75% of the varus aligned patients had a lateral positioned CoR during step up and a medial positioned CoR during step down. In contrast, there was no bias medially or laterally in the CoR position for the neutrally aligned group. The incidence of medial and lateral CoR positions were equal for both activities.

A negative correlation was found between medial-lateral location of CoR during step down and tibial slope angle (Spearmans rank r=-0.486). CoR was found to not be related to frontal plane alignment, inter-component rotation or individual component rotation.

Conclusion: CoR results show that the majority of varus aligned patients have a lateralised CoR during step up and medial CoR position during the step down activity.

It was found that CoR position correlates with tibial slope yet did not correlate with HKA or rotational alignment of components. Further analysis of the kinematic data produced from the fluoroscopy needs to be completed to fully understand the effect of alignment of TKR on biomechanical function post-surgery.

References: [1] Kempshall, P.J. et al. 2009 Review of Kinemax knee arthroplasty performed at the NHS Treatment Centre, Weston-Super-Mare. *J Bone Joint Surg Br,* 91(2), pp. 229-233

[2] Banks SA, Hodge WA. 1996. Accurate measurement of three-dimensional knee replacement kinematics using single-plane fluoroscopy. *IEEE Trans Biomed Eng* 43:638-649

Disclosure of Interest: None Declared

Bone

AS-0283

RESIDUAL STRESS OF BOVINE FEMURS IN THREE AGE GROUPS

Satoshi Yamada [1,*] Mai Onuma [2] Shigeru Tadano [1]

[1]Faculty of Engineering, [2]Graduate School of Engineering, Hokkaido University, Sapporo, Japan

Introduction and Objectives: The presence of residual stress in bone tissue, which is defined as the stress that remains in the tissue without any external forces, has been examined using X-ray diffraction techniques [1]. The residual stress can be calculated on the basis of variation in the interplanar spacing of hydroxyapatite crystals in the bone tissue using the X-ray diffraction. In previous study, the authors have proposed a measurement system using an X-ray diffraction technique with an imaging plate for obtaining the surface distribution of residual stress in the diaphysis of extremities [2]. Stress/strain state in bone tissue is essential for understanding the bone strength and bone adaptation. Especially, residual stress affects the material strength in general. In previous study, the magnitude of residual stress along the bone axis at the bone surface of adult rabbit extremities correlated with osteon population density in the transverse cross-section [3]. It appeared that the residual stress might be related to the bone formation and reconstruction, and might be a circumstantial finding of the adapted state of the bone. However, the generation mechanism and biomechanical implications of residual stresses in bone tissue are not fully understood. To enhance the understanding of generation mechanisms, the present study aimed to investigate the residual stress of bovine femurs in three age groups.

Methods: In the experiments, five specimens were obtained from bovine femurs of three age groups respectively: less than one month old (Group 1), two years old (Group 2), and 8-9 years old (Group 3). The mid-diaphysis part was cut from the femurs such that the measurement position was at both the center of the femur and the center of the specimen. The specimen lengths were 0.13 times of the femoral length. The bone marrow and the soft tissue around the surfaces were removed as much as possible. The specimens were examined under wet condition at room temperature. The residual stresses along the bone axis were measured on the surface of the specimen center at four positions: anterior, posterior, lateral, and medial. The specimen was irradiated with characteristic Mo-Kα X-rays under no external forces using a collimator with a diameter of 1.0 mm. The diffracted X-rays were detected by an imaging plate in the reflection side. The residual stress was calculated from a synthetic Debye ring of the (211), (112), and (300) lattice planes of the hydroxyapatite crystals [2].

Results: The average residual stresses of the four positions in the specimens from Group 1, Group 2, and Group 3 were 83.9 ± 53.3 MPa, 126.8 ± 62.2 MPa, and 114.7 ± 42.2 MPa, respectively. The residual stress in Group 2 was the largest in the three age groups. There was a significant difference between Group 1 and Group 2 ($p < 0.05$). Furthermore, the residual stress had a statistically positive correlation with the cortical thickness at the measured positions ($n = 54$, $r = 0.33$, $p < 0.05$). It was confirmed that the specimen cutting process had less impact on the measured residual stresses [4]. The results suggest that residual stresses may be generated under the bone formation process during growth and may be slowly released under the reconstruction process after the maturation. In general, residual stress is generated in a material by the indeterminate structure. New bone tissue may develop in a nondeformed state under in vivo loading. The stress may be generated in the tissue by the difference of deformation between the inner old and surface new tissues with

increasing the body weight and cortical thickness. Furthermore, the release of residual stress suggests that the tissue may become more uniform structure during the reconstruction process adapting to in vivo stress. In Group 3, the diaphyseal width of the anterior-posterior direction that is the bending direction in bovine femurs was much larger than that of the lateral-medial direction. The effects of nonuniformities in the micro/nano-structure related to bone adaptation on the residual stress should be investigated in further study.

Figure:
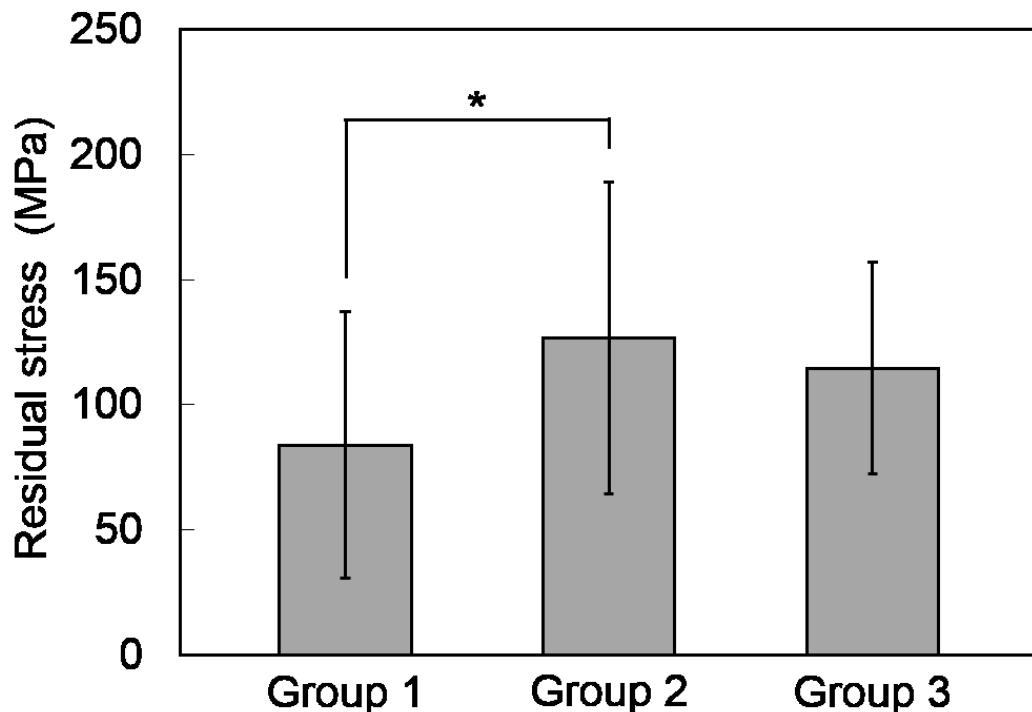
Caption: Residual stress along the bone axis at the cortical surface of bovine femurs in three age groups (<1m, 2y, and 8-9y). The values indicate the average of the four positions in the five specimens, excluding the positions that could not be examined due to remained surface soft tissue. The asterisk (*) indicates a statistical difference (p < 0.05).

Conclusion: This study shows the differences in residual stress among young, mature, and elder bovine femurs. The results of the study will be of importance in elucidating the mechanism and biomechanical implications of residual stress in bone tissue.

References: [1] Yamada et al., J Biomech Eng, 132:044503, 2010.

[2] Yamada et al., Exp Mech, 54:633-640, 2014.

[3] Yamada et al., J Biomech, 44:1285-1290, 2011.

[4] Yamada et al., J Biomech, 46:2130-2136, 2013.

Disclosure of Interest: None Declared

Bone

AS-0284

3D FINITE ELEMENT MODEL OF PROGRESSIVE DAMAGE AT MICRO-STRUCTURAL LEVEL OF CORTICAL BONE

Camila Arango [1] [1],*Eugenio Giner [1]Ana Vercher [1]F. Javier Fuenmayor [1]

[1]Materials and Mechanical Engineering, CIIM Universitat Politècnica de València, Valencia, Spain

Introduction and Objectives: In this work a numerical study of the mechanical behavior of cortical bone tissue under different loads is presented. The 3D model consists in a realistic representation of a portion of tissue containing osteons, cement lines and interstitial tissue between them. The osteon is the basic structural unit of cortical bone (200-500 μm diameter) and it is composed of mineralized collagen fibrils arranged in lamellae (3-7 μm thickness) [1]. Lamellae are concentrically arranged around blood vessels canals (Haversian canals).

The aim of this work is to apply numerical techniques for obtaining elastic anisotropic properties at different hierarchical scales and a damage model using a low computational cost method, evaluating the mechanical state of the system with composite materials failure criteria.

Methods: The material elastic properties of osteons are obtained through a finite element model at mineralized collagen fibril and lamellar levels. For the first level a numerical homogenization model is applied to a fibril configuration of collagen as matrix with hydroxyapatite crystals as reinforcement [2]. At a higher level the elastic properties of mineralized collagen fibrils grouped at different orientations and thicknesses into two types of lamellae: thick and thin.

The 3D model basic components are osteons, cement lines and interstitial tissue with a realistic geometry. The strength properties of the cement line and interstitial tissue are estimated from relations with energetic experimental data from literature. For the damage implementation, user subroutines of the finite element code Abaqus are used, varying the material properties with a stiffness degradation scheme [3]. The failure criteria for osteons correspond to interlaminar (quadratic criteria) and intralaminar stresses. In this work two different compressive load cases are analyzed (radial and axial respect to osteon longitudinal axis) and the damage patterns are compared with experimental results in bibliography [4, 5].

Results: For both load cases, the model predicts the beginning of damage at cement lines, which agrees with experimental evidence. At the same time there is damage propagation on interfaces and inside lamellae.

For the radial compression test, there is a very strong damage zone between 20 and 50 degrees from the applied load axis (Fig. 1) that is found in experimental results as well. For two different cases, thin lamellae (which have most of the fibrils perpendicularly oriented to the Haversian canals), are the less affected by the compressive load.

Figure:
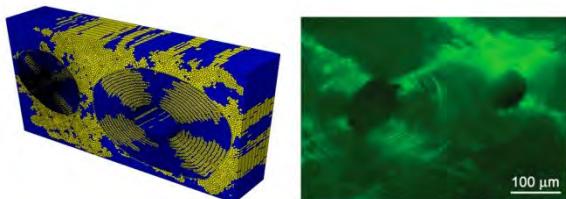
Caption: Fig. 1: Left: Advanced damage state of finite element model with compression load along the radial axis of the osteons. Right: Epifluorescence micrograph for a similar load case test from Ebacher et al. [4].

Conclusion: A 3D numerical procedure is proposed to model the progressive nonlinear damage using the finite element method. The contrast with experimental results allows validating the benefits of the model from the computational point of view. These analyses are a starting point for more complex studies incorporating bigger scale structural cases and realistic load conditions at those levels.

References: [1] Wagner HD, Weiner S. J Biomech, 25:1311-1320, 1992.

[2] Vercher A, Giner E, Arango C, Tarancón JE, Fuenmayor FJ. Biomech Model Mechanobiol, 13:437-449, 2014.

[3] Chang FK, Lessard LB. J Compos Mater, 25: 2-43, 1991.

[4] Ebacher V, Wang R. Advanced Funct Mater, 19(1):57-66, 2009.

[5] Ascenzi A, Bonucci E. Anat Rec, 161:377–392, 1968

Disclosure of Interest: None Declared

Bone

AS-0285

THE OSTEOGENIC INDEX OF FOUR COMMON CONTINUOUS AND INTERMITTENT EXERCISES USED IN OSTEOPOROSIS PREVENTION IN AN AT-RISK POPULATION

Gallin Montgomery [1,*]Will Evans [1]Luca Zoffoli [2]Grant Abt [1]Catherine Dobson [3]Michael Fagan [3]Tina Smith [4]Max Ditroilo [1]

[1]Sport, Health and Exercise Science, University of Hull, Hull, United Kingdom, [2]Department of Biomolecular Science, Universita degli Studi di Urbino, Urbino, Italy, [3]School of Engineering, University of Hull, Hull, [4]Research Centre for Sport, Exercise and Performance, University of Wolverhampton , Wolverhampton, United Kingdom

Introduction and Objectives: Information from studies designed to improve bone health is often poorly reported with regards to intensity of impacts, acceleration slope, muscular activation and stimulus frequency. These are important factors in the osteogenic index (OI) (Turner and Robling, 2003) and bone remodelling. There is a need to analyse and quantify this for a number of reported exercises within the same at-risk population so future interventions can be improved.

Methods: This study quantifies the OI of four exercises using ground reaction force (GRF) and accelerometer (ACC) data to assess which could prove the most beneficial for improving or maintaining bone health within a population of early post-menopausal women (1-5 years).

Six healthy early postmenopausal women 53.1±3.4yrs, 162.4±5.8cm, 66.2±7.5kg were recruited. Participants completed the test barefoot on a force plate recording GRF at 1000Hz. An accelerometer was attached to the sacrum whilst electromyography (EMG) surface electrodes were placed over the rectus femoris (RF) and semitendinosus (ST) muscles in accordance with SENIAM recommendations. EMG and ACC data were synchronously recorded at 1500Hz.

Four exercises were performed both continuously (CON at 15bpm) and intermittently (INT at 4bpm) for 10 cycles of each in a randomised order and included countermovement jumps (CMJ), drop jumps from a 20cm box (DJ), heel drops and unilateral stamps (one foot on the force plate).

EMG was filtered (bi-directional butterworth, 10-500Hz) and processed using a linear envelope (full wave rectification, low-pass cutoff of 8Hz). Baseline EMG was removed from the data. The EMG mean was found across the 10 cycles for each exercise and normalised to the CMJ CON trial. ACC data was filtered optimally using 95% of the signal energy from 1g before and after the 10 highest impact peaks per exercise. Peak GRF and ACC data was converted to g whilst GRF and ACC gradients (Grads) from 1g to peak, were converted to m.s^{-3}, all were averaged across the 10 cycles. OI was calculated from the GRF and ACC data using the Turner and Robling (2003) method.

Kruskall-Wallis tests were used for the analysis. Effect Size (ES) and confidence intervals (CI) were performed on percentile rank-transformed data.

Results: All variables displayed no significant differences across all exercises between CON and INT conditions.

EMG data revealed that for the RF mean CMJ was significantly higher than Heel Drops and Stamps (P<0.001, ES=3.92, CI 2.48-5.36 and P=0.012, ES=2.46, CI 1.41-3.50). DJ was also significantly higher than heel drops (P=0.043, ES=2.33, CI 0.32-4.34). The ST mean showed that CMJ, DJ and Stamps were all significantly higher than heel drops (P=0.002, ES=2.97, CI 2.25-3.70, P=0.027, ES=2.52, CI 1.22-3.82 and P<0.001, ES=3.52, CI 2.08-4.96).

Peak GRF data indicated that DJ was significantly higher than stamp with a median of 4.19gvs 2.91g (P=0.005, ES=1.3, CI 0.58-2.02) whilst CMJ and Heel Drop were higher than Stamps (ES=0.8, CI 0.1-1.51 and ES=0.75, CI 0.24-1.25). However the GRF Grads saw the Stamp give higher values than CMJ, DJ and Heel Drops (P<0.001, ES=2.02, CI 1.48-2.55, P<0.001, ES=2.04, CI 1.73-2.35 and P=0.029, ES=1.24, CI 0.73-1.75).

Peak ACC analysis highlighted that CMJ, DJ and Heel Drops were all significantly higher than the Stamp condition (P=0.001, ES=1.62, CI 0.75-2.49, P<0.001, ES=1.71, CI 0.98-2.44, P=0.005, ES=1.44, CI 0.75-2.14).

ACC Grads gave lowest values in the Stamp condition with CMJ and DJ both significantly higher (P=0.007, ES=1.67, CI 0.72-2.61, P=0.002, ES=1.84, CI 0.81-2.88).

The OI Index GRF (figure 1) showed that DJ was significantly higher than stamping (P=0.005, ES=1.3, CI 0.58-2.02) whilst CMJ and Heel Drops showed positive effects when compared to Stamps (ES=0.8, CI 0.1-1.51 and ES=0.75, CI 0.24-1.25).

OI Index SAC data (figure 1) discovered that CMJ, DJ and Heel Drop were significantly higher than stamp (P=0.001, ES=1.62. CI 0.75-2.49, P<0.001, ES=1.71, CI 0.98-2.44 and P=0.005, ES=1.44, CI 0.75-2.14).

Figure:
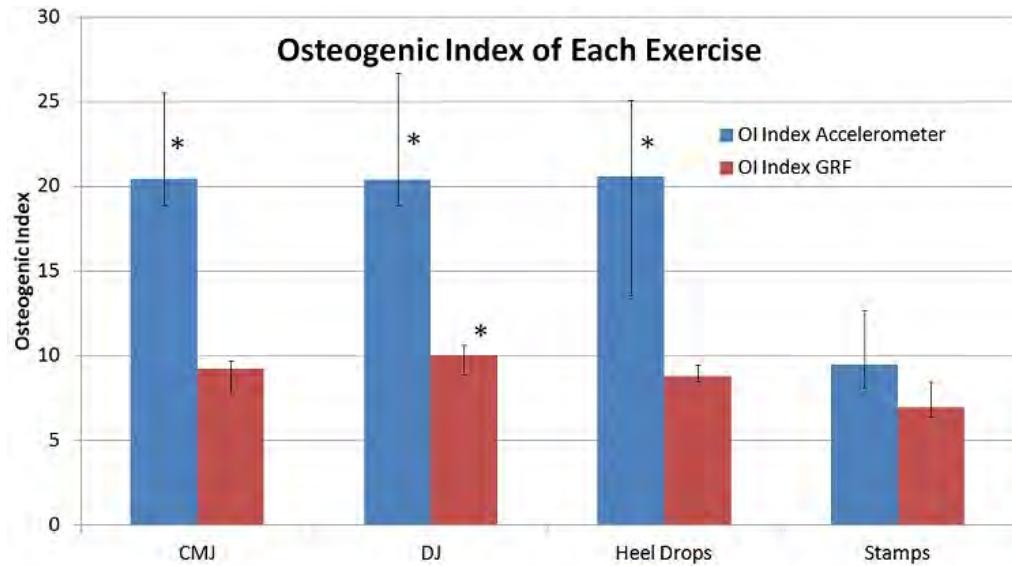
Caption: (Figure 1. Osteogenic Index.* Denotes a significantly higher value than the Stamp condition)

Conclusion: CMJ, DJ and Heel Drop conditions displayed the highest results for Peak GRF data and Peak ACC data the level of impact experienced around the sacrum. Stamp condition gives the highest acceleration slope, but fails to achieve the same level of impact experienced at the sacrum as the other exercises. For EMG the CMJ condition gave significantly the highest activation for the RF muscle and an equally high ST muscle activation along with DJ and Stamp conditions. This could imply higher concentric stress but is limited eccentrically. All exercises have their own merit for improving bone health in this population but the CMJ and DJ conditions appear to give consistently the highest results across all variables apart from the GRF Grad. The DJ appears to generate the highest OI for GRF and ACC measures combined but gives very similar results to the CMJ and Heel Drops.

Disclosure of Interest: None Declared

Bone

AS-0286

A ROBUST METHOD TO IDENTIFY CANCELLOUS BONE BEHAVIOUR:
FROM THE QUASI-STATIC TO INTERMEDIATE AND DYNAMIC STRAIN RATES.

Marianne Prot [1,*] Trevor Cloete [2] Dominique Saletti [3] Sebastien Laporte [1]

[1]Institut de Biomécanique Humaine Georges Charpak, Arts et Métiers Paristech, Paris, France, [2]Blast Impact and Survivability Research Unit , Department of Mechanical Engineering, University of Cape Town , Cape Town, South Africa, [3]3SR, Univ. Grenoble Alpes, Grenoble, France

Introduction and Objectives: Mechanical properties of cancellous bone are required over a large range of strain rate regimes to simulate injuries sustained during a car crash or a sporting accident. The majority of studies have focused on quasi-static compression loading [1], while relatively few have considered the dynamic mechanical characterization [2]. Cancellous bone is known to be strain rate dependent [3]. Recently, a specialized apparatus was developed for bone testing [4] and applied to cancellous bone [5] to address the lack of data between the quasi-static and dynamic regimes. Transient effects tend to obscure the initial phase of a compression test, which is typically recovered via linear extrapolation of apparent modulus to zero stress [6]. However, this approach can be sensitive to operator input. This paper introduces a robust method with which to determine mechanical parameters that is insensitive to toe region effect, strain rate variation and moderate noise levels.

Methods: Tests

126 cylindrical, non-defatted, bovine cancellous bone specimens were compressed in 3 strain rate regimes: quasi-static, 10^{-3}, 10^{-2}, 10^{-1} /s; intermediate, 1, 10, 100 /s and dynamic, 400 and 600 /s. Three different devices were employed as previously described in [5]. A Zwick testing machine was used for the quasi-static regime, the Split Hopkinson Pressure Bar (SHPB) implemented with a Momentum Trap system and a conical striker for the dynamic strain rates. For the intermediate regime, the behaviour was investigated using two techniques: the wedge bar apparatus for the strain rates of 1 and 10/s and the SHPB previously described for 100/s. All the tests were conducted at near constant strain rates and arrested at approximately 10% strain, so as to facilitate specimen recovery.

Data processing

Stress/strain curves were obtained. In order to consistently compare the behaviour, the following mechanical parameters were selected: the apparent Young's Modulus, E_{app}, the yield stress & strain, ε_y & σ_y, the ultimate stress & strain, ε_u & σ_u. The method used is inspired by the risk curves method. It is based on a 5 parameters logistic curve given below: two horizontal tangents (named P1 for the asymptotic minimum, P2 for the maximum), two slopes (P3, P5) and a value at the inflection point (P4).

σ=P1+P2/(1+f×g+(1-f)×h)

With:

f=1/(1+e^(-C×(ε-P4)))

C=2×P3×P5/|P3+P5|

g=e^(P3×(ε-P4))

h=e^(P5×(ε-P4))

The robust non-linear least square method is illustrated in Figure 1. E_{app} was determined as the slope at the inflexion point. The strain was set up to 0 at the intersection of this slope and the zero stress axes. An automatic process was developed to get ε_u & σ_u while the end of the elastic domain has been defined by minimizing the differences between each point of the modeled curve. The exclusion criterion is a normal distance to the slope greater than the half of the mean distance. To estimate the evaluation errors on each parameter due to the measuring noise, a bootstrap method was also implemented.

Results: The method was applied to three different regimes (illustrated in Figure 1 for quasi-static loading).

The program provides good results at every strain rate and was not biased by noise. A non-exhaustive list of the resulting data is summarized in table 1.

Data is consistent throughout the strain rates and concurs with published quasi-static data [7]. Maximum estimation errors were observed for 10/s due to load cell noise.

A distinct increase in strength is observed in the intermediate regime, especially at 10 and 100/s, which cannot be attributed to an artefact of a test method since two distinct techniques were used.

The strain rate sensitivity of the apparent Young's modulus needs to be carefully considered as 6 different bones and 3 anatomical orientations were used for sampling. Finally, there is a geometry effect due to the spongy architecture organization.

Figure:
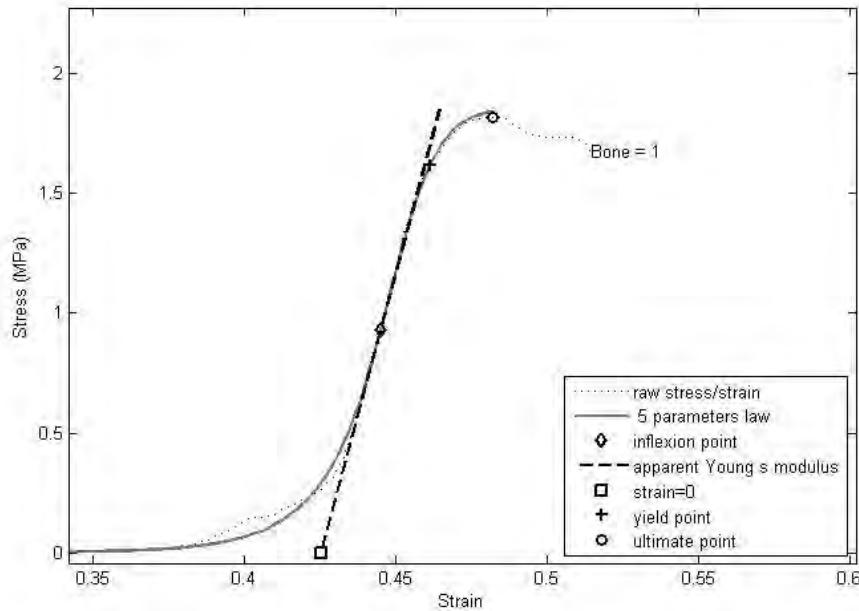
Caption: Method applied at 0.1/s

Conclusion: This study provides a robust method to determine mechanical parameters across different strain rates. The method can effectively deal with the toe region while being insensitive to moderate noise levels and quantifies the error

made on the mechanical parameters estimation. The preliminary results indicate that a distinct transition occurs in the strain rate sensitivity of cancellous bovine bone at intermediate regime.

Ongoing work focused on architectural characterization will allow the role of the porous organization in the fracture process to be investigated.

Table:

Strain Rate (/s)	Mean (MPa)	Standard Deviation	Errors (MPa)
0.001	323	217	1
0.01	365	250	1
0.1	300	192	2
1	286	172	1
10	543	319	16
100	629	480	9
400	471	34	7
600	573	314	10

Caption: Eapp's sensitivity

References: [1] Shim et al., Int J Impact Eng, 32(1), 525-540, 2005

[2] Chaari et al., Int J Crashworthiness, 12(3), 247-253, 2007

[3] Syahrom et al., Med Biol Eng Comput, 49(12), 1393-1403, 2011

[4] Cloete et al., Philos Trans R Soc Lond, A372(2015), 20130210,2014

[5] Prot et al., Comput Meth Biomec, 17(S1), 50-51, 2014

[6] Boruah et al., Proc IRCOBI, 2013

[7] Kefalas et al., J Mech Behav Biomed, 6, 41-52, 2012

Disclosure of Interest: None Declared

AS-0287

VALIDATION OF FINITE ELEMENT MODELS PREDICTING FRACTURE IN THE OSTEOPOROTIC TIBIA

Magnús K. Gíslason [1,*]Sylvie Coupaud [2] [3]Quentin Fogg [4]Stuart McNally [4]Mariel Purcell [3]Keisuke Sasagawa [5]Yuji Tanabe [5]Elizabeth Tanner [6]

[1]Institute of Biomedical and Neural Engineering, Reykjavik University, Reykjavik, Iceland, [2]Department of Biomedical Engineering, University of Strathclyde, [3]Scottish Centre for Innovation in Spinal Cord Injury, Queen Elizabeth National Spinal Injuries Unit, Southern General Hospital, [4]Laboratory of Human Anatomy, School of Life Sciences, University of Glasgow, Glasgow, United Kingdom, [5]Department of Mechanical and Control Engineering, Niigata Institute of Technology, Niigata, Japan, [6]Department of Biomedical Engineering, University of Glasgow, Glasgow, United Kingdom

Introduction and Objectives: Finite element modelling has been used to calculate the risk of fracture of the osteoporotic bone and compared to healthy bones [1]. However, it is essential to validate the computational models experimentally with real tissue. Finite element models were created using pQCT scans of two cadaveric tibiae, and were loaded in torsion and tested until failure. One specimen, CBM4, showed signs of osteoporosis but the other, CBM5 was otherwise healthy. The mechanical results were compared with the predicted risk of fracture from the FEA model.

Methods: Two fresh frozen cadaveric tibiae were obtained from the Laboratory of Human Anatomy at the University of Glasgow, following ethical approval. The specimens were thawed 24 hours prior to the experiment. Strain gauges (EA-13-062TH-120 from Vishay) designed for torque measurements were mounted 40mm from the proximal end of the specimen. The full-length tibia specimens were mounted in a custom-made square frame and methyl methacrylate (Technovit) resin was used to secure the specimens. Finally the specimens were placed in a testing machine (ElectroPuls E10,000, Instron) where the proximal end was secured to the base and the distal end subjected to rotational loading. The loading protocol was subdivided into two parts: firstly, a 50N compressive load was applied with the rate of 10 N/s for 5 s and held throughout the whole duration of the test. Secondly, the distal end of the tibia was rotated at the rate of 1°/s until failure. The finite element model was solved using Abaqus (v.6-13, Simulia). The geometry was based on multi-slice pQCT (XCT 3000, Stratec) scans of the bones. The in-plane image resolution was 0.5mm x 0.5mm and the bones were segmented using Mimics (v.16, Materialise). The material properties were based on the greyscale values of the pixels and empirical functions used to connect the greyscale values with bone mineral density and a power law connecting the bone mineral density to both Young's modulus and ultimate stress values [2].

Results: The two specimens failed at different torque levels, 36.2±0.5 Nm and 63.8±0.5 Nm respectively. Both specimens failed within the diaphysis region and with crack at 54° angle to the horizontal. The measured variables can be seen in Table 1. Figure 1 shows the torque as a function of the measured strain for both specimens. The results were in agreement with the finite element model that predicted distinct fracture in specimen CBM4 under 35Nm loading, whereas no elements exceeded the calculated fracture threshold for each element for specimen CBM5 under 35Nm loading.

Figure:

Torque as function of strain
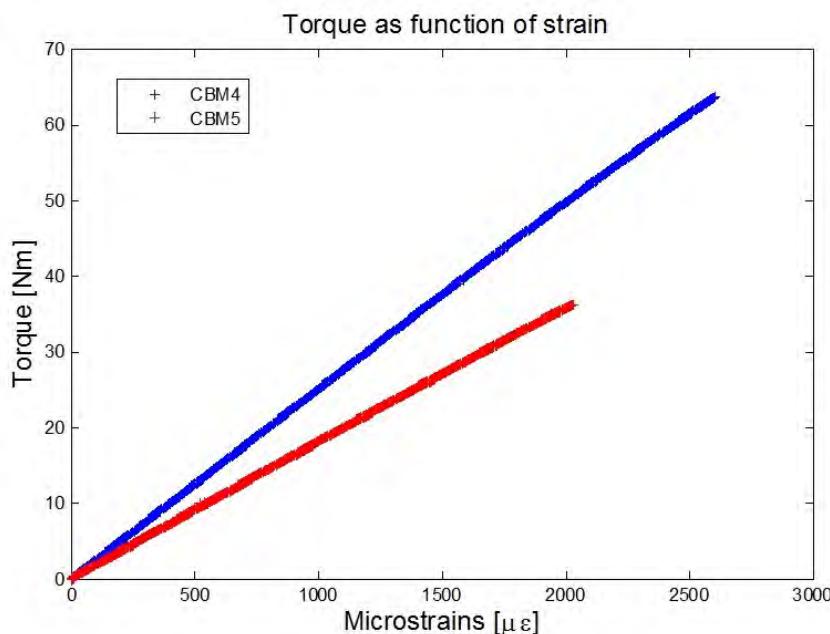
Caption: Torque as a function of strain

Conclusion: The experiment validated the finite element models and demonstrated the effects that osteoporosis has on the torsional strength of the tibia. Further understanding about the fracture mechanics will provide important information about the biomechanics and clinical relevance of the fragility of osteoporotic bone.

Table:

Specimen	Torque [Nm]	Strain [$\mu\epsilon$]	Rotation [°]
CBM4	36.2±0.5	2029±10	13.6±0.1
CBM5	63.8±0.5	2607±10	13.2±0.1

Caption: Measured variables at failure

References: 1. Gislason et al, J. Eng in Medicine Proc of ImechE, 228:165-174, 2014

2. Bessho et al, J. Biomech, 40: 1745-1753, 2007

Disclosure of Interest: None Declared

Bone

AS-0288

MORPHOLOGICAL AND MECHANICAL PROPERTIES OF DMD AND TREATED MOUSE BONES

Noor Shafini Mohamad [1,*]Jie Tong [1]Darek Gorecki [2]Matt Guille [3]

[1]School of Engineering, [2]School of Pharmacy and Biomedical Sciences, [3]School of Biological Sciences, University of Portsmouth, Portsmouth, United Kingdom

Introduction and Objectives: Duchenne Muscular Dystrophy (DMD) is caused by mutations in the dystrophin gene that gradually lead to severe muscle malfunction and eventually death [1]. Recent micro-Computed Tomography (µCT) analysis showed an effect of DMD on bone tissue morphology [2], where reduced bone mass and bone resorption was observed in dystrophic (*mdx)* mice compared with wild type. To understand the mechanisms of DMD and to develop its treatments, a receptor, P2X7, was switched off in mice. Bone morphometric and biomechanical properties were evaluated at four-week old using µCT and biomechanical testing.

Aims

To compare the morphometric and the mechanical competence of the mouse bones at 4 week old between the treated bones, the wild type and the *mdx* mouse bones, thereby to establish the role of receptor P2X7 in DMD at this early stage, when muscle function has yet fully developed.

Methods: Four-week old mice tibias (n=24) were imaged using µCT (XT H 225, X-Tek Systems) and data acquisition was performed (V=50-55kV, I=95-110µA). Genotypes included wild type (WT) (n=6), *mdx* (n=6), P2X7-/- knockout (n=6) and *mdx*/P2X7-/- double knockout (n=6). The morphometric parameters were taken at two locations (Figure 1). A three-point-bending arrangement was used to test the whole bone samples at a rate of 0.155 mm/s [3] until failure using a Bose machine (ElectroForce® 3200).

Results: In *mdx* mice, significant bone loss is evident at both proximal and midshaft levels as opposed to WT, as illustrated in Table 1, where values of statistically significant difference ($p<0.05$) from those of *mdx* are highlighted. Knocking out P2X7 in mdx mice appears to have improved the overall morphometric parameters, where most results from *mdx*/P2X7-/- show improvement over those of *mdx*, apart from maximum load at fracture and stiffness, although the differences are only statistically significant in cortical bone density and stiffness. Generally, the results from P2X7-/- are close to those of WT.

Results from mechanical testing show significantly decreased maximum load (by 38%), fracture energy (by 65%) and stiffness (by 41%) in *mdx* compared with those in WT. In P2X7-/-, the maximum load and fracture energy are comparable to those of WT but stiffness is reduced. For *mdx*/P2X7-/-, the maximum load and fracture energy are comparable to those of *mdx*, although the stiffness is reduced significantly.

Figure:

Figure 1: Locations selected for µCT scanning.

Conclusion: Morphometric and mechanical properties of mdx mouse bones differ significantly from those of WT. In treated mouse bones, the morphology analysis showed overall improved bone properties in both proximal and midshaft, although not all statistically significant.

Table:

Bone properties	WT	*mdx*	P2X7-/-	*mdx*/P2X7-/-
Morphometric properties				
BV/TV(proximal)	**0.098±0.013***	0.078±0.008	**0.093±0.119***	0.085±0.014
B.Th(proximal)	**0.140±0.025***	0.098±0.018	0.116±0.007	0.106±0.008
BV/TV(midshaft)	**0.086±0.009***	0.070±0.01	0.087±0.016	**0.093±0.006***
B.Th(midshaft)	**0.149±0.018***	0.109±0.014	**0.139±0.014***	0.121±0.021
Mechanical properties				
Maximum load (N)	**4.99±0.89***	3.10±0.90	4.32±1.63	2.43±0.45
Fracture Energy (N.mm)	**0.82±0.31***	0.29±0.12	**0.88±0.44***	0.34±0.17
Stiffness (N/mm)	**12.16±2.12***	7.19±2.58	8.64±2.73	**3.38±1.51***

Caption: Table 1 Morphometric and mechanical properties of the bones across the genotypes.

References: [1]   Nowak and Davies, *EMBO Rep.*, 5: 872–6, 2004.

[2]   Rufo et al, *J. Bone Miner. Res.*, 26:1891–903, 2011.

[3]   Finnilä et al, *J. Biomech.*, 43:1097–103, 2010.

Disclosure of Interest: None Declared

AS-0289

THEORETICAL INFLUENCE OF AGE, RUNNING SPEED, AND RUNNING DISTANCE ON THE PROBABILITY OF SECOND METATARSAL STRESS FRACTURE

Divya Budihal [1] W. Brent Edwards [2,*]

[1]Henry Wise Wood High School, [2]Human Performance Laboratory, University of Calgary, Calgary, Canada

Introduction and Objectives: Stress fractures in long bones account for approximately 15% to 20% of all overuse injuries in runners. These injuries are ultimately caused by the mechanical fatigue of skeletal tissue. Cyclical loads applied to bone during locomotion cause microdamage accumulation, i.e., small cracks in the bony matrix. If this microdamage is not repaired through the action of basic multi-cellular units, stress fractures may occur. Microdamage accumulation varies with bone quality, loading magnitude, and the number of loading cycles. Thus, the likelihood for stress fracture will depend on age, running speed, and running distance. The purpose of this study was to examine the theoretical influence of age, running speed, and running distance on the probability of stress fracture in the second (2nd) metatarsal, a major site for stress fracture development.

Methods: Stride length (SL) and ground reaction force (GRF) as a function of running speed were estimated from the literature [1]. Peak 2nd metatarsal strain for a 170 cm tall, 69 kg male was estimated using the finite element method. The finite element model consisted of 11,560 linear hexahedral elements with different material properties for cortical bone (age-specific according to [2]), trabecular bone (1 GPa), and marrow (0.1 MPa); all materials were assigned a Poisson's ratio of 0.3. The proximal end of the metatarsal was fully constrained and a distributed load equal to 24% GRF was applied to the metatarsal head at a 33° angle relative to the bone's long-axis [3]. The relationship between metatarsal strain and number of cycles to failure (N_f) was determined from a modified standard-fatigue equation, characterizing damage evolution, accumulation, and failure into a single, empirical relationship, which accounted for age-specific bone fatigue [4]. The time to failure (t_f) in days was calculated by dividing N_f by loading cycles/day, where loading cycles/day was a function of SL and running mileage. The t_f values served as inputs to a probabilistic model of bone failure, repair, and adaptation [5] to examine the influence of age (15-65 years), running speed (2.5-4.5 m/s), and running distance (3-7 miles/day) on the likelihood of 2nd metatarsal stress fracture.

Results: The cumulative probability of stress fracture with repair and adaptation (P_{fra}) for a referent scenario (i.e., 25 year old running at 3.5 m/s for 5 miles/day) peaked and plateaued at 0.15 after approximately 40 days of running (Figure). The P_{fra} increased nonlinearly with age (Figure) and running speed. In contrast, P_{fra} increased linearly with running distance. To maintain the same probability of stress fracture as a 25 year old running at 3.5 m/s for 5 miles/day, the results indicated that a 55 year old must run at 2.5 m/s for 3 miles/day (Table).

Figure:
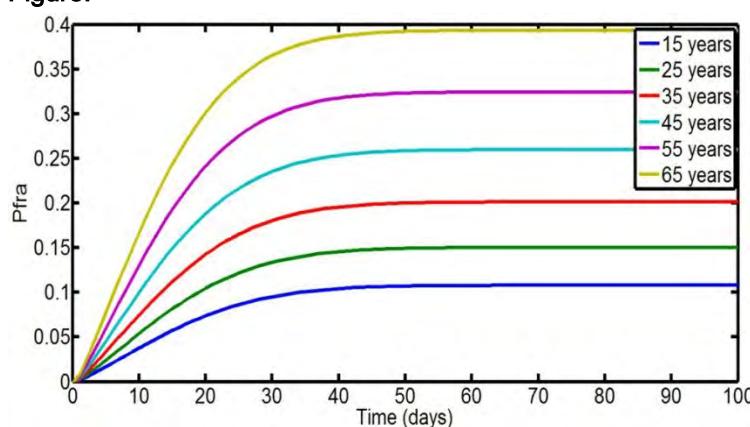
Caption: Pfra for different ages running at 3.5 m/s for 5 miles/day.

Conclusion: The probability of 2nd metatarsal stress fracture was highly dependent on age, running speed, and running distance. Whereas the probability of stress fracture increased nonlinearly with age and running speed, the probability of stress fracture increased linearly with running distance. In accordance with these findings, older runners may want to adopt a slower running speed and a lower running distance when beginning a new running regimen. As the probability of stress fracture is less sensitive to changes in running distance than running speed, new runners may want to reduce running speed rather than distance in order to minimize their likelihood for 2nd metatarsal stress fracture. Bone repair and adaptation are highly dependent on age, and a major limitation of this study was the inability to incorporate this phenomenon into the theoretical model. This study provides a comprehensive theoretical description of stress fracture probability that ultimately may aid in the prevention of this injury. It is unlikely that the theory will be able to accurately predict stress fracture risk on an individual basis, but it should be able to reasonably predict relative changes in stress fracture risk provided that subject-specific training patterns and bone strain are quantified precisely.

Table:

Age (years)	3 miles/day			5 miles/day			7 miles/day		
	2.5 m/s	3.5 m/s	4.5 m/s	2.5 m/s	3.5 m/s	4.5 m/s	2.5 m/s	3.5 m/s	4.5 m/s
15	0.0439	0.0605	0.085	0.0789	0.1078	**0.1491**	0.1148	**0.1553**	0.2116
25	0.0623	0.0856	0.1192	0.1109	**0.1501**	0.2049	0.1596	0.2131	0.2849
35	0.0857	0.1169	**0.1611**	**0.1502**	0.2011	0.2699	0.2132	0.2801	0.3663
45	0.1141	**0.1543**	0.2103	0.1966	0.2596	0.3419	0.2743	0.3537	0.4511
55	**0.1477**	0.1979	0.266	0.2495	0.3242	0.4178	0.3412	0.4308	0.5348
65	0.1869	0.2475	0.3272	0.3082	0.3932	0.4947	0.4121	0.5084	0.6135

Caption: Pfra for different ages, running speeds, and running distances. Bolded values are those within 0.01 of the referent condition probability.

References: [1] Mercer et al., J Sports Sci Med, 4: 144-152, 2005. [2] Zioupos & Curry, Bone, 22: 57-66, 1998. [3]. Gross et al., Am J Sports Med, 17: 669-674, 1990. [4] Diab et al., Eur J Morph, 42: 53-59, 2005. [5] Taylor et al., J Ortho Res, 22: 487-494, 2004.

Disclosure of Interest: None Declared

AS-0290

STRESS-MICROSTRUCTURE RELATIONSHIP IN HUMERUS OF A GOAT

Ashwij Mayya [1,*]Anuradha Banerjee [1]R Rajesh [2]

[1]Indian Institute of Technology - Madras, [2]The Institute of Mathematical Sciences, Chennai, India

Introduction and Objectives: The adaptive response of cortical bone to high mechanical stresses, depending on the anatomical site, leads to bone material having significant differences in its microstructure and mechanical properties. Haversian bone, thought to be the bone adapted to high stresses by secondary remodelling, however, has been known to have inferior tensile strength and fracture toughness [1,2]. This apparent contradiction in the understanding of bone adaptation has been the focus of a recent investigation on goat femur which presents evidence of typical Haversian adaptation only at sites under high compression [3]. It is of significance to further examine the import of these findings at anatomical sites where the stress distribution that develops within a cross-section of the bone is remarkably different from that of femur. In the present study, the humerus of a goat is chosen for characterizing the stress-microstructure relationship along the length of bone to test if Haversian bone is indeed an adaptation to high mechanical stresses that are only compressive in nature.

Methods: Humerus is primarily a load bearing bone with prominent angulation and curvature in the sagittal plane. The stress field in the humeral diaphysis is determined by applying beam theory to a simplified 2D biomechanical model of the fore leg. In the stance phase of gait cycle, the contact point with the ground is shown to be offset from the humeral head. To ensure static equilibrium, a counter clock-wise moment acts at the proximal end of the humerus as shown in Fig. 1(a). The effect of muscle forces is assumed to be restricted to contact points at the joint centres which would scale down the stress distribution of the bone. The cross-sectional area, moment of inertia, offsets from the neutral axis at the anterior and posterior regions are determined using smooth interpolation polynomials obtained from processing the binary images of cross sections. To correlate the stress field with microstructure, the sections cut along the length are polished with successively finer grit particles and observed under an optical microscope. Also, the mineral content of the microstructures is qualitatively analysed using EDS analyses by placing multiple samples on the specimen stage.

Results: At the stance phase of the gait cycle, the humerus is shown to develop significant bending stresses in sagittal plane, such that the anterior and posterior cortices are in compression and tension respectively as shown in Fig. 1(b). Maximum stresses in the bone occur at the proximal end of the diaphysis.

Microstructural examination of several sections of the bone along its length using optical microscope showed distinct variations as presented in Fig. 1(c). The authors' hypothesis that the microstructure correlates with the stress field is confirmed as Haversian systems are observed at regions of high compressive stresses while regions with low stresses have typical fibro-lamellar/plexiform structure. The regions of high tensile stress exhibit a microstructure which appears as compact layering of bone material and distinctly non-Haversian. The compact form of microstructure is shown to be significantly different from plexiform bone in the extent of calcification established from EDS line scans.

Figure:

(a) (b) (c)
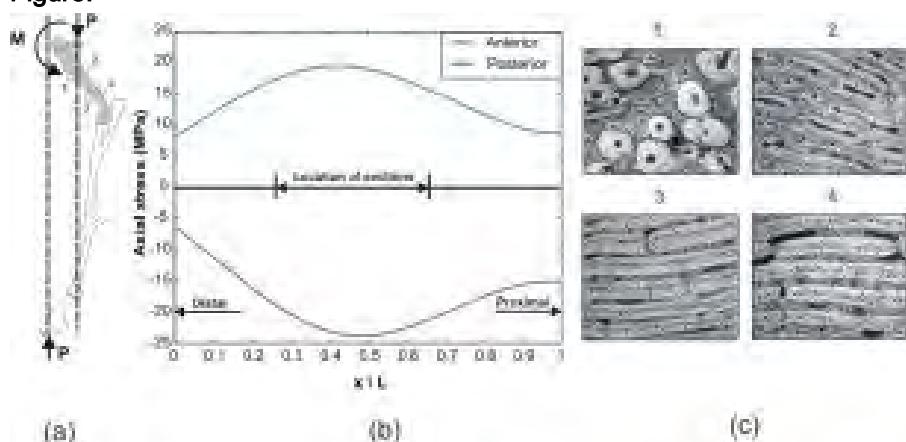
Caption: (a) Free body diagram of fore leg during the three legged stance (b) Variation of axial stresses in anterior and posterior cortices along the length (c) variation of microstructure at the anterior and posterior cortices of proximal and distal regions of diaphysis.

Conclusion: These findings support the hypothesis that Haversian remodeling is sensitive to the nature of stresses as it is an adaptive response to compressive stresses only.

References: [1]Martin et al., The relative effects of collagen fiber orientation, porosity, density and mineralization on bone strength, J. Biomech. 22:5, 419-426, 1989.

 [2]Reilly et al., The development of microcracking and failure in bone depends on the loading mode to which it is adapted, J. Exp. Biol. 202, 543-552, 1999.

 [3]Mayya et al., Mammalian cortical bone in tension is non-Haversian, Sci. Rep. 3, 2533, 2013.

Disclosure of Interest: None Declared

Computer Simulation

AS-0291

THE EFFECT OF MALALIGNMENT ON KNEE JOINT CONTACT LOADING

Franziska Reisse [1,*]Howard Hillstrom [2]Rob Walker [1]Diagarajen Carpanen [1]Mark Lenhoff [2]Carl Imhauser [3]Robert Rozbruch [4]Austin Fragomen [4]Matt Koff [5]John Dowell [1] [6]Rajshree Mootanah [1]

[1]Engineering and Built Environment, Anglia Ruskin University, Chelmsford, United Kingdom, [2]Leon Root MD, Motion Analysis Laboratory, [3]Department of Biomechanics, [4]Limb Lengthening and Complex Reconstruction Services, [5]Department of Radiology and Imaging – MRI, Hospital for Special Surgery, New York, United States, [6]Department of Orthopaedics, Ramsay Springfield Hospital, Chelmsford, United Kingdom

Introduction and Objectives: Osteoarthritis (OA) is a debilitating disease of the joint that leads to significant pain, loss of mobility and quality of life. The total annual cost of OA is estimated at $185.5 billion to the United States [1]. Lower extremity malalignment is postulated to present excessive compartment stress to the cartilage matrix and has therefore been associated with knee OA [2]. There is no known cure for OA and current therapeutic approaches cannot arrest disease progression. Malalignment correction is a surgical procedure to redistribute load in the knee joint, reduce peak pressure and delay OA progression. This is carried out by either removing or adding a wedge of bone to the proximal tibia such that the mechanical axis deviation is restored to 0 mm. The mechanical axis deviation (MAD) is the horizontal distance between the knee joint center and the line passing through the hip and ankle joint centres. However, clinical outcomes have been unpredictable. Therefore, the aim of this study is to perform virtual osteotomies on a validated knee model [3] to predict the resulting contact loading for different knee alignments. We hypothesise that the alignment correction associated with an MAD of zero does not correspond to minimum contact loading and that there is a strong correlation between MAD and knee joint contact mechanics.

Methods: Three-dimensional (3D) SPGR and 3D CUBE magnetic resonance images of a cadaveric knee joint were acquired and segmented in Mimics imaging package (Materialise, Belgium) to create accurate 3D representations of the bones, cartilage, menisci and ligaments. The solid 3D knee joint assembly model was then exported to ABAQUS V6.11-2 (HKS, USA). Bones were meshed with tetrahedral elements and all remaining parts were meshed, using hexahedral elements. Material properties of bones and cartilage were set as homogenous, isotropic structures with linear elastic behaviour; Meniscus material properties were set as transversely isotropic. Material properties of each ligament were tuned until the kinematics of the FE model matched those of the cadaveric specimen, positioned in a load-controlled robot, in 5 degrees of freedom along a 0° to 65° flexion pathway [3]. Each meniscal horn was attached to the tibial plateau by using 1D linear springs with a stiffness of 2000N/mm [4]. To evaluate the effect of alignment, the distal femur was mechanically grounded and the tibia was fixed at 18° of flexion. An axial load of 811 N, an anterior load of 100 N and a lateral load of 77 N were applied to simulate the end of weight acceptance as per normative data from the Leon Root, MD Motion Analysis Laboratory at the Hospital for Special Surgery. Different wedge geometries were then virtually removed to simulate malalignments from 14° valgus to 16° varus.

Results: The native alignment of the cadaveric knee (1° varus) gave a medial:lateral load ratio of 70%:30%. The medial and lateral peak pressure for the native aligned knee was 4.28 MPa and 2.42 MPa, respectively. Medial peak shear stress

was 2.04 MPa in the tibial cartilage and 1.67 MPa in the femoral cartilage. The lateral peak shear stress was 1.71 MPa in the tibial and 1.32 MPa in the femoral cartilage.

An increase in varus alignment substantially increased medial knee contact loading while an increase of valgus angulation substantially increased the contact loading in the lateral compartment (Figure 1). An MAD of 0 mm resulted in a medial:lateral load ratio of 60%:40%. The minimum peak pressure occurred at an angle of 0.5° valgus, which corresponds to an MAD of -1.4 mm. The lowest peak shear stress for the tibial cartilage occurred at an alignment of 0.25°, which corresponds to an MAD of 0.7 mm. For the femoral cartilage the lowest peak shear stress occurred at an alignment of -1.2°, which corresponds to an MAD of -4.25 mm. There is a very strong correlation between surgical realignment geometry, MAD and knee joint contact loading (R>0.94).

Figure:
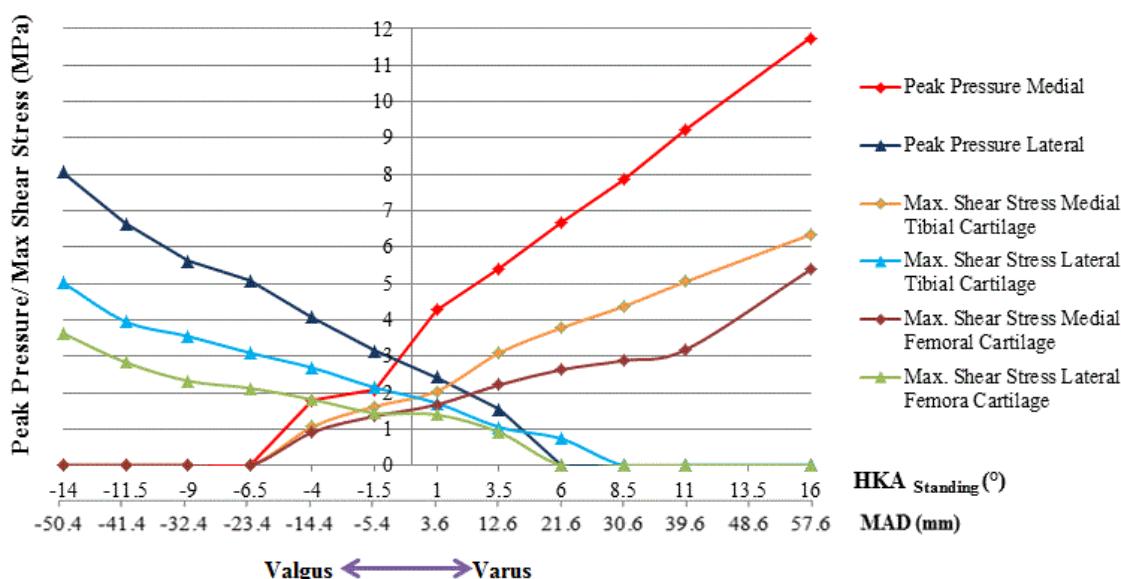
Caption: Peak contact pressure and maximum shear stress in the medial and lateral compartments

Conclusion: This study used a validated subject-specific 3D FE knee model to predict how different varus and valgus alignments influence knee joint contact loading. The hypothesis that the HTO geometry associated with an MAD of zero does not correspond to minimum contact loading was confirmed. In addition, results showed a very strong correlations (R>0.94) between knee geometry and joint contact loading. The ability of a subject-specific model to predict changes in the magnitude and location of peak contact loading within the knee as a function of alignment was demonstrated. This study serves as a foundation for the development of a surgical tool that could help surgeons make informed decisions on the degree of realignment required to minimise peak pressure, thereby delaying OA progression.

References: [1] Mathers et al., World Health, 2005.

[2] Sharma et al., JAMA, 286, 2001.

[3] Mootanah et al., CMBBE, 2014.

[4] Donahue et al, J.Biomech.Eng., 124: 273-280, 2002.

Disclosure of Interest: None Declared

Computer Simulation

AS-0292

CONTRIBUTION OF INDIVIDUAL SOURCES OF ERROR IN GYROSCOPE SIGNAL INTEGRATION FOR BODY SEGMENT ORIENTATION ESTIMATE DURING GAIT

Ilaria Pasciuto [1 2,*]Elena Bergamini [1 2]Gabriele Ligorio [3]Angelo Maria Sabatini [3]Aurelio Cappozzo [1 2]

[1]Department of Movement, Human and Health Sciences, [2]Interuniversity Centre of Bioengineering of the Human Neuromusculoskeletal System, Università degli Studi di Roma Foro Italico, Roma, [3]The BioRobotics Institute, Scuola Superiore Sant'Anna, Pisa, Italy

Introduction and Objectives: Accurate 3D orientation of body segments is a crucial aspect in human movement analysis. Among motion capture technologies employed for its estimation, inertial measurement units based on micro electro-mechanical systems (MEMS) are gaining momentum due to their easy set-up and reduced dimensions. In this context, body orientation estimation is based on the integration of the gyroscope signals, which however are affected by several sources of error that cannot always be effectively compensated for through sensor fusion approaches [1]. These gyroscope errors mainly include white noise, static bias, bias instability and miscalibration scale factors [2]. The aim of this work is to assess the contribution of these individual sources of error on the orientation estimation as obtained by numerical integration. For this purpose, a simulation approach was used, based on typical gyroscope signals associated to pelvis and tibia during walking. These sites are commonly used in human motion analysis as the former is close to the body center of mass and the latter provides robust detection of gait events and favorable conditions for sensor fusion approaches.

Methods: The simulation approach was based on modeling both the ideal gyroscope signals and the typical MEMS error sources. To obtain ideal signals representative of healthy gait, two tri-axial gyroscopes were attached to the pelvis and to the distal part of the right tibia of a healthy subject (26 years, 1.75 m, 70 kg) who walked along a 30 m straight pathway. The frequency spectra of the recorded signals, calculated over each available stride [3], were truncated at 15 Hz and averaged to produce ideal gyroscope signals of selected duration (1 minute). Mathematical models of white noise (WN), bias instability (BI), static bias (SB), and scale factor (SF) were then used to corrupt the ideal signals. In order to cover the range of typical values of commercially available sensors, ten levels were assigned to each noise source: the levels of both WN and BI differed in terms of standard deviation; SB levels were defined by the value of the offset; and SF by the gain representing miscalibration. As both WN and BI are defined stochastically, fifty simulations were performed for each level. In order to obtain the orientations corresponding to the ideal and noisy signals for each sensor, the kinematic equations [4] were integrated with an integration step representative of typical sampling frequencies (128 Hz). The difference between the ideal and each noisy orientation was then evaluated in terms of the Root Mean Square (RMS) of the orientation error defined in [4]. Finally, for each level of the two stochastic noise sources, the mean (μ) and standard deviation (σ) of the RMS over the 50 simulations was obtained.

Results: The mean errors associated to WN (Fig. a) increase with the values of the noise levels following a linear trend ($R^2=0.99$), and, in agreement with [2], a linear trend ($R^2=0.98$) is also observed for the σ of these errors. Regarding SF (Fig. d), the errors grow proportionally ($R^2>0.99$) to the gain values [2]. The slope of the curve is different for the two

sensors, as it depends on the angular velocity values. Since the tibia experiences angular velocities (μ=101.05 °/s) that are greater than those of the pelvis (μ=30.44 °/s), the former body segment is more sensitive to the SF noise. For what concerns SB (Fig. c), it presents a linear trend (R^2>0.99) in accordance with [2]. However, the two sensors present different slopes, indicating that the same offset applied to different angular velocity curves yields different variations in orientation. This result stresses the non-linear relationship between angular velocity and orientation [4] whose effects have not yet been thoroughly investigated. As suggested in [1], the cause for the difference in slopes could be related not only to the angular velocity values *per se*, but also to their distribution about the three sensor axes, which during gait was found to be much smaller in the pelvis (σ=16.11 °/s) than in the tibia (σ=106.47 °/s). Finally, the orientation error associated to BI (Fig. b) has been found to increase linearly with the noise levels (R^2=0.99) for the considered duration.

Figure:
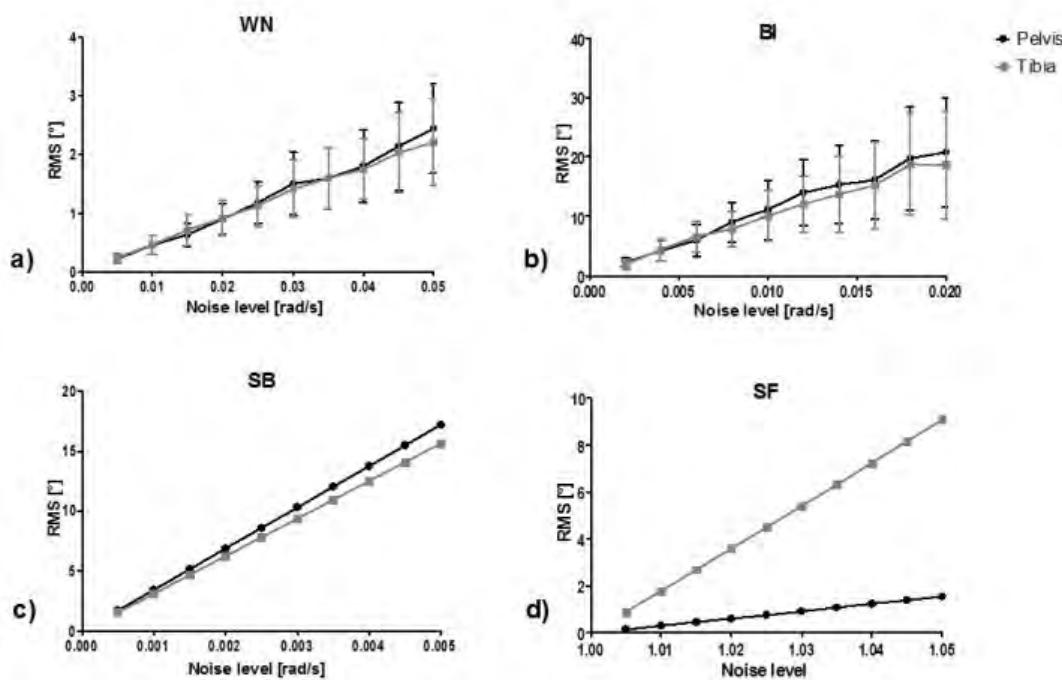
Caption: Mean RMS of the orientation error in pelvis and tibia as a function of noise source levels. The vertical bars in a) and b) represent the standard deviation of the orientation error. The noise levels in d) are dimensionless.

Conclusion: This work shows that the influence of the non-linear relationship between angular velocity and orientation is evident in the SB error and that the effect of the distribution of the angular velocities about the three sensor axes in this respect must be taken into account.

References: [1] Bergamini et al., Sensors, 14:18625-49, 2014

[2] Titterton et al., Strapdown Inertial Navigation Technology, Institution of Electrical Engineers, 2004

[3] Monaco et al., IEEE Trans Neural Syst Rehabil Eng, 20(6):845-52, 2012

[4] Sabatini, Sensors, 11:1489-525, 2011

Disclosure of Interest: None Declared

Modelling

AS-0293

THE ROLE OF ALTERED PROXIMAL FEMORAL GEOMETRY IN IMPAIRED PELVIS STABILITY AND HIP CONTROL DURING CP GAIT: A SIMULATION STUDY

Lode Bosmans [1] Karen Jansen [1] Mariska Wesseling [1] Guy Molenaers [2] Lennart Scheys [2] Kaat Desloovere [3] Ilse Jonkers [1,*]

[1] Kinesiology department, [2] Department of development and regeneration, [3] Department of rehabilitation sciences, KU Leuven, Leuven, Belgium

Introduction and Objectives: Children with cerebral palsy (CP) often present aberrant hip geometry, more specifically increased femoral anteversion (FA) and neck-shaft angle (NSA). Furthermore, altered gait patterns are present within this population, amongst which crouch gait is one of the most common. This study aimed to identify the extent to which aberrant musculoskeletal geometry on the one hand and CP gait characteristics on the other hand modify muscular control of pelvis, hip and knee kinematics. We hypothesize that the presence of proximal femoral deformities will reduce the hip and knee muscles' potentials, but that the aberrant gait characteristics themselves will also affect muscle control.

Methods: Eight subjects with diplegic CP (8-12 yrs) and one control subject were included in this study. For each subject, a clinical gait analysis was performed and magnetic resonance images (MRI) of the lower extremities were captured. For each subject, a scaled generic (based on the Gait2392_Simbody model) [1] and a personalized MRI-based musculoskeletal model with personalized bone and muscle geometry [2] were created. For each subject with CP, dynamic simulations of gait were generated in OpenSim [1] for the following kinematics-model combinations: (i) CP-MRI, (ii) CP-GEN and (iii) TD-MRI. For CP-MRI and CP-GEN, pathological kinematics were applied to the MRI-based and generic model respectively. For TD-MRI, , typically developing (TD) gait characteristics of the control subject were used and applied to the MRI-based models. For all model types and kinematics, an induced acceleration analysis [3] was used to calculate the cumulative potential of individual muscles to accelerate pelvis orientation, hip and knee joint angles during the single stance phase of gait. A Wilcoxon signed-ranks test compared the potential accelerations based on the scaled generic and personalized model (CP-MRI and CP-GEN) to identify the influence of aberrant femoral geometry during CP gait. A Mann-Whitney U-test compared the potential accelerations between the two gait patterns for the personalized models (CP-MRI and TD-MRI) to identify the additional effect of the CP gait pattern in the presence of proximal femoral deformity.

Results: As presented in figure 1, femoral deformity as well as CP-specific gait pattern have a distinct effect on muscle control. The overall muscle potential was most affected in the sagittal plane (potential difference of 894 (°/s²)/kg*m between CP-MRI and CP-GEN and 993 (°/s²)/kg*m between CP-MRI and TD-MRI), followed by transverse (432 and 460 (°/s²)/kg*m) and frontal plane (398 and 199 (°/s²)/kg*m). For specific muscles, the CP gait pattern beneficially countered the loss of muscle potential induced by the proximal femoral deformity. This was found for GMAX/GMED in the sagittal (strengthening the potential to increase pelvis retroversion, hip and knee extension) and transversal plane (increased potential to induce external hip rotation), for VAS in the sagittal plane (strengthening its potential to increase pelvis retroversion) and HAM in the frontal plane (strengthening its potential to increase pelvis tilt and decrease hip adduction). In contrast, CP gait further compromised the muscle potential of GMAX/GMED transverse plane control (increased

backward pelvis rotation), ILIOP/RF frontal plane control (increased hip adduction) and HAM sagittal plane (decreased pelvis retroversion, hip extension and increased knee flexion). Proximal femoral deformity and CP gait were found to have a contradictory effect on the potential of the hip extensors: The mono-articular GMAX (and GMED) potentials as hip extensor were augmented, whereas the potential of HAM to extend the hip decreased and the potential to flex the knee increased.

Figure:
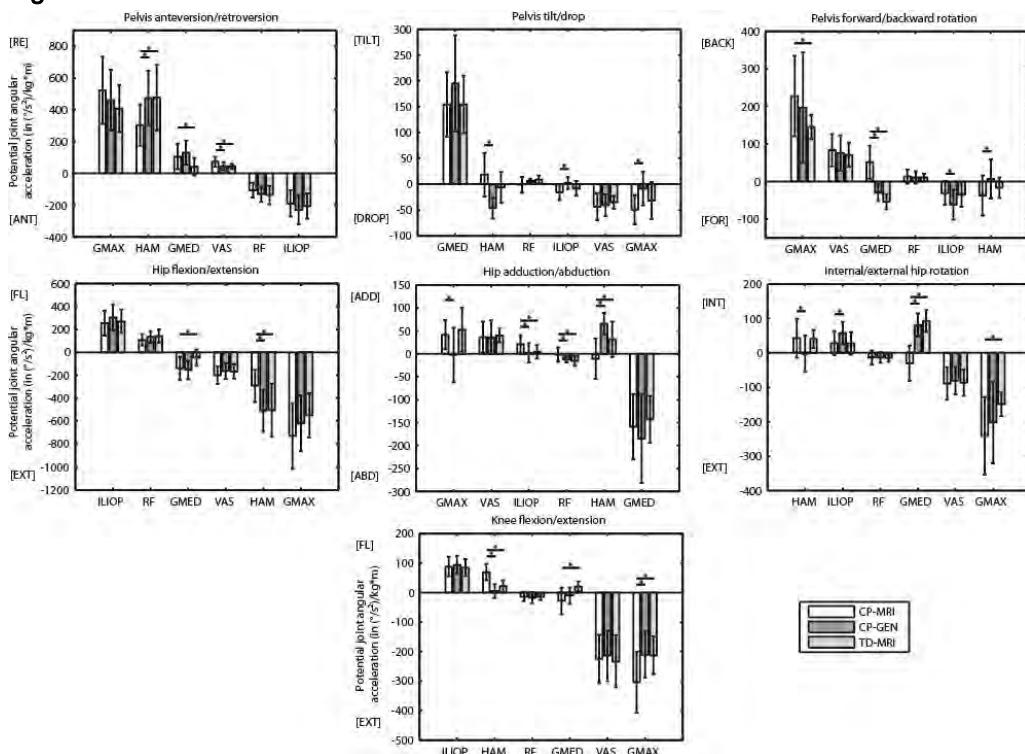
Caption: Fig 1. Potential joint angular accelerations (in $(°/s²)/kg*m$ for iliopsoas (ILIOP), rectus femoris (RF), gluteus medius (GMED), vasti (VAS), hamstrings (HAM) and gluteus maximus (GMAX). * indicates statistically significant differences ($p<0.05$).

Conclusion: Both the presence of proximal femoral deformities and the CP gait pattern substantially affect muscle control. For individual muscles, negative as well as positive effects are reported depending on the analyzed degree of freedom, indicating a complex, muscle-specific effect of the deformity. In general, CP gait affects the overall muscle potentials more than the proximal femoral deformity. The hypothesis that the muscles' potentials to control pelvis orientation and hip and knee joint kinematics were to be reduced can only be partially accepted, as muscle contributions to joint angular accelerations both increased and decreased depending on the analyzed degree of freedom. CP gait in the presence of proximal deformity appears to be a well-balanced situation optimizing muscular control in the different planes.

References: [1] Delp, SL, et al. IEEE trans biomed eng 54(11), 1940-1950, 2007

[2] Scheys, L, et al. Gait & posture, 28(4), 640-648, 2008

[3] Steele KM, et al. JOB, 43,2099-2105, 2010

Disclosure of Interest: None Declared

Modelling

AS-0294

SOFT TISSUE COMPONENTS INCREASE STABILITY AND EFFECT THE KINEMATICS OF A BIPEDAL PASSIVE-DYNAMIC WALKER

Samuel Masters [1,*]John Challis [1]

[1]Kinesiology, The Pennsylvania State University, State College, United States

Introduction and Objectives: The human body is composed primarily of soft tissue which oscillates during locomotion. As a result, ignoring soft tissue oscillation in models of human ambulation may affect the accuracy of the measurements made by said model (e.g., joint loads or muscle forces). Simulations that contain an oscillatory component may expose the benefits and impediments of soft tissue oscillation. Typically, non-rigid models are more strenuous to simulate computationally, but allow for a larger arsenal of mechanisms that increase stability (e.g., energy damper systems). Passive-dynamic walkers (PDWs) are tools for studying the underlying dynamics of human gait. A bipedal PDW with massless, rigid legs and point masses located at the hip and each foot can ambulate on an incline solely due to the energy from gravity *in silico* [1]. These systems, which capture many components of human gait, can be modified to study the dynamics of biologically inspired mechanisms (e.g., tendon energy storage and release or arm swing). A simple, bipedal PDW was modified to study the dynamical effects of a spring-damper system.

The objectives of the study were: (1) to outline the kinematic differences between a PDW with and without an oscillatory mechanism and (2) to quantify the dynamical effect of an oscillatory mass on the stability of a bipedal PDW.

Methods: A bipedal PDW with rigid, massless legs and a point mass at the hip and each foot was simulated to ambulate on an incline. There were two models: a control walker that did not contain an oscillating mass (CPDW) and a walker with an oscillating mass located at the hip (OPDW). The oscillating mass was connected to the hip via a spring-damper system. Stable gait cycles were found by keeping the damping coefficient at a constant value and incrementing the spring stiffness by 0.1 N/m until the walker failed. This was repeated for damping coefficients between 0 and 10 N/m/s in increments of 0.25 N/m/s. The conditions for foot-ground contact were such that each step was mathematically dependent upon the angular position of the stance leg exclusively. Therefore, the initial state conditions of the stance leg were perturbed to analyze the stability of the CPDW and the OPDW for varying spring-damper parameters. Furthermore, the kinematics of the CPDW and OPDWs were compared. All stable gait cycles analyzed were period-one (P1) gait cycles. That is, each step was kinematically identical and, therefore, the PDW could ambulate indefinitely if unperturbed.

Results: All results discussed were obtained for an incline of 0.009 radians.   For an OPDW without damping, stable walking cycles were found for spring stiffness values between zero and 8.6 N/m. As the damping coefficient increased, the range of spring stiffness values that resulted in stable walking increased exponentially. For example, at damping coefficients of 2 N/m/s and 4 N/m/s, stable gait cycles were found for spring stiffness values up to 11.5 N/m and 673 N/m, respectively. Compared to the CPDW, an OPDW with a spring stiffness of 61.1 N/m and damping coefficient of 4.0 N/m/s, resulted in a 2.89% decrease in step time and a 37.83% increase in step length. As a result, the average walking velocity increased by 41.87%. In general, the PDW walking velocity increased as the spring stiffness increased. Furthermore, the basin of attraction for the same OPDW (Figure 1) was 161.45% greater than the CPDW. As

the spring stiffness increased, stable gait cycles bifurcated one or more times (i.e., P1 gait cycles transitioned to period-two (P2) gait cycles, then P2 gait cycles transitioned to P4 gait cycles, etc.). Period-n gait cycles occur when the initial conditions of a step repeat every n-th step. Furthermore, this period-doubling region transitioned into a period-halving region until the gait cycles returned to stable P1 gaits.

Figure:

Basin of Attraction for Oscillating PDW (c = 4.0 N/m/s, k = 61.1 N/m)
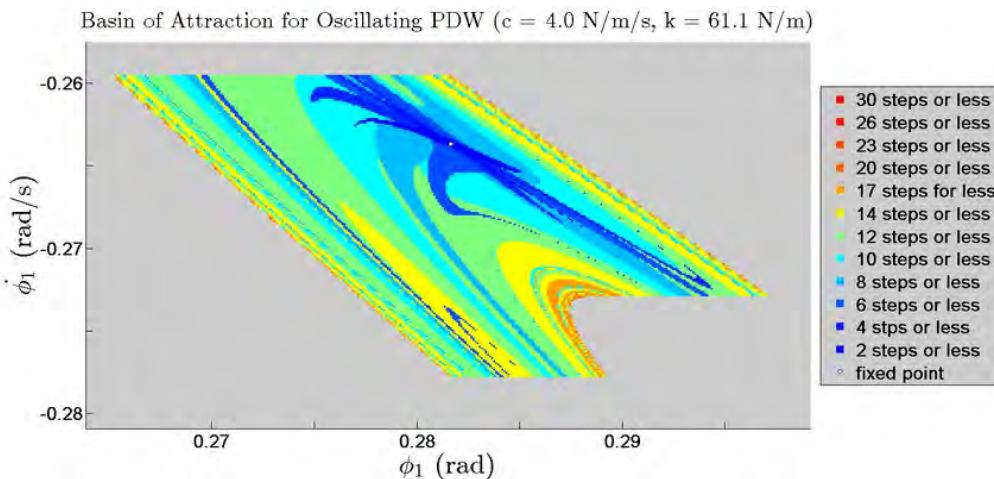
Caption: Figure 1: The basin of attraction of the OPDW (spring stiffness of 61.1 N/m, damping coefficient of 4.0 N/m/s). The initial states of the stance leg for which the OPDW returns to the period-one gait cycle (fixed point-attractor).

Conclusion: Insights into human locomotion have been obtained from PDW, here these models were extended to examine the potential role of soft tissue oscillations. The two models simulated produced gait with kinematic differences between the rigid model and the model containing soft-tissue like components. Importantly the gaits simulated with the model containing soft tissue components was much more stable than the rigid model, suggesting that in humans these soft tissue damped oscillations may, in addition to their other roles, act to make gait more stable.

References: [1] Garcia et al., J. Biomech. Eng., 120(2): 281-288, 1998.

Disclosure of Interest: None Declared

Modelling

AS-0295

HYBRID FORWARD INVERSE DYNAMICS FRAMEWORK FOR HUMAN MUSCULOSKELETAL SIMULATIONS

Mohammad S. Shourijeh [1,*] Daniel L. Benoit [1 2]

[1]Faculty of Health Sciences, [2]Faculty of Engineering, University of Ottawa, Ottawa, Canada

Introduction and Objectives: Different approaches have been used in musculoskeletal simulation studies to solve the muscle redundancy problem. Inverse dynamics, forward dynamics, and hybrid (inverse-forward [1] or forward-inverse [2]) dynamics have been applied with different optimal control techniques in static, partially dynamic, or fully dynamic approach. Focusing on the knee joint, the ideal framework would predict biomechanical quantities, such as muscle activations and joint loads, in a biofidelic manner. The goal of this research is to introduce a simulation framework that can predict knee joint biomechanical quantities, based on knee joint stability criteria, while taking advantage of the strengths of both static and dynamic optimization techniques, while maximizing the use of in vivo data to produce physiologically relevant simulations.

Methods: The workflow was developed using OpenSim-MATLAB scripting to run simulations on a variety of movements and can be used in: 1) an inverse dynamics manner (i.e. from measured kinematic data and force platform data to muscle forces/activations); 2) forward dynamics (i.e. from muscle excitations to kinematic estimations); and 3) hybrid dynamics (i.e., a combination of forward and inverse dynamics) and is shown in Fig. 1.

Several steps are included in the framework such as scaling, inverse kinematics, inverse dynamics (and residual reduction algorithm, RRA, and static optimization). These are followed by a forward inverse dynamics phase, which provides a computationally cheaper simulation compared to fully forward dynamics simulations. MATLAB optimization is used for the optimal control part, whereas other optimizations are done in OpenSim 3.2 within the specifically defined tasks, such as scaling and RRA.

The framework provides several features, including parameter identification, static or dynamic predictive simulations, noise rejection, EMG-driven simulations, partially predictive simulations, joint load calculation, and objective function alteration.

Hybrid dynamics could be used for subject-specific model tuning where the torque error between the forward and inverse dynamics sides is minimized and model parameters such as muscle-related parameters will be optimally identified, for which a dynamic optimization should be solved. This requires EMG data for all muscles in the model. Hybrid dynamics can also be used for muscle excitation optimization where the framework searches for the best muscle excitations that minimize the error as well as a physiological cost, e.g. muscle fatigue. Note that the framework starts from excitations and ends with joint torque, i.e. it does not integrate the multibody equations of the system and therefore it is more efficient than a fully forward dynamics that tracks body motion such as [3]. Finally, when some EMGs are measured, but some of the muscle signals are still unknown, hybrid simulations can be useful, in which situation optimization will be performed to find optimal values of the unknown muscle activities. As EMG measurements are prone to noise and crosstalk, minor tweaks on the known EMGs could also be done for convergence to a possibly better optimal point.

Results: The hybrid framework has simulated level walking trials using Gait2392 and Gait1018 models from the OpenSim repository. The results of using the Gait1018 along with comparison with those of static optimizations and experimental EMGs will be presented in [4].

Figure:
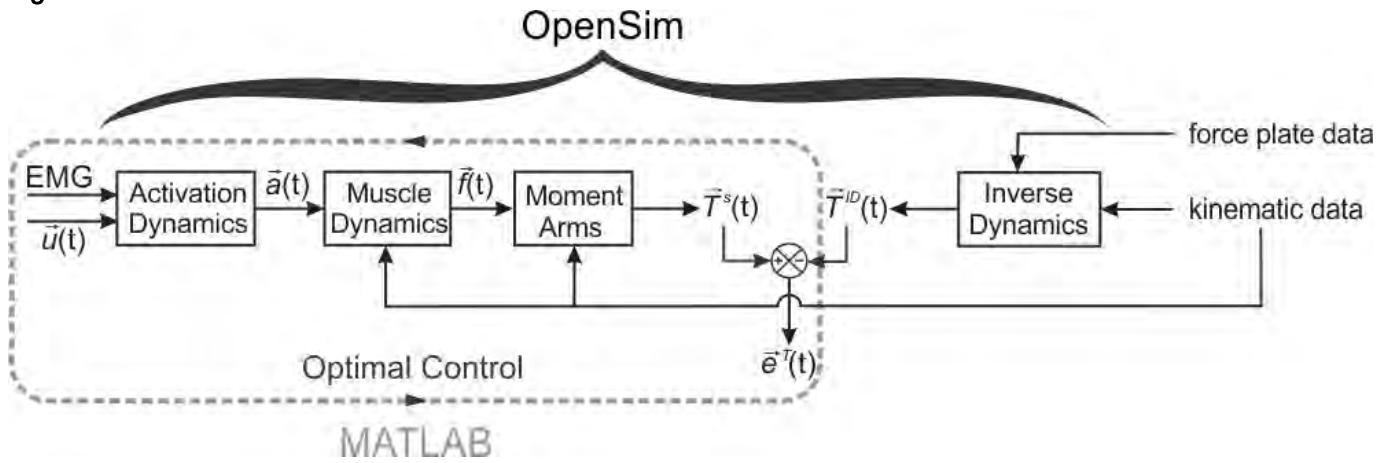
Caption: Schematic of the hybrid forward inverse dynamics musculoskeletal simulation framework. u and a are muscle excitation and activation, respectively; f represents tendon-muscle force; T is joint torque; superscripts s and ID refer to simulation and inverse dynamics; and e designates error.

Conclusion: A framework for efficiently simulating musculoskeletal models was introduced. This framework has features that use the advantages of both SO and DO, can integrate known in vivo subject characteristics making it more bio-fidelic than existing alternatives, and converges to optimal solutions within reasonable computation time. As such, it is an ideal framework to investigate the effects of population-based differences due to injury or disease. To study rehabilitation-related quantities of the knee joint, such as ACL injury, one future work will be to use a more bio-fidelic knee model that considers ligaments at the knee such as [5].

References:

[1] Shourijeh et al., *J. Comp. and Nonl. Dyn.*, 9: 031018 1-11, 2014.

[2] Sartori et al., *J. Biomech.*, 47: 3613-3621, 2014.

[3] Neptune et al., *Exerc. Sport. Sci. Rev.,* 37: 203-210, 2009.

[4] Potvin et al., Comparison of Activation Predictions of Hybrid Forward Inverse Dynamics Simulations with Static Optimization and Experimental EMG, submitted, *ISB*, 2015.

[5] Xu et al., *Comput. Meth. Biomech. Biomed. Eng.*, 18: 1217-1224, 2014.

Disclosure of Interest: None Declared

Modelling

AS-0296

TIBIOFEMORAL CONTACT LOADING IN ANTERIOR CRUCIATE LIGAMENT RECONSTRUCTED INDIVIDUALS AND HEALTHY CONTROLS DURING A RANGE OF GAIT TASKS.

David J. Saxby [1,*]Pauline Gerus [2]Bryce Killen [1]Luca Modenese [1]Tim Wrigley [3]Adam Bryant [3]Karine Fortin [3]Kim Bennell [3]Flavia Cicuttini [4]David Lloyd [1]

[1]Centre for Musculoskeletal Research, Griffith Health Institute, Griffith University, Gold Coast, Australia, [2]Laboratory of Human Motion, Education and Health, University of Nice Sophia-Antipolis, Nice, France, [3]Centre for Health, Exercise and Sports Medicine, University of Melbourne, [4]Department of Epidemiology and Preventive Medicine, Monash University, Melbourne, Australia

Introduction and Objectives: The tibiofemoral joint receives frequent high-magnitude contact loads (TCLs) during activities of daily living [1]. TCLs can cause tibiofemoral osteoarthritis (OA) in animal studies, and are implicated in human OA development [2]. Human studies have identified anterior cruciate ligament rupture and reconstruction (ACLr) as a powerful risk factor for OA. ACLr modifies joint mechanics, muscle strength and daily activity. The effect of ACLr on tibiofemoral contact loads in unknown. Instrumented prosthetic implants (IPs) allow direct measurement of tibiofemoral contact loads (TCLs), but due to cost and their invasive nature are inappropriate for most study designs. As a result, surrogate or proxy measures of *in vivo* joint contact loads are used such as the external knee adduction moment (KAM). KAM shows equivocal associations with joint health and disease, and this ambiguous nature of the KAM may arise from KAM not being an appropriate measure of medial tibiofemoral contact load (MTCL). In lieu of surrogates such as KAM, electromyogram-driven neuromusculoskeletal (EMGd NMS) models provide an alternative approach to predicting joint contact loads. EMGd NMS models incorporate experimentally measured muscle recruitment (EMGs) and external gait mechanics to estimate *in vivo* muscle forces and TCLs.

While IP studies have provided profiles of standardized net tibiofemoral contact loads during selected gait modes, healthy and disease risk (ACLr) populations perform a wide range of motions, and little is known about tibiofemoral joint contact loads across walking and sporting movements. The purpose of this study was to model TCLs in ALCr and healthy controls during walking, running and side-step cutting gait using an EMGd NMS model. We hypothesized that differences in TCLs exist across between ACLr and controls and across gait tasks, specifically that ACLr will display lower TCLs across gait tasks.

Methods: Participants (Controls n=60, ACLr = 105, age range 18-40) performed walking (W), running (R) and side-step cutting (SSc) while 3-dimensional motion capture (Vicon, UK), ground reaction forces (Kistler, Switzerland), and electromyograms (EMGs)(Zero Wire, Milan, Italy) were acquired. EMGs were acquired from 8 major knee muscles, and conditioned by band-pass filter (30-450 Hz Butterworth), linear envelope (6 Hz LP Butterworth) and scaling to functional maximum. OpenSim [3] and CEINMS [3] were used to estimate medial, lateral and total tibiofemoral contact loads (TCLs) during W, R and SSc. Repeated measures ANOVA was performed to determine differences across gait task and between groups.

Results: TCLs were significantly different between gait modes (Fig 1), with mean and peak TCLs (medial, lateral and total compartments) increasing from W to R to SSc. Lateral compartment was never unloaded, despite the presence of substantial positive external adduction moments during W and R. Similarly, medial compartment remain substantially loaded during SSc despite the presence of a positive KAM. The increase in TCLs as gait task speed and external loads increased was of no surprise although SSc which was slower than R displayed larger total TCLs. An interaction of knee injury group (ACLr or healthy) with total compartment load revealed that ACLr individuals have lower peak tibiofemoral contact loads during R and SSc, but not during walking gait.

Figure:

Total Compartment Contact Load vs. Stance Phase
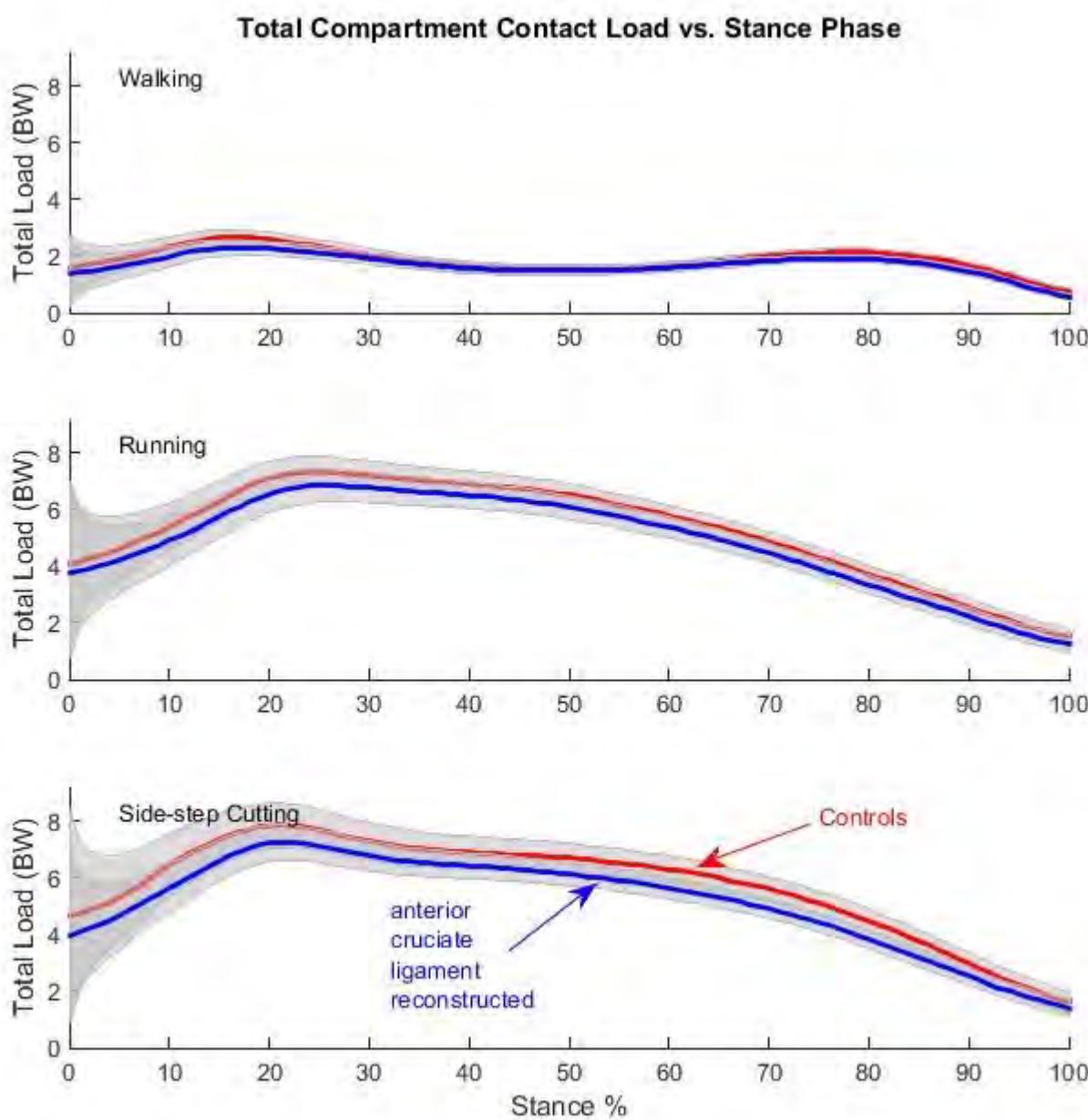
Caption: Fig 1. Total compartment load +/- 95% confidence intervals for ACLR (blue) and controls (red) during stance phase of walking, running and side-step cutting. Load is scaled to body-weight and time to 100% of stance phase.

Conclusion: Medial and lateral tibiofemoral compartments experienced substantial contact loading during walking, running and side-step cutting. Despite the presence of large positive or negative external frontal plane moments, both medial and lateral compartments experienced substantial contact forces with no periods of zero loads. Total TCLs were different across walking, running and side-step cutting gait, with a general trend of increased gait velocity resulting in increased TLCs in both compartments. For movements of similar velocities (such as running and side-stepping) TCLs were found to be larger in side-step cutting, despite running being performed at higher velocity. ACLr individuals exhibited lower TCLs during sporting tasks such as running and side-step cutting. During walking gait ACLr and controls exhibit similar TCLs. It is possible that chronic under-loading of the tibiofemoral compartment in ACLr populations could be related to their increased risk of OA development.

References: [1] Bergmann et al., PLoS One 9(1): e86035, 2014.

[2] Andriacchi et al., J Bone Joint Surg, 91: 95-101, 2009.

[3] Delp et al., IEEE Trans Biomed Eng, 54: 1940-1950, 2007.

[4] Sartori et al., PLoS One 7, e52618, 2012.

Disclosure of Interest: None Declared

A SIMULATION MODEL OF ROTATIONAL FALLS IN EQUINE EVENTING

Martin G. C. Lewis [1,*]Lauren Birkbeck [2]Cleveland Barnett [1]

[1]School of Science and Technology, [2]School of Animal, Rural and Environmental Sciences, Nottingham Trent University, Nottingham, United Kingdom

Introduction and Objectives: Rotational falls in equestrian eventing involve the horse contacting a solid fence before rotating over the fence in a somersault like action. Rotational falls present the greatest risk of death or serious injury to the rider, with nine deaths reported between 2004 and 2013, among other serious injuries such as paralysis and internal organ damage [1]. Limited research into the biomechanics of the horse and rider during jumps has attempted to understand the execution of horse jumping performance [2] and the loads imparted on fences during collisions [3]. In addition research on the mechanical conditions of a rider and horse system which result in a rotational fall does not currently exist. An investigation into the causes of rotational falls is paramount to enable investigation into methods for reducing the number of rotational falls and subsequent fall-related death or serious injury.

Methods: A rotational fall was simulated using a rigid two-dimensional, three-segment model of a horse and rider rotating about a pin joint fixed at the top near most corner of a standard dimension fence (Figure 1). One segment represented the combined properties of lower forelimb, metacarpals and digits, another segment represented the remaining forelimbs, trunk and hindlimbs and a final segment representing the rider. The rider mass centre location was given a fixed position relative to the horse trunk for each simulation. Rider whole-body mass centre location and moment of inertia were calculated from Dempster [4] according to mean digitised rider kinematics measured during competition. The segmental mass centre locations and moments of inertia of the two horse segments were calculated using data from Buchner et al. [5]. The point of contact of the horse with the fence was varied to occur between the knee (distal most end) and the elbow (proximal most end) of the antebrachium.

The effect of perturbing a number of variables was investigated including: rider position upon horse, angle between forelimb segment of the horse and trunk, angle of the horse trunk relative to the horizontal and initial rotational energy in the system. A range of initial conditions for each variable were investigated by perturbing combinations of mean kinematics for nineteen horse and rider combinations filmed successfully executing a jump for intermediate sections at a British Eventing competition.

Results: Varying the contact point of the horse with fence along the line of the antebrachium acts to change the orientation of the horse and rider where the system has sufficient energy to rotate beyond the global vertical. The orientation of the horse's trunk at this breakpoint ranges from 135° when the forelimbs are maximally flexed beneath the trunk and the contact point of horse with fence is at the knee joint, and 95° when contacting more proximal to the trunk at the elbow. This represents an angle of the horse's back relative to the horizontal of 10° and 50° respectively. Increased kinetic energy and potential energy at impact will all act to reduce the energetic requirements for a rotational fall, and increase the chance that a rotational fall may occur.

Figure:
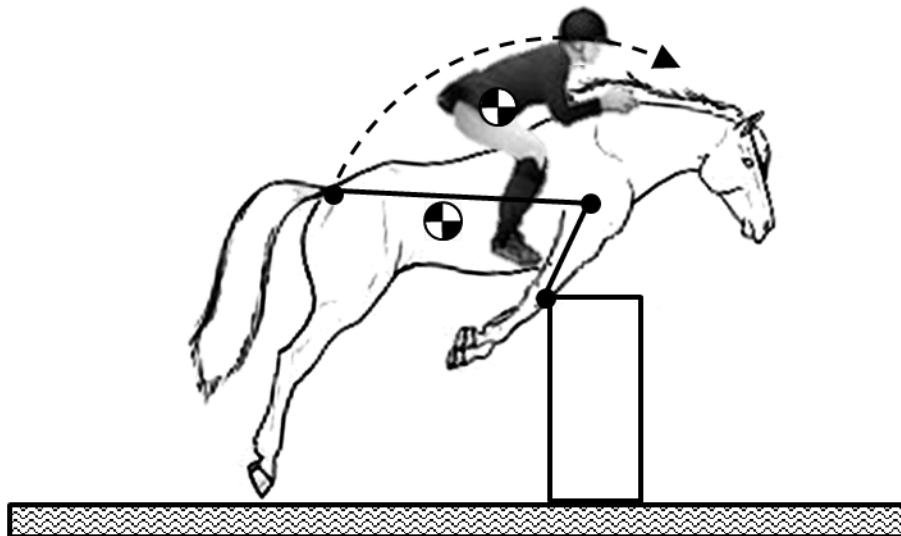
Caption: A three-segment, rigid body model of a rotational fall; segment 1 (Antebrachium) from axis of rotation at distal end at the knee to the proximal end at elbow, segment 2 (Trunk) from elbow to croup, segment 3 (Rider) with fixed mass and whole-body moment of inertia at a position relative to segment 1.

Conclusion: The effect of large initial energy in a rider and horse system makes it more likely that sufficient energy is present to cause a rotational fall. The energy requirement for a rotational fall are smallest when the forelimbs are maximally flexed and the contact point is at the most distal aspect of the antebrachium.

References: [1] Fédération Equestre Internationale. FEI Eventing final Statistics Report 2013, Fédération Equestre Internationale, 2014.

 [2] Bobbert, M.F. et al., J.Exp.Biol. 208: 249-260. 2005.

 [3] Kahmann, K.M.*,* University of Kentucky, 2010.

 [4] Dempster, W.T., Space Requirement of the Seated Operator: Geometrical, kinematic and mechanical aspects of the body with special reference to the limbs. Wright Patterson Air Force Base, 1955.

 [5] Buchner, H.H.F., et al., J.Biomech. 30: 653-658, 1997.

Disclosure of Interest: None Declared

EFFECTS OF DIFFERENT STRENGTH TRAINING PROGRAMS ON BIOMECHANICAL AND ENERGETIC PARAMETERS OF RUNNING IN TWO DIFFERENT INTENSITIES

Jorge L. Storniolo [1 2,*] Alberto E. Minetti [2] Leonardo A. Peyré-Tartaruga [1]

[1]Laboratory of Research and Exercise, Federal University of Rio Grande do Sul, Porto Alegre, Brazil, [2]Pathophysiology and Transplantation, University of Milan, Milan, Italy

Introduction and Objectives: Adding of strength to endurance training is recognized to improve the metabolic cost of running (Cr) through neuromuscular adaptations (i.e. motor unit recruitment, intra/intermuscular coordination and musculotendinous stiffness) [1, 2]. Vertical stiffness (K_{vert}) is an important variable for running because it estimates the amount of elastic energy which could be stored and released for this movement. It is known that K_{vert} is velocity-dependent and might be related to Cr due to elastic properties [3] and increase after strength training [4, 5]. However, it is unknown the response of Cr and K_{vert} after two different strength training programs. Thus, this study aims at compare the effects of maximal and explosive strength training on Cr and K_{vert} in submaximal and supramaximal intensity of running.

Methods: A total of 24 recreational runners took part in the research (mean±SD - age: 26.3±5.2 years; height: 1.75±0.9 m; weight: 75.4±15.4 kg). The subjects were assessed pre and post-training for the biomechanical and energetic variables. Indirect calorimetry data were evaluated with MEDGRAPHICS analyzer to calculate maximal oxygen consumed (VO_{2max}) and Cr on treadmill. Cr was analyzed on 60% of velocity associated to the VO_{2max}. Biomechanical data were recorded and analyzed with 6 cameras of VICON motion system with a sampling frequency of 120 Hz for 60 and 110% velocity of VO_{2max}. Video records were obtained to analyze biomechanical variables during running. K_{vert} and F_{max} were estimated from Morin et al. [5] equation. Neuromuscular parameters were evaluated such as one repetition maximal (1RM) in squat exercise and height of counter movement jump (hCMJ). The subjects were divided into tree groups: maximal and explosive strength training (MAX, n=8 and EXP, n=9) and control group (CON, n=7). MAX and EXP performed simultaneously the strength and endurance training, while CON group performed only endurance training during 8 weeks. MAX group performed exercises between 85-95% of 1RM, while EXP group performed exercises between 30-40% of 1RM in maximal velocity. A two-way ANOVA (group x time) with repeated measures was used to test for differences in K_{vert}, F_{max}, Cr, aerial time (AT), contact time (CT), velocity in 60 and 110% of velocity associated to VO_{2max} (vVO_2), 1RM and hCMJ. Paired t-test was used to compare the variables pre- and post-training. The alpha adopted was 0.05.

Results: K_{vert}, F_{max}, AT, CT and Cr did not show significant differences between the groups after 8 weeks of training (p > 0.05) at any of the measured intensities (table 1). However, vVO_2 on 60 and 110% of intensity associated to the VO_{2max} have increased for MAX group (p = 0.02; p = 0.04, respectively). Neuromuscular variables as 1RM and hCMJ increased for MAX group and was higher than CON group (p < 0.001; p = 0.01, respectively) (table 1).

Figure:
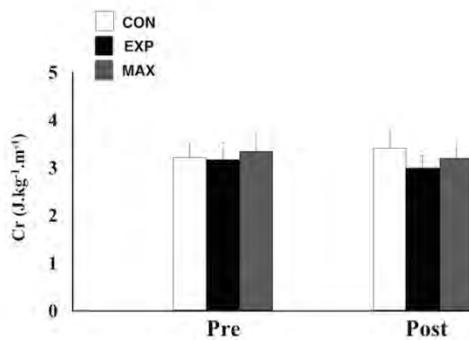
Caption: Cost of running (Cr) before and after 8 weeks of training. Where CON (white bars), control group; EXP (black bars), explosive strength group; MAX (grey bars), maximal strength group.

Conclusion: Strength training groups did not show significative differences between the biomechanical variables after 8 weeks of training at any of the measured intensities. MAX group increased the vVO_2 on both intensities and decreased the Cr, although not significant. This result, associated to maintenance of K_{vert} and F_{max} might indicate a lower energy expenditure for MAX group. Therefore, the maximal strength training through increase of force, presented at improves of 1RM and hCMJ, seems to be more beneficial to recreational runners at submaximal and supramaximal intensities.

Table:

	$\%VO_{2max}$	CON (n = 7)		EXP (n = 9)		MAX (n = 8)	
		Pre	Post	Pre	Post	Pre	Post
vVO_2 (km.h^{-1})	60	8.5 ± 0.9	8.6 ± 0.8	9.1 ± 0.8	9.5 ± 1.0	9.2 ± 1.2	$9.9 \pm 1.0*$
	110	15.6 ± 1.6	15.7 ± 1.5	16.7 ± 1.4	17.5 ± 1.8	16.8 ± 2.2	$18.2 \pm 1.8*$
K_{vert} (kN.m^{-1})	60	15.7 ± 5.2	16.5 ± 5.4	17.1 ± 5.9	18.8 ± 7.3	16.9 ± 4.9	17.1 ± 5.2
	110	$40.$	42.1 ± 17.0	$45.$	47.3 ± 19.5	$49.$	61.1 ± 18.7

		2 ± 15.9		0 ± 16.3		3 ± 16.7	
Fmax (kN)	60	1.6 ± 0.4	1.6 ± 0.4	1.7 ± 0.4	1.7 ± 0.5	1.7 ± 0.2	1.7 ± 0.2
	110	2.0 ± 0.5	2.0 ± 0.5	2.1 ± 0.6	2.1 ± 0.7	2.2 ± 0.3	2.3 ± 0.3
1RM (kg)	-	105.2 ± 22.0	105.9 ± 22.1[A]	100.21 ± 20.6	99.40 ± 20.5[AB]	103.2 ± 22.5	146.7 ± 25.4[B]*
hCMJ (m)	-	0.27 ± 0.07	0.27 ± 0.07[A]	0.28 ± 0.06	0.28 ± 0.05[AB]	0.35 ± 0.03	0.36 ± 0.05[B]

Caption: Table 1.Means ± SD values of velocity associated to maximal consumption of oxygen (VO2), vertical stiffness (Kvert), maximal force (Fmax), aerial time (AT), contact time (CT), percentage of aerial time (%AT), one repetition maximal (1RM) and height of countermovement jump (hCMJ) for maximal strength training (MAX), explosive strength training (EXP), and control training groups (CON), before (Pre) and after (Post) the training period.

References:

[1] Taipale et al., J. Appl. Physiol., 113: 325-335, 2013.

[2] Arampatzis et al., J. Exp. Biol., 209: 3345-3357, 2006.

[3] Albracht et al., Eur. J. Appl. Physiol., 113: 1605-1615, 2013.

[4] Dumke et al., Int. J. Sports Physiol., 5: 249-261, 2010.

[5] Morin et al., J. Appl. Biomech., 21: 167-180, 2005.

Disclosure of Interest: None Declared

Sport

AS-0299

PERFORMANCE OF VARIOUS NCAA FIELD HOCKEY BALLS

J.J. Trey Crisco [1,*]Kathryn Yates [1]Bethany Wilcox [2]

[1]Orthopaedics, [2]Brown University, Providence, United States

Introduction and Objectives: At the collegiate level in the United States, there is a wide range in the character of field hockey balls approved play. Colors include white and orange with smooth or dimpled surfaces.   To the best of our knowledge the performance of field hockey balls has not been previously studied. We used a motion analysis approach that we developed previously for baseball bats to examine the performance of various field hockey when hit by female colligative field hockey players.

Methods: Seven members of the Brown University women's field hockey team (NCAA Division I – Ivy League) who swung right handed were recruited. All players used the same TK Synergy 1 composite 36.5" stick which had four infrared markers attached. Markers were attached halfway down the grip (between the shooter's hands), where the grip meets the rest of the stick, halfway between the end of the grip and the end of the stick, and on the rounded end of the stick. Eleven different ball models (labeled A to K) were used in testing. Each ball tested had six square pieces of tape placed symmetrical about the ball. Ball A was defined as the reference ball as it is marketed as the NCAA approved championship ball. Four high-speed cameras (Qualisys Oqus system) were used to track the 3-D motion of the stick and ball.   For each player, the eleven ball models were randomized. Each player hit ten shots with each ball. The ball began in a stationary position, however many of the players taped the ball forward before shooting. In total, 770 total shots on goal were recorded (7 players hitting 10 shots each with 11 different balls).   The tracked data was analyzed to compute ball speed, stick linear (at point of ball contact) and rotational speed and ball performance factor. Ball performance factor was defined as ball speed divided by linear stick speed. The significance of the difference in mean speeds and performance factor among the ball models was examined with an ordinary one-way ANOVA. Differences among the various models were assessed using Dunnett's multiple comparisons test with ball model A as the reference. Mechanical testing was also performed on each ball by compressing the balls between to flat plates to a value of 6.35 mm and recording the peak compression load.

Results: Ball model A speeds averaged 46.8 m/s, with a maximum of 63.9 m/s. The linear stick speed for shooting ball model A were a mean of 47.3 m/s, with a maximum of 57.5 m/s. The rotational speeds for shooting ball model A were a mean of 40.6 radians/s, with a maximum of 57.2 radians/s. There was no difference in the mean ball or stick speeds between ball model A and any of the other ball models.

Ball performance factor of model was a mean of 1.00 for ball model A and this factor was significantly higher than ball model F (0.93) and ball model J (0.93).

The load at maximum compression did not correlate with ball performance factor (P = 0.520). However, there were substantial differences in the load at maximum compression among the various ball models. Ball model A had a mean compression load of 1274 N (SD: 70 N), while ball model F had the highest mean compression load of 2462 N (SD: 290 N) and ball model D had the lowest mean compression load of 462 N (SD: 40 N).

Conclusion: In this study the ball and stick speeds we measured were unexpectedly higher than speeds measured in baseball bat impacts or in lacrosse shooting at the collegiate level. However, we do not that the study setup was ideal, allowing the women to maximize their efforts. Across the various models we found little difference in ball performance, with ball model A only slightly outperformed the other ball models. Despite this vary narrow range of ball performance, we found a very large range, almost a factor of 5, in ball compression values. This laboratory study suggest that balls with lower compression, and thus theoretically lower injury potential, can be used in play with no significant difference in performance. However, it should be noted that what level of injury reduction this would provide is not known, nor is it known if other factors affect true field performance of the balls.

Disclosure of Interest: None Declared

Sport

AS-0300

IMPACT OF BOXING PUNCHES ASSESSED WITH WEARABLE INERTIA SENSOR AND MOTION CAPTURING

Akinori Nagano [1,*]Shoma Kudo [2]Ryosuke Akaguma [2]

[1]Faculty of Sport and Health Science, [2]Department of Sport and Health Science, Ritsumeikan University, Shiga, Japan

Introduction and Objectives: Boxing is an Olympic sport that has a long history. Because of the nature of boxing, in which a primary objective is to land punches on the head and stomach of the opponent, measures to ensure safety in boxing practice and matches are crucially required. There have been several preceding studies that pursued this goal [1] [2]. Recently with the development of high resolution, light weight and wearable sensors, biomechanical measurements have become more reliable, less restrictive and easier to conduct. We applied these latest sensing techniques to evaluate the impact of boxing punches. Specifically we utilized wearable inertia sensors, with which we measured three components of acceleration and three components of angular velocity data. We also utilized the technique of motion capturing, with which we obtained a wider variety of kinetic / kinematic data such as forces, position, velocity and acceleration of body landmarks very accurately.

Methods: Protocol: We collected punching data from right-handed experienced boxers. The punching motions were (1) jab, (2) one-two, (3) one-two-three and (4) one-two-hook. The boxers threw punches into either punching mitts held by an experienced trainer, or into a sand bag. (a) Acceleration and angular velocity of landmark points, (b) motion of the boxer, trainer who held the mitts, and sand bag, and (c) ground reaction forces were recorded. We also recorded and analyzed sparring sessions in normal boxing practice routine.

Inertia measurements: We used high resolution, wearable and light weight inertial sensors (ATR-Promotions, Japan). We attached the sensors at the wrist of boxers (Figure), at the wrist of trainer who received punches with punching mitts, and the sand back. Three components of acceleration and three components of angular velocity data were obtained at 500Hz. The sensor was quite small (slightly larger than a coin used in Japan) and light weight. The data were transferred to a mobile personal computer via Bluetooth. Restriction on the motion of boxers were minimal.

Motion Capturing: We used a system composed of 16 optical cameras (Motion Analysis Corporation, USA) and 15 force plates (Tec Gihan, Japan). Boxers threw punches in the calibrated space into punching mitts held by a trainer, or into a sand bag. Reflective markers were attached to the neck, shoulder, elbow, wrist, and fist of boxers (Figure). Position, velocity and acceleration of the landmarks were obtained. We calculated the momentum and kinetic energy of the fist/forearm.

Sparring Recording: We recorded sparring sessions in normal boxing practice with a high-speed camera (nac Image Technology, Japan). We also attached an inertial sensor on the back side of the headgear of boxers. This enabled us to directly measure the acceleration of the head component imposed by punches.

Results: Punches thrown into the mitts: Based on the data from motion capture system and force plates, the momentum of a punch was calculated as 10.00 - 19.87 kg m/s (Table). The results suggested that the impacts can be reasonably assessed in activities that include strong collisions such as boxing. The measured values from the accelerometers were found to exceed 16G.

Punches thrown into the sand bag: Acceleration of the sand bag varied according to punch type. The acceleration also varied according to the size of boxing gloves. When comparing the impulse received by the sand bag and the momentum of wrist and forearm, there was a good matching between the values. This confirmed the validity of utilizing inertial sensors for our purpose.

Sparring: In routine boxing sparring sessions, "clean hit" of punches are rare. This is because boxers usually focus on improving techniques and skills rather than knocking out the partner during sparring. Therefore in this study the inertial sensors rarely gave high acceleration values. On the other hand, even when punches were defended (blocked) by a boxer, the sensors occasionally gave moderate magnitude of acceleration values.

Figure:
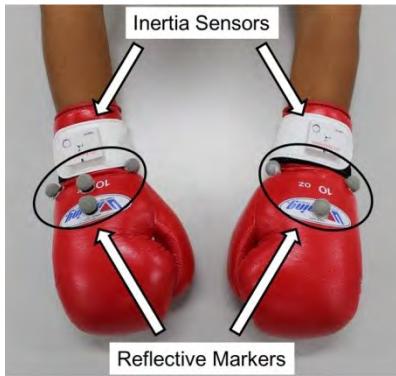
Caption: Inertia sensors and reflective markers attached on the gloves.

Conclusion: (1) We assessed the impact of boxing punches with wearable accelerometers and motion capturing. (2) We obtained consistent measures from inertia sensors and motion capture system, validating the assessment of impact using the small, light-weight and wearable sensors. (3) The momentum of punches ranged between 10.00 - 19.87 kg m/s.

Table:

	PunchSpeed (m/s)	Momentum (kgm/s)
LeftJab	7.431	13.75
OneTwo_LeftJab	6.630	12.26
OneTwo_RightStraight	8.724	16.14
OneTwoThree_LeftJab	6.213	11.49
OneTwoThree_RightStraight	8.423	15.58
OneTwoThree_LeftStraight	6.860	12.69
OneTwoHook_LeftJab	5.658	10.47
OneTwoHook_RightStraight	7.564	13.99
OneTwoHook_LeftHook	8.120	15.02

Caption: Kinetic characteristics of punches thrown by a boxer (right-handed).

References: [1] Schwartz et al., J. Neurosurg., 64: 248-252, 1986.

[2] Walilko et a., Br. J. Sports Med., 39: 710-719, 2013.

Disclosure of Interest: None Declared

Sport

AS-0301

USING POSTURE TO BOOST TILT PRODUCTION WITH ASYMMETRIC ARM ACTIONS

Joanne Mikl [1,*]

[1]ACFR, University of Sydney, Sydney, Australia

Introduction and Objectives: Tilt of the principal longitudinal axis of the body towards the angular momentum vector will produce left twist in a somersault; the twist-to-somersault ratio increases as tilt increases [1,3]. Asymmetrical arm actions may be used to produce tilt [2]. When the arms move in a plane (Fp) which is perpendicular to the principal medial axis of the body and contains the shoulder, the actions may be modelled in 2D. In a layout (L) posture, Fp will also be aligned with the frontal plane of the chest (Fc) and so coaches may use the easily understood instruction to move the arms in Fc. However, in an Entry Pike (EP) or Arch (A) posture, Fp and Fc are not aligned. EP and A may be used to increase tilt production [2], provided the arm action is still performed in Fp.

This paper seeks to describe the position of Fp to improve instruction regarding the plane in which to move the arms. Further it determines the orientation change when performing the asymmetrical arm actions "Raise", "DiverS" and "Drop" [2] and compares results between Fp and Fc in an attempt to determine if EP and A may still be used to boost tilt when using Fc.

Methods: Due to left-right symmetry in L, EP or A the transverse principal axis of the body and the transverse axis of each segment of the body are parallel. Hence the location of Fp may be described by the angle of rotation needed for the longitudinal axis of the segment of interest to reach the principal longitudinal axis of the body. A forward rotation will be positive. This angle was determined for the pelvis, abdomen, chest, upper- and lower legs.

The tilt produced by each arm action, Raise, DiverS, and Drop was determined using the conservation of angular momentum. Tilt was calculated in Fp for L, EP and A, and in Fc, for EP and A. In Fp only tilt resulted and in Fc the orientation change was split into tilt, twist, and somersault; somersault being negligible since Fc has no component perpendicular to the principal transverse axis of the body.

To determine the above values the fifteen inertial property data sets from the literature collated by Mikl [2] were applied.

Results: The pelvis' longitudinal axis was the closest of any segment to the principal longitudinal axis of the body; the median angle (Φp) was 2.1^o (EP), -2.6^o (A). Φp is small and since the frontal plane of the pelvis may be observed by eye it is helpful to use the frontal plane of the pelvis as an approximation of Fp. The angle between the longitudinal axis of the chest and the longitudinal axis of the body (Φc) had a median of -57.2^o (EP) and 27.4^o (A). Not being small angles, moving the arms in Fc rather than Fp will reduce tilt considerably, while adding twist. Attached is a sketch of EP and A with the principal axes (blue), the longitudinal axis of Fp (red), and the angles ϕp and ϕc marked.

Moving the arms in Fc rather than Fp, both EP and A show a reduction in tilt and result in less tilt than L. The reduction in tilt in EP is greater than A presumably because of a greater magnitude of ϕc. The table gives the tilt produced when the arms move in Fp for L, EP and A, and Fc for EP and A (for L, Fc and Fp are the same). Positive tilt produces a left (positive) twist.

EP and A produce opposite twist, since each Φc has opposite sign. For A the twist is in the wrong direction, putting the athlete behind in twist. Even though in EP the twist is in the desired direction it is essentially a one off bonus; the reduction in tilt will ultimately produce a lower twist rate and so twist completed will progressively fall behind.

Ranking actions in order of tilt gives Raise, DiverS, Drop in Fp and DiverS, Raise, Drop in Fc. Further DiverS produced less twist than Raise in Fc. Thus, moving both arms rather than one appears to reduce the negative effect of using Fc over Fp. Never-the-less there is still a large reduction in tilt.

Figure:
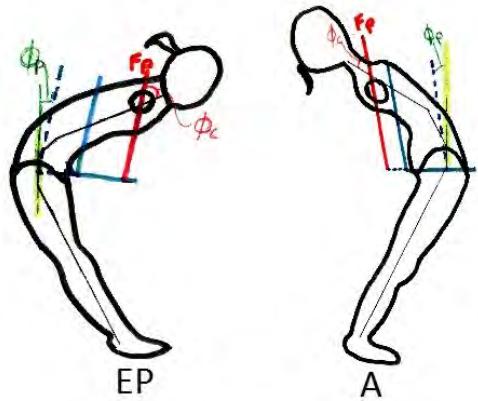
Conclusion: Using EP or A will boost tilt production if the asymmetrical arm actions used are in Fp. The location of this plane depends on the inertial properties of the body making its location difficult to explain to an athlete. It was found that the frontal plane of the pelvis was the closest anatomical plane and since this can be seen by eye, it is useful when explaining in which plane to move the arms. Moving the arms in Fc produces tilt considerably below that for L, and so using EP and A are no longer of benefit in boosting tilt. A was particularly poor since the secondary twist rotation was in the wrong direction.

Table:

Quartile			4	3	2	1	0	
Diver S	**Fp**	L	9.2	7.8	7.2	5.2	3.3	
		EP	12.6	10.0	9.9	6.3	4.1	
		A	10.0	8.2	7.8	5.4	3.5	
	Fc	EP	3.9	3.8	2.9	2.4	0.9	
		A	6.8	6.1	5.4	4.2	2.3	
Drop	**Fp**	L	8.5	7.3	6.6	4.7	3.0	
		EP	11.7	9.3	9.2	5.8	3.8	
		A	9.2	7.7	7.2	4.9	3.2	
	Fc	EP	3.5	3.4	2.5	2.0	0.7	
		A	5.9	5.4	4.7	3.8	2.0	
Raise	**Fp**	L	9.6	8.1	7.4	5.2	3.3	

		EP	13.3	10.5	10.4	6.4	4.1	
		A	10.4	8.5	8.1	5.5	3.5	
	Fc	EP	3.5	1.9	1.7	1.3	0.6	
		A	6.4	3.1	2.6	2.0	1.4	

Caption: Tilt produced by action, plane and posture

References: [1] Frohlich. AM J Phys, **47**(7): 583-592, 1979.

[2] Mikl. *ABC9*, 2014.

[3] Yeadon. *J. Sports Sci.* **11**(3): 187-198, 1993.

Disclosure of Interest: None Declared

Sport

AS-0302

PERFORMANCE ON THE FUNCTIONAL MOVEMENT SCREENTM IS RELATED TO HOP PERFORMANCE, BUT NOT TO HIP OR KNEE STRENGTH IN ATHLETES

Nienke Willigenburg [1,*] Timothy Hewett [2]

[1] OSU Sports Medicine, Sports Health and Performance Institute, [2] OSU Sports Medicine, Sports Health and Performance Institute, Departments of Physiology and Cell Biology, Orthopaedic Surgery, Family Medicine, and Biomedical Engineering, The Ohio State University, Columbus, United States

Introduction and Objectives: Pre-participation physical examinations have become common practice to screen athletes, and often include anthropometric, flexibility, and strength measures, with the aim to predict injury risk. Recently, interest has grown in screenings that reflect neuromuscular control during basic motor skills. One method to quantify fundamental movements in athletes is the Functional Movement Screen (FMSTM) [1]. The FMSTM aims to 'pinpoint deficient areas of mobility and stability that may be overlooked in the asymptomatic active population' [2]. The FMSTM consists of seven tasks which are scored on a range from 0-3, based on execution criteria, including aspects of mobility, stability, and compensatory movements. The FMSTM is currently used as screening instrument in major sport leagues, as it may be associated with the risk of athletic injuries [3]. However, from a biomechanical perspective, it can be questioned whether the selected movement tasks adequately reflect actual measures of interest, especially with respect to injury prediction. Also, the different FMSTM tasks do not appear to represent unitary constructs, which brings the use of the summed score into question [4]. Moreover, the FMSTM score depends on the subject's knowledge of the grading criteria [5]. Given these potential flaws, it may be preferable to quantify athletic performance by maximum-effort based tests that assess isolated outcome measures of interest. This study defines the relationship between FMSTM scores and hop performance, hip strength, and knee strength in a population of collegiate football players. We hypothesized that FMSTM scores would positively correlate to hop performance, but not to hip and knee strength. Our secondary hypothesis was that limb asymmetries in hip strength, knee strength and hop performance would correlate with asymmetries in FMSTM tasks.

Methods: Fifty-nine freshmen of a division I collegiate American football team (age=18±0.6 years, height=1.86 ± 0.06m, mass=106±20.2kg) participated in this study. The athletes performed the FMSTM, as well as a variety of maximum-effort hop tests, isokinetic knee strength and isometric hip strength tasks. We recorded total FMSTM score, peak strength and hop performance, and calculated asymmetries between legs on the different tasks. Spearman's correlation coefficients quantified the relationships between FMSTM scores and the other measures of strength and performance, and a chi-square analysis compared the number of athletes with asymmetries on the different tasks.

Results: We observed significant correlations (r=0.38-0.56, p≤0.02) between FMSTM scores and hop distance, but not between FMSTM scores and hip or knee strength (all p≥0.21). The amount of asymmetry on the FMSTM test was significantly correlated to the amount of asymmetry on the timed 6m hop (r=0.44, p<0.01), but not to hip or knee strength asymmetries between limbs (all p≥0.34).

Figure:
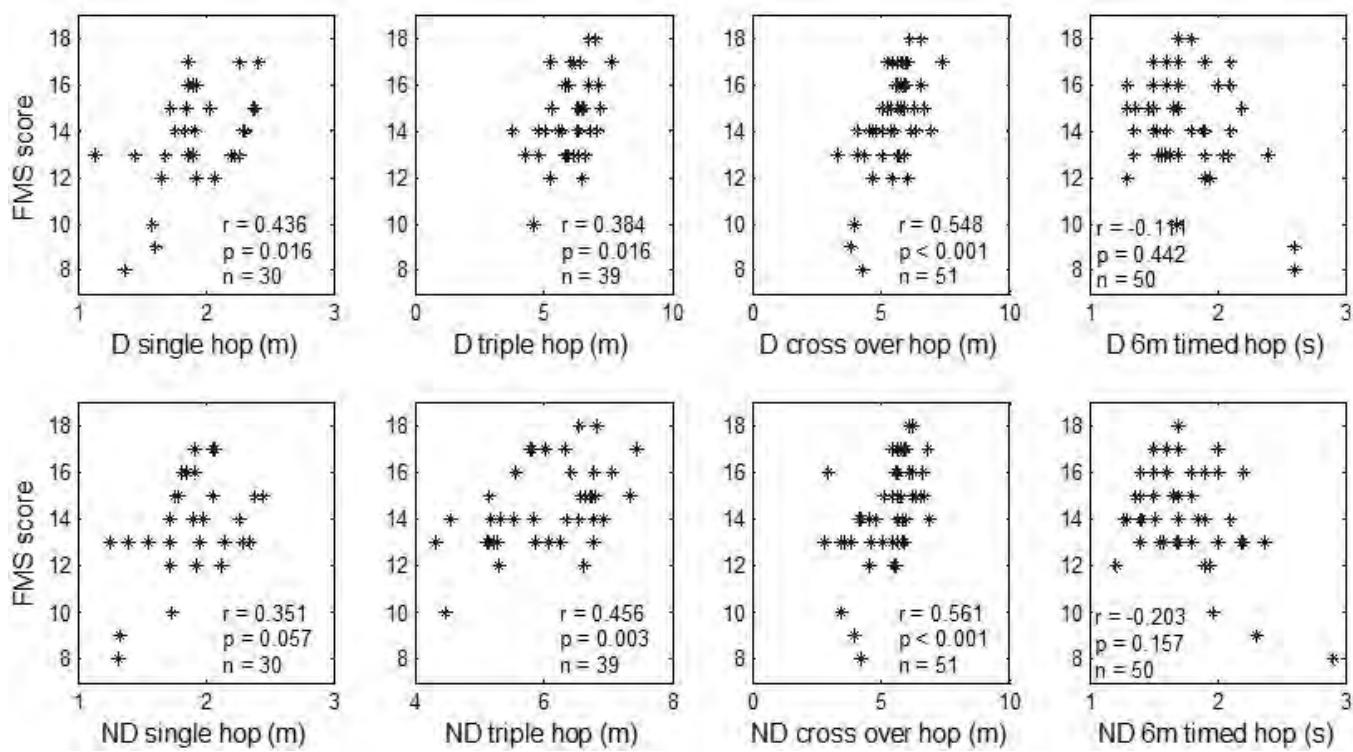
Caption: Correlations between FMS(TM) scores and the different hop tests. The upper and lower panels represent the hop performance on the dominant (D) and non-dominant (ND) limbs, respectively.

Conclusion: FMS™ total score was positively correlated to hop distance, and limb asymmetry in FMS™ tasks was correlated to limb asymmetry in 6m hop time in football players. No significant correlations were observed between FMS™ score and hip and knee strength, or between FMS™ asymmetry and asymmetries in hip and knee strength between limbs. These results indicate that a simple hop test may be a time and cost efficient alternative to FMS™ testing in athletes, and that functional asymmetries between limbs do not coincide with strength asymmetries between limbs.

References: [1] Cook et al., N Am J Sports Phys Ther, 1(2):62-72, 2006.

[2] Cook et al., N Am J Sports Phys Ther, 1(3):132-139, 2006.

[3] Kraus et al., J Strength Cond Res, 28(12):3571-84, 2014.

[4] Kazman et al., J Strength Cond Res, 28(3):672-8, 2014.

[5] Frost et al., J Strength Cond Res, DOI 10.1519/JSC.0b013e3182a95343, 2013.

Disclosure of Interest: None Declared

Computer Simulation

AS-0303

WHICH JOINT TO ASSIST? SIMULATION-BASED GUIDELINES FOR REDUCING THE METABOLIC COST OF WALKING WITH HEAVY LOADS

Christopher L. Dembia [1,*] Amy Silder [2] Thomas Uchida [2] Jennifer Hicks [2] Scott Delp [1][2]

[1]Mechanical Engineering, [2]Bioengineering, Stanford University, Stanford, United States

Introduction and Objectives: Soldiers often carry over 40 kg while on duty. These loads significantly increase metabolic cost and limit the soldiers' ability to perform their duties [1]. To alleviate this burden, engineers are designing devices to decrease the metabolic cost of walking with heavy loads ("loaded walking") [2], [3]. Many existing devices are designed to assist ankle plantarflexion, based on the rationale that the ankle typically provides half of the net positive mechanical joint work during loaded walking [3]–[6]. Alternatively, a device explicitly optimized to reduce muscle activity might lead to greater reductions in metabolic cost. Computer models of the musculoskeletal system that incorporate energy expenditure enable a systematic exploration of a range of assistance strategies (e.g., varying the joint being assisted and the timing and magnitude of actuation), without the need for time-consuming device prototyping and human testing. The aim in this work was to use musculoskeletal simulation to discover which type of joint assistance has the greatest potential to decrease the metabolic cost of loaded walking. We considered 6 types of joint assistance: ankle plantarflexion, knee flexion, knee extension, hip flexion, hip extension, and hip abduction.

Methods: We collected motion capture data for 6 individuals walking at a freely selected speed while carrying 40 kg on their torso. We generated simulations of each walking trial using OpenSim's Computed Muscle Control (CMC) algorithm [7] (the "no assist" condition). Next, we tested the 6 types of joint assistance by creating new CMC simulations in which the model could be assisted by a virtual massless torque actuator that acted at one joint and in only one direction. The kinematics of the motion remained the same, as did the objective to minimize the sum of squared muscle activations. However, CMC was free to use the virtual actuator to replace muscle actuation (the "assisted" conditions).

To estimate the metabolic cost of walking in each simulation, we used the CMC results as inputs to a modified version of the muscle metabolics model developed by Umberger et al. [8]. We used this metabolics model to compute the relative decrease in cost of transport (COT; energy required to transport a unit weight by a unit distance) that resulted from the use of each virtual actuator.

Results: All 6 types of joint assistance led to a decrease in COT (see table). Assisting hip flexion showed the greatest potential to reduce metabolic cost, with a 16% decrease in COT compared to normal walking. Assisting ankle plantarflexion reduced COT by 7.9%, which is in the same range as has been achieved experimentally [3]. Assisting knee extension had the smallest effect on COT. The torques supplied by some virtual actuators resembled the corresponding net joint moments, while others differed substantially. One reason for these differences is the fact that motion is generated by a complex coordination of both uni- and bi-articular muscles. For example, the ankle plantarflexion actuator took over the role of the uni-articular soleus muscle, but did not affect the activity of the bi-articular medial gastrocnemius (see figure).

Figure:
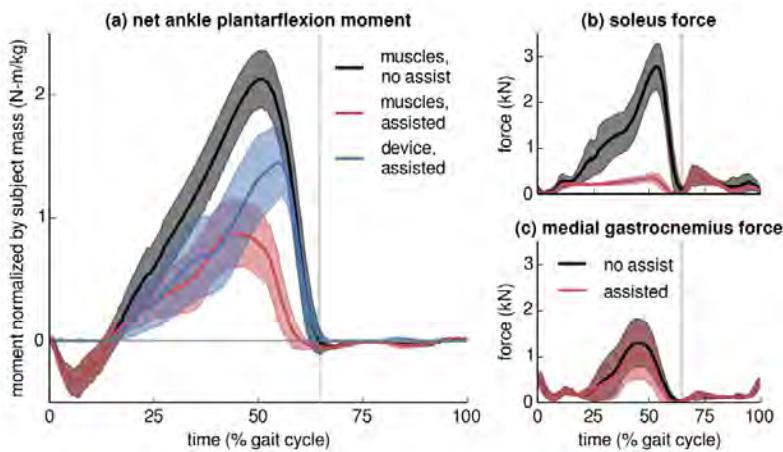
Caption: Effects of ankle plantarflexion assistance. Net ankle plantarflexion moment normalized by subject mass for the "no assist" condition (black) along with the net moment from muscles (red) and the ankle plantarflexion device (blue) in the "assisted" condition (a). Force generated by the (b) soleus and (c) medial gastrocnemius muscles, both with (red) and without (black) assistance. (solid: mean; shading: ± 1 standard deviation; vertical gray line: toe-off)

Conclusion: Assisting hip flexion, rather than ankle plantarflexion, led to the greatest potential savings in the metabolic cost of transport. Non-intuitively, some of the virtual actuator torque profiles were substantially different from the corresponding net joint moments. Both of these findings support the use of muscle-driven simulations to help design assistive devices. Our results do not account for possible kinematic adaptation—a limitation we hope to address through future work via predictive simulation.

Table:

Type of Assistance	Relative Decrease in COT ± 1 s.d.
hip flexion	16 ± 2.0 %
knee flexion	12 ± 3.7 %
hip abduction	9.0 ± 4.8 %
hip extension	8.2 ± 2.8 %
ankle plantarflexion	7.9 ± 1.7 %
knee extension	3.7 ± 1.8 %

Caption: Relative decrease in cost of transport (COT) during walking while carrying 40 kg, averaged over 6 subjects.

References: [1] Roy et al., Aviat. Space. Environ. Med., 83: 1060–1066, 2012.

[2] Walsh et al., IEEE Int. Conf. Robot. Autom., 3485–3491, 2006.

[3] Mooney et al., J. Neuroeng. Rehabil., 11: 80, 2014.

[4] Malcolm et al., PLoS ONE, 8: e56137, 2013.

[5] Sawicki et al., J. Exp. Biol., 212: 21–31, 2009.

[6] Huang et al., J. Exp. Biol., 217: 605–613, 2014.

[7] Thelen et al., J. Biomech., 36: 321–328, 2003.

[8] Umberger et al., Comput. Meth. Biomech. Biomed. Eng., 6: 99–111, 2003.

Disclosure of Interest: None Declared

Modelling

AS-0304

RUPTURE OF THE MUSCLE-TENDON COMPLEX IN TENSILE TEST USING DISCRETE ELEMENT MODELING

Anthony Roux [1 2,*] Jennyfer Lecompte [1] Laure-Lise Gras [1] Sébastien Laporte [1] Ivan Iordanoff [2]

[1]Arts et Metiers ParisTech, Institut de Biomécanique Humaine Georges Charpak, Paris, [2]Arts et Metiers ParisTech, Institut de Mécanique et d'Ingénierie, Talence, France

Introduction and Objectives: Tear of the muscle-tendon complex (MTC) is one of the main causes of sport injuries but its mechanisms are still unclear [1]. The MTC is a multi-scale, non-isotropic and non-continuous structure that is composed of numerous fascicles gathered together in a conjunctive sheath (epimysium). Many MTC models use the Finite Element Method to simulate MTC's behavior as a hyperviscoelastic material. The Discrete Element Method (DEM) used for modeling composite materials could be adapted to fibrous materials as the MTC and to model the rupture. Before modeling the tear of the MTC, the aim of the study was to model its behavior and its rupture in tensile test.

Methods: The MTC model was developed in DEM (Figure 1-a) with GranOO software (I2M, France, www.granoo.org). Mechanical properties of MTC were addressed thanks to literature values [2], [3]. Stiffness of each element was related to discrete elements' cross-sectional area, initial length of links and corresponding elastic modulus (EM). Fibers were built with spherical discrete elements linked with springs (EM=37.44 kPa). The extra cellular matrix was computed using springs between fibers. Tendon's fibers were built with respect to muscle fibers architecture (EM=800 MPa). The myotendinous junction (MTJ) was represented by multi-links between tendon and muscle. Force vs. displacement evolution was obtained during a computed tensile test. MTC was fixed on its lower extremity and the upper extremity was subjected to a linear displacement. Thus, stretch-dependent evolutions of muscle volume and pennation angle were calculated. Elongation was chosen as rupture's criterion: spring's length over 30% strain [4] leads to a break and a separation from the MTC.

Results: The computed Force-Displacement displayed a classical hyper-elastic behavior, its shape was in agreement with *in vitro* experimental data of Gras et al. [5] over the SternoCleidoMastoideus (SCM) muscle. Values of mechanical properties of extracellular matrix (EM=100 kPa) (one of the main components of the MTC) and MTJ (EM=400MPa) had to be adjusted in order to fit with experimental data due to the lack of data in the literature. Furthermore, we used elastic modulus from patellar tendon [3] which could be not directly applied to SCM tendon. The use of linear springs, added to the MTC's structural effect, leads to a hyper-elastic behavior for the MTC's response in tensile test. The decrease of pennation angle during the tensile test was in agreement with *in vivo* assessments. The variation of the volume of the MTC, calculated during the simulation, was less than 1%, as previously described in the literature. This confirms the incompressibility property of MTC thanks to springs' properties in DEM. Rupture was located in the MTJ's area of the MTC, as described in the literature [6]. Indeed, MTJ was at the interface between the stiff tendon and the soft muscle, leading to a stress concentration. MTC was broken by fibers' delamination, in agreement with in vitro data [7] (Figure 1-b).

Figure:
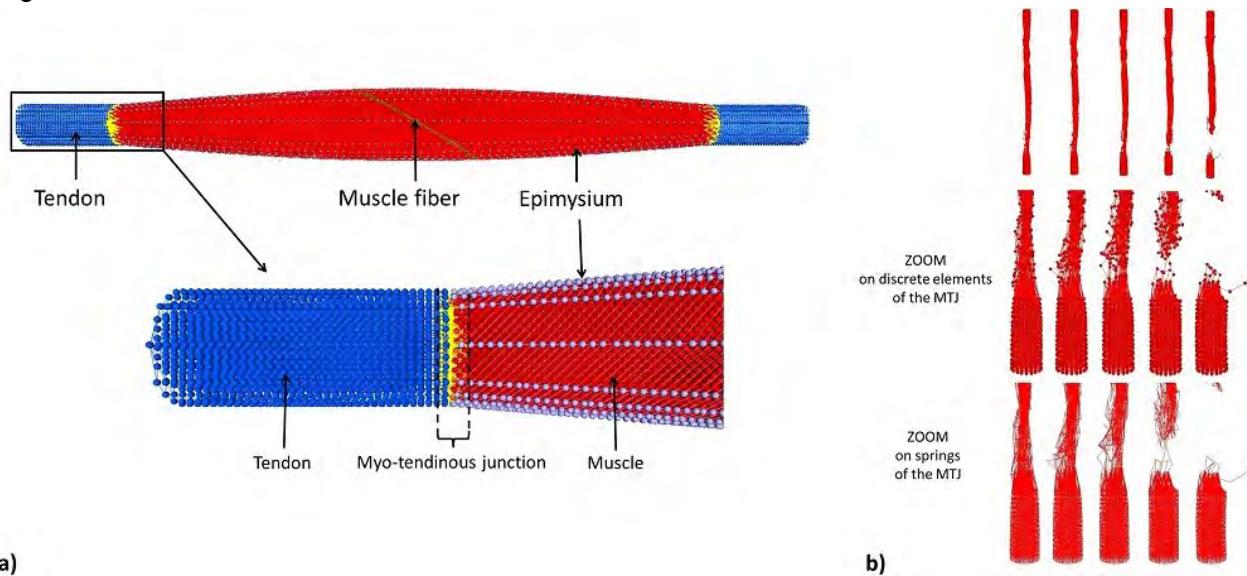
Caption: a) MTC's geometry in DEM b) Rupture in the Myo-Tendinous Junction of the MTC in tensile test with DEM

Conclusion: The DEM seems to be a promising method to model the hyper-elastic macroscopic response of MTC with simple elastic microscopic elements. In order to model the tear of the MTC, the muscle's contraction will be implemented.

References: [1] Uchiyama et al. Sports Med Arthrosc Rehabil Ther Technol, *3*, 20, 2011

[2] Regev et al. Spine (Phila Pa 1976), 36, 1666-1674, 2011

[3] Matschke et al. Sci World J 2013:514743, 2013

[4] Noonan et al. Am J Sports Med 22:257-261, 1994

[5] Gras et al., J Mech Behav Biomed Mater 15:131-140, 2012

[6] Petilon et al. Oper Tech Sports Med.13:162-168, 2005

[7] Ilaslan et al. Skeletal Radiol 36(6), 503-507, 2007

Disclosure of Interest: None Declared

AS-0305

DYNAMIC PATIENT SPECIFIC FINITE ELEMENT BREAST MODEL FOR NODULE TRACKING DURING MAMMOGRAPHY

Silvia Pianigiani [1,*] Ngan Nghiem Bich [2] Bernardo Innocenti [2]

[1]IRCCS, Istituto Ortopedico Galeazzi, Milano, Italy, [2]BEAMS Department, Université Libre de Bruxelles, Bruxelles, Belgium

Introduction and Objectives: Mammograms are commonly used to screen the breast in order to detect eventual pathologies, such as nodules. These images show a compressed breast in different deformed shapes. However, the comprehensive use of these images during surgery, when breasts are under different boundary conditions, is problematic. For example, surgeons experience difficulties not only in the identification, but also in the removal of nodules by needle aspiration. Misidentification of the nodule position could affect the patient health. Therefore, the purpose of this project is to develop and validate a patient-specific finite element model of the breast to accurately localize the position of potential breast nodules under different conditions.

Methods: First, a parametric three-dimensional breast model has been designed. By the use of this model, the patient specific breast can be obtained measuring 10 external parameters directly on the standing patient. The breast model consists of several parts, such as the fat, the glandular area and the duct. The model does not include the nipple and it is considered fully constrained to the chest. Once the patient specific model is obtained, that can be used for a finite element analysis in which several positions are considered: standing with undeformed breast, standing with deformed breast during cranio-caudal (CC) mammography, standing with deformed breast during 45° oblique mammography (MLO) and supine with undeformed breast simulating surgery conditions. Moreover, in order to track a possible nodule position from one of the deformed configurations to the surgical condition, spheres with different dimensions and positions have been inserted in the model. Different approaches to model the different materials of the breast have been used, as very few is reported in the literature. To understand which was the best modelling choice, a validation of the model is performed by comparing breast deformations in the numerical model and the mammograms. For the best matching, the tracking of the nodule has been analysed.

Results: Linear, Neo-Hookean and Mooney-Rivlin models used in this study show different outputs, in terms of shape, simulation time and displacements of the nodules. Comparing the numerical deformed shape with the ones obtained form images, the two most accurate models are the Neo-Hookean and the Mooney-Rivlin (Figure 1). The use of both models presents similar computational time. For the two models, different magnitude and trend of displacement has been shown for nodules of different dimensions and located in different part of the breast to simulate a ductal carcinoma in situ and an invasive ductal carcinoma. Generally bigger nodes move less than the smaller ones. Moreoever, the Mooney-Rivlin model shows higher displacement values, but with similar trend and position compared to the Neo-Hookean model.

Figure:
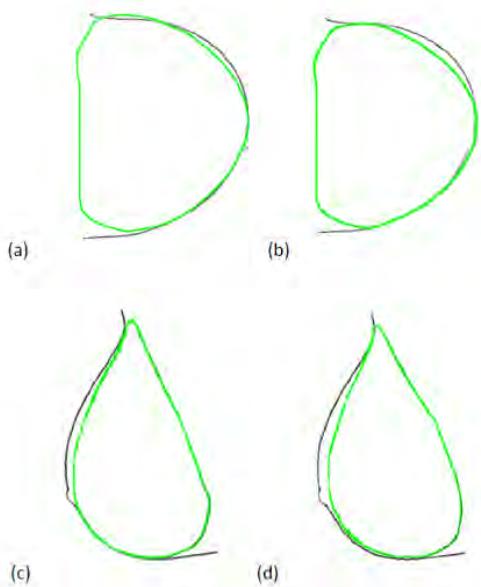
Figure 1: comparison between border deformed breast from image (black) and obtained after numerical simulation for: (a) CC view, Neo-Hookean model; (b) CC view, Money-Rivlin model.; (c) MLO view, Neo-Hookean model; (d) MLO view, Money-Rivlin model.

Conclusion: The aim of this work is to simulate breast deformation by means of finite element modeling. The use of this model has been coupled with nodule tracking information, useful during surgery to completly recover patient's health. From the obtained results, nonlinear methods provide more realistic outputs than linear methods, replicating better the hyperelastic materials behavior of the breast. There are minor differences in the outputs obtained from the two used nonlinear models.

The presented breast model presents some limitations, such as simplify geometries and the inclusion of the skin layer only throughout the friction coefficient between the breast and the mammograms plates. Although the proposed breast model presents minor limitations, it provides a valuable surgical tool to assist breast surgery.

The authors have nothing to disclose.

Disclosure of Interest: None Declared

A MODIFIED VERSION OF THE THREE-COMPARTMENT MODEL TO PREDICT FATIGUE DURING SUBMAXIMAL TASKS WITH COMPLEX FORCE-TIME HISTORIES

Michael Sonne [1,*]Jim Potvin [1]

[1]Kinesiology, McMaster University, Hamilton, Canada

Introduction and Objectives: There has been extensive research on the inclusion of fatigue models into proactive tools for the purpose of ergonomic analysis with digital human models (DHM). The end goal of this line of research is to allow for an accurate prediction of muscle fatigue during complex and/or combined industrial tasks, thus proactively reducing the risk factors related to musculoskeletal injuries before the job(s) physically exists on the assembly line.

The three-compartment model of muscle fatigue[1] ($3CM_{XFL}$) has been validated, for the prediction of endurance times for various joints in the human body, by simply modifying the fatigue and recovery rates in the model [2]. However, it is not known how well the $3CM_{XFL}$ predicts fatigue levels during intermittent tasks, consisting of repeated efforts "on" to a single force level, then "off" to complete rest. As most work tasks are more complex than on/off [3], it is not clear if the current $3CM_{XFL}$ can be used for the ergonomics analysis of the full range of occupational tasks. The purpose of this research was to validate the existing $3CM_{XFL}$, against experimental fatigue levels resulting from a variety of submaximal force patterns, and provide modifications to the $3CM_{XFL}$ to increase the accuracy of fatigue predictions in these industrially relevant tasks.

Methods: We collected 9 experimental conditions of repeated sequences of submaximal plateaus of either 12 - 15 seconds in length, varying between 0 - 45% of MVC, followed by complete rest. Fatigue was determined by comparing an MVC after each plateau to a pre-trial plateau - with the decrease representing the fatigue level. These force profiles were completed using either isometric contraction of the distal aspect of the thumb, or isometric handgrip. Changes were made to the $3CM_{XFL}$, such that: 1) the fatigue rate was scaled to the current activation level and 2) the recovery rate was scaled based on a gradient that depended on both the current activation level and current fatigue level (termed the graded motor unit 3CM, or $3CM_{GMU}$). The $3CM_{XFL}$ was also optimized ($3CM_{OPT}$), by modifying the model's fatigue (F) and recovery (R) coefficients, to predict fatigue throughout the experimental trials. We used the data from 7 of the conditions to determine the optimal F and R coefficients for the $3CM_{GMU}$ and $3CM_{OPT}$, and then tested the optimized model with data from the remaining 2 conditions. In all 9 conditions, the RMSD and R^2 between predicted and experimental fatigue was calculated, as was the error between the final experimental and predicted fatigue. The optimized models ($3CM_{GMU}$ and $3CM_{OPT}$) were also used to predict endurance times between 10% and 100% MVC, in increments of 10% MVC.

Results: The results can be found in Table 1. In general, the $3CM_{OPT}$ and $3CM_{GMU}$ were better at predicting fatigue in complex submaximal force patterns. The $3CM_{XFL}$ produced an asymptote at 6.1% MVC. Conversely, the $3CM_{GMU}$ predicted an asymptote and 29% MVC, compared to the $3CM_{OPT}$ which predicted an asymptote at 45.4% MVC.

Figure:
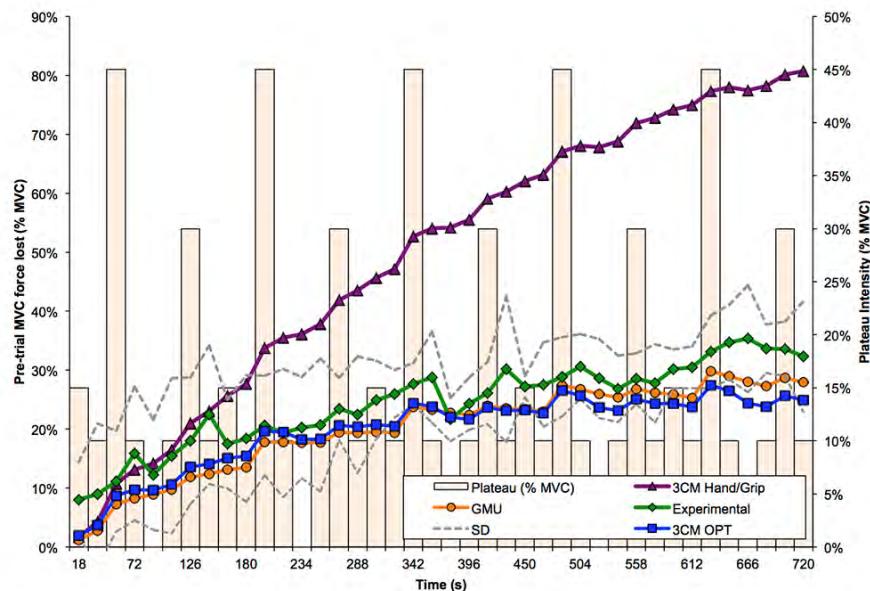
Caption: Figure 1. The mean experimental fatigue data (± SD) are plotted with the fatigue predicted with the 3CM-GMU, OPT and XFL for one of the test conditions (n = 8).

Conclusion: The 3CM$_{GMU}$ model builds on the theoretical basis of the three-compartment model of Xia and Frey-Law (2008), and aims to improve its physiological fidelity. Optimizing the F and R coefficients, for both the 3CM$_{GMU}$ and 3CM$_{OPT}$, results in strong predictions of fatigue levels during complex, submaximal force patterns. The 3CM$_{GMU}$ was able to predict muscle fatigue levels within approximately 4.1% MVC. The modifications made to the original 3CM allowed the 3CM$_{GMU}$ to provide accurate predictions of fatigue accumulation and recovery during complex, intermittent force patterns. The discrepancy between the 3CM$_{GMU}$ and 3CM$_{OPT}$ and the 3CM$_{XFL}$ in predicting endurance times indicates there are factors not accounted for between intermittent and sustained tasks. Additional research should aim to: 1) apply the findings of this model to other body parts, and 2) improve the model to allow for accurate fatigue predictions during sustained isotonic, intermittent and complex contraction patterns.

Table:

		Optimization			Test			All	
	RMSD	Mean Error	R^2	RMSD	Mean Error	R^2	RMSD	Mean Error	R^2
GMU	4.1	-0.9	0.824	4.4	-2.9	0.937	4.2	-1.3	0.849
OP	4.	-1.4	0.786	4.5	-6.0	0.916	4.1	-2.4	0.815

T	0								
X F L	29.4	45.6	0.833	31.0	49.9	0.901	29.7	46.6	0.848

Caption: Summary of results from optimization and test conditions. The GMU and OPT performed better in the submaximal complex force patterns than the XFL. There were no significant differences between the OPT or the GMU.

References: [1] Xia & Frey Law, J. Biomech, 41: 3046-52, 2008

[2] Frey Law et al., J. Biomech. 45: 1803-8, 2012

[3] Iridiastadi & Nussbaum, Ergon. 49: 344-66, 2006

Disclosure of Interest: None Declared

Modelling

AS-0307

A THEORETICAL AND COMPUTATIONAL FRAMEWORK FOR MODELING AND SIMULATING MUSCULOSKELETAL STIFFNESS DURING LOCOMOTION

Massimo Sartori [1,*] Marco Maculan [2] Claudio Pizzolato [3] Monica Reggiani [2] Dario Farina [1]

[1]Department of Neurorehabilitation Engineering, University Medical Center Goettingen, Goettingen, Germany, [2]University of Padova, Vicenza, Italy, [3]Griffith University, Gold Coast, Australia

Introduction and Objectives: Human locomotion emerges from the coordinated recruitment of musculotendon units (MTUs), which actuate multiple joints and degrees of freedom (DOFs). This underlies the continuous modulation of MTU viscoelasticity for best adapting to the mechanical demand of the performed motor task and external environment. Understanding the mechanisms regulating musculoskeletal viscoelasticity is crucial for understanding normal/abnormal locomotion. Musculoskeletal viscoelasticity can be investigated at the stiffness and damping levels. This contribution focusses on the stiffness level. Quasi-stiffness (QS) is used to derive joint elastic characteristics that are representative of entire phases of the gait cycle. However, QS may provide estimates that are biased by force responses that are not strictly associated to changes in joint kinematics. Alternatively, musculoskeletal modeling allows characterizing the elastic force response in individual MTUs/DOFs. Modelling has been used to reconstruct single-DOF stiffness from individual MTUs' stiffness in isometric conditions [1, 2]. These studies modelled the muscle elastic properties using the short-range stiffness (SRS) formulation and solved for the musculoskeletal redundancy using static optimization techniques. These factors prevent current modeling methods to be translated to the study of dynamic movement. In this context, muscle fibers would operate outside the SRS range and would underlie neuromuscular control strategies (i.e. co-contraction, reflex-based excitation) that could not be explained by a single optimization criterion chosen *a priori*. This work proposes, for the first time, a theoretical and computational framework for investigating musculoskeletal stiffness during locomotion and describes how this differs from QS and SRS.

Methods: Movement data were collected from five healthy subjects (age: 26.6 ± 1.3years, weight: 73.9 ± 11.8Kg, height: 1.77 ± 0.1m) who performed 7.8 ± 0.8 ground level walking trials (speed: 1.9 ± 0.25m/s). Collected data included EMG signals from 13 leg muscles, whole-body stereophotogrammetry data, and foot-ground reaction forces. Data were used to create and calibrate a subject-specific musculoskeletal leg model that matched each individual's anthropometry and EMG-to-force generating properties. The subject-specific EMG-driven model was validated on its ability of blindly predict experimental joint moments measured from a set of validation trials that were not used for the model calibration [3, 4]. The subject-specific model was employed to create a multi-dimensional cubic B-spline function per MTU. This described how muscle fiber force changed with respect to its states including: activation, normalized fiber length and velocity (Fig. 1A). Muscle fiber stiffness was then computed as the directional derivative from the force-length-velocity-activation surface (Fig. 1A) along the normalized fiber length directional axis, for given instantaneous states and corresponding force level. Muscle fibers stiffness was then combined with the interacting series-elastic tendon stiffness. The resulting stiffness from all MTUs in the model was then projected onto the knee flexion-extension (KneeFE) and ankle planar-dorsi flexion (AnkleFE) DOFs.

Results: Fig. 1A shows how the soleus fibers force slope at 57.6% stance can substantially differ when estimated directly from the force-length profile (i.e. see the workloop profile typically used for deriving QS) or from the instantaneous force-length-velocity-activation surface cross section (i.e. see the surface cross section used in our methods). Figs 1B-C show the instantaneous KneeFE and AnkleFE stiffness reconstructed from the individual MTUs' stiffness. Human locomotion is characterized by stiffness bursts of impulsive nature. The knee produced a stiffness peak (4.8±0.8Nm/deg) at 25±1.3% stance, followed by a minimally overlapped ankle stiffness peak (3.8±0.4 Nm/deg) at 88±2.3% stance.

Figure:
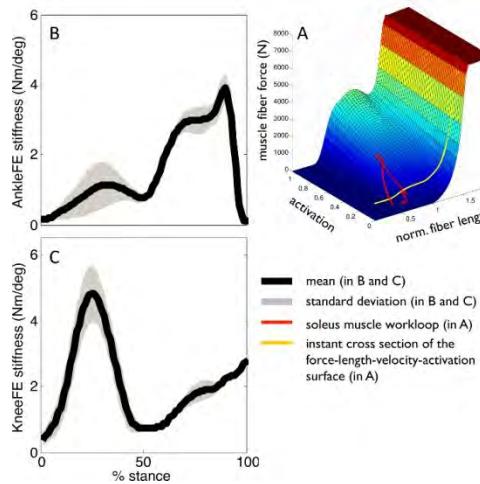
Caption: (A) Instantaneous force-length-activation surface of the soleus muscle for a given value of contraction velocity, with projected force-length work loop for one single walkig trial. (B) Ankle plantar-dorsi flexion stiffness and (C) knee flexion-extension stiffness averaged across all trials performed by one subject.

Conclusion: We proposed a subject-specific model for predicting musculoskeletal stiffness that explains both experimental EMGs and joint moments during locomotion. This provides a framework for describing how stiffness modulates as a function of muscle activation, fiber contraction, and interacting tendon dynamics as well as how this differs from QS and SRS. This could be used, in the future, to understand abnormal stiffness strategies in patients with neurological and orthopedic conditions and deliver personalized rehabilitation treatments.

References: [1]Pfeifer et al.,IEEE Trans. Biomed. Eng., 59: 2604–2612, 2012

[2]Hu et atl.,J. Neurophysiol., 105: 1633–1641, 2011

[3]Lloyd et al.,J. Biomech., 36: 765–776, 2003

[4]Sartori et al.,J. Biomech., 47: 3613–3621, 2014

Disclosure of Interest: None Declared

Modelling

AS-0308

APPROXIMATION TO THE MATHEMATICAL MODELING OF ARTICULAR CONTACT BY APPLYING THE DIFFERENTIAL GEOMETRY /KINEMATIC (DG/K) METHOD.

David L. Maldonado Guzman [1,*]Carlos Julio Cortes Rodriguez [1]

[1]Mechanical Engineering and Mechatronics, Universidad Nacional de Colombia/Biomechanics Research Group, Bogota, Colombia

Introduction and Objectives: The understanding of the physiological incongruence of the joint surface, which allows an optimal distribution of strain, it is still be a challenge for engineers, designers and health professionals whose field of work is the development of individualized joint implants. The complexity lies in the development of models capable of considering the tribological behaviour. This work presents a theoretical mathematical model of contact, which can make an approach of the kinematic behavior of a human joint. As case study is analyzed the radio cubital- proximal joint of elbow, which is a geometry entity known as trochoid. The modeling is based on the application of the method for both curves and surfaces. The method is based on the application of methods of differential geometry for the apprehension and geometrical study of identities, and basically the study of the geometry of movement or kinematics. For the study case is applied the fundamental theorem of the curves, in which it is evaluated the rigid movement joint as a control parameter of the point of instant contact, as an initial phase and are then applied the concepts of the first and second fundamental forms for the characterization of surfaces.

Methods: *Fundamental theorem or uniqueness of the curves: analysis of the instant contact.*

There is a single curve oriented to which the curvature K(s) and the torsion τ(s) a point corresponding to an arc of court with length(s). If a curve with the curvature and torsion oriented exists, then the Frenet formulas are satisfied[Toponogov, 2006]; thus the curve is parameterized in mobile reference system that moves along the same, constituting the control point of contact between the surfaces. By applying the theorem of uniqueness to the curve generated by the plane of contact between the trochlea and the olecranon, which embraces in a 50% to the trochlea and has an inclination of approximately 45 degrees,

The trochoid type is parameterized, for case between angles of 30 to 145 degrees:

$$x = bt - c \sin t \quad (1)$$

$$y = b - c \cos t \quad (2)$$

Where t is the angle variable that describes the circle of radius b, and the distance from the center to the point of contact is c.

Results: Similarly, a surface is unequivocally determined by certain values local invariants defined as first second fundamental forms. The procedure below is based on the geometric modeling of surfaces apply the following procedure gives the characterization of the contact:

1) Definition of the first fundamental form for the concave cylindrical surface (P).

   In particular, the *first fundamental form of a surface* is defined as

$I(\lambda) = I(\lambda,\lambda) = E(\lambda^1)^2 + 2F\lambda^1 \lambda^2 + G(\lambda^2)^2$ (3)

2) Definition of the metric from the first fundamental form.

$L(\gamma) = \int \sqrt{(E\,du^2 + F\,du\,dv + G\,dv^2)}$ (4)

3) Definition of the second fundamental form for the concave cylindrical surface (P)

In particular, the *second fundamental form of a surface* is defined as

$II(\lambda,\mu) = L\lambda^1\mu^1 + M(\lambda^1\mu^2 + \lambda^2\mu^1) + N\lambda^2\mu^2$ (5)

4) Definition of the fundamental factors of the second fundamental form (L, M , N) Equ (5).

Sometimes, for calculating *L*, *M*, and *N* it is more convenient to use the following Formulas:

L = −ru, nu, M = −ru, nv, N = −rv, nv,

which are obtained from the previous formulas by differentiation of the identities

ru, n= 0 , rv, n= 0.

For the cylindrical surface:

X= r cos v ;   Y= r sin v ;   Z= u

Thus , the second fundamental form :

II(λ) = (1 /r) (λ¹)² (6)

5) Identification of the natural surface

P = p(I (λ), II(λ))   (7)

6) Control of the point of instant contact coordinate transformation. Homogeneous coordinates.   Apply to theorem of Rodriguez.

Figure:
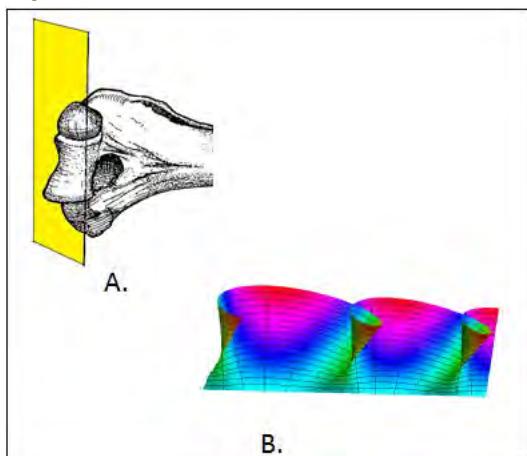
Caption: A. radio cubital- proximal joint; B. Trochoid, t =35° set the parameters defined by flat Frenet.

Conclusion: As an initial step in the process of mathematical modeling of the articular contact based on differential geometry shown to be an approximate method for the characterization and versatile, suitable for the analysis and evaluation of contact and motion geometry. In principle the DG/K method has been focused on the synthesis of machining processes, this could also be considered as a tool of synthesis and manufacturing of individualized implants.

In addition, it may be considered as instrument to support the methodology of analysis by the finite element method, likewise as implicit procedure in the development and characterization of custom implants. [Yongtae, 2010].

References: Radzevich *et la,* Mathematics and Computer Modellig, 46:1314-1331, 2007

Toponogov et la , Differential Geometry of Curves and Surfaces an concise guide, Birkhâuser 48:51, 2007

Yongtae *et la,* Advancesin EngineeringSoftware. , 41: 537–547,2010

Disclosure of Interest: None Declared

CERVICAL SPINE LOADING DURING RUGBY MACHINE SCRUMMAGING

Grant Trewartha [1,*]Ezio Preatoni [1]Timothy Holsgrove [2]Dario Cazzola [1]

[1]Department for Health, [2]Department of Mechanical Engineering, University of Bath, BATH, United Kingdom

Introduction and Objectives: Recent changes to the scrummaging laws in Rugby Union have been made to reduce the scrum engagement forces experienced by front row players [1], with the motivation of improving player welfare. However, information on the internal anatomical loading experienced by rugby players under different scrum conditions and a representation of the injury mechanisms which may act during this activity is still lacking. The purpose of the present study was to use a computational musculoskeletal modelling approach to characterise the cervical spine loading during machine-based rugby scrummaging, as an initial step in understanding more about injury mechanisms.

Methods: The 'Rugby Model', a customised OpenSim musculoskeletal model (OpenSim 3.2, SimTK) was developed, principally by merging a full body model ('OpenSim 2354') with an existing head and neck model [2]. Adjustments included providing the head and neck segments with inertia parameters from DEXA imaging to allow dynamic analyses and adding a scapulo-clavicular joint with constrained motion to permit a better representation of external loading (via the shoulders onto the spine) during scrummaging. Verification of the model for kinematic and dynamic variables was completed via referencing of residual values to literature. Nine front row rugby players (mass=102.3±14.0 kg, height=1.81±0.07 m) performed individual scrummaging trials against an instrumented scrum machine collecting external 'shoulder' forces at 500 Hz and with feet positioned on individual force plates (Kistler 9287BA, 2500 Hz). During scrum trials, a total of 52 reflective markers were positioned on the player and tracked by a motion analysis system (Qualisys Oqus, 250 Hz) and all data streams were time-synchronised.The model was scaled to the anthropometric characteristics of the participant, the Inverse Kinematics routine reconstructed the joint angles of the linked 13-segment kinematic model during the movement, the ground reaction forces and scrum machine forces were fed into OpenSim and the inverse dynamics routine was processed with kinetic and kinematic data filtered through a 3rd-order low-pass bidirectional Butterworth filter at 12 Hz.

Results: The engagement phase is the most dynamic phase of the scrum due to external load application. The OpenSim model permitted the recovery of the joint kinematics/kinetics at each individual cervical motion segment as well as between C7-T1 and C2-Head segments.The cervical spine was in an extended position from T1-C7 to C2-C3 joints prior to contact but then underwent a flexion motion during impact, whereas the C2-Head joint was initially slightly flexed but showed an extension motion throughout the engagement phase (Figure 1a). During the engagement phase, a pattern of separation between upper and lower cervical vertebrae was observed: upper vertebrae (C5 to C2) showed a high extension moment (e.g. 27.2±2.4 Nm for C4-C5 joint), whilst T1-C7 (-6.9±2.8 Nm) and C6-C7 joints showed a flexion moment (Figure 1b). These moments represent an internal load on the cervical spine that tends to straighten the neck and flatten the physiological spine curvature. Although no direct evidence of injury mechanisms can be drawn from such measures, these findings seem in line with the patterns of injury that previous authors have described in relation with scrum-related neck traumas [3]. The cervical vertebrae were all highly loaded, with magnitudes only 40% less than the

ones reported for whiplash (~40 Nm) or head compression injuries (~50 Nm). The values were considerably lower than those observed during head first impact (~100 Nm).

Figure:
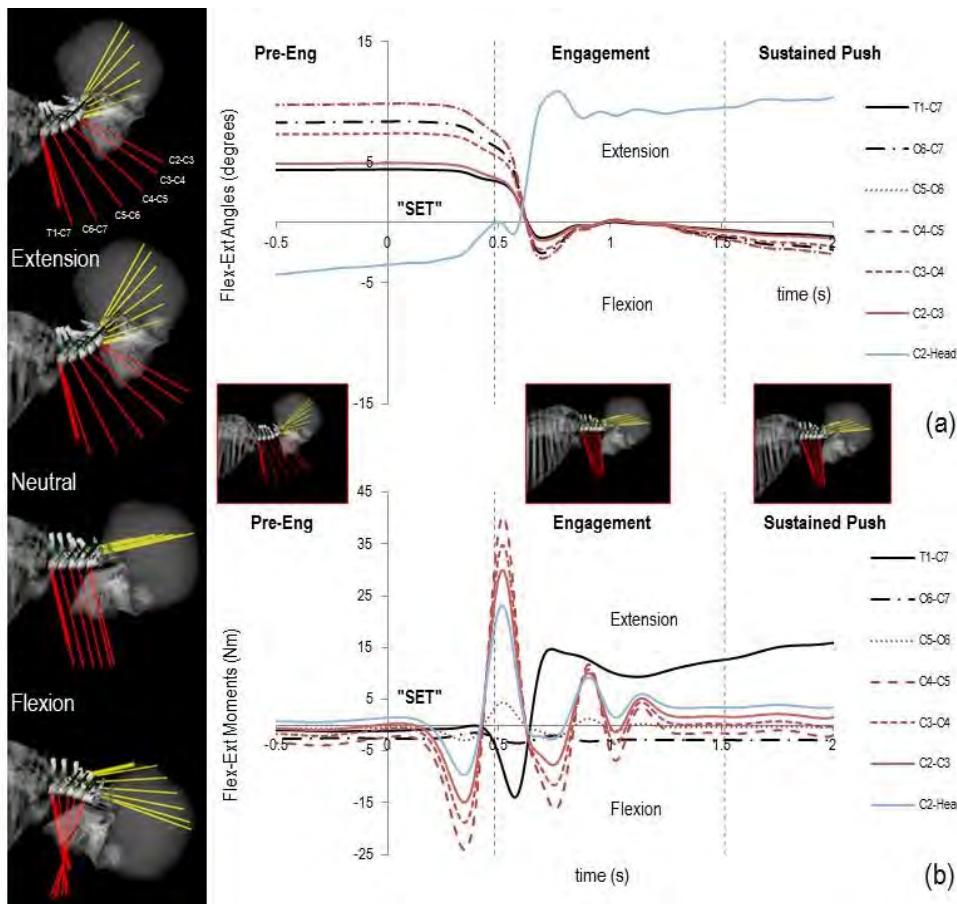
Caption: Figure 1. Cervical spine flexion/extension joint angles (a) and joint moments (b) during a single scrummaging trial.

Conclusion: This study describes the internal loading of cervical spine structures during one-player machine rugby scrummaging. This was the first 'in-vivo' study that aimed to associate the external load applied onto the player's shoulders with the internal mechanical conditions at the cervical and scapuloclavicular level. Peak magnitudes for cervical joint moments were in the region of those suggested to result in neck injuries in other contexts. During the scrummaging action there was a separation point in the loading pattern around C5 vertebra, the region known to be most at risk for catastrophic and degenerative injuries from rugby. Future work will improve the accuracy of the model representation and the ultimate goal is to perform sensitivity analyses to assess the influence of misdirected forces on cervical spine loading and to evaluate technique-based interventions for injury prevention in scrummaging.

References: [1] Cazzola et al., BJSM, 10.1136/bjsports-2013-092904, 2014.

[2] Vasavada et al. Spine, 23: 412-422, 1998

[3] Trewartha et al., BJSM, 10.1136/bjsports-2013-092972, 2014.

Disclosure of Interest: None Declared

EFFICACY OF ISOLATED ANKLE STRENGTHENING AND FUNCTIONAL BALANCE TRAINING FOR REDUCING RUNNING INJURY RISK FACTORS IN NOVICE RUNNERS: A RANDOMIZED CONTROLLED TRIAL

Jennifer Baltich [1,*] Carolyn Emery [1] Darren Stefanyshyn [1] Benno Nigg [1]

[1] Faculty of Kinesiology, University of Calgary, Calgary, Canada

Introduction and Objectives: Risk factors have been proposed for running injuries including (a) reduced muscular strength, (b) excessive joint movements and (c) excessive joint moments[1,2]. To date, many running injury prevention programs have focused on a "top down" approach to strengthen the hip musculature in the attempt to reduce movements and moments at the hip, knee, and/or ankle joints[3]. However, running mechanics did not change when hip muscle strength increased[4]. It could be speculated that emphasis should be placed on increasing the strength of the ankle joint for a "ground up" approach. Ankle strengthening techniques include isolated strengthening or movement-related strengthening such as functional balance training. There is little knowledge about the efficacy of ankle strengthening programs on gait and strength alteration or injury reduction. Therefore, the primary objectives of this study were to compare changes in ankle isokinetic strength and lower extremity running mechanics for novice runners participating in an isolated ankle strength program and a functional balance training program to an activity-matched control group. An exploratory analysis was completed to compare injury rates.

Methods: This is a randomized controlled trial. Novice runners (<2 years experience, 18-60 years) were randomized to one of three groups: an isolated ankle strengthening group (strength, n=29), a functional balance training group (balance, n=25) or an activity-matched control group (control, n=21)[4]. The isolated strengthening consisted of Thera-Band exercises at the ankle joint while the functional balance training incorporated lunges, squats, and hops using a BOSU ball. The control group completed static and dynamic stretching. All groups trained 25 minutes a day, 5 times a week for 8 weeks. Ankle strength was assessed as the peak isokinetic torque (Nm) measured using a Biodex System 3 dynamometer. Over ground running kinematics and kinetics were assessed using 3D motion analysis and a force platform. The difference in the dependent variables pre- and post-training were compared. Injuries were tracked for 6 months and defined as any physical complaint causing a restriction in running.

Results: Fifty-three participants (21 balance, 19 strength, 13 control) completed both the baseline and 8-week follow up assessment. The balance group had the fewest drop outs with 4 participants (16%) compared to the strength group with 10 drop outs (34%) and the control group with 8 drop outs (38%). Descriptive statistics are summarized in Table 1. Peak isokinetic ankle plantar flexion torque increased following training in the strength group. Both the strength group and the control group demonstrated increased ankle eversion and inversion torque. The balance group reduced the peak ankle eversion angle during over ground running. Both the balance group and the strength group reduced peak ankle inversion moments and knee adduction moments. The running injury incidence rate was 0.97 injuries/1000 hours of running exposure (95%CI: 0.48-1.74) for the balance group, 0.76 injuries/1000 hours of running exposure (95%CI: 0.28-1.66) for the strength group and 0.51 injuries/1000 hours of running exposure (95% CI: 0.14-1.3) for the control group.

Conclusion: Preliminary findings suggest that isolated ankle strength training leads to larger increases in strength at the ankle joint than functional balance training. While functional balance training was successful at reducing joint movement and moments at the ankle, both isolated ankle strengthening and functional balance training reduced joint moments at the knee. There was no significant difference in injury incidence rates between the groups. An additional 45 participants will be collected and analyzed by June 2015, bringing the final sample size to 120 runners. The results from this increased sample size will confirm whether isolated ankle strength training or functional balance training is more effective for increasing ankle strength and reducing joint movements and moments.

Table:

Outcome	Balance n=21	Strength n=19	Control n=13
Peak Plantar Flexion Torque [Nm]	2.8 [-3.7, 9.3]	17.6 [7.2, 28.4]*	8.3 [-0.78, 17.4]
Peak Eversion Torque [Nm]	0.2 [-1.2, 1.6]	2.7 [0.5, 4.9]*	2.3 [0.3, 4.3]*
Peak Inversion Torque [Nm]	0.7 [-0.17, 3.2]	6.1 [3.1, 9.2]*	5.0 [1.4, 8.6]*
Peak Ankle Eversion Angle [°]	-1.4 [-0.5, -2.3]*	0.4 [-0.7, 1.5]	0.2 [-1.0, 1.5]
Peak Ankle Inversion Moment [BWm]	-0.009 [-0.002, -0.016]*	-0.008 [-0.001, -0.016]*	-0.005 [-0.015, 0.004]
Peak Knee Adduction Moment [BWm]	-0.012 [-0.004, -0.021]*	-0.008 [-0.002, -0.014]*	-0.002 [-0.012, 0.007]

Caption: Summary of the descriptive statistics (mean change, 95% CI) for the balance, strength and control group. Significant changes are marked with an *.

References: [1] Mahieu NN, et al., *Am. J. Sports. Med.* 34: 226-235, 2006.

[2] Stefanyshyn D, et al., *Am. J. Sports. Med.* 34: 1844-1852, 2006.

[3] Willy RW, et al., *J. Orthop. Sports Phys. Ther.* 41: 625-632, 2011.

[4] Baltich J, et al., *BMC. Musculo. Skel. Dis*. In press, 2014.

Disclosure of Interest: None Declared

Injury

AS-0311

THE KINETIC IMPULSE ASYMMETRY INDEX IN THE VERTICAL JUMP PREDICTS LOWER BODY INJURY IN ELITE ATHLETES

M J Jordan [1,*] J Barnert [2] P Aagaard [3] W Herzog [1]

[1]University of Calgary, [2]Canadian Sports Institute - Calgary, Calgary, Canada, [3]University of Southern Denmark, Odense, Denmark

Introduction and Objectives: Lower body injury, including anterior cruciate ligament (ACL) rupture, occurs frequently in sport [1]. To prevent injuries, functional assessments may be useful to identify at-risk athletes [2]. The kinetic impulse asymmetry index (KIAI) obtained during countermovement (CMJ) and squat (SJ) jumping was proposed to differentiate between non-injured and ACL-reconstructed athletes [3]. However, to date, no prospective study has evaluated this approach for identifying athletes at-risk for lower body injury. Our purpose was to evaluate the use of the KIAI to predict lower body injury in competitive athletes.

Methods: Seventy-one athletes (Females: n=51, Age=20.6±2.3 years, Mass=67.8±11.5 kg; Males: n=20, Age=20.1±1.7 years, Mass=78.7±16.5 kg) from five sports (alpine skiing, luge, soccer, rugby, wrestling) were assessed at the start of the off-season preparatory period. Dual force plate analysis of the vertical ground reaction force from each limb was used to evaluate lower limb asymmetry during five bilateral CMJs and five SJs by analysis of vertical kinetic impulse in terms of phase-specific KIAI [3]. Subjects were retested weekly throughout the observation period. The closest data point prior to injury was used for the injured athletes (INJ) while baseline test values were used in the analysis of non-injured athletes (N-INJ). Injuries were classified as: muscle, bone, joint. One-way ANOVA was used to compare KIAIs between INJ and N-INJ and the absolute value of the KIAI was used in a logistic regression model for injury (α=0.05).

Results: In the follow-up period, 12 athletes suffered lower body injury (Females: n=8; Males: n=4; Muscle: n=4; Joint: n=8). Injured athletes displayed increased asymmetry in the eccentric deceleration phase of the CMJ (N-INJ = -1.1%±8.9; INJ = -11.1%±12.5, P<0.01). KIAI tended (P=0.06) to differ in the concentric phase of the CMJ (N-INJ = -1.3%±4.6; INJ = -6.2%±8.2) while no group difference was found in the late phase of the SJ (N-INJ = -3.3%±8.1; INJ = -6.3%±13.7, P=0.48). Logistic regression analysis revealed the CMJ concentric phase (Odds Ratio = 1.4, 95% CI = 1.1-1.7), and eccentric deceleration phase (Odds Ratio = 1.2, 95% CI = 1.1-1.4) to be predictors of injury (P<0.01). Retrospective injury prediction was highest using the eccentric deceleration phase of the CMJ (87.3%) followed by the concentric phase of the CMJ (84.5%), and the late phase of the SJ (84.5%).

Figure:
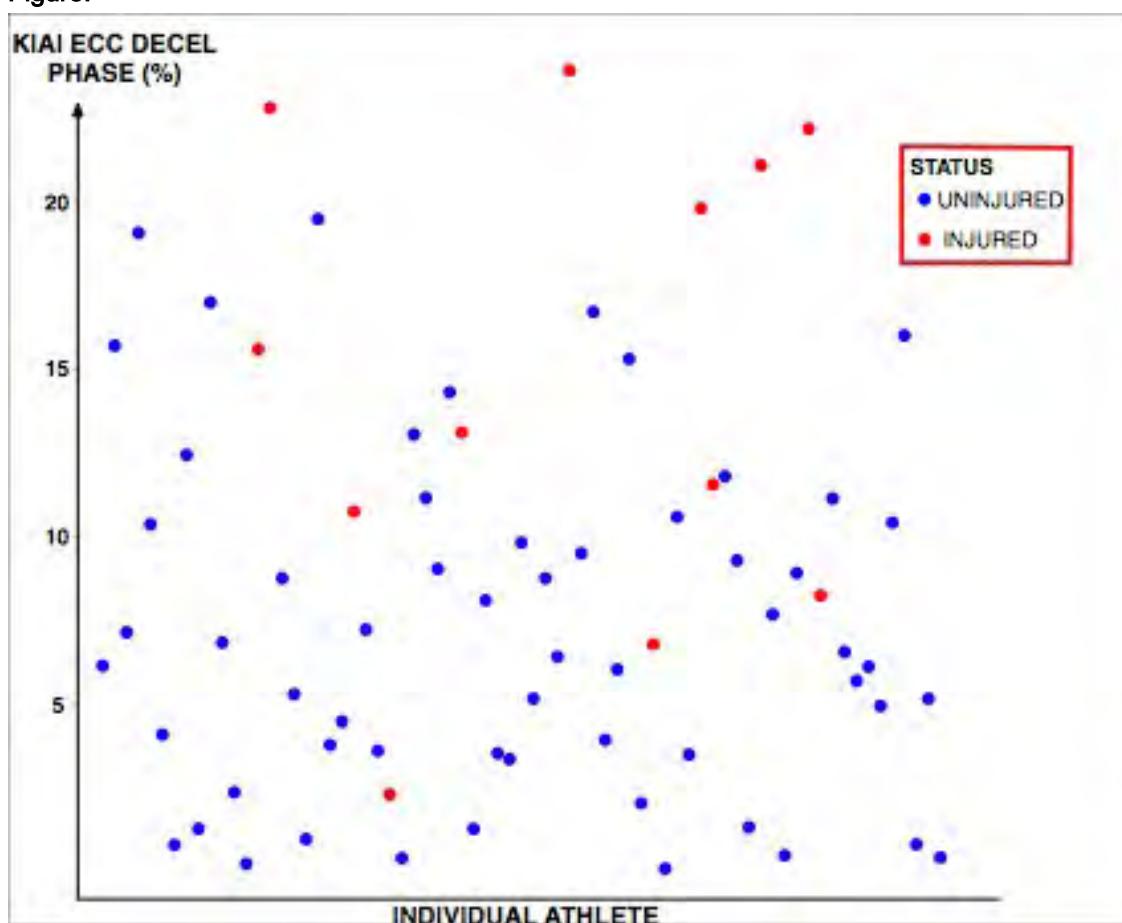
Conclusion: The present results suggest that the KIAI is an effective tool for identifying athletes at-risk for lower body joint and muscle injury. KIAI obtained for the eccentric deceleration phase of the CMJ was the strongest predictor of injury. Since the ability to decelerate the body centre of mass during many athletic movements, such as landing from jumps, is important for ACL injury prevention [2], the approach used in this study may be relevant for athletes in a variety of sports (e.g. alpine ski racing, field sports). Additionally, the KIAI can be obtained using a straightforward biomechanical approach. Combined with its high predictability for injury, the KIAI seems ideal for use in high performance sport environments. Future research will be aimed at increasing the sample size and evaluate the relationship between the KIAI and specific injury types, such as ACL rupture.

References: [1] Beynnon et al., Am J Sports Med, 1-8, 2014. [2] Hewett et al., Am J Sports Med, 33: 492-501, 2005. [3] Jordan et al., Scand J Med Sci Sports, 1-9, 2014.

Disclosure of Interest: None Declared

UTILITY OF A SHORT DURATION HIGH-INTENSITY EXERCISE PROTOCOL TO PROSPECTIVELY ASSESS BIOMECHANICAL AND MUSCULAR MARKERS OF ACL INJURY IN DYNAMIC SPORTS

Fransiska Bossuyt [1,*]Felipe Garcia-Pinillos [2]Raja Azidin RMF [1]Jos Vanrenterghem [1]Mark A Robinson [1]

[1]School of Sport and Exercise Sciences, Liverpool John Moores University, Liverpool, United Kingdom, [2]Corporal expression, University of Jaen, Jaen, Spain

Introduction and Objectives: Fatigue is suggested to play a crucial role in the mechanism of anterior cruciate ligament (ACL) injury [1]. This highlights the need for the inclusion of exercise-induced fatigue in prospective studies. Prospective studies give the highest level of evidence, but due to requiring large cohorts it is difficult to include a time consuming fatigue protocol as part of prospective screening. Therefore, the aim of this study was to investigate the effect a 5-min high intensity exercise protocol (SAFT[5]) has on biomechanical and muscular markers of ACL injury risk.

Methods: Fifteen recreationally active females completed SAFT[5] which was modified from a long duration match-play simulation (SAFT[90])[2]. Participants' non-dominant leg was analysed before SAFT[5] (PRE), immediately after (POST0), 15 min after (POST15) and 30 min after (POST30). Kinematics and kinetics were measured at these time points during the landing phase of a single leg hop (SLH) (70% body height) and a 30 cm drop vertical jump (DVJ). Maximum contractions of concentric quadriceps (Q_{con}) and concentric and eccentric hamstrings (H_{con} and H_{ecc}) were measured with an isokinetic dynamometer. A one-way repeated measures ANOVA was used to assess the dependent variables ($\alpha=0.05$).

Results: In response to SAFT[5] eccentric hamstring peak torque was significantly reduced at POST0 (7%), POST15 (13%) and POST30 (18%) compared to PRE. Functional H/Q ratio (H_{ecc}/Q_{con}) was significantly reduced at POST15 (9%) and POST30 (13%) ($p<.05$) (Figure 1). Additionally, at initial contact of a SLH, participants landed with a significantly more extended knee (2.2 ± 2.6°) at POST30 ($p<.05$) and a significantly increased knee internal rotation angle (4.1 ± 4.5°) at POST0 and POST15 (4.5 ± 3.8°, $p<.05$). There were no significant effects on conventional H/Q ratio (H_{con}/Q_{con}) and landing patterns during DVJ ($p > .05$). SAFT[5] induced detrimental effects on biomechanical and muscular markers of ACL injury risk in recreationally active females. The selective occurrence of fatigue in H_{ecc} is in agreement with previous findings of SAFT[90] in males and has been related to increased injury risk [2]. Despite the significant reduction in H_{ecc} between pre and every post-test, the functional H/Q ratio was only significantly reduced POST15 and POST30. This could be explained by the delay in peripheral fatigue (i.e. fatigue within the muscle itself) as a recent study concluded that central fatigue (i.e. alteration in the nervous system) manifests prior to reductions in knee flexor maximal torque in response to SAFT[90] [3]. The altered landing strategies in a SLH in response to SAFT[5] are thought to be associated with increased ACL injury risk [1]. Knee flexion angle was, however, only significantly reduced after 30 min passive rest. Nevertheless, this evidence supports the use of a functional exercise protocol such as SAFT[5] to identify at risk individuals in prospective screening.

Figure:
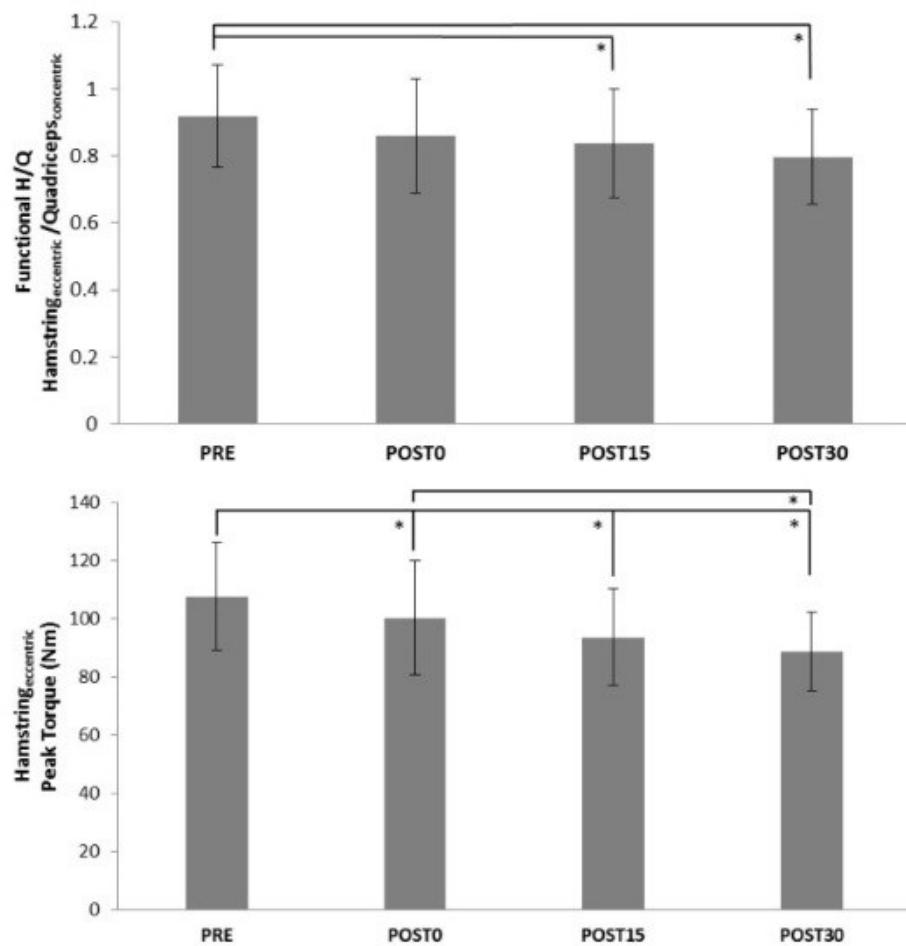
Conclusion: In conclusion, SAFT[5] altered biomechanical and muscular landing strategies that have been associated with increased ACL injury risk and are similar to observations from match simulations. Our findings therefore support the utility of such exercise protocol in the context of prospective cohort studies where time constraints apply.

References: [1] Hashemi J, Breighner R, Chandrashekar N, *et al. J Biomech*, **44**: 577-85, 2011.

[2] Small K, McNaughton L, Greig M, *et al. J Sci Med Sport,* **13**: *120-5, 2010.*

[3] Marshall PWM, Lovell R, Jeppesen GK, *et al. PLoS One,* **9**, *e102753, 2014.*

Disclosure of Interest: None Declared

AS-0313

CHRONIC ANKLE INSTABILITY ALTERS THE RELATIONSHIP BETWEEN EMG AMPLITUDE AND EVERSION PEAK FORCE OF THE FIBULARIS MUSCLES

Jay Hertel [1,*]Luke Donovan [1]Lindsy Donnelly [1]

[1]Department of Kinesiology, University of Virginia, Charlottesville, United States

Introduction and Objectives: Chronic ankle instability (CAI) occurs in approximately 40 percent of patients incurring first time ankle sprains and is characterized by persistent symptoms lasting more than 12 months after sprain, repetitive episodes of the ankle giving way, and recurrent ankle sprains.[1] Altered sensorimotor function of the fibularis muscles demonstrated in CAI patients include diminished eversion strength[2], delayed EMG activation in response to inversion perturbation[3], and arthrogenic muscle inhibition[4]. To date, the relationships between the EMG activity of the fibularis muscles and eversion force production have not been examined. Our purpose was to investigate the correlation between eversion peak force and surface EMG amplitude of the fibularis longus and brevis muscles during isometric contractions taken in neutral and plantar flexed (PF) positions in young adults with and without CAI.

Methods: Twenty-eight young adults with CAI (19 females, 9 males, age=21±3.1 years) and 28 healthy young adults without history of ankle sprain (19 females, 9 males, age=22±4.1 years) participated. Peak force was assessed with a handheld dynamometer during 5-second maximum voluntary isometric eversion contractions in two testing positions (neutral, 30° PF) while sEMG amplitudes of the fibularis longus and brevis were simultaneously recorded. Peak force was normalized to body mass. EMG signals were filtered and smoothed using a 50-sample moving window root mean square. EMG amplitude was defined as the area under the middle 3 seconds of the RMS curve. The amplitude values for each corresponding muscle were then normalized to a time-matched epoch collected during a quiet resting period. For each dependent variable, means and 95% confidence intervals were calculated for each group in each condition. Pearson correlation coefficients were calculated between the respective peak force and EMG amplitude measures within each group.

Results: The CAI group produced less eversion peak force than the control group in both the neutral and PF positions, however there were no group differences identified in any of the EMG amplitude measures (see Table). For the CAI group, there were no significant correlations between peak force and EMG amplitude for the fibularis longus (neutral: r = 0.23, P = 0.24; PF: r = 0.15, P = 0.44) or fibularis brevis (neutral: r = -0.02, P = 0.94; PF: r = -0.04, P = 0.82). In contrast, the control group had significant correlations between peak force and EMG amplitude for both the fibularis longus (neutral: r = 0.42, P = 0.03; PF: r = 0.56, P = 0.002) and fibularis brevis (neutral: r = 0.38, P = 0.05; PF: r = 0.40, P = 0.04).

Figure:

Caption of the figure shows: Fibularis Longus EMG Amplitude (y-axis, 0.00 to 100.00) vs Eversion Peak Force in Plantar Flexion (N/kg) (x-axis, .5 to 3.0). r = .56 (CAI Group, red circles); r = .15 (Control Group, blue squares).
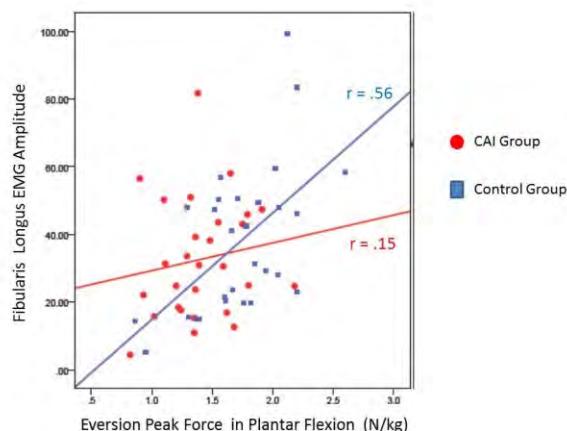
Caption: Scatter plot illustrating correlation between eversion peak force and fibularis longus EMG amplitude in the CAI and control groups.

Conclusion: The CAI group generated less isometric eversion peak force in both the neutral and PF positions relative to the control group, however there were no group differences in the EMG amplitudes of the fibularis longus or brevis muscles. The lack of EMG amplitude differences between groups could indicate that the CAI patients were able to generate adequate activity of the muscles in the leg but that activation was not translated into force acting on the ankle. An explanation for this could be lesions to the fibularis tendons or retinaculum. Unfortunately, we did not evaluate our participants for such lesions. The relationship between EMG amplitude and force production has been studied for decades[5], however this relationship has not been previously examined in CAI patients. We identified significant correlations of moderate magnitude between isometric eversion peak force and fibularis longus and brevis EMG amplitude in the healthy, but not the CAI, group. This discrepancy provides added evidence of the sensorimotor alterations associated with CAI. Further research is necessary to identify the physiological mechanisms driving the decoupling of fibularis muscle activation and eversion force output of CAI patients as well as interventions to help restore this relationship.

Table:

	Peak Eversion Force in Neutral (N/kg)	Fibularis Longus EMG Amplitude in Neutral	Fibularis Brevis EMG Amplitude in Neutral	Peak Eversion Force in Plantar Flexion (N/kg)	Fibularis Longus EMG Amplitude in Plantar Flexion	Fibularis Brevis EMG Amplitude in Plantar Flexion
CAI Group	1.64* [1.46–1.81]	27.1 [21.5-32.6]	38.3 [27.9-48.8]	1.40* [1.27–1.54]	32.7 [25.9-39.4]	38.4 [28.6-48.3]
Control Group	2.10 [1.93–2.28]	27.9 [22.5-33.3]	32.9 [27.0-38.8]	1.73 [1.60–1.87]	38.0 [29.5-46.5]	41.1 [33.0-42.3]

Caption: Means and 95% confidence intervals of eversion peak force measures in the CAI and Control groups. Significant differences are bolded.

References: [1] Hertel J. *J Athl Train*. 37: 364-375, 2002.

[2] Arnold BL et al. *J Athl Train*. 44: 653-662, 2009.

[3] Hopkins JT et al. *J Orthop Res.* 27: 1541-1546, 2009.

[4] Kim KM et al. *J Electromyogr Kinesiol.* 22: 997-1002, 2012.

[5] Stulen FB, De Luca CJ. *Electroencephalogr Clin Neurophysiol*. 45: 681-698, 1978.

Disclosure of Interest: None Declared

CHARACTERIZATION OF FUNCTIONAL CHANGES IN THE APONEUROSES OF THE RABBIT MEDIAL GASTROCNEMIUS DURING CONTRACTION IN-SITU

Christine Waters-Banker [1,*]Andrew Sawatsky [1]Azim Jinha [1]Timothy Leonard [1]Walter Herzog [1]

[1]Kinesiology, University of Calgary, Calgary, Canada

Introduction and Objectives: Previous attempts have been made to predict the stiffness of the aponeurosis in skeletal muscle by modeling the structure in-series with the tendon and fascicles. Predictions of mechanical properties of muscle elements (fascicles and aponeuroses) have been derived from force and length measurements *in vivo* using various techniques such as tendon buckle transducers, and ultrasound imaging. When aponeuroses and fascicles have been considered 'in-series', experimental and theoretical research showed a net gain of work produced by aponeuroses during full activation/deactivation cycles: a thermodynamically impossible result [1]. Therefore, the objective of this study was to record functional length changes of the aponeuroses in relation to tendon, fascicle, and whole muscle/tendon length changes during isometric and dynamic contractions *in situ*.

Methods: The right medial gastrocnemius muscles (MG) of six New Zealand White Rabbits were isolated and instrumented with 8 piezoelectric ultrasound sonomicrometry crystals while the animal was anesthetized (Figure 1a). Fascicles were isolated using a point-contact micro-stimulator and the two ends of the fascicle were marked with methylene blue dye for crystal placement. A cuff electrode was placed on the tibial nerve for electrical stimulation. A stereotaxic frame stabilized the limb at the hip, knee, and shank. The calcaneus was detached and fixed to a horizontally mounted muscle puller (MTS Inc.). The muscle was passively pulled to various predetermined lengths along the force-length relationship and then contracted either isometrically, concentrically, or eccentrically. Supramaximal stimulation was performed at 70Hz for all experiments. During contraction, total length changes for the tendon, both distal and proximal aponeuroses, fascicle, and whole muscle/tendon unit were recorded. Individual length changes of each structure were summed and compared to the absolute muscle/tendon length change during each contraction.

Results: During isometric contractions taking place at optimal length (L_0): the distal aponeurosis lengthened substantially (1.77mm ± 0.32mm (SD)) while the proximal aponeurosis lengthened slightly (0.15mm ± 0.35mm). Fascicles always shortened substantially (-3.58mm ± 1.55mm). For concentric contractions starting at L_0 and shortening onto the ascending limb: at the onset of stimulation the distal and proximal aponeuroses briefly lengthened and shortened respectively (distal: 1.4mm ± 0.06mm; proximal: -0.19 mm ± 0.23), and then shortened during the shortening phase (distal: -0.23mm ± 0.39mm; proximal: -0.37mm ± 0.36mm), while fascicles shortened throughout (-3.82mm ± 0.98mm). Eccentric contractions, traveling on the ascending limb to L_0, resulted in lengthening of the aponeuroses at the onset of stimulation (distal: 1.19mm ± 0.42mm; proximal: 0.20mm ± 0.17mm) and throughout the stretch (distal: 0.38mm ± 0.14mm; proximal: 0.21mm ± 0.16mm), while the fascicles shortened at onset (-2.06mm ± 0.76mm) and lengthened throughout the stretch (1.31mm ± 0.10mm). A counter-clockwise positive work loop (45.6 mJoules) was generated when changes in distal aponeurosis length were plotted against force production for a complete eccentric contraction from 0N force to 0N force (loading area: 47.76 Nmm, unloading area 2.12 Nmm) (Figure 1b).

Figure:

A.

B.
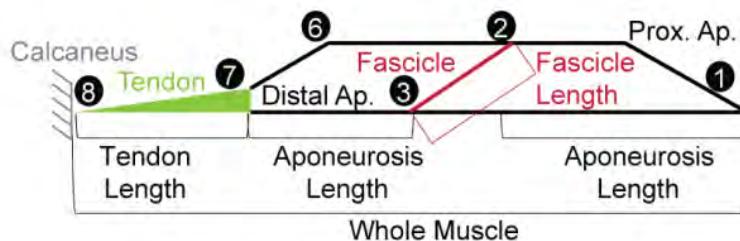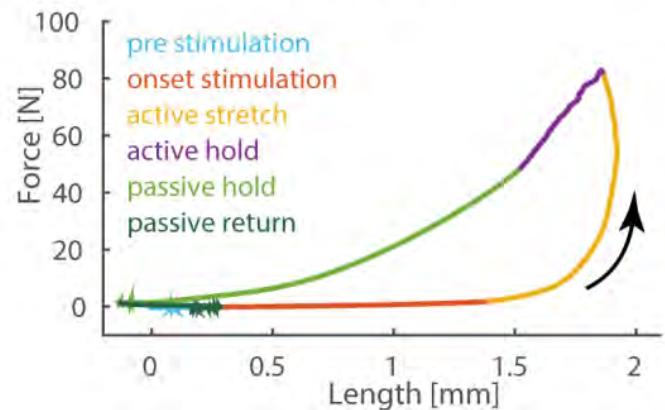
Caption: Figure 1: (A) Schematic representation of the MG muscle (side) with sonomicrometry crystal placement. (4 and 5 not pictured). (B) Counter-clockwise work loop of distal aponeurosis length vs. force production showing a creation of 45.6 mJoules energy.

Conclusion: At a first glance, changes in aponeuroses length are consistent with an in-series arrangement of aponeuroses with tendon and fascicles. However, when changes in aponeurosis length were plotted against MG forces (measured at the end of the distal tendon) during an eccentric contraction, a counter-clockwise work loop was generated indicating a net gain in mechanical work. At the onset of activation a large elongation of the aponeurosis takes place with little force, and upon stretch aponeurosis length stays virtually constant despite a great increase in force. Viscoelastic structures, such as aponeuroses, display negative hystereses with a net loss of mechanical energy. The creation of energy that results from assuming force measured at the tendon is in-series with the aponeurosis violates the Second Law of Thermodynamics, rendering the result impossible. Therefore, the force measured at the tendon is not the same force experienced across the aponeurosis, and as such it would be incorrect to model the aponeurosis as an in-series component with the tendon. Any such assumption could lead to vastly incorrect interpretations of the role of aponeuroses in the storage and release of energy in stretch-shortening cycles.

References: [1] Epstein M et al,. J. of Biomechanics, 39:2020-2025, 2006.

Disclosure of Interest: None Declared

Musculoskeletal

AS-0315

REGIONAL VARIATION IN FASCICLE STRAIN IS JOINT DEPENDENT IN A BI-ARTICULAR MUSCLE

Emma Hodson-Tole [1,*] James Wakeling [2] Taylor Dick [2]

[1]Cognitive Motor Function Research Group, Manchester Metropolitan University, Manchester, United Kingdom,
[2]Neuromuscular Mechanics Lab, Simon Fraser University, Burnaby, Canada

Introduction and Objectives: It is well documented that fascicle length changes can be uncoupled from those of the whole muscle tendon unit (MTU), within a gearing process which enables muscle fibres to operate at strain rates which are favourable for force production or mechanical power output. The strain and strain rates fibres operate at have however been reported to show regional variation within a muscle, with such variation suggested to be the result of regional differences in fascicle geometric properties, arrangement of internal connective tissue and/or neural activation patterns. In a bi-articular muscle, whether the relationship between MTU and fascicle length change can be differentially influenced by the joint moved has not been fully investigated. In addition, the potential for variation in any such relationship in different parts of the same muscle has also received limited attention. The human medial gastrocnemius muscle (MG) is a bi-articular muscle, which can contribute to ankle joint plantar flexion and knee joint flexion. Fascicles in MG are pennate, with a tendency for those in the proximal region to be shorter and more pennate than those in the distal muscle region. We therefore investigated the relationship between MTU and muscle fascicle length changes in proximal and distal regions of MG during passive rotation of the ankle or knee joint.

Methods: B-mode ultrasound images were simultaneously collected from proximal and distal regions of the right MG of eight participants (Mean±SD Height: 1.78±0.08m, Weight: 73.07±10.61kg), whilst they laid prone on an isokinetic dynamometer. Each probe was aligned to provide a clear view of complete fascicles and secured in place, for the duration of the experiment, using elasticated bandage. The dynamometer was set-up to enable passive rotation of either the ankle joint (-15° dorsiflexion to +30° plantar flexion) or the knee joint (180° extension to 90° flexion). During knee joint rotation the ankle joint was fixed at 90° using a customised brace. The ranges of motion used ensured the MTU underwent similar changes in length in each condition (knee: 0.45-0.426m; ankle: 0.45-0.42m, calculated using OpenSim v3.2).
Muscle fascicle lengths were determined from analysis of collected images, with images from the proximal portion analysed using an automated computational approach and those from the distal region assessed manually. MTU lengths for each participant were calculated, using angle data recorded from the dynamometer in each trial and participant specific knee and ankle moment arms determined from recorded MR images.

Results: The results revealed a striking and significant effect of both joint and muscle region, with differences also occurring between the MTU lengthening and shortening phase of the rotation cycle. The highest fascicle strains in both proximal and distal muscle regions occurred during ankle joint rotation, despite similar MTU lengths occurring between conditions. MTU shortening, caused by ankle joint rotation, led to the largest fascicle strains recorded in the distal muscle region while little difference occurred between proximal and distal muscle regions during the MTU lengthening phase. During knee joint rotation fascicle strains were largest in the proximal muscle region during both MTU shortening and lengthening phases of the joint rotation.

Conclusion: Knee and ankle joint rotations lead to different responses in muscle fascicles of human MG, with different responses also occurring in proximal and distal muscle fascicles. Such differences may reflect different properties in elastic structures in proximal/distal regions of MG (e.g. length of free tendon) and the association of a given joint with other muscles (e.g. soleus will have been influenced by ankle joint rotation but not knee joint rotation). These regional and joint specific differences could have implications for sensory feedback during postural control and indicate that fascicle length changes in bi-articular muscles may be influenced by the kinematics of either the joints spanned.

Disclosure of Interest: None Declared

Musculoskeletal

AS-0316

THE BIOMECHANICAL DEMANDS OF PROLONGED SITTING: AN EVALUATIVE ERGONOMIC COMPARISON OF TRUCK SEATS

Michelle Rae [1,*]Colin McKinnon [2]Dan Viggiani [3]Jack Callaghan [3]Wayne Albert [1]

[1]Kinesiology, University of New Brunswick, Fredericton, [2]University of Waterloo, Waterloo, Canada, [3]Kinesiology, University of Waterloo, Waterloo, Canada

Introduction and Objectives: The trucking industry has one of the highest claims rates for work-related injury and illness in terms of prevalence and cost. The objective of the research project was to evaluate discomfort, sitting posture and muscle activity during a prolonged driving task between a new truck seat prototype (Force-3) and an industry standard seat.

Methods: Twenty participants were recruited from a student population (10M,10F) to perform two 2-hour simulated driving sessions. Two truck seats were evaluated: Force-3's seat prototype and current market popular product "Low Ride Pro Back-Knoedler". An 8-channel surface electromyography system was used to monitor neuromuscular activity of the following bilateral muscles: Cervitis Capitis (C4), Erector Spinae (T9,L3) and the External Obliques. EMG was normalized through maximum voluntary contractions (MVCs), which included; an abdominal crunch/twist, back and neck extensions. The data was analyzed by determining the amplitude percentage change from the MVC trials. Lumbar spine flexion and lateral bend angles were measured by placing three tri-axial accelerometers on the skin over T1, L1 and S1. Angles computed from the accelerometers were expressed as a percentage of each participant's maximal range of motion. To monitor the participants perceived discomfort, ratings of perceived discomfort (RPD) and the automotive seating discomfort questionnaire (ASDQ) were given systematically (using a 100mm scale, e-VAS), every 15 minutes, throughout the simulated driving task. Following the second session, an exit survey was given to quantify which chair was preferred. **Between**. Two way repeated measure with a pairwise comparison **Within.** A one-way repeated measure with a pairwise comparison.

Results: RPD Questionnaire. *Between Chairs Comparisons (BCC)*: Participants significantly experienced more neck (Time (T)=75,90,105minutes(m)), right gluteus (T=45,105m) and right upper leg (T=45m) discomfort in the Knoedler chair compared to the prototype. *Within Comparison (WC),Knoedler:* Neck, right upper back, right/left gluteus and right/left low back significantly increased pre/post driving task (T=120m) as well as the right upper thigh(T=105m). *WC, Prototype:* Participants experienced discomfort in the low back post-driving task (T=120m). **ASDQ Questionnaire.** *BCC*: Discomfort related to seat cushion firmness was experienced in both seats, however discomfort scores were significantly greater in the Knoedler seat in comparison to the prototype (T=60m). *WC, Knoedler:* Five components of the chair were perceived as uncomfortable: Discomfort scores significantly increased in seat cushion firmness, lumbar stiffness and overall discomfort scores pre and post driving task. Discomfort scores were also found in firmness of the backrest (T=90m) and overall lumbar support (T=60,75,90m). *WC, Prototype:* Two components of the chair were perceived as uncomfortable: discomfort scores related to seat cushion firmness and lumbar stiffness significantly increase pre/post-driving task. **Exit Survey**. 90% of the participants preferred the prototype. **Accelerometers.** *BCC*: No significant differences were found between seats in flexion/extension, lateral bend lumbar angles (between L1 and S1) or thorax lateral bend (T1 and L1).

However significant increases were found in trunk (T1/L1) flexion angles when using the Knoedler seat from T=0 until T=75m. *WC, Knoedler:* Lumbar lateral bend angles (T=20, 30m) significantly increased overtime. *WC, Prototype:* A significant increase in thorax flexion/extension angles was found until T=45m. Participants also experienced more lateral bend between T=5-35m and then reverted back to baseline values throughout the rest of the driving protocol. **EMG.** *BCC:* No statistical difference was found in the comparison of neuromuscular activity between truck seats. *WC, Knoedler:* Right and left Cervitis Capitis values significantly increased overtime as well as the left Erector Spinae activity (T9) from T=5-115m and right External Obliques (T-5, 45m). *WC, Prototype:* A bilateral increase was found in the Cervitis Capitis, External Obliques and Erector Spinae(L3) activity.

Conclusion: Discomfort scores attributed to body parts and the chair was greater when using the Knoedler seat. According to the exit survey, participants preferred the Force-3 prototype. During the first 75minutes of driving, trunk kyphosis was greater when using the Knoedler seat. EMG scores did not significantly change in between chairs however neuromuscular activity did increase overtime in both seats. Biomechanical changes may be portrayed in the postural kinematic evaluation and passive lumbar flexion that has yet to be evaluated. The unsystematic patterns found in the results could be a product of compiling both genders. The Knoedler chair is designed for the 50th percentile male, which could affect female sitting patterns. Gender comparison will be analyzed and also be a pivotal focus for our future research.

Disclosure of Interest: None Declared

Musculoskeletal

AS-0317

HOW COMPLEX SHOULD LOWER-LIMB JOINT MODELS BE FOR SUBJECT-SPECIFIC SIMULATIONS OF MOVEMENT?

Lorenzo Pitto [1]Giordano Valente [1,*]Rita Stagni [2]Fulvia Taddei [1]

[1]Medical Technology Laboratory, Rizzoli Orthopaedic Institute, [2]DEI, University of Bologna, Bologna, Italy

Introduction and Objectives: Subject-specific musculoskeletal modelling can be applied to study musculoskeletal disorders, providing a valuable approach to muscle and joint loading analysis during movement. The choice of the lower-limb joint models can significantly affect force predictions [1]. However, it is not clear how different joint models affect musculoskeletal forces calculated during different motor tasks using models based on clinical imaging. Particularly, the behavior of the knee and ankle joint can be markedly variable when simulating different motor tasks, which introduce different joint ranges of motion. In addition, the identification of image-based joints is unavoidably affected by uncertainty due to the imaging quality available and operator variability. This can lead to error propagation, potentially decreasing the benefits of increased model complexity. The aim of this study is twofold: first, to evaluate the effect of different knee and ankle joint models on muscle and joint contact forces predicted during four common motor tasks, by using musculoskeletal models created from lower-body MRI; second, to analyze the sensitivity of muscle and joint contact forces to the uncertainty in the identification of subject-specific kinematics constraints.

Methods: Experimental data were collected on a healthy subject, including lower-body MRI and gait data (marker trajectories, ground reaction forces and EMG recordings) during walking, chair rise, stair ascent and descent. A baseline musculoskeletal model (M1) was created previously [2], which included a 7-segment articulated linkage with spherical joints at the hips, hinge joints at both knees and ankles, and 84 musculotendon actuators. More complex knee and ankle models were built upon the baseline model as follows: planar hinge and universal joint [3] (M2), modified spherical and universal joint [4] (M3), and anatomical 4-bar-linkage knee and ankle [5,6] (M4). To test the sensitivity to parameter identification, five operators virtually palpated the anatomical landmarks necessary to create M4 joints. The joint parameters were statistically sampled according to inter-operator palpation variability, and a set of perturbed models was then created. Simulations of movement solving a typical inverse dynamics and static optimization problem were performed using OpenSim [7]. To assess variability in model outcomes, joint contact forces from the three modified models were compared against the baseline model (absolute differences, Pearson correlation coefficients). To qualitatively assess validity of the models, predicted muscle activations predicted were compared against measured EMG. To analyze the sensitivity to the uncertainties in identifying 4-bar linkage mechanisms, standard deviations of joint contact forces predicted through the perturbed M4 models were calculated for each simulated motor task.

Results: Overall, differences in joint contact forces between the modified models and the baseline were dependent on the motor task analyzed, although they were not substantial (Figure). M2 and M4 showed mild differences and a tendency to underestimate knee loads. M3 showed the most marked differences and a tendency to overestimate loads. Predicted muscle activations were generally consistent with EMG recordings. M3 presented discrepancies in the activations of gastrocnemius and biceps femoris in stair descent and walking.

In walking, chair rise and stair ascent, the uncertainties in the identification of M4 did not have a substantial effect on joint contact forces, showing mean standard deviations over the motor task cycles below 0.26 BW. Conversely, in stair descent, there was a marked effect on knee and ankle forces, showing a mean standard deviation of 0.4 BW and a maximum of 2.66 BW at the ankle.

Figure:
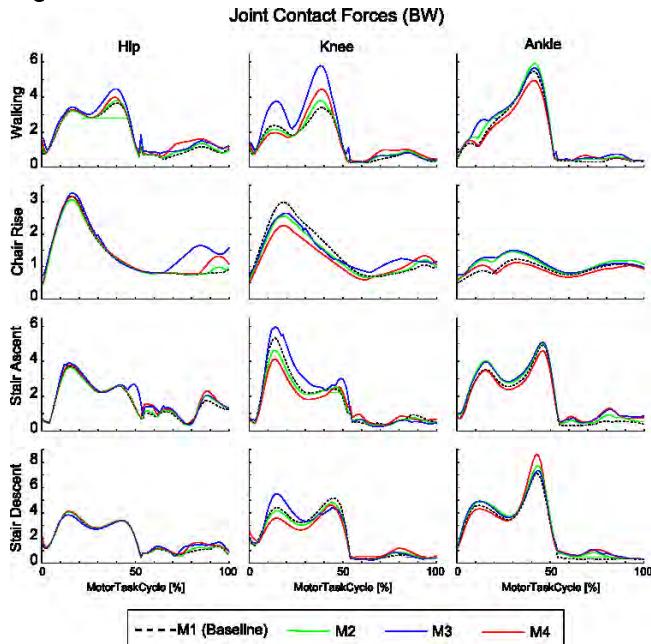
Caption: Joint contact forces (in body-weight) during the four motor tasks predicted by using the baseline model (M1) and the three modified models (M2, M3, M4) including different knee and ankle joint models

Conclusion: The models predicted different joint loads, and behaved differently in different motor tasks. In the absence of direct validation methods of the predicted forces, the implementation of complex subject-specific joints should be justified only when the predictions are robust to the uncertainties in parameter identification. Therefore, before implementing image-based kinematic constraints, it is advisable to analyze the sensitivity of predictions over the joint range of motion and, if this choice appears weak (as in the stair descent task), opting for less complex, but more robust and reproducible joint models.

References: [1] Dumas et al., Proc Inst Mech Eng Part H J Eng Med, 226: 146–60, 2012.

[2] Valente et al., PLoS ONE, 9: e112625, 2014.

[3] Delp et al., IEEE Trans Biomed Eng 37: 757–67, 1990.

[4] Donnelly et al., J Biomech 45: 1491–7, 2012.

[5] Leardini et al., J Biomech 32: 585–91, 1999.

[6] O'Connor et al., Proc Inst Mech Eng Part H J Eng Med, 203: 223–233, 1989.

[7] Delp et al., IEEE Trans Biomed Eng 54: 1940-50, 2007.

Disclosure of Interest: None Declared

Musculoskeletal

AS-0318

FASTER VS SLOWER RUNNING REDUCES TOTAL LOADS SUMMED ACROSS ALL STEPS USED TO RUN A STANDARD DISTANCE

Paul Devita [1,*]Kayla Murphy [1]Patrick Rider [1]

[1]Kinesiology, East Carolina University, Greenville, United States

Introduction and Objectives: Running is popular because it has many health benefits protecting against disability and early mortality (1,2). Running is also associated with a high rate of overuse injuries, reportedly between 19 to 79% per annum (3). Injuries occur throughout much of the musculoskeletal system but have particularly high rates in the ankle and knee regions and include achilles tendinitis, anterior knee pain, and patellar tendinitis (4). Running patterns can be modified to reduce lower extremity loads which are presumed to cause running injuries. Altering foot-strike (rear vs fore-foot strike) changes achilles tendon and ankle and knee joint loads (5,6). Shorter step length lowers patellofemoral joint forces (7-8) and running speed itself is directly correlated with the magnitude of ground forces and joint loads (9). These analyses were based entirely on individual foot steps. Alternatively, recent data supports the idea that longer steps and faster speeds reduce total lower extremity loads per unit distance (e.g. 1 km) because these gaits have fewer steps and ground contact phases per unit distance. Miller et al (10) showed that total knee joint loads summed over all steps were reduced per unit distance in running compared to walking despite having much larger per-step loads. It follows that the reduced number of steps per unit distance at faster vs slower running may also offset the larger per step loads associated with faster running. We now hypothesize that running at faster vs slower speeds reduces total lower extremity loads when summed across all steps taken to run a standard distance. The purpose of the study was to compare total ground reaction forces (GRF), achilles tendon, patellofemoral, and tibiofemoral joint forces when summed across all steps taken to run 1 km at 3 running speeds.

Methods: 3D kinematic and GRF data were collected on 16 runners (7 males; age 22 yrs; mass 65 kg) at 2.68, 3.35, and 4.47 m/s running speeds. Inverse dynamics and a lower limb musculoskeletal model (11) were used to compute per-step patellofemoral and tibiofemoral compressive forces and achilles tendon force. Step length was assessed and used to compute total steps per kilometer per limb at each speed. Total peak values for these force variables and for resultant GRF were computed as the product of their per step value and number of steps per km at each speed. 1-way ANOVA was used to identify differences in total loads followed by t-tests between sample means in the case of significant F-ratio, all $p<0.05$.

Results: Slow, medium & fast runing speeds had 486±62, 418±63, and 363±81 steps per limb per km. Total loads per kilometer and limb were significantly lower at faster compared to slower running speeds (Table 1). Total GRF and tibiofemoral force were significantly lower at each speed from slow to fast and patellofemoral and achilles tendon forces were significantly reduced from slow to both faster speeds. All significant differences were ~10% lower from each slower to faster speed.

Figure:

Table 1. Maximum Values (mean, sd)	Per Stride			Per Kilometer		
	Slow	Medium	Fast	Slow	Medium	Fast
GRF max resultant (N), 1, 2	1,520	1,588	1,677	745,946	673,428	630,768
(sd)	228	226	230	124,010	122,756	164,087
Tibio-femoral max compression (N), 1, 2	6,828	7,123	7,600	3,339,455	2,966,631	2,800,082
(sd)	1,171	1,572	1,431	521,402	463,901	528,781
Patello-femoral max compression (N), 1, 3	3,094	3,310	3,461	1,512,160	1,366,838	1,266,047
(sd)	920	1,263	1,195	423,138	467,379	439,431
Achilles tendon max force (N), 1, 3	3,390	3,602	3,871	1,652,414	1,489,334	1,458,746
(sd)	840	804	815	363,099	324,510	453,193

For Per Kilometer Data Only: 1: sig ANOVA, 2: All speeds significantly different, 3: Slow > medium & fast

Conclusion: Present data supported the hypothesis that total loads summed across all steps taken to run a standard distance are lower at faster vs slower speeds. Within the range of speeds tested, increased step length and not rate was the dominant mechanism to increase speed leading to fewer steps per unit distance. It remains to be seen whether total, summed loads are related to over-use running injuries and if reducing these loads reduces injury rates.

References: 1. Chakravarty et al., Arch Int Med, 168:1638–1646, 2008.

2. Wang et al, Arch of Intl Med, 162:2285–2294, 2002.

3. Goss et al, US Army Med Dept J, 62–71, 2012.

4. Van Mechelen, Sports Med (Auckland, N.Z.), 14:320–335, 1992.

5. Almonroeder et al, Ann Biomed Eng, 41:1758–1766, 2013.

6. Rooney et al, J Biomech, 46:2201–2206, 2013.

7. Lenhart et al, Med. Sci. Sports Exerc., 46:557–564, 2014.

8. Willson et al, Clin Biomech, 29:243–247, 2014.

9. Dorn et al, J Exp Biol 215:1944-1956, 2012.

10. Miller et al, Med. Sci. Sports Exerc, 46:572–579, 2014.

11. Messier et al. Med Sci Sports and Exerc, 40:1873-1879, 2008.

Disclosure of Interest: None Declared

Musculoskeletal

AS-0319

THE RELATIONSHIP BETWEEN MUSCLE MATERIAL PROPERTIES AND BODY MASS INDEX

Ann Marie Tullock [1] Jamie Hibbert [1] Paul Devita [1] Zachary J. Domire [1,*]

[1]Department of Kinesiology, East Carolina University, Greenville, United States

Introduction and Objectives: Obesity rates in the United States have been growing steadily over the last three decades [1]. It is well documented that obesity can lead to a wide range of other health problems [2]. One possible complication of obesity that has not been fully explored is increased accumulation of Advanced Glycation End-products (AGEs). Glycation is a non-enzymatic reaction between reducing sugars and proteins, and typically leads to the formation of covalent cross-links [3]. Tissues with greater AGE accumulation in the have been shown to have increased modulus [4]. Data collected by our lab group in aged animals has indicated that there is an inverse relationship between muscle size and modulus [5]. This indicates that increased muscle modulus may be implicated in decreased response to exercise. The purpose of this study was to identify the relationship between muscle modulus of the tibialis anterior and body mass index using elastography in a group of people with BMIs ranging from 18-44 kg/m^2. It was hypothesized that obesity may increase the rate of glycation in connective tissue and in turn result in an increase in muscle modulus.

Methods: Twenty-one participants were recruited for this study utilizing newspaper ads, flyers, and the East Carolina University listserve to reach university faculty and staff. Individuals were recruited based on BMI with the intention of testing one participant per BMI unit 18-50 kg/m^2. Inclusion criteria specified that subjects must be between the ages of 18 and 60 years old with a 18 kg/m^2 ≤ BMI ≤ 50 kg/m^2. In order to participate in this study, participants were required to be apparently healthy with the exception of high BMI. Individuals were excluded if they had any neurological, musculoskeletal, neuromuscular, or physiological disabilities. Previous surgeries to the lower limbs were also considered as exclusion criteria. This study was approved by the East Carolina University Institutional Review Board. Elastography data was collected using a SuperSonic Imagine ultrasound unit (Axe-en-Provence, France). Each participant was positioned in a HUMAC isokinetic dynamometer chair with their knees flexed at 90° and ankles in anatomical position. Participants were asked to relax and remain as still as possible during measurements. Two five-second clips were collected for the right tibialis anterior. Tibialis anterior was chosen for measurements due to its accessibility. Additionally, the tibaialis anterior typically displays a lower level of adipose tissue than other lower limb muscles despite body mass index. Modulus was established by selecting a region of interest in the middle of the muscle belly. A Q-Box 3.0mm in diameter was placed in the area determined to contain adequate wave propagation at the frame in the middle of the clip. Statistical analysis included correlations of body mass index with mean muscle modulus and body mass index with the standard deviation of muscle modulus.

Results: The primary hypothesis of this study was that an increase in body mass index might lead to an increase in glycation of connective tissues and, in turn, result in an increase in muscle modulus of the tibialis anterior. Our results showed a low correlation between BMI and muscle modulus. The lack of a relationship was a largely a result of two participants who displayed extreme levels of muscle modulus.

Figure:
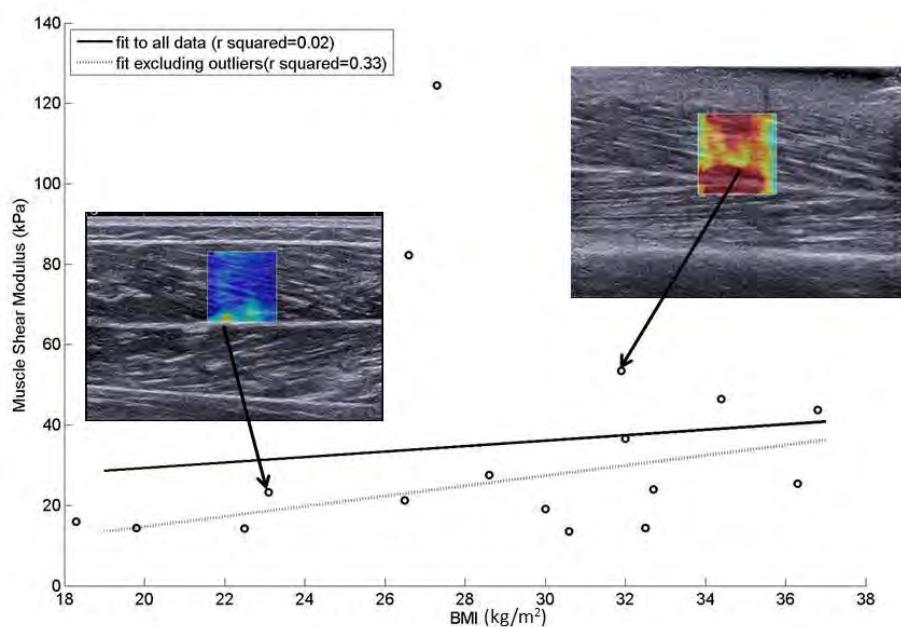
Caption: Figure 1. Relationship between BMI and shear modulus. Inset: Representative elastograms for a healthy weight and an obese participant

Conclusion: Based on the data collected during this experiment there appears to be a slight relationship between BMI and muscle modulus with higher BMI being related to increased muscle modulus. However, as mentioned above the weakness of this relationship was predominantly due to two participants who were outliers. These participants were not obese, but they were overweight. If these data points are excluded from the analysis the data show a clear relationship between increased BMI and increased muscle modulus. All participants were screened for diabetes in a pre-test questionnaire, but it is possible that the participants who were outliers are pre-diabetic or have undiagnosed type II diabetes. Increased muscle modulus may have serious implications including attenuated response to resistance exercise. Attenuated response to resistance exercise in obese individuals could be especially detrimental if it is found to interfere with exercise mediated glucose uptake. If this mechanism of glucose uptake is disrupted in individuals who have high BMIs it puts them at even greater risk of developing type II diabetes.

References: [1] Ogden et al., *JAMA*, 295:1549-1555, 2006.

[2] Wang et al., *Epidemiol Rev*, 29:6-28, 2007.

[3] Singh et al., *Diabetologia*, 44:129-146, 2001.

[4] Reddy, *Exp Diabesity Res*, 5:143-153, 2004.

[5] Pauwels et al., *J Musculosketeletal Res*, 15, 2012.

Disclosure of Interest: None Declared

A FEEDBACK CONTROLLER TO PREDICT THE POSTURAL CONTROL IN RESPONSE TO A PERTURBATION

Maarten Afschrift [1,*]Friedl De Groote [2]Ilse Jonkers [2]

[1]Human movement biomechancis, [2]Production Engineering, Machine Design and Automation (PMA) Section, Ku Leuven, Leuven, Belgium

Introduction and Objectives: Postural control is a highly relevant topic, given the high incidence of falls in the elderly. The high location of the center of mass (COM) in combination with the small base of support (BOS) necessitates continuous postural control [1]. Postural control is often divided into feed-forward control (i.e. the control that anticipates a perturbation by adjusting the intrinsic stability) and feedback control (i.e. the control that generates stabilizing forces in response to a perturbation). The three major sensory systems that provide these feedback signals are the vestibular system, the somatosensory system and the visual system [1]. However, it is still unclear how humans modulate these feedback signals to excite their muscle for postural control. We hypothesize that human modulate their feedback signals to optimize their stability state and minimize the work needed for postural control. We will combine forward simulations with experiments of perturbed posture to define and evaluate the performance of the postural controller.

Methods: During the experiments, the posture of the subjects was perturbed by a backward translation of a motion base (range 0.16m, peak acceleration 1.5 m/s^2). The kinematics, kinetics and muscle activity in response to the perturbation were measured using integrated motion capture and processed using a scaled musculoskeletal model in Opensim. The forward simulations were performed with a simplified model: the models motion is limited to the sagittal plane and has only two degrees of freedom, one at the hip joint and one at the ankle joint representing the two main postural control strategies. The maximal moment generating capacities around the joints were constrained based on the moment-angle relationship of the muscles. The initial state (i.e. the joint angles and angular velocity) was modeled by imposing the experimental state before the perturbation. During the forward simulation, the posture of this model is perturbed by imposing a similar translation of the motion base. Secondly, we have implemented a feedback controller that uses feedback of the center of mass (COM) [position,velocity,acceleration] with respect to the BOS (somatosensory system) and the orientation [angle, angular velocity] of the torso with respect to gravity (visual and vestibular system). These feedback signals were scaled by gains to control the ideal moment actuators of the hip and ankle joint. The final gains were determined in an optimization routine with a cost function that combines the margin of stability (reflecting the stability state) and the joint work needed to restore balance.

Results: In general, the forward simulation with the optimized feedback gains results in a similar response to the perturbation as in the experiments (figure 1). More specific, there is only a small difference in the hip joint angle pattern, hip joint range of motion (ROM) and maximal hip extension moment (table 1). However, there are larger differences in the ankle angle pattern, ROM and peak plantarflexion. Furthermore, the center of mass range of motion and the time needed to bring the COM velocity below 0.02 m/s are larger in the experiment compared to the simulation.

Figure:
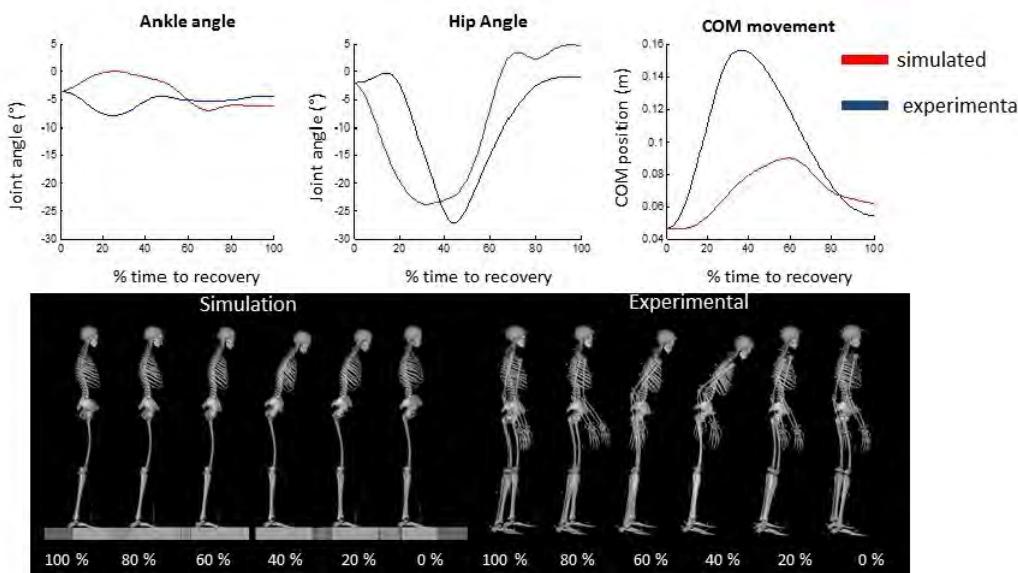
Conclusion: In conclusion, we are able to simulate the postural control in response to a perturbation using a simple feedback controller. This supports previous findings that suggest that humans use feedback of the orientation of the torso with respect to gravity and the location of the COM in relation to the BOS. Furthermore, the simulated kinematics and kinetics approximate the experimental kinematics and kinematics when we optimize the feedback gains to minimize the work needed for postural control and maximize the margin of stability. This suggests that the subject is using a similar strategy to modulate his muscle activity. However, there are still some important differences between the simulations and the experiments. Firstly, the simplifications in the simulation model will also influence the joint kinematics and kinetics. Secondly, the shorter time to stabilization and the decreased COM excursion in the simulation can be explained by the absence of a time delay on the feedback signals. In future research, we will implement a neural delay based on the first increase in muscle activity. Nevertheless, these results suggest that non-stepping postural control strategies can be approximated by a feedback controller with optimized gains. This controller could be highly relevant to predict the outcome of an intervention such as muscle strength training or the use of an assistive device on postural control. In other words, this framework allows, within the current limitation, to optimize interventions that maximize the subject's postural control capabilities.

Table:

	Time (s).	Ankle ROM (°)	Hip ROM (°)	Peak ankle moment (Nm)	Peak hip moment (Nm)	COM ROM
Experiment	1.9	4.6	26	85	50.3	0.11
Simulated	0.9	7.0	28	64.6	45.5	0.05

References: [1] Winter, Gait & Posture, 3: 193-214, 1995

[2] Welch et al., J. Neurophysiol, 99: 1032-38, 2008

Disclosure of Interest: None Declared

Balance

AS-0321

ASSESSMENT OF POSTURAL STABILITY IN MINIATURE DACHSHUNDS USING PLANTAR PRESSURE SYSTEMS AND FORCE PLATES

Aliah F. Shaheen [1,*]Thais de Mello Toledo [2]Daniela Macedo Lins de Araujo [2]Constanza Gómez Álvarez [2]

[1]University of Surrey, Guildford, United Kingdom, [2]School of Veterinary Medicine, University of Surrey, Guildford, United Kingdom

Introduction and Objectives: Miniature Dachshunds are a breed of dogs at a high-risk of developing intervertebral disc disease. This might result in spinal cord compression making them prone to developing neurological problems including paresis and paraplegia. Dogs that undergo spinal surgery will still have difficulties in walking and standing during the post-surgical recovery period, this is addressed using various rehabilitation techniques including physiotherapeutic exercises and other modalities. However, the efficacy of these rehabilitation techniques on their recovery time and musculoskeletal function is yet to be objectively assessed.

Postural stability is an important aspect of motor control which can be used as an indicator of musculoskeletal function. Objective measures of postural stability have been used in humans to assess rehabilitation programmes for patients with musculoskeletal disorders, to assess exercises used to reduce the risk of falling in older people and in stroke rehabilitation. Similarly, these measures can be used to assess the outcome of rehabilitation in dogs in the clinic, but it has not been reported in the literature.

The aim of this study was firstly to obtain measures of postural stability during quiet standing in healthy Miniature Dachshunds. Secondly, the study also aimed to assess the validity of postural stability measures obtained using plantar pressure data compared to data obtained from force plates.

Methods: 43 healthy Miniature Dachshunds of different body conditions (mean and standard deviation=5.8 ±1.7 on a scale from 1-9), gender (31 females and 12 males), hair type (smooth, long or wired) and age (6 months to 13.8 years) were recruited. The dogs' Body Condition Score were assessed by a veterinary surgeon using an established scoring system (Bartges et al. 2010). The dogs stood still on a plantar pressure mat (TekScan MatScan) placed on top of a force plate (AMTI). The two systems were synchronised and data were collected using the two systems simultaneously. Trials of 10 seconds long were collected, trials were the dog was seen to move, moved its tail or attempt to sit were discarded. A minimum of 5 valid trials were used for analysis.

Measures of Centre-of-Pressure (CoP) displacement and velocity as well as anterior-posterior and medial-lateral ranges were computed from force plate data. These were used to define normative values for healthy Dachshunds postural stability in quiet standing. Statistical analysis included t-tests, one-way ANOVA tests and Pearson correlation tests to examine the differences between gender, hair type, BCS and age. In addition, CoP measures were compared to those obtained using the plantar pressure system to assess the validity of computing postural stability measures using CoP data obtained from plantar pressure systems in the clinic.

Results: Table 1 describes the normative values for CoP measures for males and females and different hair types. There were no statistical differences between gender and hair type for any of the CoP measures. However, there was a

significant (p<0.05) negative correlation between the medial-lateral range and age (normalised to body weight). The CoP velocity was significantly (p<0.05) higher in dogs considered to be overweight (>6 from a scale 1-9) using the BCS. Finally, there were significant differences between measures obtained using the plantar pressure system and the force plate. The plantar pressure system underestimated the CoP velocity, anterior-posterior and medial-lateral ranges. However, the measures between trials and dogs were comparatively similar.

Conclusion: The study defined normative ranges of postural stability measures in healthy miniature Dachshunds. The results have shown no differences between males and females and between the different hair types. Some of the measures were different for older and overweight dogs, thus suggesting that postural stability measures are appropriate in measuring subtle differences in postural stability and may be an effective tool for rehabilitation monitoring. Future studies will focus on obtaining measurements of dogs at various stages of rehabilitation to assess the usefulness of these measures in evaluating functional improvement.

Data obtained from plantar pressure systems can be used to compute postural stability measures and are appropriate for clinical use; however, future studies using this system should note differences in the computed measures when comparisons with previous studies are carried out.

Table:

Category		AP Range (mm)	ML Range (mm)	Velocity (mm/s)
Gender	Female	22.6 ± 0.9	31.9 ± 1.4	259 ± 23
	Male	25.0 ± 2.7	37.4 ± 4.5	230 ± 36
Hair Type	Smooth	25.8 ± 1.6	36.0± 3.0	264 ± 30
	Long	20.3 ± 1.2	30.1 ± 2.0	249 ± 35
	Wire	23.8 ± 2.2	34.6 ± 3.4	236 ± 37

Caption: Normative values for CoP anterior-posterior (AP) and medial-lateral (ML) ranges and velocity, measures are divided according to sex and hair type

References: [1] Baldwin K, et al. J Am Anim Hosp Assoc. 2010 Jul-Aug;46(4):285-96.

Disclosure of Interest: None Declared

Balance

AS-0322

EFFECTS OF 45-MINUTE SOCCER MATCH SIMULATION ON BALANCE MECHANISMS FOR SINGLE-LEG HOP LANDING IN HEALTHY AND ANTERIOR CRUCIATE LIGAMENT RECONSTRUCTED FEMALES

Sean Sankey [1] [2],*Raja Mohammed Firhad Raja Azidin [3]Holly Bradburn [1]Olalla Garcia Taibo [1]Ruth Cabeza-Ruiz [1]Mark Robinson [1]Jos Vanrenterghem [1]

[1]School of Sport and Exercise Sciences, Liverpool John Moores University, Liverpool, [2]Engineering, Sport and Sciences, University of Bolton, Bolton, [3]Sport and Exercise Sciences, Liverpool John Moores University, Liverpool, United Kingdom

Introduction and Objectives: The prevalence of Anterior Cruciate Ligament (ACL) injury in sport remains a major financial and rehabilitative burden. This is particularly true for female athletes in competitive team sports such as soccer. It is widely accepted that improper mechanics during dynamic tasks can lead to the loading at the knee joint sufficient to cause ACL injury (Dempsey et al., 2009). Hof (2007) has previously proposed the use of three balance mechanisms, including, Margin of Stability (MoS), which was quantified as the difference between the base of support and the extrapolated centre of mass. Recently Oberländer et al., (2012) investigated the differences between ACL ruptured and healthy physically active participants, observing balance mechanisms suggested by Hof (2007) in a single-leg landing task. Oberländer et al., (2012) suggested that ACL injuries cause participants to present a more anterior position of the centre of mass, and therefore reduced MoS. However, limb dominance and response to a specific soccer exercise bout has not yet been observed. The present study aims to investigate, firstly, how ACL reconstructed and healthy females present MoS in their dominant and non-dominant limbs, performing a single-leg landing task; and secondly, how a soccer specific match-simulation may challenge this MoS mechanism.

Methods: Twenty-nine females, who were active in competitive team sports such as soccer, took part in the study (age 23 ± 2.7 years; height 1.67 ± 0.06 m; mass 63 ± 7 years). These participants included females who had been involved in ACL reconstructive surgery (n=11) on average 25 months post-operative, and otherwise healthy females with no reported lower limb injuries (n=16). All participants took part in a modified 45-minute soccer match simulation, which included 3D motion capture of the single-leg landing task at times '00' - preceeding the simulation; '45' after one half match simulation; and '60' following a 15-minute 'half-time' active rest. Each participant had 44 spherical reflective markers attached according to the LJMU-model - a 6-degrees-of-freedom, eight segment model including feet, upper and lower legs, pelvis and trunk. All single-leg landing trials were performed on the dominant and non-dominant sides using a force platform sampling at 1500 Hz, kinematic data were synchronously recorded using 10 optoelectronic cameras sampling at 250 Hz. It was noted that all ACL reconstructed participants had suffered injuries to their non-dominant lower limbs.

Results: No significant differences were found between ACL and healthy females for MoS in medio-lateral (X) and anterio-posterior (Y) directions, considering both limb-dominance and assessment time through the match simulation.

Conclusion: The fact that no significant differences were found between injured and healthy females, and irrespective of assessment time in the simulation, may indicate that other balance mechanisms were involved. Hof (2007) suggests the inverted pendulum and acceleration/counter-rotation of segments, may be considered, but further research is required here. Although, no significant differences were found there were some potentially important observations. MoS in the

anterio-posterior direction (Y) was noted to be higher in the ACL injured leg, and increased in response to the match-simulation to 45-minutes, and thereafter almost returned fully by time 60. This suggests ACL injured participants may try to extend their MoS, potentially as a protective mechanism on the injured side. Further to this, MoS presented in medio-lateral direction seemed to be more restricted in the injured limb of ACL participants, which is potentially a mechanism that may reduce the shear load at the injured knee joint.

References: [1] Dempsey et al., Am J Sports Med, 37(11): 2194-2200,2009.

[2] Hof, J of Biomech, 40: 451-457, 2007.

[3] Oberländer et al., J of Biomech, 45: 1387-1392, 2012.

Disclosure of Interest: None Declared

THE ABILITY TO RECOGNIZE A SLIP

Sharon Ravindran [1] [2] Yue Li [2] Tilak Dutta [2] Vicki Komisar [2] [3],*Geoff Fernie [2] [3] [4]

[1]Engineering Science, University of Toronto, [2]Toronto Rehabilitation Institute , University Health Network, [3]Institute of Biomaterials and Biomedical Engineering, [4]Surgery, University of Toronto, Toronto, Canada

Introduction and Objectives: Falls are a leading cause of injury in Canada [1], of which many result from slipping on snow or ice [2]. The ability to detect a slip is important for inducing proactive and reactive balance responses; however, the ability of a person to assess walkway slipperiness is unclear. With high variability in previous evaluations of slipperiness, no significant relationship exists between subjective evaluations with coefficient of friction or slip distance [3,4]. Further, no studies have explored the point at which people know if they have experienced a simultaneous slip of both feet (bilateral slip). The purpose of this pilot study is to quantify the range of slip distances that can be perceived, and to examine changes in gait resulting from perceived and non-perceived bilateral foot slips.

Methods: Data was collected in 'WinterLab' in the Challenging Environment Assessment Laboratory at Toronto Rehab (Figure 1). Six young women participated (age 23.7 ± 2.1y; height 162.4 ± 2.8cm; mass 58.7 ± 8.0kg).

Harnessed subjects walked back and forth along a 2m-long wet-ice walkway. All wore the same type of winter boot and walked at a self-selected pace. After each walk, subjects reported whether they perceived a slip. The walkway angle was increased by 1^0 until the researcher saw a bilateral slip.

Reflective markers on the feet and pelvis were used to quantify key gait and slipping metrics (Table 1). Bilateral slip in this study was defined as:

1)   If both feet on the ground move in the anterior-posterior (AP) direction but not in the vertical (z) direction (*vel-AP* > 0.10 m/s; *vel-z*<0.10m/s); or

2)   If one foot is in the air and grounded foot has *vel-AP*>0.10 m/s and *vel-z*<0.10m/s

Slip distance was defined as the difference between the heel position at slip termination and heel contact (HC) in the AP direction.

Slips were categorized into two groups: Perceived slips (where the subject correctly identifies a slip) and non-perceived slips (where slips were only detected from kinematic data). All variables were analyzed with a mixed model repeated measures ANOVA, with significance defined as $p<0.05$.

Results: *Seventy- eight* slips were recorded, of which 40 slips were successfully identified by participants, giving a success rate of 51% for the identification of a slip on a sloped icy surface. The main effect of direction (p= 0.43) was not significant and as a result the values from uphill and downhill were grouped together. A slip distance over 0.10 m can lead to a dangerous fall [5] and can lower a person's ability to recover should a slip occur [6]. Of the 78 slips, 17 slips had slip distances between 0.10 and 0.24m; where 13 (77%) of those slips were perceived.

Most gait parameters did not vary significantly between perceived vs non-perceived slips, except for slip distance (p= 0.004) and sliding heel velocity (p= 0.005). Perceived slips occurred with walkway inclines on average 1º higher than

non-perceived slips. Higher slopes create surfaces that are more challenging and slipperier to walk on for the participant, which may explain the increase in slip distance and sliding velocity for perceived slips.

Figure:

Wet Ice Condition

Caption: Figure 1: Subjects walked uphill or downhill along a wet ice condition inside Winterlab (left). Picture on the right shows the exterior of Winterlab.

Conclusion: Subjective assessment of perceiving a bilateral slip should be cautiously used as a method to identify potentially- dangerous slips, as only 77% of bilateral foot slips were identified by the subject when the slip distance was greater than 0.10m. Higher slip distance and sliding heel velocity may be contributors in the identification of a bilateral foot slip, thereby making it easier for subjects to perceive that they have experienced a slip [7]. Further studies with a bigger sample size are needed to examine these subjective assessments in older adults, and EMG on key leg and trunk muscles should be incorporated to quantify muscular responses. In addition, more research needs to be done to investigate the feasibility of educating or designing interventions that can help people to recognize high slip distances that could lead to dangerous falls.

Table:

	Non-perceived slip	Perceived slip	p value
Slope Angle (°)	4.0 ± 0.7	4.9 ± 0.8	0.004
Slip Distance (m)	0.05± 0.02	0.09 ±0.04	0.017
Sliding Heel Velocity (m/s)	0.12± 0.04	0.18± 0.05	0.005
Floor Foot Angle(°)	18.0±6.8	15.5±6.2	0.21
Step Width (m)	0.11± 0.04	0.11± 0.04	0.74

Caption: Table 1: Descriptive Statistics (mean+SD) for key gait parameters measured during perceived vs non-perceived slips.

References: [1] Seniors' Falls in Canada, PHAC, 2014

[2] Courtney et al, Int. J. Ergon., 44: 1118-1137, 2001

[5] Myoung et al, J. Ind. Ergon., 11: 313-319, 1993

[6] DiDomenic et al, J. Appl. Ergon., 38: 533-539, 2007

[7] Leamon et al, P. 23rd Int. Cong. Occup. Health: pp. 17

[8] Chang. Measuring Slipperiness: Human Locomotion and Surface Factors, Taylor &Francis, 2003

[9] Chang et al, J. Gait Posture, 41: 288-290

Disclosure of Interest: None Declared

Balance

AS-0324

THE ROLE OF SOMATOSENSORY PROPRIOCEPTION IN STANDING AND HANDSTAND BALANCE

Glen M. Blenkinsop [1,*]Matthew T. G. Pain [1]Michael J. Hiley [1]

[1]School of Sport, Exercise and Health Sciences, Loughborough University, Leicestershire, United Kingdom

Introduction and Objectives: The sensory organisation test was developed by Nashner [1] and is a computerised system that consists of a moveable force plate that can rotate about an axis level with the patient's ankle joint and track their sway during quiet stance. This sway referenced platform motion is intended to reduce the amount of ankle motion during normal sway to reduce sensory feedback from the surrounding somatosensory proprioceptors during quiet stance. The sway referenced platform has only been used to assess quiet stance in double leg stance as the rotation of the support surface is about a fixed point that cannot be moved. Past research has only examined the general effect of a sway referenced platform via analysis of the range and standard deviation of the centre of pressure (COP). The purpose of this study was to create a sway referenced platform on the CAREN system so that the role of visual and somatosensory proprioception could be assessed in both standing and handstand postures via a range of traditional and nonlinear analyses.

Methods: A sway referenced platform was achieved by creating a script program in the motek medical D-Flow software to control the CAREN system's Stewart platform. The platform was rotated about a virtual axis aligned with the subjects' ankle or wrist joints using the method from Barton et al. [2]. Body sway was tracked via a nine camera vicon system (200 Hz) and inputted into the D-Flow script program so that the platform could be rotated to track the subjects' body sway. Ten experienced handstanders performed balance trials with eyes open and eyes closed conditions in double leg stance and handstand on a static and sway referenced platform. Three trials of each of the eight conditions were completed for a maximum of 30 seconds duration.

Kinematic data were collected via 53 markers to divide the body into 18 segments and filtered with a fourth order zero lag, low-pass Butterworth filter with a cutoff frequency of 10 Hz, before quaternion algebra was used to calculate: segment centre of mass linear displacements, velocities, and accelerations; and segment angular velocities and accelerations. Kinetic data were collected via two Bertec strain gauge force plates (200 Hz), and raw COP data were used to assess balance via: traditional measures (trial duration, sway area, sway length, standard deviation, range, sway velocity), nonlinear dynamics (sample entropy, Lyapunov exponent), and recurrence quantification analysis (recurrence rate, determinism, Shannon entropy, divergence, trend). Kinetic and kinematic data were used to calculate 3D joint moments and forces via wrench notation, to assess balance via: estimates of neurological delay (delay, R^2, joint torque from proportional and derivative gains), and movement corrections (number of small, medium, and large corrections per second, mean torque, torque impulse, burst duration).

Results: The sway referenced platform resulted in increased sway in standing as measured by the traditional balance metrics of range, sway length, and sway velocity for eyes open, and even more so for eyes closed. Balance on a sway referenced platform resulted in reduced Lyapunov exponents, indicating trajectories became more organised with lower localised divergence. Balance on a sway referenced platform resulted in fewer corrections per second with reduced burst duration and higher mean joint torques. No significant changes were found in estimates of neurological delay.

Experienced handstanders balancing on a sway referenced platform had a loss of balance within a few seconds due to the reduced sensory information from wrist somatosensory proprioception. Handstand trials of short duration resulted in large variations in balance measures calculated from traditional and nonlinear analysis methods. Handstand balance on a sway referenced platform typically resulted in COP trajectories that were significantly less stationary, with decreased entropy and increased divergence. No significant changes were found for estimates of neurological delay, however, a significant increase in estimates of passive wrist stiffness was found for handstand balance on a sway referenced platform.

A residual effect from the sway referenced platform resulted in increased sway during static balance in standing and handstand on a stable platform compared to a previous session without any sway reference component.

Conclusion: When balancing in standing on a sway referenced platform balance becomes more regular with fewer corrections; whereas when balancing in handstand subjects tended to drift, or fall, with few corrections, leading to nonstationary signals with large divergence in local trajectories. The relationship between somatosensory and visual cue utilisation, and how this is affected by recent environmental experiences, is similar in both standing and handstand postures.

References: [1] Nashner. Biol Cybern, 10: 106-110, 1972.
[2] Barton et al., Gait Posture, 24: 510-514, 2006.

Disclosure of Interest: None Declared

Balance

AS-0325

IS THERE A CORRELATION BETWEEN WOBBLE BOARD PERFORMANCE AND STATIC BALANCE PERFORMANCE?

Jamie Parkinson [1,*]Daniel West [1]Carol Clark [1]Jonathan Williams [1]

[1]School of Health and Social Care, Bournemouth University, Bournemouth, United Kingdom

Introduction and Objectives: Wobble boards (WB) are commonly used in clinical practice to rehabilitate and enhance proprioception and balance. However the relationship between wobble board performance and balance function has yet to be determined.

The aim of this study was to explore the relationship between wobble board performance and balance performance.

Methods: Ethics approval was granted from Bournemouth University. Thirty healthy participants completed a series of WB tasks (double leg stance and single leg stance) and a series of static balance tasks (double leg stance, tandem stance and single leg stance). WB performance was measured using the SMARTwobble instrumented wobble board (which produces 5 performance metrics) and balance performance was measured using a commercially available balance sensor (produces 3 performance metrics) based on the acceleration of the sacrum. The relationship between the performance on the WB and balance performance were explored using spearman's correlation coefficients.

Results: A possible 360 correlations were explored and 45 significant correlations were identified. Of these, 7 were deemed modest correlations (r>0.50). Greatest correlations were observed for time with WB in outer tilt banding during SLS and tandem stance eyes closed (r_s = 0.60) and WB time in inner banding during SLS and tandem stance eyes closed (r_s = -0.56). Despite these specific correlations, overall, the results show little correlation between WB performance and balance performance. These results imply that WB performance and balance performance are not interchangeable. This suggests the two elements challenge different balance constructs, perhaps with the WB targeting the ability to deal with continuous balance perturbation and the balance tasks exploring the ability to maintain static balance equilibrium.

Conclusion: There was little overall correlation between WB performance and balance performance. This seems to suggest that they assess different underlying balance constructs.

Table:

Wobble board task and metric	Balance task and metric	r_s	P
SLS time in outer tilt banding	Tandem EC JERK	0.60	0.001
SLS time in inner tilt banding	Tandem EC JERK	-0.56	0.002
SLS time in inner tilt banding	Tandem EC NPL	-0.54	0.002
SLS time in outer tilt banding	Tandem EC NPL	0.50	0.005
SLS time in outer tilt banding	Tandem EC RMS	0.52	0.00

			4
SLS time on edge tilt banding	Tandem EC NPL	0.51	0.005
SLS time on edge tilt banding	Tandem EC JERK	0.54	0.003

SLS; single leg stance, RMS; root mean square, NPL; normalised path length, JERK; jerkiness of trace.

Caption: Significant Spearman's correlation coefficients >/= 0.5 between specific wobble board and balance sensor metrics.

Disclosure of Interest: None Declared

VARIABILITY OF TRUNK MUSCLE SYNERGIES DURING TARGET MATCHING TASKS

Ehsan Sedaghat-Nejad [1] Seyed Javad Mousavi [2] Mohamad Parnianpour [1] Malihe Hadizadeh [3] Bahman Nasseroleslami [4,*]

[1] Sharif University of Technology, Tehran, Iran, Islamic Republic Of, [2] University of Sydney, Sydney, Australia, [3] Tehran University of Medical Sciences, Tehran, Iran, Islamic Republic Of, [4] Academic Unit of Neurology, Trinity College Dublin, Dublin, Ireland

Introduction and Objectives: It has been suggested that the central nervous system simplifies muscle control through basic units, called synergies, to activate muscles in groups. Several authors evaluated consistency of muscle synergies during different tasks and found similar synergies across their populations. Since, trunk neuromuscular system is a complicated system with high degree of redundancy, assessing control strategies in this system will be crucial to advancing our understanding of neural control mechanisms for muscle exertions. The objectives of the present study were: (1) to examine the existence of muscle synergies - as a trunk neuromuscular system strategy - during multidirectional target matching tasks, (2) to investigate the consistency and inter-individual variability of extracted synergies in terms of their number and composition, and (3) to interpret the functional role of muscle synergies regarding their activation patterns and respective torque synergies.

Methods: We investigate the existence and inter-subject variability of trunk muscle synergies as well as torque synergies during a novel target matching task. In this regard, a population of twelve healthy participants (five female) with no history of back pain and other musculoskeletal and neuromuscular disease were studied. Generated isometric torque data at L5/S1 level and electromyographic (EMG) patterns of twelve abdominal and back muscles were recorded. Each participant performed a total number of 24 isometric target matching task in 12 different angles (0, 30... 330 degree) and 2 levels of uniaxial and biaxial exertions (45% and 70% of the Maximum Voluntary Exertion). Muscle and torque synergies were extracted using non-negative matrix factorization (NMF). Three different criteria including multivariate R^2, variance accounted for (VAF), and residual mean square error (MSE) were calculated to determine the proper number of muscle synergies. Further, a cross-validation (VAF_{cross} and R_{corr}) and reliability (ICC) procedure was assessed to verify the robustness of the extracted muscle synergies across different conditions. Also, the similarity of muscle synergies across participants was evaluated by a calculation procedure similar to VAF_{cross} and R_{corr}. Finally, torque synergies were calculated using muscle synergy activation coefficients and acquired torque data.

Results: Choosing four number of muscle synergies, the results showed mean VAF of 97.9±0.53% and mean R^2 of 94.5±1.1% which shows the efficiency of those synergies. Moreover, concerning between-subject variability of the muscle synergies, VAF_{cross} was 90.0±4.1%, and R_{corr} were 0.77±0.12, 0.86±0.08, 0.78±0.12, and 0.93±0.04 for synergy #1, #2, #3, and #4, respectively, which highlights their consistency across participants. For each set of muscle synergies, a set of four corresponding torque synergies were evaluated which had VAF_{torque} of 92.2±3.03%. Based on the torque synergies and the activation pattern of muscle synergies, functional role of muscle synergies was interpreted. As a result, synergy #1, #2, #3, and #4 were labelled as right rotation, extension, left rotation, and flexion, respectively. Each synergy was predominated in a specific direction and collaborated in other directions as well.

Figure:
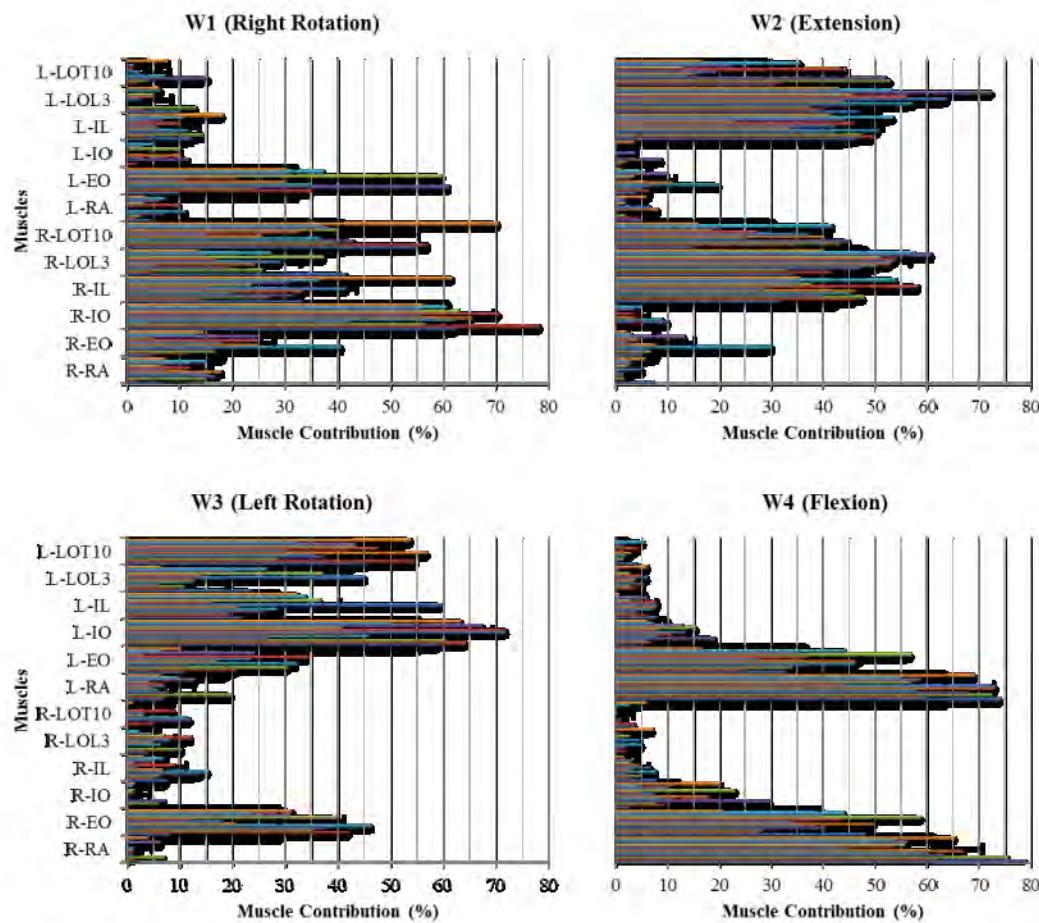
Caption: Muscle synergy compositions

Conclusion: The results showed that there is a set of four muscle and four corresponding torque synergies for a healthy person, which could efficiently break the sagittal and transverse torque planes into its main directions. Overall, our results suggested that by taking advantage of muscle synergies we could overcome the redundancy faced in control strategies of trunk neuromuscular system. In future studies, the synergies identified in patients with LBP can be compared with this set of synergies extracted from asymptomatic participants. We are now planning larger studies to identify muscle synergies in people with LBP and evaluate the effect of training to address possible altered muscle synergies.

Disclosure of Interest: None Declared

Trunk

AS-0327

EFFECTS OF VOLITIONAL SPINE STABILIZATION ON LIFTING TASK IN RECURRENT LOW BACK PAIN POPULATION

Ram Haddas [1,*] James Yang [2] Isador H Lieberman [3]

[1]Reseach , Texas Back Institute Research Foundation, Plano, [2]Mechanical Engineering , Texas Tech University, Lubbock, [3] Scoliosis & Spine Tumor Center , Texas Back Institute, Plano, United States

Introduction and Objectives: Low back pain is reported in 75-80% of the population and can significantly influence an individual's quality of life [1]. Low back pain can result from mechanical irritations of selected anatomical structures, such as the intervertebral disc, the facet joints and the associated lumbar spine nerve roots [2,3]. Lifting is a ubiquitous activity, where individuals are required to manually manage materials and loads throughout occupational tasks and activities of daily living [4]. Such lifting behaviors are used in a repeated fashion during various occupational engagements, such as healthcare, farm animal management, labor employment, and performing arts [5, 6]. A volitional preemptive abdominal contraction (VPAC) is commonly used to improve lumbar spine stabilization and reduce pelvic motion in individuals with spine dysfunction [7]. A commonly used VPAC strategy is the abdominal bracing maneuver, which produces a global trunk muscle contraction [8]. The purpose of this study was to examine the influence of VPAC and recurrent low back pain (rLBP) on pelvic and trunk mechanics, as well as neuromuscular control, during a symmetric lift task.

Methods: Thirty-seven healthy individuals and 31 rLBP individuals performed symmetric weighted box lifting trials with and without VPAC to a 1 meter height table. The VPAC condition was presented in random order. Electromyography (EMG) data from the right external oblique (EO), erector spinae (ES), multifidus (Mf), semitendinosus (ST), and gluteus maximus (GM) were measured. Three-dimensional kinematics of the lower extremity and trunk were collected. Kinematics and EMG were analyzed at two times at initial position-0.05s after lifting was initiated and again at final position -0.05s before the subject placed the box on the table. A 2 (group) × 2 (abdominal contraction) crossover mixed design was used to examine the effects of VPAC and group on biomechanical and neuromuscular control variables in lifting.

Results: The VPAC altered joint kinematic and muscle activity in rLBP and healthy individuals during symmetric lifting. A significant two-way interaction effect was observed for the ST activity in final position. The VPAC increased EO muscle activity, reduced ES, reduced Mf muscles activity at initial position, reduced Mf muscle activity at final position, greater trunk flexion angle, greater trunk side flexion angle, decrease pelvis obliquity angle at final position, and greater hip flexion angle at initial position. Recurrent LBP subjects presented reduced EO, GM, and greater Mf muscles activity at initial position, reduced EO, greater ES muscle activity and greater pelvis posterior tilt angle at final position.

Conclusion: Our results provide evidence that a VPAC strategy that is initiated during symmetric lifting decreases exposure to biomechanical factors that can contribute to lumbar spine injury. This apparent protective response is present in both healthy and rLBP individuals when lifting to a 1 meter height. Incorporating VPAC during dynamic stressful activities appears to help improve sensorimotor control and facilitate positioning of the lower extremity and the pelvis, while protecting the lumbar spine. Clinicians can use this information when designing neuromuscular control training

programs for people who have rLBP to improve lower extremity and spine control and spine stability thus potentially decreasing injury risk.

References: [1] Martin et al., Spine, 34: 2077-2084, 2009.

[2] Manchikanti et al., Pain Physician, 12: 541-559, 2009.

[3] Datta et al., Pain Physician, 12: 437-460, 2009.

[4] Ulrey et al., J Electromyogr Kinesiol, 23: 195-205, 2013.

[5] Theilmeier et al., Ann Occup Hyg, 54: 923-933, 2010.

[6] Ropponen et al., J Occup Environ Med, 54: 1330-1336, 2012.

[7] Nagar et al. Spine, 39: E89-96, 2014.

[8] Mcgill, Strength Cond J, 32, 33-46, 2010.

Disclosure of Interest: None Declared

Spine

AS-0328

CAN WE OFFER BIOMECHANICAL SUPPORT FOR LARGER BREASTED WOMEN WITH BACK PAIN?

Ambreen Chohan [1,*]Lauren Haworth [1]Jessie Janssen [1]James Selfe [1]

[1]Allied Health Research Unit, University of Central Lancashire, Preston, United Kingdom

Introduction and Objectives: It is argued that larger breasted women (D+ cup) may not receive adequate levels of support or quality of fit when measured using the traditional Warner® Alphabet system as it was initially only established for cup sizes A-C [1]. With 40% of UK females now measuring a D cup or above, many British females are at greater risk of wearing ill-fitting bras. Most bra designs take a symmetrical approach and fail to consider the high prevalence of breast asymmetry (62-82%)[2]. With a large breast exceeding 1000g in mass and no evidence to confirm that the tensile strength of the Cooper's ligaments increases in proportion with breast mass [3], failure to effectively support both breasts during dynamic activity can cause breast pain and many upper body physiological symptoms, including neck, shoulder and back pain [4]. A new innovative bra solution claims to eradicate breast-bounce and lift the breast through altered weight-distribution from the shoulders to the lower back, promoting a positive posture and lengthened abdominals (Figure). This study investigates immediate changes in pelvis, spine and breasts kinematics under three breast support conditions. In addition the quality of fit and changes in back pain, discomfort and stiffness as a result of change in breast support over a 4-week period were investigated.

Methods: Following a modified Red Flags screening process, eight females with non-specific neck/back pain (mean $\pm$ SD: age 36$\pm$9.92 years;BMI 30.60$\pm$3.91kg/m^2) were recruited. Participants with multiple red flags, those who with a history of spinal or breast surgery (such as Mammaplasty or mastectomy) Pregnant women, those that had ceased breastfeeding in the last year or were menopausal/post-menopausal were not eligible for this study. All appropriate ethical approval was gained. Body charts and Patient Reported Outcome Measures (PROMs) were used to assess pain location, pain severity, discomfort and stiffness. Participants performed 5 drop jumps off a 20cm high step and performed a computer typing task in three breast support garments (usual bra, professionally fitted bra, Optifit bra). Kinematics of the pelvis, spine and breasts were recorded using a 10-camera Oqus Qualisys motion capture system. The calibrated anatomical system technique (CAST) was used together with a multi-segment spine model and ten additional breast markers to allow analysis in the sagittal, coronal and transverse planes. All data were analysed using Visual3D (C-Motion Inc.) and SPSS. Statistical significance was set to P≤0.05. Bra fit assessments were completed based on established guidelines for each of the three bras. Nipple to sternal-notch distance, multiplanar breast deflection relative to the thorax during dynamic activity and the thoracic spinal posture relative to the pelvis in a seated and standing position was calculated.

Results: Bra-fit assessments showed that both the professional and usual bras were equally poor (0% pass rate), compared to the Optifit™ bra (100%). Common fitting issues for the usual and professional bras included a tight band and straps and incorrect cup sizes. Over the 4-week period significant improvements were seen in back stiffness in the Optifit™ bra (p<0.05). Body chart analysis for pain location showed a significant reduction in reported pain in the thoracic region (p<0.04) with the Optifit bra. Near significant reductions of over 55% were also noted for reported pain in the lumbosacral region with both the Optifit and Professional bras, compared to the Usual bra.

Nipple-sternum distances showed the Optifit™ bra provided the greatest uplift. In a standing posture, there was a trend towards significance when comparing the usual bra with the professional and Optifit™ bras, indicating both bras may open the chest, reduce slouch and bring wearers into a more upright standing position. Seated thoracic posture during the typing task showed greatest improvement with the professional bra. The dynamic task revealed a significant difference in mediolateral deflection between breasts, suggesting the need to consider breast asymmetry. Superior-inferior breast deflection showed a trend towards significance between bras with the Optifit™ bra showing the greatest level of support.

Figure:
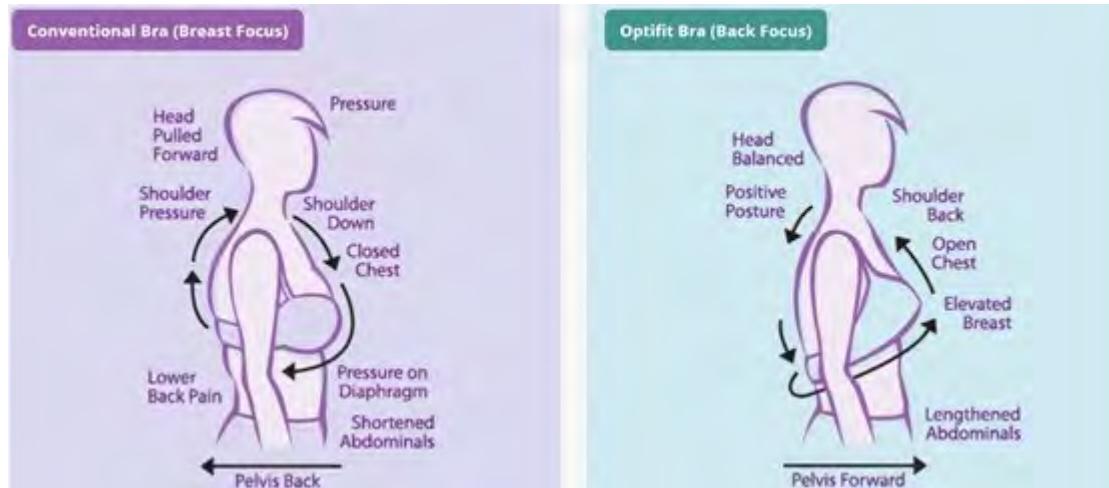
Caption: The proposed differences between a Professional bra, and the new innovative Optifit bra.

Conclusion: Overall, findings from this study support the increasing importance of bra fitting for larger breasted individuals with back pain; suggesting the need for alternative bra design and fitting guidance for these women. Further biomechanical research on alternative support solutions such as the Optifit™ bra may help to provide an alternative conservative management solution to those considering breast reduction surgery.

References: [1] Gefen, A et al. *Technology And Health Care,* 15:4, 259-271, 2007

[2] Mills, C. et al. *Journal of Sports Sciences*. 2014.

[3] McGhee, D.E. et al. *Journal of Science & Medicine in Sport,* 13:6, 568-572, 2010

[4]White, J. et al. *Ergonomics,*55: 6, 704-711, 2012

Disclosure of Interest: None Declared

Spine

AS-0329

THE GEOMETRIC CURVATURE OF THE SPINE DURING THE SIRSHASANA, THE YOGA'S HEADSTAND

Nayane Giraldi [1] Mario H. Campos [1,*]

[1] faculdade de educação física, universidade federal de goiás, Goiânia, Brazil

Introduction and Objectives: The sirshasana is one of the complex postures of yoga. Some yoga students reported that they feel a decrease of loads in the lumbar spine during this headstand position. However, the yoga postures that were most often associated with adverse events were headstand [1].

It is established that a moderate curvature minimizes the loads generated on the spine in situations where it is subjected to compressive forces [2]. The posture presented during walking may be inside the Neutral Zone [3], and appears to be a good parameter for defining this moderate curvature, ideal on sagittal plane. In the frontal plane, yet it is reasonable to assume that a rectified spine is ideal and that lateral deviations in the spinal alignment are associated with asymmetric load applications on the spinal structure. The measurement of the curvature of the spine during sirshasana is an unexplored approach that can help understand the human posture.

This study sought to analyse the behavior of the spinal posture in the sirshasana.

Methods: The study included 6 men and 5 women ($63,0 \pm 11,4$ kg; $166,4 \pm 8,0$ cm; $29,4 \pm 8,8$ years) that were able to execute the sirshasana (Figura 1). Adhesive retro-reflective markers (plane, square [8x12 mm]) were placed to mark and identify the spinous process of several vertebrae (from S2 to T1) and some another anatomical points on the back (Figure 1). Each volunteer was registered (60Hz) by 3 pre-calibrated camcorders (Mini-DV Panasonic) during: walking in a treadmill (5.0 km/h), orthostatic position and sirshasana. With Dynamic Posture system [4], the markers were identified and tracked in the movies. With DTL the 3D positions of all markers were computed in all activities.

The positions of the spinal markers were projected onto the sagittal and frontal planes. At each plane, the geometric two-dimensional curvature was computed [5]. The posture of the sirshasana was compared to the posture in the orthostatic position and with the average posture presented in all gait cycles happened between 700 frames. Kolmogorov-Smirnov (showed normally distributed data [p>0,05]), one way Anova (p<0,05) and post-hoc Tukey-Kramer tests were conducted in Matlab®.

Results: The absolute peaks of the spinal curvature of all volunteers were computed for each spinal region, in the frontal and sagittal planes, during gait, orthostatic position and sirshasana (Table 1). The frontal lumbar curvature (p=0.87) and the sagittal thoracic curvature (p=0.51) did not showed significant differences between activities. However, the sagittal lumbar curvature decreased (p=0.01) and the frontal thoracic curvature increased (p=0.04) in the sirshasana when compared to neutral postures of the gait and of the orthostatic position.

Probably, the data found at this work are associated with the position of the center of mass of the body in the erect position (near L2). During sirshasana, the mass supported by lumbar vertebrae is smaller than in the erect positions; and it is bigger for the thoracic region.

Figure:

Caption: Illustration of dorsal demarcation at sirshasana.

Conclusion: Although the number of participants in this study represents a limit to the work, the collected data are unpublished and may suggest recommendations for the practice of yoga. The findings suggest that the lumbar spine is less stressed during the execution of sirshasana. However, the sirshasana should be practiced very carefully by beginners and people who have problems in the thoracic region.

Table:

LumbarSagittal	Gait	Orth	Yoga		LumbarFrontal	Gait	Orth	Yoga
Average(m^{-1})	7.0	8.2	5.7		Average(m^{-1})	4.4	4.4	4.1
SD(m^{-1})	3.2	3.1	2.0		SD(m^{-1})	2.7	2.6	2.3
ThoracicSagittal	Gait	Orth	Yoga		ThoracicFrontal	Gait	Orth	Yoga
Average(m^{-1})	5.5	6.0	5.3		Average(m^{-1})	3.3	2.7	4.7
SD(m^{-1})	1.8	2.7	1.6		SD(m^{-1})	1.4	1.1	3.2

Caption: The average and standard deviation (SD) values of absolute peaks of the spinal curvature, for the sagittal and frontal planes, at lumbar and thoracic spine, during gait, orthostatic position and yoga.

References: [1] Cramer et al., 2013. Adverse Events Associated with Yoga... PLoS One.

[2] Adams et al., 1994. Posture and the compressive strength of the lumbar spine. Clinical Biomechanics.

[3] Scannel and Mcgill, 2003. Lumbar Posture - Should It, and Can It, Be Modified Physical Therapy.

[4] Campos M. H., 2010. Sistema de análise de movimento... PhD. Thesis, Unicamp.

[5] Brenzikofer et al., 2001. Spinal kinematics in normal walking using geometric curvature. XVIII ISB Congress.

Disclosure of Interest: None Declared

REPEATABILITY OF THE QUICK-RELEASE METHOD FOR ESTIMATING ACTIVE STIFFNESS OF THE TRUNK

Tara Diesbourg [1,*]Steven Fischer [2]Geneviève Dumas [3]

[1]School of Kinesiology and Health Studies, [2]School of Kinesology and Health Studies, [3]Department of Mechanical and Materials Engineering, Queen's University, Kingston, Canada

Introduction and Objectives:

The use of quick-release perturbations has been suggested as a method for estimating trunk stiffness. It appears to be effective for differentiating active trunk stiffness among individuals from special populations; however evidence supporting the validity of the method is limited [1]. The purpose of the current study was to examine the between-day repeatability of this process to see whether it can track changes in trunk stiffness over time.

Methods: Twenty subjects (10 male, 10 female: mean height – 174cm, mean weight – 72kg) were recruited from a university population. Trunk stiffness was estimated using a quick-release method [2]. Subjects were asked to adopt a semi-seated position with their arms crossed over their chest. Using electromagnets on cables affixed to the anterior and posterior aspects of a chest harness, weights (15% body weight) were suspended from the subject. At a random time (0-5s) and in random order either the front or the back weight was dropped (10 repetitions each), perturbing the subject in the opposite direction. A uniaxial load cell between the subject and the attached load was used to measure force. Acceleration was obtained from the force and was double-integrated to obtain displacement. It is assumed that vertical displacement of the load represents horizontal displacement of the trunk.

Trunk stiffness was estimated using least-squares optimization which used time-varying force, acceleration, velocity and displacement to estimate the system's effective mass (M), damping (B), and stiffness (K) coefficients [2]. The maximum vertical displacement (D) of the load and the time (T) required to achieve this maximum displacement were also calculated. This protocol was completed prior to and immediately following a seated 60 minute typing task (sessions = pre and post). These collections took place on 4 separate days.

For all statistical tests, coefficients obtained for forward and backward perturbations were analyzed separately. A Within-session (WS) analysis was conducted using Intraclass Correlation Coefficients (ICC(3,1)) for the 10 perturbations in each direction. The between-day (BD) analysis was completed using the mean of all perturbations in each direction and ICC(3,k) calculated across all 4 days.

Additionally, Standard Error of the Mean (SEM) were calculated for each of the WS and BD comparisons according to the method described by Weir [4] in order to better understand the test's inherent trial-to-trial noise.

Results: Due to load cell malfunctions, 46 backward sessions (23 pre and post) and 54 forward sessions (27 pre and post) were discarded prior to analysis. The ICC for all comparisons are provided in Table 1.

Repeatability within subject for stiffness in both WS was good [4] (overall mean ICC = 0.66 (Backward), 0.47 (Forward)). Repeatability for BD was moderate to good [4] (mean ICC = 0.46 and 0.38 for Backward and Forward respectively).

SEM estimates for K were 51.2% and 42.1% higher in the forward perturbation for WS and BD respectively, suggesting a larger variability exists in the data obtained from forward perturbations. Additionally, SEM estimates were 0.1 to 8 and 0.1 to 3 times greater than K for forward and backward perturbations respectively.

Conclusion: The overall results for this method indicate that it is repeatable for all types of analyses, more so for backward perturbations than forward. Therefore, this method is suitable for the desired within-subject over time comparisons, however due to the large SEM (especially for K), it may not be sensitive enough to detect minor changes in trunk stiffness over time. The SEM provides a threshold when assessing BD differences. In order to determine whether a difference should be considered real, it must surpass 2.75 times the SEM [4]. For forward perturbations, this is less likely to occur as the SEM was up to 8 times larger than the K estimate.

Table: Summary of all repeatability tests for all coefficients. WS = Within-session (pre), BD = Between-Day. M = Mass (kg), B = Coefficient of Damping (Ns/m), K = Stiffness coefficient (N/m), D = Max Displacement (mm), T = Time to Max D (ms).

		Backward				Forward			
	Var	SEM	ICC	95% CI	Sig	SEM	ICC	95% CI	Sig
WS (n=56)	M	6.63	0.792	0.723 - 0.854	0.000	31.37	0.542	0.435 - 0.660	0.000
	B	80.16	0.546	0.446 - 0.654	0.000	122.52	0.440	0.335 - 0.565	0.000
	K	770.73	0.654	0.563 - 0.747	0.000	1505.30	0.383	0.280 - 0.511	0.000
	D	7.68	0.679	0.592 - 0.765	0.000	6.54	0.546	0.440 - 0.662	0.000
	T	50.63	0.605	0.511 - 0.704	0.000	47.79	0.441	0.336 - 0.565	0.000
BD (n=7)	M	13.19	0.691	0.339 - 0.928	0.000	13.00	0.521	0.126 - 0.873	0.004
	B	134.52	0.279	-0.071 - 0.759	0.070	136.55	0.537	0.149 - 0.878	0.003
	K	1564.75	0.42	0.032	0.01	3716.69	0.14	-0.156	0.19

			3	-0.834	7		9	-0.675	5
D	15.66	0.519	0.121 -0.872	0.005	9.24	0.447	0.070 -0.841	0.010
T	101.03	0.389	0.011 -0.817	0.023	94.09	0.252	-0.074 -0.739	0.080

References: [1] Cholewicki et al, *Eur Spine J,* 8: 388-395, 1999.

[2] Hodges et al, *J Biomech,* 41: 61-66, 2009.

[3] Landis & Koch, *Biometrics,* 1: 159-174, 1977.

[4] Weir, *J Strength Cond Res,* 19(1): 231-240, 2005.

Disclosure of Interest: None Declared

AS-0331

THE GEOMETRIC CURVATURE OF THE LUMBAR SPINE DURING SQUAT EXERCISES WITH AND WITHOUT KNEE MOVEMENT RESTRICTIONS

Laizi Alaman [1] Marcelo Paula [2] Claudio Lira [1] Mario H. Campos [1,*]

[1] faculdade de educação física, universidade federal de goiás, [2] Unidade Goiânia, Instituto Federal de Educação, Ciência e Tecnologia de Goiás, Goiânia, Brazil

Introduction and Objectives: The squat is a exercise for strength training, widely used in physical conditioning programs, at rehabilitation processes and to improve sports performance.

The squat technique used can affect the distribution of forces between the knees and hips and on the kinematic properties of the exercise. The stress on the knees are minimized when the knees do not move anteriorly past the toes (restricted), but it is likely that load increases on the hips and the anterior tilt of the trunk increases [1] what could affect the lumbar posture. This study sought to analyse the behavior of the lumbar posture in the squat with and without knee movement restrictions.

Methods: The study included nine volunteers (21.7±4.1 years; 64.6±22.7 kg; 1.6±0.2 m), from both sex. All declared that were practicing strength training for one year or more than that and declared to use squat at their week training. Every one declared that had no back pain or other musculoskeletal problems. Each one indicated for the researchers the maximum (100%) load that was using at the squat training.

The volunteers wore shorts, running shoes, and for women, bikini or top with narrow straps on the back. Adhesive retro-reflective markers (plane, square [8x12 mm]) were placed to mark and identify the spinous process of several vertebrae (from S2 to T1) and some another anatomical points on the back (Figure 1).

Each volunteer was registered (60Hz) by 3 pre-calibrated camcorders (Mini-DV Panasonic) during four activities: orthostatic position; restricted squat with 100%; restricted squat with 50%; and unrestricted squat with 50%. For each squat condition, performed in a randon ordination, it was identified the most deeper position for analysis.

With Dynamic Posture system [2], the markers were identified and tracked in the movies. With DTL the 3D positions of all markers were computed in all activities.

The positions of the spinal markers were projected onto the sagittal plane and the geometric two-dimensional curvature was computed [3], in the lumbar region. The average lower lumbar posture presented in each situation was computed for analysis. Positive values indicated posterior concavities (lordosis), and negative values indicated anterior concavities (kyphosis). Kolmogorov-Smirnov (showed normally distributed data [$p > 0,05$]), one way Anova ($p < 0,01$) and post-hoc Tukey-Kramer tests were conducted in Matlab®.

Results: The results showed that the volunteers presented lordosis at the orthostatic position (5.1 ± 2.1 m^{-1}) that was higher than all squat postures ($p < 0.01$). The unrestricted squat with 50% of the load, was associated with a moderate lumbar lordosis (0.7 ± 1.6 m^{-1}) that was higher than the restricted squat postures ($p < 0.01$). The restricted squat postures were similar to each other and were associated with a moderate kyphosis at the lumbar spine (50% = -0.5 ± 1.5 m^{-1}; 100% = -0.3 ± 1.8 m^{-1}).

The data showed that happens an intense decrease of the lumbar lordosis during the squat exercise, independently of the technic adopted. However, when the knees were allowed to past ahead the toes, a posture with moderate lordosis is adopted. Differently, when the movement of the knees were restricted, the lumbar flexion was higher, and the lumbar spine presented a kyphotic posture.

Figure:

Caption: Illustration of dorsal demarcation

Conclusion: The data found at the present work shows a clear relationship between the squat technic and the spine posture. One should take into account the characteristics of each person, to choose the squat technique. To avoid kyphotic postures, one should choose a squat technique that does not restrict the forward movement of the knee.

Acknowledgements

References: [1] Fry, A. C., Smith, J. C., Schilling, B. K., 2003. Effect of knee position on hip and knee torques during the barbell squat. J Strength Cond Res.

[2] Campos M. H., 2010. Sistema de análise de movimento... PhD. Thesis, Unicamp.

[3] Brenzikofer et al., 2001. Spinal kinematics in normal walking using geometric curvature. XVIII ISB Congress.

Disclosure of Interest: None Declared

Neurological and Motor Control

AS-0332

COMPARISON OF FATIGUED AND NON-FATIGUED SQUATTING TRIALS USING MUSCLE SYNERGIES

Kenneth Smale [1,*]Mohammad Shourijeh [1]Daniel Benoit [1]

[1]Health Sciences, University of Ottawa, Ottawa, Canada

Introduction and Objectives: Humans have the ability to squat and jump with little to no conscious effort; however due to the high dimensionality of the neuromuscular system, the underlying mechanisms to perform such tasks are highly complex. Non-negative matrix factorization (NNMF) can be used to perform muscle synergy analyses, which decompose large quantities of high-dimensional EMG data into simpler components that can be used to describe the muscles' role in a certain task [1]. This procedure could be very beneficial as the shift of electrodes in relation to the underlying muscle fibres during dynamic contractions has rendered the use of traditional amplitude and frequency analyses in detecting fatigue inappropriate [2]. The **objective** of this study was to determine if muscle synergies are sensitive to detect fatigue-related changes during one and two-legged squats.

Methods: Eight healthy participants (23.8 ± 1.5y; 5 male) completed three one-leg squats on their dominant limb. To fatigue the participants, two-leg squats were completed at a pace of 35 squats/min with a standard 20.4 kg Olympic bar on their shoulders until exhaustion, which is the max value on the Borg Scale of Perceived Exertion [3]. The first three squats were used for the non-fatigued state, while the last three squats were used for the fatigued state. Once exhausted, participants completed three more one-legged squats.

Results: To account for 90% of variance in the original EMG signals, three muscle synergies (S) were needed in two-leg squats while four synergies were needed in one-leg squats. All synergy vectors had moderate to very strong correlations between fatigue states ($r = 0.6 – 0.89+$) except S4 of the one-legged squats. For both squat types, the coefficient (C) vectors showed no significant differences between the fatigue states (Figure). Interestingly, S3of the two-legged squats shifted from a general co-activation of all lower limb muscles pre-fatigue to a heavy weighting of rectus femoris and tensor fascia latae post-fatigue. This was reflected with a greater knee extensor moment throughout the entire cycle after as well as greater hip flexion moment at 35-65% of the squat after fatigue. Interestingly, the shift from a general co-activation of all lower limb muscles to knee extensor muscles (specifically the vastii) was also observed in S4 of one-legged squats, again suggested to correspond with an increase in knee extensor moment throughout the squat with significance occurring between 70-80% of the squat.

Figure:
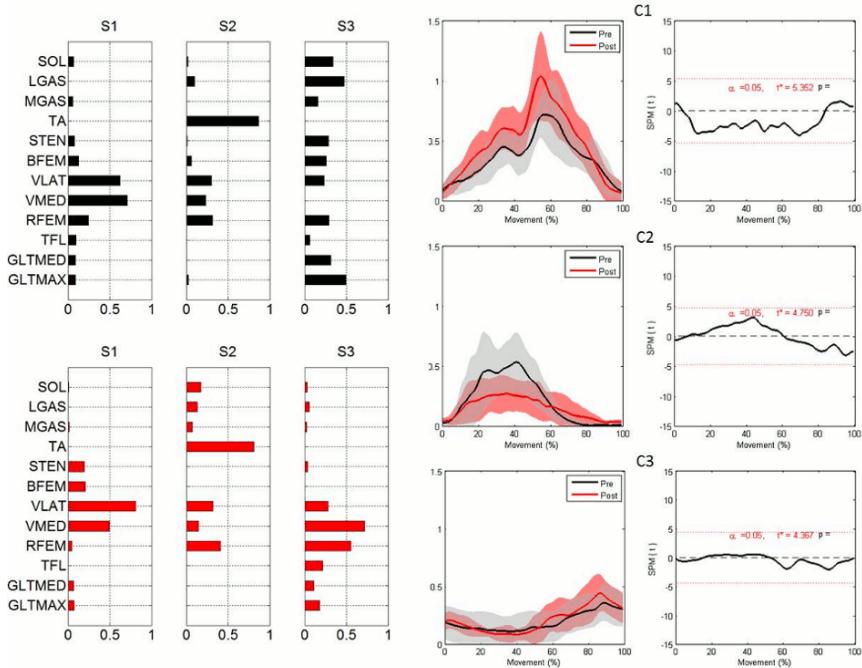
Caption: Muscle synergies (S1-S3) and coefficients (C1-C3) for two-legged squats during non-fatigued (black) and fatigued (red) states. For each coefficient, the figure on the left displays the mean and standard deviation clouds for pre and post fatigue. The figure on the right displays the t-statistic continuum determined through statistical parametric mapping. The red dotted line indicates the critical threshold and when the t-value exceeds this threshold, it is statistically significant at the α = 0.05 level. SOL: soleus; LGAS: lateral gastrocnemius; MGAS: medial gastrocnemius; TA: tibialis anterior; STEN: semitendinosus; BFEM: biceps femoris; VLAT: vastus lateralis; VMED: vastus medialis; RFEM: rectus femoris; TFL: tensor fascia latta; GLTMED: gluteus medius; GLTMAX: gluteus maximus.

Conclusion: Synergy analysis revealed the last module of both types of squatting moved from a general co-activation of muscles in the pre-fatigue state to a knee extensor dominant weighting post-fatigue, which we believe is needed when the body works against gravity during the ascending phase. It was of particular interest that the more demanding one-leg squat task elucidated a more apparent shift to knee extensors than what was seen in two-leg squats. Synergy analyses have the potential to play a critical role in a clinical setting as they have the ability to elucidate reorganization of muscle activations when their efficacy has been compromised. In particular, synergies were sensitive to detect fatigue-related differences in EMG during dynamic tasks, which were supported by differences in joint moments. This is extremely beneficial as synergy analyses focus on the holistic activation of the muscle rather than individual muscle fibres like traditional amplitude and frequency analyses. In conclusion, muscle synergy analysis can be an effective technique in decomposing complex EMG signals into rudimentary modules that can identify differences in muscle activations between fatigue states.

References: [1] Tresch et al. J of Neurophys, 95: 2199–2212, 2006. [2] Farina. Ex Sport Sci Rev, 34: 121-127, 2006. [3] Borg. Med Sci in Sports Ex, 14: 377–381, 1982.

Disclosure of Interest: None Declared

Neurological and Motor Control

AS-0333

ON THE METHODOLOGICAL IMPLICATIONS OF USING THE MUSCLE SYNERGIES CONCEPT

Alessandro Santuz [1,*]Lars Janshen [1]Antonis Ekizos [1]Adamantios Arampatzis [1]

[1]Training and Movement Sciences, Humboldt-Universität zu Berlin, Berlin, Germany

Introduction and Objectives: It has been generally accepted that the nervous system can simplify the production of movements by reducing the degrees of freedom through the creation of specific muscle activation patterns, called synergies[1]. It has been demonstrated that both human walking and running are likely to be controlled by shared synergies[2]. However, the methods used to process the EMG data, might influence the computation of muscle synergies. The purpose of this study was to investigate the outcomes and the reliability of two computational approaches ("classical" Gaussian[3] vs. Inverse-Gaussian[4] models) on muscle synergies using the non-negative matrix factorisation (NMF) approach. Furthermore, we examined the effects of the EMG processing procedures.

Methods: We recruited 20 healthy, young, adults (10 male, 10 female). The muscle activity of 24 ipsilateral muscles[5] was recorded with a wireless EMG system (myon AG, Switzerland). Ground reaction forces were recorded using a treadmill (H-p-cosmos GmbH, Germany) with an integrated pressure plate (zebris Medical GmbH, Germany). Out of the 24 recorded muscle activities, six were from the upper limb, four from the trunk and 14 from the lower limb.

The participants completed two tasks on the treadmill, in random order: shod running (2.8±0.4 m/s) and walking (1.4±0.2 m/s), both at their preferred speeds. We recorded the EMG signals during around 50 gait cycles (49±4)[6] and repeated the protocol after 15 minutes of rest, without removing the electrodes. After at least 48 h (122±84 h), the routine was repeated.

Surface EMG

The gait cycles breakdown was obtained from the pressure plate's raw data. We applied to the sEMG signals a high-pass filter (1st, 2nd and 4th order, 20, 50 and 250 Hz cut-off frequencies), a full-wave rectification and a low-pass filter (1st, 2nd and 4th order, 5, 10 and 20 Hz), creating 27 filtered and one non-filtered data sets. Each cycle was normalised to 200 data points[7] and the 50 cycles available for each trial were combined into one through averaging[6].

Motor modules extraction

We implemented (R Found. for Statistical Computing, Austria) two different NMF update rules for extracting motor modules. The first (GNMF) is based on maximising the Gaussian likelihood of reconstructing the original EMG signal[3]. The second (IGNMF) uses a special case of the generalized Inverse-Gaussian distribution[4]. To choose the minimum number of synergies required to represent the original signals, we applied two distinct methods. One is based on the cross-validation of the R^2 values used for describing the reconstruction quality[8]. The other uses the Akaike Information Criterion (AIC)[4] as an objective metric aiming to avoid over-fitting[9].

Results: The GNMF approach, consistently with previous findings[2], returns a similar number of synergies in both walking and running (5±1). The IGNMF approach, instead, can describe the original signal with only 3±1 synergies for walking and 4±1 synergies for running. The reconstruction quality, measured with R^2, is better after IGNMF (0.97±0.02 for walking and 0.98±0.01 for running) than after GNMF computation (0.86±0.04 and 0.85±0.04). Using the Pearson product-moment

correlation coefficient (r) for assessing the intra- and inter-day repeatability indicates a higher reliability of the IGNMF algorithm. As an example, the r-values for the inter-day repeatability of the motor primitives obtained using the non-filtered data set are the following ($p<0.05$): 0.48±0.34 (walking, GNMF), 0.63±0.29 (walking, IGNMF), 0.53±0.31 (Running, GNMF), 0.58±0.32 (Running, IGNMF).

Figure:
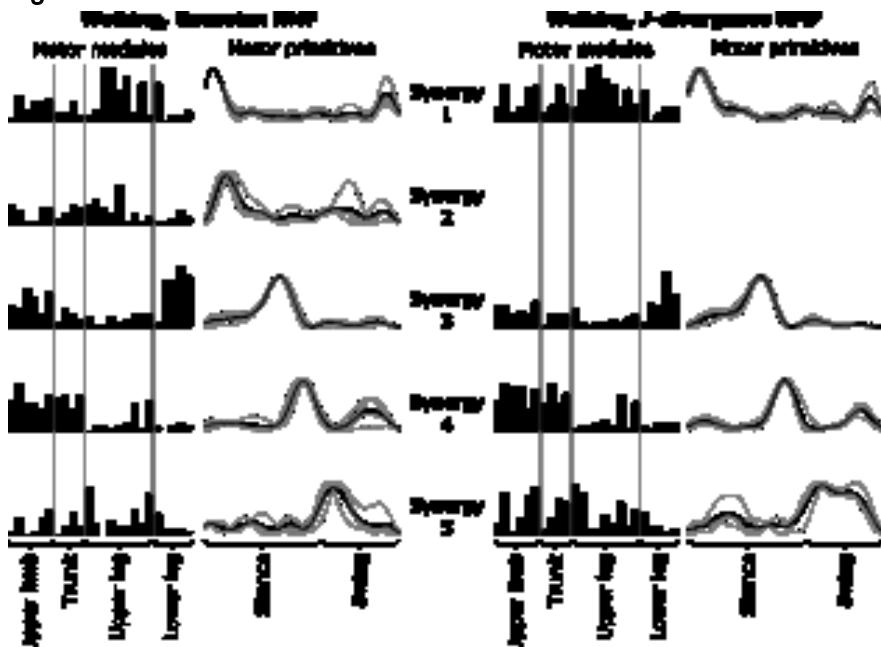
Caption: Motor modules (histograms) and motor primitives (curves) extracted with two NMF approaches for one participant during walking. The values of the motor modules are the average across four trials (two on Day1 and two on Day2). Bold curves describe the average activation patterns. Thin curves represent each single trial.

Conclusion: The filtering protocol preceding the NMF can influence both the GNMF and the IGNMF approaches. The second method shows better inter- and intra-day repeatability both in the motor modules and in the motor primitives. This is maybe due to the lower dimensionality of the resulting factorisation and it surely calls for a deeper analysis. In the future, it will be crucial to understand if the altered results are a consequence of a different description of the neurophysiological mechanisms underlying motor coordination.

References: [1] E. Bizzi et al., Brain Res. Rev., 57: 125-33, 2008.

[2] G. Cappellini et al., J. Neurophysiol.,95: 3426-37 2006.

[3] D. D. Lee et al., Nature, 401: 788-91, 1999.

[4] K. Devarajan et al., Neural Comput., 26: 1128-68, 2014.

[5] K. M. Steele et al., Front. Comput. Neurosci., 7: 105, 2013.

[6] A. S. C. Oliveira et al., Front. Hum. Neurosci., 8: 335, 2014.

[7] V. C. K. Cheung et al., J. Neurophysiol., 101: 1235-57, 2009.

[8] V. C. K. Cheung et al., J. Neurosci., 25: 6419-34, 2005.

[9] H. Akaike, Psychometrika 1987, 52, 317.

Disclosure of Interest: None Declared

Neurological and Motor Control

AS-0334

INSTRUMENTED MEASUREMENT OF NEUROMECHANICAL ANKLE PARAMETERS IN CHILDREN WITH CEREBRAL PALSY

Lizeth Sloot [1,*]Marjolein van der Krogt [1]Karin de Gooijer-van de Groep [2]Carel Meskers [1]Jurriaan de Groot [2]Annemieke Buizer [1]Jules Becher [1]Erwin de Vlugt [3]Jaap Harlaar [1]

[1]Rehabilitation Medicine, VU University Medical Center, Amsterdam, [2]Rehabilitation Medicine, Leiden University Medical Center, Leiden, [3]Biomechanical Engineering, Delft University of Technology, Delft, Netherlands

Introduction and Objectives: Spastic Cerebral Palsy (CP) is a central movement disorder and characterized by increased joint stiffness, caused by a mix of increased stretch reflex activity and muscle tone, as well as tissue stiffness. Since treatment depends on the specific cause, objective quantification of the ankle neuromechanical parameters would contribute to patient-specific treatment selection. Previously developed instrumented assessment combined with neuromechanical modeling [1,2] was extended to include background muscle tone and differentiate between the three major lower leg muscles. We examined the outcomes of the extended model and its repeatability and construct validity, i.e. the ability to discriminate between patients and controls and to measure the effect of treatment targeting abnormal muscle activation.

Methods: The most affected leg of 35 spastic CP patients (11.1±3.3 yr, GMFCS 1-3) and right leg of 35 controls (10.2±2.7 yr) was measured. Out of this population, 8 patients (10.3±3.5 yr, GMFCS 1-2) were measured again after 10±7 days to determine the inter-trial and between-day repeatability. Additionally, 6 patients (10.7±2.7 yr, GMFCS 1-3) were measured before and after treatment (4 received BTX-A in the calf muscles and 2 selective dorsal rhizotomy).

A motor driven footplate equipped with a force transducer and potentiometer applied 2 passive slow (5 °/s) and fast (100 °/s) ramp-and-hold rotations around the ankle joint. This was done at two different knee angles (20° and 70°) to discriminate between the triceps muscles, according to clinical conventions. Ankle angle and EMG of the gastrocnemius (GAS), soleus (SOL) and tibialis anterior (TA) muscles were used to optimize a nonlinear neuromuscular model to match the measured ankle torque. Tissue stiffness was based on the slow trials and taken at the highest plantar (40°) and dorsiflexion (5°) angle reached by all subjects. Root-mean-squares of baseline muscle activation and reflex torque were obtained from the fast trials. Repeatability was assessed using intraclass correlation coefficients (ICC), difference between patients and controls using non-parametric tests and treatment effect using t-tests.

Results: In CP, stiffness was increased by 70% in SOL (p=0.04), showed a trend of an increase by 80% in GAS (p=0.13) and was decreased by 37% in TA (p=0.03) compared to controls. Reflex activity was 3.5 and 3.1 times increased in CP for SOL and GAS (both p<0.01). Background muscle tone was increased by 70% in SOL (p<0.01). Variances were generally larger for CP and ratios between stiffness and reflex torque differed considerably between patients (Figure 1). Most parameters showed a good inter-trial repeatability with ICC ranging from 0.85-0.99, except for TA reflex and tonus (0.66 and 0.45) and GAS tonus (0.50). Between-day repeatability was lower, with ICC ranging between 0.54-0.96, except for SOL reflex and tonus (0.08 and 0.34) and GAS stiffness (0.32).

There was a trend of decreased reflex activity and a significant decrease in background muscle tone for the SOL (p=0.06, p=0.03) and GAS (p=0.10 and p=0.03) after treatment. Stiffness was not affected.

Figure:
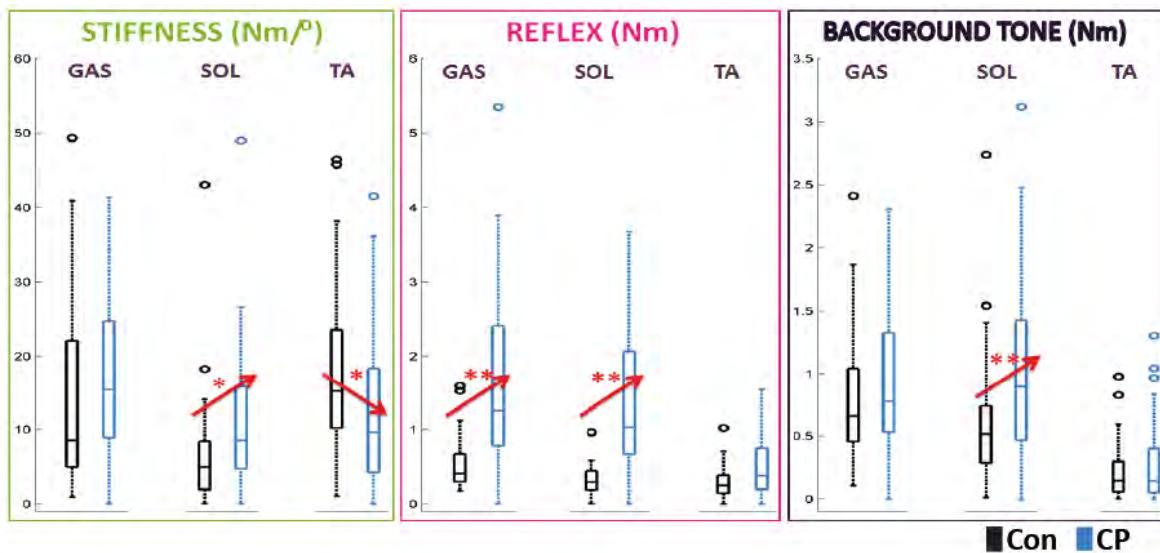
Caption: Figure 1: Stiffness, reflex and background muscle tone for CP (blue) and controls (black) for GAS, SOL and TA. Significant differences are indicated with * (p<0.05) and ** (p<0.01).

Conclusion: We developed and evaluated an extended model to quantify neurmechanical parameters for the GAS, SOL and TA. Overall, the inter-trial repeatability of these parameters was good. Their repeatability decreased between days, likely caused by the introduced variability of electrode placement and the ability to relax of a subject. The method was suitable to discriminate between CP patients and controls. In CP, reflex torque and muscle tone were increased in the triceps surae muscles, and decreased after treatment targeting abnormal muscle activation. Stiffness showed an increase for SOL, although a difference also emerged for GAS when choosing a higher dorsiflexion angle for the analysis, and was not affected by treatment. The large variance in contribution of stiffness and involuntary muscle activation in CP indicates that instrumented assessments could contribute to patient-specific therapy selection.

The limitations of the study include a small sample size for the repeatability and treatment group, as well as the assumptions of a rigid foot, i.e. no foot deformations occurred during the movements, and a strict discrimination between SOL and GAS based on knee angle. To tackle the latter, we aim to further develop the neuromuscular model in order to optimize the model parameters simultaneously for the two different knee angles. Future research will focus on the validation of the neuromechanical parameters against current clinical and manual instrumented spasticity assessment, as well as dynamic spasticity modelled during gait.

References: [1]   De Vlugt E. et al. 2010. J Neuroeng Rehabil 7:35

[2]   De Gooijer-van de Groep K.L. et al. 2014. J of NER 10:81

Disclosure of Interest: None Declared

Neurological and Motor Control

AS-0335

THE EFFECT OF ANGULAR VELOCITY ON THE MUSCULAR ACTIVATION OF ELBOW FLEXORS BICEPS AND BRACHIORADIALIS

Sylvie Von Werder [1] Catherine Disselhorst-Klug [1,*]

[1]Department of Rehabilitation & Prevention Engineering, Institute of Applied Medical Engineering, RWTH Aachen University, Aachen, Germany

Introduction and Objectives: Elbow flexion and extension movements are incorporated into various daily living activities such as eating, dressing, using a telephone or opening a door. Thereby, daily activities involve a continuous change in movement speed. However, there is a lack of detailed observations regarding the impact of movement speed on muscular activation strategies. In that context antagonistic coordination of the biceps and triceps during isokinetic concentric exercises was evaluated and found to be not dependent on angular velocity [1]. Detailed investigations of the impact of angular velocity on the force sharing of elbow flexors are missing. Spinal pathways have been identified, describing inhibitory neural connections between biceps and brachioradialis at the spinal cord level [2], while inhibitory connections of biceps differ from those of the brachioradialis [3]. Therefore this study aims to systematically investigate the coordination patterns of two elbow flexors in different movement speeds.

Methods: Elbow flexion and extension in neutral forearm position was assessed in 12 healthy subjects (age 25.9 4.9). The measuring procedure consists of two parts: guidance of targeted movement and measurement of the performed movement. With the help of a real-time visual feedback the angular velocity was guided to be in the range of 30-120 °/s. In that context a feedback path was visualized, which included ten different categories of angular velocities with 10 °/s intervals sequenced in an arbitrary order. The measurement of the performed movement included the recording of surface Electromyography (sEMG) of biceps and brachioradialis, elbow flexion angles, as well as the corresponding angular velocities. The sEMG recordings were band pass-filtered (10-500 Hz), rectified and smoothed (moving average filter, window length 100ms) in order to compute the envelope of the sEMG signal. Normalization was conducted relative to the 75% percentile of maximal amplitude of the envelope of all measurements of each subject. With the help of a decision tree at each sampling point, the processed sEMG data was categorized into combinations of angular velocity, flexion angle and contraction type categories. Thereby the contraction type was derived from the sign of the angular velocity. Positive angular velocities represented concentric contractions, whereas negative angular velocities represented eccentric contractions. The correlation of the processed sEMG signal, the angular velocity and the flexion angle was visualized in form of a three dimensional representation, containing angular velocity on the x-, angle on the y- and mean normalized sEMG envelope on the z-axis (Figure1). Finally, changes of the categorized sEMG data of both muscles were correlated to the performed angular velocity.

Results: The three dimensional representation of the biceps and brachioradialis for concentric contractions showed an increase of muscular activity with increasing flexion angles and increasing angular velocities. A change of the relation of the muscular activation of both muscles due to the angular velocity was found for flexion angles between 60-90°, only.

For eccentric contraction the three dimensional representation of the biceps showed that with increasing flexion angles the muscular activation increased, but no impact of the angular velocity on the muscular activation of biceps was found. In contrast, for the eccentric contractions of the brachioradialis the muscular activation increased with increasing angular velocity but not with increasing flexion angles. Therefore, for eccentric contractions an impact of angular velocity on the change of the synergistic relation of both muscles was found for all angles between 0-120°.

Figure:
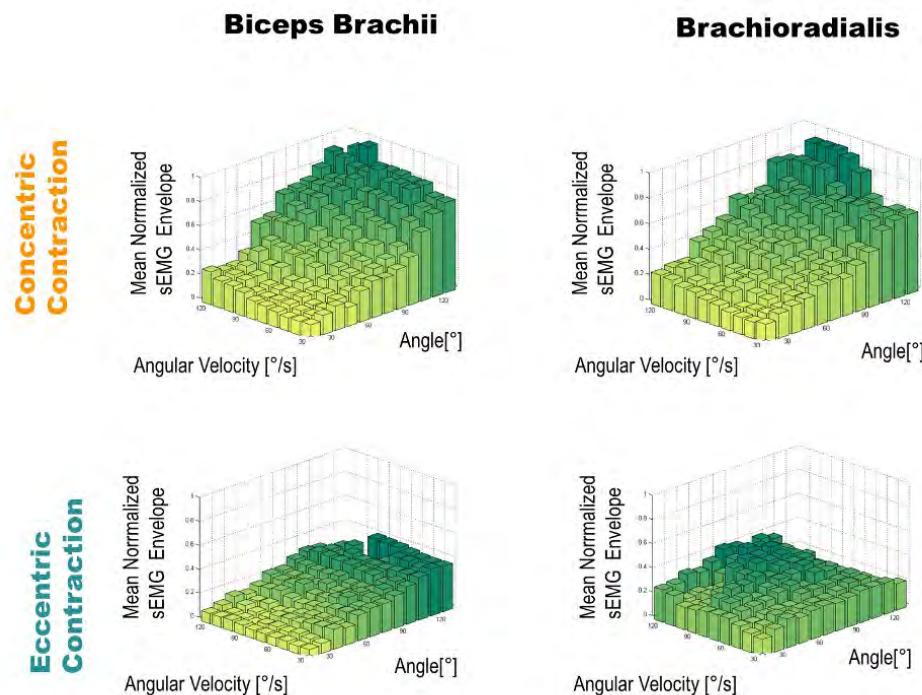
Caption: Mean three dimensional representations containing angular velocity on the x-, angle on the y- and normalized sEMG envelopes on the z-axis for biceps brachii (left column) and brachioradialis (right column) in concentric (upper row) and eccentric (lower row) contractions.

Conclusion: The present study showed that the movement speed correlates with a change in muscular activation of biceps and brachioradialis, however this effect is differently expressed for variant combinations of contraction type and flexion angle.

Due to the increased activation of brachioradialis in eccentric contractions with increasing velocities, the brachioradialis could be regarded as a controlling muscle, which helps to adapt the muscular coordination pattern of elbow flexors to the targeted angular velocity performance.

References: [1] Bazzuchhi I. et al., Muscle Nerve, 33: 191–199, 2006.

[2] Cavallari P. et al., Exp Brain Res., 78(3):465-78, 1989.

[3] Naito A, Anat Sci Int., 79(1): 11–20, 2004.

Disclosure of Interest: None Declared

AS-0336

MUSCLE SYNERGIES AND MODULARITY IN THE RABBITS DURING NORMAL HOPPING AND JUMPING

Pavan Teja Devanaboyina [1,*]Massimo Sartori [2]Thor Besier [3]David Lloyd [1]

[1]Centre Musculoskeletal Research, Griffith University, Gold Coast, Australia, [2]Department of Neurorehabilitation Engineering, University Medical Center , Gottingen , Germany, [3]Auckland Bioengineering Institute, University of Auckland , Auckland, New Zealand

Introduction and Objectives: Musculotendon forces are needed to understand the strain distribution in human and animal tendons. In animals, implantable buckle transducers are used to measure tendon forces. However, this invasive procedure causes tendon damage and abnormal movement. Alternatively, forces can be estimated by less invasive methods using neuromusculoskeletal models driven by neural signals derived from muscle synergies extracted from electromyography (EMG) [1, 2]. Muscle synergies are a low-dimensional set of synergy excitation primitives (XPs) and muscle weightings [3] that are decomposed from high-dimensional, multi-muscle set of EMGs.

We aimed to see if muscle synergies could be used to characterise the muscle activation patterns used by rabbits across different locomotion tasks, the first step to enable subsequent estimation of musculotendon forces and Achilles tendon strain. In rabbits, *in-vivo* recordings from a large number of EMG channels is not feasible. So we created a comprehensive EMG dataset that characterizes the electrophysiological activity of a larger number of muscles by combining EMG recordings from various muscles and rabbits across different motor tasks. The comprehensive EMG datasets were decomposed into low-dimensional muscle synergies XP and weightings. We then examined if the same set of XPs could be used to recompose the muscle EMG patterns across the range of motor tasks.

Methods: Four healthy rabbits performed 2 locomotor tasks: 1) normal hopping, and 2) short box jump. A Noraxon system recorded EMGs at 1000 Hz from 5-to-7 bipolar fine wire electrodes inserted in each rabbit's left hindlimb muscles. This resulted in EMGs recorded from 9 muscles in total: abductor cruris cranialis (Abd), Adductor (Add), semitendinosus (ST), vastus lateralis (VL), superficial digital flexor (SDFM), deep digital flexor (DDFM), tibialis anterior (TA), lateral gastrocnemius (LG), and soleus (Sol). EMG data were band-pass filtered (30-400 Hz), full-wave rectified, and low-pass filtered (10 Hz) to create EMG linear envelopes. These were amplitude-normalised to the peak processed value on a trial-by-trial basis and time-normalised to 100 data points. Processed and normalised EMGs across all rabbits and trials were averaged and concatenated to create 3 EMG datasets: 1) normal hopping, 2) jumping, and 3) combination of normal hopping and jumping. For each EMG dataset, non-negative matrix factorisation (NNMF) [3] was applied to extract the XPs and weightings. The number of synergy modules were increased until the variation accounted for (VAF) was greater than 95%. For each EMG dataset the corresponding XPs and weightings were linearly recombined to reconstruct the each muscles EMG patterns and were compared to the measured EMG patterns using Pearson correlations for each task.

Results: NNMF extracted 3 XPs and weightings (Fig. 1), which had VAF more than 95% for all the EMG datasets. For the hopping motor task the averaged correlation between the measured and reconstructed EMG patterns was 0.78, 0.54 and 0.77 when using hopping, short box jump and combined EMG dataset respectively (Table 1). For the short box jump

motor task the correlation values were 0.47, 0.67 and 0.55 when using hopping, short box and combined EMG dataset respectively.

Figure:
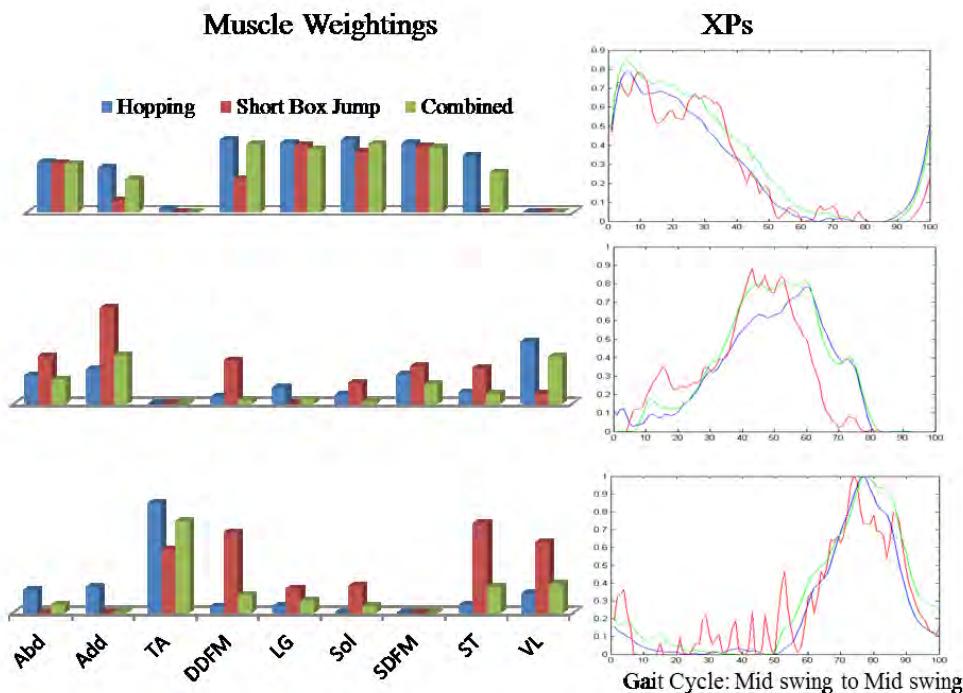
Caption: Fig 1: Muscle synergies extracted from three EMG datasets

Conclusion: We derived synergies that explain neuromuscular control strategies across 9 muscles, 4 rabbits and 2 motor tasks. The combined EMG dataset synergies were not able to improve the prediction of the measured EMG patterns when compared to corresponding task specific synergies. Therefore for the future simulations the task specific synergies should be used for calculating musculoskeletal forces and tendon strain distribution.

Table:

Tasks	Hopping EMG dataset	Short box jump EMG dataset	Combined EMG dataset
Hopping	0.78±0.23	0.54±0.39	0.77±0.22
Short box jump	0.47±0.41	0.67±0.28	0.55±0.40

Caption: Table 1: Correlation (Mean+SD) between measured EMGs and synergy reconstructed EMGs for hopping and short box jump

References: [1] Lloyd et al., J Biomech,36: p. 765-776, 2003.

[2] Sartori et al., Front Comput Neurosci, 7: p. 79, 2013.

[3] Lee et al., Nature, 401: p. 788-791, 1999.

Disclosure of Interest: None Declared

AS-0337

ANTICIPATED MUSCULAR SYNCHRONIZATION IN BAREFOOT CROSS-SLOPE WALKING

Anna S. Estermann [1 2,*]Lea Nösberger [1 2]Lukas Stammler [2]Vinzenz von Tscharner [3]Beat Göpfert [4 5]

[1]Health Division, Bern University of Applied Sciences, Bern, [2]BZG, Bildungszentrum Gesundheit Basel-Stadt, Münchenstein, Switzerland, [3]Human Performance Laboratory, University of Calgary, Calgary, Canada, [4]Center of Biomechanics, University of Basel, [5]Laboratory for Movement Analysis Basel, Children's University Hospital Basel (UKBB) Basel, Basel, Switzerland

Introduction and Objectives: Movement adaptations are necessary to perform our daily activities. These adaptations are often done automatically, like varying the walking movement while passing a cross-sloped surface. Therefore we anticipate our muscular activation pattern with a slightly alternation to accomplish the movement task in an appropriated way, that may increase safety or performance.

The goal of this study was to analyze the anticipated muscular activity and the inter-muscular synchronization while walking barefoot on flat and cross-sloped surface within each and overall subjects.

Methods: A 3D-gait-analysis (Vicon, 12 Cameras T20) with a synchronous surface electromyogram (EMG) (Myon, 2400Hz) of the right leg muscles: Tibialis anterior (TA), Peroneus longus (PL), Gastrocnemius medialis (GM) and lateralis (GL), Vastus medialis (VM) and lateralis (VL), Rectus femoris (RF), Semitendinosus (ST) and Biceps femoris (BF) was done. 10 subjects (f, 22-25y) walked at a self-selected speed on flat and cross-sloped surface (6°). 10 trials of each condition and surface were measured: flat (F), cross-slope up-side-leg (US), cross-slope down-side-leg (DS). The time was normalised over a gait-cycle, the averaged kinematic data and the normalized Wavelet-Transformed-EMG Total-Intensity (I_{tot}) of the wavelets 5 to 8 with the center frequencies: 92; 128; 170 and 218 Hz were analyzed within a gait-cycle for each subject and overall subjects while walking on the different conditions.

Results: The results show a significant difference in the stance-phase for the knee flexion and ankle dorsi-flexion between the conditions flat and cross-slope down-side-leg as well as for cross-slope up-side-leg and down-side-leg for all 10 subjects. The overall mid-stance muscular adaption of one representative subject show e.g. on the flat surface is the GM-I_{totMAX} 2.4% before the GL-I_{totMAX} (Fig. 1a left), while for the cross-slope up-side-leg condition GM-I_{totMAX} is 0.3 % ahead of the GL-I_{totMAX} (Fig. 1a right). The results overall subjects show that GM-I_{totMAX} is significant earlier than GL-I_{totMAX}: 1.8 % (SD: 1.6% p: 0.016) on the flat surface (Fig. 1b left) and 3% (SD: 2.4%, p: 0.016) for the cross-slope down-side-leg, There is no significance for the cross-slope up-side-leg with 2% (SD: 2.5%, p: 0.081) (Fig. 1b right). The intra-muscular temporal shifts between the 3 conditions are for the GM-I_{totMAX} in the cross-slope up-side-leg 1.3% (SD: 2.5%, p: 0.26) and down-side-leg 1.7% (SD: 2.8%, p: 0.19) earlier than on flat surface, and the GL-I_{totMAX} is in the up-side-leg 1.1% (SD: 2.0%, p: 0.91) and the down-side-leg 0.5% (SD: 1.9% p: 0.41) earlier than on the flat surface.

Figure:

Fig. 1a) Condition Flat, 1 Subject, 24 Gait cycles / Condition Upside Leg, 1 Subject, 30 Gait cycles

Fig. 1b) Condition Flat, 10 Subject, 266 Gait cycles / Condition Upside Leg, 10 Subject, 280 Gait cycles
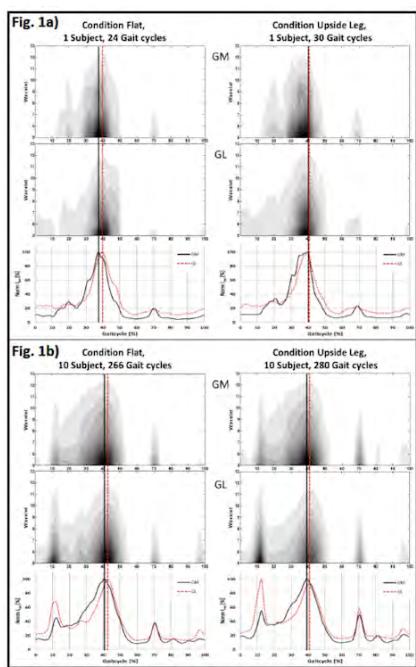
Conclusion: The results show that the movement, even with small changes in the surface condition lead to a delectable adaption in the kinematic and muscular activation pattern. The variation in the surface requires also a new synchronisation pattern of the muscular interplay similar as Wakeling [1] showed with the muscle tuning by varying the shoe elasticity. These optimising processes may be performed by a feed-forward controlling system and can therefore be seen as an anticipated muscular synchronization. This is necessary in adjusting our neuromuscular activity pattern in daily movement tasks. Further, the measured time shifts of the I_{totMAX} between the 3 conditions were small. A range of 1% corresponds to about 10 ms for the measured gait-cycle time of approximate 1s. Although it is known that small neuromuscular changes may lead e.g. to Patellofemoral Pain Syndrome due to a delayed onset of the VM vs. VL [2; 3], or increase the risk of ACL-Ruptures [4] due to a different muscular activation pattern of the ST. However neuromuscular training may increase the ability in anticipated muscular synchronization, which reduces the risk of injuries dramatically [5; 6] and increases the performance in sport [7].

Conclusion: The anticipated muscular synchronization adapts to the task and is an important aspect of neuromotor control required for performing the neuromuscular demands of everyday movements.

References: 1: Wakeling et al. J Eur J Appl Physiol. 2001 Nov;86(1):40-7.

2: Cowan et al. Arch Phys Med Rehabil. 2001 Feb;82(2):183-9.

3: Pal et al. Am J Sports Med. 2011 Mar;39(3):590-8

4: Zebis et al. Clin J Sport Med. 2008 Jul;18(4):329-37

5: Olsen et al. BMJ. 2005 Feb 26;330(7489):449

6: Pasanen et al. BMJ. 2008 Jul 1;337:a295

7: Myer et al. J Strength Cond Res. 2005 Feb;19(1):51-60.

Disclosure of Interest: None Declared

Mechanics

AS-0338

A MULTIDIMENSIONAL MODEL OF CHANGES IN KNEE JOINT MECHANICS DURING GAIT AFTER TOTAL KNEE ARTHROPLASTY

Janie Wilson [1]Jereme Outerleys [1,*]Cheryl Kozey [1]Michael Dunbar [1]

[1]Biomedical Engineering, Dalhousie University, Halifax, Canada

Introduction and Objectives: Total knee arthroplasty (TKA) surgery is the treatment of choice for those with severe knee osteoarthritis (OA). A primary aim of TKA is to improve knee joint function in daily activity. Surgery has been shown to improve knee joint kinematics and kinetics towards asymptomatic patterns, but variability and residual deficits remain post-operatively[4]. It is difficult to interpret multiple, often correlated, changes in gait mechanics simultaneously. The objective of this study was to use principal component analysis (PCA) on discrete knee kinematic and kinetic metrics to extract uncorrelated, multidimensional gait features, and to compare the gait mechanics pre-TKA to post-TKA, and relative to asymptomatic and early/moderate knee OA cohorts.

Methods: 46 patients (17M, 29F) diagnosed with severe knee OA and scheduled for primary TKA surgery underwent a 3D gait analysis 1 week prior to, and 1 year after, their TKA. Sixty asymptomatic adults and 60 with early/moderate knee OA also underwent gait analysis. Average 3D joint kinematics and kinetics were calculated at self-selected speeds and normalized to 100% of the gait cycle. TKA patients received 1 of 3 similar implant designs. Discrete gait knee mechanics metrics, reported in the literature[2], were extracted from all 166 subjects, and entered into a PCA (166 observations on 11 variables). Variables included average gait speed, stance and swing phase knee flexion angles, flexion angle range, peak flexion moment, peak extension moment (late stance), peak extension moment (early stance), peak rotation moment, first and second peak of the adduction moment, and the mid-stance adduction moment. PCscores were calculated for all subjects for the first three extracted PCs. Variables within each PC were interpreted if their coefficient was at least 50% of the maximum coefficient, and if their correlation with the PC was at least 50%[1]. ANOVA models with Tukey post hoc examined differences in PCs for the four groups ($\alpha = 0.05$).

Results: PC1, PC2, PC3 captured 43.8%, 25.5% and 9.6% respectively of the original data variability among subjects (cumulatively 79%). Gait speed, peak stance and swing flexion angle, range of flexion angle, peak early stance and late stance extension moment, and peak rotation moment in late stance had significant correlation and high, positive and equal weighing on PC1. Higher PC1 scores were associated with faster speed, more flexion, and higher peak extension and rotation moments. Thus PC1 was interpreted as a sagittal plane/speed metric, with higher scores related to higher function. Asymptomatic PC1 scores were significantly higher than all others (P<0.03), early/moderate OA were significantly higher than pre/post-TKA (P<0.0001), and post-TKA was significantly higher than pre-TKA (P<0.0001) (Table 1, Figure 1). PC2 had high correlation and high positive coefficients from the first and second peak adduction moments, and the mid-stance minimum of the adduction moment. PC2 was interpreted as capturing the overall magnitude of the knee adduction moment during stance, including not just peak values, but mid-stance as well. Asymptomatic PC2 scores were significantly lower than early/moderate OA and pre-TKA (P<0.001), meaning lower overall adduction moments throughout stance. Post-TKA PC2 scores were not significantly different than any other group (P>0.05). PC3 was

dominated by the peak flexion moment in stance, with high scores associated with higher peak flexion moments. Statistically significant differences in PC3 were observed between the asymptomatic and early/moderate OA group (P=0.017), with asymptomatic having higher peak moments.

Figure:
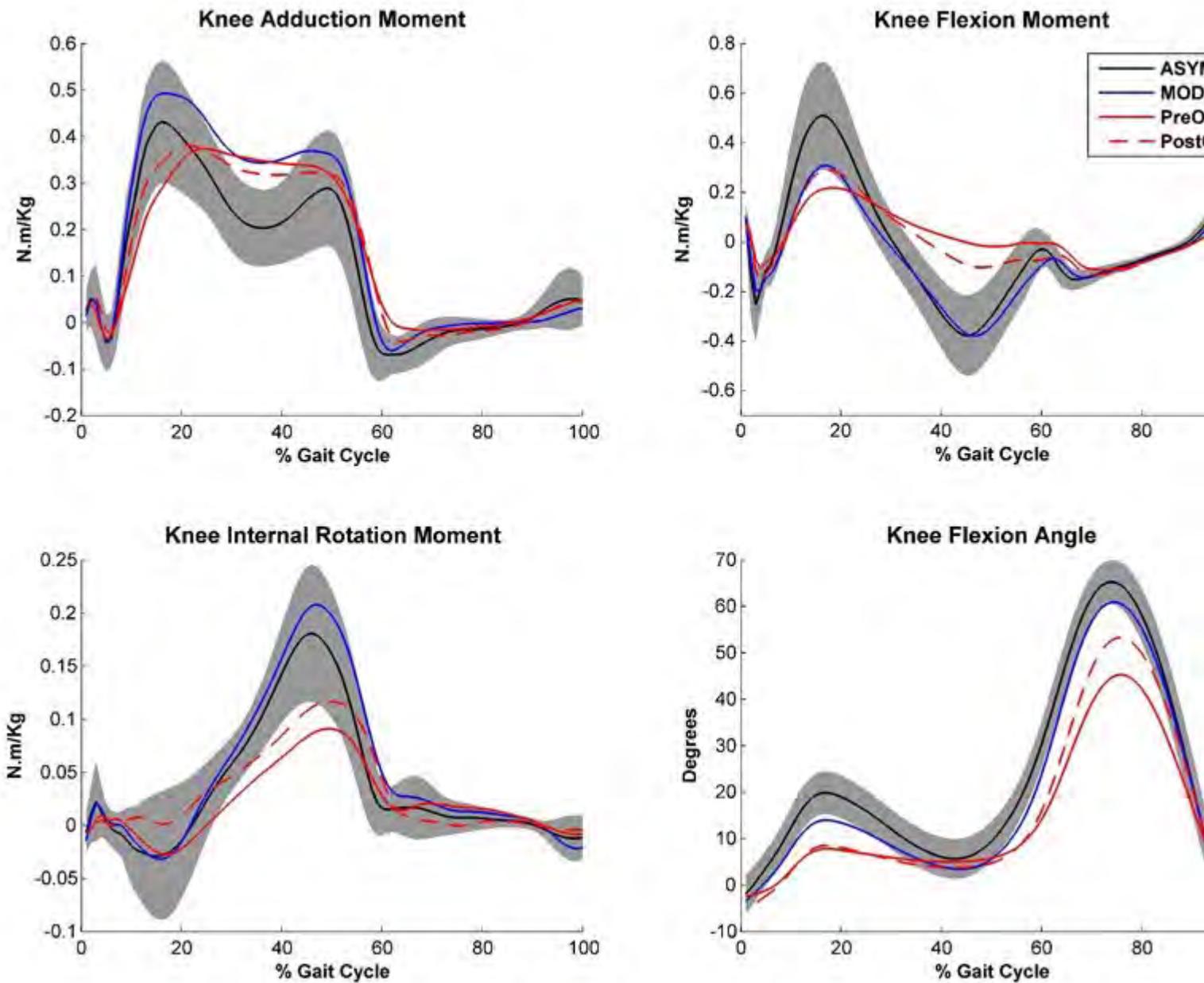
Caption: Mean gait waveforms

Conclusion: Summarizing pre to post-TKA gait mechanics changes in a few key, objectively extracted features, suggests that there is room for functional improvement post-TKA in terms of sagittal plane movement, loading and gait speed. PC1 captured significant differences among all groups, with a small, significant improvement in this metric post-TKA relative to pre-TKA. The post-TKA group was still lower than both asymptomatic and moderate OA, meaning that this aspect of gait

is not being restored. PC2 captured the overall magnitude of the adduction moment, similar to PCs from knee adduction moment waveforms[3]. The moderate and pre-TKA groups had higher adduction moments than asymptomatic, but the post-TKA group's distribution overlaps with the asymptomatic group, suggesting improvements in terms of lower adduction moments. These results also highlight that there are interrelationships among different combinations of discrete gait variables that may benefit interpretation by being combined by PCA.

References: [1]Astephen et al., Proc. Inst. Mech. Eng. H J. Eng. Med., 218(4):271-279, 2004.

[2]Astephen et al., J. Orthop Res., 26(3):332-341, 2007.

[3]Landry et al., J. Biomech., 40(8):1754-1761, 2007.

[4]Hatfield et al., J. Arthroplasty, 26(2):309-318, 2011.

Disclosure of Interest: None Declared

Orthopaedic Implants

AS-0339

NON-INVASIVE STIFFNESS ALTERATION DURING FRACTURE HEALING BY USE OF A NOVEL SHAPE MEMORY OSTEOSYNTHESIS.

Manuel Krämer [1,*] Christian Müller [2] Ronny Pfeifer [3] Sebastian Decker [2] Karen Meier [4] Christof Hurschler [1]

[1] Laboratory for Biomechanics and Biomaterials, [2] Department of Trauma Surgery, Hannover Medical School, [3] Laser Zentrum Hannover e.V., [4] Small Animals Clinic, University of Veterinary Medicine, Hannover, Germany

Introduction and Objectives: The fracture healing of bones is highly influenced by biological parameters and biomechanical stimuli. These mechanical conditions are determined by the stiffness of fixation and loading. Fixation in an optimal stiffness range stimulates bone healing by callus formation. Latest studies have shown that the progress of healing can be influenced by modulating the fixation stiffness during fracture healing [1]. In the literature concepts for the dynamization as well as for the inverse dynamization of the fracture fixation are lively discussed [1], [2]. However, alterating the stiffness of the fixation non-invasivly is so far only possible by use of a Fixateur externe. In the present study a novel Nickel-Titanium shape memory plate osteosynthesis is applied that allows contact-free stiffness modulation after fracture fixation [3]. The study was designed to test the following hypothesis: A novel shape memory plate stabilizes tibia osteotomies in rabbits and allows for fracture healing. After non-invasive electromagnetic induction heating three weeks post op. the plate changes its configuration towards a state of higher stiffness.

Methods: Prototype six-hole osteosynthesis plates were constructed and manufactured by laser based cutting and welding. The plates were manufactured from commercially available Nickel-Titanium alloy sheets. The design allows for change of shape and therewith bending stiffness. For the present study a plate which follows the concept of inverse-dynamization was realized. The modulation is triggered by warming the implant up to 50°C for a short period of time by use of electro-magnetic induction heating.

14 Rabbits were treated with prototypic plates after tibia osteotomies have been performed. Furthermore, four k-wires were implanted in each treated limb for in-vivo bending measurements.

Three weeks after procedure, animals were divided in two randomized groups. Stiffness alteration of the plate was performed only in one group by electromagnetic induction warming.

Repetitive in-vivo bending stiffness measurements were performed by use of an in-vivo bending stiffness test rig [4].

All Animals were sacrificed after six weeks. Tibiae were analysed morphologically by x-ray, µCT, and histology. The implants were explanted and bending tests of the tibiae were carried out.

Results: One rabbit died from anaesthesia during the induction warming procedure and one animal fractured its hind leg two days post op and was therefore sacrificed. The shape change of the implant in vivo could be observed radiographically during induction warming. There were no signs of implant loosening or displacement. Comparison between bending stiffness within minutes before and after induction warming confirmed a significant increase of mean bending stiffness of the tibiae ($p < 0.05$). All osteotomies healed within six weeks. However, the ex-vivo bending tests showed not significant differences in stiffness between the two groups ($p > 0.05$). The µCT showed successful bone

healing for both groups. The measured parameters such as bone volume, cortical wall thickness etc. showed no significant differences between both groups (p>0.05).

Conclusion: To the best of our knowledge, the present work is the first study applying the idea of inverse dynamization to an internal fracture fixation plate. We have demonstrated a successful application of a novel shape memory plate system for the stabilization of tibia osteotomies in rabbits. The contact-free triggering of the shape alteration of the plate could be approved and resulted in an expected increase of stiffness. Successful fracture healing was observed in all cases. These results contribute to the development of novel concepts for bone fixation that might lead to better fracture healing and less need for surgical interventions. Furthermore, in future this concept might be used for counteractions in cases of non-union.

References: [1] Claes et al., J Orthop Trauma, 25(3):169–74, 2011.

[2] Epari et al., Med Hypotheses, 81(29:225-7, 2013.

[3] Olender et al., Ann Biomed Eng, 39(5):1546-54, 2011

[4] Thorey et al., Technol Health Care, 16(2):129-40, 2008

Disclosure of Interest: None Declared

Orthopaedic Implants

AS-0340

THE INFLUENCE OF KINEMATIC CONDITIONS ON THE WEAR OF UHMWPE ARTICULATING AGAINST PEEK OPTIMA FEMORAL COMPONENTS

Raelene M. Cowie [1,*] Adam Briscoe [2] John Fisher [1] Louise Jennings [1]

[1]University of Leeds, Institute of Medical and Biological Engineering, Leeds, [2]Invibio Biomaterial Solutions, Thornton Cleveleys, United Kingdom

Introduction and Objectives: PEEK Optima has the potential for use as an alternative bearing material in joint replacement to give metal-free joints [1]. In this study, the novel bearing couple of PEEK articulating against polyethylene was investigated to ascertain whether PEEK would be a viable alternative for use as the hard bearing material in total knee replacements. The wear of all polyethylene tibial components articulating against PEEK femorals was assessed and compared to the wear against cobalt chrome femorals of similar surface topography and geometry in a knee simulator. To further investigate the appropriateness of this material, enhanced preclinical tests were carried out beyond the ISO standard.

Methods: Three cobalt chrome (initial Ra ~0.02μm) and three moulded PEEK Optima (initial Ra ~0.02μm) femoral components (Invibio Biomaterial Solutions Ltd., UK) of similar surface topography and geometry were paired with GUR 1020 all polyethylene tibial components (conventional, unsterilised) in a 6 station ProSim knee simulator (Simulation Solutions, Manchester). Experimental knee simulation was carried out under displacement control with an anterior posterior translation of either 5mm (intermediate kinematics) or 10mm (high kinematics) [2] for 3 million cycles (MC) for each condition and using 25% serum as the lubricant. Wear of the UHMWPE tibial components was assessed by gravimetric analysis with unloaded soak controls used to compensate for the uptake of moisture by the samples. Changes in the surface topography of the bearing surfaces was measured using a contacting Form Talysurf (Taylor Hobson, UK) pre-test and at each measurement point; the temperature of the bulk lubricant was monitored close to the articulating surfaces. Statistical analysis was carried out using ANOVA, data was considered significant at $p < 0.05$.

Results: Following 3MC of wear testing under intermediate kinematics, the wear rate of UHMWPE tibial components articulating against cobalt chrome femoral components was 0.97 ± 2.26 mm^3/MC, which was similar ($p=0.06$) to that against PEEK femoral components 2.45 ± 0.77 mm^3/MC (Figure 1). There was linear scratching on the surface of the femoral components in the principle direction of sliding, which was more evident on the PEEK components resulting in a mean surface roughness (Ra) of 0.03 ± 0.04μm for cobalt chrome and a significantly ($p=0.009$) higher surface roughness of 0.23 ± 0.18μm for PEEK; there was a polished region on the tibial components denoting the wear area. Following a further 3MC under high kinematics the wear rate was similar for both PEEK ($p=0.659$) and cobalt chrome ($p=0.240$) compared to intermediate kinematics (Figure 1), this may be due to the low conformity of the implant [3]. There was no significant change in the surface roughness of the femoral components following 3MC of high kinematics.

The mean temperature of the bulk lubricant under intermediate kinematics was 28.0 ± 0.7°C for cobalt chrome and for PEEK was significantly higher at 29.5 ± 0.1°C ($p<0.001$), changing from intermediate to high kinematics had no effect on

the lubricant temperature. The increased temperature may be a result of the higher friction of the PEEK bearing couple [4] but may also be an artefact caused by continuous running of the simulator.

Figure:
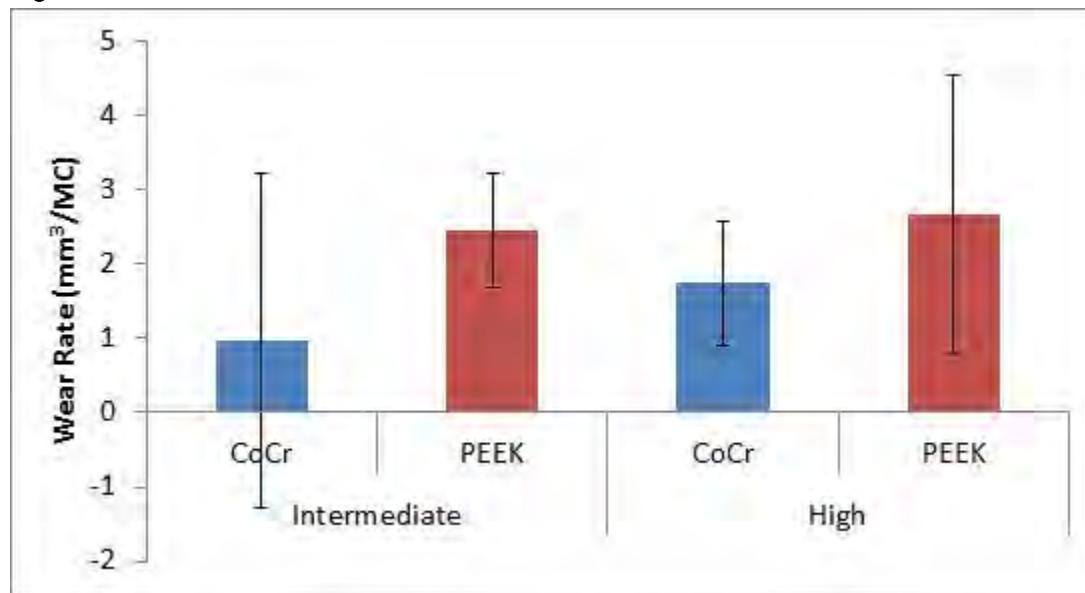
Caption: Figure 1: Wear rate per million cycles (± 95% confidence limits) of GUR 1020 UHMWPE tibial components articulating against either cobalt chrome or moulded PEEK femoral components in a knee simulator tested under intermediate and high kinematics (n=3).

Conclusion: The wear of UHMWPE tibial components was comparable when tested against PEEK and against a conventional material, cobalt chrome. This study shows that PEEK Optima has the potential for use as the femoral component in total knee arthroplasty.

References: 1.   Kurtz, S.M. and J.N. Devine, Biomaterials, **28**: 4845-69, 2007.

2.   McEwen, H.M.J., et al., Journal of Biomechanics, **38**: 357-365, 2005.

3.   Galvin, A.L., et al., J Biomech, **42**: 1898-902, 2009.

4.   Brockett, C.L., et al., J Biomed Mater Res B Appl Biomater, **100**: 1459-65, 2012.

Orthopaedic Implants

AS-0341

WEAR ASSESSMENT OF TOTAL KNEE PROSTHESES USING HIGH DEMANDING DAILY ACTIVITY WAVEFORM

Saverio Affatato [1,*]Sami Abdel Jaber [1]Claudio Belvedere [2]Alberto Leardini [2]

[1]Medical Technology Lab, [2]Movement Analysis Laboratory, Istituto Ortopedico Rizzoli, Bologna, Italy

Introduction and Objectives: Total knee arthroplasty (TKA) is a consolidated orthopaedic procedure in case of severe knee arthropathies [1]. Unfortunately, as there is a good survival rate of primary TKA (92 to 100%), failures occur for factors concerning the polyethylene composition of the implants, secondary osteolysis, and ultimately loosening of the implants are the usual causes of failure after normal use [2].

Dynamic in vitro testing of the human knee continues to be an area of interest to the orthopaedic biomechanics community. A number of different styles of machines with varied capabilities have been designed to simulate the loads and motions of the knee. For the implementation of realistic loading scenarios during *in vitro* wear testing for human joint prostheses, typical frequency and duration of daily living activities are necessary. For this reason, wear analysis is moving towards the implementation of other daily living activities, in order to better describe and investigate prosthesis wear resistance, also with the goal to offer better versatility to include those patients that are expected to recover full mobility.

The objective of this study is to perform a knee wear test applying a previous validated protocol for *in vitro* wear simulation of stair climbing [3]. A collection of pertinent real human motion data obtained by fluoroscopy and gait analyses on 15 patients operated at our Institution, were elaborated and adapted to apply onto our knee simulator in order to simulate a highly demanding daily activity (HDDA).

Methods: Four commercial cruciate-retaining fixed-bearing component prosthesis for TKA were tested in this study (Stryker®-Orthopaedics, Mahwah, NJ-USA). These were new and delivered in sterilized packages. Particularly, corresponding UHMWPE tibial inserts (size #7) were made of conventional surgical grade polyethylene resin (GUR 1020), consolidated by compression moulding (accordingly to ISO 5834/1-2), and EtO sterilized. These were tested in conjunction with corresponding CoCrMo alloy femoral components. Following a standardized protocol the UHMWPE tibial components were pre-soaked for 4 weeks prior to the wear tests in order to achieve a steady level of fluid absorption as recommended by the international standard (ISO 14243-2).

The applied kinematics was derived from a study based on fluoroscopic analysis [4], where fifteen patients that underwent TKR were analyzed during stair climbing at 6 months' follow-up using standard 3D video-fluoroscopy technique. Axial input load data were derived from a previous study based on twenty healthy patients using standard gait analysis synchronized with two force plates during the same exercise [5].

Results: The components run under HDDA-Simulation completed the planned two million cycles under bovine calf serum as lubricant. The mass loss is showed in Figure 1.

Figure:
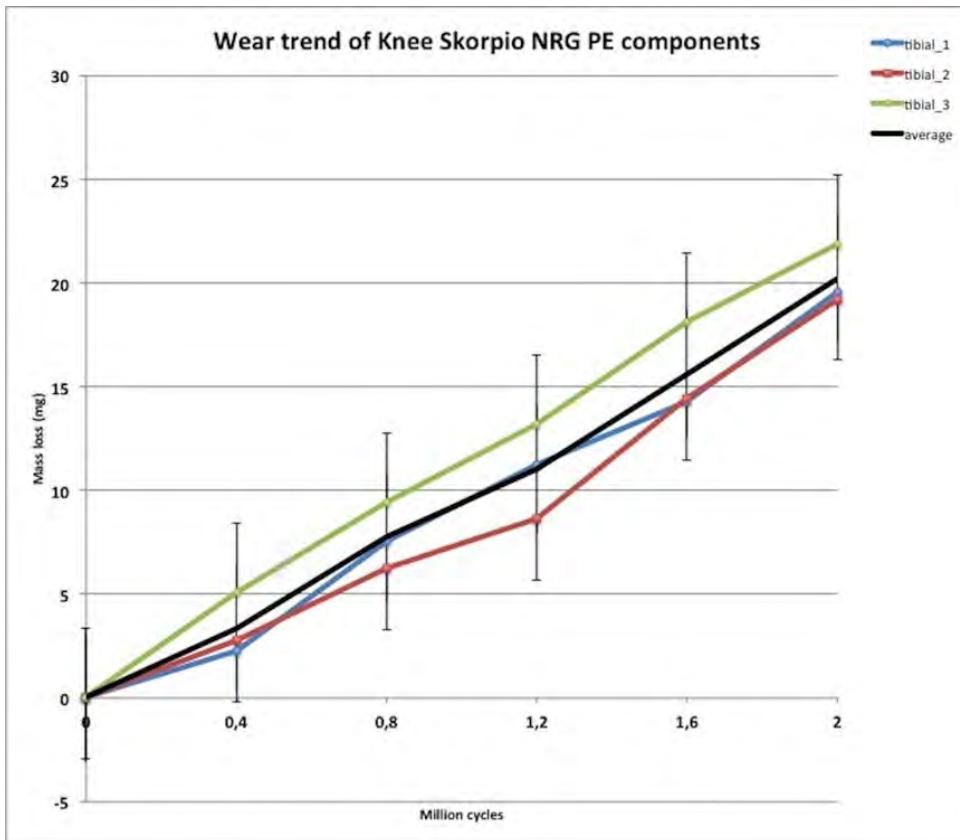
Caption: Figure 1 - Wear behaviour of the knee PE components run under HDDA motor task.

Conclusion: The knee simulator successfully executed the imposed physiological gait conditions under HDDA. To our knowledge, no previous studies have reported on a similar method. Essner et al. simulated Stair climbing activity on the Scorpio® PS tibial inserts design. However, in this study, simulation inputs were based on literature references [6]. Recently Schwiesau et al. [7] reviewed relevant published works and combined FE, AP and IE joint motion data from a number of different sources, which involved different motor tasks. The present experimental protocol and the relevant results, initially for stair climbing, may in fact open the way to understanding whether the present ISO 14243 standards, based on level walking alone, are a good representation of typical wear in TKR. Accordingly, the next step of this study might be using this new protocol to compare the results here reported with those obtained using traditional ISO 14243 applied on the same prosthesis design and size as in this study.

References: [1] Jevsevar DS. J Am Acad Orthop Surg., 21(9):571-6, 2013.

[2] Rönn K, et al. Arthritis (2011) 2011:1–9.

[3] S Battaglia et al. MedEng & Physics 36 (2014) 1605–1610

[4] Belvedere C et al. KSSTA (2013) 21:2375–83.

[5] D'Angeli V et al. (2014) 47:1198–205.

[6] Essner A. et al. (2005) AMSB 199.

[7] Schwiesau J. et al. (2013) Med Eng Phys 35:591–600

Disclosure of Interest: None Declared

Orthopaedic Implants

AS-0342

SURGICAL TRANSLATIONAL MALPOSITION AFFECTS THE LEVEL OF THE DYNAMIC MICROSEPARATION, THE SEVERITY OF EDGE LOADING AND THE WEAR IN TOTAL HIP REPLACEMENTS

Oscar O'Dwyer Lancaster-Jones [1,*]Mazen Al-Hajjar [1]Sophie Williams [1]Louise Jennings [1]Jonathan Thompson [2]Graham Isaac [2]John Fisher [1]

[1]Mechanical Engineering, Institute of Medical and Biological Engineering, [2]DePuy Synthes Joint Reconstruction, Leeds, United Kingdom

Introduction and Objectives: Hip joint replacement is a successful treatment for osteoarthritis and restores the mobility and function of the joint. However, the demands on these implants are increasing and patients want to continue with an active lifestyle. Pre-clinical testing standards assume optimal component position and do not account for the surgical and anatomical variations. Research has indicated that about 50% of acetabular cups are mal-orientated [1]. Cup malposition is a factor which has been shown to contribute to failure. Stripe wear has been observed on the surface of ceramic retrievals and has been associated with edge loading conditions [2]. It is well established that microseparation, where edge loading occurs due to translational malposition [3], increases the wear of hard-on-hard bearings [4, 5] and the possibility of failure. However, the influence of different levels of translational malposition, and the effect on wear has not been evaluated yet. Hence, it is important to understand the variables which affect the occurrence of edge loading. Many factors contribute to edge loading conditions; laxity of the joint, orientation of the cup and rim geometry of the cup. The aim of this study was to determine the effect of different surgical translational and rotational malposition on the level of dynamic microseparation, severity of edge loading and wear in total hip replacements.

Methods: Ceramic coupled bearings (36mm, BIOLOX® delta) were tested in a six-station Leeds Mark II Physiological Anatomical Hip Joint Simulator. The ceramic liners were inserted into titanium alloy shells (Pinnacle®, DePuy Synthes, UK). A standard twin peak load (3kN and a swing phase load of approximately 70N) walking cycle (flexion/extension +30°/15° and internal/external ±10° rotation) was applied. New-born calf serum (25% v/v), supplemented with 0.03% sodium azide to retard bacterial growth, was used as lubricant. Two levels of translational malpositioning were used in this study where the level of mis-match between the reconstructed rotational centres of the head and the cup were set to 2mm and 4mm in the medial-lateral axis. Two cup inclination angles were assessed; an equivalent to 45° *in vivo*, representing an optimal anatomical position, and an equivalent to 65° *in vivo*. Four conditions were investigated in total (Table 1) with three million cycles completed under each condition. The wear was determined gravimetrically using a microbalance (XP205, Mettler Toledo, UK), and the depth of the wear stripe was measured geometrically using a Coordinate Measuring Machine (CMM, Legex 322, Mitutoyo, UK) every million cycles. The dynamic microseparation was checked routinely and measured by a Linear Variable Differential Transformer (LVDT). Mean wear rates and 95% Confidence Limits (CL) were determined and statistical analysis (one way ANOVA) completed with significance taken at p<0.05.

Results: A steep angle (65°) resulted in a significantly higher level of dynamic microseparation and higher wear than the optimal cup angle for a given level of translational malposition (2mm (p=0.02) and 4mm (p<0.01)). The larger dynamic microseparation correlated with a higher wear rate for both cup inclination angles (Figure 1). The mean wear rates ±95%

CL for the 2mm translational malposition conditions for the cup inclination angle of 45° and 65° were 0.07±0.04mm³/10⁶ cycles and 0.14±0.05mm³/10⁶ cycles respectively. The final depth of the wear scar was 3±1µm and 8±3µm respectively. When a higher level of translational malposition (4mm) was applied the mean wear rate for the 45° and 65° increased to 0.32±0.04mm³/10⁶ cycles and 1.01±0.07mm³/10⁶ cycles respectively. The final depth of the scar also increased to 15±3µm and 33±6µm respectively.

Figure:
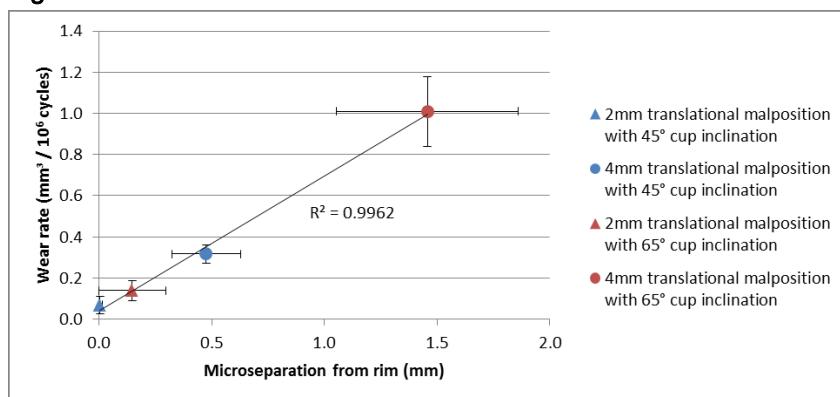
Caption: Mean wear rate of ceramic-on-ceramic bearings versus medial-lateral dynamic microseparation displacement under different testing conditions

Conclusion: This *in vitro* simulation showed the influence of cup inclination angle for a given translational malposition. The cups with a 45° inclination angle showed greater resistance to dynamic microseparation with the translational force applied medial-laterally. These results demonstrate that when a higher level of translational malposition is coupled with a rotational malposition, the damage caused due to edge loading conditions is greater than when tested with the cup in an optimal position. Future work will look into the factors which are considered to influence these results; the magnitude of the medial-lateral force, joint laxity and the magnitude of the joint reaction force during the swing phase.

Table:

	Translational malposition	
Cup inclination angle	2mm	4mm
45°	n=6	n=6
65°	n=6	n=6

Caption: The four different testing conditions investigated in this study

References: [1] Callanan et al., Clin Orthop Relat Res, 2011.

[2] Nevelos et al., J Arthroplasty, 2000.

[3] Fisher, J Bone Joint Surg [Br], 2011.

[4] Stewart et al., Journal of Material Science: Materials in Medicine, 2001.

[5] Williams et al., JBMR-B, 2004.

Disclosure of Interest: O. O'Dwyer Lancaster-Jones: None Declared, M. Al-Hajjar: None Declared, S. Williams Conflict with: DePuy Synthes, L. Jennings: None Declared, J. Thompson Conflict with: DePuy Synthes, G. Isaac Conflict with: DePuy Synthes, J. Fisher Conflict with: DePuy Synthes

AS-0343

EFFECT OF ANTIBIOTICS AUGMENTATION AND OPERATING TEMPERATURE ON IMPACT RESISTANCE OF ORTHOPEDIC BONE CEMENT

Maryam Kalantari [1,*]Ata Hashemi [1]

[1]biomedical engineering, Amirkabir University of Technology, Tehran, Iran, Islamic Republic Of

Introduction and Objectives: Bone cement has been used in joint replacement, and some surgeons advocate using antibiotic-impregnated PMMA bone cement prophylactically for all joint replacement surgeries. However, in the most cases, the mechanical strength of the bone cement is shown to be reduced by addition of antibiotic. Different mechanical tests have been utilized to characterize the mechanical properties of bone cements but there is few documents that focuses on the impact resistance of the bone cement. In the present study, the impact tests were carried out to investigate the different temperature and aging condition on the impact resistance of antibiotic loaded bone cements.

Methods: The C~ment® bone cement was used to prepare the test samples, in accordance with ASTM D256-06, the standard test methods for determining the pendulum Impact resistance of notched specimens of plastics. The bone cement components were mixed according to the medical guideline, used by surgeons. Except the control bone cement samples, bone cement samples were also mixed with gentamicin or vancomycin antibiotics. Then, the mixed bone cement was transferred to the mold. The solidified samples, i.e., the control, with gentamicin or with vancomicin groups were divided in 3 subgroups, the first were kept in ambient temperature (air) of 23°C, the second at 23°C saline, and the third one at 37°C saline. All test groups were maintained in their respective storage environments for two weeks before subsequent testing. To carry out the test, individual samples were first placed on the sample platform and centered. An impact tester with the capability of delivering energy of 3J is used to perform the tests. The specimens were carefully examined to ensure that the nominal values are in the allowable range. In addition, only samples with no surface defects were considered for testing. The tests were carried out on a bench-top impact testing machine (Ueshima IM-1100, Tokyo, Japan).

Results: The impact strength of control samples aged in air was obtained to be 3.28 ± 0.26 while that of gentamicin and vancomycin loaded samples, respectively, was 2.13 ± 0.09 and 2.13 ± 0.35. The mean impact strength of all three group samples aged at 23°C saline was slightly higher than that found for samples aged in air. That of control samples was 3.64 ± 0.31 while that of gentamicin and vancomycin augmented samples was 2.45 ± 0.4 and 2.72 ± 0.15, respectively. The mean impact strength of all samples aged at 37°C saline was found to be significantly lower for all three groups ($p<0.05$). According to the results, the control samples aged in saline at 23°C have the highest impact resistance and gentamicin loaded samples aged in saline at 37°C have the lowest resistance. Furthermore, reduction in the impact energy is minimum for vancomycin loaded samples aged in saline at 23°C.

Conclusion: Present study investigated the impact strength of antibiotic loaded bone cement at different storage conditions and temperatures. The results show that addition of 1.25 wt/wt % gentamicin/vancomycin significantly reduces the impact strength of the samples ($p<0.05$). Control samples aged in saline at 23°C have the highest impact energy and

gentamicine loaded samples aged in saline at 37°C have the lowest resistance. Reduction in the impact energy is minimum for vancomycin loaded samples aged in saline at 23°. Furthermore, it is observed that the samples aged in saline at 23ºC are more resistant than the samples aged in air at 23ºC. The effect of storage temperature was also studied showing that the impact strength decreases by increasing the aging storage temperature (p<0.05).

Disclosure of Interest: None Declared

Motion Analysis

AS-0344

EXTRACTION OF PROTECTIVE REACTION IN CASES OF INDOOR FALL BEHAVIORS USING CHANGE POINT DETECTION METHODS

Masato Ito [1,*] Akira Mano [2] Yusuke Miyazaki [1] Ryoji Watanabe [3] Yoshifumi Nishida [4]

[1]Department of Mechanical and Environmental Informatics Graduate School of Information Science and Technology, [2]Mechanical and Environmental Informatics, Tokyo Institute of Technology, 2-12-1, Ookayama, Meguro-ku, Tokyo, [3]Analysis Center, Panasonic Corporation, 1048 Kadoma, Kadoma City, [4]National Institute of Advanced Industrial Science and Technology , 2-3-26, Aomi, Koto-ku, Tokyo, Japan

Introduction and Objectives: Human falls represent daily accidents. In fact, over half of all nonfatal childhood injuries result from falls, in accordance to a report issued by the World Health Organization [1]. In addition, the elderly often suffer from fall-related accidents and in many cases these lead to fatal injuries. Therefore, methods are necessary to evaluate risks of fall for minimizing injuries and reducing associated social costs.

In earlier studies, many researchers have tried to estimate fall-related injuries, such as bone fractures, using human finite element models. However, avoidance or protective behaviors during the pre-injury phases have not been implemented in all human models that led to an overestimation of the risk probability. Therefore, for an accurate and comprehensive estimation of injury risks, the total number of fall-related injuries that involve both the pre-injury and injury phases are necessary. To clarify these mechanisms, it is important to employ methods that divide the fall-related action quantitatively into evasive, protective, and passive action phases. Therefore, the objective of our research is to develop the methods to appropriately divide the fall-related actions.

Methods: Three-dimensional motion data of child falls were captured from a fall-related motion database that focusses on unintentional daily falls occurring in a living environment [2]. The infants played freely in the room with their parents, and motions of falls naturally occurred. The latter were analyzed using a video-based motion capture system (Flame-Dias, DKH Inc.). The motion data were interpolated using cubic splines. The total number of degrees of freedom of the constructed model was fifty seven. To extract protective motions from captured data, we used the change point detection method calculated based on singular value decomposition (SVD), as proposed by Ide [3]. In this method, the degree of change of the time series data that indicates the distance between the two spaces that consisted of the backward feature motion and the current feature motion (both defined as right singular vectors) was calculated using SVD. When this value equals zero, no motion change is detected. On the other hand, when this value equals one, significant motion changes are detected. Furthermore, Ide [3] used only one-dimensional input data. In this work we improve the prior methodology extending its use to multidimensional input data.

Results: The fifty-seven multidimensional time series data, including rotation angles of whole body joints, and translational motion of hips in falling conditions were used to extract the early time periods of protective motion. Figure shows two examples of results. Both sets of results exhibit local peak values. We think that the posture may have changed drastically at the time the protective motion started. Therefore, one of the local peak values may show the early time period of the protective motion. To confirm this, we compared the results with captured motion data.

In Case 1, the maximum peak value occurs at 0.27s. Referring to the captured motion, the protective motion seems to start at approximately the same time. This indicates that the maximum peak value can be extracted from the early time period of the protective motion. On the other hand, in Case 2, similar local maximum values appear at 0.27s and 0.45s. Since protective motion also occurred at approximately 0.45s in the captured motion, the peak value at 0.27s may indicate the time when the subject lost his body balance. A total of thirteen fall datasets were investigated. We were able to extract the early data periods of the protective motion in ten cases. Furthermore, in five of the studied cases, the multilocal peak values appeared to exhibit similar patterns like that of Case 2. Because this method itself is not specialized for extracting protective motion, the input data should be selected a priori to extract protective motion. Moreover, a proper methodology is necessary to quantitatively determine which local peak value indicates protective motion. To achieve this, we need to clarify the feature motion of the fall behavior by analyzing additional motion data in the future.

Figure:
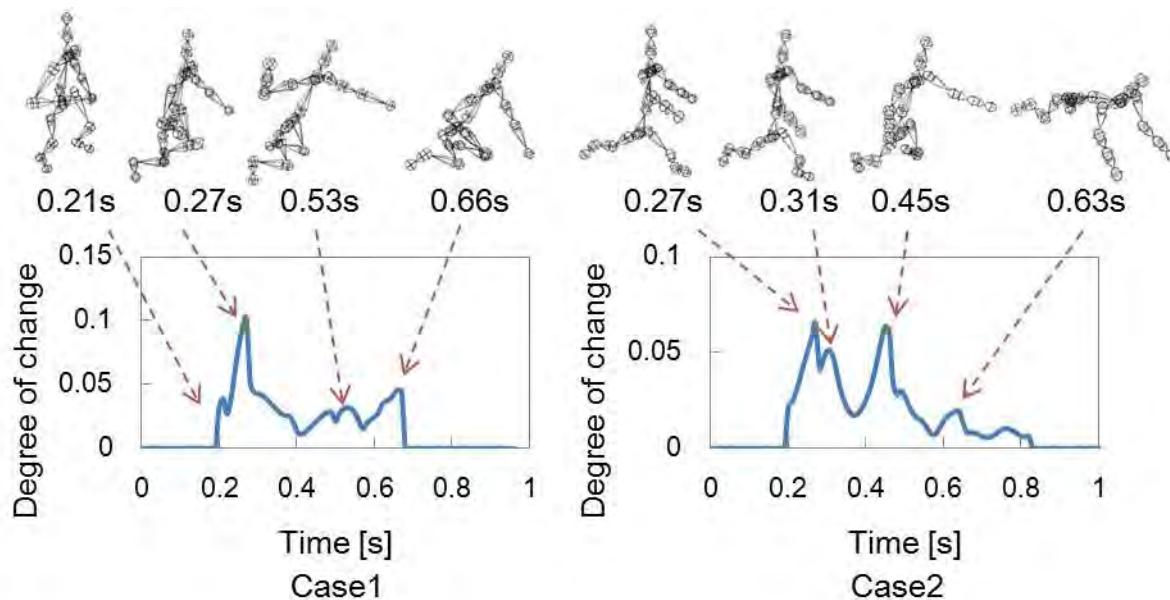
Caption: Two results of change point detection with captured motion data

Conclusion: Child falling behaviors were analyzed using the change point detection method that allowed the extraction of the early time periods of the protective action phase. The elicited results indicate that it is possible to extract these time periods of protective motion in falling conditions. On the other hand, methodologies are necessary to clarify which local peak value indicates the beginning time periods and which input data are appropriate for extracting protective motion.

References: (1) World Health Organization (WHO), 2008. World Report on Child Injury Prevention.

(2) Kakara H., *et al.*, Accident Analysis and Prevention 59, 2013, 432–442.

(3) Ide T. and Tsuda K., Proceedings of the 2007 SIAM International Conference on Data Mining, 2007.

Disclosure of Interest: None Declared

Motion Analysis

AS-0345

ASSESSMENT OF A RIB-BASED TECHNIQUE TO DEFINE THE THORACIC COORDINATE SYSTEM FOR USE WITH BI-PLANE X-RAY IMAGING

Joshua W. Giles [1,*] Tim Baumer [2] Anne Drake [2] Michael Bey [2]

[1]Mechanical Engineering, Imperial College London, London, United Kingdom, [2]Motion Analysis Lab - Bone & Joint Center, Henry Ford Hospital, Detroit, United States

Introduction and Objectives: To describe the various contributions (e.g. glenohumeral, scapulothoracic, and thoracic) to humeral motion in a physiologically relevant manner and to achieve consistency within the literature, Wu et al. [1] described standard bone-fixed coordinate systems (CS) and rotation sequences for each contributing bone and joint, respectively. The thoracic bone-fixed CS is based on anatomical landmarks on the sternum, and two vertebrae. Recently, 3D model-based bi-plane x-ray systems have been developed which can accurately track joint kinematics and contact mechanics; however, this modality has not adopted the ISB thoracic CS as it would require the midline of the body to be CT'd, greatly increasing patient dose. As a result, scapular rotations have commonly been measured relative to the ground and thus incorporated thoracic rotations into descriptions of scapular motion. To overcome this difficulty, we have developed a method to measure the 3D pose of the thorax by tracking specific pairs of ribs which are visible in both CT and during bi-plane x-ray acquisition. Therefore, our objective was to assess the accuracy of various rib-based thoracic CS compared to the ISB standard.

Methods: A thoracic CT scan was acquired for each subject (n=5) and reconstructed into a 3D bone model which was then used to create the ISB recommended thoracic CS based on anatomical landmark digitizations (Fig 1). Additional rib-based CS were constructed for all combinations of ribs 1-6 as these are consistently visible in bi-plane x-ray images. The CS were created by identifying on each rib, the costovertebral joint and the sternocostal joint. For each rib pair, the CS origin was the superior rib's sternocostal joint. The superior/inferior axis was defined as the vector between the midpoints of the inferior and superior ribs' costovertebral and sternocostal joints. The medial/lateral axis was defined as a vector perpendicular to the plane created by the two ribs' costovertebral joints and the superior rib's sternocostal joint. Lastly, the anterior/posterior axis was defined as the cross-product of the superior/inferior and medial/lateral axes.

Accuracy of each rib-based CS was assessed by determining the three Cardan angles (flexion/extension(FE), lateral rotation (LR), axial rotation (AR)) that described its orientation relative to the ISB standard. Using these data, we calculated the Root Mean Squared Error (RMSE) and precision (standard deviation) across all five subjects.

Results: Misalignment to the ISB standard was highly dependent on the rib pair used. Averaging the RMSE of the three rotations produced average rotational errors ranging between 4.6 and 22.9° across the 15 rib combinations (RMSE range: 1.4≤FE≤8.5°, 1.5≤LR≤25.2°, 4.4≤AR≤38.1°) while for precision, the error ranged from 2.3 to 6.5° (precision range: 1.1≤FE≤6.0°, 1.5≤LR≤6.5°, 4.2≤AR≤8.2°) (Table 1). Filtering for rib pairs where no rotational error was >10° left 9 potential CS (Table 1 - Bold), while filtering these for pairs with a precision <5° left four candidates; namely, ribs 3&4, 3&5, 3&6, and 4&5.

Figure:
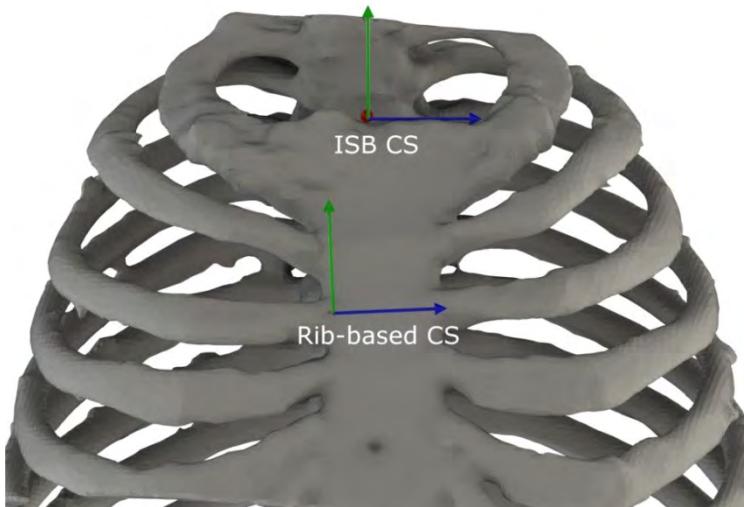
Caption: 3D reconstructed model of the thorax with ISB and one rib-based CS indicated.

Conclusion: The importance of the absolute errors is heavily influenced by the magnitude of the corresponding scapular rotation; whereby, errors that are large relative to the corresponding scapular rotation should have greater weight in selecting the best CS. Therefore, to understand their importance, the errors for the four remaining CS were calculated as percentages of published [2] scapular rotations (FE=35°, AR=25°, LR=65°) (Table 1 - % data). These data indicate that several rib-pairs yield an acceptable thoracic CS. In choosing the optimal CS, it is also critical to consider the importance of each rotation to the biomechanical question. If scapular tilting (FE) is most important, rib 3&4's CS produces the least meaningful error, while ribs 4&5 are preferable when scapular version (AR) is the critical motion. However, if both rotations are equally important, rib 3&6's CS produces an optimal compromise. Use of these new CS will greatly increase the physiologic accuracy of scapular rotations measured by bi-plane x-ray and allow thoracic rotations, which have previously been attributed to the scapula, to be independently described.

Table:

	RMSE&Precision(°)			RMSE&Precision(%)		
Ribs	FE	AR	FE	AR	LR	FE
1&2	5.4&5.5	38.1&8.2	25.2&5	-	-	-
1&3	2&2.2	21.3&6.9	11.1&4.6	-	-	-
1&4	1.4&1.5	16.4&5.1	6.3&2.5	-	-	-
1&5	2.3&1.1	14.6&4.2	4.4&1.6	-	-	-

1&6	3.3&2.2	14.2&4.2	4.1&1.7	-	-	-
2&3	7.8&4.7	10.3&7.4	5.5&5.5	-	-	-
2&4	**5.9&2.3**	**9&5.7**	**2.8&2.4**	-	-	-
2&5	**6.5&1.9**	**8&5.1**	**1.5&1.5**	-	-	-
2&6	**6.3&2**	**7.4&5.1**	**2&2.2**	-	-	-
3&4	*5.1&2.3*	*6&4.8*	*2.5&2.5*	*14.7&6.4*	*24.2&19*	*3.8&3.8*
3&5	*6.7&2.6*	*5.1&4.3*	*1.9&2.2*	*19&7.5*	*20.4&17.2*	*3&3.3*
3&6	*6.6&2.9*	*5&4.6*	*2.9&3.2*	*18.9&8.2*	*20&18.5*	*4.5&4.9*
4&5	*8.5&3.4*	*4.4&4.8*	*2.5&2.4*	*24.2&9.6*	*17.8&19.2*	*3.8&3.7*
4&6	*7.5&3.3*	*4.8&5.4*	*4.1&4*	-	-	-
5&6	*7.7&6*	*6.5&7.1*	*6.3&6.5*	-	-	-

Caption: Absolute and % RMS and Precision errors for each rotation (FE, AR, LR) across all rib-based CS.

References: [1] Wu et al., JBiomech, 38:981–992,2005.

[2] McClure et al., PhysTher, 86:1075-1090,2006.

Disclosure of Interest: None Declared

Motion Analysis

AS-0346

VALIDITY OF THE NEW KINECT-SENSOR IN MEASURING UPPER BODY KINEMATICS

Eveline Graf [1,*] Roman Kuster [2] Markus Wirz [1] Bernd Heinlein [2]

[1]School of Health Professions, Institute of Physiotherapy, [2]School of Engineering, Institute of Mechanical Systems, Zurich University of Applied Sciences, Winterthur, Switzerland

Introduction and Objectives: The quantitative description of human motion is used in various fields, e.g. in clinical settings to diagnose and assess progression of injuries or rehabilitation programs. This is mostly done using marker-based systems with accuracies of less than one millimeter [1]. However, such systems are very expensive and their usage is very time consuming, requires technical expertise and is bound to a laboratory, which severely limits their field of use. Recently, marker-less systems have been developed that are low cost and simple to use. Different studies have examined the accuracy of such systems as they, given sufficient accuracy, would provide a portable solution to quantify segmental kinematics in applied settings. While the validity and reliability of the first generation of Microsoft Kinect™ has been examined [2], there is no information about the validity of the new "Kinect for Xbox One" (Kinect) for tracking human motion. Therefore, the aim of this study was to determine validity of Kinect for measuring segment angles in upper extremity exercises.

Methods: Six subjects (31±5yrs, 1.75±0.09m, 70.0±7.77kg) provided written consent and wore tight fitting shorts and no shirt (sports bra for women). Reflective markers were placed on the skin according to the plug-in-gait model. Each subject performed unilaterally three repetitions of following tasks sitting (SIT) and standing (STAND): shoulder flexion (FLEX), shoulder abduction in frontal (ABD) and scapula (SCAP) plane. Frontal plane was defined by the vertical plane through the two shoulder centers, sagittal and scapula plane by rotating frontal by 90° and 45° around vertical axis, respectively. Inclination angle was calculated in the respective plane for the arm (AIN) and in the frontal plane for the shoulder girdle (SIN). The tasks were recorded simultaneously with a 7-camera Vicon® system and Kinect (placed according to manufacturer's recommendation). Kinect-skeleton was recorded using custom software based on "Kinect for Windows SDK 2.0", which directly provides trajectories of the joint centers. Vicon data was processed using standard pipeline from Vicon Nexus™ to calculate trajectories of the joint centers. Based on filtered data, segments were defined as the line between two joint centers (shoulder girdle: left to right shoulder, upper arm: shoulder to elbow). Data were synchronized between the systems. Resulting angles were compared between Vicon and Kinect using coefficient of multiple correlation (CMC) [3] and Bland-Altman plot.

Results: In general, there were strong correlations between the two systems. In SIT and STAND, AIN had higher CMCs compared to SIN (Table 1). For SIN, SIT resulted in higher CMCs than STAND except in FLEX.

Range of motion (RoM) was more than ten times smaller for SIN (Fig 1a) compared to AIN (Fig 1b). Figure 1 (c&d) shows differences in mean RoM between Kinect and Vicon relative to the average mean of both systems. SIN (Fig 1c) and AIN (Fig 1d) show a trend towards higher means for Kinect.

Figure:
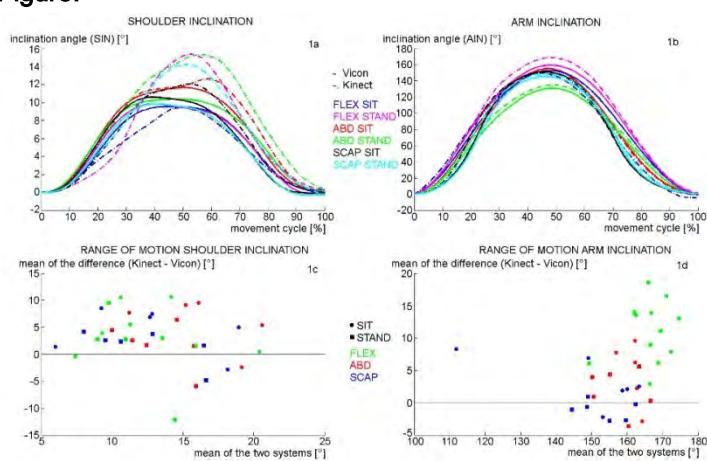
Caption: Shoulder (a) and arm (b) inclination angle; Bland-Altman plot of ROM of shoulder (c) and arm inclination (d)

Conclusion: Figure 1 (c&d) displays that there is an error (larger RoM) associated with Kinect compared to Vicon. AIN of FLEX appears to have the largest error (Fig 1d), but is also associated with a slightly larger RoM (Fig 1b), so there may be a positive relationship between size of error and absolute RoM. Since RoM is calculated based on minimum and maximum positions that are very similar for all three tasks, the difference in motion direction may not explain this result. CMCs of AIN are excellent, indicating good agreement of the angle trajectories between Kinect and Vicon, independently of the direction of motion. For SIN, the values are constantly lower, showing that Kinect is better in tracking the extremity than the shoulder girdle. Unfortunately, the body-tracking algorithm of Kinect is unknown. Therefore, it is not possible to examine where this difference comes from. For SIN, CMCs for FLEX (SIT and STAND) are lower than for the other tasks. During FLEX, the arm is elevated in sagittal plane, temporarily occluding the view of the shoulder joint. It is likely that this results in a decreased accuracy of tracking the shoulder motion.

Kinect seems to track upper body motion fairly well. In order to determine if Kinect could be used as a low-cost tool to quantitatively record RoM, e.g. during physical therapy, the between-day repeatability needs to be determined.

Table:

	shoulder inclination (SIN)		arm inclination (AIN)	
	SIT	STAND	SIT	STAND
FLEX	0.74	0.80	0.99	0.99
ABD	0.92	0.84	0.99	1.00
SCAP	0.93	0.83	1.00	0.99

Caption: Coefficients of multiple correlation (CMC) for shoulder and arm inclination (sitting: SIT, standing: STAND) for arm flexion (FLEX), arm abduction in frontal (ABD) and scapula plane (SCAP)

References: [1] Nigg et al., Biomechanics of the musculo-skeletal system, John Wiley & Sons, 2007.

[2] Bonnechère et al.,Gait Posture, 39: 593-598, 2014.

[3] Ferrari et al., GaitPosture, 31: 540-542, 2010.

Disclosure of Interest: None Declared

AS-0347

VELOCITY PROFILES OF SPATIO-TEMPORAL GAIT PARAMETERS IN LOW BACK PAIN PATIENTS: COMPARISON OF TWO REGRESSION METHODS

Clara Leyh [1,*] Véronique Feipel [1] Marcel Rooze [2]

[1]Laboratoire d'Anatomie Fonctionnelle [Laboratory for Functional Anatomy] , [2]Laboratoire d'Anatomie, Biomécanique et Organogénèse [Laboratory of Anatomy, Biomechanics and Organogenesis] , Université Libre de Bruxelles, Brussels, Belgium

Introduction and Objectives: Normalised gait velocity allows a better understanding of gait characteristics but this cannot clarify the implication of individual velocity variations on some gait parameters. Computed normalised gait velocity corridors (velocity profile) of spatio-temporal parameters (1,2) could help general practitioners to appreciate and evaluate specific locomotor disabilities and rehabilitation effects.

Low back pain patients exhibit among other a decrease of gait velocity, cadence, step length and an increase of support base, cycle time and single support time (3-7).

The aim of our study was to compute and analyse linear and polynomial velocity profiles distributions of spatio-temporal parameters of low back pain patients in gait. We also compared these profiles with those of healthy persons.

Methods: 59 low back pain patients (LBP) (females: n=30; age: 42 ± 17 years; males: n=29; age: 42 ± 15 years) and 34 healthy subjects (CG) (females: n=16; age: 45 ± 18 years; males: n=18; age: 45 ± 17 years) walked 3 times at 3 different speeds (slow, preferred and fast) over an electronic walkway (GAITRite Walkway system). The order of gait speeds was randomized and both groups were divided in 3 ages subclasses ("A": 20-40 years; "B": 41-60 years; "C": 61-80 years). Spatial and temporal parameters were computed from contact data (i.e. velocity, cadence, step length, stride length, step time, cycle time, stance time, swing time, single and double support times, stride velocity). Each parameter was then analysed using both linear and polynomial regressions to estimate "velocity profiles" in both individual and normalised gait speeds within the range of speeds achieved by all subjects (0,90 – 1,25 – 1,90 m/s). A paired sample T-test analysed the influence of laterality on each spatio-temporal parameter. ANOVA for repeated measurements was used to investigate the influence of regression modality (within-subject factors) and pathology on parameters.

Results: Best fitting results were obtained using polynomial regression for almost all parameters (cadence, step time, step length, stride length, cycle time and single support phase). Both linear and polynomial regression may be used to analyse swing time, stance time, double support time and stride velocity. It appeared that age had a significant influence on two parameters (stance time and double support time). No significant differences were observed between control and LBP groups.

Figure:

Step Time - Polynomial and Linear Regression
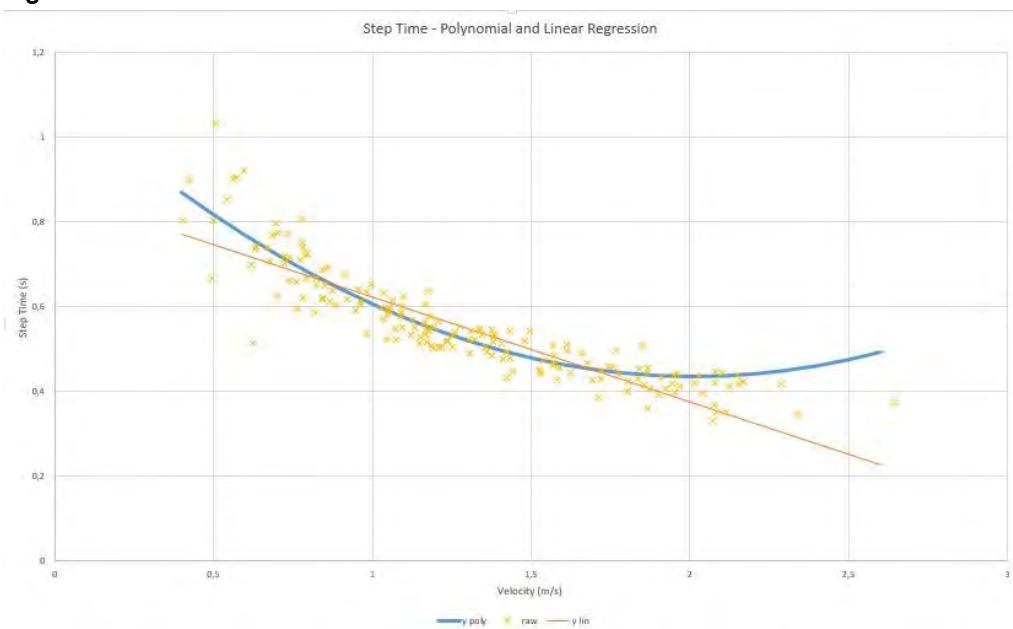
Caption: Step Time (s) polynomial and Linear regression of LBP subjects

Conclusion: The use of polynomial regression seemed to match best the distribution of most spatio-temporal gait parameters. A significant influence of age on velocity profiles was demonstrated in both groups. Nevertheless, due to the heterogeneity of low back pain definition, further studies should be extended considering various larger subgroups selected from clinical specificities such as symptoms, clinical examinations or specific spine damages.

References: [1] Moe-Nilssen et al. Gait Posture, 32: 98-101, 2010.

[2] Moe-Nilssen. Clin Biomech, 13: 328-335, 1998.

[3] Khodadaleh et al. Neuro-Orthopedics, 6: 24-7, 1988.

[4] Hanada et al. Arch Phys Med Rehab, 89: e11, 2008.

[5] Al-Obaidi et al. Int J Rehabil Res, 26: 101-108, 2003.

[6] Lee et al. Spine, 32: 1329-1336, 2007

[7] Keefe et al. Pain, 21: 153-161, 1985.

Disclosure of Interest: None Declared

TURNING KINEMATICS IN THE ASSESSMENT OF GAIT FOR CHILDREN WITH CEREBRAL PALSY

Philippe C. Dixon [1,]*Julie Stebbins [2]Tim Theologis [2]Amy B. Zavatsky [1]

[1]Engineering Science, University of Oxford, [2]Nuffield Orthopaedic Centre, Oxford University Hospitals NHS Trust, Oxford, United Kingdom

Introduction and Objectives: Turning is a crucial component of walking [1]. Kinematic changes required to successfully turn have been identified in typically developing (TD) children [2]; however, it remains unclear if children with cerebral palsy (CP) will adapt similarly to the turning condition [3]. The aim of this study was to investigate whether kinematic patterns exhibited by children with CP would be more atypical compared to their TD peers during turning gait than during straight walking given their existing neuromuscular pathologies. An understanding of turning kinematics in children with CP may be relevant in the clinical management of gait deviations.

Methods: Data from forty-four TD children (11.0 ± 2.6 years, 149.1 ± 15.5 cm) and twenty-two children with spastic diplegic CP (10 GMFCS 1 and 12 GMFCS 2) (12.4 ± 2.8 years, 149.7 ±17.7 cm) performing straight and 90° turning gait tasks were captured at 100 Hz using a Vicon system (Vicon, Oxford Metrics, Oxford, UK). For the CP group, limbs were found to have a mild (16), true equinus (9), apparent equinus (3), jump (6), crouch (2), or non-classified (8) kinematic pattern based on the algorithm of Sangeux *et al*. [4]. Kinematic data were extracted from the Plug-in Gait [5] and Oxford Foot Model [6] marker sets. Only turns about the inside limb (spin turns) are presented as both groups preferred this strategy. Left and right turns were pooled and a representative trial for each subject/condition was retained.

Inside limb kinematics were analyzed at discrete events starting at foot strike (FS) of the main turning stance phase: knee (Knee FS) and hindfoot with respect to tibia (Ankle FS) angles as well as minimum knee flexion in terminal stance (Knee TS) and maximum ankle dorsiflexion (Ankle DF) were identified as variables of interest based on clinical observation, while maximum hip adduction (Hip Add) and internal rotation (Hip IntRot), ankle maximum eversion (Ankle Eve), and forefoot with respect to hindfoot maximum supination (FFoot Sup) were extracted based on known turning gait adaptations in TD children [2]. Group differences were analyzed for each event using a 2 x 2 ANOVA (between-subject factor group and within-subject factor condition). A significant interaction would suggest that the two groups adapt differently to the turning condition (α = 0.05, no correction for multiple comparisons). Analyses of individual subjects were conducted by counting the number of children with CP outside the 95% confidence interval (CI) range of the TD group for each event/condition. These children were considered to exhibit abnormal kinematic patterns. All analyses performed using Matlab (v2012b, The Mathworks, Inc. Natick. USA).

Results: No statistically significant group by condition interactions were found; however, subject level analyses revealed that a greater number of CP subjects exhibited abnormal kinematics during turning than straight walking for Knee FS, Knee TS, Ankle DF, Ankle Eve, and FFoot Sup (Table 1). Overall, 13 children with CP (9/12 classified as having a limb with a "mild" pattern) were assessed as having normal kinematics for at least one event using CIs based on straight walking data. Of these, only 2 exhibited normal turning kinematics. Data for one child with a mild gait deviation for whom kinematics deteriorated during turning are presented (Fig. 1).

Figure:
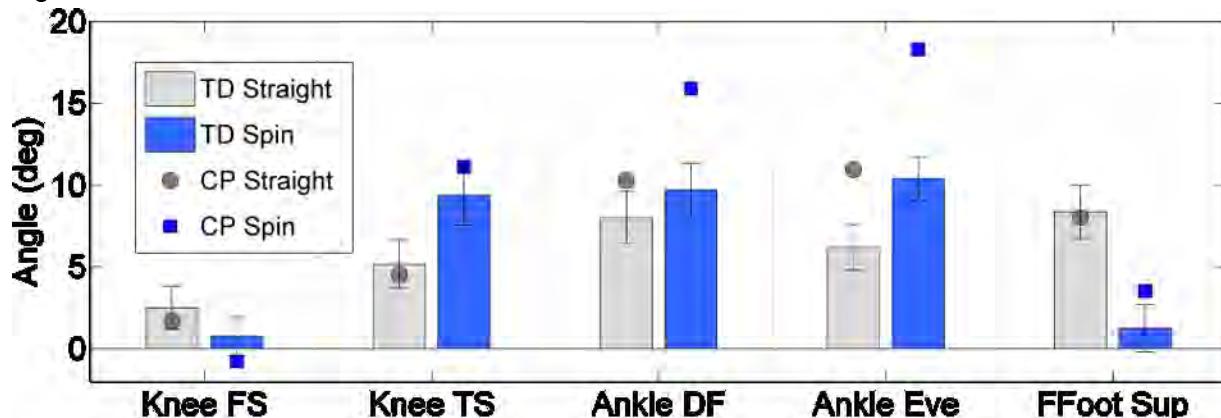
Caption: Normative range (mean ± CI) of events for straight walking and turning gait tasks derived from the TD group with data for one child with CP superimposed.

Conclusion:

This study investigated lower-limb joint kinematics during turning gait in children with CP. No significant overall group by condition differences were found, possibly due to the heterogeneity of the CP group; however, subject specific analyses showed that turning gait was a better discriminant of pathology than the standard straight walking protocol, especially for children with mild impairments. Although results are specific to the current cohort, this study outlines a simple methodology to assess individual children in a clinical setting. In practice, turning gait analysis may be conducted in cases where gait deviations exhibited during straight walking are minor, despite a child's reported difficulty in day-to-day gait activities. Future work could aim to develop a composite score for turning gait curves similar to the gait profile score [7] using these or other variables of interest such as joint kinetics.

Table:

	Hip Add	Hip IntRot	Knee FS	Knee TS	Ankle FS	Ankle DF	Ankle Eve	FFoot Sup
Straight	17	19	20	18	19	18	18	18
Spin	17	19	22	20	17	20	19	20

Caption: Number of children with CP outside the normative kinematic ranges

References:

[1] Glaister, et al. Gait Posture 25:289-94,2007.

[2] Dixon, et al. Gait Posture 38:870-5,2013.

[3] Romkes. Proceedings of ESMAC, 2012.

[4] Sangeux, et al. Proceedings of GCMAS, 2014.

[5] Kadaba, et al. J Orthop Res 8:383-92,1990.

[6] Stebbins, et al. Gait Posture 23:401-10,2006.

[7] Baker, et al. Gait Posture 30:265-69,2009.

Disclosure of Interest: None Declared

EFFECT OF A COMPRESSION GARMENT ON KINEMATICS OF JUMP-LANDING TASKS IN FEMALE RECREATIONAL ATHLETES AND PHYSICALLY ACTIVE WOMEN

Morgana A. de Britto [1,*] Andressa Lemos [2] Christielen dos Santos [2] Darren Stefanyshyn [3] Felipe Carpes [2]

[1] Center of Physical Education and Sport, Federal University of Santa Maria, Santa Maria, [2] Center of Health Sciences, Federal University of Pampa, Uruguaiana, Brazil, [3] Human Performance Laboratory, University of Calgary, Calgary, Canada

Introduction and Objectives: Previous research has shown that compressive garments can contribute to increase maximal height during vertical jumps and decrease hip flexion angles during dynamic tasks [1,2]. However, it is unknown whether movements in the frontal plane, such as hip adduction and knee valgus, can also be influenced. Knee valgus during landing is considered a major risk factor for knee ACL injury in sports [3]. Compressive garments could perhaps reduce maximum knee valgus angles during landing. Here we evaluated the effect of wearing a compressive garment on jump height and knee kinematics during a vertical jump-landing task performed by female recreational athletes and physically active women.

Methods: Eleven female recreational athletes and six physically active women participated in this study. To be in the recreational athletes group, participants had to train a team sport (with competitive goals) at least two times per week, for a minimum of 45 minutes per session. The physically active group included women that practiced walking, jogging or training at the gym. Kinematics of jump-landings were recorded using fifteen optical cameras (Vicon Motions Systems) and ground reaction forces were recorded using two force plates (OR6-2000, AMTI Inc.), one under each foot. The participants performed vertical jumps from a semi-squatted position, with the instruction to jump as high as possible and to land with one foot on each force plate. Trials were repeated if participants landed outside the force plates. Three vertical jumps were performed for each clothing condition (brand new compressive shorts or brand new regular sports shorts). Data were averaged for the three jumps in each condition. The frontal plane distance between markers on the left and right lateral femoral epicondyle at the peak of knee flexion during the landing phase was used as a measure of knee valgus angle. Also, the maximum jump height was verified through the change in vertical position of the center of mass determined based in plugin gait reference markers. A Shapiro-Wilk test was used to check whether the data were normally distributed. If they were, a paired t-test was used to test for an effect of the compressive garment and the regular sport shorts in each group.

Results: Among recreational athletes, there were no significant differences in the maximum height of jumps with and jumps without the compressive garment (p=0.311). Frontal plane knee distance was larger when recreational athletes used the compressive garment (p=0.003) compared to the regular garment. For the physically active women, there were no significant differences in maximum jump height between jumps with or without compressive garment (p=0.822). Knee distance was also not different between the conditions for the physically active women (P=0.889).

If jump height is considered as a performance marker, our data do not support the use of compressive garment as a strategy to improve performance of jumping. The increase of knee distance in the recreational athletes group calls for

explanation. It is possible that the compression above the knee (since the garments were shorts) lead to a more aligned position, helping the subjects keep their knees in less valgus positions. Our results concerning the use of compressive garments still requires a larger sample size to increase statistical power and properly address the implication for knee joint moments, frequently related to different knee injuries in sport.

Figure:
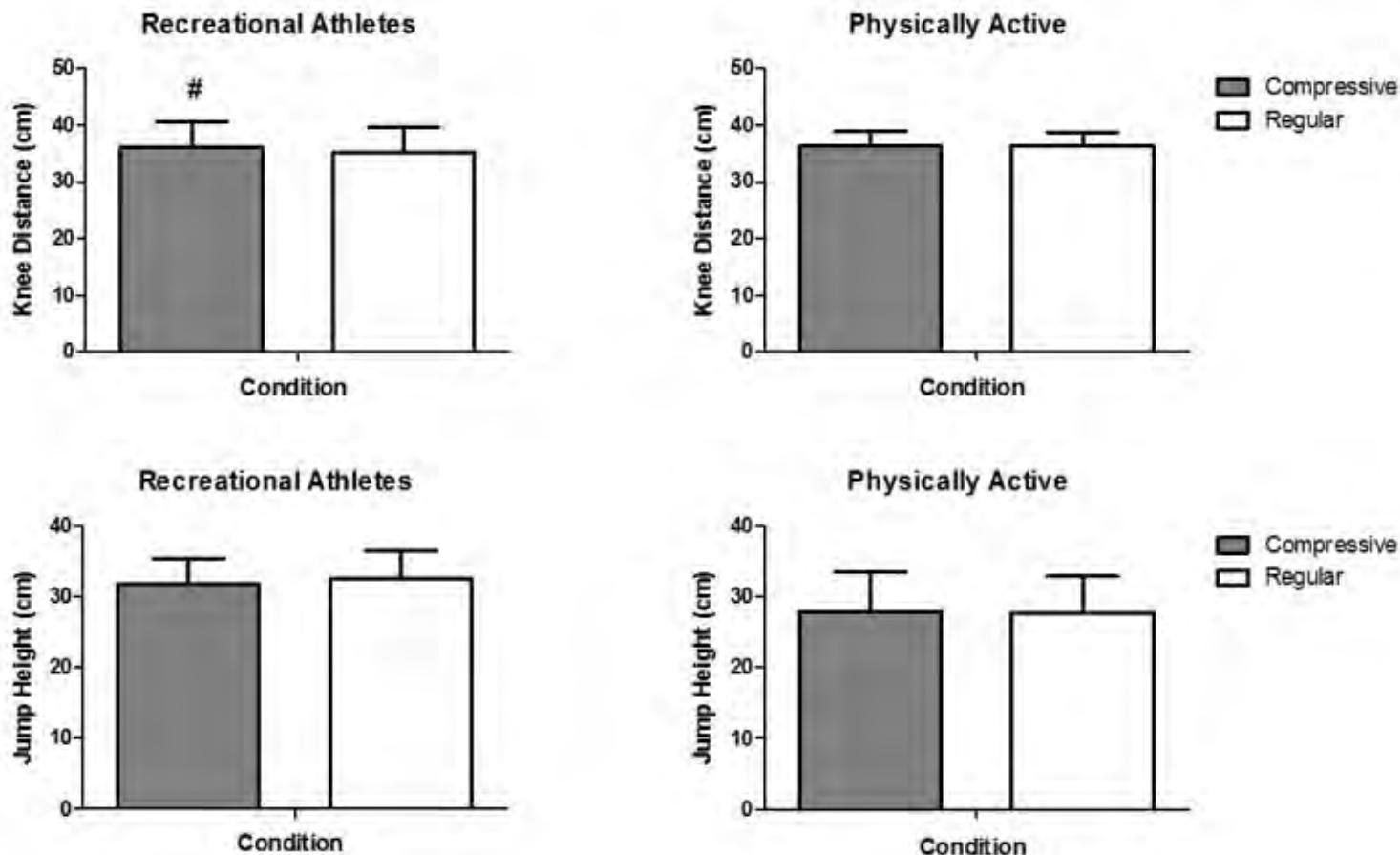
Caption: Figure 1. Means and SD values for knee distance and maximum jump height for the groups of female recreational athletes and physically active women, in two conditions (compressive or regular garment). # indicates significant difference between conditions.

Conclusion: The use of a compressive garment by female recreational athletes increased knee horizontal distance when performing vertical jump-landing tasks, in other words, decreased knee valgus.

References: [1] Doan *et al.*, J Sports Sci, 21(8):601-610, 2003.

[2] Bernhardt *et al.*, J Strength Cond Res, 19(2):292-297, 2005.

[3] Hewett *et al.*, N Am J Sports Phys Ther, 5(4):234-51, 2010.

Disclosure of Interest: None Declared

AS-0350

A THREE-YEAR LONGITUDINAL STUDY OF BIOMECHANICAL ALTERATIONS IN KNEE OSTEOARTHRITIS AND ASYMPTOMATIC CONTROLS

Janie L Astephen Wilson [1] Dianne M. Ikeda [1,*] Scott C Landry [2] William D Stanish [3] Cheryl L Hubley-Kozey [4]

[1] Biomedical Engineering, Dalhousie University, Halifax, [2] Kinesiology, Acadia University, Wolfville, [3] Dalhousie University, Halifax, Canada, [4] Biomedical Engineering; Physiotherapy, Dalhousie University, Halifax, Canada

Introduction and Objectives: The literature linking joint-level gait biomechanics with structural knee osteoarthritis (OA) has focused on individual gait metrics, mainly knee adduction moment (KAM) [1,2]. This is limited in its ability to illustrate the change of joint level mechanics and limits the interpretation of simultaneous multiple, correlated changes in gait mechanics. The objective of this study was to use principal component analysis (PCA) on discrete metrics to extract uncorrelated, multidimensional features & to compare these after three years & between asymptomatic controls (ASYM) & those with baseline moderate knee OA (MOD).

Methods: Three-dimensional (3D) gait patterns of 23 MOD & 18 ASYM adults (n=41) were recorded at baseline & approximately 3 years later. Patterns of 3D knee angles & net resultant moments were calculated. Five self-selected speed gait trials were averaged & normalized to 100% of stance, except flexion angle (KFA) that was normalized to 100% of gait. Discrete metrics reported in the literature [3] were extracted from subjects including ASYM (n=188), MOD (n=240) & severe OA before (n=108) & after arthroplasty surgery (n=91) & entered into a PCA. Variables were average gait speed, stance & swing phase peak KFA, KFA range, peak flexion moment (KFM), peak extension moment (KEM; early & late stance), rotation moment (KRM) range, first & second KAM peak & the mid-stance KAM. PCscores were calculated for the 41 subjects for the first three PCs. Variables within each PC were interpreted if their coefficient was at least 50% of the maximum coefficient for that PC [4]. A 2-way mixed model ANOVA was run on PCscores with session as a within-subjects factor & group as a between-subjects factor (α=0.05).

Results: PC1, PC2, PC3 captured 35.8%, 23.6% & 15.5%, respectively, of the original data variability (cumulatively 75%). Gait speed, peak stance & swing KFA, KFA range, peak KFM, peak early & late stance KEM & KRM range had significant correlation & high, positive, equal weighing on PC1. PC1 was interpreted as a sagittal plane/speed metric, with higher scores related to higher function. There were no significant differences in PC1 scores between groups or time, meaning that this feature remained consistent over time, with no functional difference between groups (Table 1, Figure 1). PC2 represented the first & second peak KAM, & the mid-stance KAM minimum. PC2 was interpreted as capturing the overall KAM magnitude during stance. PC2 scores were significantly higher in the MOD than ASYM group (P=0.007), meaning higher overall KAM during stance with OA. There were no time-dependent changes in PC2. PC3 was dominated by peak KFM & KFA range, with high scores related to higher peak moments & range. There was a significant time-effect for PC3 (P=0.04), with higher peak moment & range at follow-up compared to baseline.

Figure:
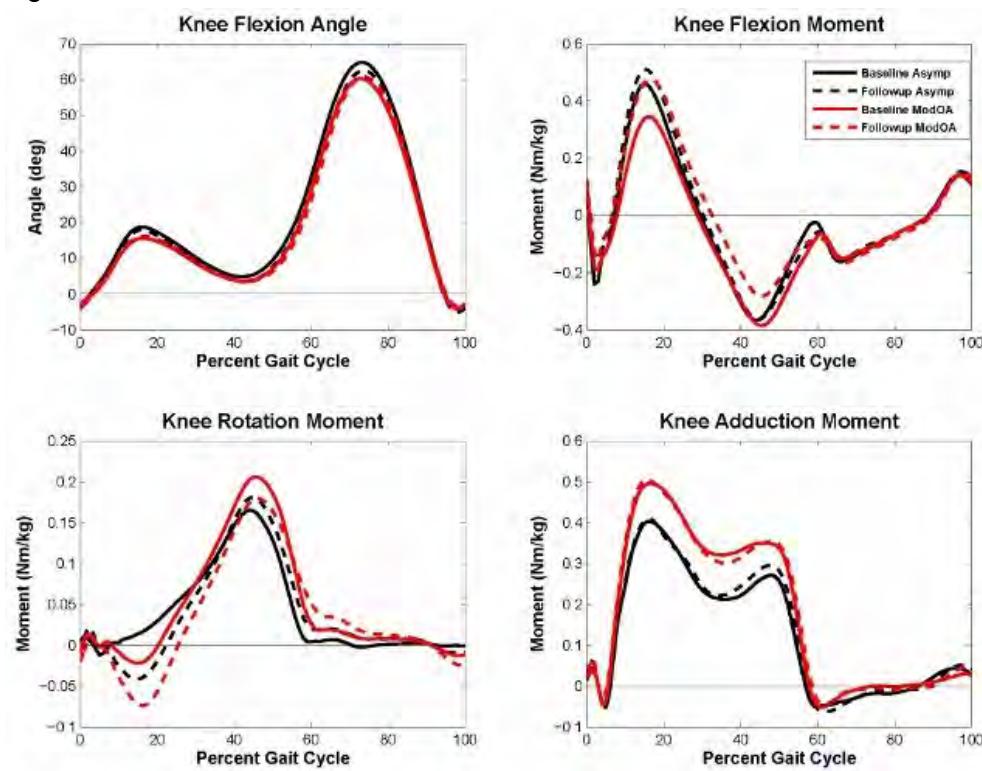
Caption: ASYM &MOD baseline & follow-up waveforms of KFA, KFM, KRM, KAM

Conclusion: Summarizing gait mechanics in some key features did not show biomechanical change over 3-years. The only statistically significant change over time reflected an improvement in gait function, with higher peak KFM & KFA range at follow-up. PC2 captured the overall KAM magnitude, similar to PCs from KAM waveforms [5]. There was a significant group difference, but no worsening of this feature over time in either group. These results also highlight interrelationships among different combinations of discrete gait variables, so combining variables into PCA may improve interpretation.

Table:

	Baseline ASYM	Baseline MODOA	Follow-up ASYM	Follow-up MODOA
BMI (kg/m^2)	27.1 (4.4)	29.8 (4.9)	28.2 (4.7)	29.8 (4.4)
Age (years)	49.8 (6.5)	56.5 (6.1)	52.7 (6.6)	59.5 (6.1)
Years from Baseline			2.9 (0.1)	2.8 (0.2)
PC1	1.13 (1.10)	0.74 (1.41)	1.03 (1.06)	0.79 (1.57)
PC2	-0.91 (0.72)	0.30 (1.44)	-0.70 (0.85)	0.20 (1.47)
PC3	-0.11 (1.10)	-0.03 (0.81)	0.27 (0.88)	0.27 (0.88)
Speed (m/s)	1.33 (0.10)	1.26 (0.18)	1.33 (0.13)	1.28 (0.15)
KFA stance peak (deg)	18.9 (3.8)	15.9 (5.9)	18.0 (5.1)	16.5 (7.8)
KFA swing peak (deg)	65.2 (5.1)	60.6 (6.7)	62.9 (5.2)	61.1 (7.0)
KFA range (deg)	46.3 (5.2)	44.7 (4.5)	44.9 (5.6)	44.6 (5.5)

KAM peak1 (Nm/kg)	0.44 (0.10)	0.53 (0.13)	0.44 (0.12)	0.54 (0.15)
KAM peak2 (Nm/kg)	0.28 (0.10)	0.36 (0.15)	0.30 (0.10)	0.37 (0.16)
KAM midstance (Nm/kg)	0.20 (0.06)	0.29 (0.14)	0.21 (0.07)	0.28 (0.13)
KFM peak (Nm/kg)	0.48 (0.20)	0.36 (0.13)	0.52 (0.18)	0.50 (0.23)
Peak early stance KEM (Nm/kg)	0.30 (0.13)	0.27 (0.10)	0.25 (0.09)	0.23 (0.10)
Peak late stance KEM (Nm/kg)	0.38 (0.19)	0.40 (0.19)	0.38 (0.16)	0.31 (0.22)
KRM range (Nm/kg)	0.20 (0.09)	0.25 (0.09)	0.24 (0.08)	0.27 (0.10)

Caption: Participant demographics & results (mean +/- standard deviation)

References: [1] Bennell et al., Ann Rheum Dis 70:1770-1774, 2011.

[2] Miyazaki et al., Ann Rheum Dis, 61:617-622, 2002.

[3] Astephen et al., J Orthop Res, 26:332-341, 2008.

[4] Astephen et al., Proc Inst Mech Eng H, 218:271–279, 2004.

[5] Landry et al., J Biomech, 40:1754-1761, 2007.

Disclosure of Interest: None Declared

PROGRESS AND BENEFITS OF SUBJECT SPECIFIC MUSCULOSKELETAL MODELING OF THE HAND

Clint Hansen [1,*]Khalil Ben Mansour [1]Pierre Devos [1]Frédéric Marin [1]

[1]Université de Technologie de Compiègne, UMR 7338 : BioMécanique et BioIngénierie (BMBI), Comipiègne, France

Introduction and Objectives: Hand movements such as reaching or grasping are performed on a daily basis, but the analysis of these movements may differ due to the joint model specifications [1]. The question arises as to how the results are affected by the model choice since previous research has highlighted differences, e.g. due to personalized model scaling and manual scaling using motion capture data [2]. In the case of musculoskeletal modeling of the hand, the definition of the model parameters becomes a critical issue due to the small size of the anatomical structures. The sensitivity of the geometrical parameters of the musculoskeletal modeling was already clearly demonstrated [2,3], and the results motivated the necessity of the subject specific procedure. The aim of this study was to evaluate the differences between generic and personalized musculoskeletal models during a functional movement task.

Methods: The musculoskeletal model consisting of 28 rigid segments, 36 joints and 14 muscles [4] was implemented in the interactive modeling software (SIMM, Motion Analysis Corporation, Santa Rosa, CA). Six subjects (age: 31.7±9.1, body mass: 72.3±13.7kg, height: 1.73±0.11m) voluntary participated in this study. The personalized models were scaled based on the internal geometry given by the MRI, while the generic models were scaled based on the positions of the 3D marker positions and the generic hand joint model. To analyze the specific features of the functional movement, both models were driven by 3D positions of 59 markers (1.5 mm) from a motion capture system (Vicon Motion Systems Ltd. UK). The internal geometry of the personalized joint model was obtained from a 3D image data visualization software (ScanIP, Simpleware©) using images from a 1.5 T MRI system (GE Signa HDx™) with a spatial resolution of 0.3x0.3x0.5 mm3. In this article, we present differences between the above-mentioned models and compare the kinematics and the force values from the personalized and generic musculoskeletal model focusing on eight hand flexor muscles (Figure 1) and four hand extensor muscles during a clinical opposition movement of the thumb.

Results: A Wilcoxon matched pairs test ($p<0.05$), Pearson correlations and nRMSE analyses were implemented in Matlab (MathWorks Inc.) to evaluate the differences between the twelve joints and the twelve muscle forces with respect to each model. While all joint kinematics differed statistically ($p<0.05$), the correlation between the models was consistently high ($r>0.7$), and the nRMSE was consistently small. The obtained muscle forces differed statistically ($p<0.05$); however, the correlation between the muscle activity pattern was consistently high ($r>0.7$). In contrast to the kinematics, the nRMSE for the forces was high. Personalizing the model demands additional material (e.g. medical imaging) and also time-consuming post processing. However, significant differences between the models have been demonstrated. Implementing in-vivo data from medical images is a first step for more detailed investigations in the field of musculoskeletal biomechanics. Personalizing musculoskeletal models using, for example, MRI or CT imaging to obtain the internal geometry can help to improve the outcome of the conducted study. This study itself provides evidence of the difficulty and delicacy of multi-body musculoskeletal modeling and, specifically, the comparability of the results.

Figure:
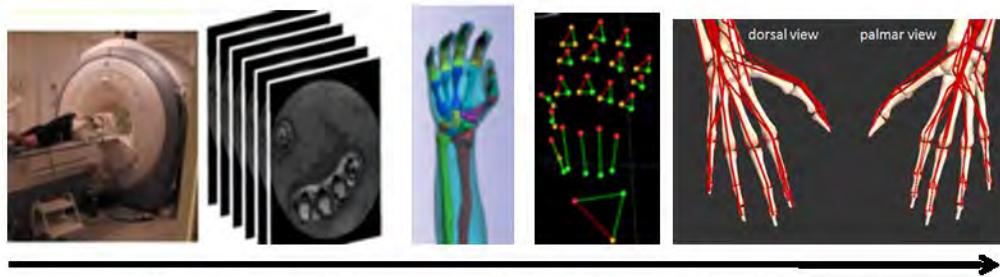
Steps to personalize musculoskeletal models of the hand

Caption: Subject specific musculoskeletal modeling of the using hand internal geometry given by the MRI and driven by 3D marker positions

Conclusion: Personalizing musculoskeletal models to obtain the internal geometry of the hand increases the complexity and the details of the musculoskeletal model. As the results show, differences in the scaling of the models led to small changes in the kinematic chain, as well as drastic changes in the computed muscle forces. Based on the aforementioned results, we emphasize the ideas of personalization of muscle-tendon paths and use of high resolution IRM. These analyses will increase the details and precision of hand modeling. However, musculoskeletal modeling of the hand remains very challenging due to the complex anatomical structures, which include 27 bones, 21 joints, 15 extrinsic and 11 intrinsic muscles. This study provides evidence of the difficulty and delicacy of multi-body musculoskeletal modeling and, specifically, the comparability of the results. In conclusion, musculoskeletal models of the hand are very valuable tools, but they must be used with caution. The outcome of this study is subject to further investigations and the necessity to improve and implement personalized models for clinical diagnoses.

Acknowledgments

References: [1] Vignais et al., Applied ergonomics 44 (4) : 566-574, 2013.

[2] Dao et al., CMBBE, 7: 745-751, 2012.

[3] Marin, Movement & Sport Sciences, in press, 2013.

[4] Gonzales et al., CMBBE, 30: 705-712, 2013.

Disclosure of Interest: None Declared

Musculoskeletal

AS-0352

SUBJECT-SPECIFIC MODELLING OF THE FOOT INTEGRATING FINITE ELEMENT MODELLING, GAIT ANALYSIS AND OPENSIM: PROOF OF CONCEPT IN DIABETIC NEUROPATHIC SUBJECTS

Annamaria Guiotto [1] Alessandra Scarton [1] Valentina Camporese [1] Claudio Cobelli [1] Zimi Sawacha [1,*]

[1] Dept of Information Engineering, University of Padova, Padova, Italy

Introduction and Objectives: Diabetes and in particular diabetic neuropathy have their main biomechanical effect on the lower limb and may lead to diabetic foot pathology and foot ulcerations.

While gait analysis allows the acquisition of the ground reaction forces (GRF) and kinematics in-vivo during gait, three-dimensional (3D) finite element analysis (FEA) allows characterizing the loads developed in the different internal structures of the foot [1]. State of art of foot FEA generally adopts both experimental kinematics and ground reaction forces as boundary conditions in order to predict plantar pressure and internal stresses distribution [2].

The aim of this study was to verify whether the inclusion of muscles forces as boundary conditions could improve foot FEA results. For this purpose subject specific muscle forces were extracted in Opensim [3] and FEA results obtained by including them or not within the boundary conditions were compared.

Methods: 3D foot gait analysis was carried out as in [4] on a diabetic neuropathic subject: age 71 years, BMI 37 kg/m^2, with type 2 diabetes, affected also by peripheral neuropathy and vasculopathy, HbA1c of 8.6%, with cavus foot, valgus heel, claw toes and callosities under the metatarsal heads. Experimental setup included a 6 cameras motion capture system (60-120 Hz, BTS S.r.l, Padova), 2 force plates (FP4060-10, Bertec, USA) and 2 plantar pressure (PP) systems (Imagortesi, Piacenza). The signals coming from all systems were synchronized. The hindfoot, midfoot and forefoot subsegments and tibia 3D kinematics, GRF and PP were calculated as in [4]. The protocol was approved by the local ethic committee. A right foot MRI (Siemens Avanto, 1.5 T, Spacing between slides: 0.7mm, Slice thickness: 1.5mm) was acquired and a FEA model was generated as in [2]: the MRI was segmented with Simpleware ScanIP (v.5.0), meshed with ScanFE module and imported into Abaqus. The muscles' insertions were identified in the MRI and then modelled as connectors in the FEA model. Material properties were obtained from the literature as in [2].

Subject-specific simulations were ran in Abaqus by conducting a quasi-static analysis on 4 gait cycle phases (initial contact, loading response, midstance, push off). Two different boundary conditions were considered: one including kinematics and both the GRF and the muscle forces (C1); one including only kinematics and GRF (C2).

Simulated PPs were extracted from Abaqus, subdivided into 3 subareas as in [4] and peak pressures were respectively calculated in C1 and C2. Errors in percentage of the experimental peak and root mean square errors (RMSE) were computed in order to compare C1, C2 and the experimental PP.

Results: The comparison between simulated and experimental data showed a good agreement in all phases of the gait cycle. Better results were obtained in C1 including kinematics with both the GRF and the muscle forces, thus confirming the important role assumed by the muscles in the modelling stage (Figure 1).

A good correspondence was also found in the identification of the peak plantar pressure's site between experimental and simulated ones.

A slight overestimation of the simulated PP resulted in both conditions.

Figure:
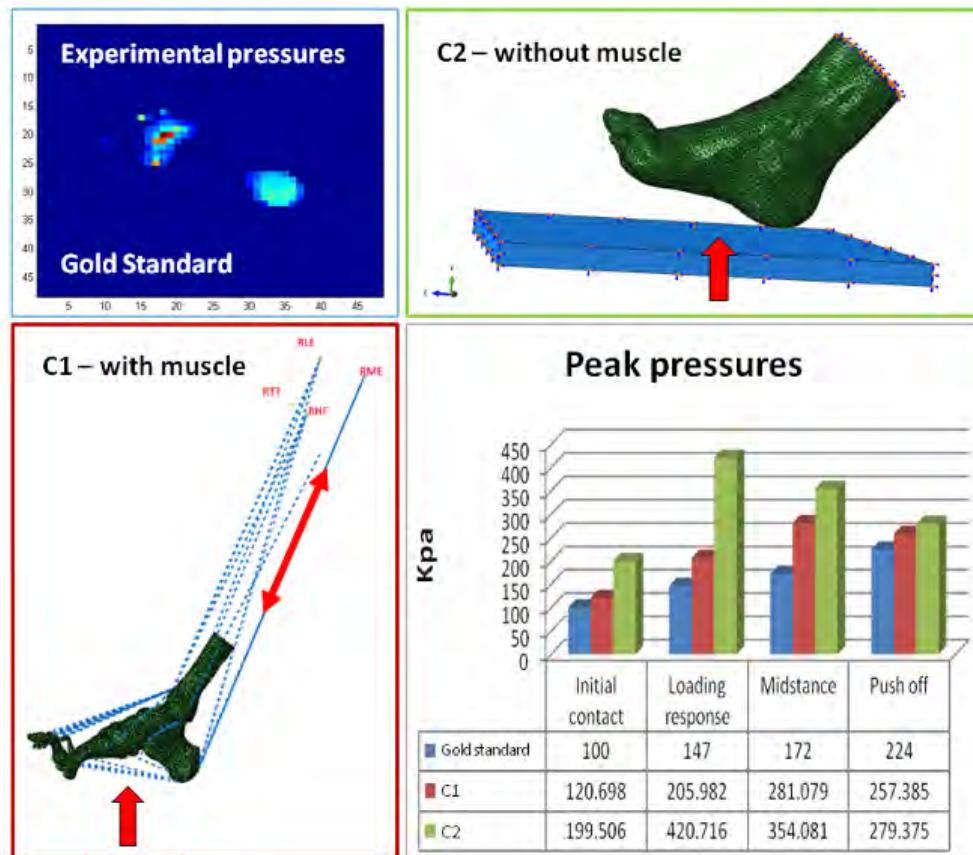
Caption: Figure 1. Experimental pressures, modelling conditions and simulated peak pressures results.

Conclusion: The differences between experimental and simulated pressures were mainly due to the non-subject-specificity of the material properties of the soft tissues applied in the FEA.

Furthermore it should be considered that muscle forces were obtained in Opensim, which adds another model within the FEA modelling procedure.

An important limitation is represented by the fact that only one subject participated in the study. However the method proposed herein, once applied to a wider subjects' cohort, may help in the management of diabetic foot pathology and in understanding its aetiology.

References: [1] Chen, W.-M., et al., Med Eng Phys, 32(4): 324–331, 2010.

[2] Guiotto, A., et al., J Biomech, 47(12): 3064–3071, 2014.

[3] Delp, S.L., et al. IEEE Trans Biomed Eng, 54(11): 1940–1950, 2007.

[4] Sawacha, Z., et al., Gait & Posture, 6(1): 20-6, 2012.

Disclosure of Interest: None Declared

Musculoskeletal

AS-0353

3-D PRESSURE-TIME DISTRIBUTION DURING PELVIC FLOOR CONTRACTION AND VALSALVA MANEUVER IN CONTINENT WOMEN

Licia P. Cacciari [1,*]Anice Pássaro [1]Amanda Amorim [1]Juliana Burti [1]Simone Silveira [1]Isabel Sacco [1]

[1]Universidade de São Paulo, São Paulo, Brazil

Introduction and Objectives: Pelvic floor (PF) muscles forces pull on the vaginal tissue is involved in bladder neck opening and closure guaranteeing urogynecological functions. PF dysfunctions affect the majority of women, for at least some time in their lives [1]. Clinicians usually evaluate PF function either subjectively by digital palpation or objectively by perineometers (intra-vaginal manometers) and dynamometers (strain gauges). Although objective evaluations assure better reliability and accuracy, the resultant force measured does not differentiate PF contraction (guaranteed by observed perineal cranial lift) from increases in abdominal pressure (leading to perineum downward movement - Valsalva maneuver). Our aim is to study the PF pressure distribution, taking into account its flexible surface with 3-dimensional deformations, objectively differentiating muscular force vectors from intra abdominal pressure raises in different regions of the vaginal cavity.

Methods: Twelve continent nulliparous woman (28.7± 5.6) were assessed in supine with knees flexed with an intra-vaginal probe (2.5cm diameter and 8cm length) introduced 7cm deep into their vaginal cavity. The probe involves 100 capacitive transducers (Pliance System - Novel, Munique, Germany) placed on a 10x10 matrix configuration. The pressure distribution map covering the whole vaginal cavity was divided into 8 sub regions (anterior, posterior, left and right; all of them cranial and caudally). Two trials of 2 different tasks were performed: (a) maximum voluntary PF muscles contraction (PFMC) and (b) maximum force in a valsalva maneuver. The data was subtracted from the passive force (acquired after one minute accommodation period inside the vaginal cavity). The maximum peak pressure and contact area were calculated and compared between tasks and regions by 2-way ANOVAs (p<.05).

Results: The interaction effect was significant between tasks and anatomical sub regions (figure). The highest peak pressure was achieved during PFMC in the anterior caudal region. The latero-lateral caudal peak pressures were smaller than the anterior caudal for PFMC, but still higher than in all regions during Valsalva. The Valsalva maneuver led to higher contact areas in the cranial anterior-posterior region than all other regions for this task, though it was similar to the contact areas during PFMC. The cranial anterior-posterior peak pressure were also not different between tasks. Considering the whole vaginal cavity area, 30% larger contact area and 4 times higher peak pressures were observed during PFMC (table). The PF muscles together with its passive structures must prevent incontinence and pelvic organ prolapse during abdominal pressure increases. The pressures observed during PFMC resulted in a pulling force up to cranial and anterior direction toward the hard surface of the pubic symphysis, what explains the higher peak pressures observed in the caudal anterior region during this task. It is interesting to note that PFMC resulted in increased pressures across the whole vaginal cavity, being more expressive in caudal regions, corresponding to its anatomical location [2]. During Valsalva, the observed increase in cranial contact area can be explained by increases in intra-abdominal pressure, pushing the pelvic organs towards the sensor probe, even though it did not result in higher peak pressures. It is also interesting to observe

that although the contact area was high in cranial regions during Valsalva, it was not higher than in any other regions during PFMC, making it easy to distinguish muscle force directions between tasks. Shifts in force-displacement-vectors of PF structures have been related to parity, mode of delivery and age [3]. This is an alternative protocol, which could help to elucidate the pathogenesis of PF dysfunctions.

Figure:
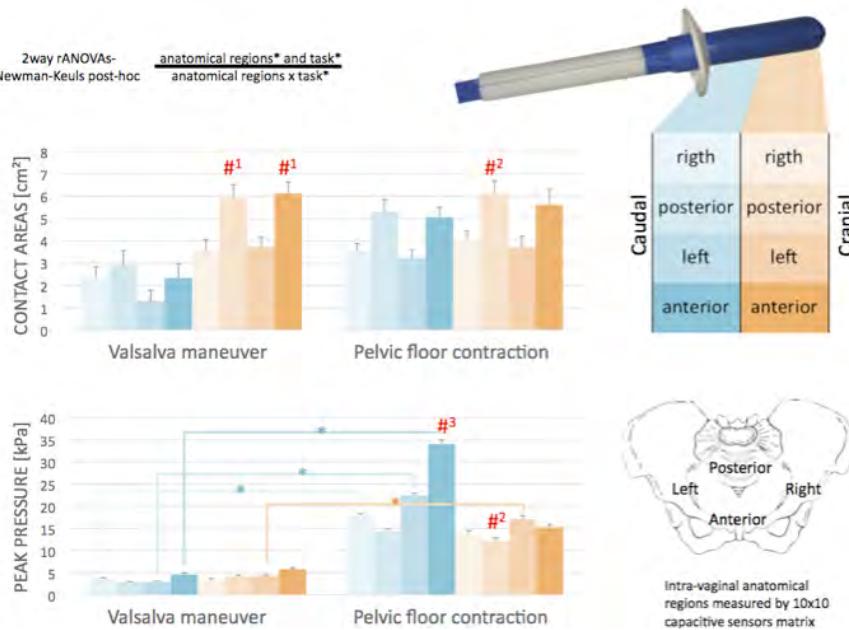
Caption: Intra-vaginal contact area and peak pressure during two tasks. Means ± standard errors. *significant differences between tasks within the same region. #differences between regions within the same task. #1- different from all caudal and cranial left/right regions. #2- different from caudal left region. #3- different from all the other regions. $p < 0.05$.

Conclusion: Pressure-time distribution during pelvic floor contraction and valsalva maneuver showed different patterns of peak pressures and contact areas across the vaginal cavity and could be used as an objective evaluation of the pelvic floor muscle function, elucidating the role of muscular force vectors on urogynecological function.

Table:

	Valsalva maneuver	Pelvic floor contraction
Contact area [cm2]*	28.2±10.2	36.6±8.4
Pressure peaks [kPa]*	10.2±9.0	50.3±18.3

Caption: Intra-vaginal contact area and peak pressures during two tasks. Means ± standard deviations. *significant differences between tasks. $p < 0.0001$.

References: [1] Dietz HP, Nrgastro, 9:113-121, 2012.

[2] Bo K et al., Neurourol Urodyn, 11(2): 107-113, 1992.

[3] Strauss C et al., Arch Gynecol Obstet, 285 (3): 741-747, 2011.

Disclosure of Interest: None Declared

Musculoskeletal

AS-0354

RELATIONSHIP BETWEEN LOADING INTENSITY AND DOSE OF PHYSICAL ACTIVITY WITH AGE AND BMI WHEN RECORDED BY ACCELEROMETRY AND QUESTIONNAIRE: POTENTIAL IMPLICATIONS FOR BONE HEALTH

Tina Smith [1,*]Sue Reeves [2]Jorg Huber [3]Lewis Halsey [2]Jin Luo [2]

[1]Institute of Sport, University of Wolverhampton, Walsall, [2]University of Roehampton, London, [3]University of Brighton, Brighton, United Kingdom

Introduction and Objectives: Fractures of the hip are an increasingly prevalent problem in an ageing population. Exercise is considered an effective measure in maintaining bone health and preventing the development of osteoporosis and hence decrease the risk of such fractures [1]. However, further clarity is required regarding how the intensity of exercise translates to mechanical stimulus at the site of the proximal femur to promote osteogenesis. In addition there is a need to identify the level of physical activity (PA) undertaken by differing individuals to accurately assess whether adequate PA is being undertaken to help maintain bone health.

Convenient and non-invasive ways of measuring PA are through questionnaires. However there could be issues around the accuracy with which participants recall and self-report previous or regular PA. Bone loading in PA can be measured more accurately by using accelerometers. Our latest research has developed a method using accelerometers to assess both loading magnitude and frequency in PA [2], which are two important parameters related to the adaptation and remodelling response of bone to mechanical stimuli [3].

The objectives of this study were to examine the relationship between loading intensity and dose at the proximal femur with age and BMI. Also to explore the relationship between PA levels determined via questionnaire with age and BMI.

Methods: A total of fifteen male and female participants (30.4 ± 7.6y (range 18-45y), 1.7 ± 0.1m, 76.7 ± 14.9kg) with a mean BMI of 25.9 ± 4.2kg/m^2 wore a tri-axial accelerometer, sampling at 10Hz, for 12 hours in order to record typical daily PA. The accelerometer was mounted directly above the hip joint as this was close to the site of typical proximal femur fractures and would therefore more accurately reflect the accelerations experienced within that region.

The 12 hours accelerometer data were filtered and then divided into 5-second long segments. Loading intensity was calculated for each segment [2] and the duration of physical activity at the following loading intensities was calculated – loading intensity of <5 BW/s, >5 BW/s, >10 BW/s, >15 BW/s, and >20 BW/s. The loading dose (BW) of physical activity was calculated at four frequency bands (0-5, 0-2, 2-4, and 4-5Hz).

Participant's usual PA levels were also measured using the short form of the International Physical Activity Questionnaire (IPAQ-SF). Accelerometer and IPAQ-SF data were correlated with age and BMI.

Results: Accelerometer and questionnaire data are provided in Table 1. Significant correlations were reported between age and loading dose for PA with frequencies ranging from 0-5Hz (overall dose: $r = 0.531$, $p = 0.041$) and loading dose for PA with a frequency range of 2-4Hz ($r = 0.547$, $p = 0.035$). Greater loading dose being associated with older age. Although not significant similar trends were observed for loading dose with a frequency range of 0-2Hz ($r = 0.487$, $p = 0.066$) and 4-5Hz ($r = 0.495$, $p = 0.061$). Questionnaire data revealed significant correlations between age and moderate ($r = 0.827$, $p < 0.001$) and vigorous ($r = -0.555$, $p = 0.049$) PA. Whilst moderate PA was significantly associated with an

increase in age, decreasing amounts of vigorous PA were associated with older age. There were no significant correlations between BMI and any of the PA measurements.

Conclusion: Acceleration data showed that the dose of mechanical loading in everyday activity tended to increase with age in the range from 18 to 45 years. It was also shown that age in this range does not seem to influence the time spent in very light (<5 BW/s) to vigorous (>20 BW/s) activity. These results suggest that people can generally maintain or increase their bone loading in daily activities from the age of 18 to early 40s. This is beneficial for the accumulation and preservation of greater peak bone mass to prevent osteoporosis. However, these results were not totally matched by questionnaire data which indicated that moderate PA increased with age, but vigorous PA decreased with age. This discrepancy could be due to the accelerometer providing only a snapshot of PA in the current cohort. However it could also reveal evidence of inaccurate reporting of levels of PA by participants.

Table:

	Variable	Mean ± SD
Accelerometer Data	Overall Dose 0-5Hz (BW)	80315.5 ± 20772.6
	Dose 0-2Hz (BW)	14206.1 ± 4095.3
	Dose 2-4Hz (BW)	42232.3 ± 11012.2
	Dose 4-5Hz (BW)	24884.5 ± 6407.4
	Loading Intensity < 5 BW/s (s)	38767.4 ± 1847.3
	Loading Intensity > 5 BW/s (s)	4432.6 ± 1847.3
	Loading Intensity > 10 BW/s (s)	1509.7 ± 1339.3
	Loading Intensity > 15 BW/s (s)	378.1 ± 465.4
	Loading Intensity > 20 BW/s (s)	199.8 ± 330.2
IPAQ-SF Data	PA Walking (MET-mins/wk)	1223.5 ± 1346.4
	PA Moderate (MET-mins/wk)	430.8 ± 420.8
	PA Vigorous (MET-mins/wk)	1224.6 ± 980.5
	PA Total (MET-mins/wk)	2878.9 ± 1462.5
	Weekday Sitting (mins/day)	420 ± 160.6

Caption: Table 1: Accelerometer and questionnaire data

References: [1] Jamsa et al., Clin Biomech. 21: 1-7, 2006.

[2] Chahal et al., Bone. 67: 41-45, 2014.

[3] Hsieh et al., J Bone Min Res. 16: 918-924, 2001.

Disclosure of Interest: T. Smith Conflict with: This study was supported by Kellogg's Company , S. Reeves Conflict with: This study was supported by Kellogg's Company , J. Huber Conflict with: This study was supported by Kellogg's Company , L. Halsey Conflict with: This study was supported by Kellogg's Company , J. Luo Conflict with: This study was supported by Kellogg's Company

Musculoskeletal

AS-0355

PASSIVE ELASTIC PROPERTIES OF HIP EXTENSORS IN SUBJECTS WITH LOW BACK PAIN

Mark Hines [1][2][*]Neale Tillin [2]Raymond Lee [1]

[1]School of Applied Sciences, London South Bank University, [2]Life Sciences, University of Roehampton, London, United Kingdom

Introduction and Objectives: Due to observed alterations in hip function, during activities of daily living in low-back pain (LBP) patients, hip range of motion (ROM) is commonly assessed by clinicians and physical therapists (Tafazzoli and Lamontagne, 1996, Parks et al., 2003, Sjolie, 2004, Davis *et al.*, 2008, Ekedahl *et al.*, 2010, Ylinen *et al.*, 2010). However, it has been proposed that an assessment of hip extensor passive properties may be a more useful indication of mechanical limitations than ROM (Hamill *et al.*, 2009, Marshall *et al.*, 2009, Gombatto *et al.*, 2008). The purpose of the present study was to compare the passive properties of the hip extensors in individuals with and without chronic, non-specific LBP.

Methods: 61 participants (back pain n = 30 (male n = 15. female n = 16), no back pain n = 31 (male n = 15, female n = 15)) volunteered for this study and were allocated to groups according to gender and presence of back pain. Participants were positioned supine on a standard treatment couch, with the knee of the test leg supported into a straight or bent angle with 1 of 4 knee braces. 2 inclinometers were secured using straps to the thigh and shank, to measure hip angle and hip angular acceleration, and to monitor knee angle, respectively. Two surface electromyography (EMG) electrodes (SX230, Biometrics, UK), were placed over the biceps femoris and rectus femoris, in accordance with the SENIAM guidelines for electrode placement. A custom-built force transducer was inserted into an ankle brace, designed to house the transducer with minimal friction, whilst maintaining the ankle in plantigrade.

The tester performed 3 leg raises with a minimum of 1 minute rest between each with each of 4 knee braces. Data from the load cell and inclinometers was used in combination with anthropometric limb segment and mass data to calculate passive hip moments, stiffness and strain energy. The passive moment calculation was based upon the dynamic biomechanical model established by Lee and Munn (2000).

Results: Figure 1 shows normalised sub-group moment-angle curves at a knee angle of 180 degrees (knee straight). A MANOVA demonstrated no significant effects between groups at any hip angle for normalised moments, stiffness or strain energy, within any of the 4 knee angle conditions ($p > 0.05$).

Normalised Moment-Angle Data of Sub-Groups (180 Degree Knee Angle)
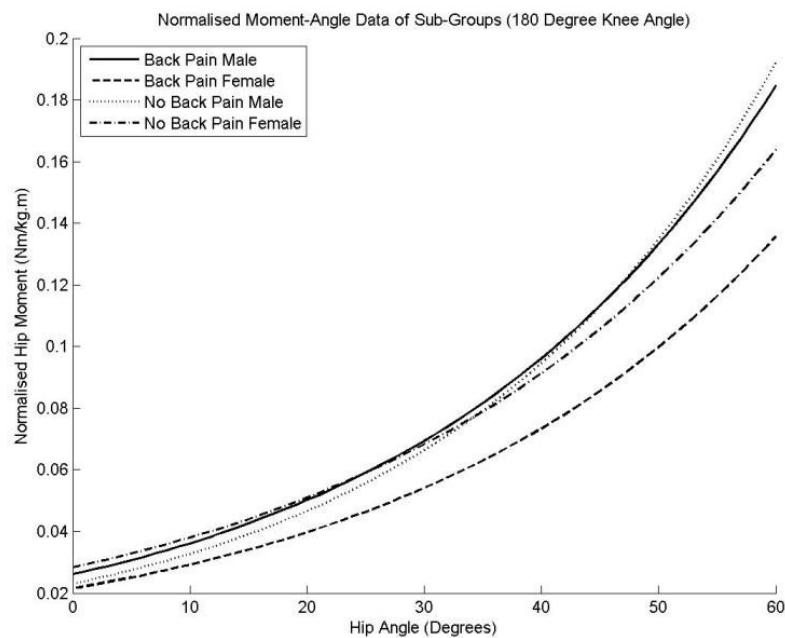
Conclusion: This study demonstrates that LBP does not significantly influence the hip extensors during passive leg raising. Observed differences during ADLs may potentially be due to alterations in active contributions to movements, such as motor control. Further research will be useful to better understand adaptations to long-term pain, and which tissues and components of movement should be targeted with clinical assessments and rehabilitation programmes.

References: DAVIS, D. S., QUINN, R. O., WHITEMAN, C. T., WILLIAMS, J. D. & YOUNG, C. R. 2008. Concurrent validity of four clinical tests used to measure hamstring flexibility. *J Strength Cond Res,* 22, 583-8.

EKEDAHL, K. H., JONSSON, B. & FROBELL, R. B. 2010. Validity of the fingertip-to-floor test and straight leg raising test in patients with acute and subacute low back pain: a comparison by sex and radicular pain. *Arch Phys Med Rehabil,* 91, 1243-7.

GOMBATTO, S. P., NORTON, B. J., SCHOLTES, S. A. & VAN DILLEN, L. R. 2008. Differences in symmetry of lumbar region passive tissue characteristics between people with and people without low back pain. *Clin Biomech (Bristol, Avon),* 23, 986-95.

HAMILL, J., MOSES, M. & SEAY, J. 2009. Lower extremity joint stiffness in runners with low back pain. *Res Sports Med,* 17, 260-73.

LEE, R. Y. & MUNN, J. 2000. Passive moment about the hip in straight leg raising. *Clin Biomech (Bristol, Avon),* 15, 330-4.

MARSHALL, P. W., MANNION, J. & MURPHY, B. A. 2009. Extensibility of the hamstrings is best explained by mechanical components of muscle contraction, not behavioral measures in individuals with chronic low back pain. *PM R,* 1, 709-18.

PARKS, K. A., CRICHTON, K. S., GOLDFORD, R. J. & MCGILL, S. M. 2003. A comparison of lumbar range of motion and functional ability scores in patients with low back pain: assessment for range of motion validity. *Spine (Phila Pa 1976),* 28, 380-4.

SJOLIE, A. N. 2004. Persistence and change in nonspecific low back pain among adolescents: a 3-year prospective study. *Spine (Phila Pa 1976),* 29, 2452-7.

TAFAZZOLI, F. & LAMONTAGNE, M. 1996. Mechanical behaviour of hamstring muscles in low-back pain patients and control subjects. *Clin Biomech (Bristol, Avon),* 11, 16-24.

YLINEN, J. J., KAUTIAINEN, H. J. & HAKKINEN, A. H. 2010. Comparison of active, manual, and instrumental straight leg raise in measuring hamstring extensibility. *J Strength Cond Res,* 24, 972-7.

Disclosure of Interest: None Declared

Sport

AS-0356

WHOLE-BODY ENERGY TRANSMISSION EFFICIENCY IN KICKING A FOOTBALL

Shoma Kudo [1,*]Ryosuke Akaguma [1]Akinori Nagano [2]

[1]Department of Sport and Health Science, [2]Faculty of Sport and Health Science, Ritsumeikan University, Shiga, Japan

Introduction and Objectives: In football games, giving effective shots that are appropriate in individual situations is so important. Experienced players are able to control the ball skillfully. Moreover, kicking is the most important attacking option and most widely studied skill in football. There are many previous researches that analyzed the motion of kicking. Sinclair et al, (2014) [1] aimed to measure the technical aspects of kicking related to the generation of ball velocity using regression analyses. This study measured angular velocity and joint moment of the hip and knee joint. Zago et al, (2014) [2] used a total body center of mass based approach for the analysis of the kinematics of inside kick. Their study focused on the control of ball kicking. Kick motion consists of not only leg movements but also movements of the whole body. Therefore, it is important for football player to convey the energy efficiently from the whole body to the ball. The purpose of this study was to evaluate the energy transmission efficiency in kicking a football with respect to the whole body.

Methods: Participants: Six male subjects (age=21±1 years old) were examined while kicking a stationary football (size 5, mass= 410g). The subjects were divided into two groups (experienced or non-experienced). The experienced person had been playing football for at least three seasons. The participants were all free from musculoskeletal pathology at the time of data collection.

Procedures: We took 3-D kinematic data from the full body of the subjects performing three ways of kicks (inside, infront and instep) by a motion capture system (Motion Analysis, MAC3D system, USA). The ball was positioned such that the support foot land on a force platform (Tec Gihan, TF-4060-B, Japan). Force data were sampled at 1000 Hz. The ball speed was measured by a high speed camera (CASIO, EX-ZR1000, 480 frames/sec). Six subjects (3-experienced and 3-non experienced) wore underwear on which 29 reflective markers were attached. The markers were attached based on Helen Hayes marker set. They wore a pair of indoor shoes. After a warm up session, the subjects performed three kinds of kick at three strength variation.

Data processing: Three-dimensional kinematic and kinetics measures were calculated using nMotion musculous (nac Image Technology Inc, Japan) (Figure). We determined the impact as the instant at which the toe velocity decreased rapidly. The mechanical energy of the ball was calculated from the velocity and the height of the ball determined using a high speed camera. We evaluated the percentage of the energy transmission efficiency. We compared the mechanical energy change of the whole body and the ball.

Results: Energy transmission efficiency in kicking ranged between 13.1% ~ 29.1%. Transmission efficiency of experienced subjects ranged between 16.8% ~ 29.1%. Transmission efficiency of non-experienced subjects ranged between 13.1% ~ 21.7%. There were not large differences in energy transmission efficiency among the three kinds of kick form. Experienced subjects exhibited high energy transmission efficiency in kicking compared to non-experienced subjects. We consider that experienced subjects could kick the ball effectively because they have high skills.

Figure:
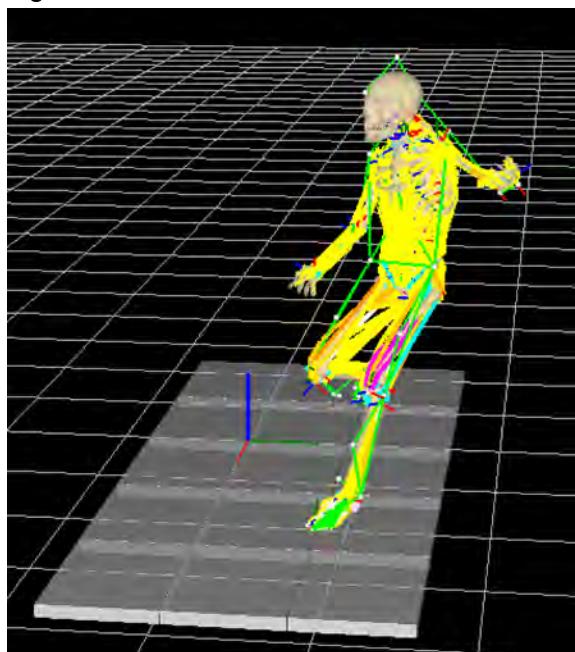
Caption: Snapshot of a kicking motion, processed with a musculoskeletal modeling software.

Conclusion: We evaluated the energy transmission efficiency of kicking a football. The experienced subjects exhibited high energy transmission efficiency in kicking compared to non-experienced subjects. The exact techniques to enhance the energy transmission efficiency need to be clarified in future studies.

Table:

		non experienced subjects		experienced subjects	
Kick	Strength	Average (%)	SD	Average (%)	SD
Inside	Weak	13.2	2.6	16.8	1.9
	Medium	18.2	4.9	29.1	2.5
	Max	21.7	5.6	25.4	1.5
Infront	Weak	16.4	7.5	26.3	2.6
	Medium	16.5	1.0	25.9	2.8
	Max	18.0	3.0	27.3	4.0
instep	Weak	18.7	3.5	25.8	4.7
	Medium	19.2	3.4	28.3	9.2
	Max	20.5	2.8	27.6	4.2

Caption: Summary of energy transmission efficiency.

References: [1] Sinclair et al., European Journal of Sport Science., 14:8, 799-805, 2014

[2] Zago et al., Journal of Human Kinetics., 42: 51-61, 2014

Disclosure of Interest: None Declared

Sport

AS-0357

HOW DOES PLAYING SURFACE AFFECT TIBIAL ACCELERATION DURING FAST BOWLING IN CRICKET?

Billy Senington [1,*] Jonathan Williams [1] Raymond Lee [2]

[1] School of Health and Social Care, Bournemouth University, Bournemouth, [2] School of Applied Sciences, London South Bank University, London, United Kingdom

Introduction and Objectives: Previous studies have suggested that repetitive exposure to high levels of ground reaction force (GRF) may correlate with the abnormally high prevalence of lumbar stress fractures, knee and ankle injuries [1-3]. GRF is typically obtained using a force plate, introducing environmental constraints to data collection especially relating to the effect of different playing surfaces. Novel methods using accelerometer derived accelerations, have been shown to strongly correlate with GRF [4]. Therefore this study aims to classify different playing surfaces and quantify the effect of different playing surfaces on peak and time to peak acceleration experienced at the front tibia during fast bowling.

Methods: A custom built impact tester was used to measure vertical acceleration across four different surfaces: Grass wicket, outdoor astroturf wicket, indoor wood and rubber composite surfaces. Variables of peak and time to peak acceleration were used to classify individual surface firmness.

To determine the effect of surface on tibial impact five trained amateur fast bowlers completed 12 deliveries on the four different surfaces whilst tibial acceleration was measured. Bowlers were recruited from local cricket clubs and instrumented with a three-dimensional accelerometer (±200g) (THETAmetrix, ADXL377) sampling at 750Hz. This was attached to the medial aspect of the mid-tibia on the subjects' 'front' leg. Peak and time to peak tibial acceleration were identified for the front-foot impact phase of the bowling action.

Intraclass correlation coefficients (ICC) were calculated from pooled data across all surfaces, standard error of measurement (SEM) and minimum detectable change (MDC) calculations for both the impact tester and tibial accelerations were calculated for all four surfaces. ANOVAs were used to analyse any differences between surfaces for both the impact tester and tibial accelerations.

Results: ICC, SEM and MDC results (seen in table 1) demonstrate high reliability between tests with ICC values between 0.716-0.932. SEM for all measures were low, consequently producing low MDC values of 2.92g and 4.21ms for tibial acceleration and time to peak acceleration and 3.52g and 1.92ms for the impact tester.

Peak and time to peak vertical acceleration results for the impact tester can be seen in figure 1.

Tibial acceleration during bowling on the wooden surface was significantly lower than grass, rubber and astroturf ($F_{(3,236)}=33.972$, $p<.001$, $p=.001$ and $p<.001$). Peak tibial acceleration was significantly greater on the astroturf surface compared with grass, rubber and wood ($F_{(3,236)}=33.972$, $p=.007$, $p<.001$ and $p<.001$). Time to peak tibial acceleration during bowling was longer on grass compared with astroturf ($F_{(3,236)}=5.231$, $p=0.001$). No other significant differences were present (seen in table 1).

Figure:
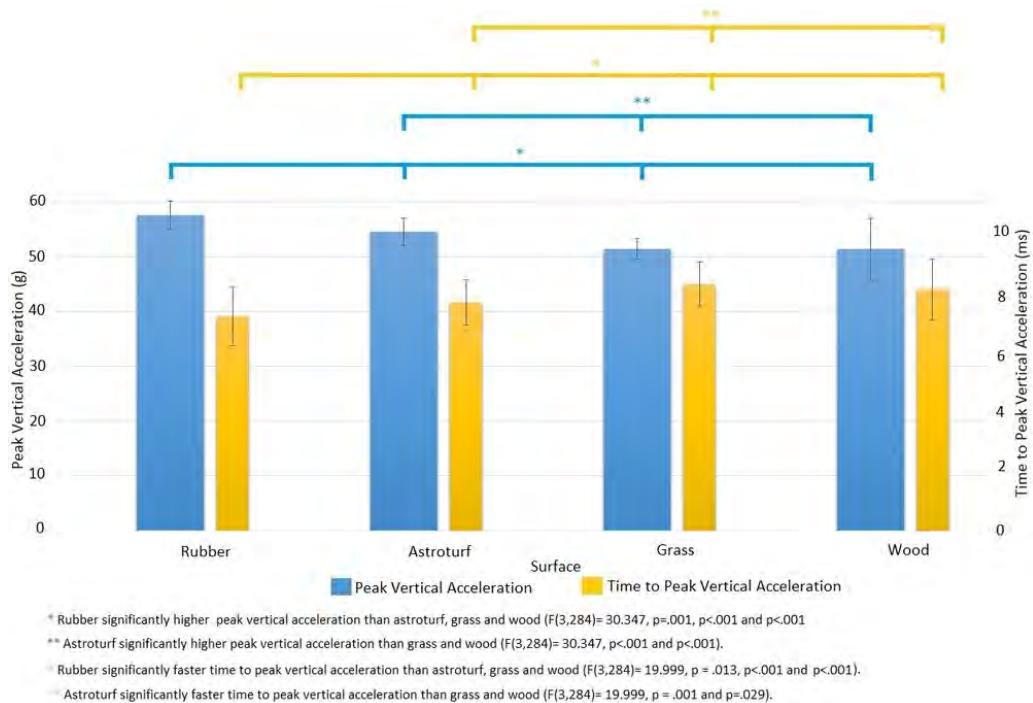
Caption: Figure 1. Peak and time to peak vertical acceleration of a custom built impact tester on four cricket playing surfaces.

Conclusion: Novel methods were used to assess the effect of surface firmness on front tibial acceleration during fast bowling. Reliability testing demonstrates the results produced were highly reliable. This study has highlighted that there was no significant difference in the tibial impact characteristics of the two most commonly used surfaces in professional cricket (grass and rubber). However, peak tibial and impact tester accelerations agree that the wooden surface produced significantly lower peak accelerations. Time to peak tibial accelerations were significantly longer on grass compared with astroturf. No other significant differences in time to peak accelerations suggests that the wooden surface produced lower peak tibial acceleration, over a similar time when compared with the other surfaces. Therefore, wooden surfaces may be beneficial if impact reduction is desired. Conversely, it may be advisable to avoid high workloads on the 'harder' astroturf surface. As no studies have investigated the effect of bowling surface on kinematics, further work may be required to analyse how these results impact bowling kinematics.

Table:

	Peak Acceleration				Time to Peak Acceleration			
Surface	Peak Acceleration (g (SD))	ICC	SEM (g)	MDC (g)	Time to Peak Acceleration (ms (SD))	ICC	SEM (ms)	MDC (ms)
Astroturf	28.14 (5.79)	.932	1.17	2.95	26.93 (13.23)	.919	1.99	3.78
Grass	24.68 (6.64)	.93	1.54	3.39	36.36 (16.11)	.91	3.68	5.24

		2				9		
Rubber	21.97 (4.89)	.93 2	0.86	2.52	30.55 (13.42)	.91 9	1.67	3.45
Wood	17.84 (5.69)	.93 2	1.04	2.82	30.00 (9.76)	.91 9	2.60	4.35
Mean (SD)	**23.16 (5.75)**		**1.15 (0.29)**	**2.92 (0.36)**	**30.96 (13.13)**		**2.49 (0.89)**	**4.21 (0.78)**

g; gravity, SD; standard deviation, ms; milliseconds, ICC; intra-class correlation coefficient, SEM; standard error of measurement, MDC; minimal detectable change.

Caption: Table 1. Acceleration and reliability measures for the front tibia during bowling.

References: [1] Spratford et al., J. Sport Sci 32: 1101-1109, 2014.

[2] Johnson et al., Phys Ther Sport 13: 45-52, 2012.

[3] Portus et al., J. Sport Sci 18: 999-1011, 2000.

[4] Sell et al., J. Appl Biomech 30: 75-81, 2014.

Disclosure of Interest: None Declared

Sport

AS-0358

HOW DOES THE SHOOTING MECHANICS CHANGE AFTER 3 MONTHS OF SHOOTING PRACTICES IN YOUNG BASKETBALL PLAYERS?

Yuki Inaba [1,*]Noriko Hakamada [1]Mitsuo Sasaki [2]

[1]Department of Sports Science, Japan Institute of Sports Sciences, Tokyo, [2]Keio University, Kanagawa, Japan

Introduction and Objectives: Improving the percentages of goals made among attempted shots during a basketball game is crucial for winning the game. Thus, optimal trajectory and spin rate of the ball that result in higher probability of shots made were investigated[1,2]. Also, shooting motion was investigated to examine intratrial variability of the shots, so kinematic analyses were conducted to investigate the variability of the joint motions [3,4]. However, since shooting mechanics how the ball is accelerated and how the back spin is applied is not investigated, the shooting motion that can improve the probability of shots made is not understood. Therefore, the first objective of this study was to investigate the mechanics of the shooting motion by conducting kinematic and kinetic analysis of upper body. In addition, in order to examine shooting motion with higher probability of shots made, the effects of shooting training that was attempted to improve ball trajectories and spin rate on shooting motion were assessed by pre- and post-training motion analysis tests, which was the second objective of this study.

Methods: Eight young basketball players who were selected to national elite academy team (height: 184.1 ± 3.7 cm, weight: 76.6 ± 10.9 kg, age: 14.2 ± 1.2 years-old) participated in this study. All participants joined five times of basketball camps in 3 months (each camp consisted of 3-days with various basketball training) and their shooting motion were assessed before and after the training program (pre- and post-test). During the camps, players went through shooting drills and were instructed to increase the maximum height of the ball and increase the spin rate. In pre- and post-tests, each participant performed 10 shots from a line 5.5 m behind a backboard. The shooting motion and the trajectory of balls were captured with VICON motion analysis system with 18 cameras (MX-series) at 500 Hz. 45 markers were attached to the whole body of the participant and 5 markers to the ball surface.

Initial velocity and acceleration of the center of the ball, release angle in the saggital plane, and maximum height of the ball were analyzed. Spin rate was also calculated as the absolute value of the angular velocity vector of the ball [5]. Theoretical optimal projection angle of the ball in saggital plane was calculated as the minimum-speed angle defined by Brancazio in 1981 [6]. Also, force exerted on the ball from shooting finger was computed from the calculated acceleration of the ball. Then, joint moment at wrist, elbow, and shoulder were calculated using standard inverse dynamics methods. Joint work at each joint was calculated by integrating the joint power from the start of the elbow joint extension to ball release.

Results: Sum of joint works or total joint works from set position to release at shoulder, elbow, and wrist joint flexion/extension axis were 17.6 ± 3.2 J at pre-test and 15.7 ± 3.6 J at post-test. Among the total work, most of the joint work was done at the elbow joint flexion/extension axis (0.5 ± 2.7 J at shoulder, 13.7 ± 2.2 J at elbow, and 3.4 ± 0.6 J at wrist joint at the pre-test). Thus, it was suggested that elbow joint extension work contributed more to accelerate the ball compared to shoulder and wrist joint.Maximum height of the ball and the projection angle increased from the pre-test to

the post-test except one subject whose arch was relatively high at the pre-test. However, there were no significant changes in the spin rate from the pre-test (562.1±138.6 deg/s) to the post-test (539.9±118.1 deg/s). In order to increase the projection angle, the direction of the force exerted to the ball from finger should be directed more upward. This result in the force application line to pass through closer to the center of the ball and the moment exerted around the ball center would be smaller. Thus, it was speculated it is difficult to increase the spin rate at the same time as increasing the ball arch if appropriate skill for applying ball spin was not acquired.

Figure:
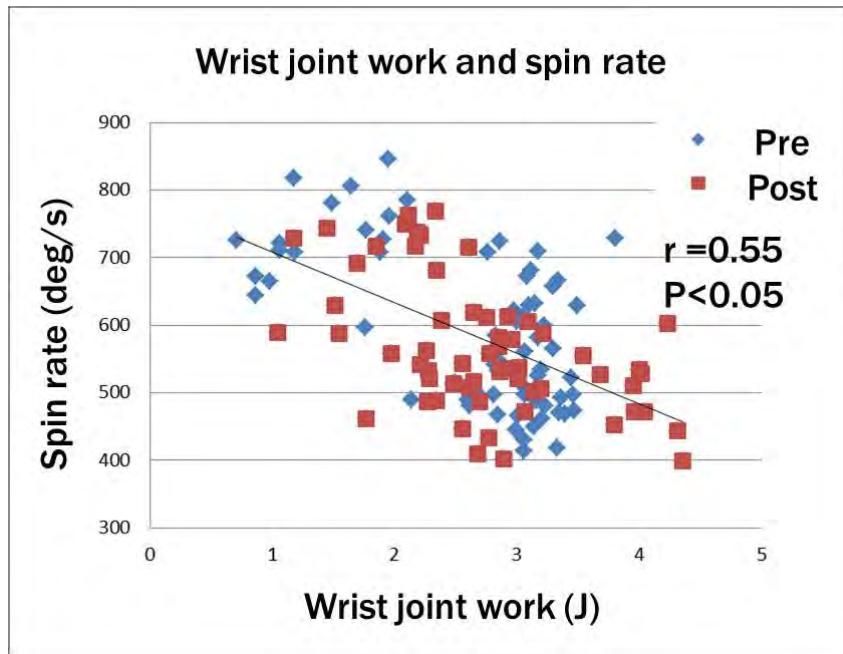
Caption: Figure: Spin rate decreased as the wrist joint work increased.

Conclusion: Firstly, it was found that joint work at elbow joint contributed more to accelerate the ball compared to shoulder and wrist joint work. After training session, even though the trajectory of the ball was improved, no improvement on spin rate was observed. It was considered that trying to increase the arch of the ball without having enough strength at elbow extension have the possibility to change the shooting mechanics and spin rate is not improved at the same time unless specific technique for increasing spin rate is learned.

References: [1] Tran et al., J Sports Sciences, 26(11): 1147-1155, 2008.

[2] Silberverg et al., J. Dyn. Sys., Meas., Control, 125(4): 531-540, 2003.

[3] Mullineaux et al., J Sports Sci., 28(9): 1017-1024, 2010.

[4] Button et al., Res Q Exerc Sport., 74(3):257-269, 2003.

[5] Craig, *Intrudoction ot robotics: Mechanics and control:* 152-186, 1989.

[6] Brancazio, Am J Ph.. 49(4): 356-365, 1981.

Disclosure of Interest: None Declared

BIOMECHANICAL AND GENDER DIFFERENCES BETWEEN SINGLE-LEGGED AND TWO-LEGGED RUNNING VERTICAL JUMPS

Masanori Sakaguchi [1,*] Ryan Madden [1] Nicole Schrier [1] Daniel Koska [1] John Wannop [1] Darren Stefanyshyn [1]

[1] Faculty of Kinesiology, University of Calgary, Calgary, Alberta, Canada

Introduction and Objectives: Vertical jump height is a crucial variable in many sports and depending on the situation, athletes may utilize either a single-legged running jump or a two-legged counter-movement jump. Interestingly, single-legged and two-legged running vertical jumps do not differ in maximum jump height despite the two-legged jump having twice the available leg musculature to produce vertical ground reaction impulse [1]. Vertical ground reaction impulse, therefore, is not sufficient to predict jump performance for a single-legged jump as it does not adequately capture the mechanical contributions of the swing leg. Furthermore, while gender differences have been studied during many athletic tasks, there is little information regarding differences for a running vertical jump. Therefore, the objectives of this study were to determine the biomechanical differences between single- and two-legged jumps, and to determine any differences in these jumps between males and females.

Methods: Twenty varsity athletes, 10 male and 10 female, were tested. Markers were attached to the athlete to determine segmental motions of the foot, shank and thigh for both legs as well as the pelvis and torso. Kinematic (240 Hz) and kinetic (2400 Hz) data were simultaneously recorded with an 8-camera motion capture system and 2 force plates. Jump heights were measured using a Vertec jump meter. To minimize the influence of footwear, all participants performed in a properly sized neutral training shoe (adipure 360, adidas). Athletes were asked to jump and reach as high as possible and contact the Vertec fins with their dominant hand using a single-legged running jump as well as a jump technique which they were free to choose with the only criteria being to reach as high on the Vertec as possible. All females and 6 of the 10 males selected a two-legged jump as the self-selected jump technique, while the remaining males selected a single-legged jump. Ten trials of each jump type were collected. Vertical ground reaction impulse and joint energetics were calculated. The net joint energy for the stance legs was calculated from the instant of the lowest position of the pelvis to takeoff. The energy from the swing leg was calculated from the same starting point to when the energy generated reached zero to account for any contributions during the flight phase. These time points were chosen as they are associated with the propulsive phase of the jump, where the energy generated is utilized to propel the athlete upwards. Paired t-tests were performed to compare between single- and two-legged (self-selected) jumps. Additionally, comparisons were made between the female and males using independent t-tests. Significance was set at $\alpha = 0.05$.

Results: A summary of the results is shown in Table 1, while joint energy contributions are shown in Figure 1. Comparing the single-legged and two-legged running jumps, results were the same regardless of gender with no significant difference in maximum jump height despite a greater vertical ground reaction impulse during the two-legged jump. The ankle and knee joint energetics were significantly greater during the two-legged jump, while the hip joint energetics were substantially greater during the single-legged jump with the influence of the swing leg becoming a significant factor, resulting in no difference in net energy of all joints combined compared to the two-legged jump. Comparing genders,

during the two-legged technique the ankle, knee and hip joints all contributed equally to the net energy between males and females (P > 0.4 for all). Conversely, during the single-legged jump males generated a greater amount of energy from their hip joint compared to the females (P < 0.001), while the females used a greater amount of energy from their knee (P < 0.05) with a trend toward significant difference at the ankle (P = 0.067).

Figure:
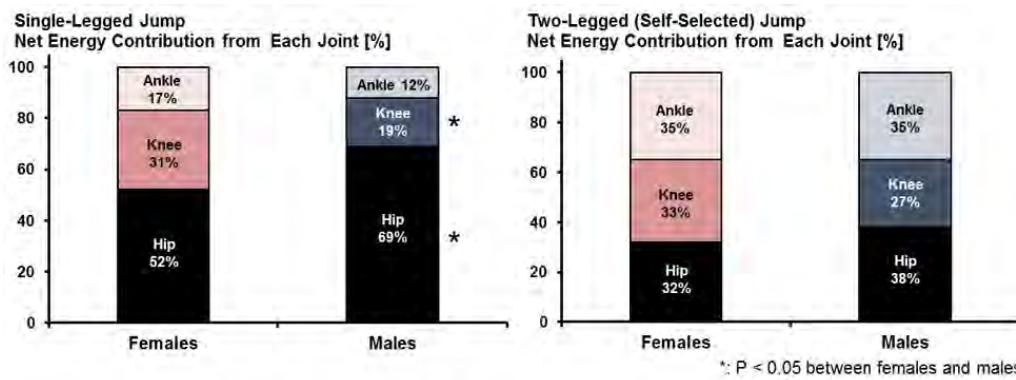
Caption: Joint Energy Contributions of Males and Females for Single- and Two-legged Jumps

Conclusion: While the maximum jump heights were similar between single-legged and two-legged running jumps, the jumping strategies employed to achieve the jumps were markedly different. Regardless of gender, the ankle, knee and hip joints all contributed equally to the net energy during the two-legged jump, whereas the hip joint energetics contributed the majority of the net energy during the single legged jump. In terms of the gender differences, males were able to generate significantly greater energy at the hip, resulting in greater net energy generation and increased jump height compared to the females.

Table:

		Female		Male	
		Single-legged	Two-legged	Single-legged	Two-legged
Maximum jump height [cm]		52	52	61	64
Vertical ground reaction impulse [Ns]		391	538 *	530	839 *
Net energy	Ankle [J]	51	110 *	45	142 *
	Knee [J]	95	103 *	83	121 *
	Hip [J]	160	101 *	269	157 *
	All joints [J]	306	314	384	407
					*: P < 0.05, Single- vs. Two-legged jumps

Caption: Kinematic, kinetic and energetic data comparing the single-legged and two-legged jumps

References: [1] Vint et al., J. Appl. Biomech, 12: 338-58, 1996.

Disclosure of Interest: M. Sakaguchi Conflict with: adidas, R. Madden Conflict with: adidas, N. Schrier Conflict with: adidas, D. Koska Conflict with: adidas, J. Wannop Conflict with: adidas, D. Stefanyshyn Conflict with: adidas

Sport

AS-0360

THE DIFFERENCES OF THE KNEE JOINT KINEMATICS AND KINETICS BETWEEN VERTICAL AND ROTATIONAL JUMP LANDING

Daisuke Bai [1][2][*] Takahiko Fukumoto [2] Munehiro Ogawa [3] Yasuhito Tanaka [3]

[1]Heisei Memorial hospital, [2]Graduate School of Health Science, Kio University, [3]Department of Orthopaedic Surgery, Nara Medical University, Nara, Japan

Introduction and Objectives: Large knee valgus angles and moments during jump landing are considered as an important predictor of non-contact anterior cruciate ligament (ACL) injury risk, particularly in females. The vertical and rotational jump training was included for ACL injury prevention program. The drop vertical jump task was commonly used to assess biomechanical performance measures that are associated with ACL injury risk. However, there are no reports to analyze the biomechanics of rotational jump landing. The purpose of this study was to assess peak knee valgus angles and moments during vertical and rotational jump landing.

Methods: Ten healthy females participated in this study. The tasks were vertical jump, clockwise 180 and 360 degrees rotational jump. Peak knee valgus angles and moments of bilateral leg were investigated during 3 different jumps with a 3-dimensional motion analysis system (Vicon) and force plate (AMTI). 3D motion was collected with a 6-camera motion capture system that sampled at 120 Hz. Vertical ground reaction force was sampled at 120 Hz and the initial ground contact was defined as the time when the vertical ground reaction force exceeded 10N. A repeated-measures ANOVA with Bonferroni post hoc analysis was used to determine whether there were any significant differences between tasks for angles and moments. Written informed consent was attained from all participants, and approval for the study was provided by the university's ethical committee.

Results: No significant differences between vertical jump landing and 180 degrees rotational jump landing were found in peak valgus angles and moments. Peak valgus angles and moments during 360 degrees rotational jump were significantly increased than the other jump landings ($P < .05$).

Conclusion: Our findings showed that knee kinematics and kinetics changed with different jump landings. Modification of high-risk movement strategies such as dynamic knee valgus angles and moment is key to the reduction of ACL injury. The results of the present study implicated that it is necessary to take into account not only vertical jump landing but also rotational jump landing to develop ACL injury prevention programs.

References: Bates et al., Clin Biomech, 28: 459-466 ,2013.

Kristianslund et al., AJSM, J. Biomechanics, 47: 193-199, 2014.

Disclosure of Interest: None Declared

AS-0361

EFFECT OF BRA STRAP STIFFNESS ON BREAST KINEMATICS AND PERCEIVED BRA PERFORMANCE DURING TREADMILL RUNNING

Steph Forrester [1,*]Laura Whittingham [1]

[1]Wolfson School oif Mechanical and Manufacturing Engineering, Loughborough University, Loughborough, United Kingdom

Introduction and Objectives: Sports bras aim to reduce breast motion during exercise and thereby eliminate pain or discomfort commonly present under lesser breast support conditions [1]. The ability of a specific sports bra to reduce breast kinematics is a function of the bra structure and the properties of the materials used. Therefore, understanding the relationship between breast kinematics and the mechanical properties of a bra can help in the development of more supportive bras, particularly for high impact sporting applications. Previous studies that have tried to link breast kinematics to bra mechanical properties have typically used commercial bras where many aspects of the bra structure and materials varied simultaneously making it difficult to isolate the individual effects, e.g. [2]. The objective of this study was to investigate the effect of strap stiffness on bra performance (breast kinematics and perceived performance) during treadmill running by manipulating the material properties of the strap whilst holding the remaining structural and material aspects of the bra constant.

Methods: Following institutional ethical approval, ten recreationally active female participants (age 25.9 ± 5.5 years; height 1.65 ± 0.09 m; body mass 67.0 ± 9.6 kg) with large breasts (underband size range 32–36 and cup size range D–F) provided informed consent. Following a short warm up, each participant completed treadmill running trials at 10 kph for each of three different strap stiffness conditions in a randomised order. Breast kinematics (relative to the torso) was captured using a seven marker set torso model and a marker on the fullest part of each breast. A marker on the right heel allowed gait cycles to be identified. Following each trial the participants were asked to rate the comfort, fit and support of the bra on a 7-point Likert scale.

Strap stiffness was modified by adapting an existing popular sports bra (Shock Absorber High Exertion N109). A section of the existing strap was removed and replaced by either a single, double or triple layer of 20 mm wide elastic (woven polyester as typically used for waistbands). The straps were connected to the bra at either end by steel hooks allowing strap changeover without removal of the bra, while the stiffness properties of each strap condition was quantified through tensile testing (Instron 5569).

Statistically significant differences between the strap conditions in three-dimensional breast displacements and participant perceptions were tested using the Friedman test with Wilcoxon post-hoc ($p < 0.05$).

Results: The single, double and triple elastic layer straps had stiffness values of 200, 550 and 800 N·m^{-1} respectively. The only significant difference in breast displacement between strap conditions was in the downward superio-inferior direction (Fig. 1). The double and triple straps reduced downward breast displacement by 7 and 15 mm respectively compared to the single strap, confirming that the principle role of the straps is in controlling downward motion of the

breasts. The lack of significant differences in medio-lateral and anterior-posterior breast displacements suggests that other aspects of bra design are more important for controlling movement in these directions.

Significant differences in perceived support were observed between the single and triple strap conditions. The values increased from 0.1±1.2 to 1.4±1.0 to 2.1±0.6 for the single, double and triple strap conditions respectively (-3 corresponded to extremely unsupportive, 0 to neutral and +3 to extremely supportive). Examining the support ratings across bra sizes, then negative ratings only occurred for the single strap and only for bra sizes of 36D and above suggesting that the single strap may still have provided adequate support for the smaller-breasted participants. Perceived comfort (overall 1.8±0.6 where 2 is very comfortable) and fit (overall 1.3±0.6 where 2 is very good fit) were high with no significant differences between strap conditions thereby supporting the method used to manipulate strap stiffness.

Figure:
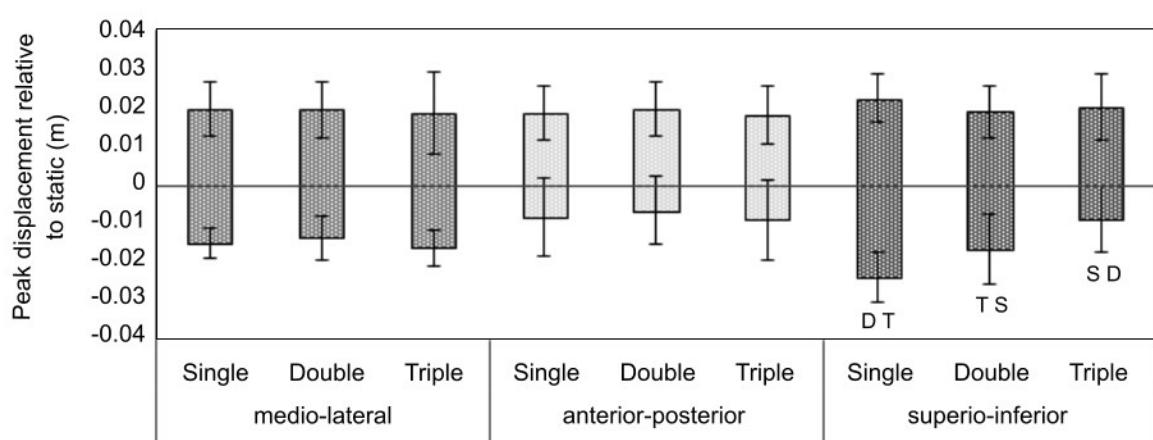
Caption: Figure 1. Three dimensional relative breast displacements for the single, double and triple strap conditions. S, D, T indicates significant differences to the single, double and triple strap conditions respectively.

Conclusion: Increasing strap stiffness improved sports bra performance with respect to reducing breast motion and improving the perceived support. However, the displacement improvements were limited to the downward superior-inferior direction reinforcing the role of the straps in controlling only this aspect of breast motion.

References:

[1] Mason BR et al. *J Sci Med Sport*. **2**: 134–144. 1999.

[2] Zhou J et al. *Text Res J*. **83**: 1500–1513. 2013.

Disclosure of Interest: None Declared

A NOVEL DEVICE FOR PROTECTING AND RESTRAINING HEAD AND NECK IN TACKLE FOOTBALL PLAYERS

Paolo Caravaggi [1,*]Alberto Leardini [1]Giada Lullini [1]Sorin Siegler [2]

[1]Movement Analysis Laboratory, Istituto Ortopedico Rizzoli, Bologna, Italy, [2]Mechanical Engineering and Mechanics, Drexel University, Philadelphia, United States

Introduction and Objectives: In tackle football, large contact and inertial forces and moments act on the player's head [1] resulting in elevated risk for traumatic head, brain, and cervical spine injuries [2]. Mandatory helmets for head protection together with a variety of rules were designed in order to minimize helmet collisions [3,4]. However, brain and spinal cord injuries resulting from large hits still persist with devastating consequences to players [1,5]. The goal of this study is the development and the evaluation of a novel customizable, visco-hyper-elastic, multi-directional Head and Neck Protective Device (HNPD, Figure 1a) providing limits to head and neck motion in order to prevent injury without compromising the athletic performance.

Methods: The HNPD (Figure 1a) consists of adjustable composite bands having low modulus of elasticity combined with a rigid non-elastic band with high modulus of elasticity, inspired by the known visco-hyper-elastic properties of biological connective tissues such as tendons and ligaments. The area between the elastic and the non-elastic bands is filled with a viscous material; when the elastic band is un-stretched, the non-elastic band is crimped and folded.

Tensile testing of the composite band was conducted at two different loading rates in order to measure its mechanical properties.

In addition, passive and active range of motion (ROM) of head and neck in all three anatomical planes was investigated using a C-ROM device in ten healthy male subjects (Figure 1a). Tests were conducted in each subject in four configurations: fully unrestrained (free motion); wearing a football gear (shoulder pads and helmet); wearing the HNPD, and wearing the HNPD under the football gear.

Results: As the composite band is initially stretched, the non-elastic band starts to unfold thus the net modulus of elasticity is very low (Figure 1b). Once the non-elastic band becomes fully unfolded, the composite band becomes stiffer and provides higher resistance to increased forces. Also, due to the presence of the viscous material, the resistance to external forces increases with increased loading rate.

The data on the effects of the HNPD on ROM of head and neck are shown in the table. All subjects experienced reduced ROM in all anatomical planes during active and passive neck motion wearing the HNPD. The decrease in head and neck motion was significantly larger (p<0.05) compared to the restraint provided by the gear alone.

Figure:
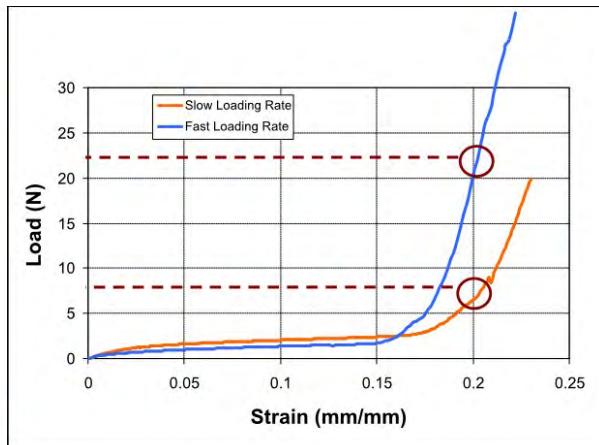
1a   **1b**

Caption: 1a A subject wearing the HNPD during testing with the C-ROM device. 1b Load/strain behavior of one of the visco-hyper-elastic bands comprising the HNPD at slow and fast loading rates.

Conclusion: A novel device for restraining head and neck excursion within safe, injury free limits in tackle football has been developed and introduced in this study. The present HNPD prototype, worn under the football gear, incorporates five adjustable hybrid bands connecting between the player's head and his torso enabling adjustable desired resistance to external forces in all planes of motion.

Testing indicate that the HNPD is capable of protecting the head and cervical spine by limiting head and neck motion. Further investigations will be performed with inertial motion units in a variety of neck motion patterns, and in the field during typical football training movements.

Table:

	gear vs. free		HNPD vs. free		gear+HNPD vs. free	
	active	passive	active	passive	active	passive
flexion	2 (17)	10 (13)	-47 (20)*	-42 (23)*	-54 (26)*	-56 (18)*
extension	-23 (8)	-21 (9)	-57 (19)*	-47 (18)*	-64 (15)*	-55 (13)*
lateral bending	-16 (11)	-21 (4)	-37 (19)*	-41 (17)*	-39 (18)*	-39 (15)*
axial rotation	-17 (9)	-7 (5)	-57 (21)*	-51 (21)*	-65 (19)*	-55 (19)*

Caption: Mean (SD) difference (%) of neck ROM between the three restrained configurations and the free neck motion during active and passive loading. * denotes statistical difference ($p<0.05$) with respect to the gear vs. free configuration.

References: [1] Viano et al., Neurosurgery, **56**: 266-280, 2005.

[2] McCrory et al., Br J Sports Med, **47**(5): 250-8, 2013.

[3] McIntosh et al., Br. J. of Sports Med, **39**:314-318, 2005.

[4] Cross et al., Clin Sports Med, **22**: 639-667, 2003.

[5] Cantu et al., Neurosurgery, **47**(3): 673-677, 2000.

Disclosure of Interest: None Declared

Lower Limb

AS-0363

DOES SELECTION OF STAIR GAIT CYCLES AFFECT RESULTING LOWER LIMB BIOMECHANICS?

Daniel Watling [1] Paul R. Biggs [1,*] Cathy Holt [1] Gemma Whatling [1]

[1] Arthritis Research UK Biomechanics and Bioengineering Centre at Cardiff, Cardiff University, Cardiff, United Kingdom

Introduction and Objectives: Stair gait is a valuable activity for the assessment of lower limb function [1]. Stair ambulation is a functionally challenging activity of daily living which can eliminate variations in gait velocity within biomechanical analysis [1] [2]. A large amount of data can be generated at the different levels of the staircase. This has resulted in a variety of different stair gait cycles (SGCs) reported in the literature and little agreement as to which SGC should be selected for analysis [3]. In order to discern differences in biomechanical data between healthy and pathological subjects these differences must be greater than the inter subject variability within groups. This study quantifies the differences and variability in bilateral hip, knee and ankle joint rotations and moments during 2 different SGC's of stair ascent and descent in healthy subjects.

Methods: Motion capture and simultaneous force plate data was collected from 37 healthy volunteers (14 male, 23 female, BMI 71k±13kg) during stair ascent and descent on a previously reported validated 4 step staircase [4]. Simultaneous, synchronised bilateral lower limb kinematics were assessed with 8 Qualisys Pro Reflex cameras (Qualisys, Sweden) sampling at a frequency of 60Hz. A modified Helen Hayes marker protocol was adopted [5] using four rigid marker clusters and an additional 22 retro-reflective markers at specific anatomical landmarks. Kinematics and inverse dynamic calculations were performed for the hip, knee and ankle within Visual 3D (C-Motion, USA).

Four stair gait cycles (SGC's) are defined for analysis. SGC 1 (ascent) was defined between foot strikes on step 1 and step 3, SGC 2 between foot strikes on step 2 and step 4, SCG3 (descent) was defined between toe offs on step 3 and step 1, and SGC 4 between toe offs on step 4 and step 2. Mean three-dimensional hip, knee and ankle kinematics and joint moment waveforms were calculated for the six trials of each SGC for each participant. Discrete parameters including range of motion (ROM) and peak joint moments were calculated from each waveform for statistical analysis.

The coefficient of variation (COV) was used to investigate variability between subjects for each of the test parameters based upon the recommendation of [6] and expressed as a percentage.

 COV=(Standard deviation/mean)*100%

Statistical analysis was carried out in SPSS using a one-way ANOVA test in SPSS using an alpha level of 0.05.

Results: Lower limb kinematics were not affected by the choice of SGC in ascent of descent. A statistical difference was identified for knee range of motion between the SGC's of stair ascent, though the difference of less than 2° falls within accepted errors associated with motion analysis techniques analysis [7, 8]. Peak ankle plantar-flexion, knee flexion and knee adduction moments were significantly different ($P < 0.05$) between SGC's in ascent. Peak knee flexion, knee adduction, hip flexion, extension and adduction moments were significantly different ($P < 0.05$) between SGC's in descent.

Conclusion: Lower limb kinematics are insensitive to SGC selection for a 4 step stair case. Hip, knee and ankle joint moments varied significantly between SGC's. The results suggest SGC's at gait initiation (SGC1 and SGC4) demand a

greater magnitude of peak sagittal plane moments than those close to gait termination. Measurements taken with force plate strikes on step1 in ascent (SGC1) and descent (SGC3) introduce less inter-subject variability and are therefore recommended for future group comparisons. While a larger staircase design might enable the subjects to reach a steady gait [9], practicalities such as cost, ceiling height, capture volume and subject fatigue have resulted in a number of researcher groups using small staircase designs [10]. These results will help ensure biomechanical, functional changes following joint pathology more are more easily distinguishable from individual variation.

References: 1. Stacoff, A., et al., . Gait & Posture, 2007. **26**(1): p. 48-58.

2. Reid, S.M., et al., Gait & Posture, 2010. **31**(2): p. 197-203.

3. Whatling, G. and C. Holt, Proc of IMechE 2010. **224**(9): p. 1085-1093.

4. Whatling, G.M., et al. *Computer methods in biomechanics and biomedical engineering.* 2009.

5. Whatling, G.M., S.L. Evans, and C.A. Holt, . Proc. IMechE Part:H Engineering in medicine, 2009. **223**.

6. Lord, S., et al., Gait & Posture, 2011. **34**(4): p. 443-450.

7. Stagni, R., et al., Clin Biomech (Bristol, Avon), 2005. **20**(3): p. 320-9.

8. Cappozzo, A., et al.,. Clin Biomech (Bristol, Avon), 1996. **11**(2): p. 90-100.

9. Cluff, T. and D.G.E. Robertson, . Gait & Posture, 2011. **33**(3): p. 423-428.

10. Andriacchi, T.P., et al., . J Bone Joint Surg Am, 1980. **62**(5): p. 749-57.

 Disclosure of Interest: None Declared

Lower Limb

AS-0364

ACHILLES TENDON MOMENT ARM GEOMETRY IN TYPICALLY DEVELOPING CHILDREN

I-Zack Lum [1] Cyril Donnelly [2,*] Siobhan Reid [2] Caroline Davis [2] Catherine Elliott [3] Jane Valentine [3] Amar El-Sallam [2]

[1] School of Sports Science, Exercise and Health, University of Western Australia, Singapore, Singapore, [2] School of Sports Science, Exercise and Health, University of Western Australia, [3] Deparment of Paediatric Research, Princess Margaret Hospital for Children, Perth, Australia

Introduction and Objectives: The ankle is one of the most important joints to absorb and generate forces and moments of force during gait. Surgeries are frequently used to correct observed differences in a patient's ankle mechanics during gait. To inform researchers and clinicians on specific mechanical characteristics of pathological gait pattern prior to surgeries, musculoskeletal models of the ankle are sometimes used. To accurately model muscle forces and joint moments about the ankle, reliable subject-specific *in vivo* moment arm estimations are required. Current 3D *in vivo* models use multiple magnetic resonance imaging (MRI) scans across the ankle's full range of motion, which is extremely time consuming with pragmatic limitations. Our aim was to develop a reliable MRI based, 3D, *in vivo* method to estimate Achilles tendon (AT) moment arms in typically developing children from a single scan sequence at a single joint posture. The secondary aim was to develop a regression equation to predict AT moment arm lengths using specific anthropometric variables.

Methods: A single time point cross-sectional design was used. Fifteen typically developing children, aged 4-12 years (mean 8.1 years, standard deviation (SD) 2.3 years), with no history of musculoskeletal conditions or injuries participated. A T1 spin echo MRI scan sequence of the lower limb was performed at Princess Margaret Hospital to obtain images of the AT and talocrural joint in the transverse and sagittal planes. Images were collected using a repetition time of 572ms, echo time of 13ms, slice thickness of 3mm, and mean inter-slice gap of 0.3mm. MR images were processed using MimicsÒ and six model combinations were used to estimate AT moment arms of participants. These include three definitions of the ankle's flexion-extension (F/E) axis of rotation (the Two-marker method (TMM), 2-point Talus method, and 3D Geometric model) (Fig. 1) each matched with two definitions of the AT line of action (the linear and polynomial methods). 3D coordinates of the talocrural joint's F/E axes and the AT were exported from MimicsÒ and processed using MATLAB to calculate the AT moment arms from each model combination.

To test the intra- and inter-rater reliability of all six AT moment arm model combinations, the first researcher processed the scans and calculated the AT moment arms twice (one week apart), and a second researcher did this once. Both researchers were blinded to the identities of participants. Intraclass correlations (ICC) and Bland-Altman plots were used to assess intra- and inter-rater reliability of all AT moment arm models. Bland-Altman plots were used to compare relative differences between methods and the limits of agreement (LoA) of their respective measurement errors (± 2 SD). A stepwise regression analysis was used to formulate a regression equation to predict AT moment arm length using the anthropometric variables foot length, tibia length and ankle plantar-flexion angle calculated during the scan sequence.

Results: Irrespective of the modelling approach, all methods displayed high intra- and inter-rater reliability (ICC = 0.957-0.990), low mean errors (-1.97-0.98) and tight LoA (1.57-2.72). A difference of 9.8mm in AT moment arm measurement was observed between the 3D Geometric model and TMM. There were minimal differences between the AT moment arm

776

measured by the 3D Geometric model and 2-Point Talus method when calculated with the AT modeled as both a straight line and fifth order polynomial. Using the 3D Geometric model and polynomial method, foot length ($p = 0.002$) and tibia length ($p = 0.002$) were significant predictors of AT moment arms, accounting for 92% ($R^2 = 0.92$) of the variance in AT moment arm length.

Figure:
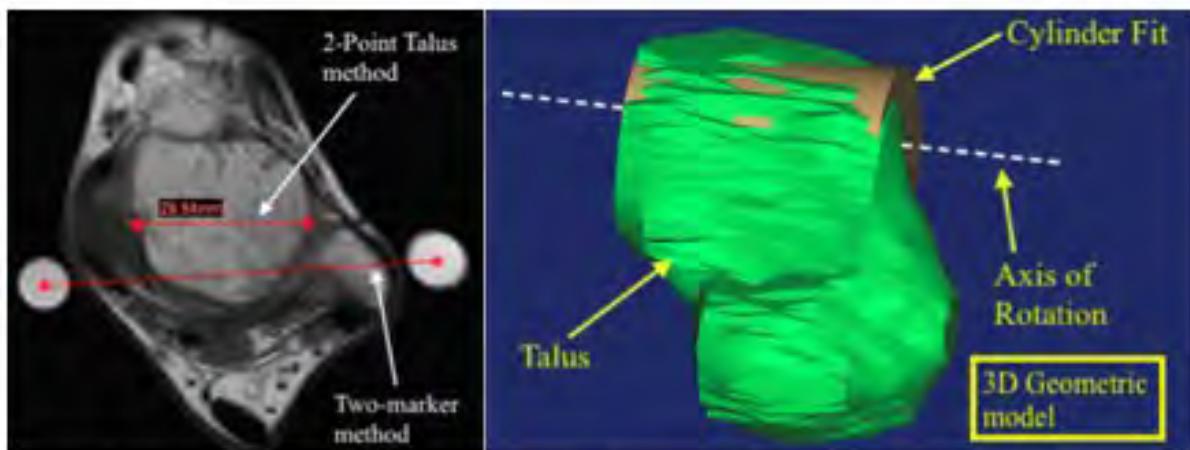
Fig. 1 The Two-marker-method, 2-point Talus method, and 3D Geometric model

Caption: The Two-marker method, 2-Point Talus method, and 3D Geometric model

Conclusion: All models for estimating 3D AT moment arms in typically developing children had high intra- and inter-rater reliability. The 3D Geometric/Polynomial model is recommended as the method of choice for three reasons; 1) it accounts for the geometry of the talus when defining the F/E axis of the talocrural joint; 2) a polynomial better represents the curved geometry of the AT, particularly during non-weight bearing tasks; and 3) a geometric cylinder to define the F/E axis of the talocrural joint may be more appropriate for populations with boney deformity where specific anatomical landmarks may be difficult to define. The current regression model predicted AT moment arm length across a wide range of foot and tibia lengths regardless of ankle position, potentially removing the need for MR images to estimate the AT moment arm in typically developing children. We recommend that the 3D Geometric/Polynomial model be tested for the measurement of AT moment arms among pathological paediatric populations with foot and ankle deformities. The current findings will have clinical relevance if used for the development of subject-specific musculoskeletal ankle models in a clinical paediatric population.

Disclosure of Interest: None Declared

Sport

AS-0365

EFFECT OF THE FOOT STRIKE PATTERN ADOPTED DURING AN INTENSE DOWNHILL TRAIL RUNNING BOUT ON LOWER LIMB MUSCLES ACTIVITY AND NEUROMUSCULAR FUNCTION

Marlène Giandolini [1,*]Nicolas Horvais [2]Jérémy Rossi [1]Guillaume Millet [3]Jean-Benoit Morin [4]Pierre Samozino [1]

[1]Laboratory of Exercise Physiology, University of Savoie, Le Bourget-du-Lac, [2]Salomon SAS, Amer Sports Footwear, Annecy, France, [3]Human Performance Laboratory, University of Calgary, Calgary, Canada, [4]Laboratory of Human Motricity, University of Nice Sophia Antipolis, Nice, France

Introduction and Objectives: Downhill running and the associated eccentric actions generate muscle damage and excitation-contraction coupling failure [1]. A significant part of the peripheral fatigue observed after ultratrail races could be attributed to the downhill sections. Minimizing musculoskeletal damage and muscular fatigue is thus considered as a determinant factor of performance in ultratrail [2]. Our purpose was to study the influence of the foot strike pattern (FSP) adopted during a downhill run on the neuromuscular fatigue at knee extensors (KE) and plantar flexors (PF).

Methods: Twenty-three runners performed a 6.5-km downhill trail run (with 1 264 m of descent). FSP and muscular activity were sampled continuously and analyzed within six sections (Figure 1). FSP was identified using two accelerometers attached to the left shoe (heel and metatarsals) by measuring the time between the heel and metatarsals acceleration peaks (THM) [3]. A positive THM indicates a rearfoot strike while a negative THM indicates a forefoot strike. Electromyographic activity was recorded from the left *vastus lateralis* (VL), *biceps femoris* (BF), *gastrocnemius lateralis* (GL) and *tibialis anterior* (TA). KE and PF neuromuscular function was assessed Pre, Post and 2 days post (Post2d). Maximal voluntary contraction (MVC), percentage of voluntary activation (%VA), high-frequency doublet force (Db100), single twitch force (Tw) and low-frequency fatigue (LFF, decrease in the ratio of stimulation peak forces at 10 Hz over 100 Hz) were measured. ANOVAs were computed from neuromuscular variables. Multiple regressions were performed with THM and the time to cover sections as independent variables, and RMS values as dependent variables (n = 138). Multiple regressions were also performed with the average THM and performance (time to cover the run) as independent variables, and Pre-Post and Pre-Post2d percent changes of neuromuscular indices as dependent variables (n = 23).

Results: The running time was 34 ± 6 min. A total of 439 ± 34 steps were analyzed per subject. The downhill run decreased MVC for KE and PF at Post (large effect) and Post2d (medium effect) (Table 1). Decreases in Db100, Tw and LFF were observed at Post for KE (large effect). PF Tw and Db100 were decreased at Post (large and medium effects, respectively). %VA was lower at Post for KE and PF (large effect) and Post2d for PF (medium effect). From the multiple regressions, THM was positively related to VL and TA RMS ($p < 0.001$), and negatively related to GL RMS ($p = 0.035$). Positive correlations were reported between THM and percent changes in PF Tw and Db100 Post ($p < 0.05$). Positive correlations were also observed between THM and percent changes in KE Db100 at Post and Post2d ($p < 0.05$). The more anterior the FSP, the greater the decreases in the peripheral indices of fatigue for PF and KE.

Figure:
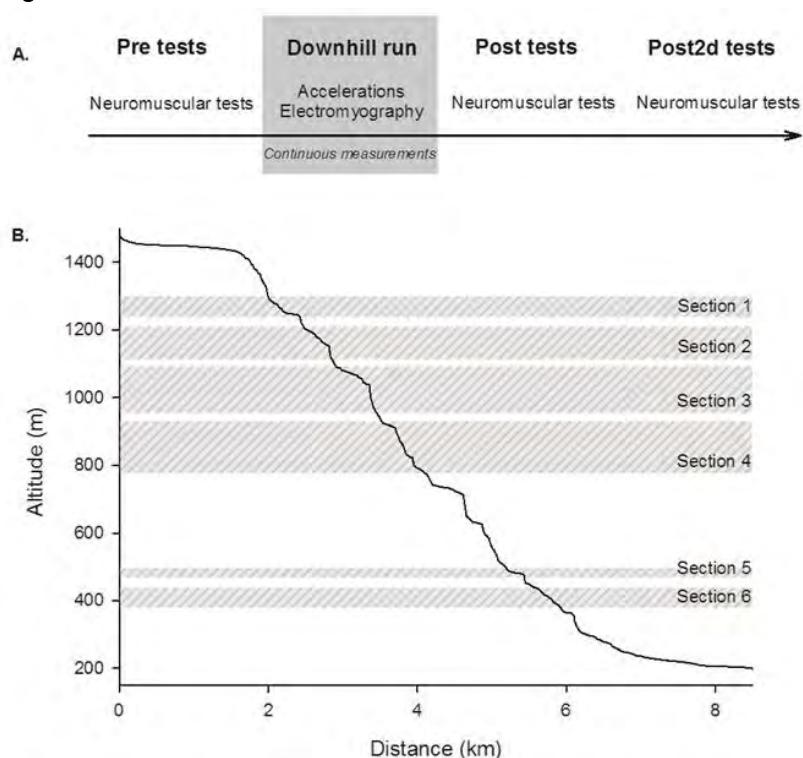
Caption: Description of the protocol design. Panel A: tests and measurements. Panel B: Profile of the downhill run, showing the six sections used for data analysis.

Conclusion: The downhill run induced peripheral fatigue for KE and PF of similar or even higher magnitude than those reported after an ultratrail [4]. This highlights the importance of eccentric mode of contraction in peripheral fatigue. Adopting a more anterior FSP led to a higher GL activity, likely explaining in part the greater peripheral fatigue at PF with this FSP. Greater severity of peripheral fatigue for KE with a forefoot strike may be attributed to a more flexed knee at initial contact, typical of this FSP [5]. This could lead (i) to lengthier lever arms between both the ground reaction force and weight vectors and the rotation axis (i.e. the knee joint), increasing thereby the torque produced eccentrically by KE preventing the lowering of the body center of mass; (ii) to greater KE lengths, which has been shown to worsen muscle damages [6]. In ultratrail, the total negative elevation (number of eccentric contractions) and the runners' speed in downhill sections (intensity of eccentric contractions) might be of greater importance for peripheral fatigue than the overall distance. Its severity could also depend on the FSP used.

Table:

	%Pre-Post			%Pre-Post2d		
KE						
MVC	-18.6	±	9.5[A]	-8.5	±	10.6 [B]
%V	-6.9	±	7.4[a]	-2	±	8.6

A						
Tw	-42.9	±	11.0^A	3.3	±	13.7
Db 100	-26.9	±	12.7 ^{a}	-2	±	12.4
LFF	-35.1	±	14.5^A	-4.3	±	17.6
PF						
MVC	-25.4	±	13.4^A	-10	±	9.6 ^{B}
%VA	-7.9	±	6.5 ^{A}	-3.8	±	6.2 ^{b}
Tw	-28.5	±	8.7 ^{A}	-1	±	11.6
Db 100	-21.6	±	8.4 ^{A}	-3.3	±	11.3
LFF	-7.4	±	5.1	0.4	±	5.8

Caption: Percent changes from Pre in neuromuscular indicators Post and Post2d. Significant changes from Pre to Post were indicated by a ($P < 0.01$) or A ($P < 0.0001$), and from Pre to Post2d by b ($P < 0.05$) or B ($P < 0.0001$).

References: [1] Feasson, et al., J Physiol, 543(1):297-306, 2002.

[2] Millet, et al., J Appl Physiol, 113(3):507-9, 2012.

[3] Giandolini, et al., J Biomech, 2014.

[4] Millet, et al., PLoS One, 6(2):e17059, 2011.

[5] Shih, et al., Gait Posture, 2013.

[6] Butterfield, et al., J Appl Physiol, 100(5):1489-98, 2006.

Disclosure of Interest: None Declared

Lower Limb

AS-0366

ASSESSING THE EFFECTIVENESS OF FIELD-BASED ACL INJURY RISK SCREENING METHODS IN IDENTIFYING HIGH-RISK LANDING PATTERNS DURING A SPORT-SPECIFIC TASK

Aaron S. Fox [1,*] Jason Bonacci [1] Scott McLean [2] Michael Spittle [3] Natalie Saunders [1]

[1] School of Exercise and Nutrition Sciences, Deakin University, Melbourne, Australia, [2] Human Performance Innovation Laboratory, University of Michigan, Ann Arbor, United States, [3] College of Sport and Exercise Science, Victoria University, Melbourne, Australia

Introduction and Objectives: Screening methods that identify those at-risk of suffering an anterior cruciate ligament (ACL) injury are vital for the development of targeted ACL injury prevention strategies. Field-based screening methods offer a simplistic and accessible method to identify dysfunction that may lead to injury. The Landing Error Scoring System (LESS) [1] and Tuck Jump Assessment (TJA) [2] assess ACL injury risk via the scoring of an athlete's landing technique. Higher scores should reflect dysfunctional biomechanical patterns during high-risk sporting tasks; however, the relationship between scores from these screening methods and lower limb mechanics during sport-specific tasks is yet to be examined. At present, the ability of these screening methods to identify poor lower limb mechanics and potential injury risk during high-risk sporting tasks is unknown. The purpose of this study was to examine the association between LESS and TJA scores to lower limb biomechanical patterns during a sport-specific landing task.

Methods: Twenty-five female netball players (23.6 ± 3.2 years; 170.4 ± 7.6 cm; 67.6 ± 9.0 kg) performed ten trials of a sport-specific landing task and had their landing technique screened as per the LESS [1] and TJA [2] protocols. The landing task chosen for this study was a netball leap landing; which involved a six-metre run-up, followed by a single-limb take-off and land on the contralateral limb while catching a pass. Three-dimensional hip and knee joint rotations and external joint moments were calculated from lower extremity kinematics and ground reaction force (GRF) data collected during the sport-specific landing task. Data were extracted from initial contact (IC) to 300 ms post IC. A vertical GRF threshold of 10N was used to detect IC.

Principal patterns (PP) in biomechanical data were identified by submitting extracted joint rotation and moment waveform data to principal component analysis (PCA). Patterns were extracted for the variables of hip flexion/extension ($H_{FLEX/EXT}$), adduction/abduction ($H_{ADD/ABD}$), and internal/external rotation ($H_{IR/ER}$); knee flexion/extension ($K_{FLEX/EXT}$), adduction/abduction ($K_{ADD/ABD}$), and internal/external rotation ($K_{IR/ER}$); and H_{FLEX}, H_{ADD}, H_{ER}, K_{FLEX}, K_{ABD}, and K_{ER} moments. Principal pattern scores (PP-Scores), which measure the degree to which the shape of the waveform corresponds to each PP [3], were computed and used for subsequent analyses. Pearson's correlation coefficients (*r*) were calculated to identify significant associations ($p < 0.05$) between LESS/TJA score and PP-Scores.

Results: LESS scores ranged from 0 to 9. Increasing LESS scores were associated with landing patterns with greater H_{ER} (*r* =-0.48), and peak K_{EXT} and K_{FLEX} moments (*r* = -0.47); and reduced K_{FLEX} (*r* = 0.42) and peak transverse plane knee moments (*r* = -0.42).

TJA scores ranged from 2 to 8. Increasing TJA scores were associated with landing patterns with reduced H_{FLEX} (r = -0.46) and K_{FLEX} (r = 0.40); and greater frontal plane knee motion (r = 0.39), and H_{ADD} (r = -0.42) and H_{ER} moments (r = 0.41).

Figure 1 illustrates the relationship between LESS and TJA scores and relevant biomechanical patterns.
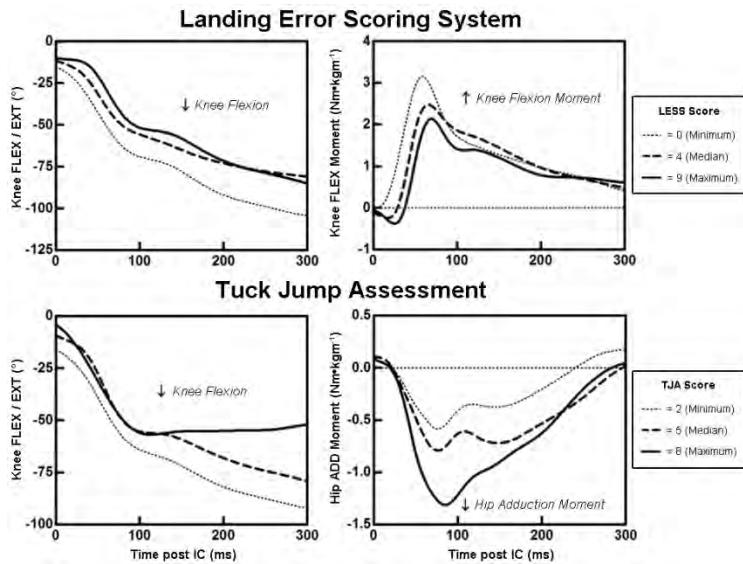
Figure:

Caption: Figure 1: Mean data from participants achieving the minimum (dotted), median (dashed), and maximum (solid) scores on the LESS and TJA for relevant biomechanical patterns.

Conclusion: Higher LESS scores were associated with reduced knee flexion, while higher TJA scores were associated with reduced hip and knee flexion, and greater frontal plane knee motion and hip adduction moments. This suggests both methods may have some utility in screening for biomechanical patterns proposed as risk factors for ACL injury [4-6] during a sport-specific task. Interestingly, higher LESS scores were indicative of reduced transverse plane knee moments; and scores from neither method were associated with frontal plane knee moments. Both transverse and frontal plane knee moments have been linked to increased ACL injury risk [7,8], therefore screening methods that identify these risk factors may be more adept in identifying athletes at-risk of ACL injury. Future work should focus on examining and maximising the capability of screening methods to identify high-risk mechanics during a range of sport-specific tasks.

References: [1] Padua et al., Am. J. Sports Med., 37: 1996-2002, 2009.

[2] Myer et al., Athlet. Ther. Today, 13: 39-44, 2008.

[3] Deluzio & Astephen, Gait Posture, 25: 86-93, 2007.

[4] Hewett et al., Am. J. Sports Med., 34: 299-311, 2006

[5] Ford et al., Clin. Biomech., 31: 33-40, 2006.

[6] Powers, J. Orthop. Sports Phys. Ther., 40: 42-51, 2010.

[7] Hewett et al., Am. J. Sports Med., 33: 492-501, 2005.

[8] Oh et al., Am. J. Sports Med., 40: 574-583, 2012.

Disclosure of Interest: None Declared

Lower Limb

AS-0367

BIOMECHANICAL CLASSIFICATION OF GAIT FOLLOWING TOTAL KNEE REPLACEMENT - COULD FUNCTIONAL RECOVERY HAVE BEEN PREDICTED?

Paul R. Biggs [1,*]Daniel Watling [1]Gemma Whatling [1]Cathy Holt [2]

[1]Arthritis Research UK Biomechanics and Bioengineering Centre, [2]Institute of Medical Engineering & Medical Physics, Cardiff University, Cardiff, United Kingdom

Introduction and Objectives: Whereas patient satisfaction of hip replacements in the UK in generally reported as 93%[1], satisfaction of knee replacements is much lower at 82% [2]. Pain is the primary indication for TKR surgery, however functional improvement still has a critical role in patient satisfaction [3].

As with all interventions, one of the keys to maximising benefits is an understanding of which patients benefit the most. This requires the use of quantifiable post-operative outcome measures and preoperative 'predictors'. A Dempster-Shafter theory (DST) classification technique has been shown to accurately discern biomechanical data between healthy and osteoarthritic (OA) knee function arriving at a degree of belief of OA, non-pathological function and uncertainty. This facilitates the objective quantification of post-operative recovery [4].

Use of three-dimensional motion analysis techniques is variable within a clinical environment – partly due to practicality and costs [5]. This study aims to retrospectively explore if recovery of biomechanical gait function could have been predicted using only variables practically obtainable during clinic, namely subjective knee outcome survey scores, temporal spatial parameters, sagittal knee angles and ground reaction force (GRF) data.

Methods: Human motion analysis was initially performed on 25 healthy (NL) and 25 subjects with late stage knee OA whom had been recommended for TKR surgery. Four marker clusters were attached to the subjects and 3D positional data was acquired using nine Oqus cameras (Qualisys, Sweden) at 60Hz. Ground reaction force (GRF) data was collected using two force plates (Bertec, USA) at 1,080 Hz. Subjects walked barefoot overground at a self-selected pace until six clean force-plate hits were observed. Kinematics and inverse dynamic calculations were performed for the hip, knee and ankle within Visual 3D (C-Motion, USA). Principle component analysis was performed in order to represent the greatest variance of each waveform as discrete variables. Twenty-seven PCs were retained, representing an average variance of 85% of the twelve waveforms. This data was used to train the Cardiff Classifier in order to characterise OA and healthy biomechanical knee function. This methodology was then repeated to quantify the pre-operative and 1 year post-operative function of 12 TKR patients. Postoperative improvement in function was calculated as the percentage reduction in the belief of OA. Statistical analysis was carried out in SPSS using a Pearson correlation and an alpha level of 0.05.

Results: The training of the classifier achieved an out-sample accuracy of 98%. 7 subjects improved significantly (Δ39-75%) and the other 5 subjects displayed very little functional recovery (Δ 0-12%).

Pre-operative age (r=0.66, p=0.02), cadence (r=0.75, p=0.005), stance percent (0.70, p=0.012), peak flexion angle during swing phase (r=0.64, p=0.026) and the anterior GRF peak (r=0.637, p=0.026) were all significantly correlated to functional improvement 1 year post TKR. Pre-operative Knee Outcome Survey and Oxford Knee Scores had weak insignificant

correlations. No significant correlations were found between post-operative recovery and peak flexion angle during stance phase, BMI, peak medial GRF, or either peak of the vertical GRF.

Conclusion: The quantification of post-operative function is based on a strong training body. The results suggest that it may be possible to predict functional outcome after surgery using solely parameters practically measurable within a clinical setting. Subjects who walked slower pre-operatively while spending less time in stance phase had reduced functional recovery 1 year following TKR surgery. Both reduction of peak flexion during swing and peak anterior GRF in poor improvers could potentially be explained by reduced gait velocity [6]. Reduced anterior posterior force could also be a sign of quadriceps weakness, which has been shown to effect post-operative recovery [7].

Findings suggest that elderly subjects who have gait adaptations associated with reduced gait velocity gained less functional benefit from TKR surgery. These predictors should be tested further on unseen data.

References: 1. Anakwe, R.E., P.J. Jenkins, and M. Moran, The Journal of arthroplasty, 2011. **26**(2): p. 209-213.

2. Baker, P., et al., . Journal of Bone & Joint Surgery, British Volume, 2007. **89**(7): p. 893-900.

3. Nilsdotter, A.K., S. Toksvig-Larsen, and E.M. Roos. Acta orthopaedica, 2009. **80**(1): p. 55-61.

4. Jones, L. and C. Holt, . Proceedings of the Institution of Mechanical Engineers, Part H: Journal of Engineering in Medicine, 2008. **222**(5): p. 647-655.

5. Wren, T.A., et al., . Gait & posture, 2011. **34**(2): p. 149-153.

6. Nilsson, J. and A. Thorstensson, . Acta Physiologica Scandinavica, 1989. **136**(2): p. 217-227.

7. Mizner, R.L., et al., . The Journal of rheumatology, 2005. **32**(8): p. 1533-1539.

Disclosure of Interest: None Declared

AS-0368

BIOMECHANICAL EFFECTS OF TAPING AND BRACING ON KNEE JOINT STABILITY IN INDIVIDUALS WITH AND WITHOUT PATELLOFEMORAL PAIN.

Jim Richards [1,*] Ambreen Chohan [1] Jessie Janssen [1] James Selfe [1]

[1] Allied Health Research Unit, University of Central Lancashire, Preston, United Kingdom

Introduction and Objectives: Over the last 30 years there has been considerable interest in different conservative treatments for patellofemoral pain. Although a consensus has emerged that low cost treatments such as taping and bracing are effective at relieving pain, there has been an ongoing debate about whether these effects are mediated by enhancing proprioceptive mechanisms. In addition few papers have been published comparing the biomechanical effects of such interventions on coronal and transverse plane knee control in normal subjects or subjects who suffer from knee pain and instability.

The purpose of this work was to explore the biomechanical effects of taping and bracing in healthy individuals and people with patellofemoral pain, and to determine the effect of different levels of conservative management on knee stability.

Methods: Twenty-four patients with patellofemoral pain and thirty-nine healthy individuals (age range:18-40 years). All healthy participants were free from lower back or lower limb problems and had not had any previous lower limb surgery. All patients had been referred for with a diagnosis of patellofemoral pain, but none had commenced treatment at the time of the study. Patient inclusion criteria were the presence of a traumatic peripatellar pain and patellofemoral pain provoked by one or a combination of the following: prolonged sitting, deep squatting, kneeling, ascending or descending stairs. Exclusion criteria were recent knee surgery (not including arthroscopy). After meeting the inclusion criteria, patients were then clinically examined to exclude referred pain from the spine and hip joint, leg length discrepancy, knee ligament, quadriceps tendon and meniscal pathology, Hoffa's and medial plica syndromes, femoral anteversion and tibial torsion. Participants were asked to perform a slow step down task. This was conducted under a range of randomised conditions including: (a) no intervention, (b) neutral patella taping, (c) tubigrip, (d) patellofemoral web brace with patellar stabilization and (e) a silicone reinforced compression sleeve. The kinematics of the pelvis and lower limbs, were recorded using a 10-camera Oqus Qualisys motion capture system. The calibrated anatomical system technique (CAST) allowed segmental analysis in the sagittal, coronal and transverse planes. All data were analysed using Visual3D (C-Motion Inc.) and SPSS.

Results: An independent samples t-test showed that the patients had a significantly greater knee coronal range of motion (ROM) than the healthy individuals, 9.5 and 6.5 degrees respectively ($p<0.01$) with no intervention (Figure 1). A mixed methods ANOVA identified changes in the knee coronal and transverse ROM between the interventions, $p=0.03$ and $p=0.01$ respectively. The brace with patellar stabilization reduced knee coronal and transverse ROM by 2.8 degrees ($p<0.01$), followed by the textured neoprene sleeve and tubigrip which reduced the knee coronal ROM by 2.7 degrees ($p<0.05$), with the neutral taping showing a 1.3 degree reduction in the patient group only ($p<0.05$). No differences were seen in peak knee flexion. At the end of the test the participants were asked to place the conditions in a rank order of which they thought helped most with joint stability and pain. The most popular order was the web brace with patellar stabilization or silicone reinforced compression sleeve, neutral tape or tubigrip and then no intervention.

Figure:
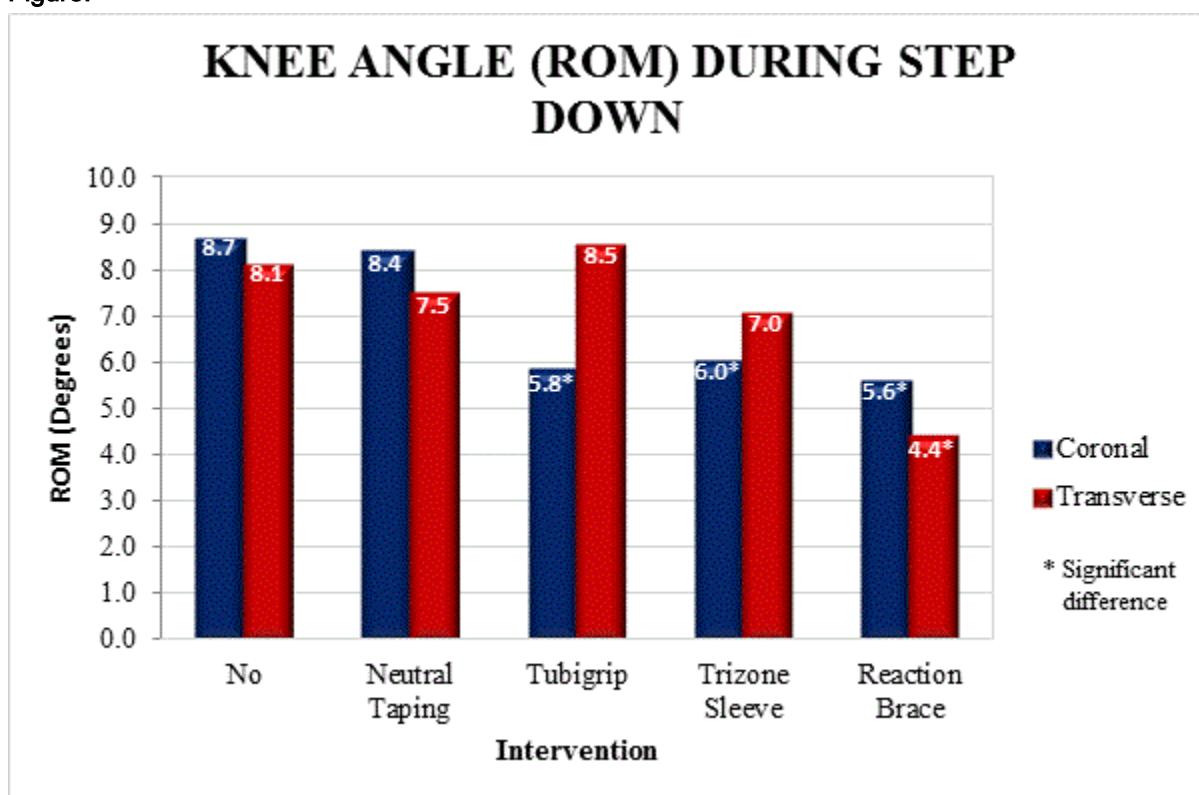
Conclusion: These changes in knee mechanics provide important evidence about the possible proprioceptive and mechanoreceptive effects of such treatments, and their role in the management of individuals with patellofemoral pain. This reinforces the view that coronal and transverse plane mechanics should not be overlooked when studying knee pain and instability.

This work provides evidence for a graduated management of knee instability, from neutral taping which produced a small improvement in coronal plane control, tubigrip and textured neoprene sleeves giving a further improvements coronal plane control and bracing producing the greatest improvement in coronal and transverse plane control. These results fit well with participants' perceptions of which they thought helped most with joint stability and pain level.

Disclosure of Interest: None Declared

ULTRASOUND BASED SUBJECT SPECIFIC MODELLING OF THE HEEL

Sara Behforootan [1,*] Panagiotis E. Chatzistergos [1] Roozbeh Naemi [1] Nachiappan Chockalingam [1]

[1] Faculty of Health Sciences, Staffordshire University, Stoke on Trent, United Kingdom

Introduction and Objectives: Foot ulcers in people with diabetes are multi-factorial and linked to a variety of clinical risk factors, like peripheral neuropathy and vascular insufficiency[1], as well as biomechanical risk factors, such as increased plantar pressure [2]. Despite that, the mechanisms behind ulceration are not yet fully understood.

Subject-specific Finite Element (FE) modelling can significantly enhance our understanding on the biomechanical phenomena that lead to ulceration but its use in the clinical setting is still impractical. Indeed the development of detailed FE models requires considerable resources and time and significant computer processing power[3]. In this study a new method for the design of simplified 3D subject-specific models of the heel based on ultrasound images and ultrasound indentation tests is presented.

Methods: Ultrasound indentation tests were performed at the heel of a healthy subject using a new device comprising a linear array ultrasound probe and a load cell[4]. The instrumented probe was mounted on a rigid metallic frame equipped with a linear actuator and adjustable foot supports. Before testing, the subject's right foot was fixed on the device and the instrumented probe was positioned to image the frontal plane of the apex of the calcaneus (Figure 1A). The subject's heel was subjected to 5 preconditioning load/unload cycles followed by 3 measurement cycles to a maximum compressive force of 80N. Heel-pad thickness and the value of the applied force were sampled at 28Hz and used to calculate the average force/deformation curve of the indentation test(Figure 1C). After the end of the tests the probe was rotated by 90° to image the sagittal plane of the heel under a compressive force of 80N (Figure 1A). Moreover the width of the unloaded heel was also measured at the site of the testing using a calliper.

The indentation test was simulated using a 3D FE model comprising a rigid calcaneus and a hyperelastic (Ogden-1st order) soft tissue (Figure 1B). The geometry of the calcaneus was reconstructed using a frontal and a sagittal ultrasound image. The boundary of the calcaneus was outlined in both images and a surface was created by dragging the frontal boundary along the sagittal one. The thickness and width of the heel-pad model was modified to correspond to the heel-pad thickness and width measured in-vivo. The ultrasound probe was modelled as a rigid body that is in frictionless contact with the soft tissue (Figure 1B) and the loading procedure was simulated by imposing a displacement to the probe (equal to the maximum in-vivo deformation). This simulation enables the numerical estimation of the force/deformation curve of the indentation test and the inverse engineering of the tissue's material coefficients. Assuming that the heel-pad is nearly incompressible ($v=0.475$) leaves only two material coefficients to be calculated: μ and α which are indirectly related to the material's initial shear modulus and strain hardening/softening respectively[5].

The aforementioned inverse-engineered material coefficients were also used in a more geometrically detailed FE model of the heel which was designed based on MRI images. This model also comprised a rigid calcaneous and a soft tissue and was used to simulate the indentation test and estimate the indentation force/deformation curve. The numerical curves

estimated using the ultrasound and MRI based FE models were compared and their difference was assessed in terms of their Mean Square Error (MSE).

Results: The values of the coefficients μ and α which were calculated using the ultrasound based model were equal to 0.12kPa and 42 respectively. The MSE between the two numerical force/deformation curves was 0.70 while their difference in terms of maximum force was only 0.5%.

Figure:
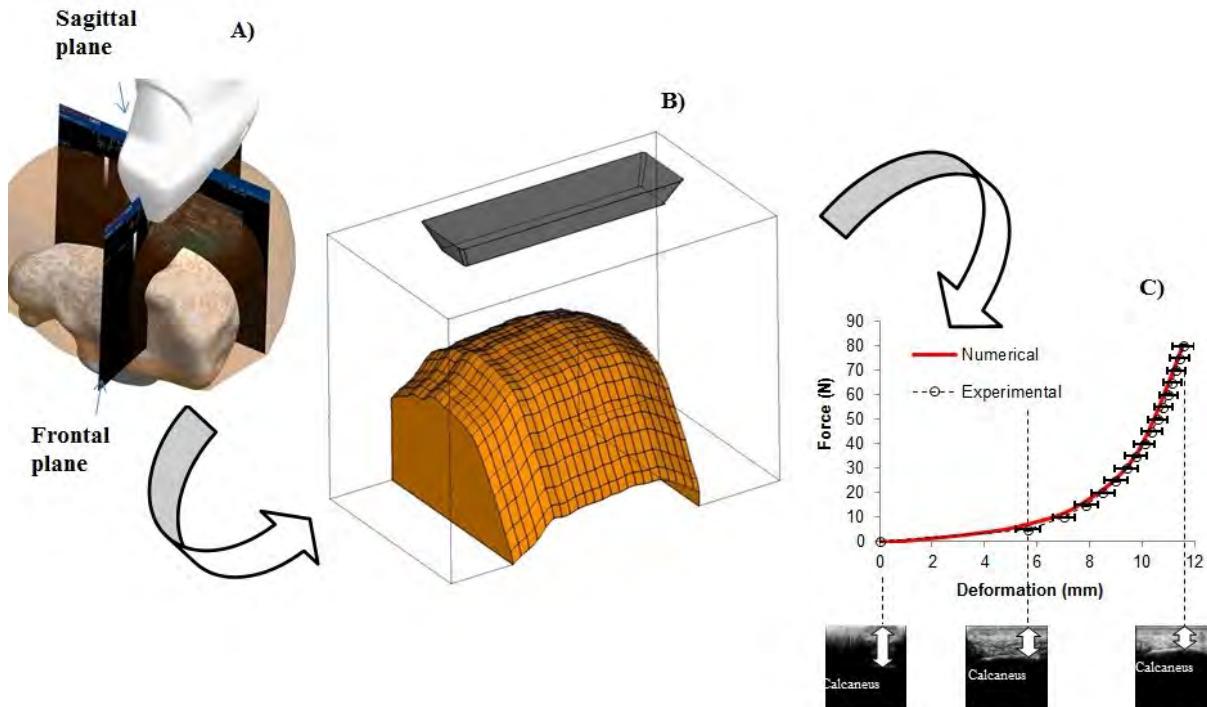
Caption: A schematic representation of the method for the design of ultrasound based FE models of the indentation test and the inverse engineering of the heel-pad material coefficients. A) The two imaging planes for the reconstruction of the calcaneus. B) The geometry of the subject-specific FE model and C) the in-vivo and the final numerical force/deformation curves for the indentation test.

Conclusion: The comparison between the simplified ultrasound based model of the heel and the more detailed MRI based one showed that they exhibit very similar behaviour. The two estimated force/deformation curves for the indentation test were very close to one another indicating that the simplified ultrasound based FE model is a good candidate for the inverse engineering of heel-pad material coefficients instead of the much more challenging and expensive to generate and solve MRI based model.

References: [1]   Crawford et al.,QJM,100:65–86,2007.

[2]   Ledoux et al.,J Diabetes Complications,27:621–6,2013.

[3]   Spirka et al.,J Biomech 47:2948-2955,2014.

[4]   Chatzistergos et al.,J Diabetes Complications,28:488-98,2014.

[5]   ANSYS Release 12 Documentation. ANSYS Inc

Disclosure of Interest: None Declared

Modelling

AS-0370

A NEW 3D RECONSTRUCTION METHOD OF THE BODY ENVELOPE FROM BIPLANAR X-RAYS

Agathe Nérot [1,2,*] Julie Choisne [2] Célia Amabile [2] Xuguang Wang [1] Wafa Skalli [2]

[1]UMR_T9406, LBMC Laboratoire de Biomécanique et Mécanique des Chocs, IFSTTAR, Bron, [2]Arts et Métiers ParisTech, Insitut de Biomécanique Humaine Georges Charpak, Paris, France

Introduction and Objectives: The consideration of both the geometry of the bones and the external body shape of an individual is of great interest in musculoskeletal modeling. The low dose radiation EOS (EOS imaging, Paris, France) system allows obtaining 3D reconstructions of the skeleton in a standing posture from biplanar radiographs of the entire body [1]. As skin contours are also visible on the radiographs the 3D reconstruction of the body shape is now under study in order to develop an innovative tool providing both the internal skeleton and the external envelope of an individual. The purpose of this study was to propose and evaluate a 3D reconstruction method of the body shape based on the visible skin contours on biplanar X-rays.

Methods: The reconstruction method consisted in projecting a generic 3D body shape model on the sagittal and frontal plane radiographs. The silhouettes obtained on both views were then adjusted with the visible skin contours of the individual. Male and female body reconstructions were differentiated.

Generic model: Two body shape meshes representing a man and a woman with a stature of 1.7m were created and were pre-positioned in an EOS standard standing posture. The two models were characterized by 16 volumetric body segments. A set of descriptors (surface points and internal joints centers) were embedded and used as controls to guide the deformation of the generic models during the reconstruction process.

Reconstruction method: The target location of a limited set of control points (mainly joints centers) was first selected on the radiographs. These points were used to project and scale the generic model to match the radiographs. Then a set of 20 points was identified on both views to initially adjust the depth and width of specific body segments (hips, calf, waist etc.)(Figure 1A). A moving least square transformation was applied to preserve shape details. A final step consisted in interactively deforming the initial solution by dragging a set of control points on the surface of the model to match the skin contours using a kriging method (Figure1B). In this preliminary approach the arms of the generic model were not deformed as they were not fully visible on the radiographs.

Method Assessment: EOS acquisitions were performed for 12 volunteers. Preliminary results were assessed only from 4 subjects (2 males, 2 females) aged from 27 to 31 years old with BMI from 20.0 to 29.5Kg/m². 140 radio-opaque markers (Ø 2 mm and 5mm) were placed on the skin of the subject from feet to head. 3D reconstructions of the body shape were performed 3 times by 3 different operators. The accuracy of the proposed method was evaluated by computing the mean distance between the reconstructed human body shape and the markers skin contact points. As the different steps of the reconstruction process require some intervention of the operator, the reliability of the method was evaluated by measuring the intra- and inter-operator variability (NF ISO-5725,1994).

Results: Thighs and Lower legs showed the smallest distance with the markers, while the head and thorax showed the greatest errors. (Table 1) This may be due to the fact that most x-rays were cut above the eyes and were too narrowed to capture the lateral sides of the thorax in the frontal view. 95% CI is below 2.6mm.

Figure:
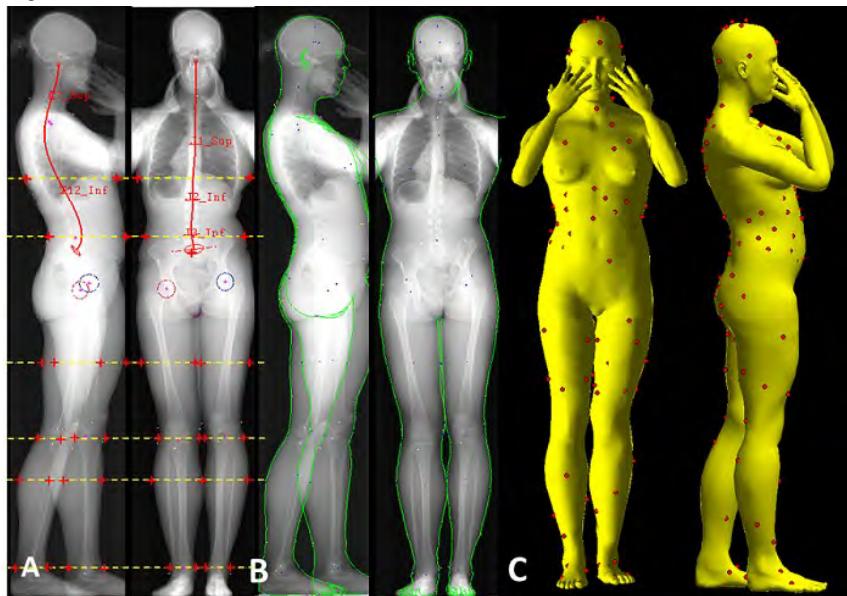
Caption: Reconstructions steps. A: Identification of points for the adjustement of body segments width and depth. B: Deformation of the generic model on the frontale and sagittal planes radiographs. C: Evaluation of the 3D reconstruction of the body shape with a set of 140 markers attached on the subject'skin.

Conclusion: This method allowed obtaining the 3D body shape from biplanar radiographs with a mean error on the geometry of 4mm on average. This method opens the way to further researches requiring both the internal skeleton and external body shape of an individual. Work is in progress to analyze the reconstructions of a higher number of subjects.

Acknowledgment

Table:

	Thorax	Head	Abdomen	Thighs	Lower legs	Feet	Body
Mean accuracy	5.6	5.5	4.5	3.0	1.4	4.4	4.0
SD accuracy	7.2	4.6	5.2	3.9	2.2	6.8	5.4
95% CI reliability	1.4	2.6	1.8	0.6	0.6	2.6	0.6

*A positive distance means that the centers of the markers are outside the reconstructed envelope

Caption: Mean and standard deviation (SD) of the distances between the 3D reconstructions and the markers on the subjects skin by region (accuracy). 95% Confidence Interval (95% CI) of the inter operator reproducibility: 2 Root-Mean-Square of the standard deviations (2RMSSD) of the distance between the markers and the reconstructed envelopes by each operator for each region (reliability).

References: [1] Dubousset J et al., *JMR* **22**, 1-12, 2010

Disclosure of Interest: None Declared

AN EFFICIENT ALGORITHM TO ESTIMATE PASSIVE FORCES IN SARCOMERES UNDER LENGTH CONTROL CONDITIONS

Gudrun Schappacher-Tilp [1,*]Getrud Desch [1]

[1]Department for Mathematics and Scientific Computing, University of Graz, Graz, Austria

Introduction and Objectives: Passive forces in sarcomeres are mainly related to the giant protein titin. Titin's extensible region consists of spring-like elements acting in series. In skeletal muscles these elements are the PEVK segment, two distinct immunoglobulin (Ig) domains (proximal and distal), and a N2A portion. Distal Ig domains are thought to form inextensible end filaments in intact sarcomeres. Proximal Ig domains, on the contrary, unfold in a force- and time-dependent manner. Force-elongation relations of single titin strands can be simulated by Monte Carlo simulations [1]. In sarcomeres where more than a thousand of titin strands are arranged in parallel numerous Monte Carlo simulations are required to estimate the sum of forces based on the elongation of all titin strands. To simplify calculations the stochastic model of passive forces is often replaced by linear or non-linear deterministic and phenomenological functions. However, new theories of muscle contractions (e.g. [2,3]) are based on a prominent role of the structural properties of titin and necessitate a detailed analysis of titin forces in length control experiments. In our study we present a simple and efficient alternative to Monte Carlo simulations. Based on a structural titin model we calculate the expected passive forces in a sarcomere under length control conditions. Moreover, our approach provides a measure for the goodness of the expectation value.

Methods: The force of a single titin strand at a given length is a discrete random variable. It can assume only a finite number of values corresponding to the number of Ig domains which can unfold. Once we know the corresponding probabilities we can calculate the expectation value which scales to the expected force of all titin strands acting in parallel in a sarcomere. However, the expression of the corresponding probabilities is not trivial since the unfolding of one domain changes the unfolding rates of all other domains and leads to integral expressions which can only be computed by expensive numerical methods. Instead, we analyze a corresponding system of ordinary differential equations which can be solved by a simple implicit Euler method in a fast and stable way. Our analysis is based on rabbit psoas 3,400-kD titin isoform with 50 proximal Ig domains, 26 distal Ig domains forming end filaments, and 800 PEVK residues [4]. Force calculations are based on the worm-like chain model of polymer elasticity for proximal Ig domains and a modified worm-like chain model for the PEVK region [5]. Finally, our approach also allows us to take into account the hierarchical structure of mean unfolding forces of proximal Ig domains [1].

Results: We compare our results to well established Monte Carlo simulations. Single simulations show the characteristic saw tooth pattern of single titin strands in length control experiments. In sarcomeres the saw tooth pattern is smoothed out. Our approach leads to a smooth expectation value where the standard error of the expectation value is assessed as well. Not surprisingly the standard error rises with longer stretches but stays within 1.5% of the expectation value for stretches up to a sarcomere length of 4.5μm.

Figure:
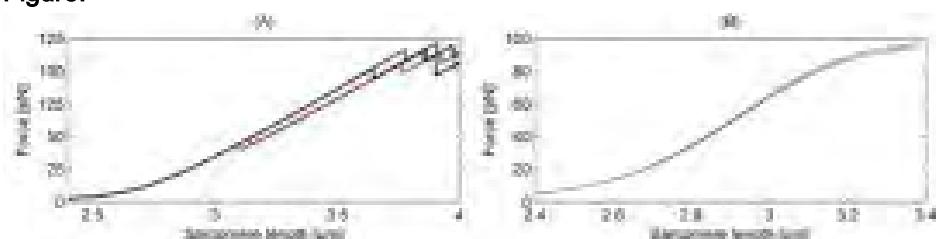
Caption: Fig. 1: (A) Four exemplar Monte Carlo simulations of a stretching experiment with controlled lengths. (B) Expectation value and standard error of the expectation value of the same experiment based on the new approach.

Conclusion: We provide an intriguingly simple approach to predict forces based on titin elongation in a sarcomere based on a structural titin model. Moreover, the goodness of the expectation value can be assessed by analyzing the standard error of the expectation value.

References: [1] Li et al., Nature, 418: 998-1002, 2002

[2] Nishikawa et al., Proc. R. Soc. B-Biol. Sci., 279: 981-990, 2012.

[3] Herzog et al., Exerc. Sport Sci. Rev., 40: 50-57, 2012.

[4] Prado et al., J. Gen. Physiol., 126: 461-480, 2005.

[5] Linke et al., Proc. Natl. Acad. Sci. U.S.A., 95: 8052-8057,1998.

Disclosure of Interest: None Declared

Computer Simulation

AS-0372

USING FEA TO DETERMINE THE SAFE CORRECTION ZONE FOR HIGH TIBIAL OSTEOTOMIES

Jennifer L. Boyd [1,*] Cameron Brown [1] Andrew Price [1]

[1]Nuffield Department of Orthopaedics, Rheumatology and Musculoskeletal Sciences, University of Oxford, Oxford, United Kingdom

Introduction and Objectives: High tibial osteotomy (HTO) is a joint-conserving surgery used to treat early-stage medial osteoarthritis. HTO shifts the mechanical axis (axis connecting the centres of the hip and ankle) from the pathological medial to the normal lateral tibiofemoral compartment [1]. It is hoped that HTO will allow patients to remain active and free from pain, as well as delay or reduce the need for joint replacement. HTO remains, however, an operation with unpredictable results [2], perhaps due to a lack of understanding of how the surgery affects the mechanics of the knee. We do not, for example, know which re-alignment will be best for individual patients. Correcting to 62% re-alignment has been suggested [3], but other correction re-alignments (for example, 50%) have also been successful. Overcorrections should be avoided; otherwise lateral tissues may become damaged (limiting future treatment options).

We used finite element (FE) models to investigate how different knee alignments (ranging from native medial to extreme lateral mechanical axis) affected the tibiofemoral stress/pressure patterns during the second ground reaction force (GRF) peak of walking (when maximum loads occur during walking).

Methods: Sets of FE models were created based on data from 3 healthy subjects: 2 female, 1 male; aged 25-32 years; BMI 20.6–21.9. Informed consent was given and absence of MRI contra-indications was verified prior to data collection.

Motion analysis data was collected first. A modified Helen Hayes marker set was used, with additional registration markers placed around the knee. Marker trajectory data (Vicon 612, Vicon Motion Systems Ltd.) and GRF data (OR6 platform, AMTI) were collected while subjects walked within a 12-camera capture volume. Data was extracted from the second GRF peak. The FE model loads were based on the forces and moments at this time point.

Next, fluid-filled registration markers were placed around the knee and 7T MRI scans (resolution 0.3mm x 0.3mm x 0.3mm, Siemens) were taken. Bone, cartilage, and meniscal structures were segmented (ITK-SNAP 2.4.0) in each MRI scan, and then smoothed (Blender 2.68a) before being assembled into the native knee geometry (SolidWorks 2014). Marker locations and ligament origins/insertions were also identified in the MRI scan.

After registering the two data sets, FE models (Abaqus 6.12) of the native knee were created. These models combined geometry from the MRI scans and loads from GRF data. The stresses/pressures on the articulating proximal tibial cartilage and meniscal surfaces were recorded. Clinically, HTO shifts the medial-lateral (M-L) location of the mechanical axis; we simulated this shift by altering the knee adduction-abduction moment. Sets of models were created which shifted the mechanical axis from the native medial alignment (~27% M-L tibial plateau width) to an extreme lateral alignment (80% M-L width) in increments of 3% M-L width. Stresses/pressures on the tibial cartilage and meniscal surfaces were again recorded.

The results from the three subjects were then analysed. Maximum stress and pressure magnitudes varied between subjects so each subject's results were first normalized according to these maximum values. Then, the normalized results of each subject were averaged.

Results: Both stress and pressure decreased in the medial compartment and increased in the lateral compartment as the mechanical axis was incrementally shifted towards the lateral compartment. Results could be split into three categories.

Category 1: native alignment (27% M-L width) to 50% M-L width. At 50% alignment, medial results decreased to nearly half their maximum results, with negligible increases in lateral compartment results. HTO corrections within this zone would be considered "safe" (though alignment changes must be large enough to merit undergoing the surgery).

Category 2: 53% to 65% M-L width. Medial and lateral results were approximately equal. HTO corrections within this zone would be considered "potentially safe". At 65% alignment, lateral results had noticeably increased, potentially enough to damage lateral tissues.

Category 3: 68% to 80% M-L width. Medial results decreased, with accompanying increases in lateral compartment results. HTO corrections within this zone would be considered "not safe" since it is likely that lateral compartment tissues would be damaged.

Figure:
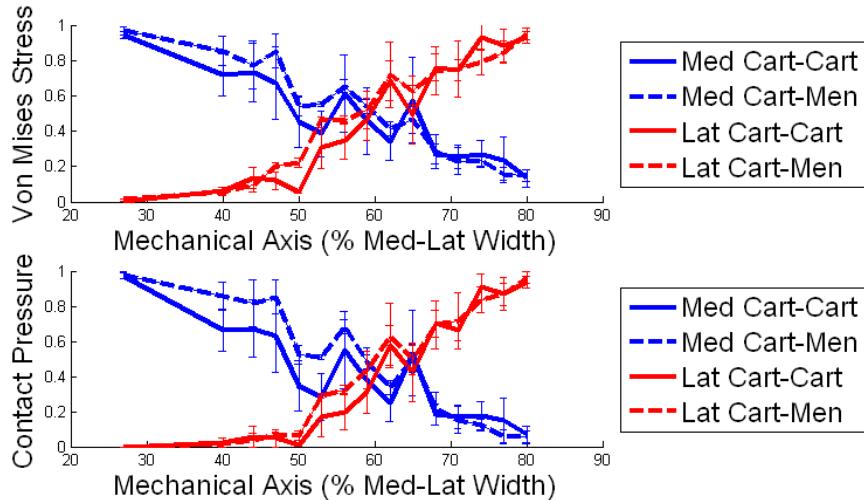
Caption: Average normalized stresses and pressures calculated for different knee alignments.

Conclusion: These results suggest a safe correction zone within which HTO can be performed. The mechanical axis should be moved far enough from the native alignment to warrant surgery, but not beyond 65% M-L width. Shifting the mechanical axis beyond 65% noticeably increased lateral compartment results, potentially damaging these tissues.

References: [1] Brouwer et al., Cochrane Database Syst. Rev., 3: 1-25, 2007.

[2] Gebhard et al., Arch. Orthop. Trauma Surg., 131: 297-302, 2011.

[3] Fujisawa et al., Orthop. Clin. N. Am., 10: 585-608, 1979.

Disclosure of Interest: None Declared

AS-0373

ACCURACY OF THE KNEE AXIS ORIENTATION AGAINST EOS, A STANDING BI-PLANE X-RAY SYSTEM

Morgan Sangeux [1] [2,*]Christophe Sauret [3]Helene Pillet [3]Wafa Skalli [3]

[1]The Royal Children's Hospital, [2]Murdoch Childrens Research Institute, Melbourne, Australia, [3]Arts et Metiers ParisTech, Paris, France

Introduction and Objectives: Gait analysis is often performed clinically to assist with decision to perform femur and/or tibia de-rotation osteotomies. However, clinicians mostly rely on the hip or knee rotation profile(s) to make such decision and these are among the least accurate outputs of gait analysis [1]. The lack of accuracy of the hip rotation profile comes from the difficulty to locate the knee axis accurately. Anatomically, the knee joint axis is considered in line with the posterior aspects of the knee condyles [2]. Conventional methods rely on manual palpation or visual alignment of a knee alignment device. Their accuracy depend on the experience of the assessor. Functional methods are considered an alternative because they do not rely on the assessor's expertise but rely on the joint movement to determine the knee axis.

EOS is a new low-dose bi-plane imaging system which allows simultaneous visualisation of the bones and external markers in 3D [3]. The aim of this study was to quantify the accuracy of conventional and functional methods to locate the knee axis against an EOS based benchmark.

Methods: Thirteen healthy adults with no history of gait pathology participated to the study. Approval was granted by the appropriate ethics committee. Light-reflective markers were attached to the subject and tracked by a 6-camera motion-capture system (Vicon Motion Systems) [3]. The knee axis was determined using a conventional, marker based, method through manual palpation of the epicondyles and three functional methods; the axis transformation technique (ATT/SARA, [4]), the geometrical method [5] and a method closely related to the dynamic KAD (DynaKAD, [6]). The functional methods were applied to two activities; open chain active or passive knee flexion-extensions, and walking.

The reference method was the condylar axis obtained from EOS. The accuracy of the methods were expressed as the angular difference of the various knee axes in the transverse plane.

Results: The conventional axis was external compared to the EOS axis, 15° (SD: 6°) on average. The DynaKAD method was the closest to the EOS axis for all calibration movements. The best results were obtained for the passive flexion-extension (0° SD: 7°). The geometrical axis performed well on the passive knee flexion-extension movement (mean: 4°) but not (mean: 15°) on the walking movement. The ATT/SARA method was, in average, more than 10° too external for all calibration movements.

Conclusion: We assessed the accuracy of various method to locate the knee axis for gait analysis against the EOS medical imaging benchmark. The DynaKAD method applied to the passive knee flexion-extension activity provided the axis closest to the EOS reference. This study was performed on healthy adults and these results need to be confirmed on those with pathology.

Table:

Family	Method	-------------------- Calibration movement -----------------		
		Active Flexion-extension	Passive Flexion-extension	Walking
Functional	Geometrical	14 (6.8)	4 (7.5)	15 (11.8)
	ATT/SARA	14 (6.5)	10 (5.5)	12 (6.0)
	DynaKAD	10 (5.7)	0 (7.3)	5 (6.1)
Conventional		15 (5.9)		

Caption: Results on accuracy of the various methods to locate the knee axis. The accuracy is expressed as the angle difference in the transverse plane in °.

References: 1.   McGinley JL, Baker R, Wolfe R, Morris ME. The reliability of three-dimensional kinematic gait measurements: a systematic review. Gait & Posture. 2009;29(3):360-9.

2.   Eckhoff DG, Bach JM, Spitzer VM, Reinig KD, Bagur MM, Baldini TH, et al. Three-dimensional mechanics, kinematics, and morphology of the knee viewed in virtual reality. J Bone Joint Surg Am. 2005;87 Suppl 2:71-80.

3.   Sangeux M, Pillet H, Skalli W. Which method of hip joint centre localisation should be used in gait analysis? Gait Posture. 2014;40(1):20-5.

4.   Ehrig RM, Taylor WR, Duda GN, Heller MO. A survey of formal methods for determining functional joint axes. Journal of Biomechanics. 2007;40:2150-7.

5.   Chang LY, Pollard NS. Robust estimation of dominant axis of rotation. Journal of Biomechanics. 2007;40:2707-15.

6.   Baker R, Finney L, Orr J. A new approach to determine the hip rotations profile from clinical gait analysis data. Human Movement Science. 1999;18:655-67.

Disclosure of Interest: None Declared

Modelling

AS-0374

OBTAINING QUICK RUNNING MACROSCALE BEAM MODELS OF WHOLE BONES FROM HIGHER RESOLUTION STRUCTURAL REPRESENTATIONS

Anantharaman Gopalakrishnan [1,2,]*Andrew T M Phillips [1,2]

[1]The Royal British Legion Centre for Blast Injury Studies at Imperial College London, [2]Civil and Environmental Engineering, Imperial College London, London, United Kingdom

Introduction and Objectives: Finite element (FE) models of whole bones have been shown to provide realistic estimates of the stress distributions induced by a variety of loading conditions, with computation times typically in the order of a few minutes. While this is acceptable for standalone evaluations of a bone's behaviour, it becomes infeasible to integrate FE models within other computationally demanding simulations such as multi-body dynamic (MBD) simulations. MBD techniques can be used to simulate limb motions and inter-limb reaction forces during blast or impact events, and the integration of a quick running, sub-simulation estimating bone stresses could give real-time predictions of fracture risk during such events. The goal of this study was to develop a quick running macroscale 'beam model' of femur to be solved using the stiffness method. The mesoscale structural model of the femur developed by Phillips et al. [1] was used as the reference model from which the beam model was derived. It was hypothesized that by (a) defining a roughly longitudinal, three dimensional trajectory for the femur, (b) obtaining cross-sections of the structural model along this trajectory at regular intervals and (c) creating a series of short beam elements with appropriate cross-sectional properties connected along the defined trajectory, an equivalent beam model could be obtained. The normal stresses induced in the beam model of the femur due to axial loading and biaxial bending were compared to results from the finite-element structural model subject to the same loading condition.

Methods: The longitudinal trajectory to the femur consisted of straight lines in the regions of the femoral head and shaft. These lines were the axes of cylinders that were fitted to the cloud of cortical surface nodes in the respective. A third degree polynomial was fitted to the femoral neck, thus connecting the two angled, straight line sections of the trajectory. The trajectory was divided into 144 intervals (5mm intervals in the shaft, 2mm in the neck and head) with consecutive points of division taken as the start and end nodes of 12 DOF beam elements, forming a series of 144 beam elements. The cross section of each beam element was determined by slicing the structural model with a plane passing through the mid-point of its corresponding beam nodes, at right angles to the trajectory tangent. The intersection of the triangular shells representing cortical bone in the structural model (taken to be triangular prisms, due to their thickness) and truss elements representing trabecular bone (taken to be of circular cross section) with the plane, constituted the cross-sectional profile of the corresponding beam element. Cross-sectional properties including the area, the second moments of area and torsion constant were computed and used to derive a global stiffness matrix for the entire beam model.

The load case presented here is a 500N point load (see Figure 1A) applied in the anterior direction on the head of the femur. All nodes below the fifth beam node from the base of the femur were constrained in all six degrees of freedom. With these loads and boundary conditions, the stiffness matrix was solved to compute the displacement and forces at each node, from which the normal stress distribution at each beam's cross section was derived. The same loading

conditions were emulated in the FE structural model where the stresses and displacements were computed using ABAQUS (3DS). The FE model's stress tensor was transformed into the corresponding beam's cross-sectional coordinate frame and the normal component of stress was compared to the values from beam theory.

Results: Figure 1B compares the normal stresses from the beam and FE structural models for points located on the outer perimeter of cortical bone, at the mid-plane of a beam from the femoral mid-shaft region. For each of the vertices of the cortical perimeter (Figure 1B) on each of the 144 beam mid-planes, the absolute errors between normal stresses from both models were expressed as a percentage of the mean normal stress (from the FE model) over all cortical points in the model. The averaged value of these errors over all the vertices was 9.5%. Analysis times were around; FE model: 90s, beam model: 0.1s.

Figure:
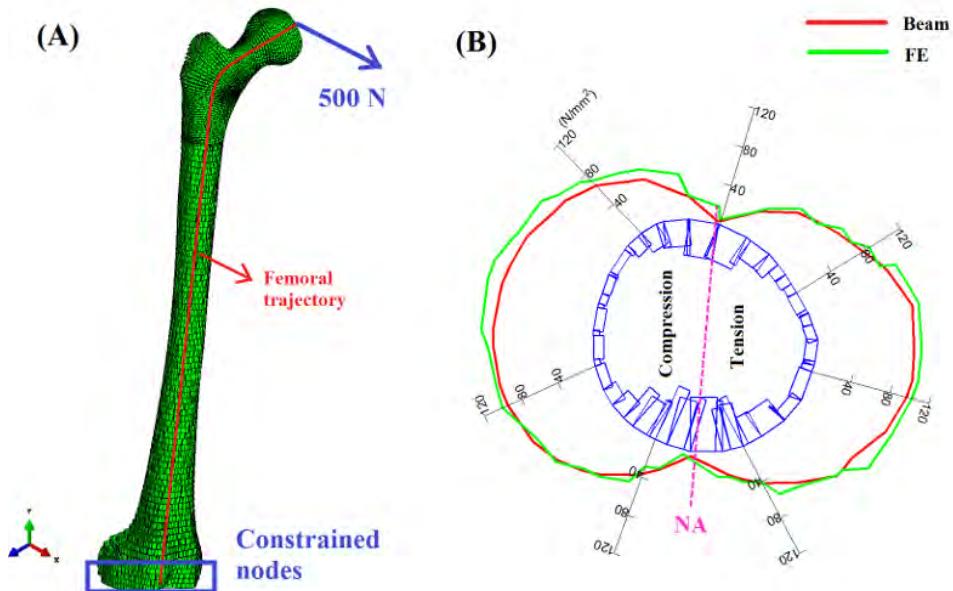
Conclusion: The simplistic beam model succeeded in computing normal stresses to a good level of accuracy compared to the more complex FE structural model. The limited loss of accuracy could be considered a reasonable trade-off for the extremely low computational time of the beam model. It is thus considered feasible to integrate the beam model into more intensive computational pipelines such as multi-body dynamic simulations of a blast event, in order to estimate the stresses in bones and predict the occurrence of fractures under dynamic motions and loads.

References: [1] Phillips et al., *International Biomechanics* (accepted).

Disclosure of Interest: None Declared

AS-0375

THE ASSESSMENT OF BALANCE IN DIFFERENT POSTURES

Glen M. Blenkinsop [1],*Michael J. Hiley [1]Matthew T. G. Pain [1]

[1]School of Sport, Exercise and Health Sciences, Loughborough University, Leicestershire, United Kingdom

Introduction and Objectives: Traditionally balance has been assessed by relatively simple analyses of the trajectory of the centre of pressure (COP) to calculate quantities such as: range, standard deviation, sway area, and sway length. Some COP signals may be considered to contain subtle structure in the form of time correlation information which may be extracted through nonlinear techniques [1]. Further information may be extracted by assessing multiple signals, such as centre of mass motion or joint angles and torques. The purpose of this research was to determine which balance metrics are best for assessing balance in different postures and providing insight into the underlying process of balance control.

Methods: Twelve experienced handstanders performed balance trials with eyes open and eyes closed conditions in double leg stance, single leg stance, and handstand. Each trial type was repeated five times and each trial was performed for a maximum of 30 seconds duration. Kinematic data were collected via a nine camera vicon system (200 Hz), using 53 markers to divide the body into 18 segments. Marker displacements were filtered with a fourth order zero lag, low-pass Butterworth filter with a cutoff frequency of 10 Hz, before quaternion algebra was used to calculate: segment centre of mass linear displacements, velocities, and accelerations; and segment angular velocities and accelerations. Kinetic data were collected via two Bertec strain gauge force plates (200 Hz), and raw COP data were used to assess balance via: traditional measures (trial duration, sway area, sway length, standard deviation, range, sway velocity), nonlinear dynamics (sample entropy, Lyapunov exponent), and recurrence quantification analysis (recurrence rate, determinism, Shannon entropy, divergence, trend). Kinetic and kinematic data were used to calculate 3D joint moments and forces via wrench notation, to assess balance via: estimates of neurological delay (delay, R^2, joint torque from proportional and derivative gains), and movement corrections (number of small, medium, and large corrections per second, mean torque, torque impulse, burst duration).

Results: Data suggests that the best balance metrics for distinguishing between each of the six conditions were the traditional balance measures of sway length and sway velocity. Nonlinear measures of sample entropy, determinism, divergence, and Shannon entropy successfully differentiated between each posture, but not between eyes open and eyes closed conditions within each posture.

Neurological delay estimates were approximately: 234 ms for double leg stance, 191 ms for single leg stance, and 176 ms for handstand. Neurological delay estimates were typically higher for trials with eyes closed compared to trials with eyes open conditions for all postures.

Movement correlation analyses show that balance in standing exhibits bursts of torque activity that are longer and with a higher torque impulse compared to balance in handstand. Lower numbers of movement corrections per second are evident in standing trials, with the largest number of corrections occurring in handstand with eyes open and single leg stance with eyes open.

Reduced mean torque and torque impulse during all movement corrections in handstand are indicative of the reduced muscular strength of the muscles found in the forearm compared to the lower leg. It would appear this leads to the requirement for a larger number of corrections per second, but with reduced burst duration, when balancing in handstand.

Conclusion: If the aim of a study is to assess balance performance, with no interest in the underlying control of balance, such as an intervention study, then the traditional measures of sway length and sway velocity appear to be sufficient. If a researcher aims to delve further into the underlying processes of balance control, more advanced analyses will be required. Nonlinear measures of balance offer insight into the underlying deterministic processes that control balance, offering measures of system determinism, complexity, and predictability. Assessments of neurological delay and movement corrections appear to provide further insight into the control of balance whilst also helping to distinguish one condition from another.

References: [1] Riley et al., Gait Posture, 9: 65-78, 1999.

Disclosure of Interest: None Declared

AS-0376

INCREASED ACTIVATION AMPLITUDE LEVELS OF GLUTEUS MEDIUS IN WOMEN DURING ISOMETRIC AND DYNAMIC CONDITIONS FOLLOWING A 4-WEEK PROTOCOL OF LOW LOAD ECCENTRIC EXERCISES

Alexandre C. Barbosa [1,*] Rafaela Carvalho [2] Douglas Bonifácio [2] Fábio Martins [2] Michelle Barbosa [3]

[1] Physiotherapy, Federal University of Juiz de Fora, Governador Valadares, [2] Physiotherapy, [3] Health Education, Federal University of Jequitinhonha and Mucuri Valleys, Diamantina, Brazil

Introduction and Objectives: Gluteal weakness is thought to contribute to greater hip adduction and internal rotation, generating a postural knee valgus during functional activity, consequently increasing the stress to the patellofemoral joint. In this regard, a body of work has emerged, utilising surface electromyography (sEMG) measurement of the gluteal muscles during functional (dynamic and isometric) tasks, reporting differences in onset times, amplitude levels and activity durations. The objective of the present study was to use a protocol involving low load eccentric exercises to observe the effects on the three subdivisions of gluteus medius (GMed) activation through surface electromyography (sEMG) and digital dynamometry.

Methods: Eleven female subjects having femoral instability participated in a four-week protocol (three sessions per week/nonconsecutive days). At each session, two low load eccentric exercises (12% of maximal isometric voluntary contraction – MVIC) in abduction, extension and external rotation were applied to the hip joint (through shin guards). The number of repetitions and series varied in each session, providing asymmetric stimuli, not allowing accommodation and providing constant neurophysiological response by the mechanoreceptors (Table 1). The sEMG of the GMed subdivisions (anterior, mid and posterior) during a squat and MVIC were assessed. The digital dynamometry was also assessed during MVIC. Parametric paired t-test was used to compare the results before and after treatment with α=0.05.

Results: The results showed an increased sEMG activity of GMed (mid and posterior portions) during isometric voluntary contraction and squat after the protocol. No difference was noted to the anterior subdivision of GMed. Another finding was the significant difference to the dynamometry results, showing improvements to generate strength to the GMed as a whole muscle in abduction with 8.15±2.34 kgf to 9.11±2.63 kgf at the final assessment (p=0.0001).

Figure:
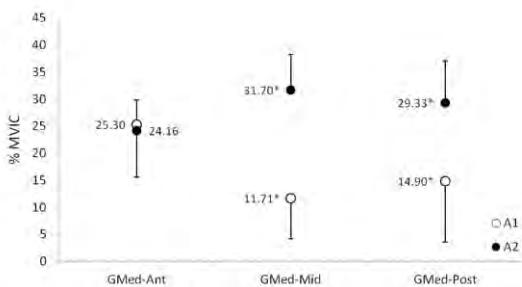
Figure 1 Normalised RMS values (mean and standard deviation) for the subdivisions of GMed muscle for pre and post assessment (isometric condition). *indicates significant difference between pre and post intervention data (p<0.05)

Conclusion: For dynamic stabilization of the hip, the ideal pattern to improve positional control seems to be a protocol that combines muscle control without exhausting the musculoskeletal system and concomitantly activates the receptors in the muscles. In this way, the sensory map may continuously be corrected by sensory feedback according to proprioceptive priority, given by the influx of afferent receptors. The four-week low load exercise protocol was effective to increase the activation of the GMed mid and posterior subdivisions, improving also the capacity to generate strength as a whole muscle during the proposed tasks.

Table: Table 1 Rehabilitation guidelines: GMed eccentric contractions. All sets and repetitions were applied to Exercise 1 and 2.

Protocol	Day 1	Day 2	Day 3
Week 1	3 sets of 8 repetitions	3 sets de 10 repetitions	3 sets de 12 repetitions
Week 2	4 sets de 8 repetitions	4 sets de 10 repetitions	4 sets de 12 repetitions
Week 3	3 sets de 12 repetitions	3 sets de 10 repetitions	3 sets de 8 repetitions
Week 4	4 sets de 12 repetitions	4 sets de 10 repetitions	4 sets de 8 repetitions

Disclosure of Interest: None Declared

AS-0377

A NEW INVARIANT PARAMETER CHARACTERIZING THE POSTURAL ALIGNMENT OF YOUNG HEALTHY ADULTS

Celia Amabile [1] [2],*Helene Pillet [1]Virginie Lafage [2]Wafa Skalli [1]

[1]LBM/Institut de Biomécanique Humaine Georges Charpak, Arts et Métiers ParisTech, Paris, France, [2]Department of Orthopaedics Surgery, NYU Hospital for Joint Diseases, New York City, United States

Introduction and Objectives: Postural troubles can have negative impact on skeleton disorders for aging adults. The first step in understanding these aging postural troubles is to observe and quantify the erected posture of young healthy adults' skeletons from radiographies. However, previous studies in the literature focused on the alignment of the spine and pelvis segments [1], rarely including the head neither the lower limbs. Our study aims to describe the postural alignment of young asymptomatic subjects from head to feet from bi-planar standing radiographies.

Methods: 69 asymptomatic subjects were included in the study: mean age 26.3years old (SD: 4.7). 3D reconstructions of the head, spine, pelvis and lower limbs segments' skeleton were performed from bi-planar radiographies (EOS Imaging, Paris, France) using well documented models [2-4] (Figure). In addition, two stereo-corresponding points localizing the acoustic meati were digitized to compute their center (CAM) [5]. Full description of the postural alignment of the volunteers was made by evaluation of parameters in 3D in the anatomo-gravital frame (frontal plane is the vertical plane going through both acetabulum centers, and transversal and sagittal planes are orthogonal to the patient frontal plane). The origin of the frame is the middle of the centers of each acetabulum (HA). Firstly, reference values for each parameter studied were computed. Secondly, relationships between these parameters were investigated.

Results: Values found for spinal curvatures, pelvic parameters and lower limbs geometrical parameters (Table) were similar to those reported in the literature [1,4,5]. Inclinations of different lines were investigated to characterize the erected posture. The closest line to the vertical passed through the following points: CAM, the most superior point of dentiform apophyse of C2 (OD), the centers of C3 to L5 vertebral bodies, and the center of the sacral plate (S1). Its inclination was in average of 3.1° (SD: 1.9°). The line joining either CAM or OD to HA are the less variable between subjects with an angle (SD) respectively of 2.9° (1.7°) and 2.9° (1.6°) with the vertical. It would be interesting to record those two inclinations for comparison with aging and pathological populations, as the head, characterized by the segment OD to CAM, might be the last one to be adjusted in compensatory mechanism to keep the head upon the pelvis. The line CAM-HA has been reported to be a good indicator to identify postural trouble [5]. Offsets from HA of both knee's center and ankles' center were in average less than 6cm (SD<2cm) ahead of HA and at less than 1cm (SD<12mm) of HA in the medio-lateral direction. This can be an estimate of the alignment of the lower limbs with the upper body. While well-known correlations were found between spinal curvatures and pelvic parameters: L1S1 lordosis with sacral slope (R^2=0.87) and with pelvic incidence (R^2=0.62); pelvic incidence with sacral slope (R^2=0.73), no other correlations were found with the lower limbs' parameters, confirming the pelvis as an independent link between the spine and the lower limbs for this population of young adults.

Figure:
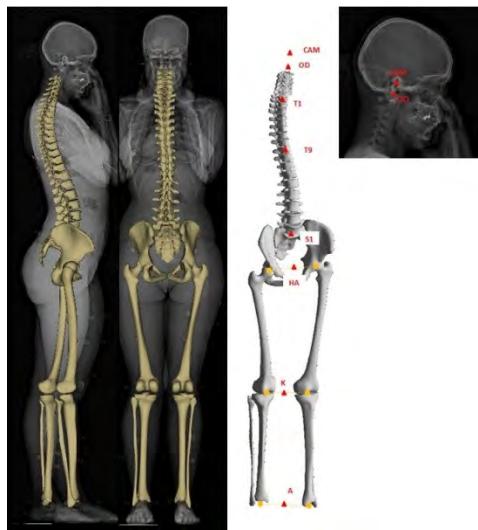
Caption: Bi-planar radiographies with 3D model: identification of CAM, OD, T1, T9, S1, HA, K (middle of both knees points) and A (middle of both ankles).

Conclusion: A description of the postural alignment in 3D, of the geometry of the spine, pelvis and lower limbs, in sagittal and frontal planes of the young healthy adult has been reported. Head upon the pelvis was an invariant. As expected, the spine is overall almost vertical (Incl close to 0°). This study would serve as a basis for future comparisons when investigating aging populations.

Table:

Ferguson C3-C7 Lordosis(°)	9(4)	
Ferguson T1-T12 Kyphosis(°)	27(7)	
Ferguson L1-S1 Lordosis(°)	30(8)	
Pelvic Incidence(°)	51(9)	
Sacral Slope(°)	41(9)	
Pelvic Tilt(°)	11(6)	
Overhang of S1(mm)	-20(10)	
Femoral torsion(°)	R: 13(10)	L: 14(11)
Tibial torsion(°)	R: 37(6)	L: 36(7)
Femoro-tibial Rotation(°)	R: 6(4)	L: 7(6)
Femoral Neck Shaft Angle(°)	R: 128(4)	L: 128(4)
Angle with the vertical of the line that best fits in the least square sense: CAM, OD, all the vertebral body' centers from C3 to L5, and S1(°)	3(2.0)	
Angle with the vertical of the line that connects CAM to HA(°)	3(1.5)	
Angle with the vertical of the line that connects OD to HA(°)	3(1.5)	
Distance between K and HA(mm)	X: -44(18)	Y: 0(7)
Distance between A and HA(mm)	X: -54(13)	Y: 1(12)

Caption: Mean (SD) of studied parameters. R (L): Right (Left) side. X: antero-posterior direction; Y: medio-lateral direction.

References: 1. Vialle, R. et al., J. Bone Joint Surg. Am., 87(2): 260–267, 2005.

2. Mitton, D. et al., Comput Methods Biomech Biomed Engin, 9(1): 1–5, 2006.

3. Humbert, L. et al., Comput Methods Biomech Biomed Engin, 12(S1): 151–163, 2009.

4. Chaibi, Y. et al., Comput Methods Biomech Biomed Engin, 15(5),: 457–466, 2012.

5. Steffen, J. et al., Eur Spine J, 19(5): 760–767, 2010.

Disclosure of Interest: None Declared

Balance

AS-0378

A NUMERICAL MODEL TO PREDICT THE 1-STEP BALANCE RECOVERY THRESHOLD AND REACTIONS FOR YOUNG AND ELDERLY

Pascal Vallee [1,*] Thomas Robert [1]

[1] LBMC, Université de Lyon - IFSTTAR, Bron, France

Introduction and Objectives: Falls are a major problem which represents 37.3 billion of medical care every year. To understand and prevent these events, it is necessary to be able to predict if a perturbation will necessarily induce a fall or, if not, what would be the most efficient balance recovery (BR) reactions. Models have been proposed to estimate which states are recoverable or not. However, these models rely on hypotheses that are too restrictive to correctly predict the risk of fall: no recovery step [1] or only instantaneous step [2] allowed, or oversimplify the ability of a human to make the desire recovery steps [3]. In this study we propose a numerical model which considers the stepping ability to predict: 1) the threshold of 1-step BR; 2) the most efficient (i.e. shortest and fastest) recovery step when perturbed beyond the threshold. This model could be unbalanced by any kind of external perturbation and will be assessed against experimental datasets from the literature for young and elderly subjects.

Methods: The human body is modeled by a 2D inverted pendulum in sagittal plan with: 1) an inertia wheel to represent hip strategy with a bang-bang acceleration profile; 2) a base of support (BoS) within which the center of pressure can be moved to represent the ankle strategy; 3) the possibility to make a step, bounded by a preparation time and constraints on the swing phase [4]. It evaluates the time evolution of the XCoM [3], considering the maximal ankle and hip reactions. It then looks if any feasible recovery steps can capture this point, which is a necessary condition to reach a steady balanced state, i.e. if it is possible to recover from the initial perturbation. This model is assessed against three experimental datasets from the literature: 1) a study which established the 1-step BR threshold line in the center of mass's state plane, by considering different kind of perturbations [5]; 2) Two tether release studies with increasing release angle (up to the 1-step BR threshold), imposing maximal step performance [6] or not [7]. All of these studies included a group of young healthy subjects and a group of elderly. For [5] we compare the 1-Step BR thresholds, while for [6] and [7] we compare the step length and timing. Model's parameters related to subject's anthropometry, set to the mean of each group of each study. Parameters related to the maximal reactions were derived from the BR characteristics reported in these studies and were identical for the three situations (see table).

Results: The proposed model predicts relatively well the 1-Step BR threshold line (see Fig., left). The main difference concerns states with small lean angle but high angular velocity for elderly. It may come, in part, from inaccurate experimental results in this area of the state plane, as they were obtained via a procedure that is really difficult to control. Moreover, the model fits well the recovery step characteristics, when performed at maximal performance. For [6], which experimental design imposes the shortest steps possible, predicted steps are between 1 cm and 8 cm shorter and between 5 ms and 40 ms quicker in average for young and elderly, respectively. For [7], results are similar for the larger release angles. However, predicted steps at smaller angles are too short and too quick (see Fig., right). As there were no explicit instructions about stepping performance, subjects were likely to perform non optimal (larger and longer) BR steps,

less difficult and safer. However, when perturbations get closer to the threshold, subjects' reaction had to get closer to the maximal performance.

Figure:
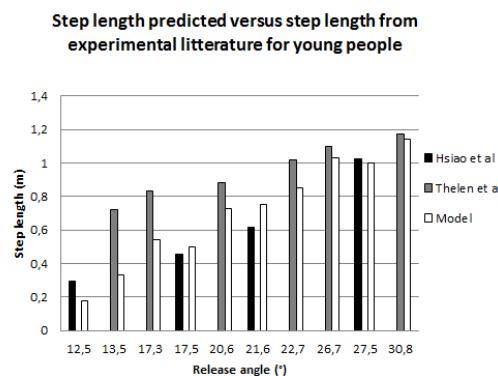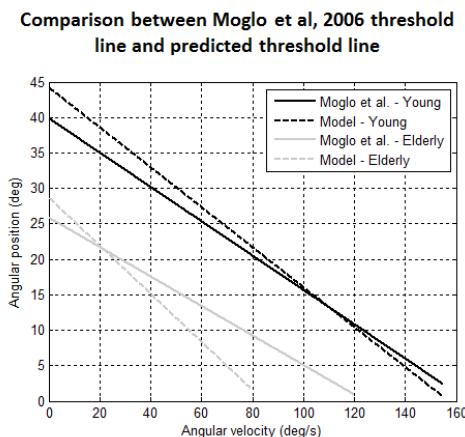
Caption: Simulated vs. experimental 1-Step BR threshold 'left) and BR step length (right)

Conclusion: Our model is able to predict the 1-step recovery threshold and the characteristics of this BR steps when performed at maximal performance, for different groups of population and for different types of perturbation. It is notable that these results were obtained against three different experimental datasets but with a single set of parameters per group of subjects. Moreover these parameters were not optimized but derived from the BR characteristics reported in these experimental studies. This model could be used to identify the potentially hazardous situations and to better understand the balance recovery mechanisms, e.g. the influence of the different BR parameters and their potential degradation with age or a disease.

Table:

Paramters	Young	Elderly
Reaction time (ms)	75	85
Step preparation time (ms)	150	170
Max Step Length (m)	1.2	0.87
Max Foot accel. (m/s²)	165	100

Caption: Model's parameters related to the maximal reactions

References: [1] Pai et al., J. Biomech., 30:347-354, 1997.

[2] Pratt et al., 6th IEEE Conf. Humanoid Robot, 2006.

[3] Koolen et al., Int. J. Rob. Res., 31:1094–1113, 2012.

[4] Aftab, PhD Thesis, 2012.

[5] Moglo et al., 30th Meeting of the American Soc. Of Biomech., 2006.

[6] Hsiao et al., Clin. Biomech. 22:574–80, 2007.

[7] Thelen et al., J. Gerontol. A. Biol. Sci. Med. Sci. 52:8–13, 1997.

Disclosure of Interest: None Declared

Balance

AS-0379

EFFECTS OF TACTILE SURFACE ON OLD ADULTS' GAIT AND PERCEPTION OF SLIPPERINESS IN A SIMULATED WINTER ENVIRONMENT

Yue Li [1,*]Sharon Ravindran [1][2]Adam Katchky [3][4]Vicki Komisar [1][5]Tilak Dutta [1]Geoff Fernie [3][4]

[1]Technology R&D Team, Toronto Rehabilitation Institute - University Health Network, [2]Division of Engineering Science, [3]Department of Surgery, University of Toronto, [4]Toronto Rehabilitation Institute - University Health Network, [5]Institute of Biomaterials and Biomedical Engineering, University of Toronto, Toronto, Canada

Introduction and Objectives: *Detectable tactile surface indicators* (tactile surfaces) are applied to the surface of curb ramps to help people with visual impairments identify street crossings. Although these surfaces do not impede rolling safety [1], the physical demands for walking have not been fully explored [2]. Snow and ice are known to impede detectability of these surfaces [3], but their effects on gait, stability and fall risk in older adults have not been examined. This study investigates whether older adults alter speed and step width on tactile surfaces compared to smooth paving in a simulated winter environment.

Methods: This study took place in WinterLab, one of Toronto Rehab's Challenging Environment Assessment Laboratories. Two types of walkway surface (simulated smooth concrete paving [concrete] and tactile paving [tactile]) and two contamination conditions (no contamination [dry] and snow covered surface [snow]) (Figure 1) were tested. The walkways were level and each walkway was 4m long and 0.5m wide. Nine able-bodied older adults (65-78 years; 3 male, 6 female) participated. All wore the same footwear (winter boots) and walked at a preferred self-selected pace. The ambient temperature in WinterLab was controlled at 9.3±1.0°C, and surface temperature was controlled at 0.8±0.9°C. The following temporal-spatial gait parameters were calculated using an optical motion capture system (Motion Analysis) tracking reflective makers placed on participants' footwear:

(1) Step time (Time between two consecutive heel strikes)

(2) Step length (Anterior-posterior distance between the heel markers of two consecutive heel strikes)

(3) Step speed (Step length/step time)

(4) Step width (Medial-lateral distance between the heel markers of two consecutive heel strikes)

Participants were asked after each trial to rate the perceived slipperiness of the surface (0 - not slippery to 10 - extremely slippery). All data were analyzed across the two surfaces and two contamination conditions with a mixed model repeated measures ANOVA ($p < 0.05$).

Results: Surface type had significant effects on step time, step length, step speed and step width (Table 1). Slower gait speed and increased step width on the tactile surface could indicate fear of falling [4]. Thies et al.[5] tested older adults on level and sloped tactile paving at room temperature and found that gait speed and step width remained comparable on smooth concrete and tactile paving as did step time. However, our study demonstrated the significant effects of tactile paving on gait when the ambient temperature was around 10°C with snow on the walkway. As anticipated, walking on snow contaminated surfaces significantly challenged stability in the direction of progression, as indicated by greater step time and reduced step speed and length as the participants felt that the snow-covered walkway was more slippery (Table

1). Interestingly, there was no significant difference in step width between dry and snow. It has been reported that increases in step time and step width, as well as decreases in step length and walking speed are used to avoid a slip on slippery surfaces [6]. No changes in step width could be due to a lack of stepping adaptability to the snow covered surface in older people. Future study with a larger sample size is needed to confirm this finding.

Figure:

Caption: WinterLab (left) and the two walkways with snow contamination (right).

Conclusion: This is the first study to examine gait on tactile vs concrete paving with snow contamination in winter-like temperatures. Older adults found dry tactile paving to be more challenging to negotiate than smooth dry concrete paving. Snow covering increased the perception of slipperiness less on the tactile paving than on the concrete paving and resulted in less of a reduction in speed. The effect of sloped tactile paving on gait measures associated with stability and falls risk in older adults will be examined in the second stage of this study. The experimental setup developed for this baseline study could be used to assess alternative tactile paving designs.

Table:

	Surface (p value)	Snow (p value)	concrete		tactile	
			dry	snow	dry	snow
Step speed (m/s)	0.001*	0.0001*	0.95 (0.03)	0.85 (0.03)	0.87 (0.03)	0.83 (0.03)
Step time (s)	0.002*	0.0003*	0.58 (0.03)	0.61 (0.03)	0.61 (0.03)	0.62 (0.03)
Step length (cm)	0.015*	0.004*	54.9 (2.50)	51.7 (2.50)	52.2 (2.50)	51.3 (2.50)
Step width (cm)	0.02*	0.09	8.3 (0.80)	7.90 (0.80)	9.5 (0.80)	8.7 (0.80)
Perceived slipperiness	0.81	0.02*	0.22 (0.37)	1.22 (0.37)	0.56 (0.37)	0.78 (0.37)

Caption: Estimated means of gait kinematic data (mean (SE)) and p-values for concrete and tactile surfaces with and without snow contamination (* = p<0.05).

References: [1]   Lee, Western Michigan University, 2007.

[2]   Bentzen, et al., FTA-MA-06-0201-94-2, 1994.

[3]   Ratelle, et al., TRANSED, 2010.

[4]   Maki, et al., J Am Geriatr Soc. 45: 313–320, 1997.

[5]   Thies, et al., J. Biomech. 44: 1599–1604, 2011.

[6]   Chang, et al., Gait Posture, 2015.

Disclosure of Interest: None Declared

EFFECT OF HANDRAIL HEIGHT ON THE TIMING AND KINEMATICS OF REACH-TO-GRASP BALANCE RECOVERY REACTIONS DURING LEVEL-GROUND WALKING

Vicki Komisar [1][2],*Alison C Novak [2]Emily C King [2][3]Brian E Maki [1][2][4][5]Karl F Zabjek [2][6]Geoff R Fernie [1][2][4][5]

[1]Institute of Biomaterials and Biomedical Engineering, University of Toronto, [2]Toronto Rehabilitation Institute - University Health Network, [3]Mechanical and Industrial Engineering, [4]Department of Surgery, [5]Institute of Medical Sciences, [6]Department of Physical Therapy, University of Toronto, Toronto, Canada

Introduction and Objectives: Handrails are often installed on stairs, ramps and in corridors of care facilities to promote balance recovery and accessibility, and reduce the risk of falls [1]. To be an effective safety feature, a handrail must be installed at a height that enables fast and accurate reactive grasping, and allows a user to generate the high forces and moments needed to stabilize their centre of mass. Handrail height significantly affects the highest voluntary forces and moments that a person can generate on a handrail while standing [2], but the effect of handrail height on the speed and accuracy of perturbation-evoked grasping is not known. This study examined the influence of handrail height on the speed and accuracy of reach-to-grasp reactions in young adults after balance loss during level-ground walking.

Methods: Data were collected in the Challenging Environment Assessment Laboratory (CEAL) at Toronto Rehab. In CEAL, a 5mx5m lab is mounted on a robotic platform to deliver support-surface perturbations (Figure 1). Data from 8 of 11 young adults (21-30y; 3M) have been analyzed.

Harnessed subjects walked back and forth with their arms at their sides beside a height-adjustable handrail, while completing a verbal counting task. Subjects wore standardized running shoes with soles covered by felt and cotton fabric. The walking surface consisted of force plates covered by fiberboard, which allowed subjects to walk normally but, with the fabric-covered shoe soles, prevented effective foot planting following balance loss due to low foot-floor friction. Balance loss was induced via sudden backward platform translation (acceleration $3.75 m/s^2$; peak velocity 1.13 m/s; displacement 0.34 m). Three handrail heights per subject were tested: 50% (LOW), 57% (MED) and 64% (HIGH) of the subjects' height. Four balance recovery trials were collected for each height.

Reach-to-grasp accuracy and hand velocity were estimated from a motion capture marker on the base of the second metacarpal; handrail contact time was measured using a handrail-mounted optical sensor. Reach onset latencies were determined using EMG from the right middle deltoid. Onset latency and contact time were defined relative to perturbation onset (platform acceleration$>0.1 m/s^2$ [3]). One-way repeated measures ANOVAs were conducted for all variables of interest (significance $p \leq 0.05$). Sphericity was checked with Mauchly's test and Greenhouse-Geisser corrections were applied where necessary. Post hoc comparisons with Bonferroni corrections were performed for metrics that varied significantly with handrail height.

Results: Descriptive statistics for key reactive graspin metrics are presented in Table 1. Middle deltoid onset latencies ($p=0.372$) and time to handrail contact ($p=0.883$) did not vary with rail height. Handrail overshoot decreased as height increased ($p =0.001$). Further, overshoot for LOW was significantly higher than MED ($p=.05$) and HIGH ($p=0.008$), but MED and HIGH did not differ significantly ($p =0.679$). Peak hand velocity in the lateral and vertical directions also

increased with handrail height, although only the vertical velocity increase was significant (lateral p=0.066; vertical p<0.001). Further, peak vertical hand velocity was significantly lower for LOW than for MED (p=0.013), and significantly lower for MED than for HIGH (p=0.015).

Figure:
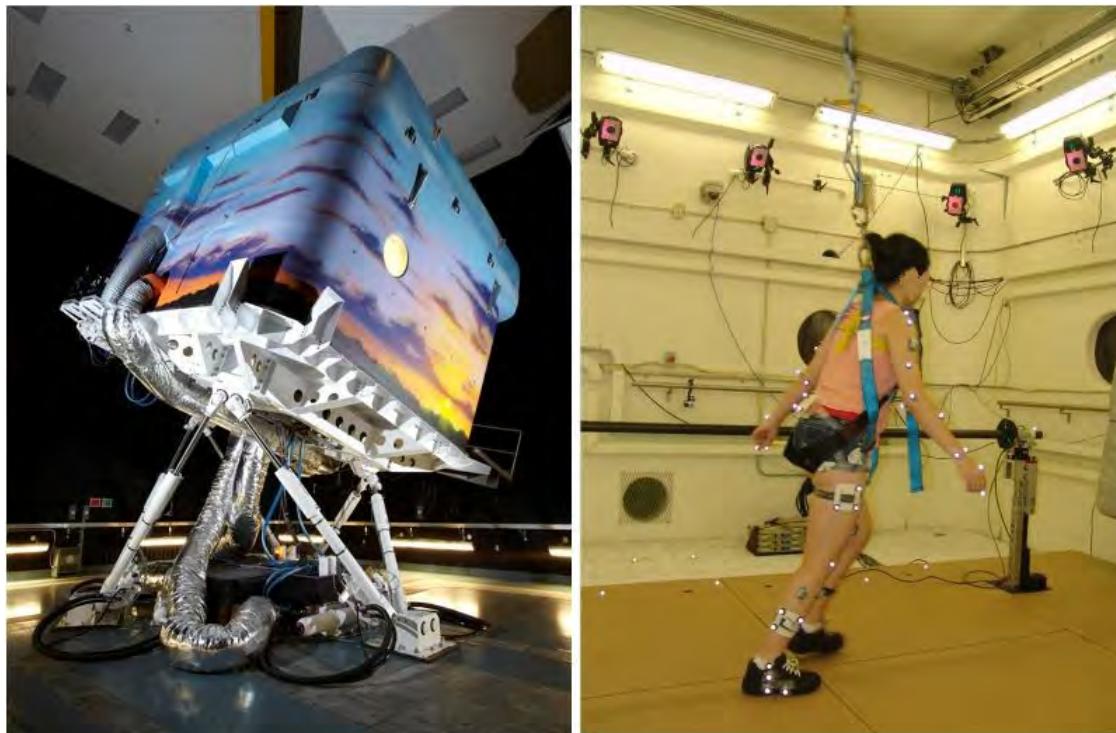
Caption: Figure 1. The Challenging Environment Assessment Laboratory. Left: The motion base. Right: Inside the lab. Motion capture cameras on the walls collect kinematic data; a handrail-mounted optical system estimates contact time.

Conclusion: Within the range tested, handrail height does not affect time to rail contact or reaching reaction onset latency following balance loss on level ground for young adults. This suggests that other balance recovery metrics such as forces and moments that a person can generate on the handrail may be more important determinants of a handrail's effectiveness in preventing falls in this population at a given installation height. The increases in both peak hand velocity and accuracy (lower rail overshoot) with handrail height may provide insights into why time to rail contact was consistent even though the initial distance between the hand and rail differed between rail heights. Repeating this experiment in older adults will improve our understanding of how handrail height affects balance recovery in broader populations.

Table:

Balance recovery metric	Handrail height		
	LOW	MED	HIGH
Middle deltoid onset latency (ms)	201 (30)	190 (24)	211 (40)
Time to handrail contact (ms)	490 (34)	483 (47)	483 (42)
Handrail overshoot (m)	0.117 (0.059)	0.061 (0.016)	0.046 (0.034)
Peak vertical hand velocity (m/s)	1.747 (0.462)	2.385 (0.405)	2.823 (0.478)
Peak lateral hand velocity (m/s)	2.375 (0.465)	2.533 (0.385)	2.628 (0.484)

Caption: Descriptive statistics (Means (SD)) for key reach-to-grasp balance recovery metrics with respect to handrail height.

References: [1] Maki et al, *Safety Science*, 28:189-206, 1998.

[2] Maki et al, *Human Factors*, 26:705-714, 1984.

[3] Cheng et al, *J. Gerontology*, 67:1238-1245, 2012.

Disclosure of Interest: None Declared

AS-0381

TIBIALIS ANTERIOR AND VASTUS LATERALIS CONDUCTION VELOCITY DURING ISOMETRIC CONTRACTION AT LOW LEVEL FORCE IN DIABETIC INDIVIDUALS WITH DIFFERENT STAGES OF NEUROPATHY

Eneida Y. Suda [1,*] Thiago Tavares Kawamura [1] Marco Kenji Butugan [1] Neli RS Ortega [2] Isabel CN Sacco [1]

[1] Physical Therapy, Speech, Occupational Therapy dept., [2] Medical Informatics, University of São Paulo - School of Medicine, São Paulo, Brazil

Introduction and Objectives: Diabetic neuropathy is one of the most prevalent complications of diabetes mellitus, affecting both sensory and motor nerve fibers. Although the most common early reported symptoms are sensorial, with neuropathic patients citing loss of tactile sensitivity, prickling sensation and pain, motor dysfunction is observed in this population. Neuromuscular impairment is related not only to nerve integrity but is also related to other factors as the state of motor end plates and skeletal muscle fibers. The diabetic neuropathy is a progressive phenomenon and related alterations could be different for earlier and more advanced stages of the disease. Therefore, the aim of this study is to investigate if different diabetic neuropathy degrees have distinct muscle fiber conduction velocity (MFCV) during isometric contraction at low level force (20%) for one proximal and one distal lower limb muscles.

Methods: Ten control subjects (49.4±9.6yrs) and 19 diabetic patients (58.6±4.8yrs, 14.8±13.1yrs of diabetes diagnosis, 196.9±79.1 mg/dL blood glucose) were evaluated. The participants were assessed for (i) vibratory perception (128Hz turning fork), (ii) tactile sensitivity (10g Semmes-Weinstein monofilament) and (iii) presence of typical neuropathy symptoms. These three groups of variables were used as linguistic inputs in a fuzzy system to determine the neuropathy degree (score 0-10). The neuropathy score was used to classify the patients into different disease severity stages. The score value was also used to classify the individuals into neuropathy classes: (a)x≤2.5: absent; (b)2.5≥5.0: moderate/severe. Multichannel Surface EMG (64 electrodes matrix: 15 x 4, OT Bioelettronica, Torino, Italy) was acquired during 20% of maximum isometric voluntary contractions (MIVC) of tibialis anterior (TA) and vastus lateralis (VL) musclesTA was evaluated during dorsiflexion performed with knee in full extension and the ankle in neutral position. VL was evaluated during knee extension performed at 90° of hip flexion and 45° of knee flexion; force levels were controlled by a knee and an ankle ergometer (strain gage load cell) and fluctuations of ±2% of the absolute torque level, controlled by a visual biofeedback system, were accepted. MFCV was determined for an epoch of 500ms using a maximum likelihood estimation method [1]. Correlation analysis were performed in order to analyze the association between MFCV and neuropathy degree, determined by the fuzzy system. The neuropathy and control groups were compared using ANOVAs, followed by Newman-Keuls post-hoc test ($p<0.05$).

Results: MFCV decreased significantly for both TA (r=-0.461) and VL (r=-0.571) muscles with neuropathy progression (Figure 1). TA muscles showed lower MFCV values for moderate/severe subjects when compared to control ones (Table). Although this difference was not observed for VL, it is clear that the disease progression leads to a higher impairment. TA muscles have higher proportion of type I fibers, that are more affected in diabetic patients, and the level of contraction evaluated (20% MIVC) probably recruited lower motor units what would explain the difference observed only for TA and not for VL muscle.

Figure:
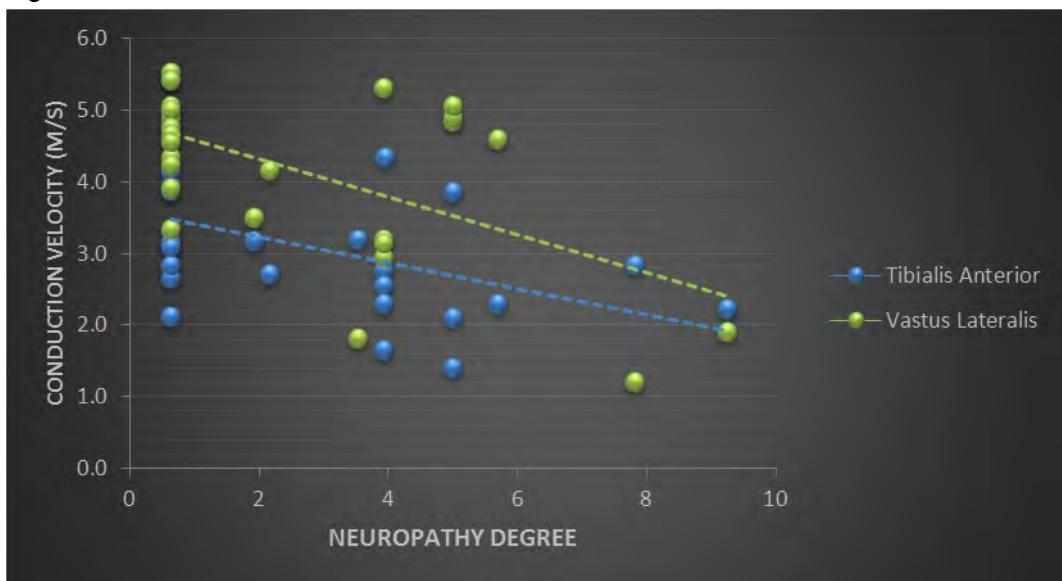
Caption: Correlation between MVIC values and neuropathy score.

Conclusion: MFCV decreases linearly and progressively with neuropathy progression in TA and VL muscles. TA muscles presented lower MFCV in later stages of neuropathy when compared to control subjects that may be related to changes in muscle fiber contractile properties since TA has a higher proportion of type I fibers that are lost in the course of the disease.

Table:

Group	MIVC – TA (m/s)	MIVC – VL (m/s)
Control (n=10)	3.86±1.05*	4.57±0.91
Absent (n=6)	3.12±0.42	4.66±0.71
Mild (n=7)	2.79±0.90	3.36±1.35
Moderate / Severe (n=6)	2.45±0.83*	3.75±1.67

Caption: MVIC values for TA and VL muscles for the neuropathy grouping classes and control individuals (*Represents the statistically different).

References: [1] Farina et al., J Neurosci Methods, 134:199-208, 2004.

Disclosure of Interest: None Declared

Neurological and Motor Control

AS-0382

SEX-RELATED DIFFERENCES IN DORSIFLEXOR RATE OF TORQUE DEVELOPMENT

J Greig Inglis [1,*] Justin Parro [1] David A Gabriel [1]

[1]Kinesiology, Brock University, St Catharines, Canada

Introduction and Objectives: Sex-related differences in the maximal rate of torque development during isometric elbow flexion persist, even after normalization with a maximal voluntary contraction (MVC). In contrast, Hannah and colleagues (2012) demonstrated that normalization with respect to MVC eliminated sex differences during maximal isometric knee extension. The purpose of this study was to determine if the findings of Hannah and colleagues (2012) extend to maximal isometric contractions of the dorsiflexors. The dorsiflexors were chosen because of their importance in ankle joint stability, balance, and the risk of falling with age (Schultz et al., 1997).

Methods: Forty-eight participants (24 males and 24 females) completed three maximal isometric contractions of the dorsiflexors. The contractions were five seconds in duration with three minutes of rest between each trial. Dorsiflexion torque and surface electromyographic (sEMG) activity of the tibialis anterior were recorded concurrently. The criterion measures were: maximal torque, maximum rate of torque development, electromechanical delay (EMD), root-mean square amplitude (RMS) during maximum torque, and the rate of increase in sEMG during the first 30 ms of activity (Q_{30}).

Results: All measures were highly stable across trials and participants were very consistent at reproducing their own scores, resulting in intraclass reliability coefficients ranging from R=0.68 to R=0.99. There were no significant differences between males and females with respect to EMD (p=0.30), Q_{30} (p=0.20) or sEMG RMS amplitude (p=0.67). However, there were significant sex-related differences with respect to maximum torque (p<0.0001) and the maximum rate of torque development (p=0.00015). An analysis of covariance using maximum torque eliminated significant differences with respect to the maximum rate of torque development (p=0.39).

Figure:
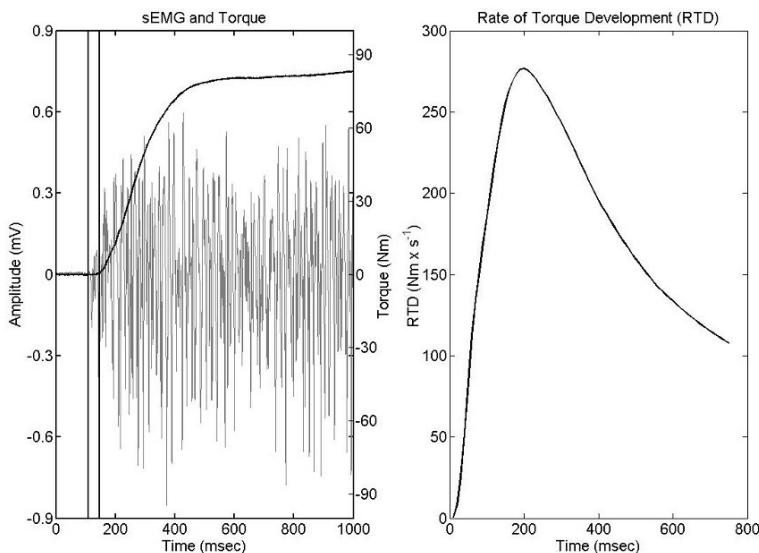
Caption: Left panel: represents the first 1000 milliseconds of a MVC. Torque (black line) onset is identified with the first vertical line, and TA sEMG activity onset (grey line) is identified by the second vertical line. Right panel: the associated dτ/dtmax of the same MVC.

Conclusion: The similarity in sEMG between males and females despite significant sex-related differences in maximal torque is consistent with our previous study (Lenhardt et al., 2009). The results support the findings of Hannah and colleagues (2012) who showed that differences between males and females with respect to the maximal rate of torque development are related to maximal torque. The sEMG results reinforce the fact that neural factors were not involved in sex differences in the maximal rate of torque development of the lower limb, which runs counter to previous observations for the upper limb (Inglis et al., 2013). Sex-related differences in the maximal rate of torque development in the dorsiflexors were related to simple differences in maximum torque, in the absence of any neural factors as assessed by sEMG activity. Understanding that sex differences in the maximal rate of torque development in the dorsiflexors is primarily determined by maximal torque suggests that standard resistive exercises may be sufficient for maintaining the ability to respond to perturbations that could lead to falls. Subsequently, more sophisticated sensorimotor training may be unnecessary.

References: [1] Hannah et al., Exp. Physiol. 97: 618-29, 2012.

[2] Inglis et al., J. Electromyogr. Kinesiol., 23: 1289-94, 2013.

[3] Lenhardt et al., Electromyogr. Clin. Neurophysiol., 49: 227-234, 2009.

[4] Schultz et al., Muscle Nerve, Suppl 5, 1997.

Disclosure of Interest: None Declared

AS-0383

HYPOTHESIS AND VERIFICATION ON COM DRIVEN CONTROL DYNAMICS DURING GAIT IN CHILDREN.

Maria Cristina Bisi [1,*]Rita Stagni [1]

[1]DEI - Department of Electrical, Electronic and Information Engineering "Guglielmo Marconi", University of Bologna, Cesena, Italy

Introduction and Objectives: The understanding of how the central nervous system (CNS) controls the numerous degrees of freedom in order to perform a specific motor task is still an open question. Recent approaches suggest that the CNS usually chooses among the infinite solutions available by optimizing a certain cost function, but sometimes uses sub-optimal choices still in full respect of the physiological constraints [1]. A recent work hypothesized that the stabilization of the centre of mass (CoM) trajectory could be a leading factor during gait in healthy and stroke patients [2]. Moreover, a recent study [3] showed that newly walking toddlers manifested characteristics of the pendulum mechanism already after one month of walking experience, even if showing strategies and patterns far from the adult-like gait. These results suggest that the control of CoM trajectory could be one of the driving factors allowing the CNS to choose among the infinite available solutions, even when not choosing the optimal one. Verifying this hypothesis on adult subjects is difficult because their gait is highly structured and repeatable, indicating that an optimal choice has been found; on the other hand, toddlers are still too variable, unstable [4] and far from showing an adult like gait. Gait maturation continues until age 6 [5]: the gait of 6-year old children can be considered stable from the motor control point of view, as they do not fall during level walking and show a good grade of coordination, but they still show higher segmental kinematic variability than adults [6]. The described aspects can facilitate the evaluation of the CoM driven CNS control dynamics. The hypothesis of the present work is that the trajectory of the CoM is a leading factor of the CNS gait control dynamics, allowing 6-year old children to reach a steady state point in gait development, despite the shown variability: if this is true, the variability of CoM kinematic should be lower than that of other kinematic variables.

Methods: 4 children [5.7±0.5y, 116±5cm, 21±3kg] and 7 young adults [22±1y, 161±6cm, 56±6kg] participated in the study. Participants were asked to walk along the gait analysis laboratory: each participant performed 15 walks, divided in groups of 5. Every 5-walk-test, participants were asked to perform some coordination exercise (e.g. standing on a foot) in order to obtain a 7 minute pause. 3D-Kinematic (SmartD, Bts, Italy) and inertial sensor data (Opal, Apdm, US) were collected during the tests (sampling frequency respectively of 200Hz and 128Hz). 18 reflective markers were positioned on anatomical landmarks according to Plug in Gait protocol. A single triaxial inertial sensor was positioned on the lower trunk approximately at approximately CoM level. For each walking test, joint angles, CoM trajectory and CoM acceleration were obtained. In order to evaluate intra-test and inter-test variability, the relative standard deviation (std%) of each estimated variable was calculated between the 5 walks of each test and among the 3 repetition of the 5-walk-test.

Results: Joint angles results showed higher variability in children than in adults both for the intra-test and the inter-test conditions: in particular children hip flexion/extension and intra/extra rotation, and ankle flexion/extension angles showed std% 6 times (or more) greater than adults' ones. CoM trajectory in the inter-test condition showed similar std% results for the two groups, while, in the intra-test, mediolateral std% was higher in the children group (5 times). In both intra-test and

inter-test conditions, children CoM acceleration showed std% similar to adults' for the antero-posterior and the vertical axis, while higher on the mediolateral axis.

Conclusion: The results of the present study supports the hypothesis that the trajectory of the CoM is a leading factor of the CNS gait control dynamics: children showed lower variability in the CoM kinematics (trajectory and acceleration) than in joint angles. Based on present results, it could be argued that, during gait, the CNS control is focused on the progression of the CoM and not on its lateral stabilization: children variability on the mediolateral axis was always higher than adults' one. In order to further verify and validate this hypothesis, an uncontrolled manifold approach can be applied [2]. Understanding control dynamics during walking is of fundamental importance both for improving basic knowledge and for enhancing rehabilitation techniques in neurologic and/or elderly patients.

References: [1] Martelli S, et al,. J Biomech 44:1716–21, 2011.

[2] Papi E, et al,. J Biomech 2014 in press

[3] Bisi MC, et al,. Gait Posture 2015 in press

[4] Bisi MC, et al,. J Neuroengineering Rehabil 11:131, 2014.

[5] Perry J, Burnifield JM, Gait Analysis, Slack Incorporated, 2010

[6] Stern KA, Gottschall JS. Pediatr Phys Ther. 24(3):285-90, 2012.

Disclosure of Interest: None Declared

AS-0384

COMPARISON OF THE ACTIVITIES MEASURED AT THREE ELECTRODE LOCATIONS ON EQUINE GLUTEUS MEDIUS MUSCLE IN WALK AND TROT

Rebeka Zsoldos [1,*]Anna Vögele [2]Björn Krüger [2]Ulrike Schröder [3]Theresia Licka [3]

[1]Department of Sustainable Agricultural Systems, University of Natural Resources and Life Sciences Vienna, Vienna, Austria, [2]Institute of Computer Science II, University of Bonn, Bonn, Germany, [3]Department for Small Animals and Horses, University of Veterinary Medicine Vienna, Vienna, Austria

Introduction and Objectives: The equine gluteus medius muscle (GMM) is the largest unsegmented muscle of the horse; its main function is to extend the hip and retract and abduct the limb. The muscle provides the visible shape of the croup, and due to its location directly under the skin, it is an ideal candidate for detecting intramuscular activation differences with surface EMG (sEMG). If present, these differences may elucidate how the anatomical and temporal distribution of activation contributes to the efficiency of muscle use. Therefore, the aim of this study is to describe the sEMG muscle activation pattern of three selected locations of the GMM during walk and trot.

Methods: Measurements were obtained in six horses without lameness, walking and trotting on a treadmill. Three electrodes were placed over the left and right GMM at the midpoint between origin and insertion about 5cm apart on the medial (GM1), middle (GM2), and lateral (GM3) part of the GMM. The resulting EMG signal was rectified and the sampling rate was reduced to 120 Hz. Butterworth low-pass filter was applied (fourth order; cut-off frequency, 20 Hz) and integrated EMG (iEMG) was calculated for each motion cycle. Only the right side results were used for this study. For each horse a minimum of 7 motion cycles at walk and a minimum of 13 motion cycles at trot was considered. Based on the vertical movement of the right hind hoof, the motion cycle was divided into the stance phase as well as the swing phase (Fig.1), and the ratio between the iEMG during those two phases was calculated by dividing the stance phase iEMG by the swing phase iEMG ("PhaseRatio"). The correlations of the values of the three electrode positions were calculated during each stance and swing phase for each horse; and for all horses correlations of the values at all three locations were also calculated.

Results: The stance phase iEMG ranged from 0.2 to 35 (mV%) in walk and from 0.1 to 41 (mV%) in trot. The swing phase iEMG ranged from 0.06 to 21(mV%) in walk and from 0.1 to 47(mV%). The cycle ratio values ranged from 0.13 to 6.77 in walk and from 0.09 to 7.53 in trot. As expected, of all correlations (100%) there were many significantly positive correlations (28%) between the three locations at walk and trot during both stance, and swing phase, as well as for the PhaseRatio. However, there were a number of significantly negative correlations (9%) between GM1 and GM2 for stance phase iEMG and between GM1 and GM3 for swing phase iEMG both in walk and trot.

For all horses in trot, there were significantly positive correlations between GM2 and GM3 for stance phase iEMG (r= 0.988, p<0.01), swing phase iEMG (r= 0.933, p=0.006), and cycle ratio values (r= 0.848, p=0.03); however, no correlation between GM1 values and the values of the other two locations was significant. For all horses, there were no significant correlations of the values obtained at the three locations in walk.

Figure:
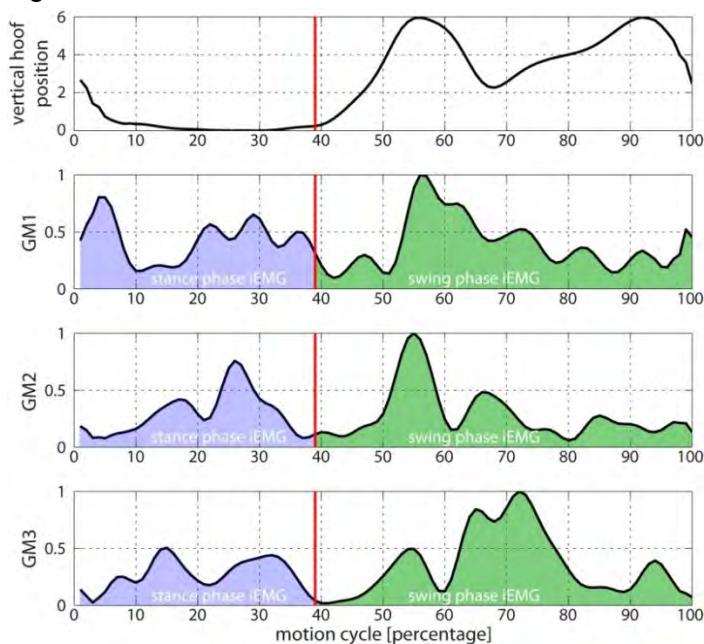
Caption: Figure 1. In Horse 1 the vertical movement of the hind hoof and iEMG of the medial (GM1), middle (GM2), and lateral (GM3) part of the gluteus medius muscle during one motion cycle (stance and swing phase) in trot.

Conclusion: In individual horses, there were both positive and negative correlations for sEMG parameters obtained at the three locations over the same muscle. This is surprising, as it indicates that the medial part of the muscle (GM1) is acting more independently than the middle and lateral parts (GM2 and GM3) and that potentially these muscle fibres act in a different way than was previously thought, but in a motion cycle related pattern. The reasons for the lack of concerted action of the medial part of the GMM may include a difference in the neuromuscular activation of the muscle fibres, as a single nerve fibre may activate a number of muscle fibres that are neither evenly distributed within the muscle, nor directly adjacent to each other. Also, the function of the GMM may be more highly differentiated than it is currently perceived to be, with the large areas of origin and insertion allowing for partially opposing functions present in a single very large muscle. Further investigations using array and needle EMG at selected locations of this large muscle are required to support these hypothetical considerations. The negative correlations observed between sEMG activities at different locations during the swing phase but not the stance phases of the GMM indicate a complex intramuscular distribution of workload. This may be due to specifics of innervation or even mechanical fascia effects; how this differential use of a single, albeit large, muscle is linked to avoidance of overexertion of muscle fibres and/or increased muscle efficiency is as yet unclear, but the prevalence of these negative correlations at trot, where more work is done by this hip extensor than at walk is pointing in this direction.

Disclosure of Interest: None Declared

Neurological and Motor Control

AS-0386

COMPLEXITY OF ISOMETRIC FORCE PRODUCTION IS ASSOCIATED WITH TIME TO ACHIEVE STEADY STATE WHEN MOVING TO A NEW FORCE LEVEL

Samantha L. Winter [1,*]Mark Burnley [1]Sarah Forrest [2]John Challis [3]

[1]School of Sport and Exercise Sciences, University of Kent, Chatham Maritime, [2]Sport and Exercise Science, Aberystwyth University, Aberystwyth, United Kingdom, [3]Department of Kinesiology, The Pennsylvania State University, State College, United States

Introduction and Objectives: Motor output and function has been shown to decline in later life, for example older adults have increased stimulus response times [1]; reduced strength [2] and changes in the variability of force production [2]. The loss of complexity hypothesis [3] suggests that a decrease in complexity is associated with ageing as the integration of complex physiological systems declines, and that this reduced complexity is associated with constrained behaviour and a loss of adaptability or flexibility in reponse. The function consequences of this loss of complexity in the fluctuations seen in isometric force records have not been investigated. However, it is possible that the reduced complexity, and more slowly repeating and constrained fluctuations in force seen in older adults [4] would limit ability to adapt to altered force requirements. It was hypothesised that reduced complexity for isometric force records in older adults would be associated with an increase in the time taken to achieve a steady state when moving to a new isometric force level.

Methods: Young (18 to 25 years) and older (65 to 72 years) neurologically healthy adults produced isometric abduction contractions of the index finger using the First Dorsal Interosseus. Participants established a steady state force at a given effort level (a percentage of maximum voluntary contraction force - %MVC) by matching a target displayed visually. A second feedback condition used both the visual display and an audible tone that varied in pitch when subjects moved below or above the target. The target was then suddenly and unpredictably increased or decreased at a randomly decided time point and participants were instructed to match this new target as quickly as they could, and to hold the new contraction intensity as steadily as possible (Figure 1). The conditions investigated were: increasing force from 5% to 25% MVC, 25% to 50% MVC, 25% to 75% MVC, and decreasing the force from 25% to 5% MVC, 50% to 75% MVC and 75% to 25% MVC. The functional reaction time was taken to be the point at which the force exceeded 3 standard deviations (SD) from the mean force in the direction of the new force level. The time to steady state was the time from the end of the functional reaction time to the start of the 3 second window with the lowest standard deviation for force. The complexity of the force record before the target change, after the target change, and during simple continuous force production with no target change was determined for the different effort levels (5%, 25%, 50%, 75% MVC) using Approximate Entropy (ApEn) [5].

Results: Confirming previous results older adults exhibited reduced complexity indicated by reduced ApEn values at effort levels >25% MVC (p<0.001) and this was the case for both the simple continuous force task (p<0.001) and the section of the force record after the change in target force (p=0.0438). There was no difference in the MVC abduction force for older and younger adults (p=0.885). There was also no difference between older and younger adults in the magnitude of the

fluctuations in force, as quantified by the standard deviation of force (p>0.05). Functional reaction time was increased by around a third in older adults (p<0.001) in both feedback conditions. Fuctional reaction time was reduced for both age groups by the addition of the audible signal. Confirming the hypothesis, the time to steady state after the function reaction time increased from a mean of 2.83s in younger adults to 3.23s for older adults (p=0.025), and this difference was unaffected by feedback condition. Post-hoc tests showed that the time to steady state differed for old and young adults at starting effort levels >5% MVC.

Figure:
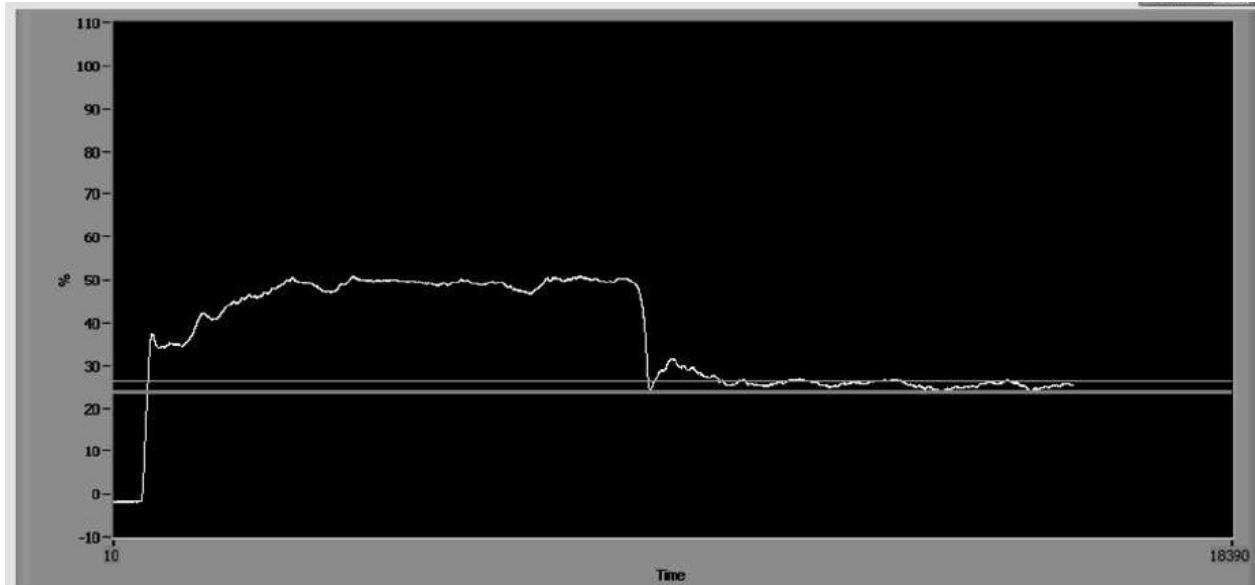
Caption: Figure 1: Display of force record showing a trial moving from an initial target of 50% MVC to a target of 25% MVC.

Conclusion: Force levels associated with reduced complexity in older adults compared to younger adults were associated with an increased time to steady state when moving from an isometric contraction at one effort level to an isometric contraction at a new effort level. This suggests that there is a change in the neuromuscular system with age evidenced by the reduced complexity that constrains response to altered force requirements. These findings have implications for the control of muscle force production in later life.

References: [1] Fozard et al., J. Gerontol., 49: P179-189, 1994.

[2] Marmon et al., Med. Sci. Sports Exerc., 43: 560-567, 2011.

[3] Lipsitz et al., J. Am. Med. Assoc., 267: 1806-1809, 1992.

[4] Vaillancourt et al., J. Appl. Physiol., 94: 903-912, 2003.

[5] Pincus, PNAS, 88: 2297-2301, 1991.

Disclosure of Interest: None Declared

AS-0387

ASSESSMENT OF AN INNOVATIVE COLLAR DESIGNED FOR PEOPLE AFFECTED BY NECK WEAKNESS

Silvia Pancani [1] [2],*Christopher J McDermott [3]Jennifer Rowson [1] [2]Wendy B Tindale [2] [4]Claudia Mazzá [1] [2]

[1]Department of Mechanical Engineering , [2]INSIGNEO Institute for in silico medicine, [3]Sheffield Institute for Translational Neuroscience, University of Sheffield, [4]NIHR D4D Healthcare Technology Co-Operative, Sheffield, United Kingdom

Introduction and Objectives: Inertial sensors are a valid tool to assess the neck range of movements [1,2]. In this study we translated methods previously used in other contexts to the assessment of a collar (Sheffield Support Snood, © Device for Dignity Healthcare Technology Co-operative) specifically designed for people affected by neck weakness caused by diseases such as motor neuron disease. Commercially available collars are designed to immobilize the neck and as such are uncomfortable and strenuous to wear for long time. The Sheffield Support Snood (SSS), developed to overcome these limits, is characterized by a less bulky structure and is adjustable with ad hoc supports according to the disease development. The aim of this study is to define a protocol for the clinical assessment of neck collars and use it to compare the performance of the SSS to those of other commonly used commercial neck collars.

Methods: Twelve healthy subjects (age 26±2) participated in the study. Inertial magneto units (IMUs) were chosen as part of the design of a protocol suitable for future clinical applications. Two IMUs (OPAL, APDM) were located on the forehead and sternum of each subject. The protocol included a series of active head movements (AHM, flexion/extension, axial rotation and lateral bending), performed first reaching the maximum amplitude and then at maximum speed.

The SSS performance was compared to two other commonly used collars, i.e. the Vista (Aspen Medical Products) and the Headmaster (Symmetric Designs, Figure 1). The SSS was tested in a stiffer (six supports: two frontal, two lateral and two posterior) and a less stiff (one A-shape frontal support) configuration. The protocol was repeated by each subject in random order wearing each collar and without any collar to have a reference measure. The sensors orientation was estimated using a functional calibration approach [2] and a quaternion-based algorithm that integrates the angular velocity [3]. The drift associated to the estimate of the orientation by integrating the gyroscope data, was corrected using a spherical interpolation [4]. The differences between AHM performed with or without collars were quantified using the maximum range of motion (ROM). Statistical analysis was performed using a one-way repeated measure ANOVA with a post-hoc Tuckey analysis.

Results: Table 1 shows the ROM obtained for the different collars. In the AHM the ROM measured with the SSS with a frontal support was significantly reduced with respect to the trials without collar only in flexion and axial rotation, showing that the support under the chin supported the neck during the flexion without affecting a subject's capability to perform extension or lateral bendings. This was confirmed in the axial rotation, where there were no significant differences between the task performed with the SSS with one and six supports: the addition of four supports to sustain the neck during extension or lateral bending doesn't affect a subject's capability to perform an axial rotation. The ROMs measured with the SSS in its stiffer configuration and the Vista were significantly lower than those observed without the collar in all tasks, but no significant differences were observed between them, suggesting that the six-supports SSS is comparable to the Vista.

Figure:
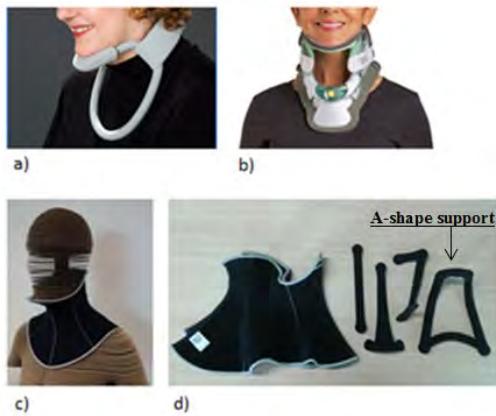
Figure 1 a) Headmaster Collar b) Vista Collar c) Sheffield Support Snood d) Sheffield Support Snood with supports.

Conclusion: The adopted protocol, which is easily translatable in a clinical context, is suitable for the assessment of neck collars. It allowed to detect significant differences in the neck motions when performed with and without collars and was highly informative in characterizing different collar performances. The SSS in its stiffer configuration was comparable to the Vista in terms of ability to support the neck and its structure appeared to be effectively adaptable to a subject specific need.

Table:

		No collar	Headmaster	SSS with one support	SSS with six supports	Vista
Extension ROM (deg)	Max Amplitude	54 (13)	50 (12)	43 (7)	35 (10)*	35 (7)*
	Max Speed	80 (12)	70 (13)	67 (11)	60 (18)*	61 (15)*
Flexion ROM (deg)	Max Amplitude	52 (9)	28 (13)*	36 (13)*	36 (12)*	27 (10)*
	Max Speed	52 (11)	30 (14)	40 (13)	37 (12)	32 (11)
Axial Rotation ROM (deg)	Max Amplitude	145 (12)	116 (21)	101 (30)*	96 (33)*	77 (30)*
	Max Speed	143 (15)	117 (23)	105 (35)*	105 (32)*	81 (29)*
Lateral Bending ROM (deg)	Max Amplitude	80 (12)	70 (13)	67 (11)	60 (18)*	61 (15)*
	Max Speed	82 (14)	72 (13)	71 (15)	63 (18)*	62 (16)*

Caption: Active head movements, maximum amplitude and speed. Mean (standard deviation) values for the ROM with collars and no collar. (*) Significantly different ($p<0.05$) from "no collar"

References: [1] Theobald et al., Man Ther., 17: 92–6, 2012.

[2] Duc et al., Med Eng Phys., 36:49-56, 2014.

[3] Favre et al., Electron Lett., 42: 612-4, 2006.

[4] Sabatini, Electron Lett., 40: 584-6, 2004.

Disclosure of Interest: None Declared

Medical Devices

AS-0388

ASSESSMENT OF ANTEROPOSTERIOR (AP) KNEE JOINT LAXITY USING NON-INVASIVE NAVIGATION IN HEALTHY VOLUNTEERS

Roberto J. Alho [1 2,*]Fraser Henderson [1]Philip Rowe [2]Jon Clarke [1 2]Frederic Picard [1 2]

[1]Orthopaedics, Golden Jubilee National Hospital, [2]Biomedical Engineering, Strathclyde University, Glasgow, United Kingdom

Introduction and Objectives: The knee joint displays a wide spectrum of laxity, from inherently tight to excessively lax even within the normal, uninjured population [1, 2]. The amount of anteroposterior (AP) laxity is dependent on the amount of force applied as well as knee positioning [2]. The assessment of AP laxity in the clinical setting is performed by manual passive tests such as the Lachman and pivot shift tests which are highly specific in the diagnosis of cruciate ligament injuries [1]. The Lachman test is usually performed at 30º of knee flexion in a clinical setting.

Non-invasive assessment based on image free navigation has been clinically validated and used to quantify mechanical alignment and coronal knee laxity in early flexion [3]. The software was further developed to allow the measure of AP laxity. When used on cadavers the software demonstrated good AP laxity results with flexion up to 40° [4].

If this technology was validated throughout flexion in live subjects, it could aid clinicians in identifying and quantifying ligamentous injuries and the planning and follow-up of total knee arthroplasty (TKA) patients in a clinical setting.

This study aimed to validate the repeatability of the assessment of anteroposterior (AP) knee joint laxity using this non-invasive system in normal, healthy subjects.

Methods: Twenty-five healthy volunteers were recruited and examined with ethical approval from the University of Strathclyde. The non-invasive system, consisting of an infrared camera, externally mounted optical trackers and computer software was used to evaluate each volunteer (Figure 1). Each of the volunteers had both legs examined by a single examiner performing two registrations. The registration included initial identification of key bony landmarks and manipulations of the volunteer's leg to achieve a virtual model of the lower limb. From this registration the supine mechanical femoral-tibial alignment (MFTA) was determined and assessment of AP laxity through flexion using the Lachman test was carried out.

Validation of the assessment of AP knee joint laxity was assessed through intra-examiner repeatability using Coefficients of Repeatability(CR) calculated with Microsoft Excel and Interclass Correlation Coefficients (ICC) using SPSS software [5]. The acceptable limits of agreement for this project were set at 3mm for anteroposterior tibial translation.

Results: Outliers were identified in the first 10 volunteers, therefore only the last 15 volunteers (30 knees) were analysed for repeatability.

The non-invasive system demonstrated consistent and comparable supine MFTA acquisition in extension consistently within the pre-validated +/-1º coronal alignment [8, 10], with a CR of 1.6° and good reliability (ICC 0.81).

The most reliable and repeatable AP laxity assessments were at 30º and 45º with both these assessments demonstrating good reliability (ICC 0.82, 0.82) and good repeatability (CR 2.5, 2.9). AP laxity at 60º demonstrated good reliability (ICC

0.79) with acceptable repeatability (CR 3.3mm). The AP laxity assessment at 0º, 15º, 75º and 90º demonstrated moderate reliability (ICC ≤ 0.75), and poor repeatability (CR ≥3.0mm) as shown in Table 1.
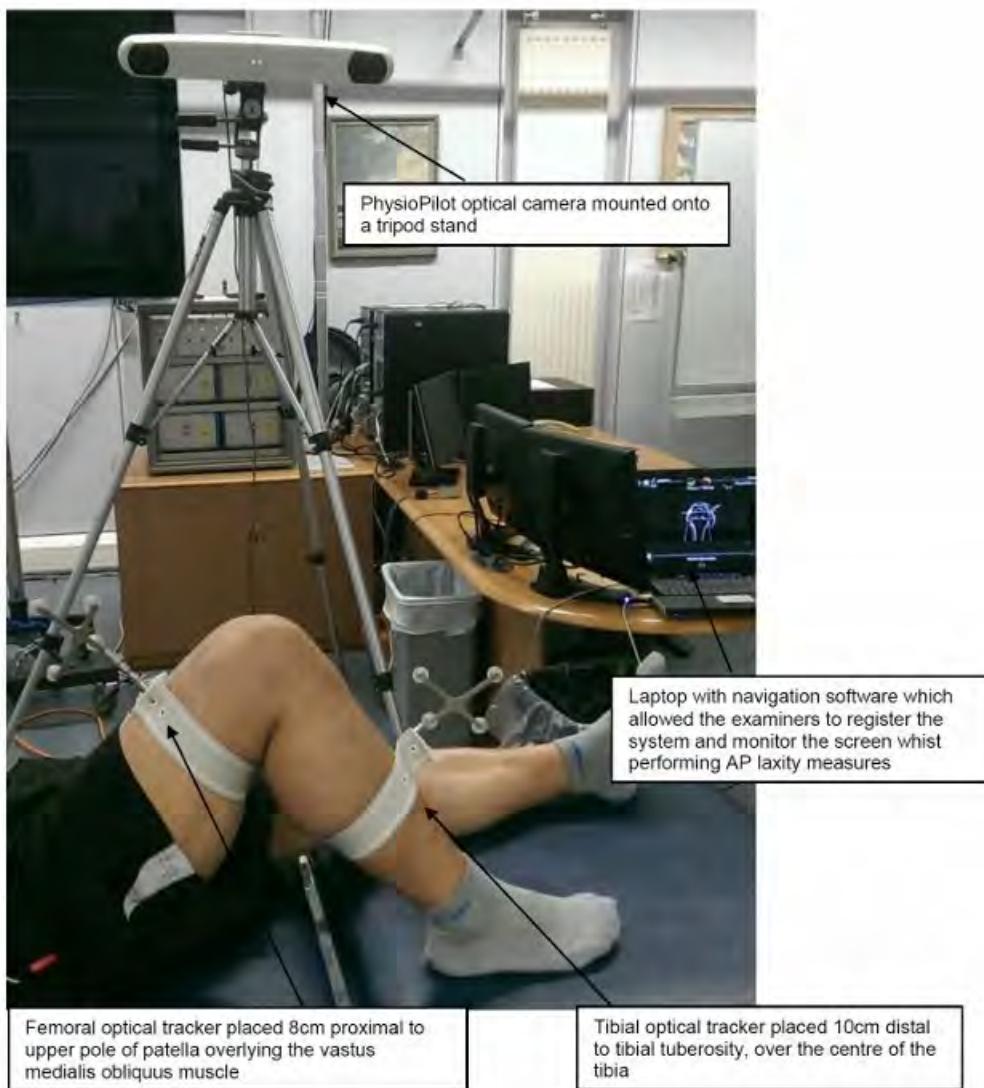
Figure:

Figure 1 An example of the set-up of each volunteer assessment; with the volunteer relaxed whilst lying supine in short trousers. Passive optical trackers mounted on the femur and tibia using fabric straps to secure the base plate holding the optical tracker in place, with the laptop visible for the examiner to perform volunteer testing.

Caption: Figure 1

Conclusion: The non-invasive system was able to reliably and consistently measures knee AP laxity between 30° and 45° flexion, which is the clinically relevant range for this assessment. This system could therefore be used to quantify abnormal knee laxity and improve the assessment of instability in the knee in a clinical setting.

Poor AP laxity results outside the limits of agreement were achieved at 0º, 15º, 75º and 90º, possibly due to difficulties in hand placement and lack of standardisation in the force used during the Lachman examination in early and late flexion. The software has been previously validated to 40º of flexion in cadavers, but due to no standardised force in AP laxity assessment in this study, the software cannot be validated throughout the whole range of flexion in living subjects.

The initial 10 outlier results seemed to indicate a learning curve, with the initial assessments showing much wider variation.

Table:

Assessment	Degrees	Coefficients of Repeatability (CR)*	Interclass Correlation Coefficients (ICC)**
Supine MFTA in extension (º)	0º	1.6	0.81
AP laxity (mm)	0º	3.7	0.70
	15º	4.8	0.72
	30º	2.5	0.82
	45º	2.9	0.82
	60º	3.3	0.79
	75º	4.6	0.76
	90º	5.6	0.73

*A CR of under 3mm for AP translation demonstrates good repeatability.

**An ICC of ≥0.9 demonstrates excellent reliability, an ICC between 0.75 and 0.9 demonstrates good reliability, and an ICC ≤ 0.75 indicates moderate to poor reliability [5].

Caption: Table 1: Summary CR and ICC results for AP laxity assessment

References: [1] JC Kupper et al., Clin Biomechs, 22: 1–13, 2007.

[2] M Cross., Sports Med Arthrosc, 4: 313–318, 1996.

[3] Clarke. The non-invasive measurement of knee kinematics in normal, osteoarthritic and prosthetic knees, Strathclyde University Press, 2012.

[4] DF Russell et al. Bone Joint Res, 2(11): 233–237, 2013.

[5] JM Bland et al., Lancet, (i): 307-310, 1986.

Disclosure of Interest: None Declared

AS-0389

A DESIGN PROCESS OF AN ARTICULAR JOINT PROSTHESIS

Michel Mesnard [1,*]Antonio Ramos [2]

[1]Institut de Mécanique et d'Ingénierie , Université de Bordeaux, Talence, France, [2]Departamento de Engenharia Mecânica, Universidade de Aveiro, Aveiro, Portugal

Introduction and Objectives: When designing a medical device (MD), the primary objective is to improve the patient's conditions. Therefore, there must be a strong focus on continuous interaction with the human elements. The procedure that has been devised to the search for concepts and the validation of an innovative temporomandibular joint (TMJ) prosthesis point out the roles and relationships between the definition of needs, the biomechanical characterization studies, modeling, mechanical and clinical validations (Fig.1).

Methods: When applying principles of mechanics and mechanical engineering to solve health-related problems by designing MDs there are some very specific requirements (interaction with human factors, implantability…) and technical solutions are specific to the field [1].

Before the design phase, the biomechanical systems have to be described. This provides the specifications, defines the functions and criteria and quantifies acceptance levels. Quantifying these characteristics, requires some very specific metrology techniques to determine the articular displacements and actions. TMJ articular displacements were described and quantified by stereo photogrammetry while muscle efforts were evaluated by electromyography and magnetic resonance imaging. The protocol was subjected to a repeatability study [2] [3].

For a healthy volunteer, three to five readings were always taken in order to evaluate the influence of changes in behavior and establish significant values. Then, for a representative sample (32 volunteers) of the population, the values followed normal distributions and the intra- and inter-individual variability of the characteristics could be described.

To complement these techniques, which can be too invasive, modeling was used. The finite element models (FEM) of the joint and jaw that were created and validated determined stresses and strains on the surface of the bone. The previous characterization study produced the input data to choose the muscular actions and the boundary conditions [4].

The search for concepts was based on functional analysis and these models of the TMJ. By building FEMs, simulations can be repeated, innovative concepts can be validated and technological solutions optimised. The models allow to predict the performance of implants and to compare behaviors of the healthy and implanted structures. Then the influence of geometry, the links between implant and bone tissues could be considered to guide the decisions when creating new technical solutions.

Results: The intra- and inter-individual variability of the characteristics may result from a range of causes: temporal, pathological, behavioral… Inter-individual variability is linked only to anatomical-physiological factors such as geometry, local distribution of tissues… Elaborating concepts, the aim cannot be to control these variations and then, the limited use in addition to difficulties in producing a custom-made prosthesis guide the designer to manage and integrate anatomical variations.

Figure:
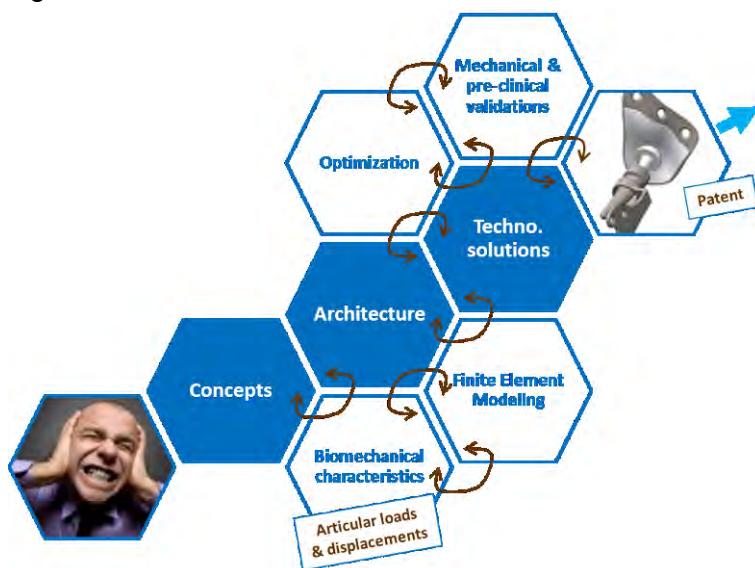
Caption: Fig.1: Design process, from needs to patent.

Conclusion: Using a modular design approach, the innovative prosthesis for the TMJ (Patent M.Mesnard & A.Ramos) presented here provides the surgeon with a range of five modules. The additive manufacturing has already been used successfully to produce finished parts in industries such as aerospace, dentistry... It will eventually be possible to produce the temporal prosthesis component that is tailor-made [5] [6].

References: [1] A. Moreau-Gaudry et al., 2010, Développement d'une innovation technologique en santé : Le cycle Concept-Recherche-Essais-Produit-Soins, IRBM, 31 (1), p.12-21.

[2] JC. Coutant et al., 2008, Discrimination of objective kinematic characters in temporomandibular joint displacements, AOB, 53 (5), p.453-461.

[3] M. Mesnard et al., 2012, Relationships between geometry and kinematic characteristics in the temporomandibular joint, CMBBE, 15 (4), p.393-400.

[4] A. Ramos et al., 2011, Straight, semi-anatomic and anatomic TMJ implants: The influence of condylar geometry and bone fixation screws, JCMS, 39(5), p.343-350.

[5] J. Ramsden et al., 2007, The Design and Manufacture of Biomedical Surfaces, CIRP Annals, 56 (2), p.687–711

[6] P. Bartolo et al., 2012, Biomedical production of implants by additive electro-chemical and physical processes, CIRP Annals, 61-2, p.635-655.

Disclosure of Interest: None Declared

Medical Devices

AS-0390

AN EXPERIMENTAL STUDY OF MECHANICAL BEHAVIOR OF POLY (LACTIC ACID) FOR STENT APPLICATION

Tianyang Qiu [1,*]Rebecca Elliott [1]Alessandro Schiavone [1]Liguo Zhao [1]Mo Song [2]

[1]Wolfson school of mechanical and manufacturing engineering, [2]Department of materials, Loughborough University, Leicestershire, United Kingdom

Introduction and Objectives: Bio-resorbable polymeric stents are developed to open plaque-blocked arteries and then disappear within specific time period, which reduces the occurrence of thrombosis, in-stent restenosis and inflammation that may happen with the deployment of metallic stents[1]. The objective of this paper is to study the mechanical behavior of poly (lactic acid) (PLA), currently used for manufacturing commercial bio-resorbable stents, through processing and testing, with a focus on creep, stress relaxation and cyclic deformation behavior.

Methods: Standard dog-bone specimens were produced by compression molding, and then used to conduct series of tests in the tensile regime. Uniaxial tensile tests were performed at a range of strain rate (0.0001 ~1) to obtain the essential material behavior. Creep tests were conducted at two constant stresses (30 and 40MPa), and stress-relaxation tests were carried out under three constant strains (1%, 1.5% and 2%) for 200 minutes. Cyclic tests were performed to understand the deformation behavior under cyclic loading. For load-controlled tests, three stress ratios (0, 0.2 and 0.5) were considered while maintaining the maximum stress level at 40 and 50MPa, respectively. For strain-controlled tests, two strain ratios (0.2 and 0.5) were considered while maintaining the maximum strain level at 2% and 3%, respectively. In addition, a multiple-step cyclic test (see Table 1) was carried out by increasing the peak strain level at each cycle while maintaining the minimum stress level at 0.1MPa.

Results: The tensile results showed that the strain rate has an effect on the stress-strain behavior of PLA, demonstrating the time-dependent deformation nature of the material. An increase of strain rate led to enhanced stress response. The creep curve under 40MPa stress showed all three stages of creep deformation (primary, secondary and tertiary), but the specimen fractured after only 3 hours of loading. The stress relaxation curves showed a rapid stress reduction at the early stage, followed by a gradual stress loss stage and the final saturation stage. Under load-controlled conditions, the cyclic stress-strain loops showed the strain ratcheting behavior, resulting in the accumulation of strain with the number of cycles. Load ratio had an effect on strain ratcheting. Under strain-controlled condition, the stress-strain loops indicated a decrease of peak stress with the number of cycle due to stress relaxation. The multiple-step cyclic test results showed the capacity of plastic deformation at variable strain ranges, which is very limited (see Figure 1) when compared to metallic stent materials.

Figure:
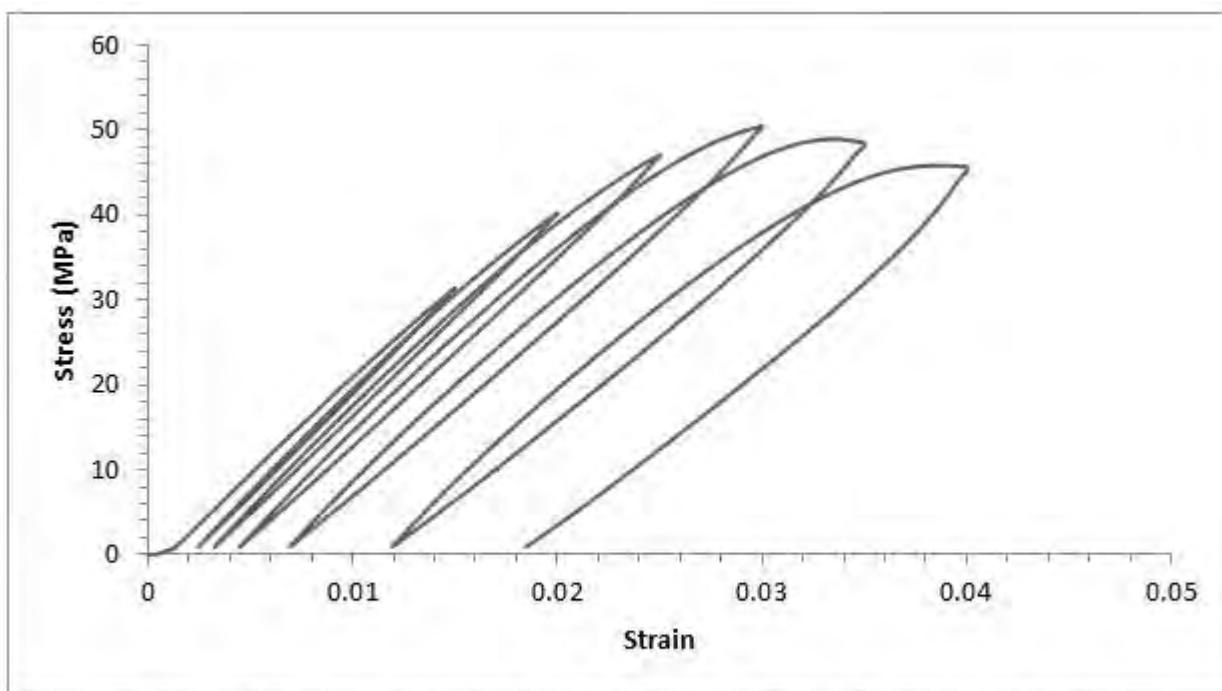
Figure 1, Stress-strain loops of PLA under multiple-step cyclic load with increasing maximum strain for each cycle (strain rate: 0.0001/s).

Conclusion: In conclusion, PLA is a brittle material that lacks significant plastic deformation behavior for stent application, as evidenced from various mechanical testing results including tensile, creep, stress-relaxation and cyclic tests. Further development of P(L)LA, through novel material processing, testing and even modelling, is required in order to improve the ductility of the material for successful stent applications.

Table:

Number of cycle	1	2	3	4	5	6
Peak strain in each cycle	1.5%	2%	2.5%	3%	3.5%	4%

Caption: Table 1, Matrix for multiple-step cyclic tests (strain rate = 0.1%/s & minimum stress = 1MPa).

References: [1] Serruys et al., J. European Heart, 33.1: 16-25, 2012.

Disclosure of Interest: None Declared

BIOMECHANICAL FUNCTION OF A PREGNANCY COMPRESSION BELT. THREE-DIMENSIONAL HIP JOINT KINEMATICS: A CASE STUDY

Merilyn Lock [1] Michael Cole [2] Paul Grimshaw [3,*] Loisa Sessman [4] Malin Tapper [5]

[1] School of Medical Sciences, University of Adelaide , Adelaide , [2] School of Exercise Sciences, Australian Catholic University , Brisbane , [3] School of Mechanical Engineering , University of Adelaide , Adelaide , Australia, [4] School of Business and Engineering, Halmstad University , [5] Physiotherapy , Halmstad , Sweden

Introduction and Objectives: Pregnancy-related pelvic girdle pain (PPGP) and low back pain (LBP) are common problems and can result in functional impairment for those who are affected. The prevalence of PPGP and LBP has been reported at around 45% during pregnancy and 25% after pregnancy (Wu et al., 2004). Although the exact causes of PPGP and LBP are not clear, they are thought to be multifactorial including biomechanical factors affecting the sacroiliac joints (SIJs) and the pubic symphysis (Kanakaris et al., 2011; Vermani et al., 2010). A review by Aldabe et al. (2012) found an association between PPGP and altered motor control and pelvic mobility in six out of seven high quality case-controlled studies. Stability of the pelvic joints is maintained by muscular forces acting perpendicular to their longitudinal axis (Arumugam et al., 2012). Pelvic compression belts (PCBs) are thought to augment this effect through application of external compression. Electromyographical studies have shown that PCBs alter neuromuscular control of hip and pelvic muscles during unilateral stance in subjects with SIJ pain (Jung et al., 2013). Recent studies evaluating the effects of PCBs in pregnant women have shown improvements in impaired balance and falls risk scores (Cakmak et al., 2014). Additionally, finite element modelling has shown altered SIJ movement and an associated decrease in strain in sacrospinous and sacrotuberous ligaments with the use of a PCB (Sichting et al., 2014). Clarification regarding the general effects of PCBs on hip and pelvis mechanics is necessary to understand their effectiveness. A review by Arumugam et al. (2012) indicated a need for in-vivo analysis of SIJ kinematics with the use of PCBs. As such, the objective of this study was to assess three-dimensional (3D) hip biomechanics in a healthy female subject during a series of movements with and without a PCB.

Methods: A 10-camera 3D optoelectronic analysis system (Vicon, Oxford, UK; 150 Hz) was used to assess the movement patterns of one healthy female subject with and without the use of a newly developed PCB (patent pending). A series of five trials (n=5 trials) for four everyday activities (walk, step, sit to stand and unilateral lift with 10% of body weight) were examined using 16 anatomical joint markers that were positioned in accordance with the Plug-in Gait model. The belt was placed covering the SIJs bilaterally. Perceived level of compression was measured using a modified Borg CR10 visual analogue scale to elicit a score of 6-7. Raw data was low-pass filtered at 10 Hz using a 4th order Butterworth routine. Three-dimensional (x, y and z) displacement, velocity and acceleration for the left and right hip joints were compared for all trials between the two conditions. During this study, it was assumed that changes in pelvic joint kinematics should result in an associated change in hip joint kinematics.

Results: See Table 1

Conclusion: Remarkable similarity was seen in the x, y and z joint position traces between the 'with belt' and 'no belt' conditions. Average vertical displacement (not shown in Table 1) in the 'with belt' condition was slightly larger during the sit to stand and walk, and smaller during the step and lift. There is insufficient data to draw any conclusions whether any differences may be a result of altered sacroiliac kinematics. The limitations of this study include the use of only one, non-pregnant subject with no history of PPGP or instability. Nevertheless, the results of this study are important as the lack of difference between these conditions may suggest that this type of testing is not sensitive enough to detect changes in pelvic joint kinematics due to the effects of a PCB. Alternatively, the effects of PCBs that have been found in previous studies may be due to neuromuscular changes, biofeedback or reasons other than changes in joint kinematics.

Future research may include controlled studies looking at hip and pelvis biomechanics of female subjects with and without PPGP during bilateral and unilateral movements.

Table:

Test/Condition	Walk	Step Left Foot First	Lift With Left Hand	Sit-to-Stand
No Belt				
Max	900.56	1123.38	902.58	898.66
Min	851.72	885.75	632.28	692.27
Mean	876.12	991.30	813.82	785.73
SD	13.54	100.85	96.81	93.47
With Belt				
Max	913.88	1139.23	916.06	914.74
Min	849.55	909.06	667.30	700.19
Mean	887.21	1001.01	835.68	795.62
SD	15.55	100.87	93.92	93.09

Caption: Table 1: Left hip vertical position (mm from zero (ground)) in the four tests, mean (n=5 trials), SD = standard deviation.

References: [1] Aldabe et al., European Spine Journal, 21: 1777-1787, 2012.

[2] Arumugam et al., Manual therapy, 17: 275-284, 2012.

[3] Cakmak et al., PM&R, 2014.

[4] Jung et al., Manual Therapy, 18: 143-148, 2013.

[5] Kanakaris et al., BMC medicine, 9: 15, 2011.

[6] Sichting et al., Pain Physician, 17: 43-51, 2014.

[7] Vermani et al., Pain Practice, 10: 60-71, 2010.

[8] Wu et al., European Spine Journal, 13: 575-589, 2004.

Disclosure of Interest: None Declared

Connective Tissue

AS-0392

DEFORMATION PATTERNS OF CRACKED ARTICULAR CARTILAGE UNDER COMPRESSION

Yasir Al-Saffar [1 2,*]Belinda Pingguan-Murphy [1]Walter Herzog [2]

[1]Biomedical Engineering, University of Malaya, Kuala Lumpur, Malaysia, [2]Human Performance Lab, University of Calgary, Calgary, Canada

Introduction and Objectives: Osteoarthritis (OA) is a common joint disease that is characterized by progressive degeneration of cartilage [1]. Among the earliest characteristics of OA is the presence of micro-fractures on the cartilage surface [2]. These micro-fractures are thought to affect the tissue mechanical properties and chondrocytes' mechanical environment [3]. While some research has started looking at possible causes of cracks in cartilage, the mechanical behaviour of cracked cartilage has not been investigated. This study aims to determine the effects of cracks on the mechanical behaviour of cartilage and its deformation pattern.

Methods: *Experimental design:*

Split line patterns of tibial articular cartilage of New Zealand white rabbits were identified using India-ink. A compression test of the cartilage at a constant rate of displacement was used to compare the mechanical properties between intact cartilage and cartilage with a defined crack. Using a custom designed 0.75 mm wide blade, a consistent full thickness crack was produced perpendicular to the cartilage surface and oriented perpendicular to the split line patterns in an attempt to induce the highest possible amount of structural damage to the cartilage [2].

Sample preparation and loading protocol:

Rabbit knee joints were dissected. Soft tissue was carefully removed from tibiae to allow secure mounting of samples in dental cement. PBS was used at all times to keep samples from drying. Once the cement was set, samples were mounted on an MTS machine for 2 compression tests. The first compression test involved lowering an indenter (2 mm diameter) towards the sample surface at a speed of 4 µm/s until reaching a force of 6 +/-0.5 N (1.75-2 MPa) where it was held steady for 20 min to measure the stress relaxation behaviour of the cartilage sample. The indenter was then removed and the tissue was allowed to recover for one hour. For experimental group cartilages, a defined crack was made at the end of the 1 hr rest period by replacing the indenter with a cutting blade. A second compression, identical to the first, followed and stress relaxation measurements were performed.

Cartilage tissues were then fixed in the loaded state and prepared for histology. Mechanical and histological differences between intact and cracked samples were quantified.

Results: The split line patterns of tibiae were found to be consistent. Control and experimental group cartilages recovered to the initial thickness at the end of the rest period. The depth of indentation for the second compression test was similar to that of the first for each sample and for the intact and cracked group cartilages. Among the cracked samples, the difference in displacement between the first and second compression ranged from 0.6% to -0.7%. Comparing the first stress relaxation curve of each sample to its corresponding second curve showed almost identical properties for control and cracked samples (fig.1).

On histology, the induced crack was difficult to identify as it closed during compression and only an S-shaped fine line was visible under polarized light microscopy. A striking feature observed at the compression site in control and cracked samples was the reorientation and crimping of collagen fibres under the applied load. The cracked samples showed a distinctly different pattern of collagen fiber reorientation under compression as a small triangular area on either side of the crack experienced less crimp than further away from the crack.

Figure:
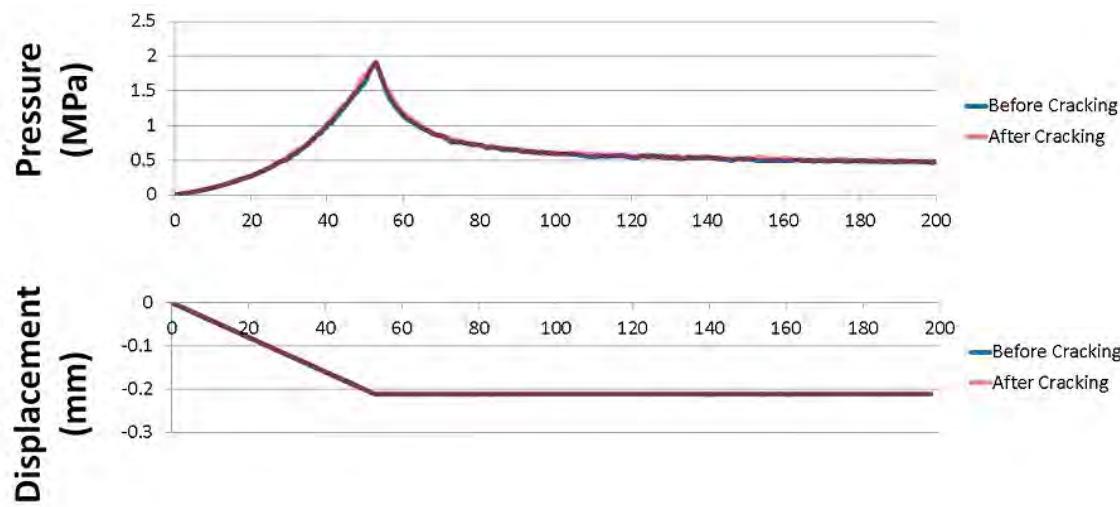
Caption: Fig.1: Example for first and second stress-relaxation curves overlapping for experimental samples.

Conclusion: The presence of a single crack did not result in detectable changes in the mechanical properties of the cartilage in terms of strain and stress relaxation behaviour. This result indicates that the cartilage's structural organisation can compensate for minimal structural damage as produced by the artificial crack, and hence may help slow the progression of OA in real life. The closure of the crack under compressive load may partially explain the preserved mechanical behaviour, and may be attributed to the swelling pressure maintained by proteoglycans. Polarized microscopy shows a distinct pattern of collagen fiber deformation in the cracked compared to the control group samples. The presence of reduced crimp at the crack's edge might indicate stress release. The difference in collagen reorientation between intact and cracked samples may provide crucial insight into the load distribution in early OA cartilage that contains cracks, and may help identify how cracked cartilage degenerates.

References: [1] Von Engelhardt et al., BMC Musculoskelet Disord, 11(1), 75, 2010.

[2] Bae et al., Osteoarthritis Cartilage, 16(7), 841–845, 2008.

[3] Waldman et al., J Orthop Res, 21(4), 590–596, 2003.

Disclosure of Interest: None Declared

Connective Tissue

AS-0393

IMAGE-BASED FINITE ELEMENT MODELING OF THE ACHILLES TENDON:
THE ROLE OF FASCICLE MORPHOLOGY AND MUSCLE FORCES IN NON-UNIFORM TENDON DISPLACEMENTS

Geoffrey Handsfield [1,*] Joshua Inouye [1] Laura Slane [2] Darryl Thelen [3] Wilson Miller [4] Silvia Blemker [1]

[1]Biomedical Engineering, University of Virginia, Charlottesville, VA, [2]Radiology, [3]Mechanical Engineering, University of Wisconsin, Madison, [4]Radiology and Medical Imaging, University of Virginia, Charlottesville, VA, United States

Introduction and Objectives: The Achilles tendon is an important tendon with a complex structure. It is composed of three to four fascicles, each controlled by a different muscle of the triceps surae group [1]. These fascicles twist 90° [2] and are capable of sliding past one another [3]. Reduced sliding of the Achilles fascicles appears to increase with aging and may be associated with tendinopathy [3,5]. Recent advances in ultrasound imaging have enabled measurement of fascicle sliding *in vivo*, as demonstrated by non-uniform tissue displacements within the Achilles tendon. These studies have shown evidence of fascicle sliding in controlled single joint tasks [4] and in walking [5]. The results of these experiments are challenging to interpret due to the complex 3D morphology of the tendon. For example, it is not clear whether it is complex fascicle geometry and/or differential muscle forces that give rise to non-uniform displacements in the tendon. The purpose of this study is to create an MRI based finite element model of the Achilles tendon fascicles to investigate the role of muscle forces and fascicle sliding on tendon tissue displacements. The specific goals are to i) build a finite element model from ultrashort echo time (UTE) MRI of the Achilles tendon, ii) predict the muscle forces necessary to replicate tissue displacements observed in the literature, and iii) use the model to understand the interactions of muscle forces and fascicle sliding on tendon displacements and strains.

Methods: We developed a novel UTE MRI approach for high contrast, high resolution imaging of the Achilles tendon. The pulse sequence, which we refer to as SUTE&TIE (Subtraction Ultrashort TE & Tendon Intensity Enhancement), obtained images with a 3D spoke-radial k-space acquisition strategy. Two complete sets of 3D images were acquired, one at an ultrashort echo time (TE: 0.08ms) and the other at a short echo time (TE: 2.5ms). Field of view was 300x300x300 mm^3 and spatial resolution was 0.8mm isotropic. Short TE images were subtracted from UTE images to maximize tendon intensity and contrast. A healthy 27 year-old female (height: 1.63m, mass: 52 kg) was scanned with this sequence on a 3T MRI scanner using a flexible RF coil wrapped around the ankle, which was manually placed in 25° of plantarflexion.

A finite element model of the Achilles tendon was created from axial image views. The tendon was subdivided into three fascicles associated with the triceps surae muscles and consistent with literature [1,6]. Two models were created—one that enabled sliding between fascicles, another with no inter-fascicle sliding. Fascicles were modeled as Neo-Hookean materials with a coefficient of 45MPa. Meshing and finite element analysis were implemented in AMPS software.

The calcaneal insertion was prescribed to rotate 25° about ankle joint center. Passive and active muscle forces on each fascicle were chosen such that the model predicted Achilles tissue displacements that were consistent with previous measurements of tendon displacements during passive and eccentric dorsiflexion experiments [4] (Fig. 1 A,B,C).

Results: Physiologically reasonable muscle forces were capable of replicating differential displacements for the "sliding" model but not the "no sliding" model. Distal displacements were inversely related to muscle forces applied to the fascicles

(Fig. 1D). Tissue strains in the MG fascicle were higher than those in the soleus fascicle for both passive and eccentric conditions. In the "no sliding" models, neither passive nor eccentric muscle forces induced differential displacements between fascicles (Fig. 1E).

Figure:
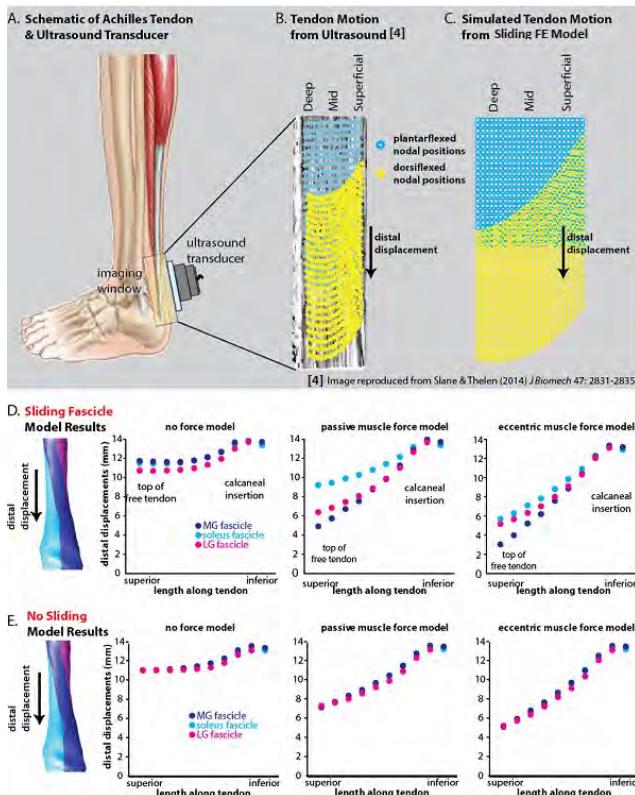
Caption: Sliding fascicle FE models replicate in vivo ultrasound results of Achilles motion (A-C). Physiological force conditions cause different displacement of the Achilles fascicles for sliding models (D) but not for no sliding models (E).

Conclusion: In this model, muscle forces and sliding tendon fascicles were necessary to replicate previously measured *in vivo* tissue displacements in the Achilles. The modeled differential tissue displacements were associated with differential fascicle stretch, with the greatest stretch in the MG fascicle. This high stretch may be due to high passive forces in the MG muscle or differences in the effective tissue compliance between fascicles. Musculotendon changes such as cross-linking of collagen between tendon fascicles and changes in muscle strength and neural activation may be the physiological mechanisms that reduce differential tendon displacements in aging subjects and runners. Further work is needed to verify these hypotheses and suggest clinical interventions to prevent tendinopathy.

References: 1. Szaro et al. *Ann. Anat.* **191,** 586–593 (2009).

2. White. *Arch. Surg.* **46,** 784 (1943).

3. Thorpe et al. *Eur. Cell. Mater.* **25,** 48–60 (2013).

4. Slane & Thelen. *J. Biomech.* **47,** 2831–5 (2014).

5. Franz et al. *Gait Posture* 1–6 (2014).

6. Sarrafian, S. K. in *Anat. Foot Ankle Descr. Topogr. Funct.* 280–282 (1993).

Disclosure of Interest: None Declared

Connective Tissue

AS-0394

A VISUAL ASSESSMENT OF HOW LOADING RATE AFFECTS THE FAILURE MECHANICS OF TYPE I COLLAGEN FIBRILS

Samuel P. Veres [1] [2],[*] Neil C. Chambers [2] Tyler W. Herod [2]

[1]Saint Mary's University, [2]Dalhousie University, Halifax, Canada

Introduction and Objectives: Overload damage to tendons can occur over a variety of strain rates, ranging from low rate injuries during lifting tasks to high rate injuries during sports activities. Because crosslinking within tendons—the major determinant of their mechanical response—varies with *in vivo* load, functionally distinct tendons may behave differently when overloaded at differing rates. In this study we present a detailed nanostructural account of the damage that occurs to individual collagen fibrils when tendons are ruptured at strain rates varying from 1 to 100%/s. We show that changes in damage morphology with strain rate are tissue specific, varying significantly between low *in vivo* load digital extensor tendons, and high *in vivo* load flexor tendons.

Methods: Digital flexor (n = 4) and digital extensor tendons (n = 4) were dissected from the forelimbs of 4 adult steers and subdivided lengthwise to produce several parallel samples. One sample from each tendon underwent crosslink analysis using hydrothermal isometric tension testing (HIT), as described previously [1]. Samples from the same tendon were assigned to the following test groups: control, 1%/s rupture, 10%/s rupture, and 100%/s rupture. All samples were first preconditioned using ten loading cycles to 10% strain. Control samples received preconditioning only. Samples in the rupture groups were pulled to rupture at their assigned strain rate (1, 10, or 100%/s). The molecular stabilities of the control and ruptured samples were analyzed using differential scanning calorimetry (DSC), conducted as described previously [2]. Collagen fibrils within control and ruptured tendons were visually assessed at magnifications of up to 90,000X using scanning electron microscopy (SEM).

Results: Extensor tendons ruptured at 1%/s showed extensive regions of well-aligned fibrils with longitudinally repeating kinks. Many of the kinked fibrils in these samples had lost their native D-banding. Extensors ruptured at 10%/s also contained aligned, kinked collagen fibrils, however, most had intact D-banding (Fig). In contrast to the 1 and 10%/s extensors, the extensors ruptured at 100%/s contained irregularly kinked and highly contorted fibrils that appeared to have undergone significant elastic recoil. Rather than a uniform loss of D-banding as in the 1%/s rupture samples, many of the irregularly kinked fibrils appeared shredded, having lost lateral cohesion among the structural subunits throughout their cross-section (Fig). At all strain rates, the damage caused to fibrils in flexor tendons was distinct from that caused to extensors. Compared to extensors, fewer regions of kinked fibrils were found in flexors that had been ruptured at 1%/s. Where kinked fibrils were found, none had lost their D-banding, indicating a greater resistance to molecular packing disruption. No plastically deformed fibrils were observed in flexors ruptured at either 10 or 100%/s, indicating a more brittle mode of failure at these higher strain rates. DSC data supported our ultrastructural observations. Compared to control extensors, endotherm onset temperatures were significantly lower in the 1%/s ($p = 0.015$) and 100%/s ($p = 0.046$) rupture samples, but not in the 10%/s rupture samples ($p = 0.23$). For flexor tendons, onset temperature was significantly lower in 1%/s rupture samples compared to controls ($p = 0.027$), but no difference was observed for either the 10%/s ($p = 0.98$) or

100%/s ($p = 0.40$) samples. Comparison of only the control extensor and flexor samples using HIT showed that significant architectural differences exist between these two tendon types, which may underlie their differing nanoscale responses to overload. HIT confirmed that crosslinking in flexor tendons was significantly more advanced than in extensor tendons. Compared to extensors, flexors had a significantly higher denaturation temperature ($p = 0.0014$), indicating greater lateral constraint among collagen molecules, and temperature of maximum force generation ($p = 0.015$), indicating the presence of significantly greater levels of thermally stable crosslinking.

Figure:
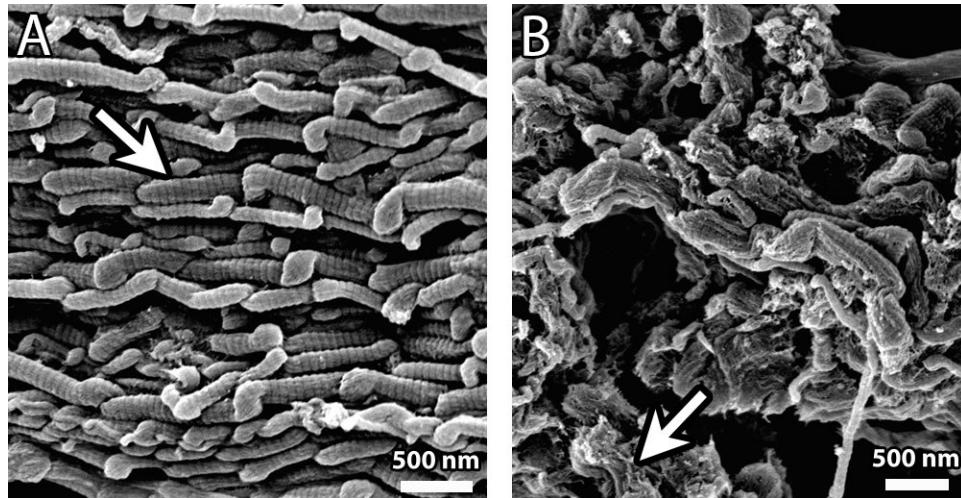
Caption: (A) Damaged collagen fibrils caused by medium speed (10%/s) extensor tendon rupture. Damaged fibrils are highly kinked, but most retain their D-banding (arrow). 25,000X. (B) Damaged collagen fibrils caused by high speed (100%/s) extensor tendon rupture. Damaged fibrils are irregularly kinked, contorted, and often shredded (arrow). 20,000X.

Conclusion: This study provides the first description of how plastic deformation of collagen fibrils varies in tendons with both strain rate and tendon type. While fibril plasticity is maintained over two decades of loading rate in low *in vivo* load extensors, fibril plasticity is lost at higher rates in high *in vivo* load flexors. The different responses to strain rate of collagen fibrils within these two tissues may affect healing potential and remodeling ability.

References: [1] Veres SP, et al. *J Orthop Res.* 31:1907–13. [2] Veres SP, et al. *Matrix Biology*. 33:54–9.

Disclosure of Interest: None Declared

Connective Tissue

AS-0395

BIOMECHANICAL PROPERTIES IN A TENDON PATHOLOGY MODEL: A ROLE FOR PROTEOGLYCANS

Rachel Choi [1,*] Joshua Martin [1] Else Jacobsen [2] Margaret Smith [3] Andrew Dart [2] Christopher Little [3] Elizabeth Clarke [1]

[1]Murray Maxwell Biomechanics Laboratory, The Kolling Institute of Medical Research, Sydney Medical School, University of Sydney, St Leonards, [2]Camden Veterinary Hospital, University of Sydney, Camden, [3]Raymond Purves Bone and Joint Research Laboratories, The Kolling Institute of Medical Research, Sydney Medical School, University of Sydney, St Leonards, Australia

Introduction and Objectives: Tendons are vulnerable to overuse and injury at work and in leisure. An often painful degenerative cascade will follow and can progressively weaken the previously healthy tendon to the point of acute rupture. While ruptures are reparable, 20% of Achilles tendon repairs experience re-rupture[1] and long-term outcomes from surgery are unsatisfactory in approximately 33% of cases[2]. No current treatments can restore the structure of degenerated tendons.

Our previous research using a focal tendon injury model confirmed that pathological tendons have decreased ultimate tensile strength (UTS) and elastic modulus. These changes extended throughout the tendon (up to 10cm from the injury site), and were associated with similar widespread increases in proteoglycans and associated glycosaminoglycans (GAGs). This indicates that "healthy" tendon tissue used in surgical repairs is in fact mechanically deficient. The aim of this study was to determine whether the accumulation of proteoglycans are responsible for the reduced modulus and UTS in pathological tendons, by assessing tendons with enzymatically reduced GAG levels.

Methods: The superficial digital flexor tendon (SDFT) was unilaterally hemi-transected (pathological) in six horses (n=6). Three control horses were sham-operated unilaterally, with the contralateral as a non-operated control (n=6, no differences found between sham-operated and non-operated controls). Animals were sacrificed after six weeks. Replicate samples (~25x1x1mm) from each tendon were harvested and allocated to three groups: (i) no treatment (*ex vivo*), (ii) incubated for 18 hours at 37°C in Tris-acetate buffer alone, or (iii) incubated in buffer with chondroitinase ABC (0.3 units/ml to remove GAGs). Specimens were biomechanically tested to failure in tension and then papain-digested for measurement of GAG content with spectrophotometry.

Biomechanics data were normalised to measured specimen cross-sectional area and gauge-length to calculate elastic modulus and UTS. The relationship between modulus, UTS and GAG content was analysed using mixed models and ranking correlation (correcting for non-independence).

Results: Ex vivo comparison of pathological versus control tendons confirmed decreased modulus (-39%, $p<0.01$) and UTS (-38%, $p<0.01$), and elevated GAG content (51%) in pathological tendons. Chondroitinase digestion reduced this GAG content to 50% ($p<0.01$) of ex vivo levels, and partially returned modulus and UTS to 73% ($p<0.01$) and 72% ($p<0.01$) of normal, respectively. GAG content was negatively correlated with both modulus ($p<0.01$) and UTS ($p<0.01$) when correcting for incubation treatment and pathological versus normal tendons.

Figure:
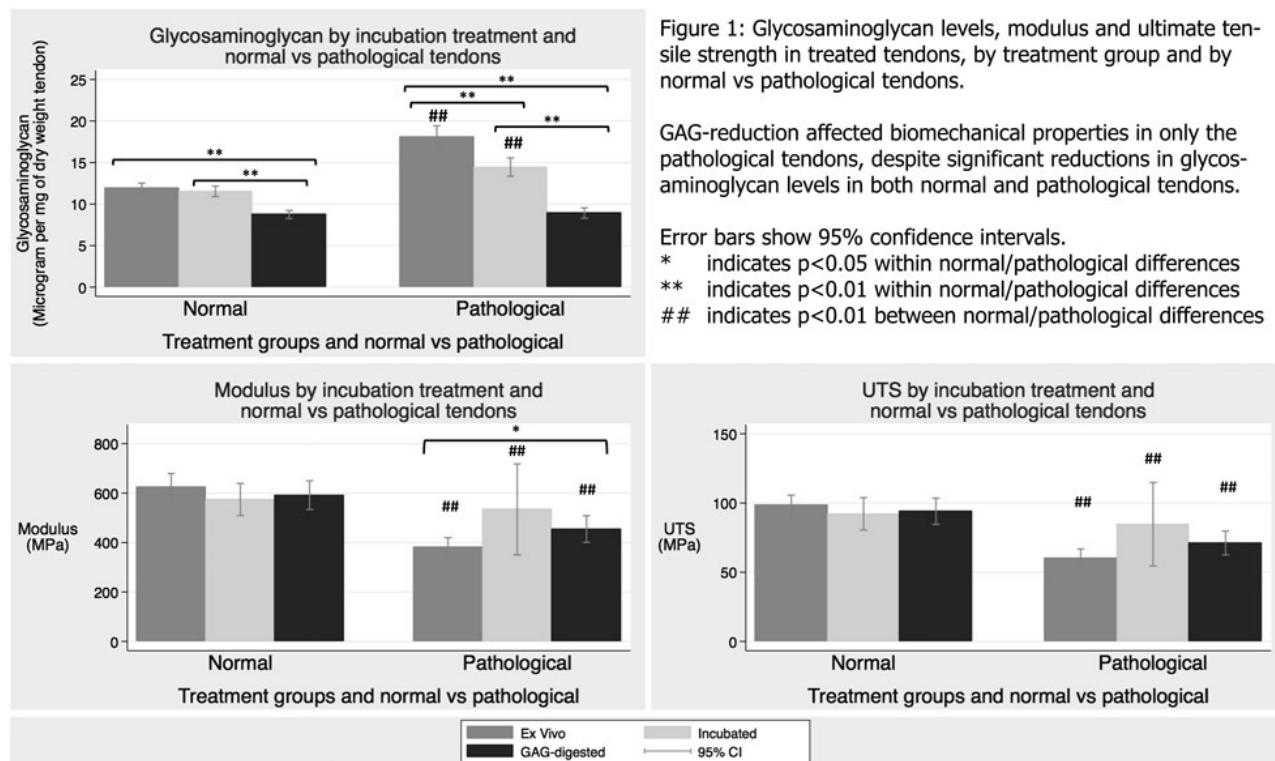
Figure 1: Glycosaminoglycan levels, modulus and ultimate tensile strength in treated tendons, by treatment group and by normal vs pathological tendons.

GAG-reduction affected biomechanical properties in only the pathological tendons, despite significant reductions in glycosaminoglycan levels in both normal and pathological tendons.

Error bars show 95% confidence intervals.
* indicates p<0.05 within normal/pathological differences
** indicates p<0.01 within normal/pathological differences
indicates p<0.01 between normal/pathological differences

Conclusion: These data demonstrate that increased proteoglycan, and specifically the chondroitin sulfate glycosaminoglycans in diseased tendons directly affects and contributes to altered biomechanical properties. Preventing proteoglycan-accumulation *in vivo* could spare the biomechanical properties of tendons undergoing degenerative changes, thus reducing incidence of rupture. Surgical repairs may also have improved outcomes if the accumulation of proteoglycans can be reversed.

References: [1] Kvist M. Achilles tendon injuries in athletes. *Sport Med*. 1994;18(3):173–201.

[2] Morberg P et al., Long-term results after surgical management of partial Achilles tendon ruptures. *Scand J Med Sci Sport*. 1997;7(5):299–303.

Disclosure of Interest: None Declared

FATIGUE DAMAGE TO POSITIONAL AND ENERGY-STORING TENDONS AT THE NANOSCALE LEVEL OF THE COLLAGEN FIBRIL

Samuel P. Veres [1 2,*] Tyler W. Herod [2] Neil C. Chambers [2]

[1]Saint Mary's University, [2]Dalhousie University, Halifax, Canada

Introduction and Objectives: The accumulation of microscale fatigue damage in tendons resulting from excessive cyclic loading has been studied previously, providing a good description of what is known as "microdamage". In this study we moved beyond microdamage, revealing the accumulation of fatigue damage to individual nanoscale collagen fibrils in two functionally distinct tendons: digital flexors and extensors. We identified two distinct forms of nanoscale fatigue damage, and show that these accumulate much faster in low *in vivo* load extensors compared to high *in vivo* load flexors.

Methods: Digital flexor tendons (n = 4) and extensor tendons (n = 4) dissected from the forelimbs of 4 adult steers were subdivided lengthwise to produce several parallel samples. One sample from each tendon underwent crosslink analysis, as described previously [1]. Samples from the same tendon were assigned to the following test groups: control, rupture, 500 cycle fatigue, and 1000 cycle fatigue. All samples were first preconditioned using ten loading cycles to 10% strain, and all tests were at a strain rate of 10%/s. Control samples received preconditioning only. Samples in the rupture group were pulled to rupture and their ultimate tensile strengths were calculated. 500 cycle fatigue samples were cyclically loaded 500 times to 30% of their ultimate stress, determined via the paired rupture sample from the same tendon. 1000 cycle fatigue samples were cyclically loaded the same way, but for 1000 cycles. After their respective mechanical interventions, the molecular stabilities of the control and fatigue samples were analyzed using differential scanning calorimetry (DSC), conducted as described previously [2], and their internal collagen fibril architectures were visually assessed at magnifications of up to 90,000X using scanning electron microscopy (SEM).

Results: Crosslinking in flexor tendons was significantly more advanced than in extensor tendons, as revealed by both denaturation temperature (p = 0.0014) and temperature of maximum force generation (p = 0.015) during hydrothermal isometric tension testing. Under SEM, control extensor tendons showed well-aligned, straight fibrils of diameter 141 ± 44 nm (40 fibrils), with clearly defined D-banding. Control flexor tendons were quite different: fibrils were significantly smaller (p < 0.0001) measuring 70 ± 30 nm in diameter (31 fibrils), and were often covered in dense filamentous webbing. In extensor tendons that had undergone both 500 and 1000 cycles of loading, collagen fibrils showed two characteristics identified as nanoscale forms of fatigue damage. First, highly localized fibrillar folds were observed, marked by a sharp discontinuity in fibril orientation caused by laterally aligned fibril kinks (Fig). Second, fibrils with longitudinally repeating, but non-aligned kinks were observed (Fig). In stark contrast, flexor tendons that had undergone 500 and 1000 cycles of loading showed little to no accumulation of fatigue damage, with minor infrequently observed fibrillar folds being the only architecture difference between the fatigue and control samples. DSC assessment of molecular stability in the control samples corroborated HIT findings: compared to extensor tendons (n = 5), flexor tendons (n = 5) had significantly higher endotherm onset temperatures (p = 0.027) and lower full-widths at half-maximum (p = 0.003) indicating that flexor tendons were composed of collagen molecules with both greater thermal stability and homogeneity. Compared to control tendons,

none of the metrics measured (onset temperature, peak temperature, full-width at half-maximum, specific enthalpy of denaturation) changed significantly with cyclic loading in either the flexor or extensor tendons, indicating that early fatigue damage, while clearly visible under SEM, does not affect enough molecules to be detectable via bulk tissue measurement.

Figure:
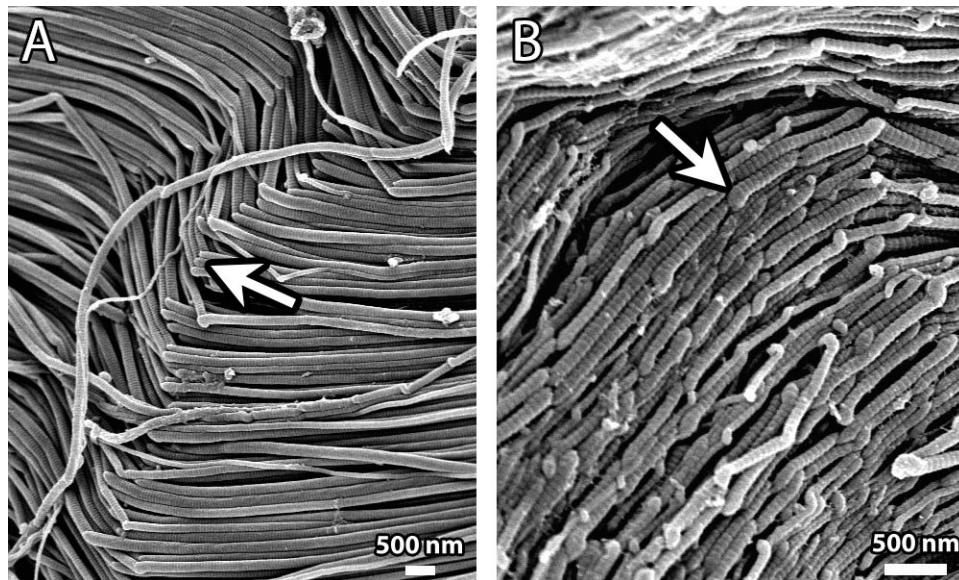
Caption: (A) Fatigue damage type I: Fibrillar folds (arrow) were commonly seen in cyclically loaded extensor tendons, but rarely seen in cyclically loaded flexor tendons. 6,000X. (B) Fatigue damage type II: Fibrils with longitudinally repeating, but non-aligned kinks (arrow) were commonly seen in cyclically loaded extensor tendons, but not flexors. 13,000X.

Conclusion: This study provides the first description of fatigue damage accumulation at the nanoscale level of individual collagen fibrils in functionally distinct tendons. Striking differences in fatigue damage to high and low *in vivo* load tendons are found, possibly arising from observed differences in collagen crosslinking and fibrillar architecture. Our findings may be important to understanding the architectural changes that tendons must undergo during development or physical training, and may have relevance to the optimal selection of allograft tissues.

References: [1] Veres SP, et al. *J Orthop Res.* 31:1907–13. [2] Veres SP, et al. *Matrix Biology*. 33:54–9.

Disclosure of Interest: None Declared

Dental

AS-0397

DYNAMIC MECHANICAL PROPERTIES OF THE BOVINE PERIODONTAL LIGAMENT

Iman Zoljanahi Oskui [1] Ata Hashemi [1,*]

[1]Faculty of Biomedical Engineering, Amirkabir University of Technology, Tehran, Iran, Islamic Republic Of

Introduction and Objectives: Periodontal ligament (PDL) has a major contribution to tooth-bone attachment [1] and also absorbs and distributes the occlusal forces on alveolar bone [2]. Owing to nonlinear and viscoelastic behavior of PDL [3], exploring its dynamic mechanical properties is necessary [4, 5]. To best of our knowledge these dynamic mechanical properties are not experimentally determined. Hence, in current study, results of tensile and compressive dynamic tests on bovine PDL are presented. Wide range of loading frequencies is applied to PDL to capture how it affects storage and loss modules in tension and compression.

Methods: Transverse sections with a thickness of 2 mm are cut from left lower bovine mandible (Figure 1.A). On these sections, eight samples of 4 mm * 8 mm dimensions are extracted from tooth-PDL-bone interface zone (e.g. S1 in Figure 1) for dynamic mechanical tests. Special attention is given to alignment of collagen fibers with longitudinal direction of the samples (Figure 1.B). These samples are imaged under light microscope and resultant images are used to measure PDL length. Our measurements showed an initial length of 0.5±0.1 mm for PDL. Subsequently, samples are mounted on TTDMA testing device (Triton Technology Inc.) such that dentin and bone are attached to jaws of testing machine. Since bone and dentin are much stiffer than PDL, any tensile or compressive force applied to the sample is transferred to PDL. Load-controlled tensile test with dynamic force of 2 N in frequency range of 0.01 to 100 Hz. Compressive tests with the same magnitude and frequencies are repeated. During the test, samples were submerged in PBS.

Results: Storage modulus is increased with elevation of frequency in either tension or compression. For a given frequency, compressive storage modulus is approximately twice of storage modulus in tension. In tensile tests, loss modulus showed an insignificant enhancement while the frequency is increased till 20 Hz and drops beyond this threshold. The same trend is seen in compressive tests with the threshold of 0.5 Hz.

Figure:
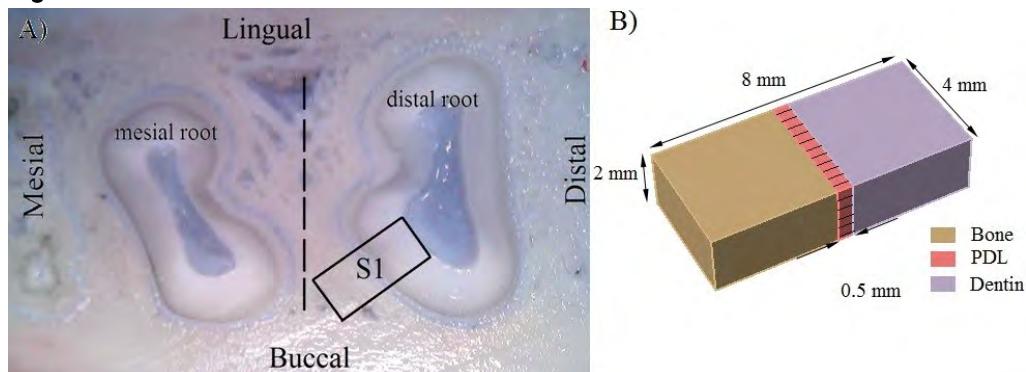
Caption: Figure 1. A) Transverse section of bovine mandible, B) Schematic of testing sample.

Conclusion: Dynamic mechanical behavior of the PDL shows different trends in tension and compression, implying that mechanical behavior of PDL is governed by collagen fibers in tension and liquid phase in compression.

References: [1] Natali et al., Connect Tissue Res, 45: 222-230, 2004.

[2] Bergomi et al., J Biomech, 43:1146-1152,2010.

[3] Tanne et al., Angle Orthod, 65: 123-128, 1995.

[4] Sanctuary et al., J Appl Physiol, 99:2369-2378, 2005.

[5] Shibata et al., Eur J Oral Sci, 114:74-82, 2006.

Disclosure of Interest: None Declared

Connective Tissue

AS-0398

MEASUREMENT OF THE EFFECTS OF 'KINESIO-TAPING' ON IN VIVO THORACOLUMBAR FASCIA MOVEMENT USING 3D ULTRASOUND: METHODOLOGICAL DEVELOPMENT AND RELIABILITY

Shihfan J. Tu [1,*]Roger Woledge [1]Dylan Morrissey [1 2]

[1]Sports and Exercise Medicine, Queen Mary University of London, [2]Physiotherapy Department, Bart's Health NHS Trust, London, United Kingdom

Introduction and Objectives: Therapeutic taping techniques are increasingly used to treat low back pain (LBP) [1, 2, 3], albeit with variable effects and unclear mechanisms. Changes in thoracolumbar fascial thickness, structure and shear strain are associated with LBP [4, 5], however methods for quantifying in vivo fascia properties are inadequate. We therefore aimed to develop a reliable in vivo measurement technique to enable exploration of taping mechanisms.

Methods: Ultrasound videos of known orientation and position were taken of 9 normal participants (male and female, aged 27.3 ± 2.04, BMI 22.98 ± 3.10) while performing velocity-guided lumbar flexion with and without taping. An automated algorithm using cross-correlation to track contiguous tissue layers across sequential frames, in two planes, was developed and applied to two movements of each subject in each taping condition. Reliability was assessed using the intra-class correlation coefficient (ICC 2, 1), limits of agreement (LOAs) were calculated for each assessment and systematic differences tested with a Student's t-test.

Results: The mean movements of thoracolumbar tissue during lumbar flexion before and after taping (figure 1) showed strong reliability within subjects ICC both when subjects were moving without tape applied (ICC = 0.82) and with Kinesio-taping applied (ICC = 0.82). No significant differences was found (No tape, p = 0.32, t = 1.00; tape, p = 0.90, t = -0.13). Intra-observer analysis revealed acceptable LOAs for both measurements when subjects were taped and not taped. The study was not powered to reveal differences between taping conditions, and none was revealed, however a sample size calculation suggested that 80 subjects would be required at 80% power and 5% significance levels. It must be noted these were normal subjects rather than those with pain.

Figure:
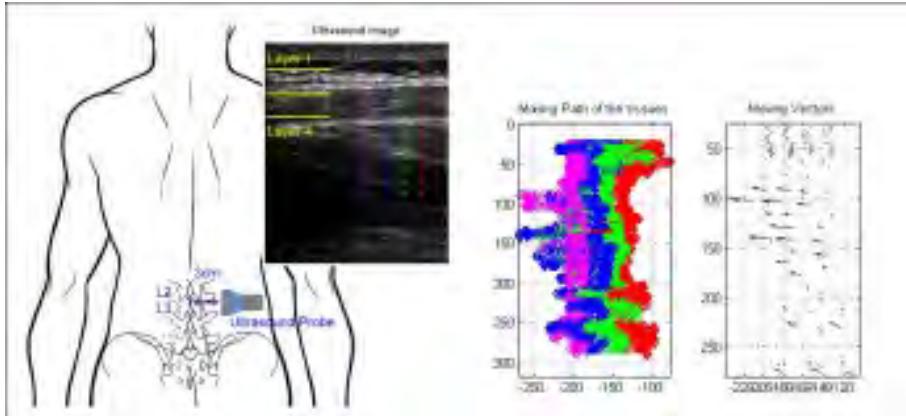
Caption: Ultrasonography tracking analysis. (A) The Ultrasound probe was placed 3 cm lateral to the midpoint of a line joining L2 and L3 spinous processes. In the tracking programme, multiple tracking targets (middle area between 4 red

dots) were drawn. (B) Movements in each position were tracked and recorded as a route map. (C) A vector field plot based on the route map was calculated to quantify tissue movements in each plane. Blue vectors indicate in-image movement direction and amount. (Plot unit = pixels)

Conclusion: Movement of relative thoracolumbar fascia, muscle and fatty tissue and underlying tissues could be reliably quantified during lumbar flexion in vivo using real-time ultrasound. The reliability was similar for both taped and untaped conditions. Next steps include validity analysis and testing in subjects with low back pain to investigate possible mechanisms of taping therapies.

Table: Table: Intra-class correlation coefficient and limits of agreement

	Analysis 1	Analysis 2	P value	ICC	MEAN$_{diff}$	SD$_{diff}$	Lower LOA	Upper LOA
without taping	2.15 ± 2.76	1.91 ± 2.3	0.32	0.82	0.23	1.97	-3.63	4.09
with taping	1.76 ± 1.78	1.78 ± 2.53	0.90	0.82	-0.02	1.69	-3.33	3.29

Caption: MEAN diff, mean difference between measurememts; ICC, intraclass correlation coefficient; LOA, limits of agreement; SD diff, SD of difference between measurements. (Figure unit = pixels, 1 pixels = 0.12 mm)

References: [1] Yoshida et al., Res Sports Med, 15: 103-112, 2007.

[2] Castro-Sánchez et al., J Physiother 58: 89-95, 2012.

[3] Chen et al., Clin Rehabil, 26: 924-933, 2012.

[4] Langevin et al., BMC Musculoskelet Disord, 10:151, 2009.

[5] Langevin et al., BMC Musculoskelet Disord, 12:203, 2011.

[6] Martin Bland et al. The lancet 327: 307, 1986.

Connective Tissue

AS-0399

DIFFERENCE IN TRAINED VS. UNTRAINED ON THE MATERIAL PROPERTIES OF SKELETAL MUSCLE

Matthew Salzano [1] Erica A Bell [1,*] Kayla D Seymore [1] Jamie E Hibbert [1] Anthony S Kulas [2] Zachary J Domire [1]

[1] Kinesiology, [2] Health Education & Promotion, East Carolina University, Greenville, United States

Introduction and Objectives: It is known that the extracellular matrix (ECM) of muscles cells plays a role in the lateral transmission of force through the whole muscle [1]. With exercise training, muscle adapts through hypertrophy and increased strength. In order for ECM to remain undamaged as a result of the muscular strength gains, its strength should also increase. ECM could become stronger by laying down more collagen and becoming bigger or by changing material properties via increased cross-links. However, existing research is conflicting on the effect training has on ECM stiffness. Endurance training was found to have no effect on the passive stiffness, measured *in vitro*, in the soleus of young rats [2]. Two studies disagree with this, showing that endurance training increases rat muscular stiffness and human joint stiffness, both measured via quick release tests [3,4]. These two studies also show that plyometric training [4] and resistance training [3] result in decreased joint and muscular stiffness, respectively. The opposite effect of resistance training on joint stiffness was found in human hamstrings [5]. The purpose of this study is to examine the effect of training on muscle material properties through comparison of ultrasound elastography measurements between elite and recreational athlete hamstrings as a representation of trained and untrained muscle, respectively. We hypothesize that modulus will be higher in the trained muscle compared to the untrained muscle.

Methods: This study used 6 elite sprinters and jumpers (3 male, 3 female) and 11 recreationally active (RA) individuals (4 males, 7 females). RA was defined as performing strength and/or cardio training for at least 5 hours per week. All subjects were free of previous injury and completed an informed consent form approved by University IRB. Ultrasound elastography measurements were taken from the mid-belly of the biceps femoris long head and semitendinosus muscles using an Aixplorer SuperSonic Imagine. Stiffness measurements were taken with a 3 mm diameter region of interest from the middle of the readable data within the Q-box. Stiffness levels were then plotted on Cleveland dot plots to compare differences between groups for each muscle.

Results: Elastography measurements show that the elite athletes had significantly higher modulus in their biceps femoris muscles than the RA individuals (avg. kPA: 20.6 vs. 14.7, respectively; $p<0.05$). There was no significant difference in stiffness values within the semitendinosus muscle between the elite athletes and RA subjects (avg. kPa: 18.9 vs. 17.4; $p>0.05$).

Figure:
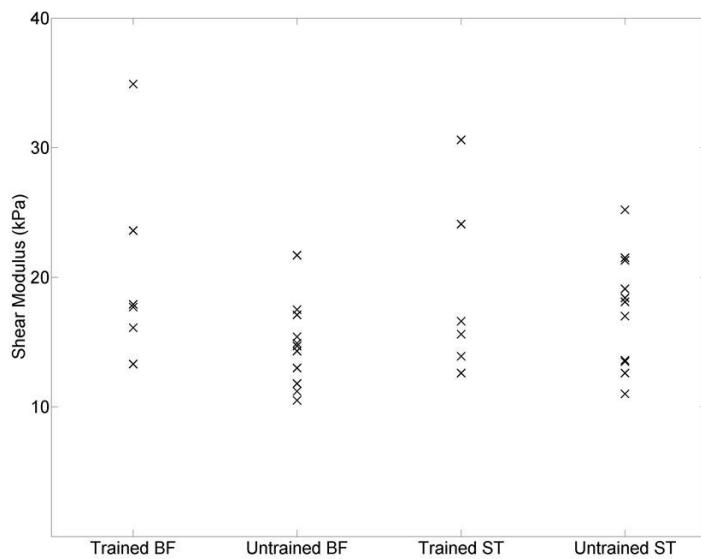
Caption: Figure 1. Trained vs. Untrained Modulus

Conclusion: The results of this study support our hypothesis that modulus in trained muscle will be higher when compared to untrained muscle. The cross-sectional nature of this study limits the ability to infer training as the cause for higher modulus. It possible that genetics plays a role, and elite athletes are predisposed to this condition, allowing for quicker and larger strength gains. The lack of information regarding the range of training volume in RA also makes it difficult to make conclusions about training effects on muscle modulus. Future work in this area could examine differences in modulus through a training protocol or by recording training volume and strength measurements. While limitations to this study exist, our work supports the idea that muscle modulus can be increased through training.

Table:

	Elite BF	RA BF	Elite ST	RA ST
Average:	20.6	14.7	18.9	17.4
Std. Deviation:	7.8	3.2	7.0	4.4

Caption: Table 1. Muscle shear modulus (kPa). BF: Biceps femoris. ST: Semitendinosus

References: [1] Jaspers et al., *J Biomech,* 32(1):71-79, 1999.

[2] Gosselin et al., *J Appl Physiol (1985),* 85(3):1011-1016, 1998.

[3] Goubel et al., *Pflugers Arch,* 410(3):321-325, 1987.

[4] Grosset et al., *Eur J Appl Physiol,* 105(1):131-139, 2009.

5. Klinge et al., *Am J Sports Med,* 25(5):710-716, 1997.

Disclosure of Interest: None Declared

THE PROBABILITY OF FINDING 0D STATISTICAL SIGNIFICANCE IN 1D TRAJECTORY ANALYSIS

Todd Pataky [1,*] Jos Vanrenterghem [2] Mark Robinson [2]

[1]Department of Bioengineering, Shinshu University, Ueda, Japan, [2]Research Institute for Sport and Exercise Sciences, Liverpool John Moores University, Liverpool, United Kingdom

Introduction and Objectives: One-dimensional (1D) kinematic and force trajectories are often summarized using 0D metrics like local extrema. One problem with this approach is that analysis of 0D metrics ultimately yields probability values which are based on classical 0D models of randomness like the 0D Gaussian distribution. Thus analyses which set a threshold for significance (α) control the likelihood that random 0D data, not random 1D data would reach that threshold. The purpose of this study was to estimate the probability with which random 1D data reach the 0D threshold for significance. Much higher 1D probabilities would imply that 0D thresholds bias analyses of 1D trajectories.

Methods: *Trajectory roughness*: We estimated the average temporal derivative λ of nine separate public 1D kinematics/force datasets from the ISB data archives and from simtk.org using an unbiased procedure [1]. Analyses below consider the full range of estimated λ values.

Theoretical probabilities: For simplicity we considered just a simple two-sample experiment design with N=10 observations per group; note that more complex designs like ANOVA would lead to greater divergence between 0D and 1D results. Basic t tables show that the critical t value (t*) for this two-sample design is t*=1.734 at α=0.05; this implies that random 0D Gaussian data would produce a t value greater than 1.734 with a probability of 5%. We computed the probably that random 1D data would reach t* as a function of λ using Random Field Theory (RFT) [2] and the open-source software: One-Dimensional Statistical Parametric Mapping (www.spm1d.org) [3].

Probability validations: We validated the aforementioned RFT probabilities by simulating 100,000 separate two-sample t tests using random 1D trajectories with controlled λ (Fig.1a,b). We repeated these 100,000 simulations across the range of λ values observed in the public datasets, and we also repeated these simulations for four separate cases: (1) scalar trajectories, (2) single three-component vector trajectories, (3) two three-component vector trajectories, and (4) six three-component vector trajectories. For conceptual purposes Case 4 could be interpreted as an experiment which measures three-dimensional joint angles from the hip, knee and ankle for both the left and right limbs.

Results: *Trajectory roughness*: Across the nine public datasets the average temporal derivative ranged from λ=0.057 to λ=8.841 (Fig.1a,b). The median value was λ=1.232.

Probabilities: For the median roughness, RFT predicts that 1D data would reach the 0D threshold for significance with a probability of 41.0%. This implies that the effective Type I error rate for 0D procedures is α=0.41 and not the presumed α=0.05. For two, three and six three-component vector trajectories, that probability increased to 79.4%, 95.8% and 99.9%, respectively (Fig.1c). This implies that, for experiments involving two or more vector trajectories, one is effectively guaranteed of observing 0D significance even when there is actually no difference between two groups. Simulations of random scalar and vector 1D trajectories validated the estimated probabilities (Fig.1c).

Figure:
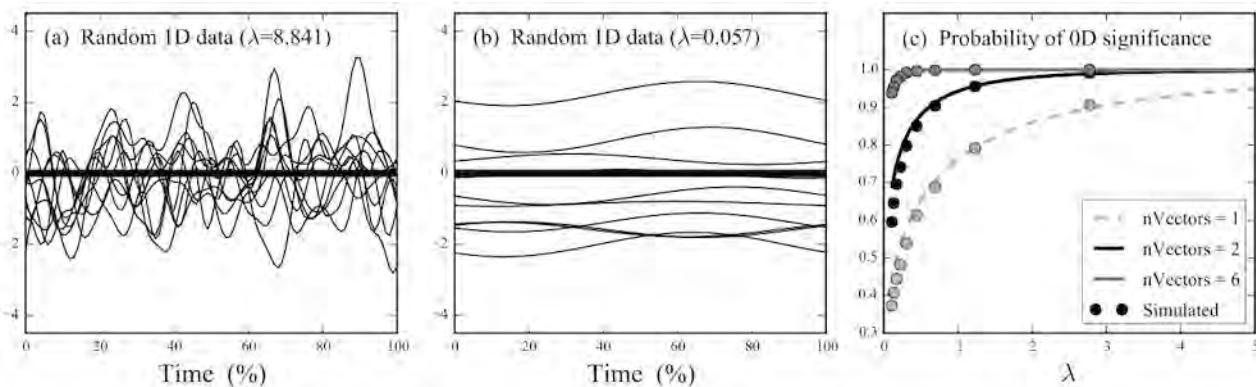
Caption: (a,b) Random 1D trajectories for different smoothness values; λ is the average temporal derivative (change in signal per percent time). (c) Analytical probability that random 1D trajectories will reach 0D significance (solid lines) and simulation values (dots).

Conclusion: This study suggests that classical models of 0D randomness may substantially underestimate the probability with which random 1D trajectories produce particular results. In particular, the current results suggest that the effective Type I error rate (α) of 0D analyses can actually be well over 90% in common Biomechanics experiments, an order-of-magnitude larger than the presumed α=0.05. Since reporting an experimental result obliges one to also report its p value (the probability with which random data would produce the same result), using a 1D model of randomness for 1D data analysis may ultimately yield more objective p values. In short, as compared to the traditional 0D Gaussian model of randomness, a model of 1D randomness may be more consistent with the experimental variability observed about mean 1D trajectories.

References: [1] Kiebel et al. NeuroImage 10: 756–66, 1999.

[2] Adler, Taylor. Random Fields and Geometry, Springer-Verlag, 2007.

[3] Pataky, Comp Meth Biomech Biomed Eng 15: 295-301, 2012.

Disclosure of Interest: None Declared

Motion Analysis

AS-0402

WHOLE BODY CENTER OF MASS VELOCITY AND DIRECTION DURING CHANGE OF DIRECTION TASK AT MAXIMUM SPEED

Daichi Yamashita [1,*] Yuki Inaba [1] Masaki Asakura [2] Yoshihiko Ito [1]

[1]Department of Sports Science, Japan Institute of Sports Sciences, [2]Athletic Performance, Deers Football Club, Tokyo, Japan

Introduction and Objectives: The ability to change of direction is important in competitive sports such as American football. To gain separation from an opponent, athletes need to run fast and change of direction quickly. Many studies have investigated biomechanical characteristics of the single foot during change of direction, however, it is difficult to achieve the required angle during a single step at high speed (Vanrenterghem et al., 2012). We compared the COM horizontal velocity and angle during straight run to change of direction over several steps.

Methods: Twelve male semi-professional and collegiate American football players (experience = 7.5 ± 4.8 years) participated in this study. They were instructed to perform two tasks: straight running (RUN) and sidestep cutting to 45° (CUT) at their fastest speed. For straight running, subjects ran for 15 yards. For CUT, subjects ran for 10 yards, then planted their left foot and change direction to the right at 45°, and continued running for 5 yards.

Three-dimensional coordinates of the anatomical landmarks were acquired using a 3D optical motion capture system with 20 cameras (250 Hz; Vicon, Oxford, UK). Thirty-one reflective markers were placed on each subject's body. The whole body centre of mass (COM) position was calculated as the weighted sum of the 14-segment model. The COM velocity and angle were defined using horizontal COM velocity vector at four flight phases; before the previous (right) foot strike (Flight -2) before the cutting (left) foot strike (Flight -1), after the cutting foot take-off (Flight +1) and after the next (right) foot tale-off (flight +2). Each flight phase was confirmed using each toe and heel markers.

Two-way repeated measures ANOVA were used to determine if differences exist between task directions (RUN and CUT) or flight phases (Flight -2, Flight -1, and Flight +1) for velocity and angle. Post hoc analyses were then examined with paired t-tests for comparison of the values measured at each flight phase between RUN and CUT. One-way repeated-measures ANOVA were conducted for velocity and angle during RUN and CUT. When the effect of flight phase was found, post hoc multiple comparison Tukey tests were conducted between flight phases ($p < .05$).

Results: A significant interaction was observed for velocity ($p < .05$). Compared to RUN, velocity was smaller during CUT at each flight phase ($p < .05$). Velocity was increased with flight phase during RUN ($p < .05$) but did not change during CUT.

A significant interaction was also observed for angle ($p < .05$). Compared to RUN, angle was greater during CUT at each flight phase (Fig.1). Angle was increased with flight phase during CUT ($p < .05$).

Figure:
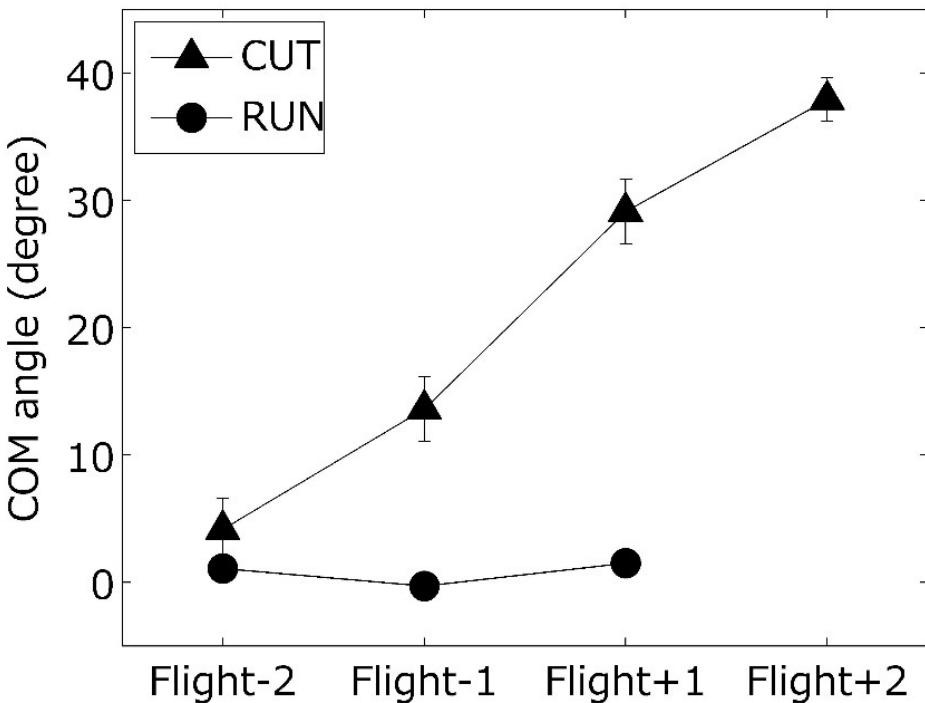
Caption: Fig.1. Average COM angle at each flight phase (mean ± SD) during CUT and RUN.

Conclusion: These results showed that change of direction motion was started before the previous foot strike. Not only the cutting leg, but also the leg before and after cutting contributes change of direction more than a bit. This study provides important insight into the whole body COM control during change of direction at maximal speed.

References: Vanrenterghem et al., J. Biomech, 45: 2444-2449, 2012

Disclosure of Interest: None Declared

Motion Analysis

AS-0403

MULTI-BODY OPTIMIZATION WITH KNEE JOINT CONSTRAINTS BASED ON THE STIFFNESS MATRIX

Vincent Richard [1 2 3,*] Giuliano Lamberto [4] Tung-Wu Lu [5] Valentina Camomilla [6] Aurelio Cappozzo [6] Raphaël Dumas [1 2 3]

[1]Université Claude Bernard Lyon 1, Villeurbanne, [2]Laboratoire de Biomécanique et Mécanique des Chocs, IFSTTAR, Bron, [3]Université de Lyon, Lyon, France, [4]Department of Mechanical Engineering, University of Sheffield, Sheffield, United Kingdom, [5]Department of Orthopedic Surgery, National Taiwan University, Taipei, Taiwan, Republic of China, [6]Department of Movement, Human and Health Sciences, Università degli Studi di Roma "Foro Italico", Rome, Italy

Introduction and Objectives: Estimation of joint kinematics using optoelectronic system and skin markers can be performed using a multi-body optimization (MBO) method [1]. With the intent to estimate the bone segments pose, MBO should compensate for the effect of soft tissue artefacts (STA), thanks to a multi-body model made of segments and articulated joints (represented by a set of constraints). When modelling the joints as simple mechanical linkages (hinge or spherical), the accuracy of the model-based kinematics is questionable [2]. Some studies have tried to improve the estimated kinematics by using a more detailed anatomical knowledge to model the joints [3,4]. Instead of a deterministic and non-physiological mechanical linkage, the present study proposes an alternative definition of the joint model thanks to a stiffness matrix introduced in MBO through a penalty-based method.

Methods: The knee stiffness matrix **S** reflects the coupling laws between passive forces and moments **F,** and joint angles and displacements of the tibia relative to the femur $\mathbf{U} = [\theta_1\ \theta_2\ \theta_3\ d_1\ d_2\ d_3]^T$ expressed in a joint coordinate system. This stiffness matrix satisfies the equation $\mathbf{F} = \mathbf{SU}$. **S** has been experimentally obtained on a cadaveric subject by measuring the forces corresponding to a known displacement imposed by means of a robotic arm [5]. **S** was measured at 30° of knee flexion and was, thereafter, assumed to be constant, independent to knee flexion.

The principle of MBO is to minimize the squared distances between model-determined and measured skin marker positions. In the present study, this distance minimization was appended with the minimization of the joint deformation energy. The optimization problem for bone pose (**Q**) estimation was the following:

min $f = 1/2[(\Phi^m)^T\ \Phi^m + w(\mathbf{U})^T\mathbf{SU}]$

subject to $\Phi = 0$

where Φ represents the kinematic constraints (other than for the knee) and the rigid body constraints of the multi-body model and w is a weighting factor. In this study, $w = 1e^4$.

The resulting model-based kinematics (Stiffness) was compared in term of root mean square errors (RMSEs) to that obtained with the model-based kinematics obtained using more classical kinematic constraints (N: no constraint; S: spherical constraints) or constraining the degrees of freedom (DoFs) of the knee with direct coupling curves (CC) between them [6]. The method was tested *in-vivo* on data from 5 running trials of 3 subjects, measured with both skin markers and intra-cortical pins [7].

Results: RMSEs were generally limited for joint angles and displacements (under 6° and 4.9 mm, respectively). For flexion/extension, RMSEs were similar for all joint models (lower than 1.6°). More discrepancy between models was observed for internal/external rotation with 2.5°, 3.4° and 6° for S, Stiffness and CC models respectively. In terms of joint

displacements, the spherical model (S), although imposing null displacements showed the smallest RMSEs, while for both Stiffness and CC models, they were between 1.6 mm and 3.7 mm. The highest RMSEs were obtained without constraints (between 3.4 mm and 4.9 mm for N).

Figure:
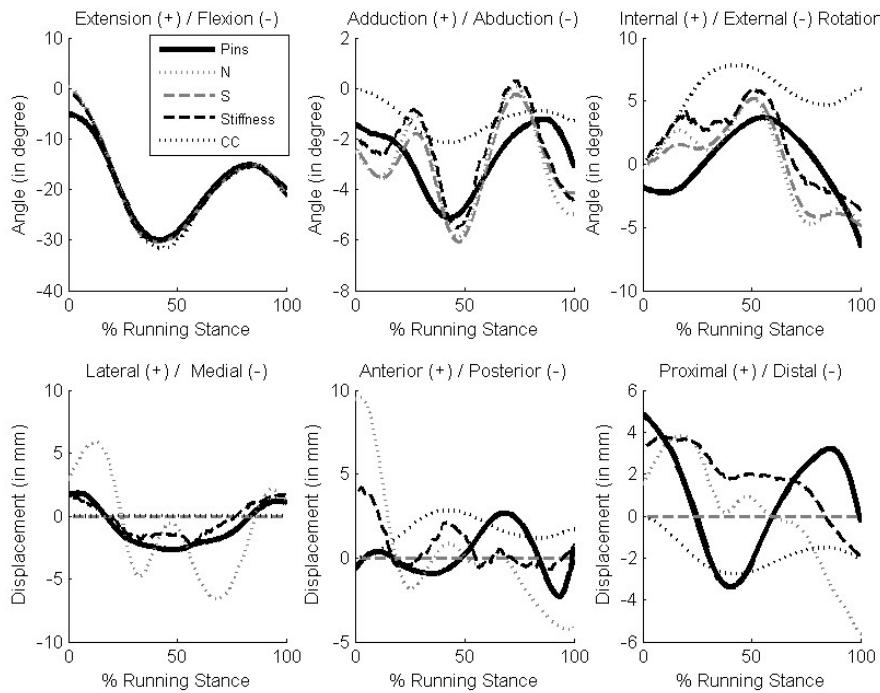
Caption: Figure 1: Knee kinematics of the mean over the 5 trials of one subject

Conclusion: Joint models based on the stiffness matrix have already been used for spine kinematics but never for limb kinematics. The present MBO results seems encouraging in comparison with the more classical models of the knee (S, CC), even though assumptions have been made (e.g., constant stiffness matrix).

The proposed method is a penalty-based method where the choice for the weight factor w is critical. It is interesting to notice that such penalty-based method does not impede the joint displacements (as S do) nor prescribe them as a function of knee flexion (as CC do). Conversely, the six DoFs rely on the stiffness matrix coefficients, and, especially the extra-diagonal coefficients that stand for couplings. To that respect, the implementation of a knee flexion dependent stiffness matrix may provide improvement. Such MBO can be a promising method for STA compensation.

Acknowledgements

Table:

Model	Ext/Flex (°)	Add/Abd (°)	Int/Ext Rot (°)	Lat/Med (mm)	Ant/Post (mm)	Prox/Dist (mm)
N	1.6±1.6	1.9±1.9	3.0±3.0	3.4±3.4	4.4±4.4	4.9±4.9
S	1.6±1.6	1.6±1.6	2.5±2.5	1.6±1.6	2.5±2.5	2.1±2.1
Stiffness	1.5±1.5	1.7±1.7	3.4±2.9	2.3±2.2	3.1±3.1	3.7±3.5
CC	1.6±1.6	1.7±1.7	6.0±2.2	1.6±1.6	3.7±3.3	2.7±1.8

Caption: Table 1: Mean RMSE (±STD) over all trials of all subjects

References: [1] Lu et al., J. Biomech. 32: 129–34, 1999.

[2] Andersen et al., Comput. Methods Biomech. Biomed. Engin. 12: 371–84, 2009.

[3] Duprey et al., J. Biomech. 43: 2858–62, 2010.

[4] Gasparutto et al., Comput. Methods Biomech. Biomed. Engin. 15: 191–193, 2013.

[5] Fujie et al., J. Biomech. 29(12): 1577-85, 1996.

[6] Walker et al., J. Biomech. 21: 965–74, 1988.

[7] Reinschmidt et al., J. Biomech. 30: 729–32, 1997.

Disclosure of Interest: None Declared

ASSESSMENT OF THE AGREEMENT BETWEEN THE SPATIO-TEMPORAL WALKING GAIT PARAMETERS FROM THE OPTOGAIT PHOTOELECTRIC SYSTEM AND THOSE FROM FORCE PLATES AND MOTION CAPTURE

Aoife Healy [1,*] Sara Behforootan [1] Nachiappan Chockalingam [1]

[1]Centre for Sport, Health and Exercise Research, Staffordshire University, Stoke On Trent, United Kingdom

Introduction and Objectives: Assessment of spatio-temporal walking gait parameters can be used to identify pathology and asymmetry in clinical populations. Instruments used to calculate these parameters include force and pressure plates and motion capture systems. Due to the high cost of some of these instruments and the space they require they may not be easily accessible to clinicians. Optogait is a portable system which consists of transmitting and receiving bars which contain LEDs; as a person walks between the bars their feet cause interruptions in the communication between the LEDs and this information is used to calculate the gait parameters. While recent research has examined the validity of the Optogait to another portable gait assessment system (GAITRite) [1, 2] no studies have compared the gait parameters calculated from Optogait to those from force plate and motion capture data. The aim of the study was to assess the level of agreement of spatio-temporal walking gait parameters calculated using a photoelectric system (Optogait) to those calculated from force plate and motion capture data (AMTI + Vicon).

Methods: Ten healthy participants (8 males and 2 females; mean age ± standard deviation: 30 ± 8 years) walked at their self-selected speed (1.33 ± 0.2 ms^{-1}) while simultaneously recorded by the two systems. The 5m Optogait system (sampling at 1000Hz; Microgate, Italy) was set up together with two force plates (AMTI OPT464508 sampling at 1000Hz; AMTI, USA) and a 14 camera Vicon motion capture system (sampling at 100Hz; Vicon, OMG, UK) for simultaneous capture. Reflective spherical markers were placed on anatomical landmarks of the participant, for use with the Plug-in-Gait Model. The force plates detected the initial foot contact and foot off gait events (using a minimum force threshold of 20N) while the movement pattern of the toe marker was used to identify the subsequent foot contact of the gait cycle. Three trials (each consisting of 1 gait cycle) were recorded with the mean values of step length and time, stride length, stance phase, swing phase, gait cycle, speed and cadence for left foot data used for statistical analysis. Agreement between the two systems was examined using 95% limits of agreement by Bland and Altman [3] and paired t-tests were used to detect any systematic differences between the systems.

Results: Six of the eight gait parameters were significantly different (p ≤ 0.05) between the systems (Table 1); with results for gait cycle, stance phase and stride length significantly higher (0.01 s, 0.02 s and 0.01 m higher respectively) for the Optogait while cadence, speed and swing phase were significantly lower (1 step/min, 0.01 ms^{-1} and 0.02 s lower respectively). Results for 95% limits of agreement showed good agreement between the two measurement systems (Table 1).

Conclusion: Consistent with previous research findings the Optogait system reports longer stance phase and shorter swing phase times than other measurement systems. This is due to the fact that the LEDs within the bars are raised 3mm with respect to the floor; thereby the measurement of stance phase time starts prior to the foot contacting the floor and the measurement of swing phase starts after the foot has left the floor. While a systematic difference between the two

measurement systems were evident for the majority of the gait parameters all parameters showed good agreement based on the 95% limits of agreement and the differences are considered small enough to be acceptable for clinical purposes.

Table:

Gait parameter	Optogait	AMTI + Vicon	95% LOA
Cadence (steps/min)	116 ± 9	117 ± 9*	-2.51 - 0.69
Gait cycle (s)	1.04 ± 0.08	1.03 ± 0.08*	-0.01 - 0.02
Speed (ms^{-1})	1.327 ± 0.2	1.335 ± 0.2*	-0.02 - 0.01
Stance phase (s)	0.65 ± 0.06	0.63 ± 0.06*	0.01 - 0.04
Swing phase (s)	0.39 ± 0.02	0.41 ± 0.02*	-0.04 - -0.001
Step length (m)	0.68 ± 0.05	0.68 ± 0.05	-0.01 - 0.01
Step time (s)	0.52 ± 0.04	0.52 ± 0.04	-0.01 - 0.02
Stride length (m)	1.37 ± 0.1	1.36 ± 0.11*	-0.01 - 0.01

Caption: Mean ± standard deviation of spatio-temporal gait parameters for both systems with 95% limits of agreement (*significant difference between the two measurement systems ($p ≤ 0.05$); LOA: limits of agreement).

References: [1] Lee et al., J Phys Ther Sci, 26: 81-5, 2014.

[2] Lienhard et al., Med Eng Phys, 35: 500-04, 2013.

[3] Bland and Altman, Lancet, 1: 307-10, 1986.

Disclosure of Interest: None Declared

Motion Analysis

AS-0405

THE ROLE OF LOWER LIMB JOINTS IN ENERGY ABSORPTION DURING DESCENT OF STAIRS AND SLOPES

Helene Pillet [1,*]Boris Dauriac [1]Coralie Villa [1] [2]Xavier Bonnet [3]Francois Lavaste [1] [2]

[1]LBM/Institut de Biomécanique Humaine Georges Charpak, Arts et Metiers ParisTech, Paris, [2]CERAH, INI, Woippy, [3]R and D Department, Proteor, Dijon, France

Introduction and Objectives: The role of lower limb joints during locomotion has classically been addressed by inverse dynamic calculation of the lower limb joints powers. This approach, focused on the function of each joint, fails in synthetizing the overall efficiency of the gait pattern. Indeed, the action of lower limb joints can be opposite, for instance, during the push off phase of gait when the ankle is generating power while knee and hip are absorbing [1]. As an alternative, the individual limb method (ILM) proposed by Kuo et al. allows a direct and simple quantification of the global mechanical work needed during gait [1]. Previous work compared the total mechanical work performed by each limb computed from both methods for able-bodied walking at different velocity on level ground [2]. Growing differences were identified during the collision period when the walking velocity increases.

When going down (stair or slope), potential energy must be dissipated. Even if previous works have addressed the quantification of joint powers independently in each condition, no study has sought to compare how negative work is made to absorb this energy according to the walking condition.

The aim of the present paper is to calculate the mechanical work performed by able-bodied subjects during the stance phase when walking downslope and downstairs using both ILM and inverse dynamics method (ID).

Methods: Thirteen asymptomatic subjects participated in the study (average age: 39.08 (±16.14) years). The protocol was approved by the local ethics committee. Data collection included a whole body motion capture with a Vicon system and force plates measurements during walking in three conditions: level ground, slopes (5% and 12% inclined) and stair (4 steps). Data processing consisted in calculating the center of gravity of the body and lower limb joints powers using the modeling described in [3] as well as the mechanical power by the ILM [1]. This second method intrinsically separates the contribution of each lower limb. Mechanical work was then computed by integration of the mechanical power provided both by the ILM and the sum of joint powers from ID to evaluate the dissipated energy during the stance phase.

Results: For one limb, the negative mechanical work obtained by ID underestimates the negative mechanical work obtained by the ILM (Figure 1, Table 1); this is particularly emphasized for the slope descent. Inverse dynamics consider segments as rigid bodies, which suggests that the remaining amount of work could be performed by soft tissue [2]. Another bias of the method is to limit the calculation to lower limb contributions. In slope, in particular, it could be useful to take into account the powers of upper body joints.

More than one third of the negative work is provided by the ankle during stair descent, which is consistent with the specific role of the ankle at strike. To ensure sufficient energy absorption, forefoot contact is required and results in increased mobility of the ankle. Depending on the stiffness of the ankle, this pattern will not be always be possible and the energy absorption would have to be made differently. The knee contributes to more than the half of the negative work performed in stairs as well as in slopes. The quantification of this negative energy can have implication in the design and the setting

of microprocessor-controlled prosthetic knee, which are able to mimic this behaviour by dissipating energy through a hydraulic system. These kind of knees must be fine tuned to avoid compensatory motion, which can have deleterious effect on residual and contralateral joints.

Figure:
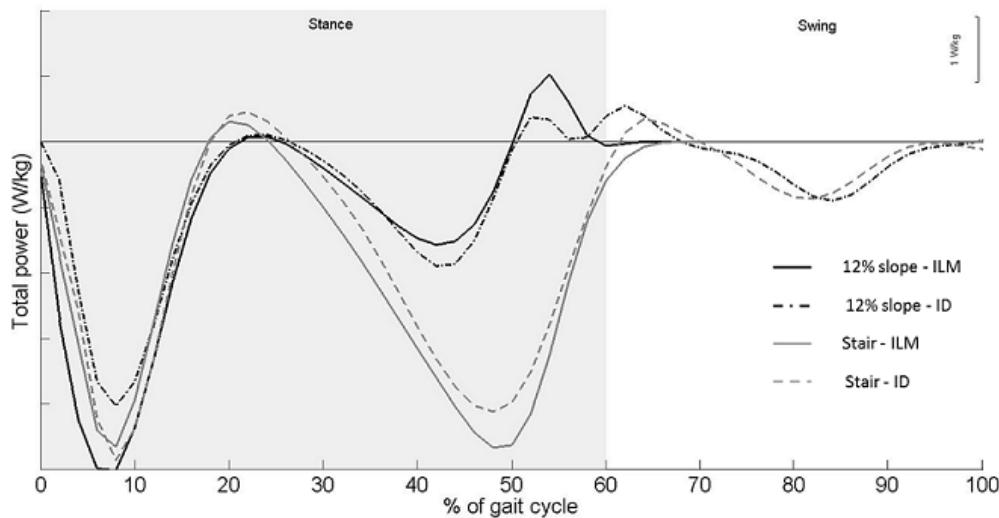
Caption: Figure 1: Total mechanical power of one lower limb over the gait cycle for stair and 12% slope descent calculated from individual limb method (ILM) and inverse dynamics method (ID).

Conclusion: The original results presented here gives reference data of mechanical power performed during stair and slope descent. They could have interesting prospects in prosthetic knee and ankle design and should be completed by a temporal analysis of the contribution of the different joints to the mechanical power absorption, which would be essential for the correct adaptation and coordination between different walking conditions.

Table:

Conditions	Negative mechanical work (J/kg)		Contribution of each joint (% of total negative mechanical work from ILM)		
	ILM	ID	Ankle	Knee	Hip
Stair descent	-1.62 (0.08)	-1.47 (0.13)	37% (9%)	59% (8%)	1% (0.5%)
12% slope descent	-0.92 (0.15)	-0.65 (0.13)	27% (7%)	51% (17%)	18% (5%)

Caption: Table 1: Average (SD) negative mechanical work over the entire stance phase for one limb given by each method (ILM and ID) and percentage of the total negative mechanical work provided by each joint of the lower limb.

References: [1] Kuo, A. D. et al. Exerc. Sport Sci. Rev., 33, 88–97. 2005

[2] Zelik, K. E. and Kuo, A. D. PLoS ONE, 7, e31143. 2012

[3] Pillet, H. et al. Gait Posture, 31, 147–152. 2010

Disclosure of Interest: None Declared

HIGHER FREQUENCY CHARACTERISTICS OF INITIAL LOADING DURING DROP LANDINGS CAN BE MASKED BY SOFT TISSUE VIBRATION ARTEFACT

Mark J. Lake [1,*]Rachel Gardener [1]

[1]Research Institute for Sport and Exercise Science, Liverpool John Moores University, Liverpool, United Kingdom

Introduction and Objectives: There is a need to improve biomechanical techniques that attempt to measure lower limb loading and movement profiles during tasks, such as drop jumping, that are used to screen for the risk of knee ligament injury [1]. Injury risk factors have focused on the initial ground contact phase of landing and turning movements [e.g. 2], but during this period there are oscillations of the lower limb soft tissues which can distort the biomechanical data.   Low-pass filtering (e.g. 10-15Hz) of lower limb kinematics during drop landings removes some of this oscillatory behavior but it is not known whether high frequency signal characteristics (>15Hz) of joint movements and loading are also removed in the process. This study examined initial lower limb loading variables during drop landings with shank motion captured using markers on two skin-mounted plates; one over soft tissue (calf muscles) and the other over bone only (tibia). We investigated the influence of plate/soft tissue vibration and data filtering on loading variables including those associated with knee ligament injury risk (early peak knee abduction moments).

Methods: Twelve young male and female subjects performed two sets of ten controlled, single leg drop (40 cm) landings onto a force platform.   In a mixed order of presentation, one session used a standard shank cluster (normal) of markers on a curved plate tightly mounted over the lateral calf (mass = 34.3 g), while the other session utilized a lighter, individually moulded plate (tibial) (mean mass = 17.4 ± 2.4 g) tightly fitted over the anterio-medial surface of the distal part of the tibia [3]. To capture possible high-frequency motion characteristics, the kinematics were sampled at 1000Hz using a six-camera opto-electronic system (Oqus 300, Qualisys, Sweden). A range of low-pass cut-off frequencies (10-45Hz) were initially used to estimate the signal frequencies present. Two-way ANOVA's were used to explore the relative importance of marker plate location and filter cut-off (15Hz or 35Hz) on loading variables during early ground contact such as peaks in angular velocities and internal knee joint moments ($p < .05$).

Results: Landing conditions (touchdown foot velocity) and initial loading (vertical ground reaction force (vGRF) peak) were not significantly different between the two sets of landings.   This suggested that a direct comparison between the biomechanical data of the two shank marker plate mountings was possible.

For both plate conditions motion of the shank had signal content up to approximately 35Hz with the normal plate providing much larger and extended oscillatory behavior (see figure 1.).   Due to the soft tissue vibration, the peak shank flexion velocities for the normal plate were 7-19% larger than the corresponding peak values when using the tibial plate. The tibial plate typically produced data that peaked earlier with a more damped oscillation (see figure 1). For both plates, extensor and abduction knee joint moment peaks were substantially increased using the 35Hz filter by 18% and 47%, respectively. The normal plate significantly increased knee extensor moments and tended to increase abduction moments for both filtering approaches.

Figure:
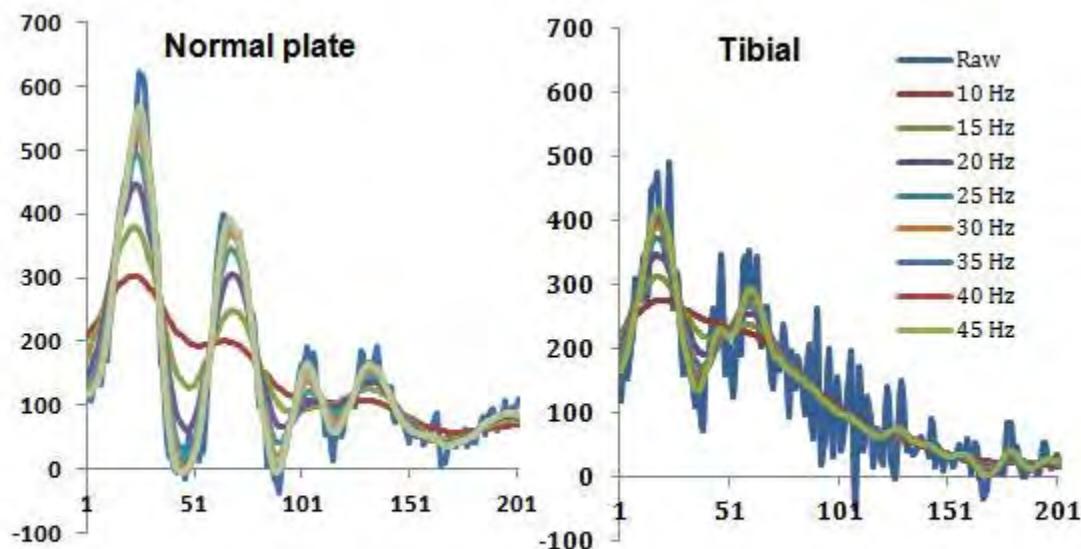
Caption: Figure 1: Shank angular flexion velocity (deg./sec) for the first 200ms

Conclusion: The substantial oscillations observed with the normal soft tissue plate had frequencies between 15Hz and 35Hz which corresponds to the range of vibration frequencies of the triceps surae muscle group after landing [e.g. 4]. Therefore, it can be reasonably assumed that soft tissue vibration was the main reason for increased values for peak segmental transients and knee joint moments during the early landing phase compared to the same data using the tibial plate. The tibial plate, which was minimally influenced by soft tissue movement, clearly demonstrated significant high frequency signal components above 15 Hz and up to 45Hz in some cases. These higher frequencies (masked by soft tissue vibration using the normal plate) agree closely with the frequency content of the vGRF during landing in this study and tibial acceleration measurements during running using bone pins [5]. The findings suggest that, unless the influence of soft tissue vibrations during initial landing can be minimised and higher frequency motion characteristics are retained in the data, injury risk factor variables determined during this phase should be treated with caution.

References: [1] Shultz et al., J. Ath. Training, 47(5):591-603, 2012.

[2] Sigward and Powers, Clin. Biomech, 21, 41-48, 2006.

[3] Digby et al., Ergonomics, 48(11-14):1623-37, 2005.

[4] Boyer and Nigg J. of Biomech, 37(10):1583-1588, 2004.

[5] Lafortune, J. of Biomech, 24(10):877-886, 1991.

Disclosure of Interest: None Declared

AS-0407

AGE AND GENDER INFLUENCE BICYCLE (DIS)MOUNTING KINEMATICS

Rosemary Dubbeldam [1,*]Chris Baten [1][2]Paul Straathoff [3]Hans Rietman [1][3]Jaap Buurke [1][2]

[1]Roessingh Research and Development, [2]Faculty of Electrical Engineering, Mathematics and Computer Science , Department of Biomedical Signals and Systems, [3]Faculty of Engineering Technology, Department of Biomechanical Engineering, University of Twente, Enschede, Netherlands

Introduction and Objectives: In the Netherlands, senior citizens continue to ride their bicycles well into old age. However, elderly cyclists have a high risk of being involved in a single-cycling accident, a cycling accident where no other party is directly involved: About 12000 elderly cyclists require medical attention each year. Most of these accidents occur at low cycling velocities and 20% occur during (dis)mounting the bicycle. Knowledge of bicycle and cyclist kinematics during (dis)mounting may provide insight in fall mechanisms. So far, accident analysis studies did not distinguish between mounting and dismounting a bicycle and no studies reported on corresponding bicycle or cyclist kinematics. This study aims to analyse bicycle and cyclist (dis)mounting kinematics and relate these findings to age, gender and fall-history.

Methods: Cycle measurements were performed outdoors. Fourteen young (18-40 years) and 33 elderly (65-82 years) cyclists were asked to get on the test-bicycle, cycle normally for about 400 m stop and wait, continue cycling for 400 m and get off the bicycle at a certain point (Fig. 1). Of the elderly cyclists, 15 had reported a fall with their bicycle in the last year. Bicycle and cyclist motions were recorded with 10 Inertial Measurement Units (IMU's). FUSION software (LABVIEW) was used to assess kinematic parameters during the (dis-)mounting phase. The mounting phase was defined from the moment the first foot was lifted from the floor till cyclic leg motion occurred, as was observed by plotting the left and right thigh angular velocity. Vice-versa defined the dismounting phase. The maximum angle, angular velocity and angular acceleration were calculated for the bicycle roll (around longitudinal axis), bicycle sway (around vertical axis), bicycle steer, cyclist left and right thigh (around transverse axis) and cyclist sternum roll (around longitudinal axis). The cycling velocity was calculated by integrating the longitudinal acceleration from the IMU accelerometer signal on the bicycle frame. By means of a linear regression model, the relationships between kinematic parameters and age, gender and fall-history were studied.

Results: All cyclists reached a cycling velocity of at least 5 km/h by the end of the mounting phase. Elderly cyclists tended to reach 5 km/h around 50% of the mounting phase while younger cyclists reached this velocity around 90% of the mounting phase. The spreading of the kinematic parameters within the older and young group was large: many older cyclists performed similar to the young cyclists. However, significant group differences were observed and significant relationships between age, gender and fall-history and cycling kinematics were assessed in the linear regression analysis. During mounting, older cyclists have 60% higher thigh angular accelerations compared to the younger cyclists (2907 vs. 1816 deg/s^2). Female cyclists have 40% higher thigh angular accelerations compared to male cyclists. Furthermore, older cyclists demonstrated 20% higher bicycle sway angular accelerations, and females demonstrated lower steer angular velocities. The older cyclists with a fall-history demonstrated 25% higher sternum angular velocities compared to older cyclists without a fall history.

Older cyclists needed about 1 second more time to dismount their bicycle compared to young cyclists (4.6 vs. 3.6 sec). During dismounting, female cyclists have 50% higher thigh accelerations compared to male cyclists, but the female cyclists showed 40% lower bicycle yaw angular accelerations compared to male cyclists. The older cyclists with a fall-history demonstrated 30% lower maximum steer angles compared to older cyclists without a fall history.

During the waiting task, these differences in dismounting thigh acceleration increase to 75% for elderly and 90% for females compared to young and male cyclists respectively.

Figure:

Caption: Figure 1. Older cyclist mounting test bicycle

Conclusion: Differences in bicycle and cyclists kinematics were observed between young and older cyclists but also between males and females. The higher thigh accelerations observed for older and female cyclists may be related to their higher risk of being injured during (dis)mounting compared to young and male cyclists which have been reported in accident analysis studies.

Disclosure of Interest: None Declared

PERFORMANCE OPTIMIZATION AND ERROR ESTIMATION OF AN OPTICAL MOTION CAPTURE SETUP FOR MEASURING SMALL DISPLACEMENTS ON THE FOOT WITHIN A FULL BODY MEASUREMENT VOLUME

Patric Eichelberger [1,*]Nicole Lutz [1] [2]Yvonne Brülhart [1]Leonore Joanna Bösch [1]Fabian Krause [3]Heiner Baur [1]

[1]Bern University of Applied Sciences, Health, Discipline Physiotherapy, Bern, Switzerland, [2]University of Salzburg, Department of Sport Sciences & Kinesiology, Salzburg, Austria, [3]University of Bern, Inselspital, Department of Orthopaedic Surgery, Bern, Switzerland

Introduction and Objectives: Foot function can clinically be assessed by the navicular drop [1], a compound measure for the talonavicular joint motion that is often taken in static conditions. It has been found that other factors than static foot posture play a role in dynamic foot mobility [2]. Therefore, a new foot model for dynamic navicular drop measurement using optical 3D motion capturing has recently been developed. The aim of this study was the optimization of an existing full body measurement setup in order to allow simultaneous foot assessments and the estimation of accompanying instrumental errors to have a quantitative landmark in the optimization process.

Methods: The examined setups consisted of six, eight or ten symmetrically arranged cameras (Vicon Bonita, 200 Hz, Vicon Motion Systems, Ltd., Oxford, UK) resulting in a measurement volume of $(5.5 \cdot 1.2 \cdot 2)$ m^3 in all cases. Spatial region of interest for performance analysis (ROI$_{PA}$) was given by two force plates centrally placed in the measurement volume. Temporal ROI$_{PA}$ was defined as the interval between left initial contact and left toe off event. For the reference object two spherical markers with a diameter of (16.14 ± 0.05) mm and an inter-center distance of (95.53 ± 0.02) mm were placed at both ends of a rigid rod. The reference object was either placed with its longitudinal axis in medial-lateral (ML), anterior-posterior (AP) or cranial-caudal (CC) direction on the left foot. AP and CC configurations were measured with reference object mounting on the foot's lateral and medial side respectively. Ten trials per reference object mounting position were captured and standard deviations (SD) from the measured marker distances calculated. The average SD from ten trials was defined as precision, the relevant performance quantity under consideration of displacement measurements. Measurement uncertainty served as outcome and was calculated as $U = 2 \cdot SD$ (95.5% CI). Following checking for normal distribution (Kolmogorov-Smirnov), outcome differences between examined camera setups were analyzed with paired t-tests.

Results: Measurement uncertainties for the initial 6-camera setup ranged from 0.78 mm to 3.31 mm. This interval decreased for the 8-camera setup (0.26 mm to 0.99 mm) and was stable when further switching to ten cameras (0.26 mm to 0.96 mm). The relative change in measurement uncertainty ranged from +9% to a reduction of -77% for the final 10-camera setup compared to the 6-camera setup. The changes of the CC-med configuration never showed statistical significance ($p < 0.05$). All other changes were significant when switching from six to eight and from six to ten cameras. Switching from eight to ten cameras never turned out to be significant.

Figure:
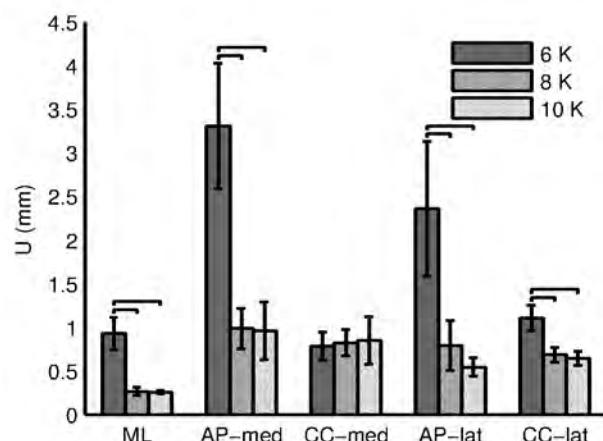
Caption: Measurement uncertainty with error bars (+/- SD) for all measured conditions with horizontal brackets indicating significant differences (p<0.05)

Conclusion: Adding two or four cameras to the initial 6-camera setup didn't influence the uncertainty in the CC-med configuration, whilst all other configurations profited from an uncertainty decrease. In the 6-camera setup, the uncertainty was more inhomogeneous for the different configurations compared to the 8-camera and 10-camera setup. Comparing six and ten cameras, ML, AP-med and AP-lat showed with (-70 to -77)% similar uncertainty improvements, whereas the uncertainty in CC-lat only decreased by 42%. In the final 10-camera setup, the smallest uncertainties were observed for ML (0.26 mm) and the highest for AP-med (0.96 mm). The estimations are spatially and temporary limited to the force plates when the foot is in stance phase. The use of ten cameras led to an optimized system performance for displacement measurements on the foot within a full body measurement volume. Relating the findings to navicular drop values of normal feet (about 8 mm), relative instrumental errors can roughly be estimated to lie between 3% and 12%, which is considered as an acceptable error range. In accordance to the requirement to keep the full body measurement volume for routine gait analysis unchanged, it is expected that the maximum measurement performance has been reached. As already reported by other authors, the influence of the laboratory setup on measurement performance was clearly demonstrated and the importance of systematic instrumental error assessment before clinical measurements is underlined.

References: [1] Menz et al., JAPMA, 88: 119-129, 1998.
[2] Dicharry et al., JOSPT, 39: 628-634, 2009.

Disclosure of Interest: None Declared

Lower Limb

AS-0409

UNILATERAL FOOT PRONATION INCREASES IPSILATERAL SHANK INTERNAL ROTATION AND CONTRALATERAL KNEE ADDUCTION MOMENT OF INDIVIDUALS WITH KNEE OSTEOARTHRITIS DURING THE STANCE PHASE OF GAIT

Renan Alves Resende [1]Kevin Deluzio [2]Renata Noce Kirkwood [3]Renato Guilherme Trede Filho [1,*]Angélica de Fátima Silva [1]Mayra Fernandes de Souza Orlandi [1]Sérgio Teixeira Fonseca [4]

[1]Physical Therapy, Universidade Federal dos Vales do Jequitinhonha e Mucuri, Diamantina, Brazil, [2]Mechanical and Materials Engineering, Queen's University , Kingston, [3]Kinesiology and Physical Education, Wilfrid Laurier University, Waterloo, Canada, [4]Physical Therapy, Universidade Federal de Minas Gerais, Belo Horizonte, Brazil

Introduction and Objectives: Increased shank internal rotation[1] and knee adduction moment[2] during the stance phase of gait increase knee osteoarthritis (OA) progression. In healthy young individuals, unilateral foot pronation increases shank internal rotation of the ipsilateral lower limb and knee adduction moment of the contralateral lower limb[3]. In addition, individuals with knee OA demonstrate increased foot pronation[4]. Therefore, this study investigated the effects of unilateral foot pronation on the biomechanics of lower limbs during the stance phase of gait of individuals with knee OA.

Methods: Kinematic and kinetic data of 20 participants (13 females) with knee OA on one or both knees were collected while they walked wearing flat sandals and laterally wedged sandals (10º medially inclined on the forefoot). Three conditions were investigated: (1) control condition - the participant walked wearing flat sandals; (2) ipsilateral side inclined condition – wedged sandal on the knee OA side and a flat sandal on the contralateral side; 3) contralateral side inclined condition - flat sandal on the knee OA side and wedged sandal on the contralateral side. The right lower limb biomechanics were analyzed for both conditions. Principal Component Analysis was used to compare differences between conditions on rearfoot eversion, shank internal rotation and knee adduction moment. The scores of the principal components retained for analysis were compared between conditions using one-way repeated measures analysis of variance (ANOVA) with pre-planned contrasts between the control condition and the two other conditions.

Results: Participants had an average age, mass and height of 67 years (SD 8.3), 87.9 kg (SD 18) and 170 cm (SD 8), respectively. Table 1 presents the results of this study. Gait waveforms represented by high (+ 1 standard deviation) and low (- 1 standard deviation) principal component scores for each significant principal component are shown in Figure 1.

Figure:

High and low single PC reconstructions (Control x ISI condition)

High and low single PC3 reconstructions (Control x CSI condition)
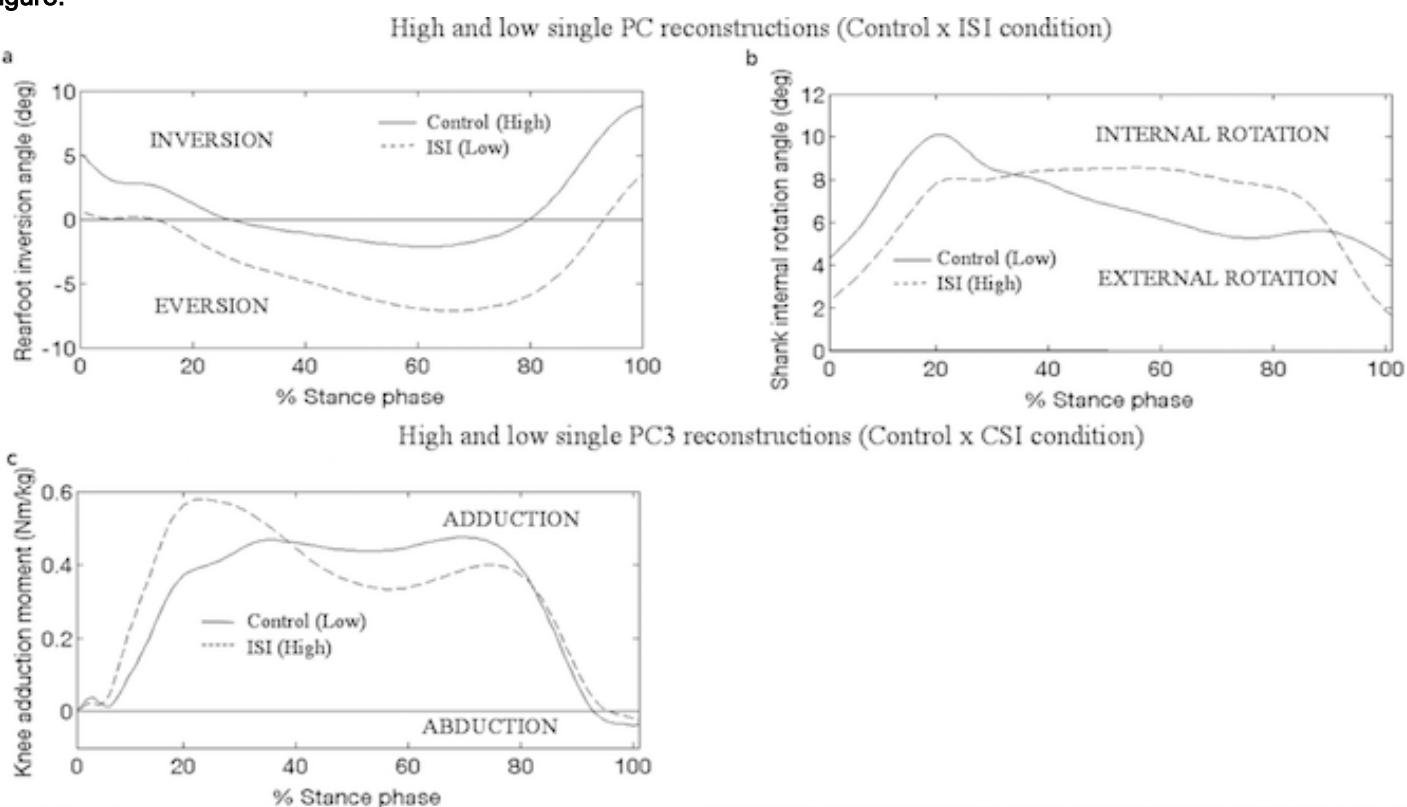
Caption: Control, ipsilateral side inclined and contralateral side inclined conditions differences demonstrated by the ANOVA. Shown in the figures are the waveforms that represent high and low principal component (PC) scores for the indicated measure and PC. In all cases, the waveform that represents the PC score (i.e. high or low PC score) that characterizes the ipsilateral side inclined (ISI) or the contralateral side inclined (CSI) conditions is shown as a dashed line; the solid line is the waveform that represents the control condition PC score. The rearfoot inversion angle PC1 (a); shank internal rotation angle PC2 (b); knee adduction moment PC3 (c).

Conclusion: The coupling mechanism between foot pronation and shank internal rotation also occurs in individuals with knee OA. Increased shank internal rotation accelerates knee OA progression, which suggests that these patients could benefit from proper evaluation and treatment of increased unilateral foot pronation. The increased knee adduction moment on the contralateral lower limb may be a compensation for the smaller knee adduction moment caused by lateral wedges on the ipsilateral lower limb[5]. Therefore, foot motion should be evaluated in individuals with knee OA and the use of lateral wedges to reduce knee adduction moment on the ipsilateral lower limb should consider the possible deleterious effects on the contralateral lower limb.

Table:

Measure	PC	Variance explained (%)	*p-value*	Effect size	Interpretation of differences between conditions
Rearfoot inversion angle	1	78.9	<0.001	0.79	ISI condition had greater rearfoot eversion throughout stance.
Shank internal rotation angle	2	3.6	<0.001	0.70	ISI condition had greater shank internal rotation during late stance.
Knee adduction moment	3	8.0	0.002	0.63	CSI condition had greater knee adduction moment in early stance.

Caption: Principal components (PCs) that demonstrated differences between conditions. Percentage of variance explained and an interpretation of each PC are also provided. ISI: ipsilateral side inclined; CSI: contralateral side inclined.

References: [1] Andriacchi et al., Rotational changes at the knee after ACL injury cause cartilage thinning. Clinical orthopaedics and related research, 442: 39-44, 2006.

[2] Miyazaki et al., Dynamic load at baseline can predict radiographic disease progression in medial compartment knee osteoarthritis. Annals of the rheumatic diseases, 61: 617-622, 2002.

[3] Resende et al., Increased unilateral foot pronation affects lower limbs and pelvic biomechanics during walking. Gait and posture, in press, 2014.

[4] Levinger et al., Foot kinematics in people with medial compartment knee osteoarthritis.Rheumatology, 51: 2191-2198, 2012.

[5] Hinman et al., Lateral wedges insoles for medial knee osteoarthritis: effects on lower limb frontal plane biomechanics. Clinical biomechancis, 27: 27-33, 2012.

Disclosure of Interest: None Declared

Lower Limb

AS-0410

THE RELATION OF LEG STIFFNESS ON PERFORMANCE IN CUTTING MANEUVERS

Sina David [1,*]Igor Komnik [1]Johannes Funken [1]Ralf Müller [1]Thomas Dupré [2]Wolfgang Potthast [1]

[1]Institute of Biomechanics and Orthopaedics, German Sport University Cologne, Cologne, [2]Karlsruhe Institute for Technology, Institut of Sports and Sports Science, Karlsruhe, Germany

Introduction and Objectives: Leg stiffness is an important component of fast sprinting or good jumping results.[1, 2] Until now, it is unclear if leg stiffness also influences the performance in fast running and sprinting including directional changes. The spring mass model is usually used to determine the absorption and generation of mechanical energy during the stance phases of walking, running and jumping. By investigating cutting manoeuvres with 90° and 180° turning angle, it is hypothesized, that higher leg stiffness also decreases the duration of the manoeuvre. Therefore the purpose of this study was to investigate the relation between leg stiffness and the performance during 90° and 180° cutting manoeuvers.

Methods: Eight healthy elite soccer players (Height: 1.79 ± 0.06m, weight: 79.5 ± 6.7 kg, age: 23 ± 3.3 years) wearing the same shoe (Under Armour Blur Carbon IV) were investigated with a 12 camera Vicon motion capturing system (200 Hz), fullbody marker set and two Kistler force plates (1000 Hz) which were covered by natural turf. They had to perform five valid trials for each, 90° and 180° cutting manoeuvres and four meter acceleration runs each at maximal effort. The approach distance of three meters and was covered by artificial turf.

Data was calculated by an Anybody AMS lower body model with 3 degrees of freedom (DOF) in the hip and knee joint respectively. Time histories of ground reaction force (GRF), center of mass (COM) and center of pressure (COP) were normalized to the contact time of the outside leg in 90° and 180° cutting manoeuvres. In sprinting, stance time of the contact leg was used for normalization. The resulting GRF (GRF_{RES}), COM (COM_{RES}) and COP (COP_{RES}) were calculated, COM_{RES} and COP_{RES} were used to define a vector between COM_{Res} and COP_{Res} (COMCOP). The GRF_{RES} was then projected on COMCOP. The total displacement of COM_{RES} in direction of COMCOP (COM_{COMCOP}) during contact time and the maximum GRF projected on COMCOP ($MaxGRF_{COMCOP}$) were calculated. The leg stiffness is the $MaxGRF_{COMCOP}$ divided by the maximum COM_{COMCOP} displacement. Further parameters are the maximum force produced to change the COM direction (Max_{DC}) which is $\sqrt{(GRF_{x^2} + GRF_{z^2})}$ for the acceleration runs, $\sqrt{(GRF_{x^2} + GRF_{y^2})}$ for the 90° cuts and for the 180° cuts GRF_x.

Results: No correlation between leg Stiffness and any other parameter was found for acceleration runs. There are only moderate correlations between the force-dependent and the velocity-dependent parameters (p=.001 to .018; r=.388 to .543). In contrast, there is a high correlation between leg stiffness and $MaxGRF_{COMCOP}$ (p<.001; r= .829) and Max_{DC} (p< .001; r=.760). Moderate correlations between leg stiffness and ground contact time (GCT) (p<.001; r=-.671) and runtime (p<.001; r=-.554). Ground contact time decreases with higher $MaxGRF_{COMCOP}$ (p<.001, r=-.717). A shorter GCT is related to shorter runtimes (p<.001; r=.836) and higher MinCOMVel (p<.001; r=-.818).

For 180° cuts leg stiffness is moderate related to GCT (p=.007; r=-.442) and the velocity-dependent parameters (p=.006 to 0.008; r=.435 to .446). Runtime increases with a higher Max_{DC} (p=.001; r=.513)(Table 1).

Figure:
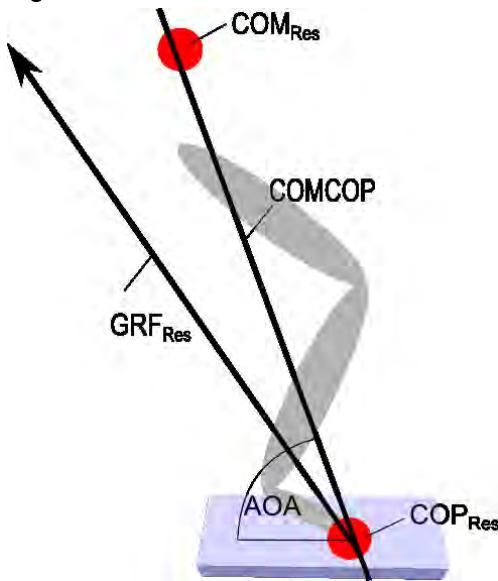
Caption: Figure 1: Schematic illustration of parameters

Conclusion: While there is a high correlation for leg stiffness and runtime in sprinting, there is no detectable relationship of leg stiffness within acceleration sprints. This may be caused by a larger AOA, and therefore higher joint angles compared to sprinting. During 90° cutting manoeuvres, leg stiffness becomes more influential, due to the necessity to change the body's orientation within a small time interval. This is also supported by the correlation of Max_{DC} and runtime, where a higher Max_{DC} leads to a shorter runtime. Contrary to the expectations, there are only moderate to small correlations within the 180° cutting values. This may be caused by a higher complexity of the movement (e.g. gaining back orientation, balance, joint stability etc.) and the role of the inner leg. Other influences on 180° direction changes like the role of countermovement in terms of energy storage[3] are also discussed. In order to further understand the movement strategies encountered in cutting manoeuvres, the role of joint stability and behaviour of muscles in the lower extremity should be investigated.

Table:

	Acceleration run	90° turning leg	180° turning leg
Leg Stiffness (kN/m)	6.55 ± 2.80	4.66 ± 1.23	8.36 ± 2.55
Max GRF_{COMCOP} (N)	1979 ± 198.77	1779.56 ± 226.73	1698.88 ± 166.56
Max_{DC} (N)	1971.49 ± 198.62	1050.25 ± 140.59	1074.68 ± 113.37
MaxCOMVel PRE (m/s)	6.57 ± 0.45	3.47 ± 0.40	4.34 ± 0.50
MaxCOMVel POST (m/s)	7.09 ± 0.44	4.27 ± 0.43	3.99 ± 0.50
MinCOMVel (m/s)	5.51 ± 0.34	1.82 ± 0.22	0.18 ± 0.97
GCT (s)	0.13 ± 0.01	0.38 ± 0.06	0.58 ± 0.17

Caption: Table 1: Means and standard deviations of the calculated parameters

References: [1]Arampatzis A. et al., J Biomech, 32(12):1349–1353, 1999.

[2]Chelly SM, Denis C. Med Sci Sports Exerc, 33(2):326–333, 2001.

[3]Harman, Everett A. et al. Med Sci Sports Exerc, 22(6):825–833, 1990.

Disclosure of Interest: None Declared

Lower Limb

AS-0411

RELATION BETWEEN PREOPERATIVELY DETERMINED STATIC LEG AXIS AND DYNAMIC KNEE ADDUCTION MOMENTS IN WALKING AND STAIR CLIMBING

Johannes Funken [1,*] Kai Heinrich [1] Ralf Müller [1] Michael Knye [1] Rüdiger Schmidt-Wiethoff [2] Wolfgang Potthast [1 2]

[1] Institute of Biomechanics and Orthopaedics, German Sport University Cologne, Cologne, [2] ARCUS Clinics, Pforzheim, Germany

Introduction and Objectives: Osteoarthritis is considered to be the most common joint disease in adult human. The varus moment of the knee (knee adduction moment, KAM) is a surrogate indicator for the loading of the medial knee compartment and an accelerated progression of gonarthritis [1,2]. High tibial osteotomy (HTO) is a surgical procedure to reduce the KAM to a normal level [3] by realigning the leg axis and shifting the loading from the medial towards the lateral compartment. Over the last decades surgical planning was based on x-rays in a static upright position and virtually shifting the mechanical leg axis through the so called Fujisawa point [4]. Durable results are strongly related to the preoperative KAM [5]. As a consequence, a high correlation between dynamic KAM and static leg axis (SLA) is essential for a positive long-term outcome of a HTO. In the international literature only correlations between SLA and KAM in very slow walking or with self-selected/unknown speed were found (r: 0.65 – 0.79) [2,6,7]. Activities of daily living (AODL), however, cover a wide range of different movements. The aim of this study was to identify the correlation between preoperative KAM and the SLA in four AODL (slow/fast walking and stair ascending/descending). In the long run this will help to optimize surgical methods and ensure a better and more stable clinical result.

Methods: Ten patients (body mass: 84.6 ± 14.0 kg; body height: 1.79 ± 0.06 m) with upcoming HTO were asked to participate in a gait analysis including slow walking (WS) and fast walking (WF) (1.2 and 1.7 m/s), stair descending (SDown) and stair ascending (SUp). Kinematic data were captured using a 3D-infrared-camera system (Vicon Nexus, 100 Hz). Kinetic data in the walking conditions were captured with two force plates (Kistler, 1000 Hz). For stair climbing a custom made staircase with five steps was used. The second and the third step were instrumented with force plates. Inverse dynamic calculations for the lower limbs were executed using a biomechanical 3D multibody model (alaska, Dynamicus). Static leg axis was calculated from x-rays in a static erect position. Peak knee joint adduction moments were then normalized to body weight and body height and correlated (Spearman) to static leg axis. Additionally ground contact time was calculated as the time between Touchdown and TakeOff.

Results: Knee adduction moment curves show different chracteristics for each condition (Figure). However, mean peak adduction moments did not differ significantly from each other (Table). Mean varus angle was found to be 8.25 ± 2.35°. In fast walking more than half of the variance of the peak knee adduction moment cannot be explained by the static leg axis, which is the main parameter for HTO planning. In stair climbing the explanation of variance is very divergent between ascending and descending. Stair descending does not differ in ground contact time to slow walking and shows a similarly high explanation of variance. Stair ascending in contrast has the longest stance phase but only 34% of the KAM can be explained by the static leg axis. All correlations were significant (p<0.05). All Ground contact times were significantly different to each other (p<0.01), except WS to SDown.

Figure:

Knee Adduction Moment
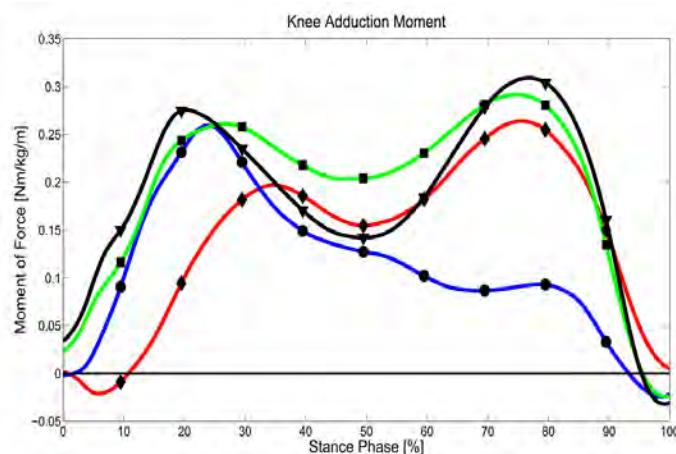
Caption: Green: slow walking, Black: fast walking, Red: stair ascending, Blue: stair descending

Conclusion: Two thirds of the peak KAM in an activity of daily living cannot be explained by the parameter HTO planning is fundamentally based on. The findings of this study indicate that preoperative planning based on static images might not be comprehensive and does not consider a wide range of daily activities. More movements of daily life should be analyzed with regards to the topic to underline the findings of this study. Future development of surgical planning might include preoperative gait analysis combined with model-based simulations to make HTO more individual and generate a more reliable long-term outcome.

Table:

	Peak Knee Adduction Moment [Nm/kg/m]	R^2 (SLA/ Peak KAM)	Stance time [s]
Slow walking	0.30 ± 0.08	0.81	0.71 ± 0.03 [a,b]
Fast walking	0.32 ± 0.09	0.45	0.59 ± 0.02 [a,c,d]
Stair ascending	0.29 ± 0.11	0.34	0.88 ± 0.10 [b,c,e]
Stair descending	0.28 ± 0.14	0.72	0.77 ± 0.11 [d,e]

Caption: Lower cases indicate a significant difference ($p < 0.05$) between two conditions.

References:

[1] Andriacchi et al., Curr Opin Rheumatol, 18, 514-518, 2006.

[2] Andrews et al., 1996, J of Ortho Research, 14 (2), 289-295, 1996.

[3] Birmingham et al., Arthr and rheuma, 61 (5), 648-657, 2009.

[4] Fujisawa et al., Ortho clinics of N America, 10 (3), 585-608, 1979.

[5] Prodromos et al., J of bone and joint surg, Am vol, 67 (8), 1188-1194, 1985.

[6] Specogna et al., Am J Sports and Med, 35 (1), 65-70, 2007.

[7] Hilding et al., Acta Ortho, 66 (4), 317-320, 1995.

Disclosure of Interest: None Declared

Lower Limb

AS-0412

BIOMECHANICAL EVALUATION OF A MICROPROCESSOR CONTROLLED PROSTHETIC KNEE MECHANISM

Anthony Crimin [1,*] Anthony McGarry [1] Stephan Solomonidis [1]

[1]Bioengineering, University of Strathclyde, Glasgow, United Kingdom

Introduction and Objectives: Manufacturers of prosthetic components claim that transfemoral prostheses incorporating microprocessor controlled prosthetic knee joints (MCPK) facilitate a more natural gait and stability compared to non-microprocessor controlled knees (non-MCPK). Furthermore, it has also been suggested that the MCPK user may reduce their cognitive effort during ambulation (Hafner et al. 2007). However, limited biomechanical evidence exists to enhance the understanding of the difference between involuntary and voluntary control that the MCPK and non-MCPK may offer (Gerzeli et al. 2009).

The objective of this investigation was to determine whether a MCPK (Blatchford Orion), compared to a non-MCPK (Otto Bock 3R80), provided participants with enhanced swing phase response and stability during stance.

Methods: The Blatchfords Orion MCPK was compared in a crossover study with six trans-femoral prosthetic users ambulating with the Otto Bock non-MCPK. Participants were considered to be outdoor ambulators (four K3 and two K2) according the Medicare Functional Classification level (MFCL) (Hafner et al.2007).

The kinematics and kinetics of six trans-femoral prosthetic users were investigated during level ambulation; a seven degrees ramp ascent/descent and stair ascent/descent activities at their self-selected walking speed (SSWS). The knee swing response was evaluated through considering the magnitude of mechanical energy absorption. The assumption was made that the magnitude of the mechanical energy absorption is correlated with the magnitude of the knee damping. Hence, with this assumption it is therefore possible to evaluate the damping response indirectly as the SSWS varies when transgressing from level walking to ramp ascent.

Results: The results on initial contact during level walking and ramp activities indicated that the MCPK provides significant (P<0.05) additional knee stability when compared to the non-MCPK as the knee extension moment on initial contact was reduced during initial contact. This result was reasoned as the hip musculature extension moment was also significantly reduced for participant A, B and C during level ambulation on initial contact, indicating that when the participants used the MCPK they felt a reduced requirement to stabilise their knee. Additionally, in contrast to the non-MCPK the two K2 participants who displayed the most significant reductions did not use the handrail for support using the MCPK during ramp descent.

The mechanical energy absorbed by the knee during swing phase, and representative of the damping response illustrated that the MCPK damping response assisted the prosthetic users' natural cadence change. This result is illustrated by the respective correlation coefficient of R=0.8 and 0.9, of the mechanical energy absorbed around the non-MCPK and MCPK (figure 1). The linear correlation indicates that mechanical energy absorption, thus damping response is correlated with walking speed. Therefore, this results illustrate that the stance period measure utilised by the MCPK microprocessor enhances the swing phase response of the knee.

Figure:
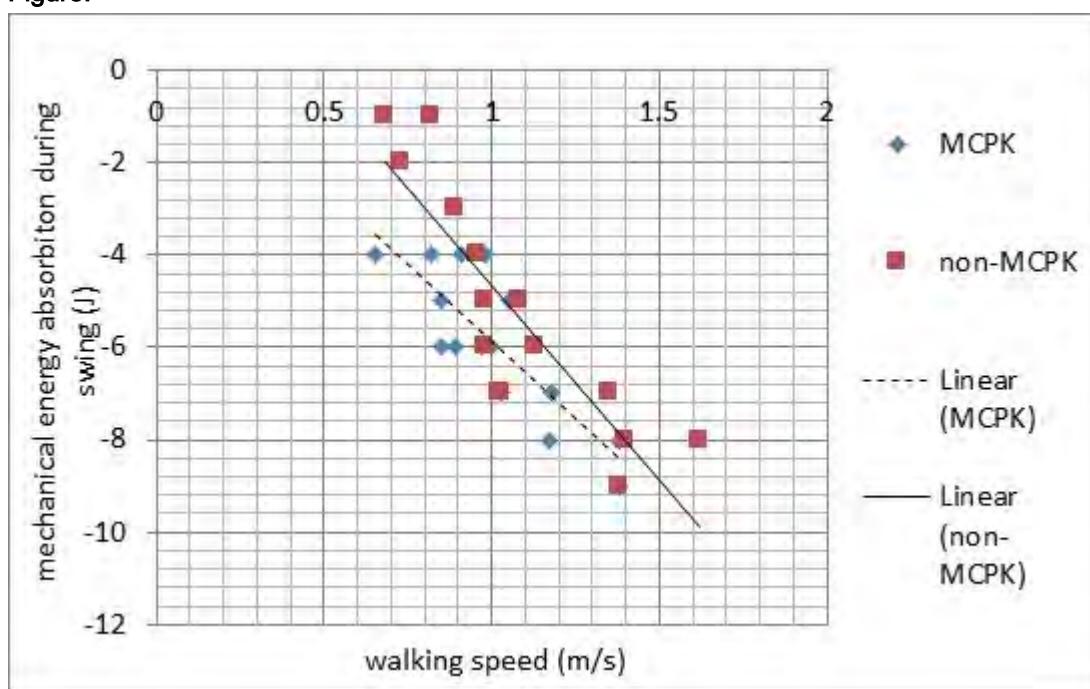
Caption: Figure 1 The mechanical energy absorbed around the knee during level and ramp ambulation

Conclusion: During ambulation with the Orion knee, the user can directly influence the flexion and extension resistance experienced around the knee through controlling the toe load, as with the 3R80 knee. However, as the microprocessor control of the Orion knee determines the relative flexion and extension moment magnitude, this sensory information may be used to determine when the user is ready to move from stance to swing. This gives the user greater voluntary control over the Orion knee compared to the 3R80 knee as high knee resistance is maintained around the 3R80 knee when they transition from stance to swing. Hence, the stance stability of the Orion knee can be maintained until the user is ready to reduce their knee security. Finally, the results also indicate that the (K2) ambulators rather the unrestricted (K3) ambulators appeared to use this additional functionally offered by the MCPK.

References: Gerzeli, S., Torbica, A. & Fattore, G. 2009. Cost utility analysis of knee prosthesis with complete microprocessor control (C-leg) compared with mechanical technology in trans-femoral amputees. *European Journal of Health Economics,* 10**,** 47-55.

Hafner, B. J., Willingham, L. L., Buell, N. C., et al. 2007. Evaluation of Function, Performance, and Preference as Transfemoral Amputees Transition From Mechanical to Microprocessor Control of the Prosthetic Knee. *Physical Medicine and Rehabilitation,* 88**,** 207-17.

Disclosure of Interest: None Declared

AS-0413

THE INTER-DAY MEASUREMENT CONSISTENCY AND PRECISION OF HAMSTRING AND LEG MUSCULO-ARTICULAR STIFFNESS

Justin P. Waxman [1,*] Randy Schmitz [1] Sandra Shultz [1]

[1]Kinesiology, University of North Carolina at Greensboro, Greensboro, United States

Introduction and Objectives: Hamstring (K_{HAM}) and leg (K_{LEG}) musculo-articular stiffness are commonly examined for their relative contribution to athletic performance and injury risk. Because K_{HAM} and K_{LEG} are neuromechanical properties that can be modified through training, it is important to know the expected day-to-day variations that are inherent in these measures before proceeding with intervention strategies. Therefore, the objective was to examine the inter-day measurement consistency and precision of K_{HAM} and K_{LEG}.

Methods: K_{HAM} and K_{LEG} were assessed on 2 separate testing occasions, separated by 2-5 days, in 15 healthy college-aged individuals (6 male, 9 female; 21.5 ± 2.5 yrs, 1.7 ± 0.1 m, 69.3 ± 11.0 kg). Participants were recreationally active and free from lower-extremity injury. K_{HAM} was assessed via the free oscillation technique, whereby the leg is modeled as a single-degree-of-freedom mass-spring system and the damping effect imposed by the hamstring musculotendinous unit on oscillatory flexion/extension at the knee joint is quantified, following a brief manual perturbation. K_{LEG} was assessed via barefoot hopping on a force platform at a frequency of 2.2 Hz under 3 separate conditions (i.e. bilateral, left leg, right leg). Inter-day measurement consistency was determined using repeated-measures analysis of variance (ANOVA) and calculating intraclass correlation coefficients ($ICC_{2,k}$ model). Measurement precision was evaluated by computing the standard error of measurement (SEM) and 68% and 95% limits of agreement (68%LOA and 95%LOA, respectively).

Results: All results are presented in Table 1. K_{LEG} demonstrated good-to-excellent inter-day measurement consistency for all three hopping conditions ($ICC_{2,3}$ range: 0.87 to 0.94) whereas K_{HAM} demonstrated only moderate measurement consistency ($ICC_{2,5}$ = 0.71). Additionally, absolute measurement error (LOA) for K_{HAM} revealed a relatively large systematic bias (9.4% of test-retest mean value), with greater values observed on Day 2 (Figure 1). When comparing the 68% and 95% LOA to the dispersion of scores (i.e. ±1 SD and ±1.96 SD, respectively), unilateral K_{LEG} had the highest measurement precision (left = 45.8%, right = 40.9% of SD), followed by bilateral K_{LEG} (65.8% of SD) and K_{HAM} (83.1% of SD).

Figure:
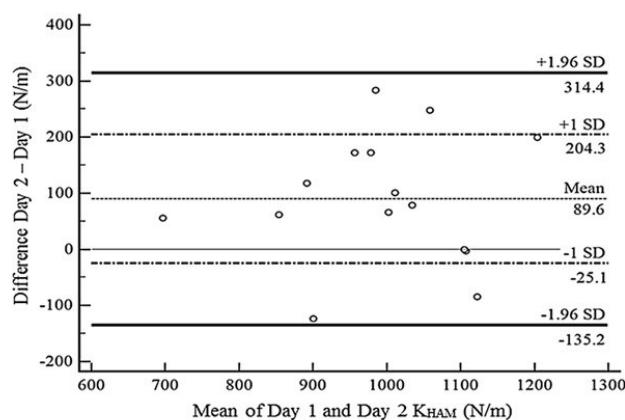
Figure 1. Bland-Altman plot showing the difference between values obtained on the first and second day of testing on the vertical axis, and the mean of the first and second day of testing on the horizontal axis, for each participant during K_{HAM} assessments. The thin dashed line represents the mean difference (bias) between testing days (Day 2–Day 1), while the thick dashed lines and solid lines represent the 68% and 95% limits of agreement, respectively. The mean difference is greater than zero, indicating systematic bias between the first and second day of testing.

Conclusion: The good-to-excellent inter-day measurement consistency observed for K_{LEG} indicates that K_{LEG} is a highly consistent measure when assessed during hopping at 2.2 Hz, and that K_{LEG} can be adequately assessed with little familiarization. In contrast, K_{HAM} demonstrated lower measurement consistency, and the systematic bias observed from the LOA analysis indicates the presence of a learning effect from Day 1 to Day 2. Thus, additional familiarization may be needed to obtain acceptable measurement consistency and precision when assessing K_{HAM}. Although K_{LEG} appears to be a highly consistent measure that can be adequately assessed with little familiarization, K_{HAM} displayed lower inter-day measurement consistency which was likely partially due to the presence of a learning effect (systematic error). As such, researchers interested in evaluating longitudinal changes in K_{HAM} should allow for adequate familiarization to the assessment procedures and include a control group. Additionally, researchers may find these results helpful for sample size estimation or when comparing day-to-day measurement consistency using alternative testing procedures.

Table:

	Day 1 m(SD)	Day 2 m(SD)	$ICC_{2,K}$	SEM	Bias	68% LOA	95% LOA
K_{LEG} (kN/m)							
Bilateral	37.2(8.1)	35.2(8.0)	0.87	2.9	-2.0	±5.3	±10.3
Left Leg	25.5(4.1)	25.1(4.2)	0.94	1.0	-0.4	±1.9	±3.2
Right Leg	25.7(4.2)	24.6(4.6)	0.94	1.1	-1.1	±1.8	±3.6
K_{HAM} (N/m)	949.0(134.1)	1038.6(141.8)	0.71	76.3	89.6	±114.7	±224.8

Caption: Inter-day measurement consistency and precision statistics for hamstring stiffness (KHAM) and leg stiffness (KLEG) measures.

Disclosure of Interest: None Declared

AS-0414

THE RELATIONSHIP BETWEEN PERFORMANCE ON A SINGLE-LEG SQUAT AND LEAP LANDING TASK: MOVING TOWARDS A NETBALL-SPECIFIC ACL INJURY RISK SCREENING METHOD

Aaron S. Fox [1,*] Jason Bonacci [1] Scott McLean [2] Michael Spittle [3] Natalie Saunders [1]

[1]School of Exercise and Nutrition Sciences, Deakin University, Melbourne, Australia, [2]Human Performance Innovation Laboratory, University of Michigan, Ann Arbor, United States, [3]College of Sport and Exercise Science, Victoria University, Melbourne, Australia

Introduction and Objectives: Screening methods that identify those at-risk of suffering an anterior cruciate ligament (ACL) injury are vital for the development of targeted ACL injury prevention strategies. The majority of ACL injury risk screening methods [1-3] utilise simplistic bilateral landing tasks, which have been shown to not adequately represent sport-specific movements [4,5]. The single-leg squat may be a useful screening movement for netball as it closely resembles the lower limb position of a leap landing; a high-risk task within the sport [6]. The purpose of this study was to determine the relationship between performance of a single-limb squat and a netball leap landing, in order to examine the utility of a single-limb squat as a netball-specific ACL injury risk screening method.

Methods: Twenty-five female netball players (23.7 ± 3.3 years; 170.9 ± 8.0 cm; 68.2 ± 9.0 kg) performed a single-leg squat task and ten trials of a netball leap landing task. The squat required the performance of one repetition on a single-limb. The leap landing involved a six-metre run-up, followed by a single-limb take-off and land on the contralateral limb while catching a pass. Three-dimensional hip and knee joint rotations and external joint moments were calculated from lower extremity kinematics and ground reaction force (GRF) data for both tasks. For the squat, data were extracted from the initiation of the squat descent to the end of the squat ascent. For the landing task, data were extracted from initial contact (IC) to 300 ms post IC. A vertical GRF threshold of 10N was used to detect IC.

Principal patterns (PP) in biomechanical data from both tasks were identified by submitting extracted joint rotation and moment waveform data to principal component analysis (PCA). Patterns were extracted for the variables of hip flexion/extension ($H_{FLEX/EXT}$), adduction/abduction ($H_{ADD/ABD}$), and internal/external rotation ($H_{IR/ER}$); knee flexion/extension ($K_{FLEX/EXT}$), adduction/abduction ($K_{ADD/ABD}$), and internal/external rotation ($K_{IR/ER}$); ankle dorsiflexion/plantarflexion ($A_{DF/PF}$), inversion/eversion ($A_{INV/EVE}$), and ankle internal/external rotation ($A_{IR/ER}$); and H_{FLEX}, H_{ADD}, H_{ER}, K_{FLEX}, K_{ABD}, K_{ER}, A_{DF}, A_{EVE}, and A_{ER} moments. Principal pattern scores (PP-Scores), which measure the degree to which the shape of the waveform corresponds to each PP [7], were computed and used for subsequent analyses. Pearson's correlation coefficients (r) were calculated to identify significant correlations (p < 0.01; r > 0.60) between squat and landing PP-Scores.

Results: Reduced peak K_{FLEX} and increased K_{IR} during the squat was indicative of reduced K_{FLEX} (r = 0.62) and increased K_{IR} (r = 0.95), respectively, during landing. Figure 1 illustrates the relationship between K_{FLEX} and K_{IR} during the squatting and landing tasks. Larger squat K_{ADD} moment was also indicative of increases in K_{IR} during landing (r = -0.82). Increased H_{IR} during the squat was associated with greater landing H_{IR} (r = 0.63). Greater frontal and transverse plane knee motion during the squat were associated with greater landing frontal plane knee motion (r = 0.74) and peak K_{ABD} (r = -0.63), respectively. Greater transverse plane knee motion and A_{EVE} during the squat were indicative of increases in peak K_{ADD}

and K_{ABD} moments (r = -0.71 and 0.65, respectively) during landing; while increases in frontal plane knee motion and K_{ADD} moment during the squat were associated with greater landing K_{ADD} moments (r = 0.67 and 0.73, respectively). Greater K_{ER} moment during the squat was associated with larger peak K_{ER} moments during landing (r = 0.71).

Figure:
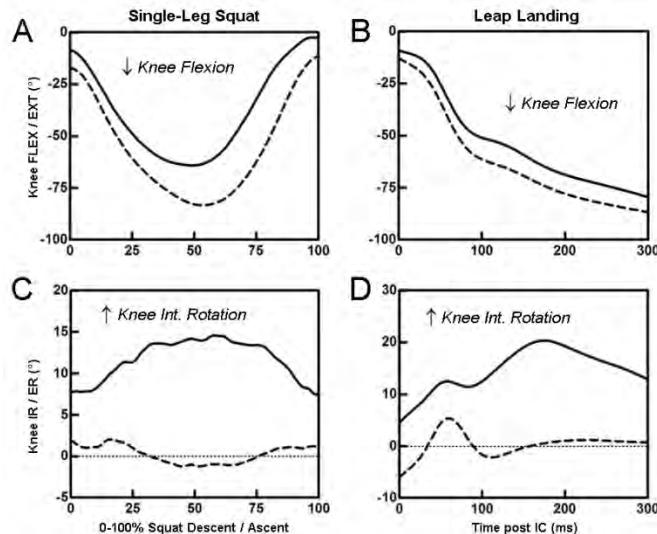
Caption: Figure 1: Effect of high (solid) and low (dashed) knee flexion and knee internal rotation PP-Scores during the squat on knee flexion (A & B) and knee internal rotation (C & D) during landing.

Conclusion: Strong associations were evident between matching joint rotations and moments between tasks, particularly at the knee (see Figure 1). A reduction in peak knee flexion during the squat was indicative of reduced knee flexion during landing. The presence of large frontal and transverse plane motion and moments at the hip and knee also transferred across tasks. The presentation of these biomechanical patterns during a single-leg squat may be useful indicators of athletes who perform leap landings with poor lower limb mechanics. Considering this type of landing is responsible for many ACL injuries in netball [6], the single-leg squat may have utility as a simplistic screening method for ACL injury risk in netball athletes.

References: [1] Myer et al., Athlet. Ther. Today, 13: 39-44, 2008.

[2] Myer et al., Br. J. Sports Med., 45: 238-244, 2011.

[3] Padua et al., Am. J. Sports Med., 37: 1996-2002, 2009.

[4] Edwards et al., Scand. J. Med. Sci. Sports, 20: 516-523, 2010.

[5] Kristianslund & Krosshaug, Am. J. Sports Med., 41: 684-688, 2013.

[6] Otago, J. Sci. Med. Sport, 7: 85-95, 2004.

[7] Deluzio & Astephen, Gait Posture, 25: 86-93, 2007.

Disclosure of Interest: None Declared

AS-0416

SAGITTAL PLANE LANDING KINEMATICS IN ATHLETES WITH AND WITHOUT PATELLAR TENDINOPATHY

Rodrigo Scattone Silva [1,*]Ana Luisa Granado Ferreira [1]Theresa Nakagawa [1]Luccas Garcia [1]José Mourão dos Santos [2]Fábio Serrão [1]

[1]Department of Physiotherapy, [2]Department of Medicine, Federal University of São Carlos (UFSCar), São Carlos-SP, Brazil

Introduction and Objectives: Patellar tendinopathy is highly prevalent in athletes engaged in sports that involve repeated jump-landings and it is considered one of the most common causes of anterior knee pain in the athletic population. Frequent application of high patellar tendon forces and poor landing biomechanics are believed to be some of the main causative factors of patellar tendinopathy [1]. Previous research has shown that asymptomatic subjects with patellar tendon abnormalities have altered jump-landing mechanics in comparison to controls without such abnormalities [2,3]. It has been demonstrated that, when landing from a horizontal jump, athletes with patellar tendon abnormalities perform hip extension, whereas athletes without tendon abnormalities perform hip flexion [2,3]. In fact, this altered hip joint movement pattern during landing was the primary risk factor that predicted both the presence and the severity of a patellar tendon abnormality [3]. However, research involving landing mechanics of athletes with symptomatic patellar tendinopathy is still scarce. The purpose of this study was to compare the sagittal plane lower limb kinematics during jump-landings between athletes with and without patellar tendinopathy.

Methods: Young male athletes, 18 to 30 years of age, were recruited from local volleyball, basketball and handball teams. They were submitted to an ultrasonographic evaluation of both patellar tendons by an experienced radiologist. Subjects presenting current symptoms in the patellar tendon during tendon-loading tasks for at least 3 months and presenting patellar tendon abnormalities [4] were included in the patellar tendinopathy group (TG; n = 7). Asymptomatic subjects without patellar tendon abnormalities were included in the control group (CG; n = 7). The Qualisys Motion Capture system with 8 cameras (Qualisys Medical, AB, SWE) was used to evaluate lower limb kinematics while the athletes performed drop vertical jumps from a box. The symptomatic lower limb was evaluated in the TG and, in case of bilateral symptoms, the most symptomatic limb was evaluated. The athletes of the CG were matched to the athletes of the TG regarding anthropometric variables and evaluated lower limb. For the kinematic evaluation, fourteen passive markers were positioned on anatomical landmarks and 3 clusters were positioned on the athlete's thigh, shank and posterior aspect of the shoe. The athletes performed 3 repetitions of a drop vertical jump task from a 31-cm box. They were instructed to drop from the box in a bipodal stance and immediately perform a maximal vertical jump to reach a ball, which was hanging from the ceiling at the maximal height the athlete could reach. The Visual3D (C-Motion, MD, USA) software was used for data processing. Mean values from the 3 repetitions of the landing phase of the task were considered for analysis. The landing phase of the task comprised the period between foot contact and peak knee flexion. The variables of interest were the peak angles of hip and knee flexion, peak ankle dorsiflexion, as well as the knee/hip, knee/ankle and hip/ankle ratios during the landing phase of the task. Independent t-tests were used for statistical analysis with a significance level of 5%.

Results: Results showed that the TG presented smaller peak hip flexion during landing when compared to the CG. No group differences were observed for peak knee flexion or ankle dorsiflexion (**Table 1**). Additionally, the TG presented a greater knee/hip ratio (P < 0.001) as well as a smaller hip/ankle ratio (P = 0.009) when compared to the CG (**Figure 1**).

Figure:
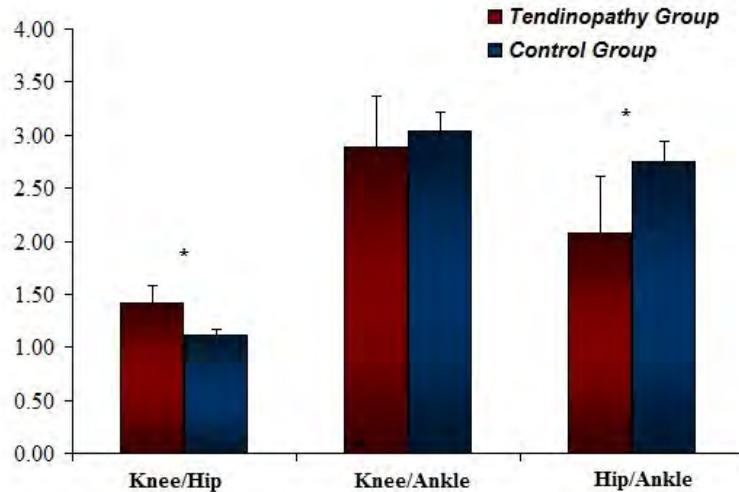
Caption: Figure 1. Sagittal plane peak angle ratios of the hip, knee and ankle during drop vertical jumps in subjects with and without patellar tendinopathy (mean and SD). * Significant difference between groups (P < 0.01).

Conclusion: The landing pattern of the athletes with patellar tendinopathy involved less hip joint flexion in proportion to knee flexion and ankle dorsiflexion when compared to controls. It is likely that this altered jump-landing mechanics results in a less efficient energy dissipation strategy, with the hip joint offering a smaller contribution for ground reaction force dissipation. This landing pattern might result in excessive overload of the knee extensor mechanism, possibly having a significant influence in the development and/or perpetuation of patellar tendinopathy.

Table:

	Tendinopathy Group	Control Group	*P*-Value
Hip Flexion	63.19 ± 10.23*	77.89 ± 9.99	0.019
Knee Flexion	88.80 ± 11.70	86.13 ± 9.98	0.654
Ankle Dorsiflexion	31.37 ± 6.35	28.49 ± 3.93	0.329

Caption: Table 1: Sagittal plane peak joint angles (deg) during drop vertical jumps in subjects with and without patellar tendinopathy (mean ± SD). *Significant difference between groups.

References:

[1] Janssen et al., Med Sci Sports Exerc, 45: 927-934, 2013.

[2] Edwards et al., Med Sci Sports Exerc, 42: 2072-2080, 2010.

[3] Mann et al., Med Sci Sports Exerc, 45: 527-533, 2013.

[4] Cook et al., Scand J Med Sci Sport, 11: 321-327, 2001.

Disclosure of Interest: None Declared

Spine

AS-0417

18F-NAF PET-CT: A MARKER FOR EARLY DETECTION OF BONE DEGENERATION AND REMODELLING IN THE LOWER LUMBAR SPINE

Justin Fernandez [1,*]Shasha Yeung [1]Andi Liu [1]Amanjeet Singh Toor [2]Ju Zhang [1]Vickie Shim [1]Thor Besier [1]Jacob Munro [2]Gerard Deib [3]

[1]University of Auckland, [2]Auckland City Hospital, [3]Mercy Private Hospital, Auckland, New Zealand

Introduction and Objectives: Chronic lower lumbar pain typically has multifactorial causes. Bone remodelling initiated by high stress has been identified as one potential source of pain [1] but there is little evidence to support this. Positron Emission Tomography (PET) is a functional imaging modality that offers an ability to measure bone metabolism for musculoskeletal disorders using a Sodium Fluoride (18F-NaF) trace marker [1,2]. While there is increasing use of 18F-NaF PET-CT for clinical diagnostics, there is no evidence to suggest that one of the major causes of vertebral endplate and spine facet degeneration, namely increased joint bone stress, correlates with NaF uptake. The primary objective of this study was to evaluate if patients who present with lower back pain have increased uptake of 18F-NaF in regions that correspond to high bone stress. The secondary objective was to see if there were any features of spine shape that are good predictors of increased bone stress and NaF uptake. These spine shape features may assist clinicians to identify suitable candidates for NaF imaging.

Methods: Twenty nine patients who presented with back pain had both CT imaging and 18F-NaF PET. Ethical approval was obtained by Mercy Private Hospital. The CT images were registered with the PET data to improve identification of NaF uptake. Those patients that showed significant NaF uptake were used to construct finite element models and compute Von Mises bone stress in the 3rd to 5th lumbar and sacrum using Abaqus. Extracted NaF uptake intensity was then mapped onto the finite element mesh for comparison between NaF intensity and bone stress. To evaluate spine shape, principal component analysis (PCA) was used to identify independent characteristics of shape; and partial least squares regression (PLSR) was used to correlate these shape modes with NaF intensity and stress in the spine.

Results: There were no significant age or BMI differences between males (age 48±19 yrs; BMI 27±4) and females (age 49±17 yrs; BMI 29±6). Of those subjects who presented significant NaF, 44% of their peak bone stress occurred in regions of high NaF uptake on average with some patients exhibiting up to 82% overlap between peak bone stress and high NaF. Further, PCA analysis revealed that the 3 key features of spine shape that influenced bone stress and NaF patterns were pelvic tilt, vertebral spine curvature and intervertebral disc spacing. A PLSR model was developed that linked these spine shape features to NaF intensity for use by both bioengineers and clinicians (as a pre-screening tool). A representative example of a PLSR model prediction of NaF intensity from shape, contrasted with the actual patient is shown in Figure 1. The model predicted the correct pattern and sites of peak NaF intensity near the vertebral endplates and at the spine facets. However, NaF intensity had errors up to 25% in magnitude near the NaF 'hot-spots'.

Figure:

Caption: Figure 1: (A) Model predicted NaF uptake versus (B) real imaged NaF uptake. Red is a peak NaF 'hot spot'.

Conclusion: NaF offers a useful clinical modality to detect early signs of peak bone stress in the lower lumbar, which is linked to bone remodelling long before advanced pathology is observable. Standard structural modalities (CT and MRI) only reflect late adaptive bone changes with reliance on bone sclerosis and marginal vertebral remodelling. Given the high radiation exposure that NaF PET-CT presents to patients the results from this study may provide both clinicians and bioengineers with a pre-screening prediction tool for vetting suitable candidates and reduce unnecessary radiation exposure for healthy patients. This study showed that 44% of peak bone stress sites on average occurred in regions of high NaF uptake and up to 82% in some patients. This suggests that peak bones stress is one important factor associated with bone remodelling and identified by NaF tracers. It is important to interpret these results as a reflection of standing posture, which does not represent the complete array of tasks that constitute a daily loading stimulus. Inclusion of different tasks is likely to increase the overlap between peak stress and NaF. The population of spine models and NaF uptake readings from this study are currently being deposited in the open-source U.S. FDA funded Musculoskeletal Atlas Project (MAP) which is available for orthopaedic evaluation (www.launchpad.net/mapclient/).

References: [1] Draper et al., J. Orthop Res, 30(2): 209–213, 2012. [2] Lotz et al., Radiology, 264(1): 6-19, 2012.

Disclosure of Interest: None Declared

Spine

AS-0418

SAGITTAL PLANE SPINE KINEMATICS DURING STOP-JUMP OF INDIVIDUALS WITH ADOLESCENT IDIOPATHIC SCOLIOSIS POST SURGICAL FUSION OF SPINE.

Rumit S. Kakar [1,*]Yumeng Li [2]Yang-Chieh Fu [3]Cathleen Brown-Crowell [2]Timothy Oswald [4]Kathy Simpson [2]

[1]Physical Therapy, Ithaca College, Ithaca, [2]Kinesiology, University of Georgia, Athens, [3]Health, Exercise Science, and Recreation Management, University of Mississippi, Mississippi, [4]Pediatric Orthopaedic Associates, Atlanta, United States

Introduction and Objectives: After spinal fusion, adolescent idiopathic scoliosis individuals (SF-AIS) often return to exercise and sport. However, the movements SF-AIS use to compensate for the loss of spinal flexibility at the fused segments during high-effort tasks like stop-jumps [1] are not known. The objective of the study was to compare the spinal kinematics in sagittal plane between SF-AIS and healthy controls (CON) groups during the stop-jump task. (Figure 1)

Methods: 10 SF-AIS (physically active; posterior-approach spinal fusion: 11 ± 2 fused segments; post-op time: 2 ± .6 yr); and 10 CON individuals, pair matched for gender, age (17.4 ± 1.3yr, 20.6 ± 1.5yr, respectively), mass (63.5 ± 12.2kg, 66.4 ± 10.9kg), height (1.69 ± 0.09m, 1.72 ± 0.08m) and level of physical activity participated. SF-AIS and CON performed 5 acceptable trials of the stop-jump task. Spatial locations of 24 retro-reflective spine and pelvis markers were recorded via a 7-camera motion capture system (240Hz). Analysis of covariance (jump height = covariate, $p < .05$) and 95% confidence intervals (95%CI) for the mean differences were used to compare the groups' sagittal plane, segmental angular displacements of the 3 spine segments (upper [UT: C7 to T8], middle [MT: T9 to T12], and lower segment [LT: L1 to L5]) and pelvis (PEL), along with relative angles UT-MT, MT-LT and LT-PEL, for the 3 phases of interest (horizontal flight: take-off to initial contact; stance: initial contact till take-off for vertical flight; and the 2nd vertical flight phase).

Results: Jump heights were not different between the two groups (mean difference: 0.013m; $p = .872$; 95% CI: -0.100m to .100m). For segmental angles during the stance phase, SF-AIS demonstrated significantly greater spinal flexion displacements of the MT (5.1°, $p = 0.009$) and LT (6.2°; $p = 0.012$) compared to CON. No other statistically significant group differences were observed for this, the two flight phases ($p > 0.104$) or any of the relative angles ($p = 0.208$-0.983). The mean difference between groups was less than 5° for most of the segmental and relative angular displacements (Table 1).

We expected that greater UT and LT angular displacements in stance phase would be displayed by the SF-AIS group to compensate for the lack of spinal motion in the MT, the segment that was fused entirely. SF-AIS did demonstrate significantly greater LT angular displacement in the compared to CON. However, not expected were the greater MT angular displacements of SF-AIS in this plane. Similar magnitudes of displacements for MT and LT and low MT-LT and LT-PEL relative angles, suggest a synchronous motion of the segments. The results supporting the predictions were contrary to those reported previously for spine kinematics in range of motion [2], gait [2-3] and side-stepping [4] studies. In the stance phase, use of LT extension range to also extend the MT as observed by their synchronous movement is one of the few compensatory adaptations used by SF-AIS during this movement that is different from CON. This adaptation likely helps achieve greater ranges of extension for the fused segments and, thus, in the spine as a whole.

Figure:
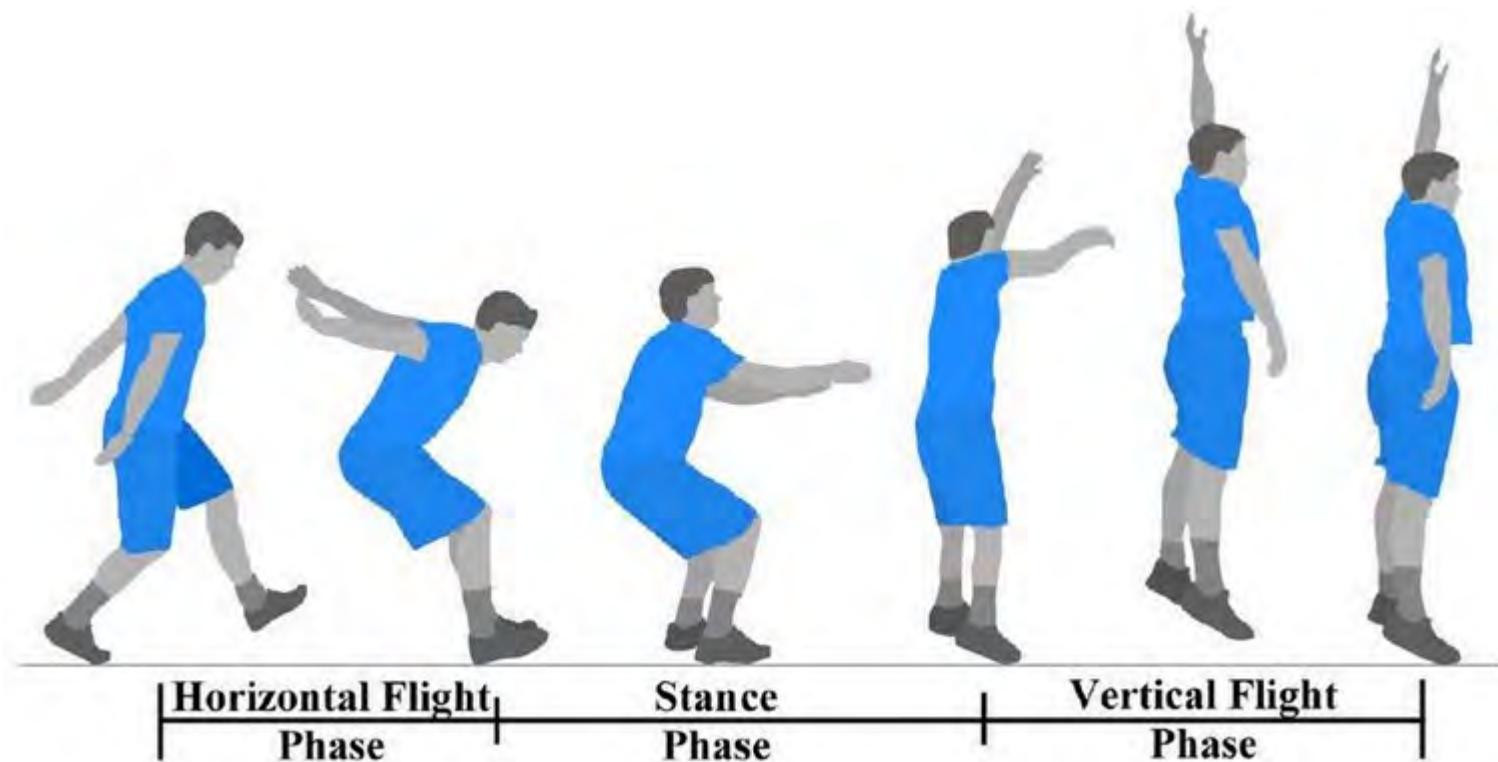
Caption: Figure 1: The stop-jump tasks and its phases.

Conclusion: Our findings suggest that these moderately-active SF-AIS individuals accomplish the performance goal of a successful jump largely through low back flexion-extension, while the fused segments synchronously move with the LT as a unit. Although this compensatory adaptation observed in SF-AIS helps achieve the performance goal during physical activities, the atypical mechanics could be clinically demanding on particular core muscles, thoracolumbar mechanics and the lumbo-pelvic rhythm [5].

Table:

Segmental Angle	SF-AIS	CON	Mean difference (°)	95% CI of the mean differences (°)		p value
	Mean ± SD	Mean ± SD		Upper limit	Lower limit	
Horizontal Flight phase						
Upper segment	18.1 ± 10.1	17.4 ± 2.6	0.7	-5.4	6.7	0.825
Middle segment	19.2 ± 10.6	14.5 ± 3.8	4.7	-1.9	11.2	0.196
Lower segment	18.5 ± 9.4	12.8 ± 3.4	5.7	-0.2	11.4	0.104
Pelvis	15.1 ± 9.6	13.1 ±	2.0	-4	7.9	0.544

		3.3				
Stance phase						
Upper segment	16.9 ± 4.1	14.1 ± 4.3	2.8	-0.7	6.3	0.187
Middle segment	18.4 ± 4.7	13.3 ± 3.0	5.1	1.8	8.3	0.009 *
Lower segment	17.5 ± 6.0	11.3 ± 2.2	6.2	2.4	9.9	0.012 *
Pelvis	13.3 ± 4.0	11.9 ± 2.7	1.4	-1.4	4.2	0.349
Vertical Flight Phase						
Upper segment	12.9 ± 3.6	15.5 ± 4.3	-2.6	-5.8	0.7	0.124
Middle segment	16.2 ± 7.2	14.4 ± 4.7	1.8	-3.3	6.7	0.487
Lower segment	14.4 ± 6.7	12.2 ± 2.8	2.2	-2	6.4	0.376
Pelvis	11.1 ± 4.5	13.1 ± 2.8	-2.0	-5.1	1.1	0.294

Caption: Group Differences (SF-AIS – CON) of angular displacements (°) of the three spine segments (upper, middle and lower) and the pelvis. *Statistically significant difference between groups ($p < .05$)

References: [1] Chappell JD et al., Am J Sport Med, 30:261-267, 2002.

[2] Engsberg JR et al., Spine, 28(17):1993, 2003.

[3] Chan PY et al., Gait Posture, 24(2):219-228, 2006.

[4] Bruyneel AV et al., Eur Spine J, 18(2):188-195, 2009.

[5] Tafazzol A et al., Clin Biomech, 29(1):7-13, 2014.

Disclosure of Interest: None Declared

Trunk

AS-0419

ACTIVE TRUNK EXERCISES REQUIRE MORE MUSCLE ACTIVITY IN MATURE THAN IN YOUNG ADULTS

Stephanie Valentin [1,*] Theresia Licka [1]

[1] Movement Science Group, Equine Clinic, University of Veterinary Medicine Vienna, Vienna, Austria

Introduction and Objectives: Reductions in muscle strength [1], changes in motor control patterns [2] and muscle morphology [3] are known to occur with ageing. However, the effect of age on trunk muscle activity during active trunk exercises has not been widely investigated, even though spinal range of motion is known to reduce with age [4]. The aim of this study was to compare the age differences in activity of the rectus abdominis (RA), obliquus internus (OI), obliquus externus (OE), and erector spinae (ES) muscles during flexion and extension exercises performed in upright (U) and 4-point kneeling (4P) postures.

Methods: Twenty-four healthy participants (12 young, aged 18-25 years; 12 mature, aged 45-60 years) were included. Reflective markers were attached over the spinous process of the 11th thoracic vertebra (T11), the head, the left and right styloid processes, and lateral femoral condyles. Three-dimensional kinematic data were collected using 10 high speed cameras (Eagle Digital Real Time System, Motion Analysis Corp., 120Hz). Surface EMG electrodes (Delsys Trigno, 1200Hz) were attached over the left and right ES, RA, OE, and OI after skin preparation. Data were collected during three repetitions of 10s of flexion and extension movements in U and 4P. Participants were instructed to perform each movement to their end range and return to the starting posture in one fluent movement. Raw EMG data were resampled, rectified, zero-mean offset, and a 4th order low pass Butterworth filter applied. Processed EMG data from 0.5s before movement onset and 0.5s after movement cessation (both based on vertical T11 movement) were included for analysis. EMG data were normalised to the maximally observed muscle activity from any trial and movement for each muscle, and the maximum and 1st, 2nd, and 3rd quartiles (Q1, Q2, Q3) calculated for the concentric phase (conc) and eccentric phase (ecc) of muscle activity. Due to non-normally distributed data, each EMG parameter was compared between the young and mature groups using a Mann-Whitney U test.

Results: There were no significant differences in T11 vertical displacement between the age groups. In the young group, median values across all muscles, postures and movements ranged from 6.91 - 33.29% for Q1, 7.17 - 42.05% for Q2, 7.53 - 66.02% for Q3, and 10.96 - 86.78% for the maximum. In the mature group, these values were 9.39 - 36.67%, 11.19 - 53.87%, 12.24 - 74.98%, and 15.33 - 89.08% respectively. In 4P, there were no significant differences between the young and mature group for any movement, muscle, or parameter, except for RA right (flexion Q2 ecc; extension Q1, Q2, Q3 ecc; $p<0.05$) which showed significantly greater values in the mature group. In U flexion, significant differences were found between the young and mature group for all muscles, however this was only in conc for ES (ES left Q1 and Q2; ES right Q1; $p<0.05$), in the maximum and Q3 ecc for left and right RA and OE, and Q3 conc for OI right (all $p<0.05$). In all these cases, values were greater in the mature group. Also, in U extension, the mature group had significantly higher values (ES left all parameters; ES right Q1, Q2 conc; $p<0.05$).

Conclusion: Differences in trunk muscle activation were observed between healthy young and mature participants, although this was dependent on movement direction and posture adopted. Interestingly, in each significant finding, the

mature group scored higher normalised EMG values compared to the young group, indicating that mature adults require greater muscle activity based on a peak dynamic normalisation method in comparison to young adults to attain similar trunk displacement. In U, differences between the age groups were found in all muscles and across all phases (concentric, maximum, eccentric). However in 4P, which is a posture considered to be relatively novel, fewer significant differences occurred between the age groups, with only RA right in the eccentric phase showing significant differences. This unilateral finding may be related to the establishment of more marked laterality with age in commonly adopted postures.

References:

[1] Singh et al., Muscle Nerve, 44: 74-9, 2011.

[2] Kanekar et al., Exp Brain Res, 232: 1127-36, 2014.

[3] Frontera et al., J Appl Physiol, 88: 1321-6, 2000.

[4] Bible et al., Spine, 33: 1793-9, 2008.

Disclosure of Interest: None Declared

AS-0420

BOTULINUM TOXIN TYPE-A INDUCED PARASPINAL MUSCLE WEAKNESS CAUSED LUMBAR SPINE DEGENERATION

Sang Kuy Han [1,*]Young Eun Kim [2]Keyoung Jin Chun [1]

[1]Advanced Biomedical and Welfare technology R&BD group, Korea Institute of Industrial Technology, Cheonan, [2]Department of Mechanical Engineering, Dankook University, Yongin, Korea, Republic Of

Introduction and Objectives: The spine is a complex anatomic structure and provides mobility and strength. The health of the spine depends on the integrities and proper functions of structural components. Paraspinal muscles and spine are mutually dependent in a functional manner, as paraspinal muscles have a role to move and stabilize the spine. It has been generally speculated that paraspinal muscle weakness is related to spinal degeneration including intervertebral disc (IVD) failure. Since experimental approaches for examining the strength of paraspinal muscle in *in-vivo* is technically difficult, most of previous studies have been conducted using an *in vitro* experiment and a computational analysis, such as, a finite element modeling, for understanding of IVD biomechanics [1-2]. Recently, a series of studies employing botulinum toxin type-A (Botox) induced muscle weakness model has been reported to investigate the relationship between adjacent muscle weakness and the synovial joint health [3]. These studies systematically demonstrated that quadriceps muscle weakness caused the degenerations of articular cartilage in a patellofemoral joint. The purpose of this study was to investigate the effects of Botox induced paraspinal muscle weakness on the degeneration of lumbar spine in an *in-vivo* animal model. We hypothesized that the paraspinal muscle weakness directly induce the lumbar spine degeneration as it breaks force balance on each motion segment in the lumbar spine.

Methods: A skeletally mature New Zealand white rabbit was obtained (N= 4, average age = 19 months). Rabbits were anesthetized for receiving intramuscular botox injections at left and right sides of the lumbar spine from 1 to 3 (average total dose = 7 units/kg). One sixth of the total botox dose was injected into each site to equalize the effect of botox injection. The botox injection sites were visually monitored by X-ray during the injection process. This study was approved by ethical committee. MRIs were taken before and at 4 weeks after the botox injection (Siemens.,1.5 T) to analyze muscle cross-section area for quantifying paraspinal muscle atrophy and to measure lumbar spine alignment for assessing spinal degenerations.

Results: Botox injections produced paraspinal muscle atrophy which was measured by the decreases of the cross-section area of muscle in MRIs (Fig. 1a). The cross-section areas of paraspinal muscle between L2 and L3 decreased 36 ± 5 % at 4 weeks after the botox injection. From the additional observations of the rabbit with the second botox injection, the cross-section area of paraspinal muscle decreased 41% at 4 weeks after the 2nd injection. As a consequence of the decrease of the paraspinal muscle, the lumbar spinal alignment shown in the coronal view of the MRI has the progress of degeneration (Fig. 1b).

Figure:
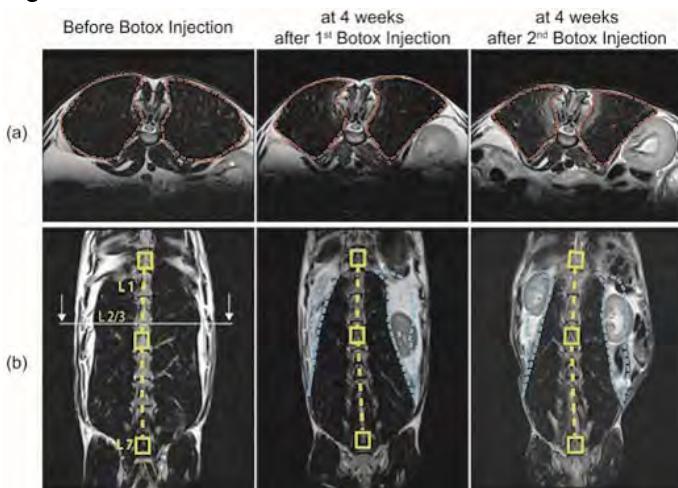
Caption: Figure 1. An example of MRI data of the changes of the botox induced paraspinal muscle and lumbar spine from multiple botox injections. (a) Transverse view of MRI for the cross-section area of paraspinal muscle around lumbar 2-3. Red dashed lines indicate the paraspinal muscle. (b) Coronal view of MRI for the lumbar spine alignment. Yellow dashed lines indicate the changes of the lumbar alignment and blue dashed area indicate paraspinal muscle decreases after Botox injections. A cross-section line points where the cross-section area shown in (a) was set.

Conclusion: To our knowledge, this is the first study to understand the effect of paraspinal muscle weakness on the degeneration of lumbar spine in an *in-vivo* animal model. Based on our results, botox can be utilized for generating an *in-vivo* lapine model of paraspinal muscle atrophy. Furthermore, the temporal progress of paraspinal muscle atrophy caused the degeneration of the lumbar spine alignment. Since paraspinal muscles have a functional role to move and stabilize the spine, we speculated that the loss of a muscular force generation and the related instability in the structural lumbar spine units could cause a breakdown of the force balance system of the spine and the degeneration of the lumbar spine alignment. Although these speculations need to be further investigated in systematic experimental and computational studies, this study suggested that the structural integrity and health of paraspinal muscles directly affect the health of the lumbar spine. Further study will aim to investigate whether the paraspinal muscle weakness directly affects the spinal degenerations or the other independent factors are associated using the biomechanical and biochemical analyses.

References: [1] Goel et al., Spine, 684-691, 1998.

[2] Panjabi et al., J. Electromyography Kinesiol. 371-379. 2003.

[3] Rehan et al., Osteoarthritis Cartilage. 1228-1235, 2009.

Disclosure of Interest: None Declared

Spine

AS-0421

A MULTI-OBJECTIVE OPTIMIZATION MODEL FOR ASSESSING SPINAL CURVATURE IN SCOLIOSIS

Simon Li [1] Daniel H. Chow [1,*]

[1]Department of Health & Physical Education, The Hong Kong Institute of Education, Hong Kong, Hong Kong

Introduction and Objectives: Previous studies have shown that the asymmetric postural adjustments had positive effect on the reduction of major spinal curvature in scoliosis [1]. However, those applications did not consider the probable negative effect on the minor region(s) of scoliotic curvature [2]. This study hypothesized that the optimal spinal loading could be achieved by controlled asymmetric load carriage for maximum correction of the affected region and minimum effect(s) on the unaffected region(s) in patients with scoliosis. The objective of this study was to develop an experimental protocol and formulate a multi-objective optimization (MOO) model [3] for determining the optimal asymmetric loading condition for scoliosis

Methods: Subjects with scoliosis were instructed to maintain a standardized and relaxed barefoot erect stance posture. A cross-chest asymmetric load was applied at the level of anterior superior iliac spines to each subject randomly at two sides (left and right) and in six different weights (0, 2.5, 5, 7.5, 10 and 12.5% of body weight). The spinal profile was palpated and identified by stickers adhered to the spinous processes [4]. Posterior-anterior view digital photos were taken to record the respective positions of the markers for determining spinal curvature. The mean spinal Cobb angles were determined [5]. Regression equations predicting the mean Cobb angles with respect to the applied load were set up. A MMO model was formulated to achieve the prioritized multiple goals of optimizing the maximum reduction in the major curvature and minimum effects on the unaffected regions(s). The subject specific optimal asymmetric loading condition was determined.

Results: Six young adults (mean age: 20.8 year, mean weight: 49.5 kg) in mild scoliosis participated in the study. The means of major and minor Cobb angles were 17.4^0 and 12.3^0 respectively. All of them had major curves at the thoracic region. Three had left curves and three had right curves. Different loads were applied to the left and right sides of the subjects. The mean Cobb angles with loading on the same and opposite sides of the major curves were 18.7^o ($+1.0^o$) and 14.2^o (-3.2^o) respectively. The effective side of the load determined by the MOO model was found to be on the opposite side of the major curve orientation. The optimal load determined by the MOO model was 3.2 kg (6.5% of BW). The predicted means of major and minor Cobb angles were 12.8^o and 13.3^o respectively. The predicted reduction in mean major Cobb angle was 4.6^o (26.4% of initial Cobb angle) and increase in mean minor Cobb angle was only 1.0^0 (8.1% of initial mean minor Cobb angle).

Conclusion: A cross-chest asymmetric load could be applied at the level of anterior superior iliac spines at the effective side opposite to the major curve orientation. The subject specific loading configuration could be determined by a multi-objective optimization model.

References: [1] Negrini and Negrini. Scoliosis 2: 8, 2007.

[2] Imrie et al. J Pediatr Orthop 31: S9-S13, 2011.

[3] Oddye et al. Eur J Operl Res 57(10): 1173-1179, 2006.

[4] Aroeira et al. Spine 36(9): 1584-1591, 2011.

[5] Weinstein et al. Lancet 371: 1527-1537, 2008.

Disclosure of Interest: None Declared

Lower Limb

AS-0422

LOWER EXTREMITY KINEMATICS DURING STOP-JUMP OF INDIVIDUALS WITH ADOLESCENT IDIOPATHIC SCOLIOSIS AFTER SURGICAL FUSION OF SPINE.

Rumit S. Kakar [1,*]Yumeng Li [2]Yang-Chieh Fu [3]Cathleen Brown-Crowell [2]Timothy Oswald [4]Kathy Simpson [2]

[1]Physical Therapy, Ithaca College, Ithaca, [2]Kinesiology, University of Georgia, Athens, [3]Health, Exercise Science, and Recreation Management, University of Mississippi, Mississippi, [4][1]University of Georgia, Athens, GA; [2]Univ. of Mississippi, USA; [3]Pediatric Orthopedic Associates, Atlanta, United States

Introduction and Objectives: Spinal fusion for individuals with adolescent idiopathic scoliosis (SF-AIS) is aimed at correcting the three-dimensional deformity of the spine. However, whether atypical lower-limb kinematics are still demonstrated postsurgically or are affected by the rigidity of the spine during high-intensity physical activities is not known. It is also important from the rehabilitation point of view to understand if interlimb asymmetry is influenced by any residual, post-surgical curvature. Therefore, the objective of the study was to compare the lower extremity kinematics between SF-AIS and healthy matched controls (CON) and to compare the mechanics of the dominant and the non-dominant lower limbs within a group displayed during the stop-jump [1]. (Figure 1a)

Methods: The stop-jump task was performed by 10 SF-AIS (physically active; posterior-approach spinal fusion: 11 ± 2 fused segments; post-op time: 2.0 ± .6 yrs; and 10 CON individuals, pair matched for gender, age (17.4 ± 1.3yr, 20.6 ± 1.5yr, respectively), mass (63.50 ± 12.2kg, 66. 40 ± 10.9kg), height (1.69 ± 0.09m, 1.72 ± 0.08m) and level of physical activity participation (International Physical Activity Questionnaire). SF-AIS and CON performed 5 acceptable trials of the stop-jump. The locations of the 24 reflective markers placed on the pelvis and lower extremities were recorded via 7-camera VICON motion capture system. 2 (Group: SF-AIS or CON) × 2 (Limb: dominant or non-dominant) mixed-model ANOVA ($p < .05$) and Tukey's HSD posthoc test were used for peak angular displacements of hip, knee and ankle joints in the 3 planes of motion displayed in the stance phase (preparation and propulsion subphase; Figure 1a). Jump heights between the two groups were compared using a one-way ANOVA ($p < .05$).

Results: Jump height was not significantly different between the two groups (mean difference: 0.013m; $p = .872$; CI (-.100m to .100m)). For the preparation subphase, a tendency for Limb main effect was observed in frontal plane, with dominant limb knee ab/adduction displacement greater than the non-dominant (5.5° –5.7°; $p = .061$). No group effects were observed. For the propulsion subphase, SF-AIS demonstrated significantly lower knee extension angular displacement than CON ($p = .02$). Similar tendencies for hip extension (3.8°; $p = .055$) and ankle plantarflexion displacement (5.0°; $p = .084$) for SF-AIS also were exhibited (Figure 1b). No other significant differences were observed. For transverse plane displacements during the propulsion subphase, tendency for Limb main effect for SF-AIS and CON demonstrated that hip joint internal rotation was greater for the dominant than the non-dominant limb (8.1° and 5.9°, respectively; $p = .089$). Discussions: Results observed in the sagittal plane are partially in consensus with those reported for AIS during level walking [2]. Reduced sagittal plane kinematics can limit the maximum vertical jump heights. Jumps repeated multiple times during sports and other activities with atypical mechanics can potentially predispose SF-AIS to lower extremity injuries, although it was not reported in this study. The interlimb differences observed in both groups can

be attributed to the non-symmetrical nature of the task where the individuals tried to reach high with on one side. Spinal fusion surgery has been reported to reduce scoliosis associated pelvic misalignments thus improving lower limb mechanics in functional activities like walking [3]. Prolonged contractions of gluteus medius and semitendinosus on the dominant side of AIS individuals during walking, as that observed by Mahaudens et al. can also be potential explanations for the observed asymmetries in the limb kinematics [2].

Figure:
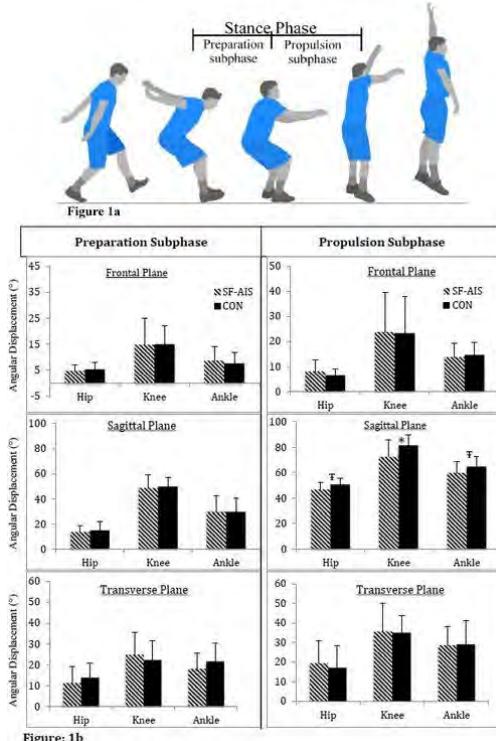
Caption: Figure 1a. Stop-jump task and the stance phase (preparation and propulsion subphase); Figure 1b: Angular displacements (°) of hip, knee and ankle joints in the two subphases of interest for the two groups, individuals with spinal fusion for adolescent idiopathic scoliosis (SF-AIS) and control (CON). * indicates significant difference between CON and SF-AIS groups (p < .05); Ŧ indicates tendency for significant difference (p = .05-.10)

Conclusion: SF-AIS display mostly comparable lower limb kinematics to that of CON to prepare and propel their body vertically to a similar jump height without losing control during high-effort tasks such as the stop-jump. Clinically, it would be essential for a physician or a rehabilitation specialist to evaluate for any atypical lower extremity kinematics post-spinal fusion surgery whcih might have an safe participation in physical activities.

References: [1] Chappell JD et al., Am J Sport Med, 30:261-267,2002.

[2] Mahaudens P et. al., Eur Spine J, 18(4):512-521, 2009.

[3] Pasha S et al., Spine, 35(17):E820-826, 2010.

Disclosure of Interest: None Declared

MECHANICAL PROPERTIES OF THE ACHILLES DO NOT RELATE TO STRENGTH OR TENDON SIZE

Stephen M. Suydam [1,*] Thomas Buchanan [2] Karin Gravare-Silbernagel [3] Daniel Cortes [4]

[1]Biomechanics, [2]Mechanical Engineering, [3]Physical Therapy, [4]Biomedical Engineering, University of Delaware, Newark, United States

Introduction and Objectives: Changes in tendon viscoelastic properties are commonly observed after injuries and during healing as a product of altered composition and structure. Continuous shear wave elastography (cSWE) is a technique to evaluate the elastic properties of soft tissue by means of the shear modulus[1]. Healthy tendon has not been previously quantified for elastic properties, nor have those properties been compared to functional or morphological measures. The aims of this study were to establish the range of shear modulus in healthy Achilles tendons, determine bilateral difference between tendons, and to show the independent nature of this measure through a lack of correlations to functional or morphological measures.

Methods: Twenty-nine subjects were evaluated for tendon health by a board certified therapist. Shear elastic modulus was measured at the free portion of the Achilles tendon using cSWE while the subjects lay prone on a plinth with their ankle in 10° of dorsiflexion. Ultrasound RF data was collected at 6450Hz while an actuator produced shear waves along the tendon. The ultrasound transducer was placed distal to the soleus myotendinous junction and the actuator was 3 cm proximal to the ultrasound probe, along the tendon. Six data sets were collected while the actuator was generating sinusoidal shear waves at each of 6 frequencies (323, 340, 358, 379, 403, 430Hz). The shear wave speed was determined in post processing with signal decomposition software. An optimization algorithm, using a Voigt model determined the shear elastic modulus with the frequencies and shear wave speeds as inputs from each of the 6 data sets. Maximum voluntary isometric contractions (MVIC) with the ankle at 90° were used to evaluate plantar flexion strength. The axial area of the free tendon was measured via B-Mode ultrasound. A Pearson's correlation determined if the shear modulus was related to the area or strength. A two, one-sided test of equivalence was used to determine if bilateral tendons were statistically equivalent. The desired detectable difference (δ) for the test of equivalence was determined by adding the possible variation caused by the measurement (mean modulus*average coefficient of variation within trial (CV)) and the minimal detectable change.

Results: The shear modulus values ranged from 37.8kPa to 67.4kPa, with a mean of 51.8kPa. The average bilateral CV was 7.2% for the shear modulus. The test of equivalence intervals δ was 6.0kPa which yielded a bilateral equivalence for the shear modulus (p=0.009). The average MVIC and area are located in Table 1. No significant correlations existed between the shear modulus of the Achilles tendons and the MVIC plantar flexion strength nor the axial area of the tendon. Tendon injuries are characterized by substantial changes in composition and structure which lead to altered tendon mechanical properties[2]. Since quantifying compositional and structural changes non-invasively is challenging, measurements of tendon viscoelastic properties can offer an alternative metric to evaluate tendon injuries and recovery. The bilateral symmetry and normative data permits this measure to be used to understand pathology and establish the severity of a case as compared to the contralateral limb. The CV between the two legs demonstrates that a 7.2%

variance bilaterally should be considered the minimum value before tendons within a subject are considered differing. Other clinical measures exist for pathological evaluation but the lack of correlation to the shear modulus from these existing metrics shows cSWE should be considered a unique method of diagnoses and recovery progress. Tendon thickening, determined through imaging techniques, and strength tests are excellent predictors of pathology and are effective diagnoses tools but may be missing the functional component.

Figure:

Caption: The arrangement of the ultrasound probe and actuator for cSWE. Note the ankle at 10 degrees dorsiflexion and the actuator 3cm proximal to the ultrasound probe.

Conclusion: The bilateral equivalence and the lack of correlation between shear modulus and clinical measures, such as strength and area, supports that cSWE has the potential to be an innovative tool for clinical evaluation.

Table:

	Mean		r
	Left	Right	(μ)
μ (kPa)	51.5	52.49	*
Area (cm^2)	0.49	0.48	0.26
MVIC (N-m)	132.2	138.5	0.01

Caption: The average shear modulus (μ), area and strength produced during MVIC. Note the lack of correlation of the area and strength to the shear modulus.

References: [1] Hoyt et al., Phys Med Biol, 53: 4063-80, 2008.

[2] Schepull et al., BMC Musculoskelet Disord, 8: 1-11, 2007.

[3] Sussmilch-Leitch et al., JFAR, 5: 1-16, 2012.

Disclosure of Interest: None Declared

Imaging / Advanced Imaging

AS-0424

MEASUREMENT AND RECONSTRUCTION OF THE GEOMETRY OF THE DISTAL FEMUR USING ROBOTIC 3D ULTRASOUND

William C. Kerr [1,*]Philip Rowe [1]Stephen Gareth Pierce [2]

[1]Department of Biomedical Engineering, [2]Department of Electronic and Electrical Engineering, University of Strathclyde, Glasgow, United Kingdom

Introduction and Objectives: Currently, computed tomography (CT) is the preferred preoperative imaging method for guided knee arthroplasty systems, such as the Makoplasty. Ultrasound imaging has the potential to provide an alternative to CT in this capacity by offering comparable accuracies, while reducing cost and eliminating the risk of ionising radiation. A system was developed which allows for imaging of the bony surface of the distal femur; serving to establish a proof of concept for a full 3D knee imaging scheme.

Methods: An artificial distal femur was imaged using a 128 element 5MHz linear probe. Following a hemispherical path, the probe was manoeuvred around the specimen by a Kuka KR5 Arc HW 6 axis robot. Bespoke probe mounts and calibration parts were designed and manufactured, allowing the probe position and orientation to be known to the robot controller. These parts were tested for accuracy using a Faro Quantum touch probe with an accuracy of 0.055mm. Using synchronised probe position and ultrasonic data capture, a total of 1611 ultrasonic data acquisitions were performed using full matrix capture. The data were processed using the total focussing method (TFM), which provided 2D images. Surface contours were extracted from each image which were translated and transformed based on the positional data. This provided a 3D point cloud representing the outer surface of the specimen. The specimen was laser scanned using a Faro Quantum, providing an accurate comparison model for the ultrasonic data.

Results: The ultrasound-derived point cloud was inaccurate relative to the reference model, with a mean error of 3.60mm, a maximum error of 32.57mm and a standard deviation of 3.06mm. While the ultrasonic data mimicked the shape of the reference model, there was an offset between the two, with the shape of the ultrasonic data generally being larger. The 2D images suffered from sidelobes of significant intensity, resulting in inaccurate contour extraction. Additionally, calibration parts were found to be inaccurate, with the calibration spike found to be as much as 1mm shorter than the intended length.

Figure:
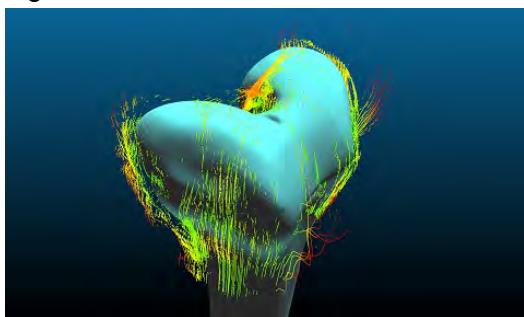
Conclusion: In principle, the system is functional, but is in need of significant improvement. The calibration parts will be redesigned and manufactured to a higher level of accuracy. In addition to this, the synthetic aperture focussing method (SAFT) will be investigated as an alternative to TFM. It is believed that the implementation of these improvements will provide a system capable of accurate bony surface imaging.

References: [1] Holmes, et al., NDT & E International, *38*(8): 701–711, 2005.

[2] Sutcliffe, et al., NDT & E International, *51*: 16–23, 2012.

[3] Torres, et al., The Fourth IEEE RAS/EMBS International Conference on Biomedical Robotics and Biomechatronics, 884–888, 2012.

Disclosure of Interest: None Declared

Imaging / Advanced Imaging

AS-0425

THE CHANGING MICROARCHITECTURE OF TRABECULAR BONE WITH HIGH STRAIN

Robert Wallace [1,*] Krishna Manda [2] Erika Sales [2] Pankaj Pankaj [2] Hamish Simpson [1]

[1] Orthopaedics, [2] Bioengineering, University of Edinburgh, Edinburgh, United Kingdom

Introduction and Objectives: Trabecular bone is a load bearing and shock absorbing material found at the ends of long bones, vertebrae and flat bones. Its complex micro-architecture and biphasic individual constituents hugely affect the macro mechanical behaviour of the bone which is largely unknown. Aging and bone disease can alter the micro-structure of the bone, which, in turn puts the bone at fracture risk. Although trabecular bone yields at small strains, large deformation analysis is necessary to understand the failure mechanisms and post-elastic nonlinear behaviour which facilitate orthopaedic implant designs.

In the current study we performed large compressive tests on trabecular bone samples from human femoral heads and assessed the microstructural indices. The specific aim of this study was to determine if there are any changes in the alignment or structure of the trabeculae during loading. Changes in the morphometry will elucidate how strain is distributed through the structure.

Methods: Human Femoral heads were harvested under ethical approval (2002/1/22) for the use of discard material in medical research. The femoral head was securely held in a submerged clamp to negate heat production as a core drill bit machined 10.64mm diameter samples. These were then cut parallel, using a Buehler Isomet low speed saw (Buehler, Illinois, USA) to a mean size of 12.15 (±0.65) mm.

Samples were inserted into a compression stage mounted in a Skyscan 1172 microCT (SkyScan, Kontich, Belgium) and scanned at a preload of 5N. Load was applied at a rate of 0.01mm/s. In 3 cases, scans were conducted pre and post loading only (2 anterior, 1 posterior). In the remaining samples (2 central and 1 posterior) the samples were held and scanned at displacements equivalent to 2%, 4%, 6%, 8% and 10% strain. After full unloading, another scan was taken for all samples. A voxel resolution of 17.22µm was used for all samples.

A region of interest of 570 pixels (equivalent to a 9.8 mm circular shape) was used to determine; Percent bone volume (BV/TV, %), Structural model index (SMI), Trabecular Thickness (Tb.Th, mm), Trabecular Number (Tb.N), Trabecular separation (Tb.Sp, mm) and Anisotropy (DM) using CTan (SkyScan, Kontich, Belgium).

Results: In order to facilitate comparison the data for each specimen was normalised with respect to the preload. The data was analysed using an ANOVA (Tukey) with a p value < 0.05 indicating a statistically significant difference (SSD). BV/TV at 2% & 4% strain were SSD to 10%. SMI revealed SSD's between the post-load and 4%>10% strain, pre load and 2% strain were SSD to 10% strain. Trabecular thickness (Tb.Th) showed SSD's between the post-load and the preload – 6% strain, preload – 4% were also SSD to 8%, 10% and post-load. The trabecular number (Tb.N) showed SSD's between 10% strain and preload up to 6%, SSD's were also seen between preload up to 4% and 8%, 10% and post-load. Trabecular Separation (Tb.Sp) and Anisotropy did not show any significant differences during loading.

On all 6 samples, a paired t-test compared the values (not normalised) pre and post compression. SSD in BV/TV (p = 0.049) was found, implying that the bone does not return to the pre deformation structure. No other property displayed a SSD when comparing preload with post-load.

Figure:
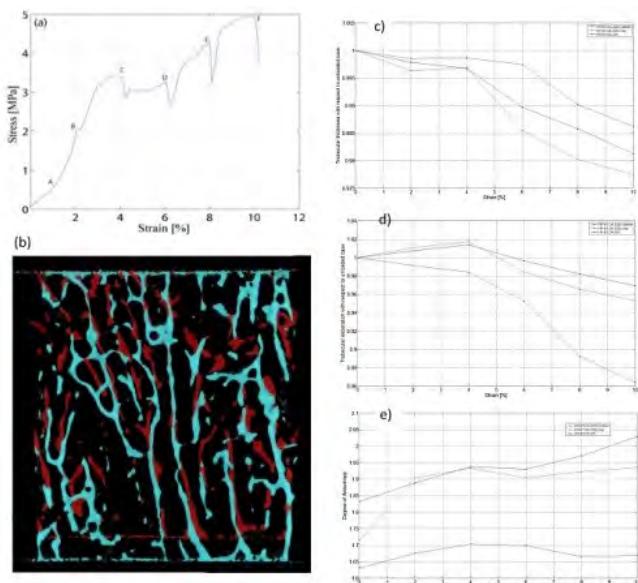
a) Stress strain curve in uniaxial compression b) Reconstructed image at preload with 10% strain superimposed
c) Tracular thickness at increasing strain d) Trabecular separation at increasing strain
e) Degree on Anisotropy at increasing strain

Caption: Sample compression and morphometric analysis

Conclusion: During loading, the alignment of trabeculae was altered with respect to its original state, resulting in a change in the degree of anisotropy. The qualitative movement of trabeculae between unloaded and 10% strain is shown in Figure 1b. The central core, extracted coincident with the principal loading axis of the femoral head, had greater trabecular alignment than the peripheral cores. The trabeculae along this axis were observed to be denser, more aligned and approaching a more plate-like structure than those in the periphery. As we move away the periphery the BVTV differs up to 3 fold and the alignment of the trabeculae (DA) becomes increasingly random.

The SMI decreased during compression. However, this does not mean that the trabecular bone is becoming a plate-like structure, rather the trabeculae are coming closer together as was registered in the images.

Frequently, implants under load in the body are considered for finite element analysis. The morphometry/bone architecture for this analysis is assessed in unloaded situations. Our data indicates significant changes in architecture under load. If trabeculae are modelled as a continuum (as in most large scale models) the changing architecture would result in different properties under load than would be derived from the unloaded scan data. This may affect how the load around an implant is distributed. This problem is magnified when we look at the bone architecture peripheral to the principal loading axis of the femoral head.

Disclosure of Interest: None Declared

AS-0426

MRI AND DTI ANALYSES COMBINED PROVIDE A POWERFUL TOOL FOR QUANTIFYING DEFORMATION ALONG HUMAN MUSCLE FIBERS IN VIVO

Uluc Pamuk [1,*]Agah Karakuzu [1]Burak Acar [2]Cengizhan Ozturk [1]Can A. Yucesoy [1]

[1]Institute of Biomedical Engineering, [2]Electrical and Electronics Engineering, Bogazici University, Istanbul, Turkey

Introduction and Objectives: Sarcomere is the basic functional element of skeletal muscle to produce muscle force. They are arranged in series within muscle fibers. Therefore, within muscles of human subjects in vivo, quantifying deformation along muscle fibers will provide invaluable information for characterizing muscle's function. Magnetic resonance imaging (MRI) analyses can quantify 3D tissue deformations in human muscles [1]. Diffusion tensor imaging (DTI) tractography allows visualizing orientation of muscle fibers [2]. With these analyses combined, we aimed at assessing fiber direction tissue deformations within the human medial gastrocnemius muscle as caused by knee angle changes.

Methods: Healthy female subjects (n=5, age=27±1 years, height=159±4 cm, body mass=50±4kg) participated. Each subject was positioned prone within the MRI scanner with the ankle angle fixed at 90°. The knee was brought to flexion (140.8±3.0°) (undeformed state) and sets of 3D high resolution MR, and DT images were acquired. This was repeated at extended knee joint position (177.0±1.0°) (deformed state). The subjects were asked to stay relaxed at all times. Demons non-rigid registration algorithm [3] was applied to the MR image sets to quantify tissue deformations in global coordinates as caused by knee angle change. After Rician filtering the diffusion weighted images from noise, Split and Merge Tractography followed by 4th order Runga-Kutta integration [4] was applied to DTI data to determine medial gastrocnemius muscle fiber tracts. Strain transformation from global coordinates to local muscle fiber direction was used to quantify deformation along muscle fibers. Undeformed state images were also transformed by a synthetic rigid body motion (10° rotation in the axial, 3° rotations in coronal and sagittal planes and 4mm translation axially) imposed. Resulting fiber direction strains calculated were used as estimates of error strains.

Results: Mean error strains (for lengthening 0.2±0.1% and for shortening 3.3±0.9%) were small and were significantly different from mean fiber direction strains (for lengthening 8.7±8.5% and for shortening 7.5±4.6%) calculated for the pooled data from all subjects due to knee extension imposed. The figure shows for two subjects, examples of "serial" strain distributions along muscle fibers (panels A-B) and "parallel" strain distributions as mean fiber strain of groups of muscle fibers represented by each tract (panels C-D). Despite globally lengthened condition of medial gastrocnemius, serial strain distributions indicate lengthening and shortening (up to locally 116.7% and 23.3%, respectively) occurring simultaneously within the same muscle fibers. Mean fiber strains of different tracts are non-uniform (e.g., in panel D they range from -0.12 to 0.15; among all subjects from -0.21 to 0.19) indicating heterogeneity of parallel strain distributions within the axial cross sections of the muscle.

In sum, knee angle changes caused substantial tissue deformations to occur along the direction of muscle fibers of the medial gastrocnemius. These deformations involve both serial and parallel strain heterogeneity such that knee extension imposed can cause sarcomeres at different parts of the same muscle fibers to attain lengths corresponding not only to the descending limb of their length-force curves but also to the ascending limb. These findings are in concert with those of

previous modeling studies and coupled animal experiments [5]. In those studies it was shown that serial and parallel heterogeneity of sarcomere lengths ascribed to intermuscular mechanical interactions can change muscle's length range of force exertion, and the size of muscle force produced at various muscle lengths including muscle optimum length. These are key properties characterising mechanics of muscle in health and disease. Ability of inferring to such properties via physiologically relevant component of muscle tissue deformation is the strength of presently developed technique.

Figure:
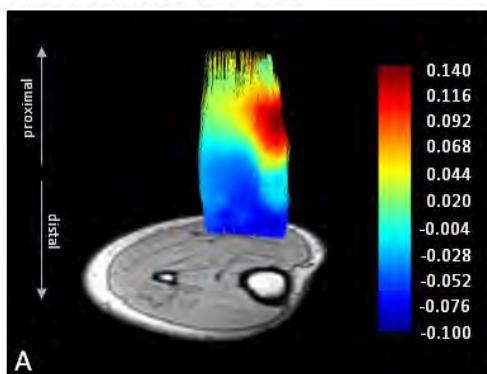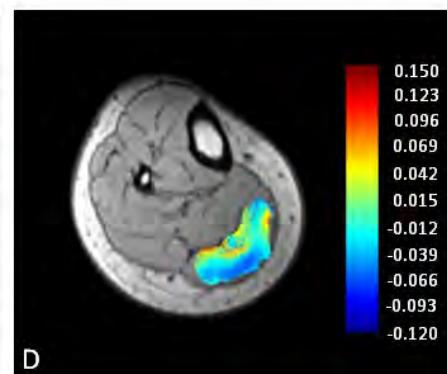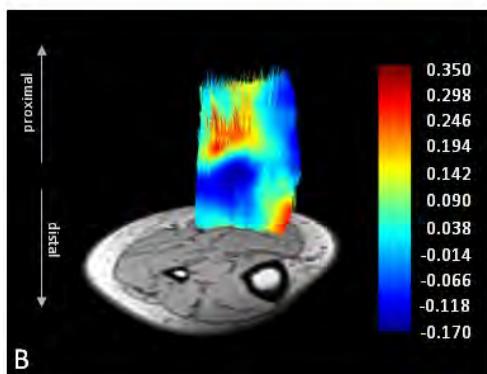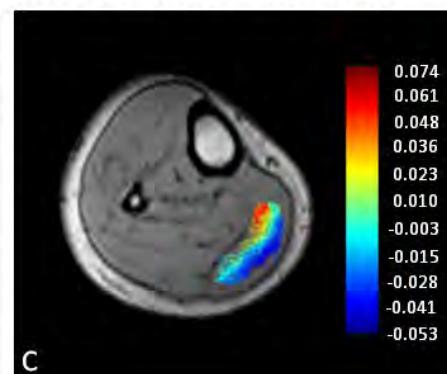
Caption: Serial (A-B) and parallel (C-D) distributions of fiber direction strains. + and - values indicate lengthening and shortening, respectively.

Conclusion: The findings show that MRI and DTI analyses combined provide a powerful tool for quantifying deformation along human muscle fibers in vivo. Such a tool considering the muscle within the context of a fascial integrity with its surrounding muscular- and nonmuscular tissues could help substantially for a better understanding of normal and pathological muscle function as well as mechanisms of treatment techniques. However, the methods should be extended to assess muscle function in active conditions and during joint movement as well.

References: [1] Yaman et al., J Biomech Eng 135: 91003, 2013.

[2] Felton et al., J Biomech 41: 1782-1789, 2008.

[3] Thirion, Med Image Anal 2: 243-260, 1998.

[4] Yoldemir et al., IEEE T Med Imaging 31: 1929-1940, 2012.

[5] Yucesoy, Exerc Sport Sci Rev 38: 128-134, 2010.

Disclosure of Interest: None Declared

Imaging / Advanced Imaging

AS-0427

VALIDITY AND RELIABILITY OF ADULT PELVIC 3D RECONSTRUCTIONS USING LOW DOSE BIPLANAR X-RAYS

Ayman Assi [1][2],*Bachir Ghostine [1][2]Christophe Sauret [2]Ziad Bakouny [1]Nour Khalil [1]Ariane Moniquet [2]Ismat Ghanem [1]Wafa Skalli [2]

[1]Laboratory of Biomechanics and Medical Imaging, School of Medicine, University of Saint-Joseph, Beirut, Lebanon,
[2]Laboratoire de Biomécanique, Arts et Métiers ParisTech, Paris, France

Introduction and Objectives: Pelvic 3D reconstructions are usually computed from CT-Scan acquisitions. However, this technique exposes the subject to high levels of radiation. A novel technique, the EOS® low dose biplanar X-Ray system, can be used to perform 3D reconstructions of skeletal structures such as the spine and the lower limbs [1,2,3]. Yet, the technique of 3D reconstruction of the pelvis, using this same system, is not fully validated, particularly when the pelvis is more or less rotated in the horizontal plane, which usually occurs because of malpositionning of patients during X-ray acquisition. The purpose of this study is to evaluate the validity and reliability of the main pelvic parameters using this new technique, in comparison with 3D reconstructions obtained by CT-Scan.

Methods: Helical pelvis CT-Scans (slice thickness: 0.6mm) of 6 adults (3 F and 3 M, age: mean 48 - SD 29) were considered. A three-dimensional reconstruction of each pelvis was obtained using the Avizo® software, by detecting the outlines of the pelvis on each slice and was considered as the reference. Lateral and Frontal Digitally Reconstructed Radiographs (DRRs) were computed from the CT-Scans, in order to simulate the lateral and frontal radiographs which would be obtained from a typical EOS exam. Then for each patient, axial rotation of the pelvis was simulated and the corresponding DRRs were calculated at 5°, 10°, 15° and 20°. The 3D reconstruction of each pelvis was obtained from each pair of X-Rays in each axial position, using the research version of the SterEOS® software (Figure 1). Four qualified observers repeated the 3D reconstruction 3 times each at each axial rotation. A total of 360 reconstructions in 3D were obtained (6 patients, 5 axial rotations, 3 operators, 3 times each).

Clinical parameters were calculated on the reference 3D scan and the biplanar X-ray reconstructions: pelvic angles (pelvic incidence, pelvic tilt, sacral slope), % of acetabular coverage of the femoral head (%ACFH), bicoxofemoral distance, frontal pelvic tilt, acetabular angles (abduction, anteversion, tilt) and center edge angle of the acetabulum (CEA). The bias was calculated as the mean difference between CT-based (reference) and biplanar X-Ray reconstructions. The 2SD of interobserver reliability was calculated in order to assess the 95% confidence interval (95%CI) of each pelvic parameter. The Intraclass Correlation Coefficient (ICC) was also used to evaluate the interobserver agreement.

Results: At 0° position, the bias was lower than 2° for all angles, lower than 3 mm for bicoxofemoral distance, and lower than 1% for the %ACFH. The 95% CI was lower than 2° for pelvic tilt and frontal pelvic tilt, between 2 measurement units (m.u.) and 4.5 m.u. for acetabular angles, pelvic incidence, %ACFH and bicoxofemoral distance, and higher than 5° for CEA. For rotated positions, the bias remained under 1.5° for pelvic angles but increased with the extent of axial rotation for CEA and acetabular angles, reaching 3.5° at 20° of rotation. The 95% CI increased with axial rotation and exceeded 7° in the 20° position for most of the studied angles. The ICC for all parameters and in all axial rotations was superior to 0.8.

Figure:
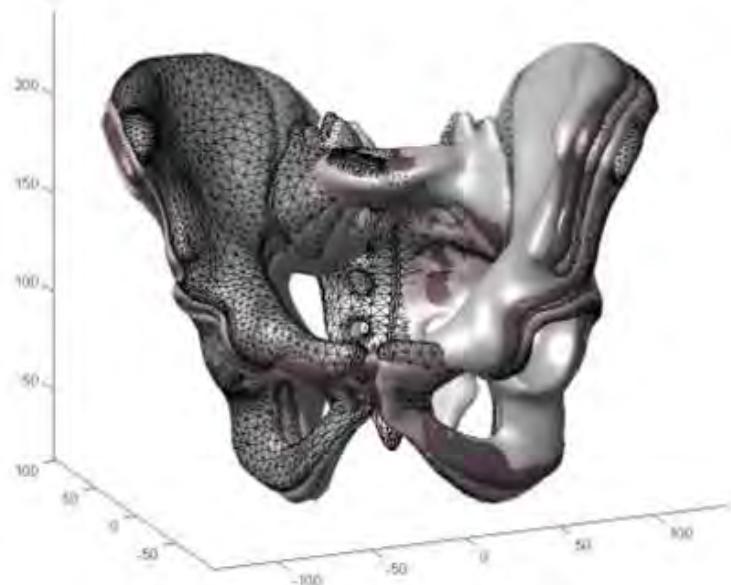
Caption: Fig 1- Superposition of 3D reconstructions obtained by SterEOS® research software for 0°, 5°, 10°, 15° and 20° of axial rotation for the same pelvis

Conclusion: Clinical measurements performed on 3D reconstructions of the pelvis from biplanar X-rays were shown to be accurate and reliable. A pelvic rotation of more than 15° significantly decreased the accuracy of CEA and acetabular angles. A pelvic rotation of more than 10° significantly decreased the reproducibility of pelvic angles, CEA and acetabular anteversion. The 3D reconstruction technique of the pelvis using biplanar X-rays was not affected by axial rotation when it did not exceed 10°, which is rarely exceeded by malpositionning of patients during X-ray acquisitions in clinical practice. Further research is underway in order to evaluate this technique on radiographs of children, where non-ossified portions of the pelvis could affect the visibility of bony landmarks and therefore the validity and reproducibility of 3D reconstructions.

References: [1] Humbert L, Med Eng Phys, 2009. [2] Baudoin A, MBEC, 2008. [3] Chaibi Y, CMBBE, 2012.

Disclosure of Interest: None Declared

Imaging / Advanced Imaging

AS-0428

IN VIVO MEASUREMENT OF BICEPS BRACHII AND TRICEPS BRACHII FASCICLE LENGTHS USING EXTENDED FIELD-OF-VIEW ULTRASOUND

Christa Nelson [1,*]Julius Dewald [1][2]Wendy Murray [1][2][3][4]

[1]Biomedical Engineering, Northwestern University, Evanston, IL, [2]Departments of PM&R and PTHMS, Northwestern University, [3]Sensory Motor Performance Program, Rehabilitation Institute of Chicago, Chicago, IL, [4]Edward Hines Jr. VA Hospital, Hines, IL, United States

Introduction and Objectives: Muscle architecture describes the number of muscle fibers and their orientation in relation to the axis of force generation. Muscle architecture is a determining factor of an individual muscle's active force-generating capacity [1]. A muscle's architecture can be quantified through measurement of specific parameters, including muscle volume, fascicle length, and the pennation angle of the fascicles. Due to the importance of muscle architecture for force generation, and consequently function, it is important to accurately measure these parameters. Architectural parameters have been shown to adapt to various conditions, such as with disuse, aging, exercise regimes, and in certain neurological conditions [1,2]. Fascicle length, in particular, is of interest, as it affects the excursion capacity of a muscle during passive and active range of motion [1]. Ultrasound is the most common imaging modality used for the *in vivo* measurement of muscle fascicle length [3]. However, due to the limited field-of-view for most ultrasound probes, static ultrasound is primarily used with muscles that have shorter fascicles and higher pennation angles, due to the ability to visualize the entire fascicle or estimate the length of a longer fascicle using trigonometric linear extrapolation.

Due to these limitations, extended field-of-view ultrasound (EFOV US) has been investigated as a method to visualize the entire muscle fascicle in one image [3]. In a gold-standard study, this method was both shown to be reliable and valid [4], and more accurate than the trigonometric method. The objective of this study was to use EFOV US to measure both biceps and triceps brachii fascicles under both active and passive conditions, determine the reliability of fascicle measurements, and evaluate the effect of joint position on fascicle length.

Methods: Biceps brachii (long head) and triceps brachii (lateral head) fascicle lengths were measured in both arms in N=11 healthy control subjects (6 female, 5 male, age range 23-71). Subjects were casted at the wrist and secured at the forearm, with the limb approximately in the horizontal plane (85° shoulder abduction, 0° shoulder rotation) and the wrist at 0°. Four EFOV US images were collected for each muscle in extended, mid-, and flexed elbow positions with the muscle relaxed, as verified by EMG. In the flexed posture, fascicles were also imaged during an isometric contraction. The level of torque held during isometric contraction was matched between limbs, and was determined as the maximum torque the subject could hold on the non-dominant limb for 10 sec., the approximate time of image acquisition. Image J was used to manually measure 4 fascicles in each image, with the best three images used for data analysis. The reliability of fascicle measurements was determined by calculating the intraclass correlation coefficient (ICC) for measurements within an image and across the three images. A two-factor repeated measures ANOVA (arm, position) was used to detect significant changes in fascicle lengths in different elbow postures. A two-factor repeated measures ANOVA (arm,

condition) was also used to detect any significant differences in fascicle lengths between the passive and active conditions.

Results: Fascicle measurements demonstrated excellent reliability for both muscles, with ICC values ranging from .831 - .949 for biceps brachii and from .812 - .919 for triceps brachii (p<.0001 for all values). As expected due to its anatomy, average biceps fascicles for all subjects *decreased* with elbow flexion (Fig. 1A), and average triceps fascicle lengths *increased* with elbow flexion (Fig. 1B). Changes in fascicle lengths between the different elbow postures were significant for both muscles (p<.0001). Measured biceps fascicles were significantly shorter in the active condition (p=.015), as were triceps fascicles (p<.0001).

Figure:
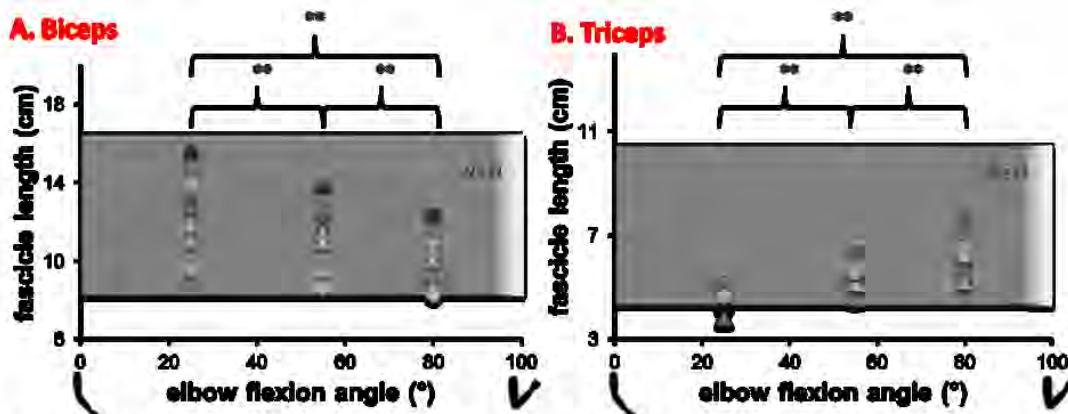
Figure 1. Biceps brachii long head (A) and triceps brachii lateral head (B) average fascicle lengths measured in N = 11 healthy control subjects using extended field-of-view ultrasound imaging. The shaded region in each plot represents fascicle measurements made in 5 male cadavers (Murray et. al 2000). Two-factor ANOVA detected a significant difference in fascicle lengths between positions (p < .0001) for both muscles.

Conclusion: Extended field-of-view ultrasound was used to measure muscle fascicles in biceps brachii and triceps brachii, under both passive and active isometric conditions. Fascicle lengths in healthy control subjects were consistent with published cadaver data [5], and significantly changed with position, as would be expected from each muscle's anatomy. Fascicle measurements were highly reliable for both muscles, with ICC values slightly higher for biceps brachii when compared to triceps brachii. Our data demonstrate the first known application of extended field-of-view US to measure longer fascicles in the upper extremity. Given the number of human muscles with fascicle lengths that are longer than the field-of-view of conventional ultrasound probes, this method is an important approach for the study of *in vivo* muscle function.

References: [1] Lieber RL. *Muscle Nerve.* 2000;23:1647-1666.

[2] Thompson LV. *J Orthop Sport Phys Ther.* 2002;32:44-57.

[3] Kwah LK. *J Appl Phys.* 2013;114:761–769.

[4] Noorkoiv M. *J Appl Phys.* 2010;109:1974–1979.

[5] Murray WM. *J Biomech.* 2000;33:943-952.

Disclosure of Interest: None Declared

COMPARISON OF 2-D AND 3-D DIRECT INVERSION ALGORITHMS IN MR-ELASTOGRAPHY FOR DIFFERENT GEOMETRICAL STRUCTURES

Lyam Hollis [1,*]Neil Roberts [2]Pankaj Pankaj [3]Peter Hoskins [4]

[1]Cardiovascular Sciences, [2]Clinical Research Imaging Centre, [3]School of Engineering, [4]Medical Physics, University of Edinburgh, Edinburgh, United Kingdom

Introduction and Objectives: Magnetic resonance elastography (MRE) is a non-invasive technique to obtain *in vivo* material property measurements. Displacements resulting from a mechanically induced shear wave are characterized by a phase-encoding gradient in the MRI scanner. An inversion algorithm is utilised to obtain local estimates of wavelength which is related to the shear modulus of the material. This can be achieved by using a direct solution to the Helmholtz equation for planar shear waves. Such inversion can be performed on 2-d or 3-d datasets, yet in both instances the solutions are limited by the assumptions made to derive the Helmholtz equation. This study utilised finite element analysis (FEA) of MRE in order to compare measurements made using the 2- and 3-d inversion algorithms whilst varying the geometry of the region of interest and the material properties of the surrounding region.

Methods: All FEA simulations were performed using *Abaqus/Explicit* using geometries of size 80x80x50mm^3. In order to investigate the geometrical dependence of shear modulus measurements a cylindrical inserts with radii 10mm have been utilised. The length of these inserts has been varied from 2-50m. The shear modulus of the background material has been defined as 3kPa and the insert as 9kPa. Viscoelastic properties have been defined in both sections using the Kelvin-Voigt model of viscoelasticity with a shear viscosity of 1Pa·s in order to reduce the effects of reflections. The lower and side surfaces were fixed using symmetric boundary conditions whilst vibrations at 100Hz were applied as a concentrated force on nodal points on the upper surface.

To investigate the effects of the material properties of the shear moduli a cylindrical insert with a diameter of 30mm and a length of 20mm was inserted into the centre of the model. The cylindrical insert was split into two: the inner 10mm radius was defined as having a shear modulus of 9kPa whilst the shear modulus of the outer 5mm was varied from 2-9kPa. The shear modulus of the background was defined as 3kPa and viscoelastic properties were assigned to all regions using the Kelvin-Voigt model of viscoelasticity. Simulations were performed with the shear viscosity equal to 0.25 and 1Pa·s.

Once simulations had run displacement data was extracted from 2-dimensional planes through the centre of the model. The 2-d algorithm required displacements in one plane and from only the vibrational direction whilst the 3-d algorithm required data from 5 parallel planes spaced 1mm apart and in all three directions. Data was exported to *Matlab* where it was analysed using with the MRE inversion algorithms.

Results: Measurements from both the 2-d and 3-d inversion algorithms were consistent with one another when the geometry of the insert was varied. The measured values for the background were consistent with those prescribed and there was little variability across all geometries. This contrasted with the measurements of the insert which were dramatically underestimated for the small inserts yet suffered from a slight overestimation for the larger insert geometries (figure).

There was a slight difference in the 2-d and 3-d measurements when the effects of varying the material properties surrounding the region of interest were studied. In this instance the 3-d algorithm tended to obtain more accurate measurements in comparison to the 2-d. in both instances the measurements were dramatically underestimated when the surrounding region was prescribed with a low shear modulus (table). The results were similar for both prescribed values for the shear viscosity.

Figure:
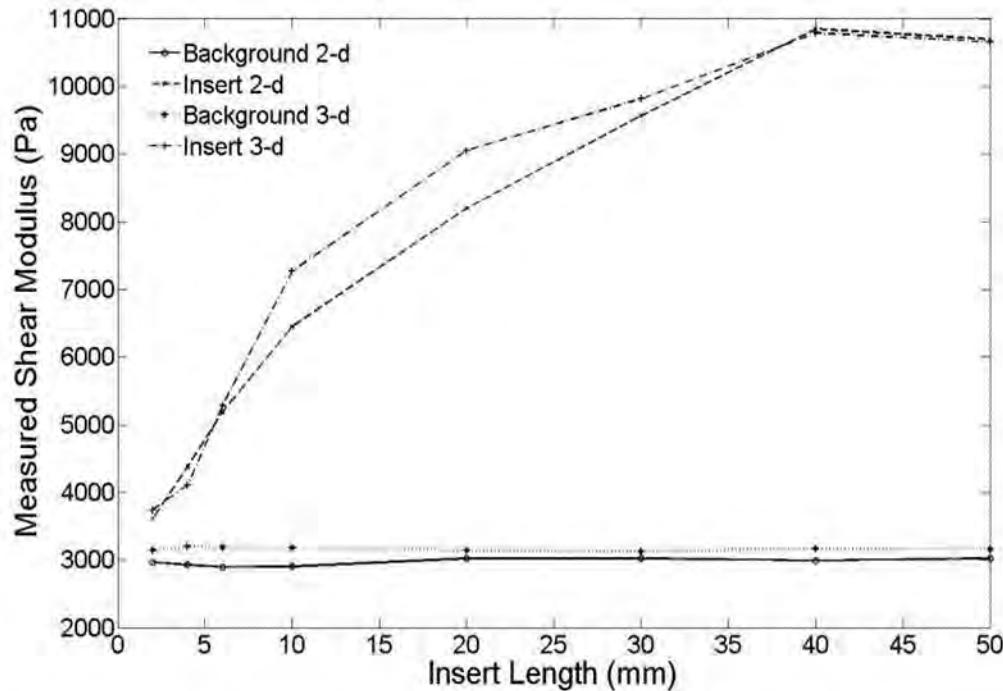
Figure: Comparison of measurements from the 2- and 3-d inversion algorithms when insert length is varied. True stiffness of the background is 3000Pa whilst the true stiffness of the insert is 9000Pa

Conclusion: This study demonstrated that measurements using both the 2-d and 3-d inversion algorithms were geometrically dependent. This suggests that whilst the direct inversion utilises local displacements to estimate local values for the shear modulus, wave propagation is dependent on the global material properties and as such this approach is limited. This implies that shear modulus measurements from different sized geometries are not directly comparable to one another. The study also showed that measurements are dependent on the material properties surrounding the region of interest. This suggests further limitations of the inversion algorithm with respect to the comparability of shear moduli from regions that have different surrounding materials. Although there was little difference between the 2-d and 3-d inversion algorithms it is likely that scattering and reflections are greatly reduced in modelling in comparison to the human anatomy and as such 3-d analysis is of greater importance *in vivo.*

Table:

	2-d Inversion		3-d Inversion	
Surrounding Shear modulus	Background	Insert	Background	Insert
2kPa	3251	5261	3121	4825
3kPa	3144	7562	3178	7439
4kPa	3143	7525	3152	7630
5kPa	3136	7499	3138	7718
6kPa	3130	7525	3129	7843
7kPa	3125	7577	3124	8005
8kPa	3125	7612	3121	8129
9kPa	3124	7585	3119	8111

Caption: Comparison of the 2-d and 3-d inverted data for a shear viscosity of 1Pas

Disclosure of Interest: None Declared

Imaging / Advanced Imaging

AS-0430

A NOVEL APPROACH TO VISUALISE THE MORPHOLOGY OF PERICELLULAR MATRIX IN LIVE CARTILAGE

Eng Kuan Moo [1,*]Scott C. Sibole [1]Walter Herzog [1]

[1]Human Performance Laboratory, University of Calgary, Calgary, Canada

Introduction and Objectives: The pericellular environment of chondrocytes plays important roles in transducing mechanical signals from extracellular matrix (ECM) to the cells, as well as protecting cells from excessive deformation [1, 2, 3]. As a result, biosynthetic activities of chondrocytes rely heavily on the mechanical behavior of the pericellular matrix (PCM). Previous studies have investigated the morphology and mechanical behaviour of PCM through immuno-staining of collagen type VI, which is highly localized in the pericellular region [2, 3, 4]. However, immuno-staining requires tissue fixation and therefore, limits PCM observation to a single time point. Conversely, multi-photon microscopy allows imaging of collagen fibers in cartilage through second harmonic generation (SHG). SHG signal originates from the fibrillar structure of type II collagen fibers, which is non-centrosymmetric in nature [5]. As PCM is characterized mainly by type VI collagen that exists in microfibrillar form [2], this pericellular region lacks the appropriate structure to generate SHG signal. Therefore, SHG imaging may localize chondron (cell and PCM) in cartilage tissue. In addition, cell can be visualised through fluorescent staining. As such, simultaneous SHG imaging and live cell imaging can conceptually highlight PCM in live cartilage. Therefore, the purpose of this study was to establish a novel approach for imaging PCM in live cartilage, and to develop an image processing protocol for morphological analysis of PCM.

Methods: Cartilage explants extracted from porcine femoral groove were used. Two experiments were performed. In the first experiment, we localized PCM by the 'gold-standard' immuno-staining approach and identify the chondron boundary from SHG image based on the immuno-stained PCM image. Briefly, cartilage layer was fixed chemically overnight and frozen. Frozen cartilage was then cut into thick sections (40μm) and processed for immuno-staining by primary antibody (anti-collagen type VI raised in rabbit, Fitzgerald) and fluorescently-tagged secondary antibody (anti-rabbit raised in donkey, Fitzgerald). The sliced samples were then simultaneously imaged for SHG signals (Ex: 800nm; Em: 400nm) and immuno-stained PCM (Ex: 488nm; Em: 515nm). In the second experiment, cartilage explant was incubated in 8μM Calcein AM for 30min. The cartilage explants were simultaneously imaged for SHG signals and cell cytoplasm (Ex: 488nm; Em: 515nm). The fluorescent immuno-stained PCM and Calcein-stained cells were identified using 'Otsu' thresholding methods (ImageJ). SHG image were analyzed using active contour model (ImageJ, AB-Snake). The parameters of active contour model determined from immuno-staining experiment were used to define chondron boundary in live tissue experiment. PCM layer can be visualised by subtracting cell from chondron.

Results: Two-dimensional (2D) SHG image showed a dark ellipse (Figure 1a[i] and 1b[i]). This dark ellipse completely encapsulates the immuno-stained PCM layer (Figure 1a[i]), thus confirming our hypothesis that SHG microscopy can image chondron region. By trial and error, a gradient threshold of 10 at 150 iterations in active contour model produced satisfactory chondron boundary (Figure 1a[iii] right). When the SHG image is overlaid with the cell image, there exists a dark ring surrounding the cells, which suggests the PCM region (Figure 1b[iii] left). Using the same parameters of active

contour models, the chondron boundary in live tissue was determined, and the PCM region can be identified by subtracting live cell from the chondron (Figure 1b[iii] right).

Figure:
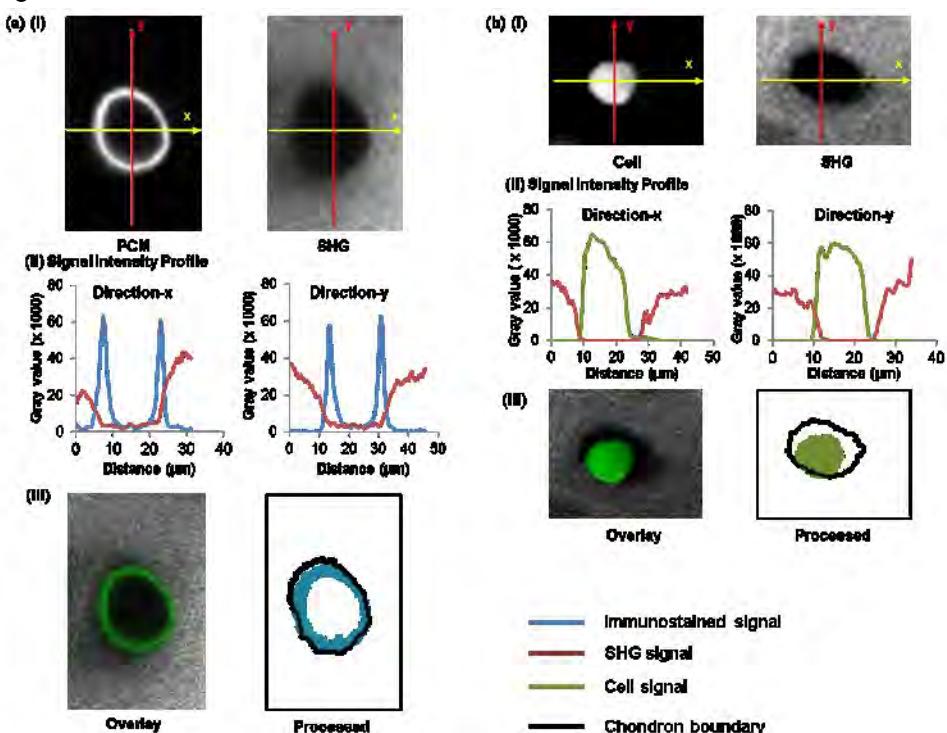
Caption: Figure 1. (a) (i)Immuno-stained PCM and the corresponding SHG image. (ii) Signal intensity profile of along x- and y-directions. (iii) Overlay of PCM and SHG images, and the processed binary image showing chondron boundary and PCM region. (b) (i) Calcein-stained chondrocyte and the corresponding SHG image. (ii) Signal intensity profile along x- and y-directions. (iii) Overlay of live cell over SHG image, and the processed binary image showing chondron boundary and live cell.

Conclusion: This study proposes a simple-to-use and novel approach for PCM imaging in live tissue. Through immuno-staining and SHG, we showed strong evidence of SHG capability in imaging chondron in live cartilage. By combining SHG imaging with live cell imaging, PCM was successfully imaged in live tissue. With the image processing protocol established in this study, future studies will focus on measuring the load-induced deformation of PCM and the role of PCM in transferring load from ECM to cells. As early osteoarthritis is related to softening of the PCM, this novel approach can enhance our understanding of the role of PCM in the pathogenesis of osteoarthritis.

References:

[1] Poole et al. J Orthop Res, 6: 408-419, 1988.

[2] Poole et al. J Cell Sci, 103: 1101-1110, 1992.

[3] Choi et al. J Biomech, 40: 2596-2603, 2007.

[4] Youn et al. Osteoarthritis Cartilage, 14: 889-897, 2006.

[5] Chen et al. Nat Protocols, 7: 654-669, 2012.

Disclosure of Interest: None Declared

Balance

AS-0431

IMPAIRED STATIC BALANCE IN CHILDREN WITH DEVELOPMENTAL COORDINATION DISORDER MAY BE EXPLAINED BY IMPAIRED CENTRAL AND PERIPHERAL CONTROL MECHANISMS

Merete B. Speedtsberg [1,*] Sofie B Christensen [1] Ken K Andersen [1] Derek J Curtis [2] Jesper Bencke [2] Bente R Jensen [1]

[1] Biomechanics and Motor Control Lab., Integrated Physiology, Department of Nutrition, Exercise & Sport, University of Copenhagen, Copenhagen N, [2] The Gait Analysis Lab., Department of Orthopaedic Surgery, Hvidovre Hospital, Copenhagen, Denmark

Introduction and Objectives: Developmental coordination disorder (DCD) affects approx. 6% of children at primary school age and is characterized by motor coordination difficulties. A recent meta-analysis on performance deficits in children with DCD suggests impaired control of postural sway as well as predictive control of action [1]. Previously reported impaired postural control in bipedal standing in children with DCD [eg.2], may interfere with activities of daily living and participation in sport. However, little is known about the underlying mechanisms. Furthermore, there are contradicting results concerning the effect of disturbance of sensory input in DCD.

The aim was (1) to study static postural control and the effect of manipulating sensory input in children with DCD compared to typically developing children (TD), and (2) to investigate if both central and peripheral mechanisms are involved in impaired static postural control in DCD.

Methods: Nine children with DCD (age: 9.0±0.5 years, body mass: 33.1±2.3 kg, height: 139.9±2.5 cm, gender: 7 boys and 2 girls) and 10 TD (age: 9.1±0.4 years, body mass: 33.7±1.8 kg, height: 141.1±3.0 cm, gender: 7 boys and 3 girls) participated. Inclusion criteria for DCD were to meet the official criteria for DCD [3], and a score below the 15th percentile in the Movement Assessment Battery for Children-2 (MABC-2), which is classified as a motor skill deficit. The MABC-2 percentile was 3±1 in the included DCD group and 73±5 in the TD group.

Static balance was performed in barefoot bipedal standing on a force plate. The child was exposed to six different combinations of visual and support surface conditions (table 1) and was instructed to stand as still as possible for 3×30 s in each condition. Visual conditions included eyes open, eyes closed and a visual-conflict dome for producing inaccurate visual input. Support surface conditions consisted of a hard and a compliant (45×45×7cm foam) surface.

Data from an AMTI force plate was sampled at 1000Hz, down sampled to 100Hz and used to calculate sway length based on centre of pressure (CoP) motion. CoP displacement was decomposed into two components, rambling and trembling in anterior-posterior (AP) and medio-lateral (ML) direction. Sway length was used to quantify static postural control. Rambling quantified the migration of a moving reference point in relation to the body's equilibrium, and represents the supraspinal component of the CoP trajectory. Trembling quantified the oscillations around the reference point, and represents the spinal and peripheral component of the CoP trajectory [4].

Results: Children with DCD showed impaired postural control expressed as 46.4±5.4% larger sway length (mean of all conditions, p=0.004). In the condition with no sensory disturbance, the DCD group had 46.8% larger sway length than TD (0.62m/30s vs. 0.42m/30s, p=0.026). Sensory disturbance did not affect DCD more than TD (p=0.942) across conditions. These results confirmed a deficit in static postural control in children with DCD. Furthermore, this impairment was present

regardless sensory conditions, which suggested a deficit in sensory organisation rather than a deficit in specific sensory systems.

Rambling in DCD was 41.4±14.5% and 30.2±15.7% larger (mean of all conditions) in AP and ML direction, respectively (p=0.002, p=0.006). Trembling in AP direction was 77.5±7.3% larger (mean of all conditions) and 81.7±24.1% in ML direction compared to TD (p=0.015, p=0.000). These results demonstrated that the larger sway length in children with DCD could be explained by impaired central as well as peripheral control mechanisms, indicating contribution of less effective automated spinal adjustments to postural control, along with a deficit in supraspinal control of the body's equilibrium in DCD.

Conclusion: Static postural control was impaired in DCD. The results indicated that the reduced postural control in children with DCD could be explained by a deficit in peripheral mechanisms as well as a deficit in central control. The spinal involvement in balance impairments could have implications for future research in static balance and treatment of DCD.

Table:

Condition	Description	Accurate sensory signals available
1	Eyes open + hard surface	Somatosensory, visual, vestibular
2	Eyes closed + hard surface	Somatosensory, vestibular
3	Eyes open + compliant surface	Visual, vestibular
4	Eyes closed + compliant surface	Vestibular
5	Eyes open in dome + hard surface	Somatosensory, vestibular
6	Eyes open in dome + compliant surface	Vestibular

Caption: Table 1: The six testing conditions.

References: [1] Wilson, PH. et al., Dev Med Child Neurol, 55, 217-228, 2013.

[2] Cherng, RJ. et al., Hum Mov Sci, 26, 913-926, 2007.

[3] American Psychiatric Association, Diagnostic & Statistical Manual of Mental Disorders V, 2013.

[4] Zatsiorsky, VM et al., Motor Control, 3, 28-38, 1999.

Disclosure of Interest: None Declared

AS-0432

A MODEL FOR ROBUSTNESS OF STANDING POSTURE BASED ON JOINT COORDINATION, JOINT VISCOELASTICITY AND INTERMITTENT CONTROL STRATEGY

Hiroko Tanabe [1,*] Keisuke Fujii [2] Yasuyuki Suzuki [3] Motoki Kouzaki [1]

[1]Graduate School of Human and Environmental Studies, Kyoto University, Kyoto, [2]Research Center of Health Physical Fitness and Sports, Nagoya University, Nagoya, [3]Graduate School of Engineering Science, Osaka University, Osaka, Japan

Introduction and Objectives: The individual differences in joint coordination during standing tasks have been reported in recent studies. The functions of these different kinematic coordinative structures and their generation mechanisms cannot be understood through experiments, and instead require computer simulations using mechanical models. Human bipedal standing is often modeled as an inverted pendulum. Intermittent control has been demonstrated to be valid for human quiet standing in recent studies using inverted pendulum models. Thus, this study has two objectives. The first is to investigate the relationships between joint coordination, passive joint viscoelasticity, and neural joint control strategies. The second is to examine whether robustness varies depending on viscoelasticity or control strategies.

Methods: The quadruple inverted pendulum model was constructed as a model of human tiptoe standing using anthropometric parameters. The PD (proportional-derivative) intermittent feedback control model was used to simulate the fluctuations of the pendulum. We used fixed P and D gains for the first objective in this study. Three pairs of joint viscoelastic parameters, 81 pairs of joint control strategies (intermittent, continuous, or no active control for each four joints; 3^4 pairs), and two values which determine the intermittent switching boundary were used for the simulations to investigate the difference in joint coordination patterns between these variables. For the second objective, we calculated the stability region of gain P for each joint, which represents the feedback gain that CNS can select to stabilize the multi-link human body, that is, the robustness of the model. We also compared joint coordination (phase distribution) with experimental data to verify the model (in this case, the Gaussian white noise was added to each joint's torque) used in this study.

Results: We found that the model could be stabilized (we defined the temporary stabilization of the model as standing for 60 seconds converging towards zero joint angles) 30 pairs of simulation variables among 246 pairs. The hip joint was intermittently controlled for all of the 30 conditions and the MP joint was under intermittent control or no active control for the stability. The joint coordination patterns shown by phase distribution varied depending on both joint viscoelasticity and joint control strategies, suggesting that the difference in joint coordination reported experimentally in previous studies might be derived from such passive or active parameters. Stability region of gain P was also dependent on viscoelasticity or joint control strategies.

Conclusion: Our study suggests that not only active joint control strategy but also passive viscoelasticity result in the difference in joint coordination patterns and the robustness of standing posture. The methodology used in this study possessed high generality to examine the robustness or stability of standing posture. This study was able to provide

specific joint control strategy that achieves more robust posture for tiptoe standing, which will afford pedagogical knowledge about balance control training to us.

Disclosure of Interest: None Declared

Balance

AS-0433

TEST-RETEST RELIABILITY OF POSTURAL CONTROL EVALUATED IN THE AQUATIC ENVIRONMENT USING A FORCE PLATFORM

João Pedro Batista Junior [1,*] Renata Campos [2] Maria Simone Barreto [2] Bruno Mazuquin [3] Jéssyca Nogueira [2] Josilainne Dias [2] Rodrigo Carvalho [4] Marcelo Taglietti [2] Felipe Moura [5] Ligia Facci [2] Jefferson R. Cardoso [2]

[1] PAIFIT Research Group, Instituto Federal do Paraná, [2] PAIFIT Research Group, Laboratory of Biomechanics and Clinical Epidemiology, Universidade Estadual de Londrina, Londrina, Brazil, [3] PAIFIT Research Group, University of Central Lancashire, Preston, United Kingdom, [4] Univervidade Federal do Vale do São Francisco, Petrolina, [5] Physical Education and Sports Centre, Universidade Estadual de Londrina, Londrina, Brazil

Introduction and Objectives: Postural control can be affected by external and internal perturbations that continually act on the body through several sensory systems such as visual, somatosensory and vestibular [1]. Immersion affect body biomechanics since water has specific properties such as hydrostatic pressure, buoyancy and density that may influence the postural control system. Force platforms are widely used to measure center of pressure variations, however, no study has demonstrated the reliability of an aquatic force plate to provide repeatable and consistent data. The aim of this study was to test the intra-subject reliability (test-retest) of postural control in the aquatic environment.

Methods: Fifty young subjects participated in the study, 32 female and 18 male, median of age Md=21 years (20-22/1°-3°), mass Md=58 kg (54-73), height Md=1.67 m (1.61-1.72) and mass in water Md=15 kg (10-23). Tests were performed in four conditions: two leg stand-eyes open (TEO), two leg stand-eyes closed (TEC), one leg stand-eyes open (OEO) and one leg stand-eyes closed (OEC) with a 48-hour interval between test and retest. The center of pressure (COP) data were collected with a 60x60x10 cm aquatic force plate (Bertec Corporation®, model FP4060-08-2000), set in a pool (15x13x1.30m) with water depth of 1.21m and water temperature of 32.5°C. The platform was connected to a computer through a 16-bit analogue to digital converter and the acquisition rate was 1000 Hz. The following variables were used: total mean velocity (TMV)(cm/s), mediolateral mean velocity (MMV)(cm/s), anteroposterior mean velocity (APMV)(cm/s), mediolateral amplitude (MLA)(cm), anteroposterior amplitude (APA)(cm) and area (cm^2). Intraclass correlation coefficient (ICC), Bland-Altman plots (and the standard error of measurement (SEM) were used to assess the reliability of data. All the procedures were approved by the local Ethical Committee (#217/2012).

Results: The test-retest results showed reliability from low to high. The MMV presented high-reliability ICC (0.75 CI 95% 0.56;0.86) with SEM of 2.58 (SD 5.16) and mean difference (of 1.44 cm/s; followed by TMV (ICC=0.73 CI 95% 0.53;0.84); SEM=3.08 (5.92) and (= 1.73 cm/s. The amplitude variable demonstrated lower reliability (ICC=0.33 CI 95% 0.16; 0.62); SEM=1.45 (SD 1.78) and = 0.18 cm.

Conclusion: Despite the large variability in the measurements derived from the COP, the aquatic environment has important physical properties such as buoyancy, which reduce body weight and change the forces acting on the joints, offering an alternative in the treatment of injuries. However, care must be taken when postural control is evaluated in the aquatic environment due to the low reliability of some measurements.

References: [1] Cupps B. Neuro Dev Treat, 1:3-8, 1997.

Balance

AS-0434

THE RELATIONSHIP BETWEEN MUSCLE QUALITY AND POSTURAL CONTROL IN OLDER ADULTS.

Gregory S. Walsh [1,*] Marco Arkesteijn [1] Daniel Low [1]

[1]Sport and Exercise Science, Institute of Biological, Environmental and Rural Sciences, Aberystwyth University, Aberystwyth, United Kingdom

Introduction and Objectives: Muscle strength decreases with age at a faster rate than muscle mass resulting in decreased muscle quality (MQ), the ratio of strength to muscle mass. The strength loss unexplained by reductions in muscle mass, result from neuromuscular and architectural degeneration in older adults [1]. Postural control (PC) requires visual, vestibular and somatosensory input and efferent neuromuscular output [2]. The neuromuscular alterations associated with declining MQ could impede somatosensory input and the output muscle activity required to maintain PC. The aim of this study was to determine if MQ and PC are correlated in older adults during quiet standing in eyes open (EO) and closed (EC) conditions. It was hypothesised that MQ would be significantly correlated with PC performance.

Methods: Twenty-five older adults participated in this study (10 males, 15 females, 66±9 years, 69.9±12.5 kg, 1.68±0.10 m). Dominant leg muscle mass was measured by dual energy X-ray absorptiometry and concentric and eccentric strength using an isokinetic dynamometer. Muscle quality was calculated as the ratio of muscle strength (summed flexor and extensor peak torques) to lean mass of the upper leg. A force plate, sampling at 48Hz, recorded quiet standing centre of pressure (COP) with EO and EC, with 5 60s trials for each condition. Traditional measures including sway length (SL), velocity (SV) and elliptical area (EA), and non-linear measures including anterior-posterior (AP) and medio-lateral (ML) fractal dimension (D_f) [3] quantified PC. The COP D_f is a measure of its complexity; a D_f of 1 is a rigidly controlled system and close to 2 as a system with little control. Pearson's correlation coefficients determined the relationship between MQ and PC and paired samples *t*-tests compared EO and EC PC, with a significance level of α=0.05.

Results: None of the traditional variables were significantly correlated with concentric or eccentric MQ (table 1). Significant correlations were found for concentric and eccentric MQ and ML D_f with EO (*r*=0.53 and 0.63, *p*<0.001 respectively) and EC (*r*=0.41 and 0.61, *p*<0.001 respectively). Sway length (*t*(24)=-4.69 *p*<0.001), EA (*t*(24)=-3.36 *p*=0.003) and ML D_f (*t*(24)=-2.1 *p*=0.04) were significantly greater in EC conditions compared with EO conditions; AP D_f remained unchanged. There was no relationship between MQ and traditional measures of PC, suggesting these methods provide descriptive understanding of COP, however stability is not reliant on constraining postural sway but on controlling it. The D_f provides an insight into the underlying mechanisms of PC [4]. The significant correlations between ML D_f and MQ demonstrates that higher MQ leads to a more complex system in the ML direction. Higher MQ allows greater freedom in postural movements whilst maintaining PC, without needing to freeze the degrees of freedom of postural adjustments creating a rigid, less complex system. The greater range of movement in the AP than ML direction means the AP direction is less stable. It is likely that control in the AP direction requires greater sensory input, whereas, ML control requires less input so neuromuscular function predominates. The changes in D_f in the present study conflict with previous findings where AP D_f increases in EC compared with EO and no change in ML [4]. This is possibly explained by differences in trial length, 2 minute trials used in previous literature [4] may lead to increased fatigue compared to 1 minute trials, resulting in altered

fractal dynamics. This highlights that further study is required to develop a greater understanding of the relationship between MQ and PC dynamics.

Conclusion: This study demonstrated a significant relationship between MQ and PC measured using ML D_f but not with SL, SV or EA. Thus, although overall sway is not affected there is an alteration in the mechanisms of PC associated with MQ. Clinically these findings suggest that high ML PC complexity, represented by D_f, should not necessarily be interpreted as a reduction in PC, merely the presence of sufficient neuromuscular control to allow greater freedom in postural adjustments.

Table: Mean(SD) and correlation coefficients MQ and PC variables.

Condition	Variable	Concentric MQ (Nm.kg^{-1})	Eccentric MQ (Nm.kg^{-1})	Mean (SD)
EO	SL (cm)	-0.12	0.02	93.78(31.11)
	SV (cm/s)	-0.12	0.02	1.56(0.52)
	EA (cm^2)	-0.30	-0.29	1.72(1.07)
	ML D_f	0.53*	0.64*	1.42(0.13)
	AP D_f	-0.06	0.02	1.46(0.08)
EC	SL (cm)	-0.16	0.02	124.18(60.06)**
	SV (cm/s)	0.04	-0.07	3.01(4.85)
	EA (cm^2)	-0.18	-0.09	2.49(1.90)**
	ML D_f	0.41*	0.61*	1.45(0.11)**
	AP D_f	-0.17	-0.01	1.46(0.07)
Mean (SD)		34.8(11.0)	43.4(12.3)	

Caption: * represents significant correlation (p<0.05), ** represents significant difference between EO and EC conditions (p<0.05).

References: 1.   Barbat-Artigas S et al., *The Journal of Nutrition Health & Aging,* **16:** 67-77, 2012.

2.   Blaszczyk J et al., *Acta, Neurobiol. Exp.*, **61**: 105-112, 2001.

3.   Higuchi T., *Physica D,* **31:** 277-283, 1988.

4.   Doyle T et al., *Int. J. Med. Sci.,* **1:** 11-20, 2004.

Disclosure of Interest: None Declared

AS-0435

BALLET DANCERS X PHYSICAL EDUCATION STUDENTS CENTER OF PRESSURE SWAYS: EFFECTS OF VISION AND FOOT POSITION

Marcus F. Vieira [1,*]Maiara Ferreira [1]Paula Lobo da Costa [2]Fernanda Nora [1]

[1]Bioengineering and Biomechanics Laboratory, Universidade Federal de Goiás, Goiânia, [2]Physical Education Department, Universidade Federal de São Carlos, São Carlos, Brazil

Introduction and Objectives: Ballet dancers practice demanding equilibrium tasks for many years and are sometimes considered experts in postural control [1,2], but this fact is controversial [3]. The aim of this study was to test the vision dependence for postural control in ballet dancers during bipedal (B) and tandem (T) standing (foot position) by analyzing the center of pressure (COP) sway.

Methods: Nine semi-professional ballet dancers (BD) and 10 physical education students (PES) gave written consent to participate in this study. COP sways for both positions were collected during 60 s by an AMTI forceplate at 100 HZ in opened (OE) and closed (CE) eyes conditions. The data was filtered by a 4th order, low pass, zero-lag Butterworth filter with a 12.5 Hz cutoff frequency. After a detrend operation, global variables (area, mean velocity-Vel, 80% power frequency-F80) were calculated to analyze COP sway in anterior-posterior (AP) and medial-lateral (ML) directions. COP power spectrum was estimated using the Welch method with 2000 samples per periodogram, resulting in a spectral resolution of 0.05 Hz. Thus, F80 power frequency, which encompass 80% of the area under the COP power spectrum, was estimated. A custom MatLab code was written to calculate the variables. Significant differences between groups, vision condition, foot position and interactions were analyzed by mixed repeated measures ANOVA (GLM 5), with $p < 0.05$.

Results: Vison condition: BD group did not show significant differences between OE x CE, except in T position, whereas PES group showed significant differences in both positions (Table 1). Position condition: there were significant differences between B x T positions for both groups, for all variables. Interaction: there was only significant difference between BD x PES groups for F80 AP in T position and CE condition. In general, all variables were larger for PES group.

Conclusion: The T position was more challenging for both groups. Despite Area was larger for BD group in T position, the other variables were larger for PES group, indicating PES group is more instable in the T position. PES group showed larger F80 AP in CE in T position and larger velocity in both positions, indicating lower sway amplitudes, increased ankle stiffness due to changes in ankle torque pattern [4,5]. The opposite observations can be done for BD group.

Conclusion BD seems to be less dependent of vision. Although not significant, BD seems to be more stable than PES in the conditions tested.

Table: Table 1 – Global variables of COP sways.

	Groups		Area		Velocity		F80	
			OE	CE	OE	CE	OE	CE
AP	BD	Bipedal	1.28 ±0.92	1.15 ±0.69	0.48 ±0.17	0.53 ±0.17	0.32 ±0.14	0.36 ±0.22
		Tande	5.77	10.51	1.48	2.13	0.51	0.49

Dir	Group	Cond.						
		m	±4.42	±6.32	±0.64	±0.71*	±0.37	±0.29
			p=0.009	p=0.002	p=0.001	p<0.001	--//--	--//--
	PES	Bipedal	1.44 ±1.03	1.47 ±0.66	0.55 ±0.15	0.67 ±0.15*	0.25 ±0.09	0.35 ±0.13*
		Tandem	3.48 ±1.67	7.91 ±3.63*	1.48 ±0.27	2.26 ±0.63*	0.77 ±0.22	0.91 ±0.18
	B x T		p=0.008	p<0.001	p<0.001	p<0.001	p<0.001	p<0.001
ML	BD	Bipedal			0.35 ±0.12	0.35 ±0.13	0.36 ±0.19	0.38 ±0.18
		Tandem			1.61 ±0.54	2.78 ±0.75*	0.55 ±0.12	0.74 ±0.23*
					p<0.001	p<0.001	p=0.014	p<0.001
	PES	Bipedal			0.42 ±0.20	0.42 ±0.18	0.45 ±0.20	0.41 ±0.19
		Tandem		1.65 ±0.34	2.95 ±0.89*	0.61 ±0.12	0.77 ±0.19*	
	B x T			p<0.001	p<0.001	--//--	p=0.001	

Caption: AP: anterior-posterior direction, ML: medial-lateral direction, BD: ballet dancers, PES: physical education students, OE: opened eyes, CE: closed eyes, *: significant differences between OE x CE conditions, p: repeated measures ANOVA.

References: References

[1] Guillou et al., Clinical Neurophysiol, 118:317-324, 2007.

[2] Kiefer et al., Gait Posture, 34:76-80, 2011.

[3] Simmons WR, Int J Neurosci, 115:1193-1203, 2005.

[4] Baratto et al., Motor Control, 6: 246-270, 2002.

[5] Loram et al., J Physiol, 532:879–891, 2001.

Disclosure of Interest: None Declared

Balance

AS-0436

IMPORTANCE OF BIARTICULAR LEG MUSCLES FOR BALANCE DURING UPRIGHT HUMAN STANDING.

Dario Tokur [1,*] Christian Rode [1] Fabian Hoitz [1] André Seyfarth [1]

[1]Sport Science, Lauflabor, TU Darmstadt, Darmstadt, Germany

Introduction and Objectives: Human bipedalism is characterized by an upright trunk posture and straight knee configuration during stance phases. The trunk must be balanced during movements like walking and running. This is an ongoing task also in standing as the body sways and has to be balanced. In order to keep an upright posture, humans can employ different control strategies such as the ankle or the hip strategy [2, 6, 7, 8]. Alternatively, they can also use the stepping strategy [4].

Ground reaction forces (GRF) during human walking intersect in a virtual pivot point (VPP) above the centre of mass. Here, simulations with a simple gait model tuning the GRFs to intersect a body-fixed VPP lead to postural stability [3].

Through activation of biarticular leg muscles humans are able to manipulate leg forces perpendicular to the leg axis with appropriate leg segment lenghts and muscle moment arms [5]. In this study we assess the relevance of this concept for humans by perturbed standing experiments.

Methods: Nine healthy male subjects (24.3 ± 1.82 years, 77.6 ± 7.5 kg and 182.1 ± 7.5 cm) took part in this study. Human upright standing was perturbed by introducing constant external pulling forces (Fig. 1A – arrows; 10, 20 and 30N) at different body locations (ankle and neck) that created external torques (Fig. 1A – dashed lines) according to the pulling direction (anterior or posterior). Subjects were instructed to maintain their upright posture resulting in re-orientation of leg forces via muscles to compensate for the external perturbation. Kinematic, kinetic and electromyographical (EMG) parameters of selected mono- and biarticular leg muscles were recorded.

EMG signals were demeaned, filtered and normalized to MVC-signal (maximal voluntary contraction) as suggested by Konrad [1]. One-second means of unperturbed and perturbed standing were calculated in order to compare EMG differences under these circumstances.

Results: Figure 1 presents the results of the data analysis for selected bi- (Fig. 1B) and monoarticular (Fig. 1C) muscles. Upper rows show predicted change (green arrow up – increase; grey, crossed out arrow – no increase) in muscle activation, lower rows show the measured muscle activation. Muscle abreviations can be found in Table 1.

In contrast to monoarticular muscles, predicted changes in EMG for biarticular muscles largely comply with measured EMG changes. Moreover, seven out of ten biarticular muscles with predicted EMG increase revealed a significant positive linear relation between pulling force and EMG increase. For monoarticular muscles, this was only the case for two out of eight muscles.

Figure:
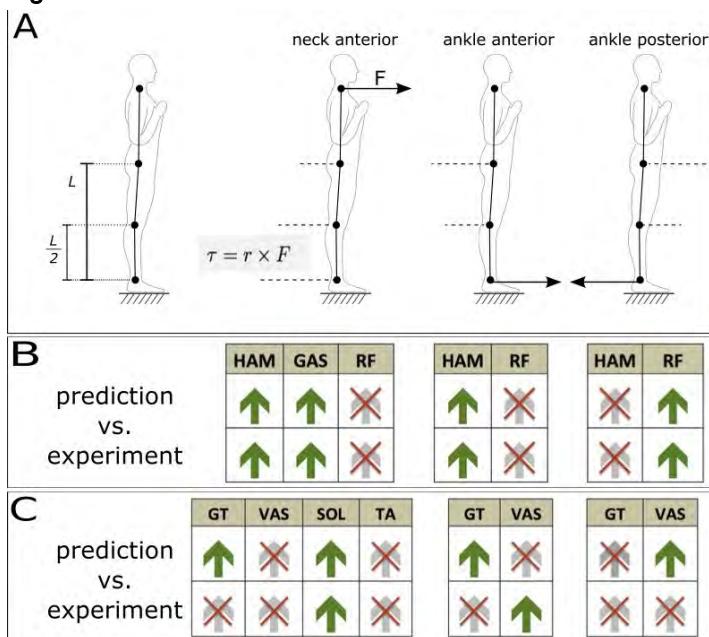
Caption: Figure1: Experimental design and results. A: experimental design with introduced external forces (black arrows), lever arm ratios (L and L/2) and resulting external torques (dashed lines) according to the perturbation location and direction (anterior or posterior). B+C: predicted (upper row) and measured (lower row) muscle activation (green arrow up – increase; grey, crossed out arrow – no increase) of biarticular (B) and monoarticular (C) muscles.

Conclusion:

Our static perturbation experiments (Fig. 1A) suggest, that upright posture can be maintained by manipulating GRF via perpendicular leg forces that are created by biarticular leg muscles. This indicates the relevance of the presented concept from Rode and Seyfarth [5] for humans.

Further data analysis comprising more sophisticated comparisons such as assessing the influence of knee angles during perturbation or a comparison with axial perturbation experiments will be done. Moreover, investigating the dynamic changes of leg force and muscle activation in response to a sudden release of the quasi static pulling force is scheduled.

Table:

Abbreviation	Muscles
HAM	Hamstrings: *Biceps Femoris long head* and *short head, Semitendinosus*
GAS	*Gastrocnemius lateralis and medialis*
RF	*Rectus femoris*
GT	*Gluteus Maximus*
VAS	*Vastus lateralis* and *medialis*
SOL	*Soleus*
TA	*Tibialis anterior*

Caption: Table 1: Explanation for abbreviations of muscles-names shown in Figure 1 (B+C).

References:

[1] Konrad. EMG-Fibel: Eine praxisorientierteEinfürhung in die kinesiologische Elekromyographie, Noraxon INC. USA, 2015.

[2]. Loram et al., *The Journal of Physiology*, *556*(3), 683–689, 2004

[3]. Maus et al., *Nature Communications*, *1*, article number: 70, 2010.

[4]. Mille, *Journal of Neurophysiology*, *90*(2), 666–674, 2003.

[5]. Rode et al, Balance control is simplified by muscle-skeletal leg design. Online proceedings – Dynamic Walking 2013: http://www.cmu.edu/dynamic-walking/files/abstracts/Rode_2013_DW.pdf

[6]. Runge*, Gait & Posture*, *10*(2), 161–170, 1999.

[7]. Winter et al., *Journal of Neurophysiology*, *80*(3), 1211–1221, 1998.

[8]. Winter, *Journal of Neurophysiology*, *85*(6), 2630–2633, 2001.

Disclosure of Interest: None Declared

AS-0437

RADIAL DISPLACEMENT ASSESSMENT OF BILATERAL SKELETAL MUSCLE ASYMMETRY

Lewis J. Macgregor [1,*]Angus Hunter [1]

[1]Health & Exercise Science Research Group, University of Stirling, Stirling, United Kingdom

Introduction and Objectives: Bilateral muscular asymmetry has been investigated in association with injuries [3] and athletic performance [1]. Muscle asymmetry has usually been quantified through differences in strength between contralateral limbs. Bilateral strength asymmetry of the knee extensors has been used in Sports Medicine to assess knee injury and inform rehabilitation programmes [8]. Asymmetry is commonly assessed by measures of peak isokinetic force [3], or through dynamic vertical jump tests [6]. Isokinetic or dynamic strength tests, provide information on isolated or multiple muscle groups, but cannot specifically identify issues in single muscles.

Assessment of muscle belly radial displacement is a sensitive [4] and reliable [7] measure of muscle contractile properties. This technique uses a portable displacement sensor to record muscle twitch response to a single submaximal electrical stimulus. The technique is passive and non-invasive and as such will not aggravate any existing skeletal musculotendinous injuries or impede recovery. Furthermore, the measure is unaffected by covariates such as volitional motivation. It is important to establish whether there is a direct relationship between asymmetry at the level of individual muscle twitch response and in the functional capability of the muscle group/ limb. Accordingly the aim of this study was to assess the relationship between bilateral asymmetry at the level of individual muscle twitch (radial displacement) and contractile function of the muscle group/ entire limb. This enabled us to establish the efficacy of a model for predicting functional asymmetry based on a passive, non-invasive and field based measurement.

Methods: Twenty volunteers (aged 17-45) reported to the laboratory following an overnight fast and rested in a supine position for 30 minutes. Then, muscle displacement, isometric and ballistic contractions were measured.

Muscle displacement responded to a 1ms electrical pulse to the muscle, through a pair of electrodes affixed to the skin directly above the muscle belly. Electrodes were located 10cm apart, with a displacement sensor (Digital-optical comparator, RLS Ltd, Slovenia) positioned perpendicular and equidistant between the two. Stimulation was progressively increased until peak muscle displacement (Dm) was achieved. This was recorded from the vastus lateralis (VL), rectus femoris (RF) andvastus medialis (VM) of both legs.

Maximal isometric voluntary contraction (MVC) of the knee extensors was assessed using an isokinetic dynamometer (Kin-Com Chattanooga Group Inc, Chattanooga, Tennessee, USA) at a knee angle of 60o (0o = full extension). Following a standardised warm up [2], three 5s MVCs were performed with 60s rest between efforts. Ballistic assessments were performed using a force platform (400 Series Force platform, Fitness Technology, Australia). Three single leg CMJs were performed on each limb. Participants performed a squat on the test leg, until a knee angle of 70o was reached, immediately a maximal vertical jump was executed, participants landed on the same single leg. For both MVC and CMJ the highest peak from the 3 repetitions was recorded for analysis. For each measurement parameter symmetry index (SI%) was calculated [4].

Using a threshold of >+10% [4] participants were categorised as asymmetric (AS) or symmetrical (SY), based on MVC and CMJ. One-way RM ANOVA with Tukey post hoc analysis was performed to explore differences in the SI% of MVC and Dm (VL, RF and VM) between SY and AS.

Results: The SI% of the SY group for MVC was significantly (p=0.032) lower than AS (3.71% compared to 11.31%). Dm in the VM was 11.27% higher in the weaker limb in AS. SI% for VM was significantly (p=0.027) different between AS and SY, as shown in figure 1.

Figure:
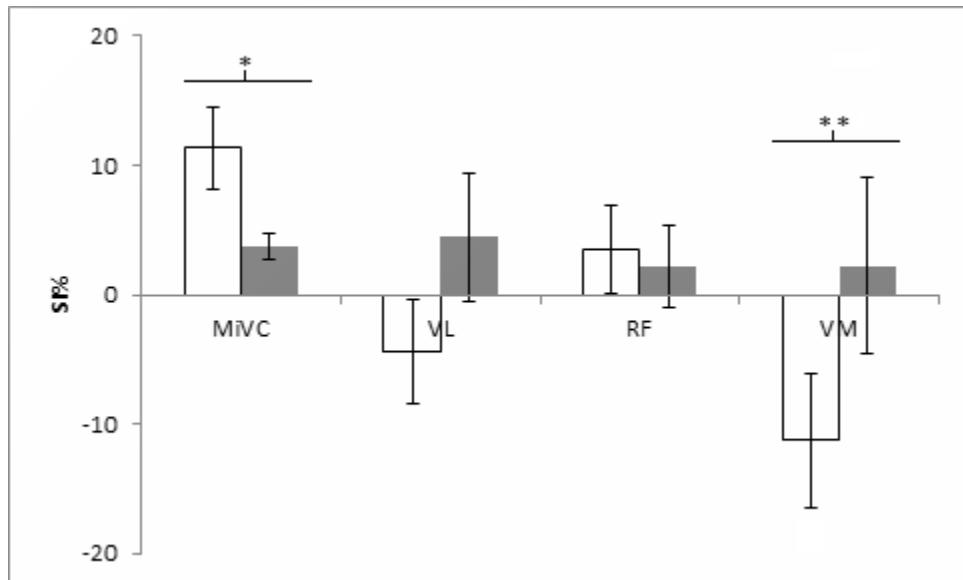
Caption: Symmetry index (%) of peak force and radial displacement, in the asymmetric (white) and symmetrical (shaded) groups. (VL: vastus lateralis, RF: rectus femoris, VM: vastus medialis). *: p = 0.032. **: p = 0.027

Conclusion: These findings suggest that asymmetries in VM twitch can predict functional asymmetries between lower limbs. Higher Dm in the VM of the weaker limb indicates decreased muscle tone in that muscle, compared to the VM in the stronger limb. Differences in muscle tone between contralateral muscles could be a primary predictor of functional asymmetry. This finding could pave the way for interventions, targeted at specific individual muscles, to manage injury and improve sporting performance.

References: [1] Bailey et al, J. Trainology, 2:1-5, 2013.

[2] Balshaw et al, J Electromyogr Kinesiol., 22:308-19, 2012.

[3] Croisier et al, Am J Sports Med., 30:199-203, 2002.

[4] Ditroilo et al, J Electromyogr Kinesiol., 23:558-63, 2013.

[5] Herzog et al, Med Sci Sports Exerc., 21:110-4, 1989.

[6] Impellizzeri et al, Med Sci Sports Exerc., 39:2044–50, 2007.

[7] Krizaj et al, J Electromyogr Kinesiol., 35:295-305, 2007.

[8] Wilk et al, Orthop. Clin. North Am., 34:107-37, 2003.

Disclosure of Interest: None Declared

Balance

AS-0438

LEARNING TO BALANCE ON ONE LEG

Jaap Van Dieen [1,*]Marloes van Leeuwen [1]Gert Faber [1]

[1]Human Movement Sciences, VU University Amsterdam, Amsterdam, Netherlands

Introduction and Objectives: We investigated changes in motor strategy in learning a novel balancing task. Balance control can be conceptualized as the control of the center of mass (CoM) in relation to the base of support. Three strategies are available to this end [1]: A) creating ankle moments to shift the centre of pressure (CoP), B) changing angular momentum of body segments around the CoM and C) creating a new base of support (e.g. by grabbing a handrail). Strategy C was considered task failure. We hypothesized that a shift in the use of strategies A and B would occur with training.

Methods: Fourteen young adults learned to balance on their preferred leg on a board mounted on a half cylinder with a 30 cm radius, which could rotate in the frontal plane. Subjects performed six 16-seconds trials standing on the board before training and six trials after 30 min training. LED markers on the board and on anatomical landmarks were tracked to determine CoM position and angular momentum time series. EMG of the adductor longus (AL) and gluteus medius (GM) muscles was measured. The sets of six trials consisted of two trials without manipulation, four trials with vestibular and visual manipulations. Motor strategies were investigated in the unperturbed trials only.

To quantify performance, the mediolateral path travelled by the CoM was determined. To assess motor strategies, we quantified the contribution of strategy B (changes in angular momentum) to CoM acceleration. In addition, we determined the means and coefficients of variation (CoV) of the EMG amplitudes. Finally, we determined the relative power of oscillations between 2.5-4.5 Hz observed in the CoM acceleration, the orientation of the board and the EMG amplitudes. Training effects were evaluated with repeated measures ANOVAs testing for effects of trial, to assess fast learning over repeated trials and for effects of 30-min training, to assess more gradual learning. In view of their distribution, EMG data were tested non-parametrically for differences between adjacent trials.

Results: Substantial postural sway and occasional loss of balance (touching the handrail) illustrated the difficulty of the balancing task. Overall angular momentum changes accounted for 70% of CoM acceleration. In most subjects angular momenta of the arms, trunk and head co-varied in-phase, apparently driven by motion around the hip of the stance leg. Substantial hip muscle activity was present in which phasic bursts were superimposed on tonic activity, sometimes reflecting reciprocal activation and sometimes reflecting co-activation. In the initial trials, strong oscillations of the CoM acceleration and the board orientation with a peak power between 2.5 and 4.5 Hz were observed in all subjects.

Performance improved with training on short and long time scales as evidenced by a significant main effects of trial and training and a significant interaction effect on CoM path. The contribution of the derivative of the angular momentum to CoM acceleration decreased over trials from on average over 100%, indicating that strategy A and B counteracted each other, to about 50%, indicating that synergistic effects of both strategies. Significant main and interaction effects of trial and training on the contribution of angular momentum changes indicated a larger decrease between pre-training trials than between post-training trials. The relative power of CoM and balance board oscillations also decreased with training,

and a significant interaction reflected a substantial decrease between trials before training and a slight increase between trials after training.

Mean muscle activity of the AL and GM decreased significantly between the two pre-training trials by 36% and 26%, respectively, but did not change significantly between later trials. The CoV of the EMG amplitudes also decreased significantly between pre-training trials from about 40 to 25% for both muscles. Relative power decreased for GM only, from 50 to 34% between pre-training trials and from 34 to 26% between pre-training 2 and post-training 1.

Figure:
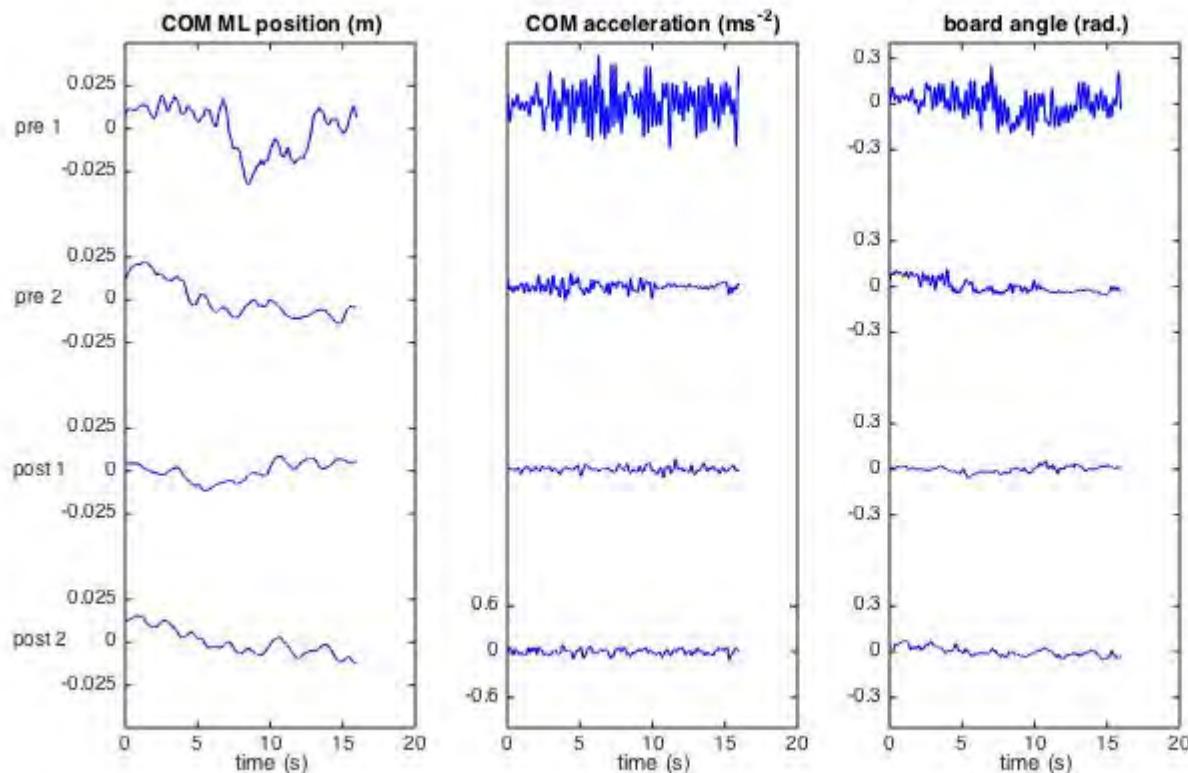
Caption: Typical example of the times series of the CoM position, its acceleration and the angle of the board with the horizontal.

Conclusion: Our results indicate that subjects rapidly improve performance in single leg balancing on an unstable object. Compared to standing on a rigid surface, standing on an unstable object changes the transfer function between ankle moment and CoM acceleration involved in strategy A. This apparently caused the oscillatory behavior, possibly due to too high feedback gains. In the initial trials, the ineffective use of strategy A had to be counteracted by means of strategy B. The oscillations were attenuated over subsequent trials, possibly by decreasing feedback gains, coinciding with a shorter sway path and less frequent balance loss, a reduced contribution of strategy B and reduced effort as reflected in decreased muscle activity.

References: [1] Hof, J. Biomechanics, 40: 451-457.

Disclosure of Interest: None Declared

Cardiovascular

AS-0440

MORPHOLOGICAL AND FLUID MECHANICS CHANGES TO THE CAROTID SIPHON OBSERVED IN MOYAMOYA DISEASE

Choon Hwai Yap [1,*]Muhammad Jamil [1]Mehnaz Haq [1]Heidi Kang Xue Han [2]Zhi Rui Lee [2]Phua Hwee Tang [3]

[1]Biomedical Engineering, National University of Singapore, [2]Hwa Chong Institution, [3]KKH Women's and Children's Hospital, Singapore, Singapore

Introduction and Objectives: Moyamoya is a cerebrovascular disease in which the distal end of the internal carotid artery is progressively occluded to cause deficiency of blood supply to the brain. Deficiency in blood supply then triggers angiogenesis and results in the formation of multiple small collateral arteries, which resembles a puff of smoke when viewed on CT scans. The disease was thus named: it was first reported in Japan in 1957, and was given the Japanese name of "Moyamoya" which translates to "a puff of smoke". Moyamoya's prevalence is 3 cases per 100,000 persons in Japan, affecting females almost twice as often than males [1], and about 0.57 per 100,000 individuals [2] in US. To date, the etiology of the Moyamoya disease is still unknown [1]. It has been hypothesized that hemodynamics plays a role in the pathogenesis of Moyamoya [3]. Canonical findings about the role of mechanical forces in vasculopathies such as atherosclerosis [4] and aneurysms [5, 6] have been presented previously. It has also been hypothesized that arteriogenesis and vascular remodeling via endothelium activation is triggered by the mechanical stimulus. Morphological aspects such as area constrictions [7], curvature [5] and torsion [8] play an important role in shaping the hemodynamics in the arteries. Study of these geometric and hemodynamic characteristics in the context of moyamoya may prove valuable in diagnosis and predicting the disease pathway.

Methods: A retrospective analysis of the Magnetic Resonance Angiography (MRA) image data from 5 Moyamoya and 10 control patients was performed. Moyamoya Data was available for both pre- and post-revascularization operations. The carotid siphon 3D geometry was segmented and analyzed for cross sectional area, curvature, tortuosity and torsion. Specific attention was paid to the proximal (B2) and distal (B1) bends of the carotid siphon. Computational Fluid Dynamics (CFD) analysis was performed to study pressure losses and secondary flows.

Results: Geometric analysis of the cross sectional area showed that Moyamoya patients had carotid siphons and internal carotid arteries which were significantly smaller in cross-sectional areas ($p<0.05$). Vessel sizes remained small even after revascularization operations. The disease also altered the relationship between the carotid siphon curvature and vascular size (Figure 1). For normal carotid siphons, the normalized curvature was found to be constant, indicating that non-dimensional shape of the siphon was retained despite growth. However, in Moyamoya disease, when the carotid siphon remodeled to change its cross-sectional area, the curvature of the siphon did not have a corresponding change, causing the vessel to deviate from having a constant normalized shape. Other geometric changes include : B2 torsion significantly increased in pre-op and post-op cases against controls, B2 tortuosity for post-op vs controls also increased significantly. Fluid mechanics analysis showed that in Moyamoya carotid siphons, the pressure drop increased and the secondary flow strength decreased as compared to the controls.

Figure:
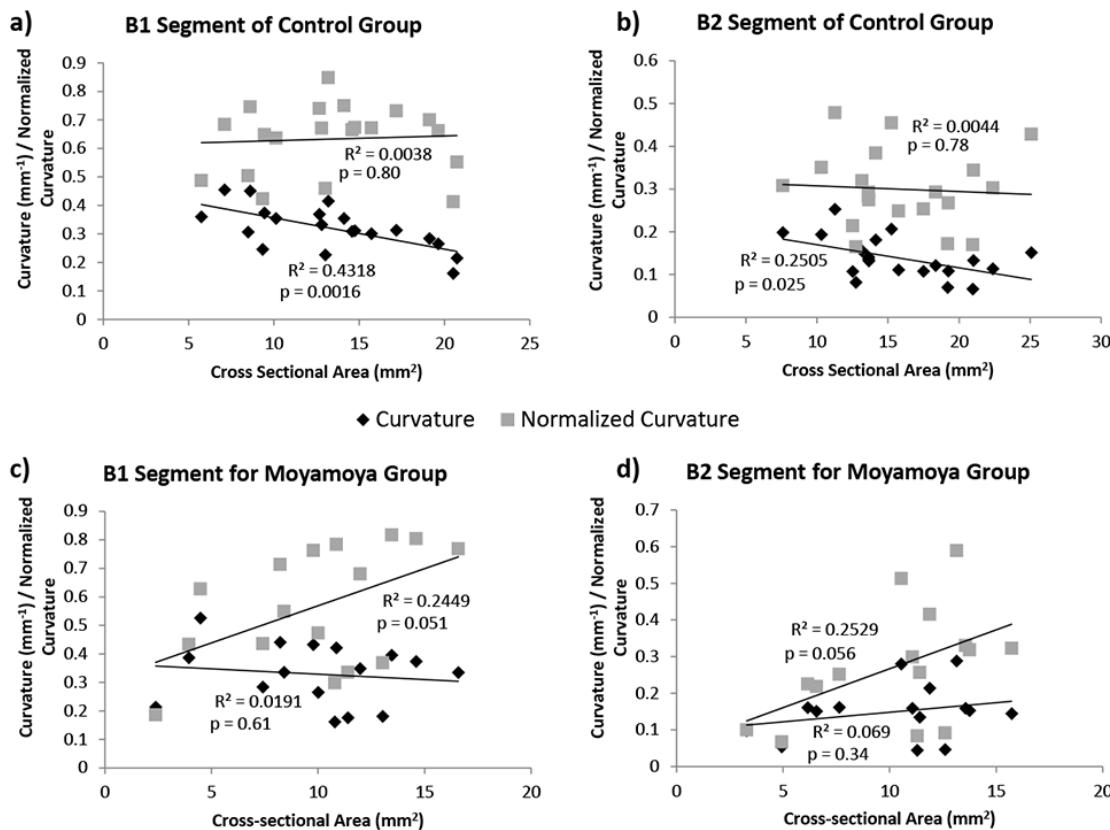
Caption: Figure 1: Scatter plots of curvature and normalized curvature versus average cross sectional area of sections B1 & B2 respectively for Control (a-b) and Moyamoya (c-d) cases

Conclusion: Geometric and computational fluid dynamics analysis was performed on the control and diseased cases. The main findings observed are: (1) Internal carotid and carotid siphon are significantly smaller in diseased cases even after the revascularization surgery; (2) Control group growth progressed in such a way so as to keep the normalized curvature constant. In Moyamoya cases, the vascular curvature (un-normalized) remained constant and didn't keep pace with the vessel growth; (3) B2 segment of the carotid siphon had significantly higher torsion in Moyamoya patients; (4) hemodynamics changes such as higher pressure drop and lower secondary flows were observed in Moyamoya patients.

References: [1] Ganesan, V., J. Ped. Neur., **8**(1): 93-95, 2010.

[2] Starke et al., Neurosurgery, **71**(1): 93, 2012.

[3] Shin et al., in *World Cong. on Med. Phy. and Biomed. Engg. 2006*, Springer Berlin Heidelberg.

[4] Peiffer et al., Vol. 99, 242-250, 2013.

[5] Lauric et al., J. Biomech., **47**(12): 3018-3027, 2014.

[6] Valen-Sendstad et al., J. Biomech., **47**(12): 3210-3216, 2014.

[7] Choi et al., Korean J. Chem. Engg., **31**(3): 402-411, 2014.

[8] Nguyen et al., J. Biomech., **41**(1): 11-19, 2008.

Disclosure of Interest: None Declared

Cardiovascular

AS-0442

A NOVEL COMPUTATIONAL MODEL FOR THE HEMODYNAMICS OF BILEAFLET MECHANICAL VALVES IN THE OPENING PHASE

Mehdi Jahandardoost [1,*]Guy Fradet [2]Hadi Mohammadi [1]

[1]Biomedical Engineering, [2]Department of Surgery , University of British Columbia, Kelowna, Canada

Introduction and Objectives: Bileaflet mechanical heart valves (MHVs) designs are known for providing a uniform flow profile and a lower incidence of structural complications. However, thrombus formation on the hinges, valve failure and leaflet escapement have been reported in certain designs. To date, in almost all of the modeling studies on the hemodynamics of bileaflet MHVs, a velocity (mass flow) based boundary condition and an axisymmetric geometry for the aortic root have been assigned which, to some extent, are erroneous. Also, the profile of velocity in downstream of leaflets has been reported contradictory. The reported values for the peak velocities range from 1 m/s to 3 m/s which highly depend on the model assumptions. The objective of this study is to demonstrate the importance of the exact anatomical model of the aortic root and realistic boundary conditions in the hemodynamics of the bileaflet MHVs. The model considered in this study is based on the St. Jude Medical (SJM) bileaflet mechanical valve in a novel modeling platform. Through a more realistic geometrical model for the aortic root and the SJM valve, we have developed a new set of boundary conditions in order to be used for the assessment of the hemodynamics of aortic bileaflet MHVs.

Methods: The present study examines both pressure- and velocity-based boundary conditions at the inlet and outlet to create the most realistic flow regime around the valve leaflets. The flow around the bileaflet MHV (SJM model) is pulsatile and encompasses the three regimes of laminar, transient, and turbulent. To predict the salient features of flow around the bileaflet MHV, the shear stress transport (SST) low-Re two-equation turbulence models were applied. There are three types of boundary conditions (BCs) considered in this study: (1) mass flow inlet and pressure outlet (MP), (2) turbulent fully developed velocity inlet and pressure outlet (UturbulentP), and (3) pressure inlet and mass flow outlet (PM).

Results: The velocity field around the valve leaflets, the vortex shedding after the leaflets, the secondary flow regions in the sinuses, etc., at three time phases of acceleration, maximum flow, and deceleration were extensively studied. In the following figure ("a" and "b"), the comparison between the velocity profiles of the current study and the study carried out by Ge et al. 2005, [1], and Nguyen et al. 2012, [2], are shown at the section downstream of the valve normal and parallel to the leaflets.

Figure:
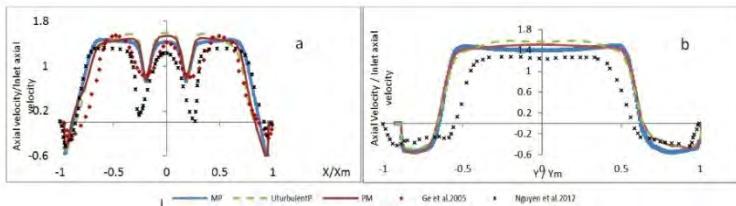
Velocity profiles downstream of the valve normal to the leaflet and at maximum area location, (a) Re=7000 at t=0.5T (Max flow phase); (e) Re=7000 at t=0.5T (Max flow phase)

Conclusion: We have developed a new computational platform by which the hemodynamics of bileaflet mechanical heart valve can be assessed precisely. We quantitatively showed the importance of realistic aortic root geometry and boundary conditions on the hemodynamics of bileaflet mechanical valves. The results of the current study are significant for the design improvement of conventional bileaflet MHVs and for the design of the next generation of prosthetic valves.

References: [1] Ge L, et al., J Biomech Eng, 127:782-97, 2005.
[2] Nguyen VT et al., J CVET, 3:88-100, 2012.

Disclosure of Interest: None Declared

Arterial Mechanics

AS-0443

MODELLING TEAR PROPAGATION IN THE ARTERIAL WALL

Lei Wang [1,*]Steven Roper [1]Xiaoyu Luo [1]N.A. Hill [1]

[1]School of Mathematics and Statistics, University of Glasgow, Glasgow, United Kingdom

Introduction and Objectives: An arterial dissection is an axial tear within the wall, which may create a false lumen through which blood flows. Propagation of the tear can quickly lead to death as a result of decreased blood supply to other organs, damage to the aortic valve, and sometimes rupture of the artery. We aim to compute the potential for tear propagation, with the ultimate aim of providing a quantitative prediction on the outcome of an existing arterial dissection, so aiding its clinical management.

Methods: To consider the propagation of an arterial dissection, we use a computational model that includes nonlinear deformation and pressure-driven failure of the arterial wall.

For failure criterion, we employ an energy approach, extending the Griffith energy balance principle [1] in linear elasticity to fibrous soft tissues with finite deformation. The material model is the Holzapfel-Gasser-Ogden constitutive law [2]. The geometry is simplified to that of an axisymmetric thick-walled cylinder and the small communicating tear is also ignored. An axisymmetric axial tear of length *a* is included in the centre of wall subject to a constant pressure *p*, assumed to be equal to the mean pressure in the lumen. Employing the finite element method through FEAP [3], we calculate the difference in the potential energy *E(a)*, before and after extending the tear from length *a* to *a+da*. If $E(a)-E(a+da)>G_c da$ where G_c is the minimum energy required for breaking the bonds of the tissue per unit length, the tear propagation is deemed to be energetically favourable.

Results: We report the effect of collagen fibre orientation and identify the regions with high risk of propagation in *(a,p)*. Similar to our early result for a two-dimensional arterial wall strip [4], the result reveals that increasing either the tear length or the pressure enhances the energetically favourable propagation. Changing the orientation of fibres can slow down the tear propagation, and a tear arrest can occur when the surrounding connective tissues with sufficient stiffness are included.

Conclusion: We have developed a computational model for predicting the tear propagation in an axisymmetric thick-walled cylinder. The results provide some insights into the behaviour of the pressure-driven tear propagation in the arterial wall and other fibrous soft tissues.

References: [1] Griffith, Philos T Roy Soc A, 221:163-198, 1921.

[2] Holzapfel, et al., J Elasticity, 61:1-48, 2000.

[3] Taylor. FEAP—A Finite Element Analysis Program: Version 8.3 Programmer manual, University of California at Berkeley, 2011.

[4] Wang, et al., J Eng Math, in press.

Disclosure of Interest: None Declared

AS-0444

ANEURYSM FORMATION: THE ROLE OF SAMPLE THICKNESS IN THE EXPERIMENTAL DATA COLLECTION

Serena de Gelidi [1,*] Gianluca Tozzi [1] Andrea Bucchi [1]

[1] School of Engineering, University of Portsmouth, Portsmouth, United Kingdom

Introduction and Objectives: Despite several experimental methodologies are available to characterize mechanical properties of soft biological tissues, a standard protocol is still missing.

In order to determine the stress achieved in the stretched materials, measurement of sample thickness represents a crucial step. Typically, the thickness is measured for each specimen by laser micrometer [1] or assumed constant for all samples tested [2]. This study aims at investigating the formation of aneurysm, using uniaxial tensile tests performed on healthy porcine descending aortas. The impact of current practice in thickness estimation is assessed by means of finite element predictions.

Methods: Porcine aortas were collected from a local farm house about one hour after sacrifice. The tissue was stored in isotonic saline solution at -20°C within 4 hours [3]. Dumb-bells shapes were cut out by means of a custom made die, ISO 37:2005(E), type 4, from thoracic aortas. Thickness and initial length were optically determined using a customised Matlab® script (Mathworks, Massachusetts, US) for each sample. In order to enhance the contrast of the region of interest (ROI), a black background was applied for the estimation of the thickness. Similarly, a white background was used for the initial length. In both cases, Sobel edge detection method is applied on the ROI, which was manually selected (Figure 1). Pixel conversion in *mm* is based on the grip dimensions, previously measured by an electronic calliper.

Six samples were pre-conditioned by 5 cycles performed at 1.2 *Hz*. Uniaxial tensile tests were carried out at 0.2 *mm/s* speed rate onto a BOSE® Electroforce (Model, Bose Corporation, USA) equipped with a 250N load cell.

Three values of thickness were considered for the stress evaluation: sample specific (through MatLab script), 1.5 *mm* and 3.5 *mm* constant. For each of them, the stiffest and the softest stress-strain responses were selected.

Filtered stress-strain data were fitted by 1st order Ogden, Neo-Hookean and Yeoh strain-energy functions and imported in a simplified artery, modelled as a tube in Abaqus® (Dassault Systèmes S.A., France). Four node shell elements with reduced integration (S4R) were adopted to mesh the tube, being the radius equal to 9.5 *mm*, thickness 1 *mm* and length 200 *mm* [4]. As boundary conditions, both ends were fully constrained and an internal inflating pressure with magnitude of 1 *kPa* was applied. Elastic instability, representing aneurysm formation, was investigated by modified Riks method [5].

Results: No critical pressure was obtained for the Yeoh strain-energy function, although this fits all the experimental data. Critical pressure values for the other two strain-energy functions are reported in Table 1.

Figure:
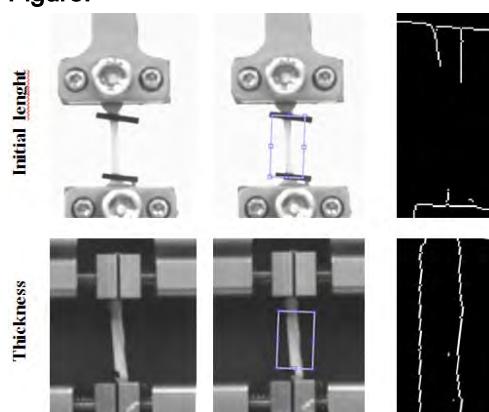
Caption: Figure 1 - Steps of Matlab script: ROI selection and application of Sobel edge detection method.

Conclusion: A novel method to estimate the sample specific thickness is presented. Differently from other works [1], the thickness value is computed as the average of all points included in the ROI (Figure 1).

Critical pressure values appear to be considerably scattered when a constant value of thickness is assumed in the stress calculation (Table 1). Comparing results related to the stiffest and the softest data for each thickness, the minimum scatter (~1kPa) is obtained for the sample specific thickness. Therefore, the most accurate prediction seems to be related to a precise thickness determination (Matlab script) as proposed in this work.

Extension of this work will include biaxial tensile tests combined with FE simulations on a model of descending aorta, as a refinement of the presented tube.

Table:

Strain-energy function	sample specific		1.5 mm		3.5 mm	
	stiffest	*softest*	*stiffest*	*softest*	*stiffest*	*softest*
1st order Ogden	8.678	no CP	2.072	no CP	6.609	no CP
Neo-Hookean	8.376	7.754	5.730	6.298	7.668	11.888

Caption: Table 1 - Critical pressure values [kPa] obtained for the stiffest and softest stress-strain behaviour calculated for three different thickness values: sample specific, 1.5mm and 3.5mm. When no critical pressure is reached, "no CP" is reported.

References: [1]Di Martino et al., *J. Vasc. Surg.*, vol. 43, no. 3, pp. 570–6; discussion 576, Mar. 2006.

[2]Choudhury et al., *Cardiovasc. Pathol.*, vol. 18, no. 2, pp. 83–91, 2009.

[3]Chow and Zhang, *J. Surg. Res.*, vol. 171, no. 2, pp. 434–42, Dec. 2011.

[4]Shi and Moita, *Comput. Methods Appl. Mech. Eng.*, vol. 7825, no. 96, pp. 265–281, 1996.

[5]Wriggers, *Nonlinear Finite Element Methods*. Berlin: Springer-Verlag, 2010.

Disclosure of Interest: None Declared

ELLIPTIC ST. JUDE BILEAFLET MECHANICAL HEART VALVES

Hadi Mohammadi [1,*]Mehdi Jahandardoost [1]Guy Fradet [2]

[1]Biomedical Engineering, [2]Department of Surgery , University of British Columbia, Kelowna, Canada

Introduction and Objectives: St. Jude Medical (SJM) bileaflet mechanical valves were approved by the Food and Drug Administration in 1977. The SJM valve design consists of two semicircular leaflets which pivot on hinges. It provides good central flow, the leaflets open completely, and the pressure drop across the valve is trivial. However, non-physiological hemodynamics around these valves may lead to red blood cells lysis and therombigenic complications. Also, the regurgitation-flow in SJM valves is almost twice that of the native valves in the aortic position. In this study, we suggest a new design for the stent (housing) of SJM valves in which 15% ovality is applied to the stent whereas its perimeter remains constant.

Methods: In a pilot study, the hemodynamic performance of the proposed design is analyzed in the closing phase and compared to that of conventional SJM models. The fluid analysis (Blood) is based on the control volume with moving boundaries in the vicinity of the leaflets. To solve governing equations in order to calculate the pressure and the related force, finite strip method has been implemented. Only 32 strips is enough to calculate the force due to pressure applied on the leaflets. To solve equations of motion Runge-Kutta in forth order has been implemented [1].

Results: Results show that while the elliptic SJM model offers a shorter closing phase (9.7% shorter), the regurgitation flow remains almost unchanged. In other words, even though the dynamic response of the valve is improved, the regurgitation flow is not decreased. Thus, a more efficient effective orifice area (EOA) is shown to be provided by the proposed model. The proposed model is shown in the following figure.

Figure:
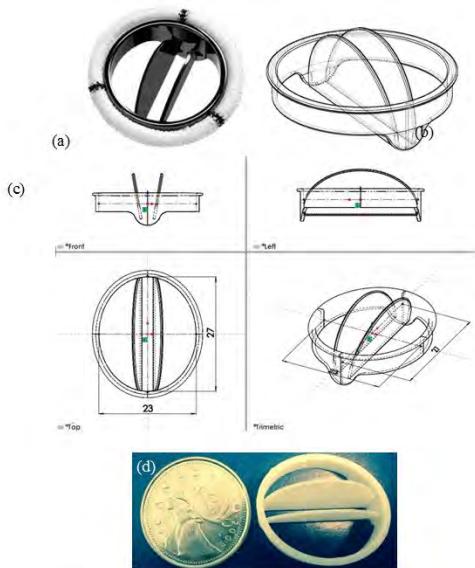
Figure: The conventional SJM valve (a); our design of conventional SJM model (b); the engineering drawing the proposed elliptic SJM valve (c); and the fabrication of the proposed elliptic SJM model (d)

Conclusion: The preliminary calculations presented in this study justify an improved hemodynamics of elliptic SJM valves compared to conventional models; the proposed design shows promise and merits further development.

References: [1] Mohammadi et al., J Med Eng & Phys, 28;122-133, 2006.

Disclosure of Interest: None Declared

Sport

AS-0446

ANATOMY OF A 2.40 METER HIGH JUMP

James Becker [1,*]

[1]Kinesiology, California State University, Long Beach, Long Beach, United States

Introduction and Objectives: As an event, the high jump has been heavily researched. Many of these studies have been performed in practice settings or controlled research environments. For competition specific jumps, there have been detailed biomechanical studies on the men's high jump conducted at the IAAF Junior and Senior World Championships. Additionally, there have been numerous competition reports from Jesus Dapena and colleagues based on data collected at the USATF National Championships in the United States. However, in all these reports, no jumps over 2.40 have been reported. In fact, there currently is no data in the literature documenting a jump over 2.40 meters.   This is not totally surprising since this feat has only been accomplished by 12 individuals. The purpose of this study is to report a detailed biomechanical analysis of three of the twelve 2.40 meter jumps which occurred during the 2014 track & field season. These jumps include Derek Drouin's (DD) 2.40 clearance at the Drake Relays in April 2014, and clearances of 2.42 by both Bohdan Bondarenko (BB) and Mutaz Essa Barshim (MEB) at the Adidas Grand Prix in June 2014.

Methods: Jumps were recorded using four HD video cameras (JVC GC-PX10, JVC Corp.), with two cameras filming jumpers approaching from the left side and two cameras filming jumpers approaching from the right side. A frame rate of 60 Hz and a shutter speed of 1/1000 was used for all recordings. A 68 point calibration frame with dimensions of 2m x 2m x 2m was used to calibrate the area encompassing the athlete's approach from approximately 6 steps out from plant through to the takeoff and flight phases. The calibration frame was placed in multiple positions and a multiphase DLT calibration was used to calibrate the full volume. Twenty body landmarks were manually digitized from five steps out from the plant through until the jumper landed on the pit. The two cameras were synchronized using the timing of foot contact and toe off for the last four steps of the approach and three dimensional coordinates were reconstructed using the direct linear transformation. Coordinates were smoothed using an interpolating quintic spline function. The whole body center of mass (COM) was calculated as the weighted sum of the individual segment center of mass locations based on Dempster's data. Finally, custom software was used to calculate commonly reported descriptors of high jump performance.

Results: COM Heights: The height of the COM when the takeoff foot touched down was 49.8%, 52.0%, and 52.6% standing height for MEB, BB, and DD, respectively. All three athletes raised their COM to over 70% of their standing height by the time their takeoff foot left the ground. In terms of overall COM trajectory, both BB and DD demonstrated their lowest point during mid-support on their penultimate step while MEB's lowest point was immediately after the takeoff foot touched down. As a result, MEB had a large negative vertical COM velocity (-0.4 m/s) when the takeoff foot touched down while BB and DD had values of -0.2 and 0.1 m/s, respectively. However, at the time the takeoff foot left ground, MEB had a vertical COM velocity of 4.8 m/s compared to 4.5 m/s for both BB and DD. This resulted in MEB's peak COM height being 2.52 m. while BB and DD only raised their COM to 2.47 and 2.42 m., respectively.

Approach Velocities: The horizontal velocities of the COM at touchdown of the takeoff foot were remarkably fast at 8.1 m/s, 8.0 m/s, and 7.9 m/s for MEB, BB, and DD, respectively. Pooling data from numerous sources in the literature suggest these velocities are in the 95th percentile for MEB and BB, and the 85th percentile for DD. All three jumpers achieved at least 70% of their approach velocity prior to entering the curved portion of the approach. During the curve, all three athletes increased their step frequencies as they got closer to the takeoff step while maintaining relatively consistent step lengths. Layout of the Approach: All three athletes showed smooth, gradual reductions in orientation relative to the bar during the curved portion of the approach. This resulted in inward leans of the torso of 14.7°, 20.4°, and 15.9° away from the bar at the time of touchdown of the takeoff foot for MEB, BB, and DD, respectively. During the takeoff the athletes rotated so they were leaning 3.2°, 6.0°, and 4.8° towards the bar, respectively.

Conclusion: These data show several common factors for elite level high jumping including using a high approach velocity, generating momentum early in the approach, and laying out the width of the curve so that it results in a smooth curve. If done correctly, the resulting postures allow for the generation of appropriate amounts of angular momentum during the takeoff which leads to an effective bar clearance. Despite these similarities, differences were observed in the way the athletes lowered their COM during the penultimate step. Functional consequences of these differences are not yet clearly understood.

Disclosure of Interest: None Declared

OPTIMUM TECHNIQUE FOR MAXIMISING HEIGHT IN A STRAIGHT HANDSPRING SOMERSAULT VAULT

Michael Hiley [1,*] Maurice Yeadon [1]

[1] SSEHS, Loughborough University, Loughborough, United Kingdom

Introduction and Objectives: The mechanics of the table contact phase of gymnastics vaulting is dependent on the initial contact conditions and the technique used during the contact phase. Although there are numerous coaching publications on vaulting, there is no general consensus about the importance of table contact technique. The aims of this study were to investigate the effect on peak post-flight height of the straight handspring somersault vault (Figure 1) arising from (a) initial conditions at touchdown and (b) joint torques during the contact phase (technique).

Methods: In order to investigate the effects of initial conditions and table contact technique on vaulting performance a torque-driven computer simulation model was developed. The model simulated the interaction between a seven-segment gymnast and a single-segment vaulting table during the table contact phase of the vault. The torque generators were defined based on the measured torque / angle / angular velocity relations and represented the maximum voluntary torques that the gymnast could produce (Forrester et al., 2011). An evaluation of the model was conducted by assessing how accurately simulations matched the recorded performances of three recorded vaults.

Three optimisations were carried out in order to maximise the post-flight height under different conditions. In the first optimisation the table touchdown configuration and orientation were varied whilst while torque activations from the matched simulation were maintained. The second optimisation used the touchdown configuration and orientation from the recorded performance and the torque activation parameters were varied in order to determine the potential improvement arising from contact phase technique changes. In the third optimisation the configuration, orientation and torque generator activation parameters were allowed to vary in order to maximise post-flight height. The model was constrained to stay on the parabola defined by the gymnast's horizontal and vertical velocity at springboard take-off in all optimisations.

Results: The peak post-flight height of the recorded vault was 2.72 m. When the configuration and orientation at touchdown were varied (optimisation 1) the peak post-flight height increased to 2.83 m (Table 1). When only the torque activation parameters were varied (optimisation 2), the peak post-flight height increased to 2.82 m. In the third optimisation where the touchdown configuration and orientation along with the table contact activations were allowed to vary the peak post-flight height increased to 3.12 m.

Figure:

Caption: Figure 1. The straight handspring somersault vault.

Conclusion: The aim of this study was to investigate the extent to which the conditions at vaulting table touchdown and the technique during table contact affected peak post-flight height during a straight handspring somersault vault. When only the initial configuration and orientation of the model were allowed to vary, an increase in peak post-flight height of 0.11 m was achieved compared to the recorded performance. When only the technique during table contact was allowed to vary, the increase in peak post-flight height was 0.10 m. These results suggest that changes in initial conditions and contact technique have a similar influence on post-flight height.

The increase in height of 0.41 m between performance (2.72 m) and optimum simulation (3.13 m) when both configuration and technique were allowed to vary may seem rather high but it is consistent with the heights reached in elite performances of handspring double front somersault vaults (3.0 ± 0.1 m) which have a similar angular momentum requirement (Takei, 2007). This suggests that the improvement is feasible.

The straight handspring somersault vault has previously been optimised for both post-flight height and distance using a passive two-segment simulation model (King et al., 1999). The optimal configuration during the instantaneous table contact was found to be with 178° between arms and torso. In the recorded performance and optimisations the configuration exhibited an angle at the shoulder and varying amounts of hip hyperextension (Table 1). Opening the shoulder angle during table contact allows the gymnast to do work and increase the post-flight height.

Table:

Simulation	Gymnast	Opt1	Opt2	Opt3
Touchdown angles				
torso [°]	5°	-21°	5°	-33°
shoulder [°]	134°	102°	134°	97°
hip [°]	187°	204°	187°	202°
Post-flight				
peak height [m]	2.72	2.83	2.82	3.13
rot. potential [ss]	1.37	1.34	1.34	1.35
time [s]	0.92	0.97	0.95	1.08

Caption: Table 1. Table touchdown and take-off variables from the recorded and optimised vaults

References: [1] King et al., J Sport Sci 17: 313-324, 1999.

[2] Takei, J Appl Biomech 23: 1-11, 2007.

Disclosure of Interest: None Declared

www.isbglasgow.com

NOVEL EVIDENCE OF SOCCER BALL KICKING TO PRACTICAL COACHING INSTRUCTIONS

Hiroyuki Nunome [1,*]Hironari Shinkai [2]Yasuo Ikegami [3]

[1]Fukuoka University, Fukuoka, [2]Tokyo Gakugei University, Tokyo, [3]Aichi Shukutoku University, Nagoya, Japan

Introduction and Objectives: In soccer kicking, ball impact is the most crucial component of the skill for determining both the quality of ball impact and the resultant ball velocity. Much practical advice exists on how to impact on the ball and handle the ball impact phase. For example, coaches often advise players to 'kick through the ball' or 'push the ball as long as possible'. However there has been limited evidence to support these types of instruction from a biomechanical perspective. The present study aimed to better develop our understanding of soccer ball impact phase, and to shed some light on the veracity of some practical coaching instructions currently used.

Methods: To illustrate representative ball impact phase kinematics, the instep kicking motion through ball impact was captured at 1000 Hz and a new time-frequency filtering algorithm which allowed changing the cut-off frequency along the time was applied to the coordinates (Study 1). Also, to clarify detailed foot--ball interaction during ball impact, a mathematical model was developed to compute the centre of gravity of the deforming ball using high-speed video records (Study 2, see Figure 1). Additionally, the relationship between the ball velocity and contact time was detected through an experiment, in which a regular soccer ball was directly fired by a soccer ball launching machine at a force platform fixed vertically on a pedestal with five different velocities (Study 3).

Results: Angular and linear velocity changes observed in Study 1 were very different from those reported previously. In fact, the shank was still angularly accelerating and the foot was still linearly accelerating up until the moment of ball impact, with both reaching their peak angular and linear velocity at, or up to 2 ms, after this moment. In Study 2, the change of the foot CG velocity, the ball CG velocity and the ball deformation during ball impact suggested interesting aspects of ball impact dynamics during kicking. First, the foot acts to deform the ball (phase I), followed by ball acceleration until foot and ball speeds are similar (phase II). The ball then begins to reform while still accelerating (phase III). The last phase shows little interaction between foot and ball suggesting no influence on ball speed. Moreover, Study 3 confirmed a strong, negative relationship between the ball velocity and contact time.

Conclusion: Our research group succeeded in providing kinematic evidence that strongly supports the practical advice of kicking like 'kick through the ball' focusing on the motion after the foot contacts with ball. On the other hand, the nature of ball impact dynamics have highlighted a gap between what players try to do and phenomena actually happening on the foot during ball impact. Study 2 revealed that it is impossible for players to intentionally lengthen ball contact time and there is a negative relationship between ball contact time and resultant ball velocity. Some coaching cues seem to be inaccurate, in particular for ball impact time, but some of them like 'kick through the ball' have recently been supported scientifically and likely work to fine tune the kicking technique.

References: [1] Nunome et al., J. Sports. Sci., 24, 11-22, 2006.

[2] Shinkai et al., Med. Sci. Sport. Exerc., 41, 889-897, 2009.

[3] Nunome et al., Footwear Science, 6, 105-118, 2014.

Sport

AS-0449

EFFECT OF REGULAR RUNNING TRAINING AND MARATHON RUNNING ON SERUM COMP CONCENTRATIONS IN NORMAL-WEIGHT AND OBESE RUNNERS

Annegret Muendermann [1] [2],*Jeroen Geurts [1]Thomas Nickel [3]Arno Schmidt-Trucksäss [4]Martin Halle [5]Henner Hanssen [4]

[1]Orthopaedics, University Hospital Basel, Basel, Switzerland, [2]Sport Science, University Konstanz, Konstanz, [3]Medizinische Klinik und Poliklinik 1, Ludwig-Maximilians-Universität München, Munich, Germany, [4]Institute of Exercise and Health Sciences, University Basel, Basel, Switzerland, [5]Department of Prevention and Sports Medicine, Technische Universität München, Munich, Germany

Introduction and Objectives: Healthy cartilage undergoes constant turnover of cartilage constituents, including collagen, proteoglycans, and cartilage oligomeric matrix protein (COMP), although at different rates. While there are a number of markers for cartilage turnover, COMP may be involved in the pathomechanics of osteoarthritis [1]. Several studies have shown that serum COMP concentration decreases in response to unloading [2] and increases in response to exercise where it returns to baseline within 30 min to 1 hour after mild to moderate exercise [3] and within 24 to 48 hours after a marathon race [4]. However, the effects of regular exercise training and acute bouts of prolonged exhaustive exercise on serum COMP concentration in obese persons—who are at a higher risk of developing osteoarthritis [5]—have not been investigated. The objective of this study was to test if changes in serum COMP concentration in response to regular running training and acute marathon running differ between normal-weight and obese runners with different fitness levels.

Methods: Forty-five subjects participated in this study (IRB approved) after providing informed consent (Table 1). Subjects were divided into three groups, obese recreational (BMI $\geq$ 30 kg/m^{2}), lean recreational and competitive runners [6]. All subjects completed a 10-week running training prior to participating in a marathon race. Blood samples were taken at the beginning of the training, and immediately before, immediately after and 24-hours after the marathon race, and serum COMP concentrations were determined using ELISA kits. Repeated measures ANOVA was used to determine the effect of running on COMP with between subject factor group and covariates BMI, age, 10-week running distance and finishing time. Because of the non-significant group effect and a significant time*finish time effect, the analysis was repeated with factor finishing time tertiles and Fisher's LSD posthoc tests (P<.05).

Results: Only small change in COMP were observed during the regular training program. COMP increased by 44% during the marathon race (P<.001). COMP did not differ between groups defined by running level, age, 10-week running distance or BMI at any time point. However, finishing time significantly influenced changes in COMP over time. COMP in subjects in the fastest (-12.8%) and middle tertile (-2.8%) decreased while COMP in subjects in the slowest tertile increased (+22.4%) within 24 hours after the marathon race (*P*<.001). Although BMI did not significantly influence changes in COMP levels, BMI was significantly greater in the slowest tertile than in the middle and fastest tertile (*P*<.001).

Figure:
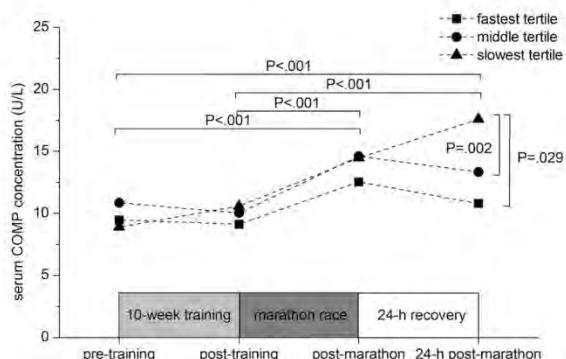
Caption: Fig 1. Serum COMP concentration before and after regular running training and marathon running in the fastest, middle and slowest runners.

Conclusion: Interestingly, finishing time appeared to be a stronger predictor of changes in COMP during the 24 post-marathon recovery than the subjects' body weight or running level. Although the running distance was the same for all subjects, those with slower finishing times presumably took more steps during the marathon. A previous study [4] has shown that COMP takes up to several days to recover after longer running races including ultramarathons. Similarly, it is possible that in the slowest runners in our study, the marathon may represent a relatively greater exercise stress compared to their regular running training than in the middle and fastest runners. These finishing time related post-marathon changes in COMP may represent differences in post-stress tissue metabolism between groups. Such differential metabolic responses in different groups of runners may explain the low prevalence of OA in former elite marathon runners [7] and warrants further investigation to understand the effect of and the recovery after acute bouts of prolonged exhaustive exercise especially in slower runners. In general, not only the response to but also the recovery from a bout of exercise may contain critical information on the health status of cartilage.

Table:

	Slowest tertile	Middle tertile	Fastest tertile	P-value
N	15	16	14	
Age (years)	40.1 (7.4)	40.9 (6.3)	38.9 (4.8)	.691
Height (cm)	182 (7)	179 (8)	181 (4)	.467
Body weight (kg)	94.6 (14.7)*	78.4 (12.6)	76.4 (4.9)	<.001
BMI (kg/m^2)	28.4 (3.3)*	24.3 (3.0)	23.3 (1.0)	<.001
Finishing time (min)	291.3 (16.5)*	244.6 (12.2)*	201.3 (14.7)	<.001

* significantly different from the faster groups (P<.05)

Caption: Tab. Mean (1 SD) demographic parameters of the subjects in this study.

References: [1] Lotz M, et al. (2013 Ann Rheum Dis 72(11):1756-1763.

[2] Liphardt AM, et al. (2009) Osteoarthritis Cartilage 17(12):1598-1603.

[3] Mündermann A, et al. (2005) Osteoarthritis Cartilage 13(1):34-38.

[4] Kim HJ, et al. (2009) Eur J Appl Physiol 105(5):765-770.

[5] Zhou ZY, et al. (2014) Obesity (Silver Spring) 22(10):2180-2185.

[6] Nickel T, et al. (2012) Atherosclerosis 220(1):219-222.

[7] Schmitt H, et al. (2006) Orthopade 35(10):1087-1092.

Disclosure of Interest: None Declared

Sport

AS-0450

ABILITY TO MODULATE MUSCLE SYNERGY IS THE KEY ASPECT THAT DISTINGUISHED COMPETITIVE ROWERS FROM NOVICE

Shazlin Shaharudin [1,*]Sunil Agrawal [2]

[1]Sports Science Unit, Universiti Sains Malaysia, Kota Bharu, Malaysia, [2]Mechanical Engineering, Columbia University, New York, United States

Introduction and Objectives: The robustness of muscle synergies have been extensively studied across different variables. However, no study has been done to determine the robustness of muscle synergies across different physiological demands which is particularly important during rowing because huge muscle mass are being recruited following the high intensity exercise. It was shown previously that muscle synergies are highly associated to rowing economy [1]. The objective of the study is to evelute the key strategy for competitive rowers to remain efficient during intense rowing events.

Methods: Ten collegiate rowers and ten physically active males were recruited. Muscle synergies were extracted from 16 rowing specific muscles using Principal Component Analysis with varimax rotation. Three specific physiological tests were conducted to examine the robustness of muscle synergies across different energy demands. Rowing performance, movement economy, kinematic and physiological variables were analyzed.

Results: Three functional muscle synergies with high indices of similarity were extracted in both groups, across three specific physiological tests. Synergy #1 which comprised of leg and back muscles and Synergy #2 which consisted of upper limb muscles were activated during drive phase, while Synergy #3 engaged during the transition of strokes. Despite equivalent level of fitness (e.g. $VO_{2\ max}$ and maximal heart rate values), the rowers performed better than novices in terms of rowing performance variables (e.g. distance covered, economy of movement, energy expenditure and power output), which ruled out physiological fitness as a bias in this study. Significant association was found between muscle synergies and rowing economy. Rowers utilized different rowing strategy with longer and slower strokes compared to the untrained subjects. The temporal adjustment of muscle synergies by rowers group enhanced their economy of movement.

Conclusion: The rowers were able to achieve better rowing economy due to their longer-slower rowing strokes which is a characteristic of practice-related adaptation that decreases energy expenditure [2]. Developing economical rowing strokes should be the focus of beginners, while the experienced rowers could achieve better rowing performance by enhancing muscles coordination. The findings of this study could be applied by fine-tuning the temporal aspect of muscle coordination in order to enhance the economy of movement which will lead to better performance in sports.

References: [1] Shaharudin et al., J Sports Sci Med, 13: 793-800, 2014.
[2] Lay et al., Human Movemt Sci, 24: 833-848, 2005.

Disclosure of Interest: None Declared

Sport

AS-0451

GUSIMBUKA URUKIRAMENDE: WERE AFRICAN HIGH JUMPERS THE REAL WORLD CHAMPIONS?

Ine Van Caekenberghe [1,*]Peter Aerts [1] [2]Wim Derave [1]Matthieu Lenoir [1]Veerle Segers [1]Dirk De Clercq [1]

[1]Department of Movement and Sports Sciences, Ghent University, Ghent, [2]Department of Biology (Functional Morphology), University of Antwerp, Antwerp, Belgium

Introduction and Objectives: Extraordinary high jumping performances of 2.30 m to 2.50 m are documented in reports, photos and films of European colonists visiting ceremonials in Rwanda during the interbellum. Some even speak of world records [cited in 1]. However, no objective height measurements were made. The reported heights are astonishing because athletes performed a typical "Gusimbuka urukiramende" technique, resembling Western roll, on bare feet. However, they pushed off on a rock, which assisted in reaching a higher bar clearance [2]. We have digitized and analyzed historical recordings (photos and films) of Gusimbuka jumps to compare them to contemporary international performances. As such, performance level of Gusimbuka athletes could be evaluated objectively.

Methods: Belgian colonial archives were searched for recordings of high jumping sequences. Of the 5 films and 85 photos retrieved, 2 films (Terres Brulées – 1938, and L'Afrique au Jeu – 1952) and 3 photos, showing bar clearance, were used for biomechanical analyses (in total of 18 jumps of 10 athletes).

After calculating a 15-segment kinematic model (mass distribution by Dempster [3]) the apex of the body centre of mass during bar clearance ($h_{BCOM\ MAX}$), the lowest point of the body in the plane of the bar ($h_{BODY\ LOW}$), take-off height on the stone ($h_{TAKE-OFF}$) and bar height (h_{BAR}) were calculated relative to ground level (Fig.). Perspective in the images was accounted for by applying scaling factors based on perspective-induced segment length changes.

For the photos in which we can scale heights to an absolute dimension (known body height, BH, of people on the photos/films), we report the absolute performance in meter. For the film images (no spatial or temporal calibration), performance is expressed relative to BH of the athlete.

Results: For results see table.

The athlete clears the bar if $h_{BODY\ LOW}$ is higher than h_{BAR}. For maximal performances at contemporary international competitions $h_{BODY\ LOW}$ could be considered equal to the reported h_{BAR} (since athletes mostly pass just above h_{BAR}). In Gusimbuka performances, $h_{BODY\ LOW}$ mostly still is a lot higher than h_{BAR}. Therefore we will compare $h_{BODY\ LOW}$ of Gusimbuka athletes to h_{BAR} of contestants in Olympic finals in the same time period. However, two corrections still need to be made:

(1) Since non-Gusimbuka athletes take off from h_{GROUND}, $h_{TAKE-OFF}$ has to be subtracted from $h_{BODY\ LOW}$ for Gusimbuka athletes (Fig.).

(2) Furthermore, pushing off from an elevated surface elicits an added beneficial effect on jumping performance (h_{GAIN}), which also has to be subtracted from $h_{BODY\ LOW}$ to obtain the net performance. Own previous research on Fosbury jumps from an elevated surface [2] enabled to quantify h_{GAIN} for the Gusimbuka technique. In contrast to the inherent downward BCOM velocity at the onset of a push-off at ground level, a Gusimbuka athlete already has an upward velocity when

initiating his push-off from the stone. This results in a larger final vertical take-off velocity and a h_{GAIN} of 0.04 m (or about 2% of BH).

To date, only jump 1 could be dated exactly. Its net performance (1.92 m) can be compared to those of the 1928 Amsterdam Olympics, in which this height would have resulted in a silver medal.

Comparison of Gusimbuka performances in the films (in BHs) to performances at Olympic finals (in meters) can be done in two ways: (1) BH of the Gusimbuka jumpers can be estimated and used to rescale the performance to meter. (2) BH of the Olympic athletes could be determined and used to rescale their performances to BH. Both pathways are being further investigated to obtain the most appropriate comparison. Nevertheless, Gusimbuka athletes are Watutsi, which are tall people. Estimating their body height at 1.90 m, we simulated the net performances, which showed that at the Olympics in between 1936 and 1952, Gusimbuka athletes could have competed in Olympic finals. Even more, the best athletes could have won a medal.

It is currently unknown whether the analyzed Gusimbuka jumps represent the maximal performances of the Gusimbuka athletes. Further analyses of (historical and present-day) Gusimbuka performances could lead to insights for sports today. Given that Gusimbuka athletes should use the present-day jumping technique (Fosbury Flop), could they perhaps still compete at international level?

Figure:
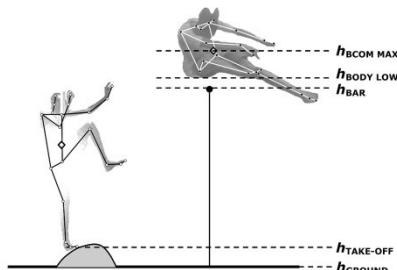
Caption: Gusimbuka urukiramende

Conclusion: During the interbellum Gusimbuka athletes could have (successfully) competed in Olympic finals.

Table:

	PHOTOS (n=3) (meter)			MOVIES (n=15) (*BH)		
	Jump 1	**Jump 2**	**Jump 3**	**M**	**±**	**SD**
$h_{BCOM\ MAX}$	2.38	2.33	2.31	1.25	±	0.08
$h_{BODY\ LOW}$	2.16	2.13	2.12	1.11	±	0.07
h_{BAR}	1.94	2.07	2.04	1.06	±	0.07
$h_{TAKE-OFF}$	0.20	0.20	0.20	0.12	±	0.02

Caption: Performance variables relative to ground level.

References: [1] Bale. *Imagined Olympians: Body culture and colonial representation in Rwanda*. U of Minnesota Press, 2002.

[2] De Wit et al. *PROCEEDINGS-XIII INT SYMP FOR BIOM IN SPORT*, 363–366, 1995.

[3] cited by Winter. *Biomechanics and motor control of human movement*. John Wiley & Sons, 2009.

Disclosure of Interest: None Declared

AS-0452

BIOMECHANICAL COMPARISON OF TIBIOTALOCALCANEAL AND TIBIOTALAR FUSION

Swati Chopra [1,*]Rayan Baalbaki [1]Maria Josina Pichonnaz [1]Julien Favre [1]Xavier Crevoisier [1]

[1]Site Hôpital Orthopédique, Centre Hospitalier Universitaire Vaudois (CHUV), University of Lausanne, Lausanne, Switzerland

Introduction and Objectives: Tibiotalar fusion/ ankle arthrodesis (AA) is an established surgical procedure to address end stage ankle osteoarthrosis (AOA). Tibiotalocalcaneal fusion (TTC) is a salvage procedure for diverse ankle-hindfoot pathologies which can also be used in combined osteoarthrosis of the ankle and subtalar joints. Biomechanical studies have already shown several drawbacks of AA due to altered gait mechanics [1],[2]. Furthermore, increased compensatory motion of the neighboring joints have been demonstrated in case of AA. Therefore, fusing not only the tibiotalar but also the subtalar joint would result in even greater biomechanical alteration. The study aims to investigate whether or not the fusion of the tibiotalar along with the subtalar joint is biomechanically detrimental.

Methods: 42 participants (14 in each group), including controls, 2-5 years TTC using retrograde intramedullary nailing, and AA patients were assessed using foot-worn inertial sensors (Physilog®) and pressure insoles (Pedar®) along with clinical questionnaires including: EQ 5D, AOFAS-hindfoot and FAAM. Each subject performed 4 walking trials of 50m, 2 trials per foot. Plantar pressure parameters (PPP) assessed included total contact duration (Tc), Max Force (Max F), Max Pressure (Max P) in 10 foot regions. Kinematics analysis included assessment of the sagittal range of motion (ROM) at MPJ1, midtarsal and tibio-calcaneal segments. Spatiotemporal parameters (STP) included cadence, stance, double support, stride, speed, peak swing speed, toe-off and heel-strike pitch angles and inner stance duration- loading, foot-flat and push-off. All together 30 PPP (3 in each of the 10 foot region), 3 ROM and 11 STP parameters were assessed. Statistical analysis included the use of Wilcoxon signed-rank and Wilcoxon rank sum tests for intra-individual and inter-individual comparison, respectively ($p < 0.05$).

Results: All three subjective scores showed no significant difference between the outcomes of the two surgical groups. Gait results with significant difference ($p < 0.05$):•

AA operated (op) foot vs TTC op foot comparison- PPP: 4 out of 30 parameters; ROM: Sagittal- all 3 joints.

• TTC op vs unop side comparison- PPP: 5 out of 30; ROM: Sagittal- MPJ1, ankle; STP 3 out of 11 parameters.

• TTC op vs control comparison - PPP: 11 out of 30; ROM: Sagittal- all 3 joints, STP 9 out of 11 parameters.

• TTC unop side vs control comparison - PPP: 11 out of 30; ROM: Sagittal: MPJ1; STP: 10 out of 11 parameters.

Figure 1 shows the difference of the median of PPP between the two sides for TTC and AA groups.

Figure:
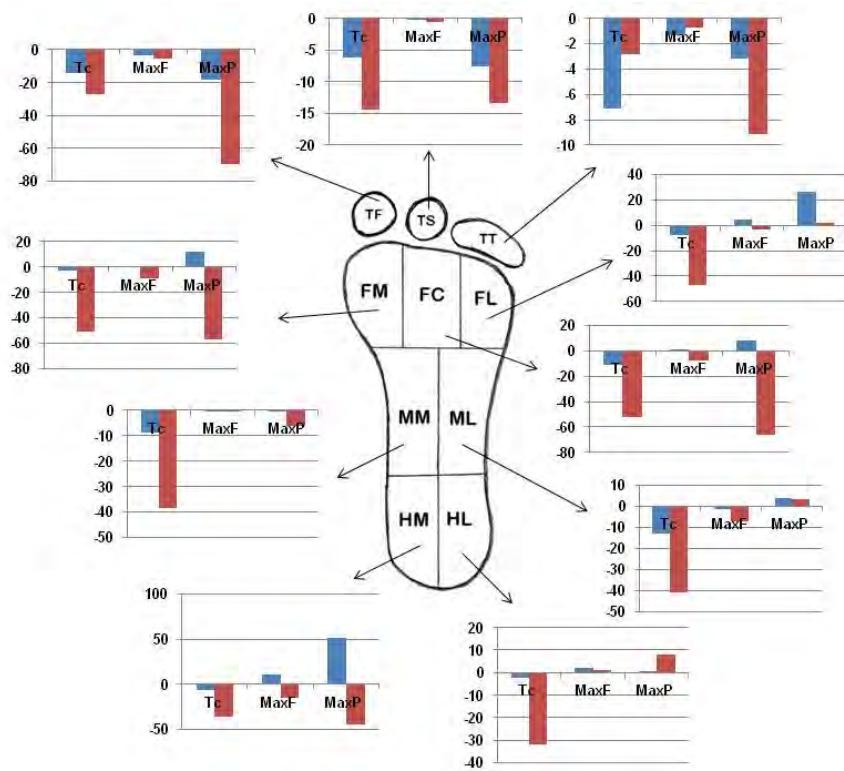
Caption: Figure 1: Plot of plantar pressure parameters, showing the difference of the median between TTC op to TTC unop side (Blue) and AA op to AA unop side (red). Results close to zero represents bilateral symmetry and negative results represent higher values on the unop sides.

Conclusion: The study reported similar gait results on the op sides of TTC and AA, however, unlike AA, TTC patients showed good bilateral symmetry with the unop side loading as much as the op side. In comparison to controls, both op and unop sides in TTC group showed a significant difference in similar gait parameters, representing an altered but near symmetrical gait pattern. Based on the results, the fusion of the hindfoot between 5-10° of valgus, along with tibiotalar, appears to result in better loading of the ankle as well as the whole foot in comparison to leaving the calcaneum free. Thus, this study concludes that the fusion of the calcaneum along with the tibiotalar joint is *not* biomechanically detrimental, and is likely an improvement.

References: [1] Chopra et al., J Orthop Res. 32(3):377-84,2014.

[2] Rouhani et al., Clin Biomech (Bristol, Avon) 26:397-404, 2011

Disclosure of Interest: None Declared

Lower Limb

AS-0453

LOWER LIMB MUSCLE ACTIVITY STRATEGY AND POSTURAL SWAY IS CHANGED DURING BALANCE TASKS IN GIRLS WITH GENERALIZED JOINT HYPERMOBILITY

Birgit Juul-Kristensen [1,*]Pia Melcher [2]Jesper Sandfeld [2]Katrine Lyders [3]Peter Hendriksen [2]Bente Rona Jensen [2]

[1]Institute of Sports Science and Clinical Biomechanics, University of Copenhagen,, Odense M, [2]Integrated Physiology, Department of Nutrition, Exercise and Sport, University of Copenhagen,, Copenhagen, [3]Institute of Sports Science and Clinical Biomechanics, University of Southern Denmark, Odense M, Denmark

Introduction and Objectives: Generalized Joint Hypermobility (GJH) in children, is defined by a Beighton score ≥ 6 positive joint tests out of 9, and the prevalence varies from 5-57% depending on tests and criteria used, in addition to the population. GJH and joint pain are major criteria for the connective tissue disorder of Hypermobility syndrome (HMS), where reduced balance has been reported in children with HMS [1]. The objective was to study knee muscle activation and postural sway during balance tasks in girls with GJH.

Methods: A total of 16 girls with GJH and 11 girls with no GJH (NGJH), aged 14 years were recruited randomly from a Danish cohort of school children. Additional inclusion criteria for GJH were at least one hypermobile knee, while for NGJH it was at least one knee without hypermobility. Postural sway, as two-legged with eyes open and closed (2EO, 2EC), and one-legged stance with eyes open (1EO), was measured on a force plate (60 s), and Rambling and Trembling of the directions medial-lateral (ML), anterior-posterior (AP), and Center of Pressure Path Length (COPL) were calculated. Surface EMG was recorded (dominant leg) on the following muscles: quadriceps (Q, mean of vastus medialis and lateralis), hamstrings (H, mean of biceps femoris and semitendinosus), and gastrocnemius (G, mean of gastrocnemius medialis and lateralis), during all balance tasks. EMG was normalized to isometric Maximum Voluntary EMG, expressed as %MVE. Co-contraction index (CCI) was calculated as the ratio of co-contracting muscle activation multiplied by the summed muscle activity (CCI = (%MVEmin/%MVEmax) * (%MVEmin+%MVEmax)), minimum and maximum muscle activity were based on mean Q-activity, mean H-activity and mean G-activity, and the final CCI was calculated (mean, medial and lateral CCI of H/Q and G/Q) over the number of balance tasks. Ratio of the medial/lateral HQ and medial/lateral GQ were further calculated. Self-reported knee related physical function was assessed with the Knee Injury and Osteoarthritis Outcome score for children (KOOS-Child). A general linear regression (mixed model) analysis was used to study between group differences.

Results: GJH did not report lower knee function than NGJH in the separate dimensions, but GJH had significantly larger sway length in 2EC (COPL 1.64 vs. 1.37 m/min, p<0.001). Furthermore, a tendency to larger values in 2EO in the anterior-posterior direction of Rambling (7.92 vs 6.05 mm, p=0.073) and Trembling (5.17 vs 3.88 mm, p=0.093) was found in GJH. There were no group differences in completion of the balance tasks.

During 2EO GJH had significantly lower muscle activity, seen in mean Q (1.29 vs 2.30%MVE, p=0.053), with a tendency also to lower activity in VM (1.15 vs 2.11%MVE, p=0.072). During 2EC and 1EO GJH had significantly lower GL activity (2EC: 2.45 vs. 3.55%MVE, p=0.005; 1EO: 9.40 vs. 13.45%MVE, p=0.010), with a tendency also to lower activity in mean

G in 1EO (12.95 vs 15.71%MVE, p=0.068). CCI of the lateral HQ was significantly lower, and the ratio of medial/lateral HQ significantly higher in GJH, during all three balance tasks.

Conclusion: During static balance girls with GJH and at least one hypermobile knee performed with larger postural sway than NGJH, and maintained the standing position with a lower muscle activity in knee extensors and plantar flexors. Furthermore, GJH had a higher medial knee muscle activity relative to the lateral activity compared to NGJH. This may contribute to the increased risk of knee injuries[2], and development of osteoarthritis in the medial knee compartment. The clinical application calls for taking this into account in prevention management strategies.

References: 1. Schubert-Hjalmarsson E, Ohman A, Kyllerman M, Beckung E: **Pain, balance, activity, and participation in children with hypermobility syndrome**. *Pediatric physical therapy : the official publication of the Section on Pediatrics of the American Physical Therapy Association* 2012, **24**(4):339-344.

2. Pacey V, Nicholson LL, Adams RD, Munn J, Munns CF: **Generalized joint hypermobility and risk of lower limb joint injury during sport: a systematic review with meta-analysis**. *AmJSports Med* 2010, **38**(7):1487-1497.

Disclosure of Interest: None Declared

Lower Limb

AS-0455

INSIGHTS INTO THE BIOMECHANICAL MECHANISMS FOR THE DEVELOPMENT OF CHRONIC EXERTIONAL COMPARTMENT SYNDROME

Andrew Roberts [1] [2],*David Roscoe [1] [3]David Hulse [1]

[1]Academic Department of Military Rehabilitation, Defence Medical Rehabilitation Centre, Epsom, [2]Department of Sport and Health Sciences, University of Exeter, Exeter, [3]Centre for Biomedical Engineering, University of Surrey, Guildford, United Kingdom

Introduction and Objectives: Chronic exertional compartment syndrome (CECS) presents as exertional pain in the lower limb as a result of elevation of intramuscular compartment pressure. Conservative treatment through biomechanical changes has recently been promoted as a viable option for CECS. Forefoot running was first described as a possible treatment in a case report by Cunningham [1] This has since been followed up by further case reports and a study of ten US military patients [2-4]. However, to date, there have been no studies examining the biomechanical differences between patients and controls in order to better define the pathophysiology and accurately inform such treatments. This study aimed to compare the kinematic and kinetic differences in cases with CECS and asymptomatic controls.

Methods: 20 men with symptoms of CECS of the anterior compartment and 20 asymptomatic controls agreed to participate. Diagnoses other than CECS were excluded with rigorous inclusion criteria and magnetic resonance imaging. Kinematic and kinetic data were collected during walking and marching. Participants were provided with military issue silver shadow training shoes for collection of shod trials. Barefoot trials were also collected.

A biomechanical model was then created in Visual3D with segments definitions based on recommendations in the literature [5-8].

Temporal-spatial variables, joint angles, moments and ground reaction forces were compared between groups. Bootstrapped t-tests and ANCOVA tests were used to investigate these differences (Matlab/SPSS). The methods described by Hof [9], and recommended by Pierrynowski [10], to normalise gait data to body size were used. Angles of the foot and the shank segments in relation to the lab were also analysed.

Results: Cases were significantly shorter (p=0.002) and took a relatively longer stride (in relation to leg length) than controls when shod. There were no differences in normalised step time, stance time and swing time. There were also no clear differences between cases and controls in any of the angles above the ankle at any point during the gait cycle. Consistent differences were identified in ankle inversion, ankle dorsiflexion and in the corresponding X and Z axes of the foot-lab angle (Table 1). The most consistent differences in joint moments were also at the ankle joint. This suggests that CECS is predominately caused by and/or affects the ankle joint system.

Cases demonstrated less ankle inversion at the end of stance and the beginning of swing. This coincided with the generation of lower ankle inversion moments. Cases also had more ankle plantarflexion from mid-stance to toe-off.

Conclusion: The differences demonstrated in the biomechanics and stature of patients provide potential mechanisms for the development of CECS in this population. The reduced stature in combination with an increased stride length may result in an excessive load on Tibialis anterior (TA), when walking/marching at high speeds. The transition from walking to

running is dependent on leg length and transfers the work from the dorsiflexor muscles to the larger proximal muscles [11]. Discomfort in the muscles of the anterior compartment can occur in healthy individuals during fast walking [12]. It follows that within the military training environment, if the anterior compartment muscles are consistently required to generate high loads, this could trigger the pathological changes seen in CECS.

The lower ankle inversion moments suggest that the TA of cases either can not generate the normal load or can not transfer the force generated as efficiently as controls. Reduced force transmission through the tendon and linked fascia would then lead to the differences observed in the ankle angles. The reasons for this are unknown although this could be a result of the reduced strength typically seen in these patients [13, 14]; or due to a mechanical disadvantage resulting in inefficient force transmission. The differences in joint angles and moments therefore indicate an impairment of the function of TA. It is unclear whether this is a cause of, or result of the condition.

Table:

Joint	Movement	Bootstrapped t-test (%)	ANCOVA (%)	Direction of effect
Ankle	Inversion (x-axis)	63-70	62-69	CON>PT
	Plantarflexion (z-axis)	55-57	NONE	PT>CON
Foot-lab	Inversion (x-axis)	83-89	87-88	CON>PT
	Plantarflexion (z-axis)	34-58	NONE	PT>CON

Caption: Table 1. Time points (% gait cycle) of significant differences (all conditions) in angular data.

References: [1]Cunningham et al., BJSM, 38(2):233-4, 2004.

[2]Diebal et al., AJSM, 40(5):1060-7, 2012.

[3]Diebal et al., IJSPT, 6(4):312-21, 2011.

[4]Gibson, IJATT, 18(6):24-6, 2013.

[5]Wu et al., JoB, 35(4):543-8, 2002.

[6]Peters et al., G&P, 29(1):42-8, 2009.

[7]Pratt et al., G&P, 36(3):434-8, 2012.

[8]Gutierrez et al., G&P, 18(2):37-46, 2003.

[9]Hof, G&P, 4(3):222-3, 1996.

[10]Pierrynowski et al., G&P, 13(3):193-201, 2001.

[11]Hreljac, JoB, 28(6):669-77, 1995.

[12]Hreljac, MSSE, 25(10):1158-62, 1993.

[13]Birtles et al., MSSE, 34(12):1900-6, 2002.

[14]Varelas et al., JOSPT, 18(5):586-9, 1993.

Disclosure of Interest: None Declared

Lower Limb

AS-0456

VALIDITY AND RELIABILITY OF HIP PARAMETERS WITH PELVIC AXIAL ROTATION DURING X-RAY ACQUISITION

Ayman Assi [1,*]Ziad Bakouny [1]Elie Saghbini [1]Fares Yared [1]Aren Joe Bizdikian [1]Sabine Esber [1]Gerard Elie Bakhos [1]Nour Khalil [1]Christophe Sauret [2]Wafa Skalli [2]Ismat Ghanem [1]

[1]Laboratory of Biomechanics and Medical Imaging, School of Medicine, University of Saint-Joseph, Beirut, Lebanon, [2]Laboratoire de Biomécanique, Arts et Métiers ParisTech, Paris, France

Introduction and Objectives: In order to assess hip disorders in children and adults, clinical parameters are measured on frontal X-rays of the pelvis [1,2]. These radiographs require standard positioning of the patient during acquisition. To our knowledge, there are no studies that have investigated the effect of axial rotation of the pelvis on the clinical parameters of adults' and children's radiographs. The aim of this study was to estimate the effect of erroneous positioning of patients, during pelvis frontal X-ray acquisition, on the reliability and validity of hip parameters.

Methods: Helical pelvis CT scans (slice thickness: 0.6mm) of 8 children (3 F and 5 M, age: mean 12 - SD 2.2) and 9 adults (5 F and 4 M, age: mean 51 - SD 26) were considered. Frontal Digitally Reconstructed Radiographs (FDRRs) were reconstructed from CTs. Then, for each patient, axial rotation of the pelvis was simulated and the corresponding FDRRs were reconstructed at 5°, 10°, 15° and 20° of axial rotation (Figure 1). Clinical parameters were measured digitally on each radiograph, for both the left and right sides of each patient: Vertical Center Edge (VCE) angle, HTE angle, Sharp's angle, Lateral Subluxation (LatSub) angle, Acetabular Fossa relative to the ilioischial line (AcetFossa), Acetabular Depth (AcetD) distance, Acetabular Width (AcetW) distance and Migration Percentage of the Femoral Head (MPFH). Three trained operators repeated the measurements 3 times each, in each axial rotation position. Intraclass Correlation Coefficient (ICC) was evaluated for intra and inter-observer agreement. The 95% confidence interval (95%CI) was calculated as 2SDs of inter-observer reliability. The bias of each clinical parameter, in each axial rotation position, was calculated as the absolute mean difference relatively to the 0° position.

Results: Intra and inter-observer agreement was shown to be very high (ICC>0.9) for all parameters and all axial rotation positions except for the AcetFossa (ICC= 0.5) in adults. In the absence of axial rotation of the pelvises (0˚), the 95% CI of HTE, VCE, Sharp's angle and MPFH were lower than 5 measurement units (m.u.) and lower than 1 cm for the AcetabD, AcetW, AcetFossa and LatSub. The 95% CI increased with pelvic axial rotation: it exceeded 5 m.u. for VCE, MPFH and reached 7˚ for HTE at 20˚ of axial rotation. However, it remained constant for the remaining parameters. All the parameters showed an increase in bias during axial rotation of the pelvis , where MPFH and VCE showed greatest bias (7.5% and 6° respectively in children and 5.5% and 4.6° in adults) at 20° position. AcetabD, AcetW, AcetFossa and LatSub exhibited a bias <1cm.

Figure:

Caption: Figure 1- Frontal digitally reconstructed radiographs of the pelvis at the different degrees of axial rotation

Conclusion: Hip parameters measured on frontal radiographs were shown to be less accurate and less reliable when pelvic axial rotation increased. The AcetFossa showed a smaller ICC in adults because the location of the ilioischial line differed from the anatomical situation with increased pelvic rotation and thus led the operators to confusion. The bias was systematically higher for all parameters in all axial rotation positions in children compared to adults. It exceeded 10% of normative values for most of the clinical parameters in both children and adults, when axial rotation exceeded 10°. This bias could significantly affect hip disorders' assessment.

References: [1] Brurås et al. , Pediatrics, 127 :661-666, 2011

[2] Anderson et al., Orthopedics, 34: 86, 2011

Disclosure of Interest: None Declared

Lower Limb

AS-0457

PREDICTORS OF MIDFOOT DEFORMITY AND FUNCTION IN INDIVIDUALS WITH DIABETES AND PERIPHERAL NEUROPATHY

Mary Hastings [1,*]Michael Mueller [1]James Woodburn [2]Michael Strube [3]Paul Commean [4]Jeffrey Johnson [5]Victor Cheuy [1]David Sinacore [1]

[1]Physical Therapy, Washington University School of Medicine, St. Louis, United States, [2]Institute for Applied Health Research, Glasgow Caledonian University, Glasgow City, United Kingdom, [3]Psychology, [4]Electronic Radiology Laboratory, [5]Orthopaedic Surgery, Washington University School of Medicine, St. Louis, United States

Introduction and Objectives: Diabetes mellitus (DM) related medial column foot deformity is a major contributor to high plantar pressure that often leads to midfoot ulceration and major lower extremity amputation.[1] However, very little is known about the quality and function of the structures that support the medial column of the foot, a critical step in halting or preventing amputation. The purpose of this study was to examine the relationship of medial column alignment and midfoot function to: intrinsic foot muscle and fat volumes, posterior tibialis and flexor digitorum tendon volumes, plantar fascia volumes, and plantarflexor peak torque in individuals with DM, peripheral neuropathy (DMPN) and controls.

Methods: Twenty-three participants with DMPN were compared to 12 age and weight-matched participants without DM, PN, or medial column deformity (control). Radiographs, kinematics, magnetic resonance imaging, and biodex were used to measure: 1) medial column standing alignment (Meary's angle- the angle formed by the line that bisects the talar head and neck and the line through the longitudinal axis of the 1st metatarsal), 2) midfoot function (forefoot relative to hindfoot plantarflexion during the heel rise task), 3) intrinsic foot muscle and fat, posterior tibialis and flexor digitorum tendon, and plantar fascia volumes, and 4) plantarflexor peak torque at 60 deg/sec, respectively. A ratio of posterior tibialis tendon (PT) volume to flexor digitorum longus (FDL) tendon volume was calculated for each participant in order to mimic standard clinical radiologist practice. Groups were compared on key variables using a two-tailed independent T-test. Simultaneous entry multiple regression was used to determine predictors of midfoot deformity (Meary's angle) and midfoot function (forefoot relative to hindfoot plantarflexion excursion during the heel rise task) in the DMPN participants.

Results: Meary's angle was not different between groups (p=.48) although the DMPN group had much higher range of measures than the control group (DMPN range= -36° to 7°, Control range=-21° to -3°). (Table 1) Compared to controls, the DMPN group had: 1) reduced plantarflexion of their forefoot relative to their hindfoot during the heel rise task (p<.01); 2) decreased intrinsic foot muscle volumes (p<.05); 3) increased intrinsic foot fat volume (p=.01); and 4) decreased plantarflexor peak torque (p<.01). The PT/FDL tendon volume ratio and intrinsic foot muscle volume were significant predictors of Meary's angle (p<.05) and accounted for 43% of the variance in Meary's angle.   Intrinsic foot fat volume and plantarflexor peak torque were significant predictors of plantarflexion excursion of the forefoot relative to hindfoot during the heel rise task (p<.05) and accounted for 37% of the variance in forefoot relative to hindfoot excursion.

Conclusion: Individuals with DMPN have marked deterioration in leg function and foot muscle quality. The deterioration of the supporting structures of the medial column (intrinsic foot muscles/fat volume, PT/FDL tendon volume, plantarflexor peak torque) predicts midfoot alignment and foot function. Additional prospective research is required to monitor

alignment, structure, and function over time to inform early intervention strategies with the goal to prevent deformity, ulceration, and amputation.

Table:

	DMPN (n=23)	Control (n=12)	P value
Lateral Radiograph (degrees)			
Meary's Angle	-13 (11)	-11 (5)	.48
Muscle Volume (cm^3)			
Intrinsic Foot	18 (11)	32 (13)	<.01
Fat Volume (cm3)			
Intrinsic Foot	18 (11)	9 (4)	<.01
Tendon and Fascia Volume (mm^3)			
Posterior Tibialis Tendon	833 (227)	800 (220)	.69
Flexor Digitorum Longus Tendon	308 (90)	287 (71)	.54
Posterior Tibialis/Flexor Digitorum Longus Ratio	2.9 (1.0)	2.9 (1.0)	1.00
Plantar Fascia	1265 (546)	1221 (465)	.86
Torque (Nm)			
Plantarflexion	45.3 (15.1)	74.2 (33.0)	<.01
Heel Rise Kinematics (degrees)			
Forefoot Relative to Hindfoot Plantarflexion Excursion	3 (6)	13 (7)	<.01

Caption: Group means and standard deviations for key study variables

References: [1] Ramsey et al. (1999). *Diabetes Care, 22:*382-387, 1999

Disclosure of Interest: None Declared

AS-0458

A CANINE GAIT ANALYSIS PROTOCOL FOR THE ANALYSIS OF THE BACK MOVEMENT: ASSESSMENT OF KINEMATIC AND KINETIC VARIABLES IN GERMAN SHEPHERD DOGS

Andrea Cereatti [1,2,*]Elif Surer [1]Maria Antionietta Evangelisti [3]Lucia Manunta [3]Gabriele Paolini [1]Ugo Della Croce [1,2]

[1]POLCOMING, University of Sassari, Sassari, [2]Interuniversity Centre of Bioengineering of the Human Neuromusculoskeletal System, Rome, [3]Pathology and Veterinary Clinic, University of Sassari, Sassari, Italy

Introduction and Objectives: Degenerative lumbosacral stenosis (DLSS) is a common disorder affecting large breed dogs and in particular German Shepherd (GS) dogs. Currently, the most common treatment is surgery, however surgical timing and techniques are still controversial [1]. In this regard, instrumented movement analysis is a powerful tool for improving the clinical intervention efficacy [2]. The majority of the gait analysis protocols proposed were devised to analyze hind limbs kinematics [3]. To authors' knowledge, only few studies focused on the movements of the back [4] and, a complete description throughout the entire gait cycle of the kinematic data variability is still lacking. Aim of the present study is two-fold: (i) to present and validate a gait analysis protocol specifically designed for the evaluation of the back motion in both sagittal and horizontal planes; and (ii) to provide normative data of the spatio-temporal parameters, kinematics and kinetics quantities during quadrupedal stance posture and level gait in healthy GS dogs.

Methods: Eight healthy GS dogs (ages: 5.6 ± 2 yrs) were enrolled in the study.

A set of 17 markers was placed as shown in Fig. 1. A virtual marker defined as the midpoint between the two iliac crests, was also defined. A multi-segmental model including ten 2D segments was used (Fig. 1).

Spatio-temporal parameters were determined from the trajectories of the markers on the paws. The joint angular kinematics were defined by projecting the markers positions on the sagittal (S) and horizontal (H) planes and then by computing the relevant angles. Sagittal angular kinematics were estimated for the tarsal, the stifle and the hip joint; the pelvis motion was described in the S plane (pelvic tilt) and the H plane (pelvic rot). The movement of the vertebral column was described by the relative angular motion in the S and H plane between the sacral and thoracic segment and the lumbar and thoracic segments.

The instantaneous positions of the markers were reconstructed using a 6-camera optoelectronic system (Vicon) acquiring at 100 Hz (6 Hz cut-off frequency). Two force platforms (AMTI) were used to record ground reaction forces (GRF) at 100 Hz. The experimental acquisition sessions consisted in a) static trials with the dog in quadrupedal stance posture; b) six gait trials during which only stereo-photogrammetric data were acquired.

Grand mean and standard deviation (*std*) values of the posturographic angles and of the GRF were computed. For each kinematics variable, grand mean, grand *std* values were computed over the subjects for each gait cycle percentage.

Results: The average cadence and *std* were 154.5 ± 18.5 step/min, stride duration and length were 0.8 ± 0.1 s and 1.0 ± 0.2 m. From the grand mean curves of the angular kinematic variables, *ROM* and the *std* values, averaged over the gait cycle, were extracted. For sake of brevity, kinetic data are not reported.

Figure:
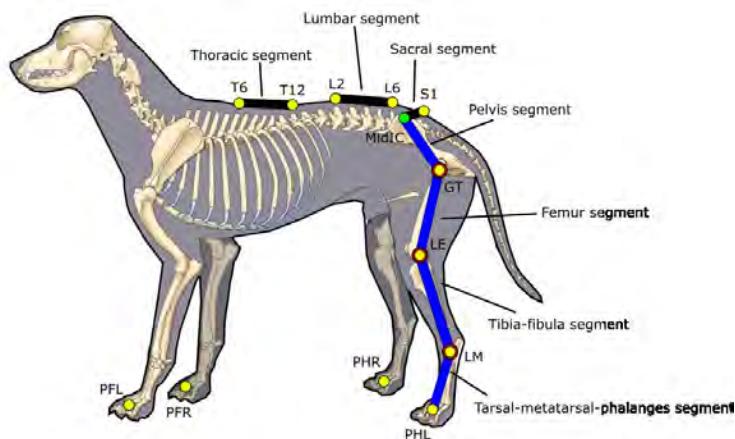
Caption: Anatomical landmarks identified by the skin markers and multi-segmental model.

Conclusion: The reliability of a novel canine gait analysis protocol was assessed on healthy GS dogs. The greater angular excursions were found, in descending order, for the hip, stifle and hock joints. Whereas the amplitude of the thoraco-lumbar movements in the H and S planes were comparable, the lumbo-sacral movement in the H plane was 3.5 times greater than in the S plane. The inter-subject joint angular variability ranged, for all segment and joints between 0.27 to 0.36. The largest variability were observed for the pelvis motion. The proposed protocol produced high repeatable kinematic data thus suggesting its effectiveness in assessing gait deviations from normality. The present protocol was specifically designed to assess functional limitations and motor impairments associated to the presence of pathologies affecting the vertebral column and in particular DLSS disease in dogs. As opposed to previous studies in which the spinal column was modeled as a single segment, the movement of the spinal column was modeled as a three segment linkage. The additional information provided by the model can improve the procedure and outcome of spinal column surgery.

Table:

Segmental and joint kinematics	ROM [°]	std/ROM
Thoraco-lumbar angle (S plane)	3.9	0.27
Thoraco-lumbar angle (H plane)	4.5	0.31
Lumbo-sacral angle (S plane)	3.2	0.29
Lumbo-sacral angle (H plane)	11.2	0.32
Pelvic tilt	8.5	0.33
Pelvic rotation	7.2	0.36
Hip flex/ex	31.0	0.30
Stifle flex/ex	27.1	0.31
Hock flex/ex	23.8	0.27

Caption: Range of motion (ROM) and inter-subject variability (std/ROM) values for segmental and joint kinematics.

References: [1] Meij et al., Vet. Clin. North Am. Small Anim. Pract. 40:983-1009, 2010.

[2] Gillette et al., Vet J. 178:165-76, 2008.

[3] Torres et al. Vet. Surg. 39:504-12, 2010.

[4] Hogy et al. Am. J. Vet. Res.;74:1164-71, 2013.

Disclosure of Interest: None Declared

AS-0459

THE USE OF FEEDBACK TO REDUCE THE ERRORS ASSOCIATED WITH PLACEMENT OF ANATOMICAL MARKERS FOR KINEMATIC GAIT ANALYSIS.

Reed Ferber [1][2],*Sean Osis [1][2]Blayne Hettinga [1][2]Ricky Watari [1]Ryan Leigh [1]

[1]Kinesiology, University of Calgary, [2]Running Injury Clinic, Calgary, Canada

Introduction and Objectives: Anatomical marker placement is the single largest source of error in gait analyses [1,2]. Previously, we developed a method that 'scores' marker placement by comparing marker coordinates to a morphometric "norm" to address this problem [2]. The outcome is an inter-quartile range ratio (IQRR), a non-parametric description of the location of a given marker placement within the distribution of normalized marker-coordinate reference data. The purpose of this study was to evaluate the use of this marker placement location feedback method, based on the IQRR, and to measure concomitant changes in peak ankle, knee, and hip joint angles during treadmill walking.

Methods: Twelve subjects (6 males; 60.0 +/- 4.5 yrs; 1.70 +/- 0.10 m; 75.3 +/- 16.4 kg) participated, as part of a larger clinical study. A single experienced examiner placed retro-reflective 9mm markers over specific anatomical landmarks of bilateral ankle, knee, and hip joints [2,3]. After the first placement and collection of a 1 second standing trial, visual feedback was given using the IQRR score for each marker with a threshold of 0.8 chosen as a cutoff. The examiner had the opportunity to correct their placement and a second standing trial was taken. Data for a single walking trial was then collected by an 8-camera Vicon system at 200Hz. Walking data were analyzed (3D GAIT software) using both standing trials (Pre Feedback vs. Post Feedback) to calculate discrete kinematic variables. Collections with these subjects were repeated again 2-7 days later, and changes in the limits of agreement (LOA) were evaluated between Pre and Post conditions, across both sessions.

Results: All but one joint angle LOA measurement was reduced after using feedback. The greatest changes were observed in ankle rotation, knee rotation, and hip adduction/extension peak angles, all with decreases greater than 5 degrees, representing more than 30% reductions in LOA (Figure 1). There were slight decreases for ankle eversion and hip rotation peak angle LOA, and a slight increase for knee flexion peak angle; however, all of these changes were less than 2 degrees, or 7%.

Figure:
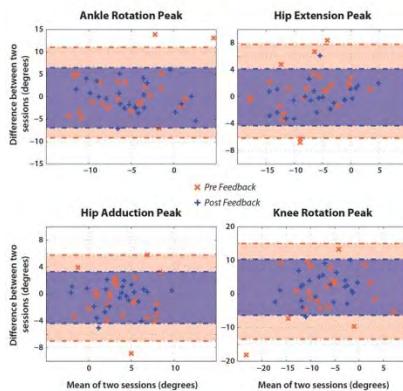
Conclusion: We quantified the use of marker placement location feedback, based on the IQRR score, and subsequently measured greater than 5-degree reductions (**> 30%**) in inter-session limits of agreement.

Caption: Figure 1 - Bland-Altman plots of joint angles, across two sessions of data collection, which displayed the greatest differences between Pre and Post. The limits of agreement Post Feedback (dark shade) have narrower ranges than Pre Feedback (light shade).

References:

[1] Gorton GE, et al., Gait Posture. 29: 398-402, 2009.

[2] Osis S, et al., Comput Methods Biomech Biomed Engin. In press, 2014.

[3] Pohl MB., et al., Gait Posture. 32: 559-563. 2010.

Disclosure of Interest: None Declared

Motion Analysis

AS-0460

POWER OUTPUT OF OAR BLADE IN CONTEXT OF ROWER LEG, KNEE AND TRUNK COORDINATION IN ON WATER SKULL ROWING

Chris T.M. T. Baten [1,*] Mats Baten [2] Fred Vuijk [1]

[1]Ambulatory 3D Analysis of Movement, Roessingh Research and Development, [2]Kottenpark College, Enschede, Netherlands

Introduction and Objectives: In varsity rowing results are obtained by skillfully delivering power to the water through the oar blades, optimally in amplitude and pattern.

This paper describes a method estimating blade power output and its application to actual on water rowing in 6 rowers in repeated sessions of multiple bouts at competition speed. The power profiles are discussed in the context of the 3D kinematics of the oar, boat and rower knee joint, trunk and elbow joint of the rower.

Methods: 6 rowers performed two 4 hour measurement sessions of 3 sets of 400m rowing on 2k competition speed and tempo, followed by 600m of light rowing before starting the next set. Experiments were conducted on the Twente Canal under mostly clear weather conditions with a slight downwind. Sessions were divided in part A and part B with 1.5 hour resting period in between.

Before, in between and after each session body segment calibrations were performed to estimate and test and/or confirm the relative orientation between the IMMU coordinate frames and the body segment coordinate frames. This was also done for the sensors on oars and boat.

17 wireless IMMUs were placed on boat, oars (2 each), upper and lower leg, pelvis, thorax, upper and lower arms and feet. Also a bow and stern camera was mounted (GoPro) and a recording tablet and wireless IMMU receiver/commander dongle were mounted in a box on the boat just behind the rower.

Power was estimated from data from 2 IMMUs on each oar. The relative angle between both IMMUs was then related to the force to the oar on the section where the blade attaches to the oar. For this a relationship is used determined by data from a separate calibration session. In this session the oar was horizontally fixated at 2 points representing hands and rig contact and different weights were applied at a point just before the of the blade attachment. Oar absolute inclination and angle around the vertical axis of the boat were taking into account. the power was split in a component in 'forward' direction and one in lateral direction.

Results: The force to bending angle α calibration procedure yielded linear relationships (R^2 = 0.99, no significance in second order term).

Figure 1 shows an example data of one piece of rowing data. Shown are from top to bottom: oar bend angle, oar forward force, forward velocity, oar angle, work, forward power and power versus knee, trunk and elbow flexion. This example illustrates clearly the consistency of amplitude and detail in the estimated entities on a similar level in power estimates as in knee, trunk and elbow kinematics estimates. This was observed throughout all experiments. Groupwise (statistical) evaluation of the rower 3D kinematics data revealed consistent high repeatability within subjects over sessions, consistent rower knee, trunk elbow coordination styles characteristics and consistent fatigue induced effects. This data behavior,

together with the consistency observed in the power data details as described above, suggests that similar observations can be made for the power data on a group level. This information is however not yet available at the moment of submission of this abstract.

Figure:
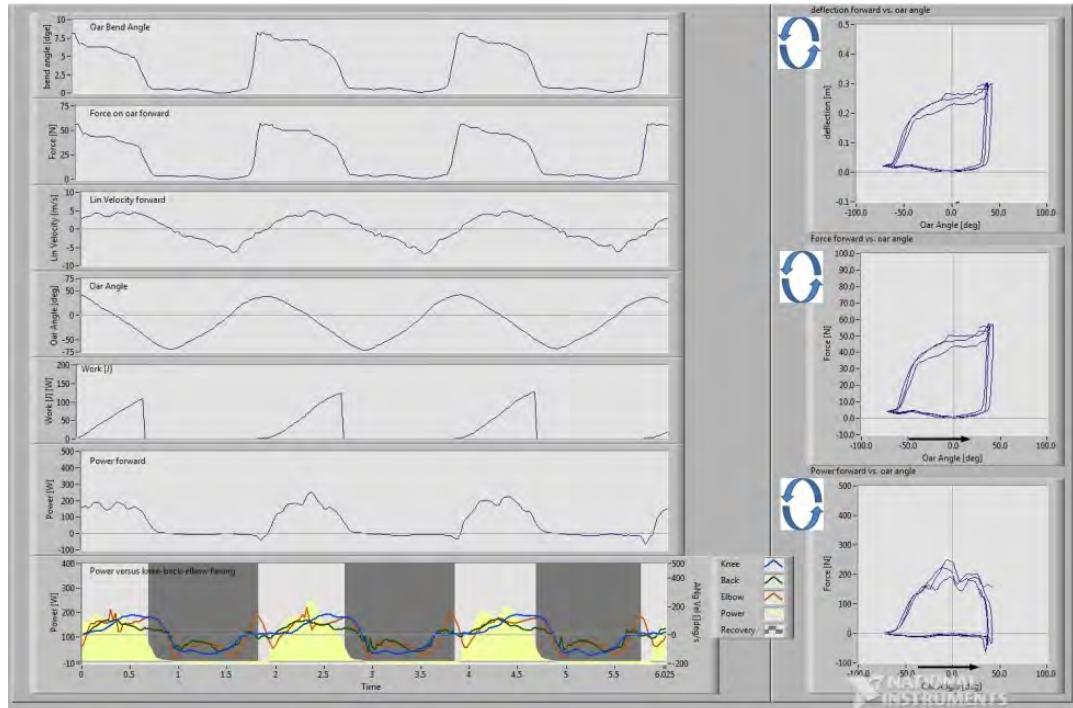
Caption: Figure 1: Example of data obtained during actual on water rowing. Top to bottom: oar bend angle, oar forward force, forward velocity, oar angle, work, forward power and power versus knee, trunk and elbow flexion.

Conclusion: It appeared feasible to synchronously record 3D kinematics of 13 body segment, boat and 2 oars with wireless IMMUs, 2 video streams. Recording of oar bending from data of 2 IMMUs on each oar and calibration of oar bending to oar force seemed possible in such a detail and consistency that oar output power could be estimated consistent in amplitude and in detail in a consistent way with the knee, trunk and elbow flexion details.

Although no absolute validation of power data is perfomed yet, studying these output power profiles in the context of the coordination details promises already to be of use for studying rower skill efficiency and effectiveness.

Disclosure of Interest: None Declared

Motion Analysis

AS-0461

ADAPTATION AND VALIDATION OF AN EXISTING FOREARM MODEL FOR CORRECTING SOFT TISSUE ARTEFACT THROUGH MULTIBODY OPTIMISATION

Alexandre Naaim [1 2 3 4,*] Florent Moissenet [4] Raphael Dumas [1 2 3] Thierry Haumont [5] Laurence Chèze [1 2 3]

[1]Université de Lyon, [2]Université Claude Bernard Lyon 1, Lyon, [3]Laboratoire de Biomécanique et Mécanique des Chocs, IFSTTAR, Bron, France, [4]Laboratoire d'Analyse du Mouvement et de la Posture, CNFR - REHAZENTER, Luxembourg, Luxembourg, [5]Chirurgie Infantile, CHU CAEN Hôpital Femme Enfant, Caen, France

Introduction and Objectives: Motion capture can be limited by Soft tissue artefact (STA) especially for upper limb motions. However, using multibody optimisation (MBO) methods can allow reducing STA. In MBO, a kinematic chain composed of rigid segments linked by joint models allows studying the limb movements. The segments positions are then optimised through the minimisation of the squared distance between model-determined (MDM) and measured (MM) markers trajectories. However, MBO is highly sensitive to the joint models. Duprey et al. [1] showed that the use of anatomy-based models allows for a better correction of STA in the lower limb. In the same idea, the model proposed by Pennestri et al. [2] was used in the present study to model forearm. This model is composed of 3 segments (humerus, radius and ulna) linked in a closed loop chain by 3 joints (humeroulnar (HU): hinge, humeroradial (HR): spherical, radioulnar (RU): sphere-in-cylinder). It presents the advantage to be simple and to require only geometrical parameters for its construction that can be easily obtained through functional methods or imaging technics. However, the joint centre positions defined by Pennestri et al. [2] remain arbitrary. The aim of the study was then to customise the geometry and to evaluate the resulting model for MBO. The general objective was to evaluate if the upper limb model can replicate a bone kinematics measured ex vivo.

Methods: A study was performed on a cadaver (man, 99 yrs) at the Laboratory of Anatomy of the CHU of Caen. Clusters of markers were rigidly fixed on hand, radius, ulna, humerus, scapula, clavicle and thorax. All anatomical landmarks recommended by ISB [3] were pointed during a static recording. Joint centres and axes were obtained with functional methods by mobilising the cadaver. Glenohumeral centre was defined using a method based on a SCoRE methods [4,5]. The SCoRE method was also used to define the RU and HR centres through respectively a pronosupination (PS) movement and a PS with elbow flexion-extension (FE) movement. Elbow FE axis was defined using the SARA method [6]. Data were recorded using a 100Hz optoelectronic tracking system (Qualysis AB, Sweden) and transferred to Matlab R2011b using the Biomechanical Toolkit [7] for all computations. Original model geometry was replaced by the geometry determined by the functional methods. Spherical joints were used to model all the shoulder joints without considering the scapulothoracic joint. Mean and standard deviation between the position of MDM and MM were calculated as indicators of goodness-of-fit. The kinematics obtained from MDM and MM for the HU FE during an elbow FE and the RU internal-external rotation (IER) during PS, following ISB recommendations [3], were compared using RMSE and R^2.

Results: The MBO was unable to converge when using the original Pennestri model and consequently no results are available in that case. The customised Pennestri model seems to fit closely to the markers (Table). Except for one marker, the difference was always less than 3.6mm. Figure shows that the model fit very well the data for HU FE during elbow FE.

However, for RU IER, the model fit well the data but not above 100° pronation where a maximum 15° difference can be found.

Figure:
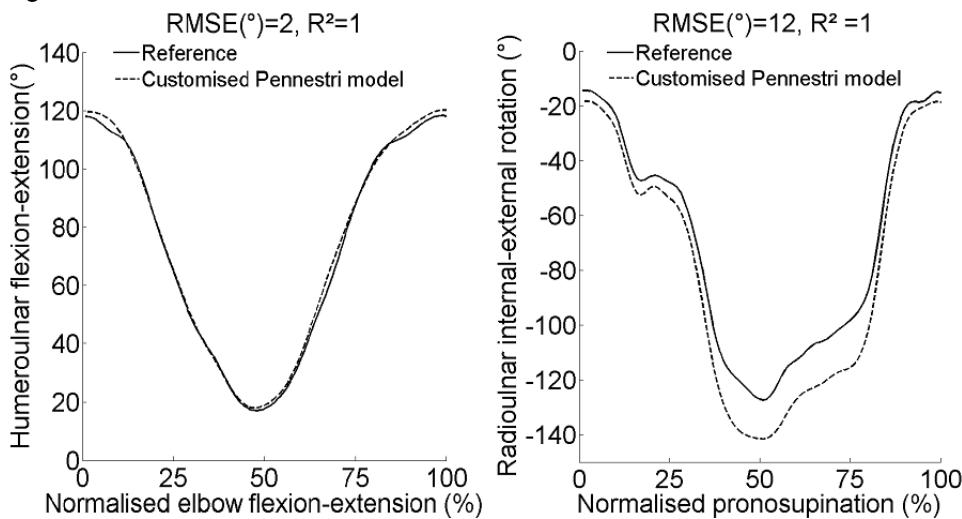
Caption: Reference and model based kinematics for humeroulnar (HU) flexion-extension (FE) during an elbow flexion–extension (FE) and radioulnar (RU) internal-external rotation (IER) during pronosupination (PS).

Conclusion: As it was impossible to obtain any result with the original Pennestri [2] model it can be concluded that it is incompatible with the bone kinematics studied and that it should be avoided to be used directly. The proposed customised Pennestri model [2] based on functional methods, seems fitting well the movements of the forearm except for high pronation. It would have been possible to obtain a better fitting by eventually adding degrees of freedom(DOF) in the model. Moreover, a more complex model including ulna translation and swaying did not show significant differences with the Pennestri model when using skin markers [8]. As a result, the proposed model could be considered as a valuable model of the forearm for MBO.

Table:

Markers		PS		Elbow FE	
		Mean(mm)	Std(mm)	Mean(mm)	Std(mm)
Humerus	1	5.0	0.7	2.7	0.8
	2	3.6	1.2	1.9	0.3
	3	3.0	0.4	3.0	0.4
	4	2.0	0.7	1.4	0.5
Ulna	1	3.4	0.7	2.5	0.8
	2	3.0	0.5	2.3	0.7
	3	3.1	1.2	1.5	0.6
Radius	1	1.2	0.4	1.3	0.6
	2	2.3	0.7	1.8	0.9
	3	2.2	0.8	1.7	0.6

Caption: Mean and standard deviation between the position of model-determined (MDM) and measured (MM) markers for a pronosupination and an elbow flexion-extension

References: [1] Duprey et al., J Biomech 43:2858–62, 2010

[2] Pennestrì et al., J Biomech 40:1350–61, 2007

[3] Wu G et al., J Biomech 38:981–92, 2005

[4] Lempereur et al., J Biomech 43:370–4, 2010

[5] Ehrig et al., J Biomech 39:2798–809, 2006

[6] Ehrig et al., J Biomech 40:2150–7, 2007

[7] Barre A et al., Comput Methods Programs Biomed 114:80–7, 2014

[8] Laitenberger et al., Multibody Syst Dyn, 2014

Disclosure of Interest: None Declared

Motion Analysis

AS-0462

COMPARISON OF TIBIAL AND FEMORAL ACCELERATIONS USING MOTION CAPTURE AND INERTIAL MEASUREMENT UNITS

Sara S. P. Marreiros [1,*] Jody Riskowski [1] Martijn Steultjens [1]

[1]School of Health and Life Sciences, Glasgow Caledonian University, Glasgow, United Kingdom

Introduction and Objectives: Measurements of joints kinematics are important for the development and validation of musculoskeletal computer models, which are often used to assess normal and pathological gait patterns [1]. Commonly, these measures are collected using a laboratory-based motion capture (MoCap) system with cameras and reflective markers. However, recent technology advances have introduced wearable measurement systems, also known as inertial measurement units (IMUs) that use accelerometers, magnetometers, and gyroscopes to measure movement and orientations [2].

Soft-tissue artefact (STA) is the main source of errors associated MoCap systems. IMUs may be better suited to addressing STA as well as provide a means for addressing joint action in everyday activities performed outside the laboratory. However, the validity and reproducibility of the joint local accelerations measured by the IMUs relative to motion capture is unknown. Therefore, the purpose of this study is to compare tibial and femoral accelerations near the knee joint obtained between a MoCap system and IMUs.

Methods: Kinematic, kinetic and accelerometer data from 8 participants were collected in 7 self-selected walking trials. Kinematic data was collected using a 14-camera MoCap system (Qualisys, Sweden) synchronized with 4 tri-axial IMUs (Opal™, APDM, USA), with both systems sampling at 128 Hz. Ground reaction forces (Kistler, USA) were collected at 2560 Hz.

IMUs were placed in an anterior and lateral position on the right thigh and shank (Femur Front and Lateral and Tibia Front and Lateral) near the knee joint, with three reflective markers on each sensor to track the IMU spatial location and orientation. A full body marker set protocol was used to collect participants' kinematic data. Markers trajectories were filtered using a 4th order low pass Butterworth filter with 20 Hz cut-off frequency; IMUs signal was not filtered.

A scaled musculoskeletal model [3], modified to allow 5 DoF (2 translations and 3 rotations) in the knee, was used to measure femoral and tibial accelerations through inverse kinematics (IK) using OpenSim v3.2 [4]. Accelerations measured by the IMUs were compensated for gravity using the IMUs self-reported spatial orientation. Acceleration in OpenSim were measured for fixed points correspondent to the IMUs origins fixed for the correspondent limb, with the assumption the IMUs' location and orientation as measured in a static trial was maintained through all gait trials. Both signals are represented in OpenSim default coordinate system (x: posterior anterior, y: vertical, z: medial lateral) and in bone local coordinate system.

Correlations between IMUs and MoCap accelerations were measured for each IMU position and axis, with means determined at both the participant- and group-level.

Results: Mean accelerations through the gait cycle were more stable when obtained through the unfiltered IMU relative to the filtered IK measure as the IMUs signal had a lower SD relative IK signal.

Mean correlations in x-axis and for the y-axis for the tibia IMUs and femur lateral IMU were high (Table; range: 0.781 - 0.836). Femur front (FFront) IMU had a moderate correlation (0.619). In the z-axis, correlations were low to moderate (range: 0.355 - 0.615).

Figure:
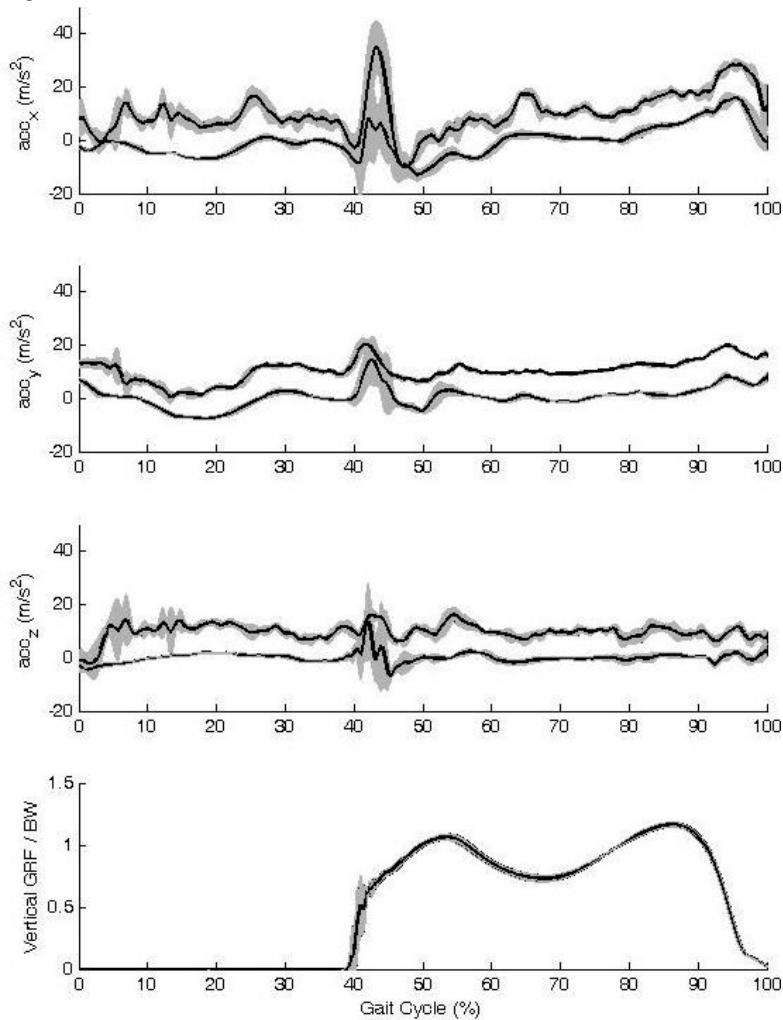
Caption: Accelerations from IMUs and IK for participant 4, TLateral point and GRF. Means and SD are represented. The acceleration from IK is off-set vertically 10 m/s2.

Conclusion: The high correlation in acceleration obtained between the IMUs and MoCap suggest that the IMUs can accurately measure accelerations and, has a portable device has the advantage of not being restricted to a laboratory. However, the lower correlations in z-axis can be related with errors in the estimation of gravity orientation suggesting that using only the hardware reported orientation may not be sufficient for this compensation.

Table:

Participant		1	2	3	4	5	6	7	8	Overall
Femur Front	x	0.685	0.901	0.871	0.899	0.742	0.868	0.900	0.869	0.836 (0.833-0.840)
	y	0.301	0.683	0.583	0.785	0.594	0.665	0.754	0.690	0.619 (0.611-0.626)
	z	0.631	0.585	0.645	0.669	0.267	0.645	0.685	0.770	0.615 (0.608-0.622)
Femur Lateral	x	0.702	0.862	0.824	0.879	0.731	0.841	0.877	0.823	0.818 (0.814-0.821)
	y	0.851	0.732	0.742	0.766	0.622	0.736	0.787	0.713	0.745 (0.740-0.751)
	z	0.491	0.266	0.245	0.287	0.231	0.575	0.418	0.358	0.355 (0.344-0.365)
Tibia Front	x	0.759	0.742	0.881	0.748	0.763	0.812	0.844	0.808	0.781 (0.777-0.786)
	y	0.813	0.707	0.893	0.702	0.494	0.759	0.831	0.790	0.742 (0.736-0.747)
	z	0.707	0.553	0.732	0.347	0.596	0.677	0.469	0.519	0.560 (0.552-0.568)
Tibia Lateral	x	0.810	0.715	0.907	0.788	0.791	0.838	0.916	0.763	0.802 (0.797-0.806)
	y	0.793	0.786	0.889	0.802	0.826	0.762	0.888	0.747	0.808 (0.803-0.812)
	z	0.521	0.475	0.684	0.367	0.710	0.567	0.458	0.391	0.496 (0.487-0.505)

Caption: Data correlations of IMUs to MoCap, with data presented as point estimate (95% confidence interval for overall).

References: [1] Akbarshahi et al., J. Biomech., 43(7):1292–1301,2010.

[2] Roberts et al., J. Eng Medicine, 227(10):1104–1113,2013.

[3] Delp et al., IEEE Trans Biomed Eng, 37(8):757–67,1990.

[4] Delp et al., IEEE Trans Biomed Eng, 54(11):1940–50,2007.

Disclosure of Interest: None Declared

Motion Analysis

AS-0463

HIP JOINT BIOMECHANICS DURING GAIT IN PEOPLE WITH AND WITHOUT SYMPTOMATIC FEMOROACETABULAR IMPINGEMENT

Laura Diamond [1,*] Tim Wrigley [1] Rana Hinman [1] Paul Hodges [2] John O'Donnell [3] Kim Bennell [1]

[1] Centre for Health, Exercise and Sports Medicine, The University of Melbourne, Melbourne, [2] Centre of Clinical Research Excellence in Spinal Pain, Injury & Health, The University of Queensland, Brisbane, [3] St Vincent's Hospital, East Melbourne, Australia

Introduction and Objectives: Femoroacetabular impingement (FAI) is a morphological hip condition that can cause hip/groin pain and impaired performance in younger active adults, plus lead to stiffness, muscle weakness, structural damage, and possibly hip osteoarthritis [1,2]. FAI results when the proximal femur abuts against the acetabular rim [1,3]. Understanding the impairments associated with FAI is crucial to guide treatment and rehabilitation strategies. Gait is the most common repetitive voluntary movement performed [4] and there is limited and conflicting evidence to suggest that hip ROM during walking is reduced in people with symptomatic FAI, despite the fact that motion in this task is generally pain free, and does not reach the end of available range [5] where painful impingement might occur. The study objective was to compare three-dimensional (3D) hip joint gait biomechanics between a symptomatic FAI and an asymptomatic control group.

Methods: Thirteen patients with FAI diagnosed clinically and with imaging features, and 15 age, gender, BMI, and activity level matched asymptomatic controls underwent a 3D gait analysis (Vicon, Oxford, UK). All patients were scheduled for hip arthroscopy surgery; patients with bilateral FAI were tested on the more symptomatic side. Subjects were required to walk along a 10-meter walkway in the laboratory six times at a self- selected speed. 3D lower limb kinematics and inverse dynamics were calculated from marker triads and the ground reaction force [6]. Joint moment data was normalised to bodyweight times body height. Peak hip angles and ROM in each plane, and peak hip moments were compared between the two groups using multivariate ANOVA. Walking speed and demographic variables were examined for between-group differences using independent t-tests ($\alpha = 0.05$).

Results: Results are shown in Table 1. There were no significant between-group differences in demographics or walking speed. The max abduction angle was significantly reduced in the FAI group compared to controls (Figure 1). There were no other significant differences between groups for hip angles or moments.

Figure:
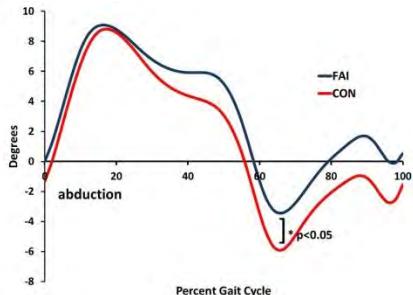
Caption: Mean hip adduction/abduction angle gait waveforms for FAI and control groups.

Conclusion: A significantly decreased peak hip abduction angle was found during gait in people with symptomatic FAI. No other variables differed between the groups. This study is limited by a small sample size and a control group that was not imaged to ensure absence of asymptomatic FAI bony changes. The clinical significance of these hip ROM differences for symptoms are unclear and requires further consideration, but might relate to an overall strategy to limit motion of the painful hip. More demanding tasks designed to target positions of impingement, such as squatting and stair climbing, might reveal greater insight into the nature of the biomechanical impairments in this population. Examination of these tasks and the function of the surrounding deep hip muscles with intramuscular electromyography is the aim of current work to better understand the neuromuscular changes in FAI as potentially modifiable targets for treatment.

Table:

Group	Age (yrs)	Males	BMI (kg/m^2)	FAI type (cam:combined)	Tegner Physical Activity Level (/10)	Walking Speed (m/s)	Max abduction (swing) (°)	Max adduction (stance) (°)	Frontal plane ROM (cycle) (°)
FAI	24.4 (5.1)	10 (77%)	24.4 (2.3)	10:3	5.3 (2.3)	1.4 (0.2)	-4.5 (2.6)*	9.7 (2.1)	14.2 (2.7)
Control	27.1 (4.4)	11 (73%)	23.5 (2.1)	N/A	6.6 (1.0)	1.4 (0.3)	-6.8 (3.3)*	9.4 (4.4)	16.2 (3.9)

Caption: Mean (SD) descriptives and frontal plane gait variables for FAI and control groups.

References: 1. Ganz R, et al. Clin Orthop Relat Res 417:112–20, 2003.

2. Beck M, et al. J Bone Joint Surg Am 87:1012–18, 2005.

3. Leunig M, et al. Clin Orthop Relat Res 467:616–22, 2009.

4. Winter DA. J Mot Behav 15:302-30, 1983.

5. Diamond LE, et al. B*r J Sports Med Online First: 2014.*

6. Besier TF, et al. J Biomech 36, 1159-1168, 2003.

Disclosure of Interest: None Declared

Computer Simulation

AS-0464

THE EFFECT OF UPPER ARM MASS ON THE THROWING VELOCITY

Patrick Fasbender [1,]*Nicholas P Linthorne [1]Thomas Korff [1]Vasilios Baltzopoulos [1]

[1]Department of Life Sciences, Brunel University, Uxbridge, United Kingdom

Introduction and Objectives: Throwing performance is important in many sports where the goal is to throw a projectile as fast or as far as possible. The most important determinant of throwing performance is release velocity, which is determined by muscular strength, inter-muscular coordination, inertial properties and transfer of angular momentum. Results from previous studies suggest that throwing performance might be improved through deliberate manipulation of the mass of the athletes' arm segments. Southard[1] found that with an additional 1.4 kg strapped on the upper arm the peak velocity of the hand when throwing a 114 g ball increased by about 5%. Similarly, Kim and colleagues[2] found that arm swing speed was slightly increased when the mass of the upper arm was increased by 25% and 50%. An interesting question arising from these results is whether there is an optimal upper arm mass that maximises release velocity. Apart from a sports performance perspective, a greater understanding of the interaction between upper arm mass and throwing performance could also be beneficial in child development, and might help to explain the gender gap in throwing performance. The aim of this study was to investigate the relationship between upper arm mass and release velocity using computer simulation.

Methods: A 2D computer simulation (Working Model 2D), consisting of two rigid bodies (upper and lower arm) and two torque generators (shoulder and elbow), was used in this study. The torques used to drive the model were obtained from experimental data. For this purpose, one subject with an upper arm mass of about 2.0 kg[3] performed a maximal throw while sitting on a chair and throwing a tennis ball at a target 3 m away. The participant was instructed to use his dominant arm in the sagittal plane without using his trunk. Kinematics were obtained using motion analysis, and joint torques at the shoulder and elbow were obtained using inverse dynamics in an OpenSim model[4]. The torque profiles were approximated by a 3rd order polynomial, which was used as the torque generator for the 2D computer simulation. In the simulations, the upper arm mass was varied between 0.5 and 12.5 kg, and the shoulder torque was varied between 80 and 120% of the experimentally determined value to investigate if the mass-dependence of throwing performance could be dependent on the capacity for muscular torque production at the shoulder.

Results: The optimal upper arm mass that produced the greatest release velocity was between 7 and 10 kg (Figure 1), with the optimal upper arm mass decreasing with increasing shoulder torque. The gain in horizontal release velocity obtained when using the optimum upper arm mass ranged from +5.0% in the highest shoulder torque condition to +13.3% in the lowest shoulder torque condition. Increasing the upper arm mass by 2 kg, similar to the maximal values used by experimental studies[1][2], resulted in increases in horizontal release velocity of between 3.70% and 8.25%. Although the maximum release velocity occurred with an additional mass of between 5 and 8 kg on the upper arm, an additional mass of only 1.5 to 3.5 kg produced a release velocity that was within 2% of the maximum velocity (Figure 1).

Figure:
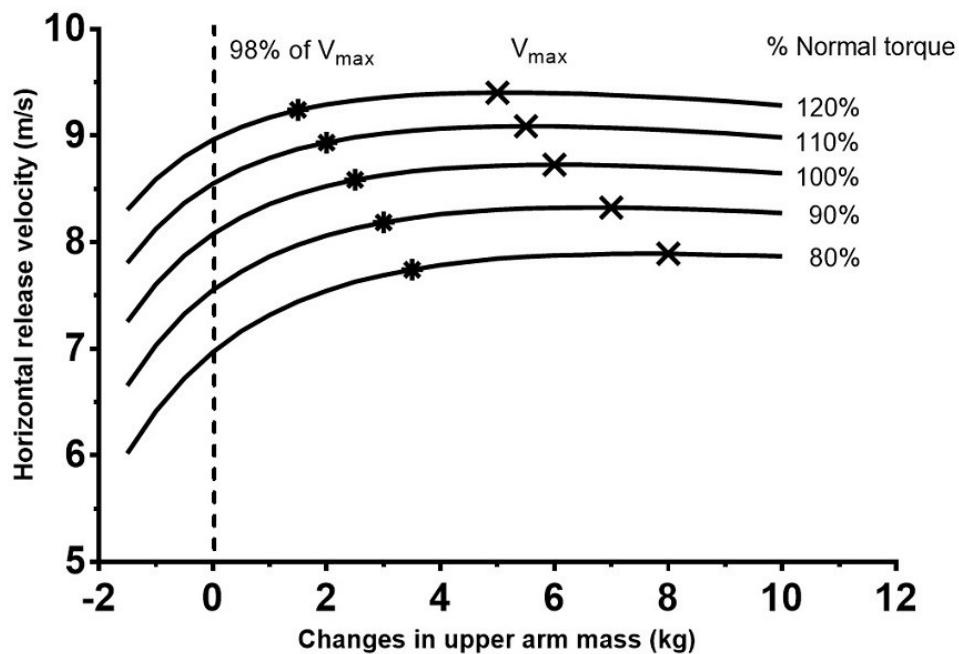
Caption: Effect of upper arm mass on horizontal release velocity for five torque conditions.

Conclusion: This study highlights the mechanical effect that upper arm mass has on throwing performance. It extends our knowledge about how the horizontal release velocity changes with upper arm mass increases that exceed the masses tested in previous studies. In sports, adding an extra 5 to 8 kg to the upper arm mass would help athletes to optimise throwing performance by maximising the release velocity. Although such a large upper arm mass is physiologically unrealistic, our results suggest that substantial improvements in release velocity can still be obtained with a more modest upper arm mass. Understanding the effect of mass distribution in the arm on throwing could have implications on child development and training. During growth, a child's forearm and hand segment reach adult proportions before the upper arm[5], and this hinders the learning of the "adult" throwing pattern. As this study used a 2D simulation, the recorded throwing movement had a number of limitations. This type of throw did not take the internal/external shoulder rotation into consideration, which is important in a maximal-effort throw. Future research should investigate if similar effects are observed in more complex simulations.

References: [1] Southard, Res. Q. Exerc. Sport, 69: 355-367, 1998.

[2] Kim et al., ISBS Conference Proceedings, 2008.

[3] Winter. Biomechanics and Motor Control of Human Movement, John Wiley & Sons, 1990.

[4] Saul et al., Comput. Method. Biomec.: 1-14, 2014.

[5] Jensen, J. Biomec., 22: 529-536, 1989.

Disclosure of Interest: None Declared

SINGLE LEG TRIPLE HOP TEST INVERSE KINEMATICS WITH DIFFERENT MARKERS WEIGHTS USING OPENSIM

Felipe Alvim [1,*]Paulo Lucareli [2]Luciano Menegaldo [1]

[1]Biomedical Engineering Program, Federal University of Rio de Janeiro, Rio de Janeiro, [2]UNINOVE, São Paulo, Brazil

Introduction and Objectives: Computer modeling in biomechanics is a widely used tool that helps understanding how neuromusculoskeletal system interact to generate movements. One of the widely used software for biomechanical analysis is OpenSim, which is an open-source platform [1]. For finding muscle activations history from kinematical data, one of the typical OpenSim applications, its workflow comprises a series of steps. Initally, a generic musculoskeletal model is used as basis, which is scaled to meet subject's anthropometry. In the sequence, inverse kinematics (IK) and inverse dynamic problems are solved. The resulting torques are then distributed among the muscles through a static optimization solution. The objective of solving an IK problem is to find a series of model positions that minimizes the distances between experimental and virtual markers placed on the model. OpenSim's User Guide recommendation is increasing the weights of markers placed at the bone landmarks for improving motion accuracy results delivered by IK tool. However, no further information is provided. The accuracy of IK results influences the subsequent steps further used in OpenSim workflow. Thus, the aim of this work is to evaluate the results of IK tool applying different groups of weights to markers placed at bone landmarks. Joint angles determined by usual rotation matrix approach [2] was used as a gold standard.

Methods: Ten female subjects were recruited to participate. They performed a single leg triple hop test (SLTHT) wile kinematic data were collected by an eight infrared camera system (SMART-D BTS®, Milan, Italy). Data were sampled at 100 Hz. Twenty five markers were attached to the skin based on Vicon Plug-in-Gait biomechanical model [3]. The markers trajectories were filtered using a Woltring filtering routine, with a 12 Hz low-pass cutoff frequency. For comparison, the joint angles were calculated by Euler angles-based rotation matrix approach [3]. The preparation phase of one attempt was selected to be analyzed for each subject. Model was scaled and the resulting scaled model was then used by a OpenSim run with IK tool. For each trial three inverse kinematic problems were solved. In the first (G1) all markers weights had the same unitary value. In second (G2) all markers placed on bone landmarks (7th cervical vertebra, anterosuperior and posterosuperior iliac spines, lateral femoral epicondyle, lateral malleolus, middle third of foot between the 2nd and 3rd metatarsals and calcaneus) have they weights defined as 10. Finally, in the third IK problem (G3), all markers placed on bone landmarks have they weights defined as 100. Hip flexion, hip adduction, hip rotation, knee flexion and ankle dorsiflexion, all corresponding to the jumping side were analyzed. Joint angles calculated by both approaches were interpolated to 101 samples and the root mean square error (RMSe) between them evaluated. Normality of dataset was verified and one way ANOVA to repeated measurements was applied to verify the existence of differences among RMS errors of the three groups of weights in the different joint angles. Tukey HSD post hoc test was applied to identify differences found in the ANOVA. Significance level of 5% was adopted.

Results: The means and standard deviations to RMSe values, of each joint angle and markers' weight group are shown in Table 1.

Statistical tests verified statistical differences only in hip flexion RMSe values between G1 and other groups. There was no difference between RMSe of G2 and G3 in hip flexion. All others RMSe values between G1, G2 and G3 weights groups in other joint angles showed no statistical differences.

Conclusion: This work have shown that increasing markers weights by one order of magnitude reduced the RMSe between hip flexion angle calculated by conventional rotation matrix approach and Opensim's IK tool. No effects were found with further increase of increasing weights of bone placed markers. In addition, no statistical differences were found in RMSe values with increased weights in other joint angles.

Table:

	G1	G2	G3
Hip Flexion (°)	31,8±5,3*	23,9±5,9	22,5±6,3
Hip Adduction (°)	6,9±3,5	5,6±3,3	5,5±3,2
Hip Rotation (°)	4,4±2,4	5,1±2,7	5,4±2,9
Knee flexion (°)	7,9±3,9	8,2±4,5	8,2±4,5
Ankle dorsiflexion (°)	10,1±2,8	9,3±2,2	9,1±2,2

Caption: Table 1: Means ± standard deviation of RMSe values to each joint angles and weights groups. (*) statistical differences.

References: [1] Delp, SL, et al. OpenSim: Open-Source Software to Create and Analyze Dynamic Simulations of Movement. IEEE Trans Biom Eng. 2006; 54:1940-50.

[2] Kadaba MP, et al. Measurement of lower extremity kinematics during level walking. J Orthop Res. 1990; 8:383-92.

[3] Winter, DA. Biomechanics and Motor Control of Human Movement. John Wiley & Sons, New York. 2009.

Disclosure of Interest: None Declared

Modelling

AS-0466

ASSESSMENT OF EFFECTS OF ENHANCED EXTRACELLULAR MATRIX STIFFNESS DUE TO BOTULINUM TOXIN ON MUSCULAR MECHANICS USING FINITE ELEMENT MODELING

Ahu N. Turkoglu [1,*]Can A Yucesoy [1]

[1]Biomedical Engineering Institute, Bogazici University, Istanbul, Turkey

Introduction and Objectives: Botulinum toxin type A (BTX) injections are commonly used to treat cerebral palsy (CP) patients. Partial muscle paralysis allows limiting hyper-excitable stretch reflexes and reducing spasticity. However, BTX also affects muscular mechanics substantially, which is functionally very important. Recently in a limited number of experiments, force measurements of muscle exposed to BTX were done over a range of muscle lengths. These studies show that the force reduction effect is not constant but variable with muscle length [1-2], and BTX can decrease muscle length range of force exertion [1]. Our previous finite element modeling study on effects of BTX on muscular mechanics indicate that a vast majority of sarcomeres attain higher lengths than identical sarcomeres of the BTX-free muscle [3]. Such *"longer sarcomere effect"* (LSE), can be considered as the characteristic determinant of effects of BTX on muscular mechanics leading to variable force reduction and decreased length range. LSE is ascribed to muscle fiber-extracellular matrix (ECM) interactions [4] and hence should be directly dependent on the mechanical properties of the ECM. Remarkably, recent experiments also show that BTX injection causes increased passive muscle forces and collagen content of the ECM [1], suggesting an increased stiffness of muscular connective tissues. Taking these in to account and using finite element modeling we aimed at testing the hypothesis that ECM stiffness increase due to BTX causes LSE to be more pronounced.

Methods: Our long existing Linked Fiber-Matrix Mesh model was used by inactivating selected muscle elements to represent partial muscle paralysis effect of BTX. Muscle modeled earlier with the middle half of its volume paralyzed [3] was chosen as the reference case. Compared to that, two manipulated ECM stiffness cases were studied: enhanced ECM stiffness in (i) muscle fiber direction only and (ii) muscle fiber and cross-fiber directions together. ECM stiffness was manipulated by changing related material properties to achieve steeper stress-strain curves (up to two fold at high strain).

Results: Manipulated ECM stiffness cases did show higher muscle passive forces (e.g. by two fold at high length) compared to the reference case. A more pronounced LSE was also found however limited to shorter muscle lengths (for approx. 60% of the length range). In contrast, for intermediate and longer muscle lengths LSE was less pronounced. See the figure for mean strain values along muscle fascicles modeled at short and long muscle lengths exemplifying this finding. Therefore, our hypothesis was confirmed only in part. However, the effects of manipulated ECM stiffness on muscular mechanics were substantial. The optimum length for the manipulated ECM cases shifted to lower muscle lengths decreasing the active length range of force exertion (up to 13%). Notably, the active force production potential of the activated muscle parts increased (up to 7%). This is because enhanced LSE at shorter muscle lengths favor active force production of sarcomeres operating at the ascending limb of their force-length curves. Similarly, reduced LSE at longer muscle lengths cause sarcomeres operating at the descending limb of their force-length curves to produce more force. Narrowing of the length range of muscle force exertion does not agree with the intention of improving joint range of

motion of treated CP patients using BTX. Therefore, it represents an inferior effect. Enhanced active force production potential of the activated muscle parts of muscle exposed to BTX compromises the force reduction effect, which can be counter-indicated in case of agonist-antagonist force imbalance. However, muscles of CP patients are known to be weak. For such patients this can offer a balance between reduced spasticity (via paralyzed muscle volume) and availability of sufficient muscle force to coop with the demands of bodily motion.

Figure:
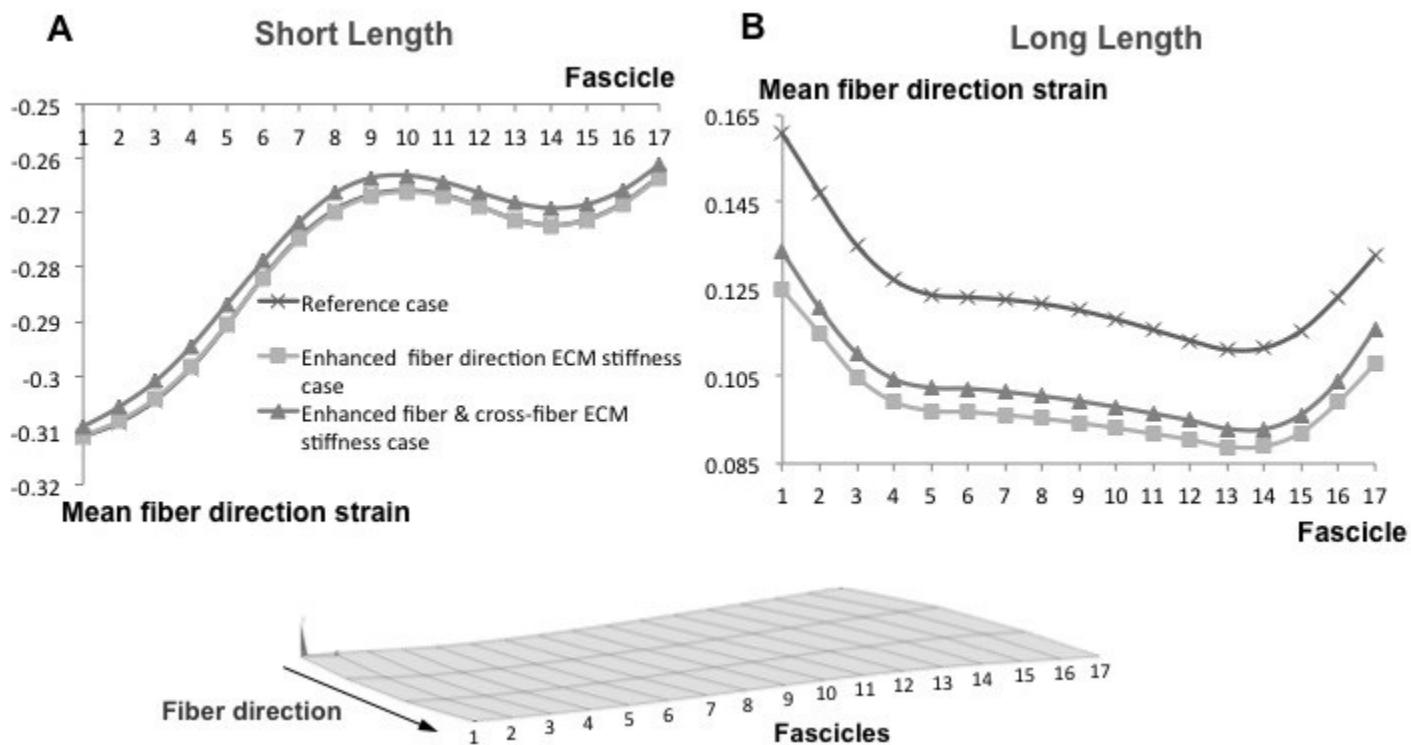
Caption: Effects of increased ECM stiffness on longer sarcomere effect (LSE). Partially paralyzed muscle model represents muscle exposed to BTX (activated muscle parts: fascicles 1–5 & 13–17; paralyzed muscle parts: fascicles 5–13). Compared to the reference case, fascicle mean fiber direction strains of manipulated ECM stiffness cases decreased at short (A) and long (B) lengths indicating more and less pronounced LSE, respectively.

Conclusion: Manipulated ECM stiffness mimicking experimental findings has complex effects on mechanics of partially paralyzed muscle representing muscle exposed to BTX. Varying LSE for different muscle lengths is the central determinant, implications of which should be further investigated also experimentally.

References: 1.   Ates et al., *Muscle & Nerve*, **49**: 866-878. 2014.

2.   Longino et al., *J Biomech*, **38**: 609-13. 2005.

3.   Turkoglu et al., *J Biomech*, **47**: 1565-71. 2014.

4.   Yucesoy, *Exerc Sport Sci Rev*, **38**: 128-34. 2010.

Disclosure of Interest: None Declared

EFFECT OF METHOD FOR DETERMINING INITIAL MUSCLE ACTIVATIONS ON SIMULATIONS OF SQUAT JUMPING

Zachary J. Domire [1,*]John Challis [2]

[1]Department of Kinesiology, East Carolina University, Greenville, [2]Department of Kinesiology, Pennsylvania State University, State College , United States

Introduction and Objectives: For most human movements there is more than one muscle that can complete the task. This redundancy has several biological advantages, but during submaximal movements this for allows infinite combinations of muscle forces that produce the same motion. A common approach for determining individual muscle forces is to perform inverse dynamics and optimize the relative contributions to the joint torque such that muscle force or muscle stress is minimized [1]. These approaches result in estimates for muscle force contributions with little or no co-contraction. If instead muscle force or stress cubed is minimized some co-contraction is typically present [2]. Performing computer simulations of movements is an alternative approach to identifying individual muscle forces. Simulations can solve for muscle forces that optimize the movement towards achieving an objective such as maximizing performance [3] or minimizing energy cost [4]. However, the initial muscle forces are still often calculated using a static optimization approach [5]. The goal of this study is to examine the effects of instead solving for the initial muscle forces such that the choice also minimizes the objective function during simulated jumping.

Methods: The model used is similar one validated previously [3]. The model is comprised of four rigid links connected by frictionless hinge joints. The initial posture of the squat was selected to be similar to what was used by experimental subjects from Challis and Domire [3]. The model is actuated by six muscle-like actuators representing the major muscle groups of the lower extremity. Each of these muscle-like actuators were Hill-type models consisting of a series elastic element and a contractile elements with nonlinear activation dynamics as well as force-length and force-velocity properties. The optimal control problem was converted to a static problem by representing the time histories of the neural excitations with discrete control nodes separated by 0.05s, with linear interpolation between nodes. The neural excitation control nodes were selected with a genetic search algorithm. The objective function for optimization was to maximize vertical energy at take-off with constraints to ensure the simulation was performed without a countermovement and the initial position was in static equilibrium. The initial muscle activations were solved for such that the choice either maximized the objective function or such that one of six static criteria was minimized: minimizing muscle force, muscle stress, relative muscle force, muscle force cubed, muscle stress cubed, or relative muscle force cubed. Jump heights and initial muscle activations were compared across the simulations.

Results: The optimal initial muscle activations included larger activations of the bi-articular muscles compared with the uni-articular muscles at each joint, and therefore, substantial co-contraction was present in the initial posture. The initial muscle activations for the linear approaches were identical. The linear approaches all included no initial contribution from bi-articular muscles, and therefore, had no co-contraction. The non-linear approaches included co-contraction to varying degrees (Figure 1). Minimizing muscle force cubed produced the largest activations in the bi-articular muscles of any of the static approaches. The activations of the gastrocnemius and rectus femoris were similar to the optimal solution. None

of the static approaches resulted in any hamstrings activity in the initial posture. The Jump heights were similar across approaches. However, jump height was largest when the initial activations were optimized for performance (Table 1). The jump height was smallest for the linear approaches and closest to optimal when minimizing muscle force cubed.

Figure:
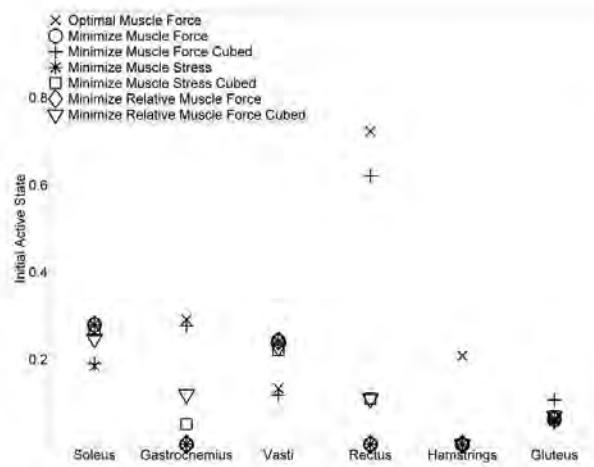
Caption: Figure 1. Initial muscle activations selected using various approaches.

Conclusion: While the impact on jump height of using various approaches to determine initial muscle activations was small, there was considerable variation among the initial muscle activations selected. The optimal solution was the only one of the simulations to include hamstrings activation at the beginning of the jump. The results suggest that athletes due to subtle sub-maximal initial activation of their muscles can influence jump performance.

Table:

Objective Function	Jump Height (cm)
Optimal Force	24.3
Min Force	24.1
Min Force Cubed	24.3
Min Stress	24.1
Min Stress Cubed	24.1
Min Relative Force	24.1
Min Relative Force Cubed	24.1

Caption: Table 1. Jump heights using various approaches for selecting initial muscle activation.

References: [1] Challis et al., Proc. Inst. Mech. Eng., 207: 139-48, 1993.

[2] Crowninshield et al., J. Biomech., 14: 793-801, 1981.

[3] Domire et al., J. Sport Sci., 25: 193-200, 2007.

[4] Anderson et al., J. Biomech. Eng., 123: 381-90, 2001.

[5] Anderson et al., Comp. Meth. Biomech. Biomed. Eng., 2: 201-31, 1999.

Disclosure of Interest: None Declared

Modelling

AS-0468

OPTIMISATION OF GLENOHUMERAL STABILITY IN A MUSCULOSKELETAL MODEL

Edward K. Chadwick [1,*]Dimitra Blana [1]Ton van den Bogert [2]

[1]Institute for Science and Technology in Medicine, Keele University, Stoke-on-Trent, United Kingdom, [2]Department of Mechanical Engineering, Cleveland State University, Cleveland, United States

Introduction and Objectives: Many clinical problems in the shoulder involve loss of stability of the glenohumeral (GH) joint, leading to loss of function and pain. Understanding the role of different structures around the shoulder is therefore important to understanding the normal function of the joint. Musculoskeletal models can provide insight into the function of musculoskeletal systems by allowing examination of internal variables that are hard to measure in vivo. A number of shoulder models have been presented [1], with varying degrees of complexity. Two models with a complete description of the shoulder girdle are the Delft Shoulder and Elbow Model [2] and the Dynamic Arm Simulator [3]. GH stability in these models is described by the joint reaction force (JRF) vector. The joint is assumed to be stable when the direction of the JRF lies inside the rim of the glenoid, modelled as an ellipse, and instability is assumed to arise when the JRF falls outside the rim. In inverse-dynamics, instability is prevented using a non-linear constraint that ensures the JRF remains inside the rim. This leads to recruitment of the rotator cuff (RC) muscles to maintain GH stability, consistent with patterns seen in vivo.

However, for movement patterns where the joint is naturally stabilised by external loads, there is no additional RC muscle force requirement, even if that results in a JRF that falls just inside the rim. If the loads suddenly change, the joint could become unstable; a hard constraint that becomes active only when the JRF reaches the rim might not best represent physiological control mechanisms. An alternative method is to include GH stability in the cost function, and minimise the deviation of the JRF from the centre of the ellipse. This may lead to a more natural and gradual increase in RC activation as GH stability is increasingly challenged. The objective of this study was to test such an approach.

Methods: The Dynamic Arm Simulator consists of seven segments, eleven degrees of freedom, and 138 muscle elements [3]. Inverse-dynamic simulations were implemented as optimisation problems and solved using Direct Collocation [4]. This method discretises both control and state variables on a temporal mesh, transforming a constrained optimal control problem into a set of algebraic constraints. The constraints are based on an implicit formulation of system dynamics, described in [3]. The optimization has an additional constraint per time node, which requires that the scapula stays on the surface of the thorax to avoid winging. The objective function consists of two terms, one that encourages the simulation to stay close to the measured kinematics, and one that minimizes muscle energy consumption, described in [5]. GH stability is included either as an additional constraint at each time node (hard constraint, HC) or as an additional term in the objective function (soft constraint, SC), weighted equally to energy consumption.

Results: As an example of a potentially destabilizing task, the model was set to 20° shoulder flexion with the arm straight, with an external force pushing the hand upwards at 0, 10 and 20N. This load does not significantly recruit the superior rotator cuff muscles (which participate in abduction) and therefore allows examination of their stabilising role in response to load magnitude changes. The direction of JRF was calculated at each force level, for HC or SC. These are shown as

empty circles in figure 1, pointing further from the center of the ellipse as the external force increases, with the HC JRF reaching the rim when the force is 20N. The muscle co-contraction required to centralize the SC JRF is evident by the higher mean force of the RC muscles (shown in the figure for the maximum force of 20N). Subsequently, the external force was removed suddenly and the instantaneous JRF direction was calculated (filled circles). In the case of the HC, this led to instability (the circle is outside the ellipse), while for the SC the joint remained stable.

Figure:
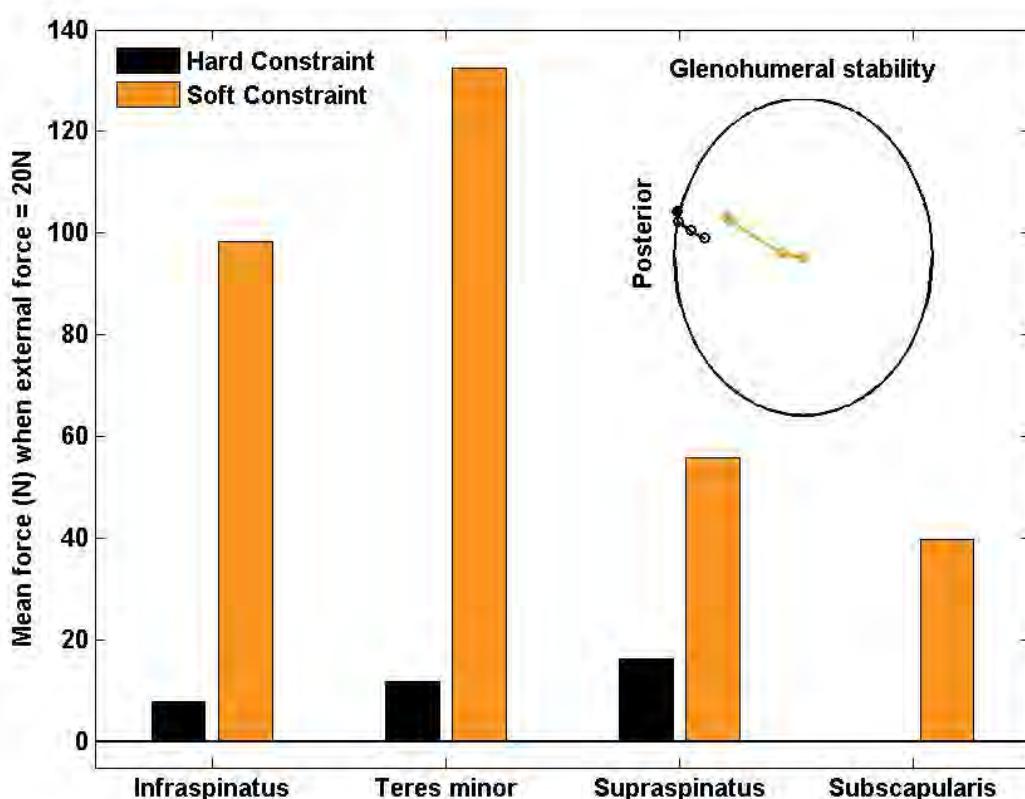
Caption: Comparison of rotator cuff forces and glenohumeral stability between hard and soft constraint methods

Conclusion: A novel approach to modelling GH stability in inverse dynamics that involves minimising instability, rather than including it as a constraint, has been presented. The method produces a pattern that maintains joint stability with a larger margin than the constraint method, and may represent a more physiological approach. Future work will involve in vivo measurements to validate the approach and identify optimal weight factors for the terms in the cost function.

References: [1] B. Bolsterlee et al. *Med Biol Eng Comput. 51(9):953-63, 2013*.

[2] F.C. Van der Helm. *J. Biomech., 27(5), 551–69, 1994*.

[3] E.K. Chadwick et al., *IEEE Trans Biomed Eng, 61(7): 1947-56, 2014*.

[4] M. Ackermann and A.J. van den Bogert. *J Biomech 43: 1055-60, 2010*.

[5] M. Praagman et al., *J. Biomech., 39(4):758–65, 2006*.

Disclosure of Interest: None Declared

Modelling

AS-0469

TOWARDS THE GENERATION OF A PARAMETRIC FOOT MODEL USING PRINCIPAL COMPONENT ANALYSIS

Alessandra Scarton [1,*]Zimi Sawacha [1]Claudio Cobelli [1]Xinshan Li [2] [3]

[1]Department of Engineering Information, University of Padova, Padova, Italy, [2]Department of Mechanical Engineering, [3]The Insigneo Institute for in silico Medicine, University of Sheffield, Sheffield, United Kingdom

Introduction and Objectives: The diabetic foot is one of the most serious complications of diabetes mellitus, which causes alterations in foot structure and leads to the development of plantar ulcers [1]. Several 3-dimensional (3D) finite element models (FEMs) have been proposed to study the behaviour of the foot own to their ability to characterise and quantify the loads developed in the different anatomical structures, and how these affect foot tissues under different loading conditions [2-3]. Current methods for the development of foot FEMs are based on individual specific MRI or CT data, which in addition of being either expensive or time consuming, requires high levels of user intervention due to the complexity of foot anatomy. The purpose of this study was to develop a method for generating a parametric foot model based on Principal Component Analysis (PCA). The procedure was first applied to the first metatarsal bone (FMTB), by taking into account that the area underneath the FMTB is one of the most subjected to plantar foot ulcers in diabetic subjects [1]. PCA has already been used for the characterisation of other bones such as the adult femur [4].

Methods: MRI scans of 6 subjects, 3 healthy (HS) (mean age 32.3 ± 10.1 years, mean BMI 21 ± 1.6 kg/m^2) and 3 diabetics (DB) (mean age 65.6 ± 5 years, mean BMI 29.4 ± 6.5 kg/m^2) feet were acquired as in [3]. The grey scale images were segmented with Simpleware-ScanIP software (v.5.0) into 30 bones and the foot skin as contour of the homogenous mass of foot soft tissues. Each foot mesh was generated as in [3] and the FMTB mesh of every subject was extracted. Then PCA was applied in order to identify the main features that characterise the anatomical variations of FMTB. Before PCA was performed, the bone FEMs were aligned to eliminate spatial variations, and the same number of elements was applied to each mesh. Two software were used to achieve these tasks: NMSBuilder for mesh co-registration and MeshLab for controlling the number of elements. The elements of the meshes were reordered using k-nearest neighbour algorithm so that the nodal numbers were consistent across all FEMs. Nodal coordinates of the meshes were extracted to form a matrix **M** where each row corresponded to one individual. The mean nodal coordinates M_{mean} across the population were then calculated and subtracted from **M** to obtain M_{adjust}= **M**- M_{mean}. The covariance matrix of M_{adjust} was evaluated and an eigenvalue analysis was performed using Matlab 2012a (7.14) (an example of the workflow is reported in Figure A) [5]. The procedure was applied first to the controls and the diabetic subjects separately (considering two distinct groups including 3 subjects each), and then by considering a whole group of 6 undifferentiated subjects.

Results: The PCA analysis resulted in a set of eigenvalues and associated eigenvectors, which represented the principle variations in the different FMTB meshes. This shape change was visualised by generating hypothesised models that contains features of the principal components by applying the following equation:

$$M_{new}=M_{mean}+U_i c \sqrt{\lambda_i}$$

Where M_{new} represents the new mesh and c is the scale factor that controls the amount of variation captured by the eigenvalues and eigenvectors (λ_i, U_i) in both positive and negative directions (see Figure B).

Figure:
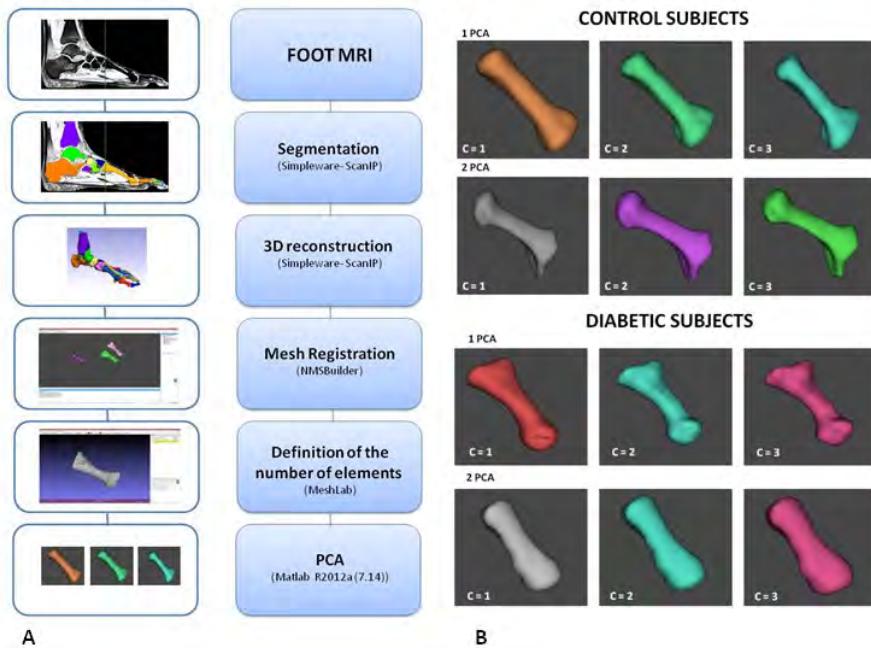
Caption: In A the workflow to run the PCA. In B the differences between the bones of the 2 groups after PCA.

Conclusion: In this study, PCA has been successfully applied to the database of 6 meshes and it has shown some preliminary results in anatomical variations within the dataset.Results showed that the most significant shape variations were located in the proximal aspects of the bones, followed by the distal ends of the bones, as shown in Figure B. When the procedure was applied to two distinct groups each containing 3 subjects, only the first two eigenvalues were significant. However, by considering a whole group of 6 undifferentiated subjects 5 eigenvalues were significant. This suggested a limited number of subjects available in the dataset. In the future, we plan to improve PCA predictions by including additional subjects into the study. Interestingly, the shape variations between healthy and diabetic patients were considerably different (see Figure B), which may provide insights into structural changes for diabetic patients in the future. Another limitation of the present study is the high computational cost considering only a single bone. However, it demonstrated that variations in FMTB morphology could be extracted using PCA. Further improvements can be made to improve computational efficiency and high performance computing resources could also be used in the future in order to apply PCA on all the foot.

References: [1] Boulton et al., Lancet 366:1719–24, 2005.

[2] Chen et al., Med Eng Phys, 32(4):324-31, 2010.

[3] Guiotto et al., J Biomech, 47(12):3064–3071, 2014.

[4] Mahfouz et al., Comput Methods Biomech Biomed Engin, 10(6):447-56, 2007.

[5] Smith et al., "A tutorial on Principle Component Analysis", 2002.

Disclosure of Interest: None Declared

Musculoskeletal

AS-0470

THE ROLE OF SARCOMERE LENGTH NON-UNIFORMITIES IN RESIDUAL FORCE ENHANCEMENT

Kaleena R. Johnston [1,*] Azim Jinha [2] Walter Herzog [2]

[1]Faculty of Kinesiology, [2]University of Calgary, Calgary, Canada

Introduction and Objectives: Residual force enhancement (RFE) is a characteristic of skeletal muscle describing the increase in isometric steady-state force following an active stretch (force-enhanced, FE), compared to the force of an isometric contraction at the final length (purely isometric, PI) [1]. It has been suggested that RFE is a result of the unstable nature of sarcomeres at lengths along the descending limb of the force-length relationship. This instability of sarcomere lengths is thought to cause long, weak sarcomeres to lengthen more than short, strong sarcomeres, when a myofibril is actively stretched. This mechanism is proposed by the Sarcomere Length Non-Uniformity Theory, and if it is the mechanism of RFE, then sarcomeres should become more non-uniform in length after an active stretch [2]. Previous research, however, has reported an inherent stability of sarcomeres following active stretching [3]. While this contradicts earlier hypotheses, it is still unclear whether sarcomere length non-uniformities play a role in the development of RFE. Therefore, the purpose of this study was to investigate the hypothesis that sarcomere length non-uniformities would increase from the PI state to the FE state.

Methods: Isolated rabbit psoas myofibrils (n = 12) were stretched passively to an average sarcomere length along the descending limb of the force length relationship [4]. Myofibrils were then activated. Five seconds after full activation, they were rapidly shortened, held for ten seconds, and then stretched back to the original length [5]. Individual sarcomere lengths and force were determined throughout the protocol and were used to identify steady state PI and FE conditions (Figure 1). Standard deviations (SDs) of the mean sarcomere lengths in each state were compared to analyze non-uniformity.

Results: Myofibril forces increased from the PI state (127 ± 44 nN) to the FE state (174 ± 52 nN), showing 39 ± 15 % RFE (p = 0.002). Mean sarcomere lengths were 2.8 ± 0.3 µm and 2.9 ± 0.3 µm for the PI and FE states, respectively. Mean sarcomere lengths in each state for each individual myofibril were compared to ensure that the force in the FE state could be compared to the force in the PI state. Mean sarcomere length SDs significantly increased from the PI state (0.7 ± 0.4 µm) to the FE state (0.9 ± 0.5 µm), (p = 0.008).

Figure:
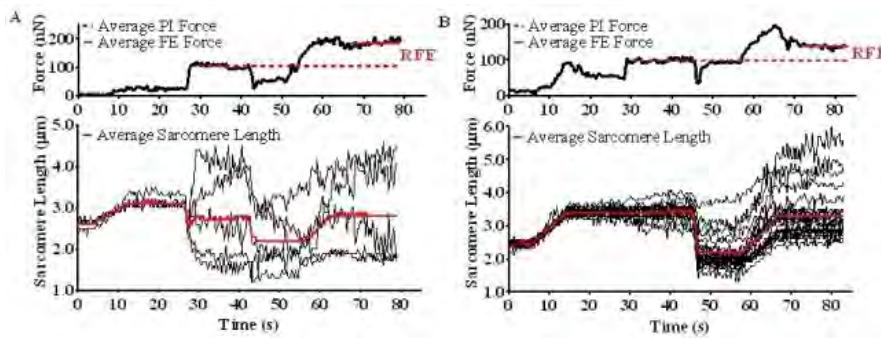
Caption: Results from two of the myofibrils indicating the force (top) and the lengths (bottom) of each individual sarcomere along the myofibril throughout each experiment. Red lines on each graph indicate average values. Myofibril A demonstrated 78 % RFE with no increase in sarcomere (n = 5) length non-uniformity (SD = 1.1 µm). Myofibril B demonstrated 40% RFE and an increase in sarcomere (n = 23) length non-uniformity from 0.2 µm to 0.8 µm.

Conclusion: While statistical analyses of the current results suggest that sarcomere length non-uniformity may play a role in the phenomenon of RFE, three of the twelve myofibrils did not show an increase in sarcomere length non-uniformity. Despite this, all of these myofibrils demonstrated RFE. Interestingly, one of these three myofibrils exhibited the greatest amount of RFE (78 %) out of all of those tested (Figure 1A). In addition, one myofibril exhibited four times more non-uniformity in the FE state (SD = 0.8 µm) compared to the PI state (SD = 0.2 µm) (Figure 1B). These results suggest that, on average, there is an increase in sarcomere length non-uniformity following active stretching of single myofibrils; however, an increase in sarcomere length non-uniformity is not essential to produce RFE following active stretching. Therefore, the development of sarcomere length non-uniformities during active muscle stretching is neither a necessary nor a sufficient condition for RFE and in order to fully understand this phenomenon, it is necessary to investigate other possible mechanisms contributing to RFE.

References: [1] Gordon, AM, et al., J. Physiol., 184: 170-192, 1966.

[2] Morgan, DL, Biophys. J., 57: 209-221, 1990.

[3] Joumaa, V, et al., Proc. R. Soc. B, 275: 1411-1419, 2008.

[3] Herzog, W, et al., Mol. Cell. Biomech., 25-31, 2010.

[4] Rassier, DE, et al., J. Biomech., 37: 1305-1312, 2004.

Disclosure of Interest: None Declared

SIMULATING SHORTEST MUSCULOTENDON PATHS ACROSS MULTIPLE BIOLOGICALLY ACCURATE WRAPPING SURFACES IN REAL TIME

Andreas Scholz [1,*]Michael Sherman [2]Ian Stavness [3]Scott Delp [4]Andrés Kecskeméthy [5]

[1]Department of Mechanics and Robotics, University of Duisburg-Essen, Duisburg, Germany, [2]Department of Bioengineering, Stanford University, Stanford, United States, [3]Department of Computer Science, University of Saskatchewan, Saskatoon, Canada, [4]Departments of Bioengineering and Mechanical Engineering, Stanford University, Stanford, United States, [5]Chair of Mechanics and Robotics, University of Duisburg-Essen, Duisburg, Germany

Introduction and Objectives: In musculoskeletal simulations, musculotendon paths are commonly modeled as locally length-minimizing strings which wrap around geometric obstacle surfaces representing bones and neighboring tissue. An accurate computation of these paths, their length and their rate of length change is essential to the correct prediction of muscle moment arms, muscle forces, and the resulting joint loads. Biological muscle typically wraps around multiple complex obstacles, yet state-of-the-art muscle wrapping methods are either limited to analytical results for a pair of simple surfaces [1], or they are computationally expensive [2]. This trade-off between accuracy and speed has limited the development of more accurate musculoskeletal models, particularly of the back and shoulder, the hip, or the hand. Here we present a method for the fast and accurate computation of a musculotendon's shortest path across an arbitrary number of general smooth wrapping surfaces, and an explicit formula for the path's exact rate of length change. We demonstrate by simulation benchmarks that the method computes high-precision solutions for path length and rate of length change, allows for wrapping over biologically accurate surfaces, and is capable of simulating muscle paths over hundreds of surfaces in real-time.

Methods: Our goal is to compute a muscle's locally shortest path between its origin point O and its insertion point I, while it wraps around a series of obstacle surfaces. Since the total path minimizes the length between O and I, it can be considered as a concatenation of length-minimizing curve segments, i.e., straight lines between the surfaces and geodesics on the surfaces. The solution approach for finding the total path consists in finding a set of geodesics on the surfaces such that all transitions between the straight lines and adjacent geodesics are collinear, i.e., the transitions have no 'kink'. The collinearity conditions at the transitions between geodesics and straight lines are used to formulate a set of nonlinear constraint equations for the shortest path. The shortest path in the neighborhood of a given configuration is computed by finding the root of the constraint equations via Newton's method using an explicit Jacobian. The Jacobian contains the partial derivatives of the path's constraints with respect to natural variations of the parameters that define each geodesic: the starting point, direction, and length. Since the constraints for each geodesic only depend on the parameters of the geodesic itself, and the parameters of the two neighboring geodesics, the Jacobian Matrix has band structure. Therefore, the computational costs of our method grow linearly with the number of wrapping surfaces which makes the method very efficient for simulating shortest wrapping paths over multiple obstacle surfaces. A muscle path's rate of length change, i.e., its contraction velocity, is an important input when computing muscle forces using Hill-type

muscle models. We have derived an explicit formula for the exact path's rate of length change to avoid nonsmooth approximations with finite differences.

Results: We demonstrate the method's ability to wrap over nonsimple, biologically accurate surfaces and its computational speed using two simulation benchmarks: (1) a force-driven simulation in which a single muscle path wraps around four (nonsimple) surfaces: a cylinder, a torus, a parametric surface patch fitted to a human ribcage, and an elliptic torus. In the literature, the geometry of the human ribcage is typically approximated by an ellipsoid (see OpenSim model in Fig.), which causes errors in muscle moment arms and muscle forces. For the shown simulation time-frame, the path length was 46.89 LU (length units) and its exact rate of length change was -3.02 LU/s; (2) we evaluated the computational costs by wrapping a single muscle path over a variable number of moving cylinders using a desktop computer with an Intel i7, 3.5GHz. For 500 cylinders, the real-time factor was 0.62 (faster than real-time) and for 1000 cylinders it was 1.34 (slower than real-time).

Figure:
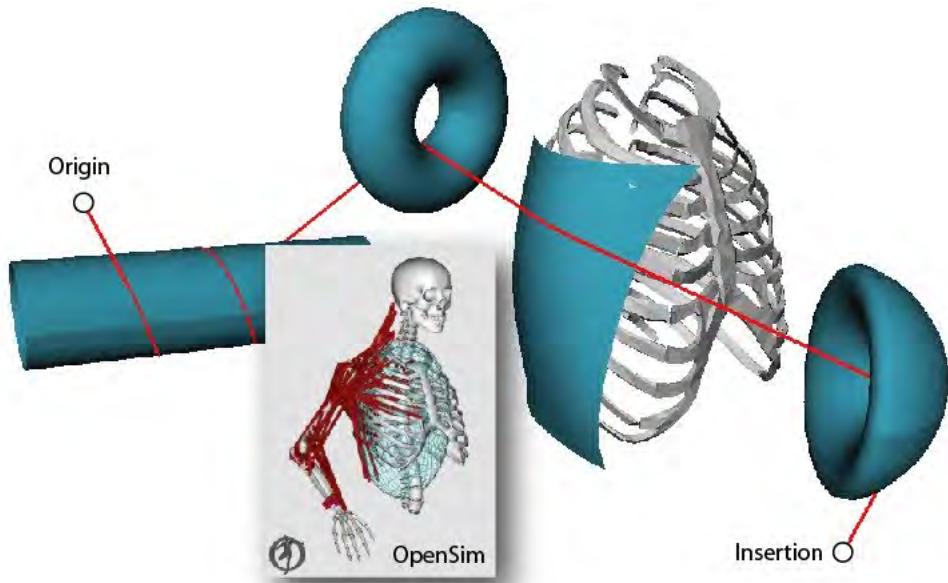
Caption: Wrapping over multiple (nonsimple) obstacles including a surface patch fitted to a human ribcage.

Conclusion: In contrast to existing methods, the presented method is both general and fast. It does not rely on special-case solutions and can handle a large number of nonsimple wrapping surfaces in real time. It computes time-continuous, geometrically smooth, and high-precision solutions for the shortest path, its length, and its rate of length change. The theoretical derivations of the method are slightly more involved compared to existing methods, yet the final methods's implementation into biomechanics software packages is straight forward. Because of its speed and its generality, we believe the method will allow biomechanists to develop more accurate yet fast musculoskeletal models.

References: [1] Garner et al., 3(1), 1-30, 2000.

[2] Marsden et al., 222(7), 1081-95, 2008.

[3] Scholz et al., 2015. (submitted)

Disclosure of Interest: None Declared

Musculoskeletal

AS-0472

A THREE-DIMENSIONAL MUSCULOSKELETAL MODEL OF THE LABRADOR RETRIEVER (CANIS FAMILIARIS) PELVIS AND HIND LIMBS

Walter Dingemanse [1,*]Ilse Jonkers [2]Lode Bosmans [2]Magdalena Müller-Gerbl [3]Jos Vander Sloten [4]Ingrid Gielen [1]

[1]Department of Medical Imaging and Small Animal Orthopaedics, Faculty of Veterinary Medicine, Ghent University, Merelbeke, [2]Human Movement Biomechanics Research Group, Faculty of Kinesiology and Rehabilitation Sciences, KU Leuven, Leuven, Belgium, [3]Institute of Anatomy, Basel University, Basel, Switzerland, [4]Biomechanics Section, Faculty of Engineering Science, KU Leuven, Leuven, Belgium

Introduction and Objectives: In veterinary medicine, canine sports medicine is one of the most recent research areas. The use of musculoskeletal computer models provides a great opportunity to further enhance our understanding of joint biomechanics and limb function [1].

As a result of the extreme variation in body types between different dog breeds, there is a need for breed-specific biomechanical research. Kinematic and kinetic gait analysis have already been applied in veterinary medicine [2,3], but current multi-body simulation models consist of limited data from mixed-breed dogs [4]. The accuracy of canine gait analysis, can greatly be improved by using breed-specific musculoskeletal models.

The objective of this study was to develop a breed-specific musculoskeletal model of the hind legs of a Labrador Retriever. To facilitate collaboration with other specialists, it was important to use readily available modelling software.

Methods: The musculoskeletal model was based on a computed tomographic (CT) scan of a healthy, adult Labrador Retriever. Bone geometry, was derived from the CT images using segmentation and three dimensional rendering (Mimics, Materialise, Leuven, Belgium).

Segment definitions were based on literature [5] and dynamical segmental parameters were determined non-invasively using CT and computer software (Abaqus, Dassault Systemes, Vélizy-Villacoublay, France).

The musculoskeletal model was based on the widely used, open-source software OpenSim [6] and included bone geometry from the last lumbar vertebra, sacrum, pelvis, femur, patella, tibia, tarsal bones, and phalanges. Left and right limb were assumed to be equal. Four different segments were defined pelvis, femur, tibia and foot. The hip joint was modeled as a spherical joint with three degrees of freedom (DOF) between the femur and the pelvis. The hip joint center (HJC) was identified by fitting a sphere to the femoral head. For the knee joint, flexion and extension was modeled by coupling rotation to translation of the tibia relative to the femoral condyles. The movement of the patella also included rotation and translation, in function of the knee angle. The ankle joint was modeled as a one DOF hinge joint between the tibia/fibula and the talus with the joint axis between the distal aspect of the medial and lateral malleolus. The tarsal bones and phalanges were assumed to be rigidly connected for simplification purposes. For each leg, 39 musculotendon units were represented. Muscle geometry was based on CT images and insertion points were checked with available literature [7] (Figure). The kinematic markers were placed on anatomical landmarks and included at least 3 markers per segment.

Results: Using the canine OpenSim model, kinematic and kinetic data was used to execute inverse kinematics and inverse dynamics, in five Labrador Retrievers, providing joint angles and moments (Figure). This model can be considered a generic model for Labrador Retrievers, a breed often studied in canine biomechanical research.

Figure:
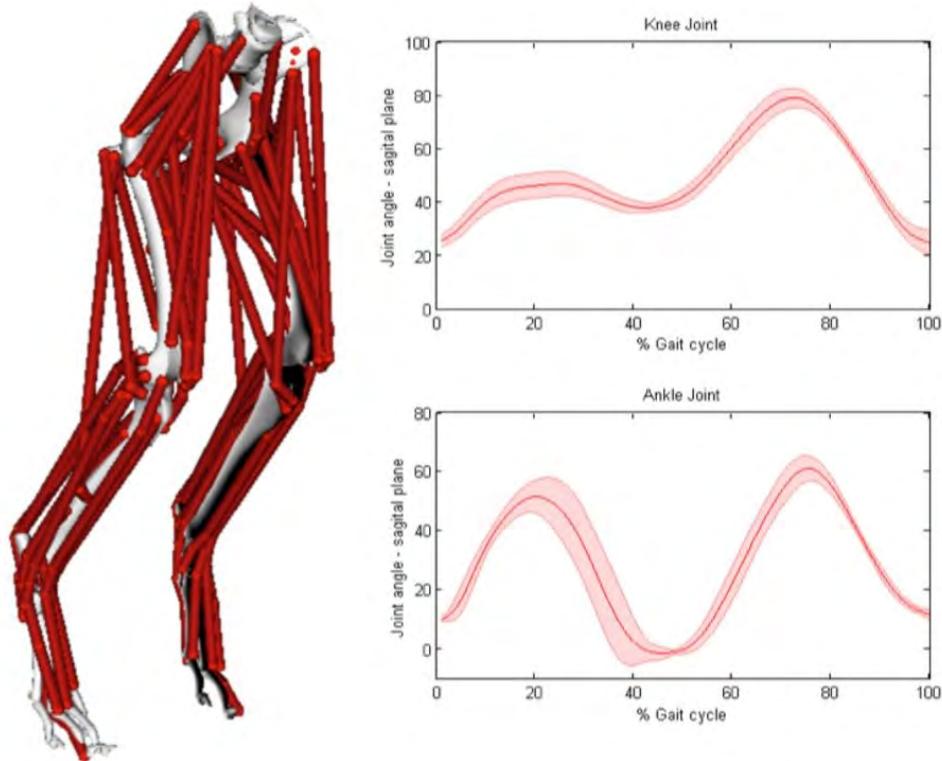
Caption: Musculoskeletal model of the hind limbs and pelvis (left) and joint angles of the knee and ankle joint (right)

Conclusion: To the author's knowledge, this is the first description of a breed-specific musculoskeletal model of the hind limbs of a dog. Although inter-subject variation will exist, the breed-specific model conformation provides a significant improvement over current multi-body simulation models. Further development of the model will include refinement of the foot-segment, and the inclusion of muscle- and tendon-specific parameters. The open-source nature of this model allows further improvements and modifications through collaboration with the whole canine biomechanical research community.

References: [1] Shahar et al,. J Biomech 37:1849-1859, 2004.

[2] Colborne et al., Am J Vet Res 66:1563-1571, 2005.

[3] Colborne et al., Am J Vet Res 72:336-344, 2011.

[4] Helms et al., Biomed Eng Online 8:36,2009.

[5] Amit et al., Vet J 182:94-99, 2009.

[6] Delp, et al., Ieee Trans. Biomed. Eng. 54:1940-1950, 2007.

[7] Shahar et al., Am. J. Vet. Res. 62:928-933, 2001.

Disclosure of Interest: None Declared

Modelling

AS-0473

BODY SEGMENT PARAMETERS AND INERTIAL PROPERTIES OF THE GERMAN SHEPHERD POLICE DOG

Yvette Jones [1][2],*Silvia Raschke [1]David Kenyon [1]Philip Riches [2]

[1]Technology Centre, British Columbia Institute of Technology, Burnaby, Canada, [2]Biomedical Engineering, University of Strathclyde, Glasgow, United Kingdom

Introduction and Objectives: In Canada, the German Shepherd (Alsatian) is the breed of choice for the majority of police forces across the country. They must maintain top physical condition to obtain success in their job and do so through regular training over the course of an average eight-year career. An injury while training or on the job will sometimes put both dog and handler out of commission and it is up to the veterinarian to get the team back on the job. But while there has been great progress in attaining knowledge of veterinary musculoskeletal disease and surgical techniques, evaluation of functional outcome from these techniques have been primarily subjective and based on the experience and observational skills of the clinician. There is little consistent data available to assist veterinarians in making clinical decisions. In fact, differences of as much as five months have been found in clinical reports quoting on the same injury[1]. For humans, biomechanical models such as the Modified Helen Hayes marker set are often used to guide rehabilitation, treatment and even surgery[2]. Anthropometry and/or mass distribution (inertial) properties are the basis of such models. Along these lines there have been numerous morphometric studies on horses and some on racing dogs however there are few that focus on the German Shepherd. Only one study provides data regarding mass distribution characteristics of the German shepherd skull, describing the principle moments of inertia and their orientation to the body and segment morphometry[3]. Therefore, the objective of this paper is to present a complete set of three-dimensional inertial properties of the German Shepherd including segment morphometrics, mass, centre of mass (COM) , inertial vectors and density of all body segments. Based on these measurements regression equations will be determined for the estimation of inertial properties in living dogs. The mass distribution characteristics obtained will be used to establish a reliable means of estimating these same properties on living animals from easily measured body parameters. The goal is to present a technique that is reasonably accurate, can be safely applied to any male German Shepherd police dog, and takes little time to acquire.

Methods: Six male German Shepherd (Alsatian) police dog cadavers (age 2 to 8yrs ; mass 36.8 +/- 1.68 kg) in good physical condition were used for the study. Each cadaver was measured and weighed, joints were placed in the midposition of the movement range and the body was frozen rigid. Joint angles were bisected in a systematic dismemberment procedure to produce 102 unit segments (17/cadaver). Each segment was weighed and segment COMs located relative to link end points using a box reference axis system (Figure 1). According to this same reference system, moments of inertia were measured about the six axes using the simple pendulum method. Finally, segment volumes were determined using the water displacement method.

Geometric models of the primary body segments have been selected to predict the principle moments of inertia. Using this method, simple morphometric measurements such as total body mass and segment length can be used in regression equations to predict the masses and moments of inertia of each segment.

Results: Morphometic data were collected for each segment (Table 1) and multiple regression equations created to predict segment mass and moments of inertia about the principle axes.

Figure:

Caption: Figure 1: Orthogonal reference box - abdominal segment

Conclusion: No previous study has provided complete data on the three-dimensional properties of the mass distribution of the German Shepherd. This paper summarizes the rationale and measurement techniques. Data from this research will be used in further study for the creation of dynamic models of canine locomotion and on the police dogs for studies on impact, training and rehabilitation.

Table:

Segment	Cranial End	Caudal End	Segment Mass/Total Mass	COM/Segment Length		Radius of Gyration/Segment Length			
				$R_{prox/cran}$	$R_{dist/caud}$	K_{cg}	K_{prox}	K_{dist}	Density
Forefoot	Carpal joint	Distal 3rd phalanx (base of claw)	0.007	0.485	0.518	0.100	0.495	0.528	0.944
Antebrachium (foreleg)	Lateral epicondyle	Carpal joint	0.014	0.394	0.608	0.120	0.412	0.619	0.983
Brachium	Glenohumeral joint	Lateral epicondyle	0.024	0.418	0.587	0.117	0.435	0.599	0.976
Hind foot	Heel	Distal 3rd phalanx (base of claw)	0.008	0.514	0.488	0.122	0.528	0.503	1.012
Crus (hind leg)	Femoral condyle	Lateral maleolus	0.015	0.366	0.636	0.110	0.382	0.646	1.011
Thigh	Greater trochanter	Femoral condyle	0.045	0.446	0.560	0.135	0.467	0.576	0.951
Head	Inion	Prosthion (nose)	0.077	0.317	0.684	0.147	0.414	0.636	0.96

									6
Neck	Atlas/axis	C7/T1	0.066	0.563	0.443	0.151	0.468	0.584	0.989
Abdomen	T13/L1	Tale base	0.241	0.467	0.535	0.171	0.544	0.518	0.971
Thorax	C7/T1	T13/L1	0.381	0.537	0.467	0.209	0.544	0.544	1.019
Tail	Tail base	Tail tip	0.008	0.313	0.689	0.212	0.477	0.618	0.984

Caption: Table 1: Summary of segment morphometry

References: [1] Canada West Veterinary Specialists. 2005.

[2] Davis et al., Human Movement Sciences 10, 575-587, 1991.

[3] Onar, V. Anatomia, Histologia, Embryologia, 28, 253-256, 1999.

Disclosure of Interest: None Declared

COMPARISON OF ESTIMATED AND MEASURED MUSCULAR ACTIVITY DURING INCLINED WALKING

Nathalie Alexander [1,*] Hermann Schwameder [1]

[1]Department of Sport Science and Kinesiology, University of Salzburg, Hallein, Austria

Introduction and Objectives: Inclined walking is associated with increased joint loading [1]. Musculoskeletal models can be used to provide information about the corresponding muscle forces causing the resulting joint loading. Direct measurement of muscle forces is generally not feasible in a non-clinical setting and in healthy populations, therefore non-invasive methods based on musculoskeletal modeling should be considered [2]. One commercially available musculoskeletal modeling system for biomechanical simulations is the AnyBody Modeling System (AnyBody, Denmark), which has been used in several different studies analyzing level walking [3,4]. Before using this model for analyzing muscle and joint forces during inclined walking, it has to be verified if the model can also be applied for this task. Therefore, the purpose of this study was to compare estimated muscle activity of the inverse dynamic musculoskeletal AnyBody model with experimentally measured EMG data during inclined walking.

Methods: Ten healthy male participants (26.5 ± 4.2 y, 1.80 ± 0.04 m, 78 ± 7 kg) were recruited and were asked to walk on a ramp (6 m x 1.2 m) with two integrated force plates (AMTI, USA, 1000 Hz) at different inclinations of -18°, -12°, -6°, 0°, 6°, 12° and 18°. Participants had to perform 3 valid trials in a constant pre-set speed of 1.1 m/s. The trial with the speed closest to the pre-set speed was used out of the 3 measured ones for further analysis. Kinematic data was captured with a 12-camera, marker based motion capture system (Vicon, UK, 250 Hz). Muscle activity of biceps femoris (BF), rectus femoris (RF), vastus lateralis (VL), tibialis anterior (TA) and gastrocnemius lateralis (GL) were recorded from the right leg using a wireless EMG system (myon AG, Switzerland, 1000 Hz).

EMG signals containing movement artefacts were excluded. In case of GL, EMG signals of all participants had to be removed for all downhill walking trials. For the other muscles a minimum of 6 participants could be analyzed per inclination. The raw EMG data were filtered using a second order Butterworth band pass filter with a frequency range of 20-300 Hz, rectified and EMG envelope curves were calculated using a fourth-order Butterworth low pass filter at 6 Hz. The processed EMG data were normalized with respect to the maximum measured EMG value for that muscle during level walking. The musculoskeletal model used in this study is a standard model (AMMR 1.6.2, MoCapModel) available in the AnyBody Modeling System (vers. 6.0). In order to compare the EMG data with the estimated muscular activity, the latter was also normalized to the maximum value during level walking. For comparison, the correlation coefficient and the mean absolute error (MAE) were calculated between the normalized EMG envelope and the estimated muscle activity [5].

Results: Both measured and estimated muscle activity of RF and VL (Figure 1) increased with increasing inclination during uphill and downhill walking compared to level walking. Muscle activity of BF and GL increased during uphill walking, being more prominent in the EMG data. During downhill walking estimated muscular activity of GL decreased and BF muscle activity remained similar. Measured and estimated muscle activity of TA during downhill walking was highest at an inclination of -18°, with the -6° and -12° condition showing similar results and was lowest during level walking. For uphill walking measured and estimated muscle activity showed minor agreement. Correlation coefficients

between estimated and measured muscular activity were in about 85% of the conditions above 0.7 and on average 0.792 (Table 1). The average MAE over all inclinations and muscle was 31%, the lowest average MAE was found for BF (20%), while the highest was found for TA (41%).

Figure:
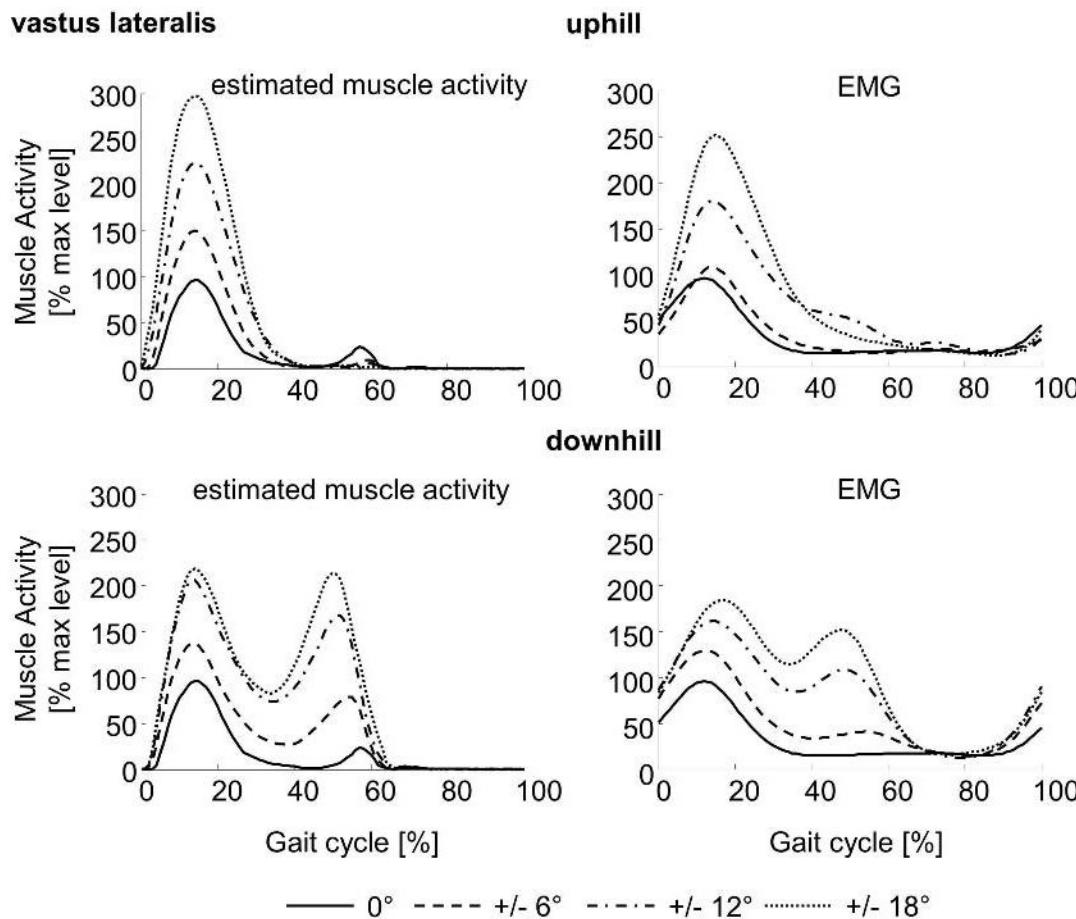
Caption: Figure 1: Estimated (left) and measured (right) muscle activity for m. vastus lateralis during uphill (top) and downhill (bottom) walking. Muscle activity is normalized to maximum activity during level walking.

Conclusion: The used model showed good agreement between the measured and estimated muscular activity for most conditions and muscles. Therefore, it might be used for further muscle force analyses in similar groups of participants.

Table:

inclination	TA	GL	VL	RF	BF	mean
-18°	0.83		0.91	0.84	0.95	0.87
-12°	0.81		0.87	0.70	0.82	0.80
-6°	0.84		0.78	0.38	0.82	0.71
0°	0.87	0.97	0.85	-0.11	0.69	0.65

6°	0.91	0.87	0.97	0.27	0.83	0.77
12°	0.77	0.92	0.96	0.71	0.90	0.85
18°	0.39	0.98	0.97	0.70	0.95	0.80
mean	0.78	0.94	0.90	0.50	0.85	0.79

Caption: Table 1: Correlation coefficients between measured and estimated muscular activity.

References: [1] Lay, A.N., et al. J Biomech, 39:1621-1628, 2006.

[2] Erdemir, A., et al. Clin Biomech, 22:131-154, 2007.

[3] Worsley, P., et al. Gait Posture, 33:268-273, 2011.

[4] Wehner, T., et al. Clin Biomech, 24:299-302, 2009.

[5] de Zee, M., et al. J Biomech, 40(6):1192-1201, 2007.

Disclosure of Interest: None Declared

SPASTIC SEMITENDINOSUS MUSCLE OF CEREBRAL PALSY PATIENTS STIMULATED ALONE CANNOT BE THE DOMINANT SOURCE OF KNEE MOVEMENT LIMITATION DESPITE BEING A PRIMARY KNEE FLEXOR

Filiz Ates [1,*]Ahu Nur Turkoglu [1]Fuat Bilgili [2]N. Ekin Akalan [3]Yener Temelli [2]Can A. Yucesoy [1]

[1]Biomedical Engineering Institute, Bogazici University, [2]Istanbul Faculty of Medicine, Department of Orthopaedics and and Traumatology, [3]Faculty of Health Science, Physiotherapy and Rehabilitation Division, Istanbul University, Istanbul, Turkey

Introduction and Objectives: Recently, by using our intra-operative experimental methods [1] in cerebral palsy (CP) patients we have shown that spastic gracilis (GRA) muscle has no abnormal mechanics representative of the patients' joint movement disorder [2]. Muscle forces as a function of knee angle showed that joint range of force production was not narrow and peak GRA forces were not available at flexed joint positions. However, the GRA is not a primary knee flexor. This suggests that the dominant source of high forces causing movement limitation at the joint may be the hamstrings. The goal was to test the hypothesis that the knee angle-muscle force characteristics of a primary knee flexor, semitendinosus (ST) muscle show abnormal mechanics representative of joint movement disorder.

Methods: Procedures in strict agreement with the guidelines of Helsinki declaration were approved by a Committee on Ethics of Human Experimentation at Istanbul University, Istanbul. Seven spastic CP patients (age 7.7±2.5 years) with no prior remedial surgery participated. The Gross Motor Functional Classification System scores (above II), popliteal angle values (PA=73.1±10.7), and clinical tests led to a decision that all patients required remedial surgery.

Knee angle-isometric ST force (KA-F_{ST}) data (n=10) were collected during muscle lengthening surgery. Under general anesthesia, after routine incisions to reach the distal ST tendon, a buckle force transducer was mounted over it. ST muscle was stimulated supramaximally using skin electrodes. F_{ST} was measured at various KA starting from 120° (maximal experimentally attainable flexion) to 0° (full knee extension). Using a least squares criterion, KA-F_{ST} data were fitted with a polynomial function.

Experimental data were used to test the hypothesis objectively based on (i) joint range of muscle force production and (ii) availability of high muscle force at low muscle length. A narrow joint range together with the availability of the peak muscle force at flexed knee positions was considered to provide an *ideal match* between the patients' impaired joint motion and the experimental KA-F_{ST} data. Spearman's Rank correlation coefficient was calculated to test if PA values are correlated with KA at which F_{STpeak} was produced (KA$_{FST peak}$) and with the ratio between F_{STpeak} and the forces measured at knee flexion (%$F_{STpeak|120°}$). Correlations were considered significant at *P*<0.05.

Results: The figure shows the KA-F_{ST} curves. F_{STpeak} (118.9N±56.8N) range between 50.9N (limb 7) and 234.2N (limb 4). None of the limbs showed an *ideal match* between the patients' impaired joint motion and the experimental KA-F_{ST} data. The operational joint range of force production for limb 9 (KA$_{FSTpeak}$=77°) was the narrowest. However, including that limb, for a majority of the limbs, spastic ST muscle operates within both ascending and descending portions of its KA-F_{ST} curve. The exceptions are limbs 8 and 10, which operate only in the ascending portion. Therefore, the operational joint range of force production of spastic ST is not narrow.

Negligible or quite low values of %$F_{GRApeak|120°}$ (0% for limbs 1-2, 5 and 10, and below 22% for limbs 3-4 and 6-8) indicate clearly that spastic ST muscle does not produce high forces at flexed knee positions. Due that, overall, the shapes of the KA-F_{ST} curves show considerable similarity with typical force-length characteristics of general healthy muscle. This is different than relatively larger values of %$F_{GRApeak|120°}$ shown previously for spastic GRA [2]. For limb 9, %$F_{STpeak|120°}$=75 is the highest however, still less than that reported for spastic GRA. No significant correlations were found between PA and $KA_{FST\ peak}$ and %$F_{ST\ peak|120°}$.

Recently published data indicate that for GRA muscle stimulated simultaneously with an antagonistic muscle, KA-F_{GRA} curves can indeed show abnormal mechanics [3]. This suggests that the role of inter-antagonistic mechanical interaction is a key determinant for joint function limitation in CP patients causing it to be the net result of simultaneous activity of different muscles, mechanics of each of which are not necessarily abnormal. This may also explain our present findings representing target muscle's activity only.

Figure:
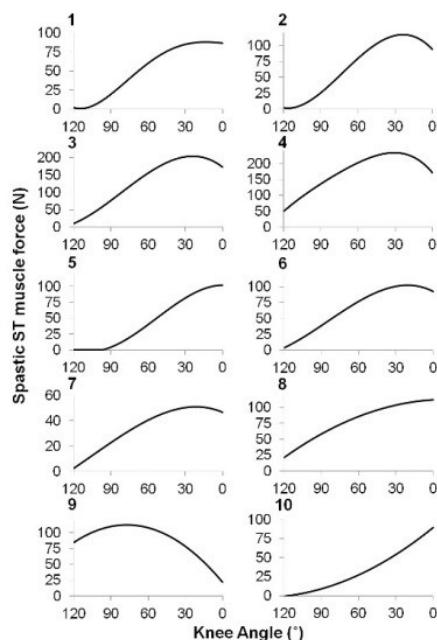
Caption: The isometric KA–FST characteristics of the spastic ST muscle.

Conclusion: Our hypothesis was rejected showing that although it is a primary knee flexor, spastic ST shows no abnormal mechanics to be the dominant source of apparent knee joint movement limitation of CP patients. Contribution of other knee flexors to such movement disorder, but particularly conditions of simultaneous activity of several muscles should be further investigated.

References: [1] Yucesoy CA, et al., J. Biomech. 43:2665-2671, 2010.

[2] Ateș F, et al., Clin Biomech, 28: 1-7, 2013.

[3] Ates, F. et al., Clin Biomech, 29: 943-949, 2014.

Disclosure of Interest: None Declared

A CRASH TEST AND CRASH TEST SIMULATION OF A NEONATE WHILST WEARING STANDARD NEONATE RESTRAINTS

Jonathan M. A. Melvin [1,*]Donal McNally [1]David Branson III [1]Don Sharkey [2]

[1]Engineering, [2]Medicine, University of Nottingham, Nottingham, United Kingdom

Introduction and Objectives:

Neonates born after less than 33 weeks gestation often require the services of specialist obstetric care units (OCU). An 11.4% annual increase in OCU admissions increased the rate of survival by 6.25% in New South Wales [1]. Because many neonatal births are unexpected, the neonate is often moved from its place of birth to an OCU. Transportation of the neonate is via an ambulance whilst inside an incubator. While most of the contents of an ambulance are designed to pass crash tests BS_EN_1789:2007 the incubator and the method of constraining the child currently do not have a corresponding test. As a result, there is an increased potential risk to the neonate in the event of an accident. In 2011/12 between 12,000 and 13,000 neonates were transported in the UK [2]. Of the 48,384 ambulances in the US over 4000 will crash each year [4] (8.27%). It is therefore reasonable to assume that an ambulance crashing whilst carrying a neonate is inevitable in the near future. Despite the risk there is no current method of simulating and evaluating crashes that include neonates, restricting the development of safer systems. The purpose of this study is to produce a madymo simulation that will enable the evaluation of injuries sustained by a neonate during a traffic collision, a result that is not possible to discover from standard test track crash investigations.

Methods:

One of the most common current constraint methods (NeoRestraint, ParAid) was tested using a dummy (LifeForm preterm manikin) on a test track, custom built at the University of Nottingham. The dummy and incubator were placed on a trolley which was accelerated to 5.8m/s at point of impact. The accelerations of the test track trolley and the dummy were recorded with an accelerometers placed on the trolley, the dummy's body and head. The crash was repeated three times and an averaged representative crash was produced from accelerometer data. The average representation data were then used within MADYMO to replicate the crash. For comparison of the MADYMO simulation to the test track crash, further accelerometers were placed in the same locations on both the crash test dummy and the MADYMO dummy. To compare the two data sets a method previously used by TNO was adapted using the following comparison criteria:

-The peak value of the curves

-The timing of the peak values

-The overall correlation of the curves

Results:

The highest peaks acceleration of the head observed in the madymo simulation was 552 m/s^2 occurring in the direction of travel. The same acceleration recorded from the track data was 459 m/s^2. The total displacement in the simulation was 0.1m whilst the track dummy moves 0.12m, thus in both cases there is a 20% difference between the track and the simulation. The head injury criterion was 163.7 with a window of 15ms.

The percentage changes observed in this investigation are greater than that previously seen in MADYMO tests but this will be reduced as the model is improved in further iterations. However, this report is still able highlight that, the scale of the accelerations exerted on the dummy are many magnitudes higher than that which a child can be expected to survive.

Figure:
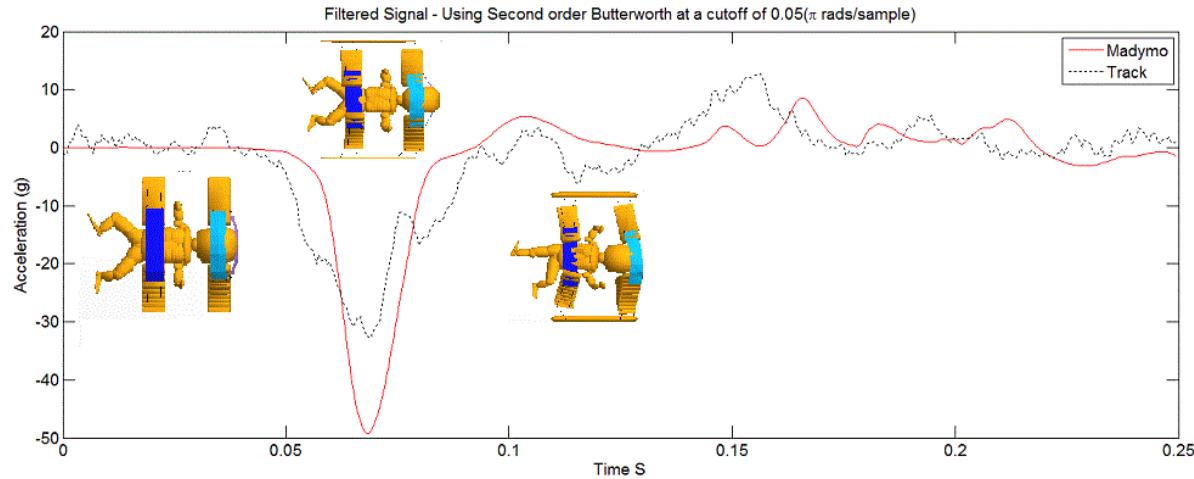
Caption: A comparison of the dummies' head accelerations (test track Vs madymo simulation). With images from the Madymo crash located at time of capture.

Conclusion: Conclusion:

A track test crash and a MADYMO simulation of a neonate being transported using a standard strapping technique were developed. The accelerations and video evidence from the track test show that the child likely sustained injury. Whilst, the use of a madymo simulation enables the investigator to provide quantitative values for the injuries sustained.

Table:

Injury	value
Combined Thoracic Index	0.76
Cumulative 3ms Maximum	581.99 (m/s**2)
HIC	163.69
Viscous Injury Response	4.58E-02 (ms)

Caption: Injuries sustained by Madymo model

References: [1] Lui et al., Pediatrics, 118: 2076-83, 2006

[2] NHS., *2013/14 NHS standard contract for neonatal critical care retrieval (Transport)*. NHS Comminssioning Board: 21, 2013

[3] Becker et al., Accis Anal prev 35: 941-8, 2003

Disclosure of Interest: None Declared

EXTERNAL KNEE MOMENTS AND LOADING DURING JOGGING POST-ARTHROSCOPIC PARTIAL MENISCECTOMY: A LONGITUDINAL STUDY

Michelle Hall [1,*] Tim Wrigley [1] Ben Metcalf [1] Flavia Cicuttini [2] Rana Hinman [1] Alasdair Dempsey [3] Peter Mills [4] David Lloyd [5] Kim Bennell [1]

[1]Centre for Health Exercise and Sports Medicine, University of Melbourne, [2]Department of Epidemiology and Preventive Medicine, Monash University, Melbourne, [3]School of Psychology and Exercise Science , Murdoch University, Perth, [4]School of Allied Health Sciences & Centre for Musculoskeletal Research,, [5]School of Rehabilitation Sciences, Griffith University, Gold Coast, Australia

Introduction and Objectives: Meniscal injury is a strong risk factor for developing medial tibiofemoral and patellofemoral osteoarthritis [1] and arthroscopic partial meniscectomy (APM) is commonly performed to treat meniscal tears. Altered external knee moments and load-related measures have been reported post-APM during walking [2,3] and potentially contribute to the increased risk of knee osteoarthrits in this population. However, there are no studies investigating external knee moments or load-related measures during jogging in these patients who are typically middle-aged. Therefore, the aim of this study was to compare the external knee moments and load-related measures during the stance phase of jogging: i) between people 3 months post-APM and healthy controls, ii) between people 2 years post-APM and healthy controls, iii) to determine if 2-year change differed between legs (ie. APM leg, non-APM leg and controls).

Methods: Seventy-eight participants (90% male; 41.1±5 yrs; BMI 27.9±3.8 kg/m^2) with medial APM were assessed 3 months following surgery (baseline) and 64 were re-assessed 2 years later (follow-up). Thirty-eight healthy controls (82% male; 40.8±7 yrs; BMI 25.1±3.4 kg/m^2) were assessed at baseline and 23 were re-assessed at follow-up. Participants jogged barefoot and performed 3 trials at a self-selected pace while kinematic data (120Hz) were collected using an 8-camera motion analysis system (Vicon) with kinetic data recorded (1080 Hz) using 3 force plates (AMTI). The first external peak knee adduction moment (KAM) and external peak knee flexion moment (KFM), were calculated using inverse dynamics (University of Western Australia model), averaged and normalised to body weight (BW) × height (HT). The first peak vertical ground reaction force (vGRF) and maximum loading rate during weight acceptance were also assessed and normalised to body weight (BW). A mixed linear model was used to evaluate differences between legs (i.e. APM leg v controls; non-APM leg v controls and APM v non-APM leg) at baseline and follow-up. Similarly, a mixed linear model was used to assess differences in change between legs and adjusted for baseline scores. For each mixed linear model, 'participant' was entered as a random effect and 'leg' as a fixed effect. Significance was set at alpha 0.05.

Results: At baseline, peak vGRF was lower in the APM leg compared to control. Peak external moments and maximum loading rate were also lower in the APM leg compared to the non-APM leg at baseline, while the peak KAM and peak vGRF was higher in the non-APM leg compared to controls (Table 1). At follow-up, the peak vGRF was higher in the APM leg compared the to the non-APM leg (Table 1). Over 2 years, the peak KFM increased in the APM leg compared to the non-APM leg (mean difference (95% CI), 1.35 (0.66 – 2.04) Nm/BW×HT, p<0.05) and the peak vGRF increased in the APM leg compared to the controls (mean difference (95% CI), 0.10 (0.00 – 0.19), BW, p<0.05).

Figure:

Table 1. Mean (SD) for the APM group and control at baseline and follow-up

	Baseline			Follow-up		
	APM group (n = 78)		Control (n =38)	APM group (n = 64)		Control (n =23)
	APM leg	Non-APM leg		APM leg	Non-APM leg	
Jogging speed (m/s)	2.46 (0.39)	2.46 (0.39)	2.48 (0.34)	2.44 (0.40)	2.44 (0.40)	2.45 (0.36)
Peak KAM (Nm/(BW×HT)%)	4.18 (2.05)[b]	4.86 (2.21)[a]	3.67 (1.46)	4.49 (2.41)	4.85 (1.92)	3.93 (1.57)
Peak KFM (Nm/(BW×HT)%)	10.91 (2.84)[b]	12.03 (2.58)	11.29 (2.17)	12.48 (2.53)	12.24 (2.37)	11.88 (2.91)
Peak vGRF (BW)	2.22 (0.26)[a]	2.28 (0.24)[a,b]	2.36 (0.18)	2.22 (0.27)[b]	2.17 (0.29)	2.19 (0.20)
Max loading rate (BW/s)	120.98 (81.95)[b]	134.02 (96.17)	103.38 (79.73)	161.42 (0.96)	157.67 (94.80)	158.51 (87.49)

[a] $p<0.05$ compared to controls; [b] $p<0.05$ compared to controls; KAM: knee adduction moment; KFM: knee flexion moment; GRF: ground reaction force; BW: body weight; HT: height

Conclusion: Individuals 3 months following APM, appear to protect the recently operated knee from excessive loads while jogging. This is evidenced by lower peak knee moments and maximum loading rate in the APM leg compared to the non-APM leg, and a reduced peak vGRF in the APM leg compared to controls. At follow-up, the peak vGRF was higher in the APM leg compared to the non-APM leg. Although the clinical implications of a higher peak vGRF are unknown, the increase in peak vGRF is of potential concern for long-term knee joint health considering the compromised function of the meniscus. Furthermore, the increase peak KFM observed in the APM leg warrants consideration given the association between a higher peak KFM and osteoarthritic changes, albeit during gait [4,5]. This study is the first to describe knee-related loads during jogging in middle-aged individuals following APM who are at risk for developing osteoarthritis. Nonetheless, our findings should be interpreted with caution as participants jogged barefoot in a laboratory environment.

References: [1] Englund M et al. Ann Rheum Dis 2005;64:1721-6

[2] Sturnieks DL et al. J Orthop Res 2008;26:1075-80.

[3] Hall M et al. Med Sci Sports Exerc 2013;45:2036-43

[4] Hall M et al. Med Sci Sports Exerc In print

[5] Chehab EF et al. Osteoarthritis Cartilage 2014;22:1833-9.

Disclosure of Interest: None Declared

HAMSTRING SHEAR MODULUS IS ALTERED PRIOR TO STRAIN INJURY: A CASE STUDY

Matthew Q Salzano [1,*]Erica A Bell [1]Jamie E Hibbert [1]Patrick M Rider [1]Zachary J Domire [1]

[1]Kinesiology, East Carolina University, Greenville, United States

Introduction and Objectives: Hamstring strains are among one of the most common sports-related muscle injuries. They are the most common injury during track and field competitions [1,2]. Over the course of a season, approximately20% ofa teamincurs hamstring injuries [3]. Though these injuries are common, the mechanism of injury is unknown. They often occur under high speed/ force movements, like sprinting [4]. It is also thought that hamstring strains, in regards to sprinting, occur as a result of the eccentric contraction during the terminal swing phase [5]. Though it is likely that it is not the force that causes the hamstring injuries to occur but it is the strain the muscles undergo during these movement that causes the damage [6]. However, the forces and strains in the muscle at the time of injury do not seem sufficient enough to cause injury [7]. It is possible that hamstring strains occur due to the accumulation of microdamage, similar to the mechanism behind stress fractures in bone. The purpose of this study is to prospectively track hamstring shear modulus over the course of a season in elite track athletes to determine if muscle material properties are altered prior to the occurrence of strain injury indicative of accumulated microdamage. We hypothesize that material properties will be locally altered prior to strain injury.

Methods: Ten elite sprinters (5 males, 5 females) are being tracked throughout the 2014-2015 track season. All subjects read and signed an informed consent form approved by University IRB. Previous injury history and leg dominance were recorded for each athlete. At this time, one athlete incurred a grade 1 strain in his right hamstring one-week post scans, allowing for a case study examination. Ultrasound lastography data was taken on 18 sites per athlete: proximal, middle, and distal portions of the biceps femoris long head (BF), semitendinosus (ST), and semimembranosus (SM) in each leg using an Aixplorer SuperSonic Imagine. Shear modulus measurements were taken with a 3 mm diameter region of interest from the middle of the scan area. Three measurements were performed at each site and the means are presented.

Results: Before scans, 3 male and 3 female athletes were found to have no history of hamstring strains. Of the remaining athletes, both females had history in both hamstrings, one male had history in his right and the other had history in his left. One of the non-injured male athletes strained his right SM one-week post-scans (S009). The athlete indicated his strain was close to the middle portion of the muscle, adjacent to the location of the middle SM measurement site. Table 1 shows his SM shear modulus measurements compared to the 3 other non-previously injured SMs. S009's distal portion was comparable to the distal portions of the 3 healthy subjects. The middle portion of S009 was ~2.5-3x higher than the middle portions of the other subjects, while the proximal region was also markedly higher. Figure 1 shows the picture of the Q-box of the mid-belly for the right BF, ST, and SM for S009 and the mid-belly of a healthy SM from a representative athlete (S007). The mid-belly of the injured SM contains more yellow and red than the other sites, indicating increased stiffness.

Figure:
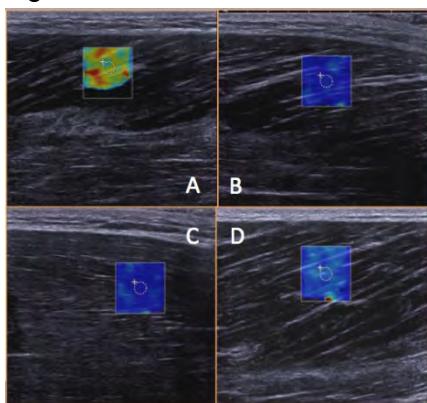
Caption: Figure 1. Elastography comparisons between the mid-bellies of S009's SM (A), BF (B), ST (C), and S007's SM. The spectrum of blue to red designates low modulus to high modulus.

Conclusion: While only one subject is used as comparison, the evidence is strong to support that muscle material properties are altered prior to strain injury. These results also support our hypothesis that material properties are altered locally between and within muscles. Increased modulus seen in the injured subject could be for a number of reasons. One possible explanation is the swelling due to edema [8]. Another possibility is that the injured site was not directly measured, and the increased modulus is a result of increased tension as a result of nearby disruptions in ECM. Further investigation will reveal if this is unique to this athlete or universal. The ability to track hamstring shear modulus over the course of a season to determine strain risk would go far in the prevention of hamstring injuries.

Table:

	S009	S004	S007	S008
Distal	16.0	15.4	13.7	16.2
Middle	51.1	17.4	21.5	17.3
Proximal	36.4	21.2	12.1	12.5

Caption: Table 1. SM shear modulus (in kPa) in the right SM for the injured subject (S009) and 3 healthy subjects

References: [1] Opar et al., *Scand J Med Sci Sports,* 24(4):254-259, 2013.

[2] Edouard et al., *Clin J Sport Med,* 24(5):409-415, 2014.

[3] Ekstrand et al., *Am J Sports Med*, 39(6):1226-1232, 2011

[4] Askling et al., *Am J Sports Med*, 35(2):197-206, 2007

[5] Schache et al., *Gait Posture,* 29(2):332-338, 2009.

[6] Lieber et al., *J Appl Physiol (1985),* 74(2):520-526, 1993.

[7] Noonan et al., *Am J Sports Med,* 22(2):257-261, 1994.

[8] Howell et al., *J Physiol,* 464:183-196, 1993

SAGITTAL PLANE KNEE KINEMATICS PREDICT NON-SAGITTAL KNEE JOINT MOMENTS IN UNPLANNED SIDESTEPPING

Mark A. Robinson [1,*] Cyril Donnelly [2] Jos Vanrenterghem [1] Todd Pataky [3]

[1]School of Sport and Exercise Sciences, Liverpool John Moores University, Liverpool, United Kingdom, [2]School of Sport Science, Exercise & Health, University of Western Australia, Perth, Australia, [3]Department of Bioengineering, Shinshu University, Nagano, Japan

Introduction and Objectives: The direct measurement of anterior cruciate ligament (ACL) strain is typically not possible *in vivo* and *in silico* estimates of ACL strain are computationally demanding with unverified reliability and validity. Instead researchers rely on surrogate measures such as net peak joint moments which reasonably predict ACL injuries [1]. In sidestepping, peak knee moments can elevate ACL strain, but it is specifically the non-sagittal moments that elevate ACL forces towards injurious thresholds [2]. Increasing knee flexion angle (KFA) is seen as an effective strategy to reduce peak knee moments and therefore ACL injury risk [3]. However, to our knowledge no-has provided an empirical rationale that increasing KFA during sidestepping can reduce peak knee joint moments. One previous study [4] attempted to relate KFA at impact to the peak knee abduction moment but found no correlation in males (r^2 = 0.21) nor females (r^2=0.1). The present study aimed to investigate the mechanical relationship between KFA and the knee joint moment vector-field throughout stance in the context of ACL injury risk in sidestepping. The hypothesis was that there was no correlation between KFA and knee joint moments during sidestepping.

Methods: The hypothesis was initially tested in a sample of 34 male Australian rules football players (dataset 1) who performed three unanticipated 45° sidesteps, whilst 3-dimensional motion and force data were recorded. An established biomechanical model with joint constraints was used to calculate the KFA at impact and estimate net knee joint moments according to the ISB X [Flex./Ext.],Y [Ab./Ad.], Z [Int./Ext. Rot.] definitions throughout stance. Canonical Correlation Analysis (CCA)[5], the vector-field equivalent of linear regression, was used to examine the correlation between the knee moment vector-field (M_{XYZ}) with the KFA at impact. Post-hoc analyses of moment couples (M_{XY}, M_{XZ}, M_{YZ}) using CCA and of individual moment components (M_X, M_Y, M_Z) using linear regression were also conducted.

We verified our results in two additional datasets. Dataset 2 was of 27 females who also performed unanticipated sidestepping according to the same protocol as dataset 1. Dataset 3 was 20 male recreational soccer players who performed anticipated sidestepping.

Results: *Dataset 1*

KFA was significantly related to the knee moment vector-field (M_{XYZ}) at around 0-10% and at ~40% stance (figure 1a). The moment couples revealed that it was the non-sagittal moment pair (M_{YZ}) that explained the result at 0-10% (figure 1d). Analysis of moment components individually failed to show the correlation at 0-10% stance (figure 1e,f,g). As the significant correlation married with the time that peak loading (~0-25% stance) and ACL injuries are believed to occur, we sought to confirm these results in two similar but independent datasets.

Dataset 2

A significant correlation between the KFA and the knee moment vector-field (M_{XYZ}) was observed within the weight acceptance phase of stance, however it occurred slightly later (~10-28% stance). Post-hoc examination showed this too was explained by the non-sagittal moment couple (M_{YZ}) only.

Dataset 3

No significant correlation between the KFA and the knee moment vector-field (M_{XYZ}) was observed in this dataset. KFA predicted non-sagittal knee joint moments in two similar but independent datasets of unanticipated sidestepping (datasets 1 & 2) but not during anticipated sidestepping (dataset 3). Examination of the knee moment vector-field revealed correlations were strong when vector combinations of moment components were considered. This suggests that the coordinate system into which the moment vector is resolved is unrelated to the moment direction of interest and may also in part, explain the weak correlations observed by McLean *et al.* [4]. These results support the recommendation to increase KFA at impact during unanticipated sidestepping as a means of reducing ACL injury risk given that high non-sagittal knee moments are known to elevate ACL strain.

Figure:
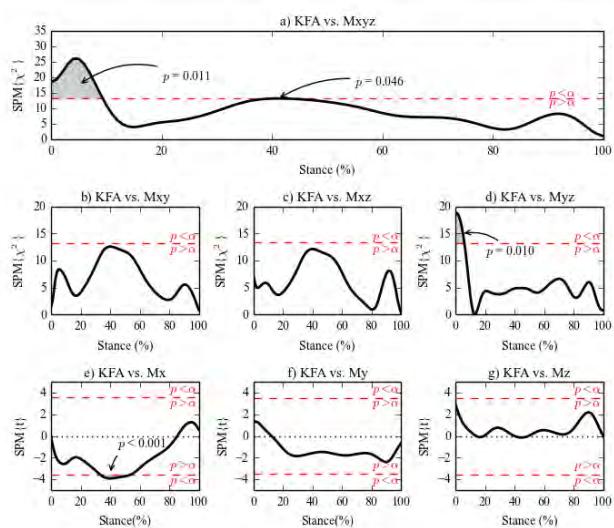
Caption: Figure 1. Relationships observed in dataset #1. (a) The relationship between knee flexion angle (KFA) and the knee moment vector-field (M_{XYZ}). (b,c,d) The relationship between KFA and moment couples. (e,f,g) The relationship between KFA and moment components.

Conclusion: KFA during unanticipated sidestepping is significantly related to non-sagittal knee moments during the weight acceptance phase of stance where ACL injuries occur. The technique recommendation to increase KFA at impact during sidestepping to reduce ACL injury risk appears sound.

References: [1] Hewett *et al.*, *Am J Sport Med* 33: 492-501, 2005.

[2] McLean *et al.*, *Clin Biom* 19: 828-838, 2004.

[3] Padua & DiStefano, *Sports Health* 1: 165-173, 2009.

[4] McLean *et al.*, *Clin Biom* 20: 863-870, 2005.

[5] Pataky *et al.*, *J Biomech* 46: 2394-2401, 2013.

Disclosure of Interest: None Declared

Injury

AS-0480

FOOT CONTACT ANGLE AND ITS VARIABILITY DURING A PROLONGED RUN IN RELATION TO INJURY HISTORY

Max Paquette [1,*]Clare Milner [2]Daniel Melcher [1]

[1]Health & Sport Sciences, University of Memphis, Memphis, [2]Physical Therapy and Rehabilitation Sciences, Drexel University, Philadelphia, United States

Introduction and Objectives: Runners most often utilize a rearfoot strike (RFS) pattern although some use non-rearfoot patterns (i.e., midfoot, forefoot, toe strike) [1]. A higher rate of running injuries have been linked with RFS runners [2] potentially due to higher loading rates of the vertical ground reaction force [3]. Strike patterns are often assessed using the sagittal plane foot contact angle (FCA; RFS have a greater positive FCA compared to non-RFS runners). Movement variability has been suggested to dissipate stresses and reduce cumulative load on musculoskeletal tissue [4]. Therefore, runners with increased movement variability may be at lower risk of developing a musculoskeletal injury. The objective of this study was to compare foot contact angle and its variability at different times during a 40 minute run between uninjured runners and runners with history of overuse running injury.

Methods: Twenty four currently uninjured runners participated in the study. Twelve runners had not suffered any injuries and twelve had suffered at least one running injury in the past year. Groups were matched for sex (8 men and 4 women), mass (72.5±12.5 vs 72.1±10.0 kg), and average weekly running mileage. Runners completed a 40 minute treadmill run at their self-selected "easy" run pace wearing their own shoes. A 9-camera motion capture system (Qualisys) was used to collect trunk, pelvis and bilateral lower extremity segments movements at the 10min, 20min, 30min and 40min time points of the run. Time of foot contact was identified using kinematic data. Visual3D software (C-Motion) was used to compute FCA measured as the absolute sagittal plane angle formed between a line joining the 5th metatarsal head and the inferior heel markers and the laboratory floor. At each time point, FCA and its standard deviation (SD) of five strides were averaged for all runners. A mixed design (2x4) repeated measures ANOVA was conducted with time as the within-subject factor and group as the between-subject factor ($p<0.05$). Due to the small sample size, Cohen's d effect sizes (ES) were also computed to compare FCA and its SD between groups and among all four time points.

Results: The ANOVA revealed no group X time interactions ($p = 0.90$) or main effects of time ($p = 0.72$) or group ($p = 0.18$) for FCA. FCA showed a moderate effect size (0.58) between groups. The injury group had greater FCA (i.e., more pronounced heel strike) than the uninjured group (Table 1). The ANOVA revealed no group X time interactions ($p = 0.64$) or main effects of time ($p = 0.87$) or group ($p = 0.93$) for FCA variability. FCA variability showed a negligible ES (0.01) between groups. FCA variability showed a small ES (0.21) for less variability at 40min compared to 10min.

Conclusion: The greater FCA in the injury group indicates that these runners utilize a more pronounced RFS pattern compared to uninjured runners. RFS runners have been associated with higher risks of injuries [2] but the current finding suggests that the degree to which runners RFS may be an important factor associated with injury risk. The lower FCA variability at the 40min time point may suggest that runners reduce their movement variability toward the end of an endurance run compared to the start. Although this difference only showed a small effect size, it suggests that more research is needed to investigate the effects of fatigue on running biomechanics variability. Overall these findings provide

further evidence of a possible association of FCA and its variability with running injuries. The implications of FCA and its variability during a run for injury risk need to be investigated in a larger group of runners and with a prospective design.

Table:

Table 1. Sagittal plane foot contact angle (degrees; mean ± SD) and its standard deviation (degrees; SD ± SD) in both groups for all four data collection times during a 40min run.

		Uninjured	Injured	Time Average
Foot Contact Angle (deg)	10 min	3.57±6.80	7.34±6.26	**5.46±6.68**
	20 min	3.52±7.02	7.12±5.34	**5.32±6.37**
	30 min	3.55±7.22	7.16±5.67	**5.36±6.61**
	40 min	4.01±6.57	7.30±6.00	**5.66±6.38**
	Group Average	**3.79±6.56**	**7.23±5.75**	
Foot Contact Angle SD (deg)	10 min	0.68±0.35	0.66±0.39	**0.70±0.33**
	20 min	0.63±0.19	0.78±0.47	**0.67±0.31**
	30 min	0.64±0.29	0.63±0.28	**0.65±0.26**
	40 min	0.69±0.31	0.61±0.0.37	**0.64±0.26**
	Group Average	**0.65±0.21**	**0.67±0.19**	

References:

[1] de Almeida, et al., Phys Ther Sport, Ahead of Press, 2014.

[2] Daoud AI, et al., Med Sci Sports Exerc, 44(7):1325-34, 2012.

[3] Milner CE, et al., Med Sci Sports Exerc, 38(2):323-8, 2006.

[4] Hamill J, et al., Clinical Biomechanics, 14: 297-308 , 1999.

Disclosure of Interest: None Declared

AS-0481

EFFECTS OF SPEED AND STEP FREQUENCY ON LOADING VARIABLES DURING RUNNING

Tomoya Ueda [1,]*Hiroaki Hobara [2]Yoshiyuki Kobayashi [3]Masaaki Mochimaru [3]Hiroshi Mizoguchi [4]Thijs A Heldoorn [2]

[1]Mechanical Engineering Faculty of Science and Technology, Tokyo University of Science, 2641, Yamazaki, Noda-shi, Chiba, [2]National Institute of Advanced Industrial Science and Technology, Aomi, Koto-ku, Tokyo, [3]National Institute of Advanced Industrial Science and Technology, Waterfront 3F, 2-3-26, Aomi, Koto-ku, Tokyo, [4]Tokyo University of Science, 2641, Yamazaki, Noda-shi, Chiba, Japan

Introduction and Objectives: Tibial stress fractures are one of the most common and potentially serious overuse running-related injuries in runners [1]. The stress fractures are thought to be related, in part, to abnormal lower extremity loading variables, such as vertical average loading rate (VALR) and vertical instantaneous loading rate (VILR). Several researchers reported that runners who developed tibial stress fractures had higher VALR and VILR than a group of age and mileage matched control subjects [2,3]. Thus, modifying these loading mechanics may decrease a runner's risk for stress fracture. Several studies have demonstrated that the loading mechanics is influenced by running speed and step frequency (f_{step}) [4,5]. However, the combined effects of running speed and f_{step} have not been systematically investigated. The purpose of this study was to ascertain which combination of running speed and f_{step} reduces the lower extremity loading variables.

Methods: Ten male individuals with no known neuromuscular disorders or lower-limb functional limitations participated in the study. The participants were instructed to run on a treadmill (PARAGON6; Johnson Health Tech) mounted on six force plates (BP400600-2000; AMTI), from which the vertical ground reaction force (vGRF) was recorded at 1000 Hz. Running speeds were four different speeds (2.6 m/s, 2.9 m/s, 3.2 m/s, 3.5 m/s). We controlled 5 f_{step}: the preferred (0%), below preferred (-10 and - 20%) and above preferred (+10 and + 20%) with a digital audio metronome to facilitate the appropriate f_{step}. The preferred step was determined by a comfortable f_{step} which subjects ran at each speed in test trial. Then, they performed running for 20 seconds at each of 5 f_{step} in a random order at each speed with 5 min rest periods in between. 10 consecutive steps from right leg were used for the analysis. A fourth order, recursive, Butterworth, low-pass filter was used to filter the force plate data at 80 Hz. Foot-ground contact was determined at a vGRF threshold of 30 N. From the measurement of vGRF, the VALR and VILR were determined. VALR was calculated as the total change in force divided by the total change in time during 20-80% of the time to impact peak [6]. VILR was peak sample to sample loading rate during this period. When no distinct impact transient was present, the same parameters were measured using the average time of impact peak as determined for other steps with an impact transient in same trial [7].

Two-way repeated measure ANOVA and Bonferroni post-hoc multiple comparison test were performed to compare the loading variables (VALR and VILR) among 5 frequencies at 4 speeds.

Results: Statistical analysis revealed that the existence of a significant main effect of running speeds and f_{step} on VALR and VILR. However, there was no significant interaction effect between running speeds and f_{step} on VALR and VILR. We found that the minimum VALR and VILR was achieved at the combination of 2.6 m/s and 0% f_{step} (Figure 1). Since loading

variables are varied by combination of running speed and f_{step}, we may be able to recommend effective training and rehabilitation strategy to reduce the risk of running-related injury for each runner.

Figure:
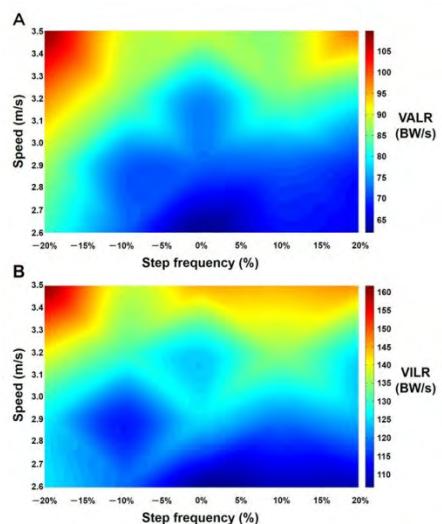
Caption: Figure 1. (A); the result of VALR among 5 frequencies at 4 running speeds. (B); the result of VILR among 5 frequencies at 4 running speeds. Blue represents the least loading variables. Red represents the highest loading variables.

Conclusion: The purpose of this study was to ascertain which combination of running speed and f_{step} reduces the lower extremity loading variables. The results of the present study suggest that a particular combination of running speed and f_{step} exhibits minimum loading variables in running. Hence, ideal combinations of running speed and f_{step} could potentially reduce the risk of running-related injury.

References: [1] Jones BH et al., Epid Rev, 24: 228-247, 2002.

[2] Davis I et al., Med Sci Sports Exer, 36: S58, 2004.

[3] Ferber R et al., Med Sci Sports Exer, 34: S5, 2002.

[4] Munro et al., J Biomech, 391987; 39: 2792-2797, 1987.

[5] Hobara H et al., Int J Sports Med, 33: 310-313, 2012.

[6] Milner CE et al., J Biomech, 38: 323-328, 2006.

[7] Lieberman DE et al., Nature, 463: 531-535, 2010.

Disclosure of Interest: None Declared

AS-0482

EFFECT OF VIRTUAL OBSTACLES NEGOTIATION ON TEMPORAL-SPATIAL GAIT IN HEALTHY YOUNG ADULTS

Mohammad Al-Amri [1,*]Omowumi Dairo [1]Robert van Deursen [1]

[1]School of Healthcare Sciences, Cardiff University, Cardiff, United Kingdom

Introduction and Objectives: Negotiating obstacles is a complex motor-control task that is described as the most common cause of falling during walking [1-2]. Successful obstacle negotiation may be compromised in individuals with gait problems [3]. Understanding how individuals negotiate obstacles while maintaining a stable and safe walking pattern is therefore important for development of interventions based on motor learning. Virtual reality can provide controlled stimuli in a meaningful, safe environment for rehabilitation and motor-control assessment [4]. This study aimed to explore how healthy individuals respond to different presentations of virtual obstacles (VOs). The expectation was that the similar changes would occur in their motor-control as seen for real-world obstacle clearance. Changes in average values of gait parameters were used as performance indicators whereas changes in variability of these parameters were used to indicate altered motor-control.

Methods: Twenty healthy subjects (Age: 25.5±3.9 years; Height: 1.71±0.07 m; Mass: 68.7±11.9 kg; Gender: 12 male & 8 female) walked on a GRAIL system (Gait Real-time Analysis Interactive Lab, Motek Medical B.V.); which consists of an instrumented dual-belt treadmill and a 12-camera Vicon tracking system. Using the self-paced mode, subjects walked under three conditions with a simple 3D endless speed-matched scene presented onto an integrated synchronised 180° screen including projection on the treadmill: 1) Free walking (WalkFR); 2) while clearing regular spaced VOs projected on the treadmill (WalkOT); 3) while clearing regular spaced VOs by controlling spheres representing the toe markers projected on the screen (WalkOS). The VOs in this study were designed in the form of a threshold across the walkway with dimensions 1.0 m x 0.2 m x 0.1 m. Each condition lasted for 3 minutes.

The average and variability (standard deviation) of 1 minute of continuous gait were calculated for: gait speed (GS), cadence (CA), stride length (SL), stride time (ST), and stance duration (SD). A repeated measures ANOVA was used to explore changes in these variables associated with the above walking conditions. The assumption was that the order of difficulty was: WalkFR, WalkOT, and WalkOS. This was tested by means of a polynomial (linear) contrast. The level of statistical significant was set at $p<0.05$.

Results: Descriptive statistics for gait parameters (GS, CA, SL, ST, and SD) are presented in Table 1. GS and CA decreased significantly whilst ST and SD increased significantly with performing the obstacle negotiation tasks. There were no significant changes for SL.

For the gait variability, the results suggest that there were significant changes for all gait variables. Polynomial contrast analysis indicated that there were significant linear differences for GS, CA, ST, and SD related to the predicted order of difficulty: WalkFR, WalkOT, and WalkOS.

Conclusion: Reported results suggest that, as hypothesised, motor-control strategies changed with demand of obstacles negotiation in young healthy subjects. Results indicate that clearing VOs projected on the screen was more difficult than while clearing VOs projected on the treadmill. It may be that differences in demand on cognition and attention can explain

why WalkOS was more difficult than WalkOT. Further studies are needed to clarify these effects and consolidate this conclusion.

Table:

	WalkFR	WalkOT	WalkOS	p-values	polynomial contrast
Average Values of Temporal-Spatial Gait Parameters					
Speed (m/s)	1.33±0.265	1.32±0.215	1.21±0.21	0.019	0.027
Cadence (step/min)	104.75±8.95	99.59±10.19	95.06±9.76	<0.001	<0.001
Stride Length (m)	1.52±0.197	1.59±0.156	1.53± 0.166	0.086	N/A (0.710)
Stride Time (s)	1.05±0.09	1.09±0.116	1.15± 0.115	<0.001	<0.001
Stance Duration (s)	0.699±0.0717	0.720±0.086	0.757±0.091	0.005	0.004
Variance Values of Temporal-Spatial Gait Parameters					
Speed (m/s)	0.13±0.01	0.15±0.016	0.157±0.022	<0.001	<0.001
Cadence (step/min)	10.19±1.07	13.54±1.869	14.36±2.9	<0.001	<0.001
Stride Length (m)	0.058±0.017	0.135±0.030	0.17±0.058	<0.001	<0.001
Stride Time (s)	0.018±0.006	0.063±0.02	0.085±0.048	<0.001	<0.001
Stance Duration (s)	0.017±0.005	0.047±0.015	0.056±0.023	<0.001	<0.001

Caption: Descriptive statistics (means and standard deviations) of gait parameters during three walking conditions: WalkFR (walking on the treadmill with 3D scene without negotiating obstacles; WalkOT (walking on the treadmill with 3D scene while clearing regular spaced VOs projected on the treadmill); and WalkOS (walking on the treadmill with 3D scene while clearing regular spaced VOs by remotely controlling spheres representing the toe markers projected on the screen). p-Values indicate the comparison between these conditions while polynomial contrast refers to the p-values of polynomial test of within-subjects contrasts.

References: [1] Galna et al, Gait & Posture. 30: 270-275, 2009.

[2] Connell and Wolf, Arch Phys Med Rehabil. 78:179-186, 1997.

[3] Kovacs, Journal of Applied Gerontology. 24:21-34, 2005.

[4] Mirelman et al, J Gerontol A Biol Sci Med Sci., 66: 234-240, 2011.

Disclosure of Interest: None Declared

Rehabilitation

AS-0483

TASK DEPENDENCE OF FRONTAL PLANE KNEE CONTROL MEASURED BY FLUENCY AND VARIABILITY DURING FIVE REHABILITATION EXERCISES.

Robert Van Deursen [1,*]Kate Button [1]Paulien Roos [1]

[1]School of Healthcare Sciences, Cardiff University, Cardiff, United Kingdom

Introduction and Objectives: Functional exercises following anterior cruciate ligament (ACL) injury are used to improve whole body motor control and local knee control. Observationally, in clinical practice this represents movement smoothness (fluency) and displacement (variability). However, alterations in knee frontal plane fluency determined in ACL studies seem to be inconsistent [1, 2]. To understand movement fluency and variability better and identify the role of knee control in the context of whole body control, five functional movements used in rehabilitation were compared in healthy participants.

Methods: Healthy participants performed four repetitions of five exercises: walking (WLK), jogging (JOG), double- and single-leg squatting (DLS & SLS), and single-leg hopping (HOP). Each task was executed at their preferred speed/distance. Quiet standing was also recorded. Motion data were collected using the VICON full body marker set. Key landmarks, COM, ipsilateral (IL; dominant/weight-bearing leg) and contralateral (CL) ankles and knees, pelvis, C7, IL and CL wrists, were used to explore whole body motor control by means of fluency and variability of each landmark whilst weight-bearing. Fluency was calculated as the inverse of the average number of times a landmark velocity in the frontal plane crossed zero (Fluency (s) = 1/frequency). Variability was defined as the standard deviation of the frontal plane movement trajectory. A repeated measures ANOVA and Bonferroni adjustment for comparisons were used to investigate COM differences between WLK and the other tasks. Subsequently, the eight other landmarks were compared to COM focussing on the weight-bearing knee.

Results: Results are reported for 29 healthy subjects (height: 1.73±0.11 m, mass: 73.5±16.4 kg, age: 28.0±6.9 years, gender: 10 female, 19 male). COM fluency and variability were significantly different between tasks ($p<0.001$). WLK COM fluency was largest; followed by HOP; SLS; JOG; DLS. Each task differed significantly from WLK ($p<0.001$). HOP COM variability was largest; followed by SLS; WLK; DLS; and JOG. Only JOG differed significantly from WLK ($p=0.004$). As expected, by comparison quiet standing COM fluency (0.01±0.003 s) and variability (0.5±0.4 mm) were substantially smaller compared to the 5 activities.

For walking all landmarks except C7 showed lower fluency compared to COM. For the other activities the pattern differed between stance leg landmarks and the rest of the body i.e. ankle fluency was lower or equal to COM whereas the knee and pelvis showed higher, equal or lower fluency depending on the task. The rest consistently showed higher fluency compared to COM.

For all activities IL ankle variability was significantly lower or equal compared to COM. All other landmarks showed significantly higher variability compared to COM (except two). Knee fluency ($p<0.01$) and variability ($p<0.001$) differed substantially between activities.

Conclusion: Whole body control was demonstrated across activities: COM variability was smallest compared to the constituent regions with higher variability, apparently compensating for each other. Fluency differed more unpredictably between activities. Knee control of the stance leg particularly seemed to adapt to task requirements. During double-leg squatting the knee was least tightly (slower, larger oscillations) and during jogging most tightly (faster, smaller oscillations) controlled. Therefore, to interpret knee fluency and variability in ACL deficiency and repair, this task-dependence needs to be considered.

Table:

Fluency (s)	WLK	JOG	DLS	SLS	HOP
COM **	0.43±0.16	0.16±0.05	0.12±0.05	0.17±0.05	0.29±0.18
Ankle IL	0.14±0.06 L	0.17±0.06	0.12±0.06	0.13±0.04 L	0.11±0.02 L
Knee IL	0.17±0.12 L	0.12±0.05 L	0.22±0.14 H	0.19±0.05	0.14±0.03 L
Pelvis	0.25±0.13 L	0.14±0.07	0.21±0.09 H	0.27±0.08 H	0.15±0.04 L
C7	0.57±0.12 H	0.25±0.04 H	0.22±0.13 H	0.38±0.13 H	0.44±0.13 H
Ankle CL	0.20±0.10 L	0.23±0.06 H	0.13±0.05	0.32±0.12 H	0.36±0.11
Knee CL	0.16±0.07 L	0.19±0.07	0.23±0.09 H	0.29±0.08 H	0.31±0.07
Wrist IL	0.40±0.14	0.27±0.03 H	0.22±0.10 H	0.37±0.15 H	0.38±0.09
Wrist CL	0.41±0.14	0.25±0.07 H	0.24±0.14 H	0.32±0.16 H	0.36±0.08
Variability (mm)					
COM **	7.0±2.7	4.5±2.4	6.3±2.6	8.8±2.7	9.1±3.7
Ankle IL	5.5±1.4 L	7.3±3.0	3.4±2.6 L	4.9±3.5 L	8.0±4.0
Knee IL	7.8±3.2	5.3±1.4 H	21.3±13.8 H	15.1±4.1 H	13.5±3.7 H

Pelvis	11.6±3.3 H	6.4±2.3 H	8.8±3.0 H	9.7±4.2	16.2±4.9 H
C7	12.1±3.0 H	8.8±2.6 H	8.9±3.2 H	24.4±11.2 H	36.9±12.5 H
Ankle CL	14.9±6.8 H	11.8±4.1 H	3.6±2.8 L	34.5±22.5 H	66.8±33.6 H
Knee CL	15.4±7.7 H	10.7±5.0 H	24.2±15.4 H	24.3±14.1 H	46.2±17.5 H
Wrist IL	24.2±13.9 H	34.8±9.7 H	20.8±14.5 H	36.6±22.1 H	86.1±34.4 H
Wrist CL	29.6±19.2 H	36.0±15.9 H	22.7±17.3 H	36.7±22.4 H	80.2±33.3 H

Caption: Fluency and variability of all landmarks used in this analysis. Differences between tasks for COM were all highly significant (**: p<0.001). Significant comparisons between landmarks and COM are indicated by coloured boxes: L= value significantly lower than COM; H= value significantly higher than COM (p<0.01).

References: [1] Button et al., Clin. Biomech. 29: 206-212, 2014

[2] Roos et al., J. of Biomech. 47: 675-680, 2014

Disclosure of Interest: None Declared

Rehabilitation

AS-0484

IS TREADMILL WALKING WITH VIRTUAL REALITY AN ACCEPTABLE AND PLAUSIBLE TRAINING MODALITY FOR STROKE SURVIVORS?

Andrew Kerr [1,*] Jennifer Dryden [2] Craig Childs [1] Madeleine Grealy [2] Andrew Murphy [1] Philip Rowe [1]

[1] Biomedical Engineering, [2] School of Psychological Sciences and health, University of Strathclyde, Glasgow, United Kingdom

Introduction and Objectives: For many stroke survivors recovering independent walking is an important objective, however, although most survivors recover some walking ability it is often insufficient to meet the challenges of community walking[1]. Treadmill walking, through forced use of the paretic side, has some evidence as an intervention but lacks transfer to community walking[2]. With the rationale of providing a more realistic, variable walking experience, the addition of virtual reality (VR) to treadmills is a recent, promising, development. This aim of this study, therefore, was to investigate the credibility and acceptability of treadmill training with VR among stroke survivors.

Methods: This was a feasibility study testing the validity of treadmill training with and without VR through comparison with overground walking. User acceptability was assessed through independent interviews. Six ambulant stroke survivors (aged 56.5±10.6years, 116±93.3months post stroke) were recruited from local stroke clubs. They attended an introductory session for baseline measurements (over ground gait biomechanics, functional mobility and cognition) and familiarisation with the treadmill VR system (MOTEKMedical, Netherlands) including wearing a harness. They then participated in two training sessions, one week apart, each session included treadmill walking without VR (TW) and treadmill walking with VR (TWVR) e.g. road and forest paths visualisations. The final session included a second measurement of gait biomechanics which provided the data for statistical comparison. Each individual was independently interviewed before and after their participation.

Results: In general minor, non-significant, differences were observed for TM, TMVR and overground walking. There was, however, a consistent, and statistically significant ($p= 0.032$) finding of greater hip flexion for TWVR, see table for details. Universally, participants found the experience acceptable and enjoyable, although "challenging".

Conclusion: This feasibility study found treadmill walking (with and without VR) to be similar enough to overground walking to justify it as a training modality for chronic stroke survivors who had already attained some independence in walking. One possible difference, greater hip flexion during treadmill walking, may be a product of harness wearing, and/or relate to the setup of the visualisations. Participants found the experience of treadmill walking acceptable. Although they preferred walking with the visualisations there were few biomechanical differences to simple treadmill walking. Further exploration of individual variability, however, should be undertaken as this may be a factor in translating gains from treadmill training to community walking. In conclusion, similarities between overground and treadmill walking (with and without VR) support its use as a training modality in stroke rehabilitation. No great advantage was evident from the use of visualisation other than participant's preference, however these findings require further testing.

Table:

Gait variable	Overground Mean (sd)	TW Mean (sd)	TWVR Mean (sd)
Preferred speed (m/s)	0.95 (0.43)	0.72 (0.47)	0.79 (0.39)
Stride length (m)	1.07 (0.39)	0.93 (0.50)	0.95 (0.39)
Step width (m)	0.08 (0.04)	0.10 (0.03)	0.09 (0.02)
Hip angle at initial contact (degrees)	23.43 (14.07)	28.86 (11.50)	31.28 (8.51)
Knee angle at initial contact (degrees)	8.83 (7.72)	13.83 (10.56)	12.39 (10.14)
Hip max flexion angle (degrees)	28.82 (14.84)	35.72 (8.68)	37.37 (7.17)

Caption: Comparison of gait variables during overground, treadmill and treadmill walking with VR

References: [1] Baer et al., Physiotherapy Research International, 6:135-144, 2001.

[2] Ada et al., International Journal of Stroke. 8, 436-444.2013.

Disclosure of Interest: None Declared

Balance

AS-0485

DEVELOPMENT OF A PERTURBATION PROTOCOL TO QUANTITY GAIT RESILIENCE USING MECHANICAL, VISUAL AND AUDITORY PERTURBATIONS: A CASE STUDY

Sanne Roeles [1,*]Georgia Tarfali [1]Frans Steenbrink [2]Craig Childs [1]Philip Rowe [1]

[1]Biomedical Engineering, University of Strathclyde, Glasgow, United Kingdom, [2]Rehabilitation products, Motekforce Link BV, Amsterdam, Netherlands

Introduction and Objectives: Falls are the leading cause of death due to injury in the elderly and therefore a major problem in our aging society. In order to prevent falls it is of great importance that clinicians are able to identify those who are at risk of falling and intervene early. However, capturing gait instability is difficult as the human body is well capable of compensating for impairments and hence it is difficult to distinguish fallers from non-fallers during steady state walking using currently available stability measures[1]. Most falls in the elderly occur during locomotion as gait resilience is compromised due to aging and therefore the ability to resist external perturbations during walking is also decreased. Measuring the response to external perturbations has been proposed to quantify dynamic stability and to identify fall-risk. However, perturbations used in these studies are unlikely to occur in everyday life and are dangerous and difficult to monitor. Little is known about the type of experimental perturbations that could be used for diagnosis of fallers . Therefore, the aim of this study is to evaluate the feasibility of a protocol that mimics perturbations encountered in daily life like, a push, a trip, a slip, sudden darkness or a loud noise

Methods: We evaluated gait resilience using spatio-temporal parameters and the margins of stability (MoS) which reflects the motion state of the center of mass (CoM) with respect to the border of the base of support[2]. One healthy young female walked in a virtual reality (VR) environment at comfortable speed on the GRAIL (instrumented dual-belt treadmill with a motion capture system; Motekforce Link BV, The Netherlands) while full body kinematics were collected. After familiarization and a two minute normal walking trial (Nrm), five perturbation types were imposed: 1) medio-lateral sway of the treadmill (Swy), mimicking a push; 2) acceleration of one treadmill belt (Acc), mimicking a slip; 3) deceleration of one treadmill belt (Dec), mimicking a trip; 4) sudden darkness in the VR environment (Viz) and 5) a loud noise (Aud). All perturbations were imposed at three different intensity levels and repeated three times. Prior to this series of perturbations one perturbation of the middle intensity was imposed as the initial perturbation affects the walking pattern more severely as compared to subsequent perturbations.

Results: In this case study, mean step length, step width, MoS in de backward direction (MoS-BW) and MoS in the lateral direction (MoS-ML) were calculated for the normal walking trial and five strides after the initial perturbation of each perturbation trial. Our subject did not fall and was well capable in completing the entire perturbation protocol. The results (see Figure 1) indicate that mechanical perturbations (i.e. Swy, Acc and Dec) are more challenging as compared to visual or auditory perturbations. In addition stability was more affected in the medio-lateral direction as compared to the anterior-posterior direction, even after anterior-posterior perturbations (i.e. Acc and Dec).

Figure:
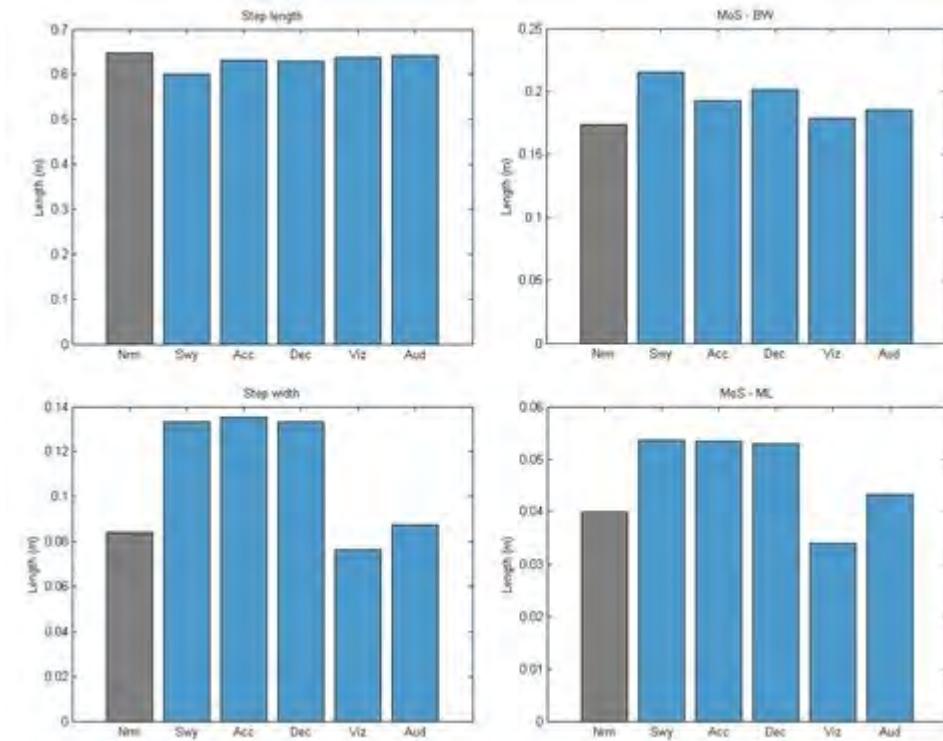
Caption: Figure 1 Mean step length (upper left corner), step width (lower left corner), MoS-BW (upper right corner) and MoS-ML (lower right corner) for the normal walking trial (gray bar) and five strides after perturbations (blue bars).

Conclusion: The aim of this study was to evaluate the feasibility of a perturbation protocol that includes various types of perturbations. The perturbations were of low intensities and our subject successfully recovered from all perturbations. The mechanical perturbations clearly affected the walking pattern suggesting that, although intensities were low, the imposed perturbations were challenging. In contrast, the visual and auditory perturbations did not seem to affect the walking pattern. Although this may expected in healthy subjects, results could be different in patients as they generally rely more on external information as compared to healthy people. Altogether, this case study shows the potential of measuring gait resilience by using a perturbation protocol. Future research should aim at finding a combination of perturbation types, perturbation intensities and stability measures that are able to accurately measure gait resilience and differentiate between fallers and non-fallers.

References: Yang F, Pai YC. (2014). Can stability really predict an impending slip-related fall among older adults? *J. Biomech.*:1-6.

2. Hof AL, Gazendam MGJ, Sinke WE. (2005). The condition for dynamic stability. *J. Biomech.* 38(1):1-8.

Rehabilitation

AS-0486

OUTCOME AND SUSTAINABILITY OF A HIPPOTHERAPY-K INTERVENTION IN ADULTS WITH CEREBRAL PALSY ON WALKING SPEED, GAIT-PARAMETERS AND MUSCULAR ACTIVATION.

Carmen Gempp [1,*] Martina Binzen [1] Julia Hayoz [1] Miriam Dousse [1] Lukas Stammler [2] Philippe Merz [2] Ruth Obrist [3] Beat Göpfert [4] [5]

[1]Physiotherapy, Health Division, Bern University of Applied Sciences, Bern, [2]BZG, Bildungszentrum Gesundheit Basel-Stadt, Münchenstein, [3]Hippotherapie Obrist, Kaiseraugst, [4]Center of Biomechanics, CMBE, University of Basel, [5]Laboratory for Movement Analysis , Children's University Hospital Basel (UKBB) Basel, Basel, Switzerland

Introduction and Objectives: Crossing a road safe on a pedestrian crossing with traffic lights needs a minimal walking speed. A common European standard is a walking speed of 1m/s (regional variation: 0.8 – 1.2m/s). Therefore the walking speed is crucial and could be used as test parameter for the outcome and sustainability of therapy interventions. Cerebral Palsy patients (CP) are often not able to accelerate there walking speed up to 1m/s, due to several reasons like, e.g. limitations in the neuromuscular control, muscular capabilities, and aerobic efficiency.

The goal of our Time-Series-Study was to analyse the outcome and sustainability of an 18 week Hippotherapy-K (Swiss Hippotherapy standard by Künzle [1]) intervention in hemiplegic adult CP-patients, with a 10m max. walking-speed-test, simulating a road crossing, and an instrumented 3D-gaitanalysis to assess changes in the gait parameters. We compared the results of the tests before and after the intervention, and 18 weeks post intervention within each subject and overall subjects. Further, during the intervention only Hippotherapy-K (once a week, 30–40min, outdoor) was done, all other physical therapies were stopped.

Methods: First, the 6 subjects with a hemiplegic CP (22-46y, 5m, 1f) were performing 3 times a 10m walking-test at max. speed with shoes [2], where the time for each trial was taken. Afterwards an instrumented 3-D gait analyses (Vicon, 12 cameras T20, 200Hz) with a synchronous surface EMG (Biovison, 2400Hz.) of the M.m. Tibialis anterior (TA), Gastroc. medialis (GM) Rectus femoris (RF) and Semitendinosus (ST) was done. 10 trials were collected using a whole body marker setup while walking barefoot at a self-selected speed. The time norm. data of the 3D-gait analyses and the norm. Wavelet-transformed EMG-data (WTEMG) were analysed within a gait-cycle for each subject for the 3 measurements: before the intervention (T1), used as a baseline, after the 18 weeks of Hippotherapy-K (T2) and 18 weeks post intervention (T3).

Results: The results show individual changes between T1, T2 and T3 for the 6 CP-subjects within the tests. The average walking speed for the 10m max. walking-speed-test overall subjects increase from T1 to T2 by 4% (SD: 14%) and decrease from T2 to T3 by 3% (SD: 16%) or is 1% faster than at T1. The time differences between the tests overall subjects are not significant.

The results of the 3D-gait analysis show that the general movement patterns of the subjects are changing too. The overall results showed a slightly faster walking speed with longer steps and smaller step width (Tab 1). The overall changes are not significant, but some changes within a single subject are.The WTEMG-intensity-pattern shows a subject-individual pattern and the changes between the 3 tests.

An example of a typical CP-intensity-pattern is seen in Fig 1. In the early swing phase a partial separation of the muscular activation (A) occurs in T2 vs. T1 and T3. Further in the loading response phase the frequency spectra shifts down (B) from T1 to T2 and T3.

Figure:
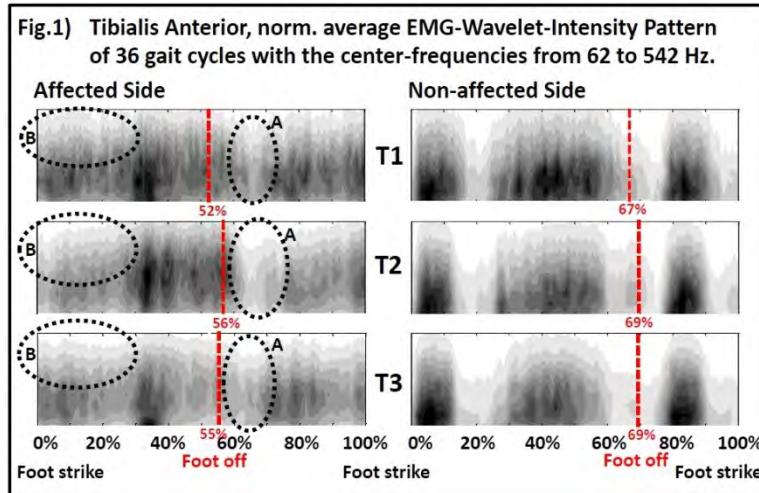
Fig.1) Tibialis Anterior, norm. average EMG-Wavelet-Intensity Pattern of 36 gait cycles with the center-frequencies from 62 to 542 Hz.

Discussion: The results of the study showed a delectable effect of the Hippotherapy-K intervention within the CP-patients for the 10m max. walking-speed-test and the overground walking. It showed, that some subject improve the neuromuscular control at a similar speed other increased the speed but walked less "controlled". A factor often mentioned in physiology exercise [3,4] to increase the speed is the core stability or core strength. Shurtleff [5] showed that Hippotherapy increased the head and trunk stability. As a result, Hippotherapy could be seen as a hidden core stability training with a high number of similar but varying 3D-movements, some may even demand fine motor skills. However strength training with varying movement patterns may support the "differential learning strategy" stated by Schöllhorn [6], and may lead to an extended movement pattern with better functional neuromuscular capabilities, e.g. functional reach [5] or higher walking speed.

Conclusion: The results of the study showed that the Hippotherapy-K intervention had an effect but just a limited sustainability. Therefore we think Hippotherapy could be a complementary strength training based on the differential learning in combination with other therapies.

Table:

Parameters	T1	T2	T3
Walking speed [m/s]	0.87	0.94	0.85
SD	*0.16*	*0.10*	*0.19*
Norm. changes [%] vs. T1		12.2	-2.8
Average stride length, affected side [mm]	957	1034	947

SD	*112*	*58*	*146*
Norm. changes [%] vs. T1		9.2	-1.3
Average stride length, non-affected side [mm]	**962**	**1032**	**954**
SD	*109*	*61*	*143*
Norm. changes [%] vs. T1		8.4	1.0
Step width [mm]	**205**	**181**	**194**
SD	*78*	*69*	*88*
Norm. changes [%] vs. T1		-11.4	-7.0

References: [1] Künzle U.: Springer, Berlin 2000

[2]Hayoz, Ruf, BSc-Thesis 2013, Physiotherapy, Health Division, Bern University of Applied Sciences, Bern, Switzerland

[3] Willardson J.M. Human Kinetics, 2014

[4] Weber, A, Bundesamt für Sport, Magglingen 2009

[5] Shurtleff TL, Arch Phys Med Rehabil. 2009 Jul;90(7):1185-95

[6] Schöllhorn WI, Medicina (Kaunas). 2010;46(6):365-73.

Rehabilitation

AS-0487

STROKE SURVIVORS ARE ABLE TO ADAPT TO A DISCRETE, UNATICIPATED DISTURBANCE DURING GAIT

Bahar Sharafi [1,*]Yasin Dhaher [1]

[1]Sensory Motor Performance Program, Rehabilitation Institute of Chicago, Chicago, United States

Introduction and Objectives: Evidence suggests that the capacity for motor adaptation is generally preserved following stroke, although the rate and magnitude of adaptation may be lower than that in unimpaired individuals. Adaptation is dependent on the development of an "internal model" of the body and the environment, driven by error feedback. A common experimental paradigm to examine the formation of internal models is through the use of a continuously applied mechanical disturbance to impose movement error. The continuous presentation of the disturbance allows the central nervous system to update the internal model so as to anticipate the requirements of movement in a perturbed environment. It remains to be seen if an internal model may be formed of a discretely applied, unanticipated disturbance. We argue that this type of disturbance simulates challenges that may be encountered during activities of daily living.

In the present study we investigated the ability to build an internal model in the presence of a discretely applied, unanticipated disturbance during gait. Given that adaptation is an essential component of motor learning, the capacity for adaptation under such conditions may be exploited to improve stroke survivors' ability to walk independently in real-world environments. We hypothesized that stroke survivors would show short-term adaptations in their response to discrete, unanticipated gait disturbances that challenge upright posture. We further explored the hypothesis that the total magnitude of adaptation is correlated with the severity of the disturbance during the first exposure.

Methods: Peak trunk inclination as a function of number of trials was well represented as an exponential decay function (Fig. 1A). Inter-subject mean of total adaptation of peak trunk inclination was 13.73 degrees ± 3.56 degrees (standard error) in the stroke group, and 17.91 degrees ± of 4.61 degrees (standard error) in the control group. Total adaptation was significantly larger than zero in both groups, with no significant differences between groups. In each group, total adaptation was linearly related to peak trunk inclination angle during the first trial (Fig. 1B) with correlation coefficients of 0.8 and 0.82 for the control and stroke groups, respectively.

Results: Peak trunk inclination as a function of number of trials was well represented as an exponential decay function (Fig. 1A). Inter-subject mean of adaptation capacity of peak trunk inclination was 13.73 degrees ± 3.56 degrees (standard error) in the stroke group, and 17.91 degrees ± of 4.61 degrees (standard error) in the control group. Adaptation capacity was significantly larger than zero in both groups, with no significant differences between groups. In each group, adaptation capacity was linearly related to peak trunk inclination angle during the first trial (Fig. 1B) with correlation coefficients of 0.8 and 0.82 for the control and stroke groups, respectively.

Figure:
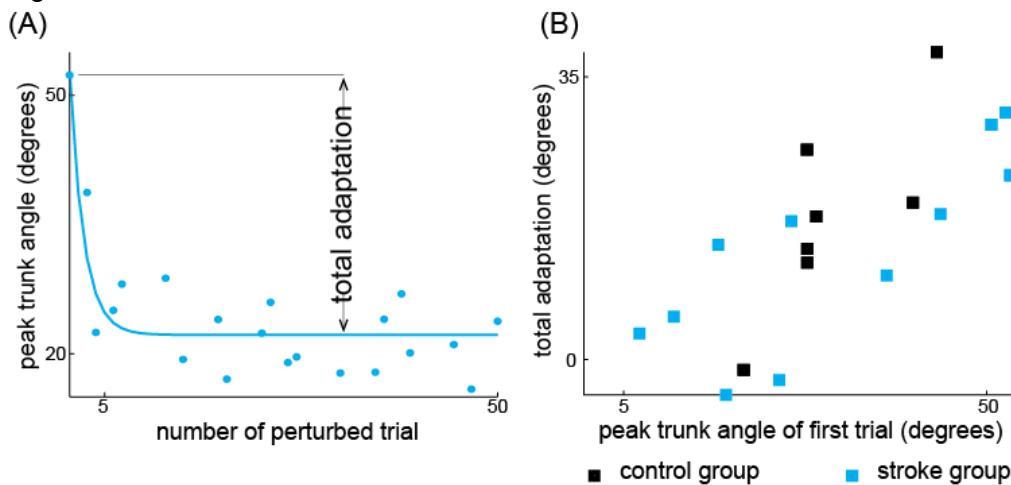
Caption: Figure 1. (A) Representative data and fit are shown for one subject. (B) Total adaptation was linearly related to the severity of deviation from upright posture following the first exposure to the disturbance.

Conclusion: Stroke survivors and healthy individuals had the ability to modulate their response to an unanticipated disturbance in order to minimize deviation from upright posture during gait. With repeated presentations of the disturbance, this deviation followed an exponential decay curve typical of error correction during a motor adaptation process. Our findings add to the evidence that motor adaptation capacity is preserved after stroke. The observed adaptation was not due to anticipatory changes in walking kinematics or lower limb EMG, as no such changes were present. Therefore we may conclude that adaptation was due to the modulation of the reactive control response. These findings suggest that the development of an internal model is possible in the presence of discontinuously applied, unanticipated, biomechanically challenging disturbances. Moreover, we found that the magnitude of adaptation was closely related to the severity of the effect of the initial disturbance, i.e., peak trunk inclination during the first trial. This finding suggests that the magnitude of disturbance may be modulated to enhance the adaptive process in individual patients.

Disclosure of Interest: None Declared

Orthopaedic Implants

AS-0488

BIOMECHANICAL ANALYSIS BETWEEN DUAL MOBILITY AND CONVENTIONAL THA DURING STAIR ASCENT AND DESCENT

Danilo S. Catelli [1,*]Sarah Reynolds [1]K.C. Geoffrey Ng [2]Mario Lamontagne [1]Paul E. Beaulé [3]

[1]School of Human Kinetics, [2]Department of Mechanical Engineering, [3]Division of Orthopaedic Surgery, University of Ottawa, Ottawa, Canada

Introduction and Objectives: THA using a dual mobility (DM) design minimizes the risks of dislocation and impingement [1-2], permitting a larger range of motion of the hip [3]. However, it is still unclear whether it would lead to an improved functional mobility.

The purpose was to compare sagittal and frontal hip angles, moments, and power of the operated limb, during stair ascent and descent, between patients who undergone THA with either a DM bearing or a standard metal-on-polyethylene (MPE) implant, along with a healthy control (CTRL) group. It was hypothesized that the improvement scores for kinematics and kinetics would be higher for the DM group than the MPE groups, during stairs ascent and descent.

Methods: Twenty-six patients (7F/19M; age: 63±5 years; BMI: 28±4 kg/m^2) and 12 CTRL participants (6F/6M; age: 61±7 years; BMI: 25±4 kg/m^2) were recruited from the orthopaedic surgeon's clinical practice. The patients for the study were randomly assigned to either a DM or MPE cementless THA. Patients agreed to undergo motion analysis prior to and nine months after their THA. The CTRL were age-, sex-, and BMI-matched with the THA group, and underwent the same motion analysis protocol.

Participants were outfitted with 45 reflective markers and performed a minimum of five trials of stair ascent and descent at a self-selected pace. Three-dimensional joint kinematics (200 Hz) of the lower limbs were captured using a ten-camera motion analysis system (Vicon, UK) and ground reaction forces were collected (1000 Hz) using two force plates (Kistler, USA) set on the first and second steps. Kinematics and kinetics data were processed in Nexus 1.8 (Vicon, UK), with a modified Plug-In-Gait model, and then exported to a custom MATLAB script (Mathworks, USA) to calculate group averages and extract relevant variables. The marker trajectories were filtered using a Woltring filter (15 MSE), and force plate data were filtered with a low-pass Butterworth filter with a cutoff of 10Hz. All trials were time-normalized based on consecutive foot strikes of the affected limb and individual averages for each participant were calculated across the five trials.

Five hip variables were included in the analysis: sagittal (θ_{sag}) and frontal (θ_{front}) angles, sagittal (M_{sag}) and frontal (M_{front}) moments, and power (P_{hip}). The percentage root mean square difference (RMSD%) was calculated between pre- and post-op conditions for each THA group, and also between each THA group and the CTRL group for pre- and post-surgery. Kinematics improvement scores (KMIS) and kinetics improvement scores (KNIS) were calculated to estimate pre- and post-op differences. They were calculated as: $KMIS = \sum_{i=1}^{n}(KM_{pre/ctrl\,i} - KM_{post/ctrl\,i})$ and $KNIS = \sum_{i=1}^{n}(KN_{pre/ctrl\,i} - KN_{post/ctrl\,i})$, where KM and KN are kinematics and kinetics RMSD% of each variable, respectively. A total improvement score was reached based on the sum of KMIS and KNIS values for each task. Wilcoxon signed-rank tests compared pre- and post-op conditions and Mann-Whitney U tests compared between groups (CI=95%).

Results: RMSD% was smaller at post/ctrl than pre/ctrl for all variables, except for the frontal angle; however, statistical significance was only observed at Θ_{front}, M_{sag}, M_{front}, and P_{hip} during stair descent. There were no differences between THA groups (DM pre/post vs MPE pre/post) (Table 1). The total scores (Fig.1) showed large improvements for MPE during ascent phase (27%) and DM during the descent phase (47%). There was no improvement to KMIS for DM during ascent and for MPE during descent; however, KNIS was improved for both THA groups in both tasks.

Figure:
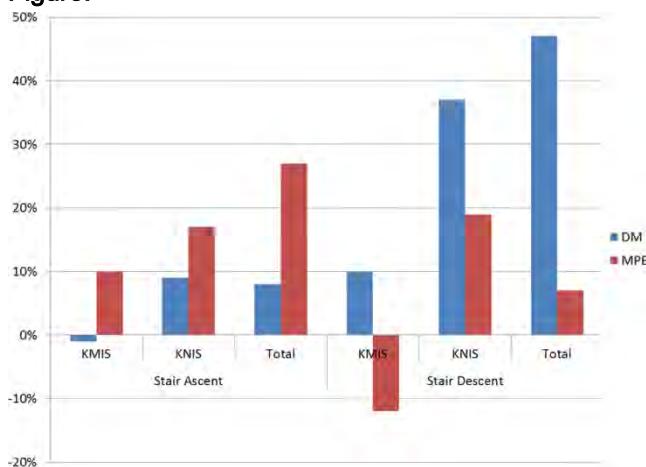
Caption: Fig.1. KMIS and KNIS for DM and MPE bearings during stair ascent and descent

Conclusion: Both the DM and MPE participants experienced post-op improvements, with kinetics variables of the THA groups closely resembling the CTRL. The only variable that increased at post-op was the Θ_{front} for MPE during descent, where patients showed larger hip abduction angles. The total improvement scores showed that the MPE group experienced greater improvements in stair ascent, while the DM bearing participants exhibited greater improvements during stair descent. The changes for KNIS among MPE and DM groups between pre-op and post-op testing also indicates that stair descent may be more sensitive to measuring outcomes for THA compared to stair ascent.

Table:

		DM pre/ctrl	DM post/ctrl	MPE pre/ctrl	MPE post/ctrl
Stair Ascent	Θ_{sag}	0.18	0.17	0.20	0.14
	Θ_{front}	0.40	0.42	0.46	0.42
	M_{sag}	0.24	0.22	0.25	0.2
	M_{front}	0.23	0.20	0.22	0.14
	P_{hip}	0.25	0.21	0.29	0.25
Stair Descent	Θ_{sag}	0.38	0.30	0.32	0.28
	Θ_{front}	0.41	0.39	0.33*	0.49*
	M_{sag}	0.42*	0.26*	0.44*	0.29*
	M_{front}	0.24*	0.14*	0.17	0.16
	P_{hip}	0.27*	0.16*	0.35*	0.32*
			* significant difference ($p<0.05$)		

Caption: Table 1. RMSD% of the sagittal and frontal kinematics and kinetics variables during stair ascent and descent

References: [1] Langlais FL et al., *Clin Orthop Relat Res,* **466**:389-95, 2008.

[2] Philippot R et al., *Orthop Traumatol Surg Res,* **95**:407-13, 2009.

[3] Guyen O et al., *Clin Orthop Relat Res,* **455**:202-8, 2007.

Orthopaedic Implants

AS-0489

REDUCED QUADRICEPS ACTIVATION AMONG TKA PATIENTS: MUSCLE INHIBITION OR EFFICIENCY?

Catriona Czyrnyj [1,*] Sarah Reynolds [2] Geoffrey Dervin [3] Mario Lamontagne [1][2]

[1]Department of Mechanical Engineering, [2]Human Movement Biomechanics Laboratory, University of Ottawa, [3]Department of Orthopedic Surgery, The Ottawa Hospital, Ottawa, Canada

Introduction and Objectives: While it is well known that total knee arthroplasty (TKA) consistently decreases pain and increases quality of life for those suffering from knee osteoarthritis (OA), it has been shown that patients do not regain joint biomechanics to fully match those of healthy individuals [1]. Studies have shown that quadriceps weakness is widely prevalent in TKA patients, along with post-surgical quadriceps inhibition, both of which have biomechanical ramifications [1]. While many biomechanical studies have been conducted on TKA patients, little is known about the effect of TKA implant designs on muscle activity (EMG) during functional tasks. This study aimed to compare operated lower-limb muscle activity of TKA patients, having either a Medial Pivot fixed-bearing (MP) or Posterior Stabilized (PS) implant, along with healthy, age-matched controls (CON) during level gait.

Methods: Unilateral TKA patients with an MP (10M/3F; age=61.9±6.4 years, BMI=29.8±4.5 kg/m^2,post-op=9±2 months) or PS (5M/1F; age=68.3±3.6 years; BMI=29.8±4.5 kg/m^2, post-op=11±3 months) implant and healthy, age-matched controls (8M/4F; age=63.4±6.2 years;BMI=26.7±4.4 kg/m^2) performed isometric contractions (MVIC), during which peak force was collected, along with five gait trials. Surface electrodes, sampling at 1000Hz with a band pass filter (Butterworth, zero lag, 4th order, 20-400 Hz cut-off frequency), were applied to the vastus lateralis (VL), vastus medialis (VM), rectus femoris (RF), biceps femoris (BF), and semimembranosus (SM) muscles of both lower limbs. Signals were high pass filtered (Butterworth, zero lag, 4th order, 20Hz cut-off frequency), rectified, bias removed, and low pass filtered (Butterworth, zero lag, 4thorder, 6Hz cut-off frequency). The MVIC signals were averaged over a 2s moving window. Gait signals were amplitude normalized by the peak MVIC and time normalized to one full gait cycle (LE). The peakLE and integrated EMG (iEMG) were then calculated. The control group limbs were averaged for each muscle. Unpaired t-tests (α=0.05) were conducted to compare MP and PS groups with the controls.

Results: Results showed that the MP group had lower total muscle activity (iEMG) throughout the gait cycle for the VM (iEMG =93.6±10V/V), VL (iEMG =96.8±8V/V), and RF muscles (iEMG =63.1±6V/V), compared to controls (VM=135.5±23V/V, VL=135.5±23V/V, RF=90.3±11V/V) (*Figure 1*). These differences reached statistical significance for the VM (p=0.05) and VL (p=0.03) muscles, and approached statistical significance for the RF (p=0.09). Analysis of the peak linear envelope revealed that the MP group also demonstrated significantly lower (p<0.05) peak muscle activity during the gait cycle for all of the quadriceps muscles (VM=0.30±0.06V/V; VL=0.33±0.05V/V; RF=0.17±0.02V/V), compared to controls (VM=0.51±0.11V/V; VL=0.55±0.09V/V; RF=0.29±0.05V/V).When this was cross examined with the MVIC data, the MP group exhibited higher peak MVIC values than the controls for the VM (p=0.21), VL (p=0.06), and RF (p=0.14) muscles for knee extension (*Table 1*). Moreover, the MP group also showed a higher peak MVIC force than the controls during the MVIC knee extension task for the quadriceps muscles; however, this did not reach statistical

significance (p=0.15). No significant differences were found for peak or integrated EMG values between the PS group and the controls.

Figure:
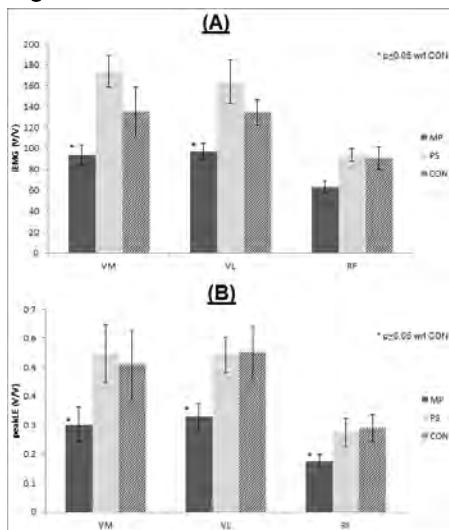
Caption: Figure 1. iEMG (A) and Peak LE EMG (B) for the vastus medialis, vastus lateralis and rectus femoris during gait

Conclusion: The lower levels of quadriceps activity in the operated limb of the MP group were initially interpreted as quadriceps weakness or inhibition during gait, similar to what has previously been reported by Mizner et al. (2005). However, when compared with the peak MVIC and peak knee extension force produced during MVIC, the MP group generated higher knee extension forces and higher peak MVIC than the control and PS groups. The MP group's lower levels of quadriceps activity during gait, combined with higher peak force for knee extension, indicated that the MP group was more efficient in performing the walking task than the PS group. Preliminary observations of pre-operative data indicate similar levels for peak MVIC knee extension forces between the MP group and the healthy controls. This quasi-normal, pre-operative quadriceps strength could be the reason for better functional outcomes post-surgery, as reported by Mizner et al. [2]. Further research is needed to investigate the relationship between muscle activation and joint kinetics for comparisons variations between PS and MP implants and controls.

Table:

Group	MVIC (mV)			MVIC Force (N/kg)
	VM	VL	RF	
MP	0.187±0.1	0.223±0.1	0.162±0.1	0.452±0.2
PS	0.092±0.03	0.165±0.07	0.119±0.06	0.282±0.1
CON	0.130±0.1	0.139±0.07	0.110±0.06	0.331±0.1

Caption: Table 1. EMG values and normalized force output during MVIC for knee extension

References: [1] Mizner and Snyder-Mackler. J. Orth. Res., 23: 1083-1090,2005.

[2] Mizner et al., J. Rheumatology, 32(8):1533-1539,2005.

Disclosure of Interest: None Declared

Orthopaedic Implants

AS-0490

PARAMETRIC ANALYSIS OF GLENOID IMPLANT DESIGN

Diogo M. Geraldes [1,*] Ulrich Hansen [1] Andrew Amis [1]

[1]Mechanical Engineering, Imperial College London, London, United Kingdom

Introduction and Objectives: Common post-operative problems in shoulder arthroplasty such as glenoid loosening and joint instability can be reduced by improvements in glenoid design, shape, material choice and fixation method [1]. Innovation in shoulder replacement is usually carried out by introducing incremental changes to existing implants, possibly overlooking other successful design combinations [2]. An automated framework for parametric analysis of different implant configurations was developed in order to efficiently sift through potential implant designs and identify the best-performing ones.

Methods: 4 different reference geometries representing the current 'gold standard' implant fixation types were generated in *SolidWorks*. Parametric variations (10 per geometry type, approximately) were automatically generated with a design table in order to assess the influence peg/keel size and position, base plate thickness or material in implant stress performance and fixation (Table 1).

The different implants were aligned and implanted with repeatability using *Rhino*. The glenoid-bone models were meshed in *Abaqus*, and boundary conditions and loading applied via a custom-made *Python* script. Finally, another *MATLAB* script integrated and automated the different steps, extracted and analysed the results. This study compared the influence of fixation type (keel vs. 2-pegged vs. 3-pegged vs. 3-pegged with central anchor peg) on glenoid components with bearing surface thickness of 3, 4, 5 or 6 mm and varying fixation feature dimensions (Table 1). A total of 40 different glenoid geometries were assigned UHMWPE (E = 1 GPa, υ = 0.46) or VITA E PE (E = 800 MPa, υ = 0.43) material properties and the bone-implant surface was tied. Fixed boundary conditions were applied at the distal surface of the cube and a contact force of 1000 N was applied as a distributed load. Four different loading scenarios were considered: a physiologically common central loading distribution and three edge-loading conditions (posterior, superior and inferior). Rocking-horse motion produced by edge loading is believed to be the most common mechanism of fixation failure in misaligned glenoid implants [3]. Two different bone qualities were looked at: healthy trabecular bone (E = 300 MPa, υ = 0.3) and rheumatoid bone (E = 30 MPa, υ = 0.3).

Results: A total of 640 models were analysed and compared over 24 hours. The data produced was filtered in order to assess how the different implant geometries ranked in bone volume preservation, implant deformation under central loading (see insert in top of Figure 1) and fixation instability due to edge loading (see insert in bottom of Figure 1) under edge loading. The influence of design parameters in the mechanical environment of the implant could be assessed. In this particular example, the normalised implant deformation under central loading (Figure 1, top) and the fixation instability (Figure 1, bottom) could be evaluated for all the different geometries simultaneously. 2-pegged geometries (2Peg) consistently produced higher deformations under central loading than the other configurations (Figure 1, top) due to lack of bone support at the centre. Thicker glenoids were shown to be less stable under all three edge loading (Figure 1,

bottom). This is thought to be due to an increase of stiffness of the whole implant, transmitting more of the displacements under edge loading to the opposite end.

Figure:
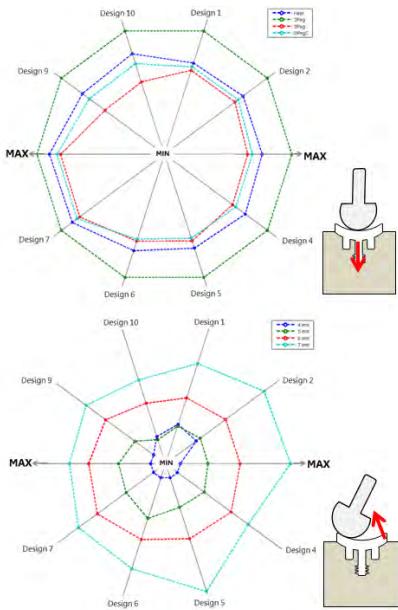
Caption: The influence of fixation type in the normalised implant deformation under central loading (Figure 1, top) and implant thickness in fixation instability (Figure 1, bottom) could be evaluated for all the different geometries simultaneously.

Conclusion: The developed method allows for simple, direct, rapid and repeatable comparison of different design features, material choices or fixation methods by analysing how they influence the mechanical environment of the bone surrounding the implant. Such a tool can provide invaluable insight in implant design optimisation by screening through multiple potential design modifications at an early design evaluation stage and identifying the best performing combinations. Future work will introduce physiological bone geometries and loading, a wider variety of reference geometries and fixation features, and look at bone/interface strength and osteointegration predictions.

Table:

Legend	Fixation Type	Nr. Fixation Features	Fixation Width (mm)	Fixation Length (mm)	Base plate thickness (mm)	Material Types	Central Peg
1	Keel	1	3, 4, 5, 6	15, 17.5, 20	4, 5, 6, 7	UHMWPE, VITAE PE	No
2	2Peg	2	7, 8, 9	7, 10, 13	4, 5, 6, 7	UHMWPE, VITAE PE	No
3	3Peg	3	4, 4.5	5, 6, 7	4, 5, 6, 7	UHMWPE, VITAE PE	Yes
4	3PegC	3	4, 5, 6	5, 7, 9, 11	4, 5, 6, 7	UHMWPE, VITAE PE	Yes

Caption: The different parametric variations analysed in this study.

References: [1] Fox et al., J Shoulder Elbow Surg, 2009. **18**(6): p. 859-63.

[2] Armstrong et al., JBJS Reviews, 2013. **1**(2): p. e2-e2.

[3] Anglin et al., J Shoulder Elbow Surg, 2000. **9**(4): p. 323-31.

Disclosure of Interest: None Declared

AS-0491

PREDICTING IMPLANT PERFORMANCE IN DISTAL FEMORAL FRACTURES: SENSITIVITY TO RESTRAINT CONDITIONS AT THE HIP

Alisdair Macleod [1,*] Hamish Simpson [2] Pankaj Pankaj [1]

[1]School of Engineering, [2]Department of Orthopaedic Surgery, University of Edinburgh, Edinburgh, United Kingdom

Introduction and Objectives: It is widely accepted that muscle contributions are key to modelling the physiological behaviour of the femur [1,2], nevertheless predictions of plate fatigue strength and the influence of screw position are made using in vitro models which neglect them [3,4]. Choosing appropriate restraint conditions to analyse a bone in isolation from the body, however, remains problematic. Speirs et al. [5] previously examined the influence of different boundary conditions on the strain environment in an intact femur; however, many studies use hinges or bi-condylar restraint and these were not considered. The influence that different restraint conditions have on predictions such as plate failure has not been examined.

The aim of the study was to examine the influence that the restraint conditions at the hip have on the prediction of distal femoral plate fixation failure.

Methods: Three-dimensional finite element models were developed and analysed using Abaqus 6.10. The femur geometry was obtained from CT data using imaging software (Living Human Digital Library). The plate was a Synthes® LISS DF. Material properties were simplified to homogeneous isotropic and were assumed to be linear elastic.

Initially, a range of hip restraint conditions commonly used in in vitro testing were examined (Fig. 1a-d). These included: clamped, pinned and hinged restraints. Three additional models were created including muscle forces acquired from Dostal et al. [6] and Sverdlova et al. [2] (Fig. 1e-g). These models were intended to be more physiological and also included healing callus within the fracture region. Hip restraint conditions in these models were selected to represent those frequently used computationally. Finally, a novel spring-based hip restraint condition was developed and evaluated.

Results: Changing the irestraint conditions at the hip dramatically influenced predictions of femoral head displacement, plate stress and joint reactions at the hip and knee. Even in the presence of physiological muscle forces and fracture callus the results are similar.

Considering an intact femur, the spring-based hip restraint produced reaction forces at the knee and hip joints that match measurements by Bergmann et al. [7] closely. Predictions of vertical and horizontal displacement at the femoral head of 0.5mm and 3.2mm respectively are very similar other recent studies [8,9].

An implanted femur with a fracture gap was found to be even more sensitive to different restraint conditions at the hip substantially altering the location and magnitude of peak stress within the plate.

Figure:
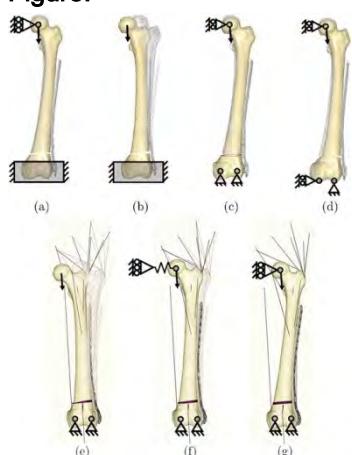
Caption: Distal femoral fracture models using different restraint conditions.

Conclusion: While we do not present the solution to the choice of boundary condition, we have shown the dramatic influence that the choice of restraint can have. The alteration in the plate stresses for different hip restraints show that predictions from in vitro tests must be treated with caution.

References: [1] A. T. M. Phillips, Med. Eng. Phys., vol. 31, no. 6, pp. 673–680, 2009.

[2] N. S. Sverdlova et al., J. Biomech., vol. 43, no. 3, pp. 387–396, 2010.

[3] H. A. Demos et al., J. Arthroplasty, vol. 27, no. 5, pp. 783–788, 2012.

[4] J. D. Granata et al., Orthopedics, vol. 35, no. 8, pp. E1210–E1213, 2012.

[5] A. D. Speirs et al., J. Biomech., vol. 40, no. 10, pp. 2318–2323, 2007.

[6] W. F. Dostal et al., J. Biomech., vol. 14, no. 11, pp. 803–812, 1981.

[7] G. Bergmann et al., J. Biomech., vol. 34, no. 7, pp. 859–871, 2001.

[8] P. Helwig et al., Comput Methods Biomech Biomed Engin, vol. 16, no. 6, pp. 669–677, 2013.

[9] K. Polgar, et al., Proc. Inst. Mech. Eng. Part H J. Eng. Med., vol. 217, no. 3, pp. 173–189, 2003.

Disclosure of Interest: None Declared

Orthopaedic Implants

AS-0492

VARIATIONS IN MORPHOLOGY OF THE ARTICULAR SURFACES OF THE ANKLE EFFECT ITS KINEMATICS AND LOAD-TRANSFER CHARACTERISTICS

Sorin Siegler [1,*] Ramya Namani [1] Claudio Belvedere [2] Jason Toy [1] Wagdi Mankarios [1] Alberto Leardini [2]

[1] Mechanical Engineering and Mechanics, Drexel University, Philadelphia, United States, [2] Laboratorio di Analisi del Movimento e Valutazione Funzionale , Istituto Ortopedico Rizzoli / Rizzoli Orthopaedic Institute, Bologna, Italy

Introduction and Objectives: Total Ankle Replacement (TAR) surgery has become a common surgical procedure for treating severe Osteoarthritis of the ankle. As TAR matures and becomes a standard of care, it is recognized that a key to its success is its ability to reproduce the natural motion of the healthy ankle. Unlike the hip or the knee, current TARs still suffer from high and premature failure rates. A key reason is believed to be their non-anatomical surface geometry design, which may produce incorrect and unnatural motion and load-transfer characteristics leading to early failure. Current TARs have articular surfaces that are either cylindrical or truncated cone surfaces following the Inman truncated cone concept postulated more than 60 years ago [1]. A recent study by the principal author demonstrated, using an image-based morphological study, that the Inman cone concept is incorrect. It indicates that each of the articular surfaces of the ankle can best be approximated by a saddle-shaped, skewed truncated cone with its apex directed laterally [2]. The goal of this study is to compare the effect of different articular surface morphology on the resulting kinematics and load-transfer characteristics through the ankle for various loading conditions and to test the validity of the hypothesis that correct surface morphology produces normal kinematics and natural load-transfer characteristics.

Methods: The study was conducted on seven cadaver ankle specimens and on three-dimensional models produced from MRI and CT scans of these specimens. Image processing software (Analyze Direct™) was used to obtain 3D renderings of the articulating bones and the regions of insertion of the surrounding ligaments. The 3D bone models were then introduced into engineering design software packages (Creo™, Geomagic™ and AutoCad™) to produce a set of three custom-fit virtual articular surfaces for each specimen: cylindrical; truncated cone with apex oriented medially according to Inman's postulate; and skewed saddle-shaped truncated cone with apex oriented laterally based on our earlier findings (Figure 1). For the simulation-based study, each of the seven 3D models, were evaluated using a dynamic simulation software (ADAMS™). The modelling and simulation details were described in earlier publications [3]. Each model was tested with the native articular surfaces and with each of the three virtual articular surfaces. Simulations were conducted with the tibia fixed and a loading/unloading moment applied to the calcaneus in the three planes of motion (dorsiflexion/plantarflexion, inversion/eversion and axial rotation). From the simulation, the following results were calculated: relative motion between the bones, distance maps describing the relative surface-to-surface distance changes and ligament forces and deformations. For the experimental validation study, the virtual TAR implants were exported to a 3D printing software and 3D physical models of each implant was produced using 3D printing. The intact cadaver was tested first in a specially design loading and measuring system [4] in which external moments were applied across the ankle and the resulting motion was measured. Each of the three implants were then surgically introduced one at a time and the test was repeated. From the results, the bone to bone motion and surface-to-surface motion were calculated.

Results: The range of motion and kinematic coupling obtained both numerically through the simulation and experimentally from the cadavers showed that an implant with surface morphology corresponding to a saddle-shaped, skewed truncated cone with apex oriented laterally produces closer to intact joint kinematics, load transfer, and ligament strain and stress then TARs with either cylindrical surfaces or those representing a symmetric truncated cone with apex oriented medially as postulated by Inman.

Figure:

Inman's cone   Natural   Saddle-shape skewed cone
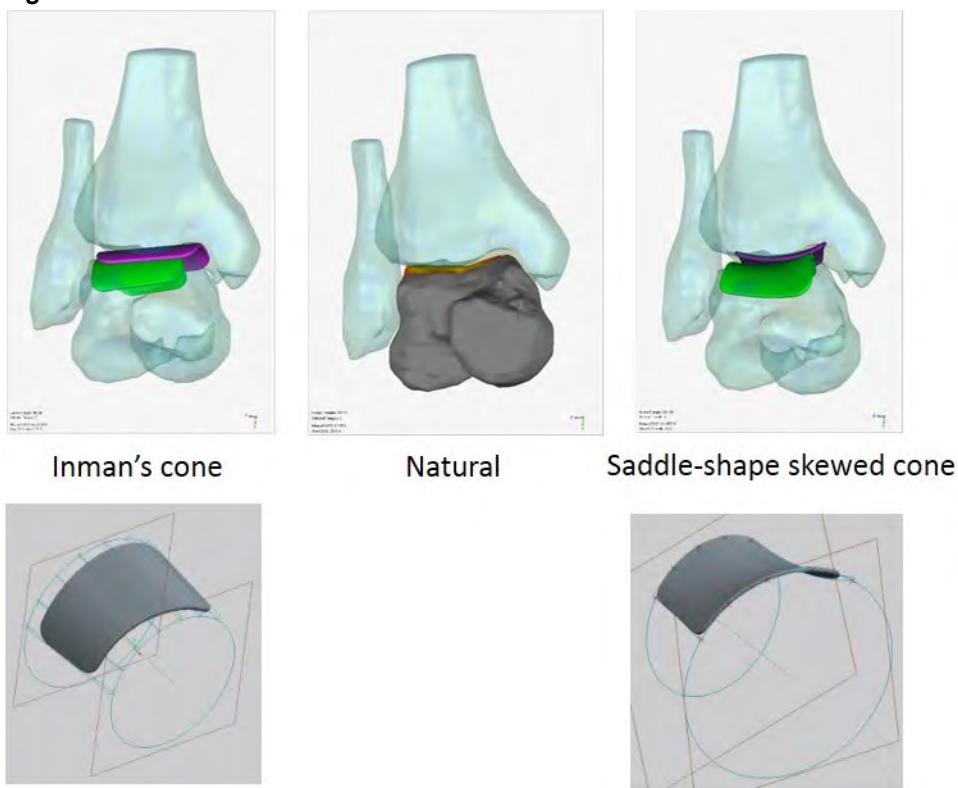
Caption: 3D models of the ankle joint for one specimen under 3 conditions: natural – center, Inman's cone – left, and saddle-shaped skewed cone – right.

Conclusion: A TAR designed with articular surfaces represented by saddle-shaped skewed truncated cone with apex oriented laterally is expected to produce closer to normal kinematic and load-transfer behavior than currently existing TARs ultimately leading to less complication and smaller failure rates than those currently available. Experiments on specimens and correspondingly designed prototypes for the artificial surfaces are planned for further validation evidence.

References: [1] Inman, V.T., The Joints of the Ankle, Williams&Wilkins, 1976.

[2] Siegler, S., et al., JCB, 29:1-6, 2014.

[3] Imhauser, C., et al., J. Biomech., 41:1341-1349, 2008.

[4] Siegler, S., et al., J. Biomech., 38:567-578, 2005.

Disclosure of Interest: None Declared

AS-0493

EFFECT OF DIFFERENT TKA TIBIAL INSERT POSTERIOR STABILIZED DESIGNS ON KNEE BIOMECHANICS: A FINITE ELEMENT STUDY

Silvia Pianigiani [1,*]Raquel Alario Bernabé [2]Héctor Robledo Yague [2]Walter Pascale [1]Bernardo Innocenti [2]

[1]IRCCS, Istituto Ortopedico Galeazzi, Milano, Italy, [2]BEAMS Department, Université Libre de Bruxelles, Bruxelles, Belgium

Introduction and Objectives: Belonging to the TKA surgery, the Posterior-Stabilized prostheses (PS) have been widely used during the last three decades reporting generally excellent results in long-term studies. Nevertheless, when the patient has non-stable knee envelope, he may require larger degree of restriction in order to manage knee instability. The Semi-Constrained version of the PS prosthesis is then introduced as revision implant by means of enlarging the size of the post, so as to be more restrictive. However, there is a lack of confidence from surgeons in this last version based on the intuitive fear that its larger post could lead to a premature failure of the post-cam mechanism of the prosthesis. Thus, the post-cam engagement of both designs has been studied under two daily activities, walking and squatting, by means of a finite element analysis (FEA). Kinematics and contact pressures have been evaluated in order to analyze the efforts supported by the prosthesis.

Methods: For the two analyzed solutions, the same femoral component has been used. A standard gait cycle and the downward movement of a squatting activity up to 120° were simulated for both situations. The tibiofemoral kinetics and kinematics have been investigated comparing the contact area between components, the internal-external rotation, the position and the magnitude of the contact forces and the Von Misses stresses on the polyethylene. Special attention to the post-cam engagement mechanism behaviour has been paid.

Results: The results obtained have shown a change on the kinematics especially along anterior-posterior direction as well as an increase of contact forces on the post of the semi-constrained design. Generally, due to the increased cross-section of the semi-constrained tibial insert, larger contact forces and pressures are experienced by lateral and medial sides of the post in the semi-constrained version compared to those in the conventional one, where no contact forces can be observed. This effect is more pronounced for the squat that for the walking task. The qualitative stress distribution is shown in Figure 1.
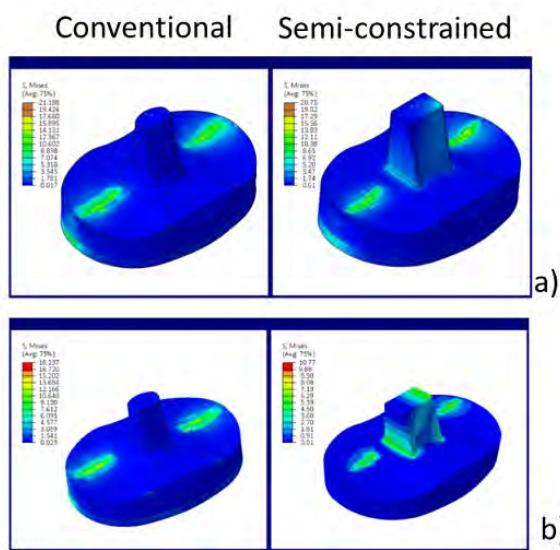
Figure:

Figure 1: a) Qualitative stress distribution for the maximum flexion reached for the low demanding task; b) qualitative stress distribution for the maximum flexion reached for the high demanding task

Conclusion: By means of this study it has been shown that the modification of the geometry of the post varies the way in which the femoral component contacts the tibial insert of a PS TKA. The results show that the enlargement of the post in the medio-lateral direction leads to the modification of the center of the total force especially along the anterior-posterior direction. Generally, the main differences in outputs for the conventional and the semi-constrained designs can be associated to the difference in shapes of the post mechanism for the two designs resulting in a higher restriction of movement for the semi-constrained design that generates also a bending moment that is exerted on the post when the rotation between both components tries to take place. Even if there are some limitations of this study, for example the soft tissues are not included in the model, results are in good agreement with the literature. Less demanding motor tasks, such as gait, have shown not achieving main differences in the outputs. However, deviation in contact outputs, especially in the post, is more evident during high demanding tasks such as squat. The reported alterations could induce earlier wear of the revision design compared to the conventional one.

The authors have nothing to disclose.

Disclosure of Interest: None Declared

Feet and Footwear

AS-0494

PATIENT SPECIFIC LEG-FOOT MODEL FOR INDIVIDUALLY DESIGNED INSOLES

Maxime LLARI [1,*]Yves GODIO-RABOUTET [1]Jean-Paul WEBER [2]Bruno VIE [2]Yves JAMMES [2]Lionel THOLLON [1]Michel BEHR [1]

[1]LBA UMR_T 24, Aix Marseille Université, IFSTTAR, [2]Ecole de Podologie de Marseille, MARSEILLE, France

Introduction and Objectives: Whether in the field of orthopedics, sports or military applications, custom orthotics is a major economic and social challenge, and prevalence of podiatric disorders is extremely common [1, 2].

Individually designed orthosis could provide a more effective treatment in case of foot disorders (metatarsalgies, diabetes, etc) or to improve performance for sport applications [3]. To reach this objective, the development of an easy-to-use technical platform which allows characterizing patient specific foot geometry and mechanical interactions is required.

This paper presents an innovative methodology that could be used by podiatrists for the design of optimized orthotics: simplified geometry data acquisition, customized a Finite element (FE) model, mechanical validation against barometric footprint.

Methods: An experimental campaign on 8 volunteers was conducted to acquire the geometry and pressure data, using a 3D optic scanner (Artec 3D) and a Novel® Emed-n50 platform. X-ray images in frontal and sagittal planes, using lead beads as markers on 10 anatomical references, were also performed for further geometrical validation (figure 1).

A finite element leg-foot model was reconstructed using Mimics® V12.1 software (MATERIALISE) from CT scans of a human male volunteer close to the 50th percentile. The model was built in order to integrate all anatomical components which have a contribution in the foot mechanical behavior for the plantar supports. All foot joints were modeled with 6 DOF elements, based on joint limits detailed in [4] to improve the overall foot kinematics. Material properties for soft tissues and bones were determined from previously published cadaver studies [5]. Muscle activations of the triceps surae and the long flexor muscles of hallux and toes were implemented to simulate the force applied on the foot during balanced standing [6]. The foot FE model was scaled to the geometry of each volunteer by kriging and then compared to X-ray data. Plantar supports were simulated for each personalized FE model with the RADIOSS® code (Altair Engineering). Computed pressures were compared to experimental barometric data. The mechanical properties of the joints and the forces applied to the muscles were then slightly tuned by optimization to obtain the closest footprint.

Results: We were able to simulate a foot print very similar to volunteers' recordings by this coupling of a simple krigging procedure a tuning of muscle tension and joints stiffness.

Figure:

Caption: Illustration of the data acquisition procedure

Conclusion: The next step of the study is to use an optimization algorithm to determine the shape and materials of the orthosis in accordance with the best footprint to prevent any particular pathology.

This innovative methodology based on using a 3D optic scanner could easily be deployed (office podiatry, sports shops...). This could lead to develop automatic technical platforms able to collect and analyse both geometric and barometric data in order to manufacture specific shoe soles.

References: [1] White and al., Age Ageing, 18(4):276-8, 1989.

[2] Ebrahim and al., Br Med J, 283(6297):949-50, 1981.

[3] Crabtree and al., Robot Cim-Int Manuf, 25:972–979, 2009.

[4] Nester and al., J Biomech, 40:1927–1937, 2007.

[5] Arnoux and al., Traffic Inj Prev, 6 (3):288–297, 2005.

[6] Gefen, J Biomech, 35:629:637, 2002.

Disclosure of Interest: None Declared

AS-0495

SPATIAL FREQUENCY CONTENT OF DIABETIC AND NON-DIABETIC PLANTAR PRESSURE AND SHEAR PROFILES

Visar Berki [1,*]Brian Davis [1]

[1]Biomedical Engineering, The University of Akron, Akron, Ohio, United States

Introduction and Objectives: The measurement of plantar pressure and shear profiles (PPSPs) is increasingly being applied to the problem of skin tissue breakdown and ulceration in diabetic patients. This study assessed the issue of sensor resolution of a custom built plantar pressure and shear measuring system and simulated the effect of increasing the transducer area (from 1.59 mm^2 up to 7.95 mm^2). Discrete Fourier Transform techniques were used to determine the spatial frequencies of PPSPs. Our objectives were to determine (i) the spatial frequency content of diabetic and non-diabetic PPSPs, and (ii) the effects of increasing the transducer sizes.

Methods: Pressure and shear stress data were collected on 28 human subjects: 16 control patients (9M, 7F; Age: 47.6 ± 5.8 years; Weight: 824 N) and 12 neuropathic, diabetic patients (7M, 5F, Age: 59.5 ± 12 years, Weight: 961 N). Each subject walked across a custom built shear and pressure system aligned in the center of a 3 m. x 0.6 m. platform. Four steps were recorded for each subject at a sampling rate of 50 Hz. Every step consisted of multiple 2-D arrays for pressure, medial-lateral shear, and anterior-posterior shear data, representing each sampled timeframe. All timeframes of a step were combined to produce unique and complete PPSPs for every step taken. A linear interpolation method of values at neighboring grid points was used to simulate the effect of increasing transducer size on PPSPs. Three transducer sizes were simulated: 1.59 mm^2, 3.18 mm^2, 7.95 mm^2. A two-dimensional Discrete Fourier Transform was performed on each data set, for each of the three transducer sizes. To quantify the difference between transducer sizes, a comparison was made using the maximum pressure and shear stress data over the entire foot-platform contact surface. The results were tested for significance using a general linear model ANOVA, including the factors of (i) group (diabetic vs. non-diabetic), and (ii) transducer size (three levels).

Results: Peak pressure data ($p = 0.002$) and peak anterior-posterior shear stress data ($p = 0.001$) showed significant difference between diabetic and non-diabetic subjects. There was no significant difference between subject groups for peak medial-lateral shear stress data ($p = 0.077$). Transducer size did not result in significant differences for the three conditions that were tested.

Figure:

Peak Pressure, ML-Shear, AP-Shear
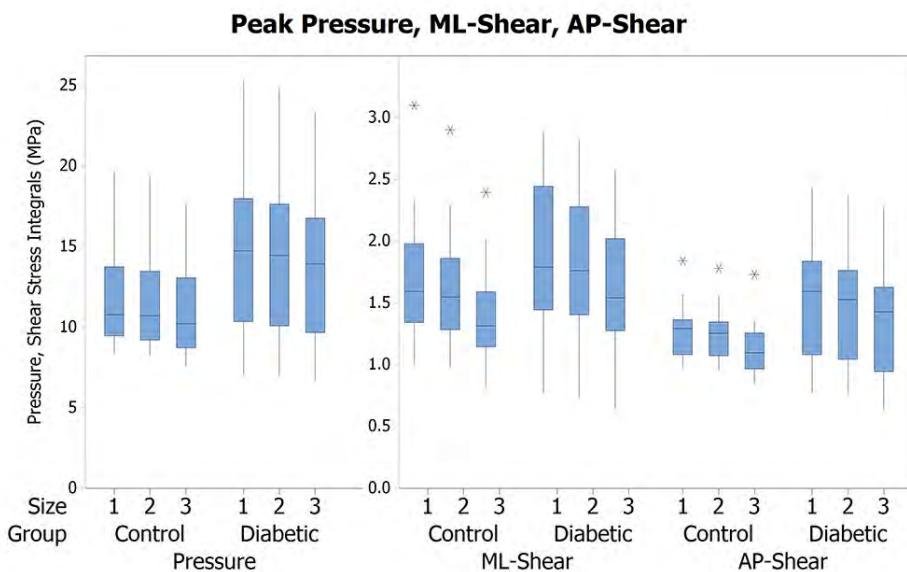
Caption: Figure 1: General linear model ANOVA, showing peaks for (i) pressure, (ii) medial-lateral shear stress, and (iii) anterior-posterior shear stress, as related to the two factors (i) diabetic vs. non-diabetic, and (ii) transducer size (smallest to largest).

Conclusion: This study showed that diabetic patients have higher spatial frequency content for both pressure and anterior-posterior shear stresses. The latter has never been shown before. These novel findings suggest that the interaction between foot and the supporting surface exhibits higher positive and negative gradients in diabetic patients compared with control subjects. While there were no significant differences when comparing sensor sizes, this is likely due to the fact that sensors that are less than 8 mm^2 can fully capture the spatial frequencies in both pressure and shear data.

Disclosure of Interest: None Declared

AS-0496

CHALLENGING FOOT ALIGNMENTS CAN INCREASE INTRINSIC FOOT MUSCLE ACTIVITY

Mahdi Pourdanial [1,*]Wen-Ming Chen [1]Rezaul Begg [2]Peter Vee Sin Lee [1]

[1]Depatment of Mechanical Engineering, University of Melbourne, [2]College of Sport and Exercise Science & Institute of Sport, Exercise and Active Living (ISEAL), Victoria University, Melbourne, Australia

Introduction and Objectives: The alignment of the human foot is a key factor in its functionality. In the pronated foot axes of mid-tarsal joints become parallel that makes the foot more compliant [1]. Extrinsic foot muscles increase their activities to compensate this reduction in the passive support of the foot arch [2]. The novel foot core system suggests that intrinsic foot muscles (IFM) provide the extrinsic foot muscles with a stable base of support to perform efficiently [3]. Balancing [4] and load bearing [5] tasks are known to affect IFM activity; however there is a lack of specific studies on the stabilizing role of the IFM. Studying frontal plane motion of the foot and its interaction with IFM may help us better understand this specific role of IFM. We hypothesize that eversion of the foot will increase the IFM activity.

Methods: Twelve healthy male subjects [Average (SD) age of 29.6 (3.8)yr, height of 175.3 (4.7)cm and body mass index of 22.5 (3.6)] performed single leg balanced stance trials. To remove the effect of balance on IFM activity, subjects held onto a tripod to maintain posture balance. We designed a platform to precisely control the frontal plane alignment of the foot for 5 specific angles (-14, -7, 0, 7 and 14 degrees; Inversion to Eversion). Each angle was tested for 10 seconds and repeated twice in a randomized order.

Surface electromyography (EMG) electrodes recorded activities of four IFM (Abductor halluces (ABH), flexor halluces brevis (FHB), abductor digiti minimi brevis (ABDM), flexor digiti minimi brevis (FDMB)). EMG signals were filtered (4th order Butterworth, band pass 5 and 30 Hz) and Root-Mean-Square (RMS) value calculated for each trial. The value was then normalized to the maximum RMS recorded over a 1 s epoch for each muscle across all loading trials [5].

Optotrak motion analysis system monitored three-dimensional foot deformations based on a multi-segment foot model (Figure) [6]. The medial longitudinal arch (MLA) height was defined as the distance of the navicular marker from the plate [5]. The MLA angle was calculated based on markers of posterior and medial calcaneus and the first metatarsal head [6] (Figure).

Results: An analysis of variance (ANOVA) showed a significant effect of frontal plane angle on The EMG activities [ABH: f=7.50, p<.001, FHB: f=10.78, p<.001, ABDM: f=3.11, p=.018]. The Tukey post hoc test yielded that the mean activity of the ABH and FHB were significantly higher in full eversion of the plate compared to the neutral posture (ABH: +72%, p=.019, FHB: +62%, p=.004). All four muscles showed higher activity as the foot moved from inverted and neutral to everted position (Table). Pearson correlation coefficients were computed to assess the inter-muscular IFM activity relationship. There was strong positive correlation between ABH and FHB(r=0.43,p<.001), FHB and ABDM(r=0.46,p<.001) and ABDM and FBDM(r=0.63,p=.07).

MLA height increased with increasing foot eversion. Mean MLA height was 51.5 mm for neutral position and the difference of means was -5.7mm (p=.001) and +6.6mm (p<.001) for 14 degrees inversion and eversion, respectively. MLA angle

decreased as the plate changed from Inversion (175.1 deg., p<.001) to Neutral (166.9 deg., comparison reference) and Eversion (157.3 deg., p<.001).

Discussion

All IFM displayed higher muscle activation in the everted foot. This increased activity was significant in medial IFM (ABH and FHB). The main reason might be associated with higher demand for stabilization of the foot, especially in the joints of the first ray, where medial extrinsic muscles also have their main insertions. IFM activity, however, reduced in the inverted foot due to a stiffer MLA and more stable foot due to mid-tarsal joint locking [1]. Although surface EMG is a reliable tool to measure activation of ABH, the main limitation of the study was the crosstalk for some IFM. However, high inter-muscular correlations in IFM activities observed during single leg stance using Intra-muscular EMG [4] suggests synergistic activation of the IFM, as we observed, in stabilizing foot structures.

Figure:
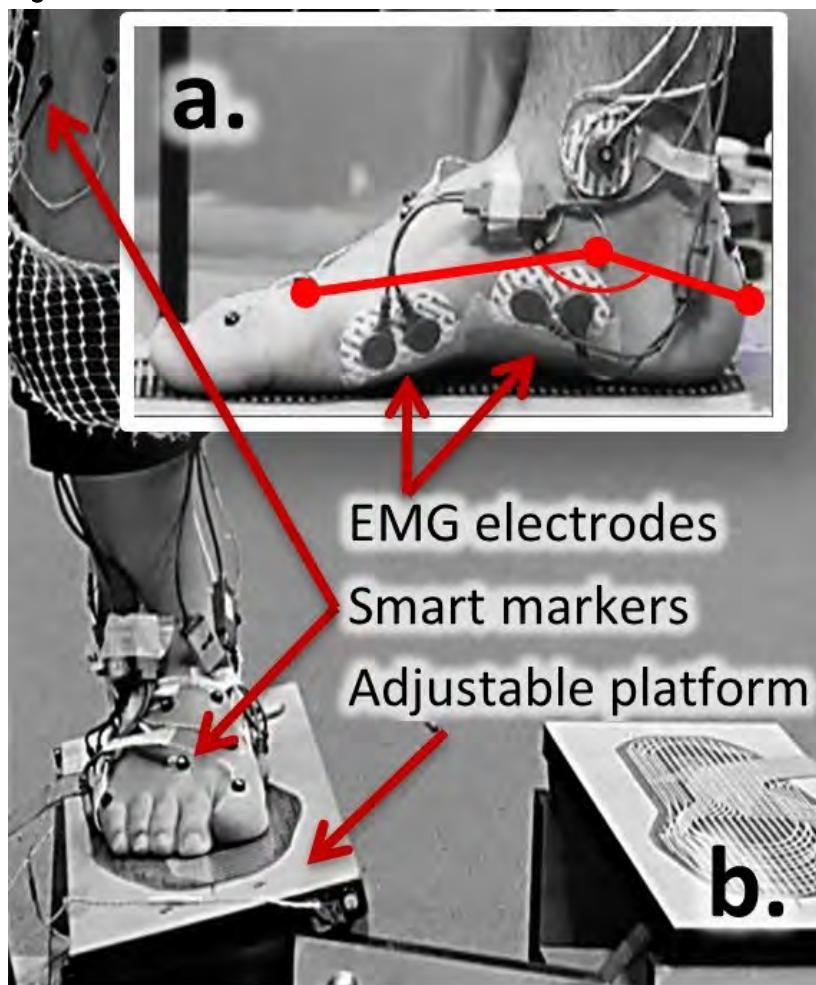
Caption: Test set up, a: Medial Longitudinal Arch (MLA), EMG electrodes for FHB (left) and ABH (right)

Conclusion: Forced over-pronation of the foot can increase medial IFM activation due to higher demand for stabilizing the joints in the first ray. IFM only come into play when the passive elements of the foot are not able to stabilize the foot on their own, otherwise they are mainly silent [4, 5].

Table:

Plate Angle (deg.)		Mean Normalized RMS EMG (%)			
		Medial		Lateral	
		ABH	FHB	ABDM	FDMB
Inversion	14	17.3	20.1	20.7	12.9
	7	22.0	19.7	20.2	12.1
Neutral	0	24.2	27.4	22.2	17.1
Eversion	7	35.2	38.1	29.1	19.1
	14	41.6	44.8	30.8	20.1

Caption: Mean IFM activities for different frontal plane angles

References: [1]Mann, J Bone Joint Surg AM, 46: 469, 1964.

[2]Murley et al., Clin Biomech, 25:728-736, 2010.

[3]McKeon et al., Brit J. sport med, 2014.

[4]Kelly et al., J. J. R. Soc. Interface, 11: 20131188, 2014.

[5]Kelly, Clin Biomech, 2011.

[6]Leardini, Gait Posture, 25:453, 2007.

Disclosure of Interest: None Declared

THE ROLE OF ARCH COMPRESSION AND METATARSOPHALANGEAL JOINT DYNAMICS IN MODULATING PLANTAR FASCIA STRAIN IN RUNNING

Kirsty Mcdonald [1,*]Sarah Stearne [1]Jonas Rubenson [1]

[1]Sport Science, Exercise and Health, The University of Western Australia, Perth, Australia

Introduction and Objectives: Elastic energy returned from passive-elastic structures of the lower limb is fundamental in lowering the mechanical demand on muscles during running. The combined elastic energy contribution of the medial longitudinal arch (MLA) ligaments has been assessed through static loading of cadaver feet [1], however the more detailed components of the arch's elastic function have not been considered during running. The purpose of this study was to investigate the two length modulating mechanisms of the plantar fascia (PLF), namely arch compression and metatarsophalangeal joint (MPJ) excursion, and to determine how these mechanisms modulate strain, and thus elastic energy storage/return of the PLF during running.

Methods: Sub-elite endurance runners (*n=18*) performed three treadmill running trials; normal shod, restricted arch compression (via an orthotic-style insert), and barefoot. Three dimensional motion capture and ground reaction force data were used to calculate lower limb kinematics and kinetics including MPJ angles, moments, powers and work. Estimates of PLF strain due to arch compression and MPJ excursion were derived using a geometric model of the arch and a subject-specific musculoskeletal model of the PLF combined with MPJ kinematics, respectively.

Results: Strain curves representing the effect of arch compression, MPJ excursion and the summation of both are presented in Figure 1 for unrestricted shod running. Peak strain for the combined effect of arch compression and MPJ flexion was significantly different between the barefoot vs. insert ($p < 0.001$), and shod vs. insert conditions ($p = 0.001$), with the barefoot condition resulting in the highest peak strain values (2.12 ±0.61%), followed by the shod condition (1.85 ±0.58%), and finally, the insert condition produced the lowest peak strain values (0.63 ±1.21%). These results were consistent with the maximum PLF strain derived from arch compression only. Maximum strain as a result of MPJ excursion did not differ between the shod and insert conditions ($p = 1.000$), however the peak MPJ-derived strain in the barefoot condition (0.32 ±0.07%) was significantly greater than both the shod (0.30 ±0.06%; $p = 0.001$) and insert (0.30 ±0.06%; $p = 0.003$) conditions.

The PLF was observed to develop strain via both arch compression and MPJ flexion. However, when we assessed the relative contributions, arch compression presented as the primary strain inducing mechanism, with the MPJ having a minor influence. Integrating the effects of arch compression and MPJ dynamics was a unique approach which led us to discover a novel function of the PLF. In the latter half of stance, arch recoil tends to shorten the PLF (positive arch power) and MPJ flexion simultaneously tends to lengthen the PLF (negative power) (Fig. 1). As a result, power is transferred between the MPJ and arch. In unrestricted shod running, we observed MPJ negative work to account for approximately 11.73% (±3.23%) of total lower limb joint energy absorption during stance phase. A component of this absorbed energy can be transferred proximally by the PLF to produce positive power in the arch.

Figure:
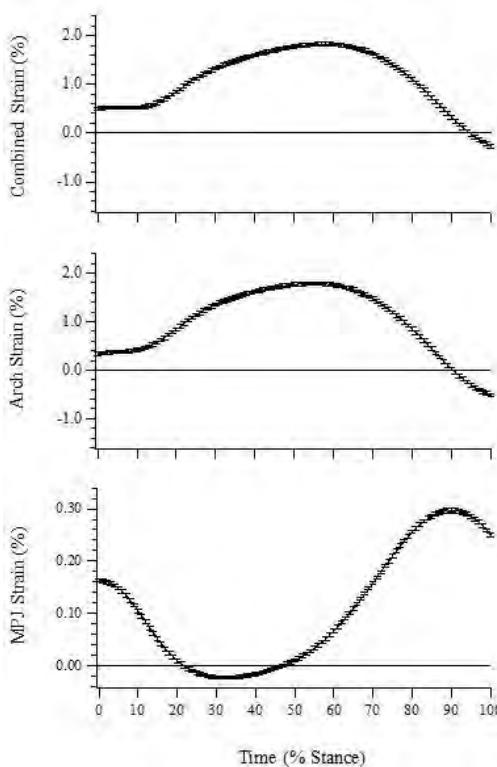
Caption: Figure 1. Estimated plantar fascia strain during stance phase for unrestricted shod running. Presented as the combined effect of arch compression and metatarsophalangeal joint (MPJ) angle, the effect of arch compression only, and the effect of MPJ angle only. Strain values ≤ 0 represent lengths at which the PLF is estimated to be slack.

Conclusion: The PLF was found to exhibit a typical elastic stretch-shortening cycle with the majority of strain generated via arch compression/recoil. Restricting arch compression, and hence spring function of the arch, was not compensated for by an increase in MPJ-derived strain. The PLF was found to transfer energy absorbed at the MPJ in the second half of stance to provide positive power generation at the arch (arch recoil). This previously unreported energy transfer mechanism has two important benefits; (1) additional energy is transferred to the MLA which assists propulsion, and (2) the risk of strain-induced PLF injury is substantially lower because the tissue is not required to lengthen excessively for the same power production.

References: [1] Ker et al., Nature, 325: 147-149, 1987

Disclosure of Interest: None Declared

Keywords: None

Feet and Footwear

AS-0499

FOREFOOT SPLAYING ACROSS THE TRANSVERSE METATARSAL ARCH IN DIABETIC PATIENTS

Mariam Crow [1] Brian L. Davis [1,*] Visar Berki [1] Daniela Ciltea [2]

[1]Biomedical Engineering, University of Akron, [2]Endocrinology, Akron General Medical Center, Akron, United States

Introduction and Objectives: The existence of a transverse metatarsal arch (TMA) across the plantar foot has long been a subject of controversy. A number of authors, using various assessment techniques ranging from plantar pressure to anatomical analyses, have reported contradictory results. The primary objective of this study was to reconcile these findings while simultaneously comparing the effects of peripheral neuropathy on forefoot splaying in diabetic subjects.

Methods: Data were collected on 29 human subjects: 16 control patients (9M, 7F; Age: 47.6±5.8 years; mean weight: 823 N) and 13 neuropathic, diabetic patients (8M, 5F, Age: 61.6±14 years, mean weight: 943 N). Each subject walked across a custom built shear and pressure system aligned in the center of a 305 cm x 61 cm platform. Four steps were analyzed for each subject with a primary focus of medial shear under the first metatarsal head (MTH) and lateral shear under the fourth and fifth MTHs. The maximum differences in instantaneous instances were determined with the greatest in magnitude chosen for comparison, as well as the difference in peak medial shear and peak lateral shear regardless of corresponding instances as a secondary approach.

Results: The maximum differences during each analyzed step between medial shear under the first MTH and lateral shear under the fourth and fifth MTHs were significantly higher for diabetic patients (143.9 ± 51.9 kPa) in comparison to control subjects (97.1 ± 25.5 kPa)(p < 0.01). A p-value of equal magnitude was obtained for the secondary analysis: the difference between peak values of medial and lateral shear under the first and fifth MTHs, respectively. The maximum difference at one time instance was also compared between men and female, regardless of subject group, resulting in higher pressure differences among men ((Diabetic Male: 159.2; Diabetic Female: 119.5; Control Male: 102.4; Control Female: 100.6 kPa)(p-value=0.01). Mean pressures were compared between the three transverse regions and averaged among each of the two groups. Both diabetic and control subjects displayed greatest pressure in the center region of the forefoot.

Figure:
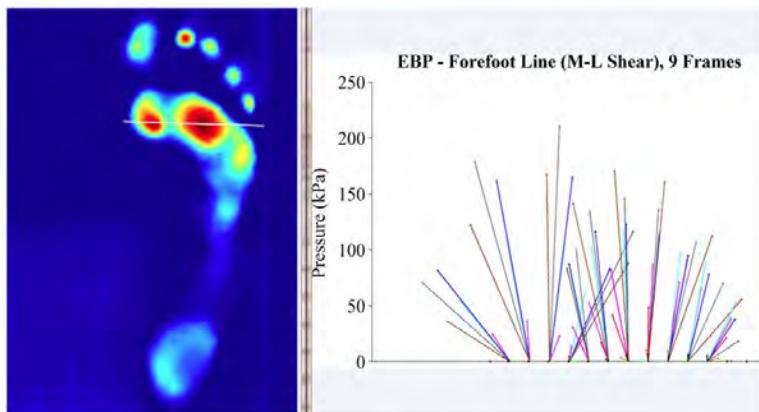
Caption: Figure 1: Shear and pressure forces mapped across the metatarsal heads of a neuropathic, diabetic subject. Height corresponds with pressure magnitude and outward vectors indicate medial and lateral shear at 9 different instants of time (0.02 s increments).

Conclusion: The difference of medial shear occurring under the first MTH coupled with the lateral shear occurring under the fourth and fifth MTHs supports the premise that the forefoot collapses at the MTHs, or 'splays' during ambulatory gait. A TMA must exist across the metatarsal heads during stance in order for the foot to exhibit these medial and lateral shear forces at the borders of the foot. Neuropathic diabetic patients are presumed to lose the ability to oppose this collapse; therefore, causing a greater splaying of the forefoot at the TMA. The notion of the foot initially resting on a tripod is supported by the evidence of splaying. When analyzing this data alongside pressure data across the TMA, it would seem that the tripod collapses during gait resulting in highest pressure under the peak of the arch as it makes contact with the floor and the forefoot splays.

Disclosure of Interest: None Declared

Computer Simulation

AS-0500

THE EFFECT OF VARIATIONS IN THE MORPHOLOGY OF THE HIP ON FEMORAL/ACETABULAR INTERFERENCE PATTERN DURING MOTION

Ramya Namani [1,*]Charanya Chandrasekaran [2]Javad Parvizi [3]Sorin Siegler [1]

[1]Mechanical Engineering and Mechanics, [2]Biomedical Engineering, Drexel University, [3]Rothman Institute, Thomas jefferson University, Philadelphia, United States

Introduction and Objectives: Femoro-Acetabular Impingement (FAI) is a clinical condition characterized by limited range of motion due to early abnormal bone-to-bone interference and is often associated with labrum and cartilage damage often leading to osteoarthritis. The surgical treatment of FAI [1] attempts to restore normal femoral morphology by removing bone regions in the femoral neck and/or the acetabular rim believed to produce early interference. Clinical experience of this procedure indicates less than favorable post-surgical results such as persistent pain or cartilage damage often leading to Total Hip Replacements [2]. This suggests that other morphological abnormalities, in addition to the ones addressed by the surgery may be contributing to early interference. The main goal of this model-based study is to explore the effect of variations in a number of morphological parameters of the proximal femur and the acetabulum on patterns of interference at the hip joint. This is achieved by systematically changing the morphology of the 3D model of the femur and studying its effect on interference patterns during motion.

Methods: Computerized Tomography (CT) images (resolution: 0.8mm*0.8mm*2mm) from seven healthy subjects were acquired. The CT images were processed through segmentation in ANALYZE™ software to produce 3D numerical models of the femur and the acetabulum. Morphological parameters such as femoral shaft angle, femoral anteversion/retroversion, alpha angle, neck offset angle, pistol grip deformity [3, 4] were measured in the 3D models. The geometry of the 3D model was virtually changed (see Figure) to produce a change in each morphological parameter from a normal to abnormal value [3, 4]. Previously developed dynamic models are used to simulate hip motion reproducing a clinical tests for FAI [1] consisting of Flexion (100^0) followed by adduction followed by internal rotation. The interference patterns were calculated using distance maps and were compared before and after the morphological change were introduced.

Results: All morphological parameters obtained from the non-modified hip models were found to fall within the normal ranges [4] for all subjects. Virtually changing the hip morphology such as to produce coxavara, coxavalga, femoral retroversion, and abnormal alpha angle, the interference at the anterior-inferior region of femoral head-neck junction increased with 100° flexion and 20° adduction followed by internal rotation. Geometrical change that produced a pistol grip deformity produced early interference on the top head of the femur with increase in adduction.

Figure:
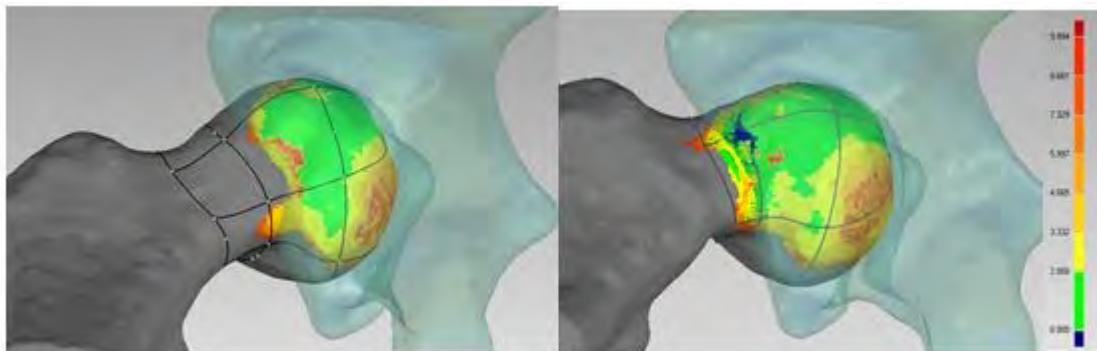
Caption: Interference of hip before (left) and after (right) inducing retroversion to femur at the simulation position of 90 degrees flexion combined with 20 degrees adduction and 30 degrees internal rotation. Blue region on retroverted femur (right) shows the region of contact

Conclusion: Morphological parameters such as femoral shaft angle, femoral anteversion, alpha angle and pistol grip deformity produce early interference at the hip and should be considered when planning FAI surgery. Future studies to validate the simulation-based results of this study will compare the morphological parameters and patterns of interference between patients with successful FAI surgery outcome and patients with post-surgical complications

References: [1] Ganz, R., et al., CORR, 417:112-20, 2003.

[2] Ilizalitturi, V., et al., CORR, 467:760-8, 2009.

[3] Beck, M., et al., JBJS, 87:1012-8, 2005.

[4] Tannast, M., et al., AJR, 188:1540-52, 2007.

Disclosure of Interest: None Declared

Modelling

AS-0501

MODELING MULTIJOINT CONTROL FOR REGULATION OF REACTION FORCES DURING IMPACT PHASE OF LANDINGS

Edward Wagner [1,*] Henryk Flashner [1] Jill McNitt-Gray [2] Veronica Eliasson [1]

[1]Aerospace and Mechanical Engineering, [2]Biological Sciences and Biomedical Engineering, University of Southern California, Los Angeles, United States

Introduction and Objectives: Modeling how individuals anticipate and control reaction forces during foot contact allows for simulation of landings under various conditions and independent modulation of variables that cannot be altered experimentally. The human body is often modeled as a system of segments with varying degrees of rigidity (Gruber, et al 1998). Our goal is to develop and experimentally validate a dynamic model of sufficient complexity enabling us to test hypotheses regarding the control and dynamics of the musculoskeletal system during flight and initial contact phases of landings. The aims of this study were to 1) validate a minimally complex 2D model that incorporates a foot and experiment-based multijoint control by comparing model-simulated and experimental peak vertical ground reaction forces (VGRF) and the vertical impulse during the impact phase of landings and 2) demonstrate the necessity of including a foot in the model by comparing the simulated and experimental forces during impact.

Methods: Modeling: Using simulation software (SimMech, MATLAB), a 2D model of the human body with 4-rigid links connected by ideal hinge joints was developed, comparable to the jumping model of Bobbert & vanSoest, 1994. Muscle actuators were replaced with joint torque actuators. Body segment parameters (DeLeva et al 1996) were scaled to the subject (female: 1.575m, 64.5kg). Link lengths were determined from segment endpoints digitized from video records. Torque actuators at each hinge accepted experimental ankle, knee, and hip torque-time curves as control inputs during simulation. The VGRF were applied at the toe and heel of the foot, modeled as Coulomb friction (horizontal coefficient of friction = 1) and a vertical nonlinear spring (C=2.17E6) and damper (D=2.89E4)(Gruber et al 1998).

Experimentation: Land-and-stop tasks were performed by former gymnast who provided informed consent and performed a series of drop landings from a 0.445m platform onto two force plates (KISTLER, 1200Hz) using self-selected normal, softer, and harder landing techniques (McNitt-Gray et al 2001). Kinematics (2D) during the landings were measured with ultra high-speed video (Phantom v711, 11,000fps).

Validation: Model-simulated (with/without foot) and experimentally measured peak VGRF and the vertical impulse during the impact phase were compared across landings. Differences between model-simulated and experimentally-measured VGRFs served to determine the ability of the model to simulate the effect of flight and impact phase control on the dynamics of the body during landing. The model was validated by comparing experimental results with the simulated peak VGRF and impulse of the VGRF during the impact phase (from contact forward to twice the time from contact to peak VGRF). If the simulated impulses match the experimental values within 10%, the model was considered sufficiently complex to establish the initial momentum conditions of the post-impact phase. Finally, the necessity of adding a foot to the model was determined by comparing the VGRF peak pattern from simulations with the experimentally observed toe-heel contact pattern.

Results: The simulated peak VGRF scaled in magnitude across the soft, normal, and hard landing cases, comparable to that observed in the experimental peak VGRF. Experimental peak VGRFs across the soft, normal, and hard landing cases ranged from 4.41-7.61 times body weight (BW), with a normal landing peak VGRF of 4.87BW(Fig b). The multijoint control model with a foot produced impulses during the impact phase accurate to within 5% of the experimental impulses for each case(Fig d). The sequential forefoot and heel contacts were qualitatively matched when the model had a foot, and they were reversed without a foot(Fig e).

Figure:
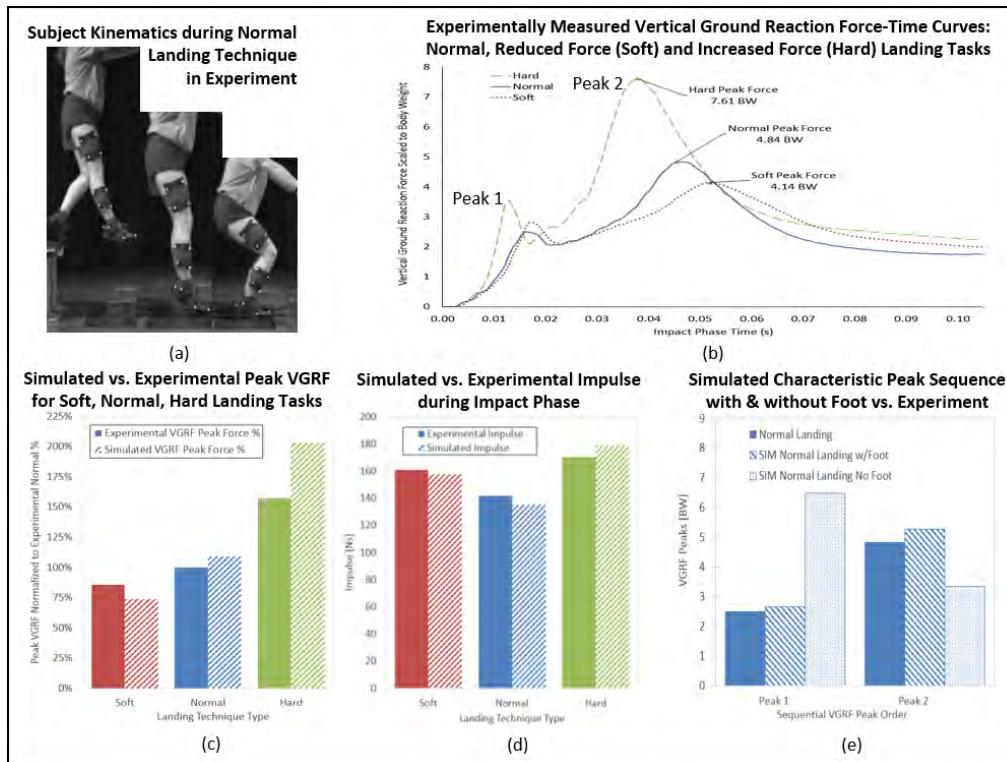
Caption: (a) Land-and-stop task (b) VGRF-time curves show decrease in peak VGRF and increase in impact-phase duration across landing tasks (c) Simulated peak VGRF show comparable scaling across tasks wrt experiment (d) Impulse during impact phase across landing tasks shows sufficiency of simulations for initial momentum conditions at post-impact. (e) Comparison of sequential VGRF peaks during impact phase for model w/ and w/o foot showing foot necessity for characteristic peak sequence found in experiment.

Conclusion: The experimental results confirmed that flight phase control affected peak VGRF and vertical impulse during the impact phase. As the other experimental parameters were held constant, the variation in peak VGRF across tasks demonstrates the necessity of including multijoint control in human body impact modelling. While not perfectly accurate to the experimental peak VGRF, which is a very sensitive value, the model provided accurate prediction of the impulse during impact, making it a sufficient model of the human body during drop landings. Finally, it is necessary to include a foot in the drop-landing model to reproduce the sequential dual-peak VGRF time curves measured experimentally.

Disclosure of Interest: None Declared

ELEMENT POSITION'S EFFECTS ON THE DEGRADATION PROCESS SIMULATION OF MAGNESIUM ALLOY STENTS IN FINITE ELEMENT ANALYSIS

Yuanming Gao [1,*]Zhaowei Chu [1]Meng Guo [1]Yubo Fan** [1] [2]

[1]Key Laboratory for Biomechanics and Mechanobiology of Ministry of Education, International Research Center for Implantable and Interventional Medical Devices, School of Biological Science and Medical Engineering, Beihang University, [2]National Research Center for Rehabilitation Technical Aids, Beijing, China

Introduction and Objectives: Biodegradable magnesium alloy stents (MAS), which have good biocompatibility and no long term health risks associated with permanent stents, have attracted intense attention in recent years. Finite element analysis (FEA) has become a powerful tool for testing stent properties due to its low costs and high efficiency compared to the conventional testing[1]. The elements located exposed exterior surfaces of the finite element models of MAS constitute the corrosion layers, and have respective number of corrosion surfaces. For example, elements on the corners of the MAS models have two or three surfaces exposed to the corrosive environment and others may have only one surface. Each of different corrosion surface numbers would cause different corrosion magnitude, especially for uniform microgalvanic corrosion processes. The objective of this study is to build up a degradable FEA model of MAS considering effects of element positions.

Methods: In this work, the corrosion of magnesium alloy is assumed to be the superposition of stress corrosion and uniform microgalvanic corrosion processes, and continuum damage mechanics was used to describe the degradation of mechanical properties during corrosion process[2,3]. Geometric model of MAS (Biotronik Magic stent) was generated based on the images in literatures. FEA models were composed of a stent, an artery vessel, a plaque and a rigid cylinder to expand the stent. Commercial code ABAQUS/Explicit, with a user material subroutine (VUMAT) devoted to calculation of the damage increment, was designed and applied in the simulations. It is assumed that uniform corrosion rate of each element is proportional to corrosion surface number of the element because the surface area exposed to corrosive environment is a very important factor for the damage rate. During simulation, once a critical amount of damage in the element is reached, the element would be removed from FE mesh of MAS. Therefor element connectivity and initial corrosion surface numbers of elements must be provided for VUMAT code and then be updated in the degradation process.

Results: In the FEA process, rigid cylinder expended the MAS and then the stent begun to be corroded and subjected to tension from the artery vessel and plaque. As damage accumulation increasing, structural weakening caused by stent degradation was shown (Figure 1). The uniform corrosion rates varied with element positions during degradation. Elements located on the corners and edges of stents, because of more corrosion surfaces, had higher rates than others. Moreover, cracks and pits appeared when fully damaged elements were removed from FE mesh of MAS, which caused neighboring elements had additional corrosion surfaces and then had higher uniform corrosion rates. Therefor the effects of cracks and pits on the degradation rate are improved by the model in this study.

Figure:
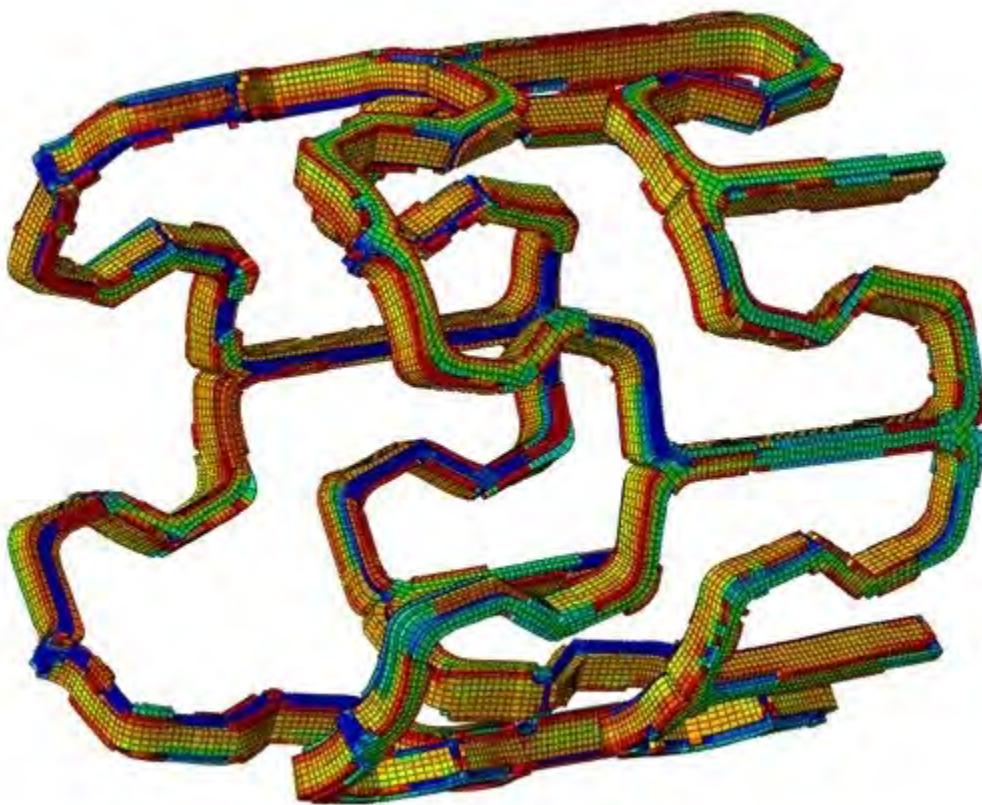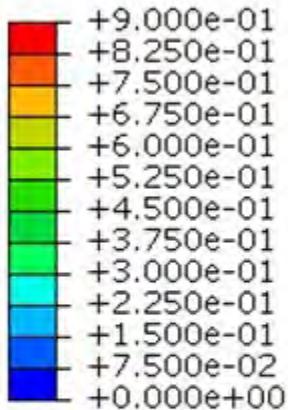
Caption: The degradation simulation of MAS. The legend is related to the uniform corrosion damage parameter.

Conclusion: The novel MAS finite element model in this work can describe more complex and precise changes of morphology and mechanical properties in degradation process. The method considering effects of element positions in FEA is helpful for not only simulations of MAS, but for simulations of other potential degradable metallic biomaterials and implants.

References: [1] Morlacchi S et al., Annals of biomedical engineering, 41:1428-1444, 2013.

[2] Gastaldi D et al., Journal of the mechanical behavior of biomedical materials, 4:352-365, 2011.

[3] Grogan JA et al., Acta biomaterialia, 7:3523-3533, 2011.

Disclosure of Interest: None Declared

Modelling

AS-0503

A NEW COMPUTATIONAL METHOD TO PREDICT THE DEVELOPMENT OF OSTEOARTHRITIS WITHIN THE KNEE JOINT

Mika Mononen [1,*]Petri Tanska [1]Hanna Isaksson [2]Rami Korhonen [1]

[1]Department of Applied Physics, University of Eastern Finland, Kuopio, Finland, [2]Department of Biomedical Engineering, Lund University, Lund, Sweden

Introduction and Objectives: One of the first signs of knee osteoarthritis (OA) is collagen fibrillation, leading to decreased collagen network stiffness and increased local tissue strains of cartilage [1,2]. It has been shown that high loading rates, i.e., impulsive loads within the knee joint are one of the most crucial risks for the onset and development of OA [3]. However, there are currently no methods to predict the progression of OA. Therefore, our aim was to develop and validate a computational finite element (FE) model, incorporating an adaptation algorithm, to predict collagen fibril degeneration regulated by altered joint loading due to overweight during gait.

Methods: MRI data of two right knee joints were selected from the Osteoarthritis Initiative (OAI) database. Subject 1 was a normal weighted person with no cartilage degeneration at the baseline or after 4-year follow-up (Kellgren - Lawrence grade 0), whereas subject 2 was an overweight person with no initial cartilage degeneration at the baseline, but after 4-year follow-up the KL grade had developed from 0 to 3. The knee joints were segmented manually by Mimics v12.3 and then the segmented tissues were imported into Abaqus v6.13, in which the final FE model geometries were constructed (Fig. 1A). Cartilage tissues were modeled as fibril reinforced poroviscoelastic materials with split-line and depth-wise fibril architectures and Menisci were considered as transverse isotropic materials [2]. Stresses in both knee joints were simulated during gait obtained from literature [4] (Fig. 1A). Then the medial compartment model was driven by the forces obtained from the whole knee joint models (Fig 1A). Cartilage responses (maximum principal stresses) were then analyzed (Fig. 1B). In the adaptation algorithm, collagen fibril degeneration (collagen softening) was regulated based on the local maximum principal stresses. The local collagen fibril softening occurred as a response when 5 MPa was exceeded, a failure stress observed experimentally for cartilage [5]. In the simulations of collagen degradation, 100 iterative steps were applied and the collagen fibril properties changed in an element-wise manner after each iteration step if the criterion of stress was fulfilled (see the iterative loop from Fig. 1B).

Results: After 100 iterative steps, the local collagen fibril stiffnesses were reduced substantially more in the model of overweight subject (subject 2) compared to the model of normal weight subject (subject 1) (Fig. 1C - top). This was consistent with the experimentally diagnosed stage of OA at 4-year follow up. At the tibial cartilage surface, the areas of degenerated cartilage tissue increased as a function of iterative steps in both models (Fig. 1C – bottom; left). The most severe changes in the degenerated surface area were observed in the overweight subject model. Collagen softening (degradation) caused substantially greater changes in stresses (decrease) and strains (increase) of cartilage in the overweight subject model compared to the model of normal weight subject (Fig. 1C – bottom; middle and right).

Figure:
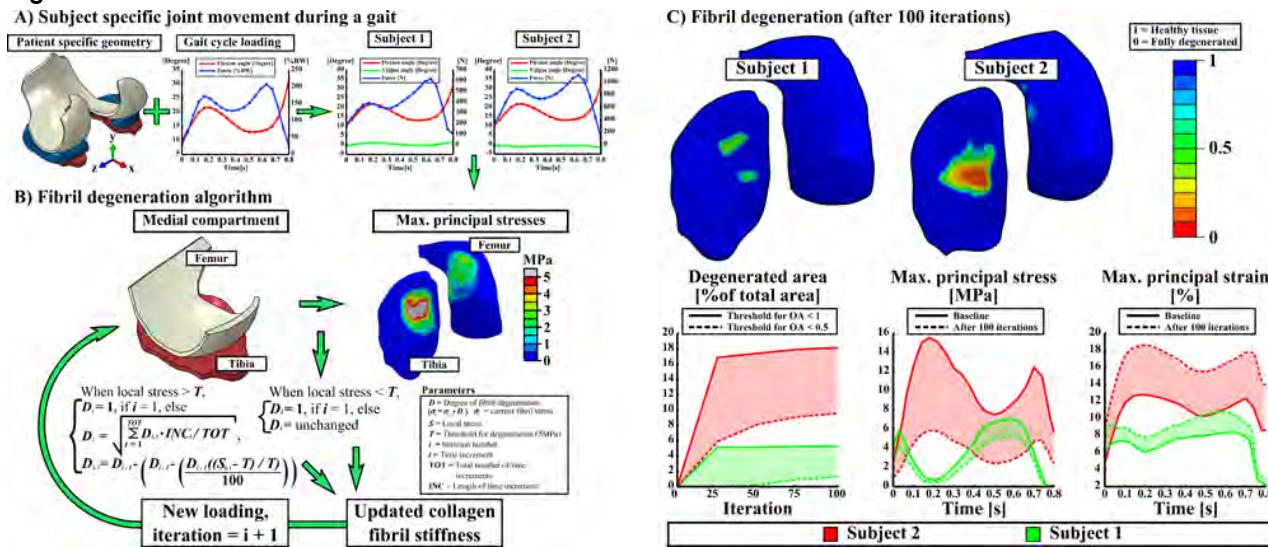
Caption: Workflow from the subject specific gait load (A) till the fibril degeneration algorithm (B) and the results after 100 iterative degenerative simulations (C). (A) subject specific knee joint loads of a medial compartment during gait, obtained from literature, were implemented into the subject specific whole knee joint models. (B) medial compartment where the fibril degeneration algorithm was applied, stress distribution is from the subject 1 during the first peak loading force of gait. (C) top figures present the rate of fibril degeneration in the subjects 1 and 2, bottom row sub-figures indicate the percentage fibril degeneration of the medial tibial surface area with two different thresholds (left), maximum principal stresses (middle) and strains (right) at the tibial surface at themost degenerated location between the baseline and adapted models (100 degenerative iterations), respectively.

Conclusion: A novel computational adaptive FE model was able to predict osteoarthritis progression (collagen softening) as a result of abnormal joint loading (overweight), while the subject under normal loading did not experience much degenerative changes. The results were consistent with experimentally diagnosed KL grades at baseline and 4-year follow-up time point. Due to substantially reduced local collagen fibril stiffnesses in the model of overweight subject, greater changes in local cartilage strains were observed. This could lead to more severe OA in the future. However, it should be emphasized that the current work presents a new theoretical method to predict cartilage degeneration for two subjects (only the other developed OA).

References: [1]Buckwalter et al., Clinical Symposia, **47**:1-32, 1995. [2]Mononen et al., J Biomech, **45:**579–87, 2011. [3]Radin et al., Arthritis Semin Arthritis Rheum, 21:3(Suppl 2):12-21, 1990. [4]Kutzner et al., J Biomech, 43: 2164-2173, 2010. [5]Danso et al., J Biomech, 47:200-206, 2014.

Disclosure of Interest: None Declared

Modelling

AS-0504

COULD FOOT KINEMATICS BE USED TO PREDICT THE DISTRIBUTION OF VERTICAL FORCE IN MULTI-SEGMENT FOOT MODELS?

Iain Hannah [1,*] Zimi Sawacha [2] Annamaria Guiotto [2] Claudia Mazzà [1]

[1] INSIGNEO Institute for in silico Medicine, University of Sheffield, Sheffield, United Kingdom, [2] Department of Information Engineering, University of Padova, Padova, Italy

Introduction and Objectives: The use of a multi-segment foot in a musculoskeletal model of human gait requires the ground reaction force (GRF) to be subdivided between the modelled foot segments. A number of foot-ground contact models have been presented in the literature [1-5] but these remain in early development. As such, no single technique has been accepted as a valid way to model the complex interaction that occurs at the foot-ground interface.

Sawacha et al. [6] found the variability of vertical load magnitudes that occur across different foot segments to be greater than that which occurs within the foot as a whole. This work thus details the development of a statistical tool which aims to use foot kinematics to predict the proportion of vertical loading that occurs in each of three foot segments during an experimental walking trial.

Methods: 20 healthy subjects (14m/6f, age: 58±5 years, weight: 74±13kg, height: 171±9cm) were recruited with each performing three walking trials at a self-selected speed. Foot kinematics, GRF and the distribution of plantar pressure were all recorded. Using the techniques reported by Sawacha et al. [6], the vertical loading that occurred during each trial was divided between the three foot segments; hindfoot, midfoot and forefoot (Figure 1b).

The subjects were randomly divided into two equally sized groups; a model testing group and a model training group. Key points on the foot segment loading curves such as the time of zero hindfoot loading, time of maximum midfoot loading and maximum midfoot load proportion were identified for each of the trials performed by those subjects assigned to the model training group. Kinematic variables were also calculated for each trial and subsequently used in a regression analysis to attempt to predict the occurrence of these points. These variables included trajectories and velocities of individual markers and marker groups, arch deformation and sole angle variation.

Results: No significant correlation could be found between the key points on the hindfoot, midfoot and forefoot loading curves and the kinematic variables measured in the experimental trials. The strongest correlation was found between the time of increased calcaneal velocity and time of zero hindfoot loading but only had an R^2 value of 42 %.   Furthermore, simply fitting the average training load curves to the testing group resulted in average RMS errors of 7.6 %, 9.7 % and 6.7 % for the hindfoot, midfoot and forefoot segments respectively (sd = 2.7 %, 3.1 %, 2.9 %).

Figure:
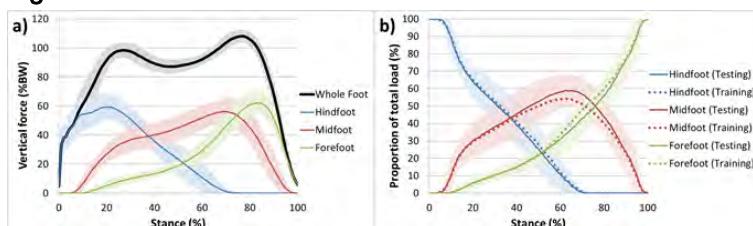
Caption: Average distribution of vertical loading between three foot segments. a) Entire cohort (±1 sd shown), and b) in training (±1 sd shown) and testing groups.

Conclusion: The high levels of inter-subject variability exhibited in the loading curves meant that foot kinematics could not be employed to predict the distribution of vertical loading that occurs across a multi-segment foot model. This inter-subject variability was higher for the three segmented force curves than for the overall vertical load. Furthermore, the variability in the distribution of the load under the foot could not be explained by the measured kinematic variables.

The high variability in the vertical forces acting under each sub-segment of the foot is in agreement with previous literature [7] where it was associated to the differences in foot shapes exhibited even amongst healthy subjects. Nevertheless, in order to characterise the complex loading scenario that occurs at the foot-floor contact interface further consideration should be given to the shear forces that occur here, and not only to the vertical component.

References: [1] Peasgood et al., Nonlinear Dyn., 2: 65–72, 2007.

[2] Barbosa et al., P. Multibody Dyn., 2005.

[3] Kecskeméthy et al., Multibody Dyn., 2011.

[4] Gilchrist & Winter, J. Biomech, 29: 795–798, 1996.

[5] Lin et al., Int. J. Numer. Meth. Biomed. Eng., 27: 436–449, 2011.

[6] Sawacha et al., Gait Posture, 36: 20–26, 2012.

[7] Guiotto et al., Gait Posture, 37: 603–610, 2013.

Disclosure of Interest: None Declared

Modelling

AS-0505

CEINMS: AN OPENSIM TOOLBOX TO INVESTIGATE THE INFLUENCE OF DIFFERENT NEURAL SOLUTIONS IN PREDICTING MUSCLE EXCITATIONS AND JOINT MOMENTS DURING DYNAMIC MOTOR TASKS

Claudio Pizzolato [1,*] David G. Lloyd [1] Massimo Sartori [2] Elena Ceseracciu [3] Thor F. Besier [4] Monica Reggiani [3]

[1]Centre for Musculoskeletal Research, Griffith Health Institute, Griffith University, Gold Coast, Australia, [2]University Medical Center Göttingen, Georg-August University, Göttingen, Germany, [3]Department of Management and Engineering, University of Padua, Vicenza, Italy, [4]Auckland Bioengineering Institute, University of Auckland, Auckland, New Zealand

Introduction and Objectives: Neuromusculoskeletal (NMS) models represent the neurological, physiological, and anatomical characteristics of an individual, and can be used to estimate the forces generated inside the human body. Individual muscle forces and their contribution to joint moments can be determined using optimisation methods, which track the external joint moments and/or kinematics to estimate muscle activations and forces [1, 2]. However, these methods cannot account for variations in muscle activation patterns used in different control tasks, and by different people. EMG-driven NMS models can overcome these problems [3] but have limitations of acquiring EMG from a limited number of muscles and errors in EMG measurement.

We have created the Calibrated EMG-Informed NMS Modelling Toolbox (CEINMS), an OpenSim [4] plug-in that enables investigators to use different neural solutions for the same NMS model and measured movements. CEINMS collects EMG-driven and EMG-informed algorithms that have been previously published and tested [3, 5-7]. CEINMS can operate with any number of degrees of freedom (DOF) and musculotendon units (MTU) and can be calibrated to the individual to better predict measured joint moments and EMG patterns. CEINMS covers neural solutions from EMG-driven to hybrids between EMG-driven and optimisation-driven, and to full optimization-driven. Also, CEINMS can use as input a set muscle synergies and scaling coefficients that are linearly combined to synthesise muscle excitations [8].

To date, it has not been possible to see if EMG-informed methods produce different muscle forces compared to static optimisation, independent of the NMS model. So we used CEINMS to examine how different neural solutions affect the predicted joint moments, muscle excitations and muscle forces using the same NMS model and motion data.

Methods: Walking data were collected from 5 subjects, using a 10-camera motion capture system and 2 force plates. Surface EMG signals were acquired from 16 muscles of a single leg. Segmental dimensions and muscle parameters of the OpenSim model were anthropometrically scaled [9] to the subjects. 3D joint angles, MTUs kinematics, and joint moments during stance phase were calculated using inverse kinematics, muscle analysis, and inverse dynamics OpenSim tools respectively. CEINMS was configured to analyse forces from 34 MTUs of the support leg, and flexion extension (FE) moments of hip, knee, and ankle. CEINMS calibrated each subjects' MTUs parameters within physiological ranges using calibration data sets. Once calibrated CEINMS estimated the joint moments using the EMG-driven [3], EMG-assisted [5], and optimisation-driven neural solutions.

Data were time-normalized and averaged across trials (6 per subject). The coefficient of determination R^2 and the root mean square error (RMSE) between the predicted and measured joint moments from the different neural solutions were used as a measure of prediction accuracy.

Results: The calibration procedure improves the estimation of hip, knee, and ankle FE moments for the EMG-driven mode (Table 1, Figure 1). The EMG-driven calibrated model well predicted the knee and ankle flexion extension moments, but poorly predicted the hip moment, while the EMG-assisted and the optimisation-driven modes both matched the experimental joint moments for the three joints (Table 1).

Figure:
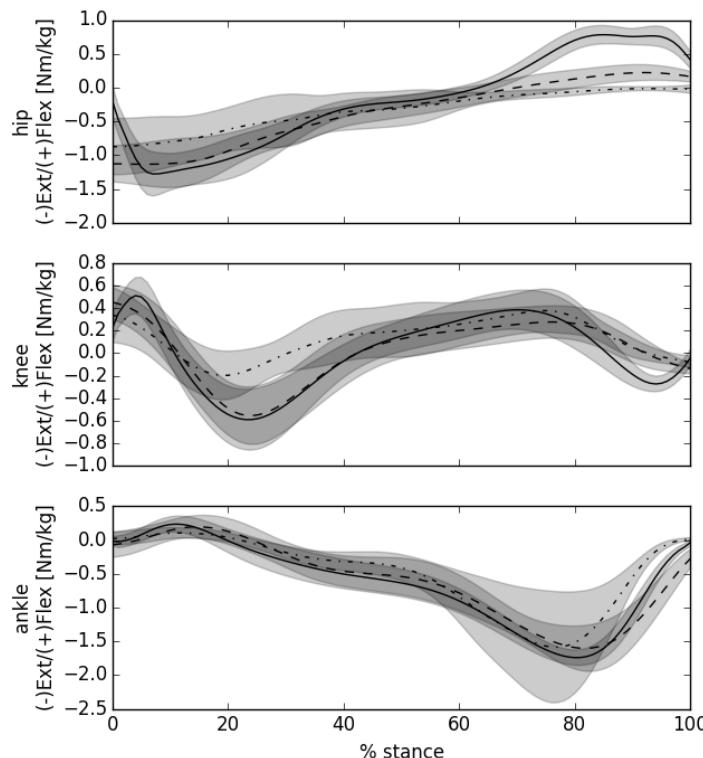
Caption: Figure 1 – External joint moments from inverse dynamics (solid), uncalibrated EMG-driven (dash-point), and calibrated EMG-driven (dashed). Curves represent ensemble averages (shaded area 1 SD) of 6 walking trials from 5 different individuals.

Conclusion: CEINMS is an OpenSim toolbox to explore the effect of different neural algorithms using a consistent NMS model. CEINMS is the first software publicly available that can be configured to work with any number of MTUs and DOFs. It includes a calibration procedure to tune the model's parameters, can be used with dynamic tasks, and provides state-of-the art EMG-informed algorithms.

Table:

	Uncalibrated EMG-driven		EMG-driven		EMG-Assisted		Optimisation-driven	
	RMSE (Nm/kg)	R^2	RMSE (Nm/kg)	R^2	RMSE (Nm/kg)	R^2	RMSE (Nm/kg)	R^2
hip FE	0.56	0.65	0.39	0.84	0.07	0.99	0.04	0.99
knee FE	0.28	0.67	0.18	0.80	0.09	0.93	0.08	0.95
ankle FE	0.44	0.86	0.24	0.88	0.10	0.97	0.06	0.99

Caption: Table 1 – CEINMS predictions for the external joint moments using the uncalibrated EMG-driven, and the calibrated EMG-driven, EMG-assisted, and the optimisation-driven modes of 6 walking trials from 5 different subjects.

References: [1] Crowninshield RD et al., *Journal of biomechanics*, 14:793-801, 1981.

[2] Anderson FC et al., *Journal of biomechanics*, 34:153-161, 2001.

[3] Lloyd DG et al., *Journal of biomechanics*, 36:765-776, 2003.

[4] Delp SL et al., *IEEE Trans Biomed Eng*, 54:1940-1950, 2007.

[5] Sartori M et al., *Journal of biomechanics*, 47:3613-3621, 2014.

[6] Sartori M et al., *Plos One*, 7:e52618, 2012.

[7] Gerus P et al., *Journal of biomechanics*, 46:2778-2786, 2013.

[8] Sartori M et al., *Front Comput Neurosci*, 7:79, 2013.

[9] Winby CR et al., *Journal of biomechanics*, 41:1682-1688, 2008.

Disclosure of Interest: None Declared

AS-0506

WHAT IS THE RELATIONSHIP BETWEEN KNEE BIOMECHANICAL FUNCTION AND PATIENT REPORTED FUNCTION BEFORE AND AFTER TOTAL KNEE REPLACEMENT?

Lucy A Bailey [1 2,]*Paul R Biggs [2 3]Chris Wilson [2 4]Cathy A Holt [2 3]Gemma M Whatling [2 3]

[1]Trauma and Orthopaedics, Southampton General Hospital, Southampton, [2]Biomechanics and Bioengineering Centre, Arthritis Research UK, UK, [3]School of Engineering, Cardiff University, [4]Trauma and Orthopaedics, University Hospital of Wales, Cardiff, United Kingdom

Introduction and Objectives: Whilst most patients have an improvement in their function following total knee replacement (TKR) and are satisfied with the surgery, around one in six will have less favourable results [1,2,3]. Risk factors have been identified[3,4,5], but reasons underlying dissatisfaction are not clearly understood. The aim of this work was to establish the relationship between measurable gait parameters and patients' subjective function, before and after TKR.

Methods: 25 subjects underwent gait analysis, before and one year following TKR. Patient reported function was investigated using the Activities of Daily Living Scale of the Knee Outcome Survey (KOS). Three dimensional motion analysis was performed using infrared cameras and reflective marker clusters to record gait (Qualisys, Sweden). Ground reaction forces (GRFs) were measured using 2 force plates (Bertec Corporation). Knee joint kinematics and GRF data waveforms were computed for each subject pre and post TKR. Metrics including the timings and magnitudes of specific events in the gait cycle were identified. Linear regression was used to assess for correlation between motion analysis data and patient reported function.

Results: At the pre-operative visit there were multiple measured gait parameters that were shown to correlate significantly with the patient's functional score, after correcting for the affect of cadence. These included the amount of extension occurring during stance after the first flexion peak (P=0.003, R^2=0.354), the internal rotation at 90% of the gait cycle (p=0.006, R^2=0.301) and the timing of the peak lateral GRF in early stance (p=0.004, R^2=0.271).

Subjects with a higher (better) pre-operative score tended to have a higher post operative score (p=0.0365, R^2=0.177), but show less of an improvement in score than subjects who had a lower pre-operative score (p=0.0058). After correction for the affect of pre-operative score, there were three measured parameters in the pre-operative gait that correlated with the extent of improvement in score that was seen after surgery. These were the rate of extension in swing (p=0.025, R^2=0.0.392), total range of motion from extension at heel strike to the maximum flexion in swing (p=0.026, R_2=0.314) and time point of maximum stance extension (p=0.019, R^2=0.384).

Post-operatively, no measured parameters correlated with KOS after correcting for the affect of cadence.

Conclusion: This work adds to our understanding of the complex relationship between biomechanical knee function and patient reported function. Before surgery the two are closely related, yet after surgery it would appear that factors other than biomechanics of gait determine patient reported outcomes. These factors might include muscle strength, pain or kinetics and kinematics of other daily activities such as climbing stairs or rising from a seated position.

The identification of elements in pre-operative gait that are associated with post-operative outcome has the potential to help guide patient treatment and could help to identify and prioritize patients that are more likely to benefit from TKR.

Patients with pre-operative gait indicative of poor outcome may warrant further investigation into causes of symptoms and alternative treatment modalities; particularly in the presence of other risk factors for poor outcome. If TKR was to be undertaken, patients could be counselled appropriately, in order that they could make an informed choice about their treatment.

References: [1] Robertsson et al., Acta Orthop. Scand., 71:262-7, 2000.

[2] Parvizi et al., Clin. Orthop. Relat. Res., 472:133-7, 2014.

[3] Scott et al., J Bone Joint Surg. Br., 92-B:1253-8, 2010.

[3] Kim et al., J. arthroplasty, 24:263-271, 2009.

[4] Baker et al., J.Bone Joint Surg. Br., 94-B:1058-66

Disclosure of Interest: None Declared

Motion Analysis

AS-0507

GAIT CHARACTERISTICS OF LOCOMOTIVE SYNDROME BY PRINCIPLE COMPONENT ANALYSIS

Baku Suzuki [1,*]Yoshiyuki Kobayashi [2]Masaaki Mochimaru [2]Hiroshi Fujimoto [3]

[1]School of Human Sciences, Waseda University, 2-579-15, Mikajima, Tokorozawa City, Saitama Pref, [2]Digital Human Research Center, National Institute of Advanced Industrial Science and Technology, Waterfront 3F, 2-3-26, Aomi, Koto-ku, Tokyo, [3]Faculty of Human Sciences, Waseda University, 2-579-15, Mikajima, Tokorozawa City, Saitama Pref, Japan

Introduction and Objectives: Aging of the population is one of the most important problems especially in Japan, but for all over the world. In this circumstance, locomotive syndrome (LS), the conditions under which people may soon need care services because of problems of the locomotive organs, was proposed by Japanese Orthopedic Association in 2007. Yoshimura et al. reported that there are over 47 million LS candidates live in Japan. Early detection of such people may decrease the number of patients needing nursing care. We aimed this study to develop the device which can discriminate whether the user is LS or not. In order to do so, first we have to know the characteristics of the LS gait pattern. The purpose of this study is, therefore, the identification of the key joint kinematics characteristics during walking that are related to LS by using principal component analysis (PCA).

Methods: Fifty-four healthy community-dwelling elderly subject (27 M & 27 F) were recruited for the study. Ten of them (6 M & 4F) were classified as the LS by using GLFS-25 questionnaire (score ≥16) [1]. The experimental protocol was approved by the local ethical committee and all the participants gave their written informed consent before participating. The experiments were performed in a room with a straight 10 meter path for the participant to walk. Three-dimensional positional data was obtained using reflective markers and a 3D motion capture system using a sampling frequency of 200 Hz. A total of 55 IR reflective markers were attached in accordance with the guidelines of the Visual 3D software. We also recorded the ground reaction force (GRF) using six force plates sampled at 1 kHz to time the gait cycle. Participants were asked to walk barefoot at a comfortable, self-selected speed. After the practice, five successful trials in which each GRF measured properly with the right foot were recorded.

The raw data was digitally filtered using a fourth-order low-pass Butterworth filter with zero lag and a cut-off frequency of 10Hz for the trajectories. The right hip, knee, and ankle joint angles on the sagittal, frontal, and horizontal planes during one gait cycle were calculated from the trajectories of the each trial. The joint angles were time-normalized by the gait cycle duration determined based on the force plate data and divided into 101 variables ranging from 0% to 100%. The calculation of the joint angles and the time normalizations were done using Visual 3D.

PCA was conducted to 54 by 1818 (AVGs and SDs for 101 time points, three joints, and three planes) matrix to identify the key joint kinematics characteristic of walking that is related to the LS. In order to confirm the stability of the analysis, the PCA were repeated with 54 surrogate input matrixes. Further, discrimination analysis with step-wise procedure was used to determine the PCVs related to the LS. All the statistical analyses were executed using SPSS Ver. 22.

Results: The PCA revealed that the first 52 PSVs explained more than 99% of the joint movement patterns. Among these 52 PCVs, PCV 7 (2.88% of the variance), PCV 12 (1.49% of the variance) and PCV13 (1.29% of the variance) were selected to the model. The results of surrogate PCAs are similar to the result of main PCA. Therefore, it is reasonable to

expect that the joint kinematics corresponding to these PCVs are the key joint kinematic characteristics of human gait related to the LS while walking on level ground. We therefore recombined the joint kinematics related to the PCV7, 12 and 13. As a result, LS group tended to show smaller ROM of hip, knee and ankle joint angles in sagittal plane, and greater joint kinematics variability of hip, knee and ankle joint angles during the swing phase in sagittal plane than non-LS group (figure 1).

These results are in agreement with those of previous studies regarding the joint kinematics related to fall risk (Kobayashi et al. 2014). Therefore, it is reasonable to expect that LS related not only risks of becoming need care services but also risks of falling.

Figure:
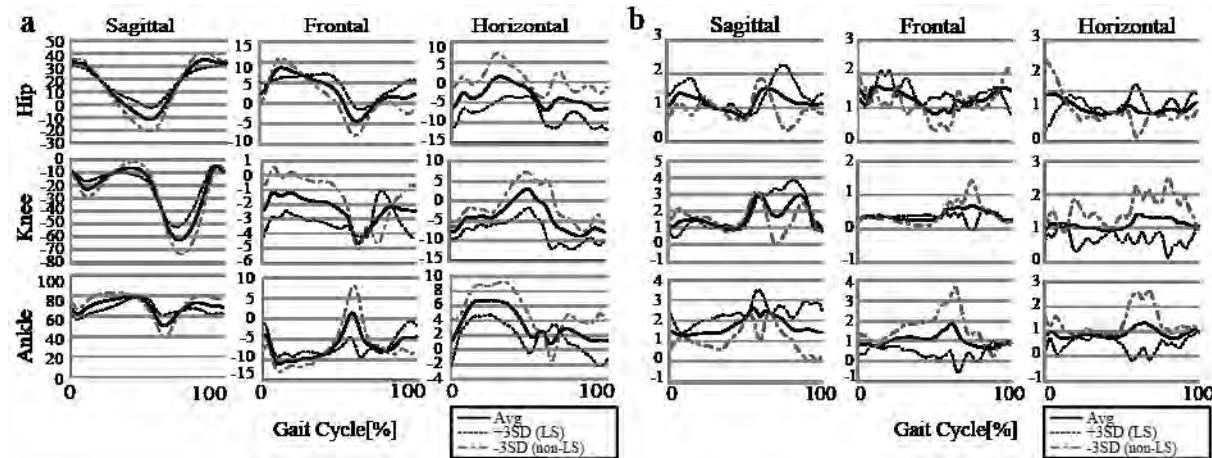
Caption: Fig.1. Joint kinematics recombined from PCV7, 12 and 13. (a) Central tendency and (b) Variability.

Conclusion: In this study, PCA was used to identify the key joint kinematics characteristics of gait related to LS when walking on level ground. Statistical analyses revealed that PCV 7, 12 and 13 among 52 generated PCVs were related to LS. The recombined joint kinematics corresponding to these PCVs indicate that LS group tend to show smaller ROM in sagittal plane and greater joint kinematics variability during the swing phase in sagittal plane than non-LS group. These observations imply us that we are able to detect people who are in LS using some sensors such as accelerometer or optical sensor to capture these features.

References: [1]JOA, The Locomotive Challenge! retrieved December 9, 2014,from https://locomo-joa.jp/en/index.pdf

[2]Yoshimura et al., J Bone and Miner Metab, 27:620-628, 2009.

[3]Seichi et al., J Orthop Sci, 17: 163-172, 2012.

[4]Kobayashi et al., J Biomech, 2014.

Disclosure of Interest: None Declared

Motion Analysis

AS-0508

ESTIMATION OF SUBJECT-SPECIFIC 3D POSITION OF THE KNEE LIGAMENT ATTACHMENT SITES AND LIGAMENT LENGTH VARIATION DURING KNEE FLEXION

Elena Bergamini [1][2],*Hélène Pillet [3]Goulven Rochcongar [3]Patricia Thoreux [3][4]Philippe Rouch [3]Valentina Camomilla [1][2]Aurelio Cappozzo [1][2]Wafa Skalli [3]

[1]Department of Movement, Human and Health Sciences, [2]Interuniversity Centre of Bioengineering of the Human Neuromusculoskeletal System, Università degli Studi di Roma "Foro Italico", Roma, Italy, [3]LBM/Institut de Biomécanique Humaine Georges Charpak, Arts et Metiers ParisTech, Paris, [4]Service de Chirurgie Orthopédique et Traumatologique, Hopital Avicenne - Université Paris 13, Bobigny, France

Introduction and Objectives: In musculoskeletal modelling and movement analysis, accurate information about the 3D position of the knee ligament attachment sites, as well their length variation during knee flexion, is critical [1]. Extensive literature exists that describes the position of both the anterior and posterior cruciate ligaments (ACL, PCL) [2], whereas few works focused on the medial and collateral ligaments (MCL, LCL) [3]. All these studies provide the attachment site positions in terms of distances to surgically relevant anatomical landmarks, rather than with respect to anatomical reference frames suitable for movement analysis applications. Furthermore, although ligament length variation during knee flexion has been dealt with in the literature [1,4], its complete characterisation along with attachment site location has not been performed yet. The purpose of this work is to provide the 3D position of the knee ligament attachment sites with respect to anatomical reference frames defined on femur and tibia bone templates, along with the ligament length variations during knee flexion. This information, associated with morphological features of the bones involved observed in a given individual, allows for subject-specific modelling of the knee ligaments.

Methods: Twelve fresh-frozen specimens (6 M, 6 F, age range: 47-79 years), consisting of femur, patella, fibula, tibia and intact joint passive structures, were analysed after a thawing period of 24 hours. Two clusters of reflective markers were secured to the femur and tibia and three tantalum spheres were embedded in each bone. The specimens were set in motion (6 flexion-extension cycles, range of motion: 0-120°) using the device described in [5] and the 3D pose of both bony segments were recorded using a stereophotogrammetric system (Polaris, CDN). Two orthogonal X-ray images of each specimen were simultaneously obtained (EOS®, FR) and a 3D model of the tibia, fibula, and femur, including markers and tantalum spheres, was obtained using the reconstruction algorithm validated in [6], which adapts bone templates to match subject-specific X-ray images. Each specimen was then dissected and the attachment sites of ACL, PCL, deep and superficial MCL, and LCL were identified and marked using a radio-opaque paint. CT scans of each bone epiphysis were finally taken (General Electric Healthcare, US) and processed to obtain the 3D geometry of each attachment site, as well as the position of the tantalum spheres. The latter were used to map the attachment sites on the corresponding bone models. The centroids of the origin and insertion of each ligament were then calculated and the distance between them was determined during the knee flexion-extension. Finally, to assess the variability of each attachment site location, all subject-specific bone models were scaled and deformed using a kriging algorithm [7] to fit the bone templates used in [6]. The same transformation was then applied to the centroids of each attachment site to map

them on the same models. Anatomical reference frames were defined for tibia and femur templates according to [1], and mean (μ) and standard deviation (σ) values of the centroid 3D coordinates with respect to the latter frames were calculated.

Results: The variability of the ligament attachment sites location are in agreement with previous literature [2,3] (Fig. 1): the variability of the origins and insertions located on the femur was, on average, lower than that on the tibia and fibula. For what concerns the tibial insertion of the superficial MCL, it should be noticed that its high variability along the y-axis can be ascribed to its critical identification due to the lack of clear-cut bony prominences [8]. The trends of each ligament length variation (Fig. 1) are in agreement with previous studies [1,4], as well as μ and σ values corresponding to the ligament maximum length [4].

Figure:

Bone	Ligament	Coordinates (mm) μ (σ)		
		X	Y	Z
Femur	ACL	-6.7 (1.4)	2.7 (3.2)	-5.6 (0.9)
	PCL	2.3 (1.6)	-7.7 (1.7)	8.4 (1.1)
	LCL	-2.5 (2.0)	3.7 (2.1)	-35.6 (0.7)
	MCL	6.9 (2.0)	6.1 (2.0)	38.4 (0.1)
Tibia/Fibula	ACL	0.2 (2.9)	-0.2 (0.1)	1.4 (1.7)
	PCL	-15.1 (1.4)	-9.9 (1.8)	3.3 (3.3)
	MCL deep	-0.5 (4.3)	-14.3 (4.3)	33.5 (0.4)
	MCL superficial	8.8 (3.1)	-63.7 (5.6)	16.8 (1.1)
	LCL	-17.3 (5.0)	-34.8 (4.0)	-39.0 (3.7)
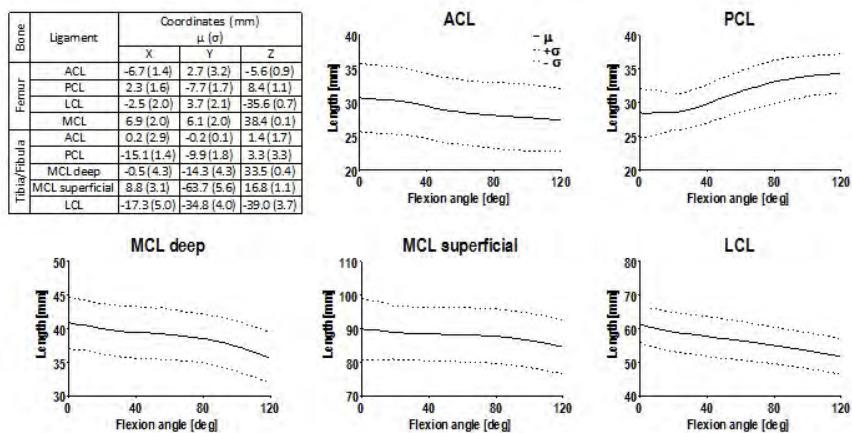
Caption: Ligament length variation patterns (μ ± σ) as a function of the flexion angle and centroid coordinates (μ and σ) in the template anatomical reference frames.

Conclusion: The present study provides the 3D coordinates of the knee ligaments attachment sites in specified anatomical reference frames of femur and tibia templates and the variation of the ligament lengths during knee flexion. By registering these templates with morphological features of the corresponding bones as observed in a given individual, subject-specific bone models with the knee ligament insertion and origin sites can be estimated with the indeterminacy provided by this investigation.

References: [1] Bergamini et al., Gait Posture, 33:706-11, 2011

[2] Kopf et al., Knee Surg Sports Traumatol Arthrosc, 17:213-9, 2009

[3] Laprade et al., J Bone Joint Surg Am, 89:2000-10, 2007

[4] Belvedere et al., J Biomech, 45:1886-92, 2012

[5] Azmy et al., Orthop Traum Surg Res, 96(1):28-36, 2010

[6] Chaibi et al., Comput Methods Biomech Biomed Engin, 15(5):457-66, 2012

[7] Trochu, Eng Comput, 9:160-77, 1993

[8] Liu et al., J Orthop Sur Res 2010, 5(1):69-77

Disclosure of Interest: None Declared

Motion Analysis

AS-0509

PLANTAR PRESSURE DISTRIBUTION DURING RUNNING IN CHILDREN

Paula R. Mesquita [1,*]Letícia Erna [1]Elias Trotti [1]Raphael Oliveira [1]Ana de David [1]

[1]Faculdade de Educação Física - FEF, Universidade de Brasília - UnB, Brasília, Brazil

Introduction and Objectives: The acquisition of fundamental motor skills such as walking and running, depends on the biological processes of maturation and growth, as well as on the experiences and motor repertoire acquired by the child. The muscle forces responsible for human locomotion together with external forces result in loads that are generated under the foot when in contact with the ground and represent an estimate of motion mechanical efficiency and can initiate changes in foot function by changing how charges are distributed.

Running results in greater mechanical stress to the musculoskeletal system than walking, creating more demands on the locomotor system, however children's plantar pressure distribution (PPD) has been studied mostly during walking and quiet standing. No studies evaluating PPD variables during running in children were found. Therefore, the aim of this study was to describe PPD during running and comparing children aged 4, 6, 8 and 10 years old.

Methods: Forty healthy children were evaluated. They were asked to run barefoot at self-selected speed across the PPD platform (Emed n-50, 50Hz, 4 sensors/cm², Novel GmbH) recording 5 trials for each foot. Data analysis was performed with database software HMFT (Novel GmbH), considering relative contact area (CA) and peak pressure (PP) values in five regions of the foot (hindfoot, midfoot, forefoot, hallux and toes) in addition to the total area. Only rearfoot strike trials were selected for analyses. Inter-groups differences were determined using the one-way Anova with significant differences analysed by Games-Howell post hoc test. All tests were performed with SPSS 21.0 ($p \leq 0,05$).

Results: No systematic differences were found between left and right feet for the parameters evaluated, therefore presented data refers to left foot trials.

Body mass (BM), body height (BH) and foot length (FL) significantly differed between groups ($p \leq 0,000$), children aged 10 years-old had increases of approximately 110% for BW and 35% for BH and FL when compared to 4 year-olds, which represents the growth of the children.

Peak pressure values in the total area of the foot were 60% lower for the 4 year-olds during running when compared to 10 year-olds ($p = 0,003$). Under the forefoot the 4 y-o group had values on average 67% lower when compared to groups aged 6 ($p = 0,011$), 8 ($p = 0,003$) and 10 ($p = 0,013$). Hindfoot and forefoot experienced the highest values of pressure. Relative contact area under the hindfoot of the 4 year-olds was on average 23% smaller during running when compared to 8 ($p = 0,039$) and 10 y-o groups ($p = 0,000$). Under the midfoot of the 4 y-o group the CA was 47% higher than for the 10 year-olds ($p = 0,024$). For the remaining foot regions the values were raised between the groups aged 4 and 6 y-o and for the 6, 8 and 10 years-old groups were either maintained or reduced.

Conclusion: Values of PP showed an upward trend through the ages, especially between 4 and 10 y-o. For some foot regions values were maintained or reduced between groups with very close ages.

A tendency for higher values with increasing age was also seen for CA under every region of the foot except for the midfoot, which had decreasing values with increasing age.

The raise in PP and CA values may be related to the increases seen in body mass, body height and foot length measures, representing the growth and development of the children. On the other way the decreasing values of CA in the midfoot region could be related to the development of the longitudinal arch.

Table:

		4 years (n= 10)	6 years (n= 10)	8 years (n= 10)	10 years (n= 10)
		Mean ± SD	Mean ± SD	Mean ± SD	Mean ± SD
BODY MASS (Kg)		18,12 ± 3,99	25,41 ± 4,16	31,38 ± 7,85	38,47 ± 7,58
BODY HEIGHT (cm)		106,20 ± 5,13	122,50 ± 5,42	129,8 ± 7,33	144,00 ± 6,70
FOOT LENGTH (cm)		17,00 ± 0,90	19,61 ± 0,96	21,04 ± 1,42	23,13 ± 1,09
PEAK PRESSURE (kPa)	TOTAL	358,80 ± 59,65*	464,80 ± 103,56	576,50 ± 230,80	576,00 ± 135,85*
	HINDFOOT	312,50 ± 83,51	292,10 ± 132,57	368,80 ± 200,09	431,20 ± 156,97
	MIDFOOT	115,90 ± 20,39	133,00 ± 38,73	154,00 ± 40,73	153,00 ± 57,92
	FOREFOOT	205,56 ± 35,47*	320,00 ±86,37*	359,60 ± 98,23*	349,70 ± 113,26*
	HALLUX	243,67 ± 45,77	362,50 ± 131,96	318,30 ± 127,32	400,20 ± 174,64
	TOES	136,40 ± 42,04	175,90 ± 45,22	172,70 ± 79,65	178,90 ± 77,81
CONTACT AREA (%)	TOTAL	100,00 ± 0,00	100,00 ± 0,00	100,00 ± 0,00	100,00 ± 0,00
	HINDFOOT	22,17 ± 1,85[a]	24,82 ± 3,19	25,37 ± 2,81[a]	27,25 ± 1,69[a]
	MIDFOOT	25,78 ± 4,53[a]	22,10 ± 2,01	20,57 ± 4,26	17,30 ± 6,91[a]
	FOREFOOT	38,03 ± 1,84	39,40 ± 0,66	39,93 ± 1,76	40,48 ± 2,71
	HALLUX	7,63 ± 0,56	8,40 ± 1,08	8,45 ± 0,88	8,75 ± 1,56
	TOES	6,27 ± 2,16	7,23 ± 2,46	6,62 ± 2,13	6,60 ± 1,87

Caption: Body mass, body height, foot length, peak pressure (kPa) and relative contact area (%) values during running (p ≤ 0,05)

Disclosure of Interest: None Declared

Motion Analysis

AS-0510

A KINEMATIC MODEL OF THE TIBIA-FIBULA-TALUS COMPLEX FROM FUNCTIONAL ADAPTATION

Michele Conconi [1 2,*] Vincenzo Parenti-Castelli [1 2]

[1]Dept. of Indusrtial Engineering - DIN, Alma Mater Studiorum - University of Bologna, [2]Health Sciences and Technologies - Interdepartmental Center for Industrial Research [HST-ICIR], University of Bologna, Bologna, Italy

Introduction and Objectives: Several direct techniques exist for the in-vivo registration of the bone relative motions [1]. However, their applicability is limited by their invasiveness and/or by the cost associated with the specific equipments and time required. Alternatively it is possible to define kinematic models based on the patient anatomy and use them for the indirect evaluation of the bones movement. A possible approach in this direction exploit the capability of the joint tissues to modify their structure in response to the mechanical environment to which they are exposed [2-4] (functional adaptation). Although there is still room for discussion [5], functional adaptation seems to produce structures that use optimally their material, providing the necessary strength with the smallest amount of tissue. If the rules governing this process are known, it is possible to revert the reasoning and reconstruct the mechanics for which a joint is optimized from its architecture. In particular, it has been hypothesized [6] that contact surfaces adapt to optimize the capability to distribute contact loads. In [7], a measure of joint congruence has been presented that allows estimating the capability to distribute an applied load from purely geometrical considerations, namely form the knowledge of the shape of the articular surfaces and their relative position and orientation (configuration). A kinematic model of the adapted motion can thus be obtained as the envelope of maximum congruence configurations evaluated at different values of the flexion angle.

This approach has been validated in vitro on the tibio-talar (TT) joint with good results [8]. The aim of this work is to evaluate if this approach holds for the tibia-fibula-talus complex as well.

Methods: As described in [9], the TT motion was registered and the articular surfaces of the talus, distal tibia and fibula were digitalized during a in-vitro experiment. The articular surfaces were thus taken from MRI of another subject, while the reference tibio-fibular (TF) motion was taken from the literature [10].

Congruence was evaluated as the ratio between peak pressure and total contact force which, within the elastic foundation contact model, becomes a purely geometrical relation, as described in [7]. The congruence of the tibia-fibula-talus complex was evaluated as the sum of the congruence of the TT, fibio-talar and proximal TF articulations.

Since the ankle joint may be considered as a single DOF joint [11], the TT and TF motions describe a spatial trajectory in which can be parameterized, for instance, by the dorsi-plantar flexion angle. The trajectory of the TT and TF adapted motion was thus found as the envelope of successive maximum congruence configurations obtained varying the flexion angle within its physiological range.

Results: Fig. 1 shows the predicted TT and fibio-talar motions (continuous lines). Dotted lines represent TT experimental motion. Tab. 1 report the mean absolute errors (MAE) between computed and experimental TT motion, with and without considering the fibula.

Figure:
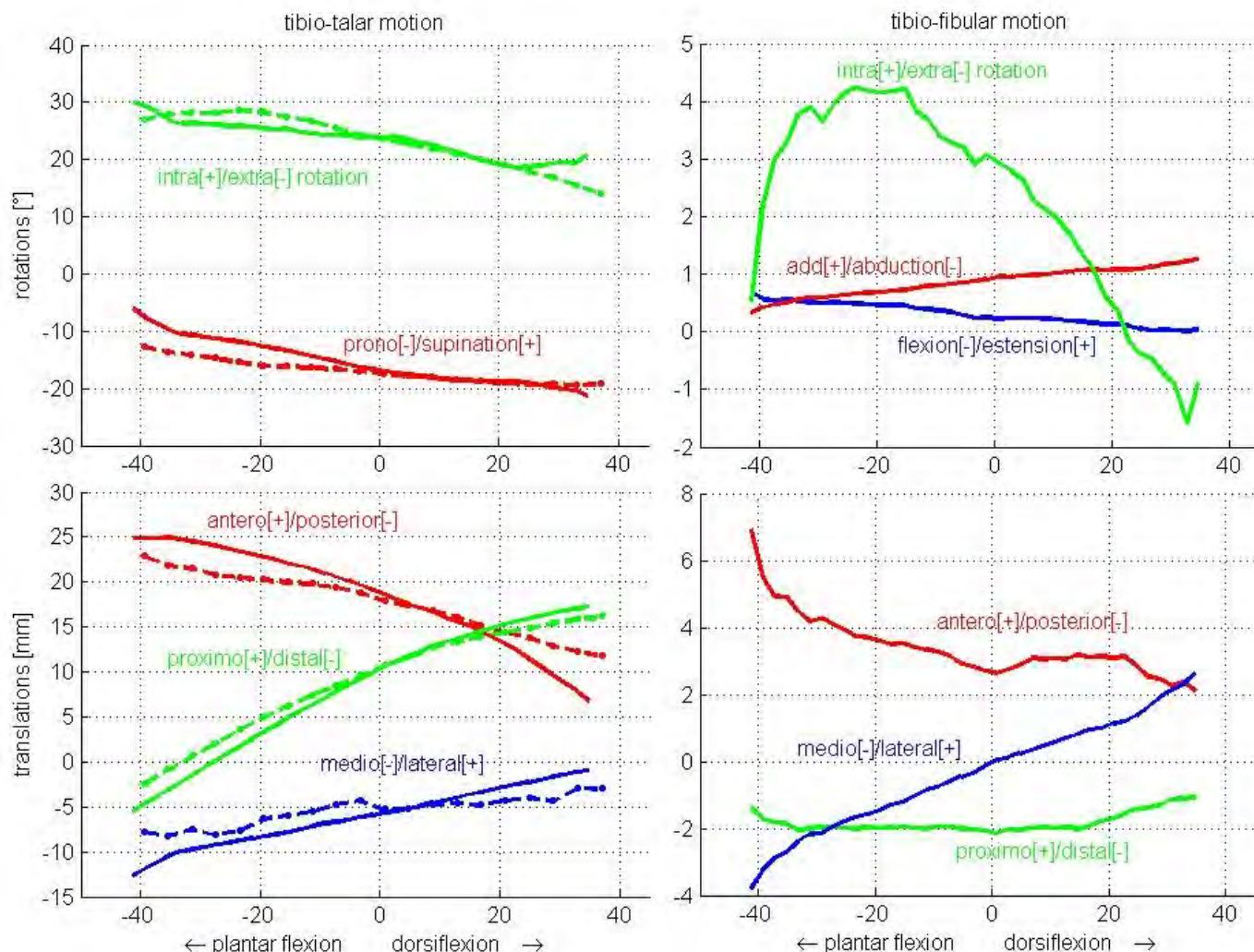
Caption: Computed (-) and experimental (.) tibio-talar and tibio-fibular motion.

Conclusion: The inclusion of the fibula did not modify the model capability to predict the TT motion. Qualitatively, the TF motion is in agree with what reported in the literature, the fibula moving posteriroly and laterally during the dorsiflexion motion, and rotating mainly about the intra-extra rotational axis. These results support the extendibility of the model to the multibone joints.

Table:

	Add/abduction	Intra/extra rotation	Antero/Posterior	Proximo/Distal	Medio/lateral
Without fibula	2.05	1.04	1.81	1.09	1.91
With fibula	1.73	1.68	1.99	1.13	1.66

Caption: MAE between computed and experimental tibio-talar motion.

References: [1] Masum, M. A. et al. ABEC 2014.

[2] Robling, A. G. et al. Annu Rev Biomed Eng, 2006, 8, 455-498.

[3] Hayashi, K. J Biomech, 1996, 29, 707-716.

[4] Plochocki, J. H. et al. Anat Rec A Discov Mol Cell Evol Biol, 2006, 288, 776-781.

[5] Bertram, J. et al. J Theor Biol, 1988, 131, 75-92.

[6] Heegaard, J. H. et al. J Orthop Res, 1999, 17, 509-517.

[7] Conconi, M. et al. J Eng Med, in print.

[8] Conconi, M. et al. App Mech Mat, 2012, 162, 266-275.

[9] Franci, R., et al. J Biomech, 2009, 42, 1403-1408.

[10] Huber, T. et al. Foot Ankle Surg, 2012, 18, 203-209.

[11] Leardini, A. et al. J Biomech, 1999, 32, 111-18

Disclosure of Interest: None Declared

DISCRIMINATION OF FALLERS AND NON-FALLERS USING THE VARIABILITY OF THE MAGNITUDE OF THE SACRAL ACCELERATION VECTOR

Yoshiyuki Kobayashi [1,*] Hiroaki Hobara [1] Thijs Heldoorn [1] Masaaki Mochimaru [1]

[1] Digital Human Research Center, National Institute of Advanced Industrial Science and Technology, Tokyo, Japan

Introduction and Objectives: Recent advancement of *Micro Electro Mechanical Systems* technology enables us to predict the potential risk of fall during daily walking in individuals. Researchers proposed various techniques to discriminate the fall risk of people using sensors. Doi et al. (2013) recently reported that the harmonic ratio of upper trunk acceleration during walking measured by tri-axial accelerometer attached on the upper trunk can discriminate the fallers and non-fallers with the sensitivity of 68.8 % and the specificity of 84.2 %.

It is quite difficult to attach the sensor accurately in practical situation; some may place the sensor in wrong location and some may place the sensor with wrong alignment. Of these errors, sensor alignment error may solve quite easily when the discrimination algorithm uses the magnitude of the acceleration vector as the input signals. Recently, we found that the variability of the joint kinematics for fallers was larger than that for non-fallers especially during the late-stance to early swing phase in gait cycle regardless of the joints and planes. Therefore, the purpose of this study was to test the hypothesis that the magnitude of the acceleration vector may predict the personal fall risk quite accurately.

Methods: Forty healthy community-dwelling elderly subjects (20 M & 20 F) were recruited for the study. Twenty of them (10 M & 10 F) experienced one or more falls during the year prior to the experiment. These participants were classified as fallers, and the others as non-fallers. The falling history of each participant was obtained before the experiment. The experimental protocol was approved by the local ethical committee and all the participants gave their written informed consent before participating. The experiments were performed in a room with a straight 10 meter path for the participant to walk. Three-dimensional positional data was obtained using reflective markers and a 3D motion capture system (VICON MX, VICON) using a sampling frequency of 200 Hz. A total of 55 IR reflective markers were attached in accordance with the guidelines of the Visual 3D software (C-Motion Inc.). We also recorded the ground reaction forces (GRFs) using six force plates (BP400600-2000PT, AMTI) sampled at 1 kHz to time the gait cycle. Participants were asked to walk barefoot at a comfortable, self-selected speed. After the practice, five successful trials in which each GRF measured properly were recorded.

The raw time series trajectory data was digitally filtered using a fourth-order Butterworth filter with zero lag and a cut-off frequency of 10Hz. The magnitude of sacral acceleration data were computed from filtered data. During this calculation, gravitational acceleration has added to the signal. The magnitude of sacral acceleration data were time-normalized by the gait cycle duration determined based on the GRFs and divided into 101 variables ranging from 0 to 100%. The intra-subject mean (AVG) and the standard deviation (SD) for each time point within the five sets of data obtained from each participant were calculated from time-normalized magnitude of acceleration data. Discrimination analysis was used to build the model to discriminate potential personal risk of falling using the data. When build the model, participants were separated into two homogeneous groups, and the accuracy was assessed each other using cross validation method.

Further, in order to ensure the robustness of the method, we calculated the average of the time-series SD data during late-stance to early swing phase of gait cycle respectively, and used these variables as the independent variable.

Results: The results of cross validation revealed the sensitivity of 80.0 % and the specificity of 85.0 % (Table 1), which is higher than the results of previous study (Doi et al. 2013). This may be due to the selection of independent variables. Indeed, Doi et al. (2013) used a harmonic ratio calculated from the acceleration data of entire gait cycle, while we used the average of the time-series SD data during early swing phase of gait cycle based on the results of previous study. Another advantage of our method is the function that users do not have to concern about the alignment of the sensors unless the location is fixed; thus, this would be strong advantage especially during the practical use, such as smart phone based system.

Caption: The results of the cross validation.

Conclusion: In the present study, we test a method to build the discrimination algorithm using the magnitude of the sacral acceleration vector to predict the potential personal fall risk during daily walking. With the assessment of the robustness and the accuracy of the proposed method, we found that the accuracy of the prediction was higher than those reported in previous study.

Table:

	Fallers	**Non-Fallers**	**Total**
High Risk	**16**	3	19
Low Risk	4	**17**	21
Total	20 Sensitivity:80%	20 Specificity:85%	40

Caption: The results of the cross validation.

References: [1] Doi et al., J Neuroeng Rehabil, 10, 2013.

[2] Kobayashi et al., J Biomech, 47, 2014.

Disclosure of Interest: None Declared

Imaging / Advanced Imaging

AS-0512

THE INFLUENCE OF TRANSDUCER ANGLE ON ULTRASOUND MEASUREMENTS OF INTER-RECTUS DISTANCE ON WOMEN POST-PARTUM

Nicole Hills [1,*]Nadia Keshwani [1]Linda McLean [1 2]

[1]School of Rehabilitation Therapy, Queen's University , Kingston, [2]School of Rehabilitation Sciences, University of Ottawa, Ottawa , Canada

Introduction and Objectives: To compensate for the expansion of the uterus in mid -to late-pregnancy, the rectus abdominus muscles must move laterally; therefore the separation between the two heads of the rectus abdominus muscle, or the inter-rectus distance (IRD), is increased [1]. An increased IRD beyond two centimeters at the umbilicus [2] is referred to as Diastasis Recti (DR), and is estimated to be present in 35 to 68 percent of women post-partum [3]. This separation can persist for many years following a pregnancy [4], and is associated with reduced abdominal strength and endurance [5] and lumbo-pelvic dysfunction [6]. Ultrasound imaging (USI) has been shown to provide valid and reliable measures of IRD at and above the level of the umbilicus when compared to measurements obtained intra-operatively [7]. However, no study has explored the effect of errors in transducer angle during these evaluations. Therefore, the purpose of this study was to determine if transducer head angle relative to the skin and underlying linea alba has an effect on the apparent IRD measured using USI in women who have previously delivered babies.

Methods: Fourteen healthy female volunteers who had previously delivered babies participated. USI images were captured at the superior border of the umbilicus by two different raters beginning with the probe held perpendicular to the anterior abdominal wall (zero degrees) and then at probe angles of 5, 10 and 15 degrees to the perpendicular both the cranially and caudally. IRD was measured from each image offline and was determined as the linear distance between the medial borders of the two heads of the rectus abdominis muscle. The data were not normally distributed, therefore a Friedman's Two-Way Analysis of Variance by Ranks was used to test for systematic differences between the two examiners and among transducer angles. A two-way repeated measures analysis of variance was performed to investigate potential interactions between examiner and angle, since such an analysis cannot be done using non-parametric tests. In this case the residuals were inspected for normality and it was determined that they were normal using the Kolmogorov-Smirnov test. An alpha level of 0.05 was used for all statistical tests.

Results: The Friedman's two-way ANOVA revealed no significant effect of transducer angle (H=2.00; $p = 0.920$), but did reveal a significant difference between examiners ($H = 7.37$, $p = 0.007$). The two-way repeated measures ANOVA revealed no significant interaction between transducer angle and examiner ($F = 0.12$, $p = 0.994$) and, consistent with the non-parametric analysis, did not show a significant effect of transducer angle ($F = 1.56$, $p = 0.162$) and did show a significant examiner effect ($F = 62.11$, $p < 0.0005$).

Figure:
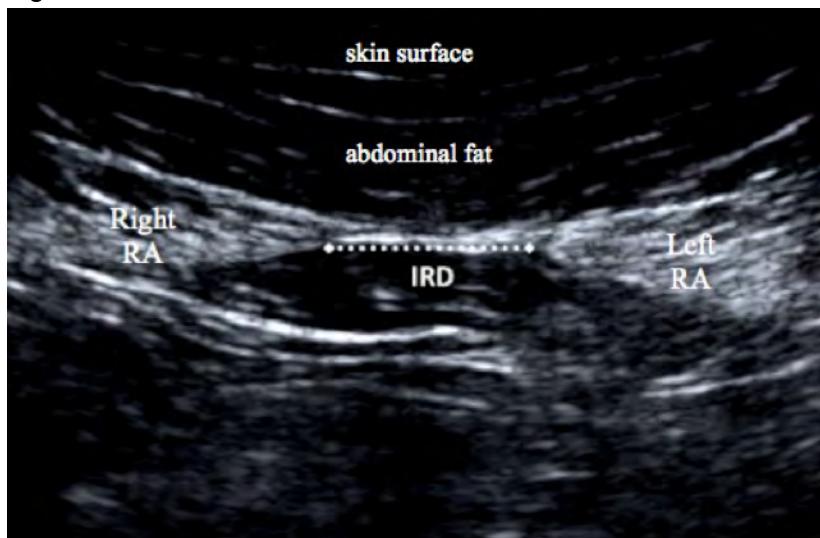
Caption: Ultrasound image of the inter-rectus distance (IRD) measurement and rectus abdominis (RA) muscle

Conclusion: The results suggest that error in transducer angle is not a major problem when measuring IRD using transabdominal ultrasound imaging. Although it appears that different examiners may induce a measurement bias. This measurement bias should be investigated further in future studies.

References: [1] Gilleard et al., Phys Ther., 76:750-762, 1996.

[2] Beer et al., Clinical Anatomy. 22:706-711, 2009.

[3] Candido et al., J Assoc Chartered Physiother Womens Health., 97:49-54, 2005.

[4] Coldron et al., Man Ther., 13:112-121, 2008.

[5] Liaw et al., J Orthop Sports Phys Ther. 41:435-443, 2011.

[6] Parker et al., J Womens Health Phys Ther., 33:15-22, 2009.

[7] Mendes et al. Acta Cir Bras., 22:182-186, 2007.

Disclosure of Interest: None Declared

Imaging / Advanced Imaging

AS-0513

THREE-DIMENSIONAL SCANNING FOR IMPROVED BRA DESIGN

Celeste E. Coltman [1,*]Julie R. Steele [1]Deirdre E. McGhee [1]

[1]Biomechanics Research Laboratory, University of Wollongong, Wollongong, Australia

Introduction and Objectives: Three dimensional (3D) scanning has potential to significantly improve bra cup design, sizing and fit by increasing accuracy in measuring parameters such as breast volume [1,2]. Accurate breast volume measurement depends on the ability of a scanner to visualize the entire breast. Inaccuracies have been reported when measuring the volume of large ptotic breasts due to the tendency of the inferior aspect of the breast to contact the abdominal wall when women are scanned in a standing position [1,3]. As this compromises the ability of the scanner to visualize the entire breast, it is likely that breast volume is underestimated. To improve breast visualization during 3D scanning, a prone position, where the breasts hang away from the trunk, has been proposed when scanning women with large ptotic breasts [3]. The objective of this study was to quantify the difference in breast volume determined when scanning women with large ptotic breasts in a standing compared to a prone position. It was hypothesized that scanning large ptotic breasts in a prone position would allow complete visualization of the breasts and, in turn, a greater breast volume, compared to scanning women while standing.

Methods: Participant's were 49 women (mean age 37.1±13.0yr; mean BMI 29.5±5.2kg/m^2; average cup size F, range D-I; average band size 16, range 8-18). Adhesive markers were placed on participants' skin around the outline of each breast. The breasts were scanned using a hand held scanner (Artec^{TM}) while participants assumed three positions: i) standing, hands on hips, ii) standing, hands on head [1,2], and iii) lying prone. A 3D model of each breast was created from each scan and breast volume was calculated (mL; Geomagic software, 3D Systems, USA). Breast visualization was rated as "complete" or "incomplete" and the level of breast ptosis was characterized by measuring sternal notch to nipple distance [4] and by grading the ptosis from 0-3 [5]. A repeated measures ANOVA with one within factor (scanning position) was used to determine any significant (p <0.05) differences in breast volume among scanning positions. Bland-Altman plots were used to determine difference in agreement between scanning position for breast volume data. Frequency of "complete" and "incomplete" breast visualizations in the scanning positions was also compared.

Results: Breast volume ranged from 302-2,265mL (mean 1,038±450mL). Ninety per cent of participants were classified as having ptotic breasts (mean stage 2; range stage 1-3) and the sternal notch to nipple distance ranged from 20.8-35.2cm (mean 28.5cm). The prone position allowed complete breast visualization in 100% of participants, compared to only 5% of participants in either standing position. Breast volume measured in the prone position was significantly greater than that measured in either standing position, which were not significantly different to each other (Table 1). Bland-Altman plots showed good agreement in breast volume data measured in the standing positions but poor agreement with a negative bias between breast volume measured in the standing position (hands on hips) and the prone position. The negative bias and consequential underestimation of breast volume in the standing positions increased as breast volume and ptosis increased (Fig 1). The error of underestimation in breast volume of both standing positions compared to the prone position was as high as 473mL at an individual level and 103mL at a group level. This equated to ~3% underestimation of breast

volume for participants at the smaller end of the breast volume (size) spectrum (volumes 400-500mL) and 7-10% for breast volume at the larger end of the spectrum (volumes >500mL).

Figure:
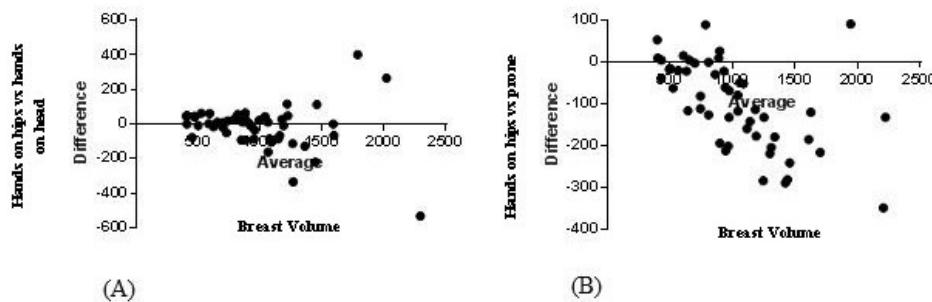
Caption: Bland-Altman plot (bias and limits of agreement ± 1.96*SD) for breast volume measured in the two standing scanning positions (A), and the standing with hands on hips and prone scanning positions (B)

Conclusion: The volume of large ptotic breasts is likely to be underestimated when women are scanned while standing, particularly for women with large breast volumes (>500mL). This error has the potential to negatively affect bra sizing, design and fit and should be accounted for when data are extracted from 3D scans to manufacture and size bras.

Table:

Scanning Position	Right breast volume (mL)	Left breast volume (mL)	
	Mean ± SD **(95% CI)**	**Mean ± SD** **(95% CI)**	
Standing hands on hips	973 ± 409 (857-1,090)	954 ± 419 (853-1,074)	
Standing hands on head	990 ± 432 (867-1,113)	963 ± 382 (854-1,071)	
Lying prone	1,072 ± 470* (939-1,206)	1,057 ± 437* (933-1,181)	

*Indicates statistically significant difference in breast volume compared to the standing positions.

Caption: Mean (SD) values for the volume of the participants' breasts in all scanning positions

References: [1]Lee et al.,Appl Ergon,35:353-359,2004

[2]Kovacs et al.,Ann Plast Surg 56:229-236,2006

[3]Thomson et al.,Plast Reconstr Surg,123:1588-1596,2009

[4]Westreich,Plast Reconstr Surg,100:468-479,1997

[5]Regnault,Clin Plast Surg,3:193-203,1976

Disclosure of Interest: None Declared

Imaging / Advanced Imaging

AS-0514

THE IMPACT OF LOADING AND BOUNDARY CONDITIONS IN FINITE ELEMENT ANALYSIS OF MR ELASTOGRAPHY

Lyam Hollis [1,*] Lauren Thomas-Seale [2] Noel Conlisk [1] Neil Roberts [3] Pankaj Pankaj [4] Peter Hoskins [2]

[1]Cardiovascular Sciences, [2]Medical Physics, [3]Clinical Research Imaging Centre, [4]School of Engineering, University of Edinburgh, Edinburgh, United Kingdom

Introduction and Objectives: Magnetic Resonance Elastography (MRE) is an MRI-based technique utilising a phase encoding gradient to track an externally induced shear wave. Local estimates of wavelength are related to the material properties using an inversion algorithm. The technique can be replicated *in silico* using finite element analysis (FEA) allowing a high level of control over input parameters and thus providing a useful pathway for testing and development of MRE post-processing software. Despite this there is limited literature investigating how variation of modelling parameters affects shear modulus measurements and how the process can optimised. This study aimed to investigate the effects that boundary conditions, loading conditions and interaction definitions between two model sections have on measurements made of the shear modulus using the MRE inversion algorithm.

Methods: All simulations were performed using *Abaqus/Explicit.* Boundary and loading conditions were investigated using a 50x50x50mm^3 box (model 1). Material properties were defined as linear elastic with a uniform shear modulus varied between 3-33kPa and a density of 1000kg·m^{-3} throughout. A set of infinite elements was applied to the lower surface to allow waves to propagate to infinity. Boundary conditions were applied to the side surfaces. The conditions investigated here were encastred and symmetric. The load was applied to the upper surface at a frequency of 200Hz over a region that varied in area from 10-40mm^2. A second model (model 2) of geometry 200x200x50mm^3 aimed to investigate how the load size affects measurements. Infinite elements were applied to both the lower and side surfaces and the load was applied over a region on the upper surface varied in area from 10-100mm^3.

To investigate interactions between regions a third model was created (model 3).This was an 80x80x50mm^3 box with a 10mm radius cylinder running through the centre. The background shear modulus was defined as 3kPa whilst the insert shear modulus was varied between 4-9kPa. Symmetric boundary conditions were applied to the lower and side surfaces. A load covering a 45x45mm^2 region was applied to the upper surface at a frequency of 100Hz. The effects of using a tie constraint, merging the two parts and defining a frictional interaction between the insert and the background were investigated. The frictional coefficient was varied from 0.5-1.25.

 In all instances once the simulation had run displacement data from a two-dimensional slice taken directly through the centre of the model was exported to *Matlab* where it was assessed using the 2-d direct inversion algorithm.

Results: Shear modulus measurements from the inversion algorithm tended to be overestimated for all prescribed shear modulus except 3kPa, which was underestimated, in both the encastred and symmetric boundary conditions. Increasing the prescribed shear modulus increased the size of the error (with encastred boundary conditions and a load size of 40mm^2 the error for the 9kPa is 4% compared with 11% at 33kPa). Whereas for the symmetric boundary conditions the size of the error decreases as the size of the load was increased, the size of the error increases with increasing load size

for encastred boundary conditions. In model 2 the size of the error increased with decreasing load size. Whilst the size of the error is larger at smaller load sizes for the symmetric boundary conditions than it is when no boundary conditions are applied, as the load size increases, the size of the error converges (figure).

Results from the tie constrained interactions and the merged insert and background parts in model 3 were almost identical to one another. In both instances increasing the prescribed value for the shear modulus resulted in an increase in the measured value for the shear modulus, whilst the measured value for the background remained consistent (table). For the frictional interaction measurements of the insert shear modulus were highly variable and often overestimated by as much as 1000%. Visual inspection of the wave images showed minimal propagation in this region.

Figure:
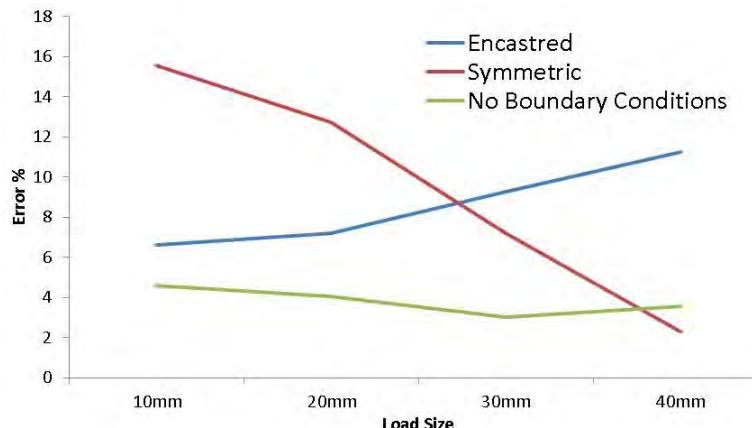
Caption: Load size dependant error in shear modulus measurement for the a shear modulus of 21kPa

Conclusion: Boundary and loading conditions have a clear influence over modelling data from MRE. For technique development it is preferable to reduce these effects to as great an extent as possible whilst maintaining short computational time. For these reasons this work suggests that using symmetric boundaries in concordance with a large loading region is optimal. With respect to interactions between two sections there seems to be little difference between merging parts and defining a tie constraint between them. In contrast defining a frictional interaction does not allow significant wave propagation in the insert and should be avoided.

Table:

	Tie		Merged	
	Background	Insert	Background	Insert
4kPa	3174	4347	3173	4340
5kPa	3171	5548	3170	5541
6kPa	3162	6775	3161	6766
7kPa	3152	8029	3152	8018
8kPa	3147	9277	3146	9264
9kPa	3134	10495	3139	10484

Disclosure of Interest: None Declared

Imaging / Advanced Imaging

AS-0515

HOW REPRODUCIBLE IS THE LOCALIZATION OF CRUCIATE AND COLLATERAL LIGAMENTS INSERTION POINTS BY USING MRI?

Silvia Pianigiani [1,*]Pasquale Salandra [2]Walter Pascale [1]Bernardo Inncoenti [3]

[1]IRCCS, Istituto Ortopedico Galeazzi, Milano, [2]Università Politecnica delle Marche, Ancona, Italy, [3]BEAMS Department, Université Libre de Bruxelles, Bruxelles, Belgium

Introduction and Objectives: The cruciate and collateral ligaments are ones of the main players in the stability of the knee joint and, for this reason; they are subjected daily to high mechanical stress. Therefore, they are more prone to injury than other soft tissues. The importance to correctly and univocally identify the ligaments position is mainly related to the clinical practice and, besides, a correct localization of them could be determinant for the surgical practice or in the development of knee specific models for biomechanical analysis. To provide information on the status of these ligaments, the use of MRI images became a common practice. However, in the literature, there are not in depth studies based on this kind of identification using MRI.

For these reasons, the aim of this study is to propose and to validate a new procedure able to localize, in a reproducible and repeatable manner, the insertion points of cruciate and collateral ligaments based on MRI.

Methods: The new proposed procedure requires to identify the insertion areas of the two cruciates and the two collaterals. In particular, two points are needed for the cruciate ligaments (the anterior and the posterior extremities of the insertion area) and one point for the collateral ligaments (considered as the mid-point of the insertion area). These points, according to literature studies, could be also considered appropriate for the correct description of the insertion footprint of these ligaments. A detailed description of the procedure to be used to identify these points has been made together with an illustrative tutorial video.

The validity, the reproducibility and the repeatability of the new technique were determined. In particular, the INTRA and INTER-Class Correlation (ICC) analysis has been performed on 10 legs, by three different operators. The operators were asked to apply the procedure in two ways: only after reading the description, instructional, manual and also after viewing the tutorial video. Moreover, the procedure has been applied on two different qualities images (MRI with magnetization at 0.4T and at 1.5T) to check if the proposed method could be considered image-quality independent. The data describing the insertion point localizations from the different operators have been collected and normalized before comparison.

Results: Results for the obtained ICC indexes, before and after watching the tutorial video, were subdivided for image–quality, for the analyzed ligament and for the location of the insertion attachment (femur or tibia).

For the highest image-quality, both intra and inter ICC indexes results higher than 0.87 with exception for the medial collateral ligament for both femur and tibia and the lateral collateral ligament for the tibia localization. All the indexes increases after the operators viewed the tutorial video (up to 127%). In general, the quality of the image improves the reproducibility in localization up to 80%.

Conclusion: The aim of this study was to develop and prove the efficacy of a new procedure to identify insertions of knee ligaments from MRI images. The obtained results of the intra and inter ICC analysis evidence that the proposed procedure

can be considered highly suitable. In particular, the cruciate ligaments insertions could be defined independently from the quality of the medical image and the operator. More attention should be taken into account for the distal insertion of the medial collateral ligament.

Disclosure of Interest: None Declared

Sport

AS-0516

AERODYNAMICS OF ISOLATED SKI JUMPING SKI

Mikko Virmavirta [1],*Juha Kivekäs [2]

[1]Department of Biology of Physical Activity, University of Jyväskylä, Jyväskylä, [2]Arteform Ltd, Espoo, Finland

Introduction and Objectives: In ski jumping the flight style changed early 1990's when V-style replaced the traditional one in which skis were held parallel and close to each other. As there was an urgent need among coaches for more information about the merit of this new flight style, several studies were conducted during these early years of V-style jumping. First and probably the most important study of V-style was published by Mahnke and Hochmuth [1]. They performed series of wind-tunnel experiments while investigating the benefits of the V-style compared with the traditional style. Cutter [2] conducted the comprehensive tests with a scale model (1:5.5) in the subsonic wind tunnel at the United States Air Force Academy Aeronautics. In this study V-angle of 22.5° with ankle angle of 20° (which was considered the maximum feasible for a ski jumper to turn skis more flat against the direction of motion) provided the best L/D ratio of 1.55. Significant improvement in L/D was found when ankle angle changed from 0 to 20 degrees especially in the lower angle of attack region (AoA). As the skis became more effective, the trim AoA (balanced pitching moment) reduced as well. Since about 2010 ski jumpers have used the curved sticks in the back part of their ski bindings in order to turn skis more flat and improve aerodynamics of the jumper/ski system. However, the true effect of edge angle of skis has not been well studied. Therefore, the purpose of this study was to examine the combined aerodynamic effect of V and edge angles of ski jumping ski in wind tunnel.

Methods: The tests were carried out in the Otaniemi LS-wind tunnel with a cross section of 3.68 m^2. Tests were done with a real 100% size ski jumping ski (Elan 242 cm) with a realistic speed around 28–30 m/s. A single isolated ski was suspended to the 6-component wind tunnel balance. The AoA and yaw-angle were automatically adjustable during the test run. These angles could be run through with a predefined script in the control computer. The edge angle was manually adjusted before each run. The balance recorded all 6 reaction components (forces and moments) and another system recorded wind tunnel speed (total and static pressures). All reaction results were converted to non-dimensional coefficients according to usual practice of aerodynamics. The suspension system was designed to slightly resemble the ankle and leg of the ski jumper but no other interactions from jumper's body were included to this test.

Results: Increasing the yaw-angle of isolated ski (0 > 20°, corresponding V-angle 0 > 40°) increased the aerodynamic lift up to 30° V-angle especially with 0° edge angle but slightly also with 10 and 20° edge angles. Increasing V-angle increased the sensitivity of ski to changes in edge angle i.e. the effect of edge angle is more negative with large V-angles. Figure shows that for maximizing L/D in the region of AoA 30° it may be reasonable to have edge angle on skis. Pitching moments (C_m) were positive but they decreased as the edge angle of ski increased.

Figure:
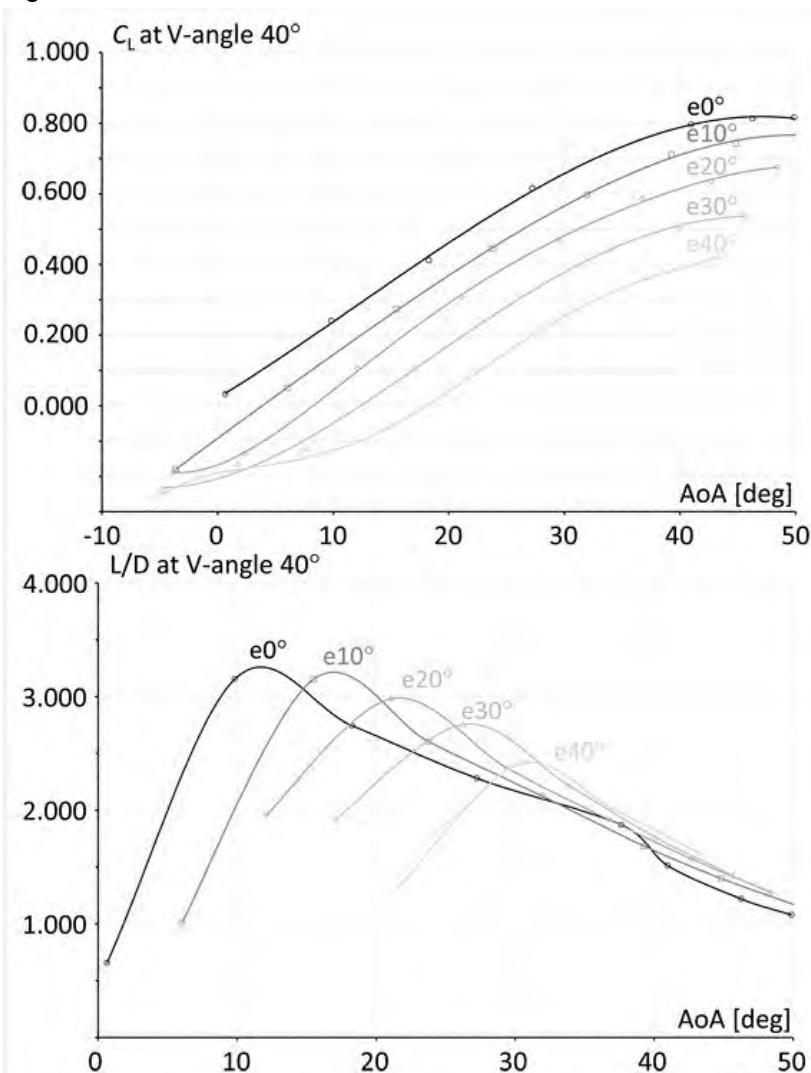
Caption: The effect of edge angle of ski (e) on the aerodynamic lift (CL) and the lift-to-drag ratio (L/D) measured through the different angles of attack (AoA) at V-angle of 40 degrees. L/D values are given only for positive CL values.

Conclusion: In ski jumping the essential region of the AoA for L/D is 20 - 30° (early flight phase) and for C_L, 30 - 45° (latter part of flight phase). It seems that edge angle decreases the aerodynamic lift (C_L) and lift-to-drag ratio (L/D) regardless of V-angle. Increase in V-angle increases the lift force and lift-to-drag ratio. Turning the skis more flat against the direction of motion may increase the positive pitching moment which may affect the stability of the flight.

References: [1] Mahnke and Hochmuth, Research Report for Forschungsinstitut für Körperkultur und Sport, Leipzig, 1990. [2] Cutter, D.A., AIAA, Aeronautical Engineering, United States Air Force Academy, Colorado Springs, Colorado, 1993.

Disclosure of Interest: None Declared

MUSCLE AND TENDON ADAPTATION IN ADOLESCENT ATHLETES: A LONGITUDINAL STUDY

Falk Mersmann [1,*] Sebastian Bohm [1] Arno Schroll [1] Heide Boeth [2] Georg Duda [2] Adamantios Arampatzis [1]

[1]Department of Training and Movement Sciences, Humboldt-Universität zu Berlin, [2]Julius-Wolff Institute, Charité - Universitätsmedizin, Berlin, Germany

Introduction and Objectives: There is evidence that on the transcriptional level of growth factors tendons feature delayed responses to mechanical loading compared to muscle [1] and differences regarding the mechanical stimuli eliciting adaptation [2]. Since adolescence may be regarded as a critical phase of tissue plasticity, as the adaptation process of the muscle-tendon unit is affected by both environmental mechanical stimuli and maturation [3], young growing athletes might be at an increased risk to develop imbalances in the time course of adaptation within the muscle-tendon unit. A recent study on the knee extensor muscle-tendon unit of adolescent volleyball athletes provided evidence for this assumption [4], reporting a marked deficit of tendon cross-sectional area (CSA) in contrast to the already adult-like muscular capacities and morphology. This might pose a risk of tendon overload injuries. The present consecutive longitudinal study investigated the development of the morphological and mechanical properties of muscle and tendon of adolescent volleyball athletes in a time period of two-years. Regarding the morphological properties, we hypothesized a non-uniform development of the muscle and tendon, with greater morphological changes in the tendon, compensating the initial deficit compared to muscle properties.

Methods: Magnetic resonance images of the dominant leg of nine female and nine male trained adolescent elite athletes (Pre: Age 16±1 years, height 188±7 cm, mass 77±10 kg; Post: Age 18±1 years, height 190±8 cm, mass 80±13 kg) were obtained with a time lag of two years. The vastus lateralis (VL), intermedius (VI) and medialis (VM) muscle as well as the patellar tendon (PT) were segmented and analysed with regard to muscle length, muscle volume, maximum anatomical CSA and tendon CSA (in 10 % intervals from 0 to 70 % of the tendon length from proximal to distal). A repeated measures analysis of variance was used to identify effects of the within-subjects factors time (i.e. pre, post) and muscle (i.e. VL, VI, VM) or tendon position (i.e. intervals) respectively. The muscle strength and tendon mechanical and material properties were assessed using a dynamometry and ultrasound approach, including kinematic and electromyographic recordings for the calculation of the knee extension moments, and are currently being analysed.

Results: There was a significant effect of time on muscle anatomical CSA ($p < 0.05$; Pre: VL 29.6±6.5 cm^2, VI 28.3±5.8 cm^2, VM 25.7±5.2 cm^2; Post: VL 30.7±6.3 cm^2, VI 29.5±6.7 cm^2, VM 27.9±6.3 cm^2), muscle volume and tendon CSA ($p < 0.05$; Fig. 1). The increase of tendon CSA (+ 27 %) in the adolescent athletes was substantially greater than the increases in muscle volume and anatomical CSA (+ 6.5 % and 5.6 % respectively). Muscle length on the other hand did not change significantly over time ($p > 0.05$; Pre: VL 38.7±2.5 cm, VI 40.9±1.5 cm, VM 36.9±2.5 cm; Post: VL 39.5±3.6 cm, VI 41.6±2.8 cm, VM 36.5±2.1 cm). Muscle length, anatomical CSA and volume differed significantly between muscles as well as the tendon CSA across the analysed length of the tendon ($p < 0.05$), but there were no significant time by muscle or time by position interactions ($p > 0.05$) on neither muscle nor tendon morphological parameters.

Figure:
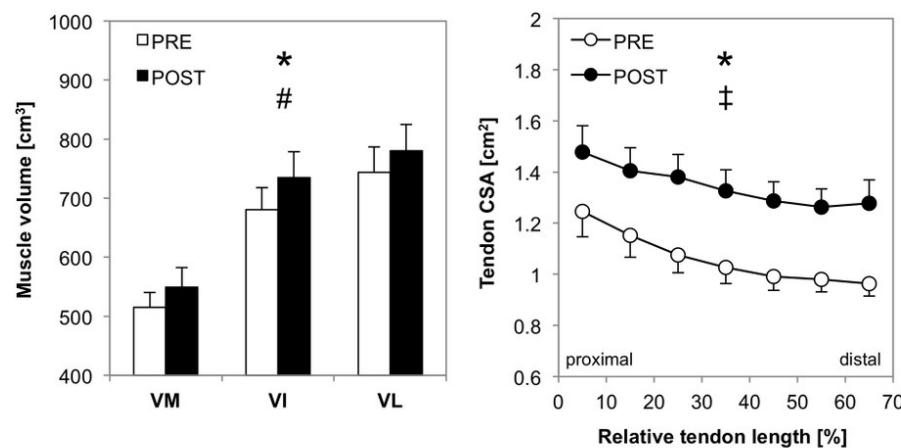
Caption: Means and standard errors (error bars) of vastus medialis (VM), intermedius (VI) and lateralis (VL) muscle volume (left) and patellar tendon cross-sectional area (CSA, right) of adolescent volleyball athletes at 16 (PRE) and 18 (POST) years of age. * significant effect of time; # significant effect of muscle; ‡ significant effect of position

Conclusion: In the present study, the relative increases in tendon CSA in the adolescent athletes exceeded the morphological changes of the muscle by factor four. With regard to the results of the preceding study [4], this indicates that during the late adolescence of elite athletes the initial morphological deficits of the patellar tendon are compensated by tendon hypertrophy and that morphologic adaptations of tendons may unfold rather long-term compared to muscle. The identified time delay of the morphological adaptation of the tendon with respect to the muscular development during adolescence may have implications for the aetiology of tendon overuse injuries. Further analyses of the dynamometry/ultrasound data will give insight into the development of the functional, mechanical and material properties of the knee extensor muscle tendon unit of adolescent elite athletes.

References: [1] Heinemeier et al., Scand J Med Sci Spor, 23: e150–61, 2011.

[2] Arampatzis et al., J Biomech, 43: 3073–79, 2010.

[3] O'Brien et al., J Biomech, 43: 1190–95 , 2010.

[4] Mersmann et al., Scand J Med Sci Sports, 24: E283-E289, 2014.

Disclosure of Interest: None Declared

Sport

AS-0518

DO FOOT ORTHOSES AND FATIGUE MODIFY IMPACT ACCELERATION DURING RUNNING?

Angel Gabriel Lucas Cuevas [1,*] Andres Camacho [2] Raul Llinares [2] Jose Ignacio Priego Quesada [1] Jose Antonio García Perez [1] Pedro Pérez Soriano [1]

[1]GIBD, Department of Physical Education and Sports., University of Valencia, Valencia, [2]Polytechnic University of Valencia, Alcoy, Spain

Introduction and Objectives: Running involves the runner striking the ground around 600 times per kilometre, where the musculoskeletal system has to attenuate the shock wave generated at each foot strike [1,2]. The repetitive and accumulative effect of this stress could overload the musculoskeletal system and lead to overuse injuries. Moreover, the ability of the body to deal with those impacts may deteriorate when the runner gets fatigued. Foot orthoses have been suggested to relieve pain, improve comfort, redistribute plantar pressure, and reduce impact acceleration and loading rate during running [3-5]. However, great controversy exists regarding the effectiveness of prefabricated orthoses in reducing impact loading compared to custom-made orthoses during running. The aim of the study was therefore to analyse the influence of custom-made insoles (CMI) and prefabricated insoles (PI) and the fatigue on impact acceleration parameters during running.

Methods: 40 recreational runners (21 males, 19 females) took part in the study. Two tri-axial accelerometers were attached firmly to the forehead and the anteromedial aspect of the tibia. Kinematic indicators (stride length, stride rate) as well as impact acceleration parameters (head and tibia peak acceleration [maximal amplitude], head and tibia impact magnitude [the difference between the positive and the negative peak], head and tibia loading rate [slope from ground contact to peak acceleration], and shock attenuation [reduction in impact acceleration from the tibia to the head]) were measured at 3.33 m/s before and after a 15-min fatigue run while using three different types of insoles: a) the original insole of the running shoe as control insoles (CI); b) prefabricated insoles (PI); and c) custom-made insoles (CMI).

Results: Effect of insoles

In the pre-fatigue state, a lower tibia and head impact rate was observed with custom-made orthoses compared to prefabricated orthoses (234.61 vs 319.99 G/s; 51.98 vs 58.33 G/s, $p < 0.05$, respectively). In the post-fatigue state, the use of prefabricated orthoses led to a higher head impact rate compared to the custom-made and the control orthoses (58.31 vs 51.47 G/s; 58.31 vs 51.34 G/s, $p < 0.05$, respectively). Also, the use of prefabricated insoles provoked a higher shock attenuation compared to the control insoles (70.55 vs 66.82 %, $p < 0.05$).

Effect of the fatigue

There was a reduction of head impact magnitude when running fatigued with the control orthoses (pre vs post: 2.43 vs 2.31 G, $p < 0.05$), as well as an increase in shock attenuation with the prefabricated orthoses (pre vs post: 67.37 vs 70.55 %, $p < 0.05$).

Neither the insole condition nor the fatigue state influenced the kinematic parameters.

Conclusion: In the present study, the use of custom-made insoles decreased head and tibial loading rate during running compared to the prefabricated insoles. Since increases in loading rate could result in a stiffened pathway along which the

shock wave has to travel, thereby leading to an increased risk of overuse injury [6], custom-made insoles could be acting as a protective mechanism. Moreover, the fatigue state did not have a strong influence on the acceleration parameters measured, except for a slight increase in shock attenuation with prefabricated insoles when running fatigued. This result is in agreement [7] and is contrary to [8] previous studies. The discrepancy among findings is believed to be due to the different type of fatigue induced.

The use of custom-made insoles were able to reduce both tibial and head loading rate during running. In long-distance races where the accumulative and repetitive loads could be deleterious for the musculoskeletal system, a decrease in impact loading at each foot strike as a result of wearing custom-made insoles could play an important role in the prevention of overuse injury prevention in running.

References: [1] García-Pérez et al. Sports Biomech, 13: 259–266. 2014.

[2] Lucas-Cuevas et al. J. Sports Sci, 32: 1712–1721. 2014.

[3] Dixon et al. Med. Sci. Sports Exerc, 35: 472–479. 2003.

[4] Lee et al. Work J. Prev. Assess. Rehabil, 41: 1114–1117. 2012.

[5] Lucas-Cuevas et al. Ergonomics, 57: 1590–1596. 2014.

[6] Milner et al. Med. Sci. Sports Exerc, 38: 323–328. 2006.

[7] Derrick, et al. Med. Sci. Sports Exerc, 34: 998–1002.2002.

[8] Mercer et al. J. Sports Sci, 21: 911–919. 2003.

Sport

AS-0519

QUANTIFYING ICE HOCKEY GOALTENDER LEG PAD KINEMATICS AND ITS EFFECT ON PERFORMANCE

Ryan J. Frayne [1,*] Jim Dickey [1]

[1]Kinesiology, University of Western Ontario, London, Canada

Introduction and Objectives: Reebok-CCM Hockey holds a large share of the goalie equipment market in the National Hockey League (NHL) and in other leagues. In part, their success is due to their multiple fit options for different body types and goaltending styles. However, personal protective equipment (PPE) design comes with technical and scientific challenges, such as the effect that it has on the human body. For example, PPE can increase: i) cardiovascular and metabolic cost [1]; ii) an individual's sweat rate leading to potential cognitive difficulties [2]; and iii) musculoskeletal demands [3]. In addition, goaltender PPE factors such as the leg channel width, pad stiffness and strap looseness may affect a goaltender's performance. Therefore, the purpose of this study was to identify how various styles of goalie pad move with respect to the goaltenders body and how this affects a goaltender's performance.

There were three main objectives of this research: 1) describe the motions of the goal pad with respect to the goaltender's leg in different styles of goal pad, 2) Quantify peak vertical butterfly drop velocity in the various goal pad styles, 3) Understand the relationship between strap looseness and butterfly drop velocity in various goal pad conditions.

Methods: Following a standard warm up, 12 junior level goaltenders (ranging from the Canadian Hockey League to Junior C) performed five butterfly drop and recoveries in three different goal pad conditions: a flexible pad with a wide leg channel, a flexible pad with a tight leg channel and a stiff pad with a wide leg channel. All movements were performed on a 3.4 m x 2.3 m synthetic ice surface while a 10 camera (Eagle, Motion Analysis Corp, CA, USA) high speed passive motion capture system recorded a custom-made reflective marker set located on the goaltender's pelvis, thigh, leg, left skate and goal pad.

Goal pad motion with respect to the leg, from initiation of butterfly drop to ice contact, and from ice contact to full recovery, were extracted for further analyses. Vertical butterfly drop velocity was calculated using the first derivative with respect to time of the uppermost-lateral marker located on the thigh section of the goal pad. To understand the effect of strap looseness on performance, a series of correlations were performed between the looseness of each strap located on the pad (boot, thigh and top and bottom calf strap) and the peak vertical butterfly drop velocity. Strap looseness was determined as the length of the strap from the most medial aspect of the pad to the subject selected strap hole. Descriptive statistics were calculated to depict the motion of the pad with respect to the leg. A one-way analysis of variance was used to analyze peak vertical drop velocity in the three goal pad conditions. Correlations between pad condition and peak butterfly drop velocity were calculated for all pad conditions.

Results: During the butterfly drop and recovery the Stiff-Wide goal pad had the greatest range of motion with respect to the leg. In particular, the transverse plane had ~26° of lateral rotation (starting at ~2° and ending at ~ 28°), during the butterfly drop. Frontal plane rotations were smaller and showed that goaltenders apply force to the medial knee riser upon initiation of the butterfly drop. The mean peak butterfly drop velocity was 3.0 m/s, 3.05 m/s and 2.98 m/s for the Flex-Wide, Flex-Tight and Stiff-Wide pad conditions respectively; however, these differences were not statistically significant.

The top calf strap was the only strap location that resulted in moderate correlation coefficients for the relationship between strap looseness and butterfly drop velocity: 0.51, 0.65 and 0.55 (Figure) for the Flex-Wide, Flex-Tight and Stiff-Wide respectively. The only significant correlation coefficient was the Flex-Tight goal pad condition P=0.024.

Figure:
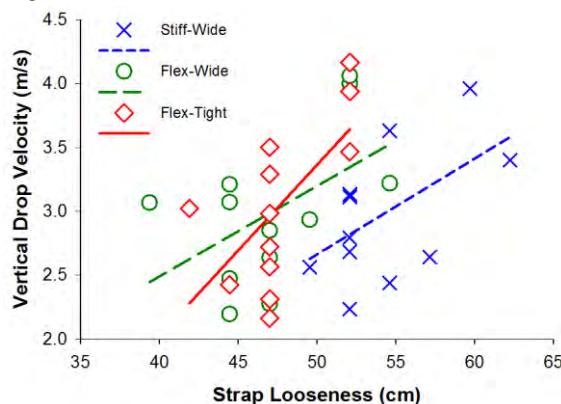
Caption: Relationship between peak vertical velocity during the butterfly drop manoeuvre and the looseness of the top calf strap.

Conclusion: The wide leg channel provides less support around the calf compared to the Flex-Tight pad condition. Therefore, the larger ranges of relative motion for the Stiff-Wide goal pad condition were expected. The less constricted Stiff-Wide and Flex-Wide pads resulted in lower correlation coefficients with butterfly drop velocity compared to the Flex-Tight pad condition. Butterfly drop velocity in the Flex-Tight pad is more sensitive to the effect of strap looseness. For example, a tight leg channel combined with a tight strap will restrict the goal pad from freely moving with respect to the goaltender's leg. Ultimately, this will slow pad velocity because the pad will be limited to the motion of the goaltender's leg. In contrast, to increase the butterfly drop velocity and improve performance, goaltenders should use a loose strap set up.

References: [1] Smith et al, Ergonomics, 55: 1243-1251, 2012.

[2] Gopinathan et al, Arch Environ Health, 43: 15-17, 1988.

[3] Son et al, Appl Ergon, 45: 1019-1027, 2014.

Sport

AS-0520

THE EFFECT OF AGE, SEX, AND HIP STRENGTH ON INTER-SEGMENT COORDINATION VARIABILITY IN RUNNERS

JJ Hannigan [1,*] Li-Shan Chou [1]

[1]Department of Human Physiology, University of Oregon, Eugene, United States

Introduction and Objectives: The majority of literature on running biomechanics and injuries has investigated individual joints without considering inter-joint or inter-segment coordination [1]. Continuous relative phase (CRP) has been suggested as a measure to quantify coordination in runners as it is a continuous variable that includes both spatial and temporal information [1]. Additionally, decreased coordinative variability in the lower extremity has been demonstrated in runners with patellofemoral pain (PFPS) [1] and iliotibial band syndrome (ITBS) [2] compared to healthy controls.

Age and sex have also been suggested as factors in developing a running-related injury [3]. However, while age- and sex-related differences in running kinematics have been studied in single joint analyses, the effect of age or sex on coordinative variability in runners has not been investigated. Additionally, while decreased hip strength has been suggested as a factor in developing knee pain [4], the relationship between hip strength and inter-segment coordination is unknown. Therefore, the purpose of this study was to quantify the relationship between age, sex, and hip strength on inter-segment coordination variability in runners.

Methods: Reflective markers were placed on 23 female (age: 27.43 ± 10.02 years) and 37 male runners (age: 29.97 ± 10.73 years). Runners ranged in age from 18 to 51 years old. Whole-body kinematic data were collected at 200 Hz using a 10-camera motion capture system (Motion Analysis Corp.) during continuous overground running.

Trunk, pelvis, thigh, and shank segment angles and velocities during stance were calculated using a custom LabView program. These values were interpolated to 100% of stance phase and normalized to values between -1 and 1. Phase portraits were constructed from these normalized segment angles (θ) (x-axis) and velocities (ω) (y-axis) so that phase angles (φ) could be calculated using the formula $\varphi = \tan^{-1}(\omega/\theta)$. Continuous relative phase (CRP) was then calculated by subtracting the phase angle of the distal segment from the proximal segment [5] in the sagittal, frontal, and transverse planes. Variability of the CRP, termed the deviation phase (DP), was quantified for each runner by averaging the standard deviation of the CRP at each data point [6]. Hip abduction, flexion, and external rotation strengths were measured isometrically using a Biodex dynamometer (Biodex Medical Systems). For each test, subjects pushed against the dynamometer with maximal force three times for five seconds. Mean peak torque was calculated for each limb and normalized by body mass for analysis. Sex differences in DP values for trunk-pelvis, pelvis-thigh, and thigh-shank coordination were calculated using independent sample *t*-tests. Pearson correlation coefficients quantified the relationship between DP values and both age and hip strength, $p < .05$ for all statistical tests.

Results: Significant weak to moderate positive correlations were seen between age and DP values (Table 1). These correlations were largest in trunk-pelvis ($r = 0.380$) and pelvis-thigh ($r = 0.299$) frontal plane variability.

No differences in trunk-pelvis, pelvis-thigh, or thigh-shank DP values were seen between sexes (Figure 1). Additionally, no significant correlations were found between hip strength and DP values.

Figure:
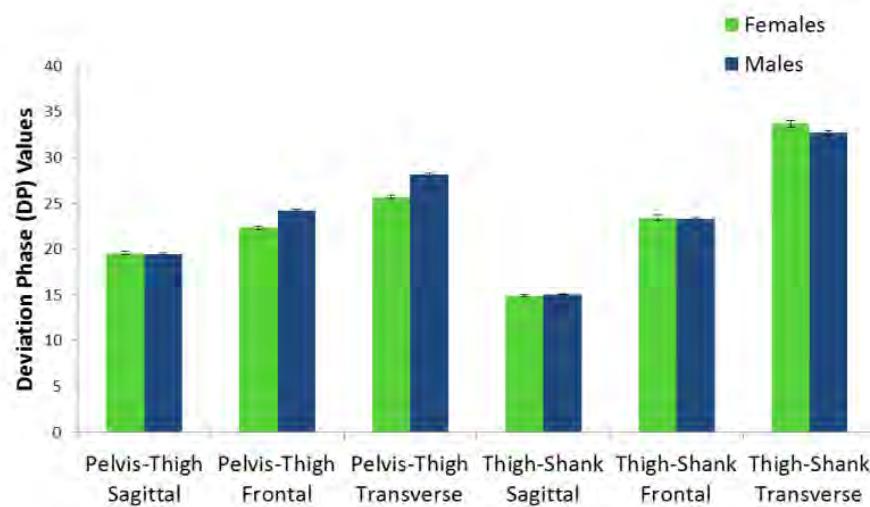
Caption: Figure 1. Mean DP values for selected couplings. No sex-differences in DP values were observed, p > .05.

Conclusion: Weak to moderate positive correlations were found between age and coordinative variability, as measured by DP values. While this suggests that coordinative variability may increase with age, previous research suggests that increased variability may be injury-protective [1,2].

While no significant differences were seen in coordinative variability between males and females, it is important to emphasize that this study only examined CRP variability, not the CRP pattern itself. Also, this study did not analyze coordinative variability of adjacent segments between different planes of motion (ex: transverse plane pelvic motion with frontal plane thigh motion). Further investigation on sex differences in inter-segment coordination appears warranted based on sex differences already cited in single-joint analyses. The relationship between hip strength and knee pain also justifies further research into the role of strength in inter-segment coordination.

Table: Table 1. Pearson correlation coefficients between age and DP values.

	Trunk-Pelvis DP	Pelvis-Thigh DP	Thigh-Shank DP
Sagittal Plane	0.226*	0.269*	0.268*
Frontal Plane	0.380*	0.299*	0.238*
Transverse Plane	0.181*	0.220*	0.125

Caption: *Indicates a significant correlation, p < .05.

References: [1] Hamill et al., Clin Biomech, 14: 297-308, 1999.

[2] Miller et al., J Appl Biomech, 24: 262-70, 2008.

[3] van Gent et al., Br J Sports Med, 41: 469–80, 2007.

[4] Cichanowski et al., MSSE, 39: 1227-32 2007.

[5] Burgess-Limerick et al., J Biomech, 26: 91-94, 1993.

[6] Chiu et al., Clin Biomech, 28: 254-58, 2013.

Disclosure of Interest: None Declared

Sport

AS-0521

GROUND REACTION FORCES IN ELITE UPPER-LIMB AMPUTEE RUNNING

Stefan Litzenberger [1,*] Franziska Mally [1] Steffen Willwacher [2] Bjoern Braunstein [2][3] Anton Sabo [1] Gert-Peter Brueggemann [2]

[1] Department for Sports Engineering & Biomechanics, University of Applied Sciences Technikum Wien, Vienna, Austria,
[2] Institute of Biomechanics and Orthopaedics, German Sport University, [3] German Research Centre of Elite Sport, Cologne, Germany

Introduction and Objectives: Whereas able-bodied athletes can easily be compared to each other without any further regulations, disabled athletes have to be ranked regarding their impairment to avoid inequality within a group. The International Paralympic Committee (IPC) mostly bases its classification process on experience and scientific work. For upper-limb amputees, however, there has been a recent change in classification, which was partly based on scientific work conducted almost three decades ago with methods no longer considered state-of-the-art and done with able-bodied athletes at running speeds significantly lower than those of disabled elite athletes [1,2,3,4,5,6]. From these studies it was concluded that no difference in net vertical momentum between impaired and sound side would be found because during running both arms act synchronously in their upward- and downward movement, respectively, which ultimately would lead to no differences in ground reaction force (GRF) between both feet. Until now no research has been done with upper-limb amputees at elite-level running speeds. We hypothesized that contrary to findings of studies so far, differences in the GRF of an upper-limb amputee athlete can be observed.

Methods: For this research an elite paralympic 400m and 800m runner (PB 400m: 0:48,45, PB 800m: 1:50,92) with a below elbow amputation on the right upper-limb was tested. GRFs were collected with four floor level mounted Kistler force plates aligned consecutively along the running track sampling at 1000 Hz. The subject was advised to do runs at two running speeds (8m/s and 5.4m/s) until four valid ground contacts were recorded for each foot and speed. Stance phase (SP) duration in ms was obtained and data for each ground contact were time normalized to 100% of SP duration and amplitude-normalized to times body weight (BW). Mean and standard deviation as well as maxima and occurrence of the maxima in the SP of vertical, antero-posterior and medio-lateral GRF were calculated and statistically evaluated.

Results: Stance phase duration between left and right foot did not differ significantly for both running speeds (5.4m/s: left: 174 ± 3 ms, right: 181 ± 8 ms ; 8m/s: left: 127 ± 2 ms, right: 125 ± 2 ms). Minor differences in the mean GRF for antero-posterior but not for medio-lateral were found for both running speeds. Maxima of vertical GRF, however, revealed statistically highly significant (alpha = 95%) differences between left and right foot for 5.4 m/s (l: 3.3 ± 0.01 BW, r: 3.1 ± 0.02 BW) and significant differences for 8 m/s (l: 3.97 ± 0.08 BW, r: 3.52 ± 0.05 BW). Furthermore the characteristics of the vertical GRF changed between the two running speeds (Fig.). Whereas the maximum vertical GRF at 5.4 m/s could be observed at approx. 40% of SP it was located at approx. 22% for a running speed of 8 m/s.

Figure:
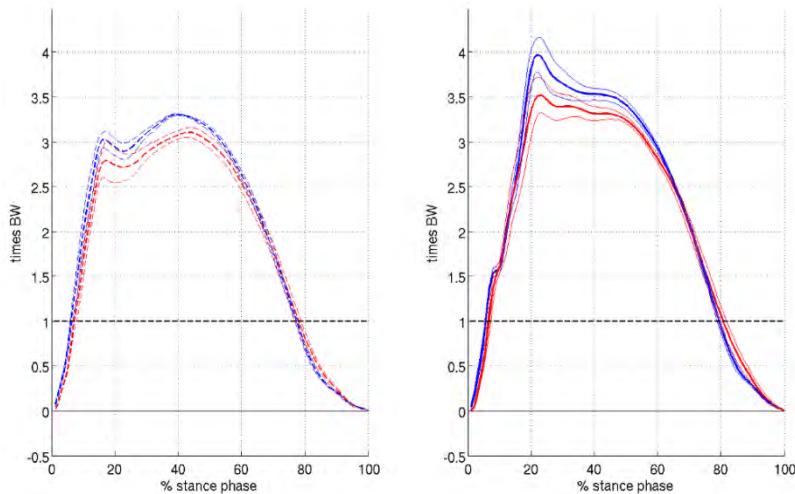
Caption: Mean vertical GRF (GRF_z) in times BW plotted over % of stance phase, thick: mean, thin: ± SD, left: 5.4m/s, right: 8m/s, blue: left foot, red: right foot

Conclusion: The data obtained in this research shows that there are significant differences in vertical GRF between the sound and impaired side of an upper-limb amputee athlete. Hence the hypothesis investigated can be verified. The data confirms that the difference is significant and increases with increasing running speed (difference at: 5.4 m/s: 6%, 8 m/s: 11%). This leads to the assumption that the vertical momentum of both arms is significantly different depending on whether the impaired or sound arm is in backward or forward motion and whether intial contact (or toe off) is made with the ipsilateral or contralateral leg, respectively.

The outcome of the presented research strongly supports the hypothesis that - especially for middle distance running - the contribution of the arms is an important factor. It is furthermore an addition and an update with state-of-the-art measurement systems to the ground-breaking work of [1] and [2].

However, it has to be pointed out that the present study was only performed with one amputee athlete and hence results cannot be generalized. A comparison of a higher number of amputee athletes is rather difficult to perform given the relatively small number of athletes competing on world-class level with this special impairment.

Nonetheless it could be shown that upper-limb amputation has a significant impact on the running mechanics which is not considered in the IPC's classificaton process.

References: [1] Hinrichs et al., Int. J. Sport Biomechanics, 3: 222-241, 1987.

[2] Hinrichs, Int. J. Sport Biomechanics, 3: pp. 242-263, 1987.

[3] Li et al., Journal of Experimental Biology, 204.1:47-58, 2001.

[4] Miller et al. Journal of biomechanical engineering, 131.12, p. 124502, 2009.

[5] Pontzer et al., J. of Exp. Biology, 212.4: 523-534, 2009.

[6] Tweedy & Bourke. IPC Athletics Classification Project for Physical Impairments: Final Report-Stage 1. *Bonn: IPC Athletics, 104,* 2009.

Disclosure of Interest: None Declared

MECHANICAL CONSTRAINTS OF FINGER INDEPENDENCE: LINKING TENDON DISPLACEMENT WITH JOINT MOVEMENT

Nathalie van Beek [1,*] Josien C. van den Noort [2] Peter Veltink [2] Ruud Selles [3] Dirk-Jan Veeger [1] [4] Huub Maas [1] Dick Stegeman [5]

[1] MOVE Research Institute Amsterdam, Faculty of Human Movement Sciences, VU University Amsterdam, Amsterdam, [2] Biomedical Signals and Systems, MIRA Institute, University of Twente, Enschede, [3] Department of Plastic Surgery and Department of Rehabilitation Medicine, Erasmus MC University Medical Center, Rotterdam, [4] Department of BioMechanical Engineering, Delft University of Technology, Delft, [5] Department of Neurology/Clinical. Neurophysiology, Radboud University Medical Centre, Nijmegen, Netherlands

Introduction and Objectives: The human hand has evolved to be able to perform skillful actions which enables us to manipulate objects. Despite this dexterity, it has been shown that we are not fully capable of independent control of individual fingers of the hand. Both peripheral mechanical factors and central neural factors can be held responsible for this limitation of independent finger control[1]. The peripheral factors include tendinous connections between the finger tendons [2] and myofascial linkages between neighboring extrinsic muscles [3]. Even though the mechanical and neural constraints are well-described, it is still unclear how much each constraint influences finger independence. The aim of this study was to quantitatively determine the effects of the mechanical connections on finger interdependence.

Methods: Subjects (n=3,age 24-27yr, another 7 subjects are being analysed) were instructed to flex their index and middle finger individually until the tip of the finger touched the palm of the hand. Non-instructed fingers were not restrained to allow involuntary finger movement. Displacement of the flexor digitorum superficialis tendon of the index and middle fingers was measured with B-mode ultrasound at wrist level. Kinematics of the metacarpophalangeal (MCP) and proximal interphalangeal (PIP) joints was measured using an instrumented glove (PowerGlove, University Twente). For both instructed and non-instructed fingers, range of joint flexion of the MCP and PIP joints and tendon displacement were calculated.

Results: Ranges of movement of MCP and PIP joints were similar for both instructed fingers (Table1). As expected, joint movements in the non-instructed fingers were observed. A lower PIP movement was found in the non-instructed middle finger compared to that of the non-instructed index finger, suggesting a higher level of independence for the index finger (Table 1). Finger interdependence was confirmed also at the tendon level, as tendon displacements of the non-instructed fingers were observed (Table1 & Fig.1A/B). To assess if mechanical factors contribute to finger independence, joint movements of the non-instructed fingers were plotted as a function of tendon displacement of the instructed finger (Fig.1C/D). Across all subjects a similar pattern was found: little to no joint change during the first phase of instructed tendon displacement followed by a steep increase of joint angle (see arrows on Fig.1C/D). Similar results were found for tendon displacements of the non-instructed fingers.

Figure:
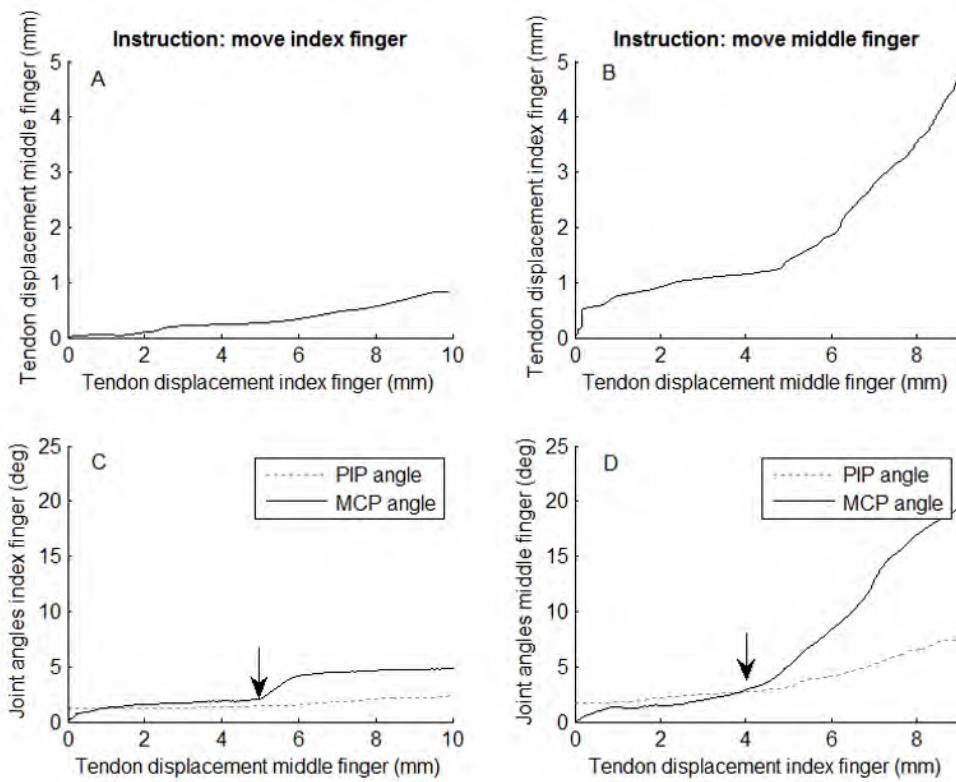
Caption: Fig.1: Tendon displacement of the non-instructed finger plotted as a function of tendon displacement of the instructed finger (A/B). Joint angle (MCP and PIP) of the non-instructed finger plotted as a function of tendon displacement of the instructed finger (C/D).Typical example (n=1), arrows = moment of joint angle increase.

Conclusion: Similar to previous studies [e.g. 4], the index finger showed a higher level of independency than the middle finger. A novel finding is that finger interdependency observed at joint level can also be observed at tendon level. When the joint angle of the non-instructed figure is plotted against the tendon displacement of the instructed finger the results first show a phase where there is hardly any joint movement. Then, a deflection of the curve was observed where the joint angle begins to increase. This pattern may be explained by the tendon interconnections first being slack but then pulled taut after a certain displacement of the instructed finger tendon. As such a pattern is not expected from neural factors, this suggests that mechanical connections between fingers play an important role. A late phase of increased displacement also suggests that mechanical connections only become of significance during larger finger movements.

Results as presented allow quantification of the mechanical connections between the index and middle finger, which may influence finger independence. For a complete picture of the factors contributing to finger interdependence , also neural factors will be addressed in future studies. Funded by the European Commission through MOVE-AGE, an Erasmus Mundus Joint Doctorate programme (2011-0015) and the Dutch Technology Foundation, part of the NWO.

Table:

	Maximum joint movement (degrees)	
	Instructed finger	Non-instructed finger
Index-PIP	78 [71-85]	12 [8-17]
Index-MCP	54 [27-86]	13 [11-14]
Middle-PIP	83 [71-93]	4 [2-7]
Middle-MCP	57 [44-79]	13 [7-20]
	Maximum tendon displacement (mm)	
	Instructed finger	Non-instructed finger
Index	11 [7-17]	3 [1-5]
Middle	9 [9-10]	3 [2-5]

Caption: Table1: Maximum joint movement (MCP and PIP) and tendon displacement of the instructed and non-instructed fingers (mean [range], n=3).

References: [1] van Duinen et al., J.Physiol., 589: 5583-5593, 2011.

[2] Leijnse et al., Acta Anat(Basel), 160(2):112-22, 1997.

[3] Maas et al., J. Appl.Physiol., 95: 2004–2013, 2003.

[4] Lang et al., J.Neurophysiol., 92(5): 2802-2810, 2004.

Disclosure of Interest: None Declared

Musculoskeletal

AS-0523

LEG FLEXION STRENGTH RECOVERS WITH MECHANICAL PROPERTIES OF THE SEMITENDINOSUS TENDON AFTER RESECTION FOR ACL RECONSTRUCTION

Stephen M. Suydam [1,*]Daniel Cortes [2]Lynn Snyder-Mackler [3]Thomas Buchanan [4]

[1]Biomechanics, [2]Biomedical Engineering, [3]Physical Therapy, [4]Mechanical Engineering, University of Delaware, Newark, United States

Introduction and Objectives: An ACL rupture is a life altering injury and more than 175,000 ACL reconstructions occur in the United States each year. Following reconstruction only 64% of patients returned to their pre-operative competitive level and 10% of patients sustain a re-rupture[1]. The semitendinosus (ST) autograft is a common, effective repair technique, but the resection of the ST tendon results in long term knee flexion strength deficits. The recovery of these hamstring strength deficits may aid in the reduction of re-injury rates and return patients to pre-injury function. Studies have shown more than 80% of patients regenerate their ST tendon and therefore the potential exists to have ST muscle function restored. While the appearance of tendon has been imaged with MRI and ultrasound, there has been no correlation between the presence of regrowth in these images and strength recovery[2]. The return of tendon elastic properties facilitates its ability to pass force from the muscle to the joint. Continuous shear wave elastography (cSWE) has been used to determine the mechanical properties in terms of shear elastic modulus of tendon *in vivo*[3]. This study aims to show that strength recovery is related to the restoration of ST tendon elastic properties using cSWE.

Methods: Ten subjects who had ST tendon resections as part of an ACL reconstruction were evaluated between 6-24 months post-op. Shear elastic modulus was determined using cSWE. Six ultrasound RF data sets were collected with an external actuator generating a sinusoidal shear wave at 6 frequencies (323, 340, 358, 379, 403, 430) and a high frame rate ultrasound. Shear wave speeds through the tendon were calculated through post processing with signal decomposition software. Shear elastic modulus was calculated through the optimization of a Voigt model using the frequencies and shear wave speeds from each of the 6 data sets as inputs. The peak torque was evaluated during an isokinetic contractions at 60 and 120°/s. The flexion angle at which peak torque was generated was used to assess remaining deep knee flexion weakness. Pearson correlations between shear modulus and strength were determined with a covariate adjustment for time. The correlation is between the percent change (involved/uninvolvedx100) of the shear modulus and the strength variables.

Results: Nine subjects of ten regrew their ST tendons. The regrown tendons had an average recovery of 59% of their shear elasticity compared to the uninvolved side. The shear modulus of the tendon was positively correlated to both the recovery of the strength and knee flexion angle at which peak torque is generated (Figure 1). The strength during the faster contraction (120°/s versus 60°/s) was more strongly correlated with the shear modulus than the slower contraction (r=0.62 vs r=0.41). The recovery of strength correlation with elastic properties demonstrates the potential to recover to pre-injury strength after ACL reconstruction. The hamstring acts to prevent tibial translation, one of the primary mechanisms of the ACL, which is bolstered by strength recovery. The recovery of the peak flexion strength at higher speeds is beneficial since the pivoting maneuvers, which typically result in non-contact ACL tears, are at these increased

speeds. The recovery of deep knee flexion strength with shear modulus may help prevent re-rupture and return pre-injury competitive levels. An increase in compressive loads at decreased flexion angle have been linked to ACL rupture. The peak torque joint angle moving from the shallow knee angles into a greater degree of deep knee flexion leads to a relatively decreased compressive load in the high risk knee flexion arrangement.

Figure:
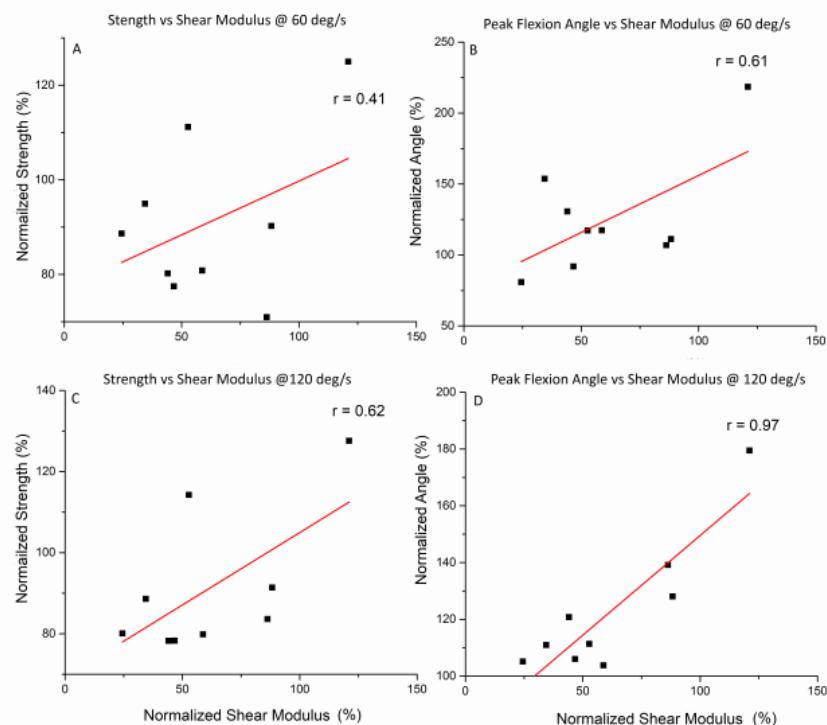
Caption: The correlations between the bilateral strength difference at 60 deg/s (A) and 120 deg/s (C) and the difference in flexion angle at which peak torque is produced for 60 deg/s (B) and 120 deg/s (D). Note the strong positive correlation for each of the graphs and the very strong correlation for flexion angle at 120 deg/s.

Conclusion: The recovery of the ST tendon is strongly correlated to the recovery of the leg flexion strength and the angle at which peak knee flexion torque is generated. The restoration of the ST tendon mechanical properties may aid in protecting the reconstructed ACL and the patients' ability to return to their previous level of sport. The knowledge that, after an ACL reconstruction involving the ST tendon, hamstring strength recovers with the mechanical properties of the tendon could influence post-operative treatment and surgical technique choice.

References: [1] Bourke et al., Am J Sports Med, 40: 1985-92, 2012.

[2] Jassen et al., Knee Surg Sports, 21: 898-905, 2013.

[3] Hoyt et al., Phys Med Biol: 53:4068-80, 2008.

Disclosure of Interest: None Declared

Musculoskeletal

AS-0524

CAN DRAWING IN AND ABDOMINAL CRUNCH EXERCISES NARROW THE INTER-RECTUS DISTANCE?

Patricia Mota [1 2,*]Augusto G. Pascoal [1]Ana Isabel Carita [3]Kari Bø [4]

[1]CIPER - LBMF, Univ Lisboa, Fac Motricidade Humana, [2]Physiotherapy, Universidade Atlantica, [3]BIOLAD, Univ Lisboa, Fac Motricidade Humana, Lisboa, Portugal, [4]Sports Medicine, Norwegian School of Sports Sciences, Oslo, Norway

Introduction and Objectives: Gestational diastasis recti abdominis (DRA) can be defined as the separation of both recti abdominis muscles (RA) starting in the last trimester of pregnancy and extends up to 8-16 weeks postpartum [1, 2]. DRA is quantified by the inter-recti distance (IRD), i.e. the horizontal distance between the internal borders of both RA. To date there is scant knowledge about the effect of the abdominal strengthening exercises on DRA particularly, about which exercises are most effective in IRD reduction. Abdominal crunch exercise has been considered a risk exercise for development DRA[3]. Lately some core training theories recommend the use of the drawing-in exercise both in general population and during pregnancy and after childbirth [4]. It has been proposed that during the drawing-in exercise the activation and training of transversus abdominis will draw the bellies of both RA together, improving the linea alba integrity and the increment of fascial tension which will allow efficient load transference and torque production [4]. However, no evidence was found in literature that supports this statement. Thus the aim of this study was to evaluate the acute effect of the abdominal isometric contraction on DRA performed in two abdominal strengthening exercises, the drawing-in and abdominal crunch exercises.

Methods: This longitudinal study following first time pregnant healthy women population (N=84) in predefined points of time from gestational week 35 till 6 months postpartum. Ultrasound images were recorded on 3 different locations on the linea alba around the umbilicus (2 cm below; 2 and 5 cm above) and on 3 conditions of the abdominal muscles contraction: at rest and in an isometric end-position of the drawing-in and the abdominal crunch exercise. The IRD was measured offline at gestational week 35 and at 3 postpartum time points: 6-8, 12-14 and 24-26 weeks postpartum. A paired sample t-test ($p<0.05$) with Bonferroni adjustment for multiple tests was used to assess the differences between the IRD on 3 condition of the abdominal muscles contraction and on the 3 locations on the linea alba, at 4 measurement time points.

Results: The results showed that during pregnancy the abdominal crunch and the drawing-in exercises induce an acute narrow effect on the IRD. In all time points of postpartum, the drawing-in exercise induced an acute widening effect on IRD when comparing with IRD in resting position. The differences were significant for all locations except for 2 cm above the umbilicus at 6-8 and 24-26 weeks postpartum, and for 5cm above the umbilicus at 6-8 and 24-26 weeks postpartum. During the abdominal crunch the IRD was reduced, and the differences were statistically significant during pregnancy and postpartum on all probe location tested except for 2 cm below the umbilicus at 24-26 weeks postpartum.

The results showed that partial recovery of DRA occurs after childbirth. For every location tested, the IRD values were narrower at 6 months compared to 6-8 weeks postpartum, which is in accordance with previous studies [1, 2].

Strengths of the study are the number of subjects followed, measurement at three abdominal locations, and the use of a reliable method to assess IRD and blinding of the investigator. We measured IRD during two commonly used exercises in pregnant and postpartum women.

A limitation of the study is the lack of pre-pregnancy assessment of the condition. However, measurement of nulliparous women planning to become pregnant is a challenge, and there are few studies in this group of women worldwide.

In our study the only structural parameter measured was the IRD, which may not reflect all of the structural changes that may take place in the fascial and muscular structures of the abdominal wall. The measurements of other structures (muscle length, thickness) could be of value in future research.

Conclusion: During the execution of the exercises, the drawing in exercise widened the IRD in postpartum women and the abdominal crunch narrowed the IRD both during pregnancy and in the postpartum period.

References: [1] Coldron Y, et al. Manual Therapy.13:112-21 2008.

[2] Mota PG, et al. Man Ther 2014.

[3] Blanchard PD. HIV Med.6:54-6 2005.

[4] Benjamin DR, et al. Physiotherapy.100:1-8 2014.

Disclosure of Interest: None Declared

Musculoskeletal

AS-0525

MULTI-SEGMENT FOOT COORDINATION VARIABILITY OF THE PONSETI TREATED CLUBFOOT

Amy Whited [1,*]George Gorton [2]David Drvaric [3]Katherine Boyer [1]Joseph Hamill [1]

[1]Kinesiology, University of Massachusetts Amherst, Amherst, [2]Motion Analysis Laboratory, [3]Shriners Hospitals for Children, Springfield , United States

Introduction and Objectives: Compared with typically developing feet (CON), long-term follow up of Ponseti treated clubfeet (PCF) report an increased prevalence of osteoarthritis (OA), limited rearfoot inversion/eversion, ankle dorsi/plantarflexion motion and reduced ankle power during late stance [1,2,3]. The underlying mechanisms that contribute to differences in biomechanics and function between PCF and CON require further characterization specifically after a prolonged period post-treatment. Coordination variability (CVar) outcomes provide an assessment of foot and lower extremity function by expressing the range of available combinations of segment coordination used to achieve an endpoint foot posture during walking. The ability to use a larger number of segment coordination combinations (greater CVar) is optimal for adaptable and pain-free movement [4,5]. A lack of CVar is associated with reduced function and adaptability and may be a strong indicator of the presence of pathology [4,5]. Differences in CVar between PCF and CON may provide information regarding the level of residual functional pathology in PCF. The objective of this study was to examine differences in forefoot-rearfoot and rearfoot-tibia CVar during walking in children with PCF compared to CON.

Methods: Eight children previously treated for a clubfoot with the Ponseti casting technique and six typically developing children were included in this analysis. All participants signed the institutional review board-approved consent form. Participants walked overground at a preferred speed while three-dimensional kinematic and kinetic data were recorded. A modified vector coding technique was used to determine CVar throughout stance for forefoot-rearfoot inversion/eversion (FF-RF) and rearfoot inversion/eversion-tibia internal/external rotation (RF-Tib) couples. CVar was averaged over early stance (ES,0-33%), midstance (MS,34-66%) and late stance (LS,67-100%) for each group. Data were analyzed with independent samples t-tests to determine if CVar was significantly different between groups. Effect Size was calculated to determine the clinically relevant differences in CVar between groups throughout stance [6]. A large effect was considered to be >0.8, a moderate effect was >0.5 and a small effect was <0.3.

Results: During ES, FF-RF and RF-Tib CVar was not significantly different between groups. There was reduced FF-RF and RF-Tib CVar for the PCF group during MS and LS (Figure 1). There was a large group effect on FF-RF CVar during MS and LS; however, differences were only statistically significant during LS (Table 1). There was a large group effect on RF-Tib CVar with statistically significant differences between groups during MS and LS (Table 1).

Figure:
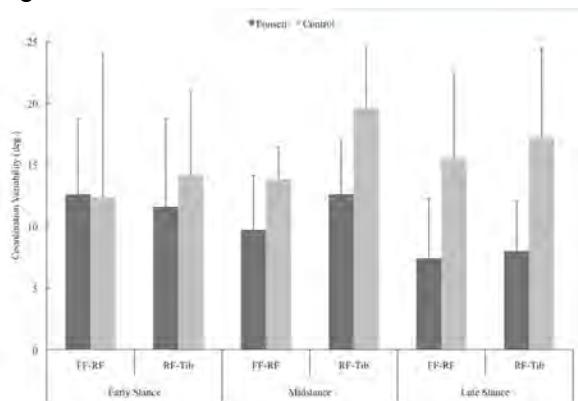
Caption: Figure 1. CVar (group mean ± SD) for FF-RF and RF-Tib coordination couples. *Significant difference between PCF and CON (p<0.05).

Conclusion: PCF demonstrated reduced CVar throughout MS and LS. This finding indicates the presence of residual clubfoot pathology in PCF and suggests a reduced functional capacity to permit adaptive foot postures during walking. Previously reported results of limited rearfoot inversion/eversion, ankle dorsi/plantarflexion motion, reduced ankle power during LS and increased OA prevalence supports the results. Limited range of motion due to joint stiffness or abnormal foot structure may inhibit the range of RF-Tib segment coordination combinations available during MS and LS and may be indicative of the lack of ankle power generation. With reduced CVar, coupling combinations are constrained and may predisposed PCF to repeated stress in the same general area resulting in degenerative changes to the soft tissue over time.

Table:

	FF-RF			RF-Tib		
	CON	PCF	Effect Size	CON	PCF	Effect Size
ES	12.33±11.68	12.64±6.07	0.03	14.22±6.67	11.59±7.07	0.38
MS	13.81±2.61	9.69±4.39	1.18	19.63±4.92	12.58±4.41*	1.51
LS	15.51±6.90	7.44±4.81*	1.38	17.21±7.19	7.97±4.03*	1.65

Caption: Table 1. CVar (group mean ± SD) and effect sizes for FF-RF and RF-Tib coordination couples. *Significant difference between PCF and CON (p<0.05).

References: [1] Smith et al., Clin Orthop Relat Res, doi:10.1007/s11999-013-3386-8, 2013.

[2] Church et al., J Child Orthop, 6:51-59, 2012.

[3] Theologis et al., J Bone Joint Surg, 85:572-577, 2003.

[4] Van Emmerik et al., (2nd ed.). Research methods in biomechanics, Human Kinetics Publishers, 2013.

[5] Hamill et al., Clin Biomech, 14:297-308, 1999.

[6] Cohen (2nd ed.). Statistical power analysis for the behavioral sciences, Lawrence Erlbaum Associates, 1988.

AS-0526

SHEAR WAVE SPEED MEASUREMENTS IN PASSIVE AND ACTIVE STROKE-IMPAIRED BICEPS BRACHII

Sabrina Lee [1,2,*]Sam Speer [2]William Rymer [2]

[1]Physical Therapy and Human Movement Sciences, Northwestern University, [2]Rehabilitation Institute of Chicago, Chicago, United States

Introduction and Objectives: Stroke survivors routinely experience long-term motor and sensory impairments. In parallel with neurological changes, material properties of muscles in the impaired limbs may also change progressively, such as muscle stiffness [1]. However, these stiffness measures are estimates derived from individual joints stiffness or whole muscle groups. Using shear wave ultrasound elastography, shear wave speed (SWS), which is related to the shear modulus, can be estimated in individual muscles[2]. Accordingly, the purpose of this study was to compare material properties, by measuring SWS in spastic paretic muscles at rest and at different activation levels with contralateral muscles in stroke survivors and in age-matched controls subjects.

Methods: Fourteen stroke survivors participated in this study (age: 58.9±7.4yrs; height: 1.68±0.10m; body mass: 85.5±18.2kg; time post-stroke: 11.4±11.6yrs.; Fugl-Meyer: 4-48, 19±15). We tested nine subjects who were gender and age-matched to the stroke survivors (age: 57.9±7.1yrs; height: 1.64±0.10m; mass: 74.4±11.2kg;).

Subjects were seated upright with their upper arm resting on a plastic support, the forearm secured in a fiberglass cast, and the wrist and forearm held in a neutral position in a ring-mount interface mounted to the table. The shoulder was positioned so that the humerus was abducted 45 degrees and the elbow positioned at 90 degrees.Subjects performed a series of isometric elbow flexion contractions at different activation levels (0, 10, 25, 50, 75, 100% maximum voluntary contraction (MVC)) while force and torque were measured at the wrist (load cell). Muscle activity (electromyography), and ultrasound images (Aixplorer, SuperSonic Imagine) of the biceps brachii were captured. Mean SW velocity was calculated from a 12mm by 12mm region of the ultrasound images.

We calculated the slope and r^2 of the linear fit between SWS and % MVC until 50%MVC as the SWS at 75% and 100%MVC reached the maximum the ultrasound system is capable of measuring (16m/s). An Analysis of Variance was used to compare the SWV at the different % MVC levels, slope, and r^2 non-paretic, paretic, and gender, age-matched controls.

Results: Our main findings show that at rest, the SWS was on average 40% greater in the paretic muscle compared to either the contralateral non-paretic muscle or the muscle of control subjects (Fig.1, p=0.003, p=0.002), and no significant difference in SWS between the non-paretic muscle and control muscle. In active muscle (10, 25, 50%), there was no significant difference in SWS between the non-paretic, paretic, and control muscles (Fig.1). The slope of SWS versus %MVC (up to 50%MVC) and R^2 values was 10% and 15% greater, respectively, in the non-paretic muscles compared to that of the paretic muscle, but was not significant (Table 1, p = 0.06).

Figure:
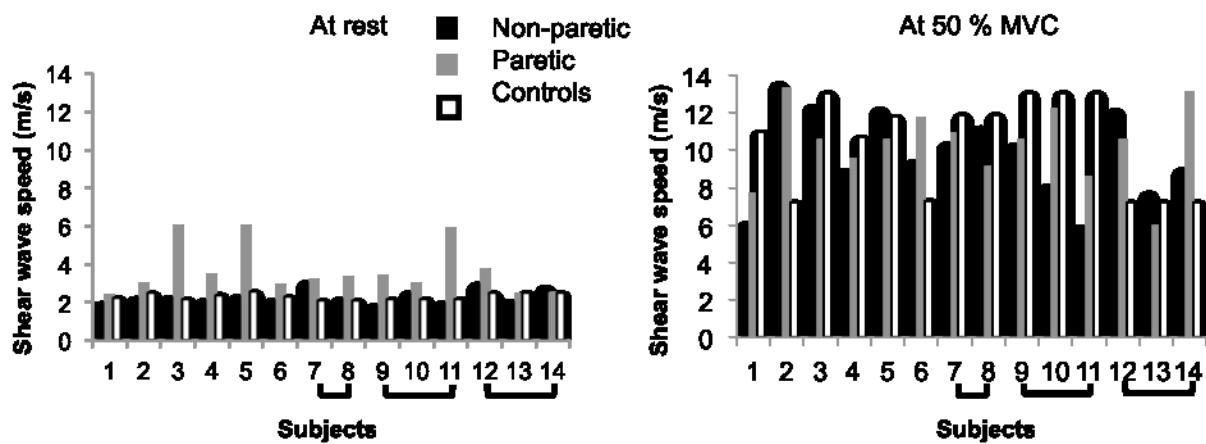
Caption: Figure 1. Mean shear wave speed at rest and at 50%MVC (force) for the non-paretic (black) and paretic (gray) muscle of individuals who have had a stroke and muscle of gender, age-matched controls (white). Brackets indicate the same control subject.

Conclusion: We demonstrate that shear wave speed is faster in the biceps brachii of the paretic limb than in the contralateral non-paretic limb of stroke survivors when the muscle is at rest. This suggests that paretic muscles have potentially altered muscle material properties, specifically stiffness in both passive and active muscles, but primarily in passive states. This can be a result of increased collagen in the perimysium and abnormal accumulation of the extracellular matrix[3].

Interestingly, this difference in SWS between three muscle groups disappears once the muscle was active. One source of active stiffness is short-range stiffness. Thus, it is possible that the non-contractile elements contributes minimally to stiffness in active muscle and the active short-range stiffness is not altered in stroke-impaired muscle.

These findings allow us to have a first glimpse into active and passive stiffness of stroke muscle. Quantitative measurements of muscle stiffness in individual muscles, is important for more accurately assess muscle function and for understanding the fundamental mechanisms of impairment that occur after a stroke, for aiding clinical decisions, and for guiding rehabilitation interventions.

Table:

Muscle	SW velocity at rest	SWV at 50%MVC	Slope (ms^{-1}%MVC^{-1})	R^2
Paretic	3.65(1.31)	10.33(2.03)	0.12(0.04)	0.73(0.12)
Non-paretic	2.30(0.38)	9.79 (2.36)	0.15(0.05)	0.81(0.12)
Control	2.29(0.18)	10.42(2.28)	0.13(0.05)	0.89(0.16)

Caption: Table 1. Mean shear wave (SW) speed at rest and %MVC, slope of SW vel and %MVC, and R2. Mean (SD).

References: [1] Katz et al., Arch of Phys Med Rehab, 70:144-55, 1989.

[2] Bercoff et al., Ultrason, Ferro and Freq Control, IEEE Transactions, 51:396-409, 2004.

[3] Lieber et al., Am J Physiol, 305:C241-C52, 2013.

Disclosure of Interest: None Declared

AS-0527

LOADING OF HIP MEASURED BY HIP CONTACT FORCES AT DIFFERENT SPEEDS OF WALKING AND RUNNING.

Georgios Giarmatzis [1,*]Ilse Jonkers [2]Mariska Wesseling [2]Sam Van Rossom [2]Sabine Verschueren [1]

[1]Musculoskeletal Rehabilitation, [2]Human movement biomechanics, KU Leuven, Leuven, Belgium

Introduction and Objectives: Exercise plays a pivotal role in maximizing peak bone mass in adulthood and maintaining it with aging, by imposing mechanical loading on the bone that can trigger bone mineralisation and growth [1]. Hip fractures are the most devastating and linked to highest morbidity rates when compared to the rest of the osteoporotic related fractures together [2]. Still, the optimal type and intensity of exercise that best enhances hip bone strength remains poorly characterized, partly because the exact loading of the hip produced by the diverse types of exercises is not known. Thus, the goal of this study was to quantify peak hip loading during walking and running at different speeds and acquire a better insight into the biomechanics of the motion in question.

Methods: 20 young healthy adults walked and run on a split-bet treadmill, in a speed range of 3 – 12 km/h, with an increment of 1 km/h. By means of integrated motion capture as an input to musculoskeletal modeling in Opensim, kinematics, kinetics and hip contact forces (HCFs) were calculated. Muscle forces were obtained by solving the static optimization algorithm. The cost function was set to minimize the squared sum of all muscle activations.

Results: Ensemble curves of HCFs during walking and running are shown in Figure 1. During walking, HCFs have a two peak profile whereby the first peak (Peak1_HCF) during heel strike increases from 4.03 BW to 5.26 BW and the second (Peak2_HCF) during toe-off from 4.1 BW to 5.4 BW, by increasing speed from 3 to 6 km/h (Table 1). During running, there is only one peak HCF (Peak_HCF) during mid-stance that increases from 7.11 BW to 9.48 BW, by increasing speed from 6 to 12 km/h (Table 1). Speed related profiles of peak HCFs and ground reaction forces (GRFs) reveal a different progression of the peaks. Larger percentage increase from 3 to 6 km/h was identified for peak HCF when compared to peak GRFs during walking and running. Larger variability of peak HCFs was calculated during walking (~ 13 – 24.5%) and running (~ 16 – 20%) than in peak GRFs (~ 3 – 8% during walking and ~ 8 – 10% during running). Regression analysis of peak HCFs and coinciding hip moments for each speed showed that hip adduction moment best predicts Peak1_HCF (mean R^2 = 0.6) during walking and Peak_HCF (mean R^2 = 0.7) during running, whereas hip extension best predicts the Peak2_HCF during walking (mean R^2 = 0.58).

Figure:
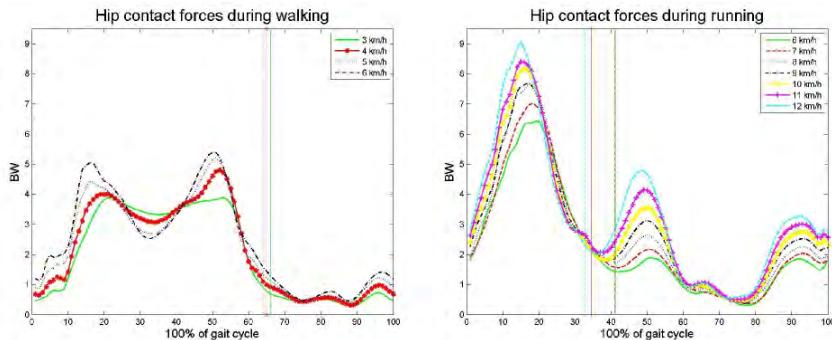
Caption: Figure 1

Conclusion: Based on our analysis, peak HCFs increase significantly with increasing speed during walking and running. Further analysis showed that speed has a stronger impact of speed on peak HCFs than on peak GRFs. Discrepancies in variability and speed progression of peak HCFs and GRFs question the notion of peak GRF as predictor of peak skeletal loading. As a consequence, clinically relevant outcomes were also investigated as possible predictors of peak HCFs. Results from regression analysis of peak HCFs and hip moments indicate the major influence of muscle activity on peak HCFs, since muscles exhibit high force output to equilibrate external moments. The present study contributes hereby to a better understanding of musculoskeletal loading during walking and running in a wide range of speeds, offering valuable information to clinicians and scientists exploring bone loading as a possible non-pharmacological osteogenic stimulus. Through modeling, a deeper insight into joint forces was established, illustrating that ground reaction forces and external moments can only partially describe the true musculoskeletal bone loading and that muscle action used to balance external joint moments is the most important factor in affecting bone loading during different exercises. In future research these results can be utilized in more elaborate techniques, such as finite element analysis, in order to fully understand the mechanisms underlying bone reaction to load.

Table:

Walking							
Velocity	3 km/h		4 km/h		5 km/h		6 km/h	
	Peak 1	Peak 2	Peak 1	Peak 2	Peak1	Peak2	Peak 1	Peak 2
Peak GRF (BW)	1.06 (0.03)	1.06 (0.04)	1.1 (0.04)	1.09 (0.06)	1.17 (0.06)	1.12 (0.09)	1.24 (0.1)	1.14 (0.08)
Peak HCF (BW)	4.03 (0.7)	4.1 (0.9)	4.15 (0.72)	4.8 (0.87)	4.58 (0.85) [4]	5.17 (0.82) [4]	8.02 (1.44)	5.4 (0.82)
Running							
	6 km/h	7 km/h	8 km/h	9 km/h	10 km/h	11 km/h	12 km/h	
Peak GRF (BW)	2.03 (0.22)	2.07 (0.22)	2.21 (0.21)	2.28 (0.19)	2.35 (0.2)	2.37 (0.25)	2.45 (0.22)	
Peak	7.1	7.3	8.0	8.6	8.41 (1.34)	9 (1.6)	9.4	

HCF (BW)	1 (1.3)	(1.44)	2 (1.44)	1 (1.58)			8 (1.53)	

References: [1] K. T. Borer, *Sports medicine (Auckland, N.Z.)*, vol. 35, no. 9, pp. 779–830, Jan. 2005.

[2] S. Boonen et al. *Best practice & research. Clinical endocrinology & metabolism*, vol. 22, no. 5, pp. 765–85, Oct. 2008.

Disclosure of Interest: None Declared

Surgical Techniques

AS-0528

KINEMATIC VERSUS NEUTRAL ALIGNMENT IN TOTAL KNEE ARTHROPLASTY: BIOMECHANICAL AND CLINICAL ASSESSMENTS

Claudio Belvedere [1,*] Andrea Ensini [2] Silvia Tamarri [1] Paolo Barbadoro [2] Michele d'Amato [2] Alberto Leardini [1]

[1]Movement Analysis Laboratory and Functional-Clinical Evaluation of Prostheses, [2]1st Orthopaedic and Traumatologic Clinic, Istituto Ortopedico Rizzoli, Bologna, Italy

Introduction and Objectives: In Total Knee Arthroplasty (TKA), one long-held tenet of prosthesis component implantation is that knee Neutral Mechanical Alignment (NMA), i.e. of 0°±3°, must be targeted to restore physiological lower limb biomechanics and to obtain better clinical results and implant survival rates. Recent studies have shown that knee natural alignment can differ from NMA and that a postoperative NMA does not improve TKA survivorship [1]. Furthermore, knee trans-epicondylar axis is questioned as the best possible reference in prosthesis alignment [2].

As a result, a novel implantation approach has been recently proposed, referred to as Kinematic Alignment (KA), based on pre-arthritic knee alignment. This is performed by suitably modeling knee posterior condyles as cylinders and by using the trans-cylindrical axis, i.e. trough the two cylinder centers, as a reference in femoral component alignment [2]. Accordingly, KA is thought to allow more natural soft tissue balance and better knee function than NMA.

Recently, patient specific instrumentation (PSI) has been introduced possibly to achieve more accurate prosthesis positioning [3] also via KA, in addition to traditional NMA. Particularly, KA via PSI seems to be more effective in restoring physiological knee kinematics and lower limb muscle activity [2], but only preliminary results have been reported.

The purpose of this study is to analyze the biomechanical behavior of the two above-cited alignment approaches. In this perspective, joint kinematics and electromyography will be assessed in two patient groups, one operated according to NMA via with the conventional instrumentation, the other according to KA approach via PSI.

Methods: 36 patients planned for TKA were divided into two equal-size groups and implanted with a cruciate-retaining fixed-bearing prosthesis (Stryker® Orthopedics, Mahwah, NJ-USA) targeting NMA via convention instrumentation (group A) or KA via PSI (group B).

Currently, 20 patients were implanted, 11 in group A and 9 in group B. These were also assessed clinically using the Knee Society Knee Scoring System, and also biomechanically at 6 month follow-up. In the latter, knee kinematics during stair climbing, chair rising and extension-vs-gravity was evaluated via 3D mono-planar video-fluoroscopy (CAT® Medical System, Monterotondo, Italy) synchronized with electromyography analysis. Relevant prosthesis component poses were reconstructed [4] to calculate knee flexion/extension (FE), ad/ab-duction (AA), internal/external rotation (IE), together with the rotation of the contact-line (CLR) on the tibial base-plate, this being the line connecting the medial (MCP) and lateral (LCP) condyle contact points. MCP and LCP antero-posterior translations were also calculated and reported in % of the tibial baseplate length.

Results: Mean postoperative knee and functional scores in group A were 78±20 and 80±23, respectively; in group B these were better, i.e. 91±12 and 90±15.

In both groups, mean AA range (see figure) was found smaller than 3° together with normal FE and IE ranges. Particularly, IE range in the 3 motor tasks was 8.0°±3.2°, 10.1°±3.9° and 7.9°±4.0° in group A, and 6.6°±4.0°, 10.5°±2.5° and 11.0°±3.9° in group B. The extension-to-flexion MCP translations were of about 13.8±5.6% anterior, 17.0±6.6% posterior and 15.4±6.6.9% posterior in group A, and 13.0±3.4%, 16.5±5.3% and 16.6±5.6% all posterior in group B; corresponding LCP values were all posterior of about 9.5±3.6%, 11.1±4.3% and 8.5±2.6% in group A, and 102±2.1%, 13.7±8.6% and 14.6±9.7% in group B. Relevant CLR was 8.2°±3.2°, 10.2±3.7 and 8.8±5.3 in group A, and 7.3±3.5, 12.6±2.6 and 12.5±4.3 in group B.

Much more consistent patterns of motion were observed in group B than in group A. In the EMG data, prolonged activation of the medial and lateral vasti muscles was observed in group A.

Figure:
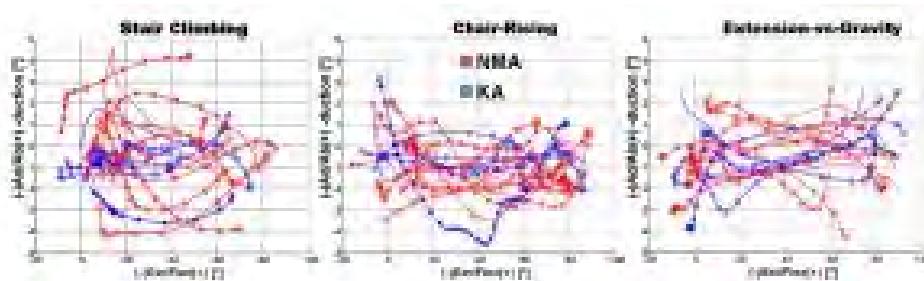
Caption: Knee ad/ab-duction during the three analyzed motor tasks in NMA and KA patients.

Conclusion: These results reveal that better biomechanical function together with clinical scores were obtained in TKA targeting KA and performed via PSI. Though irrelevant kinematic differences were observed between groups, a higher consistency in knee motion patterns was found over the KA patients. Corresponding less prolonged muscle activation suggests also a more natural stability and mobility at the knee joint, and general soft tissue balance.

These findings forecast the good biomechanical efficacy in clinics of KA via PSI, though data from of all recruited patients are necessary to establish the claimed superiority of the novel alignment approach.

References:

[1] Parratte S et al.. J Bone Joint Surg Am., 92(12):2143-9, 2010.

[2] Eckhoff DG et al., J Bone Joint Surg Am., 87(I 2):71-80, 2005.

[3] Ast MP et al., Orthop Clin North Am., 43(5):17-22, 2012.

[4] Banks SA et al., IEEE Trans. Biomed. Eng., 43: 638-649, 1996.

Disclosure of Interest: None Declared

ESTIMATION OF FEMORAL INTRA-NECK DRILLING CHANNEL FROM COMBINED PELVIC AND FEMORAL ANATOMICAL LANDMARKS: A CADAVER STUDY

Victor Sholukha [1,*]Jules Panda [2]Patrick Salvia [1]Benoit Beyer [1]Marcel Rooze [1]Serge Van Sint Jan [1]

[1]LABO, ULB, Brussels, Belgium, [2]Department of Surgery, University of Lubumbashi, Lubumbashi, Congo

Introduction and Objectives: Guiding information must be available when drilling a surgical pin through the femoral neck to reach the femoral head. While medical imaging (i.e., fluoroscopy) is widely available in developed countries, surgeons in less-favored countries do not have easy access to such technology. Accurate estimation of the femoral anteversion and inclination angles is of interest for surgical intervention. This paper proposes a new approach for the evaluation of the proximal femur morphology (e.g. femoral neck axis location). The first objective of this paper was the description of the pipeline allowing storage of bone morphological characteristics and the determination of regression relationships applicable for proximal femoral epiphysis shape and orientation prediction. The second goal was the approximation of a drilling pathway running within the femoral neck towards the femoral head without medical imaging support. It is based on a combination of 5 pelvic and 3 femoral anatomical landmarks (ALs) located on the subject-of-interest.

Methods: Fifty-seven bodies from donators were obtained from the Body Donation program of the University Libre de Bruxelles. X-ray control allowed to ensure the lower limbs of the donators did not show any osteosynthesis material that would lead to artifacts during CT imaging. After CT imaging segmentation, 3D models of the specimen pelvis and two femoral bones were obtained. Virtual palpation was then performed following strict definitions [1]. Supplementary ALs were virtually palpated on the surface of the acetabulum, femoral head and neck surfaces. These ALs were further used to characterize each surface-of-interest using shape approximation. The hip joint components (i.e., the pair including the pelvis and femoral bone) of one specimen in the database was used as reference assuming the hip joint as a ball-and-socket joint. The pose of the remaining database hip joints were adjusted by rigid transformation using the reference joint pair to obtain all available hip joints in the same joint orientation. For any new joint to be estimated, the above database procedure unification has been followed. Each hip orientation data available from the database were adjusted according to the orientation of the joint-of-interest using 5 pelvic and 3 femoral ALs. In order to complete the validation, the method has been integrated in a surgical ancillary prototype to perform a pin drilling on each available specimen. The drilling path prediction procedure was based on the computational method presented in our previous papers [2,3] and home made interactive software.

Results: Accuracy evaluation by "leave one out" (LOO) cross validation was performed on the 114 hip joints available from the database. The orientation of each available joint was sequentially flexed within the range [-30°, 30°] using 3° step. For each orientation step of the current hip joint, the location of femoral hip center (FHC) and drilling point (FDP) were compared with the prediction values obtained from the remaining 113 bone couples. Results of this LOO cross validation showed that the FHC and FDP mean prediction error was 5.1(2.1) mm and 9.6(4.1) mm, respectively.

Five cadavers from database were excluded by LOO method and selected for testing *in-situ* of nine femur drilling. Drilling results using the ancillary prototype on the 9 hip joints show good correspondence with the computed values:

discrepancies between the real drilled channel and the computed channel ("gold" values for drilling point and femoral hip center from CT image data reconstruction) was 8.9(3.7) mm and 7.1(3.8)° for the position and orientation, respectively. Results were obtained after the real drilling procedure and CT scan data reconstruction including inserted drilling pin. Examples of CT imaging 3D reconstruction after drilling procedure presented in Figure for right and left femur frontal, superior and neck axial views. Pin locations (red sticks) and size inside bone (in mm) demonstrate accuracy of the method.

Figure:
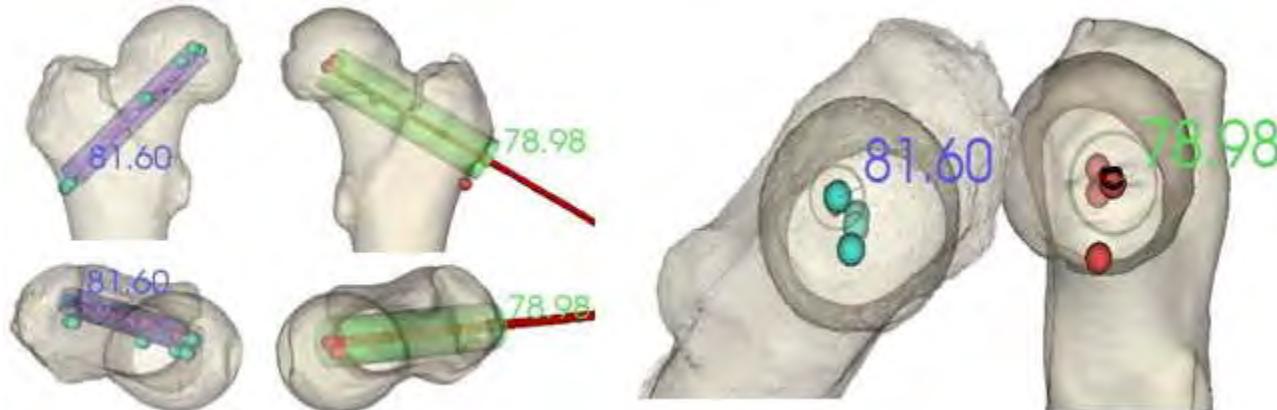
Conclusion: Results of this study show that proposed method can be used to predict parameters such as the femoral head center location and the most optimal entry point to insert a surgical pin or a trephine while remaining within an intraosseous pathway following the femoral neck. The obtained accuracy suggests that the method could be used as an alternative or complementary to fluoroscopy or computerized tomography used for pre-planning tasks. The novel method has therefore the advantage to solve the problem of radiation absorbed by surgeon and patient during medical imaging.

References: [1] Van Sint Jan, S. Churchill Livingstone - Elsevier, Edinburg, 2007.

[2] Sholukha, V., et al. *J. of Biomech.* **42**, 319-324, 2009.

[3] Sholukha, V., et al. *J. of Biomech.* **44**, 712-718, 2011.

Disclosure of Interest: None Declared

Surgical Techniques

AS-0531

SYSTEMATIC BIOMECHANICAL ANALYSIS OF TREATMENT OPTIONS FOR TIBIAL HEAD DEPRESSION FRACTURES

Stefanie Hoelscher-Doht [1,*]Martin Jordan [1]Christina Zimmermann [1]Torsten Blunk [1]Rainer Meffert [1]

[1]Department of Trauma, Hand, Plastic and Reconstructive Surgery, University Clinics of Wuerzburg, Wuerzburg, Germany

Introduction and Objectives: Tibial head fractures account for 10% of all fractures in the elderly. Due to metaphyseal bone loss, depression fractures, especially of the lateral tibial plateau, frequently occur and need to be treated operatively. After reduction of the depressed articular fracture fragment, a metaphyseal bone defect remains. Filling the defect with an autologous crest bone graft is not possible because of fatty degeneration of the crest bone. Instead, bone substitutes are used. Following operative treatment, the postoperative regime includes partial weight bearing of 15-20 kg for 3 months. Older patients, however, often do not follow this regime, resulting in a secondary subsidence of the depressed articular fracture fragment due to excessive weight bearing. A systematic biomechanical evaluation of different treatment options is needed to enable development of evidence-based recommendations for the type of bone substitute and how it is stabilized. Therefore, the aim of this study was to systematically analyse different options of osteosyntheses alone and in combination with commonly used bone substitutes for treating tibial head depression fractures.

Methods: Lateral tibial head depression fractures were created in Synbones (SYNBONE®, Switzerland) in a fracture model. After reduction, the fractures were stabilized with 8 different treatment options of an osteosynthesis alone or in combination with a bone substitute (Table 1). Two screws, 4 screws using the jail technique, and a lateral buttress plate (Figure 1) were investigated. As a bone substitute, two common clinically-used calcium phosphate cements, Norian® Drillable and ChronOS™ Inject, were applied. All specimens were X-rayed to confirm the stabilization procedures. Cyclic testing was performed using 250 N for 3000 cycles, simulating typical partial weight bearing after operative treatment of tibial head depression fractures. Displacement of the articular fracture fragment during cyclic loading (mm), the stiffness (N/mm) and the maximum load (N) in load-to-failure tests were measured.

Results: All groups with the three different types of osteosyntheses without bone substitute revealed a higher displacement compared to the control group, stabilized only with the bone substitute ChronOS™ Inject (2 Screws: 1.43±0.68 mm, 4 Screws: 1.11±0.21 mm, Plate: 3.72±3.82 mm; ChronOS: 0.53±0.20 mm; $p<0.05$). However, groups with an osteosynthesis in combination with bone substitute exhibited no significant differences compared to the control group ChronOS™ Inject only. The maximum load for the 2 screws (1957±384 N) was significantly lower compared to the jail technique with 4 screws (3067±257 N; $p=0.02$) and the buttress plate (3813±556 N; $p<0.01$). In addition, for the normalized maximum load, a significant difference was found between the jail technique (4 screws) and the buttress plate (4 screws: 231±25 %, Plate: 337±53 %; $p<0.01$). Comparing the two different bone substitutes to each other, the ChronOS™ Inject had a significantly higher stiffness than the Norian® Drillable (ChronOS: 478±149 N/mm, Norian: 307±62 N/mm; $p=0.01$). The X-rays revealed that completely filling up the defect with bone substitute depended on the

type of osteosynthesis. Using the plate, filling up was more complete compared to the 2 screws and jail technique with 4 screws.

Figure:
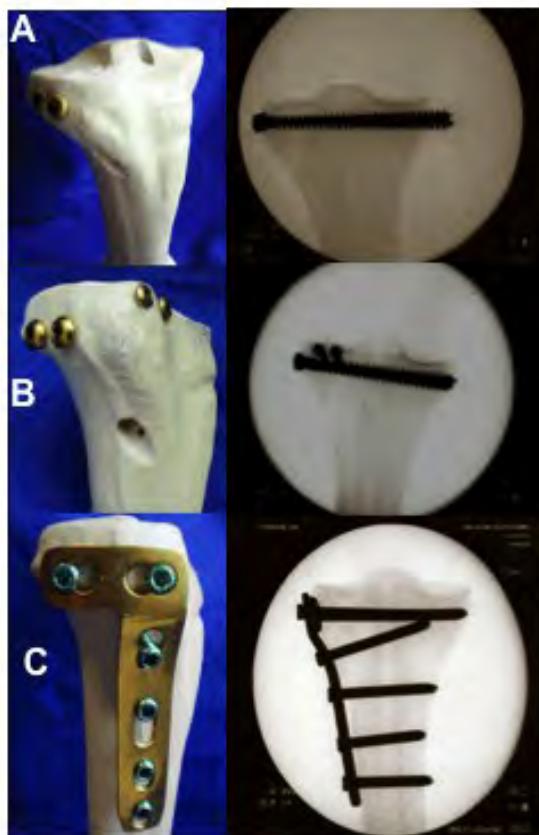
Caption: Figure 1: The three different osteosynthesis options: (A) 2 screws, (B) 4 screws in the jail technique, and (C) lateral buttress plate.

Conclusion: When treating tibial head depression fractures the fracture stabilization has to provide high stability under maximal loading, as well as to prevent a secondary subsidence of the depressed articular fracture fragment. Our study provides evidence about the mechanical performance of different osteosyntheses and bone substitutes. The buttress plate had the highest stability under maximum loading whereas the use of bone substitute was essential to limit the subsidence. Thus, the combination of both, osteosynthesis and bone substitute, is recommended to stabilize tibial head depression fractures. Interestingly, the specimens filled up with ChronOS™ Inject exhibited a higher stiffness than the ones with Norian® Drillable. Furthermore, the mode of failure differed between the two bone substitutes; under maximum loading Norian® Drillable was pressed out of the application channel, whereas ChronOS™ Inject formed a fixed contact to the synthetic bone spongiosa and the lateral tibial plateau broke completely away. Although the use of ChronOS™ Inject would be recommended based just on mechanical performance, knowledge of the mode of failure suggests Norian® Drillable is the preferred option.

Table:

Group	Osteosynthesis	Bone substitute
1	2 Screws	---
2	4 Screws	---
3	Buttress Plate	---
4	2 Screws	ChronOs
5	4 Screws	ChronOs
6	Buttress Plate	ChronOs
7	---	ChronOs
8	4 Screws	Norian

Caption: Table 1: Experimental groups: Type of osteosynthesis alone or in combination with two different bone substitutes.

Disclosure of Interest: None Declared

Surgical Techniques

AS-0532

BIOMECHANICAL COMPARISON OF THE ALL-EPIPHYSEAL AND OVER-THE-TOP TECHNIQUES FOR REPAIRING THE ANTERIOR CRUCIATE LIGAMENT USING A NOVEL ROBOTICALLY SIMULATED PIVOT SHIFT: A CADAVERIC STUDY

Tara F. Bonner [1,*]Robb W. Colbrunn [1]Joel Kolmodin [2]Paul Saluan [2]

[1]BioRobotics and Mechanical Testing Core, [2]Orthopeadic & Rheumatologic Institute, Cleveland Clinic, Cleveland, OH, United States

Introduction and Objectives:

Anterior Cruciate Ligament (ACL) injuries increasingly affect the pediatric population. The all-epiphyseal (AE) and over-the-top (OTT) are two techniques used for reconstructing the ACL in lieu of traditional techniques so as not to disrupt the epiphyseal in growing patients. Both techniques' effectiveness in restoring intact knee kinematics has been examined previously in a cadaveric study, concluding that both techniques provide anterior and rotational stability. No conclusions were made as to which technique provided more stability [1].

The robotically simulated clinical pivot shift (PS), a dynamic loading profile based on measurement of loads applied by a surgeon, was presented as a more robust test for detecting kinematic changes for evaluating ACL reconstructions [2]. This study aimed to use the simulated clinical PS to assess anterior and rotational stability provided by the AE and OTT surgical techniques.

Methods:

Six fresh-frozen, cadaveric legs were transected mid-femur and mid-tibia and mounted to the Universal Musculoskeletal Simulator capable of real-time force feedback using simVITRO™ software. Four surgical conditions were tested: Intact knee, deficient ACL, AE reconstruction and OTT reconstruction. The AE and OTT reconstruction order was randomized. For each surgical condition, three tests were performed:

1. Anterior drawer (134 N anterior, 20 N compression) at 0, 15, 30, 60, and 90° of flexion
2. Rotary loads (5 Nm internal rotation torque, 10 Nm valgus torque, 20 N compression) at 5, 15, and 30° of flexion
3. Simulated clinical PS test [2]

For each specimen, the kinematics from the intact knee for each respective test was subtracted from the kinematics of the three remaining surgical conditions to acquire kinematic response relative to the intact knee. Relative anterior tibial translation (ATT) and internal tibial rotation (ITR) were reported at each tested flexion angle for the Anterior Drawer and Rotary Loads tests and for the flexion angle initiating the shift in the simulated clinical PS test. This angle was at the peak ATT and corresponded to the start of the shift. Paired t-tests were used to determine significance ($p<0.05$). In one specimen the simulated clinical PS could not induce a shift, even in the deficient state, and thus was excluded from the analysis.

Results:

Figure 1A displays the ATT and ITR for the simulated clinical PS at the flexion angle initiating the shift. Neither surgery restored intact knee kinematics. OTT exhibited 4.2 mm more ATT compared to AE (p=0.021) and 7.2° more ITR (p=0.015). OTT had no significant kinematic difference compared to the deficient ACL.

Figure 1B displays the ATT for the Anterior Drawer test. Figure 1C and 1D display the ATT and ITR (respectively) for the Rotary Loads test. Neither surgery restored intact knee kinematics nor significantly reduced ATT or ITR compared to the other surgery, agreeing with previous work with similar loading conditions[1]. The AE surgery significantly reduced ATT compared to deficient at flexion angles of 0, 15 and 30° by 5.3, 5.3 and 4.7 mm respectively and there was no significant difference between OTT and deficient, though trending was seen (p<0.086). (Fig 1B).

Figure:
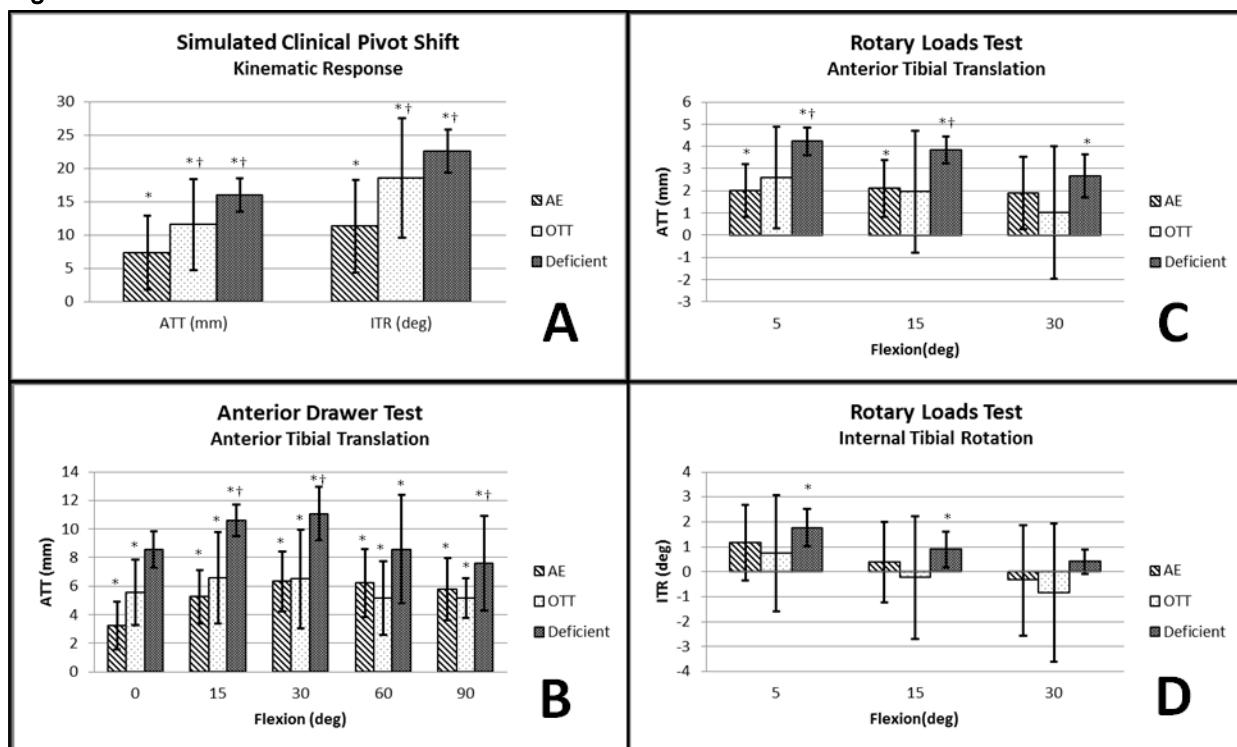
Caption: Figure 1: Kinematic responses relative to intact knee, *p<0.05 compared to intact, †p<0.05 compared to AE, (no significant results between OTT and deficient), A) Kinematic response induced by the simulated clinical Pivot Shift, B) Anterior tibial translation (ATT) induced by the Anterior Drawer, C) ATT induced by the Rotary Loads, D) Internal tibial rotation (ITR) induced by the Rotary Loads

Conclusion:

The all-epiphyseal technique, though unable to restore native kinematics, showed significantly improved stability (4.2 mm ATT, 7.2° ITR) compared to the over-the-top technique when tested with a robotically simulated clinical pivot shift. Analysis of the Anterior Drawer and Rotary Loads tests did not detect significant differences in these surgical techniques, and are in agreement with a previous study with similar loading conditions [1].

Limitations of our study include the small sample size, and the removal of one of the specimens. More work is needed on refining the loading profile to ensure it is able to induce a pivot shift in all specimens. While there is still room for improvement, it is currently still more effective than Rotary Loads, especially in its ability to detect rotational instabilities. The results from our study agree with previous studies [1,2] in that the Rotary Loads test does not induce large rotational changes amongst ACL surgical states. It also does not provide additional information compared to the Anterior Drawer test for measuring anterior laxity. It is our recommendation that the Rotary Loads test be replaced by one that can induce greater kinematic changes when comparing ACL surgical states. The simulated clinical PS is a solution that shows promise.

References:

[1] McCarthy et al., Am J Sports Med. 41,6: 1330-1339,2013.

[2] Colbrunn et al., Pro ASME SBC, SBC2013-14288, 2013.

Disclosure of Interest: T. Bonner Conflict with: The author discloses the following conflict of interest. They receive a royalty from each copy of the simVITRO software sold under a licensing agreement from the Cleveland Clinic Foundation Innovations Department., R. W. Colbrunn Conflict with: The author discloses the following conflict of interest. They receive a royalty from each copy of the simVITRO software sold under a licensing agreement from the Cleveland Clinic Foundation Innovations Department., J. Kolmodin: None Declared, P. Saluan: None Declared

BIOMECHANICS OF COMPUTER-ASSISTED VS. CONVENTIONAL THR AFTER ONE YEAR FOLLOW-UP

T Weber [1] [2],[*]T Renkawitz [2]S K Bulstra [3]J Grifka [2]G J Verkerke [4] [5]S Dendorfer [1]

[1]Laboratory for Biomechanics, OTH Regensburg, [2]Department of Orthopaedic Surgery, Regensburg University Medical Center, Regensburg, Germany, [3]Department of Orthopaedic Surgery, [4]Department of Rehabilitation Medicine, University of Groningen, Groningen, [5]Department of Biomechanical Engineering, University of Twente, Enschede, Netherlands

Introduction and Objectives: A novel, computer-assisted Femur First (CAS FF) operation method for Total Hip Replacement (THR), which incorporates various aspects of performing a functional optimization of the cup position, and comprehensively improves range of motion (ROM) as well as cup containment and alignment parameters, has been developed. To compare CAS with conventional THR a combined workflow of experimental and computational methods was used. Novel computer simulations were used to determine biomechanical outcome in terms of hip reaction forces (hrf). We assessed on hrf: are they closer to a healthy, young normal, are they distributed more symmetrically and is the hrf orientation favorable in the CAS group?

Methods: 30 CAS and 30 conventional patients were enrolled for this prospective, randomized and patient and observer-blinded clinical trial. CT-Scans from all patients were retrieved post-op and implant position and orientation were measured by an external institute (MeVis, Germany). After given written consent patients conducted 3D video based motion-capture (SimiMotion, Germany) gait analysis (self-selected speed) at three points of time (pre-op -- t0, post-op six month -- t1, post-op twelve month -- t2), recording bony landmark based marker trajectories and ground reaction forces simultaneously (Kistler, Switzerland). The recorded data were processed using a validated and commercial musculoskeletal simulation package (AnyBody A/S, Denmark). Typical signals of the hrf for either of the groups were computed using dynamic-time-warping (dtw)1. Dtw path length as well as dtw distance were used as asymmetry measures, reflecting either phase-shift symmetry or magnitude symmetry of time-series. Force orientations are quantified in the radiographic coordinate system.

Results: Hrf of both groups are increasing during the follow-up period and are at t2 closer to a healthy normal compared to t0. Hrf for the CAS FF group increased over the follow-up period, until reaching the same hrf-magnitude as young and healthy adults at t2. Phase shift and magnitude asymmetries decrease for both groups, especially in terms of phase-shift. At t1 the force orientation of the CAS FF group was significantly closer to the center of the acetabular cup compared to the conventional group, which vanished at t2. *Figure 1* The typical hrf signal of the different THR-groups. a) The hrf of the CAS FF group at the different follow up points can be seen (blue: t0, green: t1, red: t2). The x-axis denotes the stance-phase in percent; the y-axis shows the hrf in multiples of bodyweight. The dashed line is the TS of the healthy group as gathered during method verification experiments. b) Results for the CON group (blue: t0, green: t1, red: t2). c) Dimensionless walking speed at different follow-up points is displayed, as well as literature data for THR patients (point-dashed, dark red line).

Figure:
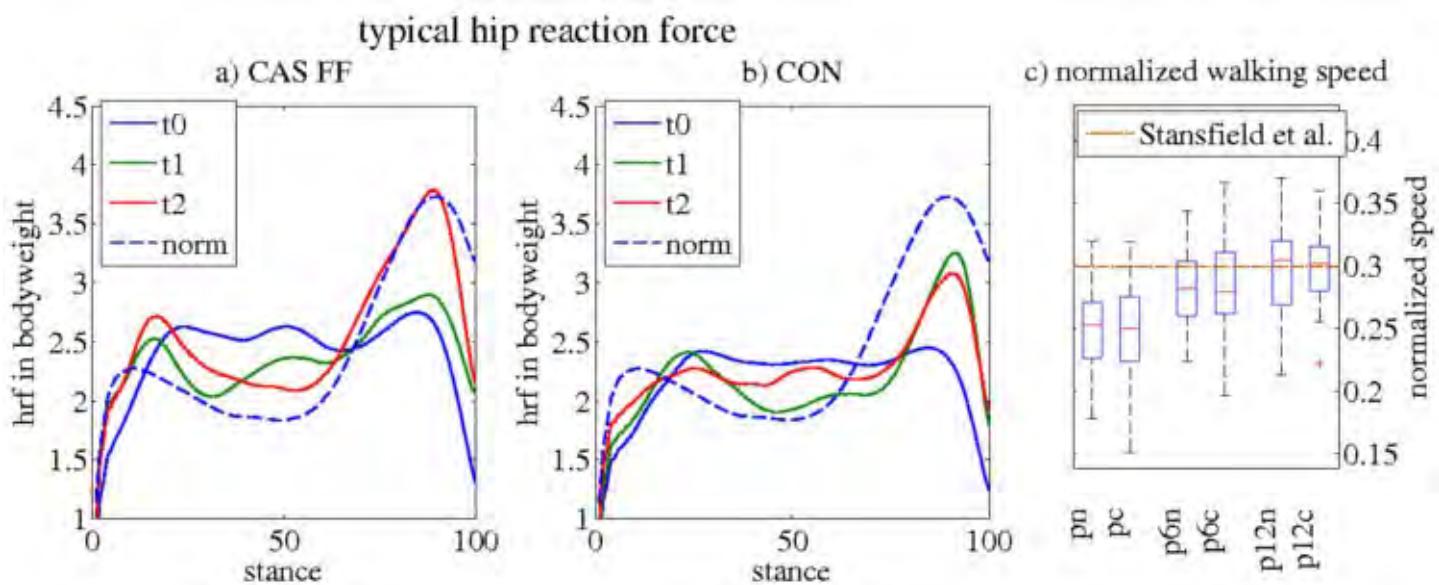
Conclusion: Patients that underwent CAS FF seem to improve more than patients that underwent conventional THR in terms of hip reaction forces. The results suggest that CAS FF leads to better performance at the artificial hip joint. At t1 the orientation of the hrf is improved for the navigated group and closer to optimum suggesting that the CAS FF operation technique decreases the propensity for dislocation and impingement in an early stage. The rather big number of patients (60) that have been analyzed using a novel computational workflow and validated models is the greatest strength of this study. The model is of a mechanical nature, therefore cancelling out psychological effects. CAS FF has the potential for an improved biomechanical outcome early after surgery. A possible long-term benefit remains to be proven.

References: [1] Bender et al (2010) Determination of typical patterns from strongly varying signals.Comput. Methods Biomech. Biomed. Engin. 15(7):761-9.

Disclosure of Interest: None Declared

STRESS-STRAIN BEHAVIOUR OF NI-TI ALLOYS USED IN ENDODONTIC INSTRUMENTS BY MEANS OF TORSIONAL SIMULATED TESTS.

Leandro A. Santos [1,*]Estevam Las Casas [1]Guiomar Bahia [1]Vicente Buono [1]

[1]Universidade Federal de Minas Gerais, BELO HORIZONTE, Brazil

Introduction and Objectives: Endodontic treatment is a clinical intervention that aims to cure infections in the pulp of the tooth, the soft tissue inside the root canal. This treatment includes a step of shaping the root canal by means of an endodontic instrument, made of stainless steel or nickel-titanium (Ni-Ti) alloy. The Ni-Ti alloy presents a property called superelasticity (or pseudoelasticity), a nonlinear elastic behaviour that allows the material to undergo large deformation without plastic residual-strain after stress removal. This behaviour is linked to a reversible solid-state transformation from stable phase austenite to a new crystallographic structure called martensite. Due their microstructure and mechanical properties, Ni-Ti endodontic instruments present several advantages compared with the stainless steel files, such as higher flexibility and less geometrical aberrations during the treatment. Despite their advantages, the fracture of rotary Ni-Ti instruments in the root canal is still an important issue in endodontics. One of the main causes of these instruments' fracture is the torsional overloading. It occurs when the instrument has its movement stopped by friction with the canal's wall whilst the shaft continues to rotate. Thus, torsion is an important loading condition to which the instruments are subjected during use. There are standard torsion tests available to evaluate the mechanical behaviour of these instruments. To improve the fracture resistance of Ni-Ti endodontic instruments, manufacturers have introduced new conditions to heat treat the Ni-Ti alloys. The resultant improvements are easily evaluated through a stress-strain curve extracted from a tensile test performed on a Ni-Ti wire. However, these new treated alloys, in general, are applied directly to the file's geometry and performing conventional tensile tests on then can be very difficult. In this case, finite element modelling (FEM) is very helpful, once by this method it is possible to simulate torsional conditions and extract stress-strain relationships as a result. Thus, the aim of this work is to simulate torsion tests on known Ni-Ti files and correlate the results with the experimental ones. Thus, it is possible to create a map of behaviour, by which one can estipulate the stress-strain curve of a unknown alloy using experimental torsion results.

Methods: A commercially available instrument with a tip size of 25 and a 0.06 taper was selected for this study. The geometric model for finite element analysis was generated by micro-CT scanning (eXplore Locus SP, GE Healthcare, Waukesha, WI, USA). Five constitutive models, based on stress-strain curves, were selected as input data. The numerical analysis was performed in ABAQUS (SIMULIA, Providence, RI, USA) with boundary conditions that were based on the ISO 3630-1 specification for torsion tests of endodontic instruments. In these tests, the instrument is locked at 3 mm from the tip and a 3 N.mm torque is applied to its shaft. As a result, a torque-angular displacement curve is obtained. The experimental torsion test was performed on an instrument with the same geometry and unknown stress-strain behaviour.

Results: Five torque-angular displacement curves were calculated by finite element simulations. Each curve was linked to its stress-strain relationship and a map of mechanical behaviour was done. The torque-displacement curve from the

experimental test was compared to the simulated ones and it was possible to estipulate the stress-strain curve of the unknown alloy.

Figure:
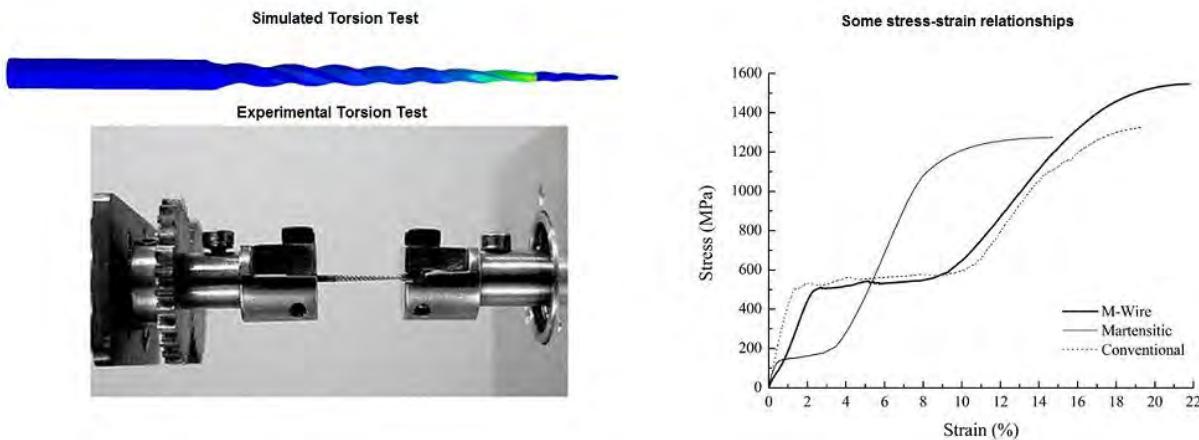
Conclusion: Stress-strain relationships are very important to characterize the mechanical behaviour of materials. Through these curves, it is possible to obtain the necessary parameters to describe the behaviour of an alloy under stress, such as elastic modulus, elongation, and yield point. In this work, it was created a method to estimate these curves for an unknown Ni-Ti alloy using torsion tests and finite element modelling.

Disclosure of Interest: None Declared

MECHANISM OF SHEAR DEFORMATION OF DEEP BRAIN DURING ROTATIONAL HEAD MOTION OBSERVED IN A THREE DIMENSIONAL PHYSICAL HEAD MODEL

Yusuke Miyazaki [1,*]

[1]Mechanical and Environmental Informatics, Tokyo Institute of Technology, Tokyo, Japan

Introduction and Objectives: Traumatic Brain Injury (TBI) occurs various impact conditions such as traffic accidents, falling accidents, and sports accidents. Therefore, it is necessary to determine the mechanism by which TBIs occur and the preventive measures that can be adopted to avoid them. Especially, rotational brain injury such as concussion or Diffused Axonal Injury(DAI) can cause shear deformation of deep brain, however, the detailed mechanism is still unknown. Moreover, the head injury criterion (HIC) is calculated by linear acceleration responses of the center of gravity of the head, it is difficult to evaluate TBI due to rotational head impacts using HIC. Therefore, it is necessary to define a new injury criterion for rotational head motion in order to minimize TBIs due to rotational head impacts. So far, some injury criterion based on peak head angular acceleration and/or angular velocity have been proposed; however, the relationship between these parameters of rigid head motion and deep brain deformation is also unclear. Research using physical or computational models has been performed to clarify the mechanism. However, the shapes of the brain models were based on simplified geometries Hence, the purpose of this study is to construct a physical head model that has a three dimensional real human shape, then examine the mechanism of shear deformation during rotational head motion, and relationship between rotational head motion and brain shear deformation.

Methods: The head model consists of an accurate 3D representation of the human head, made by assembling detailed models of the skull, falx, tentorium, CSF and brain. The skull part was made of polycarbonate and was fabricated by machining based on CAD data reconstructed from CT images. The falx and tentorium part were made of polyurethane with almost the same thickness and Young's modulus as that of the dura of cadavers, and attached to the skull model[1]. A mold of the brain was fabricated using a stereo lithography system based on the CAD data of the brain reconstructed from MR images. Subsequently, a two-tone brain model, made of black and transparent silicone gel having the same dynamic viscoelasticity of human brain[1], has a detailed shape of three dimensional brain with ventricle and cerebral sulci. White markers were painted around corpus callosum on the boundary plane. Two fiber scopes attached with high speed cameras were fixed in the intracranial space. Therefore, the model can visualize shear deformation within the depth brain at corpus callosum. Finally, the gap between the skull and brain portions was filled with water to simulate cerebrospinal fluid.

Side impacts were applied on a slider attached to the lower neck under the conditions in the case that peak angular acceleration and angular velocity were controlled. The time history of rotational impacts applied to the physical head model was calculated from the acceleration time history recorded by 3-3-3 accelerometer arrays. The displacements of the white points around corpus callosum were measured. Finally, the Green-Lagrange strain around each white point was calculated from its relative displacement.

Results: The time history of the shear strain at corpus callosum showed that the there was a time delay between the peak angular acceleration and the peak shear strain(Fig.1 c and d). From the results of the experiment, shear deformation at corpus callosum occurs because of reverse torsional deformation between right and left cerebral hemisphere along with cerebral falx(Fig.1 d and f). This reverse torsional deformation was due to relative reverse rotation between skull and brain. Moreover, the peak change in angular velocity correlated highly with the peak shear strain in the brain, rather peak angular acceleration, which has been proposed as the indicator for categorizing the severity of brain injuries or injury criterion. This was because the brain deformation was quite small at the time of peak angular acceleration of the head. Thus, brain shear deformation did not correlate with the peak angular acceleration of the head.

Figure:
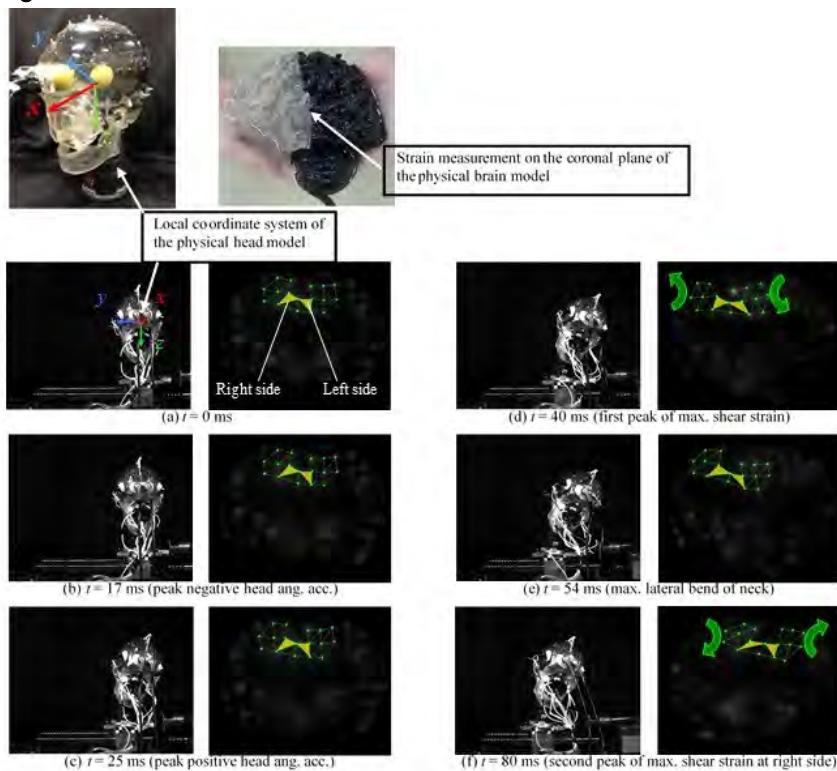
Caption: Time-histories of 3D physical Head-Neck model motion and deep brain deformation behavior at corpus callosum

Conclusion: Our results showed that relative reverse rotation between skull and cerebrum affects greatly on the mechanism of the deep brain, which was not correlated with the rotational acceleration of the head but the angular velocity. Thus, we propose that time duration of the rotational acceleration should be considered an important parameter for defining a new brain rotational injury criterion, rather than the peak angular acceleration

References: [1]Margulies et al., **J Biomech 23**:823-36, 1990

Disclosure of Interest: None Declared

CARBON-FIBER REINFORCED PEEK PLATES – A PROMISING APPROACH TO PROXIMAL HUMERAL FRACTURE PLATING?

Christoph Katthagen [1] Michael Schwarze [2,*] Mara Warnhoff [3] Christine Voigt [1] Christof Hurschler [2] Helmut Lill [1]

[1] Trauma and Reconstructive Surgery, Diakoniekrankenhaus Friederikenstift, [2] Laboratory for Biomechanics, [3] Hanover Medical School, Hannover, Germany

Introduction and Objectives: Locking-screw plating is an established and commonly used treatment for dislocated proximal humeral fractures [1]. Despite advancement of implants and a better understanding of failure mechanisms, complication rates for proximal humeral locked plate fixation remain high at up to 30% attributed to varus loss of reduction and articular screw perforation [2, 3]. Newly developed implants are regularly introduced to the market which attempt to address these issues. Carbon-fiber reinforced polyetheretherketone CF-PEEK composite plates are less stiff than stainless steel and titanium plates, with an elastic modulus similar to bone as well as the ability to withstand prolonged fatigue strain. An approach to prevent articular screw perforation is the development large diameter screws, so called locking bolts. The main purpose of the presented study was to compare the biomechanical properties of a CF-PEEK locking plate with pre-existing data of a titanium-alloy plate when used for fixation of an unstable 2-part fracture of the surgical neck of the humerus. The secondary purpose was to compare the biomechanical behavior of locking bolts and conventional locking cancellous screws.

Methods: 7 pairs of fresh frozen human humeri (female donors, mean age 59y, range: 46y to 75y) were allocated to two equal groups. All specimens were fixed with the CF-PEEK plate (PEEK Power Humeral Fracture Plate, Arthrex). Cancellous screws (group 1) were compared to locking bolts (group 2) for humeral head fixation. Stiffness, cyclic fracture gap deflection and ultimate load were assessed in a servo-hydraulic testing machine. Stiffness was determined with a load limit of 200N in axial loading, as well as 20deg abduction and 20deg adduction. Cyclic fracture gap deflection was determined during 5000 cycles at 1Hz from 50N to 250N load. Ultimate load was determined with constant displacement speed until visual observation of failure. Results were compared between groups and with pre-existing biomechanical data of a titanium-alloy plate (PHILOS, DePuy Synthes).

Results: The CF-PEEK plate featured significantly lower stiffness in all directions and more fracture gap deflection compared to the titanium-alloy plate (all p<0.001, Tab. 1). In ultimate load testing, no significant differences could be detected, although 6 out of 14 CF-PEEK plates failed due to irreversible deformation and resulted in complete loss of fixation in the femoral head. No significant difference was observed between results of groups 1 and 2 in any test configuration (p>0.05, Tab. 1).

Conclusion: The CF-PEEK plate significantly increases movement at the fracture site of an unstable proximal humeral fracture model compared to the commonly used titanium-alloy plate. The screw design however does not affect the constructs primary mechanical behavior in the constellation tested. However, the stiffness of the CF-PEEK plate was relatively low, resulting in interfragmentary displacements of ~40% strain over the 10 mm defect. These strains are sufficiently high that they could conceivably have a significant negative impact on bone healing especially in case of large

defect zones [4, 5]. This study could not find biomechanical evidence for the use of large diameter locking bolts, although clinically there might be some advantages such as reduced screw perforation in the humeral head. The utilized setup might not be appropriate to enforce screw cut-out.

As a major limitation to our findings, the results only represent initial fixation and do not reflect biological processes of in vivo healing or the loading produced by muscle forces producing moments around the shoulder joint, although the applied forces correspond to in-vivo measurements [6]. Against this background the clinical use of CF-PEEK plates should be cautious in case of remaining large fracture gaps of more than 4-5mm after fracture reduction without additional means of fracture gap augmentation.

Table:

	CF-PEEK with cancellous screws (n=7)	CF-PEEK with locking bolts (n=7)	Significance between groups	Titanium-alloy with locking screws (n=8)	Significance between plates
Axial stiffness [N/mm]	54.7 (18.8)	57.1 (15.5)	p=0.54	183.7 (26.3)	*p<0.001*
20deg Abduction [N/mm]	44.6 (7.5)	46.1 (11.8)	p=0.8	118.4 (32.2)	*p<0.001*
20deg Adduction [N/mm]	82.2 (18.1)	96.1 (29.9)	p=0.26	505.5 (321.2)	*p<0.001*
Failure load [N]	653 (133.5)	801 (201)	p=0.32	822 (143)	p=0.69

Caption: Mean stiffness and load to failure (standard deviation) of all groups and non-cyclic testing modes.

References: [1] Sproul RC et al., Injury, 42(4): 408–13, 2011.

[2] Thanasas C et al.,J Shoulder Elbow Surg, 18(6): 837–44, 2009.

[3] Hillbricht S et al., Obere Extrem, 8(3): 144, 2013

[4] Claes L et al., J Ort Res, 15(4): 577-84, 1997.

[5] Schell H et al., J Ort Res, 23: 1022-8, 2005.

[6] Westerhoff P et al., J Biomech 42(12): 1840–9, 2009.

Disclosure of Interest: None Declared

Trauma

AS-0537

A BIOMECHANICAL COMPARISON OF FOCAL TRAUMATIC BRAIN INJURY AND PERSISTENT-POST-CONCUSSIVE SYNDROME

Andrew Post [1,*]Marshall Kendall [2]Janie Cournoyer [2]Blaine Hoshizaki [2]Michael Gilchrist [3]Susan Brien [4]Michael Cusimano [5]Shawn Marshall [6]

[1]Human Kinetics, [2]University of Ottawa, Ottawa, Canada, [3]University College Dublin, Dublin, Ireland, [4]Royal College, Ottawa, [5]St. Michael's Hospital, Toronto, [6]Ottawa Hospital, Ottawa, Canada

Introduction and Objectives: Every year brain injury is a leading cause of global hospitalization. Of particular concern is defining what characteristics of the brain injury event that create a high risk of focal traumatic brain injury (fTBI), and how these differ from persistent concussive syndrome (PCS). The similarities in the biomechanics of these types of injury make it difficult for clinicians and biomechanical researchers to gain an understanding of the mechanisms contributing to these injuries. This creates a unique challenge to clinicians trying to either identify the injury at the hospital clinic or ER. For biomechanists it is important to develop an understanding of the biomechanical mechanisms that differentiate between these two types of brain injury to improve protective and preventative measures. The purpose of this study was to examine the characteristics of real-life events representing fTBI and PCS to better understand differences in event characteristics and acceleration loading profiles between these two types of brain injuries.

Methods: The subjects who sustained head impact injuries were classified into two groups by neurosurgeon: fTBI and PCS. To determine the brain injury event characteristics, each subject was interviewed and a form completed that contained information for laboratory reconstruction such as: impact location, velocity, etc [1]. The dataset involved multiple mechanisms of injury (falls, collisions, and projectiles) reconstructed using a monorail, linear impactor, or ball launcher. These devices were used to impact an instrumented Hybrid III headform under conditions as described in the Neurotrauma report. The impacts were described by linear and rotational acceleration curve characteristics [2] that have been found to have a relationship with risk of brain injury. In total 20 fTBI and 20 PCS cases were reconstructed.

Results: The linear and rotational acceleration (Table 1) curves, showed that the PCS cases had significantly lower values than the fTBI cases for all descriptors ($p<0.05$) except for duration. The average impact velocity for all the PCS cases was lower than the fTBI cases ($p<0.05$). This suggests that reduction in velocity may be an important in reducing the risk from fTBI to a PCS range. There were 3 distinct mechanisms of injury within the PCS group: falls, collisions, and projectiles. When comparing these mechanisms, significant main effects were discovered for all linear and rotational curve characteristics ($p<0.05$). Considering that all mechanisms resulted in PCS there may be at least two unique loading curve types (Figure 1) that can cause injurious damage to the brain tissue. As mechanism-related unique loading curves would create unique stress and strain conditions in different regions of the brain tissue it is possible that the loci of PCS may be different for each mechanism and it could result in different symptomologies [3]. These results also suggest that mechanisms of injury should be considered when conducting brain injury analyses and research.

Figure:
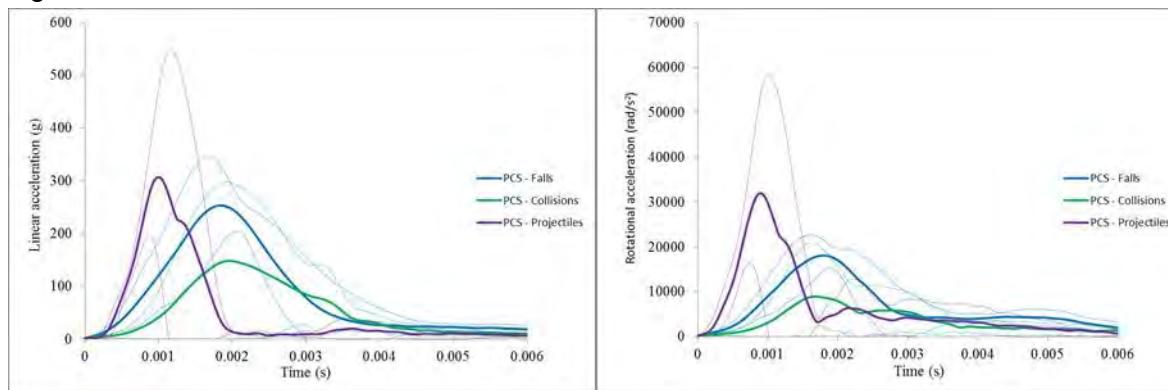
Caption: Comparison of the average linear (left) and rotational (right) acceleration loading curves for different mechanisms of the PCS cases.

Conclusion: This research examined the differences in acceleration loading curves that typify PCS and fTBI in a hospital dataset. It was discovered that other than duration of curve, the PCS group had an acceleration curve parameters of lower magnitude than that of the fTBI cases, likely due to lower average head velocity for the PCS group. When isolating for mechanism of injury, PCS was characterized by lower rotational acceleration curve characteristics than TBI, suggesting that rotational acceleration loading curves may be a better variable to distinguish between these two types of injury. Further analysis was conducted within the PCS group, revealed that mechanism of injury is an important factor in predicting brain injury. This research suggests that mechanism of injury must be considered to gain an improved understanding of injury thresholds and event characteristics that could then be applied to methods of prevention. These new technologies and innovations involving improved energy absorbing materials will need to manage the conditions of velocity, mass, and compliance linked to the mechanisms of mTBI relevant to each unique sporting or societal environment.

Table:

Injury	Velocity (m/s)	Rotational acceleration curve parameter				
		Duration (s)	Peak (krad/s^2)	Time (s)	Slope (krad/s^3)	Integral
TBI	4.17 (0.75)	0.0032 (0.0018)	34.3 (14.8)	0.0017 (0.0007)	23517.2 (14836.9)	38.8 (9.31)
PCS	3.19 (1.20)	0.0037 (0.0013)	18.1 (12.2)	0.0020 (0.0006)	11291.7 (10396.5)	25.0 (13.4)

Caption: Rotational acceleration loading curve parameters comparing the TBI and PCS cases (SD in brackets).

References: 1. Post et al., JMBBM, In Press, 2014.

2. Post et al., J Biomech, 47: 1074-1081, 2014.

3. Zetterburg et al., Nature Rev Neurol, 9(4): 201-210, 2013.

Disclosure of Interest: None Declared

Trauma

AS-0538

AN EXAMINATION OF TRAUMATIC MANDIBULAR FRACTURES USING DYNAMIC FINITE ELEMENT ANALYSIS

Gladstone Burke [1,*]Clive Neal-Sturgess [1] [2]Robert Ashford [1]

[1]Faculty of Health, Education and Life Sciences, Birmingham City University, [2]School of Mechanical Engineering, University of Birmingham, Birmingham, United Kingdom

Introduction and Objectives: The mandible is the one of the most commonly fractured bone of the facial skeleton [1][2]. The pattern of mandibular fractures is related to the magnitude, direction and duration of impact, which are features of the mechanism of injury. The multiplicity of injury mechanisms makes it difficult to determine if an anatomical sub-site has a greater propensity to fracture.

Traditionally biomechanical investigations on bony structures have involved cadaveric mechanical testing which is expensive, labour intensive and ethically questionable. Computer trauma modelling using three-dimensional finite element analysis has the advantage of avoiding such investigations. Such computer models have use in the medico-legal and forensic field where they may aid in the determination of proximate and ultimate causation of injuries[3].

The main objectives of this study were firstly to develop a three-dimensional finite element model of the adult human mandible capable of simulating mandibular fractures as a result of impact at various sites and angulations with various objects used in interpersonal violence e.g. fist. Secondly to use the finite element model to predict the anatomical fracture sub-site and temporal occurrence of mandibular fractures in a simplified traumatic simulation.

Methods: A computed tomographic scan of the facial skeleton of an adult male was used as a data source for the production of the finite element model. The images slices were segmented to identify cortical bone, cancellous bone and teeth. Finite element meshes were generated from the 3D reconstructed image slices. The assembled mandibular model was composed of 1183976 linear tetrahedral elements and 250523 nodes. The applied material properties were derived from the literature (see table).

Finite element simulations were performed with the mandible impacted at various sites (symphysis, parasymphysis, body, angle and ramus) with varying angulations with modelled objects including a pipe and a fist. Von Mises stress was used as a failure criterion. Static and dynamic 3D-finite element analyses of simplified traumatic injuries as a result of various loading situations were undertaken with in order to predict the fracture anatomical sub-site and temporal occurrence.

Results: A 3D finite element model of a human mandible was produced which allowed the examination of mandibular fracture under experimental loading conditions. Each load produced a unique cortical stress "signature". In these simplified trauma situations, non-linear dynamic analyses were able to give the disposition and temporal occurrence of fractures in addition to modelling patterns of fracture. The model did not simulate all patterns of mandibular fracture. Several patterns, especially those, which are encountered clinically, are due to indirect contacts with other parts of the facial skeleton, which was not modelled in this simulation. However, the modelled fracture patterns and loads were similar to those encountered in mechanical testing of cadaveric mandibles published in the literature (Figure 1).

Figure:

Caption: Simulated fist impact to right mandible. The lingual (inside) surface of the mandible is viewed. Fractures are indicated by asterisks. (Teeth are omitted in this simulation)

Conclusion: A finite element model used to study mandibular fracture without resorting to expensive mechanical cadaveric testing was developed. The model was capable of studying the effect of impact magnitude, direction and duration on the mandibular fracture pattern. Although this was a simplified model, the principles involved in modelling bony fractures on a macroscopic scale may be of use in larger models of the facial skeleton, which would be of clinical value. The mandibular model itself has the potential to provide useful biomechanical information for use in the forensic sciences.

Table:

	Element number	Node number	Young's modulus (MPa)	Poisson's ratio	Density (kg/m^3)
Cortical bone	454537	112273	13460	0.3	1740
Cancellous bone	217176	48898	7930	0.3	700

Caption: Model and material properties

References: [1] Haug, et al., Oral Surg Oral Med Oral Pathol Oral Radiol Endod, 90: 126–134, 2000.

[2] Hogg, et al., J Trauma, 49: 425–432, 2000.

[3] Wescott, Encyclopedia of Forensic Sciences, Academic Press, 2013.

Disclosure of Interest: None Declared

ADOLESCENT FEMORAL FRACTURE FIXATION WITH LATERAL TROCHANTERIC ENTRY RIGID HELICAL INTRAMEDULLARY NAIL - A BIOMECHANICAL EVALUATION

Darshan Angadi [1,*] Duncan Shepherd [1] Ramanan Vadivelu [2] Timothy Barrett [1]

[1]University of Birmingham, [2]University of Birmingham and Birmingham's Children's Hopsital, Birmingham, United Kingdom

Introduction and Objectives: Surgical treatment options of paediatric femur fracture include flexible or rigid intramedullary nails and submuscular plate fixation. Rigid intramedullary nailing has been suggested as a treatment option in adolescents due to the perceived advantages of stable fixation with higher union and low complication rates. However no study in the current literature has addressed the biomechanical aspects of rigid helical intramedullary nail fixation of femoral fractures in the adolescent population. Laboratory based biomechanical testing of implants is useful yet an expensive and time consuming process. Evolution of computational technology has enabled virtual testing of fracture fixation implants using finite element analysis (FEA) models of bones and implants.

Methods: 1) Development and validation of paediatric femur and helical intramedullary nail FEA models
2) Laboratory based experimental testing and FEA of femoral fracture fixation to evaluate stiffness parameters (axial/ four point bending / torsional) of common types (transverse / comminuted / segmental defect / spiral) of adolescent femoral fracture(~bodyweight of 60 kg). Methods: Experimental study involved small composite femurs implanted with helical intramedullary nail (n = 3) with (kExp Transverse, kExp Comminuted, kExp Segmental) and without (kExp Healed) fractures. Axial load (600N / 300N), four-point bending (400N / 60N), torque (4N m / 2N m) were used for healed and fractured models respectively. Femur FEA model was developed in SolidWorks using digital radiograph templates. Titanium alloy (Ti-6Al-7Nb) nail model consisted of cylinder (length 300 mm, outer diameter 11 mm-proximal, 8.2 mm-distal regions, 4.6 mm inner diameter) with helical axis. Simulation testing of fracture fixation using FEA models was performed in SolidWorks to estimate stiffness (kFEA). This validated model was subsequently used to estimate stiffness of a simulated mid-shaft spiral fracture (kFEA Spiral).

Results: Mean axial stiffness (N/mm) of femurs measured kExpTransverse = 622.84 (±36.65), kExpComminuted = 593.62 (±36.71), kExpSegmental = 562.04 (±31.51) and kExpHealed = 701.27 (±64.48). FEA model axial stiffness (N/mm) kFEATransverse = 611.97, kFEAComminuted = 602.47, kFEASegmental = 587.13, kFEAHealed = 725.46 and kFEASpiral = 576.92. Mean fourpoint bending stiffness (N/mm) of femurs was kExpTransverse = 102.53 (±16.47), kExpComminuted = 93.44 (±12.87), kExpSegmental = 88.06 (±13.76) and kExpHealed = 402.50 (±5.28) whereas FEA estimated kFEATransverse = 111.11, kFEAComminuted = 106.71, kFEASegmental = 99.01, kFEAHealed = 430.11 and kFEASpiral = 102.04. Torsional stiffness (N m/deg) (external rotation) of FEA models was kFEATransverse = 0.96, kFEAComminuted = 0.93, kFEASegmental = 0.93, kFEAHealed = 3.55 and kFEASpiral = 0.94 similar to femurs kExpTransverse = 0.96 (±0.12), kExpComminuted = 0.82 (±0.13), kExpSegmental = 0.77 (±0.14) and kExpHealed = 3.69 (±0.19). Torsional stiffness (N m/deg) (internal rotation) of FEA models was kFEATransverse = 0.96, kFEAComminuted = 0.94, kFEASegmental = 0.94, kFEAHealed = 3.56 and kFEASpiral = 0.94 comparable to experiment results kExpTransverse = 1.04 (±0.12), kExpComminuted = 0.97 (±0.20), kExpSegmental = 0.91 (±0.18) and kExpHealed =

3.86(±0.20). vonMises stress (σmax = 383.6 MPa) was noted at proximal screw in segmental fracture. Conclusions: A parametric FEA model based on simplified geometry may be used for evaluation of routine stiffness parameters of a paediatric femur. Titanium alloy rigid helical intramedullary nail used for paediatric femur fracture fixation can perform satisfactorily under physiological loading conditions experienced in the perioperative period.

Figure:

Conclusion: A parametric FEA model based on simplified geometry may be used for evaluation of routine stiffness parameters of a paediatric femur. Titanium alloy rigid helical intramedullary nail used for paediatric femur fracture fixation can perform satisfactorily under physiological loading conditions experienced in the perioperative period.

Caption: Fig 1. Composite femur specimen with a segmental defect of 10 mm and adolescent lateral entry femoral nail in situ undergoing axial compression test.

Disclosure of Interest: None Declared

AS-0540

MULTIPARAMETRIC ANALYSIS OF A PEDESTRIAN FEMUR DURING A CAR CRASH

Bernardo Innocenti [1,*]Matteo Bettoni [2]Walter Pascale [3]Filippo Begani [4]Silvia Pianigiani [3]

[1]BEAMS Department, Université Libre de Bruxelles, Bruxelles, Belgium, [2]Università Politecnica delle Marche, Ancona, [3]IRCCS, Istituto Ortopedico Galeazzi, Milano, [4]DIEF, Università degli Studi di Firenze, Firenze, Italy

Introduction and Objectives: The declaration of false injuries in the context of a car-pedestrian crash is a common problem with which the insurance companies have to face constantly. To provide them a valid support tool, this study through a finite element model wants to find out the risk of fracture (RF) associated to the femur by recreating the conditions of the impact in a collision between a car and a pedestrian.

Methods: A physiological bone model in contact with a car bumper model has been considered in this study. The femoral head has been considered fully encastred while the the distal part is unconstrained.

Due to the involvement of a high amount of parameters, the calculation of the risk for fracture of the femur was performed by a multiparametric study. The considered parameters are related to the physiological structure of the femur because its mechanical properties change greatly with the age, the thickness of the cortical bone and the presence of osteoporosis. Parameters related to the situation of the crash such as the type of bumper, the resulting impact force, the flection of the femur during the impact are also taken into account. in details, the considered parameters and their values are shown in the Table 1. The RF has been evaluated considering the maximum stress achieved by the femur after the impact. Subsequently the finite element analysis, through a statistical analysis was possible to trace what are the parameters that mostly affect the RF of the femur.

Results: The obtained results show that, among the several considered parameters, the RF is obviously mainly affected by the impact force and also by the height of the pedestrain. On the other hand, the bumper as well as the age of the pedastrian, are almost neglible factors (Figure 1).

Figure:
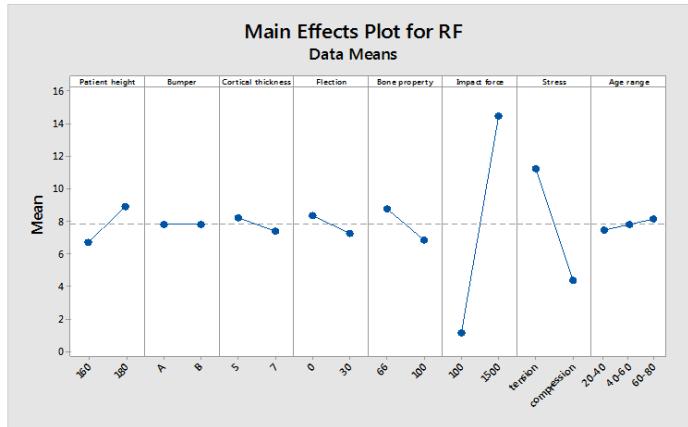
Figure 1: Influence of the analyzed parameters for the RF of the femur

Conclusion: Nowadays, insurance companies miss tools that provide help in deciding if a declaration of an injury is false after a car-pedestrian crash. This study wanted to develop a support developing a finite element model of a femur under car-pedestrian crash conditions. Several parameters have been analysed in order to consider several possible situations. The obtained results show that the features designs of a car are not decisive for the RF while the velocity of the impact is more important to be correlated with a possible femur fracture. Moreover, the age of the pedestrian, simulated as changes in the geometries and material properties of the femur bone, is not influencing the final outputs. On the other hand, the height of the patient affects the RF as the impact zone is then translated more proximally or distally. This study presents several limitations, as the complete embedment of the hip that, however, amplifies the trend of the results. Even so, the final aim of this study is not to provide a quantitative value of the induced forces and stresses during a car crash, but more to provide a tool to support decisions of insurance companies after a suspect car-pedestrian crash reimbursement request.

Table:

Parameters	Test values
Patient's height	160,180 [cm]
Impact position	lateral
Type of bumper	A,B
Impact force	100,1500 [N]
Cortical thickness	5,7 [mm]
Femur inclination	0°,30°
Bone material	healthy, osteoporotic
Age	20-40,40-60,60-80
Impact height	65 [cm]

Caption: Table 1: parameters and relative values used for the simulations

Disclosure of Interest: None Declared

Computer Simulation

AS-0541

FE MODEL OF FEMALE PELVIC FLOOR FOCUSED ON STRESS DISTRIBUTION IN LEVATOR ANI MUSCLE DURING VAGINAL DELIVERY

Linda Havelková [1,*]Ladislav Krofta [2]Luděk Hynčík [1]Jaroslav Feyereisl [2]

[1]New Technologies - Research Centre, University of West Bohemia, Plzeň, [2]Institute for the care of mother and child, Praha, Czech Republic

Introduction and Objectives: Female pelvis floor dysfunction such as organ prolapse, urinary and fecal incontinence is very often associated with damage of the levator ani muscle (LA) [1]. Muscle injuries and dysfunctions mostly occur during vaginal delivery when the muscle undergoes large deformation. Therefore, it is necessary to understand the anatomy and physiology of the LA during this process to be able to prevent and manage pelvic floor trauma. The objectives of this study were: (1) to measure the LA behavior by uniaxial test to find the material parameters; (2) to develop computer model of the female pelvic floor; (3) to analyze the stress distribution in the LA during the vaginal delivery respecting the optimal initial position and rotation of fetal head.

Methods: The passive biomechanical properties of the pig LA were measured to find the material parameters. Twenty LA samples extracted from eight pigs were used. The muscles were removed surgically during general anesthesia. Each sample was loaded by the uniaxial tensile test with a velocity of 6 mm/min until tissue rupture to obtain the stress-strain curve. The viscoelastic Ogden model was used to describe the passive behavior. The material parameters were determined by the least-square minimization method using the software called MATLAB [2].

The finite element method and the software called Virtual Performance Solution were used to develop new virtual model of the female pelvic floor. The model consists of the female pelvis, the LA, the obturator muscle and the fetal head. It was assumed that the other tissues are pushed without any significant reaction forces and thus they were neglected. The geometry is based on live subject MRI data. The model was reconstructed from axial 3T MR images. All slices were 2 mm thick. The asked subjects were a healthy, nulliparous, 25 years old female and three-day old child. The initial 3D geometric model was built using Slicer software. The final geometry and mesh were created in HyperMesh software. The boundary conditions were considered to simulate the real muscle attachments and supports. The fetal head trajectory was given by the pelvic shape - it followed the curvature of the sacrum and the coccyx to simulate the curve of Carus. The initial head flexion and rotation was also taken into account. Pelvis and fetal head were modeled by rigid bodies. During vaginal delivery, the LA performs extremely large deformations. Therefore the viscoelastic Ogden material was used to model both muscles [3]. The material parameters obtained from measurement were included.

The simulation of vaginal delivery was performed for optimal initial attitude of the fetal head –complete flexion, right occipitoposterior position. The distribution of stress von Mises in the LA was analyzed.

Results: The biomechanical properties of the LA were measured and its material parameters for Ogden model were calculated. The elastic parameters, μ and α, were $\mu_1 = 0.0082 \pm 0.0089$ MPa, $\mu_2 = 0.0216 \pm 0.0173$ MPa; $\alpha_1 = 0.1803 \pm 0.1299$, $\alpha_2 = 15.112 \pm 3.1704$.

The analysis of stress von Mises distribution in the LA during vaginal delivery was performed. The optimal fetal head position was considered. The results show, that the LA elongates almost 2.1 times in the inferior direction. The displacement of the upper arc top is about 54.272 mm in the posterior direction. Moreover, the length of the upper arc is 1.5 times higher by the biggest muscle elongation than in the initial resting position. The significant stresses were found in the upper arc of the LA, in the lower part in the middle and in the LA attachments. In summary, the maximal values were 0.094 GPa, 0.131 GPa and 0.481 GPa, respectively. To our knowledge based on clinical practice, right this stress pattern implies the highest risk of muscle stretch injury.

Conclusion: The new sophisticated virtual model of the female pelvic floor was developed to simulate the child birth. The model is primarily intended for analysis of stress generated in the LA. Nevertheless, it has wide range of applications in field of kinematics, dynamics as well as visualization. The model is now prepared for future applications. It will be used to analyze the stress distribution depending on various initial head position and rotation. In addition, the model will be used to develop the modern and efficient supporting tools preventing the urgent organ prolapse. In general, 3D pelvic floor models appear to be a promising for future mapping of pelvic trauma development. The project is co-financed by grants SGS-2013-26 and PRVOUK 32.

References: [1] DeLancey et al., Obstetrics and Gynecology, 101 (1): 46-53, 2003.

[2] Zemcik et al., Int J Gynaecol Obstet, 109: 136-139, 2012.

[3] Ogden et al., Non-Linear Elastic Deformations, John Willey and Sons, 1984.

Disclosure of Interest: None Declared

A NEUROMUSCULOSKELETAL MODEL TO SIMULATE PASSIVE WRIST EXTENSION TEST OF SPASTICITY

Ruoli Wang [1,*] Örjan Ekeberg [2] Pawel Herman [2] Johan Gäverth [3] Anders Fagergren [4] Hans Forssberg [3]

[1]Department of Mechanics, [2]Department of Computational Biology, Royal Institute of Technology, Stockholm, [3]Department of Women's and Children's Health, Karolinska Institutet, [4]AggeroMed Tech AB, Stockholm, Sweden

Introduction and Objectives: Spasticity is a motor disorder characterized by a velocity-dependent increase in tonic stretch reflexes [1], commonly seen in many neurological disorders. Clinically, spasticity is measured by an examiner rotating a joint and simultaneously estimating the resistance according to an ordinal scale. However, the limited reliability of the measurement and the impossibility to discriminate between the underlying neural (stretch reflex) and non-neural contributions have been the motivation to develop methods describing resistance joint torque quantitatively. The aim of this study is to develop a forward neuromusculoskeletal model consisting of the explicit musculotendon, muscle spindle, and motoneuron pool models, which can simulate passive wrist extension test of spasticity.

Methods: Neuromusculoskeletal model

The neuromusculoskeletal modeling includes muscle spindle modeling, motoneuron pool modeling, muscle activation dynamics and musculotendon modeling of the wrist flexors.

Muscle spindle modeling: The modified hybrid $V^{0.6}$ model was used to model the firing characteristics of the muscle spindle [2].

Motoneuron pool modeling: The motoneuron pool transformation was modeled as a sigmoid function which ranges from 0 to 1, representing the motoneuron neural excitation as a function of the muscle spindle-firing rate.

Activation dynamics: Activation dynamics can be described as the process of converting the neural excitation to muscle activation as a first order differential equation [3].

Musculotendon modeling: The musculotendon model consists of one lumped muscle actuator which represented synergistic wrist flexors and one passive plant. The passive plant can be considered as the passive viscoelastic properties of the joint. Wrist extensors were not included in the model. The Hill-type musculotendon model was used to simulate musculotendon dynamics of the lumped muscle actuator [4].

Experimental Setup and Protocol

Passive extension of the wrist at a slow (5°s-1) and a fast (236°s-1) velocity were performed using a newly developed device Neuroflexor (Aggero MedTech AB, Solna Sweden). The resistance torque induced by the passive wrist extension was measured. Range of wrist movement was set between 20° flexion and 30° extension. An example data from a chronic stroke patient (male, hand length = 0.09m, weight = 69kg) was reported.

Optimization

It is assumed that no reflex induced muscle resistant torque in the slow movement; hence the resistant torque is purely caused by the passive plant. Nonlinear least squares was used to approximate four passive parameters: elasticity coefficient K_p, viscosity coefficient B_p, and non-linear expontential coefficients k_1 and k_2. Genetic algorithm (GA) was used to identify four optimal stretch related parameter: motorneural pool parameter μ and σ, dynamic and static spindle gain G_l

and G_v, so that the root-mean-square error between the measured and predicted resistant torque in part of fast movement (approximately from 0.1 to 0.23ms, Fig 1) was minimized. Previous studies have reported that the static and dynamic gains of the spindle in the pathological group did not differ significantly from the healthy controls [6]. Therefore, constraints were set to vary ±10% from the reported values (2 and 4, respectively).

Results: Simulation results from one chronic stroke patient are illustrated in the Fig 1. Four passive parameters ([K_p = 1.54, B_p = 0.1, k_1 = 0.05, k_2 = 3.2], R^2 = 0.998) were determined. Four stretch- related (neural) parameters ([μ = 157.3, σ = 10.1, G_l = 2.1, G_v = 4.1]) were found and the minimal root-mean-square error (cost function) was 5.4.

Figure:
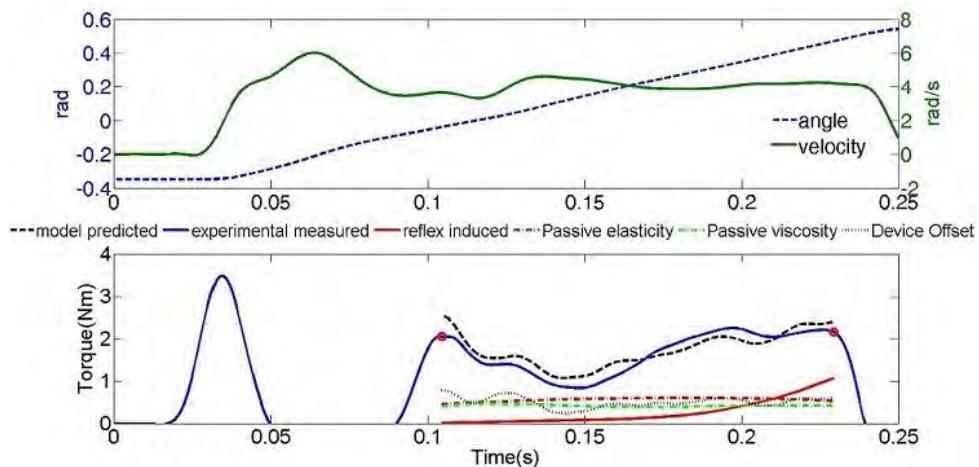
Caption: The top: the angular velocity and position were prescribed in the simulation of the fast wrist extension. The bottom: the contributions of the torques from passive muscle properties (elasticity and viscosity) and the stretch reflex to the total resistance torque were specified. The optimization was only performed during the period marked with red circles.

Conclusion: By identifying important passive and reflex related parameters using optimization, the neuromusculoskeletal model can reliably describe non-neural and neural related contributions to the total joint resistant torque. The figures illustrate a good fit between the predicted and experimental measured resistant torque. Due to the large measurement error during the period 0.05-0.09ms and the latency of the reflex, the optimization was only performed for part of the fast movement, where the angular velocity maintained stable. Due to the fact of interdependency of the parameters and the difficulties of obtaining gradient, GA was used in the current study. In conclusion, the proposed neuromusculoskeletal model can simulate the passive wrist extension test of spasticity.

References: [1] Lance, Neurology, 30: 1301-13, 1980.
[2] Prochazka et al. J Physiol, 27:21-34, 1998.
[3] Thelen, et al. ASME J Biomech Eng, 125:70-77, 2003.
[4] Winter, et al. IEEE Trans Bio-med Eng, 32:826-839, 1985.

Disclosure of Interest: R. Wang: None Declared, Ö. Ekeberg: None Declared, P. Herman: None Declared, J. Gäverth Conflict with: AggeroMed Tech AB, A. Fagergren Conflict with: AggeroMed Tech AB, H. Forssberg: None Declared

Modelling

AS-0543

INTEGRATING ULTRASONOGRAPHY INTO A SUBJECT-SPECIFIC EMG-DRIVEN MODEL TO ESTIMATE TIBIALIS ANTERIOR MUSCLE FORCE

Stuart Miller [1] [2],*Thomas Korff [2]Anthony Blazevich [3]

[1]London Sport Institute, Middlesex University, [2]Centre for Sports Medicine and Human Performance, Brunel University, London, United Kingdom, [3]School of Exercise and Health Sciences, Edith Cowen University, Perth, Australia

Introduction and Objectives: The quantification of tibialis anterior (TA) forces *in vivo* is important in order to (i) better understand its role in human movement [1], (ii) allow a more complete analysis of pathological movement [2], and (iii) provide insight into the underlying causes of overuse injuries such as chronic anterior compartment syndrome [3]. EMG-driven musculoskeletal modelling offers an interesting approach to developing a subject-specific model for estimating muscle force *in vivo*. These models incorporate the muscle's force-length and force-velocity (FV) relationships, with a scaling factor included for activation. Of importance is that the length and velocity must refer to the contractile unit [4], rather than the whole muscle-tendon unit (MTU), as changes in tendon length are rarely synonymous with changes in muscle length. To date, joint kinematics are commonly used to model the action of the contractile components. However, this approach does not allow for the differentiation of the tendon and muscle.

The aim of this study was to develop a model that allowed for the muscle properties to be recorded *in vivo* non-evasively, resulting in a more valid approach to estimating muscle force *in vivo* than previous approaches.

Methods: A set of calibration contractions were performed by four adults (age = 26±1 yr, height = 1.79±0.05 m, mass = 75.6±12.0 kg). A second set of contractions were performed that were used as a validation tool. Isokinetic dynamometry, ultrasonography and electromyography were collected. Muscle kinematics and activation were used as the model inputs, with the ankle moment providing a means to fit the model to the individual, and to allow for the validation of the model.

The model is based on a FV sub-model that is scaled to isometric force. This uses velocity as its main input. This scaled FV sub-model was then used to calculate force across muscle lengths and activation levels. Changes in the FV relationship across muscle lengths and activation levels are removed when normalising to isometric force [5] and maximal shortening velocity has been suggested to be constant across a range of intensities and muscle lengths [6]; it was thus assumed that a single FV sub-model was appropriate.

To determine the isometric force for calculation of absolute forces from the normalised FV sub-model, a second sub-model calculated isometric force for all contraction intensities and muscle lengths. This used muscle activation and length as inputs. A force-EMG relationship was produced for each muscle length, with the slope of this relationship being modelled over the full muscle length range; isometric force for all muscle lengths and contraction intensities was determined.

Direct calculation of force during the calibration procedure is needed. The only non-invasive approach is to measure joint moment. Removal of the antagonist moment is important for valid calculation of TA force from the joint moment [7]. A moment-EMG-angle relationship for the plantar flexors (PF) was developed following investigation into the optimal approach to (i) modelling moment-EMG at individual angles (i.e. linear vs curvilinear), (ii) accounting for angle within a

single model, and (iii) modelling PF (i.e. weighting of the individual muscles), whilst optimisation procedures were incorporated to investigate the optimal EMG processing procedures. This allowed for dorsiflexor moment to be calculated. The moment arm (calculated using a modified tendon excursion method [8]) was then used to calculate tendon force.

The new muscle model was compared with a more traditional ankle model in which joint kinematics were used as the input instead of muscle kinematics. Relative root mean square error (%RMSE) was used to assess the accuracy of each modelling approach.

Results: For four of the six validation conditions, small differences were found between the two approaches to modelling the contractile components of TA. For the fast concentric condition, the angle model predicted TA force better (Cohen's d=2.7) whilst the length model performed better for the slow eccentric condition (d=0.7), although this was only a difference in %RMSE of 2.8%.

Conclusion: Under controlled conditions where the discrepancy between muscle and whole MTU (estimated from joint angle change) length change is minimal, the use of ankle angle data as input into an EMG-driven model is appropriate. However, further research is required to ascertain the validity of this simplification in more complex movements where stretch-shorten cycle actions might produce a greater discrepancy between muscle and MTU length.

References: [1] Prilutsky et al., J Exp Biol, 204: 2277-87, 2001.

[2] Byrne et al., J Electromyogr Kinesiol, 17: 605-16, 2007.

[3] Birtles et al., Eur J Appl Physiol, 88: 565-71, 2003.

[4] Ito et al., J Appl Physiol, 85:, 1230-5, 1998.

[5] Bigland et al., J Physiol, 123: 214-24, 1954.

[6] Edman, J Physiol, 291: 143-59, 1979.

[7] Billot et al., Muscle & Nerve, 41: 511-8, 2010.

[8] Miller et al., Med Sci Sports Exerc, *in press*, 2014.

Disclosure of Interest: None Declared

THE EFFECT OF INTRAMUSCULAR FAT ON SKELETAL MUSCLE FORCE IN THE OBESE

Hadi Rahemi [1,*] Nilima Nigam [2] James M. Wakeling [1]

[1]Biomedical Physiology and Kinesiology, [2]Mathematics, Simon Fraser University, Burnaby, Canada

Introduction and Objectives: Obesety is a condition where excess fat accumulates in the body. While most of the excess fat is accumulated subcutaneously, some will infuse into muscle tissue. This condition affects skeletal muscle in different ways. The distribution of muscle fat can be both intra and extracellular. In addition to fat accumulation its has been shown that the proportion of type I and IIA fibre are reduced while the proportion of fatigable type IIB fibres are increased with obesity [1]. Also, a reduction in activity can lead to muscle atrophy occurring with obesity [2].

The changes to muscle structure with obesity affect its performance. This includes a reduction in both force and power output of the muscle. While experimental measurements can help us to understand the loss in the mechanical output at the level of the limb and joint, it is hard to quantify the effect of intra and extracellular fat on the performance of individual muscles. This can be done using a muscle model that allows the manipulation of intra and extracellular properties in the muscle tissue.

In this study we used variations of a 3D finite element model of human gastronemii [3] to study the effect of different intramuscular fat distribution. The effect of atrophy was also replicated by a reduction in the contractile elements (CEs).

Methods: We used a simplified geometry of unipennate muscle belly. The dimensions, boundary condition and mechanical properties of the muscle and aponeurosis were as previously described ([3], normal aponeurosis stiffness). The properties of the transversely isotropic muscle tissue were varied while the mechanical properties of the aponeuroses remained the same. Variations of the model are: [M1] Lean muscle (no fat) with 100% of CEs; [M2] muscle with a varied accumulation of X% fat (properties from [4]) in the base muscle material (BBM) and 100% CEs; [M3] lean muscle with X% reduction in CEs; [M4] muscle with X% of fat in the BBM and X% reduction in CEs; [M5] muscle with a random and sparse distribution of X% pure fat points dispersed within the lean muscle tissue; and [M6] muscle with a random and sparse distribution of X/2% pure fat points, X/2% of fat in the BBM and an X/2% reduction in CEs. M1 represented a control condition for lean muscle, M2 and M4 were models with intracellular fat, M5 represented extracellular fat, M6 contained a combination of intracellular and extracellular fat, and M3 was a lean muscle with a loss of CEs.

The concentration of intramyocellular fat for obese subjects varies between 2 to 5% depending on the fibre type [1]. In this study we have assumed that a similar amount can be accumulated extracellularly. Therefore along with an average X=10% fat level in obese people, model variants M2 to M6 were simulated in a low X=2% and an extreme X=20% fat levels.

The force at the muscle-tendon junction, mean pennation angle and mean fibre length were calculated to asses structural changes and performance of the muscle in simulated scenarios.

Results: Muscle force in model variants with intramuscular fat (M2, M4-M6) was lower than lean muscle variants (M1, M3) for equivalent activation levels. There was also a substantial reduction of the muscle force with increased intramuscular fat. For example, in an extreme 20% fat scenario, forces in models M4-M6 (~90 N) were less than half of those for the M1

model at (~205 N) at 50% activation levels. Figure 1 shows the difference in force-activity profile of M1-M6 models for 2, 10 and 20% fat levels.

The pennation increased in all model variants with an increase in muscle activity; however the pennation increased to a greater extent in the in lean models M1 and M3.

Figure:
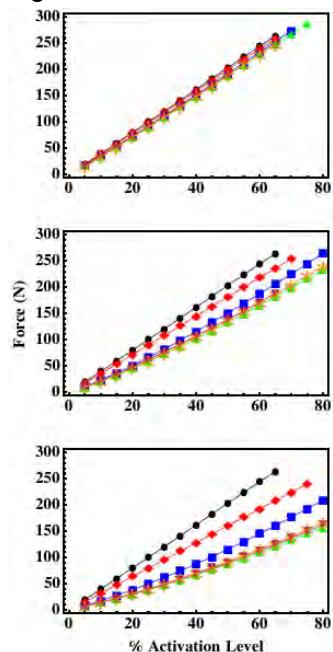
Caption: Figure 1. Force-activity plots of model variants: M1 (black), M2 (blue), M3 (red), M4 (Green), M5(purple) and M6 (orange) at 2% (top), 10% (middle) and 20% (bottom) fat levels.

Conclusion: The reduction in the fatty muscle force output compared to lean muscle may be a function of the increased stiffness of the base material properties. The stiffer tissue in the obese muscles affects the force development and transmission ability of the muscle. In addition, the results show that the loss of X% contractile elements (M3) has a smaller effect on the loss of muscle force compared to an X% intramuscular fat infusion (M2). In other words, an increase in intramuscular muscle fat is more critical to reduction in force than the decline in the contractile elements mimicking atrophy. The smaller changes in fibre pennation in the fatty muscles can affect the gearing [5] of the gastrocnemii muscles. Lowering the gearing potential of pennate muscles in general, may reduce their force and power output.

References: [1] Malenfant et al. *Int. J. of Obesity and Related Metabolic Disorders* 25.9: 1316-1321, 2001.

[2] Evans. *The Am. J. of Clinical Nutrition* 91.4: 1123S-1127S, 2010.

[3] Rahemi et al. *Frontiers in Physiology* 5: 298, 2014.

[4] Tanner et al. *Medical Physics* 33.6: 1758-1769, 2006.

[5] Azizi et al. *Proc. of the National Academy of Sciences* 105.5: 1745-1750, 2008.

Disclosure of Interest: None Declared

AS-0545

BIAXIAL COMPARISON OF AORTIC TISSUE AND CALCIFICATION BY A BUBBLE INFLATION TEST, APPLYING THE FINITE ELEMENT METHOD

Francisco Carrasco-Hernandez [1],*Richard Brooks [1]David Richens [2]Donal McNally [1]

[1]University of Nottingham, [2]The Trent Cardiac Centre , Nottingham, United Kingdom

Introduction and Objectives: Blunt Trauma Aortic Rupture (BTAR) is a significant cause of death in automotive accidents [1], up till now the internal mechanism of this trauma has not been fully understood. To further understand this, the present work is based on the hypothesis that the arterial wall has different strength or stiffness, depending on the zone of the aorta [2]. BTAR mostly initiated at the aortic isthmus, and the aortic ductus arteriosus (DA) closes forming the ligamentum arteriosos at the isthmus zone which results in a scar in the aortic wall, with fibrosis resulting from the fusion of two materials [3]. This study test the hypothesis that the fibroses scar on the wall of the aorta formed by the DA, leads to a concentration of stress and strain, at the site of the rupture in BTAR.

Methods: This research is based on experimental bubble inflation tests done by Pearson, R. et al. [2] using aortic tissue. A Finite Element Method (FEM) bubble inflation test with a specimen of 3 layers corresponding the Intima, Media and Adventitia, and geometric boundary conditions are set to reproduce the experimental test. The model can then be validated with the experimental test.

Using the verified numerical model, seven specimens were be designed with a patch of increase stiffness, with diameters of 1mm, 2mm, 3mm, 4mm, 5mm, 6mm and 7mm. In order to study the generation of stress concentration, the stiffness of the patch was also increased from the stiffness of the adventitia layer to 190%, in intervals of 10%.

Results: To understand which of the above two changes i.e. Patch size or Average of stiffness, for the greater effect, Von-Misses effective stress is compared across the inflating bubble model for varying patch sizes and stiffness. The values that are compared are in the upper element of the intima layer in the border between the patch and the aortic tissue. It is important to highlight the point that in this study there are no failure criteria.

Figure 1 with Table 1 shows the average V-M effective stress compared with the variation of patch size taking an average of stiffness across each patch. The increase in stress where a scar is introduced is considerable, on average rising to 152.7% of the stress that is given for a specimen with no patch. When the patch size is closer to the thickness of the specimen i.e. 1.03mm. After this rise is less significant

The theory of Crack Mechanics determines that a crack is the separation of material, caused by opening or sliding, with the distance of separation smaller than the length of the separation. Therefore for small diameters the concentration of strains will be bigger at certain pressure [4].

Figure:
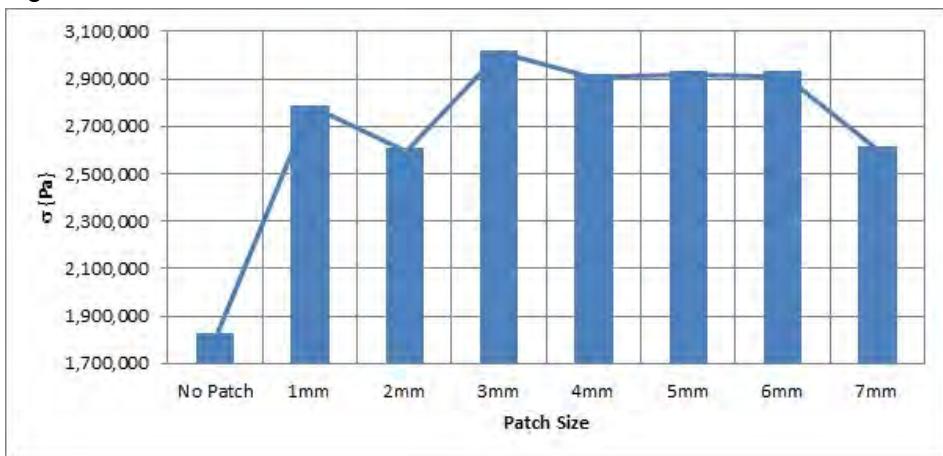
Caption: Figure 1. Comparison of the Von Misses Effective Stress of the Average Stiffness Vs Patch Size for patch stiffness.

Conclusion: The importance of this study is that with the insertion of a scar (which simulates the DA cicatrix) in the aortic tissue are found concentrations of stress and strain between the border of the aorta and the scar, if the DA forms the isthmus, this study shows that if there is a small scar or if it presents with the dimensions comparable to the thickness of the aorta, the concentration of stress and strain are above a considerable value, this could lead to a nucleation of a crack in the border of the aorta and the scar, caused by a overpressure inside of the aorta, this could be one of the reasons why the blunt aortic trauma starts with a tear in this specific region of the aorta

Table:

Pressure MPa	No Patch MPa	1 mm MPa	2 mm MPa	3 mm MPa	4 mm MPa	5 mm MPa	6 mm MPa	7 mm MPa
1.8	1.83	2.8	2.6	3.0	2.9	2.9	2.9	2.6

Caption: Table 1 Comparison of Concentration of Stress, patch size and stiffness

References: [1]   Pavlidis, et al., *Echocardiography*, 28:2, E42–3, 2011.

[2]   Pearson, et al., *Eur. J. Cardiothorac. Surg.*, 34:3, 616–22, 2008.

[3]   Moller and Hoffman, *Pediatric Cardiovascular Medicine*, Wiley-Blackwell, 2012.

[4]   Bertram Broberg, *Cracks and Fracture*. Academic Press, 1999.

 Disclosure of Interest: None Declared

Modelling

AS-0546

EFFECT OF SCALED LOWER LIMB ANATOMICAL MODELS ON FORCE PREDICTIONS DURING WALKING GAIT

Ziyun Ding [1,*]Angela Kedgley [1]Anthony MJ Bull [1]

[1]Department of Bioengineering, Imperial College London, London, United Kingdom

Introduction and Objectives: Musculoskeletal modelling studies of the lower limb require detailed descriptions of lower limb anatomical geometry. Scaled implementations of generic anatomical models (e.g., Klein Horsman et al.[1]) are often used to create customised musculoskeletal models. However, the sensitivity of musculoskeletal modelling to the choice of anatomic dataset is largely unknown. This affects the validation of musculoskeletal modelling, which normally comparing the hip and knee contact forces predicted using a scaled anatomical model against the direct measurements from instrumented prostheses on a subject. This study aims to investigate the differences between using a scaled, anatomical model and a subject-specific MRI-based model in muscle and joint contact force predictions during walking gait.

Methods: Muscle and joint contact forces were calculated using a musculoskeletal model of the lower limb [2]. The model consists of 4 segments (foot, shank, thigh and pelvis), articulated by three joints at the ankle, knee and hip. Kinematic data and ground reaction force data were collected from a single subject (male, 1.83 m, 93 kg). Musculoskeletal geometry was determined in two ways: (1) by digitising an MRI scan of the whole lower limb and (2) by linearly scaling each segment of a published anatomic dataset (male, 1.74 m, 105 kg [1]). Three-dimensional scaling factors were calculated by comparing distances between bony landmarks from the calibration trial with body landmarks from the published dataset. As complete anatomical datasets, both models provided information regarding bony landmarks, joint rotation centres, and 163 muscle elements representing 38 muscle groups of lower limb. Muscle lines of action were defined by origin and insertion points. For muscles that wrapped over underlying structures, their lines of action were defined by via points or wrapping object parameters.

Results: Differences were found between muscle force predictions using two models. There were distinct differences for muscles crossing the ankle joint. Maximum difference of the peak muscle force can be as large as 400% (i.e., extensor digitorum longus, extensor halluces longus, and peroneus longus). This interpreted the significant peak value variations for the ankle joint contact forces (see Figure). The distributions of knee and hip joint contact forces were similar. Similarities include the double peaked curve and peak values during the stance phase. However, joint contact forces predicted using the MRI-based model showed better agreement with the previous research findings [3]. [3] reported that the peak tibiofemoral joint contact force occurred at contralateral toe-off (i.e., about 15% of the gait cycle) and peak values ranged from 2.3 to 2.5 BW. The contact forces predicted using the MRI-based model agreed closely to these results.

Figure:
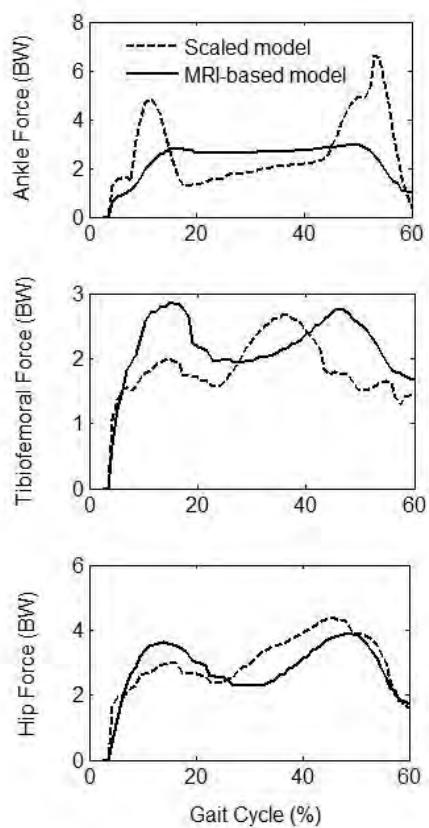
Caption: Joint contact forces predicted during the stance phase.

Conclusion: Muscle forces and joint contact forces in a stance phase were successfully predicted employing two alternative customised models. They both described lower limb muscle geometry with 163 muscle elements hence produced similar redundancy in optimisation. However, relocated joint centres and muscle origin-insertion points from the scaled model resulted in substantial variability of force solutions relative to the MRI-based model. The use of scaled models for musculoskeletal modelling validation therefore would introduce inaccuracy. This finding suggests that it is essential to establish appropriate scaling through, for example, a lower limb anatomical database. The implementation of the lower limb anatomical database would significantly improve the accuracy of musculoskeletal modelling study.

References: [1] Klein Horsman MD. et al., Clin Biomech, 22(2):239-247,2007

[2] Cleather DJ. et al., Ann Biomed Eng, 39(1):147-169, 2011

[3] Zhao D. et al., J Orthop Res, 25(5):593-602, 2007

Disclosure of Interest: None Declared

AS-0547

ASSESSMENT OF THE EFFECTS OF BODY WEIGHT UNLOADING ON KINEMATICS, KINETICS, MUSCLE ACTIVITY, AND CENTER OF PRESSURE DURING OVERGROUND GAIT

Arielle Fischer [1,*]Alon Wolf [1]

[1]Mechanical Engineering, Technion- Israel Institute of Technology, Haifa, Israel

Introduction and Objectives: Body weight unloading (BWU) on treadmills is a common method of gait rehabilitation which by alleviating load on lower joints and related pain allows patients with neurological and musculoskeletal impairments to undergo treatment at the onset or right after surgery [1,2]. However, the effects of body weight reduction on the regeneration of lower joints locomotor patterns, a vital step to regain gait functioning under normal daily conditions, were hard to assess as long as research was conducted on treadmills. The walking modality-treadmill as opposed to overground- may confound the effects of BWU [3]. Once conducted overground, gait research on the effects of BWU was facing another challenge that of controlling healthy subjects' speed variability which was easily controlled on treadmills but hard to control overground [2,4]. In this research a novel mechanical device was designed to pull the BWU system at a constant speed and thus allowed healthy subjects to maintain a comfortable speed during overground walking with a BWU system. In so doing, this study could examine the unique effects of BWU on gait biomechanical parameters under conditions that approximate daily walking. We hypothesized that partial BWU during overground walking (1) will not affect lower limbs kinematic parameters, i.e., range of motion and trajectories. We furthermore assumed that BWU will result in (2) a decrease of lower joint kinetics, (3) a decrease in electromyographic (EMG) activity and (4) a shift in the center of pressure (COP).

Methods: <u>Sample and Procedure:</u> Fifteen healthy male subjects with no prior gait impairment, included in the sample, walked overground under various levels of body weight reduction performed with a Biodex BWU system. An electric winch pulled the system at a constant speed of 4km/h. The procedure included overground walking under a control (No vest), and three 0%, 15%, and 30% BWU experimental conditions.

<u>Measures:</u> Kinematic measures of the hip, knee, and ankle joints included peak angular displacement, and range of motion in the sagittal plane and joint trajectories. Kinetic measures included the peak moments and impulses in the sagittal and frontal planes of the hip, knee and ankle. The Electromyographic measures included the duration of EMG activity, peak EMG signal, and impulse of the EMG signal for the muscles examined, the tibialis anterior (TA), lateral gastrocnemius (Lat GC) and vastus lateralis (VL).

Kinematic, kinetic and EMG data were simultaneously recorded with a Vicon Nexus motion tracking system (Oxford Metrics Ltd). The foot center of pressure was calculated by using the force plate and marker data.

Results: Findings show that healthy subjects overgound gait under 0%, 15%, and 30% BWU levels did not exhibit any significant modification in flexion and extension kinematic parameters of the joints (Figure 1a). In contrast, the increase in BWU levels resulted in a significant decrease of peak moments and impulses in the sagittal and frontal planes (Figure 1b). Additionally, paired comparisons of kinetic and kinematic trajectories under three BWU levels show high correlations between trajectories (r>0.95; p<0.001). A significant inverse relationship was also observed between BWU levels and

EMG measures (Figure 1c). As the BWU level increased, the impulse of the TA, Lat GC and VL as well as the peak EMG activity of the TA and Lat GC decreased. In contrast, the BWU level did not affect the EMG signal trajectories of the muscles which remained highly correlated (r>0.84; p<0.001) under paired comparisons of BWU levels. Increasing the BWU level resulted in modifications of the foot center of pressure (COP), with a lateral shift in the coronal plane of the COP (Figure 1d) during stance.

Figure:
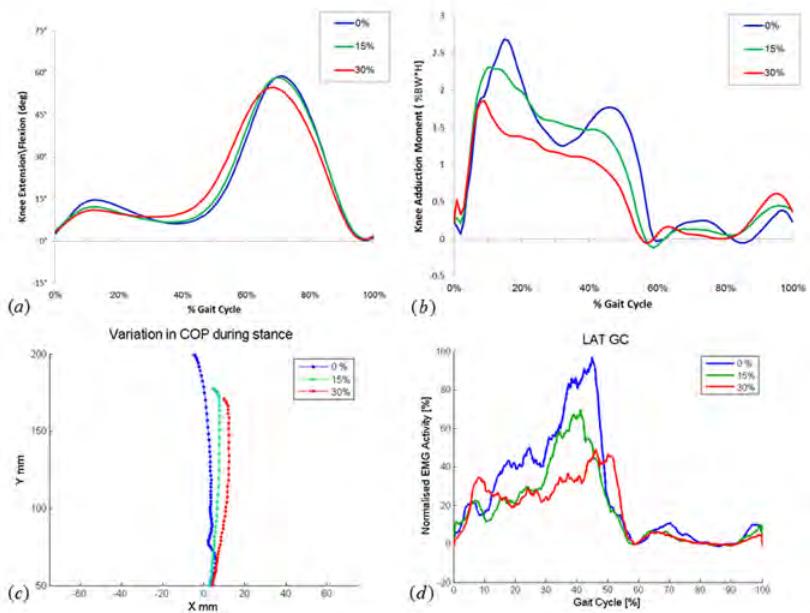
Figure 1. (a) Representative subject's Sagittal Plane Knee Flexion and Extension angle, (b) Frontal Plane Knee Adduction Moment, (c) EMG signal of the Lateral Gastrocnemius and (d) Center of Pressure under three 0% 15% and 30% BWU conditions.

Conclusion: A body weight reduction of up to 30% neither modified healthy subjects' overground gait patterns nor affected the plantarflexion needed for forward propulsion. The observed reduction in joint moments, the shift in COP and reduction in EMG activity resulting from BWU have wide implications in gait rehabilitation. These results suggest that BWU may safely be applied with clinical patients undergoing rehabilitation in situ, i.e., under conditions that replicate daily walking. This procedure is expected to reduce the load on joints and muscles without reducing the propulsive force so far observed on treadmills. As lower joints regain their functional activity with respect to balance, range of motion and locomotor patterns, patients' body weight may be gradually increased until they resume normal daily walking without any BWU. Potential applications of BWU on gait rehabilitation extend beyond clinical subjects with neurological or musculoskeletal impairments to sports injuries and/or obesity.

References: [1] Barbeau et al., Progress in motor control. Champaign (IL): Human Kinetics, 2004.

[2] Threlkeld et al., Gait Posture, 173:235-245, 2003.

[3] Ivanenko et al., J Physiol. (Lond.), 5561:267-282, 2004.

[4] Van Hedel et al., Gait and Posture, 241:35-45, 2006.

Disclosure of Interest: None Declared

CAN GAIT KINEMATICS BE USED TO PREDICT RESPONSE TO STANDARDISED EXERCISE PROGRAMS IN INDIVIDUALS WITH KNEE OSTEOARTHRITIS?

Kathryn Mills [1,*]Michael Martin [2]Sean Osis [3]Blayne Hettinga [3]Reed Ferber [3]

[1]Physiotherapy, Macquarie University, Sydney, [2]Research School of Finance, Acturial Studies and Applied Statistics, Australian National University, Canberra, Australia, [3]Kinesiology, University of Calgary, Calgary, Canada

Introduction and Objectives: Three-dimensional kinematic gait analysis is often used in the assessment of individuals with medial tibiofemoral knee osteoarthritis (OA). Patients with knee OA have been reported to exhibit varus thrust and abnormal frontal plane knee mechanics, which may be associated with disease progression [1, 2]. With increasing adoption of motion capture technologies in clinical settings, an important question is which variables best guide clinical decision-making regarding patient care. Specifically, are there kinematic variables that can predict outcome to standardised conservative management? Being able to identify those who do and do not respond to a standardised exercise program has important clinical implications. Those who respond could undertake home- or group-based strategies, while those who do not may require a more tailored approach. Therefore, the aim of this study was to investigate whether and which baseline kinematic variables could be utilised to predict OA patients' outcome to a standard management strategy.

Methods: Twenty-three participants with mild-to-moderate knee OA were recruited to participate. All individuals were ≥40 years, had a BMI ≤33 kg/ m^2 and were able to walk on a treadmill without the assistance of walking aids. Participants underwent a kinematic assessment prior to participating in a 6-week lower limb strength and balance program. Gait analysis consisted of walking on a treadmill at 1.1 m/s, wearing standard laboratory shoes (Pegasus, Nike Air, OR USA). Kinematic data of the pelvis, hip, knee and ankle were collected at 120Hz using an 8-camera VICON motion capture system (Oxford Metrics, Oxford, UK) and 9 mm reflective custom marker set.

Data were analysed in Matlab (MathWorks, MA USA). An average of 20 stance phases were used to extract maximum joint angles during the first 25% of stance and joint excursions (maximum-minimum angle). The initial 25% of stance encompasses where the external knee adduction moment is greatest [3], often interpreted as when the medial tibiofemoral compartment is under the greatest load.

The 6-week home-based exercise program focused on hip muscle strengthening. Intensity was increased weekly by either increasing the number of repetitions or the resistance of elastic bands. The balance component of the program was progressed by reducing the base of support from bilateral to unilateral stance and by increasing activity duration. Program success was measured as worst pain over the previous week on a 100 mm visual analogue scale (VAS) from 0 (no pain) to 100 (worst pain imaginable). Pain ratings at the end of the intervention were subtracted from baseline measures and participants were deemed as success or non-success using the criteria of an improvement of ≥ 50% and absolute change in pain of ≥ 20 mm [4, 5].

Two classification and regression trees were fit to identify if and which baseline kinematic variables were best able to differentiate between participants who reported success and those who did not. The first tree examined the predictive ability of maximum joint angles during the first 25% of stance (25% Tree) and the second examined joint excursion (Excursion Tree). Only kinematic variables from the most affected limb were included in each model, as well as age and BMI. This analysis aims to correctly classify as many participants as possible based on a hierarchical sequence of binary splits. Each split was subjected to a penalty that balances goodness of fit against the ability to generalise the fit to the broader population.

Results: The Excursion Tree was able to classify the 9 participants who reported success and the 14 who did not using baseline kinematics, producing a single split, which successfully classified 55.55% of successful cases and all non-successful cases. The single kinematic variable found to be the best classifier was knee frontal plane excursion and all subjects who exhibited knee frontal plane excursion <8.9° were correctly classified as successful. The 25% Tree failed to split, meaning peak angles during the initial 25% of stance are no better than chance at directing clinical decision-making.

Conclusion: Kinematic variables observed during gait analysis were able to predict which individuals with mild-to-moderate medial knee OA will and will not respond to a standardised exercise program. Specifically, exhibiting <8.9° frontal plane knee excursion was found to be the best classifier. Given the sample size of the current study, our results must be interpreted with caution. However, they represent an important step towards providing clinicians with evidence-based guidance in how to integrate kinematic gait analysis in their clinical decision-making.

References: [1] Miyazaki T, et al. Ann Rheum Dis 2002;61:617–22.

[2] Chang AH, et al. Arthritis Rheum 2004;50:3897–903.

[3] Lewek MD, et al. Osteoarthr Cartil 2004;12:745–51.

[4] Pham T, et al. J Rheumatol 2003;30:1648–54.

[5] Tubach F, et al. Ann Rheum Dis 2005;64:29–33.

Disclosure of Interest: None Declared

AS-0549

SHORT-TERM EFFECTS OF THORACIC SPINE MANIPULATION ON PAIN, FUNCTION AND SCAPULAR KINEMATICS IN SHOULDER IMPINGEMENT SYNDROME

Melina N. Haik [1,*]Francisco Alburquerque-Sendín [2]Paula Camargo [1]

[1]Physiotherapy, Federal University of São Carlos, São Carlos, Brazil, [2]Physiotherapy, University of Salamanca, Salamanca, Spain

Introduction and Objectives: Thoracic spine manipulation (TSM) has been proposed to treat individuals with shoulder impingement (SI) due to the regional interdependence among the shoulder and thoracic and cervical spines. Nevertheless, the effects on pain and function have been questioned recently and little evidence exists about the effects of TSM in scapular kinematics in this population. This study evaluated the short-term effects of a low-amplitude, high-velocity thrust TSM on pain, function and scapular kinematics during elevation of the arm in individuals with SI.

Methods: Fifty individuals with SI were randomly assigned to 1 of 2 interventions: TSM (n=25) or sham TSM (n=25). Both groups received the selected interventions twice with an interval of 3-4 days between them and were evaluated in 3 days. The assessor, who was blinded to group assignment, measured shoulder pain (Numerical Pain Rating Scale) and scapular kinematics (three-dimensional electromagnetic system) at day 1 (pre-intervention 1), day 2 (pre-intervention 2), and at day 3 (3-4 days follow-up after the second intervention) during 3 trials of elevation of the arm in the sagittal plane. All individuals also completed the Disabilities of the Arm, Shoulder and Hand questionnaire (DASH) at the beginning of each day of evaluation (pre-intervention 1, pre-intervention 2 and follow-up) to assess function of the upper limbs. An intention-to-treat analysis was carried using the average of multiple imputations for missing data (n=6) with SPSS software. The mean of the 3 trials was used for statistical analysis. Kinematic motion analysis involved selecting scapular data at 30°, 60°, 90° and 120° of arm elevation. A 2-factor analysis of variance (time and angle) was performed for each scapular kinematic in each group to identify differences along time and a 1-factor analysis of variance verified differences between time in each group for NPRS and DASH score.

Results: Numerical Pain Rating Scale following interventions did not change in any group (p>0.05) and DASH score decreased along time in both groups (p=0.02), but the change did not reach the minimal important difference of 10 points. No significant double interactions (time by angle) were found for any scapular rotation (p>0.05). However, main effects of time were found as following. In the TSM group scapular internal rotation decreased 4.1° from pre-intervention 1 to pre-intervention 2 (p<0.001) and increased 3.3° from pre-intervention 2 to follow-up (p=0.001), while in the sham TSM group it increased 2.4° from pre-intervention 1 to follow-up (p=0.001). Upward rotation increased 2.8° from pre-intervention 1 to pre-intervention 2 in the TSM group (p=0.005), while in the sham TSM group it decreased 2.4° from pre-intervention 2 to follow-up (p=0.007). Scapular tilt showed no differences in the TSM group while in the sham TSM group anterior tilt increased 2.2° and 1.8° from pre-intervention 1 to follow-up and pre-intervention 2 to follow-up, respectively.

Conclusion: Only one session of TSM produces a small, potentially non-clinically meaningful decrease in internal rotation and increase in upward rotation of the scapula in subjects with SI during elevation of the arm in a short-term. However,

these effects were neither cumulative nor lasting for about 4 days and do not seem to be related with relief in pain and improvement in function. More studies are necessary to conclude on the possible effects of TSM in individuals with SI.

References: Boyles et al., *Man Ther,* 14: 375-80, 2009.

Ludewig et al., *Phys Ther*, 80:276-91, 2000.

McClure et al., *Phys Ther*, 86:1075-90, 2006.

Muth et al., *J Orthop Sports Phys Ther*, 42:1005-16, 2012.

Orfale et al., *Braz J Med Biol Res*, 38:293-302, 2005.

Tate et al., *J Orthop Sports Phys Ther*, 40:474-493, 2010.

Disclosure of Interest: None Declared

AS-0550

PLAYING THE GOBLIN POST OFFICE VIRTUAL REHABILITATION GAME AT HOME

Andrew J. Murphy [1,*]Mohammad Al-Amri [2]Malcolm B. Hawken [3]Gabor J. Barton [3]

[1]Biomedical Engineering, University of Strathclyde, Glasgow, [2]School of Healthcare Sciences, Cardiff University, Cardiff, [3]Research Institute for Sport and Exercise Sciences, Liverpool John Moores University, Liverpool, United Kingdom

Introduction and Objectives: Cerebral Palsy (CP) may be considered "the most common physically disabling condition seen and managed by child health professionals" [1]. Children suffering from CP often display diminished control of trunk and pelvis movements, which can reduce their ability to achieve well controlled movement of the lower limbs and ultimately have a negative effect on activities of daily living [2,3]. Previous work has highlighted that it is possible to monitor trunk-pelvis coupling and core movement in children, and to enhance movement patterns via the use of a virtual reality gaming application (Goblin Post Office, GPO) in laboratory based training [2,3]. The primary aims of this study were to establish the feasibility and acceptability of conducting such training in CP children's homes, and to quantify the short term effect of GPO training.

Methods: Ethical approval for this study was granted by the University of Strathclyde Ethics Committee. Two children with Cerebral Palsy (CPC1 and CPC2) volunteered (Table 1). One typically developing child (TDC) also participated by playing a single session of the game in order to provide data against which CPC performance could be compared. All children and their parents provided informed consent.

Figure 1 illustrates the setup used in children's homes. Full detail of the adaptive algorithm that drives GPO may be found by consulting previous work [2,3], however, briefly, the aim of GPO is to use rotations of the trunk and/or pelvis to navigate a virtual dragon through a virtual cave and, using the horn protruding from the dragon's head, to "burst"/hit targets that contain virtual letters (Figure 1). Forward speed of the dragon's flight is continuously moderated based on a bespoke adaptive algorithm and thus over a training session it is possible to extract a "maximum settled speed" (MSS) which is representative of overall game performance.

On training days the investigators visited CPC's home, attached a laptop to the children's television using a VGA cable and attached a single Xsens-MTx-sensor (Xsens Technologies, The Netherlands) to CPC's trunk using a semi elastic Velcro strap; this sensor measured trunk tilt and rotation and thus navigated the flying GPO dragon shown on the television screen. CPC conducted 1-3 training sessions per training day (Table 1).

Results: All testing was conducted safely and easily; from a technical perspective all that was required of participants' homes was a television set with a VGA input. Anecdotal evidence suggested that all children and parents enjoyed the experience and did not find the process disruptive to their normal routine; further, as the days progressed the investigators' notes included comments such as "showing motivation and competition", "better controlled stance", "less sporadic arm movements". Figure 1 shows the results of data analysis.

Figure:
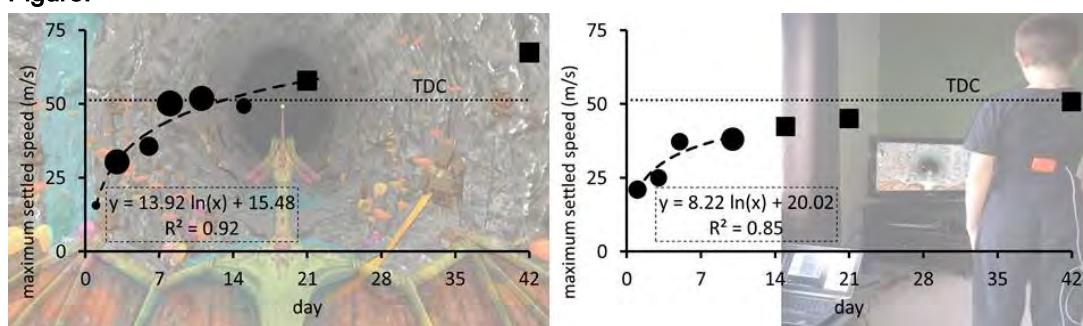
Caption: Maximum settled speed achieved by CPC1 (left) and CPC2 (right). Data is shown for the duration of the training period (circles) and as projected according to a logarithmic fit for up to six weeks of training (squares). Data points are scaled according to the duration in minutes of GPO gameplay that was conducted on each training day. The baseline data for TDC is shown by the horizontal dotted line. Semi-transparent background images show the game interface and home setup used.

Conclusion: It is acknowledged that in order to provide satisfactory evidence of the effect of GPO in the home a larger study must be carried out. However, anecdotal feedback supported the suggestion that GPO training in the home is a feasible and acceptable form of therapy for children with Cerebral Palsy and also that the investigators' subjective assessment of performance, balance and control showed improvement over the training period. Data analysis also suggested improvement in game performance; indeed CPC1 ultimately (marginally) exceeded the baseline performance of TDC. Further work is merited.

Table:

	CPC1	CPC2	TDC
age	8 years	8 years	10 years
gender	male	male	male
diagnosis	spastic hemiplegia	spastic diplegia	na
GMFCS level	GMFCS I	GMFCS II	na
posture during training	standing	high-kneeling	standing
# training sessions (mean±SD duration)	16 (9.2±1.7 min)	9 (9.6±1.1 min)	1 (16.6±na min)
# training days (mean±SD total duration)	6 (23.0±8.1 min)	4 (18.0±3.3 min)	1 (16.6±na min)
duration of training period	15 days	10 days	1 day

Caption: Participant and training data

References: [1] Morris C., Condie D. Recent developments in healthcare for Cerebral Palsy, 2008.

[2] Barton et al., International Conference on Virtual Rehabilitation, 2011.

[3] Barton et al., J NeuroEng Rehab, 10-15, 2013.

Disclosure of Interest: None Declared

AS-0551

VIRTUAL REALITY-TREADMILL COMBINED TRAINING PROGRAM TO IMPROVE GAIT IN MULTIPLE SCLEROSIS INDIVIDUALS

Agnese Peruzzi [1 2,*] Andrea Cereatti [1 2] Ignazio Roberto Zarbo [3] Anat Mirelman [4] Ugo Della Croce [1 2]

[1]POLCOMING, University of Sassari, [2]Interuniversity Centre of Bioengineering of the Human Neuromusculoskeletal System, [3]Department of Clinical and Experimental Medicine, University of Sassari, Sassari, Italy, [4]Department of Neurology, Center for the study of Movement, Cognition and Mobility, Tel Aviv Sourasky Medical Center, Tel Aviv, Israel

Introduction and Objectives: Weakness, spasticity and ataxia are common in multiple sclerosis (MS), often leading to gait abnormalities and falls [1]. Compared to healthy subjects, MS individuals show reduced stride length and walking speed, prolonged double limb support duration and greater variability in lower limb kinematics during gait [2]. Moreover, fatigue is a prevalent symptom and it can limit walking endurance. Effective gait interventions are, therefore, crucial in MS. Treadmill training (TT) has been successfully used [2]. Recently, TT has been augmented with virtual reality (VR), which allows subjects to train cognitive and motor aspects simultaneously (dual tasking), decreasing their perception of exertion and improving motivation and skill attainment [3]. The combined use of TT and VR (TT-VR) has shown promising results in neurological diseases [3, 4]. A pilot study showed that TT-VR positively affects gait of MS individuals under dual tasking [5]. The present study aims at investigating the efficacy of a six-weeks TT-VR on gait of MS subjects under single and dual task conditions and to compare its effects to TT alone. We hypothesize that both interventions will improve gait in single task, but that TT-VR will improve gait in dual task.

Methods: A parallel group controlled trial with three months follow-up is employed. The study includes 40 subjects with relapsing remitting MS (EDSS:3-5.5,MMSE≥26) with stable medical and clinical conditions in the six months prior to the study. The study is in progress: so far, 17 participants have been recruited from the Neurology Unit at Sassari University Hospital (10f, age:40±8), have been randomly assigned to the TT-VR or to the TT and are currently participating in the training. The set-up includes a treadmill with a harness, an LCD screen used to deliver the VR, two magneto-inertial sensors, attached to the subject's shoes and used to reproduce real-time feet motion in the VR, and an additional unit, placed on the subject's head and used to move the VR accordingly [6] (Figure). In the TT-VR the participants walk on the treadmill while watching a virtual tree-lined trail and are asked to pass the obstacles appearing on the trail. Successful and unsuccessful passes, as determined by the inertial measurements, are rendered to the subject with visual/acoustic feedback. Cognitive concurrent tasks are added to the VR to challenge their attention. The obstacles properties are modified according to the severity of the motor limitations and adapted during the training to increase task complexity. Trainings is provided three days/week for six weeks. Progression is based on a study of individualized TT for neurological subjects [4]. To assess training effects, a gait analysis is performed before, immediately, one and three months after the intervention with and without a concurrent cognitive task (dual and single task, respectively). Selected gait, joint kinematics and kinetics parameters are estimated using a six-cameras stereophotogrammetric system (Vicon B10, 100 frames/s), two force platforms (AMTI, 1000 frames/s) and the Vicon Plug-in Gait marker set. Five trials are evaluated for

each condition. Only data at baseline for 17 subjects are reported. Mean and standard deviation are computed across patients and a paired t-test (a=0.05) is used to compare single and dual task conditions.

Results: Lower limb joint kinematics did not show any difference between single and dual task. Both gait speed, cadence and maximum ankle muscular moment and power, significantly decreased in dual task (Table).

Figure:

Caption: Experimental set-up

Conclusion: Dual tasking is typical in everyday life and increases the burden of gait of MS subjects. The TT-VR is an intensive individualized gait intervention which trains MS individuals to better manage cognitive processes, such as reasoning, planning and problem solving during walking. We are conducting a controlled trial to assess efficacy of a six-weeks TT-VR training for patients with MS. Patients are expected to significantly improve gait in dual task, decreasing fall risk and increasing quality of life.

Table:

parameter	measurement unit	single task	dual task
ankle PF(loading response)	deg	-8(4)	-7(3)
ankle DF		12(4)	12(4)
ankle PF(swing)		-12(9)	-12(8)
knee FL(loading response)		19(8)	17(8)
knee EX		3(6)	4(6)
knee FL(swing)		57(7)	55(8)
hip EX		-14(5)	-14(5)
hip FL		31(5)	30(6)
ankle power	W/kg	1.5(0.4)	1.3(0.3)*
hip power		1.1(0.5)	1.0(0.4)
ankle DF moment	Nm/kg	1.3(0.2)	1.2(0.2)*
FE knee moment		0.3(0.2)	0.2(0.2)
gait speed	m/s	1.0(0.2)	0.9(0.2)*
cadence	step/min	104(7)	95(11)*
stride length	m	1.1(0.1)	1.1(0.1)

Caption: Gait parameters of MS subjects at baseline. PF=plantar-flexion, DF=dorsiflexion, FL=flexion, EX=extension, FE=flex/extension

References: [1]   Frohman TC et al., *Ther Adv Neurol Disord*, 4(2):83, 2011.

[2]   Swinnen E et al., *Mult Scler Int*, 240274, 2012.

[3]   Mirelman A et al., *J Gerontol A Biol Sci Med Sci*, 66(2):234, 2011.

[4]   Mirelman A et al., *BMC Neurol*, 13(1):15, 2013.

[5]   Peruzzi A et al., *Gait Posture*, 37:S7, 2013.

[6]   Peruzzi A et al., *Eur Int J Sci Technol*, 2(6):171, 2013.

Disclosure of Interest: None Declared

EFFECT AND SUSTAINABILITY OF A HIPPOTHERAPIE-K-INTERVENTION IN ADULTS WITH CEREBRAL PALSY WHILE STAIR CLIMBING.

Martina Binzen [1,*]Carmen Gempp [1]Eveline Rich [1]Julia Ruf [1]Lukas Stammler [2]Philippe Merz [2]Ruth Obrist [3]Beat Göpfert [4][5]

[1]Physiotherapy, Health Division, Bern University of Applied Sciences, Bern, [2]BZG, Bildungszentrum Gesundheit Basel-Stadt, Münchenstein, [3]Hippotherapie Obrist, Kaiseraugst, [4]Center of Biomechanics, CMBE, University of Basel, [5]Laboratory for Movement Analysis , Children's University Hospital Basel (UKBB) Basel, Basel, Switzerland

Introduction and Objectives: Stair climbing is a simple daily task for a healthy person but for someone with cerebral palsy (CP) it needs often an extra effort, additional force [1], coordination [2], and balance requirements. This is often visible in an arrhythmic and asymmetrical movement pattern with a longer stance phase [3]. The goal of this Time-Series-Study was to analyze the effect and sustainability of an 18 week Hippotherapy-K intervention in hemiplegic adult CP-patients while stair climbing and compare it before and after the intervention, and 18 weeks post intervention within each subject and with a healthy control-group. Further, during the intervention only Hippotherapy-K (once a week, 30 – 40 min, outdoor) was done, all other physical therapies were stopped.

Methods: 6 subjects with a hemiplegic CP (22-46 y, 5m, 1f, 3 to 6 trials) were performing an instrumented 3-D gait analyses (Vicon, 12 cameras T20, 200Hz) and surface EMG (Biovison, 2400Hz.), while climbing a 4 step stair at a self-selected speed and style at defined time points. The measurements were done before the intervention (T1), as a baseline, after the 18 weeks of Hippotherapy-K (T2) and 18 weeks post intervention (T3). The kinematic data of the lower body and normalized Wavelet transformed EMG-Total-Intensity (I_{tot}) of the muscles: Tibialis anterior (TA), and Gastrocnemius medialis (GM) were time normalised and averaged over a Stair Climbing Cycle (SCC) starting at the foot-off of the lower step (0%) and finishing at foot-off for the same leg at the next following step (100%). The changes were compared to T1 and with the healthy control-group.

Results: The results show individual changes between T1, T2 and T3 for the 6 CP-subjects. The changes form the measurements at T1 to T2 show that 3 subjects are climbing the stairs faster but with a less symmetrical duration of the stance phase. This is seen in the bigger difference between the duration of the stance phase for the affected and non-affected side. Further 2 other subjects are slower ascending the stairs and 1 does it at the same speed. The changes at T3 have even more variability, 2 subjects are slower than at T1 and T2, 2 are faster than at T1, but slower compared to T2, however become more symmetrical in the stance phase duration. Finally the last 2 ones climb faster than at T1 and T2, and show a more asymmetrical duration of the stance-phase.

The I_{tot} pattern changes for all subjects between the 3 measurements. An example of a subject is shown in Fig. 1a, where an increased asymmetrical stance phase duration leads to longer and higher I_{tot}-level in the other leg. This subject has the same speed at T1 and T2, and increases it at T3 by 8%, but gets less symmetrical, visible in TA-I_{tot} and GM-I_{tot}-pattern of the non-affected side at T2 and T3 (A). Further bigger angular variations occur at foot contact in the knee- and ankle joint as well as in the angle between the foot and the surface of the stairs. The effects of the changes in the gait symmetry during stair climbing are seen in another subject in Fig 1b. This one climbs at T2 and T3 slower compared to T1, further it

decreases the gait symmetry within the duration of the stance phase at T2, but increases it at T3. The result of the more symmetrical stance phase is seen in the GM- I_{tot} –pattern (B), as it gets closer to the pattern of the control group.
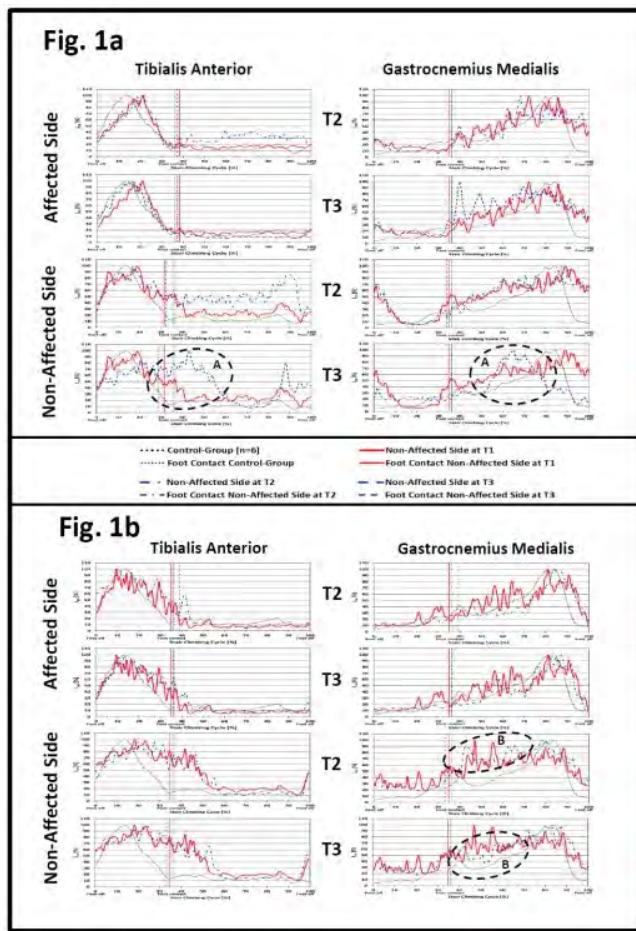
Figure:

Discussion

The results of the study showed a delectable effect of the Hippotherapy-K intervention within CP-patients while stair climbing, although we could recruit a small number of subjects in our area. The varying results in stair climbing like changes in speed and duration of the stance phase between T1 and T2, indicates an individual, but measurable effect of the Hippotherapy-K intervention. This individual effect might be linked to the "differential learning strategy" stated by Schöllhorn [4], because during a 30 to 40 min. Hippotherapy-K session a high number of similar but varying 3D-movement, some may even demand fine motor skills, have to be performed by the patients and may allow them to learn new movement patterns and also use these variations.

The changes between T2 and T3 show some sustainability of a Hippotherapy-K intervention, which are again subject individual and might be related to their daily activity and therapy program.

Conclusion

The results of the study showed that Hippotherapy-K intervention had an effect on the stair climbing, which each subject used its own way. Therefore we think Hippotherapy-K should be seen as a complementary therapy to the regular program towards a holistic approach.

References: [1] Lin, H.C., et al. Biomedical Engineering: Applications, Basis and Communications, 2004, 16(02), 101-108.

[2] Protopapadaki, A. et al. Clin Biomech. 2007;22(2):203-10, [3]

[3] Rich, E., Ruf, J. Bachelor-Thesis 2013, Physiotherapy, Health Division, Bern University of Applied Sciences, Bern, Switzerland

[4] Schöllhorn WI, Medicina (Kaunas). 2010;46(6):365-73.

RELATION BETWEEN RIB KINEMATICS AND LUNG VOLUMES: COMPARISON BETWEEN NORMAL SUBJETCS AND CYSTIC FIBROSIS PATIENTS

Benoit Beyer[* 1, 2], Véronique Feipel[1], Victor Sholukha[2], Laurence Chèze[3], Serge Van Sint Jan[2]

[1]Laboratory of functional anatomy, [2]Laboratory of Anatomy Biomechanics and Organogenesis, Université Libre de Bruxelles ULB, Brussels, Belgium, [3]Laboratoire de biomécanique des chocs LBMC, UMR_T 9406, Université Lyon1, Lyon, France

Introduction and Objectives: Relation between rib kinematics and thorax global shape variations is described in the literature but data and analysis of segmental costovertebral joint complexes (CVJ) kinematics are lacking. A thorax 3D model of breathing motion was previously obtained and rib kinematics relative to vertebra was analyzed for upper thoracic levels in a sample of asymptomatic subjects (1). This study proposes an extended description in normal subjects from thoracic levels 1 to 9 and attempts to analyse the relation between inspiratory capacity and rib kinematics. The full method is then applied to a sample of patients with cystic fibrosis.

Methods: *In vivo* computed tomography (CT) imaging was obtained at three different lung volumes (total lung capacity, middle of inspiratory capacity and functional residual capacity) calibrated according to plethysmography. Data from 9 patients with cystic fibrosis and 10 asymptomatic subjects were processed using a previously described method (1). 3D models of ribs and vertebrae were reconstructed for thoracic levels 1 to 9. Custom made software was used for virtual palpation (2) aiming to define 5 anatomical landmarks (ALs) on each vertebra and rib. Local anatomical coordinate systems were constructed following anatomical planes (figure 1a). Kinematics was processed using orientation vector and mean helical axis parameters (MHA) at each level to obtain angular displacements around each reference axis. A fusion method (2) of ALs with 3D models was used to obtain visualisation of both motion and kinematic parameters. Non parametric statistical test for independent samples was used to analyse the influence of pathological conditions on kinematics parameters. Pearson's correlation coefficient was used to analyse the link between kinematics and anthropometrical parameters in both groups.

Results: An advanced 3D model of continuous motion and kinematic parameters visualisation was achieved. Rib angular displacements occurred around dorso-ventral (i.e. pump handle motion) and medio-lateral (i.e. bucket handle motion) axes similarly at each CVJ level and MHA orientations were similar. Mean ranges of motion around both axes decreased with rib number (figure 1b) in both groups (around lateral axis: [from 12.2° to 5.7°] from level 1 to 9 in normal subjects; [from 8.7° to 3.6°] in cystic fibrosis group; around medio lateral axis: [from 9.5° to 3.8°] in normal subjects; [from 9.5 to 3.7°] in cystic fibrosis group). A correlation was found between rib kinematics around the medio-lateral axis and inspiratory capacity only in the cystic fibrosis group (r >0.7).   Significant differences in rib kinematics around the medio-lateral axis were found between groups (p<0.05) at almost all thoracic levels.

Figure:
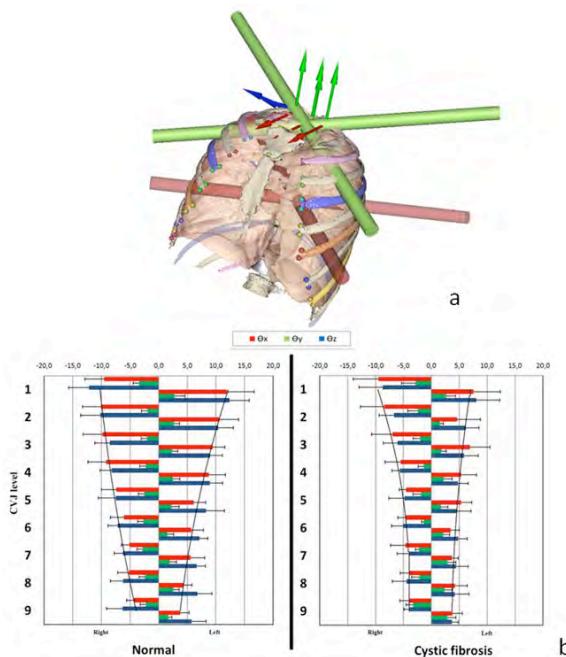
Caption: Figure 1: (a) 3D model of full thorax with mean helical axes CVJ levels 1 (green) and 7 (red).   (b) Mean ranges of motion Ө in degree around x,y and z axes at CVJ levels [1-9] in both groups.

Conclusion: The 3D model of the costovertebral joint during breathing allows visualisation and quantification of segmental kinematics parameter. The influence of a clinical condition was tested and it appeared that kinematics parameters were reduced in patients with cystic fibrosis. Correlation between segmental kinematics and inspiratory capacity was demonstrated only in the cystic fibrosis group but not in normal subjects. These results suggest the hypothesis of an influence of external parameters on volume displacement such as an increase of respiratory muscle activity in patients with cystic fibrosis (3).

References: 1.   **Beyer B. et al;** *Clin Biomech* 29: 434–438 (2014).
2.   **Van Sint Jan S. et al,** *Médecine/Sciences* 29: 529–536, 2013.
3.   **Keens TG et al;** *Am Rev Respir Dis* 116: 853–860, 1977.

Disclosure of Interest: None Declared

'BIG DATA' MOTION ANALYSIS
at Strathclyde's 'ISB EXPERIMENT'

BOOTH 21

Motekforce Link
IMPROVING HUMAN PERFORMANCE

2012 →

Motekforce Link introduced the **GRAIL**, which stands for Gait Real-time Analysis Interactive Lab. This total package solution for gait analysis and training uses dual-belt instrumented treadmill with fast pitch and sway and motion capturing in an interactive and dynamic Virtual Reality environment.

NOW →

Motekforce Link proudly introduces the **M-Gait** system: An instrumented dual-belt treadmill and the **D-Flow** software, as a start of your lab. The **M-Gait** is a modular approach, enabling various system enhancements to improve the functionality of your set-up, with options to include:

· Treadmill with fast pitch and sway
· 3D motion capturing
· Real-time biomechanical Human Body Model
· EMG, accelerometers, etc.
· Interactive Virtual Reality system (VR)
· Body Weight Support

VISIT US! →

At Booth 21 or see the **M-Gait** during the University of Strathclyde's "ISB Experiment" in the exhibition hall.

Special Sessions

Lower Limb

SS-0001

DIFFERENCES IN ANATOMICAL PARAMETERS BETWEEN THE AFFECTED AND UNAFFECTED HIP IN PATIENTS WITH BILATERAL CAM-TYPE DEFORMITIES

K.C. Geoffrey Ng [1,*]Mario Lamontagne [1] [2]Paul E. Beaulé [3]

[1]Department of Mechanical Engineering, [2]School of Human Kinetics, [3]Division of Orthopaedic Surgery, University of Ottawa, Ottawa, Canada

Introduction and Objectives: Cam-type femoroacetabular impingement (FAI), characterized by an enlarged, aspherical femoral head deformity, results in adverse hip joint loading and eventual osteoarthritis [1]. It is still unclear why many individuals with bilateral cam deformities demonstrate only unilateral symptoms. The presence of a large cam deformity, indicated by elevated alpha angles, may not be sufficient to explain symptomatology [2], thus FAI may be attributed to additional anatomical parameters [3]. The purpose was to examine patients with bilateral cam-type deformities, who demonstrate unilateral FAI symptoms, and compare the anatomical hip joint parameters between their affected (symptomatic) and contralateral, unaffected (asymptomatic) hips.

Methods: Twenty-two patients initially presented themselves with primary unilateral hip pain, clinical signs, and were confirmed to have a cam deformity on imaging data, with an axial or radial alpha angle higher than 50.5° or 60°, respectively [4]. Patients underwent pelvic and knee computed tomography (CT) imaging as well as a physical examination, evaluating their affected hip and their contralateral, unaffected hip's flexion, straight-leg raises, internal and external rotations. Patient-specific CT data were blinded and evaluated for multiple anatomical parameters associated with FAI symptoms [3, 5, 6], including: axial (AA) and radial alpha (RA) angles, femoral neck-shaft angle (FNSA), medial proximal femoral angle (MPFA), femoral head-neck offset (FHNO), femoral torsion (FT), acetabular version (AV), and centre-edge (CE) angle; for both hips, using Onis 2.4 (DigitalCore, Japan). CT measurements were performed by two readers, each performing two readings. Twenty patients (n = 20; age = 37 ± 8 years; BMI = 26 ± 5 kg/m^2) indicated elevated alpha angles for both affected (AA = 55 ± 7°; RA = 64 ± 6°) and unaffected hips (AA = 54 ± 5°; RA = 63 ± 4°), confirming bilateral cam deformities; whereas two patients were excluded for unilateral-only deformities. A paired sample t-test was computed, using SPSS Statistics v.20 (IBM Corporation, USA), to compare differences in anatomical parameters and physical examination measurements, between the patients' affected and unaffected hips (CI = 95%).

Results: Intra- and inter-reader anatomical observations were in strong to near-perfect agreement (ICC > 0.75). The affected hip demonstrated substantially reduced hip flexion, leg raise, internal and external rotations, in comparison with the unaffected hip (Table 1). There were no differences in cam deformity parameters (AA angle, RA angle, FHNO) as well as FT, AV, and CE angle, between affected and unaffected hips (Figure 1). Many patients (40%) actually had higher alpha angles on their unaffected hips. There was a significant difference in FNSA, between affected (124.8 ± 3.3°) and unaffected hips (127.5 ± 2.8°; t(19) = -4.2, p = 0.001); as well as a difference in MPFA, between affected (79.1 ± 3.5°) and unaffected hips (81.4 ± 4.5°; t(19) = -2.8, p = 0.01).
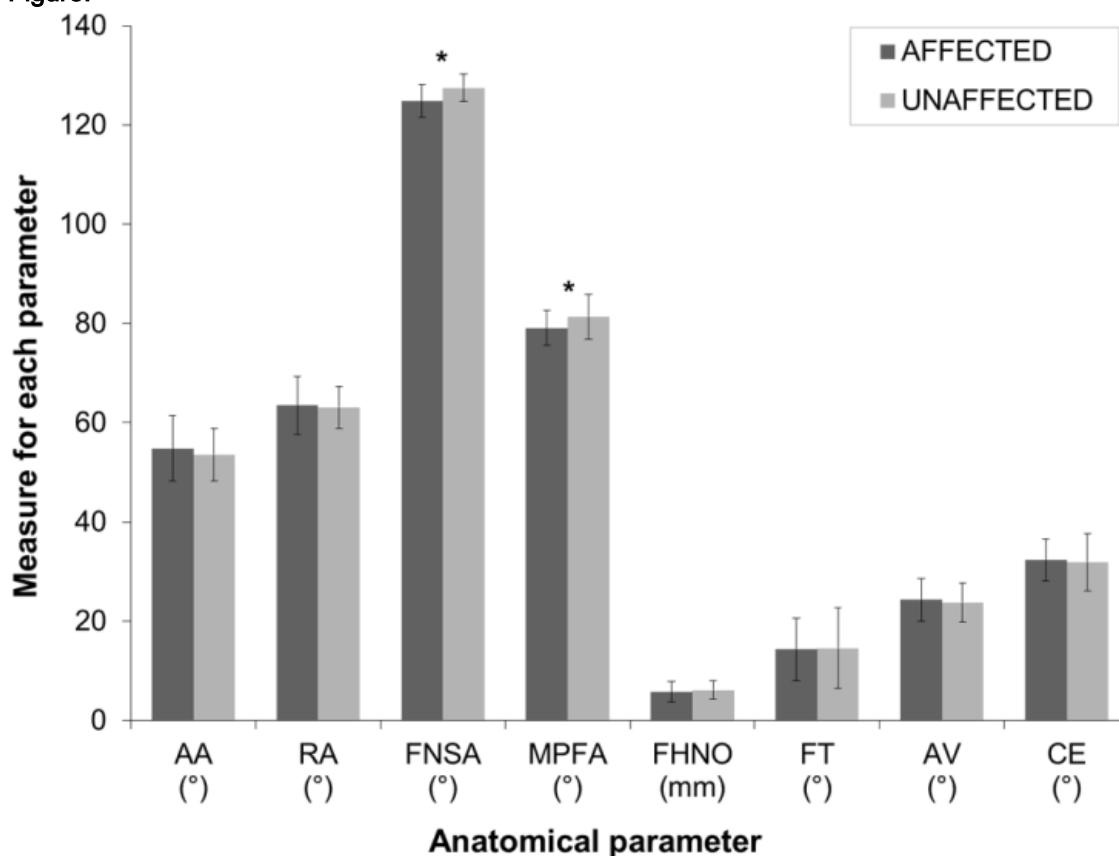
Caption: Figure 1. Patient-specific anatomical parameters, comparing the affected and contralateral, unaffected hip (*significant difference, p < 0.05)

Conclusion: To our knowledge, no study has incorporated a patient cohort with bilateral cam deformities, to examine differences in anatomical parameters. The physical examinations confirmed that the affected hip had restricted ranges of motion, indicative of FAI, which could be attributed to a combination of elevated alpha angles and decreased neck angles. Interestingly, several patients had larger cam deformities in their unaffected hip. This further supports that large cam deformity, alone, cannot explain symptomatology and does not lead to FAI [3]. The femoral neck angles (FNSA, MPFA) were the significant parameters [3, 5, 6], which can potentially predict which hip experiences early symptoms, in individuals with bilateral cam deformities. The coxa vara structure, seating the femoral head further into the acetabulum and, thus, altering the abductor moment and bringing the cam deformity closer to the anterosuperior labrum, can further explain differences in clinical signs, and as to why the asymptomatic hip does not experience early symptoms. The ongoing study will examine asymmetry and if compensatory load is applied onto the contralateral hip due to neuromuscular compensation.

Table:

Physical Examination	Affected Hip	Unaffected Hip
Hip Flexion (°)	123 ± 14	130 ± 20
Straight-Leg Raise (°)	90 ± 17	97 ± 16
Internal Rotation (°)	31 ± 15	38 ± 12
External Rotation (°)	32 ± 21	42 ± 19

Caption: Table 1. Summary of patient physical examinations, comparing the affected and contralateral, unaffected hip

References: [1] Ganz et al., Clin Orthop Rel Res, 417: 112-120, 2003.

[2] Khanna et al., Am J Sports Med, 42: 793-797, 2014.

[3] Ng et al., Clin Orthop Relat Res, 1-8, 2014.

[4] Rakhra et al., Clin Orthop Relat Res, 467: 660-665, 2009.

[5] Bardakos et al., J Bone Joint Surg Br, 91: 162-169, 2009.

[6] Ranawat et al., HSS J, 7: 115-119, 2011.

Disclosure of Interest: None Declared

MRI-BASED GEOMETRICAL DETAIL AFFECTS HIP CONTACT FORCES MORE THAN COST FUNCTION FORMULATION

Mariska Wesseling [1,*] Friedl de Groote [2] Lode Bosmans [1] Ward Bartels [2] [3] Christophe Meyer [4] Kaat Desloovere [4] Ilse Jonkers [1]

[1] Department of Kinesiology, [2] Department of Mechenical Engineering, KU Leuven, Leuven, [3] Mobelife NV, Heverlee, [4] Department of Rehalibation Sciences, KU Leuven, Leuven, Belgium

Introduction and Objectives: Modeling choices, e.g. the level of subject-specific detail included in the model, as well as cost function formulation affect calculated hip contact force (HCF). The goal of this study was to assess the relative importance of introducing subject-specific detail in bone and muscle geometry, derived from magnetic resonance imaging (MRI), in the musculoskeletal model compared to introducing minimization of hip contact forces in the optimization criterion on calculated hip contact forces during gait. Additionally, the effect of accounting for muscle wrapping around the hip joint capsule was evaluated.

Methods: Five subjects (54±6 yrs.) walked at self-selected speed (1.29±0.23 m/s). 3D marker trajectories were captured using Vicon (Oxford Metrics, UK) and force data was measured using two AMTI force platforms (Watertown, MA). MR-images were acquired (Philips Ingenia 3.0T) of all subjects while lying supine.

A musculoskeletal model consisting of 14 segments, 19 degrees of freedom and 88 musculotendon actuators was used [1] and all analyses were performed in OpenSim 3.1 [2]. Firstly, the generic model was scaled using the marker positions of a static pose. Secondly, a MRI-model was created using in house developed software and contained the subject-specific bone structures and muscle paths of all hip and upper leg muscles [3]. Thirdly, wrapping surfaces for the hip flexor muscles were added to the MRI-model, to reflect the effect of the hip joint capsule (MRIwrap). The trajectory of iliacus and psoas major around the hip joint was described using nine points in the MR-images. Two circles were fitted through these points, one defining a wrapping sphere for iliacus, rectus femoris and sartorius and one defining a wrapping surface for the psoas major. Finally, two average wrapping surfaces were created based on the five subjects and were added to the generic model (GenWrap). This model was scaled to the dimensions of each subject, resulting in a total of four models. For all models, an inverse kinematics procedure was used to calculate joint angles. Muscle forces were calculated using static optimization by minimizing squared muscle activity (SO), as well as by minimizing the weighted sum of squared muscle activity and magnitude of HCF (SOmin). Next, HCFs were calculated and first and second peak HCF, normalized to body weight (BW), were compared to contact forces measured using instrumented hip prostheses (HIP98) [4].

Results: Results show that by including MRI-based geometrical detail into the model, HCFs decrease and are more comparable to contact forces measured using instrumented prostheses (figure 1; table 1). Including MRI-based geometrical detail and wrapping surfaces have the largest effect on the magnitude of HCFs, by decreasing HCF up to 0.72 BW for the MRIwrap compared to generic model. Including wrapping surfaces results only in decreased contact forces at the second peak as at this time instant the muscles wrap over the surfaces, thereby increasing the muscle

moment arm. Including minimization of the hip contact forces in the optimization criterion also decreases HCFs, up to 0.48 BW.

Figure:
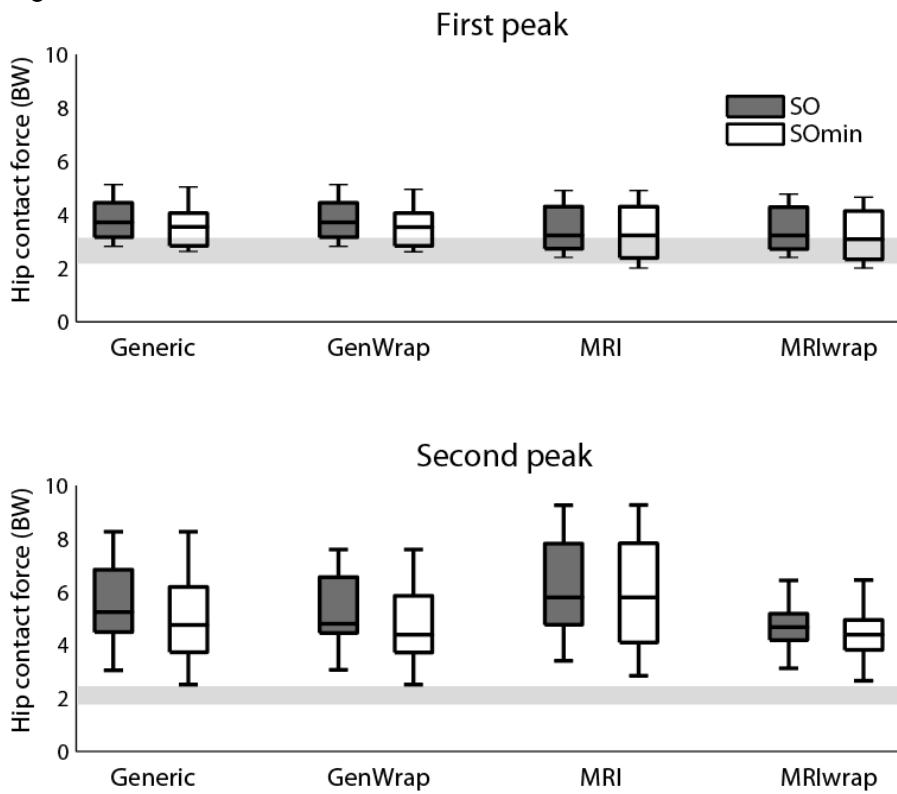
Caption: Figure 1. The magnitude of hip contact force at the first and second peak for the different musculoskeletal models using SO (dark gray) and SOmin (white). The light gray zones indicate the range of measured hip contact forces [4].

Conclusion: Inclusion of MRI-based subject-specific information in the musculoskeletal model results in HCFs that are more comparable to contact forces measured using instrumented prostheses. Including wrapping surfaces for the hip flexor muscles in the MRI model has a large effect on the contact forces. Including a minimization of HCFs in the optimization criterion also decreases contact forces, however to a lesser extent than including subject-specific wrapping surfaces. Also, when wrapping surfaces are included in the generic model (GenWrap), contact forces decreased and are closer to forces measured using instrumented prostheses (table 1). Therefore, our findings suggest that inclusion of subject-specific geometrical detail in the MRI-based musculoskeletal model is more important than altering the optimization criterion.

Table:

		Δ HCF (BW) with HIP98		Δ HCF (BW) with Generic	
		First peak	Second peak	First peak	Second peak
SO	Generic	1.17	3.01	0.00	0.00
	GenWrap	1.17	2.76	0.00	-0.25
	MRI	0.83	3.63	-0.34	0.62
	MRIwrap	0.82	2.29	-0.35	-0.72
SOmin	Generic	0.92	2.43	-0.25	-0.58
	GenWrap	0.91	2.21	-0.26	-0.8
	MRI	0.69	3.38	-0.48	0.37
	MRIwrap	0.55	2.07	-0.62	-0.94

Caption: Table 1. Average of differences in resultant hip contact force (normalized to body weight (BW)) with the contact forces measured using instrumented prostheses (HIP98) as well as with contact forces calculated for the generic model at the first and second peak hip contact force.

References: [1] Delp, SL, et al. IEEE Trans Biomed Eng 37(8), 757-767, 1990.

[2] Delp, SL, et al. IEEE Trans Biomed Eng 54(11), 1940-1950, 2007.

[3] Scheys, L, et al. Gait & Posture, 28(4), 640-648, 2008.

[4] Bergmann G, et al., J Biomech, 34(7), 859–871, 2001.

Disclosure of Interest: None Declared

Modelling

SS-0003

SIMULATION OF IMPINGEMENT AND MICRO-SEPARATION FOR TOTAL HIP REPLACEMENTS DURING STAIR CLIMBING

Amir A. Al-Munajjed [1,*]Michael Damsgaard [1]John Rasmussen [2]

[1]R & D, AnyBody Technology, [2]Department of Mechanical and Manufacturing Engineering, Aalborg University, Aalborg, Denmark

Introduction and Objectives: The total number of total hip replacements (THR) is rising in the past years particularly in younger patients. These patients have different expectations from the elderly in terms of range-of-motion and possible activities, like sports. These activities can lead to complication like impingement, separation and micro separation in the THR. The objective of this study was to analyze such complication in the THR due to the variation of the cup inclination using a musculoskeletal simulation approach for stair climbing.

Methods: A male subject was recorded climbing stairs using a motion capture system (SIMI, Munich, Germany). This data was used to build a musculoskeletal model in the AnyBody Modeling System v6.1 (AnyBody Technology, Aalborg, Denmark). The standard anatomical hip joint was replaced by a generic hip implant comprising a simple stem with ball and a cup. Different cup alignments in terms of anteversion and abduction angle of the acetabular cup have been analyzed. A mal-alignment was introduced to enforce impingement. The force dependent kinematic solver was used instead of the standard inverse dynamics solution to detect and simulate the kinetic effect of the impingement. The contact area between femoral ball and acetabular cup were computed.

Results: The contact area is shown in figure 1 during the stair climbing activity for two different cup inclinations, one normal and the other mal-aligned. This leads to impingement between stem and ball (figure 1A-C), the contact area is reduced and concentrated to the rim area, figure 1D. Additionally, micro separation could be seen in the model between ball and cup.

Figure:
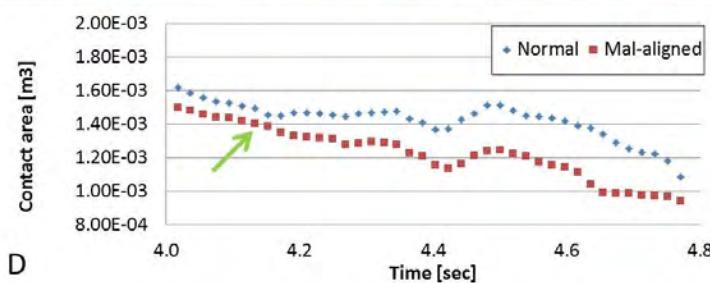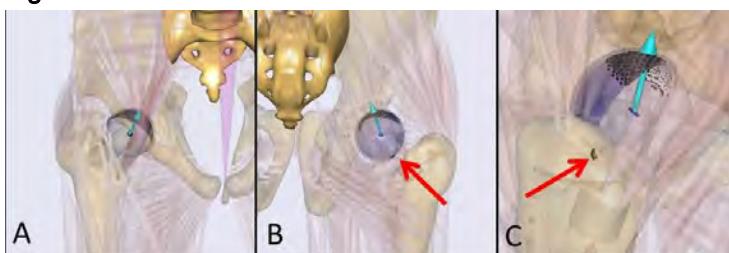
Caption: Screenshot of a mal-aligned THR during stair climbing in [A] anterior, [B] posterior and [C] magnified lateral view showing impingement (red arrow,) and [D] contact area graph for normal and mal-aligned cup with time of impingement (green arrow).

Conclusion: This study shows that complications like impingement and separation can be seen during stair climbing with a mal-aligned cup position. The mal-alignment shows even before impingement a reduced contact area, however, after impingement, a high concentration of forces at the rim area can lead to increase in wear in the THR. Even though, the mal-alignment in this subject was severe, these results can be very useful to understand clinical complication with THR. Future work will focus on including other daily activities and to include the results in wear tests simulation.

Disclosure of Interest: A. Al-Munajjed Conflict with: AnyBody Technology, M. Damsgaard Conflict with: AnyBody Technology, J. Rasmussen Conflict with: AnyBody Technology

Orthopaedic Implants

SS-0004

WEAR OF CROSS-LINKED UHMWPE HIP REPLACEMENTS USING AN ELECTROMECHANICAL HIP JOINT SIMULATOR UNDER TWO-AXIS AND THREE-AXIS OF ROTATION CONDITIONS

Murat Ali [1,*]Mazen Al-Hajjar [1]John Fisher [1]Louise M. Jennings [1]

[1]School of Mechanical Engineering, Institute of Medical and Biological Engineering, University of Leeds, Leeds, United Kingdom

Introduction and Objectives: Hip joint simulators provide a laboratory based *in-vitro* test method to study the tribology of hip implants. This has been achieved through applying a combination of loading and articulating motions using single axis or multiple axes of rotation. Although applying up to three-axis of rotation increases the complexity of the testing method, advances in technology has made the development of multi-station machines with three-axis of rotation a viable option, providing the complete anatomical range of motion during gait to be simulated. The aim of this study was to compare the wear rates of cross-linked UHMWPE (Ultra High Molecular Weight Polyethylene) under two-axis and three-axis of rotation conditions using the same hip simulator.

Methods: A ProSim Electromechanical Hip Joint Simulator (ProSim EM13, Simulation Solutions, Stockport, UK) was set up with 36 mm diameter metal-on-polyethylene (Marathon™, DePuy Synthes Joint Reconstruction, Leeds, UK) hip replacements (n = 6). The same components were used throughout this study and were lubricated with 25% new-born calf serum. For the two-axis of rotation condition, flexion-extension (F-E) and internal-external rotation (I-E) were applied, with abduction-adduction (A-A) included for the three-axis simulation as shown in Figure 1. The rotation angles and phasing under the two-axis of rotation test condition was defined to compensate for operating under biaxial rotation only, and to obtain elliptical wear paths which are physiologically relevant [1]. The same twin peak input load profile was applied during both conditions. The wear rates were compared over three million cycles for each test with gravimetric measurements carried out approximately every one million cycles (Mettler Toledo XP205, Greifensee, Switzerland). The surface roughness (R_a) was measured before testing and at the end of each test (Form Talysurf, Taylor Hobson, Leicester, UK). The mean wear rates per million cycles were calculated with 95% confidence limits and statistical analysis was carried out (one-way ANOVA) with significance levels taken at $p \leq 0.05$.

Results: The wear rates over three million cycles of testing under the two-axis and three-axis of rotation conditions were 13.1 ± 1.4 mm^3/million cycles and 12.2 ± 1.4 mm^3/million cycles respectively. There was no statistically significant difference (p = 0.29) between the wear rates of the metal-on-polyethylene bearings through two-axis and three-axis rotation simulation. The mean pre-test surface roughness (R_a) of the polyethylene liners was 0.614 ± 0.070 µm. At the end of the two-axis and three-axis rotation tests, the roughness of the liners decreased to 0.057 ± 0.018 µm and 0.070 ± 0.024 µm respectively. There was no significant difference (p = 0.30) in surface roughness of the polyethylene liners under both conditions at the end of each test.

Figure:
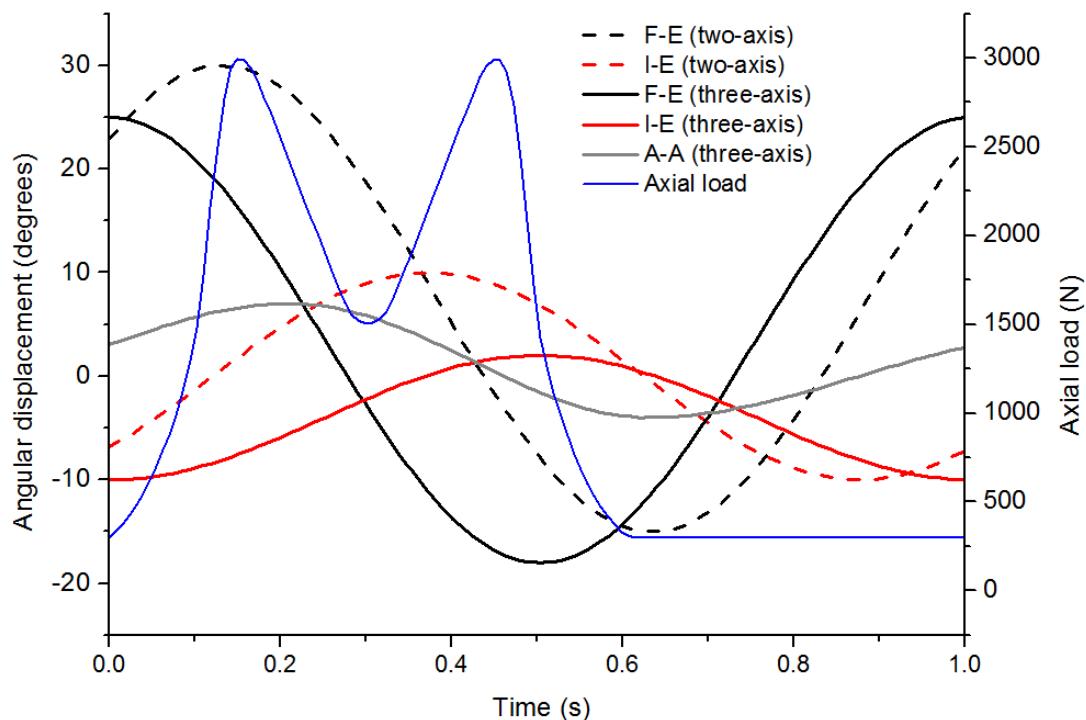
Caption: Figure 1. Angular displacements, loading profile and phasing for the standard gait cycle under two-axis and three-axis of rotation conditions. F-E: flexion-extension, I-E: internal-external rotation, A-A: Abduction-Adduction.

Conclusion: Applying three-axis of rotation during hip joint *in-vitro* testing provided the full range of motion and cross-shear to be implemented as expected to occur *in-vivo*, however, with appropriate phasing and angular displacements the cross-shear effects were also simulated using two-axis of rotation. These conditions are understood to be a contributor to the increased wear of cross-linked UHMWPE. By using a newly developed electromechanical hip joint simulator, this unique study has shown that applying angular displacements using two-axis of rotation can provide wear rates which are comparable to the volumetric wear rates when three-axis of rotation is applied.

References: [1] Barbour et al. Proc. Inst. Mech. Eng. H J. Eng. Med. vol. 213, pp. 455-467, 1999.

Disclosure of Interest: M. Ali: None Declared, M. Al-Hajjar: None Declared, J. Fisher Conflict with: Tissue Regenix Group plc, Conflict with: DePuy Synthes Joint Reconstruction, Invibio, Mathys Medical, Corin Group, Conflict with: DePuy Synthes Joint Reconstruction, Conflict with: DePuy Synthes Joint Reconstruction, L. M. Jennings Conflict with: DePuy Synthes Joint Reconstruction, Mathys Medical, Invibio, Biocomposites

GENDER DIFFERENCES IN 3D PELVIS, HIP AND KNEE KINEMATICS DURING HUMAN GAIT

Gabriel G. Zeitoune [1,*]Gustavo Leporace [1]Leonardo Metsavaht [2]Luiz Alberto Batista [3]Jurandir Nadal [1]

[1]Federal University of Rio de Janeiro, Brazil, [2]Institute Brazil of Health Technologies, [3]State University of Rio de Janeiro, Rio de Janeiro, Brazil

Introduction and Objectives: The hip range of motion in frontal plane and spatio temporal parameters differences in normal gait between women and men has been found [1-3]. Due the lower limb (LL) work as a kinematics chain, other joints can also behave in a different way, affecting the distribution of mechanical loads deriving from the initial contact. However, these papers chosen subjective parameters of gait cycle as dependent variables, which has been described as a study limitation of biomechanical signals [4]. Principal component analysis (PCA) has the advantage of allowing the whole gait cycle analysis without using subjective variables. In this perspective, the objective of this study was to compare the kinematics of the pelvis, hip and knee joints during gait between men and women.

Methods: Ten men (80,9 7,9 kg, 1,75 0,04 m) and seven women (62,9 11,4 kg, 1,62 0,07 m) composed the sample. All of participants had no recent history of low back pain and limb injuries. Subjects were oriented to walk along an eight meters long walkway. Three gait cycles for each LL were captured. The kinematic data were collected using eight cameras and a three-dimensional (3D) motion analysis system (VICON, Oxford Metrics, UK) at 100 Hz. Reflective markers were placed on the skin in trunk, pelvis and both LLs. The raw three dimensional (3D) coordinates of each marker were filtered by a low pass 2nd order Butterworth filter, applied in the forward and reverse directions, to avoid phase distortions, with a cut-off frequency of 8 Hz. After that, the pelvis, hip and knee kinematics was calculated according to [5]. To determine the beginning and final of each cycle, the Foot Velocity Algorithm [6] was used and the three joints data for the three planes of each cycle were interpolated to 51 values, representing 0% to 100% with a cubic spline algorithm. The mean of 6 cycles (three for each side) for each individual were calculated. For PCA the pelvis, hip and knee 3D kinematics of 17 subjects were inserted in nine matrices E [17 x 51] where each row corresponded to subjects and each column corresponded to the interpolated signals. The number of PC retained in the analysis from each joint 3D kinematic data were those that the cumulative sum accounted approximately 80% of the original data variance. Each PC score was compared by a non parametric Mann Whitney test ($\alpha = 0.05$). The correspondent eigenvectors of the retained PCs were analyzed in temporal correspondence to the original signals of both groups to identify the location where the variance between them could be explained [4]. The locations where eigenvectors deviate from zero indicate increased differences between groups (Figure 1).

Results: It was found significant differences between men and women for the first eigenvector of the pelvis in the sagittal plane ($p = 0.02$) and the first eigenvector of the hip and pelvis in the frontal plane ($p < 0.01$). There were no significant differences for any knee plane of motion. These findings corroborate the literature [1-3], wherein women walk with greater hip adduction. However, the first eigenvector of the hip showed that this difference is not only in load response, but also throughout the gait cycle. Additionally, during the whole cycle the pelvis remains with higher anterior tilt and pelvic contralateral drop in load response, which may explain why the hip presents increased adduction. The combination of the

pelvic and hip angular behavior generate pseudo knee valgus at this phase, visually looking like an abduction of the knee, however this does not happen indeed.

Figure:
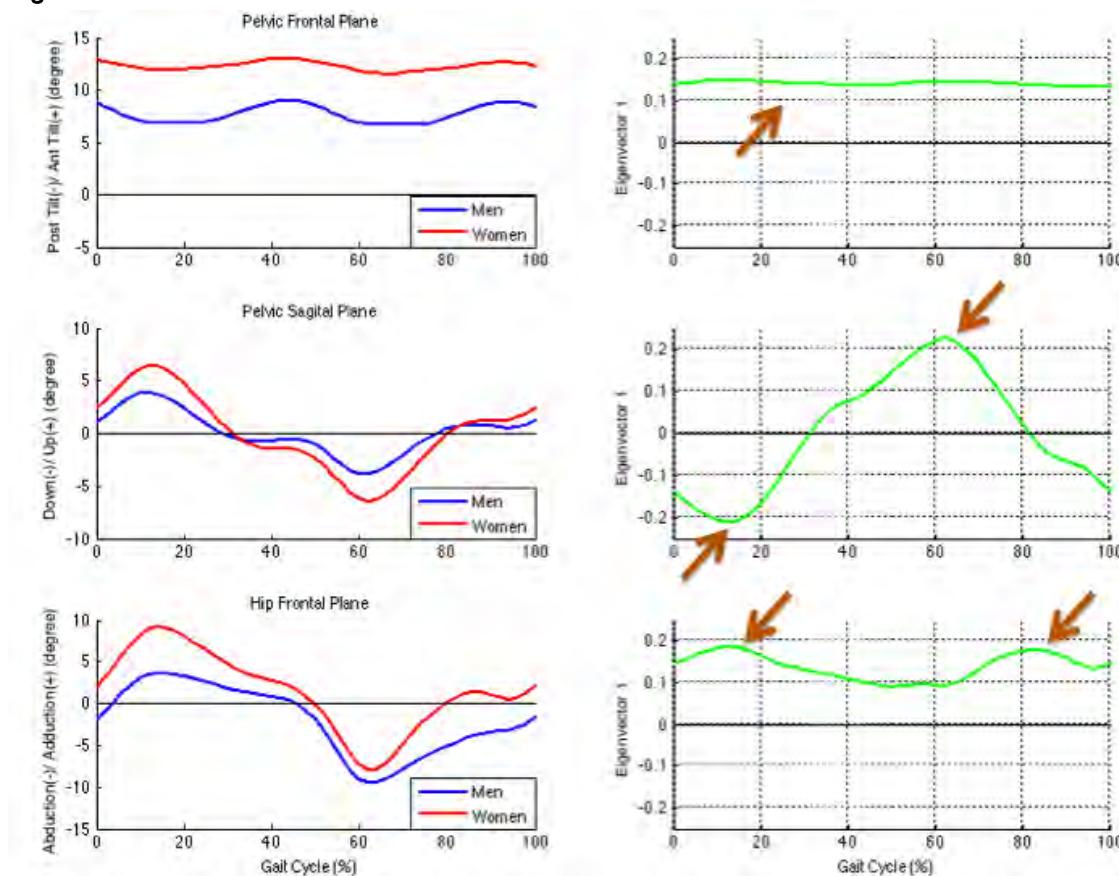
Caption: On the left there are the graphs of gait cycle kinematic of the pelvis, hip and knee joint, with red lines for the females and blue lines for the males. The plotted values are the averaged data from each gender group. On the right, with green lines there are the eigenvectors graphs that were statistically significant for each joint. The brown arrows show the largest variance of the data.

Conclusion: It was concluded that due to the observed angular behavior of the three joints in question, women appears to be more susceptible to injuries and their consequences, such as anterior knee pain, which is one of the risk factors the excessive medial collapse of knees.

References: [1] Chumanov et al., Clin Biomech, 23:1260-1268, 2008.

[2] Baldon et al., J App Biomech, 27: 223-232, 2011.

[3] Kerrigan, et al., Am. J. Phys. Med. Rehab, 77: 2-7, 1998.

[4] Leporace et al., IEEE, 2012: 6514-6517, 2012.

[5] Grood et al., J. Biomech. Eng, 105: 136-144, 1983.

[6] O'Connor et al., Gait & Post, 25: 469-474, 2007.

Disclosure of Interest: None Declared

UPPER LIMB KINEMATICS AND INERTIAL SENSORS: WHICH CALIBRATION FOR THE BEST ACCURACY?

Brice Bouvier [1 2 3 4],*Adriana Savescu [1]Sonia Duprey [2 3 4]Raphaël Dumas [2 3 4]

[1]Institut National de Recherche et de Sécurité, Vandoeuvre-lès-Nancy, [2]Université de Lyon, Lyon, [3]Université Claude Bernard Lyon 1, Villeurbanne, [4]Laboratoire de Biomécanique et Mécanique des Chocs, IFSTTAR, Bron, France

Introduction and Objectives: Magneto-Inertial Measurement Unit sensors (MIMU) are increasingly used in motion analysis as they allow monitoring ambulatory measurements. Sensor 3D orientation can be estimated by combining information from a 3D accelerometer, a 3D gyroscope and a 3D magnetometer. When focusing on joint kinematics, the definition of segment coordinate systems must be associated with MIMU [1]. International standards [2] do not provide a usable method due to the absence of position information delivered by MIMU. In the literature, three main classes of MIMU calibrations can be distinguished: segment axes equal to technical MIMU axes (TECH), and segment axes generated during a static pose (STATIC) or during functional movements (FUNCT). Despite much interest from the scientific community in this topic, two aspects of research deserve more investigation regarding MIMU-based upper limb kinematics. First, few studies have investigated the comparison of MIMU calibrations, being either focused on segment axes and not joint angles [1] or performed on an artificial arm [3]. Second, evaluations of the performance of MIMU-based upper limb kinematics often appear incomplete and disparate in terms of the protocol and validity criteria used [1,4,5]. The present study compares TECH, STATIC and FUNCT classes of calibration in terms of accuracy for the generation of wrist, elbow and shoulder (humero-thoracic) joint angles during maximal amplitude movements.

Methods: Ten subjects were equipped with four wireless MIMUs (MTw, Xsens, Netherlands) on the thorax, and right upper arm, right forearm and right hand segments. The three classes of MIMU calibration, TECH, STATIC and FUNCT were compared. STATIC consists in maintaining a standing pose with the upper arm along the body, elbow flexed at 90°, in neutral forearm pronation-supination (PS). FUNCT uses the combination of STATIC and functional movements of wrist extension, elbow flexion/extension (FE) and shoulder internal/external rotation (IER). An optoelectronic system (Eagle 4, Motion Analysis C., USA) was used as the reference measurement system for the kinematics (REF), according to the ISB standard [2]. Joint angles were compared during six separate movements of maximal amplitude (max): wrist FE, wrist abduction/adduction (AA), elbow FE, forearm PS, shoulder FE and shoulder AA (in the scapular plane). In addition, a seventh test movement consisted of a circular movement in the transverse plane (wheel) that mainly relied on elbow and shoulder DoFs. The experiment was repeated five times per subject, involving a total of fifty experimental sessions (N=50). For the seven test movements, the accuracy of the three MIMU calibrations was assessed using the mean Coefficient of Multiple Correlation inter-protocol (CMCip) [6] and the mean RMSE values calculated over the whole experiment (N=50) and compared with the REF data. Four mean CMCip thresholds were considered: very good (≥0.85), good (0.75-0.85), moderate (0.65-0.75) and bad (<0.55).

Results: The accuracy of the three MIMU calibrations was very good and equivalent (0.85≤CMCip≤0.99) for all the principal FE angles during max wrist FE, elbow FE, shoulder FE and AA, and wheel movements. The same observation

was made for the coupled PS during max forearm PS (0.93≤CMCip≤0.97) (figure 1). Lower accuracy and disparities between calibrations could be observed for the principal AA angle during max wrist AA (0.66≤CMCip≤0.86) and for the coupled AA and IER shoulder angles during max shoulder FE and AA, and wheel movements (0.53≤CMCip≤0.86), without any constant predominance of a particular calibration. Regarding RMSE values, no significant difference could be observed between MIMU calibrations for any of the movements performed (8.0°≤RMSE≤26.2°).

Figure:
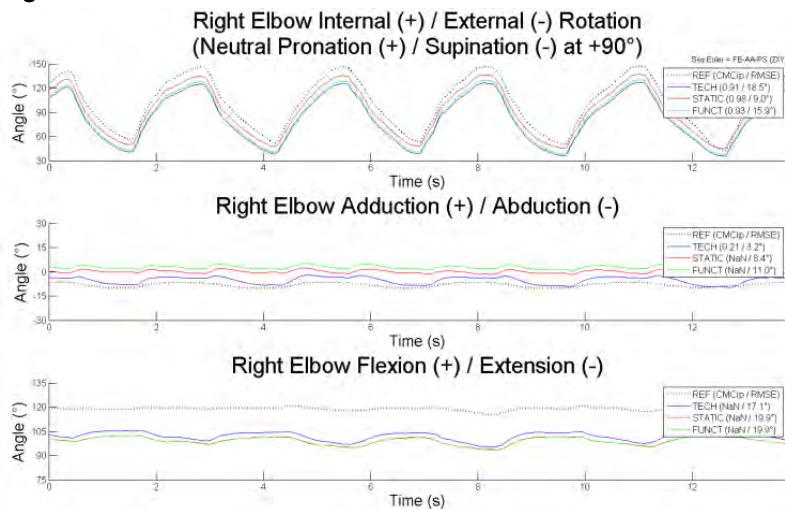
Caption: Figure 1. Elbow joint angles over time from REF (black-dotted), TECH (blue), STATIC (red), FUNCT (green) during max forearm PS

Conclusion: This study highlights that the three classes of calibration (TECH, STATIC, FUNCT) provide good level of accuracy considering CMCip, without any significant difference between them. However, it should be mentioned that the accuracy is only one aspect of the MIMU calibration performance. Indeed, differences between MIMU-based and REF joint angle always exist due to the different definition of the segment axes and the dissimilar effect of soft tissue artifact [1]. RMSE values are comparable to previous results of 20° and 10°-20° reported in the literature [1,7]. For a complete evaluation of MIMU-based upper limb kinematics, reproducibility [1] and interpretation [5,8] of joint angle should also be considered key criteria.

References: [1] De Vries et al., J. Biomech, 43:1983-88, 2010.

[2] Wu et al., J. Biomech, 38:981-92, 2005.

[3] Galinski et al., Proc. IEEE RAS EMBS, 1801-06, 2012.

[4] Coley et al., Gait Posture, 25:523-32, 2007.

[5] Cutti et al., Med Biol Eng Comp, 46:169-78, 2008.

[6] Ferrari et al., Gait Posture, 31:540-42, 2010.

[7] Luinge et al., J. Biomech, 40:78-85, 2007.

[8] Bouvier et al., CMBBE, 17:108-09, 2014.

Disclosure of Interest: None Declared

BIOMECHANICAL DOSAGE EFFECT OF KNEE BRACES ON INTERNAL JOINT MOMENT AS MEASURED BY THE E-TIBIA

Howard J. Hillstrom [1,*]Jim Tse [1]Lilly Tran [1]Darryl D'Lima [2]Shantanu Patil [2]Sherry Backus [1]Andrew Kraszewski [1]Benjamin Fregly [3]Glenn Garrison [1]Andreas Kontaxis [1]Mark Lenhoff [1]

[1]Rehabilitation - Leon Root, MD Motion Analysis Lab, Hospital for Special Surgery, New York, [2]Shiley Center for Orthopaedic Research and Education, Scripps Clinic, La Jolla, [3]Mechanical and Aerospace Engineering, University of Florida, Gainesville, United States

Introduction and Objectives: High body mass index, soft tissue injuries, and malalignment have all been associated with knee osteoarthritis (OA). Varus malalignment overloads the medial compartment of the joint and is the most common deformity in these patients. Pollo et. al. fit a strain gauge upon the hinge of an Unloader Select knee brace in a previous study and found that a portion of the load was shared with the knee via the hinge.[1] The effect of knee brace alignment upon compressive loading within the joint for treating OA is unknown. *Purpose*: Total knee moment and contact forces were measured on an individual wearing a knee brace that was adjusted for various alignments to determine the 'biomechanical dosage' effect. The test subject has been fitted with an instrumented total knee replacement (e-tibia) that can measure total knee moments and contact forces *in vivo*. Inverse dynamics and e-tibia data were simultaneously collected from the subject while wearing an Ossur Unloader Select knee brace adjusted to -8°, -4°, 0°, 4°, 8° of alignment (valgus (+) and varus (-)). Our hypotheses are: (**H1**) increasingly valgus brace alignments will more effectively decrease internal joint moment while varus brace alignments will also decrease internal joint moment and (**H2**) that the treatment mechanisms of knee bracing employs both load sharing and shifting.

Methods: A single-subject study was conducted on a female (69 years old, 81 kg) who had an e-tibia. Composed of a polyethylene insert, tibial tray, and telemetry system, the e-tibia measured three forces (F_x, F_y, F_z) and three moments (M_x, M_y, M_z) using 12 load cell strain gages that are integrated within the e-tibia.[2] The subject walked at her self-selected speed on a level walkway while simultaneously measuring e-tibia contact loading and 3D inverse dynamics (12 Eagle cameras, Motion Analysis Corp, Santa Rosa, CA; 2 Bertec, Columbus, Ohio; and 2 AMTI, Bilarica, MA force plates). The test subject walked with a knee brace (Unloader Select, Ossur Americas, Foothill Ranch, CA) adjusted to four different alignments (dosage) and an unbraced condition representing baseline (control). Each brace condition corresponded to a different frontal plane alignment (-8°, -4°, unbraced, +4°, +8°) of varus to valgus correction. Data collection was performed for five trials per condition. Total internal moment and contact forces were measured directly by the e-tibia.

Results: The unbraced condition (orange) had the largest peak moments at approximately 25% and 80% of stance phase (Figure 1). While employing 4° (light green) and 8° (dark blue) valgus brace correction, the first peak reduced by 15.8% and 29.3% respectively while the second peak reduced by 8.9% and 22.9% respectively. Increasingly valgus brace alignments more effectively decreased joint moment as measured by the e-tibia. Interestingly, 4° and 8° varus brace correction also reduced peak moments but not as much as valgus bracing. Taken together this data supports acceptance of **H1**. Since all four brace alignments reduced internal knee moment compared with the unbraced condition this data

supports the theory that the brace shares load with the knee. One plausible explanation is the load path through the hinge as described by Polo et al.[1] In the case of increasing amounts of valgus brace correction for genu varum (i.e. 4° and 8°) the internal moment progressively reduced which supports the theory that knee braces are offloading the involved compartment by reducing the total internal (varus) moment through application of a larger valgus brace moment. This load shifting in conjunction with the load sharing supports acceptance of **H2**. Since braces can provide different amounts of offloading of the involved knee compartment the treatment effect is analogous to a 'biomechanical dosage'.

Figure:
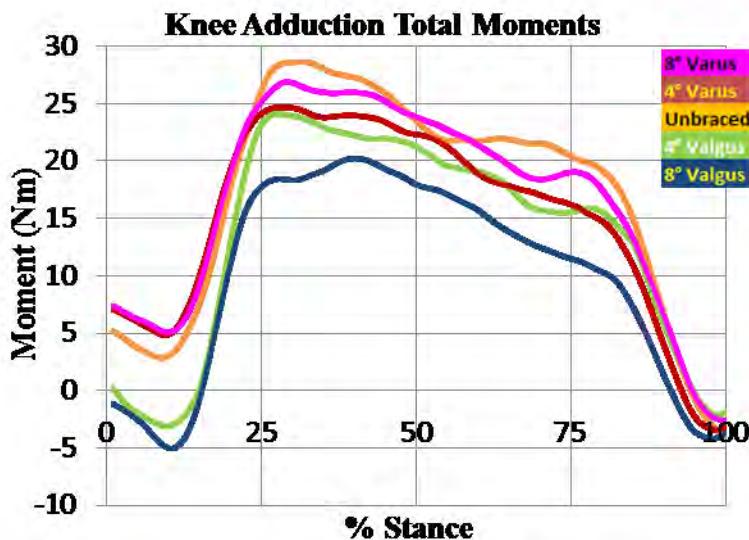
Caption: Figure 1: Knee Adduction Moments as Measured by the e-tibia

Conclusion: This study employed a test subject with an e-tibia, an electronic total knee replacement that measures internal moments and contact forces during functional tasks in vivo. Increasingly valgus brace alignments more effectively decreased internal joint moment while varus brace alignments also decreased internal joint moment. The data supports both a load sharing and shifting mechanism for treatment of knee OA knee with braces.

References: [1] Pollo, F. E. et al. *Am J Sports Med.* 30(3): 414-21, 2002
[2] D'Lima, D. D. et al. *Journal of Biomechanics* 38(2): 299-304, 2005

Disclosure of Interest: None Declared

A COMPARATIVE BIOMECHANICAL STUDY ON THE FUNCTIONALITY OF DIFFERENT ORTHOTIC CONCEPTS IN PATIENTS WITH CARPOMETACARPAL OSTEOARTHRITIS.

Timo Schmeltzpfenning [1,*]Jennifer Grunden [1]Birgit Scheib [2]Joachim Bauer [1]Jörn Heidemann [3]Kai Heinrich [4]Han Wu [4]Judith Bleuel [4]Christiane Gonska [4]Gert-Peter Brüggemann [4]Nina Hamann [4]

[1]R&D Department, [2]SA , BSN medical, Hamburg, [3]Joint Centre, Brühl, [4]Institute of Biomechanics and Orthopaedics, German Sport University Cologne, Köln, Germany

Introduction and Objectives: Osteoarthritis (OA) of the carpometacarpal (CMC) joint is a painful chronic disease, which limits the degree of thumb motion. Key element in treatment is pain reduction by stabilizing the affected joint. Patients' compliance, however, depends on daily functionality. The aim of this study was to compare orthotic concepts regarding their combination of stabilization effectiveness and functionality in daily activities.

Methods: Eighteen female subjects (mean age 63 ±3 y) diagnosed thumb CMC OA (stage II/III) were included in the study. Four orthotic concepts, differing in material and mechanical construction have been tested and compared (Rhizo Forte , BSNmedical (BSN); OrthoCMC, Push (PUSH); Rhizo-Hit, Sporlastic (SPOR); Rhizomed, Medi (MEDI)). Stabilization effectiveness was analyzed by a three-dimensional thumb kinematic model using a 6 infrared camera system at 100 Hz and retro-reflective marker arrays. Range of motion (ROM) of the thumb CMC joint was determined while hands were fixed in a custom made test bench. Sollerman test was used to examine hand functionality scoring 20 activities of daily living [1].

Results: All orthoses significantly restricted the ROM in flexion-extension, adduction-abduction and pronation-supination compared to the ROM of the thumb without external support. Significant inter-conceptual differences could be measured for all analyzed movements and for the performance of daily activities. Mean flexion-extension ROM was significantly smallest using the orthotic construction of Medi and BSN compared to the concepts of Push and Sporlastic. Mean adduction-abduction ROM was significantly largest with the minimalistic design of the Push thumb brace compared to all other orthotic concepts. The stabilization in pronation-supination direction was significantly higher with BSN and Medi compared to Push, but similar to Sporlastic. Contrary to the kinematic results, the performance of daily tasks could be managed best with Push (78 out of 80), whereas the Medi concept hindered the patients most during the execution (46 out of 80). Both differed from the other orthoses. Mean sum scores with BSN (72) and Sporlastic (75) were between the values of Push and Medi and showed no statistical differences to each other.

Figure:
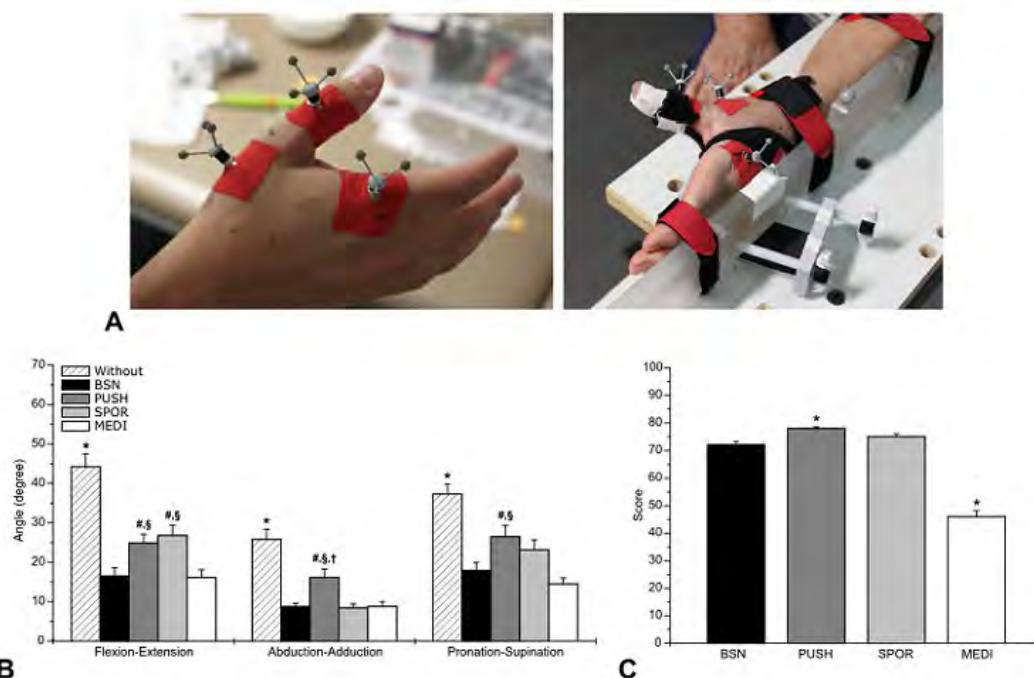
Caption: Fig. 1. (A) Hand fixed in custom made test bench during maximum active opposition-reposition with marker arrays positioned on thumb and index finger. (B) Ranges of motion of thumb CMC joint during opposition-reposition with and without orthoses. Mean ± SE. *significantly different from all orthoses p<0.05, #significantly different from BSN p < 0.05, §significantly different from MEDI p< 0.05, † significantly different from SPOR p < 0.05 (C) Mean Sollerman sum score of hand function while using the orthoses. Mean ± SE. *significantly different from all other orthoses p < 0.05.

Conclusion: The right combination of maximum functionality in daily activities and stabilization of the thumb is essential for the ideal treatment and compliance of CMC OA patients. However, our results show a negative effect on functionality by increasing the thumb stabilization. This correlation can be influenced by the conceptual design of the thumb orthotic. Best compromise of both product properties can be provided by the orthotic concept of BSN, whereas Medi and Push either lack on the functionality or stability.

References: [1] Sollerman et al., Scand J Plast Reconstr Hand Surg, 29: 167-176, 1995.

Computer Simulation

SS-0009

EVALUATING THE EFFECT OF THE STIFFNESS OF AN AFO ON GAIT IN A HEALTHY TEST SUBJECT: EXPERIMENTS VS. PREDICTIVE SIMULATIONS.

Veerle Creylman [1,*]Luiza Muraru [1]Jos Vander Sloten [2]Ilse Jonkers [3]Louis Peeraer [1][4]

[1]Mobilab, Thomas More, Geel, [2]Mechanical Engineering, Biomechanics Section, [3]Department of Kinesiology, Human Movement Biomechanics, [4]Department of Kinesiology, Musculoskeletal Rehabilitation, KU Leuven, Leuven, Belgium

Introduction and Objectives: An Ankle Foot Orthosis (AFO) is commonly used in clinical practice to assist gait of patients with different pathologies. In the past years, musculoskeletal simulations have been used to quantify the effect of AFO-stiffness on gait [1]. However, to our knowledge none of the results of these simulations were compared to experimental results.

This study quantified the effect of a varying AFO-stiffness on the gait pattern of a healthy test subject using (1) experimental gait measurements while walking with AFOs with different stiffnesses and (2) predictive simulations of the effect of varying AFO-stiffness on the kinematics and dynamics of the test subject.

The main goals of loading response are weight acceptance, shock absorption and advancing the body over the heel rocker. Therefore, the ankle plantar flexes while the knee flexes. In this study, it is hypothesized that with increasing AFO-stiffness during loading response, the ankle plantar flexion will decrease, the maximum knee flexion angle during will increase and the activation of the m. tibialis anterior will decrease.

Methods: A healthy female of 27y, mass 53 kg, is test subject for this study. Based on the scan of her lower leg, 5 patient-specific AFOs with different stiffnesses are fabricated using the SLS-method [2]. AFO-stiffness is calculated in a FE-simulation. Gait measurements are performed in six conditions: while wearing shoes and while wearing the five different custom-made AFOs combined with the same shoes. Kinematic data are collected using the CODAMOTION system. AMTI force plates are used to collect ground reaction forces. A generic musculoskeletal model of the lower limbs with 23 degrees of freedom and 92 muscles is scaled in OpenSim to match the test subject's anthropometric data [3]. The torque supplied by the AFOs is simulated as a rotational spring around the ankle joint with a constant stiffness based on the FE-analyses. The kinematic data of the person walking with the AFO with average stiffness are used as an input to the simulations to calculate the effect of varying AFO-stiffness on muscle activations using Computed Muscle Control (CMC). The muscle activations of the person walking with the AFO with average stiffness are used as an input to the simulations to calculate the effect of varying AFO-stiffness on kinematics in a forward dynamic (FD) simulation.

Results: The hypothesis is that with increasing AFO-stiffness the maximum ankle plantar flexion during loading response decreases and the maximum knee angle increases. This is not confirmed by the experimental results (table: mean results and standard deviation between brackets) where for increasing AFO-stiffness no trend in the plantar flexion is observed. In contrast, when evaluating the results of the FD-simulation, the hypothesis is confirmed.

Similar results as in the kinematics are observed for the calculated activation of the m. tibialis anterior (figure, left experimental results, mean over trials and right simulations): the hypothesis is not confirmed by the experimental results, but confirmed by the simulations.

Figure:
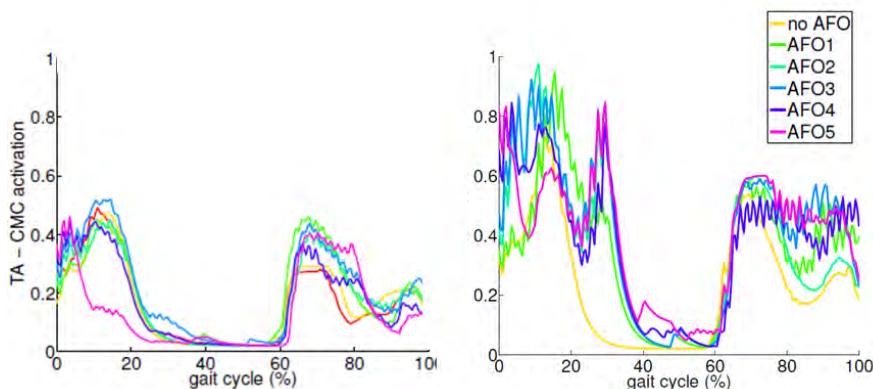
Caption: Calculated activation of the m. tibialis anterior for both the experiments (left, mean over trials) and simulations (right) for AFOs with variable stiffness.

Conclusion: The musculoskeletal simulations used here are based on a ``mechanical'' approach and from this point of view the hypotheses are confirmed: e.g., a stiffer AFO will limit plantar flexion during loading response and therefore push the knee into flexion. However, the results from the experiments do not confirm the hypotheses: it is possible that the healthy test subject attempts to maintain normal gait kinematics and therefore changes muscle activation patterns. Hence, during experiments, both the muscle activations and the kinematics of gait may be changed simultaneously while during the predictive simulations either the muscle activations or the kinematic data are varied. A further evaluation of the influence of AFO-stiffness on gait requires an elimination of the discrepancy between the experiments and the simulations by incorporation of compensating mechanisms observed.

Table:

Applied AFO-stiffness	No AFO	AFO 1 45 Nm/rad	AFO 2 69 Nm/rad	AFO 3 87 Nm/rad	AFO 4 131 Nm/rad	AFO 5 199 Nm/rad
Experimental ankle plantar flexion (°)	3.95 (0.87)	2.07 §0.83)	1.27 (0.89)	2.14 (0.36)	1.58 (0.87)	0.76 (0.51)
Experimental knee angle (°)	18.38 (2.18)	20.53 (2.69)	21.21 (1.51)	18.24 (1.96)	19.81 (2.20)	20.47 (1.90)
Simulations: ankle plantar flexion (°)	5.4	4.9	4.7	4.4	3.9	3.3
Simulations: knee angle (°)	14.0	14.0	14.0	14.1	14.2	14.5

Caption: The results of the ankle plantar flexion during loading response and peak knee angle during loading response for both the experimental results and simulations (mean results with standard deviation between brackets).

References: [1]   Crabtree et al., Gait Posture, 29: 65-70, 2009

[2]   Pallari et al., Proc SFF Symposium, Texas, 2010

[3]   Delp et al., IEEE I Bio-Med Eng, 55: 1940-1950, 2007

Disclosure of Interest: None Declared

Musculoskeletal

SS-0010

APPLICATION OF PERSONALISED FOOT ORTHOTICS FOR THE TREATMENT OF MEDIAL KNEE OSTEOARTHRITIS (MKOA)

Richard Allan [1,*] James Woodburn [1] Scott Telfer [1] Mandy Abbott [1] Martijn Steultjens [1]

[1]School of Health and Life Sciences, Glasgow Caledonian University, Glasgow, United Kingdom

Introduction and Objectives: Increased knee joint load plays play a crucial role in the pathogenesis of knee osteoarthritis. The external knee adduction moment (KAM) is commonly accepted as an indirect measure of loading of the medial compartment such that a reduction in the KAM reflects a reduction in the loading of the medial compartment. Orthotic interventions such as lateral wedged insoles are routinely prescribed to the KOA population. These are designed to reduce the KAM, effectively redistributing load, thus addressing the inadequate knee joint load patterns. Research has demonstrated a heterogeneous response to this orthotic intervention, with 23-30% of cases exhibiting an increase in the KAM [1].

Some debate remains as to whether a fully customised approach to orthotic design can provide additional benefit over prefabricated orthoses. Recently, a novel approach to 3D printing of orthotics via Computer Aided Design and Fused Deposition Modelling (FDM) has received increased attention in this area[2], providing the opportunity to allow a more personalised intervention To date these techniques have not been applied to a KOA population.

The purpose of this study is to explore a personalised approach for patients with medial KOA and assess differences in biomechanical response to alterations in two key orthotic design variables: the degree of lateral wedging (posting) and orthotic length.

Methods: Personalised foot orthotics (PFOs) were created for 9 females with symptomatic medial knee osteoarthritis (62.0±7.2yrs; 1.64±0.05m; 73.6±7.5 kg). Computer aided design (CAD) software was used to design 8 PFOs (4 full length and 4 ¾ length each with: 0° rearfoot posting; 5° rearfoot posting; 10° rearfoot posting and a combination of 5° forefoot 10° rearfoot posting) per participant based on a 3D surface scan of their feet. All PFOs were manufactured in-house using FDM methods. 14 camera motion analysis system was used to track retroflective markers at a frequency of 120Hz, and an embedded force plate measured ground reaction forces at 2400Hz. Markers were attached to the patients test leg and pelvis to define a unilateral marker model which included the pelvis, thigh, shank and full foot segments.

Quantification of the orthotic effect focused on a core set of clinically meaningful kinetic variables targeted for FO interventions. This included; Peak knee adduction moment in the 1st and 2nd half of stance (1KAM, 2KAM), KAM Impulse (KAMI) and peak knee flexion moment in the 1st half of stance (1KFM). All kinetic variables were normalised to %BW*h and defined relative to a shod test condition. Two-way mixed effect ANOVAs were performed to determine if the PFO type, PFO length and any interactions were significant at α < 0.05 level.

Results: Significant main effects were found for posting level for 1KAM (p= 0.01), 2KAM (p=0.002) and KAMI (p=0.000). Mean effect of conditions are presented in figure 1. No significant effects were found for PFO length or for group interactions. No significant effects were found for the KFM. Large between subject differences were found across all FO conditions. A mean reduction in 1KAM occurred after the introduction of lateral posting, with the greatest level of effect

occurring with a 10° level of posting (-5.7(-0.2, -11.2) %). Within subject effect of posting level was consistent suggesting that this is the most significant factor for the reduction of medial compartment loading irrespective of PFO length. Neutral PFOs increased 2KAM above shod; indicating greater medial compartment loads and was only counteracted once lateral posting was increased. As lateral posting increased, 2KAM reduced, remaining above the shod, with only the 5° forefoot 10° rearfoot PFO demonstrating an mean overall reduction, (-1.8(-8.0, 4.3)%) . Largest reductions in KAMI were found for the 5° forefoot 10° rearfoot (-4.4 (-9.2, 0.3)%) suggesting that lateral posting, irrespective of PFO length is crucial for the reduction in the cumulative loading of the medial compartment.

Figure:
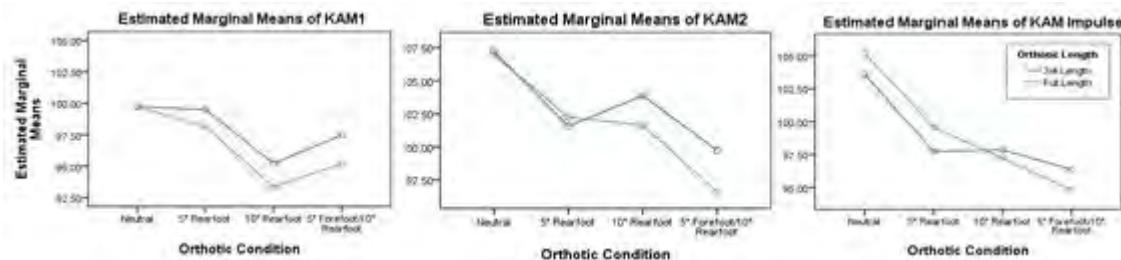
Caption: Figure 1 Estimated marginal means of selected kinetic variables relative to shod

Conclusion: Increased levels of posting provide greater reductions in KAM variables for patients with mKOA, however consistent with previous studies large between subject variability further demonstrates the responsive/non-responsive nature of the KOA population to orthotic intervention. It remains unclear whether our elevated findings related to 2KAM and to an extent KAMI are the result of the true biomechanical adaptations or could potentially be the result of systematic measurement error; however the reductions in 1KAM are consistent with previously reported findings, suggesting our results are valid. Our research further demonstrates the existing debate as to whether a personalised approach provides any additional benefits over standard orthotic interventions and requires a more in depth assessment.

References: [1] Hinman et al., Clin Biomech (Bristol, Avon), 27:27–33, 2012

[2] Telfer et al., J Biomech, 46:1489-95, 2013

Disclosure of Interest: None Declared

Assistive Technology

SS-0011

DEVELOPMENT OF AN ORTHOTIC GLOVE WITH EMG FEEDBACK FOR ASSISTIVE AND REHABILITATIVE PURPOSES

Oluwalogbon O. Akinnola [1,]*David Branson [2]Sue Cobb [2]Paul Smith [3]

[1]Mechanical Engineering, [2]Faculty of Engineering, [3] Faculty of Medicine and Health Sciences, University of Nottingham, Nottingham, United Kingdom

Introduction and Objectives: Hand rehabilitation is a priority in medical research in the UK with an estimated 550,000 people suffering from illnesses that affect the muscles, reducing grip and coordination [1]. However, current commercially available devices designed to provide assistive and/or rehabilitative solutions offer limited physical utility, such as a splint used to hold a utensil in a single grip, or they were generally cumbersome thus limiting use of some systems to fixed locations [2,3].

In response to this deficit an Orthotic Glove was designed and built to be lightweight and simple to use. It featured wrist-mounted servo motors acting as muscles that pulled on fishing line tendons attached to the front and back of the index, fore, and middle fingers. This enabled antagonistic pairings to open and close fingers for power and precision griping. The design used flex sensors to achieve amplified motion based on small finger movements and was predominantly assistive. This study investigatess the use of Electromyographic sensors as control feedback sources to improve rehabilitation quality and fidelity in the Glove.

Methods: Ten experiments, with three repeats each, were carried out to determine signal behaviour and reliability of muscle activation during normal hand motions with the glove off. There was one subject in the series of investigative trials, the author. The subject was a healthy right handed male, 23 years old, weight: 88kg, height: 186cm. Each experiment began by cleaning the arm, roughening the skin surface to encourage sensor adhesion, and placing passive 3M Red Dot 2560 electrodes on the left arm of the subject. Muscles monitored were the Extensor Indicis, Abductor Pollicis Brevis, Flecor Pollicis Longus, Flexor Digitorum Superficialis, Flexor Digitorum Profundus, and Extensor Digitorum. Muscle activity was recorded as oscilloscope plots using three Powerlab 26T data acquisition devices and LabChart 8 from ADIstruments. The plots have Time (s) on the x-axis and Voltage (mV) on the y-axis. Extra instruments, such as a dynamometer and pressure pad, were connected as needed.

Results: The experiments provided good insight into how muscle signals changed with various finger movements. It was found that signal amplitude was proportional to the force being applied by the finger irrespective of the duration of the application (Fig 1). Force and acceleration are intrinsically linked so greater acceleration meant larger signal amplitude. Results also suggested that when closing the hand flexor muscles are much more active than extensors, yet when opening the hand both muscle groups create signals similar in magnitude and nearly in phase, thus flexor activity alone cannot indicate a closing hand.

The main sources of error in the experiments were sensor noise and crosstalk – the activation of other muscles in the arm when moving a finger. Noise greatly harms the fidelity of the glove response as it can be mistaken for muscle activity resulting in unwanted motion. Action was taken to limit this, however experimental limitaions prevented complete

elimination. Thus results are only estimations of signal behaviour. The effects of crosstalk were proportional to the size of the motion; e.g. when moving the middle finger, the one most affected by crosstalk, a signal of 0.030mV in the forefinger flexion muscles accompanied a signal of 0.079mV in the middle finger flexion muscles. When the signal increased to a 0.124mV signal from the middle finger, the forefinger signal increased to 0.121mV. Whilst this does not negatively affect practical use of the Glove as natural movement is still achievable, it was experimentally difficult to determine what level of signal change was attributed to individual muscles.

Figure:
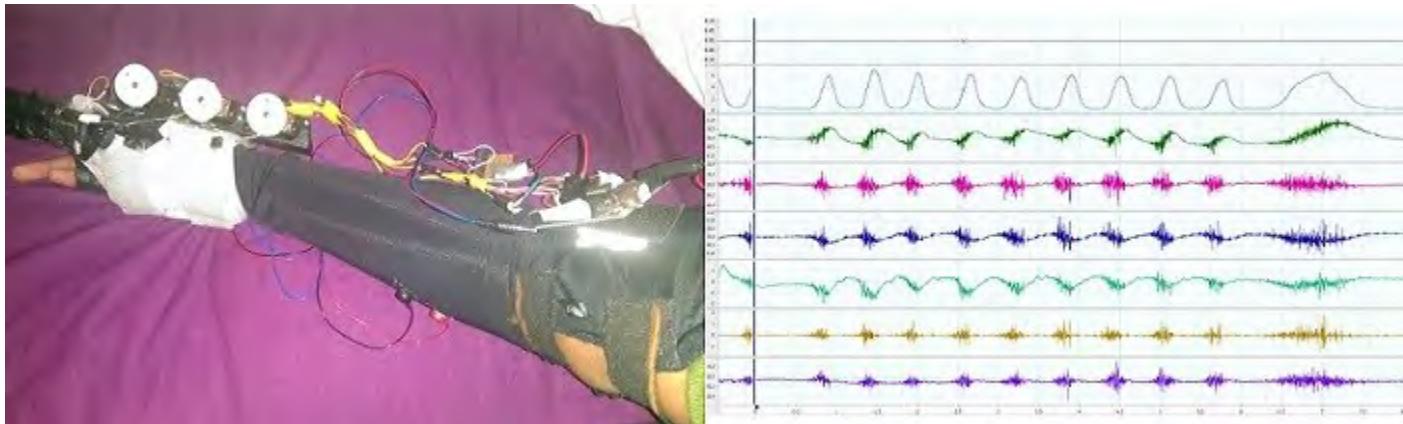
Caption: Fig1: a) Orthotic Glove MkII b) Trial 6 oscilloscope plot . Activity in muscles as force increases

Conclusion: The research produced a working prototype of a portable assistive and rehabilitative device.The results support the implementation of EMG signals as a means to initiate motion. Using these signals the rehabilitative benefits of the device will improve as the neural pathways involved in moving the fingers are also trained along with the muscles [4]. More work is needed to minimise noise and to optimise sensor location to improve the fidelity between the Glove response and the user's intention.

References: [1] Neuro Numbers, 2003 Available at: www.neural.org.uk/store/assets/files/20/original/NeuroNumbers.pdf.

[2] Radomski et al, Occ. Therapy for Phys. Dysf. 1st ed Philadelphia: Lippincott Williams & Wilkins, 2008.

[3] Hasegawa et al, *F. Finger*, 718-724, 2008.

[4] Chen et al, *Molecular genetic analysis*, 20(1), pp.157—184, 1997

Disclosure of Interest: None Declared

A BIOMECHANICAL STUDY ON EFFECTS OF FUNCTIONAL ORTHOTICS IN IMPROVING THE SWING STABILITY AND SWING PERFORMANCE

Chun-Ju Chang [1,*]Sai-Wei Yang [1]Keh-Tao Liu [2]Ching-Wei Chang [1]Siou-Ting Hsu [1]Yen-Ling Lin [1]

[1]National Yang-Ming University, Taipei, Taiwan, Department of Biomedical Engineering, [2]Global Action Inc, Taipei, Taiwan, Republic of China

Introduction and Objectives: With technology changing at such a rapid pace, there are lots of foot orthosis design in the world. An outstanding golf player not only practicing diligently, but also needs an effectively foot orthosis to help acquiring good postural control in the golf competitions [1]. In golf swinging, feet and ankles require highly static stability to give assistance for the player. Providing the functional insole may be an important intervention, it can improve the player's foot stability, increase the hitting speed and decrease clubface hitting angle variability, but the efficacy of arch support is still lack of scientific data. There are two objectives in this study, which included: (1)A golfing motion analysis will be conducted to understand effects of different foot type and lower limb alignment in golf swing; (2)The foot orthosis based on foot arch and lower limb alignment will be prescribed to evaluate the effect of new designed orthotics being able to improve performance.

Methods: Nineteen young golf players were recruited into our study, fourteen male and five female, the mean age was 17.1±8.9 years old, the height was 168.6±10.6 cm, and the weight was 61.5±16.1 kg. Considering the foot type and lower limb alignment for the foot insole, there were 11 subjects with flat arch, 8 normal arch, and no one with high arch; and 12 subjects with genu valgum, 4 straight leg, and 3 with genu varum. All of the subjects volunteered joining the foot orthosis study, and were informed the details of the study processes and singed the informed consent provided by Institutional Review Board (Taipei Veterans General Hospital, IRB No.2012-07-008ACY).

The subjects had to wear familiar golf shoes during the tests, and we recorded the swinging performance with and without foot orthosis randomly. Each of them was asked to hit the maximum distance with 5 iron club [2]. The golf foot insoles was designed by the Foot Disc (Global Action Inc, Footdisc®, Taiwan), which consist of three layers decompressed materials, arch support and adequate heel stability. mySwing Golf Swing Analyzer (Noitom Technology Ltd, China) was used to measure the hitting speed, swing ratio, path angle, and clubface angle (Fig 1). A independent t-test was used to discriminate the effect of insole.

Results: The statistic results of mean and standard deviation data (Table 1) showed there were no significant difference between the variable of hitting speed, timing of upswing and downswing phase, and the angle parameters. But in the raw data of standard deviation, we found out that the deviation decreased after wearing the foot insole in each variable. The deviation of hitting speed decreased 2.6%, downswing time decreased 4.2%, and especially at the angle of path angle, clubface angle, loft angle and lie angle, the decreased deviation was 27%, 23.4%, 22.7%, and 17.4% (Fig 2~5). Although the performance of kinematics did not change significantly, the standard deviation of angle showed the change of swinging pattern while giving the foot insole intervention.

The statistic results of coefficient of variation (CV) data (Table 2) showed there were significant difference between the variable of downing timing (3.241±2.574 vs. 2.354±0.944, p=0.034) and path angle (60.67±45.32 vs. 42.87±29.65, p=0.027). By wearing the foot insole, the subjects had less coefficient of variation compare with the no insole condition.

Figure:
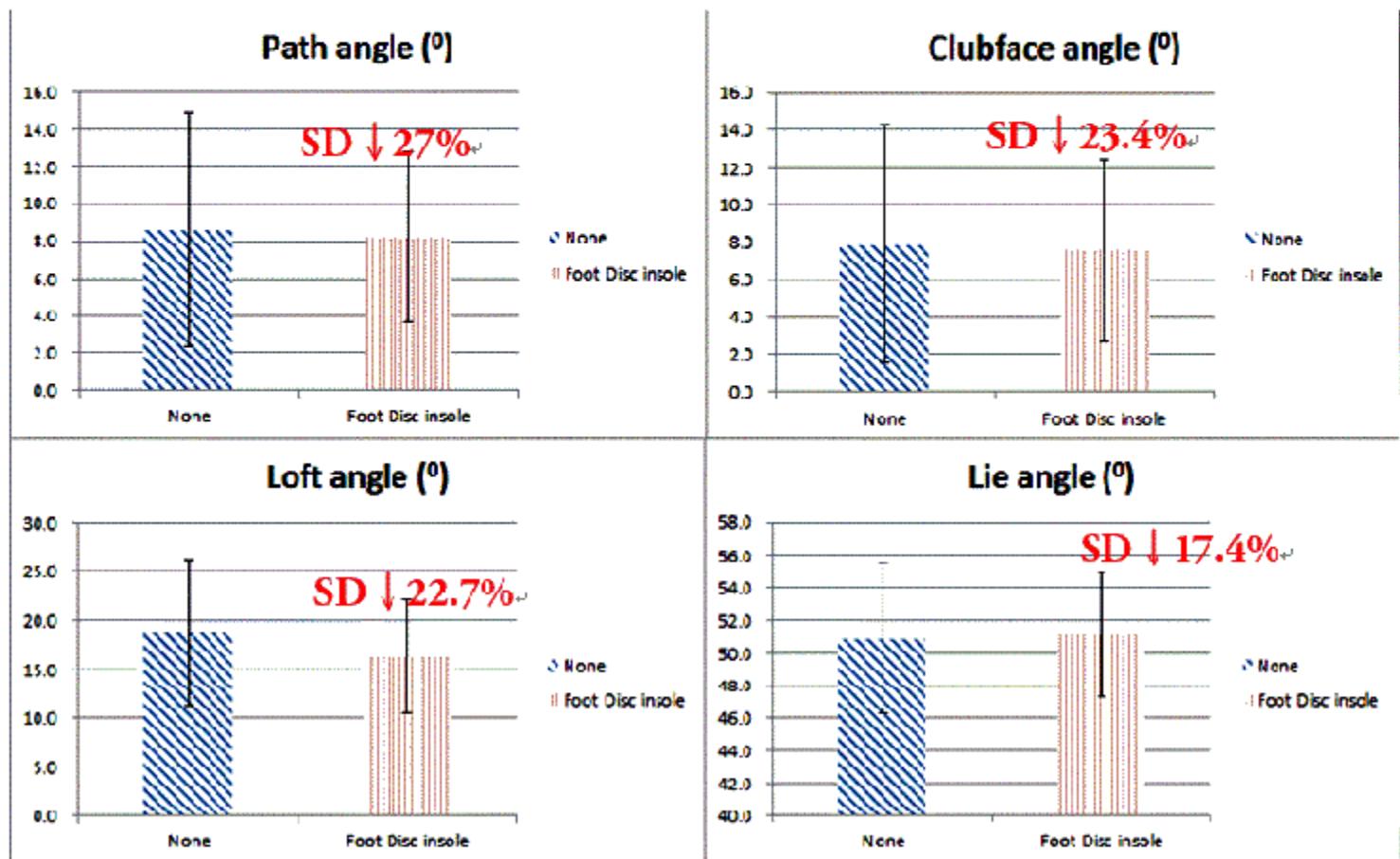
Caption: Fig 1: mySwing Golf detect device; Fig 2: Angle compare between no insole vs. Foot Disc insole

Conclusion: This study suggests the golf players wearing proper foot insole with decompressed materials, arch support and fitting lower limb alignment will improve their swinging performance and decrease the swing variability. A sports foot

insole may provide the player adequate postural stability, release foot pressure, and reduce the risk of musculoskeletal injury which results from muscle and joint motion overused [3].

Table:

Variable (unit)	no insole	Foot Disc insole	p	SD changed
Speed (mph)	82.3±7.8	82.3±7.6	0.923	-2.6 %
Upswing (s)	1.072±0.268	1.097±0.279	0.819	+4.1 %
Downswing (s)	0.284±0.071	0.282±0.068	0.976	-4.2 %
Swing Ratio	3.85±0.75	3.94±0.72	0.780	-4.0 %
Path Angle (^{0})	8.6±6.3	8.2±4.6	0.561	-27.0 %
Clubface Angle (^{0})	7.9±6.4	7.6±4.9	0.763	-23.4 %
Loft Angle (^{0})	18.7±7.5	16.3±5.8	0.723	-22.7 %
Lie Angle (^{0})	50.9±4.6	51.1±3.8	0.778	-17.4 %
Speed CV (%)	2.0±1.6	2.0±1.5	0.771	
Upswing CV (%)	4.716±4.390	3.552±2.343	0.253	
Downswing CV (%)	3.241±2.574	2.354±0.944	0.034 *	
Swing Ratio CV (%)	5.22±3.78	3.89±1.56	0.226	
Path Angle CV (%)	60.67±45.32	42.87±29.65	0.027 *	
Clubface Angle CV (%)	64.80±44.65	57.61±42.36	0.382	
Loft Angle CV (%)	19.69±16.45	21.33±14.85	0.673	
Lie Angle CV (%)	3.04±3.25	2.51±1.45	0.651	

Caption: Table 1: mean and SD of mySwing golf analyzer; Table 2: coefficient of variation (CV) of mySwing golf analyzer

References: [1] Worsfold et al., J Sports Sci Med, 8(4): 607-615. 2009.

[2] Healy et al., J Sports Sci, 29(10):1079-1088, 2011.

[3] Thériault et al., Sports Med, 26(1):43-57, 1998.

Disclosure of Interest: None Declared

Motion Analysis

SS-0013

DO SUBJECT SPECIFIC SIMULATIONS MODIFY GAIT ASSESSMENT OUTPUTS COMPARED TO THOSE FROM TRADITIONAL GAIT ANALYSIS?

Luca Modenese [1,*]Hans Kainz [1]John Walsh [2]Lee Barber [3]David Lloyd [1]Christopher Carty [1]

[1]Griffith Health, Centre for Musculoskeletal Research, Southport, [2]Queensland Children's Gait Laboratory, [3]Queensland Cerebral Palsy and Rehabilitation Research Centre, Brisbane, Australia

Introduction and Objectives: Gait analysis is a valuable tool for clinical assessment of pediatric populations with movement disorders, in particular children affected by cerebral palsy, as it provides the therapist and the surgeon with parameters (joint angles, moments and powers) that provide insight into patient's dysfunctional walking mechanics and joint energy exchange. These parameters are typically calculated in clinical practice using a marker-based model developed more than two decades ago [1], while the current musculoskeletal (MSK) modeling tools, which could now be implemented, allow the use of personalized models from medical images, e.g. magnetic resonance imaging (MRI).

The aim of this investigation was to compare the joint angles, moments and powers derived from traditional gait analysis methods against corresponding outputs obtained by using a state-of-the-art personalized model in order to determine whether a more anatomically accurate model alters typical parameters used in clinical gait assessments.

Methods: MRIs for the entire lower limb were collected on three children with cerebral palsy with mean (SD) age: 10.7 (2.3) years, height: 1.41 (0.18) m, mass: 31.3 (6.15) kg. Three dimensional bone geometries and external skin surface were obtained through segmentation and used to generate unilateral subject specific MSK models usable in OpenSim [2] using NMSBuilder [3]. In these models, joint centres and axes were defined by fitting analytical shapes to the bone structures, e.g. a sphere to the femoral head. The external skin shell volume and bones were assigned appropriate densities [4] in order to calculate the inertial properties of each body segment. Virtual markers were located on the MSK model using MRI visible markers as reference. The resulting models and experimental marker and force plate data were finally used to run simulations to calculate joint angles (via inverse kinematics), joint moment (via inverse dynamic analysis) and joint power. Alternatively, the same marker trajectory and force plate data were processed using the Plug In Gait model [5] available through Vicon (Oxford). Shapes of the curves were compared using a correlation coefficient.

Results: The joint angles, moment and power obtained from the subject-specific models showed very good agreement with the output of the standard gait analysis in the sagittal plane (Figure and Table) The variables outside the sagittal plane of motion showed moderate agreement with a minimum for hip rotation for kinematics (R = 0.68, SD: 0.04) and knee adduction for kinetics (R = 0.59, SD: 0.33).

Figure:
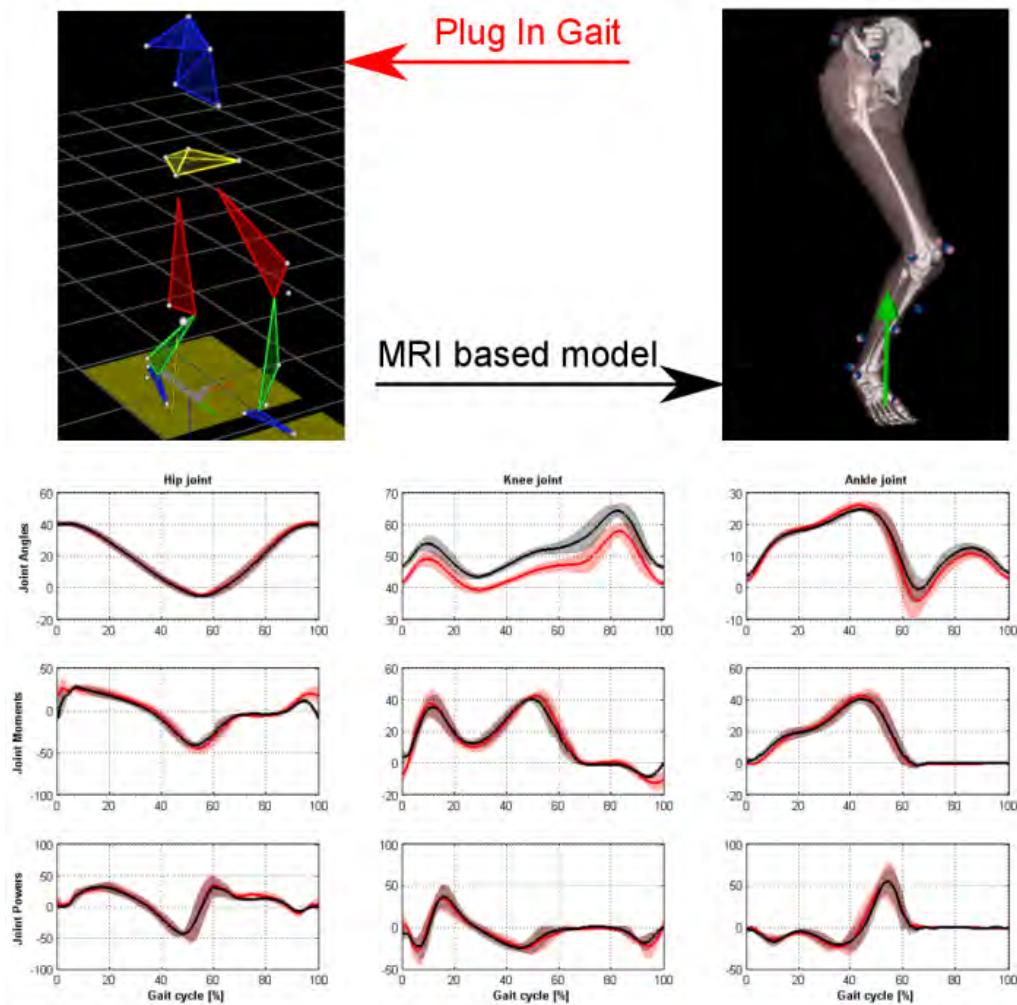
Caption: Comparison between the typical joint angles, moments and powers obtained from Plug in Gait and a musculoskeletal model generated from MRI scans in the sagittal plane. The models are visible in the upper part of the Figure.

Conclusion: We found general good agreement in clinical gait assessment outputs resulting from the current traditional model adopted in clinical practice against state of the art subject specific MSK models. The results suggest that it might not be necessary to build a personalized MSK model for the aim of a standard clinical gait assessment, as it generally produces similar outputs to the traditional gait model. However, these results also prove that there is no impediment in adopting the new subject specific MSK gait analysis methods. Importantly, developing and using these personalized MSK models is of paramount importance for introducing innovations into clinical gait analyses, such as quantitative analyses of muscle function (moment arms, muscle-tendon lengths, contributions of muscle-tendon forces to movement). Furthermore, these MSK models may enable the development of future applications like computer aided surgery and/or predictions of treatment outcome. These innovations have the potential to provide greater insight into the mechanisms causing dysfunctional walking mechanics in patient populations, thereby optimising treatments.

Table:

Considered parameters (sagittal plane)	Hip	Knee	Ankle
Joint angles	0.99 (0.001)	0.99 (0.003)	0.98(0.015)
Joint moments	0.80 (0.08)	0.89 (0.04)	0.99(0.008)
Power	0.61 (0.17)	0.80 (0.08)	0.96 (0.01)

Caption: Mean values and standard deviations (in brackets) of correlation coefficient calculated for joint kinematics, kinetics and power in the sagittal plane.

References: [1] Kadaba et al., J Orthop Res, 8:383-392 1990.

[2] Delp et al., IEEE Trans Biomed Eng, 54:940-50, 2007.

[3] Valente et al., PLoS ONE, 9:e112625, 2014.

[4] Dumas et al., IEEE Trans Biomed Eng, 52:1756-1763, 2005.

Disclosure of Interest: None Declared

SS-0014

BIOMECHANICAL-BASED CLASSIFICATION OF FLATFOOT: EFFECTIVENESS OF DYNAMIC ANGLES AND INDEXES FROM 3D KINEMATICS AND BAROPODOMETRY

Claudia Giacomozzi [1,*]Paolo Caravaggi [2]Giada Lullini [2]Lisa Berti [2]Alberto Leardini [2]

[1]Technology and Health, Istituto Superiore di Sanità, Rome, [2]Movement Analysis Laboratory, Istituto Ortopedico Rizzoli, Bologna, Italy

Introduction and Objectives: Clinical classification of flatfoot, based on morphology and function, may be effectively supported by objective measurements of footprints and joint motion during locomotion [1]. Motion analysis systems integrating 3D kinematics and baropodometry allow the detection of relevant functional parameters frequently used in the clinics to classify flatfeet: foot joints rotation, dynamic foot angles, footprint angles and morphometry, arch index, centre of pressure excursion index, etc. This study focusses on the analysis of these and ad-hoc defined parameters, their possible correlations and intra-subject variability. Main aim of the study is to identify the most appropriate and reliable subset of indicators which, in agreement with relevant clinical classifications, may deliver a deeper insight into the flatfoot functional classification.

Methods: 53 volunteers (25F/28M) were clinically screened and enrolled in the study. 3-5 consistent trials of level barefoot walking were acquired for each subject/foot – 358 trials in total - by using an integrated pressure-kinematics technique based on a VICON motion system, a NOVEL baropodometer, and the IORfoot model [2]; the model allowed the spatial registration between the two instruments [3]. 80 out of these 106 feet were clinically assessed by two expert physicians and classified as Cavus (C, high-arched, 9 feet), Normal (N, normal-arched, 25 feet), Level 1 Flatfoot (F1, 22 feet), or Level 2 Flatfoot (F2, more severe than F1, 24 feet). Preliminary analyses proved that most foot joint rotations during gait do not discriminate among the foot types; thus only range of motion of medial longitudinal arch (MLA) and its value at midstance were taken into account. The following baropodometric dynamic variables were calculated (Fig. 1A): Subarch Angle (SA); Modified Subarch Angle (SAM); Arch Index (AI); midfoot width w; Midfoot/Forefoot Ratio (RMFW), i.e. the ratio between w and A'B'; Centre of Pressure Excursion Index (CPEI). Median values and coefficients of variation (CV) were calculated for each foot over the available trials; ANOVA with Bonferroni correction was performed and correlation coefficients R^2 calculated over all median values and variables.

Results: The groups were found homogeneous with respect to age (31±15years); BMI of F2 (24.9±3.8kg/m^2) only differed from BMI in C (21.4±2.58kg/m^2). SA failed to be calculated in 19% of footprints, mostly in the C group where it remained undefined for all feet, and only discriminated F2 from the other groups. SAM (Fig 1B), AI, w and RMFW well discriminated the 4 groups, all statistically different one from the others (Table 1); SAM showed the lowest CVs (C: 0.11±0.08; N: 0.07±0.06; F1: 0.04±0.02; F2: 0.04±0.03). CPEI (Fig. 1C; Table 1) did not differ among the groups, and showed high variability within each group and high CV within each subject's trials (C: 0.72±0.52; N: 0.41±0.22; F1: 0.58±0.38; F2: 0.30±0.20). MLA range and MLA at midstance did not discriminate between F1 and F2, even though MLA at midstance had very low CV (C: 0.01±0.00; N: 0.01±0.01; F1: 0.02±0.01; F2: 0.01±0.01); they resulted statistically higher in F1 and F2 than in N and C, but with wide overlapping among the groups (Fig. 1D; Table 1). Interestingly, cluster analysis of MLA

range within each group revealed two well separated clusters, whose centroids (k1,k2) were comparable among the groups (C: 35.8, 15.3; N: 29.6, 14.6; F1: 30.5, 16.9; F2: 32.9, 16.9). Finally, SAM showed very high correlation coefficients (R^2) with AI (0.82), w (0.89), and RMFW (0.92), while CPEI, MLA range and MLA at midstance did not correlate with any variable.

Figure:
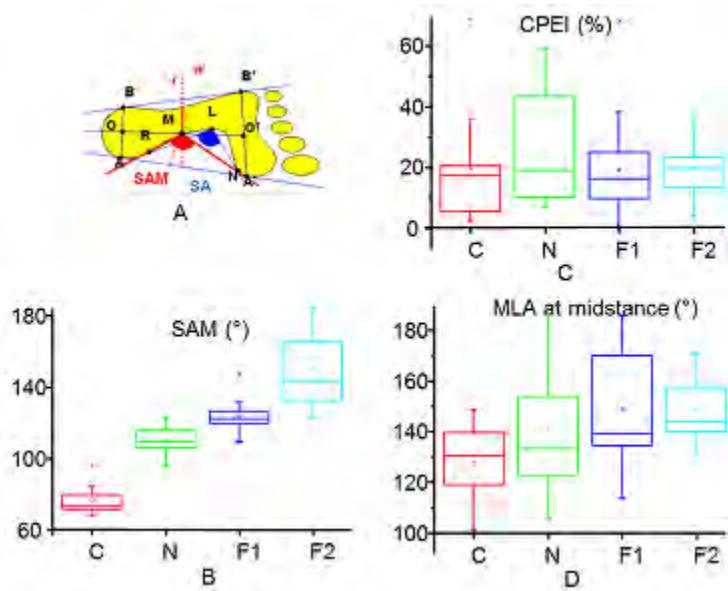
Caption: Figure 1. A: Novel dynamic footprint measures, plus ad-hoc definitions: M is the intersection point between medial midfoot and line r perpendicular to OO' through its midpoint; w is the midfoot width over r. B: SAM box chart. C: CPEI box chart. D: box chart of MLA at midstance (Legend: C: cavus foot; N: normal foot; F1: Level 1 Flatfoot; F2: Level 2 Flatfoot)

Conclusion: SAM, AI, w and RMFW seem to be the most appropriate dynamic footprint indexes for classifying flatfeet; SAM might be selected due to the lowest intra-subject CV. Within each group, MLA range seems to have high relevance to characterize the foot flexibility under load during walking.

Table: Table 1. Mean values ± standard deviations of the calculated parameters within each group

	SAM (°)	AI	w (cm)	RMFW	CPEI (%)	MLA range (°)	MLA at midstance (°)
C	77±9	0.08±0.03	0.1±0.4	0.01±0.04	20±2	18±9	127±16

				1		
N	110±8*	0.21±0.04*	2.2±0.9*	0.23±0.09*	125±16	19±9	141±22
F1	123±9*§	0.26±0.02*§	3.6±0.6*§	0.37±0.05*§	19±15	24±9	149±21*
F2	150±18*§ç	0.33±0.03*§ç	5.6±1.0*§ç	0.57±0.13*§ç	20±9	27±9*§	149±12*

Caption: ANOVA (p<0.05) with Bonferroni correction. *: stat. different from C; §: stat. different from N; ç: stat. different from F1.

References: [1] Razeghi M, Batt ME ,Gait and Posture 15: 282–291, 2002

[2] Leardini A, et al. Gait Posture 25(3):453-62, 2007

[3] Giacomozzi C., et al. J Biomech 47(11): 2654-9, 2014

Disclosure of Interest: None Declared

Motion Analysis

SS-0015

QUANTIFICATION OF HEAD AND TRUNK ACCELERATIONS DURING GAIT AS A PROXY MEASURE OF POSTURAL CONTROL DEFICITS IN PARKINSON'S DISEASE.

Christopher J. Buckley [1][2],*Brook Galna [3]Lynn Rochester [3]Claudia Mazzà [2][4]

[1]MRC-Arthritis Research UK Centre for Integrated Research into Musculoskeletal ageing (CIMA), [2]Mechanical engineering, University of Sheffield, Sheffield, [3]Institute of Neuroscience / Newcastle University Institute for Ageing, Newcastle University, Newcastle, [4]INSIGNEO Institute for in silico Medicine, University of Sheffield, Sheffield, United Kingdom

Introduction and Objectives: As a result of poor postural control when walking, people with Parkinson's disease (PD) are susceptible to falls [1]. Currently few measures exist that can quantify postural control during gait in people with PD. Lately, a selection of upper body variables have shown promise when used as sensitive measures of impaired postural control [2]. In particular, acceleration of the head relative to trunk acceleration is sensitive to the ageing process [3]. However, no investigations of gait in PD have examined head accelerations relative to trunk accelerations to quantify postural control. The objective of the current investigation was to explore whether accelerations of the head and trunk can provide a sensitive proxy measure of postural control in people with PD.

Methods: Thirteen people diagnosed with PD (70 ± 11 years, 18 to 54 months since diagnosis) and nineteen age-matched controls (70 ± 6 years) walked continuously for two minutes around a 25m circuit. Three inertial sensors (OPAL, ADPM Inc) were located on their pelvis (P), at their shoulder level (S) and on their head (H). Each sensor measured movement in the anteroposterior (AP), mediolateral (ML) and vertical (V) directions and were used to calculate: i) the magnitude of acceleration (root mean square); ii) step-to-step symmetry within a stride (Harmonic ratios normalised to gait speed) [2]; and iii) the ability to attenuate acceleration from inferior to superior located anatomical segments [3]. The ability to attenuate acceleration was measured using three coefficients designed to quantify the amount of acceleration attenuated from the P to the H (CPH), the P to the S (CPS) and the S to the H (CSH) [3]. A series of two-tailed paired *t*-tests was used to test the difference between groups and the level of significance was set at $p = 0.05$.

Results: No significant differences were found between the two groups in terms of anthropometric characteristics or spatiotemporal gait values. The magnitude of acceleration results showed no significant differences between the PD and control group with the exception of the head in the ML direction (PD 1.08 ± 0.29g vs Control 0.86 ± 0.21g, $p = 0.024$). For all sensor locations and directions, the Harmonic ratios did not show any significant differences between the two groups. In contrast, the coefficients of attenuation showed that people with PD typically did not attenuate accelerations through the trunk and neck as well as control participants (see table 1). This was most evident in the ML direction where significant differences were observed in all three coefficients (CPH: $p = 0.003$; CPS: $p = 0.009$; CSH: $p = 0.031$). In addition, a significant difference was also observed in the AP direction for CPS ($p = 0.002$).

Conclusion: People with PD walked with greater magnitude of ML head accelerations and demonstrated impaired attenuation of accelerations from the pelvis and the neck to the head. The magnitude of acceleration results must be interpreted with caution due to being gait speed and stride length dependent [4], which are both commonly effected by PD

[1]. Being speed dependent weakens the method in regards to clinical application, however, this weakness is not shared by the coefficient of attenuation [3]. Currently clinicians require objective quantifiable measures of postural control to supplement standard clinical assessments and conventional rating scales [4]. Between the three analysis techniques we present here, the coefficients of attenuation were the most sensitive to PD (particularly in the ML direction). Our findings indicate that when using inertial sensors, the inclusion of measuring the movement of the head provides unique information regarding postural control for those with PD. This information is simple to measure and is proposed to benefit clinicians seeking objective measures that are sensitive to early symptoms of PD.

Table:

	CPH %			CPS %			CSH %		
	PD	Control	p	PD	Control	p	PD	Control	p
AP	12.4±29.1	18.4±24.9		16.0±15.6	33.2±12.4	**	-0.4±19.5	4.3±11.2	
ML	0.1±34.7	33.8±21.3	**	5.5±24.5	27.9±18.6	**	-3.6±15.5	9.4±15.3	*
V	-3.6±9.8	-3.7±7.6		5.7±3.9	3.04±6.1		-5.4±8.5	-4.2±5.7	

Caption: Table 1. Mean (± SD) values of the attenuation coefficients (CPH, CPS and CSH) of the three acceleration components (AP = anterior/posterior, ML = medial/lateral; V = vertical), computed for the control and group with PD. p represents the t-test results whereby * = p < 0.05 and **= p < 0.005

References: [1] Cole et al., Mov Disord, 25:2369–78, 2010.

[2] Lowry et al., Mov Disord, 24:261–7, 2009.

[3] Mazzà et al., J Neuroeng Rehabil, 10:1–10, 2008.

[4] Latt et al., Exp Brain Res, 184:201–9, 2008.

Disclosure of Interest: None Declared

Motion Analysis

SS-0016

IN VIVO ACHILLES TENDON FORCES DURING CYCLING DERIVED FROM 3D ULTRASOUND-BASED MEASURES OF TENDON STRAIN

Taylor Dick [1,*] Allison Arnold [2] James Wakeling [1]

[1]Department of Biomedical Physiology and Kinesiology, Simon Fraser University, Burnaby, Canada, [2]Department of Organismic and Evolutionary Biology, Harvard University, Boston, United States

Introduction and Objectives: Traditional motion analysis provides limited insight into muscle and tendon forces during movement. This study used B-mode ultrasound, in combination with measured joint angles and scaled musculoskeletal models, to provide subject-specific estimates of *in vivo* Achilles tendon (AT) force.   Previous studies have used ultrasound images, tracked in 3D space, to estimate AT strains during walking, running, and jumping [1,2]. Our approach extends this work in one novel way. Specifically, we characterized AT stiffness on a subject-specific basis by recording subjects' ankle moments and AT strains during a series of isometric tests. We then used these data to estimate AT force during movement from *in vivo* measurements of tendon strain.

To demonstrate this approach, we report AT forces measured during cycling. Cycling offers a unique paradigm for studying AT mechanics. First, because the crank trajectory is constrained, joint angles and muscle-tendon unit (MTU) lengths of the gastrocnemius (MG, LG) and soleus (SOL) are also constrained. By varying crank load, subjects' ankle moments can be altered without imposing changes in MTU lengths. For this study, 10 competitive cyclists were tested at 4 different crank loads while pedaling at 80 rpm. Based on published EMG recordings (e.g., [3]) and on *in vivo* tendon force buckle data from one subject [4], we hypothesized that the cyclists' AT forces would increase systematically with crank load.

Methods: We coupled B-mode ultrasound with motion capture to estimate *in vivo* AT forces non-invasively during cycling and during a series of isometric ankle plantarflexion tests. Marker trajectories were tracked using an optical motion capture system. Joint angles and MTU lengths were calculated based on scaled musculoskeletal models [5] using *OpenSim* [6]. A 50 mm linear-array B-mode ultrasound probe was secured over the distal muscle-tendon junction (MTJ) of the MG and was tracked using rigid-body clusters of LEDs. AT lengths were calculated as the distance from a calcaneus marker to the 3D coordinates of the MG MTJ. Subject-specific AT force-strain curves were obtained from isometric tests using ultrasound to track the MTJ, markers to track both the ultrasound probe and the AT insertion, and a strain gauge to measure the net ankle torques generated by each of the subjects at ankle angles of -10° dorsiflexion, 0°, +10° plantarflexion, and +20° plantarflexion. AT strain during cycling was converted to AT force using each subject's force-strain relation. Subject-specific tendon slack lengths were calculated as the mean tendon length at 310° over all pedal cycles, based on examination of the AT length changes and on published data showing that this position in the pedal cycle precedes tendon loading across multiple pedalling conditions [4].

Results: Peak AT forces during cycling ranged from 1320 to 2160 N ± 400 N (mean± SD) and increased systematically with load (p<0.001; Fig. 1A/B). At the highest load, the peak AT forces represented, on average, 50 to 70 % of the

combined MG, LG, and SOL muscles' maximum isometric force-generating capacity, as estimated from the muscles' scaled volumes [7], the muscles' scaled optimal fiber lengths [5], and a specific tension of 20-30 N/cm². Peak AT forces occurred midway through the pedaling downstroke, at about 80°, which is consistent with the AT forces directly measured from one subject [4] and with patterns of EMG during cycling [3]. Peak AT strains during cycling were uncoupled from the MG MTU strains and ranged from 3 to 5 % across the different loads examined, measured at the MG MTJ.

Figure:
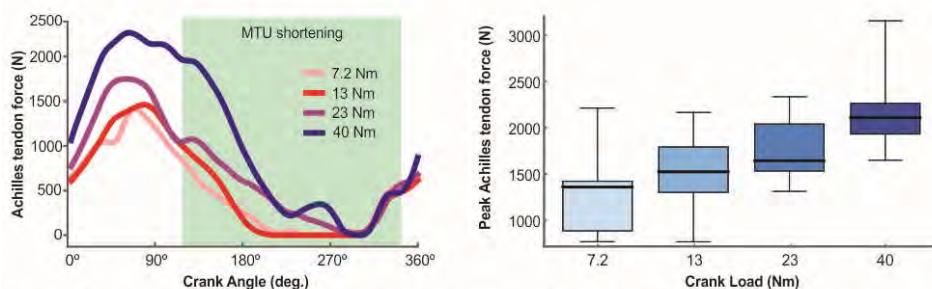
Fig 1. Evaluation of cyclists' *in vivo* AT forces using B-mode ultrasound and motion capture confirms that AT force increases with load. (A) Average AT force and MG MTU length over the pedal cycle for a representative subject cycling at 80 r.p.m and increasing crank loads. (B) Boxplots showing peak AT force for n=10 subjects cycling at

Conclusion: Our results are consistent with published data from a single subject in which AT force was measured using an implanted tendon buckle [8]; however, our results were obtained non-invasively using ultrasound and motion capture. These methods substantially augment the experimental tools available to study muscle-tendon dynamics during movement.

References: [1]Lichtwark and Wilson, 2005, J Exp Biol, 208(24), 4715-4725.

[2]Lichtwark et al., 2007, J Biomech, 40(1), 157-164.

[3]Wakeling and Horn, 2009, J Neurophysiol, 101(2), 843-854.

[4]Gregor et al., 1987, Int J Sports Med, 8(S1), S9-S14.

[5]Arnold et al., 2010, Ann Biomed Eng, 38(2), 269-279.

[6]Delp et al., 2007, IEEE Trans Bio Med Eng, 54(11), 1940-50.

[7]Handsfield et al., 2014, J Biomech, 47(3),631-638.

[8]Gregor et al. 1991, J Biomech, 24(5), 287-297

Disclosure of Interest: None Declared

Motion Analysis

SS-0017

WALKING WITH INCREASED TRUNK SWAY TO DECREASE AMBULATORY LOAD ON THE KNEE JOINT: IMPLICATIONS FOR THE LOWER BACK

Corina Nüesch [1,*] Dominik Laffer [1] Annegret Mündermann [1]

[1] Osteoarthritis Research Center, University Hospital Basel, Basel, Switzerland

Introduction and Objectives: The external knee adduction moment has been associated with the presence, severity and rate of progression of medial compartment knee osteoarthritis (OA) [1-3]. Different interventions to alter the load distribution at the knee joint during walking have been proposed. One such method – walking with increased medio-lateral trunk sway – has been shown to reduce the knee adduction moment in healthy subjects and in patients with knee OA [4,5]. However, it is unclear whether walking with an increased trunk sway alters and potentially increases the load at the lower back. Therefore, the objective of this study was to test the hypothesis that walking with increased trunk sway is associated with a reduction in the first peak knee adduction moment and an increase in the lateral bending moment at the lower back in healthy subjects.

Methods: Fifteen healthy subjects (seven males, eight females; age: 30.0 ± 8.7 years; weight: 70.5 ± 11.7 kg; height: 1.77 ± 0.08 m) participated in this study after providing informed consent. Exclusion criteria were knee pain and/or lower back pain. Three-dimensional full body kinematics and kinetics were measured using a 12-camera motion analysis system (Vicon, Oxford, UK) and two force plates (Kistler, Winterthur, Switzerland) with the full body PlugIn-Gait model [6,7]. For each subject, we collected six walking trials with normal trunk sway and six walking trials with increased medio-lateral trunk sway. Subjects walked with shoes and at their self-selected speed. For walking with increased trunk sway, subjects were instructed to increase the side-to-side motion of the upper body (with self-selected trunk-sway amplitude). For each waveform, we calculated the amplitude of the medio-lateral trunk sway, the first peak knee adduction moment, and the trunk bending moment at the time of the first peak knee adduction moment. Differences between the two walking conditions were analyzed using paired t-tests. Moreover, associations among these parameters within subjects were detected using linear regression analyses.

Results: When walking with increased trunk sway, medio-lateral trunk sway amplitude was increased six fold and the first peak knee adduction moment was reduced by 20% (Table 1). Furthermore, the mean waveform of the lateral trunk bending moment showed a prolonged greater moment that was twice as high at the time of the peak knee adduction moment than during normal walking (Figure 1). The coefficients of determination between the trunk sway amplitude and the peak knee adduction moment or the trunk bending moment respectively, were greater than 0.5 in more than two thirds of the subjects.

Figure:

Knee ab-/adduction moment

Medio-lateral trunk bending moment
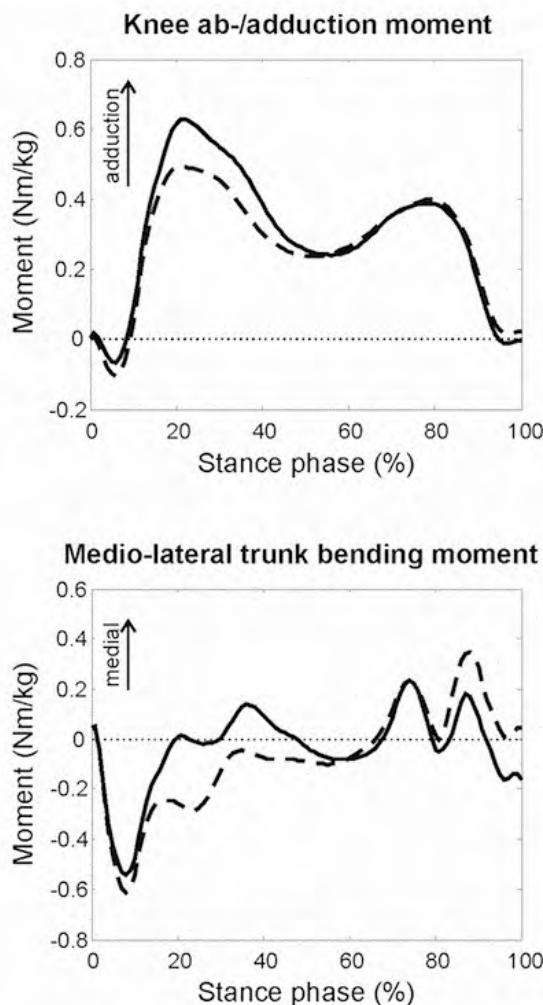
Caption: Figure 1: Mean waveforms of the knee adduction moment and the lateral trunk bending moment of the stance phase for normal walking (solid line) and walking with increased trunk sway (dashed line)

Conclusion: Similar to previous studies [4,5], walking with increased medio-lateral trunk sway decreased the first peak of the knee adduction moment compared to normal walking. At the same time however, the external trunk bending moment increased in magnitude and was still higher at the time of the first peak knee adduction moment. The altered load pattern in the first part of the stance phase together with the prolonged occurrence of the medial trunk bending moment (negative) could indicate a higher load of the lower back. To counteract these greater resultant moments, greater activation of trunk stabilizing muscles might be required and fatigue of these muscles might occur earlier. These changes might contribute to the development of low back pain or increase already existing low back pain and should be monitored in gait retraining programs with increased medio-lateral trunk sway to reduce the load on the knee joint.

Table:

	Walking	Trunk Sway	P Value
Medio-lateral trunk sway amplitude (°)	1.7 (0.7)	10.4 (3.2)	<0.001
First peak knee adduction moment (Nm/kg)	0.68 (0.15)	0.55 (0.13)	<0.001
Trunk bending moment at time of first peak knee adduction moment (Nm/kg)	0.08 (0.16)	-0.14 (0.11)	<0.001

Caption: Table 1: Mean (standard deviation) of kinematic and kinetic parameters during the two walking conditions

References: [1] Hurwitz et al., J Orthop Res, 20: 101-107, 2002.

[2] Mündermann et al., Arthritis Rheum, 50: 1172-1178, 2004.

[3] Chehab et al., Osteoarthritis Cartilage, 22: 1833-1839, 2014.

[4] Mündermann et al., J Biomech, 41: 165-170, 2008.

[5] Simic et al., Arthritis Care Res, 64: 1545-1553, 2012.

[6] Kadaba et al., J Orthop Res, 8: 383-392, 1990.

[7] Gutierrez et al., Gait Posture, 18: 37-46, 2003.

Disclosure of Interest: None Declared

INTERPRETATION OF TIBIO-FEMORAL KINEMATICS CRITICALLY DEPENDS UPON THE KINEMATIC ANALYSIS APPROACH

Maryam Hajizadeh [1][2],[*] Pascal Schütz [2] Renate List [2] Heide Boeth [3] Rainald Ehrig [4] Michael Freeman [5] William R Taylor [2]

[1] Mechanical Engineering Department, Sahand University of Technology, Tabriz, Iran, Islamic Republic Of, [2] Institute for Biomechanics, ETH Zurich, Zurich, Switzerland, [3] Julius Wolff Institute, Charité – Universitätsmedizin Berlin, [4] Zuse Institute Berlin (ZIB), Berlin, Germany, [5] ETH Zurich, Zurich, Switzerland

Introduction and Objectives: The analysis of tibio-femoral kinematics is important for understanding the functionality of the knee after total knee arthroplasty (TKA) [1] and the calculation of internal knee joint loading [2]. The most commonly used approaches for kinematic analysis of the knee joint are the geometrical knee axis [3-5], contact nearest point axis [3], and functional axis [1]. Controversial results on femoral anterio-posterior translation (APT) as well as the location of the center of rotation (CoR) in the transverse plane might be explained by the usage of different approaches for the kinematic analyses. Here, any lever arm of the analysis points around the actual "real" axis of rotation would result in an artificial APT and CoR, and therefore in an error in the interpretation of the joint kinematics. The objective of this study was therefore to assess the sensitivity of different kinematic analysis techniques used in the literature on the calculation of femoral APT as well as on the location of the CoR in the transverse plane.

Methods: A subject-independent set of tibiofemoral kinematic data was generated based on the pose data of the tibial and the femoral components of a TKA during a complete gait cycle of level walking. The original data was assessed *in vivo* using moving video fluoroscopy and simultaneous skin marker measurements [4], and then filtered with a moving average approach. Four different approaches were used to assess the joint kinematics: geometric center axis (GCA)[4], transepicondylar axis (TEA)[5], contact nearest point axis (CNPA)[3], and symmetrical axis of rotation approach (SARA) [6]. All these axes were calculated for the complete gait cycle of level walking. The GCA was defined by the position and orientation of the connecting line between the centers of spheres fitted to the medial and lateral femoral condyles. The TEA was approximated by the connecting line between the medial and lateral femoral epicondylar skin markers of a standing trial. The CNPA was created based on finding two points with the least femoro-tibial distance for each of the condyles for each frame for the entire gait cycle. Finally, the SARA local femoral axis was defined by a combination of chair-sit-to-stand and chair-stand-to-sit as a basic motion task for knee flexion/extension movement (SARA). Among all these definitions, only CNPA was an instantaneous axis, while all the others were fixed femoral component axes, being transformed to the tibial coordinate system during each frame. The two points defined by the intersection of the respective axes with the sagittal planes on the medial and lateral extremes of the tibial component were used for comparing the outcomes of analysis using the different techniques. Furthermore, CoRs were calculated as the linear least squared intersection of all axes in the transverse plane [7].

Results: The choice of the kinematic analysis technique used to assess the tibio-femoral motion showed a strong influence on the APT parameters, as well as the CoRs determined for the different time phases of the gait cycle (Figure

1). Furthermore, the ranges of motion (RoM) for APT were higher on the lateral sides for the GCA, TEA and SARA approaches, while CNPA produced a higher RoM on the medial side (Table 1).

Figure:
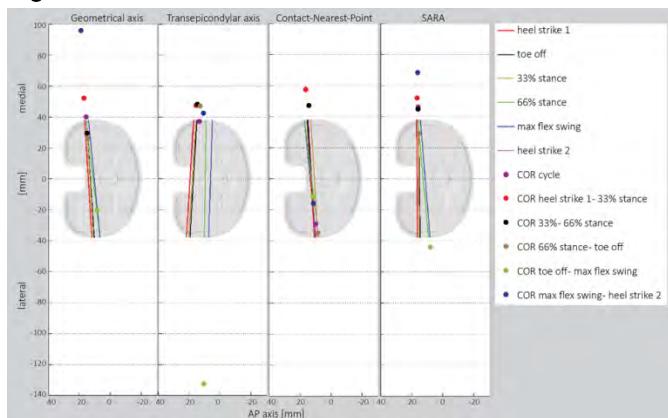
Caption: Figure 1: Knee AoR and CoR for all kinematic analysis techniques. Axes are shown at different time points within the gait cycle, while CoRs are presented for phases of cycle.

Conclusion: Even though only one single cycle of gait has been assessed, clear differences between kinematic analysis techniques in both APT and CoR were observed, demonstrating that interpretation of joint kinematics is critically dependent upon the analysis technique used. Importantly, the location of the CoR in the transverse plane shows large variance within the gait cycle for most approaches. Furthermore, not only the representation of each phase of the cycle were different between approaches, but also the average CoR for the whole gait cycle differed, possibly explaining the acute differences in tibio-femoral kinematics presented in the literature. For consistent interpretation of knee kinematics, and therefore the ability to compare the results of different studies, a clear consensus is required in the field on how to standardise analyses of tibio-femoral kinematics.

Table:

	RoM-Medial APT [mm]	RoM-Lateral APT [mm]
GCA	3.35	5.73
TEA	12.58	14.76
CNPA	5.90	3.20
SARA	3.27	8.45

Caption: Table 1: RoM for medial and lateral APT

References: 1.	Asano et al., The Journal of arthroplasty, 20(8): 1060-1067, 2005.

2.	Zheng et al., Journal of biomechanics, 47(12): 3217-3221, 2014.

3.	Hamai et al., Journal of Orthopaedic Research, 27(12): 1555-1561, 2009.

4.	Schütz P. et al., *3D AHM.* 2014. Lausanne, Switzerland

5.	Most et al., Journal of biomechanics, 37(11): 1743-1748, 2004.

6.	Ehrig et al., Journal of biomechanics, 40(10): 2150-2157, 2007.

7.	Ehrig et al., Journal of biomechanics, 39(15): 2798-2809, 2006.

Disclosure of Interest: None Declared

Feet and Footwear

SS-0019

COMPUTATIONAL SIMULATIONS AND STRESS DISTRIBUTIONS OF LANDING DURING BAREFOOT RUNNING USING FOREFOOT STRIKE PATTERN

Yu Hua Li [1 2,*]Kah Fai Leong [1 2]Yao Dong Gu [3]

[1]Nanyang Technological University, School of Mechanical and Aerospace Engineering, [2]Nanyang Technological University, Institute for Sports Research, Singapore, Singapore, [3]Ningbo University, Faculty of Sports Science, Ningbo, China

Introduction and Objectives: Barefoot running, also known as minimalism or natural running, is running without shoes or running in thin-soled shoes or 'barefoot running' shoes. Barefoot running has become very popular in last few years amongst more and more recreational as well as competitive athletes. Barefoot running encourages forefoot strike (FFS) pattern whereas majority of runners in shod running tend to use rearfoot strike (RFS) pattern. In fact, different strike patterns during running may have effects on the forces acting on the Achilles tendon, the loading rate, the magnitude of impact peak and so on. These may be the potential factors that can cause injuries in foot and lower extremity. The purpose of this study is to determine the stresses concentration and distributions in the foot and lower extremity of landing during barefoot running using FFS pattern.

Methods: In this study, a detailed three dimensional (3D) finite element (FE) model has been developed based on the manganic resonance images (MRI). 2D images were converted to 3D images in ScanIP to obtain the boundaries of the surfaces of the bones and soft tissue. These 3D images were then smoothed in Geomagics. The smoothed surfaces were then processed in SolidWorks to obtain the solid models of the foot and ankle. Finally, the FE model was developed in Abaqus (Version 6.13). Then the model was validated through comparing the current predicted plantar pressure distributions with the data collected from experiments. The current predictions showed good agreement with the experimental measurement. After validating, the model was then used to investigate the stresses concentration and distributions of landing during barefoot running using FFS pattern.

Results: The simulation results showed that the peak Von Mises stress occurred in the region of Achilles tendon, and the stress values increased with the increasing load applied to the supporting plate. The metatarsals in the forefoot region also sustained higher Von Mises stresses compared with other bone components especially the third and fifth metatarsals. The reason may be the load applied in Achilles tendon increased when landing during barefoot running using FFS pattern compared with RFS pattern.

Figure:
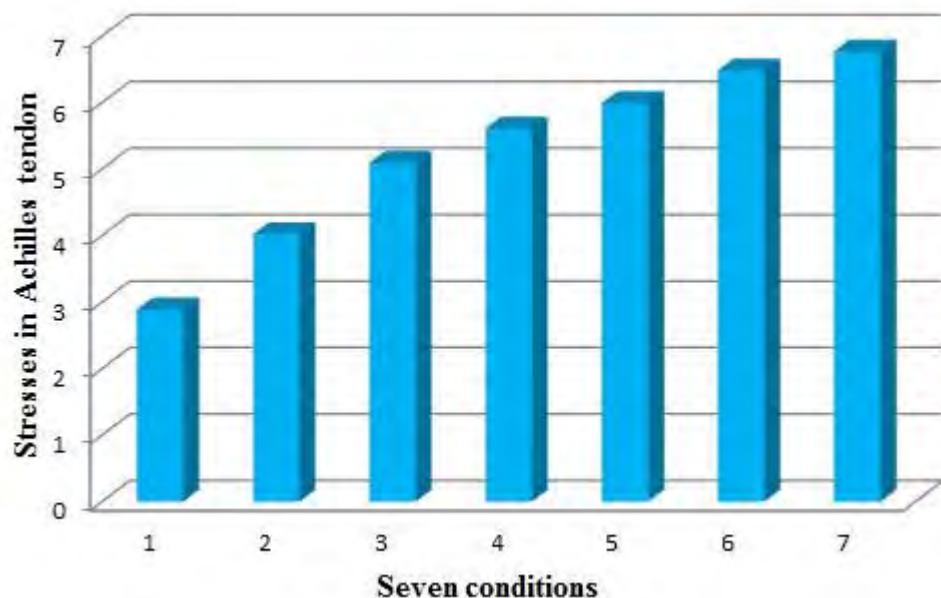
Caption: Figure 1. Peak Von Mises stresses in Achilles tendon during seven conditions

Conclusion: In summary, this study developed a detailed 3D FE model of human foot and ankle to investigate the stresses concentration and distributions of landing during barefoot running using FFS pattern. The predicted results showed good agreement with the experimental measurements. The peak Von Mises stress was found to be in the region of Achilles tendon, and these results are in good agreement with reported scientific literatures. Through the simulation results, the internal stresses and the mechanical responses to facilitate injury prevention during barefoot running can be further investigated.

References: [1] Almonroeder et al., Annals of biomedical engineering, 41:1758-66, 2013.

[2] Rothschild, The Journal of Strength & Conditioning Research, 26:2021-6, 2012.

[3] Shih et al., Gait Posture, 38:490-4, 2013.

[4] Lieberman et al., Nature, 463:531-5, 2010.

[5] Altman et al., Current sports medicine reports, 11:244-50, 2012.

[6] Rooney et al., Journal of biomechanics, 46:2201-6, 2013.

[7] Gu et al., International Orthopaedics (SICOT), 34:669-76, 2010.

[8] Giuliani et al., Orthopedics, 34:550, 2011.

Disclosure of Interest: None Declared

SS-0020

THREE-DIMENSIONAL INTERSEGMENT MOTION OF THE PAEDIATRIC FOOT DURING GAIT: ASSOCIATIONS WITH OBESITY

Ryan Mahaffey [1],*Stewart Morrison [1]Paul Bassett [2]Wendy Drechsler [1]Mary Cramp [3]

[1]Health, Sport & Bioscience, University of East London, London, [2]Statsconsultancy Ltd, Amersham , [3]Department of Allied Health Professions, University of West England, Bristol, United Kingdom

Introduction and Objectives: Childhood obesity has emerged as a major public health concern with a high level of health burden [1].   Specifically, childhood obesity has been reported to impact on the biomechanical characteristics of the musculoskeletal system [2] and is commonly associated with a pronated foot type and pes planus with implications for long-term dysfunction [3,4]. Previous research to examine relationships between childhood obesity and the foot have focused on static or two-dimensional dynamic analysis [5,6,7]. Limited information has been reported on three-dimensional (3D) dynamic intersegment foot motion in obese children [8,9]. Therefore, the purpose of this study was to explore the relationships between 3D intersegment angular foot motion during gait and obesity in boys age 7 to 11.

Methods: Fat mass (obesity) was measured in fifty-five boys (age 9.55 ± 1.18 years) using air displacement plethysmography. Gait analysis was conducted on the right foot of each participant using the 3DFoot model [10] to capture 3D angular motion of the shank, calcaneus, midfoot and metatarsals. Principal component analysis (PCA) was employed to reduce the multidimensional nature of 3D intersegment foot motion to components from which regression scores were calculated based on variation in the waveform data. Multiple linear regression analysis determined the relationships between obesity and the regression scores from PCA (representing 3D intersegment foot motion) whilst accounting for potential anthropometric and gait related confounding factors.   Second order polynomials were fitted to each predictor variable to account for curvilinear relationships. Only those regression scores that were significantly (p<.05) associated with obesity are presented in the results.

Results: PCA determined eight shank-calcaneus, three calcaneus-midfoot, and four midfoot-metatarsal components for multiple linear regression analysis. Table 1 presents the significant regression analaysis findings between components (representing 3D intersegment foot motion during gait) with obesity and confounding variables. Higher fat mass (and shorter stance phase duration) predicted greater plantarflexion of the calcaneus during the first half and end of stance and the end of swing. Greater abduction of the calcaneus throughout stance and swing was also predicted by greater fat mass. Finally, at the midfoot, higher fat mass predicted greater dorsiflexion and eversion (confounded with greater body mass index, height and step length) throughout the gait cycle.

Figure:
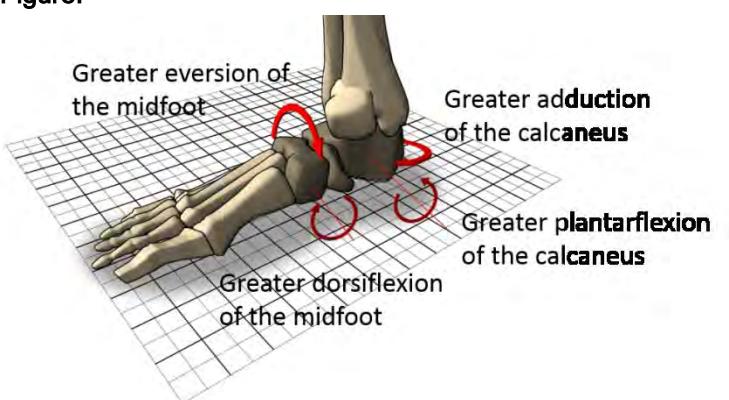
Caption: Figure 1. Representation of foot segment angular motion during gait associated with greater obesity.

Conclusion: The results demonstrated significant relationships between obesity and shank-calcaneus and calcaneus-midfoot motion during walking, summarised in Figure 1. The finding of greater calcaneus abduction concurs with previous video-based reports of externally rotated feet in obese children which may be a strategy employed to aid stability [7]. Calcaneal plantarflexion and midfoot dorsiflexion in boys with higher fat mass mirror bone alignment found in pes planus from static radiographic research [5]. Midfoot eversion in boys with higher fat mass is consistent with greater plantar pressures under the medial longitudinal arch in obese children [11]. Altered rearfoot and midfoot motion in children with greater body fat are consistent with the view that obesity affects the structural integrity and function of the foot during walking. Further research is required to understand the implications for structural dysfunction of the foot in obese children.

Table:

Dependent variable	Predictor variables β (Std Error)							Model R^2
	$Obesity_{linear}$	$Obesity_{quad}$	$BMI ZScore_{linear}$	$BMI ZScore_{quad}$	$Height_{linear}$	$Step distance_{linear}$	$Stance phase duration_{linear}$	
Shank-Calcaneus: sagittal plane								
PC1	-.04 (.02)	-	-	-	-	-	-.50 (.10)	.32
PC2	-.03 (.02)	-	-	-	-	-	-	.07
PC3	-.04 (.02)	-	-	-	-	-	-	.10
Shank-Calcaneus: transverse plane								
PC1	.21 (.09)	.01 (.00)	-	-	-	-	-	.11

PC2	.03 (.01)	-	-	-	-	-	-	.07
Calcaneus-Midfoot: sagittal plane								
PC1	.04 (.01)	-	-	-	-	-	-	.13
Calcaneus-Midfoot: frontal plane								
PC1	.23 (.10)	.01 (.00)	.38 (.13)	.20 (.06)	.06 (.02)	.01 (.00)	-	.33

Caption: Table 1. Summary of multiple regression analysis of regression score from PCA with predictor variables (Only significant results are shown)

References:

1. Ebbeling, et al. Lancet, 360/9331: 473-482, 2002.
2. Shultz, et al. Clin Biomech, 29/7: 835-38, 2014
3. Morrison, et al. J Am Podiatr Med Assoc, 97/5: 366-370, 2007.
4. Shultz, et al. J Am Podiatr Med Assoc, 102/1: 5-12, 2012.
5. Adoracion Villarroya, et al. Eur J Pediatr, 168/5: 559-567, 2009.
6. Cousins, et al, J Foot Ankle Res, 6/1: 36, 2013.
7. Hills, et al. Arch Phys Med Rehabil, 72/6: 403-407, 1991.
8. McMillan, et al. Pediatr Phys Ther, 21/2: 187-193, 2009.
9. McMillan, et al. Gait Posture, 32/2: 263-268, 2010.
10. Leardini, et al. Gait Posture, 25/3, 453-462, 2007.
11. Mickle, et al. Int J Pediatr Obes, 1/3: 183-188, 2006.

SS-0021

THE INFLUENCE OF MINIMALIST FOOTWEAR ON METATARSAL BONE STRAINS DURING RUNNING

Colin Firminger [1,*] Matthieu B Trudeau [2] Benno M Nigg [2] W Brent Edwards [2]

[1] Biomedical Engineering, [2] Kinesiology, University of Calgary, Calgary, Canada

Introduction and Objectives: Strain magnitude plays a fundamental role in the development of metatarsal stress fracture [1] and footwear type has been identified as a potential factor affecting metatarsal strain during running [2]. Minimalist footwear, characterized by a less cushioned and more flexible midsole, is becoming increasingly popular among runners. Our purpose was to quantify the effects of a traditional running shoe and a minimalist running shoe on peak metatarsal bone strain.

Methods: Forty-three participants (20 females: age 28.0 ± 9.5 yrs; height 165.5 ± 5.1 cm; mass 59.7 ± 7.3 kg; 23 males: age 31.0 ± 8.7 yrs; height 177.3 ± 6.3 cm; mass 76.7 ± 8.3 kg) ran 10 trials overground at 3.3 ± 0.5 m/s wearing either a traditional running shoe (i.e., control shoe) or a minimalist running shoe; both shoes are commercially available. Foot kinematics were collected on the left leg and insole plantar pressure data were collected on the right leg concurrently at 240 Hz and 200 Hz, respectively; symmetric gait was assumed. Kinematic data were used to determine metatarsal segment angles throughout stance. Insole pressure data were separated into specific regions of the forefoot in order to capture the forces acting underneath the five metatarsal and five toe regions. Metatarsal angles and forces served as inputs to a musculoskeletal model [3] of the metatarsophalangeal joints to quantify axial forces and bending moments at the mid-diaphysis of each metatarsal. The model assumed that: **1)** each metatarsal was rigidly attached at its base; **2)** axial forces acted through the neutral axis of the metatarsal shaft; **3)** no moment transfer occurred through the metatarsophalangeal joint; **4)** each toe was a single phalange; **5)** plantar muscles inserted inferiorly at the midpoint of the phalanges. Normal stress produced by the sum of axial force and bending moment at the mid-diaphysis was found using standard beam theory. Idealized cross-sectional bone geometry were allometrically scaled to each participant's height and weight. Metatarsal strains were calculated from stresses using Hooke's law, assuming an elastic modulus of 17.0 GPa for cortical bone. Differences in peak strains between shoe conditions were compared using Student's paired t-tests ($\alpha = 0.05$).

Results: Peak strains were significantly greater for all metatarsal bones in the minimalist shoe compared to the control shoe ($p < 0.001$); percent changes from control ranged from 6.3-23.0%, depending on bone (Figure 1). Mean absolute magnitudes in peak strain ranged from 1511-5793 µε for the control shoe and from 1647-6895 µε for the minimalist shoe (Table 1). For both shoe conditions, peak strains were consistently highest at the second metatarsal and lowest at the first metatarsal.

Figure:
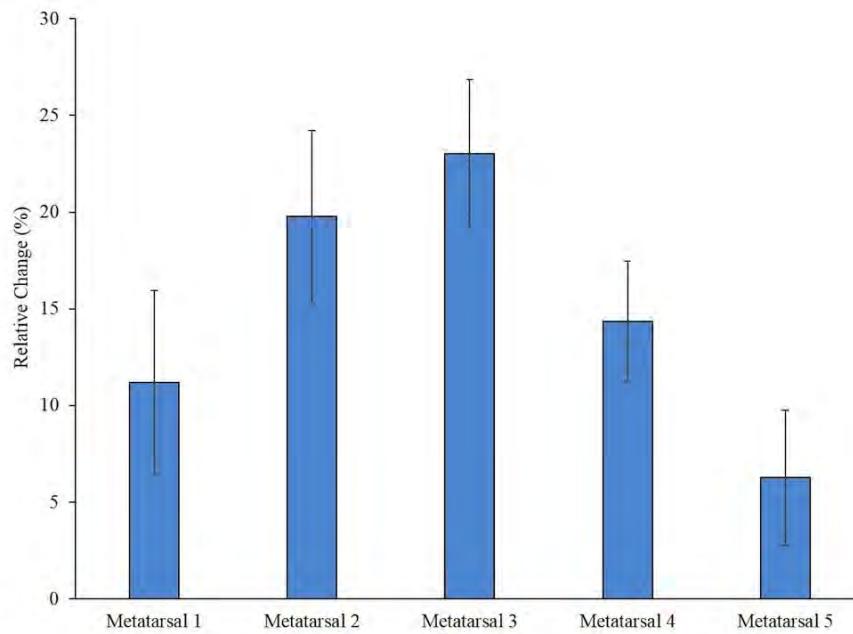
Caption: Figure 1: Percent change in subject-average peak metatarsal strains from control to minimalist shoe (± 95% confidence interval). All changes were significant at p ≤ 0.001.

Conclusion: Our findings suggest that metatarsal bone strains may be higher when running in minimalist shoes compared to traditional shoes, but whether these increased strains are associated with an increased risk of stress fracture remains unknown. Apart from the relatively high second metatarsal strains (≈6000-7000 με), the strain magnitudes calculated herein agree well with experimental strain gauge data [4]; our future work will attempt to determine the source of this discrepancy. Ultimately, this study provides valuable information beyond traditional biomechanical measures that may help to decrease metatarsal bone strain and stress fracture risk through the modification of footwear properties.

Table:

Shoe	Metatarsal 1 Strain (με)	Metatarsal 2 Strain (με)	Metatarsal 3 Strain (με)	Metatarsal 4 Strain (με)	Metatarsal 5 Strain (με)
Control	1511 (157)	5793 (501)	3431 (257)	3169 (271)	2117 (217)
Minimalist	1646 (154)	6895 (599)	4224 (356)	3622 (329)	2255 (245)

Caption: Table 1: Subject-average peak metatarsal strains (± 95% confidence interval) for control and minimalist shoes

References: [1]   Harrast et al., Clin. Sports Med., 29: 399–416, 2010.

[2]   Bergstra et al., J. Sci. Med. Sport, 2014.

[3]   Gross et al., Am. J. Sports Med., 17: 669–674, 1989.

[4]   Milgrom et al. (Ed.). Musculoskeletal Fatigue and Stress Fractures, CRC Press LLC, 2001.

Disclosure of Interest: None Declared

BODY MASS INDEX, HBA1C, AGE AND DURATION OF DIABETES AS RISK FACTORS FOR DIABETIC FOOT ULCER

Taeyong Lee [1,*]Jee Chin Teoh [2]

[1]Department of Medical Biotechnology, Dongguk University, Seoul, Korea, Republic Of, [2]Department of Biomedical Engineering, National University of Singapore, Singapore, Singapore

Introduction and Objectives: The lifetime risk to develop foot ulcers in the diabetes population is approximately 25%. 20% of them require major lower limb amputation. The mortal rate is reported to be 10% at time of amputation and 70% within 5 years. The statistics clearly explain the high fatality of diabetic foot ulcer but the early diagnosis of diabetic foot is not yet properly attended.

Diabetic foot risk is usually graded based on neurological assessment such as mono-filaments and vibration perception which are predictive methods of peripheral neuropathy. However, loss of sensation is not the direct reason. In fact, abnormally stiffened tissue that fails to withstand the impact force is a more straightforward explanation of foot ulceration. Therefore it is of utmost importance to quantify the plantar tissue stiffness which can provide the useful information to prevent foot ulcer. The objective of this study is to evaluate the relationship between plantar tissue stiffness and several parameters like age, diabetes duration (years of DM), body mass index (BMI) and HbA1c level. Understanding of these associations is certainly helpful in assigning levels of risk and in customizing foot care plan.

Methods: One hundred diabetes patients were recruited with approval from the NUS Institutional Review Board (IRB). The localized response of plantar soft tissue at hallux, 2nd sub metatarsal head (MTH) pad and heel pad were measured using the indentation system which consisted of a stylus driven by a stepper motor. One end of the stylus indented the tissue and the tissue response was quantified by the force sensor located at the other end.

Results: Two out of the four factors (BMI, HbA1c, Age and years of DM) were plotted against the plantar soft tissue stiffness. As the plantar tissue stiffness increases, the colour scale will move closer to the red spectrum. Selected factors were plotted to evaluate the contribution of each factor combination to describe the plantar soft tissue response. As shown in Fig.1A to 1F, it can be deduced that HbA1c level have a more influential role in altering the tissue stiffness in 2nd sub-MTH. The higher stiffness values, which are represented by the red spectrums, are usually observed in high BMI and high HbA1c score. Meanwhile, lower stiffness values denoted by blue spectrums are found in low BMI and low HbA1c level. Similar results are also found in hallux and heel pad. HbA1c level measures the average level of blood sugar over a period of weeks or month. Prolonged exposure to high blood glucose brings about pathological changes by enhancing reactions between reducing glucose and cellular protein that increases the formation of advanced glycation end products (AGEs) [1]. Accumulation of these compounds decreases the elasticity of tissue by the increased intermolecular cross linking and adversely modified side-chains [2]. Clinical studies have shown the stiffer plantar tissue in diabetic patients as compared to their age-matched control [6, 12]. There has been a large cohort of data showing glycated collagen to be consistent with the HbA1c level [11].

BMI also plays a key role in increasing the plantar soft tissue stiffness as shown in Fig. 1A to 1C whereby red spectrums (high tissue stiffness) are concentrated at high BMI regions. This may be explained by the strong relationship between

high BMI and DM [9, 4, 3, 7,5, 10]. It is also postulated that the loss in weight and BMI effectively improve glycemic control [8]. In other words, high BMI may cause the increase in HbA1c which may undesirably stiffen the tissue.

The results suggested that patients with BMI higher than 25kgm^{-2} or HbA1c >9%, as observed from Fig. 1A to 1F, are likely to have stiffened plantar tissue that required special attention prevent the occurrence of foot ulcer.

On the other hand, age and years of DM did not affect the tissue response much as the color spectrum obtained is not consistent and hence not conclusive. Even in young patients with short duration of diabetes, the tissue stiffness may still be adversely increased as long as the HbA1c level is high (Fig 1F).

Figure:
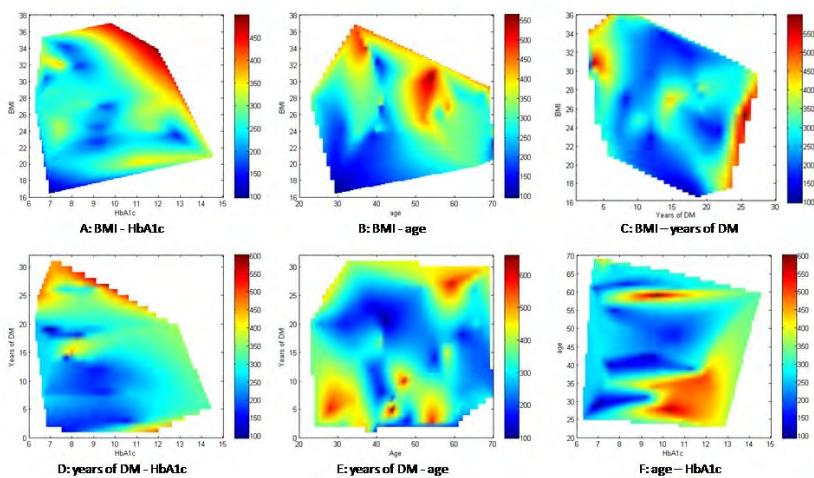
Caption: Figure 1: Triadic relationship of selected factor combination of 2ndsub-MTH pad. The color scale denotes the tissue stiffness in terms of stiffness variable, K (N/mm).

Conclusion: The results recommended that in the effort to design the foot care plan, patient's HbA1c score and BMI should be paid more attention. Special consideration should be given to the high risk diabetic foot group in high HbA1c score above 9% or BMI >25 kgm^{-2}.

References: [1] Ahmed et al. Diabetes, Obesity and Metabolism, 9: 233-245, 2007

[2] Bailey et al. Mechanisms of Ageing and Development, 122: 735-755, 2001

[3] Chan et al. Diabetes Care, 17: 961-969, 1994

[4] Colditz et al. American Journal of Epidemiology, 132: 501-513, 1990

[5] Gefen et al. Clinical Biomech, 16: 921-925, 2001

[6] Heilbronn et al. Diabetes Care, 22: 889-895, 1999

[7] Monnier et al. Diabetes, 48: 870-880, 1999

[8] Zheng et al. Ultrasound in Med and Biol, 26: 451-456, 2000

Disclosure of Interest: None Declared

REQUIRED FIDELITY OF FOREFOOT GEOMETRY REPRESENTATION FOR PRACTICAL AND ACCURATE PREDICTION OF PLANTAR PRESSURES USING FINITE ELEMENT ANALYSIS

Scott Telfer [1] [2],*Ahmet Erdemir [3]James Woodburn [2]Peter Cavanagh [1]

[1]Department of Orthopaedics and Sports Medicine, University of Washington, Seattle, United States, [2]Institute for Applied Health Research, Glasgow Caledonian University, Glasgow, United Kingdom, [3]Department of Biomedical Engineering, Cleveland Clinic, Cleveland, United States

Introduction and Objectives: Integration of patient-specific biomechanical measurements into the design of therapeutic footwear has been shown to improve clinical outcomes in patients with diabetic foot disease. The added use of computational modelling intended to optimise intervention design may help to build on these advances. However, at present, the time and labour required to generate personalised models of foot anatomy and conduct simulations restrict their routine clinical utility. We previously presented a simplified finite element (FE) model of the forefoot that was based on basic geometric shapes to represent both the metatarsals and bulk soft tissues [1]. This approach demonstrated the feasibility of a rapid model development and simulation workflow that can inform clinical decision making with regards to the prescription of footwear design. The aim of the present study is to investigate the level of geometric fidelity required to adequately predict plantar pressures under the metatarsal heads (MTHs). In addition, model development times were investigated to evaluate the feasibility of the proposed models for routine clinical use.

Methods: Dynamic plantar pressure measurements, computed tomography (CT) scans, and 3D surface scans of the right foot were obtained from 8 volunteers.

In total, four FE model designs (one authentically representing detailed anatomy (GEOM) and three simplified) representing the forefoot with varying levels of fidelity were tested for all participants (Figure 1). The GEOM model was used as the reference that the simplified models were compared against, and consisted of geometrically accurate metatarsal and bulk soft tissue components segmented from the CT data. In simplified model 1 (SM1), the metatarsals were represented as spheres scaled to the measured MTH diameters and cylinders scaled to the measured lengths of the bone [1]. The bulk soft tissue was represented as a modified rectangular block. SM2 used the same soft tissue representation, however the MTHs of the lesser metatarsals were modelled as a cylinders standing on their curved surface with width and diameter defined by the width of the MTH geometry and a circle fitted to the sagittal plane view of the MTH respectively. The sesamoids were also represented in this model. SM3 used the same metatarsal design as SM2 but the soft tissue surface geometry was taken from 3D surface scans of the foot.

All models were assembled and run in the finite element analysis package Abaqus/Standard (V6.10; Simulia, Providence, RI) using the implicit static solver. Simulations were performed for the instance of peak forefoot loading [1], and the same loading was applied for each participant for barefoot, shod and shod with insole conditions.

The predicted peak pressure across a mask on the plantar surface of the soft tissue component below each MTH was used as the primary basis for comparisons between models. Absolute differences between the anatomical and simplified

models were compared using a repeated measures analysis of variance (α=0.05) followed by post-hoc pairwise t-tests (adjusted for multiple comparisons).

Results: The best performing simplified model design was found to be the SM3 design, which gave mean differences of 13.3kPa (SD 13.4), 12.52kPa (SD 11.9) and 9.6kPa (SD 9.3) for barefoot, shod and insole conditions respectively when compared to the GEOM model. These results were significantly better than the SM2 design in the shod (p=0.017, 95% CI [1.12, 10.32]) and insole (p=0.009 95% CI [1.33, 8.42]) conditions, although there were no statistically significant differences for the barefoot conditions (F(2,8)=3.144, p=0.098). Mean build times for the GEOM and SM3 models were 194 minutes (range 161-228) and 54 minutes (range 48-58) respectively.

Figure:
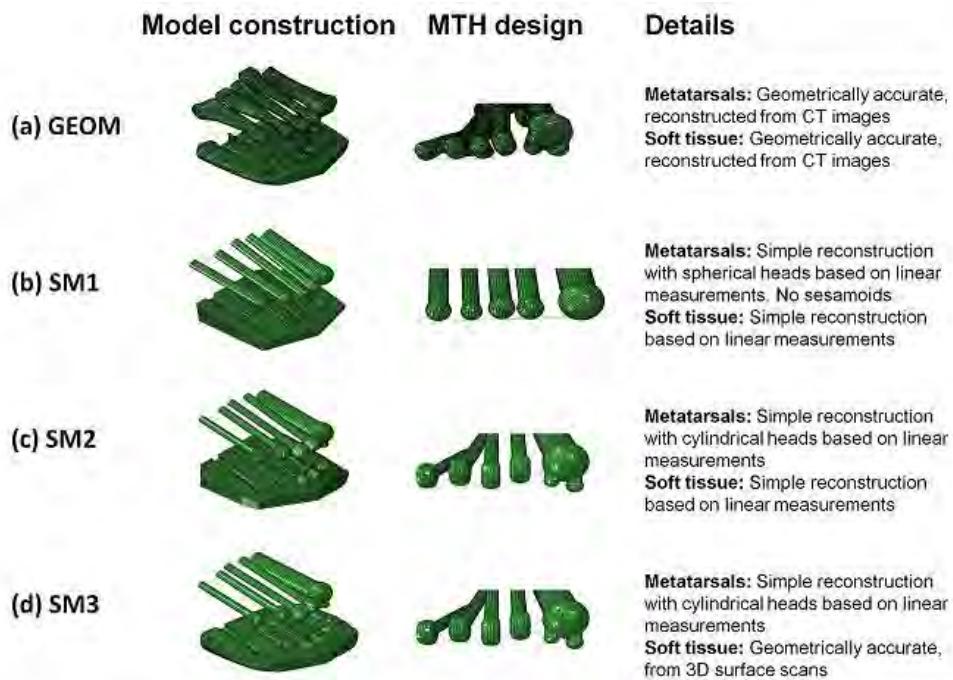
Caption: Figure 1 - FE model designs

Conclusion: A key factor in producing simplified models with direct patient utility is identifying the minimum dataset required to produce a clinically useful model of the forefoot. The best performing model here (SM3 design) required estimates of plantar tissue thickness, MTH morphology, and full soft tissue surface geometry. All measurements required to produce the simplified models presented in this paper can be obtained using easily accessible clinic-based technologies including ultrasound and 3D surface scanning.

This work has extended the concept of simplified personalised finite element model of the forefoot that can be generated through accessible clinic-based measurement techniques. These models perform adequately in comparison to more detailed FE models. The advantages of this approach, particularly in terms of build time, may improve the broad utility of the technique and bring it closer to clinical feasibility in terms of integration into the process of footwear and insole design.

References: [1] Spirka et al. J Biomech. 47: 2948-55, 2014

Disclosure of Interest: S. Telfer: None Declared, A. Erdemir Conflict with: AE has equity in innodof LLC, J. Woodburn: None Declared, P. Cavanagh Conflict with: PC has equity in DIApedia LLC

ON THE INTERACTION OF THE ACHILLES TENDON, PLANTAR HEEL PAD AND PLANTAR FASCIA

Freddy Sichting [1,*] Niels Hammer [2] Thomas Milani [1]

[1]Department of Human Locomotion, Technische Universität Chemnitz, Chemnitz, [2]Institute of Anatomy, University of Leipzig, Leipzig, Germany

Introduction and Objectives: While literature provides consistent evidence that force is transmitted from the Achilles tendon to the plantar fascia through the calcaneus, the plantar heel pad has hardly been considered in this context. However, the fibrous tethering mechanism of the heel pad gives sound evidence to hypothesize that tension of the Achilles tendon or plantar fascia influences heel pad deformation. Proving this hypothesis could shed new light on the damping mechanism of the hindfoot, but remains challenging as will be shown in this study.

Methods: Heel pad deformation of ten below-knee cadaver specimens was recorded using two simultaneous measurement methods. A uniaxial testing machine provided information of force-displacement of the foot while an ultrasound imaging system was used to measure alterations in heel pad thickness (Fig. 1). The setup allowed heel pad deformation to be differentiated from foot displacement in a range from 10 to 680 N at 134 N/s. First, heel pad deformation was measured under different Achilles tendon tensile loads, increasing stepwise from 0 to 200 N with increments of 50 N, with an intact plantar fascia. Then, this procedure was repeated with a transected plantar fascia, resulting in a total of ten different loading scenarios. Maximum heel pad deformation and load-deformation data were analyzed for all scenarios and compared statistically.

Results: Maximum heel pad deformation increased significantly ($p < 0.05$) with increasing Achilles tendon loads (at 0 N: d = 1.59 ± 0.71 mm; at 200 N: 2.41 ± 0.79 mm). Transecting the plantar fascia revealed no further change in maximum heel pad deformation in this particular experimental setup. The load-deformation curves revealed that the heel pad becomes softer with increasing Achilles tendon loads (Fig. 1). Transecting the plantar fascia had no significant effect. Besides the vertical displacement, we were able to detect corresponding horizontal displacement of the calcaneus using the ultrasound records. The horizontal displacement decreased with increasing Achilles tendon load.

Figure:
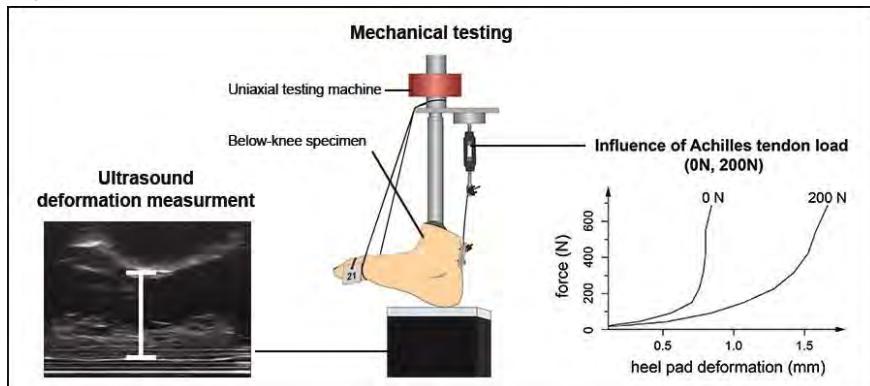
Caption: Fig. 1: Study protocol to investigate the influence of Achilles tendon and plantar fascia tension on the deformation of the plantar fat pad

Conclusion: First evidence is provided that heel pad deformation might be influenced by the adjacent connective tissues, mainly through tensile load on the Achilles tendon. The explanations for this phenomenon might be manifold and remain unclear. The Achilles tendon may interact directly with the heel pad via collagenous septa of the heel pad. Thereby, the macro chambers of the heel pad might be realigned to a more vertical position, changing its mechanical properties. Another explanation could be the change of calcaneus mobility that depends on Achilles tendon load. This explanation can be confirmed by our observations from the ultrasound measurements, showing an additional horizontal displacement of the calcaneus under load. Both approaches have barely been considered in previous studies on changes in the mechanical properties of the heel pad. The presented findings can contribute to raising awareness of the possible contributions that this functional interdependence between Achilles tendon and heel pad may have in hindfoot biomechanics.

Disclosure of Interest: None Declared

Modelling

SS-0025

THE RELATIVE IMPORTANCE OF INCLUDING PERSONALIZED HIP JOINT CENTER LOCATION AND MUSCLE LINE-OF-ACTION DEFINITION IN MUSCULOSKELETAL MODELS TO ASSESS HIP JOINT LOADING IN CP-PATIENTS WITH PROXIMAL FEMORAL DEFORMITY.

Lode Bosmans [1]christophe Van Dijck [2]Mariska Wesseling [1]Lennart Scheys [3]Ilse Jonkers [1,*]

[1]Kinesiology department, KU Leuven, [2]Materialise, [3]Department of development and regeneration, KU Leuven, Leuven, Belgium

Introduction and Objectives: Children with cerebral palsy (CP) often present proximal femoral bone deformities, such as increased femoral anteversion (FA) and neck-shaft angle (NSA). As generic musculoskeletal models (MSM) do not account for bone deformities, they are not suitable to represent the described population [1]. Personalized MSMs created based on magnetic resonance images (MRI) include the highest level of detail, such as bone geometry, muscle paths, joint center locations and joint kinematics. Different semi-automatic methods have been developed. One of the earliest methods consisted of partially deforming a generic MSM by adapting the bone and muscle geometry of a specific region of interest [2]. Recently, morphing methods have been proposed that morph bone geometry or imaging data onto personalized bone geometry and subsequently transform the muscle points [3]. These methods are more automated and less time demanding. However, the level of subject-specific geometric detail clearly differs from the image-based methods. This study investigates to what extent the approximation of subject-specific detail in these models affects the calculated hip contact forces in patients with proximal femoral deformities. If estimated hip loading only minimally differs between the different model types, this would suggest that deformed and morphed generic MSMs could serve as less time demanding alternatives for image-based MSMs to estimate hip joint loading in this patient group.

Methods: Eight subjects with diplegic CP (8-12 yrs) were included in this study. For each subject, a clinical gait analysis was performed and MRI of the lower extremities were captured. For each subject, six musculoskeletal models were created: (1) a personalized MRI-based model (MRI, [2]); (2) a morphed generic model (MOR) where the generic femur bone geometry was transformed onto the image-based femur geometry using an iterative morphing procedure [3]; (3) a deformed model (DEF) with regional deformation of the generic proximal femur to account for the subject-specific FA, NSA and neck length [4]; (4&5) for the latter two model types, a subject-specific hip joint center (HJC) definition was additionally included (MOR-HJC and DEF-HJC). For each subject, dynamic simulations of gait were generated in Opensim [1] for all models using the subject-specific kinematics. Following static optimization, first and second peak hip contact forces were calculated [5]. The contact forces of the MRI model are used as reference to compare the results between the model types. Results were compared using a Friedman test ($p < 0.05$), with posthoc Bonferroni correction.

Results: For MOR and DEF, the resultant hip contact force is overestimated at the first peak but underestimated at the second peak (Fig. 1a). For MOR, Ax and Az are overestimated at the first peak, indicating a less vertically orientated vector (Fig. 1b). For DEF, an overestimation of all three inclination angles is noticed, indicating a less vertical and posterior orientated vector. At the second peak, Ay is overestimated for MOR whereas Az is underestimated for MOR and DEF. When including the subject-specific HJC in MOR-HJC and DEF-HJC, the estimation of the magnitude of the second

peak of the resultant hip contact force improves for both models (Fig 1a). At the first peak, Ay decreased for DEF-HJC, indicating a less anterior orientation (Fig. 1b).

Figure:
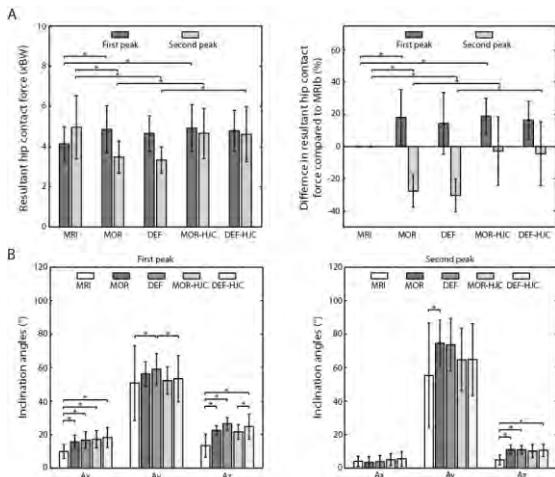
Caption: : Magnitude of (A) the two resultant peaks and (B) the inclination angles of the resultant hip contact force. Significant results (p < 0.05) are indicated with an asterix (*).

Conclusion: This study reconfirms the need to include subject-specific detail in MSMs used to estimate hip joint loading in CP-subjects with proximal femoral deformity. Inclusion of subject-specific HJC is key to introduce a relevant description of hip geometry. Nevertheless, as inclusion of subject-specific muscle lines-of-action paths still accounts for 17% and 7% of the difference in hip joint loading (for the first and second peak of the resultant loading respectively), MRI-based musculoskeletal models should remain the standard to evaluate hip joint loading in this population.

Therefore, the deformed and morphed generic MSMs in their present form cannot serve as less time demanding alternatives for image-based MSMs to estimate hip joint loading in this patient group. In future research, the use of bone-geometry based methods in combination with statistical shape modeling techniques that do account for variability in muscle line of action, should therefore be considered in this population.

References: [1] Scheys, L, et al. Gait & posture, 28(4), 640-648, 2008

[2] Arnold,AS et al. 2001 *Ann Biomed Eng,* 29:163-274, 2001

[3] Redert,A, et al. *Acta Stereologica*, 18:255-264, 1999

[4] Delp, SL, et al. IEEE trans biomed eng 54(11), 1940-1950, 2007

[5] Steele KM, et al. JOB, 43,2099-2105, 2010

Disclosure of Interest: None Declared

SS-0026

DEVELOPMENT OF A MUSCLE MODEL PARAMETER CALIBRATION METHOD VIA PASSIVE MUSCLE FORCE MINIMIZATION

Allison L. Kinney[* 1], Benjamin Fregly[2]

[1]Department of Mechanical and Aerospace Engineering, University of Dayton, Dayton, OH, [2]Department of Mechanical and Aerospace Engineering, University of Florida, Gainesville, FL, United States

Introduction and Objectives: Computational predictions of subject-specific muscle and knee joint contact forces during walking may improve individual rehabilitation treatment design. Such predictions depend directly on specified model parameter values. However, model parameters are difficult to measure non-invasively. Methods for muscle model parameter calibration have been developed previously [1]. However, it is currently unknown how the musculoskeletal system chooses muscle model parameter values. Previous studies have hypothesized that muscles avoid injury during walking by generating little passive force and operating in the ascending region of the force-length curve [2]. This hypothesis suggests that muscle model parameter values may be selected by the body to minimize passive force. The purpose of this study was to develop a method for calibrating muscle model parameter values and muscle moment arms during walking via minimization of passive force.

Methods: Experimental data were collected from a subject with a force-measuring knee implant [3-4]. A subject-specific model was created in OpenSim [5]. Muscle geometry and muscle model parameter values were transferred from a generic OpenSim model [6]. Inverse kinematics and inverse dynamics analyses were performed for one gait cycle of walking. All muscles were modeled with a rigid tendon muscle model. A reserve actuator was included at each joint. A two-level optimization-based calibration method was developed. The outer level optimization calibrated muscle model parameter values and muscle moment arms with the goal of obtaining a solution with all muscle activations between 0 and 1. Muscle model parameter values were calibrated by optimizing scale factors for tendon slack length and optimal fiber length relative to the generic OpenSim model. Muscle moment arms were calibrated by optimizing offsets that allowed deviations in the moment arms. The inner level optimization optimized the muscle and reserve actuator activations while minimizing the activation and matching the experimental inverse dynamics loads. Four calibrations were performed with the two-level optimization-based approach. During two optimizations, calibration was performed by tracking 8 inverse dynamics loads (3 hip, 3 knee, and 2 ankle) using the in vivo knee contact force data. During the remaining optimizations, calibration was performed by tracking 6 inverse dynamics loads (3 hip, 1 knee, 2 ankle). Two optimizations were performed where passive muscle force was minimized by the outer level optimization. Medial and lateral contact forces were predicted for each optimization and compared with the experimental knee contact forces.

Results: Optimizations that minimized passive muscle force increased all tendon slack length and optimal fiber length values (average: 1.2, range: $1.0 - 1.4$) and predicted smaller medial and lateral contact forces relative to the experimental measurements (Figure 1). Optimizations that did not minimize passive muscle force changed tendon slack length and optimal fiber length values minimally (average: 1.0, range: $0.8 - 1.2$) and predicted medial and lateral contact forces larger than the experimental knee contact forces (Figure 1). Muscle moment arm offsets for all optimizations were generally

small (average: 0.2 cm) but varied across muscles (range: 0 – 2.6 cm). Calibration with 6 inverse dynamics loads and no passive force minimization predicted the least accurate medial and lateral forces (Table 1).

Figure:
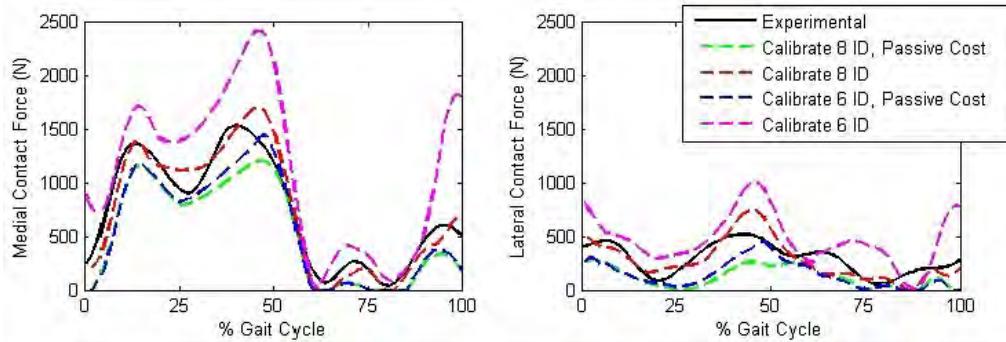
Caption: Medial and lateral contact force predictions

Conclusion: Calibration of muscle model parameter values and muscle moment arms was influenced by passive muscle force minimization. Minimization of passive muscle force caused muscles to operate only in the ascending region of the force-length curve and eliminated passive force in all muscles. Optimizations that did not minimize passive force allowed large passive force generation in some muscles. Calibration without in vivo knee contact force data and passive force minimization represents the common approach used by researchers when contact force data are not available. The high contact force predictions from this approach suggest that excessive passive muscle force may contribute to the general tendency to overpredict knee contact forces.

Table:

	Medial Contact Force		Lateral Contact Force	
	RMSE	R^2	RMSE	R^2
Calibrate 8 ID, Passive Cost	242	0.76	191	-0.84
Calibrate 8 ID	133	0.93	104	0.45
Calibrate 6 ID, Passive Cost	219	0.81	167	-0.41
Calibrate 6 ID	500	-0.02	253	-2.2

Caption: RMSE and R^2 values for medial and lateral contact force predictions

References: [1] Buchanan TS et al., J. Appl. Biomech., 20: 367–395, 2004.

[2] Rubenson J et al., J. Exp. Biol., 215: 3539–3551, 2012.

[3] Kirking B et al., J. Biomech., 39: 1744–1751, 2006.

[4] Fregly BJ et al., J. Orthop. Res., 30: 503–513, 2012.

[5] Delp SL et al., IEEE Trans. Biomed. Eng., 54: 1940–1950, 2007.

[6] Arnold EM et al., Ann. Biomed. Eng., 38: 269–279, 2010.

Disclosure of Interest: None Declared

Computer Simulation

SS-0027

A NOVEL COMPARISON OF ARTIFICIAL INTELLIGENCE METHODS FOR DIAGNOSING KNEE OSTEOARTHRITIS

Luca Parisi [1,*] Paul Robert Biggs [2] Gemma Marie Whatling [2] Catherine Avril Holt [2]

[1]School of Engineering, Medical Engineering, [2]Arthritis Research UK Biomechanics and Bioengineering Centre, Cardiff University, Cardiff, United Kingdom

Introduction and Objectives: Three dimensional motion analysis generates a great wealth of information, which has resulted in a range of mathematical techniques aimed at assisting both clinicians and researchers interpret biomechanical data [1]. Jones [2] successfully developed a technique at Cardiff University that facilitates the classification between pathological and non pathological knee function using Dempster-Shafter theory (DST), demonstrating its effectiveness in comparison to Artificial Neural Networks (ANN) and Linear Discriminate Analysis (LDA) in the classification of osteoarthritic gait. Classication techniques have advanced over the last decade with recent studies reporting high accuracies using ANN [3] and Support Vector Machines (SVM) [4]. To the best of our knowledge, this study proposes, for the first time, to compare the performance and suitability of the (i) Cardiff Classifier, (ii) ANN and (iii) SVM in discriminating between healthy and osteoarthitic knee function.

Methods: As this study involves dealing with long range data sets, a four-dimensional unsupervised Self-Organising Map (SOM) [5] and a supervised Multi-layer Perceptron (MLP) neural networks with one hidden layer having 20 hidden neurons [6], were built through the MatLab neural network toolboxes respectively named as 'nctool' and 'nprtool' (Mathworks inc., USA). The Lagrangian Support Vector Machines (LSVMs) [7] Machine Learning (ML)-based classification method and the Dempster-Shafter theory (DST)-based classifier ('Cardiff classifier') [2] were selected for pattern recognition tasks and classification purposes. Thirty-eight patients with late stage knee osteoarthritis (OA) and thirty-eight healthy volunteers were instructed to complete walking trials at speeds they deemed to be normal. Spatio-temporal gait data (stride length, cadence, body mass index) and principal components of knee kinematic and ground reaction force waveforms were averaged for five gait cycles. Eighteen selected biomechanical and clinical variables formed the input matrix for the three classifiers. After randomising the data, the physiological knee function of healthy volunteers and pathological function due to knee OA were used as desired outputs for the classifiers. In all neural network models tested for classification accuracy in this study, 70% of the data was used for training, 15% for a ten k-fold cross-validation to prevent over-fitting/overtraining [8], whilst the last 15% of the data was deployed for testing in order to assess the out-of-sample classification accuracy of the neural networks. Instead, in both LSVMs and DST-based classifier the leave-one-out cross (LOO) validation algorithm was adopted, introduced in order to maximise the utilisation of the training cohort.

Results: Table 1 below shows the out-of sample classification accuracies associated to each of the four types of classifiers being tested. In Fig. 1 a three-coordinate simplex plot referred to the patient data categorised by the Cardiff classifier is displayed.

Figure:
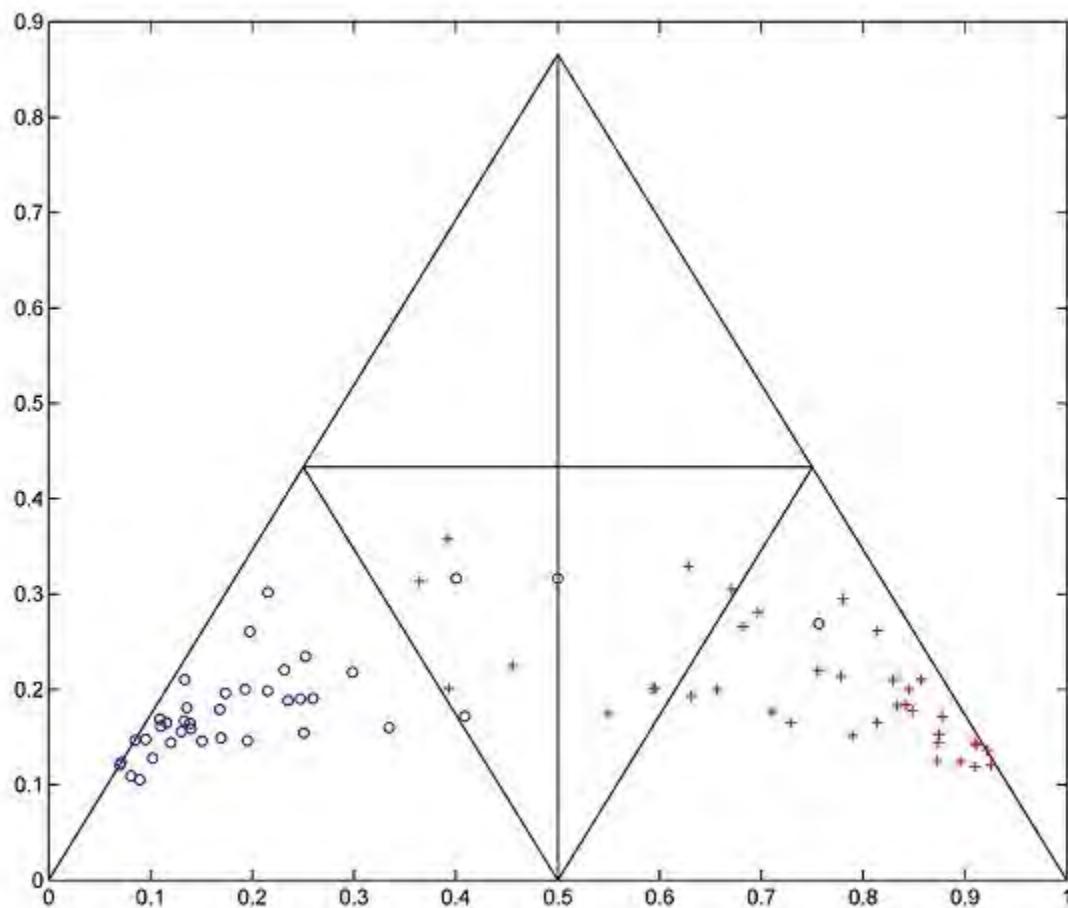
Caption: Fig. 1 Simplex plot showing how the subjects on the left (blue circles) were correctly classified as healthy subjects, whilst those on the right (red crosses) as patients with knee OA.

Conclusion: Findings indicate that, for the classified patient dataset, the DST-based classifier proved to be the most suitable method for classifying patients with knee OA (Table 1). This is due to its highest out-of-sample classification accuracy amongst the classifiers tested. This clinically relevant result partially validates the Cardiff classifier as a reliable diagnostic tool to assess the knee joint function of patients affected by knee OA. The DST-based classifier's user-friendly interface (Fig. 1) lends itself to further development into a valuable clinical tool, enabling a clinician to objectively characterise knee function without requiring any assistance from biomechanists. There is also future potential to assist with patient assessment and surgical decision making, aimed at optimising patient outcome. Future work is underway to ascertain whether the Cardiff classifier is a clinically suitable technique for improving the accuracy of the diagnosis and monitoring the effectiveness of the prognosis related to other lower limb pathologies.

Table:

Classifier	Out-of-sample classification accuracy
Multi-layer perceptron (MLP) neural network with one hidden layer	81.8%
Four-dimensional self-organising map (SOM)	71.05%
Lagrangian support vector machine (LSVM)	91%
Dempster-Shafer theory-based classifier	93.42%

Caption: Table 1. Classifiers tested and relative out-of-sample classification accuracy (on the testing set).

References: [1] Chau, Gait Posture, 13: 49-66, 2001.

[2] Jones et al., Comput Methods Biomech Biomed Engin, 11: 31-40, 2008.

[3] Kaczmarczyk et al., Gait Posture, 30: 207-210, 2009.

[4] Muniz et al., J Biomech, 43: 720-726, 2010.

[6] Anifah et al., Open Biomed Eng J, 7: 18-28, 2013.

[7] Mangasarian et al. JMLR, 1, 161-177, 2001.

[8] Taylor et al. IEEE-EMBS, 1, 339-343, 2010.

Disclosure of Interest: None Declared

Lower Limb

SS-0028

EFFECTS OF HIGH TIBIAL OSTEOTOMY ON TRUNK, HIP, KNEE AND ANKLE BIOMECHANICS DURING GAIT

Gemma M. Whatling [1 2,*]Sarah Forrest [1 2]Chris Wilson [2 3]Andrew Metcalfe [1 2 3]Salam Ismael [2 3]Cathy Holt [1 2]

[1]School of Engineering, [2]Arthritis Research UK Biomechanics and Bioengineering Centre, Cardiff University, [3]Cardiff and Vale Orthopaedics Centre, University Hospital of Wales, Cardiff, United Kingdom

Introduction and Objectives: Osteoarthritis (OA) affects 8 million people in the UK causing painful, limited movement and altered quality of life. In the case of medial compartment OA a varus deformity develops and one treatment option is a High Tibial Osteotomy (HTO). This surgery corrects varus alignment, relieves pain and shifts the location of force transmission from the diseased medial to the healthy lateral compartment. Studies have shown that this treatment modifies medial knee joint loading, evidenced through reduced external knee adduction moment (EKAM). Less however, is known about changes to overall patient biomechanics and compensatory mechanisms, or the effect of a HTO on other joints and the contralateral limb. We hypothesise that HTO affects biomechanics in other lower limb joints and this abstract reports interim findings from a large, longitudinal HTO study.

Methods: Lower limb and trunk biomechanics were evaluated during gait (n=10, BMI: 29.4 ± 3.7 kg/m^2, age: 51 ± 7 years) using 3D motion analysis. Subjects were analysed pre and post opening wedge, unilateral HTO (12 ± 1 months). The mean mechanical tibio-femoral angle was 5.8(± 3.7)$^{\circ}$. OA severity Kellgren-Lawrence scores were 3(moderate) n=8 and 4 (severe) n=2. 9 subjects received a TomoFix plate and 1 received a Puddu plate. 49 light retro-reflective markers were positioned in a modified Cleveland clinic marker set and 3D motion capture (Qualisys, Sweden and Bertec Corporation) used to record 6 trials of level gait at self-selected speeds. Biomechanical models of each subject were created in Visual3D (C-motion, Inc) to compute temporal, kinematic and kinetic data. Knee Outcome Survey (KOS) and Oxford Knee Score (OKS) were collected. Paired t-tests identified statistical differences (p<0.05) in biomechanics and patient reported scores pre and post-HTO.

Results: Biomechanical changes were evident in both lower limbs following HTO. HTO significantly reduced frontal plane knee joint loading (41% and 39% reduction in EKAM peaks 1 and 2 respectively, and 46% reduction in knee adduction angular impulse), associated with significant changes in ankle inversion moment. Both ankles had reduced inversion and dorsiflexion moments. At EKAM peak1 there was a 5% increase in medial GRF, an eversion (0.26±0.2%BW.h) instead of inversion (0.01±0.6%BW.h) moment and dorsiflexion moment reduced by 39%. The inversion moment at EKAM peak 2 reduced by 25%. Hip, knee and ankle rotations were affected in the operative limb. Trunk sway ROM reduced and both hips had increased ROM. Frontal plane trunk ROM decreased by 36% whilst frontal plane hip ROM and sagittal plane knee ROM increased significantly by 19 % and 5% respectively.

Conclusion: HTO reduces medial knee loading and patients report improved function with reduced pain, fulfilling the aims of the surgery. HTO has an effect on knee, ankle and hip biomechanics in the operative and non-operative limbs. OKS and KOS scores increased by 43% and 23% respectively indicating reduced pain, improved function and quality of life. Patients walk differently after surgery and it is important to understand the influence of HTO on other joints.

Disclosure of Interest: None Declared

Musculoskeletal

SS-0029

OSTEOARTHRITIS KNEE BRACE ABDUCTION MOMENT DOMINATES INVERSE DYNAMICS AND MUSCLE FORCE CHANGES IN REDUCING MEDIAL KNEE LOADS

Scott Brandon [1] [2],*Marcus Brown [1] [2]Adam Clansey [1] [2]Jim Richards [3]Aaron Campbell [2] [4]Kevin Deluzio [1] [2]

[1]Mechanical and Materials Engineering, Queen's University, [2]Human Mobility Research Centre, Kingston General Hospital, Kingston, Canada, [3]Allied Health Research Unit, University of Central Lancashire, Preston, United Kingdom, [4]Department of Surgery, Kingston General Hospital, Kingston, Canada

Introduction and Objectives: Braces for medial knee osteoarthritis are designed to reduce painful, and potentially injurious [1], compressive loading on the damaged medial side of the joint through application of a frontal-plane abduction moment. However, *in vivo* knee load measurements have revealed that the magnitude of load reduction varies greatly between subjects and brace designs [2]. Previous studies which investigated the mechanical effectiveness of bracing have been limited either in their musculoskeletal detail [3] or incorporation of altered external joint moments and forces [4]. Therefore, the objective of this study was to model the relative contributions of gait dynamics, muscle forces, and the external brace abduction moment to reducing medial compartment knee loads.

Methods: Nine subjects with medial knee osteoarthritis and ten healthy control subjects were recruited for this study (Table 1). Participants completed a WOMAC questionnaire and provided written, informed consent. The study was approved by the institutional ethics review board.

Subjects walked across 6 tandem force platforms, which were embedded in a 20m walkway. Synchronized motion capture (200Hz, Oqus 4, Qualisys, Gothenburg, Sweden), lower-limb electromyogram (EMG, 1000Hz, Trigno Wireless, Delsys Inc., Boston, USA), and ground reaction force data (1000Hz, Custom BP Model, AMTI, Watertown, USA) were recorded using Qualisys Track Manager. Eight gait trials were recorded in each of three brace conditions in the following order: unbraced, OA Adjuster 3 brace (DJO Global), and OA Assist brace (DJO Global). Braces were fitted according to manufacturer guidelines, and adjusted to a maximum level that would be comfortable for four hours. The abduction moment applied by the brace was computed by dynamically measuring brace deflection using motion capture, and multiplying by pre-determined brace stiffness.

For each subject, a representative stride was selected for each brace condition. A generic musculoskeletal model with two legs, a torso, and 96 muscles [5] was modified to include subject-specific frontal plane alignment and medial and lateral contact locations [6]. Inverse kinematics, inverse dynamics, residual reduction, and muscle analysis were performed using OpenSim 3.2 [7]. Muscle forces were estimated using static optimization, and tibiofemoral contact loads were estimated in Matlab [6,8]. Subject characteristics were compared using unpaired t-tests, while joint kinematics, joint moments, joint contact loads, predicted muscle activation (Act) and EMG were compared using a two-factor ANOVA and planned Sidak post-hoc contrasts between brace conditions. Significance (α) was set at 0.05.

Results: OA Assist and OA Adjuster 3 braces reduced medial joint loading by approximately 0.1 to 0.2 BW, or roughly 10%, during stance (P< 0.01, Figure 1). This decrease was primarily due to the external brace abduction moment (Figure 1). Joint kinematics and moments were significantly altered in the braced condition (P < 0.01); however, the medial knee

load reduction was independent of changes in inverse dynamic joint loads (Figure 1). Decreased quadriceps activation enhanced medial and lateral unloading, while increased gastrocnemii activation inhibited medial unloading (Figure 1).

Figure:
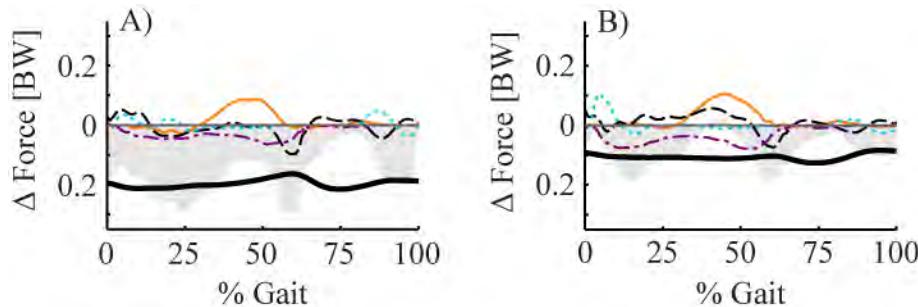
Caption: Figure 1: Contributions of quadriceps (dot-dashed, purple), hamstrings (dotted, cyan), gastrocnemii (solid, orange), inverse dynamics forces (dashed, black), and the brace abduction moment (thick solid, black) to the net change in medial knee contact load (shaded, grey) when osteoarthritis subjects were fitted with OA Assist (A) and OA Adjuster 3 (B) braces as compared with the unbraced condition.

Conclusion: In a sample of ten healthy control and nine osteoarthritis subjects, bracing reduced medial compartment knee loading by approximately 10%, as estimated using a musculoskeletal model. Gait kinematics and joint moments were relatively unaffected by bracing, while gastrocnemii activation increased; therefore, the model revealed that current unloader brace designs must apply a large knee abduction moment in order to reduce medial loading. Future braces should consider innovative designs which could enhance the unloading effect through gait modification.

Table:

Group	Osteoarthritis	Control	P-value
Age [years]	55 (3)	45 (13)	0.04
Height [m]	1.70 (0.09)	1.73 (0.11)	0.52
Mass [kg]	89 (21)	74 (15)	0.08
BMI [kg/m^2]	31 (5)	25 (2)	<0.01
HKA [deg, $^{-ve}$ varus]	-7.9 (7.3)	-1.3 (2.4)	0.02
Medial Joint Space [mm]	2.6 (2.5)	5.5 (0.8)	<0.01
WOMAC - Total	64 (17)	99 (1.6)	<0.01
Gait Speed [m/s]	1.6 (0.1)	1.4 (0.1)	<0.01

Caption: Table 1: Participant Characteristics: Mean (SD)

References: [1] Felson DT. Osteo.Cart. 21, 2013.

[2] Kutzner I, et al. J.Biomech. 44, 2011.

[3] Pollo FE, et al. Am.J.Sports.Med. 30, 2002.

[4] Shelburne KB, et al. Clin.Biomech. 2008 (23).

[5] Arnold EM, et al. Ann.Biomed.Eng. 2010 (38).

[6] Brandon SCE, et al. J.Biomech. 47, 2014.

[7] Delp SL, et al. IEEE Trans.Biomed.Eng. 54, 2007.

[8] Winby CR, et al. J.Biomech. 42, 2009.

Disclosure of Interest: None Declared

SS-0030

THE INFLUENCE OF DRILL-GUIDE ANGLE ON STRESS REDISTRIBUTION AFTER ANTERIOR CRUCIATE LIGAMENT RECONSTRUCTION

Jie Yao [1,*] Lizhen Wang [1] Yubo Fan** [1] [2]

[1]Department of biomedical engineering, School of Biological Science and Medical Engineering, Beihang University, [2]National Research Center for Rehabilitation Technical Aids, Beijing 100176, Beijing, China

Introduction and Objectives: The anterior cruciate ligament (ACL) reconstruction is the predominating treatment for ACL injury [1]. However, the tunnel enlargement and osteoarthritis are frequently reported after the surgery [2, 3]. A possible predisposing factor could be the undesirable bone remodeling due to the post-operative stress redistribution [4]. In this light, this study aims to quantify the stress redistribution in tibia after the ACL reconstruction, and to minimize the stress redistribution by adjusting tibial drill-guide angle.

Methods: The finite element model of the human knee joint was developed from the magnetic resonance images. The model was validated with the experiments and was used to simulate the anatomic single-bundle ACL reconstruction according to the routine surgical procedure. The tibial tunnel was created with the drill-guide angles ranging from 30 to 75 degrees. The stress redistributions in tibia were calculated under the compressive, valgus, rotation loadings.

Results: Among the loadings applied, the compressive loading played a leading role on the stress distribution on the tibial plateau. After the surgery, the stress was increased in the anterior region of the tunnel aperture under the compressive loading, while it was decreased in the lateral region. The severity of the stress redistribution was decreased with increasing the drill-guide angle from 30 to 55 degrees, and it slightly changed when the drill-guide angle was greater than 55 degrees.

Figure:
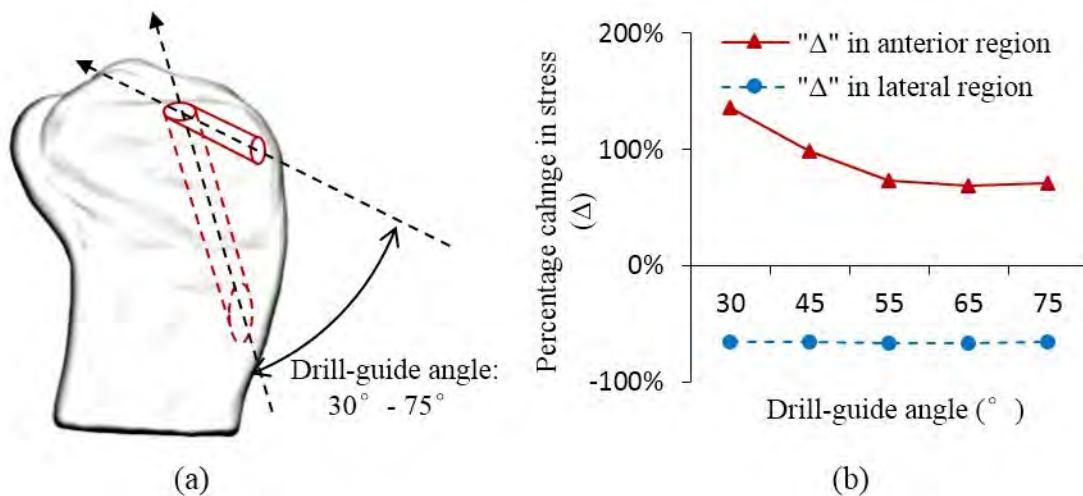
Caption: The influence of the drill-guide angle on the percentage change in stress (Δ) under the complex loadings including compression, valgus, and rotation. (a) The diagram of tibial tunnel; (b) Δs in the anterior and lateral regions of the tunnel aperture.

Conclusion: ACL reconstruction can cause the stress redistribution in the knee near the bone tunnel wall. The stress redistribution may lead to undesirable bone remodeling and contribute to tunnel enlargement and osteoarthritis. Nonetheless, the severity of the post-operative stress redistribution could be manipulated by adjusting the tibial drill-guide angle. Considering the clinical and mechanical factors together, using the drill-guide angle ranging from 55 to 65 degree could provide a beneficial mechanical environment for the rehabilitation after the ACL reconstruction.

References: [1] Woo, S.L., et al., J Biomech, 39(1): 1-20, 2006.

[2] Giron, F., et al., Knee Surg Sports Traumatol Arthrosc, 13(2): 81-91, 2005.

[3] Louboutin, H., et al., Knee, 16(4): 239-244, 2009.

[4] Yao, J., et al., Ann Biomed Eng, 40(7): 1554-1567, 2012.

Disclosure of Interest: None Declared

CARDIOVASCULAR SYSTEM RESPONSES TO ACCELERATIONS: A MODEL AND ITS VALIDATION

Yawei Wang [1,*] Jian Ma [1] Lizhen Wang [1] Yubo Fan [1] [2]

[1]Key Laboratory for Biomechanics and Mechanobiology of Ministry of Education, International Research Center for Implantable and Interventional Medical Devices, School of Biological Science and Medical Engineering, Beihang University, [2]National Research Center for Rehabilitation Technical Aids, Beijing, China

Introduction and Objectives: Accelerations generated by the high performance aircraft, spacecraft and centrifuge have complicated influences on human cardiovascular system. Such accelerations include positive acceleration (head to foot inertial loading, +Gz), negative acceleration (-Gz), positive or negative lateral acceleration (±Gy), forward acceleration (+Gx) and backward acceleration (-Gx). Influences of postive acceleration on human cardiovascular system have been research hotspots for many decades, because human performance during exposure to positive acceleration stress is limited by two primary factors: loss of vision and loss of consciousness (LOC). It is generally believed that these symptoms are caused by decreased retinal and cerebral blood flow, respectively. Many physiological parameters, such as circulating blood volume, cardiac output, cerebral and spinal cord blood flow of dogs, miniaturized pigs, baboons and human were measured at different +Gz values in several physiological experimental researches. However, insightes on global, dynamic and quantitative response of human cardiovascular system have not been gained, and the detailed mechanism of Gz induced LOC was not very clear now. Moreover, influences of multi-axial accelerations generated by new generation aircrafts when they implemented post-stall maneuvers are not been understood. In this paper, a mathematical model of human closed-loop circulatory system was established for investigating influences of the these accelerations. This mathematical model was built using a fluid-mechanical circuit representation of human closed-loop circulatory system, and was validated using physiological parameters measured in human experiments on the centrifuges from literatures.

Methods: Three basic fluid-mechanical portions of the cardiovascular system were modeled, including the heart and pulmonary system, the systemic venous system and the systemic arterial system. Left and right arms and legs were modeled respectively for including influences of Gy accelerations. Reflex regulation and effects of anti-G suit were also included in this model, as shown in Figure 1.

The heart and pulmonary system: the model of heart and pulmonary system was rather simply represented by a resistance-compliance section, a varying compliance and two valves, based on simplificaiton of a more detailed model. Right atrium, right ventricle, the pulmonary system and the left atrium were simply represented by the resistance-compliance setcion together with a valve. Left ventricle was represented by the varying compliance and another valve.

The systemic venous system: the systemic venous system was comprised of eight segments with three segments for veins in head and neck, one segment for veins in the abdominal cavity, and four segments for veins in the legs. Each segment included a variable resistance and a variable compliance. Varying values of the resistance and compliance represented the effects of venous collapse, which were calculated from nonlinear functions of transmural pressures.

The systemic arterial system: the systemic arterial system was also comprised of eight segments. Each segment included a constant resistance and a constant compliance.

Pressure differences induced by accelerations: Pressures differences induced by accelerations were modeled as electrical sources. In order to produce a net pressure around the circulatory loop, these sources were included in the arteries as well as in the veins.

Reflex regulation and effects of anti-G suit: Reflex regulation was included through using functions from literautes to control heart rate, flow resistances in the arms, legs, and organs in the abdominal cavity. Effects of anti-G suit were added by using functions to control flow resistances and compliances in the legs.

Results: Response of the model to a simulated tilt-up from 0° to a 90° head-up position was in good agreement with test data from literature. However, the recovery time after tilting back to a horizontal position was a little longer than the test data. Simulation results with and without anti-G suit were reasonable compared with physiological parameters measured in experiments of human at 3 g and 5 g +Gz conditions. Model response to a 3 g lateral acceleration showed an obvious change of heart rate but inapparent varying of blood perfusion into organs.

Figure:
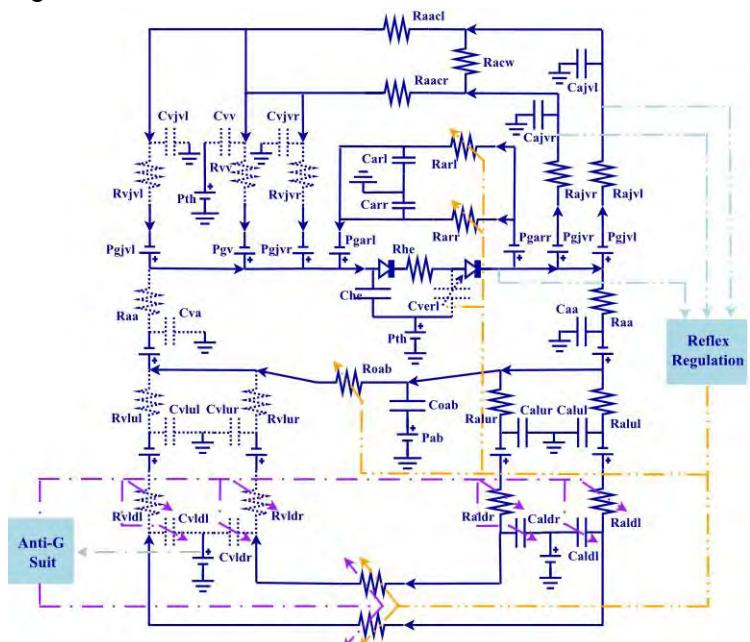
Caption: Figure 1 mathematical model of cardiovascular system

Conclusion: This model could be used to investigate influences of different accelerations on responses of human cardiovascular system.

References: [1] Snyder et al., Computer simulation studies of the venous circulation, IEEE Trans. Biomed. Eng., 4: 325-334, 1969.

[2] Gisolf et al., Human cerebral venous outflow pathway depends on posture and central venous pressure, J. Physiol., 1: 317-327, 2004.

Disclosure of Interest: None Declared

MULTI-JOINT CONTROL STRATEGY OF THE LOWER LIMB DURING RUNNING

Yuliang Sun [1] Jiabin Yu [1] Cheng Yang [1] Yu Liu [1,*]

[1] Key Laboratory of Exercise and Health Sciences, Ministry of Education, Shanghai University of Sport, Shanghai, China

Introduction and Objectives: To fully understand the control and regulation of multi-joint movements, the biomechanical properties of the moving subject, specifically intersegment dynamics, must be considered in the motor control research. A series of research results of upper-limb movement using intersegment dynamic approach have shown that the joints of a multi-articular limb play different roles in movement production according to their mechanical subordination in the joint linkage. A Leading Joint Hypothesis (LJH) has been proposed as an alternative interpretation of control of human movements[1]. However, limited attempts have been made to reveal the underlying mechanism of multi-joint control of lower limbs. This study was to understand the multi-joint control strategy of the lower limbs during running, by studying the intersegment dynamics of the hip, knee and ankle. On the basis of the current literature, we hypothesized that the control strategies were different at these three joints, and the three joints play different roles in lower-limb control during running according to LJH.

Methods: Subjects (n=16, male students) were asked to performed running at 4 different speed (2m/s, 3m/s, 4m/s, 5m/s). Three-dimensional kinematic data were collected via 16 high resolution cameras (200 Hz). The Ground reaction forces were collected by 2 recessed forceplates (1000 Hz). From the collected three-dimensional data, two-dimensional sagittal plane coordinates were extracted. Data from the right lower extremity were used for the following analyses. The lower limb was modeled as a linked-segment system (thigh, shank, foot) with frictionless joints at the hip, knee, and ankle. One of the trails containing valid force plate contacts was analyzed for each movement of the subjects. The intersegmental dynamics analysis was conducted with a customized program. Torques at each joint were separated into five categories: net torque (NET), gravitational torque (GRA), interactive torque (INT), external contact torque (EXT), and muscle torque (MUS). NET is the sum of the other four components[2]. All the torques were normalized by the product of body weight (N) and height (m). An impulse analysis was used to evaluate the contribution of each component to the NET. The positive impulse of the torque component (MUS, EXT, INT or GRA) was computed as the torque integral during intervals where the torque component acted in the same direction as the NET. Accordingly, a negative impulse of the torque component was computed during the intervals where the torque component acted in the opposite direction to the NET. All positive and negative impulses were summed for each torque component within each cycle to yield a total impulse for the entire phase. A one-way ANOVA with repeated measures was used to test the effect of speed on the kinetic data. A conservative level of significance was set at $\alpha = .05$.

Results: During the stance phase at all running speed (Figure 1a), the dominant joint torques which provided the positive contribution to the hip movement were EXT (e.g. speed level 5m/s, 2.8±1.4). EXT counterbalanced the negative effect generated by INT. But MUS at the knee (e.g. speed level 5m/s, 6.0±1.5) and the ankle (e.g. speed level 5m/s, 7.2±1.7) play the dominant role at these two joints, and provided the main positive contribution to counter the negative effect from EXT. During the swing phase (Figure 1b), the dominant joint torques which provided the positive contribution to the joint

movement were MUS (e.g. speed level 5m/s, 4.5±1.5) at the hip, but INT at the knee (e.g. speed level 5m/s, 0.9±0.4) and the ankle (e.g. speed level 5m/s, 0.1±0.01). Significant differences were found in each kind of impulses among different speed levels, especially INT (e.g. INT at knee in swing phase from speed level 2 to 5m/s: 0.4±0.1 vs 0.6±0.2 vs 0.7±0.2 vs 0.9±0.4, p<.01).

Figure:
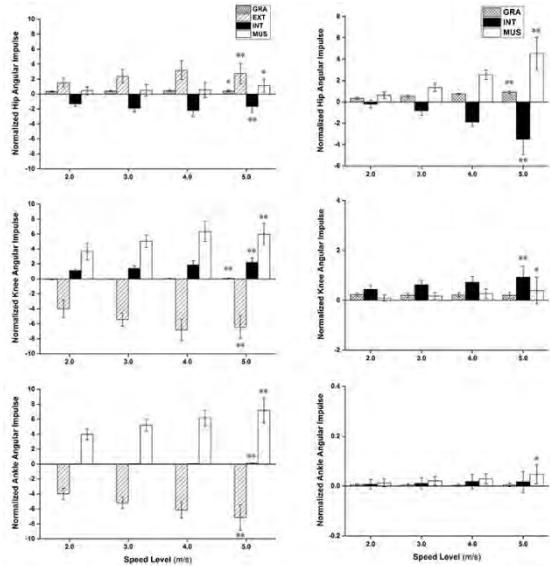
Caption: Fig.1 Impulses at hip, knee & ankle during stance (a) & swing phase (b) in 4 different speed running. Positive values indicate that the torque component had the same sign as NET and contributed to the NET impulse. The impulse was negative when the component was opposite in sign to the NET.

Conclusion: During the stance phase, the knee & ankle were the leading joints according to the Leading Joint Hypothesis (the active muscle torques were dominant for the joint movement), while the hip was the subordinate joint (passive torque was dominant for the joint movement). During the swing phase, the hip became the leading joint which accelerate or decelerate the whole limb (MUS became the dominant), while the knee and ankle were the subordinate joints, the movement of which were conducted by the INT. Therefore, the central nervous system not only exploits the muscle strength, but also the gravity of the limbs, the external contact force and the inertia force for movement organization, to perform effective and "economical" limb movement.

References: [1] Dounskaia, Exerc Sport Sci Rev, 4:201-8, 2010.
[2] Huang et al., J Biomech, 12:2018-23, 2013.

Disclosure of Interest: None Declared

SS-0033

ROBOTIC-ASSISTED PROSTATE TUMOR LOCALIZATION USING NEEDLE ROTATION FORCE

Xiaoyu Liu [1,*] Lizhen Wang [1] Wei Yao [2] Yubo Fan** [1]

[1] School of Biological Science and Medical Engineering; Yifu Building, Beihang University, Beijing, PR China., Key Laboratory for Biomechanics and Mechanobiology of Ministry of Education, Beihang University, Beijing, PR China., Beijing, China, [2] Department of Biomedical Engineering, University of Strathclyde, Department of Biomedical Engineering, University of Strathclyde, 106 Rottenrow, Glasgow, Glasgow, United Kingdom

Introduction and Objectives: Prostate cancer (PCa) is the first leading cause of male cancer dearth in the UK and many developed countries [1]. Although PCa is not so commonly found in Chinese and other Asian men, there has been a significant increase in the incidence of this cancer in these countries over recent decades [2]. Accurate localization of the prostate tumor is critical to effective early-stage PCa diagnosis and treatment. Robot-assisted technologies have been developed to guide tumor localization using TRUS and MRI imaging. Recently, force-guided technology has been introduced to localize tumors in robotic system. PCa can be identified by analyzing insertion forces on the needle. However, this technology only allow for determining the depth of a tumor on the path of needle insertion. Spatial localization of the tumor by needle forces is a significant challenge in prostate biopsy and brachytherapy. Currently, we have proposed a novel robot-assisted procedure for tumor localization by means of needle rotation forces. This procedure enables to determine the planar location of a prostate tumor, which is expected to be used in robot-assisted minimally invasive systems for prostate biopsy and brachytherapy.

Methods: We validated the robot-assisted procedure by experiment on tissue phantoms that offer simple and controllable environments for repeatable tests. A silicon material (Young's modulus 15 kPa) and a rubber button (Young's modulus 75 kPa) were used to simulate normal and harder tumor tissues respectively. A 7-DOF robotic manipulator (Cyton Gamma 1500, Robai Corporation, MA) was used to perform needle motion including vertical insertion, deviation and 360-degree rotation (Figure 1a). Firstly, a needle was driven into a prostate phantom vertically at a velocity of 1 mm/s. When an abnormality of the force data (F_z) was found during insertion, a refined analysis was conducted to determine whether the tumor is on the path of the needle insertion. If there is no indication that the tumor is inserted, the needle is then driven to perform a 2.5-mm planar deviation and a 360-degree rotation at a velocity of 1 mm/s. A 6-axis force/torque sensor (Nano17, ATI Industrial Automation, US) was used to measure the rotation needle forces.

Results: When an abnormality was found in the force data (F_x, F_y), the direction of the tumor's location can be identified since the harder tumor made a difference in the force during needle rotation. The mapping of tumor localization using needle forces by performing two needle rotations is shown in Figure 1b. It can be seen that the rotation force reached the maximum value when the needle just rotated toward the position of the tumor. The degree (θ) corresponding to the maximum needle force is the direction of the tumor location.

Figure:
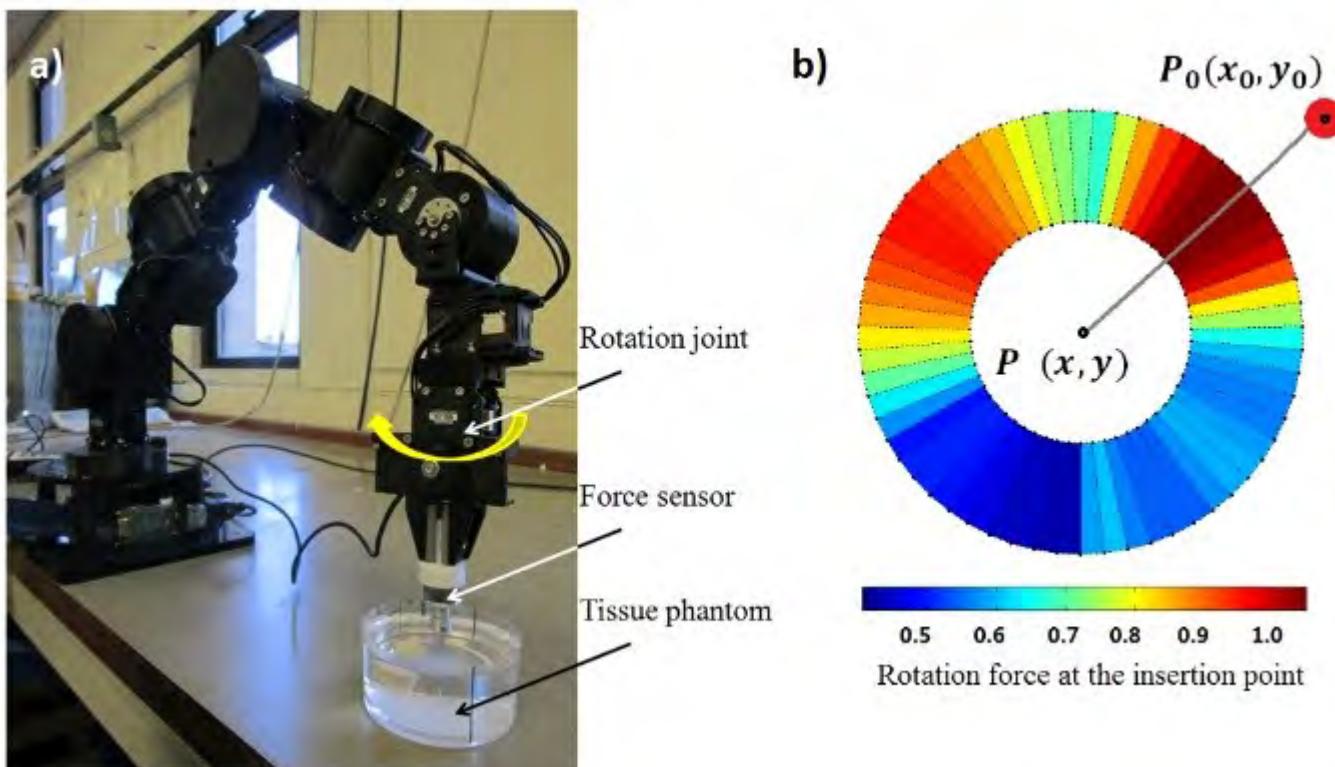
Caption: Figure 1 Robotic-assisted Prostate Tumor Localization Using Needle Rotation Force: a) Experimental setup; b) The mapping of tumor localization using needle forces.

Conclusion: The novel robot-assisted procedure, needle rotation, was validated to achieve tumor localization in the prostate phantom test. The proposed procedure is promising for further research by means of *ex vivo and in vivo* animal and human experiments. This procedure is expected to be used in robot-assisted systems for prostate biopsy and brachytherapy.

References: [1] R. Siegel, D. Naishadham, and A. Jemal, "Global cancer statistics," CA Cancer J. Clin., vol. 61, pp. 69-90, 2011.

[2] S. Han, S. Zhang, W. Chen, C, Li, "Analysis of the status and trends of prostate cancer incidence in China," Chin. Clin. Oncol., vol. 18, pp. 330-334.

Disclosure of Interest: None Declared

Mechanics

SS-0034

LOCOMOTION DYNAMICS OF GECKO: PATTERNS OF REACTION FORCES ON INCLINES?

Zhendong Dai [1,*]Zhouyi Wang [1]Aihong Ji [1]

[1]Nanjing University of Aeronautics and Astronautics, Nanjing, China

Introduction and Objectives: Locomotion is essential character of animals, and excellent moving ability results from the delicate sensing the reaction forces acting on body and modulating the behavior to adapt the motion requirement. In natural circumstance, animals have to move on various inclined surface, how animals adapt their behavior on the inclines is an interesting topic which attracted a lot of researches. In fact, there were a lot of studies were carried out when human or other mammals walk or run on shallow inclines (slope angle less than 60 degree), there were some studies when animals, such as geckos, cockroachs. Only our group measured the reaction forces of gecko moving on overall inclines, namely, floor, wall and ceiling. We found that the patter of reaction forces of gecko on the three different substrates are absolutely different, the questions we are going to ask here 1) How do the patterns of reaction forces change with slope angles and what slope angle is the critical angle at which the pattern of reaction forces change? 2) What factor induces the gecko to change the patter of reaction forces? Here we try to answer first question by measuring the reaction forces of gecko moving on various inclines and set up mechanical models to explain why the pattern change on the specific slope angle.

Methods: *Tokay geckos*, from Guangxi, China, were used in experiment (63.4±2.6g mass, snout-vent length: 138.4±6.3mm, mean ± s.d., *N*=8). The geckos were housed in two cages connected by an aisle to train them to move through the aisle of the force measuring array (FMA). The FMA was rotated step by step (30° per step) to imitate different incline surfaces. Synchronously to the force measurement (500Hz), a high speed camera (iSpeed-3, Olympus, 1280×1024 pixels) recorded each trial at 500 Hz. Moving behavior results from the continuous force action, so impulse of the forces were introduced to present the force effects. The orientation of foot in the stance phase was reflected by the orientation angle of foot between the fore-aft direction and the vertical line which is perpendicular to a line connecting the tips of the first and fifth toes.

Results: The moving speed of geckos decreased with incline angle. The duty factor of locomotion is heavily affected by the incline slope when the angle is larger than 90°, it is 0.54 when climbing on the wall (90° incline) and 0.84 when crawling on the ceiling (180° incline).

The lateral force impulses I_L acting on the front and hind limbs increased with respect to inclines, and the I_L acting on front limb increased faster than that acting on hind limb. The results suggest that lateral force become more important on larger slope inclines. The fore-aft impulse I_F acting on front limb increases with increase of incline. The front limb generated negative I_F when gecko move on non-horizontal surface, which suggests that the front limb plays an important role as a brake on horizontal surface while playing a role of propulsion on non-horizontal surface. The hind limb generated positive I_F that appeared to act as a source of propulsion over the range of the incline angle from 0° to 120°, but changed to act in the role of braking from 150° to 180°. The front limb provided negative normal impulses I_N to pull the center of mass

toward incline when inclines were larger than 90°. Alternatively, the hind limb began to provide negative I_N when the incline became greater than 120°.

The shear force impulse I_S acting on the hind limbs undergone obvious turning backwards as indicated by the solid lines in Figure 1. The change in the hind foot's orientation angle is not obvious, yet, indicated by the dotted line in Figure 1. These results may be explained by the fact that the angles between each adjacent flexible toe are noticeably different from one another.

Figure:
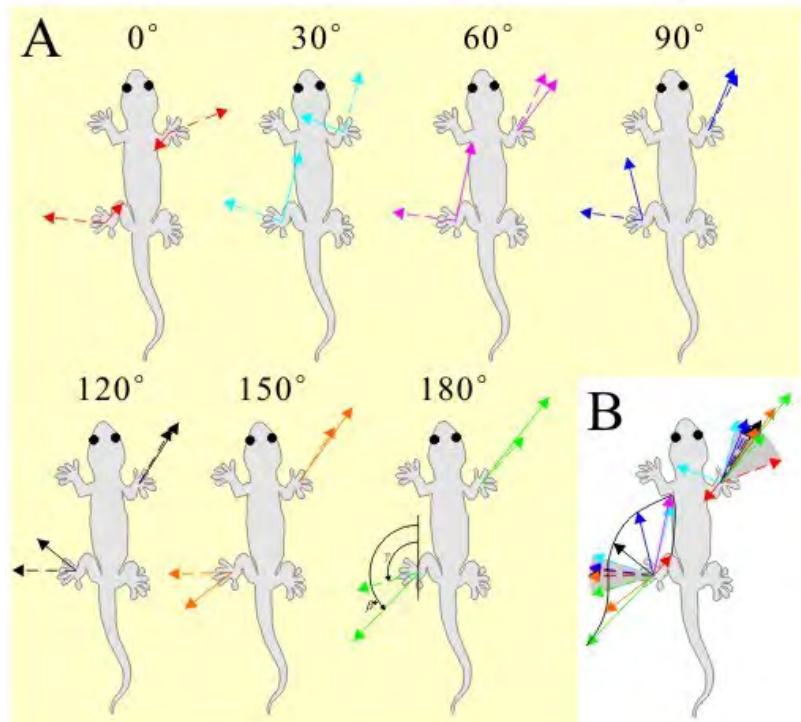
Caption: Figure 1 The relationships among the shear force impulse, orientation angle of the feet, and the incline angle. (A) Change in the shear force impulses and the orientation angle of gecko on different inclines. (B) Overprinting the shear force impulses and the orientation angle of gecko on different inclines.

Conclusion: The detailed three-dimensional reaction forces acting on an individual limb demonstrate that accurate force control is a benefit necessary to secure highly reliable attachment on inverted inclines and to enhance locomotion abilities. The pattern of reaction forces in response to inclines is directly linked to the favorable trade-off between locomotor maneuverability and stability. The geckos respond to increased inclines with a sort of threshold effect. The mechanisms revealed by above study help us to improve the performance of robots and expand its scope of application.

Disclosure of Interest: None Declared

Motion Analysis

SS-0035

AGE-RELATED CHANGES IN CENTER OF MASS TRAJECTORIES AND ACCELERATION DURING OBSTACLE CROSSING

Le Li [1,*] Na Chen [1] Yurong Mao [1] Chenming Ma [2] Lifang Li [1] Dongfeng Huang [1]

[1]Rehabilitation Medicine, First Affiliated Hospital, Sun Yat-sen University, [2]School of Engineering, Sun Yat-sen University, Guangzhou, China

Introduction and Objectives: Background: Tripping over obstacles may cause falls in the elderly while falls to the side is one of the determinant risk factors for traumatic hip fracture.

Objective: To analyzed and compared the spatial relationship of different trajectories when cross over obstacles by elder people and young group and to find the balance control mechanism.

Methods: 12 healthy elder adults and 12 healthy adults were divided to elder group and young group. Full-body three-dimension motion analysis system and force plates were used to capture and explore the characteristics of dynamic balance when crossing 10%, 20%, and 30% height of leg length of obstacles. The RMS (root mean square) value of the COM-COP distance as well as the peak COM acceleration in horizontal direction was calculated.

Results: The older adults exhibited greater average medio-lateral (ML) COM-COP distances during the leading limb stance phase after crossing the obstacle and lower anterio-posterior (AP) peak COM acceleration during the double support phase as they just about to crossing the obstacle. A moderate negative linear relationship was also found between peak AP COM acceleration and the crossing time which increased as the obstacle height increased.

Figure:
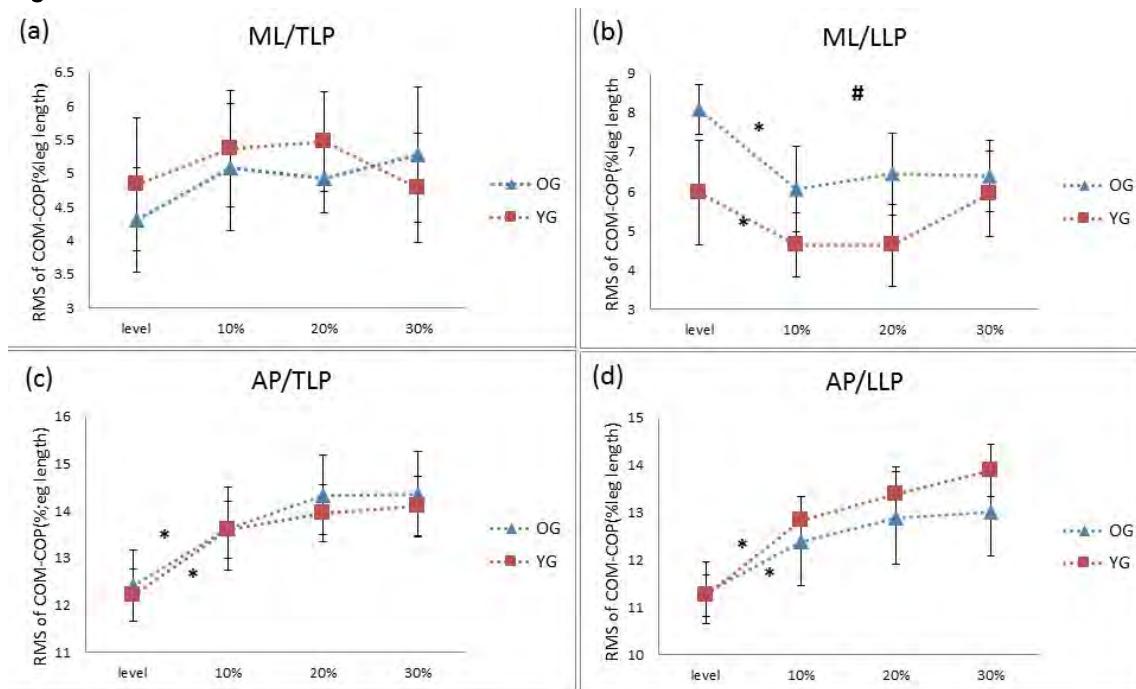
Caption: Fig. 1. Mean COM acceleration patterns in a crossing stride of 4 trials of level walking or 4 trials each of 3 heights obstacle crossing of a male young subject. ML: medio-lateral direction, AP: anterio-posterior direction.

Conclusion: Root mean square (RMS) of COM–COP divergence and peak acceleration of COM has been suggested to be a useful measurement to provide valuable insight into balance and postural control in human body. The larger average ML COM-COP distances indicate high-risk of falling sideways in elderly.

Table: Table1 The spatiotemporal parameters of the unobstructed trial of the old and young group.

	Cadence (steps/min)	step time (s)	step length	walking speed (/s)
old	100.15±9.66	0.60±0.07*	0.66±0.06	1.11±0.19
young	108.05±8.35	0.56±0.05*	0.71±0.04	1.30±0.15

* < 0.05

References: References:

 [1] Masani K, Vette AH, Kouzaki M, Kanehisa H, Fukunaga T, Popovic MR. Larger center of pressure minus center of gravity in the elderly induces larger body acceleration during quiet standing. Neurosci Lett. 2007;422(3):202-6.

 [2] Betker AL, Moussavi ZM, Szturm T. Ambulatory center of mass prediction using body accelerations and center of foot pressure. IEEE Trans Biomed Eng. 2008;55(11):2491-8.

 [3] Gschwind YJ, Kressig RW, Lacroix A, Muehlbauer T, Pfenninger B, Granacher U. A best practice fall prevention exercise program to improve balance, strength / power, and psychosocial health in older adults: study protocol for a randomized controlled trial. BMC Geriatr. 2013;13:105.

 [4] Greenspan SL, Myers ER, Kiel DP, Parker RA, Hayes WC, Resnick NM. Fall direction, bone mineral density, and function: risk factors for hip fracture in frail nursing home elderly. Am J Med. 1998;104(6):539-45.

Disclosure of Interest: None Declared

Spine

SS-0037

THE EFFECT OF CERVICAL FLEXION AND EXTENSION ON THE C5-6 AND C6-7 DISC AS MEASURED ON MAGNETIC RESONANCE IMAGING

Areej Elmaazi [1,*] Chris Morse [1] Sandra Lewis [1] Islay McEwan [1]

[1]Exercise and Sports Science, Manchester Metropolitan University, Manchester, United Kingdom

Introduction and Objectives: Cervical pain and its associated dysfunction is one of the most common musculoskeletal complaints in adults in Western society. Research suggests that one of the causes of neck pain is a sustained forward head posture [1]. This head posture is commonly adopted by people for prolonged periods while using modern technological devices such as laptops, tablets and mobile phones. The posture of the spine while in this position involves flexion of upper and lower cervical segments. One of the potential causes of pain while sustaining this posture may be the pressure this induces on the lower cervical discs which have been shown to be pain sensitive structures [2]. Research in the lumbar spine has shown that in healthy discs, there is migration of disc material away from the area of compressive force such that flexed postures (e.g. slouched sitting) causes posterior migration of disc material [3, 4]. No in vivo studies have been completed to confirm whether cervical discs also conform in a similar manner to the biomechanical pressures caused by various spinal postures. The purpose of this study was to assess, with the use of magnetic resonance imaging (MRI), whether flexion and extension of the cervical spine cause immediate, predictable changes in position of the posterior nucleus pulposus of the C5-6 and C6-7 discs.

Methods: Nineteen asymptomatic volunteers (nine males and ten females) between the ages of 21 and 49 years (mean = 33.7, SD = 9.1) were used to assess the effects of three different cervical spine postures on position of the nucleus pulposus. They were placed supine in a 0.2 T MRI scanner with sagittal images captured of the cervical spine in a neutral, followed by a flexed and finally an extended position. Position of the mid-posterior section of the disc nucleus was measured, in centimetres, relative to a line connecting the mid-section of posterior end of the vertebral bodies superior and inferior to the disc. If the mid-posterior section of the nucleus fell posterior to this line the measurement was recorded as a positive number. If it fell anterior to this line the measurement was recorded as a negative. If the posterior nucleus fell exactly on the line the measurement was recorded as zero. Measurements taken in all three cervical positions were compared at the C5-6 and C6-7 disc levels. The OsiriX Imaging Software program for Apple Macs was used for all disc measurements. A one-way repeated measures ANOVA was conducted to determine whether there were significant differences in posterior nucleus pulposus position with the cervical spine placed in neutral, flexion and extension in supine lying. Level of significance was set to 0.05.

Results: The change in cervical position elicited significant changes in position of the posterior nucleus pulposus for both the C5-6 (p = .003) and the C6-7 disc (p = .000). There were significant differences in disc position between neutral and flexion and between flexion and extension at the C5-6 disc level. There were statistically significant differences between all cervical positions at the C6-7 level (please see table 1).

Conclusion: This study examined the effects of three cervical spine postures on position of the nucleus pulposus at the C5-6 and C6-7 disc level in asymptomatic volunteers. Studies assessing healthy lumbar discs have shown that the

nucleus pulposus moves in a predictable manner when the lumbar spine is placed in various flexed and extended postures. The findings from this study also show that the cervical disc moves in a predictable manner with the nucleus pulposus in a flexed posture having a greater posterior position than in an extended posture at both the C5-6 and C6-7 disc levels. This may have implications for work and leisure activities involving sustained forward head postures. Although posterior disc prolapse has been poorly correlated with incidence of neck pain, reducing its occurrence with appropriate posture may help prevent the development of more significant disc extrusions which have been linked with pain and paraesthesia [5]. It is also important to note that cervical extension caused a reduction in posterior disc migration which may be useful as evidence to support directional therapeutic rehabilitative techniques.

Table:

Disc level	Comparison	Mean Difference	P value
C5-6	Neutral vs Flexion	.071	.010
	Neutral vs Extension	.032	.249
	Flexion vs Extension	.103	.006
C6-7	Neutral vs Flexion	.104	.000118
	Neutral vs Extension	.046	.045
	Flexion vs Extension	.058	.005

Caption: Table 1. Mean difference (cm) between disc positions and significance values for each comparison.

References:

1. Alexander, S. and Sabbahi, M., J Orthop Sports Phys Ther, 30(1): 4-12, 2000.
2. Cloward, R., Ann. Surg, 150: 1052-1064, 1959.
3. Alexander et al., Spine, 32(14): 1508-1512, 2007.
4. Parent et al., Spine, 31(24): 2836-2842, 2006.
5. Jenkins et al., Am J Roentgenol, 152(6): 1277-1289, 1989.

Disclosure of Interest: None Declared

THE EFFECTS OF EXPERIMENTALLY INDUCED LOW BACK PAIN ON SPINE ROTATIONAL STIFFNESS AND LOCAL DYNAMIC STABILITY.

Gwyneth Ross [1,*]Matthew Mavor [2]Stephen Brown [3]Ryan Graham [1 2]

[1]School of Kinesiology and Health Studies, Queen's University, Kingston, [2]School of Physical and Health Education, Nipissing University, North Bay, [3]Department of Human Health and Nutritional Sciences, University of Guelph, Guelph, Canada

Introduction and Objectives: Local dynamic stability, quantified using the maximum finite-time Lyapunov exponent (λ_{max}), and the muscular contributions to spine rotational stiffness can provide pertinent information regarding the neuromuscular control of the spine during movement tasks [1]. Studying patients with low back pain (LBP) is traditionally difficult due to: large variation in subjective pain ratings across individuals; high numbers (80-90%) of non-specific diagnoses (i.e. there is no accurate or precise diagnosis and no valid and objective diagnostic tool); no pain-free data exist to compare results to; and accurate maximum voluntary contractions are nearly impossible to obtain [2,3]. The primary goal of the present study was to assess if experimental capsaicin-induced LBP affects spine stability and the neuromuscular control of repetitive trunk movements in a group of healthy participants with no history of LBP.

Methods: Fourteen healthy males were recruited for this investigation. Participant mean age, height, and mass were 21.79 years (SD = 2.8), 180.51 cm (SD = 7.0), and 77.83 kg (SD = 9.1), respectively. Upon arrival, participants filled out two questionnaires related to kinesiophobia: 1) Tampa Scale for Kinesiophobia (TSK), and 2) The Pain Catastrophizing Scale (PCS) [4]. Each participant was then asked to complete three trials of a repetitive trunk flexion/extension task (Figure 1), at a rate of 0.25Hz for 35 cycles: 1) baseline, 2) in pain, and 3) recovery (1 hour later). Pain was induced using a heat-capsaicin model using over-the-counter topical 0.075% capsaicin cream. Throughout these trials, trunk kinematics and electromyography were monitored as per [1], and directly before and after each trial participants rated their pain on a 100mm visual analogue scale (VAS). The local dynamic stability of spine kinematics and the muscular contributions to spine rotational stiffness were extracted using published methods [1]. Local dynamic spine stability was assessed using the maximum finite-time Lyapunov exponent (local divergence exponent), λ_{max} [1]. Conversely, rotational stiffness was calculated about all three primary axes of movement by entering data into an anatomically-detailed EMG-driven biomechanical model consisting of 58 muscle lines of action representing seven bilateral muscle groups crossing the L_4/L_5 spinal joint [1]. Then, to get an estimate of total stiffness the three axes were summed, and the mean, maximum, and minimum stiffness were extracted across all cycles and averaged [1].

Results: The capsaicin cream was successful in inducing significantly higher levels of pain than those observed at either baseline or recovery (p<0.001). Local dynamic stability and the minimum muscular contributions to lumbar spine rotational stiffness were significantly impaired during the low back pain trial compared to the baseline trial (p<0.05); additionally, there was a trend for these measures to recover after one hour rest (Table 1). Strong correlations were found between increased perceived levels of pain and decreased spine stability and rotational stiffness. There were also strong

correlations between increased kinesiophobia and perceived pain levels, and decreased spine rotational stiffness and stability.

Figure:
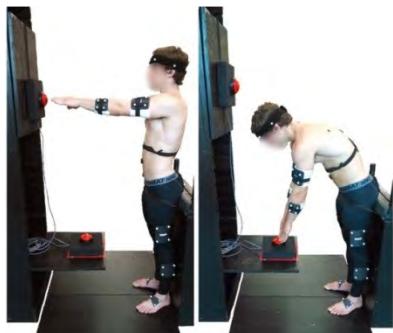
Caption: Figure 1. Experimental protocol. Participants were required to repetitively touch the instrumented targets with their hands held together to the beat of a metronome at a rate of 0.25Hz.

Conclusion: This study provides evidence that low back pain induced by capsaicin can effectively impair/inhibit spine rotational stiffness and local dynamic stability. Our current research is assessing changes to these same variables during pain induced via interspinous ligament injections, as well as further studying the relationship between kinesiophobia and LBP. An overarching goal of this research is to develop an objective diagnostic tool for assessing spine impairment and treatment effectiveness in chronic LBP patients.

Table:

Mean (SD) Results				Repeated-Measures ANOVA P-Value Results			
	Baseline	Capsaicin	Recovery	Main Effect	Baseline vs. Capsaicin	Baseline vs. Recovery	Capsaicin vs. Recovery
Local Dynamic Spine Stability (λmax)	2.00 (0.15)	2.11 (0.23)	2.06 (0.26)	**0.048**	**0.019**	0.442	0.243
Mean Total Spine Stiffness (Nm/rad)	4563.24 (137338)	4383.20 (1591.16)	4529.43 (1528.78)	0.095	0.063	0.708	0.053
Max Total Spine Stiffness (Nm/rad)	6918.61 (2068.44)	6781.27 (2885.77)	7040.21 (2907.53)	0.224	0.641	0.648	0.082
Min Total Spine Stiffness (Nm/rad)	2738.98 (933.39)	2570.83 (879.32)	2629.98 (843.80)	**0.005**	**0.009**	0.165	0.101

Caption: Table 1. Local dynamic spine stability and the total muscular contributions to spine rotational stiffness results. Bolded values indicate a significant effect at p<0.05.

References: [1] Graham et al., J. Biomech., 45: 1593-1600, 2012.

[2] Marras et al., Spine, 24: 2091-2100, 1999.

[3] Zedka et al., J. Physiol., 520: 591-604, 1999.

[4] Karayannis et al., Plos One, 8: p. e67779, 2013.

Disclosure of Interest: None Declared

Spine

THE IMPACT OF SIT-STAND WORKSTATIONS ON MUSCLE ACTIVITY AND SPINAL SHRINKAGE IN OFFICE WORKERS

Ying Gao [1,*] Neil Cronin [1] Arto Pesola [1] Taija Finni [1]

[1] Neuromuscular Research Center, Department of Biology of Physical Activity, University of Jyväskylä, Jyväskylä, Finland

Introduction and Objectives: Prolonged sitting time is adversely associated with cardio-metabolic and musculoskeletal health outcomes [1, 2]. To prevent these risks in a highly prevalent group of office workers, reducing sitting time by means of sit-stand workstations is an emerging trend but further evidence is needed regarding their health benefits. This study compared muscle activity and inactivity time, and spinal shrinkage between office workers who used either a sit-stand workstation or a traditional sitting workstation. We also quantified spinal shrinkage before and after a workday and examined whether there was an association between spinal shrinkage and locomotor muscle activity during work time.

Methods: This cross-sectional study compared work time muscle activity and spinal shrinkage between healthy office workers (aged 24-62, 58.3% female) who used either a sit-stand workstation (Sit-stand group, n=10) or a traditional sitting workstation (Sit group, n=14). During one typical workday, muscle inactivity and activity from quadriceps and hamstrings were monitored by electromyography (EMG) shorts and spinal shrinkage was measured using stadiometry before and after the workday. The differences between groups were tested by independent t-test or Mann-Whitney U and the correlation between the total muscle activity time and spinal shrinkage was studied by a partial correlation.

Results: Compared with the Sit group, the Sit-stand group had less muscle inactivity time (66.2±17.1% vs. 80.9±6.4%, p=0.014) and more muscle light activity time (26.1±12.3% vs. 14.9±6.3%, p=0.019) with no difference in spinal shrinkage (5.62±2.75 mm vs. 6.11±2.44 mm) (Table 1). Spinal shrinkage was positively associated with muscle light activity time (min) (r=0.460, p=0.041, Figure 1).

Figure:
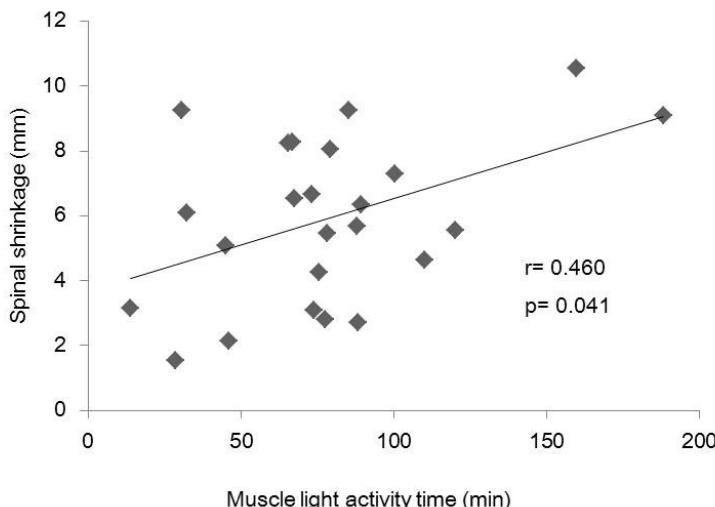
Caption: FIGURE 1. Relationship between locomotor muscle activity and spinal shrinkage during a workday

Conclusion: This study was performed in an ecologically valid setting and provides evidence that sit-stand workstations promote metabolic health by increasing muscle light activity time and reducing inactivity without harmful effects on spinal shrinkage.

Table:

Characteristics	Sit group (n=14)	Sit-Stand group (n=10)	All (n=24)	p for group difference
EMG-derived muscle activity				
Recording time (min)	392.3±23.5	420.1±65.9	403.9±47.0	0.770
Inactivity time (%)	80.9±6.4	66.2±17.1	74.8±13.9	**0.014**
Activity time (%)	19.1±6.4	33.8±17.1	25.2±13.9	**0.014**
Light activity time (%)	14.9±6.3	26.1±12.3	19.6±10.6	**0.019**
Moderate-to-vigorous activity time (%)	4.2±2.1	7.7±7.4	5.7±5.2	0.349
No of bursts	563.4±238.6	601.2±97.5	579.1±190.4	0.600
Sum of 5 longest inactivity periods (min)	60.8±37.4	41.6±17.6	52.8±31.7	0.178
Spinal shrinkage (mm)	6.11±2.44	5.62±2.75	5.91±2.53	0.653

Caption: TABLE 1. Workday EMG-derived muscle activity and spinal shrinkage in the two study groups

References: [1] Wilmot et al., Diabetologia, 55: 2895-2905, 2012.

[2] Lis et al., Eur Spine J, 16: 283-298, 2007.

Disclosure of Interest: None Declared

SS-0042

THE KINEMATIC ENVELOPE OF THE THUMB CARPOMETACARPAL (CMC) JOINT

J.J. Trey Crisco [1,*]Tarpit Patel [1]Eni Halilaj [1]Douglas Moore [1]

[1]Orthopaedics, Brown University, Providence, United States

Introduction and Objectives: The unique and important positioning of the thumb with respect to the hand is achieved through the unconstrained articulations at the thumb carpometacarpal joint (CMC). The articular surfaces of the CMC joint are considered saddle–shaped, and motion of the metacarpal is often idealized as rotation about two orthogonal axes. These primary kinematics of the CMC joint were skillfully described in a cadaver study by Hollister et al. [1], who demonstrated that the extension-flexion (FE) and abduction-adduction (AA) axes are non-orthogonal and non-intersecting. Additionally, Edmunds (2011) proposed that the soft tissues surrounding the CMC joint generate a stabilizing screw-home motion at the end of thumb flexion. A screw home mechanism requires a coupled rotation and/or translation; however, previous experimental studies have not described translation or rotational coupling of the thumb CMC joint. The purpose of this study was determine the in vivo kinematics of the thumb CMC joint during normal physiology motions and then to develop a mathematical description of the envelope of screw axes that completely defines these kinematics.

Methods: After IRB approval, CT volume images were acquired of one hand from 44 healthy subjects (20 M, age 47.9±14.2; 24 F, age 45.4±11.8) with the thumb in five positions: neutral, extension, flexion, abduction and adduction. Kinematics among all possible combinations of positions were computed and described using helical axis of motion parameters and reported with respect to a coordinate system aligned with the directions of principal curvature on the trapezium. A two-way ANOVA (sex x age) was used to evaluate differences in the mean screw axis location and position as a function of sex and age. Root mean square error (RMSE) was used to assess the validity of the mathematical model that was developed to describe the envelope of CMC kinematics.

Results: Differences in the mean kinematic variables with sex and age were small and not statistically significant. Across all subjects the FE rotation axis was offset 26.7° (1 SD = 13.1°) from the ulnar-radial coordinate axis (azimuth) and elevated 21.1° (13.1°). The AA axis was oriented 4.4° (11.2°) from the dorsal-volar coordinate axis (azimuth), and elevated 25.3° (13.5°). The minimum distance between the FE and AA axes was 9.2 mm (2.5 mm) and angle between the axes was 124.1° (18.7°). Interestingly, substantial translation was coupled with the FE and AA rotation: For every ~10° of flexion, the MC1 translated 1 mm (p < 0.0001, R^2 = 0.617) in a volar-radial direction and for every ~6° of abduction the MC1 translated 1 mm in a dorsal-radial direction (p = 0.026, R^2 = 0.1132).

Defining the azimuth angle (azi) of the HAM axis as the independent variable, each HAM variable in the set {t,ele,Qx,Qy,Qz} was a cyclic function of azi and a discrete Fourier analysis was successfully fit to each variable with RMSEs of 0.64 mm, 14.5°, 1.5 mm, 1.3 mm. and 1.3 mm, respectively.

Conclusion: This study reports the in vivo kinematics of the thumb CMC joint and demonstrates that a complete envelope of motion exists and it includes the previously reported non-orthogonal and non-interesting axes of extension-flexion and abduction-adduction. In the healthy cohort studied, sex and age were not notable factors in the kinematics. We found substantial translation coupled to the rotational DOF which has not been widely reported. Our approach to the

mathematical description was founded on the observation that the CMC joint has two primary directions of motion: extension-flexion and abduction-adduction, and all the other primary motions are components of these two motions. This observation enabled us to define the azimuth (azi) orientation of the screw axis in the articular plane as an independent variable with a cyclic domain. A harmonic function could then be fit to the elevation and position of the screw axis, as well as the screw translation as a function of the magnitude of rotation (θ). As such, once the magnitude of the thumb rotation and its direction were specified, the locations of the screw axis and the associated translations were completely defined by the reported harmonic functions.

References: [1] Hollister, A., Buford, W. et al. J. Orthop. Res., 10(3): 454–460, 1992.

Disclosure of Interest: None Declared

PHYSIOLOGICAL AND PROSTHETIC ANKLE BEHAVIOUR ON CROSS-SLOPES

Coralie Villa [1][2],*Karine Langlois [2]Xavier Bonnet [3]Pascale Fode [1]Christophe Sauret [2]Francois Lavaste [1][2]Helene Pillet [2]

[1]CERAH, INI, Créteil, [2]Institut de Biomécanique Humaine Georges Charpak, Arts et Métiers ParisTech, Paris, [3]R&D, Proteor, Seurre, France

Introduction and Objectives: Cross-slopes walking is a common situation of daily living in which one has to adapt to the transverse inclination of the ground relative to his progression direction. This situation described as limiting for lower limb amputees has yet barely been studied in the literature [1][2][3]. Dixon et al. [1] highlighted that non amputee subjects gait is mainly adjusted on cross-slopes with changes in ankle behavior in the frontal plane. The aim of the study was to investigate ankle adjustments in the frontal plane during cross-slopes walking compared to level walking in a population of non amputee people and lower limb amputees.

Methods: Seventeen non amputee subjects, thirteen transfemoral amputees and fifteen transitibial amputees wearing their own prosthetic components were asked to walk back and forth at a comfortable speed on a flat pathway and on a cross-slopes device inclined of 6° both instrumented with four force platforms (AMTI, 100Hz) in a motion analysis lab equipped with eight optoelectronic cameras (Vicon V8i, UK) [4]. Anatomical frames, segmental and articular kinematics and kinetics of lower limbs were computed according to Pillet et al. [4].

Particularly, ankle angle and moment in the frontal plane were studied during stance phase of gait cycle when the lower limb is loaded: from heel strike to the end of the single limb support. The analyses were conducted for the residual limb (amputee groups) or the left lower limb (control group) during level walking (LW), cross-slopes walking with the limb uphill (CSU) and cross-slopes walking with the limb downhill (CSD).

Results: The figure summarizes the ankle frontal plane behaviour in all situations for all groups.

In the control group, a shift of the ankle angle was observed at heel strike. This ankle angle adjustment was on average of -4.0±1.8° between LW and CSU (towards valgus) and of +3.5±1.0° between LW and CSD (towards varus). In addition, compared to LW, the maximum valgus ankle angle and maximum varus ankle moment during stance significantly increased in CSU (-6.6±1.1° and --0.06±0.08Nm/kg between CSU and LW) and decreased in CSD (6.7±1.1° and 0.03±0.10Nm/kg between CSD and LW). In addition to these adjustments, from heel strike to the end of the single limb support, the ankle internal moment remains a varus moment in all situations and the ankle showed a similar pattern of behaviour among situations.

In the transfemoral (TF) and transtibial (TT) groups, prosthetic ankles behaved in a different way. During LW prosthetic ankles reached on average very low values of ankle angle amplitude and maximum varus moment (angle amplitude TF: 1.8±1.8°, TT: 2.3±1.7°, Controls : 10.9±4.4° / max moment TF: 0.04±0.09Nm/kg, TT: -0.01±0.17Nm/kg, Controls : -0.30±0.17Nm/kg). On cross-slopes, unlike controls, prosthetic ankles were adjusted according to the slope inclination. Indeed, the ankle internal moment and angle changed sign in both groups : were observed a valgus angle and varus moment in CSU and a varus angle and valgus moment in CSD. Prosthetic ankles were passively adjusted to cross-slopes according to the changes in mediolateral direction of the ground reaction force among conditions.

Figure:
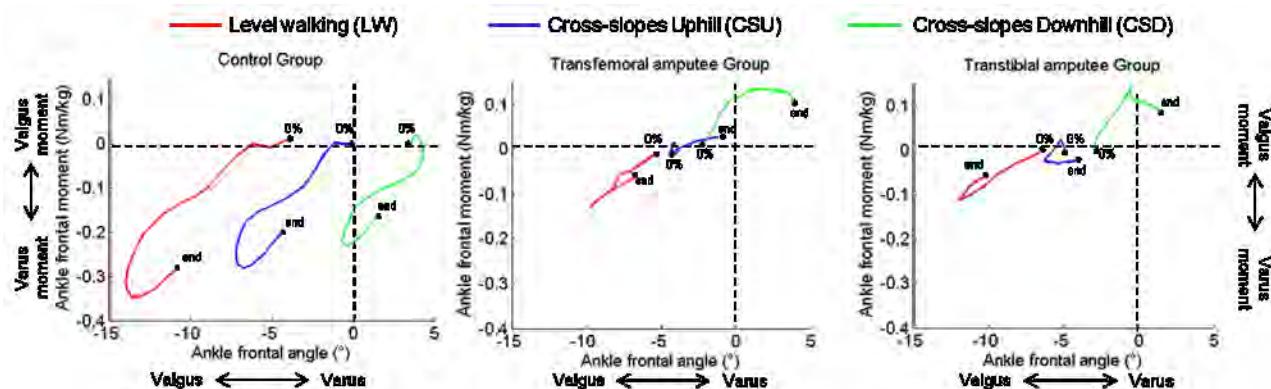
Caption: Ankle moment vs ankle angle in the frontal plane between heel strike (0%) and the end of single limb support during stance phase (end) for LW (blue), CSU (red) and CSD (green) in the two amputee patients groups (residual limb) and the control group (left lower limb)

Conclusion: Physiological ankles were in a pre-adapted position at heel strike resulting in a similar evolution of the moment during cross-slopes walking uphill or downhill and level walking. Prosthetic ankles only provided passive adjustments on cross-slopes. To facilitate amputee people locomotion on cross-slopes, prosthetic design should better reproduce physiological ankle behaviour on cross-slopes including the shift of the initial valgus angle position at heel strike according to the slope inclination.

References: [1] Dixon et al., J Appl Biomech, 26(1):17-25, 2010.
[2] Damavandi et al., Hum Mov Sci, 31(1):182-189, 2012.
[3] Starholm et al., Prosthet Orthot Int, 34(2):184-194, 2010.
[4] Pillet et al., Innov Res Biomed Eng, 35(2) : 60-65, 2014.

Disclosure of Interest: None Declared

LOWER-LIMB KINEMATICS AND KINETICS DURING AMPUTEE RUNNING: A NEW APPROACH

Stacey M. Rigney [1,*] Anne Simmons [2] Lauren Kark [1]

[1]Graduate School of Biomedical Engineering, [2]School of Mechanical and Manufacturing Engineering, University of New South Wales, Sydney, Australia

Introduction and Objectives: Recent athletics and sprinting competitions have seen lower-limb amputee athletes use carbon-fiber running specific prostheses (RSPs), which behave as leaf springs by storing and returning energy during the stance phase of running. The geometry and inherent behavior of such prostheses violate a number of assumptions utilized in inverse dynamics calculations [1]. Nevertheless, gait analysis of amputee running frequently utilizes these assumptions erroneously for a number of reasons, primarily efficiency and convenience [2]. As an alternative to the conventional two-link segment model of the shank and foot, a multiple-link segment (MLS) model consists of a number of rigid segments connected by torsional springs and dampers to represent the behavior of the prosthesis during loading. This type of model has been previously utilized in forward simulations of amputee walking gait [3], but its value in high-energy activities, such as sprinting, is yet to be determined. Therefore, the aim of this study is to assess the value of MLS models in amputee sprinting, and to optimize prosthesis modeling by determining the minimum number of segments required to best represent prosthesis behavior.

Methods: Experimental gait analysis was performed at the Australian Institute of Sport in accordance with UNSW Australia Human Research Ethics Committee approval HC13054. A 16-year-old female right-sided transtibial amputee of mass 58kg and height 163cm sprinted at maximum speed along an indoor 100m straight running track instrumented with eight Kistler 9287B 1000Hz force plates and 20 VICON MX T40-S 250Hz motion capture cameras. Both a Full Body Plug-in-Gait (PiG) and custom set of passive-reflective markers were placed on the subject, where the custom set included seven additional markers placed along the lateral side of the prosthesis, three on the posterior side and two on the lateral side of the socket.

Post-processing of the experimental data was conducted in the open-source musculoskeletal modeling software OpenSim. A generic full-body, no arms musculoskeletal model [4] was scaled according to the experimental trajectories of both the PiG and custom marker sets (Figure 1a). The MLS mathematical model of the prosthesis consisted of six rigid bodies defined by at least two markers each, connected in series via single degree-of-freedom torsional springs and dampers (Figure 1b). The PiG marker set defined the virtual foot (Figure 1c) and shank segments connected via a pin joint. A half factorial Design of Experiments analysis was used to investigate the significance of each of the five joints at a 95% confidence level, resulting in 16 configurations of the MLS model. The comparison criteria consisted of peak hip flexion during swing phase, peak hip extensor moment, minimum knee flexion during stance phase and peak knee extensor moment for both the right and left legs using each of the MLS models and the PiG model.

Results: For the hips and knees of both legs, the peak flexion angles and moments calculated using the MLS models, averaged across all configurations, were significantly different (p<0.001) in comparison to the PiG model results (Table 1, columns 3-5). When considering individual MLS configurations, every joint was found to significantly affect at least one

variable of interest (Table 1). For example, joint 1 alone did not affect right hip flexion, however when combined with joint 4 the results were significant. Overall, the calculated lower-limb kinematics and kinetics were highly sensitive to model selection.

Figure:
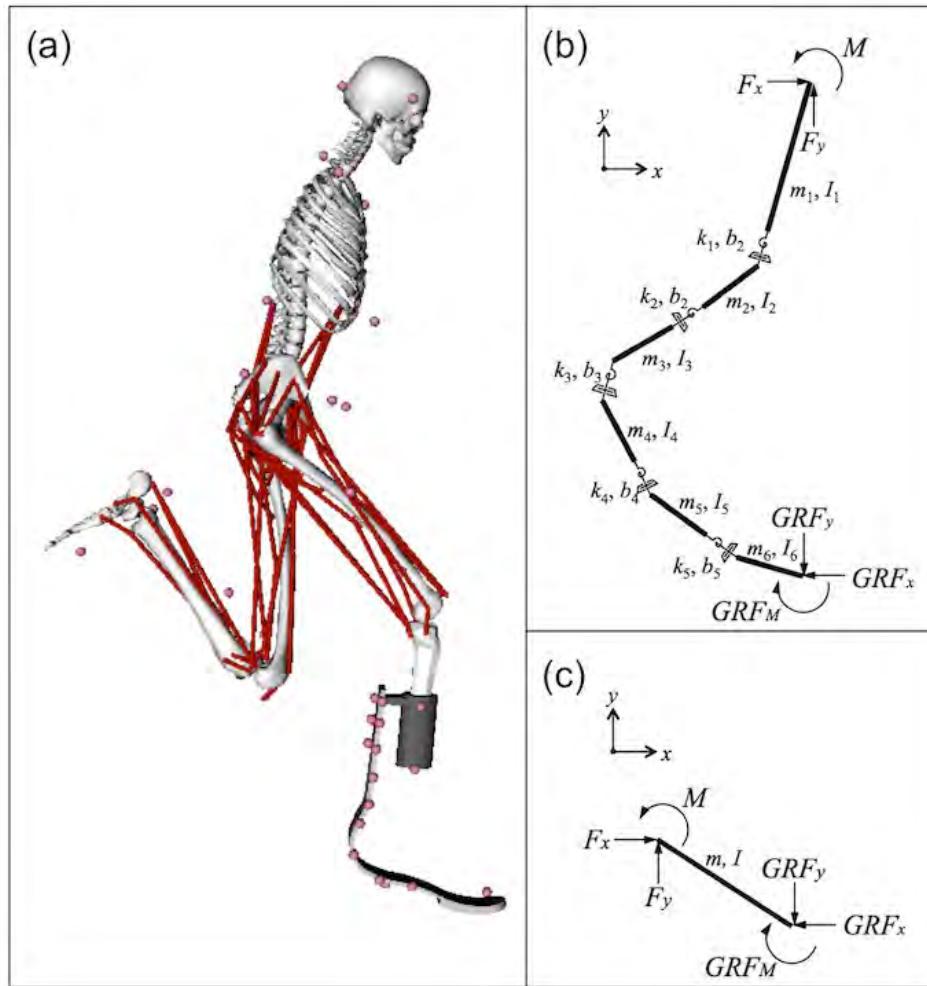
Caption: Figure 1 – Models used during gait analysis: (a) full-body musculoskeletal, (b) multiple-link segment and (c) conventional virtual foot segment.

Conclusion: During this study, the calculation of hip and knee angles and moments during amputee running has been shown to be highly sensitive to the selection of link segment model ($p<0.001$). Instead of using a traditional PiG model for gait analysis of amputee running, we recommend a MLS model consisting of at least six segments. Future work in the area should include incorporation of this MLS custom marker set directly into motion capture software for all clinical applications involving RSPs.

Table:

Limb	Variable	PiG	16 x MLS		Significant MLS joints and/or combinations of joints
			Mean	**Std Dev.**	
Right	Hip Flexion	56.8	66.3	0.26	1+4
	Hip Moment	-750.2	-656.2	20.3	2, 3+5, 4, 2+3, 5
	Knee Flexion	11.4	21.1	0.275	1+3, 4
	Knee Moment	-436.5	-469.5	12.7	Nil
Left	Hip Flexion	61.5	73.3	0.989	1+3, 3
	Hip Moment	-751.6	-728.0	12.4	Nil
	Knee Flexion	8.4	9.1	0.361	1, 2+4, 1+5
	Knee Moment	-519.6	-506.6	2.99	Nil

Caption: Table 1 – Lower-limb kinematics and kinetics calculated using the PiG model compared to the sixteen configurations of the MLS model, where joints were labeled consecutively from proximal to distal.

References: [1] Sawers et al., J Prosthet Orthot, 22: 56-61, 2010.

[2] Kent et al., J Prosthet Orthot Int, 35: 124-139, 2011.

[3] Fey et al., J Biomech, 46(4): 637-644, 2013.

[4] Delp et al., IEEE T Biomed Eng, 37: 757-767, 1990.

Disclosure of Interest: None Declared

INVESTIGATION INTO RAMP DESCENT AMBULATION FOR TRANSFEMORAL AMPUTEES WHEN USING AN INTEGRATED PROSTHESIS

Nadine Stech [1,*] Aliah F Shaheen [1] David Ewins [1]

[1]Centre for Biomedical Engineering, Department of Mechanical Engineering Sciences, University of Surrey, Guildford, United Kingdom

Introduction and Objectives: Much research has been undertaken on level ground ambulation to gain a fundamental understanding of transfemoral amputee gait. Ramp ambulation has not been considered to such an extent even though gait is highly influenced by the surface inclination, as can be seen in non-amputee gait studies [1].

This study has investigated the influence of braking actions of an integrated knee and ankle prosthesis for transfemoral amputees. The integrated prosthesis working through a single controller allows the implementation of different braking strategies at both joints. Non-amputee studies have shown a negative net energy for ramp descent where the ankle and knee joint absorb much of the energy [2]. Therefore, it was expected that incorporating a braking action into an integrated prosthesis would be beneficial.

Methods: Four established transfemoral amputees of K3 level participated in the gait study and signed consent was given. Each amputee used the integrated prosthesis, which consists of a microprocessor controlled hydraulic ankle and a microprocessor controlled hybrid knee joint working through a single controller. This controller enabled adjustment of (braking) resistance levels wirelessly. The prosthesis was aligned by an experienced prosthetist and the alignment was not changed throughout the data collection.

Kinematic and kinetic data were collected using a Codamotion Gait Analysis system and a Kistler force plate. The force plate was integrated in a 5° degree ramp. The level of declination was chosen as it falls within the guidelines of UK building regulations [3]. Data from the 4 sensors in the knee and ankle units were also collected.

The internal resistances of the knee and ankle joints were adjusted and their influence on the gait of the volunteers was investigated. Four scenarios were considered:

a)   No braking action of the limb

b)   Braking action of the ankle

c)   Braking action of the knee

d)   Braking action of the knee and ankle as an integrated limb

For each of those scenarios the optimal resistance levels at a normal self-selected speed were established before the formal data collection took place. In each case, the resistance was adjusted until the participant and the prosthetist were satisfied that it was providing sufficient but not too much support.

Additionally, subjective feedback was also collected. Each participant and the prosthetist rated the gait performance with regard to perceived safety and smoothness of each scenario independently.

Results: The ground reaction forces show clearly the influence of braking in the ankle, as the peak value and the timing of the braking impulse (posterior forces) is more pronounced.

The ankle had an impact on gait from early to mid-stance particular on the anterior-posterior ground reaction force and the sagittal plane ankle bending moment, whereas the knee showed its damping influence in mid to late stance. Most participants described the ramp ambulation using the integrated limb brake as giving more control over the prosthesis. In most cases self-selected speed as well as cadence was lower using the integrated limb brake, as illustrated in the figure below. Transfemoral amputees have the tendency to accelerate during ramp descent with increasing momentum; a lower self-selected speed therefore indicates that they have more control over their gait.

Figure:
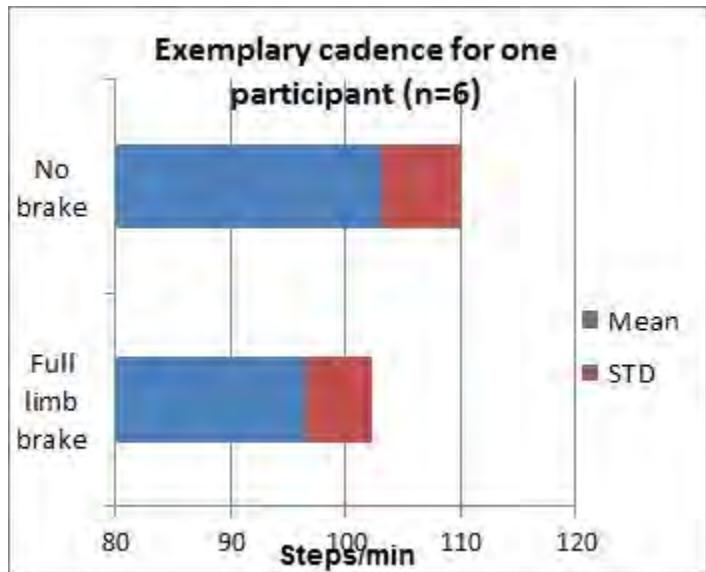
Caption: Exemplary Cadence for Ramp Descent Ambulation

Conclusion: The gait study showed that the amputees perceived a braking action in the whole limb during ramp descent as beneficial. They felt safer and that they had greater control of the prosthetic limb. The braking resistance level of the knee was found to be a very sensitive parameter.

A larger follow-up study is required to investigate in more detail the effects of the integrated limb brake and the impact of the setting of the knee and ankle braking resistance levels, e.g. on different gradients or with different self-selected speeds.

References: [1] LAY, A. N. et al. *Journal of Biomechanics,* 39: 1621-1628, 2006.

[2] SCHWAMEDER, H., et al. *SPECTRUM Suppl.,* 98-105, 2001.

[3] BSI Standards Publication. BS 8300:2009+A1:2010 Design of buildings and their approaches to meet the needs of disabled people - Code of practice, 2009-2010.

Disclosure of Interest: N. Stech Conflict with: Employee of Blatchford, A. F. Shaheen: None Declared, D. Ewins: None Declared

DIFFERENCES IN PELVIS AND THORAX KINEMATICS DURING THE STANDING TURN FOR PEOPLE WITH A UNILATERAL TRANS-TIBIAL AMPUTATION.

Tina Smith [1,]*Matthew Taylor [2]Siobhan Strike [3]

[1]Institute of Sport, University of Wolverhampton, Walsall, [2]University of Essex, Essex, [3]University of Roehampton, London, United Kingdom

Introduction and Objectives: The standing 180° turn is a common activity of daily living, however there is little biomechanical research on how this movement may be achieved, especially in people with a trans-tibial amputation. Previous research on turning while walking has indicated a reorientation of the trunk and pelvis [1] and that changing the direction of motion requires 3D motion at the ankle [2]. The simplest standing turn is made up of three turning steps. The address position prior to initiation of the turn is followed by a preparatory, turn and a depart step. It is possible that in order to execute these steps effectively a turn from standing will require even more ankle joint motion due to the increased demand to rotate about the longitudinal axis. As mobility at the ankle is compromised for amputees increased pelvic and thoracic contribution to the movement may be a compensatory mechanism adopted.

The aim of this research was to determine the contribution of the pelvis and thorax to movement about the longitudinal axis for each step of the turn when turning to either side from the intact or prosthetic limb.

Methods: Seven participants (height 1.76±0.06m; mass 85.2±9.6kg; time since amputation 16±10y) took part in the study. Participants were instructed to complete a standardised task which involved walking to a counter 3m away, picking up a slide rule and moving it 30cm, replacing it on the counter, turning through 180° and returning to the start point. This mimicked a task in which turning is embedded.

Data were collected with a 9-camera infrared system, sampling at 120Hz, recording 34 reflective markers attached to the participants according to the Vicon Plug-in-Gait model. Data was filtered using a low-pass Butterworth filter (cut-off frequency 6Hz). Pelvis and thorax transverse angular displacement for the double and single stance phase of each step of the turn, and the full turn were determined for turns from the intact and prosthetic limb. The turn direction (from intact v prosthetic limb) was determined by the stance limb during the turn step.

Results: All participants completed a turn using a prep, turn and depart step for both turn directions. Significantly greater pelvis and thorax angular displacement were exhibited in the single stance (SS) phase of the turn step (pelvis $p = .025$; thorax $p = .035$) when turning from the intact limb. When turning from the prosthetic limb significantly greater pelvis and thorax angular displacement (pelvis $p = .013$; thorax $p = .009$) occurred during the depart step when the intact limb was in SS (Table 1). No further differences were observed.

Conclusion: For turns in both directions, much of the directional change occurred when the intact limb was in stance. This meant that when the intact limb was in stance for the turn step, the reorientation was achieved mainly in that step (~74° of pelvic and thorax rotation in SS) and when the turn was completed from the prosthetic side (prosthetic limb in stance during the turn step), the reorientation mainly occurred in the depart step (~61° of pelvic and ~54° of thorax rotation in SS), when the intact limb was in stance (Table 1). Previous research on turning bias in trans-tibial amputees has

suggested no bias from the intact or prosthetic limb when repeatedly performing standing 180° turns [3]. The difference in the protocol, which adopted a shorter approach and completion of a turn embedded within a set task, may explain the turning bias evidenced here.

The adoption of the prep step and the observed strategy to favour the intact limb in order to perform much of the turn is suggestive of the amputees adopting a precautionary approach when completing a standing turn. This may have rehabilitation implications where amputees should be made aware of the restrictions when turning from the prosthetic limb and be taught how to turn effectively.

Table:

	From Prosthesis	**From Intact**
Preparatory Step	(SS on intact limb)	(SS on prosthetic limb)
Pelvis angular displacement DS (°)	4.1±4.1	5.7±5.6
Pelvis angular displacement SS (°)	16.6±7.5	19.3±8.2
Thorax angular displacement DS (°)	5.0±4.2	6.1±6.5
Thorax angular displacement SS (°)	15.1±7.6	16.5±7.4
Turn Step	(SS on prosthetic limb)	(SS on intact limb)
Pelvis angular displacement DS (°)	20.7±4.4	20.7±4.9
Pelvis angular displacement SS (°)	45.8±16.2	73.8±9.5
Thorax angular displacement DS (°)	27.2±16.1	22.2±5.6
Thorax angular displacement SS (°)	46.4±19.1	74.3±10.4
Depart Step	(SS on intact limb)	(SS on prosthetic limb)
Pelvis angular displacement DS (°)	17.9±4.7	17.9±3.6
Pelvis angular displacement SS (°)	61.6±19.0	35.6±6.5
Thorax angular displacement DS (°)	20.9±5.3	19.9±5.7
Thorax angular displacement SS (°)	54.4±18.3	28.6±7.5
Total		
Pelvis angular displacement (°)	166.3±13.6	171.8±4.8
Thorax angular displacement (°)	162.5±16.7	166.3±5.1

Caption: Table 1: Pelvis & Thorax angular displacement data (mean ± SD) during double (DS) and single support (SS)

References: [1] Patla et al., Exp Brain Res. 129:629-634, 1999.

[2] Taylor et al., Hum Mov Sci. 24:558-573, 2005.

[3] Taylor et al., Laterality. 12:50-63, 2007.

SS-0047

PRELIMINARY EVALUATION OF A MICROPROCESSOR-CONTROLLED KNEE ANKLE PROSTHESIS (MAKP) FOR ABOVE KNEE AMPUTEES.

Bonnet Xavier [1,*] Francis Djian [1] Boris Dauriac [2] Coralie Villa [3] Isabelle Loiret [4] Noel Martinet [4] Helene Pillet [2]

[1] R&D, PROTEOR, Seurre, [2] Institut de Biomécanique Humaine Georges Charpak, Arts et Métiers ParisTech, Paris, [3] CERAH, INI, Creteil, [4] IRR, Nancy, France

Introduction and Objectives: Prosthetic knees and feet design have benefited from important technical improvements over the last few decades. Microprocessor-Controlled Prosthetic knees have improved the safety and the functional outcomes of above knee amputee and became the gold standard of care in above knee prosthetics [1]. The control of the knee flexion during stance improved the walking ability both during stair [2] and slope descent [3]. In spite of these active engineering developments, patients continue to report some difficulties for ambulation, emphasized during outdoor activities [4].

Some of these difficulties could be attributed to the lack of ankle adaptations to different terrain. In literature, some authors highlighted this lack of adaptation to stairs [2] and slopes [5]. Thus, with stairs, step-by –step descent is made possible by placing the prosthetic foot on the edge of the step allowing the progression of the tibia during stance [6]. This strategy would be a consequence of the lack of mobility of the ankle resulting from the fixed stiffness of conventional prosthetic feet.

Some microprocessor-controlled prosthetic ankles are now available for both below knee and above knee amputees. In particular, some designs allow ankle movement during the swing phase. By increasing toe clearance, they reduce the risk of falling and allow adjustment of ankle position according depending on the slope [7]. Other designs including hydraulic devices were developed to adapt the ankle resistance during stance depending on the terrain [8]. Motorized design were recently presented [9-10]. Design of above knee amputee prosthesis must fit the following criteria: limited weight, reduced adaptation time and robustness.

The objective of the study was to evaluate a passive Microprocessor-controlled Knee Ankle Prosthesis (MKAP) able to mimic various adaptations quantified for asymptomatic people in slopes and stairs.

Methods: Four above-knee amputees were fitted with the prototype of MKAP. Motion capture of 54 markers placed on the patient according to the protocol described by Pillet [11]. Acquisitions were made in 3 situations of daily living simulated using instrumented devices: level ground, a ramp inclined at 12% (7°) and a 4-step staircase. From the marker set, kinetic and kinematic of 18 body segments were computed. A control group was formed with ten above-knee amputees fitted with a conventional Microprocessor-controlled Prosthetic Knee (MPK) and an Energy Storing and Return Foot (ESARF).

Results: Fig. presents the sagittal kinematic of the hip, knee and ankle of the prosthetic limb during slope ascent and descent and stair descent for the ten MPK users (shaded area) and for the four MKAP users (solid lines). Compared to MPK, MKAP allows a wider range of motion of both the prosthetic knee (especially during stair descent) and prosthetic ankle both during stance and during swing.

Figure:
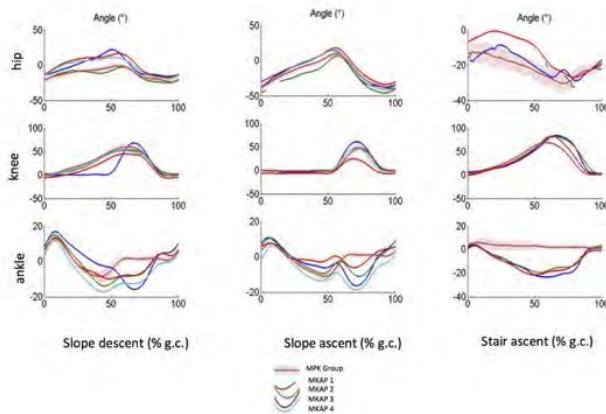
Caption: Prosthetic limb kinematics in the sagital plane

Conclusion: The limited range of ankle motion in conventional prosthetic feet does not allow amputees to keep the foot flat on the floor during ramp descent. The prototype, by allowing a reduction of the "equivalent" stiffness succeeds in restoring a large foot flat period during the single limb support phase on the prosthesis, securing this critical phase of gait. During slope ascent, the ankle dorsiflexion during swing helps the user to increase toe clearance reducing the risk of falling. During stair descent, the ankle motion range during stance avoids risky positioning of the prosthetic foot on the edge of the step. Very recent work done by Vanderbilt Unniversity have detailed the functioning of a motorized ankle/knee prosthetic system designed for above knee amputees [10]. This prototype is able to provide power to assist prosthetic movements. This power can be useful when ascending stairs but current prototypes have to be made more reliable, quieter and lighter to benefit amputees in real life [12]. Some functions (adaptation of the ankle in stance, swing dorsiflexion, knee control) can be passively achieved with a hydraulic microprocessor controlled ankle/knee system increasing the ability to walk on various terrains.

References: [1]   Sawers et al., J Rehabil Res Dev, 50: 273-314, 2013.

[2]   Schmalz et al., Gait Posture, 25: 267-278, 2007.

[3]   Burnfield et al., Prosthet Orthot Int, 36: 95-104, 2012.

[4]   Samuelsson et al., Prosthet Orthot Int, 36: 145-158, 2012.

[5]   Vickers et al., Prosthet Orthot Int, 36: 95-104, 2012.

[6]   Agrawal et al., J Rehabil Res Dev, 50: 941-950, 2013.

[7]   Fradet et al., Gait Posture, 32: 191-198, 2010.

[8]   Asha et al., Clin Biomech, 28: 218-224, 2013.

[9]   Au et al., Neural Netw, 21: 654-666, 2008.

[10] Lawson et al., IEEE Trans Neural Syst Rehabil Eng, 21: 466-473, 2013.

[11] Pillet et al., Gait Posture, 31: 147-152, 2010.

[12] Hargrove et al., N Engl J Med, 369: 1237-1242, 2013.

Disclosure of Interest: B. Xavier Conflict with: Proteor, F. Djian Conflict with: Proteor, B. Dauriac: None Declared, C. Villa: None Declared, I. Loiret: None Declared, N. Martinet: None Declared, H. Pillet: None Declared

Prosthetics

SS-0048

A LOWER-LIMB AMPUTEE MUSCULOSKELETAL MODEL FOR QUANTIFYING STUMP-SOCKET KINEMATICS AND KINETICS

Ryan Wedge [1,*] Andrew LaPre [2] Frank Sup [2] Brian Umberger [1]

[1]Department of Kinesiology, [2]Department of Mechanical and Industrial Engineering, University of Massachusetts Amherst, Amherst, United States

Introduction and Objectives: There are an increasing number of people with lower limb amputations resulting from both traumatic and vascular causes. Skin breakdown is a common problem experienced by amputees due to the motion and forces between the stump and socket. The stump soft tissues were not designed to withstand the forces they attenuate inside of the socket, which can lead to pressure ulcers[1]. The motion and forces of greatest concern are socket pistoning and flexion-extension. Pistoning refers to translational motion in the axial direction, while socket flexion-extension is the rotation that occurs in the sagittal plane, due to a bending moment created by the ground reaction force. While these loading mechanisms are known to exist[2], the actual magnitudes and patterns of loading at the stump-socket interface (SSI) over a continuous gait cycle have not been fully characterized. In previous musculoskeletal modeling studies, the SSI has usually been assumed to be rigid[3], which may be a limitation when musculoskeletal models are used to understand amputee locomotion. Explicitly modeling the SSI will provide insights as to the motion and loading at the SSI. Our long-term goal is to use this approach to aid in the development of new prostheses that can reduce these loads and decrease the incidence of soft tissue injury. The specific purpose of this study was to examine the stump-socket kinematics and kinetics during walking in transtibial (TT) amputees using a musculoskeletal model with a compliant SSI.

Methods: We created a three-dimensional unilateral TT amputee model by modifying one of the standard gait models provided with OpenSim (gait2354). We created a residual tibia/fibula (stump segment) that is connected to the socket via a joint at the most distal aspect of the stump, representing the SSI. The socket and pylon were connected to a split-toe flex foot via a pin joint. The entire model has 25 degrees of freedom, including pistoning and flexion-extension at the stump-socket joint. To demonstrate the utility of the model, results are presented for a female subject with a left-side TT amputation (height: 1.80 m; mass: 68.04 kg) who performed three overground walking trials at her preferred speed (1.31 m/s). Kinematic data were captured using a full-body marker set and were synchronized with ground reaction forces measured using three force platforms. Inverse kinematics and inverse dynamics analyses were performed in OpenSim and results were averaged over the three trials.

Results: Joint Kinematics and Kinetics: The hip, knee and ankle joint angles and moments for the prosthetic and intact limbs were in general agreement with corresponding data in the literature. For example, the magnitude of the knee extension moment in the first half of the stance phase was greatly reduced on the prosthetic side compared with the intact limb. Data collected for a second subject show similar results.

Stump-Socket Kinematics and Kinetics: There was 3.4 cm of pistoning translation and 8° of socket flexion-extension at the SSI (Fig 1). The 3.4 cm of pistoning agrees with previous studies using radiographic techniques[2]. The peak pistoning force occurred in the first half of stance and was 663 N, which is near one bodyweight (667 N). The peak extensor

moment at the SSI was 51 N m (Fig 1), which was of similar magnitude to the intact-side peak knee extensor moment. Unlike typical joint kinetics, the relatively large pistoning force and bending moment is borne by a small area of soft tissue that is not meant to withstand such loading, and may contribute to tissue damage. By directly modeling the SSI in TT amputees during locomotion, we can gain greater insights as to the motion and forces that play a role in skin breakdown. In future work, the model will be used to predict individual muscle forces, which will help reveal the accommodations made by amputees to walk. This will also provide a basis for predicting novel prosthesis designs that can reduce stump-socket loading without disrupting the way amputees naturally walk.

Figure:
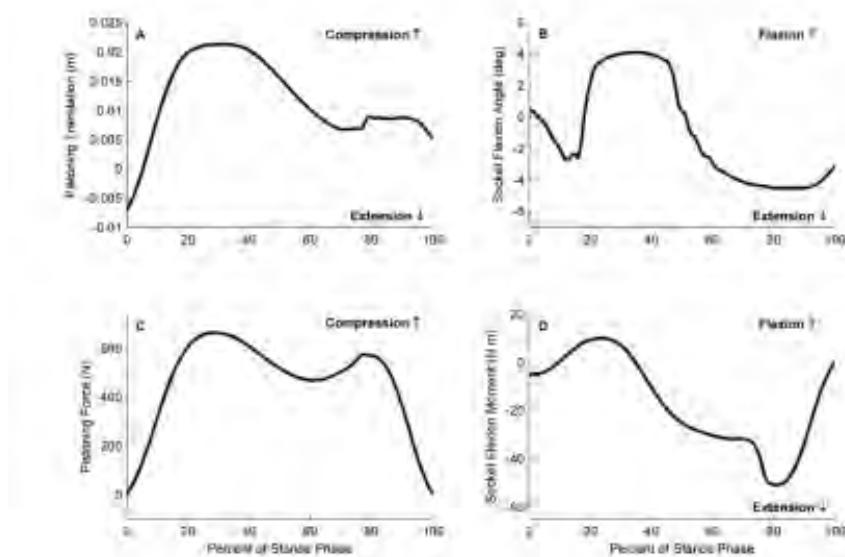
Caption: Stance Phase Socket Kinematics and Kinetics Figure 1: Pistoning motion (A), Flexion and extension motion (B), Pistoning force (C), Flexion and extension moment (D)

Conclusion: Including degrees of freedom at the SSI in a TT amputee musculoskeletal model provided potentially useful information about stump-socket mechanics, while yielding similar joint mechanics as have been previously reported in the literature.

Supported by a Pilot Project Grant from the National Center for Simulation in Rehabilitation Research.

References: [1] Dudek NL, Marks MB, Marshall SC. (1998) Am J Phys Med Rehabil 85(5), 424-429.

[2] Lilja M, Johansson T, Oberg T. (1993) Prosthet Orthot Int 17(1), 21-26.

[3] Fey NP, Klute GK, Neptune RR. (2012) J Biomech Eng 134(11), 111005/1-10.

Disclosure of Interest: None Declared

Rehabilitation

SS-0049

MULTI-PARAMETRIC EVALUATION OF MOBILITY USING SINGLE-LOCATION WEARABLE SENSOR: APPLICATION TO STROKE PATIENTS

Kamiar Aminian [1,*]Fabien Massé [1]Roman Gozenbach [2]Anisoara Paraschiv-Ionescu [1]Andreas Luft [2]

[1]Laboratory of Movement Analyisis and Measurement, EPFL, Lausanne, [2]University of Zurich, Zurich, Switzerland

Introduction and Objectives: To restore their mobility stroke survivors undergo an intensive rehabilitation program, throughout which, the patient's *capacity* is tested using clinical scores. However, these tests are not necessarily reflect the actual patients *performance* in daily life [1] and there is need for an objective evaluation of patient's performance in daily conditions. In despite of advances in wearable technologies for monitoring patients' physical activity in daily-life, for the stroke population, existing systems are limited in the number of parameters [2, 4-7] and use multiple sensor locations, which could hinder the subject. The objective of this study is to provide a system with single sensor located on the trunk and multiple parametric assessment [2, 3] of mobility in daily-life addressing 1) the characterization of (sit-to-stand and stand-to-sit) postural transitions (PT); 2) the classification/quantification of the activities and 3) a meta-analysis of these activities and PT through their temporal pattern and distribution.

Methods: The measurement system consisted of a small sensor device (Physilog®, GaitUP, CH) attached on the trunk including an inertial and a barometric pressure sensor. The data collection was carried out on 7 stroke patients (age: 52.1 ± 11.4 y.o) in their home environment and last for minimum 3 days (8 hours/day). The balance impairments and the capacity of daily-living activity were evaluated by the Berg Balance Scale (BBS) and the Barthel Index (BI). A control population of 10 elderly subjects (age: 70.8 ± 2.8 y.o) was recruited to highlight the discriminative parameters using Wilcoxon's ranksum test ($p < 0.05$). Mobility metrics were extracted in daily-life related to three categories (Figure):

- Transition (PT duration, range and peak value) [5];

- Activity (walking/posture allocation, step count, cadence [2] and number of PT [5]);

- Pattern (power-law scaling coefficient of the distribution of the number of steps per walking episodes and their duration [11] and smoothness of PT [8]).

Metrics were extracted from a PT recognition [9] and an event-based activity classification algorithm (accuracy of 90.5%)[10]. The degree of association between capacity (clinical score) and performance (mobility metrics) was computed using the Spearman's correlation coefficient (ρ).

Results: Table indicates that most of the mobility metrics are discriminative. The balance capacity (BBS) was significantly correlated with faster PT ($\rho=0.82$, $p=0.03$) and higher rate of PT ($\rho=0.79$, $p=0.04$) which are consistent with the literature [12, 13]. The percentage of time spent standing was significantly correlated with the BI ($\rho=0.80$, $p=0.04$) suggesting the overall functional capacity is associated with the ability of the patients to remain in an upright posture. The smoothness metric was significantly correlated ($\rho=0.80$, $p=0.04$) with the BI. Results are consistent with literature [2,14]. At least one metric within each category (transition, activity, pattern) was associated with clinical score showing the relevance of each category.

Figure:
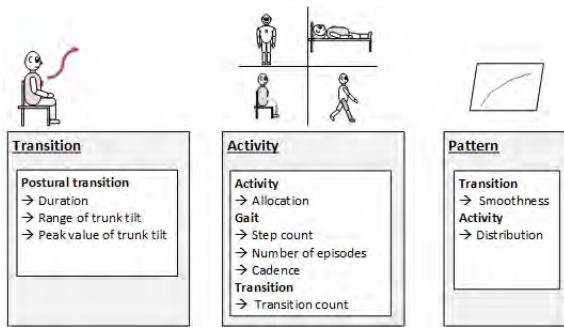
Caption: Mobility metrics extracted in daily-life related to Transition, Activity and Pattern

Conclusion: Providing the small sample size, results with stroke patients should be interpreted with care. Nevertheless, the results obtained so far, confirmed that the proposed system is convenient for long-term monitoring and the multi parametric approach provides a good picture of the performance of the patients during real world condition. The association of the proposed metrics with clinical score is a powerful tool for a personalized rehabilitation program.

Table:

	Metrics	Elderly		Stroke	
		Median	IQR	Median	IQR
Transition	Duration, sec	2.50	0.96	3.01	0.21
	Range, deg	17.6	4.08	13.0*	4.66
	Peak, deg	4.08	1.74	7.22*	2.06
Activity	Walk,%	24.1	9.52	8.2**	3.83
	Stand,%	19.4	8.78	11.3**	5.84
	Sit,%	43.9	11.74	43.8	21.1
	Lie,%	9.3	21.42	39.1*	27.8
	Rate of walking episodes, *WE/hr*	31.0	15.30	18.6**	8.18
	Average step count, *step/hr*	1263	529.52	309**	236
	Rate of transitions, *Tr/hr*	6.2	4.76	6.3	5.5

						2
	Cadence – median*, step/min*		92.5	7.11	75.8**	16.6
Pattern	Power-law coefficient	walking episode duration	1.91	0.55	2.60*	1.02
		number of steps	1.85	0.25	2.32*	0.43
	Smoothness		1.35	0.01	1.48*	0.07

Caption: MEDIAN AND IQR VALUES OF METRICS OF STROKE COMPARED TO ELDERLY SUBJECTS WITH THEIR LEVEL OF SIGNIFICANCE (* P<0.05 / ** P<0.01)

References: [1] W. H. O, 2001

[2] Lindemann et al. Phys Meas, 2012

[3] Bussmann et al, Front. Psychol. 2013

[4] de Niet et al, Arch Phys Med Rehabil, 2007

[5] Janssen et al, JNNR, 2010

[6] Alzahrani et al., JPT, 2011

[7] Prajapati et al,, JNNR, 2011

[8] Ganea. et al, Med Eng Phys, 2011

[9] Massé et al, 3DAHM 2014, 2014

[10] Massé et al, submitted to JNER

[11] Chastin et al., G&P, 2010.

[12] Ng et al., Am J of PM&R, 2010.

[13] Janssen et al., IEEE-TNSRE, 2008.

[14] Ganea et al., IEEE-TNSRE, 2012

Disclosure of Interest: None Declared

simulation solutions

BIOROBOTICS DEMONSTRATION

Simulation Solutions are pleased to be demonstrating the Siemens PLM range of robotic simulation software and its application to simulating human joint motion. The simulation software can be used in conjunction with a KUKA robot to facilitate physical testing.

Simulation Solutions are also excited to be launching the simVITRO range of products from The Cleveland Clinic Foundation. Designed as a universal musculoskeletal simulator it has the following benefits:

- Reduce cost and time to publishing your scientific discoveries
- Select the specimen module(s) that match your research program
- Utilise International Society of Biomechanics standards for joint coordinate systems

- Customise sensors and measurements unique to your particular application via the plug-in style architecture
- Build around new or existing robotic or sensor infrastructure in your laboratory or testing facility. Get the power of simVITRO while leveraging your current capital equipment.

Simulation Solutions is delighted to announce its partnership with Motion Analysis Corporation.

MotionAnalysis

Motion Analysis Corporation is the world's largest manufacturer of high performance optical instrumentation systems that test and measure movement. Their systems combine hardware, software and electro-optical techniques with standard computer and camera hardware. These systems evaluate motion in a wide variety of applications, including patient positioning, evaluation of surgical procedures, and measurement of positions and forces during cadaveric testing.

KUKA OFFICIAL SYSTEM PARTNER

Solution Partner PLM

SIEMENS

simVITRO
Cleveland Clinic   bioROBOTICS

Unit 10, Rugby Park, Bletchley Road, Heaton Mersey, Stockport SK4 3EJ
t: 0161 947 9113 | e: contact@simsol.co.uk | w: www.simsol.co.uk

KNEE AND BODY ALIGNMENT IN THE FRONTAL PLANE DURING FIVE FUNCTIONAL EXERCISES USED IN REHABILITATION

Kate Button [1] [2],*Paulien Roos [1]Paul Rimmer [1]Robert van Deursen [1]

[1]Healthcare Science, Cardiff University, [2]Physiotherapy Department, Cardiff & Vale University Health Board, Cardiff, United Kingdom

Introduction and Objectives: Frontal plane biomechanics during functional exercises are of interest in rehabilitation to evaluate recovery of neuromuscular control and re-injury prevention. Dynamic valgus is used in rehabilitation to describe knee alignment during functional exercises. External knee adductor moment (EKAM) reflects joint loading and is influenced by a number of factors including frontal plane knee and trunk alignment [1,2]. Alterations in sagittal plane knee kinematics and kinetics have been observed in individuals with anterior cruciate ligament (ACL) deficiency (ACLD) and reconstruction (ACLR) compared to controls [3, 4]. However, it is not clear whether dynamic valgus and changes in trunk alignment commonly occur and what the implications are for joint loading and knee stability. Therefore, five functional movements were compared to determine the role of frontal plane knee and trunk alignment.

Methods: ACLD, ACLR, and healthy participants performed four repetitions: walking (WLK), jogging (JOG), double and single-leg squatting (DLS & SLS), and single-leg hopping (HOP). Each task was executed at preferred speed/distance. Motion data were collected using the VICON full body marker set. Parameters calculated were: peak knee external flexor moment (PkKnFlM) and knee flexion angle at this peak (KnAngatPkM), peak EKAM (PkEKAM), dynamic valgus (DynValgus), and trunk lean. A repeated measure ANOVA and Bonferroni adjustment for comparisons were used to investigate differences between WLK and the other tasks for the three groups.

Results: Results are reported for 29 ACLR (height: 1.74±0.07 m, mass: 80.0±10.1 kg, age: 30.1±9.6 years, gender: 8 female, 21 male), 28 ACLD (height: 1.78±0.09 m, mass: 81.9±14.8 kg, age: 31.0±7.8 years, gender: 5 female, 23 male) and 29 control subjects (height: 1.73±0.11 m, mass: 73.5±16.4 kg, age: 28.0±6.9 years, gender: 10 female, 19 male). All parameters were significantly different between the five tasks ($p<0.05$), but the Group by Task interaction was only significant for PkKnFlM ($p<0.01$). Except for WLK, the ACL groups carried out the tasks with smaller moments compared to the controls. KnAngatPkM was different between groups ($p<0.05$). The ACLD group consistently used less flexion for all activities and did not depend on task requirements. The results for all the variables are summarised in Table 1. In the frontal plane, no significant differences occurred for Group*Task interactions or between groups for PkEKAM, DynValgus, and TrunkLean. Therefore, all groups seemed to use similar frontal plane movement strategies for all activities.

Conclusion: Movement adaptations in ACLD and ACLR seem to occur most obviously in the sagittal plane, i.e., a reduced peak external knee flexor moment and for ACLD a reduced knee flexion angle at this time point. No differences were found in frontal plane kinematics or kinetics between ACL groups and controls. Except for walking, it seems that regardless of task difficulty the response in ACL groups was a reduction in overall knee loading which could be considered a protective mechanism. It is not entirely clear why movement adaptations were not observed in the frontal

plane, but it may be that other aspects of frontal plane behaviour such as motor control and stability likely need to be considered.

Table:

PkKnFlM (N.m)	**Significant:** Task main effect: p<0.01 & Task*Group interaction: p<0.01 **N.S.** Group main effect: p=0.059				
	WLK	**JOG**	**DLS**	**SLS**	**HOP**
Controls	48.5±4.2	142.7±9.8	69.1±5.4	78.1±6.5	166.7±11.5
ACLR	49.3±4.2	114.3±9.8	61.4±5.4	62.0±6.6	129.5±11.5
ACLD	46.0±4.3	91.5±10.0	63.5±5.4	75.1±6.6	147.1±11.6
KnAngatPkM (degrees)	**Significant:** Task main effect: p<0.05; Group main effect: p<0.05 **N.S.** Task*Group interaction: p=0.755				
Controls	17.5±1.7	37.4±2.1	105.7±3.5	68.7±3.4	40.0±2.1
ACLR	14.5±1.7	32.8±2.0	102.7±3.2	64.1±3.3	37.4±2.6
ACLD	13.5±1.7	25.9±2.2	97.7±3.6	61.4±3.5	36.4±2.0
PKEKAM (N.m)	**Significant** Task main effect: p<0.01; **N.S.** Group main effect: p=0.769 & Task*Group interaction: p=0.704				
Controls	45.6±3.6	109.6±9.1	23.2±2.2	57.8±5.3	122.9±8.6
ACLR	48.5±3.7	113.1±9.0	24.3±2.1	61.3±5.7	134.4±8.6
ACLD	49.5±3.7	209.8±9.2	20.5±2.2	69.9±5.4	130.4±8.8
DynValgus (degrees)	**Significant** Task main effect: p<0.01; **N.S.** Group main effect: p=0.310 & Task*Group interaction: p=0.496				
Controls	1.9±0.7	1.9±1.6	14.6±2.6	6.0±1.4	7.0±1.4
ACLR	2.4±0.6	-2.1±1.0	15.5±2.2	4.5±1.9	3.9±1.4
ACLD	2.3±0.7	3.1±1.6	13.4±2.7	7.2±1.4	4.9±1.4
TrunkLean (degrees)	**Significant** Task main effect: p<0.01; **N.S.** Group main effect: p=0.718 & Task*Group interaction: p=0.174				
Controls	1.1±0.1	1.7±0.2	1.2±0.2	4.5±0.6	7.9±0.7
ACLR	1.1±0.1	1.9±0.2	1.5±0.2	3.9±0.6	6.8±0.6
ACLD	1.0±0.1	1.7±0.2	1.6±0.2	5.1±0.6	6.2±0.7

Caption: Table 1. Means and standard deviations are given for all variables for each task. Differences between tasks for all variables were significant (p<0.05). N.S is non-significant

References: 1. Takacs et al., J Biomech. 45: 2791-2796, 2012.
2. Stearns et al., Am J Sports Med, 41: 918-923, 2013.
3. Button et al., Clin Biomech. 29: 206-212, 2014.
4. Roos et al., J of Biomech. 47: 675-680, 2014.

Rehabilitation

SS-0051

DOES LONG-TERM PASSIVE STRETCHING ALTER MUSCLE-TENDON UNIT MECHANICS IN CHILDREN WITH SPASTIC CEREBRAL PALSY?

Nicola Theis [1,*] Thomas Korff [2] Amir Mohagheghi [2]

[1]St Mary's University, [2]Brunel University, Middlesex, United Kingdom

Introduction and Objectives: The aim of the present work was to investigate the effects of 6-weeks passive stretching on *triceps surae* muscle and Achilles tendon stiffness in children with spastic cerebral palsy (CP). Following the intervention, muscle stiffness decreased with no alteration to the tendon. This reduction was accompanied by an increase in muscle fascicle strain but not in resting fascicle length. Further studies should investigate the functional implications of these results.

Cerebral Palsy causes motor impairments during development. Children with CP may experience excessive neural and mechanical muscle stiffness [1]. The clinical assumption is that excessive stiffness is the main reason for reduced range of motion and functional impairments in CP [2]. As such, passive stretching is widely used to reduce stiffness, with a view to improving function for children with CP. However, current research evidence on passive stretching in CP is not adequate to support or refute the effectiveness of stretching as a management strategy to alter muscle and tendon mechanics [3]. Thus, the purpose was to identify the effect of 6-weeks passive ankle stretching on *triceps surae* and Achilles tendon mechanical properties in children with spastic CP.

Methods:

Thirteen ambulant children with spastic diplegic or quadriplegic CP (age 10.3 ± 3.0 y; GMFCS III-IV) participated in this study. Children were randomly assigned to an experimental or control group. None had received any form of lower limb surgery 24 months prior to participation in the study, and none had received Botulinum toxin injections to the legs 4 months prior to participation.

The experimental group underwent 6-weeks of passive ankle dorsiflexion stretching applied by a physiotherapist, for 15 minutes (per leg), 4 days per week, whilst the control group continued with their normal routine. Before, after and 3-weeks post intervention, the mechanical properties of the medial gastrocnemius muscle and fascicles, and the Achilles tendon were measured using a combination of motion analysis, ultrasonography and dynamometry. Briefly, a passive rotation of the right ankle joint was applied at 10 deg·s^{-1} through the available ROM. Simultaneously, medial gastrocnemius muscle belly, fascicles and Achilles tendon lengths were measured using B-mode ultrasonography (Megas GPX, Esaote, Italy; 45 mm Linear array probe, 10 MHz transducer scanning) and motion analysis (Motion Analysis, Santa Rosa, USA).

Achilles tendon stiffness was calculated as the change in passive ankle torque divided by the corresponding change in Achilles tendon length. A surrogate measure of "total *triceps surae* muscle stiffness" was also derived from the data by dividing passive ankle torque and elongation of the medial gastrocnemius muscle. Muscle and tendon stiffness were calculated from the slope of the torque-elongation curves corresponding to 20-80% of each participants peak torque. Muscle, tendon and fascicle lengths at maximum dorsiflexion were divided by their resting lengths to give strain values.

Mixed design ANOVAs with repeated measures on each dependent variable were used to assess the effects of stretching.

Results:

Following the intervention, the experimental group demonstrated a 3° increase in maximum ankle dorsiflexion. This was accompanied by a 13% reduction in *triceps surae* muscle stiffness, with no change in tendon stiffness (Figure 1). Additionally, there was an increase in fascicle strain following the intervention but with no changes in resting length. This suggests muscle stiffness reductions were a result of alterations in intra-/extra-muscular connective tissue and not due to an increase in sarcomere number. These results remained 3-weeks post-intervention but had begun to return towards baseline. Our results demonstrate that 6-weeks of passive stretching caused lasting increases in maximum dorsiflexion and reductions in muscle stiffness.

Figure:
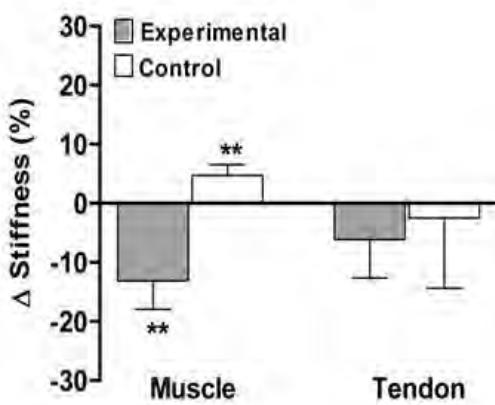
Caption: Figure 1. Change (Δ) in muscle and tendon stiffness pre- to post-intervention in the experimental and control groups (values are mean ± SD, **$p < 0.01$).

Conclusion:

Collectively, the results of this study confirm the clinical assumption that passive stretching can reduce muscle stiffness for children with CP. Moreover, the present study shows for the first time that such reductions were associated with changes in the mechanical properties of muscle but not the tendon. Future studies should investigate this from a clinically-relevant perspective as to whether this reduction in stiffness leads to improvements in gait parameters and gait efficiency in children with CP.

References: 1. Barber et al., J Biomech, 44: 2496-2500, 2011.

2. Eek & Beckung, Gait Posture, 28: 366-371, 2008.

3. Pin et al., Dev Med Child Neurol, 48: 855-862, 2006.

Disclosure of Interest: None Declared

TRAINING WITH OFF-LOADED BODY WEIGHT IN A LOWER-BODY POSITIVE PRESSURE CHAMBER IMPROVES PHYSICAL FUNCTION IN PATIENTS WITH MUSCULAR DYSTROPHY

Bente R R. Jensen [1,*]Martin P Berthelsen [1]Edith Husu [2]Sofie B Christensen [1]Kira P Prahm [2]John Vissing [2]

[1]Biomechanics and Motor Control Lab., Integrated Physiology, Nutrition, Exercise and Sport, [2]Neuromuscular Research Unit, Department of Neurology, Rigshospitalet, University of Copenhagen, Copenhagen, Denmark

Introduction and Objectives: Recent studies suggest positive effects of physical training in patients with muscular dystrophy [1]. However, patients with severe muscular dystrophies have limited possibilities to perform normal exercise protocols due to their weakness. The aim was to study functional effects of combined strength and aerobic anti-gravity training in severely affected patients with Becker and Limb-Girdle muscular dystrophies.

Methods: Eight patients (age: 36 ± 4 years, weight: 73 ± 5 kg, height: 176 ± 3 cm, gender: 6 males and 2 females) participated in a 10-week control period followed by 10-week of progressive strength and aerobic training (3 times/week, 40 min sessions) in a lower-body positive pressure (LBPP) environment, which offered weight support of up to 80% of their body weight (BW). The LBPP system consisted of a treadmill surrounded by a pressure chamber (G-trainer P200, Alter-G, USA). Strength training (treadmill at standstill), included squats, calf raises and lunges with three series of each exercise. When the patient could perform more than 12 repeats (squats and lunges) or 15-20 repeats (calf raises) at a specific %BW, then the load was increased by 5%BW to ensure training progression. Aerobic training consisted of walk/run, jogging on the spot or high knee-lift, initially at 50%BW support. Isometric knee extension and flexion strength as well as isometric rate of force development (RFD) (extension) were measured before and after the training period.

Results: Isometric knee extension and flexion torque were 0.50 Nm/kg (15% of expected value) and 0.48 Nm/kg (37% of expected value), respectively [2]. Thus, H/Q ratio was 0.96, which is more than twice of the expected value, indicating that knee extensor muscles are among the most affected muscles. Absolute knee extension RFD was 229±75 Nm/s and relative RFD was 540±49 %MVC/s. Relative RFD corresponded to values from an age and sex matched group whereas absolute RFD values corresponded to approx. 20% of expected values. These data confirm that the patients suffer from a muscle disease whereas the nervous system functions adequately. It is therefore possible that optimization through motor learning is feasible in this patient group.

Training (compliance 91%) improved functional leg muscle strength. Thus, squat series performance increased from 30%BW/leg to 38 %BW/leg, calf raises increased from 56%BW/leg to 75%BW/leg and lunges increased from 55%BW to 67%BW from week two to week 10. The first week was considered as familiarization. In contrast, neither isometric knee extension strength nor RFD increased in response to training.

Conclusion: Anti-gravity training improved functional leg muscle strength despite no change in isometric knee extension strength and absolute RFD were found. There are two possible explanations for these findings. One is that anti-gravity training, performed in LBPP, improves muscle strength of other muscles than the weak knee extensors, which we assessed. Alternatively, it may relate to a neural adaptation involving motor learning.

References: [1]. Sveen ML. et al. Muscle Nerve 47, 163-169 (2013).

[2]. Berthelsen, MP. Et al. Neuromuscular Disorders, 24(6), 492-498 (2014).

Disclosure of Interest: None Declared

SS-0053

COMPENSATION STRATEGIES FOR EXPERIMENTALLY REDUCED MUSCLE FUNCTION DURING SQUATS

Teresa Flaxman [1,*] Tine Alkjaer [2] Erik Simonsen [2] Michael Krogsgaard [2] Daniel Benoit [1]

[1] University of Ottawa, Ottawa, Canada, [2] University of Copenhagen, Copenhagen , Denmark

Introduction and Objectives: ACL injured individuals typically experience severe deficits in voluntary knee extensor muscle strength, which is thought to be a main contributor to decreased stability and self-perceived functionality [1,2]. Since the average time injured individuals participate in studies can range from 3 months – many years post-injury [2,3], results may be confounded by compensation strategies; thus, the simulation of injury-like conditions may provide more valuable insight on the effect of muscle weakness to joint stability. The aim of this study was to evaluate changes in muscle activation and joint moments with experimentally reduced quadriceps muscle function during squatting. This is achieved with intra-muscular injections of hypertonic saline, causing a perception of pain and a centrally mediated reduction in muscle activation [4]. Similar to Henriksen et al. [5], we propose that intramuscular hypertonic saline injections into the vastus medialis (VM) will cause a reduction in activation and knee extensor moments. Compensation for this deficit will be observed in the contralateral limb, evidenced by increased knee extensor moment.

Methods: 22 young healthy adults participated in this study. Each subject was tested on 2 days separated by 1 week. During a test day, one type of intra-muscular saline solution (either a hypertonic-pain inducing or isotonic-sham) was injected into VM of the dominant leg. Subjects performed 2 sets of 20 squats during 2 conditions: baseline and during experimental pain. Kinematics, kinetics and surface electromyography of 10 muscles of the dominant leg were recorded. Squats cycles were time normalized to 100% with ascent and descent phases determined by peak knee flexion angles. EMG was processed to a linear envelope and each muscle's activation was integrated for the descent and ascent phases. Between condition differences in muscle activation, peak knee joint angles, moments, and power were tested with Wilcoxon Signed Rank Tests ($\alpha=0.05$).

Results: Results of 7 subjects (4 males, 3 females) from the hypertonic session are presented. Time to peak knee joint angle and joint flexion and extension velocities did not significantly differ between conditions (T-test p > 0.05). There was a significant reduction in knee flexion angles of both legs, and knee extension moment and power of the test leg (Fig C and D). VM had significant reduction in integrated muscle activation during both descent and ascent phases (Fig A). Peak VM activation levels were reduced by an average of 43% (Fig B). During the ascent phase, a significant reduction in integrated vastus lateralis (VL) and biceps femoris (BF) was also observed.

Figure:
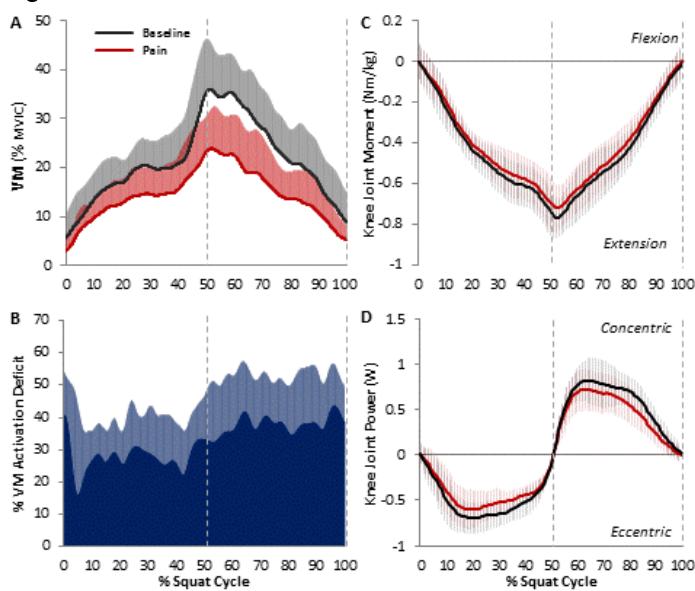
Caption: Group mean and standard deviation over entire squat cycle of: A) VM activation normalized to maximum voluntary isometric contraction (%MVIC), B) Percent (%) VM activation deficit (Baseline-Pain/Baseline*100), C) Knee joint flexion-extension moment (Nm/kg), and D) Knee joint extensor power (W).

Conclusion: This study sought to evaluate neuromuscular compensation strategies to experimentally induced muscle pain, resulting in voluntary muscle inhibition, during squatting. The hypertonic saline injections to VM caused a reduction in voluntary muscle activation, thus reducing knee extensor moments and power. Compensation for this deficit was thought to occur in the contralateral limb; however, this was not the case. Further investigation of the hip and ankle joint contributions is required. Participants with ACL deficiency commonly display increased activation of antagonistic hamstrings and gastrocnemius during functional activities[2,3]. Interestingly, no compensation strategies, as evidenced by increased activations of adjacent muscles, were observed. Rather, VL and BF were reduced ascent. Although it is unlikely to return to pre-injury activity levels, ACL deficient subject's functional stability increases over time [6]. Perhaps the lack of an acute response to muscle weakness is a main contributor to the extreme functional instability immediately after injury? Differences observed between ACL deficient and controls may rather be indicative of rehabilitation effects or chronic adaptations. However, further research on muscle weakness and its effect on knee joint stability immediately after injury are warranted.

References: [1] Hashemi et al., Exp Mech, 47:347-354, 2007.

[2] Rudolph et al., Knee Surg Sport Tr, 9:62-71, 2001.

[3]Benoit et al., Gait Posture, 18:56-63, 2003.

[4] Graven-Nielsen et al., Muscle Nerve, 26-63, 2002.

[5] Henriksen et al., J Appl Physiol, 103:132-9, 2007.

[6] Frobell et al., N Engl J Med, 363:331-42, 2010.

Disclosure of Interest: None Declared

Rehabilitation

SS-0054

SMART MONITORING OF KNEE RANGE OF MOTION AND ACTIVITY TYPE FOR KNEE REHABILITATION.

Enrica Papi [1,*]Margarita Kotti [1]Irina Spulber [1]Pantelis Georgiou [1]Alison McGregor [1]

[1]Imperial College Lodon, London, United Kingdom

Introduction and Objectives: The goal of rehabilitation in patients suffering from knee osteoarthritis is to improve knee function, minimize pain and mitigate further disease progression. The beneficial effect of rehabilitative interventions, however, is often lost due to poor compliance coupled with low levels of physical activity. The use of wearable technology to deliver rehabilitation could increase the availability and accessibility to treatment for patient populations [1]. Furthermore, the richness of information that can be acquired over an extended period of time could inform treatment for individualised and targeted interventions and, motivate patients using markers of performance. To comply with patients' preferences of unobtrusiveness and discreetness, a flexible conductive sensor unit was developed that can be integrated into clothing to create a wearable system. The aim of this study was to assess the reliability of the wearable system in monitoring the knee range of motion and its ability to classify activities of daily living.

Methods: The sensor unit consists of a conductive flexible polymeric composite material cut into a thin strip (0.02x50x100mm). This was secured to a pair of commercially available leggings to coincide with the anterior aspect of the right knee. A sensing node with embedded analogue interface circuitry for the sensor and hosting a Bluetooth module, was used to wirelessly acquire data. A data set was collected from 12 healthy adults (Age 27±5 years, Height 1.7±0.1 m, Body Mass 66±12 kg), tested twice, while wearing the smart leggings and performing four different activities: walking, running, stair ascent/descent. Data were acquired at 122 Hz and filtered with a 4th order Butterworth filter with 10Hz cut-off frequency. The sensor output range was evaluated as surrogate of knee sagittal range of motion and its test-retest reliability assessed by mean of intra-class correlation coefficient. A decision classification tree algorithm, using a splitting Gini's index, was applied for classification of the activities performed. The features used in the classifier were obtained from a power spectral density analysis of the signal output: median frequency, total power of the spectrum, and peak frequency. The data set was split into training and testing subsets with a ratio of 80:20.

Results: Sensor output time varying waveforms resemble typical knee sagittal kinematics curves. Repetitive patterns were obtained among participants in the sensor output range reflecting the knee sagittal range of motion expected for the activities performed. High reliability (ICC >0.8) was found amongst all participants. The prediction accuracy achieved with the classifier developed was as high as 89.7%.

Conclusion: The results demonstrate the overall system performance in estimating knee range of motion and activity performed. The system consisting of a flexible sensor unit interfaced with a wireless node allowed for continuous and reliable monitoring of the knee movement in unconstrained environments. Good activity discrimination was achieved via a simple classifier employing spectral features of the signal output. The ability of measuring knee range of motion in the context of the activity performed represents an advantage of the system proposed over available technology. Measuring joint function unobtrusively outside a laboratory setting in fact still represents a challenge. Objective data on mobility

function in real life environments could support the management of knee OA enhancing the clinical benefits of rehabilitation.

The reliability of the wearable system has been demonstrated. Further testing will be conducted considering more tasks, involving an osteoarthritis population and to translate sensor output to degrees quantities. The use of other classification approaches will be explored to enhance the activity recognition accuracy. Finally a feedback tool will be developed to report the information to clinicians and patients.

References: [1] Bonato. Wearable sensors and systems. IEEE Eng. Med. Biol. Mag.,29:25-36, 2010.

Disclosure of Interest: None Declared

SS-0055

ENDPOINT MOBILITY IN BIMANUAL MANIPULATION: INSIGHTS FROM GOLF BALL STRIKING

Fredrik Tinmark [1][2],[*]Anton Arndt [1][2]Maria Ekblom [1][3]John Hellström [4]Kjartan Halvorsen [5]

[1]Biomechanics and Motor Control Laboratory, GIH - The Swedish School of Sport and Health Sciences, [2]Department of CLINTEC, [3]Department of Neuroscience, Karolinska Institutet, Stockholm, [4]The School of Health and Medical Sciences, Örebro University, Örebro, [5]Department of Information Technology, Uppsala University, Uppsala, Sweden

Introduction and Objectives: The possibility of modulating the inertia (and mobility), stiffness and damping of the endpoint/end-link is a feature of redundant manipulators such as the human arm [1]. Modulation of stiffness and damping is made possible by co-activation of antagonists. Endpoint mobility (EP mobility) represents the inertial behaviour of the manipulator, and is the inverse of the inertia tensor for the endpoint [1]. Recent work suggest that human subjects are able to predict EP mobility and use these predictions to influence movement choice [2,3]. Although the concept of mobility may be used to reveal strategies of the motor control system, the experimental condition has thus far involved one upper limb only. In bimanual manipulation tasks, modulation of EP mobility is made possible by changing the configuration of not only one: but two upper limbs. Here, we attempt to gain insight into the modulation of EP mobility in bimanual manipulation using golf as model. We hypothesized that the upper limbs in golf ball striking collaborate to promote movement parallel to endpoint path and resist (unwanted) movement in other directions. In addition to test this: we determine how each arm separately and both arms together influence EP mobility; and whether endpoint mobility are dependent upon path length or skill level.

Methods: Ten male professional golf players and 10 amateurs with an intermediate skill level participated. Spatiotemporal data were collected using a Polhemus Liberty electromagnetic tracking system with a sampling frequency of 120 Hz. The experimental task consisted of striking golf balls at slow, medium and fast endpoint speeds to promote the regulation of path length. EP mobility was calculated for 2 endpoints (grip center and clubhead) and for 3 different models corresponding to: left arm + club; right arm + club; and left arm + right arm + club. The model of each arm used 6 DOFs for defining the glenohumeral joint, 2 DOFs for the elbow, and 2 DOFs for the wrist. The connection between hand and club was assumed rigid. For calculating EP mobility, methods presented by Halvorsen et al. [4] were employed. Digitized anatomical landmarks were used to define segment lengths, orientation of local coordinate frames and joint centers. Segment inertia parameters were obtained from de Leva [5]. Statistical analyses were performed using repeated measures ANOVAs and Tukey HSD tests. Significance level was set at $P < 0.05$.

Results: The major axis of the EP mobility ellipsoid (model including both left and right arm) was not aligned with endpoint path for midhands but this was the case for the clubhead. Statistical analysis revealed that 3D angles between the major axis of the EP mobility ellipsoid and movement direction for the clubhead were less than 45° (8-18°) irrespective of group, model and test condition. Projections of EP mobility ellipsoids for both groups combined at the fast test condition are illustrated in Figure 1 and are representative also for the slow and medium test conditions. Note that endpoint path increased from slow (blue circle) to medium (light blue circle) and to fast (grey circles) endpoint speeds.

Moreover, time series data (not shown) revealed that EP mobility varied substantially during movement duration. In line with our hypothesis maximal EP mobility along path and minimal EP mobility normal to path was reached at ball impact, irrespective of group, model and test condition.

Figure:

Sagittal plane   Frontal plane   Horizontal plane
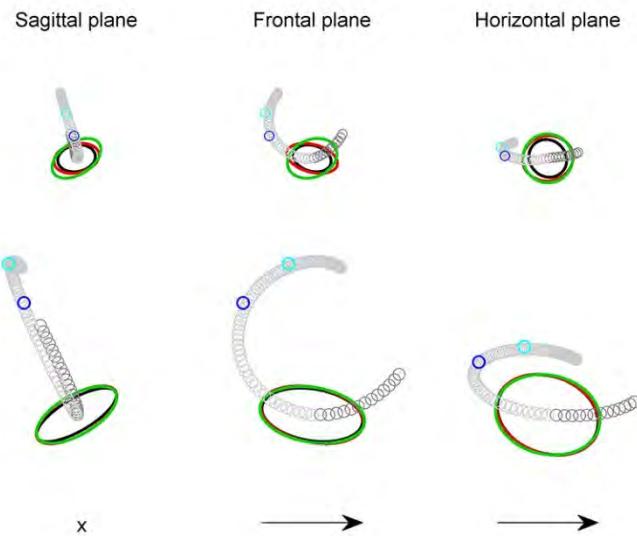
Caption: Figure 1 - Mean endpoint mobility ellipses and mean endpoint movement paths for the fast test condition. Values for both groups are combined (n = 20). The upper row depicts ellipses and paths for the endpoint – grip center. The middle row depicts the corresponding variables for the endpoint – clubhead. Black ellipses are used for the model including both arms, red ellipses for the left arm model and green ellipses for the right arm model. Endpoint paths are grey before impact and dark grey after impact. Blue and magenta circles refer to start of endpoint paths for slow and medium test conditions, respectively. The bottom row shows target direction.

Conclusion: Redundant mechanisms such as the human arm can be configured in many different ways while performing the same task. The observed alignment of the EP mobility ellipsoid support the notion that intrinsic factors with anisotropy strongly influence configuration choice. The observed alignment and approximately invariant magnitude of EP mobility between test conditions were likely chosen to facilitate endpoint control and to promote endpoint accuracy at ball impact.

References: [1] Hogan, N., J. Dyn. Sys., Meas., Control, 1985. 107(1): p. 8-16.

[2] Cos, I., F. Medleg, and P. Cisek, J Neurophysiol, 2012. 108(6): p. 1764-80.

[3] Sabes, P.N., M.I. Jordan, and D.M. Wolpert, J Neurosci, 1998. 18(15): p. 5948-57.

[4] Halvorsen, K., F. Tinmark, and A. Arndt, J Biomech, 2014. 47(14): p. 3569-73.

[5] de Leva, P., J Biomech, 1996. 29(9): p. 1223-30.

Disclosure of Interest: None Declared

IDENTIFYING BODY ROTATION FEATURES DURING THE GOLF SWING USING PRINCIPAL COMPONENT ANALYSIS

Aimee Smith [1 2,*]Jonathan Roberts [1]Steph Forrester [1]Pui Kong [3]

[1]Sports Technology Institute, Loughborough University, Loughborough, [2]Institute of Sport Research, Nanyang Technological University, Singapore, United Kingdom, [3]Physical Education & Sport Science Academic Group, National Institute of Education, Nanyang Technological University, Singapore

Introduction and Objectives: Body rotation has been identified by golf coaches [1] and in the biomechanical literature [2] as a key technical parameter during the golf swing. In particular, X-factor (the difference in axial rotation between upper thorax and pelvis) at top of the backswing and maximum values have been widely linked to measures of performance such as clubhead linear velocity [2]. However, this approach to data analysis results in portions of data being neglected and potentially important information overlooked. Furthermore, previous studies have often analysed differences in body rotation parameters between groups of golfers of different abilities and it is not known the extent to which body rotation varies between golfers of similar abilities. Techniques such as principal component analysis (PCA) can overcome these limitations and has been used to identify unique features in sporting movements [3].

Therefore, the purposes of this study were to use PCA to identify X-factor features throughout a drive in a group of highly skilled golfers and to examine the relationship with clubhead linear velocity.

Methods: Whole body kinematics were recorded for 24 low handicap golfers (handicap range +3 to 4; age = 26 ± 7; height 179.5 ± 7.3 cm; weight 79.4 ± 13.1 kg) using a 13 camera Vicon Nexus motion analysis system (250 Hz). The golfers performed ten drives towards a predefined target, from which five trials were analysed. Following data reconstruction and labelling, Visual 3D was used to build the golfer model. Clubhead linear velocity was measured using the TrackMan launch monitor.

X-factor was computed as the axial rotation between the upper thorax and pelvis segments.   Each swing was temporally aligned between, takeaway (TA) – top of the backswing (TB), TB – impact (IMP) and IMP – mid-follow through (MidFT).

A PCA was performed on X-factor using Matlab. Principal components (PCs) were considered until at least 90% of the variance in the original data was cumulatively explained. Each PC was biomechanically interpreted. The relationship between X-factor PCs and clubhead linear velocity were explored using a two-tailed Spearman's correlation ($p < 0.05$).

Results: The PCA revealed that X-factor required two PCs to explain more than 90% of the variance between golfers. Principal component one (PC1 = 70.5%) explained the difference in X-factor magnitude from mid-backswing to mid-downswing. High negative PC1 scores represented   Principal component two (PC2 = 18.9%) largely explained the variance in the rate or range of X-factor from TA to TB and the timing of the change in X-factor near TB. The scatterplot of X-factor PC1 score and clubhead linear velocity displayed a weak trend ($r = -0.33$, $p < 0.05$) (Figure 1). Golfers 7 and 19 recorded the greatest clubhead linear velocities (49.7 m.s^{-1} and 48.6 m.s^{-1} respectively) and had similar X-factor PC1 scores, however they varied greatly in PC2 scores and in X-factor profiles. Hence, this result suggests that the magnitude of X-factor alone cannot fully explain clubhead linear velocity. Brown et al. [4] also suggested that body rotation

parameters alone, in particular, X-factor at key events, could not explain differences in clubhead linear velocity in a group of low handicap female golfers.

Figure:
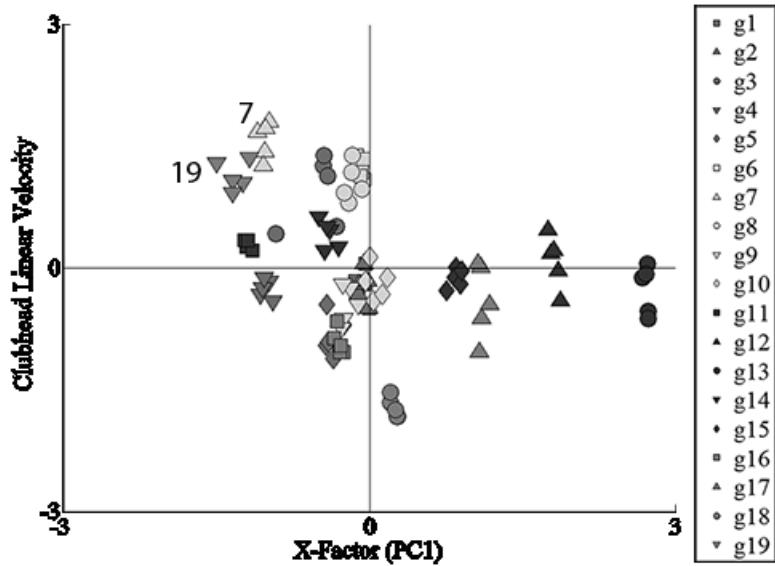
Caption: Figure 1. Scatterplot of X-factor PC1 scores (i.e. magnitude) against standardised clubhead linear velocity showing weak correlation (r = -0.33, p < 0.05)

Conclusion: The scatterplot relationship between X-factor PC1 scores and clubhead linear velocity could suggest that a greater magnitude of X-factor, throughout the swing, would lead to increased clubhead linear velocity. However, the weak linear correlation (r = -0.33) suggests there could be more explanatory factors than X-factor magnitude which influenced clubhead linear velocity. Future studies should examine the inter-relationship between further biomechanical parameters during the golf swing and examine the relationships to other measures of performance related to accuracy.

References: [1] Smith et al., Procedia Engineering, 34: 224-229, 2011.

[2] Chu et al., Journal of Sports Sciences, 28: 1251–9, 2011.

[3] Donà, G et al., Sports Biomechanics, 8: 284–301, 2009.

[4] Brown, S et al., Journal of Sports Sciences, 29: 1483–91, 2011.

Disclosure of Interest: None Declared

Soft Tissue

SS-0057

THE NEUROMECHANICAL ADAPTATIONS TO ACHILLES TENDINOSIS

Yu-Jen Chang [1,*]Kornelia Kulig [1]

[1]Division of Biokinesiology and Physical Therapy, University of Southern California, Los Angeles, United States

Introduction and Objectives: Human movement is initiated, and executed in hierarchical system. The central nervous system (CNS) plans, initiates, and sends motor command to muscle. The muscle generates force and pulls on the tendon. The tendon modulates muscle force and controls movement of bone. Components lower in the hierarchical system send feedback signals to assist CNS in planning. Therefore, a successful movement relies on the integrity of all components involved in this hierarchical system. If a component lost its integrity, the entire system has to adapt to that deficiency. Degenerated Achilles tendon exhibits lower stiffness and elastic modulus. This is partly due to disorganized collagen bundles manifested on a sonogram as quantifiable changes in the speckle structure. The descending drive from the CNS will be altered to compensate local mechanical deficit. These modulations in CNS motor commands will lead to altered agonist, synergist, and antagonist activation. The purpose of this investigation was to study the effect of tendon degeneration on its mechanical characteristics, neuromechanical behavior of surrounding musculature, and to explore the existence of CNS modulation accompanying tendinosis. We hypothesize that degenerated tendon will lead to diminished tissue mechanical properties, protective muscle activation patterns, and up-regulated descending drive from the CNS (Fig).

Methods: Nineteen individuals participated (9 with unilateral Achilles tendinosis). Tendinotic subjects were pain free at the time of study. Ultrasound images were acquired on Achilles tendons for morphological analyses. Participants performed ramped maximal voluntary isometric plantarflexion on dynamometer while torque output was recorded. The elongation of tendon was obtained by a combination of ultrasound imaging and motion capture. Evoked H-reflex and V-wave were tested on medial gastrocnemius. Kinetics and EMG data were collected while the subjects performed single-legged hopping. All data were obtained on both limbs of all subjects to allow for side-to-side comparisons.

Eight parameters were derived from the signals collected. 1) Micromorphology: obtained by performing 2D FFT on the sonogram rendering a peak spatial frequency (PSF) variable. 2) Stiffness: determined by the slope on the later 40% of the force-elongation curve obtained from ramped isometric contraction. 3) Electromechanical delay (EMD): time interval between evoked gastrocnemius EMG onset and torque output. 4) Preactivation: time interval between gastrocnemius activation and vertical ground reaction force onset during single legged hopping. 5) Maximal H-reflex: motor neuron excitability at the spinal level. 6) Maximal V-wave: H-reflex under the influence of volitional activation, hence reflects the decending command from higher center. 7) EMG based contribution index (CI). 8) EMG based Co-Contraction Ratio (CCR). Independent sample t-test with Bonferroni correction for multiple comparisons was used to test the impact of Achilles tendinosis on side-to-side discordance of those 8 variables between groups.

Results: Mean side-to-side discordances for control and tendinotic groups are presented in the Table. The independent sample t-test with correction for multiple comparisons showed significantly different side-to-side discordance in all variables. The averaged side-to-side differences in the control group were lower (variable 1, 3, and 6), very similar

(variable 2, 5, 7, and 8), and higher (variable 4) than the Standard Error of Measurement (SEM) (Table). The 2ms difference between legs in Gastrocnemius preactivation was likely due to leg dominance. In contrast, side-to-side differences in the tendinotic subject exceeded the SEM in all variables (Table). This error based analysis further supports the robustness of the findings.

Figure:
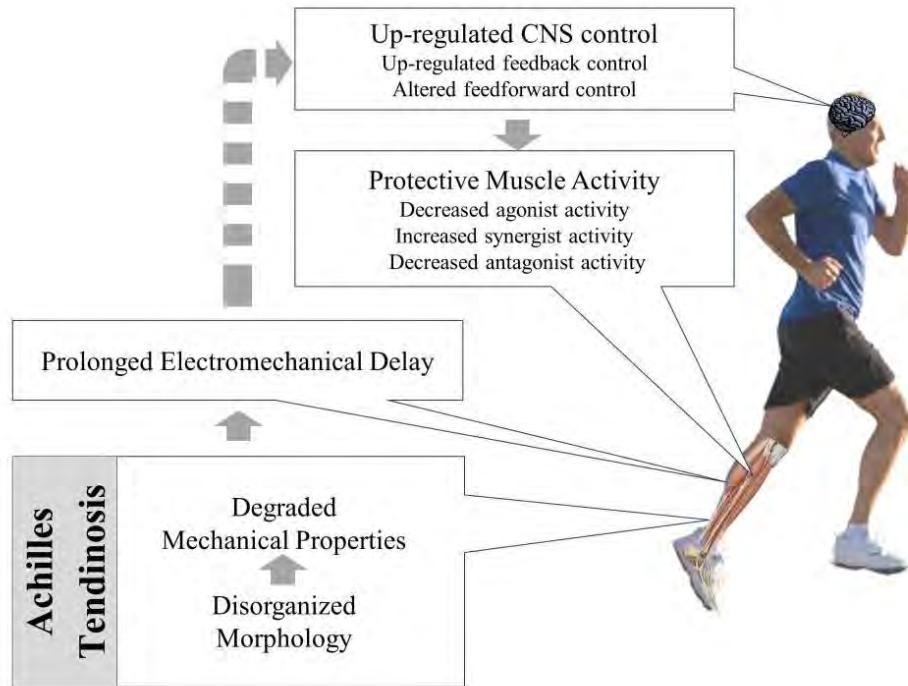
Caption: Hypothetical framework of how Achilles tendinosis affects its mechanical properties, muscle-tendon interaction, and CNS modulation.

Conclusion: This study is the first to investigate the impact of a long standing musculoskeletal degenerative disease on multiple levels of neuromuscular system. Strong evidence presented in this study indicates that long standing Achilles tendon degeneration results in a compliant tendon, which affects motor command from CNS, hence imposes changes in the activation and coordination of muscles involved in a locomotive task.

Table:

	Tendinotic (n=9)	Healthy (n=10)	SEM
Side-to-side Difference in:			
(1) Peak Spatial Frequency (mm^{-1})	0.43(0.15)	0.05(0.04)*	0.34
(2) Stiffness (N/mm)	130.58(37.97)	12.02(7.36)*	9.11
(3) Electromechanical Delay (ms)	9.99(3.16)	1.68(1.14)*	2.04

(4) Preactivation (ms)	18.37(6.58)	2.04(1.25)*	0.40
(5) H/M Ratio	0.14(0.04)	0.02(0.01)*	0.02
(6) V/M Ratio	0.16(0.09)	0.02(0.02)*	0.10
(7) Contribution Index	0.31(0.11)	0.05(0.05)*	0.04
(8) Co-Contraction Ratio	0.32(0.12)	0.10(0.11)*	0.08

*p<0.001; SEM – Standard Error of Measurement

Caption: Side-to-side differences in tendinotic and control subjects and the statistical comparison of these differences between groups. Data are Mean(SD).

Disclosure of Interest: None Declared

Bone

SS-0058

ON THE USE OF IN VIVO EQUINE DATA TO INFORM A MECHANOSTATISTICAL MODEL OF CORTICAL BONE REMODELLING

Xiaoming Wang [1,*]Helen Davies [2]David Thomas [3]John Clement [3]Raj Das [4]Justin Fernandez [1]

[1]Auckland Bioengineering Institute, University of Auckland, Auckland, New Zealand, [2]Faculty of Veterinary and Agricultural Science, [3]Melbourne Dental School, University of Melbourne, Melbourne, Australia, [4]Dpt. Mechanical Engineering, University of Auckland, Auckland, New Zealand

Introduction and Objectives: The equine model is highly suited to investigating human cortical bone behaviour. It has similar haversian structures (unlike murine models); has a fetlock joint (which is similar to the human knee); offers the ability to measure *in vivo* data; and is recommended by the U.S. Federal Drugs Administration (FDA) for comparative joint research, making it a useful animal model for translation of findings to the human. The primary objective of this study was to develop a 3D multiscale equine model of cortical bone behaviour that is informed by measured *in vivo* bone growth rates and bone strain. The secondary objective was to make this model useful in practice by developing a surrogate model to link micro cortical bone behaviour to the whole bone.

Methods: Two bone biopsies taken from the dorsal cortex of the cannon bone of size 4 mm × 3.5 mm × 2 mm were imaged at 5 μm resolution using an Xradia MicroXCT machine. The cortical structures were extracted using a snake algorithm in ITK-SNAP and voxel meshed in Hypermesh for finite element simulation in Abaqus. A cortical bone remodelling algorithm was integrated [1] that used stress stimulus to initiate bone growth and bone density responses according to the well-known 'mechanostat' developed by Frost [2]. Bone remodelling rates were adapted from biostained images taken from the equine cannon bone (Figure 1, left) during controlled periods of exercise (trot, canter, gallop, rest) with known speeds of 4 m s^{-1}, 10 m s^{-1} and 17 m s^{-1} and 0 m s^{-1}, respectively [3]. These were linked to *in vivo* bone strain measured from strain gauges placed on the dorsal cortex (Figure 1, centre) and ranged from 2.6 μm/day (trot) to 12.7 μm/day (gallop). It was observed that horses trained at galloping speeds continued to show significant bone growth during the post-gallop rest period. This motivated the development of a 'fading memory' model, whereby recent loading histories are remembered. A 3D haversian 'cutting-cone' model was included (Figure 1, right) to describe haversian tunnelling and replacement of old and damaged bone. Finally, to make this model useful in practice we trained a surrogate model using partial least squares regression (PLSR) to predict micro-architecture (shape) and homogenised Young's modulus given known whole body loads.

Results: The cortical bone model predicted the fine filamentary tunnelling behaviour that was primarily in the longitudinal direction of bone. Surrounding loads caused the haversian canals to oscillate in shape similar to that observed in synchrotron imaging and micro CT. The haversian canals showed merging behaviour and predicted formation of 'super osteons' [4] and Volkmann canal-like behaviour. This suggests that increase in porosity may be due to merging of haversian canals. The memory effect was shown to generate continued bone growth even after loading stimulus was removed. This was consistent with the data measured from horses that raced at speeds of up to 17 m s^{-1} and continued to show significant *in vivo* bone growth during post-exercise rest. The surrogate model was used to predict bone shape and

Young's modulus for bone not used in the training set. Both shape and homogenised Young's modulus were predicted with average errors of less than 1%.

Figure:
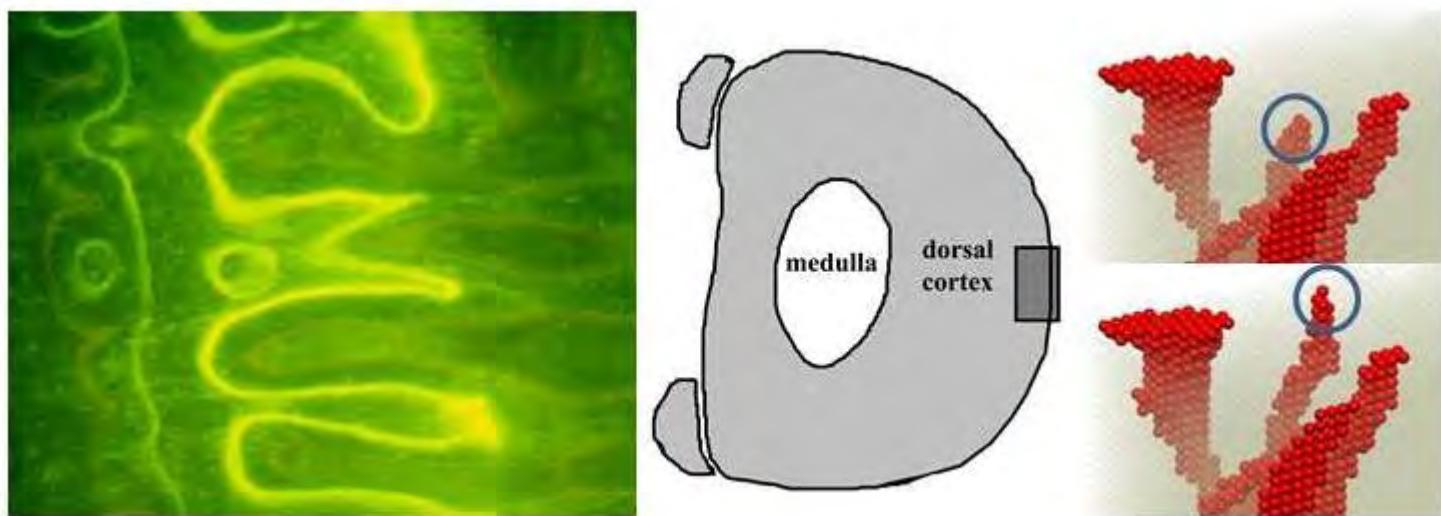
Caption: Figure 1: (Left) biostained image depicting bone growth; (Middle) equine strain gauge data; (Right) micro cortical bone remodelling.

Conclusion: The equine model provided information on *in vivo* bone growth rates and bone strain which was essential for informing computational prediction. The threshold nature that linked remodelling rates to distinct speeds and bone strains supports the use of the classical bone remodelling mechanostat. This is in contrast to other popular models, such as mice models, which do not have haversian canals and present a challenge when controlling their loading environment; and human models, which only presents limited end of life data where the history of loading is unknown.

The prediction ability of the presented surrogate model can inform whole bone strength changes rapidly and accurately without expensive computation. The influence of disease and drug effects at the micro level can also be incorporated and additional synthetic data can be generated for scenarios not experimented on. Translation to the human may be achieved by scaling the equine remodelling rates and strain thresholds, which are generally higher for horses. The results of this study are currently being developed for inclusion in the open-source IUPS Physiome project repository [5] for evaluation and sharing by the scientific community.

References: [1] Fernandez et al., Int J Numer Method Biomed Eng, 29(1): 129-43, 2013

[2] Frost, J. Bone Miner Metab, 18(6): 305-16, 2000

[3] Davies, University of Melbourne PhD Thesis, Chapter 8, 1995

[4] Bell et al., Anat. Record, 264(4): 378–386, 2001

[5] Hunter et al., Mech Ageing Dev, 126(1): 187-92, 2005

Disclosure of Interest: None Declared

SS-0059

PIEZOELECTRICITY MODULATES MECHANICS OF COLLAGEN STRUCTURES

Cameron P. Brown [1,*]Jennifer Boyd [1]Antony Palmer [1]Mick Phillips [2]Charles-Andre Couture [3]Maxime Rivard [3]Philippa Hulley [1]Andrew Price [1]Andreas Ruediger [3]Francois Legare [3]Andrew Carr [1]

[1]NDORMS, [2]Biochemistry, University of Oxford, Oxford, United Kingdom, [3]EMT, INRS, University of Quebec, Varennes, Canada

Introduction and Objectives: Collagen is the most abundant protein in the human body, and plays a dominant role in the functioning of many tissues. The complex hierarchical structure of a collagen fibril provides interesting mechanical, chemical and electrical properties, allowing it to modulate tissue structure and therefore function. Through organisation and interactions on the nanometre to micrometre scales, collagen can work effectively in a wide variety of tissue configurations to provide exceptional mechanical performance, tuned to specialised applications. Here, we examine the role of collagen piezoelectricity in the mechanical function and interactions of collagen structures in soft tissues.

Methods: Human tendon and cartilage samples were snap frozen, cryosectioned and mounted for imaging with scanning probe and interferometric second harmonic generation (ISHG) microscopy. Scanning probe microscopy (Cypher AFM, Asylum Research, High Wycombe) was performed using intermittent-contact mode and lateral piezoresponse force microscopy (PFM). ISHG microscopy was performed as described in Rivard et al. (*1*) This showed the magnitude and sign of the average second order nonlinear optical susceptibility $\chi^{(2)}$ within the focal volume of the laser, which is equivalent to the piezoelectric tensor **d**.

Modelling was undertaken in two stages. First, a model of two interacting fibrils was developed to investigate the effect of the piezoelectric property of collagen. A 2-D implicit model was developed in Abaqus (v 6.11), using piezoelectric elements. Collagen was modelled as linear elastic isotropic (E=200 MPa; (*2*) v=0.35), with the $\mathbf{d}_{15}$ coefficient of the piezoelectric tensor 1 pm/V. The two fibrils of interest were loaded in compression and shear by adjacent external fibrils to simulate a continuous boundary condition. The resulting electrical potential across each fibril was calculated for both similar and opposite polarisations.

Using the electrostatic attraction or repulsion caused by the piezoelectric response as an input, a second set of models was developed to investigate the effect of piezoelectric domains in the context of multiple fibril interfaces. These used a 2-D explicit solution with 20 fibrils of the same material properties as the two-fibril model.

Results: Using PFM we observed distinct piezoelectric domains on the tens of nanometre to micron scale resulting from the organisation of collagen fibrils (Fig 1). A constant piezoelectric property ($\mathbf{d}_{15}$ coefficient) was measured across each fibril and along its length. The magnitude of the $\mathbf{d}_{15}$ coefficient was approximately 1 pm/V. A dominant polarity was observed in any given region, broken by individual, or small groups of, oppositely polarised fibrils. Similar patterns were observed on a larger scale using ISHG. Domains of positive and negative $\chi^{(2)}$ were maintained over distances of 5 to 50 µm perpendicular to the fibrils, splitting the tissue into domains of predominant collagen fibril polarity.

Increased effective friction at interfaces caused by attractive forces within piezoelectric domains locked the fibrils together, thus increasing storage of elastic energy within each domain prior to the onset of slip. Elastic energy storage was an order of magnitude higher within a domain than at its boundary. When slipping did occur, the high friction within the domains increased the dissipation of energy. The piezoelectric domains in the 20-fibril system increased the frictional dissipation of energy by 30-50%, or 20-25% when normalised against external work. Between the domains, a slip plane with reduced friction was formed due to electrostatic repulsion, providing a mechanism for restructuring under load and relieving local stress.

The increased capacity for energy storage appears to be coupled with fracture resistance. The higher local shear stress environment inside domains will control the location of individual fibril fractures due to the 'sticking' effect. By fracturing within a domain, the attractive forces will more effectively redistribute stress across and along a domain than at an interface, protecting against the formation of a critical fracture cluster. By modulating load sharing, and increasing the effective strength distribution by forming small bundles, catastrophic failure is further suppressed due to blocking effects.

Figure:
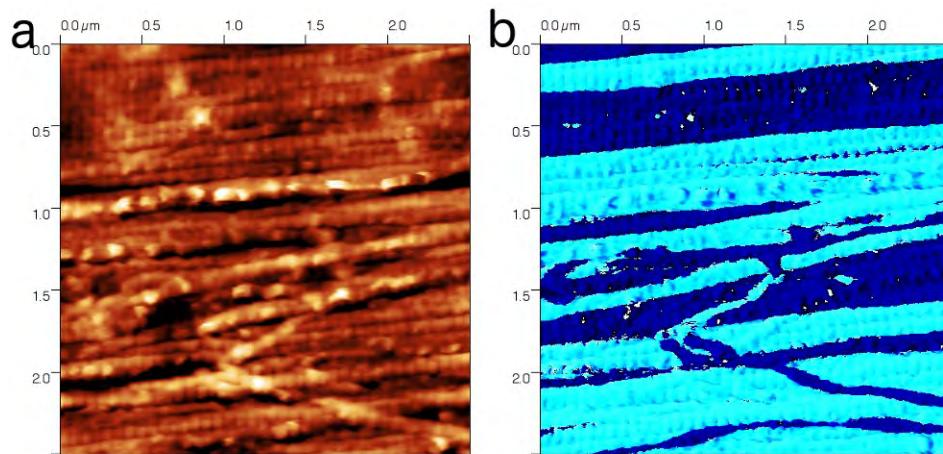
Caption: Scanning probe image of tendon showing (a) morphology and (b) piezoelectric phase, indicating piezoelectric domains as light (phase=0) or dark (phase=pi) regions.

Conclusion: Piezoelectric domains formed by collagen organisation have a distinct mechanical role, modulating fibril interactions from the tens of nanometre to the hundreds of micron scales, allowing tissues to tune energy storage, dissipation and damage resistance.

References: [1] Rivard et al., J Biophotonics 1: 233, 2013.

[2] van der Rijt et al., Macromol. Biosci. 6: 697, 2006.

Disclosure of Interest: None Declared

Connective Tissue

SS-0060

EARLY IN SITU SITE-SPECIFIC CHANGES IN CHONDROCYTE BIOMECHANICAL RESPONSES DUE TO A PARTIAL MENISCECTOMY IN THE LATERAL COMPARTMENT OF THE MATURE RABBIT KNEE JOINT

James Fick [1,*] Ari Ronkainen [1] Andrew Sawatsky [2] Ryan Madden [2] Walter Herzog [2] Rami Korhonen [1]

[1] Department of Applied Physics, University of Eastern Finland, Kuopio, Finland, [2] Facult of Kinesiology, Human Performance Laboratory, University of Calgary, Calgary, Canada

Introduction and Objectives: Although previous research[1,2] was conducted to investigate early changes in rabbit knee joint cartilage at 3 days after a partial meniscectomy (PM)[1,2], there is no study that has focused on early changes associated with *in situ* chondrocyte deformation responses as a result of a PM. Our objective was to determine if early changes in cell biomechanics are present in the superficial layer of knee joint cartilage at 3 days following a PM.

Methods: Ten skeletally mature female New Zealand White rabbits (13 ± 1 month) underwent a PM of the lateral meniscus of a randomly selected knee joint. Each meniscus had ~45% (± 15% standard deviation) of its anterior horn removed and the opposite knee was left intact. Three days after the PM, rabbits were euthanized and the knee joints were harvested. The operated knee joints formed an experimental group (n = 10) and the intact knee joints formed a contralateral (control) group (n = 10). Joint tissues were stained with fluorescein conjugated Dextran at 4°C for 5 hours prior to compression and cell imaging. Samples were mounted with dental cement into a custom built sample holder. The following sites were tested: patella, femoral groove, femoral condyles (medial and lateral) and tibial plateaus (medial and lateral).

Compression and cell imaging: A custom-designed *in situ* indentation system[3] mounted on to the stage of a confocal laser scanning microscope (Zeiss Inc.) was utilized for testing. A light-transmissible glass indenter (ϕ = 2mm) mounted on the stage with a x40-magnification objective was used to capture optical sections before and after sample compression. Sections were collected at 0.5 μm increments in the optical direction and up to 60 μm depth from the sample surface. A surface pressure (2 MPa) was applied to the samples at an average speed of 10 μm/s [4]. After reaching the desired stress level, the displacement was held constant for 20 minutes to reach an equilibrium state. The samples were then imaged in this compressed state. Cells from each set of optical image sections were identified and had their volumes and dimensions (e.g. cell height, width and depth) determined[4].

Statistics: The percentage change in cell volume, height, width and depth due to cartilage compression was determined at each site and for the experimental and contralateral knees (mean ± 95% confidence interval). Statistical differences between the experimental and contralateral knees were assessed with Student's T-tests ($p < 0.05$).

Results: Cells from both the patellar and femoral groove tissues in the experimental group experienced greater volume decreases ($p < 0.05$) expanding less in their lateral directions relative to cells from the contralateral group ($p < 0.05$ in groove). Cells from the lateral femoral condyle in the experimental group experienced greater volume decreases deforming more in the axial direction (height), expanding less in width relative to cells from the contralateral group ($p < 0.05$). In contrast, cells from the medial femoral condyle and tibial plateau in the experimental group had smaller decreases in volume, deforming less in the axial direction, relative to cells from the contralateral group ($p < 0.05$). This

finding is consistent with earlier experiments conducted on anterior cruciate ligament transected rabbits where patellar chondrocyte volumes decreased less (compared to contralateral patellar cells) and even increased relative to cell volumes before loading[4]. Interestingly, previous work utilizing a PM technique (with sectioning of ligaments) reported proteoglycan loss from knee joint tissues as early as 3 days post-surgery[1,2]. Our preliminary analysis of tissue composition indicates that the greatest proteoglycan loss occurs in medial tibial plateau cartilage (where osteoarthritic-like changes in cell biomechanics were also observed), while no proteoglycan loss occurs in the lateral tibial plateau cartilage (where cell biomechanics remained unaltered). Thus, these biomechanical changes in cell responses between groups from different sites within the knee joint likely reflect localized alterations in tissue composition/structure.

Figure:
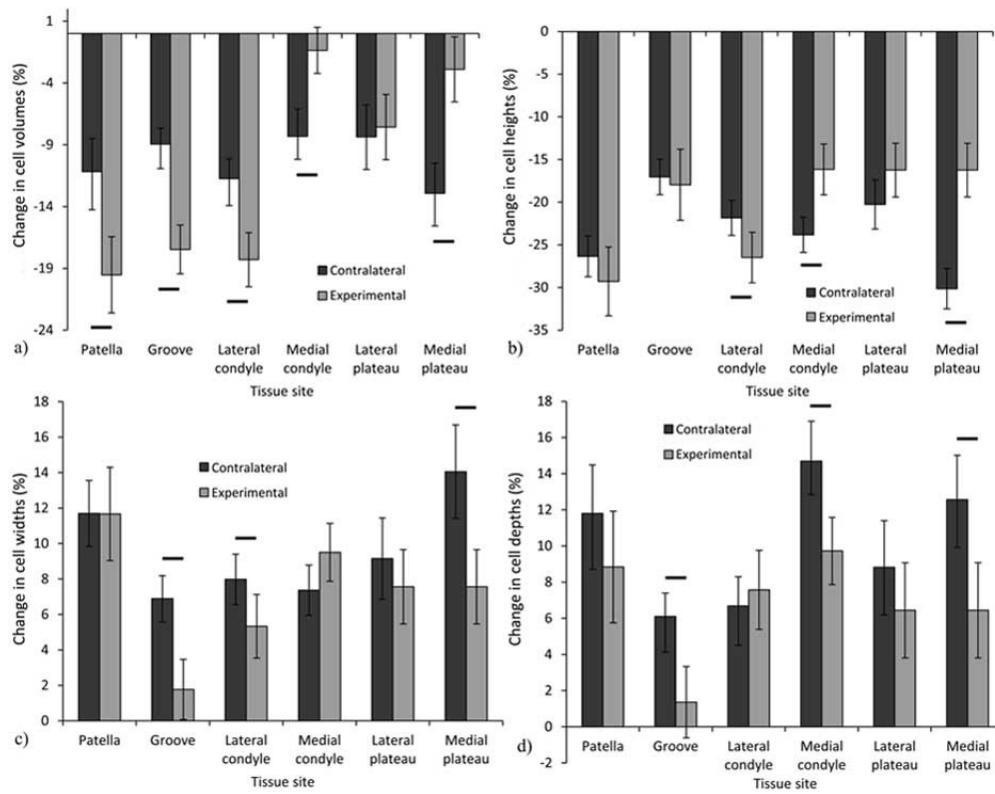
Caption: Percentage changes in cell volumes (a), heights (b), widths (c) and depths (d) due to cartilage compression across each site, between groups. Solid black bars denote significant differences ($p < 0.05$); number of cells analyzed from the contralateral group patella and lateral condyle = 90 cells/site, all other remaining sites in each group = 100 cells/site.

Conclusion: Our results demonstrate that biomechanical responses of chondrocytes within the mature rabbit knee joint are altered in a highly site-specific manner at 3 days following a partial meniscectomy of the lateral meniscus.

References: [1]Colombo et al., Arthritis Rheum., 26: 875-86. [2]Caputo et al., J. Orthop. Res., 6: 103-108, 1988. [3]Han et al., Med. Eng. Phys., 31: 1038-1042, 2009. [4]Turunen et al., Osteoarthr. Cartil., 21: 505-513, 2013.

Disclosure of Interest: None Declared

SS-0061

THE EFFECT OF IMPACT LOAD ON THE MECHANICAL PROPERTIES OF CHONDROCYTES AND ITS ASSOCIATION WITH CYTOSKELETON COMPONENTS

Zhexing Wang [1]Andrea O'Connor [1]Geoff Stevens [1]Peter V.S. Lee [2,*]

[1]Chemical and Biomolecular Engineering, [2]Mechanical Engineering, University of Melbourne, Melbourne, Australia

Introduction and Objectives: The primary cells within the articular cartilage (AC) are the chondrocytes and these cells are responsible for the maintenance of the extracellular matrix (ECM), which is the weight bearing component in AC. The activities of the AC chondrocytes are closely regulated by the mechanical forces applied to the cells. Therefore any changes to the mechanical properties (e.g. stiffness) of chondrocytes could have a significant effect on how chondrocytes sense physical forces in the AC environment. The objective of this study is to investigate whether the mechanical properties of chondrocytes can be altered by impact damage on articular cartilage, which is a leading cause of post-traumatic osteoarthritis, and its association with the cytoskeleton components within the cells.

Methods: Osteochondral explants of 8mm diameter consisting of cartilage/ subchondral bone from porcine knee joints were subjected with two different impact loads using an instrumented drop tower device. The impact energy density ($3.75J/cm^2$ and $7.5J/cm^2$) was calculated by the potential energy generated by the drop weight and height divided by the explant cross-sectional area. The chondrocytes were then isolated from the explants and the Young's moduli and viscosity of three groups of isolated chondrocytes (non impact, impact at $3.75J/cm^{2,}$ impacted at $7.5J/cm^2$) were measured using the micropipette aspiration technique[1]. The density of the cytoskeleton in the impacted and non-impacted chondrocytes was analysed by confocal fluorescence microscopy and ImageJ software by staining for F-actin.

Results: Chondrocytes from both $3.75J/cm^2$ and $7.5J/cm^2$ impacted groups exhibited a significantly higher Young's modulus ($p < 0.05$) and higher apparent viscosity ($p < 0.05$) compared with the control group (Table1). No significant difference was found in these parameters between the specimens impacted at different energies ($p > 0.05$). Moreover, we found the F-actin fluorescence intensity (Fig.1) was significantly different between the impacted and control specimens ($p < 0.05$).

Figure:
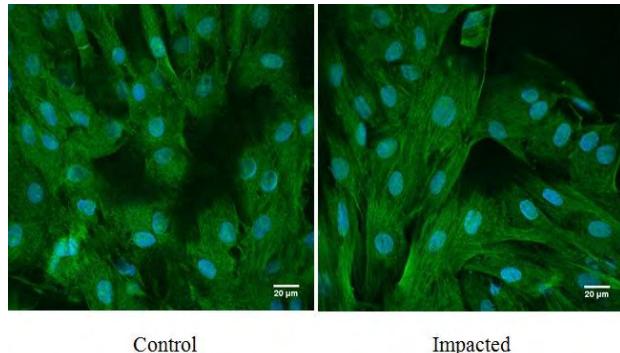
Control   Impacted

Caption: Figure 1. The fluorescence images of chondrocytes from control and impacted specimens

Conclusion: This study investigated how chondrocytes respond to mechanical loadings on a cellular level by utilising the micropipette aspiration technique and F-actin fluorescence intensity analysis. The results showed that the mechanical properties of articular chondrocytes can be altered by impact injury, but an increased impact loading did not have a measurably greater influence. The changes in mechanical properties of post-impact chondrocytes are associated with alterations in their cytoskeleton.

Table:

	Young's modulus (kPa)	Apparent viscosity (Pa·s)	F-actin fluorescence intensity (mean gray value per cell)
Control	0.23±0.022	2.19±1.16	1.24±0.08
3.8 J/cm^2 impacted	0.30 ± 0.045	3.13±1.37	1.7±0.3
7.5 J/cm^2 impacted	0.29 ± 0.032	3.19±1.58	

Caption: Table 1. Mechanical properties and F-actin fluorescence intensity of chondrocytes

References: [1] Hochmuth, R.M., J. Biomechanics,**33**(1): p. 15-22, 2000

Disclosure of Interest: None Declared

Bone

SS-0062

ANISOTROPIC NONLINEAR VISCOELASTIC MODELLING OF TRABECULAR BONE

Krishnagoud Manda [1,*]Robert Wallace [2]Erika Sales [1]Francesc Levrero Florencio [1]Pankaj Pankaj [1]

[1]University of Edinburgh, School of Engineering, Institute of Bioengineering, [2]University of Edinburgh, Department of Orthopaedics , Edinburgh, United Kingdom

Introduction and Objectives: Most musculoskeletal simulations assume that the bone to be linear time-independent elastic material though it has been previously recognized that in reality its mechanical response is time-dependent [1]. It can be hypothesized that the time-dependent behaviour can be related to its micro-architecture, but such relationships are yet to be established. Predicting the time-dependent behaviour of the trabecular bone is a significant step towards better understanding of the mechanical behaviour of the normal and diseased bone including fracture.

In the present work we modelled the trabecular bone with a nonlinear anisotropic viscoelastic material model and developed a numerical recursive iterative algorithm based on implicit stress integration principles and thereby predicted the time-dependent behaviour of the trabecular bone. The model was validated using compressive relaxation experiments on the trabecular bone samples using a loading stage in a micro-CT scanner. The nonlinear constitutive parameters were estimated based on the experimental data.

Methods: An implicit recursive iterative numerical algorithm was developed for modelling of the anisotropic time-dependent behaviour of the trabecular bone based on [2,3]. The numerical algorithm was implemented in the context of nonlinear finite element structural analysis as a user defined material subroutine (UMAT) to be used with ABAQUS (Simulia, Dassault Systemes, RI, USA) interface. The subroutine is called at each integration point of FE mesh for each global iteration with the input of state variables and converged values of stress and strain from the previous time step. The strain components are known at the beginning of each time increment and stress and consistent tangent material Jacobian are updated at the end of each time increment. The hereditary integrals are saved as state variables at the end of each increment. The iterative algorithm was presented as a flow chart, Fig. 1(a). The nonlinear stress dependent parameters (g_0,g_1,g_2 and a_σ) were expressed as polynomial function of effective stress based on the experimental data, Fig. 1(b). The transient relaxation and strain compliance functions were represented with Prony series. The anisotropic, nonlinear capabilities of the developed algorithm were verified with analytical examples of triaxial tension/compression and simple shear.

Human femoral heads were harvested and the trabecular bone samples were cored-out to the size of 10.64 mm diameter with constant water irrigation. The ends of the samples were cut parallel using low speed saw to a mean size of 12 (±0.65) mm. The compression tests were performed using a loading stage mounted in a micro-CT Skyscan 1172 (SkyScan, Kontich, Belgium) and simultaneously scanned at intermittent stopping points. The Prony series parameters representing linear viscoelastic model were estimated by nonlinear curve fitting based on the experimental relaxation curves. The observed stress relaxation curves for one of the samples are shown in Fig. 1(c) at two different strain levels equivalent to 20% and 40% of yield strain respectively, ensuring that it remains in the elastic regime. The relaxation behaviour was observed to be linear viscoelastic until strain equivalent to 20% of yield strain, and beyond that the

response varied nonlinearly. The relaxation curve at 20% of yield strain was treated as a master curve and the nonlinear parameters were obtained by shifting this master curve to match with other curves at higher strains using nonlinear curve fitting procedures.

Results: The stress relaxation curves of trabecular bone samples at different strain levels were obtained from series of compressive relaxation experiments and the viscoelastic Prony parameters were determined for each sample. The nonlinear parameters were determined and expressed as a polynomial function of effective stress, Fig. 1(b). The predicted relaxation response from the developed nonlinear viscoelastic model was in good agreement with the experimental data, Fig. 1(c), whereas linear viscoelastic model did not predict the response well and error was around 50%.

Figure:
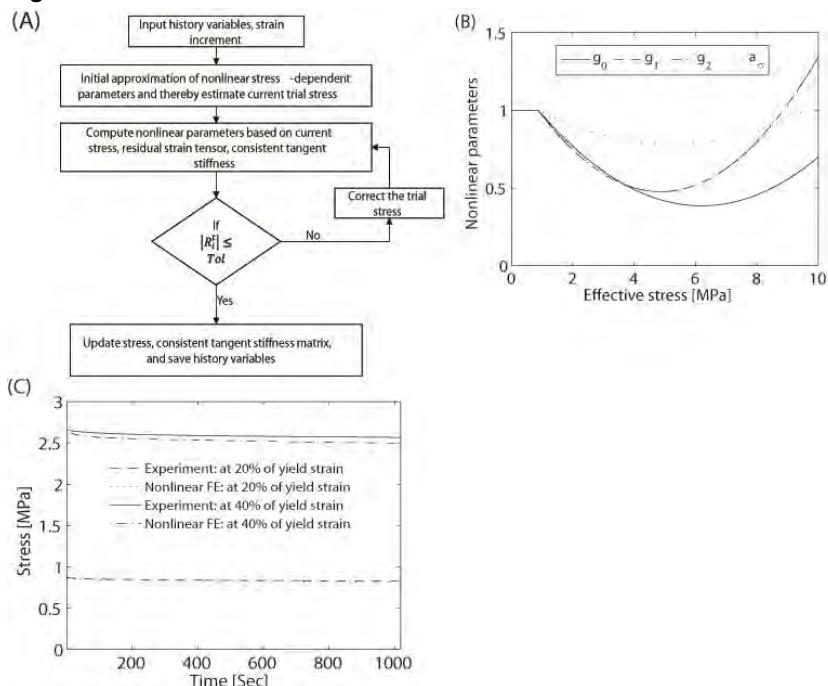
Caption: Figure 1. (A) Recursive iterative numerical algorithm, (B) Nonlinear stress dependent parameters, (C) Relaxation stress response of a cylindrical trabecular bone sample (diameter = 10.64mm, height = 12.27mm) at two different strain levels.

Conclusion: The time-dependent behaviour of the trabecular bone, observed from the experiments, was significant and the linear viscoelastic models were not sufficient to predict this behaviour. Hence, the more general anisotropic nonlinear viscoelastic material model was developed and was validated with the experiments. The results showed good agreement with the experimental data.

References: [1] Deligianni et al.,J. *Biomechanics* 27(12): 1469–1476, 1994

[2] Haj-Ali et al., *Int. J. Numerical Methods in Engg,* 59(1): 25-45, 2004

[3] Poon et al., *International Journal for Numerical Methods in Engineering,* 46(12): 2027-2041, 1999

Disclosure of Interest: None Declared

Cardiovascular

SS-0064

THE FLUID-STRUCTURE MODELLING OF THE HUMAN MITRAL VALVE USING IMMERSED BOUNDARY/FINITE ELEMENT METHOD

Nan Qi [1,*] Hao Gao [1] Xingshuang Ma [2] Colin Berry [3] Boyce Griffith [4] Xiaoyu Luo [1]

[1] School of Mathematics and Statistics, University of Glasgow, Glasgow, United Kingdom, [2] Bioengineering College, University of Chongqing, Chongqing, China, [3] Institute of Cardiovascular and Medical Sciences, University of Glasgow, Glasgow, United Kingdom, [4] Department of Mathematics, University of North Carolina, Chapel Hill, United States

Introduction and Objectives: Dysfunction of the mitral valve (MV) causes significant mortality and remains a major medical problem worldwide. MV has a very complicated anatomical structure. Although there has been significant work on developing computational models of the MV over the past 20 years, due the difficulties associated with both the finite-strain deformational kinematics and fluid-structure interaction (FSI), most MV models that include realistic anatomical geometries and constitutive models consider only the structural mechanics of the valve [2]. In this study, we develop an image-derived patient-specific dynamic model of a human MV using hybrid finite element immersed boundary method (IB/FE), incorporating a FE description of the structural mechanics. This enables us to model FSI while accounting for the nonlinear, anisotropic material response of the MV leaflets.

Methods: The IB/FE approach uses a Lagrangian description of the immersed structure along with an Eulerian finite difference description of viscous incompressible fluid modelled using the incompressible Navier-Stokes equations; interaction between Lagrangian and Eulerian variables is by integral transforms with Dirac delta function kernels [1]. Standard IB methods typically describe the elasticity of the structure using systems of elastic fibers [3]. More recently a version of the IB method that uses elasticity models with FE discretizations has been introduced [4]. Specifically, we use the first Piola-Kirchhoff stress tensor to describe the stresses generated by the immersed structure. It is determined from the passive hyperelastic properties of the leaflets by an invariant-based strain energy functional W. The leaflets of the MV are modelled as an incompressible fibre-reinforced material.

In the simulations, the MV structure is immersed in a 3D fluid box. The valve leaflets, derived from a stack of cardiac magnetic resonance images (MRI), are mounted on a housing and an outer tube that are approximately fixed in place using a penalty method. A typical physiological pressure profile is used in which the pressure waveform is rescaled to match the peak systolic pressure of 150 mmHg of the subject. The simulations employ the open-source IBAMR software framework (https://ibamr.googlecode.com), which provides an adaptive and distributed-memory parallel infrastructure for developing FSI models that use IB method.

Results: The corresponding velocity fields are shown in the Fig.; when the valve is fully opened, just closed and fully loaded at the peak pressure [5]. The valve opens at a driving pressure gradient of around 10 mmHg and we can clearly see a strong jet flow towards the outlet (the left ventricular side). As the MV closes, there is a closing regurgitation across the MV, which is responsible for the first heart sound. The complete closure of the leaflets occurs at a transvalvualar pressure gradient of around 80 mmHg, and then undergoes minor further deformation before reaching the peak transvalvular pressure drop. The opening and closing configurations of the simulated MV qualitatively show good

agreements compared to the corresponding MRI in LVOT view. The flow rate through the valve orifice is also compared, along with the measured flow rate from phase contrast MRI.

The stresses in the anterior leaflet are found to be higher than those in the posterior leaflet and concentrated around the annulus trigons and free edges of the valve leaflets. Those areas are located where the leaflet has the highest curvature. When the MV is fully opened, the fibres of the belly region are stretched, and the stress is higher compared with the trigone regions. Immediate after the MV has closed, the stresses increase in all regions, however, at this point the two trigones experience higher stress levels compared with the belly region.

Figure:
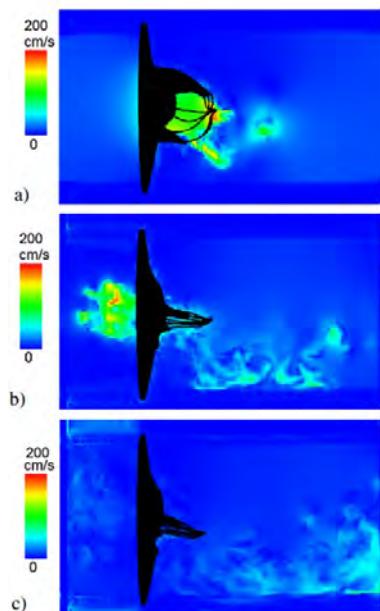
Caption: The in-plane view of the fluid velocity field parallel to the tube longitudinal axis, when the MV is (a) fully opened, (b) just closed and (c) fully loaded at the peak pressure of 150 mmHg.

Conclusion: In this study, we have developed a new human MV model using a hybrid IB/FE approach. This model is a significant step up from our previous work by providing dynamic stress distributions. The model results agree well with the simulated opening and closing leaflet configurations and the flow rate estimated from the MRI measurements. More realistic model is under development by using a more detailed chord structure and patient-specific boundary conditions. We thank for the funding provided by the UK EPSRC (EP/I1029990), the British Heart Foundation (PG/11/2/28474) and the Medical Research Scotland.

References: [1] C. S. Peskin, Acta numerica, 11:497-517, 2002.

[2] Q. Wang et.al., Ann Biomed Eng, 41(1):142–153, 2013.

[3] X. S. Ma et.al., Comput Fluid, 71:417–425, 2013.

[4] B. E. Griffith et.al., submitted

[5] H. Gao et.al., Int J Numer Meth Biomed Engng, 30(12):1597-1613, 2014.

Disclosure of Interest: None Declared

Cardiovascular

SS-0065

NOVEL METHOD FOR 3D RECONSTRUCTION OF THE CHICK EMBRYO CARDIOVASCULAR ANATOMY FROM NON-INVASIVE ULTRASOUND SCANS FOR LONGITUDINAL STUDIES

Choon Hwai Yap [1,*]Germaine Tan [1]Muhammad Jamil [1]Liang Zhong [2 3]

[1]Biomedical Engineering, National University of Singapore, [2]National Heart Research Institute of Singapore, National Heart Centre Singapore, [3]Duke-NUS Graduate Medical School, National University of Singapore, Singapore, Singapore

Introduction and Objectives: Congenital cardiovascular defects are the most common type of birth defects, affecting approximately 0.6-1.9% of newborns each year[1]. Recent small animal studies provided evidence that blood flow fluid mechanics may play a role in the pathogenesis of these malformations[2-5]. The imaging of the small animal embryonic cardiovascular anatomy is an important endeavor to support furthering these researches. To date, however, scan techniques are destructive or invasive, rendering it difficult to perform longitudinal studies on the same embryo. In the current study, the aim is to establish such a method to enable serial imaging and 3D reconstruction of cardiovascular anatomy of the chick embryo, based on high-frequency ultrasound. We show that our technique has sufficient resolution to produce geometries for Computational Fluid Dynamics simulations to quantify detailed embryonic cardiovascular fluid mechanics.

Methods: Fertilized eggs were opened at the blunt end to expose the chick embryo, and imaged in 3D over time with high-frequency ultrasound (45MHz), non-invasively. Chick embryos at Hamburger Hamilton stages 21, 25, 27 and 28 were imaged. Motion cancellation algorithms were applied to negate embryonic bodily motion for embryos past the 5th gestation day. Quadratic temporal averaging was performed in order to differentiate blood space from tissue space[6]. The vessels of interest, namely the internal carotid arteries, descending aorta and pharyngeal aortic arches, were obtained by 3D reconstruction through image-based modelling, and the accuracy of the reconstructed model was validated with stereoscopic measurements. Finally, Computational Fluid Dynamics (CFD) simulation using ANSYS Fluent software was used to model fluid flow in the generated construct of a HH27 embryo.

Results: From the raw Cine B-mode images, it was difficult to distinguish between blood and tissue (Fig. 1A), but after taking quadratic mean over time, distinction between the two was clear (Fig. 1B). The motion cancellation algorithm, when applied to the images of embryos past the 5th gestation day, played a significant role in reducing motion artifacts in the image processing. The processed images were successfully stacked and underwent 3D reconstructions of the blood space geometries (Fig. 1C).

CFD simulations show a region of low shear stress and divergent streamlines at the carotid duct, the distal connection between the 3rd and 4th pharyngeal aortic arches[7] (Fig. 1D). We hypothesize that this low shear environment play a role in the natural regression and disappearance of the carotid duct at a later stage (HH28 onwards).

Figure:
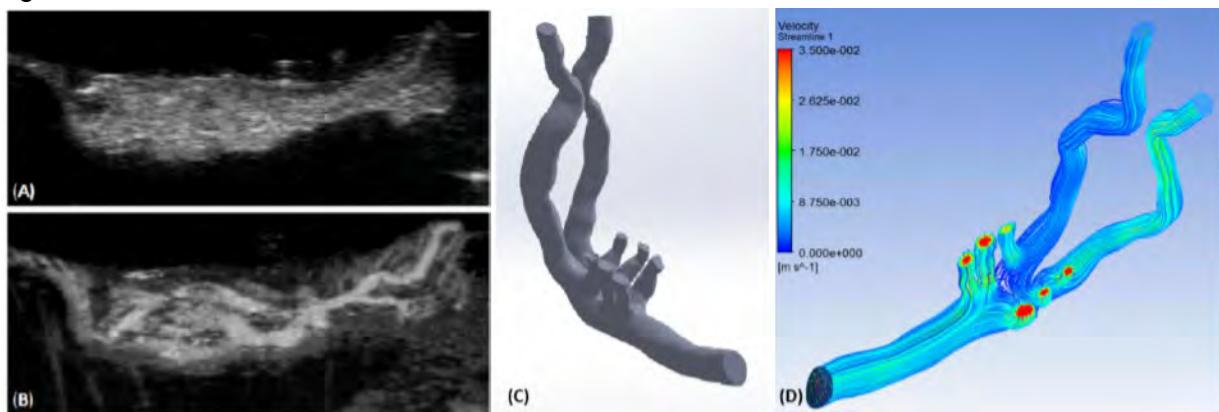
Caption: Figure 1: (A) Original UBM still-image of a HH21 embryo. (B) The same image after image processing to highlight blood space. (C) 3D reconstruction of major arteries. (D) CFD simulations of flow in the same arteries.

Conclusion: High frequency ultrasound has the potential of overcoming most limitations presented by the various imaging modalities, being non-invasive and having good scanning depth. We have established a technique for using high frequency ultrasound to obtain 3D anatomic geometry of cardiovascular organs accurately, which can enable downstream CFD analysis. Our technique allows repeated live scans of a single chick embryo, enabling embryo-specific studies of the influence of hemodynamic forces on cardiovascular development.

References: [1] Hoffman, J.I. et al., J Am Coll Cardiol, 39: 1890-1900, 2002.

[2] Hogers, B. et al., Circ Res, 76: 871-877, 1995.

[3] Tobita, K. et al., Am J Physiol Heart Circ Physiol, 279: 959-969, 2000.

[4] Jay, R.H. et al., Nature, 421: 172-177, 2003.

[5] Broekhuizen, M.L.A. et al., Ultrasound Obstet Gynecol, 13: 437-445, 1999.

[6] Qian, M. et al., Conf Proc IEEE Eng Med Biol Soc, 5127-5130, 2013.

[7] Hiruma, T. et al., Anat Embryol (Berl), 191: 415-423, 1995.

Disclosure of Interest: None Declared

Cardiovascular

SS-0066

PARAMETER ESTIMATION OF HUMAN MYOCARDIUM USING IN VIVO CMR

Hao Gao [1,*]Li Cai [2]Colin Berry [3]Xiaoyu Luo [1]

[1]School of Mathematics and Statistics, University of Glasgow, Glasgow, United Kingdom, [2]Northwestern Polytechnical University Xi'an, Xi'an, China, [3]Institute of Cardiovascular & Medical Science, University of Glasgow, Glasgow, United Kingdom

Introduction and Objectives: In general, left ventricular (LV) myocardium is considered as inhomogeneous, non-linearly anisotropic, incompressible, and even time-dependent, with fibre-enforced micro-structure. One of the centre problems in LV modelling is to identify material parameters for the constitutive equations. By employing a structure-based constitutive law [1], which takes into account the complex 3D myofibre architecture of LV myocardium, we tended to identify parameters from in vivo cardiac magnetic resonance (CMR) data.

Methods: CMR was performed on a healthy volunteer. Cine images were used for functional assessment and LV geometry reconstruction. Custom software written using Matlab was used to extract the endocardial and epicardial boundaries at early diastole, when LV pressure is lowest. Hexahedral elements were generated using a linear interpolation from endocardial to epicardial surfaces. A rule-based myocardial fibre generation method was employed to construct the fibre and sheet architecture of the myocardium. The structure-based nonlinear orthotropic constitutive law for passive LV myocardium proposed by Holzapfel and Ogden [1] was used.

Regional circumferential myocardial strain was estimated from early-diastole to end-diastole by using a deformable image registration method from cine images. The LV cavity volume at end-diastole was also calculated from the cine images, and a population-based end-diastolic pressure was assumed (8 mmHg). Material parameters were updated by forming an inverse problem to match the measured regional circumferential strain and LV cavity volume. A sensitivity study showed that there exist close correlations among the material parameters. We therefore adopted a multi-step optimization procedure by reducing the parameter space [2], shown in Figure 1(a).

Results: Myocardial material parameters of the LV model were successfully estimated using the proposed optimization procedure. The simulated regional circumferential strain and LV cavity volume were in good agreement with the measurements from cine images. We also compared the estimated myofibre stress-strain relationship with other studies, although there are necessary discrepancies due to the subject variety and different constitutive laws used, the overall trend of the mechanical response is similar, shown in Figure 1(b).

Figure:

(a)

(b)
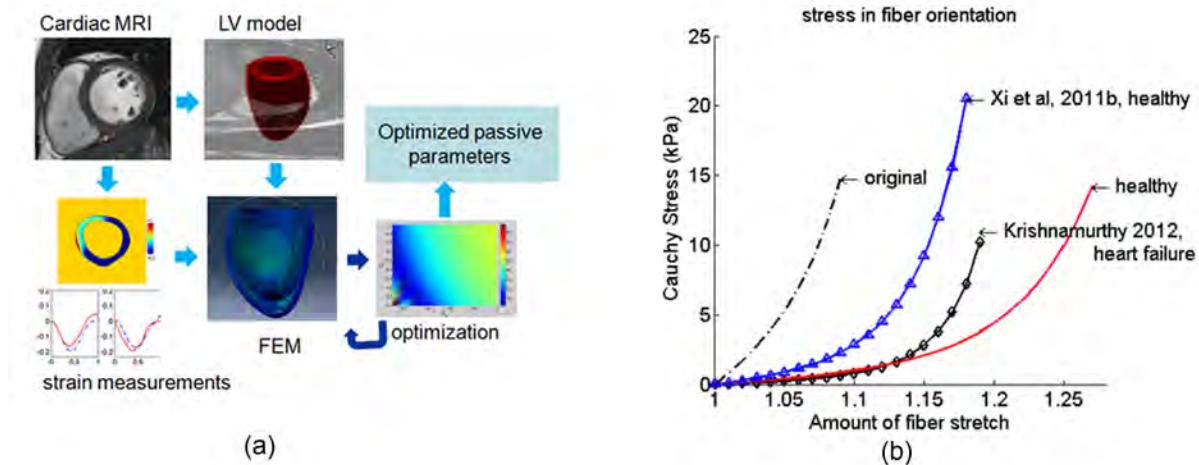
Caption: Figure 1. (a) Schematic illustration of the proposed multi-step optimization procedure; (b) estimated myofibre strain-stress relationship (indicated with 'healthy') and compared with other studies.

Conclusion: In this study, we have demonstrated, for the first time, the feasibility of inversely estimating material parameters in the orthotropic Holzapfel-Ogden constitutive law for passive myocardium by using a multi-step optimization procedure using both strain and pressure-volume data based on in vivo CMR.

References: 1. Holzapfel GA, Ogden RW, Philos. Trans. R. Soc. A 367(1902):3445–3475, 2009.
2. Gao H, Li WG, et al. J End Math, DOI 10.1007/s10665-014-9740-3, 2014.

Disclosure of Interest: None Declared

CREATING BOUNDARY CONDITIONS FOR NUMERICAL SIMULATIONS OF THE FONTAN CIRCULATION USING HEMODYNAMICS DATA OBTAINED WITH NON-SIMULTANEOUS MULTI-POINT MEASUREMENTS

Masanori Nakamura [1,*]Shinji Goto [1]Keiichi Itatani [2]Shohei Miyazaki [2]Takashi Honda [2]Tadashi Kitamura [2]Tetsuya Horai [2]Masahiro Ishii [3]Kagami Miyaji [2]

[1]Department of Mechanical Engineering, Saitama University, Saitama, [2]Department of Cardiovascular Surgery, [3]Department of Pediatrics, Kitasato University, Sagamihara, Japan

Introduction and Objectives: The Fontan circulation is the final palliative result with a single-ventricle physiology. It has two inlets (superior and inferior vena cava) and two outlets (right and left pulmonary arteries). Hemodynamics in that circulation is influenced by both respiration and heartbeat. Many computational fluid dynamics studies have been implemented so far to better surgery for the Fontan circulation [e.g. 1]. However, adequacy of boundary conditions remains debatable in a sense that the boundary conditions used actually reflect flow fluctuations caused by respiration and heartbeat. Clinically, physiological data are acquired from catheter examinations. However, it is not feasible to implement either simultaneous or synchronized measurements of hemodynamics in the related blood vessels using the catheters. Therefore, it is necessary to establish the way of creating boundary conditions for flow simulations using data measured non-synchronously at multiple locations. This study proposes a method for resynchronizing the measured data for use as the boundary conditions for flow simulations using frequency analyses, and discusses the optimal cut-off frequency to use for differentiating cardiac and respiratory variation in the hemodynamic data in the process of resynchronization.

Methods: A Fourier analysis was carried out for pressure and velocity data obtained at four locations, namely, superior and inferior vena cava and left and right pulmonary arteries. After conversion of the data into the frequency domain, a cut-off frequency was placed between two peak spectra which were thought to represent the frequencies of heartbeat and breathing to separate the data affected by heartbeat (cardiac flow) from the ones by breathing (respiratory flow). Then, temporal variations of respiratory and cardiac hemodynamics were separately restored by an inverse Fourier transform, from which representative waveforms of respiratory and cardiac flows were taken. Finally, these representative waveforms were phase-matched in reference to the minimum value of velocity or pressure to synchronize the data obtained at different locations.

Using the synchronized data, we carried out a numerical simulation of the Fontan circulation. A patient was two-year old boy who does not have abnormal collateral circulations and respiratory complications. Flow data were given to the superior and vena cava, while pressure boundary conditions were imposed on the right and left pulmonary arteries. Note that the pressures used for the boundary conditions were corrected, taking account of the characteristic impedance of the Fontan circulation.

Results: From a viewpoint of cyclic repeatability of flow waves, heartbeat effects from respiration effects was optimally separated with the cut-off frequency slightly smaller than the peak frequency of heartbeat effect.

In looking at flow patterns, a remarkable difference was not found in overall flow including velocity and pressure distributions regardless of the cut-off frequency; flow from the superior vena cava and that from the inferior vena cava collided with each other and turned to the left and right pulmonary arteries as exemplified in Fig. 1. A total energy loss during one respiratory cycle in the present geometry showed approximately 3% change for the cut-off frequencies examined. Although the energy loss in the Fontan circulation was quite small (~ 1.6 mJ) compared to that in the whole cardiopulmonary circulation, cumulative energy loss by repeated heart beats would be an indispensable load for a heart, in particular having congenital failure, addressing the importance of properly setting the cut-off frequency to evaluate hemodynamics in the Fontan circulation.

Figure:
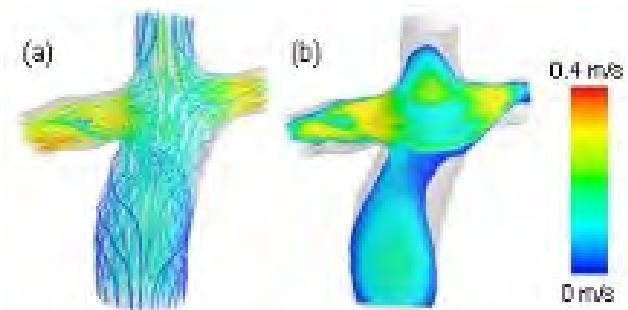
Caption: Figure: (a) Streamlines and (b) a velocity contour map at the peak of respiration.

Conclusion: In this study, we propose the way of creating boundary conditions for flow simulations using data measured non-synchronously at multiple locations for the numerical simulation of the Fontan circulation. For separating the cardiac and respiratory flows, it was best to set a cut-off frequency that gave a local minimum in the power spectrum that was slightly smaller than the peak frequency of the heartbeat. Although the overall flow patterns appeared to be similar, the energy loss that is the most important parameter for evaluating the surgery of the Fontan circulation varied with the cut-off frequency.

References: [1] Slesnick TC, Yoganathan AP. Computational modeling of Fontan physiology: at the crossroads of pediatric cardiology and biomedical engineering. Int J Cardiovasc Imaging. 30: 1073-1084, 2014

Disclosure of Interest: None Declared

Modelling

SS-0070

PREDICTIVE MESOSCALE STRUCTURAL MODELLING OF BONE INFORMED BY MICROSCALE POROELASTIC ANALYSES

Claire C. Villette [1 2,*] Andrew T. M. Phillips [1 2]

[1]Civil and Environmental Engineering, Imperial College London, [2]The Royal British Legion Centre for Blast Injury Studies at Imperial College London, London, United Kingdom

Introduction and Objectives: Bone tissue adaptation is a multi-aspect physiological process driven by interrelated mechanical and biological stimuli [1], which requires the combined activity of several populations of bone cells. Studies suggest that fluid motion in the extracellular space may be involved in cellular mechanosensitivity [2], potentially via the resulting shear stress on the cell walls. In silico studies have implemented these theories in mechanistic models with probant results [3-5]. Phenomenological approaches, based on the empirical relations between mechanical stimulus and bone adaptation are also commonly used. Such approaches are limited in scale and in scope but present tremendous computational efficiency gains.

Previously, the authors developed a mesoscale predictive structural model of the femur using truss and shell elements to represent trabecular and cortical bone respectively, and relying on a phenomenological strain-based bone adaptation algorithm [6,7]. The predicted structure showed good correlation with anatomical observations, with a high computational efficiency. However the use of truss elements was considered as a limitation as only axial strain is considered. In order to introduce a response to bending and shear, the authors considered the use of beam elements, requiring a new formulation of the bone adaptation drivers.

The primary purpose of the study presented here was to isolate phenomenological drivers based on the results of a mechanistic approach, for use in a strain-based bone adaptation algorithm to be used with a beam element representation of trabecular elements in mesoscale structural modelling [6,7].

Methods: Two distinct 2D finite element models of a single trabecula were developed. In one model the trabecula was represented by a single beam element. In the other model, the trabecula was represented by a mesh of poroelastic elements. Each model was subjected to the same selection of uniaxial loading scenarios. 42 load cases were tested, with different angles of load application, varying between 0 and π with respect to vertical, and 3 different load amplitudes.

A mechanistic adaptation algorithm was implemented to iteratively remodel the poroelastic trabecula under loading, based on fluid motion velocity through the bone matrix pores. After convergence of this iterative process, the definition parameters of a reoriented beam equivalent to the continuum remodelled poroelastic trabecula were estimated for each load case. The mechanistic adaptation algorithm was initially compared to a published bone adaptation scenario [3]. Figure 1 highlights the relationship between the phenomenological mesoscale and the mechanistic microscale approaches.

Results: Regression analyses were performed based on the initial and converged parameters of the poroelastic model, compared to the initial strain outputs of the single beam model. The ratio of remodelled trabecular thickness over initial thickness was related to the axial strain by a family of linear relationships ($R^2>0.998$). A fourth order polynomial provided a good fit ($R^2>0.98$) for the relationship between the ratio of bending strain to axial strain and the change of orientation of the single trabecula axis between initial and remodelled states.

The authors are currently implementing these relations into the phenomenological predictive algorithm for the full mesoscale femur. Challenges include nodal displacement calculation at points of multi beam junction, through weighted average, and generalisation of the derived relationships to the 3D space.

Figure:

Structural mesoscale model   Individual beam   Poroelastic microscale adaptive model
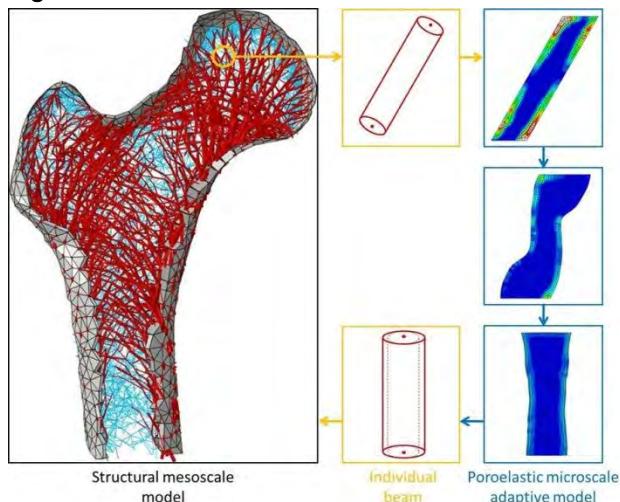
Caption: Overview of the combination of modelling techniques used in the study

Conclusion: Phenomenological drivers for predictive mesoscale structural modelling of bone architecture were derived using mechanistic microscale poroelastic analyses. It is expected that the implementation of these relationships into the phenomenological predictive algorithm for the full mesoscale femur will produce a model whose structure and mechanical behaviour are consistent with nature while maintaining a high computational efficiency.

References: [1] Wolff et al., The law of bone remodelling, Springer-Verlag Berlin, 1869, translated 1986.

[2] Temiyasathit et al., Annals of the New York Academy of Sciences 21 1192:422-428, 2010.

[3] Adachi et al., Journal of biomechanical engineering 123:403-409, 2001.

[4] Kameo et al., Acta Mechanica 225:1-10 , 2014.

[5] Pereira et al., Biomechanics and modeling in mechanobiology 13:215-225, 2014.

[6] Phillips, Engineering and Computational Mechanics 165:147-154, 2012.

[7] Phillips et al., International Biomechanics, *accepted 2014*

Disclosure of Interest: None Declared

Modelling

SS-0071

REAL-TIME ESTIMATION OF KNEE JOINT CONTACT FORCES DURING WALKING USING OPENSIM AND A CALIBRATED EMG-DRIVEN NEUROMUSCULOSKELETAL MODEL

Claudio Pizzolato [1,*]Monica Reggiani [2]Luca Modenese [1]David G. Lloyd [1]

[1]Centre for Musculoskeletal Research, Griffith Health Institute, Griffith University, Gold Coast, Australia, [2]Department of Management and Engineering, University of Padua, Vicenza, Italy

Introduction and Objectives: Real-time estimates of joint contact forces and musculotendon unit (MTU) forces can potentially enable rapid patient evaluation and biofeedback for gait retraining. MTU forces can be estimated in real-time using our calibrated electromyography (EMG)-driven neuromusculoskeletal (NMS) model (CEINMS). This uses EMG signals and three-dimensional (3D) joint angles to drive a NMS model that produces instantaneous kinematics and kinetics of individual MTUs [4, 5]. Then, the MTU forces estimated by CEINMS can be used with external joint moments to calculate the knee joint contact forces [3].

While rectified and filtered EMG signals can be directly used as input for CEINMS, joint angles and moments are estimated from motion capture data using inverse kinematics (IK) and inverse dynamics (ID) algorithms in OpenSim [1]. This is time consuming and currently precludes real-time estimation. However, using OpenSim to calculate 3D joint angles is essential to ensure consistency between motion analysis and musculoskeletal models used to estimate MTU kinematics. Furthermore, OpenSim permits personalisation of musculoskeletal models, created from imaging data to reflect an individual's specific anatomy. Therefore, we aimed to i) develop real-time OpenSim IK and ID procedures, ii) integrate these with CEINMS, and iii) compare the real-time estimates of 3D joint angles and moments, and knee joint contact forces to those from offline processing.

Methods: Custom software was written in C++ to read 3D markers trajectories, ground reaction forces (GRF), and EMG signals from a Vicon motion capture system in real-time. GRF, rectified EMG and 3D joint angles were filtered with a 6Hz low pass 4th order Butterworth filter, and processed using OpenSim IK and ID routines, which were modified to run on frame-by-frame. Multiple processing threads were used to increase the data throughput. MTU forces from CEINMS and external joint moments from ID were finally used to calculate medial and lateral knee joint contact forces [3]. CEINMS was calibrated in the background, on additional processor threads, by adjusting selected muscle parameters to reduce the error between joint moments estimated by CEINMS and ID. The real-time outputs were visualised in real-time using a Graphic User Interface (GUI).

From a single subject walking on a treadmill an 8-camera Vicon system collected motion data of a full body marker-set (68 markers) at 100Hz, and GRF and surface EMG signals from 16 muscles of a single leg at 1000Hz. Segmental dimensions and muscle parameters of the OpenSim model were anthropometrically scaled to the subject. The scaled model was then used to compute the set of multidimensional cubic B-splines that characterised the subject MTU kinematics [6] in CEINMS. During the walking trials the real-time software was used to produce and save 3D joint angles and moments from hip, knee, and ankle, and knee joint contact forces. The marker trajectories were also saved for subsequent offline

processing. The real-time and offline pathways were then compared using a modified coefficient of multiple correlation (CMC), which assessed the similarity of waveforms [2].

Results: From 6 consecutive gait cycles we found similar waveforms between the offline and real-time processing for hip, knee and ankle 3D joint angles and moments, with CMCs always greater than 0.95 (Table 1). While the computation time was about 30ms, the use of multiple threads enabled the results to be produced at the same frequency as the marker trajectory data (100Hz). The real-time estimation of knee joint contact forces is now being evaluated.

Conclusion: Our real-time system produced estimates of the 3D joint angles and moments nearly identical to those determined using offline processing. The small variations present were in the filtering and differentiation of 3D joint angles in the offline method that should not affect joint contact forces estimates. This is the first software to calculate, in real-time, 3D joint angles and moments using OpenSim coupled with an individually scaled and calibrated EMG-driven NMS model. Our framework enables real-time estimation MTU and joint contact forces that can be used for gait retraining biofeedback.

Table:

Joint	Joint angle (CMC)	Joint moment (CMC)
Hip FE	0.999	0.981
Hip AA	0.998	0.974
Hip IR	0.998	0.954
Knee FE	0.994	0.960
Knee AA	0.994	0.983
Ankle FE	0.995	0.997

Caption: Table 1: CMC for 3D joint angles and moments between offline and real-time processing from different joints and degrees of freedom (1 subject, 6 gait cycles). FE = flexion extension, AA = adduction abduction, IR = internal rotation.

References: [1] Delp SL et al., *IEEE Trans Biomed Eng*, 54:1940-1950, 2007.

[2] Ferrari A et al., *Gait & posture*, 31:540-542, 2010.

[3] Gerus P et al., *Journal of biomechanics*, 46:2778-2786, 2013.

[4] Lloyd DG et al., *Journal of biomechanics*, 36:765-776, 2003.

[5] Sartori M et al., *Plos One*, 7:e52618, 2012.

[6] Sartori M et al., *Journal of biomechanics*, 45:595-601, 2012.

Disclosure of Interest: None Declared

SS-0072

THE INFLUENCE OF DIFFERENT LOAD CASES IN ORTHOTROPIC BONE ADAPTATION IN THE FEMUR

Diogo M. Geraldes [1,*] Andrew Phillips [2]

[1]Mechanical Engineering, [2]Civil and Environmental Engineering, Imperial College London, London, United Kingdom

Introduction and Objectives: Osteoporosis is characterised by a reduction in bone mass, degradation of elastic properties and trabecular architecture increasing the risk of femoral neck fractures with an extremely high mortality rate. There is evidence that selected physical activities can increase bone mass density or reduce the rate of bone decay in affected patients [1, 2]. This work describes the importance of considering multiple load cases in bone adaptation and the topological influence of such daily activities on the region-specific material properties of the femur.

Methods: A novel 3D strain-driven orthotropic bone adaptation algorithm was developed and applied to a balanced model of the whole femur utilising physiologically relevant boundary conditions [3]. 80 frames from two different daily activities (40 for level walking and 40 for stair climbing) were considered. At each iteration an envelope containing the maximum driving stimuli was calculated by selecting the strain values for the guiding frame in each element. The guiding frame was defined as the frame in which the highest absolute normal strain value occurred. The orthotropic moduli were updated proportionally to the local principal strains and the material orientations rotated to match the local principal stress orientations. The model ran until the change in material properties and orientation was minimal.

Results: The guiding frames are shown blue to red with red being further through the cycle for each activity modelled, level walking (Figure 1 top, left) and stair climbing (Figure 1 top, right), in order to highlight the topological influence of each of the load cases on the whole femur. The percentage of elements influenced by the different instances modelled in the adaptation process is also depicted (Figure 1, bottom).

It is observed that both load cases contribute to the converged orthotropic material properties. Level walking is shown to influence the regions of the femoral head, inferior part of the femoral neck, greater trochanter, posterior-lateral aspects of the femoral shaft and posterior side of the condylar region. The stimulus produced by the stair climbing activity is shown to be dominant in the mechanical properties of the fracture prone femoral neck region, lesser trochanter, medial aspect of the cortical shaft and anterior side of the distal femur. The material properties of the femoral shaft and the femoral neck seem to be influenced by both activities.

Figure:
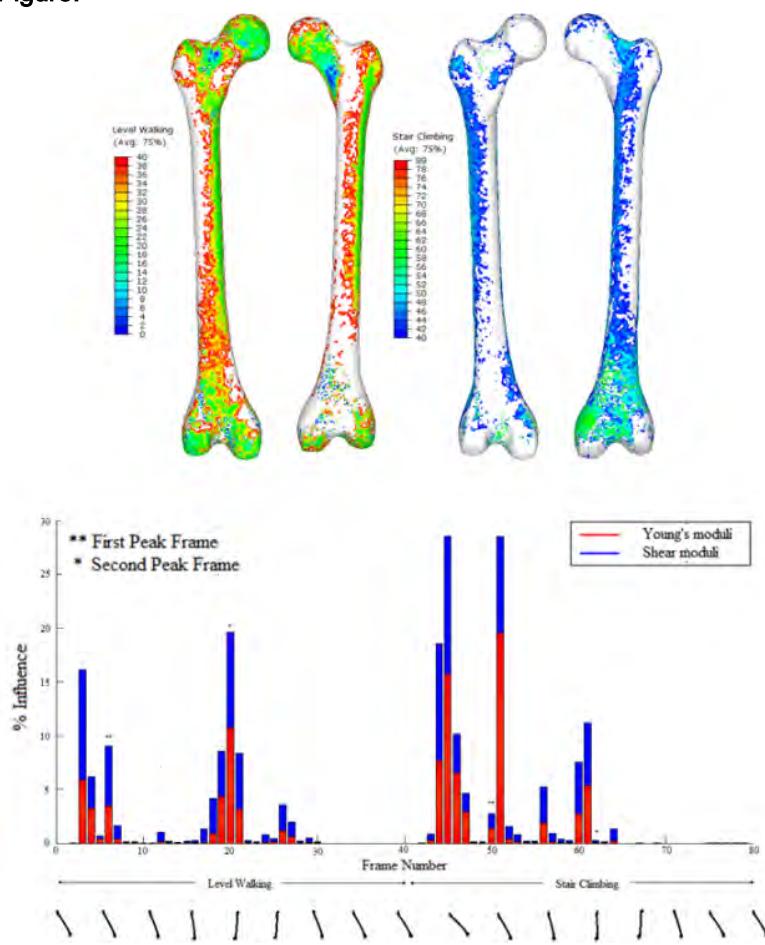
Caption: Figure 1 - Topological influence in femur's material properties of different frames for the two activities modelled: level walking (top, left) and stair climbing (top, right); percentage of elements influenced by the different instances modelled in the adaptation process (bottom)

Conclusion: The contribution of multiple frames from both activities to the converged material properties in different regions of the femur is clear. Thus, it is recommended that multiple frames from different activities are considered when predicting bone adaptation, with studies where bone adaptation was predicted by only modelling the peak frames of one of several activities ignoring the significant effect of other frames in influencing bone's material properties.

Stair climbing is highlighted as a potential beneficial non-pharmaceutical preventive intervention to prevent neck of femur fractures resulting from bone deterioration induced by sedentary lifestyles and degenerative diseases.

References: [1] Jämsä et al., Clinical Biomechanics, 21(1): 1-7, 2006.

[2] Blain et al., Calcified Tissue International 84(4): 266-275, 2009.

[3] Geraldes et al., Int J Numer Method Biomed Eng 30(9): 873-889, 2014.

Disclosure of Interest: None Declared

Surgical Robotics

SS-0073

INTRA-OPERATIVE 3D LASER SCANNING OF TIBIO-FEMORAL JOINTS FOR COMPUTER ASSISTED ORTHOPAEDIC SURGERIES

Shailesh O. Joshi [1,*] Philip Rowe [1]

[1]Biomedical Engineering, University of Strathclyde, Glasgow, United Kingdom

Introduction and Objectives: Over the last decade Computer Assisted Orthopaedic Surgery (CAOS) has emerged particularly in the area of minimally invasive Uni-compartmental Knee Replacement (UKR) surgery. Image registration is an important aspect in all computer assisted surgery including Neurosurgery, Cranio-maxillofacial surgery and Orthopaedics. It is a process of developing a spatial relationship between pre-operative data, such as Computerised Tomography (CT) scans or Magnetic Resonance Imaging (MRI) scans and the physical patient in the operation theatre. For example patient's medial or lateral femoral condyle can be visualised in the pre-operated CT scan as well the same points can be located on the actual patient during surgery using intra-operative sensors or probes. However their spatial correspondence remains unknown until image registration is achieved. Image registration is the process that generates this relationship and allows the surgeon to visualise the 3D pre-operative scan data in-relation to the patient's anatomy in the operating theatre.

Current image registration techniques for Computer Assisted Orthopaedic Surgeries (CAOS) in minimally invasive Uni-compartmental Knee Replacement surgery (UKR) are achieved using a navigated probe and by digitising points on the articulating surface of the knee joint. By using these digitised points a rigid body is formed which is then fitted to the pre-operative scan data using a best fit type minimisation. However, this manual digitisation approach is time consuming and often takes 15-20 minutes and is therefore costly. The rationale for this study was to develop a new, quick, cost effective, contactless, automated registration method which could produce an accurate rigid body model in theatre for registration from the ends of the exposed bones using 3D scans taken intra-operatively by a Laser Displacement Sensor.

Methods: Bespoke and automated 3D laser scanning techniques based on DAVID-Laserscanner were developed and were used to scan surface geometry of the knee joint in 10 cadaveric legs. The lateral compartments of all the knee joints were MRI scanned using 3D FLASH technique and were then segmented using Mimics 12.01 to generate 3D models of the articular cartilages. All the samples were then intra-operatively 3D Laser scanned using a tailored automated technique. The scanning modules were mounted on two different positioner assemblies; A six degrees of freedom haptic robotic arm manufactured by MAKO Surgicals and a customized assembly constructed using aluminium extrusion plates. In addition each sample was scanned through two different incisions; UKA of 9 cm and TKA of 18 cm. The 3D Laser scans were then registered with the corresponding MRI models in the robust digital image software package, Geomagic Qualify®. Average absolute errors between the reference MRI model and the test laser scans were evaluated using Iterative closest point, ICP algorithm. Effects of the independent variables; two setups, two incisions and two surfaces (tibia and femur) on AAE were investigated using three way repeated measures ANOVA. In addition individual effects of the independent variables on the AAE were studied using paired t-test.

Results: Average of the AAE for tibial articular cartilage surfaces ranged from 0.19 mm to 0.26 mm with its standard deviation ranging between 0.30 mm to 0.39 mm. Average of the AAE for femoral cartilage surfaces varied between 0.24 mm to 0.30 mm with a standard deviation between 0.37 mm and 0.49 mm. Repeated measures ANOVA suggested no statistically significant difference ($p>0.05$) between the types of setup used to acquire scans. AAE with TKA incisions was significantly higher than UKA incisions ($p<0.05$), whereas AAE on the femoral condylar surfaces were significantly higher ($p<0.05$) than the tibial condylar surfaces. There was no interaction effect present between the independent variables ($p>0.05$). The effects of the independent variables were confirmed by paired t-test which showed the similar pattern as that of the repeated measures ANOVA.

Figure:
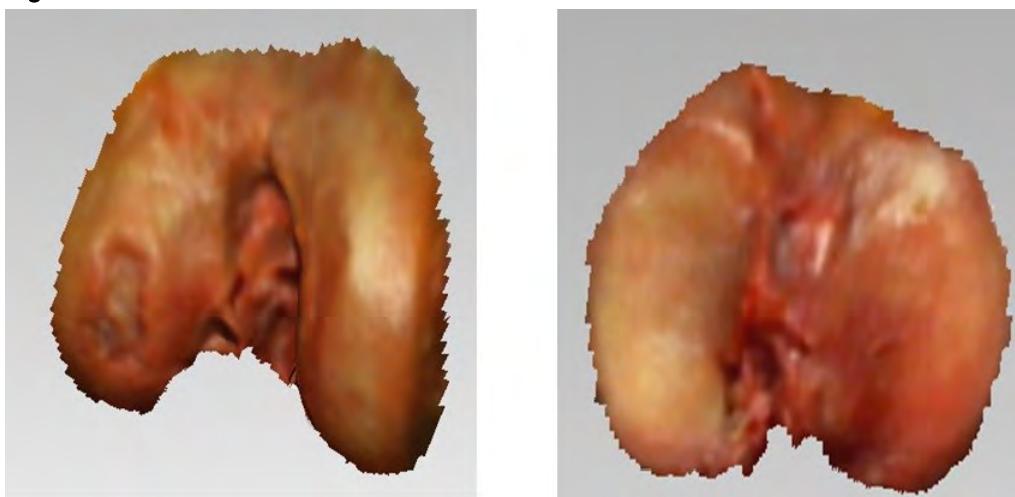
Caption: Textured 3D laser scans of the femoral and tibial condyles of the cadaveric knee joints acquired intra-operatively using developed 3D laser scanning system

Conclusion: We have demonstrated the feasibility of using a novel laser scanning technique where complete 3D models of the tibio-femoral joint in theatre along with their surface texture can be developed which can be registered with the pre-operative scan. The overall time for scanning, post-processing and the registration requires less than 5 minutes and is a non-invasive, cost-efficient approach.

This study has provided proof of concept for a new automated shape acquisition technique with the potential for providing an assessment of the articular cartilage integrity during lower limb arthroplasty.

References: 1] Kao et al., Comput Methods Programs Biomed 83:1–11, 2006.

2] Winkelbach et al., DAGM LNCS 4174, 718–728, 2006.

3] Banger et al., Bone Joint J 95(B): Supp. 28 89, 2013.

Disclosure of Interest: None Declared

AUGMENTED REALITY: SHOWING THE WAY IN ORTHOPAEDIC SURGERY

Nicholas Smith [1,*] Philip Riches [1] Vladimir Stankovic [2]

[1]Biomedical Engineering, [2]Electronic and Electrical Engineering, University of Strathclyde, Glasgow, United Kingdom

Introduction and Objectives: Computer Assisted Orthopaedic Surgery (CAOS) techniques are increasingly being applied to the challenge of ensuring accurate implant positioning during Unicondylar Knee Arthroplasty (UKA). Both commercial systems in this field use bulky infrared stereoscopic tracking systems, that restrict patient access, and standard monitors that divide the surgeon's attention away from the patient.

We present a comparison of two prototype CAOS systems which utilise significantly smaller tracking systems and provide surgical guidance through Augmented Reality (AR). AR mixes both real and virtual imagery to offer a non-intrusive and intuitive form of guidance.

Methods: Both systems are based upon six degrees of freedom tracking of fiducial markers using visible spectrum Microsoft Lifecam Studio web cameras, developed under the OpenCV library. The live video used for tracking is augmented in real-time with virtual elements, such as CT models and alignment guides, by a modern OpenGL engine. Passive control is provided by coloured resection models while additional active control is achieved through speed control of the cutting burr.

The systems differ in their tracking and display systems. The first system uses a tool-mounted monoscopic camera with the augmented video displayed on a standard monitor. The second system uses a head-mounted stereoscopic camera and a head mounted display (HMD).

The accuracy of both systems was determined by probing 108 known points on a 110x110x50 mm geometry. System latency was also measured, as the time delay between video capture and display of the final augmented frame. Finally the practicality, comfort and intuitiveness of guidance were gauged through user feedback.

Results: The monoscopic and stereoscopic systems produced an accuracy of 1.5±0.3 and 2.1±0.6 mm, respectively. However, the validity of these results is questionable as it was found the test points were inaccurate, particularly in the z axis. The monoscopic system presented an average latency of 263±55 ms compared to 293±15 ms for the stereoscopic system.

Both systems rated well for intuitiveness, with the natural view and 3D display of the stereoscopic system making some instructions clearer. The monoscopic system offered superior comfort. However, tasks such as hip centre location, which required two hands and tracking of multiple markers, were more practical with the stereoscopic system.

Figure:
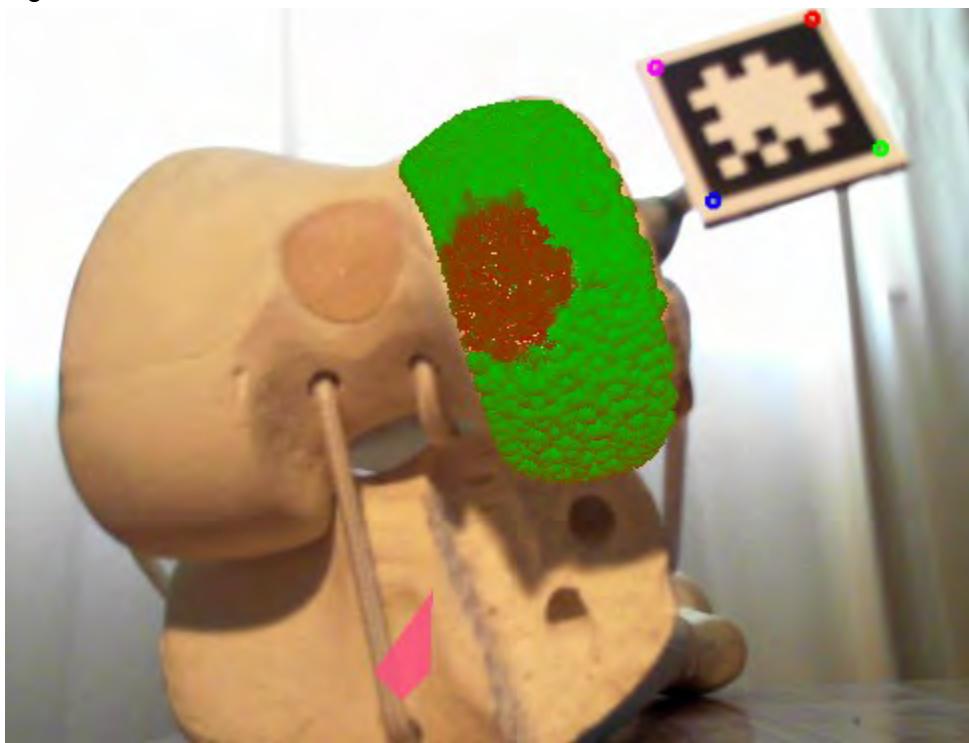
Conclusion: Due to the inaccuracies of the current target a new 3D printed target is being produced with sub-50 µm accuracy. Based on the results currently available, however, both systems produced accuracies outwith the desired sub-millimetre target. It is felt that this should be reached with several basic modifications. With the advent of USB3.0 cameras, higher resolution images may be streamed at high frame rates. This will allow more accurate marker detection and should therefore improve pose estimation. Additionally, all experiments were performed using small 20 mm markers. Larger markers would provide more data points for detection and a wider point base for pose estimation, both of which offer a potential accuracy boost.

Both systems produced latencies which were not readily perceivable to the user. This is particularly important for the HMD of the stereoscopic system, where large latencies may induce 'simulator sickness'.

It is felt that the hands-free and natural view offered by the stereoscopic system makes it the superior technology, particularly for use in a surgical environment. This is despite the inherent reduced accuracy resulting from tool to target tracking requiring an additional marker compared to the monoscopic system. If the desired accuracy is achieved it is hoped that the intuitiveness afforded by the augmented guidance will make the system appealing to healthcare professionals by keeping learning curves to a minimum. This will therefore increase the adoption of CAOS technologies.

Disclosure of Interest: None Declared

IN-VIVO PATELLAR TENDON TRACKING IN NAVIGATED TOTAL KNEE ARTHROPLASTY

Claudio Belvedere [1,*]Andrea Ensini [2]Michele d'Amato [2]Paolo Barbadoro [2]Alberto Leardini [1]

[1]Movement Analysis Laboratory and Functional-Clinical Evaluation of , [2]1st Orthopaedic and Traumatologic Clinic, Istituto Ortopedico Rizzoli, Bologna, Italy

Introduction and Objectives: The appropriate interaction between Tibio-Femoral (TFJ) and Patello-Femoral Joint (PFJ) surfaces and knee soft tissues control joint function [1,2]. Among these soft tissues, the Patellar Tendon (PT) plays important roles within the extensor apparatus [3]. The efficacy of this mechanism is enhanced by the patellar tracking [3]. Alterations at PFJ affecting normal PT functioning, as in case of Total Knee Arthroplasty (TKA), may results in-vivo in knee instability, pain and TKA failure [1,2].

An anatomy-based PT mapping is essential to assess PT functioning during knee motion [3]. PT fiber mapping and lengthening/slackening, both at the native knee and after TKA, have been investigated using several methodological approaches. Unfortunately, these generally did not allow the acquisition of reliable TFJ and PFJ knee motion data, and did not track PT mapping using robust anatomical references [3].

Among possible tracking devices, current knee navigation systems for TKA enable accurate digitization of single bony landmarks or large articular surfaces [1,2], and have the potentials for tracking also PT data.

The purpose of the present study was to evaluate in-vivo PT length and orientation changes throughout knee flexion as observed during TKA, i.e. at the original joint and after knee replacement; this was achieved via original patellar tracking, and with careful patient-specific anatomy-based mapping of PT fibers.

Methods: Ten patients recruited for TKA were implanted with Triathlon® prosthesis (Stryker®-Orthopaedics, Mahwah, NJ-USA). TKA was performed using a surgical navigation system (Stryker®-Leibinger, Freiburg, Germany; 0.5°/0.5mm accuracy).

Marker clusters were pinned onto the femur and tibia; an light cluster was fixed onto patellar anterior aspect [2]. A pointer tracker was used for system control and landmark digitations; TFJ/PFJ anatomical and articular definitions were according to recommendations [3,4] or recent proposals [1,2]. Series of 3 trials of manually driven flexions in a 0°-140° arc were recorded with the knee intact and after TKA [2].

PT fibers were recruited by point digitization along patella-to-fiber origin together with corresponding insertion on the tibial tuberosity [3]. Point strips were also collected along fibers in known anatomical position [3]. Proximal/distal attachment centroids and strips extremities were assumed as fiber origins and insertions, whose length changes over TFJ flexion were calculated and reported in % of maximum fiber length (Lmax) [3]. Fiber orientation was calculated with respect to the tibial proximo-distal axis of the tibia, both on the frontal and sagittal planes.

Results: Patient-specific PT fiber attachments were successfully accessible to the surgeon and resulted in feasible identification and digitization. Repeatable TFJ and PFJ motion patterns were observed together with PT length and orientation changes, both at intact and implanted knees: at the original knee over TFJ flexion-extension, standard

deviation over trials was smaller than 1.0 mm and 1.0° for translations and rotations respectively. Corresponding values over the patients were larger, these being about 7.5 mm and 9.3°.

As for PT lengthening, consistent patterns were observed at the intact knee in the initial 30°±5° of flexion for all fibers (see figure). This was observed also after TKA, although at near full extension all fibers were about 16% tighter than at the intact knee.

As for fiber orientation, all PT fibers at the intact knee were generally laterally and posteriorly tilted of about 12° and 26°, respectively. Further 5°, on average, of lateral and posterior tilt occurred after TKA.

PT length and orientation changes were always significantly correlated to TFJ and PFJ flexion; after TKA, only the frontal plane orientation was also correlated to medio-lateral PFJ translation shift.

Figure:
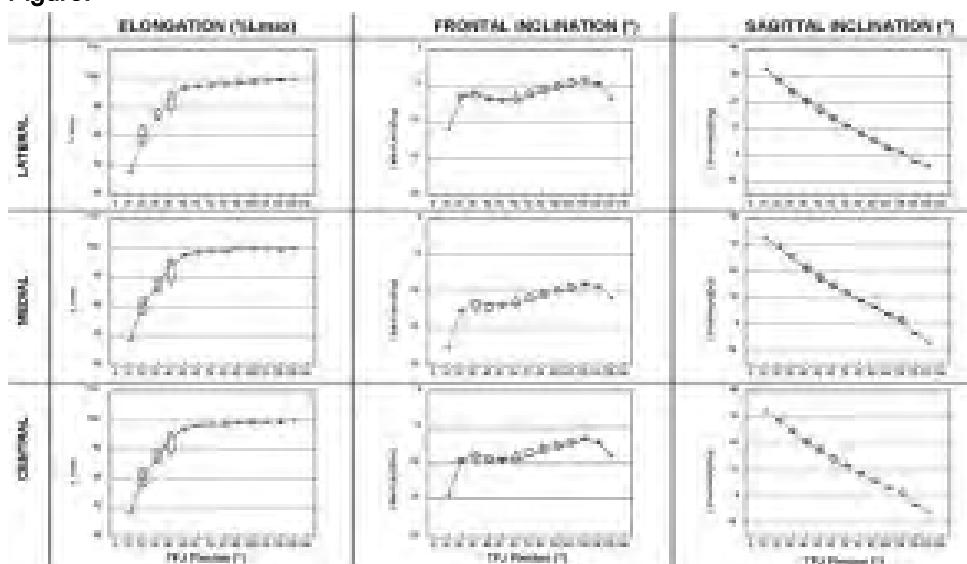
Caption: Length (elongation in %Lmax) and orientation (frontal and sagittal inclination) changes from a representative patient for the lateral, medial and central PT fibers.

Conclusion: These results show the feasibility in-vivo of patient-specific anatomy-based PT fiber mapping and tracking during TKA. This novel methodology enabled reliable data collection in consistent anatomical-based reference frames. Furthermore, this methodology allows also the possibility to monitor PT functioning intra-operatively during TKA, and this can support the complete restoration of normal knee function.

This study was aimed at contributing to the much controversial knowledge on knee soft tissue recruitment during joint motion. Relevant findings point out the importance of PT fiber recruitment and tracking in TKA.

References:

[1] Belvedere C et al., Knee Surg Sports Traumatol Arthrosc., 15(8):985-93, 2007

[2] Belvedere et al., Knee Surg Sports Traumatol Arthrosc. 22(8):1719-27, 2014

[3] Belvedere et al., J Biomech., 45(11):1886-92, 2012.

[4] Grood ES et al., J Biomech Eng., 105:136–144,1983.

[5] Cappozzo A et al., Clin Biomech (Bristol Avon), 10:171–8,1995.

Disclosure of Interest: None Declared

MUTLI-SOURCE DATABASES, MACHINE LEARNING AND MARKERLESS MOTION CAPTURE: WHY APPLIED SPORTS BIOMECHANICS NEEDS 'BIG DATA'.

Jacqueline Alderson [1,*]Amar A. El-Sallam [2]Andrew Lyttle [3]

[1]Sport Science, Exercise & Health, [2]Computer Science & Software Engineering, University of Western Australia, Crawley, [3]Biomechanics, Western Australian Institute of Sport, Perth , Australia

Introduction and Objectives: The sport biomechanist faces a number of unique challenges rarely encountered by those in clinical or lab based biomechanical research that spans research design and data collection, to analysis and reporting. Studies involving athletes are hampered by statistically small cohorts that comprise the entire available 'elite' population and which are regularly criticised for reduced ecological validity given the limitations surrounding collection of high fidelity data during match play. Critically, sporting activities generally occur at high speeds, across multiple planes of motion while utilising all degrees of freedom of the body. Subsequently, the hardware required for the collection of sporting related biomechanical data must be technologically advanced and the collection methodologies appropriate, to accurately and reliably record the unique combination of high speed and complex three-dimensional (3D) motion. The emerging solution to address such hurdles is a 'big data' approach. Though definitional ambiguity pervades the term, the description of [1] who refer to "things one can do at a large scale that cannot be done at a smaller one, to extract new insights or create new forms of value" is particularly relevant when considering its application to the field of sports biomechanics.The ideal 'big data' horizontal framework for biomechanics ideally encompasses multiple input sources such as subject specific motion, medical imaging, musculoskeletal, neurological, physiological and other complementary datasets. For the purposes of this paper we outline a motion capture procedure that fulfils the motion capture component of the framework whereby we markerlessly reconstruct 3D motion from multiple 2D camera views and also merge the dynamically reconstructed 3D visual hull (from the sporting motion) with subject specific 3D body scans.

Methods: This procedure comprises two phases. In an *offline* static phase, a static t-pose of the athlete is acquired using a high resolution 3D video scanner to create a 3D subject specific reference shape. A skeleton consisting of a number of articulated bones and joints is then fitted to the 3D model to create a reference rigged template. In the *online* motion capture phase a number of 2D video cameras are configured and calibrated to capture multi-view videos of the athlete. A background segmentation algorithm is then applied, extracting silhouettes of the athlete and then merged to reconstruct a low fidelity 3D visual hull. A number of optimisation algorithms are then used to extract geometrical data of the visual hull and identify and segment each body part. Global joint kinematics are then estimated by fitting the reference skeleton to the identified body parts of the curve skeleton. Constrained mesh deformation functions are then fed by the global joint kinematics and the resulting error between the surface of deformed model and the visual hull is employed to adapt and refine the accuracy of the initially estimated joint kinematics. A DXA scan is then registered into the final 3D hull to provide subject specific body segment inertial parameters for further application.

Results: The overall mean error between the 3D scan (reference) and the resulting surfaces (absolute mean of the difference between closest points) varied between 12cm to 16cm across three different postures selected for analysis

(Figure 1). This error is reasonable when matching two meshes of 5000 vertices each. Depending on the application or the accuracy, one may run the matching process until a desired error is achieved. GPU implementation could be a faster option for matching and deforming high resolution meshes hence accurate joint kinematics and deformed surfaces can be achieved in a shorter processing time. The overall errors between the aligned reference model and the visual hull confirm that the proposed system is capable of estimating accurate joint kinematics in diverse blind body pose estimation scenarios (i.e. sporting activities).

Figure:
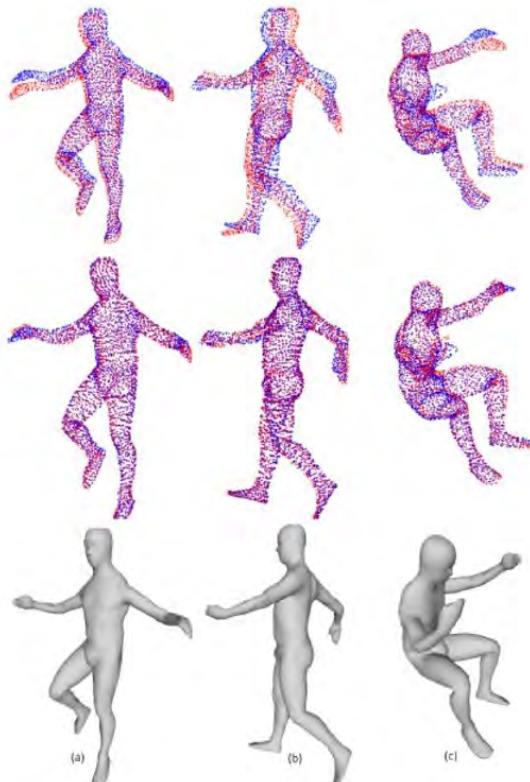
Caption: Top row: VH (blue) and the reference model (red) deformed using the estimated global joint kinematics. Middle row: the deformed reference model after refining the global joint kinematic. Bottom row: 3D meshes of the deformed model.

Conclusion: Like many scientists, sports biomechanists collect copious amounts of numerical data on often small numbers of participants, reduce the data further, to discrete key motion events and run traditional statistical analysis searching for that ever allusive significant difference. A 'big data' approach, rather than throwing out this information, implores us to collate our data and our colleagues, all of it, into a shared database, to which we can apply non-traditional analytical techniques to obtain new insights, and importantly manipulate to enhance our current collection, reconstruction and modelling methods.

References: [1] Mayer-Schönberger, V., & Cukier, K. (2013). *Big data: A revolution that will transform how we live, work, and think*. Houghton Mifflin Harcourt.

Disclosure of Interest: None Declared

Sport

AN INTEGRATED MULTISCALE ANALYSIS OF INJURY MECHANISMS IN SPORT IMPACTS: AN APPLICATION TO CERVICAL SPINE BIOMECHANICS IN RUGBY UNION SCRUMMAGING

Ezio Preatoni[* 1], Dario Cazzola[1], Tim P Holsgrove[2], Sabina Gheduzzi[2], Anthony W Miles[2], Keith Stokes[1], Richie HS Gill[2], Grant Trewartha[1]

[1]Department for Health, [2]Department of Mechanical Engineering, University of Bath, Bath, United Kingdom

Introduction and Objectives: By generating repetitive high-energy impacts (during the engagement phase) and intense sustained loads (during the sustained push phase) under unstable conditions [1], the Rugby Union scrum has been indicated as a possible risk factor for degenerative spinal injuries for forward players, and has been associated with ~40% of all catastrophic injuries in rugby [2]. However, little is known about how these external loading conditions translate into internal stresses on the spinal structures. The aim of this study was to investigate the biomechanics of cervical spine injury during rugby activities using an integrative approach: in-vivo and in-vitro experiments combined with musculoskeletal modelling.

Methods: Three levels of analysis (Levels 1-3) were integrated. Level 1 was a biomechanical study of scrummaging (N=9 experienced rugby forwards) including motion capture (Oqus, Qualisys, Sweden), force measurement (force plates: Kistler 92876BA, Switzerland; and instrumented scrum machine, [1]), and EMG of neck and trunk muscles (Delsys Trigno, Delsys Inc, USA), carried out to assess the external kinematic and kinetic conditions acting on front row players. The subsequent phases of scrummaging, initial engaggament (impact and shock absorption) and sustained push, were observed. Level 2 developed a bespoke musculoskeletal model (Rugby Model, [3]), consisting of 27 anatomical segments, 26 joints, 78 cervical muscles, and 11 torque actuators, in OpenSim (OpenSim 3.2, SimTK, USA). The Rugby Model was driven by the experimental data from Level 1 and was used to estimate joint dynamics, with a specific interest in cervical joint motions and moments. Level 3 performed an in-vitro laboratory experiment to study the injury mechanisms of porcine cervical spines subjected to impact loading conditions similar to those during scrummaging. Load (2 load cells: SLC41/005000, RDP Electronics Ltd, UK) and deformations caused by impacts (mass of 12.86 kg dropped from a height of 250 mm to give an impact velocity of ~2.2 m/s) were measured in a custom made impact rig, and high-speed videos (2 Fastcam SA3, Photron Europe Ltd, UK) were used to investigate the mechanisms of injury through digital image correlation (Vic-3D 2009.1.0, Correlated Solutions Inc, USA).

Results: Results from the biomechanical analysis confirmed that the load acting on the players, especially during the initial engagement, was of a considerable magnitude (~2.8 kN compression force in single-player machine scrummaging). Muscle activation patterns were affected by scrummaging conditions (e.g. machine vs. contested scrummaging; 'Crouch-touch-set' vs. 'Crouch-bind-set' sequence) and phases of the scrum (e.g. pre-engagement vs. engagement vs. sustaned push). For example, the activity of the *erector spinae* was significantly lower (in excess of 65%) in machine scrummaging than in contested scrummaging, and the activation of *sternocleidomastoid* and *upper trapezius* through pre-engagement and engagement were higher in the current 'Crouch-bind-set' technique than in the past 'Crouch-touch-set' one. The computational musculoskeletal model highlighted an antiphase change in movement and loading patterns between the upper and lower cervical levels (i.e. flexion load on the lower vertebrae and extension on the upper vertebrae), and resulted in a "flattening" of the lordotic cervical curve during the impact phase. The present findings do not provide direct evidence for injury mechanisms but seem in line with the patterns of injury that previous authors have described in relation with scrum-related neck traumas [2]. The patterns of strain, load and resulting damages on the cervical structures of the impacted porcine specimens were also similar to those clinically observed in injured players, with the caudal vertebrae (C4-C6) more prone to damages (6 out of 8 specimens) as a consequence of the impact. Fractures resulted from tension in the vertebral bodies due to first order buckling of the cervical spine in extension. The mean maximum load in the cranial and caudal load cells was 5.8±2.0 kN and 6.0±2.1 kN and was reached at a time of 5.1±1.0 ms and 5.6±1.1 ms after impact, respectively.

Figure:

MUSCULOSKELETAL MODEL

IN VIVO TESTING

FEM

IN VITRO TESTING

Conclusion: The proposed integrative approach provided novel and more thorough insight into how external loading conditions, muscular activity and body posture affect the internal stresses acting on the cervical spine structures. This understanding will help in elucidating injury factors related to scrummaging and represents a promising framework for future research in the area of impact-related injuries in sports. It will be further developed by including forward dynamics simulations and finite element analysis.

References: [1] Preatoni et al., BJSM, 10.1136/bjsports-2013-092938, 2014.
[2] Trewartha et al., BJSM, 10.1136/bjsports-2013-092972, 2014
[3] Cazzola et al., Proceedings of the 7th World Conference of Biomechanics (Boston, USA), 2014

Disclosure of Interest: None Declared

SS-0078

SIMULATION AND PROPHYLACTIC RESEARCH: INTERESTING BEDFELLOWS

Cyril J. Donnelly [1],*Jeff Reinbolt [2]Gillian Weir [1]Kristin Morgan [3]Jacqueline Alderson [1]

[1]School of Sport Science, Exercise and Health, The University of Western Australia, Perth, Australia, [2]Department of Mechanical, Aerospace and Biomedical Engineering, University of Tennessee, Knoxville , [3]Division of Physical Therapy, University of Kentucky, Lexington, United States

Introduction and Objectives: Modern biomechanics can be dated back to the late 1800's, with the invention of stop-action photography by Eadweard Muybridge [1], which was developed to describe animal motion that could not be observed with the human eye. Later, with the development of the force platform [2], and the application of the Newton-Euler equations of motion, the ability to calculate the forces that cause human motion became possible. With the invention of the programmable computer in the 1950's and the evolution of the silicon processor, our ability to create dynamic simulations has become an apparent reality. Now, over 100 years later, following significant scientific and technological advancements, simulation based research has firmly established its place within the field of biomechanics. The purpose of this manuscript will be to present an applied example of how simulation based research has been used to inform the development of an effective knee injury prevention training protocol.

With the use of the open-source musculoskeletal modelling framework OpenSim, our group has been using simulation based experiments to better understand how specific movements and/or muscle forces during a movement are related to an athlete's lower limb injury risk in sport. Using the residual reduction algorithm, we were able to optimize an athlete's technique to reduce their risk of knee injury during unplanned sidestepping tasks. Through simulation, we showed a causal relationship exists between an athlete's upper body mechanics, knee loading and injury risk during dynamic sporting tasks [3]. We then used computed muscle control to measure and characterize the muscle forces an athlete uses during single-leg landing tasks. Findings from this research showed that the gastrocnemius muscles are used significantly more than the hamstring muscles to stiffen and support the knee during the impact phase of single-leg landing [4]. From these simulation findings and relevant prophylactic research, we have developed and implemented a novel prophylactic training intervention designed to reduce and athlete's risk of knee injury in sport.

Methods: The Australian national field hockey team participated in a novel nine-week body-weight based training intervention. The intended focus of the intervention was to A) improve gluteal muscle strength, increasing an athlete's capacity from attaining 'dynamic-valgus' knee postures, which have been shown to predict anterior cruciate ligament (ACL) injuries in sport [5]. From our group's simulation findings, added foci were to B) improve the dynamic control of the upper body and C) improve the strength of the gastrocnemius muscles. During training, athletes' performed a range of strength, plyometric and balance exercise that continually targeted on or all of the intervention's intended foci. Prior to and following the training intervention, full-body kinematics, lower body kinetics and lower limb muscle activation were collected for 16 athletes during the UWA sidestepping protocol. All experimental methods have been described previously [6, 7].

Results: Following training, athlete's identified as 'high-risk' from their knee moments during unplanned sidestepping (n = 5) significantly reduced their peak valgus knee moments by 28% (p = 0.024), becoming consistent with valgus knee moments observed pre- post training from the 'low-risk' group (n = 11). All athletes (n = 16) were better able to utilize their hip versus their knee to generate their support moment during sidestepping, redistributing the relative contribution of their support moment from their knee to hip (Cohen's d = 0.56). For all athletes (n = 13), total gluteal muscle activation significantly increased by 27% (p = 0.006), while co-contraction of the hamstring muscle group were re-directed from the biceps femoris to the semimebranosus (Δ226%, p < 0.001). It is likely an athlete's capacity to prevent hip internal rotation, which is associated with the 'dynamic-valgus' posture would be improved. Increases in medial hamstring muscle activation would help athlete's support their knee against valgus knee moments, which is a surrogate for ACL injury risk [3, 5, 6]. We are currently analysing further motion capture data from this population to determine if these positive training effects have been preserved following 16-weeks of maintenance training.

Figure:

Figure 1: Depiction of UWA sidestepping protocol.

Conclusion: Simulation research can be used to help inform the development of effective lower limb injury prevention training protocols. The efficacy of a novel hip, trunk and gastrocnemius focused training intervention has been verified among elite level female field hockey players.

References: [1]Muybridge, *Scientific America,* 1878.

[2]Elfman, *Science*, 88(2276):152-153, 1938

[3]Donnelly et al., *J Biomech.* 45(8):1491-97, 2012

[4]Morgan et al., *J Biomech.* 47(13):3295-302, 2014

[5]Hewett et al., *Am J Sports Med.* 33(4):492-501, 2005

[6]Donnelly et al., *Br J Sports Med.* 46(13):917-22, 2012

[7]Donnelly et al., *Journal of Sci. and Med. in Sport, (In-Press)*

Disclosure of Interest: None Declared

SS-0079

THE ROLE OF GENDER ON THE VARIABILITY OF JOINT KINEMATICS AND KINETICS IN UNINJURED ATHLETES DURING A MATCH SPECIFIC LAND-CUT TASK

S Clarke [1,*] I C Kenny [2] A J Harrison [3]

[1]Leeds Beckett University, Leeds, United Kingdom, [2]University of Limerick, Lickerick, [3]University of Limerick, Limerick, Ireland

Introduction and Objectives: Higher levels of movement or coordination variability have been reported to provide flexibility and allow adaptations to complex dynamic sport environments [1]. Decreased movement and coordination variability has been previously been reported in females [2] and proposed as a risk factor for injury. The aim of this study was to compare the variability of hip and knee joint kinematics (movement) variability and lower extremity joint and segment coupling (coordination) variability in healthy males and females during a dynamic landing task. There is a scarcity of information on gender differences in coordination and movement variability during dynamic landing and cutting tasks. This information may provide valuable insight to further explain the gender bias of ACL injury, where lower levels of movement and/or coordination variability may increase injury risk.

Methods: Ten healthy males and ten healthy females were recruited for this investigation. Participants performed a dynamic task (see Figure 1) which involved dropping from a 0.30 m bench, and performing an immediate jump to touch a target and on landing perform a side cut in a randomly cued direction. Five intralimb couplings were calculated using a modified vector coding technique [3]; thigh abduction-adduction leg abduction-adduction, thigh rotation leg rotation, hip abduction-adduction knee rotation, hip rotation knee abduction-adduction, knee rotation knee abduction-adduction. Variability of the normalised coupling and joint angle timeseries was calculated point by point and averaged during the initial 40% of landing and the push off phase of cutting (70-100%). Differences in average variability were assessed using independent t-tests or Mann-Whitney U tests. Cohen's d was utilised as a measure of effect size with a 0.2=small, 0.5=moderate, >0.8=large, scale.

Results: During the initial deceleration period of landing, females demonstrated significantly less movement variability at the knee in the transverse plane on both legs (Table 1) and coordination variability in three of the five couplings examined on the dominant leg (Table 1) when compared to males. During the final push off phase of the cutting movement, females also demonstrated significantly less movement variability at the non-dominant knee and hip in the frontal plane and the dominant and non-dominant hip in the transverse plane (Table 1). No gender differences in coordination variability were noted for either leg during the final push off phase of the cutting movement for any of the examined couplings.

Figure:

*Visual Stimuli – are triggered by touching the target with a 0.03 s delay
**Area marked out for diagonal cutting maneuver
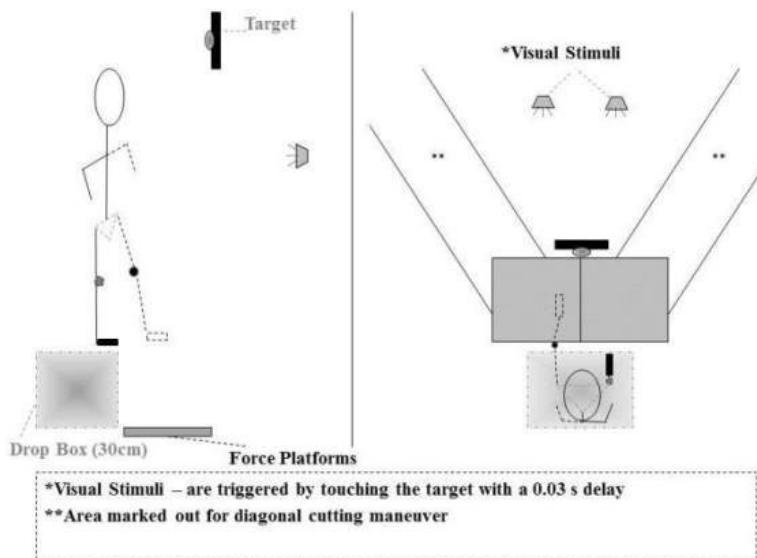
Conclusion: These findings may help explain the gender bias in ACL injury incidence. Reduced female coordination variability could also result in less flexible coordination patterns during match situations, with a decreased ability to adapt to perturbations experienced in game play. Poor adaptation to these perturbations may result in an unsafe movement response in females which are associated with the occurrence of an ACL injury. DISCLOSURE: The Irish Research Council for Science Engineering and Technology is acknowledged for its funding of the lead author for the completion of this work. All authors declare no conflict of interest.

Table:

		Dominant	Leg	Non-Dominant	Leg
MOVEMENT	VARIABILITY	MALE	FEMALE	MALE	FEMALE
Landing	Knee Internal-Ext Rot	3.26	1.53	3.10	1.52
	Knee-Rot_ Knee-Ab-Ad	23.99	22.12		
	Hip-Ab-Ad_ Knee-Rot			21.08	23.50
	Knee-Rot_ Knee-Ab-Ad	23.99	22.12		
Cutting	Knee Internal-Ext Rot			4.37	3.53
"	Hip Int-Ext Rotation	3.72	2.29	4.22	2.68
COORDINATION	VARIABILITY	MALE	FEMALE	MALE	FEMALE
Landing	Thigh-Rot Leg-Rot	26.60	23.15		
"	Hip-Rot_ Knee-Ab-Ad	20.57	19.24		

Caption: TABLE1 CAPTION: Significant gender differences in the average variability of 3D Joint Angles and joint couplings during landing & cutting..

References: Reference 1

Mullineaux, D. R., & Uhl, T. L. (2010) Coordination-variability and kinematics of misses versus swishes of basketball free throws.Journal of sports sciences, 28(9): 1017-1024.

Reference 2

Pollard C, Heiderscheit B, van Emmerik R, Hamill J. (2005) Gender differences in lower extremity coupling variability during an unanticipated cutting maneuver. Journal of Applied Biomechanics. 21(2):143.

Reference 3

Sparrow W, Donovan E, Van Emmerik R, Barry E. (1987) Using relative motion plots to measure changes in intra-limb and inter-limb coordination. Journal of Motor Behavior. 19(1):115-129.

Musculoskeletal

SS-0080

BIOMECHANICAL ASPECTS OF TRIGGER FINGER BEFORE AND AFTER PULLEY RELEASE SURGERY

Fong-Chin Su [1,2,*]Szu-Ching Lu [1,2]Li-Chieh Kuo [3]I-Ming Jou [4]Yun-Nien Sun [5]Tai-Hua Yang [2]

[1]Medical Device Innovation Center, [2]Department of Biomedical Engineering, [3]Department of Occupational Therapy, [4]Department of Orthopedics, [5]Department of Computer Science and Information Engineering, National Cheng Kung University, Tainan, Taiwan, Republic of China

Introduction and Objectives: Trigger finger is a common problem in hand clinics. "Triggering" describes the catching and sudden release phenomenon during finger extension movement. The first annular (A1) pulley release surgery has been used to treat trigger finger for over a century. The release is required to extend to the second annular (A2) pulley to completely alleviate the symptoms for certain patients. The pulley release surgery may lead to hand function change. However, the effects of the different extent of pulley release have not been well explored. Therefore, the purpose of this study was to investigate the effects of the different extent of pulley release on the tendon excursion efficiency and the changes of tendon moment arms.

Methods: To understand the effects of the different extent of pulley release, four conditions of pulley integrity were investigated, including pulley intact, A1 pulley release, half A2 pulley release, and complete A2 pulley release. Eight cadaveric hands were used in the experiment, and a total of eight middle fingers were tested. The joint rotation was measured by a motion capture system, and the tendon excursion was measured by linear position sensors. The tendon excursion efficiency was defined as the range of motion of the involved joints per unit of tendon excursion, and the tendon moment arm was determined by the slope of the linear fitting of tendon excursion versus metacarpophalangeal (MCP) joint rotation.

Results: The tendon moment arm with respect to the MCP joint was determined as 11.08mm for the flexor digitorum superficialis (FDS) and 9.29mm for the flexor digitorum profundus (FDP). The tendon excursion efficiency decreased with the increased extent of pulley release. On the other hand, the tendon moment arms increased with the increased extent of pulley release. Significant differences were found among the four conditions of pulley integrity via Friedman's test in all the evaluated parameters, including the FDS tendon moment arm ($p<0.001$), FDP moment arm ($p=0.002$), FDS excursion efficiency ($p<0.001$), and FDP excursion efficiency ($p=0.005$). The results present no significant change between A1 and half A2 pulley release in the FDP excursion efficiency, and the moment arms of FDP and FDS with respect to the metacarpal phalangeal joint.

Conclusion: This study provides the investigations of trigger finger before and after pulley release surgery from biomechanical perspectives. To relieve the discomfort, if necessary, the pulley release may extend to the half proximal A2 for trigger finger patients. Hopefully the biomechanical investigations will improve the understanding of trigger finger, provide suggestions for clinical practice, and further help in developing better assessment and treatment programs.

Disclosure of Interest: None Declared

EFFECTS OF PENNATION ANGLE ASSUMPTIONS ON THE DETERMINATION OF SUBJECT-SPECIFIC MUSCLE MODEL PARAMETERS

Youngho Kim [1,*] Jongsang Son [1]

[1] Biomedical Engineering, Yonsei University, Wonju, Korea, Republic Of

Introduction and Objectives: An EMG-driven model with a Hill-type muscle model is widely used to estimate individual muscle forces and joint moments. It includes some parameters to define muscle properties. In particular, the pennation angle is closely related to the direction of force transfer. To take the pennation angle into account, the variable pennation model has been widely used in the field of muscle mechanics [1], which assumes that (1) the muscle thickness would be constant, and thus (2) the pennation angle would be changed by the fiber length only. However, the muscle thickness varies with the muscle contraction intensity (MCI) [2]. It implies that the variable model might not be sufficient to reflect the real muscle. Therefore, this study was aimed to develop realistic pennation models of the major ankle muscles as a function of both the ankle joint angle and MCI, and to investigate effects of the developed model on the determination of subject-specific muscle model parameters.

Methods: Ten adult subjects (26.7 ± 2.1 yrs.; 70.3 ± 4.2 kg; and 172.5 ± 5.5 cm) with no history of musculoskeletal injury participated in this study. Each subject's right foot was firmly attached to the Biodex dynamometer with the knee joint at 30° flexion. The ankle joint was fixed at 15° dorsiflexion (-15°) and 0°, 15° and 30° plantarflexion. Four EMG sensors were attached to the belly of major ankle muscles (tibialis anterior, TA; gastrocnemius medialis, GCM; gastrocnemius lateralis, GCL; and soleus; SOL). For each condition, the subject was required to perform 0, 30, 70 and 100% of their maximum voluntary isometric plantar- and dorsiflexion. To measure the pennation angles, longitudinal sonography images were taken with a brightness mode real-time ultrasonic apparatus during the tests [3]. The pennation angle surface model was developed using the 'Poly22' fitting algorithm in MATLAB with average values of the measured pennation angle data corresponding each condition. Then, our EMG-driven model [4] was applied to investigate effects of the developed realistic pennation model on the determination of subject-specific muscle model parameters by comparing those of the existing variable pennation model.

Results: As a result, pennation angles increased with increases in MCI for all four major ankle muscles. The pennation angle of TA decreased as ankle plantarflexed, while the pennation angle of plantarflexors (GCM, GCL, and SOL) increased. Interestingly, the pennation angle has linear relationship with ankle angle, but nonlinear with MCI. When using the EMG-driven model with the existing pennation model, the root mean square (RMS) error between the measured and modeled joint moments was 9.41 ± 1.35, 11.44 ± 7.85, and 15.97 ± 10.79 N-m in isometric plantarflexion movements with 30, 70, and 100% MCI at neural position (0°), respectively (Figure 1A). However, the EMG-driven model with the developed pennation model showed the RMS error of 12.33 ± 1.49, 12.79 ± 8.02, and 17.18 ± 10.88 N-m in the same condition. After determined the subject-specific parameters, the existing model showed that the RMS error was considerably decreased by 1.43 ± 0.29, 5.82 ± 2.25, and 7.03 ± 1.27 N-m, but the developed model gave better results

with the decreased RMS error of 1.41 ± 0.30, 5.75 ± 2.19, and 6.97 ± 1.47 N-m in 30, 70, and 100% MCI, respectively (Figure 1B).

Figure:
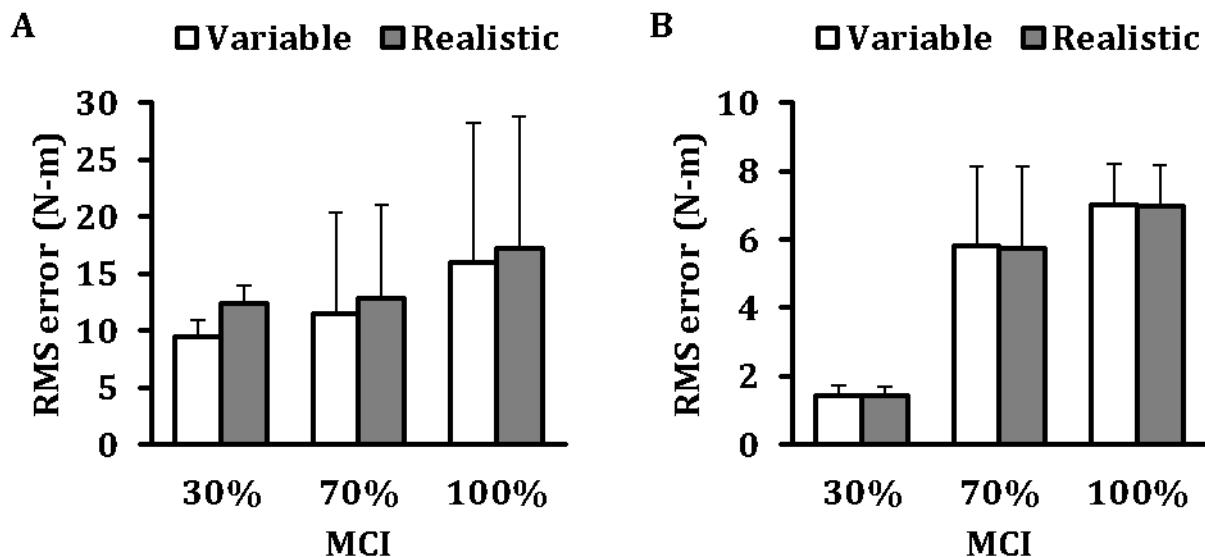
Caption: Comparison of root mean square (RMS) error at each muscle contraction intensity (MCI) between the variable and realistic pennation models. RMS errors were considerably decreased after determined the subject-specific parameters (B) compared with before (A).

Conclusion: These results implied that the existing model could better estimate joint moments compared with the realistic model when using muscle model parameters that are typically based on cadaveric studies, but the realistic model might be better for the determination of subject-specific parameters. Nonetheless, it is hard to conclude that the realistic model would be as an alternative of the existing model, because this study was simply considered the isometric condition. Indeed, the realistic pennation model was developed from the previous observation that the pennation angle is related to the joint angle and MCI. Therefore, further studies would be required to investigate the effects of the realistic model on the performance in various dynamic movements such as gait.

References: [1] White et al., J. Electromyogr. Kinesiol. 2: 217-231, 1992.

[2] Hodges et al., Muscle Nerve. 27: 682-692, 2003.

[3] Kim et al., Int. J. Prec. Eng. Manuf. 14: 855-858, 2013.

[4] Son et al., Int. J. Prec. Eng. Manuf. 13: 117-123, 2012.

Disclosure of Interest: None Declared

SS-0082

APPLICATION OF TRANSCRANIAL DIRECT CURRENT STIMULATION AND BRAIN-COMPUTER-INTERFACE-CONTROLLED ORTHOSIS FOR HAND REHABILITATION OF STROKE PATIENTS

Ming-Shaung Ju [1,*]Ko-Chieh Chao [1]Wen-Chuan Chang [1]Chou-Ching Lin [2]

[1]Mechanical Engineering, [2]Neurology, National Cheng Kung University, Tainan, Taiwan, Republic of China

Introduction and Objectives: EEG-brain-computer-interface training can modify brain potentials and change connectivity of cortical circuits. The transcraninal direct-current stimulation (tDCS) can impose stimulation on central nervous system. In our previous study [1], the power ratio of µ band in C3 and C4 was used for the BCI and the accuracy was improved using the common spatial pattern (**CSP**) method [2]. The goal of this study is to integrate tDCS and a BCI-controlled orthosis for hand rehabilitation of stroke patients. Functional magnetic resonance (fMRI) and multi-channel EEG brain connectivity analysis were used to validate effectiveness of the new method.

Methods: 8 healthy subjects (averaged age 24 years, 6 right-handed and 2 left-handed) with no history of neurological diseases and 2 stroke patients (a 35-year-old man with left hemiparesis and a 56-year-old woman with right hemiparesis) participated in this study. 19 channels of EEG signals were recorded according to the international 10-20 system. The EEG signals were band-pass filtered between 8 and 30 Hz. The CSP method was employed to extract event-related EEG features when left and right hand imagery movements were performed by the subjects [3]. A command generated according to the features was used to control right or left movement of a cursor on a screen or to drive left or right orthotic hand to extend middle and index fingers of the subjects. After a BCI pre-training session, tDCS followed by BCI training was performed twice a week for consecutive 4 weeks. The anodal tDCS (strength 2mA, ramp 5s) was applied for 20 min through 35cm^2 rectangular saline-soaked sponge electrodes. The position of anodal electrode was determined through induction of largest MEPs by using transcranial magnetic stimulation over the motor cortex area, and cathodal electrode was placed over lateral supraorbital area. 5 out of 10 subjects were randomly selected to take the sham tDCS as the control group. For the sham tDCS, the current was applied only for 30 seconds to mimic the sensation at the beginning of actual tDCS without producing any effect on the brain. The accuracy of BCI control, reaction time, and changes of brain connectivity of each session were analyzed. The cross-spectrum and phase slope index between EEG signals, within four bands, were computed. Five indices for brain connectivity, namely, global degree, global coupling strength, global efficiency, clustering coefficient, and in/out-degree were computed[4, 5].

Results: 4 healthy subjects and a stroke patient participated in anodal tDCS, and the other 5 subjects including another stroke patient participated in the sham tDCS. **Fig. 1** shows the control accuracy and reaction time of all subjects. The accuracy of anodal-tDCS group fluctuated at an average of 70% during the training and that of the sham-tDCS group increased slightly from 65% to 72%. The averaged reaction time of anodal-tDCS group decreased from 3.2s to 2.1s and that of the sham-tDCS group increased from 2.2s to 2.9s. The results showed anodal tDCS did not enhance accuracy of controlling the BCI. However, it can improve the reaction time. The brain connectivity depends on the bandwidth of EEG even for same right- or left- hand imaginary movement. Compared with the sham tDCS group, the anodal-tDCS group has higher global degree and global efficiency in latter stage of training, showing that they have more connections of nerve

signal. The anodal-tDCS could shorten the distance between the senders and recipients. The anodal-tDCS group has higher global coupling strength than the sham-tDCS group in the latter stage which means anodal-tDCS can enhance coupling strength between main nodes of signal transmission. The anodal-tDCS group has a higher clustering coefficient than the sham-tDCS group before the 6th training and get lower in the last 3 trainings.

Although BCI-control cursor training integrated with anodal tDCS does not enhance accuracy of using BCI but the reaction time does reduced after the training. Shorter reaction time implies increased transmission rate of cortex neuron signals which is consistent with the brain connectivity analyses.

Figure:
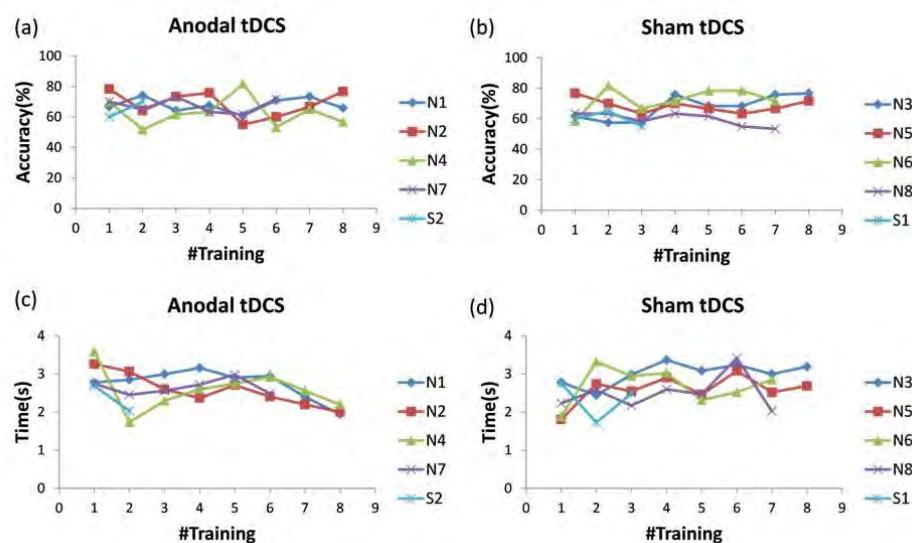
Caption: Fig. 1 Accuracy and reaction time

Conclusion: An EEG-based BCI was successfully integrated with tDCS and applied to cursor control training of healthy subjects and stroke patients. fMRI and brain connectivity analyses reveal that direct stimulation of the central nervous system do induce change of the activation of neurons in the cortex. On-going work is the control of orthotic hand to stretch the index and middle fingers of chronic stroke patients. The results will be presented and discussed in the congress.

References: [1] Pfurtscheller et al., Clinical Neurophysioly, 110(11):1842-1857.

[2] Juang, M.S. Thesis, Dept. of Mechanical Eng., NCKU, 2013.

[3] Muller-Gerking et al., Clinlical Neurophysiology, 110(5):787-798.

[4] Newman, SIAM Review, 45(2):167-256.

[5] Lu, et al., Clinical Neurophysiology, 122(8):1569-1579.

Disclosure of Interest: None Declared

MORPHOMETRIC ANALYSIS OF THE THORACIC INTERVERTEBRAL FORAMEN OSSEOUS ANATOMY IN ADOLESCENT IDIOPATHIC SCOLIOSIS USING LOW DOSE COMPUTERIZED TOMOGRAPHY.

Thorbjorn J. Loch-Wilkinson [1,*]Maree Izatt [1]Robert Labrom [1]Geoff Askin [1]Mark Pearcy [1]Clayton Adam [1]

[1]Paediatric Scoliosis Research Group, Science and Engineering Faculty, Queensland University of Technology and Mater Health Services, Brisbane, Queensland, Australia

Introduction and Objectives: The dimensions of the thoracic intervertebral foramen in adolescent idiopathic scoliosis (AIS) have not previously been quantified. During posterior approach scoliosis correction surgery pedicle screws may occasionally breach into the foramen. Better understanding of the dimensions of the foramen may be useful in surgical planning. This study describes a reproducible method for measurement of the thoracic foramen in AIS using computerized tomography (CT).

Methods: In 23 pre-operative female patients with Lenke 1 type AIS with right side convexity major curves confined to the thoracic spine the foraminal height (FH), foraminal width (FW), pedicle to superior articular process distance (P-SAP) and cross sectional foraminal area (FA) were measured using multiplanar reconstructed CT. Measurements were made at entrance, midpoint and exit of the thoracic foramina from T1/T2 to T11/T12. Results were correlated with potential dependent variables of major curve Cobb Angle measured on X-ray and CT, Age, Weight, Lenke classification subtype, Risser Grade and number of spinal levels in the major curve.

Results: The FH, FW, P-SAP and FA dimensions and ratios are all significantly larger on the convexity of the major curve and maximal at or close to the apex. Mean thoracic foraminal dimensions change in a predictable manner relative to position on the major thoracic curve. There was no significant correlation with the measured foraminal dimensions or ratios and the potential dependent variables. The average ratio of convexity to concavity dimensions at the apex foramina for entrance, midpoint and exit respectively are FH (1.50, 1.38, 1.25), FW (1.28, 1.30, 0.98), FA (2.06, 1.84, 1.32), P-SAP (1.61, 1.47, 1.30).

Conclusion: Foraminal dimensions of the thoracic spine are significantly affected by AIS. Foraminal dimensions have a predictable convexity to concavity ratio relative to the proximity to the major curve apex. Surgeons should be aware of these anatomical differences during scoliosis correction surgery.

Disclosure of Interest: None Declared

Arterial Mechanics

SS-0084

DORSAL-VENTRAL DIFFERENCE IN BIOMECHANICAL AND BIOCHEMICAL PROPERTIES IN THE RABBIT THORACIC AORTAS

Takeo Matsumoto [1,*]Shukei Sugita [1]Takahiro Shirono [1]Shintaro Iijima [1]Kazuaki Nagayama [1] [2]Akio Matsumoto [3]

[1]Department of Mechanical Engineering, Nagoya Institute of Technology, Nagoya, [2]Department of Intelligent Systems Engineering , Ibaraki University (current), Hitachi, [3]Department of Pharmacology, Chiba University School of Medicine, Chiba, Japan

Introduction and Objectives: Aortic walls have long been assumed to be uniform in the circumferential direction in most of the studies on blood vessel wall biomechanics. However, it gradually becomes clear that they are heterogeneous in the circumferential direction in humans [1] and rabbits [2]. Sugita et al. [2] observed the deformation of an aortic segment during inflation in the longitudinal direction to find that the wall of rabbit thoracic aorta is more compliant in the ventral side than the dorsal. This indicates that cyclic deformation of aortic wall during heart beat is higher in the ventral side than the dorsal, which may cause difference in the properties of smooth muscle (SM) cells not only in biomechanical but also in biochemical aspects. In this study, we observed the dorsal-ventral (DV) difference in the SM contractility and RNA expression levels with a microarray analysis in rabbit thoracic aortas.

Methods: *DV difference in the biomechanical properties:* Thoracic aortas were obtained from matured male Japanese white rabbits weighing 2.5–3.0 kg. The aortic segments were stretched to their in vivo length and pressurized to 80 mmHg in an aerated Krebs-Henseleit solution at 37°C. Four small needles were stuck perpendicularly into the aortic wall at almost equal intervals on a circumference. Displacement of the needles during pressurization from 0 to 200 mmHg and during isobaric SM contraction at 80 mmHg induced with norepinephrine (NE) was observed in the longitudinal direction with a CCD camera and laterally with two digital cameras placed in an opposite direction across the aorta. The images taken by the cameras were used to identify the point at penetration of each needle. Circumferential length between the needles was obtained assuming that the aortic segment had circular cross section.

SM contractility at cellular level: SM cells isolated from dorsal or ventral quarter of rabbit thoracic aortas with enzymatic digestion were used. Length of the isolated cells was measured in an aerated Ca2+-free Krebs-Henseleit solution at 37°C before and after contraction induced with 2.3mM of CaCl2 and 10-5M of NE.

DNA Microarray analysis: To study the dorsal-ventral difference of SM cells in biochemical properties, dorsal and ventral quarter of aortic segments were analysed with a Rabbit Gene Expression Microarray (G2519F, 020908, Agilent) based on the manufacturer's standard protocols. Microarray expression data was validated by real-time PCR.

Results: Circumferential stretch ratio at 120 mmHg in reference to length at 40 mmHg was significantly lower in the dorsal side (1.3±0.1, mean±SEM, n=5) than in the dorsal (1.6±0.1), indicating that thoracic aortas are stiffer in the dorsal side than in the ventral as shown in the previous study [2]. The circumference of the aortic specimens contracted significantly more in the ventral side (24±4%, n=5) than in the dorsal (16±3%) upon SM contraction. Similar results were obtained for isolated cells. The amount of contraction was 37±4% (n=20) for cells isolated from the ventral side and was significantly

higher than that of the dorsal side (22±2%). These results indicate that the more compliant side of the aorta is more contractile.

In the microarray analysis, there were 392 genes of 43,603 found to express more than twice in the ventral side as much transcript as in the dorsal side, besides 296 genes were found to express less than half as well, indicating that gene expression profile is also different between dorsal and ventral sides. Several genes with DV difference were confirmed by real-time PCR, including osteopontin with higher expression in the dorsal side and actin with higher expression in the ventral. Osteopontin stimulates DNA synthesis of SM cells [3] and actin is one of the most important contractile proteins. Thus, SM cells in the dorsal side may have more synthetic phenotype and those in the ventral side more contractile.

Conclusion: DV difference in the smooth muscle contractility and gene expression profile may be explained by the DV difference in the mechanical properties.   Higher compliance in the ventral side causes higher cyclic strain during a cardiac cycle. Such higher mechanical stimulation may induce higher contractility to the SM cells, i.e., more contractile phenotype in this side. However, the reason for the DV difference in the mechanical properties remains unknown. The ventral side of the thoracic aortas is connected with the vertebral column via collagen fibers. This might induce accumulation of collagen fibers in the dorsal side. Since collagen fibers are much stiffer than other components in the aortic wall, accumulation of collagen fibers may induce wall stiffening.

References: [1] Draney et al., Ann. Biomed. Engng., 30: 1033-45, 2002.

[2] Sugita et al., Trans. JSME, Ser. A, 69: 43-8, 2003.

[3] Takemoto et al., Arterioscler. Thromb. Vasc. Biol., 20: 624-8, 2000.

Disclosure of Interest: None Declared

Musculoskeletal

SS-0087

THE SKINNY ON OSTEOARTHRITIS -- DOES BODY FAT AFFECT QUADRICEPS MUSCLE COMPOSITION?

K H Collins [1,*] R A Seerattan [1] W Herzog [1]

[1]University of Calgary, Calgary, Canada

Introduction and Objectives: Western-type diets, high in fat and sugars, often lead to obesity. Obesity in turn is associated with chronic inflammation thought to be a risk factor for the onset and increased rate of progression of metabolic osteoarthritis (OA) in joints [1]. Aside from affecting bones and cartilage, obesity-induced metabolic OA may affect muscle structure and function, causing weakness, thereby increasing risk for OA development [2]. However, the relationships between diet-induced obesity, muscle structure and weakness, and OA remain poorly understood. The purpose of this study was to determine these relationships in a pre-clinical model of metabolic OA.

Methods: Thirty-two male rats (8-12 weeks) were randomized into a high fat/high sucrose diet (DIO) (n=21, 40% fat 45% sucrose) or control (n=11 lean chow (LFD, 13.5% fat) group. After a 12-week obesity induction period, DIO animals were stratified into Obesity Prone (DIO-P, Top 33% of animals by change in body mass over twelve weeks, n=7), Obesity Resistant (DIO-R, bottom 33% n=7). Animals were euthanized after a total of 28 weeks when all outcomes were measured: body fat (Dual Energy X-Ray Absorptiometry), knee OA severity (Modified Mankin score) [3], and vastus lateralis muscle (VL) mass (g) and intramuscular fat infiltration (LFD n=6). Vastus lateralis muscles were frozen, stained with Oil Red O, imaged and quantified under 10x magnification using a custom MatLab program. Kruskal-Wallis tests and Spearman correlations were performed at $\alpha=0.05$.

Results: DIO-P and DIO-R animals had increased body fat when compared to LFD (DIO-P: 56.7±1.7%, DIO-R: 42.8±1.5%, LFD: 29.5±2.5%, p<0.001). However, DIO-P animals were heavier than both DIO-R and lean animals (DIO-P: 1207±66g, p<0.001), but DIO-R and lean animals had similar mass (DIO-R: 896±43g, LFD 823±19g, p=0.25). All DIO animals had greater Modified Mankin scores than LFD (Median and {Interquartile range}: DIO: 50 {40-63}, LFD: 26 {22-38} p=0.002). Despite being heavier, DIO-P and DIO-R animals had similar Mankin Scores (p=0.805). Conversely, DIO-R animals had more joint damage than LFD animals, (DIO-R: 47{40-64}, LFD: 26{22-38}, p=0.004). There was a strong positive relationship between body fat and Modified Mankin score (r=0.6, p=0.001), but not body mass. All DIO animals had decreased VL mass compared with LFD (2.1±0.05g, 2.3±0.07g), and despite having similar body mass, DIO-R had decreased VL mass compared with LFD (2.0±0.06g) (p<0.05). VL intramuscular fat was increased in DIO animals (DIO: 22.7±1.3%, LFD: 3.3±0.9%) and despite having similar body mass, DIO-R animals had increased VL intramuscular fat compared with LFD (DIO-R: 20.7±0.8%) (p<0.001). There was a significant negative relationship between body fat and VL mass (r=-0.50, p=0.03) and Modified Mankin Score and VL Mass (r=-0.40, p=0.04). Positive relationships were calculated between body fat and VL fat (r=0.80, p<0.001), and Modified Mankin Score and VL fat (r=0.45, p<0.05).

Conclusion: Body fat is associated with increased intramuscular fat accumulation in the vastus lateralis muscle. Quadriceps intramuscular fat is a novel link between systemic inflammation, muscle composition and metabolic OA. This work is a first step towards understanding the crucial mechanical and inflammatory signatures of metabolic OA in skeletal muscle.

References: Reference 1

Zhuo et al. (2012) Metabolic Syndrome Meets Osteoarthritis. Nat. Rev. Rheumatol., 12, 729-737

Reference 2

Lee et al. (2012) Sarcopenic obesity is more closely associated with knee osteoarthritis than is nonsarcopenic obesity: a cross-sectional study. Arthritis Rheum., 12, 3947-3954

Reference 3

Mankin et al. (1971) Biochemical and metabolic abnormalities in articular cartilage from osteo-arthritic human hips. II. Correlation of morphology with biochemical and metabolic data. J Bone Joint Surg Am., 3, 523-537

Disclosure of Interest: None Declared

Musculoskeletal

SS-0088

USING ADVANCED MRI TECHNIQUES FOR ESTIMATING STRAIN DISTRIBUTIONS ALONG MUSCLE FIBERS DURING ISOMETRIC PLANTAR-FLEXION ACTIVITY OF HUMAN MEDIAL GASTROCNEMIUS, IN VIVO

Agah Karakuzu [1,*]Uluc Pamuk [1]Burak Acar [2]Can A. Yucesoy [1]

[1]Institute of Biomedical Engineering, [2]Electrical and Electronics Engineering, Bogazici University, Istanbul, Turkey

Introduction and Objectives: Magnetic resonance imaging (MRI) enables identifying orientation of muscle fibers through coupled implementation of diffusion tensor imaging (DTI) [1]. MRI analyses also allow quantifying 3D local tissue deformations in human muscles, in vivo [2]. These analyses combined are capable of determining deformation along muscle fibers. This is physiologically highly relevant information. Previously it was shown that skeletal muscle is not independent from its surroundings, because myofascial connections provide linkages from the muscle belly to adjacent muscular and non-muscular structures [3]. Finite element modeling designed to study mechanics of activated skeletal muscle within the context of a fascial integrity suggests presence of inhomogeneous deformations along the muscle fibers indicating sarcomere length heterogeneity [3]. Using MRI and DTI analyses our aim was to quantify fiber direction deformations in human subjects, in vivo, and to test the hypothesis that sustained plantar-flexion activity of the medial gastrocnemius causes heterogeneous length changes.

Methods: Five healthy female subjects (age=26±3 years, height=162±7 cm, mass=51±5 kg) participated in this study. The subjects were positioned prone in a 3T clinical MRI scanner with their right leg constrained using a custom design apparatus: the ankle was fixed at 90° and the knee was kept extended (175.6°±3.3°) (reference state). Maintaining these positions, the subjects were asked to sustain isometric plantarflexion activity corresponding to 15% maximum voluntary contraction (MVC) with the help of a visual feedback (deformed state). DTI and high-resolution 3D MRI anatomic image sets were acquired in both states, separately. To quantify tissue deformations occurring in global coordinates due to such contraction, the image sets were registered using non-rigid Demons algorithm [4]. DTI data were denoised [5] prior to Split and Merge Tractography [6]. Streamline integration using 4th order Runge-Kutta algorithm allowed determining muscle fiber tracts of the medial gastrocnemius. Strain transformation from global coordinates to local muscle fiber direction was used to quantify deformation along muscle fibers. Undeformed state images were also transformed by a synthetic rigid body motion (10° rotation in the axial, 3° rotations in coronal and sagittal planes and 4mm translation axially) imposed. Resulting fiber direction strains calculated were used as estimates of error strains.

Results: For the pooled data of all subjects, mean fiber direction strains (16.0±9.3% for lengthening and 4.0±3.7% for shortening) calculated were significantly greater than mean strain errors (1.9±1% for lengthening and 1.8±0.9% for shortening). The figure shows for two subjects, examples of "serial" strain distributions along muscle fibers (panels A-B) and "parallel" strain distributions as mean fiber strain of groups of muscle fibers represented by each tract (panels C-D). The serial strain distributions indicate that along the same tract, shortening and lengthening (up to locally 108.9% and 23.6%, respectively) occurs simultaneously. Mean fiber strains of different tracts are non-uniform (e.g. in panel D they range from -0.01 from to 0.16; among all subjects from -0.02 to 0.33). Therefore, parallel strain distributions within axial

sections of the muscle are also heterogeneous. These findings confirm our hypothesis and are in concert with the expectations from the previous studies of our research group [3].

At reference state, extended knee position conceivably imposes stretch on the medial gastrocnemius proximally. On activation at 90° of ankle angle, shortening along the muscle fiber direction is plausible. However, instead of such uniform strain distributions, our findings indicate that locally along groups of muscle fibers represented by each tract, lengthening occurs at parts, whereas shortening occurs at different parts and at varying amplitudes. This is explained by epimuscular myofascial loads acting on the muscle belly via the muscle's connections to the surrounding muscular and non-muscular structures and further mechanical interaction between neighboring muscle fibers [3].

Figure:
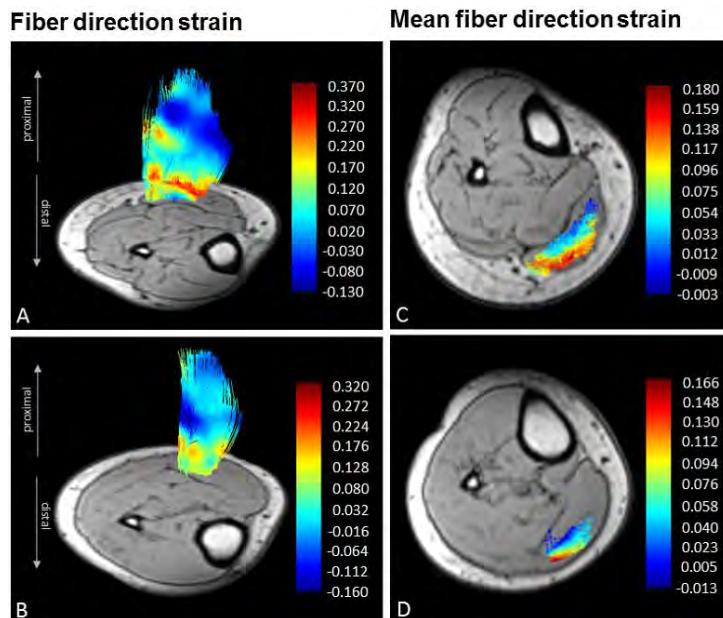
Caption: Serial (A-B) and parallel (C-D) distributions of fiber direction strains. + and – values indicate lengthening and shortening, respectively.

Conclusion: MRI and DTI analyses combined provide a powerful tool for quantifying deformation along activated human muscle fibers, in vivo. Estimating length changes of bigger groups of sarcomeres is quite relevant for characterization of the muscle's contribution to joint mechanics.

References: [1] Froeling et al., *J Magn Reson Imaging* **36**:237-248,2012.

[2] Yaman et al., *J Biomech Eng* **135**:910003,2013.

[3] Yucesoy, *Exerc Sport Sci Rev* **38**:128-134,2010.

[4] Thirion, *Med Image Anal* **2**:243-260,1998.

[5] Tristán-Vega et al., *Med Image Anal* **14**:205-218,2010.

[6] Yoldemir et al., *IEEET Med Imaging* **31**:1929-1940,2012.

Disclosure of Interest: None Declared

Musculoskeletal

SS-0089

EFFECTS OF BOTULINUM TOXIN TYPE A ON MUSCULAR MECHANICS APPEAR TO BE MUCH MORE INVOLVED THAN KNOWN SO FAR

Can A Yucesoy [1,*]Ahu N Turkoglu [1]Filiz Ates [1]

[1]Bogazici University, Istanbul, Turkey

Introduction and Objectives: Botulinum toxin type A (BTX-A) is widely used in treating cerebral palsy (CP) patients. Partial muscle paralysis helps blocking the hyper-excitable stretch reflexes. This also decreases active force production. Therefore, through reduced spasticity and decreased muscle tone BTX-A is considered to improve function by acting against an agonist-antagonist force imbalance and increasing joint range of motion. Although this mechanism can reflect positively on function, a comprehensive understanding of the effects of BTX-A requires more critical and specific testing. (I) BTX-A is not contained only within the muscle injected and (II) active force reduction is not invariable for different muscle lengths [1]. (III) BTX-A is considered to decrease passive resistance to stretch via the mechanism described however, its effects on muscle passive forces and tissue structural properties need to be studied. (IV) If BTX-A actually increases muscle length range of force exertion should be assessed. (V) Intra-operative tests on CP patients show that spastic muscle activated alone has a regular muscle force-joint angle relationship [2]. However, if an antagonistic muscle is co-activated, the muscle's mechanics become representative of the patients' joint movement disorder [3]. This suggests that intermuscular mechanical interaction [4] is improper in CP patients. Therefore, it is important to test whether BTX-A affects such interaction. In order to address these issues, a broader scale than just the injected muscle should be considered. Active and passive forces of neighboring muscles should be measured simultaneously and at various muscle lengths and positions. Keeping the target muscle compartment intact allows preserving intermuscular interactions. The goal was to quantify the effects of BTX-A accordingly.

Methods: The tibialis anterior (TA), extensor digitorum longus (EDL) and extensor hallucis longus (EHL) muscles of the intact anterior crural compartment of the rat were studied 5 days post injection. 0.1U BTX-A in 20μl of saline (BTX-A group) or only 20μl of saline (control group) was injected into the mid-belly of the TA. (i) The TA was lengthened (BTX-A, n=8, body mass 312.5±14.6g; control, n=8, body mass 318.5±12.5g). (ii) The EDL was lengthened both proximally and distally and, (iii) the relative position of the EDL was changed (BTX-A, n=8, body mass 315.0±6.3g; control, n=8, body mass 300.0±6.9g). In (i) and (ii) muscles other than the one lengthened and in (iii) all muscles were kept at constant length. Gomori trichrome stain was used to assess intra- and intermuscular connective tissue content histologically.

Results: (1) Substantial force decreases (peak force drops range from 47.3% to 85.6%) for all compartmental muscles indicate spread of BTX-A. (2) Force reductions are length dependent and more pronounced at shorter lengths (e.g., for the TA, force reductions increase from 46.6% to 55.9% with decreasing length), (3) BTX-A does not increase muscle length range of force exertion, but can decrease it (for the EDL both proximally and distally, by up to 26.1%), (4) BTX-A causes increased passive forces (for all lengthened muscles, minimally three-fold). (5) Unlike the sizable intermuscular interaction effects shown in the control group, EDL forces of the BTX-A group measured at the most proximal position did not change significantly with the muscle's position changes and proximo-distal force differences vanished. This shows

compromised intermuscular interactions. Histological analyses show an increased intramuscular collagenous tissue content and a contrasting decrease in intermuscular connections. Spread of BTX-A and length dependent force reduction implies complex nature of effects on joint mechanics. Narrowed length range of active force production suggests that BTX-A can worsen already limited joint range of motion of CP patients. Increased passive forces can compromise intended reduction in passive resistance to stretch as obtained by reduced hyper-excitable stretch reflexes. These effects are contraindicated. Highly diminished intermuscular mechanical interactions is remarkable and can be clinically relevant if in future studies the role of such interaction on mechanics of spastic muscle can be further established.

Conclusion: BTX-A does not increase the length range muscle produces force, but can reduce it. Moreover, it causes increased muscle passive force, but diminished intermuscular mechanical interactions. In sum, our experiments reveal remarkable new effects of BTX-A worthwhile further testing in clinically representative conditions.

References: [1] Yaraskavitch et al., J. Biomech, 41: 897-902, 2008.

[2] Ates et al., Clin Biomech, 28: 48-54, 2013.

[3] Ates et al., Clin Biomech, 29: 943-949, 2014.

[4] Yucesoy, Exerc Sport Sci, Rev. 38: 128-134, 2010.

Musculoskeletal

SS-0090

PEAK FORCE AND HYSTERESIS IN ACTIVELY AND PASSIVELY LENGTHENED SKELETAL MUSCLE MYOFIBRILS AT VERY LONG SARCOMERE LENGTH.

Tim Leonard [1,*] Jens Herzog [1] Azim Jinha [1] Walter Herzog [1]

[1] University of Calgary, Calgary, Canada

Introduction and Objectives: The molecular spring titin is a giant protein found in muscle sarcomeres and is the primary source of passive force in myofibrils [1]. The extensible region of titin contains spring-like domains arranged in series with visco-elastic properties that come into play in a prescribed sequence with increasing sarcomere length (SL). Within the physiologically relevant SL range, sarcomeres that are lengthened will initially align and straighten the Ig domains, followed by stretching the PEVK region. These two events are known to be essentially elastic. Beyond the physiological range (> 3.5μm), Ig domains unfold, and this unfolding is thought to be highly visco-elastic. Active muscle lengthened not only from SL of 1.8μm to 4.0μm but also beyond 4.0μm (region of loss of myofilament overlap) will produce more force than passively lengthened muscle at the same SL [2].We hypothesize that the rate of Ig domain unfolding in titin is increased with higher force. If so, then activated myofibrils will exhibit greater hysteresis during stretch-shortening cycles (SSC) compared to passive myofibrils because the increased force for the actively stretched myofibrils will cause a greater number of Ig domains to unfold compared to passively stretched myofibrils.

Methods: Rabbit psoas myofibrils were used for these experiments, activated and lengthened (n=6) and passively lengthened (n=5). Single myofibrils with an initial mean sarcomere length (SL) of 2.8μm were either actively (pCa+2=3.5) or passively (pCa+2=8) lengthened to approximately 4.5μm and then immediately subjected to 10 small amplitude SSC of 0.5μm/sarcomere before returning to SL of 1.8μm. All length changes were done at 0.1μm/sarcomere/second. Forces are expressed as stresses so that comparisons between myofibrils of different diameters can be made. Materials and apparatus are reported elsewhere for brevity [2]. All descriptive results are reported as mean ± standard deviation Institutional ethics approval was obtained for these experiments. The primary outcomes measures reported here are: 1.Peak force at the end of the initial lengthening to 4.5μm, or at the stretch segment of the SSC for each subsequent cycle. 2. The hysteresis measured for each of the small amplitude SSC, calculated as stretch energy -- return energy in units of nN*μm. 3. The percent energy loss calculated as (energy returned-energy input)/energy input x100.

Results:

Mean 1st peak force (force achieved at the end of the initial stretch to 4.5μm) was higher in active versus passive myofibrils (see Figure 1) at 339±137nN/μm2 versus 103±17nN/μm2, as expected. Mean peak force for each subsequent SSC fell continuously from the 2nd to the 10th cycle in active, while the peak force stabilized in passive tests by the 4th cycle. Hysteresis was greater in the active tests; mean 1st SSC hysteresis was 18±1nN*μm (active) versus 4±2nN*μm (passive). By the 10th SSC, the hysteresis in active was still 9±4nN*μm while in passive it was only 0.4±0.3nN*μm The mean percent energy loss per cycle was initially high for both test conditions; active = 26±14% versus passive = 28±8% and by the end of the 10th cycle, active was 17±4% while passive was only 5±4%. The mean energy loss across all 10 SS cycles for active was 18±11% and for passive 11±8%.

Figure 1: Stress as a function of sarcomere length for two different conditions. One exemplar active (red) and passive (green) experiment are shown here. The black arrow shows the direction of the trace with respect to time. The active data shows initial activation and then a stretch to about 5 µm and then the 10 small stretch-shortening (SS) cycles. The forces are much higher in the active experiment than the purely passive lengthening experiment.

Figure:
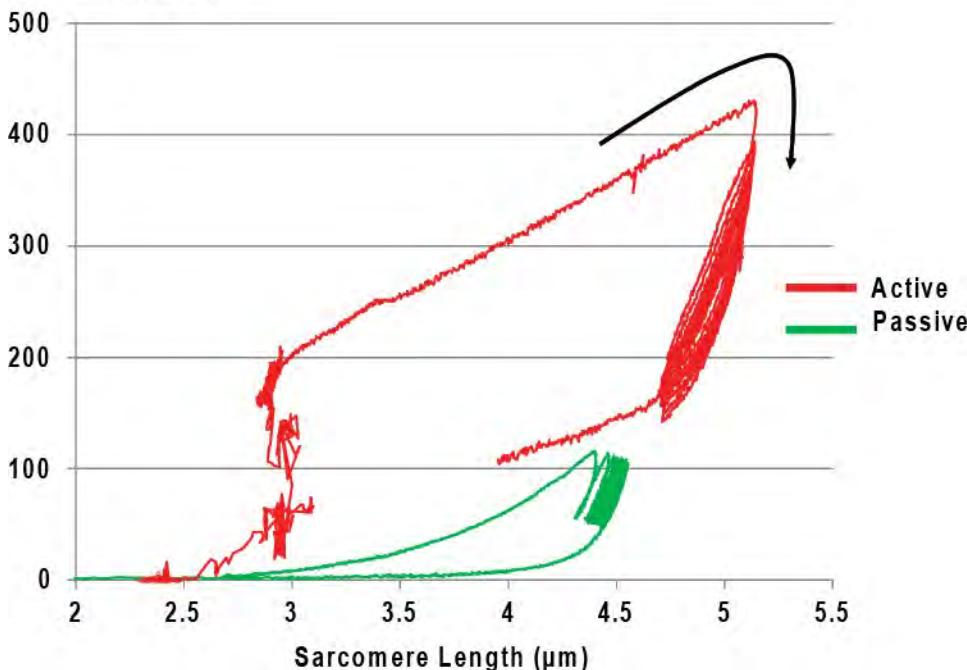
Conclusion: Hysteresis was greater for active compared to passive SSC and while the hysteresis was reduced by the 10th cycle, it remained higher in absolute and relative terms for active compared to the passive tests, indicating that higher forces promote greater Ig domain unfolding, resulting in a more visco-elastic (and less elastic) behaviour of titin. The much higher active force beyond myo-filament overlap (> 4µm) can only be attributed to titin [2] and a stiffer (possibly due to a shorter) free region of titin results in greater Ig domain unfolding at long sarcomere length, producing a greater hysteresis compared to passively lengthened myofibrils. The continuous drop in peak force across the 10 SSC in active is not seen in the passive tests, indicating that the higher force in active results in the recruitment and unfolding of new Ig domains during the entire test. The large hysteresis in active at the 10th SSC (at 50% of the 1st SSC) was not seen in passive (only 10%) indicating that the passive myofibrils exhibited a more elastic behaviour by the end of the tests, compared to the active samples.

References: Reference 1

[1] Tskhovrebova L et al. 1997, Nature 387: 308-312.

Reference 2

[2] Leonard and Herzog, 2010, AJP-(Cell) 299:14-20.

Disclosure of Interest: None Declared

Musculoskeletal

SS-0091

APPLICATION OF A PSEUDO-INVERSE METHOD FOR THE ESTIMATION OF INDIVIDUAL MUSCULO-TENDON FORCES CONTRIBUTIONS TO THE GROUND REACTION 3D FORCE AND MOMENT AND TIBIOFEMORAL CONTACT FORCES

Florent Moissenet [1,*] Laurence Chèze [2 3 4] Raphaël Dumas [2 3 4]

[1]CNRFR - Rehazenter, Laboratoire d'Analyse du Mouvement et de la Posture, Luxembourg, Luxembourg, [2]Laboratoire de Biomécanique et Mécanique des Chocs, IFSTTAR, Bron, [3]Université Claude Bernard Lyon 1, Villeurbanne, [4]Université de Lyon, Lyon, France

Introduction and Objectives: Besides giving access to an estimation of individual musculo-tendon forces (iMTFs), musculoskeletal (MS) models now allow studying interactions between the different MS structures [1,2]. In this sense, the study of iMTFs contribution to forces and accelerations is possible during different tasks and may provide insights about either pathologic gait patterns or the progression of joint disorders (e.g., osteoarthritis). However, to estimate the contributions of iMTFs, most of the studies require a high computational time since they are based on a forward dynamics approach with an induced acceleration analysis [3] or a perturbation analysis [4]. Recently, Lin et al. [5] proposed an inverse dynamics approach with the use of a pseudo-inverse. Yet, even if inverse dynamics was used, a 5-point rigid contact was used to model contact forces between the foot and the ground. The aim of this study was thus to extend this approach to estimate the iMTFs contributions to the ground reaction 3D force and moment (GRFM) at the centre of pressure. The procedure was applied to a 3D lower limb MS model during gait, and the contributions of iMTFs to the GRFM and to tibiofemoral contact forces (TBCF) were computed and compared to the literature.

Methods: A previously described 3D lower limb MS model [1], consisting of pelvis, thigh, patella, shank and foot segments and 43 muscular lines of action was used. The following procedure was then applied on one gait cycle provided in the dataset of the "First Grand Challenge Competition to Predict in Vivo Knee Loads". For details relating to the subject and dataset, see [6].

The dynamics equation of the whole lower limb was used, introducing the iMTFs and Lagrange multipliers standing for the bone, contact and ligament forces [7]. The iMFTs were first estimated by a static optimization procedure [1]. In order to estimate the iMTFs contributions to the GRFM, a parameter reduction was applied in order to cancel all Lagrange multipliers [7,8]. The GRFM due to each iMTF were then computed using the pseudo-inverse approach [5] by setting all other iMTFs to zero. For that, the ground reaction 3D moment was replaced by six equivalent forces [9]. Similarly, for the iMTFs contribution to TBCF, a partial parameter reduction [1] was applied in order to cancel all the Lagrange multipliers except the ones standing for the contact forces. The same pseudo-inverse was used with the unique, above-mentioned, iMTF, and the corresponding contribution to GRFM as well as to the segment accelerations.

Results: The contributions of iMTFs to the GRFM obtained meet the estimations reported by Lin et al. [6]. Similarly, the contributions of iMTFs to the axial, medial and lateral TBCF are close to the estimations reported by Pandy et al. [2]. A selection of these results is reported in Figure 1.

In each case, the sum of the contributions of all iMTFs (SUM) obtained from the proposed pseudo-inverse method was near to the magnitude of the measured GRFM and TBCF (i.e., the root mean square errors were respectively 0.06BW and 0.54BW). This was expected for the GRFM that are one of the inputs for the MS model. Conversely, while the TBCF is an output of the model, the sum of the contributions matches reasonably well, especially at the first peak, the prosthetic measurement.

Figure:
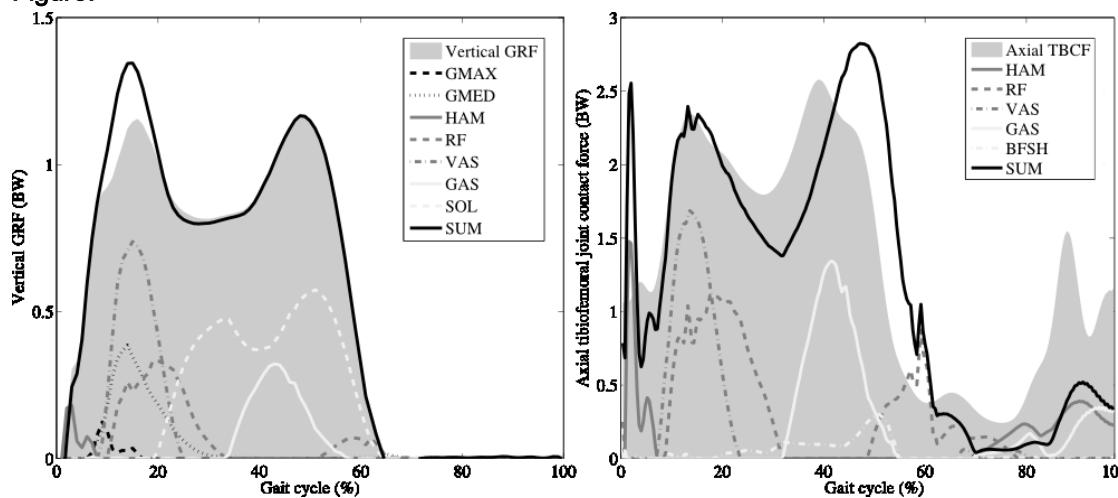
Caption: Left: Contribution of gluteus maximus (GMAX), gluteus medius (GMED), hamstrings (HAM), rectus femoris (RF), vastii (VAS), gastrocnemii (GAS), soleus (SOL) and the sum of all musculo-tendon forces (SUM) to the measured vertical ground reaction force (GRF) expressed in body weight (BW). Right: Contribution of RF, VAS, GAS, biceps femoris short head (BFSH) and SUM to the measured axial tibiofemoral contact force (TBCF) expressed in BW.

Conclusion: This study confirms that the iMTFs contributions to different forces in the lower limb can be obtained through an inverse dynamics and static optimisation procedures using a pseudo-inverse. Moreover, a rigid foot contact model is not required. The contribution to the GRFM can be directly computed at the centre of pressure.

Thanks to the proposed MS model and the partial parameter reduction [1], it is now possible to analyse the contribution of iMTFs to many different forces in the lower limb (e.g., ligament, patellar contact) and to better understand the interactions into the MS system.

References: [1] Moissenet et al., JBiomech 47:50-8, 2014

[2] Pandy and Andriacchi, Annu Rev Biomed Eng 12:401-33, 2010

[3] Anderson and Pandy, Gait Posture 17 :159-69, 2003

[4] Liu et al., JBiomech 41 :3243-52, 2008

[5] Lin et al., Int J Numer Meth Biomed Engng 27:436-49, 2011

[6] Fregly et al., J Orthop Res 30:503–13, 2012

[7] Moissenet et al., Multibody Syst Dyn 28:125–41, 2012

[8] Garcia de Jalon and Bayo, Springer-Verlag, New-York, 1994

[9] Dumas and Chèze, Med Biol Eng Comput 45:315-22, 2007

Disclosure of Interest: None Declared

SPEED-ACCURACY TRADE-OFF IN GOLF DRIVING: A KINEMATIC AND PERFORMANCE ANALYSIS OF A GROUP OF LOW HANDICAP GOLFERS

Dr Susan Brown and Michael Davidson

Edinburgh Napier University

UK

Introduction: Research studies which consider kinematics within golf driving are numerous, although differences in data collection and processing methods can directly influence findings. Researchers have investigated the role of major segments such as the pelvis and torso (presented and analysed as a single segment), using the principle of the X-Factor (the separation of the pelvis and torso/shoulder segments) albeit used differently across studies. It is argued that an increase in club head speed can be attributed to an increased X-Factor which has a positive impact on driving performance [1]. However, the methods used for trial selection are also inconsistent, for example using a single measure of club head or ball speed to determine suitability for inclusion [1,2,3]. Recently researchers demonstrated the effect of different parameters on accuracy in driving confirming the interaction between club head and ball launch conditions as being paramount in driving success [5]. Furthermore, driving accuracy has been shown as a more robust predictor of scoring average than driving distance [6,7].

Objectives: To identify specific pelvis and torso segment differences when participants were asked to drive the ball for distance and for accuracy; to determine if driving for distance has an impact on driving accuracy; and if driving for accuracy caused a significant decrease in driving distance.

Methods: A 12-camera, 3D motion capture system operating at 500Hz (Oqus 3+, Qualisys AB) was used to capture 20 drives from 15 low handicap golfers (mean (±SD) self-reported handicap 0.7±1.76 strokes) using a TrackMan™ Pro radar (Trackman A/S) to directly measure club head and ball data set up according to the Manufacturer's guidelines. There were two randomly ordered conditions; driving distance and driving accuracy using analogies of hitting the longest drive down a par 5 wide fairway and hitting the fairway on a tree-lined par 5 respectively. 37, 19mm diameter retro-reflective markers were used following the definitions presented within the Qualisys Project Automation Framework (PAF) reduced marker set for golf analysis to identify each segment coordinate system (SCS) (head, pelvis, torso, left upper arm, left lower arm, left hand, right and left feet, club shaft and club head). Mean (±SD) data were extracted after processing (Visual 3D™, C-Motion Inc. through PAF) for both conditions for the following: peak X-Factor (z-component of torso orientation with respect to the pelvis); peak X-Factor rate of change (z-component of angular velocity of the torso relative to the pelvis, expressed within the pelvis SCS); peak angular velocity for the pelvis and torso (with respect to the GCS). TrackMan™ data was extracted for club head and ball speed, spin rate, smash factor (ratio of ball to club head speed), carry distance (distance) and side distance (accuracy). Paired sample t-tests were used to identify differences between the conditions.

Results: See Table 1. Comparison between the two conditions showed a significantly greater peak pelvis–torso separation (X-Factor) when hitting for distance compared to accuracy but no significant differences for peak X-Factor angular velocity, peak pelvis or peak torso angular velocity. Significant differences were seen for club head speed, ball speed, carry distance and side distance with all variables greater for the distance condition ($p<0.05$). **Conclusion:** The analysis

demonstrates a speed-accuracy trade-off within the golf drive in terms of the performance outcome, with greater carry distance, but an increase in side distance or in other words, a reduction in accuracy. There is a certain amount of sense in this given a shot hit with spin could deviate further offline the further it travels. Within this study, the golf drives for accuracy generated 95.8% of the carry distance of those which were struck under the speed/distance condition. This is in contrast to previous studies which found a decrease of around 15-20% in ball velocity during kicking for speed and accuracy [8,9,10]. The increase in driving distance may be attributable to the increase in peak pelvis-torso separation (X-Factor) as previously described. It would seem that where other studies have shown an important performance related reduction in accuracy with an increase in segment speed, this may not apply to the same extent in golf.

References

1. Meister et al., 2011. *J App Biomechanics,* 27, 242-251
2. Egret et al., 2006. *Intl J Sports Med,* 27, 463-467
3. Myers et al., 2008. *J Sports Sci,* 26, 181-188
4. Chu et al., 2010. *J Sports Sci,* 28, 1251-1259
5. Betzler et al., 2014. *J Sports Eng & Tech,* 1-8
6. Quinn, 2006. *Teach Stat*, 28, 3-10
7. Wiseman & Chatterjee, 2006. *Percept Motor Skills*, 102, 109-117
8. Teixeira, 1999. *Percept Motor Skills,* 96, 423-434
9. Lees & Nolan, 2002, *Sci & Football IV Proc,* 16-21
10. Andersen & Dorgë, *Scand J Med & Sci in Sports, 21, 79-84*

Table: Mean (±SD) data for pelvis and torso segments, club head and ball flight

	Peak X-Factor (deg)	Peak X-Factor ang vel (deg·s⁻¹)	Peak pelvis ang vel (deg·s⁻¹)	Peak torso ang vel (deg·s⁻¹)	CH speed (m·s⁻¹)	Ball speed (m·s⁻¹)	Smash factor (ratio)	Spin (rpm)	Carry dist (m)	Side dist (m)
Distance	**-55.5 ±8.6**	223.5 ±75.5	494.6 ±80.3	723.3 ±52.3	**47.1 ±2.8**	**68.3 ±4.2**	1.46 ±0.03	3085.2 ±485	**241.4 ±12.4**	23.6 ±10.4
Accuracy	**-53.3 ±9.1**	214.7 ±53.8	484.1 ±76.1	703.0 ±61.5	**45.4 ±2.7**	**66.6 ±3.3**	1.47 ±0.03	2989.8 ±576.2	**231.1 ±12.4**	18.3 ±9.5

Values in **bold** denote significant difference between conditions (p<0.05).

PERFORMANCE DIFFERENCES BETWEEN BLADE AND CAVITY BACK 5-IRONS

Tom Corke[a,b,*], Eric Wallace[a], Steve Otto[b]

[a]Sport and Exercise Sciences Research Institute, Ulster University, Northern Ireland

[b]R&A Rules Ltd, St Andrews, Scotland

*Presenting author

Introduction and Objectives: The topic of 'perimeter weighting' was discussed half a century ago [1], which entailed positioning of a clubhead's discretionary mass so as to maximise moment of inertia (MOI) about specific axes, and thus its resistance to twisting. The cavity resulting from this design gave rise to the archetypal 'cavity back' iron, which is commonly perceived to offer different performance characteristics to the more traditional 'blade' iron. Whilst efforts have been made to understand the effect of relocating this discretionary mass [2,3], the effect of mass distribution on shot outcome has generally remained confined to modelling [4,5,6]. These factors motivated the current study to experimentally determine the performance differences between a blade and cavity back 5-iron.

Methods: Representative blade and cavity back 5-iron clubhead models were chosen based on their physical properties. The clubs were matched for clubhead mass, overall length, static loft and static lie. Inertia properties and centre of gravity (CG) location were determined manually relative to a hosel coordinate system. Three motion tracking cameras were used to track opto-reflective passive markers positioned on the clubheads at 1000Hz; a bespoke clubhead tracking system [7] was used to process this data, returning clubhead presentation variables at the point of first contact with the ball. Developments were made to the system to include tracking of the leading edge of the club face. The two studies discussed herein involved a golf robot and a sample of 96 participants, comprising both male and female golfers ranging in ability from touring professional to high-handicapped amateurs. Stereoscopic and Doppler radar launch monitors were used to measure launch conditions for robot and player tested respectively. The robot testing was designed to measure the relative performance of irons when impact location was systematically varied, whilst the sample of golfers – each performing 12 shots from natural turf with both irons – established whether any observed differences remained tangible once human variation had been introduced. A paired *t*-test was used to determine whether within-player differences between club medians differed significantly from zero.

Results: The robot testing indicated that the effective loft with which the cavity back was presented to the ball was 1.56° greater than that of the blade, even though the static lofts were matched. This agreed in principle with research concerning shaft bending [8] and the relative CG locations of the two clubheads. Vertical launch angle and total spin were 0.27° and 390 rpm greater for the cavity back relative to the blade respectively. Comparable differences arose from the player testing, as can be seen in Table 1. Dependency of ball launch variables on impact location yielded further differences. A greater disparity in horizontal launch angle between toe and heel shots was evident for the blade relative to the cavity back. Figure 1 illustrates the change in spin axis tilt as horizontal impact location is varied. Although relatively weak, the positive relationship exhibited by the cavity back is consistent with the 'gear effect' as observed in driver studies [5,6], whereas an 'angle effect' [9] appears to dominate for the blade. Figure 1 also shows a more rapid decay in efficiency

(ball speed normalised to clubhead speed) for eccentric impacts with the blade; indicating that missing the location of peak efficiency on the club face by 5 mm in the horizontal direction will cause the blade to lose 0.43 mph of ball speed, whereas the cavity back will lose only 0.34 mph, at a clubhead speed of 90 mph. Due to the non-linearity of this relationship, a miss of 15 mm in the same direction equates to a larger disparity: a loss of 3.85 mph for the blade and 3.04 for the cavity back. The higher average efficiency of the cavity back (Table 1) for the player testing suggests that this difference may be tangible to the golfer, and was further supported by the cavity back's more consistent efficiency ($p <$ .05), as indicated by subsequent analyses.

Conclusion: The cavity back 5-iron tested as part of this study was found to consistently launch higher, and with greater total spin than the statically-matched blade 5-iron. Both effects could, to some extent, be attributable to the greater effective loft of the cavity back at impact. Robot testing revealed that ball launch variables such as efficiency and launch angle varied less with impact location for the cavity back than the blade. Relationships supporting the likely presence of the 'gear effect' in cavity back impact mechanics were also observed, although strength of association was relatively weak. Although average performance differences between the club types were found at the group level for the player tests, inspection of differences at the participant level indicated that the relative performance of the clubs was far from universal.

References: [1] Cochran, A. J. & Stobbs, J. (1968). *Search for the Perfect Swing*. Chicago, IL: Triumph Books.

[2] Whittaker, A., Thomson, R., McKeown, D., & McCafferty, J. (1990). The application of computer-aided engineering techniques in advanced clubhead design. In A. J. Cochran (Ed.), *Proceedings of the World Scientific Congress of Golf* (pp. 286–291). St Andrews, Scotland.

[3] Nesbit, S. M., Hartzell, T. A., Nalevanko, J. C., Starr, R. M., White, M. G., Anderson, J. R., & Gerlacki, J. N. (1996). A Discussion of Iron Golf Club Head Inertia Tensors and Their Effects on the Golfer. *Journal of Applied Biomechanics*, *12*, 449–469.

[4] Whittaker, A. (1998). A study of the dynamics of the golf club. *Sports Engineering*, *1*(2), 115–124.

[5] Iwatsubo, T., Kawamura, S., Miyamoto, K., & Yamaguchi, T. (2000). Numerical analysis of golf club head and ball at various impact points. *Sports Engineering*, *3*, 195–204.

[6] Iwatsubo, T., Kawamura, S., Furuichi, K., & Yamaguchi, T. (2002). Influence of Characteristics of Golf Cub Head on Release Velocity and Spin Velocity of Golf Ball after Impact. In *Proceedings of the World Scientific Congress of Golf* (pp. 410–425). St Andrews, Scotland: Routledge.

[7] Betzler, N. F., Monk, S. A., Wallace, E. S., & Otto, S. R. (2012). Variability in clubhead presentation characteristics and ball impact location for golfers' drives. *Journal of Sports Sciences*, *30*(5), 439–448.

[8] Horwood, G. P. (1994). Golf shafts - a technical perspective. In A. J. Cochran & M. R. Farrally (Eds.), *Proceedings of the World Scientific Congress of Golf* (pp. 247–258). St Andrews, Scotland.

[9] Penner, A. R. (2001). The physics of golf: The convex face of a driver. *American Journal of Physics*, *69*(10), 1073. http://doi.org/10.1119/1.1380380

Figure: Efficiency and spin axis tilt for blade and cavity back 5-irons for systematic variation of horizontal impact location. The measured vertical impact location of all plotted points were within the range of 10±1mm below the geometric centre of the sandblasted area of the club face.
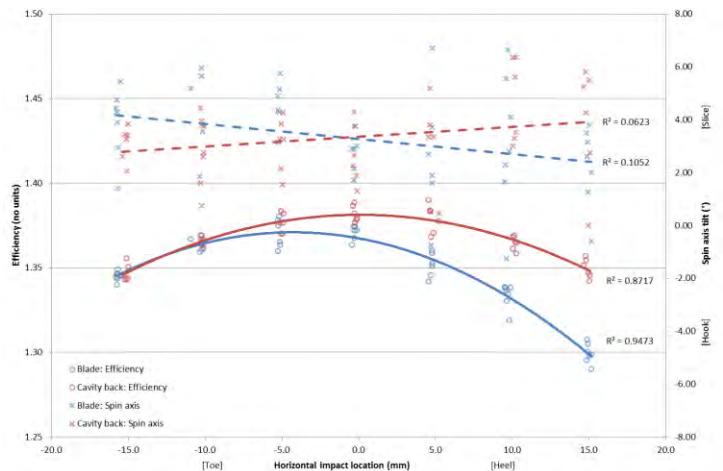
Table: Blade grand mean ($\bar{x}_{blade}$), mean of the differences ($\bar{x}_{cavity - blade}$) between blade and cavity back, standard deviation (*SD*) of the mean difference, significance level (*p*) and effect size (Cohen's *d*) for a paired t-test comparing within-player medians of selected clubhead presentation and ball launch variables. A positive difference between the clubs indicates that the cavity back was greater than the blade, and vice versa. All values in degrees unless otherwise stated.

	$\bar{x}_{blade}$	$\bar{x}_{cavity - blade}$	SD	p	Cohen's d
Clubhead speed (mph)	85.45	.54	.71	.000	.772
Face angle	-1.02	-.03	1.45	.854	.019
Path	-0.61	.00	.82	.989	.001
Attack angle	-4.04	-.05	.48	.333	.099
Effective loft	20.21	.78	1.96	.000	.399
Efficiency (no units)	1.350	0.010	0.031	.002	.324
Vertical launch angle	12.63	.46	.86	.000	.531
Horizontal launch angle	-1.12	-.10	1.10	.379	.090
Total spin (rpm)	5193	327	299	.000	1.093
Spin axis tilt	2.81	-.17	2.90	.570	.058

Golf

SS-0094

ANALYSIS OF THE DELIVERY PLANE IN THE GOLF SWING USING PRINCIPAL COMPONENTS

Morrison, A, McGrath, D, Wallace, E

SESRI, Ulster University, UK

Introduction and Objectives: Although the swing plane has been a popular area of golf biomechanics research, the movement of the club relative to the swing plane has yet to be shown experimentally to have a relationship with performance. Recent studies have shown that only the trajectory of the clubhead near impact can fit to a single plane, while the remainder of the swing deviates from this plane (Kwon et al., 2012; Morrison et al., 2014). As many popular golf coaching texts advocate keeping the club either on or parallel to a particular plane, the movement of the club relative to the delivery plane needs to be explored further.

This study used principal components (PC) and multiple regression analysis to investigate the relationship between the movement of club relative to the delivery plane, and the impact conditions between club and ball. As a delivery plane was calculated for every shot, it was the route by which the club arrived at the plane that was under investigation.

Methods: Fifty-two male golfers of handicap between+4 and 18 participated in this study (handicap 6.6±6.9). Twelve Oqus 300 cameras operating at 1000Hz through Qualisys Track Manager were used to collect and calculate 3D coordinate data (Qualisys AB, Gothenburg, Sweden). Five markers were attached to the face of the club for static capture, and were referenced to 3 dynamic markers attached to the crown of the club. Two pieces of retro-reflective tape 20cm apart were attached near the top of the shaft. Participants hit 40 shots with their own driver into a net situated 10m away from the player, onto which a fairway was projected. The clubhead model was identical to that of Betzler et al (2012), and had been previously validated.The delivery plane was defined as per Morrison et al (2014), and was calculated for every shot. The perpendicular distance of the club face centre from the delivery plane was calculated at specific swing events, along with the angle the two shaft markers formed with the delivery plane. The swing events used were takeaway, mid-backswing, late backswing, top of the backswing, early downswing and mid-downswing (Kwon et al., 2012). Maximum and minimum values of the displacement and angle of the shaft to the plane within each swing were also included in the PC analysis. Diagnostics were carried out and outliers and highly correlated variables were removed according to recommendations by Field (2009).The PCs extracted from the data were then used as predictor variables in a multiple regression analysis. A total of 16 impact related outcome variables were used along with handicap. The impact variables were the same as those used by Betzler et al (2012), in addition to impact location of the ball relative the mean impact location of the player. A further 8 regression models were created for the median absolute deviation (MAD) values of these impact variables. Statistical analysis was carried out using SPSS (Release 22, IBM).

Results: Three PCs were extracted which accounted for 84.7% of the variance in the original data, with individual components accounting for 42.8%, 26.8% and 15.1% respectively. Using the rotated component loadings (fig. 1), the PCs appear to group the variables by swing phase. PC1 appears to represent variables from the top of the swing and the downswing, while PC2 represents the backswing. PC3 appears to account for the remaining maximum and minimum values.

The multiple regression analysis suggested that the PCs account for the most variance in the impact location related variables. Interestingly, it was the variability in impact location rather than the distance from the club face centre that was most highly correlated (table 1).

Conclusions: The movement of the golf club relative to the delivery plane during the golf swing was investigated in relation to the impact characteristics. The results suggest that when the club makes fewer deviations during the swing to arrive at the final trajectory, the precision of ball striking improves. Simplicity in the route and alignment of the club to the final trajectory are important in better ball striking, and should be considered by coaches in their analysis.

Table: Coefficients for multiple linear regression fits between principal components and selected output variables and R2 values for the models

Outcome variables	Constant	PC1	PC2	PC3	R^2
Handicap	6.440	2.630	-3.617	2.376	53.2%
Distance from face centre (mm)	12.666	1.605	-2.232		32.7%
Distance from impact cluster centre (mm)	9.315	1.299	-1.433	1.024	55.9%
Horizontal impact location MAD (mm)	6.720	1.007	-1.404		57.4%
Vertical impact location MAD (mm)	5.113	0.709	-0.680	0.503	43.5%
Distance from face centre MAD (mm)	4.910	0.492	-0.869		34.6%
Distance from impact cluster centre MAD (mm)	4.304	0.533	-0.667	0.466	45.5%

Figure: Graph of the data from the rotated component matrix with variables ordered chronologically through the swing (correlations with a magnitude below 0.4 have been removed) (MBS = mid backswing, LBS = late backswing, Top = top of the backswing, EDS = early downswing, MDS = mid downswing)
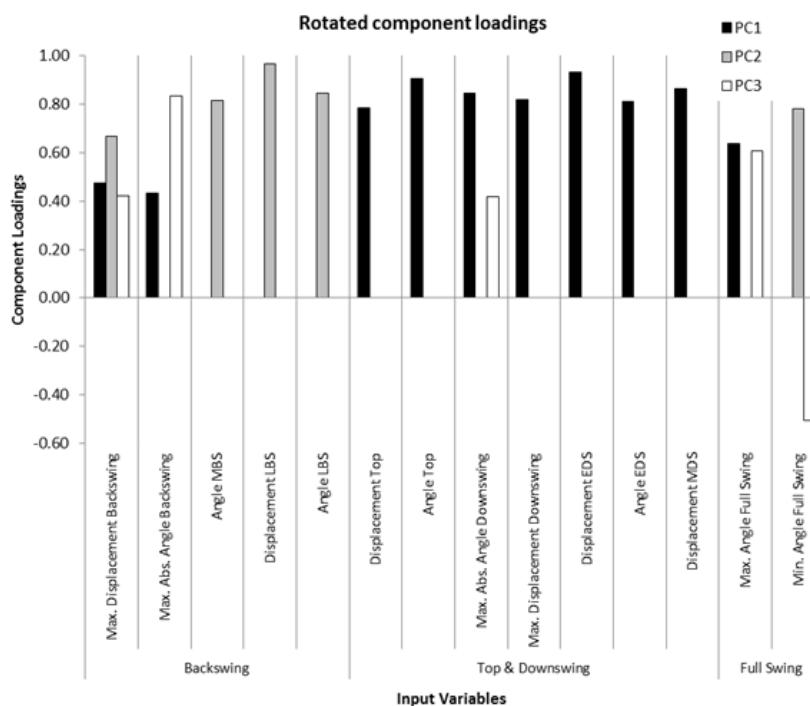
References:

Betzler, N. F., Monk, S. A., Wallace, E. S., & Otto, S. R. (2012). Variability in clubhead presentation characteristics and ball impact location for golfers' drives. *Journal of Sports Sciences*, *30*, 439–448.

Field, A. (2009). *Discovering statistics using SPSS* (3rd ed.). London: Sage.

Kwon, Y.-H., Como, C. S., Singhal, K., Lee, S., & Han, K. H. (2012). Assessment of planarity of the golf swing based on the functional swing plane of the clubhead and motion planes of the body points. *Sports Biomechanics*, *11*, 127–148.

Morrison, A., McGrath, D., & Wallace, E. (2014). Changes in club head trajectory and planarity throughout the golf swing. *Procedia Engineering*, *72*, 144–149.

SS-0095

BIOMECHANICAL CONSIDERATION FOR IVD TISSUE ENGINEERING

Puay Yong NEO, James C H GOH

Department of Biomedical Engineering

National University of Singapore

The intervertebral disc (IVD) can be found between two vertebrae bodies and consists of i) the gelatinous nucleus pulposus (NP) in the central region, ii) the fibrous annulus fibrosus (AF) surrounding the NP, and iii) the endplates interfacing the disc with the adjoining vertebral columns. During loading conditions, the IVD absorbs and disperses loads - an ability that is intimately related to its capability to absorb and release water. While the interconnected network of collagen and elastin provide the elasticity and general morphology of the NP, the proteoglycans maintain the osmotic pressure, and in turn confers compressive strength, stiffness and viscoelasticity properties to the IVD as a whole. During loading, lateral expansion of the NP is confined by the surrounding AF through i) tension of the AF in the circumferential direction, and ii) compression of the AF in the radial direction.

Tissue engineering (TE) offers a promising treatment alternative for degenerative disc disease (DDD) as current options do address the pathophysiology of the clinical problem. With a TE approach, the biology and structural architecture of the IVD can be taken into consideration and perhaps mimicked. Eventual success in clinical translation of a TE strategy for IVD is in turn heavily contingent upon recapitulating not only the structure and composition of the healthy IVD, but in particular its mechanical properties. For example, the AF experiences complex loading conditions, and possesses residual stresses even when the spinal column is unloaded. Hence AF TE strategies not only should target mending the damaged AF to prevent disc herniation and further AF degeneration, but take into consideration the biomechanical compatibility of the TE AF with the native IVD tissue. Another case in point would be TE of the NP. Given the role of the NP in the native IVD, a TE NP strategy considering the relevant mechanical properties such as swelling pressure and confined compression modulus would be paramount in determining its eventual success in clinical translation.

The native IVD is a composite tissue with complex mechanical requirements. For eventual success at the bedside, TE strategies targeting the repair of the IVD as a whole disc or its individual components (NP, AF) not only have to consider the biochemical and mechanical properties of the biomaterials used, but also should take into consideration the appropriate mechanical properties and biomechanical compatibility of the TE construct when integrated with the native IVD tissues.

Mimics® Innovation Suite

Software & Services for Engineering on Anatomy™

With 25 years of expertise, Materialise offers software and services for patient-specific treatment and biomedical research. The Mimics Innovation Suite allows researchers to quickly segment even the most complex anatomical structures. This results in an accurate 3D model which can be used to simulate orthopaedic interventions, optimize your FEA or CFD mesh or prepare musculoskeletal simulations, and all of this within the same software package.

Key Advantages:

- **High geometrical accuracy:** Benefit from the accurate and consistent segmentation in the Mimics Innovation Suite, used by leading researchers

- **Flexible:** Customize the modular software to your unique R&D needs

- **Product quality:** Enjoy the comfort of working with validated, stable software

- **User-friendly:** Segment, measure, design and model directly on your anatomy of interest within one software suite

- **Technical support:** Access our experts for training and further optimizing your workflow

Contact us:

Daniel Daryaie
Daniel.daryaie@materialise.co.uk
+44 (0)1143 997847

or biomedical.materialise.com

Materialise
innovators you can count on

Poster Presentations

Arterial Mechanics

PO-0000

NUMERICAL ANALYSIS OF THE RESIDUAL STRAIN IN ARTERY WALL

Tongtong Guo [1,*]Xueming XIAO [1]

[1]Nature Science Department, Harbin Institute of Technology Shenzhen Graduate School, SHENZHEN, China

Introduction and Objectives:

There exist residual strain in artery wall, which can avoid stress concentration under blood flow and be decided by the vascular material actually. In this paper, we considered the impact of the residual strain and blood pressure in our arterial model, discussed the mechanical response of the arterial wall in different mechanical parameters.

Methods:

We firstly established the three layers anisotropic elastic artery model with fiber reinforced(G.A.Holzapfel, 2000). By applying the displacement boundary conditions, the distribution of the residual strain was simulated under different opening angles; Then altering the two material parameters, C10 and k1, to explore the impact to the residual strain, so do the circumferential stress after loading blood pressure.

Results:

With the addition of the two material parameters under the same opening angle, the residual strain increased as well; As C10 and k1 increased 3 times, the maximum residual stress value increased 2.58 times, the maximum residual strain increased 17.48%(Figure 1). Circumferential residual strain curve along radial direction of artery wall behaved as quasi-linear distributions, taking cubic polynomial fitting, R2=0.943; Keep the parameter abiding to a value, with the increment of opening angle, both of the residual stress and strain increased; The circumferential stress of arterial wall with residual strain varied slowly and deliberately after loading blood pressure, which got in line with the physiological characteristics of the real arterial wall, As C10 and k1 increased 30 times, the circumferential stress of the inner layer increased 1.38times, outer wall is 17.2.

Figure:
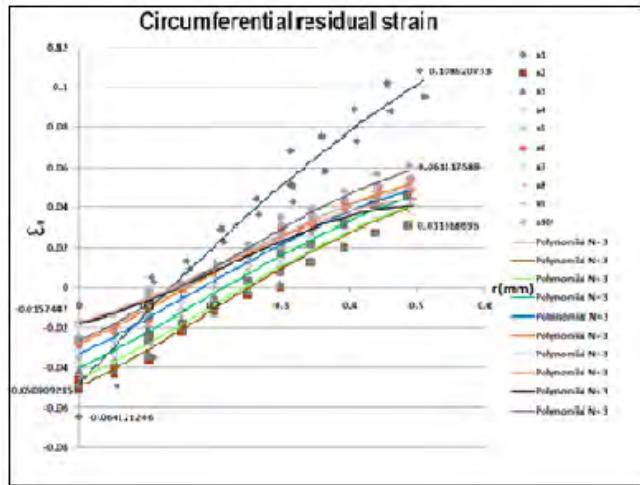
Caption: Figure 1

Conclusion:

The material parameters of the arterial wall have a significant effect on the residual strain, which mainly due to the larger parameters reflect the bigger strain energy value. The study shows that individual differences tremendous impact on arterial mechanical environment.

References: [1] G.A.Holzapfel et al, Journal of Elasticity, 61:1-48, 2000.

Disclosure of Interest: None Declared

REQUIREMENTS AND LIMITS OF A PERSONAL REHABILITATION DEVICE FOR UPPER LIMB

Federico Casolo [1,*]

[1]Dipartimento di Meccanica, Politecnico di Milano, Milan, Italy

Introduction and Objectives: The functional motor recovery is a fundamental pillar for the rehabilitation[1]. The evolution of cognitive disorders, as well as other pathologies directly affecting muscle mechanics, can be profitably countered by intensive physiotherapy or assisted recovery of physiological movements[2].Only personal devices may allow patients intensive care at reasonable costs, psychological and economic. The present work aims to identify clinical-functional requirement of a device for the neuro-motor rehabilitation of the upper limb and to propose a prototype of a simple multifunctional robotic system suitable to equip a standard wheelchair. The project is mainly focused on the needs of neuromuscular patients, but the robotic device may have a much wider field of use. Until now it has been tested by two patients affected by Duchenne muscular dystrophy who collaborate in the research. Assistive devices can be classified as exoskeletons or end-effectors depending on whether they are connected to the arm: at several points or at a single location. The basic requirements of a personal assistive device are: ease of use, set-up and wear, avoiding to overstress natural joints, limited dimensions and cost. Only end-effector devices can fulfill these conditions. Our prototype is an end-effector where a robotic arm is connected to a point of the subject forearm, constraining 3 d.o.f. . A consequence of this architecture is the impossibility to place each segment at any arbitrary position but it is a minor problem because the arm segments always reach physiological positions[3]

Methods: In order to minimize complexity and cost, only three axes of the system, are active. A dynamical model of the whole system hallows to use the gravitational forces of the limb to obtain the correct arm posture. The device is equipped with three brushless motors powered by four electronic boards appositely designed and communicating via I^{2}C protocol; one board works as master for the other three, which have simpler tasks. Most of the driving software has been developed with Matlab and the code has been translated into C++. To save weight and volume two of the little flat motors have been coupled with harmonic drives and the other with a planetary gear; a cable transmission is also used. For the same reason a system of spring and cables working against gravity helps to minimize the torque needed and consequently motors size and weight.

The working principle of the device is related to the enabled working model (w.m.) A first w.m. helps the patient to repeat a stereotyped action and is mainly used for physiotherapy, if the subject cooperate his effort is measured and used to monitor the the disease evolution. A second w.m. actively compensates the gravity in order to facilitate autonomous arm movement of weak subjects. With a third w.m. the device helps the subject during the activities of daily living (ADL). For the first and the third w.m.s a mechanical impedance control have been implemented to smoothly follow the hand target. One of the most difficult problems for the second w.m. is related to the efficiency of the transmissions that oppose different resistances at start and during motion. Since it is not possible to predict in which direction the subject would like to move, to compensate the resistance of each transmission in that direction, a new algorithm has been implemented in the control software: it basically applies harmonic torques varying between the values of the two opposite resistance to

the motion until the system start moving and than torques related to the velocity ranges are applied. On the other hand the third w.m. requires to interpret the patient intention to move the upper limb. A simple solution of this problem requires to add force sensors at the arm-machine interface and moreover requires a patient able at least to vary even slightly the force exchanged with the robotic armrest of the wheelchair. Since those sensors are not present in the prototype, the problem has been solved linking the hand motion to the head movement. Some of the already tested algorithms to connect hand target to head kinematics can solve the problem, but their suitability changes subject by subject and can be judged according to the subjects learning curves

Results: Look up tables have been built with many experimental test [fig] to compute the extra torque required to the motors - and the resultant I - in order to balance the resistance of the transmissions to be moved from any angular position, in both directions and with a wide range of possible loads. Some learning curves built for few subject highlight the subjective attitude to drive the hand target with the different algorithms implemented for the third w.m

Figure:
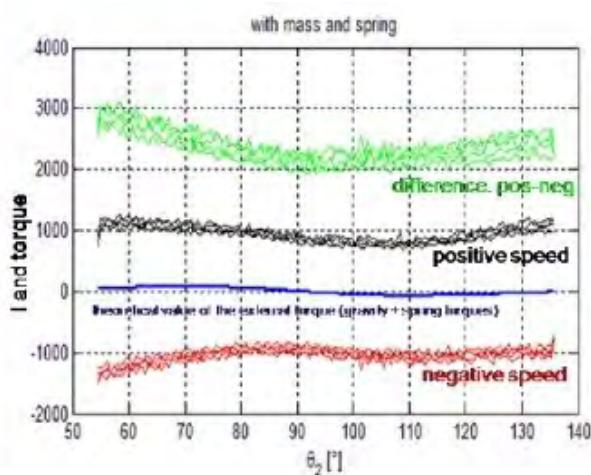
Caption: data to build lookup tables

Conclusion: All three w.m. have been positively tested but the third requires to be refined adding new force sensors

References: [1] Krebs J Rehab. Res.& Dev.37(6), 2000

[2] Kahn J.Neuro Eng.& Reh. 3, 2006

[3] Tao Exp Brain Res 252-361, 2005

Disclosure of Interest: None Declared

Assistive Technology

PO-0003

MOTION ANALYSIS OF SIT-TO-STAND ASSISTED BY A WEARABLE ROBOTIC EXOSKELETON IN PATIENTS WITH SPINAL CORD INJURIES

Hsing-Po Huang [1,*]Wu Cheng-Hua [2]Ting-Ming Wang [3]Mao Hui-Fen [4]Jia-Da Li [1]Hong Shih-Wun [1]Hu Jwu-Sheng [2]Tung-Wu Lu [1][3]

[1]Institute of Biomedical Engineering, National Taiwan University, Taipei, [2]Institute of Electrical Control Engineering, National Chiao Tung University, Hsinchu, [3]Department of Orthopaedic Surgery, School of Medicine, National Taiwan University, [4]School of Occupational Therapy, National Taiwan University, Taipei, Taiwan, Republic of China

Introduction and Objectives: Decreased or loss of mobility in people with spinal cord injuries (SCI) is a key factor associated with their quality of activities of daily living, and the impact on patients is enormous, including their participation in social, vocational, and recreational activities. Sit-to-stand (STS) is a prerequisite to locomotion, recovery of the function of sit-to-stand will help patients with SCI gain their ability to walk [1]. Patients with SCI need assistance to stand up, either by the great effort of the upper extremities or by other people [2]. Wearable robotic exoskeletons have been proposed to provide assistance to patients with SCI in walking but the performance of such devices in assisting STS has not been documented. Motion analysis has been used widely in the study of human motion and the assessment of assistive technology. The purpose of the current study was to study STS assisted by a wearable robotic exoskeleton in patients with SCI by motion analysis techniques.

Methods: Three patients with complete SCI below T4 participated in the current study with written informed consent as approved by the Institutional Research Board (Table 1). A wearable robotic exoskeleton (WRE) developed by Mechanical and Systems Research Laboratories, Industrial Technology Researcher Institute, Taiwan was used to provide controlled torques to the hip and knee joints to assist STS in patients with SCI (Fig. 1). Thirty-nine retroreflective markers were used to track the motions of the body segments and the WRE, and measured using 8-cameras motion analysis system (Vicon T-40S, Oxford Metrics Group, UK), and measuring the ground reaction forces with 3 forceplates (AMTI, U.S.A.). Ninety degree of hip initial angles and 1400 rpm of angular velocity of WRE were selected. The hip, knee and trunk joint angle and angular velocity was acquired by camera, and internal joint moments of hip and knee normalized to body weight were calculated using inverse dynamics analysis. The energy consumption was calculated by summation of potential energy related to center of mass, translational kinetic energy and rotational energy [3]. The time-varying COP positions were measured by two forceplates during quiet standing. The sway area of the COP was described by an equivalent ellipse, the two principal axes of which were obtained by using principal component analysis [4]. The center of mass position was acquired by the data of Dempster's coefficients.

Results: There were no significant differences of extensor moments of the hip and knee among the SCI subjects (fig. 1e and 1f). Greater sway area of the COP was found in the patient with higher injury level of SCI (S1). The S1 subject also showed greater trunk flexion during sit-to-stand (fig. 1b). In addition, greater trunk angle angular velocity were also found in the S1 subject. The patient who were unexperienced with the wearable robotic exoskeleton showed greater posterior COM related to COP motion during sit-to-stand (fig. 1c). The patient with a higher injury level (S1) had larger COP

traverse (580), whereas patients with lower injury level (S2, S3) had smaller COP traverse (320, 53) (fig. 1(a)).　The higher level (S1) can complete the task by a trunk flexion compensatory strategy (fig. 1(b)).　Patient with no previous powered HKAFO using experience (S3) had a backward position of COM than S1 and S2 (fig. 1(c)).　Greater trunk angle angular velocity were found in S1 (fig. 1(d)).

Figure:
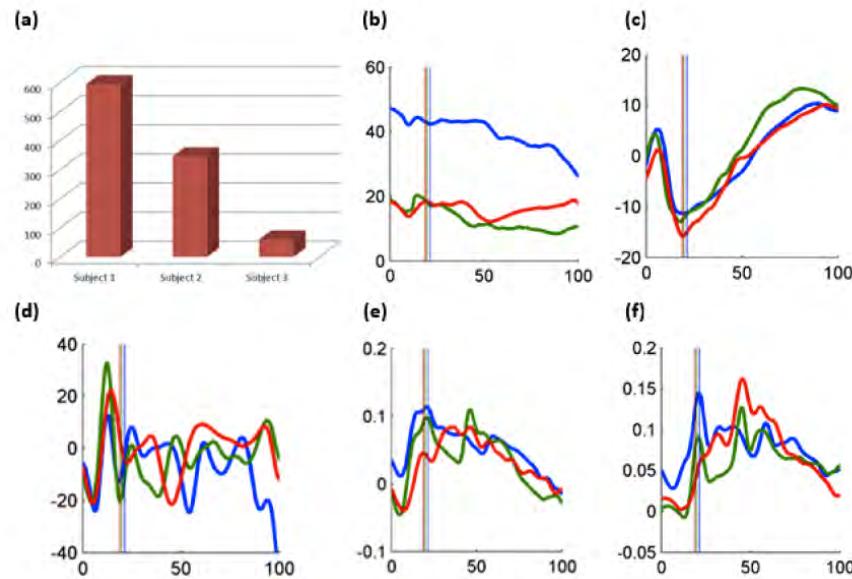
Caption: (a) The 95% confidence ellipse area of the traverse of center of pressure of quiet standing. (b) The trunk flexion angle during sit-to-stand (Blue line: S1/ Green line: S2/ Red line: S3). (c) The inclination angle of COM-COP during sit-to-stand. (d) The trunk angular velocity during sit-to-stand. (e) The hip joint moment during sit-to-stand. (f) The knee joint moment during sit-to-stand.

Conclusion: The results of the current project could help the therapist for designing the training plans for the patients who would use the powered HKAFO.　In addition, it was suggested that a subject specific training program is needed according to the patient's physical ability, including the injury level, balance reaction and muscular strength.　The adjustment of trunk angle and angular velocity of the powered HKAFO was also helpful for the efficiency of sit-to-stand.

Table:

Code	Height	Weight	Age	Medical history	ASIA level	Injury level	Onset years	Muscle tone	HKAFO training
S1	170	60	36	Force impact	A	T4-7	4.83	Hypotonic	yes
S2	180	59	37	Force impact	A	T10-12	2.5	Hypotonic	yes
S3	170	68	35	Force impact	A	T10-12	1	Hypotonic	none

Caption: Detail information of three typical patients with SCI enrolled in this study

References: [1] Aissaoui et al., IEEE SMC '99 Conference Proceedings, 1999.

[2] Bahrami et al., Clin Biomech, 15:123-133, 2000.

[3] Winter, BIOMECHANICS AND MOTOR CONTROL OF HUMAN MOVEMENT SECOND, John Wiley and Sons, Inc, 1990.

[4] Doyle et al., Gait Posture, 25: 166-171, 2007.

Disclosure of Interest: None Declared

Assistive Technology

PO-0004

NEUROMUSCULAR ELECTRICAL STIMULATION TOLERANCE DURING AN EIGHT-WEEK TRAINING PROTOCOL IN ELDERLY WITH KNEE OSTEOARTHRITIS

Matias Fröhlich [1,*] Matheus Joner Wiest [2] Fábio Juner Lanferdini [1] Alexandre Mayer [1] Marco Aurélio Vaz [1]

[1] Neuromuscular Plasticity, Federal University of Rio Grande do Sul, Porto Alegre, Brazil, [2] University of Alberta, Edmonton, Canada

Introduction and Objectives: Neuromuscular electrical stimulation (NMES) is largely used in knee osteoarthritis (OA) treatment aimed at preserving and/or improving knee extensor muscles strength [1-5]. However, NMES treatment effectiveness shows large variability mainly due to the different stimulus parameters used, especially NMES intensity or amplitude. Increases in NMES amplitude are necessary to maintain target muscle strength levels in order to produce the desired muscle adaptions during NMES training. However, increases in NMES amplitude often result in increased discomfort or pain. Knowing the optimal NMES amplitude is important to increase its effectiveness in knee OA treatment. The purpose of this study was to determine the tolerance to increases in stimulation amplitude during eight weeks of NMES training in adults with knee OA.

Methods: Sixteen knee OA patients (♀=14, ♂=2; age = 59.13±8.47 years) participated of an eight-week knee extensor NMES training program. A portable stimulator delivered a symmetrical biphasic current with a frequency of 80 Hz and pulse width of 400 µs to the knee extensors motor point. NMES protocol started with 10 s stimulation trains, with 50 s intervals between stimulation trains. Inter-train interval was reduced in 10 s every two weeks. Treatment time was set at 18 min in the first training week and two minutes per session were added per week up to a total of 32 min. Treatment frequency was set to three times per week. Patients were seated with the knee flexed at 90°. The ankle joint was fixed to the legs of a chair by a strap, allowing for isometric knee extensor contractions during NMES. NMES amplitude was set at the maximum level tolerated based on subject's comfort level, and was increased throughout the session by the subject. The stimulator recorded the mean NMES amplitude values during each session. The mean and standard deviation NMES amplitude (mA) values were calculated for each treatment week.

Maximal isometric knee extensor torque was recorded before and after the NMES training program on an isokinetic dynamometer. Subjects performed three 5 s maximal voluntary isometric knee extensor contractions at 60° of knee flexion (full knee extension=0°). A 2-min interval was used between contractions. Maximal torque was determined from the highest absolute torque achieved during the three contractions. Peak torque values were reported as a percentage increase from pre-training values.

Mean weekly NMES amplitudes were compared using a one-way ANOVA, with a Bonferroni *post hoc* test to identify specific differences (significance level = 5%). Baseline and post-training torque values were also compared with a two-tailed T-Test.

Results: No between-weeks differences were observed for the NMES amplitude for the first four weeks ($p \geq 0.153$), but NMES amplitudes increased from week 4 to week 8 ($p \leq 0.048$; Figure 1A). A 46.47 ± 26.07% increase in NMES amplitude

was observed from the beginning to the end of the NMES training program. The torque showed a 17.02 ± 31.58% increase after the NMES training program (p=0.0001; Figure 1B).

Conclusion: Eight weeks of NMES training increased knee extensor torque by 17%. These results are in agreement with a previous study that evaluated the effects of NMES training on knee extensors torque production capacity [3]. This torque increase is evidence that the stimulation parameters and protocol were adequate and can be used in future NMES training protocols aimed at increasing or maintaining muscle strength.

The accommodation time-course to the NMES amplitude of weeks 1-4 was probably due to skin pain receptors activation and/or afferent neurons adaptive adjustment during the first four training weeks. The 46% increase in NMES amplitude from weeks 4-8 is probably related to increase in pain threshold due to activation of endogenous pain inhibitory systems, generally by local spinal mechanisms, according to the gate control theory [6]. Endogenous opioids, such as dynorphins, enkephalins and endorphins, working mainly at the end-receptors, are among the mediators suggested to play a key role in hypoalgesia during NMES [7].

References: [1]   Rosemffet MG, et al. J Clin Rheumatol. 10: 246-249, 2004.

[2]   Durmuș D, et al. J Clin Rheumatol. 26: 674-678, 2007.

[3]   Walls RJ, et al. BMC Musculoskeletal Disorders. 11: 119-128, 2010.

[4]   Talbot LA, et al. J of Rheumatol. 30(7): 1571-1578, 2003.

[5]   Vaz MA, et al. J Orthopaed Res. 31: 511-516, 2012.

[6]   Lund I, et al. Neurosci Lett. 375: 75-80, 2005.

[7]   Liebano RE, et al. Pain. 152: 335-342, 2011.

Disclosure of Interest: None Declared

PO-0005

EVALUATION OF CENTER-OF-PRESSURE DISPLACEMENT IN A STANDING POSITION WITH EYES OPENED AND CLOSED IN OLDER ADULTS

Lindomar Mineiro[1], Suzane K. Martello[2], Elisangela V. Rodrigues[1], Luiza H. Gallo[1], Liliana L. Rossetin[1], Eduardo M. Scheeren[2], Anna R. S. Gomes[*][1]

[1]PPGEDF, Universidade Federal do Paraná, [2]PPGTS, Pontifícia Universidade Católica do Paraná, Curitiba-PR, Brazil

Introduction and Objectives: Senescence is associated with a general deterioration of many biological systems, mainly in the locomotor system [1]. Some studies have reported that older adults have greater difficulty in detecting the direction and magnitude of disturbances and they are more dependentof visual input. It limits the generation of appropriate neuromotor action to keep the balance when compared to youngers [2]. Thus, alteration in the visual input is considered an important factor for risk of fall and fractures in aged [3]. Understanding the changes in the postural control of older individuals is important to prevent the loss, reduction, or reverse specific age-related impairments and improve reactive postural control [4]. The aim of the present study was to investigate the visual input in the postural control displacement of female community-dwelling elderly.

Methods: The study sample consisted in 12 elderly women (74.25 ±5.46 years old) from local community. The postural control was assessed by the center-of-pressure (COP) displacement with the participant in a static standing position through a force plataform (AMTI, OK6-7-2000) [5]. It was performed two experimental conditions, in a standard standing position: the first with eyes opened (EO), looking forward to a fix point 3 m from the plataform; and the second with eyes closed (EC). The participants were oriented to stay in a quite standing position for 30 s. The signals were sampled at 100 Hz and were low-pass filtered using a fourth-order dual-pass Butterworth filter at 10 Hz prior to processing.

It was used MatLab (v.7.10.0) software to calculate COP displacement. Shapiro-Wilk's test revealed data were not normally distributed, considering non-parametric. Wilcoxon was used to compare the two experimental conditions. A significance level of $p < 0.05$ was adopted for all statistical procedures, which were performed using SPSS (v.20.0).

Results: The COP trajectories showed an increase in the displacement when eyes were closed in comparison with opened eyes (0.771±0.476 cm *vs* 0.437 ± 0.203 cm, p=0,041). The data are demonstrated in the Figure 1.

The mean values of COP with eyes opened found in the present study were similar to those described in literature for community-dwelling elderly. However, in the condition with eyes closed the mean values of the present study were under that reported by the literature, showing a better postural control, probably because they presented moderate level of physical activity [6].

Figure:
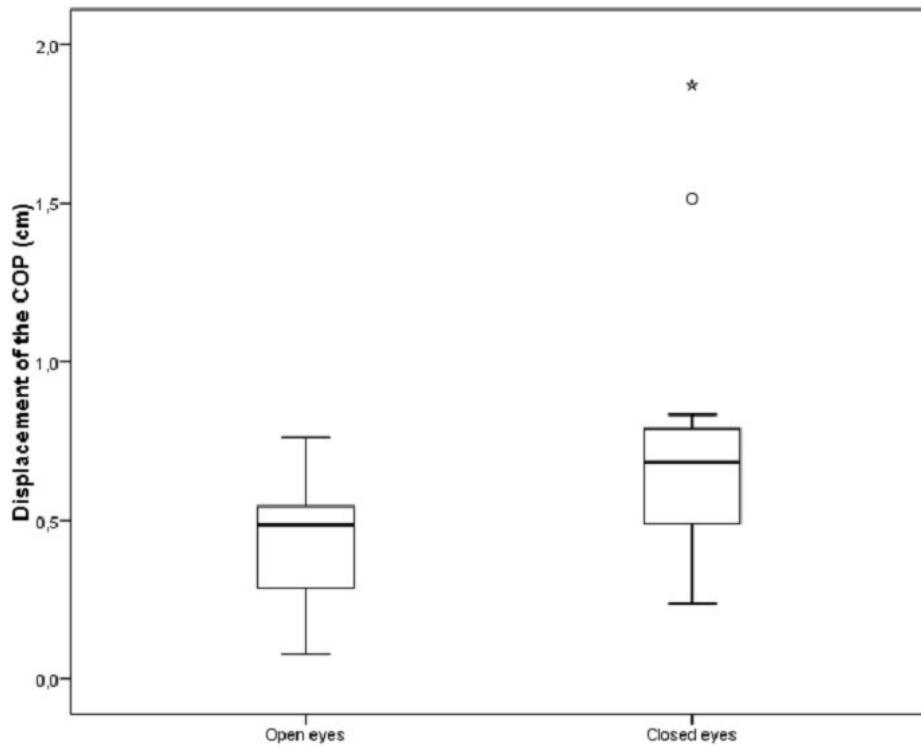
Caption: Figure 1 - COP displacement with open eyes and closed eyes.

Conclusion: It can be concluded that when eyes were closed the absence of visual input impaired the control of standing balance which increased center-of-pressure displacement for female community-dwelling elderly.

References: [1] Konrad et al. The Laryngoscope, 109: 1454-60, 1999.

[2] Freitas et al. Gait & posture, 35: 83-7, 2012.

[3] Abdelhafiz et al. Age and Ageing, 32: 26-30, 2003.

[4] Pijnappels et al. Exp. brain research, 160: 326-33, 2005.

[5] Melzer et al. Clinical Biomechanics, 25: 984-8, 2010.

[6] Melzer et al. Age and ageing, 33: 602-7, 2004.

Disclosure of Interest: None Declared

Balance

PO-0007

THE EFFECTS OF CORE STABILITY TRAINING ON DYNAMIC BALANCE IN HEALTHY YOUNG STUDENT

Yenting Wang [1] [1,*]Alex, J. Y. Lee [2]

[1]Graduate Institute of Athletics and Coaching Science , National Taiwan Sport University, Taoyuan City, [2]Department of Physical Education, National HsinChu University of Education, HsinChu City, Taiwan, Republic of China

Introduction and Objectives: Core stability is the ability to control the position and movement of the central portion of the body. Greater core stability may benefit sports performance by providing a foundation for greater force production in the upper and lower extremities [1]. Core stability training (CST) targets the muscles deep within the abdomen which connect to the spine, pelvis and shoulders, to assist in the maintenance of good posture and provide the foundation for all arm and leg movements [1,2]. On a more significant note, muscle power is derived from the trunk region of the body and a properly conditioned core helps control that power, allowing for smoother, more efficient and better coordinated movement in the limbs.

Methods: Twenty-four healthy collegiate female students (height: 162.3 ±6.0 cm, weight: 54.1 ± 16.3kg, age: 20.1 ± 1.4 yrs) from university participated in this study. All participants completed a self-report health history questionnaire and signed a written informed consent before testing.

The CST was combined the pilates and Swiss ball exercise altogether in ninety minutes, twice per week, for six weeks. Guidelines from the United States aerobic fitness association was followed, including warm-up exercise, the main movement along with three phases in order promote a progressive manner, and impose different intensity at different stages of the training protocol as well as strengthen the abdominal muscle strength and lower limb muscle strength.

The dynamic balance was evaluated by the 8-direction limits of stability (LOS) test. Subjects were tested bilaterally at two levels of difficulty: 3 and 6. To control for the learning effect and fatigue, the order of the tests was randomly assigned. The subject was instructed to start moving the cursor which accurately moves the display toward the flashing target at eight different directions. The LOS score was calculated for each direction according to the percentage between the straight line distance to target and the number of samples.

Repeated-measures *t* test were used to examine the differences in each parameter before and after training. For all analyses, the level of statistical significance was set at $P < .05$.

Results: The LOS performance in right (26.6 ± 14.4 vs. 32.1 ± 14.2) and backward-right (29.8 ± 14.7 vs. 37.5 ± 17.0) directions at level 3 was significant improved in post-training than pre-training. Furthermore, The LOS performance in overall (27.7 ± 9.2 vs. 38.9 ± 11.3), right (30.9 ± 12.3 vs. 40.9 ± 13.3), forward-right (32.3 ± 12.4 vs. 43.9 ± 14.3), backward-right (32.9 ± 9.6 vs. 40.2 ± 14.5), and backward-left (32.5 ± 12.7 vs. 43.4 ± 17.3) directions at level 6 was significant improved in post-training than pre-training (Figure 1)

Figure:
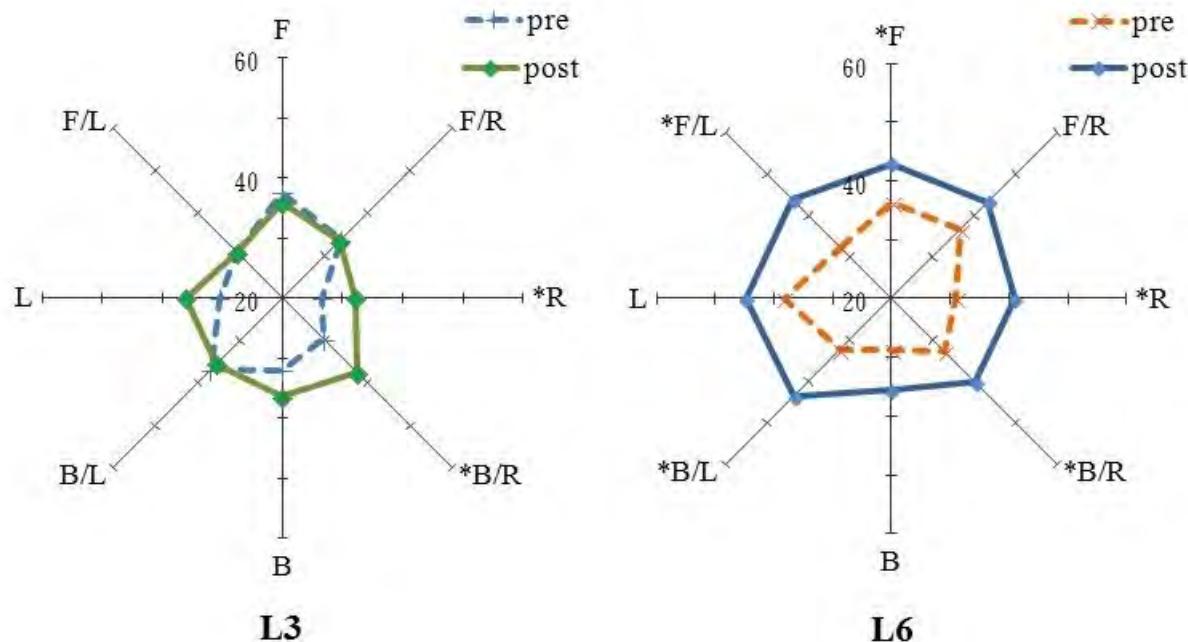
Caption: Comparisons of the LOS scores in each direction between groups before and after training.

Conclusion: Finding of this study showed significant improvement in the overall performance on the stable, level 6 LOS test indicates that a 6-week period of Core training can improve dynamic postural stability. This study provided support for this hypothesis, since it showed that CST could facilitate voluntary active postural and lower extremity corrections during the unstable LOS test.

The CST appears to be effective in improving flexibility, dynamic balance in healthy young students.

References: [1] Omark et al., J Bodyw Mov Ther, 13: 98-103, 2009.

[2] Akuthota et al., Curr Sports Med Rep, 7: 39-44, 2008.

Disclosure of Interest: None Declared

Balance

PO-0008

COMPARISON OF THE EFFECT OF NEUROMUSCULAR BALANCE TRAINING AND EXTERNAL ANKLE SUPPORTS ON BALANCE PERFORMANCE IN NETBALL

Alice Fisher-Edwards [1] Saeed Fayaz [1] Dawn Ridgway [1] Eddie J. Bradley [1,*]

[1] Sport, University of Sunderland, Sunderland, United Kingdom

Introduction and Objectives: Netball is a fast-paced goal-scoring ball sport with a demand for high-intensity movements such as running, jumping, passing, and shooting. The game is characterised by rapid changes in acceleration to break free from the opposition or to change direction suddenly. As such, netball has a high injury rate. McManus et al [1] reported an incidence of 14 injuries per 1000 player hours with an overall lower limb injury rate of 92.4%. Between 30% and 84% of injuries sustained by elite netball players occurred in the ankle [1-3], with 34% to 71% being ligamentous injuries. The application of prophylactic ankle devices are commonplace in netball, usually a semi-rigid brace or tape, that are designed to increase stability at the ankle by restricting range of motion[4,5] and improving proprioception [6,7]. The benefit of proprioceptive training in reducing injury incidence in previously injured athletes has been identified [8] but it is not known if it has the same effect in netball players with no history of ankle injury. Balance training is an effective way of improving stability and can easily be incorporated into regular training sessions. The aim of the study was to determine if balance training was effective as routinely used prophylactic ankle devices in maintaining stability in a group of netball players.

Methods: Experimental cross-sectional design. 15 previously uninjured female university netball players (aged 18-21) were randomly assigned to a training, semi-rigid brace or tape group (each n=5). The participants in the training group completed a six-week balance training regime, three times a week on a Biodex Balance Trainer. The training consisted of a unipedal postural stability test, an athlete single leg stability test, a bipedal limits of stability test, and maze test that increased in dificulty over the six-week period each session. Participants in the device groups were instructed to wear a semi-rigid brace or zinc oxide tape in a figure of 8 technique on the weaker ankle, identified using a Lafayette Manual Muscle Tester, during normal training and matches. Antereo-posterior (AP) and mediolateral (ML) displacement and centre of pressure velocity (CoPVel) measures were recorded on a Pasco force platform pre, immediately following application of brace or tape or after the first training session, and at the end of the six-week training program. Differences in balance measurements were compared between ankle stability conditions and time periods using a two-way ANOVA (ρ=0.05).

Results: No significant differences were found for AP sway or CoPVel between the groups at any time period. Mediolateral sway improved in the tape condition, however this was not significantly lower than the training group after six weeks (Figure 1).

Figure:
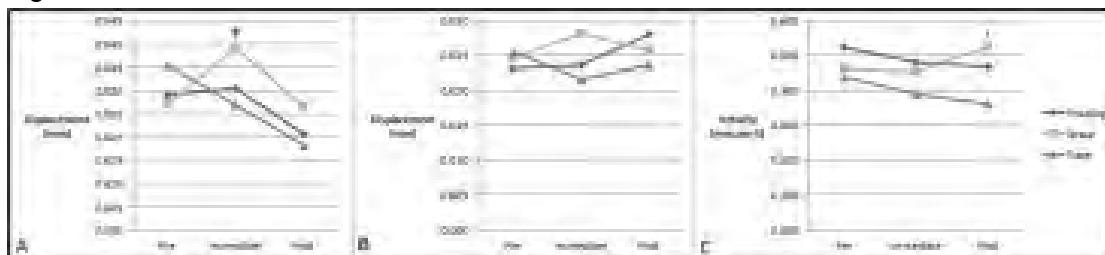
Conclusion: The use of tape and braces is routine in netball but the current literature is undecided on its effectiveness, especially in previously uninjured players. This study compared the effects of a neuromuscular balance training program with common prophylactic ankle supports on balance performance in an uninjured sporting population. The training group displayed similar changes in stability as both the brace and tape groups over the six week period. The findings of this study are similar to the 10% improvement in Star Excursion Balance Test (SEBT) composite scores after an eight-week neuromuscular training program applied to a group of female soccer players [9]. While Ozer et al [6] identified that neuromuscular balance performance, including single leg balance and proprioception assessment, were similar between bracing, tape, and barefoot conditions in a group of non-sporting males, balance was exclusively used as a measurement tool and no neuromuscular training was involved. The six-week training program provided similar proprioceptive and mechanical benefits around the ankle joint as the brace and taping, resulting in comparable improvements in balance performance. In conclusion, a six-week proprioceptive training program was as effective in improving balance as the application of tape or brace in a cohort of netball players and the necessity of such devices, especially if previously uninjured, should be reconsidered.

References: [1] McManus A et al., *J Sci Med Sport*, 9: 119-124, 2006.

[2] Hopper, D.M., et al., *Sports Med*, 16(2): 148-162, 1993.

[3] Hopper, D.M., et al., *Br J Sports Med,* 29(4): 223-228, 1995.

[4] Hardy, L., et al., *J Athl Train*, 43(4): 347-351, 2008.

[5] Cordova, M.L., et al., *J Sports Rehabil*, 19(2): 136-148, 2010.

[6] Ozer, D., et al., *Foot (Edinb),* 19(4): 205-210, 2009.

[7] Delahunt, E., et al., *Arch Phys Med Rehabil*, 91(9): 1383-1389, 2010.

[8] Verhagen, E.A., et al., *Clin J Sport Med*, 10: 291-296, 2000.

[9] Filipa, A., et al., *J Orthop Sports Phys Ther*, 40(9): 551-558, 2010.

Disclosure of Interest: None Declared

Balance

PO-0009

ANALYSIS OF BALANCE CONTROL BY MEANS OF COM AND COP FLUCTUATIONS DURING SUSTAINED SWISS PRESS HAND STAND MOVEMENT

Kazuo Funato [1,*] Hisashi Mizutori [2] Yu Kashiwagi [1] Noriko Hakamada [3] Tsuyoshi Nobukuni [4]

[1]Graduate School of Training Sciences, Nippon Sports University, Tokyo, [2]Keio University, Fujisawa, Kanagawa-pref, [3]Japan Institute of Sports Sciences, Tokyo, [4]Hiroshima Senior High School, Hiroshima-city, Japan

Introduction and Objectives: Hand stand Swiss press movement is one of the fundamental and important techniques in gymnastics. This study was designed to examine how to get stable balance during isolated Swiss press by comparing Japanese world class and junior national gymnasts. As one of the research on the balance control of hand stand, frequency analysis on center of mass (COM) during hand stand indicated the greatest power spectrum existed below 1Hz (Clement and Rezette, 1985). This study focused on the balance control by means of COM as well as center of pressure (COP) fluctuations in the A-P direction during 10s sustained hand stand movement.

Methods: Hand stand movement was performed on a force platform (9287B, Kistler Co., sampling rate: 1 kHz) and was recorded with high speed camera (A602fc-2, BASLER, H6x8- 1.0, SPACE Inc., 100fps). X-Y coordinates of COP was recorded from force platform as long as sagittal plane X-Y coordinates of COM from video analysis. Reflective makers were positioned on the left side of the subject. Body segment angle (thigh, trunk, and forearm), joint angle (shoulder and hip), center of mass (COM), center of pressure (COP), moment arm of COM, and moment around COM were calculated. COM was calculated by Winter's method based on Dempster (1955) body segment data. Subjects were male Japanese junior high class gymnasts (n=44, age: 15.4 +/- 1.9 years old, height: 154.3 +/- 11.5cm, weight: 48.7 +/- 10.4kg). Each subjects performed twice sustained hand stand movements for 10 seconds, one of two trials was taken for the analysis. Frequency analysis in A-P fluctuations of COP and COM were examined by Fast Fourier Transform (FFT) methods.

Results: Skilled subjects had larger trunk segment angle, larger shoulder joint angle, smaller hip joint angle, and smaller moment around COM than unskilled subjects. COM of skilled subjects positioned upon COP vertical line even at the beginning of toe-off phase. This could be suggested that enough flexibility of shoulder and hip joints, as well as sufficient muscle strength to keep the stretched position might essential to stabilize the Swiss press. Mean frequency in maximum power spectrum in COP and COM were shown at around 0.47 +/- 0.36 Hz and 0.30 +/- 0.15 Hz, respectively. Whereas mean frequency in COP fluctuations have characterized as another high power spectrum at around 1.21 +/- 0.51 Hz. This result was similar to previous study by Clement and Rezette (1985) describing the COP fluctuation around 3.0Hz during hand stand. Higher frequency component in COP might contribute to minimize the fluctuation of COM.

Figure:
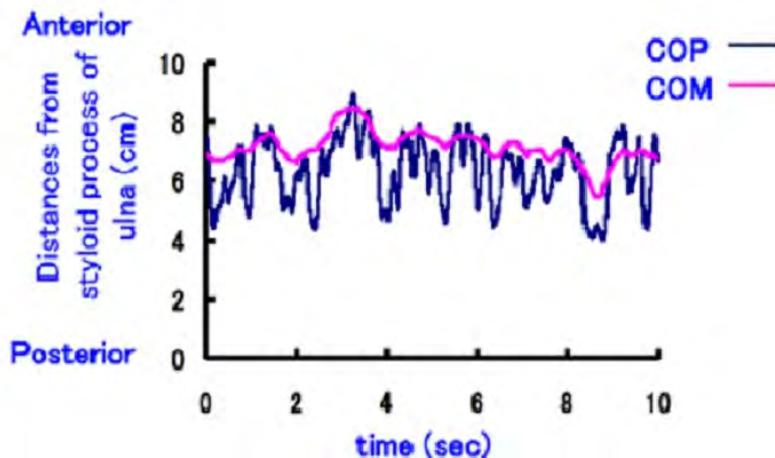
Caption: Typical example of COP and COM fluctuations during Swiss press hand stand in A-P direction.

Conclusion: It was estimated that the high power spectrum frequency band of COP might contribute to control the balance during sustained hand stand movement. Wrist strategy as well as high flexibility of shoulder and hip might be stressed in order to keep the balance in stable during hand stand Swiss press.

References: Clement ,G. & Rezette ,D.. (1985). Motor behavior underlying the control of an upside-down vertical posture. Experimental brain research, 59,478-484Kerwin, D.G. & Trewartha ,G. (2001) Strategies for maintaining a handstand in the anterior-posterior direction. Med. Sci. Sports Exerc., 33(7), 1182-1188.Yeadon, M.R. & Trewartha, G. (2003) Control strategy for a hand stand balance. Motor control, 7, 411-430.

Disclosure of Interest: None Declared

Balance

PO-0010

CHRONIC EFFECT OF FLEXIBILITY TRAINING ON POSTURAL BALANCE IN ELDERLY WOMEN PRACTITIONERS WATER AEROBICS

Elciana D. P. L. Vieira [1,*]Flávia Porto [2]Edmundo Drummond Alves Júnior [1]Jonas Lírio Gurgel [1]

[1]Physical Education, Federal Fluminense University, Niterói, [2]Physical Education, University in the State of Rio de Janeiro, Rio de Janeiro, Brazil

Introduction and Objectives: The aging process involves a series of changes that may lead to impairment of performance of daily activities and increase the risk of falling. Among the various risk factors, weakness of postural balance and the loss of flexibility were chosen for study because of a possible relationship between them. This study aimed to examine the chronic effect of flexibility training on postural balance in elderly women practitioners of water aerobics belonging to the Prev-Quedas Project. The other objective was to identify correlations between the values of Δ goniometric those concerning testing of postural balance in both groups.

Methods: The subjects consisted of participants only in a water aerobics program, selected from non-probabilistic way meeting the eligibility criteria. Were excluded those with diseases, diagnosed by a doctor, that compromised postural balance. Also were excluded from the study participants who had two or more consecutive missing sessions weekly on proposed training without replacement had occurred in the same week or at least on week after missing. Two groups were formed: the intervention group (IG) comprised of 25 elderly women who participated in a program with flexibility exercises, in addition to water aerobics and the control group (CG) comprised of 21 elderly women who underwent only in water aerobics. The flexibility training lasted three months, with a weekly frequency of two non consecutive days. The static range of motion exercises involving trunk and lower limbs. The two groups underwent an evaluation: anthropometric (body mass index and circle measures of chest, waist, abdomen and hip), cognitive capacity, handgrip strength, the ability of functional and lateral reach, static stabilometry, the time spent on one foot and maximum range of motion of trunk, hip and ankle joints (goniometry). Both groups were assessed before the intervention began (pre-intervention) and after (post-intervention). Shapiro-Wilk test was used to analyze the normality of data. To compare the two groups, Student t test for paired and independent samples (parametric data) or Mann-Whitney and Wilcoxon for nonparametric data were used. Pearson correlations were used to correlate for the parametric and Spearman for nonparametric data. The level of significance was $p \leq 0.05$ for all tests.

Results: The IG showed significant improvement in the maximum range of motion of the hip and ankle joints, before and after the intervention, when compared to CG who got the same result only in the ankle joint. However, the CG demonstrated significant improvement in the ability to reach for both sides beyond the average speed and total displacement of the COP in the anteroposterior axis (COPy) with eyes open. However, the same group showed a reduction in the time spent on one foot. Also, no significant correlations were found between the values of Δ goniometric for those regarding testing of functional and lateral reach, static stabilometry and one leg support for both groups.

Figure:
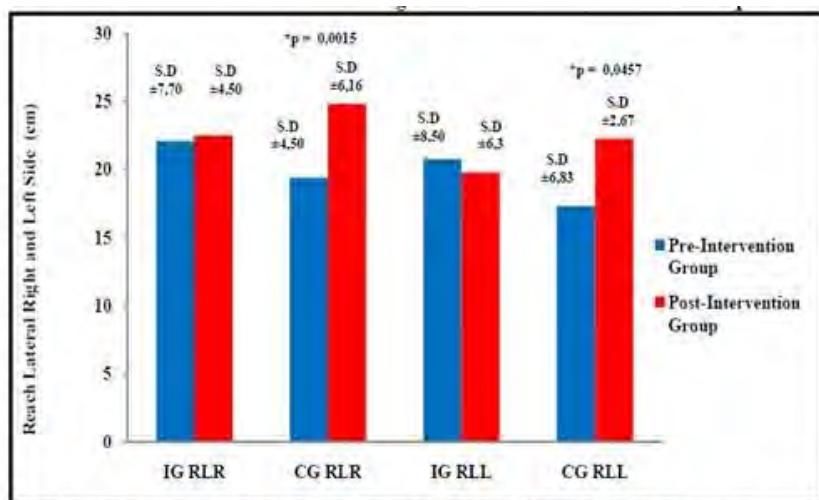
Legend: IG= intervention group; CG= control group; RLR= reach lateral right; RLL= reach lateral left; S.D=standard deviation; p = comparison t Student test for two dependent parametric sample and Wilcoxon for nonparametric sample; * p ≤ 0,05.

Caption: Results of Functional and Lateral Reach

Conclusion: Therefore, flexibility training associated with the practice of water aerobics not had significant results on postural balance in elderly women, although promoted increases on the maximum range of motion on the hip and ankle joints. According to the results of this study, the water aerobics exercises appears to contribute for improvements of postural balance and increases the range of motion on ankle joints.

Table:

		IC		CG		
		x	IR	x	IR	p
	Pre	6,77	2,07	7,40	1,89	0,8686 †
Average.Speed.COPy	Post	6,98	2,50	6,61	2,12	0,6512 †
EO (cm/s)	p	0,0926 †	-			
	Pre	304,22	93,11	332,39	85,12	0,8686 †
Total.Displacement.COPy	Post	313,50	112,29	297,04	95,25	0,4873 †
EO (cm)	p	0,0926 †	-	0,0406†*	-	-
	Pre	30,00	11,16	30,00	9,53	0,6512
Time Spent On One Foot	Post	30,00	15,07	21,05	18,99	0,2799
(s)	p	0,7299	-	0,0092	-	-

Legend: n = sample size; x = median; IR= interquartile range; IG = intervention group; CG = control group; p= comparison t Student test for two independent parametric sample and Mann Whitney for nonparametric sample; p = comparison t Student test for two dependent parametric sample and Wilcoxon for nonparametric sample; pre = assessment pre-intervention; post = assessment post-intervention; EO = eyes open; cm = centimeters; cm/s = centimeters per second; cm^2 = square inches; s = seconds; †= nonparametric data; * p ≤ 0,05.

Caption: Static Stabilometry and One Foot Support Results

References: [1]ACHOUR JÚNIOR (Ed.2) Flexibilidade e Alongamento: Saúde e Bem-estar, Manole, 2009.

[2]SHUMWAY-COOK et al., (Ed. 3).Controle Motor: Teoria e Aplicações Práticas,Manole, 2010.

[3]LUSTOSA eta al., Rev.bras.fisioter, 14:497-502, 2010.

[4]GAJDOSIK et al., Clin Biomech, 20:973-83, 2005.

[5]DUNCAN et al., J Gerontol, 45: 192-97, 1990.

[6]FELAND et al., Phys Ther, 81: 1110-17, 2001.

[7]GODOI et al., Rev Bras Ciên Esporte, 23: 9-22, 2002.

[8]JONSSON et al., J Rehabil Med, 35: 26-30, 2002.

[9]KLEINER et al.,Rev Neurocien, 19: 349-57, 2011.

[10]LEWIS et al., Arch Phys Rehabil, 90: 454-62, 2009.

Disclosure of Interest: None Declared

PO-0011

TWENTY MINUTES SEEMS TO BE NOT ENOUGH TO RECOVERY QUADRICEPS MUSCLE FATIGUE FOR WALKING

Fabio A. Barbieri [1,*]Stephannie Beretta [2]Victor Beretta [2]Lucas Simieli [2]Diego Orcioli-Silva [2]Paulo Santos [2]Jaap van Diëen [3]Lilian Gobbi [2]

[1]Physical education, Univ. Estadual Paulista - Bauru - Brazil, Bauru, [2]Physical education, Univ. Estadual Paulista - Rio Claro , Rio Claro, Brazil, [3]MOVE Research Institute Amsterdam, Faculty of Human Movement Sciences, VU University Amsterdam, Amsterdam, Netherlands

Introduction and Objectives: Quadriceps muscle fatigue reduces gait stability [1,2] by changes in the spatial-temporal [1-4], kinetics [3-4] and muscle activity [4,5] parameters. Around 23 to 30% of falls in the job occur because the fatigue [6]. Given the negative effects of muscle fatigue on gait, it is important to understand the recovery period of spatial-temporal, kinetics and electromyography parameters after muscle fatigue. The aim of the study, therefore, was to investigate the effect of different recovery periods after quadriceps muscle fatigue on gait in young adults.

Methods: Forty individuals aged between 20 and 40 years old (age: 28.85±5.00 years old; body weight: 78.61±14.00 kg; body height: 1.76±0.06 m) participated in this study. The participants performed the following tasks: i) walking in regular environment: the participants performed 3 trials at preferred velocity and walked 8 meters on each trial, ii) maximal isometric voluntary contraction protocol (MVC): 2 trials in each period performed on a Leg Press instrument; iii) fatigue induction protocol: quadriceps muscle fatigue was inducted by repeated sit-to-stand task until voluntary exhaustion; iv) the first and second items were repeated after muscle fatigue, and after 5, 10 and 20 minutes of passive rest. The spatial-temporal (stride length, stride duration, stride velocity, step width and double support time), kinetic (braking and propulsive anterioposterior impulses) and electromyography (root mean square of vastus lateralis and biceps femoris of the right limb) parameters were analyzed before and after the muscle fatigue protocol and after 5, 10 and 20 minutes of passive rest. These parameters were measured in the central stride on each trial. Data were compared by ANOVA with repeated measures for time periods (before muscle fatigue X after muscle fatigue X 5 minute of rest X 10 minutes of rest X 20 minutes of rest).

Results: The MVC decreased after muscle fatigue protocol ($p<0.001$) and after the 5, 10 and 20 minutes of recovery compared with before muscle fatigue protocol. For gait parameters, step width ($p<0.001$) and RMS of biceps femoris ($p<0.05$) increased immediately after muscle fatigue and remained increased after the recovery periods – 20 minutes (Table 1). In addition, for the stride duration ($p<0.001$) there was a decrease in the value immediately after fatigue induction when compared with the period before muscle fatigue and 10 and 20 minutes of rest. The anteroposterior propulsive impulse ($p<0.001$) was also decreased after the muscle fatigue protocol and remained low after 5, 10 and 20 minutes of rest.

Conclusion: We concluded that 20 minutes is not enough to recover the gait parameters, especially parameters related to gait stability. The findings indicate that the modulations of gait, caused by muscle fatigue, are quite persistent and may be an effect of the persistent decline of muscle strength.

Table: Table 1. Means and standard deviations of the spatial-temporal, kinetics and electromyography parameters before (BF) and after (AF) muscle fatigue and after 5 (AF5), 10 (AF10) and 20 (AF20) minutes of rest. * - before fatigue is significantly different the other muscle fatigue period; # - before fatigue is significantly different the after fatigue and 10 and 20 minutes of rest.

	BF	AF	AF5	AF10	AF20	
Maximal isometric voluntary contraction						
Muscle force (kg/f)	375.65±13.23*	318.34±25.90	330.79±12.02	326.62±14.76	333.25±46.11	
Spatial-temporal parameters						
Stride length (cm)	134.96±10.85	135.38±11.98	134.72±10.93	135.45±11.83	135.60±11.74	
Step width (cm)	11.45±2.31*	12.76±2.66	12.18±2.38	12.33±2.72	12.82±2.78	
Stride duration (s)	1.07±0.08#	1.05±0.08	1.06±0.07	1.07±0.09	1.07±0.09	
Stride velocity (cm/s)	127.31±15.16	129.39±15.29	128.15±14.05	127.99±18.63	127.83±17.97	
Double support duration (%)	26.79±2.99	26.69±3.29	27.84±3.93	26.43±2.93	26.43±2.84	
Kinetics parameters						
Braking AP impulse (BW)	-0.04±0.04	-0.05±0.04	-0.05±0.04	-0.05±0.04	-0.05±0.04	
Propulsive AP impulse (BW)	0.04±0.02*	0.03±0.01	0.03±0.01	0.03±0.01	0.03±0.01	
Electromyography parameters						
RMS vastus	23.06±5.09	24.89±13.18	24.61±14.01	23.38±15.55	21.8±9.89	

lateralis (%)					
RMS biceps femoris (%)	21.13±5.63*	23.63±9.77	24.89±12.25	24.12±11.21	25.01±11.67

References: [1] Parijat et al. Gait Post, 28: 568-73, 2008.

[2] Helbostad et al. J Gerontol Biol Sci, 62: 1010-1015, 2007.

[3] Barbieri et al. Gait and Post, 38: 702-701, 2013.

[4] Barbieri et al. Gait and Post, 37: 542-546, 2013.

[5] Murdockt et al. Eur J Appl Physiol, 112: 439-449, 2012.

[6] Swaen et al. Occup Environ Med, 60: 88-92, 2003.

Disclosure of Interest: None Declared

Balance

PO-0012

PRE-IMPACT FALL DETECTION WITH THE REMOVAL OF GRAVITY EFFECT

Soonjae Ahn [1,*] Isu Shin [1] Jaesung Ryu [1] Youngho Kim [1]

[1]Department of Biomedical Engineering, Yonsei University, Wonju, Korea, Republic Of

Introduction and Objectives: Falling is a major cause of injuries and deaths in older adults [1]. Even though most falls produce no serious injury, 20-30% of fall-related patients will suffer moderate to severe injuries. Furthermore, some of them require hospitalization to continue living in community and have an increased risk of death [2]. As for intervention strategies, one of the important problems in preventing or reducing the severity of injury in the elderly is to detect falls in its descending phase before the impact [3, 5]. Many studies have been performed to detect pre-impact falls using accelerometers [3-5], but did not remove gravity effect, since the gravity can some errors.

In this study, six different protocols based on different sensor configurations and with/without the gravity removal were tested in order to detect falls before impact. Three different protocols used acceleration with gravity effect removed. Then, lead time, sensitivity and specificity were also compared among different protocols.

Methods: Forty healthy male volunteers (23.4 ± 4.4 years, 68.7 ± 8.9 kg, 172.0 ± 7.1 cm) participated in the present study. In faint fall simulations, the subjects were told to stand on the floor beside the mattress. Then they fell by simply relaxing to the front, back, and lateral. All falls were conducted on the soft foam mattress for five times respectively. A chair and the mattress were used for ADL trials (sitting, sit–stand transitions, walking, stand–sit transitions and lying). Each activity was conducted for three times.

MPU-9150 (Invensens®, USA) containing a 3-axis accelerometer and a 3-axis gyro sensor was used for the pre-impact fall detection sensor module. It was attached on the middle of the left and the right anterior superior iliac spines. Data was sampled at 100Hz. Totally six different protocols were tested: acceleration, acceleration (gravity effect removed), acceleration + angular velocity, acceleration + angular velocity (gravity effect removed), acceleration + angular velocity + vertical angle, acceleration + angular velocity + vertical angle (gravity effect removed). To remove the gravity, the algorithm proposed by Moe-Nilssen [6] was applied to the raw acceleration signal. This algorithm is based on a simple trigonometric computation and transforms. When using raw acceleration signals, the detection threshold was set 0.4g, but 0.6g when the gravity effect was removed. When acceleration and angular velocity were used, thresholds of acceleration and angular velocity were set to 0.4g, 30°/s but 0.6g when the gravity effect was removed. When acceleration, angular velocity and vertical angles were used, thresholds of acceleration, angular velocity and vertical angle were set to 0.9g, 30°/s and 30° respectively.

Results: Table 1 showed the sensitivity and the specificity for six different protocols. Most false-positive errors occurred during stand-sit transition without considering vertical angle. However, when considering vertical angle, results showed 100% sensitivity and 100% specificity. Means and standard deviations of lead times for three types of falls were shown in Figure 1. When the vertical angle was not considered, with gravity effect removed, the longer lead time was observed. When using vertical angle, the lead time was the longest and no effect was found for gravity removal.

Figure:
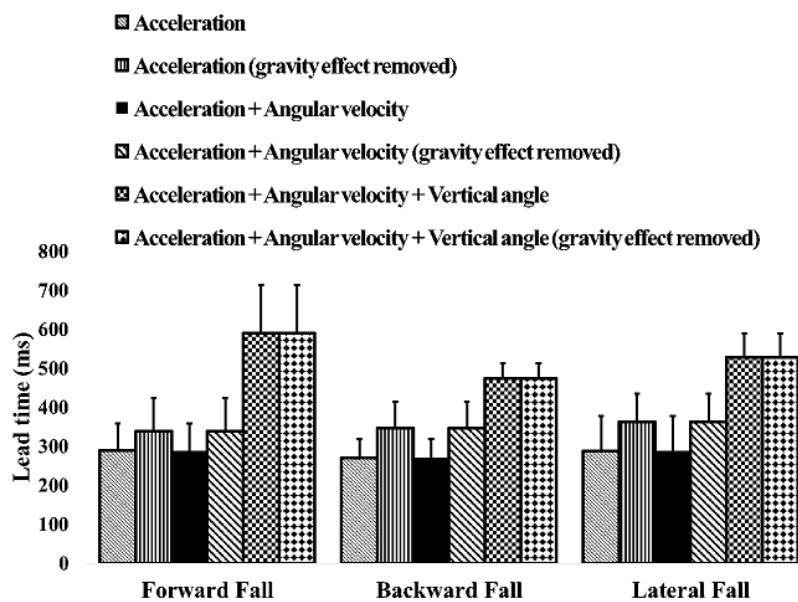
Caption: Lead time

Conclusion: In this study, six different protocols based on different sensor configurations and with/without the gravity removal were tested in order to detect falls before impact. For a long lead time, it is necessary to use acceleration and to remove gravity effect in pre-impact fall detection. 100% sensitivity, 100% specificity and the longest lead time were found when vertical angle data was used in addition to acceleration and angular velocity data. Consequently, for the faster and more accurate detection, vertical angle data is required.

Table:

Protocols	Sensitivity (%)	Specificity (%)
Acceleration	100.0	89.7
Acceleration*	100.0	91.2
Acceleration + Angular velocity	100.0	89.7
Acceleration* + Angular velocity	100.0	91.2
Acceleration + Angular velocity + Vertical angle	100.0	100.0
Acceleration* + Angular velocity + Vertical angle	100.0	100.0
*Gravity effect removed		

Caption: Sensitivity and Specificity

References: [1]   Annekenny et al., Clinics in Geriatric Medicine 18: 13-14, 2002.

[2]   Nevitt et al., Journal of Gerontology 46: M164–M170, 1991.

[3]   Wu et al., Journal of Biomechanics 33: 1497–1500, 2000.

[4]   Nyan et al., Medical Engineering & Physics, 28:842–849, 2006.

[5]   Kim et al., Journal of Foot and Ankle Research, 7:A124, 2014.

[6]   Moe-Nilssen., Clinical biomechanics, 13:320-327, 1998.

Disclosure of Interest: None Declared

Balance

PO-0013

THE RELATIONSHIP BETWEEN DYNAMIC AND STASIC ABILITY OF POSTURAL STABILITY AND BODY COMPOSITION IN JAPANESE OBESE CHILDREN

Noriyuki Yamamoto [1,*] Yoshiya Ito [1] Sharon Hanley [2] Hitoshi Yanagi [3] Tadashi Wada [4] Fumiko Takenoya [5] Yukinori Shintaku [6]

[1] Japanese Red Cross Hokkaido College of Nursing, Kitami, [2] Hokkaido University, Sapporo, [3] Kitami Institute of Technology, Kitami, [4] Kokushikan University, [5] Hoshi University, Tokyo, [6] Biwako Seikei Sport College, Ohtsu, Japan

Introduction and Objectives: Overweight in children leads to decreased ability to balance the body. In childhood and adolescence fractures of the distal forearm (wrist) are extremely common, affecting 1% of the pediatric population aged 3–15 years annually [1]. A previous study has shown that overweight children and adolescents have a greater risk of sustaining these fractures than leaner children [2]. Although neural regulation of the plantar flexor muscles is essential in the control of postural sway as mentioned above, the muscle properties, such as muscle volume and strength, around the ankle joint can also affect postural stability as the muscle is the effector of the neural command. Studies have shown that muscle strength is associated with the incidence of falls [3,4], and that the muscle strength of the plantar flexors is correlated with the limit of stability [5]. However, the relationship between postural stability during quiet standing and muscle volume in obese children has not been explored at all. The purpose of this study was to investigate relationship between dynamic and static ability of postural stability and body composition in Japanese obese children.

Methods: Twenty-two obese children (male:16, female:6, age 8-12yrs, height 141.0±9.9cm, body weight 46.8±10.4kg, BMI 23.2±2.6kg/m^2, %fat 33.0±6.0%) subjects participated in this study. Before the experiment, all procedures and any potential risks were explained to each subject, and an informed consent document was signed previous to participation. This study was approved by Japanese Red Cross Hokkaido College of Nursing Review Board for Health Sciences Research Involving Human Subjects. The body composition of the subjects was measured by bio-impedance method (BC-612, TANITA, Tokyo, Japan). Postural sway was recorded by detecting the body's center of gravity continuously with a force platform equipped with a data processor (Gravicorder G-5000, Anima, Tokyo, Japan). Subjects were requested to stand on the platform with their feet parallel, gazing at a target, a black circle with a diameter of 10cm on a white background, fixed at a 2.0m distance and at the height of each subject's eyes. This arrangement of the visual target produced a visual angle of 5°. The body sway of each subject was recorded for 30 seconds, first with the eyes open (EO$_{two legs}$) and next with eyes closed (EC$_{two legs}$). Similarly, the subjects were asked to keep one leg on the platform and the other leg elevated, aligned with the contralateral malleolus and with the hands placed on the waist. The subjects were instructed to stand as still as possible, first with the eyes open (EO$_{one legs}$) and next with eyes closed (EC$_{one legs}$). The one leg task was recorded duration of the first contact to grand and contact times during 30 seconds. During each task, the foot center of pressure (COP) position and horizontal ground reaction force were measured. The path length of COP and area of body sway were registered. All data are expressed as means ± SD. Correlation analysis was also performed between the variables with the subjects to investigate the effect of body composition on a wider range of postural stability. Significance level was set at the $p < 0.05$.

Results: A significant negative correlation was found between the skeletal muscle volume and the path length of COP in $EC_{two legs}$ (r = -0.590, p < 0.05). In contrast, there was no significant correlation between the skeletal muscle volume and the path length of COP in $EO_{two legs}$. A significant negative correlation was obtained between the skeletal muscle volume and the path length of COP in both eye condition of one leg task ($EO_{one leg}$: r = -0.574, p < 0.05, $EC_{one leg}$: r = -0.654, p < 0.05). Therefore, there was found a significant negative correlation between the %fat and the path length of COP in $EC_{one leg}$ (r = -0.547, p < 0.05). On the other hand, there was no significant correlation between %fat and the path length of COP in $EC_{two legs}$, $EO_{one legs}$, $EO_{one legs}$.

Conclusion: The present study compared postural sway measures, such as the path length of COP and area of body sway during one leg and both feet standing, and the correlation between postural sway and body composition in Japanese obese children. The main findings were that the muscle volume was negatively correlated the path length of COP in $EC_{two legs}$, $EO_{one legs}$, $EC_{one legs}$. However, as the correlation does not necessarily indicate a causal relation, further physiological studies are required. In the present study, we indicated that one leg and both feet standing ability of the obese children depends on the skeletal muscle volume. The present study suggested a high risk of fall into the obese children during the exercises.

References: [1] Jones IE, et al, NZ Med J, 113: 443–445, 2000.

[2] Goulding A, et al, Int J Obes, 24: 627–632, 2000.

[3] Perry MC, et al, Eur JAppl Physiol, 100: 553–561, 2007.

[4] Pijnappels M, at al, Eur J Appl Physiol, 102: 585–592, 2008.

[5] Melzer I, et al, Age Ageing, 38: 119–123, 2009.

Disclosure of Interest: None Declared

PO-0014

EFFECT PROPRIOCEPTIVE TRAINING IN THE POSTURE BALANCE OF GYMNASTICS RHYTHMIC ATHLETES

Rodrigo F. D. Oliveira [1,*]Deise A A Pires-Oliveira [1]Larissa D Bertin [1]Stheace K F Szezerbaty [1]Juliana Serpeloni Almeida [1]Ana Claudia S. Hirata [1]

[1]Centro de Pesquisa em Ciências da Saúde, Universidade Norte do Paraná - UNOPAR, Londrina, Brazil

Introduction and Objectives: Rhythmic gymnastics (GR) is a sport that Brazil has gained significant results, a process of expansion in international competitions in the last years[1], [2]. The good results are coming from the organization and implementation of a multidisciplinary approach, which aims at the harmonious development of the gymnast, as well as the adaptation of his body to the requirements of modality.[1,2]

Physical demand movements, lack of concentration, poor posture and insufficient or incorrect physical preparation can cause great risk of injury to athletes. The higher incidence of injuries in GR are the joint, knees, ankles and some cases in hand ends. Lesions also vary according to their severity and can occur from tendonitis (tenosynovitis) to a more serious injury with ligament ruptures and fracture[3].

The proprioceptive re-education aims to develop joint protection through conditioning and reflective training, one of the final steps of the whole rehabilitation process and fundamental in functional recovery. Studies show that instability and imbalance are related to this type of training situations and are essential in order to have activation of proprioceptors, and result in a muscular response to the reorganization and posture stabilization. [4], [5]

Due to the increasing number of sports injuries and mainly the high incidence of injuries in the ankle joint GR practitioners athletes, evolving into frames of joint instability, there is a need for evaluation programs and proprioceptive intervention.

The objective of the project is to evaluate the influence of proprioceptive training on postural balance Rhythmic Gymnastics athletes - GR.

Methods: Nine subjects participated in this research, female, mean age between 13 to 16 years, from the GR team UNOPAR, Londrina / PR. Subjects were excluded undergoing surgical procedures or who had musculoskeletal injuries in the lower limbs and / or who were in clinical and physical therapy.

After the explanation and signing the Consent and Informed by the legal guardian of each athlete, began the exercise protocol. The protocol was performed twice in the week prior to GR training in order preventing any muscle fatigue.

The first parameters in the force platform BIOMEC400 (EMG System of Brazil, SP Ltda) were measured; called pre-intervention. Then the application of a specific proprioceptive protocol lasting 4 weeks, and reviewed in force platform called post intervention.

The protocol consisted of a circuit with the following devices: step down; balance beam; bosu; proprioceptive inflatable disc, trampoline, slide. Where the athletes performed the sport movements under appliances

Results: When evaluated the COP area, the three tested positions, it was observed that after the intervention there was an improvement in the balance of one leg right and onde leg left positions, as well as bipedal balance also showed a significant improvement. According to the results, we can see that according to the variables analyzed, there was an

improvement of proprioceptive mechanism after 4 weeks of intervention in the area of the COP and Vel AP and ML, noting that the lower the values found, the better the result.

All statistical procedures were performed using the SPSS 17.0 has been established at the 95% confidence interval and 5% significance level software for all tests (P <0.05). We used the Shapiro-Wilk test to establish the normality of the sample, T Wilcoxon test was used to compare the two times for the same individual. The respective data are presented as median and the quartiles.

Figure:

Task	Variable	Pré	Post	P>0,005
BOA	COP	1,73 (1,03; 2,51)	1,03 (0,84; 2,21)	0,038[*]
	VEL_AP	0.95 (0,90; 1,02)	0,90 (0,81; 1,02)	0,018[*]
	VEL_ML	0,81 (0,74; 0,89)	0,76 (0,65; 0,80)	0,008[*]
UNID	COP	8,42 (7,00; 11,6)	7,97 (6,69; 9,95)	0,008[*]
	VEL_AP	2,80 (2,45: 3,07)	2,69 (2,23; 2,80)	0,008[*]
	VEL_ML	3,13 (2,74; 3,50)	2,93 (2,43; 3,16)	0,008[*]
UNIE	COP	8,63 (7,37; 10,0)	7,94 (6,15; 8,39)	0,008[*]
	VEL_AP	3,02 (2,33; 3,17)	2,37 (2,18; 2,85)	0,008[*]
	VEL_ML	2,82 (2,68; 3,54)	2,57 (2,37; 3,09)	0,008[*]

BOA (Bipedal with open eyes); UNI D/E (One leg right / left); COP (Pressure center area); Vel (Average speed of COP sway); A/P (Ântero-posterior); M/L (Average / Side).

* P < 0.05 T WILCOXON test values expressed as presented in mediana and quartiles.

Caption: Table 1: Results of the Force Platform Test

Conclusion: CONCLUSION

The application of a specific protocol for proprioceptive mode, produces significant effect on balance and postural disorders in amending this mechanism in Rhythmic Gymnastics athletes.

References: REFERENCES

[1] Vieira LF, Botti M, Vieira JLP. Ginástica rítmica – Análise dos fatores competitivos motivadores e estressantes da Seleção Brasileira Juvenil. Maringá 2005;27(2):207-215.

[2] Gonçalves LAP, Barros Filho AA, Gonçalves HR. Características antropométricas de atletas de ginástica rítmica. Arq Ciênc Saúde Unipar, Umuarama 2010 jan/jun;14(1):17-25.

[3] Oliveira MMM, Lourenço MRA, Teixeira DC. Incidências de lesões nas equipes de ginástica rítmica da UNOPAR. UNOPAR Cient, Ciênc Biol Saúde. Londrina 2003/2004 out;5/6:(1)29-40.

[4] Antunha EL, Sampaio P. Propriocepção: um conceito de vanguarda na área diagnóstica e terapêutica. Boletim Academia Paulista de Psicologia.2008;02(08):278-283.

[5] Johgnson EO, Babis GC, Soultanis KC, Soucacos PN. Functional Neuroanatomy of Proprioception. J Surg Orthop Adv. 2008;17(3):159-64.

Disclosure of Interest: None Declared

PO-0015

THE EFFECT OF BAREFOOT COBBLESTONE WALKING ON PATTERNS OF LIMB MOVEMENT

Bruno G. Straiotto [1,*]Darren C. James [1]John P. Seeley [1]

[1]School of Applied Science, London South Bank University, London, United Kingdom

Introduction and Objectives: Understanding how individuals adapt their gait when walking over different surfaces can have important implications in relation to locomotion generally and for individuals whose movement is compromised by disease or ageing. The objective of this study was to examine body segment coordination of human gait for movement over two different surfaces. This was achieved using standard kinematic analysis techniques and through application of principal component analysis (PCA) to the data obtained.

Methods: Eight subjects (2 females, 6 males; age 33±5 years; mass 76±14 kg; height 1.7±0.1 m (mean±SD)) performed barefoot walking trials across a flat surface (FS) and a destabilizing cobblestone surface (CS). Movements in each condition were recorded in three dimensions from a set of reflective markers placed over 35 anatomical landmarks. Marker positions were recorded using an eight-camera, motion-capture system at 60 Hz. The walking data were normalized to a constant gait cycle using a standard method ("normalized to 101%"). The marker coordinates were interpreted as 105-dimensional posture vectors. These vectors were centred and re-scaled to unit variance for each trial and submitted to PCA to identify the principal movement components (PMCs) for each condition.

Results: The first four principal components covered approximately 90% (FS) and 92% (CS) of data variability. The PMC eigenvalues in % were as follows (FS then CS): PMC1, 46.4±2.1, 52.6±4.9; PMC2, 22.6±4.9, 21.7±5.1; PMC3, 14.2±2.2, 12.4±2.5; PMC4, 9.1±2.1, 7.2±1.9 (mean±SD). PCA decomposition of the main movement patterns of gait allowed identification of significant differences in PMC1 (p=0.02), PMC3 (p=0.04) and PMC4 (p=0.01) between FS and CS. The eigenvector coefficients provided information about the contribution of different body segments to particular movement components. For both conditions, several of the PMCs were related to forward movement, and for CS bodily adjustments in relation to posture and balance were recorded.

Conclusion: In this study, the spectrum of eigenvalues that quantify the strength of individual movement components in the data set provided only limited insight into the changes in movement patterns. Different PMCs were used by the subjects as means to control their stability for movement over the destabilizing surface. The approach of PCA has theoretical benefit as the PMCs describe the behaviour of the whole system without use of pre-selected variables and may access "hidden variables" inherent to the body's movement patterns. There were differences in PMCs associated with the subjects' strategies to control their stability when the system was affected by external factors - in this case the uneven nature of the cobblestone surface. In this study it appeared that eigenvalues were somewhat insensitive to movement change.

Disclosure of Interest: None Declared

Balance

PO-0016

THE EFFECT OF AGE ON THE SOMATOSENSORY, VISUAL AND VESTIBULAR CONTRIBUTIONS TO THE MAINTENANCE OF POSTURAL EQUILIBRIUM

Lisa Alcock [1,*]Thomas O'Brien [2]Natalie Vanicek [3]

[1]Institute of Neuroscience, Newcastle University Institute for Ageing, Newcastle upon Tyne, [2]School of Sport and Exercise Sciences, Liverpool John Moores University, Liverpool, [3]Department of Sport, Health and Exercise Science, University of Hull, Hull, United Kingdom

Introduction and Objectives: Adequate postural control relies on maintaining equilibrium and correct orientation relative to three dimensional space and time[1]. Age-grouped comparisons have indicated increased latency in response to external perturbations and increased sway in older adults when visual, somatosensory and vestibular input where removed or inaccurate[2-4]. However, little is known about the accumulative changes that occur with older age. Postural sway of older women is particularly increased when support surfaces are unstable or when multiple balance systems are challenged, compared to males[4], making them more vulnerable to postural unsteadiness and falls[5]. Understanding the nature of this decline will help to guide timely intervention and the development of balance strategies. Therefore, the aim of this cross-sectional study was to quantify the postural responses of older women across an age-continuum using the NeuroCom EquiTest®.

Methods: Postural control was assessed from 39 non-falling community-dwelling women [Age 71.9(±7.2)y, range 60-83 years]. The relative contribution of systems responsible for balance was assessed across six conditions on the Sensory Organisation Test (Figure 1) and the *Equilibrium (EQ) score* (angular difference between measured anterior-posterior sway limits and the theoretical maximum sway limit) and *Composite score* were calculated. The ability to respond to unexpected perturbations that were graded in magnitude was evaluated using the Motor Control Test during which *response latency* and *weight symmetry* were evaluated. Linear regression quantified the changes in balance that occurred with older age.

Results: Significant yearly declines in *EQ score* and *Composite score* were estimated for conditions when somatosensory information was inaccurate (Conditions 5 and 6 on the Sensory Organisation Test; Table 1). The largest annual change was estimated for Condition 5 when somatosensory information was inaccurate and visual input was also removed. From the Motor Control Test, annual increases in response latency were observed with older age across all conditions, however only line gradient for the medium backwards translations were significant (R^2=16%, B=0.76, p=.013). Analysis of correlations between *weight symmetry* and age (data not presented) revealed small positive relationships (r≤0.33) for all backwards and forwards translations with the strongest, significant correlation for the medium backward translation (R^2=11%, B=0.28, p=.044).

Figure:
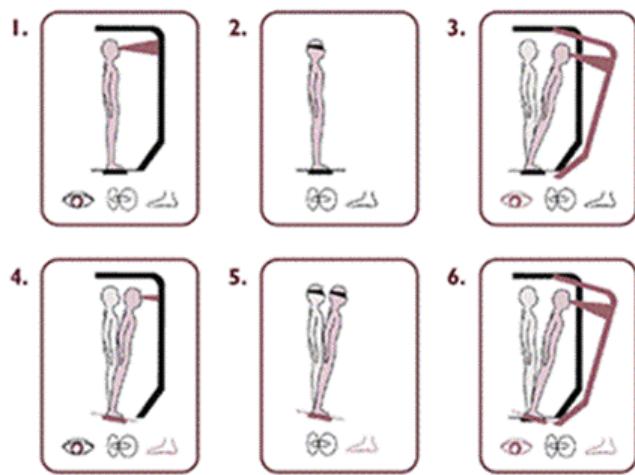
Caption: Figure 1: Schematic illustrating the SOT conditions. Condition 1: control condition. Condition 2: restricted visual input. Condition 3: inaccurate visual feedback (sway-referenced surround). Condition 4: eyes open, inaccurate visual feedback (sway-referenced surround). Condition 5: eyes closed and inaccurate somatosensory cues (sway-referenced support). Condition 6: eyes open and inaccurate visual and somatosensory cues (sway-referenced support and surround).

Conclusion: The magnitude of postural sway increased throughout older age in a cohort of women particularly when visual input was removed and somatosensory cues were inaccurate. This indicated that with advancing age, women were less able to utilise vestibular feedback to maintain balance, and increasingly relied on visual input and somatosensory information even when inaccurate. Increased asymmetric weight loading, as observed during the Motor Control Test, indicated that participants distributed their body weight unilaterally in preparation for a perturbation. This may be considered an anticipatory mechanism prior to initiating a stepping strategy needed to compensate for age-related increasing response latency. Participants were informed prior to the Motor Control Test that they would experience a perturbation to balance and anticipatory responses may have been elicited. Balance disturbances are generally unknown and may be multidirectional thus anticipatory responses are not always possible. The unexpected nature of postural disturbance would increase the motor planning and response complexity, and therefore the Motor Control Test may underestimate the motor responses executed.

Table:

Condition	1	2	3	4	5	6	Composite Score
Mean EQ score [SD]	95.0 [2.4]	89.8 [4.0]	87.1 [9.2]	81.0 [9.7]	41.5 [21.4]	36.1 [22.1]	65.5 [10.7]
Pearson's r correlation	-0.10	-0.30*	-0.08	-0.23	-0.46**	-0.34*	-0.43**
R^2 (%)	-	9	9	5	21	11	18
Line gradient	-	-0.17	-0.20	-0.31	-1.37	-1.01	-0.63

Caption: Table 1: Explained variance (R2) and line coefficients for the EQ scores of the Sensory Organisation Test. * p<0.05, ** p<0.001

References: [1] Horak, F., *Phys Ther,* 1881-1885, 1987.

[2] Mackey & Robinovitch, *Gait & Posture,* 59-68, 2006.

[3] Cohen, J., *Age & Ageing,* 39-44, 1996.

[4] Hageman et al., *Arch Phys Med & Rehab,* 961-965, 1995.

[5] Wolfson et al., *Gerontol,* M160-167, 1994.

Disclosure of Interest: None Declared

Balance

PO-0017

DETERMINATION OF AN OPTIMAL THRESHOLD LEVEL FOR A THRESHOLD-BASED FALL DETECTION METHOD

Jongsang Son [1,*]Soonjae Ahn [1]Isu Shin [1]Jeseong Ryu [1]Jongman Kim [1]Baekdong Cha [1]Eunkyoung Choi [1]Youngho Kim [1]

[1]Biomedical Engineering, Yonsei University, Wonju, Korea, Republic Of

Introduction and Objectives: Fall-related injuries can cause a long-term hospitalization which may lead to a loss of independence, morbidity and mortality [1]. For these reasons, the automatic (pre-impact) detection of a fall could be a promising approach to prevent the fall-related injury. To accomplish this aim, many researchers have been interested in specific changes in the acceleration of a human segment under a fall condition, and generally used a wearable sensor to measure the acceleration data due to its great portability. Most fall detection algorithms are typically based on the threshold of the acceleration, and show a possibility of application to the related-field [2]. Although the threshold could directly result in the performance of the sensitivity and specificity, it has been less studied in determining the threshold which is empirically done before [3]. In this study, a novel method determining an optimal threshold level is introduced to suggest a guide for a threshold-based fall detection.

Methods: Total twenty healthy male (23.4 ± 1.3 yrs.; 176.1 ± 7.6 cm; and 69.3 ± 9.5 kg) participated, who have no clinical history of musculoskeletal injury. They were categorized into two different groups performing: (1) typical activities of daily living (ADLs) such as normal gait, sit-to-stand, stand-to-sit, and stand-to-lying (6 subjects); and (2) simulated falls to the front, back, and side (14 subjects). All ADLs were conducted for five times, and all falls on soft foam mattress for three times. The experimental protocol was approved by the Yonsei University Research Ethics Committee (1041849-201308-BM-001-01). During the tasks, three-axis accelerations were obtained from the middle of two anterior superior iliac spines at the sampling rate of 100 Hz, and then the signal vector machine (SVM) was calculated from the measured acceleration data. By using the SVM data, an optimal threshold was determined from the optimization based on the maximum sensitivity and specificity criteria subject to the constraint that the lead time is equal to or longer than the pre-defined time. Because the longer lead time would be favorable to take an action to prevent fall-related injuries before the contact. To investigate changes in the sensitivity and specificity according to the lead time, the pre-defined time was arbitrarily set with 100, 200, 300, 400, or 500 ms.

Results: Table 1 shows the changes in the sensitivity and specificity according to the pre-defined lead time. The optimal threshold values increased as the pre-defined lead time decreased. The sensitivity and specificity were the best (100%) with the lowest optimal threshold value (i.e., 0.41 g), and were decreased with the increase in the optimal threshold value. These results suggested that the performance of the threshold-based algorithm might have a trade-off relationship between the sensitivity/specificity and the lead time. This means that the longer lead time, the lower sensitivity and specificity in our database at least.

Conclusion: The purpose of this study was not to develop an automatic pre-impact detection algorithm, but to develop a quantitative determination algorithm of a threshold for a guidance to a threshold-based detection algorithm. Indeed, it might be insufficient to expect a perfect fall detection algorithm with only accelerations, because the acceleration signal is sensitive to an external impact. Therefore, many researchers have tried to combine other sensors such as gyro sensor or

inclinometer to improve the sensitivity and specificity [4]. In this regard, we expect that the developed algorithm would be useful to determine the threshold satisfying a desired lead time.

Table:

Lead time (ms)	Optimal threshold (g)	Sensitivity (%)	Specificity (%)	Accuracy (%)
100	0.41	100	100	100
200	0.52	100	94.7	97.1
300	0.70	100	64.7	80.8
400	0.81	100	50.7	73.2
500	0.87	100	35.3	64.9

Caption: Changes in the sensitivity and specificity according to the pre-defined lead time

References: [1] Haentjens et al., J. Bone Joint Surgery Am. 83: 493–500, 2001.

[2] Bourke et al., Med. Eng. Phys. 30: 937–946, 2008.

[3] Ahn et al., J. Foot Ankle Res. 7(Suppl 1): A124, 2014.

[4] Kulkarni et al., J. Biomed. Eng. Tech. 1: 36–39, 2013.

Disclosure of Interest: None Declared

PO-0018

MUSCLE CONTRIBUTIONS TO CENTER OF MASS ACCELERATION DURING BALANCING AGAINST EXTERNAL PERTURBATION.

Shinya Ogaya [1,*]Koutatsu Nagai [2]Yusuke Okita [3]Koji Nonaka [1]Satoshi Fuchioka [1]

[1]Physical Therapy, Osaka Prefecture University, Habikino, [2]Physical Therapy, Hyogo University of Health Sciences, Kobe, [3]Physical Therapy, Kyoto University, Kyoto, Japan

Introduction and Objectives: Loss of standing balance leads to a fall, which results in fractures in older people. Muscle activations have a crucial role to control the center of mass (COM) against perturbation and to recover balance. However, the muscle that mainly contributes to prevent perturbation is unknown. In previous reports forward musculoskeletal simulation analysis revealed contributions of the muscle on joint accelerations during gait. We used this method to analyze recovering balance after a platform translation and investigated muscle contributions to the COM acceleration.

Methods: This study has two steps, namely 1) motion capture and 2) analysis using forward simulation. For the motion capture, 1 older female subject aged 70 years old who had no serious dysfunction participated. Six reflective markers were attached to the subject's bony landmarks (acromion, greater trochanter, lateral knee, lateral malleolus, heel, and fifth metatarsal). The participant was instructed to stand on a computer-controlled moving platform and maintain balance with foot fixed to the platform. Ankle, knee, and hip sagittal angles were measured using a video camera during anterior platform translations, with a velocity of 15 cm/s and amplitude of 6 cm. Before the measurements, 10 practices were performed to improve familiarity with the device. The motion data were low-pass filtered at 15 Hz. Next, a standing model, which included 4 segments (foot, shank, thigh, and trunk), 3 joints (ankle, knee, and hip), and 9 muscles in the lower limb (tibialis anterior, soleus, gastrocnemius, vastus, rectus femoris, short hamstrings, long hamstrings, gluteus maximus, and iliopsoas), was constructed for the forward simulation analysis. The model was scaled to the subject's height and weight. The parameters of the segments (segment weight, inertia, and position of segment COM) and musculo-tendon units (force-length and force-velocity relation, maximum force, optimal fiber length, pennation angle, and tendon slack length) were referred to previous studies. Sinusoidal-shaped acceleration induced by the platform translation was applied to the model in the same experimental manner. Time series muscle forces were determined using the Lagrange formation with an optimization process to minimize the sum of square muscle activations to track measured angles. The linear translational spring damper was applied to the foot-floor pressure. The spring-damper parameters were determined by the fifth metatarsal marker acceleration. To evaluate muscle contributions to the COM acceleration, decomposition of the horizontal COM acceleration into contributions by muscles, platform translation, gravity, and centrifugal components was accomplished. At each instance of the simulated motion, an induced acceleration method was applied for the angular acceleration in each joint to decompose net angular acceleration into the individual components. Next, the horizontal acceleration of the COM was calculated from the joint accelerations by taking the segment mass and length. The muscle component was also divided into individual muscles.

Results: The individual contributions of the major components to the COM acceleration are shown in Figure. The strongest component to induce the COM acceleration was the platform translation, especially posterior COM acceleration

during the first 100 ms after perturbation. However, the contribution of the muscle component gradually increased after 100 ms. Acceleration induced by gravity did not show a remarkable change in the time series. The centrifugal component had little effect on the COM acceleration. For individual muscles, the tibialis anterior and vastus muscles mainly activated within 100–200 ms during the early recovery phase to resist the platform translation. The tibialis anterior greatly contributed to induce the anterior COM acceleration against the posterior acceleration perturbed by the platform translation. In contrast, the vastus muscle induced posterior COM acceleration. The other muscles had little contribution or activated during the later stage after 200 ms.

Figure:
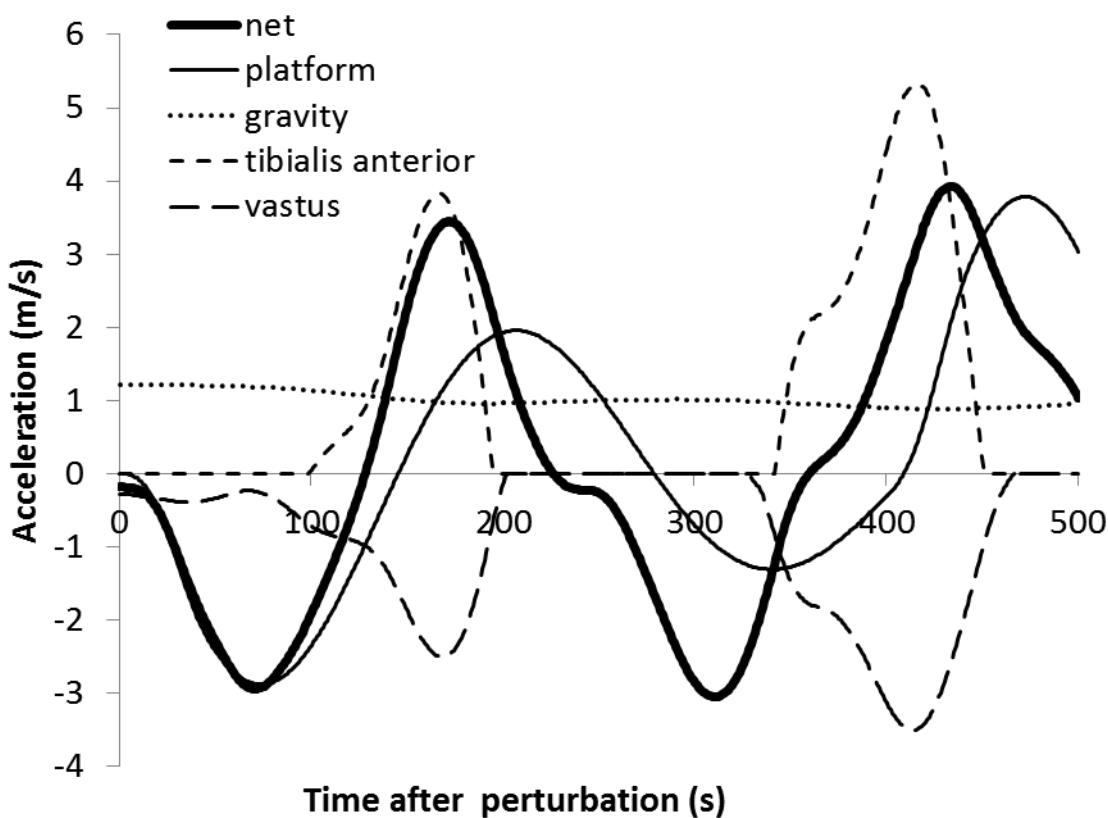
Caption: Contributions to center of mass acceleration

Conclusion: Against the backward loss of standing balance perturbed by a platform translation, COM acceleration is strongly affected by the magnitude of the platform translation during the early phase. After the muscle reaction time, the muscle can gradually increase its contribution to the control of COM acceleration. The tibialis anterior has an early response and resists backward COM acceleration. These results indicate that the tibialis anterior may play an important role in recovering COM against backward balance loss.

Disclosure of Interest: None Declared

Balance

PO-0019

QUANTIFYING PERFORMANCE AND EFFECTS OF LOAD CARRIAGE DURING A CHALLENGING BALANCING TASK USING AN ARRAY OF WIRELESS INERTIAL MEASUREMENT UNITS

Stephen M. Cain [1 2,*]Ryan S. McGinnis [3]Steven P. Davidson [1]Rachel V. Vitali [2]Noel C. Perkins [2]Scott G. McLean [1]

[1]School of Kinesiology, [2]Department of Mechanical Engineering, University of Michigan, Ann Arbor, MI, [3]MC10, Inc., Cambridge, MA, United States

Introduction and Objectives: Understanding how human movement is affected by load is critical for designing the equipment that warfighters and emergency responders must carry during missions or rescues. Advancements in inertial measurement unit (IMU) technology have made it possible for researchers to easily and unobtrusively measure body segment kinematics in real-world environments. In this study, we utilize an array of wireless IMUs to measure the movements of subjects traversing an outdoor zigzag-sloping balance beam as quickly as possible, both with and without load. Our objectives are: 1) to use data recorded by the IMU array to calculate metrics that quantify performance (e.g. speed and stability) and 2) to investigate the effects of load on performance. We hypothesize that added load significantly decreases subject speed yet increases the stability of subject movements.

Methods: We tested 30 subjects (11 females, 19 males; age = 20.8±2.6 years; body mass = 75.4±11.1 kg; height = 1.75±0.08 m; mean ± standard deviation). The University of Michigan IRB approved the study, and all subjects gave informed consent. Subjects completed an outdoor obstacle course both with and without a 20.5 kg load (body armor and tactical assault panel); the order of trials was random. In this study, we focus on a balance beam obstacle composed of five elevated aluminum planks (0.15 m wide, 3.05 m long). The first plank is level, whereas the other planks alternately slope up or down at 9 degrees. The junction between the first and second planks is straight, whereas the other junctions are alternating right and left 90 degree turns.

We secured eight APDM Opal wireless IMUs (APDM, Inc.) to each subject's feet, shanks, thighs, sacrum, and torso. Each IMU contains a 3-axis accelerometer, angular rate gyro, and magnetometer; a proprietary Kalman filter estimates the directions of gravity and magnetic north relative to sensor-fixed axes. Subjects performed calibration movements prior to testing, allowing us to deduce body segment-to-sensor alignments in post-processing. Foot-strikes and push-offs are identified via a wavelet analysis applied to foot segment angular velocities, allowing calculation of the duration of double support for each stride. Sacrum accelerations are resolved in an inertial frame and integrated to obtain vertical velocity of the sacrum; peaks in the vertical velocity signal reveal the jumps onto and off of the beam, which define the time required to traverse the beam. The ratio of the RMS acceleration in the medial-lateral (M-L) to the RMS acceleration in the anterior-posterior (A-P) direction for the sacrum measures the magnitude of lateral balance corrections (M-L) relative to propulsive/braking accelerations (A-P). Orientation of the torso-mounted IMU relative to gravity is used to calculate M-L tilt (left-right lateral flexion) of the torso.

We focus our analysis on four metrics: 1) time to cross beam (less time = more speed), 2) percentage of total time spent in double support (more double support = more stable), 3) ratio of sacrum M-L to A-P RMS acceleration (lower ratio = less lateral balance corrections = more stable), and 4) M-L torso range of motion (smaller range of motion = less balance

corrections = more stable). We used paired t-tests with a Bonferroni correction (α = 0.05/4 = 0.0125) to test for significant differences between loaded and unloaded conditions.

Results:

As hypothesized, speed decreased significantly with load, as quantified by an increase in the total time needed to cross the beam (mean diff=1.28s, t=4.85, p<0.001). Stability metrics also changed significantly with load, suggesting increased stability; double support time increased (mean diff=4.64%, t=6.04, p<0.001), the ratio of sacrum acceleration RMS decreased (mean diff=-0.19, t=-5.56, p<0.001), and the M-L torso range of motion decreased (mean diff=-5.41 degrees, t=-2.82, p=0.009). Figure 1 illustrates the trade-off between speed (time to traverse beam) and stability (percentage of total time spent in double support). The two subject data points highlighted in Figure 1 demonstrate that some subjects are able to maximize speed while simultaneously maintaining high stability.

Figure:
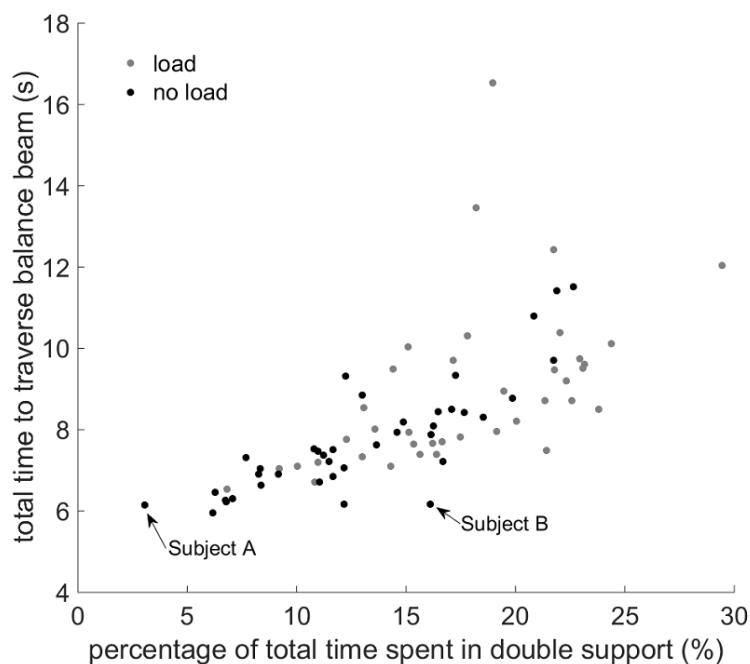
Caption: Figure 1. Time to traverse beam versus double support time. Subjects A and B traverse the beam in a similar amount of time (6.14 versus 6.16 seconds). However, Subject B spends much more time in double support (16.1%) than Subject A (3.1%), allowing Subject B to maximize both speed and stability.

Conclusion:

Using data from an array of IMUs, we developed metrics for quantifying the performance of subjects during a challenging balance task. Load carriage had a significant effect on the performance of the subjects, decreasing their speed while increasing their stability (increasing caution). Future work will explore additional performance metrics (e.g. foot trajectories) and quantify differences in technique between high and low performing subjects.

Disclosure of Interest: None Declared

Biodynamics

PO-0020

MUSCLE RATE OF TORQUE DEVELOPMENT IN FEMALE FUTSAL PLAYERS

Ana Carolina de Mello Alves Rodrigues [1,*]Nathália Arnosti Vieira [2]Sergio Augusto Cunha [2]Sérgio Rocha Piedade [1]

[1]School of Medical Science, [2]University of Campinas, Campinas, Brazil

Introduction and Objectives: Futsal players are known by developing maximum strength in a short periodof time, providing greater efficiency in tasks such as sprints and change of direction. In the early stages of muscle contraction (1), the strength development ratio (SDR) is a useful parameter to evaluate the dynamic of muscle contraction in sports activities (2), as well the joint stability in order to promote actions to prevent injuries (3).In clinical practice, the SDR is the ratio of Δstrength / Δtime calculate between 0 ms and 500 ms (1,2,4-7), resulting in an average value. However, in athletes the maximum SDR occur in the beginning of movement, due to its important for performance of the tasks in game. Thus, it is necessary to know the maximum of the acceleration of dominant and non-dominant member of these athletes, instead of the average value, to assist in the training of prescription. Therefore, the aim of this study was to analyze the maximum torque developmentratio (maximum TDR) of knee extensors in dominant and non-dominant member.

Methods: We analysed the performance of the best trial of 18 amateur female futsal players aged 21.0±2.8years (mean±SD), body mass of 56.4±6.1kg and height 160±0.1m. A Biodex system-3 was used for the isokinetic testing of knee extension torque. Each subject performed 1 set of 5 knee extension and flexion repetitions at $180°·s^{-1}$ with dominant (DM) and non-dominant (NDM) member.After find the peak torque for extensors it was possible calculate the maximum TDR by the derived, torque as a function of time derivation in the corresponding time interval. This variation interval goes from the beginning of the movement till the instant at which the maximum torque is reached. So, the maximum TDR ($N·m·s^{-1}$) was calculated for knee extensors of DM and NDM of athletes. As the data had normal distribution, ANOVA was performed to compare maximum TDR between DM and NDM adopting, $p<0.05$.

Results: Table 1 showed no difference ($p=0.97$) between the maximum TDR of extensor muscle group and the DM ($646,96 N·m·s^{-1} ± 155,14$) and NDM ($648,82 N·m·s^{-1} ± 144,45$). This may be due to the training that athletes are subjected, which consisted in improving muscle performance and promotion of joint stability in order to prevent injuries. Thereby, the athletes showed symmetry between the lower limbs, results consistent with those found in the literature (8,9).

Conclusion: The symmetry between the lower limbs corroborates to the achievement of greater efficiency of the tasks performed in futsal.

Table:

Subjects	Maximum TDR of Extensors (N•m•s⁻¹)	
	DM	NDM
S1	441,77	624,33
S2	586,51	464,77
S3	494,33	501,73
S4	593,18	710,68
S5	770,94	801,10
S6	801,52	765,18
S7	499,76	597,18
S8	727,92	801,26
S9	547,17	682,58
S10	642,97	413,50
S11	665,70	657,16
S12	500,35	516,32
S13	789,43	784,76
S14	912,71	831,15
S15	480,02	466,70
S16	638,87	702,35
S17	1010,40	863,98
S18	541,80	494,01

Caption: Table1. Values of maximum TDR of knee extensors from dominant (DM) and non-dominant member (NDM) at 180°•s-1.

References: [1] Aagaard et al., J. ApplPhysiol, 93: 1318-1326, 2002.

[2] Greco et al., Clinical Physiology and Functional Imaging, 33: 18-23, 2013.

[3] Andersen et al., Scand J Med Sci Sports, 20:162-169, 2009.

[4] Mebes et al., Arthritis & Rheumatism-Arthritis Care & Research, 59: 1665-1669, 2008.

[5] Holtermann et al., European J. of Applied Physiology, 101:301-312, 2007.

[6] Blazevich et al., Muscle & Nerve, 38: 1133-1146, 2008.

[7] Heggelund et al., European J. of Applied Physiology, 113: 1565-1573, 2013.

[8] Pinczewski et al., The American J. of Sports Medicine, 35: 564-574, 2007.

[9] Ageberg et al., Knee Surgery, Sports Traumatology, Arthroscopy, 17: 162-169, 2009.

Disclosure of Interest: None Declared

Biodynamics

PO-0021

LEVEL OF SYNERGIES IN SIMPLE, REPETITIVE TOOL USE

Chris Baber [1] Sandra Starke [1,*]

[1]Electronic, Electrical and Systems Engineering, University of Birmingham, Birmingham, United Kingdom

Introduction and Objectives: From a systems perspective, the coupling of human-tool-material, in a specific environment for a specific task, sets constraints for performance. However, variability might arise as a result of the degrees of freedom problem, or as a result of noise in movement control, or as a result of noise in the 'system'. Here, we focus on the manner in which variability in simple, repetitive tasks is managed using the example of sawing. Our objective was to quantify sawing frequency and cycle duration across a range of conditions and participants. Specifically, we wondered whether individuals would operate a saw in a random manner, in a task-specific manner or as the result of some form of internal timing (as predicted by Bernstein's level of synergies).

Methods: Data were recorded for two sawing tasks. For task #1, five participants were asked to use a wood saw (blade length 10 cm) and cut into a piece of wood, holding the saw horizontally or vertically. Each participant repeated the activity five times. A Qualisys motion capture system was used to track markers attached to the saw tip in 3D space at 200 Hz. For task #2, 18 participants recruited from a School of Jewellery were asked to use a piercing saw (blade length 14 cm) and, holding the saw vertically, cut lines into a piece of copper. The saw was instrumented with sensors, including an accelerometer aligned with the primary movement direction of the saw's handle. Each participant repeated the task five times.

For task #1, displacement components for a single axis in global space (horizontal/vertical component for horizontal/vertical sawing) were extracted. For task #2, calibrated accelerometer signals corresponding to movement in the direction of the long-axis of the saw were extracted. Individual sawing cycles were detected by identifying minima in the data stream for each trial. For each participant and trial, median and interquartile ranges (iqr) were calculated across cycle durations corresponding to one trial. After initial inspection, k-means clustering was performed for a group size of 3 (task #1, vertical and task #2) and 2 (task #1, horizontal) to report central tendencies while reflecting banding of data. A Friedman test was performed to examine whether median sawing duration changed as a function of trial number. For task #1, within-trial iqr was compared between horizontal and vertical sawing using the Wilcoxon signed-rank matched-pairs test.

Results: For task #1, mean (SD) cycle duration were 379 (69) ms for horizontal and 442 (272) ms for vertical sawing. The identified cluster centers across all trials and participants were 318 ms (11 cases) and 428 ms (14 cases) for horizontal sawing and 238 ms (11 cases), 506 ms (12 cases) and 1179 ms (2 cases) for vertical sawing. There was increased variation between participants for vertical sawing resulting from sawing at distinct, widely spaced bands. There was an effect of trial number on sawing cycle duration for horizontal sawing (P = 0.028) but not for vertical sawing (P = 0.246). Variation within participants' sawing frequency during a trial was significantly greater for vertical compared to horizontal sawing (P < 0.0005), with a mean (SD) participant-specific iqr of 58 (54) ms for horizontal sawing and 314 (369) ms for vertical sawing. For task #2, the mean (SD) cycle duration was 439 (71) ms while the identified cluster centers across all

trials and participants were 319 ms (10 cases), 434 ms (52 cases) and 550 ms (13 cases). There was a significant effect of trial number on median sawing cycle duration (P = 0.046).

Conclusion: In this study we found that use of a saw resulted in highly constrained operation across tasks and participants: the sawing motion was executed within specific cycle duration bands that were near-multiples, the most common cycle duration corresponding to a frequency of around 2.5 Hz. This suggests that saws were not operated in a random or task-specific manner, but rather under global constraints. A possible explanation for the observation stems from the notion of level of synergies, in which the response patterns arise from the internal coherence of movement dynamics. The observation is that participants attempt to produce consistent sawing actions, irrespective of material or posture, suggests that this activity might be independent of system components and more a matter of endogenous timing of this activity.

Disclosure of Interest: None Declared

EFFECT OF MECHANICAL PARAMETERS HAIR CAUCASIAN PREGNANCY WOMEN

Marie Skřontová [1,*] Lucie Šimková [1] Josef Zeman [2] Karel Jelen [1] Bohumil Chalupa [2]

[1]Department of Anatomy and Biomechanics, Faculty of Physical Education and Sport, Charles University Prague, Czech Republic, [2]Department of Physics, Faculty of Engineering, Czech University of Life Sciences Prague, Czech Republic, Prague, Czech Republic

Introduction and Objectives: The objective of this report is to show the changes of mechanical parameters of hairs found that come up during gravidity. The hair shaft consists of three concentric layers: the cuticle, the cortex and the medulla. Each of these components has different structure and function. The cuticle protects the inner parts from the outer environment and from derogation caused by daily treatment. The cortex (90 % of the hair) determines mechanical properties of the hair, and the medulla can sometimes be completely absent [1].

Methods: Samples of hairs have been taken from 50 Caucasian women's scruff each month of their pregnancy. The age of the women ranged from 23 to 43 years. Other samples have been taken after confinement end. Four hairs have been analysed from each taking; 3 samples have been subjected to tensile test and the last one to a relaxation test. Following mechanical parameters have been determined from the measured data: Diameter, modulus of elasticity, elastic limit, yield limit, relaxation times τ_1 and τ_2 and the total percentage of relaxation in the elastic region.

Results: Detectable trend that the gravid women have embodied in mean value has been found for some of these parameters. Although by far not all women display the trend that is valid for mean population, the trend is significant in the whole set e.g. for the hair diameter. It turns out that the hair diameter increases during gravidity, with a rate of 0.4 µm per month, the mean diameter being 84 ± 16 µm.

Figure:
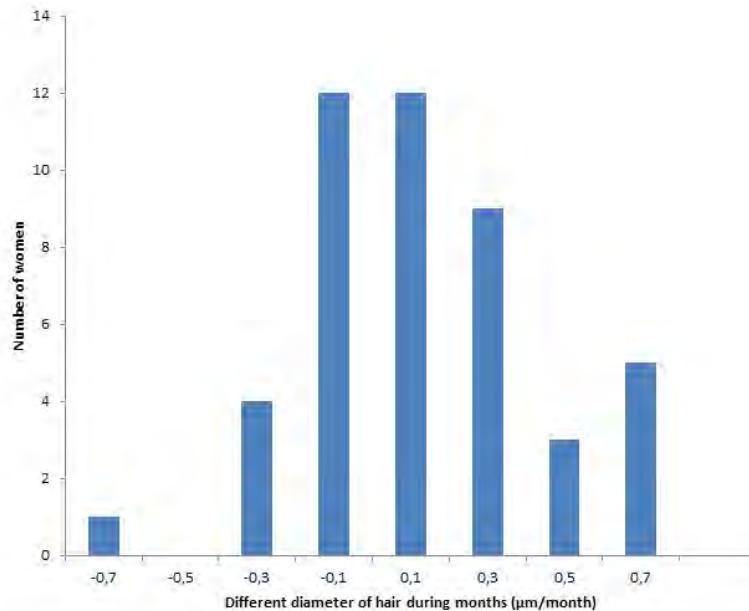
Conclusion: The distribution of the hair diameter change during gravidity can be seen in fig. 1. No dependence between the diameter, standard deviation and the women's age has been found in the age range given.

References: [1] Benzarti et al., World Academy of Science, Engineering and Technology, 74: 471 – 477, 2011.

Disclosure of Interest: None Declared

MODULATION OF H REFLEX AMPLITUDE DURING MENTAL TASKS IN ABLE BODIED VOLUNTEERS

Mohammed S. Jarjees [1 2,*] Aleksandra Vuckovic [1]

[1]Biomedical Department, University of Glasgow, Glasgow, United Kingdom, [2]Technical College of Mosul, Foundation of Technical Education, Mosul, Iraq

Introduction and Objectives: The H reflex is the monosynaptic reflex evoked by percutaneous electrical stimulation of the Ia sensory fibers [1]. It is considered as a measure of integrity of spinal pathways [2]. Research showed that it is possible to modulate H reflex from the higher centres, e.g. during imagination of movement [3] or even during mental math. By providing a biofeedback based on electromyogram (EMG) it is possible to increase or decrease the amplitude of H reflex [4]. Although it is believed that H reflex can be voluntarily modulated, cortical activity during H reflex modulation task has never been measured. The objective of this study was to explore whether the amplitude of the H reflex can be modulated by voluntary increasing or decreasing the amplitude of the sensory-motor rhythm (SMR, 8-12 Hz), which is a brain rhythm closely related to voluntary control of movements. Voluntary modulation of H reflex amplitude by modulating SMR might be beneficial for creating novel neurorehabilitation strategies for motor control.

Methods: Fifteen able bodied volunteers (9 M, 6 F; 27.9 ± 4.2 years) with no known neurological deficit or injury to their legs performed three different tasks: Motor Imagery (MI), Mental Math (MM) and Neurofeedback (NF). During MI, participants were asked to imagine dorsiflexing their feet for 60% of the maximum voluntary contraction and they were allowed 5s to perform MI before evoking H reflex. During MM, participants were asked to subtract numbers in steps of 7 starting from 100. While both MI and MM resulted in decreasing of SMR, it is believed that only MI directly modulates the activity of cortico-spinal pathways. NF was used to enable participants to voluntarily increase their SMR. In order to learn NF strategy, participants had 3 training pre-experimental session. Participants' EEG was recorded from electrode location Cz located over the primary motor cortex of legs. H reflex was evoked from right leg's tibial nerve and recorded over the soleus muscle. H reflex was evoked 5 times with at least 15 s interstimulus interval in each task (MI, MM and NF) and in the resting state before (PreBL) and after (PostBL) neuromodulation tasks. H reflex was evoked when the Power Spectral Density (PSD) of SMR was for at least 0.5s: 60% above the baseline for NF, 80% under the baseline for MM and MI. The stability of background EMG was confirmed by calculating Root Mean Square Value (RMS) of the EMG for 1s before the stimulation. Modulation of H reflex was considered significant if it was larger than 5%.

Results: The ratio of peak-to-peak H reflex amplitude to peak-to-peak muscle wave amplitude (H/M) with respect to the baseline during MI, MM, NF and PostBL are presented in Figure1. No differences were noticed in M wave amplitudes with respect to the baseline. Fourteen out of 15 participants achieved modulation of H reflex larger than 5% in at least one task. On the contrary, the modulation of H reflex in 14 volunteers varied less than 5% in PostBL. Statistically significant change in H/M ratio in all subject and overall tasks was noticed (P<0.0001) and NF showed the larger change than MM and MI. H reflex amplitude was modulated in 11 participants during NF (9 increase and 2 decrease), in 11 participants during MI (6 increase, 5 decrease) and in 7 participants during MM (6 increase). The average absolute value

of H reflex modulation was 20(±3.7) for NF, 16(±2.1) for MI and 12(±1.8) for MM. No increases in RMS values of the background EMG were observed (RMS under 7.5 µV).
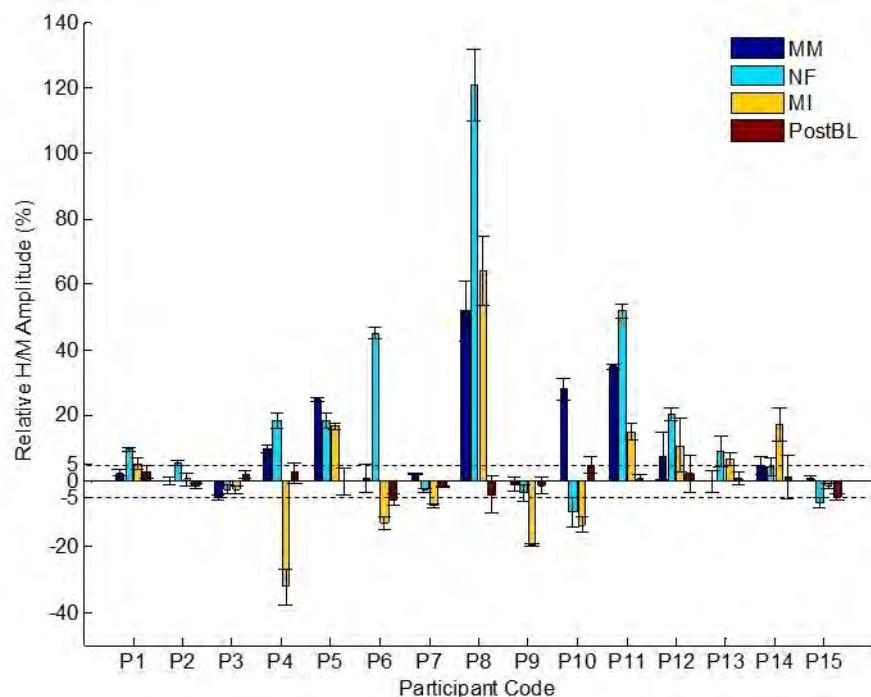
Figure:

Caption: Figure 1: Relative H/M ratio with respect to the baseline (PreBL) values. The two horizontal dashed lines mark the 5 % change of the H reflex amplitude compared to the PreBL; any change larger than 5% was considered significant.

Conclusion: Modulation of SMR results in modulation of the H reflex, but its effect is mostly excitatory independent on the direction of modulation of the SMR rhythm. While NF and MM dominantly increased the H reflex, results on the influence of MI on H reflex are inconclusive. Previous studies showed that MI increased H reflex in general population [3] and decreased H reflex in elite athletes [5]. In this study the level of fitness was not measured but participants were mostly healthy young adults corresponding to volunteers in [3]. The decrease of H reflex is believed to be related to the decrease of spasticity in people with spinal cord injury [6], but in healthy people it does no influence locomotion [6]. Further analysis of cortico-muscular coherence and analysis modulation of EEG signal in different frequency band would be needed to better understand the relation between modulation of H reflex and related brain rhythms.

References: [1] Palmieri, et al., J Athl Training, 39:268-277,2004.

[2] Misiaszek, J. E., Muscle Nerve, 28:144-160,2003.

[3] Hale et al., Behav. Brain Res, 142: 81–87, 2003.

[4] Thompson A. K. et al., Neuroscientist, 1:13, 2014.

[5] Oishi K. et al., Behav. Brain Res, 62: 55-61, 1994.

[6] Makihara Y. et al., J Neurophysiol, 112:1439-1446, 2014.

Disclosure of Interest: None Declared

Bone

PO-0024

FOREFOOT MORPHOLOGICAL PARAMETERS FOR ASSESSING INTRINSIC RISK FACTORS OF HALLUX VALGUS

Chien-Chung Kuo [1][2],*Hsuan-Lun Lu [2]Horng-Chaung Hsu [1]Tung-Wu Lu [2][3]

[1]Department of Orthopedics, China Medical University Hospital, Taichung, [2]Institute of Biomedical Engineering, [3]Department of Orthopedic Surgery, School of Medicine, National Taiwan University, Taipei, Taiwan, Republic of China

Introduction and Objectives: Hallux valgus (HV) is a common foot pathology in the modern society. The deformities diminish the function of the hallux and first metatarsophalangeal (MTP) joint in transmitting forces during locomotion, resulting in the progression of lesions beneath the 2nd/3rd metatarsal heads [1]. Footwear has been considered to be the main extrinsic factor of the development of HV. However, HV was also reported in the unshod population in South Africa [2]. This suggests that apart from the extrinsic factors HV is also affected by intrinsic factors such as heredity, ligamentous laxity and Achilles contracture, etc. However, previous studies have focused mostly on the 1st MTP without considering effects of the forefoot morphology [3] that may predispose the foot to HV when subject to improper external loads. The purpose was thus to identify forefoot morphological parameters that may be the intrinsic risk factors of HV.

Methods: Forty patients with HV and forty normal subjects participated in the current study. Both groups were evaluated by the standard weight-bearing anteroposterior radiography of the foot. Selected bony landmarks of the forefoot, namely heel, 5th metatarsal head, and 1st & 2nd proximal phalanx bases and metatarsal heads, were identified by an experienced surgeon on each radiograph image in a house-developed program in MATLAB. The lengths of the foot (L), 1st toe (L_1) and 2nd toe (L_2), forefoot width (W) and 1st web space (W_{12}) were then calculated using the relevant landmarks. Five morphological parameters were defined, namely normalized toe lengths (L_1/L and L_2/L), length-to-width ratios (L/W, L_1/W and L_2/W) and length-to-web ratios (L/W_{12}, L_1/W_{12} and L_2/W_{12}). Mean values and standard deviations of these parameters were calculated and their differences between HV and normal groups were compared using an independent t-test. The statistical analysis was performed using SPSS with a significant level set at $\alpha = 0.05$.

Results: Normalized toe lengths for the 1st and 2nd toes did not have significant differences between groups. In contrast, patients with HV showed significantly reduced ratios between toe lengths and the forefoot width, as a result of wider 1st web space, increased forefoot width and thus larger space between 1st and 2nd toes. The normal subjects had greater values of all the ratios (Table 1).

Conclusion: Morphological parameters based on toe lengths did not appear to be risk factors for HV because no significant differences of the normalized toe lengths were found when compared with the normal group. People with greater length-to-width and length-to-web ratios may be at a higher risk of developing HV if subject to improper medially applied external forces such as shoes with a narrow toe box for a long period of time. Therefore, proper and careful fitting of shoes is suggested for those with this specific forefoot morphological feature.

Table:

	L_1/L	L_2/L		L/W	L_1/W	L_2/W		L_1/W_{12}	L_2/W_{12}
Normal	0.22 (0.02)	0.22 (0.02)		3.19 (0.20)	0.71 (0.06)	0.69 (0.07)		2.05 (0.22)	2.00 (0.23)
HV	0.22 (0.01)	0.22 (0.02)		2.94 (0.22)	0.66 (0.05)	0.64 (0.08)		1.78 (0.20)	1.74 (0.26)
p-value	0.49	0.64		<0.001	<0.001	0.01		<0.001	<0.001

Caption: Means and standard deviations of the forefoot morphological parameters for HV and normal control groups, and the p values for between-group comparisons using independent t-test.

References: [1] Coughlin (8th Ed.). SURGERY OF THE FOOT AND ANKLE, Philadelphia, 2007.

[2] Wells, Am J Phys Anthropol, 15: 185-289, 1931.

[3] Mancuso et al., J Foot Ankle Surg, 42: 319-326, 2003.

Disclosure of Interest: None Declared

PO-0025

THE ASSESSMENT OF TOXICITY OF HYDROXYAPATITE (HAP) AND BORON NITRIDE (BN) NANOPARTICLE USING ATOMIC FORCED MICROSCOPY

Mohammad Alim I. Rasel [1,*]Trung Dung Nguyen [1]YuanTong Gu [1]

[1]Chemistry, Physics, Mechanical Engineering, Queensland University of Technology, Brisbane, Australia

Introduction and Objectives: Nanoparticles have considerably found practical applications in the field of biotechnology in recently. The large surface to volume ratio and the flexibility to deliver in desired positions makes them more attractive than any other nanomaterials. Because of their unique physical and chemical properties researchers have proposed sophisticated applications of nanoparticle ranging from biosensing, molecular imaging to drug delivery, optical storage and so on. Despite all these exciting applications and prospects, one thing has always bothered researcher about nanomaterial, their toxic nature. No matter how appealing the nanoparticle is, it can't be used for clinical treatment unless it's safety is properly assessed. This study focuses on two nanoparticles, Hydroxyapatite (HAP) and Boron Nitride (BN), which gained much popularity for their exceptional properties. A number of researchers have already proposed a wide variety of application of HAP and BN. However, as always their toxicity is a great concern. Several researchers have adopted traditional methods to quantify their toxicity. In this study, we tried to adopt a completely different approach. The idea is to quantify the mechanical property of cells and compare the properties between normal cells and cells with nanoparticles. The aim is to investigate whether there is any change in mechanical property due to the cellular uptake of nanoparticles and assess the cellular response in terms of mechanical property.

Methods: Confocal microscopy imaging is utilized to ensure cells are successfully uptaking the nanoparticles. The osteocytes, osteoblasts cells are cultured with both HAP and BN nanoparticles for 24 hours. After that, the attached cells are fixed with 4% Paraformaldehyde (Sigma-Aldrich). The cells are then stained with DAPI, and Alexa Fluor 568 Phalloidin (GIBCO, Invitrogen Corporation, Melbourne, Australia) for 15 minutes to observe the cells' nuclei and actin filament network, respectively. The samples were then properly washed and imaged on a confocal microscope (Nikon A1R confocal, Japan) using a 40X Nikon oil immersion objective lens.

Once the cellular uptake of nanoparticle is ensured, Atomic Forced Microscopy (AFM) is used to quantify the mechanical property of cells. AFM is a state of the art facility to study the mechanical and topological property of nanoscale materials. The AFM used in the current study is a Nanosurf FlexAFM (Nanosurf AG, Switzerland), which is mounted on a Leica DM IRB (Leica Microsystems). Nanosurf C3000 software is used to conduct AFM experiments. A colloidal probe SHOCONG-SiO2-A-5 (AppNano) cantilever is used. The diameter of the colloidal probe is around 5 µm and its spring constant is around 0.224 – 0.3114 N/m.

Results: From the confocal images, it can be confirmed that both HAP and BN can successfully go into the cells, therefore they can be used as a drug delivery vehicle or any other advanced biomedical application. This is the first to report that Boron Nitride nanoparticles successfully going into the cells.

From the preliminary AFM results it is observed that, for both BN and HAP, there is no significant difference between cells with and without nanoparticles. The nanoparticle does not seem to alter the mechanical property of cell much.

Conclusion: As confocal report confirms that both HAP and BN can go into the cell successfully, therefore they both can be used for a wide range of advanced biomedical applications. Although there are several reports about HAP going in the cell, this is the first report revealing that BN can also successfully going into the cell. This opens a new door in the field of biotechnology with huge potential.

The AFM experiment results demonstrate that both HAP and BN fails to alter the mechanical property of cells. This signifies that, it does not matter whether the particles are in or outside of the cells; mechanically they are still functioning at the same level. Therefore, it is perfectly safe to use them in the recommended amount.

Disclosure of Interest: None Declared

PO-0026

STUDY ON THE LOADING RATE BEHAVIORS OF ARTICULAR CARTILAGE UNDER COMPRESSIVE LOAD

Yan Bao [1,*]Chunqiu Zhang [2]Zhidong Liu [2]Wei Yao [1]

[1]University of Strathclyde, Glasgow, United Kingdom, [2]Tianjin University of Technology, Tianjin, China

Introduction and Objectives: Articular cartilage is a connective tissue that locates between the articular and bone, bearing and transmitting load while allowing low-friction and low-wear joint articulation depending on its special structure. It is difficult to repair the damaged cartilage by itself when cartilage has experienced trauma or degeneration, which may affect people's activity and will be inconvenient to human life. Therefore, it is vitally important to study the mechanical properties of articular cartilage, in particular its structure and different composition. Articular cartilage is divided into three layers from above to below, and the biomechanical property of different layers show diversity. So it is difficult to completely reveal the biomechanical property while regarding articular cartilage as a whole for researching. The study is focused on the rate behaviors of different layers for fresh pig articular cartilage under compressive load.

Methods: An optimized digital image correlation (DIC) technique was applied to investigate the rate behaviors and the micro mechanical properties of cartilage were obtained. Iron-oxide nanoparticles were embedded in the cartilage samples as tracer elements and the change of the relative position of nanoparticles under loading shows the sample deformation.

Results: Compressive stress-strain curves under different loading rates (0.1N/s, 0.3N/S, 0.5N/S, 1N/S, 3N/S) show the mechanical property of cartilage changes along its depth from surface to deep layer and this property is related to the loading rate. Under constant loading rate, the strain amplification in the surficial layer is the largest and the deep layer is the smallest, which is related to the microscopic structure of different layers. Under the same compressive load, the Possion's rate is smaller in the surficial layer than that in the deep layer of articular cartilage.

Conclusion: Persistent low stresses also can cause large deformation in cartilage, which will damage its inner structure. Therefore, persistent loading should be avoided in order to prevent injury caused by chronic stress.

References: [1] Gao LL, Zhang CQ, Dong LM, et al. Description of depth-dependent nonlinear viscoelastic behavior for articular cartilage in unconfined compression, Master Sci Eng C, 2012.

[2] Federico S, Grillo A, Rose GL. A transversely isotropic, transversely homogeneous microstructural-statistical model of articular cartilage, Journal of Biomechanics, 2005.

[3] Wilson W, van Donkelaar CC, Huyqhe JM. A Comparison Between Mechano-Electrochemical and Biphasic Sweelling Theories for Soft Hydrated Tissues, J. Bimmech. Eng., 2005.

Disclosure of Interest: None Declared

Bone

THE IMPORTANCE OF THRESHOLDING IN MICRO-CT FOR THE HISTOMORPHOMETRIC ANALYSIS OF MAMMALIAN BONE TISSUE

George Adams [1]Richard Cook [2]John Hutchinson [3]Peter Zioupos [1,*]

[1]Cranfield forensic institute, Cranfield Univeristy, Swindon, [2]National Centre for Advanced Tribology at Southampton, Univeristy of Southampton, Southampton, [3]Department of Veterinary Basic Sciences, University of London, Hatfield, United Kingdom

Introduction and Objectives: In recent years the use of micro-computed tomography (µCT) has become popular in the assessment of bone microstructure. There are 2 main considerations that need to be addressed when assessing samples by µCT; the material surrounding the samples during the scan and where the threshold is drawn when evaluating the scan data. Determining which method of scanning and thresholding provides the truest and most accurate value is important to validate the use of µCT in the assessment of bone morphology.

Methods: 31 Samples of bone from an elephant femur of varying porosities were scanned with the ambient medium being water and air. Before scanning each sample had a slice of bone tissue removed and demineralized using EDTA leaving behind only the organic phase of the bone. Each sample was then scanned in both conditions and with the presence of the demineralized slice.

Results: The results showed that scanning the samples in water gave an average difference of 6.3% from results obtained by conventional densitometry, but when the samples were scanned in air the difference was reduced to 5.7%. In determining where the threshold should be drawn to determine morphology 3 different "backgrounds" were used; air, water, and collagen (from the demineralized slice). The results showed that there was little difference between the samples with air and water taken as the background, however when collagen was considered to be the background the morphology varied significantly.

Figure:
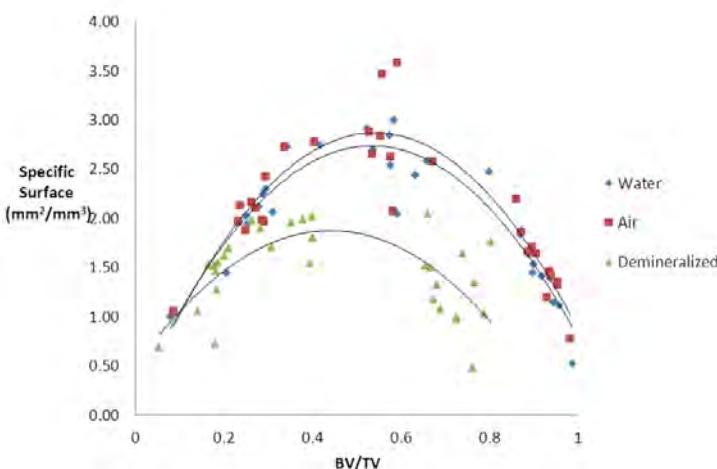
Caption: Specific surface distribution for all three thresholds

Conclusion: Contrary to popular protocol our results suggest that scanning samples in air rather than water produce results more similar to other conventional histomorphometry methods such as the Archimedes principle. One argument for scanning in water over in air scanning could be that the results are likely to be more similar to clinical scanners. However this is flawed as the type of scanner (cone beam or spiral), voxel size, volume of soft tissue between source and target as well as many other factors vary to such an extent that they make this a redundant point. In the interest of obtaining the most accurate morphological data it is suggested to scan the samples in air rather than water.

Disclosure of Interest: None Declared

Cardiovascular

PO-0028

ENERGY COST AND PHYSIOLOGICAL RESPONSES IN UPPER LIMBS EXERCISES PERFORMED WITH DIFFERENT POSTURES

Yomara L. Mota [1,*]Renato Silva [1]Guilherme Molina [1]Ciro Brito [1]Flávio Pires [1]

[1]Department of Physical Education, Universidade Católica de Brasília, Taguatinga, Brazil

Introduction and Objectives: It is not well described in the literature the influence of the variation in position on the physiological responses and the energy cost of exercises performed with the upper limbs. Therefore, the aim of this study was to characterize the physiological responses during upper limbs exercises performed with different postures.

Methods: Eight men physically active for at least 1 year, with no experience in upper limbs exercises, with 28.2 (± 5.7) years old, 173.7 (± 7.4) cm of height, 74.1 (± 11.4) kg of body weight, 30.2 (± 2.09) ml $\cdot$ kg $\cdot$ min-1 VO2peak and 24.4 (± 2.5) kg / m2 of BMI were recruited to participate in this study. All subjects were instructed for an initial cardiopulmonary exercise testing, two familiarization sessions andtwo upper limbs exercises sessions lasting for 30 minutes have been applied on different days. Themetabolic and hemodynamic responses obtained in sitting postures (SP) and vertical positions (VP) werecompared.

Results: The results demonstrated that the upper limbs exercises session performed in a VP generated energy expenditure 14.3% higher than during the SP ($p = 0.014$) and significantly increased the lipid catabolism ($p = 0.004$) compared to the SP session. In vertical exercise the pressure rate product was higher ($p = 0.037$).

Conclusion: The upper limbs exercises performed in VP modify the VO2 responses and increase ventilation. This way, the cost energy and cardiovascular load associated with orthostatic position.

Disclosure of Interest: None Declared

Cardiovascular

PO-0029

IDENTIFICATION OF ORTHOTROPIC MATERIAL PARAMETERS FOR HEALING MYOCARDIAL INFARCTS IN THE RAT

Mazin Sirry [1,*] Laura Dubuis [1] Neil Davies [1] Jun Liao [2] Thomas Franz [3]

[1]Cardiovascular Research Unit, Chris Barnard Division of Cardiothoracic Surgery, University of Cape Town, Observatory, South Africa, [2]Tissue Bioengineering Laboratory, Department of Agricultural and Biological Engineering, Mississippi State University, Mississippi , United States, [3]Division of Biomedical Engineering, Department of Human Biology, University of Cape Town, Observatory, South Africa

Introduction and Objectives: Myocardial infarction (MI) is one of the major causes of mortality globally. Research has been devoted to study the biomechanical aspects of MI and its emerging intramyocardial injection treatment [1]. Finite element (FE) models have been effectively utilized in such research. Although the rat is a widely used animal model for MI, there is a lack of data on material models for rat infarcts in the literature. This study aimed at identifying the parameters of Fung orthotropic constitutive model for different healing stages of rat infarcts through inverse FE analysis utilizing biaxial (cardiac circumferential and longitudinal axes) tensile mechanical data obtained in a related study. The temporal stages of healing infarcts included immediate (0 day), 7, 14 and 28 days.

Methods: Four 3D models of the infarct sample (square sample dissected from the infarcted left ventricle wall) were developed in Abaqus CAE 6.12-2 (Dassault Systèmes, Providence, RI, USA) utilizing the average physical dimensions of samples in each stage and mimicking the setup of the biaxial tensile experiment. Models were meshed using C3D8RH elements. Through a user-defined subroutine, 14 transmural layers of fibre angles ranging linearly from -50° (epicardium) to 80° (endocardium) were incorporated. The orthotropic case of the generalized Fung constitutive model was utilized to model the material properties of the infarct. The parameters of Fung model were optimized so that the FE solution best fitted the biaxial experimental stress-strain data. Three simulations were run for each infarct stage to fit the experimental data which were obtained with three different biaxial loading ratios; namely 1:1, 2:1 and 1:2. The computed stress data were compared to the experimental data at predefined strain values. The objective function (OBJ) utilized in the optimization was developed so that it returns the mean absolute percentage error. A genetic algorithm (GA) was used to minimize the objective function (SCILAB 5.4, Scilab Enterprises S.A.S, Versailles, France).

Results: The identified Fung orthotropic material parameters for different infarct stages are shown in the table. The FE model predictions best approximated the experimental data of the 28 days infarct stage with 3.0% error. The worst approximation was for the 7 days stage with 3.6% error. The figure illustrates the best fit of FE model predictions to the experimental data for the 28 days infarct stage in circumferential and longitudinal directions from three loading conditions.

Figure:
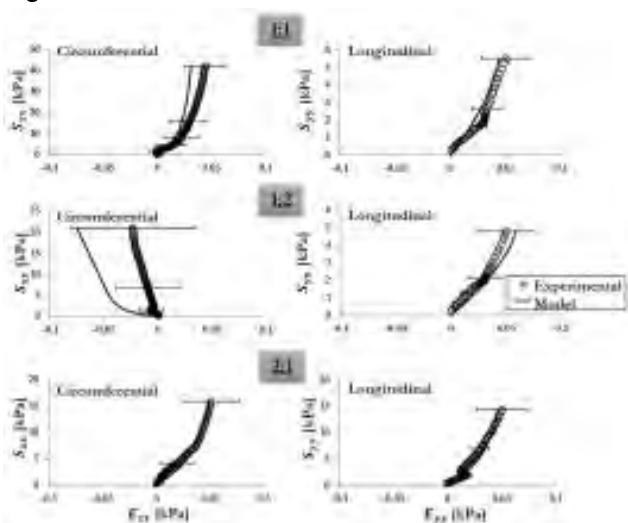
Conclusion: The experimental stress-strain data of healing rat infarcts could be successfully approximated using inverse FE methods and genetic algorithms. The material parameters identified in this study will provide a new platform for FE investigations of biomechanical aspects of MI and the development of therapies.

Table:

Material parameter	0d	7d	14d	28d
b_{1111}	64.31	176.09	16.38	159.65
b_{1122}	14.08	-70.92	-16.16	-25.52
b_{2222}	48.60	83.95	128.78	38.15
b_{1133}	20.51	81.15	-11.62	1.10
b_{2233}	-39.35	-84.99	-6.94	-31.44
b_{3333}	152.06	175.57	172.58	116.40
b_{1212}	68.31	176.54	77.86	18.56
b_{1313}	111.94	175.11	130.73	127.89
b_{2323}	63.54	158.40	189.56	65.77
c (kPa)	0.201	0.133	0.146	0.695
(%)	3.2	3.6	3.2	3.0

Caption: Identified Fung orthotropic material parameters for immediate (0d), 7, 14 and 28 day infarct stages.

References: [1] Kichula, E., et al., Ann. Biomed. Eng., 42(7): 1546-1556, 2014.

Disclosure of Interest: None Declared

Cardiovascular

PO-0030

THE EVALUATION AND CHARACTERISATION OF THROMBIN-INDUCED MAMMALIAN THROMBI MODELS FOR THE INVESTIGATION OF VASCULAR OCCLUSION IN ACUTE ISCHEMIC STROKE.

Fiona Malone [1,*]Patrick Delassus [1]Eugene McCarthy [2]John Thornton [3]Paul Fahy [1]Liam Morris [1]

[1]GMedTech, [2]Marine and Freshwater Research, GMIT, Galway, [3]Neuroradiology Dept., Beaumont Hospital, Dublin, Ireland

Introduction and Objectives: A lack of blood supply to any part of the brain for an unknown period of time may lead to brain tissue necrosis, commonly known as stroke. Stroke remains the third most common cause of death worldwide and kills more than 2,000 people a year in Ireland. Stroke is also the leading cause of acquired long-term disability and is almost twice as prevalent among women as men. Over 80% of all strokes are ischaemic that can result from a thrombus occlusion of a major cerebral artery.

Thrombosis is an important repair mechanism within the human body but also occurs if blood flow becomes stagnant. In vivo, erythrocyte rich thrombi are generally formed in relatively static, low flow-regions, as with arterial fibrillation. On the other hand, fibrin rich thrombi arise in areas of rapid moving blood flow and often originate from damaged endothelia. Animal thrombi models[1] have played a unique role in understanding the pathophysiology, morphology and mechanical characteristics of thrombi underlying the vascular occlusion in acute ischemic stroke. This project concerns the histological and mechanical examination and characterisation of thrombin induced, erythrocyte rich mammalian thrombi. Such thrombi models will be used to experimentally model and simulate ischemic stroke.

Methods: Mammalian blood (ovine and bovine origin) was harvested from a local abattoir. Samples were induced immediately using bovine thrombin. Haemotoxylin and Eosin (H&E) and Martius, Scarlet and Blue (MSB) stains were completed on ovine and bovine thrombi specimens at day 1 and day 33 (n=35). The presence of nuclei and erythrocytes correlated significantly with stained human thrombi samples reported from literature. Compositional differences were noticed in the thrombi after 33 days.

9 patient specific scans of the aortic arch in DICOM format were imported into Mimics Version 16.0 to generate 3D models using segmentation techniques. Models were geometrically characterised and differentiated for flexible model production. These models will be incorporated into a cerebral test facility for releasing the animal thrombi and tracking the trajectory within the cerebral vasculature. This test will further characterise the thrombi behaviour and lodgement morphologies within the cerebral vasculature.

Results: Figure 1(A) displays H&E stain of thrombin induced ovine thrombus (6NIH Units/ml blood). Figure 1(B) displays MSB stain of thrombin induced bovine thrombus (9 NIH Units/ml blood). The presence of fibrin and collagen was determined in high concentrations of thrombin induced mammalian thrombi.

Tensile and compression tests were conducted at day 1 at varying strain rates. Initial results indicate a possible increase in elasticity with increase in thrombin concentration (NIH units/ml blood).
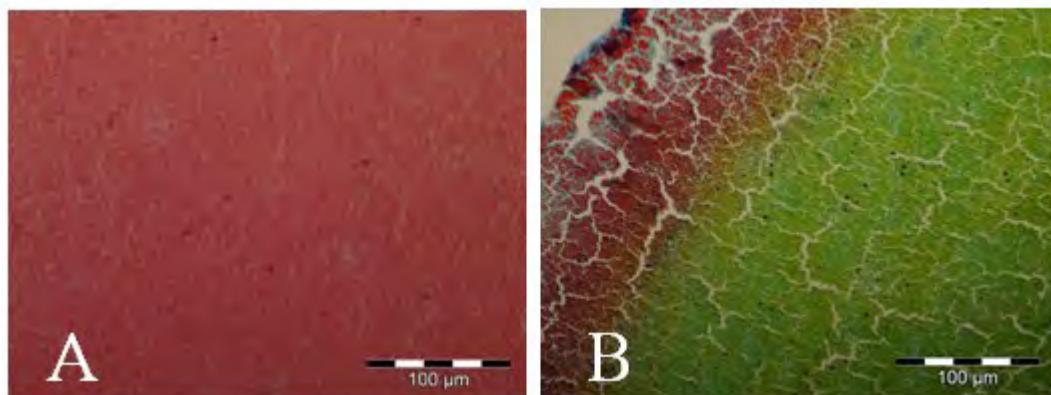
Figure:

Caption: Figure 1: H&E stain ovine thrombus at day 1 (A), MSB stain bovine thrombus at day 33 (B)

Conclusion: The successful development of such thrombus models and future clot flow studies may provide a basis for the characterisation of post-operative thrombi removed from humans. Knowledge about the histological characteristics and lodgement morphologies of thrombi may provide a means for improving current endovascular therapies and the development of new treatment strategies for revascularisation in patients with acute ischemic stroke. These findings could indicate that the composition of thrombi is a potential key variable regarding the selection of the appropriate treatment options for ischemic stroke patients and in predicting the performance of mechanical thrombectomy devices and thrombolytics

References: [1] Chueh, J.Y., (*et al.*), American Journal Neuroradiology, 32: pp 1237-1244, 2011

Disclosure of Interest: None Declared

PO-0031

AN IN VITRO STUDY OF CONFIGURATION DEFORMATION OF TRANSCATHETER HEART VALVE

Wentao Feng [1 2 3,*] Xianda Yang [1 2 3] Yang Liu [1 2 3] Yubo Fan [1 2 3 4]

[1]School of Biological Science and Medical Engineering, Beihang University, [2]International Research Center for Implantable and Interventional Medical Devices, [3]Key Laboratory for Biomechanics and Mechanobiology of Ministry of Education, [4]National Research Center for Rehabilitation Technical Aids, Beijing, China

Introduction and Objectives: Currently, percutaneous transcatheter aortic valve implantation (TAVI) has evolved into a safe, effective therapy for aortic valve replacement (AVR). However, TAV devices have had serious leakage and durability problems. Some of these problems are associated with geometric configuration deformation of TAV stent implantation in the calcified aortic annulus that has a non-concentric geometry. This study evaluated the hydrodynamics of different geometric configurations with different leaflet tissue thickness.

Methods: Three 22mm sized TAV devices with the same self-expanding nitinol stents with different leaflet tissue thickness's (0.25mm, 0.4mm, 0.55mm) were tested on pulse duplicator system. Six vary configurations were simulated as nominal, undersized (20mm), elliptical with commissure along minor axis, elliptical with commissure along major axis, triangle with commissures in edge and triangle with commissures in vertex. Hydrodynamics patterns such as traxnsvalvule pressure, regurgitant fraction and effective orifice area (EOA) were tested to analyze.

Results: The nominal shape had the smallest transvalvule pressure (15.4mmHg) and regurgitant fraction (6.83%) with the largest EOA (1.569cm^2) while the triangle shape had opposite results. The elliptical configuration with commissure along the major axis had a larger EOA (1.496cm^2) and lower regurgitant fraction (8.35%) than the same shape. There is no statistically significant differences between the undersized type and the elliptical tape with commissure along the minor axis. The triangle with commissures in side had a largest regurgitant fraction (15.02%) and smallest EOA (1.218cm^2). The regurgitant fraction and EOA of 0.55mm thickness valve were the smallest in all configurations.

Conclusion: The results showed significant hydrodynamics performances are impact by valve stent deformation and leaflet thickness. The triangle deformation should be neglected in TAVI procedures.

Disclosure of Interest: None Declared

Cardiovascular

PO-032

12-WEEK SUPERVISED EXERCISE REHABILITATION IMPROVES SKELETAL MUSCLE CONTRACTILE FUNCTION AND STRENGTH IN PATIENTS WITH CARDIAC DISEASE.

Yumna Albertus [1,*] Angus Hunter [2] Wayne Derman [1]

[1]Human Biology, University of Cape Town, Cape Town, South Africa, [2]Sports Studies, University of Stirling, Stirling, United Arab Emirates

Introduction and Objectives: Patients with cardiac disease are shown to have secondary structural and functional changes that occur in the skeletal muscle, which can result in decreased functional capacity and exercise intolerance. Previous studies have shown that supervised exercise rehabilitation programs result in improvements in functional capacity [1; 2] but the exact effect of exercise training on skeletal muscle activity in these patients is unknown. Therefore the aim of the study was to determine the effect of a supervised 12-week exercise rehabilitation program on skeletal muscle activity and muscle fiber conduction velocity (MFCV) during static, dynamic muscle contractions and during the 6 min walk test.

Methods: 9 patients with cardiac disease and 9 age matched healthy controls undertook testing before and after a 12-week period. During the 12 weeks the patients underwent exercise rehabilitation whereas the controls continued with normal daily activities. An electrode array (4 electrodes, 4 mm inter-electrode distance) was placed on the Vastus lateralis of the right leg to measure MFCV. Both groups performed two 5 s isometric maximal voluntary contraction on the Biodex dynamometer, followed by 5 s submaximal contractions at 20 %, 40%, 60 % and 80% MVC. Three maximal concentric isokinetic contractions were then performed at 60, 120 and 180 deg.s^{-1}. For the 6 min walk test, surface electrodes were placed on the vastus lateralis, vastus medialis, medial and lateral gastrocnemius muscles of the right leg. Resting heart rate (HR) and blood pressures (BP) were taken. They then walked around a 70 m track for 6 min, trying to cover as much distance as possible. HR and rating of perceived exertion (RPE) were measured every minute during the test. Post 1 min recovery HR and BP was recorded. After 12 wks the same protocol was repeated. The EMG was normalized to the participants walking at a normal pace over 10 m.

Results: Patients had significantly lower muscle strength (191 ± 27 Nm) compared to controls (230 ± 38.8 Nm) (p=0.026) and their strength significantly improved after 12 weeks of rehabilitation (218 ± 50 Nm) (p=0.038). MFCV has shown no difference between Controls (2.8 ± 0.7 – 3.3 ± 0.9 m.s^{-1}) and Patients (3.1 ± 0.7 – 3.6 ± 0.7 m.s^{-1}) in the Pre and Post Intervention trials during MVCs and dynamic contractions. Interestingly, the patients had significantly greater EMG activity during dynamic contractions (p < 0.03) before rehabilitation, whereas Post Rehab the EMG returned to levels of the controls, but with a significant increase in muscle strength. Similarly during the 6 min walk test, EMG activity was not significantly different between the Controls and Patients nor did EMG change, however patients showed a significant improvement in distance covered Post rehabilitation of 17.7 % (± 107 m) (p=0.00), whereas the Controls did not improve. Patients average HR increased significantly from 97 ± 5 bpm to 112 ± 7 bpm during the 6 min walk test Post rehabilitation (p=0.007). RPE remained similar Pre and Post rehabilitation in both the Patients and Controls.

Figure:
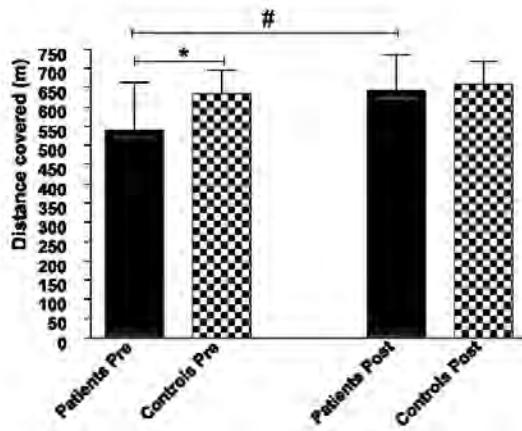
Caption: Distance walked in the 6-minute walk test by patient and control group Pre and Post intervention.

Conclusion: The findings of this study suggest that skeletal muscle contractile function was altered so as to produce greater force output but with unchanged relative EMG activity and conduction velocity. This suggests that patients become more efficient in performing the required exercise task following exercise rehabilitation training.

Table:

	Pre Intervention (0 weeks)			*Post Intervention (12 weeks)*		
	Patients (n = 9)	**Controls (n = 9)**	**p**	**Patients (n = 9)**	**Controls (n = 9)**	**p**
Male	8	8		8	8	
Female	1	1		1	1	
Age (years)	60 ± 10	63 ± 5	0.374	60 ± 10	63 ± 5	0.374
Height (cm)	169 ± 8	174 ± 5	0.114	169 ± 8	174 ± 5	0.114
Weight (kg)	83 ± 21	82 ± 10	0.943	83 ± 22	81 ± 9	0.808
BMI	28 ± 5	27 ±	0.	28 ± 5	26 ±	0.3

(kg.m²)		3	460		3	84
Body fat %	29 ± 5[#]	26 ± 4	0.187	27 ± 4[#]	26 ± 4	0.887
Resting HR (bpm)	70 ± 14	76 ± 9	0.203	71 ± 15	71 ± 13	0.914
Resting SBP (mmHg)	119 ± 7	124 ± 15	0.377	116 ± 10	125 ± 12	0.123
Resting DBP (mmHg)	69 ± 7	79 ± 10	0.0300*	69 ± 8	80 ± 10	0.022*

Data represented as mean standard deviation, except for gender.

*Significant difference between patient and control group.

[#] Significant difference between patients Pre and Post intervention.

BMI - Body mass index, HR – Heart

Caption: Descriptive characteristics of participants in both patient and control groups at zero weeks and following 12-weeks of the exercise intervention

References: 1) Derman et al. Healthy lifestyle interventions in general practice. Part 2: Lifestyle and cardiovascular   disease. South African Family Practice 2008.

2)Streuber et al Heart rate recovery in heart failure patients after a 12-week cardiac rehabilitation program. American Journal of Cardiology 97:694-698, 2006.

Disclosure of Interest: None Declared

PO-0032

RELIABILITY OF A FASCIAL MODEL CONNECTIVITY IN VIVO BETWEEN THE PELVIS POSITION AND MEDIAL GASTROCNEMIUS

Carlos M. Cruz-Montecinos [1,*] Mauricio Cerda [2] Antonio Cuesta-Vargas [3]

[1] Kinesiology, [2] SCIAN-Lab. ICBM, University of Chile, Santiago, Chile, [3] Psychiatry and Physiotherapy, University of Malaga, Málaga, Spain

Introduction and Objectives: Different authors proposed the existence of myofascial tissue connectivity at a distance [1,2]. However, models that show the level of connectivity myofascial tissue in vivo are scarce. For example, the thoracolumbar fascia, responds to mechanical traction induced by muscular activity, in order to effectively transfer the load between spine, pelvis, legs and arms [1]. Other authors have questioned the existence of myofascial force transmission in response to physiological motion of joints [3,4]. In this context, an important step toward understanding distant myofascial tissue connectivity is to validate measurement methodology. The objective of this study was to evaluate the reliability of fascial model connectivity automatic measurement in vivo between the pelvis position and deep fascia displacement of medial gastrocnemius (DFMG) during anteversion of pelvis (AP) motion from retroversion position with the hip at 80 degrees, knees blocked in extension and ankles at 90 degrees.

Methods: With the approval of the local Ethical Service, 17 asymptomatic, sedentary young male were recruited. Each individual was asked to perform the motion AP three times. Measurement was performed by 3 stages automatic method: (i) DFMG tracking, (ii) AP Tracking, (iii) Variable synchronization, and a manual method to compare. (i) DFMG tracking was evaluated by Lucas-Kanade Tracker method with pyramid and iteration (LKPI), using real-time ultrasound. Within the range of interest (ROI), 9 pixels of greater representation were automatically detected. (ii) Angular variation of the AP was determined by 2D kinematic analysis; in order to tracking the markers Lucas-Kanade affine template method (LKAT) was used. (iii) Synchronization between the variables of interest, was performed offline with pressure sensors. All of the data had a normal distribution. In order to establish reliability of the proposed model in our study, intrasubject reliability for displacement DFMG and AP was determined by using Intraclass Correlation Index (ICC). To establish displacement reliability of DFMG and AP tracking, the maximum value obtained by automated tracking was compared to manual tracking in 20 videos using the Blant-Almant method (BAM) to verify their agreement.

Results: All of the participants were males, aged 22.76 ± 1.8 years old. Intrasubject reliabililty ICC of the DFMG model was of 0.903 (IC95%0.782 to 0.962) with a $p<0.001$.The intrasubject reliability ICC for AP of the pelvis was of 0.781 (IC95% 0.509 to 0.914) with a $p<0.001$. Reliability between manual tracking and tracking with the LKPI algorithm was of 0.973 (IC95% 0.993 to 0.989) with a $p<0.001$. Using BAM, an average difference of 0.034 mm could be observed between the two methods, with an according percentage <0.95%. LKAT tracking reliability for determining maximum AP motion during execution, was of 0.967 (IC95%0.917 to 0.987) with a $p<0.001$. An average difference of 0.879 degrees was observed with the BAM between both methods, with an according percentage <0.95%.

The result of a normalized simple linear regression at each 10% of the total cycle between AP motion and displacement of DFMG was r= 0.791 with a $p<0.001$.

Figure:

Range of anteversion of the pelvis

Displacement the deep fascia of GM
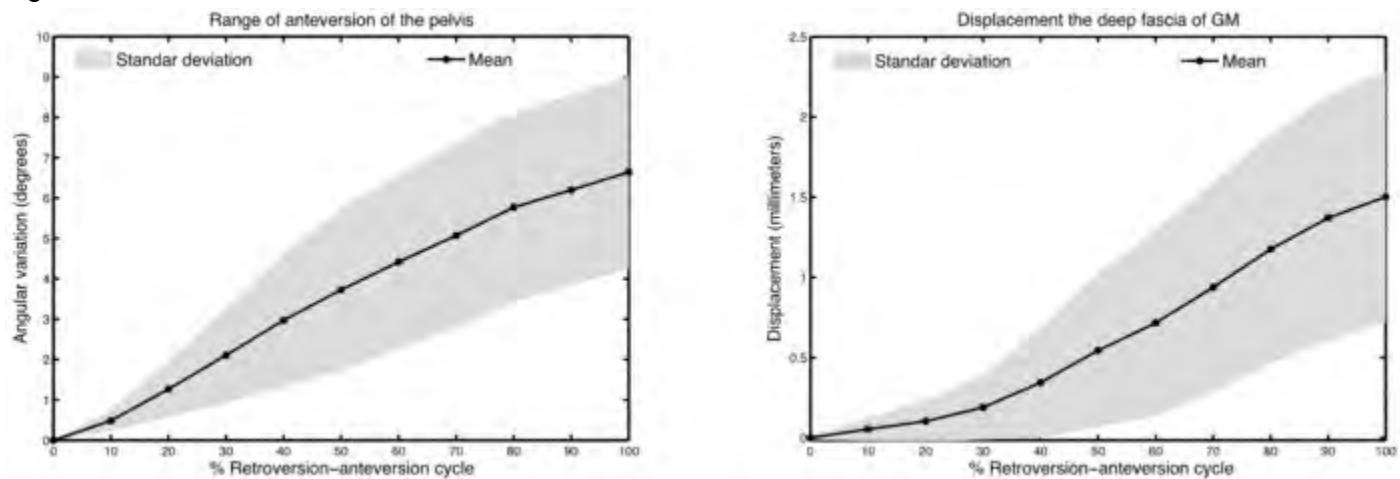
Conclusion: The present model of myofascial connectivity at a distance between the pelvis and leg, presents a good reliability. The results confirm and support the concepts of myofascial tissue connectivity. Future work will include to study other in vivo human movements.

References: [1] Vleeming A et al., Spine, 20:753-758,1995.

[2] Carvalhais VO et al., J Biomechanics, 46:1003-1007,2013.

[3] Herbert RD et al., J Appl Physiology,104:1549-1550, 2008.

[4] Maas H et al., J App Physiology, 104: 1549-1550,2008.

Disclosure of Interest: None Declared

Dental

PO-0033

VALIDATION OF FINITE ELEMENT MODEL OF DENTAL PROSTHESIS USING EXPERIMENTAL DATA

Bruno Agostinho A. Hernandez [1,*]João Paulo de Oliveira Freitas [1]Edson Antonio Capello Sousa [1]Cesar Renato Foschini [1]Max Laurent Albarracín [2]José Henrique Rubo [2]

[1]Mechanical Departament, Engineering College of Bauru - São Paulo State University (Unesp), [2]Dentistry, Prosthesis and Dental Materials Department, Dentistry College of Bauru – São Paulo University (USP), Bauru, Brazil

Introduction and Objectives: The bioengineering field consists in applying the engineering methods on the developing of devices that will support the life. One of areas that bioengineering acts is in the field applied on dental prostheses studies. The dental prostheses are typical biomechanical structures because they have an objective to restitute the mastication functions and they are responsible for replacement the original dental component that was damaged. In the last few years, many studies have been realized and big achievements have been noticed in this area. However, clinical studies, experimental procedures or analytical stress studies for these conditions are sometimes impractical, due to the biological nature of these components and their non-linear conditions. Consequently, many researchers have applied the Finite Element Method (FEM) in their researches. This method allows the evaluation of non-linear situations (e.g. biomechanical interactions), with complex geometries where experimental tests are usually difficult to be conduct. But in dental prostheses studies, the development of a model that simulates and predicts the real life condition of the mechanical behavior becomes very complicated, since the prosthesis structure is composed of many parts, with distinct geometries, materials and mechanical functions. Then, in order to improve the modeling techniques and the quality in Biomechanical studies, improved models have to be generated, studied and validated. As reliable the model is, more accurate the results will be. Therefore, this project aims to develop a tridimensional finite element model of dental prosthesis and validate this model using an experimental data.

Methods: A geometric model from a single dental prosthesis will be generated from Micro CT and Scanning data. Then, the geometry will be exported to finite element software where a finite element model will be created. After that, boundary conditions and loads will be applied in order to simulate an experimental procedure. Finally, the simulation results (strains) will be compared with experimental results (strains) so that the model can be validated.

Results: Comparing the results between the methodologies (numerical and experimental), it can see that the model is reliable because the strains results of numerical simulation were similar to the experimental results.

Conclusion: The results obtained in this study illustrate the accuracy of Finite Element Method has in simulate the biomechanical conditions, mainly in dental prosthesis. In this study, modeling techniques were improved and a reliable model was developed. In the next studies, this model will be used in the evaluation of fatigue problem in dental prostheses.

Disclosure of Interest: None Declared

AGE EFFECTS ON INTER-JOINT LOAD-SHARING AND MUSCLE ACTIVITIES DURING CYCLING

Jia-Da Li [1,*] Hsing-Po Huang [1] Hsuan-Lun Lu [1] Tung-Wu Lu [1][2]

[1]Institute of biomedical engineering, [2]Department of Orthopaedic Surgery, School of Medicine, National Taiwan University, Taipei, Taiwan, Republic of China

Introduction and Objectives: Deterioration of the musculoskeletal system due to geriatric degeneration has been studied in recent decades. Reduced muscular strength [1], ability of dynamic balance control [2], joint coordination, and sensory feedback would increase the risk of injuries and decreased quality of life. Cycling has been widely applied in the rehabilitation of lower extremities and also played an important role in transportation, recreation, and sport in our daily lives. Previous studies on the lower limb mechanics during cycling have focused mainly on young subjects. However, it remains unclear how the elderly would adapt their lower extremities to meet the demands during cycling. Knowledge of such adaptation strategies will be helpful for preventing injuries, improving rehabilitation efficacy and designing bicycles for the elderly. Therefore, the current study aimed to identify the changes of inter-joint load-sharing and muscle activities in the elderly during cycling when compared with the young.

Methods: Fifteen healthy older adults (Age: 77.4 ± 7.7 years, height: 164.9 ± 9.6 cm, mass: 68.7 ± 9.9 kg) and fifteen young healthy controls (Age: 25.0 ± 4.4, height: 171.4 ± 5.5 cm, weight: 72.1 ± 16.5 kg) participated in the current study. Each subject wore 30 skin markers on the pelvis and bilateral lower extremities, and performed cycling movement on a self-developed ergometer at an average resistance of 20Nm mimicking rehabilitation conditions. A metronome was used to control the cycling speed at 35 rpm. The 3D marker trajectories were measured using an 8-camera motion capture system at a sampling rate of 120Hz (Vicon Motion System Ltd., UK) and the pedal reaction forces were measured by a 6-component load-cell installed on the left pedal. Electromyography (EMG) of the rectus abdominis, erector spinae, left iliacus, gluteus maximus, rectus femoris, biceps femoris, tibialis anterior and gastrocnemius were measured (ZeroWire, Aurion S.r.l.). Maximum voluntary contractions (MVC) were also acquired for each muscle. Joint moments were calculated using inverse dynamics analysis. Inter-joint load-sharing was indicated by joint contributions defined as the ratio of the extensor moment of a single joint to the summation of the extensor moments of the three lower limb joints when the maximum crank torque occurred. The maximum value of the MVC-normalized EMG envelope was used to indicate the muscle contribution. An independent t-test was used to compare the calculated variables between groups at a significant level of 0.05.

Results: Significant differences in joint contributions were found at the hip and knee, the older adults showing increased hip contribution (older: 37.0%, young: 24.5%) but decreased knee contribution (older: 45.4%, young: 56.7%) although the knee extensor moments were the biggest among all the joints (Table 1). Significantly increased muscle activities were also found in the older group for most of the muscles except for the rectus abdominis, maximum EMG values ranging from 7.0% to 29.4% in the older group and from 4.3% to 18.8% in the young group. Both groups showed the highest activity in the rectus femoris muscle.

Figure:

Caption: An older subject was performing cycling

Conclusion: Under the same resistance and pedaling speed during cycling, the older group was found to increase their muscular activation when compared to the young, which may be related to the age-related reduction in muscle strength [1] when trying to maintain the pedaling speed. With this strategy, the older subjects increased the hip contribution to reduce the knee contribution because the knee extensor moments were the highest among the lower limb joints. This was achieved by increasing activations in most of the muscles, avoiding high contraction levels in a single muscle. The current results show that proper bike fitting (e.g., via changing the seat positions) is critical in the elderly to reduce knee extensor loadings and prevent overuse injuries.

Table:

	Elderly	Young	P-value
Joint Contribution (%)			
Hip	37.01 (10.11)	24.48 (7.65)	0.003*
Knee	45.37 (11.49)	56.69 (9.93)	0.019*
Ankle	17.62 (8.64)	18.84 (6.62)	0.707
Muscle Activity (%MVC)			
Iliacus	19.47 (8.27)	12.46 (5.97)	0.027*
Gluteus maximus	16.38 (6.98)	6.00 (2.64)	<0.001*
Rectus femoris	29.35 (13.09)	18.78 (9.39)	0.034*
Biceps femoris	20.40 (7.07)	8.02 (4.90)	<0.001*
Tibialis anterior	24.41 (8.30)	13.98 (4.00)	0.001*
Gastrocnemius	16.27 (6.34)	7.15 (2.59)	<0.001*
Rectus abdominis	6.95 (5.64)	4.29 (4.48)	0.219
Erector spinae	9.86 (4.75)	4.81 (3.40)	0.008*

Caption: Means (standard deviations) and P-values of the variables. * indicates statistical significance (p<0.05).

References: [1] Roos et al., Muscle & Nerve, Age-related changes in motor unit function, 20 (6): 679-690, 1997.

[2] Manchester et al., J Gerontol, Visual, vestibular and somatosensory contributions to balance control in the older adult, 44 (4): M118-M127, 1989.

Disclosure of Interest: None Declared

EXERCISE TRAINING IN OLDER PEOPLE CAUSES JOINT MOMENT REDISTRIBUTION DURING STAIR DESCENT

James P. Gavin [1,*]Neil Reeves [2]David Jones [2]Vasilios Baltzopoulos [3]Irene Di Giulio [4]Michael Roys [5]Costis Maganaris [1]

[1]Research Institute for Sports and Exercise Sciences, Liverpool John Moores University, Liverpool, [2]School of Healthcare Science, Manchester Metropolitan University, Manchester, [3]Centre for Sports Medicine and Human Performance, Brunel University, [4]Sobell Department of Motor Neuroscience and Movement Disorders, University College London, London, [5]Building Research Establishment, Watford, United Kingdom

Introduction and Objectives: Stair descent presents a physically demanding task, routine to everyday life, which is made more challenging by age-related deteriorations in lower-limb musculoskeletal capacities. Decline in functional mobility is particularly limiting in built environments, where stairs comprised of increased rise steps may be encountered. Stair descent involves mainly eccentric contractions, and with the old operating at higher maximum eccentric ankle capacities than the young [1], exercise training may allow older adults to meet the varying biomechanical demands of descent [2]. This study examined the effects of lower-limb exercise training on the biomechanics of older adults when descending standard, and increased rise stairs.

Methods: Fifteen older adults (age, 75±3 years) descended a four step stair adjusted to standard rise (170 mm), and 50% increased rise (255 mm) higher than those common to public and residential buildings [3]. Trials were on separate visits before, and after 16 weeks of either: resistance exercise and stretching training (n = 8), or no training (n = 7). Three, unaided trials were performed on each visit, at a self-selected pace. Kinematic and kinetic data were measured during a single gait cycle, referring to the left leg [4].

Kinetic data were measured from step-mounted force plates (Kistler type Z17068, Kistler Instruments, Winterthur, Switzerland), and kinematic data from motion-capture cameras at 120 Hz (VICON 612 system, VICON Motion Systems Ltd., Oxford, UK). Trials were calculated with a 'plug-in-gait' model, and processed by running a static and dynamic model using Workstation software (VICON Motion Systems Ltd., Oxford, UK).

Training involved two sessions per week of resistance exercises (three sets of ~8 repetitions for: leg-press, knee extension and calf-press, at ~80% three-repetition maximum), and static plantarflexor stretching (45 s holds, with three repetitions per leg). Eccentric, maximum voluntary contractions of the knee extensors (angular velocities of 60, 120, 180 and 240°·s^{-1}) and plantarflexors were assessed before, and after 16 weeks for training and control groups using an isokinetic dynamometer (Cybex NORM, New York, USA), as was maximum dorsiflexion angle. Repeated, two (time) x two (step rise) measures ANOVAs compared changes after 16 weeks for both groups on standard and increased rise stairs. Bonferroni Adjustments were used to identify step rise-specific training effects in each group. Data analysis was performed using IBM SPSS Statistics Version 21 (IBM Corp, Armonk, NY), with statistical significance as 0.05.

Results: Maximum eccentric torques increased at the knee (by 29.8% at 60°·s^{-1} and 43.2% at 180°·s^{-1}; P<0.001) and ankle (by 35.3% at 60°·s^{-1}; P=0.001) after exercise training, as did maximum dorsiflexion angle. Training did not alter ankle angles when descending either stair. Training decreased knee flexion angle in single-leg stance (P=0.03) on standard

stairs, and increased flexion angle upon final foot contact on increased rise stairs (P=0.001). Training did not affect hip flexion angle for either stair, but hip abduction angle increased in double support for increased rise stairs (P=0.04). Descending increased rise stairs required higher ankle and hip joint moments, and lower knee joint moments, when compared to standard stairs (P<0.001). Training reduced ankle joint moment (P<0.001), but increased knee joint moment (P=0.01), on increased rise stairs; training increased ankle joint moment (P<0.001), but reduced knee joint moment (P<0.01), on standard stairs. Training did not alter hip joint moments on increased rise stairs; upon standard stairs, hip flexion moment increased (from foot contact to double support, P<0.001) and hip abduction moment decreased (from single-leg stance to double support, P<0.05; Figure 1).

Figure:
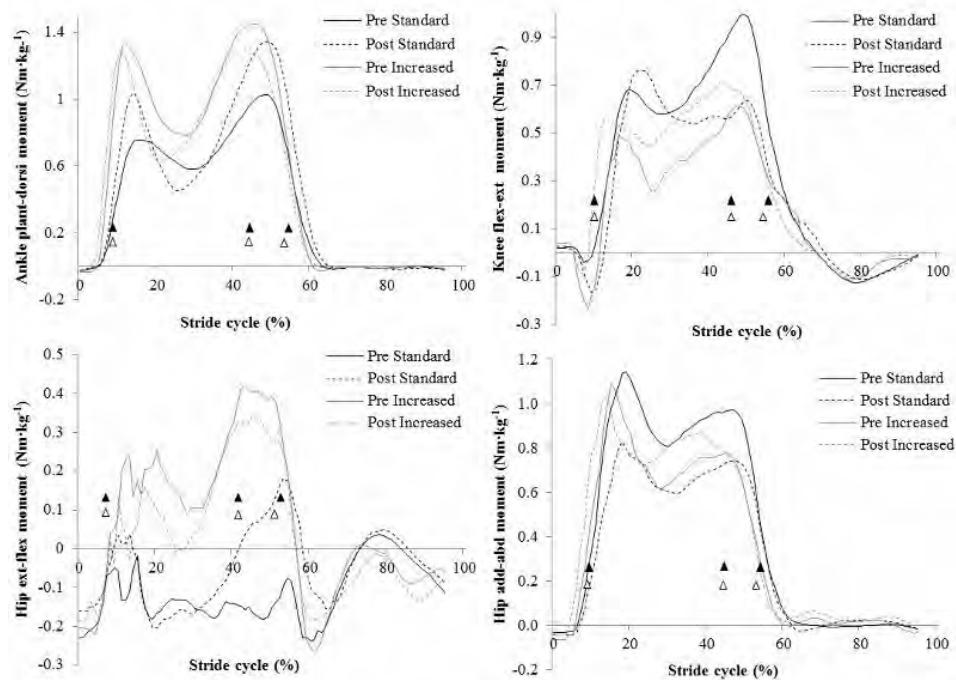
Caption: Figure 1. Lower-limb joint moments of older adults descending standard and increased rise stairs, pre and post-exercise training. Gait cycle events (· standard, · increased) refer to initial foot contact (0%), single-leg stance, double support, foot off and final foot contact with the above step (100%). Positive = abduction, negative = adduction.

Conclusion: Older adults after training descended i) standard rise stairs, by increasing ankle and hip joint moments, and reducing knee joint moments; and ii) increased rise stairs, by increasing knee joint moments and reducing ankle joint moments. These findings suggest older adults adopt neuromuscular strategies to meet the demands of stair descent, and strength improvements from exercise training can reorganise these strategies.

References: 1. Reeves ND, et al. *J Electromyogr Kinesiol*, 18: 218-27, 2008.

2. Capodaglio P, et al. *Age Ageing*, 34: 141-7, 2005.

3. Government HM. *Approved Document K - Protection from falling, collision and impact*, 2013.

4. Nadeau S, et al. *Clin Biomech*, 18: 950-9, 2003.

Disclosure of Interest: None Declared

Elderly

PO-0036

ASSOCIATION OF THE LENGTH OF INSTITUTIONALIZATION WITH OLDER ADULTS' BALANCE AND RISK OF FALLS

Gabriel Espinosa [1,*]Flávia Porto [2]Wagner Batista [1]Edmundo Drummond [1]Waldyr Castro [1]Jonas Gurgel [1]

[1]Fluminense Federal University, Niterói, [2]Rio de Janeiro State University, Rio de Janeiro, Brazil

Introduction and Objectives: The increase in longevity has raised various questions for the management of public policies, among which there is the increase in demand for Homes for the Aged (HAs). Living in these institutions, however, can promote social isolation, reduction in mental and physical activities, and a worsening in the older adults' quality of life. Moving to HAs is strongly associated with a decline in the abilities to undertake activities of daily living (ADLs) and a progressive reduction in opportunities for mobility. Consequently, this contributes to the failure to perform ADLs, inducing a hypokinetic routine for them, which becomes an intervening factor for falls. This study was realized in order to ascertain the association of the length of institutionalization with older adults' balance and risk of falls.

Methods: All subjects of this study live in a home for aged in a municipality of Três Rios, RJ, Brazil. From a total of 96 aged institutionalized, 40 subjects were eligible to take part in this study. Nevertheless, 4 of them were lost during the study (1 death; 2 bead resting and 1 returned for the family). The final sample size was composed by 36 elderlies. They were 75.44 years old, and havd Body Mass Index 22.67 kg/m². Subject's Length of Institutionalization varied between 07 and 231 months. The balance was assessed by three different methods. For the Berg Balance Scale, it was used the Brazilian-Portuguese validated version of the protocol. The test consists in a set of 14 different balance-related daily tasks. Each one classified between 0 and 4 (0 for the worst and 4 for the best performance). The maximal score is 56 that indicate the minor risk of fall. It was adopted the 41 value as a cutoff. The Get up and Go test was applied as proposed on the original protocol. Volunteers had to get up from a chair, walk 3 meters and then return fast as they could to the starting position, sited on the chair. The time was registered, and 20 seconds was considered as cutoff value. For the stabilometric tests, it was used a force plate. For the opened eyes test, subjects were requested to stand during 45 seconds at the center of the plate on orthostatic position, barefoot (30° between feet). There was a reference marked point 2.5 meters from de center of the plate on the wall to keep viewing fixed. The signal was processed and analyzed in a computer through the software LabVIEW (National instrumetns, 2012, for windows) and MATLAB (MathWorks, R2012a, for windows) respectively. After processing of the signal, the statokinesigram was analyzed considering the Elliptical Area as 95% (1.96 standard deviation of x and y axis) and mean velocities on the x and y axes of center of pressure displacement. The normality of data was tested by Shapiro-Wilk test, thus parametric (Pearson) and nonparametric (Spearman) correlations were used. The significance level was set at $\alpha \leq 0.05$.

Results: There was no significant correlation between the length of institutionalization and the tests for evaluation of risk of falling. The stabilometric parameters, on the other hand, demonstrated significance in the negative correlations between the elliptical area and the speed of the COP in the x axis (Table).

Conclusion: In the evaluation of the risk of falls proposed by the BBS and TUG clinical tests, a leveling effect was observed which was below the minimum established for their respective cutoff points. In the stabilometric behavior, a

reduction was noticed of the parameters of the COP whenever there is an increase in the LI of the older adults in the HAs, suggesting different strategies for postural control. These discoveries suggest the existence of an association of the LI with postural balance and the risk of falls; difficulty in undertaking motor tasks which require postural control is also indicated. These findings suggest that the length of residence in HAs negatively influences postural balance and, consequently, the risk of falls. This points out to the need to rethink health policy for institutionalized older adults, as well as to restructure the methods and strategies used in the care for the health of these individuals.

Table: Correlation of the lenth of institutionalization with balance and the risk of falls in older adults resident in Homes for the Aged. Três Rios, RJ, Brazil, 2012 (N=36)

Variable	Correlation	P
Berg Balance Score (0 to 56 points)	-0.264[‡]	0.119
Timed Get up and Go Test (s)	0.297[§]	0.077
Elliptical Area (cm²)	-0.597[‡]	0.003[*]
Mean speed of the COP in the x axis (cm/s)	-0.446[‡]	0.03[*]
Mean speed of the COP in the y axis (cm/s)	-0.279[§]	0.16

p=Level of significance; ‡Pearson Correlation; §Spearman Correlation; *Significant correlation ($p \leq 0.05$)

Disclosure of Interest: None Declared

Elderly

PO-0037

CHANGING OF MUSCLE FIBER CONDUCTION VELOCITY ON VASTUS MEDIAL MUSCLE WITH AGING

Kazuyuki Mito [1,*]Noriyasu Ota [2]Satoko Soga [2]

[1]Graduate School of Informatics and Engineering, The University of Electro-Communications, Tokyo, [2]Kao Corporation, Tochigi, Japan

Introduction and Objectives: A decrease of muscle due to aging is associated with the atrophy of fast twitch (Type II) muscle fibers [1]. The aim of this study is to elucidate the difference of muscular activity by aging with the use of muscle fiber conduction velocity (MFCV).

Methods: The subjects were 42 healthy male volunteers 22-77 years of age, and they provided a written informed consent to participate in this study after a detailed explanation including the purpose and procedures of the experiment. The subject was seated in a chair and knee joint angle of dominant foot was fixed at 90-degrees, and maintained an isometric contraction force of 20%, 40% and 60% of the maximum voluntary contraction (MVC) for 5 seconds.

The surface myoelectric signals were measured by an electrode arrays which were installed on on vastus medial muscle. The electrode arrays were composed 5 silver-silver chloride poles each with a diameter 2 mm and a height of 3 mm attached on a silicon rubber plate (Unique-medical Co., Japan). The inter-electrode distance was 5 mm. The myoelectric signals detected between adjacent silver-silver chloride bars was amplified with use of differential bioelectric amplifiers. The frequency range and the gain of amplifier were set from 5 Hz to 1000 Hz and 60 dB, respectively. The amplified myoelectric signals of 4 channels were stored on a personal computer through an A/D converter with a 16-bit resolution and with a sampling frequency of 10 kHz. The muscle fiber conduction velocity (MFCV) was calculated by cross-correlation methods [2]. The cross correlation coefficient was evaluated from the two myoelectric signals in the neighboring channels. In each contraction force, Peason's correlation coefficient (r) was used to study the relationship between MFCV data and age.

Results: A significant statistical negative correlation was observed in 40% and 60% MVC between MFCV and age as shown in Figre 1. Peason's correlation coefficient (r) and corresponding P values for those correlation in 20, 40, 60%MVC were r = -0.224, -0.556, and -0.635, and P=0.153, 0.001, 0.001, respectively. As the muscle force is large, the MFCVs were significantly reduced depending on the age.

Figure:
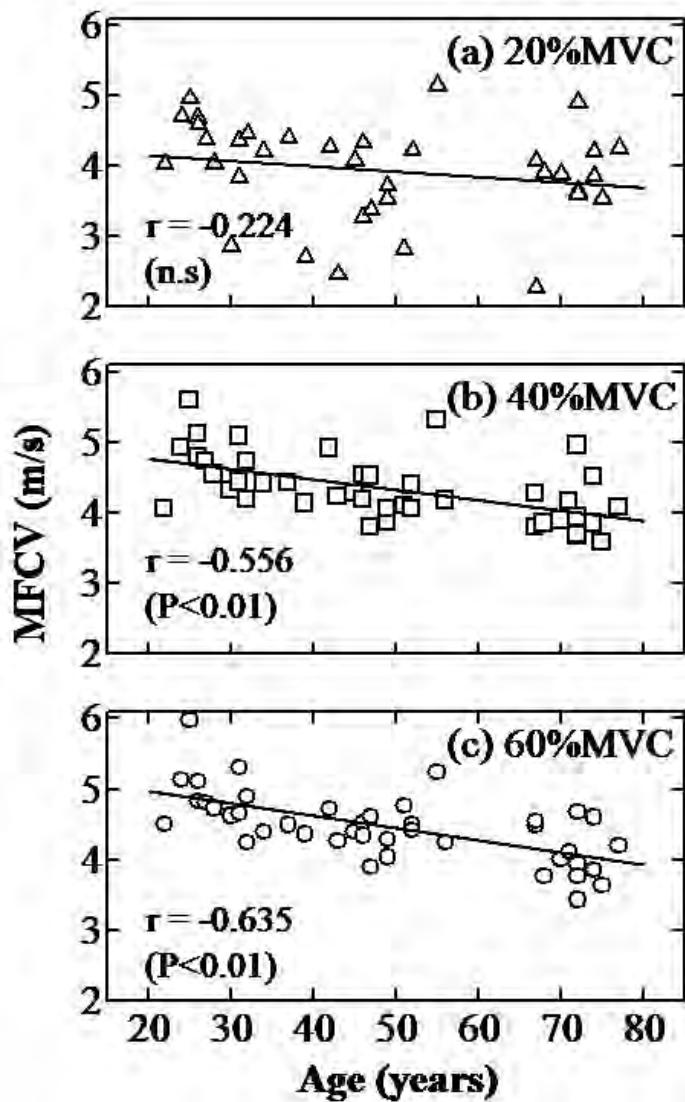
Caption: Relationship between MFCV and age in (a) 20%, (b) 40%, and (c) 60%MVC.

Conclusion: In high contraction force, the values of MFCV were decreased in according to age. The fast twitch muscle fiber which MFCV is faster than slow twitch muscle fiber are mainly active in strong muscle contraction.

Therefore, the reduction of MFCV at 40% and 60% MVC due to aging might reflect the atrophy of fast twitch muscle fiber.

References: [1] Lexell et al., Journal of the Neurological Sciences, 84, 275-294, 1988

[2] Roy et al. J. Appl. Physiol., 61, 1510-1517, 1986

Disclosure of Interest: None Declared

Elderly

PO-0038

ELDERLY WOMEN'S QUADRICEPS ACTIVATION IN RESPONSE TO A POWER KNEE EXTENSION TASK: A CONTINUOUS WAVELET ANALYSIS APPROACH

João P. Pinho [1,*]Bruno Mezêncio [1]Desidério Porras [2]João Claudino [1]Rafael Soncin [1]Ana Azevedo [1]Juliana Pennone [1]Julio Serrão [1]Alberto Amadio [1]

[1]Laboratory of Biomechanics, University of São Paulo, [2]Department of Physical Therapy, School of Medicine, São Paulo, Brazil

Introduction and Objectives: Among the main qualitative muscle changes in aging muscle power loss is the one that early occurs suggesting it as the most striking muscle alteration in the senescent locomotor system. Corroborating this statement, TSCHOPP et al. [1] pinpoint muscle power as the main independence determinant in the elderly. The authors showed that when compared with maximum muscle strength this parameter presents an earlier and abrupt reduction. Moreover, GREENLUND & NAIR [2] showed that between the third and the eighth decades the knee extensors ability to generate peak torque suffers a significant decline. The functional capacity diminution multifactorial origin makes the ideal exercise protocol to increase this ability to perform everyday tasks unclear. Notwithstanding, TSCHOPP et al. [1] suggest power training as the best nonpharmacologic strategy to attenuate, or even reverse, that functional capacity declining over one's life. A problem that arises alongside with this new protocol is the one related with the optimum training load. In fact, although for athletes the ideal training load to produce maximum power is known, for the elderly this is still to be found. Therefore, this study's aim was to investigate the training load that permits sedentary elderly women to produce the maximum peak power as well as examine their knee extensors electromyographic activation by a continuous wavelet analysis.

Methods: Thirteen sedentary elderly women aged between 65 and 70 years old (69,3 ± 4,06 years) took part in the study. The participants were previously informed of all of the operational procedures and gave their Written Consent informing that their involvement in the study was voluntary. The study was approved by the local Ethics Committee. The experiments were conducted in a conventional knee extensors machine (Gervasport Fitness Equipment) ensuring that the participants' trunk and thigh remained immovable. To avoid any risks to the participants' physical integrity a sub-maximum test was conducted. After estimating the maximum load effort by Brzycki [4] equation 3 load regimes were calculated: 30%, 50% and 70%. In a randomized order the participants executed 6 repetitions of each load condition with the concentric phase of the knee extension movement as quickly as possible. Reflexive markers were attached to the participants' ankle and knee axis being the knee aligned with the leg extensor machine axis. A digital video camera (Casio EX-ZR10) with an acquisition rate of 240Hz and a shutter speed of 1/2000s recorded the trials. The markers were digitized by the *Ariel Performance Analysis System* (*Ariel Dynamics, INC*). An external trigger was used to synchronize the video capture with an electromyography system (Lynx technology). Using the SENIAM procedures vastus lateralis and rectus femoris were monitored. A continuous wavelet analysis was used as a time-frequency transformation strategy of our EMG data. Daubechies 44 was selected to perform the transformation since it was found to be the most similar mother wavelet function to EMG signal [5]. All mathematical procedures were performed in MatLab (Mathworks, Inc).

Results: The repeated measures ANOVA showed an increased peak power in the 70% (221±84 W) and 50% load conditions (217±94 W) when compared with the 30% regime (185±78 W). Although no differences were seen between the conditions in the total median frequency (MF) of the studied muscles, the MF 200 milliseconds before the peak power in the 70% (69±23 Hz) condition was found to be different (p=0.009) that the 30% condition (58±17 Hz).

Figure:
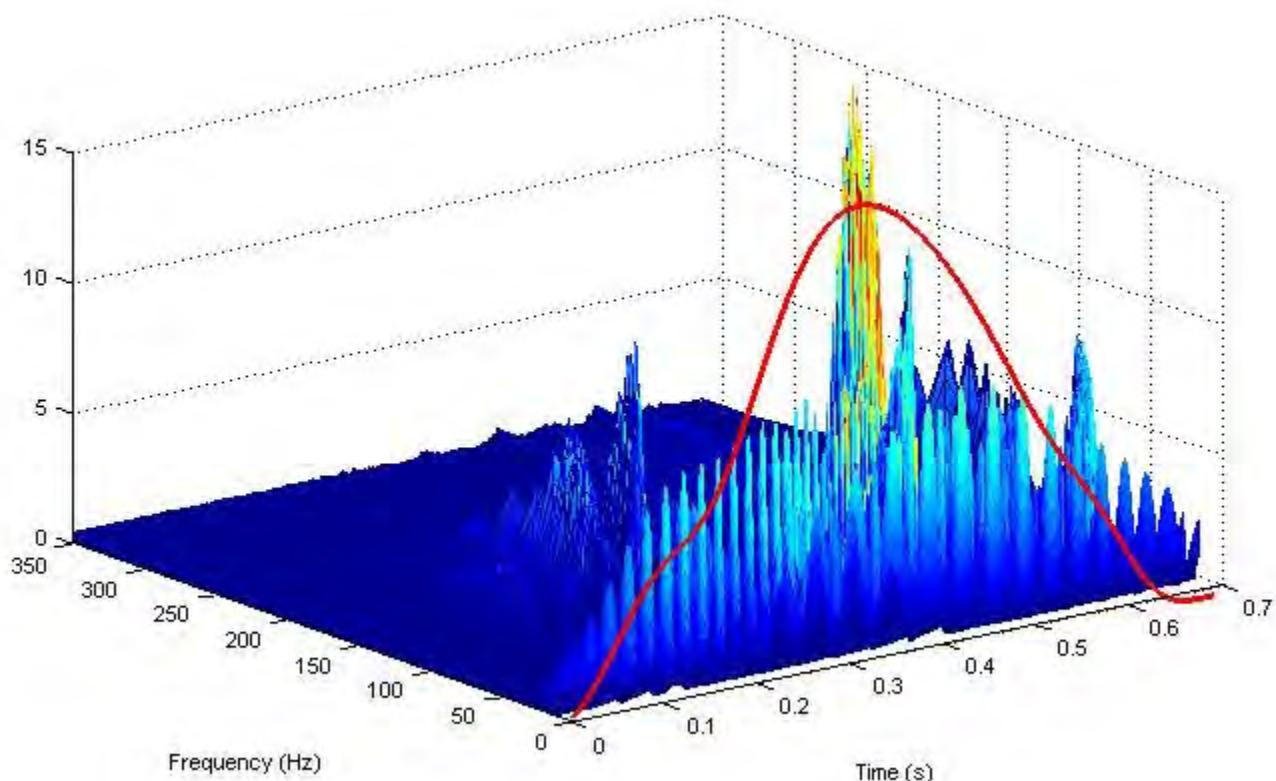
Caption: Example data of the continuous wavelet transform db44 (3D graph) and knee extensors power (2D red line).

Conclusion: The results of the present study showed that in order to obtain higher peak power older adults need to exercise with higher loads. The wavelet analysis approach that allowed to obtain time as well as frequency resolution suggests that the load increment activates muscle fibers with higher frequency rates which could mean a better fast twitch fibers recruitment, which in turn have a close relationship with elderly's functional capacities. To the authors' best knowledge this is the first study to explain how the elderly's knee extensors are able to generate greater knee extension power with higher load regimes.

References: [1] Tschopp et al., *Age Ageing*, 40,5:549–556, 2011.

[2] Greenlund et al., *Ageing Dev.*,124,3:287–299, 2003.

[3] Brzycki, *J. Phys. Educ. Recreat. Danc.*, 68:88–90, 1993.

[4] Rafiee et al. Expert Syst Appl, 38:6190–6201, 2011.

Disclosure of Interest: None Declared

PO-0039

INFLUENCE OF THE LENGTH OF INSTITUTIONALIZATION ON OLDER ADULTS' POSTURAL CONTROL

Wagner Batista [1,*]Flávia Porto [2]Gabriel Espinosa [1]Edmundo Alves Junior [1]Waldyr Castro [1]Jonas Gurgel [1]

[1]Fluminense Federal University, Niterói, [2]Rio de Janeiro State University, Rio de Janeiro, Brazil

Introduction and Objectives: In human aging, postural control changes are perceived. These changes are related to a reduction of sensorial capabilities of the locomotor system and the interactions of different systems to realize adequate actions and reactions to maintain balance. The longevity increase have brought a number of relevant questions to the public health policies, among others, an increase of demand for Homes for the Aged (HAs). Otherwise, to reside in an HAs may contribute to social isolation, a reduction of mental and physical activities and a decrease of quality of life among elderly. The institutionalization of elderly in an HAs may be accelerating the physiological decline what shows restrictions to the maintenance of cognitive and motor abilities, essential to postural control. The aim of this study was to verify the effects of the length of institutionalization in HAs on postural control and stability limits of elderly subjects.

Methods: To evaluate the center of pressure (COP) behavior during the quasi-static stabilometry was utilized a force plate. The analyzed variables were COP velocities (cm/s) (in both, x axis and y axis) and 95% of COP elliptical area (cm2). The groups were stratified using the variables: residential time on HAs, age, fallers and non-fallers. Data were analyzed using independent Student´s t-test (parametric data) or Mann-Whitney test (non-parametric data). Each test was used to compare the different groups, stratified by length of institutionalization in HAs (7-63 months LI1 e 65-231 months LI2) and fallers and non-fallers. One way ANOVA with Tukey post-hoc test (parametric data) or Kruskal-Wallis with Dunn post-hoc test (non-parametric data) were used to compare the subgroups stratified by age and length of institutionalization in HAs (LI1AG1, LI1AG2, LI2AG1 and LI2AG2). For all tests, the significance level adopted was $\alpha \leq 0.05$.

Results: The data shows (Table) a reduction on the COP variables analyzed when the length of institutionalization in HAs increases. Mainly, this reduction can be perceived on the COP velocity in both axes and in the 95% of elliptical Area, comparing the LI1 e LI2 groups. Fallers and non-fallers presented significant differences on all COP variables, showing smaller valor on fallers group. The results did not show significant differences between the age groups with the same length of institutionalization in HAs, showing only significant differences between the groups with different length of institutionalization in HAs.

Conclusion: The presented results of the variables analyzed suggest a not usual COP behavior, what is in the opposite direction of classical scientific evidence. Otherwise, the same behavior was found by some researchers investigating debilitated population. What can be explained by a change on postural control strategies of the more debilitated elderly subjects, decreasing the limits of stability and the possible area for COP oscillation. The age does not appear to be an issue to change the COP behavior, but the length of institutionalization in HAs appears to be.

Table:

Variable	LI1 (7-63 months)	LI2 (65-231 months)	p	Faller (n=19) 52.77%	Non-faller (n=17) 47.23%	P
Elliptical Area (cm^2)§	22.06 (10.9)$^{\|}$	9.10 (7.8)$^{\|}$	0.003¶	10.71 (4.1)‡	20.30 (7.3)‡	0.022¶
Mean speed of the COP in the x axis (cm/s)§	1.99 (0.8)$^{\|}$	1.32 (0.8)$^{\|}$	0.032¶	1.08 (0.8) $\ddagger$	1.88 (1.1) $\ddagger$	0.006¶
Mean speed of the COP in the y axis (cm/s)†	2.84 (1.36)‡	1.47 (1.4)‡	0.848	1.42 (1.3) $\ddagger$	2.84 (1.4) $\ddagger$	0.016¶

§Student t test, ||Mean and (standard deviation), †Mann-Whitney non-parametric test, ‡Mean and (standard deviation), ¶ Significant difference (P≤0.05)

Disclosure of Interest: None Declared

PO-0040

THE EFFECTS OF TAI-CHI EXERCISE ON COUNTERMOVEMENT JUMP IN OLDER ADULTS

Bo-Jen Ko [1,*]Chen-Fu Huang [1]Po-Chieh Chen [1]Tai-Yen Hsu [2]

[1]Physical Education, National Taiwan Normal University, New Taipei City, [2]National Taichung University of Education, Taichung, Taiwan, Republic of China

Introduction and Objectives: Lower limb muscle strength has great impact on functional performance of daily activities. Weakness lower limb muscle strength may cause fall risk. Previous research has been reported that muscle power decline 1.2%~2% per year after 65 years old [1]. Regular exercise is essential for older adults in order to maintain muscle function.

   Many studies has been confirmed that Tai Chi exercise has advantages on people such as pain reduction, fall prevention and improvement on balance, strength and flexibility[2][3], but the advantage of lower limb biomechanics on elderly is still unclear. The counter movement jump (CMJ) is an efficient physical performance test which is common used for young adults and can be used to estimate lower limb biomechanics in older adults.

The purpose of this study was to investigate the biomechanical effects of Tai-Chi exercise in older adults by using CMJ test.

Methods: Nine older adults with regular Tai Chi exercise experience (age: 60.56 ± 2.4 yrs; height: 158.22 ± 6.53 cm; weight: 60.28 ± 6.07 kg) and nine older adults without regular and systematic physical training (healthy elderly: age: 62.22 ± 1.71 yrs; height: 155.89 ± 9.03 cm; weight: 58.78 ± 8.12 kg) participated in this study.

Ten cameras (Vicon MX13+, Oxford, UK, 250Hz) were used to record CMJ data. Two Kistler force plates (Kistler Instrumente AG, Winterhur, Switzerland, 1000Hz) were used to record the ground reaction forces (GRF) while the subjects performed 3 maximal effort CMJs. Vicon Nexus 1.81 and Visual3D V5 software were used to analyze kinematics and kinetics data. All data were analyzed by using an independent sample t-test ($\alpha = .05$).

Results: The results in table 1 showed that Tai Chi group had greater jump height. ($p<.05$). Tai Chi group also had greater peak vertical force as well as peak hip, and ankle moments in jump phase ($p<.05$).

These results showed Tai Chi group had greater lower limb muscle strength in hip and ankle and thus muscle strength could be enhanced by training Tai Chi exercise. Tai chi exercise usually used lower center of gravity pose to move their body and it could be the possible reasons for these results. It was concluded that older adults participated in Tai Chi exercise training had better performance in a maximal effort CMJ.

Figure:
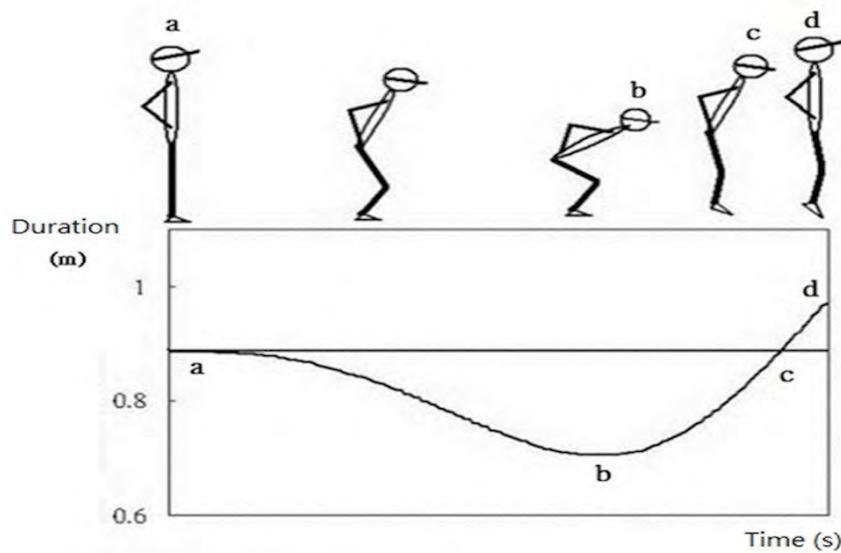
Caption: CMJ Phase (a~ b: Countermovement phase; b~ c: Jump phase; c~ d: Air phase)

Conclusion: The Tai Chi group exhibited a better ability to generated energy to increase the CMJ jump height which indicated that Tai Chi exercise might be able to enhance muscle strength of lower extremity in older adults. These performance enhancements might also influence the functional performance of elder daily life and reduce fall risk.

Table:

Parameter	Tai Chi		Healthy elders		
	M	*SD*	*M*	*SD*	*P*
Countermovement phase					
Duration (ms)	632.80	58.10	674.42	143.24	0.375
COM displacement (cm)	24.46	10.70	25.54	9.86	0.715
Hip degree (deg)	80.85	23.21	75.60	15.72	0.842
Knee degree (deg)	74.06	23.44	77.47	10.53	0.183
Ankle degree (deg)	23.66	7.75	20.46	6.71	0.260
Jump phase					
Duration (ms)	302.3	68.20	334.62	69.53	0.320
COM displacement (cm)	35.01	10.40	35.34	9.66	0.840

Peak vertical force (N/Kg)	22.54	4.44	20.61	3.95	0.032 *
Peak hip moment (N-m/Kg)	0.71	0.39	0.57	0.21	0.021 *
Peak knee moment (N-m/Kg)	0.98	0.29	0.92	0.28	0.328
Peak ankle moment (N-m/Kg)	0.33	0.19	0.29	0.15	0.014 *
Air phase					
Jump height (cm)	28	4.20	20.90	3.40	0.001 *

Caption: Tai Chi and the healthy group CMJ data

References: [1] Grieg et al., Age and Ageing, 23: 371- 377, 1995.

[2].Gatts et al., Gait posture, 25: 205-214, 2007.

[3].Li et al., Journal of Biomech, 42: 967–971, 2009.

Disclosure of Interest: None Declared

ESTIMATING THE EFFECT OF ERGOMETRIC PEDALING EXERCISE IN ELDERLY PERSONS BY USE OF EMG

Kenichi Kaneko [1,*]Masako Shisido [1]Kazuyuki Mito [2]Hitoshi Makabe [3]Kazuyoshi Sakamoto [4]

[1]Industrial Engineering and Management, Fuji University, Hanamaki, [2]Informatics and Engineering, The University of Electro-Communications, Chofu, [3]Physical Therapy, Yamagata Prefectural University of Health Science, Yamagata, [4]Activation Research, The University of Electro-Communications, Chofu, Japan

Introduction and Objectives: Japan has the highest proportion of older adults in the world. It is called "Super-Aging Society". The population of person requiring care has been over four millions since 2005 in Japan. A fall and born fracture is one of the main causes of requiring care. Resistance trainings of muscles on the lower limbs are required to prevent the fall and born fracture. We studied on an effect of ergometric pedaling exercise as the resistance training of lower limb muscles in elderly persons. To estimate the effect of ergometric pedaling exercise, electromyographic activities of lower limb muscles in elderly persons were compared with the pre-ergometric pedaling exercise and the post-ergometric pedaling exercise (after a month). Furthermore, the ergometric pedaling exercise was carried out on young competitive road cyclists and young non-cyclists. The EMGs for the lower limb muscular activations were evaluated by using of values of RMS and Wavelet Transform. The comparisons of these values were useful to understanding the effect of ergometric pedaling exercise from the view point of kinesiological motor skills.

Methods: The subjects were three elderly females (ages 60-90 yr), five young competitive road cyclists (ages 18-22 yr) and five young non-cyclists (ages 21-22 yr). All subjects had an ergometric pedaling exercise (for 15min with 50% MVC) twice a week for a month. The electromyographic activity during ergometric pedaling was measured in the Rectus femoris (RF), the Biceps femoris (BF), the Tibialis anterior (TA), and the Gastrocnemius medialis (GM) by using of the wireless EMG sensors (Trigno Wireless System, DELSYS, U.S.A.). The EMG signals were stored on a personal computer through an A/D converter with a sampling frequency of 1 kHz. The EMG activities were evaluated by RMS, %RMS, and dimension of frequency. Firstly, the RMSs were calculated for the generating EMG relation to the ergometric pedaling on four muscles (RF, BF, TA, and GM). The starting time and the ending time for the generation of the EMG waveform were defined here as the amplitude reached and stabilized at 10% of the peak to peak. Secondly, the %RMSs were calculated as follows. The pedaling dynamics divided into two phases were the "down phase" and the "up phase" from the view point of the crank angle (down phase; 0 to 180 degree, up phase; 180 to 360 degree, respectively). The %RMS values for the EMG during the pedaling were calculated at a ratio of the RMS for the down phase to the RMS for the up phase. Finally, the Time-frequency analysis of the EMG signals were conducted using continuous wavelet transform (CWT). In addition to the CWT, the EMG data segments were also processed with a Daubechies 4 wavelet algorithm. The EMG data were decomposed into six separate scales (j=-1; 125-250 Hz, j=-2; 62.5-125 Hz, j=-3; 31.25-62.5 Hz, j=-4; 15.625-31.25 Hz, j=-5; 7.8125-31.25 Hz, and j=-6; 3.906-7.8125 Hz).

Results: Figure 1 showed that the values of RMS of the RF and the TA were increased by the ergometric pedaling exercise for a month in elderly persons. On the other hand, the young competitive road cyclists have decreased the muscle activities of the RF, the BF, and the TA in the post-ergometric pedaling exercise (after a month). The only muscle

activity of the GM was increased by the ergometiric pedaling exercise in young competitive road cyclists. The means of %RMSs for the BF and the GM were higher than 100% in the pre-ergometric pedaling exercise. In contrast, the mean of the %RMSs for the RF and the TA were lower than 100%. The individual differences of the %RMSs for the BF and the GM were larger than that for the RF and the TA in the young competitive road cyclists. There was no difference between the elderly persons, young competitive road cyclists, and the young non-cyclists about all %RMS values, though, the %RMS values at the TA and the GM were significantly difference between the three subject groups. The mean power of wavelet decomposition (Ej) are compared. The values of Ej for the young competitive road cyclists were significantly larger than that of the elderly persons and the young non-cyclists at j=-1, -2, -3, -4, -5 (from 7.81 Hz to 250 Hz).

Figure:
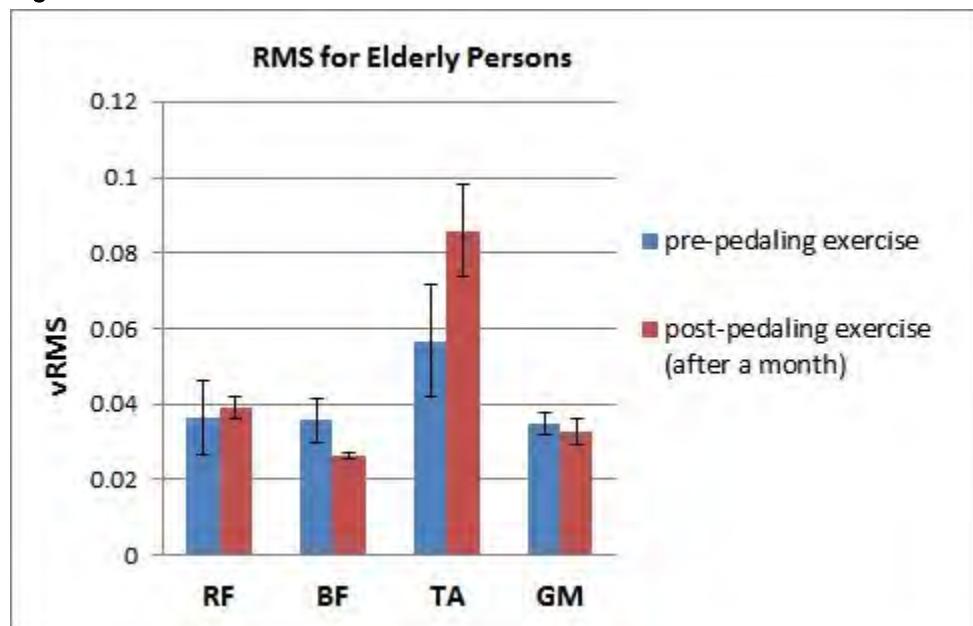
Caption: Figure 1. Root mean square (RMS) for EMG activities of four lower limb muscles relation to pedaling load in elderly persons.

Conclusion: These results suggested that the value of RMS, %RMS, and Ej at the TA and the GM were useful indices to evaluate the effect of the ergometric pedaling exercise in elderly persons.

References: [1] Hug F., Dorel S., J Electromyogr Kinesiol,19: 182-198, 2009.

Disclosure of Interest: None Declared

Elderly

PO-0042

CHARACTERISTICS OF THE GAIT IN ELDERLY PEOPLE WITH EXERCISE HABITS

Kentaro Takahashi [1,*]Minato Kawaguchi [1]

[1]College of Science and Technology, Kanto Gakuin University, Yokohama, Japan

Introduction and Objectives: While many studies on elderly people have analyzed the reduction in walking ability with increasing age, most of them were performed in the elderly population as a whole; few studies have assessed the gait of elderly people with exercise habits. This study aimed to analyze gait in elderly people with exercise habits and thereby elucidate its characteristics. This study aimed to analyze gait in elderly people with exercise habits and thereby elucidate its characteristics.

Methods: This study was performed in healthy young people and healthy elderly people who exercised once in a week. The subjects were instructed to walk on a path with a normal gait over 5 trials such that one foot passes each of the 2 force plates at least once during an analysis; these analyses were performed using a VICON system. A gait cycle, which was recorded in the middle of the measurement period, was obtained from the measurement data that were normalized to 100%. The muscle activities at 6 sites during walking were simultaneously recorded by performing electromyography for the right leg of each subject.

Results: In elderly people with exercise habits, the hip-flexion moment in the pre-swing phase was high and the hip-flexion angle from the initial swing phase to the terminal swing phase after the pre-swing phase was also high. Therefore, in comparison with younger people, these individuals show greater utilization of their hip and hamstring to elevate the lower extremity during outward motion of the extremity of the swing side. In the elderly people with exercise habits, the knee-extension moment and knee-flexion moment were high in the terminal-stance and terminal-swing phases and in the pre-swing phase, respectively, during elevation/forward movement of the lower extremity of the swing side; these findings indicate that in comparison with younger people, elderly people with exercise habits show greater utilization of knee-extension muscles in the terminal stance and terminal-swing phases and of the knee-flexion muscles in the pre-swing phase during the abovementioned movement. And, the RMS values for several muscles during a gait cycle were significantly higher than the corresponding values in young people.

Conclusion: Our results suggest that due to the habituation associated with training, the gait in elderly people with exercise habits is consciously modified to achieve motional effects as high as that achieved during walking training. Therefore, in such elderly people, the hip/knee/ankle have a wider range of motion during elevation/forward motion of the lower extremity of the swing side in comparison with the range of motion in general elderly or young people, and the hip flexion or knee extension/flexion muscle activation in these elderly people are more than those in young people or in elderly people with no exercise habits, thereby permitting a gait in which the said hip flexion and knee extension/flexion was achieved with a high motional effect. Furthermore, the results also suggested that biarticular muscles successfully compensate for the age-associated strength reduction of monoarticular muscles.

Disclosure of Interest: None Declared

AGE-RELATED REDUCTIONS IN THE LENGTH AND NUMBER OF SERIAL SARCOMERES CONTRIBUTE TO SHORTENED FASCICLE LENGTHS: A SOURCE OF ELEVATED PASSIVE TENSION IN THE ELDERLY?

Geoffrey A. Power [1],*Sean Crooks [1]Jared R. Fletcher [1]Brian R. MacIntosh [1]Walter Herzog [1]

[1]Human Performance Lab, University of Calgary, Calgary, Canada

Introduction and Objectives: With natural adult aging, there is a loss of muscle mass and alterations to the structural components of the human muscular system that results in impaired contractile function and performance [1, 2]. Muscle weakness associated with old age contributes to declines in neuromuscular function and is associated with impairments in activities of daily living [3]. On the other hand, older adults maintain force production during lengthening contractions (i.e. eccentric contraction) relative to other contraction modes [1]. The age-related maintenance of eccentric strength is evident in whole muscle and skinned single fibre preparations [1]. In addition to many of the mechanisms proposed for the preservation of eccentric strength, alterations to the structural properties of the muscle fascicle leading to elevated passive force have not been investigated [4]. A potential unexplored mechanism for increased passive force in old age could be decreased muscle fascicle lengths owing to either a decrease in the number of sarcomeres in series and/or shorter sarcomere length [5]. Thus for a given joint angular rotation, decreased fascicle length will result in greater sarcomere length change of muscles from old as compared to young rats, resulting in increased stiffness in the aged muscles, contributing to elevated passive tension and higher relative forces during lengthening. The purpose of this study was to compare the medial gastrocnemius (MG) of young and old rats to determine fascicle length, serial sarcomere numbers and the sarcomere length at which peak force is obtained (i.e. plateau of the force-length relationship; L_o). It was hypothesized that fascicle length in old rats would be shorter compared with young owing to fewer sarcomeres in series, however, the sarcomere length at L_o in old rats will remain unaltered as compared with young.

Methods: Two groups of Fisher344x Brown Norway hybrid rats ($n = 17$) were used in this experiment, a young cohort (7-8 months ≈20 human years) ($n = 9$) an old cohort (30-35 months; ≈75-80 human years) ($n = 8$). The MG from the right leg was surgically isolated, attached to a custom made muscle puller and force transducer. For whole muscle activation, the tibial nerve was isolated and electrically stimulated via a nerve cuff. The L_o was determined by performing a standard force-length relationship. Contractions were evoked at 200 Hz of 250 ms duration separated by 2 min rest across muscle lengths corresponding to the: ascending, plateau, and descending limb of the force-length relationship. The animals were then sacrificed and the hind limb was immediately placed in a VWR 10% Formalin (fixative) solution at the muscle length corresponding to L_o. After a 1 h period of fixation, the MG muscle was firmly secured to a wooden applicator stick at L_o and allowed to fix for a 2 week period in a VWR 10% Formalin solution. The muscles were then dissected into 4 lengthwise sections medial and lateral of the center of each MG muscle belly. After a 4 hour, 30% nitric acid digestion process, 5 individual fascicles from each muscle section were isolated and placed on slides for sarcomere length measurement at 5 locations along the fascicle by laser diffraction. In this method, the laser beam (1mm wide, λ=630 nm) penetrated through the thin actin filaments, but not the thick myosin filaments, creating a superposition of gratings of

aligned myofibrils [7]. The first order diffraction distance was used to mathematically determine the average sarcomere length in the measured area (Figure 1A).

Results: A reduction in muscle fascicle length of ~14% was observed in the old rats (average = 11.3 ± 1.0 mm) when compared to young rats (average = 13.1 ± 1.1 mm), $P < 0.05$. There was a reduction in average sarcomere length of ~4 % observed in the old rats (average = 2.22 ± 0.11 μm) versus the young rats (average = 2.31 ± 0.05 μm), $P < 0.05$. The MG of old rats showed ~10% fewer sarcomeres in series (average = 5087 ± 465 sarcomeres) when compared to young rats (average = 5684 ± 440 sarcomeres), $P < 0.05$ (Figure 1B.).

Figure:
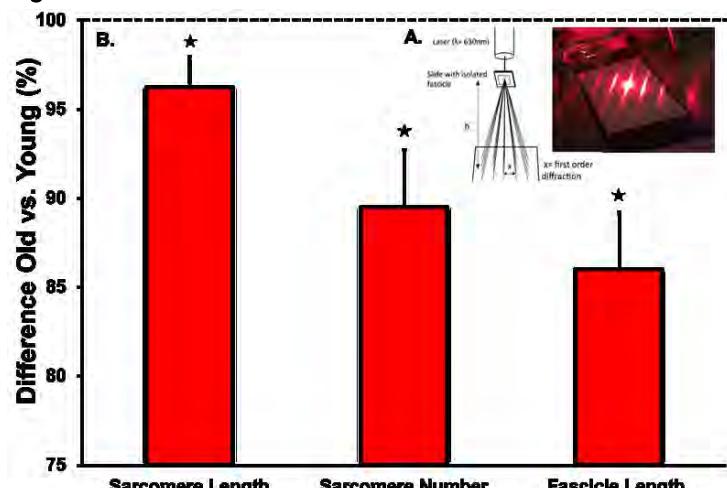
Figure 1. **A.** Laser diffraction set up and diffraction pattern. **B.** Percent difference in sarcomere length, sarcomere number and fascicle length from the MG of young rats (100%-dashed line) vs. old rats (red bars) measured at L_o. Bars indicate standard error. Significance indicated by ★ ($P<0.05$).

Conclusion:

The results of this study were in accordance with the hypotheses that as individuals age, not only are sarcomeres lost in parallel but are also lost in series, resulting in shorter fascicles. But quite unexpectedly average sarcomere length was shorter at L_o in the old compared with young muscle. The functional consequences of these age related changes could be a reduced range of motion for older adults and less force production capacity throughout that range of motion to perform activities of daily living. These results may also help to explain the increased passive tension observed for muscles of older individuals.

References:

[1] Power, Dalton & Rice. *J Sport Health Sci.* **2**:215-226, 2013.

[2] Narici, Maganaris, Reeves, & Capodaglio, *J Appl Physiol.* **95**:2229-2234, 2003.

[3] Li et al. *J Gerontol.* **58**:283-290, 2003.

[4] Roig, et al. (2010). *Exp Gerontol.* **4**:400-409, 2010.

[5] Lieber et al. (1984). Biophys. J **45**:1007-1016, 1984.

Disclosure of Interest: None Declared

DOES A PROLONGED WALKING SESSION IMPAIR STAIR NEGOTIATION IN THE ELDERLY?

Marcos R. Kunzler [1],*Emmanuel Rocha [1]Maarten Bobbert [2]Felipe Carpes [1]

[1]Applied Neuromechanics Research Group, Federal University of Pampa, Uruguaiana, Brazil, [2]University Amsterdam, Amsterdam, Netherlands

Introduction and Objectives: Elderly self-report climbing up and down stair as being a difficult activity in daily life [1], and difficulty with stair locomotion serves to predict functional decline in the elderly [2]. A routine of chronic aerobic exercise can improve mobility and stability in the elderly [3, 4]. However, single sessions of exercise eliciting fatigue in the lower extremity were shown to impair performance in both unobstructed level ground walking and obstacle crossing in the elderly [5, 6]. Here we set out to determine whether prolonged walking also has an acute effect on foot clearance during stair ascent in elderly.

Methods: Thirty elderly (age 67 ± 5 years, height 1.55 ± 0.05 m, body mass 65.4 ± 11 kg) participated in this study. Participants wore casual street shoes in order to achieve natural gait patterns. After 3 min of familiarization with walking on a treadmill, they walked during 30-min on the treadmill at their preferred speed, which was on average 4.05 ± 0.9 km/h. Before and after the prolonged treadmill walking, the participants performed at least 10 trials of locomotion on a three-step stairs built according to the recommended standards in Brazil (rise height 17 cm for each step, tread depth 30 cm, without nosing, and width 90 cm). The ascent phase of stair locomotion was considered in this study. Kinematic data were recorded using a motion analysis system (Vicon Motion Systems, Oxford, UK) with fifteen cameras sampling at 120 Hz. Retroreflective markers were attached to the participants' body and to the stairs. Positional data were processed using the Nexus 1.5.2 software and foot clearance (FC), defined as the vertical distance between foot and stair when the foot was right over the edge of each step. Foot clearances were analyzed for steps with the preferred foot leading. Leg preference was determined using the revised Waterloo inventory. Normality of data distribution was checked using Shapiro-Wilk and with the data considered parametric, to compare foot clearance pre versus post walking in each step of the stairs we used t-test for paired samples (SPSS version 21.0) at a 0.05 level of significance.

Results: After exercise, foot clearance was lower for step 1 ($t_{(29)}$= 2.074, p= 0.047) and 2 ($t_{(29)}$= 2.082, p= 0.046). However, the differences were very small in amplitude (on average less than 5 mm).

Figure:
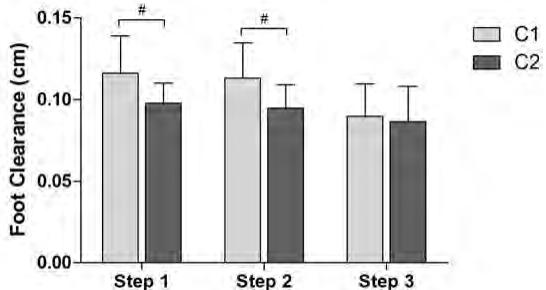
Caption: Figure 1. Foot clearance before (C1) and after prolonged walking (C2), considering the three steps of the stairs. # Indicates significant difference between before and after walking (P<0.05).

Conclusion: Walking at preferred speed during 30 minutes on a treadmill decreased foot clearance in the elderly during negotiation of stairs. From the three steps analyzed, decreased foot clearance was observed in the first and second steps. We were not able to measure force output before and after exercise. Most likely the prolonged exercise caused a reduction in force output, like it did in other studies [5, 6], causing a reduction in lower limb elevation during stair negotiation. The marker on the top of the shoe makes it difficult to assess the actual clearance, but does not interfere with the difference pre-post. Considering that foot contact with an obstacle or with the step of a stairs is one of the determinants of stumbling, participants in our study may have experienced an increased risk of stumbling after the walking exercise.

References: [1] Verghese, J., et al., Arch Phys Med Rehabil, 89: 100-4. 2008.

[2] Oh-Park, M., et al., Arch Phys Med Rehabil, 92: 2006-11, 2011.

[3] Chou, C.H., et al., Arch Phys Med Rehabil, 93: 237-44, 2012.

[4] Chodzko-Zajko, W.J., et al., Medicine & Science in Sports & Exercise, 41: 1510-1530, 2009.

[5] Hatton, A.L., et al., Gait Posture, 37: 506-10, 2013.

[6] Barbieri, F.A., et al., Gait Posture, 39: 985-90, 2014.

Disclosure of Interest: None Declared

Elderly

PO-0045

QUANTITATIVE EVALUATION OF FALL RISKS USING A DIMENSIONALITY REDUCTION METHOD

Yi-Horng Lai [1] [2] Bo-Ching Yang [1] I-Ching Lin [3] Lan-Yuen Guo [1,*]

[1] Department of Sports Medicine, Kaohsiung Medical University, [2] Department of Mechanical and Electro-Mechanical Engineering, National Sun Yat-Sen University, Kaohsiung, [3] Changhua Christian Hospital, Changhua, Taiwan, Republic of China

Introduction and Objectives: Lately instrumented versions of the motor performance tests in which objective sensors were used as the measurement system are being considered. Similar to the biomechanical laboratory-based measurements, a very high number of the measurements can be computed from the modified tests [1]. Although the interdisciplinary collaboration of objective measurements has the strongest effects in fall risk assessment, high dimensionality gait and balance measurements often confound the interpretation [2].

We hypothesized that the high dimensionality objective parameters, followed by a feature selection and dimension reduction process, could promote the capability of discriminating fallers from non faller group among the elders.

The aims of this study are to select a reduced subset of informative features by using dimensionality reduction method and compare the ability of discrimination with other traditional functional measurement.

Methods: Twenty nine community-living elders (faller: n=13; non faller: n=16) were recruited. The fallers were included only if they reported one or more falls with no obvious reasons in the previous year. Subjects with a history of stroke, dementia, major depression, Parkinson's disease, or any diseases likely to have an impact on gait were excluded. The interdisciplinary measures include both gait and balance assessment. For instrument time up and go (iTUG) test: Subjects wore the custom made Arduino based 9-axis motion tracking device and performed two TUG trials with their own preferred comfortable pace. For center of pressure assessment (COP): Subjects stood barefoot 30 seconds on a force platform (Kistler 9286AA, USA) with eyes open and eyes close respectively. Based on our review, a total of 12 scalar measures were extracted from the both test. Mann–Whitney U-tests were used to investigate the effect of 12 scalar measures. Only the p-value less than or equal to 0.05 was considered as candidate feature.

Linear discriminant analysis (LDA) which is easy to interpret and visualize was selected. LDA cast multidimensional features into a single dimension for best classification. Receiver-Operator Characteristic (ROC) curves were constructed to compare the predictive quality of the candidate features and LDA feature. The sensitivity was defined as the percentage of correctly identified fallers. Area under ROC curve (AUC) was used as a filter feature quality metric.

Results: Candidate features extracted from iTUG and COP test are amplitude of sit-to-stand, slope of stand-to-sit and velocity of COP in eye close trail.

The ROC curves were shown in Fig 1. The AUC of all the features were LDA dimension reduction feature (0.937), amplitude (0.721), slope (0.716) and velocity (0.712). The LDA feature has the best predictive quality (sensitivity: 0.875; sepecificity: 0.923).

Figure:
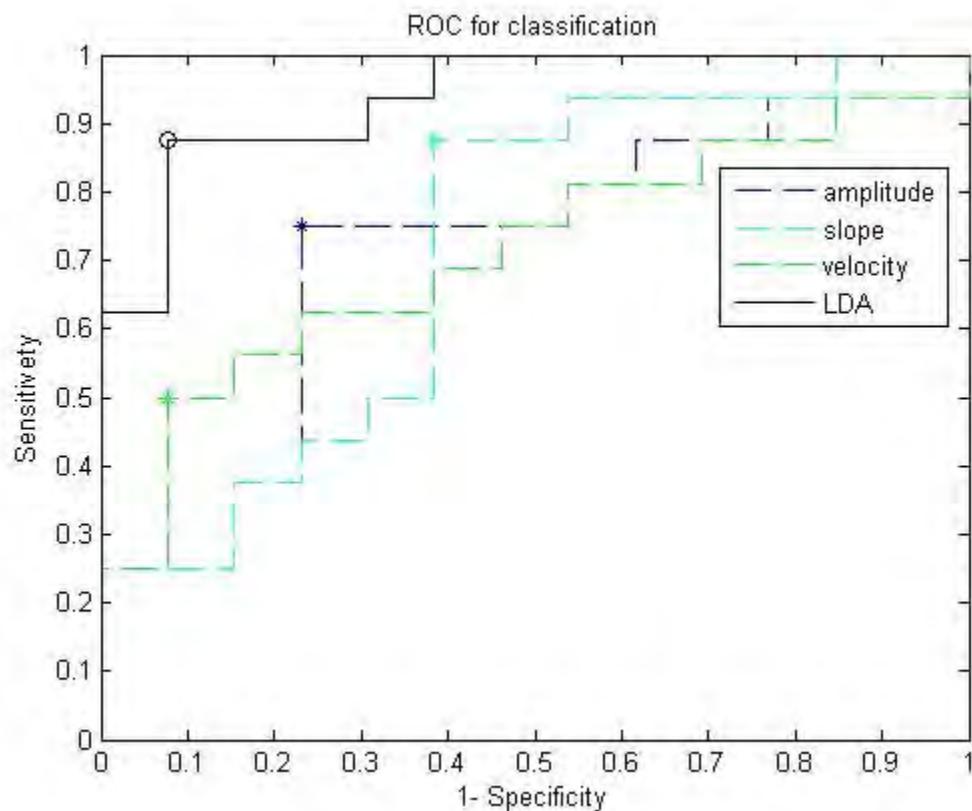
Caption: The ROC curves of all features

Conclusion: For community-dwelling elder, Single functional measures usually lack the ability to capture all gaits and balance impairment at its early phase. Because of the complex nature of falls, effective approaches should include interdisciplinary assessment. However, high dimensional quantitative parameters assessments are challenging. The LDA dimension reduction method has the additional advantage in interdisciplinary collaboration measures.

References: [1] Palmerini, L., et al., Neural Systems and Rehabilitation Engineering, IEEE Transactions on, 21(4):664-673, 2013.
[2] Saripalle, S.K., et al., Human Movement Science, 33(0): 238-250, 2014.

Disclosure of Interest: None Declared

PO-0047

WAVELET ANALYSIS OF MULTI-CHANNEL SURFACE EMG ACTIVITY OF THE LOWER BACK DURING THE BACK SQUAT

Richard Twycross-Lewis [1,*]Dylan Morrissey [1]Roger Woledge [2]

[1]Centre for Sports & Exercise Medicine, Queen Mary University of London, [2]Comparative Biomedical Science, The Royal Vetinary College, London, United Kingdom

Introduction and Objectives: Muscle fatigue in the lower back during the back squat results in decreased vertebral load tolerance and abnormal loading of the spine, which is, in turn, associated with acute muscle injury. We determined focal regions of EMG activity within the lumbar erector muscles which occur during the performance of the back squat.

Methods: Ten resistance trained men (age = 23.8 ± 1.9 years; height = 1.75 ± 0.1 m; weight = 82.8 ± 14.7 kg; years lifting = 2.7 ± 0.9 years) volunteered to take part in the study. High surface area, low density EMG data was collected using 16 differential EMG channels placed on the lower back (Figure 1). Lift phase was determined using marker height from active infra-red motion analysis markers placed above, below and around the EMG markers. Raw rectified EMG was subjected to a wavelet transform algorithm.

Results: Analysis of interactions between channel, phase of momvement and frequency by 3 factor ANOVA revealed significant interactions between lumbar region and movement phase (F = 30.92, $p < 0.01$) and with frequency band (F = 58.81, $p < 0.01$) . The greatest interaction was obsrved between movement phase and frequency band (F = 212.07, $p < 0.01$) (Figure 1).

Figure:
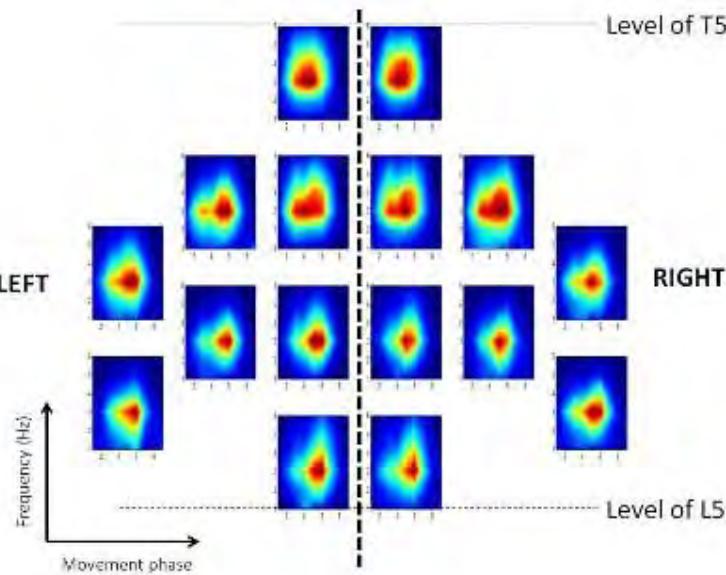
Caption: Figure 1: EMG placement during the squat and wavelet activity throughout the movement across the lower back either side of the spine from the level of T5 to L5.

Conclusion: : There is notable asymmetry in the patterns of activtion from the top to the bottom of the back. This seems to suggest the addition of faster motor units in the lower back as the squat progresses from eccentric mechanical movement to concentric activity in the lower back, whereas faster motor unit recruitment appears to occur throughout both the eccentric and concentric phases of the lift towards the upper region of the area of measurement. Finally, whilst there are characteristic patterns within different areas of the upper and lower back, there is notable left to right symmetry either side of the spine.

Disclosure of Interest: None Declared

SPATIAL DISTRIBUTION OF THE GASTROCNEMIUS MEDIALIS ACTIVITY FROM EXTENDED TO FLEXED KNEE JOINT IS UNSENSITIVE TO MUSCLE ARCHITECTURE CHANGES

Liliam Oliveira [1] [2],[*]Carolina Avancini [1]Luciano Menegaldo [1]Taian Vieira [2]

[1]Programa de Engenharia Biomédica, [2]Escola de Educação Física e Desportos, Universidade Federal do Rio de Janeiro, Rio de Janeiro, Brazil

Introduction and Objectives: The gastrocnemius muscles produce greater plantar flexion torque withthe knee inextended than flexed position. At flexed knee positions, the reduced plantar flexion torque is typically explained by the gastrocnemius tension-length relation [1]. Bipolar EMGs with low amplitude have also been documented for the gastrocnemius muscle during isometric plantar flexion contractions with knee flexed; this has been conceived as a strategy of the nervous system to more efficiently distribute the neural drive across plantar flexors [2]. Anatomical and electrophysiological evidence suggest however the changes in architecture and activation may distribute unevenly within the gastrocnemius muscle [3-5]. In this study we use ultrasound and a large array of surface electrodes to investigate how knee joint angle affects the distribution of activity and of fibres' length within the medial gastrocnemius (MG) muscle.

Methods: The muscle architecture was estimated for knee flexed and extended positions from ultrasound (US) panoramic images taken during rest and with the ankle joint held in neutral position (Figure 1). MG muscle was divided into proximal and distal portions and pinnation angle, fibre length and fat thickness were measured at each region. Surface EMGs were detected from the MG muscle of 16 healthy participants with a linear array of 16, silver bar electrodes (1 cm inter-electrode distance) positioned to cover as much as possible the muscle longitudinal axis. Subjects were asked to exert isometric plantar flexions at 60%MVC for 5 seconds, with the ankle joint at 90º. Submaximal efforts were performed with the knee fully extended (180º) and flexed at 90º. The channels detecting RMS amplitudes greater than 70% of the maximal amplitude were considered*active channels*. The barycentre coordinate of *active channels* was calculated, indicating where the RMS amplitude is mainly distributed along the muscle proximo-distal axis.

Results: Marked differences in MG architecture were observed when subjects moved their knee from extended to flexed position but the proximo-distal differences in MG architecture were not significantly associated with knee position. Regardless of the MG region considered, the proximal (32.0 ± 5.6 mm) and distal (34.0 ± 5.4 mm) values obtained for MG fibre length with knee flexed was significantly smaller than those observed for the proximal (42.0 ± 6.8 mm) and distal (43.2 ± 8.5 mm) MG regions with knee extended. No significant interaction or additive effect of knee position and/or muscle region was observed for the MG pinnation angle. The distribution of EMG amplitude along the skin surface changed markedly. When flexing the knee the amplitude of surface EMGs decreased and the barycentre coordinate shifted to the MG proximal region. For the knee flexed and extended conditions, the barycentre mean position was located at respectively 39-53% (interquartile interval) and 50-74% of the distance from the femoral condyle to the distal extremity of the MG superficial aponeurosis.

Figure:

Figure 5

Knee fully extended
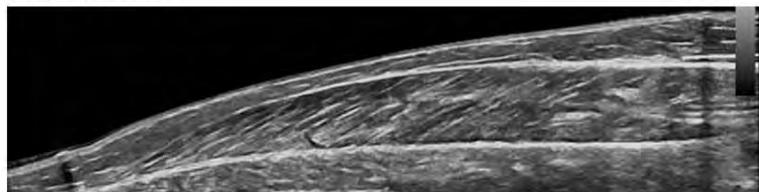
Knee flexed at 90 deg
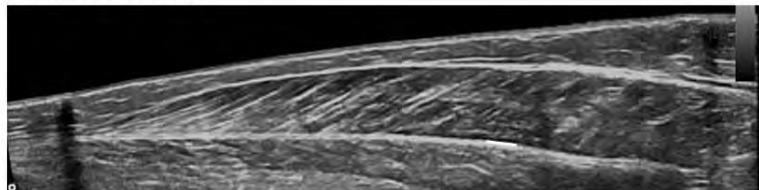
Caption: Figure 1. Panoramic ultrasound images of the gastrocnemius muscle. The images shown in the top and bottom panels were collected with knee fully extended and flexed at 90 deg, respectively.

Conclusion: These results indicate that RMS amplitude was mainly distributed distally when plantar flexion contractions were exerted with knee extended whereas, during knee flexed, EMG amplitude distributed at more proximal, skin regions. These results suggest knee position greatly affect the redistribution of activity within the MG muscle. Changes in MG proximo-distal activity were unlikely explained by regional changes in MG fibre length, pinnation angle and fat thickness. Finally, if detected locally, either proximally or distally, EMGs may provide different indication on the degree of MG activity for different knee positions.

References: [1] Hahn et al., J. Biomechanics, 44:2059-2065, 2011.

[2] Kennedy et al., Experimental Brain Research, 137:58-64, 2001.

[3] Lichtwark et al., J. Biomechanics, 40:157-164, 2007.

[4] Vieira et al., J. Applied Physiology, 108: 85-94, 2010.

[5] Hodson-Tole et al., J. Electromyography Kinesiology, 23: 43-50, 2013.

Disclosure of Interest: None Declared

EFFECT OF THE INSTRUCTION FOR CONSCIOUS ACTIVATION OF ABDOMINAL MUSCLES ON THE SCAPULAR MUSCLES ACTIVATION – PRELIMINARY DATA

Angie S. Vega [1] Anamaria Oliveira [1,*] Ann Cools [2]

[1]Programa de Pós-Graduação em Reabilitação e Desempenho Funcional, Universidade de São Paulo, Ribeirão Preto (São Paulo), Brazil, [2]Department of Rehabilitation Sciences and Physiotherapy, Ghent University, Ghent, Belgium

Introduction and Objectives: Functional relationship between trunk and periscapular muscles can be explained from different approaches.One is the Anatomic Trains Theory(1) that considers serratus anterior and the external oblique muscles as forming a lateral myofascial meridian in the trunk chain.Other one is the interdependence between the control of the distal segments and the stability of proximal ones according to the concept of functional kinetic chains(2).Posture and movement are refined by feedback and feedforward mechanisms.Feedback(biofeedback) could be represented by verbal, visual, auditory or kinesthetic stimulus(3).Although biofeedback mechanisms applied to scapulothoracic muscles have been already studied, there are no studies that have investigated whether biofeedback applied to muscles of trunk muscle results in more activation in during exercises for motor control and strengthening focused on the serratus anterior muscle(4).The aim of this study is to investigate the effect of verbal instruction and manual tapping for consciously increasing activation of the abdominal muscles voluntary contraction on the surface myoelectric activity of the scapulothoracic muscles.

Methods: Twenty healthy asymptomatic individuals(10 female and 10 male) aging 24±3.9 years old were evaluated.Three repetitions of wall press,knee push,wall slide,inferior glide,and isometric low row exercises were performed during 5 sec,with 5 sec of rest interval between each repetition(FIGURE1).Surface electromyographic amplitude was obtained from serratus anterior and external oblique muscles during exercises without and with verbal commands consciously activation of the abdominal muscles and manually tapping on the abdominal muscle.The familiarization was performed with abdominal training exercises as abdominal bracing e abdominal hollowing using verbal commands based on *Pilates* and *Core* techniques (5).EMG amplitude values are represented by normalized root mean square(RMS) for isometric exercises and by integrated EMG(iEMG) for dynamic exercises.Raw data was normalized by EMG RMS amplitude of the maximal voluntary isometric contractions,for each muscle.Data analysis was performed to compare amplitude averages between with and without instruction conditions using Student's *t*-test, with significance level set at 5%.

Results: Verbal instruction for consciously activation of the abdominal muscles significantly increased activation of the serratus anterior and external oblique muscles during wall slide,wall press,knee push,inferior glide and isometric low row exercises($p>0,05$)(TABLE1).Preliminary results showed an increase of the periscapular muscles activation as resulting of the biofeedback applied to trunk muscles.Those results support neuroanatomical linkage and functional interdependence between trunk and shoulder girdle as as suggested before by the Anatomic Trains Theory and functional kinetic chain concept(2,6,7).Kibler(2010) also proposed that synergistic muscle activation between trunk and periscapular musculature contributes for a normal scapulohumeral rhythm.Our results require confirmation by increasing the sample sizes and checking prospectively effect size for analysis comparing with and without biofeeback EMG amplitude means.

Figure:
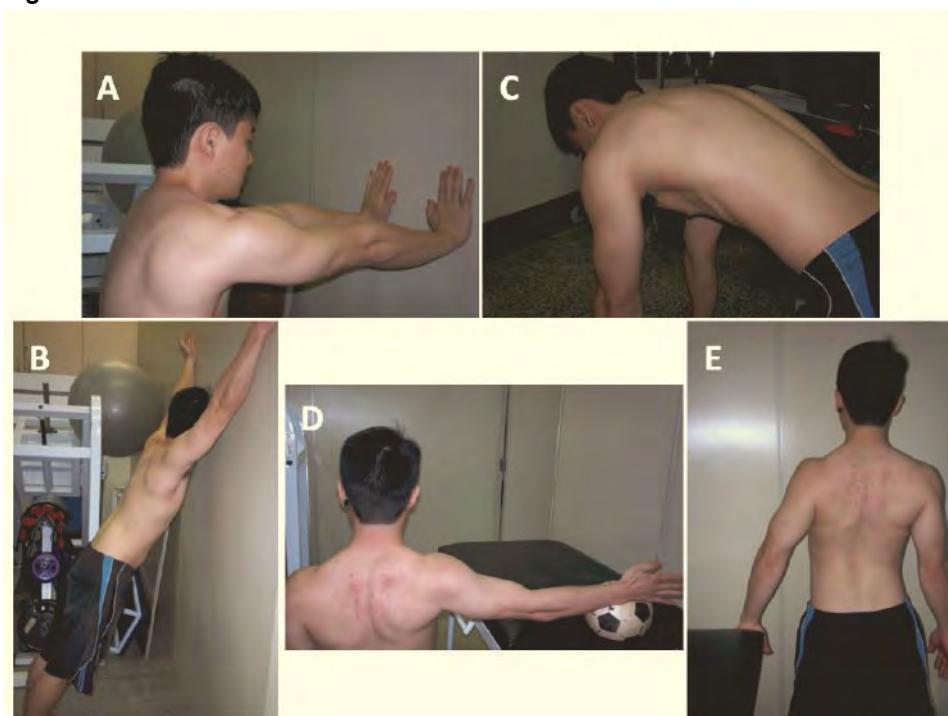
Caption: FIGURE1.Wall slide(A),wall press(B),knee push(C),inferior glide(D) and isometric low row(E)

Conclusion: Preliminary results demonstrated that verbal instruction for consciously activation of abdominal muscle and manual tapping increased the activation of the serratus anterior muscle during exercises for motor control and strengthening focused on the serratus anterior muscle.

Table:

Exercises	Muscles	Not Instruction	With Instruction	P Value
Wall Slide	RSA	16.27±8.30	27.95±11.19	0.00
	LSA	18.87±9.30	31.13±18.05	0.00
	ROE	11.73±7.45	30.02±28.84	0.01
	LOE	10.61±8.31	20.41±11.36	0.00
Wall Press	RSA	10.81±4.93	28.14±12.78	0.00
	LSA	14.24±10.21	31.09±16.91	0.00
	ROE	5.02±3.04	14.36±6.94	0.00
	LOE	4.16±2.46	10.79±5.45	0.00
Knee Push	RSA	14.94±7.56	33.13±13.84	0.00
	LSA	18.97±10.63	34.89±18.94	0.00
	ROE	6.88±3.36	18.45±11.03	0.00
	LOE	5.59±3.08	14.46±10.54	0.00
	RSA	61.19±44.19	89.10±61.37	0.00

Inferior Glide	**LSA**	68.68±54.90	88.47±64.51	0.00
	ROE	26.29±14.37	44.86±21.34	0.00
	LOE	31.20±18.94	41.62±20.76	0.04
Isometric Low Row	**RSA**	58.81±54.31	82.79±67.07	0.00
	LSA	53.21±39.04	83.80±50.47	0.00
	ROE	20.66±11.91	38.26±21.04	0.00
	LOE	16.36±10.47	27.99±13.97	0.00

Caption: TABLE1.Mean normalized EMG amplitude(± standard deviation) of the serratus anterior and oblique external muscles in five exercises performed.RSA,right serratus anterior;LSA,left serratus anterior;ROE,right oblique external;LOE,left oblique external

References: [1]Myers,Thomas W.*Elsevier Health Sciences*,2013

[2]Rubin,B.D e Kibler,W.Ben.*The Journal of Arthroscopic and Related Surgery*,18,9:29-39, 2002

[3]Mey,Kristof,et al.*Journal of orthopaedic & sports physical therapy*,43,1:3-10, 2013

[4]Cricchio,Mike e Frazer,Cindy.*J Hand Ther*,24,322–34,2011

[5]Kibler,WB,Press,Joel e Sciascia,Aaron.Sports Med,36:3,189-198,2006

[6]Cools,Ann M.,et al.*The American Journal of Sports Medicine*,35,2007

[7]Kibler,W Ben,et al.*Br J Sports Med,*1-12,2013

Disclosure of Interest: None Declared

EMG

PO-0051

NONNEGATIVE MATRIX FACTORIZATION TO ASSESS SPATIOTEMPORAL MUSCLE ACTIVATION

Didier Staudenmann [1,*]Dick F. Stegeman [2]Jaap H. van Dieen [3]

[1]Movement and Sport Science, Department of Medicine, University of Fribourg, Fribourg, Switzerland, [2]Donders Institute, Radboud University Medical Centre, Nijmegen, Nijmegen, [3]MOVE Research Institute Amsterdam, Faculty of Human Movement Sciences, VU University, Amsterdam, Netherlands

Introduction and Objectives: Changes in the distribution of activity across a muscle has been observed. Spatial heterogeneity of muscle activity has been assessed by comparing EMG amplitudes between channels within a grid of electrodes [1]. This procedure, however, averages amplitudes over time and hence discards temporal information. As an alternative method a k-means clustering algorithm was applied considering both temporal and spatial information [2]. However, this approach requires predefining the amount of clusters and if this amount does not correspond with the true spatial distribution, this method will not provide an adequate representation. The aim of this study was to explore the utility of nonnegative matrix factorization (NMF) in the quantification of temporal and spatial variability of muscle activation.

Methods: In eight subjects we measured surface EMG (49±8 electrodes covering the entire biceps brachii) during two contraction types: 1) pure elbow flexion and 2) elbow flexion with a superimposed forearm supination. The monopolar EMGs were spatially filtered with principal component analysis [3], rectified, smoothed and normalized to maximum voluntary contraction. We used NMF [e.g. 4] to decompose spatiotemporal muscle activation and represent it by W ('common mode' signal) and H (spatial gain of W over the muscle) Furthermore, we propose a method to quantify: i) the contribution of the common mode to spatio-temporal pattern as the variance in the signals accounted for (VAF) by W and ii) the spatial distribution over the muscle of the common mode correlations to W (spatial correlation).In eight subjects we measured surface EMG (49±8 electrodes covering the entire biceps brachii) during two contraction types: 1) pure elbow flexion and 2) elbow flexion with a superimposed forearm supination. The monopolar EMGs were spatially filtered with principal component analysis (Staudenmann 2006), rectified, smoothed and normalized to maximum voluntary contraction. We used NMF [e.g. 3] to decompose spatiotemporal muscle activation and represent it by W ('common mode' signal) and H (spatial gain of W over the muscle) Furthermore, we propose a method to quantify: i) the contribution of the common mode to spatio-temporal pattern as the variance in the signals accounted for (VAF) by W and ii) the spatial distribution over the muscle of the common mode correlations to W (spatial correlation).

Results: VAF was significantly (43%) larger for flex+sup than for pure flex (89±3% vs. 51±9%, p<0.01), whereas the spatial gains showed a marginal and non-significant difference between contraction types (p>0.882). The standard deviation of the spatial correlation was significantly (-57%) lower for flex+sup than for pure flex (0.08±0.05 vs. 0.18±0.07, p<0.01). The correlations with W showed a clear topographical distribution for pure flexion (see Figure) indicating that the variation in the EMG amplitudes captured by W was representative for one head of the biceps only, whereas it represented coactivation of the whole biceps in the combined contraction.

Figure:

pure flexion flexion + supination
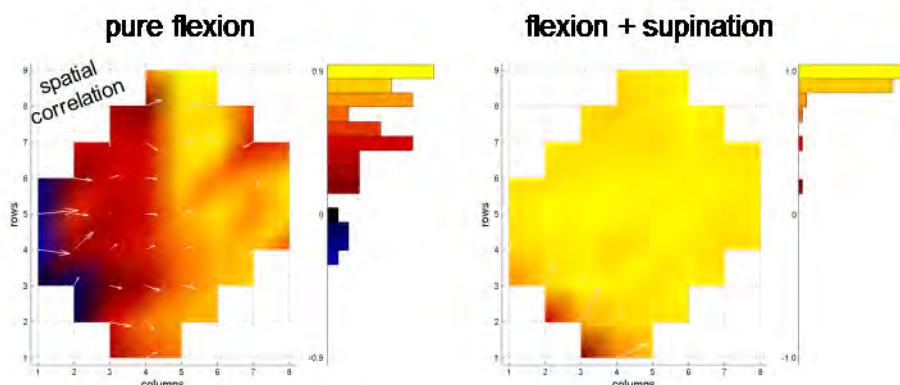
Caption: Spatial correlation shows how the time signal W correlates over the muscle surface of biceps brachii. Note that the flex+sup contraction showed higher correlations and lower variability compared to pure flex contraction.

Conclusion: This study shows that NMF is a powerful method to quantify spatiotemporal muscle activation. The advantages of NMF are that it is unbiased and directly provides temporal and spatial information. The VAF and spatial correlation were sensitive to the contraction type, while the spatial gain represented by H was not. It can be concluded that the outcomes proposed were sensitive to contraction types and can be interpreted in a physiologically meaningful way.

References: [1] Farina et al., J Electromyogr Kinesiol, 18: 16-25, 2008

[2] Staudenmann et al., J Electromyogr Kinesiol, 19: 882-895, 2009

[3] Staudenmann et al., IEEE Trans Biomed Eng, 53: 712-719, 2006

[4] Lee et al., Nature, 401: 788-791, 1999

Disclosure of Interest: None Declared

EMG

PO-0052

PATTERN CLASSIFICATION ACCURACY AND HIGH DENSITY EMG COLOUR MAPS FOR IMPROVED PROSTHESIS CONTROL

Usha Kuruganti [1,*]Victoria Chester [1]Yves Losier [2]Craig Prime [1]

[1]Faculty of Kinesiology, [2]Mechanical Engineering, University of New Brunswick, Fredericton, Canada

Introduction and Objectives: Myoelectric prosthetic limbs have evolved over several decades. While these systems have improved significantly over several decades, challenges remain. Traditionally, surface electromyography (EMG) has been used to investigate muscle activation patterns to determine which areas of a residual limb would be appropriate for electrode placement and control. Pattern recognition-based controllers have the potential to significantly improve myoelectric control systems for prosthesis control by increasing the number of controllable movements. These systems involve using pattern classifiers to analyze the neural signals produced by the muscle (EMG) and classify the movement produced based on predetermined settings. The effectiveness of the classifier is measured by its classification accuracy. Recently, high-density EMG (HDEMG) systems have allowed for non-invasive collection of myoelectric signals from many closely spaced electrodes. The data obtained can be examined through the use of 'colour maps,' which provide a visual indication of the distribution and intensity of muscle activation. The increased volume of data produced from HDEMG systems has not been extensively utilized in relation to classification accuracies. The relationship between pattern classification accuracy and HDEMG based colour maps is unknown, however understanding this relationship may help to better understand muscle activation patterns with applications in prosthesis development as well as imaging muscle activity in rehabilitation (e.g. in stroke or sport injury).

Methods: A HDEMG system (REFA, TMS International) was used to evaluate four different hand movements (hand open, hand closed, pronation, and supination) at a self-selected medium contraction level. Twenty able-bodied individuals (mean age = 31.6 ± 12.0 years, 9 females and 11 males) participated in this study. Sixty-four channels of EMG were collected and the electrodes were placed in an 8 by 8 grid formation over the forearm region to collect EMG data. The areas on the forearm that experienced muscle activity during given movements were illustrated in topographical (colour) maps for each trial. Pattern recognition was performed to determine how well each contraction could be distinguished using a Linear Discriminate Analysis (LDA) classifier. The colour maps were visually inspected to determine any changes in intensity (amplitude) and pattern repeatability between trials. Pattern classification accuracies were computed for all movements.

Results: The mean classification accuracies for each movement are shown in Table 1. Upon examination of each colour map it appears as both pattern and intensity changes differ in relation to classification accuracy with those with higher classification accuracy having (visually) more consistent colour maps (i.e. shape and intensity of the image). A mathematical relationship between classification accuracy and colour map changes is yet to be established, however the data collected in this work will help to investigate that relationship.

Conclusion: The results suggest that classification accuracy differ according to both pattern and intensity changes, however the exact relationship remains elusive. Understanding this connection may help to provide better understanding

of muscle activity for improved prosthetic control as well as develop new imaging techniques for those with reduced muscle activation due to injury or disability.

Table:

Mean Pattern Classification Accuracy	HO	HC	PR	SP
	87.9 ± 14.5	95.7 ± 11.1	86.4 ± 17.1	92.2 ± 13.6

Caption: Table 1: Classification accuracies for hand open (HO), hand closed (HC), pronation (PR) and supination (SP). All values are %.

Disclosure of Interest: None Declared

EMG

PO-0053

SUBCUTANEOUS FAT THICKNESS IS NOT CORRELATED TO THE MAGNITUDE OF MEASURABLE TRUNK MUSCLE ACTIVITY IN SURFACE EMG OF NORMAL WEIGHT HEALTHY ADULTS

Stephanie Valentin [1,*] James Elliott [2] Theresia Licka [1]

[1]Movement Science Group, Equine Clinic, University of Veterinary Medicine Vienna, Vienna, Austria, [2]Feinberg School of Medicine, Northwestern University, Chicago IL, United States

Introduction and Objectives: Surface Electromyography (sEMG) is a non-invasive tool from which muscle activation parameters can be investigated during a variety of static and dynamic conditions. However, subcutaneous fat overlying a muscle of interest can reduce the amplitude of the signal obtained, as fat can act as a low pass filter [1,2]. The effect of subcutaneous tissue and skinfold thickness on measurements of muscle activity has been evaluated in previous studies using ultrasound and calipers [2,3]. However to our knowledge, magnetic resonance imaging (MRI) assessment, which is a more precise method of determining subcutaneous fat thickness, has not been compared to sEMG values of trunk muscle activity. Therefore, the aim of the study was to compare the sEMG output of two trunk muscles with skin/subcutaneous fat thickness determined from MRI.

Methods: From data obtained previously, EMG and MRI values of two separate measurement sessions from 12 healthy participants aged 18-25 years (female n=6) with a BMI of <25 were correlated. Muscle activity had been obtained through sEMG electrodes (Delsys Trigno, 1200Hz) attached over the left and right erector spinae (ES) 2cm laterally from the thoracolumbar junction, and rectus abdominis (RA) 2cm above the umbilicus and 1cm lateral to midline. Data had been collected during 3 trials of 10s at natural stance. For the present study, raw sEMG data were processed using two methods: (1) resampling, rectification, zero-mean offset, and a 4th order low pass Butterworth filter applied, followed by the mean activity being calculated from the middle 6s of each 10s trial, and (2) EMG integration by cumulative summation of the rectified values. For the MRI aspect of the study, transverse images were obtained from the distal thoracic spine to the pelvis using a T1-weighted sequence (1.5T Philips Achieva; slice thickness 10mm, gap 1mm, repetition time 9.3ms, echo time 4.6ms, flip angle 15 degrees, field of view (FOV) 345mm, rectangular FOV 78%). Total skin and subcutaneous fat thickness (termed SC) of the abdomen was measured at L2-L3 disc level, equating to the RA sEMG site, and SC of the back was measured at T12-L1 disc level equating to the ES sEMG site (Sante DICOM viewer freeware, v4.0.5). For both locations, this was performed for the left and right side separately. Normal distribution of the data was confirmed using a Shapiro-Wilk test and Pearson's correlations were carried out between the total thickness of skin and subcutaneous fat and the respective sEMG value for each muscle, separately for each EMG processing method.

Results: Mean BMI of the participants was 21.7 ± 2.2. The means and standard deviations of the MRI and EMG data are shown in Table 1. Negative correlations were found between the SC values and EMG output in all muscles and from both EMG processing methods, although none of these findings were significant (all p>0.05).

Conclusion: The findings from the present study show that, although an inverse relationship i.e. negative correlation between SC and sEMG values was expected, this was not significant in either of the two muscles. Therefore, in healthy people who are not classed as being overweight, the effects of skin/subcutaneous fat thickness on resultant measurable

muscle activity with sEMG can be considered negligible in static, minimal effort conditions, based on the two different EMG processing methods described here. Identifying whether this also applies during dynamic and isometric contractions should be further investigated, however during dynamic activities the effect of the increased skin displacement with increased subcutaneous fat thickness should be considered.

Table:

	mean EMG (mV)			
	ESL	ESR	RAL	RAR
mean	0.69	0.75	0.69	0.77
stdev	0.21	0.32	0.20	0.25
	integrated EMG (mV/s)			
	ESL	ESR	RAL	RAR
mean	6.76	7.24	6.86	7.66
stdev	2.01	3.24	1.97	2.47
	SC (mm)			
	ESL	ESR	RAL	RAR
mean	9.13	9.47	10.25	11.22
stdev	2.79	3.15	5.58	6.07

Caption: Mean EMG from low pass filter (top), integrated EMG (middle), and skin and subcutaneous fat thickness (SC) (bottom) for the muscles erector spinae left (ESL), erector spinae right (ESR), rectus abdominis left (RAL) and rectus abdominis right (RAR)

References:

[1] Petrofsky J. Med Eng Phys, 30: 1168-76, 2008.

[2] Minetto et al., J Electromyogr Kinesiol, 23: 285-295, 2013.

[3] Cooper et al., J Electromyogr Kinesiol, 24: 207-213, 2014.

Disclosure of Interest: None Declared

PO-0055

DIFFERENTIATION CAPABILITY OF FREQUENCY AND TIME DOMAIN ELECTROMYOGRAPHY PARAMETERS IN WOMEN WITH PATELLOFEMORAL PAIN

Ronaldo Briani [1,*]Danilo Silva [1]Marcella Pazzinatto [1]Carlos Albuquerque [2]Deisi Ferrari [3]Fernando Aragão [2]Fabio Azevedo [1]

[1]Physical Therapy Department, University of São Paulo State, Presidente Prudente, [2]Physical Therapy Department, University of West of Parana, Cascavel, [3]bioengeneering department, University of Sao Paulo, Sao Carlos, Brazil

Introduction and Objectives: Patellofemoral pain (PFP) is one of the most common complaints in orthopedic practices and accounts for 25% to 40% of all knee problems in sports medicine centers. Despite its high incidence, PFP etiology remains unclear. A commonly accepted PFP etiology hypothesis is Vastus Medialis (VM) and Vastus Lateralis (VL) contraction dysfunction. Surface electromyography (sEMG) analysis, such as onset determination, of VM and VL has been widely reported in order to verify this hypothesis, however, onset has yielded controversial results[1]. sEMG frequency analysis, instead, has been recently proposed as a promising tool for PFP differentiation and, to the best of our knowledge, no prior study has compared sEMG frequency domain parameters and sEMG time domain variables. Therefore, the aim of this study was to determine the diagnostic accuracy of two different analyzes, sEMG in the frequency and time domain, on the VM and VL of individuals with PFP, compared to matched control.

Methods: 31 individuals with PFP and 28 control individuals (18–30 years) participated in this study. Data collection included a sEMG evaluation of each participant's symptomatic limb (those with unilateral symptoms) or most symptomatic limb (in those with bilateral symptoms) during stair descent. Data were collected using a conditioner module (Lynx®, Sao Paulo, SP, BRA; model EMG 1000-8-4I). The raw EMG signal was recorded at a sampling rate of 4000 Hz. A force plate (AMTI, OR6, Watertown, MA, USA) was positioned in the center of the fourth step and used to obtain ground reaction force data and, thus, to establish the moment when the subject was passing over the step. Each participant was asked to descend the stairs at their natural comfortable speed across the staircase and five successful trials were collected. The power spectrum density (PSD) of the frequency domain parameters were divided in bands: low (15-45Hz) (B1), medium (45-96Hz) (B2), and high (96-400Hz) (B3); and the onset analyzes were realized in 3 different manners: automatic algorithm, visual inspection and cross-correlation. Receiver operating characteristic (ROC) curves were done to assess the capability of differentiation (diagnostic accuracy) of each variable and the Younden index was used to identify the point when sensitivity (Sn) and specificity (Sp) were both maximized.

Results: ROC curves were performed (Figure 1), and the results of Sp and Sn for the optimal cut off and area under the curve values were obtained (Table 1). Regarding area under the curve, medium frequency bands were classified as moderately accurate for the VM (0.71) and VL (0.71), whereas other parameters were categorized as less accurate and non-informative. Similarly, the B2 presented the best Sn and Sp combination according to the Youden index, 72% and 69% for VM and 68% and 62% for VL, respectively. In spite of not presenting the best results compared to what has been shown in the literature when observed Sn and Sp separately[2], B2 demonstrated to be the most equally weighted variable presented for this goal. On the other hand, results from this study showed cross-correlation onset and visual onset AUC with non-informative values (.47) and (.49), respectively, and automatic onset with a fair AUC value (.60).

Concerning onset Sn and Sp, only automatic onset demonstrated an acceptable Sn (68%), yet, Sp as not suitable (55%). Other onset variables presented low values of sensitivity and specificity, as shown in table 1.

Figure:
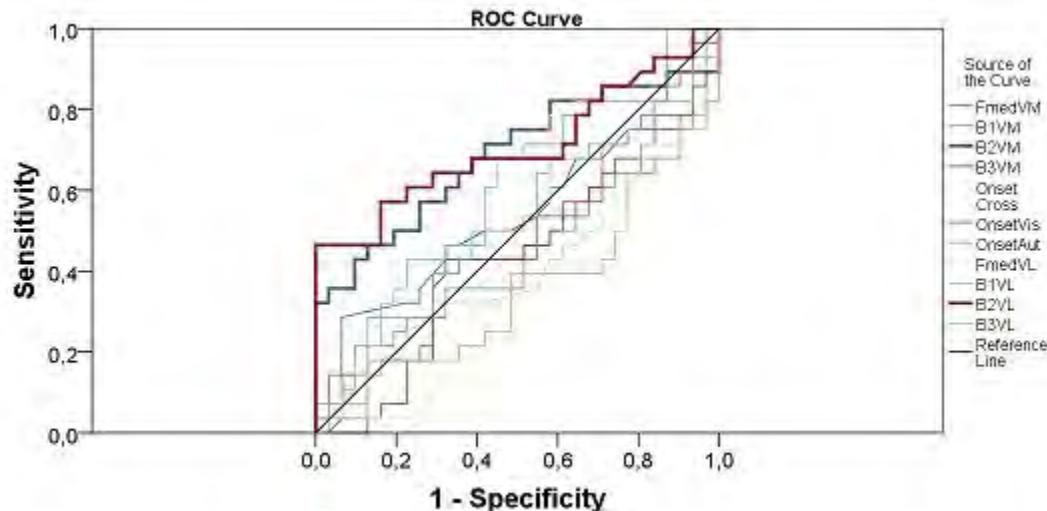
Caption: Receiver operating characteristic curves for the sEMG frequency and time domain parameters.

Conclusion: This study provides some evidence on the behavior of sEMG parameters associated with PFP. Results from the present study provide an accurate new approach, able to differentiate individuals with this disorder.

Table:

Variables	Sensitivity %	Specificity %	AUC (95%CI)	SE	P-value
B1 VM	50	43	0.43 (0.30;0.60)	0.078	0.466
B2 VM	72	69	0.71 (0.54;0.82)	0.072	0.014*
B3 VM	46	58	0.45 (0.27;0.57)	0.076	0.335
FM VM	61	43	0.53 (0.37;0.68)	0.078	0.733
Cross Onset	54	53	0.47(0.31;0.62)	0.078	0.693
Aut Onset	68	55	0.60 (0.44;0.74)	0.075	0.832
Vis Onset	54	45	0.49 (0.33;0.63)	0.077	0.219
B1 VL	50	61	0.53 (0.37;0.67)	0.07	0.785

				7	
B2 VL	68	62	0.71 (0.56;0.84)	0.071	0.006*
B3 VL	42	52	0.46 (0.37;0.68)	0.073	0.058
FM VL	46	38	0.41 (0.21;0.50)	0.076	0.219

Caption: Values of sensitivity and specificity for the best balanced cut off according to the Youden index and area under the curve (AUC) values.

References: [1]   Uliam Kuriki H, Mícolis de Azevedo F, de Faria Negrão Filho R, Alves N. Comparison of different analysis techniques for the determination of muscle onset in individuals with patellofemoral pain syndrome. J Electromyogr Kinesiol 2011;21:982–7. doi:10.1016/j.jelekin.2011.08.002.

 [2]   Nunes GS, Stapait EL, Kirsten MH, de Noronha M, Santos GM. Clinical test for diagnosis of patellofemoral pain syndrome: Systematic review with meta-analysis. Phys Ther Sport 2013;14:54–9. doi:10.1016/j.ptsp.2012.11.003.

Disclosure of Interest: None Declared

EMG

PO-0056

MUSCLE ACTIVITY PATTERN COMPARISON BETWEEN TWO FILTERING METHODS DURING PRONE HIP EXTENSION IN CHRONIC LOW BACK PAIN INDIVIDUALS

Carlos V. Cruz-Montecinos [1,*]Rodrigo Nuñez [1]Giselle   Horment [1]Pablo Letelier [1]Claudio Tapia [2]

[1]Kinesiology, [2]Electrical Engineering, University of Chile, Santiago, Chile

Introduction and Objectives: Analysis of muscle pattern during prone hip extension has been proposed as a clinical tool for assessment of musculoskeletal dysfunction [1]. However, some researchers have reported a consistent pattern [2], whilst others have concluded that no pattern exists [3]. Possible explanations for the differences include methodological issues. Different methods have been proposed for muscle onset determinations. Previous studies reported improvement of onset detection accuracy after using Teager Kaiser Energy Operator (TKEO), compared to other popular methods [4]. Recently, several advanced signal processing algorithms have been proposed for Independent Component Analysis (ICA) in order to remove noise from EMG recordings [5]. On the other hand, Emprirical Mode Descoposition (EMD), has been proposed for noise filter [6]. Both methods remove noise without removing frequency components of the muscle. The selection method for filter signal, can influence the determination of muscle patterns.

The objective of this study is to compare muscle pattern recruitment and onset muscle during prone hip extension (PHE) using Butterworth filter combined with TKEO versus (ICA) filter and combination with (EMD).

Methods: With the approval of the local Ethical Service, 9 chronic low back pain (CLBP) individuals were recruited. The surface electromyography (SEMG) electrodes were located in Semitendinosus (ST), Gluteus Maximus (GM), Erector Spinae ipsilateral (ESI) and contralateral (ESC) at L3 level. Each subject performed a PHE with knee in full extension, from neutral position to 20 degrees of hip extension. Movement speed was regulated with a metronome and all patients received training in order to adjust their motion speed to that rhythm. Each patient was asked to perform 6 repetitions. The starting movement was considered when velocity of execution reached 5% peak value during PHE. Muscle onset was calculated as the difference between the time lapse of the starting movement and the time lapse of muscle activation. Signal processing was compared between two methods. The first method consisted in high-pass Butterworth filter 10 Hz [7], which was later smoothed by a root mean square (RMS) with a window of 250 milliseconds, then TKEO was applied [4]. The onset of the EMGs burst was identified as the point in which the smoothed signal exceeded the threshold of the mean adding 3 standard deviations of the baseline signal. [1]. The second method consisted in filter processing using ICA and then using EMD, with a soft-threshold of the mean added by 2 standard deviations of the baseline signal. For the statistical analysis, Student *t*-tests and ANOVA were employed (when P value $p<0.05$ was considered statistically significant).

Results: 4 males and 5 females of the age 46 ± 12 were evaluated. All variables distributed normally. Comparing the onset between the two methods, significant differences were observed only in the onset of ESI ($p> 0.017$). On the other hand, the onset between the muscles, only presented differences in the first method. Differences between muscle onset could be observed in GM-ST ($p<0.009$) and ESI-GM ($p<0.019$).

Figure:

Comparison between filtering methods in muscle activation pattern during PHE
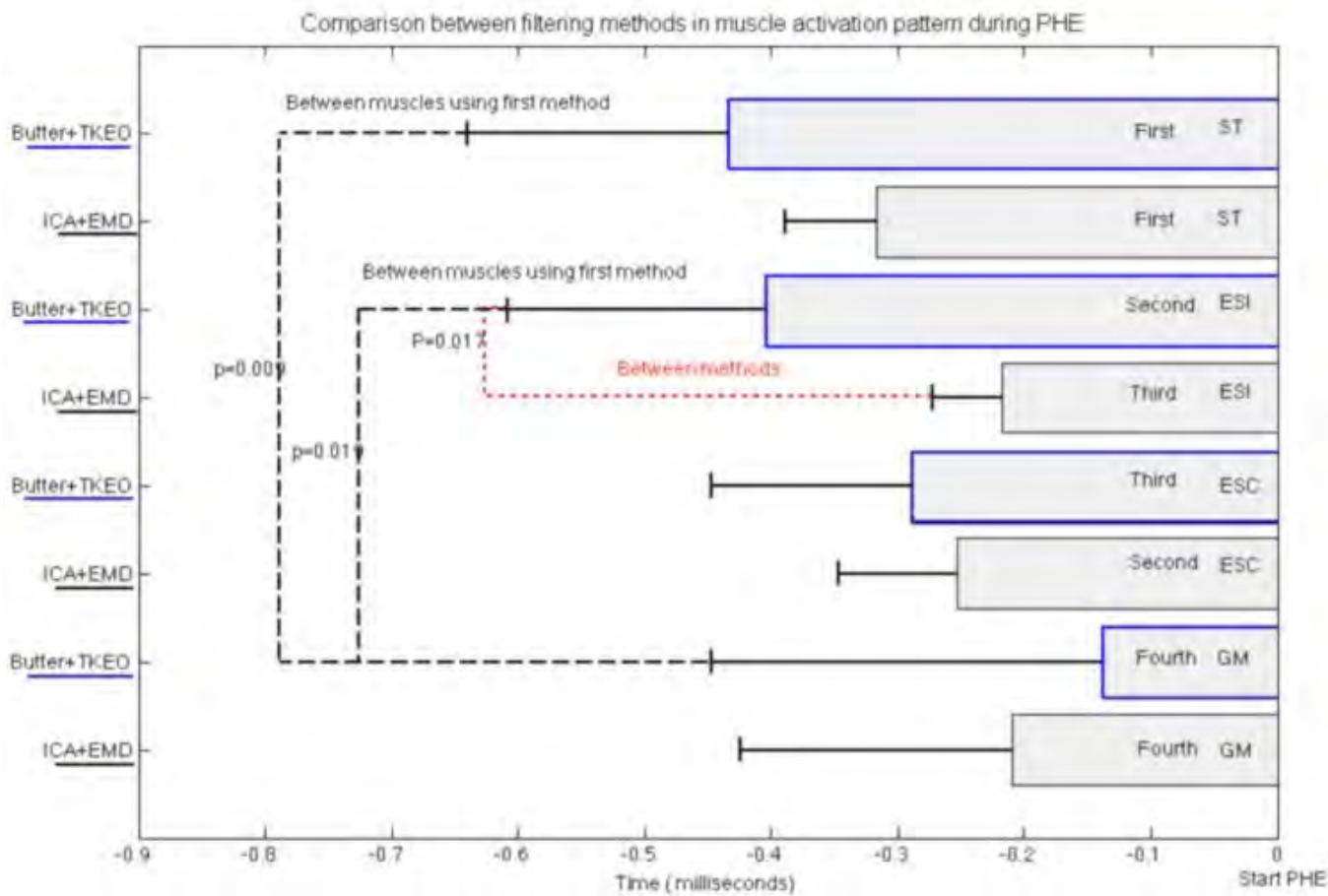
Caption: Figure.Comparison between filtering methods. Abbreviations: Butterworth filter (Butter); Teager Kaiser energy Operator (TKO); Independent Component Analysis (ICA) ; Empirical Mode Descomposition (EMD) .

Conclusion: Depending on the filtering methods used, our results proposed changes in the patterns during PHE. Therefore, for activity pattern detection, future studies using filter methods that do not remove frequency components of muscle are necessary.

References: [1].-Lewis, C. L et al., J. Athl. Train, 44: 238, 2009.

[2].-Vogt L et al., Clin Biomech, 12:122–127, 1997.

[3].-Lehman GJ et al ., BMC Musculoskelet Disord, 5:3, 2004

[4].- Lee, Angela S et al ., J biomech 40: 3521-3526, 2007.

[5].- G. Lu, J.S et al., Neurosci Lett, 462:14-19, 2009.

[6].-Andrade, Adriano O et al., Biomed Signal Proces 1: 44-55,2006.

[7].-Guimarães, Cristiano Q., et al. Braz. J. Phys. Ther 14: 351-357, 2010.

Disclosure of Interest: None Declared

PO-0057

SPATIAL DISTRIBUTION PATTERN OF SURFACE ELECTROMYOGRAPHY WITHIN HUMAN RECTUS FEMORIS MUSCLE ON OVERGROUND VS. TREADMILL WALKING

Kohei Watanabe [1,*]Motoki Kouzaki [2]Toshio Moritani [2]
[1]Chukyo University, Nagoya, [2]Kyoto University, Kyoto, Japan

Introduction and Objectives: Based on its unique anatomy, it was previously thought that proximal and other regions of the human rectus femoris (RF) muscle act independently during human movements (1). Recently, we demonstrated differences in neuromuscular regulation between proximal and other regions of the RF muscle during walking on a treadmill (2). The objective of this study was to compare neuromuscular activation of the whole RF muscle during treadmill and overground (normal) walking.

Methods: Seven healthy young men performed overground and treadmill walking. The gait speed on the treadmill walking was to be the same as that on overground walking, being comfortable for each subject. During walking, surface electromyography (EMG) was recorded from the RF muscle with 24 electrodes, arranged along the longitudinal axis of the muscle. Central locus activation (CLA) of the surface EMG amplitude was calculated to quantify the spatial distribution pattern of surface EMG within the muscle. CLA in each phase and the surface EMG amplitude in each phase and at each electrode were compared between the two different walking conditions. Heel contact and toe-off timings were identified using a foot switch. The knee joint angle was also measured using an electrical goniometer.

Results: No significant differences were noted between the two walking conditions in the gait speed, toe-off timing, cadence, maximum knee joint angle, or timings of the minimum knee joint angle. Significant differences were demonstrated in the minimum knee joint angle and timing of the maximum knee joint angle between the two conditions ($p < 0.05$).

There were no significant differences in CLA between the overground and treadmill walking throughout a stride. Significant differences in the surface EMG amplitude were observed around the heel contact phase between the two walking conditions in middle to distal regions ($p < 0.05$). On the other hand, there were no significant differences in the surface EMG amplitude between two conditions in the proximal regions during a stride.

Figure:
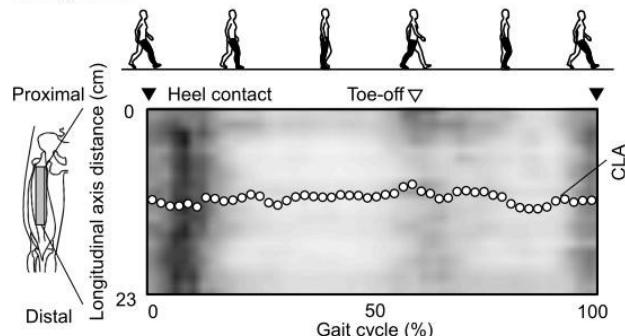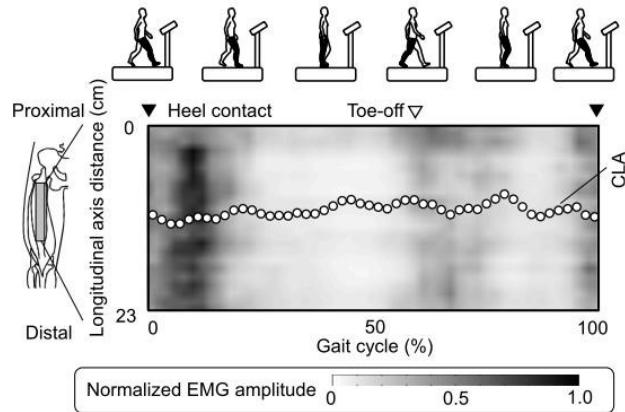
Conclusion: Our previous study demonstrated activation of the whole muscle around heel contact and selective activation in the proximal regions around stance-to-swing transition (2). In the present study, differences in surface EMG between overground and treadmill walking were shown in middle and distal regions, but not in proximal regions. This suggests that neuromuscular activation of the RF muscle is regionally regulated based on changes in the walking condition. Also, the unique activation pattern of proximal regions is independent of the walking condition.

References: [1] Hasselman et al., *Am J Sports Med* 23: 493-499, 1995.
[2] Watanabe et al., *J Biomech* 47: 3502-3508, 2014.

Disclosure of Interest: None Declared

EMG

PO-0058

EFFECTS OF NIGH NEUTRAL WRIST SPLINTING THERAPY IN THE ELECTROMYOGRAPHIC ACTIVITY OF SHOULDER AND FOREARM MUSCLES, GRIP STRENGTH, AND PINCH STRENGTH: A CARPAL TUNNEL SYNDROME CASE STUDY

Helga T. Tucci [1,*]Mariana Fogaça Leme [1]Vanessa Diogo [1]Maria Santos [1]

[1]Department of Human Motion Science, Federal University of São Paulo, Santos, Brazil

Introduction and Objectives: Treatment of Carpal Tunnel Syndrome could be conservative or surgical, according to the level of disease. Between conservative rehabilitation methods for the treatment of carpal tunnel syndrome, the use of wrist splint is one of the most common indication. Orthosis could stabilize or restrict movements, helping to align the segment in a functional position in order to correct existing deformities

The purpose of this case study was to investigate whether the conservative treatment consisted of the use of night neutral custom-molded thermoplastic resin wrist splint, associated with neural gliding exercises could alter electromyographic activity of shoulder and forearm muscles, and to improve grip and pinch strength in a person with CTS after 45 days of treatment.

Methods: Participation in this case study a women diagnosed with moderate carpal tunnel syndrome in the right hand through electrodiagnosis exam. CTS was also confirmed based on physical findings, and clinical evaluation. Patient was instructed to wear a neutral custom-molded thermoplastic resin wrist splint only at night; and to perform gliding exercises every day during 45 days. A booklet was given to the patient, containing the gliding exercises instructions, and places to note if she had used splint at night, and if she had done the exercises. Experimental procedure consisted in an evaluation of grip and pinch strength, and an evaluation of electromyographic activity of selected muscles before and after the treatment. Electromyographic activity was sampled with the patient performing an upper extremity functional activity in the scapular plane holding a halter with 0,028% of total upper extremity weight. Patient was sit in a chair, with 30° of arm flexion in the scapular plane, forearm on the desk. The desk had 2 scapular plane aligned markers: point 1 (near) and 2 (far). Functional activity consisted in to hold the halter ("reach phase") in the position 2, brings it to the position 1 ("flexion phase"), return it to the position 2 ("extension phase"). Once in the position 2 again, arm was elevated ("elevation phase) and lowered ("lowering phase") with elbow full extended. Thus, movements of elbow, wrist and shoulder were done to activated the selected muscles. Three maximal voluntary isometric contractions of each muscle were done in the muscular function position to posterior signal normalization. Three channels of a 16-bit A/D converter board suit were used to record electromyographic signal, with simultaneous acquisition and sample frequency of 2 kHz per channel (Miotec©, Rio Grande do Sul, Brazil. Myoelectric signal were sampled by a disposable bipolar electrode (Ag/AgCl, 20 mm inter-electrode distance) made of polyethylene foam and medicine hypoallergenic adhesive gel, connected to a sensor. Sensors have input impedance of 10 GΩ, Common Mode Rejection Ratio of 130 dB and gain of 20 times (Miotec©, Rio Grande do Sul, Brazil). A circular disposable electrode was fixed in the sternum for reducing acquisition noise. Electrode placement on the upper trapezius was oriented according to SENIAM recommendations [1], and placement of flexor carpi ulnaris and extensor carpi ulnaris were defined according to Perroto et al. [2]. After data collection, SEMG signal was

filtered at a frequency bandwidth of 20-1000Hz. An additional channel was used as a trigger to mark phases of functional activity. Three maximum isometric handgrip and pinch measurement of dominant upper extremity were performed using Jamar© and Pinch Gauge© dynamometers, respectively. Descriptive analyzes of normalized electromyography, grip and pinch strength were done before and after treatment.

Results: Lower grip strength, and greater pulp-to-pulp, and lateral pinches strength were found after treatment. Normalized electromyogtraphic were lower after treatment. Extensor carpi ulnaris normalized electromyographic activity in the "reach phase" was [0,40(0,12)] before and [0,15(0,03)] after; "flexion phase" [0,84(0,28)] before and [0,62(0,02)] after; "extension phase" [1,03(0,53)] before and [0,48(0,02)] after. Extensor carpi ulnaris in the "reach phase" was [0,26(0,14)] before and [0,13(0,07)] after, "flexion phase" [0,47(0,11)] before and [0,33(0,09)] after, and "extension phase" [0,37(0,17)] before and [0,25(0,06)] after. Upper trapezius in "elevation" was [0,61(0,04)] before and [0,53(0,01)] after, and "lowering" [0,49(0,10)] before and [0,47(0,05)] after.

Conclusion: The treatment showed to be effective in reducing the electromyographic activity, and improved pulp-to-pulp, and lateral pinch strength.

ACKNOWLEDGEMENT: CNPq (458837/2013-0).

Table:

Dynamometry [kgf mean (SD)]						
	Grip Strength		Lateral Pinch Strength		Pulp to pulp Strength	
	Before	After	Before	After	Before	After
Right Hand	23,3 (5,03)	22,6 (4,04)	8 (0)	9 (0)	9,6 (0,58)	10 (1)

Caption: Mean (standad deviation) of grip strength, lateral pinch strength, and pulp-to-pulo strength bafore and after treatment

References: Hermens et al. J Eletromyogr Kinesiol. 10(5): 361-74, 2000

Perroto et al. 2004

Disclosure of Interest: None Declared

EMG

PO-0059

DETERMINING THE ENERGY COST OF INDIVIDUAL LEG MUSCLES IN HUMAN WALKING

Neil Cronin [1,*]Patricio Pincheira [1]Lauri Stenroth [1]Janne Avela [1]

[1]Department of Biology of Physical Activity, University of Jyväskylä, Jyväskylä, Finland

Introduction and Objectives: Economy is a fundamental concept in human movement, and can be expressed as oxygen consumption normalised to body mass and speed (oxygen cost of transport, COT). The COT value reflects the net energetic cost of all active muscles, so changes in COT denote changes in the economy of some or all muscles. In walking, COT exhibits a U-shaped curve when plotted against walking speed; it is lowest at intermediate speeds of ~4.5 km/h and dramatically increases at speeds faster or slower than this optimum[1]. The aim of this study was to estimate the energy cost of individual leg muscles in young and older individuals in an attempt to determine which muscle(s) contribute to walking speed-dependent changes in COT.

Methods: 26 participants were recruited (13 young aged 18-30 and 13 old aged 70-80). Participants were equipped with an oxygen mask, and electromyography (EMG) electrodes were placed over 10 muscles of the right leg (vastus lateralis, vastus medialis, rectus femoris, semitendinosus, biceps femoris, tibialis anterior, lateral gastrocnemius, medial gastrocnemius, soleus, and flexor hallucis longus). Participants then walked on a motorized treadmill at seven different speeds for four minutes each in a random order: at the preferred speed (previously determined in overground walking) and 15, 30, and 45 % faster and slower than the preferred speed. A force-sensitive resistor placed under the right heel was used to synchronise data sources and detect gait events. Both groups wore a harness attached to the treadmill frame for safety purposes.

Mean oxygen consumption during the fourth minute of each walking speed was used to calculate COT. EMG data from the fourth minute of each walking speed were used for analysis on a stride-by-stride basis. The cumulative activity required to traverse a unit distance (CMAPD) was calculated for each muscle, speed and participant according to the method of Carrier et al[2], as this value has been suggested to be an indicator of muscle metabolism. To facilitate comparisons between muscles and subjects, CMAPD values were normalized to the value from the fastest walking speed for each subject and muscle.

Results: At the group level, speed-dependent changes in COT occurred in parallel with changes in mean CMAPD of all tested muscles for both young and old groups (Figure 1). In the young group, r^2 values for the correlation between CMAPD and COT ranged between 0.003 to 0.250 across all muscles. Proximal muscles such as vastus lateralis exhibited higher CMAPD at speeds faster and slower than the energetically optimal speed, whereas, for example, soleus CMAPD was relatively independent of speed. In the old group, COT was higher at all speeds, and preferred speed was slower. Regarding CMAPD, similar findings were observed as in the young group.

Figure:
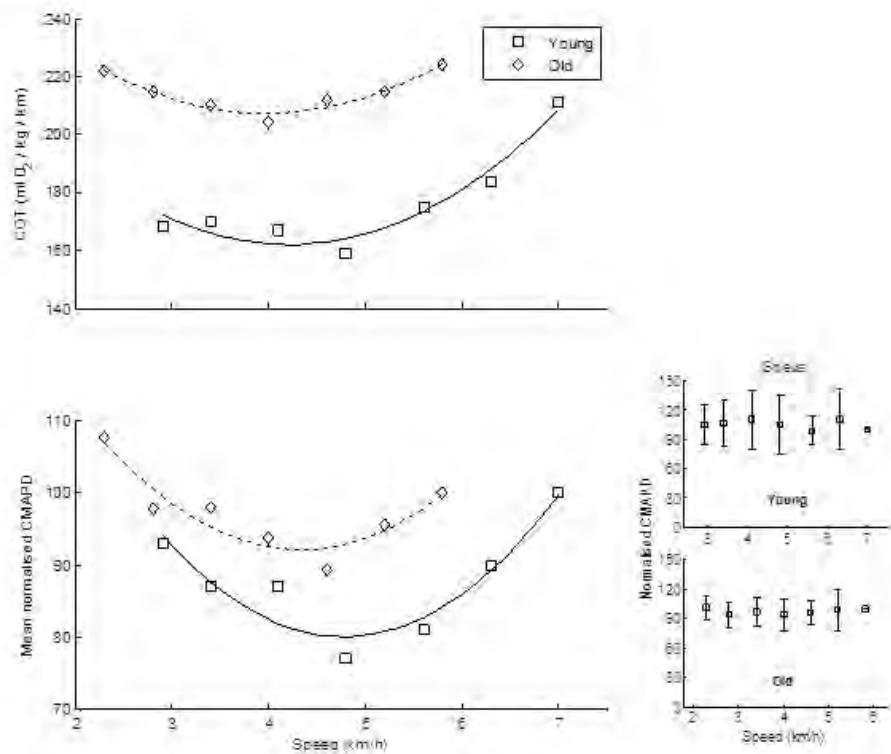
Figure 1. Walking speed versus group mean COT (upper panel) and group mean CMAPD from all muscles combined (lower panel). Inset: CMAPD values for soleus muscle only in both age groups. Note that due to the fact that values are normalised to the fastest walking speed within each group, absolute CMAPD values are not directly comparable between groups

Conclusion: In young individuals, speed-dependent changes in energetic cost of walking are reflected in the estimated metabolic cost of individual muscles. In general the quadriceps showed the largest changes in CMAPD with changes in speed, whereas soleus functioned at a constant CMAPD regardless of speed. Results were similar for older individuals. These results suggest that soleus may be an important target muscle in interventions aiming to maintain economy in old age. Moreover, in both age groups, the metabolic cost of contraction in proximal leg muscles such as the quadriceps seems to increase dramatically when walking at speeds faster or slower than the energetic optimum.

References:

1. Bramble DM & Lieberman DE (2004). Nature 432(7015):345-52.
2. Carrier DR, Anders C & Schilling N (2011). PNAS 108(46):18631-18636.

Disclosure of Interest: None Declared

EMG

PO-0060

ACUTE EFFECTS OF LOW EMISSION PHOTOTHERAPY ON ELECTROMYOGRAPHIC FATIGUE OF BICEPS BRACHII IN YOUNG MEN

Kamila Verlene S. G. Vieira [1,*] Ana Cláudia Rennó [2] Paulo Henrique Azevedo [1] Carlos Eduardo Pinfildi [1] Emilson Colantonio [1] Helga Tatiana Tucci [1]

[1]Department of Human Movement Science, [2]Department of Biosciences, Federal University of São Paulo, Santos, Brazil

Introduction and Objectives: Low emission phototherapy (low level laser therapy and light-emitting diode therapy) has been studied as a resource for reducing fatigue onset during physical activity, and their positive effects could also be observed through electromyographic analysis done during physical exercise. However, to date there is not a consensus about the acute effects of low emission phototherapy in reducing electromyographic fatigue.

The purpose of this study was to analyze the acute effects of low emission phototherapy in the electromyographic fatigue of long head of biceps brachii muscle of young males.

Methods: Twenty males [mean (standard deviation) 22.5 (3.52) years; body mass 69.3 (0,04) kg; and height 1.74 (9.47) m] were randomized in Active and Placebo Group. Subjects were submitted to a fatigue protocol that consisted of 30-seconds of maximum voluntary isometric contraction biceps brachii performed in a Scott bench. Before experimental fatigue protocol, phototherapy was applied over biceps brachii of dominant upper extremity according to group randomization using a cluster with seven 850nm wavelength diodes (GaAlAs), 100 mW output power, and 4 J per diode. Due to cluster´s size, one application was necessary to cover the muscle, totalizing 28J for all diodes in 40 seconds of application (LEAL JUNIOR et al., 2009). Thus, subjects underwent a surface electromyographic sample of long head of biceps brachii muscle during the fatigue protocol. Before placing the electrode, the skin was shaved and cleaned with alcohol. Electrode placement on the biceps was oriented according to Surface ElectroMyoGraphy for the Non-Invasive Assessment of Muscles recommendations (HERMENS et al., 2000). Myoelectric signals from the biceps brachii were sampled by a disposable bipolar electrode (Ag/AgCl, 20 mm interelectrode distance) made of polyethylene foam with medicine hypoallergeni adhesive gel connected to a sensor that has input impedance of 10 GΩ, Common Mode Rejection Ratio of 130 dB and gain of 20 times (Miotec®, Rio Grande do Sul, Brazil). A circular disposable electrode was fixed on the sternum as a reference for reducing acquisition noise. SEMG signals were sampled by a 16-bit A/D converter board with 2 kHz frequency. After, 30-seconds raw signal was digitally filtered at frequency bandwidth of 20-1000Hz, and divided in 3 windows with 10-seconds each. Median frequency (MDF) of signal was used to data analysis. Electomyographic fatigue of biceps brachii (FB) was determined by dividing MDF obtained from the third 10-seconds window by MDF obtained from the first 10-seconds window. FB was compared intra-groups. Statistical analysis was done using a paired-samples t-test, with level of significance set at $P<0.05$.

Results: Results showed that there were not found statistical difference of FB obtained from Active Group [FB mean (standard deviation) 0.67 (0.08); $p=0.30$] when compared to the FB obtained from Placebo Group [0,72 (0,11); $p=0.30$]. The aim of this study was to analyze the acute effects of low emission phototherapy on electromyographic fatigue of the long head of the biceps muscle in young males. Researches has suggested that the low emission phototherapy acts on

muscle bioenergetics, helping to reduce muscle fatigue, blood lactate concentrations and inflammatory markers (LEAL JR et al., 2009; DE MARCHI et al., 2012). Thus, the effects of this resource could help to delaying the development of muscle fatigue, and allowing to improve the muscle performance during exercise. This result may be justified through the fact of the phototherapy parameters of this research could not be the more appropriate for this aim. However, there is not not an ideal parameters described to improve muscle performance, which suggest that new studies comparing different phototherapies could help to adjusted parameters.

Conclusion: In this experimental procedure, phototherapy did not show an acute effect in delaying electromyographic fatigue of biceps brachii muscle in young males.

References: [1] De Marchi et al. Lasers Med Sci. 27(1): 231-6, 2012

[2] Hermens, et al. J Eletromyogr Kinesiol. 10(5): 361-74, 2000

[3] Leal Junior et al. Lasers Surg Med 2009. 41:572–577, 2009

Disclosure of Interest: None Declared

EMG

PO-0061

EFFECTS OF LOW EMISSION PHOTOTHERAPY IN THE RATE OF FORCE DEVELOPMENT AND ELECTROMYOGRAPHIC FATIGUE OF QUADRICES FEMORIS IN ELDERLY WOMEN

Helga Tatiana Tucci [1,*] Patrícia Gabriele Vassão [2] Ana Carolina de Souza [2] Luis Henrique da Silva [2] Larissa Neves [1] Ana Claudia Rennó [2]

[1]Department of Human Movement Science, [2]Department of Biosciences, Federal University of São Paulo, Santos, Brazil

Introduction and Objectives: Aging is responsible for several biochemical and structural changes in the body that leading to a decline in the function of various tissues, with musculoskeletal system being the most affected. Low emission phototherapy (Low-level laser therapy and Ligth-emitting Diodes therapy), by its biomodulation effects, could be a resource to improve muscle performance [1, 2].

The objectives of this experimental procedure were to analyze the acute effects of low emission phototherapy in the rate of force development (Q_RFD) and Fatigue Index (FI) of quadriceps femoris in elderly women.

Methods: Eight females were randomized [mean (standard deviation) 65,60 (3,44) years; body mass 66,98 (6,93) kg; and height 156,60(3,78) m] in Active Group (n=4) and in Placebo Group (n=4). Quadriceps femoris fatigue protocol was performed in a leg extension chair, and consisted of 30-seconds quadriceps femoris maximum isometric voluntary contraction (MIVC) with subject sit in a leg extension chair with knee at 90° of flexion. From group randomization, phototherapy was applied over quadriceps femoris of dominant lower extremity immediately before experimental fatigue protocol using a cluster with seven 850nm wavelength (GaAlAs) diodes, 100 mW output power, and 4 J per diode. Due to cluster´s size, 4 applications were necessary to cover the muscle, totalizing 112J in 120 seconds. Before placing the electrodes, skin was shaved and cleaned with alcohol. Then, surface eletromyography (SEMG) was sampled from vastus medialis, rectus femoris, and vastus lateralis according to SENIAM recommendations[3]. Myoelectric signals from the vastus lateralis, rectus femoris, and vastus medialis of dominant lower extremity were sampled by a disposable bipolar electrode (Ag/AgCl, 20 mm inter-electrode distance) made of polyethylene foam and medicine hypoallergenic adhesive gel, connected to a sensor. Sensors have input impedance of 10 GΩ, Common Mode Rejection Ratio of 130 dB and gain of 20 times (Miotec®, Rio Grande do Sul, Brazil). A circular disposable electrode was fixed in the tibial plateau of dominant lower extremity for reducing acquisition noise. A load cell was used to sample force during fatigue experimental procedure (Miotec®, Rio Grande do Sul, Brazil). SEMG and load cell signals were sampled simultaneously by a 16-bit A/D converter board with 2 kHz frequency (Miotec®, Rio Grande do Sul, Brazil), and after filtered at a frequency bandwidth of 20-1000Hz. SEMG 30-seconds raw signal was windowed in 3 parts of 10-seconds each, and median frequency (MDF) was used to data analysis. Fatigue Indexes were determined by dividing MDF of third 10-seconds window by MDF of first 10-seconds window. Quadriceps femoris rate of force development (Q_RFD) was calculated through load cell signal, as a derivation of maximal force in its corresponding time interval, determined from the beginning of MCIV until the instant which maximum force was reached. Q_RFD, fatigue index of vastus lateralis (FI_VL), fatigue index of rectus femoris (FI_RF), and fatigue index of vastus medialis (FI_VM) were compared between groups. Student t test for not related sample was used as statistical analysis, with level of significance set at $p<0.05$.

Results: Results showed that there were not found statistical difference between Q_RFD of Active Group [mean (standard deviation) 25,69 (13,97); p=0.28] compared to Placebo Group [mean (standard deviation); 15,85 (8,29); p=0.28]. Also, there were not significant difference for FI_VM of Active Group [mean (standard deviation); 1,10 (0,39); p=0.37] compared to Placebo Group [0.90 (0.09); p=0.37]. The comparison of FI_RF between Active Group [0.87 (0,24) p=0.94], and Placebo group [0.88 (0.23); p=0.94] was not statistically different. Lastly, FI_VL [1,02 (0,15); p=0.76] of Active Group, when compared to Placebo Group [0.99 (0.90); p=0.76], was not statistically different. Small sample size, and photherapy parameters chosen could be possible explanations to absence of significant results between groups. Results could be justified to the small sample size, and through the fact that phototherapy parameters of this research are not the best choice to improve muscle performance in elderly women. However, there is not a consensus at the literature about the more appropriate photherapy parameters aiming to reduce or prevent muscle fatigue, and to improving RDF.

Conclusion: Low emission phototherapy has not effect on reducing FI_VM, FI_RF, FI_VL, and in improving Q_RFD in elderly women submitted to this experimental procedure. Results should be viewed with caution because sample is too small to have accurate conclusions.

References: [1] de Marchi et al. Lasers Med Sci. 27(1): 231-6, 2012

[2] Hermens et al. J Eletromyogr Kinesiol. 10(5): 361-74, 2000

[3] Leal Junior, et al. Lasers Surg Med. 41:572–577, 2009

Disclosure of Interest: None Declared

EMG

PO-0062

MAXIMUM TRUNK MUSCLE ACTIVATION DURING DIFFERENT CONTRACTION MODES IN HEALTHY SUBJECTS

Stephan Kopinski [1,*] Tilman Engel [1] Jimmy B. Lawrence [1] Juliane Mueller [1] Steffen Mueller [1] Frank Mayer [1]

[1] Department Sports & Health Sciences, University Outpatient Clinic Potsdam, Potsdam, Germany

Introduction and Objectives: Isokinetic strength measurements and electromyographic activation measures of trunk muscles are widely used in research and clinical context. In general, normalization of EMG data is recommended to be done by maximum voluntary contractions (MVC) in isometric contraction mode. However, if the reference EMG should be taken preferably of the same contraction type as the task EMG, e.g. as in a dynamic trunk strength task, is of continual discussion. Therefore, the purpose of this study was to compare the activation of trunk muscles during isometric, and concentric and eccentric isokinetic strength tests in healthy adults.

Methods: Seventeen healthy participants (10 M, 7 F; 25 ± 7yrs, 71 ± 12kg, 1.78 ± 0.11m; VAS back pain ≤ 0.1) performed a MVC trunk extension/flexion (ext/flex) test sequence. They were measured in a dynamometer (Con-Trex MJ, TP-module, Physiomed AG, Germany) in standing position, equipped with a 12-lead bilateral sEMG (myon RFTD-32, myon AG, Suisse) on Mm. erector spinae (ES, L3 and T9 level), latissimus dorsi (LD), rectus abdominis (RA), and obliquus internus (OI) and externus (OE). After an extensive warm-up the protocol consisted of two isometric trials (ISM; ext and flex, both in $17.5°$ flex for 5s) and four isokinetic trials (ROM: $45°$ flex to $10°$ ext) - three in concentric ($CON_{30/60/120}$; $30°$/s, $60°$/s and $120°$/s, each 5 repetitions) and one in eccentric mode (ECC; $30°$/s, 5 repetitions). All trials were separated by 60s rest. Peak torque in ext and flex ([Nm], for CON and ECC mean of 3 highest) was analysed (mean$\pm$SD). After the EMG signal was averaged for sides and moving average filtered (50 points), peak EMG activity [V] during agonist muscle work (ISM: time of peak torque $\pm$ 0.5s; CON/ECC: whole ROM) was evaluated (mean$\pm$SD). A one-way repeated measures ANOVA with Bonferroni correction was used to test for differences in agonistic muscle activity between the five contraction modes ($\alpha=0.05$).

Results: Peak torque ranged from 281 ± 87 Nm (ECC) to 200 ± 71 Nm (CON_{120}) during ext, and from 144 ± 52 Nm (CON_{30}) to 135 ± 49 Nm (ISM) during flex, respectively. Maximum absolute muscle activity ranged from 0.80 ± 0.31 V (ES at L3, during CON_{120}) to 0.28 ± 0.18 V (LD, during CON_{60}) during ext, and from 0.87 ± 0.49 V (OE, during ISM) to 0.66 ± 0.33 V (OE, during CON_{60}) during flex (Figure 1). For trunk extensor muscles effect of contraction modes was found statistical significant only for ES at T9 ($p<0.05$, no statistical significant post-hoc result), with non-significant values for ES at L3 ($p=0.460$) and LD ($p=0.238$). During trunk flexion a statistical significant effect of contraction modes was present only for OI ($p<0.01$), but not for RA ($p=0.190$) and OE ($p=1.197$). Post-hoc pair-wise comparison for OI identified statistical significant differences between CON_{30} and each CON_{60}, CON_{120} and ECC modes (all $p<0.01$).

Figure:

Peak EMG Activity of Trunk Muscles
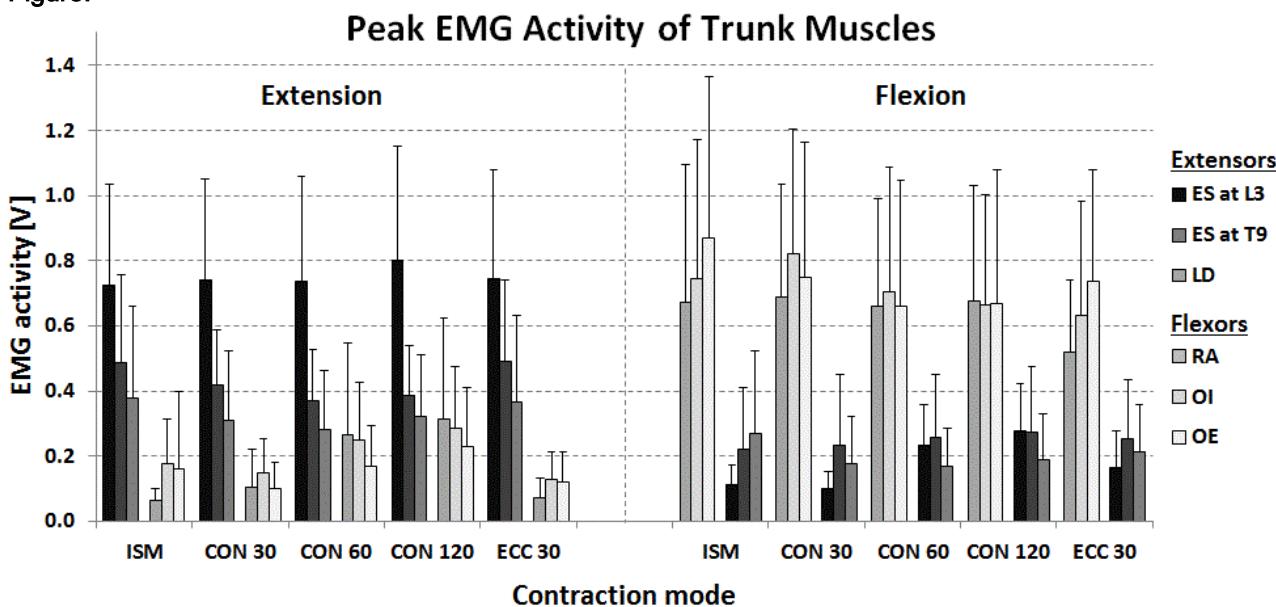
Caption: EMG activity of trunk extensors Mm. erector spinae (ES, at L3 and T9 level) and latissimus dorsi (LD), and trunk flexors Mm. rectus abdominis (RA), and obliquus internus (OI) and externus (OE) during isometric trials (ISM), isokinetic concentric (CON, 30 to 120°/s) and eccentric (ECC, 30°/s) contractions. Bars represent peak muscle activity of 17 healthy subjects (mean±SD).

Conclusion: Trunk muscle activation during trunk flexion and extension in general was not affected systematically by contraction mode. The high variability of absolute EMG activity between participants contributed to this inconsistent outcome. Peak torque values were highest during ECC and non- to low velocity muscle contraction modes (ISM, CON$_{30}$). The usage of isometric MVC may be favourable concerning higher EMG signal stability, with low relative movement of electrodes over detected muscle fibres. On the other hand, isokinetic MVC may be more conclusive when normalizing results of dynamic strength testing. To conclude, the choice of contraction mode for MVC normalization of dynamometer supported muscle strength and activation tests is more a substantive question than a matter of method.

Disclosure of Interest: None Declared

EMG

PO-0063

SURFACE ELECTROMYOGRAPHY AS A TOOL IN THE TREATMENT OF TEMPOROMANDIBULAR DISORDERS.

Fabiola Spolaor [1,*]Francesco Coccilovo [2]Claudio Cobelli [1]Antonio Gracco [2]Zimi Sawacha [1]

[1]Department of Information Engineering, [2]Department of Neuroscience, University of Padova, Padova, Italy

Introduction and Objectives: The clinical usefulness of the use of surface electromyography (SEMG) in diagnosing and treatment of temporomandibular disorders (TMDs) is still debated [1,2]. Temporomandibular disorders (TMD) is a complex disease affecting the Temporo-mandibular joint, the masticator muscles, or both, and its nature is not completely understood yet [3].

The aim of this work is to verify weather subjects with CrossBite display different Temporo-mandibular joints muscles activation patterns than controls during consecutive chewing task, maximum teeth clenching with and without cotton rolls.

Methods: 30 subjects participated in the study: 10 healthy (control group (CG), 20 with CrossBite (CB) who had not south any treatment. Subjects were asked to perform repeating chewing task (while eating a cookie), and surface electromyography (sEMG) activity was recorded. Afterword 2 maximum voluntary contractions (MVC) were performed through maximum teeth clenching either with or without cotton roll. Kinematics data (glabella, right and left Temporo-mandibular joints markers trajectories) were acquired together with sEMG signals of Right Temporalis (RT), Right Masseter (RM), Left Temporalis (LT) and Left Masseter (LM). A BTS motion capture system (6 cameras, 60-120 Hz) synchronized with a Free EMG system (8 channels SEMG system, BTS, Srl) were used. Ten consecutive chewing cycles and 10 consecutive seconds within the central part of each MVC trial were extracted and analysed. sEMG linear envelopes were estimated and the following parameters were determined: peak of envelope position (PoE) and Peak of Envelope (PE) [4]. Markers trajectories were used in order to define different chewing tasks. Welch's t test was performed (SPSS, version 19.0) in order to compare the data of the of the TMD and the CG groups.

Results: CB group showed a significant higher value of PE (Figure 1) and a delay in PoE when compared to CG (0.007

Figure:
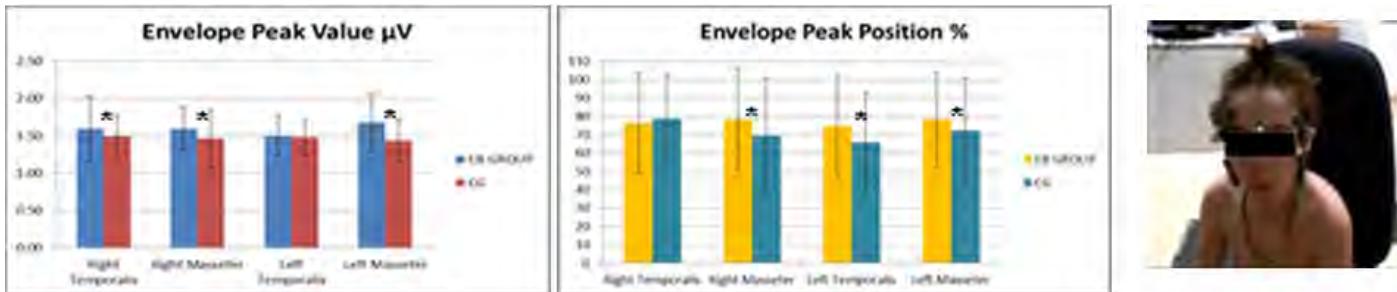
Figure 1. a,b: Each muscles PoE and PE (mean and standard deviation) estimated during the 10 consecutive chewing trials (Red=CG; Blue=CB) . *= Significant p<0.05; c: a patient while executing the chewing task.

Conclusion: Delay in PoE and higher PE values can be justified by considering that CB subjects exhibit neuromuscular alterations that can lead to functional alterations. The latters may determine delayed muscle activation accompanied by larger amplitude of the muscle activity in order to cope with the underling deficit.

Preliminary results showed that sEMG allowed to highlight differences in timing of muscles activation between TMD and CG subjects. Future development will include increasing the number of subjects in order to differentiate between subjects affected by monolateral and bilateral crossbite.

Table:

Groups	CB	CG
Number	20	10
Age	9±2	9±2
BMI	18±3	20±1

Caption: Table 1 Clincal Data

References: REFERENCES

[1] Klasser GD and Okeson JP. Am Dent Assoc. 2006 Jun;137(6):763-71.

[2] Ferrario et al, Manual Therapy 12 (2007) 372–379

[3]Manfredini D., et al. Journal of Oral Rehabilitation 38; 101–119, 2011

[4] Sawacha Z. and Spolaor F., et al Gait & Posture 35 (2012) 101–105.

Disclosure of Interest: None Declared

EMG

PO-0064

THE NON-INVASIVE MEASUREMENT OF DEEP FOREARM MUSCLE ELECTROMYOGRAPHY USING SURFACE ELECTRODES

Jeremy D. Pitman [1,*] Lester R. John [1]

[1]MRC/UCT Medical Imaging Research Unit, Division of Biomedical Engineering, Dept. of Human Biology, University of Cape Town, Cape Town, South Africa

Introduction and Objectives: It is commonly accepted that surface EMG (sEMG) is limited to the measurement of superficial muscle activity. Deep muscle EMG detection is only considered possible through the insertion of intramuscular electrodes into the muscle, an invasive and inherently risky procedure. A method for non-invasive deep muscle EMG measurement combining monopolar EMG, an un-mixing method such as Independent Component Analysis (ICA) and an activation or movement protocol specific to the muscle being investigated[1] has been tested on Brachialis[2] and Tibialis Posterior[3], successfully detecting activity in both deep muscles. This technique was extended and applied to 4 deep forearm muscles (Flexor Pollicis Longus (FPL), Extensor Pollicis Longus (EPL), Extensor Pollicis Brevis (EPB) and Abductor Pollicis Longus (APL)) and two superficial forearm muscles (Flexor Digitorum (FD) and Extensor Digitorum (ED)) during isometric contractions of the thumb and index finger.

Methods: Monopolar EMG was recorded from two concentric rings, consisting of 20 electrodes each, placed at the distal and proximal thirds of the forearm from fifteen healthy male participants. The participants performed 10 repetitions of isometric thumb flexion (TFl), thumb extension (TEx), thumb abduction (TAb), thumb adduction (TAd), index finger flexion (IFFl) and index finger extension (IFEx). The isometric contractions (<30% of the Maximum Voluntary Contraction-verified by strain gauges) were performed in a randomized order and interspersed with rest periods for each experimental run. Contraction timing and sequence adherence information was derived from the strain gauges. The isometric contractions were selected to independently activate and thereby isolate the target muscles within the area encircled by the electrode bands. fastICA was used to un-mix the 40 monopolar EMG waveforms (containing EMG activity attributable to both superficial and deep muscles) and resolving the signals into 40 constituent components, known as the Independent Components (ICs). The ICs were root mean square (RMS) smoothed using a 250ms moving window and normalised to range from 0 to 1. A contraction sequence specific predicted EMG pattern was created for each muscle (based on corresponding intramuscular measurements[4,5]) and was correlated with the processed ICs using Pearson's Correlation Coefficient (ρ). The IC which best correlated with the predicted EMG waveform for each muscle was considered to represent the recovered EMG activity from that particular muscle (shown for a typical experimental run for one participant in Figure 1).

Results: Good correlation, of the predicted EMG with the processed ICs, was found for the deep FPL, EPL, EPB and APL (summarised for all experimental runs in Table 1). This indicated the ICs were highly likely to represent the activity of those muscles. Low correlation was found for the superficial FD and ED, due to either co-contraction that was un-accounted for in the predicted EMG waveforms or poor separation of the monopolar EMG by fastICA for these particular muscles. Occasionally, fastICA recovered activity when no EMG activity was predicted (ie during TAd for FPL; TFl for

APL). This phenomenon was seen across multiple experimental runs and was likely due to unintended co-contractions (due to poor contraction sequence adherence) or inaccurate estimation of the muscle activity by fastICA.

Figure:
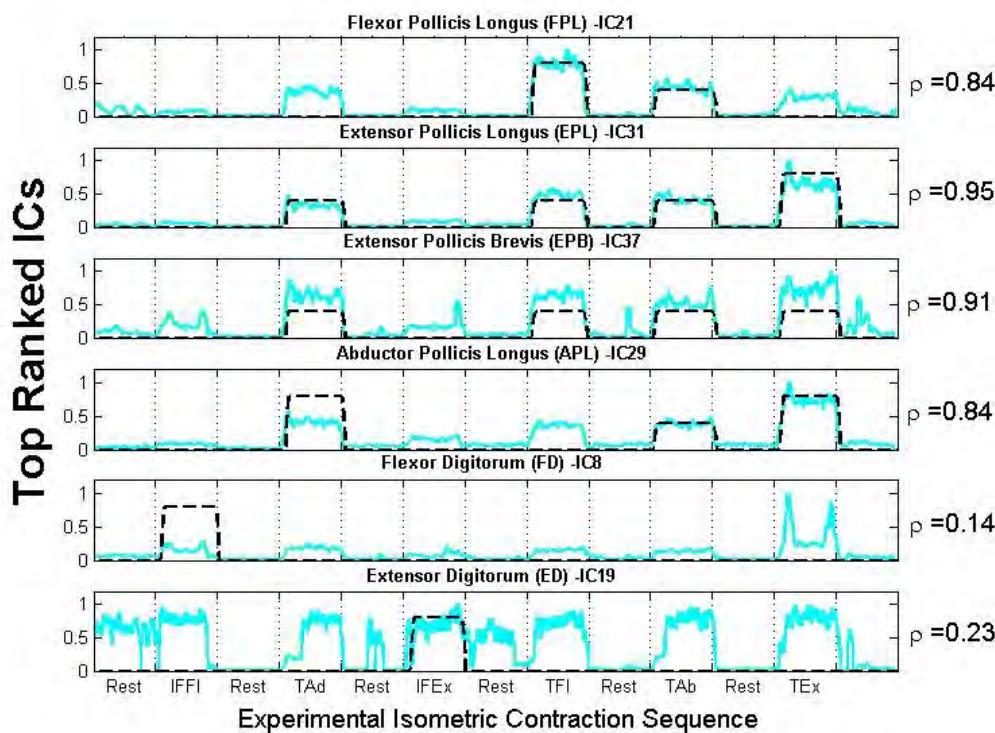
Caption: The predicted EMG waveforms (dashed line) and processed ICs (solid line) with the highest correlation coefficient (ρ) values for one experimental run for one participant. The vertical dotted lines demarcate the waveforms into intervals according to the contraction performed and each rest period.

Conclusion: The ρ values in Table 1 for the 4 deep muscles indicate that the correlation of the predicted EMG with the ICs was consistent over all experimental runs, especially for EPL and EPB. The large variation of the ρ values for the 2 superficial muscles indicated the technique was largely inadequate in detecting activity from these muscles. The results indicate that EMG activity from FPL, EPL, EPB and APL is detectable using surface electrodes. Research verifying this technique is ongoing.

Table:

Muscles		Mean (Min - Max) ρ
Deep	FPL	0.80 (0.58 - 0.96)
	EPL	0.88 (0.72 - 0.96)
	EPB	0.92 (0.80 - 0.96)
	APL	0.83 (0.56 - 0.96)
Superficial	FD	0.40 (-0.07 - 0.88)
	ED	0.38 (-0.07 - 0.85)

Caption: Average (Fisher-transform corrected) ρ values between the predicted EMG and best-fit ICs for each muscle over all experimental runs (15 participants, 10 repetitions per participant)

References: [1] John, L.R., PCT/IB2010/001876, priority date: July 30 2009.

[2] Moroaswi S. et al., MScMed thesis (unpublished), Dept. Human Biology, Univ. Cape Town, 2010.

[3] Sayed, A. et al., presented at Int. Soc. Electromyogr. Kinesiol. Conf., Rome, 2014.

[4] Kaufman, K.R. et al., Clin. Biomech., **14**(2): 141–50, 1999.

[5] Birdwell, J.A. et al., J. Neurophysiol*., * **110**(6): 1385–92, 2013.

Disclosure of Interest: J. Pitman: None Declared, L. R. John Conflict with: the non-invasive deep muscle electromyography method and device is patented (inventor: co-author L.R. John; assignee: University of Cape Town and the South African Medical Research Council) in China (201080030787.6) and South Africa (2011/09253), and patent-pending in the USA (13/387,897), Europe (10803972.8), Japan (J2012-522271), India (2823/MUMNP/2011)

PO-0065

UNGRADED MUSCLE CONTRACTION IS THE SOURCE OF TENDON PERTURBATIONS OBSERVED DURING IN VIVO TRICEPS SURAE LOADING

Saira Chaudhry [1,*] Hazel Screen [2] Dylan Morrissey [3] Dan Bader [3] Roger Woledge [3]

[1] Centre for Sports and Exercise Medicine, [2] School of Engineering and Material Science, [3] QMUL, London, United Kingdom

Introduction and Objectives: Achilles tendinopathy is a most common overuse injury in recreational and professional sports participants [1]. It is difficult to treat and prone to recurrence, with current treatments achieving only partial success. Eccentric loading (eccentric) has shown to promote significant healing in Achilles tendinopathy [2] as compared to concentric loading (concentric). However, the mechanisms underpinning its effects are unclear. Recent in vivo studies in healthy humans have reported no difference in the peak Achilles tendon force during applied eccentric and concentric [3], instead reporting that the primary difference between eccentric and concentric is 10 - 12 Hz tendon perturbations occurring during eccentric [4]. In order to establish the region specific origin of these perturbations, a study was carried out to characterise the pattern of muscle activity across the surface of the triceps surae during eccentric and concentric exercises. From this, it was aimed to investigate the anatomical origin of the 10 - 12 Hz perturbations observed during eccentric.

Methods: Nine healthy subjects participated in the study. Subjects performed eccentric or concentric on a step mounted on a force plate. EMG data was recorded in synchrony with motion analysis data. For mapping calf muscle EMG, 32 EMG electrodes were used on the leg, divided across the three compartments of the triceps surae muscle; the medial gastrocnemius, lateral gastrocnemius and soleus. Each muscle was further divided into proximal, middle and distal sub regions. EMG frequency components were calculated by taking the fast Fourier transform (FFT) of the raw EMG data from each electrode pair.

Results: Tendon perturbations were significantly higher during eccentric than concentric exercises (P = 0.024). Graded EMG magnitudes were found to be higher overall in concentric than eccentric EMG data (particularly at very high frequencies). For concentric, higher intensities of graded EMG were present from 10 Hz upwards, focused in the distal gastrocnemius. There was a less uniform spectrum of frequencies present across the triceps surae during eccentric. However, considering 10 - 12 Hz region, the highest graded EMG was observed during eccentric (Figure 1) mainly recorded from the distal, middle and proximal medial soleus, as well as the distal medial gastrocnemius and proximal lateral gastrocnemius. It is evident that certain triceps surae regions, clearly shows a 10 - 12 Hz peak in eccentric data only.

Figure:
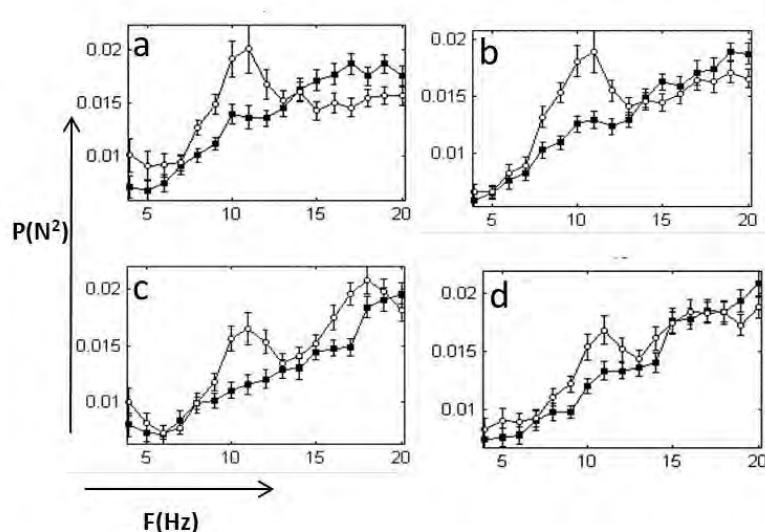
Caption: Example data set for the Fourier transform of the calf EMG ± SE (filled circles concentric, empty circles eccentric). a) distal medial soleus. b) proximal medial soleus. c) mid medial gastrocnemius. d) proximal medial gastrocnemius

Conclusion: During eccentric, 10 - 12 Hz frequency peaks were observed in the soleus and the medial gastrocnemius regions of the triceps surae, indicating that these areas of the muscle are likely to be responsible for the specific 10-12Hz vibrations. These findings signify the importance of these regions in the triceps surae; It has been reported recently that tendon rupture mainly occur in the posterior-mid tendon [5], where the load bearing is maximal from the medial soleus and gastrocnemius; if 10 - 12 Hz stimulation is important in treating tendinopathy [6], these are the source. It is still unclear whether perturbations are a beneficial stimulus for tendon repair, or in fact indicate a muscle weakness or poorly synchronized muscle activity in the triceps surae, both of which may be risk factors for tendinopathy. It may be that eccentric treats tendinopathy by training the triceps surae to function more effectively and minimize perturbation, with a progressive load and speed challenge incorporated as the triceps surae adapts to the training stimuli.

The relevance of 10-12Hz perturbations remains unclear; however, finding the origin is an important step towards understanding if perturbations do have a beneficial effect on tendon healing.

References: 1.   Jonge et al., *Br J Sports Med.* 45(13):1026-1028, 2011.

2.   Rowe et al., *Sports Med.* 42(11):941-967, 2012

3.   Rees et al., *Rheumatology (Oxford).* 47(10):1493-1497, 2008.

4.   Chaudhry et al., *Journal of applied biomechanics,* 2014.

5.   Alfredson et al., *Br J Sports Med.* 45(5):429-432, 2011.

6.   Grigg et al., *Med Sci Sports Exerc.* 45(3):520-526, 2013;

Disclosure of Interest: None Declared

EMG

PO-0066

ELECTROMYOGRAPHIC AND SUBJECTIVE RESPONSES DURING LOAD CARRIAGE IN GRADED UPHILL AND DOWNHILL WALKING

Sohini Paul [1,*]Tirthankar Chatterjee [1]Anilendu Pramanik [1]Deepti Majumdar [1]Madhusudan Pal [1]Dhurjati Majumdar [1]

[1]Ergonomics, Defence Institute of Physiology and Allied Sciences, Delhi, India

Introduction and Objectives: Thousands of Indian army soldiers are deployed in the mountainous border areas in the eastern and the western Himalayas. Execution of military objectives often demands patrolling and marches in this terrain with different intensities of load that include communication gear, weapons, ammunition, food, water and others. Load carriage in uphill and downhill gradient is always stressful, fatiguing and affects soldiers'combat performance. It is hypothesized that uphill and downhill walking continuously with load increases the muscular responses linearly while walking up the slope and almost in all cases decreases while walking down the slope. It is also hypothesized that this form of exercise affects the lower limb and back muscles differently. This study examined the effect of increasing load and incremental and decremental gradients during uphill and downhill treadmill walking on different muscle activities as electromyographic (EMG) responses and subjective responses using the Borg's scale of rating of perceived exertion (RPE).

Methods: Twelve physically fit Indian soldiers with mean (± SD) age- 26.8 (± 3.9) yrs, height- 170.6 (± 3.2) cm and weight 66.2 (± 6.8) kg volunteered for this study. All the experiments were conducted in controlled laboratory conditions with temperature ranging from 25-28^{0}C and 35-40% relative humidity. The subjects walked continuously for 1 hr in both uphill (30 mins) followed by downhill gradients (30 mins) at 3kmhr^{-1} speed carrying 0.0kg, 10.7kg and 21.4kg load. At first they walked uphill at 0%, 5%, 10%, 15% and 20% gradients followed by walking at downhill gradients of 20%, 15%, 10%, 5% and 0%. For each gradient the subjects walked for 6 mins. The EMG activity for all the load conditions at each of the gradient were normalised with the EMG data of the 0% gradient for the respective load conditions. All the experiments were conducted at random to avoid any biasness. During the experiment the electromyographic responses of Erector spinae(ES), Vastus medialis(VM), Gastrocnemius medialis(GM) and Soleus(SOL) of both sides were monitored continuously along with RPE.

Results: Significant effects of gradient on all the four pairs of muscles for all the conditions were observed. It was found that the activities of the right Erector spinae (RES) and the left Erector spinae (LES) increased as the load mass increased. Both the ES muscles showed an average increase of about 26% activity at 5% gradient while walking unloaded and about 250% increase in activity at 20% gradient in comparison to their respective load at 0% gradient. While walking downhill from 20% to 0% it was observed that the activities of RES and LES muscles decreased in comparison to their respective uphill gradients. There was an average increase in activity of the knee extensors [RVM (right Vastus medialis) and LVM (left Vastus medialis)] by 24% at 5% gradient while walking unloaded and about 272% increase at the highest uphill grade and load combination compared to their respective load at 0% gradient. On the other hand when the subjects started walking downhill an average 284% increase in muscle activity was observed at 20% downhill and carrying 21.4kg load. There was a significant effect of grade on these muscle pairs. A significant increase in

the RGM (right Gastrocnemius medialis) and the LGM (left Gastrocnemius medialis) activity in response to progressive increase of load and increasing and decreasing gradients were noticed. The GM muscles of both the sides increased linearly to about 9% while carrying no load at 5% gradient. At 20% gradient while carrying 21.4kg load at the same walking speed the muscle activity increased to about 72% as compared to the 0% gradient. At downhill gradients the muscle activity decreased compared to the uphill gradients. The SOL muscles showed an average increase of about 8% activity at 5% gradient while walking unloaded and that for carrying 21.4kg at 20% gradient there was 80% increase. It was observed that the activity of the RSOL (right Soleus) and the LSOL (left Soleus) was significantly affected by load and grade.

Conclusion: The present study indicated that while walking up the slope the ES and VM muscles were affected the most. On the other hand walking down the slope affected the knee extensors activity more in comparison to the other muscles. RPE was also significantly affected by the load and grade with the maximum rating of 16.5 out of 20 while walking with 21.4 kg load and 20% uphill grade. The Indian military personnel when subjected to similar exercises in routine military operations in higher altitude, the prevailing hypoxic condition there may further exaggerate and accelerate the risk of muscle injuries, soreness and fatigue to a larger extent affecting the combat fitness of the individual. Hence, adequate preventive measures are required by the individual while traversing at steep gradients with load.

Disclosure of Interest: None Declared

THE USE OF INDEPENDENT COMPONENT ANALYSIS ON EMG DATA TO EXPLORE CROSSTALK

Róisín M Howard [1,*]Richard Conway [1]Andrew J Harrison [2]

[1]Electronic & Computer Engineering, [2]Physical Education & Sports Science, University of Limerick, Limerick, Ireland

Introduction and Objectives: Cross talk is a common problem associated with surface Electromyography (sEMG). Multiple muscles contribute to a movement which may cause multiple signals to be picked up by the sEMG sensor from neighbouring muscles. The combined signal is gathered and analysed, with the user being unaware if cross talk is contained and how much. ICA is a dimension reduction technique which can return data that was originally hidden from the larger data set. The data should be non-Gaussian and components should be statistically independent. EMG data fits the criteria for ICA and therefore has been used in studies to isolate EMG data. Willigenburg et al. makes use of ICA to remove ECG contamination from EMG recordings of the trunk muscles [1]. Similarly Azzerboni et al. uses a combination of techniques, ICA being one of them, in EKG artefact removal from EMG recordings [2]. The aim of this study is to explore the use of ICA on EMG signals to reduce cross talk from the gathered data, isolating individual muscle contributions.

Methods: Seven volunteers, four males and three females, who were injury free at the time of testing, participated in this study. Ethical approval was granted by the local University Research Ethics Committee and all participants provided informed consent in writing before testing. The Delsys Trigno Wireless EMG system was used, EMG electrodes were attached according to SENIAM recommendations (with extra electrodes attached in unideal locations so as to gather cross talk data) [3]. Participants performed five reps of split squat which isolates the quadriceps muscle group.

EMG data was imported into Matlab. A mixed signal matrix was created with data from 3 of the combination of sensors for each movement, in multiple combinations. Each mixed matrix was analyzed using the ICA algorithm and subsequently compared to the signals gathered from the sensors in recommended locations. The integrated EMG (iEMG) of the analysed signals and the original ideal signals were compared using interclass correlation coefficients (ICC) with 95% Confidence Intervals (CI) [4].

Results: Table 1 shows the mean muscle activations (±SD) for the Rectus Femoris (RF), Vastus Lateralis (VL) and Vastus Medialis (VM) for the split squat exercise. The RF returned an ICC of 0.478 when compared with iEMG from the EMG signal gathered at the ideal sensor location and the iEMG of the average output from the ICA algorithm for the RF using sensors from other locations on the quadriceps. Similarly the VL returned an ICC of 0.359 and the VM returned an ICC of -0.006. In a comparison of iEMG on all the outputs from the ICA algorithm, the RF returned an ICC 0.941, the VL returned an ICC of 0.958 and the VM returned an ICC of 0.721. The systematic bias observed between the ideal EMG signals and the ICA output signals was significant; however the percentage difference was very small.

Figure 1 shows an image of the signals gathered in ideal sensor locations vs one set of output signals from the ICA algorithm. It can be seen that there are many similarities visually between both sets. Note must be made that ICA does not keep scaling properties but the signal profile remains the same.

Figure:
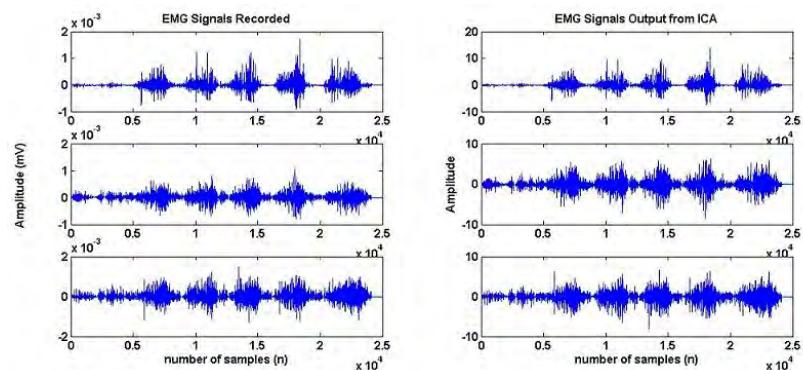
Caption: Figure 1. Comparison of ideal EMG signals to output from ICA algorithm

Conclusion: Results of this investigation identified that the ICA algorithm is a successful tool which can be used to distinguish between individual muscle activations. Results showed moderate agreement between the output from the ICA algorithm and the ideal EMG signals. However, these ideal EMG signals may still be picking up cross talk from neighbouring muscles groups. A moderate to high agreement was found between all the outputs from the ICA algorithm which leads to the conclusion that the results of the ICA algorithm may be returning the actual ideal EMG signals for the specific muscle groups. Further research into the use of this algorithm can be done to make results more accurate and reliable.

Table:

	Rectus Femoris	Vastus Lateralis	Vastus Medialis
iEMG ideal ± SD (mV)	1.17 ±0.56	1.89 ±1.14	2.09 ±1.04
iEMG of ICA output ± SD (mV)	1.50 ±0.22	1.59 ±0.79	1.60 ±1.01
% Difference	0.32	-0.30	-0.50
Systematic Bias	6	6	6
ICC (between ideal and ICA output)	0.478	0.359	-0.006
(95% CI)	(-0.782 - 0.898)	(-2.174 - 0.887)	(-3.195 - 0.815)
ICC (on all outputs of ICA)	0.941	0.958	0.721
(95% CI)	(0.816 - 0.989)	(0.868 - 0.992)	(0.138 - 0.946)

Caption: Table 1: Comparison of Integrated EMG (iEMG) for ideal EMG signals and outputs from ICA algorithm

References: [1] Willigenburg, N.W, et al., JEK 22:485–493, 2012.

[2] Azzerboni, B. et al., 2004 IJCNN, 4: 3223 – 3228, 2004.

[3] European Recommendations for Surface Electromyography, Roessingh Research and Development, 1999.

[4] Atkinson, et al., Sports Medicine, 26:217-238, 1998.

Disclosure of Interest: None Declared

EMG

PO-0068

EFFECT ON SIDE RATIOS OF ERECTOR SPINAE MUSCLE DURING ISOKINETIC TRUNK EXTENSION USING ABSOLUTE OR NORMALIZED EMG AMPLITUDES

Martin Wolter [1,*] Stephan Kopinski [1] Monique Wochatz [1] Steffen Mueller [1] Frank Mayer [1]

[1] Sport and Health Science, University Outpatient Clinic Potsdam, Potsdam, Germany

Introduction and Objectives: EMG is a valuable tool to assess neuromuscular impairments in patients e.g. suffering from chronic low back pain. Numerous studies have shown alterations in the neuromuscular activation of trunk muscles. Side differences in EMG amplitude between muscle pairs are present in patients as well as in healthy controls, though to a lesser degree. Usually normalization of EMG to maximum exertion (MVC) is used to account for confounding factors like differences in electrode placement. But normalization could also mask the distinctions that would be associated with pathology and it depends on maximum voluntary contractions (MVC). The aim of this study was to evaluate the effect of EMG amplitude normalization on calculation of contralateral side ratios in m. erector spinae (ES) in an isokinetic trunk extension.

Methods: In 42 healthy subjects (21 males/21 females, 27±3 years, 69±12 kg, 1.74±0.09 m) muscular activity of the lumbar ES (LES) at L3 level and thoracic ES (TES) at Th9 level were measured bilaterally via 4-lead-EMG during concentric isokinetic back extension at 45 °/s and a ROM of 45° flexion to 10° extension. Warm-up was followed by 5 maximum voluntary contractions (MVC). Afterwards each 5 isokinetic contractions were performed with 20, 40, 60 and 80% of the MVC peak torque. Root mean square (RMS) for the isokinetic phase of all 5 repetitions was averaged within each condition and normalized to MVC. Side ratios were calculated for raw RMS (Δ_{raw}) and normalized RMS (Δ_{norm}) with the formula │1-(left side/right side)│*100. Differences of both calculations (Δ_{raw} vs Δ_{norm}) were tested for significance with a paired t-test ($\alpha=0.05$). Agreement between both was tested with Bland-Altman-Analysis (BAA) with bias ± limits of agreement (LoA; SD*1.96). Additionally repeated measure ANOVA (Bonferroni adjusted) was conducted to assess load dependency of the site ratios.

Results: Statistical significant differences between Δ_{raw} and Δ_{norm} were present for LES in 40, 60 and 80% with 18 vs 14%, 15 vs 11% and 14 vs 7%, respectively (Tab.1). ANOVA revealed significant differences for site ratios of the LES regarding load in both normalized and raw data. Post-hoc tests of Δ_{raw} showed just significant differences between 40 and 60%, whereas pair-wise comparisons of Δ_{norm} showed significant differences in 4 of 6 comparisons.

Figure:

Load	TES			LES		
	Raw RMS vs Normalized [%]		Bias±LoA	Raw RMS vs Normalized [%]		Bias±LoA
20%	24±17	25±21	-2±50	21±16	18±16	3±29
40%	22±21	23±19	-3±53	18±13	14±11 *	4±24
60%	23±22	21±16	1±43	15±11	11±7 *	4±20
80%	21±17	17±12	4±40	14±9	7±5 *	6±19

Caption: Side differences (mean ± SD) between left and right side of each muscle pair (* indicates significant differences between Δraw and Δnorm with $p<0.05$) and BAA.

Conclusion: Side ratios calculated with normalized RMS data reveal lower values and LES site ratios were affected by the applied load. But Δ_{raw} seem to be more stable for load effects than Δ_{norm}. Whether the significant difference between both ways of calculating side ratios has practical relevance needs to be discussed. IfΔ_{norm} is more reliable than Δ_{raw} and able to distinguish between healthy and LBP patients needs to be investigated. Since EMG amplitudes can be influenced by several factors one should weigh carefully the advantages and disadvantages of raw RMS data.

Disclosure of Interest: None Declared

EMG

PO-0069

EVIDENCE FOR MUSCLE-SPECIFIC PIPER RHYTHM OF LOWER LIMB MUSCLES DURING WALKING

Gregor Kuntze [1,*]Vinzenz von Tscharner [2]Cam Cummings [3]Carol Hutchison [3]Janet Ronsky [1]

[1]Mechanical and Manufacturing Engineering, [2]Kinesiology, [3]University of Calgary, Calgary, Canada

Introduction and Objectives: Electromyographic (EMG) signals of skeletal muscles display a temporal rhythmicity [1, 2] representing a cortical drive that tends to synchronize the activity of motor units. The Piper rhythm (30-60Hz) can be resolved during cyclic movements using wavelet analysis [3] and has been shown to be sensitive to changes in running speed [4]. While the general frequency range of the Piper rhythm has been defined, it is feasible that modulation of this rhythm occurs in response to task demands. Further, differences in activation rhythmicity may exist between different muscles of the lower limbs. However, there remains a lack of information concerning potential inter-muscular differences in this activation rhythmicity. The aim of this study was to investigate the Piper rhythm of seven lower limb muscles during a walking task. It was hypothesized that lower limb muscles display Piper frequencies between 30-60Hz and that significant inter-muscular differences in the Piper rhythm can be identified during a walking task.

Methods: Nine healthy female subjects (61.4±7.4 years; BMI 25.6±2.4) volunteered for participation in this study. Approval was received from the local ethics board. Subjects walked at a self-selected pace on a raised wooden walkway. Gait velocity was recorded using a pair of timing lights (Banner, USA) positioned immediately before and after two forceplates (AMTI, OR6-6, USA; Kistler, 9286AA, Switzerland). Following recommendations by SENIAM (www.seniam.org) EMG data of seven lower limb muscles of a randomly selected limb were collected: vastus lateralis (VL), vastus medialis (VM), rectus femoris (RF), semitendinosus (SEM), biceps femoris (BF), lateral gastrocnemius (GAS) and tibialis anterior (TA). The skin was shaved, cleaned with rubbing alcohol and bipolar Ag/AgCl EMG electrodes (diameter 10mm, inter-electrode distance 20mm; Noraxon, USA) were affixed. All data were normalized to stance phase using force-plate measures. EMG signals were wavelet transformed [5], time normalized to 501 data points and visually inspected for movement artifacts. The lowest number wavelet was removed to minimize effects of signal noise. Five trials per subject were taken forward for analysis in Matlab (MathWorks, USA). Total intensity (TI) patterns were calculated for each muscle and trial by computing the sum of intensities of the wavelet pattern at each time point. Peaks, apparent in the TI patterns, were identified in Matlab and all peaks <5% of the maximum intensity were rejected. Between peak intervals (ms) were computed and histograms of all subject data were generated. Data distributions were obtained using a gamma fit. The peak and mean of each gamma distribution was computed for analysis purposes.

Data were tested for normality (Shapiro-Wilk) and log transformed if necessary. Multivariate ANOVA were performed in SPSS (IBM, USA) with Bonferroni correction ($p \leq 0.05$).

Results: Gamma distribution peak and mean data are presented in Figure 1. A significant effect of muscle was observed ($p<0.001$) with VL displaying longer between-peak intervals compared to all other muscles ($p<0.001$ throughout). These results indicate a Piper frequency range of 25-32Hz for VM, RF, BF, SEM, GAS, and TA and 16-19Hz for VL. Variations in frequency estimates based on peak and mean data may be explained by the distinct and consistent positive skew of the distribution curves. Peak data therefore would tend to result in a higher frequency estimate, while mean data would tend

to result in a lower frequency estimate. If the Piper frequency is modulated to meet exercise demands (Maurer et al. 2013) peak data may be more sensitive to such changes. However, this remains speculation at this time and will be investigated further in future studies.

Figure:

Between Muscle Comparison (w5-10)
Gamma Distribution
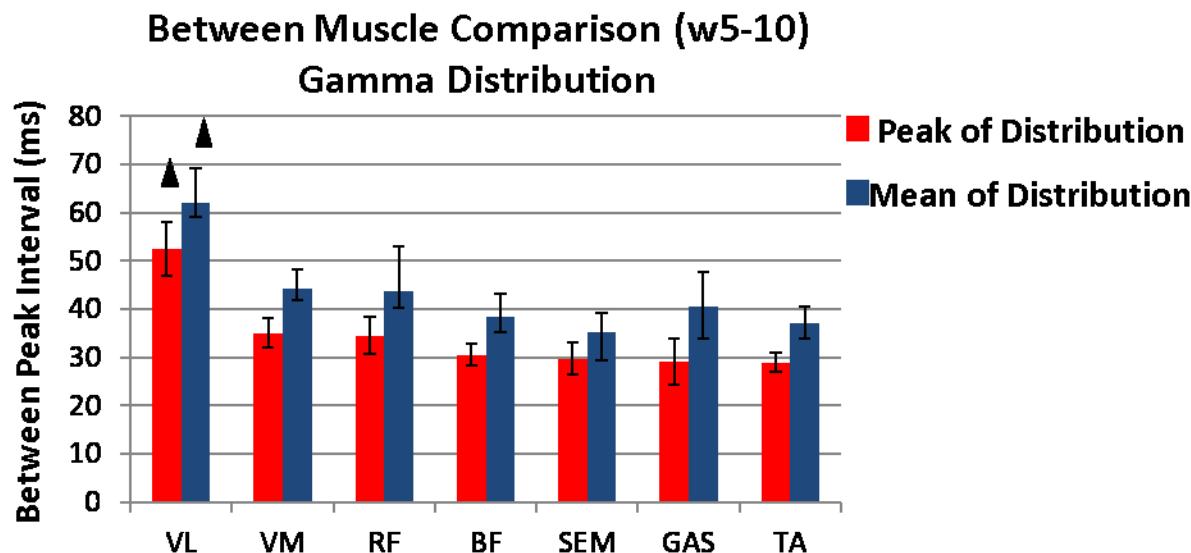
▲Significantly different from all other muscles (p<0.001)

Caption: Figure 1. Peak (red) and mean (blue) distributions of intensity peak intervals of the activations of 7 superficial lower limb muscles.

Conclusion: The observations of this study indicate significant differences in the Piper frequency between muscles of the lower limbs. While the exact causes for these differences remain to be elucidated, this may be an indication that not all muscles receive the same cortical synchronization stimulus but that this input is indeed customized to the activity of the muscle.

This study was supported by Alberta Ingenuity Fund (AITF), NSERC, and AHFMR.

References: [1] Piper, J. (1907). Über den willkürlichen Muskeltetanus. Pflueg Gesamte Physiol. 119:301–38.

[2] Brown, P. (2000). Cortical drives to human muscle: the Piper and related rhythms. Prog Neurobiol. 60(1):97-108.

[3] Stirling, L.M. et al. (2011). Piper rhythm in the activation of the gastrocnemius medialis during running. J Electromyogr Kinesiol. 21:178-183.

[4] Maurer, C., von Tscharner, V. and Nigg, B. (2013). Speed-dependent variation in the Piper rhythm. J Electromyogr Kinesiol. 23:673-678.

[5] von Tscharner, V. (2000). Intensity analysis in time-frequency space of surface myoelectric signals by wavelets of specified resolution. J Electromyogr Kinesiol. 10(6):433–45.

Disclosure of Interest: None Declared

EMG

PO-0071

THE IMPORTANCE OF KNEE MUSCLE COORDINATION THROUGH DIFFERENT STAGES OF OSTEOARTHRITIS.

Aseel Ghazwan [1,*]Cathy Holt [1]Gemma Whatling [1]

[1]Arthritis Research UK Biomechanics and Bioengineering Centre, Cardiff University, Cardiff, Wales, United Kingdom

Introduction and Objectives: Literature has shown that people with knee Osteoarthritis (OA) tend to walk with greater muscle co-contraction to compensate for joint instability. This in turn increases knee contact load, and may contribute to the progression of OA. The ideal strategy to understand this scenario is to explore how the coordination between quadriceps, hamstrings, and gastrocnemii are affected at different stages of knee OA. Accordingly, this study was initiated which aims to determine the changes in co-contraction index with the severity of OA.

Methods: Fifteen, fully consented subjects formed three groups: five healthy subjects, five with medial OA awaiting high tibial osteotomy (pre-HTO), and five with late stage OA awaiting total knee replacement (pre-TKR). The mean and SD of weight and height for healthy, pre-HTO and pre-TKR cohorts were (81.7±8.7 kg, 88.5±11.4 kg, 91.6±17.7 kg), (173.2±3.4 cm, 169.3±8.2 cm, 161.9±4.5 cm), respectively.

Muscle electromyographic (EMG) data were collected bilaterally for seven muscles: Rectus Femoris, Vastus Lateralis, Vastus Medialis, Biceps Femoris, Semitendinosus, Gastrocnemius Lateralis, and Gastrocnemius Medialis. The electrodes were placed longitudinally over the muscle bellies after standard preparation of the skin.

Individuals were then asked to walk at their comfortable speed. Meanwhile, information regarding muscle EMG, ground reaction force and three dimensional movement were collected using motion analysis (Qualisys, Sweden). 6 trials of level gait were recorded for each subject.

EMG data, through stance phase, were analysed in Matlab version R2013a. The raw EMGs were band-pass filtered using a Butterworth 4th order filter at 40_450 Hz to remove the movement artefacts, rectified and finally low-pass-filtered with a 4th order Butterworth filter at 6 Hz, to create a linear envelope for each muscle. Linear envelopes were normalized to peak values obtained through the walking cycle by using the Peak Dynamic Method (PDM), as that adopted by Knarr et al 2012 [1]. The EMG data were normalized to 100 data points though the stance phase and an average of six trials for each participant were calculated, thus representing the mean muscle activity through stance. Finally, the co-contraction index (CCI) was calculated for each muscle through stance according to Rudolph et al.[2].

CCI was calculated for the following muscle sets: Vastus Lateralis- Gastrocnemius Lateralis (VLLG), Vastus Lateralis-Lateral Hamstring (VLLH), Vastus Medialis- Gastrocnemius Medialis (VMMG), and Vastus Lateralis-Medial Hamstring (VMMH).

CCI was calculated for each subject during stance phase. Group means and standard deviations are presented in Figure1. One-way ANOVA was used to reveal statistically significant differences between the three cohorts ($p < 0.05$).

Results: Figure 1(A, B, and C), shows the CCI for healthy, pre-HTO, and pre-TKR subjects, respectively. As expected, patients with OA (Figures 1-B and 1-C), have a higher CCI compared to healthy subjects (Figure 1-A). Significant differences in the CCI were identified between the three cohorts, as indicated in Figure 1.

Interestingly, this study shows an almost two-fold increase in gastrocnemii CCI in the pre-HTO group as compared to healthy subjects ($p<0.05$). For the pre-TKR group, the gastrocnemii indices are increased further. The hamstring muscle indices are also significantly increased compared to the pre-HTO cohort, indicating that they also have a potential to provide stability for the knee joint. The Hamstring indices increased almost 60% on the lateral side and 25% on the medial side, as compared to healthy individuals. The statistically significant increase in VLLH CCI for the pre- TKR group as compared to the healthy cohort, may contribute to a reduction in the medial contact force.

These findings are consistent with previous literature, where patients with OA co-contracted significantly higher than that of healthy individuals. It has found a strong relationship between CCI and the stage of OA, i.e., the index is higher among the pre-TKR group, which represent the end stage of OA, than for the pre-HTO group.

Figure:
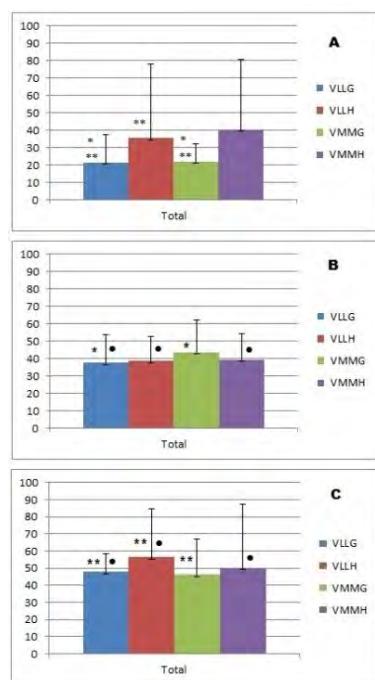
Caption: Figure-1: Co-contraction index during stance-phase for healthy subjects - A, pre-HTO subjects – B, pre-TKR subjects - C. Values represent mean and standard deviation. (*) means the difference is significant ($p < 0.05$) between Pre-HTO and healthy groups. (**) means the difference is significant ($p < 0.05$) between Pre-TKR and healthy groups. (●) means the difference is significant ($p < 0.05$) between Pre-HTO and Pre-TKR groups.

Conclusion: In conclusion, hamstring and gastrocnemii muscles play a significant role in stabilizing the knee joint and they altered their coordination through different stages of OA.

References: 1.Knarr et al, J Electromyogr Kinesiol, 22(4):607-611, 2012.

2.Rudolph et al. Knee SurgSports Traumatol Arthrosc, 9(2):62-71, 2001.

Disclosure of Interest: None Declared

PO-0072

IDENTIFICATION METHOD OF INNERVATION ZONE BY SURFACE ELECTROMYOGRAM DURING DYNAMIC CONTRACTIONS USING ELECTRODE ARRAYS

Aya Shirai [1,*]Tota Mizuno [1]Naoaki Itakura [1]Kazuyuki Mito [1]

[1]Graduate School of Informatics and Engineering, The University of Electro-Communications, Tokyo, Japan

Introduction and Objectives: During dynamic contraction, Innervation zone (IZ) shifts according to change muscle length in surface electromyogram (sEMG)[1]. Visual identification of IZ location is major method, but it is a matter of lack of objective assessment.

 This study provided the new identification method of IZ location during dynamic contraction in order to identify that objectively, and compared with the traditional method.

Methods: 1. Experiment

 Five healthy male subjects (mean of age was 21.6 years) maintained static (isometric) and dynamic contractions of right arm to the limit during 40% of maximum voluntary contraction (MVC). Isometric contractions were at right elbow joint angles 50°, 90° and 130°, and dynamic contraction was at the joint angle from 40° to 140° and the speed was set 10 °/s.

 sEMG was recorded from the right biceps brachii muscle. Electrode arrays were composed of fifteen silver wires with diameter of 1 mm and a length of 10 mm, and attached on the muscle belly. The distance between neighboring electrodes was 5 mm. Fourteen sEMG signals were derived bipolarly from paired neighboring wires filtered by bandpass from 5 Hz to 1 kHz. The sEMG signals were digitized with sampling frequency of 10 kHz and stored on computer.

 sEMG data for the isometric contraction (ISO) was analyzed at 0.4 seconds. sEMG data for the dynamic contraction was divided into concentric and eccentric contraction (CON, ECC), and each data analyzed at 0.4 seconds on the joint angles 50°, 90° and 130°.

2. New identification method

 In visual identification, most of measurers focus on waves of large amplitude values. Thus in the new method, the waves were paid attention to similarly, and identification was conducted using sEMG data at 0.4 seconds and electrode arrays including fourteen channels.

 First, sEMG data was divided in section between points of electrical potential crossing zero from negative to positive. For each section, maximum amplitude absolute values were calculated, and for each channel, sections which were ten of top the values or more were extracted. After that in any sections other than extracted sections, amplitude values were defined as 0 V.

 Next for each channel, Cross-correlation Coefficient (CC) was calculated for extracted section and both neighboring channels. After that, rate of CC which was -0.7 or less (uRATE), and rate of CC which was 0.7 or more (oRATE) were calculate, and means of the rates between same channels were calculated.

 Finally IZ location was determined from the following two cases. In first case, if channels which the highest uRATE and the lowest oRATE were identical channels, IZ location was defined as the channels. In second case, if channels which the

highest uRATE and the lowest oRATE were consecutive channels, IZ location was defined as the middle channel. If there were not implement all the above cases, IZ locations were defined as impossible identification.

Results: In visual identification, IZ is located on reversed peak action potential of neighboring channel (Figure). Results of visual identification of IZ location by three experts were defined as correct result, and concordance rates of the new method and visual identification were calculated.

Table shows mean concordance rate of three experts in three contractions each five subjects. The mean was 80 % in all contractions of all subjects, and it is useful to identify IZ location by new method. Compared with contractions, concordance rates at CON and ECC in subject A were showed 50%. The result was related to sEMG amplitude values. With decreasing amplitude value, it was difficult to extract characteristic wave. Amplitude values of subject A were lower than other subjects, therefore it led to low rate.

Figure:
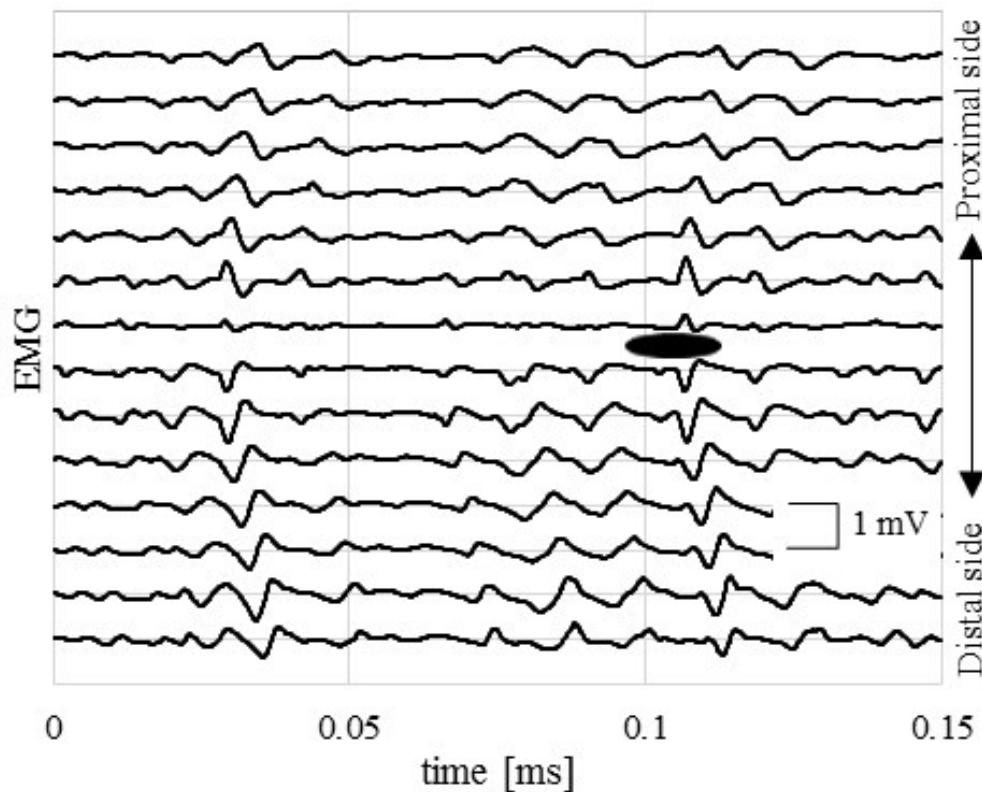
Caption: Example of IZ location by sEMG using electrode arrays, and ellipse shows IZ location in visual identification.

Conclusion: In identification of IZ location using sEMG, visual identification is major, and it is a matter of lack of objective assessment. Therefore, this study provided new objective identification method of IZ location. In the new method, characteristic waves were extracted, and similarities of the waves and neighboring channels were determined using CC. After that, by rate of CC was low and high each channel, IZ location was defined. Result of comparing the new method with visual identification, mean concordance rate was over 80 %, and it was useful to identify IZ location objectively.

Table:

Subject	ISO		CON		ECC	
	mean	±SD	mean	±SD	mean	±SD
A	83%	0%	50%	0%	50%	0%
B	83%	0%	72%	10%	78%	10%
C	78%	10%	100%	0%	100%	0%
D	83%	0%	100%	0%	83%	0%
E	67%	0%	83%	0%	89%	19%

Caption: Mean concordance rate of three experts of new identification method each subject (accuracy range is ± 0.5 channel), and standard deviation (number of samples was 18)

References: [1]Kazuyuki MITO et al., J. Jpn. Soc. Welfare Eng., 9(2): 40-46, 2007.

Disclosure of Interest: None Declared

EFFECT OF NUMBER OF TRIALS IN GROUND REACTION FORCES RELIABILITY DURING RUNNING

Andrea N. Onodera [1 2,*] Licia Cacciari [1] Ana Paula Ribeiro [3] Maria Isabel Roveri [1] Isabel C N Sacco [1]

[1]Physical Therapy, Speech and Occupational Therapy Dept. School of Medicine, University of São Paulo, São Paulo, [2]Dass Nordeste Calçados e Artigos Esportivos Inc., Ivoti, [3]Universidade de Santo Amaro, Universidade de Santo Amaro - Campus I, São Paulo, Brazil

Introduction and Objectives: The ground reaction forces during running and its impact are very studied area especially for running shoes researches [1,2,3]. Particularly, the number of trials needed to reduce the variability has been questioned between researchers studying highly variable parameters, such as the human locomotion [4]. The Brazilian National Standards Organization [5] recommends 20 trials to determine shoe-cushioning rates during gait, what results in a long data acquisition time and a large amount of acquired data, delaying the development of sports shoes. It can also represent discomfort for the runners. Diss [6] compared the reliability of ground reaction force (GRF) data of running for one and 10 trials, predicting that 10 trials were enough to achieve high level of confidence. However, only the Intraclass Correlation Coefficients (ICC) score was analyzed. Our study purpose to analyze the ICC and the Standard Error of Measurements (SEM) along the series of tested trials for 6 GRF parameters in healthy runners, intending to optimize the biomechanical test protocols, yet assuring high confidence levels.

Methods: Ten healthy runners (39.0±9.3 years old, 70.0±6.1 kg, 170±6 cm) with rearfoot strike pattern ran over a 25 meters walkway in constant and natural velocity (2.64 to 2.92 m/s). All runners used the same commercially available sport shoes. Ten valid trials were acquired by a force platform sampled at 1200 Hz (AMTI BP600600, Watertown, USA), and data was filtered at 300Hz by Butterworth 4th order zero-lag filter. The leg side was randomly chosen. Kinetic variables from vertical and antero-posterior GRF were analyzed. The Reliability tests were performed after confirming normal data distribution (Kolmogorov-smirnov). The Standard Error of Measurements (SEM = SD$\sqrt{1-ICC}$) were calculated along 2 to 10 trials, as well as the intraclass correlation coefficient (ICC(1,1) = (MSb-MSw)/(MSb + (k-1)MSw)) corresponding to the one-way model with single measurements reliability [7].

Results: All kinetic variables analyzed in this study presented the highest ICC scores for number of repetition with the lowest SEM, which means that the highest consistency of data is followed by the lowest absolute error in the measurements (figure 1). Biomechanical studies usually record 5 to 10 trials to guarantee data consistency. Our results show that for 10 subjects running 10 or 20 trials as recommended by the Brazilian National Standards Organization would be a waste of experiment time and also would reduce the consistency of the data, probably because the increasing chance of error. The first vertical force peak presented the highest reliability and lowest error at 6 trials. For loading rate and the median frequency of the first vertical force peak 3 trials corresponded to the optimal reliability rate and low SEM. On the other hand, variables related to the second vertical force peak presented optimal reliability rates and low SEMs for 2 trials. And lastly, the one variable related to the first antero-posterior peak presented higher reliability with 5 trials.

Figure:
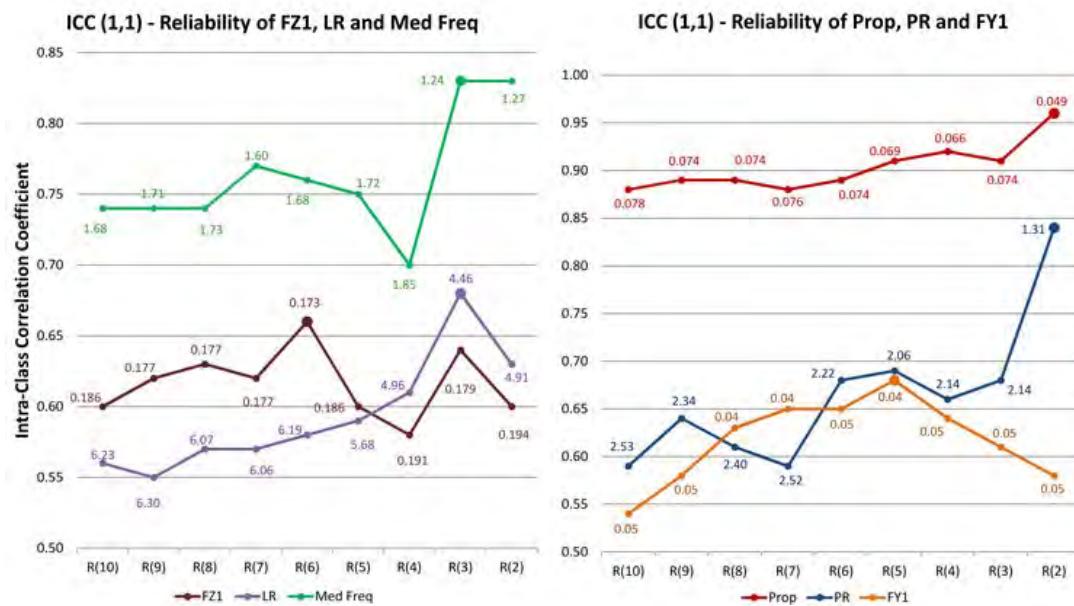
Caption: Ilustration of Intraclass correlation coefficient (lines) and Standard Error of Measurement (numbers above or under each mark) of ground reaction force parameters during 2 to 10 trials.

Conclusion: The ideal number of trials needed in biomechanical studies differ according to the running event on focus. When studying the vertical GRF 3 trials seems to be enough, guarantying good reliability rates, except for the first peak. In cases in which horizontal GRFs are the main focus of the study, at least 5 trials are necessary to optimize the reliability and the standard error of measurements.

Table:

Variables	Mean	sd
First Impact Force (BW) - FZ1	1.66	0.29
Loading Rate (BW/sec) - LR	42.38	9.35
Median Frequency (Hz) - Med Freq	14.07	3.27
Propulsion Force (BW) - Prop	2.59	0.22
Propulsion Rate (BW/sec) - PR	17.92	3.98
Horizontal Breaking Force (BW) - FY1	-0.38	0.08

Caption: Means and standard deviations of all variables for 10 trials

References:

[1] Azevedo A et al., J Sports Sci 30(9): 929-35, 2012.

[2] Kersting UG and Bruggemann GP, Res Sports Med 14(1): 1-17, 2006.

[3] Hennig EM et al., J Applied Biomech 12: 143-50, 1996.

[4] McGinley JL et al., Gait Posture 29: 360-9, 2009.

[5] ABNT, NBR14839, 2011.

[6] Diss CE, Gait Posture 14: 98-103, 2001.

[7] Wier JP, J Strength Cond Res 19(1):231-40, 2005.

Disclosure of Interest: None Declared

GROUND REACTION FORCE IMPULSES DURING FIRST ATTEMPT OF BAREFOOT RUNNING IN HABITUAL SHOD RUNNERS

Ana Paula D. S. Azevedo [1,*]Juliana Pennone [1]Bruno Mezêncio [1]Rafael Soncin [1]João Claudino [1]João Pinho [1]Alberto Amadio [1]Julio Serrão [1]

[1]Laboratory of Biomechanics, School of Physical Education and Sport - University of São Paulo, São Paulo, Brazil

Introduction and Objectives: Running has been a very important expression of movement. However, your practice has been related to an increasing injury rate [6,8]. Parameters of the vertical component of Ground Reaction Force (GRF), as the impulses, have been associated to these injuries [2,4,8]. Evidences suggest barefoot running decreases impact forces [3,5,7]. Thus, the belief that barefoot running could be an effective strategy to improve mechanical load control has been reinforced. Other evidences suggest barefoot running increases external load and could be harmful to human body [1,9]. Nevertheless, few studies analyzed the influence of barefoot running upon GRF in habitually shod athletes in their first attempt in this mechanical condition. Therefore, the purpose of this study was to analyze the effect of barefoot condition upon the impulse of the first 50ms and total impulse of GRF in habitually shod runners in their first attempt of barefoot running.

Methods: Fourteen habitually shod runners (12 men and 2 women; age = 28.4 ± 7.3 years; mass = 72.7 ± 7.8 kg; height 1.74 ± 0.06 m) ran during 10 minutes at 9 km.h^{-1} on a treadmill in two conditions: using conventional running shoes and barefoot. An instrumented treadmill (GAITWAY Instrumented Treadmill System 9810S1; and TROTTER Treadmill Model 685, 01-06560201) with two piezoeletric force plates (KISTLER Inc.) was used to obtain the vertical component of GRF. Nine acquisitions (10 seconds each) of GRF were performed for each experimental condition at 2600 Hz. The impulse of the first 50ms (Imp50, area under the curve GRF x time of the first 50ms) and total impulse (ImpTot, area under the curve GRF x time) were calculated.

GRF data was low pass filtered by a Butterworth filter (4th order, 90 Hz cutoff frequency). The start and end of each left and right step was determined using 30N threshold. GRF data was normalized by individual body weight, while time was normalized by total support time. Statistical analysis of data was performed in SigmaStat 3.5 (Systat, Germany) software. Data normality was verified using the Kolmogorov-Smirnov test, while homoscedasticity was checked by Levene's test. For means comparison, an analysis of variance (ANOVA) for repeated measures was performed. The level of significance adopted was $p \leq 0.05$.

Results: Significant differences were observed between shod and barefoot running for the variables analyzed. The Imp50 was 29.2% higher ($p < 0.001$) for barefoot running (33.83 ± 11.20 BW.ms) compared to conventional shoe (26.19 ± 7.94 BW.ms). However, the ImpTot was 17.2% smaller for barefoot (328.30 ± 3.23 BW.ms) than conventional shoe (396.30 ± 4.12 BW.ms).

Conclusion: Habitually shod runners seem to have higher energy propagated through human body in the impact phase during running barefoot. When the entire stance phase is considered, barefoot running imposed less energy propagation than conventional shoe. This result can indicate a less efficient mechanical load control and higher external force in a

critical moment of gait cycle in habitually shod runners during their first attempt barefoot. Such results corroborate with evidences reported by literature [1,9]. Therefore, although barefoot running presents a smaller total impulse of GRF, the impulse of 50ms, related to the impact phase of running, seems to be increased in habitually shod runners in their first attempt in this mechanical condition. A cautious use of barefoot condition in habitually shod runners is suggested to minimize injury risk.

References: [1] Bergstra et al., J Sci Med Sport, 21:S1440-2440(14), 2014;

[2] Cavanagh et al,. J Biomech, 13:397-406, 1980

[3] Divert et al,. International Journal of Sports Medicine, 26:593-598, 2005

[4] Komi et al., Int J Sports Med, 8:196-202, 1987

[5] Lieberman et al,. Nature, 463:531-535, 2010

[6] Milner et al., Med Sci Sports Exerc, 38:323-328, 2006

[7] Squadrone et al., J Sports Med Phys Fitness, 49:6-13, 2009

[8] van Gent et al., Br J Sports Med, 41:469-480, 2007

[9] Willy et al., Med Sci Sports Exerc, 46:318-323, 2014

Disclosure of Interest: None Declared

Feet and Footwear

PO-0075

BAREFOOT AND SHOD WALKING IN VIRTUAL REALITY ENVIRONMENT WITH OXFORD FOOT MODEL

Craig R Childs [1,*] Vicki Cameron [2] Andrew J Murphy [1]

[1]Biomedical Engineering, University of Strathclyde, Glasgow, [2]StEPS Podiatry, Troon, United Kingdom

Introduction and Objectives: The Oxford Foot Model (OFM) [1] was developed to get accurate measurement of foot movement during gait as the bone pin method [2] is not practical for most clinical situations. It has been validated in adults [3] and children [4]. However, since barefoot walking on a treadmill is not recommended there is a question over whether the OFM can be usefully applied in facilities such as the Motek CAREN (Computer Assisted Rehabilitation Environment - motekmedical.com). Consequently, there is an interest to see if applying OFM markers to shoes can give useful results when measuring human walking on treadmills. This study looks at the differences in measurements using the OFM between walking over-ground (barefoot and with shoes) and on a treadmill (with shoes).

Methods: Nine boys (mean age 13.5±0.5yrs, height 1.59±0.09m, mass 47.8±8.3kg) were recruited. Retro-reflective markers were attached bilaterally following the Plug-in-Gait lower limb and OFM models. The over-ground (barefoot and with shoes) trials were recorded in a standard gait laboratory (12 camera Vicon T-Series). Barefoot trials were performed first to minimise the need to reattach markers. The treadmill walking trials were recorded in the CAREN immediately after the over-ground trials (12 camera Vicon Bonita10). The treadmill speed was set to match the speed of over-ground walking in the gait laboratory. Gait events were determined from force plate contacts. All the boys wore light indoor training shoes. Data was captured using Vicon Nexus 1.8.5 and processed using Plug in Gait and OFM models in Nexus 2.1.

Results: There was no difference in ankle kinematics between over-ground (barefoot and with shoes) and on a treadmill (with shoes). Although Forefoot-Hindfoot angles were comparable to the literature in the barefoot condition, this was not the case with shoes (Table 1). Barefoot, there was a steady dorsiflexing motion throughout stance until push off which was signified by a rapid plantar-flexing motion. With shoes on, the same model segments show rapid dorsiflexion, then plantar flexion during early stance followed by neutral position held until push-off.

Conclusion: Reinschmidt and colleagues [2] reported that the shape of the calcaneal motion curves was similar for shoe mounted markers and bone markers, but that the shoe-mounted markers overestimated joint angles. In this study, the shape of the curves was quite different. This paper will discuss the practicalities and limitations of this technique, and where it may be usefully applied.

Table: Forefoot-Hindfoot Model Segment Dorsiflexion during Stance

	range (degrees)	time of peak (% of stance phase)	rate of change (degrees per second)
Stebbins [4]	12	82	25
Barefoot	11	87	22
Shoe over-ground	9	11	150
Shoe treadmill	8	23	130

References: [1] Carson, et al. J Biomech **34**(10): 1299-1307, 2001.

[2] Reinschmidt, et al. Clin Biomech (Bristol, Avon) **12**(1): 8-16, 1997.

[3] Wright, et al. Gait Posture **33**(1): 108-112, 2011.

[4] Stebbins, et al. Gait Posture **23**(4): 401-410, 2006.

Disclosure of Interest: None Declared

PO-0076

BIOMECHANICAL EVALUATION OF TWO SHOE DESIGNS FOR FOREFOOT OFFLOADING

Paolo Caravaggi [1] Alessia Giangrande [1] Lisa Berti [1] Giada Lullini [1] Alberto Leardini [1,*]

[1] Movement Analysis Lab, Istituto Ortopedico Rizzoli, Bologna, Italy

Introduction and Objectives: Forefoot offloading shoes (FOS) are special orthopedic footwear designed to protect and unload the injured part of the foot after surgery and for conservative treatments. While these shoes are intended to be worn only for short periods, a compromise must be found between offloading and comfort from one hand, lower limb functionality and stability on the other hand. In this study therefore, the traditional baropodometric measurements were integrated with joint kinematics and kinetics from standard gait analysis to assess the effects of a traditional half-shoe and a novel FOS (Podartis, Treviso, Italy), in a comparison to a standard comfortable shoe (control).

Methods: Ten healthy female participants (28.2±10.0 years; BMI 20.4±1.2 kg/m2) were asked to walk in three different footwear conditions for the left/right foot: control / traditional half-shoe, control / novel, and control / control. State-of-the-art gait analysis with three-dimensional rotations and moments at the hip, knee and ankle joints [1] was obtained from three walking trials for each participant in each condition. Simultaneously a sensor insole system (Pedar, Novel GmbH, Munich, Germany) recorded plantar pressure at 100 Hz. Rearfoot, midfoot and forefoot regions, along with the whole foot, were defined a-priori by selecting corresponding pressure capacitive sensors among the 99 available. Normalized root mean square error, determination coefficient, and frame-by-frame statistical analysis were used to assess differences between kinematic and kinetic time-histories.

Results: No significant differences were detected in walking speed and ground reaction force between the three shoes, nor in the spatio-temporal parameters with the exception of the stride length, this being on average 86 mm shorter in the half-shoe condition. From baropodometry, the time-histories of peak pressure (kPa) for each shoe condition at rearfoot, midfoot, forefoot and total foot (Figure 1) revealed different patterns between these three shoe conditions. Wearing the traditional and the novel FOS resulted in smaller peak pressure at forefoot (kPa, half-shoe 178±90; novel 186±45; control 244±75: p<0.05). The half-shoe showed also the smallest mean and maximum force and force-time integral at forefoot. At rearfoot, mean and peak pressure were the largest in the novel shoe. novel FOS design showed less compensation at the more proximal lower limb joints. Motion at the lower limb joints was similar to control for the two FOS designs, but at the pelvis the normalized root mean square error was 68% for the half-shoe, 27% for the novel design. At the ankle, sagittal-plane rotation in the novel FOS had a pattern more similar to control (half-shoe r2=0.85; novel r2=0.93). With respect to joint moments, the largest discrepancy from the control was observed in the sagittal and frontal planes at the ankle joint, the root mean square error being 16% for the half-show, 4% for the novel design.

Figure:
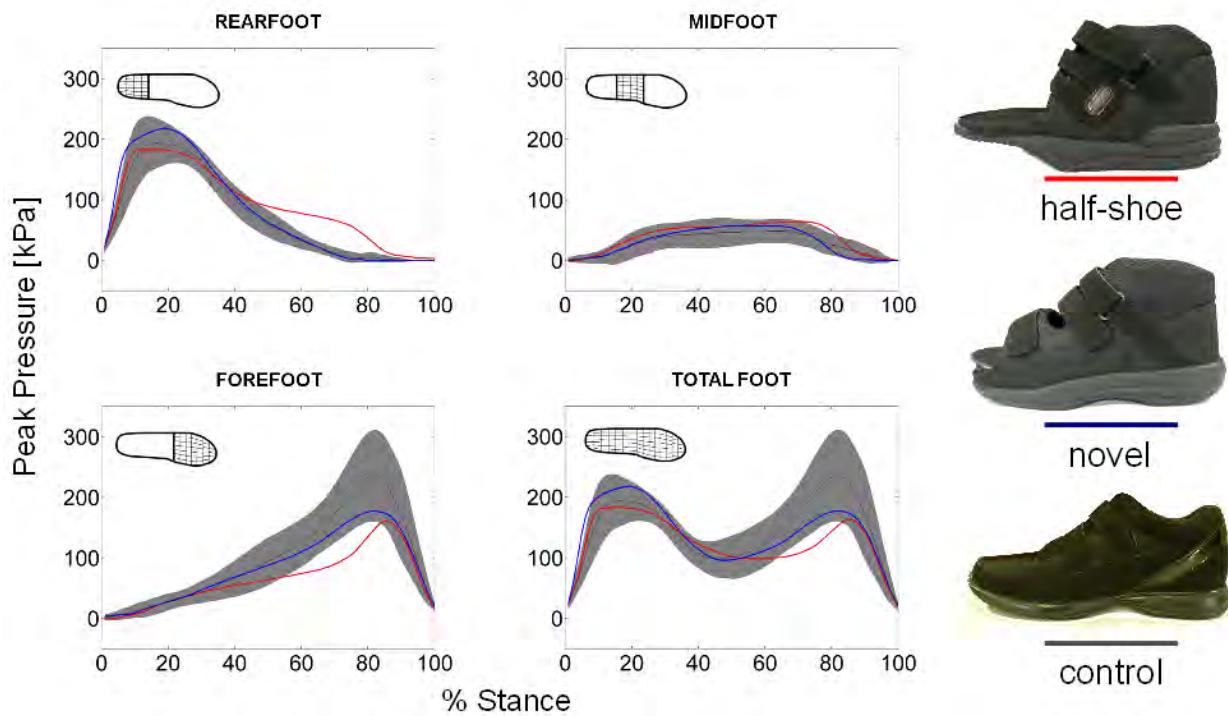
Caption: Patterns of peak pressure [kPa] at the three regions and at the entire footprint; mean values according to the color code shown on the right, grey bands showing standard deviation of the control.

Conclusion: The novel FOS appears capable, though less effective than a traditional half-shoe, in reducing considerably forefoot pressure. However, the good forefoot offloading provided by the traditional half-shoe was associated to more kinematic and kinetic alterations at the proximal lower limb joints with respect to the control, likely associated to the necessary compensation mechanisms for the peculiar shape of the outsole. The prescription of these forefoot offloading shoes should take into consideration both the required offloading and the overall restoration of normal gait function.

References: [1] Leardini et al., Gait & Posture, 26:560-71, 2007.

Disclosure of Interest: None Declared

COMPARISON OF THE FOOT KINEMATICS DURING WEIGHT LOADING BETWEEN NORMAL FOOT AND THE FLATFOOT

Shintarou Kudo [1][2],[*]Yasuhiko Hatanaka [3]

[1]Graduate school of Suzuka university of medical science, Mie, [2]physical therapy, Morinomiya university of medical sciences, Osaka, [3]physiotherapy, Suzuka university of medical science, Mie, Japan

Introduction and Objectives: The foot kinematic of the flat foot is important to make a foot orthosis. Three dimensional foot kinematics analysis during the gait is showed that forefoot abduction movement and rear foot pronation movement were increased, and peak plantar flexion moment were increased in the late stance phase using oxford foot model. However, forefoot is calculated as one segment in this model, although forefoot is consisted five metatarsals. Therefore, it has a limitation which can't be analyzed in detail forefoot movements. The purpose of this study is to be clarified difference the foot kinematics including mid- and forefoot between normal foot and the flat foot.

Methods: Sixty-one feet of fifty-two young normal volunteers were participated in this study. All subjects were categorized two groups which were normal foot group and flat foot group using both Foot Posture Index-6 and medical history of the pain were related to the flat foot. The fifteen color markers were mounted over the anatomical landmarks which were five metatarsal head and bases, navicular, the cuboid, the peroneal trochlea (cal-lat), the sustentaculum tali (cal-med), and posterior tip of the calcaneus (cal-p). The foot motion when measurement foot was stance forward, and body weight loaded on the forefoot as well as possible with lower leg forward inclined and whole plantar surface in contacted with the floor was recorded using the four hi-definition digital video cameras. And all markers were manually digitized using Flame DIAS4 software program. Three dimensional displacement of the each marker were calculated. And each directional markers movement were compared normal foot group with flat foot group using Man-Whitney test. Moreover, discriminant functional analyses were performed on all combinations if significant differences existed between the normal foot and the flat foot using SPSS statistics ver.18 (IBM).

Results: In the medial direction, flat foot is significant smaller than normal foot at the first, third, fourth metatarsal head, first to third metatarsal base, navicular and cuboid. In the forward direction, flat foot is significant larger than normal foot at the first metatarsal head and base, second and third metatarsal base, cuboid and cal-p. In the vertical direction, flat foot is significant smaller than normal foot at first, fourth and fifth metatarsal head, fifth metatarsal base, navicular and cuboid, and it was larger second metatarsal head and cal-p. In the discriminant analysis between the groups the Cub-y and the MTB3-x were the most powerful variables in distinguishing between normal foot and flat foot (fig.1). Based on these two variables 90.48% of the patients were correctly classified (Wilk's lambda 0.3; kai square 37.7; p<0.01). If the step height was additionally included in the discriminant analysis, 70% of the flat foot were correctly classified.

Figure:
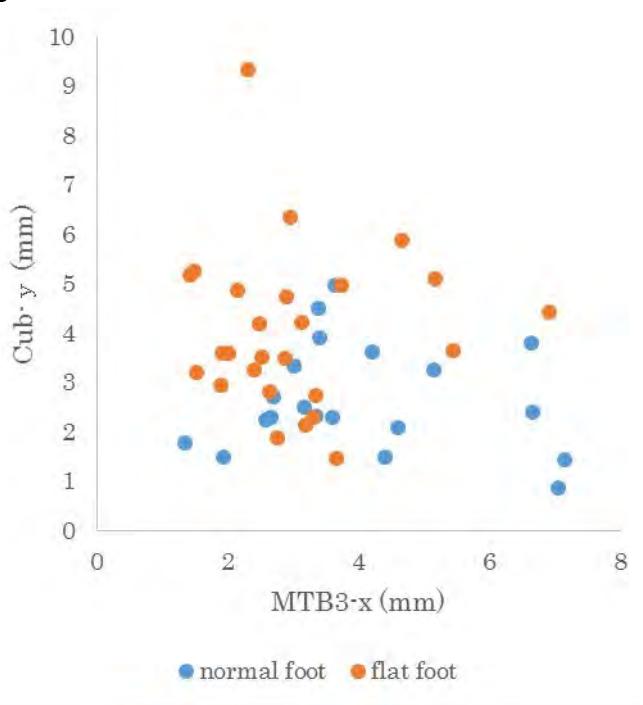
Conclusion: In the normal foot, some anatomical makers showed larger medial movement than that of the normal foot. While, some anatomical makers of the flat foot showed larger forward movement than those of the normal feet. Therefore we considered that normal foot showed medial inclination with maintaining the arch structure, however flat foot showed that forward splaying with collapsed arch structure. Moreover, it may be key movements which are forward movements of the cuboid and medial movement of the third metatarsal base.   Lundgren[1] showed that the mobility of the lateral side of the foot was greater than medial side of the forefoot such as medial cuneiform and first metatarsal. Therefore, results of this study were indicated that it might be important for the treatment of the flatfoot to control the stability of the lateral longitudinal arch.

References: [1]   Lundgren et al.,Gait and Posture. 28(1): 93-100, 2008.

Disclosure of Interest: None Declared

PO-0079

INFLUENCE OF FOOTWEAR IN POSTURAL BALANCE OF YOUNG WOMEN

Estele C. W. Meereis [1,*] Patrícia Dorneles [1] Gabriel Panke [1] Carlos Mota [2]

[1]Federal University of Rio Grande do Sul, Porto Alegre, [2]Federal University of Santa Maria, Santa Maria, Brazil

Introduction and Objectives: Postural balance involves a complex connection mechanism of the afferent and efferent pathways and their integration into the central nervous system (CNS). Postural balance is influenced by proprioceptive, vestibular and visual sensory inputs [1]. The proprioceptive affereces and the cutaneous-plantar discrimination mechanism facilitate CNS to detect the center of gravity projection, and thereby, seems to decrease body sway in posture maintenance [2]. The aim of this study was to analyze the body balance of young women in three situations: barefoot, with sport shoe and with high heel shoe, to identify possible influences of using different shoes.

Methods: The study included 16 women with mean age of 22,94 ± 1,91 years. The postural balance was assessed through the center of pressure (CoP) displacements with a force platform in all three situations: for the subject barefoot, wearing sport shoe, and wearing high heel shoe. ANOVA with post hoc Bonferroni test was used to perform statistical analysis, $p < 0.05$ was considered significant.

Results: Regarding the postural sway, statistically significant differences were found between situation using high heel shoes and the others in the three CoP variables analysed: antero-posterior amplitude os displacement (CoPap), medial-lateral amplitude displacement (CoPml), and mean velocity (CoPmv). The subjects showed higher postural sway when using high heel shoes.

Conclusion: It was ound that high heel shoes negatively affected the postural balance of the partipants of the study. It were found larger displacements amplitudes and velocity of CoP in the high heel shoes situation. It suggests that high heel shoes affect the postural control performance.

Table:

	Barefoot (n=16)	Sport shoe (n=16)	High heel (n=16)	*p*-valor	*f*
CoPap (cm)	1.77 ± 0.53 [a]	1.86 ± 0.62 [ab]	2.33 ± 0.64 [c]	0.030	3.76
CoPml (cm)	1.01 ± 0.37 [a]	0.92 ± 0.32 [ab]	1.37 ± 0.44 [c]	0.003	6.45
CoPmv (cm/s)	0.86 ± 0.20 [a]	0.89 ± 0.20 [ab]	1.41 ± 0.29 [c]	0.001	9.01

Caption: Young women postural balance in different footwear situations.

References: [1] Hatzitaki et al. Gait Posture, 29:296-299, 2009.

[2] Bernard-Demanze et al. J Integr Neurosci, 3:433-451, 2014.

THE RELATIONSHIP BETWEEN ARCH FLEXIBILITY AND MEDIAL-LATERAL GROUND REACTION FORCES

Regina Parker [1,*] Rebecca A. Zifchock [1] Willahelm Wan [1] Howard Hillstrom [2] Jinsup Song [3] Michael Neary [4]

[1]Civil & Mechanical Engineering, United States Military Academy, West Point, [2]Leon Root, MD Motion Analysis Laboratory, Hospital for Special Surgery, New York, [3]School of Podiatric Medicine, Temple University, Philadelphia, [4]Keller Army Hospital, United States Military Academy, West Point, United States

Introduction and Objectives: Several authors have analyzed extrinsic causes of foot and leg injuries, such as the relationship between the magnitude of vertical impact force and susceptibility to bone fracture. However, few have analyzed the role of intrinsic biomechanical factors on the magnitude of ground reaction forces, which may be indicative of injury susceptibility. Foot structure may be described by a number of features, such as arch flexibility. Greater three-dimensional flexibility of the foot may facilitate force redistribution from the vertical to the medial-lateral or antero-posterior directions. It is plausible that medial-lateral ground reaction force (GRF) may contribute to injuries in the knee joint [1]. Therefore, the purpose of this study is to examine the relationship between arch flexibility and the relative proportion of medial-lateral to vertical GRF impulse. We expect that there will be a difference in the distribution of medial-lateral GRF between individuals with flexible and stiff arches. In order to characterize the entire stance phase, the impulses of the GRFs were used to describe the distribution of force in each direction.

Methods: Ten subjects have participated in this ongoing study (all male, 19±1yrs, 176.5±6.4 cm, 73.5 ± 13.4 kg). All participants were injury-free, and wore the same clothing and shoes during testing. Participants ran for 8 minutes on a single belt of an instrumented treadmill (Bertec Corp; Columbus, OH) at 7 mph. Kinetic data were collected at 1000 Hz during the final 10 seconds of running. From these data, the medial, lateral and vertical impulses were determined for each of ten sequential left foot strikes. These impulses were related to participants' left foot arch height flexibility (AHF), which was determined a year prior (as part of a larger study). AHF is defined as the difference between arch height in the seated and standing positions normalized to body weight [2]: AHF = (AH(standing) – AH(sitting))/(40%BW)

Participants were categorized into one of two groups—stiff (AHF<14.9 mm/kN) and flexible (AHF>14.9 mm/kN). The criterion of 14.9 mm/kN was based upon the median value of AHF for a large sample size (n = 1124). According to this categorization method, 6 participants had stiff arches and 4 had flexible arches.

The ratio of medial-lateral to vertical GRF impulse was calculated for each participant, and an independent t-test was used to detect a difference in the measure between the stiff and the flexible groups. Additionally, the ratios of medial to vertical GRF impulse and lateral to vertical GRF impulse were calculated independently for each participant. A mixed-effect ANOVA model was used to analyze the difference between the directional ratios, and between the stiff and flexible groups. All analyses were conducted in SPSS (IBM SPSS Statistics, v19).

Results: The independent t-test suggests that there is no significant difference in the ratio of medial-lateral to vertical GRF impulse between groups ($p = 0.27$). However the calculated moderate effect size of 0.77 suggests that there may be a significant difference between the groups given a larger sample size.

The results of the mixed-effect ANOVA model suggests that there is no interaction between the direction of GRF impulse (medial vs lateral) and between group membership (stiff vs flexible) (p = 0.25). Further, neither the main effect of direction nor group membership were significant (p = 0.22 and p = 0.27, respectively). However, there was a moderate effect size of 0.66 for the main effect of direction and 0.55 for the main effect of group. Descriptive statistics are shown in Table 1.

Conclusion: While this study does not support any statistically-significant findings, the moderate effect size for all analyses suggests that the hypotheses may have merit. The descriptive statistics demonstrate that individuals with flexible arches have a greater portion of impulse in the medial-lateral direction than the individuals with stiff arches. Further analysis of the data suggests that this disparity is due to the medially-directed force, and not the laterally-directed. Individuals with flexible arches have twice the GRF impulse in the medial direction as compared to individuals with stiff arches. However both groups have similar magnitudes of lateral GRF impulse.

With only ten subjects, this study does not have the power to support our hypothesis. However, with a larger data set, there may be evidence to suggest that individuals with flexible arches may direct a larger proportion of their GRF medially. This may suggest a mechanism for injury susceptibility based upon foot structure.

Table:

	T-Test	ANOVA	
	Medial-Lateral : Vertical	Medial: Vertical	Lateral : Vertical
	Mean ± SD	Mean± SD	Mean± SD
Stiff	0.06± 0.03	0.02± 0.01	0.04± 0.02
Flexible	0.07± 0.02	0.04± 0.02	0.04± 0.02

Caption: Table 1: Descriptive Statistics

References: [1] Sculco and Martucci. *Knee Arthroplasty.* Italy: Springer-Verlag/Wien Press, 2001.

[2] Zifchock et al. Foot Ankle Int 27(5): 367-372, 2006.

Disclosure of Interest: None Declared

PO-0081

CAN FOOT STRUCTURE PREDICT RUNNING KINETICS?

Willahelm Wan [1,*] Rebecca A. Zifchock [1] Regina Parker [1] Howard Hillstrom [2] Jinsup Song [3] Michael Neary [4]

[1]Civil & Mechanical Engineering, United States Military Academy, West Point, [2]Leon Root, MD Motion Analysis Laboratory, Hospital for Special Surgery, New York, [3]School of Podiatric Medicine, Temple University, Philadelphia, [4]Keller Army Hospital, United States Military Academy, West Point, United States

Introduction and Objectives: Stress fractures are one of the most common lower extremity injuries – accounting for 4 to 16 percent of running injuries [1]. While our bones are built to adapt to strains, there are extrinsic risk factors such as training changes and inappropriate footwear, and intrinsic risk factors such as muscle inflexibility that may increase the incidence of stress fracture. There is evidence to suggest a relationship between stress fracture and elevated values of the vertical ground reaction force (vGRF) [2]. However, very few studies have examined the intrinsic foot characteristics that may be related to those elevated values. In their study of the relationship between arch mobility and GRF, Williams et al. found that runners with high arch structure but differing arch mobility exhibited differences in select lower extremity movement patterns and forces [3]. However, their description of foot characteristics was limited to arch mobility in high-arched individuals.Therefore, the goal of this study was to examine the relationship of foot length and flexibility with vGRF during running. In order to characterize the vGRF, both the overall peak and the average value over the entire stance phase were considered. It was hypothesized that longer and more flexible feet would have lower average and peak vGRF.

Methods: As part of a larger ongoing study, the foot structure data on over 1100 individuals have been collected. A subset of that cohort was invited to participate in the current study. To date, 9 volunteers have been included in this sub-study (all male, 19±1 year, 176.5±6.4 cm, 73.5±13.4 kg). Participants were asked to run on an instrumented treadmill (Bertec FIT; Bertec Corp; Columbus, OH) at 7mph for 8 minutes. All participants wore the same shoes and clothing while running. Kinetic data were collected at 1000 Hz from the final 10 seconds of the run. The average and peak vGRF from the left-side stance phase of 10 sequential foot strikes were extracted from the raw data using a custom-written Python program (Python Software Foundation). These data were then compared to the participants' left foot length and arch flexibility, AHF: AHF = AH(standing) – AH(sitting)/(40%BW)

Step-wise regression, with a backward elimination method, was used to identify the foot structure variable(s) that best predicted the peak and average vGRF (Microsoft Excel). The model was generated separately for peak and average vGRF.

Results: When both foot structure measures were entered into the model, the R^2 value was calculated to be 0.21 and 0.14 for peak and average vGRF, respectively. The models were then re-run, entering the foot structure measures independently to predict both peak and vGRF, as shown in Figure 1. Both kinetic variables only showed weak relationships with foot structure. The relationships suggest that increased arch flexibility may lower the peak vGRF and increased foot length may increase the peak vGRF but neither structural variable has an effect on the average vGRF.

Figure:
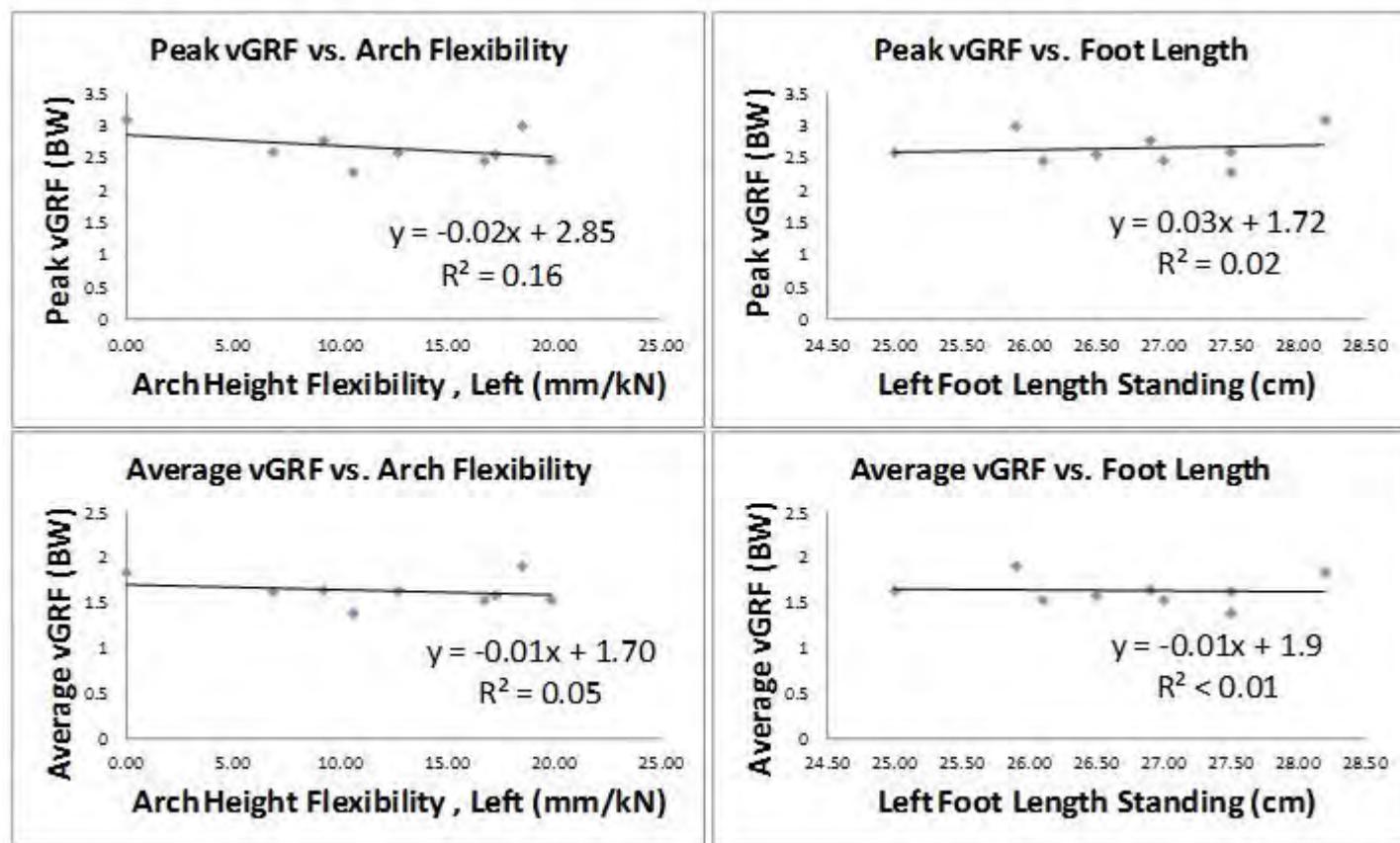
Caption: Figure 1. Relationship between individual foot structure measurements and vGRF

Conclusion: With the inclusion of both foot structure measures into the model, they were able to account for 21% of the variance in peak and 14% in average vGRF. On their own, arch flexibility accounted for 16% of the variance in peak vGRF and only 5% of the variance in average vGRF. Foot length showed a weaker relationship, accounting for only 2% of the variance in peak vGRF and less than 1% of the variance in average vGRF. These results suggest that intrinsic characteristics of a runner's foot can have a moderate influence on the magnitude of their ground reaction forces. There may be additional foot structural measurements that could account for additional variability in the measure. Further, with the inclusion of additional participants, the predictive capacity of these structural measures on vGRF, and the relationship between kinetics and foot structure, may be strengthened.

References: [1] Jones BH et al. Oxford Journals. 24(2): 228-47, 2002.

[2] Zadpoor AA et al. Clin Biomech 26(1): 23-8, 2001.

[3] Williams DS et al. J Athl Train 49(3): 290-6, 2014.

Disclosure of Interest: None Declared

Feet and Footwear

PO-0082

VERTICAL IMPACT PEAK OCCURRENCE IN HABITUALLY SHOD RUNNERS UNDER DIFFERENT CONDITIONS OF RUNNING.

Juliana Pennone [1,*] Ana Paula Azevedo [1] Bruno Mezêncio [1] Rafael Soncin [1] João Claudino [1] João Pinho [1] Alberto Amadio [1] Júlio Serrão [1]

[1] School of Physical Education and Sport - University of São Paulo, São Paulo, Brazil

Introduction and Objectives: Running can be most injurious at the moment the foot collides with the ground [6]. Patellofemoral pain, plantar fasciitis and tibial stress fractures are examples of injuries that have been associated with a high vertical impact peak of ground reaction force (GRF), as well as to its load rate [7].

Previous studies that compared barefoot and shod running showed increased mechanical loads in barefoot condition [2,3,4]. Nevertheless, barefoot running has been suggested as a means to reduce impact forces, since habitually barefoot runners presents a suppression of the first vertical peak (Fy) of GRF[6]. However, it is not known if habitually shod runners also present this pattern when running barefoot. For many runners, barefoot running may be impractical due to unsafe running surfaces and potential performance limitations [1,5,7]. The minimalist shoes were designed to allow runners to employ the same mechanics of barefoot running, but minimizing the risk of injury due to direct contact of the foot with the ground. Thus, the aim of this study is to investigate the incidence of vertical peak of GRF in subjects not adapted to barefoot condition during shod, barefoot and minimalist running and to verify if the minimalist shoe provides the same mechanical condition of barefoot running.

Methods: Fourteen habitually shod runners (12 men and 2 women; age = 28.4 ± 7.3 years; mass = 72.7 ± 7.8 kg; height 1.74 ± 0.06 m) ran during 10 minutes at 9 km.h^{-1} on a treadmill in three conditions: using conventional running shoes, using minimalist shoes and barefoot. An instrumented treadmill (GAITWAY Instrumented Treadmill System 9810S1; and TROTTER Treadmill Model 685, 01-06560201) with two piezoeletric force plates (KISTLER Inc.) was used to obtain the vertical component of GRF. Nine acquisitions (10 seconds each) of GRF were performed for each experimental condition at 2600. The mean occurrence of the first vertical peak of GRF (Fy1) was calculated.

GRF data was low pass filtered by a Butterworth filter (4th order, 90 Hz cutoff frequency). The start and end of each left and right step was determined using 30N threshold. Statistical analysis of data was performed in SigmaStat 3.5 (Systat, Germany) software. Data normality was verified using the Kolmogorov-Smirnov test, while homoscedasticity was checked by Levene's test. For means comparison, an analysis of variance (ANOVA) for repeated measures was performed. The level of significance adopted was p ≤ 0.05.

Results: No significant difference was observed between shod and minimalist running, while barefoot running was significant different from both conditions for first peak occurrence. Barefoot condition showed 39,6% (p<0,001) and 34,75% (p<0,001) lower Fy occurrence when compared to shod and minimalist conditions, respectively.

Conclusion: Barefoot running seems to induce a decrease in Fy1 occurrence even in subjects not adapted to this condition. The lower occurrence is probably related to changes in running technique and foot strike pattern, providing reductions in GRF as observed in habitually barefoot runners [5,6]. Corroborating with other studies, the minimalist shoes

was not capable to induce the same mechanical condition found in barefoot running for Fy occurrence [1,7]. These results suggest a less mechanical load and reduced risk of injury in barefoot running.

References: [1]   Bonacci et al., Br j sports med, v.47, n.6, p.387-392, 2013.

[2]   Cavanagh et al., Biomechanics vii. A. F. Morecki, k.; kedzior, k.; wits, a. Baltimore, university park press: 151-156, 1981.

[3]   Clarke, et al., Int j sports med, v.4, n.4, p.247-251, 1983.

[4]   Komi, et al., Int j sports med, v.8, n.3, p.196-202, 1987.

[5]   Lieberman. Exerc sport sci rev, v.40, n.2, p.63-72, 2012.

[6]   Lieberman et al., Nature, v.463, n.7280, p.531-535, 2010.

[7]   Willy et al., Med Sci Sports Exerc. v46,n.2,p.318-23, 2014.

Disclosure of Interest: None Declared

Feet and Footwear

PO-0083

IS PLANTAR PRESSURE A GOOD INDICATOR OF FOOT JOINT MOBILITY?

Paolo Caravaggi [1,*] Alberto Leardini [1] Claudia Giacomozzi [2]

[1]Movement Analysis Laboratory, Istituto Ortopedico Rizzoli, Bologna, [2]Department of technology and health, Istituto Superiore della Sanità, Rome, Italy

Introduction and Objectives: The foot is generally regarded as a flexible structure which can adjust its flexibility in response to various external conditions and variable dynamic states within the motor tasks of daily living. In gait, both joint kinematics and plantar pressure have shown to be affected by functional and structural factors [1]. In fact, pressure distribution can be seen as the effectiveness of the musculoskeletal system in absorbing the ground reaction forces and managing propulsion via the foot and its joints. Excessive repetitive load may develop into calluses, which become sites of peak pressure and pain. While an association between limited joint mobility and increased plantar pressure has been shown in the diabetic foot [2,3], no study has hitherto investigated the relationship between in-vivo joint mobility and pressure in the normal foot. Aim of this study was to combine a multi-segment kinematic model [4] with advanced baropodometric analysis based on anatomical masking [5], to investigate correlations between intersegmental kinematics and regional baropodometric parameters in the normal-arched healthy foot.

Methods: Ten able-bodied subjects (26.8 ± 6.9 years; 67.5 ± 12.6 Kg; BMI 22.0 ± 2.7) with normal-arched feet (foot arch index 0.15 ± 0.02) volunteered in the study. An eight-camera motion system (Vicon, UK) was used to track foot segments during the stance phase of level walking, according to an established protocol [4]. This implied tracking fourteen 10mm reflective spherical markers attached to relevant anatomical landmarks of the shank and foot over three walking trials. Simultaneously, a pressure plate (Novel Gmbh, Germany) recorded foot plantar pressure. An anatomical-based masking [5] was employed to divide the pressure footprints in six subareas (Fig. 1a). Maximum of mean and peak pressure, of vertical force, contact-area and -time, and pressure- and force- time integrals, were determined for each subarea. The relationship between range of motion (ROM) of the foot joints in each anatomical plane and baropodometric parameters in each subarea was investigated using Pearson's and Spearman's coefficients.

Results: Walking speed was consistent across subjects and trials (1.41±0.14 m/s). Most of the statistically significant correlations between foot joints ROM and baropodometric parameters were moderate (Pearson's |r| =0.36 – 0.67). In general, motion at the foot joints was negatively correlated with pressure and pressure-time integral at rearfoot and forefoot (see Fig. 1b) and positively correlated at midfoot.

Figure:
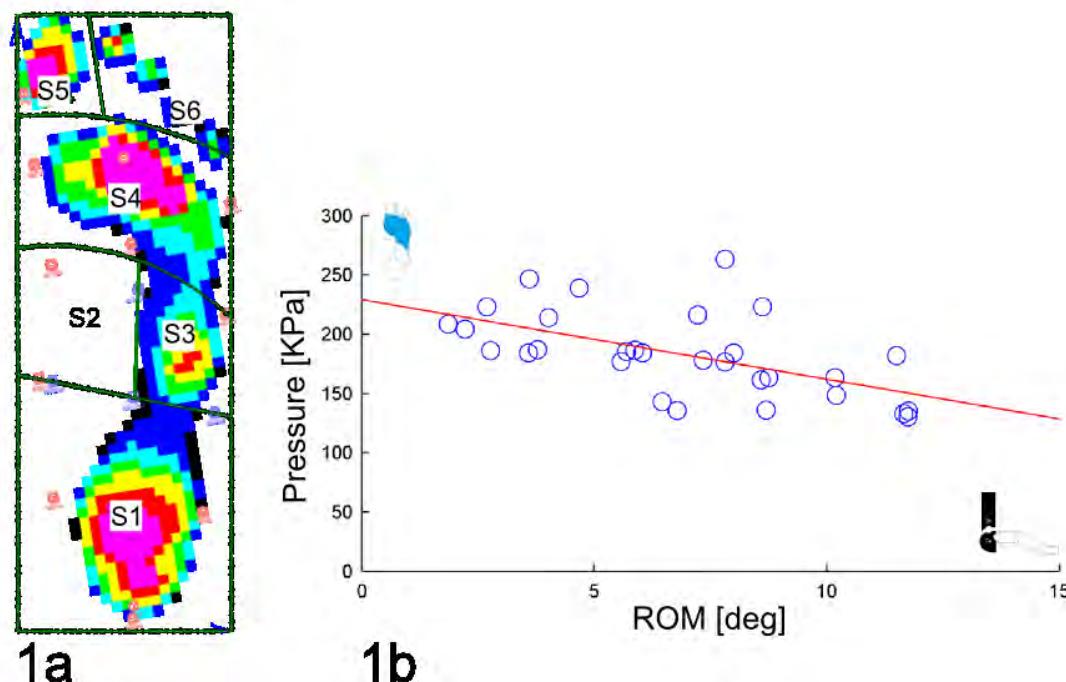
Caption: 1a. A typical footprint pressure image from a walking trial of one of the subjects. Where S1-S6 are the six subareas according to the projection of the foot anatomical landmarks on the footprint image. 1b Negative correlation (r=-0.57, p=0.001) between between peak pressure at the forefoot and frontal-plane ROM at the ankle joint across all walking trials.

Conclusion: According to the sample of normal feet analyzed in this study, those feet presenting smaller joint mobility are associated with larger pressure at the rear- and fore-foot. A trend for decreased pressure at the midfoot was also detected in those feet presenting a stiffer medial longitudinal arch. A more flexible foot may allow better distribution of pressure at the plantar foot surface during gait, with greater involvement of the midfoot region. Additional factors worsening joint mobility, such as age, weight and foot pathologies, may even magnify the impact on plantar pressure and increase the tissue damage; therefore they should be carefully considered in the identification of at-risk subjects.

References: [1] Morag et al., *J of biomech*, *32* (4), 359-370, **1999**

[2] Fernando et al., *Diabetes care, 14* (1), 8-11, **1991**

[3] Rao et al., *Gait & Posture*, *31* (2), 251-255, **2010**

[4] Leardini et al., *Gait & Posture*, *25* (3), 453-62, **2007**

[5] Giacomozzi et al., *J of biomech*, *47 (11), 2654-9*, **2014**

Disclosure of Interest: None Declared

Feet and Footwear

PO-0084

SOCCER SHOES STRUCTURE AND ITS CORRELATION TO PLAYERS INJURY RISKS : A LITERATURE REVIEW

Sylvain blanchard [1]Jerome Palestri [2]Jean-Luc GUER [2]Marta-Catalina Harnagea [2]Benoit Cheyrou [2]Michel Behr [1,*]

[1]Laboratoire de Biomécanique Appliquée, IFSTTAR/Aix-Marseille Université, [2]Wizwedge SARL, Marseille, France

Introduction and Objectives: Soccer is the most popular sport in the world, the one generating greatest financial incomes, and whose practice has evolved the most in terms of intensity and commitment, with a particularly high inherent risk of injury [1]. The cleated shoe seems to play a major role in this high exposure to injury [2]. Despite the increasing interest of the scientific community in this regard, soccer shoes have experienced small changes in their design and mechanical structure, as compared to other sports such as running, tennis, basketball.

Based on an in-depth literature review, an analysis of the modern soccer shoe design and its adequation with regards to injuries protection is proposed.

Methods: The articles were selected by a review of the literature conducted on PubMed and ScienceDirect research gates between 1970 and october 2014, focusing on 6 different aspects of the structural characteristics of the shoe, in order to identify possible links between biomechanical characteristics and sport-specific pathologies. These axes are:

(1) Ankle dorsiflexion

(2) Medio-lateral plantar constraints

(3) Ergonomics, comfort and proprioception

(4) Types of ground surfaces and studs

(5) Uppers height of cut

(6) Minimalism and weight of the shoe.

Results: (1) Fitting and outsole configuration should help ensure sufficient range of motion of the ankle dorsiflexion, minimizing exposure to the many pathologies associated with the limitation of this parameter.

(2) The geometry and material used for the outsole should reduce the harmfulness of mediolateral stresses observed in soccer-specific movements.

(3) Adding plantar arch supports and systematic customized outfit would significantly improve the ergonomics of the soccer shoe. In addition, cushioning materials integrated in the outsole could reduce peaks of potentially pathogenic stress and improve comfort.

The integration of proprioceptive stimulation elements should also help preventing instabilitiesrelated accidents.

(4) Given the conflicting data in the literature, those cleats offering moderate resistance to rotational movements should be preferred. In addition, counseling strategies must be developed to help players to choose a reliable type of footwear and cleats type corresponding to the specifics of their practice.

(5) A low-cut shoe model does not seem to induce increased risk of ankle injury, while ensuring sufficient lightness and freedom of movement. This trend is in a certain way supported by the fact that even basket-ball seems to come back to low cut shoes. New high-cut soccer shoe models have appeared on the market, but authors are not aware of any previously published scientific evaluation of their efficiency.

(6) There is no major argument in favor of drastic reduction of the soccer shoe weight. On the opposite, many authors tend to prefer heavier products as long as they would integrate technical devices to enhance protection, comfort and performance. As such, one should seek the right balance between weight and technicality.

Conclusion: This study underlines the possible link between characteristics of the soccer shoe in its current design and the specific injuries related to the practice of this sport. It also reveals the sometimes contradictory developments proposed by some soccer shoe manufacturers. From this analysis, some possible technical solutions to design a safer soccer shoe were also identified.

References: [1] Ekstrand et al., Br J Sports Med, *45(7)*:553-561, 2011.
[2] O'Connor et al., Foot Ankle Clin, 18(2): 369-380, 2013.

Disclosure of Interest: None Declared

Feet and Footwear

PO-0085

THE RELATIONSHIP BETWEEN THE FLEXIBILITY OF THE TRANSVERSE ARCH OF THE FOREFOOT AND GAIT IN HEALTHY SUBJECTS

Takashi Kondo [1,*]Tsutomu Fukui [1] [2]

[1]Sports Management Center, [2]Health Care Science, Graduate School, Bunkyo Gakuin University, Tokyo, Japan

Introduction and Objectives: To measure the transverse arch of the forefoot (; TAF) is important, because a low transverse arch may lead to forefoot deformity (hallux valgus) and decrease balance ability of elderly people. TAF have been examined by plantar pressure measurements [1], ultrasonography [2], and X-ray photography [3]. Recently, using 3D foot-scanner [4] has been getting easy to measure TAF. As the evaluation of foot posture is complicated by the existence of both static foot posture and foot mobility, it has been still unclear how to evaluate the foot posture. Therefore, the relationship between flexibility of TAF and human movement has not been revealed. Clinically, it is important to establish a simple method of the foot evaluation. The purpose of this study is to investigate the relationship between the flexibility of TAF and gait in healthy subjects.

Methods: Fifteen healthy subjects (8 men and 7 women) participated in this study. Their mean age was 23.4 ± 3.2 years, body weight was 60.5 ± 12.5 kg, height was 165.2 ± 9.7 cm. Foot posture evaluations were recorded using a 3D foot-scanner INFOOT (I-Ware Laboratory, Osaka, Japan). Three conditions of TAF were measured. Condition1: sitting. Condition2: standing. Condition3: foot forward and lower leg tilting anteriorly to the maximum position with heel contact. Width and height of TAF of dominant foot were measured in respective condition. Rates of the width (%width) and height (%height) of TAF among three conditions were calculated. Gait kinematics was recorded using a Vicon motion system (Vicon Motion Systems Ltd, Oxford, UK) and a force plates (AMTI, MA, USA). Reflective markers were attached by the definition of the Vicon Plug-in Gait (full body). Subjects were asked to walk at self-selected speed for 5 trials to detect the gait variables (gait speed, stride length, hip, knee, ankle angles, moments, and ground reaction forces). Firstly, the peak values of the joint angle, moment in the sagittal plane and ground reaction force were calculated during last half of mid-stance, terminal stance, and pre-swing phases. Secondly, the averages values of the five repetitions of peak values were analyzed. Partial correlation coefficients between the flexibility of TAF and the gait variables adjusted for gait speed and stride length were used to evaluate. The statistical significance was set at the level of p <0.01.

Results: In the case of the differences in between condition2 and condition3, there was a significant correlation between the gait variables and the flexibility of TAF. The flexibility of TAF width(%) significantly related to anterior component of ground reaction force (r = 0.53) and TAF height(%) significantly also related to vertical component of ground reaction force (r = 0.61) and ankle plantar flexion moment (r = 0.60) .

Conclusion: We found that the relationship between the differences in standing and foot forward and lower leg tilting anteriorly and some gait variables. When the body moved anteriorly, abilities of both mobility and stability of TAF might be crucial for gait performances. These results indicated that evaluation of TAF might be useful for patients with hallux valgus and the elderly people with impaired balance ability. The evaluations of TAF in the differences standing and foot forward and lower leg tilting anteriorly to the maximum had some relationships with gait variables.

References: [1] Kanatli U, Yetkin H, Bolukbasi S.: Evaluation of the transverse metatarsal arch of the foot with gait analysis, Arch Orthop Trauma Surg, 123(4), 148-50, 2003.

[2] Daentzer D, Wulker N, Zimmermann U.: Observations concerning the transverse metatarsal arch, Foot and Ankle Surgery, 3(1), 15-20, 1997.

[3] Suzuki J, Tanaka Y, Takaoka T.: Axial radiographic evaluation in hallux valgus: evaluation of the transverse arch in the forefoot, J Orthop Sci, 9(5), 446-51, 2004.

[4] Mochimaru M, Kouchi M: Shoe customization based on 3D deformation of a digital human, The Engineering of Sport 4th International Conference, 4, 595-601, 2002.

Disclosure of Interest: None Declared

PO-0086

FOOT CHARACTERISTICS OF INDIAN RURAL SCHOOL CHILDREN

Rajani Mullerpatan [1,*] Yuvraj Singh [1] Stacey Pinto [1] Anila Paul [1] Amit Maurya [2] Robert VanDeursen [3]

[1] Physiotherapy, MGM Insitute of Health Sciences, Navi Mumbai, [2] Mechanical Engineering, Indian Institute of Technology Bombay, Mumbai, India, [3] Physiotherapy, Cardiff University, Cardiff, United Kingdom

Introduction and Objectives: Foot anthropometry varies across populations. Limited information on morphological characteristics of feet among tribal children walking bare foot motivated this study. The objective was to study foot characteristics of Indian rural school children using a foot-print based approach.

Methods: This study was approved by the Institution Review Board of MGM Institute of Health Sciences. Consent was sought from all parents by the school. A convenience sample of 112 healthy children aged 5-15 yrs with no history of foot pain was studied. 55 rural children (24 females and 31 males) were matched on marginal distributions for age and body mass with 57 urban children (24 females and 33 males) for comparison.

Bilateral static footprints were obtained for all subjects resulting in a total of 224 feet for analysis. Foot characteristics were studied in terms of foot surface area and medial longitudinal arch height (Cavanagh & Rodgers, 1987). A foot-print based approach was used to calculate total surface area of foot (sq.cm), forefoot, mid-foot and hind-foot and medial longitudinal arch height using Arch Index (AI). Foot prints were scanned and MATLAB software was used for image processing and further computation. Arch height was also calculated with Staheli's Index (SI) (Staheli & Chew, 1997) and Chippaux-Smirak Index (CSI) (Forriol &Pascual, 1990) for comparison using a standard protocol.

Following an overall one-way Anova, independent sample t-test was used for between group comparisons.Paired t-test was used for within group analyses to compare left and right side.

Results: Arch height increased with advancing age on AI (r=-0.247; p=0.020).Total foot surface area (p=0.001), fore-foot area (p=0.000) and mid-foot area (p=0.043) were greater for the right foot compared to left foot in all children (pooled).Total surface area in males was greater compared to females on both right (p=0.027) and left side (p=0.006).

Total foot surface area of rural children was greater than urban children on both sides. Forefoot and hind foot area was significantly greater on right side; however differences on left side were not significant.Medial longitudinal arch height did not differ between rural and urban children as measured by all 3 indices on both sides.

Conclusion: Increasing arch height with advancing age from 5 yrs to 15 yrs suggested continued development of medial longitudinal arch in both rural and urban children. All children presented with wider right foot compared to left side and males presented with wider foot compared to females.

Rural children presented with wider feet compared to urban children, particularly the forefoot which may relate togreater demand on prehensile function of feet to adapt to uneven terrain while walking barefoot. Whereas in urban children the presence of footwear leads to less interaction between the feet and irregular walking surfaces. In the absence of longitudinal studies, clinical judgments on implications of such foot characteristics of rural children on lower limb function are difficult.

Table:

Foot characteristics	Rural children (n=55) Mean (S.D.)	Urban children (n=57) Mean (S.D.)	p value
Right Total surface area (sq.cm)	86.9(20.9)	74.7(19.1)	0.006 *
Right Fore-foot area (sq.cm)	43.4(11.4)	34.9(8.6)	0.000 *
Right Mid-foot area (sq.cm)	20.5(6.2)	19.1 (8)	0.345
Right Hind-foot area (sq.cm)	22.9 (5.3)	20.7 (4.6)	0.036 *
Right Arch index (AI)	0.24 (0.04)	0.25 (0.05)	0.16
Right Chippaux-Smirak Index (CSI)	0.45 (0.12)	0.49 (0.19)	0.29
Right Staheli's Index (SI)	0.75 (0.24)	0 .80 (0.29)	0.31

p≤0.05 significance level

Caption: Summary of foot characteristics on right side for rural and urban children matched for height and mass.

References: [1]   Cavanagh et al., J Biomech, 20: 547-51, 1987.

[2]   Forriol et al., Foot Ankle, 11:101-4, 1990.

[3]   Staheli et al., J Bone Joint Surg Am, 69:426-8, 1997.

Disclosure of Interest: None Declared

Feet and Footwear

PO-0087

THREE-DIMENSIONAL KINEMATIC ANALYSIS OF THE HUMAN CADAVER FOOT IN WEIGHTBEARING CONDITION USING BIPLANAR X-RAY FLUOROSCOPY

Kohta Ito [1,*]Koh Hosoda [2]Masahiro Shimizu [2]Shuhei Ikemoto [2]Takeo Nagura [3]Hiroyuki Seki [3]Masateru Kitashiro [3]Nobuaki Imanishi [3]Sadakazu Aiso [3]Masahiro Jinzaki [3]Naomichi Ogihara [1]

[1]Department of Mechanical Engineering, Keio University, Kanagawa, [2]Graduate School of Engineering Science, Osaka University, Toyonaka, [3]School of Medicine, Keio University, Tokyo, Japan

Introduction and Objectives: The human foot is a complex musculoskeletal structure consisting of many bones, muscles, ligaments, and soft tissues that directly interact with the ground during locomotion. In attempt to clarify the behavior and internal loading of the human foot for biomechanical, orthopedic and ergonomic applications, finite element (FE) models are employed recently as foot bone kinematics and internal forces are generally difficult to measure experimentally. However, the predictive ability of the FE model certainly depends on experimental validation. A method to comprehensively and quantitatively validate the FE model is essential for realistic emulation the human foot behavior that mechanically interacts with the ground. In the present study, therefore, we developed an experimental framework to precisely measure three-dimensional bone kinematics of the human cadaveric foot under a variety of loading conditions using biplanar X-ray fluoroscopy.

Methods: We developed a custom-made X-ray biplanar fluoroscopy system, consisting of two sets of X-ray sources and flat panels positioned in a quasi-orthogonal arrangement (Shimadzu, Kyoto, Japan). A human cadaveric foot was fixed to a vertical shaft supported by a linear motion rolling guide and 10 levels of axial force up to 60kg were applied by putting weight. Paired radiographic images of the foot under different axial loading conditions were obtained using the biplanar fluoroscopic system. We determined the motion of the tarsal and metatarsal bones by a model-based registration technique. Specifically, 3D surface models of foot bones were generated prior to motion measurement based on computed tomography, and the bone models generated were registered to fluoroscopic images such as to maximize similarity measures between occluding contours of the bone surface models with edge-enhanced fluoroscopic images, while avoiding mutual penetration of bones. The accuracy of bone registration was evaluated as 0.27 ± 0.19 mm and 0.24 ± 0.19 degree (mean ± standard deviation) in translation and rotation, respectively. To describe the change in the relative positions and orientations of each of the bones due to axial loading, a local coordinate system was defined by anatomical landmarks. In the present study, two fresh frozen cadaveric feet were investigated.

Results: By automatic registration technique, three-dimensional movements of the tarsal and metatarsal bones under axial loading conditions were precisely quantified. With higher axial loads, larger downward displacement of the talus, plantar flexion of the calcaneus with respect to the talus and overall flattening of the medial longitudinal arch were observed. The 1st and 5th metatarsals were everted and abducted, respectively, with increasing the axial loading. The change in the length of plantar aponeurosis, defined as the distance between metatarsal heads and calcaneal tuberosity, was also measured. The strain of the PA due to 60 kg of axial loading was found to be 6.9 and 1.1 % in the medial side

and 2.0 and 0.6 % in the lateral side, suggesting that the mechanical property of the human foot has considerable individual variability as suggested elsewhere [1-3].

Figure:
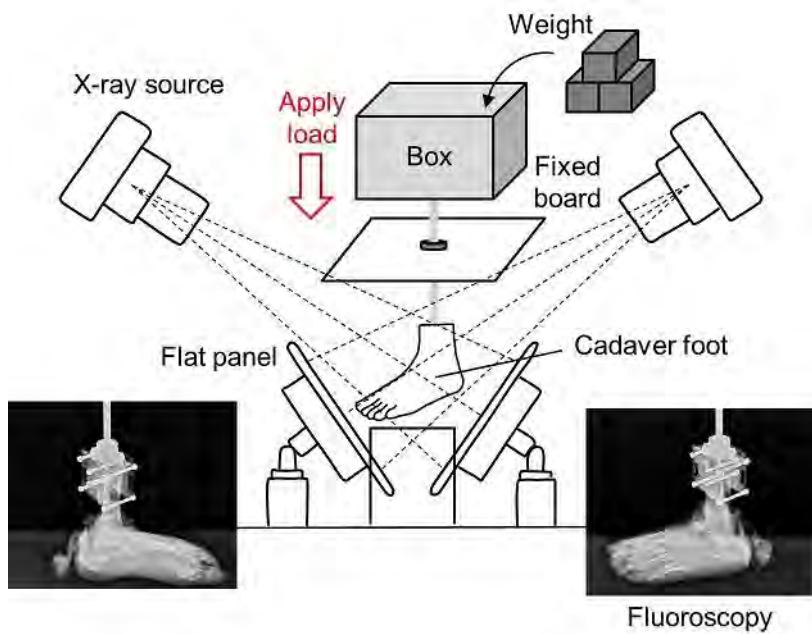
Caption: Biplanar X-ray fluoroscopy system and loading system

Conclusion: We developed an experimental framework to precisely measure human foot kinematics in weight bearing conditions using a biplane fluoroscopy for rigorous validation of foot FE model.

References: [1] Gefen et al., Foot Ankle Int, 24: 238-244, 2003.

[2] Kogler et al., Foot Ankle Int, 22: 433-439, 2001.

[3] Caravaggi et al., J Exp Biol, 212: 2491-2499.

Disclosure of Interest: None Declared

CHARACTERIZING FOOT TOTAL DEFORMATION USING HELICAL ANGLE: REPEATABILITY OF THE METHOD.

Claude Pothrat [1,*]Laurent Vigouroux [1]Marvin dufrenne [1]Elke Viehweger [2]Eric Berton [1]Guillaume Rao [1]

[1]Institute of Movement Sciences, Aix Marseille Université, MARSEILLE cedex 09, [2]Pediiatric orthopedic department, APHM La Timone Hospital, 13005 MArseille, France

Introduction and Objectives: The foot specific architecture gives this segment high adaptive skills that allow handling both long-term locomotor solicitation as well as sudden direction or support changes[1]. As the foot motion results from the combination of motions coming from numerous intrinsic joints, a global approach is necessary to investigate the solicitations while respecting its anatomy. This study aims to propose a global approach to characterize the total intrinsic foot motion during walking, running, lateral cutting, and 180° U-turn movements. The helical angle has been calculated to express the movement between forefoot and rearfoot segments[2]. The outcomes have been analyzed in terms of repeatability[3] and relevance of the results. We hypothesized that the helical angle (HA) would be representative of foot solicitation to give consistent clues in the understanding of its behavior. In this line, HA should differ depending on the movements.

Methods: Twelve subjects, 6 men and 6 women volunteered for this study. Each subject performed 5 repetitions of each movement along a 12m pathway, equipped with embedded force plates and an optoelectronic 8 cameras system (Vicon, Oxford UK). Six retro-reflective markers were placed on the forefoot and rearfoot segments of the right foot (Fig. 1) to calculate local coordinate systems.Twelve subjects, 6 men and 6 women volunteered for this study. Each subject performed 5 repetitions of each movement along a 12m pathway, equipped with embedded force plates and an optoelectronic 8 cameras system (Vicon, Oxford UK). Six retro-reflective markers were placed on the forefoot and rearfoot segments of the right foot (Fig. 1) to calculate local coordinate systems.

Results: Results concerning the maximum and the amplitude of the helical angle are presented in table 1 (values and ICCs), with repeated measure ANOVA showing significant differences in between all the movements. ICCx on the HA patterns for walking, heel running, and forefoot running were respectively 0.66±0.21, 0.69±0.15, and 0.61±0.20 whereas sport movements showed much smaller ICCx coefficients (90° cutting: 0.33±0.29 and 180° U-turn: 0.0±0.0).

Figure:

Caption: . Marker placement on the forefoot and rearfoot. Local coordinated systems definition.

Conclusion: The purpose of the study was to assess foot deformation by quantifying the helical angle, representative of the total intrinsic foot motion through the stance phase, for five sport movements. This measure is less prone to error than cardan angles can be, as it is free from sequences resolution. Maximum and amplitude values of the HA were representative of foot intrinsic solicitations and are sufficiently sensitive to statistically differentiate movements between them. As expected, cyclical locomotor movements that require more flexibility from the foot reached the highest values of HA. Opposite to that, non-cyclical movements as 90° cutting and the U-turn got less amplitude in HA, related to a more stiff foot. According to our results, the chosen movements allowed to obtain different foot solicitations that are fairly represented by a significantly different maximum and amplitude values of HA. The use of HA is then a suitable method when studying foot function in a global approach.

The ICCx methods allows considering the variables behavior over the entire time course of the dataset. From this perspective, ICCx performed on the helical angle can be used as a signature of the movement expertise. Repeated measure ANOVA confirmed these differences, as cutting and U-turn movements were reported with significant poorer repeatability compared to daily movements. The use of over time ICCx on the HA brought out a new and objective tool for the understanding of foot response to different solicitations. Indeed, a well-mastered movement will lead to a higher repeatability of the foot deformation pattern.

Table:

	Walking	Heel impact run	Fore foot impact run	90° cutting	180° U-turn
	Value (°)± sd	Value (°)± sd	Value (°)± sd	Value (°)± sd	Value (°)± sd
Maximum	20.8±6.7°*	13.0±6.7°	16.4±8.4°*	12.54±7.8°	4.4±4.6°*
Amplitude	26.5±5.2°*	20.2±4.1°*	23.6±5.5°*	16.5±5.0°*	9.9±4.1°*
	ICC	ICC	ICC	ICC	ICC
Maximum	0.8	0.9	0.8	0.8	0.5
Amplitude	0.7	0.7	0.8	0.8	0.3

Caption: Maximum and amplitude values of the helical angle during the stance phase of each movement are given in °± standard deviation. corresponding ICC values are presented. * means the related result is significantly different from all other conditions. $p < 0.05$

References: [1] Elftman H, Artif Limbs, 13(1):49-58, 1969.

[2] Graf ES et al., Comput Math Methods Med, 2012:368050, 2012.

[3] Duhamel A et al., Gait Pos, 20(2):204-212, 2004.

Disclosure of Interest: None Declared

Feet and Footwear

PO-0090

EVALUATION OF THE MEASUREMENT OF REARFOOT MOTION USING DIFFERENT MARKER PLACEMENT TECHNIQUES

Yousef Shanib [1,*]Anmin Liu [1]Andrew Findlow [1]Richard Jones [1]

[1]Health Sciences, The University of Salford, Salford, United Kingdom

Introduction and Objectives: Quantifying rearfoot motion in barefoot and shod using loose skin/shoe mounted markers can lead to artefacts and inaccurate tracking of the segment. Therefore, an optimal method that allows both to be obtained without the need for removal of markers is required. A rigid heel cup cluster with three markers attached firmly to the skin of the heel has frequently been utilised to track the 3D movement of the heel in barefoot biomechanical studies (Nester *et al.*, 2014). In addition to this, a skin mounted 4-marker heel pin cluster secured to the lateral aspect of the rearfoot (fig. 1) has also been utilised (Schultz and Jenkyn, 2012). If there is agreement in these two methods of estimating rearfoot motion during barefoot, then it may be possible to use a heel pin cluster through an aperture in footwear (to prevent shoe interference); thus allowing the motion of the rearfoot in a shod experimental condition to be compared to the barefoot data directly. The aim of this study was to investigate the difference in rearfoot motion using two different attachment methods; the heel cup cluster and a heel pin cluster.

Methods: Fifteen healthy participants (7 male, 8 female) were recruited to take part in this study in the gait laboratory at The University of Salford using sixteen OQUS infrared cameras (Qualysis AB, Sweden) sampled at 100Hz. Three retro reflective markers were attached to the heel cup and four were fixed on to a heel pin cluster, both attached independently of each other to the skin of the heel with double sided tape (fig. 1). A cluster was attached to the leg for the calculation of rearfoot motion. Five walking trials were conducted for each participant with the data captured simultaneously for both attachment methods.

The error between the heel cup cluster and the heel pin cluster was determined by root mean squared deviation (RMSD) in the three planes of motion relative to the tibia. Paired t-tests were undertaken to determine significant difference at the 95% confidence interval.

Results: The angular movement of the heel about the tibia indicated no significant difference (P>0.05). The RMSD differences were identified as less than ±1.5 degrees between the two methods.

Figure:

Caption: Figure 1 – Heel cup cluster and heel pin cluster markers.

Conclusion: The heel pin cluster marker was identified as a reliable and non-invasive method to capture rearfoot kinematics during walking. The small difference that was identified may be due to skin movement artefact. Therefore, either method could be used for the collection of rearfoot motion during barefoot walking. Rearfoot motion is difficult to quantify in shod conditions without modifying the heel counter extensively, therefore using a heel pin cluster with a small hole appears to be a potential solution for comparison studies of barefoot to shod experimental conditions.

The findings of this study will be of benefit to investigations into rearfoot motion whilst wearing footwear and its part in the lower limbs function, particularly to those during the assessment of orthotic interventions.

Table:

R_Relative_Tibia	Mean					
Barefoot	Heel Cup	Pin Cluster	STD Cup	STD Pin	P value	RMS D
Plantar Flex (X)	-1.21	-2.01	2.29	2.86	0.133	0.88
Eversion (Y)	-2.35	-2.43	2.43	2.13	0.897	1.37
Abduction (Z)	-0.75	-1.11	5.26	4.44	0.662	1.21
Dorsi Flex (X)	15.31	15.30	3.45	3.41	0.984	
Inversion (Y)	7.86	8.81	3.75	4.32	0.068	
Adduction (Z)	8.27	8.94	4.87	4.63	0.470	

Caption: Table 1- Comparison of the heel cup cluster and the heel pin cluster

References: [1] Nester et al., J. Foot and Ankle Research, 2014. In press.

[2] Shultz et al., Medical Engineering and Physics, 34: 118-122, 2012.

Disclosure of Interest: None Declared

Feet and Footwear

PO-0091

INVESTIGATION OF BENCH METHODS FOR DETERMINING STIFFNESS OF SOLID ANKLE-FOOT ORTHOSES

Dimitrios Sokratis Komaris [1,*]Stephanos Solomonidis [1]Andrew James Murphy [1]

[1]Biomedical Engineering, University of Strathclyde, Glasgow, United Kingdom

Introduction and Objectives: The prescription of ankle-foot orthoses (AFOs) is one of the most common and effective treatments for the compensation of neuromuscular disorders, for example stroke and spinal cord or peripheral nerve injuries (Bregman et al., 2010). The biomechanical functions of plastic AFOs are determined by their thickness, the material selection and their geometry. The geometry, also known as trim-line, reflects the stiffness in relationship to the range of motion that the AFO allows at the talocrural joint (Lin and Bono, 2010). Their design, however, is mainly empirical due to a lack of evidence-based research on their geometrical characteristics (Papi, 2012). Therefore, experimental data are critical for the optimization of AFOs' characteristics.

This project aimed to investigate the different experimental methods currently utilized for determining the stiffness of homo-polymer and co-polymer polypropylene AFOs with different trim lines.The experimental procedure had two aims.

    1. To design and fabricate an artificial leg suitable for the stiffness testing of an AFO.

    2. To measure and compare the stiffness of an AFO with/without the presence of the artificial leg by means of different stiffness-measuring methods.

Methods: The strengths and weaknesses of eight experimental bench testing methods were analysed and two different techniques (Figure 1) were implemented in order to determine the relationship between the AFOs' mechanical properties and their geometry: the bending test by Ross et al. (1999) in a custom-made rig and the mechanical test by Major et al. (2004) in the Instron ElectroPuls E10000 testing machine. Three AFOs were tested in total: a 4.6mm black co-polymer solid AFO (4.6BCP), a 6mm homo-polymer solid AFO (6HP) and a 4.6mm co-polymer solid AFO with carbon fibre shape corrugations (4.6CP).

Results: Table 1 demonstrates the different dorsiflexion angles when a constant moment of 20Nm about the ankle joint is applied to the AFOs. During the Instron test and when a moment of 20Nm about the ankle joint was applied, adopting the mathematical equations that were described by Major et al. (2004), an error equal to 1.05° was found when the distance between the lower jig and the medial malleolus prominence of the 4.6BCP AFO and the distance connecting the medial malleolus and the upper jig were considered as constants.

Figure:

Caption: Figure 1 Left, the mechanical testing of the 4.6 BCP AFO in the Instron E10000 as described by Major et al. (2004), and (right) the dorsiflexion test of the 4.6CP AFO in a custom-made rig with the presence of the artificial leg as described by Ross et al. (1999).

Conclusion: The results of this investigation indicates, particularly in relation to the 4.6CP AFO, that the difference in stiffness when a leg is introduced in an AFO is noteworthy and it is suggested that the outcomes of a study utilizing an artificial leg cannot be compared with the results obtained when testing isolated AFOs. Additionally, comparing the 4.6BCP and the 4.6CP, and as suggested by Ross et al. (1999), colour additives in the copolymer polypropylene sheets will affect the stiffness of the AFO resulting in a more flexible orthosis.

The difference between the two methods is also considerable and it is believed that the cause of this variation is that the manual methods are more sensitive to creep and thus the AFO seems to be more flexible when measured manually than in materials testing machines.

Finally, the mathematical data processing of the Instron testing that exists in the literature (Major et al., 2004) was found to be imprecise and it is suggested that a camera system (such as the Bluehill software) should be used in order to measure accurately the deformation of the AFOs.

Table:

AFO	With the artificial leg		Without the artificial leg	
	Custom-made rig/ Dorsiflexion Angle (°)	Instron E10000/ Dorsiflexion Angle (°)	Custom-made rig/ Dorsiflexion Angle (°)	Instron E10000/ Dorsiflexion Angle (°)
4.6BCP	3.49	3.35	3.84	3.56
6HP	3.28	1.81	3.30	2.19
4.6CP	4.20	1.96	5.29	3.48

Caption: Table 1 Comparison of the dorsiflexion angle when a moment of 20Nm about the ankle joint was applied.

References:

[1] Bregman et al., Prosthet Orthot Int, 34(3), 293-304, 2010.

[2] Lin et al., Spinal cord medicine, 1st ed, Demos Medical, 2010.

[3] Major et al., Prosthet Orthot Int, 28(1), 44-48, 2004.

[4] Papi, *An investigation of the methodologies for biomechanical assessment of stroke rehabilitation*. Ph.D thesis, University of Strathclyde, 2012.

[5] Ross et al., Prosthet Orthot Int, 23(1), 63-71, 1999.

Disclosure of Interest: None Declared

Feet and Footwear

PO-0092

COMPARATIVE FUNCTIONAL MORPHOLOGY OF THE HUMAN FOOT BASED ON THREE-DIMENSIONAL FINITE ELEMENT ANALYSIS

Tomoya Nakamura [1] Ryo Suzuki [1,*] Kohta Ito [1] Naomichi Ogihara [1]

[1] Department of Mechanical Engineering, Keio University, Yokohama, Japan

Introduction and Objectives: The anatomy of the human foot complex is distinctive from that of the apes owing to specialized morphological adaptations for habitual bipedal locomotion. However, the functional significance of the human unique morphological features that differentiate the human foot from those of apes and other primates still remains unclear due to the complexity of structure and mechanics of the foot. In this study, we developed three-dimensional finite element models of the human and chimpanzee feet in order to comparatively investigate the functional morphology of the human foot.

Methods: Each bone and the whole foot surfaces were extracted from computer tomography images. The volume enclosed by each surface was meshed with tetrahedral elements. The bones were represented as a linear elastic material. The articular cartilage was also assumed to be linear elastic and the contact between the articular surfaces was considered frictional. The encapsulated soft tissue was defined as a hyperelastic Ogden material. Ligaments and plantar fascia were represented by tension-only spring elements. The foot-ground contact was modeled using rigid contact surfaces. The mechanical interactions of the human and chimpanzee feet with the ground during balanced standing were simulated by applying compressive force on the tibia and tension along the Achilles tendon due to muscle contraction. The size of the foot is normalized by the total volume of the foot bones for comparisons between the human and chimpanzee feet.

Results: Our results demonstrated that the center of pressure was situated more anteriorly in the human foot because of the presence of the longitudinal arch. It was also demonstrated that the calcaneocuboid joint was less mobile in the pronation-spination direction in the human foot due to locking mechanism of the articular morphology. Furthermore, the human foot is probably more capable of storing elastic energy during foot-ground contact for effective generation of propulsive force in the late stance phase.

Conclusion: We developed a computational framework for comparatively investigating the causal relationship among the morphology, behavior, and internal loading of the human foot, leading to a better understanding of morphofunctional relationships between the foot architecture and human bipedal walking.

Disclosure of Interest: None Declared

Feet and Footwear

PO-0093

THE INFLUENCES OF THREE-TYPES OF FOOT STRIKE PATTERNS ON THE MECHANICAL ADVANTAGE AND THE FORCES APPLIED TO FOOT

Satoru Hashizume [1][2],[*]Toshio Yanagiya [1]

[1]School of Health and Sports Science, Juntendo University, Chiba, [2]Japan Society for the Promotion of Science, Research Fellowship for young Scientists, Tokyo, Japan

Introduction and Objectives: Distance running sometimes induces musculoskeletal injuries. One of common injured parts of running-related musculoskeletal injuries is foot and ankle, such as the Achilles tendon (AT) and the tibia. Effective prevention method, therefore, is required to reduce the rate of running-related musculoskeletal injuries occurring at foot and ankle.

The influence of different foot strike patterns on the risks of running-related musculoskeletal injuries occurring at foot and ankle was previously discussed. Lieberman et al [1] reported that the smaller vertical ground reaction force (GRF) was found for fore-foot strike than for rear-foot strike during early stance phase. They suggested that fore-foot strike may reduce the risk of running-related musculoskeletal injuries occurring at foot and ankle as compared with rear-foot strike. However, the GRF does not coincide with the forces applied to common injured parts of foot and ankle such as the AT and the tibia. The influence of different foot strike patterns on the forces applied to common injured parts should be confirmed to prevent running-related musculoskeletal injuries occurring at foot and ankle.

The mechanical advantage, which is defined as the ratio between the AT moment arm and the moment arm of the GRF influences on the relationships between the GRF and the AT force and between the GRF and the joint reaction force. The mechanical advantage varies depending on ankle angles [2], suggesting that the AT and joint reaction forces may also vary among foot strike patterns even if the GRF is constant. The purpose of this study, therefore, was to confirm the influences of the different foot strike patterns on the mechanical advantage and the forces applied to foot.

Methods: Seven male runners voluntary participated. Reflective markers were attached to skin overlaying the medial and lateral malleoli, the calcaneal tuberosity, the distal muscle-tendon junction (MTJ) of the soleus, the heads of first and fifth metatalsal bones and the toe. Subjects were asked to perform barefoot running along a 15 m runway at 3.33 ± 0.16 m/s by using fore-foot strike, mid-foot strike and rear-foot strike. The three-dimensional coordinate of each marker and the GRF were recorded by using the motion capture system (250 Hz) and the force platform (1000 Hz), respectively. The position of the center of mass of foot was calculated by using the three-dimensional coordinate of markers attached to the calcaneal tuberosity, the heads of first and fifth metatalsal bones and the toe. The talocrural joint axis was defined as the line passing through the markers attached to the medial and lateral malleoli. The line of action of the AT force was defined as the line passing through the markers attached to the calcaneal tuberosity and the distal MTJ of the soleus. The AT moment arm and the moment arm of the GRF were calculated as the shortest distance between the talocrural joint axis and the line of action of each force, respectively. The mechanical advantage was calculated as the ratio of the two moment arms. The AT and joint reaction forces were calculated by solving the equations of motion of foot.

Results: The means and standard deviations of each parameter were represented in Table. The AT moment arm was not different among each foot strike pattern. Meanwhile, the moment arm of the GRF was significantly greater for fore-foot strike than for others foot strike patterns, and greater for mid-foot strike than for rear-foot strike. The mechanical advantage was significantly smaller for fore-foot strike than for others foot strike patterns, and smaller for mid-foot strike than for rear-foot strike patterns. The GRF was not different among each foot strike pattern. Meanwhile, the AT and joint reaction forces were significantly greater for fore-foot strike than for others foot strike patterns, and greater for mid-foot strike than for rear-foot strike.

Conclusion: Present results showed that the mechanical advantage was significantly different among foot strike patterns, and this induces in the significant differences in the AT and joint reaction forces among each foot strike pattern. The largest AT and joint reaction forces were found for fore-foot strike, suggesting that the risks of running-related musculoskeletal injuries occurring foot and ankle may be higher than others foot strike patterns.

Table:

	fore-foot strike	mid-foot strike	rear-foot strike
AT moment arm (mm)	55 ± 3.8	54 ± 3.7	54 ± 4.1
GRF moment arm (mm)	111 ± 4.7	98 ± 8.1	83 ± 3.9
mechanical advantage	0.491 ± 0.037	0.552 ± 0.038	0.648 ± 0.058
GRF (N)	1085 ± 151.3	1064 ± 112.0	1037 ± 108.5
AT force (N)	2318 ± 236.1	1995 ± 249.0	1599 ± 128.3
joint reaction force (N)	3292 ± 364.6	2971 ± 342.7	2565 ± 150.3

Caption: Table. The means and standard deviations of each parameters.

References: [1] Lieberman et al., Nature, 463: 531-535, 2010

[2] Hashizume. Structure of foot and ankle -biomechanical risk factor of Sever's disease- (Doctoral thesis), Waseda University, 2014

Disclosure of Interest: None Declared

PO-0094

DEVELOPMENT OF A LARGE-SCALE SUBJECT-SPECIFIC FINITE ELEMENT MODEL OF HUMAN FOOT COMPLEX

Mohammad Akrami [1,*] David Howard [2] Chris Nester [2] Zhenmin Zou [1] Lei Ren [1]

[1] School of Mechanical, Aerospace and Civil Engineering, University of Manchester, [2] School of Health Science, University of Salford, Manchester, United Kingdom

Introduction and Objectives: Human foot, as the only component of the human body in contact with the ground during locomotion, has different roles in absorbing the shocks, bearing body weight and generating propulsive powers during locomotion [1]. In the past years, a large amount of experimental and computational studies have been conducted to investigate the biomechanical structures and functions of the human foot complex. However, due to the complexity of the foot musculoskeletal structure, our current understanding of the fundamental biomechanical mechanism of the human foot structure is still very limited. The objective of this study is to develop a large-scale subject-specific finite element model of the human foot complex with high bio-fidelity so that the delicate foot structure and function interplay during different activities could be investigated.

Methods: The anatomical and geometrical structures of the model were constructed based on the individualised Magnetic Resonance Images (MRI) of the right foot of a healthy male subject (age: 27 years, weight: 75 kg; no history of the foot abnormalities or lower limb injuries). Totally 28 foot bones and also tibia and fibula were modelled. All the possible relative motions among the 28 foot bones have been modelled as connecting joints constrained by contacts between 52 cartilage layers and 80 ligament groups. A three dimensional (3D) plantar fascia structure was constructed to represent the load transfer between rear foot and phalanges. All the bones, cartilages, ligaments and the plantar fascia structure are embedded into a 3D structure of the encapsulated soft tissues. In this study, 3D gait measurement for the same subject used for modelling, was conducted to record the major foot bone motions, ground reaction forces and moments and plantar pressure distribution during normal level walking. The in vivo force data of 12 major ankle/foot muscles around talocrural, subtalar and metatarsophalangeal joints were calculated using a scaled OpenSim foot musculoskeletal model driven by the gait measurement data.

Results: FE simulations were conducted to analyse the mechanical behaviour of the foot complex in the mid-stance of normal level walking. The simulations were driven by the in vivo muscle forces of 12 major foot muscles and also the bone-to-bone contact forces between tibia and talus calculated based on gait measurement data. The model simulation results were rigorously validated against the measured region specific peak plantar pressure data, and also the relative 3D orientations and positions of major foot bones. The simulated peak plantar pressure data showed a good agreement with the pressure plate data. The predicted relative 3D angle changes of the major foot bones agreed reasonably well with the in vivo measurement data. The experimental validation results indicated that the developed FE foot model is capable of predicting the plantar pressure distribution, load transfer and foot bone motions reasonably well.

Figure:
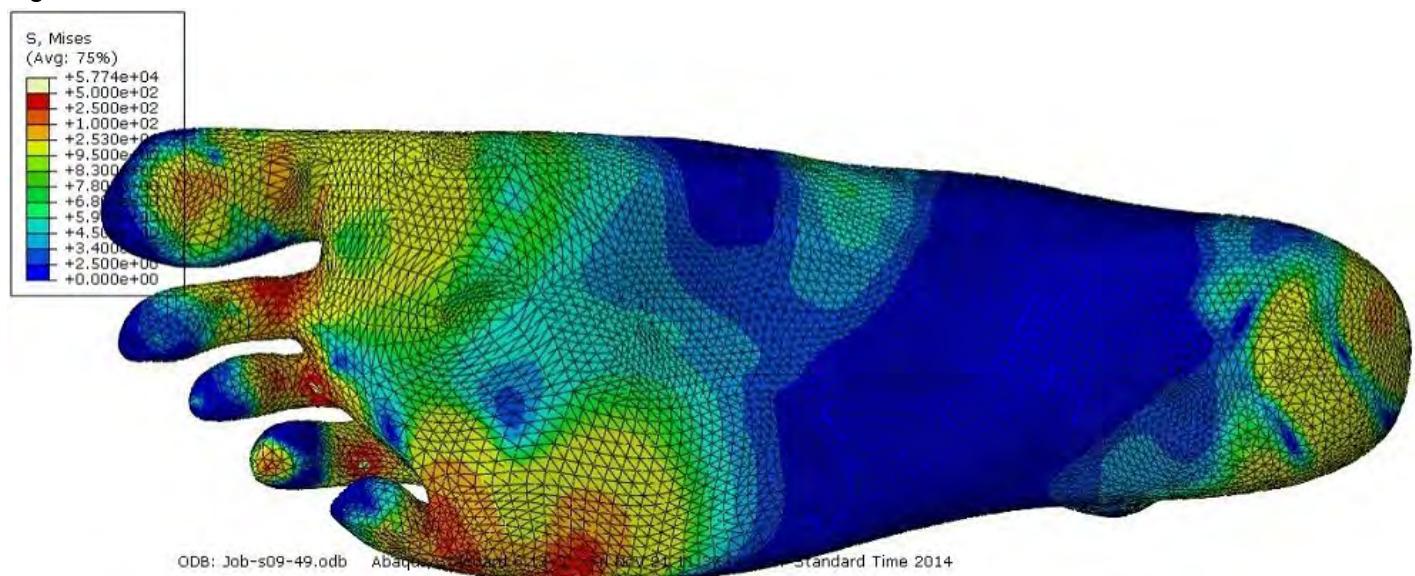
Caption: Fig 1: Plantar pressure distribution of the human foot (Von Mises stress)

Conclusion: A large-scale subject-specific 3D FE musculoskeletal model of the human foot complex was developed to represent the bio-realistic behaviour of the foot during in the stance phase of normal walking. The peak pressures were found in the heel region and the area underneath the five metatarsal bones in the middle stance. This pattern is reasonable considering the ankle joint force role in transmission the force from rear foot to the fore foot through talonavicular and cuneonavicular joints in which showing high stress values in the heel region and under the five metatarsal bones. Future works involve the investigation of the contribution of different foot structure components to the weight bearing, load transmission and power generation capacities of the human foot complex during different motor activities.

References: [1] Qian ZH et al., PLoS One, 8 (11): e79424, 2013

Disclosure of Interest: None Declared

Feet and Footwear

PO-0095

A CORRELATION STUDY BETWEEN THE DYNAMIC FOOTPRINT AND STATURE USING PEDOGRAPHY

Raghad Mimar [1,*]Hossien Nabavi Nik [2]Hadi Mohammadi [1]

[1]Biomedical Engineering, University of British Columbia, Kelowna, Canada, [2]Physical Education and Sport Sciences, Kharazmi University, Tehran, Iran, Islamic Republic Of

Introduction and Objectives: One of the established methods to effectively assess the size of the human body is using anthropometric techniques. The objective of this study is to estimate standing height or stature by pedography using a dynamic footprint.

Methods: Measurements of the dominant footprint of 40 subjects were assessed using pedography. In order to collect data, a two-step protocol in which the participant walked barefoot at a self-selected pace was implemented. Five trials of the right foot were recorded and the average was calculated for the analysis (Fig. 1). The Pearson correlation coefficient was then used to determine the relationship between the variables followed by the implementation of the linear regression test to estimate the subject's stature.

Results: Results showed a high correlation between standing height and foot length from heel to the second toe ($p < 0.01$, $R = 0.472$) and a low correlation with the width of the foot in metatarsal phalangeal area ($p < 0.05$, $R = 0.016$). As to the models available to predict the stature, the foot length equation from the base of the heel to the tip of the second toe offered the highest coefficient of determination ($R^2 = 0.48$), (Tbl. 1).

Figure:

MPJ Width (Metatarsophalangeal joints Width)
Arch Width
Calc Width (Calcaneus Width)
Clarke's Angle
Arch Index (Mid Area/ Forefoot Area+Mid Area +Rearfoot Area)
Calc-A1 (base of heel to First Toe)
Calc-A2 (base of heel to Second Toe)
Calc-A2 (base of heel to Third Toe)
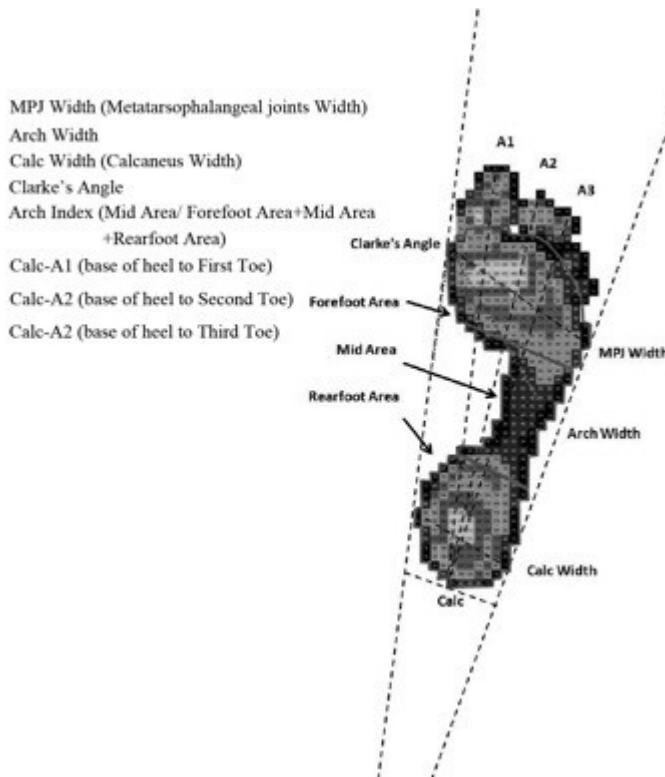
Conclusion: Results of this study showed a strong correlation between the different footprint sizes and stature. Thus, a person's height can be estimated by different footprint sizes left at a crime scene with different regression models. Depending on the quality of the footprints recovered at a crime scene, the regression models developed in this study may effectively estimate the stature with an error of the order of a few millimeters.

Table:

Variables	Maximum (mm)	Minimum (mm)	Mean (mm)	Standard Deviation	Correlation Coefficient
MPJ Width	11.3	9.1	10	0.46	0.174
Arch Width	7.6	1.9	3.47	1.04	0.172
Calc Width	7	4.8	6	0.45	0.016
Arch Index	0.29	0.18	0.24	0.02	0.171
Clarke's Angle	61	22.8	46.38	9.26	-0.063
Calc-A1	27.1	23.3	25.01	0.76	0.440*
Calc-A2	26.1	22.8	24.78	0.75	0.472**
Calc-A3	25.1	22.1	23.82	0.77	0.337

Caption: •Statistical significance at $P<0.05$; ** Statistical significance at $P<0.01$

References: [1]. Sen et al., *J. Forens.* Sci., 56(Suppl 1):S148-153, 2011.

[2]. Reel et al., *Forens. Sci. Int.,* 219(1-3):283.e1-283e5, 2011.

Disclosure of Interest: None Declared

USING TOPOLOGY OPTIMISATION TO GENERATE PERSONALISED FOOTWEAR MIDSOLE GEOMETRIES

Iain Hannah [1,*]Andy Harland [1]Dan Price [2]Tim Lucas [2]

[1]Sports Technology Institute, Loughborough University, Loughborough, United Kingdom, [2]adidas AG, Herzogenaurach, Germany

Introduction and Objectives: Studies have shown that adding mass to a runner's shoes increases oxygen uptake [1] and thus the metabolic cost of running. However, further studies have also suggested that shod running may provide an energetic advantage over a barefoot condition for habitual rearfoot runners [2]. As a result of these findings, lightweight performance footwear that still offers some degree of cushioning represents a large segment of the running shoe market [3].

Lieberman et al. [4] have conducted a significant number of studies into different running footstrike styles and concluded that "…runners who forefoot or midfoot strike do not need shoes with elevated cushioned heels to cope with [the] sudden, high transient forces that occur when you land on the ground." This suggests that footwear could be optimised to a runner's individual footstrike pattern, providing support under the areas of the foot that are highly loaded with material omitted elsewhere. Based on the "Material Distribution Method" [5], this paper details the use of finite element analysis and topology optimisation to output lightweight footwear midsole geometries optimised for an individual subject's personal footstrike loading profile.

Methods: Biomechanical running trials were performed by three healthy, male subjects (two habitual rearfoot strikers, one habitual forefoot striker) whilst wearing a pair of simple athletic shoes. The plantar surface of the foot was segmented into 20 discrete regions with the triaxial loads exerted on each sub-area of the foot estimated by combining the data output by the force platform and pressure insole using an "assumption of proportionality" [6].

A generic finite element midsole geometry was created, meshed with linear hexahedral elements and assigned an isotropic linear elastic material model. The 20 sub-sections of the foot's plantar surface were represented by rigid plates with the maximum 3-D load predicted to occur in each area applied to its respective plate. The objective function of the optimization task was to minimise strain energy whilst satisfying a constraint defined to ensure the midsole volume remained below a defined threshold. This approach resulted in a robust model capable of outputting midsole geometries optimised to be stiff but lightweight.

Results: As expected, material was retained in areas of high loading but removed in areas that experienced lower strains. This is highlighted by the clear differences in the optimised geometries output for the rearfoot (Subject A and Subject B) and forefoot (Subject C) strikers. The midsole geometries output for Subject A and Subject B were similar but Subject B exhibited comparatively greater loading in the lateral rearfoot and under the metatarsal heads. This is reflected by a higher level of material retention in these areas. Geometric restrictions were also applied in subsequent analyses.

Figure:
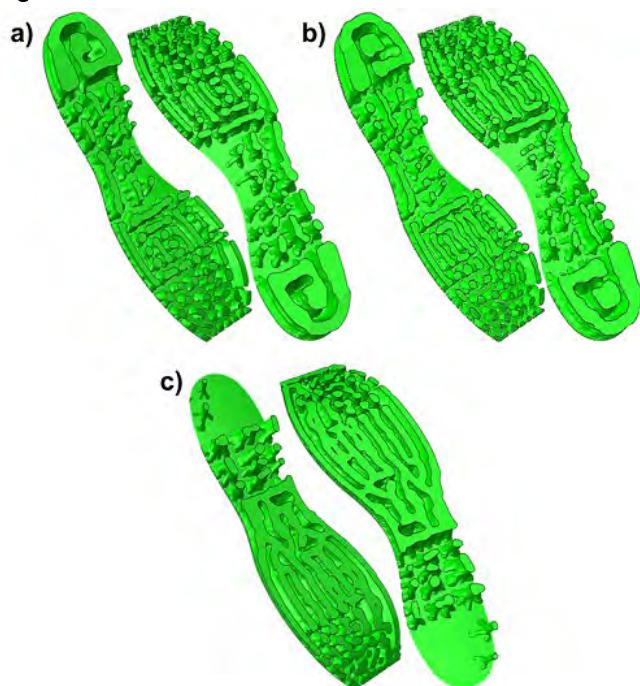
Caption: Optimised midsole geometries output for each subject. a) Subject A (rearfoot striker), b) Subject B (rearfoot striker), and c) Subject C (forefoot striker).

Conclusion: This study demonstrated that topology optimisation methods could potentially be employed to automatically generate lightweight midsole geometries optimised for a subject's individual footstrike loading pattern. However, the primary role of the midsole is to dissipate footstrike impact forces but the task was defined such that the stiffest structure was considered optimal. To address this, some degree of "engineered compliance" [7] should be introduced in future optimisation tasks. Furthermore, significant advances in manufacturing technology would also be required before the mass customisation of functional footwear midsoles could become a feasible reality.

References: [1] Nigg & Kerr (Ed.). Biomechanical Aspects of Sport Shoes and Playing Surfaces, The University of Calgary, 1983.

[2] Kerdok et al., J. Appl. Physiol., 92: 469-478, 2002.

[3] Nigg, Footwear Sci., 1: 73–79, 2009.

[4] Lieberman et al. Biomechanics of Foot Strikes & Applications to Running Barefoot or in Minimal Footwear, 2010

[5] Bendsøe & Sigmund. Topology Optimization: Theory, Methods and Applications, Springer, 2003.

[6] MacWilliams et al., Gait Posture, 17: 214–224, 2003

[7] Sigmund, Mech. Struct. Mach., 25: 493–524, 1997.

Disclosure of Interest: None Declared

PO-0097

FOOT ANTHROPOMETRY AND SHOE SIZE OF BRAZILIAN ELDERLY: A LONGITUDINAL STUDY

Thais R. Aurichio [1,*] Eliane Manfio [2] Alessandra Castro [3] Juliana Ansai [1] José Rubens Rebelatto [1]

[1]Federal University of Sao Carlos, Sao Carlos, SP, [2]FEEVALE, Novo Hamburgo, RS, [3]Federal University of Espirito Santo, Vitória, ES, Brazil

Introduction and Objectives: The use of unsuitable shoes is a common problem among elderly and has been highly associated with deformities in toes, presence of calluses, symptoms of pain and falls in this population. An appropriate shoe is composed of functional qualities, aspects related to comfort and safety and according to trends of current fashion. The purpose of this study was to identify foot anthropometry parameters in order to highlight the importance of manufacturing different profiles for each size; to verify influence of aging on foot anthropometry of elderly women over four years.

Methods: 101 community-dwelling elderly women with a mean age of 69.4 (±6.1) years were assessed in two moments within a range of four years. Foot anthropometric variables (foot length (FL), instep circumference (IC), foot breadth (FB), dorsal arch height (DAH) and height of top of ball girth (HTBG)) were measured through analog instruments, such as caliper, fiberglass tape and height gage. Body weight and height were measured to calculate body mass index (BMI). The volunteers were questioned about their shoe size. To investigate the relationship between FL and other anthropometric variables, they were transformed into discrete variables, according to the French system (each size corresponds to intervals of 6.666mm of FL) and previous studies of anthropometric characterization (perimeters and widths change every 5mm and height every 2.5mm). The highest concentration of subjects for FL was in intervals of 240.0mm, 246.7mm and 253.3mm, corresponding to 36, 37 and 38 brazilian size, respectively. These subjects were kept in these subgroups for longitudinal analysis. Paired t-test and its corresponding nonparametric test (Wilcoxon) were used to assess differences in anthropometric variables in each size over four years and a 5% significance level was used.

Results: At baseline 65 (64.3%) elderly were at FL intervals corresponding to 36 (26.7%), 37 (17.8%) and 38 (19.8%) shoe sizes. After four years, only 61.4% volunteers were at FL intervals corresponding to the 36 (22.8%), 37 (20.8%) and 38 (17.8%) sizes. At baseline, for 36 size there was a change of 30mm (217 to 247mm) in IC and three IC profiles (235 to 245mm) were required to attend 59% volunteers in this subgroup. After four years, this variability remained (220 to 253mm) and three IC profiles were also required. The biggest change (41mm) occurred for 37 size, in both assessments, and three profiles (230 to 240mm) were required to attend 57.2% elderly. For 38 size, the IC variation was initially 34mm and two profiles (235 and 240mm) were required to attend 55% elderly. After four years, the variation was 29mm and two profiles (245 and 250mm) were required to attend most volunteers. At baseline 52.3% used unsuitable shoes according to FL and after four years the use of unsuitable shoes reduced to 50.8%. There was a decrease of FL over years for 36, 37 and 38 sizes. Also, the FB for 37 size and the HTBG for 38 size reduced in aging. The BMI reduced only for elderly with 37 and 38 sizes.

Conclusion: These results suggest the need of manufacturing different profiles for each size in order to provide a comprehensive and more suitable shoe for Brazilian elderly population. The constant adjustment of shoe models and sizes are needed in elderly population to prevent injuries and falls.

Table:

			BMI	FL (mm)	IC (mm)	FB (mm)	DAH (mm)	HTBG (mm)
36 size	Baseline	Min - Max	23.55-41.14	234-240	217-247	93-106	60-80	25-35
		Mean (SD)	29.18 (±1.15)	236.50 (±0.44)	231.94 (±2.01)	99.06 (±0.90)	66.22 (±1.39)	29.39 (±0.82)
	After four years	Min - Max	22.93-39.12	231-241	220-253	89-104	56-77	26-33
	Mean (SD)		28.75 (±1.20)	235.94 (±0.62)	233.39 (±2.26)	97.61 (±0.96)	67.06 (±1.31)	30.67(±0.48)
	P value		0.254	**0.032**	0.392	0.141	0.749	0.101
37 size	Baseline	Min - Max	21.49-39.05	241-246	224-265	93-108	57-83	19-36
		Mean (SD)	28.37 (±0.89)	243.78 (±0.35)	238.27 (±2.59)	100.22 (±1.23)	70.06 (±1.61)	30.50 (±1.00)
	After four years	Min - Max	21.50-40.53	236-247	220-261	91-107	59-80	26-38
	Mean (SD)		27.37 (±1.01)	241.94 (±0.65)	237.06 (±2.30)	99.06 (±1.25)	69.78 (±1.65)	31.11(±0.74)
	P value		**0.037**	**0.008**	0.517	**0.006**	0.812	0.796
38 size	Baseline	Min - Max	21.05-33.77	247-253	220-254	87-112	62-77	29-37
		Mean (SD)	27.47 (±1.05)	249.72 (±0.53)	235.58 (±2.00)	100.72 (±1.45)	68.83 (±0.83)	32.61 (±0.61)
	After four years	Min - Max	20.72-35.55	242-253	221-250	91-112	61-76	27-36
	Mean (SD)		27.21 (±1.02)	247.39 (±0.66)	235.74 (± 2.05)	100.56 (±1.48)	68.06 (±1.09)	30.89 (±0.55)
	P value		**0.043**	**0.000**	0.889	0.739	0.538	**0.005**

References: [1] Scott, G., Menz, H.B., Newcombe, L. Age-related differences in foot structure and function. Gait Posture, 2007;26,1:68-75.

[2] Manfio, E.F., Avila, A.O.V., A study of anthropometric parameters of the Brazilian female foot (in Portuguese). Rev Bras Biomec, 2003;4(1).

Disclosure of Interest: None Declared

PO-0098

PLANTAR PRESSURE AND FOOT TEMPERATURE RESPONSES AFTER BAREFOOT RUNNING

J I Priego [1,*] M R Kunzler [2] E S da Rocha [2] A S Machado [2] F P Carpes [2]

[1]University of Valencia, Valencia, Spain, [2]Federal University of Pampa, Uruguaiana, Brazil

Introduction and Objectives: Benefits or inconveniences of barefoot running still are controversial in the literature. Barefoot running was associated to higher plantar pressure in forefoot region (Squadrone and Gallozzi 2009), which can result in more friction therefore impacting foot temperature. However, the relationship between plantar pressure and skin temperature still is unclear. Skin temperature helps to investigate the efficiency of thermoregulatory system during exercise. Foot temperature can help to understand the effect of footwear insulation. Here we examined the immediate effects of barefoot running on foot plantar pressure and temperature.

Methods: Eighteen participants (age 23.9 ± 3.6 years, body mass 64.8 ± 16.6 kg, and height 1.70 ± 0.11 cm) completed two protocols of running (shod and barefoot) following two days. They ran during 15 min at preferred and comfortable speed in a treadmill. Preferred speed was determined in the first trial and kept constant for the second. Plantar pressure during bipedal standing was recorded before and after running using a pressure mapping system (Matscan, Tekscan Inc). Foot temperature was quantified using an infrared thermography (camera E60, FLIR). Pressure and temperature were analyzed for whole foot, forefoot, midfoot and rearfoot regions. Plantar pressure in each foot region was normalized by the total pressure. Skin absolute temperature and its percentage variation between pre and post running were quantified. A 2x2 analysis of variance for repeated measures was applied to analyze the differences in plantar pressure and temperature before *vs* after running and barefoot *vs* shod. Pearson correlation was used to verify the relations between skin temperature and plantar pressure. Significance level was set at 0.05 using SPSS.

Results: The average speed was 7.3 ± 1.6 km/h. No significant differences were found in plantar pressure after running barefoot and shod (p>0.9). Regardless of the shoe condition, pressure in midfoot increased (p=0.003, 95%CI [0.8-3.1%]) whereas pressure in rearfoot decreased (p=0.004, 95%CI [0.8-3.7%]), after running. Shod running resulted in higher temperature in forefoot (p=0.003, 95%CI [0.5-2.2°C]) and midfoot (p<0.001, 95%CI [0.9-2.4°C]). Barefoot running resulted in higher variation of temperature in rearfoot (p=0.04, 95%CI [0.1-10.4%]). Any significant correlations were observed between skin temperature and plantar pressure (p>0.05 and r<0.5 or r>-0.5)

Conclusion: The main findings in our study were the lack of difference in static plantar pressure distribution after barefoot and shod running, higher temperature in forefoot and midfoot regions after shod running, larger variation of temperature in rearfoot after barefoot than shod running, and finally, no correlation between skin temperature and plantar pressure. Changing running technique towards a barefoot running may change rearfoot landing strategy to a midfoot and forefoot technique, producing higher dynamic plantar pressure in forefoot (Squadrone and Gallozzi 2009). We did not find differences in static plantar pressure after running between shod and barefoot running. Despite this, running in any of the conditions increased plantar pressure in the midfoot and decreased plantar pressure in the rearfoot, which is also in accordance with previous findings (Willems et al. 2012). These changes in plantar pressure may result from fatigue of plantar musculature (Willems et al. 2012). Shod running produced higher temperature in forefoot and midfoot than

observed for barefoot running, which may result of the footwear insulation. No significant correlation between plantar pressure and temperature were observed. These results could mean that the effect of footwear insulation can be greater than possible higher dynamic forefoot pressure produced by barefoot running. It was observed a higher variation of temperature in rearfoot after barefoot running. One possible reason to explain these results is that barefoot running can produce more vascularization due to activation of foot musculature, and higher mechanical work and stride frequency (Divert et al. 2008). More vascularization in one region can lead to higher temperature variation.

References: [1] Divert et al. (2008) Int J Sports Med, 29 (6), 512-518.

[2] Squadrone et al. (2009) J Sports Med Phys Fitness, 49 (1), 6-13.

[3] Willems et al. (2012) Gait Posture, 35 (3), 405-409.

Disclosure of Interest: None Declared

Impact

PO-0099

EFFECTS OF FALLING WITH AND WITHOUT KNEE PROTECTION: AN IN-VITRO STUDY

Michael Schwarze [1,*]Bastian Welke [1]Christof Hurschler [1]

[1]Laboratory for Biomechanics, Hanover Medical School, Hannover, Germany

Introduction and Objectives: Falling on the knees is a hazard prevalently occurring during various sports or in the elderly. For some sports the usage of protective devices such as pads is mandatory. In the elderly, special padding on the hips can reduce the effect of an unexpected fall [1]. To our knowledge, the mechanics of such padding was not investigated in high-force real life scenarios to date. The presented study illustrates the effect of wearing knee pads compared to unprotected impact on a hard surface.

Methods: Eight human knee cadaver specimens were acquired (mean age: 68y). The skin and subcutaneous soft tissue were removed at the proximal and distal end leaving the muscles, articular capsule, tendons and ligaments intact. The tibia and femur were embedded and fixed with a flexion angle of 90 deg in a custom made drop testing device (75kg including the knee). A commercially available knee pad was attached to the knee when required. Specimens were lifted 10, 20, 30 and 40mm from a force sensor and subsequently released to fall along guiding rods onto a rigid, even aluminium plate. Falling speed was continuously monitored by a displacement transducer at 1000Hz.

Results: The usage of a knee pad lead to an average attenuation of peak forces on impact by about 15% (Fig.1). As contact time on the plate was higher with a knee pad, the observed impulse was also increased. The effect diminished with increasing falling height. Energy dissipation, defined as the difference between kinetic energy pre-impact and peak potential energy post-impact, was slightly higher without a knee pad. The difference between pad or no pad was negligible at 10mm height, while difference was 75% at 40mm falling height.

Figure:
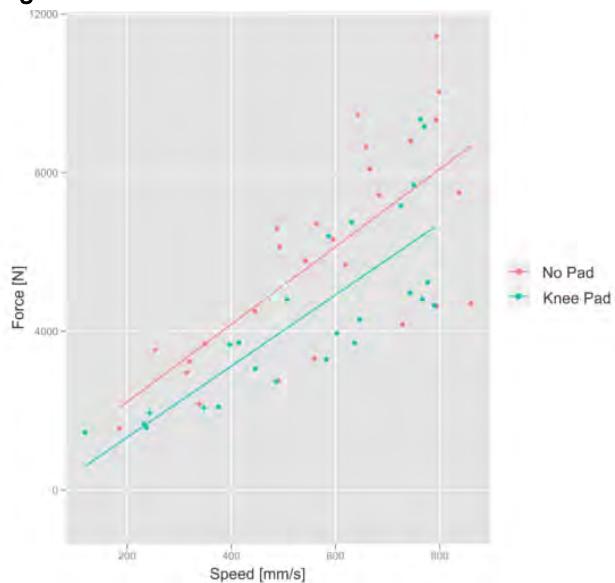
Fig.1: Maximum forces at impact over maximum falling speed of the specimen. Specimen with pads are colored in blue, specimen without pads are colore in red.

Conclusion: Despite several limitations, the results from this study illustrate the magnitude of influence of knee pads on peak forces, transmitted impulse and energy transfer. Contrary to expectations, the knee pad did not act as a mechanical damper. The mechanical behavior was more closely to a spring that temporarily stored energy and therefore reduced peak forces on impact. Possible indications for development of innovative pad designs will be the subject of further research.

References: [1] Laing, AC et al., J Orth Res, 24 (7): 1405–11, 2006.

Disclosure of Interest: None Declared

PO-0100

THE PARAMETERISATION OF THE CAVITY FORMATION IN SUBSTITUTE MATERIALS FOR NORMALISED AND SPECIAL MILITARY AMMUNITION

Richard Billich [1,*]Ondrej Fanta [1]Frantisek Lopot [1]Petr Kubovy [1]Pavel Stursa [2]Karel Jelen [1]

[1]Department of Anatomy and Biomechanics, Faculty of Physical Education and Sport, Charles University in Prague, [2]Department of Radiology, Na Homolce Hospital, Prague, Czech Republic

Introduction and Objectives: The issues of gunshot injuries and their consequences are at the forefront of the interest of a wide spectrum of various fields of science – medical and technological. Our study sets the goal of giving precision and accuracy to the description of bullet behavior in the human organism. Among parameters crucial for the assessment of the effect of a gunshot is not only the shape of the bullet path after the stabilization of the whole process, but also during the penetration of the material by the bullet. The bullet path with its permanent cavity defined by its shape, proportion and orientation within tissue is unique for every penetrating gunshot. Tissue damage provokes a wide range of reactions in the affected organism. The main nature of biological material is its reactibility through innervation.

Methods: Experimental shooting uses 20% gelatine blocks kept at the temperature of 4°C and glycerine soap. The size of blocks used in our experiment is 20x20x35 cm. Weapon systems used to shoot through the substitutive material were of 9 mm calibre for a pistol cartridge. Impact velocity was determined using optical light gates (LS-04 Intelligent Light Gates). Exiting velocity of bullets was measured with a radar (DRS-1 Doppler Radar System). Parameterization of shape transformations within the test blocks was done methods of computed tomography (CT) and magnetic resonance imaging (MRI). Experimental data was acquired using computer software CURVE EXPERT DATA.

Results: Most substantial changes happened on bullet .357 Magnum-GOLD DOT. During the penetration of the substitutive material it passed on 91% of its kinetic energy. Diagnostic methods calculated for this weapon system a difference of more than 48,2 mm in diameter between the entry and exit hole. While preserving its original weight the bullet reached its maximal average temporary cavity in the distance of 142 mm.

Conclusion: The weight of a bullet, the impact speed, bullet shape and construction constitute the determinating characteristics of a bullet's wounding effect. Specific profiles of the bullet path help constitute an image of what gunshot wound can be anticipated of each respective weapon system. It is apparent from the performed comparison that advantages and disadvantages of both substitutive materials used are approximately balanced. The results of these experiments have further significance also for the construction of ballistic protective systems.

Disclosure of Interest: None Declared

Impact

MODELING THE INFLUENCE OF PAD STIFFNESS AND DAMPING PROPERTIES ON SKULL-BRAIN MOTION DURING BALLISTIC IMPACTS

Wenming Chen [1] Melanie Franklyn [1] Peter Vee Sin Lee [1],*

[1] Department of Mechanical Engineering, University of Melbourne, Melbourne, Australia

Introduction and Objectives: Brain injury studies involving military helmets have primarily focused on the effects of head acceleration; however, recent findings support the idea that Traumatic Brain Injury (TBI) is more likely to be caused by rapid deformation of the brain tissue [1]. To date, experimental approachs for military helmet evaluation have predominately been limited to tests using standard headforms, for example, the Hybrid III dummy head. However, the Hybrid III headform does not give a sufficient or realistic view of the intrinsic brain responses; hence there are limitations to the changes which can be made to enhance helmet performance and improve head protection.

Methods: The aim of this study was to develop a simplified mathematical model of the combined helmet/head system and then simulating a ballistic impact loading scenario. Firstly, a model of the human head represented by a spring-damper-mass system was developed by modifying Stalnaker's head model [2] where an additional soft tissue mass known as the "wobbling mass" was added to include the effect of brain oscillation within the skull under impact load. Secondly, a bi-layered subsystem consisting of nonlinear spring-damper units was constructed to model the helmet's shell and padding. The physical properties of contact between the pad and the skull were described by the Hertz type contact law, and experimentally obtained using an impact test to determine the stiffness and damping parameters of the helmet pad (ZAP PADs, Zorbium Foam, Cleveland, USA). The helmet subsystem was then coupled onto the head model to form an integrated helmet/head system (Fig. 1). The system governing equations were derived by applying the Newton's Second Law of motion and implemented using Matlab/Simulink (MathWorks Inc).

Results: Typical traces of the helmet-head contact force predicted by the model exhibited double peaks, i.e. forces peaked rapidly at 1~2 ms, then followed by a second peak with slightly a lower magnitude. This force trace resembled those measured contact forces reported in the literature. In addition, the movement pattern of the wobbling mass was also similar to a recent study on tagged magnetic resonance images (MRI) which demonstrated that the brain matter shifts relative to the skull and "wobbles" in a complex damped manner upon impact. A parametric analysis further revealed that the maximum displacement of the brain varies from 1.23 to 2.52 mm at different padding conditions simulated. The maximum brain acceleration decreased from 372.5 to 192.4 m/s^2 when padding properties were altered from hard to soft conditions.

Figure:
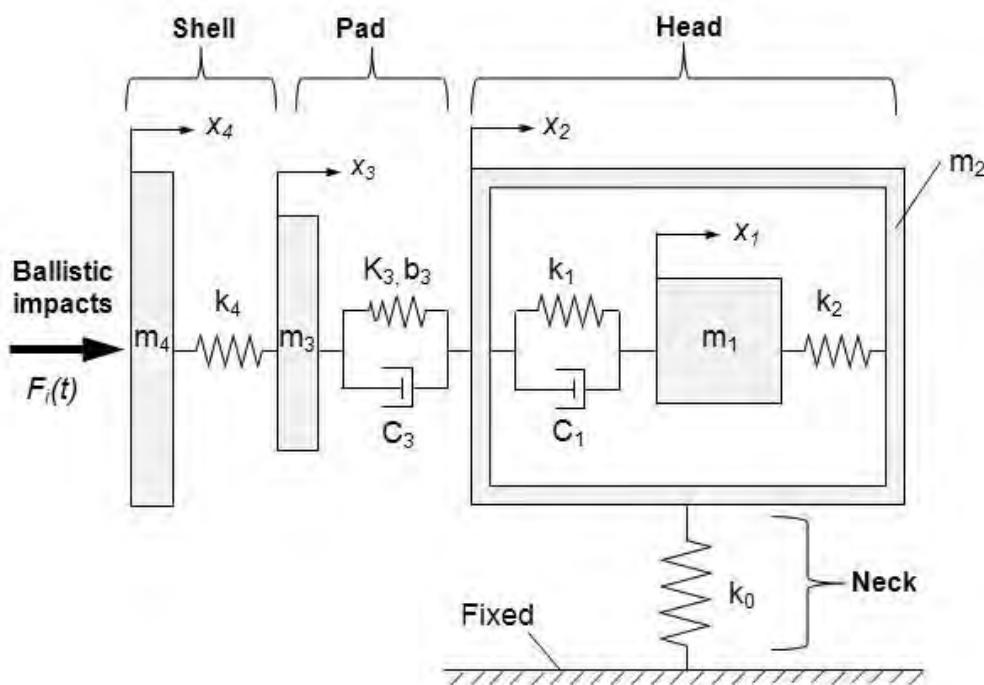
Caption: Figure 1. The schematic of the head model with a bi-layered subsystem attached.

Conclusion: In this study, a mathematical model to investigate impact biomechanics of the head-helmet system was developed and validated. The model facilitates efficient evaluation of military helmet designs on helmet-head contact forces and intrinsic brain responses under ballistic impact conditions. It was shown that brain motions were strongly influenced by the padding stiffness properties, which should therefore be considered as an essential parameter in helmet designs.

Table:

Helmet parameters		Predicted responses by the model		
Shell (K4)	Padding (K3/C3)	Fc (N)	Ds (m)	Acc (m/s^2)
550 kN/m	Soft	1480	0.0015	245.8
	Hard	2490	0.0024	451.4
4400 kN/m	Soft	2150	0.0012	192.4
	Hard	3620	0.0025	372.5

Caption: Table 1. Model predicted helmet-head contact force (Fc), maximum skull-brain displacement (Ds), and maximum brain acceleration (Acc) as a function of different helmet properties.

References: [1] Monea AG et al. 2012. J Neurotrauma 29:2305-17.

[2] Stalnaker, R.L. et al. 1971. ASME Paper No. 71WA/BHF-10;

Disclosure of Interest: None Declared

Impact

PO-0102

THE INFLUENCE OF IMPACT DIRECTION ON BRAIN TISSUE RESPONSE FROM REAL-WORLD HUMAN PCS INJURY RECONSTRUCTIONS

Marshall Kendall [1,*]Andrew Post [1]Janie Cournoyer [1]Thomas Blaine Hoshizaki [1]Michael D. Gilchrist [2]Susan Brien [3]Shawn Marshall [4]

[1]Human Kinetics, University of Ottawa, Ottawa, Canada, [2]University College of Dublin, Dublin, Ireland, [3]Hull Hospital, Gatineau , [4]Ottawa General Hospital, Ottawa, Canada

Introduction and Objectives: Persistent post-concussive syndrome (PCS) is a major concern as it leads to long term disability and lost productivity. In a clinical setting, PCS is characterized by long term symptoms (6 weeks +) that are representative of mechanical damage to tissues in regions of the brain that are responsible for the affected brain functions. It is possible that PCS injury is affected by impact direction as brain tissue is anisotropic and inhomogenic by nature and directional dependency of brain tissue damage in anatomical research has been shown [1]. This anatomical research has yet to be quantified in real-world human PCS cases. Thus, the purpose of this study is to investigate the influence of impact direction on the location of the peak magnitude of strain within the brain for real-world human PCS reconstructions cases.

Methods: Subject data collection for the PCS cases took place at three hospitals in Canada. Fourteen PCS cases were used for reconstruction of which: eight were in the rear direction, four in the frontal direction, and two in the side direction. Subject inclusion criteria for this study required; PCS symptoms lasting longer than six weeks with no lesions evident on medical imaging. The injury cases in this study resulted from three mechanisms of injury (falls, collisions, and projectiles) and were thus reconstructed using a monorail for falls, linear impactor for collisions, or pneumatic ball launcher for projectiles. A Hybrid III headform instrumented with a 3-2-2-2 accelerometer array was impacted under conditions as described. The three-dimensional linear and angular acceleration loading curves were used as input for the University Dublin Brain Trauma Model (UCDBTM) in order to calculate brain tissue responses (MPS). The UCDBTM was analyzed according to nine regions of the brain linked to PCS symptomology. The influence of impact direction was characterized in MPS and compared using an ANOVA.

Results: The largest magnitude MPS value for each impact direction occurred in a different location of the cerebrum (Table 1). Statistical analysis for the frontal impacts reported no significant differences between location of the largest magnitude MPS and values in the other locations of the cerebrum. Significant differences were found in rear impact direction where the peak magnitude MPS were larger than those values reported in the other areas of the cerebrum ($p < 0.05$). Significant differences were found between the location of the peak MPS for side impacts (Primary somatosensory cortex) and the values in the Prefrontal cortex and Visual cortex ($p < 0.05$). Overall, there was no significant difference between the peak MPS in the cerebrum between the three impact directions ($p > 0.05$).

All PCS cases clearly demonstrated brain tissue deformation values above the 50% risk of concussive injury threshold for the entire cerebrum (MPS 0.19) [3]. This result may be characteristic of PCS in these cases, where large strain fields in

the brain would cause a multitude of symptoms, and the large strains may indicate severity in terms of duration of ill effects.

Figure:
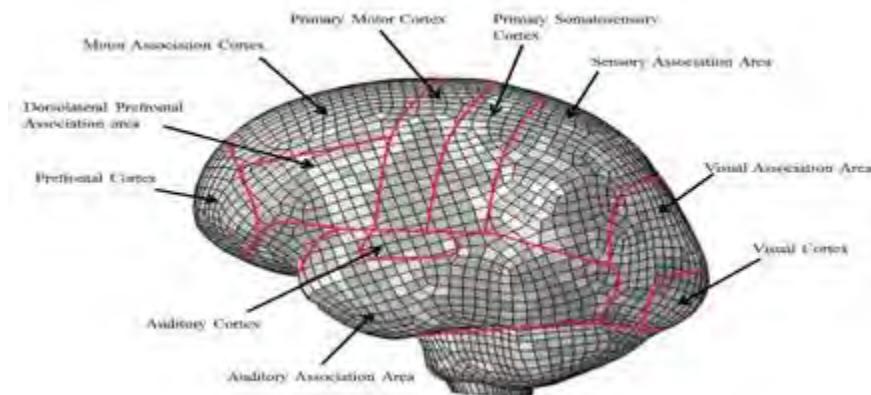
Caption: Figure 1. Image of the UCDBTM segmented into regions for analysis.

Conclusion: This study investigated whether impact direction influenced the location of MPS in the brain from real-world PCS injury reconstructions. Maximum principal strain between impact directions was not found to be significantly different. In addition, while where the peak MPS was located in the brain was different, this was inconsequential in terms of risk of injury because the strain levels were so high throughout the entire cerebrum. These results suggest that for these PCS cases, the characteristics of the impact were so severe that factors such as impact direction may not have been influential in the location of peak strain that might have been able to indicate symptoms of PCS.

Table:

Impact Direction	MPS for nine requions of the cerebrum								
	1	2	3	4	5	6	7	8	9
Front	0.454 (0.199)	**0.488 (0.254)**	0.435 (0.214)	0.454 (0.222)	0.423 (0.049)	0.332 (0.056)	0.234 (0.034)	**0.488 (0.126)**	0.289 (0.072)
Back	**0.531* (0.074)**	0.441 (0.054)	0.405* (0.038)	0.431 (0.071)	0.401* (0.134)	0.334* (0.061)	0.247* (0.058)	0.440 (0.085)	0.269* (0.036)
Side	0.261* (0.131)	0.430 (0.231)	0.342 (0.161)	0.458 (0.235)	**0.519* (0.269)**	0.369 (0.240)	0.302 (0.197)	0.333 (0.202)	0.186* (0.108)

Caption: Table 1. Maximal principle strain for nine regions of the cerebrum resulting from impacts in the front, back and side direction.

References: [1] Prange et al. 2002. Defining brain mechanical properties: Effects of region, direction and species. 44th Stapp Car Crash Conf.

[2] Post A. 2013. The influence of dynamic response characteristics on traumatic brain injury. PhD thesis, University of Ottawa.

[3] Kleiven, S. 2007. Predictors for traumatic brain injuries evaluated through accident reconstructions. Proc. of the 51st Stapp Car Crash Conference, San Diego, CA, pp. 81-114.

Disclosure of Interest: None Declared

PO-0103

COURT SURFACE EFFECT AND PLANTAR LOADING ASYMMETRY DURING A BASKETBALL JUMPSHOT LANDING

Darren Z. Nin [1,*]Raymond Quek [1]Pui Wah Kong [1]

[1]Nanyang Technological University, Singapore, Singapore, Singapore

Introduction and Objectives: Basketball is a sport which places a considerable amount of stress on the lower extremities of players and an inability to attenuate these forces might lead to injury[1]. Outdoor (asphalt) and indoor (wood) playing surfaces have different cushioning properties which might affect the level of attenuation from impact forces during landing movements. Previous studies have examined the impact attenuation properties of different playing surfaces (e.g. grass, artificial turf) for a variety of sports[2, 3] but less is known about basketball court surfaces.

Movements such as the jumpshot result in a double-leg landing and it has been assumed that the bilateral symmetry of such a landing reduces the risk of lower limb injury.[4] There are, however, no available data of plantar loading between the two feet in basketball-specific movements. Therefore, the purpose of this study was to investigate the court surface effect and bilateral asymmetry in plantar loading variables during the landing of a basketball jumpshot.

Methods: Thirteen university basketball players (23.0 ± 1.4 years, 1.75 ± 0.05 m, 68.4 ± 8.6 kg) were recruited for this study. The Novel Pedar-X system (Novel GmbH, Munich, Germany) with 99 sensors within each insole was used to measure plantar loading. A randomised cross-over design was used. Each participant performed 10 trials of a basketball jumpshot on an ashpalt- and wood-surface basketball court from the free-throw line. Trials were considered valid if (i) the shot was successful, (ii) the ball made contact with the rim or (iii) the ball made contact with both the back-board and the rim. The jumpshot landing steps were analysed using the Novel Pedar-X Step Analysis software (Novel GmbH, Munich, Germany). The shooting side was defined as the leg on the same side of the shooting arm. The three variables recorded from the software were peak force (PF), peak pressure (PP) and pressure-time integral (PTI). A predefined mask of eight regions, created using the Novel Multimask software was applied to obtain the values of each region for PF, PP and PTI. Variables were compared using a two-way repeated measures ANOVA (court surface × side) ($\alpha = .05$). Post-hoc analysis was conducted with Bonferroni-correction for significance level.

Results: When landing from a jumpshot, there was no difference in any plantar loading variables between the asphalt- and wood-surface courts. Bilateral asymmetry was observed in some variables. PF was higher at the medial forefoot (21.8%, $p = .038$) and heel (39.1%, $p = .002$) in the non-shooting than shooting sides. PP was higher at the heel (10.8%, $p = .001$) while PTI was higher for the whole foot (35.5%, $p = .021$), at the hallux (47.8%, $p = .021$), lateral arch (50.6%, $p = .009$) and heel (62.1%, $p = .020$) in the non-shooting side. A significant court surface × side interaction (show p-value) for PP was found at the lateral arch (Figure 1). Post-hoc analyses did not reveal any significant pairwise comparisons.

Figure:
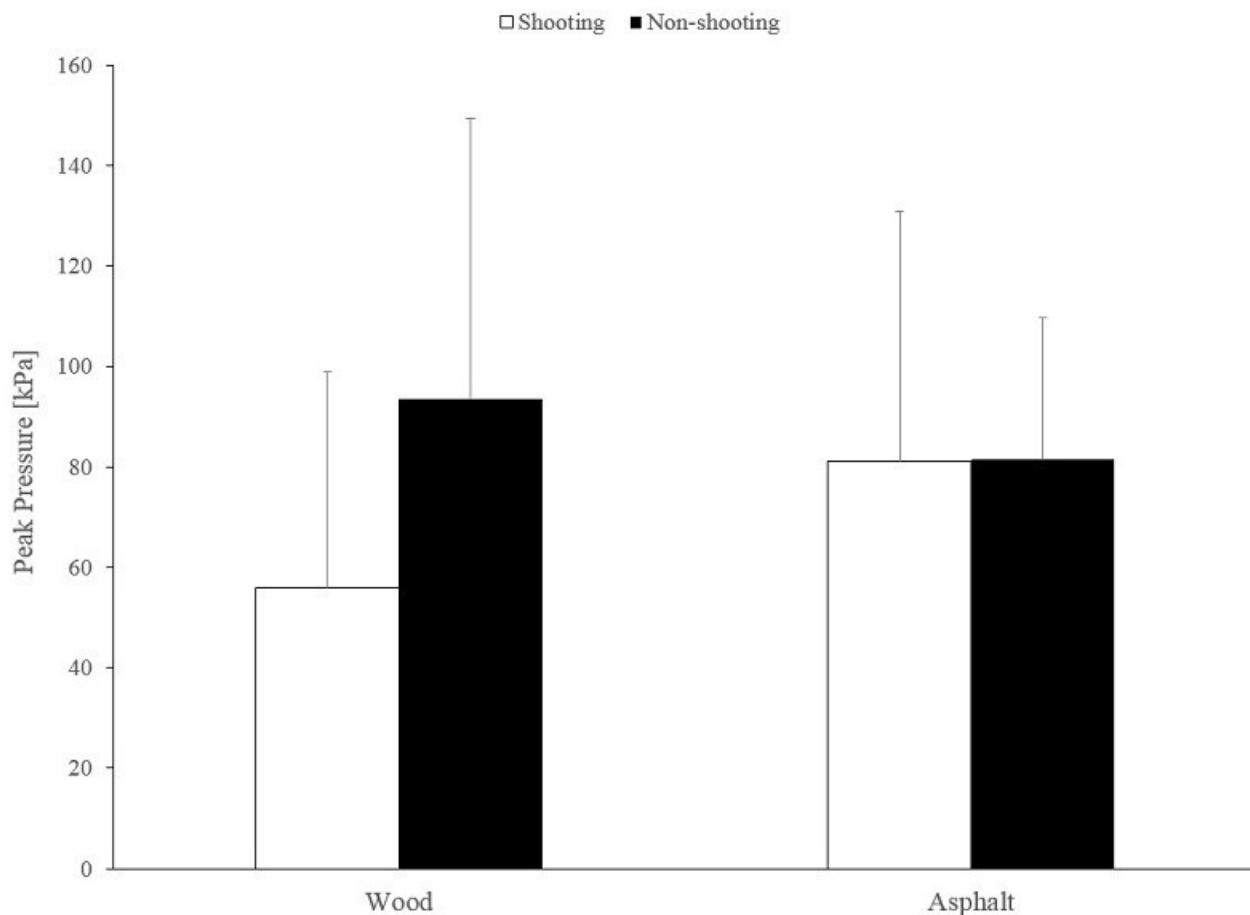
Conclusion: The foot loading associated with landing from a jumpshot did not differ between asphalt and wood surfaces. This suggests that playing surface does not have an effect on impact force attenuation during landing. Players and coaches should be aware of the loading asymmetry between the shooting and non-shooting side, predominantly at the heel region. Future studies could investigate whether this asymmetry is associated with lower limb injuries.

References: [1] McClay et al., J Appl Biomech, 10: 222-236, 1994.

[2] Dragoo et al., The Knee, 20: 191-195, 2013.

[3] Fuller et al., Br J Sports Med, 41: 20-26, 2007.

[4] Wang H K & Cochrane T., J Sports Med Phys Fitness, 41: 403-410, 2001.

Disclosure of Interest: None Declared

LEG DOMINANCE DIFFERENCES EXIST IN MUSCLE ACTIVATION PATTERNS IN PRE- OR EARLY-PUBESCENT SOCCER PLAYERS PERFORMING UNANTICIPATED SIDE-CUTS: RELEVANCE TO NON-CONTACT ACL INJURIES.

M J Del Bel [1,*]M L Jones [1]A K Fairfax [1]K Steele [1]S C Landry [1]

[1]Acadia University, Wolfville, Canada

Introduction and Objectives: It has been well established that female athletes have an increased risk of sustaining a non-contact ACL injury in sport compared to males. The increased occurrence of ACL injuries in females may be influenced by neuromuscular patterns at the knee joint that are not yet fully understood. Studies examining sex/leg differences in the muscle activity of muscles surrounding the knee joint have typically focused on athletes competing at the high school or collegiate level (1). This study set out to identify if sex and/or leg dominance differences exist in male and female soccer players under the age of 12 years, while performing unanticipated side-cut maneuvers on artificial turf.

Methods: Neuromuscular patterns during the stance phase of 45o side-cut maneuvers were analyzed under unanticipated conditions to closely emulate a true game-like scenario where non-contact ACL injuries most likely occur. Thirty-four youth soccer players (17 male and 17 female) with no history of lower limb injuries had muscle activity measured for the following muscles: lateral and medial gastrocnemii, lateral and medial hamstrings, and vastus lateralis and medialis. Mean muscle activation waveforms during the stance phase of the cutting stride were amplitude normalized to a series of maximal voluntary isometric contractions. Principal component analysis was performed on the individual mean waveforms of each athlete, with PC1 and PC2 capturing differences in overall magnitudes and phase shifts, respectively. A two-way mixed model ANOVA was used to test for sex, leg or interaction effects.

Results: Significant findings ($p \leq 0.05$) were found in five of the six muscles tested. All significant differences found were leg effects with both sexes displaying i) greater activation magnitudes in their dominant leg compared to their non-dominant leg for the lateral gastrocnemius, lateral and medial hamstrings, and vastus lateralis muscles and ii) earlier peak activations in their non-dominant leg compared to their dominant leg for the lateral and medial gastrocnemii, medial hamstrings and vastus lateralis muscles. No differences were observed in the vastus medialis or between sexes.

Conclusion: Few studies have evaluated neuromuscular differences between legs in athletes performing unanticipated side-cut maneuvers. It has been demonstrated that in older populations (ages 14-38), females are more at risk of injuring the ACL in their non-dominant leg, while males are more likely to injure the ACL in their dominant leg (2). Both males and females in this study displayed similar differences with respect to leg dominance, suggesting that leg differences are not influenced by sex in a young population. Furthermore, it has generally been reported that female collegiate athletes, compared to males, display greater activation magnitudes in the vastii muscles, potentially putting them more at risk of sustaining an ACL injury. However, in the population in this study, there were no sex differences found in neuromuscular patterns of muscles crossing the knee joint. Conclusion: Completing further studies considering sex and leg dominance differences could provide additional insight into the mechanisms behind non-contact ACL injuries. It is essential to determine how muscle activity across the knee joint occurs in a population that rarely experiences non-contact ACL

injuries and where no sex-bias is present (3) to help improve injury prevention programs aimed at reducing the rate of non-contact ACL injuries.

References: Reference 1

Benjaminse et al. (2011) What is the true evidence for gender-related differences during plant and cut maneuvers? A systemic review. Knee Surg. Sport Tr. A., 19, 42-54.

Reference 2

Brophy et al. (2010) Gender influences: the role of leg dominance in ACL injury among soccer players. Br. J. Sports Med., 44, 694-697.

Reference 3

Barber-Westin et al. (2006) Jump-land characteristics and muscle strength development in young athletes: A gender comparison. Am. J. Sports Med., 34, 375-385.

Disclosure of Interest: None Declared

PO-0105

SEX AND AGE EFFECT ON MUSCLE ACTIVITY PATTERNS IN THE DOMINANT AND NON-DOMINANT LEGS OF EARLY PUBESCENT AND POST-PUBESCENT SOCCER ATHLETES DURING THE PERFORMANCE OF UNANTICIPATED SIDE-CUT MANEUVERS: IN RELEVANCE TO NON-CONTACT ACL INJURIES

Kendal Steele [1,*] Michelle Jones [1] Michael Del Bel [2] Alana Fairfax [1] Scott Landry [1]

[1]School of Kinesiology, Acadia University, Wolfville, [2]School of Human Kinetics, University of Ottawa, Ottawa, Canada

Introduction and Objectives: Recent studies regarding non-contact ACL injuries show that female athletes have a significantly increased risk of sustaining this injury in sport compared to their male counterparts (1). During puberty, it has been suggested that females undergo unfavorable alterations in their neuromuscular control patterns that can lead to an increased risk of ACL injuries (5). Previous research has also shown that female athletes are twice as likely to tear their ACL in their dominant leg as opposed to their non-dominant leg (2). This study set out to identify if sex differences exist in male and female soccer athletes at two different age groups: under 12 year old male and female athletes (U-12), and above 17 year old male and female athletes (AB-17) in unanticipated side-cutting conditions.

Methods: All athletes, 20 males and 16 females (U-12) and 20 males and 19 females (AB-17), had no history of major lower limb injuries. Participants performed 45 degree unanticipated side-cut maneuvers, at 75% of their maximum speed, on an artificial turf surface. Unanticipated conditions were used to simulate a true game-like scenario, where non-contact ACL injuries are most likely to occur. Neuromuscular control patterns were recorded and analyzed during the stance phase of the side-cut maneuvers for the vastus lateralis (VL) and medialis (VM), lateral (LH) and medial hamstrings (MH), and lateral (LG) and medial gastrocnemius (MG). A series of maximal voluntary isometric contractions were used to normalize the magnitude of muscle activation waveforms during the side-cut maneuvers. A separate principal component analysis (PCA) was performed on each of the different muscle groups, with a two-way ANOVA being used to test for a sex, age and interaction effect on both the dominant and non-dominant leg of the athletes.

Results: Significant differences ($p \leq 0.05$) were identified in all six muscles tested for the dominant leg. AB-17 athletes had greater magnitudes (PC1) than U-12 athletes for all six muscles. AB-17 athletes had earlier peak muscle activity (PC2) compared to U-12 athletes in the MH. All female athletes demonstrated greater magnitudes in the VM and earlier peak activity in the VM and VL compared to males. For the VL of the dominant leg, there was an interaction effect for phase shift, where AB-17 males peaked earlier than AB-17 females.

Significant differences ($p \leq 0.05$) were found in four of the muscles tested for the non-dominant leg. AB-17 athletes had greater magnitudes than U-12 athletes in the LG, MG, and MH. AB-17 athletes had earlier peak muscle activity compared to U-12 athletes in the LG and MG. U-12 athletes had earlier peak muscle activity compared to AB-17 athletes in the VL. AB-17 female athletes, and U-12 male athletes peaked earlier than their sex counterparts for the VM. Both groups of female athletes showed greater magnitudes than male athletes for the LG and VL.

Conclusion: Research has shown that female athletes display greater magnitudes of activation in the vastus medialis and lateralis than their male counterparts (4). In this study, AB-17 athletes displayed greater magnitudes for all muscles in the dominant leg and in three of the muscles for the non-dominant leg. This finding requires further investigation but the

increased activity level required to execute the cutting maneuvers in post-puberty athletes could lead to greater strains on the ACL in this population who are at greater risk of injury. A sex effect was apparent as females demonstrated significantly greater magnitudes in the VM of the dominant leg and in the LG and VL of the non-dominant leg. These findings combined with joint loadings and body positioning during the maneuvers could help explain the higher incidence of ACL injuries seen in the AB-17 female athletes. Activation of both the gastrocnemii and vastii muscles without appropriate activation of the hamstring muscles has previously been shown to increase the strain on the intact ACL, while a balanced synergistic activation between muscle groups is essential in protecting the ACL from injury (3).

Future studies considering each of the factors presented in this study (sex, age, leg dominance) will provide additional and important insight into the mechanisms behind non-contact ACL injuries and why collegiate female athletes are more prone to injuring their ACL. It is essential to determine what neuromuscular patterns are occurring in a population before puberty, allowing researchers to further understand how neuromuscular patterns change as an individual ages and how prevention programs can be developed to help reduce the incidence of this devastating injury post-puberty.

References: [1] Agel et al., *Am. J. of Sports Med.,* 33(4): 524-531, 2005.

[2] Hewett et al., Am. J. Sports. Med., 33(4): 492-501, 2005.

[3] Li et al., J. of Biomech., 32(4): 395-400, 1999.

[4] Malinzak et al., *Clin. Biomech.,16*: 438-445, 2001.

[5] Renstrom et al., *Br. J. of Sports Med.*, 42: 394-412, 2008.

Disclosure of Interest: None Declared

Injury

PO-0106

FATIGUE PROGRESSION CAUSES A TRANSITION FROM SOFT TO STIFF LANDING

Mianfang Ruan [1,*]Qiang Zhang [2]Xie Wu [3]

[1]Physical education, Ningbo University, Ningbo, [2]Kinesiology, Shanghai University of Sport, [3]kinesiology, Shangh University of Sport, Shanghai, China

Introduction and Objectives: Although tremendous research efforts have been made to understand risk factors for noncontact ACL injuries [1] and a few prevention programs have been developed, the annual incidence of ACL injuries has increased by 1.3% in jump-landing sports [2] and the magnitude of the difference between male and female athletes has remained constant or even widened [3], which suggests that critical risk factors in ACL injury may have been ignored [4]. Most ACL injuries occur in the late phase of the match [5] and landing biomechanics showed significant changes throughout fatiguing. However, the changes in landing biomechanics associated with fatigue are inconsistent in the literature which may be due to distinct fatigue protocols. Considering that the neuromuscular fatigue is a progressive process and there is no standardized fatigue level in studies, the prefatigue-postfatigue testing model, which was used in most studies, may be another factor contributing to controversial results in the literature. This study aimed to investigate the progressive changes in landing biomechanics during a fatiguing exercise protocol.

Methods: Nine females and nine males were recruited to perform landing tasks throughout the fatigue protocol. A variety of movements including sidestep cutting, running, pivoting and jumping were incorporated in the fatigue protocol. The subject was requested to stand in the center of a 6 m diameter circular region and six lights were equally placed on the circle. When a light was illuminated randomly by a program, the subject ran to touch the active light to turn it off and trigger illumination of next lights. Males chased a series of 35 lighting intervals and females completed a series of 25 lighting intervals, followed by 8 CVJ trials to complete one fatigue drill cycle. Pilot testing revealed this would ensure both male and female subjects achieve the severe fatigue (SF) level in approximately 9 sets, which would take approximately 40 minutes. The average jumping height of the last 3 jumps was used to calculate the reduction of jumping height compared to the pre-fatigue (NF: no fatigue) jumping height. The medium fatigue (MF) level criterion was a reduction of 20% in jumping height and the severe fatigue (SF) criterion was a reduction of 30%. The fatigue drill was repeated until that threshold was met. At that point, the drop landing test was applied. Three-dimensional lower-limb-joint kinematics and kinetics during the drop landing testing were recorded by a 16-camera motion analysis system (100 Hz, Vicon Motion Analysis Inc., Oxford, UK) and two force platforms (1000 Hz, Kistler Instruments AG Corp., Winterthur, Switzerland) simultaneously during the testing. A 2-way (fatigue level × gender) mixed-design analysis of variance (ANOVA) was performed to determine any significant effects and interactions of fatigue levels and gender. A Bonferroni *post hoc* analysis was applied for further evaluation when a main effect was present. The αlevel was set at .05.

Results: Non-progressive patterns were observed: landing duration time (main fatigue effect, P= .007), peak knee flexion angle (main fatigue effect, P= .001) and peak hip flexion angle (main fatigue effect, P= .039) increased, and knee joint stiffness (main fatigue effect, P= . 033) decreased from NF to MF and all remained unchanged from MF to SF. Reversal patterns were observed: peak ankle dorsiflexion angle (main fatigue effect, P= .001) increased and then decreased from

NF to MF to SF, whereas peak VGRF (main fatigue effect, P= .001) and peak hip extension moment (main fatigue effect, P= .001) decreased and then increased across fatigue levels. Peak hip abduction angle (fatigue *gender, P= .021) in female subjects at SF was less than it at NF and MF, but this parameter in male subjects was not influenced by fatigue.

Figure:
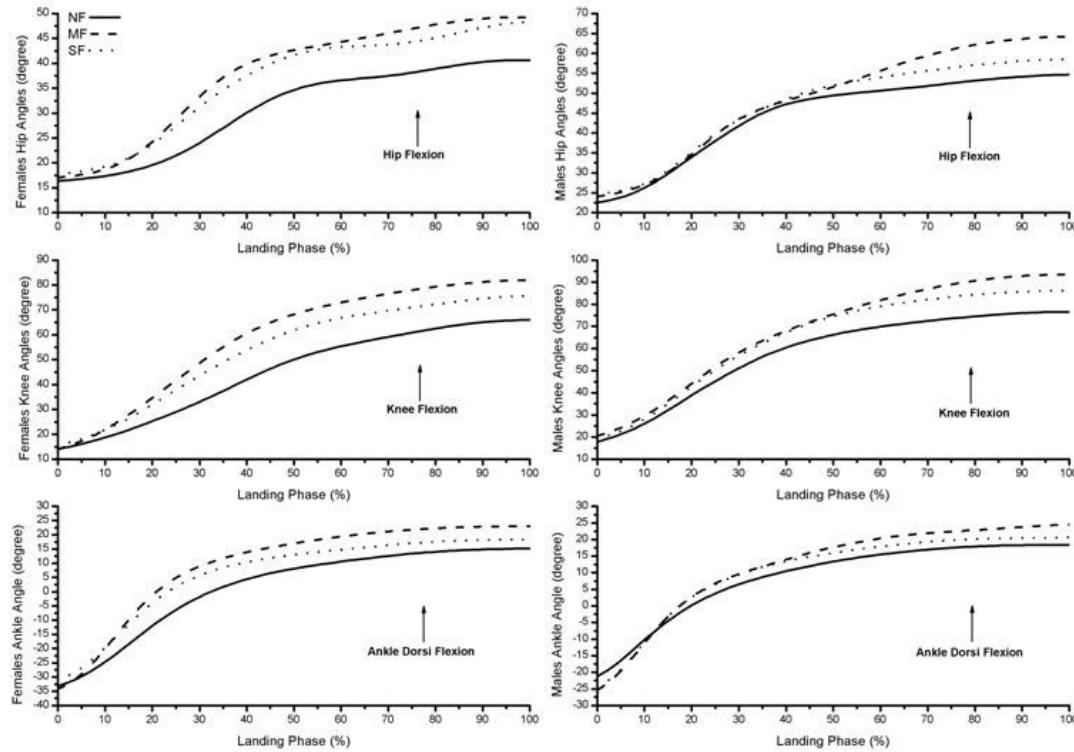
Caption: Figure 1.The time history of hip, knee, and ankle joint in sagittal plane during landing for females (left) and males (right).

Conclusion: Over all, we observed non-progressive or reversal patterns in landing biomechanics during fatigue progression. The results indicated that fatigue progression would cause a transition from soft to stiff landing, which could eventually increase ACL injury risk. Additionally, fatigue may potentially further increase females' risk in ACL injury.

Table:

	Females				Males		
	NF	MF	SF		NF	MF	SF
Landing Duration Time β	0.13±0.04	0.20±0.06	0.18±0.05		0.20±0.09	0.21±0.06	0.23±0.06
Knee Joint Stiffness Index β	4.07±0.35	3.39±0.61	3.91±0.93		3.66±1.17	3.08±0.72	3.19±0.47

β Denotes statistically significant difference between NF and MF

Caption: TABLE 1. The landing time (s) and knee joint stiffness index (/body mass) at different fatigue levels.

References: 1. Yu, B. et al., Br J Sports Med, **41 Suppl 1**: 47-51.2007.

2. Alentorn-Geli, E., et al., Knee Surg Sports Traumatol Arthrosc, **17**: 705-729. 2009.

3. Agel, J., et al., Am J Sports Med, **33**: 524-530,2005.

4. McLean, S.G., et al., Med Sci Sports Exerc, **39**:502-514.2007

5. Hawkins, R.D. et al.,Br J Sports Med, **32**:326-332.1998

Disclosure of Interest: None Declared

PO-0107

INVESTIGATION OF THE BIOMECHANICS OF BRUISING

Heather Black [1,*]Niamh NicDaéid [2]Philip Riches [1]

[1]Biomedical Engineering, University of Strathclyde, Glasgow, [2]Centre for Anatomy and Human Identification, University of Dundee, Dundee, United Kingdom

Introduction and Objectives: In legal cases involving physical injury, assessment of bruising can prove vital. Yet the mechanics of bruise formation and whether force of impact or age of injury can be inferred from bruise appearance, are not completely understood. One study is currently known to have focussed on the mechanical parameters of bruise formation [1]. Impact stresses of 1720 kPa to 5560 kPa were applied to one person, finding that increased tissue stiffness did increase the likelihood of bruising. Red, green and blue (RGB) value tracking has been used to quantify bruise analysis with little success, although showing potential [2, 3]. Infrared (IR) and ultraviolet (UV) wavelengths have also shown limited success [4]. Such colour analyses have not yet been related to the stress required for bruise formation, thus this study investigates the biomechanics of bruise initiation, RGB value tracking and use of IR and UV for bruise analysis.

Methods: Using custom built apparatus, three impact forces were generated by dropping a 2.7 kg mass from heights of 3, 4 and 5 cm onto an impactor resting on the forearm of 5 volunteers. An accelerometer (MicroStrain®, G-Link®, Wireless Node) was attached to the mass and its recordings used to derive the impacting pressure, displacement and tissue stiffness for each impact. Colour, IR and UV images were taken prior to impact and then daily for up to 2 weeks. The colour images were standardised and RGB values for each bruise obtained.

Results: Average impact stresses were 679.24±115.94 kPa, 577.61±95.98 kPa and 619.99±76.25 kPa for the 5 cm, 4 cm and 3 cm drop heights respectively. Unexpectedly, constant pressures were not recorded for each drop height. This was primarily due to the anatomical variation of impacting location.

Displacement varied with drop height and position with significant intra- and inter-subject variation. Skin displacement generally decreased from proximal to distal areas while tissue stiffness increased. Increased tissue stiffness was also observed as drop height increased.

For each drop height, both red (Fig. 1a) and green values followed a similar pattern inter- and intra-person. Blue values followed an intra-person pattern only (Fig. 1b). These patterns indicate colour timelines may be reproducible and comparable.

Colour photography provided clearest contrast between skin and bruise. IR failed to provide positive results while UV showed minor contrast between skin and bruise. Neither IR nor UV detected bruising once no longer visible to the naked eye. Skin tone influenced all imaging techniques and bruise appearance differed for all individuals.

Figure:
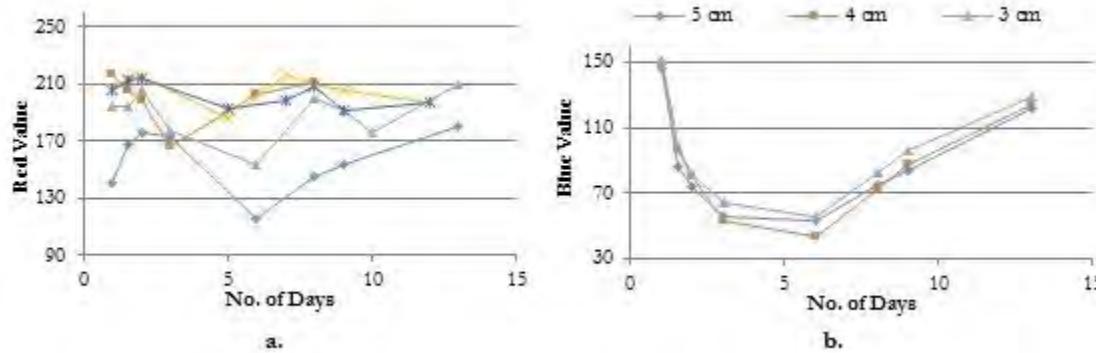
Caption: Figure 1. a. Example of red inter-person pattern b. Example of blue intra-person pattern

Conclusion: This study found that the mechanics of bruise formation and how impacting conditions influence bruising, could not be determined. RGB values could not be linked to impacting conditions, though did show potential. IR and UV imaging were not successful in bruise analysis.

Future work will aim to develop a repeatable and reliable method of bruise initiation, then use a larger group of volunteers to investigate bruise characteristics. If bruise biomechanics and colour development can be successfully understood, their use as evidence would cease to be subjective, thus having a major impact on forensic injury investigations.

References: [1] Desmoulin et al., J. Forensic Biomech, 2: 1-10, 2011.

[2] Georgieva et al., Comp Sys Tech, 1-6, 2005.

[3] Grossman et al., Med Sci Law, 51: 170-176, 2011.

[4] Baker et al., J. Forensic Ident, 63: 103-125, 2013.

Disclosure of Interest: None Declared

Injury

PO-0108

KINEMATIC AND DYNAMIC BIOMECHANICAL VALUES IN RELATION TO MUSCLE ACTIVITY DURING CONTACT HEAD IMPACT

Ondrej Fanta [1,*]Karel Jelen [1]Daniel Hadraba [1]Richard Billich [1]

[1]Department of Anatomy and Biomechanics, Faculty of Physical Education and Sport, Charles University in Prague, Praha 6, Czech Republic

Introduction and Objectives: For the evaluation of neck injury the relative distance was observed between a marker placed on the forehead and a marker placed on the shoulder and also by change of the angle. To compare the severity of head injury a value of maximum head acceleration was used, HIC and a 3 ms criterion. All criteria were related to the activity of musculus sternocleidomastoideus and musculus trapezius in a situation of expected or unexpected contact impact.

Methods: The situation was recorded using a Qualisys system, head acceleration of probands in three axes was recorded using the accelerometer, activity of neck muscles was monitored by a mobile EMG.

Results: Maximum head acceleration was 5.61 g for non-visual and 5.03 g for visual. HIC36 was 6.65 non visual and 5.97 for visual. 3-ms criterion was 5.37 g for non-visual and 4.89 g for visual and max. force was 291 N for non-visual and 314 N for visual. The average time of muscle activation of the observed group without visual perception is 0.355 s after hitting an obstacle, with visual perception 0.085 s before the crash.

Conclusion: Kinematic values indicate more favourable parameters for neck injuries for visual. Head injury criteria show an average decrease of about 10% for visual. We can conclude that the visual perception means a significant increase in pre-activation of the observed muscle group of almost 745 % and lower activation in following phase of approximately 90 %.

Disclosure of Interest: None Declared

PO-0109

IS THE 45 DEGREE LAB-BASED SIDE-CUT TASK EVER ACHIEVED? IMPLICATIONS FOR ACL INJURY RISK SCREENING

Grace Smith [1,*] Mark Robinson [2] Jos Vanrenterghem [2]

[1]Sport and Exercise Sciences, University of Chester, Chester, [2]Research Institute for Sport and Exercise Sciences, Liverpool John Moores University, Liverpool, United Kingdom

Introduction and Objectives: The side step cutting manoeuvre has been used extensively as a screening tool for ACL injury risk in laboratory-based biomechanical research. Rapid decelerations in single-leg support, combined with a change in direction, generate high joint loading and have been identified as a common mechanism of noncontact ACL injury in athletes during game situations. A variety of approach speeds and cutting angles have been reported, possibly reflecting the diverse range that athletes will perform during a game [1]. Whilst the 45 degree side step cut has been used more extensively than other angles, there has been little evidence that this task is actually being achieved in a lab-based environment. However, a clear trade-off between task achievement and mechanical loading with increasing running speed in a 45 degree cut has been reported previously [2]. The purpose of the present study was to investigate task achievement of a side cut at different cutting angles: 45, 90, 135 and 180 degrees.

Methods: Ten male footballers (20.6 ± 0.8 years; 182.0 ± 6.5 cm; 73.9 ± 4.3 kg) performed five trials of an anticipated side cut in each cutting angle condition. Angles of 45, 90, 135 and 180 degrees were marked on the floor with tape and subjects were asked to follow these lines. A run-up speed of 3.45 – 4 ms^{-1} was required, monitored using timing gates/ Kinematic data were recorded using 10 opto-electronic cameras (Oqus 300, Qualisys, 250 Hz) and 44 reflective markers [3]. Each side cut was completed on a Kistler force platform (9287C, Kistler Instruments Ltd, 1500 Hz). Marker and force data were filtered using a 4th order low pass Butter-worth filter with a cut off frequency of 18 Hz and analysis was undertaken in Visual 3D (v.4.83, C-Motion). For the evaluation of task achievement, a one-way repeated measures ANOVA (α=0.05) was used to determine statistical differences between COM velocity, transverse plane angle of progression, contact time, and peak horizontal and medio-lateral ground reaction forces [2].

Results: Only the 45 degree cutting task was performed at the prescribed touchdown running speed, other cutting angle tasks were performed significantly slower (Table 1). The prescribed change in angle was not achieved during the observed support phase by any of the four tasks, with the actual cutting angle deviating from the prescribed angle by up to 34 degs. The inability to achieve the required change may be explained by the significantly lower contact times. For side cuts that require a larger change of direction, this comes with a clear trade off in the velocity of the athlete. As participants had to slow down substantially before touchdown, they were unable to perform a 180 degree turn at high velocities. Peak posterior GRFs were significantly lower for the 45 degree cutting task, but peak medial GRFs were different between all cutting task conditions, demonstrating that each task elicited different GRF loading responses.

Conclusion: In none of the conditions was the task achieved, both in terms of obtaining the required velocity and change, in agreement with some previously reported data on task achievement [2]. This questions whether these lab-based tasks can suitably mimic the changes in directions experienced in real-time competition situations, which likely occur at higher

and varying approach velocities. Previous studies have failed to standardize cutting angle or speed of task execution, raising questions about the legitimacy about the task.

The successful execution of a side stepping task is dependent on cutting angle, however for a 45 degree side cut, the change in angle achieved is far from 45 degrees. If clinicians are to move towards a gold-standard method of ACL injury risk screening, which will inevitably require a task which mimics competition situations, they must be aware that the side cutting protocol needs standardizing and task achievement needs assessing.

Table:

Variable	45°	90°	135°	180°	F	p
Touch-down speed (m s $^{-1}$)	4.87± 0.53	3.46± 0.27	2.70± 0.30	2.67± 0.25	79.8	<0.001***
Toe-off speed (m s $^{-1}$)	4.5 ± 0.62	2.81± 0.23	2.00± 0.11	1.78± 0.24	108.2	<0.001***
Touch-down angle (deg)	10.1 ± 2.4	10.7 ± 2.7	6.7 ± 3.0	1.4 ± 1.4	36.7	<0.001*
Toe-off angle (deg)	30.9 ± 3.7	67.0 ± 3.5	127.4± 9.8	169.7± 4.3	1243.2	<0.001*
Actual cutting angle (deg)	20.6 ± 4.2	56.3 ± 5.1	120.5±12.2	168.4±5.3	1036.5	<0.001*
Contact time (s)	0.21± 0.02	0.33± 0.04	0.47± 0.05	0.49± 0.06	98.3	<0.001***
Peak posterior GRF (N/kg)	12.1 ± 1.5	15.0 ± 1.9	15.8 ± 0.8	15.8 ± 0.9	18.4	<0.001**
Peak medial GRF (N/kg)	11.8 ± 1.2	10.4 ± 1.8	4.8 ± 0.8	2.3 ± 0.6	225.5	<0.001*

*Indicates all cutting angles significantly different from each other **45 significantly different from other angles ***All cutting angles significantly different with the exception of 135° to 180°

Caption: Table 1. Mean ± SD Task achievement data for four side cutting angles.

References: [1] Bloomfield et al., J. Sports. Sci. Med., 6: 63-70, 2007.

[2] Vanrenterghem et al., J. Biom., 45: 2444-49, 2012.

[3] Vanrenterghem et al., Gait Posture., 31: 517-21, 2010.

Disclosure of Interest: None Declared

Injury

PO-0110

ACL RECONSTRUCTION RESULTS IN INCREASED INSTABILITY DURING VISUAL FEEDBACK OF MULTIDIRECTIONAL FORCE PRODUCTION.

Amelia A. Lanier [1 2,*] Thomas Buchanan [2 3]

[1]Biomechanics & Movement Science, University of Delaware, [2]Delaware Rehabilitation Institute, [3]Mechanical Engineering, University of Delaware, Newark, United States

Introduction and Objectives: After anterior cruciate ligament (ACL) rupture most will undergo reconstructive surgery. Within the first year after surgery 25% of patients will re-tear their ACL. Most of those injured attempt to return to sports which include running and cutting. The ability to produce appropriate ground reaction forces may be crucial for the successful return to sports without re-injury. Understanding stability of multidirectional ground reaction force (mGRF) production in healthy and ACL reconstructed (ACL-r) patients can lend insight to the high instance of re-injury. Typically, stability has been measured using linear analyses, but these analyses cannot capture the subtle time varying changes that can occur. Recently, research using nonlinear techniques, such as the Lyapunov exponent (LyE), have been able to overcome these issues. Recent studies using this measure to quantify the stability of knee flexion during gait found that there are significant increases in LyE measured after ACL injury and reconstruction when compared to healthy control subjects [1, 2]. The purpose of this study was to understand the ability of those with ACL reconstruction to produce specific mGRFs stably. We hypothesized that there would be more instability, noted by greater LyE values, after ACL reconstruction when compared to healthy uninjured controls. Secondarily, we hypothesized that LyE values measured during the medial/lateral (ML) task would be greater compared to the anterior/posterior (AP) task.

Methods: Our study included 7 (2M) healthy uninjured individuals and 2 (1M) who have undergone ACL reconstruction. We provided visual feedback of GRF production in the AP and ML direction to the subjects. Subjects stood on two force plates (AMTI OR-6) with a foot on each plate. Subjects were instructed to alternatively and continuously produce ±50 % of their max force in the AP or ML direction to the beat of a metronome set at 60 beats per minute. For the LyE analysis, AP and ML GRFs were the variables of interest. Calculating LyE requires two input parameters time lag (tau) and embedding dimension (m), used to transform the AP and ML GRF into phase space. Tau & m were calculated using an average mutual information (AMI) algorithm and global false nearest neighbor (GFNN) algorithm respectively. Once in this format maximum LyE was calculated using the Wolf algorithm. Detailed descriptions of the AMI, GFNN, and Wolf algorithms can be found in previously published work [3, 4]. Largest LyE in bits/sec was reported as it indicates maximum divergence/instability of force production.

Results: ACL-r subjects had larger LyE values when compared to healthy uninjured controls (Fig.1). Additionally, the uninvolved limb of ACL-r subjects exhibited larger LyE values when compared to healthy uninjured controls. When comparing the ML and AP task there were no differences in all three limbs: healthy, involved, and uninvolved (Fig.1). While there was instability between groups there was no instability specific to direction of force production.

Figure:
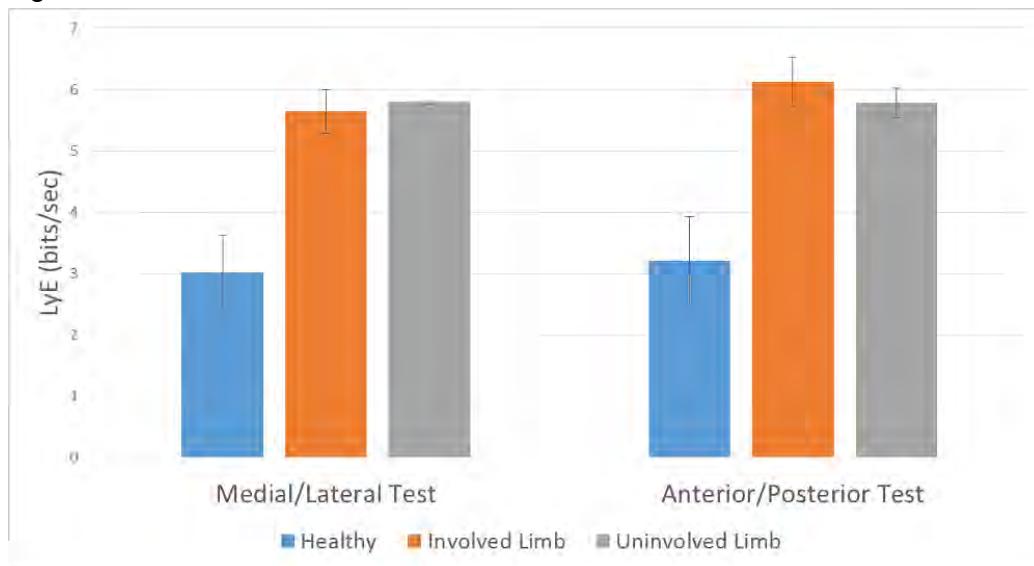
Caption: Figure 1: Avg. LyE ± SD (bits/sec) for healthy uninjured and ACL-r subjects. Lower values for LyE imply greater stability.

Conclusion: After ACL reconstruction, patients produce less stable multidirectional ground reaction forces when compared to healthy controls. Instability is present in both the AP and ML directions, suggesting this phenomena is not limited to a single direction. Given that the ACL primarily limits anterior tibial translation we initially predicted the AP direction would exhibit greater instability, however, this was not the case. Instability in both AP and ML directions may be a result of reduced proprioception and neuromuscular control commonly seen after ACL injury. Previous studies have observed reduced stability in ACL injured [1]and reconstructed[2] populations during gait using LyE analysis of knee flexion/extension, when compared to healthy controls. Interestingly, increased LyE values are present in both the involved and uninvolved limbs during both gait[2] and for the mGRF task performed in this study. For those who have undergone ACL reconstruction and plan to return to sport instability during GRF production may be an important factor contributing to re-injury. Approximately, 70% of ACL tears are noncontact which include activities like landing or cutting maneuvers. Instability when generating ML ground reaction forces may lead to reductions in performance and subsequent injury. Overall, after ACL reconstruction patients are unable to produce stable ground reaction forces, but this is not confined to the involved limb or direction (AP & ML). Instability during force production may be contributing to ACL injury as it may affect performance during cutting maneuvers.

References: [1] Stergiou et al., Clin Biomech, 19:957-963, 2004.

[2] Moraiti et al., Gait Posture, 32:169-175, 2010.

[3] Dingwell et al., Chaos, 10:848-863, 2000.

[4] Wurdeman et al., Ann Biomed Eng, 41:806-813, 2013.

Disclosure of Interest: None Declared

Injury

MECHANOMYOGRAPHIC DETECTION CAPABILITIES POST FATIGUE IN THE BICEPS BRACHII AGAINST THE BICEPS FEMORIS: A COMPARATIVE STUDY

Christian A. Than [1,*]Mark Gorelick [2]Mark Brown [1]

[1]School of Biomedical Science, The University of Queensland, Brisbane, Australia, [2]Department of Kinesiology, San Francisco State University, San Francisco, United States

Introduction and Objectives: Mechanomyography (MMG) is a developing analytical technique with the ability to assess the contractile properties of muscle non-invasively. Its capacity to quantify changes in muscle contractile performance suggests it might have utility as a clinical diagnostic tool. The aim of this study was to determine whether the MMG technique was sensitive to changes in muscle contractile properties following eccentric muscle injury in an upper (biceps brachii) and lower (biceps femoris) limb muscle.

Methods: 12 subjects (6 male and 6 female; mean age 24.3 ± 3.7yrs) were recruited and performed an eccentric exercise protocol to volitional cessation using their biceps brachii. A further 12 subjects (9 male and 3 female; mean age 21.1 ± 1.1yrs) performed a similar exercise protocol using their biceps femoris muscle. Subjects were monitored for 5 days total post exercise using MMG and psychological measurements of pain (VAS scores) to follow the onset of fatigue and recovery between the two groups.

Results: VAS scores in both groups significantly changed on day 2 post exercise, with resolution on day 4 for the biceps brachii group and no resolution in the biceps femoris group by the 6th and final day of the experiment ($P<0.05$). Contraction time of the biceps brachii was found to be significantly slowed post exercise on days 2 and 3 ($P<0.05$) while those in the biceps femoris group showed no significant change despite similar trends of slowing. Relaxation time of the biceps brachii group was found to be significantly slowed post exercise on days 2, 3 and 4 ($P<0.05$) while relaxation time in the biceps femoris group showed no significance.

Conclusion: MMG was able to detect changes in contractile properties in the biceps brachii group during the onset and resolution of muscular fatigue, but was not able to detect significant changes in the biceps femoris group. This could be in part attributed to the different fiber compositions of the two muscles, with the biceps femoris group consisting of a substantially higher number of slow twitch fibers that are fatigue resistant. Nevertheless, the MMG technique continues to show potential for clinical application in detecting muscular changes that may be beneficial for predictive, diagnostic or rehabilitative purposes.

Disclosure of Interest: None Declared

THE FATIGUE EFFECT IN ANTECIPATORY AND COMPENSATORY POSTURAL CONTROL IN FEMALES INDOOR SOCCER ATHLETES WITH ANKLE INSTABILITY

Thiago T. Teruya [1,*] Alex Sandra Oliveira Cerqueira [1] Vinicius Andre Soares [1] Julio Cerca Serrão [1] Luis Mochizuki [2] Alberto Carlos Amadio [1]

[1] School of Physical Education and Sport, [2] School of Arts, Sciences and Humanities, University of São Paulo, São Paulo, SP, Brazil

Introduction and Objectives: The ankle sprain a common injury in indoor soccer. This injury affect a sports and locomotion performance. Despite widely studied in biomechanics and motor control areas, the postural adjustments in people with a history of ankle sprain were few studied. The purpose of this pilot study was to analyze the anticipatory and compensatory postural control in female athletes soccer athletes.

Methods: 8 female college indoor soccer athletes were divided into 3 groups: functional instability (3 subjects), mechanical instability (2 subjects) and control (3 subjects). Before and after a fatigue protocol, 20 inversion movements were simulated on an inversion platform [1] on both legs and the electrical activity of the mm. tibialis anterior (TA), fibularis longus (FL), fibularis brevis (FB) and gastrocnemius lateralis (GL) were recorded. The root mean square (RMS) from two EMG epochs (the anticipatory, APA; and compensatory postural, CPA, adjustments) were calculated. The APA was defined as the interval between 200 ms before and 51 ms after start of the fall of the inversion platform. The CPA was defined as the interval between 51 and 251 ms after start of the fall of the inversion platform. The movement start of the inversion platform was measured with a 3D accelerometer. The raw EMG signal was demeaned, filtered (4th order 200hz Butterworth low-pass filter), and rectified. The analysis of variance (ANOVA) was applied to check de differences among the groups. The level of significance was 5%.

Results: APA: TA: There was not effect of fatigue ($F_{2,191}=0.3$ p=0.74), group ($F_{2,191}=2.4$ p=0.09) and interaction ($F_{4,191}=1.9$ p=0.10). FL: There was effect of group ($F_{2,191}=43.4$ p<0.001). The post hoc Tukey test showed that the control group showed the highest RMS; and it decreased after the fatigue protocol. FB: There was effect of group ($F_{2,191}=17.2$, p<0.001). The post hoc test Tukey showed that the mechanical instability presented the highest RMS. GL: There was effect of group ($F_{2,191}=12.6$ p<0.001), fatigue ($F_{2,191}=4.7$ p=0.01) and interaction ($F_{4,191}=5.7$ p<0.001). The post hoc test Tukey showed that for the mechanical instability presented the lowest RMS; and fatigue increased the RMS at the functional group.

CPA: TA: There was effect of group ($F_{2,191}=8.3$ p<0.001) and interaction ($F_{4,191}=3.0$ p=0.01) between group and fatigue. The post hoc test Tukey showed that the functional instability showed the highest RMS. FL: There was effect of group ($F_{2,191}=4.8$ p=0.009), fatigue ($F_{2,191}=4.7$. p=0.01) and interaction ($F_{4,191}=2.9$ p=0.02). The post hoc test Tukey showed that the RMS was higher in control group than mechanical instability group; and the RMS was lower in dominant leg after the fatigue protocol for the mechanical and functional instability group. FB: There was effect of group ($F_{2,191}=5.3$ p=0.006). The post hoc test Tukey showed that the mechanical instability showed the highest RMS. GL: There was effect of group ($F_{2,191}=28.5$ p<0.001). The post hoc test Tukey showed that the functional instability presented the highest RMS.

Conclusion: The ankle sprain simulation induces different muscle activation before and after the mechanical stimulus. The results suggest that postural control during APA and CPA is instability-dependent. For APA, the functional instability group presented the lowest activity of FL and FB; and the mechanical instability presented the lowest activity of GL. The fatigue decreased FL activity and increased GL activity at the functional group. For CPA, the ankle instability groups presented the highest TA (functional) ,GL (functional) and FB (mechanical) activities; and presented the lowest FL activity. The fatigue decreased the FL activity in the dominant leg for the mechanical and functional instability groups.

Table:

Epoch	Group	Leg	RMS (% maximal activity)			
			Tibialis Anterior	Fibularis Longus	Fibularis Brevis	Gastrocnemius Lateralis
APA	Control	Non dominant	16.4+ 2.6	35.4+2.4	2.7+5.2	19.9+2.5
		Dominant	14.2+2.5	34.9+2.3	2.3+5.1	14.3+2.4
		Fatigue Dominant	10.6+2.5	35.9+2.3	2.3+4.9	13.1+2.3
	Functional instability	Non dominant	7.8+3.0	22.8+2.8	1.2+6.0	20.36+2.9
	Dominant	16.9+4.7	32.7+4.3	1.4+9.4	7.9+4.5	
	Fatigue Dominant	13.9+2.5	20.9+2.4	1.5+5.1	29.9+2.4	
	Mechanical instability	Non dominant	12.3+2.7	18.3+2.5	27.1+5.4	10.7+2.6
	Dominant	7.3+2.4	17.2+2.2	27.9+4.8	8.4+2.3	
	Fatigue Dominant	8.7+2.5	18.1+2.0	16.4+4.5	6.5+2.1	
APC	Control	Non dominant	35.1+6.2	30.0+2.5	2.7+39.0	24.6+2.1
		Dominant	25.2+6.1	33.0+2.5	2.7+38.2	21.5+2.1
		Fatigue	25.1+5.8	29.8+2.4	3.3+36.7	17.5+2.0

	Dominant				
Functional instability	Non dominant	36.2+7.2	28.2+3.0	2.0+45.4	22.3+2.5
	Dominant	33.7+11.2	34.8+4.6	2.1+70.7	28.7+3.9
	Fatigue Dominant	65.9+6.1	21.3+2.5	3.0+38.2	27.9+2.1
Mechanical instability	Non dominant	24.8+6.5	31.4+2.6	45.2+40.8	12.4+2.3
	Dominant	17.1+5.7	21.3+2.3	167.5+36.0	12.2+2.0
	Fatigue Dominant	21.0+5.3	21.4+2.2	66.0+33.6	10.9+1.9

References: [1] Myers et al., A. J. Sports Medicine, 31:498-506, 2003.

Disclosure of Interest: None Declared

DOES A HALF TIME RE-WARM UP INFLUENCE THE MARKERS OF ANTERIOR CRUCIATE LIGAMENT INJURY RISK DURING MULTI-DIRECTIONAL SIMULATED SOCCER MATCH-PLAY?

Raja Mohammed Firhad Raja Azidin [1 2,*] Sean Sankey [2] Ruth Cabeza-Ruiz [2 3] Fransiska Bossuyt [2] Barry Drust [2] Mark A Robinson [2] Jos Vanrenterghem [2]

[1] Faculty of Sport Science and Recreation, Universiti Teknologi MARA, Shah Alam, Malaysia, [2] School of Sport and Exercise Sciences, Liverpool John Moores University, Liverpool, United Kingdom, [3] Department of Physical Education and Sports, University of Seville, Seville, Spain

Introduction and Objectives: An inactive (passive) half-time interval during soccer matches has been shown to impair physical performance, imposing an increased risk of injuries during the early stages of the second half [1,3]. The main aim of this study was to investigate markers of anterior cruciate ligament (ACL) injury risk related to knee and hip mechanics and isokinetic muscle strength imbalance during a soccer match simulation, and the effect a half-time re-warm up has to reverse increased risk in the second half of play.

Methods: In a single-group repeated measures design, 14 male recreational soccer players completed a 90-min lab-based multi-directional overground match-play simulation, comprising two 45-min halves separated by a 15-min half-time interval. During the half-time period, players either remained seated (passive, CON), or performed an intermittent agility exercise at ~70% of maximal heart rate during the last 5-min of half-time (re-warm up, RWU). Kinematics and kinetics of the support leg during unanticipated 45° side cutting manoeuvres were recorded as part of the simulated match-play, providing multiple trials over the 45 minutes which were subsequently grouped into 15 minute blocks. Participants also performed five maximal dominant-limb isokinetic contractions for concentric quadriceps (Q_{con}) and eccentric hamstrings (H_{ecc}) prior to exercise (time 0 min), at the beginning and end of half-time (time 45 min and 60 min), and post-exercise (time 105 min). A two-way ANOVA was used to identify significant differences, with α=0.05.

Results: Significant reductions in H_{ecc} (*P*< .010) and functional H_{ecc}:Q_{con} ratio (*P* < .020) were observed at all times during match-play compared to pre-exercise values, for both conditions, with no significant difference observed between conditions (Figure 1). Similarly, significant increases in Q_{con} angle of peak torque at all times (P<.030), compared to pre-exercise values and H_{ecc} angle of peak torque (P=.037) in the last 15 minutes of match-play were observed. A trend towards increased hip extension angles at initial contact (P=.076) was observed in the last 15 minutes of simulated match-play. No significant differences between conditions or over time for Q_{con}, knee abduction moments and knee extension angles were observed.

 The main findings revealed RWU did not offset impairments in all the markers of ACL injury risk. Reduced eccentric hamstrings strength and muscle imbalances, a shift in angle of peak torques and a trend towards more erect hip landing posture at initial contact, suggested a greater risk of ACL injury during the latter stage of match-play, supporting epidemiological observations [2]. A reduced muscle temperature due to passive rest during half-time has been associated with a reduction in physical performance during the second half of match-play [3]. Whilst RWU has been shown to

increase muscle temperature, increased nerve conduction rate, and increased contraction velocity [3], RWU had no reversal effects on markers of ACL injury risk in this study.

Figure:
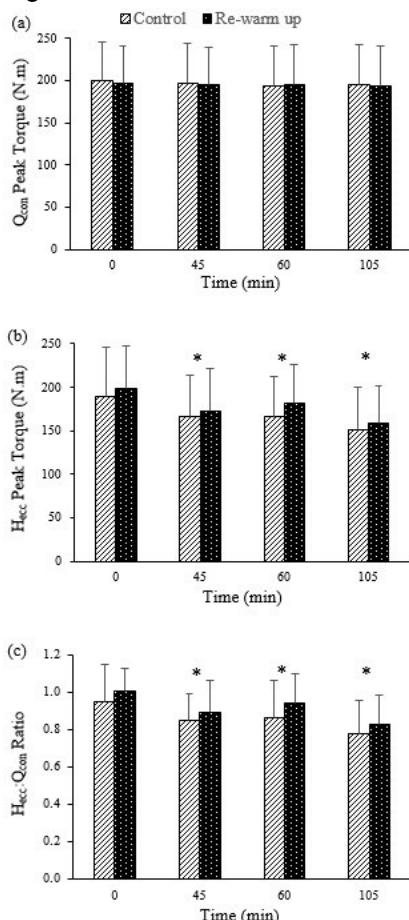
Caption: Quadriceps concentric peak torques (a) hamstrings eccentric peak torques (b) and functional hamstring eccentric: quadriceps concentric strength ratio (c) during simulated match-play. *Indicate significant difference from pre-simulation (time 0 min).

Conclusion: Despite the growing evidence of physical performance improvement after RWU in soccer players, the efficacy of this intervention towards reducing ACL injury risks remains unknown and requires further investigation.

References: [1] Edholm et al., Scan J Med Sci Sports, doi: 10.1111/sms.12236, 2014.

[2] Hawkins et al., Br J Sports Med, 35(1): 43-47, 2001.

[3] Mohr et al., Scand J of Med and Sci Sports, 14(3): 156-162, 2004.

Disclosure of Interest: None Declared

AGE AND GENDER EFFECT ON MUSCLE ACTIVATION PATTERNS IN THE DOMINANT AND NON-DOMINANT LEGS OF SOCCER PLAYERS DURING UNANTICIPATED SIDE-CUTS: RELEVANCE TO NON-CONTACT ACL INJURIES

Michelle L. Jones [1,*]Kendal Steele [1]Michael J Del Bel [1]Alana K Fairfax [1]Scott Landry [1]

[1]Acadia University, Wolfville, Canada

Introduction and Objectives: Recent literature demonstrates that females are more susceptible to non-contact anterior cruciate ligament (ACL) injuries compared to males, though muscle activity differences in age and gender are not yet completely understood. While a number of studies exist examining gender effects on non-contact ACL injury risk, very few consider gender as well as the effect of age (1). The purpose of this study was to determine if gender and age differences exist in lower limb muscle activation patterns between pre-pubescent and post-pubescent male and female soccer players while performing maximum effort unanticipated side-cutting maneuvers off both the dominant and non-dominant leg.

Methods: A series of 45 degree unanticipated side-cutting maneuvers were performed at a maximum effort by 33 pre-pubescent (17 male age 10.4 ± 1.4 yrs, and 16 female age 9.1 ± 1.2 yrs), and 39 post-pubescent (20 male age 21.3 ± 1.9 yrs, and 19 female age 19.5 ± 2.3 yrs) soccer athletes who had no significant lower limb injury in the past 6 months or that required surgery. A timing reaction system was used to guide the athletes to cut either to the left or right of their dominant or non-dominant leg in an unanticipated maneuver, thereby more closely replicating a true game-like situation where this injury is most likely to occur. Muscle activation patterns during the stance phase of the side-cutting maneuvers were analyzed for the following muscles: lateral and medial gastrocnemii, lateral and medial hamstrings, and vastus lateralis and medialis. Mean muscle activation patterns for the stance phase of the side-cutting maneuvers were amplitude normalized to a series of maximum voluntary isometric contractions. For each muscle separately, the participants' individual mean waveforms were analyzed using principal component analysis (PCA), with PC1 and PC2 capturing overall magnitude and timing features (phase shift) in the activation waveforms, respectively. Gender, age, and/or interaction effects were tested for using a two-way ANOVA for each muscle group. Analyses of the dominant leg and the non-dominant leg were each completed separately.

Results: The analysis on the dominant leg revealed that the post-pubescent group had significantly greater ($p < 0.05$) muscle activation magnitudes over the pre pubescent group for all muscles examined. The vastus medialis showed gender and age differences, with higher activation magnitudes demonstrated in females compared to males, and post-pubescent males reaching peak muscle activation closer to initial contact (IC) compared to pre-pubescent males. Peak muscle activation occurred earlier for the post-pubescent males compared to post-pubescent females in the vastus lateralis, with trends ($p < 0.1$) evident in the vastus medialis. The analysis of the non-dominant leg indicated significantly higher activation magnitudes for the post-pubescent athletes compared to pre-pubescent athletes in the lateral and medial gastrocnemii and the vastus lateralis. Trends of similar differences were also observed in the lateral and medial hamstrings. Greater activation magnitudes earlier in stance or earlier peak activation (phase shift) for the lateral hamstring were observed in males compared to the females. For the medial hamstring, however, greater activation magnitudes

earlier in stance were observed for pre-pubescent athletes compared to post-pubescent athletes. The vastus lateralis showed earlier peak activation for the post-pubescent males in comparison to the post-pubescent females.

Conclusion: Findings that include earlier peak muscle activity for the vastus lateralis and medialis muscles in males may play a role in better stabilizing the knee and decreasing the risk of injury for males (2). Gender differences were more evident in the post-pubescent group and this goes along with findings in the literature that indicate females are more likely to injure their ACL in post-pubescent athletes, with no gender differences in non-contact ACL injuries existing for pre-pubertal athletes (3). Trends or significant age differences in muscle activation magnitudes were found to exist in all but one muscle, with post-pubescent athletes having higher activation magnitudes compared to pre-pubescent athletes. Further research is recommended to determine the role that these age and gender differences may have on the risk of non-contact ACL injury risk.

References: [1] Walden M et al. (2011) Knee Surg. Sport Tr. A., 19, 3-10.

[2] Beaulieu ML et al. (2009) Knee Surg. Sport Tr. A., 17, 968-976.

[3] Alentorn-Geli E et al. (2009) Knee Surg. Sport Tr. A., 17, 705-729.

Disclosure of Interest: None Declared

Injury

PO-0115

THE EFFECT OF PERIPHERAL FATIGUE ON KNEE JOINT POSITION SENSE.

N S Relph [1,*] L C Herrington [2]

[1]University of Cumbria, Carlisle, [2]University of Salford, Salford, United Kingdom

Introduction and Objectives: Muscular fatigue is the inability to maintain a power output or force during repeated muscular contractions due to changes in physiological processes. Joint position sense (JPS) is the awareness of position in space. Exercising when fatigued increases the risk of injury, which may be due to a reduction in knee position sense. Indeed, evidence suggests more injuries occur in the final third of sports matches than in earlier periods. The aim of this study was to measure the effect of peripheral muscular fatigue on knee JPS.

Methods: 20 healthy participants provided informed consent. Knee JPS was recorded before and after a fatiguing protocol. The JPS measurements were taken using a previously validated method (Relph and Herrington, 2014a, 2014b). This involved open chain, passive-active reproduction of a target angle into both flexion and extension. Absolute error scores (AES) were taken as the absolute difference between target and reproduction angles. Angles were measured using image capture and manual digitising techniques. Fatiguing protocol was conducted on an isokinetic dynamometer and involved concentrically extensions and flexions of the dominant knee maximally at 60°/s until they reached 50% of their maximum voluntary contraction on three consecutive trials in both flexor and extensor muscle groups.

Results: The mean (±SD) maximum voluntary contraction into knee flexion and extension was 78.7N.m (±22.8) and 177.1N.m (±39.0) respectively. Results of the analysis revealed no effect of the fatiguing protocol on either JPS flexion (p=0.729) or JPS extension (p=0.492). Knee JPS flexion error scores reduced by 0.17° and JPS extension error scores reduced by 0.14°. Discussion - One viable explanation of the results of this study is the fatiguing protocol was not severe enough to induce a fatigued state. For example the anterior shear loads imposed on the knee joint during isokinetic contraction at 180°/s are equivocal to that of walking and compressive loads equivalent to stair climbing. This suggests studies using isokinetic fatiguing may not create representative fatiguing of the joint as would occur during exercise. The method of measuring fatigue levels using 50% of MVC may also have limitations. It may be more appropriate to use blood analysis techniques to confirm fatigue. However, it would appear peripheral fatigue occurred to some extent as MVC performance did reduce. Another explanation for the lack of JPS decline may be compensatory techniques in the central nervous system, central processing may have adjusted efferent information to ensure continued to provide accurate joint position sense.

Conclusion: In conclusion, peripheral fatiguing protocols may not induce fatigue to an appropriate level to illustrate the effects on knee JPS. Alternatively, knee JPS may not be affected by fatigue and hence a reduction in knee static proprioception may not be a mechanism of the increased risk of injury during the latter stage of exercise and sport. Future research should consider the effect of central fatiguing on knee proprioception. Disclosure -This data is new and has not been submitted elsewhere.

References: Reference 1

Relph et al. (2014a). Inter-Examiner, Intra-Examiner and Test-Retest Reliability of Clinical Knee Joint Position Sense Measurements Using an Image Capture Technique. J. Sport Rehabil., In Press.
Reference 2
Relph et al. (2014b). Criterion-Related Validity of Knee Joint Position Sense Measurement Using Image Capture and Isokinetic Dynamometry. J. Sport Rehabil., In Press.

Disclosure of Interest: None Declared

PO-0116

SACROILIAC JOINT CARTILAGES BIOMECHANICAL ANALYSIS AFTER DIFFERENT PERCUTANEOUS SCREW FIXATIONS: A FINITE ELEMENT ANALYSIS

Peng Ye [1,*]tang peifu [1]zhang lihai [1]

[1]Department of Orthopaedic Surgery, General Hospital of Chinese People's Liberation Army, Beijing, China

Introduction and Objectives: Sacroiliac screw fixation are widely applied in the pelvic fractures and sacroiliac joint dislocations. Many cadaver biomechanical study have been done for the stability of fixations. However, many patients feel uncomfortable and low back pain after fixations which may be cause by the biomechanical change on cartilage. At the same time, the information of stress distribution and changes are difficult to be obtained from cadaver studies. Therefor the three-dimensional finite element model of pelvic was developed for this study to analyze the biomechanical change of sacroiliac joint cartilages after different percutaneous screw fixations.

Methods: Finite element pelvic models reconstructed, bones, cartilages, and ligaments of FE model were developed. The Tile type-B and type C sacroiliac joint disruption were analyzed based on fixation with a single S1 screw (S1-1), single S2 screw (S2-1), two S1 screws (S1-2) and a combination of a single S1 and a single S2 screw (S1-S2). The stress of cartilage and pelvis change were compared and analyzed in bilateral stance.

Results: The largest difference values between both cartilages was in the S1-1 fixation of type C dislocation (2.79Mpa). The smallest difference values between both cartilages was in the S1-2 fixation of type B dislocation (0.51Mpa). The differences of same fixations in type C were larger than in type B. The dislocation more stable, the stress closer between left and right sacroiliac joint cartilages. In the S2-1 fixations, both side of cartilage stress increased (5.25Mpa and 4.45Mpa in type B, 7.68Mpa and 5.10Mpa in type C). In the S1-S2 fixations, both side of cartilage stress is the minimum value (0.79Mpa and 2.94Mpa in type B, 1.07Mpa and 3.06Mpa in type C). The difference of stress in 4 kind of percutaneous fixation in type B disruption and normal pelvis are very small. The normal pelvis stress range from 0-2.347 (Mpa). The S1-1 fixation stress range from 0-2.989(Mpa) in type B and 0-3.234(Mpa) in type C. The S2-1 fixation stress range from 0-2.646(Mpa) in type B and 0-3.945(Mpa) in type C. The S1-S2 fixation stress range from 0-2.854(Mpa) in type B and 0-2.862(Mpa) in type C. The S1-2 fixation stress range from 0-2.832(Mpa) in type B and 0-2.930(Mpa) in type C.

Figure:
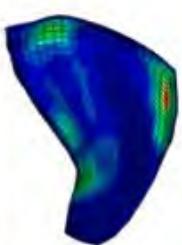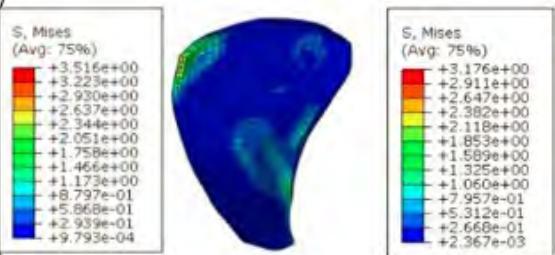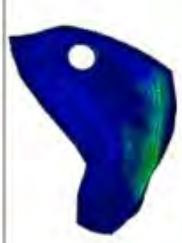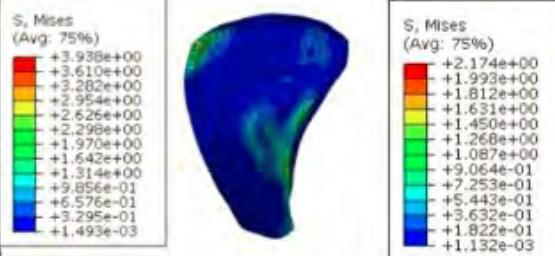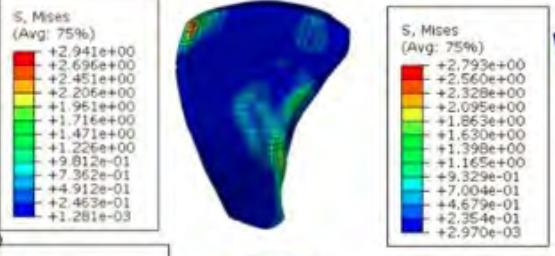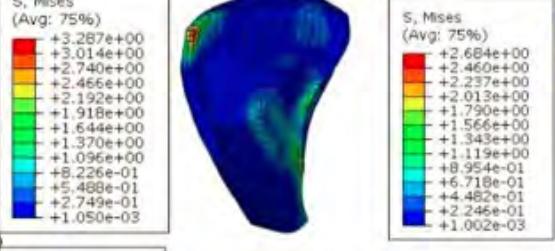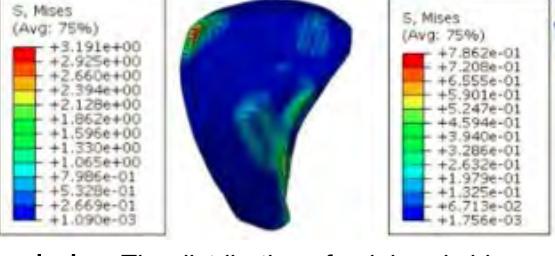
Conclusion: The distribution of uninjured side were mainly located at the posterior sacroiliac region and anterior horn. The fixation will increased one side rigidity which will cause the increased wear of the other side. So that, the biomechanical of trans-sacral fixation will be better than the unilateral screw fixations. The differences of same fixations in type C were larger than in type B. The dislocation more stable, the stress closer between left and right sacroiliac joint cartilages. The S2-1 fixation were recommended in type B fractures, and the S1-S2 fixation were recommended in the type C dislocations.

Table:

	Stress of left SIJ cartilage(Mpa)	Stress of right SIJ cartilage(Mpa)	Difference between left and right
Normal	3.18	3.52	0.34
B S1	1.60	3.00	1.40
B s2	5.25	4.45	-0.80
B S1S2	0.79	2.94	2.15
B S1*2	2.68	3.19	0.51
C S1	1.31	4.10	2.79
C S2	7.68	5.10	-2.58
C S1S2	1.07	3.06	1.99
C S1*2	2.10	3.29	1.19

Caption: Stress of left and right SIJ cartilages

References: [1] Routt et al., J Orthop Trauma. 11:584–589,1997.

[2] Shuler et al., J Trauma. 38:453–458,1995.

[3] Mullis et al., J Orthop Trauma. 22(5):293-8,2008.

[4] Gorczyca et al., Injury. 27:561–564,1996.

[5] Hearn et al., In Proceedings of the 13th International Conference on Biomechanics, 1991.

[6] Simonian et al., Orthop Clin North Am. 28:351–367,1997.

[7] Tile et al. Fractures of the Pelvis and Acetabulum, Lippincott Williams &Wilkins, 2003

[8] Camp et al., Spine 15(9):932-941.1990.

[9] Routt et al., J Orthop Trauma 9(3):207-214,1995.

[10] Giannoudis et al., J Bone Joint Surg Br. Feb;89(2):145-54,2007.

[11] Leighton et al., J Orthop Trauma.5:313–317,1991.

[12] Simonian et al., Clin Orthop. 323:202–209,1996.

[13] Varga et al,. Injury. 26:75– 80,1995.

[14] Comstock et al., J Orthop Trauma.10:517–522.1996.

[15] Mason et al., Eur Spine J. Oct; 22(10):2325-31,2013.

[16] Goel et al., Comput Biol Med 8:91–104,1978.

[17] Oonishi et al., J Biomech 16:427–44,1983.

[18] Dalstra et al., J Biomech Eng 117:272–8,1995.

[19] McLauchlan et al., Rheumatology (Oxford). Apr; 41(4):375-80.2002.

[20] Gray. Anatomy of the human body. 2000.

[21] Miller et al., J Orthop Res 5:92–101,1987.

[22] Eichenseer et al., Spine 36(22): E1446e52,2011.

[23] Kim et al., J Korean Neurosurg Soc 47(6):446e53, 2010.

Disclosure of Interest: None Declared

Injury

PO-0117

PLAYER LOAD MONITORING IN SPORT: PREDICTING CENTRE OF MASS ACCELERATION FROM BODY-WORN ACCELEROMETRY

Niels J. Nedergaard [1,*] Paulo Lisboa [2] Mark Robinson [1] Jos Vanrenterghem [1]

[1]School of Sport and Exercise Sciences, [2]School of Computing & Mathematical Sciences, Liverpool John Moores University, Liverpool, United Kingdom

Introduction and Objectives: GPS data from units positioned on the upper trunk are frequently used for player monitoring in team sports, yet these devices also include accelerometers and gyroscopes. The accelerometer data can be used to estimate the external load on players (e.g. PlayerLoad™, a cumulative summation of change in resultant accelerations) and to monitor the risk of overuse injuries [1]. The relationship between energy expenditure and PlayerLoad™ has been documented recently [2], but an understanding of the relationship between PlayerLoad™ and the whole-body centre of mass (CoM) acceleration is required to judge how well PlayerLoad™ may relate to the external ground reaction forces. The aim of this study was to investigate the relationship between body-worn accelerometry and whole-body centre of mass (CoM) acceleration during a 45-degree side-cutting task at different intensities.

Methods: Twelve team sports athletes volunteered to participate in this study (age: 23 ± 3 years, mass: 73 ± 11 kg, height: 179 ± 7 cm). All participants completed four anticipated 45-degree side-cutting tasks on their dominant leg at four different approach speeds 2, 3, 4 and 5 m/s (± 5%). Approach speed was measured from photocell timing gates 2 m from where the cut was performed. A 6-degress-of-freedom eight segment model including feet, upper and lower legs, pelvis and trunk was created from kinematic data recorded with 10 optoelectronic cameras (Qualisys AB, Gothenburg, Sweden) sampling at 500 Hz. Trunk acceleration was measured from a triaxial accelerometer within a GPS unit (MinimaxX S4, Catapult Sports, Melbourne, Australian) sampling at 100 Hz. This was positioned as typically worn; on the upper part of the trunk in an elastic vest. Additional acceleration data was collected from three triaxial accelerometers (Noraxan USA Inc., Scottsdale, USA) sampling at 1000 Hz, positioned directly onto the GPS unit, on the hip (between the left and right PSIS) and the anterior tibia.

PlayerLoad™ and resultant peak accelerations were determined during the foot-ground contact and Pearson's correlation coefficients were used to determine any relationships between CoM accelerations and accelerometry data across the different approach speeds.

Results: Stronger relationships were observed between peak CoM acceleration and peak accelerometry data compared to CoM PlayerLoad™ and accelerometry data PlayerLoad™ (Table 1), whereas accelerometry location had little effect on the relationship with CoM acceleration.

Conclusion: Body-worn accelerometers measure the accelerations of the segment they are attached to, while the CoM acceleration represents the accelerations of the whole body, this may explain the moderate relationship. As the acceleration signals were unprocessed, this data may not be best suited to the estimation of external ground reaction forces acting on the players' body in the field. Accelerometer specification, data processing and relative movement of the trunk accelerometer compared to the Catapult trunk accelerometer may explain the difference observed within the trunk.

Further studies and other approaches using body-worn accelerometry are needed to better estimate the peak and accumulated external ground reaction forces acting on the body during team sports in the field.

Table:

	CoM Acceleration	Catapult (Trunk)	Trunk	Hip	Tibia
Peak acceleration (g)					
2 m/s	1.5 (0.3)	2.7 (0.5)	3.6 (1.0)	4.4 (1.1)	8.4 (2.4)
3 m/s	1.9 (0.4)	3.4 (0.7)	4.5 (1.1)	5.8 (1.5)	12.0 (3.9)
4 m/s	2.7 (0.7)	4.2 (1.0)	5.5 (1.5)	8.3 (2.9)	17.1 (4.4)
5 m/s	3.0 (0.6)	4.3 (0.8)	5.7 (1.5)	10.1 (4.3)	19.7 (5.2)
Pearson's r	-	0.732*	0.650*	0.711*	0.709*
PlayerLoad™ (au)					
2 m/s	6 (1)	9 (2)	17 (7)	19 (7)	59 (17)
3 m/s	7 (1)	10 (3)	20 (6)	27 (9)	88 (25)
4 m/s	10 (2)	13 (4)	26 (9)	43 (15)	134 (31)
5 m/s	10 (2)	14 (3)	26 (6)	50 (22)	158 (40)
Pearson's r	-	0.683*	0.658*	0.660*	0.698*
Denotes a significant correlation, p<0.01.					

Caption: Means (± SD) for peak accelerations and PlayerLoadTM for the different approach speeds and Pearson's correlation coefficient across approach speeds between CoM acceleration and accelerometry data.

References: [1] Boyd et al., Int J Sports Physiol Perform, 6(3): 311-321, 2011.

[2] Boyd et al., Int J Sports Physiol Perform, 8(1): 44-51, 2013.

Disclosure of Interest: None Declared

PO-0118

VARIABILITY IN THE PEAK OF PLANTAR PRESSURE IN CHILDREN, ADULT AND ELDERLY DURING WALKING

Pedro S. Franco [1] [2] Emmanuel da Rocha [1] [2] Caio da Silva [2] Gislaine Santos [2] Mariane Figueiredo [2] Renato Azevedo [2] Felipe Carpes [1] [2],*

[1] Graduate Program in Physical Education, Federal University of Santa Maria, Santa Maria, [2] Applied Neuromechanics Group, Federal University of Pampa, Uruguaiana, Brazil

Introduction and Objectives: Plantar pressure is a biomechanical measure commonly used to quantify mechanical loads in the foot during standing and walking. Occurrence of peak pressures on specific foot sites can be related to foot injuries and skin damages. Such conditions are especially investigated in the elderly. Although previous studies addressed average plantar pressures in different foot regions in people of different ages, variability of plantar pressure is briefly considered. Considering that elderly are subjected to foot injuries most likely due to higher plantar pressure, it could be possible that in the elderly a lower variability in the peaks of plantar pressure result in repetitive loads leading to higher risk of injury. Therefore, in this study we quantified and compared the variability in the peak of plantar pressure between able-bodied children, adults and elderly during walking.

Methods: Participants were 7 children (mean age ± SD 10 ± 1 years old, body mass 46 ± 14 kg and height 1.45 ± 0.16 m), 7 adults (age 39 ± 5 years old, body mass 71 ± 21 kg and height 1.64 ± 0.09 m), and 7 elderly (age 74 ± 2 years old, body mass 64 ± 11 kg and height 1.59 ± 0.06 m). For data acquisition, participants walked barefoot in a 9 m walkway. Walking was performed at self-selected speed. Plantar pressure (PP) was recorded at 400 Hz by using a pressure mapping system (Matscan, Tekscan Inc, USA). Data from 5 steps were recorded for determination of the peak of pressures in the forefoot (FF), midfoot (MF) and rearfoot (RF) [1] and normalized by the individual body mass. The coefficient of variation was determined as the ratio between the standard-deviation and the mean. Data normality was verified using Shapiro-Wilk's test. One-way ANOVA for repeated measures was used to compare the coefficient of variation in each foot region between the groups. Tukey post-hoc was applied when suitable. Significance level was set at 0.05 for all analyses using the SPSS 20.0.

Results: We found an effect for the group in all foot regions [FF ($F_{(2)}$=6.729; p=0.007), MF ($F_{(2)}$=3.862; p=0.040) and RF ($F_{(2)}$=4.372; p=0.28)]. Elderly present greater variation in peak of plantar pressure than adults in the FF (p=0.005), MF (p=0.032) and RF (p=0.025), but similar to observed in the children (p=0.083; p=0.439; p=0.623, for FF, MF and RF, respectively). Adults were similar to children for FF (p=0.395), MF (p=0.304) and RF (p=0.152). Results are presented in the Figure 1.

The higher variability in plantar pressure observed in the elderly compared to adults can be resultant of variability inherent to the aged gait and that make them in higher risk of falling [2].Rather, it would be important to identify if such variability is consistent enough to elicit some risk to the elderly health.

Figure:
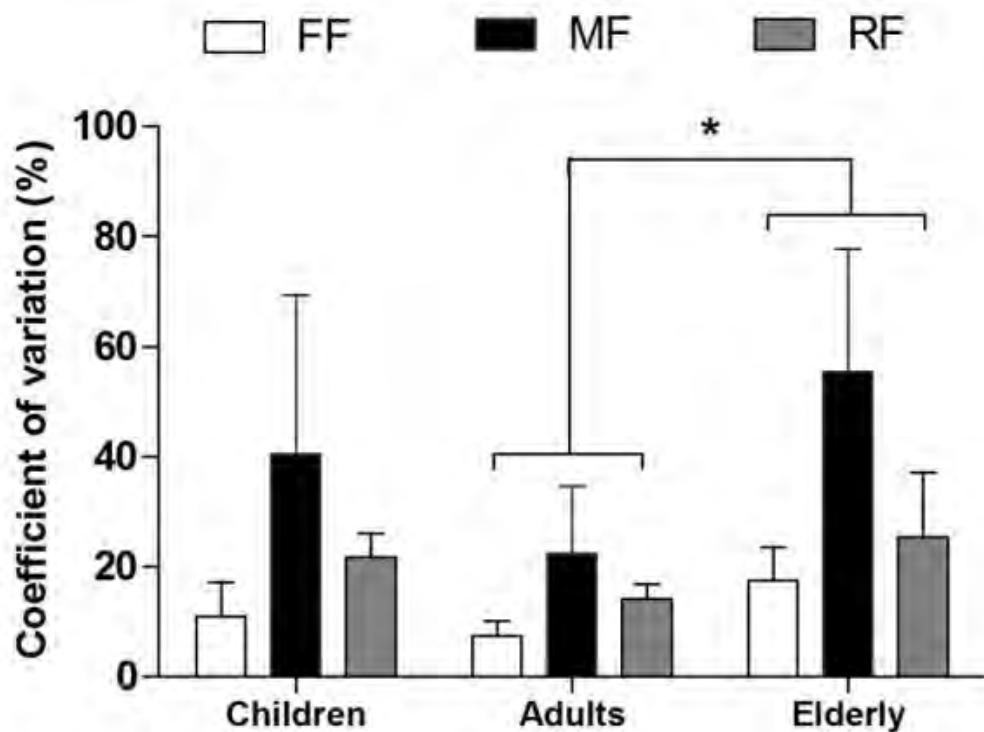
Caption: Figure 1. Coefficient of variation for the peak of plantar pressure in the elderly, adults and children in each foot region. FF means forefoot; MF, midfoot; and RF, rearfoot. * indicates statistically significant difference ($p<0.05$).

Conclusion: Elderly presented higher variability in the peak of plantar pressure than observed among adults. Next step in this research will be dedicated to verify if such pattern is consistent when elderly are assessed in repeated days.

References: [1] Burns et al. Clin Biomech, 20(9): 877-882, 2005.

[2] Nigg et al. Gait Posture, 2(4): 213-220, 1994.

Disclosure of Interest: None Declared

THREE DIMENSIONAL KINEMATICS OF THE HUMAN METATARSOPHALANGEAL JOINT DURING LEVEL WALKING AND RUNNING

Sivangi Raychoudhury [1,*] Dan Hu [1] Lei Ren [1]

[1]Biomechanics, Mechanical engineering, University of Manchester, Manchester, United Kingdom

Introduction and Objectives: The human foot plays many important roles in maintaining stability, generating propulsive powers and attenuating ground impacts during locomotion. However, our understanding of the biomechanical function of the forefoot is very limited. So far, little is known about the in vivo orientation and position of the functional rotation axis of the metatarsophalangeal (MP) joint during locomotion and how it changes with varying speed. The objective of this study is to investigate the three-dimensional (3D) kinematics of the functional rotation axis of the human MP joint during level walking and running at different speeds.

Methods: Six male subjects with no medical history of foot injury participated in this study. The subjects walked and ran at their self-selected slow, normal and fast speeds. To record the 3D motions, marker clusters were attached on the foot. A 12 infrared camera motion analysis system (Qualisys, Sweden) was used to capture the motions at 150 Hz. Six force plates (Kistler, Switzerland) were used to record the ground reaction forces (GRFs) and moments at 1000 Hz. A set of static calibration procedures were undertaken to locate the anatomical landmarks. Five rigid segments were defined to represent the lower limb: pelvis, thigh, shank, tarsometatarsi and phalanges. The 3D anatomical coordinate system was defined for each individual segment. We have assumed that the five phalanges form a single rigid segment and the MP joint is a single hinge type joint. The anatomical axis (AA) of MP joint was defined as an oblique line connecting the 1st and 5th metatarsal heads. While the functional axis (FA) was defined as the rotational axis between the hindfoot and forefoot segments (see Figure 1). Raw data were processed using GMAS (Generalised Motion Analysis Software), a MATLAB based software package for 3D kinematic and kinetic analysis of biomechanical multi-body systems. Statistical analyses were conducted using SPSS 20.0 software (IBM, Armonk, New York, USA) to investigate the 3D position and orientation differences between the AA and FA, and the effect of locomotor speed on the axes of MP joint by considering subjects and trials as random effects. Difference between AA and FA, and between each pair of speeds were tested using Fisher's least significant difference multiple comparison based on the least-squared means, considering probability $p<0.05$ as statistically significant.

Results: Statistically significant differences were found for all the orientation and position parameters across all three speeds, except for the vertical position parameter y at slow walking speed. The FA of MP joint has a more anterior and superior position than the AA across all speeds. The FA remains anterior to AA with an average distance of about 16% of the foot length. The FA is superior to AA with an average distance about 2% of the foot length during normal and fast walking. The FA shows an anteriorly more medial and more superior orientation than the AA. The joint orientation angle difference is more significant in the sagittal plane than in transverse plane. The joint position in the anterior posterior direction shows statistically significant difference when walking speed changes from slow to fast. The FA moves forward,

towards a more anterior position. Also the FA moves upwards towards a more superior position appreciably with increasing speed.

Figure:
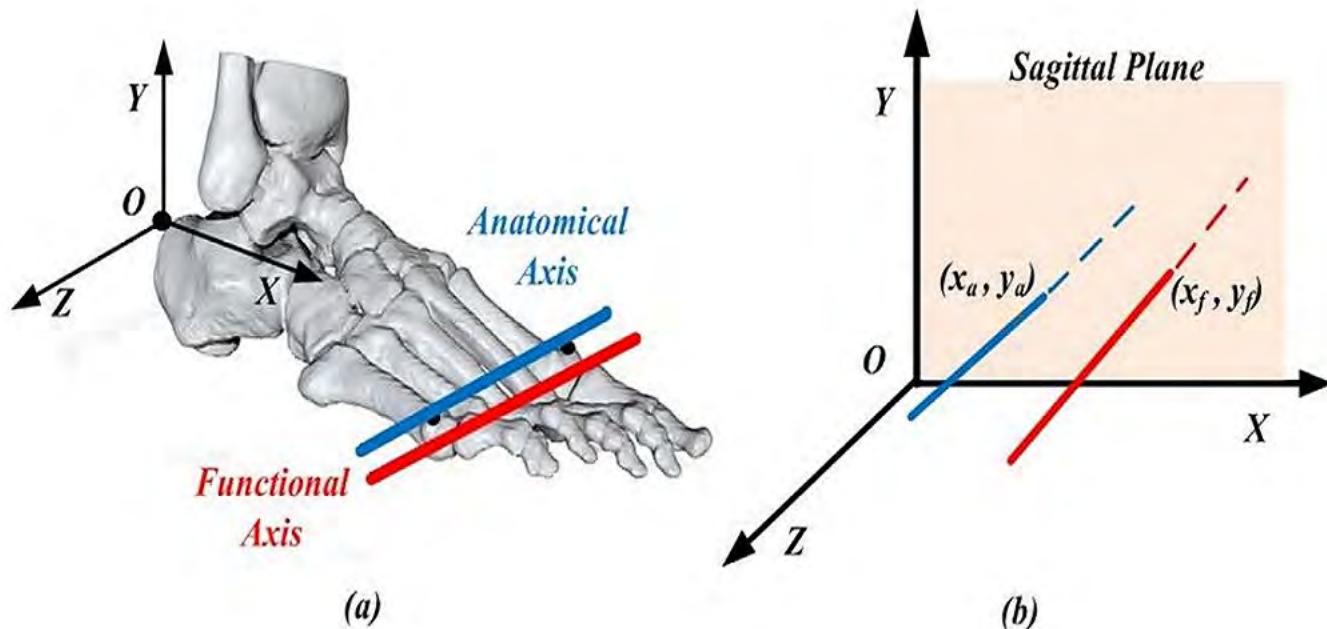
Caption: Figure 1. (a) The FA (red) and AA (blue) of the MP joint (b) The position of the FA is defined by its intersection point (xf, yf) and the location of the AA by (xa, ya) with the XOY plane of the foot coordinate system.

Conclusion: The position and orientation differences found between AA and FA suggests that using AA to represent the MP joint, as normally used in previous studies, may result in overestimated joint moment and power and underestimated muscle moment arms for MP extensor muscles. The joint axis shift towards the GRF vector in the late stance of walking will result in decreased moment arm of GRF and simultaneously increased moment arm of MP extensor muscles, hence will increase the effective mechanical advantage (EMA) of MP extensor muscles. The forward shift of the MP joint axis will result in an increased lever distance to the ankle joint and may moderate the angular velocity increase with increasing speed. The forward and upward FA shift may help to maximise the locomotor efficiency and reduce the risk of injury. This study may help us to better understand the contribution of the intrinsic foot structure to the propulsive function of the foot during locomotion at different speeds. Furthermore, this may also help in improving the design of sports and therapeutic footwears, prosthetic lower limbs and robotic legs.

References: [1] Stefanyshyn et al., Mechanical energy contribution of the metatarsophalangeal joint to running and sprinting. *Journal of Biomechanics* 20, 1081-1085, 1997.

Disclosure of Interest: None Declared

DIFFERENCES IN LOWER LIMB KINEMATICS AND KINETICS BETWEEN OLDER MALES AND FEMALES WITH OSTEOARTHRITIS

Olivia Zajdman [1,*]Daniel Benoit [1]

[1]Human Kinetics, University of Ottawa, Ottawa, Canada

Introduction and Objectives: Osteoarthritis (OA) is a slow, progressive degradation of articular cartilage and subchondral bone, most commonly found in the knee [6]. OA affects 13% of Canadian adults and is 2-3 times more prevalent in females than males [1]. Differences in strength and muscle activation patterns are present between sexes [4]. These factors will affect the biomechanics of the lower limb and may cause kinematic differences in squatting strategies between males and females. Males with OA have been shown to display lower limb gait kinematics similar to healthy populations, while females demonstrate different biomechanical tendencies [3]. Lower limb kinematics during a counterbalanced and two-legged squat have previously been compared between young, healthy, active male and female subjects [2], but not in an OA population. It is unclear what the kinematic differences between sexes are in an OA population during a two-legged squat despite being an essential activity of daily living. The purpose of this study is to characterize differences in peak sagittal plane hip, knee, and ankle moments (M) and sagittal plane peak knee flexion angle between male and female older adults with osteoarthritis.

Methods: Nine male [62.9 $\pm$ 8.6 years; BMI 24.5 $\pm$ 4.1; KOOS: 72.25$\pm$ 14.8] and eight female [60.3 $\pm$ 8.3 years; BMI 26.8 $\pm$ 3.0; KOOS: 63.94$\pm$ 11.02] adults with knee OA have participated in this study. No subject had a significant lower limb musculoskeletal injury within six months of participation or a BMI $\geq$40kg/m2. Subjects completed the Knee injury and Osteoarthritis Outcomes Score (KOOS) and affected limb(s) were recorded before data collection. Subjects performed 3 two-legged squats on two force platforms, and were instructed to squat down to 90° knee flexion, if possible, at a self-selected pace. Squat range was not standardized due to range of motion variability within the participant population. Ground reaction force data were recorded from the platform at 1000Hz. Marker trajectories were captured at 200 Hz with a ten-camera infrared Vicon motion analysis system. Lower limb kinetic and kinematic data were recorded and outputted using *Nexus* software. Peak sagittal plane hip, knee, and ankle moments, body weight normalized, and sagittal plane peak knee flexion were determined for the affected leg(s) through custom-made *MatLab* software. A one-way repeated measures ANOVA was performed for peak sagittal plane hip, knee, and ankle moments and sagittal plane peak knee flexion using SPSS at an alpha level of 0.05.

Results: There were significant ($p < 0.05$) differences seen in peak hip moment and knee flexion angle at a self-selected squatting speed between sexes (Table 1). Males exhibited statistically significant larger peak hip moment (M =-0.755 Nm/kg; F= -0.528 Nm/kg) and peak knee flexion angle (M= 102.32 ^{o}; F= 77.61 ^{o}) than females.

Conclusion: Males and females with knee OA exhibited differences in kinetic and kinematic squat parameters. Differences in lower limb mechanics between sexes may cause kinematic variations in squat execution and play a role in the greater incidences of OA in females [1]. Males showed greater peak hip moments, suggesting a more hip dominant squat strategy. This is known to decrease knee loading [2] and may have allowed males to increase peak knee flexion by using

a more efficient squatting technique that was less painful. A similar pattern was seen in adolescents performing single leg squats, where males exhibited greater eccentric hip torque [5]. Knowing the sex differences in joint kinetics and kinematics of a squat could allow for more targeted and successful rehabilitation interventions in persons with OA.

Table:

Variable	Sex	Mean	Standard Deviation	P value
Peak Hip M (Nm/kg)	F M	-0.528 -0.755	0.169 0.169	0.014*
Peak Knee M (Nm/kg)	F M	-0.615 -0.667	0.140 0.180	0.522
Peak Ankle M (Nm/kg)	F M	-0.332 -0.328	0.139 0.124	0.955
Peak Knee Flexion Angle (^{o})	F M	77.61 102.32	13.18 18.6	0.007*

Caption: Table 1: Males and Females with knee OA show significant (p< 0.05) differences in squat parameters (*).

References: [1] Badley E.M. *J. Rheum.* **22**:19–22, 1995.

[2] Lynn, S. K. et al. *J Strength Cond. Res.*, **26**(9): 2417–2425, 2012.

[3] McKean, K. et al. *Clinical Biomechanics*. **22**(4): 400–409, 2007.

[4] Petterson, S. C. et al. *J. Bone Joint Surg.* **89**(11): 2327–33, 2007.

[5] Silva, R. et al. *Computers Biol. Med.,* **29**: 1063–1069, 2014.

[6] Van Baar, M. E. et al. *Arthritis and Rheumatism*, **42**(7): 1361–9, 1999.

Disclosure of Interest: None Declared

Lower Limb

PO-0122

CHARACTERISTICS OF JOINT TORQUE DURING WALKING WITH PUSHING A WHEELCHAIR

Tetsu Yamada, Masami Hidaka

Introduction: Transportation using a wheelchair is a commonly used method for a person with lower limb disorder, an elderly person, and others. Most person who use a wheelchair need support by another person to drive the wheelchair. Although such support to drive a wheelchair is important, there has been little research to investigate the kinetics of walking with pushing a wheelchair.

The purpose of this study was to investigate joint torques of lower limbs during walking while pushing a wheelchair.

Methods: Five healthy male subjects (age: 20.6 ± 1.0 years, height: 1.71 ± 0.07 m, mass: 56.2 ± 5.2 kg) volunteered for participation. All the subjects signed an informed consent form. All experimental protocols were approved by the research ethics board of Hyogo University of Health Sciences.

An 8-camera motion capture system (Vicon MX, Vicon Motion Systems; Oxford, UK) operating at 100 Hz was used to collect all kinematic data. On each subject were attached 34 retroreflective markers, at bony landmarks of the Plug-in-gait model (Vicon Motion Systems; Oxford, UK). Kinematic and kinetic parameters were then calculated by using the Plug-in-gait model.

Analysis of variance (ANOVA) was performed for spatial and temporal descriptors and joint torques. Post hoc analyses for significant parameters were performed using Tukey's multiple comparison test. The level of significance was set at less than 0.05.

Results: Stride time (normal: 1.03±0.05 s; wheelchair: 1.03±0.08 s; weighted wheelchair: 1.10±0.07 s) and stride length (normal: 1.43±0.08 m; wheelchair: 1.39±0.15 m; weighted wheelchair: 1.38±0.16 m) were not significantly different among three conditions. Velocity of walking while pushing the weighted wheelchair (1.25±0.10 m/s) was significantly smaller than that of normal walking (normal: 1.39±0.09 m/s; wheelchair: 1.35±0.13 m/s) ($p < 0.05$).

The patterns of joint torque of the hip, knee, and ankle were mostly similar among three conditions. The peak flexion torque of the hip of normal walking (1.30±0.26Nm/kg) was significantly greater than when pushing a wheelchair (wheelchair: 0.83±0.19Nm/kg; weighted wheelchair: 0.79±0.21Nm/kg), either with or without the weight ($p < 0.05$). The peak extension torques of the hip were not significantly different among three conditions. The peak extension torque of the knee of normal walking (0.74±0.19Nm/kg) was significantly greater than when pushing a wheelchair (wheelchair: 0.55±0.13Nm/kg; weighted wheelchair: 0.40±0.12Nm/kg), either with of without the weight ($p < 0.05$). The peak flexion torques of the knee were not significantly different among three conditions. The peak plantar flexion torque of the ankle of normal walking (1.52±0.15Nm/kg) was significantly greater than when pushing a wheelchair (wheelchair: 1.28.83±0.09Nm/kg; weighted wheelchair: 1.16±0.19Nm/kg), either with of without the weight ($p < 0.05$). The peak dorsiflexion torques of the ankle were not significantly different among three conditions.

The walking velocity and thigh segment angle of the normal walk were great (normal: 63.3±5.3 deg.; wheelchair: 38.2±12.9 deg.; weighted wheelchair: 33.0±13.3 deg.), therefore the hip flexion torque of the normal walk had to been greater than the other conditions.

During walking with pushing a wheelchair, subjects could support part of themselves weight by pushing a wheelchair downward. The peak extension torque of the knee and the peak plantar flexion torque of the ankle during pushing a wheelchair were developed smaller than normal walking, because these support pushing a wheelchair decreased load that need to support by lower limbs.

Conclusion: This study investigated joint torques of the lower limbs during walking while pushing a wheelchair. The hip flexion torque, the knee extension torque, and the ankle plantar flexion torque were developed smaller during the pushing a wheelchair than normal walking. These changes were affected by the support with hands pushing a wheelchair downward.

ISOKINETIC STRENGTH OF LOWER LIMB MUSCLES IN RECREATIONAL RUNNERS WITH CHRONIC LOW BACK PAIN

Congcong Cai [1]Pui W. Kong [2,*]

[1]Physiotherapy, Rehabilitation Department, Alexandra Hospital-Jurong Health Service , [2]Physical Education and Sports Science Academic Group, Nanyang Technological University, Singapore, Singapore

Introduction and Objectives: Back injuries are common among runners but little is known about the strength characteristics of lower limb muscles in runners with chronic Low Back Pain (LBP). This study aimed to compare the isokinetic strength of the hip and knee muscles between chronic LBP and healthy recreational runners.

Methods: Using a retrospective design, 18 [9 males, age = 27.8 (5.6) yr) recreational runners with chronic LBP and 18 [9 males, age = 24.6 (3.5) yr) healthy runners were recruited. Maximum concentric torque of bilateral hip extensors and abductors, and knee extensors were measured using an isokinetic dynamometer at 60˚/s. Peak torques were normalized to individuals' body mass by ratio scaling. A general linear model with repeated measures was used to detect differences in the lower limb strengths between the chronic LBP and healthy runners (between-subject factor: LBP condition, within-subject factor: side of the body, age was used as a covariate).

Results: The LBP runners presented lower knee extensors peak torque than the healthy runners (P = .020, Table 1). There were no significant differences found in hip extensor and abductor isokinetic strength. No bilateral differences were observed in any strength variables.

Runners with chronic LBP are characterized by weaker knee extensor strength compared with healthy runners. In literature, there is no information on lower limb strength in chronic LBP runners but the association between isokinetic knee strength reduction and trunk weakness in patients with disc herniation and other chronic LBP populations has been reported [1,2]. Knee extensor inhibition and trunk muscle endurance reduction as detected by EMG were also found in golfers with chronic LBP.[3] In a study specifically on runners, increased knee joint stiffness during running has been reported in chronic LBP runners comparing to the healthy controls.[4] During running, the quadriceps contract eccentrically following initial contact, playing an essential role as shock absorbers.[5] Weakness and inhibition of the knee extensors may increase knee joint stiffness during running and therefore reducing its capacity for shock attenuation. The shock from ground may then transmit to the low back, increasing lumbar spine stress.

Conclusion: Chronic LBP runners showed lower knee extensor isokinetic strength. Assessing knee extensor strength may contribute to the screening, diagnosis and rehabilitation of chronic LBP runners.

Table:

Torque	Side	LBP	Healthy		*P*-value	
				Condition	Side	Condition × side
Knee extensor (Nm/kg)	D	2.19 (0.43)	2.49 (0.39)	**.020**	.240	.389
	ND	1.96 (0.38)	2.41 (0.36)			
Hip extensor (Nm/kg)	D	1.19 (0.36)	1.43 (0.50)	.223	.615	.734
	ND	1.25 (0.30)	1.43 (0.45)			
Hip Abductor (Nm/kg)	D	1.28 (0.46)	1.30 (0.40)	.437	.051	.235
	ND	1.27 (0.47)	1.39 (0.45)			

Data are in mean (standard deviation). D = dominant, ND = non-dominant.

Caption: Table 1. Comparison of lower limb isokinetic strength between chronic low back pain (LBP) and healthy runners

References:

[1] Ho et al., *Spine*, 30: E528-533, 2005.

[2] Lee et al., *Spine,* 20:1994-1996, 1995.

[3] Suter et al., *Spine*, 26: E361-366, 2001.

[4] Hamill et al., *Res Sports Med*, 17:260-274, 2009.

[5] Novacheck, *Gait Posture*, 7:77-95, 1998.

Disclosure of Interest: None Declared

Lower Limb

PO-0124

AN APPROACH TO SIMULATING OVERGROUND ACCELERATIVE LOCOMOTION MECHANICS ON A TREADMILL

Dominic J. Farris [1 2,*] Glen Lichtwark [1] Andrew Cresswell [1]

[1] School of Human Movement & Nutrition Sciences, The University of Queensland, Brisbane, [2] Australian Institute of Sport, Canberra, Australia

Introduction and Objectives: van Ingen Schenau [1] described how the mechanical demands of constant speed treadmill locomotion are the same as for overground. However, the same cannot be said for accelerative locomotion overground vs. treadmill locomotion while the belts are accelerated. As shown by van Caekenberghe et al. [2], on an accelerating treadmill belt one is not required to produce the same propulsive impulse as for overground. This is owing to a component of acceleration coming from the acceleration of the reference frame and not acceleration of the body centre of mass (COM) [2]. This results in a theoretical missing component of fore-aft force. Considering the use of wired measurment systems and the advent of instrumented treadmills for biomechanics research, it would be useful to reproduce the mechanics of accelerative movements on a treadmill.

Therefore, we applied a horizontal force proportional to body mass and belt acceleration via a spring element to participants as they walked and ran on the accelerating belt of an instrumented treadmill. The aim was to induce a net fore-aft impulse and net mechanical work demand similar to what would theoretically be required overground. We hypothesised that providing the additional force would result in more similar mechanical demands to overground acceleration than providing no additional force.

Methods: Nine males (mean ± s.d. age = 26 ± 4 years, height = 1.81 ± 0.5 m, mass = 81 ± 9 kg) participated in the study. Each walked and ran on a fore-aft split belt instrumented treadmill (AMTI, USA) as the belts were linearly accelerated at 0.09, 0.26, 0.42 and 0.67 m·s^{-2} from 0.8 to 2.75 m·s^{-1}. For every acceleration the task was completed with and without a horizontal (fore-aft) force applied to participants. This force was applied via a harness worn on the torso and rubber tubing that was anchored to a winch situated 4 m behind the treadmill. A load cell measured the force and the force magnitude was adjusted using the winch to equal the product of body mass and belt acceleration. The instrumented treadmill recorded ground reaction forces (GRF) at 2000 Hz that were filtered using a low-pass cut-off of 25 Hz.

Data were processed on a step-by-step basis. For each step we calculated an experimental value of net fore-aft GRF impulse (I_{net}) and net mechanical work done on the COM (W_{net}). I_{net} was calculated as the integral of the fore-aft GRF and W_{net} as the integral of COM power. COM power was the dot product of the sum of all external forces (including load cell force) and the velocity of the COM. We computed COM velocity as the integral of COM acceleration, which was determined by dividing net external force by body mass. This was an adaptation of the Combined Limbs Method of Donelan et al. [3]. For the trials where a force was applied (LH), the average load cell force (F_{LC}) was also calculated. For comparison to experimental measures, we also computed theoretical values for I_{net}, W_{net} and F_{LC}. Theoretical I_{net} was the product of body mass and the change in velocity of the treadmill belt. Theoretical W_{net} was calculated as: 0.5 x body mass x (final belt velocity^2 - initial belt velocity^2). We multiplied the acceleration of the treadmill belt by body mass to determine

theoretical F_{LC}. Theoretical I_{net} and W_{net} values for each step for all participants were linearly regressed against experimental values from LH and when the harness was not loaded (NH).

Results: The average experimentally achieved F_{LC} at each acceleration rate is compared to the theoretical F_{LC} in Fig. 1A. The experimental F_{LC} proved a reasonable approximation of the theoretical values. Figures 1B & C shows the regressions for I_{net} and W_{net}. For I_{net}, the regression produced a slope of 0.94 ($R^2 = 0.41$) for LH and 0.003 ($R^2 < 0.00$) for NH. For W_{net}, a slope of 1.01 ($R^2 = 0.44$) was observed for the LH condition and only 0.004 ($R^2 < 0.00$) for NH. Regressions produced highly significant (P<0.0001) correlations between theoretical and experimentally derived I_{net} and W_{net} for LH but, non-significant (P = 0.88 and P =0.90) for NH.

Figure:
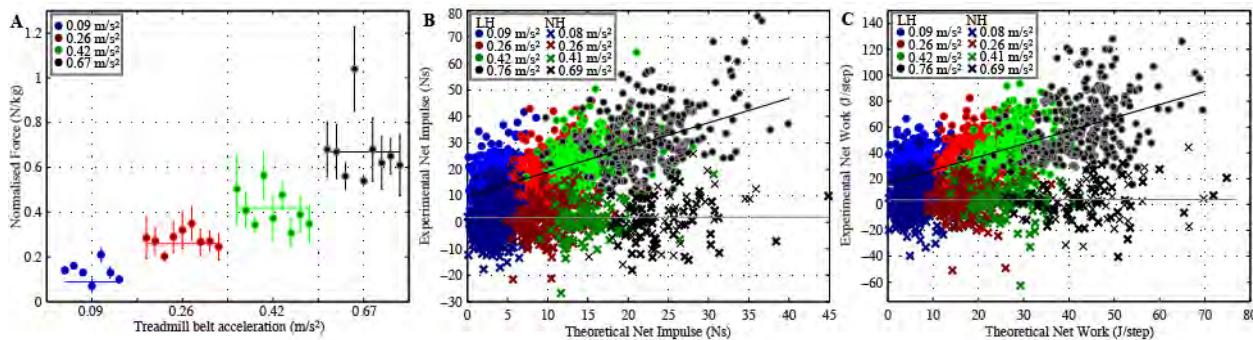
Caption: Fig. 1. (A) Participant normalised load cell force (o) vs. theoretical force (lines). (B) Regression for net fore-aft GRF impulse - LH (o, black line), NH (x, grey line). (C) Regression for net mechanical work - LH (o, black line), NH (x, grey line)

Conclusion: Our hypothesis was supported by the regression results that showed significant and moderate correlations between theoretical and experimental I_{net} and W_{net} values when an appropriate force was applied, but not when no force was applied. For future experiments this could be improved upon by removing outlying steps where the experimental F_{LC} did not match the theoretical F_{LC} well, or by developing a more accurate method of applying the appropriate force.

References: [1]Van Ingen Schenau, Med Sci Sports Exerc,12:257-61,1980. [2]Van Caekenberghe et al., Gait & Posture,38:125-31,2013. [3]Donelan et al., J Biomech,35:117-24,2002.

Disclosure of Interest: None Declared

Lower Limb

PO-0125

THE EFFECT OF GAIT VELOCITY ON JOINT MOMENTS AFTER ANTERIOR CRUCIATE LIGAMENT RECONSTRUCTION

Karine J. V. Stoelben [1,*] Mateus Silveira [1] Evangelos Pappas [2] Carlos Mota [1]

[1]Laboratory of Biomechanics, Federal University of Santa Maria, Santa Maria, Brazil, [2]Faculty of Health Sciences, University of Sidney, Sidney, Australia

Introduction and Objectives: Compensatory gait adaptations after an anterior cruciate ligament reconstruction (ACLR) can indicate individual protection mechanisms to avoid overload on the affected knee [1]. Asymmetries generated by these compensatory changes can lead to injuries and degenerative diseases [2].

Even two years after ACLR neuromuscular deficits persist [3]. However, the effect of increasing gait speed in patients who had ACLR at least four years ago has not been investigated. Therefore, the objective of this study was to analyze joint moments of the lower limbs in adults who had ACLR at least 4 years ago while walking at two different velocities.

Methods: Six men between 30 and 45 years old took part in the study. All of them had ACLR between four and eight years ago. KOOS and IKDC questionnaires were completed before the measurement of gait biomechanics. Then, participants were asked to walk on a 10m walkway at two different velocity conditions: their preferred walking speed and 30% faster than the preferred speed.

Six infrared cameras (VICON system) captured the motion of 16 markers (PlugInGait Model) attached to body landmarks with acquisition frequency set at 200 Hz. Two force plates (AMTI) recorded the kinetic data at 1000 Hz sampling rate. Kinematic and kinetic data were filtered by a 4th order Butterworth low pass filter, with cut-off frequency of 6 Hz. Walking speed was monitored during the data collection using two photocells positioned six meters apart but also assessed by tracking the average velocity of one marker attached to the participants' hip. Joint moments were calculated with inverse dynamics equations of motion (NEXUS 1.8.5, VICON).

Three successful trials (total landing of the foot upon the force plate and gait velocity within 5% of target) for each condition were used in the analysis. Joint moment data were normalized to the stance phase of the gait cycle and statistically compared between limbs and velocities at 10% increments of the stance phase of the gait cycle (Fig. 1). Data normality was verified by Shapiro-Wilk test and the limbs (ACLR vs. intact) were compared with independent Student t test or with U Mann Whitney, accordingly. The comparison between velocities was performed with a paired t test or Wilcoxon. The significance level was set at $\alpha = 0.05$ a priori.

Results: The participants' characteristics were (mean ± standard deviation) age of 36.67 ± 4.57 years; height of 174.8 ± 6.97 cm, mass of 90.82 ± 6.18 kg, time since ACLR of 70.17 ± 15.12 months, IKDC score of 84.48 ± 7.47. KOOS scores were: 85.71 ± 10.71 for symptoms, 92.13 ± 5.42 for pain, 96.82 ± 2.15 for activities of daily living, 85 ± 11.55 for sport and recreation function and 62.5 ± 11.97 for knee-related quality of life. Two subjects had the ACLR on the right limb.

No differences were found between ACLR and intact limb for any moments ($p>0.11$).

In respect to the sagittal plane moment, both ACLR and intact limbs showed higher ankle plantarflexion moments at mid stance ($p≤0.025$) during walking at preferred speed compared to the fast speed. At the beginning of the stance phase,

larger knee moments were observed at faster speeds for both limbs (p≤0,01). The ACLR limb showed larger knee moments in mid stance at the preferred speed (p=0,019) and the intact limb in the final stance (p=0,018). Larger hip extension moments at the beginning (p≤0,018) and larger hip flexion moments at the end of the stance (p≤0,03) were found when walking faster for both limbs. In respect to the frontal plane moment, there were no differences in ankle moments (p>0,17). In the knee, the intact knee showed larger adduction moments at the beginning of the stance when walking faster (p=0,043). Similarly, hip adduction moments were larger at beginning (p≤0,014) and immediately after heel strike (p≤0,028) when walking with faster velocities for both limbs. Schaefer et al. [4] found more symmetrical gait patterns when young adults without injuries increase their velocities. The current results demonstrate different behavior, with greater compensatory patterns when walking faster. Joint moments at the hip showed larger adduction moments for both limbs, suggesting a possible compensatory mechanism to avoid overload on the ACLR knee.

Figure:
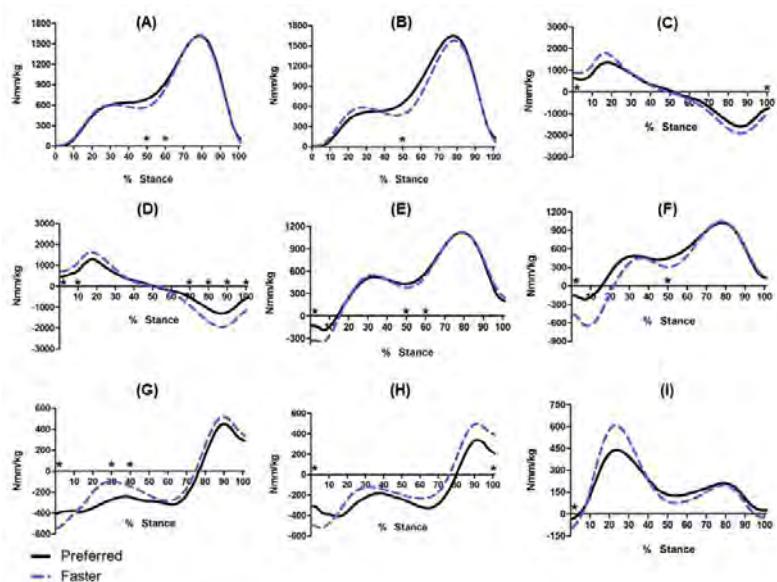
Caption: Figure 1: Joint moments of ankle on sagittal plane (A;B); hip on sagittal (C;D) and frontal (E;F) planes and knee on sagittal (G;H) and frontal (I) planes during walking at preferred and faster speeds. ACLR limb: A;C;E;G. Intact limb: B;D;F;H;I. *Different for p<0.05

Conclusion: Faster walking velocities are associated with increased joint moments (mainly around the hip) suggesting possible compensatory mechanisms that may provide insight into the biomechanical mechanisms of the development of post-traumatic knee osteoarthritis.

References: [1] Orishimo et al., *Knee* Surg *Sports* Traumatol Arthrosc, 18:1587-93, 2010.

[2] Roewer et al., J Biomech, 44:1948-53, 2011.

[3] Castanharo et al., J Orthop Sci, 16:531-5, 2011.

[4] Schaefer et al., Gait Posture, xx: xx–xx, 2014.

Disclosure of Interest: None Declared

Lower Limb

PO-0126

GAIT RESPONSE TO AN ACUTE PHYSICAL ACTIVITY STIMULUS IN INDIVIDUALS WITH OSTEOARTHRITIS PAIN.

Katherine A. Boyer [1,*] Carl Jewell [1] Jocelyn Hafer [1]

[1] Kinesiology, University of Massachusetts-Amherst, Amherst, United States

Introduction and Objectives: Musculoskeletal pain related to osteoarthritis (OA) is a major cause of disability in older adults. Despite significant effort to improve pain management in OA, there has been limited success as current therapies provide only mild to moderate pain relief.[1] A contributing factor to this variable success may be a lack of information regarding changes in the mechanical environment of the joint with pain. Weight bearing activity is known to exacerbate OA pain on a short term basis [2]; however, very little is known about patient gait compensations to acute flares of OA pain. This acute increase in pain in response to a mechanical stimulus (i.e. weight bearing activities) presents an opportunity to probe the motor system adaptation to pain in the absence of changes in disease severity. The aim of this study was to test the hypotheses that, in response to a 20 minute moderate paced walking stimulus (20MWS), there would be an increase in pain for knee OA patients and there would be a significant difference in the change in ambulatory function and gait mechanics for knee OA patients compared with pain free, healthy younger and older adults.

Methods: Thirty subjects including 14 healthy younger adults (HY) (24.36 ± 3.7 yrs; 23.8 ± 2.8 kg/m^2; 10 healthy older adults (HO) (63.9 ± 5.0 yrs; 22.7 ± 2.8 kg/m^2) and 7 older adults with knee pain (OA) (62.3 +/- 6.2 years; 24.8 +/-2.8 kg/m^2) were enrolled after completing the informed consent process and a Physical Activity Readiness Questionnaire (PAR-Q+). For the OA group, the Knee Osteoarthritis Outcome Score (KOOS) was used to assess knee symptom severity. Gait mechanics data were collected before and after the 20MWS while subjects walked at a preferred and faster than preferred speed over a 20m long walkway with embedded forceplates. External joint moments were calculated for the lower limb using an inverse dynamics procedure. For the 20MWS, subjects walked on a treadmill at a pace similar to the faster than preferred overground speed, or "fitness" pace. For the OA group perceived pain was evaluated on an 11 point verbal numeric pain rating scale (vNRS) in the first and final 2 minutes of the 20MWS. Primary outcome measures were walking speed, stance time, 1st and 2nd peak ground reaction forces (GRF1, GRF2), maximum external knee flexion (KFM), adduction (KAM1, KAM2), external rotation (KERM) and internal rotation (KIRM) moments. Significant group differences in the change in gait outcomes following the 20MWS were tested for using a one-way analysis of variance with least significant difference adjusted post-hoc testing and alpha level of 0.1.

Results: The mean KOOS pain score for the OA group was 62.7 ± 23.1. The initial and final vNRS were 2 ± 1.7 and 2.4 ± 2.2, respectively (p=0.19). At the preferred walking speed there were significant differences in 1st peak KAM between HO and OA and Y and OA and in the stance time for Y and OA in response to the 20MWS (Figure 1). At the faster than preferred speed there were significant differences in the change pre-post 20MWS for the 1st and 2nd peak KAM between the HO and OA and Y and OA (Figure 1). There were also significant differences in the change pre-post 20MWS in the KIRM between the HO and OA and Y and OA for both speeds. No differences in the change in walking speed or GRF magnitudes were found with the 20MWS.

Figure:

Change at preferred speed

Change at faster than preferred speed
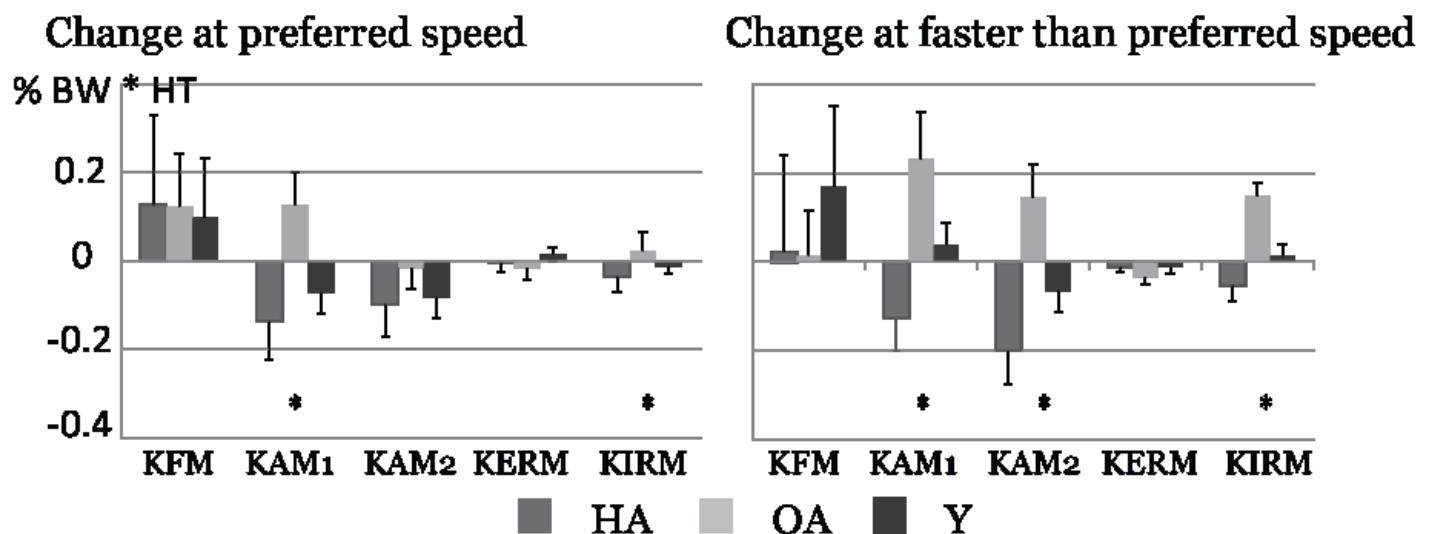
Caption: Figure 1: Changes in joint kinetic parameters in response to the 20MWS for the healthy older (HA), knee OA (OA) and healthy younger (Y) groups. * indicate a significant difference with $p < 0.1$.

Conclusion: In contrast to the hypothesis, the OA patients did not report a significant increase in pain in response to the 20MWS however, as expected, there were significant differences in the gait response to a 20MWS between the healthy older, younger and chronic knee OA pain groups. While there was a decrease in the KAM magnitude for the healthy groups following the 20MWS, there was an increase in the KAM, as well as the KIRM for the OA group. The KAM is a surrogate measure for the distribution of loading at the knee joint and this OA group response would thus indicate a possible increase in the load acting across the medial compartment of the knee. In response to the 20MWS, mild muscle fatigue in combination with pain-related inhibition of the knee extensor muscles may combine to alter coordination of movement and the ability to maintain a "protective" gait pattern that individuals with chronic pain may have adopted. The changes in joint kinetics could exacerbate an acute pain flare in response to weight bearing activity. This suggests a need for more complex pain adaptation theories for chronic pain conditions such as knee OA[3]. Given that weight-bearing physical activity is often recommended for management of OA, there remains a need to understand the mechanisms of the unexpected changes in gait.

References: [1]Reid MC et al, *HSS J*;8:159-164, 2012
[2]Focht BC et al, *Ann Behav Med*;24:201-210, 2002
[3]Hodges PW,*J Electromy Kines*;21:220-228, 2011

Disclosure of Interest: None Declared

KINECT-BASED LOWER LIMB MOTION ANALYSIS

Shikha Sarkar [1,*]Lina Stankovic [1]Andrew Kerr [2]Philip Rowe [2]

[1]Electronic and Electrical Engineering, [2]Biomedical Engineering, University of Strathclyde, Glasgow, United Kingdom

Introduction and Objectives: This paper investigates the viability of using the Kinect sensor for the purposes of gait analysis in patients recovering from stroke. Use of Kinect has been studied, with little success, for recording of clinical data using analysis [1, 2]. Posture, gait, and mobility data can be produced from 3D point cloud sequence. Physiotherapy programs based on optical movement analysis systems are the norm, and they require large facilities and expensive installations comprising several cameras such as the Vicon. The proposed Kinect based solution, JAFAKEC system, provides a marker-less inexpensive alternative for gait analysis at home or at care homes. Capture of human movements is the primary application of the Kinect but the Kinect SDK does a quick and approximate computation of joint positions, which are not accurate enough for clinical gait monitoring. This paper details the mathematical algorithms applied on the point cloud to improve accuracy of the joint angle calculation.

Methods: The proposed approach starts with an investigation of the achievable accuracy and suggests using some low-complexity algorithms as given in table 1 to improve the accuracy of joint positions. The captured depth frame from the Kinect recorder is compressed via run length encoding to allow storage of more frames in a limited memory. The stored point cloud is then used to perform body part labelling and pattern recognition in order to detect the limbs of interest. This process is followed by feature extraction via multiple geodesic distance labelling, shortest path algorithm and model fitting on specific subsets of points once the geodesic distances are attached to the points. With these features attached to each point, points are classified in the space of the features as belonging to specific limbs. Finally, the principal axes of the limbs are computed and the joint angles are calculated as angles between the principal axes.

Experiments:

Two different healthy males and one female were instructed to walk across a 10 meter walkway in the laboratory for the recording using the Kinect at different speeds for the gait data capture of both the left and right legs for approximately 1 to 2 minutes for a few trials. Spatiotemporal data were collected simultaneously using a 12 camera Vicon system with reflective markers placed according to the Vicon requirement.

Results: Experiments were performed to evaluate the proposed system, and results are benchmarked with the state-of-the-art Vicon optical movement analysis system. Figure 1 shows that the calculated angles obtained using the Kinect version 1.8 are a good match with the Vicon results.

Figure:
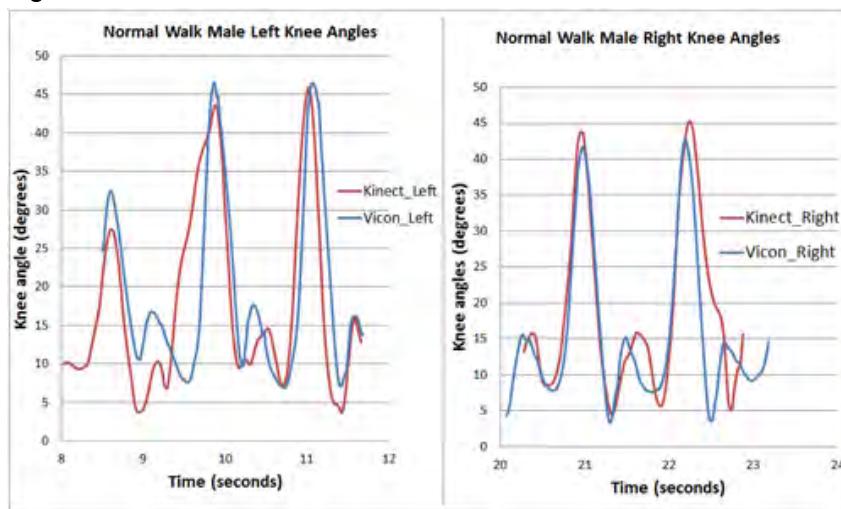
Caption: Figure 1: Kinect 1.8 vs Vicon, normal person, walking in moderate speed

Conclusion: The joint angles obtained from the skeleton computed by Microsoft Kinect SDK were inaccurate, but the depth frame is shown to achieve better accuracy in capturing the gait cycle of a subject walking at a distance of about 3m from the Kinect sensor. An assortment of geometric algorithms has been used to improve the accuracy of gait capture. Figure 1 shows that the accuracy of Kinect 1.8 results using the proposed JAFAKEC system is within a range of 5 degrees from the angle computed by Vicon. JAFAKEC, using a suite of customised mathematical algorithms, enables marker less gait capture for healthy and post-stroke patients, inexpensive in home application, easy to use GUI and fast. Using the proposed algorithms, the swing phase knee angles in the gait cycle are getting computed accurately but the stance phase knee angles are relatively inaccurate. The system works reasonably well with healthy males but needs to be improved for female gait data as the peak results have a higher difference of gait angle as compared with Vicon.

Table:

Algorithm	Application in JAFAKEC
Geodesic distance labelling	Forming a mesh representing the surface
Shortest path algorithm	Defining features of points for limb classification
3D Convex hull	Assembling the classified points for a single limb into a polyhedron so that point-density does not have an effect on axis calculation
Least-square line fitting	Determining the principal direction of an oblong polyhedron or point-set corresponding to the limbs of interest.
Sectioning of point cloud	Segmenting into sub regions such as for specifying source regions for shortest path and for feature definition.

Caption: Table 1: Algorithms used in the JAFAKEC system

References: [1] R.A. Clark et al., Gait and Posture, 36: 372–377, 2012.

[2] T.Dutta, Applied ergonomics, 43: 645-649, 2012.

Disclosure of Interest: None Declared

Lower Limb

PO-0128

ASSESSMENT OF POWER LOWER LIMBS IN WOMENS WITH LOW BONE MINERAL DENSITY

Diane Hartmann [1] Sandra Morais [2] Estele C. W. Meereis [3,*] Luiz Fernando Rodrigues [1] Rafael Gobbato [1] Jaqueline Biazus [1] Carla Mai [1]

[1]University Franciscano Center, [2]Federal University of Santa Maria, Santa Maria, [3]Federal University of Rio Grande do Sul, Porto Alegre, Brazil

Introduction and Objectives: Osteoporosis is the deterioration of bone mass, which leads to a growth of bone fragility and a higher risk of fractures. It may happens to both men and women, being more predominant among women. Therefore, this research aimed to verify if the aquatic exercises influence the cases of low bone mineral density (BMD).

Methods: The research had a quantitative almost-experimental approach with pre and post tests. Samples of 14 women, aged 55 to 80 years old. Project approved by the CEP: 162.843. Muscle Strength Test was applying in lower members were done through the dynamometer MIOTOOL® 400. The Hydrotherapy protocol was made in two sessions of 50 minutes a week, in total 8 weeks. For dynamometry analysis was used Wilcoxon test, the data were typed at an Excel data base and the statistics analysis was done in the SPSS Program, version 15.0.

Results: Muscle Strength evaluation showed meaningful improvement on right quadriceps (p= 0,005099) and left quadriceps (p= 0,00004423).

Conclusion: Hence, it was observed that the hydrotherapy protocol has significant influence on the power from osteopenic patient's lower limbs.

Disclosure of Interest: None Declared

COORDINATION VARIABILITY AND OVERUSE RUNNING INJURIES: A PROSPECTIVE INVESTIGATION

Julia Freedman Silvernail [1,*]Katherine Boyer [2]Joseph Hamill [2]

[1]Kinesiology and Nutrition Sciences, University of Nevada, Las Vegas, Las Vegas, [2]Kinesiology, University of Massachusetts, Amherst, United States

Introduction and Objectives: Coordination variability has been viewed as a metric of musculoskeletal health in human movement research[1]. Both injured and disease states have been tied to lower values of coordination variability compared to healthy individuals [1,2]. It has been suggested that, in a healthy system, variability contributes to adaptability, protecting the individual from injury [1,2]. Yet there is a dearth of prospective research to determine if lower values of variability may lead to injury or is instead a result of injury. Therefore, the purpose of this investigation was to test the hypothesis that prospective running data would show that coordination variability would be greater in individuals who remain healthy compared to those who become injured.

Methods: 110 runners were enrolled to the study after providing informed consent. Participants ran at 3.5 m/s (±5%) in a neutral laboratory shoe while three-dimensional kinematics and kinetics were collected.   Runners were tracked for one year after the gait analysis was performed and information on injuries incurred was gathered. Participants were asked via email to report if they had sustained an injury which was defined as anything that forced them to alter their normal training for more than two days. Participants who reported an injury completed a questionnaire clarifying the nature and location of the injury. Eleven participants reported overuse injuries during the data collection period (Table 1). Twenty-five participants who reported remaining healthy over the data collection period were selected as the control group.

Five trials for each participant were used for further analysis. Foot, Shank and Thigh segment angles were calculated relative to the laboratory coordinate system using a cardan sequence (X-Y-Z). Segment angles were time normalized for the stance phase of gait and were divided into sub-phases of early stance (1-33%), mid-stance (34-66%) and late stance (67-100%). A modified vector coding technique [3] was used to determine the movement coordination variability during stance for the following segment couplings: Sagittal plane foot and shank rotation, foot eversion and shank internal rotation, sagittal plane thigh and shank rotation, transverse plane thigh and shank rotation and thigh flexion and shank internal rotation. Trial to trial variability was calculated as the circular standard deviation of the coupling angle calculated at each percentage of stance for each participant. Variability was averaged over each sub-phase of stance and was compared between healthy and injured groups using independent t-tests ($\alpha = 0.05$).

Results: During all phases of stance coordination variability was similar between healthy and injured runners for all measured segment couples ($p > 0.05$).

Figure:
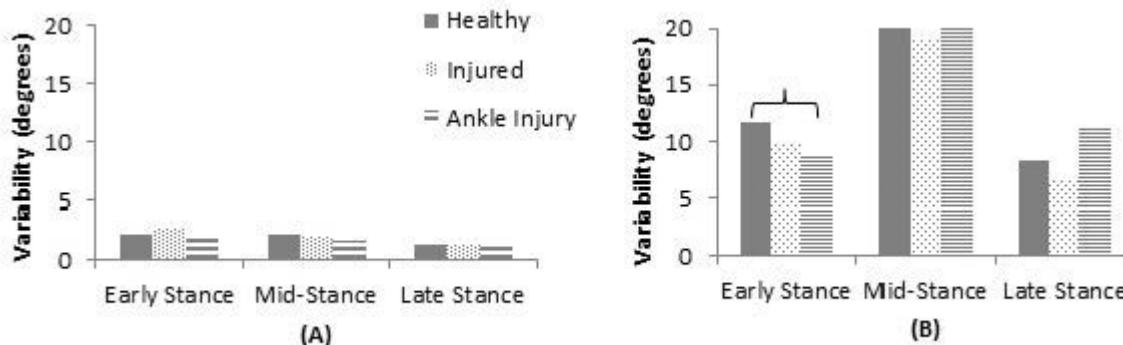
Caption: Figure 1: Coordination Variability of the Foot-Shank Couple: (A) Sagittal plane motion, (B) Foot eversion-Shank internal rotation

Conclusion: It appears that individuals who will become injured do not exhibit overall lower coordination variability when running than individuals who remain healthy. With only a 10% injury rate, this study was limited in the injury data available. Furthermore, the injuries sustained by the participants varied. This suggests that if coordination variability plays a role in injury risk, it is likely specific to the injury location and cannot be generalized to overall changes in variability. To investigate this further, the variability of a subgroup of injured participants (n=4) whose injuries were sustained at the ankle/shank level was analyzed. These individuals had significantly less coordination variability during early stance in the couple of shank internal rotation and foot eversion (Figure 1). With such a small number of participants it is difficult to generalize overall conclusions regarding this information. However, these findings suggest that when looking at applicable segment couplings, individuals at risk may be able to be identified prior to injury.

Table:

Injuries Reported	Number
ankle/shank	4
hip/thigh	4
knee	1
back	1
forefoot	1

Caption: Table 1: Breakdown of Injury Location in Injured Group

References: [1] Van Emmerik et al. (2nd ed.). Research Methods in Biomechanics, Human Kinetics Publishers,2013.

[2] Hamill et al. *Clinical Biomechanics,14*(5): 297-308, 1999.

[3] Chang et al. *Journal of Biomechanics*, 41: 3101-3105, 2008.

Disclosure of Interest: None Declared

Lower Limb

PO-0131

INTRALIMB JOINT COORDINATION IS AFFECTED BY DIABETES MELLITUS EVEN BEFORE PERIPHERAL NEUROPATHY IS INSTALLED

Liu C. Yi [1,*] Cristina Sartor [2] Francis Trombini-Souza [2] Isabel Sacco [2]

[1]Human Movement Science, Federal University of São Paulo, Santos, [2]University of São Paulo, São Paulo, Brazil

Introduction and Objectives: Diabetes Mellitus (DM) is cause of impairments to stability, mobility and locomotor tasks, especially due to polyneuropathy. It affects distal segment tissues and functions, especially in the ankle. This might induce compensatory mechanisms in intralimb coordination, especially between ankle and hip joints that has seldom been addressed in this population. When associated with increased time-space depreciation and altered loading distribution that are consequences of the disease, they may lead to major comorbidities such as ulcers and falls. Its constant repetition may cause overuse injuries or can be associated with lower mobility and poor capacity of adaptation [1]. Our aim is to describe changes in lower limb coordination in different groups of patients with and without DM to identify how the disease affects the gait cycle. Besides that, we are interested in identify if there would be a pattern of coordination that could distinguish between healthy and different stages of DM installation.

Methods: Sixty subjects between 45 and 65 years-old were evaluated and divided into 4 groups by using Fuzzy Logic Model [2]: Control (CTRL=13, 55±7 years-old, BMI 24±2), Diabetic (DIAB=18, 59±6 years-old, BMI 28±6, DM for 11±7 years, MNSI score 5±3), Mild Diabetic Neuropathy (MILD=7, years-old 56±4, BMI 27±2, DM for 19±7 years, MNSI score 10±3) and Severe Diabetic Neuropathy (SVRE=22, 57±5 years-old, BMI 29±4, DM for 14±8 years, MNSI score 12±4). Patients walked in a 10m walkway, barefoot, in a constant speed monitored by a metronome. Continuous relative phase (CRP) was calculated on each stride [3]. Hip, knee and ankle segmental angular velocities were calculated as the first derivative of segment angular position. Angular position and velocity were normalized to 101 data points. These normalized position and angular velocities vectors were plotted relative to each other for each of the 3 joints. The Phase Angle for hip and ankle joint during gait cycle were calculated ($\theta_{i} = \tan^{-1}[y_i/x_i]$). Afterwards the Relative Phase Angle was calculated, that consist the difference between distal and proximal joint Phase Angle ($\theta_{relative\ phase} = \Phi_{distal\ segment} - \Phi_{proximal\ segment}$). CRP was defined for the joint pairs of (a) ankle and hip, (b) ankle and knee and (c) knee and hip, at each instant of the stride. CRP variability was defined as the standard deviation of the CRP at each time point across the trials. The gait cycle was divided in 5 phases: early stance (0-10%), early midstance (11-40%), late midstance (41-60%), propulsion (61-80%) and balance (81-100%). The mean and standard deviation were calculated and one-way ANOVAs between groups were performed to each frame of the resulting time series. One-way ANOVAs between groups were also calculated for standard deviation of the 5 stance phases to compare the CRP variability (α = 5%).

Results: For the ankle-hip CRP, the SVRE presented increased variability in the early stance and remains more anti-phase ratio during late midstance compared to other groups. During propulsion, all diabetic groups remain with more in-phase ration than the CTRL, that also had increased variability. For the ankle-knee CRP, the 3 diabetic groups had more anti-phase ratio than during the early and late midstance, with decreased variability in early midstance. In propulsion phase, the same groups had more anti-phase at the end of balance phase. Finally, for the knee-hip CRP, the MILD

showed more in-phase ratio at the beginning of stance and all the diabetic groups again were more in-phase at early midstance (with lower variability) and at the end of balance phase, especially the MILD that had lower variability than the others.

Figure:

Continuous Relative Phase of Ankle - Hip

Continuous Relative Phase of Ankle - Knee

Continuous Relative Phase of Knee - Hip

Severe neuropathy
Mild neuropathy
Diabetic
Control

* Control is different from the others
# Control, diabetic and severe are different from each other
& All groups are different from each other
$ Mild is different from the others
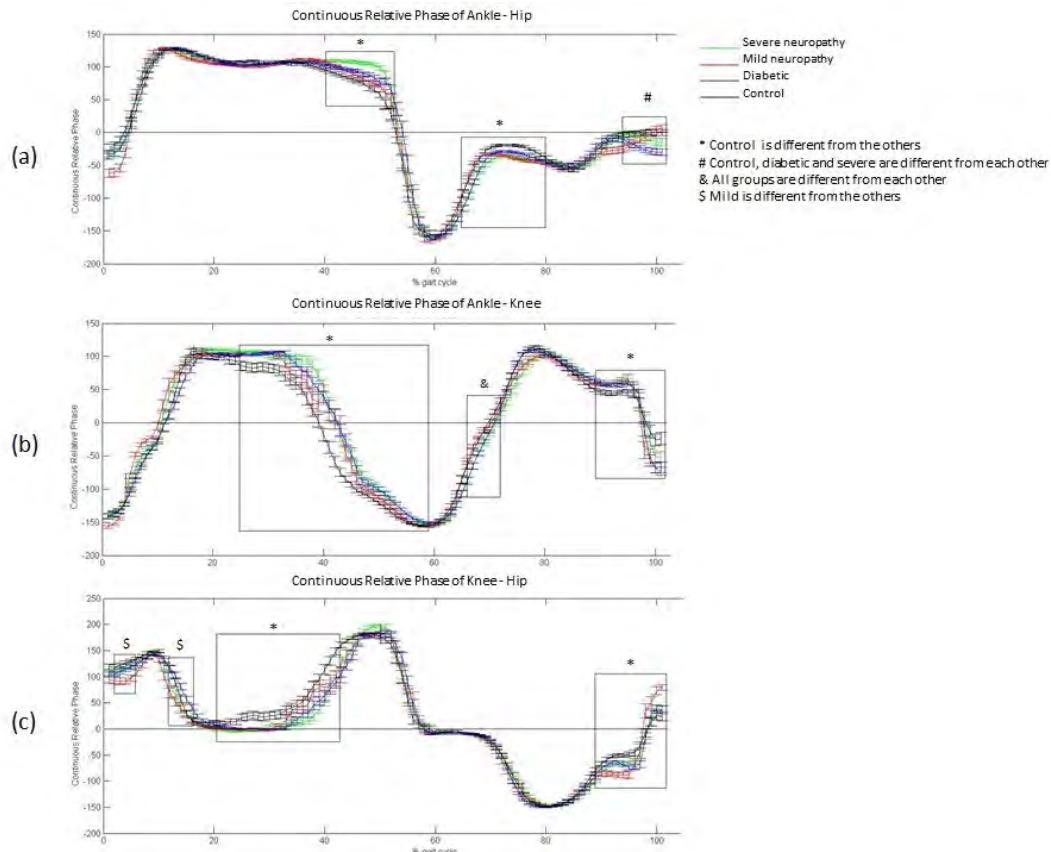
Conclusion: The three CRP were able to distinguish between the control and the diabetic groups, showing that DM can influence on the lower limb coordination during gait. Those differences in coordination were present mainly during the midstance, when the lower limb has to deal with loading transferring in unipedal support. Related to diabetes complications, only the ankle-hip CRP could distinguish the SVRE from the others in late midstance, and only the knee-hip CRP could distinguish the MILD in the beginning and at the end of balance phase. It is expected that the SVRE would have the distal segments more compromised by polyneuropathy, and therefore the hip could deal with the distal insufficiency since it is a more proximal and preserved joint. The low variability and differences in CRP of the MILD was not expected, but could represent an early adjustment of coordination as soon as the disease installation starts to change the sensorimotor intra-limb relations.

References: [1] Esposito et al., Gait&Posture, 40(4): 640-6, 2014.
[2] Watari et al., J Neuroeng Rehabil, 8: 11-11, 2014.
[3] Hamill et al., Clin biomech (Bristol Avon), 14: 297-84, 1999.

Disclosure of Interest: None Declared

PO-0132

RELIABILITY OF ANKLE MUSCLE ACTIVITY IN HEALTHY AND FUNCTIONAL INSTABLE ANKLES DURING PERTURBED TREADMILL WALKING

Antje Reschke [1,*]Steffen Mueller [1]Martin Wolter [1]Tilman Engel [1]Stephan Kopinski [1]Heiner Baur [2]Frank Mayer [1]

[1]Sports & Health Sciences, University Outpatient Clinic Potsdam, Germany, Potsdam, Germany, [2]Health Division, Bern University of Applied Sciences, Bern, Switzerland

Introduction and Objectives: Reflex reaction of ankle muscles can be evaluated by unexpected stumbling trials on a treadmill. In individuals with functional ankle instability (FAI), inter-session reliability of ankle muscular activity during normal (NW) and perturbed walking (PW), performed on a split-belt treadmill, is unclear. The aim of this study was to assess inter-session reliability of ankle muscle EMG amplitude (EMG-A) in adults with and without FAI during NW and PW on a split-belt treadmill.

Methods: Fourteen participants (6 M, 8 F, 26±5 yrs, 1.80±0.09 m, 76±15 kg) were included in a test-retest (M1, M2) design with 6 weeks in between. By means of three criteria (never sprained, score ≥28 pts on "Cumberland Ankle Instability Tool" [CAIT] and ≥80% on "Foot and Ankle Ability Measure" [FAAM], left and right ankle were categorized into healthy ankles (H, n=12). Criteria for functional instable ankles (FAI, n=11) were at least 2 sprains in the past and 1 of 2 scores (CAIT≤27 pts, FAAM<80%). Tests were performed on a split-belt treadmill (WOODWAY): after warm up (walking at velocity of 1 m/s), 30 stumbling stimuli (each 15 left and right belt; time- and side randomized; 100 ms duration [50 ms deceleration to -1 m/s; 50 ms acceleration back to 1 m/s]) were applied 200 ms after initial heel contact (IC). Bilateral sEMG (myon RFTD-32, myon AG, Suisse) was recorded from M. tibialis anterior (TA), M. peroneus longus (PL) and M. gastrocnemius medialis (GM). For EMG-A, RMS was calculated within 200-400 ms post IC, normalized to MVC (%, mean of 15 steps) and presented descriptively (mean±SD of M1 and M2). Reliability was analyzed by ICC (2.1), test-retest variability (TRV, %) and Bland-Altman analysis with bias and limits of agreement (bias±1.96*SD).

Results: EMG-A ranged from 10.1±7.0% (TA, NW) to 93.6±39.4% (PL, PW) in H and from 10.4±4.8% (NW) to 75.7±34.3% (PW) in FAI. For H, TRV varied from 25.8±20.6% (TA, PW) to 57.3±45.2% (PL, PW) and ICC ranged from 0.59 (GM, PW) to -0.24 (PL, PW). For FAI, TRV varied from 35.7±22.3% (GM, PW) to 51.7±45.3% (PL, PW) and ICC ranged from 0.78 (GM, PW) to -0.20 (TA, NW). Bias±1.96*SD ranged from -1.0±24.9% (PL, NW) to -14.8±106.6% (PL, PW) in H and from -2.4±12.2% (TA, NW) to 6.0±97.8% (PL, PW) in FAI (detailed results in table 1).

Figure:

Group	Muscle	NW/ PW	M1, M2 Mean±SD (%)		TRV Mean±SD (%)		Bias	± 1.96*SD	ICC (2.1)
H	TA	NW	10.1	7.0	54.3	44.1	1.6	21.7	-0.03
		PW	70.4	20.3	25.8	20.6	3.6	41.0	0.59
	PL	NW	25.6	12.6	42.7	27.0	-1.0	24.9	0.33
		PW	93.6	39.4	57.3	45.2	-14.8	106.6	-0.24
	GM	NW	46.9	19.2	42.4	48.2	4.3	46.4	0.37
		PW	49.8	27.2	32.9	26.0	13.2	56.9	0.59
FAI	TA	NW	10.4	4.8	48.5	36.1	-2.4	12.2	-0.20
		PW	70.5	22.5	42.0	38.7	-4.6	58.6	0.03
	PL	NW	29.5	19.3	44.7	39.7	4.4	27.4	0.35
		PW	75.7	34.3	51.7	45.3	6.0	97.8	0.12
	GM	NW	37.1	22.6	47.5	57.0	-6.0	29.1	0.69
		PW	46.0	24.0	35.7	22.3	-4.1	28.7	0.78

Caption: Table 1: RMS normalized to MVC (mean±SD, %) of M1 and M2 for both groups (H or FAI), all muscles (TA, PL, GM) and both walking conditions (NW or PW); reliability values of RMS normalized to MVC (%)

Conclusion: Inter-session reliability of ankle muscular activity resulted in poor to moderate values in healthy adults and poor to good values in adults with FAI, depending on walking condition and ankle muscle tested. Large random error and high variation for reliability may reflect the physiological variability in muscle activation during gait and have to be considered with regard to follow-up investigations.

Disclosure of Interest: None Declared

EFFECT OF KNEE TAPING ON LOWER LIMB KINEMATICS IN SIDE-HOPPING TASK

Kuang-Wei Lin [1,*] Yu-Lun Huang [2] Sai-Wei Yang [1] Ying-Fang Liu [3]

[1]Department of Biomedical Engineering, National Yang-Ming University, Taipei, Taiwan, Republic of China, [2]Department of Kinesiology, University of Texas at Arlington., Arlington, United States, [3]Office of Physical Education, Hsin Sheng College of Medical Care and Management, Taoyuan, Taiwan, Republic of China

Introduction and Objectives: Anterior cruciate ligament deficiency (ACLD) is a common injury of knee joint in the sports field. The incidence rate of knee ACL injuries was reported as of 45.4%[1]. In clinical practice, the protective strapping on knee is applied to protect the ACL, however, it is difficult to determine when the ACLD patients are safe to return to strenuous physical activities. Gustavsson et al. (2006) reported that the side hopping task could effectively discriminate the abnormal function of ACL from the normal one [2]. The aim of this study was to biomechanically evaluate the effect of the protective taping on ACLD in kinematics.

Methods: Seven male and ten females (24.65±6.32 years) with one knee ACL injured over 6 months were recruited. Vicon T40 motion analysis system with ten infrared cameras sampled in 100 Hz rate were used. The surface markers were attached on the segments; two force platforms with sampling rate of 1000Hz were used to synchronically record the ground reaction forces during the task.

Before testing, subjects were asked to perform a standard warm up protocol for 20 minutes, then, thoroughly familiarize the experimental procedure with few times of practices. The modified side-hop testing protocol described by Gustavsson et al. (2006) [2] was used. Each subject stood on the injured leg, hopped between two force platforms from side to side, then repeated the same procedure after tapping. The ACL protective strapping method adapted from Anderson et al. (2004)[3]. A static reference measurement was used to measure the locations of the markers (tibial tuberosity, fibular head and both medial and lateral epicondyle) with respect to the cluster markers and to define the neutral joint orientations. Subjects were asked to hop to highest repetition within 30 seconds. The distance of side-hop was determined by the subject's height multiplied by 0.22.

The data reduction of 3D marker trajectories were processed using a MatLab program of 4th order zero-lag Butterworth low-pass filter with a cut off frequency of 8 Hz (The Mathworks Inc., Natick, USA). The calculation of knee Eulerian joint angles was in the rotation sequence of z-x-y. Data were checked the normality first, then used paired t-test to discriminate the efficacy of tapping with the significance of the α level 5%.

Results: Table 1 showed the knee joint angles in the frontal and transvers planes of three different phases. In all phases, taping reduced the knee abduction angle significantly; and significantly increased the knee external rotation angle at the initial contact and take-off phases.

ROM of knee joint with taping in sagittal plane was greater than without taping significantly. In fontal plane, ROM of knee joint with taping was smaller than without taping significantly. However, there was no significant difference in transverse plane (Fig1).

Taping technique aims to restrict excessive joint movements. We combined two taping techniques to provide support and stability to the ACL and collateral ligaments of the knee. Anderson et al. (1992) used cadaver specimens to evaluate the effects of taping and bracing, they found the tape and brace combination reduced knee translation and rotation. However, the tape method used individually restricted translation and rotation better than the Stabler brace along[4]. The primary findings of this study were similar to the effects of taping on healthy knee[5]. It reduced abduction angle and led to the tibia rotation externally. In addition, it decreased the ROM of knee joints in frontal plane that could reduce the risk of ACL tear. However, this study did not calculate the forces acting on knee with taping. Future research should also investigate the reaction forces of the knee joint or muscle activation patterns during the side hop task.

Figure:
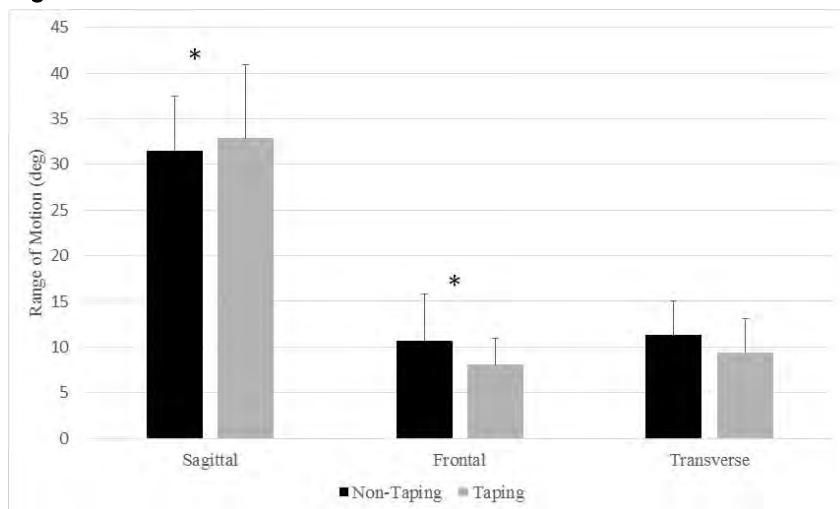
Caption: Average and standard deviation values for ROM of knee joint in three different planes with and without taping during side hop (* $p<.05$).

Conclusion: The findings suggest that taping on ACLD knees contributed to limit the knee joint angle of frontal and transverse plane. Moreover, taping may provide restraining capabilities to prevent ACL injury.

Table:

Phase	Direction	Non-taping	Taping	p
Initial contact	Adduction(+)/Abduction(-)	-6.77±5.01	-3.14±4.43	.00**
	Internal(+)/External(-) rotation	-3.91±5.35	-7.30±5.51	.00**
Max flexion	Adduction(+)/Abduction(-)	-4.46±7.34	-2.66±6.58	.02*
	Internal(+)/External(-) rotation	-1.42±7.19	-2.46±8.24	.25
Take-off	Adduction(+)/Abduction(-)	-8.83±5.18	-5.45±3.98	.00**
	Internal(+)/External(-) rotation	-3.07±5.13	-6.01±5.75	.00**

Caption: Average value with standard deviation of knee joint adduction (+) / abduction (-) and internal (+) / external (-) rotation angle at initial contact, maximum knee flexion, and take-off during jumping outward.

References: [1] Majewski et al., The knee, 13(3): 184-188, 2006.

[2] Gustavsson et al., Knee Surg Sports Traumatol Arthrosc, 14: 778-788, 2006.

[3] Anderson et al., Am. J. Sports Med., 20(4): 416-421, 1992.

[4] Lin et al., DSR proceeding, 2011.

Disclosure of Interest: None Declared

Lower Limb

PO-0134

REPRODUCIBILITY OF KINEMATICS MEASURED WITH INERTIAL MEASUREMENT UNITS (IMU) DURING TREADMILL RUNNING

Jasmin Gaudel [1,*]Anna Dannemann [1]Doris Oriwol [1]Christian Maiwald [1]

[1]Department of Research Methodology and Data Analysis, Institute of Kinesiology, Chemnitz, Germany

Introduction and Objectives: Over the past few years, use of inertial measurement units (IMU) to measure running-specific features has increased [1, 2, 3]. The advantages compared to stationary kinematic systems (e. g. 3D-motion-capture-systems, force plates) are the possibility to use inertial sensors in field test based on the low weight, small size and wireless mounting [4].

To use inertial sensors in field conditions, data reproducibility should first be tested in a laboratory setting, particularly on the treadmill. Expected variations in the measurement setup and participants must be known to make predictions about kinematic running parameters, e. g. interventions and shoe-specific demands. However, there are currently no scientific studies in this area.

Therefore, the purpose of this study is to analyze the reliability of kinematic parameters during treadmill running and to determine variation ranges.

Methods: Eleven well-trained runners (3♀; 8♂, age: 25 ± 3 y; height: 1.78 ± 0.09 m, weight: 71.4 ± 9.7 kg) performed two running trials over 50 minutes on a treadmill. There was a resting period of 3 days between each trial. On day 1 (MD1), the participants ran at a self-selected, comfortable running speed (10.29 ± 1.08 km/h) with their own running shoes. On day 2 (MD2), the measurements were repeated using the same procedure. Maximum eversion velocity (EVmax [°/ s]) and stride duration (StrD [ms]) were acquired using inertial sensor (Achillex©; 3-axial; acc., mag., gyr.; 400 Hz) at the heel cap on the left side. The first 2000 strides were analyzed minus a warm-up period of 40 strides. The statistical analyses include mean differences ($diff_{mean}$ (absolute); $diff_{norm} = (Mean_1 - Mean_2)/\ Mean_{all} * 100$ (relative)), limits of agreement ($LoA = \pm\ 1.96 * SD_{diff}$ (absolute); $LoA_{norm} = \pm\ 1.96 * SD_{diff}/\ Mean_{all} * 100$ (relative)) and Bland & Altman plots with pooled standard deviation (SD_{pool}) used as a measure for intra-subject variability.

Results: The data analyses revealed high inter-subject variability for both parameters, which illustrated the high ranges on the two measuring days (Table 1).

EVmax showed high intra-subject variability (Figure 1). Individual running cycles of some participants were clearly beyond the limits of agreement. The inter-subject variation of EVmax will likely be underestimated when only a limited number of stride cycles is available for analysis. Nevertheless, the characteristic of intra-subject variability was similar for all participants, which is illustrated by the pooled standard deviation (Figure 1).

Both parameters, EVmax and StrD, are distributed homoscedastically around the average of the differences. This means that there was no systematic bias between the two measurement days.

During treadmill studies, maximum deviations from a participant's true value between repeated measurements is expected to be up to 57.16 °/ s (EVmax).

For Stride duration, the inter-subject variation range may be up to 32.44 ms, which corresponds to 4.3 % (normalized).

Inertial sensors achieve a high degree of reliability for selected parameters in comparison to stationary and other transportable kinematic systems [5].

Figure:
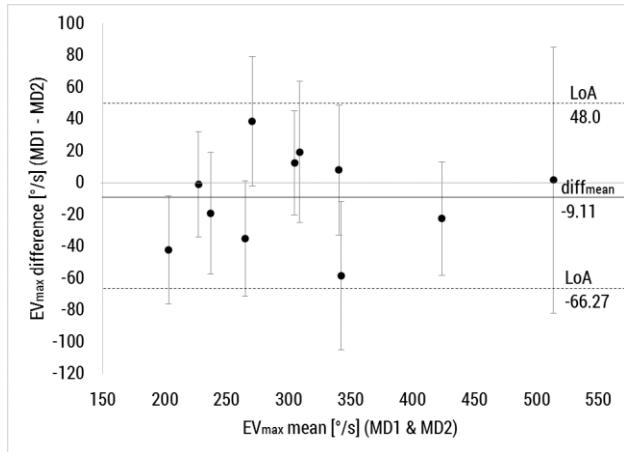
Caption: Fig. 1. Bland & Altman plot for EVmax with error bar of all participants (SDpool)

Conclusion: Inertial sensors can be used to generate kinematic parameters (e. g. EVmax and StrD) as an alternative to stationary systems. The deviations of the true values of a participant should be noted to make statements about previous differences with regard to interventions, shoe-specific demands, etc.

Table:

	Mean 1	Mean 2	R_1	R_2	diff$_{mean}$ ± LoA	diff$_{norm}$ ± LoA [%]
EVmax [°/s]	307.04	317.05	182-514	224-512	-9.11 ± 57.16	-2.92 ± 18.3
StrD [ms]	754.18	753.74	692-801	690-803	-0.44 ± 32.44	0.06 ± 4.3

Caption: Tab. 1. Average value (Mean1; Mean2) and ranges (R1; R2) for MD1 & MD2, diffmean with LoA and diffnorm with LoAnorm for EVmax [°/s] and StrD [ms]

References: [1] Lee, J.B. et al. *Journal of science and medicine in sport / Sports Medicine Australia, 13* (2): 270–273, 2010.

[2] Rønved, S.M. et al. *Footwear Science, 3* (sup1): S133, 2011.

[3] Yang, S. et al. *Gait & posture, 34* (4): 462–466, 2011.

[4] Norris, M. et al. *Journal of Sports Engineering and Technology, 228* (1): 3–15, 2014.

[5] Brauner, T. *Rückfußbewegung beim Laufen. Einflussfaktoren, Messmethodik und innovative Messsysteme*. Dissertation: TU Chemnitz, 2010.

Disclosure of Interest: None Declared

GAIT ANALYSIS FOLLOWING PROXIMAL MEDIAL GASTROCNEMIUS RELEASE – A PILOT STUDY

Alex Humphries [1,*]Aliah Shaheen [1]Derek H Park [2]Daniel McCaffrey [3]Dionysios Trigkilidas [3]Matthew Solan [3]

[1]Mechanical Engineering Sciences, University of Surrey, Guildford, [2]Barnet and Chase Farm Hospital, Royal Free London, London, [3]Orthopaedic department, Royal Surrey County Hospital, Guildford, United Kingdom

Introduction and Objectives: Tightness of the gastrocnemius has been shown to affect dorsiflexion of the ankle [1], leading to increased pain in the forefoot. Gastrocnemius release is shown to improve the dorsiflexion of the ankle [1] and is commonly used in the treatment of gastrocnemius contracture in paediatric patients with neuromuscular conditions [2]. However, relatively little is known about how the surgery affects the kinematics of the foot and the patient's gait.
The study aims to assess the kinematics of the forefoot and hindfoot during walking before and after proximal medial gastrocnemius release surgery, allowing changes in the gait pattern to be identified. This will improve understanding of the effects of the procedure on patients' walking and how it helps in treating conditions causing foot and ankle pain.

Methods: Four patients were recruited for the study who had been offered a proximal medial gastrocnemius release as part of the routine management of their condition. Patients were excluded from the study if they had neuromuscular or rheumatological conditions or bilateral gastrocnemius contracture. Each patient attended a pre-operative gait analysis session and a postoperative session three to four months after their surgery.
Kinematic data and plantar pressure data were collected during each session for four barefoot 10 metre walks. To minimise the influence of pain on the patient's walk, they were asked to take their regular anaesthesia prior to the sessions. Kinematic data was collected using an optoelectronic system (Qualisys, Sweden), where reflective markers were attached to the patient's skin according to the Oxford foot model [3] on the symptomatic side and a standard 6DoF marker set on the non-symptomatic side. During each walk, ground reaction forces were measured using force-plates whilst pressure data of the symptomatic side was collected using a pressure mat (Tekscan, USA). The data was then used to describe the kinematics of the foot, quantify the loading of the forefoot and to evaluate the temporal-spatial parameters during each session, allowing changes in the gait characteristics to be identified. These included the angles of rotation of the forefoot relative to the hindfoot and tibia, rotation of the hindfoot relative to the tibia, knee kinematics, centre of pressure trajectory, peak forefoot pressure and forefoot loading time. A visual analogue scale (VAS) was collected during each session to obtain a measure of the patient's pain whilst walking during the previous week.

Results: Following surgery there was increased dorsiflexion of the forefoot during stance and swing and increased plantarflexion at toe-off when the forefoot was measured relative to the tibia. Consequently, there was a larger range of ankle dorsiflexion-plantarflexion during stance and swing, where these rotations were comparable to a non-pathological group [4]. Rotations of a patient's symptomatic forefoot relative to the tibia during one gait cycle before and after surgery are shown in the figure with standard deviations, illustrating how gastrocnemius release affects the kinematics of the forefoot. The symptomatic forefoot is also shown to pronate during single stance and has reduced supination throughout the gait cycle following surgery, which is also comparable to a non-pathologic group [4]. These characteristic changes in the kinematics of the foot are also shown when the forefoot rotations are measured relative to the hindfoot. There were

also improvements in the knee kinematics following surgery, showing a reduced abduction during stance and increased adduction during swing. When considering the temporal-spatial parameters there were no differences between the symptomatic and non-symptomatic sides and there were no changes to these measures as a result of surgery. Each patient also reported less pain whilst walking after the surgery compared to their levels of pain before, which was reflected in the patient's VAS score. Forefoot loading was shown to increase following gastrocnemius release, demonstrated by an increased symptomatic forefoot plantar pressure during the toe-off phase of the gait cycle.

Figure:
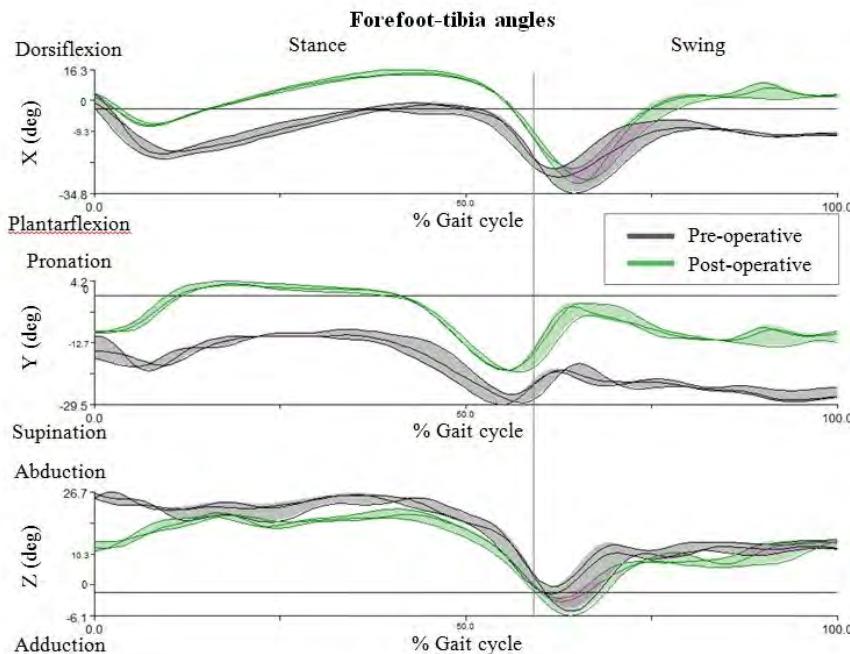
Caption: Mean rotations of a patient's symptomatic forefoot relative to the tibia before and after surgery

Conclusion: The study shows that gastrocnemius release improves the patient's gait by restoring the range of motion of the forefoot. The reduced pain and increased range of motion following gastrocnemius release could subsequently allow for an increase in loading of the symptomatic forefoot during toe-off. It is important to note that the results presented here are based on a small number of patients, however, these results will help in understanding the effects of gastrocnemius release on gait.

References: [1] Rose *et al.*, *J Pediatr Orthop*, 13(6):727-32, 1993.

[2] Craig *et al.*, *J Bone Joint Surg [Br]*, 58(1):84-7, 1976.

[3] Wright *et al.*, *Gait & Posture*, 33(5):108-12, 2011.

[4] Stebbins *et al.*, *Gait & Posture*, 23:401-10, 2006.

Disclosure of Interest: None Declared

PO-0136

ASSOCIATION BETWEEN THIGH MUSCLE COACTIVATION AND MOVEMENT PRECISION OF LOWER LIMBS ON THE DYNAMIC LEG PRESS

Sophie Rabe [1,*]Konstantina Intziegianni [1]Josefine Stoll [1]Frank Mayer [1]

[1]Department Sports & Health Sciences, University Outpatient Clinic Potsdam, Potsdam, Germany

Introduction and Objectives: Muscular coactivation provides joint stability and plays an important role for the coordination of movements. Coactivation has been found to be a motor control strategy for precision of arm movements [1]. The Dynamic Leg Press (DLP) aims to train sensorimotor control and strength of the lower limbs while giving visual feedback to control the movement precision of a task. The user performs extension and flexion movements in a closed kinetic chain at the device. To our knowledge no study before has investigated the association between muscular coactivation and movement precision at the lower limbs on the DLP. This study aimed to test for an association between muscular coactivation and movement precision in a set of exercises for the lower limb on the DLP.

Methods: Nineteen healthy subjects (10 male, 9 female, age 28 ± 3 years, weight 68.2 ± 12.4 kg, height 173.8 ± 8.3 cm,) participated in the study. Subjects had to perform different tasks of 30s in a randomized order on the DLP. Exercises where performed with both legs in an isometric or dynamic movement and differed in terms of load (half/ whole bodyweight) and velocity (slow/ fast). EMG amplitudes were assessed of the agonist M. vastus lateralis (VL) and antagonist M. biceps femoris (BF). RMS of EMG amplitudes were normalised to their MVIC on an isokinetic Leg Press (Con-Trex LP) at a knee angle of 50°. Outcome measure for coactivation was the coactivation index (CI: VL / BF). Movement precision was measured by the deviation of the predefined line (degrees [°]). Data of left/ right leg and time windows of 0-10s/ 20- 30s were analysed for all tasks. Spearman correlation coefficient (ρ) was used to test for a statistically significant association ($\alpha \leq 0.05$) between muscular coactivation and movement precision.

Results: Taking the different DLP tasks: load conditions, velocity conditions, legs (left/ right) and time windows into account, 48 conditions were investigated. Out of those 4 conditions showed a statistically significant association (ρ= 0.472 to 0.563) between coactivation and movement precision. All 4 significant conditions occurred in the time window of 20-30s. The conditions differed in terms of load, velocity and legs. Averaged CI ratio values were 0.7±0.6.

Figure:
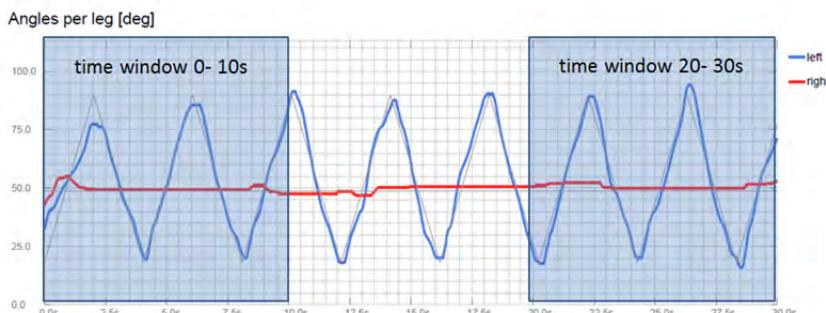
Caption: Figure 1 screen of DLP with deviation of predefined line [°] and analysed time windows

Conclusion: Due to a large majority of not statistically significant results and only 4 moderately significant associations within all 48 testing conditions no association between muscular coactivation and movement precision at the lower limbs on the DLP could been detected in this study. High variability of coactivation values and possible person- and gender-specific coactivation strategies may have influenced the results.

References: [1] Gribble et al., J. of Neurophysiology, 89: 2396–2405, 2003

Disclosure of Interest: None Declared

Lower Limb

PO-0137

RELATIVE MUSCLE EFFORT OF THE ANKLE AND KNEE JOINTS ACROSS DIFFERENT MODES OF HUMAN LOCOMOTION IN YOUNG AND OLD MEN

Juha-Pekka Kulmala [1,*]Marko Korhonen [2]Luca Ruggiero [1]Sami Kuitunen [3]Harri Suominen [2]Ari Heinonen [2]Aki Mikkola [4]Janne Avela [1]

[1]Department of Biology of Physical Activity, [2]Department of Health Sciences, University of Jyväskylä, University of Jyväskylä, [3]Research Institute for Olympic Sports, Jyväskylä, [4]Department of Mechanical Engineering, Lappeenranta University of Technology, Lappeenranta, Finland

Introduction and Objectives: The force generation requirements of the muscles depend on speed and mode of locomotion and substantially vary between different muscle groups [1]. However, knowledge of operating muscle effort of different lower limb muscle groups during human locomotion is limited and stems predominantly from studies, which have compared joint moments generation during walking in relation to maximum force production in isokinetic dynamometers [2]. The findings of these studies suggest that during walking ankle plantarflexors are working closer to their performance limit compared to knee and hip extensors.

However, switching gait from walking to running has been shown to increase peak joint moments more at the knee (approximately by 3-fold) than ankle level (by 2-fold) [3]. Furthermore, Biewener et al. (2004) reported much greater increase in estimated active muscles volume at the knee extensors compared with ankle plantarflexors as humans changed gait from a walk to a run [4]. On the other hand, our recent study [5] examining age-related changes in locomotion mechanics found that reduced ankle plantarflexor output contributes most to the locomotor decline among old adults, while no age-related deterioration was present in the muscular output of the knee joint. Hence, it can be postulated that despite running increase muscular demands more at the knee than ankle level, it seems that limited muscular output from the ankle rather than from knee may limit the human locomotor performance. Furthermore, assuming that the muscular force production capacity is better in young than old adults, it appears that the knee extensor muscles in young adults are working well within their performance limit even during running and maximal sprinting. However, experimental study of the relative muscular efforts is needed to evaluate these assumptions.

The objective of this study was to investigate relative muscle effort of the ankle plantarflexors and knee extensors during walking, running and sprinting in young and old adults. For that purpose, explosive hopping task was used to quantify maximum effort of the ankle and knee joints which was then used to normalize joint moment generation during locomotion. It was hypothesized that (i) the relative muscle effort would be higher in the ankle versus knee joint in both groups during all modes of locomotion, and that (ii) old adults would demonstrate higher relative efforts in both joints across all measured activities excluding ankle joint during sprinting.

Methods: Eleven young (age 27 ± 6 yr.) and 11 old (age 70 ± 8 yr.) male athletes performed walking trials at 1.6 m/s, running trials at 4 m/s and 60 m sprinting trials at maximal effort. Maximum force generating capability of the ankle and knee joints were quantified during explosive two leg hopping task which has been shown to enable athlete to produce the

greatest mechanical output from the ankle and knee joints amongst several other plyometric exercises [6]. Inverse dynamics was used to calculate joint moments across measured activities.

Results: Within subject comparison showed that relative effort of the ankle was significantly higher compared with the knee in the young group across all measured activities (Fig.1). A trend towards higher ankle effort was observed also in the old group. In addition, between group comparison showed that the old group exhibit higher relative effort in the ankle and knee joint level compared with the young group (Fig.1).

Figure:
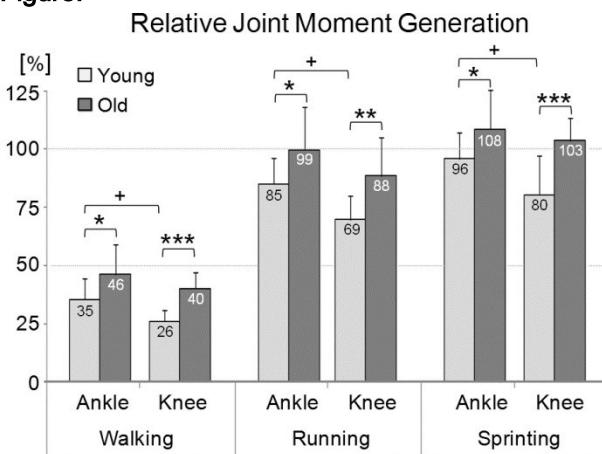
Caption: FIG 1. Relative muscle effort across different modes of locomotion in young and old groups.

Conclusion: This study demonstrates that human locomotion requires greater effort from the ankle plantarflexors than knee extensors. It was also found that the old adults exhibit higher relative efforts in the ankle and knee joint level across all measured activities. These findings support previous suggestions that muscular capacity of the ankle plantarflexors plays a key role in locomotor performance as well as help to understand why age-related loss of muscle force capacity first challenges normal function of ankle joint during locomotion. Furthermore, higher muscular effort of the ankle than knee during running may explain why only minor portion of the runners exhibit forefoot striking pattern, which further increases the muscular demand on the ankle joint [7].

Table:

	Walking		Running		Sprinting		Hopping	
	Y	O	Y	O	Y	O	Y	O
Ankle moment (Nm/kg)	1.67±0.34	1.50±0.14	4.09±0.65***	3.34±0.55	4.60±0.62***	3.63±0.46	4.84±0.69***	3.46±0.86
Knee moment (Nm/kg)	1.20±0.19	1.28±0.25	3.22±0.43	2.85±0.65	3.76±0.88	3.35±0.58	4.70±0.66***	3.25±0.59

Caption: Joint moments across different modes of locomotion in young and old groups.

References: [1] Farris et al. J R Soc Interface 9: 110–118, 2012

[2] Beijersbergen et al. Ageing Res Rev 12: 618–627, 2013.

[3] de David AC et al. J Sports Sci 8: 1-7, 2014.

[4] Biewener et. al. J Appl Physiol 97: 2266–2274, 2004.

[5] Kulmala et al. J R Soc Interface 11: 2014.

[6] Sugisaki et al. J Sports Sci 31: 894-906, 2013.

[7] Kulmala et al. Med Sci Sports Exerc 45: 2306-13, 2013.

Disclosure of Interest: None Declared

REPRODUCIBILITY OF RUNNING PARAMETERS MEASURED WITH INERTIAL SENSORS DURING FIELD TESTING

Anna Dannemann [1,*]Jasmin Gaudel [2]Doris Oriwol [2]Christian Maiwald [2]

[1]Department of Research Methodology and Data Analysis, Institute of Kinesiology, [2]Department of Research Methodology and Data Analysis, Institue of Kinesiology, Chemnitz, Germany

Introduction and Objectives: Reasons to measure running related features are manifold and include clinical as well as sport related questions. Due to new developments and advancements of measuring systems like inertial measurement units (IMU), data collection is no longer limited to spatial and temporal limitations in a laboratory [1]. This allows for the collection of large quantities of real world data – e. g. of an entire endurance run. However, detecting effects that stem from training, footwear, or injury related mechanisms will only be traceable if a sufficient amount of reproducibility can be attributed to this type of data collection and the amount of natural variance is known. Therefore, the purpose of this study is to determine the variability of biomechanic variables within and across two sessions of outdoor overground running.

Methods: Eleven subjects (3 f.; 8 m., 25.7 ± 2.6 years; 178.5 ± 7.5 cm; 70.6 ± 9.8 kg) with running experience performed two fifty-minute endurance runs at an individual, self-selected and constant running speed (3.2 ± 0.5 m/s) at least 24 hours apart. Data were collected using an inertial sensor (Achillex©; 3-axial; acc., mag., gyr.; 400 Hz) fixed at the right heel cap of subjects own running shoes. To avoid any artifacts when initiating the run, the first 40 strides of each run were discarded and analysis was limited to the subsequent 1500 strides. Maximum eversion velocity (EVvel [°/s]) and stride duration (StrDur [ms]) were calculated for each stride interval.

Statistical analyses included mean differences ($diff_{mean}$, absolute and $diff_{rel}$, relative: $(mean_1 – mean_2) / mean_{all} * 100$), Limits of Agreement (LoA, $diff_{mean} \pm 1.96 * SD_{Diff}$) and Bland-Altman plots.

Results: EVvel revealed large inter-subject differences between days (Figure 1). The bias of 19.8 °/s (EVvel) is negligibly small compared to its absolute values. Data of all subjects fell within the LoA and were distributed homoscedastically around the mean difference. However, the range of 172.8 °/s between LoA is substantial and relative differences up to 17.6% were found (Table 1). Data for StrDur was found to be less variable than EVvel. The range between LoA was 86 ms, and relative differences varied from 0.3 % to 6.7 %. It appears questionable whether any type of effect (e. g. based on training or footwear interventions) can exceed the natural variability found in this type of data.

Ultimately, future studies should address the question whether the assessment of means is an adequate way to analyze timeseries of biomechanic data of running, data or whether there is a benefit of non-linear methods [2].

Figure:
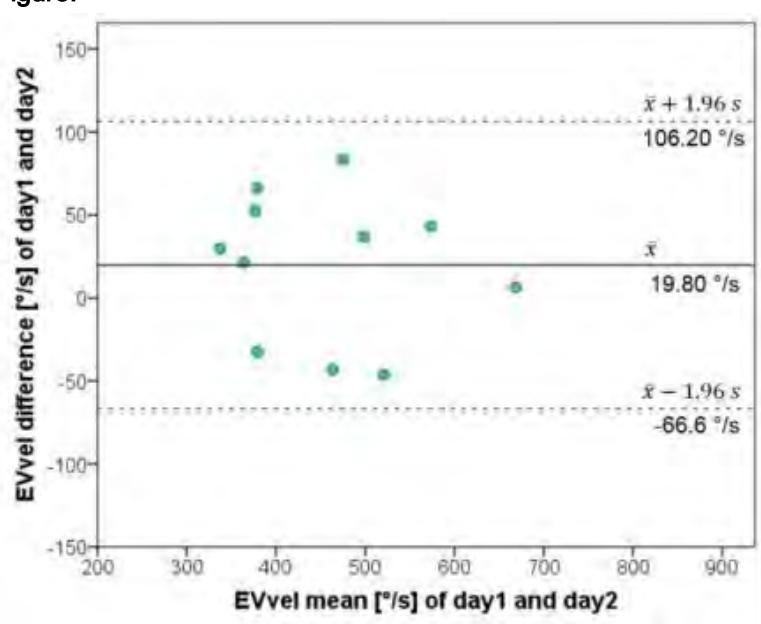
Caption: Figure 1: Bland-Altman plot for EVvel

Conclusion: The recording of biomechanic variables in a natural running environment using IMU is advantageous in many ways. Nevertheless, large variances in EVvel can be expected in this type of protocol, whereas StrDur appears to be more reliable even under field testing conditions. The application of non-linear analysis techniques may be beneficial for this type of data.

Table:

	Mean$_{Diff \pm LoA}$	Diff $_{rel}$	Diff $_{rel}$Min	Diff$_{rel}$Max
EVvel [°/s]	19.8 ± 86.4	11.9	0.9	17.6
StrDur [ms]	-5.1 ± 43.0	1.9	0.3	6.7

Caption: Table 1: Mean differences with LoA; mean, minimal and maximal relative differences of EVvel and StrDur

References: [1] Norris et al., *Journal of Sports Engineering and Technology,* 228(1): 3-15, 2014.

[2] Meardon et al., *Gait & Posture,* 33: 36-40, 2011.

Disclosure of Interest: None Declared

Lower Limb

PO-0139

THE EFFECT OF LIMB PREFERENCE ON KNEE MECHANICS DURING UNANTICIPATED SIDESTEPPING

Kaitlyn Weiss [1,*]Scott Brown [1]

[1]Sports Performance Research Institute New Zealand, Auckland University of Technology, Auckland, New Zealand

Introduction and Objectives: Anterior cruciate ligament (ACL) injuries are the most costly with respect to both the cost of care and the by cost per hour of participation [1]. Previous studies [2, 3] note that 70-84% of all ACL injuries are non-contact in nature and that the majority of these injuries occur during changes of direction, rapid deceleration while running, cutting manoeuvres combined with deceleration, landing after a jump with the knee in or close to full extension, and pivoting on a planted foot with shallow knee flexion [4, 5]. Compared to male athletes, female athletes have been shown [2] to be four to six times more prone to injure their ACL. Additionally, research [6-9] has shown that leg preference is related to the risk of anterior cruciate ligament injury and athletic performance. Most recently, Brown et al. [10] observed important mechanical differences between the preferred and non-preferred legs during planned sidestepping in female footballers (soccer players). While previous research [11] has assessed both planned and unplanned sidestepping and its impact on knee mechanics, to our knowledge, the effect of leg preference on biomechanics during unplanned sidestepping has not been assessed. The purposes of this research were to observe the mechanical differences between the preferred and non-preferred legs during unplanned sidestepping and to assess the magnitude of the mechanical differences between legs during sidestepping.

Methods: Three-dimensional data were collected with 12 female collegiate football and field hockey players during unplanned sidestepping with their preferred and non-preferred kicking leg. Knee kinetics and kinematics were analysed for both legs during initial contact, weight acceptance, peak push-off, and final push-off phases of sidestepping [10].

Results: In comparison to the preferred leg, the non-preferred leg showed moderate decreases in knee flexion angle at initial contact (ES=-0.63); moderate decreases (ES=-0.71) in knee abductor moment and moderate increases (ES=0.75) in knee rotator moment during initial contact, small decreases (ES=-0.52) in knee flexion during weight acceptance, small decreases (ES=-0.51) in abductor moment and small increases (ES=0.58) in rotator moment at peak push-off, moderate decreases (ES=-0.63) in abductor moment and small increases (ES=0.41) in rotator moment at final push-off.

Conclusion: The results of this research indicate that differences exist between the preferred and non-preferred legs during unplanned sidestepping such that the preferred limb was observed to be at a greater risk of knee injury. This increased probability of knee injury is due to differences in knee frontal plane loading experienced by the preferred limb while in a position that decreases stability and the ability to attenuate this increased load. The combination of shallow knee flexion angles of <30 at initial contact and final push-off and greater internal rotation moments make the ACL of the preferred limb more likely to experience greater loading. It is possible that we did not see these mechanics in the non-preferred limb because the non-preferred leg acting as the primary stance leg during various tasks in field sports. The results of this research will augment what is currently known of knee injury in female athletes and can facilitate the design of injury prevention strategies and protocols in the future. Future studies may seek to examine the impact of leg preference on knee mechanics during unplanned sidestepping in males.

References:

[1] de Loes et al., Scand J Med Sci Sports, 10: 90-7, 2000.

[2] Yoo et al., Knee Surg Sports Traumatol Arthrosc, 18: 824-30, 2010.

[3] Shimokochi et al., J Athl Train, 43: 396-408, 2008.

[4] Boden et al., Orthopedics, 23: 573-8, 2000.

[5] Fauno et al., Int J Sports Med, 27: 75-9, 2006.

[6] Negrete et al., J. Str Cond Res, 21: 270-273, 2007.

[7] Matava et al., J. Knee Surg., 15: 11-16, 2002.

[8] Harrison et al., Phys Ther, 74: 245-52, 1994.

[9] Cowley et al., J. Ortho & Sport Phys Ther, 35: A75, 2005.

[10] Brown et al., Sports Biomech, 1-11, 2014.

[11] Brown et al., Sport Med, 44: 1573-1588, 2014.

Disclosure of Interest: None Declared

Lower Limb

PO-0140

GENDER DIFFERENCES AMONG MALES AND FEMALES WHILE PERFORMING ROUTINE TASKS - A PRECURSOR TO OSTEOARTHRITIS RISK

Sudip Paul [1],*Dinesh Bhatia [1]

[1]DEPARTMENT OF BIOMEDICAL ENGINEERING, NORTH-EASTERN HILL UNIVERSITY, SHILLONG, India

Introduction and Objectives: Osteoarthritis (OA) is characterized by the degradation of hyaline cartilage in the joints affecting smooth locomotion. OA is the most common form of arthritis and one of the most important causes of long-term disability in adults. OA mainly affects the elderly population > 60 years and its prevalence > 50%. OA of the knee is also associated with obesity, trauma, history of inflammatory arthritis and certain metabolic diseases. Recently, it has been observed that symptoms of OA are being observed in the younger healthier age group which is an alarming sign. The common sites of joints to develop OA include the knee, hand, hip, spine and foot. Of these, OA of the knee is most commonly found. Patients with knee osteoarthritis often have decreased thigh muscle strength originating from brain centers and spinal cord restricting recruitment of fibers responsible for muscle contraction. This impairs patients' abilities to perform activities of daily living (ADL) and may even contribute to further joint degeneration. Treatment options include various pharmacological and non-pharmacologic interventions but none of them has been successful till date with several side-effects. The most commonly used device available for short-term relief from knee OA pain is the Transcutaneous electrical nerve stimulator (TENS) device. It offers greater relief initially, but is less effective in treating knee arthritis and with time its ability to heal starts diminishing.

The aim of the present study is to understand development of OA symptoms in age group 20-40 years across genders to determine whether there has been a fall in age barrier for OA development in healthier age group. This would aid in understanding predominant factors leading to development of the disease and whether they are related to lifestyle disorders. This would support the development of devices aimed at increasing muscle strength, restoring normal function, and possibly slowing down progress of knee OA to enhance the patient's quality of life plagued with this disease.

Methods: In this study, we conducted the experiments in quadriceps and hamstring muscle for 10 healthy female and male volunteers and 5 paraplegic subjects suffering from UMN as these are prominent muscles leading to OA development as per available literature studies. The study was ethically approved and all subjects gave their written consent. Studies on the right and left leg were done for each of these volunteers and they were asked to perform daily routine tasks such as stepping, normal walking tasks and under voluntary condition. The data was collected by employing 4 channel wireless Biopac Nomadix system available.

Results: As per results, obtained from the experimental data of 10 healthy female for left leg, the EMG values for performing stepping task were 0.011 mV, for normal walking was 0.0076 mV and under voluntary condition was 0.004 mV. The right leg values in these subjects were for stepping task was 0.009 mV, normal walking was 0.006 mV and under voluntary condition was 0.0036 mV. These results were consistent with those available in literature for normal subjects. Again, we have performed with 10 healthy male volunteers for the left leg for the stepping task was 0.0089 mV, for normal walking was 0.0046 mV and under voluntary condition was 0.289 mV. For the right leg for the stepping task was 0.005 mV, for normal walking was 0.004 mV and for voluntary condition was 0.004 mV. It shows that during stepping and voluntary conditions for the healthy male the results show few variations from the normal values. If we look into the paraplegic condition (upper motor neuron paraplegia), we found for the left leg for stepping condition is 0.0034 mV, during normal walking with assistance is 0.0037 mV, and under voluntary condition is 0.0034mV. For the right leg for stepping

condition it is 0.0032 mV, for normal walking with assistance it is 0.004 mV, and under voluntary condition is 0.004 mV. All these values were compared with the MVC values of the respective muscles of the volunteers. Hence, we can say that in, paraplegic condition, the results from both the legs or limbs are almost of equal amplitude during stepping condition however, difference exists during normal walking and voluntary conditions, which shows that their muscle movement is not normal.

Conclusion: We can conclude that this study must be helpful for the understanding the mechanism of muscle functioning during performance of routine tasks. Moreover, it can provide insight for understanding development of osteoarthritis (OA) condition in the knees for this population group at an early age.

Disclosure of Interest: None Declared

CAN HEIGHT AND FLEXIBILITY OF FOOT ARCH MAINTAINED IN OBESITY?

Yuichi Takata [1,*]Yuki Saito [2]Tomoaki Kamiya [2]Takako Chikenji [2]Eiichi Uchiyama [3]

[1]Department of Physical Therapy, Hokkaido Bunkyo University, Eniwa, [2]Sapporo Medicel University, [3]Department of Orthopaedic Surgery, Hitsujigaoka Hospital, Sapporo, Japan

Introduction and Objectives: Overweight may lead to mechanical trauma, degeneration, and eventually posterior tibial tendon dysfunction. Flexibility of the foot arch aids human gait by supporting the body weight against gravity. The tibialis posterior muscle is believed to be the most important dynamic support of the arch of the foot. However, no previous experimental studies have examined the influences of the obesity to the dynamic function of tibialis posterior tendon and *flexibility of the medial longitudinal arch* (FA).The aim of the present study was to investigate the FA which was calculated by the change of the *medial longitudinal arch height* (AH) during cyclic axial loading with obesity compared to the non-obese condition.

Methods: 14 normal fresh frozen cadaveric legs were used. The mean age at the time of death was 82 years (range, 59 to 93). Each leg was cut at the proximal third of the crus. The proximal edge of each specimen was fixed with 2-mm Kirschner wires and mounted by a 5-cm-diameter acrylic tube filled with polymethylmethacrylate resin. The leg was set at the neutral position on the custom jig.

A total of 10,000 cyclic axial loadings of 500 N or 1,000 N (1Hz) were applied to the longitudinal axis of the tibia using the Materials Testing Machine (AG-1, SHIMADZU, Kyoto, Japan). The 32 N dynamic muscle loadings were applied to the tibialis posterior tendon. The experiments were divided into two groups. The 500 N cyclic axial loadings and 32 N dynamic muscle loadings were applied to the tibialis posterior tendon by the servomotor (normal group, n=7). The 1,000 N cyclic axial loadings and 32 N dynamic muscle loadings (obese group, n=7). A 1 mm^2 square red light emitting diode (LED) was attached to the medial aspect of the navicular with minimum disruption. The displacement of the LED light was monitored via a charge-coupled device (CCD) camera (Figure 1) [1] . The image from the CCD camera was converted to the coordinate system. The translational accuracy was 0.06 mm (0.2% full scale).

One cycle was determined that the period of over 5 N axial load applied. The navicular heights with initial 5 N axial load and a peak of axial load were recorded in each cycle. It means that the navicular height with minimum and maximum weight bearing, respectively. The arch change was evaluated using the bony arch index (BAI) [2]. The BAI was determined by the navicular height to foot length ratio. A low arch was defined as a BAI with weight bearing of less than 0.21. The BAI with maximum weight bearing (BAI_{max}) and minimum weight bearing (BAI_{min}) were calculated for each 1,000 cycles. FA was defined as (BAI_{min}- BAI_{max}). Results were expressed as a mean ± standard deviation (SD). We compared BAI with maximum and minimum weight bearing and FA for each 1,000 cycles between normal and obese group by using a t test. A p value of 0.05 was chosen as the level of significance. This study was approved by our institutional review board (IRB).

Results: The height of the navicular decreased with cyclic axial loading. The initial BAIs with maximum weight bearing were 0.242±0.011 (normal group), and 0.234±0.012 (obese group). The BAI of obese group decreased less than 0.21 after 1,000 cyclic axial loadings. On the other hand, the mean BAI of normal group were remained over 0.21. After 10,000 cyclic axial loadings, the mean BAIs with maximum weight bearig were 0.213±0.009 (normal group) and 0.180±0.023 (obese group). The initial BAIs with minimum weight bearing were 0.283±0.007 (normal group), and 0.276±0.018 (obese group). After 10,000 cyclic axial loadings, the mean BAIs with maximum weight bearing were 0.258±0.012 (normal group) and 0.197±0.025 (obese group). The initial value of FA were 0.045±0.011 (normal TP group) and 0.042±0.014 (obese TP group). After 10,000 cyclic axial loadings, FA were 0.046±0.013 (normal TP group) and 0.017±0.006 (obese TP group). Statistical significances were found between normal TP group and obese TP group in the mean BAI with maximum and minimum weight bearing after 1,000 cyclic axial loadings(Figure 2,3) and the FA after 2,000 cyclic axial loadings(Figure 4).

Figure:
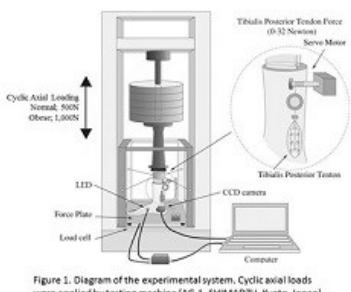
Figure 1. Diagram of the experimental system. Cyclic axial loads were applied by testing machine (AG-1, SHIMADZU, Kyoto, Japan).
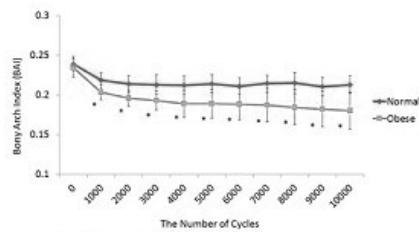
Figure 2. Bony arch index with maximal weightbearing
* The BAI of obesity was significantly lower than normal(p < 0.05)
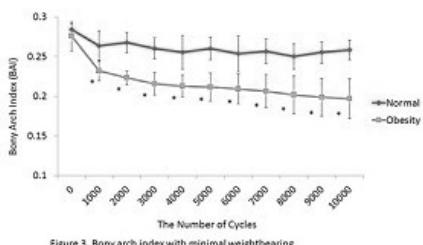
Figure 3. Bony arch index with minimal weightbearing
* The BAI of obesity was significantly lower than normal(p < 0.05)
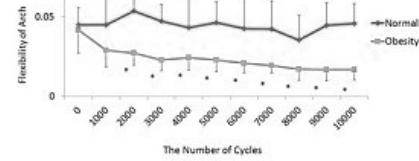
Figure 4. Flexibility of arch (FA, BAI$_{min}$-BAI$_{max}$)
* The FA of obesity was significantly lower than normal(p < 0.05)

Conclusion: We investigated the influence of the overweight to the arch height and flexibility during cyclic axial loadings with tibialis posterior muscle force. The present results showed that the BAI with obese group was significantly decreased after 1,000 axial cyclic loading and the flexibility of arch (FA) with obese group was significantly decreased after 2,000 axial cyclic loading. Energy which is received by foot arch is proportional to flexibility (energy=κ*flexibility). Therefore, our results suggested that the decreased flexibility in the obese foot might diminish the energy absorption at the foot arch, and increase the load to the proximal weight bearing joint including ankle joint.

References: [1] Kamiya, T et al , Clin Biomech,27:962-966,2012   [2] Cowan, DN et al, Arch Fam Med,2,773-777,1993

Disclosure of Interest: None Declared

PO-0142

SYMMETRY/ASYMMETRY BETWEEN THE LOWER LIMBS BASED ON GENDER AND DOMINANT LIMB

Alireza Rastegarpanah [1,*]Mozafar Saadat [2]

[1]School of Mechanical Engineering, Doctoral researcher - University of Birmingham, [2]School of Mechanical Engineering, University of Birmingham, Birmingham, United Kingdom

Introduction and Objectives: The term "gait symmetry" is used to define the differences between the lower extremities in relation to kinematic parameters and it has been defined as an ideal harmony between the actions of lower extremities[1]. Term of asymmetry often was used by researchers to show structural and functionality disparities, although asymmetries in the brain`s functional map and cytoarchitecture have been associated with asymmetrical behavioural traits such as handedness and footedness[2]. In a number of previous studies asymmetry has been used to show a pathological case, while in many others, gait symmetry has been used for simplifying the data analysis. In this paper experimental gait measurements have been used in conjunction with statistical tests to provide a unique investigation in functional differences between the lower limbs during normal walking.

Methods: As it can be seen in Figure1, gait analysis was performed with anthropometric measurements and measurement of leg segmental motion characteristics of 28 subjects, including 14 male (7 left footers and 7 right footers) and 14 female (7right footers and 7left footers), 7 left female footers, and 7 male right footers. Vicon system was used as the tracking system. The experimentation was performed in two modes: the first part (Normative mode), participants unaware about existence of force plate along the walkway, while the second part, Targeting mode, participants aware of the existence of the force plate. Based on the obtained data, the values for Joints rotations between the first and second foot strikes for each leg were extracted after normalization of cycle time. Statistical ANOVA tests were applied in order to compare the symmetry/asymmetry of angular rotations of the hip, knee and ankle joints using IBM SPSS software. Initially the data between the male and female participants were investigated in two modes. Then, the symmetrical/asymmetrical behaviour of the joints for the male and female was investigated based on the dominant limb.

Results: In this study, force plate has been utilized as a key parameter in determining the effect of laterality on asymmetry/symmetry of angular rotation of the hip, knee and ankle joints between the right limb and the left limb when the brain is not cognizant and does not have any understanding of the existence of an object along the walkway. Therefore, in the Normative mode the context of laterality is modest and no limb predominance observed, specially for males. To study the relation of the these differences, gender investigation was performed and it was concluded that symmetry between the angular rotations of the lower limbs joints appeared in Targeting mode for the right footers females who struck the force plate with their right foot, while asymmetry happened for right and left footers males, with right and left foot strikes, in both Targeting and Normative modes.

Figure:
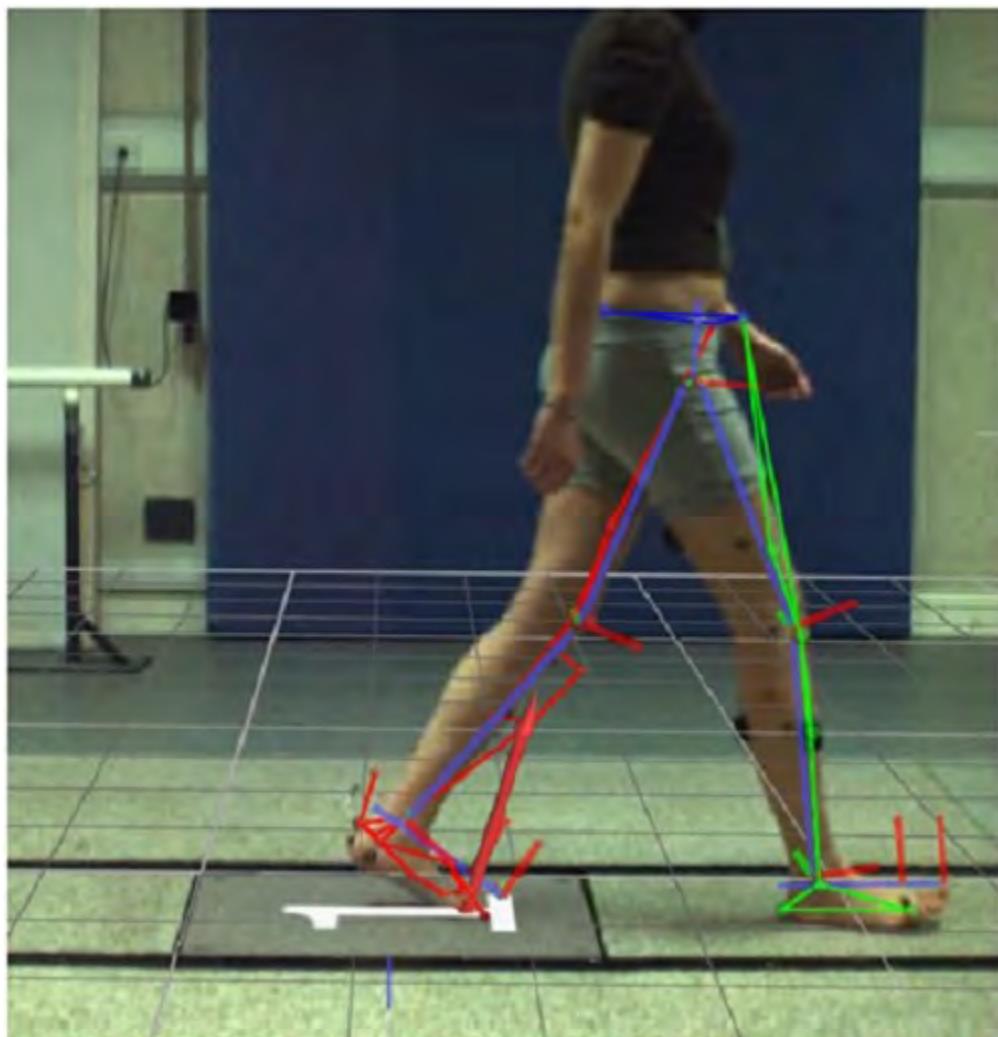
Caption: Gait analysis and overlay 3D simulation of lower limb

Conclusion: The results suggest that female participants achieved more symmetrical gait motion signatures, between the rotation of the joints of left leg and right leg than their male counterparts in Targeting test. The outcome of this pilot study will provide an improved understanding about human motor function, and will specifically be useful in applications concerned with robotic rehabilitation.

References: [1]Hesse S, Reiter F, Jahnke M, Dawson M, Sarkodie–Gyan T, Mauritz KH. Asymmetry of gait initiation in hemiparetic stroke subjects. Arch Phys Med Rehab ,78(7):719–24, 1997.

[2]Gabbard C. Coming to terms with laterality. J Psychol-,131(5):561–4, 1997.

Disclosure of Interest: None Declared

PO-0143

KNEE AND HIP STRENGTH PROFILES CHARACTERISE FUNCTIONAL NEEDS IN RUGBY ATHLETES

Scott R. Brown [1,*]

[1]Sports Performance Research Institute New Zealand (SPRINZ), Auckland University of Technology, Auckland, New Zealand

Introduction and Objectives: Rugby union is an intermittent high-intensity contact sport requiring maximum strength and power performances, interspersed with low-intensity efforts [1]. Rugby forwards utilise strength for success in contact situations such as front-on tackling, rucks, mauls and scrums; whereas backs utilise power for success in high-speed side-on tackling and contact evasion [2]. Unique force-producing attributes are developed in specific joints and angles between the two positions for efficiency. Lower-extremity strength assessment techniques should shift their importance to multi-joint assessments in conjunction with the angles of peak torque for a complete representation of an athlete's lower-extremity strength [3]. Bilateral single-joint or unilateral multi-joint strength deficits may increase risk of lower-extremity injury; especially when unique positional attributes can further accelerate strength differences [4]. We assessed rugby athletes through multi-joint and multi-speed isokinetic actions to illuminate any position specific strength profiles.

Methods: Twenty-nine male academy (development-level) rugby athletes (age 22±4y, body-height 1.9±0.1m, body-mass 97±11kg), separated into forwards (n=15) and backs (n=14), performed bilateral isokinetic strength assessments at the knee and hip with concentric ($60°·s^{-1}$ and $180°·s^{-1}$) actions and at the knee with eccentric ($60°·s^{-1}$) actions. Fourth-order polynomial curve fitting was used to identify peak torque and angle of peak torque. Hamstrings-to-quadriceps (H:Q) ratios and knee flexion-to-hip extension (KF:HE) ratios were calculated.

Results: Backs were smaller in stature (MDiff=-0.032m; ES=-0.45) and lighter in body-mass (MDiff=-13kg; ES=-1.3) compared to forwards. Strength comparisons at the knee showed small decreases in strength of the backs compared to forwards during concentric knee extension and flexion at $60°·s^{-1}$ (MDiff=-19N·m; ES=-0.37 and MDiff=-11N·m; ES=-0.48 respectively) and small to moderate decreases at $180°·s^{-1}$ (MDiff=-23N·m; ES=-0.59 and MDiff=-15N·m; ES=-0.85). Eccentric peak extension and flexion torques showed unclear and small decreases in strength of backs compared to forwards (MDiff=1.07N·m; ES=0.018 and MDiff=-10.7N·m; -0.30). Compared to forwards, backs showed moderate decreases in peak concentric flexion angles at $60°·s^{-1}$ and $180°·s^{-1}$ (MDiff=-10°; ES=-1.004 and MDiff=-3.3°; ES=-0.65) and moderate to small changes in peak eccentric extension and flexion at $60°·s^{-1}$ (MDiff=-5.7°; ES=-0.78 and MDiff=4.4°; ES=0.58). At the hip, strength comparisons between forwards and backs showed unclear to small decreases in strength during hip extension and flexion at $60°·s^{-1}$ (MDiff=-10N·m; ES=-0.12 and MDiff=-11N·m; ES=-0.33) with differences between the groups unclear at $180°·s^{-1}$ (MDiff=4.2N·m; ES=0.046 and MDiff=-5.0N·m; -0.16). Backs showed a small increase in angle of peak torque during $60°·s^{-1}$ hip extension (MDiff=1.1°; ES=0.29) and a large decrease during hip flexion (MDiff=-2.7°; ES=-1.2) compared to forwards.

Conclusion: It was not surprising that forwards had greater peak torque values at the knee and hip compared to backs considering the conceptual positional requirements of each group [2]. Strength differences between forwards and backs were similar to those reported for professional rugby athletes [1]; with the exception of an overall decrease in strength,

likely a result of the age, competition level and strength training history. Backs possessed more desirable angles of peak torque during extension and flexion actions (i.e. larger extension and smaller flexion angles) and speeds given the types of movement patterns they use in match play. Adequate strength at long muscle lengths are more desirable in sports with sprinting bouts as hamstring injuries are suggested to occur near full knee extension [5]. Forwards and backs showed substantially smaller H:Q ratios (0.54 vs 0.67 forwards; 0.53 vs 0.64 backs) and KF:HE ratios (0.39 vs 0.58 forwards; 0.37 vs 0.61 backs) compared to professional rugby athletes [1]; most likely resulting from overactive quadriceps and/or weak hamstrings. Meaningful strength differences were present in academy rugby forwards and backs at the knee and hip which became more substantial during faster assessment speeds. While rugby forwards had superior lower-extremity strength compared to backs, their associated angle of peak torque occurred at inferior degrees; potentially lending way to lower-extremity injury. Bilateral single-joint and unilateral multi-joint lower-extremity strength assessments can facilitate more informed recommendations on whether athletes would be more advantaged to perform specific movements aimed to improve strength at longer muscle lengths.

References: [1] Brown et al., Int J Sports Physiol Perform, 9: 358-61, 2014.

[2] Gamble, Strength Cond J, 26: 10-23, 2004.

[3] Brown et al., NZ Sports Med Sci, 42, 2014.

[4] Brown et al., Phys Ther Sport, 15: 211-5, 2014.

[5] Mendiguchia et al., Brit J Sports Med, 46: 81-5, 2011.

Disclosure of Interest: None Declared

Lower Limb

PO-143

DEFINING A CUT-OFF THRESHOLD FOR JOINT POSITION SENSE IN INDIVIDUALS WITH PATELLOFEMORAL PAIN

Ambreen Chohan [1,*]Michael Callaghan [2]Denis Martin [3]Jim Richards [1]James Selfe [1]

[1]Allied Health Research Unit, University of Central Lancashire, Preston, [2]Arthritis Research UK, Institute of Inflammation and Repair, University of Manchester, Manchester, [3]Health and Social Care Institute, Teeside Univeristy, Middlesborough, United Kingdom

Introduction and Objectives: The importance of measuring proprioception status has increased to help explain the clinical effect of interventions such as knee braces, patellar taping and exercise. In the absence of a reference standard, various measurement techniques have been used for joint proprioception. The most common is joint position sense (JPS) using active angle reproduction (AAR). To date there has been no consensus defining a threshold above or below which proprioception status can be classified. Cut-off thresholds can be based upon the absolute difference between the target angle and achieved angle during AAR testing. To date studies on either healthy people or those with knee pathology had a target angle for JPS tests of absolute difference of ≤5 degrees to differentiate good/poor proprioception though this had no supporting evidence. If a JPS test such as AAR is to be used it is necessary to set a cut-off threshold, below and above which people would be considered to have good/poor proprioception respectively. Defining the threshold may help in the sub-classification of knee conditions such as patellofemoral pain (PFP) and knee osteoarthritis and help decide appropriate treatment if proprioceptive deficits are found.This study aimed to determine the optimum cut-off threshold and test angle that most accurately classifies those with poor proprioception using target angles of 20° and 60° in individuals with and without PFP and explored the possible use of AAR tests as a diagnostic test for PFP participants with poor proprioception.

Methods: Twenty healthy adults (26.8±8.2years old) and thirty adults with PFP (32.1±11.2years old) were recruited. The study was performed in accordance with the 2008 Declaration of Helsinki and appropriate ethical approval was gained from all relevant bodies. JPS was assessed through AAR using an Isokinetic Dynamometer. An ipsilateral position matching activity was performed at target knee flexion angles of 20° and 60° as studies have suggested that functionally these angles are clinically important when assessing patellofemoral disorders. The lever arm passively extended the leg to a target angle of 20° or 60° of knee flexion, without resistance and was held for 10 seconds to enable participants to memorise the position. After the limb was passively returned to 90° there was a 5-second pause before participants actively moved the limb at a self-selected speed, to the target angle, stopping when they thought the target had been perceived. Participants were not permitted to correct the angle. The absolute difference between the perceived angle and the target angle was calculated for each trial. AAR testing was repeated 5 times at each angle in accordance with previous recommendations. The Diagnostic Odds Ratio (DOR) has been determined as a good single indicator of test performance, to define an optimum cut-off threshold. Fig.1, illustrates a cut-off threshold below which tested participants may be determined as healthy, or with good proprioception and above which are individuals with poor proprioception and PFP. An optimum cut-off threshold was determined by maximising the True Negative and Positives (TN, TP), whilst

minimising the False Negatives and Positives (FN, FP). A minimal grey overlap is the ideal situation, minimising the percentage chance of being wrongly classified through AAR testing. Performance of the DOR for AAR testing was compared to the cut-off threshold determined by the Youden's index. Both DOR and Youden's index determine the strength of association between proprioception and a diagnosis of PFP.

Results: For AAR joint position sense testing at 20° there was an agreement between the two test performance indicators (DOR and Youden's index) for a 2° cut-off threshold. However, at 60°, results were similar but not identical (DOR=10°,Youden's Index=11°). Taking each of the test angles separately, at 20° a 2° cut-off threshold shows 62% accuracy and a 38% chance of falling into the "grey area" requiring further assessment, sub-classification or sub-grouping. The previous arbitary threshold of ≤5° would lead to this figure being 52%. At 60°, a 10° cut-off threshold shows lower accuracy at 58%, leaving a larger chance of incorrect identification of PFP through this form of proprioceptive testing.

Figure:
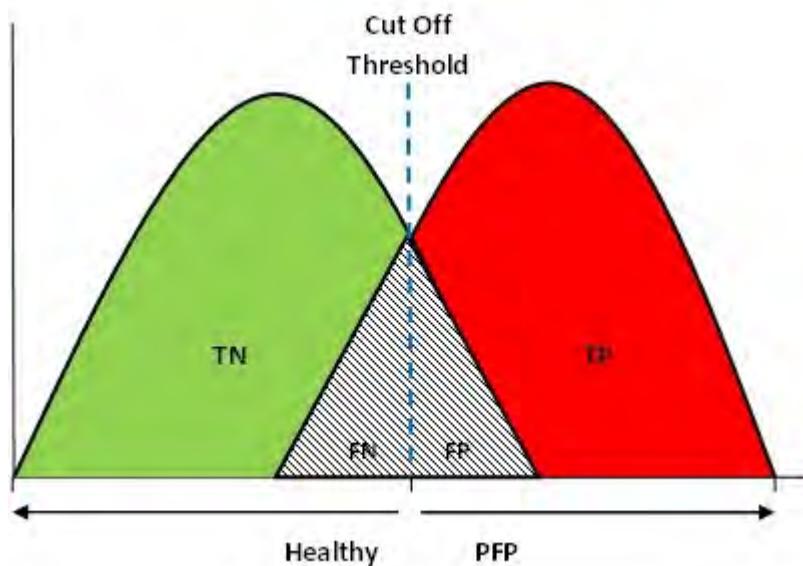
Caption: Graphical representation of a cut-off threshold

Conclusion: Proprioception status has been shown to play an increasingly important role in the effect of clinical interventions. This study suggests that independent tests for proprioception may not be solely relied upon for accurate diagnosis of proprioceptive deficit and PFP. A cut-off threshold for JPS testing may help to optimise treatment in light of proprioceptive deficits. It is suggested that for adults with PFP the previously used arbitrary cut-off threshold of ≤5° is revised to 2° and that 20° is the more clinically appropriate test angle as a greater degree of accuracy is required when approaching full extension in order to optimise control of the knee joint.

Disclosure of Interest: None Declared

PO-144

ACUTE EFFECTS OF WHOLE BODY VIBRATIONS ON LANDING LOAD DURING DROP JUMPS FROM A 40 CM HEIGHT

I.Lin Wang [1,*]Sheng-Wun Siao [2]Tzu-Chieh Chang [2]Yuan.Mei Sun [2]Mu.San Chang [3]Li.I Wang [2]

[1]National Dong Hwa University, Department of Life Science and the Institute of Biotechnology, [2]National Dong Hwa University, Department of Physical Education and Kinesiology, [3]Tzu Chi University, Center of Physical Education, Hualien, Taiwan, Republic of China

Introduction and Objectives: Drop jumps (DJ) are a common plyometric exercise, and many studies have confirmed that drop jump task training can improve sports performance [2,8]. However, drop jump task movements carry a potential risk of injury [1,9]. The proper use of drop jump tasks to effectively train and reduce the risk of injury is an important issue given that enhanced muscle strength may help to reduce the loading during landing [11]. Whole body vibrations (WBV) could stimulate the muscle spindle and increase muscle action to enhance muscle strength and provide power immediately [4,10]. Hence, the purpose of this study was to investigate the acute effects of WBV on landing load.

Methods: Fifteen male college students from the physical education (19.47±0.59 yrs, 1.73±0.04 m, and 64.67±4.22 kg) from the physical education department voluntarily participated in the study. Subjects were excluded if they experienced any lower body orthopedic injuries or musculoskeletal injuries within the past six months. The Institutional Review Board approved this study.

A standard warm-up was performed before testing. The subject performed a pre-test involving a drop jump from a 40 cm drop height (pre-DJ40). All subjects were subject to a WBV process (1 min*3set, 30Hz, 3 mm) [3,6]. A 4-min rest time after WBV occurred [7] before the post-test involving a drop jump from a 40 cm drop height (post-DJ40).

The Qualisys Track Manager (QTM) motion capture system with 8 infra-red cameras (200 Hz) was used to capture motion data. Two AMTI (60 cm×90 cm) force plates (1000 Hz) were used to collect ground reaction forces. The data were analyzed by using the Motion Monitor analysis software.

The SPSS 14.0 statistical program was used for statistical analysis. A repeated measures t-test was used to compare the difference between the pre-DJ40 and post-DJ40. The significance level was set at α=0 .05.

Results: The results of this study are shown in Table1. The peak VGRF and vertical loading of post-DJ40 were significant less than pre-test (p<.05). The knee joint angular displacement of post-DJ40 was significantly greater than the pre-DJ40 during landing phase (p<.05). There were no significant different in ankle and hip joint angular displacement during landing phase between pre- and post-DJ40 (p>.05).

Conclusion: In summer, we conclude that WBV reduced the landing load acutely during 40-cm drop jump tasks. WBV could be applied during plyometric training with drop jump to reduce the risk of injury.

Table:

Group	pre-DJ40	post-DJ40	*p*-value
Peak VGRF (BW) *	2.98±0.78	2.66± 0.65	0.005
Loading Rate (BW/s*)	83.80± 61.43	69.49±42.31	0.039
Ankle joint angular displacement during landing (degree)	40.94±5.73	40.87±4.69	0.931
Knee joint angular displacement during landing (degree) *	43.80±9.57	47.01±10.03	0.029
Hip joint angular displacement during landing (degree)	15.70±7.09	17.07±6.80	0.171

* Significant differences between pre-DJ40 and post-DJ40 , *p*<0.05

Caption: Table 1. The GRF parameters and joint kinematics of pre-DJ40 and post-DJ40 during landing phase (Mean±SD)

References: [1] Blattner, S.E., et al. *American Allianc for Health, Physical Education, Recreation and Dance,* **50**, 583-588.1979.

[2] Bosco, C., et al. Electromy Clin Neur, 22 : 549.1982.

[3] Cardinale, M., et al. J Strength Cond Res, 17: 621-624.2003.

[4] Cardinale, M., et al. Brit J Sport Med, 39: 585-589. 2005.

[5] Decker, M.J., et al. Clin Biomech, 18: 662-669. 2003.

[6] Issurin, V. B., et al. J Sport Sci, 17: 177-182.1999.

[7] Lamont, H. S., et al. J Strength Cond Res, 24: 3433-3442. 2010.

[8] Matavulj, D.,et al. J Sports Med Phys Fit, 41: 159-164.2001.

[9] Wang, L. I., et al. Int J Sports Med, 35 : 522-527.2014.

[10] Warman, G., et al. Aviat Space Envir Md, 73: 119-127.2002

[11] Wilkerson, G. B., et al. J Athl Training, 39: 17.2004.

[12] Zhang, S. N., et al. Med Sci Sport Exer, 32 : 812-819.2000.

Disclosure of Interest: None Declared

PO-0144

QUANTIFYING WARFIGHTER PERFORMANCE ON A TARGET ACQUISITION AND AIMING TASK USING WIRELESS INERTIAL SENSORS

Steven P. Davidson [1,*]Stephen M. Cain [1] [2]Ryan S. McGinnis [3]Rachel V. Vitali [2]Noel C. Perkins [2]Scott G. McLean [1]

[1]School of Kinesiology, [2]Department of Mechanical Engineering, University of Michigan, Ann Arbor, MI, [3]MC10, Inc., Cambridge, MA, United States

Introduction and Objectives: In a combat scenario, the performance of a warfighter is paramount to the safety and success of a mission. In these situations however, a warfighter is expected to carry over 18kg of advanced armor, weapons, ammunition, and support gear, while simultaneously maneuvering through a complex and often random environment. These additional load constraints often restrict/alter key movements and increase fatigue rate, contributing to a rapid decay in warfighter performance. A key aspect of warfighter performance is the ability to aim a rifle and to successfully acquire and hit a target. Overall aiming performance rests on the ability to react, identify, and stabilize on a target before accurate shot execution. It is understandably a challenge to quantify overall aiming performance, particularly given the random (real) environments that a warfighter negotiates. However, a promising means to do so is summarized herein by employing an array of wireless inertial measurement units (IMUs) that measure 3D rifle and body segmental movements in in simulated combat environments. By employing IMUs, this study aims to quantify explicit warfighter aiming performance metrics pre- and post-fatigue in a simulated target acquisition (TA) task.

Methods: Thirteen participants (7 Male/6 Female, 20.4±1.5 years old) were recruited from an athletic collegiate student population. Participants were outfitted with three IMUs (Yost Engineering), attached to the barrel of a mock rifle, the sacrum, and the sternum. Participants wore a military issue generation III improved outer tactical vest (IOTV-III) equipped with mock-ballistic plates and mock- tactical assault panel attached to the IOTV-III anteriorly. A mock-M4 assault rifle outfitted with a laser aiming system provided visual confirmation of target acquisition. The TA task consisted of two targets (6.35cm black circles on white sheets of paper) spaced 11.6m apart and 0.9m high. At the beginning of the TA task, the participant was verbally commanded to pick up the rifle and stabilize the laser within the black circle of one target. Once stabilized, the participant was instructed to perform a 180° turn and stabilize the laser within the black circle of the second target. The participant performed a final 180° turn, again stabilizing the laser in the circle. The participant then performed a fatiguing circuit (~5 minutes) before repeating the task. The fatigue circuit consisted of vertical jumps, box step ups, and modified shuttle run requiring two standing to prone transitions between runs. Participants continued to perform the TA task and fatigue circuit until maximum fatigue, defined by a drop in vertical jump height equal to 70% of the subjects' maximum non-fatigued weighted vertical jump height. Kinematic measures of aiming performance (deduced from the IMU array) were compared between the first (pre-fatigue) and final (post-fatigue) TA task trials. Specifically, maximum angular velocity (MAV) and total turn time (TT) of the rifle, sacrum, and sternum IMUs were compared (Figure1). Significant differences between pre- and post-fatigue performance were revealed using paired t-tests (α=0.05).

Results: Fatigued MAV was significantly less than pre-fatigue levels during turn 1 by an average (±std) of 64.87±46.43deg/s, 54.98±54.48deg/s, and 80.83±62.03deg/s, for the sternum, sacrum, and rifle IMUs, respectively.

Similarly during turn 2, fatigued MAV was significantly less for the sternum (56.49±39.45deg/s), sacrum (50.54±33.23deg/s) and rifle (53.48±43.93deg/s) IMUs, respectively. Fatigued TT was significantly longer during turn 1 for the sternum, sacrum, and rifle IMUs by an average of 0.372±0.282s, 0.471±0.404s, and 0.256±0.304s, respectively (Figure1). However, fatigued TT was significantly longer in Turn 2 only for the rifle sensor by an average of 0.139±0.195s.

Figure:
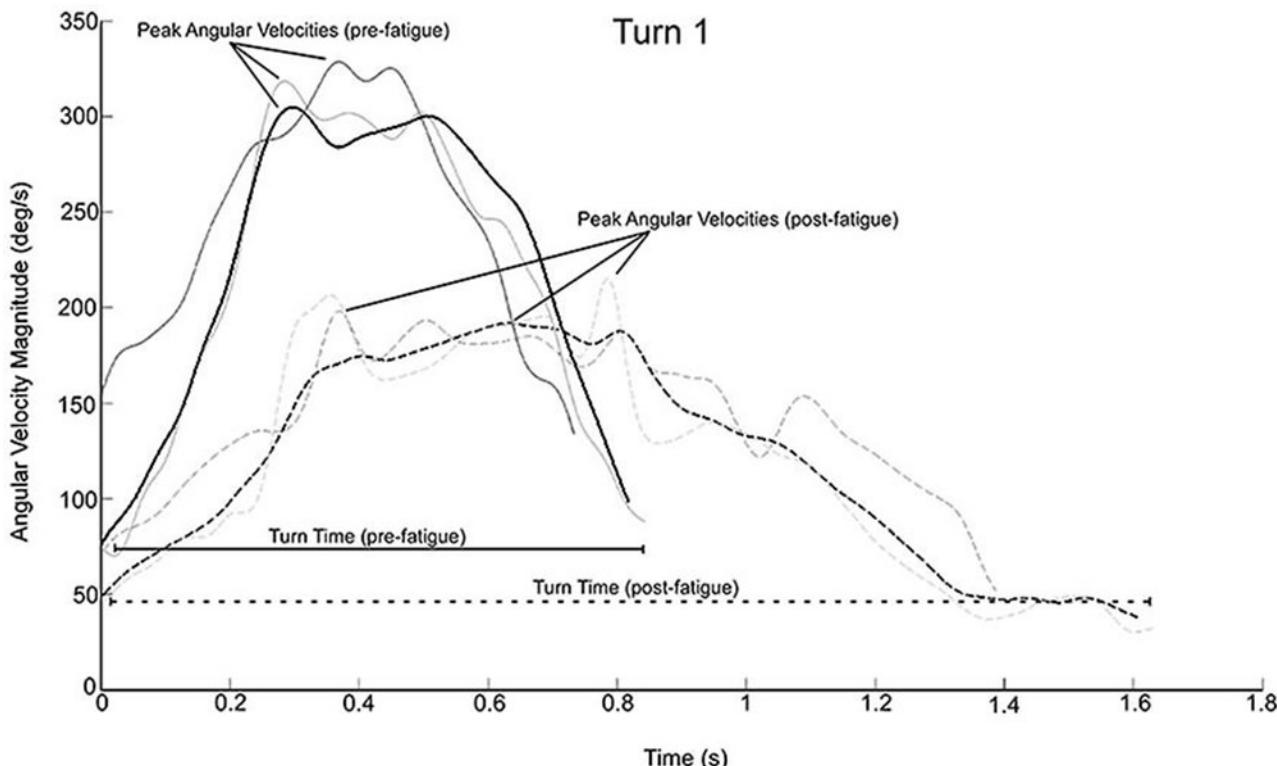
Caption: Figure1: Representative data from a single trial, showing maximum angular velocity and turning time differences in the first turn of a target acquisition task before and after fatigue.

Conclusion: Fatigue-induced decreases in MAV for the rifle, sacrum and sternum sensors evident for both turns likely represent a decreased ability to successfully react and perform the given task. The associated increase in TT may be particularly critical for warfighter performance, suggesting an increased vulnerability during the movement and an inability to react quickly for an extended period. Additionally, decreased MAV during the turning motion suggests a reduced ability to maneuver the body when fatigued; leading to low shot success even if a target is visually identified and acquired. Current outcomes suggest that fatigue associated with realistic warfighter movements under load degrades the ability to acquire and aim at a target in the battlefield, therefore reducing warfighter performance and increasing risk. The study also confirms the promise of IMU arrays as a means to quantify warfighter performance in realistic warfighter environments.

Disclosure of Interest: None Declared

PO-0145

BIOMECHANICAL RESPONSE OF SCAFFOLD ON MECHANICAL LOADING.

Jana Anděrová [1,*] František Lopot [1] Karel Jelen [1]

[1] Anatomy and Biomechanics, Charles University in Prague, Prague, Czech Republic

Introduction and Objectives: Many authors encounter problems associated with insufficient mechanical properties, as the formed tissue is actually not strong enough/resistant, or even earlier, when the cells are not forming optimally or do not grow adequately. This is caused by number of factors, such as suboptimal chemical - biological properties of the scaffold as well as its mechanical properties.

While electrospinning the nanofibers, many parameters can be adjusted, affecting the final properties of the nanofibers (manufacturing solution viscosity, voltage, collector type ....)

The properties of the scaffolds are also adjusted by the post-production processes, such as. cross-linking ect. It is evident from the available literature, that there is not a linear dependence on the properties of the nanofibres and the complex nanofibrous structure. These are characterized by their rheological inhomogenity and the available approaches used to study deformations omit detailed structural changes inside the material.

The aim of this work is the detection of mechanical properties through basic viscous, plastic and elastic components with a clear physical interpretation, and effects of hydration on the properties of the scaffolds.

Methods: The research subject were polyvynilalcohol scaffolds produced by electrospinning technology NanospiderTM 2nd generation. The molecular weight of a solution of 40 kDa, 220 kDa, and for measuring the scaffolds were produced with the following ratios of solutions: 1:3, 1:2, 1:1, 2:1, 3:1.

A single-axis tensile test was utilised, where controlled variable was displacement, velocity $1,5 mms^{-1}$. Evaluation of the measured data takes place by evaluating the measured software stress-strain response curve. A lateral deformation had been detected by HD camera recording, which was used for the calculation of Poisson's ratio.

Samples were adjusted to the dimensions of 70x20 mm. The thickness of the samples was very small due to substantial non-uniformity of the materials and measurement difficulties. Instead of the cross-section area, the width of the sample was determined to be the standardized dimension. By default, the normalization values of the material applied relative to the initial cross-sectional samples. However, since one of the cross-sectional dimensions of the test scaffolds approaching zero as a limit, is not only for the purpose of this work is designed to standardization initial width sample b_0 [mm]. This approach introduced stiffness and damping coefficient unit, for which the following equation:

$K = K '/ b_0$ [N / ($mm_x.mm_b$)]

$B = B '/ b_0$ [Ns / ($mm_x.mm_b$)]

where the index x indicates mm in the length direction and the index b mm in the width direction of the sample. Measured data passed the evaluation software, and the force deformation response curve was fitted by equation of selected rheological model. The monitored parameters were the damping coefficient and normalized stiffness in areas of small deformations (units %) as well as large deformations (from 20%).

Samples were measured in a dry and hydrated state (Ringer's solution).

Results: The data was processed into the visual charts comparing the ratios for individual production solutions for the samples measured in dry and hydrated state.

As for the dry samples, it has been found that the damping coefficient and the stiffness in both fields retain deformation character. Large deformations led to an increase in standardized damping coefficient values, on average by 30%, and an increase in standardized stiffness values in average by 43%.

For wet samples large deformation led to a very significant increase in normalized damping coefficient values on average by 278%. Large deformations do not cause significant change, an increase on average of 7% has been recorded.

The smallest changes in both parameters for the dry measurement have been observed for the solution ratio of 1:1. The highest increase in damping coefficient values for the hydrated state had been detected also at the solution ratio of 1:1, on the contrary the smallest change of stiffness has been recorded.

Conclusion: Detection of the scaffolds mechanical parameters can be used to stabilize the production conditions, and their adaptation of specific usage and application of scaffolds.

There is no linear relationship between the manufacturing solution rations and monitored parameters.

Hydration sample causes a value decrease in damping coefficient and decrease stiffness values.

Ratio 1:1 solution constitutes a landmark from which have values for other ratios of solutions either increase or decrease in value, both when measured in the dry and wet state. Also while simply observing macroscopically, the Poisson points change indicates that the structure of the samples scaffolds changes under strain.

Only just detailed analysis of changes in the internal organization of the influence of deformation is the key to the generally applicable methodology for measuring nanofibrous structures.

Disclosure of Interest: None Declared

Mechanics

PO-0146

MOTION AXIS OF SUBTALAR JOINTS

Takahiko Fukumoto [1 2,*]Kenrin Shi [3]Kazuomi Sugamoto [2]

[1]Department of Physical Therapy, Faculty of Health Science, Kio University, Nara, [2]Department of Orthopedic Biomaterial Science, [3]Department of Orthopedic Surgery, Osaka University Graduate School of Medicine, Osaka, Japan

Introduction and Objectives: There have been many studies on the kinematics of the subtalar joint accompanying the ankle motion. It is reported that the subtalar joint is associated with varus-valgus among foot parts. And it is reported that the motion axis internally rotates for the long axis of the foot part. Most of these studies were cadaveric studies. Alternatively, it was the in vivo study that rotated the ankle joint in varus-valgus. However, the movement of the subtalar joint is unclear when an ankle dorsi-plantar flexion. The purpose of this study was to analyze the subtalar joint kinematics during plantar-dorsiflexion of the ankle, using multi-positional low-dose CT imaging.

Methods: After informed consent, 20 ankle joints of 10 healthy male volunteers (age, 32.5±5.0 years; height, 170.9±3.2 cm; weight, 65.3±2.1 kg) underwent low-dose CT in 3 positions (40° plantar flexion, neutral, and 20° dorsiflexion). 3D pose of the fibula relative to the tibia in each position was analyzed by our originally developed software, and was calculated by Euler's method. Then 3D motion of the ankle was visualized in animation.

Results: When the ankle was in plantar flexion, the calcaneus was rotated varus in all case. The rotation angle of the calcaneus against the talus were varus; 5.1±1.7°, plantar flexion; 1.0±0.8°, external rotation; 0.8±0.7°. The motion axis were 48.3±5.8° for a tibial long axis (fig.A) and 75.8±6.1° for a medial-lateral malleolous line (fig.B)

Figure:
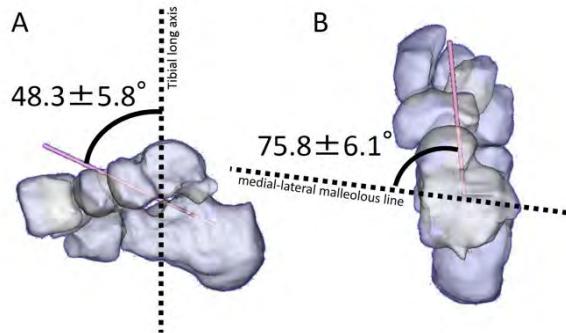
Conclusion: When an ankle dorsi-plantar flexed, the subtalar joint turned a foot part varus-valgus. The motion axis internally rotated from the anterior-posterior axis of the foot part. This motion axis is similar with a conventional report very much. The subtalar joint seems to make a constant move regardless of the movement of the ankle joint like a midcarpal joint makes a constant move regardless of the movement of the wrist. This is very useful for orthopedics and physical therapy.

Disclosure of Interest: None Declared

EFFECTS OF INTERNAL AND EXTERNAL ATTENTION ON GAIT IN ELDERLY

Jonathan De Melker Worms [1,*] John Stins [2] Erwin van Wegen [3] Peter Beek [2] Ian Loram [1]

[1]School of Healthcare Science, Faculty of Science and Engineering, Manchester Metropolitan University, Manchester, United Kingdom, [2]MOVE Research Institute Amsterdam, Faculty of Human Movement Sciences, VU University Amsterdam, [3]Department of Rehabilitation Medicine, MOVE Research Institute Amsterdam, VU University Medical Center, Amsterdam, Netherlands

Introduction and Objectives: The aging population is confronted with the problem of mobility loss. It has been suggested that individuals with increased fear of falling have heightened conscious attention to their own movements (e.g., control of locomotion), which otherwise would require little attentional control. The process of switching from a more automated implicit form to a more conscious form of motor control has been termed reinvestment [1]. Using the Movement Specific Reinvestment Scale (MSRS), Wong et al. have found higher reinvestment scores in elderly with a history of falling compared to elderly non-fallers [1]. Related to reinvestment, one might distinguish between external and internal focus of attention during motor performance. Based on a growing body of literature [2], an external focus of attention appears to facilitate performance on challenging motor tasks, as it allows more 'automatic' or 'efficient' control mechanisms to come into play, compared to an internal focus of attention. To assess walking stability as a function of attentional focus one could study kinematic properties of walking. We studied whether an external focus of attention leads to a temporary less variable gait pattern (indicative of greater stability) than internal attention. Effects of gait perturbations, fall history and falls efficacy on spatiotemporal gait parameters and fear of falling were studied as well.

Methods: 28 healthy older adults (8 males, 20 females) aged 65 or above were recruited. Participants walked on the Gait Real-time Analysis Interactive Lab (GRAIL) system (Motek Medical b.v., Amsterdam, The Netherlands). The GRAIL system consists of an instrumented split belt treadmill in combination with a Virtual Environment (VE) projected on a 180° semi-cylindrical screen (see the figure). Temporary unilateral treadmill decelerations at random time intervals were used to perturb gait. Using Motek Medical's Human Body Model (HBM) and D-flow software full body kinematics was collected. In this abstract reported data is limited to unperturbed gait episodes. Perturbation data is analysed at the time of abstract submission. Participants filled out Dutch versions of the Falls Efficacy Scale International (FES-I), the Movement Specific Reinvestment Scale (MSRS, consisting of 2 subscales) and details about their fall history. 5 Minutes of unperturbed and two 5-minute trials of perturbed gait were recorded, one internal and one external attention condition, in counter balanced order. For the internal attention condition participants received the verbal instructions: "Look ahead at the screen and concentrate on the movement of your legs". For the external attention condition the instruction was: "Look ahead at the screen and concentrate on the movement of the treadmill". Instructions were repeated every 30 seconds during the trials using a speaker system. We calculated variability (coefficient of variation [CV]; SD∕mean × 100) for the following gait parameters: step width, step length, swing time and stance time.

Results: 12 out of 28 participants had experienced a fall within the last 12 months and were labeled as fallers, while the remaining subjects were labeled as non-fallers. A one way ANOVA with FES-I and MSRS scores as dependent variables

and fall history as independent variable showed significantly higher FES-I scores for fallers, $F_{1,28}$ = 7.15, $p < 0.05$. MSRS scores were not significantly different between fallers and non-fallers, $F_{1,25}$ = 0.74, $p = 0.40$ (MSRS part 1) and $F_{1,25}$ = 0.61, $p = 0.44$ (MSRS part 2). For the CVs of step width, step length, swing time and stance time no significant difference was found between conditions, neither for fallers, nor for non-fallers.

Figure:
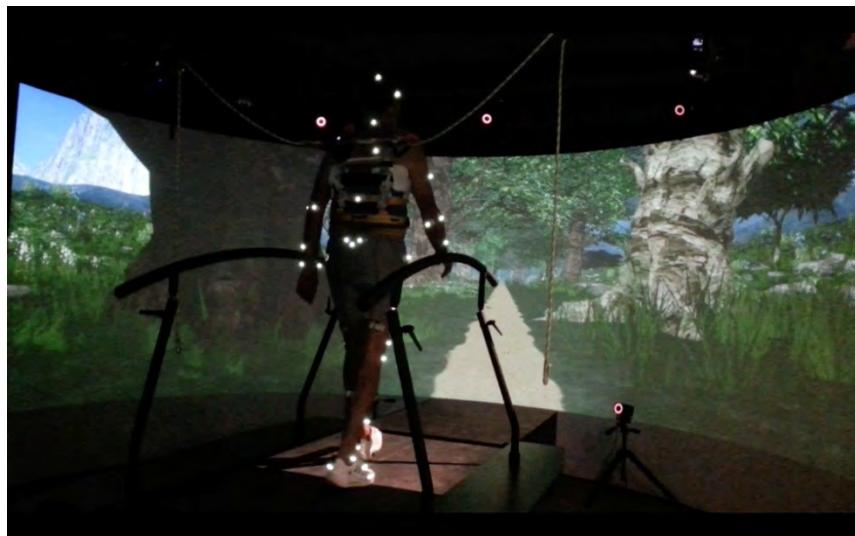
Caption: Virtual walking environment.

Conclusion: Variability of our selected gait parameters did not show a significant difference between internal and external attention. Possible limitations of conventional spatiotemporal gait parameters are the strong emphasis on location of the feet, neglecting the rest of the kinematic chain. Currently we are analyzing centre of mass velocity and body segment angular velocity time series as described by Bruijn, S.M., et al. [3]. With this multivariate analysis of the perturbation response a more detailed assessment of stability in perturbed gait could be produced. However, our results of spatiotemporal gait parameters indicate that effects of internal and external attention on motor control, as observed in other studies with challenging motor tasks, are not found in healthy elderly gait.

Table:

	Step width	Step length	Swing time	Stance time
External	34.2 (13.9)	12.4 (2.5)	6.3 (1.7)	14.4 (4.2)
Internal	35.3 (10.4)	11.3 (3.1)	6.4 (2.1)	14.3 (4.9)
Difference	1.1 (8.1)	-1.1 (3.9)	0.1 (1.5)	-0.1 (2.9)

Caption: Mean coefficient of variation of spatiotemporal parameters (SD) per condition, and for the difference between conditions.

References: [1] Wong, W.L., et al., Neurorehabil Neural Repair, 22(4) 410-4, 2008.

[2] Wulf, G., Int Rev Sport Exerc Psychol, 6, 77-104, 2013.

[3] Bruijn, S.M., et al., J Exp Biol, 213, 3945-52, 2010.

Disclosure of Interest: None Declared

PO-0148

FORCE CONTROL STRATEGY FOR ACCURATE GENERATION AND RELAXATION

Chiaki Ohtaka [1,*]Motoko Fujuwara [2]

[1]Department of Human Sciences, Graduate School of Human and Sciences, Nara Women's University, [2]Faculty of Human Life and Environment , Nara Women's University, Nara, Japan

Introduction and Objectives: All physical movements consist of the coordination of muscle contractions and relaxations, and a wide variety of movements is possible by changing their amplitudes, velocities, and directions. To move as intended, it is essential to accurately control both the generation and relaxation of the force, which is considered a basic and key element.

However, the vast majority of studies have focused on force generation. Although a previous study reported that controlling the force relaxation is more difficult than controlling the force generation, the reason and a motor strategy for controlling the force relaxation remain to be elucidated.

Therefore, the purpose of this study was to investigate a motor strategy for force generation and force relaxation, utilizing grading tasks during isometric force control. A comparison of the force generation and force relaxation strategies is used to elucidate the difficulty of force relaxation.

Methods: Fifteen healthy right-handed subjects participated in the study. They accurately controlled the force of their isometric elbow flexion response to a go signal to reach a target force level as quickly as possible.

They performed the following two tasks: a generation task, in which they increased their force from 0% maximum voluntary contraction (MVC) to 20% MVC (0–20%), 40% MVC (0–40%), or 60 %MVC (0–60%), and a relaxation task, in which they decreased their force from 60% MVC to 40% MVC (60–40%), 20% MVC (60–20%), or 0% (60–0%). The subjects performed the tasks under two conditions: a simple reaction (SR) condition, and choice reaction (CR) condition. The force output by each subject was recorded, and the following items were analyzed. The difference between the peak force and each target force level was evaluated using the absolute error, constant error, and variable error. The time element was evaluated using the reaction time (RT), adjustment time (AT), and total adjustment time (TAT). The velocity of the force control was calculated using the peak velocity (Peak V) and time needed to reach the Peak V (time to Peak V).

To determine the difference in the mean value for each magnitude of force controlled (20%, 40%, and 60%) and each condition (SR and CR), a two-way repeated measures analysis of variance (ANOVA) was conducted for all the parameters in both tasks.

Results: In the generation task, no difference in the error was observed among the three magnitudes of force controlled (following the 20%, 40%, or 60% magnitude). Under the relaxation task, the error for 20% and 40% was greater than that for the 60% magnitude (Fig.1).

As for the time, under both tasks, AT increased with the magnitude, whereas RT tended to decrease with an increase in the magnitude.

With regard to the strategy (Peak V, time to Peak V), under the generation task, as the magnitude increased, Peak V and the time to Peak V both increased. On the other hand, under the relaxation task, as the magnitude increased, Peak V was increased, although the time to Peak V was constant. A comparison showed that, Peak V was greater for the relaxation task than the generation task under all the magnitudes, and the time to Peak V was greater for the generation task than the relaxation task under the 60% magnitude.

Figure:
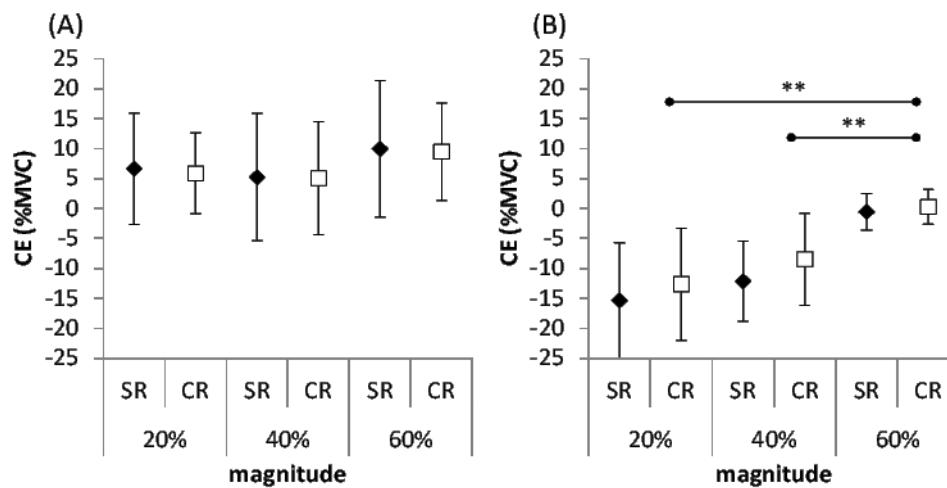
Caption: Fig. 1. Mean and standard deviations of constant error for the generation task (A), and relaxation task (B). *: a significant level of difference between magnitudes, **: p< .01.

Conclusion: The result of this study showed that it is difficult to accurately of control the force relaxation with a slight magnitude, and under both force generation and relaxation the adjustment time depended on the magnitude of the force controlled.

Moreover, in relation to the strategy, under the force generation, Peak V came in the latter half of the adjustment time. On the other hand, under the force relaxation, Peak V came at an early stage of the adjustment time and was greater than that under the force generation. Therefore, this suggested a factor in the difficulty of force relaxation compared with force generation: when the force control speed was great and the peak velocity was reached quickly.

Disclosure of Interest: None Declared

PO-0149

MULTI-OBJECTIVE OPTIMAL CONTROL STRATEGIES OF THE LOCOMOTOR SYSTEM DURING OBSTACLE-CROSSING IN PATIENTS WITH PARKINSON'S DISEASE

Hsuan-Lun Lu [1,*] Bing-Chang Wu [1] Tung-Wu Lu [1] [2]

[1]Institute of Biomedical Engineering, [2]Department of Orthopedic Surgery, School of Medicine, National Taiwan University, Taipei, Taiwan, Republic of China

Introduction and Objectives: Locomotor changes are one of the most obvious clinical symptoms of Parkinson's disease (PD). It can be a great challenge to patients with PD to perform daily activities such as walking and obstacle crossing. A successful obstacle-crossing requires not only sufficient toe clearance but also the body stability provided mainly by the stance limb. Failure to cross the obstacle can lead to falls and serious injuries [1]. Previous motion analysis studies of obstacle-crossing in PD have focused mainly on individual joint variables such as joint angle and moments. However, it is not clear how the overall control strategy is affected by the disease. The purposes of this study were to study the overall control strategies of obstacle-crossing in healthy older adults and older patients with PD.

Methods: Fifteen healthy older adults (NO) and 15 patients with 1st stage PD participated in the current study with informed written consent. The motions of the body segments were meaureed using a skin marker-based motion capture system when they crossed obstacles of 10%, 20%, and 30% of each subject's leg length. A 7-link sagittal-plane model of the whole body was developed, including the feet, shanks and thighs of both the stance and swing limbs, and the pelvis, upper torso, head, neck and hand as a single segment. The joints were modeled as frictionless hinge joints. Inertial properties of the segments were determined using Dempster's coefficients. The obstacle crossing cycle was discretized into twenty time instances. During each time instance, given the kinematics of the stance limb, the positions of the swing ankle in space and thus the motions of the swing limb were determined by solving a multi-objective optimal control (MOOC) problem with 3 objectives, anmely energy expenditure (f_1), toe clearance (f_2), and heel clearance (f_3) [2]. The weighting method was ued to convert the MOOC problem into a single objective one with the new objective as the weighted sum of the original objectives, i.e., ($W_1f_1 + W_2f_2 + W_3f_3$), where W_1, W_2, and W_3 were weighting factors satisfying the condition $W_1 + W_2 + W_3 = 1$ [2]. The best-compromised solution to the MOOC problem was one that minimized the root-mean square error (RMSE) between the model predicted ankle trajectories and those experimentally measured. The corresponding weighting set is called the best-compromised weighting set, which indicates the control strategy adopted during obstacle-crossing [2]. A two-way ANOVA was used for statistical analysis. Once a significant main effect was found, the Duncan's post-hoc test was used to compare the differences in the best-compromised weighting sets between groups and heights. The significance level was set at 0.05. All statistical analyses were performed using SPSS 13.0 (Chicago, USA).

Results: The energy expenditure weighting for the older group was 0.54 (0.01), much smaller than 0.68 (0.07) for young subjects previously reported [2], suggesting that the older people adopt a more conservative strategy with increased emphasis on foot clearance but reduced emphasis on energy expenditure, which was helpful for reducing the risk of tripping over the obsacle. The energy expenditure weightings in PD were significantly smaller than those in NO,

suggesting that patients with PD increased their emphasis on toe and heel clearances more than the healthy older people did for successful obstacle crossing.

Conclusion: Patients with PD were found to have adopted a control strategy significantly different from that of the healthy older people as expected, with more emphasis on the foot clearance than energy expenditure. These between-group differences were not affected by obstacle height. The findings of the current study provide a better understanding of the control of obstacle crossing in patients with PD from a system-level perspective, which will be helpful for the rehabilitation and design of fall prevention strategies for this patient group.

Table:

Group	Obstacle Height	Energy Expenditure	Toe Clearance	Heel Clearance
Healthy control	10%	0.52	0.24	0.24
	20%	0.51	0.24	0.24
	30%	0.53	0.23	0.24
PD	10%	0.49	0.26	0.26
	20%	0.46	0.27	0.27
	30%	0.49	0.26	0.26
Height Effect		p=0.55	p=0.72	p=0.74
Group Effect		p=0.03	p=0.02	p=0.02

Caption: Average values of the best-compromise weightings for healthy older group (NO) and patients with PD (PD) when crossing obstacles of different height. The last two rows show the P-values for height and group effects, respectively.

References: [1]. Tinetti et al., N Engl J Med, 320: 1055-1059, 1989.

[2]. Lu et al., Gait Posture, 36: 552-556, 2012

Disclosure of Interest: None Declared

PO-0150

ANODAL MOTOR CORTEX TRANSCRANIAL DIRECT CURRENT STIMULATION IMPROVES FORCE STEADINESS IN POST-STROKE HEMIPARETIC PATIENTS

Rafael Montenegro [1] [2],[*] Adrian Midgley [2] Wendell Bernardes [1] Renato Massaferri [1] Paulo Farinatti [1]

[1] Physical Activity and Health Promotion Laboratory, State University of Rio de Janeiro, Rio de Janeiro, Brazil, [2] Department of Sport and Physical Activity, Edge Hill University, Ormskirk, Lancashire, United Kingdom, Ormiskirk, United Kingdom

Introduction and Objectives: Relative imbalance in interhemispheric motor cortex excitability is observed in post-stroke patients due to an ipsilesional motor cortex hypo-excitability with concomitant contralesional motor cortex hyper-excitability. As a consequence, high coefficient of variation of muscle strength induced by high force variability was showed in stroke patients while performing submaximal dynamic strength exercises. Transcranial direct current stimulation (tDCS) is a simple and non-invasive technique widely used in neurological rehabilitations programs. Enhances in affected motor cortex plasticity as well as improvements in maximal and isometric submaximal strength exercise performance in hemiparetics and healthy subjects have been showed when bi-hemispheric motor cortex tDCS is applied. The main purposes were to investigate and compare the acute tDCS effects on peak muscular torque as well as the force steadiness during maximal and submaximal dynamic leg isokinetic exercise protocols, respectively, in hemiparetic and healthy subjects.

Methods: In a double blind, crossover, randomized sham controlled experimental design, 10 chronic stroke hemiparetic patients and 09 healthy subjects performed bilateral knee extension and flexion isokinetic tests at submaximal and maximal workloads [2 sets of 10 repetitions at 50% peak torque and 1 set of 3 reps at 100% peak torque, respectively] with and without bihemispheric tDCS over motor cortex [2mA during 20 min]. First of all, the participants were invited to perform one or, if necessary, two familiarization sessions aiming to avoid apprehensible behavior and learning effect within experimental protocols. The range of motion varied between 0° to 90° with execution speed fixed in $60°.s^{-1}$ for maximal and $120°.s^{-1}$ for submaximal exercise tests. The peak muscular torque and the coefficient of variation between repetitions and sets were used as an indicator of force production and force steadiness, respectively. All participants got information to keep their food diet routine normally prior to perform the visits but were discouraged to consume ergogenic beverages like coffee and soft drinks.

Results: After tDCS the peak torque in stroke patients increased only for the knee extension in the non-affected leg (P = 0.008), while no difference was found in the affected leg (P > 0.05). For healthy subjects, no difference was found for the peak torque in both dominant and non-dominant legs (P > 0.05). The force steadiness reflected by the coefficient of variation during the knee extension phase decreased in tDCS *vs.* sham condition in both affected (P = 0.01) and non-affected legs (P = 0.04). However, in the knee flexion phase, the coefficient of variation after tDCS decreased only in affected leg (P = 0.05). For healthy subjects, the force steadiness during both knee extension and flexion phases decreased in tDCS *vs.* sham condition only in non-dominant leg (Knee extension phase: P = 0.04; Knee flexion phase: 0.03).

Figure:

Hemiparetics / **Healthy**
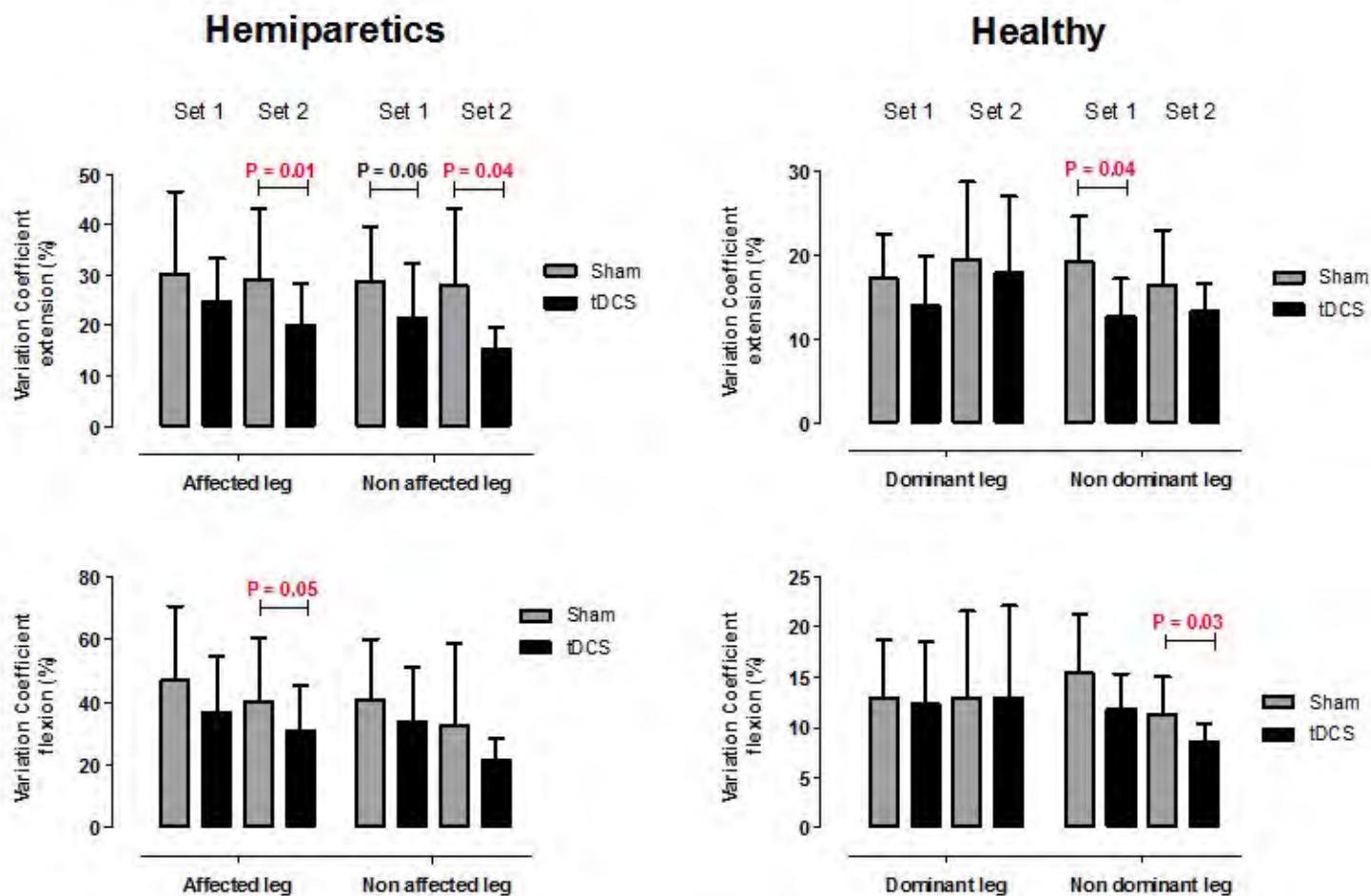
Caption: Variation coefficient (Mean ± SD) between two sets of 10 repetitions at 50% of peak muscular torque) after anodal motor cortex tDCS (black bars) or sham condition (gray bars) in both hemiparetics and healthy subjects

Conclusion: A single session of bihemispheric tDCS might enhance the maximal strength in chronic stroke patients but not in healthy subjects. Furthermore, the force steadiness might be attenuated in both chronic stroke and healthy individuals. These findings warrant additional research to ratify the potential role of bihemispheric tDCS to improve motor performance in stroke patients.

References: Tanaka S et al. Single session of transcranial direct current stimulation transiently increases knee extensor force in patients with hemiparetic stroke. Neurorehabil Neural Repair. 25(6):565-9, 2011.

Okano AH, Fontes EB, Montenegro RA, Farinatti PD, Cyrino ES, Li LM, et al. Brain stimulation modulates the autonomic nervous system, rating of perceived exertion and performance during maximal exercise. Br J Sports Med. 2013.

Disclosure of Interest: None Declared

Neurological and Motor Control

PO-0151

DIFFERENTIAL EFFECT OF VISION GUIDING ON ARCHIMEDES SPIRAL DRAWING BETWEEN PATIENTS WITH ESSENTIAL TREMOR AND PARKINSON'S DISEASE

Kai-Hsiang Chen [1]Yu-Jung Chen [2,*]Po-Chieh Lin [2]Bing-Shiang Yang [2]

[1]Neurology, National Taiwan University Hospital, Hsinchu Branch, Hsinchu, [2]Mechanical engineering, National Chiao Tung University, Taiwan, Hsinchu City, Taiwan, Republic of China

Introduction and Objectives: Tremor is the most common movement disorder seen in general neurological outpatient clinics. There are many diseases that could have tremor as a main clinical phenotypes, including Parkinson's disease (PD) and essential tremor (ET). Because of the similar symptom, it is usually difficult to differentiate between PD and ET in an early stage using current clinical assessments, which could result in inappropriate diagnoses or treatments. Therefore, the aim of this study was to develop a clinical assessment to better distinguish tremor between patients with PD and ET.

Methods: Archimedes spirals are commonly used in the evaluation of patients with pathologic tremor. Thus, we employed a digitizing tablet with sampling rate 50 Hz to quantify the performance of drawing Archimedes spirals. Six patients with ET (ages: 73.8±6.64) and three with PD (ages 71.6±3.51) signed informed consents to participate in the study. Spiral drawing was recorded under two tasks - *task 1*: patients were instructed to draw the spiral along printed spiral loops from inside to outside; and *task 2*: patients were instructed to follow a guiding point with a constant velocity (3cm/sec). Drawing velocities were quantified during each test.

Results: Figure 1 shows the distribution of drawing velocity in one typical PD and one typical ET patents during the two tasks. We found that distributions of task 2 were significantly different between ET and PD, with the mean velocity as 1.94±1.34 in PD cm/sec, and 2.77±2.33cm/sec in ET($p<0.05$). Besides, Jaccard's similarity coefficients of PD patients are less than 0.4, while those of ETs are more than 0.5 (Table 1).The interquartile range the velocity distribution of guiding task is about three times as the non-guiding task in PD, but less than two times in ET patients (Table 1).

Figure:
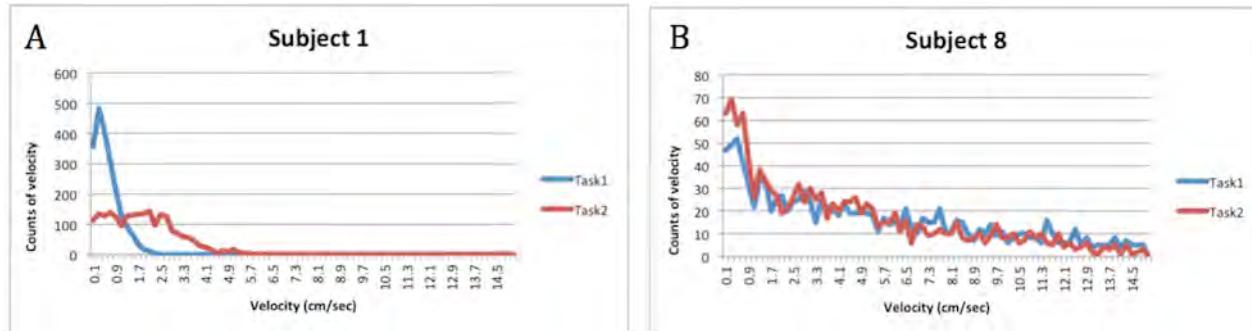
Caption: Figure 1 Distribution of velocity in task 1 and 2. The Jaccard's similarity coefficient defined as the size of the intersection divided by the size of the union of the sample sets. A: data from one PD patient. B: data from one ET patient.

Conclusion: A visual guiding could bring different performance in ET and PD in spiral drawing. Patients with ET have the similar distribution of velocity between the guided and non-guided tasks. However, the velocity distribution of PD patients is significantly changed during the guiding task (p<0.05). In addition, the Jaccard's similarity coefficient and interquartile range of velocity indicate that frequency profile of drawing velocity between two tasks in ETs are with more similarity than those in PD patients. It appears that patients with PD were affected by the guiding point. These findings can be used to develop a standardized test for early diagnosis for patients with tremor, to distinguish essential tremor from Parkinson's disease, in clinical environment.

Table:

	Jaccard's similarity coefficient	Interquartile range of velocity		
		Task 1	Task2	Ratio (Task1/Task2)
PD (N=3)	0.34±0.05	0.67±0.08 (cm/s)	1.93±0.17 (cm/s)	2.87±0.17
ET (N=6)	0.64±0.14	3.08±1.88 (cm/s)	3.34±1.33 (cm/s)	1.29±0.55

N=number of subject

Caption: Table 1 Jaccard's similarity coefficient, interquartile range of velocity and the ratio between task 1 and task 2 in PD and ET patients.

References: [1] Mansur PH et al., A review on techniques for tremor recording and quantification. Crit Rev Biomed Eng. 2007; 35(5): 343-62.

[2] Haubenberger D et al., Validation of digital spiral analysis as outcome parameter for clinical trials in essential tremor. Mov Disord. 2011; 26(11): 2073-80.

[3] Saunders-Pullman R et al., Validity of spiral analysis in early Parkinson's disease. Mov Disord. 2008; 23(4): 531-7.

[4] Pullman SL., Spiral analysis: a new technique for measuring tremor with a digitizing tablet. Mov Disord. 1998; 3: 85-9.

Disclosure of Interest: None Declared

PO-0152

LOW OBSTACLE INCREASES VARIABILITY OF GAIT TEMPORAL PARAMETERS IN APPROACHING PHASE IN PATIENTS WITH PARKINSON'S DISEASE

Lucas T. B. Simieli [1,*] Fabio Barbieri [2] Diego Orcioli-Silva [1] Paulo Cezar Rocha Santos [1] Victor Spiandor Beretta [1] André Macari Baptista [1] Vinicius Alota Ignacio Pereira [1] Lilian Teresa Bucken Gobbi [1]

[1] Department of Physical Education, Univ Estadual Paulista "Julio de Mesquita Filho" - Rio Claro, Rio Claro, [2] Department of Physical Education, Univ Estadual Paulista "Julio de Mesquita Filho" - Bauru, Bauru, Brazil

Introduction and Objectives: The literature reports that obstacles change gait parameters during gait of elderly people, mainly in individuals with Parkinson's disease (PD) (1,2). Variability of temporal parameters is an important factor on gait during obstacle crossing (4). Patients with PD present alterations on gait, such as longer double support phase (1,3) and greater variability (4), which seems to indicate a deficit on programming, mainly during challenging tasks, such as crossing an obstacle (1,4,5). These modulations during obstacle crossing may explain the greater number of falls in this population. However, there is little information in the literature about the effects of different obstacles height on gait parameters, mainly related to approaching to the obstacle (approaching phase) (5). Therefore, the aim of this study is to investigate the influence of three different obstacle heights during the approaching phase in patients with PD and neurological healthy elderly (control group).

Methods: Fifteen patients with PD (70.61±9.82 years) and 13 neurological healthy elderly (70.5±15.4 years) participated in this study. All subjects performed ten trials for each condition: gait without obstacle, gait with low obstacle, gait with intermediate obstacle and gait with high obstacle. The conditions were randomized by block, but the first condition for all participants was the gait without obstacle. The obstacle heights were customized according to leg length (low = ankle height; intermediate = (low obstacle height + high obstacle height)/2; high = knee height/2). The obstacles were positioned in the middle of a pathway (8 meters). The temporal parameters were recorded by a carpet with sensors of pressure (GAITRite® (CIR System, Clifton, NJ, USA). The parameter analyzed was the variability (standard deviation) of step time, double support time, swing time, stance time and single support time of the STEP BEFORE OBSTACLE CROSSING.

Results: MANOVAs with factor for group and condition were performed, with repeated measures for condition, to answer the questions of the study (α = 0.05). The groups were similar at age ($t_{1,26}$ = 0.70), mental status ($t_{1,26}$ = 0.76), body weight ($t_{1,26}$ = 0.98) and body height ($t_{1,26}$ = 0.20). The MANOVA revealed main effects of group (p = 0.001) and condition (p = 0.001) and interaction (p = 0.001) between group and condition. About the interaction, PD group showed a greater variability of all temporal parameters than control group, mainly in low obstacle condition. Low obstacle changed the approaching phase of PD group, increasing the variability of step time (p<0.001) and swing time (p<0.001) compared to other conditions and with control group (p = 0.001).

Conclusion: Interesting, these findings were against our initial hypothesis: high obstacle will increase the variability of temporal gait parameters compared to other conditions, mainly for PD group. Less attention driven to the obstacle seems to explain the greater variability during approaching phase in low obstacle condition (5). This behavior induces the individuals to adjust gait parameters during obstacle approaching, increasing the variability. In addition, patients with PD

needs more time to process environmental information and seems to judge this incorrectly, which could also explain the greater variability. In conclusion, the presence of obstacle increased variability of temporal parameters on approaching phase of individuals with PD, regardless its height. In addition, low obstacle influenced the temporal gait variability of patients with PD more than other obstacle height.

Table:

	Without obstacle		Low obstacle		Intermediate obstacle		High obstacle		
	PD	Control	PD	Control	PD	Control	PD	Control	
Step time	0.018±0.00	0.013±0.001	0.052±0.007	0.013±0.008	0.022±0.001	0.015±0.001	0.021±0.001	0.015±0.001	
Swing time	0.015±0.001	0.011±0.001	0.021±0.001	0.013±0.001	0.019±0.001	0.015±0.001	0.017±0.001	0.013±0.001	
Stance time	0.016±0.006	0.089±0.006	0.075±0.004	0.048±0.005	0.070	0.065±0.004	0.083	0.068±0.008	

					±0.004		±0.004		
Single support time	0.017±0.001	0.013±0.001	0.062±0.003	0.047±0.003	0.065±0.003	0.062±0.004	0.073±0.004	0.062±0.004	
Double support time	0.009±0.001	0.009±0.001	0.016±0.001	0.010±0.001	0.013±0.001	0.012±0.001	0.016±0.001	0.013±0.001	

Caption: Table 1. Variability of temporal parameters of each condition for PD group and control group.

References: References

[1]VITÓRIO et al.Gait Post, 143–146, 2010.

[2]SIMIELI et al. J Alz Dis, 43, p. 435-441, 2015.

[3]MORRIS et al. Brain, 119, part 2, p. 551-568, 1996.

[4]HAUSDORFF, et al. Mov Dis, v.13, n. 3, p. 428–437, 1998.

[5]PIERUCCINI-FARIA et al., J Mot Beh,2013 (*online)*

Disclosure of Interest: None Declared

Neurological and Motor Control

PO-0153

THE INFLUENCE OF BODY WEIGHT SUPPORT ON COORDINATION OF LOWER LIMB IN STROKE PATIENTS WITH SLIGHTLY PARALYSIS DURING TREADMILL WALKING

Takuma Yawata [1][2] Hitoshi Makabe [1],*Shinjiro Saito [3]

[1]Physical Therapy, Yamagata Prefectural University of Health Sciences, Yamagata, [2]Physical Therapy, Oizumi Kinen Hospital, Shiroishi, [3]Yamagata City Hospital SAISEIKAN, Yamagata, Japan

Introduction and Objectives: On discharge from rehabilitation, 60% to 80% of stroke patients walk at insufficient speed and poor inter-limb coordination [1]. It is known that body-weight supported walking training on a treadmill (BWSTT) improve walking performance [2]. However, it is not clear whether or not the BWSTT is effect to coordination of lower limb. The purpose of this study was to investigate the influence of body weight support (BWS) on the coordination of lower limb during treadmill walking in stroke patients with slightly paralysis.

Methods: Subjects were 10 healthy individuals (control group: age = 64.3±7.5 years, height = 166.9±7.2 cm, weight = 71.7±11.7 kg) and 10 stroke patients (patients group: age = 64.8±8.2 years, height = 163.2±8.6 cm, weight = 64.6±11.4 kg, NIH stroke scale=0~2). Experimental task was walking on treadmill with body weight support (BWS) system. BWS was set in 0%, 10%, 20%, and 30% of the body weight. The subjects walked at a comfortable speed estimated on the basis of Froude velocity for 30 seconds. Kinematics of walking was recorded by 3D motion analysis system (Vicon). Muscle activities of lower limb and trunk acceleration at L3 level were recorded by wireless EMG and acceleration system (Trigono Wireless System). Continuous relative phases (CRP) of thigh-shank and shank-foot, %EMG (vastus medialis = VM, lateral hamstring = LH, tibialis anterior = TA, and gastrocnemius = GAS; ratio of RMS EMG to 0% BWS,), and %ACC (ratio of RMS acceleration to 0% BWS) at L3 level were calculated from 10 stride data. Means and variance of relative phase were calculated by circular statistics (Oriana 3.0). Analysis of variance was used to determine the effect of BWS (R ver.2-8-1). Significant level was set at $p < .05$. This study was undertaken in accordance with the Declaration of Helsinki Ethical approval and all participants gave informed consent. The present study was approved by the Institutional Review Boards of the Yamagata Prefectural University of Health Sciences and the Yamagata City Hospital Saiseikan.

Results: Thigh-shank CRP of the stroke patients at heel-contact during 10%, 20%, and 30% BWS were significantly greater compared with that of the healthy individuals at heel-contact during 0% BWS. Shank-foot CRP of the stroke patients at toe-off during 0% BWS were significantly greater compared with that of the healthy individuals at toe-off during 0% BWS. Shank-foot CRP of the stroke patients at toe-off during 10%, 20%, and 30% BWS decreased to the value of the healthy individuals at toe-off during 0% BWS. %EMG of VM and TA for the stroke patients during 10%, 20%, and 30% BWS were significantly lower than those for the stroke patients during 0% BWS. No significantly difference was in %ACC between the healthy individuals and the stroke patients.

Figure:

Thigh-shank CRP at 0%BWS

Healthy subjects (n=10)
(Mean± SD=26.6±9.8)

Thigh-shank CRP at 0%BWS

Stroke subjects (n=10)
(Mean± SD=32.3±9.7)
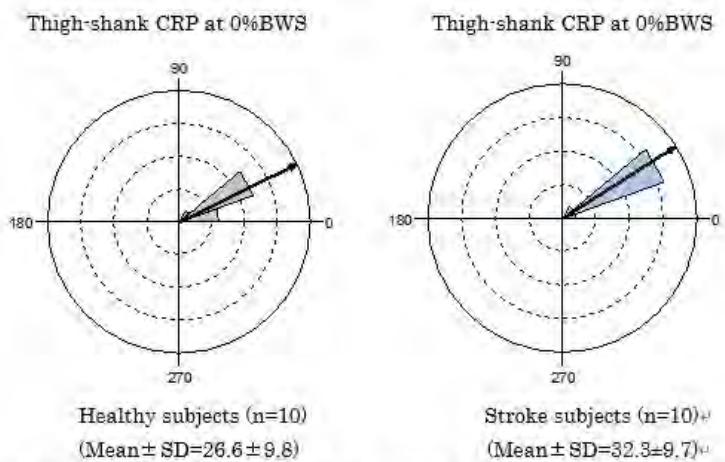
Thigh-shank relative phase of stroke patients at toe off during 0%, 10%, 20% and 30% of body support weight.

Shank-foot CRP of the stroke patients at toe-off during 0% BWS were significantly greater compared with that of healthy individual at toe-off during 0% BWS.

Conclusion: BWS for the stroke patients with slightly paralysis made thigh-shank CRP at heel-contact delay and made shank-foot CRP at toe-off fast. These changes may result from reducing muscle effort around knee and ankle joints during treadmill walking with BWS. We need to use the treadmill walking with BWS for the stroke patients with slightly paralysis in consideration of the merit and demerit of the treadmill walking with BWS.

References:

[1] Green et al., Lancet, 359: 199-203. 2002.
[2] Pohl et al., Stroke, 33: 553-558, 2002.

Disclosure of Interest: None Declared

Neurological and Motor Control

PO-0154

NEUROMUSCULAR CONTROL OF FREELY CHOSEN CADENCE DURING SUBMAXIMAL CYCLING

Karl Grainger [1,*]Lee Romer [1]James Martin [2]Thomas Korff [1]

[1]Centre for Sports Medicine and Human Performance, Brunel University, London, United Kingdom, [2]College of Health, The University of Utah, Salt Lake City, United States

Introduction and Objectives: Previous research has shown that crank length has little effect on metabolic cost and joint power distribution once the effects of pedal speed (the mathematical product of cadence and crank length) are accounted for. Pedal speed (PS) is indicative of muscle shortening velocity, and it would be intuitive to hypothesise that the central nervous system would seek to preserve this variable when perturbed by changes in crank length. Alternatively, the central nervous system may seek to preserve cyclic velocity when crank length is changed. Cyclic velocity (CV) is the product of pedal speed and pedalling rate, and it is therefore a measure which is indicative of both muscle shortening velocity and activation/deactivation dynamics. The purpose of this study was therefore to determine the effect of crank length on freely chosen cadence (FCC), PS and CV during submaximal cycling. Based on previous research [1] [2], it was hypothesized that PS would be preserved across crank lengths.

Methods: Ten volunteers (6 male and 4 female) cycled at 90% of ventilatory threshold using three different crank lengths (150-, 170- and 190-mm), and a range of set cadences and FCC. ANOVAs were performed to examine differences in FCC, PS and CV across crank lengths. In addition, we predicted the FCC for the extreme crank lengths based on the cadence chosen at a crank length of 170 mm assuming that PS would remain constant. Similarly, we predicted FCC at the extreme crank lengths based on the assumption that CV would remain constant. The predicted values were then correlated with the actual values for FCC by means of a linear regression with a forced zero intercept.

Results: As predicted by our hypothesis, increasing crank length resulted in significantly reduced FCC ($p < .001$). However, contrary to the hypothesis, increasing crank length resulted in a significant increase in PS ($p < .001$), but had no significant effect on CV ($p = .805$). FCC was strongly correlated with FCC predicted from CV ($r = .992$) but less strongly with FCC predicted from PS ($r = .708$) (Figure 1, Table 1).

Figure:
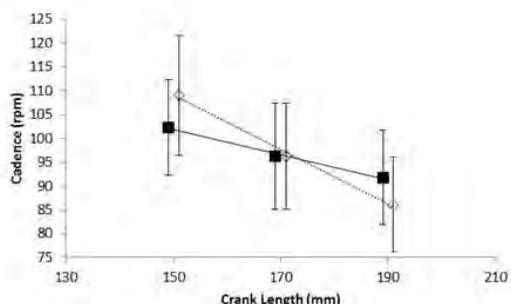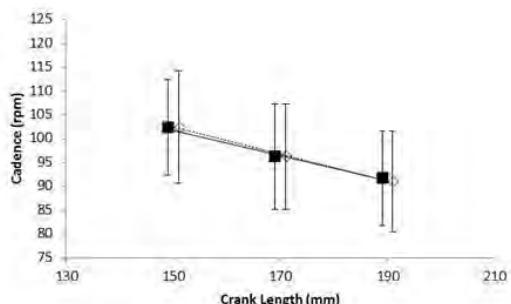
Caption: Cadence (modeled and freely chosen) - crank length comparison for submaximal cycling. A = pedal speed model, B = cyclic velocity model. Note: ◇ MPC, ■ FCC. Error bars show FCC and model predicted standard deviation. Points are offset horizontally so that error bars are visible.

Conclusion: Contrary to our hypothesis, the participants did not select FCC to preserve PS but rather to preserve CV. These results suggest that when perturbed, the central nervous system does not solely seek to preserve muscle shortening velocity. They further suggest that it is a combination of muscle shortening velocity and activation/deactivation dynamics which is important in the selection of FCC. These results lead us to speculate that FCC is selected to find an optimal trade-off between the minimisation of metabolic cost and neuro-muscular stress. From an applied perspective, our findings add to the body of evidence that crank length is not an important determinant in submaximal cycling performance.

Table:

Crank length (mm)	Actual cadence (rpm)	Pedal speed model predicted cadence (rpm)	Cyclic velocity model predicted cadence (rpm)
150	102.3 ± 9.5	109.1 ± 12.6	102.4 ± 11.8
170	96.2 ± 11.1	96.2 ± 11.1	96.2 ± 11.1
190	91.8 ± 9.4	86.1 ±9.9	91.0 ± 10.5

Caption: Comparison of actual cadence and predicted cadences from pedal speed and cyclic velocity (values are mean ± s.d.)

References: [1] Martin. Exerc Sport Sci Rev, 35(2):74-81, 2007.

[2] Martin et al., J. Biomech, 33:969-974, 2000.

Disclosure of Interest: None Declared

Neurological and Motor Control

PO-0155

DEVELOPING CONCUSSION TESTING IN A COMPUTER ASSISTED REHABILITATION ENVIRONMENT (CAREN)

Matthew Pain [1,*]Louise Burnie [1]Glen Blenkinsop [1]

[1]School of Sport, Exercise and Health Sciences, Loughborough University, Loughborough, United Kingdom

Introduction and Objectives: Concussion is becoming accepted as a major problem in many sports, e.g. American football, ice hockey, soccer, rugby, judo, road cycling, and better testing methods are needed to track and improve rehabilitation. Neurocognitive deficits may be observed following a concussion and can be used to help diagnose concussion and monitor recovery. Previous research, using visual only virtual reality (VR) systems, has shown that athletes can pass common test but fail when taking visually based VR tests. With the CAREN system we can also add movement perturbations to the sensory input or require the athlete to take the test using actual whole body movements as the control method. This latter format would replicate the real world needs of athletes where decision making, cognitive function and movement control are needed simultaneously in many instances. The purpose of this project was to develop a neuropsychological testing procedure using a motion sensing CAREN system to assess cognitive function whilst incorporating simultaneous balance assessment and whole body motion as the controller to develop a more sensitive and sport specific concussion testing, monitoring and rehabilitation methodology.

Methods: Variants of standard neuropsychological tests were created using D-Flow software that allowed the tests to be taken using a video games controller or via two force plates with an immersive 2D screen. CAREN based tests were: word memory, pattern memory, reaction time and pattern recall, visual-motor processing speed, colour response and Stroop test, letter recall and trail making. These were variants or adaptations of standard paper and computer based neuropsychological tests. Validity, reliability and test-retest reliability, including using the Reliable Change Index (RCI), were determined against "gold standard" pen and paper tests for a total of 17 healthy subjects. The effect of taking the test in two different conditions, controlled via force plates and games controller, or only a games controller was investigated. To examine if just standing, as needed for the force plate tests, would alter performance subjects took the games controller only tests both standing or seated at a regular computer screen was investigated. Test order was randomised across subjects. Practise and retention effects with test – retest intervals of 10 minutes and 1 week were also assessed. Pearson's product correlation compared pen and paper tests to CAREN tests. One-Way Anova with Bonferroni correction compared test scores in different conditions, significance at $p < 0.05$. Subjective feedback from the subjects was also recorded.

Results: The CAREN tests had moderate to strong correlations with the pen and paper equivalents. There were no significant differences between standing and sitting for games controller only. There were significantly different scores between force plate control and games controller for time based scores. Pen and paper showed a large number of significant differences for test-retest, while the CAREN tests showed less. RCI measures only gave a significant result on one pen and paper test on the retest interval of 10 minutes, Hopkins verbal learning test. There was no difference in subjective ranking of difficulty of the pen and paper tests or the CAREN tests.

Conclusion: The motion sensing CAREN based tests are a reliable and repeatable set of tests whilst allowing: balance metrics to be simultaneously analysed, postural movements as a controller, visual and physical perturbations to be introduced for greater diffuse sensory input during testing. The next step is to begin testing of concussed subjects with this system to determine an overall system scoring system for assessing concussion, and then to introduce further refinement via introducing perturbation affects during testing.

Disclosure of Interest: None Declared

PO-0156

THE EFFECTS OF PAIRED ASSOCIATIVE STIMULATION -INDUCED BRAIN PLASTICITY CHANGES ON VISUOMOTOR LEARNING TASK

Janne Avela [1,*] Susanne Kumpulainen [1] Jussi Peltonen [1] Ilona Ruotsalainen [1]

[1] Department of Biology of Physical Activity, University of Jyväskylä, Jyväskylä, Finland

Introduction and Objectives: Brain can adapt in response to motor learning by changing its neuroanatomical and functional properties. A simple repetitive motor activity does not; however induce this reorganization (representational map plasticity). Instead, skill acquisition, learning or practice of a novel motor task does induce map plasticity. Thus, specific patterns of motor activity are required to produce functional motor cortex plasticity. One proposed model for these changes is long lasting enhancement of synaptic strength called long-term potentiation (LTP) (Hebb 1949). LTP-like changes in motor cortex are possible to induce artificially with paired associative stimulation (PAS). Some evidence exists that PAS can enhance specific types of motor learning (Ziemann et al. 2004). The aim of this study was to examine the effects of PAS-induced LTP-like plasticity on early acquisition phase of brief visuomotor learning task.

Methods: Twenty healthy volunteers (8 females, 12 males; age = 26.6 ± 4.3; height = 174.4 ± 8.7; weight = 75.5 ± 12.5) participated in this study. The measurements were conducted during two separate sessions. During the first session, measurements of maximal isometric plantarflexion contractions (MVC), motor evoked potentials (MEP), maximal compound muscle action potentials (Mmax) and H-reflexes preceded the PAS intervention (PAS). Five minutes after PAS, learning task one (L1) was conducted. There was a 15 minutes break between the next two consecutive learning tasks (L2 and L3), during these breaks MEPs, Mmax and H-reflexes were measured (POST1, POST and POST3).

PAS consisted of 200 electrical stimuli delivered to the posterior tibial nerve at popliteal fossa, paired with a single TMS pulse of the soleus area over the contralateral M1. The rate of paired stimulation was 0.2 Hz. The interstimulus interval between electrical stimuli and TMS was calculated as the latency time of the sensory evoked potential + 18ms (Kumpulainen et al. 2012).

Learning task performance was calculated as a magnitude of an average error throughout the task. Subjects were divided into three different groups: control group (CON, n=6), group of responders (RES, PAS induced MEP facilitation, n=8) and group of non-responders (NON, PAS did not increase MEP size, n=6).

Results: All groups improved their learning task performance between L1 and L2 as expected (figure 1). However, there was an additional improvement between L2 and L3 for the RES group only. This improvement was significant when compared to CON and close to significant when compared to NON. MEP amplitudes following PAS increased in the RES group by 138.0 ± 98.6 % (POST1), 227.8 ± 130.2 % (POST2, $p < 0.022$) and 228.4 ± 152.9 % (POST3, $p < 0.012$). In the NON group MEP amplitudes were 83.0 ± 35.2 % (POST1) 70.7 ± 21.7 % (POST2, $p < 0.020$) and 72.0 ± 15.5 % (POST3) when compared to PRE. There were no changes in MEP size in CON when compared to PRE measurement. Both the H-reflex and Mmax did not change significantly between the conditions in neither of the groups.

Figure:
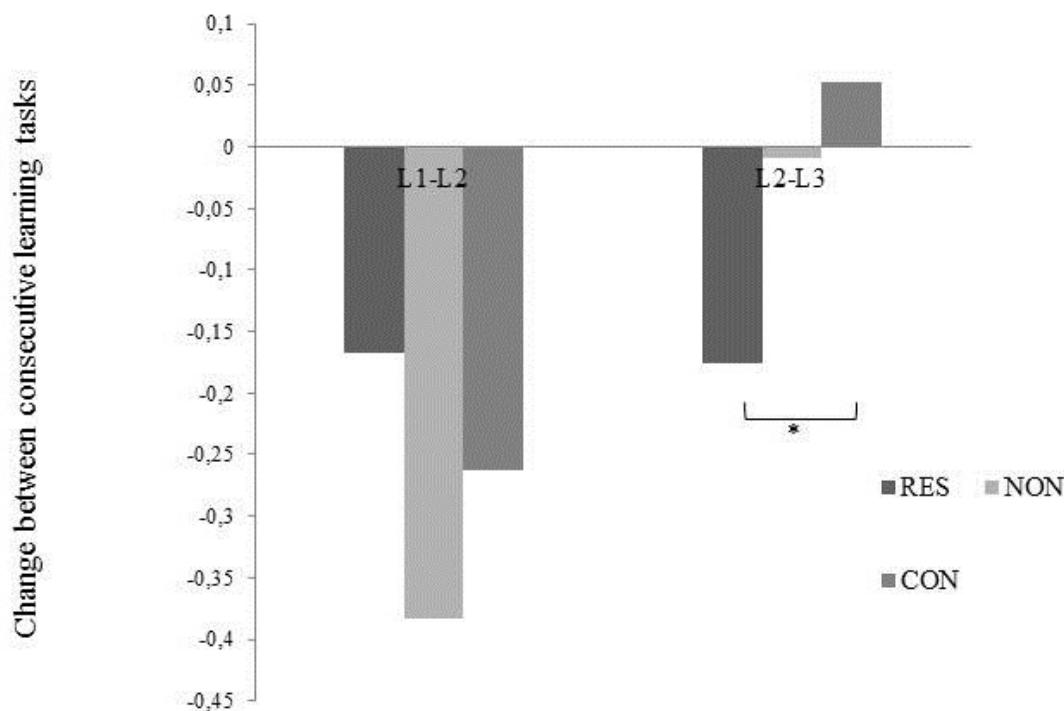
Caption: Change in average errors between consecutive learning tasks L1-L2 and L2-L3. Asterisk represent a significant (p < 0.05) difference between RES and CON groups. Data expressed as mean.

Conclusion: The present findings showed that PAS-induced LTP-like plasticity did not improve visuomotor learning immediately after the PAS intervention (between L1 and L2). However, as the learning proceeded PAS might have had a beneficial effect on learning (between L2 and L3). This could be due to delayed effects of PAS, which was shown as significantly higher MEP values in POST2 and POST3 than in POST1. This is in line with some previous experiments which have shown that is usually takes some 10 to 15 minutes for LTP to evolve after PAS (e.g. Kumpulainen et al. 2012). Since there were no changes in H-reflexes or Mmax between the different conditions in neither of the groups, it is very likely that the changes took place at the cortical level. However, since the visuomotor learning alone (CON) did not affect the MEP amplitudes, it is difficult to identify the cortical networks that could have affected the visuomotor learning.

References: (1) Hebb, D.O. (1949) Wiley, New York, USA.

(2) Ziemann, U., Iliać, T.V., Pauli, C., Meintzschel, F. & Ruge, D. (2004) J Neurosci 24(7) 1666–1672.

(3) Kumpulainen, S., Mrachacz-Kersting, N., Peltonen, J., Voigt, M. & Avela, J. (2012) Exp Brain Res 221: 241–249.

Disclosure of Interest: None Declared

HIGH-DENSITY SEMG FOR THE OPTIMIZATION OF MOTOR EVOKED POTENTIAL DETECTION ON TIBIALIS ANTERIOR MUSCLE DURING TRANSCRANIAL MAGNETIC STIMULATION

Niklas König [1,*] Navrag Singh [1] Marco Gazzoni [2] Nicole Wenderoth [3] William Taylor [1]

[1]Institute for Biomechanics, ETH Zürich, Zürich, Switzerland, [2]Laboratory of Engineering of Neuromuscular System and Motor Rehabilitation , Politecnico di Torino, Turin, Italy, [3]Neural control of movement laboratory, ETH Zürich, Zürich, Switzerland

Introduction and Objectives: Integrated effects of central & peripheral neuromotor entities are required for effective motor control [1]. Transcranial magnetic stimulation (TMS) is a tool for assessing the causal influence of cortical areas on motor control by evaluating changes in task performance in response to induced neural perturbations [2]. Until now TMS has been used primarily to investigate upper limb function due to limited magnetic field penetration depth. However, recent developments in coil designs provide accessibility to lower extremity muscle representations [3]. TMS application requires determination of subject-specific parameters based on evoked responses measured via surface EMG. Typically, lower limb muscles are large, allowing for variability in positioning the EMG electrodes during TMS. Furthermore, bipolar EMG amplitude is sensitive to electrode location, with locations over the muscle innervation zone resulting in significantly lower EMG amplitudes [4]. The rest motor threshold (RMT) is defined as the lowest stimulation intensity (%maximum stimulator intensity [MSO]) needed to evoke 5/10 motor-evoked potentials (MEPs) with an amplitude > 0.05mV [5]. Thus, the RMT is dependent on the EMG amplitude. However, for application of TMS to lower limb muscles, it remains unclear whether location of the surface EMG can alter the subject-specific RMT. Therefore the aim was to assess if optimised EMG location would result in decreased RMT.

Methods: Five subjects (29±5yrs, 70±13kg, 171±10cm) were seated relaxed with their knees and ankles at 90°. Bipolar EMG (Delsys, USA) was placed on the right tibialis anterior muscle belly after preparing the skin. MEPs were induced with a double-cone coil connected to a Magstim 200 stimulator (Magstim, UK) while EMG responses were sampled at 4kHz (CED, UK). Initially, the coil location resulting in the largest and most consistent MEPs was determined. Firstly the RMT for each subject was determined using the bipolar EMG located centrally on the muscle belly (RMT_Norm) [5], followed by 20 MEPs recorded at 130% RMT_Norm. A high-density surface EMG (HD-sEMG) with a grid of 16x4 electrodes (LISiN, Turin) was then attached covering the whole muscle surface. This HD-sEMG grid was connected to a 64 channel amplifier (W-EMG, LISiN-Bitron). A 15s ramp isometric contraction was then recorded, as well as 20 MEPs at 130% RMT_Norm. The electrode pair resulting in the largest MEP amplitude was identified and the corresponding location was marked on the muscle. Finally, the HD-sEMG was replaced by a bipolar electrode located at the identified optimised muscle location before RMT was again evaluated (RMT_Opti) and 20 MEPs recorded at 130% RMT_Opti.

Results: The RMTs remained unchanged when the bipolar sEMG was located at the centre of the muscle belly compared to the optimal location. The change of MEPs between MEP_Norm and MEP_Opti was inconsistent with 3/5 subjects revealed lower MEPs at MEP_Opti. Cross-correlation of amplitude and shape between the action potentials in the ramped contraction and the MEPs in a revealed that TMS only recruits a fraction of motor units within the pool (Figure 1).

Figure:
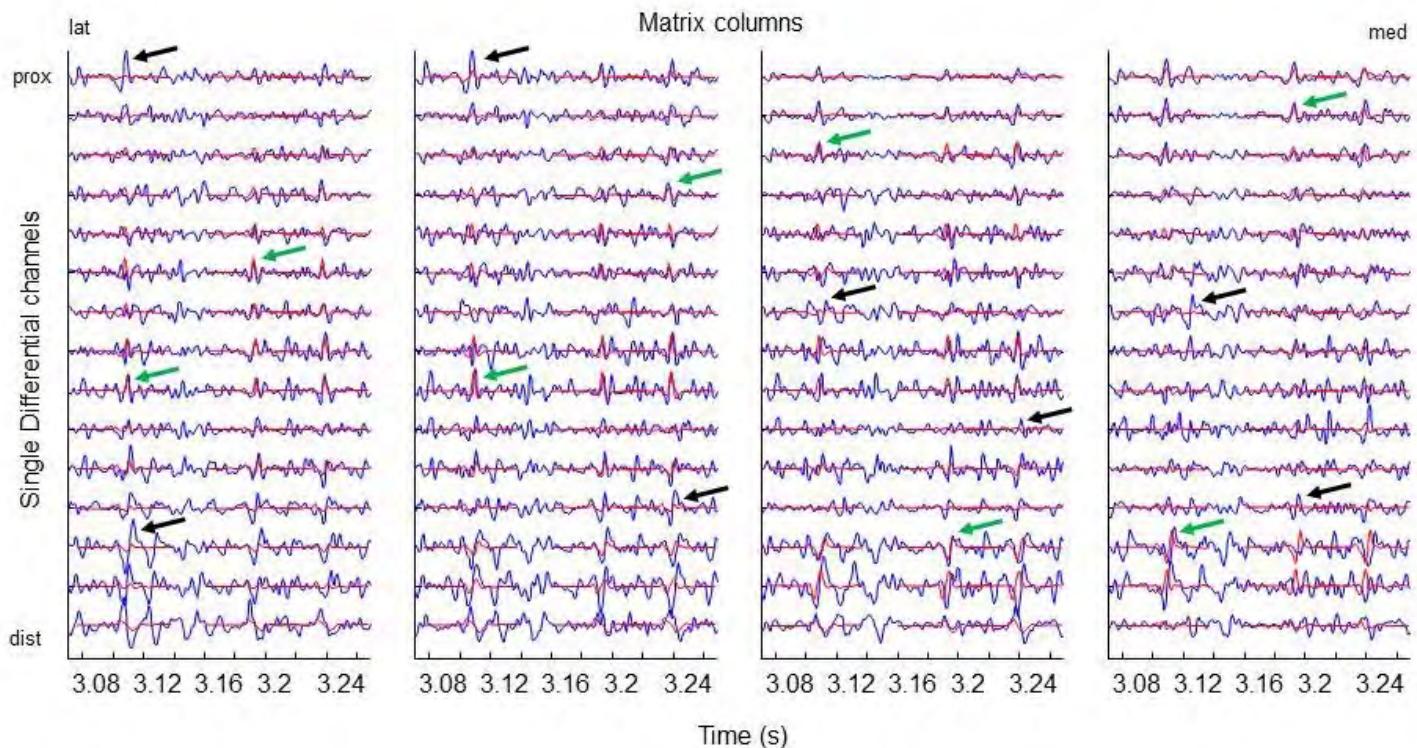
Caption: Cross-correlation between motor-units during ramped contraction and the MEP during TMS. Blue traces: ramped contraction. Red traces: MEP template. High (green arrows) and low (black arrows) correlation between both signals

Conclusion: The RMTs were insensitive to the location of the bipolar EMG. Although in a small sample size, a comparison between action potentials during the ramped contraction and the MEP showed that TMS at 130% RMT innervated only few motor units. The amplitudes at MEP_Opti were not larger than at MEP_Norm, which is in contrast to the increased MEPs identified for the optimised location in the HD-sEMG. This might be due to differences in the electrode geometry, or that the TMS quasi-randomly innervates motor units [6], which would result in the optimal location moving with every iteration. Finally, it appears that although the average MEP_Opti was reduced in 3/5 subjects, the RMT remained stable, which implies that the central effect in the primary motor cortex is larger than the local effect of amplitude change on the muscle. In conclusion, the current RMT method is a robust measure to assess subject-specific TMS intensity irrespective of local muscular effects. The effects of TMS on motor unit recruitment are interesting but require further investigation.

Table:

Subject	RMT_Norm [%MSO]	RMT_Opti [%MSO]	MEP_Norm [mV]	MEP_Opti [mV]
1	44	44	0.49	0.86
2	37	39	0.91	0.50
3	43	43	0.48	0.15
4	32	32	0.45	0.35
5	34	34	0.21	0.24

Caption: Change in RMT and MEP between the two electrode positions

References: 1.Hausdorff et al., Exp Brain Res, 164(4): 541-8, 2005.

2.Chouinard et al., Front Hum Neurosci, 4: 173, 2010.

3.Barthelemy et al., Prog Brain Res, 192: 181-97, 2011.

4.Barbero et al. *Atlas of the muscle innervation zones*, Springer, 2012.

5.Rossini et al., Electroencephalogr Clin Neurophysiol, 91(2): 79-92, 1994.

6.Enoka, J Electromyogr Kinesiol, 5(3): 141-9, 1995.

Disclosure of Interest: None Declared

PO-0158

EVIDENCE FOR SPINAL CORD ACTIVATED MOTOR UNITS IN SPASTIC MUSCLES AFTER STROKE

Kathrin Koch [1,*] Catherine Disselhorst-Klug [1]

[1]Rehabilitation and Prevention Engineering, RWTH Aachen, Institute of Applied Medical Engineering, Aachen, Germany

Introduction and Objectives: About 15 million people suffer from stroke each year worldwide and approximately 10% subsequently remain with spastic impairments. A spastic impaired muscle shows a velocity dependent increase in muscle tone. The changes in the muscular activation are caused by the lesion in the cerebral tissue after the stroke incident, whereas the muscle structure itself is not impaired.

Since the insult the regulating effect of the brain, which controls the activation of the muscle, is missing and changes in the activation of motor units can be expected. Spasticity is often linked with hyperreflexia what leads to the suggestion that the activation of the spastic muscle is now controlled by mechanisms on spinal cord level. In order to get evidence for a spinal cord controlled activation of spastic muscles, the activation of single motor units is analyzed with surface electromyography.

Methods: For an evaluation the changes in the activation of the smallest excitable units (motor units) of a muscle will be analyzed. By measuring muscular activation on motor unit level important information about the recruitment and firing strategies can be gained. The activation of motor units is measured with grid electrodes in combination with a two-dimensional Laplacian filter (high spatial resolution electromyography) which was used already for the distinction between different neuromuscular disorders. Measurements have been performed at the abductor pollicis brevis of 10 stroke patients at maximum voluntary contraction for one second. From the measured data the number of action potentials per time, the firing frequency of all motor units and the distance between peaks were extracted, which describe the special characteristics of spastic muscles.

Results: The HSR-EMG signal of patients who suffer from stroke shows significant changes compared to the signal of healthy subjects. The most dominant feature is a constant appearance of action potentials (Figure 1). The constant firing is a common feature for all patients with spasticity. The main frequency of the firing rate is about 8 to 16 Hz. The distance between single peaks is extraordinarily uniform. Additionally the shape of the repeated, isolated peaks is similar. Further characteristics of the HSR-EMG signal of spastic muscles are sparsely distributed, isolated peaks and rarely background activity. The total number of peaks per second is much less than in healthy muscles.

Figure:
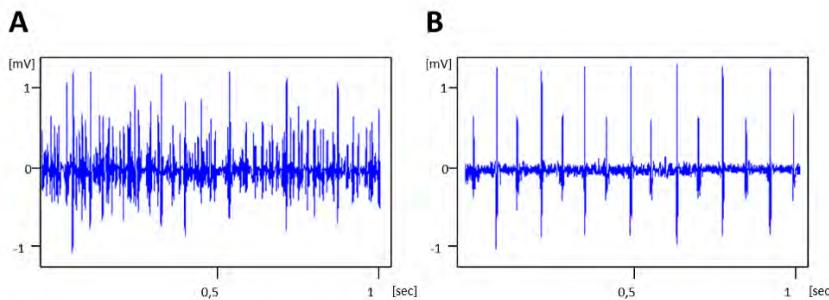
Caption: Figure 1: HSR-EMG signals of a healthy muscle (A) and spastic muscle (B)

Conclusion: The activation of single motor units in spastic muscles shows constant firing rates. The underlying mechanism for this activation pattern might be an autonomously oscillating circuit on spinal cord level. A trigger frequency which is developed after central lesions could be responsible for the special firing frequency. Additionally it could contribute to the increased muscle tone in spastic muscles. A sparse appearance of action potential indicates less active motor units than in a healthy muscle. After the brain insult the innervation of the complete pool of motor units is no longer possible, so the compensation strategy of this deficit results in less active motor units activated at a constant frequency. The regular activation strategies for force generation of a muscle controlled by the brain, like increase of firing rate and increase of activated motor units, cannot be provided by the mechanism on spinal cord level.

In conclusion possible evidence for muscle controlling mechanisms on spinal cord level can be found in the activation pattern of spastic muscles.

Disclosure of Interest: None Declared

Neurological and Motor Control

PO-0159

INVESTIGATION OF A CAUSAL MODEL LINKING CORTICOMUSCULAR COHERENCE TO MOTOR PRECISION INCLUDING ANTAGONIST MUSCLE EFFECTS

Nikhil V. Divekar [1,*]

[1]Exercise Science and Sports Medicine, University of Cape Town, Cape Town, South Africa

Introduction and Objectives: The relationship between cortico-muscular-coherence (CMC) and motor-precision is unclear: a within-task direct relationship [1] and a between-task inverse relationship [2 3] were found previously. The latter was explained using a proposed causal model: higher beta (15-35-Hz) CMC induces higher beta oscillations in the agonist electromyogram (EMG) which cause higher beta and low-frequency (<5Hz) fluctuations in joint-torque (leading to lower precision). We aimed to examine this proposed causal model in the within-task scenario to control for the confounding task factor. Furthermore, previous studies applied to agonists only, but antagonist muscles would also affect precision and hence were also included.

Methods: EEG, EMG and wrist-joint-torque were recorded from 15 subjects performing 10 repetitions of 2 isometric tasks (wrist flexion, extension) using multiple co-contracting agonists-antagonists. Data was segmented, re-ordered and bifurcated into high-precision (HP) and low-precision (LP) groups within each task.

Results: Within both tasks, both beta CMC and beta EMG of certain agonists and antagonists were significantly higher for HP; while both beta and low-frequency (<5Hz) fluctuations in wrist-joint-torque were significantly lower for HP.

Conclusion: Hence contrary to the causal model, lower joint-torque fluctuation (higher precision) was found despite the higher beta EMG that was induced by the higher beta CMC. We propose the annulled task confound and also co-contraction of agonists-antagonists to have facilitated this result. We hence confirm a direct CMC-precision relationship and also reveal the significance of antagonist CMC in this relationship. An extra observation suggests the extent of the CMC-precision relationship varies with the role (ant/agonist) of certain muscles.

References: [1] Kristeva R, Patino L, Omlor W. Neuroimage. 2007;36(3):785–92.

[2] Divekar NV, John LR. Clin Neurophysiol. 2013 Jan;124(1):136–47.

[3] Ushiyama J, Katsu M, Masakado Y, Kimura A, Liu M, Ushiba J. *J Appl Physiol.* 110: 1233–1240, 2011.

Disclosure of Interest: None Declared

Transform the way you think
about motion capture.

See a demo at the Vicon booth

VICON

VICONVANTAGE

Intelligence in motion

ISB 2015 GLASGOW | XXV CONGRESS OF THE INTERNATIONAL SOCIETY OF BIOMECHANICS

Platinum sponsors of ISB 2015

PO-0160

THE EFFECTS OF LONG-TERM FIELD TENNIS PRACTICE ON POSTURAL ADJUSTMENTS AND MOVEMENT PLANNING AND EXECUTION DURING A TARGET-POINTING TASK

Alethéa G. Nardini [1,*] Luis Vicente [2] Igor Souza [3] Paulo Freitas [4] Sandra Freitas [1]

[1]Programa de mestrado e doutorado em fisioterapia, [2]Graduação em Fisioterapia, Universidade Cidade de São Paulo, [3]Graduação em Educação Física, [4]Programa de Pós Graduação em Ciências do Movimento Humano, Universidade Cruzeiro do Sul, São Paulo, Brazil

Introduction and Objectives: One of requirements to be a good tennis player is to be able to quickly use visual cues from the opponent's movement to plan and execute an appropriate move. But before that, the tennis player should have a good body control to perform the movements of the upper limbs. Thus, the aim of study was to examine the effect of long-term tennis practice on the anticipatory postural adjustments (APAs) and on reaction time (RT) and movement time (MT) during a pointing to a target task.

Methods: Eight right-handed adolescent tennis players (6 males and 2 females) with at least two year of intensive practice (three or more days per week) and eight sex- and age-matched controls participated in the study. The standing participant placed each foot on a force platform (AMTI OR6-7), and pressed with the index finger of the dominant hand a force sensor (ATI Nano 17) attached to a tripod located in front of and aligned with the participant's midline. They were instructed to point one of two targets displayed on a 32-inch touch screen monitor ELO placed at a distance of 85% of the participant's arm length. The two 2.5-cm diameter circular targets were set at left and right extremities of the screen, respectively defined as contralateral and ipsilateral to the arm used to perform the movement. At the beginning of each trial both targets were displayed as dark green. The sign indicating that the pointing movement should be performed was the target changing of color (from dark to light green) changed the color. They were asked to start moving as soon as the target changed its color, to perform the movement towards the target as fast as possible, and be as accurate as possible pressing the screen at the center of the target. Ten trials were performed for each target location under a certainty condition (participant knew what target he/she should move to) or uncertain condition (movement direction was unknown until one to two targets change its color). APAs were assessed from changes in weight bearing and center of pressure (COP) displacement and movement planning and execution by RT and MT.

Results: Before starting the movement, participants presented symmetry in their weight bearing independent of the target and direction and no difference between tennis players and controls was found. Also, the COP displacement on the left limb was higher when participants had to reach the contralateral target during uncertain condition and this effect was more evident for tennis players, suggesting a greater preparation of this group for more complex condition (i.e., contralateral target on the uncertainty condition). Regarding movement planning, participants in both groups spent more time to start their movement in the uncertainty condition compared to the certainty condition (≈50 ms), but no difference between tennis players and controls was found for RT. For movement execution, results revealed no effect of direction and condition but revealed that the MT for tennis players was shorter than for controls, but only when the target reached was the contralateral one.

Conclusion: The findings indicate that long-term tennis practice did not improve individual's ability to detect the visual stimulus and plan the target-directed movement in a pointing task. However, tennis practice can cause little changes in movement execution, principally when someone has to contact a target placed contralateral to the moving limb. This increase in movement velocity could be directly related to the higher amplitude postural adjustments found in tennis players in this condition. A plausible explanation for this increased movement velocity when moving towards the contralateral target is that tennis players are more accustomed to move their upper-limb to the contralateral side of their dominant limb when they use a backhand stroke and this kind of movement is not common for individuals who do not play any racket sports.

Disclosure of Interest: None Declared

Neurological and Motor Control

PO-0161

MOTOR UNIT SYNCHRONIZATION BETWEEN QUADRICEPS MUSCLES IS TASK-DEPENDENT

Maurice Mohr [1,*]Marius Nann [2]Vinzenz von Tscharner [1]Benno Nigg [1]

[1]Human Performance Laboratory, Faculty of Kinesiology, University of Calgary, Calgary, Canada, [2]University of Erlangen-Nuremberg, Nuremberg, Germany

Introduction and Objectives: Motor unit (MU) synchronization within and between individual muscles as a result of a common synaptic input has commonly been investigated during isometric contractions[1]. Recently, it has been suggested that MU synchronization within a muscle is task-dependent and is higher during concentric muscle contractions than during isometric contractions[2]. In consequence, MU synchronization, particularly with respect to its physiological function, should be investigated under dynamic and more natural conditions. However, for MU synchronization between two individual muscles, the presence of a task-dependence is unknown. Further, the influence of balance tasks that may require independent muscle contributions rather than synchronized muscle function is poorly understood. Therefore, the purpose of this study was to compare the synchronization of MUs between two quadriceps muscles during isometric and dynamic squats with and without balancing elements. We hypothesized (1) that concentric muscle contractions during dynamic squats demand a higher degree of MU synchronization than an isometric contraction and (2) that synchronization is reduced during balancing tasks.

Methods: Healthy, male (n=13) and female (n=5) participants (age: 25±4 years) completed an isometric squat (IS), a series of dynamic bipedal (BPS) as well as single-leg squats (SLS) and a single-leg balance task (SLB). A recently developed current amplifier[3] was used to record monopolar surface electromyograms (EMGs) from the *vastus lateralis (VL)* and *medialis (VM)*. As a measure of synchronization, coherence spectra between the raw EMGs of *VL* and *VM* were calculated between 15–100 Hz and averaged across subjects. Coherence spectra were considered significant if they were different from a random coherence spectrum (RD) that was computed between two similar but unrelated signals. Statistical differences between coherence spectra were determined using a one-way repeated measures ANOVA and Bonferroni corrected post-hoc tests ($\alpha=0.05$).

Results: The coherence between *VL* and *VM* during BPS, SLS, and IS was significantly higher than the random coherence ($p<0.001$). Coherence during SLB was not significantly different from the random coherence ($p=0.416$). The highest coherence was found during BPS and decreased significantly for SLS ($p=0.008$) and IS ($p<0.001$) (Figure 1).

Figure:
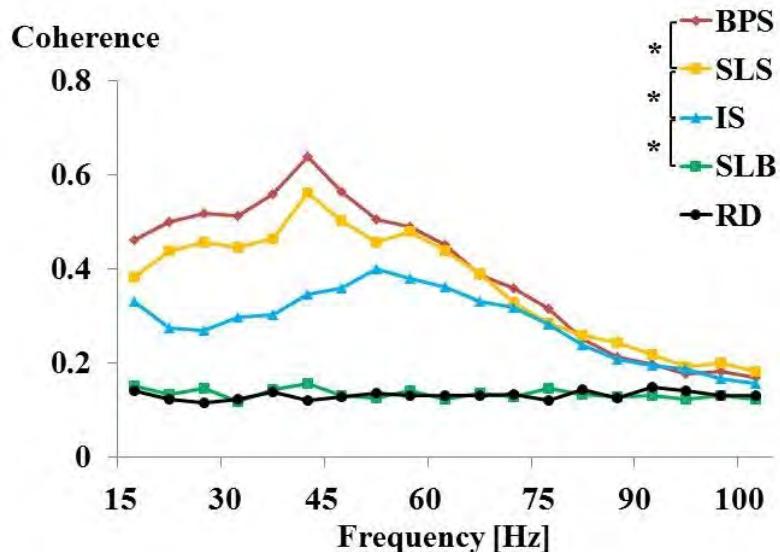
Caption: Figure 1: Mean coherence spectra for bipedal squat (BPS), single-leg squat (SLS), isometric squat (IS), single-leg balance (SLB), and random coherence (RD) (n=18)

Conclusion: During BPS, IS, and SLS, MUs of *VL* and *VM* were significantly synchronized. The degree of synchronization during dynamic squats (BPS, SLS) was higher compared to an isometric squat, supporting our first hypothesis. It is assumed that the higher degree of synchronization during dynamic squats originates from an increased common synaptic input to the motor neurons of the quadriceps muscle. This might reflect a basic strategy of the central nervous system to produce force more rapidly and to simplify the execution of more complex movements[4]. The synchronization during SLS was smaller compared to BPS and there was no synchronization during a SLB, supporting our second hypothesis. We speculate that reducing the common motor input may be a central strategy to promote a more independent function of the individual quadriceps muscles in order to maintain the stability around the knee joint during a balance task[4]. The results of this study underline the importance of investigating MU synchronization during dynamic tasks rather than isometric contractions. Future research has to use similar approaches to further elaborate the functional role of synchronized quadriceps activation with respect to performance and injury outcomes.

References: [1] Bremner et al. J Physiol, 432: 381-399, 1989.

[2] Von Tscharner. J Exerc Sports Orthop, 1: 1-7, 2014.

[3] Von Tscharner et al. J Electromyogr Kines, 23: 1044-1051, 2013.

[4] Semmler. Exerc Sport Sci Rev, 30: 8-14, 2002.

Disclosure of Interest: None Declared

Orthopaedic Implants

PO-0162

BIOMECHANICAL COMPARISON OF ANCHORING STRENGTH OF DIFFERENT EXPANDABLE PEDICLE SCREWS IN SEVERE OSTEOPOROSIS

Ching-Lung Tai [1,*]Yi-Lu Chen [1]Cheng-Syuei Lin [1]Lih-Huei Chen [2]

[1]Graduate Institute of Medical Mechatronics, Chang Gung University, [2]Department of Orthopaedic Surgery , Chang Gung Memorial Hospital, Taoyuan, Taiwan, Republic of China

Introduction and Objectives: Pedicle screw fixation for patients with severe osteoporosis remains a challenge for the orthopedist. To solve this problem, the common surgical technique is to inject cement into vertebrae, and then secure the screw to improve the screw/bone interfacial strength. Recently, cement-injectable cannulated screws and expandable screws are used to enhance the screw holding power. To improve screw pullout strength in cannulated screw, the PMMA bone cement was squeezed to the osteoporotic bone, via the central hole of screw, and thus enhances the screw/bone interfacial strength [1]. For the expandable screws, however, the screw also has a cannulated center in which an expansion pin is placed. The anterior end of the screw is divided lengthwise to form separated wings that expand at the posterior tip after pin insertion, and hence increase the screw holding power. Expandable screws are demonstrated to significantly improve the axial pullout strength as compared to conventional screws in osteoporosis. However, previous studies addressing the influence of design parameters such as the degree of screw expansion, number of the lengthwise wings, cement augmentation or not, on the axial pullout strength of the expandable screws are lacking. This study aims to explore the effects of the above-mentioned parameters on expandable pedicle screws.

Methods: Four screw designs were employed in the present study: 4 slits and 6 slits with 16 mm or 22 mm in effective expansion length. The effective expansion length was defined as the length from the point of diameter change of the screw central hole to the screw tip. Commercially available test block (model #1522-507, Pacific Research Laboratory Inc., Vashon Island, WA, USA) was used as a substrate for vertebrae with severe osteoporosity, which eliminated the experimental errors caused by the variability of bone properties and morphometry. Prior to screw insertion, a pilot hole was drilled into the test block using a 3-mm drill bit, and a cannulated screw was then inserted into the test block through the prepared pilot hole. For screw without cement augmentation, a pin was inserted into the screw central hole to achieve screw expansion. Whereas for screw with cement augmentation, cement was injected via the central hole prior to the insertion of central pin. Pedicles screws with or without cement augmentation were then tested for axial pullout failure using an Instron testing machine (model 5544, Instron Inc., Canton, MA, USA). Screw pullout test was conducted according to ASTM F543-02 testing standards [2].

Results: The 6-slit screw with 16 and 22mm of effective expansion length after expansion was shown in Fig. 1A. The expansion diameters at the screw tip for screws with 16 and 22mm effective expansion length were 11 and 15 mm, respectively. The results revealed that the screw with a longer effective expansion length achieved a larger expansion range. The radiological examination of the screws inserted into the test blocks was shown in Fig. 1B. The radiological photograph indicated that the cement was exuded from the slits closest to the very beginning of its flow path. The mean pullout strength of various types of expandable screw was shown in Fig. 1C. Solid screw without cement augmentation

presented the lowest pullout strength (27.6±12 N). Regardless of screw designs, a significant increase of pullout strength was found for expandable screw combined with cement augmentation. Although previous literatures have shown expandable pedicle screws effectively enhance screw holding power, our results further demonstrated that expandable screw combined with cement augmentation may enormously increase screw fixation as compared to the use of expandable screw alone. The increase in both screw slit number and the degree of screw expansion has little impact in increasing screw anchoring strength.

Figure:
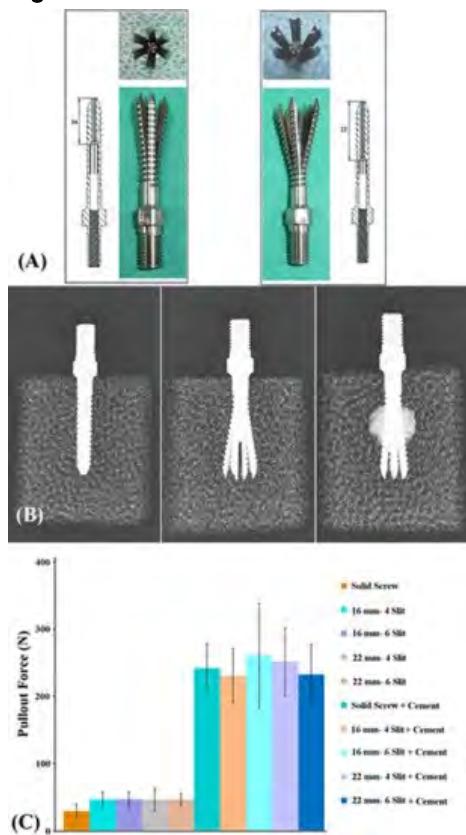
Caption: Fig. 1. (A) Photograph showing the pedicle screw after expansion. 6-slit screw with 16 mm of effective expansion length (left); 6-slit screw with 22mm of effective expansion length (right). Screw with 22 mm effective expansion length presents a large expansion range. (B) Radiological photograph showing pedicle screws inserted into test block. Solid screw with cement augmentation (left); Expandable screw without cement augmentation (middle); Expandable screw with cement augmentation (right). (C) The mean pullout strength of various types of expandable screw.

Conclusion: Cement augmentation is the most influential factor in improving screw pullout strength in application of expandable pedicle screws.

References: [1] Chen LH et al. *BMC Musculoskelet Disord.* **12**:33, 2011.

[2] ASTM F 543-02

Disclosure of Interest: None Declared

Orthopaedic Implants

PO-0163

STABILITY ASSESSMENT OF STAND-ALONE CAGE WITH VARIOUS DESIGN PARAMETERS FOR DIRECT LATERAL INTERBODY FUSION USING FINITE ELEMENT ANALYSIS

Yong Woo Kim [1] Won Man Park [1] Dae Kyung Choi [1] Kyungsoo Kim [2] Yoon Hyuk Kim [1,*]

[1] Mechanical Engineering, [2] Applied Mathematics, Kyung Hee University, Yongin, Korea, Republic Of

Introduction and Objectives: Direct lateral interbody fusion (DLIF) is an effective surgical method to treat low back pain because it could be performed by a minimally invasive option. Furthermore, this method could avoid complications such as posterior bony resection, wide muscle dissection in posterior approach, and vascular injury in anterior approach. In addition, it can preserve all the ligamentous structures which were considered to be one of the major stabilizing components of the lumbar spine [1, 2]. However, a biomechanical study has reported that stand-alone cage system for DLIF could not provide enough stability at the operated level and suggested the utilization of supplementary fixations to improve the stability [3]. In order to increase stability without utilization of supplementary fixations, we investigated the effects of design parameter of stand-alone cage system for DLIF on stability at the operated level by using finite element analysis.

Methods: A validated three-dimensional finite element model of the lumbar spine from L1 to S1 was used [4]. Two kinds of stand-alone cages, which are a cage with two internal screws (Int_Screw) and a cage with two external screws (Ext_Screw), were used (Figure). In case of Int_Screw, the cage was completely inserted between vertebrae and screwed to upper and lower vertebrae through inferior and superior planes of vertebrae. In case of Ext_Screw, the inserted cage between vertebrae was screwed to the vertebrae with external plate on right lateral side of vertebrae. Each stand-alone cage was inserted at L4-L5 motion segment. About 68% of annulus fibrosus was removed for applying DLIF on the lumbar spine model. The initial screw angle and length were 25° and 45 mm in Int_Screw, and 5° and 45 mm in Ext_Screw. Screw angle varied from 20° to 35° and from 5° to 30° in Int_Screw and Ext_Screw cases with increments of 5°. Screw length of both types of stand-alone cages varied from 35 mm to 45 mm with increments of 5 mm. The sacrum of the healthy lumbar spine was rigidly fixed and bending moments of 10 Nm along flexion, extension, lateral bending and axial rotation were applied on the superior plane of the L1 vertebra with a compressive force of 500 N along the follower load direction. Hybrid loading conditions which generate the same overall rotation angle to the healthy lumbar spine were applied for the implanted models. The predicted ranges of motions (ROMs) at the operated level were compared with each other to evaluate the stability.

Results: The ROMs at operated level in Int_Screw decreased from 4.4°, 2.3°, 0.4°, 1.3°, 0.5°, and 0.5° to 3.8°, 2.2°, 0.4°, 1.0°, 0.5°, and 0.5° in flexion, extension, right lateral bending, left lateral bending, right axial rotation and left axial rotation, respectively, with increase in screw fixation angle from 20° to 35°, while those in Ext_Screw changed from 1.9°, 1.2°, 0.2°, 0.6°, 0.4°, and 0.5° to 1.6°, 1.0°, 0.2°, 0.5°, 0.4°, and 0.5° in case of with increase of fixation angle from 5° to 30° (Table). The ROMs in flexion and extension in Ext_Screw increased from 1.9° and 1.2° to 2.2° and 1.3°, respectively, when the length of screw was reduced from 45 mm to 35 mm. All but these two analysis cases showed slight changes in ROMs.

Figure:
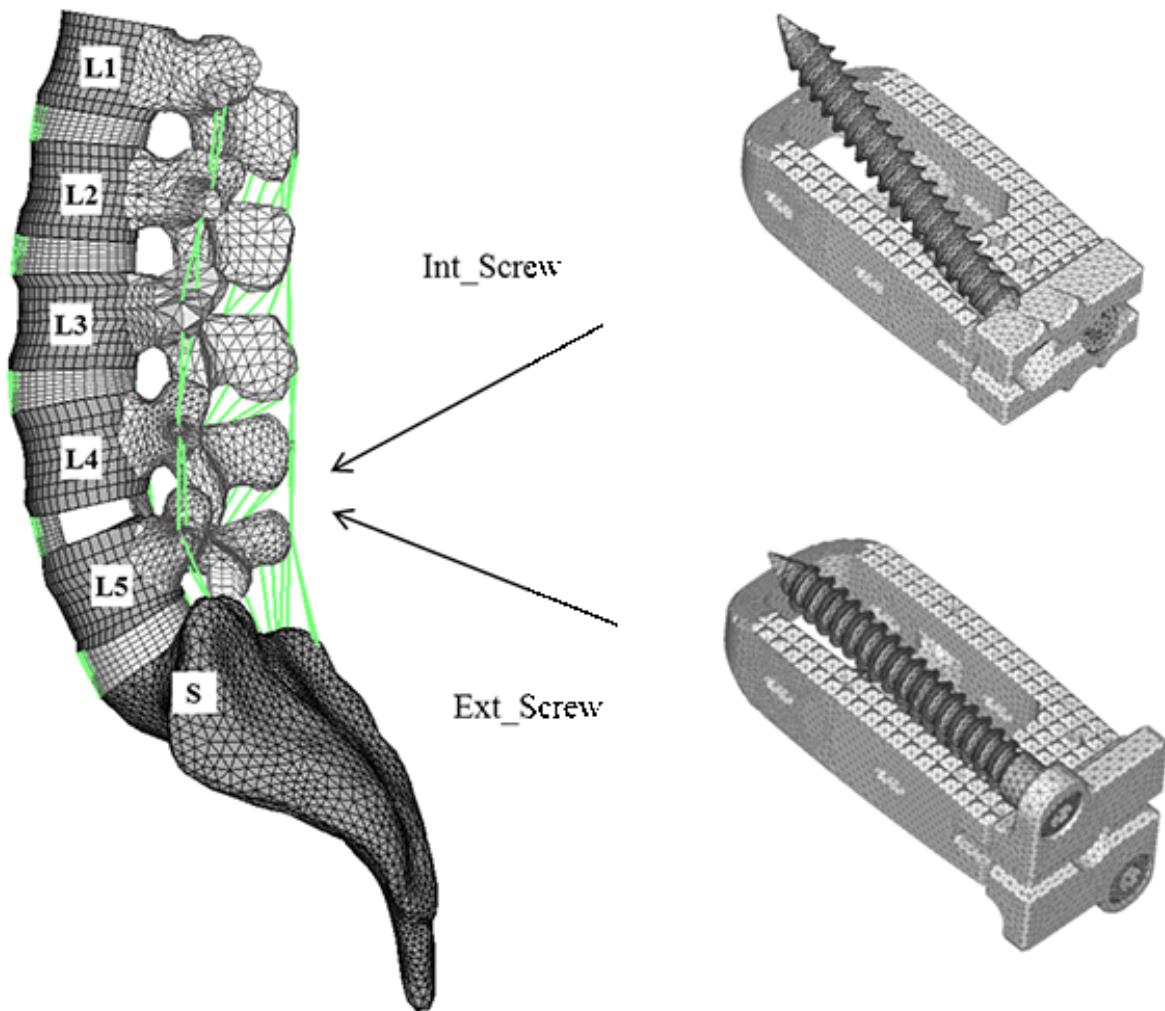
Caption: Finite element models of the lumbar spine and cages with internal or external screws

Conclusion: The results of this study showed that high screw fixation angle is beneficial for stability at operated level, especially in flexion, extension and left lateral bending both in Int_Screw and Ext_Screw. The longer screws generated the higher stability only in flexion and extension in Ext_Screw. In addition, the Ext_Screw case showed quite higher stability at operated level than the Int_Screw case in all loading conditions, where this finding might be explained as the penetration of cortical bone in Ext_Screw could improve the stability. This study could present basic biomechanical information to enhance the stability in terms of screw fixation angle, screw length, and types of stand-alone cage system for DLIF, because primary stability is essential for successful surgery in the spinal fusion even if stand-alone cage system for DLIF has many advantages.

Table:

Screw fixation angles		Flexion	Extension	Right lateral bending	Left lateral bending	Right axial rotation	Left axial rotation
Int_screw	20°	4.43	2.34	0.42	1.28	0.52	0.48
	25°	4.21	2.30	0.42	1.19	0.50	0.48
	30°	3.95	2.24	0.40	0.98	0.51	0.49
	35°	3.76	2.20	0.39	0.97	0.52	0.48
Ext_screw	5°	1.91	1.19	0.17	0.58	0.37	0.53
	10°	1.89	1.16	0.17	0.57	0.37	0.54
	15°	1.79	1.09	0.17	0.56	0.37	0.53
	20°	1.71	1.06	0.17	0.55	0.37	0.53
	25°	1.66	1.00	0.16	0.54	0.37	0.53
	30°	1.56	0.96	0.16	0.54	0.37	0.53

Caption: ROMs at the operated motion segment in various screw fixation angles (°)

References: [1] Cappuccino et al., SPINE, 35: 361-367, 2010.

[2] Marchi et al., Sci. World J., 2012: 1-7, 2012.

[3] Huec et al., Eur. Spine J., 11: 130-136, 2002.

[4] Park et al., Comput. Biol. Med., 43: 1234-1240, 2013.

Orthopaedic Implants

PO-0164

SQUAT ASYMMETRY IN PATIENTS WITH TOTAL HIP ARTHROPLASTY: COMPARISON BETWEEN DUAL MOBILITY AND STANDARD PROSTHESES

Danilo S. Catelli [1,*] Robert Little [1] Mario Lamontagne [1] Paul E. Beaulé [2]

[1]School of Human Kinetics, [2]Division of Orthopaedic Surgery, University of Ottawa, Ottawa, Canada

Introduction and Objectives: Dual mobility (DM) bearings have shown their capacity to increase hip range of motion (ROM) and stability while minimizing the risk of impingement [1-3]. However, it is unclear whether the improved hip ROM will lead to better functional mobility, especially during eccentric movements. Symmetry analyses in joint kinetics and kinematics have shown to be useful in highlighting potential imbalances between limbs of a patient [4] using the symmetry angle (SA), which avoids artificial inflation of results and provides a standardized scale (±100%) for interpretation [5]. The aim of this study was to compare ground reaction forces (GRF) patterns in the operated and non-operated limbs during squat descending phase, in patients having undergone either DM or a standard metal on polyethylene (MPE) bearings and healthy control participants to provide a reference for symmetry values. It was hypothesized that the DM group would get better improvement than the MPE.

Methods: A total of 20 patients and 9 control participants (CTRL) were recruited from the orthopaedics clinic at the local hospital (Table 1). The patients who volunteered for the study were randomly assigned to either a DM or a MPE cementless total hip replacement. They also agreed to undergo to motion analysis before and nine months after THA. All surgeries were performed by the same surgeon using the direct anterior approach. The healthy participants were matched by age and BMI.

Participants performed a minimum of five squatting trials, at a self-selected pace, on two force plates (1000HZ, Bertec Corp., USA). Ground reaction force (GRF) data were processed in Nexus 1.8 (Vicon, UK) and exported to a custom MATLAB script (Mathworks, USA) to extract the variables. All trials were time-normalized during the squat descending phase, starting at maximum hip extension to maximum hip flexion angles, and individual averages for each participant were calculated across the five trials.

The method of Zifchock et al. (2008) [5] was used to calculate the SA values for all variables: $SA = (45º – arctan(X_{operated}/X_{non\text{-}operated}))/90º * 100\%$. A SA value of 0% indicated perfect symmetry, ±100% indicated that the two values were equal and opposite in magnitude. Therefore, if $(45º – arctan(X_{operated}/X_{non\text{-}operated})) > 90º$, the following equation was substituted by: $SA = (45º – arctan(X_{operated}/X_{non\text{-}operated}) – 180º)/90º * 100\%$. For the CTRL group, the dominant and non-dominant legs were considered. A Wilcoxon signed-rank test, comparing pre- and post-op conditions, and a one-way ANOVA, comparing post-ops and control, were conducted for both hip kinematic parameters and SA (CI = 95%).

Results: The SA calculations show that the CTRL group remains around 0% during all task, with an average of -0.3%, while both pre-op affected groups (DM: 4.7%, MPE: 5.7%) were consistently higher than the post-ops (DM: 2.1%, MPE: 2.3%). These measures show that the operated groups still exhibited higher SA compared to the CTRL. A paired comparison between the pre and post conditions did not show a statistical difference for DM or MPE groups (p = 0.13 and 0.26, respectively). Also, the ANOVA among post-op and CTRL groups did not show differences (p = 0.40).

Figure:
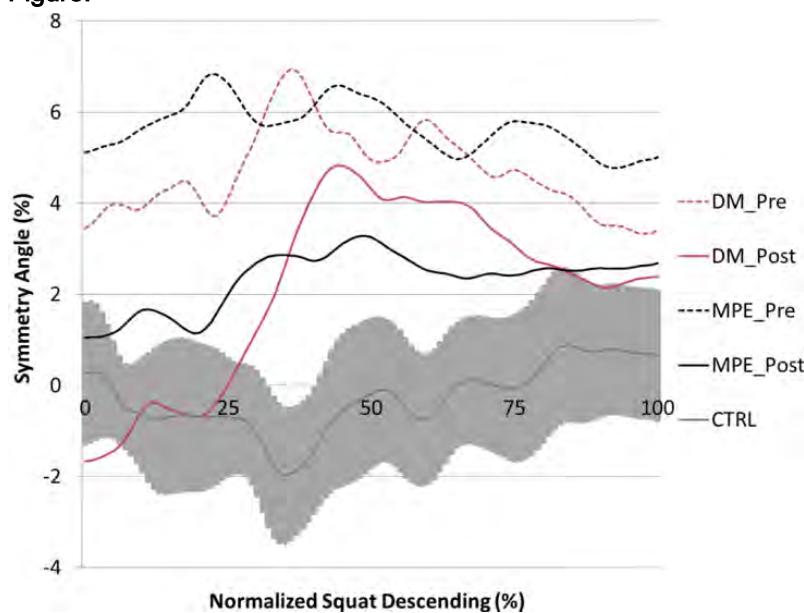
Caption: Fig. 1. Symmetry angles during squat descent. The light gray shadow indicates the standard deviation around the CTRL group mean.

Conclusion: Despite the pre- and post-op paired analysis not showing a statistically SA improvement after THA, the reduction obtained in both post-THA groups could be clinically important. Interestingly, this SA reduction on post-ops was also not different from the CTRL. Post-op THA symmetry did not reach the level of the CTRL. The squat descending phase was chosen because it would represent a controlled, lower limb eccentric contraction, however, further investigations must also include concentric phase and a longer follow-up.

Table:

Group	Pre-op (n)	Post-op (n)	Age (yrs)	BMI (kg/m^2)	Sex ratio (F/M)
DM	10	10	63 ± 6	28 ± 3	4/6
MPE	9	10	61 ± 4	29 ± 5	2/8
Control	9	NA	63 ± 7	25 ± 4	2/7

Caption: Table 1. Summary of participants demographics

References: [1] Langlais FL et al., Clin Orthop Relat Res, 466:389-95, 2008.

[2] Philippot R et al., Orthop Traumatol Surg Res, 95:407-13, 2009.

[3] Guyen O et al., Clin Orthop Relat Res, 455:202-8, 2007.

[4] Beyaert C et al., Gait & Posture, 28:278–84, 2008.

[5] Zifchock RA et al., J Biomech, 39:2792–7, 2006.

Disclosure of Interest: D. Catelli: None Declared, R. Little: None Declared, M. Lamontagne Conflict with: Medacta International SA, P. E. Beaulé Conflict with: Medacta International SA, Conflict with: Medacta International SA

Orthopaedic Implants

PO-0165

THE MELBOURNE PROSTHETIC TOTAL JOINT REPLACEMENT SYSTEM FOR THE HUMAN TEMPOROMANDIBULAR JOINT

David Ackland [1,*]Adrian Moskaljuk [1]Chris Hart [2]Peter Lee [1]George Dimitroulis [3]

[1]Mechanical Engineering, University of Melbourne, Parkville, [2]Orthopaedic Surgery, [3]Maxillofacial Surgery, St Vincent's Hospital, Melbourne, Australia

Introduction and Objectives: Painful disorders involving the temporomandibular joint (TMJ), including osteoarthritis, have a prevalence ranging from 16-59% [1]. Total prosthetic TMJ replacement surgery is the established treatment for end-stage TMJ osteoarthritis; however, current TMJ prosthetic implant designs face a range of problems including fracture from metal fatigue; screw loosening; and difficulty in placement of the prosthesis to avoid screw-related damage to the mandibular nerve. The aim of this study was to develop a musculoskeletal finite element model of the TMJ based on the Visible Human Male (VHM) dataset, and to use this model to evaluate joint contact mechanics after implantation of a novel 'Melbourne' TMJ prosthetic total replacement system designed at the University of Melbourne. Unlike current prosthetic TMJ designs, the shape of the Melbourne prosthetic TMJ condyle conforms to the mandibular anatomy to make intra-operative placement more accurate, while condylar screw locations avoid the mandibular nerve.

Methods: Axial images from the Visible Human Male dataset were digitally segmented and combined to reconstruct 3-D surfaces of the mandible, glenoid fossa and articular cartilage and discs. The major muscles of mastication – the masseter, temporalis (anterior and posterior), lateral and medial pterygoids – were also digitally reconstructed. Muscle lines of action, volumes and muscle fiber lengths were measured and used to calculate maximum isometric muscle force for each muscle. Using the measured muscle lines of action, and assuming ideal actuators, muscle forces during a normal chewing bite were computed by summing moments in three-dimensions about the TMJ joint centre. A static optimisation routine was used with a cost function chosen to minimise the sum of the squares of muscle activation subject to a bi-lateral bite force of 200N positioned at the second molar. TMJ contact forces were subsequently computed.

The calculated muscle forces were used as boundary conditions in a finite element model of the human jaw. The anatomy of the jaw included the three-dimensional surfaces of the mandible, glenoid fossa, articular cartilage and discs generated from the Visible Human Male dataset. A simulation of a normal chewing bite was performed and articular cartilage and disc contact stresses were calculated. The Melbourne prosthetic TMJ system was then implanted into the left TMJ of the finite element model in a virtual TMJ arthroplasty. The condylar component was fixed with three screws (superior, mid and inferior), while the fossa component was rigidly fixed to the temporal bone. Muscle and joint forces were re-calculated without the lateral pterygoid, since this muscle is severed intraoperatively. A finite element model simulation was performed to calculate implant stresses and strains during a chewing bite.

Results: The pre-operative joint reaction forces were 98.9N and 86.3N at the left and right TMJ, respectively. Pre-operatively, the maximum contact stress in the left and right condylar cartilage was 1.1MPa and 1.5MPa, respectively (Fig. 1). Post-operatively, the TMJ joint reaction force magnitudes on the left and the right TMJ were 79.1N and 78.3N, respectively. At the TMJ joint prosthesis, the maximum contact stress at the condylar component and the fossa

component was 85.0MPa and 166.1MPa, respectively. The maximum stress and strain magnitudes in the condylar component were 279.9MPa and 2253.7×10^{-6}, respectively, occurring in the region of the screw hole closest to the implant condyle head. The maximum stress of the screw at this location was 338.2MPa. Screws placed superiorly experienced higher stresses than those of all other condylar fixation screws.

Figure:
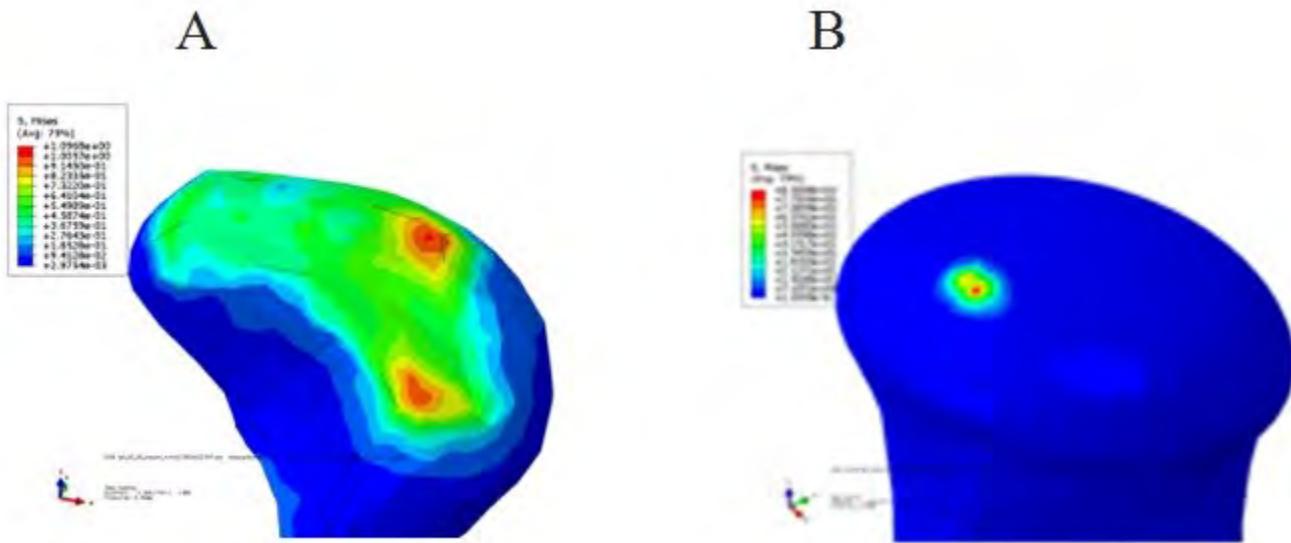
Caption: Pre-operative contact-stress distribution on condylar cartilage (A) and post-operative contact stress distribution on prosthetic condyle (B)

Conclusion: This study describes a new prosthetic TMJ, and provides estimates of muscle and joint-contact loads in the TMJ both before and after TMJ arthroplasty. While contact forces at the TMJ were of lower magnitude post-operatively, the contact stresses in the TMJ components were orders of magnitude higher than those in the pre-operative condylar cartilage. This finding indicates a potential mechanism for wear in the TMJ prosthesis. High stresses in the most superior screw-hole (closest to the condyle head) indicate risk of early screw loosening at this location if this screw is not placed carefully, or with enough fixation. This is clinically significant, since intra-operative placement of the superior screw is most difficult for the surgeon as he/she must avoid the facial nerve by working through an incision below the angle of the mandible.

References: [1] Carlson GE and LeResche L. (1995). Temporomandibular Disorders and Related Pain Conditions. IASP Press, Seattle

Disclosure of Interest: None Declared

Orthopaedic Implants

PO-0166

IN VITRO WEAR TESTING OF THE MATORTHO® PIPR™ PROSTHESIS

Andrew Naylor [1,*] Ian. A Trail [2] Thomas. J Joyce [1]

[1]School of Mechanical and Systems Engineering, Newcastle University, Newcastle upon Tyne, [2]Upper Limb Research Unit, Wrightington Hospital, Lancashire, United Kingdom

Introduction and Objectives: The MatOrtho® PIPR™ (figure 1) is an anatomical surface replacement used for arthroplasty of the proximal interphalangeal joint. The articulating surface materials are: Cobalt-chromium (CoCr) for the proximal component; and Ultra High Molecular Weight Polyethylene (UHMWPE) for the medial component, both of which are mounted on CoCr stems with a hydroxyapatite coating. The PIPR™ was first implanted in 2006 in patients who predominately have osteoarthritis. Nearly 800 have been implanted worldwide to date. The key objectives of this study were to evaluate the wear and surface roughness characteristics through testing of the PIPR™ in-vitro.

Methods: A pneumatic finger rig was used to simulate two biomechanical functions: 1) to cycle the prosthesis through flexion and extension with dynamic loads of 10-15 N; 2) to apply a static load of approx. 100N to simulate a 'pinch' (applied at 3000 cycle intervals). The simulator is described in greater detail elsewhere [1], and it has previously been used to evaluate other designs of two-piece finger prostheses [2-4]. In this study one CoCr-UHMWPE prosthesis 'test' pair was subjected to five million cycles of flexion and extension, with a 'control' prosthesis pair submerged within the test chamber to account for lubricant uptake. Wear was measured gravimetrically at one million cycle intervals using a Denver Instruments TB215D balance, measured to the nearest 0.1 mg. Roughness average (Ra) values of the articulating surfaces were obtained using a non-contacting profilometer, also at one million cycle intervals.

Results: There was a distinctive correlation between the ascending cycles of flexion-extension and gravimetric change in weight (Δm) (Table 1). The CoCr test component gradually decreased in weight over the five million test cycles, at a rate of approx. 0.7 mg per million cycles. By comparison, the weight of the CoCr control component varied only by a small amount, less than 0.1 mg per million cycles. The UHMWPE test component decreased in weight over the five million test cycles, at a rate of approx. 0.3 mg per million cycles. In contrast the UHMWPE control component increased in weight at a rate of approx. 0.1 mg per million cycles. The surface roughness results (Ra values) were inconclusive. There was no distinctive correlation between the ascending cycles of flexion-extension and Ra values. This indicates that the level of wear that occurred at articulating surfaces was negligible. Micrograph images taken at the end of testing exhibited large sections of the test prosthesis stems where little hydroxyapatite coating was present. This is in contrast to the control prosthesis stems which exhibit a more uniform coating. This loss of hydroxyapatite may explain the decrease in weight of the CoCr test component.

Figure:
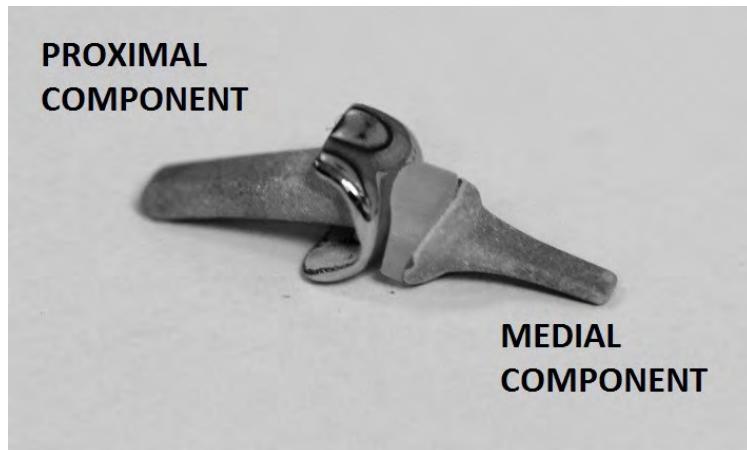
Caption: Figure 1 – The MatOrtho® PIPR™

Conclusion: Both the CoCr and UHMWPE test components exhibited clear signs of gravimetric wear. Both test components decreased in weight while there was very little change for the control, in the case of CoCr, or even an increase in weight for the UHMWPE control. The inconclusive surface roughness trends provide little evidence to support that wear occurred at the articulating surfaces. The micrographs do however indicate that the hydroxyapatite coating was removed across large sections of the test prosthesis stems in-vitro. This accounts for the observed gravimetric loss.

Table:

	CoCr (Proximal) - Test	CoCr (Proximal) - Control	UHMWPE (Medial) - Test	UHMWPE (Medial) - Control
Cycles	Δm (mg)	Δm (mg)	Δm (mg)	Δm (mg)
0	0.0	0.0	0.0	0.0
1.E+06	-1.5	-0.2	-0.3	0.2
2.E+06	-2.2	-0.2	-0.5	0.4
3.E+06	-2.8	-0.3	-0.8	0.5
4.E+06	-3.2	-0.2	-1.0	0.5
5.E+06	-3.5	-0.3	-1.4	0.5

Caption: Table 1 – Summary of Gravimetric Results

References: [1] T. J. Joyce et al., Proc Inst Mech Eng H., 214: 519-526, 2000.

[2] T. J. Joyce., J Mater Sci Mater Med., 21: 2337-2343, 2010.

[3] T. J. Joyce et al., Biomed Mater Eng., 16: 1-10, 2006.

[4] T. J. Joyce et al., J Appl Biomater Biomech., 2: 136-42, 2004.

Disclosure of Interest: None Declared

Bone

PO-0167

BIOMECHANICAL COMPARISON OF THE DORSAL FEMUR CONDYLES AND THE ILIAC CREST IN TERMS OF FAILURE BEHAVIOR

Rainer Penzkofer[* 1], Stephan Grechenig[2], Richard Kujat[2], Peter Angele[2], Sebastian Dendorfer[1]

[1]Biomechanics, Regensburg Center of Biomedical Engineering, [2]University Hospital Regensburg, Regensburg, Germany

Introduction and Objectives: 10 to 12 % of the population suffer from cartilage damage in the knee joint, which in many cases leads to osteoarthritis (OA). OA is partially caused by increased forces which result from obesity. The resulting increased moments acting in the knee joint in combination with a defective position of the extremities accelerates this process even further. In addition to that, impacts resulting from accidents or overuse exercise may induce local damage altering the stress distribution on the joint surface. Beside bone marrow stimulation and autologeous chondrocytes transplantation, osteochondral transplantation is performed to replace minor subchondral defects using extracts from the iliac crest. Little is known about the treatment options for large and deep osteochondral defects. Currently it is still unclear if the mechanical properties of the iliac crest meet the biomechanical loading situation of the knee joint.

The aim of the current study was to compare the subchondral layer of the femur condyles with the cortical layer of the iliac crest concerning their biomechanical properties.

Methods: From five donors (3 male, 2 female) left and right Thiel embalmed sections of the iliac crest and the femur condyles were prepared and embedded into PU. CT scan was performed on all specimens and the Bone Mineral Density (BMD) was measured via QCT. None of the donors had signs of previous injury, abnormality or disease. The maximal strength in Newtons (N) and the failure behavior were investigated using an indenter testing procedure by loading the bone's surface with a 2mm cylindrical indenter until passing the subchondral bone zone and cortical layer, respectively. The load was applied displacement controlled at a test speed of 0.1 mm/s. A custom made clamping system guaranteed the orthogonal orientation of the area currently tested to the indenter. For each pair of specimen three kinds of tests were conducted. First (i), the iliac crest was tested. After that, the femur condyles were tested with (ii) and without (iii) the articular cartilage layer. One test again consisted of 8 subtests. From each test mean and standard deviation were calculated.

Results: The failure load of the iliac crest samples ranges from 53.3N to 180.5N. Specimen that still had an intact cartilage layer showed failure loads between 118.3N to 260.4N. Removing the cartilage layer of the femur condyles leads to a reduction of the failure load of about 20% to 80%. Concerning failure load, no significant difference could be found for samples of the iliac crest and femur condyles having their cartilage removed. Especially the condyle samples with an intact cartilage layer showed a different failure behavior in terms of an almost linear load increase until failure. Iliac crest and condyle samples without cartilage layer failed stepwise. Samples offering a low BMD showed minor load to failure values compared to those offering high BMD levels. In general specimen from male donors tend to show higher load levels than the female ones.

Figure:
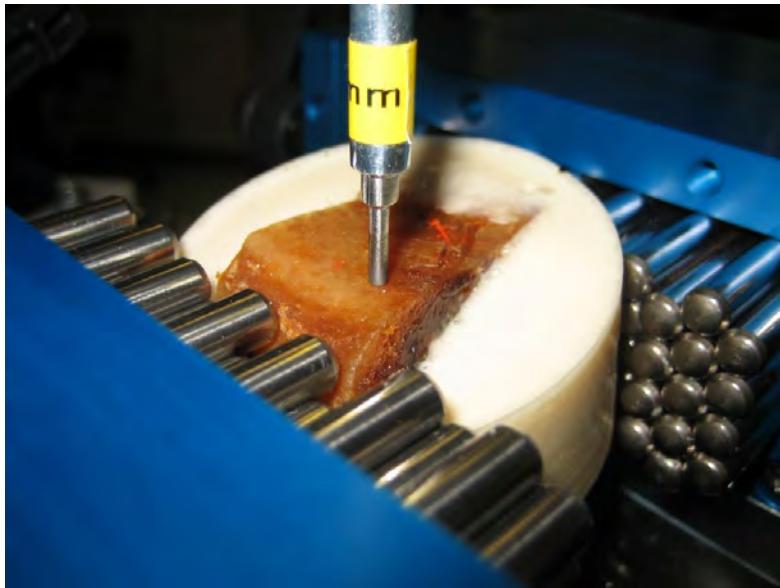
Conclusion: This study showed promising results in terms of biomechanical properties of a bone block from the iliac crest compared to the subchondral layer of the femur condyles. From a mechanical view, the cortical layer of the iliac crest seems to fulfill the requirements of the subchondral bone without cartilage in the knee joint. Removing the cartilage layer leads to a decreased failure load and different failure behavior. Hence, the cartilage layer seems to be mainly responsible for the stability of the femur condyles compared to the iliac crest samples. The articular cartilage was removed from the condyle's surface by a surgeon using a scalpel. The possible damage of the bony surface may contribute to the lower failure forces compared to specimen with remaining cartilage.

Although, the histologic structure of subchondral bone of the knee joint without cartilage differs from the structure of the iliac crest material, both show comparable mechanical properties in a macroscopic local compression test performed in this study. Using autologous bone grafts for bone augmentation seems to be a good option for the regenerative therapy of large osteochondral defects.

Disclosure of Interest: None Declared

Orthopaedic Implants

PO-167

FRONTAL PLANE KINEMATICS AND KINETICS AFTER UNICONDYLAR KNEE ARTHROPLASTY DURING ACTIVITIES OF DAILY LIVING

Igor Komnik* [1], Michaela Wehrstein[2], Sina David[1], Wolfgang Potthast[1]

[1]Institute of Biomechanics and Orthopaedics, German Sport University, Cologne, [2]Instiut für Sport und Sportwissenschaft, Karlsruher Institut für Technologie, Karlsruhe, Germany

Introduction and Objectives: Currently, 4 007 400 adults older than 50 years live with a total knee Arthroplasty (TKA) in the U.S. [1]. Even though unicondylar knee arthroplasty (UKA) represents a small proportion of all knee arthroplasties, there is an increase in UKA-surgeries in the recent years [2]. Among other potential benefits of UKA compared to TKA, UKA is stated to show more normal knee kinematics and kinetics e.g. due to preservation of both cruciate ligaments [3]. Only few articles investigate UKA-patients performing activities of daily living (AODL) with optoelectronic systems. Especially high adduction moments are connected to increased polyethylene wear primarily in the medial compartment and are there of particular interest [4]. Hence, the aim of this case study is to describe frontal plane kinematics and kinetics of three UKA-patients and three healthy subjects performing four AODL.

Methods: Six male subjects participated in this case study. Three patients underwent an unilateral unicodylar knee arthroplasty (UKA-Group) at least 22 months prior to testing. The initial diagnosis was osteoarthritis with nondiseased contralateral limbs and no musculoskeletal disabilities. Three healthy subjects build the control group (CG) that was matched according to age, sex, height and BMI of the UKA-group (Table 1). Motion analysis was performed using an optoelectronic eleven-camera motion capture system (Vicon, Oxford, UK). Two force plates (Kistler, Winterthur, Switzerland) were embedded in the floor and one in the second as well as in the third step of a staircase consisting of five steps. Fifty retroreflective markers were attached to subject's feet, shank, thighs, pelvis, thorax, upper arm, lower arm and head to create a 17-segment rigid model. Kinematics and kinetics calculations were performed with AnyBody (AnyBody Technology, Aalborg, Denmark). Knee Adduction moments are presented as external moments normalized by body weight and height. The subjects completed four tasks of AODL: level walking (1.38 ±0.07 m/s), level walking + 90°-sidestep turning(1.38 ±0.07 m/s), stair ascent/descent. For each motor task five trials were averaged for data analysis. Due to the small sample size, descriptive statistics of the affected knee joint frontal plane kinematics and kinetics are presented as median (range).

Results: The following results are presented as a descriptive approach and should therefore be considered with caution. Both groups showed similar range of motion (ROM) values in the frontal plane and peak knee adduction moments during level walking. The sidestep-turning condition showed highest knee adduction moments (0.41 Nm/kg/m, range 0.28-0.57 Nm/kg/m) in the first 50% of stance phase compared to other locomotor tasks. Furthermore greater knee adduction moments occurred to the CG (0.45 Nm/kg/m, range 0.37-0.56 Nm/kg/m) than to the UKA-group (0.33 Nm/kg/m, range 0.28-0.44 Nm/kg/m) as shown in Figure 1. The UKA-group negotiated the stair ascent task with greater ROM (9.82°, range 8.99-10.23°) in the frontal plane and positioned the knee in a more abducted manner compared to the CG (CG 6.87 °, range 5.09-8.74°). In this regard the UKA-group presented in the first 50% of stance phase modest higher knee

adduction moments, but wider dispersion (UKA 2.5 Nm/kg/m, range 0.14-0.35 Nm/kg/m; CG 0.217 Nm/kg/m, range 0.216-0.218 Nm/kg/m).

Figure:
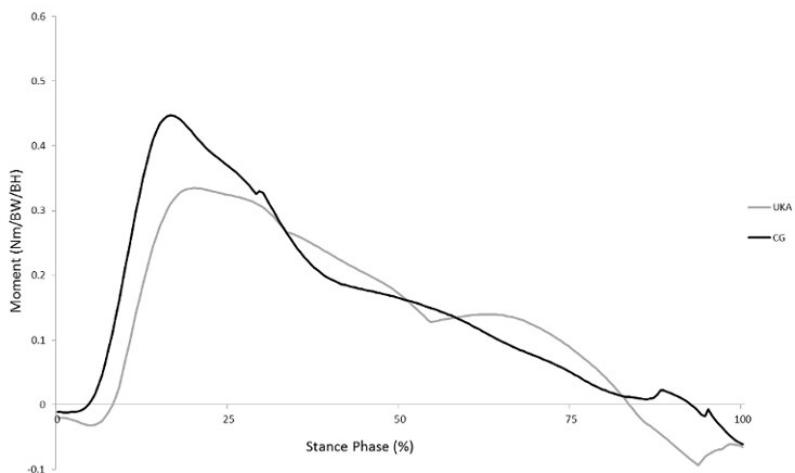
Caption: Figure 1 Median knee adduction moments course of the UKA-group and CG.

Conclusion: The results of the current case study emphasize the importance of researching besides level walking physical more demanding activities like stair negotiation and turning tasks. No kinematic and kinetic differences between the two groups were observed during level walking. Indeed, in the turning task condition the CG tended to perform this task with higher knee adduction moments, although both groups walked pre-turning with nearly the same speed of 1.38 m/s. Potential reasons for this difference could be the persistence of a pre-surgery movement pattern or unconscious avoidance of high knee loads. Further variables like e.g. angle of attack and limb-symmetry could clarify the mentioned observation and should be calculated in future studies. In general, there is a lack of knee arthroplasty articles investigating knee adduction moments during turning tasks. Only McClelland et al. [5] presented frontal plane kinetics but in patients with TKA. Future studies should involve more subjects and additionally TKA-groups.

Table:

Group	Age	BMI (kg/cm²)	Height (m)	UKA-Side	Compartment	Post-surgery (months)
KA	56	28.37	1.837	Left	Lateral	22
	56	26.45	1.83	Right	Medial	22
	57	28.72	1.77	Left	Medial	22
CG	58	27.47	1.81			
	50	26.06	1.85			
	50	25.35	1.72			

Caption: Table 1 Subjects characteristics

References: [1] Weinstein et al., J Bone Joint Surg Am., 95:385–392, 2013.

[2] Riddle et al., J. Arthroplasty, 23: 408-412, 2008.

[3] Andriacchi et al., J Bone Joint Surg, 64A: 1328-1335, 1982.

[4] Collier et al., J Bone Joint Surg, 89: 1306–1314, 2007.

[5] McClelland et al., Gait & Posture, 30: 288-295, 2009.

Disclosure of Interest: None Declared

Orthopaedic Implants

PO-0169

DIAGNOSTIC OF ACETABULAR CUP LOOSENING WITH A NON-INVASIVE DIAGNOSTIC TECHNIQUE BASED ON VIBRATION ANALYSIS

Abdullah A. Alshuhri [1,*] Anthony W. Miles [1] James L. Cunningham [1]

[1]The Centre for Orthopaedic Biomechanics, Department of Mechanical Engineering, University of Bath, Bath, United Kingdom

Introduction and Objectives: Well over one million total hip replacements (THR) are carried out annually around the world; a number which is only likely to increase [1]. Aseptic loosening remains a significant clinical problem, in particular associated with the acetabular cup. Current techniques for diagnosing early loosening of the acetabular cup in THR are ineffective [2]. Accordingly, the aim of this study was to investigate the viability of using vibrational analysis for accurately detecting early acetabular component loosening.

Methods: A simplified acetabular model was constructed using a Sawbone® foam block into which an acetabular cup was fitted. Loosening of 1 mm was simulated by the interposition of thin layer of silicon between the acetabular component and the Sawbone block. A constant amplitude sinusoidal excitation with a sweep range of 100–1500 Hz was used. Output vibration from the model was measured using an accelerometer and an ultrasound probe. Loosening was determined from output signal features such as the number and relative strength of the observed harmonic frequencies.

Results: Both measurement methods were sufficient to measure the output vibration; however the ultrasound measurements were of a clearly higher magnitude than accelerometer readings throughout the frequency range. Different patterns in the output signal spectra were visible when comparing the stable cup with the 1mm of simulated loosening at the higher frequency range.

Figure:
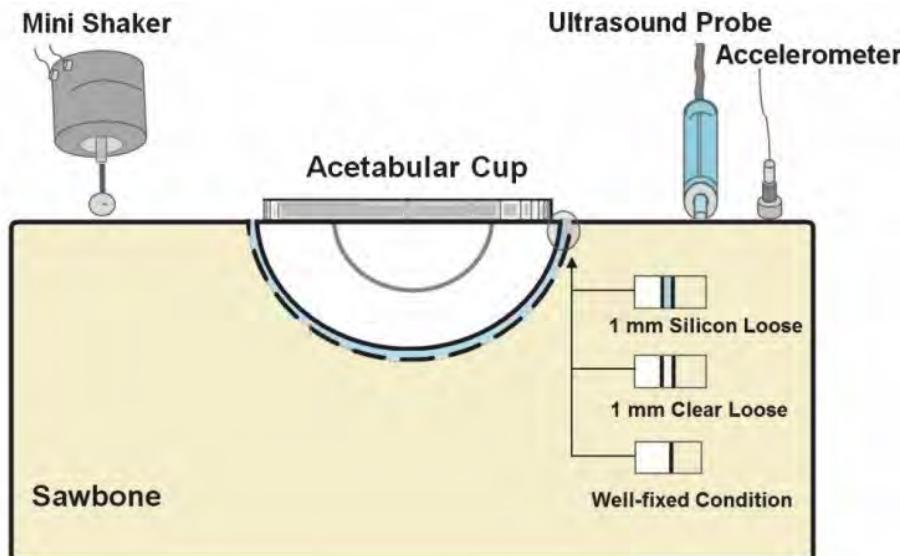
Caption: The Sawbone block showing the excitation and measurement methods.

Conclusion: These preliminary findings show that vibration analysis could potentially be a reliable method for detecting acetabular component loosening using either an accelerometer or ultrasound probe. However, the capacity of ultrasound to overcome the attenuating effect of the surrounding soft tissues and its high signal to noise ratio suggest it has the best potential for clinical use.

References:

[1] Pivec et al. 2012, Hip arthroplasty. The Lancet, 380, 1768-1777.

[2] Ruther et al. 2012, InTech, ISBN: 978-953-307-990-5.

Disclosure of Interest: None Declared

Prosthetics

PO-0170

THE EVALUATION OF BONE REMODELING AROUND TWO TYPES OF ACETABULAR CUPS

Tongtong Guo [1],*Yan Wang [1]

[1]Nature Science Department, Harbin Institute of Technology Shenzhen Graduate School, SHENZHEN, China

Introduction and Objectives:

The design of acetabular cups is essential for THA operation results. The main purpose of this study is to compare long-term bone remodeling results around two kinds of acetabular cups after THA operation.

Methods:

Hip geometry model applied in this study is from CT scan [Ho Ba Tho, 2003]. The elements of cortical bone and acetabular cup in this model are defined as solid elements, the ones of cancellous bone are shell elements. Hip is divided into 18662 elements. Ischium and ilium are fixed constraints. One type acetabular cup is from the patent (Type A)[Ho Ba Tho, 2004], the other is the general type (Type B). The contact between hip and acetabular cup is defined as a rigid - elastic contact body, and friction coefficient is 0.25. Bone remodeling algorithm is applied to predict long term THA results in two types of hip - acetabular models.

Results: The long-term bone density of two hips with prosthesis implantation is obtained at 135 months after THA operation. From the distribution graphs of total density and cancellous bone density, we can see that the number of elements being absorbed of prosthesis B is more than that of prosthesis A; after 135 months implantation of prosthesis, acetabular bone with prosthesis B is absorbed 1310 units, whereas the one with prosthesis A is absorbed 1203 units. The hip with prothesis A is about to reach a bone remodeling equilibrium after 130 months, however, acetabular bone mineral density with prothesis B is still in declining (Figure 1).

Figure:
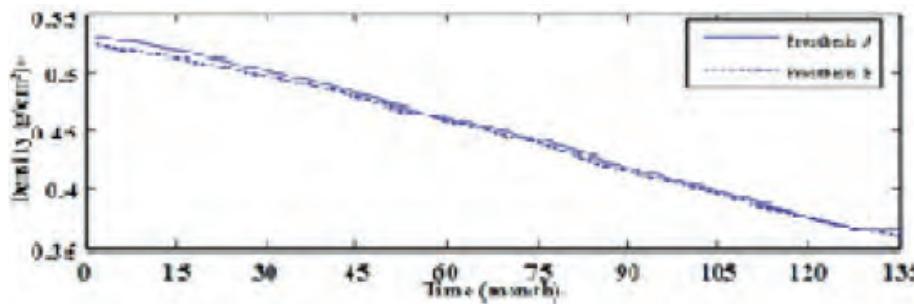
Caption: Figure 1

Conclusion:

The stress concentration of prosthesis B is more serious than prosthesis A, and the initial maximum and average strain energy density energy density of prosthesis B is larger than prosthesis A.

The number of being absorped elements of prosthesis B is more than prosthesis A, and the absorption speed of prosthesis B is faster. From the total density variation figuer, when bone remodeling with prosthesis type A reaches equilibrium, the one with prosthesis type B is still in the process of bone resorption.

References: [1] Ho Ba Tho et al, CMES, 4(3&4):489-496, 2003.

Disclosure of Interest: None Declared

MUSCLE MECHANICS OF UPPER LIMB INVOLVED IN THE DESIGNING OF PROSTHETIC HAND WITH MOVING FINGERS

Nitin Sahai [1,*]Sudip Paul [1]Dinesh Bhatia [1]Angana Saikia [1]

[1]DEPARTMENT OF BIOMEDICAL ENGINEERING, NORTH EASTERN HILL UNIVERSITY, SHILLONG, MEGHALAYA, INDIA, SHILLONG, India

Introduction and Objectives: Rehabilitation has long lacked a unifying conceptual framework. Rehabilitation is a set of measures that assist an individual who experience, or are likely to experience, disability to achieve and maintain optimal functioning in interaction with their environments. An "ideal" upper limb prosthesis should be perceived as part of the natural body by the amputee and should replicate sensory-motor capabilities of the amputated limb. However, such an ideal "cybernetic" prosthesis is still far from reality. Current prosthetic hands are simple grippers with one or two degrees of freedom (DOF), which barely restore the capability of the thumb index pinch. Upper-limb amputations are most often the result of sudden trauma to the body, although they also can be caused by malignancy, congenital deficiencies, and vascular disease. This paper describes muscles involvement during movement of fingers, thumb and the development of a cost-effective and acceptable prosthetic hand which can restore the lost function and bear resemblance to natural hand having a long life span with maximum load bearing capacity. There are 35 muscles involved in movement of the forearm and hand, with many of these involved in gripping activities. Bio-signals based natural gesture recognition is one of the most active thrust area of rehabilitation robotics.

Our objectives are:-

1. To find out whether signals from these muscles are helpful in development of prosthetic hand with moving fingers This study is a part of research grant sponsored by government to develop low cost artificial prosthetic hand with moving fingers for amputees.

Methods: In the present work, individuals of different sex and age group were employed for studying the muscle activity of upper limb. The EMG signal was recorded from the selected muscles of human hand of these subjects by placing surface electrodes (Ag-Agcl), as they performed fingers and palm motion like flexion and extension, abduction and adduction of hand. Here we have used AD Instruments Power Lab 4/ 25T for signal acquisition. Signal conditioning of muscle signals obtained was performed post signal amplification to determine the actual activity of individual muscles involved during the motion of fingers and thumb. These signals would help in developing the proposed myoelectric arm.

Results: The observations were made after concluding from the data obtained, that the following muscles showed higher percentage movements of index finger, namely as, Extensor Digitorum muscle for Extension of finger, Flexor Digitorum Superficialis muscle for the flexion of finger, Dorsal Interossei muscle for the adduction of finger and Plamar Interossei muscle for the abduction of finger. In second phase of this paper, we will correlate how these findings would help us in designing of prosthetic hand with moving fingers.

The following are the recognition rates of the four types of muscles for the movement of the index finger (Figure 1)

The experimental results shows that the movement of the index finger using the four different muscles mentioned above showed the highest recognition rate. Further, it has been found that the overall detection accuracy rates obtained are in the acceptable range of the clinical tests. These results could be employed for the design of the prosthetic hand with moving fingers. The classified signal can be efficiently used to develop a human computer interface to help the people with disabilities who wish to interact with computer devices and outside world.

Figure:
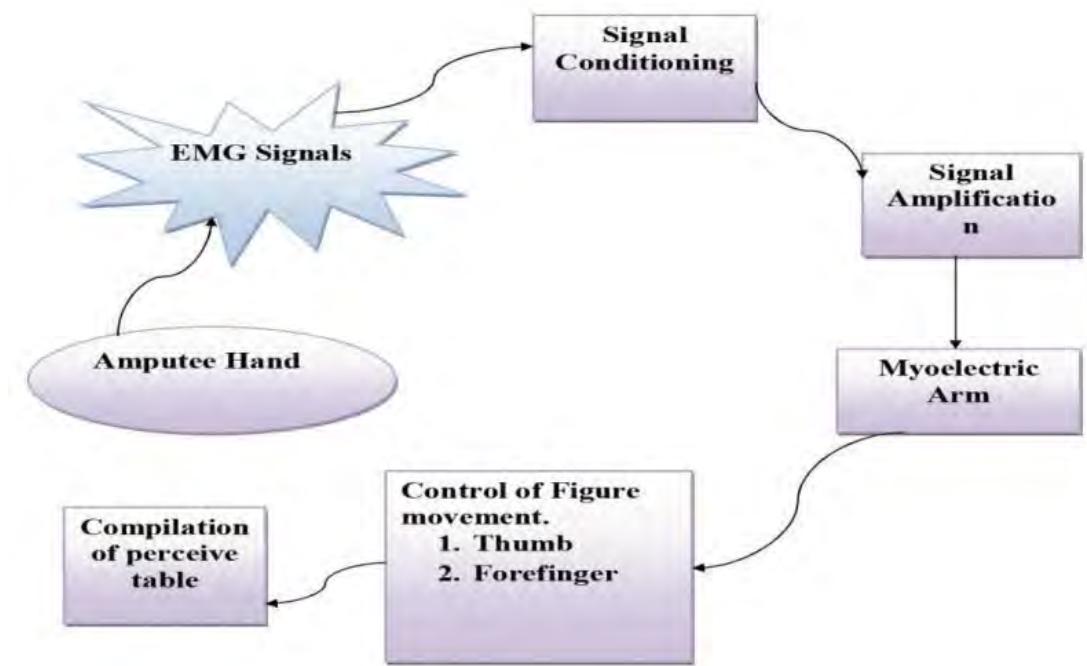
Caption: Study protocol with experimental model

Conclusion: The presented research article will conclude that economical cost effective myoelectric arm can be developed which can restore overall functions of a normal human hand, thus improving the quality of life of individual.

Table:

MOVEMENTS	MUSCLES	RECOGNITION RATE
Flexion	Flexor Digitorum Superficialis muscle	75%
Extension	Extensor Digitorum Muscle	80%
Adduction	Dorsal Interossei Muscle	85%
Abduction	Plamar Interossei Muscle	90%

Caption: The following are the recognition rates of the four types of muscles for the movement of the index finger

Disclosure of Interest: None Declared

Rehabilitation

PO-0172

COMPARISON ON NONLINEAR REGRESSION ALGORITHMS FOR PREDICTION OF SKIN TEMPERATURE IN LOWER LIMB PROSTHESES

Neha Mathur [1,*] Ivan Glesk [1] Arjan Buis [2]

[1]Electronic and Electrical Engineering, [2]Biomedical Engineering, University of Strathclyde, Glasgow, United Kingdom

Introduction and Objectives: Monitoring and predicting the residual limb skin health in amputees is of principal importance as the socket of the prosthesis creates an airtight, warm and damp environment that encourages growth of bacteria and skin breakdown.Elevated stump skin temperatures are one of the major factors that affect the tissue health in that region [1].Monitoring interface temperature at skin level is notoriously complicated as embedding wires and sensors in an elastomer eventually results in elastomer failures because of the high strain induced when donning a liner. Another reason is because placing sensors and wires directly against the skin could cause irritation and chaffing over just a short period of time.The heat dissipation in prosthetic sockets is greatly influenced by the thermal conductive properties of the socket and interface liner materials [2].This leads to a hypothesis that if the thermal properties of the socket & liner materials are known then the in-socket stump temperature could be accurately predicted by just measuring the prosthetic socket or liner temperature.A mathematical model using the Gaussian processes for machine learning to predict the residual limb skin temperature of the amputee by measuring the in-socket temperature has been developed [3].Here we compare the performance of Gaussian processes for regression (GPR) to the other computational method namely support vector machines (SVM).

Methods: To investigate the correlation between the position of thermocouples (skin and in-socket), one trans-tibial traumatic amputee was recruited to perform in a 35 minute laboratory protocol (see Table). To monitor and record the skin and in-socket temperatures, four K–type thermocouples via a data logger were used.Two thermocouples were taped onto the residual limb in lateral and medial position.The other two thermocouples were put on the corresponding positions on the liner (in-socket).The temperature profiles of the liner and the residual limb skin were recorded for ambient temperatures of 10°C, and then the same protocol was repeated for 15°C, 20°C, and 25°C. All experiments were conducted in a climate controlled chamber with zero wind velocity and 40% humidity level.It was seen that at any given ambient temperature, the trace of the liner temperature follows that of the residual limb skin.This suggested a possibility to model the liner temperature as a function of skin temperature and create a mathematical model of the same.Different modelling techniques for machine learning were utilized and the results from the Gaussian processes model and support vector regression technique are compared in this study.

Results: The results (Figure) indicate the predictive capability of both Gaussian Processes and SVM modelling techniques at the lateral side at an ambient temperature of 10ºC.The key assumption in Gaussian Process modelling is that our data can be represented as a sample from a multivariate Gaussian distribution. A Gaussian process model infers a joint probability distribution over all possible outputs for all inputs.This form enables the implementation of Bayesian framework where the covariance function is taken in the squared exponential form which specifies the set of hyperparameters.After optimizing the hyperparameters, the predictions lie in the 95% confidence interval (±2 standard deviations).This is

indicated in (a) in the figure.The SVM modelling technique relies on defining the loss function that ignores errors, which are situated within the certain distance of true value.This epsilon intensive loss function measures the cost of the errors on the training points. In order to optimize it, the least squares cost function is used.This enables the predictions from the model to lie in 95% confidence interval (see (b) in figure).

Figure:
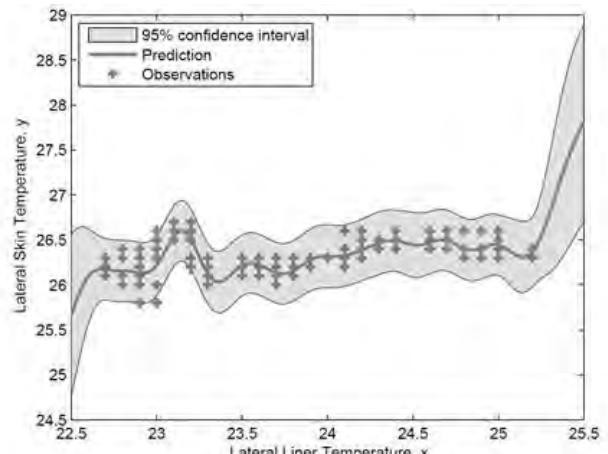
(a)
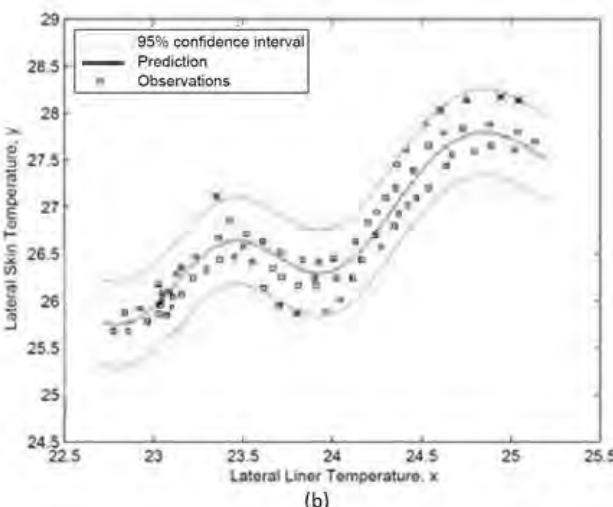
(b)

Caption: Illustration of prediction of residual limb skin temperature at 10°C with (a) Gaussian Processes (b) Support Vector Machine

Conclusion: The results presented in this work show the feasibility of non-invasively monitoring the residual limb skin temperature by utilizing two mathematical regression algorithms.The accuracy of predictions of residual limb temperature estimated by SVM with least squares kernel and GPR with squared exponential covariance function is 95%.For all the experimental data sets, estimation with GPR yielded values that closely matched the true values, whereas SVM showed comparable performance only for temperatures of 10ºC and 15ºC.These results indicate that GPR with a squared

exponential covariance function is better suited than SVM to reliably determine residual limb temperature from liner temperature experimental data.Furthermore the GPR based determination requires less computational time.

Table:

Activity	Time (minutes)
Resting/Sitting	10
Walk at self-selected pace of 0.62 metres/second on a treadmill	10
Final rest	15

Caption: Experimental Protocol

References: [1] J.T. Peery et al., JRRD, 42: 147 – 154, 2005.

[2] G.K. Klute et al., POI, 31: 292 – 299, 2007.

[3] N. Mathur et al., IEEE-JBHI, in press, 2014

Disclosure of Interest: None Declared

Rehabilitation

PO-0173

RELATIONSHIP OF LOWER-LIMB MUSCLE STRENGTH AND STANDING ABILITY TO WALKING SPEED AND GAIT CYCLE VARIABILITY IN COMMUNITY-DWELLING OLDER PEOPLE

Wakako Inoue [1][2],*Tome Ikezoe [1][2]Ikuya Sato [1][2]Katarzyna Malinowska [1][2]Takahisa Kawaguchi [2][3]Yasuharu Tabara [2][3]Takeo Nakayama [2][4]Fumihiko Matsuda [2][3]Tadao Tsuboyama [1][2]Noriaki Ichihashi [1][2]

[1]Human Health Sciences, Kyoto University Graduate School of Medicine, [2]The Nagahama Study group, Kyoto University, [3]Center for Genomic Medicine, Kyoto University Graduate School of Medicine, [4]Department of Health Informatics, Kyoto University Graduate School of Public Health, Kyoto, Japan

Introduction and Objectives: Decreased walking speed and increased gait cycle variability have been associated with the risk of falling in older adults. Therefore, therapeutic exercises aimed at improving walking speed and reducing gait cycle variability may help to prevent falls in this population. However, few studies have focused on the relationships between walking speed, gait cycle variability, and muscle strength including the strength of the hips, knees, and toes. The purpose of this study was to determine the relationship of gait speed and gait cycle variability to lower-limb muscle strength and standing ability in community-dwelling older adults.

Methods: The subjects comprised 205 community-dwelling, healthy, older adults (69 men, 136 women, aged 67.5±5.0 years). Subjects with physical dysfunctions that could potentially have influenced measurements, such as acute neurological impairment, severe musculoskeletal impairment, or severe cognitive impairment, were excluded.

Lower-limb muscle strength was determined by measuring the maximal isometric strength of hip flexion, extension, and abduction, knee extension (at 90-degree flexed position), quadriceps muscle setting, and toe grip strength. Strength during quadriceps muscle setting was measured with a specialized device (Locomoscan, Alcare Co., Ltd. Tokyo, Japan) that utilized a force sensor placed in the popliteal region while the subject sat with their knees fixed at 20° flexion and their hips and ankles held in place with belts. One-legged standing time with the eyes open was considered to represent standing ability.

Walking speed and gait cycle variability were evaluated at a comfortable walking pace and while walking as quickly as possible. Walking speed was measured over 12 m, with the subjects allowed 2 m to accelerate before measurements began. Gait cycle variability was assessed using a wireless sensor consisting of a triaxial accelerometer, magnetic sensor, and triaxial gyroscope (G-walk, Bertec Japan Co., Ltd. Kanagawa, Japan) to detect the heel contact during each step. The coefficient of variation (CV) was calculated from the mean value and standard deviation (SD) of the duration of eight steps (from the fourth through the eleventh step; $CV = 100 \times SD / mean\ value$). This CV was used as the index of gait cycle variability.

Stepwise regression analysis was performed with walking speed and CV as dependent variables and lower-limb muscle strength and one-legged standing time as independent variables. P values of < 0.05 were considered statistically significant.

Results: Walking speed was 1.5 ± 0.2 m/s at a comfortable pace and 2.0 ± 0.3 m/s at maximum speed. The CVs were 3.4 ± 1.7% and 4.6 ± 2.8% at a comfortable and maximum pace, respectively.

At a comfortable walking speed, stepwise regression analysis showed that only quadriceps muscle setting strength (standardized coefficient = 0.23) was a significant and independent determinant of speed (R^2 = 0.06). Only one-legged standing time (standardized coefficient = −0.21) was a significant and independent determinant of CV (gait cycle variability) during comfortable walking (R^2 = 0.04).

At maximum walking speed, stepwise regression analysis revealed that one-legged standing time (standardized coefficient = 0.26), knee extension strength (standardized coefficient = 0.22), and quadriceps muscle setting strength (standardized coefficient = 0.16) were significant and independent determinants of speed (R^2 = 0.21). No variables were identified as significant determinants of CV during walking at maximum pace.

Conclusion: This study showed that quadriceps muscle setting strength was a significant and independent determinant of both comfortable walking speed and maximum walking speed. Thus, strength of quadriceps setting among lower-limb muscle strength may be associated with walking speed in community-dwelling older adults. In addition, our results suggest that gait cycle variability during comfortable walking may be more closely related to one-legged standing ability than to lower-limb muscle strength.

Disclosure of Interest: None Declared

PO-0174

SONOGRAPHIC ASSESSMENT OF SUPRASPINATUS TENDINOPATHY AS A FUTURE DIAGNOSTIC AND EFFECT MEASURE – A RELIABILITY STUDY OF THE ASSESSMENT METHOD

Kim G. Ingwersen [1 2,*] John Hjarbaek [3] Henrik Eshoej [1] Camilla Marie Larsen [1] Jette Vobbe [4] Birgit Juul-Kristensen [1 5]

[1] Institute of Sports Science and Clinical Biomechanics, Faculty of Health Sciences, University of Southern Denmark, Odense M, [2] Department of physiotherapy, Hospital Lillebaelt, Vejle Hospital, Vejle, [3] Department of radiology, Musculoskeletal section, Odense University Hospital, Odense, [4] Orthopaedic Department, Shoulder Unit, Hospital Lillebaelt, Vejle Hospital, Vejle, Denmark, [5] Institute of Occupational Therapy, Physiotherapy and Radiography, Department of Health Sciences, Bergen University College, Bergen, Norway

Introduction and Objectives: Rotator cuff tendinopathy is a common condition in the shoulder, most often involving the supraspinatus tendon. The causes are numerous and pathogenesis unclear, but during recent years it has been proposed that tendinopathy should be regarded as a continuum of stages, where structural changes in the tendon can range from a normal to a pathologic tendon [1]. The stage of tendinopathy has great influence on the rehabilitation that is considered appropriate. Anamnesis and combinations of special clinical orthopaedic tests are often used when diagnosing rotator cuff tendinopathy, but these tests are often lacking good specificity and sensitivity. Sonographic visualization of structural changes in the rotator cuff is therefore often used to confirm rotator cuff tendinopathy, and can possibly aid in deciding the specific stage of tendinopathy.

Sonography is an operator dependent technique, and is highly influenced by the performers expectations, experience and technique. Therefore, a standardized procedure is necessary in order to obtain reliable assessments.

Thus, we sought to develop a standardised sonographic method to assess and classify pathological changes in the supraspinatus tendon, which may be associated with supraspinatus tendinopathy, and test inter-examiner reliability of this assessment method.

Methods: A standardized procedure for obtaining sonographic pictures and movie sequences of the supraspinatus tendon was developed, ensuring that relevant changes regarding tendon thickness, hypoecchoic areas, fibrillar disruption, calcification and neovascularity were visualized optimally. A modified version of a grading scale, proposed by Poltawski et al. 2012 [2], was developed for grading the potential pathological characteristics. The modified scale consists of a 0-1 score for assessing the presence of fibrillar disruption, calcification and neovascularity. A grey-scale picture was obtained at a fixed point for evaluating tendon thickness.

Five healthy participants and five participants with shoulder discomfort were used in the development and training phase. Afterwards, in the inter-tester reliability study a sample of 10 participants with no shoulder discomfort and 10 participants diagnosed with supraspinatus tendinopathy were included. The primary investigator (rater A) performed all sonography scans. Demographic information regarding age, gender, arm dominance and Self-reported shoulder function scored on "Disability of the Arm, Shoulder and Hand questionnaire'' (DASH), was obtained at the same time as the sonography scan. In order to secure blinding of rater A, all data were stored for at least four weeks, before they were analyzed. Two

raters (A and B) independently viewed the obtained picture and movie sequences, measured tendon thickness and assessed the presence of calcification, fibrillar disruption, and neovascularity.

Cohen's Kappa statistics were used for the dichotomized scale of fibrillar disruption, neovascularization and calcification. ICC statistics were used for measurement of tendon thickness. MDC for tendon thickness was calculated based on the ICC-value. The difference in height between rater A and B was tested with a paired t-test in order to evaluate potential systematic differences between rater A and B.

All statistics were performed in Stata/IC 13.1 (StataCorp, Texas, USA).

Results: There was no statistically significant difference in age, gender, height or hand dominance between participants with and without shoulder discomfort. A significant difference was, as expected, found on the patient reported outcome score "Disability of the Arm, Shoulder and Hand questionnaire'' (DASH) between participants with and without shoulder discomfort. Kappa-values were substantial for calcification (0.76), perfect for neovascularization (1.0), but poor for fibrillar disruption (0.08). The ICC was 0.73 for tendon thickness and MDC was 1.7mm. A non-significant (p=0.23) difference of 0.25mm (SD 0.9) in measured tendon thickness was found between rater A and B.

Conclusion: The standardized method for assessing supraspinatus tendinopathy showed good inter-examiner reliability in measuring thickness, calcification and neovascularization, and the MDC indicates that even small changes in tendon thickness are detectable. The standardized protocol for assessing fibrillar disruption needs to be reevaluated and retested before further research with this assessment methode can be performed.

In order to increase the likelihood of clinicians choosing the most appropriate rehabilitation strategy, based on the specific stage of tendinopathy, the assessment method must be reliable and sensitive. This trial takes a step towards using a standardized method for sonographic scanning of the supraspinatus tendon and a standardized assessment of the observed changes that relate to the stages of tendinopathy.

References: [1] Cook et al., Br. J. Sports Med., 43(6): 409-416, 2009.

[2] Poltawski et al., Skeletal Radiol., 41(1): 83-89, 2012.

Disclosure of Interest: None Declared

Rehabilitation

PO-0175

EFFECTS OF DIFFERENT METATARSAL PAD DESIGNS AND PLACEMENTS ON PLANTAR PRESSURE DISTRIBUTION

Weng-Pin Chen [1,*]Shih-Cherng Lin [2]Sih-Chen Huang [1]Fuk-Tan Tang [2]

[1]Mechanical Engineering, National Taipei University of Technology, Taipei, [2]Physical Medicine and Rehabilitation, Chang-Gung Memorial Hospital, Taoyuan, Taiwan, Republic of China

Introduction and Objectives: Due to the load transfer mechanism, the propulsive ground reaction force is often concentrated on the area beneath the first and second metatarsal heads during human ambulation. The pain and discomfort resulted at this area are known as metatarsalgia. In order to relieve this symptom, metatarsal pad is commonly prescribed for patients with metatarsalgia in clinical practice. Although the effectiveness of metatarsal pad on the plantar pressure reduction had been investigated in previous studies using plantar pressure measurement system, the experiment itself is very difficult to eliminate the relative motion between the foot sole and insole, and to define the location precisely. For this reason, no clear conclusion on the metatarsal pad design and placement that can achieve best effectiveness in plantar pressure reduction so far. Due to the finite element analysis has the advantages in modifying the model and adjusting the parameters easily, this study aimed to investigate the effects of different placements and geometrical designs of metatarsal pad on the plantar pressure distribution through dynamic finite element analysis.

Methods: A three-dimensional finite element model of the foot-shoe complex, including the foot bony and ligamentous structure, soft tissue, metatarsal pad, insole, outsole and shoe cover, was adopted in this study. The trajectory of the reflective markers and the kinematic data of the foot obtained from gait analysis were used to define the boundary condition in the finite element analysis. After validation of the model, the effects of metatarsal pad on the plantar pressure distribution beneath the metatarsus and the second metatarsal head were investigated by changing five different placements, two different heights, and three different sizes of the metatarsal pad.

Results: According to the results from the dynamic finite element analysis, when the pad was placed 10 mm proximal to the second metatarsal head, better efficacy of pressure reduction than other placements was found. Under the appropriate placement, the efficacy would be further improved by raising the height of the pad from 5 mm to 10 mm, but causing high pressure concentration beneath the metatarsus. However, increasing the pad size by 10% would relieve the concentrated high pressure.

Figure:
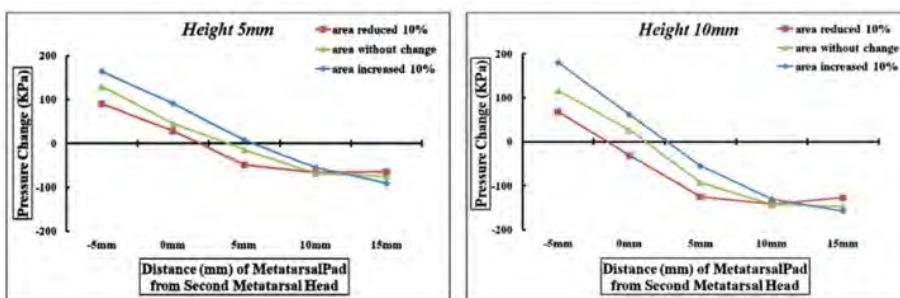
Caption: The changes in peak pressure under five different placements, three different bottom areas and two different heights, compared with the condition without using MT pad beneath the region of second MT head.

Conclusion: As a result, increasing the height as well as area of metatarsal pad properly may enhance the efficacy of plantar pressure reduction beneath the second metatarsal head, and relieve high pressure concentration beneath the metatarsus. The current results from the dynamic finite element analysis were focused on one single subject. Different foot dimension and structural classification were not considered in this study. More subjects with different size and structure of foot should be recruited in the future in order to provide a more comprehensive recommendation on the prescription of metatarsal pad.

References: [1] Fadel et al., Curr Orthopaed, 16:193-204, 2002.

[2] Bardelli et al., Foot Ankle Sure, 9:79-85, 2003.

[3] Espinosa et al., Foot Ankle Int, 29:871-879, 2008.

[4] Budhabhatti et al., J Biomech, 40:s176, 2007.

Disclosure of Interest: None Declared

Rehabilitation

PO-0176

ASSESSMENT OF SCAPULAR POSITIONING AND FUNCTION AS FUTURE EFFECT MEASURE OF SHOULDER INTERVENTIONS – AN INTER-EXAMINER RELIABILITY STUDY

Henrik Eshoj [1,*]Camilla Marie Larsen [1]Kim Gordon Ingwersen [1]Karen Sogaard [1]Birgit Juul-Kristensen [1 2]

[1]Institute of Sports Science and Clinical Biomechanics, Faculty of Health Sciences, University of Southern Denmark, Odense M, Denmark, [2]Department of Health Sciences, Institute of Occupational Therapy, Physiotherapy and Radiography, Bergen University College, Bergen, Norway

Introduction and Objectives: Scapular dyskinesis, defined as an abnormal positioning, and/or altered function of the scapular is often present in subacromial impingement syndrome (SIS). SIS is one of the most common shoulder disorders, potentially leading to degenerative conditions and/or osteoarthritis in the glenohumeral joint. Treatment of SIS primarily consists of physical therapy aiming at reducing signs of scapular dyskinesis. However, no consensus exists regarding which clinical tests to use for identifying and measuring scapular positioning and function. As a first step acceptable clinimetric measures of reliability is important, although, several tests have only been tested for intra-examiner reliability. The objective was to investigate the inter-examiner reliability of an extended battery of clinical tests for assessing scapular positioning and function.

Methods: A standardized three-phase protocol for clinical reliability studies was conducted, containing a training, an overall agreement and a study phase. The index condition (scapular dyskinesis) was defined as a clearly obvious scapular winging (pseudo or margo medialis winging) observed during bilateral repeated active flexion's of the upper extremity. A total of 24 clinical assessment variables were compiled into three categories; static (6), semi-dynamic (7) and dynamic assessment variables (9), besides assessment of external rotational strength (2). Testers were blinded to the status of subjects, the results of each test round and each others´ test results. Intra-class correlation coefficients (ICC) and kappa values were interpreted as: 0.0-0.40 (poor); 0.40-0.75 (fair to good); and 0.75-1.00 (good to excellent).

Results: A total of 41 subjects (23 males, yrs 25±9), were recruited among adult overhead athletes from the municipality of Odense, DK. Prevalence of the index condition was 54 %. Data was tested and found to have normal distribution for all continuous variables and Bland Altman plots showed no funnel effects. Bland Altman plots found no systematic bias and good to excellent ICC values in four of the static assessment variables. The ICC values ranged from "fair to good" (n=2 assessment variables, av) and "good to excellent" (n=6 av) in the static and external shoulder rotation strength (n=2 av); from "poor" (n=3 av) to "fair to good" (n=4 av) in the semi-dynamic av, with; from "poor" (n=4 av) to "fair to good" (n=3 av) in the dynamic av, and no kappa statistics computed in three tests due to constant measurements from one of the testers.

Conclusion: An extended assessment battery to investigate the inter-examiner reliability for assessing the scapular positioning and function were compiled. Systematic bias between testers appeared in some, but not all assessment methods, questioning the overall accuracy. However, within the static assessment methods, four of these had ICC values within "good to excellent" and no systematic bias. Improvements of clinimetric properties of assessment methods for measuring scapular dyskinesis are needed.

Disclosure of Interest: None Declared

PO-0177

THE ADDITION OF MANUAL THERAPY TO AN EXERCISE PROTOCOL DOES NOT AUGMENT THE EFFECTS ON PAIN, FUNCTION AND SCAPULAR KINEMATICS IN INDIVIDUALS WITH SHOULDER IMPINGEMENT – RANDOMIZED CONTROLLED TRIAL

Paula Camargo [1,*] Francisco Alburquerque-Sendín [2] Mariana Avila [3] Melina Haik [3] Amilton Vieira [3] Tania Salvini [3]

[1] Physical Therapy, UFSCar, [2] University of Salamanca, [3] UFSCar, São Carlos, Brazil

Introduction and Objectives: Many conservative treatments have been proposed to manage shoulder impingement (SI). Systematic reviews have indicated that stretching and strengthening exercises are effective to improve pain and disability in individuals with SI, however there is still conflicting evidence for the effectiveness of manual therapy as an add-on therapy to exercises. More studies are necessary to determine if adding manual therapy techniques into a standardized exercise program is better than exercises alone. The aim of this study was to evaluate the effects of stretching and strengthening exercises associated or not with manual therapy on pain, function and scapular kinematics in individuals with SI.

Methods: Forty-six patients participated in this study and were randomly assigned to one of the 2 groups: exercise only group (14 males and 9 females, 32.65 ± 10.73 years, 68.35 ± 10.79kg, 1.69 ± 0.02m) and manual therapy + exercises group (10 males and 13 females, 35.96 ± 12.08 years, 67.04 ± 13.12Kg, 1.69 ± 0.12m). Pain during movement and greatest pain at last week were measured by a visual analogue scale. All participants also completed the DASH questionnaire to assess function of the upper limbs and scapular kinematics was assessed during elevation of the arm in the sagittal plane. The outcomes were measured 3 times over a period of 5 – 6 weeks. Individuals were first evaluated and then, started the intervention period up to 1 week after the first evaluation. Second and third evaluations were carried out after 2 and 4 weeks of intervention, respectively. Both groups were treated with stretching exercises targeting the upper trapezius, pectoralis minor and posterior shoulder, and strengthening exercises targeting the external rotators of the arm, lower trapezius and serratus anterior muscle. These exercises were selected based on alterations already identified in the SI condition. The manual therapy + exercises group also received techniques of manual therapy focused on the shoulder complex, shoulder girdle, cervical spine and upper thoracic spine. A 2-factor ANOVA (group x evaluation) was conducted for the pain and DASH, and a 3-factor ANOVA (group x angle x evaluation) for each scapular rotation. Alfa level was set at .05.

Results: Pain during movement, the greatest pain at last week and the DASH score decrease ($P<0.05$) along time independent of the intervention applied. Few improvements in scapular motion were also observed along time in both groups ($P<0.05$). Scapular internal rotation decreased ($<3.7°$) at 120° of arm elevation and upward rotation increased ($<2.5°$) at 90° and 120° of arm elevation. No significant changes were found for scapular tilt ($P>0.05$).

Conclusion: The findings indicate that the addition of manual therapy to an exercise protocol is not superior than exercises only to improve pain, function and scapular kinematics in individuals with SI. Both groups improved independent of the intervention received. Improvements in pain and function are not likely explained by changes in scapular motion once these alterations in scapular motion are not clinically relevant.

Rehabilitation

PO-0178

TREADMILL TRAINING AND TRANSCRANIAL DIRECT CURRENT STIMULATION OVER THE CEREBELLAR REGION IN SIX CHILDREN WITH ATAXIC CEREBRAL PALSY

Luanda Greco [1][2] Natália Duarte [1] Manuela Galli [3] Felipe Fregni [2] Claudia Oliveira [1,*]

[1]Rehabilitation Sciences, UNINOVE, São Paulo, Brazil, [2]Department of Physical Medicine & Rehabilitation, Harvard Medical School, Boston, United States, [3]Department of Electronics, Information and Bioengineering, DEIB, Politecnico di Milano, Milan, Italy

Introduction and Objectives: Previous studies have demonstrated that anodal transcranial direct current stimulation (tDCS) over primary motor cortex can regulate corticospinal excitability.(1) Stimulation applied to the motor cortex during motor training is associated with improved performance and motor learning.(2-5) In children with cerebral palsy, the combination the motor training and anodal tDCS has demonstrated beneficial effects on gait and motor function.(4, 5) The aim the present study was to analyze the effects of anodal tDCS over the cerebellar region combined with treadmill training for improving balance in children with ataxic cerebral palsy.

Methods: Six children with ataxic cerebral palsy received two interventions separated by four months. The order of the interventions (experimental or control) was determined by simple randomization. The experimental intervention involved anodal tDCS and the control intervention involved sham stimulation over the cerebellar region (Oz) during treadmill training. The patients underwent the same intensive gait training program. Five weekly 30-minute sessions were performed over two consecutive weeks. Evaluations of static (oscillations of the center of pressure in the anteroposterior and mediolateral directions with eyes open and eyes closed) and functional balance (Pediatric Balance Scale) were performed before and after the interventions as well as at follow up.

Results: The experimental intervention achieved better results regarding anteroposterior oscillation with eyes open (experimental intervention: 26.2±3.7 to 20.4±4.19 mm; control intervention: 25.7±4.1 to 20.9±2.9 mm), anteroposterior oscillation with eyes closed (experimental intervention: 40.1±8.0 to 24.0±2.8 mm; control intervention: 47.7±8.6 to 52.6±9.7 mm), mediolateral oscillation with eyes open (experimental intervention: 54.7±4.9 to 34.1±4.9 mm; control intervention: 56.6±5.8 to 53.7±5.4 mm), mediolateral oscillation with eyes closed (experimental intervention: 42.9±6.7 to 30.7±2.9 mm; control intervention: 40.4±7.3 to 38.6±8.1 mm) and functional balance (experimental intervention: 38.2±2.1 to 44.2±2.3; control intervention: 40.1±3.5 to 43.2±4.1). A significant decrease in all oscillations with eyes closed was achieved with the experimental intervention in comparison to the control intervention (Figure 1).

Figure:

Oscillation of the center of pressure with eyes closed
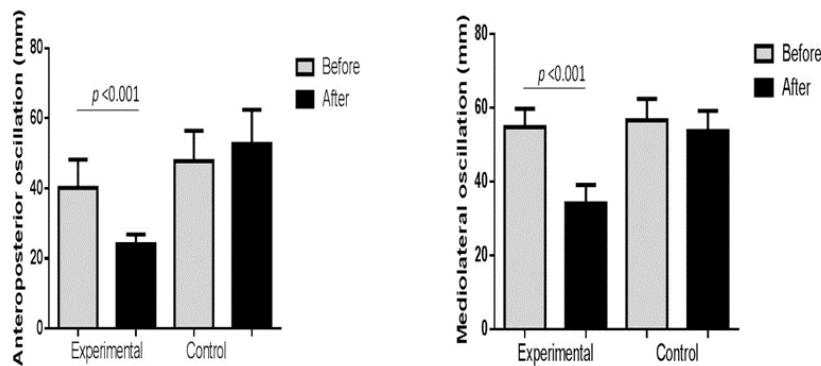
Caption: Results of the oscillation of the center pressure with eyes closed before and after control and experimental intervention.

Conclusion: The present findings support the hypothesis that anodal tDCS over the cerebellar region (Oz) combined with treadmill training could be a useful tool for improving static balance in children with ataxic cerebral palsy.

References:

1. Stagg et al, Neuropsychologia, 49(5):800-4, 2011.
2. Lee et al, Archives of physical medicine and rehabilitation, 95(3):431-8, 2014.
3. Viana et al, NeuroRehabilitation. 2014.
4. Grecco et al, Research in developmental disabilities, 35(11):2840-8, 2014.
5. Duarte et al, PloS one, 9(8):e105777, 2014.

Disclosure of Interest: None Declared

PO-0179

EFFECTS OF TRANSCRANIAL DIRECT CURRENT STIMULATION COMBINED WITH FUNCTIONAL UPPER LIMB TRAINING IN A CHILD WITH HEMIPARETIC CEREBRAL PALSY: A CASE REPORT

Renata Moura [1,*]Cibele Santos [1]Roberta Lazzari [1]Arislander Dumont [1]Veronica Cimolin [2]Claudia oliveira [1]

[1]Rehabilitation Sciences, UNINOVE, São Paulo, Brazil, [2]Department of Electronics, Information and Bioengineering, DEIB, Politecnico di Milano, Milan, Italy

Introduction and Objectives: Cerebral palsy (CP) is the most prevalent form of physical disability in children. Nearly 50% of children with CP have impaired upper limb function. Children with hemiparetic CP seldom use their paretic hand spontaneously in daily activities. Thus, increasing attention in the last decade has focused on upper limb rehabilitation in this population.[1] Transcranial direct current stimulation (tDCS) can be used during motor therapy sessions and involves the administration of a weak electrical current and induces lasting changes in cortex excitability in both animals and humans. In rehabilitation programs, the aim of tDCS is to enhance local synaptic efficiency, thereby altering the maladaptive plasticity pattern that emerges following a brain lesion. Stimulation is used to modulate cortex activity by opening a pathway to increase and prolong functional gains achieved in physical therapy.[2]

The aims of the present study were to determine the effects of tDCS applied over the primary motor cortex combined with functional upper limb training in a child with hemiparetic cerebral palsy.

Methods: This study received approval from the Human Research Ethics Committee of the UNINOVE (Brazil) under process number 525935/2014. The 12-year-old child had a diagnosis of left hemiparetic spastic CP, Manual Ability Classification System II, no history of surgery or neurolytic block in the previous 12 months, absence of orthopedic deformities, absence of epilepsy and no metal implants in the skull or hearing aids. The kinematic evaluation of the upper limb was performed using the SMART-D 140® system and using SMARTAnalyser software (BTS, Italy). The child was asked to reach an object on a desk in front of the patient at a normalised distance (80% of subject's arm length); the subject is seated with flexed arm flexed on the desk. The task was repeated 12 times (six movements, right and left). Kinematic analysis was conducted identifying and computing specific parameters of movement duration, velocity, smoothness and upper limbs angles[3,4]. The patient was assessed before and after training. A control Group (CG) of ten healthy children was included[4]. The child underwent the 10-session intervention protocol involving functional upper limb training combined with tDCS stimulation. The anodal electrode was positioned over the primary motor cortex of the hemisphere with the lesion following the 10–20 International Electroencephalogram System[5] and the cathode was positioned in the supra-orbital region on the contralateral side. A 1-mA current was applied over the primary motor cortex for 20 minutes as the child performed upper limb training, which involved motor strategy reach and move objects while maintaining the elbow extended.

Results: Table 1 displays the variables analyzed for the paretic upper limb (left side) at baseline (trial 1) and after training (Trial 2) in terms of kinematics. From these data, it is possible to observe a reduction of going and returning phase duration, an improvement of NJS and NMU parameters after training; mean velocity and its peak increased in the Trial 2, too

Conclusion: Studies involving use of tDCS in the rehabilitation of patients with cerebral palsy suggest that this method is safe and clinically relevant[2]. The findings of the present study demonstrate that the combination of functional upper limb training and tDCS is capable of potentiating improvements in children with CP.

Table: Table 1: Values of the analyzed parameters for the paretic upper limb.

Time parameters	Trial 1	Trial 2	Control Group
Going Phase (s)	0.9+ 0.02	0.648+ 0.06	0.6+0.1
Adjusting phase (s)	0.126+ 0.037	0.11+ 0.24	0.28+ 0.15
Returning Phase(s)	0.9 + 0.021	0.616+ 0.025	0.7+0.2
Smoothness			
IC(mean)(Index of Curvature)	1.04	1.046	1.1 +0.1
NJS (Normalised Jerk Score)	222.43	97.452	226.89+124.78
NMU (Number of Unit Movement)	5.2	2.2	2.4+1.56
Velocity			
Mean Velocity (m/s)	0.582+ 0.015	0.768+ 0.07	0.64+0.16
Peak Velocity (m/s)	1.004+ 0.053	1.258+ 0.102	2.2+0.2
Accuracy			
End Point Error (mm)	9.1+ 0.8	18.8+ 2.1	14.2+7.5
Adjusting Sway (mm)	12	20.8	9.87+7.32

Legend: Data on mean ±st.dev.

Caption: Table 1: Values of the analyzed parameters for the paretic upper limb.

References: References: [1] Arnould et al., Front Neurol., 5: 48, 2014.

[2] Duarte et al., PLoS One, 9(8), 2014.

[3] Menegoni et al., Eur J Neurol., Feb;16(2):232-9, 2009.

[4] Cimolin et al., J Head Trauma Rehabil., May-Jun;27(3):177-87, 2012.

[5] Homan et al., Electroencephalography Clin Neurophysiol, 66: 376–82, 1987

Disclosure of Interest: None Declared

Rehabilitation

PO-0180

A BIOMECHANICAL EVALUATION OF THE COMBINED ELEVATION TEST

Sam Allen [1,*]Steve McCaig [2]Gemma Phillips [1]

[1]Loughborough University, [2]England and Wales Cricket Board, Loughborough, United Kingdom

Introduction and Objectives: The Combined Elevation Test is a widely recognised musculoskeletal (MSK) screening tool, used across a variety of sports including, but not limited to, cricket, rugby union, swimming and triathlon [1]. The Combined Elevation Test is thought to identify impairments in strength and range of motion during synchronised thoracic extension, glenohumeral joint (GHJ) flexion, and retraction and upward rotation of the scapula [2]; however its efficacy has not yet been quantified. The outcome of the Combined Elevation Test is recorded in one of two ways. One technique adopted by [1] uses the angle created between the raised humerus and the horizontal; a more widely adopted technique is measurement to the nearest 0.1 cm, of the perpendicular height between the resting surface and the base of the first metacarpal [2]. The objectives of this study were to evaluate the Combined Elevation Test biomechanically in terms of the relationship between the outcome and its component joint motions and thoracic spine angles between test positions, genders, and different methods of measurement.

Methods: Eighteen subjects participated in the study: eleven males (age: 24.5 ± 3.1 yrs, height: 1.82 ± 0.05 m, weight: 75.3 ± 7.4 kg); and seven females (age: 23.6 ± 4.1 yrs, height: 1.73 ± 0.04 m, weight: 62.8 ± 6.8 kg). Subjects were all either elite swimmers or elite triathletes. Performance in the Combined Elevation Test was measured in two head positions: forehead in contact with the ground; and chin in contact with the ground. Individual contributions to the test outcome of: shoulder joint retraction (used as a proxy for scapular retraction and rotation); glenohumeral joint flexion; and elbow joint flexion were calculated using automatic motion capture (Figure 1). Upper, lower, and total thoracic spine angles were also calculated. Both perpendicular height of the wrist, and humeral angle were measured. Relationships between individual test components and outcome, and the effects of gender, head position, and measurement method were investigated statistically.

Results: There were no differences in any variables between males and females in any of the test components, or between head positions. Subjects scored more highly on the test in the forehead position than the chin position (34.3 cm vs 30.2 cm; p<0.001). The variables most strongly associated with test performance in both head positions were glenohumeral joint flexion (r = 0.86 – 0.97), shoulder retraction (r = 0.75 – 0.82), and total thoracic spine angle (r = -0.40 – -0.44). The use of humeral angle as a test measure was strongly, but not perfectly, related to wrist height (r = 0.93; p<0.001).

Figure:
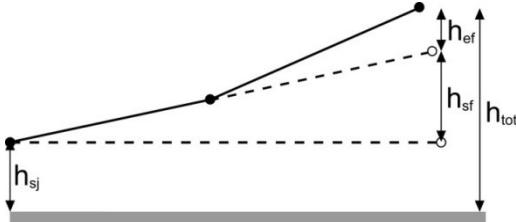
Caption: Figure 1. The contributions of each joint to test performance: hsj is the height of the shoulder joint centre; hsf is the contribution of shoulder flexion, assuming no elbow flexion; hef is the contribution of elbow flexion; and htot is the total vertical displacement of the WJC. (n.b. hsf and hef values can be negative).

Conclusion: Within the group in this study none of the combined elevation test outcomes were different in any way between genders, therefore males and females within this subject group can be assessed using the same norms. Performance in the test was greater in the forehead than chin position due to increased shoulder retraction. The results of the correlations between test components and outcomes indicated that the component with the strongest relationship to test outcome was glenohumeral joint flexion, the second strongest predictor of test outcome was shoulder joint retraction, whilst elbow joint flexion was not related to test outcome. Total thoracic spine angle was related to test outcome but this relationship was not statistically significant. These results lend weight to the claim that the test measures GHJ flexion, and retraction and upward rotation of the scapula, and that it may also relate to thoracic extension. Humeral angle represents a good predictor of test performance but does not incorporate some aspects of the test, such as shoulder retraction, so perpendicular height of the wrist is a more suitable measure if this information is required.

Table:

	forehead		chin	
measure	male (n=11)	female (n=7)	male (n=11)	female (n=7)
h_{tot} (cm)	34.0 ± 10.0	34.8 ± 11.7	30.5 ± 10.9	29.8 ± 12.2
h_{sj} (cm)	21.3 ± 2.0	20.0 ± 2.3	19.8 ± 2.5	18.5 ± 3.0
h_{sf} (cm)	7.8 ± 9.9	9.6 ± 9.8	6.6 ± 10.5	7.0 ± 10.3
h_{ef} (cm)	4.9 ± 3.0	5.2 ± 1.5	4.1 ± 5.9	4.3 ± 3.0
T_1-T_{12} (°)	12.2 ± 5.3	13.3 ± 3.7	12.6 ± 4.9	12.8 ± 4.4
T_1-T_8 (°)	10.2 ± 4.9	8.9 ± 5.4	9.9 ± 4.7	8.6 ± 4.2
T_4-T_{12} (°)	10.5 ± 3.6	11.7 ± 2.5	11.1 ± 3.3	12.0 ± 3.2

Caption: Table 1. Test measures (mean ± SD) between positions and genders

References: [1] Blanch, P., Phys Ther Sport, 5: 109-124, 2004.

[2] Dennis et al., Phys Ther Sport, 9: 25-33, 2008.

Disclosure of Interest: None Declared

Rehabilitation

PO-0181

FUNCTIONAL EVALUATION OF PEDIATRIC CANCER PATIENTS AFTER A 4-WEEK CLINICAL REHAB PROGRAM

Dieter Rosenbaum [1,*] Carsten Müller [1] Konstantin Krauth [2]

[1]Movement Analysis Lab, Inst. Exp. Musculoskeletal Medicine, University Hospital Münster, Münster, [2]Klinik Bad Oexen, Bad Oeynhausen, Germany

Introduction and Objectives: Children that are affected by oncologic diseases experience a life-threatening situation and have to undergo a long intensive treatment that might involve chemotherapy, radiation, resection surgery with subsequent limitations in functional capacity and quality of life. In order to help them to recover a stationary rehabilitation is part of the treatment plan in Germany. Such a rehab program aims to improve potential functional deficits and strengthen physical, psychological, and social resources.

The present project set out to evaluate the functional status, level of activity and quality of life of pediatric cancer patients before and after a 4-week rehab program with a maximum follow-up of 12 months. More specifically, we wanted to evaluate the long-term effects of the rehab program, and to determine which patient groups would benefit more or less.

Methods: Pediatric patients between 4 and 18 years of age who had been treated for brain (n=63), bone and soft tissue tumors (n=38) as well as leukemia and lymphoma (n=109) were contacted before admission to 4-week stay in the rehab clinic Bad Oexen. If time allowed for it, they were asked to wear a step counter for a week before admission to the clinic. In the clinic, patients were asked to complete a questionnaire regarding quality of life and to wear a step counter (SAM Stepwatch Activity Monitor, Orthocare Innovations, USA). Furthermore, patients with a potentially impaired gait function were also evaluated with 2-dimensional gait analysis (2 video cameras and analysis with TEMPLO 6.0, Contemplas, Germany) and foot loading measurements (emed-m/R, Novel GmbH, Germany) in the beginning and at the end of the rehab program.The measurements were analyzed with respect to the symmetry of gait or foot loading by determining a symmetry index for temporal-spatial, kinematic and kinetic parameters.

Results: The gait analysis revealed no major changes in the overall gait parameters but indicated a decrease of the degree of asymmetry during the rehab program with respect to the step length, single-leg stance and swing duration, and maximum knee flexion angle.

The foot loading parameters remained stable but the slightly increased maximum forces indicated a more dynamic gait pattern. Again, the asymmetry indices were reduced.

The balance tests showed a significantly improved function with a longer single-leg stance duration (8.6à9.6 s; p=.001) and less sway velocity (6.8à6.4 cm/s; p=.010). Analysis of the different diagnostic groups indicated that bone tumor patients are likely to have more pronounced functional deficits than brain tumor patients.

Conclusion: In general, the results demonstrated the effectiveness of the 4-week stationary rehab program and allowed for an objective evaluation of the individual progress or deficit. Patients improved the overall gait symmetry and especially bone tumor patients with an affected lower extremity benefitted from the therapy. The functional assessments might help to personalize the treatment regimens to the patient's individual needs.

Disclosure of Interest: None Declared

STRENGHT AND HEALTH RELATED QUALITY OF LIFE IMPROVEMENT OF INDIVIDUALS WITH SHOULDER IMPINGEMENT SUBMITTED TO MOTOR CONTROL AND STRENGTHENING EXERCISES – PARTIAL RESULTS

Gisele H. Hotta [1]Adriane Santos [1]Anamaria Oliveira [1,*]

[1]Biomechanics, Medicine and Rehabilitation of Locomotor System, University of São Paulo, Ribeirão Preto School of Medicine, RIbeirão Preto, São Paulo, Brazil

Introduction and Objectives: The adequate scapular motion is important to shoulder's function. Subjects with shoulder impingement have decrease upward rotation and posterior tilt, and increase in medial rotation of scapula relative to the thorax [1]. These alterations are associated with less recruitment of scapulothoracic muscles [1,2] and less health related quality of life [3]. Objective this study is to evaluate the isometric force and quality of life the subjects submitted to protocol of motor control and muscle strengthening for scapulothoracic muscles.

Methods: Inclusion criteria were painful arc and Neer or Hawkins-Kennedy positive test, dyskinesis type I or II and a history of shoulder pain lasting more than a week in the anterolateral proximal region of shoulder. The study was approved by the Ethics Committee of the Clinic's Hospital of the Ribeirão Preto School of Medicine of the University of São Paulo. The subjects were submitted to the motor control exercises protocol for scapula and strengthening muscle, specific to serratus anterior, middle and lower trapezius and rhomboids strengthening (Figure 1). Exercises were performed three times a week for eight weeks and each session consisted of three sets of ten repetitions with initial load of 60% of 1 repetition maximum recommended by American College of Medicine Sports [4]. The protocol is specific for serratus anterior, middle trapezius, lower trapezius and rhomboids strengthening.

The evaluations were carried out before and after eight weeks of motor control and strengthening program. Assessment the strength muscles performed with load cell. Subjects were positioning according Kendall et al. (2007) and performed three repetition maximum voluntary contractions. For assessment health related quality of life was used the Shoulder Pain and Disability Index – SPADI Brazil. The SPADI contains 13 items that assess two domains; a 5-item subscale that measures pain and an 8-item subscale that measures disability. A mean is taken of the two subscales to give a total score out of 100 and higher score indicating greater impairment or disability [6]. Only data from painful shoulder were used for analysis. The Student's t-test was used to compare mean values isometric force and SPADI-Brazil total score, pre- and post-eight weeks of treatment. Level of significance was set at 5%.

Results: Twenty five volunteers were submitted to protocol. They presented mean age of 47.3 (±9.4) years old. Fourteen subjects were male. After protocol, subjects presented lesser score in the SPADI, indicating less impairment and disability and consequently improvement quality of life. The SPADI scores improved above ten points. These changes were statistically significant (p<0.00; Table 1) and met the minimally clinically important difference (MCID) [3]. Worsley and colleagues (2012) performed a training of motor control for scapula during ten weeks in subjects with shoulder impingement and also found clinically important quality of life improvement after treatment.

Strengthening muscle was observed for middle trapezius and serratus anterior (p<0.05; Table 1). The trapezius and serratus anterior have been recognized as muscles wich can stabilize and rotate the scapula and they are the prime

movers for scapular upward rotation [8]. The middle trapezius is ideally suited for scapular external rotation and serratus presents substantial mechanical advantage for upward rotation, posteriorly tilt and externally rotate the scapula [9].

Figure:

Caption: Figure 1: Motor control exercises (A-B) and muscle strengthening (C-D)

Conclusion: According to the partial results of this non-controlled study, the motor control and strengthening program could change the strength muscle and improvement health related quality of life, however, effect sizes in the complete sample should be calculated to estimate the power of the final findings.

Table:

Table 1: Comparison of pre and post treatment of Shoulder Pain And Disability Index – SPADI Brazil (total score) and muscle isometric force (Kgf) variables.			
	Pre treatment	Post treatment	p value
SPADI - Brazil	48.10 ± 17.94	12.61 ± 14.39	0.000
Middle Trapezius	7.07 ± 4.85	14.10 ± 17.97	0.045
Lower Trapezius	8.00 ± 6.48	14.85 ± 17.81	0.077
Serratus Anterior	11.28 ± 5.48	19.27 ± 15.97	0.024
Rhomboids	6.68 ± 4.81	13.58 ± 17.74	0.055
Values expressed as mean ± standard deviation. Kgf: Kilogram-force			

References: [1] Ludewig et al. *Physical. Therapy*, 80(3): 276-291, 2000.

[2] Lin et al. *J Electromyogr Kinesiol* 15.6: 576-586, 2005.

[3] Roy et al. *Arthritis Care Res*, *61*(5), 623-632, 2009.

[4] American College of Sports Medicine. *Med Sci Sports Exerc*, 41(3); 687-708, 2009.

[5] Kendall (Ed). Músculos: Provas e Funções, Manole, 2007

[6] Martins et al. *Rev. Bras., Fisioter*, 14; 6; 527-536, 2010.

[7] Worsley et al. J Shoulder Elbow Surg, 2012.

[8] Inman VT, Abbott LC. *Clin. Orthop. Relat. Res*, *330*, 3-12, 1996.

[9]Phadke et al.. *Braz. J. Phys. Ther.*, *13*(1), 1-9, 200

Disclosure of Interest: None Declared

COMPENSATORY MECHANICS DURING STAIR ASCENT IN PATIENTS WITH MEDIAL KNEE OSTEOARTHRITIS; AN ANALYSIS OF MECHANICAL ENERGY TRANSFER IN THE LOWER EXTREMITY.

Yumiko Koyama [1,*]Hiroshige Tateuchi [1]Xiang Ji [1]Riho Nhishimura [1]Hiroki Umegaki [1]Masashi Kobayashi [2]Noriaki Ichihashi [1]

[1]Human Health Sciences, Graduate School of Medicine, Kyoto University, [2]Kobayashi Orthopedic Clinic, Kyoto, Japan

Introduction and Objectives: Patients with knee osteoarthritis (knee OA) often complain about their difficulties in stair negotiation, which would limit their mobility independence and increase the risk of falls. Stair ascent requires much energy generated in the lower extremities compared to level walking. Although these patients are supposed to climb stairs with certain compensatory mechanics, there is no study that disclose such compensatory strategies regarding mechanical energy efficiency. The purpose of this study was to evaluate mechanical energy efficiency during stair ascent in order to clarify the compensatory strategies in patients with knee OA.

Methods: Twenty-one females with medial knee OA (age: 64.8±7.8years, height: 154.9±3.4cm, weight: 59.7±6.6kg) and six young heathy volunteers (age: 23.8±1.0years, height: 162.7±6.2cm, weight: 55.4±5.3kg)were included in this study. Patients were classified into two groups based on Kellgren-Lawrence grade, with eleven patients allocated to the mild group and the others allocated to the severe group. Each participant was instructed to ascend a 20cm-hight step by the involved limb, that is the more affected side in patients with knee OA and the dominant side in healthy volunteers. Three trials per participant were analyzed with 3D motion analysis system (Vicon Nexus; Vicon Motion Systems Ltd., Oxford, England) and force platforms (Kistler Japan Co., Ltd. Tokyo, Japan). All participants performed these trials in their self-selected speed without using any walking aids.

Data processing was conducted for the period from the timing when the involved limb touched down on the step to the timing when the center of body mass (CoM) reached highest position during single limb stance. Segmental power was calculated at the pelvis, femur, shank, and foot segment of involved limb, and net joint power at each joint of the involved limb was also collected. All kinetic data were normalized to body mass and height of each participant. Mechanical Energy Expenditure (MEE) and Mechanical Energy Compensation (MEC) were determined at each joint by the method described previously [1]. MEE was calculated by the integral of net joint power curve at each joint, and MEC was defined as the proportion of muscle energy compensated by inter-segmental energy transfer. MEE and MEC were determined separately in three phases, according to the previous study [1], as follows ； concentric transfer phase, eccentric transfer phase, and no-transfer phase. Wilcoxon rank-sum test was applied to compare MEE and MEC at each phase and joint between each pair from three groups. The time taken for ascending a step were also compared between each group. Holm correction was applied to take into account multiple comparison. The significance level was set at 5%.

Results: Healthy and mild groups could climb the step faster than severe group, while there were no significant difference between healthy and mild group (Figure (a)). Healthy group performed stair ascending with higher MEE at the knee during non-transfer phase, which corresponds to the phase when the CoM was steadily elevated, compared to both patient groups (Figure (b)). It was also shown that both patient groups ascended with higher MEE at the hip during concentric transfer phase, which corresponds to the phase when the CoM starts rising, compared to healthy group (Figure (c)).

Increased hip MEC during this phase was observed in severe group in comparison to that observed in healthy group (Figure (d)). There were no significant differences in any other parameters between any pairs.

Figure:
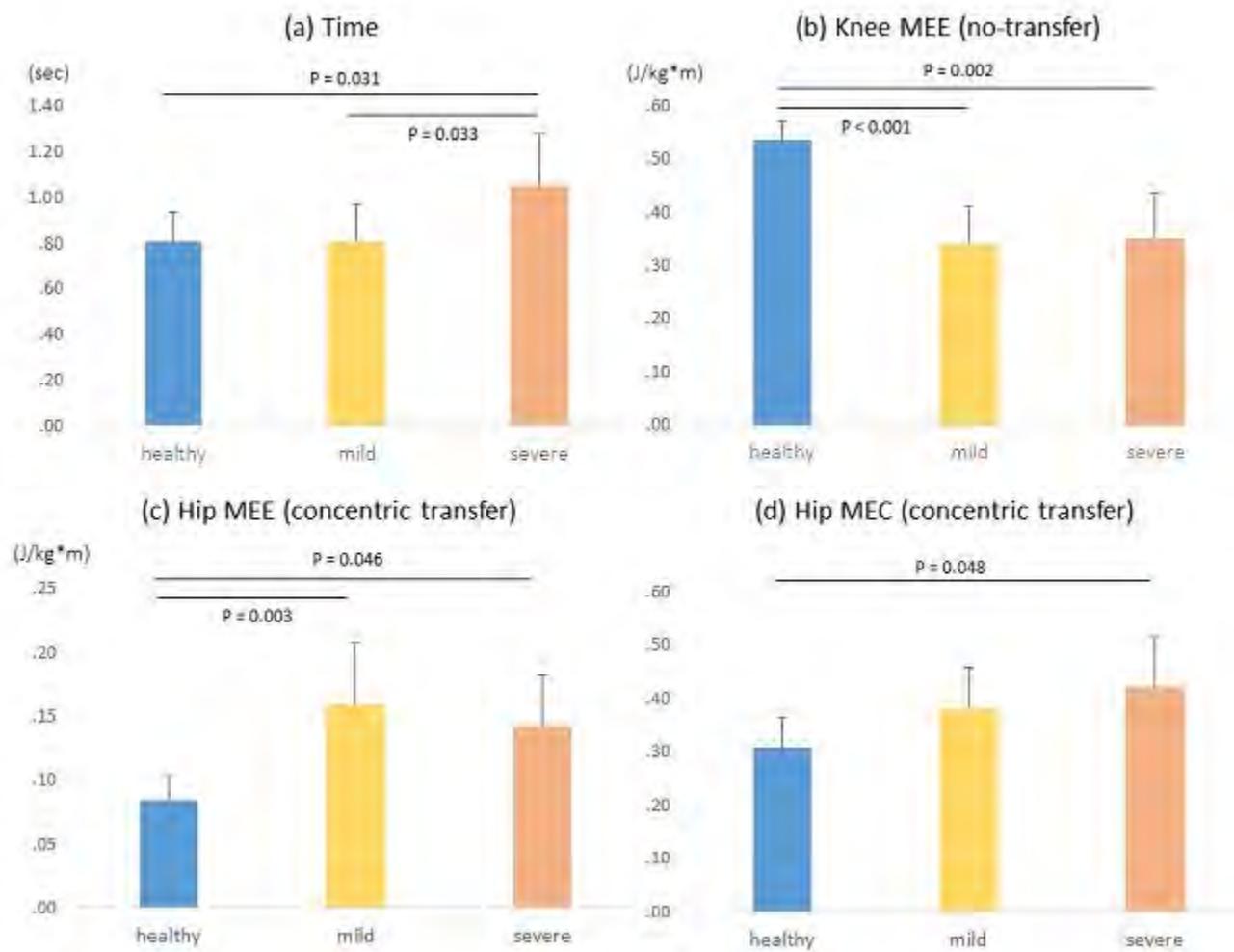
Caption: Comparison of (a) time taken for ascending a step, (b) mechanical energy expenditure at the knee during no-transfer phase, (c) mechanical energy expenditure at the hip during concentric transfer phase, and (d) mechanical energy compensation at the hip during concentric transfer phase between each pair from three groups

Conclusion: Though patients with knee OA have difficulties in stair ascending, most them manage to do it with certain compensatory strategies. This study clarified that patients with knee OA generated much mechanical energy at the hip instead of the less energy generated at the knee when they elevated their body to the upper step. It is also suggested that severe OA patients transferred much mechanical energy generated at hip into the femur segment in order to compensate for the less energy generated at the knee.

References: [1] McGibbon CA,et al. Clin Biomech (Bristol, Avon). 16(4):324-33, 2001.

Disclosure of Interest: None Declared

PO-0184

BIOMECHANICAL ASSESSMENT OF CONGENITAL TALIPES EQUINOVARUS WITH AN ALTERNANT CORRECTIVE METHOD

Wei Chen [1,*]Fang Pu [1]Yang Yang [1]Yubo Fan** [1] [2]Hong Liu [3]

[1]Key Laboratory for Biomechanics and Mechanobiology of Ministry of Education, International Research Center for Implantable and Interventional Medical Devices, School of Biological Science and Medical Engineering, Beihang University, [2]National Research Center for Rehabilitation Technical Aids, [3]Rokab Pedorthic Center, Beijing, China

Introduction and Objectives: Congenital talipes equinovarus (CTEV) is a common foot deformity, with the behavior of equinus, varus, cavus and adductus[1]. Many children present with obvious forefoot adduction deformity by using the previous corrective methods after they begin to walk. The objective was to introduce a new corrective method which consist of day use and night use orthopedic shoes, and explore the effect of this new correction manner on the outcome for CTEV children.

Methods: 18 CTEV children with moderate grade according to the Dime´glio classification were recruited to have the alternant correct method when they began to walk. Orthopedic shoes were applied for day use and Forefoot abduct shoes (FAS) which especially designed to correct forefoot adduction were applied for night use. The corrective treatment were last for 3-4 years with regularly follow-up visit. A 3D scanner and a high resolution pedobarograph were used to record morphological characteristics and plantar pressure distribution. The value of bean-shape ratio, bimalleolar angle and pressure ratio were analyzed.

Results: The average bimalleolar angle is 77.55 with the range from 75.57 to 79.53. The average bean-shape ration is 0.27 with the range from 0.25 to 0.28. The average heel/forefoot pressure ratio is 0.73 with the rang from 0.61 to 0.86. The average heel/lateral arch pressure ratio is 1.98 with the range from 1.68 to 2.29.

Conclusion: This alternate corrective method can effectively improve forefoot adduction for children with CTEV. In addition, this corrective method could also correct equinus and varus. CTEV children with this alternate corrective method obtain better corrective outcome in clinic and their parents were satisfied with the corrective outcome. (This work is supported by National Natural Science Foundation of China No. 11421202, 11120101001 and 11202017)

References: [1] Yapp L.Z et al., J. The Foot, 22(2): 90-94, 2012.

Disclosure of Interest: None Declared

Rehabilitation

PO-0185

PATTERNS OF ACTIVATION OF THE CORE MUSCLES DURING DIFFERENT INTERMEDIATE EXERCISES FROM MAT PILATES IN HEALTHY INDIVIDUALS

Ivye L. Pereira [1,*]Bergson Queiroz [1]Isabel Sacco [1]

[1]Pysiotherapy, Speech Therapy and Occupational Therapy Department, Universidade de Sao Paulo, sao paulo, Brazil

Introduction and Objectives: The Pilates method is an exercises repertoire that aims to improve body awareness, control of movement and posture(1). In chronic low back pain treatment a range of therapeutic possibilities are considered as possible massage therapy, acupuncture, physical therapy (2), yoga (3), and Pilates (4). Pilates has been frequently prescribed for patients with low back pain, due to its central focus on the training of the lumbopelvic stabilizing muscles.The goal of this study is to describe and compare the core muscles electromyographic pattern during intermediate Mat Pilates exercises.

Methods: We performed an electromyography analysis assessing the multifidus, external oblique, internal oblique and rectus abdominis muscles during adapted intermediary exercises of the Pilates classical repertoire (Single leg stretch, Criss-cross and Dead bug). Nineteen healthy subjects (28.1 ± 8.2 years old; 64.5 ± 10.2 kg; 1.60 ± 0.91 m), performed each exercise 6 times. The EMG was acquired unilaterally on the right side of the body and the signal was synchronized with electrogoniometric data placed on the hip. The frequency of sampling was 2000Hz and the raw EMG signals were filtered with the digital band-pass filter Butterworth 4th order with frequency 10-500 Hz. For each movement cycle (lower limb flexion+extension) and for each muscle, the root mean square (RMS) was calculated, normalized by maximum voluntary isometric contraction(MVIC) of each individual and muscle. EMG linear envelopes normalized by the MVIC were calculated to obtain temporal pattern of activation during the exercise cycle. From the linear envelopes, we calculated the peak of activation of each muscle and the time of the peak activation in the exercise cycle.

Results: The magnitude of the muscle activity (RMS and peak activation) showed to be higher in the Criss-cross exercise, followed by the Single Leg Stretch and Dead bug, respectively. Thus, despite the exercises are classified as intermediary, they have different activation patterns.Criss-cross exercise can be suitable to strengthen the obliques muscles and rectus abdominis in healthy people, the Single Leg Stretch promoted gain of strength of the three muscles working during its performance and the Dead bug exercise would favour the stability ability of the rectus and obliques strengthening.The time of peak activation of the external oblique and rectus abdominis showed to be anticipated for the Dead bug and Single leg stretch, compared to the Criss-cross. This result reinforces that Dead bug exercise would be best for early stages of treatment and, as treatment progress, one can introduce the Single Leg Stretch and then Criss-cross in a more advanced stage.

Figure:

Caption: Sequential performance of Single let Stretch (A), Criss-Cross (B) and Dead Bug (C) exercises.

Conclusion: We conclude that the three Mat exercises presented different patterns of activation in terms of magnitude and timing of EMG peak, even with the same classification in the Pilates method, as intermediate exercises, and in terms of treatment progression, we may start with the least challenging exercises (Dead bug, Single leg stretch) and only then progress to more complex exercises that require greater lumbopelvic stabilization (Criss-cross). The Pilates method allowed the activation of the lumbopelvic stabilizing muscles even in a first session, and may therefore be indicated in cases of chronic nonspecific low back pain rehabilitation with proper progression.

Acknowledgements to CAPES for the finatial support

Table:

RMS	Single leg strech	Criss-cross	Dead bug	p
Rectus Abdominis	53,93±27,47	85,55± 21,79	85,55±21,79	<0,0001*
External Oblique	71,13±34,54	94,46±41,68	81,9 ± 41,97	<0,0001*
Internal Oblique	95,6±30,54	107,68±28,03	84,97±36,16	<0,0001*
Multifidus	19,8±13,4	23,99±15,54	21,77±17,02	0,075

Caption: Normalized Root Means Square (RMS) values and standard deviations (%MVIC) of healthy individuals in the exercises analyzed. P values *represents significant differences between exercises.

References: [1]Rydeard, R., Leger, A., Smith, D. Pilates-based therapeutic exercise: effect on subjects with nonspecific chronic low back pain and functional disability: a randomized controlled trial. J Orthop Sports Phys Ther. 2006; 36(7): 472-84.

[2]Rached, R.D.V.A., Rosa, C.D.P., Alfieri, F.M., Amaro, S.M.C., Nogueira, B., Dotta, L. Lombalgia inespecífica crônica: reabilitação. Rev Assoc Med Bras. 2013; 59(6): 536-53.

[3]Sorosky, S., Stilp, S., Akuthota, V. Yoga and pilates in the management of low back pain. Curr Rev Musculoskelet Med. 2008; 1(1): 39-47.

[4] La Touche, R., Escalante, K., Linares, M.T. Treating non-specific chronic low back pain through the Pilates Method. J Bodyw Mov Ther. 2008; 12(4): 364-70.

Disclosure of Interest: None Declared

SHAPE AND MOBILITY OF RIBCAGE IN CHILDREN WITH HEMIPLEGIC CEREBRAL PALSY

Raquel P. Carvalho [1,*]Ricardo Machado Leite Barros [2]Soraia Libório Cabó [1]

[1]Human Movement Science, Federal University of Sao Paulo, Santos, [2]Laboratory for Instrumentation for Biomechanics, Campinas State University, Campinas, Brazil

Introduction and Objectives: Cerebral palsy (CP) refers to a group of permanent disorders due to a non-progressive disturbance during the process of brain maturation[1]. Children with CP have predominant motor impairment, with different degrees of trunk control and level of functionality. The respiratory system is influenced by disturbances of tone, posture and movement[2]. CP children with severe impairment show lower tidal volume, forced vital capacity and diaphragm movement[3]. This lower respiratory capacity in severe CP is also related to ribs, vertebrae and sternum deformities, and muscle weakness[4]. There are few evidences about ribcage shape and mobility, and if ribs motion is influenced by CP in children with mild impairments like hemiparetic CP children. This knowledge will enable to verify changes on the normal patterns of trunk deformations during tidal capacity breathing in mild CP children. The purpose of this study was to analyze the shape and mobility of thoracic cage in children with mild CP during quiet breathing.

Methods: Eighteen children aged from 8 to14 years old participated of this cross-sectional study. Nine children with spastic hemiparetic CP (levels I and II of the Gross Motor Function Classification System) were included in the group of CP (CPG) and paired by age and gender with nine children with typical motor development who were included in the control group (CG). A three-dimensional kinematic analysis system (Dvideow) with six video cameras was used to describe spatial trajectories of 60 markers attached on anatomical landmarks[5]. The children remained seated on a chair without back support, with abduction of shoulders, knee flexion and feet on the ground. They were asked to avoid any movement while performing quiet breathing during 20 seconds. The linear distances between the markers on the lateral extremities of each right and left rib and between the markers on the thoracic vertebrae and on the sternum were calculated. The experimental variables obtained for the first to tenth ribs were anteroposterior (APD) and transverse diameters (TD). T-Student tests and boxplot analyzes were performed to compare CG and CPG and the lower and higher ribs for each group. This study was approved by the Federal University of São Paulo Ethics Research Committee (nº 275.276). The parents gave permission for the participation of infants in the study by signing a consent form.

Results: There were no significant differences among CG and CPG for mean of APD and TD from the first to tenth ribs, showing similar ribcage shape (table 1). CG and CPG showed higher APD than TD in first, second and third ribs and equal APD and TD in inferior thorax. For CG, the mean of APD increased from first to fifth rib and remained a plateau from sixth to tenth rib. The mean of APD of the first and second ribs were lower than sixth to tenth ribs. The mean of TD increased from first to sixth rib and remained a plateau from seventh to tenth rib. The TD of first, second and third ribs were lower than fifth to tenth ribs. For CPG, the mean of APD increased from the first to sixth rib and remained a plateau from seventh to tenth rib, similar to GC. The mean of APD of first rib was lower than third to tenth rib; the second rib was lower than fourth to tenth rib; and third rib was lower than sixth and seventh ribs. The mean of TD increased from the first to fifth rib and remained a plateau from sixth to tenth rib. The TD of first, second and third ribs were lower than fifth to

tenth ribs, similar to GC. Therefore, both groups showed lower mean of APD and TD in superior than inferior thorax. In relation to mobility, there was no difference among CG and CPG for APD. CPG showed lower absolute variation for fifth, eighth, ninth and tenth ribs for TD.

Conclusion: Children with mild hemiparetic CP showed similar ribcage and lower mobility in lower ribs when compared to typical developmental children. For future researches we suggest to analyze forced breathing to verify possible respiratory dysfunctions during active tasks.

Table:

Group	CG	CPG	CG	CPG
Ribs	**APD(SD)**	**APD(SD)**	**TD(SD)**	**TD(SD)**
1st	14,4(2,1)	14,3(3,6)	10,3(1,0)	11,3(0,7)
2nd	16,4(1,9)	16,3(3,5)	12,7(1,5)	13,1(1,8)
3nd	17,7(2,0)	17,6(3,5)	14,7(1,7)	14,7(2,3)
4nd	18,9(2,0)	18,6(3,6)	16,8(2,0)	16,7(2,7)
5nd	19,8(2,1)	19,5(3,5)	24,0(4,1)	23,3(3,2)
6nd	20,6(2,2)	20,3(3,5)	23,8(3,6)	23,1(2,9)
7nd	20,7(2,2)	20,2(3,7)	23,7(3,4)	22,9(2,7)
8nd	20,8(2,2)	20,1(3,9)	23,5(3,3)	22,7(2,6)
9nd	20,9(2,2)	20,0(4,1)	23,5(3,3)	22,5(2,6)
10nd	21,0(2,2)	20,1(4,3)	23,3(3,3)	22,4(2,6)
Mean (SD)	19,1(2,2)	18,7(2,1)	19,6(5,4)	19,2(4,7)

Caption: Table 1: Mean and standard deviation (SD) for anteroposterior (APD) and transverse diameters (TD) in control (CG) and cerebral palsy group (CPG) during quiet breathing

References: [1]Rosenbaum et al., Dev Med Child Neurol, 109:8-14,2007.

[2]Frownfelter(ed)Chest Physical Therapy and Pulmonary Rehabilitation, 1987.

[3]Ersoz et al., Turk J Pediatr, 48:344-50,2006.

[4] Massery, Pediatr Phys Ther, 3:3-8,1991.

[5]Sarro et al., J Appl Biomech,25:247-52,2009.

Disclosure of Interest: None Declared

Soft Tissue

PO-0187

A METHOD FOR QUANTIFYING HEEL PAD VISCO-ELASTIC REACTION MODEL PARAMETERS

Roozbeh Naemi [1,*]Panagiotis Chatzistergos [1]Nachiappan Chockalingam [1]

[1]Centre for Sport Health and Exercise Research, Faculty of Health Sciences, Staffordshire University, Stoke on Trent , United Kingdom

Introduction and Objectives: Heel pad represents a shock attenuating interface underneath the calcaneus with a structure of fatty tissue separated by septa (1).This gives the heel pad a unique capacity to attenuate the impact during heel strike(2,3).As the mechanical properties of this interface affect the loading on the entire body(4), the mathematical models that describe force-deformation relationship of the heel pad are used to determine loading on the musculo-skeletal system. While some models only considered the stiffness of the heel pad(5,6)a number of models considered both elasticity and viscosity(7,8,9)to reflect the visco-elastic behaviour of the heel pad. From these models, non-linear visco-elastic model proposed by Scott and Winter(10)proved to adequately represent the plantar fat pad reaction force-deformation relationship(7).Despite this there has been no set method for quantifying the subject-specific model parameters. The objective of this study was to develop a method of quantifying the nonlinear visco-elastic behaviour of the heel pad under load.

Methods: A customised ultrasound indentation device comprising a18 MHz Esaote linear array ultrasound probe connected in series with a 3kN INSTRON load cell was used to extract force deformation data during a compression loading cycle.During loading the instrumented probe was pressed against the plantar aspect of the heel through which the heel pad was compressed between the probe and the calcaneus.

The synchronised force-deformation data was collected at 28 Hz over 10 load/unload cycles at constant target deformation rate of 1.25 mm/s with the actual deformation rate was 0.96 mm/sec ± 0.14 mm/sec. The target stress was 150 kPa, and the first seven load cycles were used for pre-conditioning and the last three were recorded for assessment. The stress-strain data was deducted by normalising the force deformation data to contact area (3.8 cm2 as the probe footprint-area) and the initial heel pad thickness. 9th order Polynomials were fitted to the 3 stress-strain curves during loading and unloading separately. These two loading and unloading polynomials were used to reconstruct the stress during loading and unloading for strains from 0 up to 0.5 strain with 0.01 increment.

In a visco-elastic model that consists of a nonlinear spring parallel to a nonlinear damper (15) during loading the spring and damper both resist deformation (Equation 1).

$\sigma l = a.\varepsilon b + c.\varepsilon d.\dot{\varepsilon}$. Equation 1

While during unloading the spring works in favour of and damper resists rebound (Equation 2), the parametric elastic and viscous stress components were deducted.

$\sigma u = a.\varepsilon b - c.\varepsilon d.\dot{\varepsilon}$. Equation 2

The elastic component can be deducted by adding the two sides of equations 1 and 2 as follows:

$(\sigma l + \sigma u)/2 = a.\varepsilon b$ Equation 3

By fitting a power function to the average of stress during loading and unloading parameters a and b were calculated.

The viscous component can be deducted by subtracting the two sides of equations 1 and 2 as follows:

$(\sigma l - \sigma u)/(2. \ \varepsilon.)= c.\varepsilon d$ Equation 4

By fitting a power function to the difference in stress during loading and unloading over twice strain rate parameters c and d were calculated.

Curve fitting was performed using a bisquare method that minimises the summed square of the residuals and downweight outliers (Matlab, Mathworks, 2010). The fit goodness statistics were calculated using R-square and RMSE.

Results: The strain rate was calculated as 0.051 s^{-1} , the elastic scaling factor (*a*) was 1.719 MPa and the elastic exponent (*b*) was 3.801 . The elasticity power function provided a good fit to the elastic stress-strain data with R^2=0.985, RMSE = 2569Pa.The viscous scaling factor (*c*) viscous exponent (*d*) were found as 4.117 MPa.s and 2.477 . The viscosity power function provided a good fit to the elastic stress-strain data with R^2 = 0.9866 and RMSE = 934 Pa .

Figure:
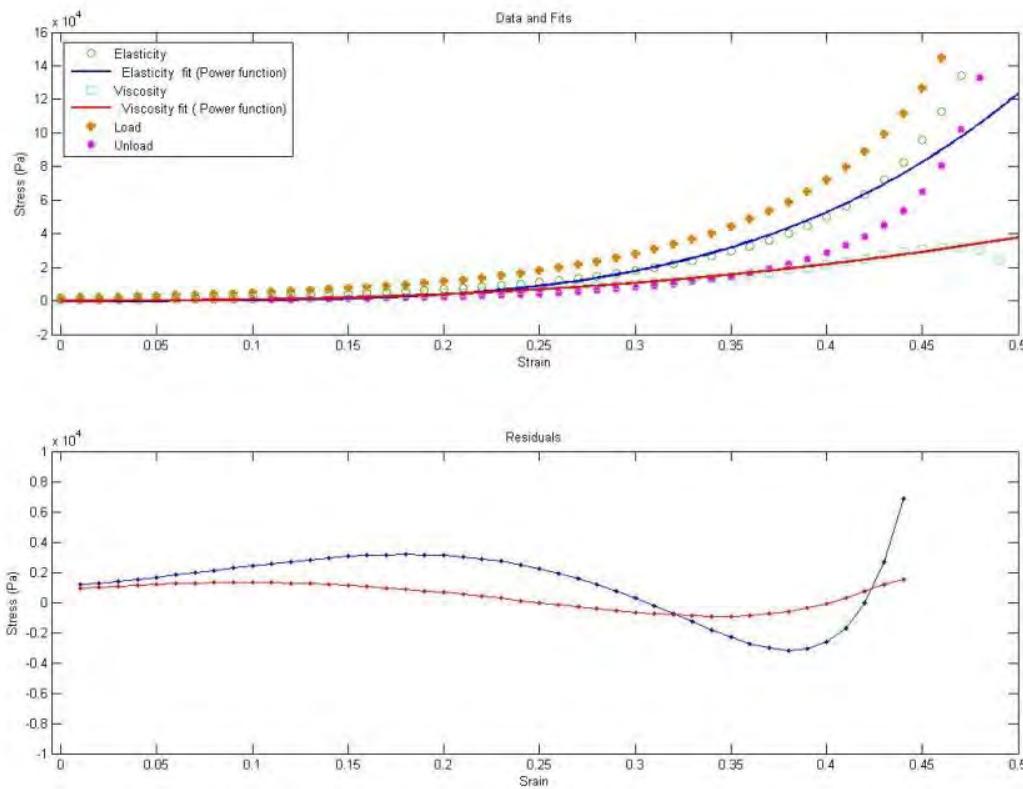
Caption: Top: Loading and unloading data together with the elasticity and viscosity components and the corresponding power function fits.

Conclusion: The proposed method allowed differentiating between the elastic and viscous components of the heel pad response to loading. The curves that represent the elasticity and viscosity functions provided a good fit to the elastic and viscous stress components which indicate that the model can adequately reflect the corresponding stress-strain of the plantar soft tissue during loading and unloading. This method has potential implications in quantifying the mechanical behaviour of the heel pad and can provide a detailed understanding of plantar soft tissue behaviour under load.

References: [1] Jahss et al., Foot Ankle 13:233–42, 1992

[2] Bennett and Ker RF. J Anat 171:131–8, 1990

[3] Whittle. Gait Posture 10:264–75. 1999

[4] Jørgensen, Bojsen-Møller. Foot Ankle 9:294–9, 1989

[5] Challis et al. J Appl Biomech 24:377–81, 2008

[6] Chao et al., Clin Biomech 25:594–600, 2010

[7] Cole et al., Clin Biomech 11:181–193, 1996

[8] Gilchrist, Winter. J Biomech 29:795–8, 1996

[9] Gerritsen et al., J Biomech 28:661–8, 1995

[10] Scott, Winter, J Biomech 26:1091–1104, 1993

Disclosure of Interest: None Declared

PO-0188

RELATIVE EXCURSION OF FLEXOR DIGITORUM SUPERFICIALIS AND PROFUNDUS TENDONS DURING TENDON GLIDING EXERCISE AND FIST

Hsiao-Feng Chieh [1,*] Chien-Ju Lin [2] Li-Chieh Kuo [3] Shu-Chi Liu [1] I-Ming Jou [4] Fong-Chin Su [1 2 5]

[1]Department of Biomedical Engineering, [2]Musculoskeletal Research Center, [3]Department of Occupational Therapy, [4]Department of Orthopedics, [5]Medical Device Innovation Center, National Cheng Kung University, Tainan City, Taiwan, Republic of China

Introduction and Objectives: Adhesion formation following surgery is demonstrated to reduce the normal gliding function of tendons and nerves, causing nerve compression and impairing motion. Recently, adhesion prevention has been paid more attention and indicated as the need for early post-operative mobilization of digits after tendon injury or repair. Several strategies including physical, surgical, and pharmacological treatments have been explored in order to reduce peritendinous adhesion and achieve a better gliding function of the digital tendons [1]. It is generally accepted that tendon excursion could avoid adhesion; however, current knowledge of the rehabilitation protocol is mostly focused on the total tendon excursion [2]. Therefore, the purpose of the current study was to evaluate rehabilitation protocols, tendon gliding exercise and full fist motion, on the total tendon excursion and the relative motion between flexor digitorum superficialis (FDS) and flexor digitorum profundus (FDP) using high-resolution ultrasound images.

Methods: Ten healthy subjects (5 male, 5 female) with a mean age of 25.2 ± 3.3 years were recruited in this study. Each participant was asked to sit beside the custom forearm clamp, and then eleven reflective markers with a diameter of 2 mm were set on the dorsal surface of the middle digit. The motion of flexor tendon gliding exercises is to posture hand sequentially with straight, duck, straight fist, full fist, and hook. Fist motion is from straight to full fist and then from full fist to straight. The Images of tendon movement and finger motion were acquired by an ultrasound scanner (S2000, SIEMENS) and motion capture system (Motion Analysis Corporation), respectively. Manual tracking was used to measure the excursion of the FDS and FDP tendons. All tests repeated 3 times for both FDS and FDP tendons.

The tendon excursions during motion were measured and correlated with the corresponding finger joint angles. In order to identify the characteristic pattern during different motion, the process of tendon gliding exercise was divided into five phases, straight-duck (Phase I), duck-straight fist (Phase II), straight fist-full fist (Phase III), full fist-hook (Phase IV), and hook-straight (Phase V). Meanwhile, the process of active fist motion was divided into five phases according to the corresponding total joint angle in the tendon gliding exercise. Tendon excursions of FDP and FDS were measured and the normalized relative tendon excursion between FDP and FDS were calculated during the whole movement and individual phases. The calculation of normalized relative tendon excursion (R_d) is shown as follows,

$R_d = [(E_{FDP} - E_{FDS})/\text{Hand Length}] \times 100\%$

where E_{FDP} and E_{FDS} are the excursions of FDP and FDS, respectively.

The maximum tendon excursion and the normalized relative tendon excursion for both motions were compared using a paired t-test (SPSS 17, SPSS Inc., Chicago, IL). $p \leq 0.05$ were considered statistically significant.

Results: Results showed that the total tendon excursion of FDP and FDS during fist were 40.23±5.29 and 24.69±2.83 mm, respectively. During modified exercise, the total tendon excursion of FDP and FDS tendons were 40.04±6.11 and 23.64±2.74 mm, respectively. Our statistical analysis indicated that the maximum FPS excursion, maximum FDP excursion, and the maximum relative excursion of FDP and FDS between two motions showed no significant difference. In this study, the gliding process of tendons was analyzed to distinguish the relative motion of tendons. Results showed the greater normalized relative motions between FDP and FDS during phase I, Phase III, and Phase V during the modified exercise than that during pure fist motion (Figure 1). Furthermore, the greater difference between two continuous phases during the modified exercise demonstrated the greater relative motion between tendons and showed a higher potential for adhesion prevention.

Figure:
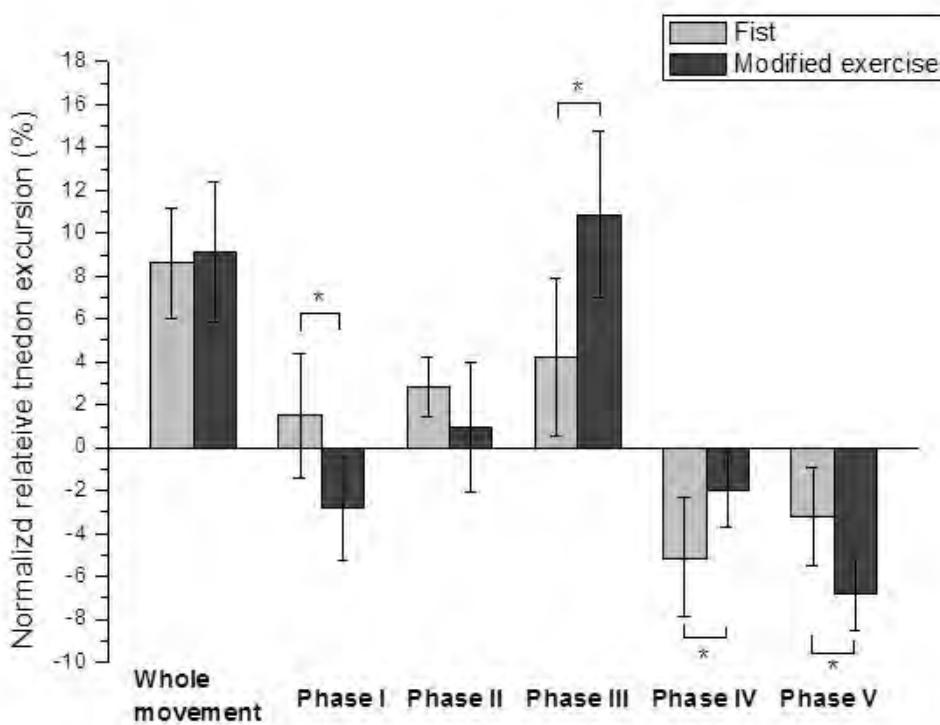
Caption: Normalized relative tendon excursions between tendons during whole movements and individual phases.

Conclusion: Our findings demonstrated that the modified tendon gliding exercise could achieve a better solution of adhesion prevention than pure fist motion. These data suggested that in addition to the total tendon excursion, the relative tendon motion during the process should be taken into account while evaluating the efficacy of rehabilitation protocols.

References: [1] Gelberman, R. H. et al., Hand Clinics, 1(1): 35-42, 1985.

[2] Korstanje, J. W., et al., J Hand Surg Am, 35(4): 559-65, 2010.

Disclosure of Interest: None Declared

PO-0189

GROWING LOW COST BACTERIAL CELLULOSE – THE LUMPS MATTER

Nicola Everitt [1] Christopher Mariani [1] Donal McNally [1,*]

[1]Faculty of Engineering, University of Nottingham, Nottingham, United Kingdom

Introduction and Objectives: Bacterial cellulose has been the subject of a great deal of research since 1989, when the first research was published on a pellicle from Acetobacter Aceti [1]. The high mechanical properties observed on sheets of cellulose prepared by the bacteria has attracted the attention of a variety of different research fields including its use as an artificial medical tissue such as scaffolding for the tissue engineering of cartilage[2].

The objective of this study was to produce cellulose sheets using a low cost water bath culture and air dry method, mechanically characterise them and relate the behaviour to the observed microstructure.

Methods: Gluconacetobacter xylinum ATCC®700178 was initially provided by Dr. Stuart Thompson at the University of Westminster. 100 ml of fresh culture medium was inoculated with 1ml of seed bacteria. The bacteria were statically cultured in a water bath at 27°C, without any disruption. After 9 to 12 days the pellicles were harvested from the culture, washed with distilled water and then were stored under refrigeration, floating in distilled water. Harvested pellicles had a diameter of 75 mm and a thickness of approximately 0.5 mm. Test samples were produced by cutting into strips 5 mm wide and 30 mm long. The samples were air dried for 48 hrs between filter papers, with a steel mesh and then a mass on top (applying a pressure of ~5 MPa).

Tensile testing was conducted using a Deben Microtest 200 machine with a 200 N load cell. The tests were conducted at an extension rate of 0.2 mm/min.

Results: 7 of the 12 (58%) cultures carried out produced pellicles, of which 5 produced a useable pellicle, giving an overall success rate of 42%. Reasons for a pellicle not being produced included culture infection and bacterial mutation.

Analysis of scanning electron microscopy (SEM) images showed the pellicles were comprised of randomly distributed cellulose microfibrils (Fig 1), as expected from previous studies. Using Environmental SEM the fibril diameter was measured at between 90 - 110nm. This agrees with previously published data measuring the diameter of fibrils to be less than 130nm [1].

Figure 1 (a and b), shows large scale crystal formation formed throughout the sample. Figure 1(d) shows the size of the crystal in comparison to the cellulose sheet clearly. The crystal measured 36 µm compared to the sheet thickness of 5.7 µm. The crystal formation causes significant disruption to the fibril network. The crystals have grown from within layers of fibrils and forced the fibrils away from the main plane. Broken fibrils can also be seen. The corners of the crystals will also act as stress concentration sites across the sheet, further reducing the tensile stress the sheet can withstand as well as the fibrils mobility in the structure. More vigorous washing saw a reduction in crystal formation during the air drying, with a much smoother and flatter sheet produced Fig 1(e and f). Figure 1(f) shows how the crystals were forming from within the sheet and not on the surface. The crystals were still present but were much smaller, at approximately 5 um, and no longer breaking the surface of the sheet and breaking fibrils.

The stress strain curves for the bacterial cellulose were what would be expected from their structure. Namely a region of relatively low stiffness as the fibrils move over one another and align to the stress, followed by a stiffer region as the fibrils are loaded to failure. The mechanical properties of the samples from pellicles A and B are presented in Table 1. The strength and stiffness of the two pellicles are significantly different (p>0.95), demonstrating that the crystals in the structure cause significant deterioration in the mechanical properties.

Figure:
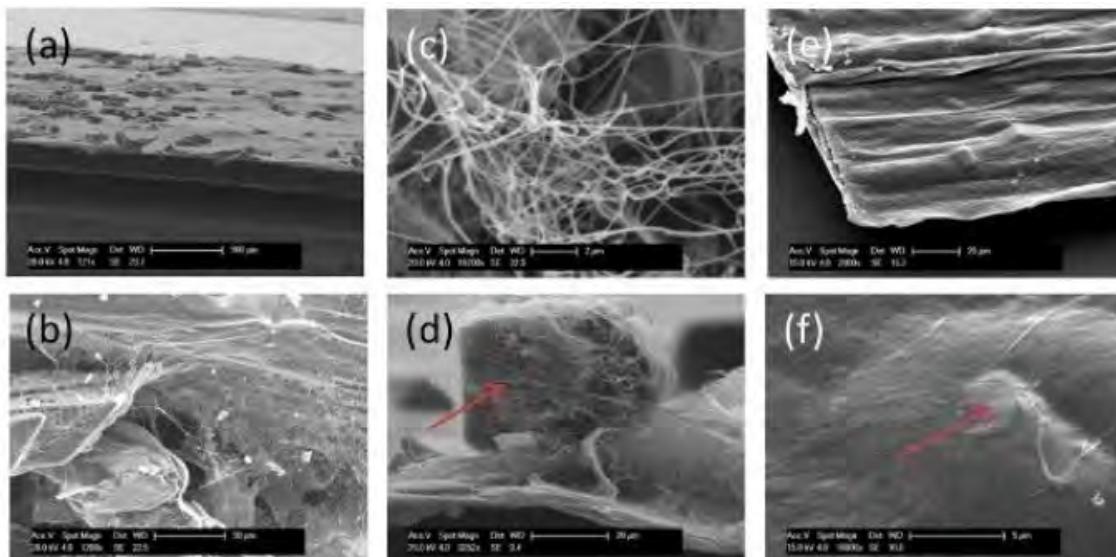
Caption: Figure 1 – Scanning electron micrographs of dried cellulose sheets. Pellicle A (a-d). (a) crystal formation on the surface, (b) crystal disruption of the fibril network, (c) amorphous fibril network, (d) crystal size in relation to cellulose sheet thickness. Pellicle B (e-f). (e) sheet, (f) crystal within the structure. Red arrows indicate crystals.

Conclusion: The water bath culturing method selected for the project was driven by cost and availability. The water bath method provided a low initial cost route to culturing the bacteria but infection is higher than incubator culture. The mechanical properties, whilst lower than other methods of production, are appropriate to musculoskeletal soft tissue. Crystal formation in the cellulose structure has proven to be extremely damaging to the mechanical properties.

Table:

Pellicle	Ultimate tensile strength (MPa)	Strain to failure (%)	Young's modulus (GPa)
A	12.4	0.43	2.96
B	68.8	1.27	6.26

Caption: Table 1: Mechanical properties of pellicles A and B

References: [1] Yamanaka, S et al., J. Mater. Sci. 24: 3141-3145, 1989

[2] Svensson, A et al., Biomaterials, 26: 419-431, 2005

Disclosure of Interest: None Declared

Soft Tissue

PO-0190

BIOMECHANICAL PROPERTIES OF RAT CERVIX IN THE LAST TRIMESTER OF PREGNANCY

Alireza Ashofteh Yazdi [1,*] Ali Esteki [2] Mohammad Mehdi Dehghan [3] Farhad Tabatabai Ghomsheh [4]

[1]Department of Biomechanics, Science and Research Branch, Islamic Azad University, Tehran, Iran, [2]Department of Biomedical Engineering, Shahid Beheshti University of Medical Sciences, Tehran, Iran, [3]Department of Veterinary Surgery, University of Tehran, Tehran, Iran, [4]Department of Ergonomics, University of Social Welfare and Rehabilitation Sciences, Tehran, Iran, Islamic Republic Of

Introduction and Objectives: Cervical Insufficiency refers to a condition in which the cervix dilates in the absence of contractions from the uterine smooth muscles and results in a spontaneous pregnancy loss between the second and third trimester of pregnancy [1]. Quantitative measurements of its mechanical properties may lead to a more accurate description of cervical remodeling and prediction of preterm birth [2]. The results of this research provides an insight to the stiffness of the pregnant cervix and allows us to investigate the mechanical changes that lead to a premature delivery in the beginning of the last trimester of pregnancy.

Methods: Cervices were harvested from Wistar rats early in the last trimester of pregnancy (15-17 days). The distal halves were taken immediately to the laboratory for mechanical testing. Samples were subjected to a series of tensile, cyclic and relaxation tests to measure both linear and nonlinear mechanical properties of the pregnant tissues. Strain controlled tensile loadings were implemented to the samples in the circumferential direction. In the tensile test, tissue was stretched at the rate of 0.01 mm/sec to the rupture point. In cyclic test, tissue underwent 10 cycles of loading and unloading at the rate of 1 mm/sec up to 60% strain. The relaxation test was fulfilled at the rate of 0.01 mm/sec up to 60% strain and was held for 10 minutes untill the tissue relaxed. Stress and strain were measured as functions of time and curve fitting tool in Matlab was used to model the results.

Results: Tensile linear results revealed a Young's modulus of 0.014 MPa, as well as an ultimate stress and strain of 0.3 MPa and 79.9%, respectively. Failure stress and strain was measured as 0.085 MPa and 190.1%. Cyclic and Relaxation tests indicated a nonlinear, time-dependent behavior of tissue with a large range of plastic deformation in the last trimester of pregnancy.

Conclusion: According to previous studies [2, 3], Cervix becomes more compliant as compared to the former two trimesters and virgin ones. This is related to the nonlinear viscoelastic behavior of the pregnant tissue which is due to its compositional and microstructural changes in the last trimester of pregnancy.

References: [1] Anastassia P. Paskaleva, Biomechanics of cervical function in pregnancy-case of cervical insufficiency, Doctoral Dissertation, Massachusetts Institute of Technology, 2007.

[2] M. J. Poellmann, E. K. Chien, B. L. McFarlin, A. J. Wagoner Johnson, Mechanical and structural changes of the rat cervix in late-stage pregnancy, Journal of the Mechanical Behavior of Biomedical Materials, vol.17, 2013, pp.66-75.

[3] W. R. Barone, A. J. Feola, P. A. Moalli, S. D. Abramowitch, The effect of pregnancy and postpartum recovery on the viscoelastic behavior of the rat cervix, Journal of Mechanics in Medicine and Biology, Vol. 12, No. 1, 2012, 1250009 (17 pages).

MECHANICAL STRAIN REQUIREMENT FOR SUCCESSFUL DECELLULARISATION OF PORCINE BLADDER

Ashley Ward [1,*] Jen Edwards [1] John Fisher [2] Jenny Southgate [3] Helen Berry [4] Eileen Ingham [1]

[1]School of Biomedical Sciences, [2]Institute of Medical and Biological Engineering, University of Leeds, Leeds, [3]Department of Biology, University of York, [4]Tissue Regenix, York, United Kingdom

Introduction and Objectives: Current surgical bladder augmentation procedures have limitations [1]. A decellularised xenogeneic bladder biomaterial may have utility as an augmentation device. Previously, a process was developed for porcine bladders that required bladders to be distended to achieve successful decellularisation [2]. This process was found to be incompatible with scalable manufacturing processes. This project aims to develop a new process for the decellularisation of porcine bladder which avoids distending intact bladders, for translation to commercial manufacture.

Methods: Two porcine bladders were decellularised using low concentration SDS and proteinase inhibitors as described previously [2]. Throughout the process each bladder was distended with 500 ml of solution. Bladder filling experiments were carried out on fresh bladders in order to find a relationship between required bladder fill volumes and initial bladder dimensions. Bladder decellularisation was repeated using these fill volumes, rather than the 500 ml volume specified by the original process. In order to determine the state of deformation in the bladder walls when bladders were successfully decellularised, bladders (n = 12) were immersed in and distended with PBS at the required volumes. Volume, pressure, strain and stress were measured and calculated throughout the distension process.

Results: One of the bladders decellularised using the original process, which was considerably larger than usual, was not fully decellularised. The filling experiments then established a relationship between the initial dimensions of bladders and their fill volumes. Bladders decellularised using these revised fill volumes were successfully decellularised, and all were filled with volumes larger than 500 ml during the process. When bladders were immersed and distended, the strains in the bladder walls at the calculated fill volumes were found to be 1.97 ± 0.11 and 1.39 ± 0.06 [Figure 1] in the transverse and apex-to-base directions respectively (mean ± standard error of the mean). The pressures and stresses in bladders at the fill volumes were highly variable.

Figure:
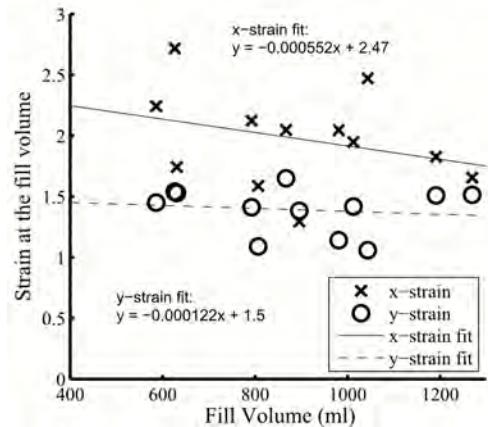
Caption: The wall strain of bladders filled to their fill volumes. Strain at the fill volume does not vary substantially with fill volume.

Conclusion: Bladders decellularised using the modified fill volumes were acellular. The strains found in distended bladders that resulted in successful decellularisation will now be applied to flat sheets of porcine bladder tissue as part of a decellularisation manufacturing process.

References: [1] Biers, S. M. et al., BJU Int., 109: 1280-1293, 2012.
[2] Bolland, F. et al., Biomaterials, 28: 1061-1070, 2007.

Disclosure of Interest: A. Ward Conflict with: Tissue Regenix Group Plc, J. Edwards: None Declared, J. Fisher Conflict with: Tissue Regenix Group Plc, J. Southgate: None Declared, H. Berry Conflict with: Tissue Regenix Group Plc, E. Ingham Conflict with: Tissue Regenix Group Plc, Conflict with: Tissue Regenix Group Plc

Surgical Techniques

PO-0192

COMPARISON OF NAVIGATED TOTAL KNEE REPLACEMENT INTRA-OPERATIVE COMPUTER GENERATED DATA WITH ACTUAL PATIENT ANATOMY

C Govind [1,*] A H Deakin [1] [2] P E Riches [1] F Picard [1] [2]

[1]Faculty of Biomedical Engineering, University of Strathclyde, Glasgow, [2]Department of Orthopaedics, Golden Jubilee National Hospital, Clydebank, United Kingdom

Introduction and Objectives: Failure to correct lower limb alignment in total knee replacement (TKR) is known to increase the risk of implant failure [1]. The use of computer navigation systems in TKR is reported to reduce the number of outliers for coronal lower limb alignment [2]. These navigation techniques determine hip, knee, and ankle centres and then establish the mechanical axes between them and provide this information to the surgeon. Based on this virtual lower limb model the position and orientation of resections can then be calculated. For these computer models to be accurate the patient anatomy must be properly defined. This project aimed to compare the location of anatomical and kinematic points as calculated by navigation software to anatomical points in a CT scan.

Methods: This retrospective study was approved by an NHS Research Ethics Committee and all patients consented to the use of their data. Data from 21 navigated TKRs (OrthoPilot, Aesculap, Tuttlingen, Germany) were included in the study. For each patient, data on the anatomical and kinematic points were collected from the computer navigation file. Post-operative lower limb CT images were analysed using Mimics (Materialise, Leuven, Belgium) to give the anatomical coordinates of lower limb landmarks and joint centres from the navigation data. The landmarks found in both datasets were the medial and lateral malleolus, the medial and lateral epicondyles, the distal medial and lateral condyles and the hip joint centre. From this information the relative ankle and knee widths and the femoral and tibial lengths were calculated. To determine the relationship between the kinematic and anatomical knee centre, an anatomical knee centre midway between the distal condyles as described by Moreland et al. [3] was used as. A local coordinate system was created from CT and navigation data to enable comparisons. Basic patient demographics were collected. The post- and intra-operative mechanical femorotibial (MFT) angles from both systems were provided as a result of a previous study. Comparisons between the navigation and CT measurements for widths, length and knee centre were made by using two-tailed paired T tests to see which differences were significant. To investigate the influence of patient demographics (BMI and age) on these findings, regression analysis was used.

Results: The kinematic knee centre was on average 34.1 ± 7mm away from the anatomical centre. The major component being along the longitudinal axis of the leg meaning that the kinematic knee centre was on average 33.8 ± 7mm proximal to the anatomical. The relative error corresponded to a $12 \pm 2\%$ difference when normalised with respect to CT leg length. No significant changes were present between the ankle widths, knee widths, tibial length and alignment angles. Only the femoral length in both data sets showed any significant difference (p=0.03) with the navigation data giving a shorter femur. Overall, there was no statistically significant difference between MFT angle values in the CT and the navigation data (p=0.182).The effects of age and BMI had no effect on outcome measures.

Conclusion: To the authors' knowledge this is the first time anatomic and kinematic knee centre data have been compared in osteoarthritic patients.The difference in knee centre position is likely to be a result of the differing definitions of the anatomical knee centre. As the differences in knee centre position along the longitudinal axis were found to be significant, it is likely that this would have a further effect on the femoral length. The consistent difference (12± 2%) between the anatomical and kinematic knee centres facilitates the prediction of the kinematic centre from CT data. The limitations of this study include the small number of subjects, a lack of a pre-operative CT scan which would have allowed more points to be compared and also a lack of known points (fiducials) in the navigation data and CT scans that would have allowed direct comparison of location. We conclude that the navigation system was able to create an appropriate lower limb model. The kinematic knee centre relates well to the anatomical centre in the transverse and sagittal planes although there is a large difference in the coronal plane. Further work would be to assess a larger sample of patients with pre-operative CT scans.

References: [1] SCUDERI, GR. & TRIA., AJ. 2006. Knee Arthroplasty Handbook- Techniques in Total Knee and Revision Arthroplasty. Springer, New York.

[2] JENNY, J. Y. & BOERI, C. 2001. Computer-assisted implantation of total knee prostheses: a case-control comparative study with classical instrumentation. Comput Aided Surg, 6, 217-20.

[3] MORLAND JR, BASSETT LW, HANKER GJ (1987) Radiographic analysis of the axial alignment of the lower extremity, J Bone Joint Surg Am;69-A:745-749

Disclosure of Interest: C. Govind: None Declared, A. H. Deakin Conflict with: BBraun Aesculap, P. E. Riches Conflict with: BBraun Aesculap, F. Picard Conflict with: BBraun Aesculap, Conflict with: BBraun Aesculap

Surgical Techniques

PO-0193

THERMAL DAMAGE DONE TO BONE BY BURRING AND SAWING WITH AND WITHOUT IRRIGATION IN KNEE JOINT REPLACEMENT

G Tawy [1,*]P Rowe [1]P Riches [1]

[1]University of Strathclyde, Glasgow, United Kingdom

Introduction and Objectives: Orthopaedic tools which resect bone in procedures such as total knee replacement (TKR) generate heat, causing a temperature rise at the resected surface[1]. When bone temperature exceeds 47°C for >60 seconds irreversible changes known as osteonecrosis develop[2]. Osteonecrosis has been found to increase rates of aseptic implant loosening and implant failure by causing cell death at the cut surface, thus reducing the likelihood of bone-implant incorporation[2]. With computer assisted surgery becoming more common in orthopaedics, burrs are being increasingly used. This study aimed to compare the traditional oscillating saw to the burr (NavioPFS, Blue Belt Technologies Inc.) in terms of temperature generation, and thermal damage done to bone health. The effectiveness of irrigating bone to reduce bone temperature was also investigated.

Methods: Bovine femora (n=17) were burred and sawed with or without irrigation, and bone temperatures were recorded with a visual infrared thermometer. Two cooling agents were used; one at room temperature, and a second at 4°C. After cutting, samples were removed for histomorphometric analyses. Percentages of non-viable osteocytes at the cut surface were calculated, and minimum depths of thermal damage done by both cutting tools were estimated. Statistical analyses were carried out to test differences between groups (α = 0.05).

Results: We found some evidence that burring produced temperatures of >47°C for >60 seconds more often than sawing. The mean and maximum temperatures also tended to be higher when burring. However, there were no statistical differences between the temperatures generated when sawing and burring (p > 0.05). Irrigated bone had lower temperatures, higher percentages of viable osteocytes, and smaller thermal damage depths (p < 0.05). Uncooled saline was successful at reducing mean temperatures <47°C in sawed bone, however cooled saline was needed when burring (p < 0.05).

Conclusion: Temperatures recorded in this study whilst burring and sawing reflected those quoted in similar studies. Despite this, it was not possible to fully reproduce the surgical scenario in the laboratory as no blood supply was present. For this reason the results should be treated with caution when considering resecting bone in theatre. It is believed that uncooled saline was able to lower the temperature of sawed bone to <47° as the irrigation was directly applied to the bone. This was not the case when burring, as the tubing which conveyed the fluids to the cutting site was attached to the drill, which becomes heated with use. This could have increased the temperature of the saline solution, thereby affecting the results, and requiring cooled saline to be used. As expected, lowering the temperature at the cutting site reduced the extent of histological damage done to the bone. Despite these positive results, further research needs to be carried out to determine whether these results are replicated in theatre.

Conclusion: The results suggest that thermal damage is done to bone tissue during surgery, and could be reduced with the use of irrigation (especially cooled saline). This may be most beneficial in procedures which involve implanting

cementless prosthetic parts, where the only heat source comes from the cutting tools. By reducing the level of osteonecrosis, rates of implant loosening and failure could be lowered.

References: [1] Toksvig-Larson et al., J. Bone Joint Surg., 73-B: 13-15, 1991.

[2] Birkenfeld et al., Ann Anat., 192: 227-231, 2010.

[3] Lee et al., Med Eng Phys., 33: 1234-1244, 2011.

Disclosure of Interest: G. Tawy Conflict with: Blue Belt Technologies Inc., P. Rowe Conflict with: Blue Belt Technologies Inc., P. Riches Conflict with: Blue Belt Technologies Inc.

Trauma

PO-0194

EFFECTS OF ANTENATAL EXERCISE WITH OR WITHOUT BALL ON BACK PAIN AND PERINEUM STATE

LAWANI Mansourou [1,*]DUMAS Geneviève [2]HOUETO Gratien [3]

[1]INJEPS, UAC, PORTO-NOVO, Benin, [2]Mechanical and Materials Engineeringi, Queen's University, Kingston, Canada, [3]Laboratoire de Biomécanique et Performance, INJEPS, PORTO-NOVO, Benin

Introduction and Objectives: Pregnancy is an important period of postural changes in women. Indeed, the spine is subjected to severe physical stresses that alter the normal biomechanics of the body. Several offsets occur due to the change in the body mass and its distribution among pregnant woman. These changes create imbalances in the muscles and ligaments of the back, pelvis and lower limb and changes in the posture of the woman. The prevalence of low back pain during pregnancy varies between 40% and 90%, with an incidence of back pain by 61% [1-3]. This prevalence is 56% among pregnant women in Benin. [4]

During pregnancy, women are looking for natural approaches, different treatments those offered by conventional medicine and remedies that can relieve their back pain [5]. This is what justifies this comparative study of the effects of exercise programs with or without gym ball on back pain and childbirth.

Methods: This study is transversal, analytic and comparative, conducted in 69 pregnant women with back pain who have voluntarily agreed to participate regularly in the execution of training programs. The experiment was conducted over a period of 5 months (February-June 2014). Women were randomly assigned to one of the three groups: 1) no training, 2) training without exercise ball, 3) training with exercise ball?

Ethical considerations : All participants signed an informed consent form. The study was approved by scientific committee of sectorial Sciences and Technics of Physical Activities and Sport of Abomey-Calavi University.

Data analysis : Data were collected before and after the implementation of the different programs, postpartum and recorded on the cards for data collection. These data were then processed with Microsoft Office Excel 2007 software and STATISTICA version 5.5 Stat Soft Inc. For each variable, the mean and standard deviation are calculated. The ANOVA test allowed us to globally compare continuous variables. When the probability is less than 0.05, the final statistical decision is taken on the basis of binary tests. The significance level was set at $p < 0.05$.

Results: The analysis of the results reveals that the lumbar region (69.56 %) is the area most exposed among pregnant women suffering from back pain while the other parts of the body are pelvis (18.84 %), groin (8.69 %) and leg (2.89 %). Significant reduction (50.79 %) of the intensity of pain was noticed among women trained in gymnastics with ball, compared to the other two groups.

Table I show that the majority of women who participated in the study were involved in domestic activities such as sweeping, washing clothes, washing dishes, fetching water and cooking. They cook mostly in sitting position (84.05%), draw water standing (92.85%) and 80.59% of women sweep in bent position. Figure 1 shows that the largest number of intact perineum (20 women on a sample of 23 women or 86.95%) was observed in the group of women trained in prenatal gymnastics with ball against 30.43% for women untrained and 73.91% for women trained in prenatal gymnastics without the ball. Women in the training programs experienced a significant reduction in back pain. These results corroborate

several studies regarding the effect of gymnastic exercise on back pain [6,7]. The ball exercises help prepare the deep muscles, support the lower back and spine so as to have better posture and less subjects with back pain [8]. Regarding the state of the perineum our results corroborate those of Delgado et al. [9].

Figure:
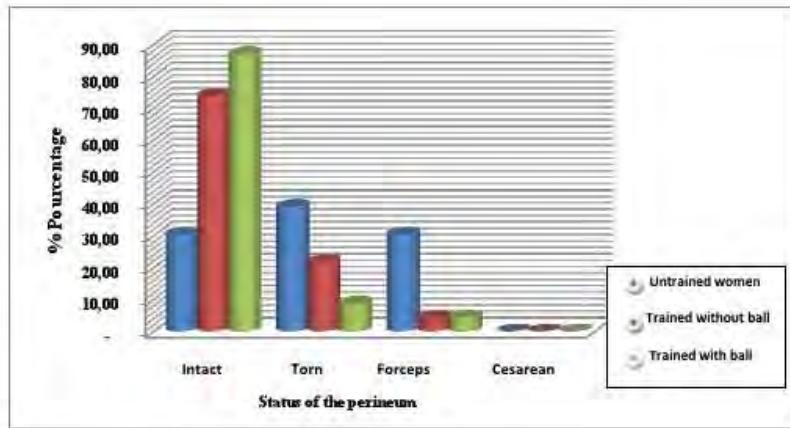
Figure 1 : Status of the perineum after childbirth

Conclusion: Pain decreased significantly in women in the training programs with better advantage among women trained in prenatal gymnastics with ball compared to those trained without the ball. Antenatal gymnastics with ball is an effective way to treat back pain and promotes an uncomplicated delivery.

Table I: Distribution of Women according postures during housework

			Postures					
			Sitting		Bent		Standing	
	E	%	E	%	E	%	E	%
Housework Sweeping house	67	97.10	00	00	54	**80.59**	13	19.40
Laundry	65	94.20	32	49.23	24	36.92	09	13.84
Dishes	48	69.56	29	60.41	15	31.25	04	08.33
Draw water	42	60.86	00	00	03	07.14	39	**92.85**
Cook	69	100	58	**84.05**	05	07.24	06	08.69

E : Effective

References: [1] Berg & al. J. Obstet Gynecol. 1988;(71):71-5.

[2] Svensson HO, Andersson GJ, Hagstad A, Jansson PO. Spine. 1990;(15):371-5.

[3] Östgaard HC, Anderson GBJ, Karlsson K. Spine. 1991;16(5):549-52.

[4] Tigri T. [Mémoire]. Maîtrise STAPS 2012. 83p.

[5] Connie JG, Mid CMM, Colleen SM. J Perinat Educ. 2001;10(1):1-12.

[6] Garshasbi A, Faghih Zadeh S. Int J Gynecol Obstet. 2005;(88):271-5.

[7] Suputtitada al. J Méd Thaïlande. 2002;85(1):170-9.

[8] Taavoni & al. J Mid la santé des femmes. 2011;56(2):137-40.

[9] Delgado & al. Enferm Clin. 2012;22(1):35-40.

Disclosure of Interest: None Declared

Computer Simulation

PO-0195

HOW TO GENERATE INJURY PRONE SITUATIONS FOR NONCONTACT ACL INJURIES BY MONTE CARLO SIMULATION

Robert Eberle [1][2],*Dieter Heinrich [1]Peter Kaps [2]Michael Oberguggenberger [2]Werner Nachbauer [1]

[1]Department of Sport Science, [2]Unit for Engineering Mathematics, Department of Engineering Science, University of Innsbruck, Innsbruck, Austria

Introduction and Objectives: ACL injuries are one of the most common knee injuries in sports. If video sequences of injury situations are available the kinematics can be obtained by video analyses to study injury mechanisms (e.g. [1]). But these video sequences are rare and because of ethical reasons it is not feasible to imitate injury prone situations experimentally. Musculoskeletal computer simulations allow to simulate injury situations on the computer and to predict ACL loads (e.g. [2]). Musculoskeletal simulation models combined with Monte Carlo simulation have been applied successfully. In addition certain injury mechanisms were investigated (e.g. [3]). In these studies Monte Carlo simulation was applied to generate repeated forward dynamic simulations. These approaches neglected the task-oriented adaptive behavior of the athlete. A formulation as optimal control problem allows considering this task. In this work an optimal control problem formulation was applied to generate injury prone situations for ACL injuries by using measured kinematics of a non-injury situation. The approach is demonstrated for jump landing in downhill skiing.

Methods: The musculoskeletal simulation model was written as a system of implicit differential equations [2]

$$f(x,x',u)=0 \quad (1)$$

with state variables $x=[q,q',L_{CE},a]$ and control variables u. Here, the state variables q, q' denote the generalized coordinates and velocities of the model, L_{CE} denotes the muscle fiber lengths and a the active states of the muscles. A measured reference movement was reproduced by the musculoskeletal simulation model. This was formulated as an optimal control problem. The goal was to minimize an objective function with respect to muscle excitation patterns u:

$$J=J_1+J_2+J_3 \rightarrow min \quad (2)$$

subjected to constraints given by equation (1). The objective function J consisted of three terms. The term J_1 was used to fit the generalized coordinates q to data of a measured reference movement, J_2 represented the mean of spared muscle excitations u and J_3 was used to avoid exceeding physiological limits as hyperextension or hyperflexion. Direct collocation was used to transform the optimal control problem in a Nonlinear Programming Problem (NLP), which was solved using IPOPT [4].

Injury prone situations were generated as follows. The initial kinematics of the reproduced reference movement was n times randomly perturbed and the optimal control problem was recomputed. The ACL loads were calculated for all n simulations and the simulations with ACL forces higher than a threshold of 1689 N were collected. The threshold was determined by the 3-sigma rule using measurement data of the maximal traction force of the ACL obtained by Woo et al. [5]. These simulations were classified as injury prone situations.

This approach was applied to generate injury prone landing situations during jump landing in downhill skiing. The data of a non-injury landing situation were taken from Nachbauer et al. [6].

Results: The series of 1500 Monte Carlo simulations results in 527 injury prone landing situations (405 simulations for right ACL, 122 simulations for left ACL). The mean values of trunk orientation and joint angles 100 ms before impact were calculated for the injury prone landing situations. In the injury prone landing situations the skier had compared to the reference jump a more backward trunk orientation, the ski tails impacted first and the skier landed on one leg with a more extended knee.

Conclusion: The presented approach can be used to generate injury prone situations for ACL injuries on the computer using measured kinematics of non-injury situations. The conventional investigations with musculoskeletal simulation models were done by forward simulations and neglected the task-oriented adaptive behavior of the athlete. The formulation as optimal control problem in this work considered this task.

The approach was successfully applied to study jump landing in downhill skiing. The results are consistent with video recordings obtained in Senner [7].

The computer generated injury prone situations can be used to study injury mechanisms or the effects of equipment and muscle parameters on ACL loads during injury prone situations.

References: [1] Krosshaug et al., J Biomech, 38: 919-929, 2004.

[2] Heinrich et al., Scand J Med Sci Sports, 24: 180-187, 2014.

[3] McLean et al., J Clin Biomech, 23: 926-936, 2008.

[4] Wächter et al., Math Program, 106: 25-57, 2006.

[5] Woo et al., Am J Sports Med, 19: 217-225, 1991.

[6] Nachbauer et al., J Appl Biomech, 12: 104-115, 1996.

[7] Senner (Ed.). Thesis, TU Munich, 2001.

Disclosure of Interest: None Declared

NUMERICAL STUDY OF THE ANKLE OSTEOARTHRITIS AFTER ACUTE INVERSION ANKLE SPRAIN ON NORMAL WALKING

Ji Yong Bae [1,*]Kyung Soon Park [2]Jong Keun Seon [2]Gunhee Kim [1]Insu Jeon [3]

[1]Korea Basic Science Institute (KBSI), Center for Analytical Instrumentation Development, Daejeon, [2]The Center for Joint Disease, Hwasun Hospital, Chonnam National University, Hwasun-Gun, Jeonnam, [3]School of Mechanical Engineering, Chonnam National University, Gwangju, Korea, Republic Of

Introduction and Objectives: Ankle sprains are a common musculoskeletal injury in which the ligaments of the ankle partially or completely tear due to sudden stretching. It mainly occurred by an excessive inversion or eversion of ankle joint, and caused a damage of the lateral collateral ligament (LCL), which is consisted of anterior talofibular ligament (ATaF), calcaneofibular ligament (CF) and posterior talofibular ligament (PTaF). Damage of the LCL includes rupture of ATaF or often to the combined with CF. Most treatment for injury of the LCL is performed using conservative methods. However, when adequate treatments are not applied, injury of the LCL can be developed into chronic ankle instability. It induces to the damage of the articular cartilage and finally can be led to osteoarthritis [2]. In present study, three dimensional finite element model of the ankle joint was developed to investigate the causal link between lateral ankle instability and osteoarthritis. Altered kinematics of the ankle joint, contact pressure of articular cartilages and strain pattern of LCL were calculated through finite element analysis using developed finite element model. Based on the results, the causal links between lateral ankle instability and osteoarthritis are clearly elucidated.

Methods: A. 3D reconstruction of the ankle joint

T1 MR images were obtained from healthy left ankle joint of a 33-years-old male in the axial plane at neutral foot position. The MR scan was performed using a 3TMR scanner (Signa Excite 3.0T; GE HealthCare, USA) at intervals of 0.7mm. In order to keeping non weight bearing situation, the volunteer maintained the supine position at least 30 min before scan. The acquisition parameters for the MR scan were determined as a field of views of 250×250 mm, an optimal pixel size of 0.566mm, and a resolution of 512×512. Using obtained MR images, 28 bony structures (including tibia, fibula, talus, calcaneus, cuboid, navicular, cuneiforms, metatarsals and components of the phalanges), their articular cartilges and enveloped soft tissue were 3 dimensionally reconstructed using the commercial software MIMICS (v10.1, Materialise, Belgium).

B. Finite element modeling and material properties

Based on the reconstructed ankle joint model, 3D Fe meshes were generated including ligament, tendon and plantar fascia using the commercial software PATRAN (v2008, MSC Software Corporation, USA). The tetrahedral solid element was used for all the bony structure models and cartilages, and the tetrahedral hybrid continuum element, which is suitable for hyperelastic material, was used for the enveloped soft tissue. The bony structures, cartilages and ligaments were assumed to be homogeneous, isotropic and linear elastic material. (5,6) The enveloped soft tissue was considered as 2nd order polynomial hyperelastic model. The ligaments were modeled as 1D truss elements considering a physiological cross

sectional area (PCSA) (Fig.1) [7,8]. Based on the intact model, 3 types of LAI model such as without ATaF, without CF and without both ligaments were developed, and used in our simulations.

Results: Contact pressure and strain on the talus articular cartilage and anteroposterior translation of the talus increased gradually as the walking phase progressed. The values increased rapidly at the push off (PO) stance phase. Peak contact stress and strain and translations were higher in anterior talofibular ligament (ATFL)-deficient models than in the intact ankle joint model at each stance phase, and they were highest in the ruptured LAL models.

Figure:
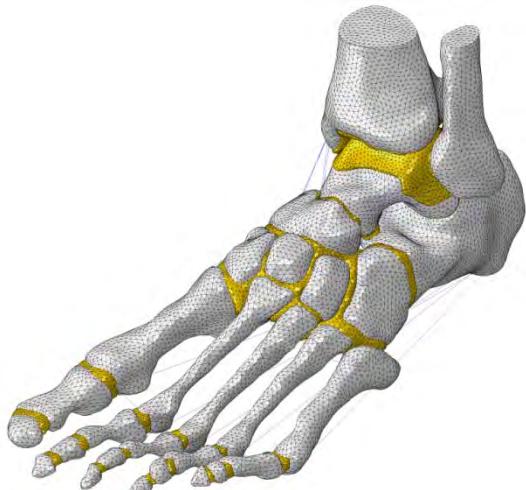
Caption: 3D FE model of ankle joint without enveloped soft tissue.

Conclusion: The LAL injury increased the contact pressure and strain on the talus articular cartilage and the translations of the talus during normal walking. Therefore, the injured LAL, under normal walking conditions, could be a significant cause of ankle joint osteoarthritis. Ankles with ruptured ATFLs had a higher likelihood of experiencing the osteoarthritis than ATFL laxity ankles. In particular, ankles with ruptured ATFL+calcaneofibular ligament (CFL) and all ruptured ankles had a similar likelihood as the ruptured ATFL ankles. The PO stance phase was the worst situation for ankle joint osteoarthritis in the LAL injury ankles.

References: REFERENCES

[1] Fallat et al., J Foot Ankle Surg, Vol. 37, pp. 280~285, 1998.

[2] Valderrabano et al., Am J Sports Med, Vol. 34, pp. 612~620, 2006.

[3] Hirose et al., J Orthop Sci, Vol. 9, pp. 37?43, 2004.

[4] Omori et al., Knee Surg Sports Traumatol Arthrosc, Vol. 12, pp.457~462, 2004.

[5] Gefen et al., Clin Biomech, Vol. 16, pp. 921~925, 2001.

[6] Athanasiou et al., Clin Orthop Relat Res, Vol. 348, pp.269~281, 1998.

[7] Siegler et al., Foot Ankle, Vol. 8, pp.234~242, 1998.

[8] Wright et al., J Bone Joint Surg Am, Vol. 46, pp. 482~492, 1964.

Disclosure of Interest: None Declared

Computer Simulation

PO-0197

MODELLING STERNOTOMY VIA FINITE ELEMENT ANALYSIS

Nicholas Farrugia [1]Kevin Schembri [2]Zdenka Sant [1,*]

[1]Department of Mechanical Engineering, University of Malta, [2]Department of Cardiothoracic Surgery, Mater Dei Hospital, Msida, Malta

Introduction and Objectives: Median sternotomy is a surgical procedure in which access to the vital organs is obtained by sternum dissection. Despite the low occurrence, the postoperative complications are associated with a high mortality rate[1]. Thus the interaction between the suture and the sternum bone requires further studies. The presented work aims to increase this knowledge pool.

Sternal wire fixation is a commonly used technique as it is easier than the rigid-plate technique. Excessive tensioning of the sutures cuts through the bone while lack of tensioning would not promote the bone healing process. Number of tests carried on animal or cadaver bone as well as on the foam model are reported in the literature but none provides analysis of bone-wire interface behaviour[2].

Computational modelling has increased in the past years as it is rapid, provides relative inexpensive evaluation, and reasonable comparison of different closure techniques. Its main drawback is the extent of present knowledge translated in a mathematical model of the bone microstructure into a macrostructure model. Another drawback specific to this approach is the load simulation relying on a mathematical model or experimental data.

The objective of this study was to obtain a stress-strain distribution after median sternotomy using a locally used wire closure technique.

Methods: The three-dimensional sternum geometry was obtained by manual segmentation of CT scan data. An incision along the midline of the sternum model and a suture technique were modelled based on the practice of a local cardiac surgeon as shown in Figure 1a.

Considering that the strain at the cortical bone would not exceed 0.2%, it was possible to create a material model with linear isotropic behaviour. An analysis of the CT scans resulted in an average thickness of cortical bone of 1.38mm. The Young's Moduli of the bone tissues of the sternum were estimated to be 5000MPa and 50MPa for the cortical and cancellous bone respectively[3]. Testing of the stainless steel suture evaluated Young's Modulus to be 193GPa[4].

The application of loading and boundary conditions were then assigned. Published results indicate a range for the forces experienced by the sternum starting from 160N to 400N[2] for breathing up to 1650N for coughing[5]. The simulation carried out was based on a mathematical model of the thorax as an ellipsoid pressure vessel with varying chest wall thicknesses. This model provides varying loads at different rib levels increasing from around 250N to 480N, which seem to be reasonable and correspond to *in vitro* experiments[6].

A Finite Element (FE) model was obtained following discretisation and then finalised by setting the contact at the bone-wire interfaces.

Results: The results indicate that the gap between the two halves varies from 0.125 ±6.25e-4mm at the manubrium to 0.904±4.52e-3mm near the xiphoid. This degree of micromotion in response to the dynamic loading promotes the healing

of the wound. The highest von Mises' stress on the sternum cortical bone is observed to be 25.102±0.125MPa at the xiphoid while at the location of the wire sutures, the von Mises' stress on the cortical bone is 11.15±0.056MPa as shown in Figure 1b. Thus all stresses on the cortical bone are below the assumed yield strength of 170MPa[7]. The majority of the uppermost sutures experience a stress below the yield strength of 290MPa[4]. The stress in the sutures is increasing in the caudal direction reaching a von Mises' stress of 446MPa at the bottommost suture as shown in Figure 1c.

Figure:
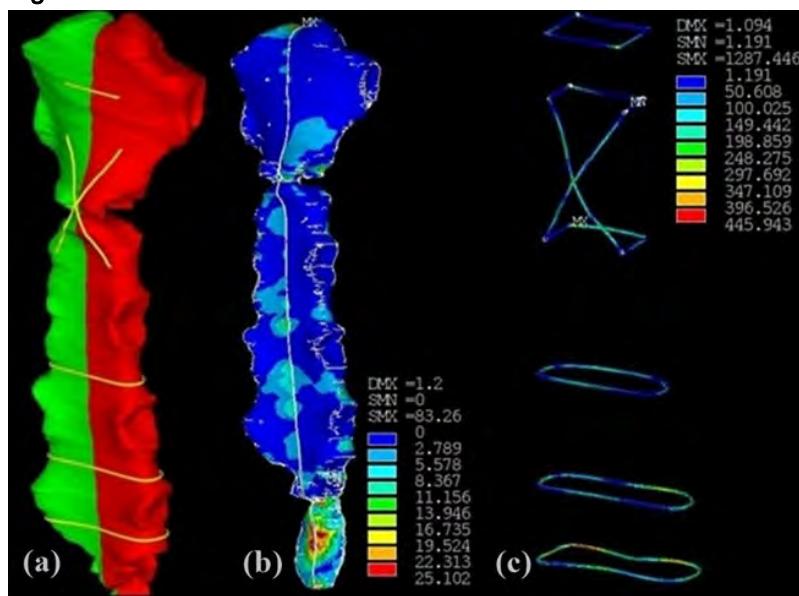
Caption: Geometrical model of the human sternum with the suture technique; (b) Von Mises' stresses on the two sternal halves, (c) Von Mises' stresses on the sutures

Conclusion: The stress results on the lower region of the sternum are mainly due to the load model and its application at connection of the false ribs. This corresponds to the similar results obtained from a computation prior to incision thus confirming the necessity to provide a correct evaluation of the chest load model. Also the stresses in the suture at the inferior region are much higher than the yield strength of the suture material, which confirms our conclusion mentioned above. The application of this study is to increase the knowledge pool about the bone-wire interface in median sternotomy and to identify the problematic areas on the sternum following such procedure.

References: [1] Schimmer et al., Ann Thorac Surg, 86:1897-904,2008.

[2] S. Pai, In vivo characterisation of respiratory forces on the sternal midline following median sternotomy, Faculty of Worcester Polytechnic Institute, 2005.

[3] J. Cilia, Analysis of Stress-Strain Distribution within the Sternum (Foam Model), University of Malta, 2010.

[4] AKSteel, 3116/316L Stainless Steel Bulletin, 2013

[5] Casha et al., Eur J Cardiothorac Surg, 15:365-9, 1999.

[6] Casha et al., Interact Cardiovasc Thorac Surg, 14: 283-7, 2012

[7] Murugan (Ed.). Tissue Engineering and Regenerative Medicine: A Nano Approach, CRC Press,2012.

Disclosure of Interest: None Declared

Computer Simulation

PO-0198

POST IMPLANTATION DESIGN OPTIMIZATION OF CORONARY ARTERY STENT

Dimitrios Drougkas [1] Serafim Chatzimoisiadis [1,*]

[1]Optimization Applications, Beta Cae Systems S.A., Thessaloniki, Greece

Introduction and Objectives: The use of stents is an effective and trusted solution for coronary artery stenosis. Their principle of design offers immediate results with minimal recovery time. But how do they stand in terms of reliability after their implantation? Clinical experiments in combination with FEA analysis are performed in order to define the optimal design of coronary stents since it is very important the maintenance of their final shape for the rest of the patient's life, against the complex loading conditions within the arterial walls.

From the engineer's point of view the most crucial loading condition is the cyclic bending of the stent. During which the stent not only has to flex without traumatising the arterial walls, but it has to maintain its effective diameter in order to prevent a restenosis due to mechanical failure.

Methods:

The optimum design and thickness of a flexible metal stent has been determined through an optimization process. Stent shape parameters were defined as morphing parameters in the Pre-Processor and used as design variables for the optimization case. The desired responses were automatically extracted from the results with the aid of the Post - Processor and used as design objectives and constraints. The load cases included crimping (reducing stent diameter), blowing pressure (increasing stent diameter) and also a 3point bending test to ascertain the flexibility of the stent design. The final step was the coupling of the optimizer, the Pre- and Post- Processors and the solver employing the respective build in nodes to set up the optimization process.

Results: The optimum design that was suggested by the optimizer achieved the maximum possible value for the objective variable , the diameter of the stent after the bending test. The design achieved 20.47% larger diameter for the inflation step and 22.15% larger diameter after the bending test in comparison to the initial mode. The optimum design also complied with the defined design objectives providing an overall viable solution to the optimization problem.

Figure:
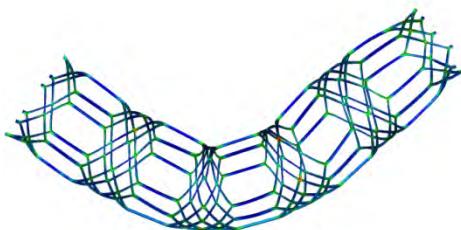
Conclusion: Concluding, the coronary artery stent design optimization problem was successful in acquiring optimum design using FE mesh morphing techniques, complying with both constraints and achieving optimum results.

Disclosure of Interest: None Declared

FORWARD DYNAMICS SIMULATION OF 3D RUNNING MOTION USING A NEURO-MUSCULO-SKELETAL MODEL

Kazunori Hase [1,*]

[1]Mechanical Engineering, Tokyo Metropolitan University, Hachioji, Tokyo, Japan

Introduction and Objectives: Forward dynamics simulation is important in the research fields of biomechanics, because it autonomously generates human movement such as walking and running in a computer without any motion data collected from actual human, and can complement limitation of the experimental approach. Running includes flying phase, i.e., the entire body floats on the air, which walking does not include, so motor control of running is more difficult than walking. If human running is precisely synthesized by a computer simulation, biomechanical principles of the motion might be clarified computationally and the simulator might become a useful tool for the research field of sports biomechanics. The purpose of this study is to simulate three-dimensional running in humans using a neuro-musculo-skeletal model based on forward dynamics. This study especially focused on synthesizing faster running motion to improve locomotive stability.

Methods: The inertia properties of the whole body were represented by three dimensional 14-rigid-links system with 23 degrees of freedom of the joints. The musculoskeletal model was constructed by 70 muscle models that included mechanical and physiological properties of the muscle. The geometric path of each muscle was expressed by a series of line segments. The interaction between the foot and the ground was modeled as a combination of springs and dampers. The basic motion controller consisted of artificial neural network models including 23 neural oscillators. The neural oscillator mathematically represents the central pattern generator (CPG) in the nervous system. This generates the combined neuronal stimulus for each degree of freedom by receiving a nonspecific stimulus from the higher center of the neuronal system and feedback signal from the sensory feedback system. This feedback system corresponds approximately to the reflexes.

   The above-mentioned CPG-based controller was thought to correspond to the lower level function of the central nervous system such as the spinal cord. On the other hand, the cerebellum has been thought to work involuntarily to maintain locomotive balance. We constructed an attracting controller modeled after the involuntary control functions of the brain to maintain locomotive balance. There were two main features of the design of the attracting controller. First, this controller was designed in the reduced-order space composed by the principal components of the joint angles and angular velocities. Second, the attracting controller generated torque signals to maintain regular or desired locomotion patterns only when locomotion was perturbed by some disturbance. The attracting controller was placed in parallel to the CPG-based controller. The CPG-based controller receives somatic sensation signals and generates an oscillatory pattern for the locomotive motion, while the attracting controller receives each joint angle and outputs the signals to return to the regular locomotive trajectory by canceling the disturbance. The signals from the attracting controller and the CPG-based controller are summed for delivery to the peripheral nerve model to stimulate the muscles.

   Furthermore, the simulation system included a numerical search method to modify the characteristics of the model according to the purpose of the simulation. The parameters in the neuro-musculo-skeletal model can be changed using genetic algorithms as optimization techniques with evaluative criteria of locomotion and parallel computing techniques.

Running motion was generated by transition from a normal gait using the numerical search. The transition process was divided into two stages. The first stage of the process was the acquisition of the flying phase in which minimizing the period of foot-ground contact was employed as the evaluative criterion. After realizing a running motion with a flying phase, the second stage aimed at maximizing the both of locomotive speed and energy efficiency. Such numerical search process was thought to correspond to learning process of human movement.

Results: In the search process to obtain the desired running motion, solving of the differential equations of the neuro-musculo-skeletal system was conducted until the model walked or ran for only the prescribed six steps. Figure 1 shows synthesized running motion using the proposed model. The running speed was 6.0m/s, the stride length was 2.95 m, and the running cycle period was 0.49 s. The final running pattern agreed closely with that of a human. However, locomotive motion was still unstable and easy to fall down, so it was difficult to realize running speed over 6 m/s.

Figure:
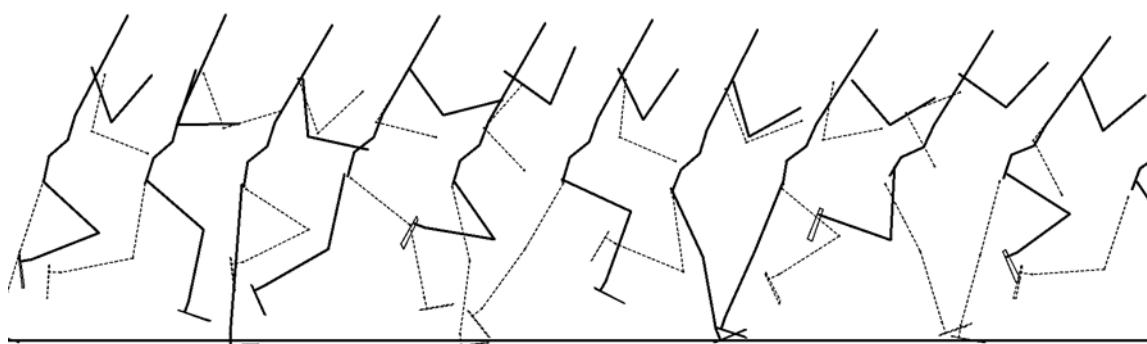
Caption: Fig. 1 Stick pictures of simulated running motion. Each stick picture is traced at 0.1 sec intervals.

Conclusion: In the present study, running motion at a speed of six meters per second was realized using the forward dynamics simulation with a three-dimensional entire-body neuro-musculo-skeletal model.

Disclosure of Interest: None Declared

Computer Simulation

PO-0200

EFFECT OF ALTERED MUSCLE ACTIVATION PATTERNS ON THE LOADING OF THE ACL DURING JUMP LANDING IN DOWNHILL SKIING

Dieter Heinrich [1,*]Antonie J. van den Bogert [2]Werner Nachbauer [1]

[1]Department of Sport Science, University of Innsbruck, Innsbruck, Austria, [2]Department of Mechanical Engineering, Cleveland State University, Cleveland, United States

Introduction and Objectives: Injury data in alpine skiing highlight that competitive skiers face a high injury risk. In particular, jump landing in downhill skiing has been identified as a common situation leading to ACL injury [1]. During landing maneuvers muscle forces have been shown to significantly contribute to the loading of the ACL either as agonist or as antagonist (e.g., [2]). However, it is unknown how altered activation of individual muscles affects the loading of the ACL taking into account compensatory effects of the other muscles. Therefore, the purpose of the present study was to determine the changes in ACL loading during jump landing in downhill skiing due to altered muscle activation patterns and to determine the muscles with the highest influence.

Methods: A 25 degrees of freedom sagittal plane musculoskeletal model of an alpine skier with two skis was used to study jump landing in downhill skiing [3]. The motion of the skier was actuated by 16 three-element Hill-type muscles, eight for each lower extremity: iliopsoas (ILI), glutei (GLU), hamstrings (HAM), rectus femoris (RF), vasti (VAS), gastrocnemius (GAS), soleus (SOL) and tibialis anterior (TA). The model had 82 state variables $x=[q,q',a,L_{CE}]^T$, where q and q' denote the generalized coordinates and velocities, and a and L_{CE} denote the activations and the contractile element lengths of the muscles. Furthermore, the model had 16 control variables u representing the muscles excitation patterns.

We developed a dynamic optimization framework to study the effect of altered muscle activation patterns on peak ACL loading. Measured kinematic data of a jump landing maneuver served as reference data and were taken from a previous study [4]. In particular, the following performance index was minimized

$J = J_1 + J_2$

with

$J_1 = 1/(N_d\,N_f)\,\sum_i\sum_k((q_i(t_k) - q_{i,data}(t_k))/\sigma_i)^2$

and

$J_2 = 1/(N_m\,T)\,\int_0^T(\sum_j w_j\,u_j(t)^2)dt$

subject to constraints due to system dynamics and unity bounds on u. The first term J_1 represents the deviation of the simulation with respect to experimental data. The second term J_2 was used to account for muscle redundancy similar to [5]. The optimal control problem was transformed into a nonlinear programming (NLP) problem [6] and solved using the NLP solver IPOP. Setting the weighting contants w_j to 10 for all muscles resulted in a reasonable weighting between J_1 and J_2. Sagittal knee joint loading was calculated similar as in [3].

The change in ACL loading due to altered muscle innervation was determined by performing two optimizations with different weighting constants w_j for each muscle. A similar approach was used in [7] to study the change in tibiofemoral forces. In the first optimization the weighting constant w_j of a single muscle was set to 0 to encourage activation of the

selected muscle. The weighting constants of the other muscles were not changed. In the second optimization the weighting constant w_j was set to 1000 to penalize activaiton of the selected muscle.

Results: The measured jump landing maneuver of the downhill skier could be successfully simulated. Peak ACL forces reached 1046 N in the right leg after about 35 ms of initial ground contact. Peak ACL force was sensitive to altered activation of the VAS, SOL, GLU and ILI of the right lower extremity (Figure 1). In particular, encouraging activation of the VAS and GLU as well as penalizing activation of the SOL and ILI increased peak ACL force. On the other hand penalizing activation of the VAS and GLU as well as encouraging activation of the SOL and ILI decreased peak ACL force. Furthermore decreased activation of the VAS in the left lower extremity increased the peak ACL force in the right knee transferring additional load to the right lower extremity. Only a small influence on peak ACL force was observed by altered activation of the HAM. The main reason was compensatory activation of the VAS to track the measured kinematics.

Figure:
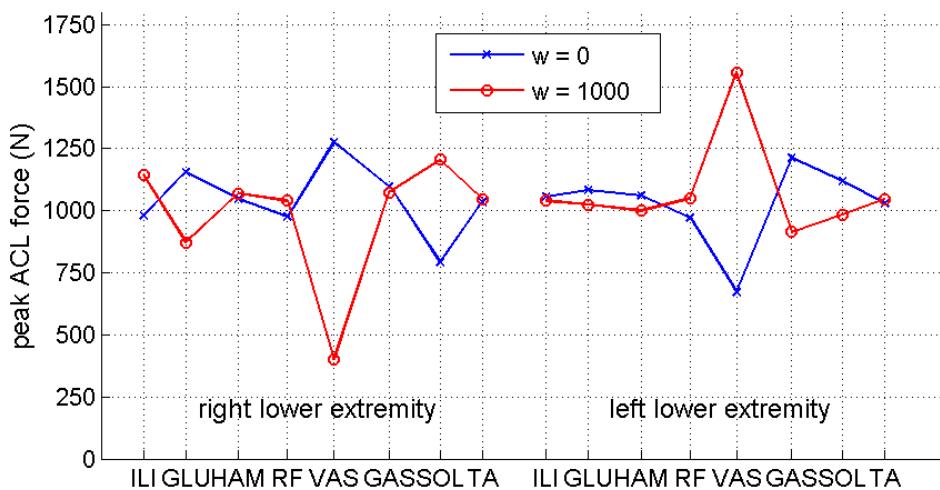
Caption: Change in peak ACL force due to altered muscle activation of individual muscles. Setting the weight constant w to 0 and 1000 was used to encourage and penalize the activation of a selected muscle, respectively.

Conclusion: A planar musculoskeletal model of an alpine skier was applied to study the effect of altered muscle activation of individual muscles on peak ACL loading in downhill skiing. While peak ACL force was primary affected by the VAS also muscles not spanning the knee joint affected peak ACL force significantly. Peak ACL force was insensitive to altered activation of the HAM due to compensatory activation of the VAS.

References: [1] Bere et al., Am J Sports Med, 39: 1421-1429, 2011.

[2] Pflum et al., Med Sci Sports Exercise, 36: 1949-1958, 2004.

[3] Heinrich et al., Scand J Med Sci Sports, 24: 180-187, 2014.

[4] Nachbauer et al., J Appl Biomech, 12: 104-115, 1996.

[5] Spägele et al., J Biomech, 32: 521-530, 1999.

[6] van den Bogert et al., Procedia IUTAM, 2: 297-316, 2011.

[7] DeMers et al., J Orthop Res, 32: 769-776, 2014.

Disclosure of Interest: None Declared

Computer Simulation

PO-0201

HUMAN CENTERED CAD SYSTEM WITH BIOMECHANICAL ANALYSIS

Younguk Kim [1,*]Yeounghun Kim [1]Sangjun Lee [1]Dooyoung Lee [1]Kunwoo Lee [1]

[1]Mechanical Aerospace Engineering, Seoul National University, Seoul, Korea, Republic Of

Introduction and Objectives: As the market becomes competitive, it is more difficult to sell products with price strategy or development of function. Therefore, human-oriented design system is in the spotlight of manufacturer to satisfy the various demands of consumer. Unfortunately, there is no proper product design system which adequately applies the human factor into the design phase. The conventional design system is time consuming and costly, because a repetitive process is required on producing a prototype to test it on human subjects and then changing the design parameters based on the test results.

According to [1], development costs and time can be reduced by using a digital human model. Moreover, a study by Chaffin et al. [2] implemented a digital human model called 3DSSP or Jack (Siemens, Germany), which is widely used in the industry. In addition, Jung [3] converted a CAD design into an AnyBody Modeling System (AnyBody Technology A/S, Denmark) [4] and executed analysis. However, these studies do not provide an integrated simulation in one system or not specialized in product design.

In order to improve upon the existing studies, this study proposes a method of transplanting a musculoskeletal analysis into a CAD system; therefore, users can evaluate the product model by performing musculoskeletal dynamic analysis during the design process.

Methods: The entire system of this research can be divided into three parts - CAD, motion generator and biomechanical analyzer. In the CAD part, user designs a product and generates a human-product model using the integrated modeling system [5]. For integrated model, human model data are exported from an OpenSim 6 Degree of freedom upper-body model [6].

In the motion generator part, users can calculate the each segment motion with the product's target motion. Also they can achieve the interaction forces between the human and the product. "Independent joint control" method is used by motion generation which considers each joint as an independent object. This method determines each joint control, then it controls the difference with feedback control. [7] The target trajectory x_d is decomposed by the joint control input with a Jacobian relationship. In addition, the actual joint position x can be derived by solving the forward dynamic equation with the joint control input. With this information, we can define the control error for feedback control as follows:

$$\tilde{x}(t) = x_d(t) - x(t) \quad (Eq.1)$$

The PD control input for error compensation is expressed with gain factor k_p, k_D

$$F(t) = k_p \, \tilde{x}(t) + k_D \, \dot{x}(t) \quad (Eq.2)$$

According to (Eq.2), each joint control input can be acquired by decomposition of the joint space with a Jacobian J_A

$$u(t) = J_A^T F(t) = J_A^T (k_p \, \tilde{x}(t) + k_D \, \dot{x}(t)) = J_A^T (k_p \, \tilde{x}(t) + k_D \, J_A \, \dot{q}(t)) \quad (Eq.3)$$

The motion is generated by this process with RoboticsLab [8], and the human-product interaction orce is calculated by dynamic equation of motion.

In the biomechanical analyzer part, based on motion and force information, analyzer can calculate each joint torque and muscle activation of the musculoskeletal model. With the OpenSim API, inverse dynamics equation is solved with the motion and interaction-force information. After the interaction force is converted to an external force, it is substituted into the dynamic equation. Joint moment is obtained the by calculating the dynamic equation with force and motion information. Furthermore, we perform optimization to achieve the muscle activation results and metabolic cost.

Results: As shown in (Fig.1), a human-product integrated model is created with product information, which is designed in a CAD system. Integrated model motion and interaction force information are derived from the objective motion and integrated model. In addition, the constructed system performs calculation of inverse dynamics and optimization with the musculoskeletal information. This result is reflected in CAD system. It allows the user to access biomechanical information with one complete system.

Figure:
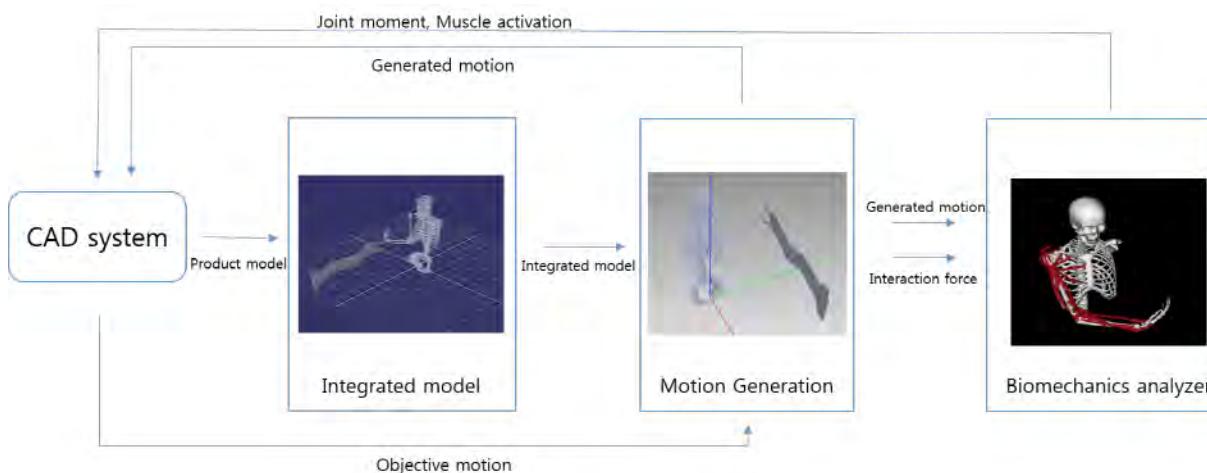
Caption: Fig 1. System overview

Conclusion: The significance of this research is integration of biomechanics into a CAD system. It allow us to predict the biomechanical effect during the design process without manufacturing. Therefore, it could reduce the time for iterative experiments during the process and possible to suggest the optimal biomechanical design conditions

References: [1] Chaffin B., Digital human modeling for vehicle and workplace design. Society of Automotive Engineer, 2001.

[2] Chaffin B. et al, Occupational Biomechanics,2nd Edition,Wiley, 1991.

[3] Jung M. et al., ACDDE (2010), pp.883-897.

[4] AnyBody 4.2, AnyBody Technology A/S, Aalborg, Denmark, 2010.

[5] Delp SL. et al. IEEE Transactions on Biomedical Engineering. 2007,pp. 1940~1950.

[6] Kim Y. et al.,ACDDE (2014),pp21~22.

[7] Spong, MW. et al. Robot modeling and control.Vol.3 Wiley, 2006.

[8] Park J. et al, KRS (2010), 7(2), pp. 29-39.

Disclosure of Interest: None Declared

Computer Simulation

PO-0202

STUDY OF THE STRESS AND TEMPERATURE OF CORTICAL BONE CUTTING BY MICRO-TEXTURED TOOL

Weihua Fu [1,*]Hongyin Cui [2]Chao Wang [2]Yahui Hu [2]

[1]General Surgery Department, Tianjin Medical University General Hospital, [2]Tianjin Key Laboratory of the Design and Intelligent Control of the Advanced Mechatronical System, Tianjin University of Technology, Tianjin, China

Introduction and Objectives: In bone cutting operations, severe friction exists when the tool is in contact with the workpiece. It causes an increase in bone temperature, and a temperature above 47°C is critical because it causes thermal bone necrosis. In this paper, three kinds of tools with micro textured rake face were fabricated. The purpose of this research is to investigate the improvement of cutting performance in cutting of cortical bone with the micro textured tools and seek the conformable cutting parameters for exertion of the advantages of these tools.

Methods: Numerical models of cortical bone and cutting tool was used to simulate the cutting process by ABAQUS6.11. Parameters of the micro-texture tools and the common tool were selected respectively by single factor analysis. Dry friction tests on the pin-on-disc tribological tester were carried out with these micro textured surfaces and conventional surfaces for comparison. A prediction model of temperature was set up according to a orthogonal experiment design.

Results: The simulated experiment indicated that morphology and geometric parameter differences of the micro-texture cutter caused different temperature changes in the third deformation area, cutting temperature was proportional to spacing and depth of micro-texture, but was inversely proportional to width. Width of micro-texture played a key role in temperature variation . Through the analysis of variance, A prediction model of temperature was proved to be right.

Conclusion: The finite element model and experimental model has the same change trend. The stress and temperature in dry cutting of cortical bone with the micro textured tools was reduced compared with that of the conventional tool. The prediction model of temperature can assist in the selection of favorable cutting conditions for the operations of micro-textured tools.

References: [1] Hillery MT,et al. Journal of Materials Processing Technology, 92-93:302-308,1999.

[2] Wu Ze Deng,et al. Journal of Tool Technology, 45 (7) : 18-21,2011.

[3]Augustin,et al. Archives of Orthopaedic & Trauma Surgery 128(1):71-77,2008.

[4]Wang lei,et al. Drilling Process,1: 8-12,2007.

[5]T.Udiljak, et al. Advance Production Engineering & Management,2: 103-106 ,2007.

[6]Wu Ze,et al. Int J Adv Manuf Technol, 62:943–951,2012.

[7]Anis Fatima, et al. Int J Adv Manuf Technol , 69:771–776,2013.

[8]JinXie,etal.International Journal of Precision Engineering and Manufacturing,13(10):1845-1852,2012.

[9]Augustin,et al. Archives of Orthopaedic & Treuma Surgery 129(5):703-709,2008.

Disclosure of Interest: None Declared

Computer Simulation

PO-0203

DEVELOPMENT OF A MUSCULOSKELETAL MODEL FOR THE ANALYSIS AND SIMULATION OF CERVICAL SPINE LOADING DURING RUGBY ACTIVITIES

Dario Cazzola [1,*] Ezio Preatoni [1] Timothy Holsgrove [2] Richie Gill [3] Grant Trewartha [1]

[1]Department for Health, University of Bath, Bath, United Kingdom, [2]School of Engineering and Applied Science, University of Pennsylvania, Philadelphia, United States, [3]Department of Mechanical Engineering, University of Bath, Bath, United Kingdom

Introduction and Objectives: Musculoskeletal modelling is widely used in biomechanics for the analysis and simulation of human motion, especially to investigate the variables that are not directly measurable through *in-vivo* or *in-vitro* experimental design. An example is the analysis of hazardous situations, such as vehicle crashes or injury scenarios in sports, where direct measures of loading conditions on internal anatomical structures are not feasible or ethical. Musculoskeletal modelling needs to be based on *in-vivo* or cadaveric kinematics and anatomical measurements, to provide reliable analysis and simulation outcomes that are relevant for understanding real-word problems. The aims of this study were to: i) establish a full body OpenSim musculoskeletal model, optimised for simulating rugby activities such as scrummaging and tackling; and, ii) verify the model's suitability during machine scrummaging trials.

Methods: The 'Rugby Model' was developed using OpenSim software (OpenSim 3.2, SimTK) and Notepad++ XML editor. The Rugby Model (Figure 1a) is an upgrade of a refined head/neck OpenSim model [1] embedded into a full body model [2], and consists of 29 rigid anatomical segments divided into lower limbs (femur, tibia, talus, calcaneus and toe), pelvis, trunk (thorax and spine), seven cervical spine vertebrae (C1-C7), scapula, clavicle, humerus and head (skull and jaw). Additionally, 78 upper and lower cervical muscles divided into 19 muscle groups inherited from Vasavada's model [3] were included, along with 17 torque actuators representing lower limb and upper limb muscle actions. Motion between body segments was permitted via 26 joints and 30 joint constraints. Body anatomical segment inertial properties were obtained from a combination of literature [3; 4] and DEXA scan data from a front row rugby player (height 1.84 m, 120.4 kg). DEXA imaging enabled improved mass distribution for the anatomical segments, while the local centre of mass locations and inertia moments were obtained from anthropometric tables [4]. The verification of model suitability for rugby scrummaging analysis was carried out through its application in OpenSim software. The scaling, inverse kinematics and inverse dynamics procedures were performed and the residuals values were compared with reference values in the literature.

Results: A new set of inertia parameters was provided. The Rugby Model includes an existing lower limb model, and comprises two custom scapuloclavicular joint (SCJ) to model the coupled motion of scapula and clavicle with respect to humeral elevation [1]. The model was scaled in OpenSim and a RMS value of 12 mm discrepancy between model marker and marker positions was produced. Inverse kinematics analysis of scrummaging trials showed an RMS value, across all movement phases, of 20 mm. An inverse dynamics analysis was performed and both ground reaction forces and external forces were applied respectively on model lower limb and scapula-clavicular region (Figure 1b). The relation between moment arm and anatomical segment motion, used in the Rugby Model were compared with values in literature [5],

showing that the inclusion of SCJ did not stretch or shorten the cervical spine and upper trunk muscles over their physiological limit. In this way any dynamic analysis including the contribution of muscles to the net joint moment is not negatively affected by non-physiological values of muscles moment arm due to SCJ movements.

Figure:
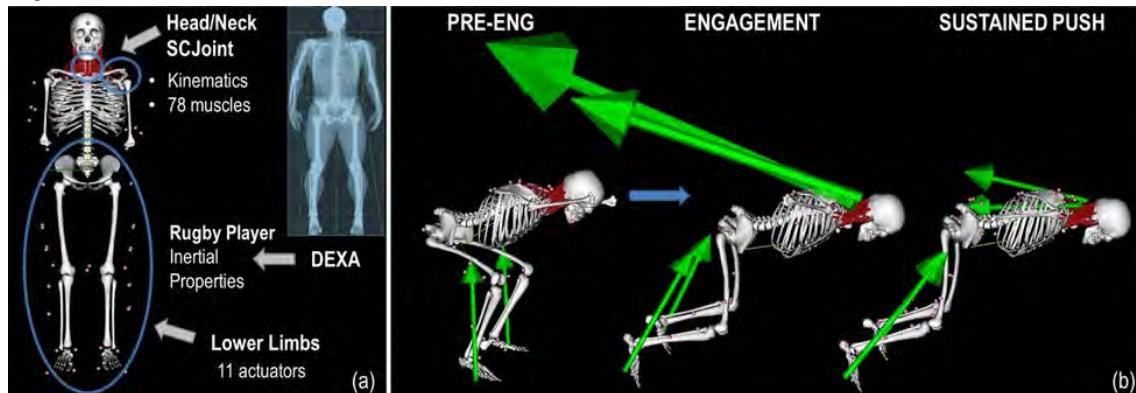
Caption: Figure 1: (a) Rugby Model includes Head/Neck and scapuloclavicular (SCJ) joints, and inertial parameters from a DEXA scans. (b) Inverse dynamic analysis during scrummaging.

Conclusion: The Rugby Model is the first full body model that provides the foundation for further applications in rugby activities and other sports impacts involving upper body contacts. The Rugby Model includes i) a refined estimation of model inertial properties, and ii) the inclusion of lower limbs in order to allow the simultaneous application of multiple external loads. The model was optimised to provide the kinematics of the cervical spine and scapula-clavicular segments, with coupled joint motion relationships based on cadaveric data. The inclusion of inertial values from DEXA scans enabled inverse dynamics analysis and an improved scaling procedure based on rugby-specific participants. The model will be used to calculate muscle lengths and moment arms, as well as the forces and moments around the cervical spine during rugby activities, such as scrummaging and tackles. The model will be used to investigate cervical spine injury mechanisms during rugby scrummaging. Further modelling developments will integrate MRI data into the construction of subject-specific models.

References: [1] Cazzola et al., Proceedings of the 7th World Conference of Biomechanics (Boston, USA), 2014

[2] Hamner et al, J Biomech. Oct 19;43:2709-2716, 2010

[3] Vasavada et al, Spine. Feb 15;23:412-422, 1998

[4] de Leva, Journal of Biomechanics.29:1223-1230, 1996

[5] Ivancic et al, Traffic Inj Prev. Dec;7:389-399, 2006

Disclosure of Interest: None Declared

DIFFERENCES IN MORPHOLOGICAL PARAMETERS AND PATTERNS OF INTERFERENCE AT THE HIP IN NORMAL AND FAI PATIENTS

Ramya Namani [1,*] Charanya Chandrasekaran [2] Javad Parvizi [3] Sorin Siegler [1]

[1] Mechanical Engineering and Mechanics, [2] Biomedical Engineering, Drexel University, [3] Rothman Institute, Thomas Jefferson University, Philadelphia, United States

Introduction and Objectives: Femoro-Acetabular Impingement (FAI) is a clinical condition characterized by limited range of motion due to early abnormal bone-to-bone interference and is often associated with labrum and cartilage damage leading to osteoarthritis [1]. Previous studies [2, 3] suggest that the early interference at the hip joint and FAI are due to abnormal morphology of the bones. The purpose of this study is to further test this assumption by comparing the morphology and the patterns of bone interference during motion of the hip between healthy subjects and patients diagnosed with FAI.

Methods: Computerized Tomography (CT) images (resolution: 0.8mm*0.8mm*2mm) from seven healthy, non-symptomatic subjects and ten age-matched FAI patients were acquired. The CT images were processed through segmentation in ANALYZE™ software to produce 3D numerical models of the femur and the acetabulum. Twenty seven morphological parameters representing common clinical parameters for the acetabulum, femur, and acetabulum-femur relations were measured from the 3D bone models. These morphological parameters were compared between the healthy and FAI subjects using statistical analysis based on t-test. For each subject, a 3D hip model was produced in which the assumed center of rotation of the hip was taken as the average location between the femoral head center and acetabular center. Motion of the hip model was produced and analyzed in a software environment ADAMS™. For the simulation, boundary conditions consisted of a fixed acetabulum and a free femur to which moments were applied in various anatomical directions to simulate clinical tests of FAI [1] consisting of Flexion (100^0) followed by adduction followed by internal rotation. An Interference Detection Algorithm (RAPID™) was used to detect when and where during the simulated motion contact between the proximal end of the femur and the acetabulum occurred. In order to compare the patterns of interference the femoral head was divided into 18 zones. 6 zones starting from anterior-inferior to anterior-superior and each further divided into medial, superior and lateral regions to produce the 18 zones. The interference patterns were calculated using distance maps and were compared within the subjects and between the normal and FAI subjects at each simulated position.

Results: The following parameters were found to be significant different between normal and FAI subjects: Acetabular diameter (FAI: 52.52±3.87mm, normal: 45.93±3.5mm), acetabular width (FAI: 18.84±4.3mm, normal: 14.54±2.22mm), peak-edge distance (FAI: 18.84±4.3mm, normal: 14.54±2.22mm), femoral neck length (FAI: 105.50±6.00mm, normal: 28.49±3.45mm), femoral head diameter (FAI: 48.73±4.2mm, normal: 3.055±1.15mm), alpha angle (FAI: 65.60^o±14.68^o, normal: 39.98^o±18.70^o), two tear drop distance (FAI: 112.59±7.16mm, normal: 128±4.522mm).

The FAI subjects had interference at the anterior-inferior region of femoral head-neck junction starting at 100° flexion with 20° adduction and going through 100° flexion combined with 20° adduction and 40° internal rotation. In contrast, for the

normal subjects, 3 subjects did not have interference in any of the simulated positions and 4 subjects have interference only at the extremes of motion such at 100° flexion with 20° adduction combined with 30° at the anterior-inferior region of femoral head-neck junction.

Figure:
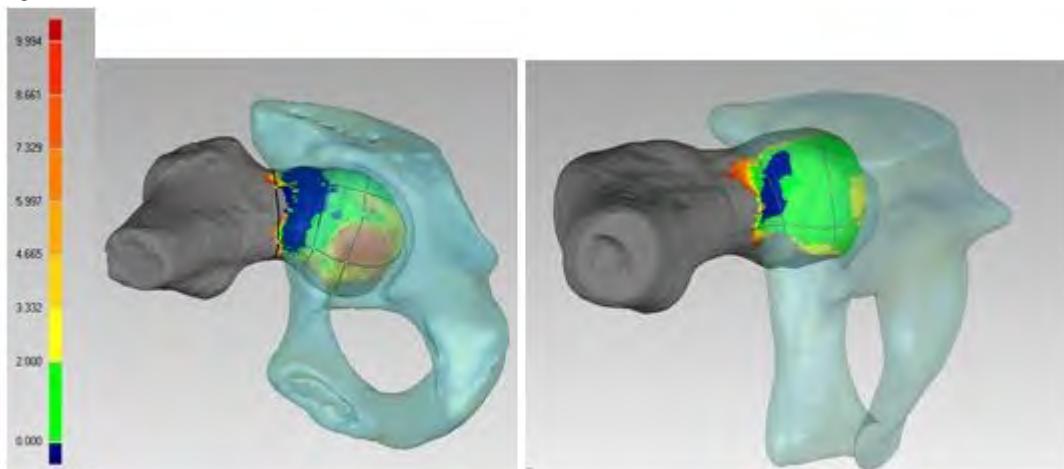
Caption: Interference in FAI hip (left) and normal hip (right) at the simulated position of 100 degrees flexion combined with 20 degrees adduction and 30 degrees internal rotation. Blue region on FAI joint shows the region of contact.

Conclusion: Some common morphological parameters were found to differ significantly between normal and FAI subjects. The early interference observed in the FAI subjects support the earlier studies documenting restricted range of motion in FAI. The results also suggest, that several morphological parameters may be related to FAI and these should be considered when evaluating and planning surgery.

References: [1] Ganz, R., et al., CORR, 417:112-20, 2003.

[2] Beck, M., et al., JBJS, 87:1012-8, 2005.

[3] Tannast, M., et al., AJR, 188:1540-52, 2007.

Disclosure of Interest: None Declared

Computer Simulation

PO-0205

CONTROL SIMULATION OF 5D AND CYLINDRICAL GRASPING BASED ON PCA

Javier Andres [1,*] Marta C. Mora [1] Joaquin L. Sancho [1]

[1] Mechanical Engineering, Universidad Jaume I, Castelló de la Plana, Spain

Introduction and Objectives:

Human hand grasping is a very complex process that has been studied for years under different perspectives in the field of hand biomechanics [1-3]. Its characterization is the key for hand prosthetic control. In a previous work [4] the use of kinematic reduction as a rational generalized method for studying grasping postures was proposed. In particular, Principal Component Analysis (PCA) was applied to reduce the hand kinematics while grasping cylinders, and to study the effect of the cylinder diameter and weight, as well as that of the subject, on the grasping posture for cylindrical (C) and 5-digit pinch (5dP) grasps. The PCA showed that the hand kinematics is actually low-dimensional for grasping tasks, and can be efficiently described by a small number of Reduced Kinematic Variables (5 RKVs) for C and 5dP grasps with all fingers. In [5, 6] we proposed a self-contained hand biomechanical model for grasping simulation. Here, we extend the previous work and tackle grasp posture planning with Artificial Neural Networks (ANN).

The present research initially reviews the previously cited RKVs by means of an ANN. Then, electromyography prosthetic control is simulated by means of a real time modulation of those RKVs as inputs of an ANN. The outputs are the hand joint angles during the grasping trajectory. Graphical validation is done in a hand model with Opensim® software.

Human hand grasping is a very complex process that has been studied for years [1-3]. Its characterization is the key for hand prosthetic control. In a previous work [4] the use of kinematic reduction as a rational generalized method for studying grasping postures was proposed. In particular, Principal Component Analysis (PCA) was applied to reduce the hand kinematics while grasping cylinders for cylindrical (C) and 5-digit pinch (5dP) grasps. The PCA showed that the hand kinematics is actually low-dimensional, and can be described by 5 Reduced Kinematic Variables (RKVs) for C and 5dP grasps.

In [5, 6] we proposed a self-contained hand biomechanical model. Here, we extend the previous work and tackle grasp posture planning with Artificial Neural Networks (ANN).

The present research initially reviews the RKV concept by means of an ANN. Then, electromyography prosthetic control is simulated by means of modulation of those RKVs. The outputs are the hand joint angles during the grasping trajectory. Graphical validation is done with Opensim®.

Methods: In the kinematic model in [5] the human hand is considered to be composed of 5 open chains connected to the carpus through different joints (25 DOFs).

Grasping experiments were performed with 8 right-handed subjects and 4 cylinders of various diameters. Subjects carried out transportation tasks with C and 5dP grasps. Each test was repeated 3 times and the 3D positions of 32 markers were recorded using a motion capture system (infrared Vicon© system). The evolution of 25 joint angles describing the hand grasping posture was computed from the markers' positions over time, using the method described in [7].

Pattern recognition and control are implemented by using a 2-layer feed-forward ANN with 100 neurons in the hidden layer, as in [6]. A training set is established by identifying and associating min/max numerical intensity values of the postures associated to each RKV described in [4]. The resulting ANN manages to identify the same patterns and their intensities in new sets. Thus, a new ANN is trained to control the evolution in hand posture, by varying the intensity modulation of the RKVs value.

Results: ANNs are a powerful method that allows modeling cumbersome dependencies. They are recognized as the most effective and appropriate artificial intelligence technology for pattern classification and control.

After the appropriate ANN has analyzed the dataset (network training), it can make predictions based on hidden dependencies.

Figure:
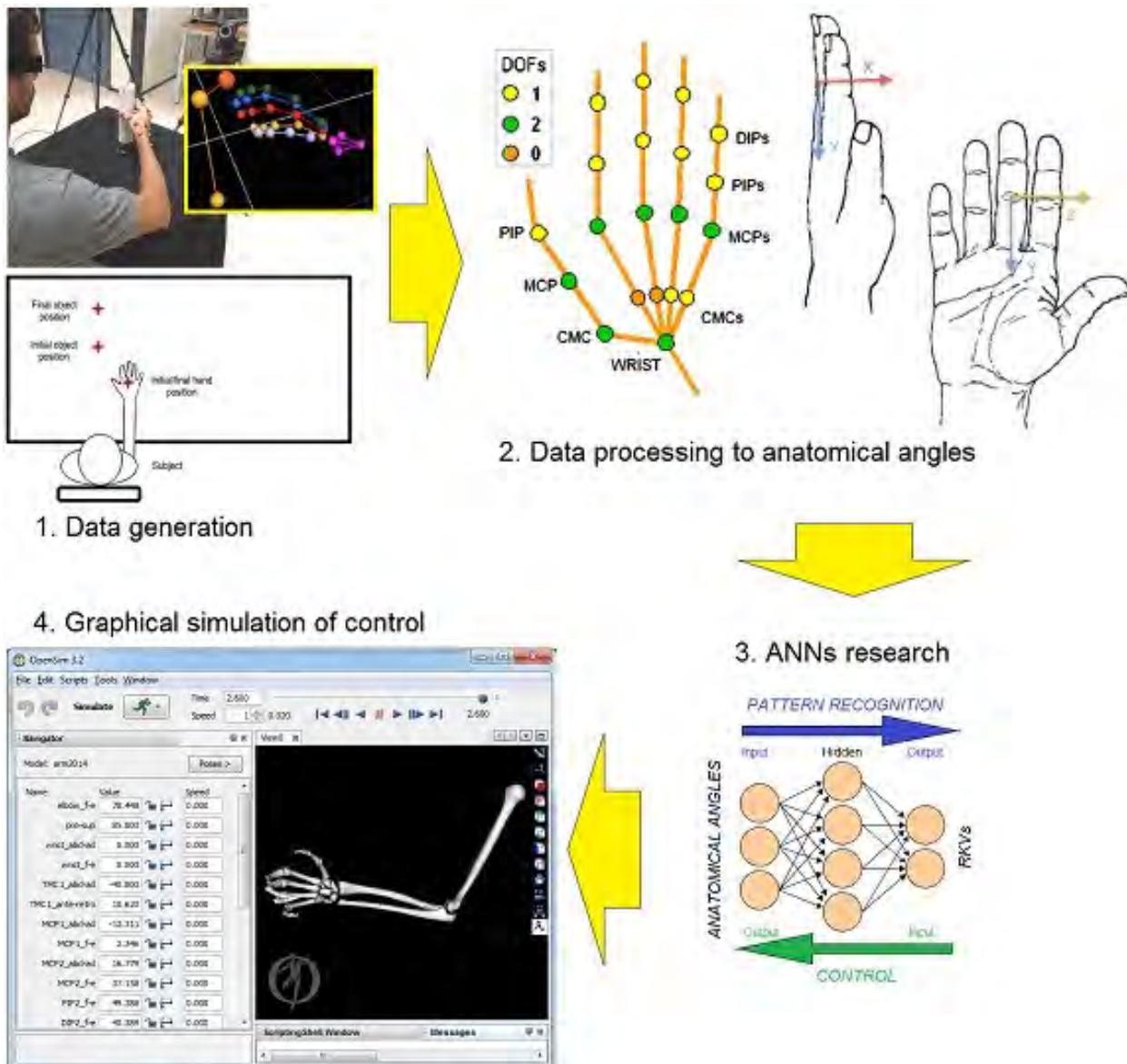
Caption: Flow process from data acquisition to ANN control simulation

Conclusion: The proposed studies are of high interest for the control of prostheses by a few electromyography signals in real time.

References: [1] Buchholz B., et al.; J. Biomechanics 25: 149-62, 1992.

[2] Santello M., et al.; J. Neurophysiology 79(3): 1307-20, 1998.

[3] Valero-Cuevas F.J., et al; J. Biomechanics 36: 265–70, 2003.

[4] Jarque N., et al.; III Reunión del Capítulo Español de la Sociedad Europea de Biomecánica (ESB), 24 de Octubre 2013, Barcelona, Spain

[5] Sancho-Bru J.L., et al; , (Ed.). Theoretical Biomechanics¸ InTech, 2011.

[6] Mora M.C., et al.; Int. J. Adv. Robotic Systems 9: 139, 2012.

[7] Sancho-Bru J.L., et al; Proc Inst Mech Eng H. 228(2):182–9, 2014.

Disclosure of Interest: None Declared

Computer Simulation

PO-0206

PROPOSAL OF A THREE-DIMENSIONAL TENNIS FOREHAND MODEL

Takuya Otsu [1,*]Norihisa Fujii [2]

[1]Health and Sport Sciences, University of Tsukuba Graduate School, [2]Faculty of Health and Sport Sciences, University of Tsukuba, Tsukuba, Japan

Introduction and Objectives: The tennis forehand groundstroke is one of the most important techniques in rallies. Elite players dictate games by using the powerful and precise forehand (Landlinger et al., 2010). In the real world, it is impossible to adapt various factors for various objectives and to induce ideal results simultaneously and instantaneously. Thus, in order to clarify the optimal forehand, an optimization technique including forehand simulations is essential. In the optimization studies, the simulations which meet some objectives reasonably were presented in ball pitching (Fujii and Hubbard, 2002) and high jump (Wilson et al., 2007), and such methods have been proven to be very useful. But very few researches on the optimization of the forehand have been reported. Moreover virtually no investigation on the forehand simulation model has been implemented. The objectives of this study were to formulate the forehand simulation model for the optimization and to evaluate the model.

Methods: One Japanese varsity-level tennis player participated in this study. The forehand motion was captured with twelve high-speed video cameras (500 Hz; VICON). The 3-D coordinates of the body land marks were collected to calculate the joint torques of an upper extremity. The racket-side arm was modeled by four segments: upper arm, forearm, hand, and racket. (1) The equations of motion, (2) the kinematic constraint equations, (3) the equations representing the degree of freedom for each joint (Fujii and Hubbard, 2002) were formulated as a matrix form $Ax = b$, where A is a coefficient matrix, x is a column vector comprising the variable to be calculated, and b is a column vector comprising the known values (Casius et al., 2004). The equations were solved with the Runge-Kutta method. To calculate a segment's orientation from its angular velocity, its angular acceleration and velocity were converted into Eulerian angles before integrations. The control variables of the model were time sequences of a shoulder horizontal adduction/abduction torque, adduction/abduction torque, and internal/external rotation torque; elbow flexion/extension torque; hand and racket angular accelerations. The control variables for hand and racket angular accelerations enabled the simulated motion to be proper for forehand. The output variables were motions of upper arm and forearm, elbow varus/valgus torque and pronation/supination torque, wrist flexion/extension torque, radial/ulnar flexion torque, and internal/external rotation torque. In order to evaluate this model, a matching simulation, which is the simulated forehand motion with the measured torques and angular accelerations, was compared with the captured motion. The simulation was carried out for the forward swing phase which was the phase from a completion of backswing to an impact. Then simulations with different conditions were implemented in order to check the sensitivity of the control variables. In condition 1, the peak timing of shoulder horizontal adduction torque was hastened by 5% of forward swing phase time. In condition 2, the peak timing of shoulder internal rotation torque was hastened by 5% of forward swing phase time.

Results: RMSs between the matching simulation and the captured motion were 0.12 rad/s^2 for angular accelerations and 0.003 Nm for output torques. Good consistency was observed between these two motions. It is considered that this model

represents the real forehand properly. Figure shows the stick figures of simulations in different conditions. The change in the shoulder internal rotation torque largely affected the motion. Table indicates the impact parameters, maximums and minimums of the constraint torques. In condition 2, it is observed that the much larger torque was needed to maintain the orientations of hand and racket.

Figure:
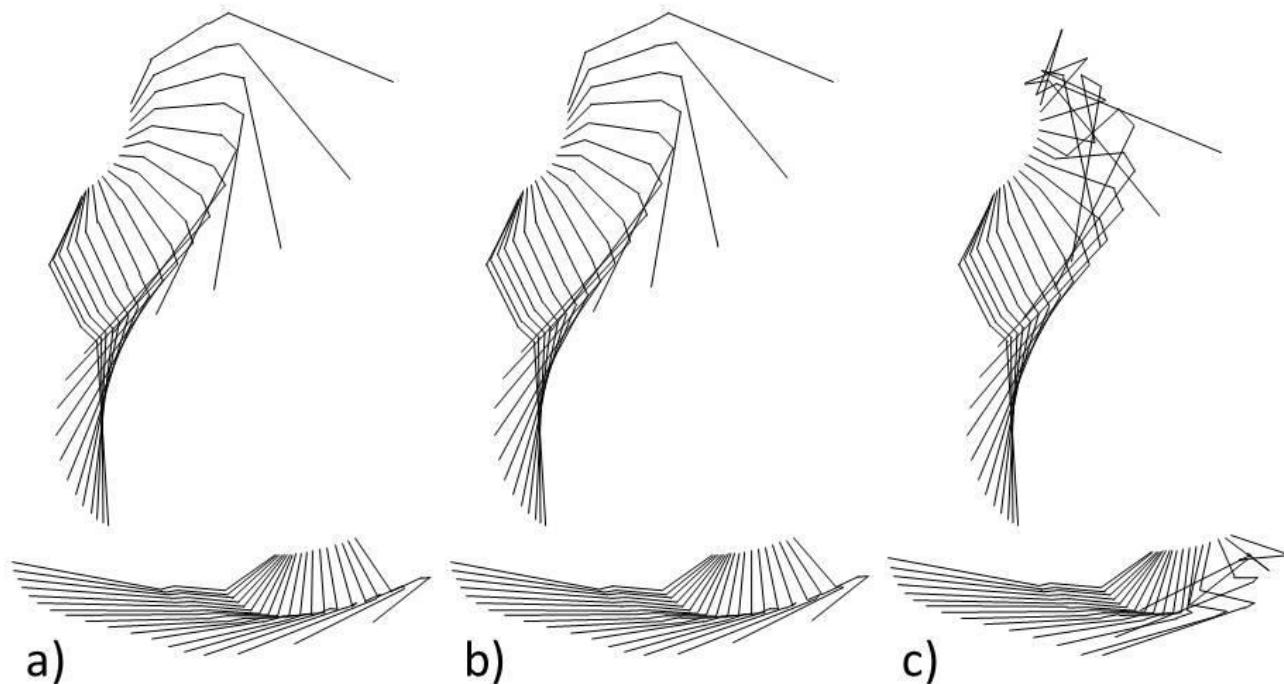
Caption: Stick figures of the matching simulation and the simulations with different conditions. Upward = bird's-eye view. Downward = lateral view. (a)Matching simulation; (b)Condition 1: The peak timing of the shoulder horizontal adduction torque was hastened.; (c)Condition 2: The peak timing of the shoulder Internal rotation torque was hastened.

Conclusion: The 3-D forehand simulation model was formulated for the steady integration and easy estimation of a success shot. The simulation model in this study can reduce the computational cost because of its fewer control variables.

Table:

Simulation	Racket face speed (m/s)	Swing direction difference (degrees)	Elbow varus(+)/ valgus(-) torque	(N·m)	Wrist internal(+)/ external(-) rotation torque	(N·m)
			Maximum	Minimum	Maximum	Minimum
Match	32.5	0.0	95.4	-125.4	17.6	0.7
Condition1	32.4	1.2	94.9	-124.0	19.3	0.7
Condition2	28.0	22.2	628.6	-184.6	318.7	-156.2

Caption: The impact parameters, maximums and minimums of the constraint torques.

References: [1] Casius et al., J. Appl. Biomech., 20: 421-449, 2004.

[2] Fujii and Hubbard, J. Appl. Biomech., 18: 135-154, 2002.

[3] Landlinger et al., Sports Biomech., 9(4): 280-295, 2010.

[4] Wilson et al., J. Biomech., 40: 3155-3161, 2007.

Disclosure of Interest: None Declared

Computer Simulation

PO-0207

THE SENSITIVITY OF OCCUPANT INJURY OUTCOME TO ERRORS IN DELTA-V PREDICTION

Rebecca Pride [1,*]Donald Giddings [1]David Richens [2]Donal McNally [1]

[1]The University of Nottingham, [2]Cardiothoracic surgery, Nottingham University Hospitals NHS Trust, Nottingham, United Kingdom

Introduction and Objectives: The aim of this study is to identify the variance in predicted occupant injury due to expected errors in the calculated delta-V (ΔV). The ΔV value is a descriptor of vehicle motion during a collision and its accuracy is dependent on the accuracy of input parameters used in its calculations. The Abbreviated Injury Scale (AIS), a non-linear severity scoring system, is used to describe injury severity and can be predicted by use of injury criteria.

Methods: In all selected collisions the occupant sustained a fatal aortic rupture allowing them to be broadly comparable in terms of known injury outcome and as there are two well documented thoracic injury criteria, Viscous Criterion (VC) and Combined Thoracic Index. The nature of each collision was such that the ΔV calculation was valid. The ΔV value was either obtained from the police collision reports or calculated using standard protocols. A confidence interval for the value of ΔV was determined using the sensitivity values of ΔV to its input parameters. MADYMO® software was used for the simulations with a triangular crash pulse to represent a typical collision. The injury criteria used to predict AIS injury severity included the Head Injury Criterion (HIC_{15}), Neck Injury Criterion (Nij) and the Combined Thoracic Index (CTI). The Maximum Abbreviated Injury Score (MAIS) is the highest assigned AIS level across all body regions.

Results: The variance of ΔV had little effect on the predicted AIS score for each of the regions documented; 87% of low and the high run predictions were within 1 AIS level to the mid run (Table 1). The occupant in one simulation sustained a 3 point increase in thoracic AIS level in the high ΔV run due to impact with the steering wheel, this indicated that the two lower ΔV were not representative of the actual collision due to the low ΔV values. ΔV variance had little influence on the location of the most serious injury, and the locations with AIS > 3. Thoracic and head injuries with AIS > 3 were predicted over a large range of ΔV values whereas this only was seen in high ΔV in the neck region. The results show valid representation of collisions with a ΔV > 8ms^{-1} but indicated that collisions with lower values require more precise measurement and calculation.

Conclusion: The expected errors in the calculation of ΔV did not result in significant variance of predicted occupant AIS; this indicates that the data collection methods for the calculation of ΔV are of sufficient accuracy to successfully predict occupant injury through simulation.

Table:

	ΔV (ms⁻¹)	AIS value					MAIS	Location of MAIS	Areas of AIS > 3
		Head	Neck	Thorax	Femur	Tibia			
Peugeot	16.1	3	5	4	3	3	5	Neck	Neck, Thorax
	19.23	5	5	5	3	3	5	Head	Head, Neck, Thorax
	22.3	5	5	6	3	3	6	Thorax	Head, Neck, Thorax
MG	4.411	1	1	1	1	1	1	Thorax	
	7.297	1	1	2	1	1	2	Thorax	
	7.587	2	1	5	1	3	5	Thorax	Thorax
Fiat	10.79	6	3	5	3	3	6	Neck	Head, Thorax
	12.84	6	1	6	3	3	6	Thorax	Head, Thorax
	14.89	6	1	5	3	3	6	Head	Head, Thorax

Caption: Table 1 - Results

Disclosure of Interest: None Declared

PO-0208

FINITE ELEMENT SIMULATION OF DRILLING FORCE IN CORTICAL BONE WITH EXPERIMENTAL VALIDATION

Yahui Hu [1,*]Jianbo Sun [1]Qingyun Zhang [1]Weihua Fu [2]

[1]Tianjin Key Laboratory of the Design and Intelligent Control of the Advanced Mechatronical System, Tianjin University of Technology, [2]General surgery Department, Tianjin Medical University General Hospital, Tianjin, China

Introduction and Objectives: Bone drilling causes an increase in bone temperature, and a temperature above 47°C is critical because it causes thermal bone necrosis. Prediction and control of
drilling force is critical to the success of operations involving bone drilling. This paper studied the changes of drilling force in the process of drilling cortical bone, and a prediction model of drilling parameters about drilling force was built.

Methods: A numeric approach was adopted. The three-dimensional finite element model with Abaqus6.11 was used to simulate bone force. A prediction model was set up according to a orthogonal experiment design. By comparing the finite element model with the experimental results, the influence of the drilling parameters on drilling force was gotten, and further the reliability of the finite element model and the prediction model of drilling force were verified.

Results: Results of analysis indicated that the bit diameter affected drilling force most, feed rate was the second, and drilling speed was the smallest. The increase in drill diameter and feed rate caused increase in drilling force, the increase in drilling speed caused decrease in the drilling force. The predicted results were also
proven to be in accordance with the experimental results, but it was always greater than experimental. There were some deviations which was within 15% between finite element model and experimental model.

Conclusion: The drilling force of finite element model and experimental model has the same change trend. The FE model can predict the drilling force with reasonable accuracy. The prediction model of drilling force
can assist in the selection of favorable drilling conditions and drill-bit geometries for bone-drilling operations.

References: [1]Abukhshim NA,et al. Int J Mach Tools Manuf,782:800–46,2006.

[2]Bachus KN, et al. Med Eng Phys ,22(10):685–91,2000.

[3]Bono M,et al. Int J Mach Tools Manuf ,901:907–46,2006.

[4]Brisman DL. Int J Oral Maxillofac impl ,11:35–7,1996.

[5]Hamade RF,et al. Int J Mach Tools Manuf ,387:396–446,2005.

[6]Mukherjee I,et al. Compute Ind Eng ,15:3–5,2006.

[7]Shin HC,et al. J Biocmech ,33:39-139,2006.

[8]T.U.Diljak,etal.AdvancesinProduction Engineering&Management ,2:103-106,2007.

[9]Ueda T,et al. Manuf Technol ,93:56–96,2007.

[10]Wang lei, et al. Tool technology,1:8-12,2007.

[11]Yuan-Kun Tu,et al. ICBBE,1268-1271,2008.

[12]Yuan-Kun Tu,et al. Bio-informatics and Biomedical Engineering, (ICBBE),1-4,2011.

Disclosure of Interest: None Declared

Computer Simulation

PO-0209

MRI-BASED PARALLEL MECHANISMS TO MODEL SUBJECT-SPECIFIC JOINT KINEMATICS

Simao Brito Da Luz [1,*] Luca Modenese [1] Nicola Sancisi [2] Peter Mills [1] Belinda Beck [1] Thor Besier [3] David Lloyd [1]

[1] Center for Musculoskeletal Research, Griffith University, Gold Coast, Australia, [2] DIN, University of Bologna, Bologna, Italy, [3] ABI, University of Auckland, Auckland, New Zealand

Introduction and Objectives: Subject-specific musculoskeletal (MSK) computer models can estimate muscle and joint articular forces, enabling the identification of mechanical factors causing joint injury or disease. MSK models include models of skeletal anatomy and joint kinematics that can be created in OpenSim [1]. These models are generic and undergo simple linear scaling to a subject using markers from motion analysis. However, generic scaled MSK models produce less accurate estimates of measured knee articular forces compared to those that are subject-specific [2]. Thus, methods are needed to readily create subject-specific models.

Passive tibiofemoral (TFJ), patellofemoral (PFJ) and talocrural (TAJ) kinematics measured in cadavers are well predicted using 3D parallel mechanisms [3,4]. These models integrate the cadaver's measured bone, ligament and tendon geometries to constrain the joints' degrees of freedom (DOFs). Using TFJ flexion angle as input, TFJ and PFJ models estimate the tibia's and patella's remaining Flex-Extension (FE), Abd-Adduction (AA), Int-External (IE) rotations and Ant-Posterior (AP), Prox-Distal (PD) and Med-Lateral (ML) translations. Similarly, TAJ models use talus flexion angle to estimate kinematics from the other TAJ DOFs. However, these models have only been used in cadavers where the kinematics were accurately measured and used to tune the models geometrical parameters.

We aimed to use MRI images of *in vivo* lower limb bones, cartilages and ligaments to create models' geometrical parameters. Using previously described mechanisms [3,4] we estimated subject-specific kinematics for use in OpenSim. However, without measured kinematics to tune the model, we created specialized algorithms to solve the mechanisms and then compared the results with those from cadaveric studies.

Methods: TFJ, PFJ and TAJ models were modified from [3,4] so that parameters could be determined from MRI. Participants (n=14) were scanned in a 3T MRI scanner with axial slices of the complete limb and sagittal slices of the hip, knee and ankle. Segmentation, alignment and smoothing were performed generating 3D surfaces (Fig.1) and bones' coordinate frames according to ISB standards. Spheres were fitted to the articular surfaces of the femur, tibia, fibula and talus. Two spheres were also fitted to the femoral trochlea with their centers defining the PFJ hinge axis. Ligament and tendon attachment points were initially represented by the centroid of each attachment surface.

For TFJ flexion angles from 0° to 90° the other TFJ and PFJ DOFs were determined using the mechanisms, by minimizing the changes in 1) distance between the spheres' centers, and 2) ligament lengths. TAJ model was a similar mechanism, using FE angles from -25° to 15°. For each subject, model parameters were tuned via simulated annealing including constraints to 1) avoid mechanism singularities, 2) match cadaveric kinematics patterns, and 3) minimize the difference between tuned and initial measured parameters. Our algorithm also ensured the tuned 1) ligaments' attachments remained within their bone attachment areas, and 2) sphere centers and radii well matched the cartilage surface point clouds.

Pearsons' correlations were calculated between the mechanisms derived kinematics and those from cadaveric studies. Sensitivity analysis was performed to verify how robust results were to the tuned parameters.

Results: Derived kinematics had no singularities and were very similar to the cadaveric data (Table.1). Differences in participant's anatomy compared to cadavers may explain some of low correlations. Nevertheless, good overall correlations indicate that models can be used to reproduce subject-specific kinematics. Sensitivity analysis suggested that TFJ, PFJ and TAJ models' were more dependent respectively on tibia's MCL insertion, tibia's patella tendon insertion and tibia's distal-lateral sphere center.

Figure:
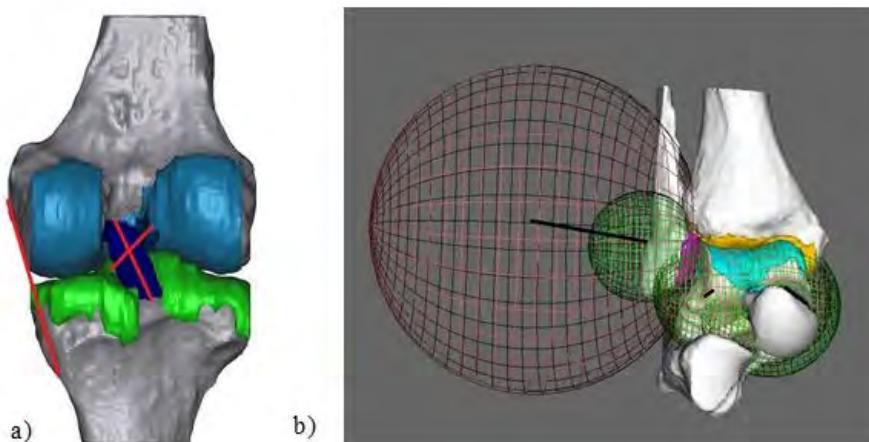
Caption: Figure 1-a) TFJ surfaces with ligament links, b) Spheres fitted to TAJ surfaces

Conclusion: TFJ, PFJ and TAJ kinematics can be estimated using 3D mechanisms with parameters obtained from MRI. These can be used in OpenSim and MSK models and may improve estimates of muscle and joint contact forces.

Table:

	DOF					
	FE	AA	IE	AP	PD	ML
TFJ	-	0.87±0.07	0.88±0.01	0.93±0.02	0.99±0.005	0.67±0.33
PFJ	0.99±0.0	0.67±0.31	-0.09±0.58	0.99±0.006	0.99±0.004	0±0.58
TAJ	-	0.93	0.98	0.98	0.57	0.83

Caption: Table 1 - Correlation (mean±SD) between subject-specific kinematic and cadaveric results

References: [1] Delp et al., IEEE Trans Biomed Eng, 54:1940-1950, 2007.

[2] Gerus et al., J Biomech, 46:2778-2786, 2013.

[3] Sancisi et al., J Mech Robot, 3:041003-1-041003-7, 2011.

[4] Franci et al., J Biomech,42:1403-1408, 2009.

Disclosure of Interest: None Declared

Computer Simulation

PO-0210

PROTECTION OF ANKLE BRACE ON ANKLE SPRAIN DURING PARACHUTE LANDING

Junchao Guo [1,*]Lizhen Wang [1]yubo fan** [1]

[1]Key Laboratory for Biomechanics and Mechanobiology of Ministry of Education, School of Biological Science and Medical Engineering, Beihang University, Beijing, China

Introduction and Objectives: Ankle injuries were the most common injuries in running and jumping. Ligament injuries of ankle in US army paratroopers were reported annually [1]. 74% of all ankle injuries were ankle ligament sprains, and 85% of ligament sprains were caused by an inversion trauma. Ankle injuries accounted for 30 to 60% of all parachuting injuries. This study was aim to investigate the protection of ankle brace for lateral ankle joint during parachute landing.

Methods: A group of 16 adult male participated in this study. They had no acute lower extremity injury and previous ankle injury or surgery. Average weight was 71.3Kg at 25years old. Subjects with ankle brace stood the predefined platform, and jumped from the different height of platform (152cm, 82cm and 52cm) [2] on force plate (FP4060-08-100, Bertec, Inc, USA) (Fig.1). The data of ground reaction force in landing experiments was recorded at 1000Hz sampling frequency. To establish the outer ankle brace profile, point cloud was obtained by 3D Scanner (Tianyuan, Inc, China). Impact time and plantar pressure were measured during parachute landing on 20°slope. Then a finite element model of the complex foot structures including bones, cartilage, ligaments, fascias, soft tissue and skin was developed to contrast the effect of no ankle brace and outer ankle brace on lateral foot ankle (Fig.1).

Results: Peak plantar pressure of 11.12MPa in F-Scan measurement was predicted at the lateral forefoot region when volunteer loaded on 20°slope. This was consistent with the results in FE prediction. Plantar pressure after the outer ankle brace was redistributed in medial and lateral of forefoot and heel region. To some extent, peak plantar pressure was decreased. Whilst the strain of calcaneofibular ligament and anterior talofibular ligament reduced 32.6% and 32%, respectively.

Figure:
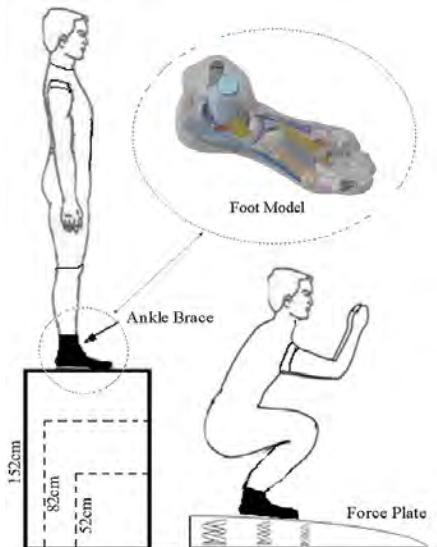
Caption: Simulation landing on force plate from the different height of platform and foot model

Conclusion: Protection of ankle brace could be important to protect the lateral ankle joint during parachute landing on slope. In particular reduced the risk of lateral ankle ligaments sprain.

References: [1] Schmidt et al., Injury Prevention, 11:163-168, 2005.

[2] Niu et al., Aviat Space Environ Med, 82:1118-1124, 2011.

Disclosure of Interest: None Declared

STREAMING FLOW FROM MICROBUBBLES ACTIVATED BY ULTRASOUND IN A BLOOD VESSEL MODEL

Kyehan Rhee [1,*]Eun Jin Cho [1]Gon Khang [2]

[1]Mechanical Engineering, Myongji University, [2]Biomedical Engineering, Kyung Hee University, Yongin, Korea, Republic Of

Introduction and Objectives: Recently, ultrasound contrast agents (UCAs) have been applied to therapeutic purpose in order to increase the specificity and efficiency of drug delivery. Ultrasound enhances drug delivery incorporating UCAs can induce temporary increase of tissue and cellular membrane permeability, which is achieved by the pressure and stress fields caused by cavitation of microbubbles. Transport of UCAs towards vessel walls is desirable because therapeutic compounds attached to UCA shells can binds more efficiently to the vessel well as well as near wall bubbles generate strong wall stress field. Most studies on bubble oscillations, translation and streaming induced by oscillating bubbles were limited to a single bubble, and bubble cluster formation and streaming from microbubble foam have been studied less. The formation of bubble clusters and streaming from them may be of interest in therapeutic application of UCAs. In this study, we analyzed the streaming flow induced by bubble cluster motion and oscillation, and observed UCA cluster formation and translation by ultrasound sonication.

Methods: An elastic tube with the inside diameter of 3 mm was manufactured from a silicone resin (Sylgard 184, Dow Corning, NH). The silicon tube was inserted into the polycarbonate container (150x120x35 mm^3), and filled with distilled water for ultrasound transmission. A 15.5 mm diameter hole was drilled for ultrasound probe (1.0 MHz, i3-0108-P, Panametrics-NDT, Waltham, MA) insertion. Acoustic pressure was measured using a calibrated 0.2 mm PVDF needle hydrophone (Precision Acoustics Ltd, Dorchester, UK) at the tube surface. The UCA Sonovue® (Bracco, Milano, Italy) was mixed in 5ml of deionized water, resulting in 2×10^8 mirobubbles per milliliter solution. Fluorescent particles with a diameter of 7 μm were also mixed with the solution for flow visualization. The UCA and fluorescent particle mixture in distilled water was infused to the silicon tube using a syringe pump (KDS Legato100, KD Scientific, MA). The test section was place on top of a microscope (BX51, OLYMPUS Co., Japan) equipped with a high-speed camera (MIRO EX4, Vision Research Inc., NJ). Particle image velocimetry (PIV) was used to measure the streaming flow fields. In order to obtain the particle images, the fluorescent images of particles were captured at a frame rate of 1,000 fps. They were processed with commercial PIV software (Insight-3G, TSI Inc., MN) for velocity field measurement. The field of view was 4.5 mm×3.5 mm, and the interrogation window size was 16×16 pixels with a 50% window overlap. Because time interval of two consecutive images was much longer than the period of incident pressure wave, measured velocity showed mean nature of flow streaming for 1 ms.

Results: The ultrasound probe was activated by a continuous sinusoidal voltage signal. The signal was amplified up to 50 volts, and incident pressure amplitude at the tube surface was 500 kPa. The UCAs were unevenly distributed over the test section before sonication. When 1 MHz ultrasound of sonication started, microbubbles attracted and repelled by secondary radiation forces and formed clusters near the pressure nodes within 100 ms. These clusters coalesced to form microforms, and translated in the direction of the ultrasound field owing to primary radiation forces. The resulting microfoams further moved to the tube wall, and remained in the stable position afterwards. Further movement of

microforms was not observed, because radiant and drag forces on the microforms were balanced. This observation agreed with the UCA cluster formation in a capillary with diameter of 200 micrometers. Movement of micro clusters and microform induced the vortical flow fields, and the center of clockwise vortex moved to the lower region of an image frame. Streaming velocity was order of 10 mm/s, and the maximum velocity of 15 mm/s was also observed at some locations. Once microforms stayed in a stable position, coherent vortical streaming flow over the tube was not observed. Local streaming from the oscillating bubbles or small clusters was detected, and local streaming velocity was less than 10 mm/s.

Conclusion: In this study, UCA coalescence, cluster formation and translation by ultrasound sonication was observed, and flow streaming induced by micro bubbles and foams were measured. Microbubbles formed clusters within a few hundred microseconds and translated to the wall by primary radiation force of 500 kPa acoustic pressure, and remained in the position where primary radiant force balanced with the drag force. Bubble cluster motion in a tube induced vortical flow with the streaming velocity of about 10 mm/s. Once the bubble clusters located in a stable position, this vortical streaming was disappeared and local streaming from small oscillating bubbles was observed. Streaming velocity from stably oscillating bubbles was less than 10 mm/s.

Disclosure of Interest: None Declared

Imaging / Advanced Imaging

PO-0212

A DUAL SLICE-TO-VOLUME REGISTRATION METHOD FOR MEASURING THREE-DIMENSIONAL KNEE KINEMATICS IN VIVO USING REAL-TIME MRI

Cheng-Chung Lin [1]Tung-Wu Lu [1][2],*Chao-Yu Hsu [3]Ting-Fang Shih [3]

[1]Institute of Biomedical Engineering, National Taiwan University, [2]Department of Orthopaedic Surgery, School of Medicine, National Taiwan University, [3]Department of Radiology, College of Medicine, National Taiwan University, Taipei, Taiwan, Republic of China

Introduction and Objectives: Accurate knowledge of the three-dimensional (3D) kinematics of the tibiofemoral and patellofemoral joints *in vivo* are essential for a better understanding of the function of the joints and for relevant clinical applications. However, radiation free methods for such information are limited. Recently, our group has developed a method based on the registration of 3D MRI volume and single-slice real-time MR images at a high spatiotemporal resolution obtained by a novel real-time MRI technique [1] (WIP 610, Siemens) to measure 3D kinematics of the femur and tibia [2]. But, this approach did not enable accurate measurement of the 3D kinematics of the patella. To bridge the gap, the current study aimed to develop a new approach based on the novel real-time MRI with dual slice scheme. This new method was evaluated for the accuracies in measuring 3D poses of the tibiofemoral and patellofemoral joint during knee flexion/extension.

Methods: Four healthy adults (age: 23 ± 0.0 years) participated in the current study with informed written consent as approved by the Institutional Research Board. The subject was examined at a prone position in a 3-Tesla MRI system (Verio, Siemens, Erlangen, Germany) with the thigh and shank fixed to a purpose-built jig, allowing passive knee flexion/extension as the thigh remained stationary. A neck matrix coil was applied for imaging the knee joint.

Static multi-slice 3D images and dual slice real-time images of the knee joint were acquired separately at five static positions using MRI. The parameters of the MRI sequences followed our previous study [2]. The positions of dual slice images were adjusted to intersect with both the femoral and tibial shafts with an inter-slice distance of approximately 22 mm. Real-time images of the knee were then acquired at each of the static positions with an effective temporal resolution of 3 frames/s, giving 46 × 2 images per position.

The MR-derived models of the femur, tibia and patella were segmented from the 3D MRI data set. The proposed dual slice-to-volume registration method (DSVR) was based on the registration of a 3D volumetric bone model to the dual slice real-time images. That is, the six degrees-of-freedom of an individual bone at each instance were determined when two reformed images interpolated from the bone model [2] best matched the two real-time MRI slices according to a gradient difference criterion.

The accuracy of the proposed DSVR was evaluated using the data from the static trials. The gold standard poses of the tibiofemoral and patellofemoral joints were obtained from the static 3D image data set. The measurement errors were determined as the differences between the gold standard and the DSVR-determined poses. The accuracy of the method was expressed in terms of the bias and precision over all trials and all subjects.

Results: The bias and precision of the DSVR-determined tibiofemoral joint poses were all within 0.51 mm and 0.64 degree for translations and rotations respectively (Fig. 1). The performance of the method for the patellofemoral joint poses were slightly worse, with the bias and precision within 0.64 mm and 0.92 degree for translations and rotations respectively (Fig. 1). Compared with previous fluoroscopy-based methods [3], the DSVR method has much better medial-lateral translational precision while maintaining comparable accuracies in the rotational components. When compared with our previous single slice-to-volume registration method [2], current DSVR method was found to have slightly reduced errors for the tibiofemoral joint poses, which can be explained by the nature of dual slice registrations. For example, if the center of rotation of a bone is placed on one slice, a slight out-of-plane rotation of the bone would lead to a significant change in the intersection region between the bone and the other slice owing to the inter-slice distance, giving the high sensitivity of the objective function to the out-of-plane rotations.

Figure:
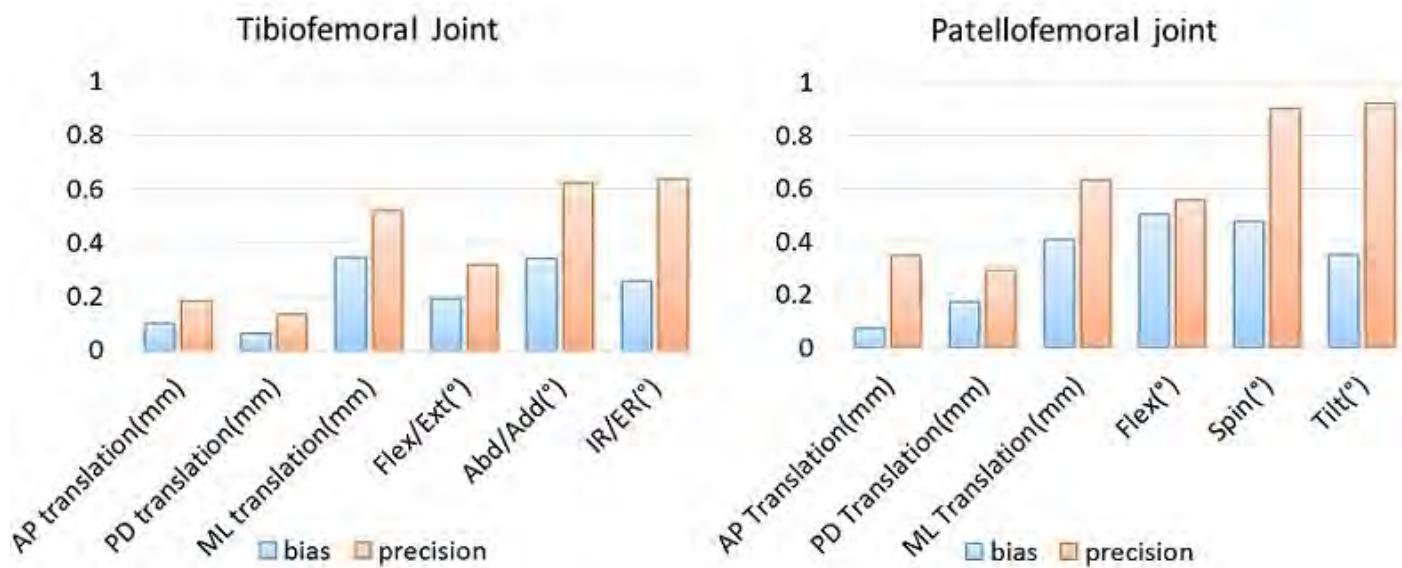
Caption: Fig. 1: The bias and precision of the DSVR measurements of the tibiofemoral and patellofemoral joint poses.

Conclusion: A new non-invasive method based on dual slice real-time MRI was developed and evaluated for accuracies in measuring *in vivo* the 3D poses of the tibiofemoral and patellofemoral joints. With the accuracies achieved, and without the use of ionizing radiation, the proposed method promises to be a valuable tool for studying 3D kinematics of the knee joint in a non-invasive way.

References: [1] Zhang et al., J Magn Reson Imaging, 31:101-9, 2010.

[2] Lin et al., Med Phys, 40:102302, 2013.

[3] Tsai et al., Med Phys, 37:1273-84, 2010.

Disclosure of Interest: None Declared

PO-0213

INVESTIGATING THE OCULAR SURFACE TEMPERATURE IN PRESENCE OF UVEAL LESIONS

Sara Matteoli [1,*]Giulia Pieretti [2]Cinzia Mazzini [2]Andrea Corvi [1]

[1]Department of Industrial Engineering, [2]Department of Translational Surgery and Medicine, University of Florence, Florence, Italy

Introduction and Objectives: The presence of a tumor inside biological bodies is known to cause an increase in the temperature of the surrounding healthy tissues [1]. Such phenomena have been observed in the human breast and skin [1]. In the field of ophthalmology, the effects of tumor on the ocular temperature distribution appear to be rarely investigated [2-4]. So far, the use of ocular thermography has offered great opportunities for both monitoring the temperature of the anterior eye and analyzing the effects of some pathology in the OST [5-9]. The aims of this study were to evaluate the ocular surface temperature (OST) in patients affected by uveal lesions and to investigate any correspondence between OST and uveal lesions.

Methods: Nineteen (9M/10F, 30-91 years) affected by uveal lesions were included in the study. Table 1 shows the lesion characteristics of all subjects. They all underwent a comprehensive clinical evaluation in order to investigate the presence of other ocular or systemic pathologies other than uveal lesions. All eyes were investigated by infrared thermography (FLIR A320) and ultrasound. Specifically, the ultrasound scans were always performed after thermography as both dilating drops and acoustic gel could interfere with the temperature measurement. In case of malignant lesions, thermographic acquisitions were performed even after treatment, if given. OST values were calculated by means of an image processing technique, which allowed extracting the OST from the selected frames independently of the eye geometry. This kind of normalization allowed avoiding confounding factors when comparing both eyes of the same subject.

Results: The analysis of the OST showed that patients affected by primary or secondary choroidal melanoma had the pathological eye warmer (0.5-2°C) than the contralateral healthy one. Moreover, the treatment lowered the OST of the affected eye (up to 0.9°C). This effect was shown also in case of treated choroidal hemangioma. In case of choroidal nevi, the OST of the affected eyes were always lower than the contralateral.

Figure:
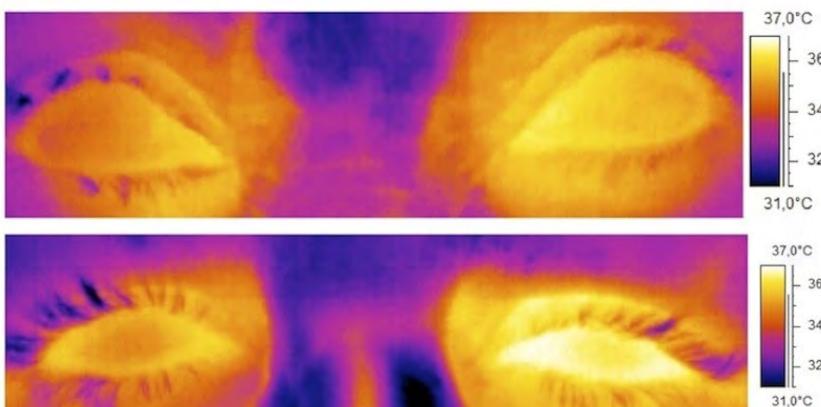
Caption: Choroidal nevus (right eye, up); choroidal metastasis (left eye, low).

Conclusion: The main hypothesis of this study was to find a temperature increase in case of malignant lesions. This hypothesis was satisfied within the investigated subjects. Indeed, patients affected by choroidal melanoma had the pathological eye warmer than the opposite healthy one. Especially in case of suspect melanoma, this finding may help the clinician to be more suspicious about the malignant nature of the lesion, as its diagnosis was still uncertain. Patients who underwent thermographic measurements after treatment showed, as expected, a decrease in temperature in the treated eye, which can demonstrate a reduced blood perfusion to the lesion (reduced in dimensions itself). The OST measurements may represent a cheap, not-invasive and not-time-consuming test to evaluate ocular vaso-regulation, and to relate those measurements with the presence of intra ocular uveal lesions. This approach paves the way to make thermography a useful tool in differentiating benign from malignant lesions.

Table:

N°	M/F	Age (aa)	Eye	Kind of lesion	Lesion (mm)*	Site of lesion (area)	Treatment
1	F	82	OS	choroidal nevus	5.5x1.5	I	-
2	F	65	OD	choroidal nevus	3.1x1.26	T	-
3	F	75	OS	choroidal nevus	6.4x1.1	PP (supero-macular)	-
4	M	58	OS	choroidal nevus	4,3x0,8	Para-papillary	-
5	F	73	OD	choroidal nevus	minimum thickness	S-N	-
6	M	46	OD	choroidal hemangioma	2 x 7.7	PP (S-T arcade)	3 PDT
7	M	30	OD	choroidal hemangioma	8.3x3.7	Supero-papillary	3 PDT (August 2011, June 2012, September 2013)
8	M	47	OS	choroidal hemangioma	flat lesion	PP (I-T arcade)	PDT (September 2013)
9	M	91	OD	choroidal melanoma	7x2	PP	-
10	M	72	OD	choroidal melanoma	5X5	PP (I-T arcade)	-
11	F	72	OS	ciliary body melanoma	12x5	N	Proton-beam(2002)
1	F	77	O	ciliary body	3.1x1	I	Proton-beam (2004)

2			D	melanoma			
1 3	F	72	O D	choroidal melanoma	4x0.5	para-papillary	Brachitherapy I125 (February 2009)
1 4	F	72	O S	choroidal melanoma	3.4x0.4	I-T	Proton-beam (2004)
1 5	M	49	O S	choroidal melanoma	8.3x4.8	S-N	Brachitherapy l125 (January-February 2011).
1 6	F	77	O D	choroidal melanoma	9.5x3.8	PP (I-T-arcade)	Brachitherapy (2011)
1 7	M	61	O D	choroidal melanoma	7.7x7.7x3.6	T	Laser (June 2012)
1 8	M	80	O D	choroidal metastases	whole vitreous cavity	whole vitreous cavity	-
1 9	F	53	O S	choroidal metastases	13x3.5	I-T	-

*basal diameter x thickness; I=inferior, T=temporal, S=superior, N=nasal, PP=posterior pole.

Caption: Characteristics of the lesions of each patient examined

References: [1] Ooi EH et al., Comput Biol Med, 39: 667-677, 2009.

[2] Popescu MP et al., Rev Chir Oncol Radiol O R L Oftalmol Stomatol Ser Oftalmol, 23: 271-274, 1979.

[3] Wittig I et al., KlinMonatsb. Augenheilkd, 201: 317–321, 1992.

[4] Bourjat P and Gautherie M. Mod Probl Ophthalmol, 14: 278-285, 1975.

[5] Fujishima H et al., Br J Ophthalmol, 80: 29-32, 2006.

[6] Sodi A, et al. Eur J Ophthalmol, 17: 755-759, 2007.

[7] Martin D and Fatt J. Acta Ophthalmol (Copenh), 64: 512-518, 1986.

[8] Betney S et al., Cornea, 16: 158-161, 1997.

[9] Corvi A et al., Physiol Meas, 27: 371-384, 2006.

Disclosure of Interest: None Declared

DEVELOPMENT AND IMPLEMENTATION OF A METHOD USING OPENSIM TO CALCULATE GLENOHUMERAL JOINT CONTACT FORCE DURING MANUAL WHEELCHAIR PROPULSION ACCESSIBILITY TASKS

Andrew Symonds [1,*]Stephen Taylor [1]Tatsuto Suzuki [2]Peter Smitham [3]Angela Gall [4]Catherine Holloway [2]

[1]Biomedical Engineering, [2]Civil, Environmental & Geomatic Engineering, [3]Orthopaedic Surgery, University College London, [4]London Spinal Cord Injury Centre, Royal National Orthopaedic Hospital NHS Trust, London, United Kingdom

Introduction and Objectives: Manual wheelchair propulsion is known to cause shoulder injury, with repetitive joint loading and a high level of muscle activity suggested as causative factors [1]. High Glenohumeral (GH) joint contact forces during ramp propulsion and weight relief manoeuvres have been reported [2]. Further work is required to investigate the demand placed on the shoulder joint during accessibility tasks including propulsion on cross slopes and ascending bus access ramps. The aim of this study was to develop and test a method of collecting experimental data from wheelchair users during accessibility tasks, to enable calculation of GH joint contact force using OpenSim musculoskeletal modelling software. The methods of data collection chosen reflect the aim to enable analysis of such tasks away from the laboratory setting.

Methods: An experienced Spinal Cord Injured (SCI) manual wheelchair user (L1 incomplete, 75kg body weight (BW)) attended University College London's Pedestrian Accessibility and Movement Environment Laboratory. The laboratory houses an adjustable platform which enables the set-up of accessibility challenges similar to those experienced by manual wheelchair users in the built environment. The participant was required to propel a manual wheelchair on a stretch of level paving, a 2.5% cross slope (wheelchair tilted to the left when moving forwards), 6.5% incline and 12% incline. The 12% incline was set to recreate the length and slope of a London Bus access ramp.

Trunk, left shoulder and elbow kinematics were obtained using the XSens MTw system. Euler angles to animate the model coordinates were derived from the rotation matrix that determined the relative position of XSens units on adjacent body segments either side of the joint [3]. Push rim kinetics were recorded on the left side using the Sensewheel, a lightweight instrumented wheelchair wheel measuring 3-dimensional force, and moment about the wheel axle.

Measured joint kinematics and push rim reaction forces were applied to an adapted OpenSim model of the upper limb and trunk named 'Dynamic Arms 2013', a version of the Stanford VA Upper Extremity Model [4]. The model consists of rigid bodies representing the trunk, upper arm, forearm and hand and was constrained to allow trunk lean, 3 degrees of freedom at the GH joint and flexion/extension at the elbow joint. The actuator set comprised 29 muscles crossing the GH and elbow joints. A reserve actuator was added to the thorax ground joint; otherwise all other model muscle properties were maintained.

The model was manually scaled to participant characteristics. The muscle forces required to generate joint torques were calculated using the OpenSim (Version 3.1) static optimisation analysis, which utilises an objective function that minimises muscle activation. The results of the static optimisation analysis were used to calculate shoulder joint contact force during a representative push phase for each of the conditions. The peak and mean resultant propulsion force and GH joint contact force, and force magnification ratio were calculated [5].

Results: The results from the single SCI participant show that increasing peak and mean resultant propulsion force resulted in an increase in peak and mean GH Joint contact force (Table 1, Figure 1). The contact force results for the level condition were similar to those previously reported involving similar propulsion forces [6]. Increasing forces occurred as the slope of the footway increased.

Figure:
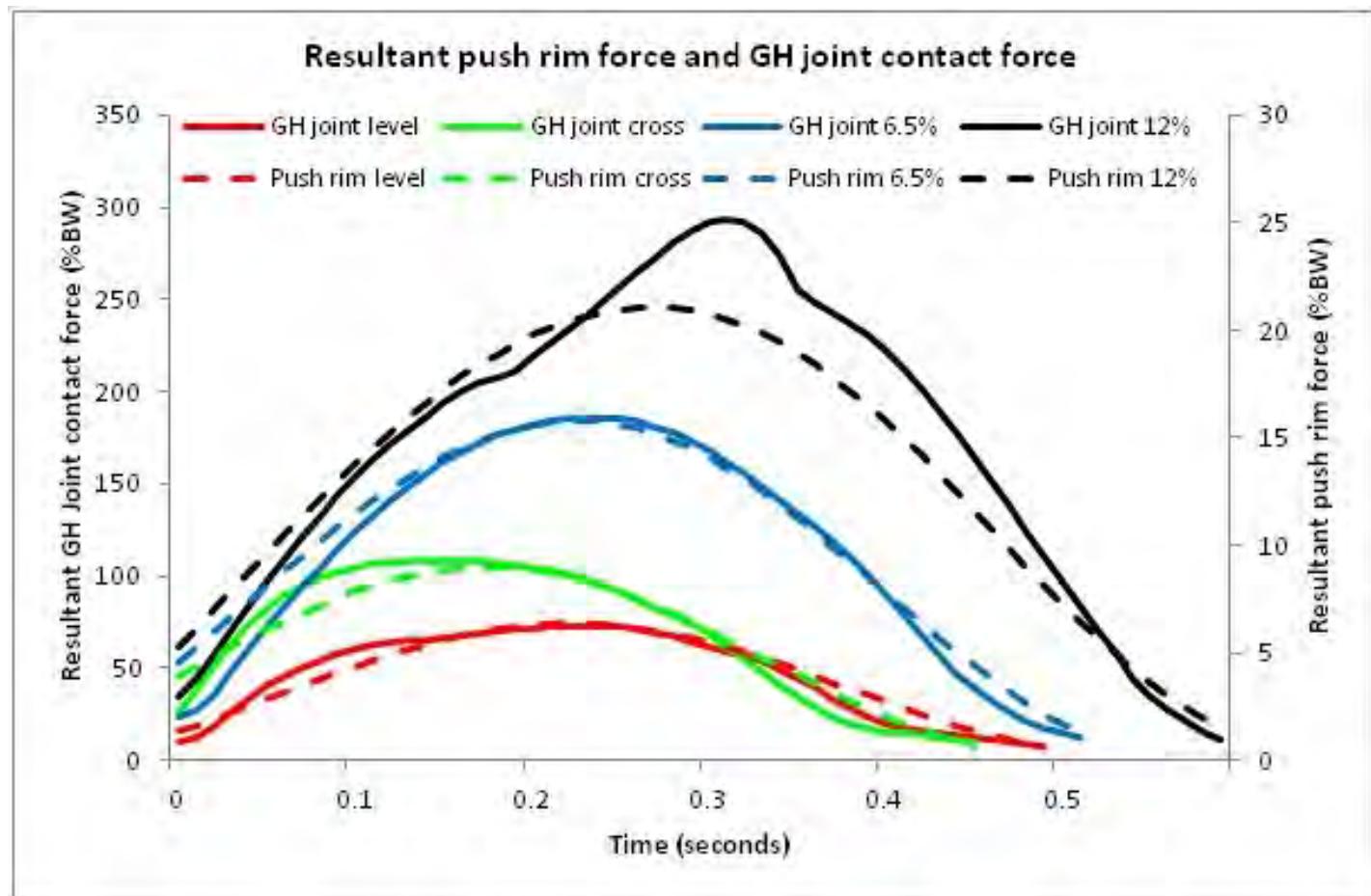
Caption: Figure 1: Resultant push rim and GH Joint contact forces from a representative push phase during different conditions

Conclusion: The experimental method used enabled calculation of GH joint contact force during activities representing accessibility challenges for manual wheelchair users. Negotiating the 12% incline representing the bus access ramp resulted in GH joint contact force 4 times greater than during level propulsion. This indicates that great stress is applied to the shoulder during such activities, potentially leading to injury. Analysis of propulsion during functional tasks to enable optimisation of technique is required.

Table:

Condition	Level	2.5% Cross slope	6.5% incline	12% incline
Peak resultant propulsion force (%BW)	6.4	9.0	15.8	21.0
Mean resultant propulsion force (%BW)	4.0	5.9	10.3	13.6
Peak resultant GH Joint contact force (%BW)	73.1	108.4	185.9	294.0
Mean resultant GH Joint contact force (%BW)	46.0	69.2	113.8	168.4
Peak force magnification ratio	14.6	16.5	12.0	14.5

Caption: Table 1: Push rim forces and GH Joint contact forces during a representative push phase for each condition

References: [1] Boninger et al., J Spinal Cord Med, 28(5): 437-470, 2005.

[2] Morrow et al., J Biomech, 43: 2487-2492, 2010.

[3] Kobrick et al., 63rd International Astronomical Congress, IAC-12-A1.6.6, 2012.

[4] Holzbaur et al., Ann Biomed Eng, 33(6): 829-840, 2005.

[5] Lu et al., J Biomech, 30: 1101-1106, 1997.

[6] Veeger et al., Clin Biomech, 17: 211-218, 2002.

Disclosure of Interest: None Declared

Modelling

PO-0215

FES SIMULATION TO REDUCE KNEE MEDIAL COMPARTMENT LOADING BASED ON MUSCULOSKELETAL MODELLING

Rui Xu [1] Ziyun Ding [2] Dong Ming [1] Anthony M.J. Bull [2,*]

[1]Department of Biomedical Engineering, Tianjin University, Tianjin, China, [2]Department of Bioengineering, Imperial College London, London, United Kingdom

Introduction and Objectives: Joint loading is believed to contribute to the development of Osteoarthritis (OA). According to the report of National Institute for Health and Care Excellence, knees are the joints most often affected by OA for people over 45 years old. Compared the medial and lateral compartment of the knee, the medial compartment burdens more loading than the lateral one. Therefore, medial knee OA is nearly 10 times more common than lateral knee OA [1]. Quadriceps, Hamstrings and Gastrocnemius are reported to be the main contributors to the knee adduction/abduction moment [2], which is highly related to the medial-lateral force distribution.

Functional Electrical Stimulation (FES) system is a device that can induce a current in specific motor neurons to generate muscle contractions [3]. It's widely used for individuals with Spinal Cord Injury (SCI).

In this study, FES is expected to reduce the medial compartment loading for medial knee OA patients by increasing certain muscle forces. The objective is to verify this expectation using a lower limb musculoskeletal model with two optimisation methods.

Methods: The data used is normal walking data of one subject, including the motion data and the ground reaction force data. The muscle geometry data is from [4]. Two methods were proposed to increase the muscle forces by revising the static optimisation part and they were used to simulate the situation that certain muscles were stimulated by an FES system. The first method is to add a parameter c into the original objective function:

$$\sum (c_i \cdot (f_i/Max_i)^3) \tag{1}$$

where f_i is the muscle force of muscle element i (i=1,…,163) and Max_i is the maximal muscle force of muscle element i. For stimulated muscle elements, c_i=0.25; for others, c_i=1. Compared to the original optimisation without the parameter c, this new optimisation will assign larger forces to the muscles with a smaller c.

The second method is to assume that the muscle forces of the stimulated muscle elements are a (a=1.5) times of the forces obtained by the original model. In this case, the stimulated muscle forces are known parameters for the optimisation.

Results: The knee joint reaction forces during stance phase are shown in the figure. For both methods, the medial reaction forces are effectively reduced 0.389BW and 0.147BW, while the total reaction forces are increased 0.125BW and 0.271BW, respectively.

Figure:
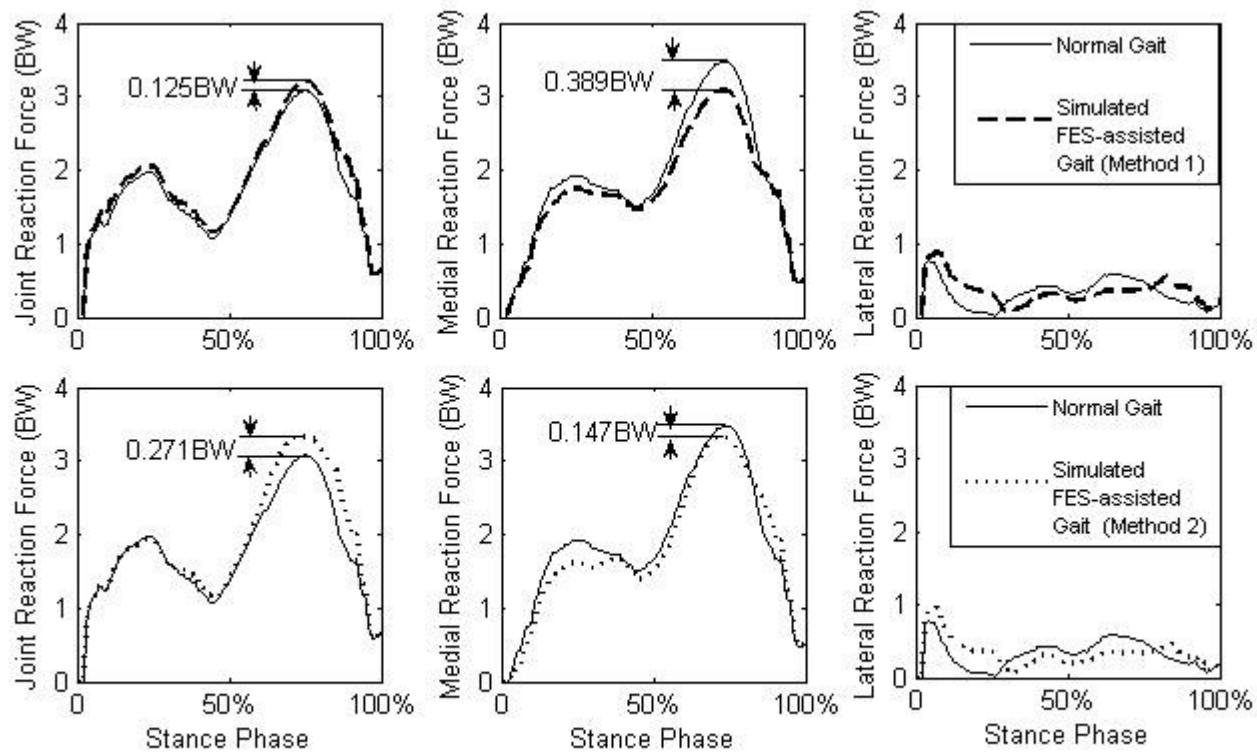
Caption: The comparison of the knee loading of FES simulation

Conclusion: Two methods were proposed based on the lower limb musculoskeletal model to simulate FES-assisted walking. The medial loading of knee can be reduced during FES simulation based on these two methods. The result shows a potential application of FES system to reduce the knee medial forces for medial OA patients. However, more data sets need to be considered and the model will be validated based on obtained EMG data. Furthermore, the stimulated muscles will be analysed in details in order to achieve better results.

References: [1] Fisher DS et al., J. Orthop Res, 25: 540-546, 2007.

[2] Winby CR et al., J Biomech, 42: 2294-300, 2009.

[3] Lynch CL et al., IEEE Contr Syst, 28: 40-50, 2008.

[4] Klein Horsman et al., Clin Biomech, 22: 239-247, 2007.

Disclosure of Interest: None Declared

COMPARISON OF ACTIVATION PREDICTIONS OF HYBRID FORWARD INVERSE DYNAMICS SIMULATIONS WITH STATIC OPTIMIZATION AND EXPERIMENTAL EMG

Brigitte M. Potvin [1,*] Mohammad S. Shourijeh [2] Kenneth Smale [3] Daniel L. Benoit [2]

[1]Faculty of Engineering, [2]Faculty of Health Sciences, [3]Department of Human Kinetics, University of Ottawa, Ottawa, Canada

Introduction and Objectives: The knee joint is the one most affected by osteoarthritis (OA) and musculoskeletal modelling and simulations are now starting to be used to better understand the effects of knee injury and OA in order to implement evidence based medical decisions[1,2]. Simulations typically use either inverse or forward dynamics, combined with optimization techniques to solve for muscle redundancy surrounding human joints[3,4]. To solve such a system in a model simulation, optimization is used to minimize predicted muscle activations or metabolic energy expenditure for a given movement. However, these functions may not be applicable in higher intensity motions such as jumping or running, or in individuals with muscle disorders [7]. Using a hybrid forward-inverse dynamics simulation framework could allow for the otherwise costly optimization of muscle model parameters while remaining computationally frugal since it is using the inverse dynamics of the recorded multibody system [5,6]. The purpose of this study was therefore to evaluate the effect of changing the objective function within the hybrid framework by comparing the muscle activation results to those of standard static optimization (SO) and experimental electromyography data (EMG).

Methods: Kinematic and kinetic analysis data of two healthy young adults (P1: 162cm, 61kg; P2: 185cm, 85kg) performing self-selected pace overground gait were used to run hybrid and inverse dynamics simulations with a simplified musculoskeletal model "gait10dof18musc" available from simtk.org.

We developed a simulation framework which, although similar to the recent Sartori framework [5], also allows any combination of muscle excitations to be treated as known variables (i.e.: from EMG) or unknowns, and the framework is then able to seek optimal excitations using optimization. The objective functions tested in the hybrid framework were minimization of error in torque calculations between the inverse and forward dynamics calculations of the model (Tmin) and of a combination of both minimization of torque error and a physiological cost function, overall muscle activation squared (T+Amin). The inverse dynamics SO process used minimization of total muscle activation squared. Predicted muscle activations from the hybrid simulations were compared to results from the inverse dynamics SO process and to the linear envelope of normalized experimental EMG data from the gluteus maximus(GM), biceps femoris(BF), medial gastrocnemius(MG), rectus femoris(RF), soleus(SL), tibialis anterior(TA) and vastus lateralis(VL). Correlation analyses were used to compare predictions and experimental data.

Results: Tmin hybrid results were generally larger in magnitude than those using the T+Amin cost function (Figure 1). Curve shapes between Tmn and T+Amin results correlated well for the SL (R=0.75 and 0.97), MG (R=0.83 and 0.88), RF (R=0.92 and 0.75) and iliopsoas (R=0.99 and 0.93) muscles for P1 and P2, respectively. EMG profiles of the SL, MG and RF muscles followed those of hybrid results. However the hybrid excitations preceded EMG data despite the EMG being dual-pass filtered, leading to poor correlations. The TA muscle showed a moderate (R=0.45 and 0.37) relationship with

hybrid results, while the gluteus maximus had no correlation or visual trends between any tested conditions or with experimental data. SO results did not follow experimental EMG profiles, but did show visual parallels with the T+Amin hybrid results for the VL and BF muscles, although SO results had smaller value magnitudes.

Figure:
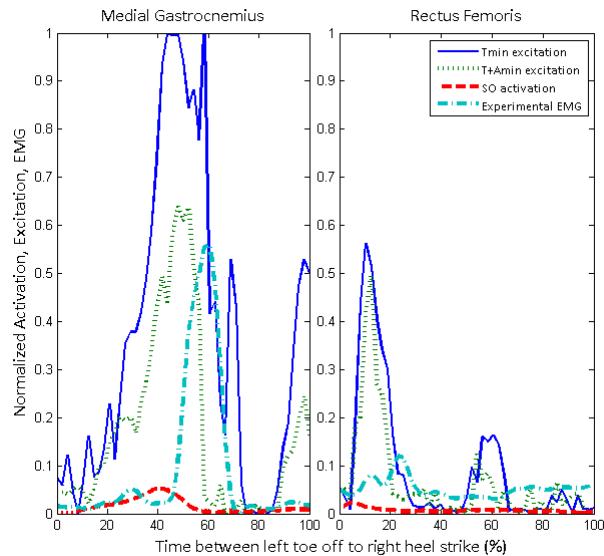
Caption: Figure 1: Examples of predicted muscle excitations (hybrid model) and activations (Inverse dynamics static optimization) in comparison to experimental EMG data for the right medial gastrocnemius and right rectus femoris muscles.

Conclusion: Similarities were found between some muscle predictions from the hybrid framework and experimental EMG data, more so than between static optimization results and EMG. Hybrid results differed when the physiological cost function was added to the torque error. The choice of optimization criterion is important when running musculoskeletal simulations. Modifying this optimization to a more physiologically appropriate goal, as well as increasing the complexity of the modeled knee to include a multiple degree-of-freedom joint and more muscles, could improve model predictions in gait as well as in other motions.

Caption: Figure 1: Examples of predicted muscle excitations (hybrid model) and activations (Inverse dynamics static optimization) in comparison to experimental EMG data for the right medial gastrocnemius and right rectus femoris muscles.

References: [1] Mansouri et al., J. Biomech., 45,1517–1521,2012.

[2] Fregly et al., J. Orthop. Res., 2011.

[3] Cao et al., J. Biomech. Sci. Eng., 8(1), 2013.

[4] Lloyd et al.,J. Biomech. Eng., vol. 118, 1996.

[5] Sartori et al., J. Biomech., 47(15),3613-3621, 2014.

[6] Shourijeh et al.,Abstract submitted to the ISB Conference, Glasgow, 2015.

[7] Winby et al., J. Biomech., 42, 2294–2300, 2009.

Disclosure of Interest: None Declared

ESTIMATION OF LOWER LIMB MUSCLE FORCES IN CHILDREN'S GAIT

Filipa Joao [1,*]Vera Bagao [1]Silvia Cabral [1]Vera Moniz-Pereira [1]António Veloso [1]

[1]Laboratório de Biomecânica e Morfologia Funcional, CIPER, Faculdade de Motricidade Humana, Universidade de Lisboa, P-1499-002 Cruz Quebrada, Portugal

Introduction and Objectives: Pathological walking patterns are frequently assessed in children with different gait abnormalities. The observed gait patterns are the result of the forces generated by the muscle-tendon unit structures, which drive the skeletal to a certain motion. However, these internal forces are not trivial to quantify. Moreover, the lower limb muscle forces estimation in children is scarcely reported[1,2]. In order to better understand these gait deviations from the normal pattern, a normative database of the pediatric population should be used for correct comparison. Therefore, the aim of this study was to estimate the individual muscle forces of the lower limb during gait in normal children, in order to create the normative database for our laboratory.

Methods: The gait data from ten children (5 male, 5 female, age: 7.5±0.8 yrs old and mass: 27.06±5.42 kg) were analyzed for this study. Motion capture was collected using an optoeletronic system of 14 cameras Qualisys (Oqus-300) operating at 100Hz. 17 reflective markers and 4 marker clusters were used for the reconstruction of eight body segments (trunk, pelvis, thighs, shanks and feet). Ground reaction force (GRF) was collected with 3 force plates and joint moments were calculated by inverse dynamics. Kinematic and kinetic data were processed with a lowpass Butterworth filter with a cut off frequency of 6 Hz. All data processing and model building were done in Visual 3D. Electromyography (EMG) was collected for the gluteus medius, rectus femoris, semitendinousus, gastrocnemius lateralis and tibialis anterior. The EMG was highpass filtered (Butterworth with a frequency cut of 30Hz) and a linear envelope (moving frame of 51) was applied. All children walked at their self-selected speed and the analyzed gait periods were selected from the cycles where the subjects achieved two consecutive force plate strikes during which only one foot contacted each force plate. A generic musculoskeletal model with 19 degrees of freedom and actuated by 92 Hill-type muscle-tendon units[3,4] was scaled to match the anthropometric characteristics of the subjects. Subtalar and metatarsophalangeal joints remained at neutral angular position. Residuals reduction was performed to compensate for dynamic inconsistencies between the measured kinematics and ground reaction forces. Individual muscle forces and activations were estimated using a static optimization algorithm[4] during the unilateral stance (USt) period corresponding to the time interval from 10% to 50% of the gait cycle. All muscle forces were normalized to each subject body weight (BW). To assess whether muscle activations estimated in the static optimization were similar to the subjects EMG activity, we visually compared them with the experimentally obtained EMG.

Results: In order to facilitate the muscle force analysis we grouped some of the model actuators: the 3 vasti and rectus femoris (Quadriceps); the semitendinosus, semimebranosus and biceps femoris (Hamstrings); the gastrocnemius medialis and lateralis (Gastrocnemius); the 3 actuators of the gluteus maximus (GLTmax) and the 3 actuators of the gluteus medius (GLT med). We have selected only the muscles which generated force above 0.4 BW and the results are presented in xBW ± SD. We observed that during the initial USt period, the GLTmed, Quadriceps, GLTmax and Tibialis

Posterior exerted the greatest amounts of force, reaching 1.72±0.45 BW, 1.25±0.42 BW, 0.58±0.17 BW and 0.90±0.53 BW respectively. From the middle period until the end, the hip flexors (psoas and iliacus), gastrocnemius and hamstrings increased their force production, generating a peak force of 1.04±0.40 BW, 0.90±0.34 BW, 1.89±0.36 BW and 0.44±0.13 BW, respectively. Soleus muscle generated a force peak of 1.74±0.38 BW in the final phase of the USt (see Fig.1 for a representative subject).

Figure:
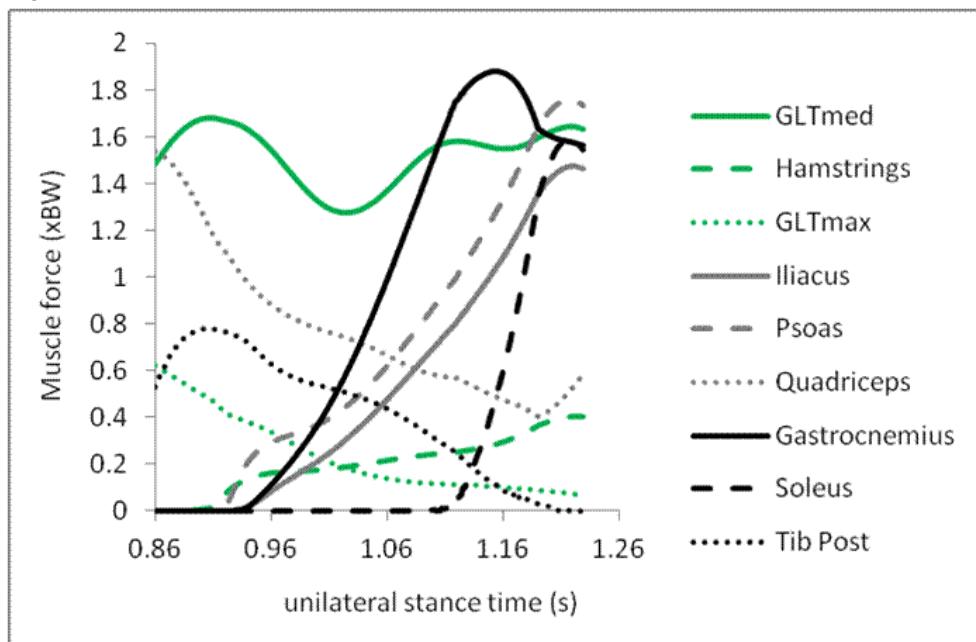
Caption: Fig.1 - Estimated muscle forces of one representative subject

Conclusion: The estimated muscle forces and activations show similar patterns to the collected EMG of some of the muscles (especially gastrocnemius, rectus femoris and GLT med). Our results are in accordance with the studies that report muscle force in children with the same age[1,2]. This indicator give us confidence for the next step, that is to use these estimated muscle forces to calculate the joint reaction forces at the hip, knee and ankle joints and also the contribution of each muscle to accelerate the body forward during locomotion (induced acceleration analysis). It is also in process the increasing of the normative children's gait database which will allow us to establish the comparison between the normal and different types of abnormal gait.

References: [1] Bosmans L et al., J Orthop Res, 32(11): 1406-15, 2014.

[2] Steele K et al., Gait Posture, 35(4): 556-560, 2012.

[3] Delp SL et al., IEEE Trans Biomed Eng, 54(11): 1940-1950, 2007.

[4] Thelen DG, Anderson FC, J Biomech, 39: 1015-1107, 2006.

Disclosure of Interest: None Declared

IMPROVED CONTACT AND MENISCUS PROPERTIES IN MULTIBODY DYNAMICS MODELING OF THE KNEE

Stephen Wilson [1] Jerome Hausselle [1,*] Trent Guess [2] Roger Gonzalez [1]

[1]Mechanical Engineering, University of Texas at El Paso, El Paso, [2]Physical Therapy, University of Missouri, Columbia, United States

Introduction and Objectives: Understanding knee joint biomechanics during daily activities is a critical step towards preventing degeneration. Since *in vivo* measurements are very difficult to perform, computer models are a popular method to achieve this understanding. One of the largest barriers to progress in this area is the high developmental and computational cost required by finite element models which include meniscus and simulate dynamic motions with multiple contacts. Although less popular than finite element modeling, multibody dynamics modeling is another approach and shows promise since multibody models do not require time-consuming meshing steps and are less computationally expensive. Guess et al. [1] have developed a meniscus model that includes radial deformation. However, meniscus material properties were optimized to match a finite element solution, which is undesirable for a method meant to capitalize on efficiency. Although, cartilage-to-cartilage contact parameters have also been implemented [2], they suffer from being imprecise for cartilage-to-cartilage contact and optimization-based for cartilage-to-meniscus contact. The current work addresses these issues while studying vertical loading of a straight knee joint with and without menisci.

Methods: A knee model was constructed in MSC Adams (Newport Beach, California) using geometries derived from magnetic resonance images of a cadaver specimen. We implemented an Adams routine to segment the menisci cirumferentially by 15deg increment relative to meniscus volume centroid and implement specific physically-based stress-strain equations between adjacent meniscus segments. Horn attachments were modeled using a translational spring with a stiffness of 180N/mm [3], whereas corronary ligaments that connect the tibia to the meniscus element closest to the collateral ligament path were modeled using a translational spring with a stiffness of 50N/mm. Stress-strain equations for the menisci were taken from Moran [4]. A custom contact subroutine was implemented which calculates contact forces from contact strains and areas using a physically-based third-order stress-strain polynomial relationship for each of the two contacting bodies of interest. Stress-strain polynomials for tibial and femoral cartilage were computed from values recommended by Deneweth [5]. The menisci stress-strain polynomial equation was determined from Moran [4]. All degrees of freedom were constrained except vertical displacement and a compressive load of 1000 Newtons applied to the knee with and without menisci.

Results: Addition of the mensici greatly increased contact area and thus noticably reduced peak and overall pressure (see figure). Results are similar to experimental findings by Fukubayashi and Kurosawa [6,7] (see table). However, they found smaller contact area without menisci and thus had higher average and peak pressures. This could be due to individual geometry variance and the use of generalized and non-region-specific cartilage and mensicus material parameters. Peak pressure in the current model could also be lower due to contact being discretized into 3x3mm elements.

Figure:
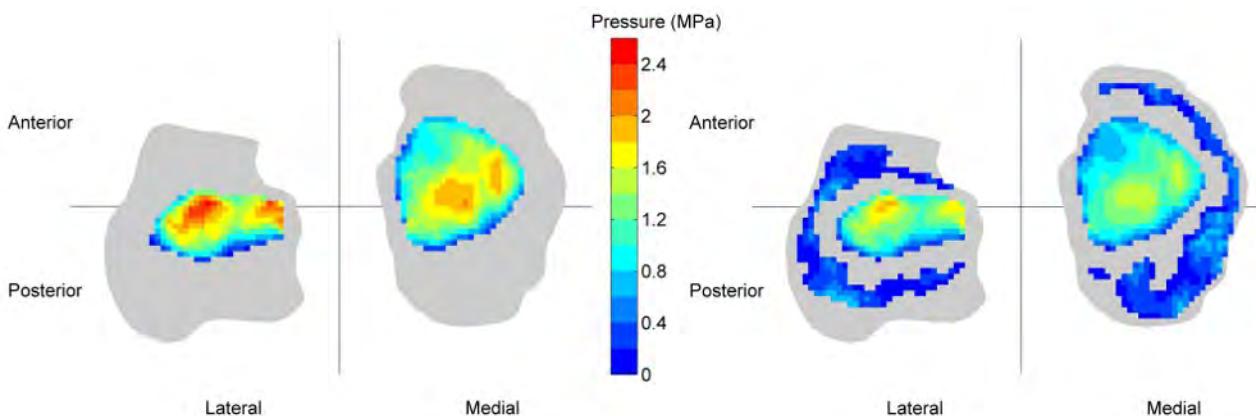
Caption: Pressure map of tibial cartilage during 1000N vertical load with (right) and without (left) menisci.

Conclusion:

Multbody dynamics modeling of the knee has relied on oversimplified material properties which require optimization. In the current model, we implemented experimentally determined mechanical equations to better simulate contact and meniscus properties. This work is a promising development which enables efficient simulation of the consequences of cartilage and mensicus degeneration during a variety of daily activities.

Table:

	Without Menisci		With Menisci	
	Model	Experimental [6,7]	Model	Experimental [6,7]
Contact area/Total area	38%	26%	64%	62%
Average Pressure (MPa)	1.27	1.97 ± 0.56	0.71	0.8 ± 0.2
Peak Pressure (MPa)	2.41	6	1.93	2-3

Caption: Comparson of model contact results to experimental.

References:

[1] Guess et al., Med Eng Phys, 32(5):505-515, 2010.

[2] Guess et al., Comput Method Biomec, 16(3):256-270, 2013.

[3] Hauch et al., J Biomech, 43(3):463-468, 2010.

[4] Moran, Univ of Edinburgh, 2001. **VIA** Fraser, Univ of Edinburgh, May 2011.

[5] Deneweth, Univ of Michigan, 2013.

[6] Fukubayashi et al., Acta. orthop. scand., 51:871-879, 1980.

[7] Kurosawa et al. , Clin Orthop Relat R, 149:283-290, June 1980.

Disclosure of Interest: None Declared

Modelling

PO-0219

DEVELOPMENT OF A SUBJECT-SPECIFIC THREE-DIMENSIONAL WHOLE-BODY MODEL TO PREDICT HUMAN WALKING

Dan Hu [1,*] David Howard [2] Lei Ren [1]

[1]Mechanical Aerospace and Civil Engineering, University of Manchester, Manchester, [2]Computing Science and Engineering, University of Salford, Salford, United Kingdom

Introduction and Objectives: Over the past decades, intensive studies have been carried out toward an understanding of the biomechanics of human walking using state-of-the-art three-dimensional (3D) motion analysis and biomechanical modelling techniques. Although these studies have greatly deepened our understanding of the biomechanical mechanisms underlying human walking, the majority of the outcomes have been descriptive in nature as they are based on measurements, which by its very nature tells us what happens but not why it happens. Very few studies have been devoted to predictive modelling (i.e. not based on measurements), which has the powerful feature of being explanatory because the reasons for particular model behaviours can be interrogated [1,2]. The objective of this study is to develop a 3D subject-specific 3D whole-body human model to predict walking kinematics and kinetics with minimal measurement inputs.

Methods: A 3D whole-body multi-segment model was constructed consisting of 13 segments (head, torso, pelvis, right and left upper arms and forearms, right and left thighs, shanks and feet) with total 25 degree of freedoms (DoFs). Three-dimensional whole-body gait measurement for a healthy male subject (age: 25; weight: 68.8kg; height: 177cm) was conducted to support and validate the modelling. The anthropometric data of the model were estimated based on the test data collected in the gait measurement. The subject-specific positions and axis orientations of the anatomical joints in the model were defined using the functional method conducted in the gait measurement. Quaternions were used to define the 3D motions of each joint, of which the time traces were represented by using parameterised spline curves. In the model, the feet were represented as effective rollover components over the ground surface without slipping. The 3D kinetics of the whole-body system was evaluated using a 3D inverse dynamics approach. In this study, the human walking behaviour was formulated as an optimal control problem by minimising certain criteria whilst subjected to multiple constraints. Those kinematic and kinetic constraints define human walking include joint motion range, segment motion range, swinging leg condition, stance leg condition, double support condition, ground reaction force and moment condition and task constraints etc.

Results: The optimization simulations were implemented in MATLAB programming environment. Three gait parameters: average walking velocity, gait cycle period and double stance duration were used as the only inputs to drive the model. In the current stage, we set the ankle, knee, hip and waist joins to move freely in the sagittal plane with the shoulder, elbow and neck in their neutral standing positions, and minimising the mechanical energy cost was used as the criterion. The predicted lower limb joint motions and ground reaction forces were compared to the measurement data (see Figure 1). Over most of the gait cycle, the predicted results are in reasonably good agreement with the measured data. The predicted mechanical energy expenditure for the whole gait cycle was 229.65 J, which was close to the previous result [2].

However, there are still some discrepancies between the prediction results and measurement data especially torso rotations, which may be because that the model was confined to the sagittal plane and the upper limb motions were neglected.

Figure:
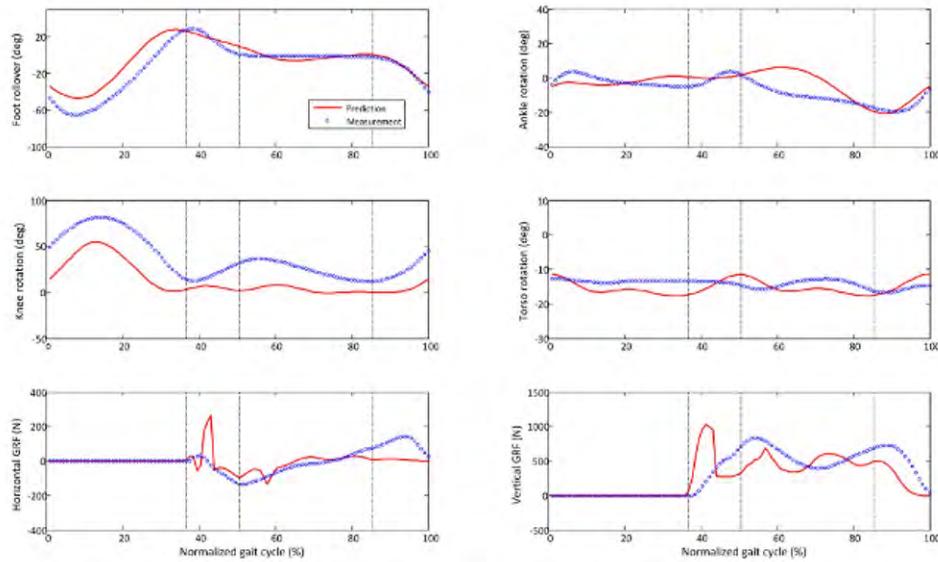
Caption: Figure 1 Predicted rotations of the right foot rollover, right ankle, right knee and torso in the sagittal plane (red line), compared with measured data (blue point) for one subject (age: 25; weight: 68.8kg; height: 177cm); Predicted horizontal and vertical ground reaction force (GRF) (red line), compared with recorded force plate data (blue point) for the subject.

Conclusion: In this study, we have established a computational framework to predict the 3D whole-body human walking based only on three simple gait descriptors. Promising results have been achieved in terms of predicted joint motions and ground reaction forces compared with the measurement data. Future work involves the 3D whole-body simulations by releasing all the joint motions in all the three planes, and also by introducing multiple criteria into the optimisation scheme.

References: [1] Anderson et al., J. Biomech. Eng., 123: 381–390, 2001.
[2] Ren et al., J. Biomech., 40: 1567-1574, 2007

Disclosure of Interest: None Declared

Modelling

PO-0220

THE AFFECT OF BODY SEGMENT PARAMETER CHOICE ON ESTIMATES OF INTERNAL WORK IN A TOTAL BODY ACTION.

Gary Doyle [1,*]Wendy Drechsler [1]Ryan Mahaffey [1]Mary Cramp [2]

[1]School of Health, Sport and Bioscience, University of East London, London, [2]HAS - Allied Health Professions, University of the West of England, Bristol, United Kingdom

Introduction and Objectives: Internal work is estimated by the change in kinetic energy from the velocity and mass of a given system and is suggested as a descriptor of movement proficiency [1]. Whilst the internal work estimates are influenced by the chosen body segment parameter (BSP) data set there is little research examining how this choice influences the results.

Regression based BSPs are often used due to simplicity and time constraints. Dempster's [2] data is commonly used but has a small sample size based on an elderly population. de Leva's [3] data set is based on a more recent, larger population, yet is less commonly used. These data sets differ in their values for segmental mass, position of centre of mass and moment of inertia.

The aim of the research was to examine the differences and repeatability in calculated values of internal work for two different BSP data sets using the same kinematic data on a total body movement at different exercise intensities.

Methods:

Ten male participants (mass 81±7 kg; stature1.77±0.06 m, age 31±8 yrs) familiar with a rowing ergometer but without formal training volunteered and rowed at 50,100 and 150 W, within a three-dimensional motion capture system (Vicon, OMG, Oxford). From the Vicon Plug-in-Gait model, joint centres position, with respect to time, were exported to a custom written LabVIEW code (National Instruments) for the drive phase of 8 strokes, at each intensity. From a 13 segment body, internal work was calculated as the change in translational and rotational kinetic energy from the start to the finish of the drive phase of the stroke data and were analysed using both the data sets of Dempster [2] and de Leva [3]. Intra-trial repeatability was assessed using Intraclass Correlation Coefficients (ICC). Statistical differences were assessed using pairwise comparisons and effect sizes (Cohen's *d*).

Results: Internal work data was normally distributed and considered reliable (ICC 2,1 > 0.7). Internal work increased with respect to exercise intensity. The mean difference in work done with respect to intensity was 3.0 J, 4.6 J and 8.0 J for 50 W, 100 W and 150 W, respectively, representing changes in internal work between BSP data sets approaching 10%. The Dempster condition demonstrated larger estimates and variability of internal work, at all intensities (see table 1). Statistical differences ($p < 0.05$) between the de Leva and Dempster conditions at each intensity were supported with moderate to large effect sizes (Cohen's *d* = 0.48, 0.30, 0.8, respectively).

Figure:
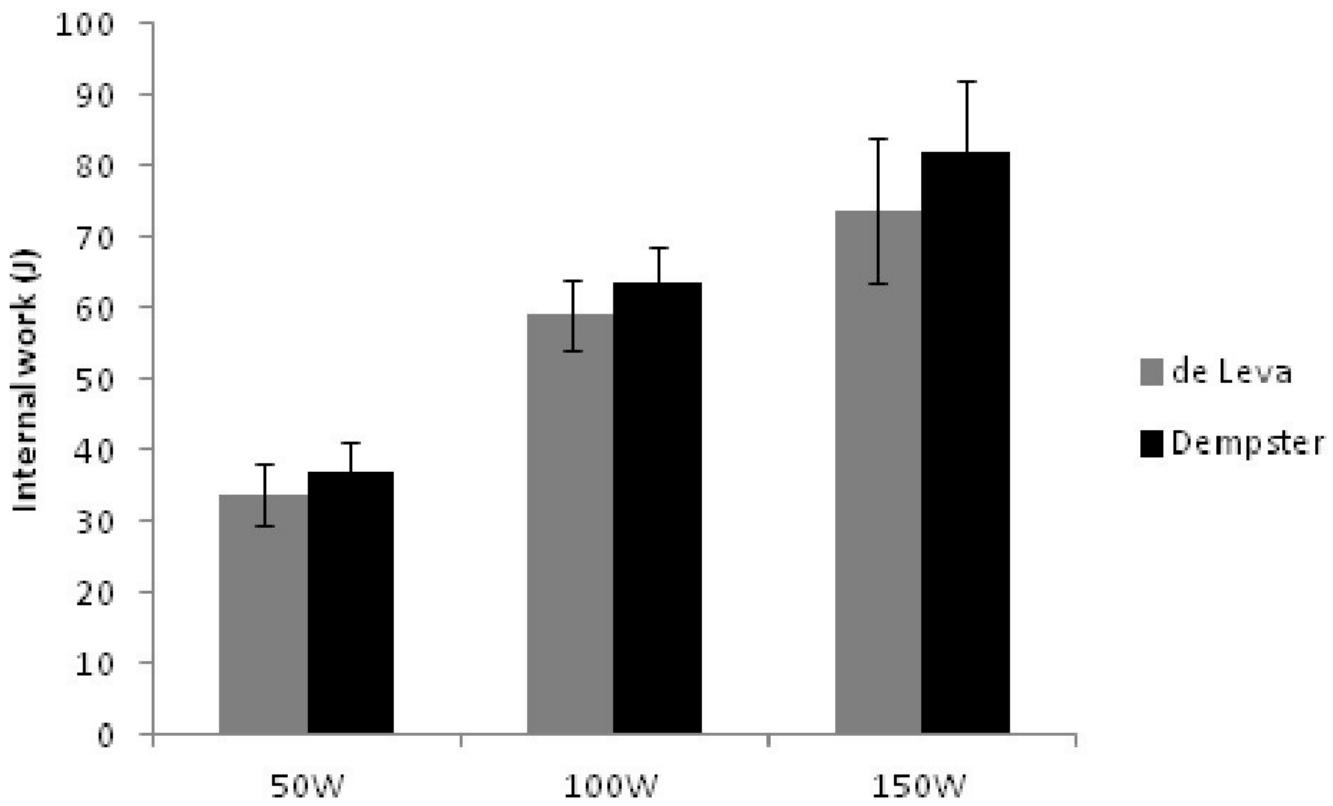
Caption: Figure 1 Average internal work against rowing intensityfor each BSP

Conclusion:

Identical kinematic data for a total body action was modelled with two different BSP data sets across 3 exercise intensities, to examine the effects of calculations of internal work. The differences approximated 8-10%, were statistically different and were supported by moderate to large effect size statistics which may indicate some importance to the results of mechanical calculations. However, the overlap of confidence intervals suggested little difference to the sample variability for internal work between the two models.

It is not possible to suggest that one BSP data set yielded more accurate results than the other. However, the ability of models to predict outcomes is based on the assumptions used. Whilst de Leva (1996) data set, which is based on a larger cohort, and was completed on more recently living participants returned smaller values of internal work, it demonstrated less variability in the results which is attributed to the differences segmental mass, position of centre of mass and moment of inertia between data sets.

The results of this study indicate small but potentially important differences in internal work calculations dependent upon choice of data set. Careful consideration of the BSP data sets needs to be given when calculating internal work matching the participants with the regression cohort.

Table:

	Mean (J)	95% CI	SD	$ICC_{(2,1)}$	SEM
de Leva 50W	33.8	4.40	5.8	0.78	2.72
Dempster 50W	36.8	4.98	6.4	0.80	2.90
de Leva 100W	59.1	10.07	14.0	0.92	4.08
Dempster 100W	63.7	11.46	16.6	0.91	5.10
de Leva 150W	73.8	12.09	9.3	0.70	5.06
Dempster 150W	81.8	13.64	10.7	0.71	5.83

Caption: Table 1. Measures of variation in internal work

References: [1] Purkiss and Robertson Gait Posture, 18:149-149. 2003.

[2] Winter. Biomechanics and Motor Control of Human Movement. Wiley. 2005

[3] de Leva. J. Biomech. 29:1223-1330

Disclosure of Interest: None Declared

PO-0221

DEVELOPMENT OF MOLECULAR-BASED NON-LINEAR VISCOELASTIC MODEL OF COLLAGEN FIBRILS

Andrzej Mlyniec [1,*]Tadeusz Uhl [1]

[1]Department of Robotics and Mechatronics, AGH-University of Science and Technology, Krakow, Poland

Introduction and Objectives: Collagen is the most abundant protein in mammals. Biomechanical properties of fibrous collagenous tissues result from the molecular structure of collagen fibrils. Collagen fibrils consist of staggered array of tropocollagens, connected to each other by covalent cross-links as well as hydrogen bonds. The viscous friction mediated by the hydrogen bonds results in fibril stiffening with the increase of the loading rate. This effect known as a collagen viscoelasticity can be studied by means of Molecular Dynamics (MD) simulations [1], although predicted by MD values of elastic moduli are overestimated. This results from extreme high loading rates and very short simulation times. The temporal and spatial limitations of atomistic methods can be partially overcome by the use of Coarse-Grained model [2–4], but predicted stress-strain curves still do not correspond to the behavior at a macro-scale.

The goal of our study is to create the molecular-based viscoelastic material model which can be directly used in Finite Element Analysis of collagenous tissues. Moreover, we aim to enhance our model by denaturation kinetics. This allow to predict the influence of thermal denaturation on biomechanical behavior of collagen fibrils.

Methods: The molecular models were built using the collagen-like peptide structure obtained with X-ray diffraction. For this model we performed shear and tensile tests, which were used for calibrating parameters of Coarse-Grained (CG) model. Using this CG model we created a fibril model incorporating three-dimensional staggered array of tropocollagens (Fig.1). Created CG models were used to investigate the viscoelastic behavior of collagen fibrils, resulting from hydrogen bonds network [4]. Results of meso-scale CG analysis have been used to calibrate the non-linear viscoelastic model which consist of hyperelastic Arruda-Boyce model and rate dependent Arruda-Boyce model disposed parallel (Fig.1). Moreover, proposed model has been enhanced by reaction kinetics using Arrhenius equation. This enhancement allow one to predict influence of thermal treatment on mechanical behavior of collagen fibrils.

Results: The proposed nonlinear viscoelastic model allow to predict mechanical behavior of collagen fibrils for deformation rates ranging from 0.1 to 1e9. Additionally, incorporation of denaturation kinetics in constitutive model, has allowed to predict drop of mechanical properties resulting from thermal treatment. Elevated temperature leads to decrease of elastic behavior as well as decrease of viscoelasticity of the fibrils. Predicted values of Young's modulus are in good quantitative agreement with results of experimental observations[5-6].

Figure:
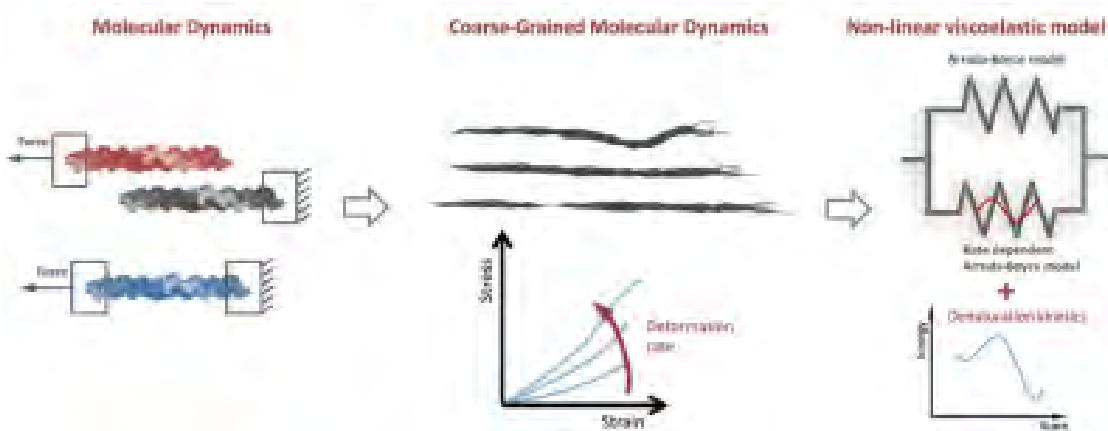
Caption: Modeling methods used in development of molecular-based nonlnear viscoelastic model

Conclusion: The proposed model allows to predict biomechanical behavior for real deformation rates, thus can be successfully used in micro Finite Element modeling or other homogenization methods [7]. Our model takes into account changes of rigidity as well as viscosity of the fibers exposed to elevated temperatures. The thermal cleavage of collagen leads to reduced influence of a deformation rate on the fibrils stiffness. Further development of proposed constitutive model includes taking into account influence of the proteoglycans and elastin as well as external loading.

References:

[1] Buehler, *J. Mech. Behav. Biomed. Mater.*, 1: 59–67, 2008.

[2] Karimi-Varzaneh et al., *Top. Curr. Chem.*, 307: 295–321, 2012.

[3] Gautieri et al., *J. Chem. Theory Comput.*, 6: 1210–1218, 2010.

[4] Mlyniec et al., *Soft Mater.*, under review, 2014.

[5] Aksan et al., *J. Biomech. Eng.*, 125: 700–708, 2003.

[6] Chen et al., *J. Biomech.*, 31: 211–216, 1997

[7] Spiesz et al., *J. Mech. Med. Biol.*, 14: 1450013-1-15 , 2013.

Disclosure of Interest: None Declared

MODELING PARAMETERS TO CALCULATE REALISTIC INVERSE DYNAMICS MUSCULAR ACTIVITY IN RUNNING

Allison H. Gruber [1,*] Ross Miller [2] Brian Umberger [3] Shane Murphy [1] Joseph Hamill [3]

[1] Kinesiology, Indiana University Bloomington, Bloomington, [2] Kinesiology, University of Maryland, College Park, [3] Kinesiology, University of Massachusetts, Amherst, United States

Introduction and Objectives: Modeling parameters, such as tendon slack length (Lslack), maximum isometric force production (Fmax) and series elastic strain at maximum isometric force production (Umax), are typically taken from experimentally measured values of cadavers or non-human mammalian muscle tissue. Modeling parameters from those sources often result in simulated activation of the plantar flexors over 1.0 when modeling muscle-tendon mechanics from experimental inverse dynamics data. One solution is to increase Fmax to account for the difference in muscle size between elderly cadavers and healthy, young subjects performing dynamic tasks. Although adjusting parameter values can allow for simulated muscle forces to correspond with experimental joint moments produced in running, the resulting muscle-tendon dynamics comparable to ultrasound measurements [1]. Purpose: to examine the sensitivity of gastrocnemius (GAS) muscle activation in running estimated from inverse dynamics to muscle model parameters, and determine parameter ranges that predict realistic activations.

Methods: Eighteen rearfoot runners (26.8±6.3 yr, 71.3±9.2 kg, 1.8±0.1 m) ran at a target speed of 3.5 m•s^{-1} ±5% as 3D kinematics and ground reaction forces were collected and processed into sagittal plane knee angle, ankle angle, and resultant ankle moment. GAS muscle-tendon unit (MTU) length, velocity, and moment arm were estimated from the joint angles [2]. GAS muscle force was calculated assuming ~34.5% of the active joint moment was attributed to the GAS then dividing the GAS moment by the GAS moment arm. A two-element Hill muscle model was used to determine the GAS contractile element (CE) and the series elastic element (SEE) lengths and velocities. Activation (Act) was then calculated as a function of the instantaneous CE force, length, and velocity. This calculated was repeated with Fmax values adjusted by changing the specific tension (ST) from 10-100 N•cm^{-2} in 10 N•cm^{-2} increments, and with Umax values adjusted in 1% increments from 3%>10% at each level of Fmax. When Umax was changed, Lslack was adjusted to maintain a constant ankle angle at which the maximum isometric moment was produced. The CE and SEE kinematics of simulations that resulted in a maximum act <1.0 were compared with literature values.

Results: 31 simulations resulted in a peak act of <1.0 (ST 40-100; Umax 1%>7%). All but 4/31 simulations resulted in a peak CE shortening velocity less than 8 Lo/s (ST(N•cm^{-2}):Umax(%)= 40:3, 80:3, 90:2, 100:2). Only 5/31 simulations resulted in CE lengths within the range measured with ultrasound (ST(N•cm^{-2}):Umax(%)= 70:3, 80:1, 80:2, 80:6, 90:5)[1].

Conclusion: Lower Umax values resulted in more reasonable simulated GAS activations and CE length simulated with an inverse dynamics-based musculoskeletal model regardless of the specific tension, thus Fmax. These Umax values were slightly lower than the gastrocnemius tendon/aponeurosis strains measured with ultrasound during running [3]. Caution should be made when using higher values for Umax or specific tension to account for parameters measured from cadavers or non-human mammalian muscle.

References: [1] Ishikawa & Komi, *Gait Posture*, **25**: 380-384, 2007.

[2] Arnold et al., *Ann Biomed Eng*, **38**: 269-279, 2010.

[3] Lichtwark et al., J Biomechanics, **40**: 157-164, 2007.

Disclosure of Interest: None Declared

Modelling

PO-0223

SCALING MUSCLE PARAMETERS IN A CANINE MUSCULOSKELETAL MODEL.

Billy Dries [1,*] Ilse Jonkers [2] Wim Van den Broeck [3] Walter Dingemanse [1] Ingrid Gielen [4]

[1]Faculty of Veterinary Medicine - Medical Imaging and Small Animals Orthopaedics, University of Gent, Gent, [2]Faculty of Kinesiology and Rehabilitation Sciences - Human Movement Biomechanics Research Group, University of Leuven, Leuven, [3]Faculty of Veterinary Medicine - Department of Morphology, [4]Faculty of Veterinary Medicine - Department of medical imaging and orthopedics of small animals, University of Gent, Gent, Belgium

Introduction and Objectives: Recently, veterinary institutions have taken an interest into the possibility of creating musculoskeletal computer models of domestic animals.To use these musculoskeletal models for the analysis of musculoskeletal loading, incorporation of muscle structures is essential. Apart from defining the geometry of the muscle line of action, parameters describing the muscle force generating capacity need to be defined. To do so, experimental measures of optimal fiber length, maximal muscle force, pennation angle and tendon slack length need to be acquired in dogs. Furthermore, a dedicated method for scaling these parameters needs to be established and tested. This study reports on a first data set of optimal fiber length and muscle volume acquired in 3 canine hind limbs and evaluates the use of weight versus limb length (LL) as scaling factor for the muscle-tendon parameters.

Methods: Muscles were dissected from the right hind limb in three dogs weighing 30kg, 35kg and 52kg.
The limb bones were placed caudally on a table and a calibrated photograph was taken. LL was calculated in ImageJ based on the summed length of the individual limb bones.Fat and connective tissue was removed as much as possible without damaging the muscle. Muscles were then weighed on a scale with a sensitivity up to 0,001g. Immediately afterwards the muscles were placed in a neutral-buffered 10% formaldehyde solution for 48-72h, after which they were placed in a 0.4M phosphate-buffered saline solution with a pH of 7.2 for 24-48h. Subsequently muscles were placed in a 20% sulphuric acid solution to loosen the muscle fibers for 3-7 days. Once the muscle fibers were loosened, 3-8 individual muscle fibers (or small bundles of fibers of equal length) were removed, depending on the size of the muscle. Muscle fibers were taken from different sites in the muscle to ensure a representative sample. The extracted muscle fibers were then photographed upon grid paper for scale.The pictures of the muscle fibers were analysed in ImageJ to measure fiber lengths. Fiber length was measured from end to end following the curvature of the fiber.
A correlation matrix using Pearson product moment was constructed to analyse the relationship between the different muscles fiber lengths and volumes with the dogs weight and LL.

Results: There are clear relationships between the LL and weight with both muscle fiber length and muscle volume for at least 70% of the measured canine hind limb muscles. However, these correlations were not clearly more pronounced for LL or weight (fig 1). Nevertheless, muscle fiber length correlated more strongly with LL than with dog weight and inversely muscle volume correlated more strongly with dog weight. The correlation coefficient between LL dog was that strong weight. In specific muscles the fiber length and/or muscle volume correlated negatively with the scaling parameters. For example, the internal obturator fiber length scales and strongly negatively with LL and weight, meaning that a heavier dog with longer limbs would have a shorter muscle fiber in the internal obturator muscle. This is mostly found in very small

and/or short muscles and could be related to measurement error. Therefore, these results were omitted from the calculations.

Figure:
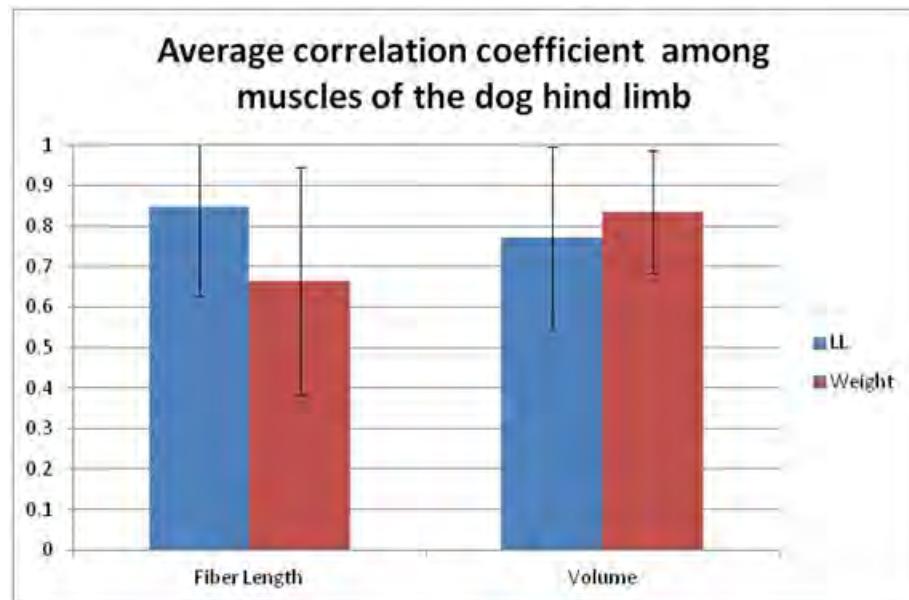
Caption: fig 1: correlation coefficient of muscle fiber length and volume with LL and Weight, averaged over the different muscles of the dog hind limb

Conclusion:

As dogs can vary widely in size and shape, it is important to develop procedures to scale musculoskeletal models for dogs in order to allow sufficient flexibility of the muscle model parameters to adequately represent dogs of different sizes and body proportions. This study evaluated LL based on the hind limb dimensions and weight to normalise hind limb muscle parameters in dogs.

The (relative) weakness of the correlation between dog weight and LL can be expected from the variability in dog body conformations.

Leg length appears a better normalising factor than weight for fiber length, but not for muscle volume. Although LL could not unambiguously be identified as a better normalising factor than weight, there is evidence to suggest that muscle parameters for different muscles may scale differently depending on the scaling factor used. Further research will be needed to investigate how a generic (dimensionless) model may be scaled to fit specific dog breeds.

Disclosure of Interest: None Declared

PROPOSITION OF AN ALGORITHM FOR SIMULATING NATURAL VARIABILITY IN ARM GRASPING POSTURE WHEN ROTATING A SPHERICAL OBJECT

Julien Lardy [1] [2] Thomas Robert [2] Xuguang Wang [2,*]

[1]MIP (EA 4334), Université de Nantes, Nantes, [2]LBMC (UMR-T 9406), Ifsttar, Bron, France

Introduction and Objectives: Digital human models are being more and more used in early phase of a product/workplace design. However, human motion simulation still faces the well-known problem of motor redundancy, implying that humans have more degrees of freedom than necessary to perform a given task. As a consequence, humans have an infinite number of possibilities to do one task. Solutions used nowadays in motion simulation are mainly based on optimization trying to find a unique solution that satisfies a set of constraints while minimizing an objective function (see [1] for review). Nevertheless, some authors suggest that redundancy should be considered as an advantage rather than a problem to be solved. Indeed, Latash considers the human redundancy as an ability to adapt to the environment [2]. Moreover, studies showed that different ways to perform a task can coexist, questioning the pertinence of looking for a unique solution. Then, natural motion variability should also be simulated. Grasping and manipulating an object with the hand is one of the routine tasks of human beings and is frequently encountered in workplace evaluation and product design. In case of rotating a spherical object, a recent study showed a large variation in arm posture when grasping the object for a given rotation amplitude [3]. The work presented here aims at proposing a stochastic algorithm to predict the grasping posture as a function of the intended manipulation.

Methods: The rotation task consists in grasping and rotating a sphere. Rotation amplitudes range from -315° in counter-clockwise direction (CCW) to 270° in clockwise direction (CW). Actual subjects performed this task in order to compare our simulation results to real data.. Experimental results and details of the protocol have been published in [3].

Hand palm is considered as a rigid plan formed by the head of the second metacarpal bone and the wrist styloids. Although there are multiple contact points between the palm and the sphere, we choose to limit our analysis to a unique contact point on the sphere, where the sphere and the palm share the same normal vector. From the shoulder to the palm, seven degrees of freedom are defined (3 for the shoulder, 2 for the elbow and 2 for the wrist).

Joint limits avoidance is based on Wang's work [4] which takes into account coupling effect of joint axes allowing us to have more natural simulated postures. Shoulder and wrist circumduction cones are based on data from the literature ([4] for the wrist and [6] for the shoulder), while axial limits of the upper arm are from [5].

The definition of the grasping posture is done as follow: 1- estimation of all the possible grasping points allowing an amplitude of rotation required by task; 2- a uniform probability distribution is attributed to these admissible points; 3- a grasping point is selected randomly; 4- the palm orientation around the selected grasping point is defined in order to maximize the shoulder-wrist pivoting angle margin at the beginning of the rotation, given the constraint that it must be inferior or equal to the pivoting margin at the end of the rotation; 4bis- if this constraint cannot be satisfied, another point is selected (step 3); 5- the elbow position is compute in the middle of the pivoting margin once the palm orientation is determined.

Results: Simulations were based on one subject's anthropometric data. Due to simulation constraints (rigid hand and no shoulder motion), we were only able to simulate grasping postures for the rotation amplitudes from -315° to 270°. Twenty simulations were performed for each amplitude. Figure represents the forearm (prono-supination) and shoulder-wrist (pivoting) angles for simulated and real postures. Globally, one can observe a similar evolution between the simulated and actual angles. Also, we have to note a tendency to have higher values for simulated pivoting angle in counter-clockwise rotations, i.e. a lower elbow position. Finally, as for the real data, simulated pivoting margins at the beginning and end of rotation show same behavior described in one of our previous work [3].

Figure:
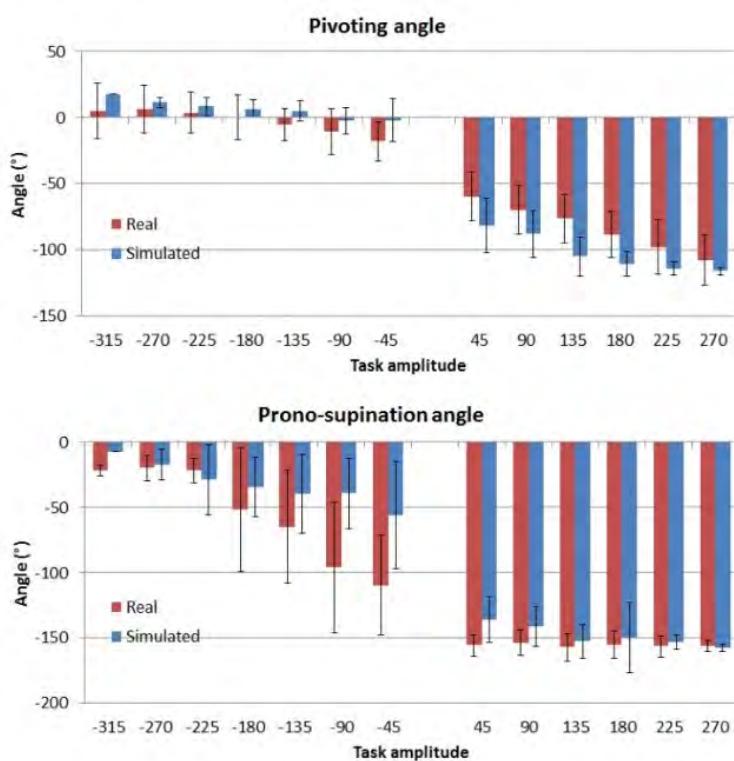
Caption: Comparison of simulated and real arm angles

Conclusion: First conclusion of this work is the ability of our algorithm to simulate arm grasping postures in agreement with experimental data. Moreover, despite a quite simple probability distribution, simulations show interesting results in term motion of variability. Nevertheless this model could be improved taking into account individual joint limits. Finally, other probability distributions should also be tested.

References: [1]Gielen et al., Hum. Movement Sci., 14: 487-509, 1995

[2]Latash, Fundamentals of Motor Control, Academic Press, 2012

[3]Lardy et al., Ergonomics, 55 (12): 1524-1534, 2012

[4]Wang, J. Biomech. 32: 453-460, 1999

[5] Wang et al., J. Biomech. 31: 899-908, 1998

[6]Engin et al., J Biomech. Eng. 108: 215-227, 1986

Disclosure of Interest: None Declared

PO-0225

COMPARISON OF MECHANICAL PARAMETERS OF TISSUE ENGINEERED AND NATIVE CARTILAGE: A NUMERICAL STUDY

Antonio Completo [1,*]Cátia Bandeiras [1]Antonio Ramos [1]

[1]Mechanical Engineering, University of Aveiro, Aveiro, Portugal

Introduction and Objectives: One of the main difficulties associated with tissue engineered cartilage is the unability, so far, to obtain tissues with homogeneous mechanical properties and similar to the native cartilage ones [1]. We will simulate the effects of biphasic mechanical properties obtained from simulation of free swelling culture of tissue engineered cartilage on the mechanical behaviour of the tissue in comparison to homogeneous tissue engineered cartilage and native cartilage with homogeneous mechanical properties.

Methods: Axisymmetric 2D slices of tissue engineered cartilage and native cartilage (2mm width x 2.34 mm height) were modelled in Abaqus v 6.12.1 (Dassault Systèmes, France). A biphasic model with isotropic neo-Hookean solid phase was implemented [2,3]. The mechanical properties of tissue engineered cartilage were calculated by replicating the experimental conditions in [1] and using the tool presented in [2]. The mechanical properties of the middle zone of articular cartilage were taken from [4]. Stress-strain compressive mechanical tests were simulated until 20% compression (0.05%/s) in all the samples.

Results: The distributions of the unloaded mechanical properties of tissue engineered cartilage are shown in Figure 1A. The average mechanical properties of tissue engineered cartilage are compared with the middle zone articular cartilage properties in Table 1. The nominal stress and pore pressure simulated for each case are shown in Figure 1B.

Table 1: Average mechanical properties of tissue engineered cartilage and native cartilage.

Figure:
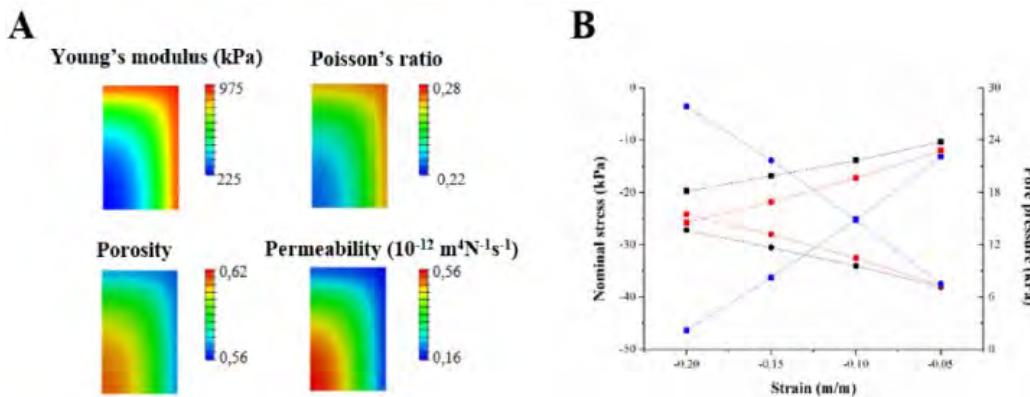
Caption: Figure 1. A: Mechanical properties of tissue engineered cartilage obtained from simulation of the experimental conditions of [1] during 56 days. B: Average nominal stresses (squares) and pore pressures (circles) for heterogeneous TE cartilage (black), homogeneous TE cartilage (red) and native cartilage (blue).

Conclusion: The lack of nutrient supply to the cores of TE cartilage resulted in maximum/minimum relative differences of 23, 82, 90 e 29% for the Young's modulus, Poisson's ratio, porosity and permeability respectively. Heterogeneous TE cartilage has nominal stresses and pore pressures 23 and 12% inferior to the homogeneous TE cartilage and 57 and 51% inferior to the native cartilage. This is essentially due to the high average permeability of TE cartilage, approximately 6 times higher than the native cartilage one. Research on experimental procedures and materials that allow for a more optimal reduction of permeability and that allow to reduce the heterogeneity in the distribution of the parameters is important to obtain TE cartilage with mechanical behaviour more similar to the native cartilage one.

Table:

Property	TE cartilage	Native
E (kPa)	653.5	364
υ	0.205	0.24
φ	0.59	0.75
k (10^{-12} $m^4.N^{-1}.s^{-1}$)	0.0967	0.0172

Caption: Table 1: Average mechanical properties of tissue engineered cartilage and native cartilage.

References: [1]   L. Bian *et al* Osteoarth. Cartil. 17 (2009) 677-685.

[2]   C. Bandeiras, A. Completo Comput. Methods Biomech. Biomed. Eng. 16 (Sup 1) (2013) 262-263.

[3] C. Bandeiras, A. Completo Comput. Methods Biomech. Biomed. Eng. 17 (Sup 1) (2014) 262-263.

[4] F. Boschetti *et al* Biorheology. 41 (2004) 159-166.

Disclosure of Interest: None Declared

PO-0226

CHEST MODEL FOR BLUNT AORTIC TRAUMA MODELLING CREATED USING MULTIPLE MODES OF IMAGING

Alan Parish [1,*]Francisco Carrasco-Hernandez [1]Donal McNally [1]

[1]Engineering, Nottingham University, Nottingham, United Kingdom

Introduction and Objectives: For finite element modelling of blunt aortic trauma in car crashes it is important to model not only the aorta but its surrounding tissues. As forces involved in the crashes interact with all the different tissues and are likewise affected by their varying mechanical properties.

To this end to ensure that the correct anatomical geometry of the tissues and the aorta was correct, multiple medical imaging models were used of a single cadaver taken from the visible human project [1].These data sets have the unique advantage that the subject was scanned in multiple modes post-mortem, (CT, MRI and photographically as the body was ground down). Also as the subject did not die from a heart related problem the aorta is in healthy condition.

The use of multiple data sets is important as segmenting out the body from a single data set such as CT is only feasible for dense tissues such as bone and not for soft tissue such as the heart, while the MRI data is good for soft tissue but not for dense. Therefore by combining the CT and MRI data as well as unique photographic data this data set also possesses, it is possible to build up a whole model of the chest area which would not be possible when using just a single data set.

This segmented model is advantageous over a simplified geometric model as it does not rely on assumptions about the shape and represents directly the relative position of all the different tissue types.

Methods: The three data sets were taken from a 38 year old male [1] and were all segmented using the software Mimics (Materialise) with the resultant 3D models being post processed in 3-Matic (Materialises). All the models were segmented directly, except for the aorta, which because of the thickness of its layers was constructed from the blood within it and then wrapped with layers of 0.27, 0.36 and 0.40mm to create a 3 layer model [2].

The different tissue contrast of the three data sets were used to create the model:

The bone, cartilage on the ribs, lungs and intestines were segmented from the CT data.

The heart was segmented from the MRI data.

The aorta and liver were both segmented from the photographic data.

This combined imaging method provides the novel advantage of this model, namely as all the imaging data was collected post mortem all the tissue is stationary so unlike in a living subject the image data from all the different image sources can be over laid (on the photographic data set) to create a model which takes into account the different tissue types.

Once the different tissue types were segmented and meshed, the meshes were then cleaned and the number of elements reduced for the non-aorta meshes.

Results: The model created retains the anatomically determined geometry while having below 1.5 million elements, with the layers of the aorta possessing a higher proportion of the elements to size because they are the regions of interest.

Figure:
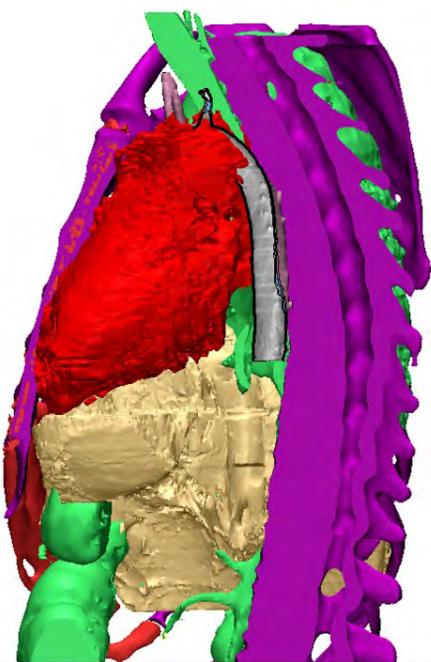
Caption: Cross section along the sagittal plane of the chest model, showing the complete heart and the layers in the aorta.

Conclusion: With the utilization of a unique post mortem data set and cutting edge segmentation software, it is possible to create a model for FEM which retains both the anatomically determined geometry as well as the segmenting out the different tissue types. Because of the different tissue's types properties, this would not be possible by using only a single data type such as CT, as such this multiply imaging types data set model allows for highly in-depth FEM to be performed in the future; which takes into account the actually shape and differing properties of the tissue types in the chest.

References: [1] Holzapfel, G. a, Sommer, G., Gasser, C. T., & Regitnig, P. (2005). Determination of layer-specific mechanical properties of human coronary arteries with nonatherosclerotic intimal thickening and related constitutive modeling. *American Journal of Physiology. Heart and Circulatory Physiology*, *289*(5), H2048–58. doi:10.1152/ajpheart.00934.2004

[2] Spitzer, V., Ackerman, M. J., Scherzinger, a L., & Whitlock, D. (1996). The visible human male: a technical report. *Journal of the American Medical Informatics Association   : JAMIA*, *3*(2), 118–30.

Disclosure of Interest: None Declared

DEVELOPMENT OF A BILATERAL UPPER LIMB MUSCULOSKELETAL MODEL TO INVESTIGATE MUSCLE CONTRIBUTIONS DURING DIFFERENT PUSH-UP VARIATIONS.

Julie Ellis [1,*] James Johnston [2] Jon Farthing [1] Alison Oates [1] Joel Lanovaz [1]

[1]College of Kinesiology, [2]Dept. of Mechanical Engineering , University of Saskatchewan, Saskatoon, Canada

Introduction and Objectives: The ability to estimate upper limb muscle forces during dynamic tasks can improve understanding of bone and joint loading in both normal and pathological conditions. The push-up is a common and important exercise movement which provides dynamic loading to the arms. To date biomechanical analysis of push-ups have been limited to external force [1] and inverse dynamics analysis [2], and EMG based estimation of muscle activation [3]. Musculoskeletal models utilizing muscle-tendon representations allow estimations of muscle and joint contact forces but currently no published upper limb models have been applied to push-up loading tasks. The purpose of this study was to 1) develop a bilateral dynamic upper-limb musculoskeletal model capable of simulating loaded movements and 2) evaluate the model by simulating three push-up variations with different expected loading patterns.

Methods: In this case study, a musculoskeletal model is used to estimate individual muscle contributions to net joint moments at the elbow and shoulder joints during push-ups with three different hand positions. A unilateral computational model of the upper limb [4], constructed in OpenSim [5], was adapted for this application. The original model was modified to include both arms which was required for simulating push-up movements and included 12 degrees of freedom (DOF) in each arm representing the sternoclavicular (SC), acromioclavicular (AC), glenohumeral, elbow and wrist joints. Movement of the SC and AC joints were constrained as a function of shoulder elevation based on de Groot & Brand [6]. Muscle moment arms from the original model [4] were maintained. A lower limb model was also included with 10 DOF representing the back, hips, knees, ankle, subtalar and metatarsophalangeal joints. The resulting bilateral whole body model included 100 Hill-type muscle representations in the upper extremities and ideal torque actuators controlling torso and lower extremity DOF.

Experimental data driving the analysis were obtained from a single male participant performing push-ups with three different hand widths (wide, neutral and narrow) and similar shoulder positions. Using a metronome, the timing of the push-ups were controlled at 0.5Hz. Kinematics of each variation were recorded using a 54-marker set with a three-dimensional motion analysis system (VICON, Denver, CO). External loads were measured by three force platforms, one under each hand (AMTI, Watertown, MA) with a third under both feet (Bertec, Columbus, OH). The OpenSim modelling platform [5] was used for analysis. The model was scaled and inverse kinematics and dynamics were performed. Single representative trials from each variation were selected for static optimization analysis to estimate individual muscle force contributions to the recorded movements. The estimated muscle forces and moment arms from static optimization were used to calculate moment contributions throughout the push-up movements. Muscle moments were averaged across the push-up cycle to calculate mean muscle moment contributions for comparison between hand position variations.

Results: Experimental net joint moments at the elbow were comparable to previously published data [2]. Simulations found the triceps brachii (elbow), anterior and middle deltoids and pectoralis major (shoulder) muscles to be the major

contributors during the push-up (Figure 1). Triceps were most active in the narrow hand position and least active in the wide position. Both anterior and middle deltoids followed an opposite pattern being most active in the wide hand position and least active in the narrow position. The anterior deltoids were always dominant over the middle deltoids. Pectoralis major produced the highest mean moment in the neutral hand position, followed by the narrow and wide positions. The patterns of individual muscle moment contributions between the three hand positions agreed well with previous EMG based estimations of muscle activation during similar push-ups [3].

Figure:
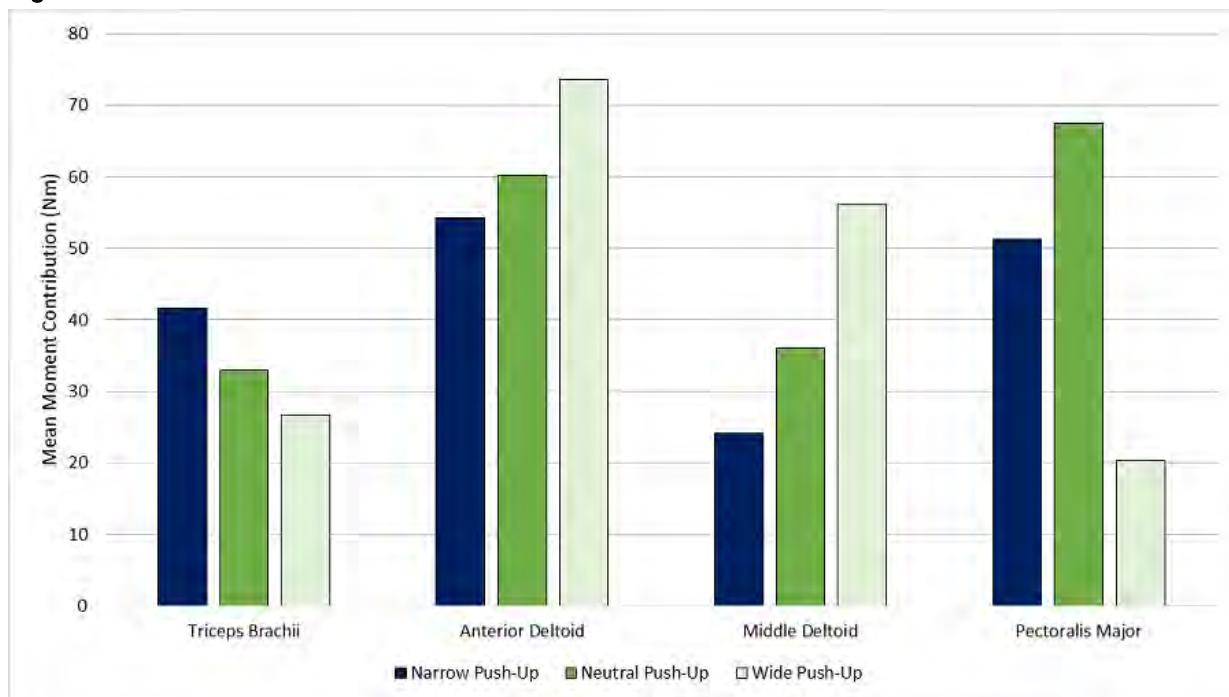
Caption: Figure 1: Mean muscle moment contributions to push-ups with narrow, neutral and wide hand positions.

Conclusion: The current study demonstrates an application of a novel bilateral upper extremity musculoskeletal model, simulating a relatively complex whole body dynamic task with external loading. Future work will include a range of participants and a sensitivity analysis investigating the effect of model parameter variation on outputs.

References: [1]Ebben et al., *J Strength Cond Res,* 25: 2891-2894, 2011.

[2]Donkers et al., *J Biomech,* 26: 625-632, 1993.

[3]Cogley et al., *J Strength Cond Res,* 19: 628-633, 2005.

[4]Saul et al., *Comput Methods in Biomech Biomed Engin,* ahead of print, 2014.

[5] Delp et al., *IEEE Trans Biomed Eng,* 54: 1940-1950, 2007.

[6] de Groot et al., *Clin Biomech,* 16: 735-743, 2001.

[7] Delp et al., *IEEE Trans Biomed Eng,* 37: 757-767, 1990.

Disclosure of Interest: None Declared

PO-0228

RELATING FEMORAL CONDYLE GEOMETRY TO ANTERIOR CRUCIATE LIGAMENT LENGTH

Melissa A. Boswell [1]Brian Davis [1,*]Michael Kelly [2]Danielle Filipkowski [2]John Elias [2]

[1]Biomedical Engineering, The Univeristy of Akron, [2]Akron General Medical Center, Akron, United States

Introduction and Objectives: A relationship between femoral condyle geometry and ACL length, although not currently quantified, would facilitate optimal knee reconstructive surgery. In this study, the relationships between the radii of the femoral lateral and medial condyles and the length of the ACL bundles were evaluated using knee computational models.

Methods: Ligaments and muscles were modeled as described previously [1], with the models used to simulate dynamic knee flexion with eccentric muscle contractions. The anterior and posterior ACL bundle lengths were measured from tibial to femoral insertion points.   For each condyle, anterior and posterior cylinders were used to represent the distal femoral anatomy. The models were run with the contact between the femur, or cylinders, and the tibia guiding the motion. ACL force vs. flexion angle of the tibia for the two contact conditions was compared to confirm that the radii of the fitted cylinders matched those of the patients' knees.

Results: In one knee model, both the tibiofemoral contact model and cylinder contact model had an ACL posterior bundle force starting at 350N and steadily decreased to 0N at 25° flexion and an ACL anterior bundle starting at 150N and reaching 80N at 50° flexion. A similar pattern for the other knees indicates that the radii of the cylinders fitted matched that of the condyles and the radii length could then be compared to the ACL bundle lengths.

Figure:
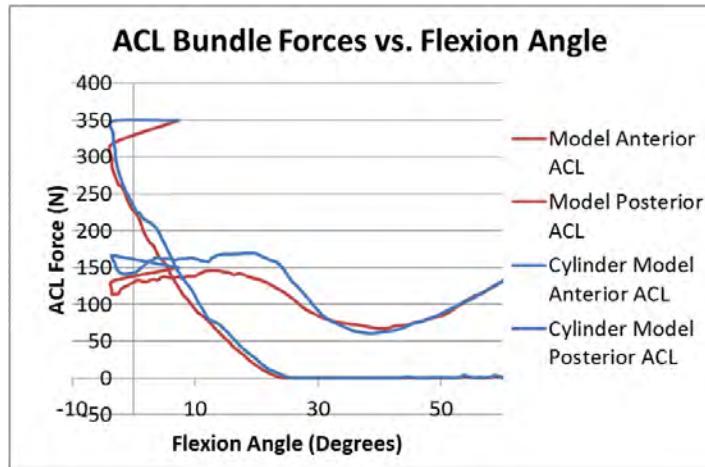
Caption: A similar pattern in ACL bundle forces before and after the cylinders were fitted to the model indicates that the cylinders closely resemble the femoral condyle geometry.

Conclusion: The results supported the hypothesis that there is a close synergy between condyle geometry and ACL length.

References: [1] Purevsuren T, Elias JJ, Kim K, Kim YH. Comput Methods Biomech Biomed Engin, 15:1-5, 2014.

Disclosure of Interest: None Declared

Modelling

PO-0229

SIT-TO-STAND PREDICTION FOR A RIGID LINK HUMAN MODEL

Valerie Norman-Gerum [1,*] John McPhee [1]

[1] Systems Desgin Engineering, University of Waterloo, Waterloo, Canada

Introduction and Objectives: Decreased capacity to perform sit-to-stand (STS), often due to effects of aging, disease, or injury, limits patient mobility and independence. Available interventions are evaluated based on past outcomes and performance in the clinic. A better option is to first assess interventions in silico, by creating computational patient and intervention models to support predictive simulation of motion.

A model of a healthy patient was created from the literature and experiments. Its motion is driven by Bézier curves, optimized to minimize joint torques. The predicted motion is evaluated against normative events of STS. This work will be used as a foundation for predictive simulation with models and performance criteria more closely tied to human physiology, including muscle dynamics, for greater fidelity in motion prediction.

Methods: A biomechanical model was constructed in MapleSim (Maplesoft, Canada) to represent a typical adult Caucasian female (61.9kg, 1.735m) (Fig.). The model's three links, HAT (head, arms, and torso), thigh, and leg, are connected by two planar revolute joints at the hip and knee, and to the ground by a revolute joint at the ankle. Thus, the model moves in the sagittal plane only. Forces between the chair and seat of the patient were modelled using a nonlinear spring-damper and hyperbolic tangent Coulomb friction. The parameters of this model are taken from the literature [1, 2] as well as from experiments.

Sit-to-stand dynamics and kinematics of one subject were measured using AccuGait force plates (Advanced Mechanical Technology, USA) and MVN Biomech motion capture system (Xsens, Netherlands). Seat contact parameters were estimated using an optimization routine executed in MATLAB (The MathWorks, USA), which minimizes the difference between measured ground reaction forces and those calculated when driving the model with measured kinematics. The kinematics also provided the orientation of body segments used to calculate the inertial parameters of the HAT.

The model was then simulated independently of experimental data. The hip angle and vertical and horizontal locations of the hip were modelled as Bézier curves, with the first and last knots constrained to describe static sitting and standing poses, respectively. The locations of these knots were optimized to minimize the sum of squared joint torques required for the model to achieve STS. The number of knots was increased sequentially until the solutions converged to an optimal motion.

Dynamics and kinematics of the patient model were calculated for the predicted STS. From these, the markers of STS events [3] were calculated as a percent of the total time taken to complete the motion and compared to normative data.

Results: Sit-to-stand as predicted for the human model is presented in the Figure and Table. The six phases of the STS cycle, quiet sitting, initiation, seat unloading, ascending, stabilization, and quiet standing [3], are present in the prediction. The events defining the phases are in proper sequence. The spacing of the events is uncharacteristic when examined in context of the statistics in the Table. Predicted vertical acceleration begins early and terminates late, seat off is early, and the stabilization phase is short. The predicted motion is analogous to STS; however it is not typical.

Figure:
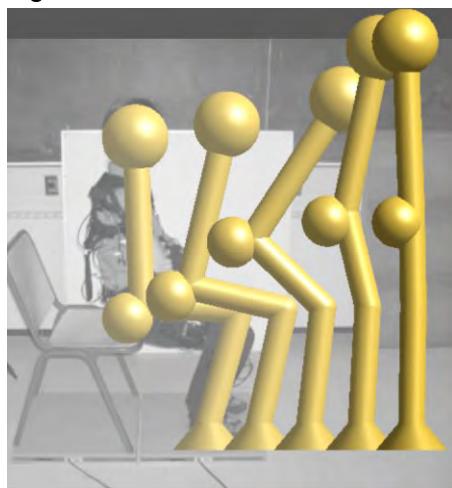
Caption: A photo of the experiment behind a series of images of the model performing the predicted STS.

Conclusion: Predictive simulation of human motion requires a model that appropriately represents the human body with a physiologically representative optimal control formulation. The rigid link model created is clearly not a human and the cost function used, minimizing a function of joint torques, is abstract; however the predicted STS resembles that of a human. This model will soon be supplemented with models of muscles; this step toward biofidelity will provide the context to enforce achievable joint torques and specify more physiological performance criteria including functions of muscle forces and joint contact forces.

The current model has been used to predict STS with the normative sequence of phases and events. The objective of future modelling is to predict event occurrence within the range of event times in the healthy human population.

Table:

	Event					
	Initiation	Start of vertical acceleration	Seat off	End of vertical acceleration	Start of stabilization	Standing on
Prediction	0.0	1.4	21.3	76.9	97.2	100.0
Average	0.0	26.5	33.2	45.3	72.7	100.0
Standard Deviation	0.0	6.1	5.7	5.3	4.1	0.0
Minimum	0.0	41.2	47.1	56.1	82.2	100.0
Maximum	0.0	18.3	25.7	35.9	66.3	100.0

Caption: Comparison of predicted and experimental [3] event times as a percent of the total time taken to complete STS.

References: [1] de Leva, J. Biomech. 29: 1223-1230, 1996.

[2] Yamaguchi, Dynamic modelling of musculoskeletal motion, Springer Science+Business Media, 2006.

[3] Kraij et al., J. Biomech. 23: 1123-1138, 1990.

Disclosure of Interest: None Declared

KINEMATICS AND DYNAMICS OF FOUR R-TYPE JOINT ANTHROPOMORPHIC FINGER

Anil Kumar Gillawat [1]Hemant J Nagarsheth [1,*]Mansi H. Nagarsheth [2]Nirmal Kumar Kushwaha [3]

[1]Department of Mechanical Engineering, Sardar Vallabhbhai National Institute of Technology, [2]Department of Physiology, Surat Municipal Instiute of Medical Education & Research, Surat, [3]Department of Mechanical Engineering, Babaria Institute of Technology, Vadodara, India

Introduction and Objectives: Kinematic and Dynamic analysis of human hand, end effectors, desired trajectory and output power has derived the interest of many researchers in the field of designing [Fukui et al], analysis [Butz et al] and modeling [Yamane et al.] of anthropomorphic fingers. This paper presents the study of kinematics and dynamic analysis of an anthropomorphic finger with four revolute joints (R- joints). The torques are derived and plotted against the angle of rotations. The results are analyzed and justified. Kinematic Analysis is used to find out the position, velocity and accelerations without considering the forces causing the motion. Denavit-Hartenberg table (D-H Table) is generally used for kinematic analysis. Dynamic equation is used to derive the torques and forces which are used as inputs for designing the controllers. Two formulations: Newton-Euler formulation and Lagrange-Euler formulation are used to derive the dynamic equations. In this paper, Lagrange Euler formulation is used for deriving the torque equations.

Methods: Kinematic Analysis of finger joints is carried out in order to find the position, velocity and acceleration, which are used as inputs to the dynamic equations. The Dynamic equations are derived to find out the torques and forces which are again useful in designing controllers. D-H table is used for kinematic analysis and Lagrange-Euler formulation is used to derive the dynamics equations. MATLAB is used for obtaining the torque results which are used to depict the relation between the rotated angle and the torque encountered for both lifting conditions (with and without load). The Dynamic analysis is carried out at all the joints of finger considering flexion only. All the joints: Metacarpophalangeal joint (MCP), Proximal interphalangeal joint (PIP) and Distal interphalangeal joint (DIP) are assumed to be revolute and able to produce flexion and extension motion of the fingers only.

Results: The torque results are obtained from the dynamic equations and graphs for Torque vs Angle are plotted for both the cases: (i) no load condition and (ii) lifting load of 50 gm having diameter of 50 mm. For the particular case, all motors are assumed to be in unconstrained motion. remaining motors are assumed to keep the links stationary, which requires some torque at these joints. The rotation of one joint had some effect on the other joint on the same finger, which is depicted in the figures. Joint torque behaviour is studied for unconstrained rotation of joints. When all joints are rotating with no load, DIP joint has minimum torque and maximum torque for CMC joint. All joint torques have depicted same behaviour within the restricted range of motions. Figure 1 shows that the maximum torque is required at the starting as it has to overcome the static forces. The torque reduces drastically and then adopts the sinusoidal behaviour, with peak value less than the starting torque. The maximum torque is experienced by CMC joint as it has to sustain the load of the complete finger as depicted by kinematic model. The maximum torque is experienced by CMC joint, which is responsible for lifting of complete finger and is minimum for DIP joint, which is responsible for lifting only last link (Distal Phalange). CMC joint torque has to balance the remaining joint torques and hence rapid increase in joint torque is observed. CMC

joint has negative starting torque which is different from the remaining joint torques. Starting torque for theMCP, PIP and DIP joints is found to be maximum and reduces drastically and then adopts the sinusoidal behaviour, which has peak value less than the starting torque. All the four joint torques exhibit the sinusoidal behaviour. The negative joint torque suggests that resisting torque is greater than the applied torque for lifting other links and payload attached to the joint torques and acts against the gravity to keep the links stable. Initial high positive torque obtained indicates that obtained torque is positive and the resisting force is zero.

Figure:
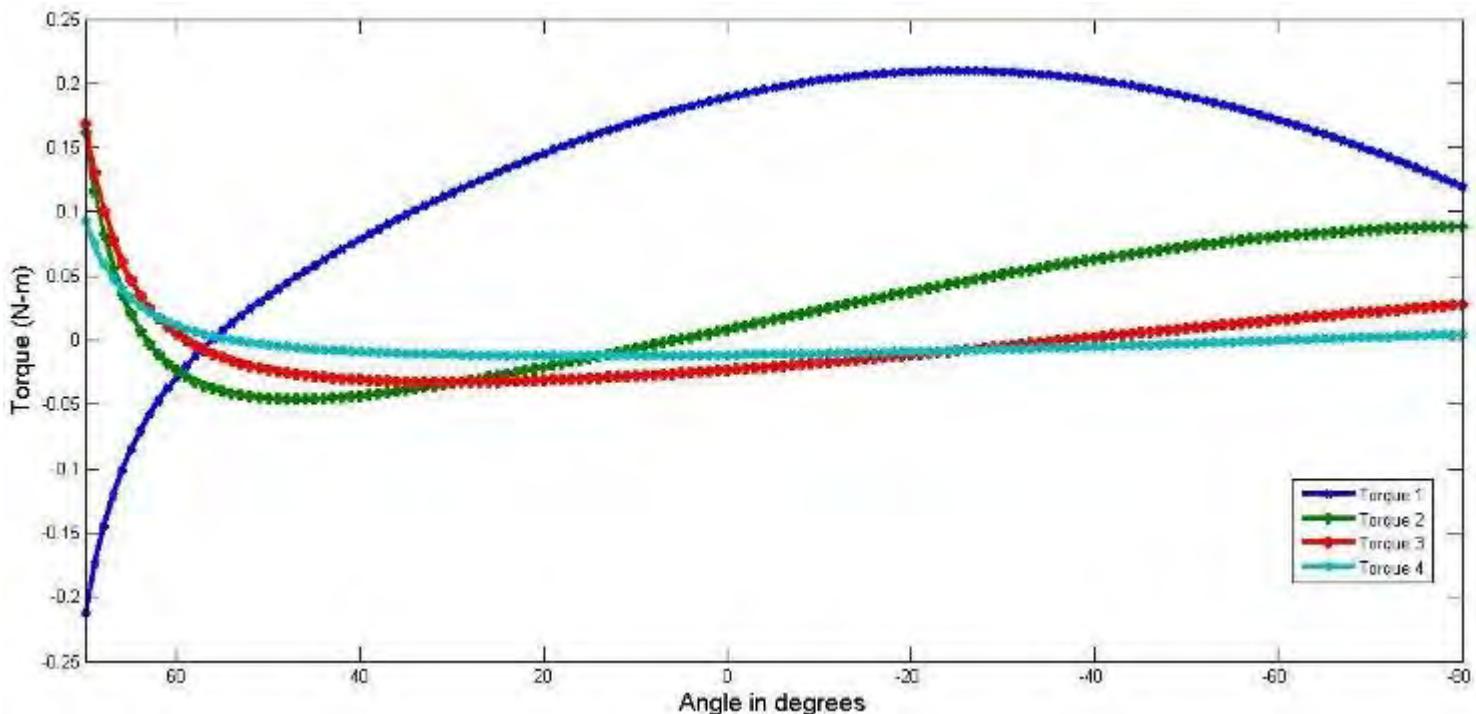
Conclusion: Mathematical modeling for joint torques are derived using D-H approach and Lagrange-Euler approach. The torque results are obtained by using MATLAB and the relations are depicted. The results are found to be satisfactory. The results can be useful for physical therapy and rehabilitation of hand with minimum load on the joints. The effect of rotation of one finger on other can be considered for further study.

References: [1] Butz K D, et al. Computer Methods in Biomechanics and Biomedical Engineering, 15(2): 131–140, 2012.
[2] Fukui W, et al. The future of Humanoid Robots Research and Applications, 2012.
[3] Yamane K and Nakamura Y. Springer Tracts in Advanced Robotics, 66(4): 49-60, 2011.

Disclosure of Interest: None Declared

Motion Analysis

PO-0232

EFFECTS OF SURGICAL BREAST CANCER TREATMENT ON THREE-DIMENSIONAL SCAPULAR KINEMATICS DURING UPPER-LIMB MOVEMENT

Ivana Ribeiro [1,*]Paula Camargo [1]Angelica Ferrari [1]Maíra Lixandrão [1]Tania Salvini [1]

[1]Departament of Physical Therapy, Universidade Federal de São Carlos, São Carlos, Brazil

Introduction and Objectives: The residual effects of surgery treatment for breast cancer may affect upper limb function, strength and movement. Patients report shoulder pain, weakness, tightness and reduced functional capacity. Limited shoulder motion and function are consistently identified following surgical breast cancer treatment and subsequent both axillary lymph node dissection and sentinel node biopsy. These procedures can decrease functional activities, particularly overhead reaching and quality of life in breast cancer survivors. Normal scapular motion during arm elevation consists of upward rotation, posterior tilt and external rotation. In breast cancer survivors, altered motion patterns can be presented in the affected side. However, it is not known yet if the type of surgery procedure associated to axillary lymph node dissection can contribute to abnormal scapular movement. Therefore, the purpose of this study was to assess the scapular kinematics in women who had undergone a surgical breast cancer treatment.

Methods: Seven women who had surgical breast cancer treatment were evaluated (42.8± 5.6 years; 72.2±18.3 kg; 1.64±0.01m; Disabilities of arm, shoulder and hand questionnaire: 36.3±29.6). Most of them had undergone mastectomy surgery (5 participants) than quadrantectomy procedure (3 participants) both associated to axillary lymph node dissection.The period of surgery was closer to 2 years (mean: 24.7±16.8 months) and all participants had taken chemotherapy after surgery in the non-affected side. The Flock of Birds® electromagnetic tracking system was used to evaluate scapular kinematics during elevation and depression of the arm in the scapular plane. Local coordinate systems were established for the trunk, scapula, and humerus using the digitized landmarks following the protocol recommended by the International Society of Biomechanics (Wu et al., 2005). Three repetitions were recorded with the individual in the standing position. Kinematic motion analysis involved selecting scapular data at 30°, 60° and 90° of arm elevation. The results were analyzed using the SPSS statistical package. A two-way ANOVA was used to identify angle x group interaction or main effect of group. The level of significance was considered 5%.

Results: For scapular internal rotation, the interaction side × angle was not significant as well as main effect of group for elevation ($p=0.75$, $p=0.93$, respectively) and lowering ($p=0.31$, $p=0.95$, respectively) of the arm. For scapular upward rotation, the interaction side × angle was not significant as well as main effect of group for elevation ($p=0.79$, $p=0.76$, respectively) and lowering ($p=0.10$, $p=0.55$, respectively) of the arm. For scapular tilt, the interaction side × angle was not significant as well as main effect of group for elevation ($p=0.22$, $p=0.34$, respectively) and lowering ($p=0.13$, $p=0.58$, respectively) of the arm. The mean difference between sides was 0.37° ± 4.31°, 1.21° ± 3.93° and 2.18° ± 2.21° for scapular internal rotation, upward rotation and tilt, respectively, during arm elevation. For lowering of the arm, the mean difference between sides was 0.21° ± 3.66°, 2.55° ± 4.17° and 1.32° ± 2.34° for scapular internal rotation, upward rotation and tilt, respectively, during arm elevation. The absence of altered scapular kinematics may represent compensatory responses for scapular function improvement during arm elevation. In fact this is according to Shamley and colleagues

(2012) who concluded that shoulder morbidity after surgical breast cancer treatment is bilateral. In addition, this could be related to chemotherapy exposure in the non-affected side after surgical treatment.

Conclusion: Scapular kinematics during elevation of the arm do not differ between affected and non-affected sides in woman who had undergone surgical breast cancer treatment. Besides, it is important to consider the small sample size in this study. Futures studies are needed, especially with a large sample size to verify possible alterations in scapular kinematics.

References: Borstad JD, Szucs KA. Three-dimensional scapula kinematics and shoulderfunction examined before and after surgical treatment for breast cancer. Human Movement Science. V. 31, p. 408–418, 2012.

Shamley D et al. Shoulder morbidity after treatment for breast cancer is bilateral and greater after mastectomy. ActaOncologica. v.51, p. 1045–1053, 2012.

Crosbie J et al. Effects of Mastectomy on Shoulderand Spinal Kinematics During Bilateral Upper-Limb Movement. Physical Therapy. v. 90, p. 679-692, 2010.

Wu G, van der Helm FC, Veeger HE, et al. ISB recommendation on definitions of joint coordinate systems of various joints for the reporting of human joint motion--Part II: shoulder, elbow, wrist and hand. JBiomech. 2005;38:981-992.

Disclosure of Interest: None Declared

Motion Analysis

PO-0233

COMPARISON OF KNEE JOINT KINEMATICS AND KINETICS BETWEEN ANTERIOR CRUCIATE LIGAMENT DEFICIENT AND HEALTHY SUBJECTS DURING RUNNING

Saud M. Alarifi [1,*] Lee Herrington [1] Richard Jones [1]

[1] Knee Biomechanics and Injury Research Programme, University of Salford, Salford, United Kingdom

Introduction and Objectives: Anterior cruciate ligament (ACL) and patellofemoral joint (PFJ) injuries are common and cause significant time loss to sports participation, as well as the reported increased risk of osteoarthritis (OA) from ACL and PFJ injuries. There is little data on why individuals with an ACL-deficient (ACL-D) or ACL-reconstructed knee consequently develop OA but altered kinematics and kinetics are one of the hypothesised reasons. Numerous studies investigating walking gait have found significant reductions in knee flexion moment and small reductions in peak knee flexion angle, with individuals adopting a quadriceps avoidance gait pattern during walking. One of the most common activities pre- and post-surgery is running and it is not known if individuals with an ACL-D knee have different knee kinematic and kinetic patterns to healthy runners. In the absence of typical function of the ACL, the ACL-D individuals may subconsciously avoid contraction of the quadriceps to avoid displacing the tibia anteriorly during jogging where dynamic loads are greater. This may then increase the risk of development of generative diseases due to excess loading so understanding if there are differences is of utmost importance. Therefore, the purpose of this study was to compare the knee kinematics and kinetics between a group of ACL deficient individuals and healthy non-injured subjects during running. We hypothesised that the ACL-D individuals would have differences in knee kinematics and kinetics compared to the non-injured healthy group.

Methods: Eight individuals (2 female, mean +/- standard deviation age, height and mass are 22.5 ± 4.72 years, 1.73 ± 0.08 m, 74 ± 16.4 kg) who had sustained an ACL injury and were on the waiting list for reconstruction were recruited to the study, were compared with Eight healthy subjects (6 males, 29.2±4.89 years; mean height, 1.69±0.03m; mean mass, 68.4±8.39Kg). Each participant underwent a single assessment. A twelve-camera Qualisys motion analysis system (240 Hz), with an AMTI force platform (1200 Hz) embedded in the running track floor, was used to collect the kinematic and kinetic data.

Subjects ran along a twenty two metre runway at a self-selected speed, which was recorded with timing gates. Each subject performed five successful trials. The contact phase (initial contact to toe off) of five trials was normalised to 100% of stance and averaged for each condition.

Data were post-processed with Visual 3D software (C-motion Inc. USA) where the marker trajectory data were filtered at 12 Hz, and force data were filtered at 25 Hz using a fourth-order Butterworth low-pass filter. Euler angles to calculate three-dimensional angular motions between segments, and joint kinetics were calculated using a six-degree of freedom, inverse dynamics model. The outcome variables included peak knee valgus angle, peak knee flexion angle during early stance (first 30%), peak sagittal and coronal moments and peak vertical ground reaction force at stance phase.

Statistical analysis was performed with SPSS Version 22.0 (IBM SPSS, Chicago, IL), using a t-test to compare between ACL-deficient injured patients and the healthy subjects at the 95% confidence interval ($p < 0.05$).

Results: The running speeds were not significantly different between the two groups ACL-D 3.28±0.13 m/s, non-injured 3.02±0.29 m/s (p > 0.05). For the knee kinematics and kinetics, none of the outcome variables were significantly different to one another during the running activity (P > 0.05).

Figure:
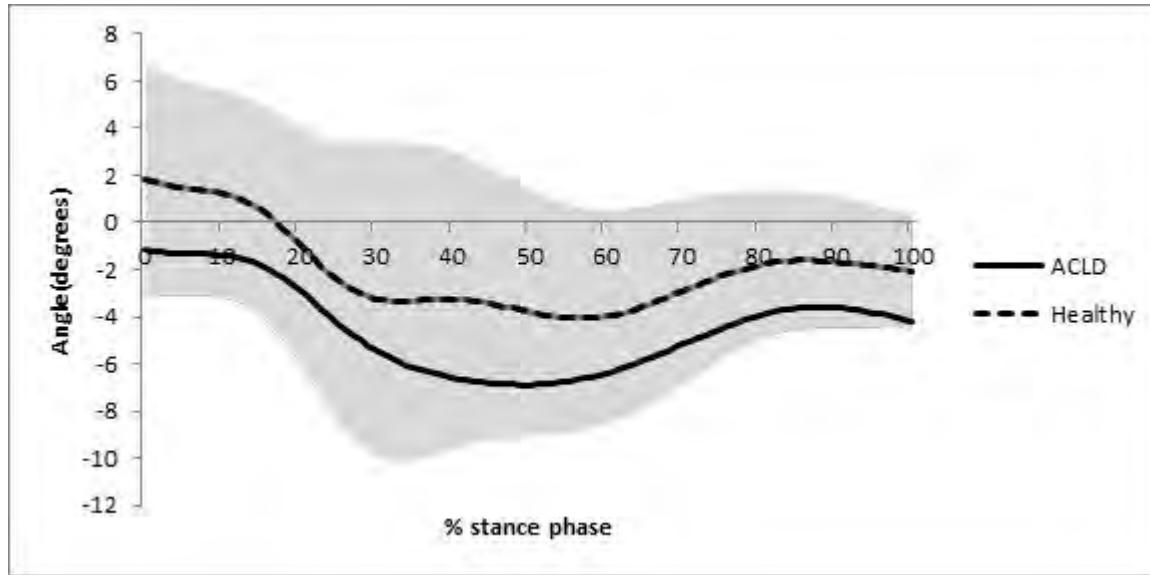
Caption: Figure 1: Knee valgus angle (-) during running for the ACL-D and healthy subjects (mean ± standard deviation).

Conclusion: This study showed no significant differences in knee kinematic and kinetic variables during running between the ACL deficient and healthy non-injured subjects. It would appear that ACL deficiency does not have a significant effect on the knee in how an individual runs in a straight line pre-ACL reconstruction. Further investigation is warranted to determine if these variables differ once reconstruction has occurred, as this may impact on the aetiology of degenerate joint disease found commonly post surgery.

Table:

Events	Peaks at stance phase			Peaks at early stance	
	KVA (°)	**KVM**(Nm/Kg)	**VGRF**(BW)	**KFA** (°)	**KFM**(Nm/Kg)
	X±SD	X±SD	X±SD	X±SD	X±SD
Healthy	-5.9±4.7	0.49±0.19	2.43±0.08	46.3±5.45	2.7±0.30
ACLD	-8.5±3.2	0.48±0.26	2.44±0.25	41.6±9.18	2.3±0.76
P-value	0.21	0.92	0.9	0.23	0.26

KVA: Knee Valgus Angle, KVM: Knee Valgus Moment, KFA: Knee Flexion Angle, KFM: Knee Flexion Moment, ACLD: Anterior cruciate ligaments Deficits, X±SD: Mean ± Standard Deviation, SEM: Standard Error of Mean, Sig: (Significance level), NS: non significant

Caption: Table 1: Knee kinematics and kinetics during running for ACL-D and healthy subjects.

Disclosure of Interest: None Declared

Motion Analysis

PO-0234

DIFFERENTIATION CAPABILITY OF DYNAMIC AND STATIC KINEMATIC MEASUREMENTS OF REARFOOT EVERSION IN PATELLOFEMORAL PAIN

Danilo Silva [1,*] Ronaldo Briani [1] Marcella Pazzinatto [1] Deisi Ferrari [2] Fernando Aragão [3] Carlos Albuquerque [3] Fábio Azevedo [1]

[1] Physiotherapy, University of São Paulo State, School of Science and Technology, Presidente Prudente, [2] Bioengineering, University of São Paulo, São Carlos, [3] Physiotherapy, State University of West Parana, Cascavel, Brazil

Introduction and Objectives: One of the most common knee disorders affecting young individuals is Patellofemoral Pain (PFP)[1]. Excessive rearfoot eversion is thought to be a risk factor for patellofemoral pain development, due to the kinesiological relationship with ascendant adaptations. Individuals with PFP are often diagnosed through static clinical tests[1], however, the adaptations seem to appear in dynamic conditions. Thus, the aim of this study was to determine the differentiation capability of three rearfoot eversion measures: rearfoot range of motion, static clinical test and static measurement using a 3D system.

Methods: 29 individuals with PFP and 25 control individuals (18–30 years) participated in this study. Motion analysis was collected using a three-dimensional motion-analysis system (VICON MX, Vicon Motion Systems Inc.; Denver–EUA) combined with 4 cameras (type Bonita®B10) operating at a sampling frequency of 100 Hz with a resolution of 1 megapixel. Ground reaction forces were collected using a force plate (AMTI, OR6, Watertown, USA) at a sampling frequency of 200Hz. To perform kinematic evaluation of each participant during stair climbing the Oxford Foot Model was used associated with a plug-in gait model to perform static calibration. A static trial was collected to verify the rearfoot eversion angle measured by the system. Each trial was filtered with a fourth-order Butterworth low pass filter with a cut-off frequency of 6 Hz. The retro reflective markers were identified and labeled within the Vicon Nexus® 1.8 for reconstruction. Gait events (heel strike and toe off) were identified using the force plate data. In addition, one rater has performed a rearfoot static clinical test, which is a classical measure in PFP evaluation. Receiver operating characteristic (ROC) curves were done to show the differentiation capability (diagnostic accuracy) of each variable.

Results: In the sequence, the results of specificity and sensitivity for the optimal cut off and area under the curve values (Table 1). Regarding area under the curve, the rearfoot range of motion was classified as moderately accurate (0.71), whereas the static variables were classified as less accurate (0.63; 0.60), in addition, the only dynamic variable showed the best combination of sensitivity and specificity values at 72% and 63%, respectively. Despite growing evidence that excessive rearfoot eversion is one of the PFP etiological factors, instruments used to enable this evaluation are not well-established. Foot posture has been frequently evaluated in individuals with PFP under the assumption that measuring static structure will provide insight into the dynamic function, although this is unproven[2]. Comparing static measures, the best was rearfoot eversion measured by a 3D system, however, Area under the curve = 0.63, Sensitivity = 59% and Specificity = 59% values do not characterize this variable as a confident differentiation tool.

Conclusion: This study provides some evidence on the behavior of rearfoot eversion kinematics theoretically associated with PFP. Therefore, rearfoot range of motion alterations are not seen in static measurements which could be a reasonable explanation for the lack of success of orthotic treatment. The rearfoot range of motion during stair climbing

variable presented the best results in terms of differentiation capability. Static variables seem not to be related to individuals with PFP, due to low accuracy values. Therefore, the results were not better than other biomechanical variables in the literature, questioning the importance of distal factors in PFP.

Table:

Variable	Sensitivity %	Specificity %	Area Under the Curve (95%CI)	Standard Error	P-value
REROM	72	63	0.71 (0.55 – 0.86)	0.078	0.014
RESM	59	59	0.63 (0.47 – 0.80)	0.082	0.106
Clinical Rater	63	45	0.60 (0.42 – 0.78)	0.091	0.091

Caption: Table 1 – Kinematic variables: REROM (Rearfoot Eversion Range of Motion), RESM (Rearfoot Eversion System Measurement), Clinical Rater (Clinical evaluation of rearfoot eversion).95%CI (95% Confidence Interval).

References: [1]   Lack S, Barton C, Malliaras P, Twycross-Lewis R, Woledge R, Morrissey D. The effect of anti-pronation foot orthoses on hip and knee kinematics and muscle activity during a functional step-up task in healthy individuals: a laboratory study. Clin Biomech (Bristol, Avon) 2014;29:177–82.

[2]   Barton CJ, Menz HB, Levinger P, Webster KE, Crossley KM. Greater peak rearfoot eversion predicts foot orthoses efficacy in individuals with patellofemoral pain syndrome. Br J Sports Med 2011;45:697–701.

Disclosure of Interest: None Declared

Motion Analysis

PO-0235

CRITICAL FLUCTUATIONS OF POSTURAL STABILITY AS A FUNCTION OF OSCILLATORY PLATFORM MOVEMENT

Aviroop Dutt-Mazumder [1,*] Karl M Newell [2]

[1]Kinesiology, The Pennsylvania State Uiversity, State College, [2]Kinesiology, The University of Georgia, Athens, United States

Introduction and Objectives: Addressing self-organization coordination processes involved while standing on an oscillatory platform is one avenue that reflects the emerging behavior of phase transition at the critical fluctuating point with respect to higher oscillating frequencies. Such experimental setup gives an insight to investigate the degenerate ways of maintaining stability despite encompassing the numerous degrees of freedom of the movement system in action[1]. In a simple rhythmic movement the fundamental elastic and frictional functions limit the ways in which the body's multiple subset can be assembled into a comprehensive rhythmic unit of few degrees of freedom[2].

We investigate how the postural system regulates the joint space degrees of freedom when subjected to lateral oscillating perturbation through the lens of phase portraits and relative phase. The aim was to investigate the coordination changes of a ML stance on a moving platform. It was hypothesized that center of mass(CoM)-center of pressure(CoP) and Head-CoP would abruptly shift from in-phase (low platform frequencies) to anti-phase (higher frequencies)[3].

Methods: Twelve healthy male participants were recruited, according to the experimental protocol approved by Pennsylvania State University IRB.3-D motion analysis system (QTM, Sweden) was enabled to record 13-segment model reconstructed from an 18-marker system[3]. A force platform (AMTI, OR 6-5-1000) was used to derive the displacement of the CoP and was mounted on a moving platform that translated sinusoidally in the M-L direction. The participant were instructed to maintain their postural balance when they stood on the moving platform with bare feet placed side-by-side comfortably and kept their arms folded across their chest. The moving platform was controlled by a motor that generated oscillated at six frequencies (0.2, 0.4, 0.6, 0.8, 1.0 and1.2) Hz with a constant amplitude of 20 cm. Each day had a six trial block that had 1 min of intra-trial recovery.

Results: Fig.1 presents the phase portraits of the joint angular trajectories[4]. Qualitatively inferred, that there is a definite frequency and amplitude relationship with the oscillating platform frequency. Lower frequency (e.g. 0.2 Hz) all the lower limb joints (ankle, knee and hip) exhibits overlapping phase plane trajectories, indicating small amplitude but higher frequency and large variability in the joint angular motions. However, the joint motions exhibit a different shape of phase plane trajectories with increasing oscillating frequency of the moving platform. Between 0.4 Hz-0.6 Hz which is our predicted phase transition frequency band, we can see that the oscillations being unwrapped and moving towards larger amplitude, hence there is significant amount of less overlapped trajectories in the joint space giving rise to smoother limit cycles. The knee angular motion has less angular space exploration than ankle or hip joint across both feet as a function of increasing oscillating platform frequency.

CoM-CoP coupling moves from in-phase (36º) to anti-phase (142º) (Table 1). The SD peaks at 0.4 Hz (which is the phase transition frequency) and decreases as the frequency is increased further. This could reflect that the coordination of CoM-CoP is undergoing large instability during the phase transition region. CoM-Platform and CoM-Head remain largely

unchanged and stays in-phase irrespective of the increasing frequency conditions. The Head-CoP coupling shows a similar trend that of CoM-CoP, which is a shift from in-phase mode to an anti-phase mode after undergoing a phase transition at 0.4 Hz. The joint angular coupling of at the local level (Hip-Knee and Knee-Ankle) reflect that there is a gradual increase to anti-phase mode during 0.6-0.8 Hz before retreating back to in-phase mode. In other words, the local joint synergies are strongly coupled at a lower and higher frequency in order to maintain stability whereas they are loosely coupled (large M and high SD) during the unstable region of the phase transition period in order to accommodate postural balance.

Figure:
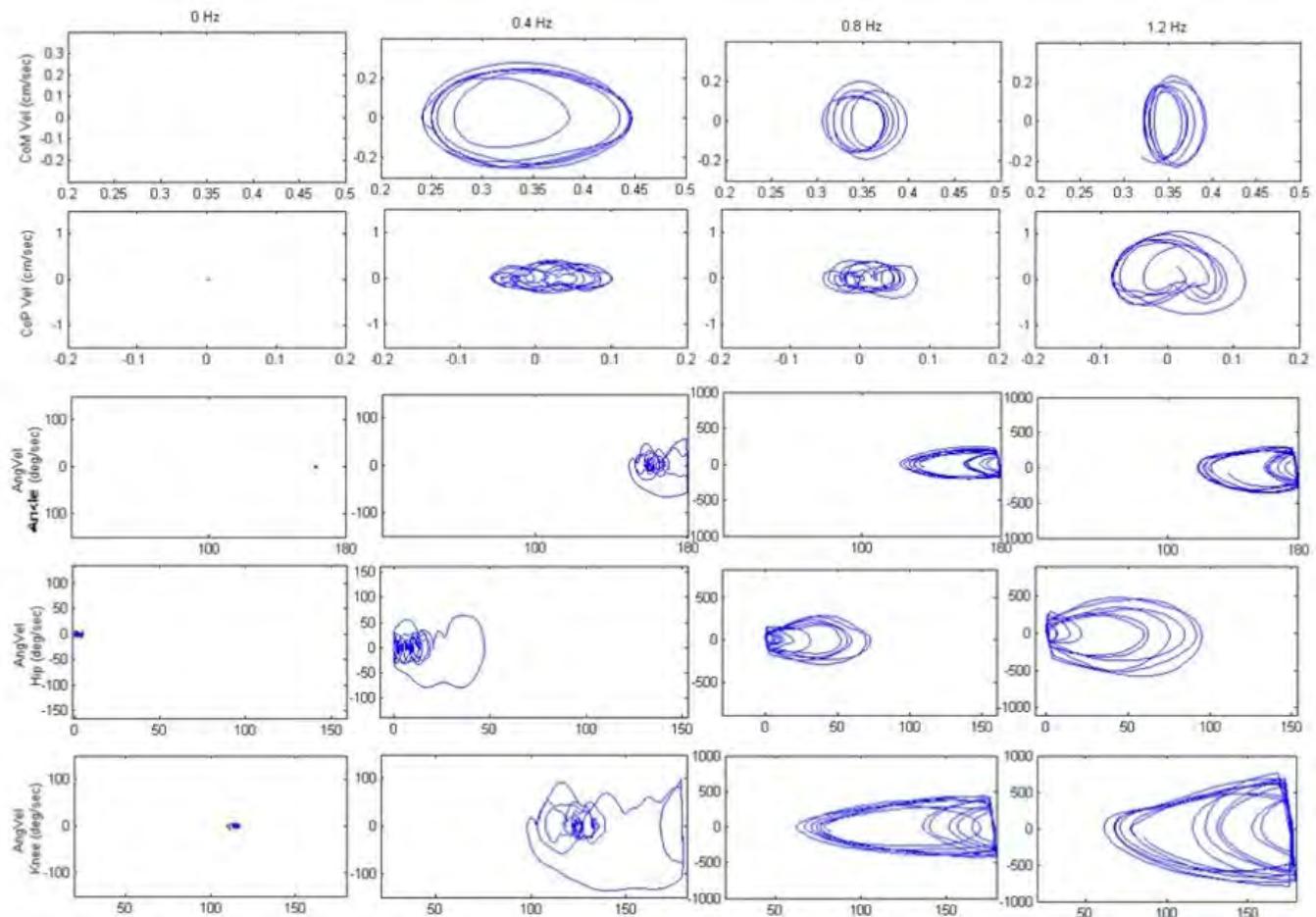
Caption: Phase portrait of global (x-axis: cm, y-axis: cm/sec) and local variables (x-axis: deg, y-axis: deg/sec)

Conclusion: CoM-CoP was considered as a candidate of collective variable of multi-segmental whole body postural system based on coordination dynamics perspective[2] we extend such proposition further by suggesting Head-CoP to be an alternative control variable candidate as well.

Table:

Frequency	Mean & SD	CoM-CoP	CoM-Plat	CoM-Head	Head-CoP	Head-Plat	Hip-Knee	Knee-Ankle
0.2 Hz	M	36	3	2	39	5	1	1
	SD	37	6	4	27	8	9	8
0.4 Hz	M	142	10	2	157	12	2	4
	SD	54	6	7	56	13	15	3
0.6 Hz	M	153	5	3	159	2	96	98
	SD	34	6	4	48	8	79	91
0.8 Hz	M	107	16	12	108	40	176	101
	SD	25	10	38	63	53	43	135
1.0 Hz	M	132	27	14	153	167	96	95
	SD	19	10	40	63	111	35	68
1.2 Hz	M	136	31	13	152	155	37	9
	SD	19	8	39	33	43	15	14

Caption: Relative Phase of global and local variables

References: 1. Ko et al.,*Experimental Brain Research*, *226*, 183–91, 2013.

2. Kelso. *Dynamic patterns: The self-organization of brain and behavior*. Cambridge, MIT Press, 1995.

3. Winter. *Biomechanics and motor control of human movement*. NJ, Wiley, 2009.

Disclosure of Interest: None Declared

STRENGTH AND SCAPULAR KINEMATICS IN ASYMPTOMATIC NON-THROWERS WITH AND WITHOUT POSTERIOR CAPSULE TIGHTNESS

Dayana P. Rosa [1,*] Paula Camargo [1] John Borstad [2]

[1] Physicaltherapy, UFSCar, São Carlos, Brazil, [2] Physicaltherapy, Ohio State University, Columbus, United States

Introduction and Objectives: Posterior capsule of the shoulder is an important restraint during movements of the upper limb mainly when horizontal adduction is associated to internal rotation. Studies have indicated that posterior capsule tightness can be related to deficit in strength of the external rotators of the shoulder and alterations in scapular kinematics in overhead athletes, especially throwers. It was described that high stress loads are transferred to posterior capsule in the deceleration phase of the arm during the throwing motion, which can lead to tightness of this structure. However, it is not known yet if same alterations are present in a general population of non-throwers. Therefore, the purpose of this study was to assess the strength of the shoulder external rotators and scapular kinematics in asymptomatic non-throwers with and without posterior capsule tightness.

Methods: Sixteen individuals with no shoulder pain were evaluated and divided in 2 groups: with posterior capsule tightness (6 women and 1 man; 26.28 ± 2.69 years; 59.42 ± 7.39 kg; 1.63 ± 0.09 m) and without posterior capsule tightness (7 women and 2 men; 25.66 ± 3.08 years; 64.05 ± 10.77 kg; 1.67 ± 0.08 m). All of them were not involved to overhead sports. The posterior capsule tightness was determined by the low flexion test as described by Borstad and Dashottar (2011). This test was performed with the individuals in the standing position. They were passively positioned in 60° of arm elevation in the sagittal plane, and then the evaluator measured the bilateral internal rotation range of motion with a digital inclinometer aligned with the radial styloid. A difference of at least 7° in internal rotation between both arms was used to classify individuals with tightness. All individuals from the posterior capsule tightness group presented tightness in the dominant side. The group without posterior capsule tightness was paired to the side to be evaluated. Strength of the external rotators was measured unilaterally in the sitting position with a handheld dynamometer. Two repetitions were performed and the evaluator was blinded for measurements. The Flock of Birds® electromagnetic tracking system was used to evaluate scapular kinematics during elevation of the arm in the sagittal plane. Local coordinate systems were established for the trunk, scapula, and humerus using the digitized landmarks following the protocol recommended by the International Society of Biomechanics (Wu et al., 2005). Three repetitions were recorded with the individual in the standing position. Kinematic motion analysis involved selecting scapular data at rest, 30°, 60°, 90° and 120° of arm elevation. The results were analyzed using the SPSS statistical package. For external rotation strength, an independent t-test was used to identify differences between groups. For scapular data, a two-way ANOVA was used to identify angle x group interaction or main effect of group. The level of significance was considered 5%.

Results: The posterior capsule tightness group presented a difference of 9.11° ± 1.25° of internal rotation between sides while the group without posterior capsule tightness presented 3.11° ± 1.27°. No differences were detected in the strength of the shoulder external rotators (p=0.50) between groups (posterior capsule tightness: 1.31 ± 0.14 N/kg; no posterior tightness 1.35 ± 0.32 N/kg). The two-factor interaction of group x angle and the main effect of group were not significant

(p>0.05) for scapular internal rotation, upward rotation and tilt. The mean difference between groups was 1.73° ± 1.94°, 0.76° ± 2.96° and 0.69° ± 2.62° for scapular internal rotation, upward rotation and tilt, respectively. The lack of difference between groups in the present study can be due to the small sample size analyzed. The increased posterior muscle tension and humeral retroversion have also been described as possible contributors for posterior capsule tightness. The threshold of 7° to determine the tightness of the posterior capsule may not be ideal because it does not take into consideration the humeral retroversion. This difference between limbs may be different due to humeral retroversion instead of being a real tightness of the capsule. Although the low flexion test has not been validated in vivo yet, this test demonstrated greater tension of the posterior capsule in a cadaveric study compared to other tests (Borstad and Dahsottar 2011).

Conclusion: Strength of the shoulder external rotators and scapular kinematics during elevation of the arm do not differ between asymptomatic non-throwers with and without posterior capsule tightness.

References: [1]Borstad and Dashottar, J Orthop Sports Phys Ther, 41:90-99, 2011.
[2]Wu et al., J Biomech. 38:981-992,2005.

Disclosure of Interest: None Declared

INFLUENCE OF FATIGUE ON THE VARIABILITY OF THE GROUND REACTION FORCES DURING A PROLONGED RUNNING ON AN INSTRUMENTED TREADMILL

Sang-Kyoon Park [1] Sihyun Yoo [2] Hea Lee Park [2] Ji-Seon Ryu [3,*]

[1]Physical Education, [2]Motion Innovation Centre, [3]Health and Exercise Science, Korea National Sport University, Seoul, Korea, Republic Of

Introduction and Objectives: Ground reaction force (GRF) is a good indicator for observing the changes in velocity of the body during human locomotion. Recent technologies using an instrument treadmill allow us to measure both impact and active GRF with prolonged running on a treadmill (Jean-Benoit et al., 2011; Ryu, 2012).The investigation of GRF is essential in biomechanical research associated with injury risk and decreased stability of movement resulting from fatigue during a period of prolonged running. However, little research has examined variability of GRF that occurs with prolonged running. Variability of movement is critical and natural in human movement and it may actually be an adaptation needed for the flexibility to respond to the altered circumstance of the task (Preatoni et al., 2014). Therefore, the purpose of this study was to investigate the variability of GRF presented in timed series via a nonlinear analysis during prolonged running at three different lapsed times. It was hypothesized that an increase in running time will affect the variability of GRF during a period of prolonged running.

Methods: Nineteen healthy young males participated in this study. The subjects ran on an instrumented treadmill (Bertec, USA) at their preferred running speed (mean=2.5m/s) for 2.16 hours. GRF data (Fx: medial-lateral, Fy: anterior-posterior, and Fz: vertical) were collected for forty continuous footfalls at five, sixty-five, and one hundred and twenty-five minutes, respectively. Approximate Entropy (ApEn) technique after surrogate time series on the GRF data was applied to assess the variability for each of the running time conditions. A one-way repeated measure (ANOVA) was performed to compare the differences in ApEn values of GRF components between the running time conditions. The level of significance was set at $P < .05$.

Results: The findings indicated that among three GRF components the mean variability of Fz showed significant decreases after 2 hours running (p<.05). However, there were no significant changes in mean variability for the Fx and Fy components (Fig.1). Thus, it appeared that movement of segments occurring in a vertical direction after 2 hours of running during a prolonged run may be less flexible and adaptable to unpredictable environmental changes. In other words, fatigue resulting from increasing running time is linked to more regularity, but less complexity in vertical movement during prolonged running (Lipsitz, 2002). We hypothesized that this may be one of a runners' movement strategies to adapt to increased fatigue during running.

Figure:
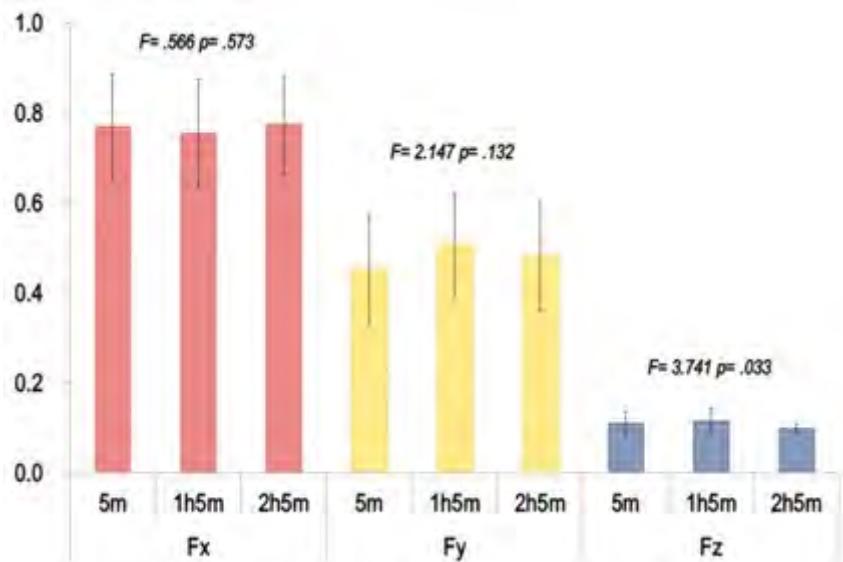
Caption: Figure 1. Average variability (ApEn) of GRF at three time intervals (Fx: medial-lateral, Fy: anterior-posterior, Fz: vertical).

Conclusion:

Our findings indicated that Fz is more easily reproduced, whereas the reliability in Fx and Fy components are less effective because of a higher frequency compared with Fz (Ryu, 2012).Finally, among the three GRF components, Fz is the most reliable biomechanical variable when it is used to discriminate a certain abnormality of motion among different clinical populations because of the high repeatability of the signal (Preatoni et al., 2014).

References: [1] Jean-Benoit, et al., MSSE, 43: 5 829-836, 2011.

[2] Lipsitz, L. A., J. Gerontology, 57A: 3, B115-B125, 2002.

[3] Preatoni, et al., Sports Biomech., 12: 2, 69-92, 2014

[4] Ryu, J.S., Korean Journal of Sport Biomechanics, 23: 3, 225-233, 2012

Disclosure of Interest: None Declared

PO-0238

DEVELOPMENT OF AN ADVANCED COMPUTER-BASED GAIT TRAINING TOOL

H John Yack [1,*]

[1]Physical Therapy & Rehab Sci, University of Iowa, Iowa City, United States

Introduction and Objectives: In spite of observational gait analysis being commonly used by clinicians to assess gait deviations, previous research has shown that the reliability and validity of observational gait analysis is not very good. While a number of strategies have been developed to document observed deviations, we are not aware of any training tools with the goal of improving observational skills.   The goal of this collaborative effort is to develop a training tool that will improve the observational skills of clinicians performing gait analysis.

Methods: Conventional 3-D MoCap walking data was capture on a variety of patients, seen at the Military Performance Laboratory and the Orthopedic Gait Analysis Laboratory, representing a spectrum of gait deviations. These data were translated for input into the digital human avatar (Santos™, Center for Computer-Aided Design), which allows image form and view manipulations.Testing and training modules were developed that provided a dedicated environment. Testing environments enabled the viewing of multiple gait deviations with question sequences that assessed the user's observational skills. Training environments enabled the viewing of multiple gait sequences with the user manipulating static images that represented specific temporal events in the gait cycle. Immediate feedback is provided on how successful these manipulations were compared to the actual images. Thus far, a limited number physical therapy students and clinicians have tested various aspects of the testing and training tools in a web-based environment.

Results: Testing modules, assessed before training, showed clinicians were not able to consistently assess range of motion changes of less than 10 degrees. This was verified in analyses that showed associations between the magnitude of the deviation and the ability to detect the deviation (R^2=.25). These modules also demonstrated a sensitivity that should enable the detection of improvements resulting from using the training tool, something that is currently under investigation.

Conclusion: The development of a training tool offers the possibility of improving the observational skills of clinicians who perform gait analysis.

References: 1. Kawamura, et al. (Gait & Posture, 25(1), 18–24, 2007.

2. Viehweger, E., et al, Annals of Physical and Rehabilitation Medicine, 53(9), 535–546, 2010.

3. Ferrarello, F., et al, Physical Therapy, 93(12), 1673–1685, 2013.

4. Toro, B., et al, Physiotherapy Theory and Practice, 19, 137–149, 2003.

5. Eastlack, et al, Physical Therapy, 71(6), 465–472, 1991.

6. Perry, J., & Burnfield, J. M. Gait analysis: normal and pathological function (2nd edition.). Thorofare, NJ: SLACK Incorporated, 2010.

Disclosure of Interest: None Declared

Motion Analysis

PO-0239

VARIABILITY, ASYMMETRY AND BILATERAL COORDINATION OF GAIT IN WOMEN WITH FIBROMYALGIA

Jose Heredia-Jimenez [1,*] Maria Eva Orantes-Gonzalez [1] Victor Soto-Hermoso [1]

[1]Physical Education & Sports, University of Granada, Granada, Spain

Introduction and Objectives: Fibromyalgia (FM) is characterized by widespread musculoskeletal pain of at least three months' duration, fatigue, poor sleep and tenderness on palpation in at least 11 of 18 specific tender point sites[1]. Measurements of temporal and spatial parameters of gait are of recognized clinical relevance in the assessment of motor pathologies [2] and commonly used for the identification of gait disorders[3]. But there are a few studies that utilized the gait disorder in patient with FM, reporting that the FM syndrome also affects several gait parameters and different muscle recruitment patterns. [4,5]

 The aim of the present study was to assess if there are differences in spatio-temporal variables, variability, asymmetry and bilateral coordination of gait (PCI) between women affected by FM and healthy women.

Methods: We studied 55 FM women and 44 healthy women. Gait analysis was performed using an instrumented walkway (GAITRite system) at a confortable walking speed. Spatio temporal variables, variability of gait, gait asymmetry index and bilateral coordination of gait (PCI) were measured.

We calculated the coefficient of variation (CV) of swing time (CV_SW), stride length (CV_SL) and Step width (SWth) using the formula:

 CV = 100 X standard deviation/mean

gait asymmetry was evaluated according to Patterson et al. [6] and coordination index according to Plotnik et al. [7]

Results: FM patients present significant differences in kinematics variables. In relation with variability and PCI, the FM patients present worse values. Gait asymmetry not presented differencess between groups (table 1).

Conclusion: We consider that variability and bilateral motor control of gait may be particularly sensitive to the effects of FM at any walking speed condition than kinematics variables. Variability and PCI should be a strong test that complemented the evaluation of FM patients and confirm the motor dysfunctions of those patients across of diagnosis and gait evaluation.

Table:

Variables	FM Mean (SD)	C Mean (SD)	p value
Gait velocity (cm/s)	109.0 (20.5)	139.2(16.8)	< 0.001
Cadence (steps/min)	109.5 (12.6)	124.5(8.7)	< 0.001
Stride length (cm)	119.1 (14.7)	134.2(11.7)	< 0.001

Swing phase (%)	36.6 (2.2)	39.0(1.4)	**< 0.001**
Stance phase (%)	63.4 (2.2)	61.0(1.4)	**< 0.001**
Single support (%)	36.6 (2.2)	39.0(1.4)	**< 0.001**
Double support (%)	26.7 (4.4)	22.1(2.8)	**< 0.001**
CV Stride Length	2.9 (1.4)	2.4(0.9)	**0.04**
CV Swing time	4.9 (1.7)	3.6(0.8)	**< 0.001**
CV Step width	3.4 (1.4)	2.7(0.8)	**0.004**
PCI	3.8(1.5)	3.2(1.1)	**0.01**
Swing GA	3.24 (3.66)	2.08(1.37)	0.18
Stance GA	1.71 (1.82)	1.31 (0.76)	0.94
Step GA	2.21 (2.06)	1.84 (1.55)	0.58

Caption: Table 1. Spatio-Temporal, asymmetry, variability and coordination index of gait between Fibromyalgia and healthy women

References: [1] Wolfe et al., Arth & Rheum, 33: 160-172, 1990.

[2] Macellari et al., Gait Posture, 10:171-182, 1999.

[3] Dobbs et al., Age Ageing, 22:27-30, 1993.

[4] Auvinet et al., Joint Bone Spine, 73:543-546, 2006.

[5] Pierrinowsky et al., Gait Posture, 22: 210-218, 2005.

[6] Patterson et al., Gait Posture, 31: 241-246, 2010.

[7] Plotnik et al., Exp Brain Res, 181: 561-570.

Disclosure of Interest: None Declared

PILOT STUDY: SCAPULAR KINEMATICS DURING OSCILLATORY ARM MOVEMENTS USING FISIO FLEX SANNY™ EXERCISE DEVICE

Camila C. Biazotto [1,*]Kevin McQuade [2]Anamaria Oliveira [3]

[1]Department of Rehabilitation Medicine, School of Medicine, University of São Paulo, Ribeirão Preto Medical School, Ribeirão Preto, Brazil, [2]Department of Rehabilitation Medicine, School of Medicine, University of Washington, Seattle, WA, USA, Washington, United States, [3]Graduation Program Rehabilitation and Functional Performance, University of São Paulo, Ribeirão Preto Medical School, Ribeirão Preto, Brazil

Introduction and Objectives: Low frequency vibration transmitted through the human body is used in different areas to achieve goals of physical training and rehabilitation [1,2]. An oscillatory pole is a device (similar to Bodyblade™, USA) with elastic properties that provides oscillation through rhythmic movements with low frequency vibration directly delivery to upper limb. The device operates like a mass spring oscillator, where person pushes and pulls the center of the pole while the distal ends flex back and forth providing inertial resistance based on the pole stiffness. This results in rapid eccentric and concentric contractions, of distal and proximal musculature [2,3,4]. Despite widespread use of this device in training and rehabilitation, and claims for improved scapular stability, there are no studies that have examined the acute effect of these types of oscillatory exercises on scapular kinematics. The aim of this pilot study is to analyze acute effect of exercises with oscillatory pole on scapular kinematics. Secondary aim is verify the oscillatory pole median frequency and the frequency delivery to upper limb during exercises.

Methods: Four volunteers without any symptoms in the upper limbs, or previous history of trauma or surgery in the joints of the shoulder/cervical/thoracic spine participated. Three-dimensional kinematics were recorded using Liberty^{TM} electromagnetic tracking system (Polhemus Inc, Colchester, VT). To verify the pole frequency three sensors EMG TrignoTM Wireless System (Delsys Inc. Boston, MA) configured like accelerometers were used attached to the central grip, the extremity of the pole and to participant dominant hand. Statistical analyses were performed using the IBM SPSS software v.16.0 (Chicago, IL, USA) and Excell program (Microsoft Corporation). Exercises were performed with oscillatory pole Fisio Flex Sanny ™, Brazil. Device manual was consulted and virtual contact was made but no oscillation frequency information was provided by device manufacturer. First exercise was performed bimanually with both hands holding pole in front of chest at 90º shoulder flexion, forearms pronated and pole horizontal oscillating in transverse plane parallel to the ground. Second exercise was unilateral with the shoulder at 90° flexion, forearm neutral and pole vertical oscillating in sagittal plane, perpendicular to the ground. The exercise was repeated for both left and right sides. Three repetitions of each exercise were performed for 10 seconds each. Scapular kinematics relative to the thorax was defined using YX'Z" Euler rotations following International Society of Biomechanics recommendations [5]. To evaluate scapular kinematics during the exercises the amplitude of movement in degrees of internal/external rotation, upward/downward rotation, and anterior/posterior tilt were described with median values and standard deviation. Student t-test was used to evaluate differences between dominant and no-dominant limb during the same exercise and between the two exercises with the same limb. A confidence interval of 95% was assumed with a significance level of $p \le 0.05$.

Results: Median oscillatory frequencies during exercises were 4.5 Hz on the pole distal ends, 4.3 Hz on the central grip and 3Hz on the hand during exercise 1 and 2. Other studies with different oscillatory devices show similar results [3,4]. No statistical differences between dominant and no-dominant limb during the same exercise and between the two exercises with the same limb were observed (p≥0.05). Table 1 summarizes the scapula rotation amplitudes and Student t-test results to comparisons between dominant and no-dominant limb.

Conclusion: According to preliminary analyses of means and standard deviations values, results suggest that effects of exercises with oscillatory pole are different according to three scapulae movement axes. No differences between dominant and no-dominant scapulae during the exercises were found. During three exercises both scapulae had more variation on superior and inferior rotation, however this rotation had the larger standard deviation. While the lowest variation was observed to anterior and posterior tilt.

Table:

	Exercise 1			Exercise 2		
	Dominant limb	No dominant limb		Dominant Limb	No dominant limb	
	(Mean±SD)	(Mean±SD)	p value	(Mean±SD)	(Mean±SD)	p value
Upward/Downward rotation	8.05 ± 4.54	8.46 ± 4.52	0.587	9,67 ± 3.73	10,56 ± 7.85	0.123
Internal/external rotation	6.94 ± 4.46	5.55 ± 2.81	0.605	6,41 ± 1.43	9,66 ± 2.96	0.816
Anterior/Posterior tilt	3.65 ± 1.40	3.92 ± 0.79	0.516	3,07 ± 0.91	4,41 ± 0.96	0.162

Caption: Table 1. Amplitude values of scapular rotations in degrees (º) during exercises with oscillatory Fisio Flex Sanny™ pole and Student t-test results. (SD: Standard Deviation)

References: [1] Rubin et al.,Spine, 28(23): 2621–2627,2003

[2] Mileva et al., J Strenght Cond Res,24(3):737-748,2010

[3] Hallal et al., Rev Bras Fisioter,15(2):89-94,2011

[4] Arora et al., Int J Sports Phys Ther,8(4):370-380,2013

[5] Wu et al., J Biomech,38(5);981-992,2005

Disclosure of Interest: None Declared

Motion Analysis

PO-0241

SPEED MODELLING OF RELATIVE GAIT PHASE DURATIONS

Felix Hebenstreit [1 2 3,]*Andreas Leibold [1]Sebastian Krinner [3]Götz Welsch [3]Matthias Lochmann [2]Bjoern Eskofier [1]

[1]Digital Sports Group, [2]Institute of Sport Science and Sport, Friedrich-Alexander University Erlangen-Nürnberg (FAU),
[3]Department of Trauma Surgery, University Hospital Erlangen, Erlangen, Germany

Introduction and Objectives: Gait speed is an important factor to consider when performing biomechanical studies or diagnosing gait disorders. As an example, Andriacchi et al. showed that healthy subjects could be distinguished from injured and rehabilitating patients by evaluating spatiotemporal parameters such as stance and swing time during gait at different speeds [1].

Perrys common definition of the gait cycle separates the gait cycle into functional sub phases [2]. However, Perry stated no specific speeds for the definition of these sub phases. Other studies indicated that biomechanical parameters depend on gait speed. One study showed the dependency of kinematics and kinetics on self-selected speeds in five different speed ranges [3]. They described changes of the double support, single support and swing phases in these speed ranges. A recent study investigated gait sub phase variations for three different self-selected speeds [4].

As detailed analyses of the changes of all stance sub phase durations with speed are still missing, we quantitatively determined the durations of the loading response, mid stance, terminal stance, pre swing, total stance and total swing phase. These phases can be separated by the events "heel strike", "toe off" and "heel off" [2] (figure 1).

The purpose of this study was then to model the relative durations of the gait sub phases (as % of one gait cycle) with speed in a large speed range at a high resolution and based on a large dataset of steps.

Methods: 21 healthy subjects (10 male, 11 female, age: 23.8 yrs ± 3.3 yrs, height: 172.8 cm ± 9.4 cm, mass: 66.6 kg ± 10.9 kg) gave informed consent before participating. The local ethical committee approved this study. We attached six reflective markers to each foot above the first, second and fifth metatarsal heads, on the calcaneus and on the lateral and medial malleoli. All subjects wore the same type of shoe. We acquired the markers' positions using a Qualisys infrared system (8 cameras, 200 Hz sampling rate) and the ground reaction forces using a Bertec instrumented split-belt treadmill (1000 Hz sampling rate).

The subjects walked for two minutes on the treadmill for accommodation. Thereafter they walked without stopping at 12 speeds in the range of 0.6 m/s to 1.7 m/s with 0.1 m/s increments. We randomized the speed order with a trend to higher speeds at the end of the session to minimize fatigue effects. Each trial at one speed lasted 60 s.

Pre-processing was performed in Visual3D (C-Motion) and consisted of force drift correction and force and marker position filtering using a 2nd order Butterworth filter (6 Hz cut-off frequency). A 20 N threshold on the vertical component of the ground reaction force yielded the events "heel strike" and "toe off". We applied a threshold of 0.1 m/s to the vertical velocity of the calcaneus marker to detect the "heel off" event [5]. The relative sub phase durations were then calculated in MATLAB R2013b. We calculated the mean for each walking trial and foot of every individual subject, performed a linear regression with these averaged durations (model: $f(x) = ax+b$, $f(x)$: duration, x: gait speed) and determined the coefficient of determination R^2.

Results: We acquired 25306 steps in total with 615 steps being excluded by hand when the subject stepped on both belts. The results of the regression are stated in table 1. The stance phase duration decreased by 0.3 % and the swing phase duration increased by 0.3 % absolutely per 0.1 m/s speed increase. The loading response and pre swing phase decreased by 0.3 %, the mid stance decreased by 1.6 % and the terminal stance phase increased by 1.8 % per 0.1 m/s speed increase. The general trend of decreasing stance and increasing swing time is consistent with the literature. The regression parameters indicate a redistribution of the mid stance phase towards the terminal stance phase.

Figure:
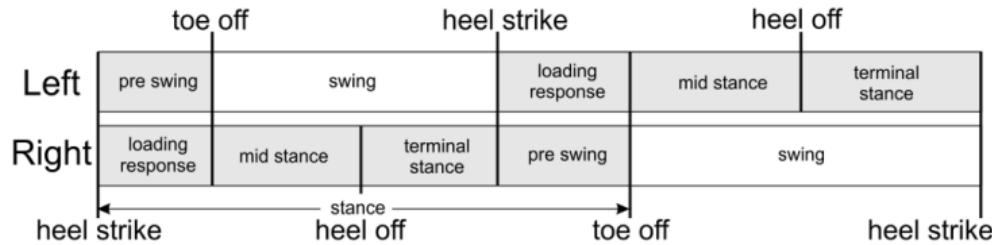
Caption: Gait cycle and the analyzed sub phases.

Conclusion: This study showed an effect of gait speed on the relative gait sub phase durations. The linear modelling indicated an empirical rule of thumb that can be used to estimate gait phase durations. The results show that the individual gait speed should be regarded in biomechanical investigations. The results from this study may be used as a reference for interpreting gait data or in orthopedic applications. In the future, the determination of model parameters for different patient populations might help to characterize and understand biomechanical mechanisms of specific diseases.

Table:

Phase	a [%/(m/s)]	b [%]	R^2
Stance	-3.2	68.0	0.52
Swing	3.4	31.7	0.56
Loading response	-3.2	17.9	0.56
Mid stance	-15.7	41.4	0.39
Terminal stance	17.7	-10.3	0.79
Pre swing	-3.1	17.9	0.56

Caption: Results of the regression of the sub phase durations.

References: [1] Andriacchi et al., J. Biomech., 10: 261–8, 1977.

[2] Perry. Gait Analysis: Normal and Pathological Function. SLACK, 1992.

[3] Schwartz et al., J. Biomech., 41: 1639–50, 2008.

[4] Liu et al., Gait Posture, 39: 756–60, 2014.

[5] Ghoussayni et al., Gait Posture, 20: 266–72, 2004.

Disclosure of Interest: None Declared

Motion Analysis

PO-0242

SMOOTHING OR FILTERING MARKER TRAJECTORIES? THE EFFECTS ON CALCULATED JOINT MOMENTS

Annaclaudia Montanino [1,*]Luca Modenese [2]Anantharaman Gopalakrishnan [3 4]Nicola Petrone [5]Andrew T. M. Phillips [6]

[1]Department of Information Engineering DEI, University of Padova, Padova, Italy, [2]Centre for Musculoskeletal Research, Griffith University, Griffith, Australia, [3]Department of Civil and Environmental Engineering, Imperial College London, [4]The Royal British Legion Centre for Blast Injury Studies at Imperial College, London, United Kingdom, [5]Department of Industrial Engineering, University of Padova, Padova, Italy, [6]Structural Biomechanics, Department of Civil and Environmental Engineering, Imperial College London, London, United Kingdom

Introduction and Objectives: In the field of biomechanical analysis, it is common practise to use motion capture systems to quantify the motion of body segments based on the trajectories of skin markers. The obtained measurements, even if accurate, include a noise component that is necessary to take into account especially when investigating the dynamics of the system. This evaluation includes a derivation process to calculate accelerations which is known to amplify the noise content.

Many filtering techniques have been proposed in literature. The most traditional one is the low-pass Butterworth filter [1], which relies on an arbitrary choice of a cut-off frequency since the signal and noise bandwidth are unknown a priori and the nature of the signal of interest is non stationary. Another feasible approach is based on singular spectrum analysis (SSA) in its sequential version [2]. This smoothing algorithm is free from assumptions on the original signal and does not involve any arbitrarily set parameters apart from the parameter which describes the stopping criterion.

It has been demonstrated that 6Hz is an appropriate cut-off frequency for walking data [1], but there is no analogous evidence for the appropriate cut-off frequencies for the analysis of other daily living activities such as stair climbing. The objective of this study is therefore to compare the SSA and standard low-pass filter based on joint moments calculated for daily living activities.

Methods: To compare the SSA and the standard low-pass approaches applied to marker trajectories, an inverse dynamics analysis using OpenSim [3] was performed on the same original dataset.

The dataset includes data collected during 10 walking trials and 8 stair climbing trials of a healthy female subject. A Vicon System of 10 cameras (sampling rate: 100Hz) was used to track the markers and 3 Kistler 9286BA platforms were used to measure the ground reaction forces (sampling rate: 1000Hz). The given 3D trajectories of 57 markers were first labelled and gap filled using Vicon Nexus software and cloned: the trajectory components of the first clone were filtered using a 4th order zero-lag low-pass Butterworth filter with cut-off frequency set at 6Hz, while the trajectory components of the other clone were iteratively smoothed with the SSA algorithm presented in [2] until the stopping criterion was met, that is when the difference between the RMS of the accelerations computed in two consecutive iterations is less than 1%, to avoid over smoothing of the acceleration.

Joint angles for a full body model based on [4] were obtained for both cloned datasets using the inverse kinematics tool available in OpenSim. In the adopted model the hip joint is represented as a ball socket joint and has 3 degrees of freedom, whereas both knee and ankle joints are modelled as hinge joints.

The computed joint kinematics and measured ground reaction forces, were inputted to an OpenSim inverse dynamics analysis to calculate the joint moments. The similarity between the obtained curves was quantified by computing cross-correlations for each pair of corresponding moments.

Results: The mean cross-correlation coefficient for the 10 walking trials is 0.98 ± 0.01 while for the 8 stairs trials is 0.99 ± 0.01, denoting practically equivalent results between the two processing methodologies. Hip joint average curves and standard deviations are presented in the Figure. Additional activities from the dataset (stair descending, sitting and standing from a chair) are currently being processed.

Figure:
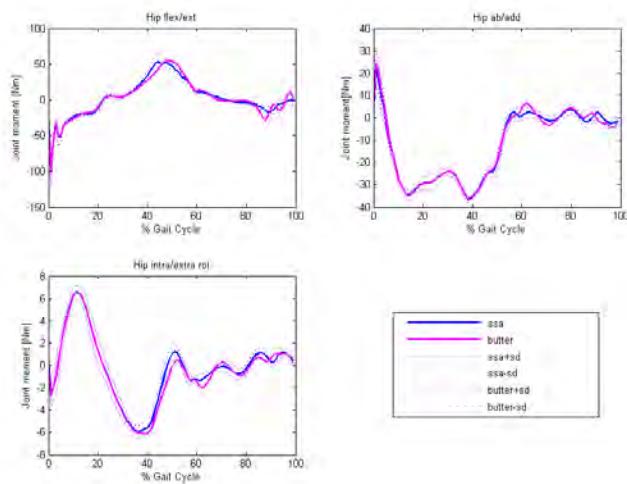
Conclusion: The purpose of this study was to compare inverse dynamics results obtained from 3D marker trajectories processed either with a low-pass Butterworth filter or with a SSA smoothing.

Our results did not indicate a significant difference between the SSA and the low-pass filtering approaches for the inspected activities, however, it must be noted that the inverse kinematics algorithm [5] calculates joint angles searching for the optimal pose of the multibody model thus relying not only on the position of the global markers, but also on the joint constraints. As a consequence, differences between the two approaches under consideration may be mitigated.

Although SSA does not rely on arbitrary choices, as the resulting moments obtained by the two approaches are close to equivalent both for walking and stair climbing, the use of the traditional filtering procedure with cut-off frequency of 6Hz seems justified for these activities. Further study could take into account other daily living activities such as running, whose derived joint moments could potentially be more affected by the computed accelerations, with the inertial contribution being more significant.

References: [1] Winter et al., Journ. Biomech., 7:157-159,1974.

[2] Alonso et al.,Lecture Notes in Computer Science, Springer, 2004.

[3] Delp et al.,IEEE Trans. Biomed. Eng, 54, 1940-1950, 2007.

[4] Modenese et al., Journ. Biomech., 44:2185-2193, 2011.

[5] Lu et al., Journ. Biomech., 32:129-134,1999.

Disclosure of Interest: None Declared

Motion Analysis

PO-0243

EFFECTS OF LEADING LIMB AND OBSTACLE HEIGHT ON THE CONTROL OF THE END-POINT AND BODY'S CENTER OF MASS MOTION DURING SIDE-LOADED OBSTACLE CROSSING

Chih-Chung Hu [1][2] Tung-Wu Lu [1][3],* David Tzewei Lin [1] Ching-Ru Chen [1]

[1]Institute of Biomedical Engineering, National Taiwan University, [2]Department of Mechanical Engineering, Ming Chi University of Technology, [3]Department of Orthopaedic Surgery, School of Medicine, National Taiwan University, Taipei, Taiwan, Republic of China

Introduction and Objectives: Tripping and loss of balance are two major causes of falls during obstacle-crossing, especially in the elderly. Precise end-point control (sufficient foot clearance over the obstacle) and good balance control (body's center of mass (COM) control) are critical for crossing obstacles safely. Under side-loaded conditions such as carrying a handbag, the control of the end-point and COM may be more difficult owing to the asymmetrical mechanical challenges of the side-loads. Proper choice of the leading limb (ipsilateral or contralateral to the loaded side) may be helpful for better control of obstacle crossing. The current study aimed to investigate the effects of leading limb and obstacle height on the control of the end-point and body's COM motion during side-loaded obstacle-crossing in young healthy adults.

Methods: Ten young healthy adults (age: 24.4±4.71 years, height: 168.6±5.97 cm and mass: 62.7±4.71 kg) walked and crossed obstacles of heights of 10%, 20% and 30% of their leg lengths (LL) while carrying a constant load (dumbbell) of 4.5 Kg by their right hand. All subjects were judged to be right-handed by the Edinburgh Handedness Inventory. Forty-three infrared retroreflective markers were placed on specific anatomical landmarks to track the motions of the body segments and two markers were attached to the ends of the dumbbell. A 7-camera motion analysis system (Vicon 512, Oxford Metrics, U.K.) and three force plates (AMTI, U.S.A.) were used to measure the marker trajectories and ground reaction forces. The body's COM position was calculated as the weighted sum of those of all the body segments. Toe clearances were calculated as the vertical distance between the toe marker and the obstacle when the toe was directly above the obstacle. The positions of the center of pressure (COP) were calculated from the forceplate data. The COM-COP inclination angles (IA) were calculated as the angles between the COM-COP vector and the vertical in the sagittal and frontal planes, giving sagittal IA and frontal IA respectively. Two-way mixed-model ANOVA with one between-subject factor (obstacle height) and one within-subject factor (leading limbs) was performed for the toe clearance and IA ($\alpha=0.05$). SPSS was used for all statistical analysis.

Results: No interactions between the main factors were found. Toe clearances decreased significantly with increasing obstacle height (p = 0.004) but no significant differences were found between the ipsilateral and contralateral limb conditions (p = 0.419) (Table 1). The frontal IA during crossing with the contralateral limb leading was statistically greater than that with the ipsilateral limb leading (p = 0.025) but no significant height effect was found (Table 1). No significant height or limb effects were found for sagittal IA (p>0.05).

Conclusion: The height of obstacle has significant effect on toe clearances, but not on body's COM motion during side-loading obstacle crossing, suggesting that balance control is maintained with compromised end-point control when facing

higher obstacles. Different strategies were found when crossing with different limb leading. During obstacle crossing with the contralateral limb leading, when the COM and the side load were on different sides of the trailing stance limb, the COM was displaced away from the stance limb to counteract the effects of the side load, leading to larger frontal IA. On the other hand, with the ipsilateral limb leading, when the COM and the side load were on the same side to the trailing stance limb, the COM was displaced towards the stance limb to decrease the lever arms of the COM and the side load in order to maintain the body's stability. It appears that with less frontal inclinations ipsilateral limb leading is preferable to contralateral limb during side-loaded obstacle crossing.

Table:

Height (LL)	Ipsilateral limb leading			Contralateral limb leading		
	Toe Clearance (mm)	Fontal IA (degree)	Sagittal IA (degree)	Toe Clearance (mm)	Frontal IA (degree)	Sagittal IA (degree)
10%	201.77 (9.08)*	3.23 (0.65)**	2.56 (0.38)	211.54 (13.09)*	4.39 (0.37)**	0.67 (0.21)
20%	188.66 (11.31)*	3.27 (0.58)**	1.06 (0.35)	186.07 (14.85)*	4.90 (0.22)**	0.78 (0.42)
30%	153.11 (10.26)*	3.61 (0.38)**	1.29 (0.60)	168.32 (16.13)*	3.85 (0.34)**	1.42 (0.48)

* indicates a significant height effect on toe clearances (p = 0.004)

** indicates a significant leading limb effect on frontal IA (p = 0.025)

Caption: Table 1: Means and standard deviations of the toe clearance, frontal IA and sagittal IA when crossing obstacles of three different heights with the ipsilateral or contralateral limb leading.

References: [1] Chou et al., Gait Posture 13:17-26, 2001.

[2] Chien et al., Gait Posture 38:391-396, 2013.

Disclosure of Interest: None Declared

Motion Analysis

PO-0244

METHODOLOGY FOR COMPUTING NEW SEGMENT ROTATION AXIS

Yuta Kawamoto [1,*]Takahito Suzuki [2]Shinsuke Yoshioka [1]Senshi Fukashiro [1]

[1]Department of Life Sciences, The university of Tokyo, Tokyo, [2]Department of Human Sciences, Kanagawa University, Kanagawa, Japan

Introduction and Objectives: Most of segment movements consist of translation and rotation, and the position of rotation axis was debatable. In many cases, the body segment rotation axis was placed on its center of mass (COM). However, a body segment usually does not rotate about its COM, and the rotation axis changes position on the segment. When axis was placed on instantaneous screw axis (ISA), it was able to change position on the segment [1], but the translation perpendicular to ISA was incorporated into the rotation about ISA. Therefore the new rotation axis, about which segment actually rotated and which was able to separate translation, was needed. The purposes of this study were to define new rotation axis and to develop the searching procedure for computing it. The procedure based on mathematical predictions was confirmed by simulation.

Methods: A point that moved straight in the global coordinate system (straight moving point: SMP) was defined as the new rotation center, in two-dimensional segment movement. SMP would be searched with the location of instantaneous center of rotation (ICR), which is the point with zero velocity for a particular instant and which ISA passes thorough in two-dimensional movement. This searching procedure was based on following mathematical predictions. First many points which moved almost straight were distributed on the circle with a gap. Second ICR existed at the gap of the circle. Third, SMP was on the circle. The prediction was confirmed by the following simulations. In simulation 1, velocity and angular velocity of the segment were constant. In simulation 2, they were varied linearly. Position of SMP was selected as below. When a point attached to the segment coordinate system passed certain points on the global coordinate system at specific time interval, the sum of distances between the pass points and regression line of them was computed as the objective function value of the point attached to segment coordinate system. Then, a point that had the minimum value was selected as SMP. In the three-dimensional movement, axis was able to be defined as below. First, to compute ISA and to eliminate the translation along ISA, the three-dimensional movement reduces to two-dimensional one. And then, SMP position was computed and axis was on SMP along ISA. The movement was represented with linear movement of SMP, rotation about SMP and translation along ISA.

Results: Figure 1 showed a typical graph of objective function values in simulation 1. X and Y coordinates coincided with local coordinates of the segment. The graphs in both simulation 1 and 2 always formed a circle with a gap as seen in the figure. The circle meant there were many points which moved almost straight. ICR and SMP existed on the gap of the circle and on the circle, respectively. Therefore, using ICR the position of the circle was searched easily and SMP position was able to be computed as the point that has the minimum objective function value on the circle. SMP position was accurately computed and the error of SMP was within 1% of the square-shaped segment height.

Figure:
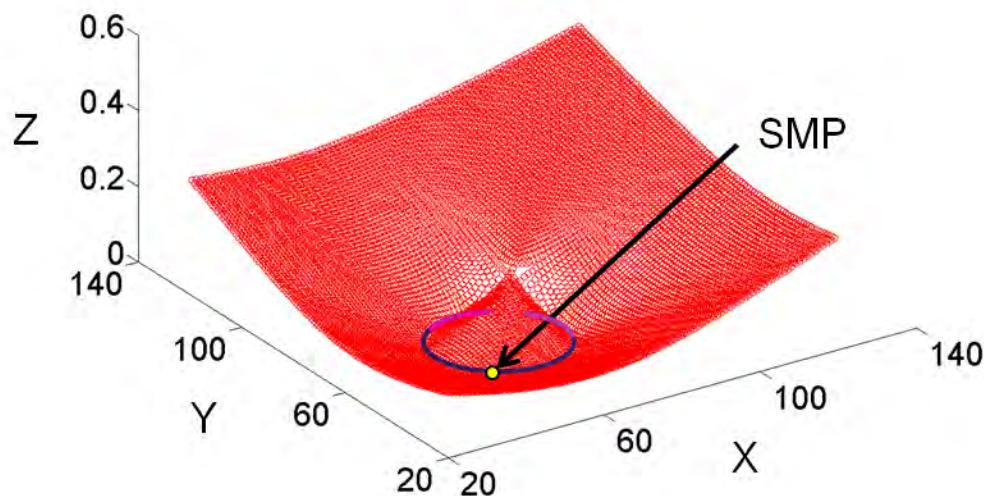
Caption: Figure 1 Typical graph of objective function values in simulation 1

Conclusion: SMP was defined as a position of segment rotation axis. Mathematical predictions were confirmed by the simulation. Based on the predictions, SMP position was accurately computed. SMP represented the position about which segment actually rotated and could separate translational component. On the other hand, COM was not the position about which segment actually rotated and with ISA translation was incorporated into simple rotation. Therefore SMP had advantage over COM and ISA in representing the rigid body movement. Segment movements in various sports consist of translation and rotation. SMP can apply to those movements and it would offer new insight into segment kinematics.

References: [1] Woltring et al., J Biomech, 18(5):379-389, 1985

Disclosure of Interest: None Declared

PO-0246

GAIT PATTERN RECOGNITION IN CEREBRAL PALSY PATIENTS AND NORMAL CHILDREN USING NEURAL NETWORK MODELLING

Jan Muhammad [1] Sheila Gibbs [1] Rami Abboud [1] Weijie Wang [1,*]

[1] University of Dundee, Dundee, United Kingdom

Introduction and Objectives: Interpretation of gait patterns from 3D gait data is challengeable as there are many kinematic and kinetic parameters involved. Artificial neural network is a type of computer model which works similar to human's central nervous system capable of learning from input data and then use the obtained knowledge to predict gait patterns. The aim of this study was to build neural network models which can recognise gait patterns from the pre- and post-treated patients and normal children.

Methods: Twenty-eight patients with cerebral palsy were recruited as subjects whose gait data were collected in pre- and post-treatment. Twenty-six normal children participated in this study as control group. All subjects' gait data were analysed to obtain the gait parameters and kinetic and kinematic parameters of hip, knee and ankle joints in three planes of both limbs. The gait data were collected using a Vicon® 12 FX digital camera motion capture system (Oxford, UK). Three best trials were chosen for each patient from pre- and post-treatment sessions, respectively and three for each healthy one as well. The gait data were categorised as three patterns, i.e. normal, pre- and post-treatments and used as input to construct neural network models. A total of 350 trials were split into 70% and 30% to train and test the models, respectively. Different models were built using different combinations of gait and joint parameters.

Results: The neural network models created using all parameters in both injection and surgical groups produced the high quality results, both being over 95% correct ratio in training samples and over 90% correct ratio in testing samples, respectively. The results showed that the models using all parameters or using the joint angles and moments could predict the gait patterns with approximately 95% accuracy. The models using joint power and moments had lower rate in recognition of gait patterns with approximately 70% - 90% successful ratios. The models created using kinetic parameters (force, power & moment) in injection group and the model created using angles and gait parameters in surgical group, yielded approximately 95% correct prediction in training samples and 90% in testing samples. In surgical group, the model created using joint angles and gait parameters predicted with 95% and 90% accuracy in training and testing samples, respectively.

Conclusion: The neural network models can be constructed using joint and gait parameters in cerebral palsy patients in pre- and post-treatments and healthy subject. The built neural network models show highly correct ratios in predicting gait patterns for CP patients in both injection and surgery groups and in different treatment periods. We can conclude that the neural network modelling is a robust and a reliable method which could help clinicians to interpret and assess patient gait in clinical gait analysis.

Disclosure of Interest: None Declared

ANALYSIS OF ACTION SPORTS WITH A MOTION RECORDING SYSTEMS BASED ON 9-DEGREES SENSORS AND GPS

K Ishida [1,*]

[1]Hiroshima Institute of Technology, Hiroshima, Japan

Introduction and Objectives: We develop a new motion recording systems based on GPS and 9-degrees sensors which is composed of 3 axis accelerometer, 3 axis gyroscope, and 3 axis digital compass. Deploying the systems, we analyze turn maneuver on a half-pipe with skateboard, inline skate, and BMX (Bicycle Motocross).

Methods: We put the recording device on an athlete's head, waist, right foot, and left foot. The device is composed of microcomputer (Arduino Fio), accelerometer and gyroscope (MPU6050), digital compass (HMC5883L), and GPS (MTK3339). The motion and location data is stored in micro SD-card. The recording data is processed by a pre-processing software. The software converts date and time into timestamp in the data. It also synchronizes and normalizes the timestamp on the data collected from multiple devices on head, waist, right foot, and left foot. After the normalization, it detects time series of each action automatically. Based on the pre-processed data, we define a distance function between each pair of time series of two runs in order to identify varieties of turn maneuver on a 13 feet halfpipe. The function is defined by sum of squared difference between pair of autocorrelation functions of two action time series data. In terms of turn skill on a halfpipe, we find three types of riding level on a halfpipe, i.e, beginner, intermediate, and advanced. Beginner is defined as turning on the concave of a halfpipe. Intermediate is defined as turning on the vertical surface of a halfpipe. Advanced is defined as making air turn over the coping of a halfpipe. We can observe different type of autocorrelation function between different riding levels.

Results: An experiment was conducted on a 13 feet halfpipe with skateboard, inline skate, and BMX. There were total of 18 athletes who participated the experiment. They did three or four ridings. Each riding is composed of 6 to 8 round trips on the halfpipe. We got 57 riding data excluding unsuccessful ridings. All distances between each pair of time series of runs is calculated based on the proposed method of autocorrelation. For comparison, we also calculated ordinal distances measure based on statistical indexes, i.e. average and standard deviation on each time series of riding data. In order to evaluate the two distances measure, we defined precision of ranking based on each distance. The precision is defined by s / n, where n is the total number of same type riding data in the data set and s is the number of same type riding data in the top n ranking list. In terms of the precision, the average score based on proposed distance is 0.72563 and standard deviation is 0.187456. On the other hand, the average score based on the ordinal distance is 0.674764 and the standard deviation is 0.20836. Furthermore, to have a visual confirmation of the advantage of the proposed method, we illustrate two dendrograms of hierarchical clustering with ward method for the proposed method and ordinal method. According to the dendrogram of the proposed method, same type of riding data is properly classified into a same cluster. While, in that of the ordinal method, 17 riding time series were not classified into proper clusters.

Conclusion: We developed a new motion recording systems based on GPS and 9-degrees sensors which is composed of 3 axis accelerometer, 3 axis gyroscope and 3 axis digital compass. Deploying the systems, we analyzed turn maneuver on a half-pipe with skateboard, inline skate, and BMX.

Table:

References: Reference 1

Akin Avci, Stephan Bosch, et al., : Activity Recognition Using Inertial Sensing for Healthcare, Wellbeing and Sports Applications - A Survey, Architecture of Computing Systems (ARCS), 2010 23rd International Conference, Hannover, Germany, (2010).
Reference 2
5) Benjamin A. Crockett, Randall L. Jensen : Kinematic Analysis and Muscular Activity of Skateboard Propulsion in Experienced Participants, 25 International Symposium on Biomechanics in Sports, 602, Ouro Preto, Brazil, (2007).
Reference 3
7) Jason W. Harding, Colin G. Mackintosh, Allan G. Hahn, Daniel A. James : Classification of Aerial Acrobatics, Proceedings of 7th Snowboarding Using Inertial Sensors ISEA CONFERENCE 2008, Biarritz, June 2-6, (2008).

Disclosure of Interest: None Declared

A DYNAMIC MODEL TO COMPUTE TORQUES GENERATED BY THE SHOULDER AND THE ELBOW TO PRODUCE FORCES DURING HANDCYCLING

Abdelmajid Ousdad [1,*]Matteo Lancini [1]Giovanni Legnani [1]

[1]department of mechanical and industrial engineering, university of Brescia, Brescia, Italy

Introduction and Objectives: Handbikes are three wheel vehicles used for transportation and recreation, but also widely used in rehabilitation programs for people with reduced mobility, and in sport field for disabled persons.

In the last decades, researches have showed interest in different aspects of synchronous handcycling. Literature analyzes physiological responses with oxygen uptake, ventilation and respiratory rate to identify the mechanical efficiency [1]. Furthermore, some studies performed a biomechanical and force analysis, which conducted to the identification of two main efficiency indices. The first one is the fraction of effective force (FEF) [2], associated with the effectiveness of the force application. The second one is the postural force production index (PFPI) [3], which evaluates the force generation capacity in all directions. However, these indices do not take in account gravity, inertia and the Coriolis effects, thus presenting a limitation in the efficiency evaluation.

The aim of this study is to present a dynamic model that takes in account the contributes of gravity, inertia and Coriolis effects, in order to associate the forces measured on handles to the corresponding shoulder and elbow torques, and to determine the force manipulability ellipsoids during handcycling. This allows to correct the definition of the mentioned indices to give them more relevance.

Methods: Five wheelchair dependent subjects, after giving their written informed consent, participated in the experiments. All subjects, experienced in handcycling, were asked to performe tests at a constant power. The tests were conducted in an adjustable recumbent sport Handbike which was converted in ergometer, integrating a control system that guarantees a constant output power. This device, designed and built by the university of Brescia, is equipped by two bi-axial load cell mounted on handles to measure radial and tangential components of the applied force, and an encoder to measure the angular position of the crankshaft in order to relate the measured force to the crank position (figure1). The 3D coordinates of the elbow and shoulder were determined by a vision system using passive markers. Then, anthropometric data was used to identify the dynamic parameters of arm and forearm. Finally, a dynamic model of the arm was defined [4], considering three rotations for the shoulder joint, one rotation for the elbow joint, pronosupination and two degrees of freedom (DoF). The angular position and forces were measured in cycling tests at constant power propulsion.

Results: The posture of the arms, the crank position and the force at the handle are measured with respect to the time, while velocities and accelerations are assessed by numerical differentiation. By using the dynamic model it was possible to compute torques generated by the human joints.

In order to determine the maximum voluntary joint torques that a subject may generate, we locked the crank in different angular positions and asked the subject to exert the maximum possible force. The maximum joint torques were used to determine the force manipulability ellipsoids.

In the end, we modified the definition of the mentioned indices (FEF and PFPI) by including the effect of dynamic contributions, and of the force weight, obtaining the Fraction of Effective Torque (FET) index, which assesses the efficiency of torque generation in joints, and the Inertial and Postural Force Production (IPFP) index, which evaluates the effect of inertia and the posture on the generation of force.

Figure:
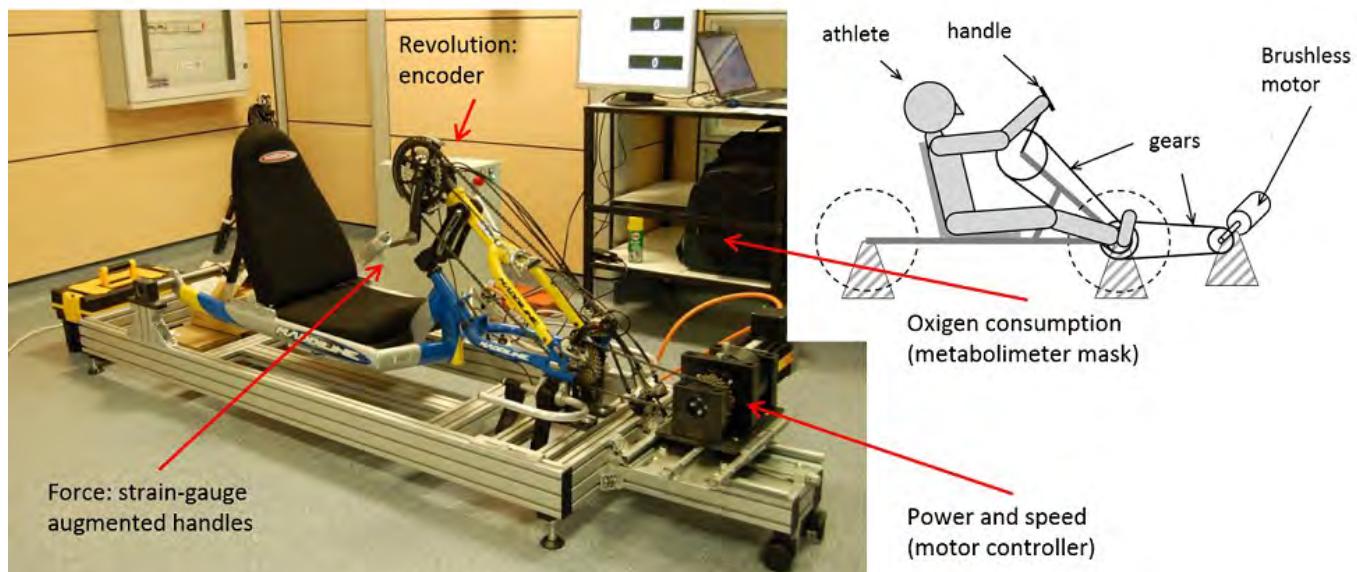
Caption: Figure 1: Details of the ergometer used for the tests.

Conclusion: This study had developed an analytic method to compute joints torques generated during handcycling. The method takes into account inertia, gravity and the Coriolis effects. Furthermore, it has identified two new indices that could be used to describe and understand the performance of handbike athletes. Experimental tests confirm the effectiveness of the approach.

References: [1] Powers S.K., Beadle R.E. and Mangum M., Exercise efficiency during arm ergometry: Effects of speed and work rate, 1984.

[2] Van Drongelen S. , Arnet U., Van Der Woude L.H.V., Veeger H.E.J., Propulsion effectiveness of synchronous handcycling, 2010.

[3] Jacquier-Bret J., Faupin A., Rezzoug N., Gorce P.A., New postural force production index to assess propulsion effectiveness during handcycling, 2013.

[4] Arnaud Faupin, Philipe Groce, Effects of crank adjustment on handbike propulsion: a kinematic approach, 2008.

Disclosure of Interest: None Declared

PO-0249

VALIDATION OF AN ACCELEROMETER EMBEDDED ON SMARTPHONE AGAINST A DYNAMIC LINEAR ACTUATOR

Natália Carneiro Badaró [1,*]Amanda Pe López [2]Alberto Luiz Serpa [2]Ricardo M.L Barros [1]

[1]Faculty of Physical Education, [2]Faculty of Mechanical Engineering, University of Campinas, Campinas, Brazil

Introduction and Objectives:

Inertial sensors have been increasedly used in motion analysis in clinical or performance contexts with a great variability of purposes. Sensors inside smartphones have also been proposed and tested. Most of the studies found in the literature evaluated the feasibility [2] or the validity [1] of such devices testing the measurements against the results of kinematical analysis system, commonly used to measure human motion. Considering the complexity of such kinematical systems and the problems related to define common coordinate systems, simpler and more controlled mechanical tests could provide useful information. The purpose of this study was to validate the use of the linear accelerometer embedded in a Smartphone testing those measurements against a dynamic linear actuator. The variables evaluated were the main frequency and the amplitude of acceleration of the measured signals. The smartphone was attached in a linear actuator to measure the signal. The idea of this work is to validate the smartphone sensor in order to evaluate the potencial of this device to measure human body motions.

Methods:

In order to validate the measurements of the smartphone, a linear actuator was used as reference (Gold Standard). A linear actuator is a device that creates motion in a straight line under very controlled conditions. In this test, a dynamic linear actuator INSTRON (model PL25) with nominal range of 50 mm was used. The actuator was regulated to work at different frequencies (0.5, 1, 2, 3, 4, 5, 6, 8 and 12 Hz) and amplitudes (0.3, 5.0 and 10 mm). A smartphone Samsung Galaxy SII GT-I9100 was tested. The Acceleration Sensor inside was the model K3DH with range of 19.6133 m/s^2 and a resolution of 0.0047884034 m/s^2. The Sensor Insider Pro application software was used to acquire data and export to a Matlab file format. A special device was designed to fix rigidly the smartphone to the actuator and to orient the coordinate systems of both devices accordingly. The motion in only one direction was analyzed (Y-direction in the smatphone). The experiment was performed at the Dynamic Testing Laboratory in the University of Campinas, Brazil.

The signals were processed using spectral analysis (Fast Fourier Transform) to obtain the signal decomposition in terms of frequency. The frequency with the higher power spectral density was selected and used for comparisons. Afterward a fourth order butterworth filter with a cutoff frequency twice the selected frequency was applied to both signals. The displacement signal generated by the actuator was initially filtered and after that differentiate twice. The main frequency of motion and the average amplitude of the acceleration from both devices were compared in terms of absolute and relative errors.

Results:

Figure 1 show the single-sided amplitude spectrum of the signals recorded by the smartphone in three different tests with 2, 4 and 8 Hz and an amplitude of 10, 10 and 5 mm respectively.

The average amplitude of 1500 samples of the signal measured by the smartphone was compared with the amplitude of the actuator signal in each condition. The results are showed in Table 1.

Figure:
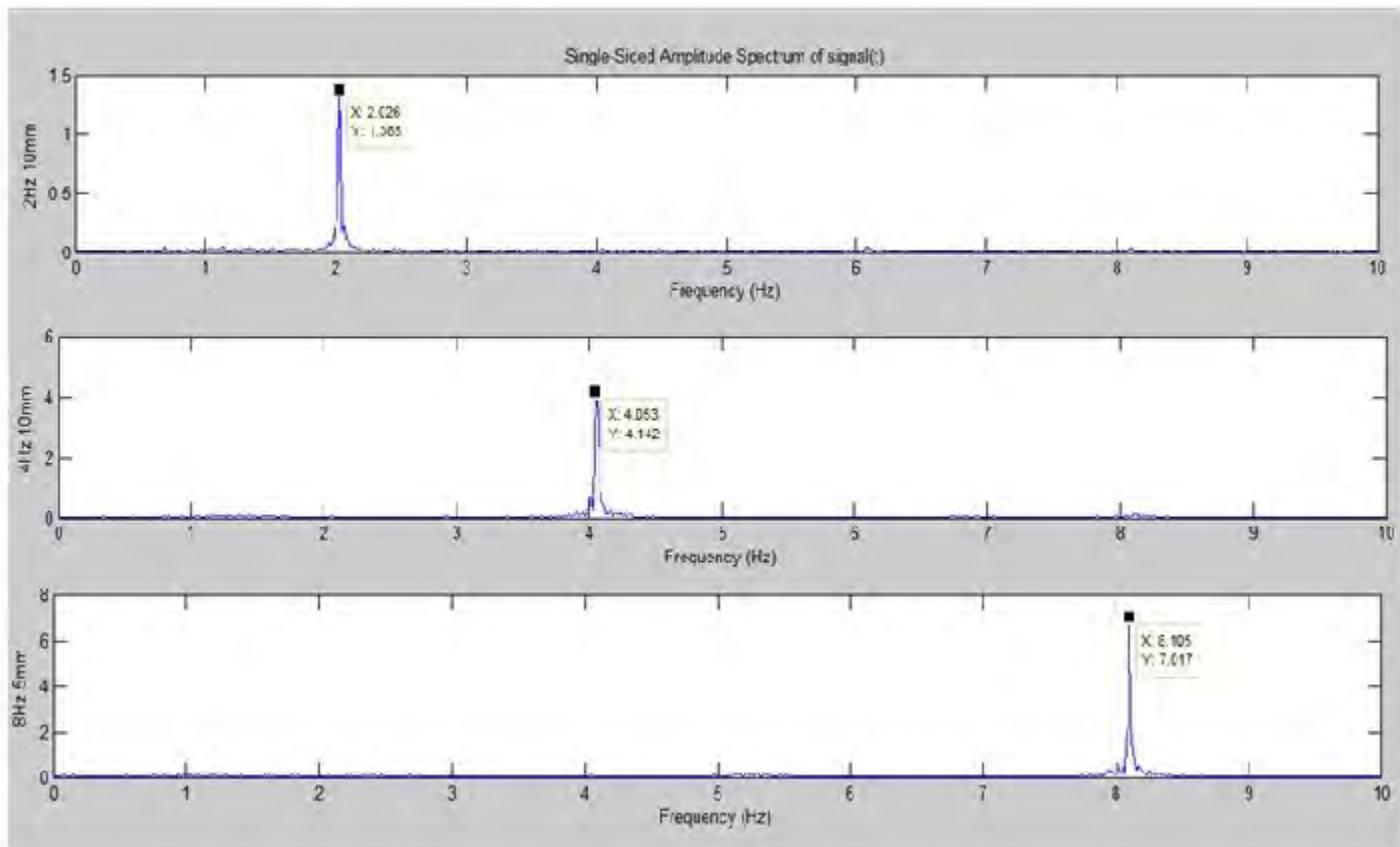
Caption: Figure 1: Frequency analyses of the signal with 2Hz, 4 Hz and 8 Hz and an amplitude of 10 mm, 10 mm and 5 mm respectively to obtain the main frequency.

Conclusion:

The estimates of frequency of motion provide by the smartphone are close to the expected values with relative error around 2%. However, the accelerations provided by the smartphone presented inconsistent values. It is important to take carefully these outcomes considering the possible influence of filtering and derivative procedures on the results of acceleration comparisons. It is possible that further improvements in the data processing provide measurements closest to the expected values of acceleration. In conclusion, the test designed in the present study revealed that the smartphone can measure the main frequency of motion properly however the acceleration measurements were not acceptable.

Table:

Amplitude of the actuator signal (mm)	Frequency of the actuator signal (Hz)	Frequency observed by the smartphone (Hz)	Frequency relative error (%)	Acceleration amplitude of the actuator signal (m/s^2)	Acceleration amplitude of the actuator signal (m/s^2)	Amplitude relative error (%)
10	0.5	0.51	2.00	0.099	0.102	3.03
10	1	1.01	1.00	0.395	0.663	67.84
10	2	2.02	1.00	1.573	1.881	19.58
10	3	3.05	1.66	3.505	3.475	0.86
10	4	4.05	1.25	6.077	5.699	6.22
10	5	5.06	1.20	9.288	7.740	16.66
10	6	6.07	1.16	12.982	10.369	20.12
5	8	8.10	1.25	11.166	8.808	21.11
0.3	12	12.17	1.41	1.305	1.198	0.53

Caption: Table 1: Results of the amplitude and frequency analyses.

References:

[1] NISHIGUCHI, Shu et al. Reliability and validity of gait analysis by android-based smartphone. Telemedicine and e-Health, 18(4): 292-296, 2012.

[2] MATHIE, M. J. et al. Classification of basic daily movements using a triaxial accelerometer. Medical and Biological Engineering and Computing, 42(5): 679-687, 2004.

Disclosure of Interest: None Declared

Motion Analysis

PO-0252

TRUNK REFERENCE FRAMES AND THE CALCULATION OF TRUNK AND BREAST KINEMATICS IN HUMAN MOVEMENT ANALYSIS

C Mills [1,*] A Loveridge [1] A Milligan [1] J Scurr [1]

[1]University of Portsmouth, Portsmouth, United Kingdom

Introduction and Objectives: The use of the female cohort presents a unique challenge as the design of the bra used to support the breasts during physical activity compromises the positioning of the International Society of Biomechanics (ISB) recommended marker set used to create the trunk reference frame [1]. The need to develop a new trunk marker set has been highlighted [2] and should consider the location and design of the underband and bra straps; and other bra features such as neckline height. This study aimed to compare trunk and breast kinematics calculated using two existing and one new trunk marker set.

Methods: Following institutional ethical approval twelve females (mean (SD): age 23.8 (3.5) years, height 1.68 (.06) m, body mass 61.0 (5.8) kg, 32 to 34 underband with a B to D cup size) volunteered for this study. Eight trunk markers were used to define the three trunk reference frames (Figure) and an additional marker on the right nipple represented gross breast motion. Three dimensional movement of the markers were tracked using 15 optoelectronic cameras (Oqus, Qualisys, Sweden), positioned around the treadmill, sampling at 200 Hz. The participants stood statically in the anatomical position for a 2 second trial for use in the segment estimation algorithm before running bare-breasted at 2.8 m/s. Marker coordinates were recorded for five gait cycles. Markers were identified and reconstructed in Qualisys Track Manager; no data interpolation was used as marker capture success was utilised in this study to assess the suitability of each marker set. Marker coordinates from both the static and dynamic bare-breasted trials were imported into Visual 3D (C-Motion Inc, USA) and the three trunk reference frames (segments) were created. To simulate the underband when wearing an everyday or sports bra [3] both the PX and T8 markers (Figure) were removed from the raw data files (dynamic trials). These modified files were imported into Visual 3D where it was noted that the Trunk 2 segment failed to be constructed due to an insufficient number of markers, limiting its use during trials that include females wearing a breast support garment. Trunk segment capture success (%), segment origin instability (cm), segmental residual (cm), trunk kinematics (°) and breast ROM (cm) relative to each trunk segment, were calculated for the three trunk segments.

Results: Segment capture success varied from 88 % to 100 % depending on the marker set. Segment origin instability ranged from 1.5 cm to 0.2 cm, which represented up to 35 % of superio-inferior breast ROM. Maximum trunk extension differed by 7° depending upon the marker set used and finally breast ROM varied by 41 % in the anterioposterior (A-P), 54 % in the mediolateral (M-L), and 21 % in the superioinferior (S-I) direction (Table).

Figure:
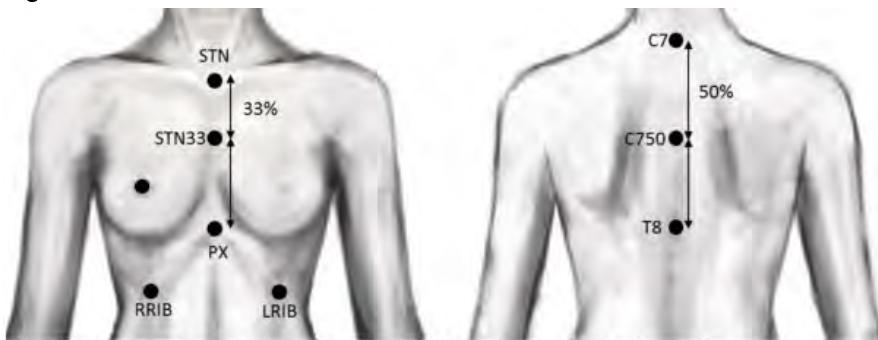
Figure: Marker locations on the trunk segment used to define the trunk reference frames
(Trunk 1 - STN, RRIB, LRIB; Trunk 2 - STN, PX, C7, T8; Trunk 3 - STN, PX, C7, T8, STN33, C750)

Conclusion: Key findings show that Trunk 1 marker set achieved less than 100 % capture success and was also the marker set with the greatest origin instability. Qualitative inspection of optoelectronic data suggests that arm swing during running tended to alternately obscure the rib markers reducing capture success. Furthermore the majority of origin instability occurred in the superioinferior direction, possibly due to motion of the subcutaneous fat at the distal marker locations used for the Trunk 1 segment. Trunk segments with markers restricted to the anterior aspect of the trunk (Trunk 1) caused a backward tilt of the trunk segment relative to the global vertical axis. Within the local coordinate system of the trunk, this tilt altered the directional distribution of the breast. Trunk 2 marker locations (PX, T8) are obscured by a bra's underband therefore preventing its use when female participants are wearing breast support garments. The Trunk 3 marker set maximises capture success and minimises origin instability whilst also having sufficient markers to avoid obstruction from current bra designs and arm swing mechanics. This trunk marker set is recommended when investigating trunk and breast kinematics using the female cohort during running with and without breast support.

Table:

Marker Set	Segment Capture Success (%)	Origin Instability (cm)	Segment Residual (cm)	Trunk Maximum Tilt (°)	Trunk Maximum Flexion / Extension (°)	Trunk Maximum axial rotation (°)	Breast A-P ROM (cm)	Breast M-L ROM (cm)	Breast S-I ROM (cm)
Trunk 1	88	1.5	0.5	-3.5	-5.8	-13.2	3.9	3.5	4.3
Trunk 2	100	0.2	0.4	-4.1	7.9	-18.5	2.6	1.8	5.2
Trunk 3	100	0.2	0.4	-4.1	8.0	-19.4	2.3	1.6	5.0

Caption: Table: Breast and trunk kinematics

References: [1] Wu et al., J. Biomech, 38: 981-992, 2005.

[2] Mills et al., J. Biomech, 47: 2606-2610, 2014.

[3] Scurr et al., J. Sports Sci, 28: 1103-1109, 2010.

Disclosure of Interest: None Declared

CHANGES IN MULTISEGMENT FOOT KINEMATICS AS A FUNCTION OF GAIT SPEED

Victoria Chester [1,*]Jeffrey Grant [1]Usha Kuruganti [1]Gwyneth de Vries [2]

[1]Kinesiology, University of New Brunswick, [2]Orthopaedics, Horizon Health, Fredericton, Canada

Introduction and Objectives: The majority of gait research has modeled the foot as a single rigid segment with few degrees of freedom. Recently, there has been an increase in the number of studies using multisegment foot models to examine motion between segments of the foot. While it is known that walking speed influences ankle kinematics derived from simplistic foot models [1-3], relatively little is known about the effects of walking speed on multisegment kinematics. During pathological gait, individuals may walk slower or faster than typical walking speeds. As a result, speed-mediated effects may be difficult to distinguish from those due to an injury, disease and/or disorder. A greater appreciation of the effects of walking speed on multisegment foot kinematics in control groups is needed. Therefore, the purpose of the present study was to examine differences in multisegment foot kinematics as a function of walking speed using healthy controls.

Methods: Twenty-two (n=22) adult participants (11 male, 11 female) were recruited between the ages of 18-30 years (age=23.0±2.6 yrs; height: 1.73±0.1 m; weight: 72.1±10.1 kg). A 12 camera T160 Vicon motion capture system (Oxford Metrics Group, Oxford, UK), sampling at 100 Hz, was used to track the three-dimensional trajectories of 32 reflective markers placed on the participant's skin. Six force plates (Kistler Instruments, Winterhur, Switzerland), embedded in the lab floor, were used to aid in the identification of gait cycle events. The foot model consisted of the 6 rigid segments, including the tibia, hindfoot, midfoot, forefoot, hallux, and total foot. A static capture of the participant during was recorded to permit the calculation of offset values for all joint rotations. Joint offset values were subtracted from the gait cycles of each participant. Planar angles were calculated and reported without any offsets. Participants were asked to perform at least 6 gait trials for the left and right limbs. Displacement data were filtered using a zero phase lag, second order Butterworth filter with a cutoff frequency of 6-9Hz. Relative joint angles were computed using Euler angles. Joint angle data were normalized to 100% of the gait cycle. Gait speed was rendered dimensionless in accordance with Hof [4]. Repeated measures ANOVAs were used to test for significant differences in the mean values of the temporal-spatial values and peak joint angles across 5 walking speeds (very slow, slow, typical, fast,and very fast, Table 1). Data was analyzed using custom software created in Matlab (Mathworks, Inc. Natick, MA, USA).

Results: Significant differences ($p<0.002$) were found in the mean values of temporal-spatial gait variables across gait speeds. Variation in walking speed significantly ($p<0.002$) affected the magnitude and timing of the relative and absolute angles of the foot. All significant changes in the magnitude of angles occurred in the sagittal plane only. Changes in speed altered the angular kinematics of the calcaneus vs tibia, midfoot vs calcaneus, and forefoot vs calacaneus (Figure 1). In addition, planar angles of the hallux, metatarsals, and medial longitudinal arch also varied with speed.

Figure:
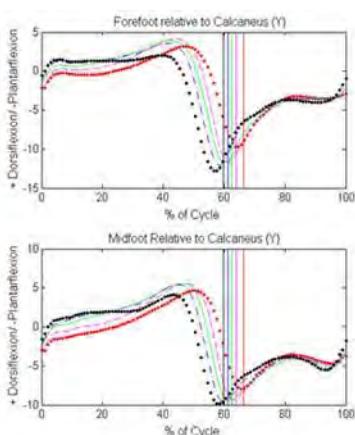
Figure 1: a) Picture of multisegment marker system, b) Example of changes in multisegment angles as a function of speed (black = very fast; red = very slow)

Conclusion: Similar to the single rigid body model, walking speed was found to affect multisegment foot kinematics. These results have important implications for studies examining foot and ankle function in typical and atypical populations. The results suggest that speed-matched control data should be used for the analysis of multisegment kinematics, especially in clinical populations where walking speed is altered by pathology. Such data will also facilitate a greater understanding of gait deviations and the effects of treatment interventions. Future studies should examine the effects of walking speed on multisegment foot kinematics in varying age groups and clinical populations. In addition, changes in multisegment foot kinematics as a function of speed may be further understood through the examination of kinetic, EMG, and plantar pressure data.

Table:

Speed Groups	Dimensionless Speed	Number of Trials
Very Slow	v <= 0.382	43
Slow	0.382 < v <= 0.495	41
Free	0.495 < v <= 0.581	42
Fast	0.581 < v <= 0.721	43
Very Fast	v >0.721	39

Caption: Post hoc classification of normalized walking speeds

References: [1] Crowninshield et al., J Biomech., 11: 75–85, 1978.

[2] Kirtley et al., J Biomed Eng., 7: 282-288, 1985.

[3] Van der Linden et al., J Pediatr Orthoped. ,22 : 800–806, 2002.

[4] Hof. Gait Posture, 4: 222-223, 1996.

Disclosure of Interest: None Declared

Motion Analysis

PO-0254

AGE-RELATED DIFFERENCES IN UPPER EXTREMITY MOVEMENTS DURING ACTIVITIES OF DAILY LIVING

Victoria Chester [1],*Brian Beaudette [1]

[1]Kinesiology, University of New Brunswick, Fredericton, Canada

Introduction and Objectives: While gait patterns have been studied extensively across the life span, few researchers have examined age-related differences in upper extremity (UE) kinematics during activities of daily living (ADLs) [1-3]. The movement of the upper extremities is a critical component of many ADLs, such as feeding, drinking, dressing and perineal care. Knowledge of changes in UE movement patterns as a function of age is needed to establish valid control databases for the identification of movement deviations in clinical populations (e.g., cerebral palsy). Therefore, the present study examines age-related differences in three-dimensional UE kinematics between young adult and pediatric groups while performing drinking and eating tasks.

Methods: Fifteen young adults (5 male, 10 female), aged 18-24 years (mean age: 20.2 years), and fifteen paediatric participants (5 male, 10 female) aged 7-9 years (mean age: 8.3 years) participated in the study. An eight-camera Vicon MX motion capture system (Oxford Metrics Ltd., UK) was employed to track the three-dimensional trajectories of eighteen (n=18) reflective markers placed on the participants' skin at a sampling frequency of 60 Hz. Rigid body segments included the head, trunk, and the left and right upper arm, forearm, and hand. Each participant was asked to perform a standardized eating task, which involved scooping pudding from a bowl with a spoon, and drinking task, which involved drinking water from a cup. The participants performed the drinking task using both the dominant and non-dominant arms. Joint angles were then computed from the relative orientations of embedded coordinate systems using Euler angles. Two-way ANOVAs were used to test for significant ($p<0.05$) differences in mean maximum joint angle data across age groups and dominant/non-dominant arms.

Results: Significant differences ($p < 0.004$) in mean maximum values of joint angle parameters were found between age groups for both tasks. No significant interactions or differences in mean maximum joint angle parameters were found between the dominant and non-dominant arms. No significant differences in temporal-spatial data were found for the tasks. The young adult had a significantly larger mean maximum elbow flexion than the paediatric group during phase 1 of the eating task (lift spoon to mouth). The young adult group also had a significantly larger mean maximum elbow flexion angle than the paediatric group during phase 2 of the eating task (return spoon from mouth to bowl). The paediatric group showed significantly greater shoulder abduction throughout the task. Both groups showed similar movement variability; however, the young adult group showed more consistent elbow flexion patterns. For the drinking task, the paediatric group had significantly larger mean maximum angles for neck flexion in phases 1 (period between grasping of the cup to the peak of cup sipping) and phase 2 (the period following peak cup sipping to the return of the cup to the table). In addition, the paediatric group had significantly larger mean maximum shoulder abduction in phase 2 compared to those for the young adult group. Significantly lower mean maximum shoulder flexion angles were also found during phase 2 in the paediatric group (see Figure). While the variability of movement was very similar across age groups, the young adult group had consistently lower variability.

Figure:
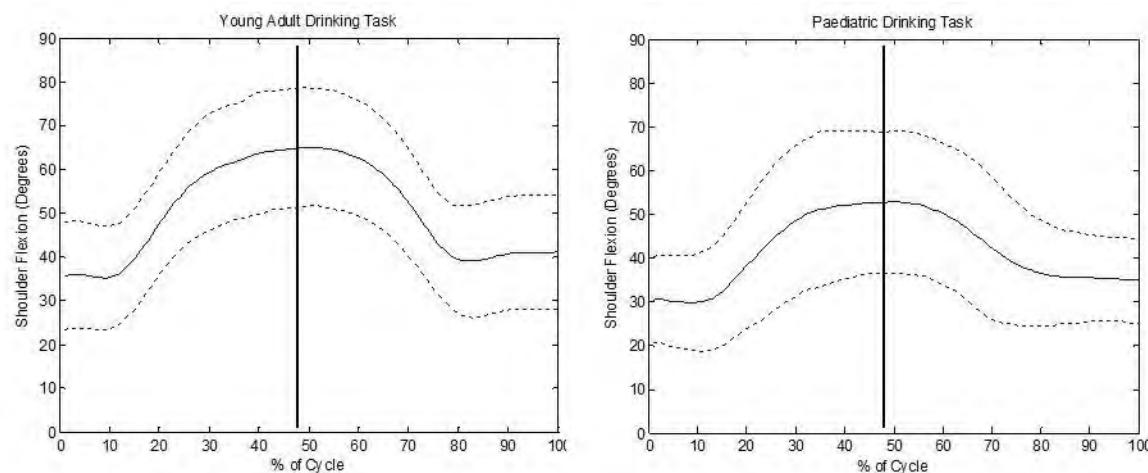
Conclusion: The results of this study suggest that age-related differences exist in movement patterns between pediatric and young adult age groups during the performance of ADLs. Differences in experience with the task, anthropometrics, techniques used to complete the task, and neuromaturational levels likely contributed to the varying movement patterns. Information on age-related differences in UE kinematics is critical to our understanding of typical movement patterns and future clinical studies involving the UE. The identification of movement deviations and their underlying causes in clinical populations is dependent on the availability of well-defined control data. Differences in UE kinematics between pediatric and young adult age groups demonstrates the importance of using age-matched control groups in future clinical studies. Future work will focus on increasing sample sizes and examining additional age divisions for comparative purposes.

References: [1]   Petuskey et al., Gait Posture, 25: 573-579, 2007.

[2]   Boone et al., J. Bone Joint Surg., 61-A: 756-759, 1979.

[3]   Maitra et al., Occup. Ther. Int., 11: 67-81, 2004.

Disclosure of Interest: None Declared

Motion Analysis

PO-0255

THE EFFECT OF SPRING RESISTANCE AND KNEE SUPPORT ON SHOULDER MECHANICS DURING THE LONG STRETCH EXERCISE ON THE REFORMER IN PILATES

Heiliane D. B. Fontana [1,*]Ana Paula Moratelli Prado [1]Caroline Ruschel [1]Helio Roesler [1]

[1]Health and Sports Science Center, University of the State of Santa Catarina, Florianópolis, Brazil

Introduction and Objectives: Among Pilates equipments, the most frequently used is the reformer, which employs spring tension exerted on a movable carriage. Typically, exercise progression on the reformer can be easily made by increasing spring resistance. However, in some exercises, such as the long stretch, resistance will also depend on the subjects body weight and gravity, partly resembling the floor work resistance in Pilates. Despite the frequent use of the long stretch exercise in clinical practice and the increasing popularity of Pilates, the effect of different body alignment and spring resistance on shoulder mechanics remains unknown. The interaction of gravity result in a complex relationship between spring resistance and exercise demand, which challenges the perception of the instructor and patient in order to achieve a proper exercise progression. Therefore, the aim of this study was to analyze the effect of spring resistance and knee support on the shoulder range of motion and torque during the long stretch exercise on the reformer. In this experiment, we chose to evaluate the initial and final position of each movement cycle, as they represent the minimum and maximum spring resistance imposed to the exercise.

Methods: A certified Pilates instructor with seven years of practice (29 years, 50.8 kg and 1.60 m) was invited to take part in the experiment. The subject performed five repetitions of the long stretch exercise in six onditions based on different spring resistances - no spring; one spring (linear resistance $R^2>0.99$, K=255.65 N/m) and two springs - with and without knee support. In order to collect force data, a recently developed instrumented reformer was used (Figure 1). It contains two specially designed three-axial force plates in parallel (150 x 300 mm each) [1], connected to an acquisition system (ADS2000-IP, Lynx LTDA). All executions were recorded by a synchronized camera (EX-FH20, Casio) placed 3.0 m from the left shoulder sagital plane. Markers were placed at the following anatomical landmarks: ulnar styloid process, acromion, and great trochanter. Images were processed using Kinovea 8.15. From the segment angle of the upper limb and the vertical and antero-posterior forces measured at the reformer instrumented bar, radial and tangential forces to the upper limb were calculated on the sagital plane for both the initial and final position. Tangential forces were multiplied by the upper limb length (0.46 m) to obtain an estimate of shoulder torque on the sagital plane.

Results: In Table 1, the mean values of the analyzed variables are shown. Shoulder net torque varied from 17.6 Nm towards flexion to 50.3 Nm towards extension. At the initial position, shoulder net torque was always directed towards flexion, being negligible when the exercise was performed with knee support, but, similarly to the compressive radial forces, increasing with increasing spring resistance and in the absence of knee support. At the final position, however, all conditions, apart from the two-spring with knee support, resulted in a extensor torque effort, which decreased with increasing spring resistance and with knee support. Shoulder range of motion decreased with increasing spring resistance in the knee support condition; while an opposite trend was observed for the no knee support condition. The changes in range of motion were mainly due to differences in shoulder angle at the final position.

Figure:
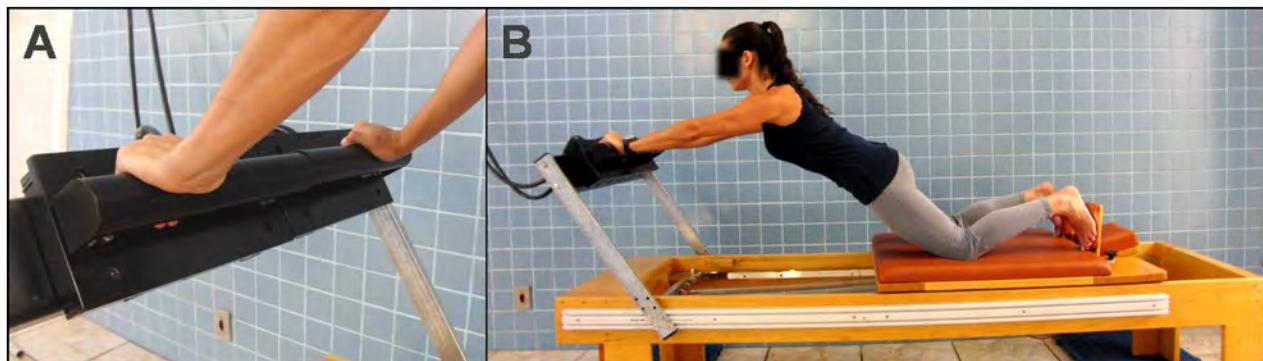
Caption: A. Upper limb position on the reformer instrumented bar. B. Long stretch exercise on the reformer.

Conclusion: The relationship between spring resistance, gravity and shoulder mechanics is complex and the common sense that the long stretch exercise is mainly directed to shoulder flexors is misleading. In fact, from the zero to the two-spring condition, the addition of springs provides assistance to shoulder extensors rather than resistance to shoulder flexors, at least in the position in which spring resistance is maximum.

Table:

		WITH KNEE SUPPORT			WITHOUT KNEE SUPPORT		
		NO SPRING	1 SPRING	2 SPRINGS	NO SPRING	1 SPRING	2 SPRINGS
SHOULDER TORQUE(Nm)	INITIAL	-1.1(-1.0)	0.4(1.7)	3.2(0.4)	1.6(-2.0)	7.0(-3.8)	17.7(-7.0)
	FINAL	-39.5(-2.3)	-16.3(2.6)	8.8(8.2)	-50.3(0.6)	-29.8(1.3)	-2.3(2.1)
RADIAL FORCE (N)	INITIAL	39.68(-6.45)	64.59(-13.21)	70.76(-21.59)	162.81(-34.13)	151.04(-32.45)	150.80(-35.18)
	FINAL	-6.87(9.27)	96.06(5.31)	166.35(0.64)	84.46(-38.53)	102.30(-19.04)	171.77(-32.4)
SHOULDER ANGLE (°)	INITIAL	42	51	50	54	55	55
	FINAL	144	140	127	103	130	134
SHOULDER ROM (°)		102	89	77	49	75	79

Caption: Shoulder net torque, radial force, angle and range of motion (ROM) at the initial and final position of the long stretch exercise on the reformer. Data are expressed in mean values and mean absolute difference (in parenthesis) between left and right upper limbs. Mean positive torque and radial force are in the direction of shoulder flexion and compression respectively. Positive absolute differences (in parenthesis) indicate higher forces on the right upper limb.

References: [1] Machado et al.Corpus et Scientia, 9: 101-114, 2013.

Disclosure of Interest: None Declared

Motion Analysis

PO-0256

NORMAL RUNNING GAIT PATTERNS EXAMINED BY HIERARCHICAL CLUSTER ANALYSIS

Angkoon Phinyomark [1,*]Sean Osis [1]Blayne Hettinga [1]Reed Ferber [1]

[1]Faculty of Kinesiology, University of Calgary, Calgary, Canada

Introduction and Objectives: Previous studies have demonstrated distinct clusters of walking gait patterns in both healthy and pathological groups, suggesting that within samples of walkers, different movement strategies may be represented [1-2], and comparative outcomes may be influenced by these strategies [3]. However, no studies have investigated whether distinct clusters exist for gait patterns in running. Therefore, the first purpose of this study was to determine if running gait patterns for healthy subjects could be classified into homogenous subgroups. The second purpose was to identify differences in joint kinematics between these groups, and then to investigate the practical implications of clustering healthy subjects by comparing these kinematics with runners experiencing patellofemoral pain (PFP).

Methods: Three-dimensional kinematic data from ankle, knee, and hip joints in 121 healthy runners (40 males, 81 females, age 39.45 ± 12.61 years) and 56 PFP runners (20 males, 36 females, age 31.43 ± 8.66 years) were collected in frontal, transverse, and sagittal planes of motion. A principal component analysis (PCA) was used to reduce the dimensionality of the entire gait waveform data from both stance and swing phases of running gait cycle, and then a hierarchical cluster analysis (HCA) determined group sets of similar gait patterns and homogenous clusters based on the Euclidean distance and the Ward's linkage method. The optimal number of clusters was determined using the inflection point on a plot of agglomeration coefficient as a function of cluster number and was confirmed by verifying the consistency and inspecting the dendrogram. Differences in running kinematics between clustering healthy subjects and runners with PFPS were examined based on PC scores and gait waveforms using the analysis of variance and effect size *d*.

Results: The first 4 PCs, which explained 87.86-96.12% of the total variance in the original data, were retained for each of the waveforms, such that the 36 PC scores (4 PCs x 3 planes x 3 joints) comprised the columns and the 121 subjects comprised the rows of the input matrix for the HCA approach. Two distinct running gait patterns: Cluster 1 (C1) with 36 subjects and Cluster 2 (C2) with 85 subjects were found using the HCA approach, as shown in the Figure, and no significant differences were found between clusters with respect to age, height, weight and running speed ($p > 0.05$). Seven out of the 36 PC scores demonstrated significant differences between the two clusters ($p < 0.05$, $d > 0.8$). Specifically, differences between the clusters in frontal and sagittal plane knee angles were found in PCs 1 and 3 (75.79% of total variance in the data) and PC 2 (23.52% of total variance in the data), respectively. C1 exhibited greater knee abduction angles during 14-35% and 76-96% of running gait cycle compared to C2 and in the sagittal plane knee joint, C1 exhibited greater knee flexion angles during 76-88% of running gait cycle and reduced knee flexion angles during 39-58% and 97-100% of running gait cycle in comparison to C2. Other significant differences between C1 and C2 were present, but explained less than 20% of the total variance, including transverse and sagittal plane ankle joint, transverse plane knee joint, and frontal and sagittal plane hip joint kinematics. Conversely, no differences were found for frontal plane ankle and transverse plane hip joint kinematics.

When these two groups were compared to runners experiencing PFP, one cluster exhibited greater (-7.97° vs -5.49°, p = 0.03; d = 0.49) while the other exhibited reduced peak knee abduction angles (-4.44° vs -5.49°, p = 0.02; d = 0.40). In contrast, no differences in peak knee abduction angles were found for all 121 healthy runners as compared to PFP (-6.04° vs -5.49°, p = 0.43; d = 0.13).

Figure:
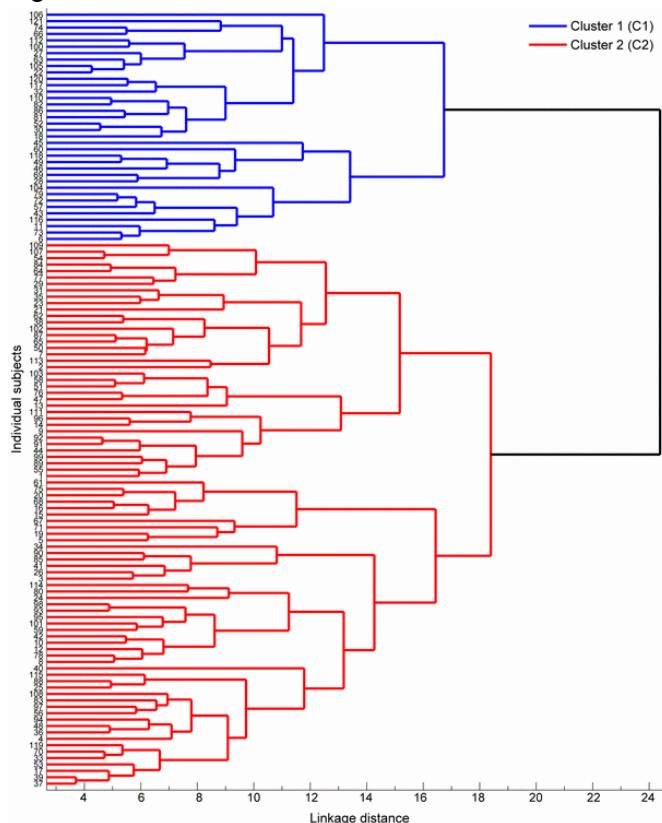
Caption: Ward's minimum variance linkage dendrogram of the hierarchical cluster analysis of the normal running gait patterns representing the two-cluster solution. Two groups are highlighted by blue color for Cluster 1 (C1) and red color for Cluster 2 (C2). Participant numbers are indicated.

Conclusion: This is the first study to experimentally demonstrate that the homogeneity of running gait patterns in a pain-free control group could significantly influence the results of a clinical investigation. The variability observed in running patterns across a sample could be the result of different gait strategies. Therefore, it is possible that movement strategies included within a traditional "control" group may influence any biomechanical differences found. These results suggest care must be taken when selecting samples of subjects in the investigation of gait pathomechanics and the biomechanical aetiology of running injuries.

References: [1] Simonsen et al., Med. Eng. Phys., 34: 219–224, 2012.

[2] Toro et al., Gait Posture, 25: 157–165, 2007.

[3] Grau et al., Res. Q. Exerc. Sport, 79: 450–457, 2008.

Disclosure of Interest: None Declared

Motion Analysis

PO-0257

TRAJECTORY BASED ANALYSIS, A NEW METHOD FOR MOTION ANALYSIS USING THE KINECT™ SENSOR

Victor Sholukha [1,*]Bruno Bonnechère [1]Serge Van Sint Jan [1]

[1]LABO, ULB, Brussels, Belgium

Introduction and Objectives: Lots of studies have been done in order to validate Kinect™ sensor as a Markerless System (MLS) for various uses (e.g. motion analysis, posture analysis…) [1,2,3]. Interesting results have been found in term of accuracy (compared to gold standard Marker-Based System (MBS)) and especially in term in precision. Due to the information provided by the Kinect SDK (a simple skeleton model composed by 20 points) it is not possible to directly obtain three-dimensional joint orientation position [4]. Another issue related to motion analysis is the different conventions used (e.g. Euler's sequences) making comparison and interpretation of the results difficult. The objective of this paper was developing advanced (PiG like) MLS model [5] and a new method for motion analysis based on joint trajectories instead of joint angles. Results of this new method are more easy to interpret and could therefore be used in clinics to assess patients status and monitor follow up.

Methods: Twenty healthy adults (26±8 years old, 173±8 cm height, 70±11 kg weight, 23±3 kg/m² BMI, 8 women) were recruited to participate to this study. MLS (Kinect™) and MBS (Vicon™) simultaneously captured motion data from in total 97 trials (per ten repetitions each type of motion) were processed. Four different type of test motion were selected for method testing: squat motion; right hip and shoulder abductions; right elbow flexion.

Each frame of the MLS motion data was available as 3D coordinates of crude approximation of the main human joints, e.g. presented in Figure by 20 red circles reconstructed by Kinect™ SDK. The major lack of this approach is the inability of allowing anatomically correct descriptions of the joint angular motion according to today clinical conventions.

To amend this stick-based model we improved the standard linear model to obtain a final model including three points for each segment link depicted in Figure. The new model architecture therefore allows proper anatomical and clinical motion representations. The final enriched model is similar to current standards in clinical motion analysis (such as the Vicon™ PiG model). In total 19 local coordinate systems (LCS), following ISB recommendations for axis orientation, were located in the origins indicated by numbers (1-19) in Figure. Then 33 LCS origin trajectories relative to parent LCS were evaluated. Each of 33 trajectory plots was processed to assess different properties of the shape created by hodograph and also processed (as a point clouds) to assess principal and supplementary axes origin and orientation in parent LCS (see Table for parameter list).

Results: All source motion data were processed and statistic was evaluated for each type of four motions. In total 30 parameters were collected and saved for each of 33 trajectories of processed 97 trials for MLS and MBS captured data. Then for each type of four trials mean and SD value of each of 30*33 parameters were assessed. These parameters could be used for motion analysis and scoring. Most of the parameters show SD variability within 10-20% from mean value.

Finally, absolute and relative difference between correspondent MLS and MBS parameters were evaluated. Mean relative error deviates from 1 to 22%. The best similarity show hip and elbow flexions and shoulder abduction. Hip abduction shows lager difference mainly due to bigger error of pelvis point recognition by MLS when pelvis rotates in frontal plane.

Figure:
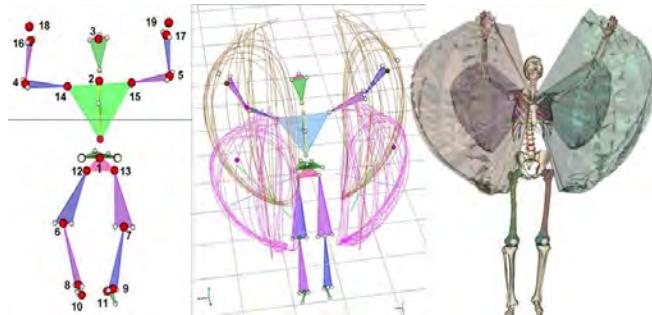
Conclusion: Two major results were presented in this paper. First is method for development an advanced model from crude MLS data to get full 3D motion data similar to Vicon™ PiG like protocol. Second, we suggested an alternative way of motion kinematics representation by mainly analysis trajectories of the selected points.

Table:

Parameter #	Units	Parameter value
1	m	Total length of the trajectory
2	degr	Total angle of the trajectory (hodograph) radius
3,4,5	m/s	Mean, SD and max of the hodograph velocity
6,7,8	degr/s	Mean, SD and max of hodograph angular velocity
9	degr/s	Mean hodograph angular velocity from parameter 3 and mean radius
10	cm^2	Square of cross sectional rhomboid, defined by first and second principal axis
11	cm^3	Volume of two pyramids (diamond) constructed from three principal axes end points
12,13	degr	Angles of view of two main axis from parent LCS origin
14,15	mm	Size of two main axes
16-18	mm	Position of principal axes origin in parent LCS
19-30	mm	Positions of the end points on the first two principal axes in parent LCS

Caption: List of parameters evaluated from trajectory analysis.

References:

[1] Bonnechere, B., et al. Gait & Posture 39, 593-598, 2013

[2] Clark, R., et al. J. of Biomech. 46, 2722-2725, 2013.

[3] Pfister, A., et al. J. of Med.Eng.&Techn. 38, 274-280, 2014.

[4] De Rozario, H., et al. J. of Appl. Biomech. 30, 294-299, 2014.

[5] Sholukha, V., et al. J. Biomech. 46, 2363-2371, 2013.

Disclosure of Interest: None Declared

Motion Analysis

PO-0258

THE COORDINATION MODE ANALYSIS DURING WALKING FORWARD AND BACKWARD

Luis Mochizuki [1,*]Karine Külkamp de Souza [2]Vanessa Herber [2]Fernanda Romaguera [2]Stella Maris Michaelsen [2]

[1]Physical activity sciences, Universidade de São Paulo, São Paulo, [2]Physioterapy, Centro de Educação Física, Fisioterapia e Saúde, Universidade do Estado de Santa Catarina, Florianopolis, Brazil

Introduction and Objectives: The information about how joints are coordinated is provided by several methods which tell about the similarity in the time, frequency or space domain of the data. During a motor task, there is a very simple and important question: what movement joint B performed when joint A was moving? This information is necessary to understand the risk for injury. The aim of this study is to describe how to perform coordination mode analysis (CMA) e discuss the importance of this novel analysis to understand the motor coordination during gait analysis.

Methods: Eight healthy adults participated in this study. One camera (HSC 180, 30 Hz frequency sampling) were used to shut the task. For the image digitalization, it was used the Ariel Performance Analysis System, APAS 1.4. The body markers were placed on acromion, greater trochanter, lateral condyle of tibia, and lateral malleolus of fibula. The participant walked forward and backward freely a treadmill at its self-selected speed. The hip and knee angles were calculated for the sagittal plane. The time series of those angles was low-pass filtered (2th order Butterworth, 20 Hz) and smoothed with quintic spline function. The coordination modes analysis (CMA) is based on the modified vector coding analysis [1] and the calculation of the inclination angle *f* of vector defined by a pair of consecutive points (a_i, b_i) and (a_{i+1}, b_{i+1}). Then, the time series of the coupling angles is codified with numbers (1 inphase, 2 antiphase, 3 a phase, and 4 b phase) which represents each coordination mode, this is the coordination mode sequence (COMOS). The COMOS is a *m* x 2 matrix, where *m* coordination modes and their relative times are provided. The COMOS variability is quantified by the CMS polymorphism, considering the variability within each COMOS and among COMOS. The variability along the positions is the polimorphism of the coordination. The polymorphism on each site of *n* COMOS is calculated by the heterozygosity *h* at the site *i* and the relative frequency of each coordination mode c_{ij} (*j*=1,2,3,4).

$h_i=n(1-\Sigma c_{ij}^2)/(n-1)$

The heterozigosity is calculated for COMOS of the same size. The COMOS of same size are called as codon# and # identifies how many coordination modes exist in that codon#. For example, codon2 is a COMOS with two coordination modes. The structure of the codon# reveals the coordination strategy applied to perform the task. The set of diferent codon# builts the motor coordination codex index (MOCX), the descriptor of the motor coordination strategy. Other information provided by the COMOS is how a coordination mode shifts to another. There are three type of coordination mode transition (COMOTA): a) inversion: from inphase to antiphase or from antiphase to inphase, from phase a to phase b, or from phase b to phase a; b) restriction: from inphase or antiphase to phase a or phase b; c) synchronization: from phase a or phase b to inphase or antiphase.

Results: The amount of coordination modes was affected by walking (H=5.4 p=0.01). Walking forward presented more coordination modes than walking backward (p<0.05). The inphase (H=1.4 p=0.22) and antiphase (H=2.6 p=0.10) modes were not affected by the type of walking. The knee phase (H=18.7 p<0.001) and hip phase (H=5.5 p=0.01) modes were

affected by walking. Walking forward presented the highest quantity of knee phase mode during the gait cycle. The type of walking affected the quantity of invertions (H=3.9 p=0.04), but the amount of synchronizations (H=3.7 p=0.05) and restrictions (H=3.4 p=0.06), during the gait cycle. From the codon2 to codon9, the mean h indexes calculated for walking forward and backward were similar. From codon10 to condon13, the diference between walking forward h indexes increases because the variability of the coordination modes decreases in walking backward.

Conclusion: The CMA is a novel method to describe the coordination between two joints. We showed how the hip and knee are coordinated during walking forward and backward. It provides information about the coordination rules and it is potential tool to describe how two joints move together.

Table:

Coordination mode	Walking type	Quantity of coordination modes (median [25%,75%])				
		Gait cycle	Stance			Swing
			Early	Middle	Late	
Phase	Backward	3 [2,3]	1 [1,1]	0 [0,0]	1 [0,1]	1 [1,1]
	Forward	3 [3,3]	0 [0,0]	1 [1,1]	0 [0,0]	2 [1,2]
Antiphase	Backward	3 [3,3]	1 [1,1]	1 [1,1]	0 [0,0]	1 [1,1]
	Forward	3 [3,3]	1 [1,1]	1 [0,1]	0 [0,0.75]	1 [1,1]
Knee	Backward	2 [2,3]	0 [0,1]	0 [0,1]	1 [0,1]	1 [1,1]
	Forward	3 [3,3]	1 [0,1]	0 [0,0]	1 [1,1]	1 [1,1]
Hip	Backward	3 [3,3]	1 [1,1]	1 [1,1]	0 [0,0]	1 [1,1]
	Forward	3 [3,3]	1 [1,1]	1 [1,1]	0 [0,0]	1 [1,1]

Caption: Quantity of coordination modes during walking forward and backward.

References: [1] Chang et al., J Biomech.,41:3101-5, 2008.

Disclosure of Interest: None Declared

THE EFFECT OF TRUNK OVERWEIGHT IN GAIT BIOMECHANICS DURING PREGNANCY

Liliana Aguiar [1,*]Rita Santos-Rocha [2]Filomena Vieira [3]Marco Branco [2]Andrade Carlos [1]António Veloso [1]

[1]Faculty of Human Kinetics, University of Lisbon, Oeiras, [2]Sport Sciences School of Rio Maior , Polytechnic Institute of Santarém , Santarém, [3]Faculty of Human Kinetics, Polytechnic Institute of Santarém, Oeiras, Portugal

Introduction and Objectives: The main purpose of this study was to understand the effect of the increased mass in the trunk associated to gait during pregnancy, on joint range of movement (ROM) and moments of force (M_f), by comparing three loading conditions: 2nd trimester pregnant women (PG); non-pregnant women (NPG); non-pregnant women carrying an additional load of 5 kg placed in the abdomen and breasts.

Methods: The PG walked during non consecutive three minutes. The NPG performed two trials of gait at a self-selected speed, one of them carrying 5 kg extra load. This value was calculated based on IOM recommendations for weight gain during pregnancy [1,2], which was 0.42 kg/week, and its distribution was 46% located in the belly and 32% in the upper trunk [3], resulting in 4 kg on the belly and 0.5 kg in each breast for this group (load carrying group, LCG).

Motion capture was performed with an optoelectronic system of twelve cameras Qualisys (Oqus-300) operating at a frame rate of 200Hz, synchronized with two force platforms (Kistler AG, Winterthur, Switzerland) and one AMTI (Advanced Mechanical Technology, Inc, Watertown, MA), which collected ground reaction force data.

To reduce the effect of soft tissue artifact, a global optimization on the data processing algorithm was performed [4]. The model also assumed a universal joint to the ankle, a revolute joint to the knee and a spherical joint to the hip.

The inverse dynamics method was used to estimate net M_f produced by the muscular action. To calculate ankle, knee and hip ROM and M_f, the 3D biomechanical models were constructed, using the software Visual 3D C-Motion, Inc.

Results: The average joint angles and moment curves were obtained for each participant as well as the mean curve for the three groups.

Caption: Figure 1- Ankle, knee and hip joints and pelvis range of motion (ROM) in sagittal (first row), frontal (second row) and transversal planes (third row) for the non-pregnancy (NPG), pregnancy (PG) and load carrying (LCG) groups.

Conclusion: A set of variables is defined when there are significant differences in a variable in (NPG_PG) and (NPG_LCG), and no difference in (PG_LCG), which has a clear relation with the trunk weight.

Thus, we find the variables: maximum hip extension, maximum pelvic right obliquity, pelvic obliquity ROM, maximum transversal left rotation and peak hip flexion Mf. The trunk weight gain increases both stance phase duration and DLST in both LCG and PG subjects. The body's response to the external hip flexor M_f is related to a higher extensor activity to support the anterior additional mass of the trunk and to the forward translation of the center or mass. The pelvis amplitude on the frontal and transversal planes, may be reduced due to the surrounding constraints, once it supports the belly weight. The hip joint and pelvis are adjacent to the trunk and can be more affected by the weight gain and its distribution.

The relation between anterior trunk extra weight and gait modifications needs further research since weight gain during pregnancy provides higher biomechanical joint loads during walking that can cause injuries by overuse of certain specific muscles.

Acknowledgements

Table:

Normalized peak M_f (N.m/kg)	NPG	P G(1)	LCG (2)	P value
ankle dorsiflexion	1.08±0.16	1.21±0.16	1.13±0.19	1) p=0.021[a] 2) p=0.211 1-2) p=0.239
ankle plantarflexion	-0.63±0.40	-0.52±0.32	-0.06±0.03	1) p=0.371 2) p=0.528 1-2) p=0.839
ankle eversion	-0.06±0.03	-0.05±0.02	-0.07±0.03	1) p=0.571 2) p=0.031[a] 1-2) p=0.054
ankle inversion	0.06±0.03	0.10±0.04	0.07±0.05	1) p=0.012[a] 2) p=0.617 1-2) p=0.068
knee flexion	0.54±0.28	0.53±0.20	0.50±0.28	1) p=0.904 2) p=0.528 1-2) p=0.424
knee extension	-0.17±0.06	-0.17±0.09	-0.18±0.07	1) p=0.989 2) p=0.089 1-2) p=0.562
hip flexion (hip)	0.43±0.12	0.43±0.09	0.54±0.16	1) p=0.971 2) p=0.000[b] 1-2) p=0.023[a]
hip extension	-0.91±0.16	-0.79±0.18	-0.84±0.16	1) p=0.050 2) p=0.022[a] 1-2) p=0.391
hip adduction	0.71±0.17	0.76±0.11	0.78±0.21	1) p=0.254 2) p=0.017[a] 1-2) p=0.700
hip abduction (valley)	0.40±0.13	0.52±0.09	0.49±0.16	1) p=0.003[a] 2) p=0.003[a] 1-2) p=0.485
hip internal rotation	-0.11±0.0	-0.12±0.0	-0.15±0.0	1) p=0.658 2) p=0.020[a]

	7	5	7	1-2) p=0.171
hip external rotation	0.07±0.03	0.08±0.04	0.07±0.04	1) p=0.407 2) p=0.286 1-2) p=0.003ᵃ

Caption: Table 1. Comparison of ankle, knee and hip peaks Mf mean and standard deviation between 1) non-pregnancy (NPG) and pregnant (PG) groups and 2) non-pregnancy and load carrying (LCG) conditions.a-level of significance p<0.05;b-level of significance p<0.001.

References: [1] IOM, NRC. Weight gain during pregnancy. Reexamining the guidelines. Washington, D.C.: The National Academies Press; 2009.

[2] Paisley J, Mellion M. Exercise during pregnancy. Am Fam Physician 1988; 38(5), 143 – 150.

[3] Pitkin R. Nutritional support in obstetrics and gynecology. Clin Obstet Gynecol 1976; 19(3), 489-513.

[4] Lu TW, O'Connor JJ. Bone position estimation from skin marker coordinates using global optimization with joint constraints. J Biomech 1999; 32, 129-134.

Disclosure of Interest: None Declared

Motion Analysis

PO-0261

A COMPARISON OF METHODS TO ESTIMATE FOOTSTRIKE, TOE-OFF AND CONTACT TIME USING KINEMATIC DATA DURING OVERGROUND RUNNING

Laura C. Smith [1] Stephen Preece [1,*] Duncan Mason [1] Christopher Bramah [1]

[1]School of Health Sciences, University of Salford, Salford, United Kingdom

Introduction and Objectives: The gait cycle is frequently divided into stance and swing phase; identification is reliant upon accurate detection of the gait events footstrike and toe-off. This is typically achieved using force plates, however in some situations force plates cannot be used [1], it is therefore necessary to use kinematic algorithms to estimate events. Published algorithms for detecting gait events during running are based around timing of kinematic events, such as minimum shank and foot angular accelerations [2]. Although relatively good estimation accuracy of algorithms has been reported [1,2], some algorithms fail to accurately determine the timing of footstrike [3], alternatively have not been shown to estimate gait events as accurately when implemented in subsequent studies [1,2]. Furthermore, previous research has not reported associated errors in contact times [1,3,4] and has only tested algorithms at relatively slow speeds [1]. It is therefore unknown how published algorithms perform at higher speeds, characteristic of competitive races. The aim of this study was to propose a new custom-designed kinematic algorithm and compare its accuracy with established algorithms for footstrike, toe-off and contact time estimation at a relatively fast running speed.

Methods: Twenty elite runners (16 male and 4 female; age 24.3±4.4 years, mass 63.3±8.5 kg and height 177.3±6.8 cm) ran along a 35 m track at 5.6 m/s (±2.5%), contacting an AMTI force plate (1200 Hz) with their right foot. Synchronised three-dimensional kinematic data (240 Hz) were collected using a twelve-camera motion capture system (ProReflex, Qualisys). Kinematic data were filtered with a fourth order Butterworth low pass filter with a cut-off frequency of 10 Hz. Segmental kinematics were derived using a global optimisation approach [5]. Ground reaction forces determined true footstrike (>20N) and toe-off (<20N) events. Four existing algorithms (detailed in [1]) and one custom-designed algorithm were implemented to estimate footstrike and toe-off. The custom-designed algorithm estimated footstrike at the first maximum in vertical displacement between the heel and PSIS marker (Fig. 1a) and toe-off at the maximum vertical displacement between the second metatarsal head and PSIS marker, which was closest to the second peak knee extension (Fig. 1b). Errors for each algorithm were calculated as True Error (TE) (mathematical difference between estimated and true gait event time) and Root Mean Square (RMS) error. Differences between true and algorithm contact times were examined in SPSS 20 using repeated-measures ANOVA, with Bonferonni post hoc analysis ($p \leq .05$).

Results: The results show there were differences in accuracy between algorithms (Table 1). The custom-designed algorithm (Smith) provided the most accurate estimation of footstrike, demonstrating the lowest TE (1.2±17.1 ms) and RMS errors (14.1 ms). The Alton algorithm most accurately estimated toe-off (TE -3.8±4.2 ms and RMS 6.1 ms), however this was only marginally better than the custom-designed algorithm (TE 4.7±5.9 ms and RMS 9.2 ms). The custom-designed algorithm produced the most accurate estimate of contact time which was not significantly different to true contact time ($P > .05$). All other algorithms were significantly different to true contact time.

Figure:
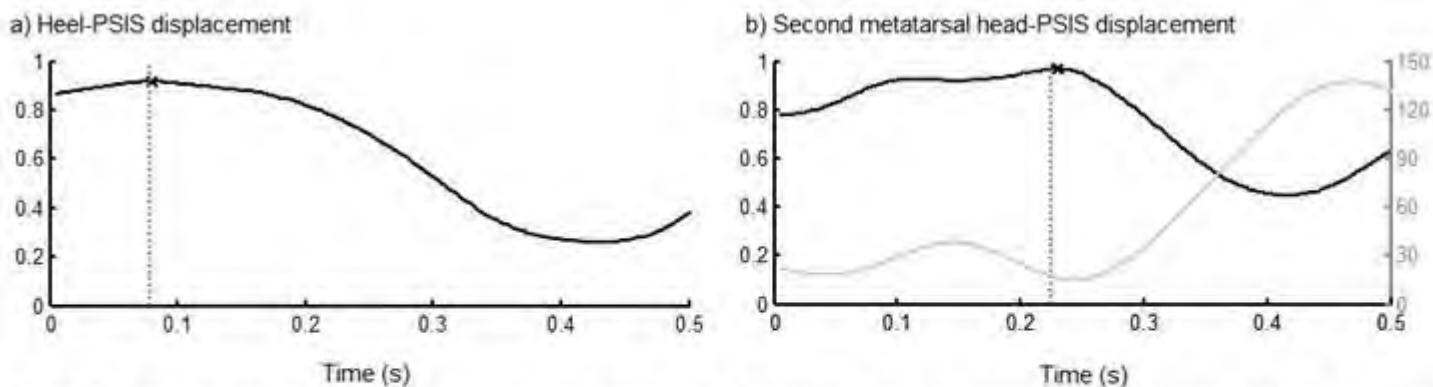
Figure 1. Representation of the custom-designed algorithm (Smith). a) Vertical displacement between the heel and PSIS marker is plotted against time and footstrike estimated to occur at the first maximum (denoted with an **x**). The dashed line shows footstrike time derived from the vGRF. b) Vertical displacement between the second metatarsal head and PSIS marker is plotted against time and toe-off estimated to occur at the local maxima closest to the second peak in knee extension. This estimate is marked on the graph with an **x**, in which the black line represents the custom-designed algorithm, whereas the grey line represents knee flexion-extension and again the dashed line represents vGRF derived toe-off.

Conclusion: There were differences in accuracy between the algorithms. The results showed the accuracy of contact time estimation varied between different algorithms, due to a combination of under and over estimations in footstrike and toe-off. The results illustrate that compared to the other tested algorithms, the custom-designed algorithm provided an accurate estimation of footstrike, toe-off and contact time; therefore provides a simple but effective method to accurately estimate footstrike, toe-off and contact time from kinematic data. In instances whereby ground reaction force data is not available we would recommend the use of the new algorithm for estimating gait events from kinematic data at faster speeds; however further work is required to confirm whether it would be equally effective at slower speeds.

Table:

		Smith	Alton	Dingwell	Hreljac	Zeni
Footstrike	TE	1.2±17.1	32.0±14.1	-27.4±7.4	-20.0±8.6	18.7±81.4
	RMS Error	14.1	32.3	27.9	23.1	151.7
Toe-off	TE	4.7±5.9	-3.8±4.2	13.8±10.5	34.1±50.7	91.4±22.5
	RMS Error	9.2	6.1	19.7	66.6	106.4
Contact	Contact Time	171.1±21.6	131.8±19.8*	208.7±13.4*	221.7±50.8*	240.3±81.0*
	TE	3.5±18.2	-35.8±16.0	41.1±10.8	54.1±48.8	72.7±78.0
	RMS Error	18.4	36.8	44.6	74.1	202.0

Caption: Table 1. Mean±SD Error between estimated and true gait events (in ms).Positive and negative values indicate algorithm overestimation and underestimation respectively. * denotes algorithm contact time is significantly different (p <0.05) to true contact time (167.6±8.9 ms).

References: [1] Fellin RE et al., J Sci Med Sport, 13: 646-50, 2010.

[2] Hreljac et al., Med Biol Eng Comput, 38: 503–6, 2000.

[3] Leitch et al., Gait Posture, 33: 130-2, 2011.

[4] Zeni et al., Gait Posture, 27: 710–4, 2008.

[5] Lu et al., J Biomech, 32: 129-34, 1999.

Disclosure of Interest: None Declared

PO-0262

INFLUENCE OF UPHILL WALKING ON SPATIO-TEMPORAL PARAMETERS OF GAIT DURING LOAD CARRIAGE OPERATIONS IN INDIAN SOLDIERS

Anilendu Pramanik [1,*] Deepti Majumdar [1] Bodhisattwa Chowdhury [1] Sohini Paul [1] Tirthankar Chatterjee [1] Madhusudan Pal [1] Dhurjati Majumdar [1]

[1] Ergonomics, Defence Institute of Physiology and Allied Sciences, Delhi, INDIA, Delhi, India

Introduction and Objectives: Soldiers are often expected to carry heavy loads over long distances through undulating and mountainous ranges. They may need to walk uphill with load while maintaining stability of gait at the same time. Though such load carriages on inclined surfaces are frequently encountered in a soldier's everyday life but their effects on the gait is relatively less understood. Treadmill walking has been shown in literature as an appropriate simulation of uphill and downhill locomotion at a common laboratory setup. The present study hypothesized that undertaking uphill treadmill walking with military load should result in alteration of gait pattern.

Indian soldiers generally carry loads in existing ensembles (ELCe) comprising of backpacks (BP, 10.7kg), haversack (HS, 4.4kg) on waist, WEBB (2.2 kg) on chest and rifle (4.2kg) in hand or on shoulder, resulting a total load of 21.4 kg. Depending on the operational requirement, either they carry these ensembles in single unit or in combinations.

Methods: Twelve healthy male Indian Infantry soldiers with mean (SD) age 26.8(3.8) yrs, height 170.6(3.3) cm and weight 66.4(6.8) kg, volunteered for the study. They walked on a treadmill at comfortable speed (3.0 km/hr), without load and with carrying 10.7kg (HS, WEBB and Rifle, 16.1% of body weight) and 21.4kg (ELCe, 32.2% body weight) load respectively. Total duration of walk was 30 mins, with every 6 mins each at 0%, 5%, 10%, 15% and 20% positive gradients. Their gait data was collected using 6 Camera based 3D Motion Analysis System. The temporal parameters (total support time, initial double support time, single support time) and spatial parameters (cadence, swing phase) of subjects data have been reported for each condition.

Results: Results shows that cadence decreased with uphill walking while total support time increased and the changes were significant with increasing gradients. These observations indicate that even low magnitude loads (10.7 kg, 21.4 kg) cause significant changes in spatio-temporal parameters of gait while uphill walking.

Conclusion: These changes may be explained as adaptive phenomena to counteract the effects of gradient and load on gait.

Disclosure of Interest: None Declared

BIOMECHANICAL STRATEGIES FOR SUCCESSFUL OBSTACLE-CROSSING IN PATIENTS WITH ANTERIOR CRUCIATE LIGAMENT DEFICIENCY

Horng-Chaung Hsu [1,*]Tung-Wu Lu [2] [3]Shih-Wun Hong [1]

[1]Department of Orthopaedics, China Medical University Hospital, Taichung, [2]Institute of Biomedical Engineering, National Taiwan University, [3]Department of Orthopaedic Surgery, School of Medicine, Taipei, Taiwan, Republic of China

Introduction and Objectives: Identification of movement deviations and compensations in patients with anterior cruciate ligament deficiency (ACLD) during daily activities is helpful for the rehabilitation of such patients. Obstacle-crossing is a common motor task in our daily living, requiring both stability of the stance limb and accurate end-point control of the swing limb. Therefore, it can be a great challenge to those with ACLD because both the structural stability and sensory feedback of the ACL are impaired. It remains unclear whether specific strategies exist in such patients in coping with obstacles during gait. The purpose of the current study was to identify the biomechanical strategies adopted by patients with ACLD in crossing obstacles of different heights.

Methods: Twenty unilateral ACLD patients and seventeen healthy subjects were recruited in the current study. Each subject walked and crossed obstacles of heights of 10%, 20% and 30% of their leg lengths at a self-selected pace. Kinematic and kinetic data were measured with a 7-camera motion analysis system (Vicon, Oxford Metrics, U.K.) and two force plates (AMTI, U.S.A.). The leading and trailing toe clearances were calculated as the vertical distances between the toe markers and the obstacle when the toe was directly above the obstacle. Joint angles of both limbs, and joint moments of the trailing limb, were calculated. Peak extensor moments at the knee during stance phase and the corresponding joint angles were extracted for statistical analysis. Two clusters of the ACLD patients were identified by a hierarchical cluster procedure of Ward's method with peak joint moment as a cluster variable. A 3 by 3, 2-way mixed-model analysis of variance with one between-subject factor (group) and one within-subject factor (obstacle height) was performed (α=0.05). SAS version 9.2 was used for all statistical analysis.

Results: The two clusters of the ACLD patients according to the peak knee extensor moments were Group A (N =9) and Group B (N =11). No significant differences in the toe clearances were found between Group B and the control group (Table 1). Significantly reduced leading and trailing toe clearances and peak knee extensor moments on the affected limb were found in Group A when compared with those of the other groups (Table 1). Group A showed significantly reduced knee flexion in the stance limb when peak knee extensor moments occurred.

Conclusion: Two distinctive gait patterns were identified in the ACLD subjects during obstacle crossing. Differentiation of the subtle differences in the strategies adopted by the ACLD population may help improve the efficacy of the rehabilitation efforts in different ACLD subgroups. The ACLD patients with decreased extensor moments of the knee (Group A) appeared to be at a higher risk of stumbling over the obstacle. Advanced rehabilitation program or reconstruction of the ACL is suggested for this subgroup.

Table:

Limb	Variables	Obstacle Height (%)	Group A (N=9)	Group B (N =11)	Control (N =17)
Affected	Leading Toe Clearance (mm)	10	117.35 *	137.28	149.58
		20	99.00 *	145.14	143.25
		30	103.71 *	152.70	136.52
Affected	Trailing Toe Clearance (mm)	10	104.69 *	129.31	145.57
		20	94.42 *	128.00	135.58
		30	106.49 *	144.08	130.62
Affected	Peak Knee Extensor Moment (% LL*BW)	10	6.09*	7.24	7.51
		20	6.12*	7.27	7.70
		30	6.68*	7.79	8.22
Unaffected	Leading Toe Clearance (mm)	10	118.12 *	130.84	149.58
		20	100.99 *	136.28	143.25
		30	105.14 *	138.48	136.52
Unaffected	Trailing Toe Clearance (mm)	10	108.60 *	124.73	145.57
		20	92.27 *	121.95	135.58
		30	91.21 *	140.37	130.62
Unaffected	Peak Knee Extensor Moment (% LL*BW)	10	7.54	9.12	7.51
		20	8.84	9.46	7.70
		30	9.95	9.41	8.22

* indicates a significant group effect; LL: Leg Length; BW: Body Weight

Caption: Means of toe clearances and peak knee extensor moments in the patients with ACLD (Group A and Group B) and the Control group when crossing obstacles of heights of 10%, 20% and 30% of their leg lengths.

Disclosure of Interest: None Declared

Motion Analysis

PO-0264

THE EFFECT OF DIFFERENT LATERAL JUMP SMASH CONDITIONS DURING LANDING PHASE IN BADMINTON

Po-Teng Huang [1,*]Jia-Hao Chang [1]

[1]Physical Education, National Taiwan Normal University, Taipei, Taiwan, Republic of China

Introduction and Objectives: Overhead striking, like lateral jump smash, used to apply in competition of badminton. The footwork training has been used in badminton, but it is no ball strike in this training. To improve the reality in training, the purpose of this study was to understand the lower limb biomechanics between contralateral footwork (CF), contralateral hitting (CH) and contralateral target (CT) lateral jump smash.

Methods: Six male elite badminton players (13 ± 2.2 years training experience, aged; 22.6 ± 2.7 years, height: 177.4 ± 2.8 cm, mass; 72.3 ± 6.2 kg) participated in this study. All the participants were stood in the center of court and performed three times lateral jump smash in three conditions (CF, CH and CT). After landing, participants were quick returned to the center of court. A Vicon motion capture system (ten cameras, 300 Hz) and a Kistler force plate (1500 Hz) were used to collect biomechanics data during the landing phase. Vicon Nexus and Visual3D software were used to analyze kinematic data. All data were compared by using SPSS 22.0 in three conditions. Repeated measures ANOVA was used to test the differences of CF, CH and CT in the initial contact joint angle and maximum range of motion (ROM) ($\alpha = .05$).

Results: CF hip flexion was significantly larger than CH and CT, CT hip flexion was significantly larger than CH and at the initial contact. CF knee ROM was significantly larger than CH, CF ankle ROM was significantly smaller than CH and CT at touchdown to leave floor ($p < .05$).

Conclusion: The footwork training had the different kinematic in landing. The hip flexion increased in initial contact in CF group. The knee ROM increased and ankle ROM decreased in CF group during landing phase. We concluded that training with ball had the different landing kinematic with only footwork training.

Table:

Table1 Mean ± SD (degree) of hip, knee and ankle joint kinematics at initial contact				
	CF	CH	CT	p
Hip Flexion(+)/Extension(-)	12.87 ± 4.67	6.09 ± 7.00	11.317 ± 5.13	.001 *
Knee Flexion(-)/Extensio(+)	-13.51 ± 3.35	-14.24 ± 3.66	-13.78 ± 3.10	.375
Ankle Dorsiflexion(+)/plantar flexion(-)	-26.76 ± 3.85	-27.76 ± 2.75	-27.39 ± 4.00	.528
*CF > CH, CT; CT > CH				

References:

[1] Kimura, Yuka, et al. *British journal of sports medicine* 46.3: 207-213, 2012.

Disclosure of Interest: None Declared

PO-0265

DOES A DIFFERENCE IN THE LOCATION OF WEIGHT IN A BACKPACK AFFECT HUMAN GAIT?

Takashi Nakayama [1,*]Keio Ishiguro [1] [1]Tomokazu Muto [1]

[1]Physiotherapy Department, Tokyo University of Technology, Tokyo, Japan

Introduction and Objectives: Backpacks have varying designs, sizes, and functions, and are currently considered to be very useful for carrying luggage, while dispersing pressure appropriately and maintaining a suitable load on the back, when walking. In the present study, we aimed to assess the effect of weights loaded at different locations in a backpack on human walking on level and sloping surfaces.

Methods: Eleven healthy male volunteers, aged 19 to 22 years, participated in this study. None of the subjects had any impairments in walking due to orthopaedic diseases or conditions of the spine and legs. The aim and method of the study were described to the participants prior to study initiation, and their consent was obtained. The subjects were asked to walk on a flat surface and an ascending slope (6°) without any weight and while wearing weighted backpacks with weights placed randomly at different locations such as the anterior, upper posterior, and lower posterior locations. The loaded weight was set as 15% of the subject's body weight, based on previous reports. While walking, the three-dimensional angular displacements and moments of the hip, knee, and ankle, as well as lateral displacement of the centre of gravity (LDCOG) were obtained using the VICON Nexus system and 4 force plates. The electromyography (EMG) activities of the gluteus medius, rectus femoris, biceps femoris, tibialis anterior, and gastrocnemius were recorded using surface electrodes at a sampling rate of 1000 Hz, and were sequentially processed as %integrated electromyograms (%iEMGs) according to the ratio of the maximum voluntary contraction volume of each muscle.

Results: Compared with no-weight walking, the flexion ranges of motion of the hip and knee as well as the dorsiflexion of the ankle in the sagittal plane and maximal flexion moment during the stance phase when walking on an ascending slope were significantly larger than when walking on a level surface ($p < .05$, table). Although there was no significant difference among the three different loading conditions, the flexion range of the knee during anterior-loaded backpack walking was significantly larger than that during the other two loading conditions. However, no significant difference was noted in the LDCOG, moments, and %iEMG results for the muscles examined among the different loading conditions.

Figure:

angles

(°)	maximum		minimum		range	
	no loading vs post.loading		no loading vs post.loading		no loading vs post.loading	
slope — hip	25.0 ± 3.8 *	28.6 ± 3.4	−18.1 ± 2.4 *	−19.8 ± 2.4	43.1 ± 3.0 *	48.4 ± 1.0
slope — knee	18.1 ± 5.3 *	27.5 ± 5.6	3.0 ± 4.5	3.2 ± 4.9	15.1 ± 2.8 *	24.3 ± 0.8
slope — ankle	−3.0 ± 7.0	−3.4 ± 6.8	−21.8 ± 8.4 *	−35.4 ± 9.0	18.9 ± 3.6 *	31.9 ± −2.3
	slope vs flat		slope vs flat		slope vs flat	
post.loading — hip	28.6 ± 3.4 *	18.7 ± 4.0	−19.8 ± 2.4	−20.1 ± 2.3	48.4 ± 1.0 *	38.8 ± 3.8
post.loading — knee	27.5 ± 5.6 *	31.1 ± 6.3	3.2 ± 4.9 *	1.2 ± 4.5	24.3 ± 0.8 *	29.9 ± 5.3
post.loading — ankle	−3.4 ± 6.7 *	−5.8 ± 6.0	−35.3 ± 9.0 *	−31.4 ± 7.2	31.9 ± −2.3 *	25.6 ± 5.4
	ant.loading vs post.loading		ant.loading vs post.loading		ant.loading vs post.loading	
flat — hip	18.3 ± 4.4	18.5 ± 3.2	−18.0 ± 2.7	−20.2 ± 2.4	36.3 ± 3.9	38.7 ± 2.8
flat — knee	35.9 ± 5.9	30.2 ± 4.9	0.1 ± 4.5	0.6 ± 5.1	35.8 ± 5.8 *	29.6 ± 4.0
flat — ankle	−5.8 ± 6.0	−6.2 ± 6.2	−32.9 ± 6.4	−31.9 ± 6.9	27.0 ± 4.5	25.7 ± 3.6

moments

(mmN)	maximum		minimum		range	
	no loading vs post.loading		no loading vs post.loading		no loading vs post.loading	
slope — hip	26.1 ± 6.8	27.3 ± 6.0	−49.3 ± 7.5 *	−61.2 ± 9.9	75.4 ± 9.9 *	88.5 ± 9.3
slope — knee	14.9 ± 5.1	15.0 ± 4.3	−41.0 ± 12.4 *	−62.4 ± 18.4	55.8 ± 13.1 *	77.4 ± 16.2
slope — ankle	87.9 ± 11.0 *	101.3 ± 11.4	−9.4 ± 3.0 *	−11.2 ± 4.6	97.3 ± 9.6 *	112.6 ± 6.9
	slope vs flat		slope vs flat		slope vs flat	
post.loading — hip	27.3 ± 6.0 *	12.9 ± 13.6	−61.2 ± 9.9 *	−69.4 ± 11.5	88.5 ± 9.3	82.3 ± 15.7
post.loading — knee	15.0 ± 4.3 *	4.1 ± 8.2	−62.4 ± 18.4	−61.6 ± 22.8	77.4 ± 16.2 *	65.7 ± 18.3
post.loading — ankle	101.3 ± 11.4 *	87.8 ± 16.8	−11.2 ± 4.6	−18.1 ± 13.5	112.5 ± 6.9 *	105.9 ± 10.0

Caption: A comparison of angles and moments at the hip, knee and ankle with and without loading backpacks during walking.

Conclusion: The study results suggest that loading of the backpack with weights at different locations (15% of body weight) may not affect the kinematic and kinetic body mechanics during walking. However, larger angular displacements in the lower extremity joints may be needed for the body to move forward when walking with a loaded backpack on an ascending slope. [A2] However, further studies, including assessments of the movement and muscular activity of the trunk under more-specific and precise biomechanical settings may, be needed to clarify the mechanism underlying different gaits when carrying a backpack.

References: [1]Tarkeshwar S et al, Gait Posture, 29:49-53, 2009.

[2]Al-Khabbaz YS et al., Gait Posture, 28:297-302, 2008.

Disclosure of Interest: None Declared

Motion Analysis

PO-0266

DATA CONSISTENCY ACROSS MULTIPLE GAIT LABORATORIES

Kenton Kaufman [1,*] Emily Miller [1] Trevor Kingsbury [2] Elizabeth Russell Esposito [3] Erik Wolf [4] Jason Wilken [3] Marilynn Wyatt [2]

[1]Orthopedic Surgery, Mayo Clinic, Rochester, MN, [2]Naval Medical Center-San Diego, San Diego, CA, [3]Center for the Intrepid, Brooke Army Medical Center, San Antonio, TX, [4]Walter Reed National Military Medical Center, Bethesda, MD, United States

Introduction and Objectives: Data reliability is of utmost importance when attempting to share data across sites to evaluate patient progress or to pool research data for comparative effectiveness studies. Twelve motion analysis laboratories found an average 15 degree difference for all parameters measured across sites and, between testing days at one site, five of eight parameters measured were significantly different [1]. This study raised concerns about comparing gait data across different laboratories. More recently, it has been demonstrated that it is possible to pool normative data between two gait analysis services [2]. However, the concern about inter-lab reliability still remains. Therefore, the purpose of this study was to evaluate consistency in 3-D gait measurements across three motion analysis laboratories.

Methods: Ten subjects (6 male/4 female, age 30 ± 6 years, BMI 24 ± 4 kg/m^2) without any neuro-musculoskeletal impairments were studied after signing an IRB approved consent form. Subjects traveled to the three foremost Department of Defense Medical Treatment Facilities to be studied. The marker set was applied by a single examiner at each site. The marker configuration, camera systems, and examiners differed across sites. Subjects walked at self-selected and Froude (0.16) speeds. Data were collected for five strides per side during a single session, and then this procedure was repeated for three separate sessions at each site. Data were processed with Visual 3D (C-Motion, Germantown, MD) at each site, de-identified, and sent to an independent evaluator for analysis. Inter-trial, inter-session, and inter-lab errors were quantified [3].

Results: It was possible to collect reliable data across labs for Froude walking speeds (see Table 1). Mean kinematics errors were <5 degrees and peak errors were <6 degrees. Mean kinetic data differed by <10% for the hip sagittal and frontal plane, 16% for the knee sagittal plane, and 4% for the ankle sagittal moments. Similar results were obtained for the self-selected walking speed.

Conclusion: This study demonstrates that high quality data can be collected from multiple gait laboratories, even while using different testing methodology. Previous work demonstrates that it is possible to minimize between session variability within a laboratory with quality assurance techniques and training [3]. This study demonstrated that differences in marker placement, marker sets, testers and collection environments between sites did not preclude the collection of consistent data.   A key to similarity between sites was use of identical anatomical segment definitions for the respective gait models. Measurement consistency across sites participating in multi-center research studies directly influences required sample size, level of detectable difference, and statistical power.

Table:

		Mean across Gait Cycle			Peak during Gait Cycle		
		Inter-trial	Inter-Session	Inter-lab	Inter-trial	Inter-Session	Inter-lab
Kinematics (degree)	Pelvic Tilt	0.67	1.14	2.21	0.80	1.27	2.45
	Pelvic Obliquity	0.41	0.73	1.18	0.52	0.90	1.77
	Pelvic Rotation	1.00	1.04	1.50	1.20	1.27	1.88
	Hip Flex/Ext	0.90	1.50	3.15	1.25	1.92	4.16
	Hip Ab/Ad	0.58	1.10	1.85	0.81	1.42	2.49
	Hip ER/IR	1.09	2.53	4.69	1.69	3.19	6.09
	Knee Flex/Ext	1.48	1.63	3.96	2.76	2.80	5.74
	Knee Var/Val	0.48	0.99	2.10	0.95	2.14	4.45
	Ankle PF/DF	0.93	1.10	2.50	2.00	2.09	4.16
	Foot Progression	1.39	1.69	2.41	2.34	2.60	3.80
Kinetics (Nm/kg)	Hip Flex/Ext	0.04	0.04	0.08	0.13	0.13	0.20
	Hip Ab/Ad	0.04	0.04	0.06	0.09	0.09	0.13
	Hip ER/IR	0.01	0.01	0.03	0.04	0.04	0.06
	Knee Flx/Ext	0.03	0.03	0.09	0.08	0.08	0.21
	Knee Var/Val	0.03	0.03	0.04	0.06	0.06	0.09
	Ankle PF/DF	0.04	0.03	0.05	0.10	0.09	0.13

Caption: Inter-lab Data Reliability: Mean and Peak Differences during the Gait Cycle

References: [1] Gorton GE et al. *Gait & Posture* 29:398-402, 2009

[2] Pinzone O et al. *Gait & Posture* 40:286-290, 2014

[3] Schwartz MH et al. *Gait & Posture* 20:196-203, 2004

ACKNOWLEDGMENTS

DISCLOSURE STATEMENT

Views expressed are those of the authors and do not reflect the official policy or position of the Department of the Army, Department of the Navy, Department of Defense, or the U.S. Government.

Disclosure of Interest: None Declared

Motion Analysis

PO-0267

INTRA-LIMB COORDINATION AS A VALUABLE PARAMETER TO DISTINGUISH GAIT ALTERATIONS IN DIABETIC INDIVIDUALS: A PRINCIPAL COMPONENT ANALYSIS APPROACH

Liu Yi [1,*]Cristina Sartor [2]Francis Trombini-Souza [2]Isabel Sacco [2]

[1]Federal University of Sao Paulo, Santos, [2]Physical Therapy, Speech and Occupational Therapy, University of Sao Paulo, Sao Paulo, Brazil

Introduction and Objectives: The more typically discussed biomechanical variables used to describe gait alterations in diabetic patients are: the reduced joint motion, mainly at the ankle, and the increased peak plantar pressure, commonly associated to ulcerations. Particularly the kinematic variables are usually interpreted alone, without considering their dynamical links between joints. In addition, some other motor aspects of diabetic gait could be exploit and thus revealed to be altered due to the global and symmetrical nature of the neuromuscular impairments of the diabetic neuropathy (DN). Intra-limb joint coordination during gait can offer valuable information about the changes that the diabetes might produce into the system, but it has seldom been addressed in diabetic population. Our aim is to identify the most representative kinematic and coordinative variables among patients with and without DN to identify how the disease affects the gait cycle. We are also interested in identifying if there would be variables that could distinguish between healthy and different stages of diabetes progression.

Methods: Thirty nine subjects between 45 and 65 years old were analyzed. According to the clinical evaluation of signs and symptoms of DN, the subjects were classified based in the Fuzzy model previously developed [1] into 3 groups: Control Group (CG = 13), Diabetic Group (DG = 13), Diabetic Neuropathic Group (DNG= 13). The Phase Angle for hip, knee and ankle joints during gait cycle were calculated ($\theta_{i = tan}^{-1} [y_i/x_i]$). Afterwards, the Relative Phase Angle (rpa) was calculated, consisting of a difference between distal and proximal joint Phase Angle ($\theta_{relative\ phase} = \Phi_{distal\ segment} – \Phi_{proximal\ segment}$). Principal Components Analysis (PCA), were performed from the data set enrolled by 101 points of the gait cycle x 88 cycles x 9 variables. The variables: (1-2-3) sagittal ankle, hip and knee angular displacements, (4-5-6) sagittal ankle, hip and knee velocities, (7) rpa ankle-hip, (8) rpa ankle-knee, (9) rpa knee-hip were considered. According to Kaiser criteria, a sample of 85 cycles could explain 60% of the variability of the data. In the present study we had 88 cycles per group. Therefore, the sum of the eigenvalues of the first two principal components was set at 70% [2,3]. To compare PCA´s eigenvectors between groups, two-way ANOVAs and Newman-Keuls post-hoc were applied ($p<0.05$).

Results: The variables that represented the largest variance of the gait cycle were: for the DG in the first PC - hip velocity (-0.15) and rpa ankle-hip (0.16); for the DNG in the second PC - rpa ankle-knee (0.15) and ankle velocity (-0.13); for the CG in the second PC – ankle velocity (0.14), rpa ankle-knee (0.17) and rpa knee-hip (-0.13). For PC1, CG was different from DG in the ankle, hip and knee velocities, rpa ankle-hip, rpa ankle-knee. We also found differences for the PC 1 between DG and DNG in the rpa ankle-angle, ankle and knee velocities. For PC2, CG was different from DG in ankle and knee angles, and rpa knee-hip. We found differences between DG and DNG in the rpa knee-hip for the PC 2.

Figure:

	PC1			PC2		
	CG	DG	DNG	CG	DG	DNG
	(a)	(b)	(c)	(d)	(e)	(f)
ankle angle	0.09(0.34)°	0.07(0.33)°,¶	-0.01(0.32)¶	0.01(0.016)?	0.04(0.20)?	-0.02(0.21)
knee angle	-0.09(0.34)	-0.09(0.35)	0.41(0.04)	0.08(0.26)?	-0.06(0.31)?	0.03(0.21)
hip angle	-0.04(0.21)	0.02(0.16)	-0.05(0.14)	0.12(0.35)	0.02(0.36)?	0.12(0.40)?
ankle velocity	-0.01(0.15)°	0.09(0.20)°,¶	0.01(0.21)¶	0.14(0.27)	0.06(0.28)	0.11(0.28)
knee velocity	0.06(0.23)°	-0.07(0.27)°,¶	0.04(0.18)¶	-0.12(0.41)	-0.04(0.40)	-0.14(0.44)
hip velocity	0.01(0.44)°	-0.15(0.42)°	0.06(0.47)	0.03(0.30)	-0.07(0.27)	-0.02(0.19)
relative phase ankle-hip	-0.01(0.41)°	0.16(0.42)°	0.06(0.46)	0.02(0.26)	0.08(0.20)	0.05(0.18)
relative phase ankle-knee	-0.06(0.25)°	0.1(0.28)°	-0.02(0.23)	0.17(0.43)	0.07(0.43)	0.15(0.45)
relative phase knee-hip	0.04(0.37)	0.04(0.31)	0.07(0.33)	-0.13(0.31)?	0.01(0.40)?,?	-0.1(0.35)?

O condition a is different from b; # condition a is different from c; ¶ condition b is different from c; ? condition d is different from e; π condition d is different from f; ?condition e is different from f;
For all interactions p = 0.05.
Letters a, b, c, d, e and f represent the groups conditions.

Caption: Mean, standard deviation and Eigenvectors values, in different groups of patients, for PC1 and PC2.

Conclusion: The most representative variables that can explain differences between gait of healthy, diabetic and diabetic neuropathic patients are related to the hip and ankle velocities, and also the coordination pattern between the ankle-hip and ankle-knee. The hip velocity and its coordination coupled with the ankle could be identified in diabetic patients, which still do not have the typical ankle and foot impairments. On the contrary, in the DN group, the coordination between ankle-knee and ankle velocity characterizes more their pattern. Sagittal kinematics of the lower limb is not a good variable to distinguish the studied groups, even in the most severe neuropathic patients. Since our sample was composed by patients that did not had an ulceration history, preventive actions should take into account the altered coordination between lower limbs that have not been described yet in this population. The traditional and expected restriction of joint motion, especially at the ankle, may be more relevant in patients that have major foot comorbidity.

References: [1] Watari et al., J Neuroeng Rehabil, 8: 11-11, 2014.
[2] Hair et al., Multivariate Analysis, 6ºed, 2009.
[3] Federaolf et al., J Biomech, 46(13): 2173-8, 2013.

Disclosure of Interest: None Declared

PO-0268

HOW DOES THE TOE STEP AFFECT BIOMECHANICAL CHARACTERISTICS OF LOWER LIMB IN PINNACLE TRAINER STEPPING?

Yu-Lin You [1,*] Yu-Chi Hsu [1] Hsiao-Feng Chieh [1] Chien-Ju Lin [1] Li-Chieh Kuo [2] Fong-Chin Su [1 3]

[1] Biomedical Engineering, [2] Occupational Therapy, [3] Medical Device Innovation Center, National Cheng-Kung University, Tainan, Taiwan, Republic of China

Introduction and Objectives: Exercise with fitness equipment is more popular in the recent years. Some of these fitness equipment acted as a close kinetic chain exercise [1], such as stationary bicycle, elliptical trainer and stair climber. Close kinetic chain exercise was performed as the foot fixed and knee motion is accompanied by motion at the hip and ankle [2]. This kind of exercise produced greater compression force and a greater antero-posterior force on knee compared with the open kinetic chain exercises [2]. In our previous study, we found participants stepped the pinnacle trainer (S770, SportsArt Fitness, Taiwan) at their comfortable and faster than comfortable speed appeared toe step movement during stepping at the terminal stepping phase rather than heel toe step together. Stepping the pedal with the toe only may involve more ankle strategy during stepping. The different strategies during stepping may result in different training effects and the biomechanical characteristics. The subjects had greater knee valgus moment during stepping pedal with trunk kept in a central position than the trunk medial-lateral shift [3]. Thus, the training effects of this stair climber on knee medial compartment osteoarthritis needs to be verified. However, in order to design proper exercise prescription for specific subject group, the investigation of biomechanical characteristics on different stepping strategies is needed.

Purpose: Thus, the purpose of this study was to investigate the differences of biomechanical characteristics between toe step and heel toe step together during stepping pinnacle trainer.

Methods: This study recruited 6 healthy participants who were excluded from musculoskeletal diseases. The mean age was 24.75 (1.50) years old, the mean height was 164.75 (11.70) cm, and the mean weight was 59.50 (15.33) kg. The stair climber (S770, SportsArt Fitness) was used. The loading level of this fitness equipment was set a level 1. The 3-D motion capture system (Raptor, Motion Analysis Corporation) was used to collect motion data during stepping the stair climber. A 6-axial force and torque sensor was used to collect foot contact force (Mini 85, ATI). Participants stepped this fitness equipment at their comfortable speed. There were two conditions, foot full contacts on the pedal (FC), and the other one condition was toe stepping (TS) at the terminal stepping phase. Every condition performed 5 trials and 15 seconds per trial. The cycle period contained the stepping phase which is a period when the pedal was at the highest position to the lowest of the track and the recovery phase which movement of pedal is inverse to the stepping phase.

Results: The ankle joint angle in sagittal plane showed a plantar flexion during TS condition at the terminal stepping phase. However, the FC condition showed a dorsiflexion at the terminal stance phase. The TS condition showed greater knee flexion angle than the FC condition. Both conditions showed a similar tendency in the hip joint angle in sagittal plane. In frontal plane, the TS condition had a greater inversion angle and a greater knee valgus angle. However, both conditions have a similar tendency in the hip joint angle in frontal plane. In joint moment comparison, the TS condition showed a greater plantar flexor and a greater hip extensor moment. Nevertheless, the knee extensor moment was smaller in the TS

condition compared to the FC condition. In the frontal plane, the TS condition showed a greater knee varus moment and a greater hip abductor moment, but a similar magnitude of ankle eversion moment.

Conclusion: This study investigated the differences of the biomechanics of the lower extremity between the TS and FC conditions. The current study identified the better stepping posture for exercise training for the different subject group. According to the results of knee joint moment in frontal plane, which showed a greater varus moment at terminal stepping phase in the TS condition than the FC condition. Thus, for the knee medial compartment osteoarthritis subject group, step with foot full contact on pedal may be recommended in order to decrease the medial compartment loading.

References: [1] Batte et al., J Sports Med Phys Fitness, 43: 300-305, 2003

[2] Michael et al., The American Journal of Sports Medicine, 24: 792-799, 1996

[3] Tsai et al., Int J Sports Med, 32:712-719, 2011

Disclosure of Interest: None Declared

A TEMPORO-SPATIAL EVALUATION OF A STANDARDISED REHABILITATION REGIME DESIGNED FOR AN ADULT CEREBRAL PALSY PATIENT

Ukadike C. Ugbolue [1,*]Fiona Henriquez [1]Philip Rowe [2]

[1]School of Science and Sport, University of The West of Scotland, Hamilton, [2]The Department of Biomedical Engineering, University of Strathclyde, Glasgow, United Kingdom

Introduction and Objectives: Cerebral Palsy (CP) is a perinatal disorder that is idiopathic in nature. As a consequence of growth this abnormality can progressively lead to secondary deficits such as bony deformities, muscle contractures, and gait abnormalities. [1] Although majority of the research in CP have been focused on children [1,2,3], there is a need to evaluate CP in adults so as to understand what changes occur with respect to their ambulation and joint mobility as they go about performing functional activities of daily living. Within our laboratory, a low cost two dimensional augmented video based portable system has been developed which can be used to evaluate CP gait as well as provide functional outcome measures that have strong clinical significance useful to clinicians and the allied health professionals. Indeed, there is still a dearth of knowledge with respect to how CP adults respond to functional activities of daily living. For that reason, it is necessary to design studies that can evaluate purposeful parameters leading to restoration of normal function and ability that describe functional deficits in response to routine activities of daily living. Therefore, the purpose of this pilot study was to evaluate a prescribed physiotherapy program designed for a cerebral palsy patient with mild walking difficulties.

Methods: This pilot study involved only one adult CP female patient aged 38 years old. The study monitored the patient throughout a rehabilitation process of prescribed exercise administered by a qualified physiotherapy practitioner. The study commenced from the onset of the rehabilitation process right through to the follow up session ten weeks after the baseline measurement. The study was laboratory based and performed at the biomechanics laboratory located at The University of The West of Scotland. The participant walked across a 6 metre long, high-contrast-grid vinyl mat while being video-filmed in the sagittal plane. Bi-directional temporo-spatial gait analysis and the production of sagittal plane estimates of joint kinematics were measured. This test was carried out on two occasions / time points (TP). TP1 was carried out prior to starting physiotherapy. TP2 was carried out ten weeks after starting physiotherapy. Seven strategically placed bulls-eye markers were placed on each heel, ankle, toe, knee and hip, covering ipsilateral and contralateral sides (Figure 1). Anthropometric measurements were obtained. The participant performed three gait cycles up and down the walkway grid mat barefoot at a self-generated walking speed. A three minute rest was observed. The participant performed three gait cycles up and down the walkway grid mat, this time wearing comfortable shoes (with splint) at a self-generated walking speed. The task orders were randomised. Video data was processed using the ProTrainer system (Sports Motion Inc®, Cardiff, CA) software. Descriptive statistics was applied. Step length variability was determined using the coefficient of variation (CV), where CV = (standard deviation / mean) x 100. The CV for the temporo-spatial measurement parameters were calculated using the mean of both legs averaged over all evaluated gait cycles.

Results: Both walking with splints and comfortable shoes and walking barefeet scenarios showed an increase in walking speed at TP2 for the left and right limbs (Figure 1). For the walking with splints and comfortable shoes task at TP2, the

percentage stance time reduced by 5% but increased by 0.5% during swing time. Conversely, the barefoot task showed a percentage stance time increment of 1.3% and a 1.3% swing time reduction at TP2. During the walking with splints and comfortable shoes task the CV for the left and right limb step length at TP1 (TP2) were 4.69% (2.13%) and 2.60% (4.53%) respectively. The CV for the left and right limb step length at TP1 (TP2) were 0.47% (4.97%) and 0.93% (10.39%) respectively for the barefoot task.

Figure:
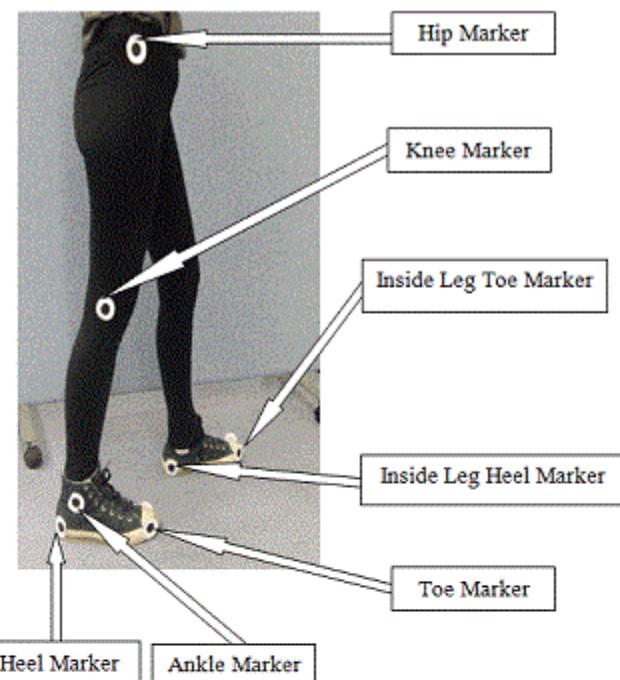
(a)

Parameters for TP1 and TP2	Walking with Splint and Comfortable Shoes	Walking Barefoot
Walking Speed (m/s) for Right Limb (Mean (SD))	TP1: 0.952 (0.001) TP2: 0.977 (0.001)	TP1: 0.821 (0.001) TP2: 0.881 (0.001)
Walking Speed (m/s) for Left Limb (Mean (SD))	TP1: 0.921 (0.003) TP2: 0.968 (0.001)	TP1: 0.843 (0.003) TP2: 0.868 (0.001)
Percentage (%) Stance Time	TP1: 67.18 TP2: 66.18	TP1: 65.38 TP2: 66.68
Percentage (%) Swing Time	TP1: 32.82 TP2: 33.32	TP1: 34.62 TP2: 33.32
Right Limb Step Length (cm)	TP1: 58.15 (1.50) TP2: 60.48 (2.74)	TP1: 53.49 (0.50) TP2: 55.43 (5.76)
Left Limb Step Length (cm)	TP1: 58.37 (2.74) TP2: 57.71 (1.25)	TP1: 52.60 (0.25) TP2: 50.30 (2.50)

(b)

Caption: Figure 1: (a) Volunteer marked with black-and-white bull's eye markers (b) Measurement outcome parameters for Adult CP pilot study at different time points (TP).

Conclusion: The spatial parameters showed low levels of CV. The percentage stance and swing time temporal parameters showed variable results at TP1 and TP2 when both tasks were performed. In terms of consistency between tasks and TPs, walking speed appears to be a variable outcome measure useful for evaluating the efficacy of the administered standard rehabilitation regime.

References: [1] Gage JR et al., J Pediatr Orthop B, 10, 265-74, 2001.

[2] Massaad A et al., Gait Posture, 39, 354-8, 2014.

[3] Domagalska M et al., Gait Posture, 38, 1038-43, 2013.

Disclosure of Interest: None Declared

PO-0270

THE EFFECT OF SCHOOL TROLLEY LOAD ON SPATIOTEMPORAL GAIT PARAMETERS OF CHILDREN

Eva Orantes-González [1,*] Jose Maria Heredia-Jiménez [1] Victor Manuel Soto-Hermoso [1]

[1]Physical Education and Sport, University of Granada, Granada, Spain

Introduction and Objectives: Every day children have to carry a backpack full of books to school, which has traditionally been the most common modality of transport(1). Transporting a backpack over one or two shoulders has been widely studied. Changes in gait, energy expenditure and balance have been analysed with backpacks of different loads(2-6). Recently, a new form of carrying backpacks has appeared on the market: wheeled backpacks or school trolleys(7). Our research in the literature has not found any investigation in respect to gait when using school trolleys. The increase in the use of school trolleys has made a deeper and wider knowledge about this mode of school transport children. It becomes more important as children experience significant growth and motor development(6). Therefore, the purpose of this study was to determine the effect of using a school trolley with different loads on spatio-temporal gait parameters of children on students of a primary school.

Methods: Fourteen students of a primary school(aged 11.43 ± 0.51 years) participated in this study. The average body weight was 35.06 ± 10.07kg and average body height was 1.42 ± 0.09m. To analyse the effect of increased loading on school trolleys, we used four conditions: without trolley (represented 0% body weight)(0%BW), 10%, 15% and 20%BW. The different loads were achieved filling the trolley with books of different weights. Each child was weighed and measured(SECA769,Hamburg,Germany). After, subjects completed 5 trials walking comfortably along a pressure mat(GAITRite system;CIR Systems Inc.,NJ,USA) without trolley and 5 trials walking with the 3 load conditions (10%,15% and 20%BW) in a randomized order. The mat was positioned on the centre of the walkway and cones were placed at 3 metres from the start and the end of the mat to be sure that arrived with a stable gait. Spatiotemporal parameters were analysed: velocity(cm/s); cadence(steps/min); stride length(cm), swing (%Gait Cycle)(%GC), stance (%GC), single support (%GC) and double support phase(%GC). Analysis of data was done with SPSS(SPSSv.20, SPSS Inc., Chicago IL). The Shapiro Wilk´s test was used to test normal sample and repeated measures ANOVA to compare the different load conditions.Bonferroni test was applied for pair comparison. Level of significance was set at $p < 0.05$.

Results: Results showed a non-significant difference in velocity and stride length when children walked without a school trolley compared with pulling it with the different loads($p=0.116$;$p=0.773$ respectively). With respect to cadence, showed significant increase comparing 10, 15 and 20%BW load conditions with control level(0%BW)($p<0.001$;$p=0.002$;$p<0.001$respectively).Comparing with control level, swing and single support phase decreased significantly when load increased and stance and double support phase significantly increased when load increases(fig.1). None of the gait parameters studied showed significant differences between load conditions(10% and 15%>20% nor between 15% and 20%BW).

Figure:
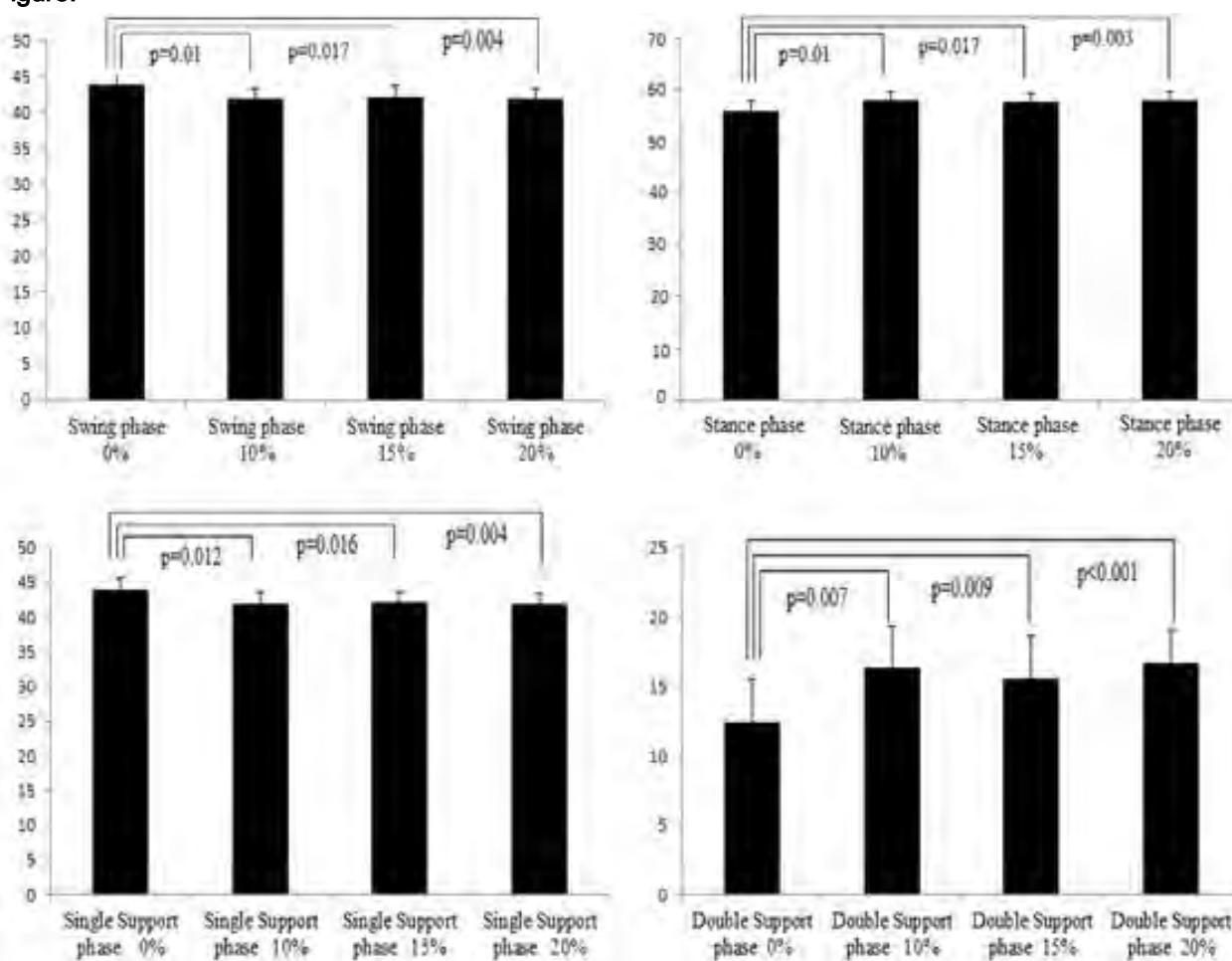
Caption: Figure 1. Swing phase (%); stance phase (%), single support (%) and double Support (%).

Conclusion: Gait parameters related to pulling school trolleys with different loads have not been investigated before to our knowledge. Pulling a school trolley with 0%,10%,15% and 20%BW did not affect velocity and stride length.Previous studies have analysed the transport of asymmetrical loads obtaining lower velocity when children walked with 17%BW in a backpack carried in their hands(8).Cadence significantly increased when children carried 10, 15 and 20%BW when compared with no load conditions. That motivated a non-significant increase in velocity because the children used to adjusted their cadence to effect the change in speed. Stance and double support phase were higher when children walked in the three load conditions compared with no load. Kellis and Arampatzi(8) explained this increasing because when children walked with a loaded school trolley increase the instability and they have to increase the stance and double support phase to maintain their balance (9). Consequently it produced a decrease in the swing and single support phase when load was higher compared with no load conditions. We would highlight that in none of the spatio-temporal gait parameters analysed in this study showed significant changes between 10% and 15%BW,10 and 20%BW and nor between 15 and 20%BW conditions. So carrying a school trolley with a load produces significant changes with respect to normal gait, but increasing load(range to 10-20%BW)did not produce significant differences in gait parameters.

References: [1]Pau et al.,HFES,57:501-505,2013.

[2]Hong et al.,Gait posture,17:28-33,2003.

[3]Hong et al.,Gait posture,22:63-68,2005.

[4]Hong et al.,Ergonomics,43:717-727,2000.

[5]Motmans et al., Ergonomics,49:127-138,2006.

[6]Pascoe et al.,Ergonomics,40:631-641,1997.

[7]Forjuoh et al.,Am J Phys Med Rehabil,82:261-266,2003.

[8]Kellis et al.,J Pediatr Orthoped,18:275-282,2009.

[9]Hillman et al.,Gait posture,29:81-85,2009.

Disclosure of Interest: None Declared

Motion Analysis

PO-0271

RELIABILITY OF A MARKER-BASED LOCATOR FOR MEASURING IN VIVO THREE-DIMENSIONAL SCAPULAR POSES USING STEREOPHOTOGRAMMETRY

Mei-Ying Kuo [1] [2],*Tung-Wu Lu [2] [3]Jia-Da Li [2]

[1]Department of Physical Therapy, China Medical University, Taichung, [2]Institute of Biomedical Engineering, [3]Department of Orthopaedic Surgery, School of Medicine, National Taiwan University, Taipei, Taiwan, Republic of China

Introduction and Objectives: Accurate measurement of the three-dimensional (3D) scapular kinematics is essential for a better understanding of the mechanical interactions between the scapular and the other segments of the shoulder complex. However, precise measurement of the scapular kinematics is difficult because the scapular moves greatly underneath the skin during dynamic activity. Previous studies have used magnetic tracking devices with a scapular locator to measure the poses of the scapula [1]. Since skin marker-based stereophotogrammetry has been widely used for motion analysis in basic research and clinical applications, there is a need to develop such locators for measuring scapular poses. Therefore, the purposes of the study were (1) to development a marker-based scapular locator for measuring scapular poses and (2) to determine the intra-rater and inter-rater reliability of the locator.

Methods: An adjustable marker-based scapular locator was developed and used to measure the scapular poses by pointing to the root of spine (RS), the inferior angle (IA) and the acromial angle (AA) of the scapular with its three legs (Fig. 1). Twenty-two healthy volunteers without shoulder pathologies participated in the current study with informed written consents as approved by the IRB. Each subject was tested separately by two raters (A and B) using the marker-based scapular locator while performing static shoulder flexion at 20, 40, 60, 80, 100 and 120 degrees in the sagittal plane. The marker positions were measured using a seven-camera motion analysis system (Vicon 370, Oxford Metrics, U.K.) at 60Hz. The reliability models, ICC $_{(2, k)}$ and ICC $_{(3, k)}$, were used to analyze the intra-rater and inter-rater reliability for scapular of positions of the AA, RS and IA and the three scapular rotations. An ICC value of 0.8 to 1.0 indicates a very good reliability, 0.61-0.8 good, 0.41-0.6 moderate, and below 0.2 is a poor reliability. All statistical analysis was performed using SPSS 13.0 (SPSS Inc., Chicago, USA).

Results: For the intra-rater reliability, the ICC ranged from 0.81-0.97 and 0.89- 0.99 for rater A and rater B for the scapular rotations in each arm elevation position. The ICC ranged from 0.88 to 0.99 by the two raters for the positions of the AA, IA and RS for shoulder flexions at 20, 40, 60, 80, 100 and 120 degrees in the sagittal plane. For the inter-rater reliability, the values of the ICC ranging from 0.92 to 0.99 were found for scapular rotations and positions for shoulder flexion at 20, 40, 60, 80, 100 and 120 degrees in the sagittal plane.

Figure:

Caption: The three legs of the marker-based scapular locator can be moved to point to the AA, RS and IA of the scapula, and then fixed by the bolts.

Conclusion: The results showed that very high intra- and inter-rater reliability for scapular rotations and for the AA, RS and IA positions were achieved using the locator. Two main reasons led to this effect: (1) design of the scapular indicator and (2) careful palpation of the bony landmarks over the scapula. The new design of the marker-based scapular locator overcame the limitation of three-point scapular locations [1], which was unable to adjust three pointers to adapt different size of the scapula. The current results show that the new locator is helpful and reliable in the measurement of the scapular poses for research and clinical applications.

References: [1]   Johnson et al, Clinical Biomechanics. 8: 269-273, 1993.

Disclosure of Interest: None Declared

Motion Analysis

PO-0272

THE EFFECTS OF LOAD CARRIAGE AND SPEED ON THE BIOMECHANICAL RESPONSES OF THE SOLDIER DURING UPHILL, DOWNHILL AND LEVEL WALKING

Caley Chaplin [1,*]Heinrich Nolte [1]

[1]Research and Development, Ergonomics Technologies, Pretoria, South Africa

Introduction and Objectives: Load carriage systems (LCS) are used to transport equipment and supplies over extensive distances and unpredictable terrain, especially in a military application. The advancement in technology has resulted in soldiers carrying loads that very often exceed 50% of body weight. LCS impact soldier performance and combat readiness and therefore an understanding of the physiological and biomechanical impact on the soldier is crucial in preventing injuries and enhancing performance. The majority of load carriage research has focused on the physiological effects but more recently there has been a shift in focus to the biomechanical impact. There is a lack of evidence however explaining the linear kinetics of walking downhill with a load and how this compares to walking level and uphill. Increases in ground reaction forces (GRF) and changes to the typical gait pattern as a result of additional loads and change in gradient have been linked to the cause of overuse injuries such as shin splints, blisters and stress fractures (Birrell et al., 2010). The objective of this study is to therefore determine the effects of load, speed and gradient on the biomechanical responses of the soldier. These findings will contribute to understanding the mechanisms of gait and reducing biomechanical stress placed on the body to prevent injuries specifically during downhill walking.

Methods: Sixteen soldiers (14 males and 2 females) walked on an instrumented treadmill at two speeds of 4km/h and 5km/h with and without a load on their back at decline (-10%), flat (0%) and incline (+10%) gradients. The load consisted of a military type backpack external frame with shoulder straps and a hip belt and 35kgs of barbell weights placed between the shoulder blades at the level of the 4th thoracic vertebra. The Qualisys Motion Capture System was used in conjunction with the Bertec™ Instrumented Treadmill to obtain the kinetic and kinematic responses of the soldiers. However, this paper will only discuss the linear kinetics during downhill walking. All force data was normalized according to body mass and additional load carried and analyzed using STATISTICA Version 12.

Results: Decline walking resulted in significant increases in peak loading rates, impact peak loads, braking forces and significant decreases in propulsive forces when compared to level and incline walking. Decline walking resulted in the first peak GRF to be 11% higher than incline walking and the second peak GRF to be 16% lower than incline walking. Walking at 5km/h compared to 4km/h resulted in significant increases in peak loading rates and impact peaks. The peak loading rates, vertical impact peak and anterio-posterior braking forces were significantly lower during the loaded condition compared to the unloaded condition during downhill walking. In addition, the first half of the stance phase was found to be significantly longer when carrying a load during level and decline walking which explains the reduction in forces during load carriage.

Caption: Figure 1: The mean peak loading rate (N/s/kg) during level, uphill and downhill walking with and without a load

Conclusion: Previous research (McNally, 2010) has identified uphill walking as significantly more physiologically taxing than downhill walking and therefore a key factor in regulating walking speed during a military route march. However the

significantly larger GRFs measured during downhill walking suggest that a reduction in speed can be used as an effective strategy in reducing these high forces and risk of injury. The findings from this study highlight the importance of pacing strategies as an effective technique to mitigate forces especially during loaded downhill walking. An increased stance time was found during load carriage when walking downhill suggesting that individuals adopt protective mechanisms to mitigate additional force. Additional strategies such as increased muscle activation; greater joint flexion (Polcyn et al., 2002) and postural adaptations may also be used to increase absorption of force when carrying additional loads. LCS design should focus on reducing the impact peak and maximum braking force as this has been strongly associated with the development of acute and overuse injuries (Birrell et al., 2010). These findings can be used to provide recommendations on safe load carriage practices to the military in order to enhance soldier performance and reduce the risk of injuries to the lower body.

References: [1] Birrell, S. et al., 2010. The effect of load distribution within military load carriage systems on the kinetics of human gait. Applied Ergonomics, 41: 585-590.

[2] Polcyn, A.F et al., 2002. The effects of weight carried by soldiers: combined analysis of four studies on maximal performance, physiology and biomechanics. US Army Research Institute of Environmental Medicine, Natick.

[3] McNally, M.P. 2010. Positive vs negative muscle work of non-level walking in lean and obese adults. Master thesis, Department of Exercise and Sport Science.

Disclosure of Interest: None Declared

DEVELOPMENTAL PROCESS OF "FORESEE-MOVEMENT" IN YOUNG CHILDREN CATCHING A BOUNCING BALL

Mami Umemoto [1,*]Chiaki Ohtaka [2]Motoko Fujiwara [3]

[1]Human Behavioarl Sciences, Guraduate School of Humanities and Sciences, [2]Human Sciences, Guraduate School of Humanities and Sciences, Nara Women's University, [3]Faculty of Human Life and Environment, Nara Women's University, Nara, Japan

Introduction and Objectives: The period of childhood is important for the development of fundamental movement. Exercise during this period promotes nervous system development for exercise performance and can affect movement abilities in adolescence. Young children acquire a variety of movement through play and activity in their daily lives. Children also acquire the abilities to anticipate the movement of a target or to estimate their own movement. We define "foresee-movement ability" as the abilities to anticipate and estimate. The purpose of this study was to examine the developmental process of "foresee-movement" in young children catching a bouncing-ball.

Methods: The participants were 139 children between 3 and 5 years old (3-year-old children: 23, 4-year-old children: 56, 5-year-old children: 60). The tasks were to catch a bouncing ball in following two manners. One was a straight-line task. In this task, an experimenter dropped the ball from a height of about 1.6m from the floor at a point 1m in front of the participant. The participant was told to move to the drop point and catch the ball after the first bounce. The other task was parabolic-line task. In this task, an experimenter threw the ball to a height of about 1.6m from the floor toward a drop point 2m in front of the participant. The participant was told to move forward 1m and catch the ball after the first bounce.
The participants' catching movement was recorded from the right side by video cameras.

We analyzed four items in the data. First, we divided catching movement by success or failure. If the participants were able to catch the ball before the second bounce, it was considered a success; the other trials were classified as failures. Second, we analyzed "Total motion time" between the beginning of the motion to catching the ball. "Total motion time" was divided into two phases, "Estimate time" "Movement time" with a border, the beginning of the participant's motion. Third, we checked the distance of the catching point. Finally, we classified "Catching Movement-pattern" into some categories based on active or still, success or failure to catch the ball, and manner of catching.

Results: The catching rates increased with age in both tasks. The straight-line task had a higher success rate than the parabolic-line task (Figure 1).
The catching movement-pattern was classified into six patterns: (1) no movement, (2) the ball bounced once and passed over the head, (3) the ball was caught after two bounces, (4) an attempt was made to catch the ball after one bounce, but the ball could not be touched, (5) an attempt was made to catch the ball after one bounce, but the ball was knocked away, and (6) the ball was caught after one bounce.
In the straight-line task, the total motion time and the movement time shortened in accordance the participant's age of the moon. Patterns 3–5 accounted for many aspects of the movement-pattern of 3-year-old and 4-year-old children.

In the parabolic-line task, the total motion time and the movement time shortened with participant's age of the moon, and the estimate time lengthened. The movement-pattern of the 3-year-old and 4-year-old children was classified into patterns 1–3. Many of the movement-patterns in the 5-year-old children, on the other hand, were classified as pattern 5.

In both the straight-line and parabolic-line tasks, the catching movement was done around the highest point after the first bounce. Movement-pattern 6 was significantly increased from 4-year-old through 5-year-old children.

Figure:
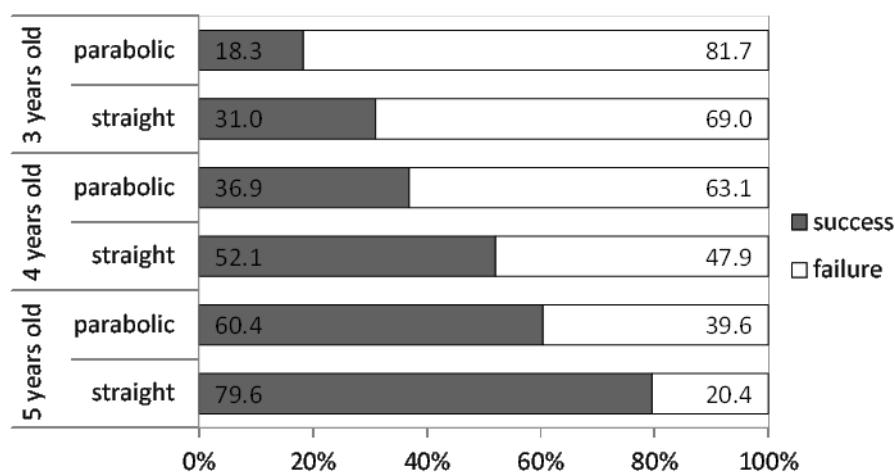
Caption: Figure 1. The catch success rate with the age in parabolic- and straight-line tasks.

Conclusion: The specific characteristics of young children's movements include catching at the high point above the neck. It is obvious that young children are able to anticipate the track of the ball and estimate their own movement increasingly with age. Foresee-movement is gradually developed along with age even if catching movement is classified as failure-pattern.

Multi-dimensional spatial expectation—for example, the parabolic-line task—is difficult for 3-year-old. We suggest that 3-year-old children start simple tasks or interact with the ball and that ball play should be adopted with orbital prediction after 4-years-old.

Disclosure of Interest: None Declared

KINETIC ANALYSIS OF ROTATIONAL MOVEMENT OF LOWER TRUNK IN BASEBALL TEE-BATTING

Kazumichi Ae [1,*] Sekiya Koike [2]

[1]School of Sport, Exercise and Health Sciences, Loughborough University, Loughborough, United Kingdom, [2]Faculty of Health and Sport Sciences, University of Tsukuba, Tsukuba, Japan

Introduction and Objectives: A baseball batter is required to increase bat-head speed as much as possible to hit a long ball. The bat-head speed is generated by utilizing a kinetic link transferring energy up from the lower extremities through successive body segments (Welch et al., 1995). In order to make clear the effective movements of the lower extremities, kinetic analyses of the lower extremities have been reported by evaluating the pattern of ground reaction forces. Although, Takagi et al. (2010) analyzed the kinetic features of the lower extremities on torso motion under different ball speeds condition in order to clarify the mechanisms of the trunk rotation; the study focused on the mechanical power at the individual hip joints. It is, therefore, still unclear how the individual hip joints contribute the rotational movement of the lower trunk. The purpose of this study was to investigate the kinetic mechanisms of the trunk rotation in baseball tee-batting.

Methods: Ten male collegiate baseball players (age: 20.7±1.1 yrs., height: 1.75±0.05 m, weight: 76.3±7.1 kg, athletic career: 12.7±2.7 yrs.) participated in this study. They performed baseball tee-batting with a middle ball height (belt height) condition. Three-dimensional coordinate data were captured with a motion capture system (VICON MX+, 16-cameras, 250 Hz). Ground reaction forces of individual feet were measured with force platforms (1000 Hz). The joint kinetic data of the individual lower extremities were calculated using inverse dynamics. The equation of rotational motion of the lower trunk segment can be expressed as follows:

$$I_{LT}\alpha_{LT}+\omega_{LT}\times(I_{LT}\omega_{LT})=N_{PS,Hip}+N_{SS,Hip}-N_{Trk}+N_a+N_b+N_c$$

$$N_a=r_{LTcg-PS,Hip}\times F_{PS,Hip}, \ N_b=r_{LTcg-SS,Hip}\times F_{SS,Hip}, \ N_c=-r_{LTcg-Trk}\times F_{Trk}$$

(LT: lower trunk, PS: pivot side, SS: step side, Trk: trunk, cg: center of gravity)

where I_{LT} is the moment of inertia of the lower trunk segment, α_{LT} is the angular acceleration of the lower trunk segment, ω_{LT} is the angular velocity of the lower trunk segment, r_{LTcg-i} is the vector from the cg of the lower trunk segment to individual joint center, $I_{LT}\alpha_{LT}+\omega_{LT}\times(I_{LT}\omega_{LT})$ is the inertial moment, $N_{PS,Hip}$, $N_{SS,Hip}$, N_{Trk} are individual joint torques, and N_a, N_b, N_c are individual moment caused by the joint forces. In addition, the coupled force ($r_{LTcg-i}\times F_{cf,i}$, CF: coupled force) of the joint force at the individual hip joints was estimated.

These kinetic data of all subjects were normalized by the time of the step-side foot contact to the ball impact as 0 to 100%. The period was divided into two phases (1st phase: 0-50%, 2nd phase: 50-100%) for the analysis and description of data.

Results: Figure 1 shows the averaged patterns of Z axial moment about the lower trunk segment. The trunk joint torque (N_{Trk}) had a significant negative value among the other joint torques, and the peak value was observed at 40% time. The pivot-side hip joint torque ($N_{PS,Hip}$) was almost constant value. The step-side hip joint torque ($N_{SS,Hip}$) increased until around 30% time and decreased gradually around 70% time, and then changed to a negative value. The moment caused

by the step-side hip joint force ($r_{LTcg\text{-}SS,Hip} \times F_{SS,Hip}$) increased from 40% to 80% time and became the greatest value among the moments caused by other joint forces. Table 1 indicates the averaged values of Z axial components of moment exerted on the lower trunk segment in the phases. In the first phase, the joint torques were greater than the moments caused by joint forces, and trunk joint torque (N_{Trk}) showed a significant negative value. The coupled force at the individual hip joint force terms was small and was similar to the value of the trunk joint force term. In the second phase, the trunk joint torque also had a significant negative value, and the step-side hip joint torque decreased significantly. The moments caused by the hip joint forces and the coupled force included in the hip joint force were greater than those values in the first phase.

Figure:
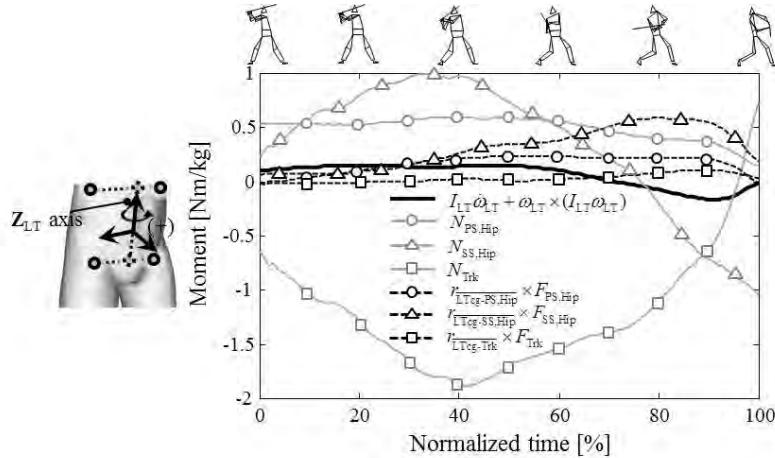
Caption: Figure1 Averaged patterns of the Z axial moment about the lower trunk segment ((+): batted ball's direction, (-): catcher's direction).

Conclusion: We focused on the relationship between the individual hip joints and the rotational movement of the lower trunk segment because the hip joint torques were greater than the other joint torques. It was clear that the torques of both hip joints contributed largely to the generation of Z axial moment of the lower trunk segment.

Table:

	1st Phase	2nd Phase
$I_{LT}\alpha_{LT}+\omega_{LT}\times(I_{LT}\omega_{LT})$	0.124	0.002
$N_{PS,Hip}$	0.535	0.442
$N_{SS,Hip}$	0.723	0.077
N_{Trk}	-1.303	-1.177
$r_{LTcg\text{-}PS,Hip} \times F_{PS,Hip}$	0.090	0.195
$r_{LTcg\text{-}SS,Hip} \times F_{SS,Hip}$	0.097	0.423
$r_{Trk} \times F_{Trk}$	-0.017	0.041
$r_{LTcg\text{-}PS,Hip} \times F_{CF,PS,Hip}$	0.019	0.166
$r_{LTcg\text{-}SS,Hip} \times F_{CF,SS,Hip}$	0.019	0.166

Caption: Table 1 Averaged values of the Z axial components of moment exerted on the lower trunk segment in the phases (Unit:Nm/kg, (+): batted ball's direction, (-): catcher's direction).

References: [1] Welch and Draovich, J. Orthop. Sports Phys. Ther., 22(5): 193-201, 1995.

[2] Takagi et al., J. Society of Biomechanisms, 34(2): 216-224, 2010 (in Japanese).

Disclosure of Interest: None Declared

Motion Analysis

PO-0275

DEFINING MIDSTANCE IN DIFFERENT POPULATIONS

Catriona M. Kerr [1,*] Julie Stebbins [2] Amy Zavatsky [1]

[1]Engineering Science, University of Oxford, [2]Oxford Gait Laboratory, Nuffield Orthopaedic Centre, Oxford, United Kingdom

Introduction and Objectives: Event-driven analysis of the gait cycle avoids the effects of time averaging. Midstance is one such event; however, this event has many definitions:

- Halfway between foot contact and foot off. This may not represent a comparable point in different subjects, particularly those with pathology. Also, patients who drag their feet do not show clean foot strike and foot off events.
- The instant where the long axis of the tibia is vertical.
- The time at which the foot is most flat, though this may represent an extreme posture.
- The Vertical Ground Reaction Force (VGRF) allows the finding of a local minimum (which closely corresponds to the maximal vertical body height).

The aim of this study was to compare these definitions as applied to data from different populations seen in a clinical gait laboratory and to identify an event-driven, kinematically-repeatable time-point during the foot flat period of midstance.

Methods: Six populations (n=203) were included in this study (Table). Retro-reflective markers were applied to the feet and limbs at known anatomical landmarks [1]. 12-16 infra-red cameras (Vicon-MX, Oxford, UK) were used to track the marker positions (100 Hz), alongside 3 AMTI force-plates (Advanced Mechanical Technology, Inc., Watertown, MA, USA) collecting VGRF data (1000 Hz). Data was recorded for at least three separate walking trials with clean force-plate strikes per limb. Trials were processed using Vicon Nexus software. Small gaps were handled by interpolation using cubic splines [2] or by assuming constant distance between markers on the same segment [3]. A Woltring filtering algorithm was used [4]. Foot strike and foot off events were determined using VGRF where possible (else manually). Thigh wand offsets were iteratively determined (minimising ab-/ad-duction occurring at the knee) [5].

Halfway between foot strike and foot off was defined as 50% stance. The vertical tibia event was when the tibial segment first became vertical in the sagittal plane. The time at which the vertical sum of all foot mounted markers was closest to zero was defined as the flattest foot event. The first and second VGRF peaks closest to 25% and 80% stance were identified from VGRF data smoothed with a moving average filter with a span of 5 frames. The minimum VGRF between these events was the fourth definition. For each definition, 14 lower-limb kinematic angles and the intra-subject and inter-subject variability were calculated:

Intra-subject variability$_{event, population}$ = Σ_{angle} (mean$_{subject}$ (s.d.$_{trials}$(x)));

Inter-subject variability$_{event, population}$ = Σ_{angle} s.d.$_{subject}$ (median$_{trials}$(x));

Where *x* refers to the kinematic angle found for a subject, event, and trial. The sub-scripts indicate to which set of data the operation should be applied.

Results: All events in all populations occurred on average prior to 50% stance (Figure), especially vertical tibia and flattest foot. Adult females demonstrated most intra-subject variability, adults with crouch gait the least. Idiopathic toe walkers were the most variable inter-subject.

Figure:
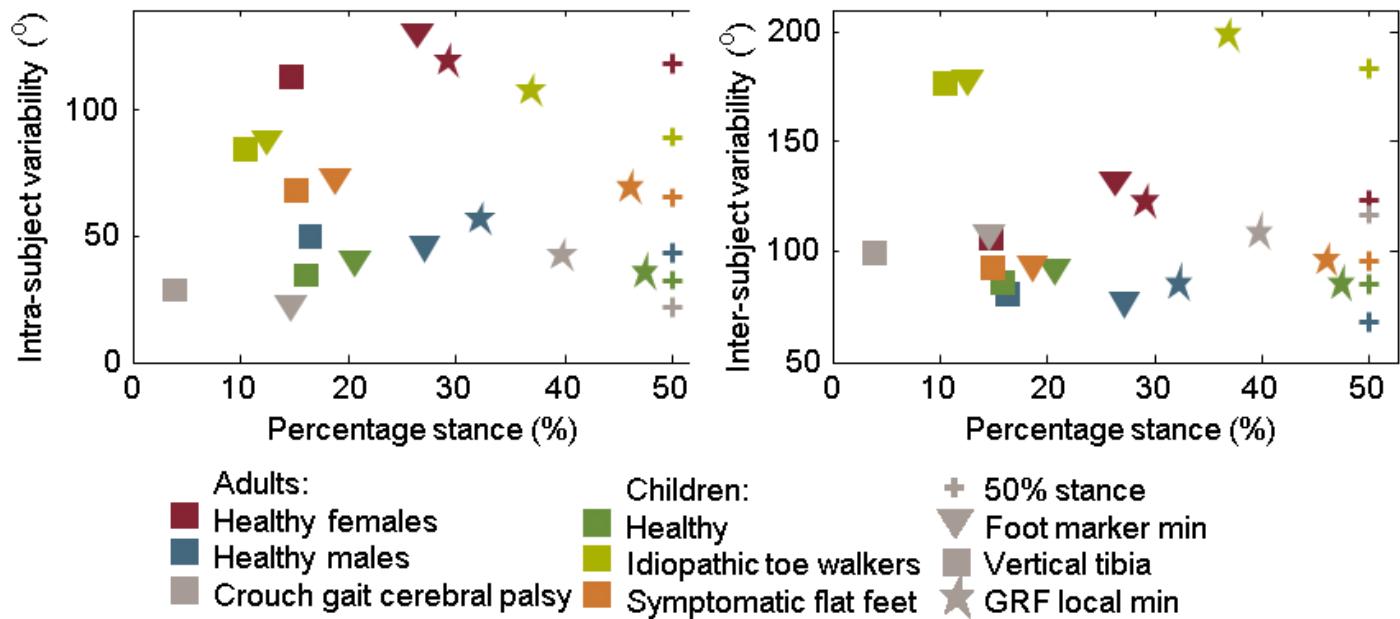
Caption: Intra- and inter-subject variability per group.

Conclusion: This study investigated the timing and variability of lower-limb posture using 4 midstance definitions and 6 subject groups.

The timing of vertical tibia was the earliest, particularly amongst those with crouch gait (probably due to knee flexion). The foot marker sum also occurred early in stance; this may be related to the larger VGRF in early stance. The VGRF minimum timing was closer to 50% stance.

Intra- and inter-subject variability was more different between groups than between midstance definitions. Adult females had the most intra-subject variability; mostly in ankle and foot angles. Those with crouch gait had least variability across all midstance definitions. This may reflect differences in angular range of motion. Inter-subject variation was greatest for toe walkers; this was due to ankle and hallux flexion variation. The increased variability may reflect differing degrees of equinus severity.

This investigation into the variability and timing of four midstance definitions revealed the study group to be an important factor. Vertical tibia and flattest foot midstance definitions describe a point early in stance, sometimes within the double support phase, making them less suitable midstance events. VGRF minimum and 50% stance are closer in time, and similar in variability.

Table:

Adults		Children	
Healthy_Female	n=22	Normal	n=88
Healthy_Male	n=21		
Crouch_Gait_Cerebral_Palsy	n=22	Idiopathic_Toe_Walker	n=31
		Symptomatic_Flat_Feet	n=19

Caption: Groups in the study.

References: [1] Stebbins et al., Gait & Posture, 23(4):401410, 2006.

[2] Muijtjens et al. J. Biomech., 30(1):95-98, 1997.

[3] Desjardins et al., Medical Eng. & Physics, 24(6):437-440, 2002.

[4] Woltring, Adv. in Eng. Softw., 8(2):104-113, 1986.

[5] Baker et al., Hum. Mov. Sci., 18(5):655-667, 1999.

Disclosure of Interest: None Declared

EFFECTS OF OBSTACLE HEIGHT ON THE JOINT MOMENTS OF THE LOWER EXTREMITIES WHEN CROSSING OBSTACLES WITH HIGH-HEELED SHOES

Kao-Shang Shih [1] [2],[*]Hui-Lien Chien [3]Tung-Wu Lu [3] [4]

[1]Shin Kong Wu Ho-Su Memorial Hospital, Department of Orthopedic Surgery, Taipei City, [2]School of Medicine, Fu-Jen Catholic University, New Taipei City, [3]Institute of Biomedical Engineering, National Taiwan University, [4]Department of Orthopaedic Surgery, School of Medicine, National Taiwan University, Taipei City, Taiwan, Republic of China

Introduction and Objectives: In modern society, many women wear high-heeled shoes in both professional and social settings. High-heeled shoes with a reduced support base increase the difficulty of maintaining balance, and thus the risk of falling, leading to injuries such as fracture and ankle sprains. This challenge is increased by the presence of obstacles. Apart from the precise end-point control for sufficient foot-obstacle clearance of the swing limb, a successful and safe obstacle-crossing also requires the stability of the body provided mainly by the stance limb. Loss of balance is one of the major causes of falls during ambulation while negotiating obstacles. The purpose of the present study was to investigate the influence of obstacle height on the joint moments of the lower extremities when crossing obstacles with high-heeled shoes.

Methods: Twelve female wearers (age: 24.3±3.8 years; height: 157.3±4.8 cm; mass: 48.8±4.6 kg) participated in the current study with informed written consent, as approved by the Institutional Research Board. They crossed obstacles with heights of 10%, 20% and 30% of their leg lengths when wearing high-heeled shoes. The high-heeled shoes were narrow-heeled (heel base: 2.0 cm x 1.6 cm; heel heights: 6.3 cm) and were commercially available. Each subject wore 39 retroreflective markers for tracking motions of the body segments. The kinematic data were measured using a 7-camera motion capture system (Vicon 512, OMG, UK) and the ground reaction forces were measured using two forceplates (AMTI, USA) placed on each side of the obstacle. Six successful trials, three for each limb, were obtained. With the measured GRF and kinematic data, inverse dynamics were used to calculate the intersegmental moments at the lower limb joints. Inertial properties for each body segment were obtained using Dempster's coefficients. The joint moments of the trailing limb when the leading toe was above the obstacle were extracted and analyzed using one-way repeated measures ANOVA. Whenever a height effect was found, a polynomial test was performed to determine the linear trend. All significance levels were set at α=0.05. SPSS version 17.0 (SPSS Inc., Chicago, USA) was used for all statistical analyses.

Results: When the leading toe was above the obstacle, subjects showed linearly increased knee extensor moments but linearly reduced ankle plantarflexor moments with increasing obstacle height (Table 1). Abductor moments at the hip and knee were also reduced linearly.

Figure:
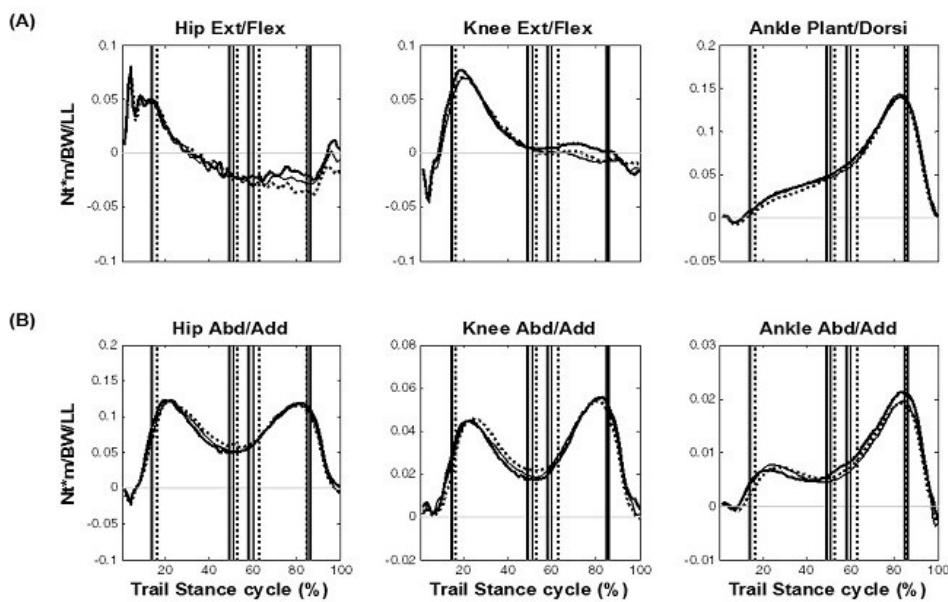
Caption: Ensemble-averaged joint moments of the hip, knee and ankle joints of the trailing limb in the (A) sagittal and (B) frontal planes when crossing obstacle of 10% (dashed lines), 20% (solid lines, thin) and 30% (solid lines, thick) conditions with high-heeled condition. Vertical lines indicate the time when the leading swing toe above the obstacle. Ext/Flex: extensor/flexor; Abd/Add: abductor/adductor; Plant/Dorsi: plantarflexor/dorsiflexor; Pro/Sup: pronator/supinator)

Conclusion: With increasing obstacle height, the mechanical demands to the ankle plantarflexors, and hip and knee abductors were all reduced linearly, primarily because the stance limb became more extended. In contrast, the knee extensor moments of the trailing stance limb was increased. This strategy relies on the knee extensors to provide the whole body support when facing obstacles with increasing height. Therefore, inability to recruit the knee extensor muscles or weakness of the knee extensors, such as resulting from aging, may lead to an increased risk of unsuccessful obstacle-crossing. Further study on the older population is needed. The current results may be helpful for the development of strategies aiming at minimizing the risk of falls during obstacle-crossing in high-heeled shoes.

Table:

	Obstacle height (% leg length)			Effects
	10%	20%	30%	
Knee extensors	0.2 (1.2)	0.4 (1.4)	0.7 (1.2)	increase
Ankle Plantarflexors	5.0 (1.3)	4.8 (1.5)	4.8 (1.6)	decrease
Hip abductors	5.9 (1.2)	5.2 (1.1)	5.0 (1.2)	decrease
Knee abductors	2.2 (0.9)	1.9 (0.9)	1.8 (1.0)	decrease

Caption: Means (standard deviations) of the joint moments in the sagittal and frontal planes for the trailing stance limb when the leading toe was above the obstacle with high-heeled condition. 'Increase' indicate linearly increasing trend while 'decrease' arrows indicate linearly decreasing trend (p<0.05). Units: %BW*LL.

Disclosure of Interest: None Declared

CHARACTERIZATION OF SURF POP-UP SIMULATED MOVEMENT

Marcio Borgonovo-Santos [1] Sara Morais [2] Marcelo Castro [3] Pedro Fonseca [2] Pooya Soltani [1] Andréia Flores [2] João Paulo Vilas-Boas [1,*]

[1]Biomechanics Laboratory of Porto - LABIOMEP, Faculty of Sports - University of Porto (FADE-UP), [2]Biomechanics Laboratory of Porto - LABIOMEP, Porto, Portugal, [3]School of Physical Education, Sport and Exercise Science, University of Otago, Dunedin, New Zealand

Introduction and Objectives: The pop-up is one explosive movement executed to stand up quickly on the surfboard. This movement defines the transition from the horizontal to vertical phase of surfing. After paddling the hands are supported in parallel on the surfboard, under the chest. An extension of the arms is held to promote a strong impulse to take-off, the feet are guided to the back deck and front deck of the surfboard, after that stabilize the body. The pop-up movement separates the successful surf riding or not. Because this is important to understand how this technic works. The main objective of this study is to characterize the pop-up simulated movement on dry land (laboratory conditions). Kinematic analysis was used to explore the best way to divide the movement, and kinetic analysis was used to explore differences between dominant and non-dominant upper and lower limbs.

Methods: The Ethics Committee of the Faculty of Sport from the University of Porto approved this project with the process CEFADE 27-2014. Seven recreational surfers, who practice the activity regularly (age = 31±6yrs, height = 1.77±0.03m, mass = 72±9kg, surf experience = 17±3yrs, frequency of training = 3 times/week) were evaluated performing a pop-up maneuver over force platforms on dry land. This was done on a drawn surfboard layout (6 foot and 2 inches size) over four Bertec force plates (Fig. 1.a.), synchronized with 12 Oqus cameras from the 3D motion capture system (Qualisys AB, Gothenburg, Sweden). Movements were tracked with 48 retro-reflective markers (full body setup) and recorded at 200 Hz. Data analysis was performed with Visual 3D Professional (Visual3D, C-Motion, Kingston, Canada). Forces were normalized according to the subject's body weight. The following outcomes were calculated: upper limbs impulsion peak force percent, lower limbs land peak force percent. Paired T-tests were applied to verify differences between forces applied by the dominant and non-dominant upper limbs, as well as between the lower limbs (front and back on the surfboard).

Results: The movement began when the surfer's hand touched the force plates, the results indicated that the subjects took 1.40±0.52s to perform the movement (touch the hands on the force plates, stand-up and stabilize). The dominant upper limbs contribute to an impulsion force 50±6% of the body mass, and the non-dominant limb 49±5%, while both upper limbs exert a impulse force that represent 98±9% of the body mass. Non-statistical significant differences confirm that the movement was executed in balance (p=0.43). The front foot reaches the surfboard with a force that represent 118±29% of the body mass, and the back foot with 36±14%. When both feet land, they apply a force on the surfboard that represents 153±35%. Statistical significant differences were observed between lower limbs (p<0.001).

Figure:
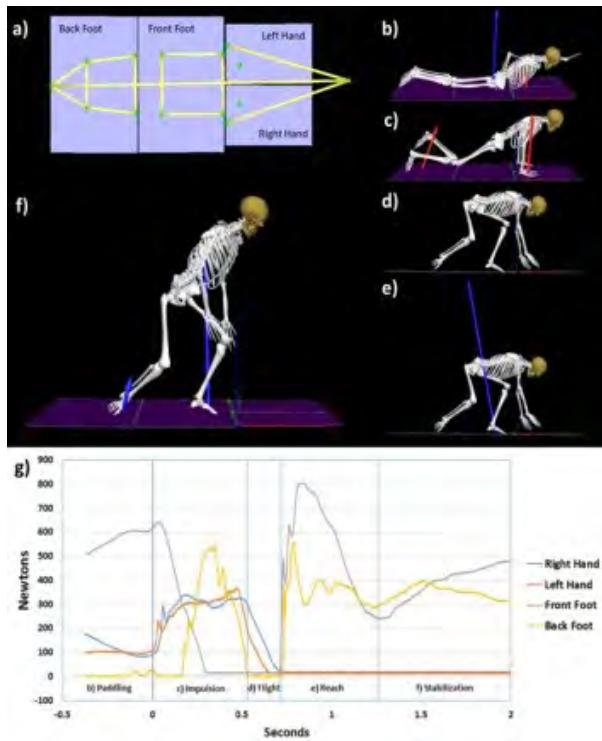
Caption: Pop-Up Movement - a) Force plates setup. b) Paddling simulation on the floor. c) Impulsion. d) Flight. e) Reach. f) Stabilization

Conclusion: It was possible identify some didactical (Fig. 1.b-f) and analytical (Fig.1.g.) phases of the Pop-Up movement, and analyze the forces in an independent way for each limb of the body, also verify the proportion of the force exerted on the surfboard during this process. The movement was divided in impulsion (Fig 1.c.), flight (Fig. 1.d.), reach (Fig. 1.e.), and stabilization (Fig. 1.f.) phases. We can conclude that the upper limbs needs to perform approximately the full body mass of force on the surfboard, to impulse the movement and stand-up. As well, when the body reaches the surfboard, the force applied represents about 150% of the body weight.

The force difference between the legs are expected, because when more force are applied in the front deck of the surfboard, the surfer increase the velocity on the wave, while if the force are applied on the back deck the board breaks. The low standard deviation shows values suggest that experienced recreational surfers show a similar way of performing the pop-up.

References: Acknowledgments

Disclosure of Interest: None Declared

Motion Analysis

PO-0278

HUMAN GAIT USING LOCKED AND STANCE CONTROL MODE KNEE ANKLE FOOT ORTHOSES: OPTIMISING DATA ANALYSIS TECHNIQUES TO DETECT AND QUANTYIFY GAIT DEVIATIONS

James J. Skivington [1,*]Mairi Mackay [2]Andrew J Murphy [1]Karyn Ross [2]Craig Childs [1]

[1]Biomedical Engineering, [2]National Centre of Prosthetics and Orthotics, University of Strathclyde, Glasgow, United Kingdom

Introduction and Objectives: Knee-Ankle-Foot Orthoses (KAFOs) potentially benefit a large range of patient populations with quadriceps weakness and knee instability. In the UK the most common prescribed is a locked-knee device, where the knee is locked in extension at all times, which have been shown to introduce secondary gait deviations, such as vaulting, hip hiking and circumduction. Stance control KAFOs, which lock the knee during stance but permit flexion during swing have been shown to reduce gait deviations as well as increase walking speed and efficiency.[1] The Gait Deviation Index (GDI)[2] is a metric distilled from a walking dataset to indicate the extent to which a person's gait deviates from a control. To our knowledge the GDI has not previously been demonstrated to quantify the effects of assistive devices, such as KAFOs. In addition, calculation of the GDI has often required substantial manual processing of data, which is time consuming and subject to human error.

The aims of this study were to conduct a comparison of walking biomechanics whilst using a KAFO in both locked and stance control modes, and also to develop a data processing utility to automatically calculate and report the Gait Deviation Index, as well as more traditional kinematic and spatial temporal data.

Methods: Sessions used a 12 camera Vicon B10 motion capture system installed in a Computer Assisted Rehabilitation Environment (Motek Medical CAREN extended suite) with a Becker Orthopaedic PreStride 2007, which can be set to both locked or stance control mode, and adjusted to fit the majority of participants. It is worn with sandals to accommodate the bulk of the device.

The participants were age 25±6.03 years and screened to ensure that they had no conditions which would affect the results or endanger them then provided with a 15 minute acclimatisation period to ensure correct knee operation.

Each person completed a 30s trial in the following randomised conditions walking at a self-selected speed:

- Own footwear – used to generate control group data for GDI calculations
- KAFO footwear – used as the normal gait condition to mitigate any deviations caused by the footwear
- Locked mode
- Stance control mode

The analysis tool was created using Microsoft Excel 2010 and Schwartz's GDI template.(2) The template allowed a single step's GDI to be calculated, but the developed tool allowed up to 15 steps of kinematic, spatial temporal and GDI data for both legs to be found.

Heel velocity was used to calculate step and swing phase status - sensitivity adjustments were incorporated to mitigate heel movement during stance phase.

Steps with sample sizes outside of 0.5 std. dev. of the mean were excluded whilst valid steps were downsampled to ensure compatibility with the GDI calculator. This resulted in an output of a 16-metric analysis for each valid step. Results were subjected to a K-S test to determine distribution. Where data was normally distributed an ANOVARM was used to determine significance, whilst data which was non-parametric was subjected to a Wilcoxon Signed Ranks test.

Results: Fig 1 shows velocity, cadence and stride length increase when going from locked to stance control to normal modes. Davis[3] and McMillan[4] found increases from locked to stance whilst Zissimopoulos[5] reported increases from stance to normal modes. The reduction in KAFO leg swing phase from locked to stance was also observed by Davis. Contralateral plantar flexion (vaulting) and pelvic obliquity (hip hiking) decrease from locked to stance mode whilst KAFO leg hip abduction (circumduction) and knee flexion increases from locked to stance to normal modes. Zissimopoulos found a similar reduction in pelvic obliquity.

All GDI metrics increase from locked to stance to own footwear trials – showing an increase as joint restriction decreases. This presents similar findings to Molloy [6] who used GDI to evaluate Cerebral Palsy patients and found a linear relationship between the GDI and the patient's GMFCS.

Figure:
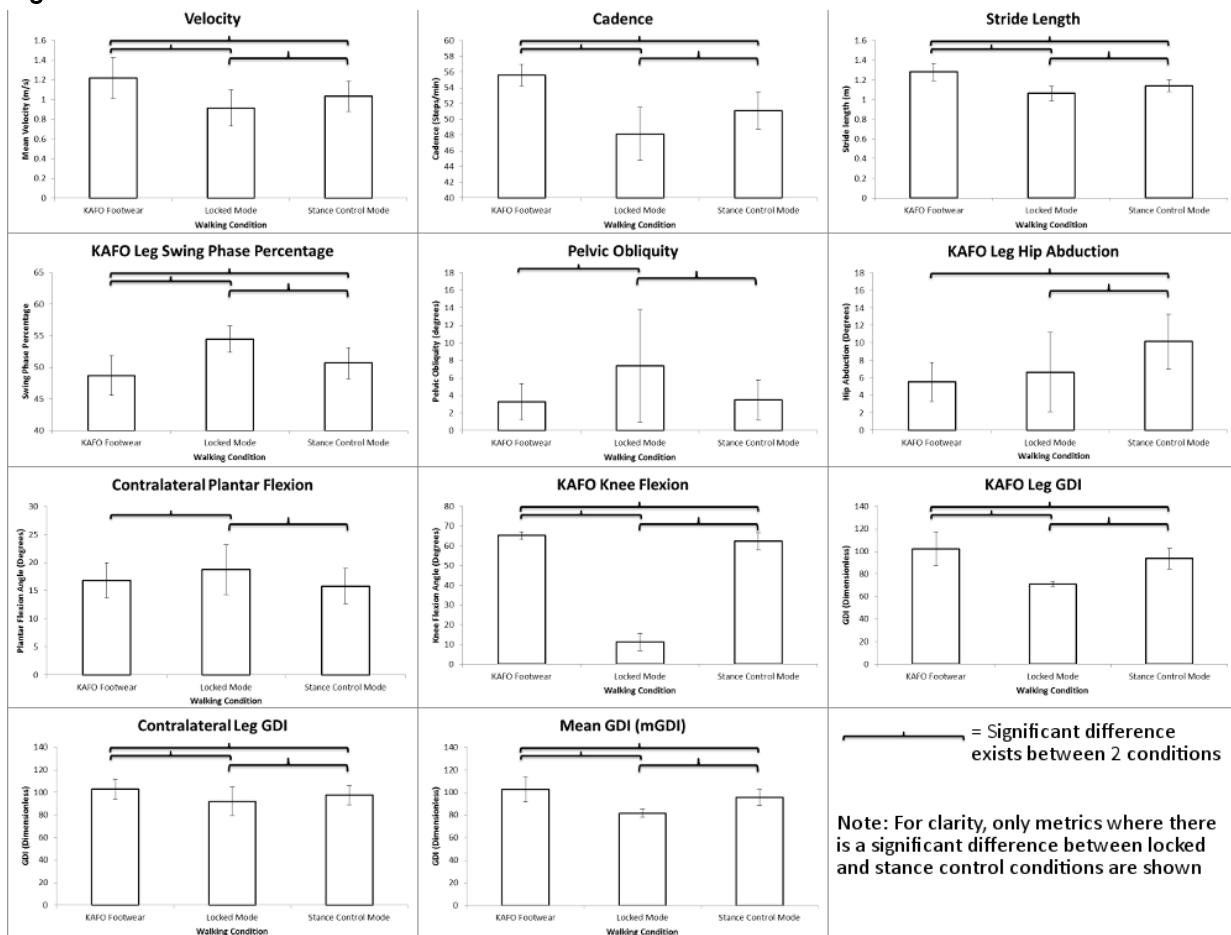
Caption: Fig 1: Trial Data

Conclusion: Overall, the device presents improved spatial temporal and kinematic performance in stance mode compared to locked mode. There is, however, a reduction in performance from the normal trials to stance control mode, showing there are still gait deviations present.

The GDI score shows a linear relationship with the mode of the device – as the device becomes more restrictive the GDI decreases. This shows that the GDI may be considered a useful tool for quantifying the effect of devices.

The author found that the tool created allows processing to be cut down from 30-40 minutes per participant to 1-2 minutes. This presents a large potential time saving, easier access and lower likelihood for error.

References: [1]Arazpour et al., P&O Int, 37(5):411-414, 2013.

[2]Schwartz, Rozumalski, Gait & Pos, 28(3):351-357, 2008.

[3]Davis et al. P&O Int, 34(2):206-215, 2010.

[4] McMillan et al. J of P&O, 16(1):6-13, 2004.

[5] Zissimopoulos et al. J of Reh. R&D, 44(4):503-514, 2007.

[6] Molloy et al. Gait & Pos, 31(4):479-482, 2010.

Disclosure of Interest: None Declared

PO-0279

SPATIAL VARIABILITY IN NORMAL OVERGROUND GAIT

Christoph Mickel [1,*]Gerrit Kollegger [2]Dietmar Schmidtbleicher [3]

[1]Exercise Physiology and Human Movement Science, Institute for Sport Science, Frankfurt, [2]Institute for Sport Science, Darmstadt, [3]Exercise Physiology and Human Movement Scinece, Institute for Sports Science, Frankfurt am Main, Germany

Introduction and Objectives: There are plenty of measures in gait like step width, step length and so forth [1] and all of those are useful also for looking at the variability, but until now there is no common way to determine the spatial variability in the three dimensional space.

Methods: 48 students of the Institute for Sports Sciences (height 178 cm ± 11,3, weight 72,1 kg ± 12, age 23,5 years ± 3,92) that had no acute or chronic lesions or diseases of the lower extremities carried four 3D accelerometers (Analog Devices ADXL 326), which were mounted to the distal end of Os metatarsale III and below the Malleolus lateralis of each foot. Sampling frequency was set to 2000 Hz. Subjects were instructed to walk at their preferred walking speed for consecutive 20 to 25 minutes. Two double-photoelectric barriers measured locomotion velocity several times during the trial. Average locomotion velocity for the group was 1,57 m / s ± 0,16 with an average SD for the single subject of 0,02 m / s.

After separating the accelerometer time-series into stride intervals, stance, swing and double-support times the data was normalized in time (2000 data points) and a point-to-point ensemble-average-curve was determined for each subject in each of the three axis. Therefore the standard deviation (SD) was calculated for each point in time. To obtain the total amount of variability at every point in time the SDs of the different axis were multiplied. The result is a variability cuboid. From these volumes the mean value and SD for the stance, swing and double-support-times was calculated. This procedure was performed for both feet. The data was tested for normal distribution with the Shapiro-Wilk-test. As this condition was not fulfilled the Friedman's test with post-hoc Wilcoxon test was applied (p < 0,05).

Results: Friedman's test showed significant (p=0,000) differences between the different gait phases for each foot. The post-hoc Wilcoxon-tests showed significant differences between the variability of stance and swing (p=0,000), stance and double-support-time (p=0,000) and swing and double-support-time (p=0,000). The applied Wilcoxon-tests between each phases right with left showed no significant differences (stance right vs. stance left: p=0,713; swing right vs. swing left: p=0,778; double-support-time right vs. double-support-time left: p=0,544).

Conclusion: The significant differences between swing and the other two phases may be explained through the restriction of the movement trajectory in the vertical direction by the ground and the anatomic-morphological and mechanical limitations [2, 3]. The significant difference between stance and double-support-time may be lead back to the fact that in double-support-time an even stronger stability exists since there is only very limited time to shift the weight from one leg to the other. The safety margin may be very small to accomplish that task. Further studies are necessary to clarify this finding.

Table:

Parameter	foot	N	Average	Min	Max	SD
V Stance	right	41	144443,3	36348,9	1423491,6	217489,9
	left	35	138052,9	36580,5	1419056,7	231640,4
V Swing	right	41	221645,2	18699,8	1726695,3	287717,6
	left	35	224402,6	54431,1	1734879,7	284890,8
V DST	right	34	9288,3	482,7	40728,4	9939,0
	left	34	9685,3	794,3	42136,5	10448,4

Caption: Deskriptive Statistics (V = Volume; DST = Double-Support-Time)

References: [1] Perry / Burnfield. Gait analysis - normal and pathological function, Slack Inc., 2010

[2] Geyer et al., Proc R Soc B, 273: 2861-2867, 2006

[3] Scafetta et al., Chaos, 19: 026108

Disclosure of Interest: None Declared

3D SHOULDER ROTATION USING ISB EULER ANGLE ALGORITHMS

Simon Thwaites [1] Paul Grimshaw [1,*] Michael Cole [2] Merilyn Lock [3]

[1]School of Mechanical Engineering , University of Adelaide , Adelaide , [2]School of Exercise Science, Australian Catholic University , Brisbane , [3]School of Medical Sciences , University of Adelaide , Adelaide , Australia

Introduction and Objectives: Describing anatomical movements easily is a problem for clinicians, scientists and engineers. Shoulder girdle movements are complex and promote a high degree of difficulty for analysis. This can be attributed to the shoulder's multiple articulating segments. Comprehensive evaluation of the shoulder must take these articulations into consideration. The International Society of Biomechanics (ISB) developed an approach utilizing sequence-dependent Euler angles to describe anatomical motion (Wu et al 2005). This method orientates a given anatomical segment's local coordinate system (LCS) with reference to another segment's LCS. However, insufficient bony landmarks exist on the humerus to define its LCS (i.e. the origin of which is at the glenohumeral (GH) joint rotation centre). The position of the GH joint rotation centre (GH-r) is required to define the longitudinal, y-axis of the humerus LCS. Hence, the position of the GH-r requires estimation, as it is not a bony landmark (Van der Helm 1996; Meskers et al 1998). The LCSs of the humerus and thorax combine to construct the thoracohumeral joint coordinate system (JCS) such that motion of the humerus is defined in a Y-X′-Y″ rotation sequence. For the thoracohumeral JCS, these rotations are defined as *Plane of Elevation*, *Elevation* and *Axial Rotation*, respectively. Currently, the manner in which motion data is collected and presented is at the discretion of the researcher. This lack standardization inhibits comparison of results between studies. Adopting a standard would aid assessment of shoulder injuries and degeneration, inform rehabilitation techniques and have implications for robotic applications (Rosso et al 2013). This study modeled the shoulder joint throughout simple and complex movement patterns, via an anatomical marker-based approach (ISB recommendations). The study also assessed the reliability and effectiveness of this approach in describing shoulder motion with a focus on ease of clinical interpretation.

Methods: Testing was conducted with a 16-camera motion capture system (OptiTrack, Corvallis, USA, 100Hz) and AMASS software (C-Motion Inc., Germantown, Maryland, USA). Twenty-two optoreflective markers (5 markers to define the GH-r centre) were placed on ISB-specified bony landmarks. Data were post-processed in AMASS and then imported into MATLAB (The MathWorks, Natick, MA, USA) for further processing. The approach was evaluated on one subject by analyzing three clinical range of motion (ROM) movements (humeral abduction, flexion and extension), forming the foundation for the development of the MATLAB code. This was then extended to analyze six subjects (2 female and 4 male) and five clinical ROM movements (humeral abduction (AB), flexion (FL), extension (EX), horizontal flexion (HF) and horizontal extension (HE)) at three different orientations (full external (EXT), full internal (INT) and neutral (N) orientations; 15 ROM tests in total). An easily repeatable and complex movement pattern (throwing) was also analyzed.

Results: Time series plots of the three Euler angles required to describe thoracohumeral rotation for left humeral AB, FL, EX HF and HE are presented at all three orientations (EXT, INT and N). This subplot sequence is consistent with the order of the Euler angle rotations according to ISB guidelines (Wu et al 2005), i.e., *Plane of Elevation* (γh−1), *Elevation*

(βh), and *Axial Rotation* (γh−2). The γh−1, βh, and γh−2 values between the start and end of movement were mapped to 0% and 100%. This allowed for averaging and comparison for a given ROM between the male and female subjects. Similarly, each subject's dominant (right) shoulder motion was plotted for the throws. Mean and standard deviation values are presented at 0, 25, 50, 75, and 100% of the movement cycle for the female and male groups and statistical significance of any differences between the groups was assessed. Figure 1 shows the results for the abduction ROM tests for the female subjects (n=2).

Figure:

AVERAGE FEMALE: ABDUCTION

Elevation Plane, γ_1 ($0°$ = abduction, $\pm 90°$ = flexion/extension)

Elevation, β ($-180°$ = vertical elevation)

Axial Rotation, γ_2 (positive° = internal rotation, negative° = external rotation)
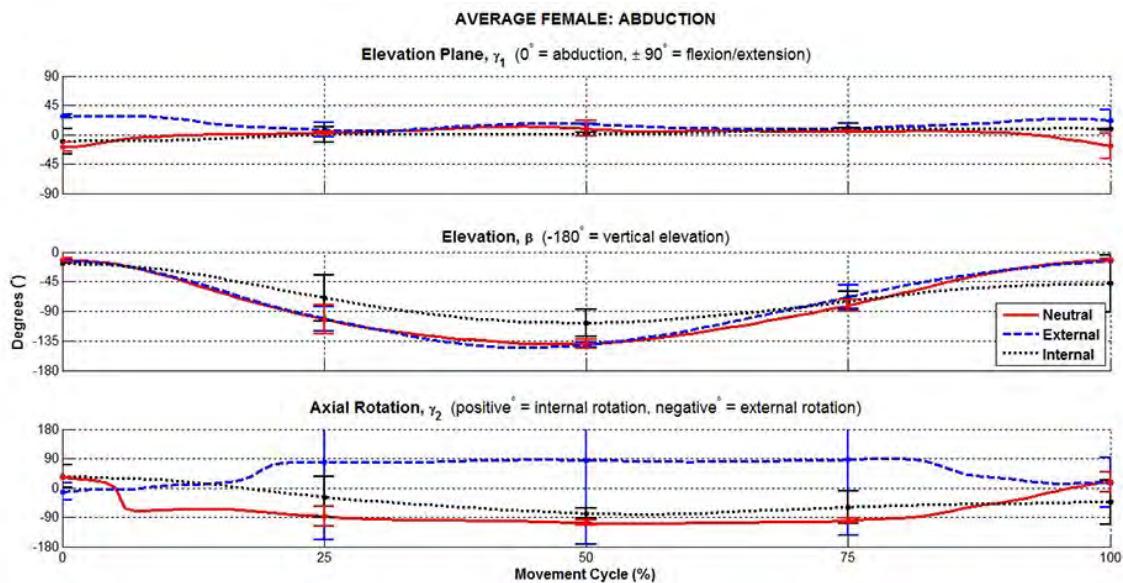
Caption: Fig 1   Abduction ROM test for n=2 female subjects

Conclusion: These movements were described using guidelines proposed by the ISB. Thoracohumeral rotation was decomposed into three sequence-dependent Euler angles via well-known vector mathematics techniques and Rodrigues' rotation formula. A mathematical regression based on the location of five bony landmarks about the scapula was incorporated into the analysis in order to define the humeral coordinate system. It is concluded that the approach would provide a quantitative assessment of mobility and identification of underlying causes of movement disability. However, further work needs to be conducted in order to provide a clinically meaningful assessment of *Axial Rotation* of the humerus.

References: [1] Van der Helm, In: Veeger et al (eds)., Proc of 1st Conf Int Shoulder Group. 1-7, 1996.

[2] Meskers et al., Journal of Biomechanics 31: 93-96, 1998.

[3] Wu et al., Journal of Biomechanics 38: 981-992, 2005.

[4] Rosso et al., Journal of Orthopaedic Surg. and Research 8:24, 2013.

Disclosure of Interest: None Declared

EFFECT OF ALTERED WALKING SURFACE AND VISUAL CONDITION ON SELECTED KINEMATIC AND KINETIC GAIT PARAMETERS OF YOUNG HEALTHY WOMEN AND WOMEN WITH ANKLE SPRAIN.

Raghad Mimar [1,*] Roya Hoveizavi [2] Hadi Mohammadi [1]

[1]Biomedical Engineering, University of British Columbia, Kelowna, Canada, [2]Physical Education and sport sciences, Kharazmi University, Tehran, Iran, Islamic Republic Of

Introduction and Objectives: Maintaining balance while walking involves coordination of response from multiple sensory systems including the vestibular, somatosensory, and visual systems. The objective of this study is to investigate the effect of altered walking surface, and consequently, the altered plantar proprioception on selected kinematic and kinetic gait parameters of both young healthy women and women with ankle sprain.

Methods: 22 young healthy women (age range?) and women with ankle sprain participated in this study. Subjects performed 3 trials of walking on 6 different conditions: natural surface with natural light, natural surface with low light, soft surface with natural light, soft surface with low light, irregular surface with natural light, and irregular surface with low light. Gait timing, stride length, gait velocity, cadence, whole body acceleration and both vertical and shear forces were measured from a two-dimensional motion analysis system and force platform. For data analysis, MATLAB (version 6.5) and SPSS (version 21) were implemented in this study.

Results: Results showed no significant difference between the normal and ankle sprain group in all conditions. However, the ankle sprain group showed less mean value and greater standard deviation (SD) in force and acceleration. However, within groups, there was a significant (word missing?) within subject effect of surface on walking velocity (only between soft and irregular surfaces, sig=0.036), strongly on vertical and A/P shear whole body acceleration (between all three surfaces, sig=0.000), force of the loading response phase (sig= 0.002) and maximum and minimum A/P shear forces (sig= 0.000). Also, vision had a significant effect on whole body acceleration of the loading response phase (sig=0.000). The combined effect of surface and vision was significant only on the whole body acceleration of the loading response phase (sig=0.000), (Tbl. 1)

Conclusion: It is concluded that surfaces (especially soft surfaces) have greater effect on walking kinematics and also, soft surfaces have greater stimulation on proprioception. Walking on irregular surfaces also needs greater propulsive shear force, which could result in faster muscular fatigue. With the exception of the acceleration of loading response phase, the low light condition had no significant effect on steady state walking, which appears to be one of the restrictions of this investigation.

Table:

Effect of surface and vision (sig)	Effect of vision (sig)	Effect of surface (sig)	Parameter
0.955	0.900	0.036*	Walking velocity
0.000*	0.000*	0.000*	Vertical whole body acceleration of early stance
0.540	0.276	0.002*	Vertical whole body acceleration of late stance
0.664	0.341	0.000*	Maximum A/P Shear acceleration
0.897	0.987	0.000*	Minimum A/P Shear acceleration
0.540	0.295	0.002*	Vertical force of late stance
0.600	0.341	0.000*	Maximum A/P Shear force
0.890	0.975	0.000*	Minimum A/P Shear force

Caption: Results summery

References: [1] Thies SB et al., Gait Posture, 22: 40-5, 2005.

[2] Menz HB et al., Gait Posture, 18: 35-46, 2003.

[3]   Curtze C et al., Gait Posture, 33: 292-6, 2011.

Disclosure of Interest: None Declared

MEASUREMENT OF 3D FOOT DEFORMATION DURING HUMAN WALKING BY DIGITAL IMAGE CORRELATION METHOD

Kohta Ito [1,*] Ikumi Fujiwara [1] Koh Hosoda [2] Takeo Nagura [3] Naomichi Ogihara [1]

[1]Department of Mechanical Engineering, Keio University, Kanagawa, [2]Graduate School of Engineering Science, Osaka University, Toyonaka, [3]School of Medicine, Keio University, Tokyo, Japan

Introduction and Objectives: Human walking is a mechanical phenomenon to move the centre of body mass forward without falling by appropriately generating the ground reaction forces by the feet. Detailed understanding of the deformation of the foot during walking is important for elucidating how the structure of the human foot facilitates appropriate mechanical interaction with the ground in generation of robust bipedal walking. However, the nature and degree of foot deformation during human walking have not been fully investigated. In this study, we aimed to clarify the three-dimensional (3D) deformation of the human foot during bipedal walking by means of digital image correlation (DIC) method, an optical method to measure 3D deformation of an object surface by using the stereo-triangulation and the image correlation of speckle pattern on the object surface [1].

Methods: Two adult male participants were asked to walk along a walkway at a self-selected speed and the surface of the right foot during the stance phase (from heel-contact to toe-off) were filmed at 1000Hz using two synchronized high speed cameras (MEMRECAM GX-3, NAC Image Technology, Japan) with a resolution of 1280 x 1024 pixels. Dorsolateral and medial surfaces were filmed separately. The right foot was sprayed with aqueous black ink to draw the speckle pattern on the distribution of the magnitudes and directions of the principal strain on the surface of the foot in the stance phase. The skin strain distribution was calculated by taking the foot shape at the middle of the stance phase as the reference shape configuration. Digital image correlation method software Vic-3D (Correlated Solutions, Columbia, SC, USA) was used for quantification of the foot deformation.

Results: The figure represents the principal strain distribution of the foot during stance phase. Our results demonstrated that in the early stance phase, the dorsal surface around the ankle was stretched and that around the metatarsophalangeal joint was contracted in the anteroposterior direction due to the plantarflexion and dorsiflexion, respectively. In the late stance phase, the lateral surface of the rear foot is stretched, while the medial surface is contracted, both in dorsopalmar direction, suggesting that the calcaneus was inverted with respect to the talus. At the same time, the lateral surface of the midfoot was stretched in the anteroposterior direction, suggesting the pronation of the forefoot. Inversion of the heel and pronation of the forefoot produce the rigid structure of the foot (locking mechanism [2]) for generating propulsive force in the late stance.

Figure:
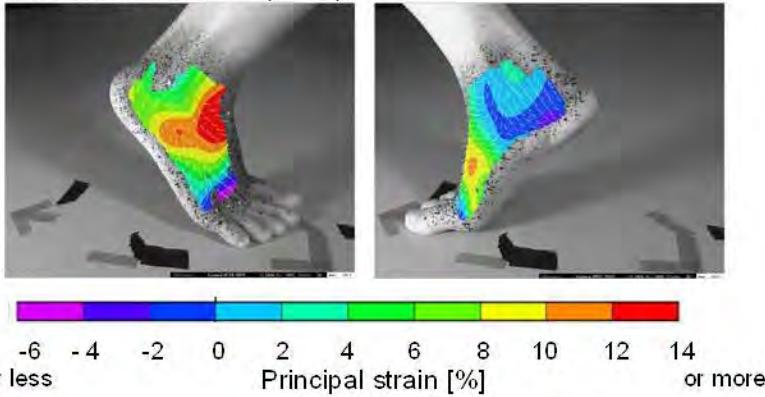
Caption: Principal strain distribution of the foot during walking (Left: dorsolateral, Right: medial)

Conclusion: The present study demonstrated that the DIC method can be successfully applied to capture and quantify the 3D deformation during bipedal walking. Although this methodology has some limitations and must be undergone further evaluation, the present framework may serve as an effective tool for understanding the morphofunctional roles of the human foot structure during walking.

References: [1] Sutton et al., Image correlation for shape, motion and deformation measurements, Springer, 2009. [2] Blackwood et al., Foot Ankle Int, 26: 1074-1080, 2005.

Disclosure of Interest: None Declared

Motion Analysis

PO-0283

JOINT BIOMECHANICS AND BALANCE ISSUES DURING COMMON REHABILITAITON EXERCISES IN OBESE FEMALES

Bhupinder Singh [1,*]Ashley Artsdalen [1]H. John Yack [1]

[1]Physical Therapy, California State University , Fresno, United States

Introduction and Objectives: Obese individuals may have difficulty performing basic rehabilitation exercises like squat and lunge. Balance and adipose tissue restriction, are major issues for obese individuals, which could have implications on joint biomechanics. Despite potential for biomechanical differences from normal weight subjects, the influence of obesity on the performance of squat and lunge has not been documented. The purpose of this study was to analyze and compare the joint biomechanics of obese females, as measured by joint moments and balance, as measured by sway area of center of pressure (COP) while performing squat and lunge exercises. It is hypothesized that obese females will have higher joint moments and poorer balance control than their normal weight counterparts, and that as the difficulty of the exercises increase, the increase in joint moments and balance control deficits will be more apparent.

Methods: Ten obese (BMI > 30 kg/m2) females 37.4�3.7 years, BMI 39.2�3.7 kg/m2 and ten normal weight (BMI

Results: For the squat, hip and knee extensor moments in obese females were not different than normal weight females for all three levels. However, ankle extensor moments were higher in obese females (p=0.04). The support moment was higher in obese females for squat 70 (p=0.03) and squat 80 (p=0.01), but not different for squat 60 (p=0.07) (Table 1). Sway area was not different between obese and normal weight females for squat 60 (p=0.62) squat 70 (p=0.16) and squat 80 (p=0.11) (Figure 1). There was no within group differences for squat 60, 70 and 80. For the lunge, hip extensor moments were greater in obese females for level 1, 1.1 and 1.2 (p-values: 0.004, 0.003 and 0.007 respectively). Knee and ankle extensor moments were not different (Table1). Support moments showed an overall group effect between obese and normal weight subjects (p=0.01). Sway area was higher for obese females for all three levels of lunge, lunge 1 (p=0.004), lunge 1.1 (p=0.002) and lunge 1.2 (p=0.001). The lunge had greater sway area as compared to standing as well as squat activities (p

Figure:

	Stand 30s	Stand 3s		Squat 60	Squat 70	Squat 80		Lunge 1	Lunge 1.1	Lunge 1.2
■Obese	6.63	2.36		3.95	4.46	5.07		14.51	16.23	16.91
■Normal Weight	3.91	0.97		3.64	3.23	2.96		5.7	4.82	6.55
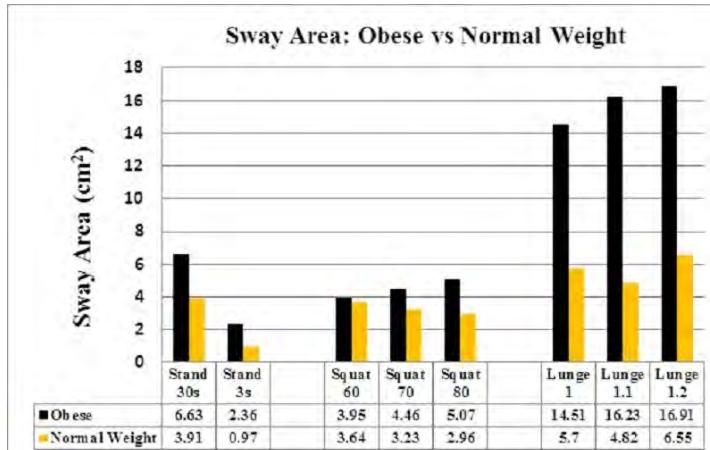
Caption: Mean sway area for standing eyes open 30 s, standing 3 s, squat and lunge levels. The asterisk (*) shows significant differences between activities (p<0.05).

Conclusion: The lunge activity was more challenging for obese females than squatting and standing, as shown by greater sway area and hip joint moments. It could be argued that the excess adipose tissue in obese subjects caused an increase in hip moment. When compared to standing 3 s, squat and lunge have greater sway area, although significant differences are only seen for lunge, which could be attributed to the greater base of support and more effort needed to stabilize the mediolateral shift of the trunk in obese individuals. There were no differences in the three squat depths, indicating that squat may be a better exercise choice for obese individuals with fall risk or joint pathologies like hip arthritis. To conclude, identifying the underlying biomechanical issues and the strategies used by obese individuals during these common rehabilitation exercises can provide a rationale to set different recommendations for the obese population.

Table:

Moment(Nm/kg)		Squat 60	Squat 70	Squat 80	Lunge 1	Lunge 1.1	Lunge 1.2
Hip	Obese	0.22 (.24)	0.29 (.28)	0.37 (.30)	1.32 (.27)	1.41 (.28)	1.48 (.32)
	Normal	0.12 (.17)	0.17 (.18)	0.24 (.18)	0.96 (.39)	1.07 (.38)	1.14 (.39)
Knee	Obese	0.67 (.10)	0.73 (.12)	0.82 (.12)	0.53 (.15)	0.53 (.16)	0.50 (.22)
	Normal	0.59 (.22)	0.66 (.23)	0.75 (.26)	0.64 (.30)	0.56 (.29)	0.52 (.24)
Ankle	Obese	0.28 (.16)	0.31 (.19)	0.34 (.19)	0.42 (.20)	0.43 (.20)	0.47 (.21)
	Normal	0.19 (.10)	0.20 (.13)	0.20 (.11)	0.45 (.26)	0.42 (.25)	0.40 (.22)
Support	Obese	1.18 (.25)	1.33 (.32)	1.53 (.36)	2.33 (.36)	2.44 (.42)	2.52 (.47)
	Normal	0.92 (.27)	1.03 (.30)	1.18 (.34)	2.07 (.65)	2.05 (.64)	2.07 (.59)

Caption: Mean (SD) hip, knee, ankle extensor and support moment for different levels of squat and lunge exercises

Disclosure of Interest: None Declared

Musculoskeletal

PO-0284

EFFECT OF CRYOTHERAPY ON ECCENTRIC EXERCISE-INDUCED MUSCLE DAMAGE: A RANDOMIZED CLINICAL TRIAL

Liane B. Macedo [1,*]Caio Lins [2]Daniel Borges [1]Jamilson Brasileiro [2]

[1]Department of Physiotherapy, [2]Universidade Federal do Rio Grande do Norte, Natal, Brazil

Introduction and Objectives: Exercise-induced muscle damage provokes the installation of an inflammatory process that results in a sensation of pain and discomfort in individuals [1]. Recently cryotherapy has been used in many sports as a strategy to recover from exercise-induced muscle damage, such as after training or competition [2, 3]. Its effects on damaged tissue help relieve pain, inflammation and oedema, since it provokes local vasoconstriction, which reduces capillary, lymphatic and cell permeability, lowering inflammatory response and oedema associated to trauma [4,5]. It has been observed that cooling decreases secondary hypoxia, with a consequent decline in muscle necrosis. Furthermore, deceleration of cell metabolism and nerve conduction velocity would occur, limiting injury secondary to lesion and pain [5]. This positive effects caused by cooling, individuals would manage to continue their training, with no decrease in performance, in the days following injury [4]. However, are necessary more studies to evaluate these effects on muscle recovery. Thus, the present study aims to assess the effect of cryotherapy on eccentric exercise-induced muscle damage.

Methods: This is a randomised clinical trial composed of 40 women (22.8±2.2 years). Participants were randomly divided into two groups: control group and cryotherapy. Both groups underwent three assessments: pre, immediately after and 48 hours after intervention, all composed of algometry, dynamometry (peak torque normalized by body weight) and electromyography (root mean square and median frequency). After initial assessment, all the participants were submitted to an eccentric exercise protocol on an isokinetic dynamometer (2x10 maximum eccentric contractions of non-dominant elbow flexors at 60°/s). Next, participants were submitted to the interventions: the control group did not undergo any intervention and remained at rest for 25 minutes; to cryotherapy group a 1kg ice pack was strapped over the entire brachial biceps muscle and adjacent muscles of the arm under study using a bandage. Application lasted 25 minutes and a digital thermometer with interface was used to measure cutaneous temperature and ensure cooling level [6]. After the interventions each subject underwent two assessments: Immediately (post) and 48 hours after the interventions, identical to the first assessment. SPSS for Windows (version 20.0) was used for all statistical analyses. A test t was used to investigate baseline differences between groups. A mixed design ANOVA (3x2) was used to investigate changes in algometry, peak torque normalised for body weight, median frequency and RMS with one between-subjects variable, *group*, with two levels and one within-subject variable, *time*, with three levels. The effect of group, time, and group by time interactions were tested. When the assumption of sphericity was violated, significance was adjusted using the Greenhouse-Geisser method. When the effect of test was significant, the analysis using the multiple comparison Bonferroni post-hoc test was applied. A 5% significance level was used ($p < 0.05$).

Results: No initial differences in anthropometric measures or variables analysed were observed between the groups. In relation to algometry, a significant difference was observed for the control and cryotherapy groups, with a statistical difference at 48hr compared to pre and immediate post ($p<0.01$). However, no intergroup difference was observed

(p=0.15). Analysis of peak torque normalised for body weight had altered values for both groups, demonstrating a difference at pre to immediate post and 48hr (p<0.01), but no intergroup difference (p=0.77). Analysis of electromyographic variables shows that median frequency was a significant difference in cryotherapy group, demonstrating an intragroup difference at post to pre and 48hr (p<0.01) and intergroup difference between post (p<0.01), probably due to reduction in nerve conduction velocity from cooling [7]. The electromyographic amplitude revealed no significant pre, immediate post and 48hr difference after intervention in the two groups assessed for RMS (p>0.05), or any intergroup variation (p=0.76) (Figure 1).

Figure:
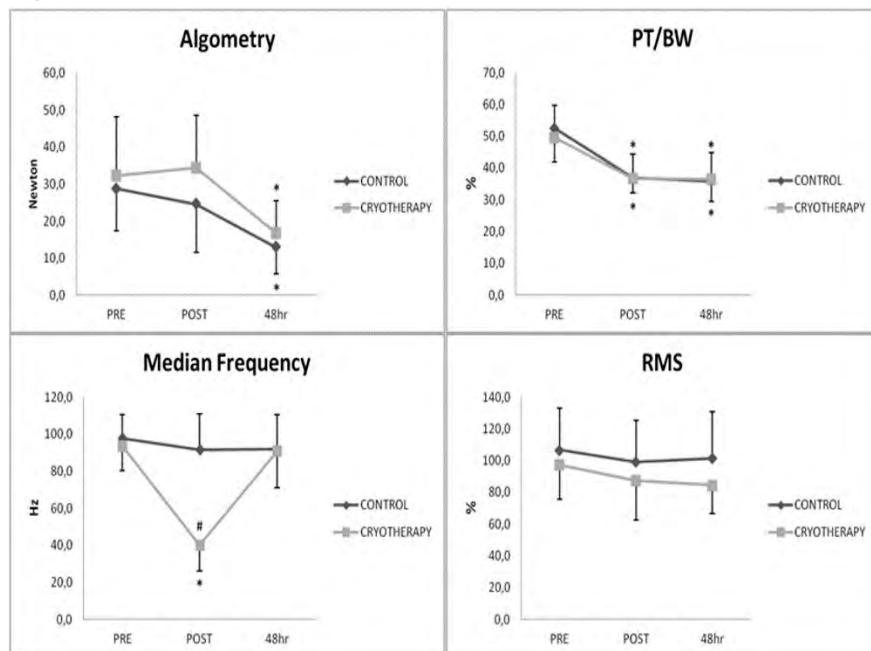
Caption: Figure 1. Means of algometry, peak torque normalized by body weight (PT/BW), median frequency and root mean square (RMS) to control and cryotherapy groups. * indicates significant change compared to baseline values. # indicates significant change between groups.

Conclusion: The results of the present study suggest that cryotherapy do not interfere in the response to eccentric exercise-induced muscle damage to any variable analysed.

References: [1] Abad, C.C.C. et al. Rev Bras Med Esporte, 16: 36-40, 2010.

[2] Bailey, D.M. et al. J Sports Sci, 25:1163–70, 2007.

[3] Pointon, M et al. Eur J Appl Physiol, 111:2977–86, 2011.

[4] Sellwood, K.L. Br J Sports Med, 41:392–7, 2007.

[5] Ascensão, A. J Sports Sci, 29(3): 217-25, 2011.

[6] Bleakley, C.M. Phys Ther Rev, 15(4): 344-50, 2010.

[7] Herrera E. Physical therapy, 90(4): 581-91, 2010.

Disclosure of Interest: None Declared

NONINVASIVE MUSCLE FORCE EVALUATION OF THE PSOAS MAJOR DURING ISOMETRIC HIP FLEXION

Hiroshige Tateuchi [1,*]Yuta Kondo [1]Tadao Tsuboyama [1]Noriaki Ichihashi [1]

[1]Kyoto University, Kyoto, Japan

Introduction and Objectives: The psoas major (PM) has an important role in motion and stabilization of the hip joint and lumbar spine. Activity of the PM can be recorded using an intramuscular fine-wire electrode since the muscle is situated deeply. However, such invasive evaluation is difficult for clinical application. Shear-wave elastography is a reliable noninvasive technique for evaluating individual muscle force by measuring shear elastic modulus. Previous studies have shown that the relationship between torque and shear elastic modulus of the muscle differs according to the muscle [1]. The purpose of this study was to determine the relationship between exerted muscle force and shear elastic modulus of the PM using shear-wave elastography.

Methods: Nineteen healthy men (mean age, 22.1 ± 1.5 years) participated in this study. All subjects provided informed consent, and the protocol was approved by the local ethics committee. Participants sat on a lifting chair with hips flexed at 45°. The pelvis was fixed by a belt to prevent pelvic posterior tilting. Prior to data collection, maximum isometric strength of hip flexion was measured in above-mentioned posture. Shear elastic modulus of the PM was measured just distal to the inguinal ligament using shear-wave elastography (Aixplorer; Supersonic Imagine, Aix-en-Provence, France). The PM was identified by using B-mode imaging, and the transducer was placed longitudinally with respect to the direction of the muscle fibers. Participants were instructed to perform isometric hip flexion at 0%, 10%, 20%, and 30% of maximum strength, keeping the foot off the floor (0% represents active hip flexion at 45° without external load). Measurement at 40% was excluded from analysis because maintaining stable isometric contraction was difficult. The examiner confirmed the exerted force using the force sensor and a screen on which the force was displayed in real time. Two regions of interest for measurement of shear elastic modulus were set on the PM, and their mean was calculated. All measurements were performed three times, and the mean shear elastic modulus value was used in the analysis. The conditions (0%>30%) were measured in random order. For shear elastic modulus values of the PM, a paired t test with Shaffer correction for multiple comparisons was used to determine differences among rest and 0% to 30% conditions. A P value of <0.05 was considered statistically significant.

Results: Shear elastic modulus of the PM increased significantly in 0%, 10%, 20%, and 30% conditions compared with that at rest. Furthermore, shear elastic modulus of the PM increased significantly in 10%, 20%, and 30% conditions compared with that in the 0% condition. However, there were no significant differences among 10%, 20%, and 30% conditions. The external load measured 5 cm proximal to the patella in the 10% condition was 4.4 ± 1.0 kg.

Our findings indicate that shear elastic modulus of the PM increases with an increase in muscle force within a limit of 10% of maximum strength. Our previous study showed that muscle thickness of the PM did not change with an increase in muscle force. Therefore, the method used in this study would be useful for evaluating PM function during light-load motion in the patients with muscle weakness. However, the results suggest that muscle force of the PM at more than 10% of

maximum strength cannot be evaluated because of a technical limitation. Change in shear elastic modulus of the PM at different hip joint angles still needs to be investigated.

Figure:
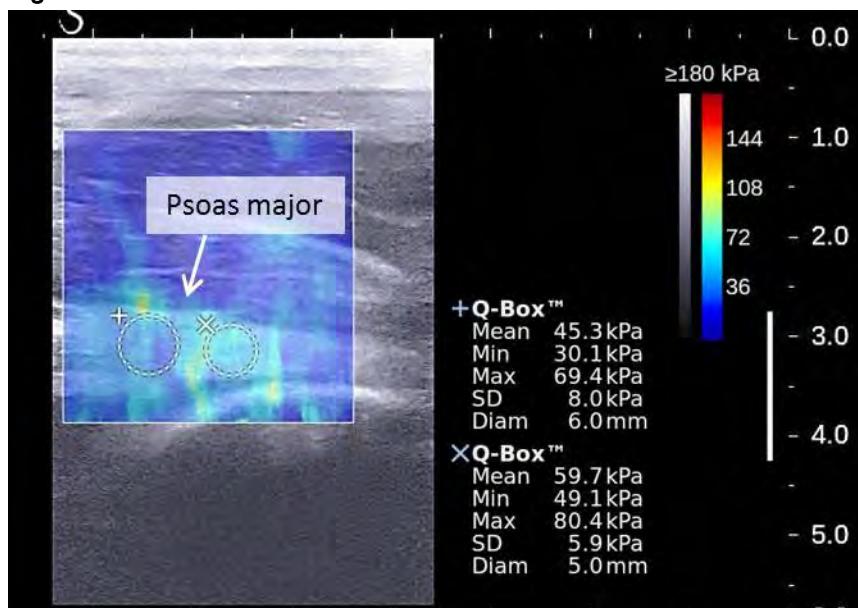
Caption: A typical example of shear elastic modulus measurement at the psoas major. Young's modulus of the 2 regions of interest (Q-box), arranged in the psoas major, was calculated. The shear elastic modulus was obtained by dividing Young's modulus by 3.

Conclusion: Muscle force of the PM during isometric hip flexion can be evaluated using shear-wave elastography within a limit of 10% of maximum strength (i.e., hip flexion with up to an approximately 4.4-kg load).

None of the authors have any conflicts of interest associated with this study.

Table: Shear elastic modulus (kPa) of the psoas major

Rest	0%	10%	20%	30%
10.8±2.6	13.7±2.5†	15.0±3.3†‡	16.1±3.9†‡	15.6±3.4†‡

Caption: All values are mean ± SD. † Significant difference to value at rest. ‡ Significant difference to value in 0% condition.

References: [1] Bouillard et al., J. Biomech, 45: 1424-1429, 2012

Disclosure of Interest: None Declared

Musculoskeletal

PO-0286

DEVELOPMENT OF THE PORCINE KNEE MODEL FOR PRE-CLINICAL TRIBOLOGICAL ASSESSMENT OF CARTILAGE REPAIR INTERVENTIONS

Aiqin Liu [1,*]Louise Jennings [1]Eileen Ingham [2]John Fisher [1]

[1]School of Mechanical Engineering, [2]School of Biomedical Sciences, Institute of Medical and Biological Engineering, University of Leeds, Leeds, United Kingdom

Introduction and Objectives: To date, the success of early-stage cartilage repair interventions in the knee has been constrained by a lack of biomechanical and biological consideration in the design of the therapeutic interventions. This stems from an inadequate understanding of functional cartilage biotribology in the natural knee joint. Therefore, the aim of this study was to develop and validate a porcine knee model using a whole joint knee simulator investigating tribological and biomechanical properties of the natural knee, which could then be used to assess the restorative function and tribology of cartilage repair interventions before they are assessed *in vivo*.

Methods: Porcine knee joints (N = 6) were dissected by removing soft tissues leaving only the cartilage and meniscus in place, and mounted into a single station knee joint simulator (Simulator Solutions). The tribological behaviour in terms of frictional shear force between the femur and tibia was ascertained under 3 conditions, each of which induced different frictional sliding and rolling behaviours. These conditions were achieved through varying the constraint in the anterior-posterior (AP) axis as follows: 1) Sliding condition, which was created by constraining the tibial AP carriage; 2) Rolling condition, which was created by decoupling the tibial AP carriage (unconstrained); 3) A combination of sliding and rolling conditions were created by the incorporation of springs (K=2.69 N.mm^{-1}). The mean frictional shear force with 95% confidence limits was determined under the three AP conditions.

Results: As shown in Fig. 1a, under 'simple input' kinematic conditions, the AP constrained condition displayed increased shear force with increased flexion angle, resulting in a triangular shear force profile with a peak anterior value of 97.4±43.8 N at maximum flexion. The shear force under spring condition showed a smaller magnitude triangular wave pattern than constrained condition with a peak value of 23.4±11.8 N at maximum flexion. A shear force profile with constant low values (1.6±3.0N) was observed under AP unconstrained condition.

During a clinically relevant gait cycle, the AP constrained condition caused a higher shear force response with a range from 45.1±22.8 N (at 0.04 s) posteriorly to 29.2±15.8 N (at 0.55 s) anteriorly, compared to the shear force values ranging from 11.2±11.6 N (at 0.03 s) posteriorly to 14.7± 6.4 N (at 0.79s) anteriorly under spring condition (Fig. 4b). The spring condition showed increased shear force values compared to the AP unconstrained condition, specifically during swing phase of the gait cycle (in the region 0.62 s-0.8 s).

Figure:
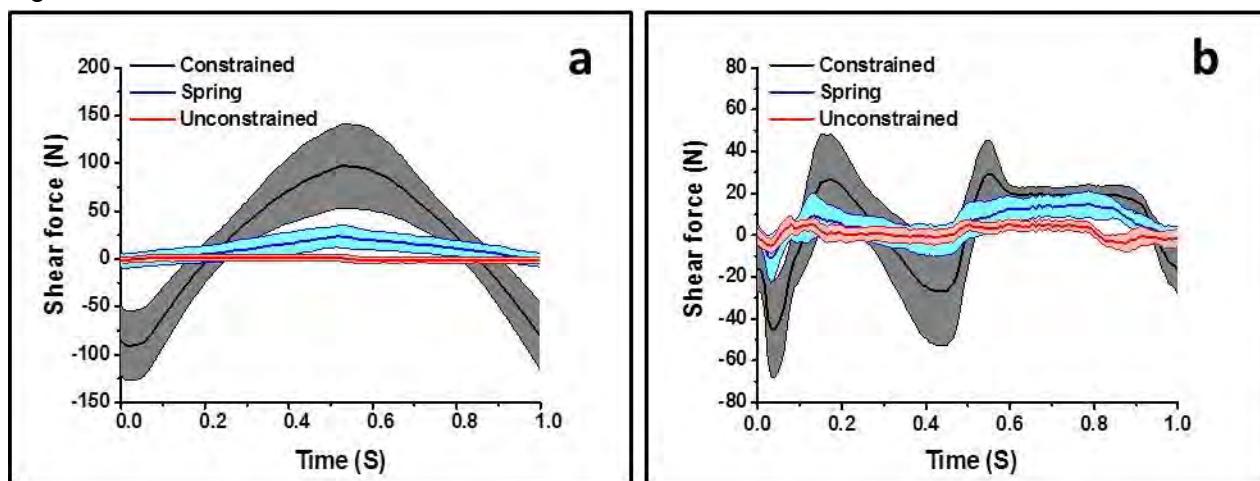
Caption: Fig. 1. Average shear force of porcine knee joints (n=6) testing under a) simple profile with a constant load and flexion/extension only and b) complex profile inputs based on a standard gait cycle and appropriately scaled for a porcine joint. The grey, blue and red regions indicate 95% CI of the mean of shear force under AP constrained, spring and AP unconstrained conditions.

Conclusion: The shear force measurements under both simple input profile and clinically relevant gait cycle input showed higher values under the AP constrained condition where sliding motion occurred, compared to the AP unconstrained condition where rolling motion occurred. The results indicated that the in vitro simulation model was able to simulate and measure different tribological behaviours when the femoral and tibial bearing was entrained to slide or/and roll. Therefore, the porcine knee model showed the potential capability to investigate the effect of knee structural, biomechanical and kinematic changes, on the tribological function of different cartilage substitution therapies.

Disclosure of Interest: None Declared

Musculoskeletal

PO-0287

THE MAGNITUDE OF STRETCH-INDUCED FORCE ENHANCEMENT FOLLOWING SHORTENING IS TIME-DEPENDENT

Rafael Fortuna [1,*] Geoffrey A. Power [1] Walter Herzog [1]

[1]Faculty of Kinesiology, university of Calgary, Calgary, Canada

Introduction and Objectives: Force production is influenced by history-dependent properties of muscle. Following an active lengthening or shortening contraction, the steady-state isometric force is distinctly different than a purely isometric contraction at the same muscle length and activation level[1]. These properties are referred to as residual force enhancement (FE) following active lengthening and force depression (FD) following active shortening. Force enhancement and FD properties have been observed at all structural levels[1,2] and have also been found in human voluntary and electrically stimulated muscles[2]. However, the detailed mechanisms causing FE and FD remain unknown. During functional tasks, muscles usually undergo shortening-stretching cycles (SSCs) while activated. It has been shown that active shortening preceding a stretch reduces the stretch-induced FE, but this reduction disappears if shortening and stretch are separated by sufficient time in frog single muscle fibers[3]. However, it is unclear whether this time-dependent effect is present in intact human muscles, and thus might play a role in every day movements. The purpose of this study was to evaluate the effect of time between active shortening and lengthening on the stretch-induced FE in the adductor pollicis of healthy young adults.

Methods: Twelve healthy male participants (age: 28±5 years; height: 180±6cm; weight: 75±5kg) gave free written informed consent to participate in this study. The left forearm was placed in a custom-designed dynamometer to assess thumb adduction forces[4]. Full thumb adduction was defined as 0° and abduction angles were defined as positive up to 30°. The adductor pollicis was electrically stimulated at a frequency of 50Hz via the ulnar nerve with a current intensity that produced 50-60% of each subject's maximum voluntary force. First, FD was determined by shortening the muscle at an angular velocity of 60°/s from 30° to 0° and comparing the steady-state isometric force following shortening to the corresponding purely isometric force. Next, three shortening-stretching cycles were randomized and performed with intervals of 0s (SSC_0s), 0.5s (SSC_0.5s), and 1s (SSC_1s) between the shortening and the stretching phase. Shortening and stretching were performed at an angular velocity of 60°/s and ranged from 0° to 30° and from 30° to 0°, respectively. Lastly, FE was determined using active stretching of the muscle at 60°/s from 0 to 30°. To minimize fatigue, a 5min interval was given between consecutive contractions. Each contraction was preceded by an isometric reference contraction (Ref) at the corresponding final thumb angle. The magnitude of FD (SSC_0s/0.5s/1s), and for FE were normalized relative to the corresponding isometric reference contractions. A repeated measures ANOVA was performed for comparisons between the different contractions with $\alpha < 0.05$. When significance was observed, a Bonferroni post-hoc test was performed to identify differences.

Results: FD following active shortening was ~22% (result not shown), and FE following active stretching was ~20%. When zero (SSC_0s) and half a second time intervals (SSC_0.5s) were given between shortening and stretch, FE was significantly reduced to ~10 and 11%, respectively. However, when a one second interval (SSC_1s) was given, the effect

of shortening on the stretch-induced FE was abolished and FE was similar to the FE measured without shortening preceding the stretch (Fig. 1).

Figure:
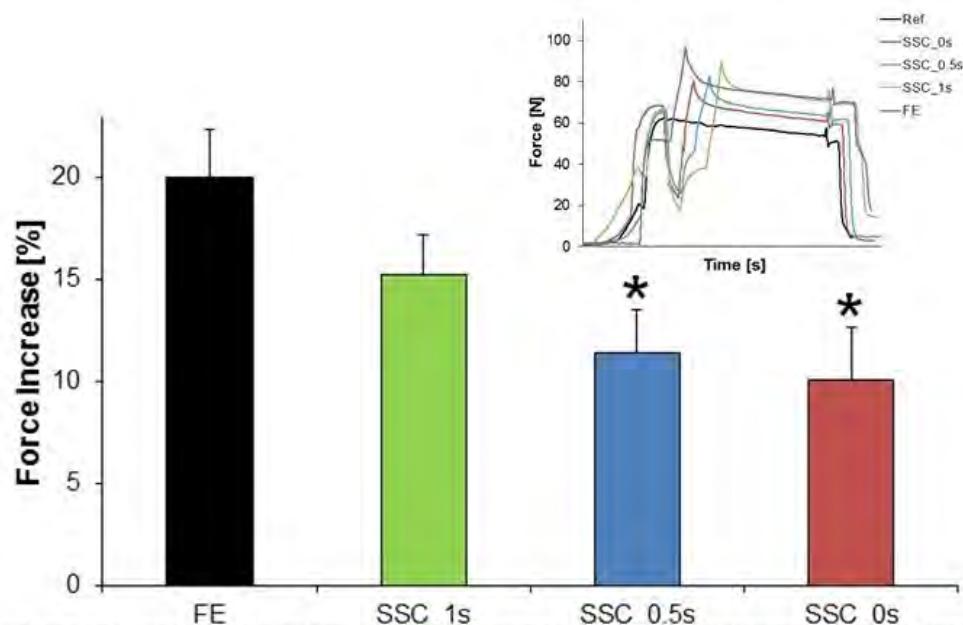
Fig 1 Mean values of force increase (+/-SE) normalized relative to the values of the isometric reference contractions. Inset: Seven second raw force traces for the different experimental conditions. Force enhancement for pure stretch conditions was ~20%, SSC_0s and SSC_0.5s produced significantly less FE (~10%) compared to the FE for the pure stretch condition. When a 1s interval (SSC_1s) was introduced between shortening and stretch, the effects of shortening on FE were abolished and the forces between the two conditions were similar. * Compared to FE ($p<0.005$).

Conclusion: From the results of this study, we conclude that active shortening preceding an eccentric muscle contraction affects the subsequent force enhancement, but only if the shortening and stretch follow each other within a sufficiently short time (less than 1s). Immediately after active shortening, the proportion of attached cross-bridges is reduced, but this reduced cross-bridge state is abolished with time. It appears therefore that the stretch-induced force enhancement is affected by the proportion of attached cross-bridges at the beginning of the stretch, and that this proportion is smallest when stretching immediately follows shortening, but is restored to its full capacity within about 1s of shortening. The molecular details of this observation need to be identified using a reduced (single fibre or myofibrillar) preparation.

References:

[1] Abbott et al., J Physiol, 117(1):77-86, 1952.

[2] Lee et al., J Physiol, 545(1):323-330, 2002.

[3] Rassier et al., J Biomech, 37:1305-1312, 2004.

[4] Fortuna et al., J Electromyogr Kinesiol, 22(2):228-233, 2012.

[5] Marechal et al., J Gen Physiol, 73:453-467, 1979.

Disclosure of Interest: None Declared

PO-0288

EFFECT OF WHOLE BODY VIBRATION ON ISOKINETIC PERFORMANCE OF THE QUADRICEPS FEMORIS

Daniel T. Borges [1,*]Liane Macedo [1]Caio Lins [1]Jamilson Brasileiro [1]

[1]Department of Physotherapy, Federal University of Rio Grande do Norte, Natal, Brazil

Introduction and Objectives: Whole body vibration (WBV) has become a popular practice in training and rehabilitation centers[1]. These are devices that produce vibrations in a wide range of frequencies and amplitudes that are transmitted in the form of mechanical energy to the body in order to create instability[2]. The mechanism by which the vibrating platform acts on body is based on the excitatory neuromuscular response. The vibratory stimulus acts on myotendinous structures, causing changes in the length of the fibers inducing excitation of the muscle spindles. Finally, the Ia afferent neurons facilitate the activation of alpha motor neurons causing a reflex muscle contraction[3].Although this is a widely used resource, there is a lack of consensus in the literature regarding the protocols to be applied, and the real benefits and immediate physiological responses triggered by vibration. Therefore, the present study aims to analyze the acute effects of an exercise protocol with WBV, in different frequencies, on the isokinetic performance of the quadriceps in healthy women.

Methods: This is a randomized controlled trial where 60 healthy and active women were randomly divided into three groups with 20 members each: control group (CG)-performed an exercise protocol without WBV; group 30 Hz - performed the exercise protocol with WBV, with frequency set at 30Hz and 4mm of amplitude, and 50 Hz group - performed the same WBV protocol at a frequency of 50 Hz and 4mm of amplitude. Initially volunteers performed a warm-up exercise on a stationary bicycle (5 min; 15 W; 20 km/h). Performance measurements were started 3 min after the warm-up. For isokinetic evaluation, volunteers were positioned on the dynamometer, stabilized by braces and with the device axis aligned with the evaluated knee. The machine's lever arm was attached to the distal region of the non-dominant leg. They were instructed to perform 5 maximal contractions only for knee extension at 60°/s, starting from 90° flexion up to full extension. Variables analyzed were peak torque normalized by body weight (PT/BW), total work, power and time of peak torque (TPT). Immediately after the isokinetic evaluation, intervention protocols were carried out. The 30 and 50 Hz groups performed an exercise protocol on the vibration platform, which was composed of an unilateral isometric semi-squat with the knee held in 40º[4], both arms extended at shoulder height and the trunk in upright position. Participants performed a total of 10 sets of 30s, with rest intervals of 30 s between sets[4, 5]. The knee angle was monitored with a universal goniometer to ensure that there were no changes in the amplitude during the protocol. The platform was turned on at the beginning of each series, established with a vibration frequency of 30 Hz or 50 Hz (depending on the group) and an amplitude of 4mm[6]. Volunteers of the CG group performed the exercise with the platform turned off and familiarization was allowed for all participants. After the application of the exercise protocols in the respective groups, all volunteers underwent a reassessment identical to the evaluation performed at baseline. Software SPSS (20.0) was used for statistical analysis. A One-way ANOVA was used to investigate baseline differences between groups. A Two-way repeated measures ANOVA was calculated to identify differences within and between pre- and post-tests. In the case of significance, post hoc comparisons (Bonferroni) were calculated additionally. A significance level of 5% was chosen.

Results: No significant differences in anthropometric measures or variables analysed were observed on the baseline evaluation between the groups. There was no significant difference in the values of PT/BW, total work and power regardless of the adopted frequency. There was a significant reduction in the values of TPT on the CG, 30Hz e 50Hz groups (P=0,18;P<0,001;P=0,003 respectively), but with no significant differences between them (Figure 1).

Figure:
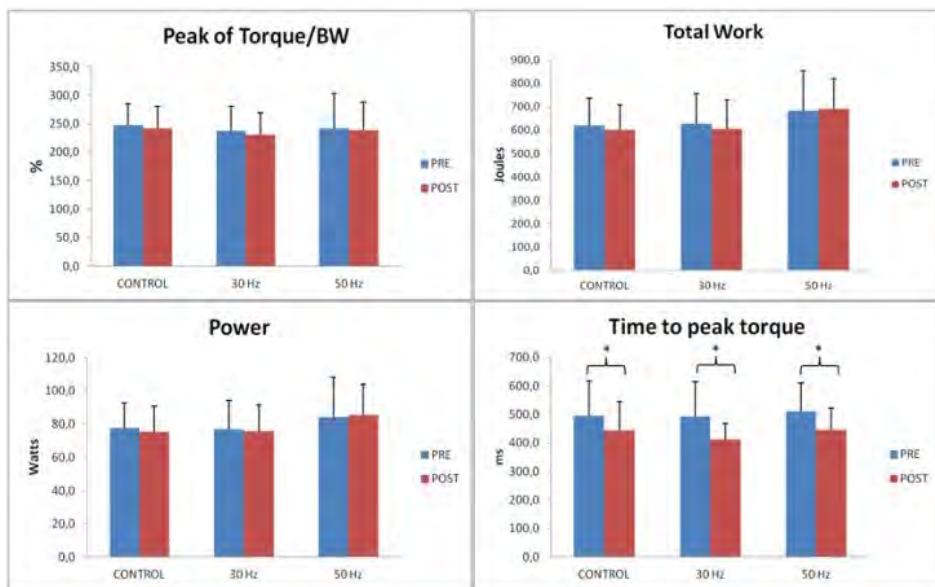
Caption: Figure 1 - Means and standard deviation of peak torque normalized by body weight (PT / BW x 100), total work, average power and time to peak torque, pre and post implementation of the protocol on three groups: control, 30 Hz and 50 Hz.

Conclusion: The results of this study suggest that the exercise protocol associated with WBV is not able to significantly improve the isokinetic performance of the non-dominant quadriceps femoris of healthy and active women.

References: [1] Siu P.M., et al., Arch of phys med rehab, 91: 1608-15, 2010.

[2] Albasini A., et al., Using whole body vibration in physical therapy and sport - clinical practice and treatment exercises, Elsevier, 2010.

[3] Cardinale M., Lim J., J of strength cond res, 17(3): 621-4, 2003.

[4] Caryn R.C., et al., Int J sports med, 35: 330-8, 2014.

[5] Shinohara, M. Med Sic sport exer. 37(12): 2120-5, 2005.

[6] Hazell T. J., et al., Appl. Physiol. Nutr. Metab, 32: 1156-63, 2007.

Disclosure of Interest: None Declared

Musculoskeletal

PO-0289

A PREDICTIVE EQUATION FOR ESTIMATING THE CONTRIBUTION OF BIARTICULAR MUSCLES TO PASSIVE JOINT MOMENT

Mark Hines [1] [2,*]Neale Tillin [2]Raymond Lee [1]

[1]School of Applied Sciences, London South Bank University, [2]Life Sciences, University of Roehampton, London, United Kingdom

Introduction and Objectives: Hip joint moments during dynamic tasks are commonly modelled using the inverse dynamics method, based upon the Newton-Euler equations. In the inverse dynamics approach, the hip joint is considered to behave as a frictionless line-hinge (Koopman *et al.*, 1995), without appreciable interaction of passive structures. However, investigators have reported that passive structures about the hip joint can contribute considerably to the net moments measured during dynamic tasks, such as gait (Yoon and Mansour, 1982, Silder *et al.*, 2008, Whittington *et al.*, 2008).

The purpose of the present paper is to demonstrate the contribution of the posterior hip tissues to hip moments during passive flexion, and to develop an equation for the prediction of passive hip moments during active tasks, at various hip and knee angles.

Methods: Hip moment-angle data from 52 subjects, measured during supine passive leg raising tests, was reassessed for development of the predictive equation. In the initial investigation, the knee had been supported in each of 4 angles from 180 (leg straight) to 140 degrees. Passive hip moments were measured using a custom-built force transducer.

To establish a predictive equation for passive moments, based upon a combination of hip and knee angles, plots were generated for assessing the changes in hip moments with hip angle, and at different knee angles independently. In agreement with other researchers, passive hip moments were found to increase exponentially as a function of hip angle. By introducing a variable knee angle component, it was found that this contributed a linear component to the model. A surface fitting programme was written for Matlab, and visual and residual analyses used to determine the most appropriate equation for the individual datasets.

Results: For both absolute and bodyweight-normalised moments, the mean adjusted r-squared was 0.894 (0.077), with a range of 0.603 to 0.995. For absolute moments, the mean RMSE was 2.059 (0.891), with a range of 0.588 to 4.8. For bodyweight-normalised moments, the RMSE was 0.029 (0.013), with a range of 0.007 to 0.062.

Figure 1 shows a surface plot of the ensemble mean of 3 passive moment curves at each of 4 knee angles, for a typical test participant. Table 1 shows the average, standard deviation and ranges for the equation coefficients. The coefficients interact for a given participant and therefore mean values should not be used to estimate passive moments.

Figure:
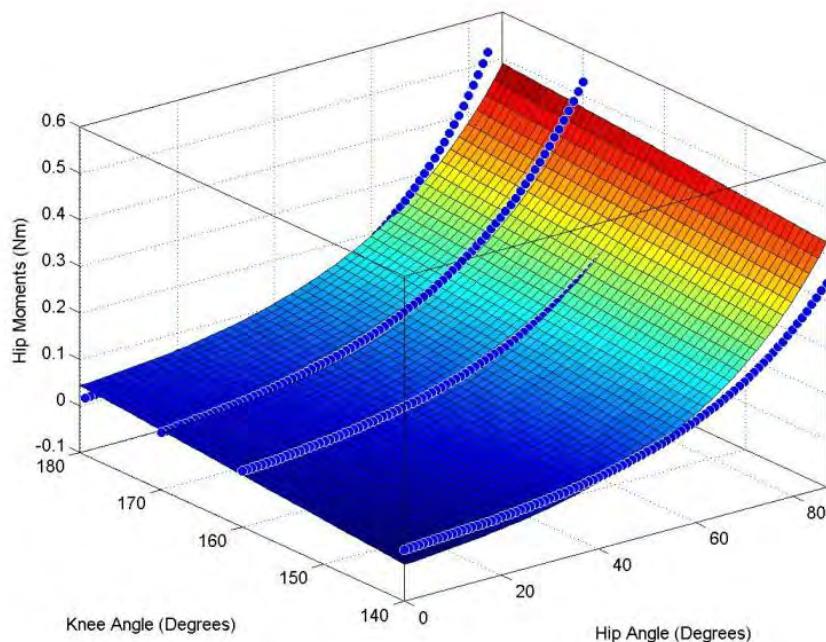
Conclusion: Models of dynamic movements that do not include a measure of passive contributions are at risk of overlooking an important biomechanical component. The following equation should be used to derive the contribution of passive moments about the hip during flexion, in dynamic movements utilising a variety of hip and knee angles

$$M(Passive) = a*theta(knee)+b*exp(c*theta(hip))+d$$

Table:

	Equation Coefficients			
	a	*b*	*c*	*d*
Mean	0.002	0.068	0.022	-0.307
Median	0.002	0.067	0.021	-0.302
SD	0.001	0.942	0.014	0.942
Min	-0.001	-8.644	0.000	-3.594
Max	0.005	3.359	0.085	8.182

References: Koopman, B., Grootenboer, H.J., & de Jongh, H.J., 1995. An inverse dynamics model for the analysis, reconstruction and prediction of bipedal walking. *J Biomech*, 28(11), 1369-76

 SILDER, A., HEIDERSCHEIT, B. & THELEN, D. G. 2008. Active and passive contributions to joint kinetics during walking in older adults. *J Biomech,* 41, 1520-7.

 WHITTINGTON, B., SILDER, A., HEIDERSCHEIT, B. & THELEN, D. G. 2008. The contribution of passive-elastic mechanisms to lower extremity joint kinetics during human walking. *Gait Posture,* 27, 628-34.

YOON, Y. S. & MANSOUR, J. M. 1982. The passive elastic moment at the hip. *J Biomech,* 15, 905-10.

Disclosure of Interest: None Declared

Musculoskeletal

PO-0290

WEBINARS SERIES AND INTERNET BROADCAST: A STRATEGY TO PROVIDED EDC REGIONS WITH ACCESS TO BIOMECHANICS

Emmanuel S. Da Rocha [1 2,*] Marco Vaz [2 3] Felipe Carpes [1 2]

[1]Applied Neuromechanics Group, Federal University of Pampa, Uruguaiana, [2]Brazilian Society of Biomechanics, [3]Biomechanics and Kinesiology Research Group, Federal University of Rio Grande do Su, Porto Alegre, Brazil

Introduction and Objectives: Access to education is still one of the main challenges in economically developing countries (EDC). In Academia, it is very common to hear from EDC members about their difficulties to travel abroad to attend international scientific conferences that gather scientist of the field. In the other hand, Internet access has significantly increased in EDC regions in the last years. The use of Internet for science divulgation is not a novelty, but in the field of Biomechanics there are very few online courses and materials available.

The purpose of this study was to show how internet-based tools are being used to divulgate Biomechanics, how the distance between the scientists and the academic apprentices in EDC can be decreased and what is the participants' perception on the themes presented by invited speakers and the importance of these themes for their academic lives.

Methods: Internet tools were used since 2011 to divulgate Biomechanics through online broadcasting tools provided by the Federal University of Pampa and the Federal University of Rio Grande do Sul, both Brazilian Universities. Using these tools, lectures were recorded and broadcasted online, and the records were later made freely available online worldwide. The recordings were made from webinars and lectures given by invited speakers, in Portuguese, English or Spanish. These activities were related to:

Monthly webinars

The monthly webinar involved lectures on topics of exercise and rehabilitation that were live broadcasted through the Internet. Upon speaker's agreement, lectures were recorded. This activity was developed since 2011 and is currently listed as an EDC project at the ISB webpage (isbweb.org/component/content/article/127-edc-projects/434-unipampa-brazil). Every January, an annual agenda of the invited lectures topics is made available on the Internet (porteiras.s.unipampa.edu.br/gnap/webinar). To watch the lecture online people interested should visit a specific URL (webconf.unipampa.edu.br/gnap). There is no need for previous registration and there is no fee to be paid. The University supports the webinar system. To watch recorded lectures the visitant needs to open the link (porteiras.s.unipampa.edu.br/gnap/webinar) and wait until the system loads the class. At the end of each live webinar people are requested to answer some questions concerning the experience online. Part of these answers are summarized in Figure 1. There was a positive feedback for all questions regarding the webinar.

Online broadcast

Using the same method used for the webinars, live broadcast was used for MSc and PhD defenses and for other scientific events. One of the relevant examples that made scientific knowledge accessible worldwide was the broadcasting of the V Annual Symposium on Applied Neuromechanics, in October 23rd-25th 2014, where all lectures were live broadcasted and recorded for subsequent display. A special website was created where any person can access the lectures and watch

them online. The website link (sites.google.com/site/symposiumneuromechanics/neuromech-tv) does not require any login or registration.

Results: The webinar series consists of 36 online lectures in different topics since 2011. The average number of participants in each lecture ranged from 20 to 35, with some lectures bringing more attention than others. For example, a lecture on scientific writing had 45 participants and the lecture with the highest number of participants had 56 people online the same time. If we look at the total number of participants, in the last three years more than 700 logins were made on the webinar online system. Most of the participants attending the online lectures were from Brazil and South America, especially when the lecture was in Portuguese or Spanish. When lectures were in English, we observed a higher number of participants from other continents. Finally, a continuous interest was observed for accessing former lectures recorded, which also happens due to the different time zones. In Figure 1 a summary of the feedback received is shown.

Figure:
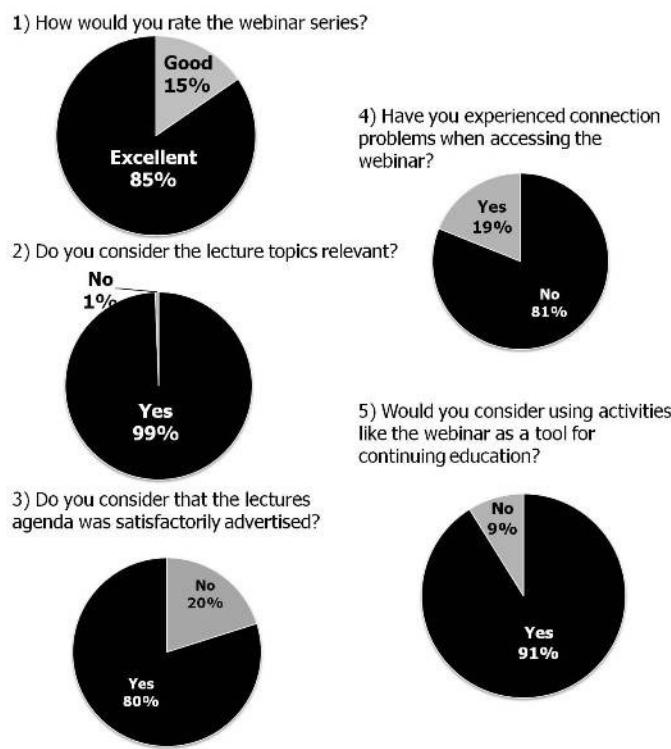
Caption: Figure 1. Feedback received from the participants.

Conclusion: The use of Internet to spread the knowledge in the field of Biomechanics is an efficient strategy to provide people from different places with access to information. Online lectures bring attention of a significant number of people, but it is still lower than the number of people we want to reach. Different time zones and the language barriers are some of the challenges to overcome when promoting strategies to increase access to online education in EDC.

Disclosure of Interest: None Declared

Musculoskeletal

PO-0291

EXPLORING THE CONSISTENCY OF MUSCLE CO-ACTIVATION ACROSS ACTIVITIES OF DAILY LIVING IN INDIVIDUALS WITH KNEE OSTEOARTHRITIS

Stephanie L. Smith [1,*]James Woodburn [1]Martijn Steultjens [1]

[1]School of Health and Life Sciences, Glasgow Caledonian University, Glasgow, United Kingdom

Introduction and Objectives: Individuals with knee osteoarthritis (KOA) exhibit different movement and muscle activation patterns compared to matched controls. These changes in muscle activation can be seen in muscle co-activation levels, whereby individuals with KOA demonstrate high levels of muscle co-activation compared to controls. High co-activations levels are thought to be neuromuscular adaptations to promote dynamic joint stabilisation; however, it is also thought that high muscle co-activation increases joint load and may therefore be detrimental to the progression of KOA. The purpose of this study was to explore the consistency of muscle co-activation across different activities and explore specific areas of co-activation during different phases of walking.

Methods: Neuromuscular performance of 25 symptomatic KOA (60.9 ± 9.5 yrs; 30.4 ±5.9 kg/m^2) participants and 4 controls (50.8 ± 2.0 yrs; 25.8 ±4.8 kg/m^2) was assessed using electromyography (EMG) and ground reaction forces recorded during a series of walking, stair ascent and descent and sit to walk trials at self-selected speed. Gait was split into phases (pre loading, loading response, early, mid and late stance). EMG was recorded from 7 sites (medial/lateral gastrocnemius, biceps femoris, semitendinosus, vastus lateralis/medialis and rectus femoris). All trials where normalised to maximal voluntary isometric force contractions (MVC). Peak force and muscle co-activation index (CI) were calculated from the normalised EMG for all activities using the following equation CI = (lowerEMGi/higherEMGi)*(lowerEMGi+higherEMGi) where lowerEMGi is the antagonist (least active muscle) and higherEMGi is the agonist (most active muscle) [1,2]. Pearson's correlations where performed to assess the relationship between muscle co-activation across different activities.

Results: Table 1 shows the CI for hamstring-quadriceps (H:Q) co-activation across different activities for both the KOA and control group. CI's were higher in the KOA group than among controls. Within the KOA group, correlation for the H:Q CI between activities was r = 0.558. Similar patterns were observed for the other muscle combinations (range of correlation r = -0.140 to -0.602). There was a strong negative correlation between MVC and CI in the KOA group. When comparing CI's within one activity for different muscle combinations, again a moderate positive correlation was observed between the CI's r = 0.372. High CI's (r = -0.660 - -0.628) were found for medial-lateral co-contraction within the same muscle group (i.e., between vastus medialis and lateralis, semitendinosus and biceps femoris respectively).

Conclusion: Participants with KOA demonstrated high muscle co-activation compared to controls. When muscle co-activation was correlated between activities it demonstrated that individuals with high muscle co-activation remained high across all activities. When looking at muscle combinations participants with KOA high muscle co-activation was most prevalent in the H:Q and medial - lateral muscle groups and most pronounced in the vastus lateralis – vastus medialis muscle co-activation. Although it remains unclear whether high muscle co-activation may be detrimental or beneficial to

KOA disease progression, high muscle co-activation may indicate loss of neuromuscular control in participants with knee osteoarthritis.

Table:

	KOA	Control
Stair dscent	-0.629	0.584
Stair descent	-0.675	0.308
Sit to walk	-0.660	0.863
Gait (stance)	-0.376	-0.624
Pre loading	-0.605	0.295
Loading response	-0.623	0.548
Early stance	-0.490	0.520
Mid stance	-0.620	0.638
Late stance	-0.564	0.511

Caption: Table 1. Hamstrings-quadriceps muscle co-activation correlated with muscle strength during different activities for KOA participants and controls (r values).

References: [1] Rudolph et al., KSSTA, 8: 262-269, 2000.

[2] Schmitt et al., Arthritis Care Res, 42: 1018-1026, 2007.

Disclosure of Interest: None Declared

SHORTENING-INDUCED FORCE DEPRESSION IN HUMAN ADDUCTOR POLLICIS DURING FATIGUE

Ian C. Smith [1,*] Geoffrey A. Power [1] Rafael Fortuna [1] Walter Herzog [1]

[1] Human Performance Laboratory, University of Calgary, Calgary AB, Canada

Introduction and Objectives: Muscle force production is highly history-dependent. For example, a muscle which has undergone active shortening produces less force than a purely isometric contraction at the same final muscle length and activation level. This intrinsic property of muscle, known as shortening-induced force depression (FD), is thought to result from stress-induced changes to the actin filaments inhibiting cross-bridge formation. However, the precise nature of these changes is not well understood. The torsional and flexural rigidity of the actin filament is known to be affected by the specific entity occupying the specific metal cation (K^+, Mg^{2+}, Ca^{2+}) and nucleotide (ADP, ATP) binding sites located on actin, with greater flexibility when Mg^{2+} and ADP are bound [1]. It is possible that the higher Mg^{2+} and ADP concentrations associated with muscle fatigue could affect the entities present at these sites, imparting greater susceptibility of stress-induced deformations to the actin filament, and increase the amount of shortening-induced FD. Thus, the present study was aimed at determining if shortening-induced FD is affected by fatigue during electrically-evoked contractions in the human adductor pollicis muscle.

Methods: Contractions were electrically induced in the adductor pollicis of healthy young participants via Ag-AgCl electrodes placed over the ulnar nerve. Stimulation was applied at 50 Hz with current sufficient to elicit 50-60% of maximal voluntary force. Shortening-induced FD was measured by passively stretching the thumb to a 30° adduction angle prior to the onset of stimulation, and then actively shortening the muscle at a rate of 20° s^{-1} to 10°, with total contraction duration of 4 s. Purely isometric contractions were performed at a thumb adduction angle of 10° for 4 s and served as a reference. In the unfatigued state, the shortening-induced FD and pure isometric measurements were performed 3 minutes apart. Fatigue was then induced by occluding blood flow to the arm via a pressure cuff, and then applying constant 50 Hz stimulation until force was reduced to 40% of the initial value. Prior to cuff deflation, shortening-induced FD was measured and compared to the average results of isometric contractions applied before and after the shortening contraction. The transient nature of fatigue made it necessary to test the shortening and isometric contractions in rapid succession (~10 s apart). Recovery of FD was similarly monitored at 5 and 10 minutes following cuff deflation. Stiffness of the adductor pollicis was measured using a rapid 2° increase in adduction angle (500° s^{-1}). Sample recordings are shown in Figure 1.

Results: The fatigue intervention resulted in a 31±2% decrease in force and a 27±4% reduction in stiffness during the isometric reference contractions (P<0.05). Similarly, work performed during the 20° shortening contraction was 27% lower in the fatigued state (P<0.05). While the absolute magnitude of shortening-induced FD was lower in the fatigued state than the unfatigued state, the relative level of FD was not different between conditions (Table 1). Despite the force differences, no differences in muscle stiffness were detected between the purely isometric and force depressed state. Ten minutes following cuff release, isometric force and stiffness had returned to 88±1% (P<0.05) and 90±4% (not significant), respectively of the values seen in the unfatigued state.

Figure:
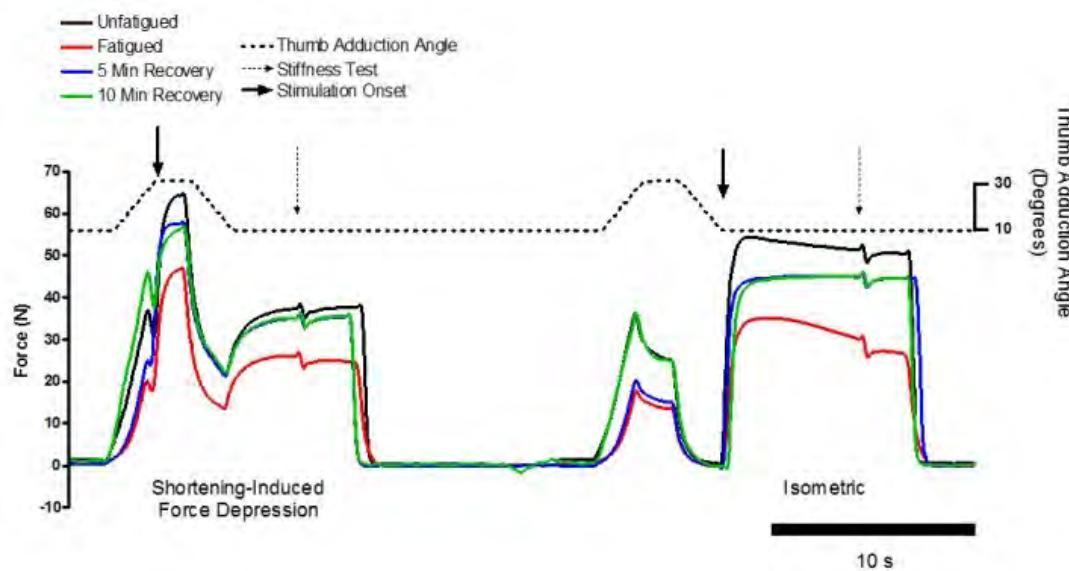
Caption: Figure 1: Sample tracings from human adductor pollicis angle displacement (top) and force production (bottom) for the different conditions tested. Isometric and shortening contractions were performed 3 minutes apart in the unfatigued state. All other conditions were performed approximately as shown with minor temporal shifts (<5 s) to synchronize the records.

Conclusion: The reduced absolute magnitude of shortening-induced force depression during fatigue is consistent with the well documented effects associated with lower stress during shortening, and shortening-induced FD does not appear to be otherwise modified by fatigue. Future work should focus on examining the structure of the actin filament during shortening contractions.

Table:

Condition	50 Hz Force (N)	Work Performed During Shortening (mJ)	Force Following Shortening (N)	Force Depression (N)	Force Depression (% 50 Hz Force)
Unfatigued	55.2 ± 1.4	80 ± 3	37.9 ± 0.5	17.3 ± 1.0	31.2 ± 1.1
Fatigued	38.0 ± 0.8 *	58 ± 6 *	29.9 ± 2.8 *	8.2 ± 2.6 *	21.4 ± 6.7
5 min Recovery	50.7 ± 2.3 †	81 ± 12 †	39.3 ± 4.9 †	11.4 ± 2.8	22.6 ± 6.3
10 min Recovery	48.7 ± 1.8 * †	82 ± 9 †	37.3 ± 4.2 †	11.4 ± 2.6	23.6 ± 5.9

Caption: Table 1: Effects of fatiguing protocol on force and force depression characteristics * - Different from unfatigued (P<0.05) † - Different from fatigued (P<0.05). All values are mean±SEM.

References: [1] Orlova et al., J Mol Biol 232: 334-341, 1993.

Disclosure of Interest: None Declared

Musculoskeletal

PO-0293

FINGERTIP FLEXION FORCE AND MINIMIZATION OF THE SECONDARY MOMENTS AFTER TENDON TRANSFERS FOR RADIAL NERVE PALSY.

Florent PACLET [1,*]François MOUTET [2]Franck QUAINE [3]

[1]INCIA, Bordeaux University, Bordeaux, [2]Unit of Hand Surgery, Grenoble CHU, [3]GIPSA-Lab, Grenoble University, Grenoble, France

Introduction and Objectives: High radial nerve palsy induces the loss of extension in the thumb, fingers and wrist. Tendon transfer surgery uses remained active flexor muscles to restore these lost functions by rerouting the tendon paths. The aim of this study was to investigate how the fingertip forces change following a tendon transfer surgery when performing a finger pressing task. In this study, the transfer procedure corresponds to the Tsugé technique. The principle of minimization of the secondary moments is described as a simple rule to understand the hand biomechanics [1]. It's used by the CNS to solve musculoskeletal redundancy: during the application of four-finger task, a stable force sharing among fingers is adopted to minimize unnecessary rotational moments of the hand. Since High radial nerve palsy and tendon transfer surgery modify the number of muscles crossing the finger and wrist joints, our objective was (i) to characterize the flexion and extension resultant force changes following the transfer, and (ii) to determine if the principle of minimization of the secondary moments of the hand remains valid after tendon transfers for flexion and extension forces.

Methods: 19 asymptomatic subjects and two patients (A and B) with high radial nerve palsy performed four-finger pressing task (i.e. I M R L for Index, Middle, Ring and Little fingers) with the distal phalanx (P3) and four-finger extension task with the proximal phalanx (P1) at maximal intensity. Patients were followed before (M-1) and after (from M+1.5 to M+6) the surgery for a total of 6 months. 4 Kistler force sensors were used to record vertical forces applied by each fingertip in flexion and extension with fingers in a neutral posture. Resultant force in flexion and extension corresponds to algebraic sum of each fingertip force.

Results: Fig. 1 (Top) illustrates fingertip force patients applied in flexion and extension during the follow-up. Results showed both patients have recovered the extension force after the surgery, with an increase during the follow-up (force doubles in 6 month). This force was always inferior to the one observed in asymptomatic subjects. Flexion force reduces just following the surgery, and then increases until three month after the surgery. From three to six month, no significant change was observed in both patients. One can note the force applied by patient B was superior to the asymptomatic subjects force before the surgery (red line), and almost equal after the surgery. The principle of minimization of the secondary moments is presented in Fig.1. Flexion force value (Middle) for each finger changes after the surgery, but it tends to go back to the flexion force sharing pattern computed before the surgery. This pattern is very similar to the one computed for asymptomatic subjects (red dotted line). Concerning extension (Bottom), we observed force distribution is different for each patient with no obvious stable sharing.

Figure:
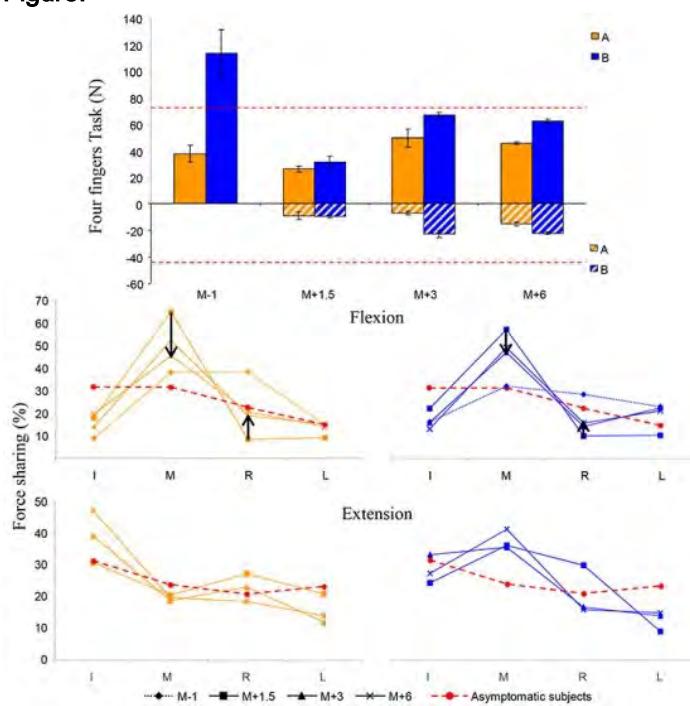
Caption: Fig 1: (Top) Fingertip force 1 month before the surgery (M-1), and after the surgery (M+x) for patient A and B. (Middle) Force sharing pattern for flexion force in both patients (A left, and B right). The black arrow indicates the tendency during the recovery phase. (Bottom) Force sharing pattern for extension force in both patients (A left, and B right). For each graph, red line represents the results for asymptomatic subjects

Conclusion: We observed extension force recovery after the surgery. For one patient (B) this force equals half the force of the asymptomatic group. In the same time, the flexion force drastically reduces just after the surgery, but in spite of the reduction of the number of flexor muscles involved in the task (donor muscles), the force increases in a second time. This force may be still improved since it is superior to the one applied before the surgery. This result confirms the rule in tendon transfer surgery meaning that the procedure used for the transfer does not deteriorate the force production in flexion. For flexion force, force sharing pattern across finger is changed after the transfer, but tendency seems to be the comeback to the initial value during recovery period. We can thus conclude rerouting several flexor muscles for tendon transfers for radial nerve palsy does not modify the way the subject shares the force at the fingertips in flexion. In extension, comparison is more hazardous since this pattern doesn't dependent on the subject motor strategy. In fact, only one muscle is grafted on the finger extensor tendons and theoretically the force sharing pattern should be fixed by the initial tensioning and should remain stable without any possible change. We conclude the principle of minimization of the secondary moments may apply in flexion for hand biomechanics after tendon transfer. It may thus be considered as a simple tool to characterize restored hand biomechanics after tendon transfers.

References: [1] Li et al., Exp. Brain Res., 119: 276-286. 1998

Disclosure of Interest: None Declared

Musculoskeletal

PO-0294

BEHAVIOUR OF HUMAN GASTROCNEMIUS MEDIALIS MUSCLE ARCHITECTURE FOLLOWING MAXIMAL ISOMETRIC FATIGUING CONTRACTIONS

Neil M. Thomas [1,*]Susan Dewhurst [1]Theodoros Bampouras [1]

[1]Department of Medical and Sports Sciences, University of Cumbria, Lancaster, United Kingdom

Introduction and Objectives: By combining ultrasound measures of muscle fascicle length changes with estimations of muscle-tendon unit (MTU) length, researchers have been able to examine the interactions between the contractile and elastic components of MTUs [1]. This method, however, assumes fascicles imaged in a specific region of a muscle exhibit the same magnitude of shortening as fascicles throughout the muscle. Although uniform fascicle behaviour has been demonstrated in the non-fatigued human *gastrocnemius medialis* (GM) [2], widely studied in the literature, there has been no consideration of the potential modification of fascicle homogeneity following fatigue. This raises important questions for the accuracy of GM MTU modelling implemented under the assumption of homogenous fascicle behaviour, in fatigued conditions. The aim of the present study, therefore, was to assess the effects of fatigue on human GM fascicle behaviour.

Methods: With Institutional ethical approval, fifteen male participants (age 21.9 ± 4.1 years, mass 84.0 ± 13.6 kg) performed repeated isometric plantar flexion maximal voluntary contraction (MVC) until peak force fell 30% below an initial baseline MVC. Force from the isometric contraction was measured with a force gauge (Myometer, MecMesin, West Sussex, UK), with the ankle joint at 90°. B-mode ultrasonography (Voluson-i, GE Medical Systems, Zipf, Austria) was used to measure GM muscle fascicle length and pennation angle at distal, middle, and proximal regions at rest and during MVC prior to and following the fatiguing contractions. The middle region of the muscle was defined as the middle of the mediolateral width, at the point with maximal anatomical cross-sectional area, with distal and proximal regions 35mm longitudinally from this point [2]. The effects of muscle region and fatigue state on fascicle length and pennation angle at rest and during MVC were assessed using a 2x3 RM ANOVA protocol. Bonferroni corrected pairwise comparisons were used where applicable.

Results: There was a significant increase in fascicle length during MVC in the distal (2.8mm, 8.1%, $p<0.05$) middle, (4.9mm, 14.1%, $p<0.05$), and proximal (5.2mm, 14.7%, $p<0.05$) regions post-fatigue compared to pre-fatigue. There was also a significant reduction of pennation angle during MVC in the distal (3.3°, 8.8%, $p<0.05$), middle (3.9°, 9.4%, $p<0.05$), and proximal (2.9°, 6.9%, $p<0.05$) regions post-fatigue compared to pre-fatigue. These changes, however, were not region specific. There were no alterations of GM architecture at rest post-fatigue compared to pre-fatigue.

Conclusion: Repeated fatiguing contractions caused a significant reduction of fascicle shortening during isometric MVC, and this reduction was uniform at all regions of interest. The maintained fascicle shortening uniformity following fatigue supports the assumptions of biomechanical models of muscle-tendon interaction in fatigued conditions. The reduction of fascicle shortening indicates that fatigue induced a change in the behaviour of the fascicles which, owing to previous literature [3], may reflect the effects of some of the peripheral mechanisms of muscular fatigue.

References: [1] Fukunaga et al., Proc.R. Soc. Lond. B, 268: 229-233, 2001.

[2] Lichtwark et al., J. Biomech, 40: 157-164, 2007.

[3] Kawakami et al., J. Appl. Physiol, 88: 1969-1975, 2000.

Disclosure of Interest: None Declared

BIOMECHANICS OF CHILDBIRTH AND UPRIGHT POSITIONING DURING LABOUR: GLOBAL HEALTH IMPLICATIONS

Andrea Hemmerich [1,*] Geneviève Dumas [2] Rajani Mullerpatan [3]

[1] Economically Developing Countries (EDC) Programme, International Society of Biomechanics, Ottawa, [2] Dept. of Mechanical and Materials Engineering, Queen's University, Kingston, Canada, [3] School of Physiotherapy, MGM Institute of Health Sciences, Navi Mumbai, India

Introduction and Objectives: Positions of labour are often culturally dependent. In non-Western settings including most developing countries, upright postures such as squatting or kneeling are often naturally adopted. Despite recommendations from the World Health Organization against routine use of a supine position during childbirth, this is still the most common delivery position of women in heath centres, which may be attributed to caregiver preference and Western ideals rather than comfort of the mother.

Upright birthing positions are associated with several benefits such as greater ease and positive perception of the mother, shorter labour, and fewer episiotomies and assisted deliveries [1]. Researchers have suggested numerous biomechanical distinctions associated with upright birthing positions, including stronger uterine contractions and gravity, improved alignment, and greater pelvic outlet area which increase the effectiveness of the passage of the fetus for a shorter labour [1,2]. Using non-medicalized approaches to improve birth outcome would be especially beneficial in developing countries where access to medical resources are often scarce. The biomechanical mechanisms of birth positioning that contribute to specific physiologic outcomes have yet to be adequately explored and understood, however.

The primary purpose of this research was, therefore, to conduct a review of birth complications originating from biomechanical difficulties that could potentially be addressed by mobility and change in birth position during labour and delivery. The secondary objective was to compare incidence of these birth complications in developed and developing countries and the underlying reasons (related to risk factors) for observed differences.

Methods: Scientific and clinical knowledge on the mechanics of the second stage of labour and associated complications in various populations was synthesized to explore potential links between maternal positioning and birth outcome. A review of available data in the fields of biomechanics, clinical medicine, epidemiology, and anthropology was conducted. Due to the lack of rigorous, scientific publications on related material, in particular in developing countries, additional resources were examined, including guidelines and reports produced by global health institutions, informal online literature, and interviews with experts.

Results: The primary biomechanical complication of childbirth is obstructed labour, in which the maternal propulsive power is inadequate to overcome forces opposing delivery, resulting in the inability of the foetus to pass through the birth canal. Resistance is most often due to cephalopelvic disproportion (a geometric mismatch in pelvis and presenting part of the foetus), which may be caused by several maternal and/or foetal irregularities (Figure 1).

Obstructed labour may result in serious consequences and even death if untreated. Trauma in the form of tearing or stretching of the perineum, bladder, or rectum can cause vaginal or uterine prolapse or incontinence in the longterm. If

neglected for too long, obstructed labour could result in impaction of the presenting part of the foetus causing pressure necrosis leading to obstetric fistula. A ruptured uterus may result in haemorrhage, shock, and maternal death.

Poor outcomes in the newborn include fractures of the clavicle, brachial nerve damage, and in severe cases hypoxia leading to brain damage or death.

The prevalence of these outcomes is typically greater in developing countries due to both a lack of skilled birth attendants and/or sterile instruments that could facilitate delivery (e.g. Caesarean section) or repair the trauma that may ensue. In addition, several risk factors are more prominent in developing countries, such as malnutrition and early age of pregnancy, which may both account for smaller maternal pelvic dimensions [3].

Figure:
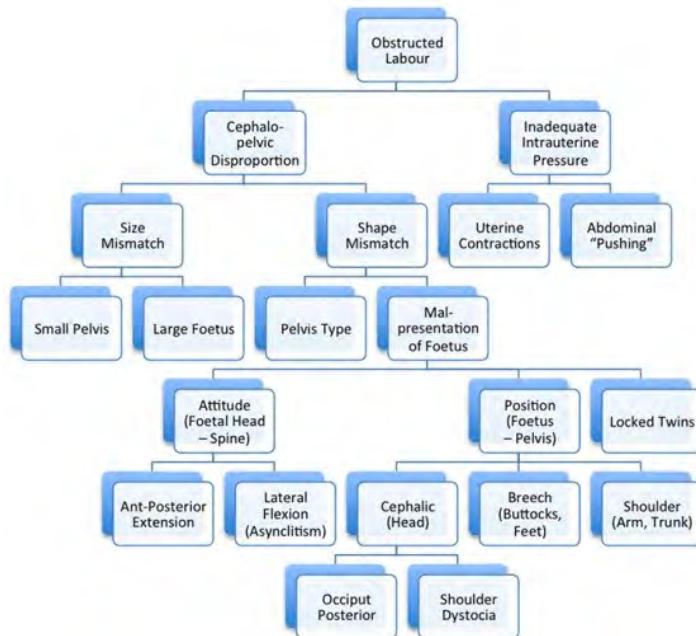
Caption: A biomechanical frame of reference for major complications of childbirth.

Conclusion: In this study we have highlighted an area of women's health that could greatly benefit from further biomechanical research in order to positively influence clinical practice. Although mobility and changing position during labour and delivery has potential to improve maternal and neonatal birth outcome while concomitantly demedicalizing perinatal care, many care providers are reluctant to change practice due to insufficient evidence and insight into the link between dynamic musculoskeletal mechanics and clinical outcome. Implications of childbirth biomechanics research, specifically on maternal positioning, may be greater in developing countries due to associated risk factors and lack of available resources for treatment.

References: [1] Gupta JK et al., Cochrane Database Syst Rev. 5:CD002006, 2012.

[2] Reitter A et al., Am J Obstet Gynecol. 211:662.e1–662.e9, 2014.

[3] Dolea C et al., Global Burden of Obstructed Labour in the Year 2000. Evidence and Information for Policy (EIP), 2003.

Disclosure of Interest: None Declared

KNEE JOINT STRUCTURE FORCES IN INCLINED WALKING AT SELF-SELECTED AND PRE-SET SPEED

Hermann Schwameder [1,*]Nathalie Alexander [1]

[1]Sport Science and Kinesiology, University of Salzburg, Hallein, Austria

Introduction and Objectives: Uphill and downhill is associated with increased knee joint loading compared to level walking [1,2,3]. Inclined walking typically leads to reduced walking speed indicating a clear correlation with the amount of inclination. When investigating the effect of the magnitude of the inclination on joint loading parameters one approach is keeping the walking speed constant for all conditions in order to provide comparative conditions, however, this does not correspond with the typical speed adjustment on inclined surfaces. Another approach is to allow self-selected speed, but in this case the comparison between the inclination conditions is restricted. Thus, the purpose of this study was to compare knee joint structure forces in inclined walking at differently inclined surfaces while walking at a pre-set and self-selected speed. Furthermore, it was investigated if differences in knee joint loading regarding the two conditions can be explained by the differences in walking speed.

Methods: 18 healthy male participants (27.0 ± 4.7 y, 1.79 ± 0.05 m, 74.5 ± 8.2 kg) were recruited for this study. The participants were asked to walk on a ramp (6 m x 1.2 m) with two integrated force plates (AMTI, USA, 1000 Hz) at different inclination angles of -18°, -12°, -6°, 0°, 6°, 12° and 18°. They had to perform three valid trials both with a constant pre-set speed of 1.11 m/s and a self-selected walking speed. In the pre-set condition the trial with the speed closest to the aimed speed and in the self-selected condition the median trial were used for further analysis. Kinematic data were captured with a twelve-camera, marker based motion capture system (Vicon, UK, 250 Hz). The knee structure forces were calculated using a 2D, quasi-static knee model [2] and were normalized to body weight (BW). ANOVA with repeated measures were used to check for statistical significance. The magnitude of the walking speed effect on the differences was determined using correlation and ANCOVA approaches.

Results: Table 1 shows the tibio-femoral contact force (Ft), the patella-femoral compression force (Fcp) and the quadriceps tension force (Fq) in the self-selected (-s) and pre-set (-p) conditions. As expected the knee structure forces in both conditions increase continuously and significantly with inclination, while the magnitude of increase is more pronounced in downhill (up to 6.9 BW) compared to uphill walking (up to 4.2 BW). The differences of the knee structure forces between the two conditions are rather small and do not exceed 0.51 BW. The largest deviations can be observed for the level walking conditions. Due to the low forces the relative differences in this condition reach magnitudes of about 25%, though. While the structure forces for the -18° and -12° inclinations are higher in the pre-set condition, the opposite relation has been observed for the remaining inclinations. The correlation and ANCOVA analyses showed that more than 80% of the differences between the two walking conditions can be explained by the differences in walking speed.

Conclusion: Walking with self-selected and pre-set speed leads to relatively low differences regarding the knee joint structure forces. To conclude, depending on the purpose of the study each of the walking speed approaches is applicable without causing pronounced changes of the structure forces in the knee. Due to the high correlation between the walking speed and the differences of knee structure forces a normalization of structure forces on walking speed is a reasonable measure to make diverse walking conditions better comparable.

Table:

inclination	Ft-s	Ft-p	Fcp-s	Fcp-p	Fq-s	Fq-p
-18°	5.48	5.91	5.63	5.96	6.50	6.94
-12°	5.16	5.17	4.96	5.09	5.99	6.09
-6°	3.34	3.07	2.94	2.65	3.94	3.66
0°	2.91	2.40	1.97	1.57	2.79	2.29
6°	3.43	3.23	2.22	1.97	2.69	2.42
12°	3.94	3.72	3.38	3.04	3.70	3.36
18°	3.93	3.92	4.06	3.95	4.21	4.12

Caption: Table 1: Tibio-femoral contact force (Ft), patello-femoral compression force (Fcp) and quadriceps tension force (Fq) in self-selected (-s) and pre-set (-p) speed conditions in walking on differently inclined surfaces (values in BW).

References: [1] Lay, A.N., et al. (2006). J Biomech, 39(9):1621-1628.

[2] Schwameder, H., et al. (2005). Sports Biomech, 4(2):227-243.

[3] Kuster, M., et al. (1994). Clin Biom, 10: 79-84.

Disclosure of Interest: None Declared

Musculoskeletal

PO-0297

EVALUATION SACROILIACA TEENS IN A PUBLIC SCHOOL OF THE SANTA MARIA, RS, BRAZIL

Estele C. W. Meereis [1,*]Sandra C. Morais [2]Mithielle A. Machado [3]Veronica J. Casarotto [4]Tatiele Zulian [3]

[1]Postgraduation in Human Movement Sciences, Federal University of Rio Grande do Sul, Porto Alegre, [2][1]Graduation in Biological and Behavioral Aspects of Physical Education and Health, [3]Specialist, Federal University of Santa Maria, [4]Physiotherapist, Franciscan University, Santa Maria, Brazil

Introduction and Objectives: Obesity and overweight in adolescence are global public health issues (Catenacci, HILL, WYATT, 2009; ENES, SLATER, 2010) including Brazil. Thats factors such as musculoskeletal discomfort, general lack of mobility and poor lower limb alignment are more common in overweight children and collaborate to perpetuate the accumulation of fat (Taylor et al, 2006). Thus, this study aimed to verify the relation between central adiposity and mobility and structural problems in the iliac sacrum region in adolescents in the city of Santa Maria (RS).

Methods: This research is a cross-sectional descriptive study with High School students from a public school in Santa Maria, RS. For the analysis of body composition: portable digital scale, waist circumference, and hip circumference. The physical therapy evaluation was performed following the evaluation criteria for iliac using active physiological mobility test of bending forward and the iliac placement test. The intrapelvic movement was detected as follows: the teenager was made stand with his or her weight evenly distributed on both legs, while the physiotherapist removed with thumbs the excess of skin so the fingers could stay in the best position, with better sensitivity of bone process. Also, the physiotherapist fingered the underside of the posterior superior iliac spine (PSIS), on both sides. The teenager would bend the trunk forward so that the symmetry of the two PSIS could be observed. Both of them were to perform the same movement downward, therefore showing normal movement. Data were analyzed using simple descriptive statistics (average, standard deviation and percentage). In comparing the groups with presence or absence of hipomobility, we used the Student T test. For comparison between genders the chi-square test was performed. Statistically significant differences were considered when the P value was lower than 0.05. The software used was SPSS version 15.0.

Results: 103 adolescents were evaluated with an average age of 15.35 + 0.84 years, of which 53.4% (n = 55) were female. Of the total sample 74.7% (n = 62) were considered non-obese (eutrophic and thinness). In tests for mobility of the iliac, it was observed similarity in the number of adolescents (n = 103) who have demonstrated alignment and those who have demonstrated to have some changes, as described in Figure 1. These data are considered worrisome, since the iliac reflects not only bad posture from students, but also deficiencies that may be related to the movement. When comparing the anthropometric variables among adolescents (n = 103) with and without the changes in the iliac, it is observed that the students who had pelvic alignment in the active test had weight and waist and hip circumference statistically higher than those who did not show abnormalities. When the test result was the presence of left hipomobility (HE) there were no statistical differences in anthropometric variables between students with and without this alteration, except for the hip circumference (HC), in which those with this change showed higher HC, as shown in Table 1.

Figure:

103 students

51%   49%

■ Satisfatória

▨ Insatisfatória
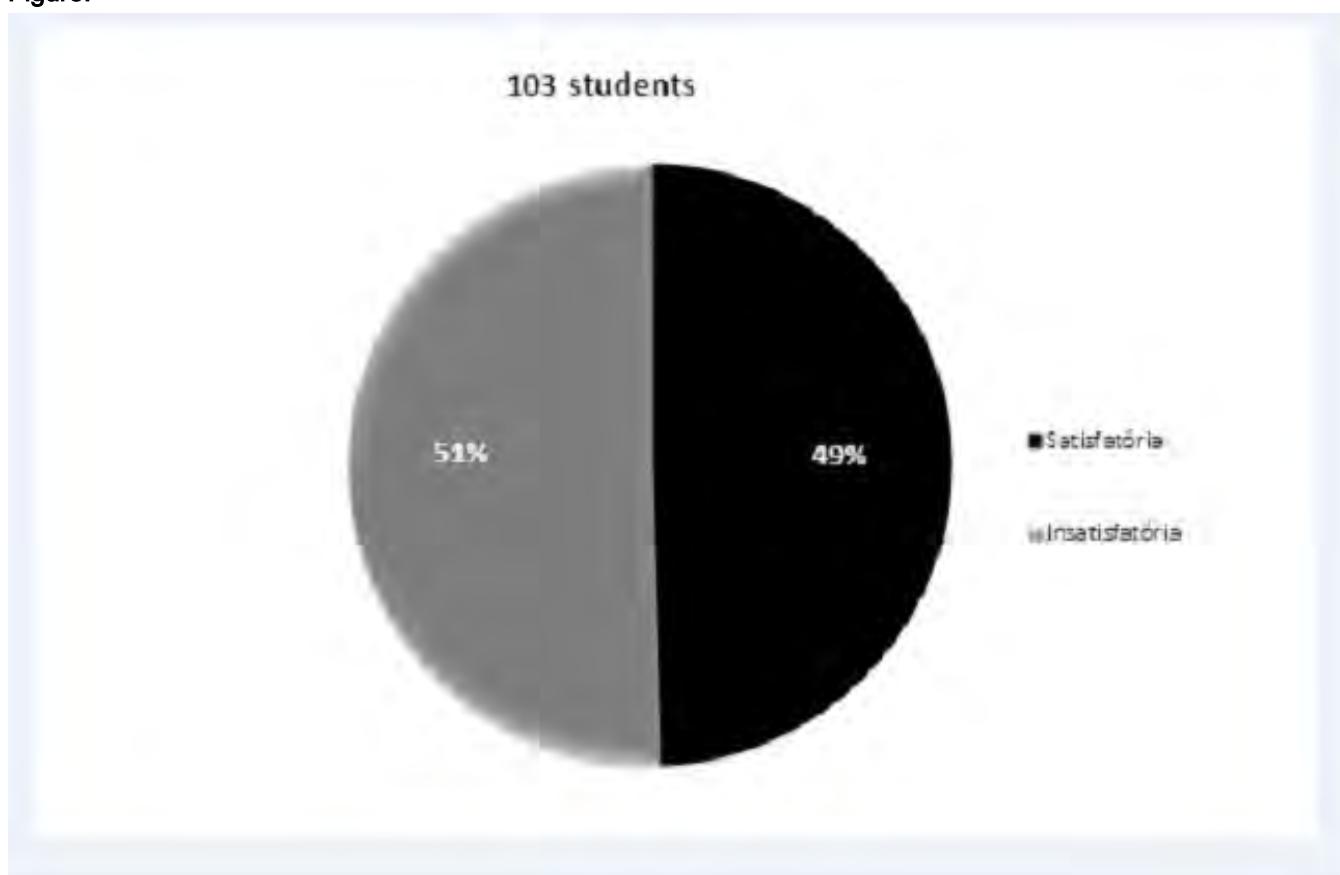
Caption: Iliac positioning Assessment adolescents from a public school in Santa Maria-RS

Conclusion: Half the population had dysfunction in the iliac mobility, showing an unsatisfactory result. There was prevalence of changes in the iliac mobility tests with predominance of hipomobility to the right. We observed that the students who had pelvic alignment in the active test had weight and waist and hip circumference statistically higher than those who did not have any change

Table:

ACTIVE TEST - MATCHING GIFT			
	NOT Mean ± DP	YES Mean ± DP	P
HEIGHT (cm)	167,9 ± 8,7	165,4 ± 8,9	0,87
WEIGHT (kg)	63,6 ± 16,4	58,3 ± 9,4	0,01
CC (cm)	73,6 ± 11,2	71,4 ± 6,4	0,03
CQ (cm)	98,9 ± 10,1	96,1 ± 6,1	0,03

Caption: Comparison of anthropometric variables among adolescents with and without changes in the mobility of the iliac (active testing), Santa Maria-RS. P = Student's t test; cm: centimeters; kg: kilogram; SD: standard deviation; WC: waist circumference; HQ: hip circumference

References: BIENFAIT, M. Summus, 2000. CAMPOS, F. SILVA, A. S. FISBERG, M. o. Braz Pedriatr News, 2002. DETSCH, C. et al. Revista Panamericana de Salud P�blica, 2007. DETSCH, C.; CANDOTTI, C. T. Revista Movimento, 2001. FOLLE, A. BRUM, C. F. POZZOBON, M. E. Revista Digital - Buenos Aires, 2008. NORMAN, P. et al. The Journal of Pediatrics, 2011. MARTELLI, R.I C.; TRABERT, J. Revista Brasileira de Epidemiologia, 2006. VOLPON, J. Ribeir�o Preto Medical Journal, 1996.

Disclosure of Interest: None Declared

PO-0298

THE INFLUENCE OF RESIDUAL FORCE ENHANCEMENT ON MUSCLE OXYGENATION STATUS DURING SUBMAXIMAL VOLUNTARY CONTRACTION OF M. QUADRICEPS FEMORIS

Florian K. Paternoster [1,*] Wolfgang Seiberl [1] Daniel Hahn [2] Ansgar Schwirtz [1]

[1] Biomechanics in Sport, Technische Universität München, Munich, [2] Human Movement Science, Ruhr-University Bochum, Bochum, Germany

Introduction and Objectives: When an active muscle is stretched the resulting post-eccentric steady-state force at a given level of activation is known to be greater than the isometric force at the corresponding muscle length or for a given force less muscle activation is required at the same muscle length. Especially the characteristics of activation reduction of this so- called residual force enhancement (RFE) were associated with possible reduced metabolic costs compared to a pure isometric contraction. Recently, Joumaa and Herzog [1] could show a reduction in the ATPase activity per unit of force for the isometric contraction after active stretch, compared to the purely isometric contraction for a skinned fibers from rabbit psoas muscle. However, it is unclear if these findings of stretch-induced energetic savings can be transferred to human muscle function. Therefore, oxygen consumption of human quadriceps femoris was measured during and after submaximal voluntary lengthening and pure isometric reference contractions.

Methods: Unilateral submaximal isometric-eccentric-isometric (iso. -ecc. -iso.) and purely isometric knee extensions of n=10 subjects were measured using a motor-driven dynamometer (IsoMed 2000, D&R Ferstl, GmbH). The stretch amplitude was 20° (80°-100° knee flexion, 0° refers to full knee extension) and angular velocity was set to 60°s^{-1}. Muscle activation from mm. rectus femoris (RF), vastus medialis (VM) and vastus lateralis (VL) were measured using a sEMG system (OT Bioelecttronica, 4000Hz). For the calculation of the voluntary activation (VA) and the assessment of fatigue, the interpolated twitch technique was used. Muscle oxygenation status of m. VM and m. VL was measured by means of near infrared spectroscopy systems (PortaMon/PortaLite, artinis medical systems, 10 Hz).

First experimental session started with 3 MVCs, followed by a 60s fatiguing, isometric contraction at a submaximal torque level of 60% MVC, controlled via biofeedback software. Directly afterwards an additional MVC was performed to evaluate fatigue. The second session contained an iso.-ecc.-iso contraction, with an identical experimental protocol. Test sessions were separated by 4 hours to fully recover prior to the second session. If the differences between MVCs before sessions one and two exceeded 5%, subjects were excluded from the study.

Statistical analysis of baseline parameters contained MVC torques, VA level and resting twitches (RT). For the sustained contractions torque, muscle activation and oxygen consumption was analyzed during 6 time windows, one every 10 seconds after the onset of the contraction. The muscular oxygen consumption was defined by the maximum slope of the tissue saturation index. Data was tested for normality and repeated measures ANOVA with post-hoc comparisons were used for statistical analysis ($p < 0.05$).

Results: There were no significant differences of baseline values before the sustained contractions of the first and second session. PT level ranged between 148Nm ± 38.36Nm and 147.50Nm ± 38.8 Nm, VA was between 96.49% ± 3.43% and 95.75% ± 4.22% and RT was 44.46Nm ± 20.12Nm for the first and 44.96Nm ± 20.68Nm for the last session. Also during

the 60s fatiguing contractions of first and second session there were no differences in muscle activation and oxygen consumption between purely isometric and lengthening contractions (p> 0.05). After the sustained contractions sessions one and two, there was a significant decrease in MVC torque and RT of about 30%.

Conclusion: The results are not in accordance with previously published findings. Seiberl et al. [2] found AR in the quadriceps femoris with an identical setup at the same submaximal MVC level. Although baseline values at the beginning of the two sessions did not reveal differences, the lack of RFE in our setup might still be due to the uncompleted recovery after the first session. VA and RT provides some information about central and peripheral fatigue, but as the complete mechanisms of RFE are still not understood, there might be other factors sensible to fatigue that are responsible for the absence of RFE in this study. Despite high torque level of 60% MVC in our setup, some subjects showed a reoxygenation of the VL and VM during the endurance contractions, which might has biased the relation of consumed oxygen in muscles. An increased time of recovery as well as the use of a mechanical cuff to create full occlusion of thigh muscle thereby suppressing reoxygenation is planned for future work in order to investigate possible energetic benefits of stretch-induced AR.

References: [1] Joumaa et al., J Biomech 46 (6): 1135–1139, 2013.
[2] Seiberl et al., J Electromyogr Kinesiol 22 (1): 117–123, 2012.

Disclosure of Interest: None Declared

Musculoskeletal

PO-0299

CAN PATELLA TENDON SLACK LENGTH BE MEASURED IN VIVO?

Taija Finni [1,*]Johanna Toivonen [1]Neil Cronin [1]

[1]Department of Biology of Physical Activity, University of Jyväskylä, University of Jyväskylä, Finland

Introduction and Objectives: Muscle-tendon slack length is an important parameter in muscle models but it is difficult to estimate in vivo. The muscle-tendon unit is at slack length when it does not exert any passive tension. Slack may be associated with curvature in some structures that can be visualized but force measurements are very difficult. This study assessed changes in patellar tendon length using curved and linear paths, while also measuring the tendon's resistance to compressive forces using a myotonometer. If initial tendon lengthening occurs without an increase in resistive force, this method could potentially be used to identify patellar tendon slack length.

Methods: Twelve physically active healthy female volunteers (age 23.3 ± 2.8 years, height 165.9 ± 5.4 cm and mass 61.3 ± 6.2 kg) lay supine on a custom-made table with the knee joint at 120° (Fig.1A). Patellar tendon length was measured using ultrasonography (both linear and curvilinear paths were assessed, within-analyser reliability >0.965, Fig 1B), and tendon force response to perpendicular compression was assessed using a myotonometer (probe area of 1 cm, speed 1 mm/sec, protrusion 3 mm) first in a relaxed condition and then at 2.5%, 5%, 10%, 15%, 20% and 30% maximal voluntary contraction (MVC) levels.

Results: At rest (P<0.001, Fig. 1B) and at 2.5% MVC (P=0.019), the curved path of the tendon provided longer lengths than the linear one. Already at 5% MVC the patellar tendon followed a linear path and thus linear distance between patellar and tibial attachment sites may be used when assessing e.g. mechanical properties of tendon, which are typically examined at forces above 10% MVC. Myotonometer peak force correlated with the level of knee extension torque (r=0.90, P<0.001). Based on knee extension torque a linear trendline through 2.5%-30% MVC levels suggested that tendon slack ends at a length which is approximately 4.4% greater than that found at rest. However, a similar estimation based on the myotonometer force suggests only 2.8% tendon elongation at the point when it starts to resist force (Fig. 1).

Figure:
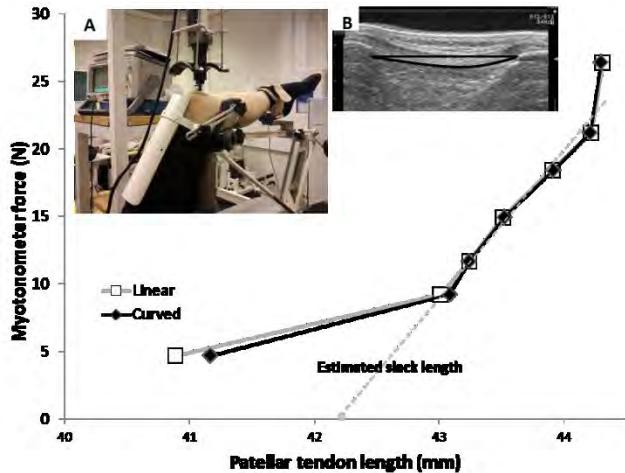
Conclusion: The study showed that estimates of patellar tendon slack length differ depending on whether knee extension torque or myotonometer force is used in the estimations. These results suggest that myotonometry is potentially useful for assessing patella tendon slack length. Moreover, the data suggest that force levels lower than 2.5% MVC are required to further examine this issue; these experiments are currently ongoing.

Disclosure of Interest: None Declared

PO-0300

NEW TAPING METHODS FOR INCREASING THE MUSCLE STRENGTH.

Tsutomu Fukui [1,*] Takashi Kondo [2] Yuko Otake [2]

[1]Health Care Science, Graduate School, [2]Sports Management Center, Bunkyo　Gakuin University, Tokyo, Japan

Introduction and Objectives: While the application of Kinesio tapes may have some therapeutic benefits, the usage of these tapes does not promote strength gains in healthy adults [1]. Kinesio taping did not result in changes in maximal grip strength in healthy subjects [2]. Meanwhile, application of therapeutic Kinesio taping is effective in improving isokinetic quadriceps torque [3]. Although there were lots of researches used the Kinesio Taping for muscle strength, the results have not coincided. It is still uncertain and controversial how to use the taping for muscle strength. We have researched skin movement during joint motion by three dimensional motion analysis system. It was called skin movement artifact and exhibited movement difference between markers on the skin and underlying bone. One of the factors of the artifact may be caused by the sliding at the superficial myofacial layer. In clinical settings, these sliding could be used for muscle exertion by using the new taping technique. We have used this new taping methods named *skin taping* for some years and have lots of effects to facilitate the muscle strength. For facilitating muscle strength, taping direction which should accommodate to the direction from insertion to origin of the muscle was critical importance. The aim of this study is to certain the effects of *skin taping* methods for increasing muscle strength.

Methods: Thirteen healthy male subjects participated in this study. Average age was 23 ± 2.3 years old, height was 171.6 ± 2.5 cm, weight was 58.0 ± 3.9 kg. Gluteus Maximus (; GM) of them used for the evaluation. We applied right GM to ascertain the application of the facilitative taping by *Primus* RS [BTE technologies, Baltimore, USA]. After getting used to the isokinetic contraction, subjects were asked their hip extend maximally at 30deg/sec, concentric mode, three times with five minutes interval. Four condition of Isokinetic evaluation were fulfilled. Condition1: Elastic tape was applied from insertion to origin direction and skin on the Gluteus was stretched. Condition2: Elastic tape was applied from origin to insertion direction and skin on the GM was slacked. Condition3: Dummy tape with no direction. Condition 4: No tape, the order of the condition was randomized. Differences in mean value were assessed with one way ANOVA and Bonferroni multiple comparison procedure.

Results: Mean value of Condition1 was significantly greater than any other conditions ($p < 0.01$) .

Figure:
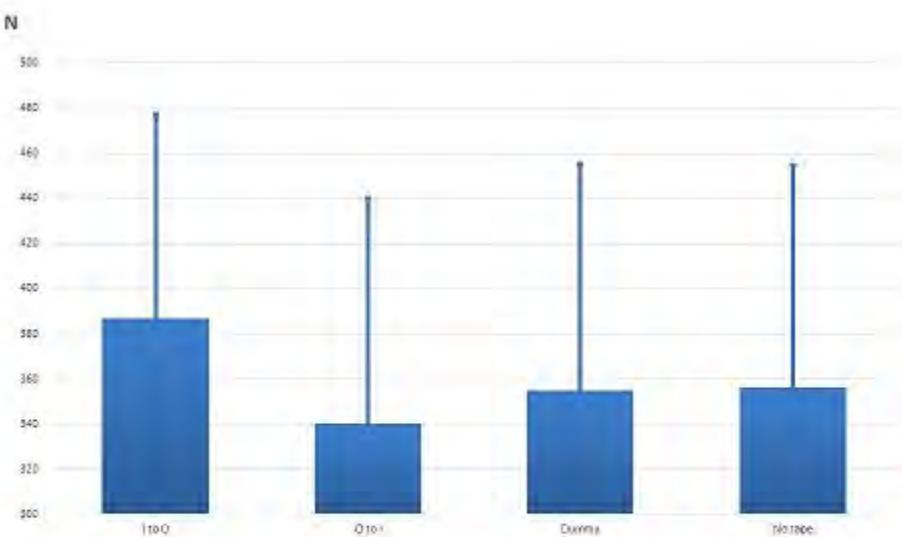
Fig. 1 Isokinetic strength of Gluteus Maximus
I to O was greater than any other taping conditions (*P*<0.001)

I to O: taping direction was from Insertion to origin O to I: taping direction was from origin to insertion.
Dummy: taping with no direction

Conclusion: New taping methods; *skin taping* facilitated the muscle strength. Skin taping direction run from insertion to origin direction may help the sliding of GM contraction. We could observe the sliding between GM and subcutaneous tissue at superficial myofacial layer by ultrasonography. We believe this direction is crucial and also reverse direction had a tendency of inhibition of muscle strength. New taping which run from insertion to origin direction increased the isokinetic GM muscle strength.

References: [1] Csapo, R. Alegre, L. M.: Effects of Kinesio taping on skeletal muscle strength-A meta-analysis of current evidence, J Sci Med Sport: 10.1016/j.jsams.2014.06.014.
[2] Chang, HY. Chou, KY, Lin, J J: Lin, CF, Wang, CH: Immediate effect of forearm Kinesio taping on maximal grip strength and force sense in healthy collegiate athletes, Phys Ther Sport: 11,122-127,2010.
[3] Anandkumar, S, Sudarshan, S, Nagpal, P: Efficacy of kinesio taping on isokinetic quadriceps torque in knee osteoarthritis: a double blinded randomized controlled study, Physiother Theory Pract, 30:375,383,2014.

Disclosure of Interest: None Declared

Musculoskeletal

PO-0301

IMPACT OF FATIGUE ON CONSTANTS OF MOVEMENT FROM FORCE-VELOCITY RELATION AND ACTIVATION DYNAMICS

Harald Penasso [1,*] Sigrid Thaller [1]

[1] University of Graz, Institute of Sport Science, Graz, Austria

Introduction and Objectives: Muscles have properties that determine their characteristics at various conditions. From experience we know that the performance of muscles alters in the course of fatigue [1], and we generally assume that the physical condition of the muscles plays a major role to maintain a certain muscular performance. Therefore, the fresh state of the muscle should contain information about how the properties of the muscles change in the course of fatigue. The aim of this study is to calculate neuromuscular properties from non-invasive measurements in vivo. To identify these constants of movement we use nonlinear parameter identification strategies. A mathematical knee-extensor model is fitted to measured data sets containing data from explosive dynamic and isometric knee-extension maximum voluntary contractions (MVCs). The fatigue protocol is designed to allow the calculation of the constants minute by minute. At each stage we calculate a set of parameters that characterizes the force-velocity relationship (FV) of the knee extensors and its activation dynamics.

Methods: The original approach was introduced by Sust [2] and an improved method was published later [3]. Our recent modifications have enabled an automatized processing routine [4,5].

The model of a single leg-extension consists of an anthropometric-geometric function G(X) that transfers externally measured values to the corresponding values of the muscle and of a muscle force function including activation: A(t) · fm(vm). According to the individual FV the muscle force depends on the contraction velocity (vm) [6]. G(X) depends on position data (X) (distance from greater trochanter to lateral malleolus). The model output is the external force as a function of time.

Force data are measured at an inclined leg-press (9.8°) with a force plate mounted onto a sledge. The position of the sledge (X) is recorded by a high frequency position sensor. The anthropometric lengths of the leg used in G(X) are measured with a tape measure.

The parameter identification routine (Matlab) uses solvers for nonlinear functions to calculate the values of the arbitrary constants by minimizing the sum of the squared differences of measured force data and model output [5]. The constants are the maximum excitation (umax), the excitation rate (U), the maximum isometric force (fiso), the maximum contraction velocity (vmax), and the maximum efficiency (etamax). The final goodness of fit is determined via the normalized mean squared error (NMSE). The constants' confidence intervals, the correlation matrix, and the variance of each residual are calculated as well.

After briefing, familiarization, preparation, and warm up the experiment starts with four explosive dynamic concentric MVCs against the sledge (heels only)(2 conditions: 2x 53.5 kg and 2x 73.5 kg) and is followed by the fatigue protocol: n · [9 · (3 s isometric MVC followed by 3 s rest) plus two explosive dynamic contractions (73.5 kg and 53.5 kg) in quick succession]. The last series is reached individually when the decline of force stabilizes at around n = 15 repetitions.

For each series the constants of movement are calculated from data sets containing the 9th isometric MVC and the next two dynamic MVCs. The initial state is calculated from the first seven contractions where at least one of the two conditions is used.

Results: One subject completed n = 17 series where 13 series matched the inclusion criteria (no constant stuck in a constraint, NMSE greater than 0.96). From the initial state, umax increased by a factor of 4.5 whereas U declined to 58%, vmax to 73.4%, fiso to 40.5%, and etamax to 52.4%. This means that the curvature of the FV (a/fiso) increased to 239%. The mean of all included NMSE was 0.983 ± 0.00903.

Figure:
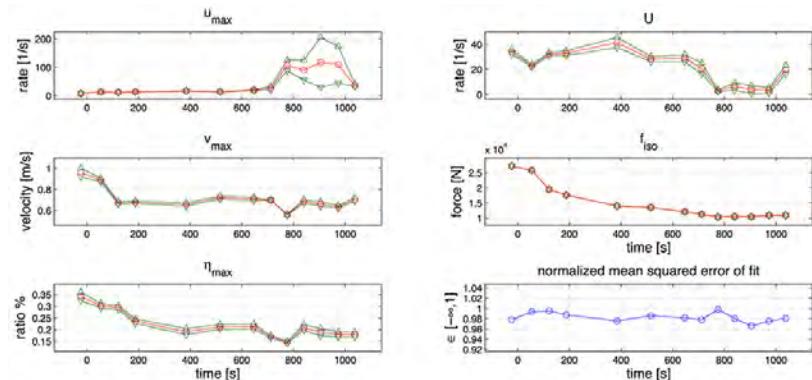
Caption: Fatigue related changes of constants of movement. U and umax refer to the activation dynamics and vmax, fiso, and etamax characterize the FV. Red o: final value, green Δ∇: 95% confidence level.

Conclusion: We found that the model is able to reproduce fresh and fatigued states from non-invasive measurements at natural conditions of the movement. The findings in vmax and fiso are in accordance with literature but our findings show a different behaviour of the curvature of the FV (etamax, a/fiso) (cf. [1]). The planned combined analysis of kinematic data, EMG-data and the pooling of multiple subjects will lead to a better understanding of this fact.

Table:

	umax [1/s]	U [1/s]	vmax [m/s]	fiso [N]	etamax [-]	a/fiso [-]
fresh	8.08	34	0.959	27190	0.342	0.208
fatigued	36.2	19.7	0.704	11010	0.179	0.498

Caption: Fresh vs. fatigued values of the constants of movement.

References: [1] Jones, at al., J. Physiology, 576(3): 913–922, 2006.

[2] Sust, Beitrag zum Aufbau einer axiomatischen Theorie der Biomechanik und Beispiele ihrer Anwendung, University of Jena, 1987.

[3] Siebert et al., Human Movement Science, 26: 320–341, 2007.

[4] Penasso, European College of Sport Science, 19: 241, 2014.

[5] Penasso, Proceedings MATHMOD, Vienna, submitted, 2015.

[6] Hill, Proceedings of the Royal Society (B), 126: 136–195, 1938.

Disclosure of Interest: None Declared

Musculoskeletal

PO-0302

EFFECTS OF STATIC STRETCHING AND PILATES METHOD IN ELDERLY WOMEN FLEXIBILITY: COMPARATIVE STUDY

Deise Aparecida de Almeida Pires-Oliveira [1,*]Rodrigo Franco de Oliveira [1]Raphael Gonçalves de Oliveira [1]Laís Campos de Oliveira [1]

[1]Masters and doctoral program in Rehabilitation Sciences, University of Northern Paraná, Londrina, Brazil

Introduction and Objectives: For the elderly, adequate levels of flexibility contributing to the achievement of activities of daily living independently. Among the possibilities of exercises for the development of this capacity, are static stretching and Pilates. However, there are no studies showing the differences between static stretching and Pilates on the flexibility of the elderly. Thus, the objective of this study was to compare the flexibility of elderly women subjected to static stretching and Pilates on flexibility variable.

Methods: This study is characterized as a randomized controlled trial, blind mono, with elderly residents in the community of the city of Jacarezinho, Paraná-Brazil. The project was approved by the Ethics Committee for Research involving human beings of North University of Paraná (Brazil) under the protocol 513.001.

Inclusion criteria were age between 60 and 65, are not practicing any kind of physical exercise in the last six months and agree not to do another type of exercise during the search. Exclusion criteria were: cognitive deficit>19 according to the Mini Mental State Examination, use of assistive devices for gait and/or presentation of musculoskeletal dysfunction.

After the initial selection, 32 volunteers were evaluated for their flexibility, and submitted to the randomization process, which distributed the volunteers in the stretching group (GA) and Pilates (GP), with 16 members each. After the speeches, they were reassessed.

To measure the flexibility we used a fleximeter assessing flexibility in degrees (°) in flexion (TFM) and trunk extension (EMT), hip flexion (HFM), plant (PFA) and dorse flexion of the ankle (DFA) in three attempts, and considered only the best.

The GA and the GP received 12 weeks of intervention carried out twice a week on nonconsecutive days lasting 60 minutes. The GA held 20 static stretching exercises for the major muscle groups, actively, in three sets of 30 seconds. The GP held 20 Pilates exercises, equipment: Combo Chair, Cadillac Trapeze, Universal Reformer and Ladder Barrel.

Statistical analysis was performed with SPSS 20.0 program, with a significance level of $p<0.05$. Verification of normality occurred using the Shapiro-Wilk test. The initial physical characteristics were compared using the Mann Whitney U test. Since it was not rejected normal distribution hypothesis, applied analysis of variance for repeated measures (ANOVA two way) to verify the intra and inter-group comparisons, at different times of the study. The post hoc Tukey was used for the identification of specific differences in variables.

Results: The groups showed no significant differences at baseline, the variables, age, weight, height and flexion and trunk extension, hip flexion and plant and dorse ankle flexion.

Table 1 shows the comparing pre and post intra-group intervention. The GA had a significant improvement to the TFM and HFM variables. For GP elderly significant improvement for all tests (TFM, EMT, HFM, PFA and DFA).

In the post-intervention comparison (between groups) there was no significant improvement to the TFM (p=0.553), HFM (p=0.873), PFA (p=0.623) and DFA (p=0.333). Only the assessment of EMT significantly different (p<0.001).

Conclusion: It was observed that older who underwent Pilates showed increased flexibility when compared to elderly who performed stretching and may be considered in clinical practice, when the objective is to increase the flexibility of older women.

Table:

Variables		Stretching Group (GA) n=16			Pilates Group (GP) n=16		
	Pre test	Post test	p-value	Pre test	Post test	p-value
TFM (°)	83,12±10,74	91,87±11,93*	0,0247	76,87±11,91	89,62±12,59*	0,0015
EMT (°)	21,32±6,92	24,06±6,60	0,0828	21,87±5,08	30,12±4,11*	<0,001
HFM (°)	88,81±11,73	98,37±7,24*	0,0473	81,56±20,16	99,12±17,48*	<0,001
PFA (°)	26,25±3,89	28,81±3,98	0,0977	24,56±6,03	28,06±5,76*	0,0255
DFA (°)	16,37±3,09	18,06±2,54	0,1057	16,81±3,51	19,06±2,64*	0,0328

Caption: Table 1. Mean values, standard deviation and α, when comparing pre and post-intervention (intragroup). Legend: TFM= trunk flexion movement, EMT= extension movement of the trunk, HFM= hip flexion movement, PFA= Plant flexion movement of the ankle, DFA= dorse flexion movement of the ankle, * = Statistically significant difference (p <0.05).

Disclosure of Interest: None Declared

Musculoskeletal

PO-0303

NEUROMUSCULAR, BIOMECHANICAL AND COGNITIVE STRATEGIES: HOW CAN TAPE ALTER CONTROL?

Steven Lindley [1 2,*] Jim Richards [1] James Selfe [1]

[1]Allied Health Research Unit, University of Central Lancashire, Preston, United Kingdom, [2]Delsys Inc., Natick, United States

Introduction and Objectives:

Patellofemoral pain (PFP) is a musculoskeletal condition that has been described as "the Loch Ness monster of the knee" and the "black hole of orthopaedics" due to its indefinable and expansive nature when addressing the aetiology, management and treatment of pain in and around the knee cap. Although significant and clinically important changes have been observed with joint biomechanics, psychosocial factors, brain activity and neuromuscular activity there still remains a lack of understanding in the control of the knee and the efficacy of common clinical interventions.

This study aimed to provide a unique and multifaceted investigation into understanding the movement control of PFP subjects and the response to a common clinical intervention; explicitly studying the novel aspects of motor unit and neuromuscular control in combination with 3D joint kinematics and kinetics and complimentary clinical measurements of psychosocial characteristics. Consequently providing insight into the muscle force and control strategies both within and between muscle groups in and around the knee, including their response to a clinical intervention, whilst concurrently monitoring the knee joint biomechanics and cognitive measures.

Methods: Both non-symptomatic (n=13) and symptomatic subjects (n=13) performed a single limb isometric squatin two conditions, no tape and with a medial glide tape application. Motor unit data from the Vastus Medialis (VM) and Vastus Lateralis (VL) was recorded using sEMG Decomposition technology (Delsys dEMG). Muscle activity of the Gastrocnemius (GAS), Rectus Femoris (RF), Biceps Femoris (BF) and Gluteus Medius (GMed) were collected using sEMG (Delsys Trigno). Lower limb joint kinematics and kinetics was recorded at 200Hz and 2000Hz respectively, modelled using the CAST method. Measures of conscious motor processing were made using the Movement Specific Reinvestment Scale and pain levels recorded using the Numerical Rating Scale for the symptomatic subjects.

Results: Grouped Tape Response: Regression analysis of the mean motor unit firing rate against the knee joint sagittal joint moment showed the motor unit recruitment intercept was significantly higher and the recruitment slope significantly steeper in the VM for the non-symptomatic subjects with no change in the VL and no change in the symptomatic subjects. Both subject groups demonstrated significant reductions in transverse plane knee joint range of moment, no significant changes in the coronal or sagittal joint mechanics were found. Symptomatic subjects demonstrated a propensity to consciously control their movements and exhibited pain scores of 4.2/10 on the numerical rating scale.

Comparison of groups: Regression analysis comparing the subject groups, demonstrated that symptomatic subjects had a significantly flatter slope for the VM and VL compared to non-symptomatic subjects, and thus significantly different motor unit recruitment strategy. Symptomatic subjects demonstrated a lower common drive in the VM and higher common drive in the VL compared to non-symptomatic subjects. Symptomatic subjects also exhibited significantly lower muscle activity in the GAS, BF, RF and GMed. No changes were seen in the joint biomechanics between the groups.

Individual Tape Response: Exploration of individuals' response to tape exhibited a non-uniform response with variable increases, decreases and no changes across all the different measurements taken.

Conclusion: These findings suggest that the nervous system has various schemes to control the motor unit pool to the Vasti and how it responds to a taping intervention. However, it is evident that the motor unit firing rate, common drive and motor unit recruitment present variable responses amongst individuals, offering a portfolio of solutions to achieve the same goal; increasing the force and its control within the muscle. The underlying mechanism for the observed findings are unable to be expressed definitively, however it can be deduced that the application of tape presents feedback to the muscle that alters the motor unit pool; consequently adjusting the force and its control within and across muscles leading to an increase in knee stability.

The key clinical implications is that the application of tape can offer clinically meaningful change to the sensory-motor control system. However, researchers and clinicians should consider the individualistic responses with data analyses and clinical decision processes respectively.

INSERTION OF A PRESSURE SENSOR MINIMALLY AFFECTS HIND FOOT JOINT KINEMATICS DURING IN-VITRO GAIT SIMULATIONS

Tassos Natsakis [1,*] Josefien Burg [2] Greta Dereymaeker [1] Ilse Jonkers [2] Jos Vander Sloten [1]

[1]Biomechanics section, [2]Faculty of Kinesiology and Rehabilitation Science, KU Leuven, Leuven, Belgium

Introduction and Objectives: Investigating joint loading is of high importance, as several pathologies of the hind-foot (e.g. ankle Osteoarthritis) have been linked to mechanical overloading. Different techniques exist to estimate the contact area or joint contact forces in-vivo, however when a direct measurement of the intra-articular pressure distribution is needed, it must be assessed with the insertion of a pressure sensitive array in the ankle joint. As this requires a highly invasive technique, it might potentially influence the biomechanical behaviour of the joint, more specific altering the kinematics and therefore changing the pressure distribution. Currently, however, the influence of a pressure sensitive array insertion on the resulting kinematics of individual joints was not previously documented. We therefore evaluated the influence of inserting the sensing array in the ankle joint on the range of motion (ROM) of individual joints of the hind-foot during in-vitro gait simulations.

Methods: Gait simulations were performed in 7 cadaveric specimens, amputated mid-tibially [1,2]. The tibial kinematics in the sagittal plane were imposed and the force on nine tendons was applied simulating roll-offs of one second duration. The kinematics of hind-foot bones were captured by an optoelectronic camera system (Krypton K600, Metris, Leuven, Belgium). Active LED markers were mounted on intra-cortical pins that were inserted in the tibia, talus, calcaneus, cuboid and navicular bones of each specimen. Gait simulations were performed before and after the insertion of a Tekscan #5033 (Tekscan Inc, Boston, MA) pressure sensor in the ankle joint. The ROM of each joint was calculated for each direction and a non-parametric rank sum test (Wilcoxon) for each joint and direction was performed between the two sets of measurements. Finally, the relevance of the difference in ROM was evaluated by comparing it with the normal variability in ROM measured in the specimens before the sensor insertion

Results: The maximal difference in ROM measured found in the talo-navicular joint for the transverse and coronal planes (3.2 and 1.6 degrees decrease respectively) and for the talo-calcaneal joint (1.2 degrees decrease). The difference in ROM measured for the tibio-talar joint was less than 1 degree in all three planes. None of these differences was statistically significant and was within the normal variability in ROM that was measured during the simulations before the sensor insertion.

Figure:
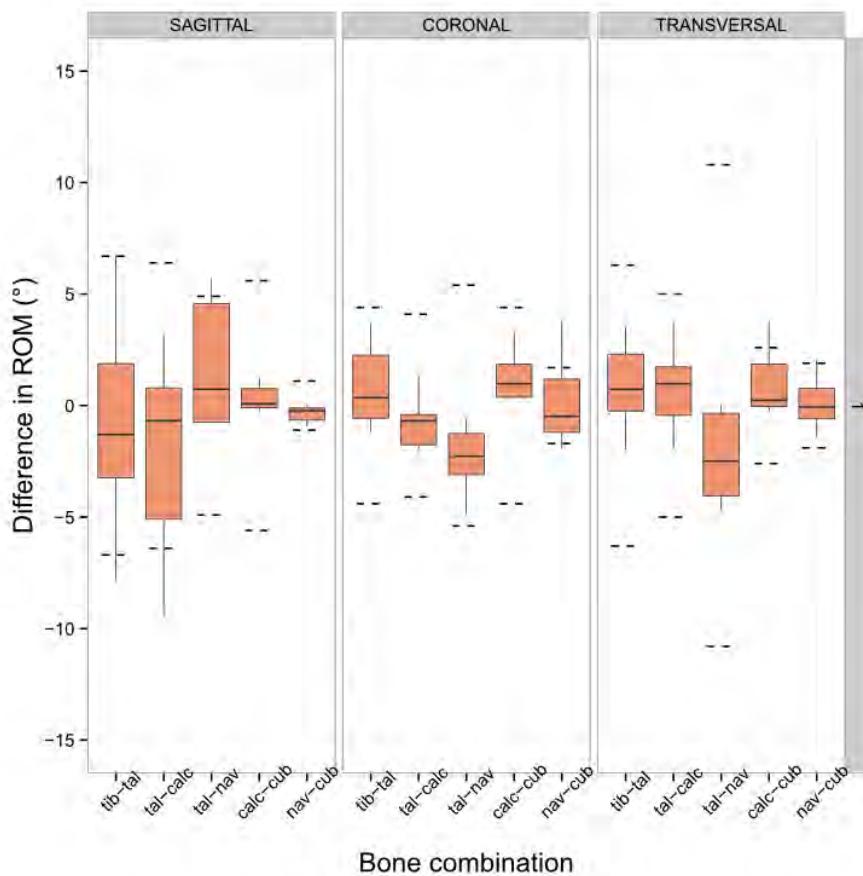
Caption: Difference in range of motion (ROM) for all specimens for each bone combination and plane of motion (positive means increase). The width of each box represents the interquartile range, while the bottom and top end of the whiskers represent the lowest and highest value still within 1.5 of interquartile ranges respectively. The horizontal line inside the box represents the median. The horizontal dotted lines represent the one standard deviation of the ROM in all the measurements without the sensor.

Conclusion: After sensor insertion , differences in ROM are non significant and fall withing the normal variability of the ROM. This, suggests that the kinematics of the hind-foot are not affected by the insertion of the pressure sensing array used in this study. Therefore, such sensing devices can be used to accurrately assess representative joint loading conditions during simulated gait.

References: [1] Peeters et al. J. Eng. Med. 9; 955-967,2013

[2] Natsakis et al. J. Biomech., 2014 (in print)

Disclosure of Interest: None Declared

Musculoskeletal

PO-0305

GLUTEAL MUSCLE ACTIVATION PATTERNS AND HIP JOINT MOTION ARE ALTERED IN THOSE WITH MODERATE AND SEVERE HIP OSTEOARTHRITIS COMPARED TO ASYMPTOMATIC COHORT

Janice Moreside [1 2,*]Derek Rutherford [1 2 3]Ivan Wong [4]

[1]Kinesiology, [2]Physiotherapy, [3]Biomedical Engineering, [4]Orthopaedic Surgery, Dalhousie University, Halifax, Canada

Introduction and Objectives: End-stage (severe) hip osteoarthritis (OA) has been the focus of much biomechanical research, yet little is known as to how joint mechanics alter with increasing severity during gait. Similarly, motor patterns of the surrounding musculature has not been explored among those of increasing hip OA despite increasing support for the role of such musculature to maintain hip function during functional activities. Thus, the purpose of this study was to compare gluteal muscle activation patterns and 3-dimensional hip joint kinematics between 3 groups: those with 1) advanced, 2) moderate unilateral hip OA, and 3) an asymptomatic cohort.

Methods: 60 participants were recruited: 20 with moderate OA and 20 with severe OA, as determined by requirement for surgical management by an orthopaedic surgeon (arthroscopy (moderate) vs. arthoplasty (severe)). Kellgren-Lawrence classifications were used for radiographic OA grading. 20 age-matched asymptomatic participants were recruited from the community. Preferred walking speed was determined using the Gaitrite™ instrumented walkway, followed by approximately 10 minutes of treadmill walking at the determined speed, during which 3 - twenty second trials were collected.

Gluteus maximus and medius electromyograms (EMG) were recorded according to a standardized protocol at 2000 Hz using a custom LabVIEW™ program. Raw signals were processed using custom MATLAB™ script resulting in a linear enveloped signal, normalized to peak amplitude obtained during the gait cycle.

Hip joint 3D kinematics were collected at 50 Hz using a Qualisys® motion capture system. Joint angles were calculated using a 6 degree of freedom model with Cardan/Euler rotations (sagittal, frontal, axial sequence). Heel strike events were determined using an established kinematic method.

Joint angles and EMG were time normalized to 100% of the gait cycle and ≥40 individual waveforms were ensemble averaged to create one waveform per individual. Principal component analysis (PCA) extracted electromyographic waveform features. From 3D hip motions, discrete measures (maximum, minimum) and angular excursions were calculated. A series of one way ANOVAs determined between group differences ($α=0.05$) for 3-dimensional hip motions and principal component scores, with Tukey's post-hoc tests when appropriate.

Results: The severe OA group used a smaller range of total motion (maximum – minimum range) in all 3 planes, compared to both the asymptomatic and moderate groups ($p<0.026$). In the sagittal plane, total motion utilized by the moderate OA group was also significantly different than the asymptomatic group ($p=0.002$) (Figure 1a). The severe OA group demonstrated less hip extension and adduction than either of the other groups ($p<0.001$), and less hip external rotation than the asymptomatic group ($p<0.019$).

In the severe OA group, gluteus medius demonstrated less dynamic response to changing loads throughout the gait cycle, compared to the other 2 groups (Figure 1b). Instead, the gluteus medius initial peak response to heel strike was

lower, followed by higher levels throughout the rest of the cycle, especially mid-stance. This was corroborated by significant differences between the severe and other two groups for both PC1 and PC2 (p<0.005), identifying temporal between-group differences. Average EMG patterns indicate the moderate OA group also showed a trend towards the gluteus medius pattern seen in the severe group (Figure 1b).

Similarly, gluteus maximus activation in the severe OA group showed an initial lower response to heel strike, following by higher activation throughout stance, especially mid-stance. PCA indicated temporal differences between the severe and asymptomatic groups (p=0.05).

Figure:
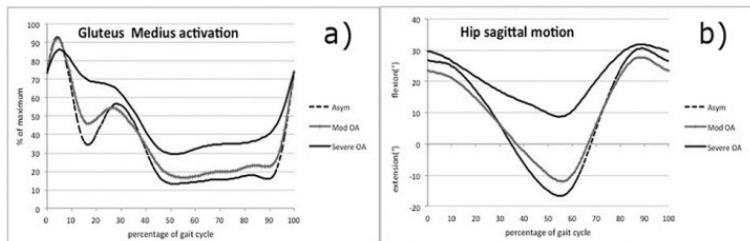
Caption: Figure 1: a) Average amount of hip flexion (+ve) and extension (-ve) utilized during the gait cycle by the 3 groups studied. b) Gluteus medius activation throughout the gait cycle as a percentage of maximum amplitude obtained during the gait cycle.

Conclusion: As 3-dimensional hip motion during gait diminishes with increasing hip OA severity, gluteal muscle activation patterns also change, particularly during early and mid-stance. While these findings occur in those with severe OA, the moderate OA group also showed similar changes in gluteus medius. These increased contraction levels during gait would likely increase compressive forces within the hip joint, potentially hastening further joint deterioration and diminished function during gait.

Table:

	age	BMI[a]	velocity[b]	KL score
Asym	62.6(6)	25.6(5)	1.5(0.2)	-----
Mod OA	59.1(8)	28.7(4)	1.3(0.2)	2
Severe OA	63.4(8)	30.5(5)	1.1(0.2)	4

Caption: Table 1: Participant demographics and average Kellgren-Lawrence (KL) score. a= significant difference between the asymptomatic and severe groups (p=0.026). b= significant differences between all groups (p<0.015)

Disclosure of Interest: None Declared

Musculoskeletal

PO-0306

TEXTURE ANALYSIS OF ULTRASOUND IMAGES ON THE QUANTIFICATION OF THE MUSCLE DAMAGE INDUCED BY ECCENTRIC EXERCISE

Thiago T. D. Matta [1,*]Wagner Pereira [1]Regis Radaelli [2]Ronei Pinto [2]Liliam Oliveira [1]

[1]Biomedical Engineering Program, Federal University of Rio de Janeiro, Rio de Janeiro, [2]Laboratório de Pesquisa do Exercício, Federal University of Rio Grande do Sul, Porto Alegre, Brazil

Introduction and Objectives: High intensity or volume eccentric muscle contractions induce skeletal muscle damage, mainly when the subject is untrained (1). There are many techniques to evaluate the physiological effects of those types of exercises and to quantify of consequent muscle damage (2). Ultrasound echo intensity is commonly used as a local and non-invasive method, and it is based on the histogram of the greyscale pixels of a region-of-interest (ROI) (3). However the small order of the image unidimentional analysis and impaired spatial assessment of the ROI must be considered technical limitations (4). Image texture analysis is a mathematical procedure used to inform the relative position between pixels of the ROI and quantified by many statistical techniques (e.g. grey-level of co-occurrence matrix – GLCM or complexity curve – CC) (5). Therefore, texture analysis can be a promising method for muscle damage studying, which has not been reported in literature yet. The aim of the present study is to analyze the time changes of the complexity curve and grey-level co-occurrence matrix texture parameters and echo intensity on ultrasound images of Brachialis muscle during volume eccentric muscle contractions.

Methods: Thirteen healthy young women performed two sets of ten elbow flexors eccentric contractions by elbow joint extensions at 30 degrees/second, with a 60-second rest interval. The images were acquired by B-mode ultrasound (Nemio XG, Toshiba, Japan, 7.5 MHz, 38 mm linear probe), at 8 cm above the elbow joint. Ultrasound images were acquired at baseline, immediately after, 24h, 48h, 72h and 96h after exercise. Ten texture parameters were calculated: five for GLCM: entropy(*coo*), second angular moment (*asm*), standard deviation (*std*), contrast (*con*)and correlation (*cor*); and five for CC: maximum value (*mv*), average value (*av*), sample mean of grey-level (*sm*), sample standard deviation of the grey-level (*ssd*) and entropy (*ent*). The echo intensity value was considered de mean and median values of the gray distribution (0: black and 255: white). All parameters were calculated on a ROI of 25 x 25 pixels of the brachialis muscle.

Results: Significant value increase was found for the *cor, sm* and echo intensity average at 48, 72 and 96h from baseline, and 96h from immediately before and 24h (Figure 1). Other parameters do not differ statistically. The *cor* increasing presented a high similarity between grey levels, and this response can be visually assessed by changes in brightness on ultrasound images after few days of high intensity eccentric exercises. The *sm* emphasizes grey levels that present large number of transitions on binary image. A heterogeneous texture tends to result in high *sm* values and is dependent on grey-level adopted on image processing, and it is clearly numbers of grey-level dependent.

Figure:
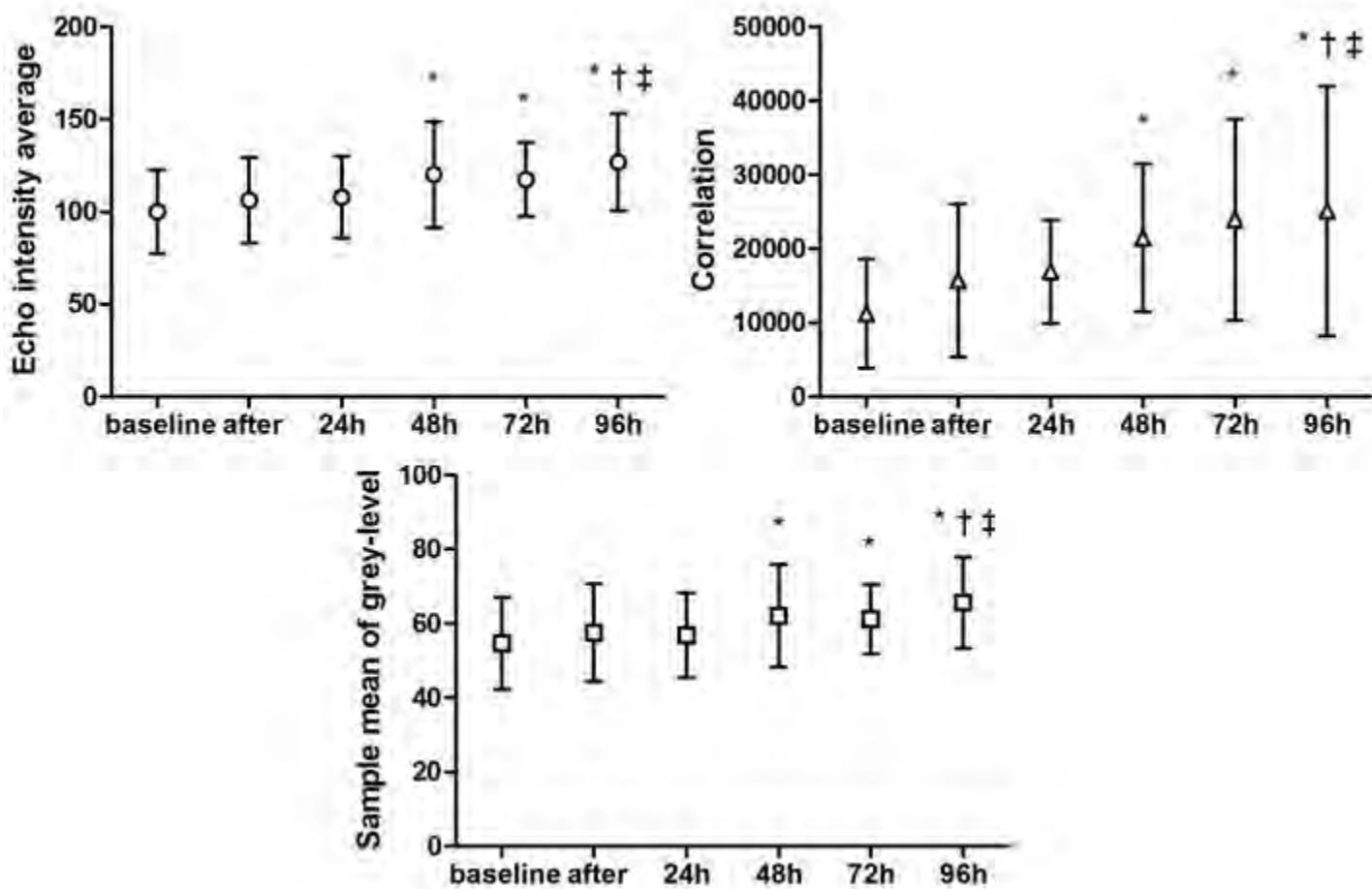
Caption: Figure 1: Mean and SD of correlation, sample mean of grey-level and echo intensity average. * for $p < 0.05$ from baseline; † for $p < 0.05$ from after; ‡ for $p < 0.05$ from 24h.

Conclusion: The texture analysis by the GLCM and CC seems to be a useful tool of assessing muscle damage as well as different biological tissues. The *cor* and *sm* proved to be the most sensitive and promising single texture parameters to study time changes of muscle damage as verified after 48h. Additional studies must include the evaluation performance for associated parameters as well as for different number of grey levels and ROI sizes and site selection, muscles with different fiber arrangement or ultrasound probe orientation.

References: 1. J. Friden, R. L. Lieber, Acta Physiol Scand 171(3): 321-326 (2001).

2. T. C. Chen, K. Y. Lin, H. L. Chen, M. J. Lin, K. Nosaka, Eur J Appl Physiol 111(2): 211-223 (2011).

3. S. Pillen et al., Muscle Nerve 39(6): 781-786 (2009).

4. M. H. Bharati, J. J. Liu, J. F. MacGregor, Chemometrics and intelligent laboratory systems 72(1): 57-71 (2004).

5. A. V. Alvarenga, W. C. Pereira, A. F. Infantosi, C. M. Azevedo, Med Phys 34(2): 379-387 (2007).

Disclosure of Interest: None Declared

MULTI-JOINT MODELING: EFFECT OF KNEE MUSCLE IMBALANCE ON SACROILIAC JOINT STRESS LEVELS DURING THE STANCE PHASE OF GAIT

Jerome Hausselle [1,*] Roger V. Gonzalez [1]

[1]Mechanical Engineering, The University of Texas at El Paso, El Paso, United States

Introduction and Objectives: Degenerative joint diseases such as osteoarthritis (OA) usually lead to the development of compensatory mechanisms to limit pain. For example, knee OA often increases the risk of comorbidities such as low back pain and OA onset in adjacent joints [1]. Although many current studies focus on understanding OA onset and development, to our knowledge, none focuses on comorbidity issues. There is for example a dearth of information regarding potential effects of knee compensatory mechanisms on hip and sacroiliac joints. To bridge that gap, we developed a computational multi-joint model to study the effect of knee extensor and flexor individual muscle forces and co-contractions on the sacroiliac joint stress levels during the stance phase of gait.

Methods: We developed a finite element model of the hip-pelvis system in FEBio [2]. Our model included the hip, pubic symphysis, and sacroiliac joints; and nine muscles crossing the hip and/or knee joint. The bones (femoral head, ilium, and half of the sacrum) were considered as rigid bodies and were joined by the hip, sacroiliac, and pubic symphysis cartilages. Cartilage was defined as an isotropic elastic material and seven sacroiliac ligaments were modeled using tension-only springs [3]. The sacrum bone was fully constrained, as well as the medial face of the pubic symphysis cartilage. Input kinematics and kinetics data were taken from published studies [4-6] and we computed the muscle force orientations throughout the motion by combining the femoral kinematics data with a lower limb model previously developed [7]. The mean von Mises stress of reference throughout the motion was computed with all the muscle forces scaled at 100%. Then, for each of the four muscles of interest (Rectus Femoris, Biceps Femoris, Semimembranosus, and Semitendinosus), eleven simulations were performed by scaling the force curve between 50 and 150%, with 10% increment. Then, co-contractions were simulated by modifying he contraction timing of the Biceps Femoris muscle, *i.e.* increasing the duration of the maximum force developed from 10 to 50% of the stance phase of gait, with 10% increment (see figure). Relative stresses were computed as the percentage of the difference between each mean von Mises stress with the mean stress of reference divided by this reference value.

Results: Results on individual muscle force showed that only the Biceps Femoris muscle force levels influenced the sacroiliac joint stress level (see Table). This result can be explained by the location of its insertion on the ilium, combined with the fact that it developed the highest force of all the muscles included in the model. Co-contraction simulations highlighted the fact that joint stress levels seemed to be as sensitive to co-contractions as to individual muscle forces, at least regarding the Biceps Femoris.

Figure:
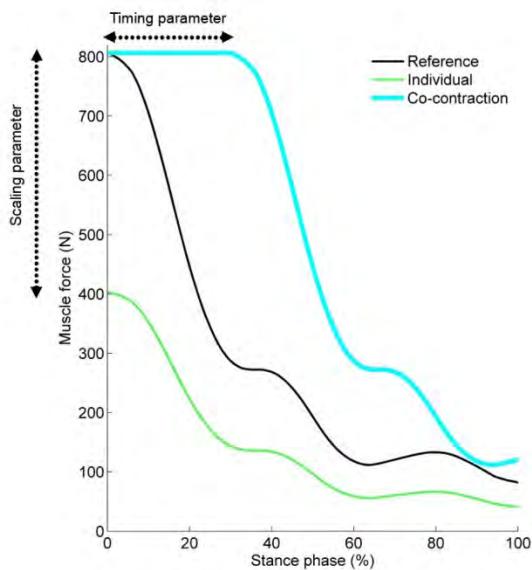
Caption: Examples of Biceps Femoris muscle force curves: reference (black), individual contraction curve (dashed green) with a scaling parameter of 50%, and co-contraction curve (cyan) with a timing parameter of 30%.

Conclusion: There is a need to understand potential consequences of compensatory mechanisms due to degenerative joint diseases at the whole body level. We showed that individual muscle force modifications and co-contractions developed to cope with a specific joint issue affect stress levels in adjacent joints. We believe that this multi-joint approach will pave the way for novel computational studies focusing on modeling entire kinetic chains. Follow-up work will include taking into account kinematic changes due to muscle force changes, adding more muscles, and studying more in details the effects of co-contractions. Such models will enable us to assess the efficiency of rehabilitation protocols and pain management strategies at the whole body level, and minimize the risk of comorbidities.

Table:

Scaling parameter (%)									
50	60	70	80	90	110	120	130	140	150
-8 (16)	-7 (13)	-5 (10)	-4 (8)	-3 (4)	4 (3)	7 (4)	15 (10)	18 (13)	23 (15)

Timing parameter (%)				
10	20	30	40	50
4 (6)	10 (7)	12 (9)	16 (11)	20 (13)

Caption: Relative sacroiliac joint stress level (mean (standard deviation)) over the stance phase of gait with respect to scaling and timing parameters of the Biceps Femoris muscle.

References:

[1] Suri et al., Arthritis Care & Research, 62: 1715-1723, 2010.

[2] Maas et al., Journal of Biomechanical Engineering, 134: 011005, 2012.

[3] Shi et al., Medical Engineering & Physics, 36: 745-753, 2014.

[4] Besier et al., Journal of Biomechanics, 42: 898-905, 2009.

[5] Bergmann et al., Journal of Biomechanics, 34: 859-871, 2001.

[6] Delp et al., IEEE Transactions on Biomedical Engineering, 54: 1940-1950, 2007.

[7] Hausselle et al., Computer Methods in Biomechanics and Biomedical Engineering, 17: 480-487, 2014.

Disclosure of Interest: None Declared

PO-0308

IN VIVO STATIC AND DYNAMIC DEFORMATION OF ARTICULAR CARTILAGE

Ziad Abusara [1,*] Markus Kossel [1] Walter Herzog [1]

[1]Human Performance Lab, University of Calgary, Calgary, AB, Canada

Introduction and Objectives: *In vivo* movement of bones comprising synovial joints has been evaluated in various ways and has been calculated theoretically to understand joint biomechanics. In order to assess joint loading and bone movements accurately, the deformation behavior of articular cartilage has been investigated in confined and unconfined compression experiments and indentation tests, but to date there exist no data on dynamic *in vivo* deformation of articular cartilage in intact joints loaded through controlled muscular contraction. Therefore, the aim of this study was to measure in vivo, real time articular cartilage deformations for precisely controlled static and dynamic muscular loading in intact joints.

Methods: In order to achieve the purpose of this study, we developed a novel *in vivo* testing system that allows for controlled loading of mouse knees through muscular contractions and quantification of the associated, cartilage and chondrocyte deformations. Mice (n=12) were fixed in a custom-built jig onto the stage of a dual photon microscope. Controlled forces of the knee extensor muscles were produced through direct muscle stimulation using indwelling fine wire electrodes and a Grass (S8800) stimulator. Static loading was applied over an 8s period using muscular forces of up to 80% of the maximal possible knee extensor force. Dynamic loading was applied using 15 repeat contractions lasting 0.5s each and repeated every 4s using forces ranging from 40-80% of maximal. The medial meniscus was excised to provide a direct view of the medial tibio-femoral joint. Imaging of articular cartilage deformation across the entire medial compartment of knees was performed using a Zeiss 40×0.95 NA water-immersion objective coupled with a Coherent Chameleon IR laser tuned at 780 nm for two-photon excitation.

Results: *Single static load*

The average overall cartilage thickness was 32±2 μm on the femoral condyles. Increases in muscular loading of the knee caused increases in articular cartilage deformation (Figure 1c). 80% of the maximal muscular forces (equivalent to twice body weight) produced average peak articular cartilage strains during an 8s contraction of 18.3±1.5% (Mean ± SD) (Figure 1a). Cartilage peak deformation was reached at the end of force application. Cartilage tissue recovered to its original thickness within approximately 45s following force removal (Figure 1a).

Dynamic cyclic load

Articular cartilage compressive strain increased as a function of muscular load (Figure 1c). 80% of the maximal muscular forces produced average peak articular cartilage strains of 10.7±1% (Mean ± SD) (Figure 1b). Cartilage deformation, for these conditions, started at the 4th muscular contraction and reached its maximum by the end of the last pulse. Cartilage tissue recovered to its original shape within approximately 35s following force removal (Figure 1b).

Figure:
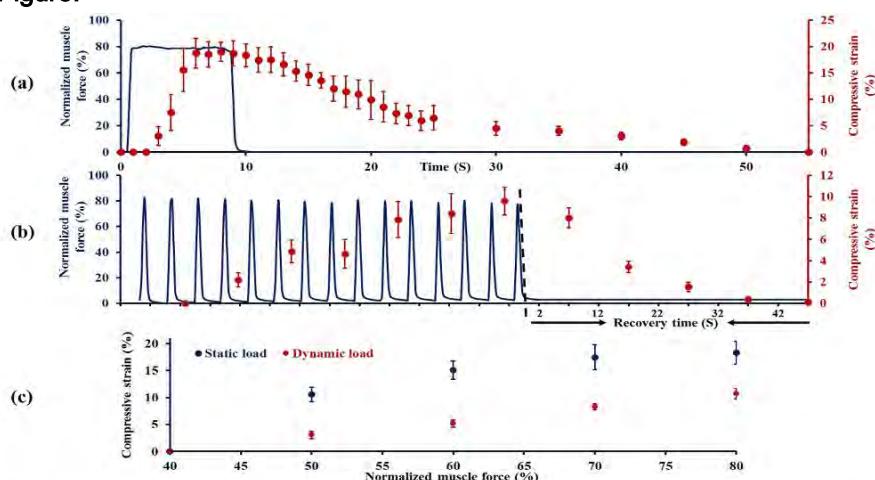
Figure1: (a) Normalized (relative to maximum =100%) knee extensor forces as a function of time. Muscles were stimulated for 8s at a voltage and frequency producing approximately 80% of the maximal isometric force. Cartilage deformation changes during loading and recovered to its original shape within approximately 45s following force removal (n=7) (b) Normalized muscle force as a function of time. Muscles were stimulated for 0.5s every 4s using a current and frequency producing approximately 80% of the maximal force. Cartilage strain increased with increasing the number of muscular force pulses. Cartilage tissue recovered to its original shape within approximately 35s following force removal (n=5) (c) In the static load condition, Articular cartilage strain increases exponentially between about 40 – 70% of the maximal force, and remains almost constant beyond about 70 - 80% of maximal force. In case of dynamic load, cartilage strain increases almost linearly. No sign of cartilage deformation was noticed at a 40% of maximal force or less.

Conclusion: The results of this study suggest that tibio-femoral contact between the articulating surfaces is only achieved with relatively high muscular forces (about 40% of maximal). This may be an artifact of the current setup where the medial meniscus was removed, and physical contact between the two articulating surfaces may occur for lower forces if the meniscus had been left intact. This finding will need to be investigated further. However, this result suggests, that in the presence of medial meniscectomy, high forces are required to obtain physical cartilage to cartilage contact in the medial tibio-femoral compartment of the mouse knee. Cartilage behaves highly visco-elastically. Specifically, peak cartilage deformation is reached much later than peak joint loading through the muscle forces. Here, we found that peak cartilage deformations were always reached at the end of the 8s loading time or at the end of the 15th muscular contraction, suggesting that cartilage deformation would have been greater than found here had joint loading been applied for longer than 8s or more than 15 loading cycles. This visco-elastic cartilage deformation behavior suggests that in normal cyclic movements, such as walking (loading time of approximately 800ms) peak steady-state cartilage deformation corresponding to the applied force is not reached within a few loading cycles. Similarly, full cartilage thickness recovery following load removal takes approximately 40s, suggesting that deformation recovery within cyclic movements such as walking, with an unloading time of about 1s, may be neglected. Finally, peak cartilage deformation for the static loading conditions seems to reach its maximum at muscle forces of about 70% of the maximal isometric force, with further deformations with higher forces not detected by our system. This begs the question of stiffness changes in cartilage with increasing loads and the mechanisms underlying extreme deformation of cartilage under very high joint loading conditions.

Disclosure of Interest: None Declared

DEVELOPMENTAL DIFFERENCES IN MUSCLE FASCICLE BEHAVIOUR DURING WALKING: IMPLICATIONS FOR MOVEMENT EFFICIENCY?

Charlie M. Waugh [1,*] Nicola Theis [2] Thomas Korff [1] Bill Baltzopoulos [1]

[1]Sport, Health and Exercise, Brunel University, Uxbridge, [2]School of Sport Health and Applied Sciences, St Mary's University, Twickenham, United Kingdom

Introduction and Objectives: Children perform cyclic motor tasks less efficiently than adults; however, the mechanisms underlying such differences are not fully understood. One mechanism that may contribute to age-related differences in task efficiency is the fascicle behaviour of key muscle groups in relation to the velocity of the movement outcome, as this can influence the muscle's energy expenditure and power output. Differences between children and adults have been identified in both tendon stiffness and the interaction between muscle and tendon within a muscle-tendon unit, both of which may affect fascicle mechanics and could influence movement efficiency. The primary aim of this study was to examine muscle fascicle length changes during steady-speed preferred walking velocity between children and adults to elucidate the mechanisms of muscle energetics

Methods: 4 children (9.5±1.5 years) and 4 adults (27.9±2.7 years) walked unshod on an instrumented treadmill at 80% of their preferred over-ground walking speed (0.66 and 1.07 ms-1, respectively; [1]) for a 10-minute period. Reflective markers placed on the hip, knee and foot provided lower body movement kinematics. Gastrocnemius Medialis (GM) fascicle length changes were visualised using ultrasonography and quantified using an automatic tracking algorithm [2, 3]. Fascicle length changes were averaged over six consecutive walking steps for each participant, determined by the treadmill ground reaction forces, and normalised to the average fascicle length of the trial (Figure 1). Peak shortening, peak lengthening and mean fascicle velocities were calculated from the stance phase data of the gait cycle (0 – 70% gait cycle) only. Group means of velocity data were examined using an independent t-test (p<0.05).

Results: Mean fascicle length for children and adults was 38.5 ± 6.8 and 47.9 ± 4.4 mm, respectively. Children appeared to demonstrate a greater fascicle lengthening, relative to normalised fascicle length at heel strike (0% gait cycle), during the ground contact phase of the step cycle. Despite this, peak shortening, peak lengthening and mean fascicle velocity was not different between children and adults (Table 1).

Figure:
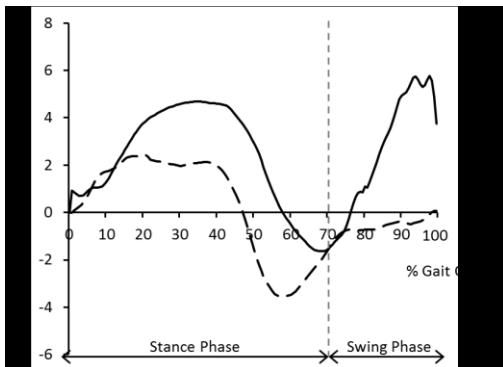
Caption: Figure 1. GM fascicle length changes in children (solid line) and adults (dashed line) during treadmill walking. Fascicle length changes are expressed in relation to gait cycle and as a percentage of the mean fascicle length calculated across the duration of the walking trial.

Conclusion: The present data demonstrate that GM fascicle velocities are similar in children and adults during unshod treadmill walking, which might indicate that the muscle's energy expenditure during preferred walking velocity is comparable between groups, in relation to fascicle length effects. The overall behaviour in GM fascicle mechanics may be different between groups, indicated qualitatively by their different lengthening and shortening profiles. These results may have implications for muscle power and so may influence movement strategies and sporting performance.

Table:

	Children	Adults	P-value
Peak Shortening Velocity	-0.46 ± 0.16	-0.55 ± 0.15	0.935
Peak Lengthening Velocity	0.71 ± 0.33	0.82 ± 0.09	0.449
Mean Fascicle Velocity	0.02 ± 0.02	0.02 ± 0.05	0.526

Caption: Group mean ± SD of fascicle velocities

References: [1] Dal et al. Gait Posture, 31(3):366-9, 2010.

[2] Cronin et al. J Appl Physiol, 111:1491–6, 2011.

[3] Gillett et al. Comput Methods Biomech Biomed Engin, 16(6):678-87, 2013.

Disclosure of Interest: None Declared

PO-0310

DYNAMICS OF NEWTS LOCOMOTION ON INCLINES

Aihong Ji [1,*]Benzheng Dong [1]Zhendong Dai [1]

[1]College of Astronautics, Nanjing University of Aeronautics and Astronautics, Nanjing, China

Introduction and Objectives: In the learning of locomotion behavior of newts, the seeked principle of its locomotion can be an important inspiration on the design of robot of wet adhesive mechanism. To achieve this goal, in this paper, locomotion behavior of newts on surfaces of 0^0 , 30^0 , 60^0 and 75^0 are recorded. Hereby, variation in spatial and temporal kinematics of different surfaces' locomotion is analyzed.

Methods: Newt (*Pachytriton labiatus*), from Guangxi, China, were used in experiment (4.82±0.73g mass, snout-vent length: 53.76±2.34mm, mean ± s.d.,N=10). The newts were train to move through the aisle of the force measuring array (FMA). The FMA was rotated step by step (30° per step) to imitate different incline surfaces. Synchronously to the force measurement (500Hz), a high speed camera (iSpeed-3, Olympus,1280×1024 pixels) recorded each trial at 25 Hz. Moving behavior results from the continuous force action, so impulse of the forces were introduced to present the force effects. The microstructure of pad observed by SEM is used to analyze its role for wet adhesion.

Results: The moving speed of newts decreased with incline angle. The duty factor of locomotion is gradually increased by the incline slope, it is 0.73 when climbing on the level and 0.92 when crawling on 75^0 surface. The lateral force impulses I_L acting on the front and hind limbs increased with respect to inclines, and the I_L acting on front limb increased faster than that acting on hind limb. The results suggest that lateral force become more important on larger slope inclines. The fore-aft impulse IF acting on front limb increases with increase of incline. The front limb generated negative F_F when newt move on horizontal surface, which suggests that the front limb plays an important role as a brake on horizontal surface while playing a role of propulsion on non-horizontal surface. The hind limb generated positive IF that appeared to act as a source of propulsion over the range of the incline angle from 0° to 75°. The front limb provided negative normal impulses F_N to pull the center of mass toward incline when inclines were larger than 60°. The microstructure of newts' pad be similar with tree frogs', this structure contributes to increase shear force and reduces the stiffness to increase contact area.

Conclusion: The climbing velocity gradually decreases with increasing the degree of slope, but step lengths no significant difference, so newts mainly moderate the pace by stride frequency rather than step length. Duty factor growing shows that newts need more contact time to maintain the stability and continuity for locomotion. The front and hind legs' function vary with increase of degree of slopes, forelimbs change from complementary role to main exporter of driving force. Lateral force toward body sides can form adduction force being similar to newt's pattern, this is beneficial to increase shear force and reduce the height of mass center to decrease the pitching moment. Adhesion force is far less than peeling force, so newts can't climb on a vertical surface.

Disclosure of Interest: None Declared

Musculoskeletal

PO-0311

ULTRASONIC SHEAR-WAVE ELASTOGRAPHY STUDY ON THE EFFECT OF ELEVATION ANGLE IN CROSS-BODY STRETCH

Jun Umehara [1,*]Satoshi Hasegawa [1]Satoru Nishishita [1]Masatoshi Nakamura [2]Hiroki Umegaki [1]Takuya Kobayashi [1]Hiroki Tanaka [1]Kosuke Fujita [1]Noriaki Ichihashi [1]

[1]Human Health Sciences, Graduate School of Medicine, Kyoto University, [2]Faculty of Health and Sports Science, Doshisha University, Kyoto, Japan

Introduction and Objectives: Cross-body stretch, which induces horizontal adduction of the shoulder, is often performed to prevent posterior shoulder tightness, as it is thought that such tightness is a contributing factor of shoulder injuries. Wilk et al. (2013) reported that cross-body stretch with stabilized scapula is more effective than that without stabilized scapula. However, there has been no investigation of the effect of the elevation angle of the cross-body stretch on posterior shoulder tightness.

Recently, a new ultrasound technology called ultrasonic shear-wave elastography (SWE) has allowed noninvasive and reliable measurement of the shear elastic modulus of a muscle. Nakamura et al. (2014) reported that the shear elastic modulus measured by SWE is a reliable index of the flexibility of an individual muscle.

The aim of the present study is thus to investigate the effect of the elevation angle on cross-body stretching using the shear elastic modulus measured by SWE as an index of muscle flexibility.

Methods: The nondominant shoulder of eighteen healthy male (age: 23.7 ± 3.4 years) subjects were evaluated. While side-lying on their dominant side, the subjects randomly performed cross-body stretch at three elevation angles; i.e., horizontal adduction at 60° elevation (60Ele), 90° elevation (90Ele), and 120° elevation (120Ele). This cross-body stretch was repeated five times for 30 s at 20 s intervals, over a total period of 150 s. The horizontal adduction angle during the cross-body stretch was defined as the maximum angle that the subjects could achieve without discomfort or pain. Before (Pre) and after (Post) cross-body stretch, the shear elastic modulus of the superior and inferior portions of the infraspinatus muscle (ISPs and ISPi), the teres minor muscle (TM), and the posterior portions of the deltoid muscle (Deltoid) were measured. Measurements were made using ultrasonic SWE (Axiplorer; SuperSonic Imagine, Axi-en-Provence, France). An ultrasound transducer (SL-10-2 linear ultrasound transducer) was positioned on measurement points parallel to the direction of the muscle fiber, which was confirmed by tracing several fascicles without interruption across the B-mode image. During the measurement, the subjects were in a seated position with their arm held at 90° shoulder forward elevation.

The shear elastic modulus of each muscle was analyzed by two-way analysis of variance (ANOVA) with repeated measures (factors: time ´ elevation angle). When a significant interaction or main effect of time was found, the level was assessed as the significance of difference using the paired Student's *t*-test with Bonferroni revision as a post-hoc test. Differences were considered statistically significant at an alpha level of $P < 0.05$.

Results: The results for the shear elastic modulus of each muscle at Pre and Post are given in Table. In the cases of ISPs and ISPi, ANOVA showed no significant interaction between time and elevation angle, but indicated a significant main

effect of only the time factor. The post-hoc test for time indicated that the shear elastic modulus of Post was lower than that of Pre for all elevation angles. In the case of TM, ANOVA showed significant interaction between time and elevation angle. The post-hoc test for the time factor indicated that the shear elastic modulus of Post was lower than that of Pre for 120Ele, whereas no significant difference between Pre and Post was found for 60Ele or 90Ele. The post-hoc test for the elevation angle factor indicated that the shear elastic modulus of 120Ele was lower than that of 60Ele and 90Ele for Post, whereas no significant difference between 60Ele and 90Ele was found for Post. In the case of Deltoid, ANOVA showed no significant interaction or main effect.

Conclusion: This current examined the effect of cross-body stretch on posterior shoulder structures, and showed that shear elastic moduli of ISPs and ISPi significantly decreased after cross-body stretch at all elevation angles. In the case of TM, the shear elastic modulus of Post for 120Ele was significantly lower than that of Pre. However, the shear elastic modulus in the case of TM for 60Ele and 90Ele showed no significant difference between Pre and Post. In the case of Deltoid, the study showed that the shear elastic modulus did not significantly decrease after stretching.Our study thus revealed that the flexibility of ISPs and ISPi increased after cross-body stretch at all elevation angles. However, only cross-body stretch at an elevation angle of 120° increased TM flexibility.

Table:

Muscle	Angle	Pre(kPa)	Post(kpa)	Interaction
ISPs	60°	6.6±1.6	4.9±1.6*	P=0.53
	90°	6.3±1.6	4.4±1.1*	F=0.66
	120°	7.2±2.1	5.1±1.4*	
ISPi	60°	6.1±3.4	4.6±1.6*	P=0.84
	90°	5.5±1.2	4.3±1.1*	F=0.18
	120°	6.0±2.0	4.5±1.0*	
TM	60°	6.2±2.1	5.8±1.9	P<0.01
	90°	6.4±2.1	6.1±2.5	F=9.78
	120°	5.9±1.6	4.0±1.4*†	
Deltoid	60°	13.8±4.5	12.8±3.7	P=1.00
	90°	14.1±4.1	13.0±3.8	F=0.00
	120°	14.1±3.5	13.2±2.8	

 * :P<0.05:significant difference vs Pre

†:P<0.05:significant difference vs 60Ele and 90Ele

Caption: The shear elastic modulus of each elevation angle in muscle.

Disclosure of Interest: None Declared

Spine

PO-0313

CHANGES IN BIOMECHANICAL BEHAVIORS OF THE CERVICAL SPINE AFTER DEGENERATION OF THE INTERVERTEBRAL DISC AND FACET JOINT

Won Man Park [1] Dae Kyung Choi [1] Kyungsoo Kim [2] Yoon Hyuk Kim [1,*]

[1] Mechanical Engineering, [2] Applied Mathematics, Kyung Hee University, Yongin, Korea, Republic Of

Introduction and Objectives: Cervical disc degeneration is one of the most common causes of neck pain [1] and there is evidence that disc degeneration often accompanies facet joint degeneration [2]. It has been reported that facet joint degeneration is also considered an important source of pain in the cervical spine [3]. In this study, we developed finite element (FE) models of the cervical spine with various grades of intervertebral disc and facet joint degeneration. Then, changes in biomechanical behaviors including ROM, intradiscal pressure, and facet joint force at the degenerated and adjacent segments were investigated using the developed FE models.

Methods: A three-dimensional finite element model of the healthy cervical spine from C2 to C7 was developed based on a series of computed tomographic images. Then mild, moderate, and severe degenerations of the intervertebral disc and facet joint were described at the C5-C6 motion segment based on the clinical classification [4, 5]. Disc height and artificial cartilage thickness decreased by 20%, 50% and 80% for mild, moderate and severe degeneration, respectively (Figure). Annulus fibrosis and ligaments were pre-stressed and/or buckled by the loss of disc height. And compressibility of nucleus pulposus increased with progress of degeneration. The developed FE models of the healthy and degenerated cervical spine were examined in hybrid loading conditions for flexion, extension, lateral bending, and axial rotation. Changes in segmental rotations, intradiscal pressures and facet joint forces at the degenerated and adjacent segments were investigated in this study.

Results: Segmental rotation of the C5-C6 motion segment during flexion-extension, left-right lateral bending, and left-right axial rotation decreased with progression of degeneration by 33% on average. Segmental rotations at the inferior and superior motion segments to the degenerated segment increased with progression of degeneration for compensating the decreased motion at the degenerated segment (Table). While intradiscal pressure at the degenerated segment in all motions decreased with progression of degeneration, the pressures at the adjacent segments slightly increased during flexion (Table), and slightly decreased during extension and lateral bending. During axial rotation intradiscal pressures at the superior segments slightly decreased while the pressure slightly increased at the inferior segment. Facet joint forces at all but one motion segment steadily increased with progression of degeneration in extension, lateral bending, and axial rotation; the force at the C4-C5 slightly decreased in early stages of degeneration during axial rotation.

Figure:
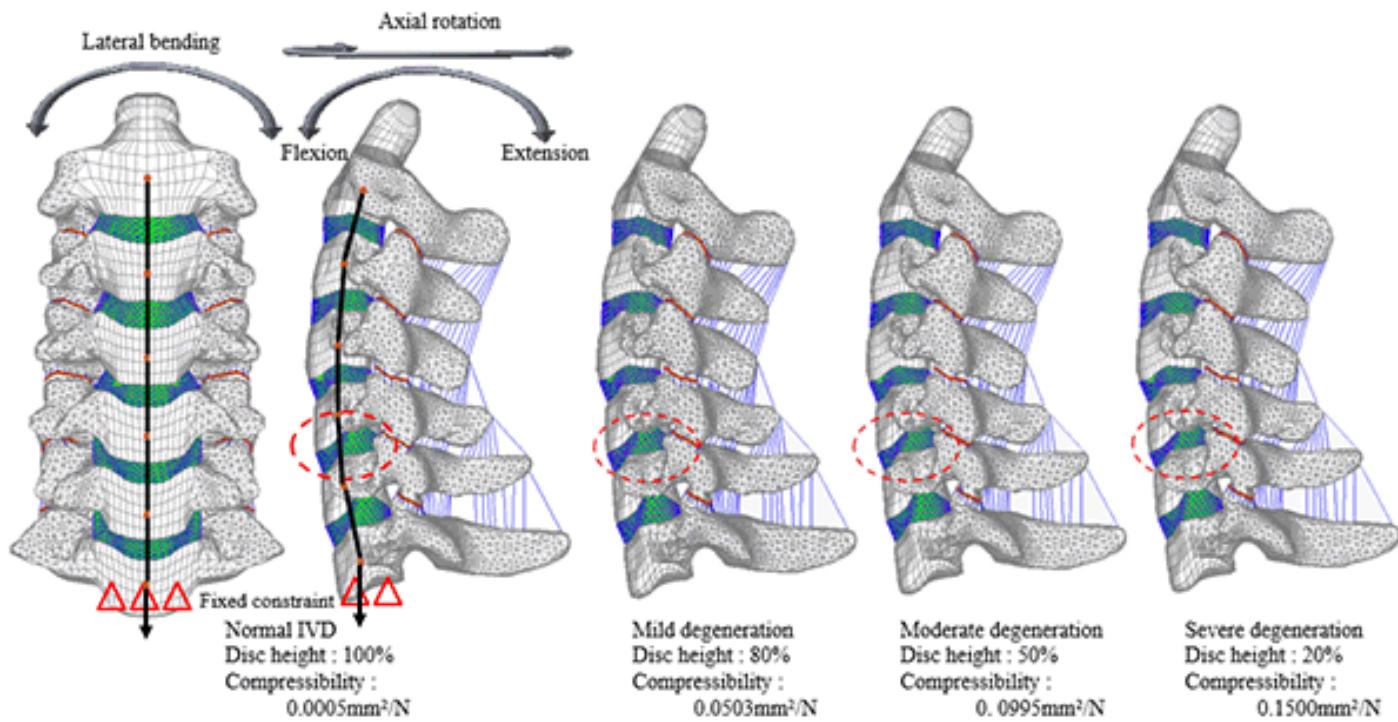
Caption: Developed FE models of the healthy and degenerated cervical spine. Boundary and loading conditions are represented for the healthy cervical spine

Conclusion: The results of this study showed that segmental motion and intradiscal pressure at the degenerated segment decreased with progression of degeneration, whereas the facet joint force increased. Segmental motions and facet joint forces at the adjacent segments increased with progression of degeneration, whereas intradiscal pressure slightly increased in flexion and slightly decreased in extension and lateral bending. These changes in spine biomechanics caused by intervertebral disc and facet joint degeneration would be a possible reason for accelerated disc degeneration at the healthy adjacent segments and worsening osteoarthritis at the degenerated segment. The results of this study could be used to understand the mechanism of injury caused by intervertebral disc and facet joint degeneration.

Table:

		C2-C3	C3-C4	C4-C5	C5-C6	C6-C7
Segmental rotation during flexion-extension (°)	Healthy	7.8	7.9	7.5	7.9	9.6
	Mild degeneration	7.9	7.9	7.6	7.6	9.7
	Moderate degeneration	8.0	8.1	7.7	6.8	10.0
	Severe degeneration	8.2	8.3	7.9	5.8	10.4
Intradiscal pressure during flexion (MPa)	Healthy	0.28	0.41	0.39	0.34	0.32
	Mild degeneration	0.28	0.41	0.39	0.26	0.32
	Moderate degeneration	0.28	0.41	0.40	0.18	0.33
	Severe degeneration	0.28	0.42	0.40	0.09	0.33
Facet joint force during extension (N)	Healthy	52.5	53.6	49.7	45.4	37.6
	Mild degeneration	55.0	56.1	51.9	48.2	39.0
	Moderate degeneration	59.9	61.1	56.3	59.3	42.2
	Severe degeneration	64.6	66.2	60.7	67.1	45.5

Caption: Changes in segmental rotation during flexion-extension, intradiscal pressure during flexion, and facet joint force during extension with progression of intervertebral disc degeneration and facet joint degeneration

References: [1] Avery, Int J Ther Massage Bodywork, 5: 41-46, 2012.

[2] Butler et al., Spine, 15: 111-113, 1990.

[3] Lewinnek et al., Clin Orthop Relat Res, 213: 216-222, 1986

[4] Kettler et al., Eur Spine J, 15: 732-741, 2006.

[5] Kettler et al., Eur Spine J, 16: 987-992, 2007.

Disclosure of Interest: None Declared

Spine

PO-0314

AXIAL ROTATION IN THE LUMBAR SPINE AND ITS EFFECT ON ASSOCIATED NERVE TISSUE

Graham Mayberry [1,*] Janessa Drake [1]

[1]Kinesiology and Health Science, York University, Toronto, Canada

Introduction and Objectives: The lumbar spine has been characterized under a variety of different conditions, providing researchers with a strong understanding of its functional anatomy. The relationship between the intervertebral foramen (IVF) and the spinal nerve root (NR) that exits through it has not been quanitified, though it may play a significant role in how or whether individuals experience LBP (Lee et al, 2009). Nowicki et al (1996) conducted an invitro study using magnetic resonance imaging (MRI) to measure compression of the nerve root by ligamentum flavum or the intervertebral disc, while more recently Senoo et al (2014) used computerized tomography to quantify the heights and widths of the lumbar foramen invivo. These works did not quantify the IVF-SNR relationship in various postures invivo using MRI . The specific research goals of the current invivo study were to quantify the cross-sectional area (CSA) and volume of the IVF and NR in both neutral and axially-rotated positions in the lumbar spine.

Methods: Two healthy males (24.0 +/- 2.0) were recruited for this study with no history of LBP over the previous 12 months and successfully passed the MRI screening process. During the imaging session, the participants were asked to lie in a supine position with their shoulders strapped down while 3D MRI scans were acquired (Siemens MAGNETOM 3T Trio MRI scanner). The participants then moved to their maximal axially-rotated position (with their knees pointing to the left). Wedges were placed at the hips and between the knees, and straps were fastened around the shoulders, knees and hips to ensure they were comfortable and would not move during imaging. The lumbar spine was imaged, focusing on the levels of L4-L5, providing a complete functional spinal unit (FSU). The imaging protocol was T2SPC, with a slice thickness of 0.781mm, lasting six minutes per scan. The images were analyzed using OsiriX (© Pixmeo Sarl, V 5.0.1) and TurtleSeg (V 1.3.0.1777) for CSA and volume, respectively. The CSA for both the NR and IVF were calculated by averaging the seven smallest CSAs from the entire series of slices along an axis that was manipulated to run directly through the center of the IVF perpendicular to the saggital plane. The volume of both the IVF and NR was measured from the medial side to the lateral side of the pedicles of the FSU (see Figure 1).

Results: The right IVF and SNR of the L4-L5 FSU were quantified in both the supine (SUP) and axially-rotated (AR) positions in terms of the volume, CSA, and ratio of IVF to NR (see Table 1). The CSA of the IVF in Subject A increased from supine to axially-rotated while decreasing in the Subject B, however the CSA of the SNR decreased in both subjects. The IVF:NR ratio increased from supine to axial rotation for both subjects when using CSA analysis. When using the volumetric analysis, the SNR decreased for both subjects, while the IVF and IVF:NR ratio got larger for Subject A but got smaller for Subject B.

Figure:
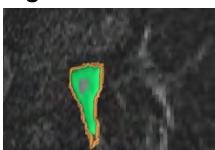
Caption: Figure 1. Example of volumetric segmentation of the IVF (green) and SNR (purple).

Conclusion: Although the two subjects demonstrated different patterns in some aspects of this analysis, there were some important findings that could help direct future studies and improve our understanding of the body's response to various movements. We believe that the decrease in SNR cross-sectional area and volume when comparing a supine to an axially-rotated position is likely due to stretching and may be why individuals are susceptible to LBP if that position is maintained. Despite the consistency in the NR, the IVF was not consistent between subjects and we suspect it could be due to a pelvic tilt accompanying the axially rotated position, as participant's were instructed only to get comfortable in their maximal position. Anecdotally, in pre-trials where subjects were asked to remain in the supported-rotated position until comfortable, Subject A (increased IVF) time was much longer than Subject B (decreased IVF). In light of the opposite IVF size changes at the L4-L5 level, future research will examine more lumbar levels to see whether these differences hold along the spine. The findings of the current study are valuable, as no previous research has investigated this relationship invivo and in both neutral and deviated positions. If we are to understand the epidemic of LBP, a neurological understanding is critical.

Table:

			S 1	S 2	Ave
CSA (cm^2)	SUP	IVF	1.053	0.988	1.020
		NR	0.135	0.214	0.175
		IVF:NR	7.801	4.610	6.206
	AR	IVF	1.143	0.955	1.049
		NR	0.118	0.164	0.141
		IVF:NR	9.723	5.825	7.774
Volume (cm^3)	SUP	IVF	0.134	0.134	0.134
		NR	0.049	0.051	0.050
		IVF:NR	2.741	2.604	2.672
	AR	IVF	0.192	0.126	0.159
		NR	0.04	0.05	0.04

			1	1	6
		IVF:NR	4.64 5	2.46 5	3.55 5

Caption: Table 1. The CSA (cm2) and volume (cm3) of the IVF and SNR of the subjects and the ratio of IVF:SNR are displayed below.

References: Lee, Y. et al. (2009) *Am J Neuroradiol*, 30, 1062-67.

Nowicki, B. et al. (1996) *Am J Neuroradiol* 17, 1605-14.

Senoo, I. et al. (2014) *Spine* 39, 929-35.

Disclosure of Interest: None Declared

PO-0316

THE EFFECT OF THE PILATES PRACTICE ON YOUNG ADULTS´ POSTURE

Alessandra B. Porto [1,*] Túlio Moura [1] Celina Qurino [1] Victor Okazaki [1]

[1] CEFE, Londrina State University, Londrina, Brazil

Introduction and Objectives: The muscle and bone balance maintains a good posture that protects the body from damage and pain [1]. Some daily habits of bad posture can develop deformities [1]. On the other hand, the practice of physical exercises may help to prevent and treat some posture problems [2]. Pilates has shown to be efficient on the treatment of low back pain and some postural disorders [3].

Pilates has become a progressively popular method of exercise to achieve a better postural alignment [4,5]. Pilates exercises can be floor-based that uses the gravity to resist and assist the movement execution and can involve the use of specialized equipment [6]. This method can be also used in treatment of rehabilitation, emphasizing the core stability and posture [7].

Emery et al [3] studied the effect of the Pilates (using mat and equipment) and verified that 12-weeks of training was effective in posture. However, it is important to verify if those changes that happened with the Pilates method during all those decades still brings benefits to the practitioner´s posture and if the floor-based Pilates method, which is not an expensive method and can be instructed in any place without equipment, can improve postural disorders. Thus, the aim of this study was to verify the effect of the Pilates method on young adults´ posture.

Methods: The research was conducted in the Laboratory of Biomechanics at Londrina State University. Volunteered in the study 10 women, mean age of 40 years old (SD=12.8). They had their posture assessed before they started the Pilates classes and after 10 weeks of practice. The practice consisted on 50 minutes of mat Pilates, performed twice a week, for 10 weeks, totaling 20 sessions.

The 50 minutes Pilates´ session consisted in 10 minutes warm up, 30 minutes of Pilate´s exercises on the floor, using a mat and a professional Pilates´ ball, and 10 minutes of light exercises to finish the session. The Pilate´s exercises was medium and high intensity and varied between the sessions.

The posture assessment was realized by Photogrammetry, in which the spinal processes of the C7, T12 and L5 vertebras were identified by the palpation method [8] and external markers were attached on the skin with double-sided tape. After that, the participants positioned in orthostatic position, than 3 photos were taken in sagittal plane. The external markers were taken off and a marker made of half sphere of Styrofoam were placed in the same place as the other marker. Three more photos of the back were taken in frontal plane.

All the photos were unloaded into a computer and were analyzed in SAPO software. The software provided the thoracic angle formed by the C7 and T12 markers, the lumbar angle formed by T12 and L5 from the photos on sagittal plane. From the photos on frontal plane, the SAPO provided the angle between the C7-T12 and T12-L5, both in relation to a vertical line.

As the normality was assumed by the Shapiro Wilk´s test, the Student´s T test for paired measures was used to identify differences between the pre and post assessment. Statistical significance adopted was 5% ($P<0.05$).

Results: The analysis showed differences only for the C7-T12 assessment on frontal plane in pre and post evaluation (P=0.03) in which the mean of the angles in pre were greater (1.88^0, SD=0.96) than in the post assessment (1.05^0, SD=0.75). For the thoracic angle there was a tendency of decreasing the mean of the angles from the pre to the post assessment, but without statistical significance (P=0.083). The frontal plane analysis of the region T12-L5 showed no significant effect (Table 1).

The results of the present study corroborated with Emery´s [3] study that showed an improvement on posture with the Pilates after 12 weeks training. In the present study, only 10 weeks of floor-based Pilates training, was enough to show some modification on posture (thoracic region). Perhaps, a prolonged period of floor-based Pilates training would even maximize its effects on posture.

Conclusion: The Pilates practice used in the present study seems to influence subjects posture (thoracic portion of the spine mainly on frontal plane) and might help to correct the scoliosis problem. It was suggested for future studies a prolonged time of Pilates training in both technique and more participants performing the intervention.

Table:

	Pre	Post	P
Thoracic angles	39.84°(7.74)	38.54°(13.62)	0.083
Lumbar angles	32.39°(11.81)	28.98°(13.62)	0.130
C7-T12	1.88°(0.96)	1.05°(0.75)	0.037*
T12-C7	1.71°(1.68)	1.82°(0.94)	0.779

*significant difference

Caption: Table 1: Angles(SD) pre and post assessment

References: [1] Kendall et al, Músculos, Provas e Funções, Manole,2005.

[2] Rossi et al, Fisioter Mov, 24:255-263, 2011.

[3] Emery et al, Clin Biomech, 25:124-130,2010.

[4] Latey, JBMT, 8:94-101,2002.

[5] Blum, J Manip Physiol Ther, 25,2002

[6] Wells et al, Complement Ther Med, 20:253-262,2012

[7] Gagnon, Doctoral dissertation. The University of Tennessee, Knoxville, 2005

[8] Tixa, Atlas de anatomia palpatória do pescoço do tronco e do membro superior. Manole; 2009.

Disclosure of Interest: None Declared

IN VITRO COUPLED MOTIONS IN THE ELDERLY HUMAN VERSUS THE YOUNG PORCINE SPINE IN CYCLIC AND CREEP LOADING

Idsart Kingma [1],*Iris Busscher [2]Albert J. van der Veen [3]Gijsbertus J. Verkerke [4]Albert G. Veldhuizen [2]Jasper Homminga [4]Jaap H. van Dieën [1]

[1]Faculty of Human Movement Science, VU University Amsterdam, Amsterdam, [2]Department of Orthopedics, University Medical Center Groningen, Groningen, [3]Department of Physics and Medical Technology, VU University Medical Center, Amsterdam, [4]Department of Biomechanical Engineering, University of Twente, Enschede, Netherlands

Introduction and Objectives: When a spine segment is loaded about a single axis, this causes rotations about other axes as well. Such motions, which are often described as coupled motions, are partly induced by orientations of the facet joints, which vary along the spine. Furthermore, spinal asymmetry likely enhances coupled motions. This asymmetry may be larger in elderly and degenerated spines than in young spines. As young human spines are hard to retrieve, we used porcine spines as a proxy for young human spines, to compare with elderly human spines. We hypothesized that, compared to young porcine spines, human spines would show larger coupled motions, and that this difference would depend on spinal level and loading direction.

Methods: Six elderly human (55-84 years of age) and six young porcine fresh frozen cadaveric spines were dissected. Each spine was sectioned in high thoracic, mid thoracic, low thoracic and lumbar segments, consisting of 4 vertebrae each. The top and bottom vertebrae of each segment were embedded in neutral orientation in an alloy (Cerrolow-147) and positioned in a custom-made four-point bending device. After 1-hour preloading at 250 N compression, specimens were cyclically loaded (3 cycles, 0.5 degrees/sec) up to 4 Nm (human spines) or 2 Nm (porcine spines) in Flexion-Extension (FE), Lateral Bending (LB), and Axial Rotation (AR). Subsequently, spine segments were continuously loaded at half of these loads for 30 minutes in LB, AR, flexion and extension. Three-dimensional motions of the middle two vertebrae were recorded and decomposed into FE, LB and AR using Euler decomposition, starting with the loaded direction. Motions about the non-loaded (coupling) axes were expressed relative to motions about the loaded axes.

Results: In cyclic loading of human spines, relative coupled motions averaged over spines ranged from 11% (for FE coupling in LB loading of the lumbar segment) to 68% (for FE coupling in AR loading of the lumbar segment), and were up to 60% in FE loading. Averaged over spine sections, loading directions and coupling axes, relative coupled motions were larger in human than in porcine segments (27% vs 14%, P<0.001). In creep loading, relative coupled motions in human spine segments, ranged from 19% (for LB in extension loading of high thoracic spine sections), to 148% (for AR in extension loading of mid thoracic spine sections). The average was 46 % of the creep in the loaded direction, which was much larger (P<0.001) than for porcine spines (15%). In both creep loading and cyclic loading, differences with porcine spines depended on spine level and loading direction (P<0.02).

Conclusion: As anticipated, coupled motions varied highly with loading direction and with spine level. More importantly, coupled motions were about twice as high in elderly human spines compared to young porcine spines in cyclic loading, and these effects were even more pronounced in creep loading. Even in FE loading, large coupled motions were seen in

human spines. These findings suggest that asymmetry in stiffness and/or geometry contribute substantially to coupled motions in elderly human spines.

Disclosure of Interest: None Declared

Spine

PO-0315

USE OF INERTIA SENSORS TO MEASURE THREE-DIMENSIONAL TRUNK MOMENT AND MOTION DURING WALKING

Jordan Berceville [1] Raymond Lee [2] Jin Luo [3,*]

[1]National Institutes of Applied Sciences (INSA), Strasbourg, France, [2]London South Bank University, [3]Department of Life Sciences, University of Roehampton, London, United Kingdom

Introduction and Objectives: Walking is a popular exercise to enhance musculoskeletal health and physical function in ageing population. To ensure that walking exercise can be conducted both effectively and safely, especially for people with osteoporosis and obesity, it is important to quantify the mechanical loading applied to the spine during walking. Current methods of measuring spinal loading have their limitations as they require the use of laboratory bound equipment such as force platform or video camera system [1,2]. The objective of this study was to develop a method that uses inertia sensors to measure trunk moment and motion during walking.

Methods: A biomechanical model of trunk consisting of three segments (head and trunk, left arm, and right arm) was created. Each segment was treated as rigid body. Head and trunk articulated with lower body at L5/S1 joint. Left and right arms articulated with trunk at left and right shoulder joints respectively. The dynamic equilibrium equations that described the moment about the L5/S1 joint were developed in sagittal, frontal, and transverse plane.

In order to obtain these moments, the 3-D orientation of each segment and the 3-D coordinates of its centre of mass (COM) at any time point during walking were determined by measurement and calculation. The 3-D orientation angles were measured by attaching four inertia sensors to the skin surface at locations corresponding to COM. The 3-D coordinates of COM were determined by the following method: first, a Fastrak system was used to digitize the 3-D coordinates of the four inertia sensors at time zero which were used as the stationary initial position of COM in the model. The 3-D coordinates at any following time points were then calculated through matrix transformation method by using 3-D orientation angles at that time point and 3-D coordinates at time zero [2]. All 3-D coordinates and moments were expressed in an anatomical reference system defined by ASIS and PSIS.

Ten adult male (Age: 45.5 ± 21.8 years) took part in the experiment. Their anthorpometric measurements were taken in order to estimate segment mass and moment of inertia. They were then asked to walk in a straight line with their normal walking speed for about 20 meters in a biomechanics lab. The walking trial was then repeated after 1-min rest. The data were analyzed by a customized MATLAB program to obtain 3-D trunk moment and motion. Maximum and minimum of trunk moment and motion during one full stride (from right heel contact to the subsequent right heel contact) were determined. Trunk moments were normalized to percentage of the product of body weight and height (joint moment/(body weight x height)) x100).

Results: As seen in table 1, trunk moment and motion obtained in the present study are in good agreement with a previous study [2] which used a bottom up rigid link segment analysis method.

Conclusion: The current study has successfully developed a method using inertia sensors to measure trunk moment and motion during walking. The strength of our method is that it can be easily implemented in the natural environment as it does not require laboratory bound equipment such as video camera system or force platform.

Table:

	Flexion/extension		Lateral bend		Axial rotation	
	min	max	min	max	min	max
Moment						
This study	-0.64(0.29)	0.62(0.23)	-0.61(0.28)	0.59(0.38)	-0.55(0.54)	0.46(0.31)
Callaghan et al.	-0.98(0.51)	0.48(0.53)	-0.56(0.38)	0.74(0.67)	-0.26(0.23)	0.25(0.18)
Motion (degree)						
This study	-5.02(1.90)	4.38(2.31)	-4.79(1.88)	4.75(2.00)	-7.96(3.52)	7.70(3.72)
Callaghan et al.	-3.34(3.36)	3.12(3.42)	-4.90(3.49)	3.11(2.19)	-4.55(3.64)	4.21(2.07)

Caption: Table 1. Minimums and maximums of trunk moment and motion (mean (S.D.))

References:

[1] Cappozzo, J. Biomech,16:265-277,1983.

[2] Callaghan et al., Clin Biomech, 14:203-216,1999.

[3] Zatsiorsky. Kinematics of human motion. Human Kinetic Publisher, 1998.

Disclosure of Interest: None Declared

Spine

PO-0312

CHANGES IN THE STANDING LUMBAR SPINE AT ABOVE BODYWEIGHT LOADING

Gary Dougill [1,*]Neil Reeves [2]Christine Le Maitre [3]Glen Cooper [1]

[1]Engineering, [2]Healthcare Science, Manchester Metropolitan University, Manchester, [3]Biomedical Research Centre, Sheffield Hallam University, Sheffield, United Kingdom

Introduction and Objectives: Understanding the mechanical response of the spine and intervertebral disc to various loading situations is vital to predicting its behaviour, to verify computer models of the spine and to gaining insight in to how loading and spinal posture may cause or exacerbate injury.

Studies of the lumbar spine and intervertebral disc under compression have typically been carried out in vitro; those which have used in vivo methods have mostly been conducted in the supine position at loading equal to or below static bodyweight. This study measures the lumbar spine response to above bodyweight loading in the standing position at loads equivalent to walking.

Methods: Sagittal plane magnetic resonance imaging scans of the spine were taken of nine asymptomatic male subjects (22-32 years of age, 167-195 cm, 66.3-93.2 kg) in the supine and standing positions with a third scan taken in the standing position with additional loading. Additional load was applied by having subjects hold two 6 kg kettlebells, one in each hand, enough to increase loading on the IVD to levels experienced during walking.

Disc heights were measured as the average of anterior and posterior distance between adjacent vertebrae in the mid-sagittal plane. Change in lordosis was measured in two ways; the relative angle between the lumbar spine and pelvis was measured as the posterior angle between L5 and S1 vertebrae whilst change in the upper lumbar spine was measured by the angle between the superior facet of L3 with the vertical plane.

Results: Increased axial loading resulted in reduced disc height and lumbar lordosis. Initial disc heights in the supine position for L3/L4, L4/L5 and L5/S1 were found to be 10.7(1.6), 12.0(2.8) and 11.4(1.9) mm respectively (Fig. 1a). These heights were reduced to 10.4(1.9), 11.4(2.1) and 10.8(1.6) mm in the standing position and 10.3(1.4), 11.4(2.0) and 10.4(1.8) mm with additional loading but these changes were not statistically significant (P>0.05). Lumbar angle in supine, standing and with additional loading was found to be 140(9), 145(11) and 145(12) degrees respectively (Fig. 1b) with L3 angled 0.7 (3.5), 4.4 (4.4) and 4.8 (4.2) degrees posteriorly from the horizontal in the three loading positions (Fig. 1c). In all cases disc height change was greater posteriorly as loading increased lumbar lordosis.

Figure:
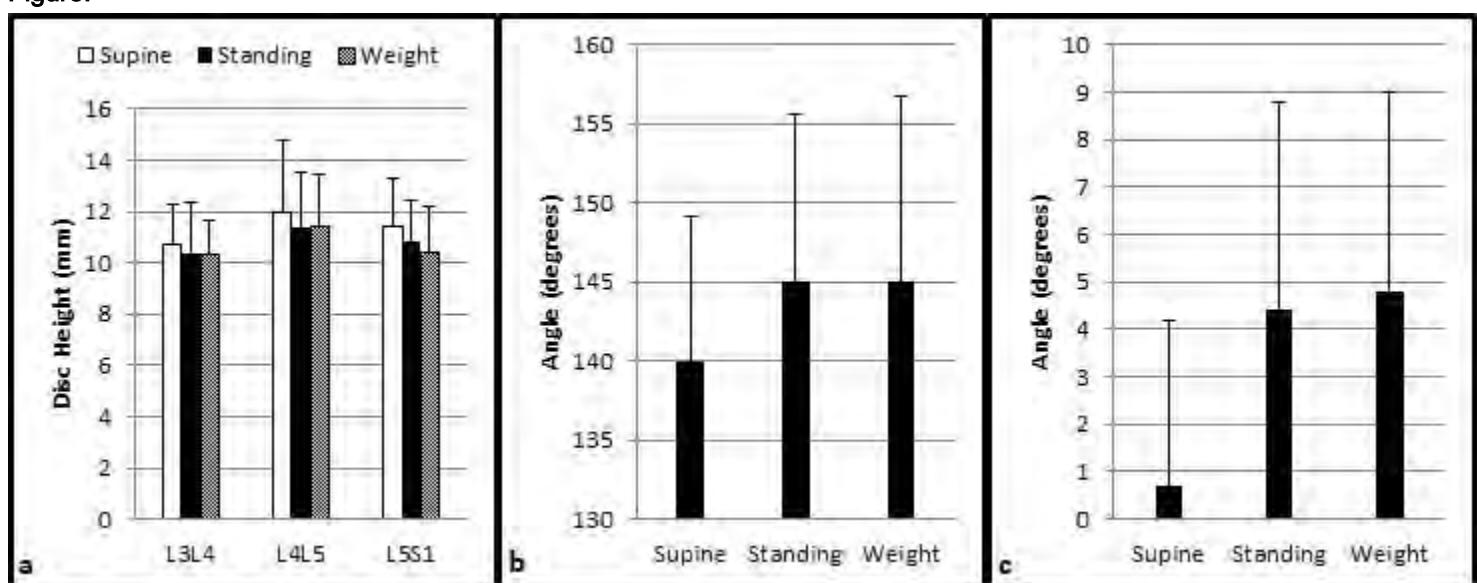
Caption: Figure 1 - (a) Average IVD height of lower Lumbar discs in three loading positions. (b) Angle between Lumbar and Sacral spine in three loading positions. (c) Posterior tilt of L3 vertebrae in three loading positions.

Conclusion: Increased axial loading was found to progressively decrease intervertebral disc height; this change in height was not equal across the disc with reduced compression in the anterior region of the disc. Lordosis in the lumbar spine was found to increase with progressive loading; L5/S1 angle was greater in the standing position than supine whilst the superior facet of the L3 vertebrae was increasingly rotated posteriorly. Increased lumbar lordosis and compression in the posterior region of the disc with increased loading suggests that moderate axial loading in the upright position typical of that found during walking is not a risk factor in acute herniation of the intervertebral disc.

Disclosure of Interest: None Declared

PO-0317

THE CHARACTERISTICS OF REGIONAL BONE QUALITY IN CERVICAL SPINE

Dai-Soon Kwak [1,*] In-Beom Kim [1] Moon-Kyu Kim [2]

[1]Catholic Institute for Applied Anatomy, The Catholic University of Korea, Seoul, [2]Department of Neurosurgery, Gangneung Asan Hospital, Gangneung, Korea, Republic Of

Introduction and Objectives: Pedicle screw fixation has biomechanical advantages, but it was considered very risky due to neurovascular complications. Thus, a lot of anatomical studies were conducted. However, the anatomical study has still limitations about the individual shape difference of the vertebra. The freehand technique for cervical pedicle screw fixation was a method to complement these limitations. For performing a safety freehand technique, the strength or quality of bone at the cortical wall of the spinal canal (adjacent of the lateral mass), the medial and the lateral wall of pedicle have to be quantified to lead the probe. In this study, we evaluated the regional bone quality in cervical vertebra for safety guidance on freehand technique and related applications.

Methods: In this study, we used 99 patients' data (female: 51, male: 43, mean age: 64) of the cervical CT. The Hounsfield unit (HU) numbers and the thickness of cortical bone (T) in the vertebral canal (cHU/cT), the medial (mHU/mT) and lateral (lHU/lT) wall of pedicle were measured on the axial CT images in the middle of pedicle from C3 to C7 (fig.1). Then, we evaluated the difference in the thickness of cortical bone and the HU number among these regions.

Results: There was no statistical difference between the left and right side of cortical bone thickness and HU number. The largest cortical bone thickness was found in the vertebral canal (cT). And the smallest thickness was the lateral wall of the pedicle (lT). The mean thickness were 1.49 ± 0.27 mm (cT), 1.40 ± 0.22 mm (mT), and 1.02 ± 0.25 mm (lT) ($p<0.01$). The HU No. was showed the highest value in the vertebral canal. The mean number of HU in vertebral canal, the medial wall and the lateral wall of pedicle 1083.43 ± 202.15, 1031.13 ± 206.89, and 688.65 ± 233.41 respectively ($p<0.01$).

Figure:
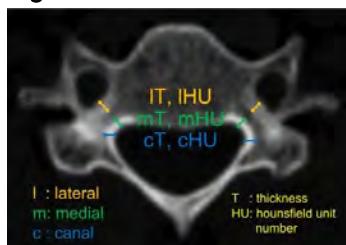
Caption: Fig.1 Measurement parameters, thickness and mean Hounsfield unit numbers at each region

Conclusion: The cortical bone thickness in the vertebral canal and the medial wall of pedicle was thicker than the lateral wall. Moreover, the mean Hounsfield unit number in the vertebral canal wall and the medial wall of pedicle was larger than the lateral wall. Thus, the vertebral canal wall and the medial wall of pedicle were strong structure among these regions. And these structures could support the probe to make a safety trajectory for pedicle screw.

References: [1] Park J.H. et al., Spine (Phila Pa 1976), 39(4): 280-285. 2014

Disclosure of Interest: None Declared

Spine

PO-0319

LIFTING AND BENDING DEMANDS OF THE VARIOUS TASKS PERFORMED BY DAYCARE WORKERS

Genevieve A. Dumas [1,*]Adam Labaj [1]Tara Diesbourg [2]Andre Plamondon [3]Hakim Mecheri [3]

[1]Mechanical and Materials Engineering, [2]SKHS, Queen's University, Kingston, [3]Ergonomie, IRSST, Montreal, Canada

Introduction and Objectives: Research from the 1990s identified that daycare workers are subjected to high postural and lifting demands, and made recommendations concerning furniture and work organisation [1], but few studies have quantified these demands with physical measurements. The objective of this study was to quantify bending and lifting demands on current daycare workers and identify the tasks for which these demands are the highest and should be first considered for improvement.

Methods: Caregivers from five daycares were recruited to participate in the study. They were recorded by video camera for ~ 3.3 hours in the morning of their shift. All children and objects (>1kg) lifted were weighed. Participants' trunk posture was monitored with a dosimeter designed at IRSST [2]; absolute trunk orientation with respect to the vertical and relative flexion-extension between T1 and S1 were continuously recorded.

Video recordings were observed to identify the main tasks performed by the workers. All lifts for which there was a good quality video image were analysed with 3D-SSPP and compression and shear at L5/SI determined. Posture was analysed using APDF and Exposure Variation Analysis (EVA) [3]. Summary scores along the flexion angle amplitude axis (FAA) and the flexion duration axis (FD) were computed to find the average position of the EVA distribution on each axis [4] and used as a measure of postural exposure.

Results: Of the 24 participants (23 females, 1 male; mass - 70.9±25.0 kg, height - 163±8cm), 7 worked with infants (0 - 1.5 yr), 7 with toddlers (1.5 - 2.5 yr), and 10 with pre-school children (2.5 - 4 yr). Eleven tasks were identified and their percentages of collection time computed (Fig. 1).

Workers lifted on average 501 kg during collection time with one lift every four minutes; 54% of the lifts involved children. Most of the weight was lifted during two tasks (Table 1): "**Preparation**" when workers get children (e.g. putting on snowsuits) and room ready for an activity (e.g. setting up for arts and crafts) and "**Changing diapers**" when they lift children to the changing table. The average weight lifted during these two tasks was 7.7 and 12.2 kg, and the average lifting frequency was 0.60 and 0.78 lifts per minute respectively. Compression(C) and shear(S) were highest in "Bathroom" (i.e. helping children in the bathroom) with C= 2858 N and S= 386N and putting children to sleep or "Nap", with C=2735 N and S=371 N, two tasks when few lifts were performed. Though these levels of exposure may not exceed recommended limits for lifting, it must be considered that other factors such as stability are not taken into account. The majority of lifts consisted in lifting a child who, unlike a box, may move in unpredictable ways.

For flexion angle from the vertical, APDF 90 reached 55º showing that workers experienced flexion angles greater than 55º more than 10% of collection time. For flexion between pelvis and upper trunk, APDF 90 was 50.5º. Based on the EVA summary score FAA, the most demanding tasks were "**Nap**" and "**Cleaning**" for absolute flexion and "**Activity**" (children performing an organised activity such as crafts), "**Playing**" and "**Nap**" for relative flexion. For these tasks, the summary score of FAA fell in the EVA class of 20º to 30º which is far from a safer erect posture (0-10 º). "**Activity**" and "**Nap**" were

also the tasks with the highest duration summary scores falling in EVA classes of 2 to 4 and 4 to 8 seconds respectively. During these tasks, the workers were bending over for substantial periods of time to either help the children with their activity ("Activity") or pat their backs to induce them to sleep ("Nap").

Figure:
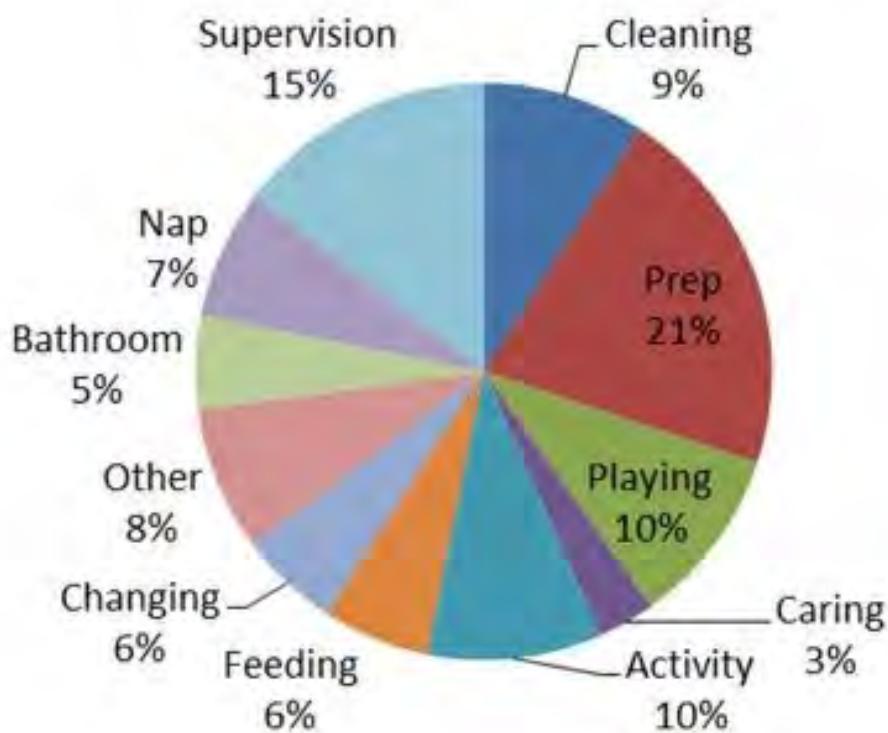
Caption: Percentage of collection time spent in each task.

Conclusion: The results showed that the tasks **"Preparation"** and **"Changing diapers"** were the most demanding in terms of lifting. For trunk posture, "**Activity**" and "**Nap**" were the most demanding both in amplitude of flexion and in duration for holding postures, while **"Cleaning and "Playing"** were demanding in amplitude of absolute or relative trunk flexion. In questionnaire data also collected in this study, the highest ranked and scored tasks identified by the workers were: **Outdoor Preparation**, **Diaper Changing**, **Playing**, **Cleaning**, **Moving Furniture** and **Nap** which shows a good overlap with the tasks identified above for their high demands either in lifting or trunk posture. The results are limited by the small number of daycares considered.

Table:

TASKS	TOTAL WEIGHT (kg)	AVERAGE TOTAL NUMBER OF LIFTS/WORKER	AVERAGE FREQUENCY (#lift/min)
PREPARATION	186	24.1	0.60
CHANGING DIAPERS	182	14.4	0.78
PLAYING	75	6.0	0.45
SUPERVISION	68	6.8	0.24
OTHER	36	3.5	0.30
CARING	33	2.9	0.47
ACTIVITY	32	2.7	0.10
BATHROOM	29	2.3	0.17
CLEANING	27	4.4	0.23
FEEDING	20	2.2	0.10
NAP	17	1.4	0.31

Caption: Lifting demands during data collection duration ordered by total weight lifted.

References: [1] King PM et al., *Work*, 6: 25-32, 1996.

[2] Plamondon A et al., *Appl.Ergon,* 38: 697-712, 2007.

[3] Mathiassen SE and Winkel J, *Ergonomics*. 34(12):1455-68, 1991.

[4] Delisle A, et al, Ergonomics, 49: 139-160, 2006.

Disclosure of Interest: None Declared

Spine

PO-0320

EFFECTS OF HEEL INSERTS ON SPATIO-TEMPORAL LOCOMOTION PARAMETERS IN ATHLETES WITH AND WITHOUT LOW BACK PAIN

Sophie Gondry [1] Clara Leyh [1 2] Marcel Rooze [1 2] Veronique Feipel [1 2,*]

[1]Laboratory of Functional Anatomy, [2]Laboratory of Anatomy, Biomechanics and Organogenesis, Université Libre de Bruxelles, Brussels, Belgium

Introduction and Objectives: In the literature, the relationship between leg length discrepancy (LLD) and low back pain remains controversial and the existence of a causal relationship between LLD and low back pain remains unknown [5]. Nevertheless, LLD is frequently corrected by the use of heel inserts or other types of foot orthoses, and foot orthoses are frequently prescribed for the treatment of low back pain, including in athletes [5]. The mechanisms advanced to explain their potential efficacy in thre prevention or treatment of low back pain include a change in spinal muscle activity during jogging [2, 7] or shock absorbing properties [3]. The efficiency of foot orthoses in the treatment of low back pain remains, however, insufficiently explored [8]. The same review indicated that evidence does not support the efficacy of orthoses in the prevention of low back pain. A few studies [e.g. 4], probably of insufficient quality, showed however positive effects of heel inserts in patients with low back pain.

Our study was designed to compare the spatial and temporal parameters during gait and running, with and without heel inserts in healthy athletes and in athletes with low back pain.

Methods: 15 healthy athletes (6 females, mean age of 23 (SD 2) years) and 15 athletes with low back pain (11 females, mean age of 22 (SD 3) years) were invited to walk over the GAITRite instrumented walkway at various speeds (slow gait, preferred gait speed, fast gait, jogging) with different heel insert conditions (without heel inserts, wearing a unilateral 5 mm heel insert, wearing heel inserts bilaterally, wearing a double unilateral heel insert). Three trials were sampled for each condition. The order of heel insert conditions and locomotion speeds were randomized. The software associated with the GAITRite walkway computes spatial and temporal parameters from foot contacts on the embedded pressure sensors. It was shown to be reliable and valid [1, 6, 9]. Gait velocity, cadence, step length, cycle length, step width, step time, cycle time, stance time, swing time, and for gait trials single and double support times were extracted and averaged across trials. A repeated measures ANOVA was used to compare speeds and heel insert conditions (within-subject factors) and groups (between-subject factor).

Results: Wearing heel inserts, in subjects with low back pain and healthy subjects, significantly altered each parameter studied. An increased gait velocity, stride velocity, cadence, swing time, single support time and step length, as well as a reduced step time, cycle time, stance time, and double support time (for gait trials) were observed in the presence of heel inserts. For most of these variables, no significant group effect nor group x insert interaction was observed.

Figure:
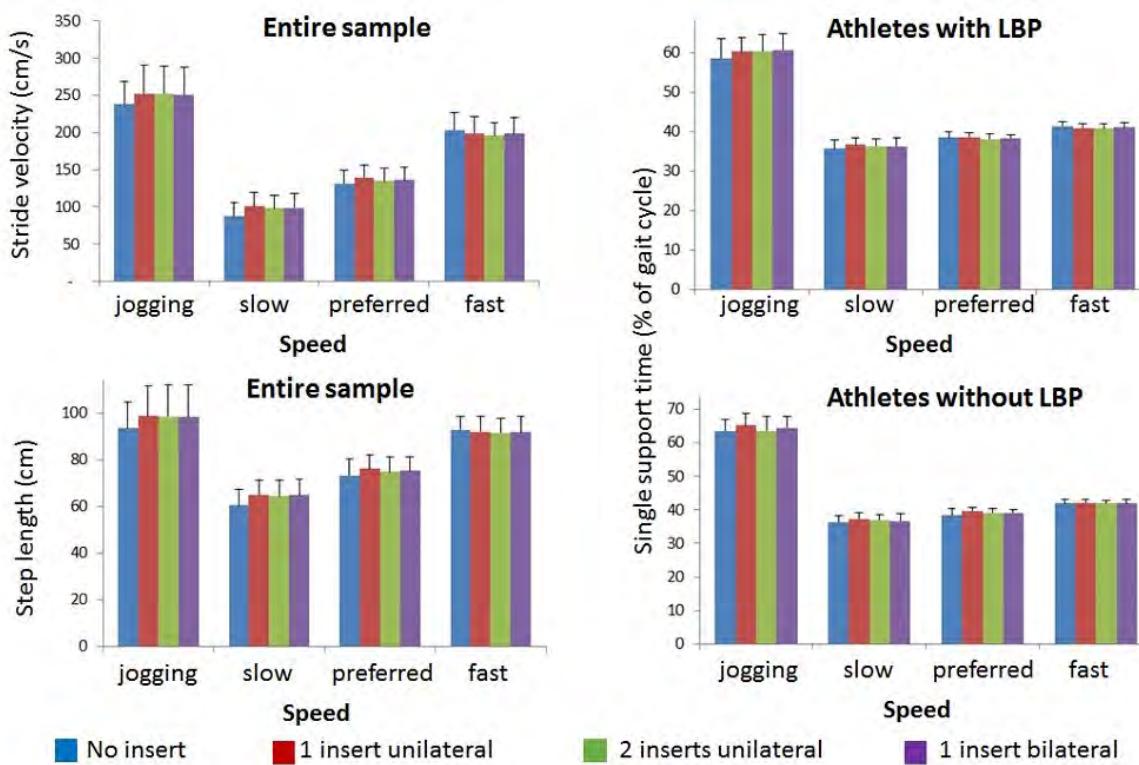
Caption: Stride velocity, step length and single support time in both samples at different locomotion speeds.

Conclusion: In athletes, wearing heel inserts, whatever the configuration, changed the spatio-temporal locomotion parameters in the same direction as does an increase of gait speed. The results of the study do not allow to conclude that these heel changes related to heel inserts have an effect on reducing or preventing low back pain.

The hypotheses of a better restitution of elastic energy, better shock absorption [3] and an anterior imbalance modifying spinal muscle activities [2, 7], even if the heel inserts were used to correct leg length discrepancy are advanced and deserve further investigation, including the effect of wearing heel inserts in the longer term. The absence of familiarization with the wear of heel inserts might indeed be responsible for some of our observations.

References: [1] Bilney et al., Gait Posture, 17: 68-74, 2003.

[2] Bird et al., Gait Posture, 18: 81–91, 2003.

[3] Folman et al., Prev. Med., 39: 351–354, 2004.

[4] Golightly et al., JOSPT, 37: 380-388, 2007.

[5] Kendall et al., Foot, 24: 75–80, 2014.

[6] Menz et al., Gait Posture, 20: 20-25, 2004.

[7] Ogon et al., Int. J. Sports Med., 22: 414-419, 2001.

[8] Sahar et al., Cochrane Db. Syst. Rev., 4: CD005275, 2007.

[9] van Uden et al., BMC Musculoskelet. Disord., 17:13, 2004.

Disclosure of Interest: None Declared

WHOLE SPINE ALIGNMENT IN AUTOMOTIVE SEATED AND SUPINE POSTURES BY USING AN UPRIGHT OPEN MRI SYSTEM

Fusako Sato[* 1], Mamiko Odani[2], Yui Endo[3], Mitsunori Tada[3], Yusuke Miyazaki[2], Taichi Nakajima[1], Koshiro Ono[4], Shigehiro Morikawa[5], Mats Svensson[6]

[1]Safety Research Division, Japan Automobile Research Institute, Ibaraki, [2]Tokyo Institute of Technology, [3]National Institute of Advanced Industrial Science and Technology, Tokyo, [4]Japan Automobile Research Institute, Ibaraki, [5]Shiga University of Medical Science, Shiga, Japan, [6]Chalmers University of Technology, Gothenburg, Sweden

Introduction and Objectives: Whiplash associated disorder (WAD) caused by rear-end car accidents is a worldwide problem. Many aspects of WAD are still unknown and further research to understand the injury causation and prevent WAD more effectively is needed. Human body finite element models have been used to study injury biomechanics in vehicle crashes. Those studies reported cervical spine kinematics which was considered to be related to WAD was affected by initial positions of thoracic-lumbar spine as well as cervical spine[1]. Therefore, the accurate knowledge of alignment of whole spine is important. However, alignment of whole spine in automotive seated posture has not been well reported in literature, particularly in females[2], generally due to availability of image data in supine[3].

The purpose of this study was to provide the alignment of whole spine in automotive seated posture by analyzing image data acquired with an upright open magnetic resonance imaging (MRI) system. Furthermore, this study showed the comparison of vertebral alignment between seated and supine postures in order to provide reference data to estimate spine alignment in seated posture by using conventional computed tomography (CT) or MRI data in supine.

Methods: Five female and two male subjects were scanned in seated and supine postures by an upright open MRI system (0.5T GE Signa SP MRI system) at Shiga University of Medical Science. Subjects were laid on their back on a horizontal table in supine. In seated posture, subjects were seated in a wooden rigid seat with a seatback angle of 20 ° from the vertical and seat pan angle of 10° from the horizontal. Then, the subjects were asked to face forward and relax. The specifications of the seat were defined based on the previous volunteer sled testing which simulated occupant kinematics during rear-end accidents [4]. The MRIs from the bottom of skull to coccygeal bone were acquired with 4 serial images changing the height of the seat. All subjects had no history of spine injury and provided informed consent.

MRI images were analyzed to extract the whole spine alignment. The spine curvature was determined by the vertebral angle relative to lower adjacent vertebra in the sagittal plane from C2 to sacrum in this study. The vertebral angles were defined as the angle of the mid-plane between superior and inferior endplates of each vertebral body. The angle measurements of sacrum were taken at its superior endplate.

Results: From C2 to C5, intervertebral angles varied a great deal due to different types of cervical spine alignment. Four female and one male subjects had kyphosis and one female and male subjects lordosis.

C6 angle of all subjects and C7 angle of females exhibited lordosis. Then, thoracic spine from T1 to T7 showed kyphosis. Previous studies analyzed spine alignment in cervical and thoracic spine separately[5]. In addition, thoracic spine is commonly described in T4-T12 kyphosis angle[6]. Therefore, there was lack of information of connectivity between

cervical and thoracic spine[7]. However, results showed intervertebral angles from C7 to T3 were not so small as to be negligible and those values have a significant role in defining cervical spine orientation.

In the lumbar spine, intervertebral angles in supine were greater than that in seated posture. In this study, MRI scans of sagittal sections were obtained in 100mm width around spine, and the pelvic angle was extrapolated with the superior endplate angle of sacrum. Peleg[8] reported the angle between the line joining the anterosuperior iliac spine and the anterosuprtior edge of the symphisis pubis and the line along the sacrum superior endplate was 48.5±10.2°. The superior endplate of sacrum in seated posture was inclined at 1.6° for females and 9.3° for males from the horizontal. Therefore, the angle of line joining the anterosuperior iliac spine and the anterosuperior edge of the symphisis pubis in seated posture of this study was estimated at approximately 50.1° for females and 57.8° for malets from horizontal plane.

Figure:

(a) MRI images of a female volunteer
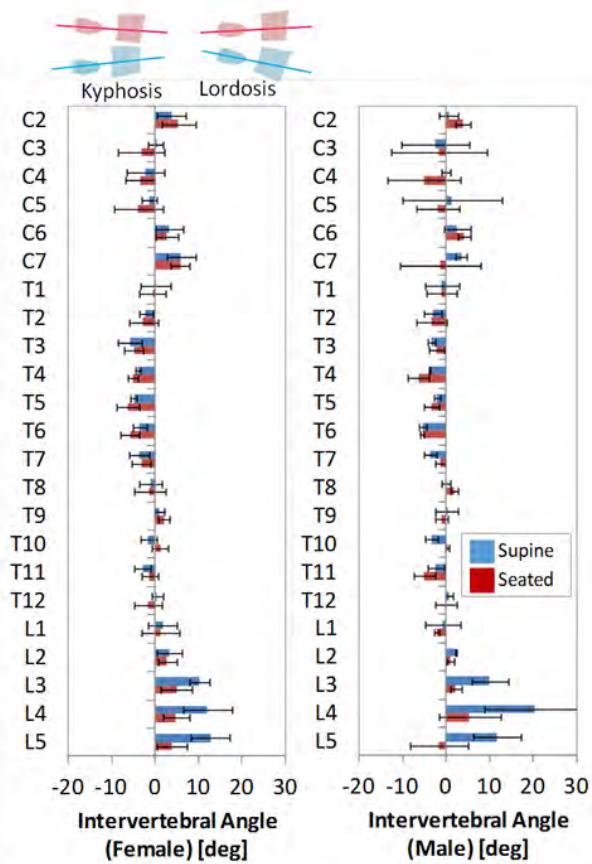
(b) Average of intervertebral angles

Caption: Fig. 1 MRI images and average intervertebral angles relative to each lower adjacent vertebra in seated and supine postures.

Conclusion: This study showed the whole spine alignment in seated posture by using an upright open MRI system which could take a scan without the risk of ionizing radiation. Results provided useful information to determine the whole spine alignment in seated posture. This will enable a more accurate starting posture and result in improved computer simulations of vertebral kinematics to investigate neck injury mechanisms.

Table:

ID	Sex	Height [m]	Weight [kg]
1	F	1.58	47
2	F	1.56	41
3	F	1.58	44
4	F	1.57	54
5	F	1.69	55
6	M	1.71	68
7	M	1.72	60

Caption: Table 1 Characteristics of subjects

References: [1] Sato, IRCOBI, 41-58, 2010

[2] Chabert, ESV, 2073-9, 1998

[3] Parenteau, Traf Inj Prev, 15:66-72, 2014

[4] Ono, IRCOBI, 103-13, 2006

[5] Klinich, J. Biomech. Eng., 134(11):114503, 2012

[6] Beillas, Stapp, 53:127-54, 2009

[7] Lee, Spine J, 14:2628-38, 2014

[8] Peleg, Am J Phys Anthropol 133:967-77, 2007

Disclosure of Interest: None Declared

EFFECTS OF THE SWIMMING PRACTICE ON SCAPULAR KINEMATICS IN CHILDREN AND ADOLESCENTS

Fernanda A. P. Habechian [1,*]Ana Leticia Lozana [1]Elisa Pires [1]Livia Pogetti [1]Paula Camargo [1]

[1]Physiotherapy, Federal University of São Carlos, Piracicaba, Brazil

Introduction and Objectives: Swimming is among the most popular sports worldwide. Ninety percent of the propulsive force is performed by the upper limb, requiring a great demand of the shoulder complex [1]. Adult elite swimmers are used to practice all week an average of 10,000 to 14,000 meters per day, which causes an overuse in the shoulder complex leading to shoulder pain and injuries [2]. In the current literature on this topic, most of the studies were conducted with adult swimmers. However, the number of children and adolescents participants in youth sports has increased as well as the injuries in their shoulder complex [3]. A better comprehension of the biomechanical aspects of the shoulder complex afforded by the swimming in this young population is warranted. Thus, the objective of this study was to evaluate the effects of the swimming practice on the 3-dimensional scapular kinematics in children and adolescents.

Methods: Twenty-eight male children/adolescents were evaluated and divided in 2 groups: 14 swimmers competitors (12.00 ± 1.95 years) and 14 non-swimmers (12.84 ± 1.35 years). All participants had no history of shoulder/cervical dysfunction and at least 150° of arm elevation. The swimmers had to practice the sport for a minimum of 1 year, at least 3 times per week and to participate in professional level competitions. The non-swimmers could not be involved to the practice of other sports involving the upper limb. Scapular kinematics was assessed with the electromagnetic tracking device Flock of Birds® integrated with the MotionMonitor™ software. Local coordinate systems were established using the digitized landmarks following the International Society of Biomechanics recommended protocol [4]. The dominant arm was evaluated and the individuals had to maintain light fingertip contact with a flat planar surface to keep positioning of the arm in the scapular plane. Three repetitions were performed of elevation of the arm. Scapular kinematics was analyzed at 30°, 60°, 90° and 120°. The data were averaged over the 3 repetitions. Shapiro-Wilk test was used to check the normality. A 2-way mixed model analysis of variance (ANOVA) was used for the 3 scapular rotations, in separate, considering humeral angle (30°, 60°, 90° and 120°) as within factor and group (swimmers and non-swimmers) as between factor. The Bonferroni test for post hoc analysis was used when necessary. A $p < 0.05$ was considered significant.

Results: Both groups had same pattern of scapular movement: increase internal rotation and upward rotation, and progression from anterior to posterior tilt during arm elevation. A 2-factor interaction was found where swimmers showed more internal rotation ($p < 0.05$) at 90° and 120° of arm elevation compared to non-swimmers (mean difference: 6.34° and 8.28°, respectively). The non-swimmers presented slight external rotation at the end range of arm elevation while internal rotation continued until the end of elevation in the swimmers. It is important to remember that one of the most important modality of swimming is the crawl, and during this modality the internal rotation of the humerus is essential and probably the scapular internal rotation is needed as well [5]. For scapular upward rotation no differences were found ($p > 0.05$) between groups. With regards to the scapular tilt, the swimmers had more posterior tilt at all angles of arm elevation (average mean difference: 5.9°). The literature has already showed that the serratus anterior is one of the most active muscle during the swimming in adults and it is also known that this is the only scapulothoracic muscle with the

capability to both upwardly rotate and posteriorly tilt the scapula on the thorax making its contribution to normal scapular kinematics very significant [2]. Its line of action will directly approximate the scapula to the thorax, which can serve as a stable base, which is extremely necessary during the swimming strokes.

Conclusion: The scapular kinematics pattern was similar between the groups, however the swimming practice seems to affect it. Swimmers have higher internal rotation at the end range of the arm elevation compared to non-swimmers and a higher posterior tilt at all angles of arm elevation. A more comprehensive understanding of scapular kinematics in the young population of swimmers can help in the development of appropriate evaluation, treatment and preventive protocols focused for children and adolescents swimmers.

References: 1. Mountjoy et al. *Br J Sports Med*, 44: 522-526, 2010.

2. Pink & Tibone. *Orthop Clin*, 31:247-261, 2000.

3. Tarkin et al. *The Americ J Sports Med*, 33:596-601, 2005.

4. Wu et al. *J Biomech,* 38:981-992, 2005.

5. Whiteley et al. *J Orthop Sports Phys Ther*, 39:256-263, 2009.

Disclosure of Interest: None Declared

Sport

PO-0323

EFFECTS OF DIFFERENT KNEE JOINT TAPING TYPE DURING A JUMP-STOP TASK

Po-Han Chang [1,*]Chen-Fu Huang [1]Tzu-Lin Wong [1]Min-Hao Hung [1]

[1]Physical Education, National Taiwan Normal University, Taipei, Taiwan, Republic of China

Introduction and Objectives: Sport taping was used to prevent injure [1, 2], and it was popular on today's sport fields. Many sports had some common movements like jump-stop. This movement had to decrease speed quickly and maintain balance that make follow-up movement more easily and stability [3]. But jump-stop movement may increase the loading rate of anterior cruciate ligament (ACL) [4, 5, 6]. The purpose of this study was to investigate the effects of stability by using different types of taping on knee joint during a jump-stop task.

Methods: Eight healthy males (aged = 19.5 ± 1.2 year, height = 174.3 ± 5.9 cm, weight = 65.9 ± 4.2 kg) participated in this study. All the participants performed a jump-stop task under three knee taping conditions (traditional taping (TT), Kinesio taping (KT) and non-taping (NT)). A high speed camera (Mega Speed 30 Ks, 100Hz), two AMTI force plates (1000Hz) and four Biovision electromyography (EMG, 1000Hz) systems were used synchronously to collect kinematic, kinetic and EMG data during the landing phase. The Kwon3D and DASYLab 6.0 software were used for further analyses of the data. One-way repeated measures ANOVA and Scheffe methods was performed to compare the parameters among three conditions (a=.05).

Results: The results indicated that lower peak anterior-posterior ground reaction force (A-P GRF) and shorter displacement of anterior-posterior center of pressure were observed under the TT and KT conditions than the NT condition. A smaller average loading rate was reported with the KT compared to the NT. Regarding kinematic parameters, an increased knee flexion angle at peak impact was observed under the TT and KT conditions than the NT condition. A larger knee flexion ROM angle was reported under the KT compared to the NT. Furthermore, smaller mean EMG amplitudes were found in the rectus femoris and gastrocnemius muscles under the TT and KT conditions.

Conclusion: The study concluded that the traditional and Kinesio taping techniques effectively increases the stability by giving a strong support and limiting the forward displacement of the anterior cruciate ligament at a jump-stop task. The Kinesio taping is also beneficial to increase the range of motion of knee joint.

Table:

	NT (1)	TT (2)	KT (3)	F	Post hoc
Peak of A-P GRF (B.W.)	0.570 ±0.045	0.504 ±0.043	0.490 ±0.059	5.953*	(1)>(2) (1)>(3)
Knee joint ROM (°)	53.60 ±9.50	61.38 ±8.37	65.49 ±8.16	3.855*	(1)<(3)
Knee joint ROM at peak of A-P GRF (°)	39.70 ±5.75	46.47 ±3.97	48.11 ±4.97	6.486*	(1)<(2) (1)<(3)
Mean EMG of rectus femoris (%MVC)	71.82 ±3.48	63.73 ±7.53	63.02 ±4.21	6.642*	(1)>(2) (1)>(3)
Mean EMG of gastrocnemius (%MVC)	19.19 ±11.08	17.34 ±9.33	15.90 ±9.58	10.983*	(1)>(2) (1)>(3)
*p<.05					

Caption: The difference of taping types during a jump-stop task

References: [1] Callaghan et al., J ATHL TRAINING, 37: 19-24, 2002.

[2] Huang et al., BIOMED ENG ONLINE, 10, 2011.

[3] Chappell et al., AM J SPORT MED, 30: 261, 2002.

[4] Yu et al., CLIN BIOMECH, 21: 297-305, 2006.

[5] Nagai et al., J ATHL TRAINING, 48: 31, 2013.

[6] Schmitz et al., CLIN BIOMECH, 22: 681-688, 2007.

Disclosure of Interest: None Declared

VARIABILITY IN JOINT DYNAMICS IN CHILDREN AND ADULTS DURING COUNTERMOVEMENT JUMPS

Peter C. Raffalt [1,*]Tine Alkjær [1]Erik Simonsen [1]

[1]Department of Neuroscience and Pharmacology, University of Copenhagen, Copenhagen, Denmark

Introduction and Objectives: Variability in inter-limb (between limbs) and intra-limb (within limbs) joint dynamics during whole body movements like vertical jumps can be used to evaluate both the limb-synchronization and consistency of movement pattern. It has recently been observed that the amount of variability in vertical ground reaction force during countermovement jump without arm swing does not differ between girls and adult women [1]. However, it is unknown if the coordination with respect to variability in limb-synchronization and movement pattern differs between children and adults. The purpose of the present study was to estimate the amount of variability in inter- and intra-limb synchrony of joint dynamics during countermovement jump in children and adults. We anticipate, that the adults show less variability in both inter- and intra-limb joint dynamics compared to children.

Methods: Nine boys (mean ± SD age: 11.8 ± 1.7 years, height: 157.1 ± 14.1 cm and mass: 41.7 ± 12.8 kg) and eight adults (25.6 ± 3.7 years, 181.7 ± 6.6 cm, 77.4 ± 11.0 kg) completed 9 consecutive maximal countermovement jumps without arm swing. Three-dimensional lower limb kinematics and ground reaction force from each foot were recorded. Inverse dynamics were used to calculate concentric and eccentric sagittal hip, knee and ankle joint power. Joint power was normalized to body mass. Right leg joint power from each jump of each subject was plotted against left leg joint power (figure 1A and 1B). Based on this plot three variables for each joint on both legs of each subject were calculated: 1) the average perpendicular distance from the coordinates from each joint to the line of identity as a measure of inter-leg joint power synchrony, 2) coefficient of variation (CV1) of the perpendicular distance from the coordinates from each joint to the line of identity as a measure of variability of inter-limb synchronization and 3) coefficient of variation (CV2) of the distances between the origin and the projection of each point on the line of identity as a measure of variability in intra-limb joint power generation. In addition, the relative variability of each joint contributing to the total power generated was calculated.

Results: No group differences were observed in inter-leg joint power synchrony or variability of inter-limb synchronization. The children had a significant higher variability in intra-limb eccentric and concentric power generation for the hip joint (p <0.05) but not for the knee and ankle joint. This was confirmed by a higher variability in relative joint contribution of concentric power (table 1).

Figure:
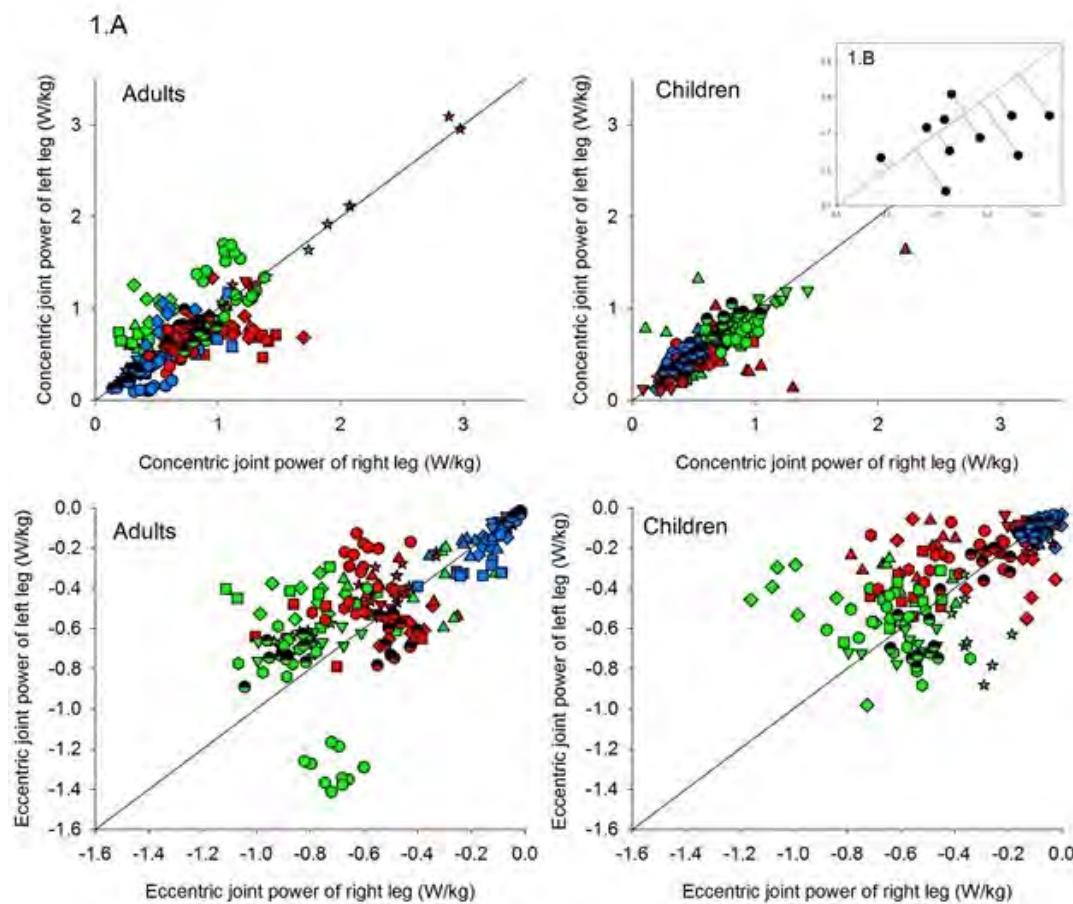
Caption: Figure 1A: Concentric (top graph) and eccentric (bottom graph) joint power of right leg plotted against concentric joint power left leg (top graphs) for adults (left side) and children (right side). Each symbol represents a jump and each symbol type represents each subject. Red symbols are hip joint power, green symbols are knee joint power and blue symbols are ankle joint power. 1B: CV1 is calculated as the coefficient of variation of the perpendicular distances between each point and line of identity. CV2 is calculated as the coefficient of variation of the distances between the origin and the projection of each point on the line of identity.

Conclusion: The present study shows that children are capable of performing maximal countermovement jumps with the same level of joint power synchronization as adults [2]. However, children have a less consistent hip power generation compared to the adults. The present study supports previous studies, that have observed adult-like movement pattern in children during vertical jumps [1,2]. Based on the results presented in figure 1, it is clear that large individual differences exist in the variability of power contribution. This suggests that some individuals accomplish the movement according to a variety of different solutions while other individuals utilize a more consistent movement pattern.

Table:

Adult subject number	CV right hip	CV right knee	CV right ankle	CV left hip	CV left knee	CV left ankle
1	7.3	25.4	12.7	13.2	10.4	14.5
2	14.2	37.8	12.4	15.0	18.9	18.8
3	13.8	30.9	17.2	19.7	21.0	15.2
4	10.4	7.4	13.1	12.2	3.8	20.2
5	16.8	20.5	24.0	18.9	18.4	18.4
6	22.1	15.2	33.7	20.2	13.6	33.3
7	19.0	6.9	21.5	8.0	3.7	23.8
8	9.8	7.5	23.2	8.1	10.0	24.8
Group mean ± SEM	14.2 ± 1.8	18.9 ± 4.1	19.7 ± 2.6	14.4 ± 1.7	12.5 ± 2.4	21.1 ± 2.2
Child subject number	CV right hip	CV right knee	CV right ankle	CV left hip	CV left knee	CV left ankle
1	24.0	40.5	27.7	48.0	53.9	30.2
2	26.2	18.5	11.8	23.8	14.0	17.8
3	17.0	14.6	14.5	14.7	15.0	19.5
4	29.5	12.1	7.2	32.2	14.2	6.1
5	32.8	6.0	17.7	33.0	3.7	12.9
6	21.0	12.4	12.8	21.8	9.4	16.2
7	12.9	10.0	11.9	8.6	11.9	25.9
8	19.5	7.9	14.7	16.2	9.6	16.0
Group mean ± SEM	22.8 ± 2.3 *	15.2 ± 3.9	14.8 ± 2.1	24.8 ± 4.5 *	16.5 ± 5.5	18.1 ± 2.6

Caption: Table 1: Coefficient of variation (CV) of percentage joint power contribution for right and left leg in adults and children. * indicates significant group differences ($p < 0.05$).

References: [1] Floria et al., J Appl Biomech, Jul 9[Epub ahead of print], 2014.

[2] Jensen et al. Res Q Exerc Sport, 63(3), 258-268, 1994.

Disclosure of Interest: None Declared

HIP, TRUNK AND SHOULDER STRENGTH IN THROWING ATHLETES WITH AND WITHOUT SHOULDER PAIN

Lívia S. Pogetti [1,*] Theresa Nakagawa [1] Elisa Pires [1] Paula Camargo [1]

[1] Physical Therapy, Federal University of São Carlos, São Carlos, Brazil

Introduction and Objectives: The dynamics involved in the throwing motion can be best understood by adopting the concept of force development through sequential segments of the kinetic chain. The kinetic chain is a coordinated sequence of activation, mobilization and stabilization of body segments, which places the distal segment in a great position, speed and time to produce the desired task.The majority of force required to propel the ball forward is developed in the hips and trunk. This force is sequentially transferred through the trunk, to the scapulohumeral complex to be transferred to the arm. Any change in a segment of the kinetic chain can increase the stress on the distal segments resulting in soreness or anatomic lesion. Thus, the objective of this study was to evaluate the muscle performance of the hip, trunk and shoulder of throwing athletes with and without shoulder pain.

Methods: Eight throwing athletes without shoulder pain (1 female and 7 males; 20.62±2.13 years; 84.87±18.69 kg; 177.25±7.28 cm) and 5 with shoulder pain (4 females and 1 male, 21.20±1.92 years; 59.8±8.64 kg; 161.6±8.82 cm) participated in this study. All of them were athletes in the college level of handball (n=8), baseball (n=2) and softball (n=2) modalities. Isokinetic concentric peak torque of the extensor muscles of the hip was measured at 60°/s for the impulsion leg; which is the ipsilateral leg to the throwing arm. The average of 5 repetitions was used to determine the peak torque. The trunk flexor muscle strength was measured in the supine position with a hand dynamometer. The average of 3 maximum voluntary isometric contraction repetitions was used for analysis. Isokinetic concentric peak torqueof the dominant arm was also analyzed by the average of 5 repetitions during internal and external rotation of the shoulder at 90º/s and 180º/s.The Student t-test for independent samples was used for group comparisons. An alfa level was set at .05.

Results: The group with shoulder pain showed lower isometric trunk flexor strength (pain group, 1.34±0.34N/kg; no pain group, 1.97±0.50N/kg; P=0.03); lower peak torque during external rotation at 90°/s (pain group,0.51±0.10 Nm/kg·m; no pain group, 1.01±0.21Nm/kg·m; P=0.03) and internal rotation at 90º/s (pain group, 0.63±0.10 Nm/kg·m; no pain group 0.93±0.29Nm/kg·m; P=0.03) when compared to the group with no shoulder pain. No significant differences were found between groups during external rotation at 180º/s (pain group, 0.56±0.14 Nm/kg·m; no pain group 1.02±0.20 Nm/kg·m; P=0.10), internal rotation at 180º/s (pain group, 0.64±0.15 Nm/kg·m; no pain group0.89±0.27 Nm/kg·m; P=0.07) and for the hip extension peak torque at 60°/s (pain group, 3.79±1.89Nm/kg·m; no pain group, 3.50±1.38 Nm/kg·m; P=0.77). The shoulder pain did not affect the ability to reach high velocity, possibly because all athletes continued with their regular routine of training, despite the pain. Considering the concept of integrated kinetic chain, the shoulder is the receiver and transmitter of the forces generated in the trunk, pelvis and hip. Therefore, the current results suggests that the appropriate function of the shoulder in throwing athletes with shoulder pain is impaired being potentially influenced by the weakness of the trunk flexors. These results provide a better understanding of possible changes in the segments of the kinetic chain

and can help the development of most appropriate and comprehensive protocols for assessment, treatment and prevention of injuries in this population.

Conclusion: The throwing athletes with shoulder pain showed lower trunk and shoulder strength compared with athletes without pain. Strengthening of the shoulder and trunk should be considered in the rehabilitation of these athletes.

References: Kibler et al. Operative techniques in sports medicine, 20:103-112, 2012.

Kibler et al. Sports Med, 36(3):189-198, 2006.

Sciascia et al. Sports Med Arthrosc, 20:16-21, 2012.

Disclosure of Interest: None Declared

PO-0326

THE KINETIC CHAIN ANALYSIS IN DIFFERENT LEVELS OF SOCCER PLAYERS DURING INSTEP KICK

Yo Chen [1,*]Wu-Yeh Chang [2]Yao-Ting Chang [1]Jia-Hao Chang [1]

[1]Department of Physical Education, National Taiwan Normal University, [2]Department of Ball Sports, University of Taipei, Taipei, Taiwan, Republic of China

Introduction and Objectives: Kicking is a natural fluid motion and a fundamental activity in soccer[1]. Elite players have a better kicking skill than general players. The ratio of ball-foot velocity and the kinetic chain have been used to understand the efficiency in soccer kicking. The purpose of this study was to improve the kicking skill in general players, thus we compared the kicking kinematics and measured the kinetics chain between elite and general soccer players.

Methods: Fourteen Taiwanese soccer players were recruited as participants in this study (elite group, EG: N= 7, Aged: 20.2 ± 1.0, Height: 173.3 ± 5.9 cm, Mass: 71.5 ± 15.7 kg; general group, GG: N= 7, Aged: 24.6 ± 2.4, Height: 169.1 ± 5.8 cm, Mass: 64.1 ± 8.9 kg). A VICON motion capture system (sampling rate at 200 Hz) was used to capture the kicking motions, and the plug-in-gait marker set was use to build full-body model. A radar gun was used to measure the peak ball velocity. Participants were asked to kick a ball three times in instep kick, and the kicking data with the fastest ball velocity was selected to analyse. The Visual3D was used to calculate the kicking kinematics. The ratio of ball-foot peak liner velocity was used to understand weather the ball was kicked on the centre of a ball. The measurements of foot peak liner velocity in back swing and forward swing, and the duration of kinetics chain transmit in segments were used to understand the kicking strategy between different levels of soccer players. The paired t-test (α = .05) was applied to assess significant difference in this study.

Results: The greater ball velocity (EG: 27.4 ± 0.7 m/s; GG: 20.9 ± 1.0 m/s) and ball-foot ratio was found in elite grope (EG: 1.7 ± 0.1; GG: 1.4 ± 0.1). No differences were found in foot peak liner velocities. In back swing, the foot velocity was 7.20 ± 0.77 in EG and 7.28 ± 0.51 in GG. In forward swing, the foot velocity was 16.45 ± 1.69 in EG and 15.06 ± 0.92 in GG. The total time of kicking (from back swing to ball contact) was averaged 0.25 s in both group, and no differences were found in kinetic chain. It was 0.043 ± 0.012 s in EG and 0.038 ± 0.012 s in GG from the peak velocity of foot back swing to the peak velocity of thigh forward swing. Also, the similar duration was found from the peak velocity of thigh to the peak velocity of shank, it was 0.043 ± 0.010 s in EG and 0.038 ± 0.013 s in GG. From peak velocity of shank to peak velocity of foot it was 0.023 ± 0.008 s in EG and 0.016 ± 0.011 s in GG.

Conclusion: Elite and general players had similar characteristic of kinetic chain. According to the ball-foot ratio, elite players can kick a ball in the right position. To have a higher ball velocity, general players should improve their accuracy in ball-foot contact position.

References: [1] Clagg et al., Sports Biomechanics, 8: 141-153, 2009.

Disclosure of Interest: None Declared

PO-0327

BILATERAL DIFFERENCE IN TRUNK MUSCLE VOLUME IN MALE COLLEGIATE GOLF PLAYERS

Youka Izumoto [1,*]Michio Wachi [1]Tadashi Suga [1]Toshiyuki Kurihara [1]Tadao Isaka [1]

[1]Sport and Health Science, Ritsumeikan University, Kusatsu, Japan

Introduction and Objectives: Asymmetric activation of the bilateral trunk muscles is essential for effective golf swing (Marta et al., 2012). Such asymmetric activations were seen in the erector spinae and abdominal oblique (Watkins et al., 1996), muscles responsible for trunk twist and lateral bending. Therefore, recurrent golf swing practices could cause asymmetric hypertrophy on these trunk muscles. The purpose of this study was to investigate the degree of asymmetric hypertrophy on trunk muscles by measuring the muscle volume between left and right sides in male collegiate golf players.

Methods: Ten male right-handed collegiate golf players (golf players: age 20.5 ± 1.0 yrs, height 171.9 ± 5.7 cm, weight 64.8 ± 5.0 kg) and nine physically active right-handed college students who had never played golf (non-golf players: age 22.3 ± 0.6 yrs, height 172.0 ± 5.0 cm, weight 66.8 ± 9.3 kg) participated in this study. Golf players had at least 4 years of experience in golf practice (8.8 ± 3.6 yrs). They regularly practiced at a golf training center (1.5 ± 0.4 hours for 3.9 ± 1.4 days / week), and played on a golf course (1.4 ± 0.7 rounds / week). The MR images were obtained with a 1.5-T magnetic resonance system (Signa HDxt; GE Medical Systems) while the subjects lying supine. Serial transverse MR images (1cm slice thickness) were obtained from the intervertebral space between the 4th and 5th thoracic vertebrae to the lower part of the sacrum. With the use of the intervertebral space between the 5th lumbar and 1st sacral vertebrae as the point of origin (0cm), the images of every 3 cm slice to the head (e.g. +3cm, +6cm…) and to the caudal regions (e.g. -3cm, -6cm…) were used to estimate muscle volume. Cross-sectional area of the trunk muscles (rectus abdominis, abdominal obliques, psoas major, quadratus lumborum, and erecror spinae) was determined (SliceOmatic ver.5.0 rev-4b2, Tomovision), and was then multiplied by 3cm to estimate muscle volume for each slice. As for the erector spinae, the muscle volume was divided into the lumbar (levels from 0cm to 18cm) and thoracic regions (levels higher than +18cm). The degree of bilateral asymmetry for each trunk muscles was calculated as the left to right volume ratio (= (right - left) / right * 100).

Results: There were no significant differences in the volume of each muscle between the golf players and non-golf players. In the golf players, the muscle volume on the right side was significantly larger than that on the left side for the rectus abdominis, while the muscle volume was significantly larger on the left side for the abdominal oblique and psoas major. Moreover, although no significant difference was observed in the total muscle volume for the erector spinae, the opposite side was larger in muscle volume between the thoracic and lumbar regions for the golf players: the right side was significantly larger than the left side in the thoracic region, whereas the left side was larger in the lumbar region. For the non-golf players, there was no such bilateral difference between the thoracic and lumber regions within erector spinae.

Figure:

Right and left asymmetry of trunk muscles on golfers/non-golfers
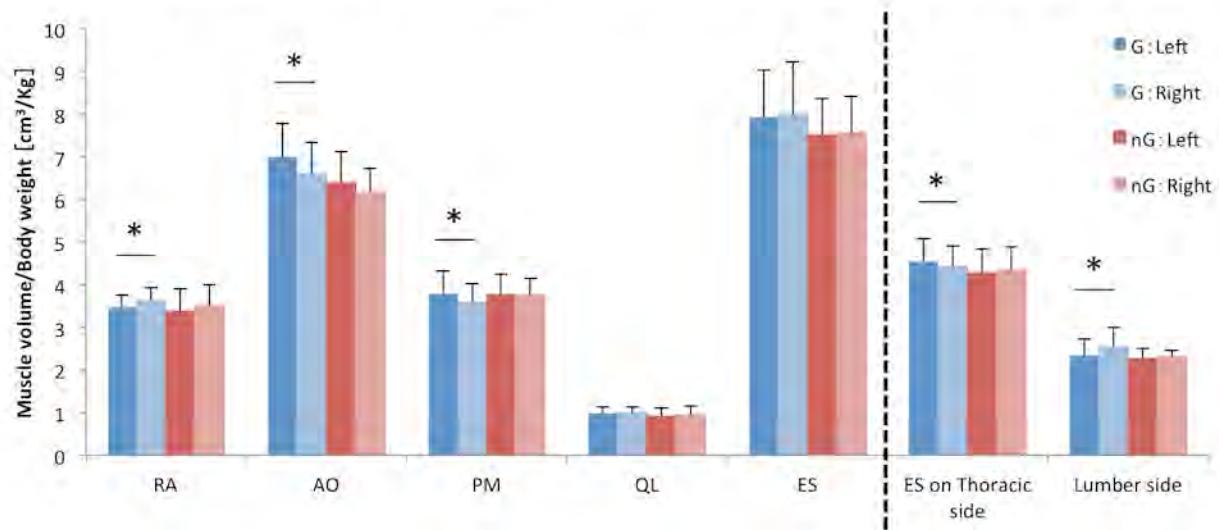
Caption: * < 0.05. G : golf player, nG : non-golf player, RA : rectus abdominis, AO : abdominal obliques, PM : psoas major, QL : quadratus lumborum, ES : erecror spinae. Thoracic side is 0cm~+18cm of ES, Lumber side is +18cm~ of ES.

Conclusion: The male collegiate golf players demonstrated bilateral difference in muscle volume in the rectus abdominis, abdominal oblique, and thoracic and lumber regions of the erector spinae. Right-handed golf players are known to twist their trunk to the left and bend it to the right (Okuda et al., 2010; Sugaya et al., 1996). Larger muscle volume obtained in the left abdominal oblique and right erector spinae seem to result from such trunk motion. These findings suggested that recurrent golf practice could cause asymmetric hypertrophy in the left abdominal oblique and right erector spinae for right-handed golfers. Such asymmetric muscle hypertrophy in the bilateral trunk muscles would also be seen in the other sports that require asymmetric trunk motion, such as cricket, tennis, and field throwing events.

References: Marta et al., J. Electromyography and Kinesiology, 22: 803-813, 2012.

Okuda et al., J. Sports Science and Medicine, 9: 127-133, 2010.

Sugaya et al., Ja J. Clinical Biomechanics, 17: 157-161, 1996.

Watkins et al., Am J. Sports Med, 24(4): 535–8, 1996.

Disclosure of Interest: None Declared

Sport

PO-0328

STUDY ON THE DOUBLE ROUNDHOUSE KICK FOCUSED ON THE BRINGING DOWN LEG AFTER THE FIRST IMPACT

Madoka KINOSHITA [1,*]Norihisa FUJII [2]

[1]Graduate School of Comprehensive Human Sciences, [2]Health and Sport Sciences, University of TSUKUBA, Tsukuba, Japan

Introduction and Objectives: Taekwondo is an Olympic event characterized by a diverse array of kicking techniques. Because the rules were changed recently, accurate and continuous kicks to the opponent are required instead of kicks with strong impact forces to win the competition. According to previous studies (Falco et al., 2012; Kim et al., 2011), roundhouse kick (RHK) was one of the most critical and basic kicks. Some researches were focused on a single RHK. There are few researches about a multiple RHK. As mentioned above, multiple RHK is required to win the game. Our previous studies about double RHK (Kinoshita et al., 2014) showed that the trial time of the phase from the 1st impact to the 2nd toe off the floor (DOWN phase) was accounted as 30% of total trial time (from start to 2nd impact). Technique of DOWN phase had a relation to shortening the total trial time, and to the fast and quick kicking in 2nd kicking phase because of long time and the characteristics as preparatory phase. They also showed that there were some types of way to bring down the kicking leg based on the path of knee (I-type and S-type, Figure 1 b)).

The purpose of this study was to analyze the double RHK in the phase from 1st impact to the 2nd toe off in order to get the some knowledge of mechanisms that gives a reason for the type of way, and to find the way to bring down the leg suitable for taekwondo.

Methods: Ten male Japanese Taekwondo athletes (with age: 21.4±3.2 [yr], height: 1.72±0.04 [m], body mass: 66.7±12.7 [kg], and experience: 6.5±5.9 [yr]) participated in this study after informed consent. The participants had the diverse skill levels (national game level - not in particular). Experiment trial consisted of double RHK to a target with preferred leg and non-preferred leg alternately. The 3D coordinates of reflective markers on the body and the target were captured by a motion capture system (Vicon MX+, 250 Hz), and filtered the captured data with a Butterworth digital filter (12.5-25.0 Hz) (Wells et al., 1980). The ground reaction forces were obtained for both legs by force platforms (Kistler, 1000 Hz). The total analysis trial was 28 trials (0-4 trials per subject). To normalize a kicking motion, the trial motion was divided at 0% (start to kick, STR), 50% (1st toe off the floor, 1st TOF), 100% (1st impact, 1st IMP), 150% (2nd toe off the floor, 2nd TOF), and 200% (2nd impact, 2nd IMP) as figure 1 a). The analysed phase was from 100% (1st IMP) to 150% (2nd TOF) termed "DOWN phase". Both averaged I-type and S-type motions about two segments (pelvis-thigh and shank-foot in bringing down leg) were reconstructed for inverse and forward dynamics simulation based on hip joint coordinate value in support leg. Four type (II-type, IS-type, SI-type, and SS-type) of motion data were produced by reconstructed data to investigate the reason why the type of motion were divided.

Results: Figure 1 c) showed that the angular velocities of hip internal-external rotation in the bringing down leg. The magnitudes of external angular velocities were different among 4 types about 110% time. After that, the angular velocities branched off into two patterns (II-type, SI-type and SS-type, IS-type).

In this report, there is no figure on the position of each segments, angular velocity of knee joint, torque, and etc. In view of the kinematics results, both IS-type and SI-type (combined type) were considered as a feasible motion. Among all types, motions of hip external rotation and knee flexion-extension had the relations to the shank motion. On the other hand, for the kinetics results, the combined types showed that larger constrained torque of knee joint was required to perform. Original types (II-type, SS-type) showed almost same magnitude of torque nevertheless their motions were quite different.

Figure:
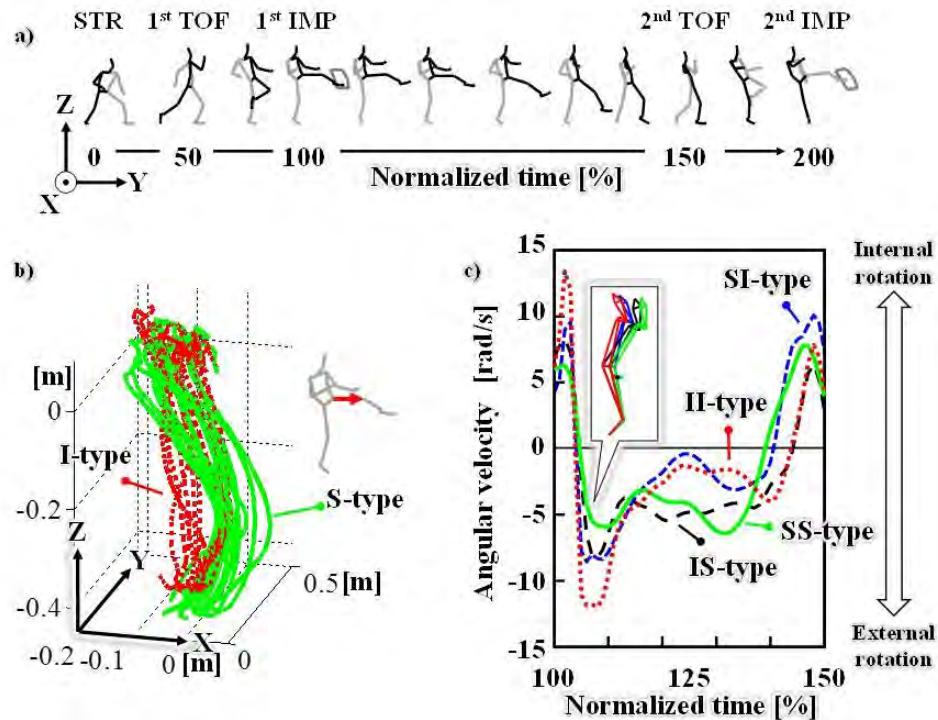
Caption: Figure 1 a) Motion of double roundhouse kick. b) Locus of the knee joint based on hip joint. c) Angular velocity of internal-external rotation.

Conclusion: This study provided a new insight into the mechanism of the motion about bringing down leg in DOWN phase. GOOD athletes bring down their leg by the same way, that is the same joint torque. However, the type of way to bring down their leg with the movement of hip external rotation was settled by the knee position at the 1st impact. It is our view that the coaches should pay more attention to the DOWN phase in which there are many suitable types of way for bringing down the leg.

Table:

Type	Thigh-data	Shank-data
II	I	I
IS	I	S
SI	S	I
SS	S	S

Caption: Table1 Reconstructed data type

References: [1] Falco et al., *Adv Physical Educ*, 2, 28-31, 2012.

[2] Kim et al., *J Sports Sci Med*, 10, 31-38, 2011.

[3] Kinoshita et al., Proc SOBIM2014, 41-44, 2014 (in Japanese).

[4] Wells et al., (1980). Proc *Human Locomotion*, 1, 92-93.

Disclosure of Interest: None Declared

INFLUENCE OF UNILATERAL AND BILATERAL ANKLE BRACING ON JOINT KINEMATICS OF THE BRACED AND NON-BRACED ANKLE JOINT.

Andrew Greenhalgh [1,*]Victor Lonchuk [1]Amey Kolekar [1]Jonathan Sinclair [2]

[1]London sports Institute, Middlesex University, London, [2]University of Central Lancashire, Preston, United Kingdom

Introduction and Objectives: In many sports ankle sprain is the most common injury reported (Fong et al., 2007). During jogging, significant inversion and external rotation have been associated with Chronic ankle instability (Drewes et al., 2009). Ankle bracing is widely used in many sports as a way of reducing the prevalence of such injuries (Dizon and Reyes, 2010; McGuine et al., 2012). Whilst the effects of bracing on an ankle joint appear to have a body of evidence supporting a change in movement, little is known on the effects of a braced foot on the opposite ankle movement. Due to changes in movements on one side of the body there may well be an effect on the other.

There is a paucity of research comparing the same bracing system used in a bilateral or unilateral approach. Therefore the aim of this study was to investigate the influence of unilateral bracing on the dominant ankle joint in both the braced foot and unbraced foot during running shod. The results will be compared to bilateral braced and non-braced conditions. The hypothesis of the study was that the movement of both a braced and a non-braced ankle joint would be affected by the bracing condition on the other foot.

Methods: Seven participants (height 1.81 ± 0.08 m, mass 77.3 ± 6.0 Kg Age 22.8 ± 2.9 y)who were all recreational soccer players with no history of ankle injury in the past 6 months were recruited for the study. Participants ran in a laboratory along a runway with an embedded force plate at the centre, at 4.0m/s ±5% in three different conditions; non-braced, braced dominant foot, and bilaterally braced. Running velocity was quantified using infrared timing gates Newtest 300 (Newtest, Oy Koulukatu, Finland). All kinematic data was captured by a 14 camera opto electric motion capture system (Qualisys™ Medical AB, Goteburg, Sweden). The marker configuration for this investigation used the calibrated anatomical systems technique (CAST) technique (Cappozzo et al., 1995). In order to define the segment co-ordinate system axes of the shanks and feet, retro-reflective markers were positioned on the 1st and 5th metatarsal head, and posterior calcaneus positions on the footwear, medial and lateral malleoli, medial and lateral epicondyle of the femur. Quad marker tracking clusters were securely attached to each of the shank segments. A static reference trial was obtained prior to the commencement of dynamic data collection with the participant in the anatomical position, allowing the positions of the anatomical markers to be referenced in relation to the tracking clusters, which allowed for the removal of Malleolus markers to fit the braces. Participants all wore their own shoes which they would normally wear when playing soccer. The order in which participants ran in each condition was randomized. The force plate allowed identification of foot strike and toe off and only strikes where suitable contact with the force plate were accepted for analysis (Sinclair et al., 2014).

In order to test the hypothesis of the study kinematics of the unbraced non-dominant foot with no brace on the dominant foot was compared to the unbraced non-dominant foot with a brace on the other foot. Then the kinematics of the dominant

braced foot with the other foot braced was compared to the dominant braced foot with the other foot non-braced. Paired sample t-tests were used for the specific comparisons.

Results: No significant differences ($P < 0.05$) were found between the non-braced foot conditions and the braced foot conditions for peak external rotation, peak inversion and peak dorsiflexion.

Conclusion: The results suggest that the braced condition on the other foot do not influence the movement of the ankle joint in question. This research therefore suggests that ankle joints should be continued to be assessed separately when it comes to deciding whether or not to use bracing to protect the ankle from potential injury.

References: Cappozzo et al., Clin. Biomech, 10: 171–178, 1995.

Dizon et al., J. Sci. Med. Sport, 13: 309–317, 2010.

Drewes et al., J. Sport Rehabil, 18: 375–388, 2009.

Fong et al., Sport. Med, 37: 73–94, 2007.

McGuine et al., Am. J. Sports Med, 40: 49–57, 2012.

Sinclair et al., Appl. Biomech, 30: 166–172, 2014.

Disclosure of Interest: None Declared

Sport

PO-0330

OPTIMIZATION OF DUAL COMPLEMENTARY BIOMECHANICAL VARIABLES ON STRETCH-SHORTENING CYCLE

Carlos M. B. Rodrigues [1,*]Miguel Correia [1]João Abrantes [2]Marilú Gomes [3]Marco Benedetti [4]Jurandir Nadal [5]

[1]C-BER - Centre for Biomedical Engineering Research, INESC TEC - Technology & Science Associate Laboratory, Porto, [2]MovLab – Laboratório de Tecnologias e Interfaces, Universidade Lusófona de Humanidades e Tecnologias, Lisboa, Portugal, [3]Departamento de Engenharia Biomédica, [4]Departamento de Eletrônica e Sistemas, Universidade Federal de Pernambuco, Recife, [5]PEB - Programa de Engenharia Biomédica, COPPE/UFRJ - Universidade Federal do Rio de Janeiro, Rio de Janeiro, Brazil

Introduction and Objectives: Stretch shortening cycle (SSC) is a natural form of muscle action usually observed in gait, running and jumping as a specific and independent form of muscle action controlled by the neuromuscular system for impact anticipation, protection of structural integrity, efficiency on sub-maximal actions and potentiation on maximal actions [1]. SSC consists in a pre-stretch of activated muscle before its reversible shortening action, optimizing levels of force production and synchronizing them according to intended action.

SSC has been assessed using well-defined protocols based on maximum vertical jumps (MVJ), originally introduced by Asmussen et al. [2] and followed by numerous authors as Komi et al. [3], Bobbert et al. [4], Aragon-Vargas et al. [5] and these procedures still used today, because of its standard nature, reproducibility and simplicity. Three types of jumps are commonly analyzed, the Squat Jump (SJ), the Counter Movement Jump (CMJ) and Drop Jump (DJ) [2].

The aim of this study was to explore dual behavior of two complementary biomechanical variables, force and displacement of body center of gravity (BCG), and the resultant developed mechanical work to assess human optimization of different lower limb SSC's. In connection with this assessment, other dual biomechanical variables of BCG were analyzed for the same purpose namely force and push time for impulse analysis and force – velocity for evaluation of developed mechanical power.

Methods: Selected subjects are a small sample of n=6 healthy male students of sports and physical education degree, without any relevant sports past or previous specific training. Each subject was weighted (76.7 ± 6.7)kg, measured his height (178.9 ± 4.9)cm and performed a total of 3 trials of SJ, CMJ and DJ. During the tests, ground reaction forces were acquired with force platform AMTI BP2416-4000CE at frequency acquisition of 1000 Hz and coupled amplifier AMTI Mini Amp MAS-6.

Based on vertical ground reaction force $GRF_z(t)$ during the impulse phase it was was obtained the resulting vertical force $RF_z(t) = GRF_z(t) - Fg$ and vertical acceleration $a_z(t) = RF_z(t) / m$ of the BCG. From null initial velocity at inversion of vertical movement ($v_{zi} = 0$) and numerical integration of $a_z(t)$ it was obtained the vertical velocity $v_z(t)$ and numerical integration of $v_z(t)$ yielded vertical displacement $Dz(t)$ of the BCG from the initial position for each jump. By numerical temporal integration the force impulses $I[GRF_z(t)]$ and $I[RF_z(t)]$ were obtained. The propulsive mechanical power $P(t) = RF_z(t) \, v_z(t)$ and mechanical work $W(t) = RF_z(t) \, Dz(t)$ of the BCG were calculated as well as the GRF_z / Fg and RF_z / Fg.

From the above physical quantities, there were extracted a set of discrete, instantaneous and cumulative parameters with interest for this study. These were statistically analyzed with parametric and non-parametric tests, despite normality tests

due to small sample size. For this purpose IBM SPSS 9.5.0.0 was used and decisions were taken on statistical significance differences (SSD) $p<0.05$.

Results: Despite > values of *P mean up / m* at DJ than CMJ and at CMJ than SJ the values *W imp up / m* are > at CMJ than DJ and > at CMJ than SJ without SSD. This can be explained based on the fact that despite *P mean up / m* is > at DJ than CMJ and at CMJ than SJ, the time period Δt_{up} during which energy is transferred by means of mechanical power is much < at DJ than CMJ and slightly < at CMJ in relation to SJ, explaining > values of *W imp up / m* at CMJ than DJ despite > values of *P mean up / m* at DJ than CMJ and non-SSD of *W imp up / m* between CMJ and SJ despite > values of *P mean up / m* at CMJ than SJ. The same is observed with *GRF$_z$ mean up*, Δt_{up} and *I(RF$_z$) imp up / m* since, although *GRF$_z$ mean up* presents > values at DJ when compared to CMJ and SJ the impulse *I(RF$_z$) imp up / m* is > at CMJ than DJ and > at SJ than at DJ in this case without SSD, which can be explained by the differences at the action time interval Δt *up* of the vertical forces at the upward phases on different MVJ.

Figure:
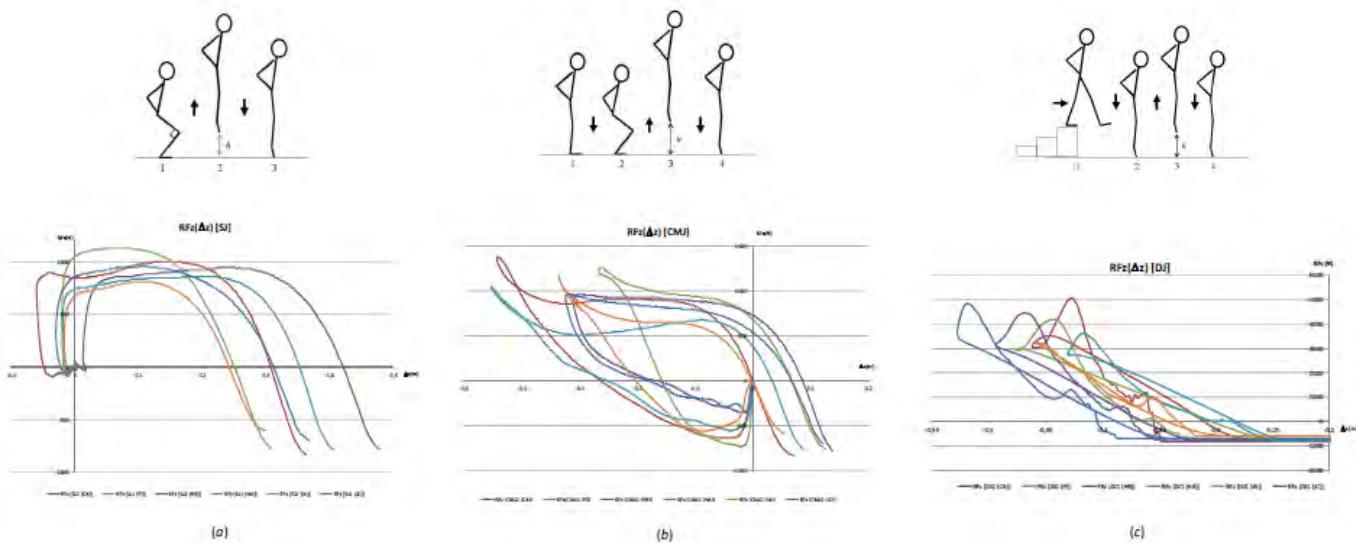
	SJ	CMJ	DJ
P mean up / m (W/kg)	10,59 ± 0,96	12,50 ± 1,51	24,41 ± 3,60
W imp up / m (J/kg)	3.04 ± 0.45	3.45 ± 0.29	2.75 ± 0.34
Δt_{up} (s)	0.283 ± 0.042	0.278 ± 0.039	0.113 ± 0.012
GRF$_z$ mean up (N)	1421.39 ± 162,82	1474.93 ± 156.28	2357.73 ± 205.12
I(RF$_z$) imp up / m (Ns/kg)	2,457 ± 0,186	2.620 ± 0,109	2,336 ± 0,139
v$_z$ up (m/s)	1.365 ± 0,075	1.638 ± 0,061	1,735 ± 0,100
Δz up (m)	0.408 ± 0.075	0.459 ± 0.062	0.200 ± 0.027
h (flight) (m)	0.332 ± 0.045	0.364 ± 0.042	0.274 ± 0.032

Caption: Stick-figures and vertical resultant force - displacement graphs of body center of gravity for SJ (a), CMJ (b) and DJ (c)

Conclusion: By itself the higher levels of force and vertical velocity found in DJ and the larger displacements and push time found in CMJ are not sufficient to explain the differences in optimization of MVJ results expressed by h (*flight*) at each MVJ type. The current analysis shows that the process of human optimization of BCG movement at different lower limb SSC on MVJ cannot be explained based on a single discrete variable separately considered, but rather a dual optimization of complementary physical quantities such as (F_z, Δt), (F_z, Δz) or (F_z, v_z).

References: [1] Komi et al., Portuguese J. Sports Sciences, 11(2): 31-33, 2011.

[2] Asmussen et al., Acta Physiol. Scand., 91: 385-392.

[3] Komi et al., Med. Sci. Sports, 10(4): 261-265.

[4] Bobbert et al., Eur. J Appl Physiol., 54: 566-573.

[5] Aragón-Vargas et al., Eur J Appl Physiol., 13: 24-44.

Disclosure of Interest: None Declared

Sport

PO-0331

GOLF DRIVING PERFORMANCE: THE EFFECT OF DYNAMIC AND STATIC STRETCHING WARM UP ROUTINES

Graeme Sorbie [1,*]Ukadike C. Ugbolue [1]Fergal Grace [1]

[1]School of Science and Sport, University of The West of Scotland, Hamilton, United Kingdom

Introduction and Objectives: Biomechanics has been used in an attempt to find the model golf swing, with emphasis on improving performance and reducing the rate of injury [1]. Swing mechanics are described by many golf professionals as the most important factor for optimal golf driving performance [2]. Biomechanically, a high level of flexibility and ROM at specific joints and soft tissues is required to achieve the desired golf swing movement patterns [3]. Despite there being a number of different stretching techniques available to adopt as routine warm up protocols prior to competition and practice, it still remains unclear what the optimum warm up protocol should be in terms of improving the biomechanical efficiency of the golf swing. Among the various warm up protocols, dynamic and static stretches are two of the most popular stretching techniques [4]; that have been chosen to be investigated. Therefore the purpose of this study was to investigate the effect of dynamic and static stretching warm up routines using shot accuracy, distance, angle of deviation and percentage clubface contact as performance outcome measures.

Methods: A total of 12 subjects (age: 22.5 ± 3.0 years; mass: 80.3 ± 6.4 kg; height: 1.84 ± 0.1 m), volunteered to take part in the study. All subjects held a Council of National Golf Unions (CONGU) handicap of 5 or less (1.4 ± 1.9). Prior to commencing testing, approval for the study was obtained from the School of Science & Sport, University of the West of Scotland, UK, Ethics Committee. Each subject was required to attend 2 separate sessions on non-consecutive days. The testing lasted an average of 2 hours over a 3 / 5 day period. The three different components tested were carry distance, accuracy and ball contact using a driver. Each subject was randomized to either a dynamic stretching or static stretching routine on their first day of testing. The opposite routine was then performed on the final testing session. Each testing session began with a 5 minute run at 40% of their perceived maximum running speed around the practise area. This was based on a study by Yamaguchi et al. [5]. The stretching protocols consisted of 9 stretches targeted at the upper and lower body. The markings on the fairway ranged from 150-300 yards. Accuracy was measured by the absolute distance each shot deviated, left or right, from the predetermined target line. Measurement recordings were taken from the teeing area to the final resting position of the ball. Club contact with ball data was based on how well the ball was hit. Participants responded either with "yes" for good contact or "no" for poor contact. Descriptive statistics and paired t-tests were performed (P = 0.05) between the dynamic and static stretching protocols.

Results: Within participants there was a significant difference between driving distance after performing the dynamic stretch and static stretch (P = 0.012). Driving accuracy produced a significant difference between participants after the dynamic and static warm up (P = 0.049). Within participants the driving distance coefficient of variation after the dynamic and static stretch protocols were- range: 2.55% - 7.09% and range: 1.88% - 7.37% respectively. Also within participant there was a greater variability in the shot accuracy after the dynamic stretch protocol (Mean (SD): 55.77 (9.29) %) compared with the static stretch protocol (Mean (SD): 49.83 (12.18) %). The results also showed no significant differences between the angle of deviation outcome measure.

Figure:

Participants	Handicap	Distance after Dynamic Stretch (Yards) Mean (SD)	Distance after Static Stretch (Yards) Mean (SD)	Shot Accuracy after Dynamic Stretch (Yards) Mean (SD)	Shot Accuracy after Static Stretch (Yards) Mean (SD)	Angle of Deviation after Dynamic Stretch (°) Mean (SD)	Angle of Deviation after Static Stretch (°) Mean (SD)	Percentage Clubface Contact after Dynamic Stretch (%)	Percentage Clubface Contact after Static Stretch (%)
A	+1	255.30 (16.08)	250.00 (17.62)	7.30 (2.83)	6.30 (3.47)	1.64 (0.64)	1.44 (0.82)	80	70
B	2	250.50 (16.47)	242.30 (17.18)	8.40 (2.67)	8.20 (5.05)	1.97 (1.28)	1.91 (0.57)	70	70
C	4	220.50 (13.02)	220.40 (11.35)	9.50 (4.25)	9.50 (3.37)	2.52 (1.26)	2.47 (0.89)	60	60
D	0	249.30 (8.72)	249.20 (10.68)	4.50 (2.01)	7.00 (4.24)	1.61 (0.98)	1.04 (0.48)	90	70
E	1	256.90 (7.33)	247.30 (11.70)	5.40 (2.59)	7.30 (3.06)	1.21 (0.58)	1.69 (0.70)	70	70
F	+2	253.40 (9.49)	249.70 (14.11)	4.90 (3.37)	5.20 (3.61)	1.22 (0.89)	1.11 (0.86)	80	70
G	4	238.90 (15.17)	234.20 (16.38)	5.70 (3.06)	7.90 (3.84)	1.40 (0.82)	1.98 (1.08)	80	70
H	3	253.60 (12.10)	248.90 (8.78)	5.70 (3.34)	8.20 (5.25)	1.92 (1.30)	1.31 (0.80)	70	80
I	0	227.90 (8.49)	224.70 (7.30)	4.40 (2.07)	4.60 (2.67)	1.10 (0.51)	1.17 (0.68)	90	80
J	3	247.00 (4.64)	243.70 (6.22)	5.90 (3.18)	5.70 (3.37)	1.35 (0.83)	1.38 (0.76)	90	70
K	2	253.80 (6.49)	248.00 (12.48)	6.90 (2.85)	8.10 (5.15)	1.87 (1.21)	1.56 (0.65)	100	60
L	1	229.00 (7.09)	229.10 (11.35)	5.10 (3.00)	5.80 (3.37)	1.28 (0.75)	1.46 (0.77)	60	70

Caption: Summary of Driving Performance Results

Conclusion: The current study is the first to report that with a driver a dynamic general warm up will enhance driving performance over a static general warm up routine. It is worth noting, that Moran et al. studied dynamic stretching versus static stretching and no stretching prior to testing similar variables with a 5 iron. Their protocol was different and outcome measures were club head speed and ball speed [4]. A more scientific approach was adopted where the distance of each shot, clubface angle and swing path were calculated to measure accuracy. The results demonstrate that dynamic stretch could significantly increase driving distance and accuracy in comparison to static stretch. However, no significant difference was displayed in club contact with the ball between the dynamic and static stretching protocols. Although the sample size was small and no control group was used, we anticipate that the outcome of this research study provides useful data to amateur and professional golfers who engage in stretching techniques during training.

References: [1] Hume PA et al., *Sports Med, 35*(5), 429-449, 2005a.

[2] Keogh JW et al., *Sports Biomech, 11*(2), 288-309, 2012.

[3] Tilley NR et al., *Int J Sports Phys Ther, 7*(4), 388-395, 2012.

[4] Moran KA et al., *Int J Sports Med, 30*(2), 113-118, 2009.

[5] Yamaguchi T et al., *J Strength Cond Res, 21*(4), 1238-1244, 2007.

Disclosure of Interest: None Declared

Sport

PO-0332

EQUINE SURFACE ROTATIONAL RESISTANCE MEASUREMENT

Johannes P. Schramel [1,*]Christian Peham [1]

[1]Equine clinic, Movement Science Group, Vienna, Austria

Introduction and Objectives: In recent years, manufacturers and embodiments of equine arena surfaces and floorings for horse caring have increased significantly. Surface functional properties and methods for their assessment are still under discussion and subjective opinions of riders and experts replace missing guidelines. It is commonly accepted that some surface characteristics assist in achieving optimal performance but may also reduce or enhance the risk of injuries. The interaction between hoof and ground is complex and varies depending on gait and riding discipline. In particular, horse races and show jumping exerts high loads to the horse´s legs that may be strongly influenced by surface attributes. Many studies investigate shock absorption and energy restitution with equipment that mimics the footing of a horse. Some apply vertical forces in combination with tangential (shear) forces to simulate slipping after impact. However, also the rotational resistance (RR) between the surface and the hoof is an important functional property. It mimics loads occurring in show jumping where heavy landings together with sharp turns happen frequently. The latter is considered a major stress for joints, tendons and ligaments and may result in even fatal injuries. On the other hand a too small RR can cause unsafe movements and ligamental strain. Moving repeatedly on a circle in horsewalkerswith a high RR rubber floor may compromise soundness in the long term. The same holds for performing canter pirouettes on high friction grounds where excess loading may occur from a rotating limb and fixed foot. Aim of the study is the development of a RR test equipment that enables assessment of the maximum torque between a surface and a loaded hoof.

Methods: Rotational resistance was measured with a custom-made device (Fig. 1). A weight- loaded lever (1) applies a constant force of 1000N vertically to a natural horn capsule (2) of representative size and shape (15cm x 12cm). The latter was pivoted in the midline to achieve flat contact with the surface. The probe to be tested (3) was located on a turntable (4) that can be adjusted in height to set the lever (1) to a horizontal position. Granular material like sand was filled into a bucket up to about 15-20 cm height and then put on the turntable. A digital torque wrench (5) with max-hold function (DTW-100f CHECKLINE Europe) was attached to the turntable to measure the maximum torque (Nm) at the transition from static to kinetic friction between surface and hoof. Each sample was measured six times (turf 11 times) to derive mean value and standard deviation with Microsoft Excel. The value of the first rotation was discarded. Moisture content of granular material was measured with a TRIME PICO 64 HD2 (IMKO Germany) sensor. Compliant surfaces were levelled before every measurement and the hoof was reset to plane position. The angle of rotation was between 15 ° and 45 ° until a stable reading of the torque meter was achieved.

Descriptive statistics was applied and results were compared with turf by ANOVA. Level of significance was set to $p<0.05$.

Results: Nineteen surfaces for riding areas and for horse caring have been measured. The results of the RR in comparison to turf are depicted in table 1. Moisture content was between 8% and 15%. Turf had a higher RR than some surfaces designed for equitation. High RR was also recorded for dry wooden shavings used for horse bedding.

Sands without supplements showed smaller RR. Rubber based surfaces revealed greater or equivalent RR than turf. In contrast, a piece of oak wood and plastic grid not filled with grit showed low RR revealing a slippery surface.

Figure:

Caption: Test equipment for rotational resistance of surfaces

Conclusion: The proposed method to determine RR of equestrian surfaces seem to be suitable to compare sand and rubber - based materials with turf and may assist the design of suitable riding surfaces by combining versatile materials and supplements. The equipment may also be used to test horse shoeing concepts on multiple grounds.

Table:

Surface	Mean	SD	Significance
Turf	370.1	50.2	Reference
SF1	267.6	15.0	
SF2	292.4	14.1	
SF3	243.8	5.0	SD
SF4	163.2	13.6	SD
Grit	151.6	8.7	SD
S1	239.2	17.6	SD
S2	157.8	8.8	SD

S3	83.8	7.8	SD
WC	314	27.9	
Concrete	281.8	18.5	
R1	392	18.8	
R2	408.8	10.0	
R3	525.6	31.7	
Wood dry	120.4	17.9	
RG1	444.8	6.0	
RG2	322	15.0	
RG3	263	3.1	SD
RG4	176.6	13.9	SD

Caption: Rotational resistance of surfaces. Legend: SF = sand with fibre; S = sand; WC = wooden chips, dry ; R = rubber; RG = rubber granules with binder. Results are compared to turf .

Disclosure of Interest: None Declared

PO-0333

KINEMATIC CHANGES DURING A 30-REPETITION BOUT OF THE BARBELL POWER CLEAN

Paul Swinton [1,*] Katherine Burgess [1] Eimear Dolan [1] Rodrigo Aspe [2]

[1]School of Health Sciences, Robert Gordon University, Aberdeen, [2]School of Sport and Exercise, University of Gloucestershire , Gloucestershire , United Kingdom

Introduction and Objectives: Recently, there has been increased popularity of high intensity training programs performed with technically demanding resistance exercises. Despite improvements in fitness and body composition that can be obtained over short time periods with such training practices, many exercise professionals and researchers have raised concerns regarding the safety of performing complex resistance exercises during states of extreme fatigue. The purpose of this study was to quantify and compare the kinematics of the lower extremity when well-trained athletes perform a fatiguing and non-fatiguing protocol with a technically demanding resistance exercise to provide mechanical insights into the associated injury potential.

Methods: Sixteen male and four female resistance trained participants performed 30 repetitions of the power clean using a gender specific absolute load (males: 62 kg, females: 41 kg) in as short a duration as possible. To provide a baseline assessment of kinematics, a non-fatiguing protocol comprising 6 repetitions (with inter-repetition rest periods of 10 seconds) was performed with the same absolute load. Kinematics were quantified using 2-dimensional video analysis of the hip, knee and ankle in the sagittal plane. Discrete kinematic variables comprised joint angles measured at the beginning (start of the first pull) and end of each repetition (the point where the barbell touched the shoulder during the catch phase). In addition, the coordinated action of the hip and knee were quantified using angle-angle plots and a vector coding method that produced a coupling angle describing the relative movement as: 1) Hip dominant; 2) In-phase; 3) Knee dominant; or 4) Anti-phase. To assess the effects of fatigue on kinematics, the variables measured were averaged across blocks of six repetitions. The first block comprised the baseline assessment (BASE), the second block comprised the first six repetitions of the fatiguing protocol (F1-6), the third block comprised the thirteenth to eighteenth repetitions of the fatiguing protocol (F13-18), and the fourth block comprised the final six repetitions of the fatiguing protocol (F25-30). Potential differences between the blocks of repetitions were analysed using a one-way repeated measures ANOVA. Effect sizes were calculated using the eta squared statistic (n^2), with values of 0.02, 0.13 and 0.26 used to indicate a small, medium and large effect, respectively.

Results: Analysis of the discrete kinematic data identified significant differences in joint angles adopted at the start and end of the power clean (Table 1). The results demonstrated that as fatigue accumulated participants reduced the amount of knee flexion ($p<.001$, $n^2=.045$) at the beginning of the movement and reduced the amount of hip flexion ($p<.001$, $n^2=.040$) and ankle dorsiflexion ($p=.036$, $n^2=.044$) at the end point of the movement. Analysis of coupling angles demonstrated no significant differences in the distribution of the coordination phases across the repetition blocks ($p=0.199$ to $p=0.069$; $n^2=.040$ to $n^2=.097$, Table 1).

Figure:
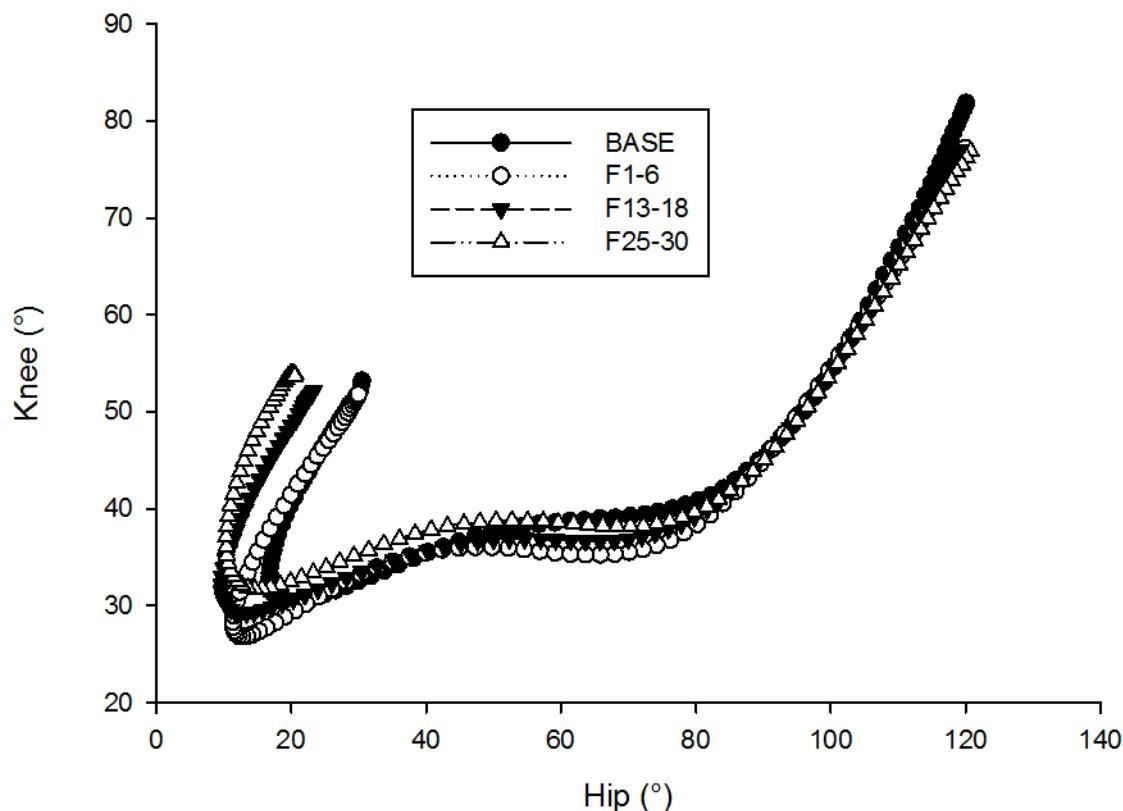
Caption: Figure 1. Angle-angle diagram displaying the relative hip and knee motion averaged across subjects.

Conclusion: The results of the present study demonstrate that a fatiguing protocol representative of that used in popular high intensity resistance training programs has the potential to cause statistically significant changes in the kinematics associated with a complex exercise. It appears that the kinematic changes observed occur as a result of the fatigue developed and potentially the task constraint of attempting to complete the prescribed number of repetitions in as short a duration as possible. However, it is important to note that the change in kinematics observed were relatively small in magnitude compared with the variation across individuals performing the same movement. That is, effect sizes calculated for all kinematic variables demonstrating statistically significant differences were classified between small and moderate. Interestingly, the majority of participants demonstrated the ability to maintain the salient feature of coordinating the action of the hip and knee despite the fatigue elicited. Collectively, the results suggest that well trained athletes can perform complex resistance exercises in states of extreme fatigue and still maintain appropriate kinematics to reduce the likelihood of incurring injury.

Table:

	BASE	F1-6	F13-18	F25-30	p	n²
Initial hip (°)	121±8	120±9	119±8	120±8	.58	.004
Initial knee (°)	83±11	77±11	76 ± 12	73± 9	.000	.045
Initial Ankle (°)	95±6	98±6	97±5	97±7	.06	.036
Final hip (°)	31±18	30±20	23±18	20±18	.000	.040
Final knee (°)	52±16	52±18	52±17	54±15	.95	.002
Final Ankle (°)	93±7	92±7	87±5	85±5	.03	.044
Inphase (%)	50±15	55±14	48±14	48±16	.19	.099
Hip D (%)	29±9	31±14	36±17	32±15	.21	.097
Knee D (%)	14±8	10±5	9±6	11±6	.12	.102
Antiphase (%)	7±4	5±4	7±4	8±6	.13	.114

Caption: Table 1. (mean ± SD) Comparison of joint angles and coupling angles between repetition blocks

Disclosure of Interest: None Declared

Sport

PO-0334

PEDALING SYMMETRY DURING TWO TYPES OF INCREMENTAL MAXIMAL CYCLING PROTOCOLS

Rodolfo A. Dellagrana [1,*]Luis Antonio Pereira de Lima [1]Felipe P Carpes [2]Fernando Diefenthaeler [1]

[1]Biodynamic Research Group, Federal University of Santa Catarina, Florianópolis, [2]Applied Neuromechanics Research Group, Federal University of Pampa, Uruguaiana, Brazil

Introduction and Objectives: Pedaling asymmetry was observed among mountain bike (MTB) cyclists performing protocols of simulated cycling [1,2]. For both prolonged [1] or incremental workload [2] MTB cyclists presented pedaling asymmetries related to exercise intensity, in which higher intensities elicited smaller asymmetry indexes. It is know that MTB and road cycling are very different cycling disciplines and although they share some characteristics, there are some important biomechanical differences between them [3]. It is not clear if pedaling asymmetries that may exist among road cyclists could be related to exercise intensity as observed in MTB. In this study, we investigated if pedaling asymmetry in peak torque is observed among road cyclists and analyzed whether asymmetry can be related to exercise intensity.

Methods: Eighteen road cyclists with more than two years of training experience volunteered for this study (age: 25 ± 8 years; body mass: 70.6 ± 7.7 kg; height: 177 ± 4 cm; body fat: 9.3 ± 4.7 %). Cyclists performed two incremental cycling trials (step and ramp) to exhaustion in two separate days within 48h. Protocols were randomized and both trials were performed on an electromagnetically braked cycle ergometer. Both tests started at initial workload of 100 W. In the step type test, workload was increased 30 W every 3 minutes, whereas in the ramp type workload continuously increased resulting in 30 W every minute. Pedaling cadence was their preferred. Leg preference was determined by using the Waterloo inventory. The maximum crank torque average (MT) of 11 subsequent pedaling cycles were bilaterally determined using a pair of instrumented cranks for every workload stage. Asymmetry index (AI) was calculated using equation by Chavet [4]. Data normality was verified by Shapiro-Wilk test. Descriptive statistics (mean and standard deviation), and both independent t-test and Mann-Whitney test were utilized to compare preferred and non-preferred limbs. Significance level was set at 5%.

Results: In general, road cyclists were symmetric for MT regardless of the testing protocol. A single pedaling asymmetry was observed during the ramp protocol at stage of 250 W (Figure 1). Additionally, average AI in each stage presented ranged from 3.35 to 4.85 % in the step test, and 3.90 to 6.70 % in the ramp test. Different results were found to MTB cyclists, in which pedaling asymmetry was intensity dependent [2]. This difference may be explained by the competition and training configuration. For example, MTB presented different pattern of sagittal plane kinematics at the ankle when compared to road [5], which may have implication for maximal as measure here.

Figure:
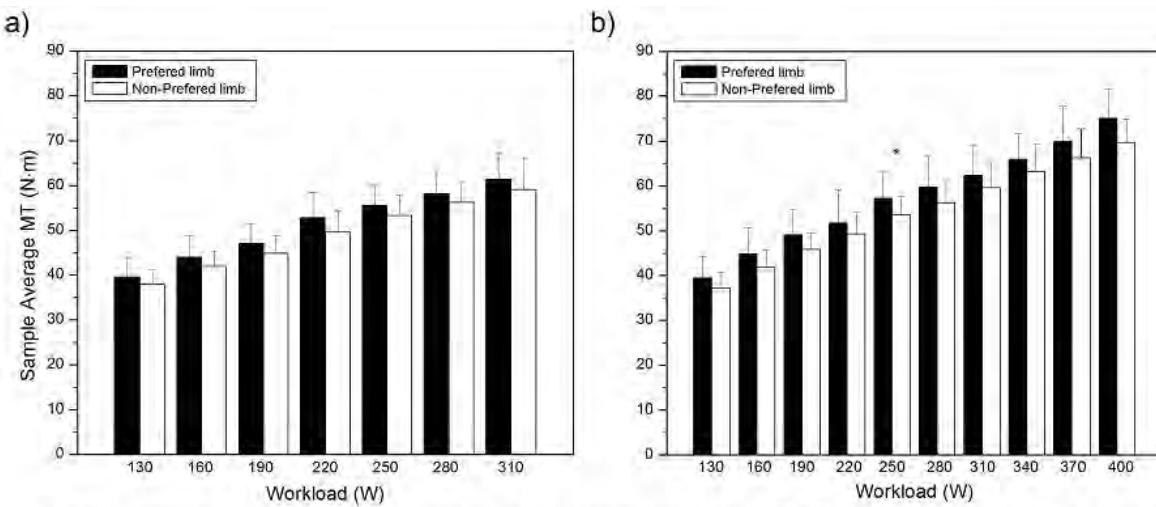
Figure 1. Maximum crank torque average (MT) for preferred and non-preferred leg during the step (a) and ramp (b) trials. * significant difference in MT between preferred and non-preferred leg.

Conclusion: Road cyclists submitted to incremental cycling testing with different condition of load delivery were symmetric concerning MT. A single asymmetry was observed at stage of 250 W for one of the test and its meaning needs further investigation. Moreover, AI was less than 10% in all stages to both incremental tests.

References: [1]   Carpes et al., J Sports Med Phys Fitness. 47(1): 51-57, 2007.

[2]   Carpes et al., Brazilian Journal of Biomotricity. 2(3): 155-159, 2008.

[3]   Impellizzeri et al., Eur J Appl Physiol. 102: 335-341, 2008.

[4]   Chavet et al., Hum Mov Sci. 16: 391-406, 1997.

[5]   Carpes et al., Rev Port Cien Desp. 6(1): 7-14, 2006.

Disclosure of Interest: None Declared

Sport

PO-0336

FOUR WEEKS OF HIGH-INTENSITY INTERVAL TRAINING USING CONTINUOUS VERTICAL JUMPS INCREASES THE POWER OUTPUT AND JUMP HEIGHT

Jonathan Ache Dias [1,*]Rodolfo André Dellagrana [1]Anderson Santiago Teixeira [2]Antônio Renato Pereira Moro [1]

[1]Biomechanics Laboratory, [2]Physical Effort Laboratory , Federal University of Santa Catarina, Florianópolis, Brazil

Introduction and Objectives: Several types of jumps has been routinely used in athletic evaluation and training. In general, have been suggested that vertical jump training increases the jump height [1]. The continuous vertical jumps test was proposal initially to measure mechanical power output [2] and recently to evaluate the anaerobic fitness [3]. However, in our knowledge, no studies have evaluated the use of continuous vertical jump as a mode of high-intensity interval training, like used in other exercise modes such as cycling [4]. The objective of this study was to verify the effect of continuous jump interval training on kinetic and kinematic variables of continuous jump test.

Methods: Eighteen recreational runners (age = 27.8 ± 4.4 years), ten women and eight men, participated of this study. They were divided randomly in two groups according to peak velocity, determined in a maximal incremental test performed in treadmill. Groups: Control (body mass = 66.3 ± 13.9 kg) and Experimental (body mass = 63.1 ± 10.1 kg). The training program was conducted in four weeks. During this time all participants performed, three times for week, a basic training consisted of 40 minutes of treadmill running at 70% of peak velocity. In separate days, the experimental group underwent to a complementary training that was consisted of eight sessions, distributed in the four weeks, of four to six repeats of 30 s of continuous vertical jumps. The repeats was performed with maximal effort (all-out) and five minutes of recovery between repeats (active = 2:30 of treadmill walking at 4 km/h and 2:30 of passive recovery) was adopted. Two days before and after the training program one repeat of 30 s of maximal continuous vertical jumps was performed as evaluation using a force platform (Quattro Jump 9290BD, Kistler, 500 Hz) and a video camera (Canon SX510B, 120 Hz). From vertical ground reaction force of each jump was measured the peak force (PF) and peak power output (PP). From kinematic analysis was analyzed the jump height (JH) and the lowest point of maximal vertical displacement of center of mass (hc). The vertical stiffness was calculated as follow: Kvert = PF/hc. All variables were analyzed from the mean of all jumps performed in 30 s. A mixed model ANOVA (Split-plot) with a between participants (groups: experimental and control) and within participants (time: before and after training) variables was used with a level of significance of 5%. The simple effects was analyzed by independent and paraded t-test with a level of significance of 1% (Bonferroni correction).

Results: The participants performed approximately 25 jumps during each repeat of 30 s of continuous jumps in both training and evaluations. Table 1 shows the descriptive statistics of the continuous jumps test and indicate the significant paired comparisons. The analysis of variance revealed main effect of time (μ_{JH} = 0.28; F_{JH} = 6.48; p_{JH} = 0.02; μ_{PP} = 0.38; F_{PP} = 9.83; p_{PP} = 0.06) and interaction groups *vs* time (μ_{JH} = 0.4; F_{JH} = 10.9; p_{JH} = 0.004; μ_{PP} = 0.36; F_{PP} = 9.28; p_{PP} = 0.08) for JH and PP. These results suggest that four weeks of the jump training increases the JH (10.1%) and PP (9.6%). PF and Kvert do not presented any effect of group (F_{PF} = 0.77; p_{PF} = 0.39; F_K = 2.13; p_K = 0.16), time (F_{PF} = 0.5; p_{PF} = 0.48; F_K = 0.86; p_K = 0.36) or interaction (F_{PF} = 2.1; p_{PF} = 0.16; F_K = 0.33; p_K = 0.56).

Conclusion: The continuous jump interval training is able to increase the jump height and power output without alterations in peak force and stiffness. This training mode may be an alternative to improve the power output of athletes from different sports.

Table:

	JH (cm)	PP (w)	PF (N)	Kvert (kNm)
Control BT	32.92 ± 5.68	2586.00 ± 893.50	1354.55 ± 465.41	5.29 ± 2.21
Experimental BT	30.15 ± 5.69*	2191.05 ± 679.43*	1142.38 ± 367.19	4.28 ± 1.37
Control AT	32.52 ± 5.22	2589.01 ± 868.60	1358.93 ± 324.92	5.23 ± 1.51
Experimental AT	33.21 ± 4.12*	2400.88 ± 676.56*	1243.12 ± 327.80	4.03 ± 1.29

JH = jump height; PP = peak power output; PF = peak force; Kvert = stiffness; * Significant differences between BT and AT in experimental group ($p \leq 0.01$).

Caption: Table 1. Biomechanical variables (mean ± SD) of 30-s continuous jumps test before (BT) and after (AT) training.

References: [1] Markovic, Br J Sports Med, 41: 349–355, 2007.

[2] Bosco et al., Eur J Appl Physiol, 50: 273-282, 1983.

[3] Dal Pupo et al., J Sci Med Sport, 17: 650-5, 2014.

[4] MacDougall *et al*. J Appl Physiol, 84: 2138–2142, 1985.

Disclosure of Interest: None Declared

Sport

PO-0337

RELATIONSHIP BETWEEN SWIMMING MEAN VELOCITY ANT TWO DYNAMOMETRY TESTS: THE TETHERED SWIM TEST AND THE PARTIALLY SWIMMING TEST.

Bruno Mezêncio [1,*]Rafael Soncin [1]Joao Claudino [1]Joao Pedro Pinho [1]Juliana Pennone [1]Ana Paula Azevedo [1]Alberto Carlos Amadio [1]Julio Serrão [1]

[1]Laboratory of Biomechanics, USP, São Paulo, Brazil

Introduction and Objectives: The propulsive force as well as the swimming technique, are determinants factors on swimmer performance [1]. Among the methods used to evaluate this force during the swimming, the tethered swimming test can be highlighted like a valid and specific test [2,3]. Nevertheless, in this test swimmers are not affected by the drag force. Another way to test swimming force, which incorporates the effect of a drag force, is by the partially tethered swimming. However there is a disagreement in the scientific literature about the relationship between the partially tethered swimming and swimming performance [4,5]. Thus the aim of the study was compare the relationship between these tests (tethered and partially tethered swimming) and the swimming performance.

Methods: Twelve male swimmers with experience higher than five years on swim (22.6 ± 3.8 years, 1.75 ± 0.06 m, 74.3 ± 4.9 kg e 26.1 ± 1.3 s as best time on 50m free style) performed five repetitions of free swim tests, tethered swim test and partially tethered on random order with 5' of rest interval between the tests.

On free swim test a maximal 25 m crawl sprint without breathing was performed starting from inside the pool, and was recorded by a camcorder (A602fc-100fps, *Basler*, Germany). On tethered swim test, each swimmer used a waist belt connected to a steel cable fixed on a load cell with sampling frequency of 1000 Hz (Interface, Noraxon, USA). In the partially tethered swimming test the system used in the tethered swimming test, composed by the steel cable and load cell, was attached to another steel cable passing through a pulley fixed at a starting block, which worked by a geared motor (RX-400, Ringcone, Brazil). This configuration allowed the test velocity to be controlled in 0.6 m/s. In both dynamometry tests the swimmer should perform the higher possible effort without breathing for 10 stroke cycles. The force data was registered during all tests, however it was analyzed the fourth to the eighth stroke cycle.

The video data was analyzed on software SIMI *motion* 7.0 (SIMI Reality Motion Systems, Germany). The force data was treated on software Matlab 2009b (Math Works, EUA) where was filtered with low pass filter type Butterworth 6ª order with cut-off frequency of 16Hz. There was calculated the mean propulsive force of the stroke cycles for both dynamometry test and the mean velocity for free swim test. In order to relate the force data with the swimming mean velocity a linear regression was performed for each dynamometry test. The correlation coefficient (r) and the determination coefficient (r²) were calculated for each equation. The significance level adopted was ρ<0.05.

Results: The mean velocity on free swim test was 1.83 ± 0.16 m/s, the mean force during the tethered swim was 111.91 ± 17.12 N and during the partially tethered swim was 97.43 ± 16.11 N. The regression analysis results are presented in Table 1.

Conclusion: The force evaluated by both tests presented significant correlation with the mean swimming velocity, however the intercept coefficient of both tests are high. This indicates that both tests are very influenced by unknown factors. The detection of these factors can improve the effectiveness of the tests to evaluate the swimming performance.

Table: Table 1 – Intercept, Slope, correlation coefficient (r), coefficient of determination (r^2) and confidence interval (CI 95%) for the regression equation

Models	Intercept (CI 95%)	Slope (CI 95%)	r - (r^2)
Tethered Swim	0.774 (0.328 - 1.231)	0.010 (0.006– 0.014)	0.847* - (0.717)
Partially Tethered Swim	1.011 (0.542 - 1.431)	0.082 (0.031 – 0.126)	0.791* - (0.625)

 * P<0.05

References: [1] Smith et al., Sports Med., 32: 539–554, 2002.

[2] Dopsaj et al., Facta Univ Phys Educ Sport, 1: 15–20, 2003.

[3] Kjendlie et al., Rev Port Cien Desp, 36: 231–233, 2006;

[4] Klentrou et al., J. Swimming Research, 7: 13–18, 1991.

[5] Costill et al,. J. Swimming Research, 2: 16–19, 1986.

Disclosure of Interest: None Declared

Sport

PO-0338

COMPARISON OF CENTER OF PRESSURE TRAJECTORY CHARACTERISTICS IN TABLE TENNIS DURING TOPSPIN FOREHAND LOOP BETWEEN SUPERIOR AND INTERMEDIATE PLAYERS

Y Zhang [1,*] Y Gu [1] J S Li [1] J Baker [2]

[1]Faculty of Sports Science, Ningbo University, Ningbo, China, [2]Faculty of Science and Technology, University of the West of Scotland, Glasgow, United Kingdom

Introduction and Objectives: Several previous studies have reported that momentum generation depends on foot drive largely in striking motions. Based on this case, the purpose of this study was to investigate the differences in the center of pressure (COP) trajectory under the dominant foot during forehand loop between superior and intermediate players. The whole motion was divided into two key events: backswing and forward swing corresponding to the stage from preparation to backward-end and the stage from backward-end to forward-end, respectively. Variables as COP anterior-posterior displacement (D_x), medial-lateral displacement (D_y), and velocity ratio between forward swing and backswing ($R_{f/b}$) were included.

Methods: Thirteen superior (national Division I) and thirteen intermediate (national Division II) male table tennis players volunteered to participate in this study. Novel Pedar insole plantar pressure measurement system (Novel GmbH, Munich, Germany) was used to record COP trajectory. A ball machine projected topspin balls directly to the foreside of the subject's court. All subjects were required to perform single crosscourt forehand loop with maximal power wearing unified training footwear. At least five successful trials were performed for one subject. Independent samples t-test were taken for each dependent variable. The level of significance was set at $p < 0.05$.

Results: Dx of superior players at backward-end located more laterally compared with that of intermediate players. No significant difference was found in Dx at forward-end between two skilled levels. Dy of superior players was obviously smaller at backward-end and forward-end. The data of Rf/b for superior group was significantly higher than the intermediate group. At backward-end, superior players transferred body weight more sufficiently to the racket-side resulting in larger Dx, which may facilitate momentum generation and distal velocity. Dy for the intermediate group located closer to the forefoot region, suggesting that the heel was off the ground, and this may decrease stability of players during this stage. At forward-end, D_x would not be influenced by skilled level. The smaller D_y of superior players contributes to resume to preparation for the next stroke. In addition, for superior players, the slower COP shift velocity during backswing provided a more stable basis for the following stage. While the faster velocity during forward swing related to a forceful lower limb drive which was considered as the "starting point" of kinetic chain.

Figure:
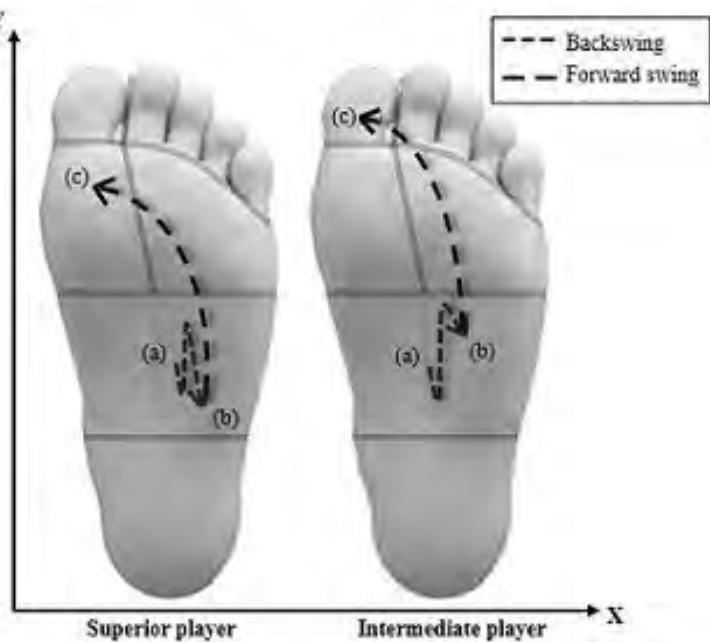
Conclusion: Significant differences between two skilled levels were found in D_x during backswing, D_y during both backward and forward swing and $R_{f/b}$. The key results indicated that superior players possessed better ability of motion control and technique manipulation. Table tennis coaches and players should pay more attention to stability training and enhancing push-off effect.

References: [1] Elliott, Brit J Sport Med, 40: 392-396, 2006.

[2] Bonnet et al., J Biomech, 47: 1603-1608, 2014.

Disclosure of Interest: None Declared

PO-0339

HOW CAN WE MONITOR PASSIVE DRAG IN COMPETITION SETTINGS?

Tiago M Barbosa [1,*] Jorge E Morias [2] Henrique Neiva [3] Pedro Forte [3] Nuno D Garrido [4] Daniel A Marinho [3]

[1] Nanyang Technological University, CIDESD, Singapore, Singapore, [2] Polytechnic Institute of Braganca, CIDESD, Braganca, [3] University of Beira Interior, CIDESD, Covilha, [4] University of Tras-os-Montes and Alto Douro, CIDESD, Vila Real, Portugal

Introduction and Objectives: Swimming rules do not allow instrumenting the swimmer during an official event. Therefore there is the need of a valid, straightforward, quick and affordable way to monitor the passive drag in competition settings. The aim was to compare the passive drag assessed with experimental and analytical procedures

Methods: Sixty young swimmers (30 boys and 30 girls with approximately 12-13-y) part of a national talent ID scheme were assessed. The passive drag was assessed experimentally with inverse dynamics of the gliding decay speed [1]. Swimmers were invited to perform a maximal push-off on the wall fully immersed and glide in the streamlined position. A speedo-meter cable (Swim speedo-meter, Swimsportec, Hildesheim, Germany) was attached to the swimmer's hip and the gliding velocity decay was acquired (f=50Hz). After numerical differentiation of the filtered speed-time curve, with the anthropometrical and inertial parameters collected beforehand (height, body weight, surface areas), the passive drag (Dp) and passive drag coefficient (CDp) were computed. The theoretical modeling included a set of analytical procedures based on naval architecture [3]. The Dp is the sum of friction drag and pressure drag. The friction drag was estimated based on its coefficient determined from the ITTC-57 correlation line for turbulent flow and the wetted surface. Pressure drag was assumed to be due to bluff body separation, with viscous pressure resistance due to boundary layer growth negligible. Pressure drag was calculated based on the frontal surface area measured with a photogrammetric technique and retrieving the pressure drag coefficient from numerical simulation studies [2]. Simple linear regression models and Bland-Altman analysis were computed between experimental and analytical procedure.

Results: Linear regression models showed a high adjustment for both Dp (R^2=0.64; R^2a=0.63; SEE=16.436; P<0.001) and CDp (R^2=0.79; R^2a=0.78; SEE=0.021; P<0.001). On average the bias between procedures was -7.002N (95%CI: -40.480; 26.475) for the Dp and an overestimation of 0.127 (95%CI: 0.007; 0.247) for the CDp. Figure 1. Comparison between experimental and analytical procedures to assess the passive drag (Dp and Df+pr, respectively) and the passive drag coefficient (CDp and CDf+pr, respectively).

Figure:
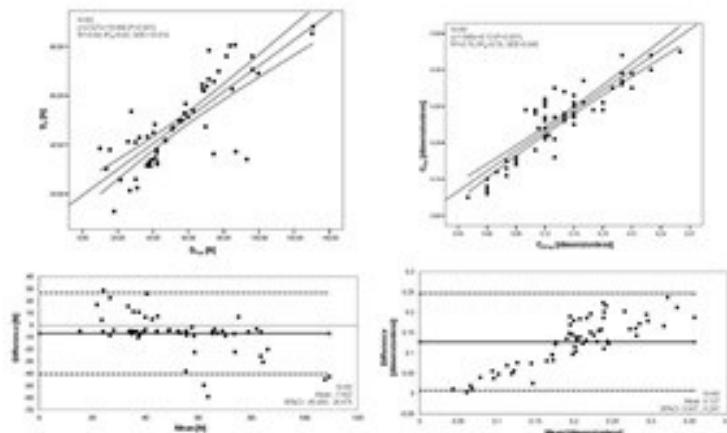
Conclusion: As a conclusion, there is a strong relationship in the Dp and CDp between experimental and analytical procedures. Analytical procedures are a novel, feasible and valid way to gather insight about one's passive drag during competition settings.

References: Reference 1

Barbosa et al. (2014) Hydrodynamic profile of young swimmers: changes over a competitive season. Scan J Med Sci Sports. doi: 10.1111/sms.12281

Reference 2

Marinho et al. (2011) The Hydrodynamic Study of the Swimming Gliding: a Two-Dimensional Computational Fluid Dynamics (CFD) Analysis. J Hum Kinetics, 29, 80-88

Reference 3

Webb Aet al. (2011) Prediction of passive and active drag in swimming. Procedia Eng, 13, 133-140

Disclosure of Interest: None Declared

COMPARISON OF CLASSICAL KINEMATICS, VARIABILITY AND NONLINEAR PARAMETERS FOR THE FOUR COMPETITIVE SWIMMING STROKES

Tiago M Barbosa [1,*] Mario J Costa [2] Jorge E Morais [3] David Prendergast [4]

[1]Nanyang Technological University, CIDESD, Singapore, Singapore, [2]Polytechnic Instiute of Guarda, CIDESD, Guarda, [3]Polytechnic Instiute of Braganca, CIDESD, Braganca, Portugal, [4]University of Buffalo, Buffalo, United States

Introduction and Objectives: The aim of this research was to compare classical kinematic and nonlinear parameters in the four competitive swimming strokes.

Methods: Twenty-one national level swimmers (11 boys and 10 girls; 13.61±1.3-y) performed a set of 4×25 m swims from a push-off start with the front-crawl, backstroke, breaststroke and butterfly stroke in random order. A speedo-meter (Swimsportec, Hildesheim, Germany) was attached to the subjects' hip (f=50Hz) to determine instantaneous velocity. Data were exported to a signal processing software (AcqKnowledge, Santa Barbara, USA). Velocity fluctuation (dv) was selected as a classical kinematic parameter and based on previous studies, is also considered an energy cost estimator [1]. For the non-linear analysis, ApEn was calculated for at least 700 pairs of speed-time, an embedding dimension of $m=2$ and the maximum tolerance value of $r=0.1$ [2]. The D was calculated by the Higuchi's method (D_ Huijing) from the speed-time pairs and complemented with the Box-count method (D_Box-count) [3]. Repeated measures (within-subjects ANOVA) analysis was performed ($P \leq 0.05$).

Results: Fractal properties were 1.80±0.86 - 1.93±0.02 for D_ Huijing and 1.24±0.07 - 1.42±0.03 for D_Box-count (Fig 1). There were significant variations among the four swimming strokes for dv [$F_{(1,21)}=620.99$; $P<0.001$], ApEn [$F_{(1,21)}=296.50$; $P<0.001$], D_Huijing [$F_{(1,21)}=87.86$; $P<0.001$] and D_Box-count [$F_{(1,21)}=207.81$; $P<0.001$]. Post-hoc testing showed that all possible pairwise combinations were significantly different ($P<0.001$). Overall, the lowest values were observed for front-crawl; followed by the backstroke, butterfly stroke and breaststroke (Fig 1). Conversely, within-subject testing controlling the effect of velocity (ANCOVA) did not demonstrated significant interactions for the dv [$F_{(1,20)}=0.12$; $P=0.91$], D_Huijing [$F_{(1,20)}=0.001$; $P=0.97$] and D_Box-count [$F_{(1,20)}=0.05$; $P=0.83$] but did for the ApEn [$F_{(1,20)}=4.96$; $P=0.04$].

Figure:
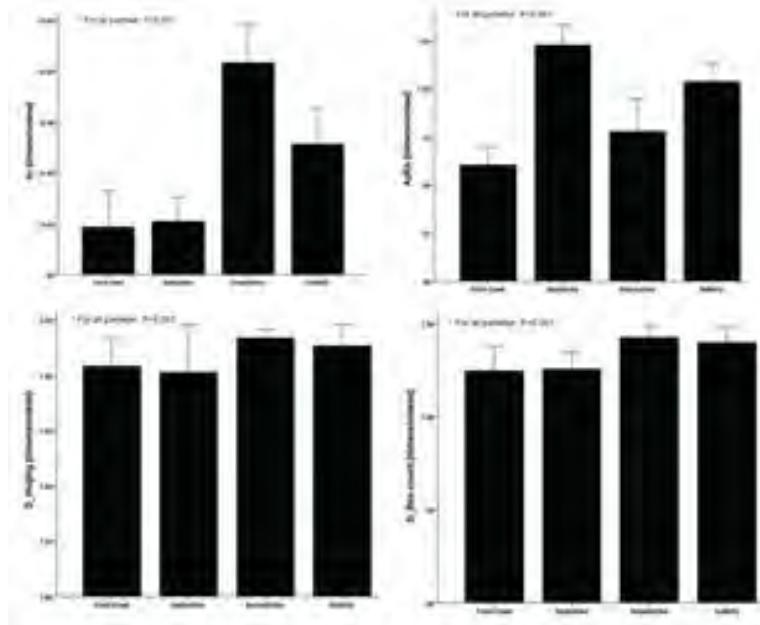
Conclusion: Human swimming with all four competitive strokes showed fractal properties (1≤D≤2). More predictable swimming patterns (i.e. ApEn) have a lower level of complexity (D) and this might have an effect on the energy cost of swimming based on the observed dv.   Figure 1: Comparison of the classical and nonlinear parameters between the swim strokes (mean±2SD).

References: Reference 1

Barbosa et al. (2005). Energy cost and intra-cyclic variations of the velocity of the centre of mass in butterfly stroke. Eur J Appl Physiol, 93, 519-523

Reference 2

Barbosa et al. (2014) Hydrodynamic profile of young swimmers: changes over a competitive season. Scan J Med Sci Sports. doi: 10.1111/sms.12281

Reference 3

Higushi (1988). Approach to an irregular time series on the basis of the fractal theory. Physica, 31, 277-283

Disclosure of Interest: None Declared

PO-0341

THE RERATIONSHIP BETWEEN THE GLIDE DISTANCE AND SWIMMING SPEED IN THE COMPETITIVE SWIMMERS

Tadashi Wada [1,*]Yuya Horihata [2]Noriyuki Yamamoto [3]Yukinori Shintaku [4]Yu Kashiwagi [2]Kazuo Funato [2]

[1]Kokushikan University, [2]Nippon Sport Science University, Tokyo, [3]Japanese Red Cross Hokkaido College of Nursing, Hokkaido, [4]Biwako Seikei Sport College, Ohtsu, Japan

Introduction and Objectives: Improvement in swimming performance is not only associated with stroke technique but also with the gliding movement during the start and turn phases. Furthermore, it is important that the momentum created by a swimmer in swimming direction is larger than against swimming direction. Passive drag is produced by measuring the force necessary to tow a swimmer through the water at a constant speed with his body in a prone position [1]. The underwater gliding and dolphin kick movement during the start and turn phases are important for the total race time in modern swimming [2, 3]. The study was designed to analyze the findings of underwater electromyography of lower limb muscles during the underwater dolphin kick movement in competitive collegiate swimmers.

Methods: Seven healthy male competitive swimmers volunteered to participate in this study (age: 22.0±3.8yrs, height: 173.4±6.9cm, body weight: 71.3±7.9kg, athletic career: 13.7±3.9yrs). The subjects performed underwater gliding movement at maximum speed after pushing off from the start wall. In addition, three types of underwater gliding movement [Prefer distance, Short distance and Long distance] were performed with maximum effort. The subjects were monitored through an underwater video camera with a sampling frequency of 60 Hz in the sagittal plane to measure the angular displacement of their different joints. A wireless electromyography system (Biolog DL-5000, S&ME, Japan) was used to collect the muscle activities from the vastus lateralis, hamstrings, tibialis anterior, and gastrocnemius. Speed Meter (Vine Co., Japan) was used to measure swimming speed, and a motion analysis system (Frame-DIAS4; DKH, Japan) was used to digitize body landmarks.

Results: Among the underwater gliding movement distance types, the swimming speed of the prefer distance was the fastest (prefer distance: 2.22 m/sec; long distance: 2.10 m/sec; and short distance: 2.19 m/sec, $P < 0.05$). The rectified EMG findings showed that gastrocnemius and hamstrings muscle activities of elite swimmers were higher than non-elite swimmers during these movements. However, elite swimmers had no muscle activity in the tibialis anterior.

Conclusion: The main finding of this study is that the gliding movement of long distance was significantly slower in the swimming speed than short and prefered distance. In addition, prefered glide distance was the fastest swimming speed. The present study results suggested that there was the most prefered glide distance to get the maximum swimming speed after a start and a turn.

References: [1]   Adrian et al., Biomechanics of Human Movement. Brown & Benchmark, 1995.

[2]   Marinho et al., J Appl Biomech, 25(3): 253-257, 2009.

[3]   Wada et al., Biomechanics and Medicine in Swimming XI: 185-187, 2010.

Disclosure of Interest: None Declared

Sport

PO-0342

PREDICTION OF INJURY RATES USING TURNOUT VARIABLES IN CONTEMPORARY DANCERS

Joanna Jenkins [1,*] Matthew Wyon [2] Alan Nevill [2]

[1]London Metropolitan University, London, [2]Wolverhampton University, Wolverhampton, United Kingdom

Introduction and Objectives: Turnout has both an aesthetic appeal and functional implications and over the past two decades has been the subject of some debate as to the requirements and implications of "appropriate" turnout. To achieve the 180° of turnout, which dancers strive for, other structures of the lower limb, in addition to the hip, contribute. Research has suggested that dancers may be more at risk of injury when they excessively utilise non-hip components of turnout to compensate for deficits in hip external rotation when trying to achieve maximal total turnout. However, numerous different measures of turnout have been cited in the literature as well as suggestions for derived variables to account for shortfalls in particular components of turnout. The objective of this study was to assess whether measurements of turnout can predict the number of injuries ([0 or 1 injury] or [2+ injuries]) incurred over a 10 month period.

Methods: At the beginning of the academic year 47 female, full-time contemporary dance students (age 19.9 ± 2.51 years; height 1.65 ± 0.05 cm; weight 56.23 ± 6.51 kg) were screened as part of a bi-annual screening process. Measurements, summed of both legs, were obtained for passive hip external rotation (pER), total passive turnout (TPT) and total active turnout (TAT). From these, three further variables were derived; compensated turnout, muscular turnout and active ER lag. At the end of a 10 month period the number of injuries reported by the dancers to a physiotherapist were obtained for the previous 10 months.

Results: Binary regression carried out on all six turnout variables identified a significant positive effect of both compensated and muscular values, on the probability/odds of being in the 2+ injury group. For every 1% increase in compensated and muscular values, there was a corresponding 9% and 8.4% increase, respectively, in the odds that the dancer would sustain 2 or more injuries compared to 0 or 1 injury.

Conclusion: The findings of this study support previous findings that dancers with a greater difference between passive hip ER and total lower limb turnout are more at risk of injury. However, the present study quantifies this risk. It also emphasises the need to assess not only the hip pER but ensure comparisons are made with TPT and TAT. Screening compensated and muscular values may be useful to address shortfalls to prevent injuries in the future.

Disclosure of Interest: None Declared

A BIOMECHANICAL INVESTIGATION OF THE USE OF HEEL WEDGES DURING SQUATS PERFORMED BY RECREATIONALLY TRAINED MALES WITH OR WITHOUT LIMITED DORSIFLEXION

Paul Swinton [1],[*]Swatik Mahendra [1]

[1]School of Health Sciences, Robert Gordon University, Aberdeen, United Kingdom

Introduction and Objectives: The squat is one of the most frequently used forms of lower body resistance exercise in both athletic and rehabilitation settings. The widespread use of the movement is primarily based on its similarity to activities performed in daily living and in various sports. A large number of research studies have previously investigated kinematics and kinetics of the squat from both a performance enhancement and injury risk perspective. To perform the squat appropriately, substantial excursion at joints of the lower body is required. Previous research has demonstrated that restriction in ankle joint dorsiflexion range of motion (ROM) is associated with increased stress experienced at the knee and lower back. As a consequence, many individuals perform the squat with a wedge located under the heel to position the ankle initially in plantarflexion and thereby enable greater joint excursion during the squatting movement. The purpose of this study was to investigate the associated kinematics and kinetics of the squat performed on a level surface and with heel rises of different heights in participants with and without restricted ankle dorsiflexion.

Methods: Twelve recreationally active males (age: 27±3.9 years; height: 170.7±5.5 cm; mass: 69.7±13.8kg) volunteered to participate in the study. Ankle dorsiflexion ROM was assessed in two positions (knee extension and 30° knee flexion) with the foot moved passively from a neutral position until resistance was noted. If the ROM was found to be less than 20° and/or 10° with the knee in full extension or 30° of flexion, respectively, the participant was classified as exhibiting restricted ankle dorsiflexion. Six of the twelve participants were subsequently identified as exhibiting restricted ankle dorsiflexion. Therefore, the participants were sectioned into two groups each comprising six individuals.

All squats were performed with a bar of negligible mass positioned across the upper trapezius. Three dimensional kinematics and kinetics of the ankle and knee were quantified using inverse dynamics in a motion analysis laboratory, with models processed using Vicon Nexus 1.8.5 software (Oxford Metrics, Oxford, UK). Each participant performed squats barefoot under five different conditions, including: 1) level surface, 2) 1.5cm heel rise, 3) 2cm heel rise, 4) 2.5cm heel rise and 5) 3cm heel rise. For each condition, participants performed six repetitions of the squat under a set cadence with the average value over the six repetitions selected for further analysis. Data were analysed using a mixed between-within factorial ANOVA (group × 2, heel height × 5).

Results: No significant interaction effects were noted between group and heel height for peak ankle dorsiflexion and knee joint ROM ($p=0.73$ and $p=0.98$, respectively). A significant main effect of heel wedge height was noted for peak ankle dorsiflexion ($p<0.01$). No significant interaction effects were noted between group and heel height for ankle and knee kinetics ($p=0.31$ to $p=0.81$). Significant main effects were obtained for heel wedge condition on knee medio-lateral shear forces ($p=0.03$) and knee compressive forces ($p<0.01$). The results showed that knee joint forces increased with greater heel elevations. In addition, a significant group main effect was obtained for compressive forces at the knee ($p<0.001$),

with larger forces experienced by the group with restricted ankle dorsiflexion. Finally, ankle antero-posterior shear forces were found to increase with greater heel elevations for both groups of participants (p=0.01).

Conclusion: The results of the study demonstrate that the use of a wedge underneath the foot to raise the heel can cause a number of biomechanical changes in individuals with and without limited dorsiflexion ROM when performing the squat. In particular, the results demonstrate that the use of heel wedges decreases peak dorsiflexion as the ankle is placed in an initial plantarflexed position and joint excursion remains relatively constant. In contrast, the results of the study demonstrate that the use of heel wedges significantly increase various forces experienced at the ankle and knee joint, with larger force values measured with greater heel elevation. Coaches and clinicians should be aware of these changes, particularly with individuals in a rehabilitation setting where increased skeletal forces may be of practical significance.

Table:

Variable	Restricted Dorsiflexion			Non-restricted Dorsiflexion		
	Level	HW (2cm)	HW4 (3cm)	Level	HW (2cm)	HW4 (3cm)
Peak dorsiflexion(°)	34.1±7	28.8±8	23.9±6	34.4±6	29.5±6	28.5±6
Knee ROM(°)	117±4	125±6	125±5	120±6	122±8	126±10
Ankle AP force (N)	13±5	20±5	26±11	10±2	17±4	24±12
Knee ML force (N)	16±9	28.4±26	22±19	15±2	21±12	17±9
Knee COMP force (N)	133±8	252±31	362±25	122±10	220±16	337±26

HW = heel wedge, AP = antero-posterior, ML = medio-lateral, COMP = compressive.

Caption: Table 1: Selection of kinematic and kinetic variables for the level and two specific heel wedge conditions.

Disclosure of Interest: None Declared

Sport

PO-0344

COMFORT ASSESSMENT IN BIKE FITTING

Jose Ignacio Priego [1,*]Angel Gabriel Lucas-Cuevas [2]Rosario Salvador-Palmer [1]Pedro Pérez-Soriano [2]Rosa Mª Cibrián Ortiz de Anda [1]

[1]Department of Physiology, [2]Department of Physical Education and Sports, University of Valencia, Valencia, Spain

Introduction and Objectives: Comfort has a strong effect on injury prevention and enhancement of performance in different sports. However, it is still unclear how different postures may influence the cyclist's perception of comfort on the bike during cycling. Furthermore, an adequate posture in cycling is essential to improve performance and reduce the risk to suffer an overuse injury [1]. The aim of the study was therefore to assess the influence of different positions on the bike on the perception of comfort during cycling.

Methods: Twenty participants (30.9 ± 11.1 years, 75.5 ± 9.9 kg, 178.5 ± 6.8 cm, 207 ± 133 km/week) completed one pre-test and three main tests. The pre-test consisted of an incremental cycling test to exhaustion using a stationary cycle ergometer in order to determine the individual workload for each participant. The three mains tests consisted of 45 minutes of cycling at 90 rpm at their individual 50% peak power output. Each test was performed with a different knee flexion angle (20º [Knee20º], 30º [Knee30º], 40º [Knee40º] when the pedal crank was at 180º) and trunk flexion angle (35º [Trunk35º], 45º [Trunk45º], 55º [Trunk55º] with respect to the transverse plane). Angles were measured using 2D motion analysis during cycling. Knee angle was defined as the degrees of knee flexion with respect to the anatomical reference position (static upright standing posture) considered zero degrees [2]. Perception of comfort of the limbs and of the trunk was reported one minute before the end of each test using a 5-point Likert scale ranging from very uncomfortable (-2) to very comfortable (+2). A repeated measures ANOVA was used to examine the difference in trunk and limb comfort between the different postures.

Results: Knee30º was significantly perceived as the most comfortable posture of the limbs (with scores between "neither comfortable nor uncomfortable" and "very comfortable"). Knee20º was reported to be "neither comfortable nor uncomfortable" ($p=0.1$, 95%CI [-0.5, 0.6]). This position was considered more comfortable than Knee40º (95%CI [-1.7, -0.9], ES=1.36 and $p<0.01$) but more uncomfortable than Knee30º (95%CI [0.6, 1.5], ES=0.94 and $p<0.01$). Knee40º was perceived the most uncomfortable posture of the limbs (with scores between "neither comfortable nor uncomfortable" and "very uncomfortable"). Knee fitting significantly affected trunk comfort, Knee30º (x=0.9, 95%CI [0.5, 1.3]) was considered more comfortable for the trunk than Knee40º (x=0.1, 95%CI [-0.4, 0.6], ES= 0.83 and $p=0.03$).

Trunk55º (x=1.0, 95%CI [0.6, 1.4]) was considered more comfortable than the most flexed position Trunk35º (x=0.0, 95%CI [-0.5, 0.5], ES= 1.1 and $p<0.01$). Trunk position did not have any effect on limb comfort.

Conclusion: The main findings in our study were that cyclists perceived the limb intermediate flexion posture (30º of knee flexion) and the trunk in the most upright position (55º of trunk flexion) as the most comfortable postures. Also, the posture with the highest knee flexion (40º) was perceived as the most uncomfortable and it also produced discomfort in the trunk. A knee flexion angle of 25º to 30º when the pedal crank is at 180º during static assessment has been recommended to prevent overuse injuries and improve performance [1]. However, Ferrer-Roca et al. [3] also suggested that during dynamic

assessment, the recommended range of knee flexion angle is between 30º to 40º, but with absolute values and without static correction. The limb postures that were within the recommended flexion range (Knee30º) and outside of this range (Knee40º) with the static correction [2] and in absolute angle values (39.8± 4.0º and 50.4 ±3.5º, respectively) [3], were considered the most comfortable and uncomfortable postures, respectively. The saddle position with the highest knee flexion (40º) resulted in greater trunk discomfort. This result showed that the posture of the limbs affects the perception of trunk comfort due to changes in the hip flexion angle during exercise. This interaction between the pelvic and the spine is in agreement with a previous study [4]. Finally, an upright position was perceived more comfortable than a position where the trunk is flexed forward. This should be taken into account depending on cycling purpose. For recreational cycling, the upright position is recommended in order to improve comfort as shown in the present study. For competitive cycling, on the other hand, a more flexed position is recommended in order to decrease air resistance and improve speed. In conclusion, cyclists' perception of comfort on the bike should be taken into account when it comes to choosing the most beneficial position since it can play a major role when aiming to enhance performance and reduce injury occurrence in cycling.

References: [1] Bini et al., Sports Med, 41: 463–76, 2011.

[2] Peveler et al., J. Strength Cond. Res., 26: 3004–9, 2012.

[3] Ferrer-Roca et al., J. Strength Cond. Res., 26: 3025–9, 2012.

[4] Jobson et al., J. Sports Sci., 26: 1269–78, 2008.

Disclosure of Interest: None Declared

UPPER BODY POWER AND FLEXIBILITY AFFECT RUNNING THROW-IN PERFORMANCE IN YOUNG FOOTBALL PLAYERS

Dale Azzopardi [1] Susan Dewhurst [1] Theodoros Bampouras [1,*]

[1] Medical and Sport Sciences, University of Cumbria, Lancaster, United Kingdom

Introduction and Objectives: Throwing performance is crucial to success in many sports and a considerable amount of literature has been published with regard to overarm throwing performance [1]. The two-handed overhead throw, used in football, has received little attention, however, despite its importance to the game as throw-ins contributed to 4% of the goals scored in the 2006 FIFA World Cup [2]. The literature that is available around throw-ins reveals that power has been the main component of interest [3]. Moreover, studies to date have only focused on the upper-body and therefore the extent that other factors could contribute to throw-in performance such as leg power or flexibility are not known. In addition, the scarce literature on football throw-in examines the adult population while studies on youth populations are even fewer, despite the established different physical demands between the two age groups. The aim of the current study was to determine the relationship between maximum throwing distance and height, shoulder flexibility, upper- and lower-body power in youth team football players. It was intended that the results will provide information to help coaches design appropriate and effective training programmes for increasing football throw-in distance.

Methods: With Instituitnal Ethics approval, thirty-nine male youth team football players volunteered for the study (age 16.6 ± 0.9 years; height 1.74 ± 0.06 m; body mass 71.3 ± 13.4 kg). All participants had a minimum of 3 years competitive playing experience, were currently playing for a football club and familiar with taking football throw-ins. Goalkeepers were excluded from the study as they typically do not perform this skill. A running throw-in was performed indoors using a FIFA approved football. The running distance was standardised and within the distances allowed by football pitch restrictions. Height was measured according to the ISAK protocol. Shoulder flexion was measured using video analysis. Upper-body power was assessed using a 3 kg medicine ball seated chest pass while lower-body power was assessed from a countermovement jump without arm swing. For both throw-ins and measurement variables, two trials were performed and the best performance was used for further analysis. Following examination of data multicollinearity and residuals' homoscedasticity, correlation and distribution normality a hierarchical multiple regression was used to examine the variables that would better predict running throw-in distance.

Results: Mean results for running throw-in distance was 18.91 m ± 3.47 while shoulder flexion, upper-body power , and lower-body power results were 181.68 ± 6.16 º, 3.97 ± 0.38 m, and 3377.8 ± 613.5 W, respectively. The regression model indicated that the only significant predictors of throw-in distance were upper-body power ($p < 0.001$, adjusted $R^2 = 0.373$) and flexibility ($p < 0.001$, adjusted $R^2 = 0.637$). Regression coefficients of the measured variables can be found in Table 1.

Conclusion: The results indicate that upper-body power and shoulder flexibility are the major contributors to running throw-in performance in younger football athletes form the variables used in the current study. Their impact, although moderate, could be sufficient in achieving true performance changes . Youth coaches should consider these results when designing training programmes for younger athletes rather than following suggestions based on studies for adults, as well

assist them in throw in tactics. In addition, future studies should attempt to examine additional factors that could contribute to running throw in performances.

Table:

	B	SE B	β
Constant	-41.977	15.179	
Lower body power	-0.001	0.001	-0.136
Upper body power	4.908	1.081	0.577*
Flexibility	0.306	0.064	0.523*
Height	-0.066	0.056	-0.126

Caption: Coefficients the regression model. The order of the variables in the table reflects the entry order to the model.

References: [1] van der Tillaar et al., J Appl Biomech, 23: 12-19, 2004

[2] Acar et al., J Sport Sci Med, Supplement, 10: 2-5, 2007

[3] van den Tillaar et al., J Strength Cond Res, 25: 2316-2321, 2011

Disclosure of Interest: None Declared

Sport

PO-0346

THE SIX-WEEK SWISS BALL TRAINING AND DETRAINING EFFECT ON FUNCTIONAL PERFORMANCE FOR HIGH SCHOOL BADMINTON PLAYERS

Chung-Lin Wu [1,*] Chen-Fu Huang [2] Min-Hao Hung [2]

[1]Biomechanics Laboratory, Department of Physical Education NTNU, NEW TAIPEI CITY, Taiwan, Republic of China,

[2]Department of Physical Education NTNU, NEW TAIPEI CITY, -

Introduction and Objectives: Swiss ball trainingwas applied as rehabilitation therapy for a long time, and now has been widely used in physical fitness and sports training. The principle of Swiss ball training is to balance body on an unstable surface in order to achieve better proprioception, balanceperformance and muscle coordination(Fuller, 2002; Robert, Peter, & Brendan,2004).Many studies stated that Swiss ball is a good tool for training or rehabilitation equipment. Recent studies found that incorporating of short-term Swiss ball training into the abdominal training program was more effective than general resistance training. (Cosio-Lima,Reynolds, Winter, Paolone, & Jones, 2003). Previous researches have proved the effects of Swiss ball training on sports performance, but the studies did not put emphasis on the maintaining effect. The purpose of this study was to determinate the training and detraining effect on functional performance in high school badminton players while 6-weeks Swiss ball training performed.. The purpose of this study was to determinate the training and detraining effect on functional performance in high school badminton players while 6-week Swiss ball training performed. The functional performance assessments were carried out before, immediately after 6-weeks training, and after the 6-weeks of training termination.

KEYWORDS: instability training, dynamic balance, footwork, non-dominant leg

Methods: Sixteen high school badminton players with experience of three years or more were participated in this study. Those subjects were randomly divided into

control(n=8,age=16.63±0.48years,height=172±3.24cm,weight=68.13±3.06kg)and training group(n=8,age=16.880.78years,height=172.75±4.58cm

,weight=63.5±3.20kg).

The functional performance, including distance of standing long jump, height of vertical jump,dynamic balance, and timed left-to-right footwork and timed diagonal step footwork, were measured before, after6 weeks of trainingimmediately, and after the 6-weeks of training termination. Then the training group received Swiss ball training, which has contains eight movements of trunk, four of lower limbs training, and one of balance training, twice a week for 6-week. After 6-week training, the training group terminated Swiss ball training for another 6-week, and then reassessed the functional performance. The repeated-measures ANOVA were used to analyze the functional performance variables between two groups for three time assessments.

Results: The left-to-right footwork and dominant leg dynamic balance instantly after training was better thanbeginning and reached significant difference(P<0.05). The dynamic balance performance of non-dominant leg instantly after training was thebest (P<0.05). The performance of long jump and vertical jump after detraining for 6-week was better than the time

after training and reached significant difference(P<0.05). The times diagonal footwork was the best performance in the detraining. Others functional performance was not statistically significant differences.

Figure:
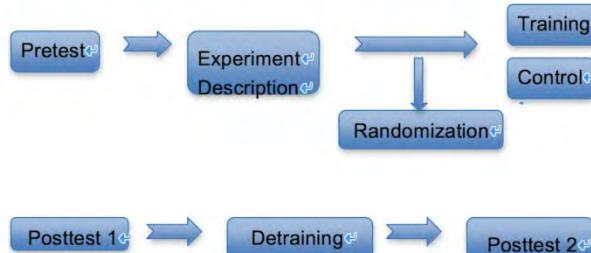
Conclusion: The 6-week Swiss ball training could contribute to left-to-right footwork and the dominant leg dynamic balance. For both training group and control group were not statistically significant difference, it was maybeless numbers of participants andthe shorter length of training period. We suggested that the future research wouldfocus on more   training periods to understand appropriated training effect.According to the results of this study, we suggested that Swiss ball training could be brought into conditioning and power phase to enhance the some functional performance of badminton player.

Table:

Variables	Pretest	Posttest 1	Posttest 2	Contrast
Long jump (CG)	232.13±32.1	231.00±17.61	237.50±18.97	
Long jump (TG)	249.50±11.76	243.00±13.77	247.63±11.40	A > B
Vertical jump (CG)	55.88±9.88	53.13±7.04	56.00±9.09	
Vertical jump (TG)	60.12±4.55	57.88±5.17	61.50±5.40	A > B
Left-right footwork (CG)	27.48±1.56	26.79±1.76	26.89±1.58	
Left-right footwork (TG)	26.75±1.16	25.34±1.49	25.84±0.99	B > A
Diagonal footwork (CG)	58.91±2.74	56.13±1.88	53.30±1.97	
Diagonal footwork (TG)	59.19±2.07	55.37±2.47	50.50±4.03	C > B > A
DDB (CG)	10.00±3.16	8.5o±4.00	8.88±3.79	
DDB (TG)	9.38±5.90	5.75±3.99	7.13±4.99	B > A
NDDB (CG)	9.50±3.51	7.25±4.10	8.75±3.92	
NDDB (TG)	9.75±5.55	4.13±3.48	9.13±6.88	B > A B > C

References: [1] Paterno, M. V., Myer, G. D., Ford, K. R., and Hewett, T. E.(2004).Neuromuscular training improves single-limb stability in young female athletes. *Journal of Orthopaedic& Sports Physical Therapy*, 34, 305-316.

[2] Cosio-Lima, L. M., Reynolds, K. L., Winter, C., Paolone, V., and Jones, M. T. (2003). Effects of physioball and conventional floor exercises on early phase adaptations in back and abdominal core stability and balance in women. *Journal of Strength and Conditioning Research*, *17*, 721-725.

[3] Liang,K. H., and Wu, H.W. (2010). Application and benefit of the Swiss ball exercise. *The University Physical Education and Sports*, 109, 93-99.

Disclosure of Interest: None Declared

Sport

PO-0347

A BIOMECHANICAL INVESTIGATION OF THE USE OF THE STRETCH SHORTENING CYCLE WHEN PERFORMING THE KETTLEBELL SWING

Paul Swinton [1,*]Deborah Jason [1]

[1]School of Health Sciences, Robert Gordon University, Aberdeen, United Kingdom

Introduction and Objectives: Kettlebell training has gained popularity over the last decade as a form of resistance training. A small number of studies have recently investigated the acute physiological and biomechanical effects created when performing kettlebell exercises. Research has demonstrated that the kettlebell swing, the most commonly performed kettlebell exercise, results in large force and power outputs and therefore it is suggested that repeated bouts of the exercise has the potential to chronically improve strength and muscular power. The kettlebell swing comprises rhythmic phases where the kettlebell and body mass are lowered under control and then rapidly elevated. This phasic movement pattern is common in sporting actions such as running and jumping where the presence of a phenomenon referred to as the stretch shortening cycle describes the storage of elastic energy during the lowering phase and subsequent release of the stored energy during the elevation phase. Exercises that prominently feature the stretch shortening cycle are frequently included in the power training of athletes. Therefore, the purpose of the present study was to investigate the extent to which the stretch shortening cycle phenomena featured during performance of the kettlebell swing.

Methods: Six male and three female recreationally trained participants with a minimum of six months experience performing the kettlebell swing were recruited for this study. Participants performed kettlebell swings with, and without a lowering phase. For each condition, the participants performed six repetitions with a 16 kg and 24 kg kettlebell. The condition with a lowering phase replicated standard practice and six repetitions were performed continuously. In contrast, swings performed without a lowering phase were initiated with the kettlebell resting on a wooden box with the participant adopting the same posture used in the other condition. Repetitions performed without a lowering phase were interspersed with a ten second rest period to ensure the effects of the stretch shortening cycle did not influence the subsequent elevation phase. Three dimensional kinematics and kinetics of the ankle knee and hip were quantified using inverse dynamics in a motion analysis laboratory, with models processed using Vicon Nexus 1.8.5 software (Oxford Metrics, Oxford, UK). A repeated measures ANOVA with two within factors (load * condition) was used to test for differences.

Results: To assess the effects of the stretch shortening cycle, the primary variable utilised was peak joint power summed at the hip, knee and ankle. A significant main effect of load ($p<0.01$) and condition ($p<0.01$) was obtained (Table 1). The results demonstrated that the inclusion of a lowering phase increased peak joint power by 45% and 17% during swings performed with the 16 and 24kg load, respectively. A significant main effect of load ($p<0.01$) and condition ($p<0.01$) was also observed for the peak joint force experienced at the hip (Table 1). The results also demonstrated larger forces experienced for the heavier load and when the movement was performed with a lowering phase.

Conclusion: The results of the present study demonstrate that the stretch shortening cycle features prominently during performance of the kettlebell swing. Increases in peak joint power of up to 45% were noted between the movement performed with and without a lowering phase. In addition, the differential for force measured at the hip joint was even

larger, with a 110% increase in force measured for the heaviest kettlebell load when including a lowering phase. The results of the study provide further evidence that the kettlebell swing is likely to produce a mechanical stimulus that is closely aligned with the power training goals of athletes.

Table:

Load/Condition	Peak Joint Power (W.kg)	Peak Hip Force (N.kg)
16 kg - lowering phase	46.0±15.7	54.5±71.3
16 kg + lowering phase	66.5±15.1	76.9±99.71
24 kg - lowering phase	71.3±24.4	78.7±126.3
24 kg + lowering phase	83.7±24.02	165.3±65.7

Caption: Table 1: (Mean±SD) Peak joint power and peak hip force

Disclosure of Interest: None Declared

Sport

PO-0348

BIOMECHANICAL COMPARISON OF LONG HEAD OF BICEPS TENODESIS WITH KNOTLESS SCREW AND INTERFERENCE SCREW TECHNIQUES

Wei-Ren Su [1,*]Chih-Hsun Chang [2]Florence Y Ling [3]Chih-Kai Hong [2]I-Ming Jou [1]

[1]Orthopaedic Surgery, National Cheng Kung University Hospital, [2]Department of Medicine, National Cheng Kung University College of Medicine, Tainan, Taiwan, Republic of China, [3]University of Texas Health Science Center at San Antonio School of Medicine, San Antonio, United States

Introduction and Objectives: The purpose of this study was to biomechanically evaluate a new technique of knotless screw fixation for suprapectoral biceps tenodesis and to compare it with the interference screw fixation[1,2].

Methods: Twenty-four fresh-frozen human cadaveric shoulders with a mean age of 63.3±8 years were studied. The specimens were randomly divided into 3 experimental biceps tenodesis groups (n=8): single knotless screw, double knotless screw and interference screw (Figure). Each tenodesis specimen was mounted on a mechanical testing machine, preloaded for 2 minutes at 5 N, and followed by a test of axial load to failure (1 mm/s). We evaluated the mode of failure and computed the ultimate failure load and stiffness.

Results: The interference screw group had the highest ultimate failure load (215.8±43.1 N), significantly higher than that for the single (70.1±13.6 N) and double (148.8±13.1 N) knotless screw groups ($P < .0001$). In addition, the interference screw group had the greatest stiffness (25.7±5.2 N/mm), significantly higher than that for the single (7.1±1.5 N/mm) and double (11.9±1.9 N/mm) knotless screw groups ($P < .0001$). The double knotless screw group had the second greatest ultimate failure load and stiffness, significantly greater than that of the single knotless screw technique ($P < .0001$ and $P = 0.024$, respectively) (Table). The most common mode of failure was suture slippage for both the single (6/8) and double knotless screw (7/8) groups and biceps tendon tearing for the interference screw groups (6/8).

Figure:
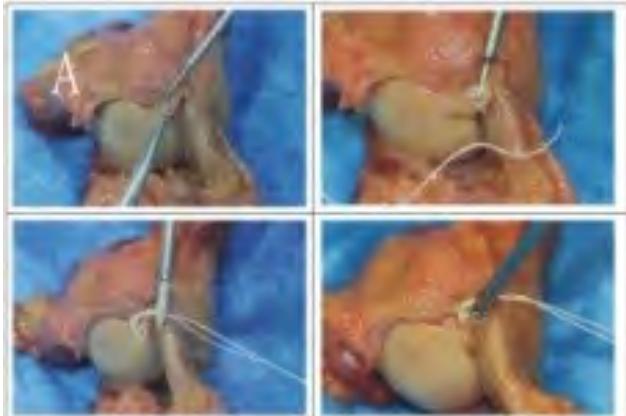
Suprapectoral tenodesis with single Footprint PK anchor (Smith & Nephew) on a right proximal humerus.

Conclusion: In this biomechanical study, double knotless screw fixation was found to have a significantly greater ultimate failure load and stiffness than the single knotless screw fixation, but values lesser than the interference screw fixation.

Table:

Table : Results for All Testing Parameters			
	Single Knotless Screw	Double Knotless Screw	Interference Screw
Age (yr)	68±8	66±5	65±11
BMD (g/cm^2)	0.73±0.17	0.68±0.16	0.72±0.13
Failure Load (N)	70.1±13.6 P< 0.0001	148.8±13.1 P= 0.0002	215.8±43.1
Stiffness (N/mm)	7.1±1.5 P< 0.0001	11.9±1.9 P< 0.0001	25.7±5.2
NOTE. P values are presented for comparison between interference screw and the other 2 knotless screw techniques.			
BMD, bone mineral density.			

References:

[1] Song et al., *Arthrosc Tech.*, 1:e43-46, 2012

[2] Su et al., *Arthroscopy,* 29:1498-1505, 2013

Disclosure of Interest: None Declared

A FOOT MORPHOLOGY-RELATED LOADING CHARACTER OF HABITUALLY UNSHOD AND SHOD RUNNERS

Qichang Mei [1,*] Lin Yu [1] Julien Baker [2] Ukadike Ugbolue [2] Yaodong Gu [1]

[1]Faculty of Sports Science, Ningbo University, Ningbo, China, [2]School of Science and Sport, University of the West of Scotland, Hamilton, Lanarkshire, Scotland, United Kingdom

Introduction and Objectives: Feet morphological characteristics have been proven to be closely linked with ethnicities (Hoffmann, 1905). One unique difference between habitually unshod running feet and shod running feet is that the great toes of habitually unshod runners are quite separate from the other toes compared with habitually shod runners. It is aimed in this study to investigate the separate hallux's function of habitually unshod runners and shod runners while running under shod and unshod conditions.

Methods: A total of eighteen habitually male barefoot (Indian) runners and twenty habitually male shod (Chinese) runners participated in the running test. Each participant conducted six trials of running test with the speed of 3.0±0.2m/s. The in-shoe plantar pressure measurement system (Novel Pedar-X System, Germany) was employed to measure the pressure and force exerted on the pressure sensors of the insole, and the insole was divided into eight anatomical parts, including medial rearfoot (MR), lateral rearfoot (LR), medial midfoot (MM),lateral midfoot (LM), medial forefoot(MF), lateral forefoot(LF), hallux (H) and other toes (OT). The peak pressure, contact area and force time integral were collected to analyze the difference while pushing off between habitually unshod feet and shod feet.

Results: Under unshod condition, the peak pressure and force time integral in the medial forefoot and lateral forefoot parts of habitually unshod and shod runners' running are significantly larger than those under shod conditions. However, the peak pressure and force time integral in the hallux part of habitually unshod runners' shod running are significantly larger than that under unshod condition. And the peak pressure and force time integral in the medial and lateral forefoot parts are significantly reduced compared with those of unshod conditions. The figure shoes the peak pressure in the forefoot and toes part while pushing off.

Figure:

Habitually unshod runners running under unshod(left) and shod(right) conditions

Habitually shod runners running under unshod(left) and shod(right) conditions
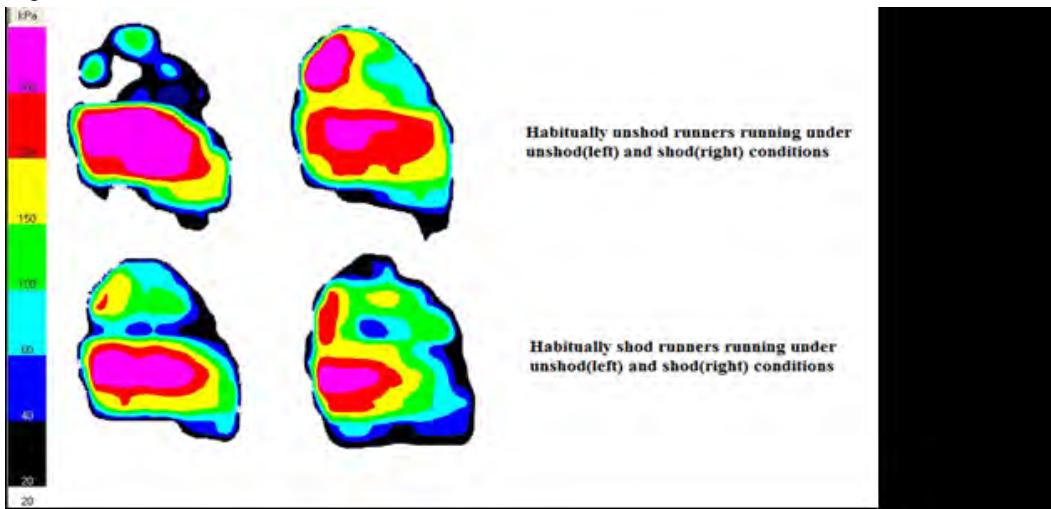
Conclusion: The increased peak pressure and force time integral in the hallux part of habitually unshod runners under shod condition could be explained with the hallux's prehensile function like fingers (Lambrundi, 1932). While shod running, the separate hallux of habitually unshod runners could grip the ground in the pushing off phase. Owing the gripping function of hallux, the loading to the forefoot was correspondingly reduced, thus lowering the risks of injuries to the forefoot (metatarsal) part. Conclusions and Disclosure The separate hallux shared parts of foot loading and reduces the loading focused in the forefoot region during push-off phase under shod condition. It will be beneficial for the prevention of feet injuries like plantar fasciitis and metatarsal stressed fracture.

References: [1] Hoffmann, P. The American Journal of Orthopedic Surgery, 3(2):105-136, 1905.

[2] Lambrinudi, C. Postgraduate Medical Journal., 8(86):459-464, 1932.

Disclosure of Interest: None Declared

Sport

PO-0350

DO SUCCESSIVE JUDO MATCHES PROVOKE DECLINE IN LOWER-LIMB MUSCLE POWER?

Daniele Detanico [1,*]Saray Giovana dos Santos [1]

[1]Physical Education Departament, Federal University of Santa Catarina, Florianópolis, Brazil

Introduction and Objectives: Muscle strength is considered potential predictor of judo performance, since high muscle power is required mainly for the execution of throwing techniques [1]. Thus, considering that judo players performed several matches during a tournament day with a minimum recovery [2], this study aimed to investigate the acute effects of successive judo matches on lower-limb muscle power.

Methods: Twenty male judo athletes (20.7 ± 4.6 years old; 72.8 ± 12.6 kg; 174.0 ± 8.7 cm; 13.9 ± 3.1% of body fat) volunteered to participate in this study. All athletes participated in several national and state tournaments and were regularly training 3–4 times a week during the evaluation period. Judo athletes performed three 5-minute judo matches with 15 minutes interval of passive rest among the matches. Before the first match and after each match the athletes performed three maximal countermovement jumps (CMJs) on a piezoelectric force platform (Quattro Jump, model 9290AD, Winterthur, Switzerland) at a frequency of 500 Hz in order to analyse the lower-limb muscle power. Analysis of variance for repeated measures (within-subjects ANOVA) and Bonferroni post-hoc tests were used to compare the CMJ performance among the matches.

Results: Table 1 shows the jump height and power output of CMJ in pre-match and post-match 1, 2 and 3. According to the analysis of variance, jump height showed significant reduction in post-match 2 when compared to the baseline and post-match 1. Similarly, the jump height in post-match 3 decreased when compared to the baseline and post-match 1. No significant effect of power output was detected in the matches. The simulated judo matches induced fatigue in the lower limbs, as indicated by the decline in CMJ height (3.6% after match 2 and 3.2% after match 3 when compared to baseline). This finding may be explained by the high eccentric-concentric load (SSC) in the actions performed by the lower limbs during the judo-specific techniques. It has been documented that prolonged and intense eccentric exercise, mainly involving SSC, induces immediate and prolonged reductions of function in several muscles, such as stretch-reflex sensitivity, joint stiffness regulation and jump performance [3].

Conclusion: We conclude that three successive judo matches induced fatigue in lower limbs. These findings may provide important information for coaches and physical trainers to delineate specific training to improve physical performance. It is recommended that the training design should be directed to power-specific resistance training in the lower limbs, aiming to maintain optimum levels of neuromuscular performance during successive judo matches.

Table:

	Pre-match	Post-match 1	Post-match 2	Post-match 3
H (cm)	45.38 ± 5.24	44.96 ± 5.56	43.74 ± 5.81*#	43.93 ± 6.13*#
P (W.kg^{-1})	27.73 ± 3.92	27.89 ± 3.63	27.50 ± 4.40	27.39 ± 3.94
Data are expressed as mean ± standard deviation; H: jump height; P: power output. *Significantly different from pre-match ($p<0.05$). # Significantly different from post-match 1 ($p<0.05$).				

Caption: Table 1. Jump height and power output of CMJ in pre-match and post-match 1, 2 and 3.

References: [1] Franchini et al. Int J Perform Anal Sport, 13:626-643, 2013.

[2] Bonitch-Domínguez et al. J Sport Sci, 28:1527-1534, 2010.

[3] Horita et al. Eur J Appl Phys, 79:160-167, 1999.

Disclosure of Interest: None Declared

Sport

PO-0351

ACUTE EFFECT OF KINESIO TAPE ON KNEE JOINT BIOMECHANICS DURING SIDESTEP CUTTING TASK

Chuanpis Boonkerd [1,*]Weerawat Limroongreungrat [1]Jos Vanrenterghem [2]

[1]College of Sports Science and Technology, Mahidol University, Nakronpathom, Thailand, [2]School of Sport and Exercise Sciences, Liverpool John Moores University, Liverpool, United Kingdom

Introduction and Objectives: Kinesio tape (KT) has been widely used for different purposes including structural support, reducing swelling and inflammation, stimulating and inhibiting muscle activity, and improving blood and lymph flow [1]. Anterior cruciate ligament (ACL) injury commonly occurs during non-contact situations particularly during deceleration, sidestep cutting and landing [2]. KT has also been used to support the knee after ACL injury to prevent tibial translation. It is believed that KT allows more functional activity as compared to other types of support such as functional knee braces and prophylactic tape. However, no previous studies have investigated the effect of KT on knee joint motion during sidestep cutting tasks. Therefore, the purpose of this study was to investigate the acute effect of KT on knee joint motion during sidestep cutting task.

Methods: Five healthy males (age 21 ± 0.9 years; weight 69 ± 8.5 kg; height 1.7 ± 0.8 m) volunteered in the study. Subjects performed sidestep cutting tasks at $45 \pm 5°$ of approach direction with running speed at 4.5 ± 0.5 m·s^{-1}. A 10 camera motion analysis system (BTS Bioengineering, Italy) synchronized with force plate (Piezoelectric pressure sensors, Kistler, Switzerland) were used to record kinematics and kinetics. The LJMU lower limb and trunk model was applied [3]. Each subject was randomly tested two times; 1) with a standardized KT technique for ACL injury (Taping group: TG) and 2) with the same tape and technique but without tension (Placebo group: PG). Three trials per condition were averaged and analyzed. Knee joint angles and moments from initial contact (IC) to the first 100 milliseconds of foot contact were analyzed using Visual3D software (C-motion, Inc., USA). Multiple t-tests were performed with Bonferroni correction adjustment of the alpha level by dividing the conventional alpha of 0.05 by the number of t tests.

Results: No significant differences of knee joint angles between TG and PG were found (Table 1). For knee moments, only internal rotation at IC between was found significant difference (Fig. 1).

Figure:

*Significant difference between two conditions $p=0.013$
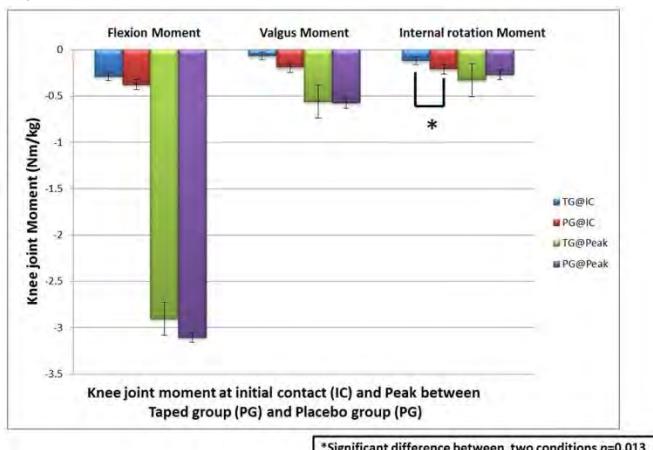
Conclusion: Although the results did not show significant differences between the two conditions, the TG had smaller peak knee flexion and valgus angles which may indicate that the tape tension provide some support for joint stability. However, whether the tape is strong enough to help prevent ACL injury, it is still questionable since knee flexion and valgus moments were similar in both conditions. Nevertheless, further research with a large sample size is warranted to clarify the beneficial effect of KT on movement control.

Table:

Knee joint angles at the initial contact (IC) and peak knee joint angles during sidestep cutting task

Angle (∘)	TG (N=5)Mean±SEM	PG (N=5)Mean±SEM	p-value
Knee flexion at IC	23.9±1.90	23.6±2.73	0.94
Knee valgus at IC	-2.2±1.07	-3.9±0.67	0.23
Internal rotation at IC	4.4± .25	5.2±1.71	0.68
Peak knee flexion	45.2±2.28	49.6±2.23	0.12
Peak knee valgus	-5.5±1.20	-7.6±1.45	0.20
Peak knee internal rotation	14.0±0.96	15.71±5.20	0.11

References: [1] Williams et al., Sports Med, 42(2): 153-164, 2012.

[2] Kristianslund et al., Am J Sports Med., 41(3): 684-688, 2013.

[3] Robinson et al., Journal of Biomechanics, 45: 941-1946, 2012.

Disclosure of Interest: None Declared

Sport

PO-0352

CENTER OF PRESSURE VELOCITY DURING TRUNK MOTION ARE ASSOCIATED WITH PERFORMANCE IN WHEELCHAIR RUGBY-SPECIFIC SKILLS

Thiago Lemos [1,*] Jeter Freitas [1] Miriam Mainenti [1] [2] Patrícia Vigário [1]

[1]Graduate Program in Rehabilitation Sciences, UNISUAM, [2]Escola de Educação Física do Exército, Rio de Janeiro, Brazil

Introduction and Objectives: The aim of the present study was to investigate the relationship between trunk stability measures and the performance in sport-specific skills in wheelchair rugby players.

Methods: Eight male subjects were recruited from a local wheelchair rugby team of the main division of the Brazilian wheelchair rugby championship. Seven subjects had spinal cord injuries at the level of C5-C7, and one had Guillain-Barre syndrome. All subjects provided their own International Wheelchair Rugby Federation classification. The classification scores were 0.5 (n=2), 2.0 (n=1), 2.5 (n=4) and 3.5 (n=1). The Beck Battery of Quad Rugby Skills Tests was employed to assess sports-specific skills performance (pass for accuracy; pass for distance; maneuverability with the ball; picking and sprinting). The tests took place at the same court used for athlete's training, and each subject used his own rugby wheelchair. For trunk motion assessment the subjects were placed in a sitting position on a force platform embedded in a stiff wooden block, with their feet unsupported. They were asked to lean the body in a selected direction, indicated by dot markers separated by 45 degrees interval from each other (Fig. 1a). The subjects should lean as far as they could and return to the initial position, in a comfortable self-selected speed. The center of pressure (COP) coordinates were measured with a force platform (AccuSwayPLUS, AMTI) sampled at 100Hz and low-pass filtered at 10Hz. The average velocity of COP displacement was computed. Spearman correlation (rho) analysis was applied to investigate the relationship among the results of the Beck Battery tests and COP velocity in the different directions.

Results: COP average velocity during trunk motion showed strong association with performance in the Beck Battery tests. Specifically, skill of maneuvering with the ball was associated with faster lateral COP motion (right and left motion, Fig. 1b). Also, faster right-posterolateral and forward COP displacement were correlated with performance in picking and sprinting tests, respectively (Fig. 1c and 1d). Finally, there was trend to perform better in the pass for distance test when subject showed a higher COP average velocity during backward motion (rho=0.70, p=0.06).

Figure:
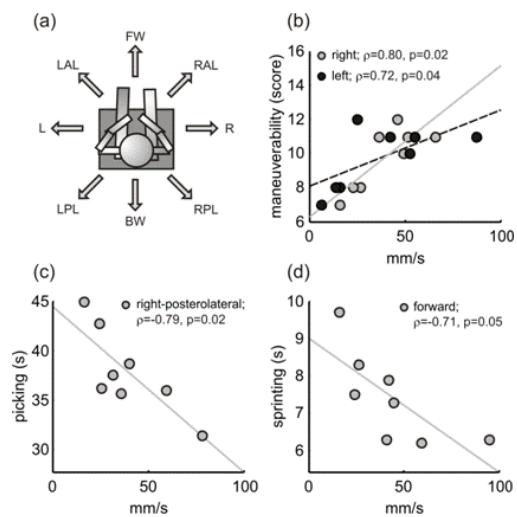
Caption: Fig 1. (a) Schematic illustration of the experimental procedures indicating the eight directions in which subjects must lean their body during trunk motion trials. Directions were assigned in a clockwise orientation as: FW, forward; RAL, right-anterolateral; R, right; RPL, right-posterolateral; BW, backward; LPL, left-posterolateral; L, left; LAL; left-anterolateral. Spearman correlation coefficient (rho) and the corresponding p-values (indicated as inset in the panels) showed a strong association between COP average velocity in a particular direction (also indicated as inset) and performance in the maneuverability with the ball (b), picking (c) and sprinting (b) tests. Least-squares regression lines are shown to emphasize the relationship between postural and sports skills performance.

Conclusion: Faster trunk motion in specific directions was correlated performance in locomotor/sport specific-related skills in wheelchair rugby players. Seated postural stability measures, in particular those related with the velocity of trunk motion, should be considered for sports classification and for monitoring of the training status of wheelchair rugby players.

Disclosure of Interest: None Declared

Sport

PO-0353

AGE-RELATED DIFFERENCES IN LOWER EXTREMITY MECHANICS DURING RUNNING

Mariana Souza [1,*]Ana Flávia Dos Santos [1]Bruna Luz [1]Jéssica Souza [1]Theresa Nakagawa [1]Fábio Serrão [1]

[1]Physiotherapy Department, Federal University of Sao Carlos, Sao Carlos, Brazil

Introduction and Objectives: The increase in life expectancy and the benefits that physical activity brings to health resulted in an increase in middle-aged and elderly individuals who practice run[1]. However, studies show that the incidence of injury in older individuals is higher than in young individuals[2]. In addition, older runners take longer time to recover from an injury and thus, take more time to return to practice physical activities[3]. This higher incidence may be partly due to changes in the running kinematics[4]. However, there are few studies evaluating the effect of aging on the kinematics of the lower limbs and comparing young, middle-aged and elderly runners. The aim of this study was to evaluate the kinematics of the hip and knee in young, middle-aged and elderly runners at touchdown in the fontal plane during running on a treadmill to have a better understanding of the biomechanical changes that occur due the aging process.

Methods: Twelve subjects were separated into three groups. Group 1 (H1) included four men aged between 18 and 35, group 2 (H2), with four men aged between 36 and 60 years and Group 3 (H3), with four men aged over 61 years. As inclusion criteria, the subjects should run more than 16 kilometers per week and be a rearfoot striker during running[5]. The exclusion criteria were any incidences of injury in the three months prior to the experiment, and musculoskeletal alterations in the lower limbs that could affect the running biomechanics[6]. Kinematic evaluation was performed during 5 minutes running on a treadmill using Qualisys Motion Capture System (Qualisys Medical AB, Sweden) with six cameras and a sampling frequency of 240Hz. At least five consecutive steps were recorded for analysis of knee and hip angle at touchdown in the frontal plane. The data were smoothed with a 12Hz low-pass Butterworth filter of fourth order and zero lag. One-way ANOVA test was performed to comparison between groups and *post hoc* comparisons were performed using Bonferroni adjustments ($\alpha = 0,05$).

Results: Significant differences were found for knee abduction between H1 and H2 (higher values for H2, $p = 0.012$) and between the H1 and H3 (higher values for H3, $p = 0.007$). In addition, significant differences were found for hip adduction between H1 and H2 (higher values for H2, $p = 0.007$) and H1 and H3 (higher values for H3, $p = 0.032$). There were no significant differences between groups H2 and H3 for the variables evaluated. Studies have shown that an increase of hip adduction and knee abduction is associated with an increase in the quadriceps angle (Q angle) and this contributes to dynamics knee valgus[7]. As the Q angle reflects the frontal plane forces acting on the patella, kinematic changes of the lower limb in the frontal plane may affect the patellofemoral joint[7]. Thus, excessive knee valgus resulting from hip adduction and/or knee abduction would increase the Q-angle as the patella would be displaced medially[7]. Therefore, there is an increase in the lateral forces acting on the patella, which can lead to a maltracking and can result in an increased contact pressure between the lateral facet and the lateral femoral condyle, leading to articular cartilage degradation and pain over time[8].

Conclusion: Therefore, the older runners showed an increase in hip adduction and knee abduction which are risk factors for certain injuries. These kinematic changes can generate an overload, especially in the knee joint, and might predispose these runners to injury.

Table:

Variables	Groups	Mean	Standard Deviation	ANOVA (p-value)	Bonferroni
	H1	-3.06	3,84		H1-H2 0.012*
Knee Abduction(+)	H2	5.66	2.53	0.004*	H2-H3 1.000
	H3	6.48	3.17		H3-H1 0.007*
	H1	-2.18	3.16		H1-H2 0.007*
Hip Adduction(-)	H2	-14.57	2.8	0.006*	H2-H3 0.998
	H3	-11.69	5.78		H3-H1 0.032*

Caption: Mean values and standard deviation of the analysed kinematic variables for young, middle-aged and elderly runners during running and P-values of the one-way ANOVA test and the Bonferroni adjustments (*significant difference (p<0.05)).

References: [1] Young A; Dinan S, BMJ, 330: 189-191, 2005.

[2] McKean et al., Clin J Sport Med, 16: 149-154, 2006.

[3] Matheson et al., Med Sci Sports Exerc, 21: 379-385, 1989.

[4] Bus SA, Med Sci Sports Exerc, 19: 1167-1175, 2003.

[5] Willson et al., Clin Biomech, 27: 1052-1057, 2012.

[6] Fukuchi RK; Duarte M, Can J Sport Sci, 26: 1447-1454, 2008.

[7] Powers C, JOSPT, 40: 42-51, 2010.

[8] Dierks et al., JOSPT, 8: 448-456, 2008.

Disclosure of Interest: None Declared

Sport

PO-0354

THE RELATIONSHIP OF RELEASE FACTORS ON THROW DISTANCE OF FEMALE HAMMER THROWERS

Suzanne Konz [1,*]

[1]Kinesiology, Marshall University, Huntington, WV, United States

Introduction and Objectives: Release angle, release height, and velocity at release are the most influential factors on throw distance according to previous research. No literature statistically has investigated the relationship of release factors on throwing distance of female hammer throwers. The aim of this study was to determine relationship of the release factors on throw distance for female hammer throwers.

Methods: The best performances of the top 10 female throwers at the 2014 USA Track and Field Nationals and 2014 USATF CV OTC meet were examined. Video was captured using two 60 Hz cameras. The best throw of each athlete was digitized and analyzed using the Contemplas Motus 10.0.1 motion analysis system.

Results: No correlations between the release factors and the distance thrown existed in the data set. However, the correlation matrix revealed that variables did correlate with other variables. A stepwise linear regression of the release factors indicated that none of the variables can predict distance thrown. A stepwise linear regression of all factors ($p<.000$ $r=.1.00$) indicates that the separation of the feet and hips at release and the vertical position of the hammer at the take-off during Turn 4 are predictors of throw distance.

Conclusion: The lack of a correlation of release factors with throw distance is interesting. Previous research has correlated release angle, release height, and velocity at release with throw distance. The most important of these typically is velocity at release. Correlation of individual factors with each other was present. Even the lack of representation of release factors within the stepwise linear regression is interesting.

Disclosure of Interest: None Declared

PO-0355

THE EFFECT OF CHANGES TO FORCE LOADING DIRECTION ON CERVICAL INTERVERTEBRAL DISC STRESS DISTRIBUTION DURING A RUGBY SCRUM

Eddie J. Bradley [1],*

[1]Sport, University of Sunderland, Sunderland, United Kingdom

Introduction and Objectives: In rugby union, a front-row player's neck is subjected to repetitive impact forces during scrum engagement. The scrum is one of the most powerful physical encounters in any sport, where up to 9000 N force may be exerted by the pack [1]. The formation of the scrum results in contact between the two opposing front rows. The forces are transmitted through the neck of the front-row players on engagement that occur up to 29 times per game [2]. Berge et al [3] reported early degenerative changes in the cervical region in 47 front-row forwards compared to 48 controls, while Scher [4] found 40 out of 150 rugby players aged 20-35 years displayed signs of osteoarthritic degeneration. Hogan et al [5] identified significant radiographic evidence of degeneration in experienced front-row players compared to non-rugby controls. O'Brien [6] termed this rugby neck, with repeated loading in the scrum identified as the cause. The purpose of this study was to quantify the effect of changes in loading application due to body position adjustments during the scrum on the stress response within a cervical intervertebral disc.

Methods: A finite element model of a C5-C6 cervical spine unit was created (Figure 1 L) with region-specific Young's modulus [7] applied to represent cortical and cancellous bone, endplates, annulus fibrosis and nucleus pulposus. Spinal ligaments and facet joint were modelled as spring elements. Force was applied to the C5 spinous process at nine angles progressing at 5° intervals in the sagittal plane (±20° to a neutral vector perpendicular to the spinal column longitudinal axis). Force application represented contact between the cervical region of one front-row player and the superior shoulder region of the opposing front-row player due to engagement in the scrum, and can be considered as a posterior-anterior directed force vector across the neck in the neutral position with increased superior-inferior force component as the angle varied. Equivalent von Mises stress along the mid-transverse plane of the disc and displacement of the disc were analysed.

Results: In a neutral scrum position (0° loading angle) the maximum equivalent von Mises stress in the intervertebral disc would be 1.7GPa. When the loading angle was altered to +20°, simulating the heads of the front row rising, the maximum stress decreased to 0.78GPa, and increased to 2.48GPa at -20°, with a near linear response (R=-0.988) to the loading angle range. The decrease in the loading angle occurs due to the shoulders of the front-row dropping below the hips, a manoeuvre used by the front row to get underneath the opposite player to gain an advantage. The findings show that this technique is placing the cervical spines of the whole front-row at an increased risk of degenerative injury as it increases the stress within the intervertebral disc. A back slope of 5° [8] produced the best scrummaging performance, which supports the finding that a higher head position is safer and more effective. Distribution of stress throughout the disc was found to be uneven (Figure 1 R), with the maximum stress 3mm from the anterior edge and a secondary peak 2mm from the posterior edge of the disc (Table 1). This agrees with the findings of Panjabi et al. [9], who reported that in the cervical spine the load is borne on the anterior edge of the vertebral body below C4-C5. As the force is transmitted through the

vertebrae, it causes rotation of the superior vertebrae around the facet joint. The disc is compressed anteriorly and the force is transmitted into the disc The distribution of stress in the intervertebral disc may be one of the main causes of disc degeneration reported by Berge [3] and O'Brien [6].

Figure:
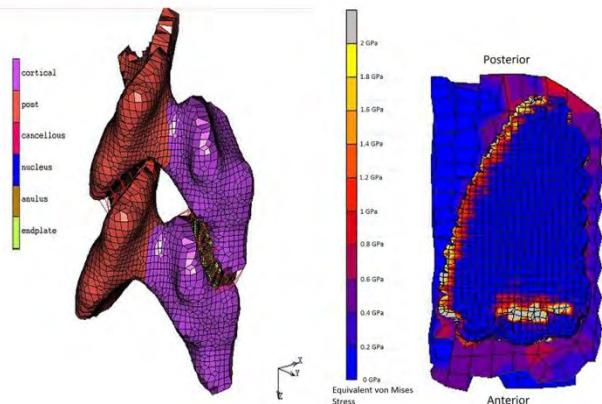
Caption: Figure 1. Finite element model of the C5-C6 vertebraal unit with material identification (Left) and Stress distribution in the intervertebral disc after loading at the 0· loading angle

Conclusion: The study indicates the magnitude of the loads that are placed on the cervical spine at different force applications, and repeated exposure may lead to serious injury. These findings may help inform the laws of the game by limiting the body angles of the front row at engagement.

Table:

Angle	-20	-15	-10	-5	0	5	10	15	20
Posterior Peak (GPa)	1.79	1.66	1.53	1.38	1.22	1.22	0.88	0.70	0.51
Anterior Peak (GPa)	2.48	2.32	2.13	1.94	1.72	1.72	1.26	1.02	0.78

Caption: Table 1. Stress distribution within the intervertebral disc

References: [1] Quarrie, K.L., et al., J Sports Sci, 18: 237-246, 2000.

[2] Fuller, C.W., et al., Br J Sports Med, 41: 862-867, 2007.

[3] Berge, J., et al., Am J Sports Med, 27(4): 422-429, 1999.

[4] Scher, A.T. Clinics in Sports Med, 17(1): 195-205. 1998.

[5] Hogan, B.A., et al., Irish J Med Sci, 179: 259-263, 2010.

[6] O'Brien, C.P. Clinical J Sports Med, 6: 56-59, 1996.

[7] Kumaresan, S., et al., Clinical Biomech, 14: 41-53, 1999.

[8] Mills, S., et al., Proceedings of the 18th International Symposium in Sports. Chinese University of Hong Kong, 2000.

[9] Panjabi, M.M., et al., Spine, 26(24): 2692-2700, 2001.

Disclosure of Interest: None Declared

Sport

PO-0356

THE FATIGUE EFFECT OF SIMULATED FUTSAL MATCH PROTOCOL ON STRENGTH BALANCE OF THE KNEE FLEXORS AND EXTENSORS MUSCLES

Juliano Dal Pupo [1,*]Saray dos Santos [2]

[1]Physical Education Departament, [2]Federal University of Santa Catarina, Florianópolis, Brazil

Introduction and Objectives: Fatigue in team sports is noticeable during a match, reducing the muscles' capacity to generate force. This fatigue effect may causes alterations in the strength balance between knee flexors and extensor muscles [1]; thus, it has been considered as a predisposing factor to muscle strains [2,3]. Thus, the objective of this study was to investigate the fatigue effects induced by a futsal-specific shuttle-run protocol on the conventional concentric quadriceps-to-concentric hamstrings and functional eccentric hamstrings-to-concentric quadriceps torque ratios.

Methods: Twenty-one under-17 and under-20 male futsal players (age = 17.2 ± 1.0 years; body mass = 68.2 ± 4.5 kg; height = 1.75 ± 0.05 m; body fat = 11.0 ± 1.9%) volunteered to participate in this study. Futsal players performed a futsal-specific intermittent shuttle-run protocol (FIRP) designed to replicate the activity profile of a futsal match. It comprises two blocks of 20-minute activities performed around a shuttle-run along a 15-m distance. The activities performed in the protocol were divided into the following categories: standing (0 km/h), walking (6 km/h), jogging (8.5 km/h), medium-intensity running (13 km/h), high-intensity running (17 km/h), and sprinting (>18 km/h). At pre-protocol, half-time, and post-protocol, the isokinetic torque of the knee flexors (concentric and eccentric actions) and extensors muscles (concentric action) were measured using an isokinetic dynamometer (Biodex System 3, Biodex Medical, Shirley, NY, USA), only in the participant's dominant leg ('kicking leg'). From the peak torque values, the traditional concentric flexor-to-concentric extensor and functional eccentric flexor-to-concentric extensor torque ratios were identified. Analysis of variance (ANOVA) with repeated measures using Bonferroni post hoc tests was used to compare the variables over the time points.

Results: Significant differences in the torque ratios were observed among the tested conditions (Table I). Lower values of conventional torque ratio were observed at the end of the FIRP when compared to pre-protocol; the values at half-time did not differ from the values measured pre-protocol and post-protocol. Regarding the functional torque ratio, lower values were observed at the end of the FIRP when compared to pre-protocol (as occurred with the conventional torque ratio); the values at half-time did not differ from the values measured pre-protocol or post-protocol.

Conclusion: It was concluded that the protocol designed to replicate the demands of a futsal match induced fatigue in the players, reducing the conventional and functional torque ratios at the end of the protocol, indicating a muscular imbalance at the end of exercise. This means that fatigue affected more pronounced the torque production of knee flexors than the knee extensors. Thus, fundamentally exercises focusing on the eccentric strength of hamstring muscles should be privileged aiming to at least reduce the deleterious effects of fatigue, and thereby reduce the chance for the predisposition of hamstring-strain injury in futsal players.

Table:

	Pre-protocol	Half-time	Post-protocol	p
Conventional torque ratio	0.631 ± 0.081	0.603 ± 0.089	0.578 ± 0.088[a]	<0.01
Functional torque ratio	0.955 ± 0.143	0.991 ± 0.121	0.919 ± 0.162[a]	0.01
[a] Significantly different from the pre-protocol value				

Caption: Conventional and functional torque ratios obtained pre-protocol, at hal-time and post-fatigue protocol

References: [1]Camarda et al. J Sci Med Sports, 15:355-360, 2012.

[2] Rahnama et al. J Sports Sci, 21:933-942, 2003.

[3] Greig. Am J Sports Med, 36:1403, 2008.

Disclosure of Interest: None Declared

PO-0357

A NEW KINEMATIC METHOD TO CLASSIFY ALL FOOT STRIKE PATTERNS DURING RUNNING

Max Paquette [1,*]

[1]Health & Sport Sciences, University of Memphis, Memphis, United States

Introduction and Objectives: Rearfoot strike patterns are most often studied in biomechanics due to the higher prevalence of rearfoot runners compared to non-rearfoot runners (e.g., midfoot, forefoot and toe strike). Toe striking is less common but observed in some competitive and elite runners but is often lumped into a classification with forefoot runners. There is currently a kinematic (i.e., foot contact angle [1]) and a kinetic (i.e., strike index [2]) method to classify strike patterns and these methods can effectively differentiate rearfoot and non-rearfoot strike patterns. However, non-RFS patterns can often be more difficult to classify with these methods. Correct classification of strike patterns in non-rearfoot runners is important to understand biomechanical differences between all running styles as scientists continue to study running injury risk factors. The objective of this study was to compare a new kinematic method to classify strike patterns with currently accepted methods.

Methods: Six young adults (4 men) completed five over-ground running trials at 3.5m/s±5% using a rearfoot, midfoot, forefoot and toe strike. Subjects warmed up on a treadmill before testing and completed practice trials before each condition. Strike patterns were randomized and verbal instructions were given for each pattern. Strike patterns were visually monitored by the same researcher. 3D motion capture data of the right shank and foot (Qualisys AB) and, 3D ground reaction force data were collected to identify time of foot contact (AMTI, Inc). A new kinematic method to differentiate strike patterns was computed as the ratio of the sagittal plane foot contact angle and ankle range of motion to midstance (Foot-Ankle Ratio; FAR). Foot contact angle (FCA) was measured as the absolute sagittal plane angle formed between a line joining the 5th metatarsal head and the inferior heel and the laboratory floor. Ankle range of motion was measured as the sagittal plane angular excursion of the ankle from foot contact to peak dorsiflexion. Strike index (SI) was computed as the ratio of anterior center of pressure location at foot contact relative to the length of the foot. The means of the five running trials for FAR, SI and FCA were computed and used for analysis. Cohen's d effect sizes (ES) were computed to compare mean differences for each strike pattern classification methods among strike patterns.

Results: All strike patterns showed different FAR (ES = 2.82 – 10.08), FCA (ES = 1.27 – 14.72) and SI (ES = 4.08 – 12.60; Table 1). The ranges of subject means for all methods did not overlap when comparing RFS with MFS and FFS and, MFS with FFS (Table 1). However, when comparing the ranges of subject means between FFS and TS, only the ranges of FAR and FCA did not overlap between these strike patterns (Fig 1).

Figure:
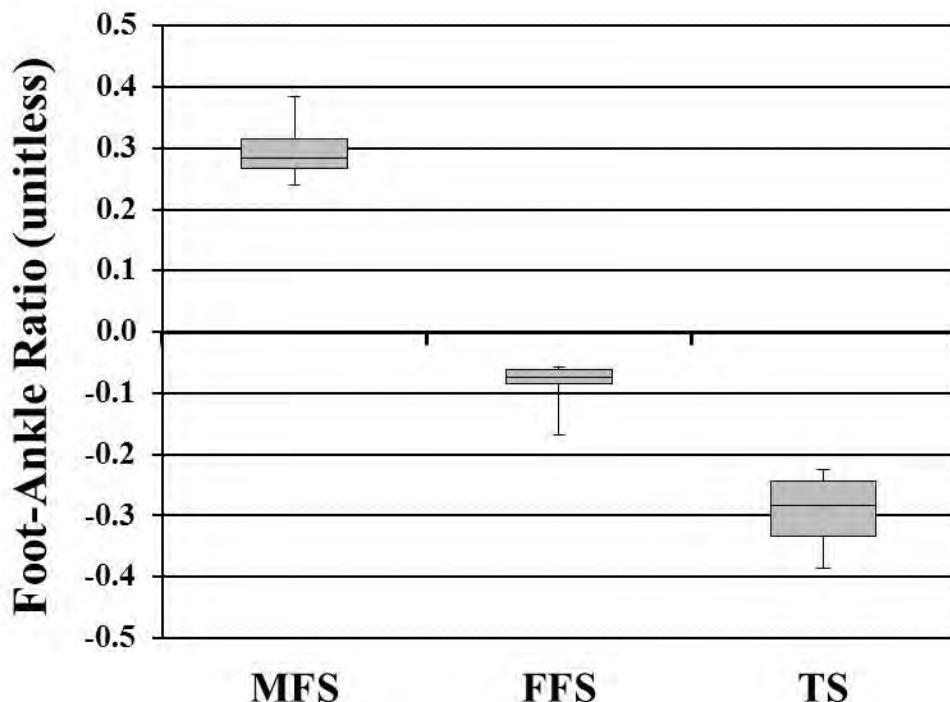
Caption: Fig 1. Boxplot for midfoot (MFS), forefoot (FFS) and toe strike (TS) for the foot-ankle ratio (FAR): the ratio of the sagittal plane foot contact angle and the sagittal plan ankle range of motion (Maximum, 3rd Quartile, Median, 1st Quartile, Minimum).

Conclusion: The findings indicate that FAR, SI and FCA can successfully classify rearfoot, midfoot and forefoot strike patterns, but SI failed to clearly differentiate forefoot and toe strike patterns. The FCA and a new kinematic method to classify strike patterns, FAR, can effectively differentiate all strike patterns including forefoot and toe striking. This preliminary analysis with a small sample size indicates that the two kinematic methods are more effective than a kinetic method (SI) to classify all strike patterns in running. Based on these findings, the FCA would be the most effective method as data collection and computation are simple. A larger sample size will be used to further confirm the effectiveness of these methods in classifying all strike patterns during running.

Table:

	RFS	MFS	FFS	TS
FAR (unitless)	3.14 (1.58,5.14)	0.30 (0.24,0.38) [a]	-0.09 (-0.06,-0.17) [a,b]	-0.30 (-0.23,-0.39) [a,b,c]
SI (%)	12.21 (4.54,22.04)	67.86 (45.15,81.29) [a]	109.24 (98.43,122.75) [a,b]	102.46 (107.04,128.47) [a,b,c]
FCA (deg)	23.68 (17.51,29.93)	6.41 (5.68,7.31) [a,b]	-2.72 (-2.02,-6.79) [a,b]	-9.65 (-7.90,-11.62) [a,b,c]

Notes: [a]: large ES compared to RFS; [b]: large ES compared to MFS; [c]: large ES compared to FFS (ES > 0.8).

Caption: Table 1. A comparison of the foot-ankle ratio (FAR), strike index (SI) and foot contact angle (FCA) strike pattern classification methods for all four strike patterns: rearfoot (RFS), midfoot (MFS), forefoot (FFS) and toe strike (TS). [mean (minimum, maximum)]

References: [1]. Altman A.R., Davis I.S. Gait & Posture. 2012. 35(2):298-300

[2]. Cavanagh, P. R., & Lafortune, M. A. J Biomechanics. 1980. 13(5), 397-406.

Disclosure of Interest: None Declared

Sport

PO-0358

THE BIOMECHANICS OF THE LATERAL JUMP SMASH AND FOOTWORK TRAINING IN BADMINTON

Min-Hao Hung [1,*]Jia-Hao Chang [1]Po-Han Chang [1]Yao-Ting Chang [1]
[1]Physical Education, National Taiwan Normal University, Taipei, Taiwan, Republic of China

Introduction and Objectives: To have an advantage in the competition, the lateral jump smash has been used in the badminton. The footwork training improves the skill in lateral jump smash, but only footwork training (without ball) is not accordance with real competition[1]. **Purpose:** to improve the reality in training, this study was measuring the differences between lateral Jump smash training (with ball) and lateral Jump smash footwork training (without ball) in biomechanics.
Methods: Eight players with 13 ± 2.9 years badminton training experience, all participants were right hand dominant (n=8,23.6 ± 3.3 years, 176.5 ± 3.1 cm, 70.5 ± 8.2 kg). Eight Vicon infrared high-speed cameras (300 Hz) and a Kistler force plate (1500 Hz) were used to collect kinematic and kinetic data respectively. Players were asked to jump three times in lateral Jump Smash Footwork (without ball) and three times laterals Jump Smash (with ball). After smash, they were landing on the force plate and returned to the original position. The Visual3D software was used to process and analyze biomechanics. The Dependent sample t test was performed to compare the joint angle, ground reaction force between two conditions by using SPSS 22.0 (α = .05).
Results: No difference was found between the two conditions at ground reaction force. The main finding was focused on the landing moment. Spike had greater hip abduction (38.4 ± 5.7°) and greater knee flexion (15.5 ± 3°), footwork training had a greater hip flexion (11.6 ± 5.4°). In landing phase footwork had a greater knee flexion and extension range of motion (60 ± 6.1°).
Conclusion: The differences between two training were the joint angles and landing strategy in landing. Hard landing strategy was found in a spike with a ball, and soft landing strategy was found in footwork training.

Table:

Table Mean ± SD (degree) of joint angle			
	footwork	Spike	p value
Hip（initial contact）Abduction (+)/Adduction (-)	33.98 ± 7.79	38.42 ± 5.65	.007 *
Hip（initial contact）Flexion(-)/Extension(+)	-11.56 ± 5.35	-6.38 ± 4.52	.001 *
Knee（initial contact）Flexion(-)/Extension(+)	-11.84 ± 2.96	-15.51 ± 3.01	.02 *
Hip（range of motion）	60± 6.1	51.23 ± 6.72	.03 *
* p < .05			

References: [1]Kimura, Yuka, et al. *British journal of sports medicine* 46.3 : 207-213, 2012.

Disclosure of Interest: None Declared

USING A DYNAMIC SYSTEM APPROACH AS A MEASURE TO DISCRIMINATE RUNNING WITH DIFFERENT FOOT STRIKE PATTERNS

I.Lin Wang [1] Li.I Wang [2,*]

[1]National Dong Hwa University, Department of Life Science and the Institute of Biotechnology, [2]National Dong Hwa University, Department of Physical Education and Kinesiology, Hualien, Taiwan, Republic of China

Introduction and Objectives: Running is a popular recreational sport. While running, the foot repeatedly contacts the ground. This movement can cause repeated impact forces that result in lower extremity injuries [5;6]. Running exhibits a high proportion of lower extremity injury rates, especially in the knee joint. Three types of foot contact with the ground are observed: rear-foot strike (RFS), mid-foot strike (MFS), and fore-foot strike (FFS) [3]. Different landing patterns cause different impact characteristics. Past studies suggest that FFS method produces a smaller impact force [1;3]. Thus, the purpose of this study was to determine the effect of the strike pattern coordination on lower extremity landing while running to provide information regarding the risk of injury.

Methods: Sixteen habitual RFS runners (height: 1.71 ± 0.10 m; weight: 62.44 ± 9.70 kg; age: 21.44 ± 1.67 years) and four habitual FFS runners (height: 1.67 ± 0.10 m; weight: 57.50 ± 11.70 kg; age: 21.00 ± 0.82 years) served as the subjects. All subjects were university students from the physical education department who volunteered to participate in the study. Kinematic data were collected using an eight-camera motion analysis system (Qualisys motion system, Gothenburg, Sweden) (200 Hz). Ground reaction forces were collected using two AMTI force plates (1000 Hz). Joint angles and angular velocities were interpolated to 100% of the breaking phase. The dynamic system approach was used to analyze the pattern of the inter-joint coordination with the mean absolute value of the ensemble relative phase angle curve value (MARP) [2]. Statistical analysis was performed with SPSS 14.0 for Windows. The significance level was set at $\alpha=0.05$. Independent t-test was used to detect differences among groups with different foot strike pattern.

Results: The results are revealed in Table 1. The MARP of knee flexion/extension – ankle inversion/eversion in habitually RFS runners was significant smaller than habitually FFS runners ($P<0.05$). There were no significantly different in MARP of knee flexion/extension – ankle plantar flexion /dorsiflexion and hip flexion/extension - knee flexion/extension between two groups ($P>0.05$).

Conclusion: In the dynamic systems approach, analysis of the MARP values yields an understanding regarding the motion of the two joints, i.e., whether the joints are moving in phase with low individual independence or out of phase with high individual independence [2;4;6]. The present study revealed that the RFS group exhibited relatively in-phase patterns for knee flexion/extension-ankle inversion/eversion inter-joint coordination compared with the FFS group. This in-phase (low-independence) coordination pattern may be associated with increased collision forces [6]. This at-risk motion pattern predisposes runners to injuries. Additionally, Stergiou, et al. [7] revealed that a relatively out-of-phase motion pattern during the stance phase is potentially associated with the desire to reduce the landing load. Inappropriate lower extremity coordination is likely to limit the impact-absorbing capacity of the lower extremities during the stance phase, thus predisposing runners to running injuries [6;7].

Habitual RFS runners potentially decrease the independence of knee flexion/extension-ankle inversion/eversion during the breaking phase of running. This inappropriate lower extremity inter-segment coordination may increase the risk of lower extremity injury.

Table:

Group	RFS	FFS
MARP of knee flexion/extension – ankle inversion/eversion *	0.662±0.21	1.006±0.11
MARP of knee flexion/extension –ankle plantarflexion /dorsiflexion	1.108±0.21	1.058±0.30
MARP of hip flexion/extension – knee flexion/extension	0.848±0.08	0.808±0.09

Caption: Table 1: Inter-joint coordination parameters with different foot strike pattern

References: [1] Arendse, R.E., et al. Med Sci Sports Exerc, 36, 272-277.2004.

[2] Burgesslimerick, R., et al. J Biomech, 26, 91-94.1993.

[3] Lieberman, D.E., et al. Nature, 463, 531-535.2010.

[4] Lu, T.W., et al. Gait Posture, 27, 309-315.2008.

[5] Stergiou, N., et al. Med Sci Sports Exerc, 31, 1645-1655.1999.

[6] Stergiou, N., et al. Clin Biomech, 16, 213-221.2001.

[7] Stergiou, N., et al. Gait Posture, 13, 210-220.2001.

Sport

PO-0360

EFFECTS OF EXTERNALLY DAMPING ON IMPACT-INDUCED SOFT TISSUE VIBRATIONS AND MUSCLE RESPONSES IN LANDINGS

Weijie Fu [1,*] Yu Liu [1] Rui Xia [1] Lingyan Huang [1]

[1] Key Laboratory of Exercise and Health Sciences of Ministry of Education, Shanghai University of Sport, Shanghai, China

Introduction and Objectives: Numerous studies have shown that most physical activities including running and jump/landing experience impacts during ground contact. These impact forces cause large transient shocks that act upon the lower body and excite local vibrations that are either absorbed or transmitted through the soft tissues [1]. A reduction in soft tissue oscillation is considered to be one of the benefits of wearing compression garments in enhancing performance. Theoretically, damping the soft tissue vibrations would decrease the muscle activity and, thus, decrease the needed energy [2]. Therefore, the purpose of this study was to investigate the effect of compression shorts on soft tissue vibrations, and muscle activity in the lower extremity during a drop jump landing task.

Methods: Twelve trained male volunteers (age: 23.7±2.7 years, height: 178.3±2.5 cm, mass: 70.1±4.6 kg) were recruited for this experiment. All were requested to wear two types of shorts [nylon-elastane compression shorts (CS) vs. loose fitting shorts (as a control condition, CC)] to execute three trials of maximal effort drop jump (DJ) from each of height (30, 45, and 60 cm) from a platform. Vibrations of the quadriceps and hamstrings in the dominant leg through the accelerometers were collected using two Biovision biaxial accelerometers (1200 Hz). A Biovision EMG system (1200 Hz) was used to record the EMG signals from the rectus femoris (RF) and biceps femoris (BF) synchronously. The main variables used in this study characterizing the vibration signal included peak soft tissue acceleration (a_{peak}) and the damping coefficient (c) following landing impact for each condition. They were determined using a least-squares minimization method (Levenberg–Marquardt). Meanwhile, root mean square of the muscle activity (EMG_{RMS}) was calculated during the pre-activation, post-activation, eccentric, and concentric phases of the drop jump. A repeated measures ANOVA was used to determine the effects of compression shorts and drop heights on soft-tissue vibrations and EMG activity.

Results: For the soft tissue vibrations, the CS condition showed a significant decrease in the vibration amplitude of quadriceps and hamstring, and an increase in damping coefficient of the corresponding muscles (Table 1). For the muscle activations, the EMG_{RMS} of the RF and BF muscles both showed a significant decrease in wearing compression shorts compared to control condition (Figure 1). Specifically, the EMG_{RMS} of RF when wearing CS was significantly lower compared to CC during pre- & post-activation and eccentric (downward) phases from all heights of DJ; similarly, the EMG amplitude wearing CS compared to CC also showed a decrease in BF during the post-activation of DJ45 and eccentric (downward) phase of DJ60, respectively.

Figure:
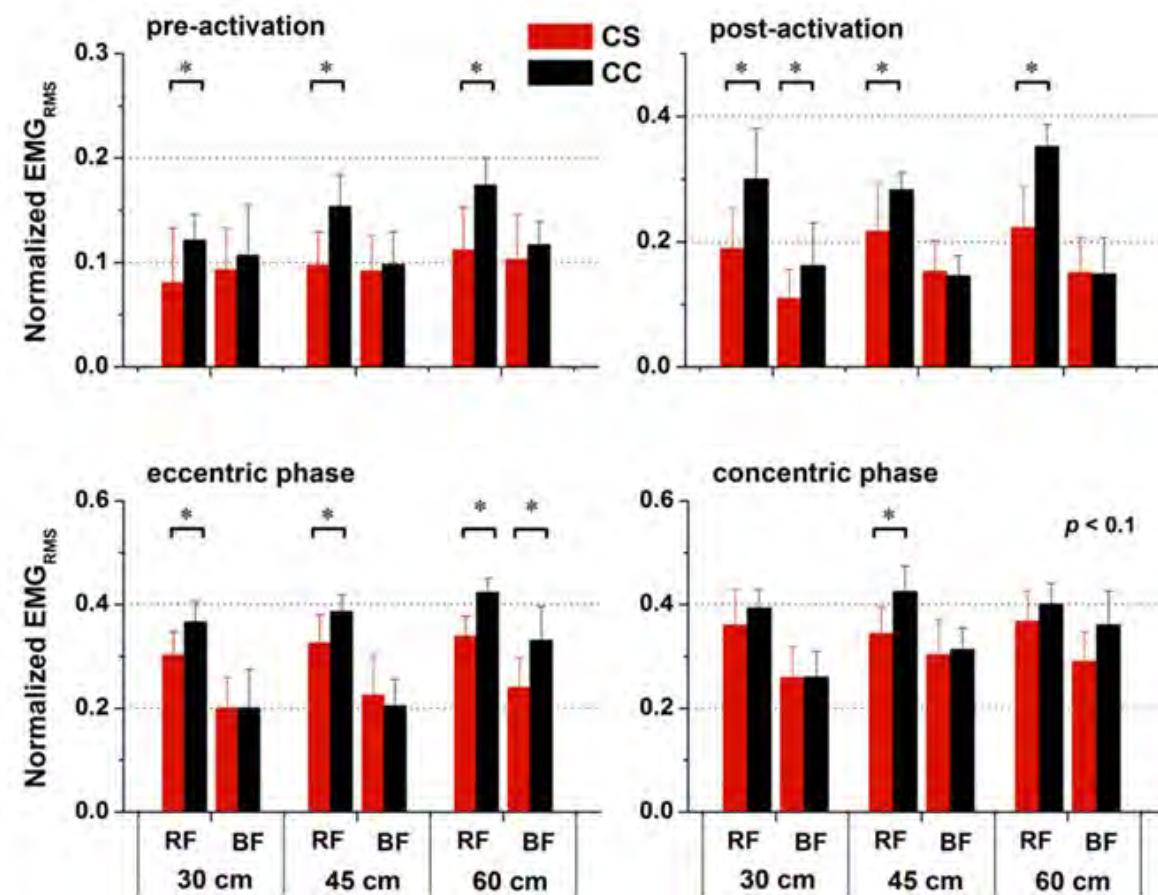
Caption: Figure 1 Influence of externally damping (CS: compression shorts; CC: control condition) on the EMG amplitude of rectus femoris (RF) and biceps femoris (BF).

Conclusion: Our results suggest that soft tissue vibration can be reduced by wearing compressive shorts without generating additional muscle activation during drop jump landing. Contrarily, externally induced soft tissue vibration damping might be associated with a decrease in muscular activity of the rectus femoris and the biceps femoris muscles. However, future studies should focus on the possible relationship between soft tissue vibration damping, muscle activity and energy consumption.

Table:

Variables	Muscle groups	Shorts conditions	Landing heights			
			30cm	45cm	60cm	
a_{peak} (g)	Quad	CS	6.85±3.1	10.25±4.9*	11.18±4.1*	
		CC	7.82±3.2	13.16±4.4	14.31±4.2	
	Hams	CS	3.18±1.2*	4.07±1.5	5.01±1.1†	
		CC	4.42±1.9	4.85±1.0	5.92±2.4	
c (s^{-1})	Quad	CS	15.57±1.2	17.21±2.7	19.22±3.5*	
		CC	13.86±3.5	15.67±5.4	16.80±3.1	
	Hams	CS	11.68±5.7	12.93±6.7	13.88±5.7*	
		CC	13.17±5.3	14.69±5.6	16.82±5.7	

* Significantly different between shorts in the same landing height with $p < 0.05$.

† Significantly different between shorts in the same landing height with $p < 0.1$.

Caption: Table 1 Influence of externally damping (CS: compression shorts; CC: control condition) on peak accelerations (apeak) and damping coefficient (c) of the quadriceps femoris (Quad) and hamstring (Hams) muscles.

References: [1] Coza et al., Med Sci Sport Exer, 43: 509-515, 2011.

[2] Friesenbichler et al., J. Biomech, 44: 116-20, 2011.

Disclosure of Interest: None Declared

Sport

PO-0361

THE PLANE OF ROTATION AT DIFFERENT BASEBALL BATTING HEIGHT

Tang-Yun Lo [1,*]Po-Yao Chuang [1]Yao-Ting Chang [1]Jia-Hao Chang [1]

[1]Department of Physical Education, National Taiwan Normal University, Taipei City, -

Introduction and Objectives: Many researches investigated the difference of body motion in varying hitting conditions and focused on joint angle and angular velocity. But few researches investigated the changes of trajectory which directly affect batting. The aim of this study was to observe motional variation between different batting tasks (high, middle, low) by analysing the plane of rotation.

Methods: Sixteen collegiate baseball players (aged: 22.70 ± 2.05 yr, height: 174.7 ± 2.0 cm, mass: 70.6 ± 6.1 kg) participated in this study. A Vicon 3D motion capture system (250Hz) was used to collect the motion data. Markers were placed on participants in accordance with the plug-in gait marker set, and markers also placed on batting tee, bat head and bat tail. Batting tees are adjustable to simulate the batting situation in different heights (high, middle and low). After warming up, every player was asked to bat 3 times successfully and the trail which has the fast velocity of bat head while ball-bat contact was chosen during each height of task. In order to reduce individual unstable batting motion in interference, the swing phase was defined from the angle between X axis of *global* coordinate system and the line passing through the right shoulder and left shoulder in XY plane was zero to ball-bat contact Kwon3D XP was used to calculate the kinematic parameters. We calculated normal vectors to the plane of rotation by bat (N_B) and upper trunk (N_T) trajectory. The one-way ANOVA with repeated measures ($\alpha = .05$) was used to test the angle between normal vectors so as to observe the relationship between segments (upper trunk and bat) motion in different batting tasks.

Results: The angle between N_B and global Z axis(θ_{BZ}) in high hitting condition was less than in middle condition and in middle condition was less than in low condition. The angle between N_T and global Z axis(θ_{TZ}) in high hitting condition is less than in middle condition andθ_{TZ} in middle was less than in low condition. The angle between N_B and N_T(θ_{BT}) in high batting task was less than in middle and low batting task.

Conclusion: In order to batting successfully, player's motion will be changed with batting height. Many studies indicate that the motion of upper lime is the key factor to batting, nevertheless, upper trunk may also play an improtant role. In this reserch, we observe that the rotation plane of upper trunk and bat are change similarly with batting height.

Table:

Table 1. Angle between vectors in different batting tasks.		
	Batting Task	Mean±SD (degree)
θ_{BZ}	High	18.5 ± 5.8^{ab}
	Middle	37.4 ± 7.1^{ac}
	Low	50.5 ± 5.2^{bc}
θ_{TZ}	High	17.7 ± 5.8^{ab}
	Middle	24.1 ± 6.1^{ac}
	Low	33.0 ± 7.8^{bc}
θ_{BT}	High	12.7 ± 5.6^{ab}
	Middle	16.8 ± 6.7^{a}
	Low	19.9 ± 5.5^{b}
significant difference ($p < .05$) : a: high vs.middle, b:high vs. low, c: middle vs. low		

Disclosure of Interest: None Declared

PO-0362

SINGLE-CAMERA DEPTH-SCANNING TO MEASURE REAL-TIME PELVIC POSITION AND ORIENTATION DURING TREADMILL GAIT: IMPLICATIONS FOR RISK FACTOR MODELLING

Tom Macpherson [1,*] Jonathan Taylor [1] Tom McBain [1] Matthew Weston [1] Iain Spears [1]

[1] Sport and Exercise, Teesside University, Middlesbrough, United Kingdom

Introduction and Objectives: The pelvic region forms the proximal end of the lower kinetic chain and is routinely assessed due to its reputed relationship with pelvic, spinal and lower limb pathologies (Liebenson, 2004; Sahrmann, 2002; Herrington, 2011). The surrounding musculature provides the control and stabilization necessary for efficient gait (Saunders et al., 2005), and large linear and/or angular oscillations of the pelvis during gait are implicated in musculoskeletal injuries (Saunders et al., 2005). However, these reputed risks and causal pathways are not well understood (Laird et al., 2014).

Several studies have presented protocols to quantify pelvic movements during gait (Schache et al. 2002a; Bickham et al., 2000; Schache et al., 2000). However, they are generally lab-based and time-consuming, which may limit the practicality for use in large-scale trials. Depth sensing cameras, such as the Kinect sensor (Microsoft™, USA), may offer an affordable and pragmatic alternative (Dutta, 2012). The key feature of this technology is the real-time measurement of camera-object distances (depth) on a pixel-by-pixel basis. The raw data from this module is more precise than the better known skeletal tracking module (Dutta, 2012).

Therefore, the aims of this study were to develop techniques and evaluate a single-camera depth scanning approach to the 3D measurement of linear and angular oscillations of the pelvis during treadmill gait.

Methods: Three participants volunteered for the study (age 27.7 ± 1.9 y, height 87.7 ± 2.9 cm and mass 78.0 ± 8.7 kg). Participants undertook a baseline incremental treadmill test to determine their maximal oxygen uptake (O_2max) followed by trials (180s each) at 3 different speeds of locomotion (walking: 5.1-6.0 km/h; jogging: 10.5-11.2 km/h and running: 13.5-14.4 km/h).

Four retro-reflective disks were positioned bilaterally on the posterior and anterior iliac spines. Pelvic movements were captured concurrently using a single RGBD camera (Kinect™, Version 1, Microsoft, USA) and a 6-camera motion capture system (Vicon MX13 and Vicon Nexus 1.7, Vicon Motion Systems). Depth data for the single camera system was used to reconstruct a surface on the posterior of the lumbo-pelvic complex. The surface was then processed to estimate pelvic orientation position and angular position.

The time-series for the triaxial linear positional (Figure 1a, b and c) and triplanar angular (Figure 1d, e and f) data were used to determine the amplitudes of oscillations for the 6 degrees of freedom on a stride-by-stride basis. These were compared with the data from the 'gold standard'. Individual strides were determined by processing the superior-inferior movements (Figure 1b). The within-trial typical errors (reported with 90% Confidence Limits [90% CL]) of measurement were derived using a custom-written spreadsheet (Hopkins, 2000).

Results: Typical errors for the single-camera system, expressed as a CV (%) were 1.4 (90% CL: 1.0-2.4), 4.3 (3.0-7.8) and 1.4 (1.0-2.6) for the amplitude of oscillation in the anterior-posterior, superior-inferior and medial-lateral directions.

Typical errors of the angular measurements were 9.8 (6.8-18.2), 13.9 (9.6-26.4) and 41.1 (27.5-85.6) in the frontal, transversal and sagittal planes, respectively.

Figure:
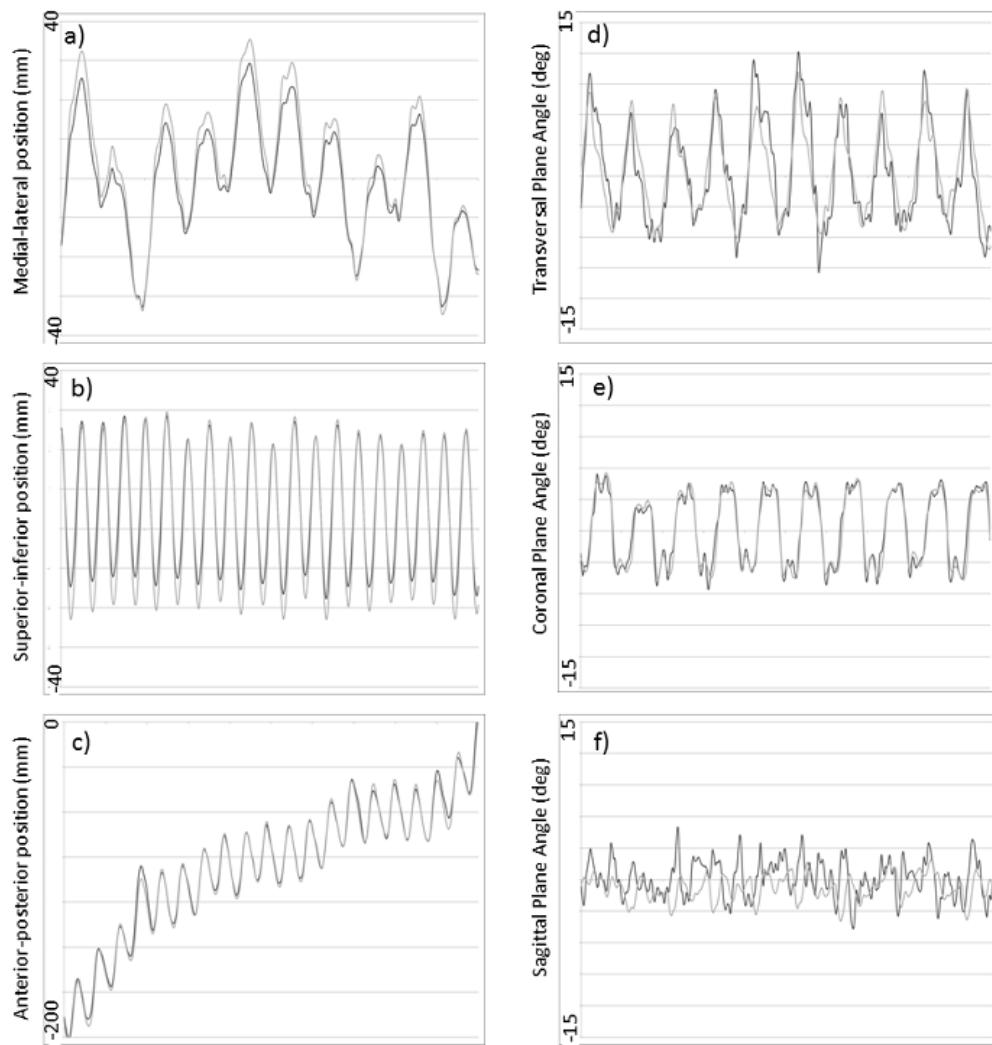
Caption: Figure 1. Time-series of data points taken over a 10second interval for self-selected walking in one of the participants. The single-camera system (black line) and the six-camera system (grey line). Positional data in the medial-lateral (a), superior-inferior (b) and anterior-posterior directions (c). Angular rotations are in the transversal (d), coronal (e) and sagittal (f) planes.

Conclusion: The single-camera system offers a safe, rapid, easy-to-use and portable kinematic system as the data it produces compares well with the criterion data for five of the six degrees of freedom tested. This study has shown the single-camera system offers a pragmatic method for kinematic data capture that is suitable for large-scale data collection on the pelvis and risk-factor modelling. However, the system needs to be tested in a much wider populations, which may include clinical or obese populations, for whom small abnormal movements and skin movements may be much more problematic (Schache et al., 2002b).

References: [1]   Bickham et al., J. Sport Rehab, 9: 219–228, 2000.

[2]   Dutta, App Ergo, 43: 645-649, 2012.

[3]   Herrington, Man therapy, 16: 646-648, 2011.

[4]   Hopkins, Sports med, 30: 1-15, 2000.

[5]   Laird et al., BMC musculoskeletal disorders, 15: 229, 2014.

[6]   Liebenson, J bodywork movement therapies, 8: 43-45, 2004.

[7]   Sahrmann, Diagnosis and treatment of movement impairment syndromes, Elsevier Health Sciences, 2012.

[8]   Saunders et al., Clini Biomechs, 20: 784-793, 2005.

[9]   Schache et al., Brit j sports med, 34: 279-283, 2000.

[10] Schache et al., Human Movement Sci, 21: 273-293, 2002a.

[11] Schache et al., Gait posture, 15: 136-145, 2002b.

[12] Van den Herrewegen et al., J biomechs, 47: 2531-2539, 2014.

Disclosure of Interest: None Declared

Sport

PO-0363

A BIOMECHANICAL EVALUATION OF THREE NEEDLELESS GRASPING SUTURE TECHNIQUES FOR GRAFT FIXATION

Wei-Ren Su [1,*] Chih-Kai Hong [1] Chih-Hsun Chang [1] I-Ming Jou [1]

[1]Orthopaedic Surgery, National Cheng Kung University Hospital, Tainan, Taiwan, Republic of China

Introduction and Objectives: The purpose of this study was to evaluate the tendon graft holding strength of needleless grasping suture techniques, namely the modified Prusik knot, Wittstein suture loop and modified rolling hitch.

Methods: 30 fresh-frozen porcine flexor profundus tendons were used and randomly divided into 3 groups of 10 specimens. The experimental procedure was designed to assess elongation of the suture-tendon construct across three different needleless tendon-grasping techniques (Figure). All suture configurations were completed with a No. 2 FiberWire suture (Arthrex). Each tendon was pre-tensioned to 100 N for three cycles, cyclically loaded to 200 N for 200 cycles, and then finally loaded to failure. Elongation, load to failure and mode of failure for each suture-tendon construct were measured.

Results: During the pre-tension phase, the modified rolling hitch had the smallest suture-tendon construct elongation ($P<0.001$) ($16.9 \pm 5.8\%$) compared with the modified Prusik knot ($31.2 \pm 6.9\%$) and Wittstein suture loop ($25.5 \pm 8.1\%$). During cyclic loading, there were no significant differences in elongation for any of the tested suture-tendon constructs (modified rolling hitch ($21.2 \pm 9.6\%$), modified Prusik knot ($21.4 \pm 9.9\%$), and Wittstein suture loop ($26.2 \pm 4.5\%$)). Similarly, the failure load and cross-sectional area were not significantly different across all tested suture groups (Table).

Figure:
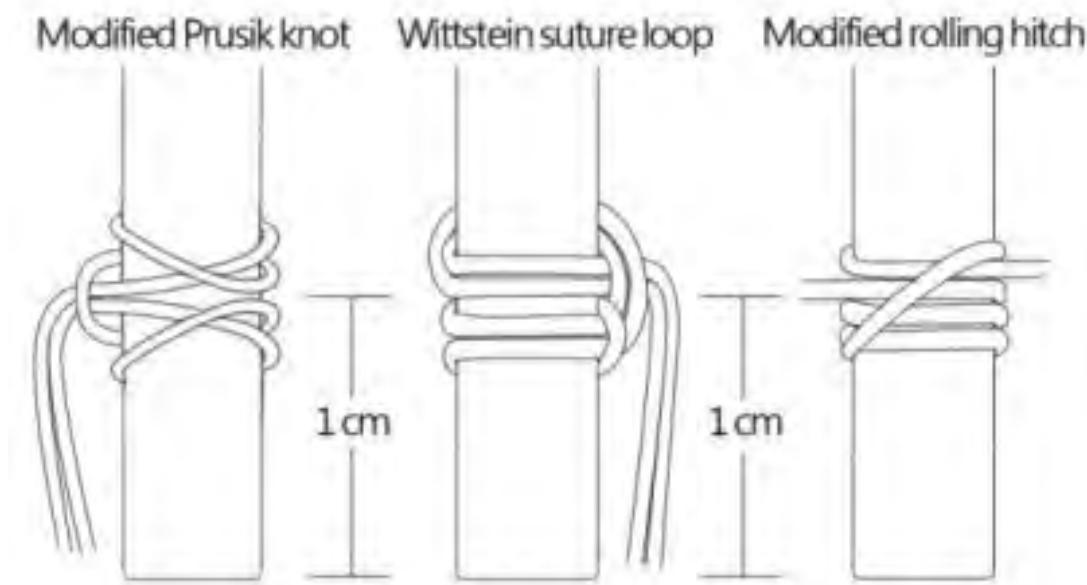
Conclusion: The modified rolling hitch technique provided lesser elongation after pretensioning and equal elongation after cyclic loading as well as loading to failure when compared with the modified Prusik knot and Wittstein suture loop techniques tested in this in vitro biomechanical evaluation.

Table:

	Modified Prusik Knot	Wittstein Suture Loop	Modified Rolling Hitch	p-value
Elongation after pre-tensioned, mm (%)	16.1 ± 3.1 (31.2 ± 6.9)[b]	14.2 ± 4.6 (25.5 ± 8.1)[c]	9.8 ± 3.7 (16.9 ± 5.8)[b,c]	<0.001[a]
Elongation after cyclic loading, mm (%)	11.1 ± 4.9 (21.4 ± 9.9)	14.5 ± 2.3 (26.2 ± 4.5)	12.2 ± 5.5 (21.2 ± 9.6)	0.275
Load to failure, N	348 ± 19	356 ± 15	341 ± 14	0.107
Cross sectional area, mm^2	42.4±4.8	43.3±6.1	41.3±3.9	0.235
Failure mode	Suture breakage at the knot	Suture breakage at the knot	Suture breakage at the knot	
[a] Significant difference among the groups with one-way ANOVA test: $P < 0.05$. [b,c] Significant difference between the groups with Bonferroni post hoc test: $P < 0.05$				

Disclosure of Interest: None Declared

Sport

PO-0364

THE PLANTAR PRESSURE CHARACTERISTICS OF RIGHT-FORWARD LUNGE STEP OF PROFESSIONAL-LEVELLED AND AMATEUR-LEVELLED BADMINTON PLAYERS

Lin Yu [1,*]Qichang Mei [1]Julien Baker [2]Ukadike Ugbolue [2]

[1]Faculty of Sports Science, Ningbo University, Ningbo, China, [2]School of Science and Sport, University of the West of Scotland, Hamilton, Lanarkshire, Scotland, United Kingdom

Introduction and Objectives: Badminton has gained large amount of participants with its effect of participants' whole body physical capacity exercising (Jérgensen et al., 1987). Lunge as one of the most basic and important footworks in badminton movement has been studied (Fu et al, 2009). The study was aimed to investigate the plantar pressure characters of both professional-levelled and amateur-levelled badminton players. Comparative analysis were made to illustrate the different loading features while performing the right-forward lunge step between badminton players of two levels.

Methods: A total of twelve badminton players, with six professional-levelled and six amateur-levelled badminton players, participated into the test. The Novel pedar-X plantar pressure measuring system was taken to collect the force and pressure on the plantar insole. And the insole was divided into eight anatomical parts, with medial heel (MH), lateral heel (LH), medial midfoot (MM), lateral midfoot (LM), medial forefoot (MF), lateral forefoot (LF), big toe (BT) and other toes (OT). Peak pressure and force time integral were utilized to show the different plantar pressure characteristics of two group badminton players while performing the right forward lunging step.

Results: The peak pressure and force time integral were analysed in the eight anatomical parts. As the result turns out and figure (* indicates the significance level below 0.01) shows, the peak pressure in the medial forefoot (MF) and lateral forefoot (LF) show great significance (with p<0.01) between professional-levelled and amateur-levelled badminton players. The peak pressure in the medial forefoot (MF) of professional-levelled players are obviously higher than that of amateur-levelled players. And the peak pressure in the lateral forefoot (LF) of professional-levelled players are significantly smaller than that of amateur-levelled players.

Figure:
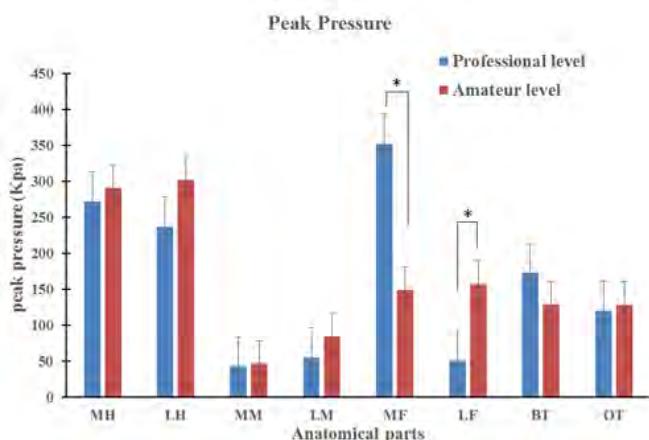
Conclusion: The peak pressure difference in the forefoot were linked with badminton players' performance in the court. While finishing the lunging step, the next movement is the preparing action for a defence or strike depending on the competition situations. The higher peak pressure in the medial forefoot part reflected the accurate and fast pushing-back movement of badminton players.

References: [1] Jérgensen, U., & Winge, S. International Journal of Sports Medicine, 8:379–382, 1987.
[2] Fu et al., Footwear Science, 1(S1):113-115, 2009.

Disclosure of Interest: None Declared

UPPER EXTREMITY KINEMATICS & KINETICS IN YOUTH BASEBALL CATCHERS AND PITCHERS

Gretchen D. Oliver [1,*]Wendi Weimar [1]Hillary Plummer [1]

[1]School of Kinesiology, Auburn University, Auburn, United States

Introduction and Objectives: Biomechanical analysis of youth throwing continues to evolve and has taken on a new resurgence. Up to this point, a majority of research on youth throwing has focused on baseball pitchers. However, another player throws the ball nearly as much as the pitcher but has gone mostly overlooked. The catcher throws the ball back the pitcher after every non-hit pitch, down to second, and even has plays at first. Furthermore, they make all of these throws after rising from a squatting position. Therefore it was the purpose of this study to quantify upper extremity mechanics of youth baseball catchers and pitchers. It was hypothesized that due to the catcher's squat position, and timing demands, that the overhead throwing motion of catchers would be different from the throwing motion of the pitchers.

Methods: A total of 78 youth baseball catchers (N= 25; 10.7 ± 1.9 yrs; 149.4 ± 12.3 cm; 44.5 ± 9.7 kg) and pitchers (N= 53; 11.1 ± 1.2 yrs; 152.6 ± 9.8 cm; 46.6 ± 10.2 kg) volunteered. All participants were tested during the fall baseball season and had not thrown for two days prior to testing. The MotionMonitor™ (Innovative Sports Training, Chicago IL) synched with an electromagnetic tracking system (Flock of Birds Ascension Technologies Inc., Burlington, VT) was used to collect data. Sensors were attached to the following locations: [1] the posterior/medial aspect of the torso at C7, [2] posterior/medial aspect of the pelvis at S1, [3-4] bilateral distal/posterior aspect of the upper arm, [5] the flat, broad portion of the acromion of the scapula, [6-7] bilateral distal/posterior aspect of the forearm, [8-9] bilateral distal/posterior aspect of the lower leg, and [10-11] bilateral distal/posterior aspect of the upper leg. Participants were given an unlimited time to perform their own pre-competition warm-up. Then the catchers were instructed to catch a pitched ball and throw maximum effort to a position player at second base (84.85 feet; 25.86 meters) as they would if trying to throw out a runner stealing. Pitchers were instructed to throw maximal effort fastball for a strike over a regulation distance (46 feet; 14.02 meters) to a catcher. Kinematic & kinetic data were analyzed at the events of foot contact (FC), maximal shoulder external rotation (MER), ball release (BR), and maximum shoulder internal rotation (MIR). The fastest throw for each participant was chosen for analysis.

Results: A one-way ANOVA revealed significant differences ($p \leq 0.05$) between upper extremity kinematics and kinetics in youth baseball catchers and pitchers. At FC, the catchers had significantly greater shoulder distraction forces. At the events of BR and MIR the pitchers displayed significantly greater shoulder elevation (see Table 1).

Conclusion: It was hypothesized that catchers and pitchers would utilize different throwing mechanics, due to the different demands of the specific throws. For example, pitchers have a target and a motion that is below the starting position of the throw, while catchers have a target and motion that is above the starting position. Further, pitchers are able to control the time to release, while catchers have the constraint of the base runner. It is clear that pitchers and catchers do use different kinematics and kinetics to achieve the respective throwing motions. Further analysis is needed to determine whether it the timing demand or the elevation demands that bring about these results.

Table:

	FC				
	S_PlaneEl	S_Elev	S_Rotation	E_Valgus	S_Dist*
Catchers	18 + 3.2	87.8 + 2.5	33.8 + 4.4	2.5 + 0.6	-1.5 + 0.8
Pitchers	20.3 + 3.6	86.7 + 1.9	35.5 + 3.1	3.0 + 0.5	2.0 + 0.7
	MER				
	S_PlaneEl	S_Elev	S_Rotation	E_Valgus	S_Dist
Catchers	17.9 + 2.8	73.0 + 9.4	73.8 + 10.2	10.5 + 1.8	2.2 + 1.2
Pitchers	19.4 + 2.2	76.5 + 5.9	86.5 +2.2	8.8 + 1.4	1.8 + 1.2
	BR				
	S_PlaneEl	S_Elev*	S_Rotation	E_Valgus	S_Dist
Catchers	16.6 + 3.0	64.5 + 8.6	54.5 + 6.0	5.8 + 2.1	9.3 + 3.3
Pitchers	9.4 + 3.1	80.3 + 1.5	53.5 + 2.2	3.5 + 1.7	5.8 + 1.5
	MIR				
	S_PlaneEl	S_Elev*	S_Rotation	E_Valgus	S_Dist
Catchers	31.0 + 3.2	64.1 + 8.6	17.9 + 4.0	12.8 + 2.1	21.3 + 1.8
Pitchers	32.8 + 2.6	84.2 + 1.4	13.0 + 2.5	10.1 + 1.7	20.2 + 1.6
means and standard error presented					
* = significance at p< 0.05					

Disclosure of Interest: None Declared

Sport

PO-0366

A BIOMECHANICAL CASE STUDY ON THE TAKEOFF MOTION OF A JAPANESE WOMAN JUNIOR LONG JUMPER - POSSIBILITY OF THE EFFECT MUSCLE STRENGTH TRAINING ON THE JUMPER'S TAKEOFF MOTION -

Ikko Omura [1,*] Hiroyuki Koyama [2] Akira Iiboshi [3] Michiyoshi Ae [4]

[1]Kagoshima Women's College, Kagoshima, [2] Kyoto Univ. of education, Kyoto, [3]Kagoshima Univ., Kagoshima, [4]Tsukuba Univ., Ibaraki, Japan

Introduction and Objectives: We studied the takeoff motion of the long jump for the various level athletes from views point of kinematic data and the standard motion obtained by averaging the motion of the elite athletes. As for the Japanese junior women long jumpers, their motion of the upper body (trunk) during the takeoff phase was remarkably different from that of Japanese men junior long jumpers (Omura.2012). Although the Japanese junior women long jumpers leans the trunk backward during the takeoff phase, the Japanese Junior men jumpers leans the trunk forward during the takeoff phase. Such trunk motions observed in the Japanese junior women jumpers might be due to poor muscle strength of the trunk, resulted in a lower horizontal velocity at the touchdown and release of the takeoff phase. Therefore, focusing muscle training on the trunk of the women junior jumpers might be effective to improve the trunk motion and horizontal velocity during takeoff phase. The purpose of this study was to investigate the effect of the trunk muscle strength training on the takeoff motion of a Japanese junior woman long jumper.

Methods: The subject was a Japanese woman junior long jumper with her personal best record of 6.16m and the second place at the final of 2014 Japan High School T & F Championship. To investigate the effect of the trunk muscle strength training on the long jump takeoff motions, two competitions were filmed. The 1st competition held at September in 2013 and the best trial was 5.76m (Trial-5.76m). After that, we suggested to her coach to introduce the muscle training emphasized on the upper body muscles. Then, she executed upper body muscle training such as six types of abdominal and back muscles, Bench press and Chin up six times per week for seven months. The 2nd competition held at May in 2014 and best trail was 6.16m (Trial-6.16m). In both competitions, the digital video camera was placed at perpendicular to the takeoff board, and filmed the takeoff motion of the jumper with 60f/s. Best trial of each competition was analyzed using FRAME DIAS system (DKH Co., Japan).

Results: The total number of Sit up within 30 seconds increased 13 reps. Bench press and Chin up improved to 25kg and 5 reps, respectively. Percent FAT of the body at Trail-6.16m was 2.2% lower than that of Trial-5.76m. These results suggested the effect of muscle strength training.

The horizontal velocity at the touchdown and the release of the takeoff for the Trial-6.16m was greater than that of Trial-5.76m (touchdown velocity were 9.15m/s vs 8.56m/s, release velocity were 7.45m/s vs 7.30m/s). And also, the vertical velocity at the release of the takeoff for the Trial-6.16m was greater than that of Trial-5.76 (2.83m/s vs 2.68m/s). Furthermore, the takeoff angle of the Trial-6.16m tended to be greater than those of the Trial-5.76m (20.8 deg. vs 20.1 deg.). According to these results, Trial-6.16m, personal best record, might be due to the greater values of the horizontal velocity at the touchdown of the takeoff, the vertical velocity at the release of the takeoff, and the takeoff angle.

Interesting changes observed in the trunk segment during the takeoff phase between Trial-5.76m and Trial-6.16m. Trunk segment angle at the touchdown of the takeoff foot for Trial-5.76m showed large negative value (i.e. the trunk leans backward) compared to Trial-6.16m. If the jumper keeps lean the trunk backward at the takeoff, the horizontal velocity will decrease remarkably due to huge mass of trunk. Therefore, smaller horizontal velocity at the touchdown of takeoff for Trial-5.76m might be caused by the large negative trunk angle. The trunk segment angle during the takeoff phase for Trial-6.16m showed positive value (i.e. the trunk leans forward) at the middle of the takeoff phase, resulting in greater release velocity. The maximum knee joint angle of the supporting leg for the Trial-6.16m during the takeoff phase showed small value (i.e. more knee joint flexion) compare to the Trial-5.76m. In this study, the subject did not execute special long jump practice emphasized on upper body during the takeoff phase except for upper body muscle strength training during seven months training session. Seven months muscle training improved the muscle strength of the upper body, and the subject gave us following comment: "I feel that my upper body becomes stronger than before by the strength training. So, I could maintain the approach velocity during the takeoff and do the takeoff motion more powerfully".

Conclusion: Based on this study, to strengthen the upper body for the junior woman jumper with weak muscle strength might be more effective way to improve the takeoff motion and enhance the athletic performance.

References: [1] Omura, et al. *Kyushu J. Phys. Educ. Sport.*27.40.2012.

[2] Omura, et al. 62th *Kyushu Society of Physical Education and Sport.*57.2013.

Disclosure of Interest: None Declared

Sport

PO-0367

RUGBY SCRUMMING SUCCESS IS RELATED TO THE SCRUMMING KINETICS BUT NOT TO THE ANTHROPOMETRY OF THE PLAYERS IN A SCRUM

Sam Kerr [1,*]Andrew Green [1]Chloe Dafkin [1]Warrick McKinon [1]

[1]School of Physiology, University of the Witwatersrand, Johannesburg, South Africa

Introduction and Objectives: The rugby scrum is an integral part of the game of rugby used to restart the game after a minor transgression. The scrum contest consists of the forward packs from opposing teams involved in a physical push for the ball. The effectiveness of different scrumming techniques and the physical and anthropometric characteristics of individual rugby players have previously been studied to optimize successful scrummaging. However, the specific factors that contribute to scrumming success are currently uncertain. Therefore, the aim of this study was to determine predictors of a winning scrum by testing whether anthropometric variables, pushing force and direction, subjective ratings of fatigue and effort, prior injury and experience are related to scrumming success.

Methods: Sixteen amateur male rugby players (age: 19-48 years) competed in ten successive scrums; each with a different permutation of player positions. The cumulative properties for different scrums with the following recorded variables were compared between winning and losing scrums: scrum force and direction (recorded for each player individually using a customised scrumming machine equipped with four load cells so that the kinetics of pushing [pushing force magnitude and centre of pressure] could be calculated); anthropometric measures (height, mass, body mass index (BMI), muscle mass and fat mass); injuries and playing experience (obtained from questionnaire data) and subjective ratings of exertion and fatigue (measured using the Borg scale and Visual Analogue Scale respectively).

Results: Winning scrums consisted of players that produced a significantly greater force (2061.05 ± 110.13kg vs. 1890.88 ± 110.13kg, $P < 0.05$) than the losing scrums. Winning scrums were also directed in a more upward and lateral direction, than losing scrums. There were also significantly more concussions in the winning scrum compared to the losing scrum (3.40 ± 0.84 vs 1.60 ± 0.84, $P < 0.05$). In contrast, body mass, body fat and body muscle percentage, BMI, playing experience, subjective ratings of effort and fatigue as well as current injuries did not significantly contribute to winning scrums ($P > 0.05$).

Conclusion: Scrum success, was directly related to a forward packs' larger cumulative scrumming force (both as a total force and relative to the scrum mass) as well as scrumming force directed to the right, in an upwards direction, and a greater number of total concussions. In contrast, body mass and playing experience, which previous studies have attributed to scrum success, were not proven in this study. The current study has important relevance for rugby players, as it highlights factors players may want to focus on, giving one player an advantage over another in team selection and scrum success. For greater scrumming success coaches should focus on force production optimization in players involved in the scrum.

Disclosure of Interest: None Declared

Sport

PO-0368

FUNCTION OF THE ADDUCTOR MUSCLES DURING MAXIMAL VELOCITY SPRINTING

Yuji Ohshima [1,*] Norihisa Fujii [2]

[1]Doctoral Program in Physical Education, Health and Sports Sciences, [2]Faculty of Health and Sport Sciences, University of Tsukuba, Ibaraki, Japan

Introduction and Objectives: The hip joint torque around flexion-extension axis has an important role on sprint running ability (Dorn et al, 2012). In addition, Sugisaki et al. (2012) indicated the larger adductor muscles were advantageous for achieving higher sprint performance because those muscles act as a hip flexor at extended position. On the other hand, Ohshima et al. (2014) indicated that during the terminal support phase, the hip adductor torque drove forward the hip joint of support leg. But, it is not clear that how much the adductor muscles produce the hip flexion torque and the hip adduction torque.

Therefore, our objectives were (1) to quantify that how much the adductor muscles produce the hip flexion torque and the hip adduction torque during the terminal support phase by estimating muscle force, and (2) to clarify the function of the adductor muscle during the terminal support phase.

Methods: Eight male sprinters volunteered for the present study. The participants ran 60m with the maximal effort from a standing start position. Ground reaction forces (GRFs) of the right support phase was obtained with a force platform (Kistler, Wintherthur, Swiss), operating at 1000Hz, which was placed at the 50m mark from the start. At the same time, 3D coordinates of 47 reflective markers on a body were recorded with a motion analysis system (Vicon, Oxford UK.) using 20 cameras (MX-T20), operating at 250Hz. Coordinates of the markers were smoothed using a fourth-order Butterworth low-pass-digital-filter at cutoff frequencies based on the residual method of Wells and Winter (1980). The cutoff frequencies ranged from 7.5Hz to 15.0Hz.

In order to estimate muscle forces about support leg, the musculoskeletal model of support leg comprised 43 Hill-type muscles was developed by using OpenSim (Delp et al., 2007). The problem regarding distribution of the total torque between muscles was resolved by using optimization. The objective function (J) was to minimize activation cubed, summed across all joints. The constraint condition was to match the net joint torques of all muscles with those estimated by an inverse dynamics approach. The time series data of support phase were normalized to the time of a step as 100%.

Results: Running velocity at the 50m mark was 9.24 ± 0.33 m/s. As shown in Figure 1, sprinters exerted the hip flexion torque and adduction torque during the terminal support phase (80-100%). The hip flexion torque was generated mostly by iliopsoas, but hardly by adductor muscles. And the hip adduction torque was generated by iliopsoas and adductor muscles. From these results, it is obvious that the adductor muscles do not act as the hip flexor. The causes we speculated were as follows. First, the adductor muscles' moment arm about the hip flexion torque is very short during the terminal support phase. Second, if the adductor muscles exerted the larger muscle force to enhance the contribution of hip flexion torque, the constraint condition to estimate muscle forces would not be satisfied because the hip adduction torque by the adductor muscles would be large. Furthermore, the objective function would not be minimum value because

the abductor muscle group would exert the larger muscle force to match the hip adduction torque by forces of all muscles with that estimated by an inverse dynamics approach.

Therefore, during the terminal support phase, it is possible that the hip adductor muscles do not act as the hip flexor, but have the function that drives forward the hip joint of support side.

Figure:
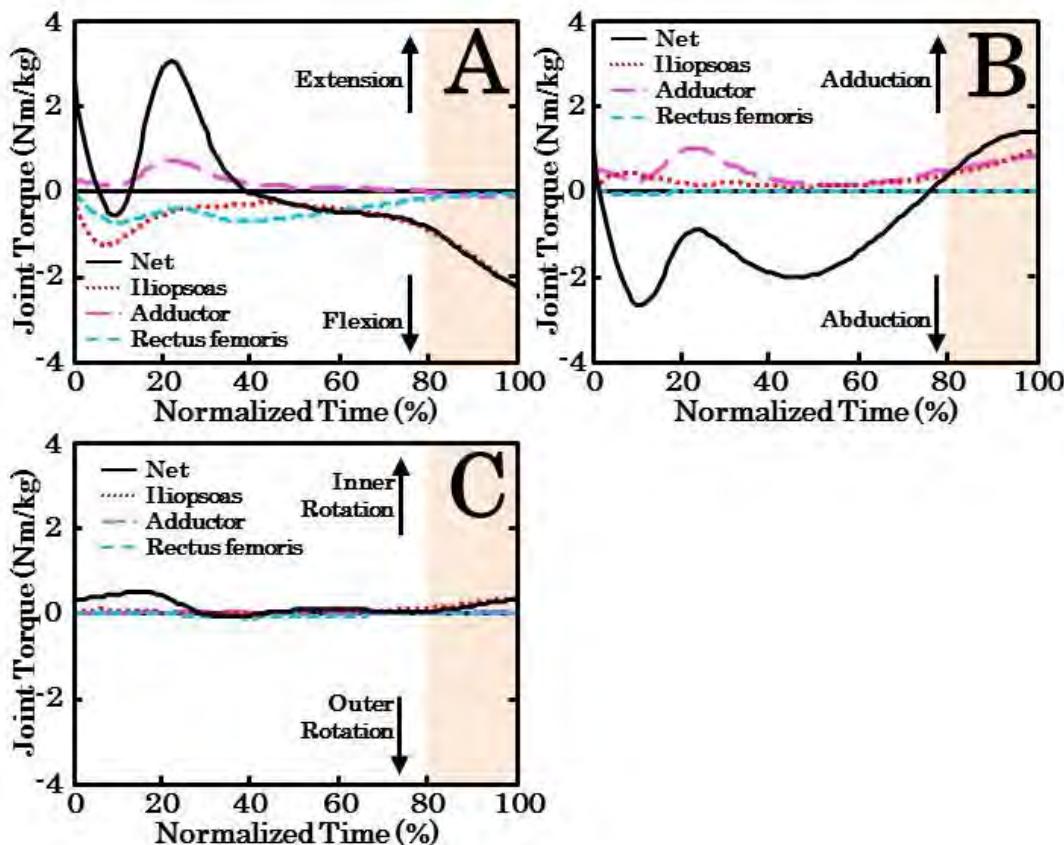
Caption: Averaged pattern of hip joint torque during support phase. A: Flexion-Extension, B: Adduction-Abduction, C: Inner-Outer Rotation

Conclusion: The important results of this study are as follows: (1) the hip flexion torque was generated mostly by iliopsoas, and the adductor muscles did not act as the hip flexor. (2) The hip adduction torque was generated by iliopsoas and adductor muscles. (3) The function of adductor muscles was to drive forward the hip joint of support side.

References: [1] Dorn et al., J. Experimental Biology, 215: 1944-1956, 2012.

[2] Sugisaki et al., Int. J. Sports and Health Sci. 9: 1-7, 2011.

[3] Ohshima and Fujii, Proceedings of ISBS, 2014.

[4] Delp et al., IEEE Trans. Biomed. Eng. 54(11): 1940-1950 2007.

Disclosure of Interest: None Declared

THE BENEFITS OF TAI-CHI EXERCISE ON BALANCE CONTROL DURING STAIR-TO-FLOOR TRANSITION

Chenfu Huang [1,*]Tzu-Hsiang Yang [1]

[1]Physical Education, National Taiwan Normal University, TPE - Taipei, Taiwan, Republic of China

Introduction and Objectives: Downstairs walking was in turns consisted of forward walking and downward descending. The transition strides were constituted two discrete walking patterns, and as such were inherently variable and unstable. Increased falls were occurred during the transition strides before and after stair walking [1]. Injuries related to falls included muscle strains, fractures and even more serious complications.

Center of pressure (CoP) has been defined as the neuromuscular response to shifts in the body's center of mass (CoM), and evaluation the CoP trajectory and CoM-CoP separation during stair negotiation have been used as indicators of dynamic stability on stairs among the elderly [2]. Due to the decline of physiological function, the safety precautions were utilized in older adults, such as lesser A-P and M-L CoP displacement, lower average CoP velocity compared with young adults [2]. Tai-Chi (TC) exercise has been found to improve the abilities of functional movement in daily life in elderly. The purpose of this study was to investigate differences in CoP characteristics during stair-to-floor transition between TC and normal elders.

Methods: The CoP data of 12 Tai-Chi elderly practitioners (Tai-Chi training experience: 10.2±3.3 years; age: 73.0±6.0 years; height: 1.67±0.06 m; weight: 58.5±6.0 kg) and 14 matched control elders (age: 65.6±2.1 years; height: 1.64±0.07 m; weight: 65.6±2.1 kg) were obtained by a Kistler force plate (1000Hz), with negotiating stair descent transiting to level walking at self-selected speed. Participants were aksed to place oly one foot on each step (foot-over-foot). The average CoP velocity was defined as total CoP displacement dividing by stance duration. The peak A-P and M-L CoP displacement were also analysed. Differences in variables between two groups were assessed using t-test (α=.05).

Results: Results revealed as table 1, TC group had wider M-L CoP displacement and faster average CoP velocity. TC group descended at faster speed and had larger stride length. There were no differences in A-P CoP displacement and stance duration.

The backward displacement of the CoP during stair descent generates the forward momentum necessary to initial gait [3]. In previous studies, increased A-P CoP displacements were observed during level walking, stepping over an obstacle and stair descent after TC training. In the study, there were similar in A-P CoP displacement between two groups. However, the benefits of TC exercise reflected on faster descending speed and larger stride length, instead of the possible greater A-P displacement.

In frontal plane, TC group showed greater M-L displacement during stair-to-floor transition. The greater M-L displacement is likely the results of improved coordinated action of the hip abductor and adductor muscles after TC training [3]. It is important for the maintenance of lateral stability in elderly subjects.

The CoP velocity provides valuable important information about how individuals modulate gait when negotiating various stairs [3]. TC groups showed faster CoP velocity, may reflect enhancement in the maintenance of dynamic balance. The

current study was a cross-sectional study, differed from previous longitudinal studies. The benefits of long-term TC exercise (over 7 years) might be slightly different.

Conclusion: TC exercise influenced generation of forward momentum via greater stride length instead of A-P displacement, and improved the maintenance of balance via greater M-L displacement and CoP velocity.

Table:

	TaiChi (n=12)	Normal (n=14)	*P*
A-P displacement (cm)	10.79 ± 2.03	10.44 ± 3.82	
M-L displacement (cm)*	8.16 ± 1.31	4.22 ± 1.68	0.00
CoP velocity (cm/s)*	51.9 ± 18.0	35.1 ± 9.6	0.01
Duration (ms)	663 ± 77	678 ± 103	
Stride length (m)*	0.50 ± 0.06	0.34 ± 0.06	0.00
Descending velocity (m/s)*	0.68 ± 0.08	0.62 ± 0.07	0.02
Male / female	9 / 3	8 / 6	

Caption: CoP parameters during stair-to-floor transition between two groups

References: [1] Sheehan & Gottschall (2011). J. Electromyogr. Kinesiol.,21, 533-541.

[2] Kim (2009). J. Phys. Ther. Sci., 21, 129–134.

[3] Kim, et al. (2009). Ther. Sci., 21, 317–323.

[4] Reid, et al. (2011). Gait & Posture, 34, 529–532.

Disclosure of Interest: None Declared

Sport

PO-0370

BIOMECHANICAL AND PHYSIOLOGICAL PREDICTORS OF FALLS IN HORSE RIDERS

Sam Kerr [1,*]Andrew Green [1]Chloe Dafkin [1]Yoshin Barnabas [1]Warrick McKinon [1]

[1]School of Physiology, University of the Witwatersrand, Johannesburg, South Africa

Introduction and Objectives: In horse riding, the rider's seat and posture play an important role in the communication with the horse and balance of the horse and rider. The incorrect seat, whilst being uncomfortable for both the horse and rider, also disrupts effective control over the horse and puts both the horse and rider at risk of injury. Falling from the horse is the most common cause of injury in equestrian sports. Literature suggests that improving elements of posture, balance, flexibility and synchronized movement between the horse and rider enhances rider skills thus should subsequently reduce the risk of falls and injury. Therefore, the aim of this study was to determine whether the incidence and frequency of equestrian sports related falls could be predicted by various biomechanical, anthropometrical and physiological attributes of the riders.

Methods: Thirteen experienced horse riders each rode the same horse at the trot and the canter. Retro-reflective markers were attached to anatomical landmarks of the horse and rider and tracked using a 6 camera kinematic system at 250 frames/second. The kinematically calculated variables included head straightness and back straightness. Horse-rider movement phase delay (an objective measure of horse-rider synchrony) was also determined for each horse and rider for each gait. Incidence of falls and their causes were retrospectively documented for the previous 12 months. Anthropometric and physiological measurements of the riders included: height, weight, balance (the standing stork test), flexibility (sit and reach test), grip strength (hand held dynamometer), lower leg power (vertical jump test) and reaction time. Correlations were run to determine relationships between the variables and number of falls/ incident rate ratios (IRRs) for falls per ride respectively. A stepwise multiple regression model was generated for the most predictive variables of falls.

Results: Age ($r=-0.60$, $p=0.03$), balance ($r=-0.64$, $p=0.02$), flexibility ($r=0.59$, $p=0.04$) and back straightness whilst cantering ($r=0.61$, $p=0.03$) were significantly correlated to the number of falls. Body mass ($r=0.55$, $p=0.04$) and phase delay for trot ($r=-0.80$, $p<0.01$) were significantly related to IRRs for falls per ride. Grip strength, lower leg power and reaction time were not related to the number of falls or IRRs. Back straightness ($r=0.59$) and BMI ($r=0.58$) were positively related to horse shying behaviour ($p<0.05$). Back straightness was also significantly correlated to horse refusal at a jump ($r=0.60$, $p=0.03$). A greater phase delay was found to be the most predictive variable of falls ($\beta=0.541$, $p<0.001$).

Conclusion: Various physiological attributes and biomechanical variables of the rider were able to predict equestrian sports related falls. This study demonstrated the importance of improved balance and flexibility as well as optimizing the synchrony of movement between horse and rider while maintaining the correct upright seat (back straightness) to minimize the risk of falls.

Disclosure of Interest: None Declared

Sport

PO-0371

RELIABILITY OF DOLYO CHAGUI KICK IN TAEKWONDO DESCRIBED BY HIP AND KNEE JOINT ANGLES

Afonsa J. Silva [1,*]Ricardo ML Barros [1]Jerusa PR Lara [1]

[1]Faculty of Physical Education, University of Campinas, Campinas, Brazil

Introduction and Objectives: Taekwondo (TKD) is martial art which uses kicks and punches as offensive techniques in combat. Biomechanical analyses of kicks in TKD are usually described in the literature and commonly use kinematic variables such as hip and knee joint angles [2,4].

Therefore it is important to establish the reliability of the measurement procedure to know how strongly measurements of the same group resemble each other [3].

Thus the aim of this study was to evaluate the reliability of joint angles of kicking and supporting legs during the execution of Dolyo Chagui in Taekwondo.

Methods: Seventeen black belt male athletes of TKD with age 26 (7.5) years, height 1.77 (0.08) m, mass 76.3 (10.3) kg and 12 (5.6) years of experience, voluntarily participated in the study.

The DVideo kinematic analysis system was used to obtain the three dimensional coordinates of markers [1]. The system consisted of five Basler cameras (A602fc) working at 100 Hz. Sixteen anatomical markers were tracked, modeling the athlete's body with five segments: pelvis, thighs and shanks (right and left). The hip joint was represented with three degree of freedom and the knee joint with only one (flexion/extension). An extra marker was located at the sparring doll head.

The athlete performed three repetitions with the preferred limb. As a target was used a sparring doll positioned in front of the athlete. The kick movement was analyzed in three conditions: Start, Execution Phase and Contact. An algorithm based on the analysis of the anterior-posterior velocity of the lateral malleolus was designed to objectively determine those conditions. The Start Condition was assumed to be the moment previously to the first detectable malleolus movement towards the target. The Contact was defined at the moment of the first detectable movement of the doll's head marker. The Execution Phase was defined between the Start and the Contact. The minimum and maximum values of each variable during the execution phase were analyzed in terms of reliability.

Sixteen variables were tested. Hip three joint angles and angular velocities; knee flex-extension angles and the corresponding angular velocities, these in supporting and kicking legs. In order to test the absolute agreement of variables between subjects and observations the intraclass correlation coefficient (ICC) was used. A two-way variance model was adopted, which assumed the random row and column variable as sources of variance. In this way the ICC case 2A1 was used, which is interpreted as the degree of absolute agreement among measurements [3]. ICC classification: Poor (ICC≤0.4); Satisfactory (0.4<ICC<0.75); Excellent concordance (ICC≥0.75)

Results: Table 1 presents the results obtained. The majority of knee and hip joint angles presented ICCs with excellent concordance with the exception of the knee angle at contact. The angular velocity rarely presented excellence concordance, ranging from poor to satisfactory.

To the best of our knowledge a study comparing the reliability of such variables in Taekwondo kicks was not yet published in the literature. The results pointed out to an excellent reliability of joint angles. The angular velocities analyses revealed not so good, but satisfactory results. The reasons for that can be due to increased intra-subject variability or also due to the possible error propagation related to the numerical procedures to obtain the derivate. In this study, the subjects were all well-trained black belt athletes that can explain the low variability in the execution detected by the ICC analysis. Future studies are necessary to establish the reliability of kinematic variables among different age or level groups.

Conclusion: The reliability of Dolyo Chagui in Taekwondo in well-trained athletes was excellent with relatively worst reliability to the variables related to angular velocities. The study suggests that kinematical analyses of aekwondo kicks can provide reliable results.

Table: Table 1 Intraclass correlation coefficients - ICC of hip and knee joint variables during the execution of Dolyo Chagui in Taekwondo.

COND	LEG	JOINT ANGLES				JOINT VELOCITIES			
		HIP			KNEE	HIP			KNEE
		Flex-Ext	Add-Abd	Int-Ext Rot	Flex-Ext	Flex-Ext	Add-Abd	Int-Ext Rot	Flex-Ext
Start	K	0.87	0.86	0.98	0.75	0.59	0.56	0.71	0.36
	S	0.90	0.91	0.99	0.78	0.34	0.43	0.57	0.27
EP-Max	K	0.95	0.92	0.97	0.86	0.49	0.45	0.40	0.66
	S	0.94	0.91	0.97	0.86	0.57	0.70	0.54	0.45
EP-Min	K	0.89	0.88	0.93	0.77	0.79	0.80	0.69	0.55
	S	0.92	0,89	0.94	0.87	0.64	0.74	0.71	0.63
Contact	K	0.95	0.85	0.98	0.20	0.75	0.58	0.40	0.33
	S	0.91	0.82	0.95	0.79	0.74	0.55	0.36	0.60

Caption: Legend: COND - Condition; EP-Max - Execution Phase-Maximum; EP-Min - Execution Phase-Minimum; S - Supporting Leg; K - Kicking Leg; Flex-Ext - Flexion/Extension; Add-Abd - Adduction/Abduction; Int-Ext Rot - Internal/External Rotation.

References: [1] FIGUEROA et al. Computer Methods and Programs in Biomedicine. 72: 155-65, 2003.

[2] KIM et al. Sports biomechanics. 9 (2): 98-114, 2010.

[3] McGROW et al. Psychological Methods. Vol. I, No. 1,30-46, 1996.

[4] SULLIVAN et al. J. of Sports Science and Medicine 8(CSSI III), 13-16. 2009.

Disclosure of Interest: None Declared

Sport

PO-0372

RELATIONSHIP BETWEEN GROUND REACTION FORCE AND LOWER LIMB MUSCLE PRE-ACTIVATION AFTER AN 8-WEEK BAREFOOT TRAINING PROGRAM

Nicholas Tam [1,*]Janie Astephen Wilson [2]Ross Tucker [1]

[1]Human Biology, UCT/MRC Research Unit for Exercise Science and Sports Medicine, University of Cape Town, Cape Town, South Africa, [2]School of Biomedical Engineering, Dalhousie University, Halifax, Canada

Introduction and Objectives: Previous research has suggested that muscle activation strategies and resultant kinematics prior to initial ground contact influence loading rate. This has been shown with neuromuscular modelling of muscle activity and lower limb segment velocity prior to ground contact to determine its influence on the loading of structures . This may be practically relevant as clinicians may be able to focus on modulation of certain muscle groups to affect treatment or prevention of injury.

As initial loading rate occurs early during stance, it may be of value to consider muscle activation immediately prior to ground contact. The modelled effect of muscle activation during the swing phase on the initial loading rate found that increased hip flexor activity throughout swing phase decreases initial loading rate and the impact peak by modulating mid-swing kinematics and reducing landing velocity.

The aim of this study was to describe the neuromuscular activity and examine the initial loading rate, before and after a systematic and progressive 8-week pure barefoot training programme. We hypothesised that posterior muscle groups including ankle plantarflexors would display increased muscle activity during the pre-activation in runners with lower loading rates. Further, we hypothesised that the muscles around the hip that both mobilise and stabilise this joint and the lower limb would be related to the initial loading rate. This would be the result of learned neuromuscular responses prior to landing that modulates the landing posture, joint moments and energy absorption of the lower limb prior to ground contact in response to the barefoot training programme.

Methods: Twenty-one runners completed an 8-week progressive barefoot running training programme. Before and after this intervention, ground reaction force and surface electromyography data were collected in the barefoot and shod condition. Pre-activation and stance phase activity of the gluteus medius (GM), ;biceps femoris (BF);rectus femoris (RF);peroneus longus (PL);tibialis anterior (TA) and gastrocnemius lateralis and medialis (LG and MG) were assessed, along with initial loading rate.

The raw EMG signal was processed using a 15–500 Hz band pass filter. The data were smoothed using route mean squared analysis, (50ms). The processed EMG from the fastest sprint was analysed. The sub-maximal EMG data from clamped speed trials were expressed as a percentage of the fastest sprint (%sprint max). Average EMG activity was calculated for pre-activation and stance phase, reported as a percentage of maximal sprint activity (%sprint max).

To explore the individual response to the progressive barefoot training programme, individuals were segmented in three groups according to a change >1 SD of the initial barefoot loading rate group mean. This produced the groups, namely non-responders (<20 BW·s-1 in loading rate pre- and post-training programme), positive responders (decreased >20 BW·s-1) and negative responders (increase >20 BW·s-1).

A 2-factor ANOVA was used to investigate differences between variables pre- and post-training programme factoring for footwear condition. Further analyses between different group responses for the variables were also assessed. A Tukey's post-hoc analysis was used when appropriate. Relationships between EMG and initial loading rate variables were further assessed with Pearson correlations. Differences were deemed statistically significant at p<0.05

Results: LG and MG pre-activation were greater in the barefoot condition before and after the training intervention. This difference was also seen in the LG during stance phase. GM activity during stance phase was increased post-training intervention in both footwear conditions. MG pre-activation was associated with lower initial loading rates before the training programme, while after GM, PL and TA pre-activation when barefoot were associated with initial loading rate after training. Runners who decreased loading rate after training displayed increased BF and GM activity and decreased RF activity when barefoot

Figure:
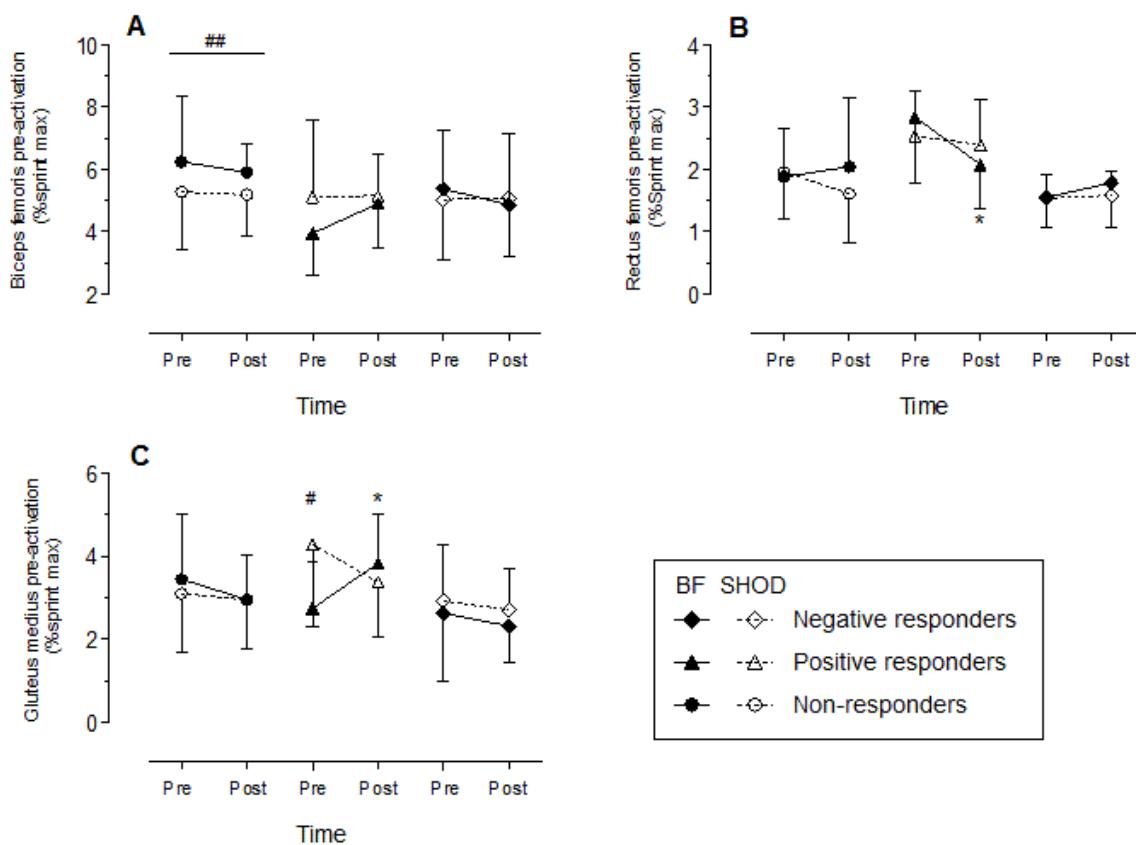
Caption: Changes in biceps femoris (A), rectus femoris (B) and gluteus medius (c) pre-activation in the responder groups

Conclusion: The inverse relationship between loading rate and posterior muscle group pre-activation and the positive relationship with TA activation suggests that a neuromuscular strategy, which presumably alters the stiffness and kinematics of the lower limb joints, contributes to ground reaction forces. Training-induced changes in GM activity, and the specific changes occurring in the positive responders who reduce loading rate, suggest that neuromuscular strategies can be acquired through training, though the extent and nature of these changes requires further investigation.

Table:

Mean(SD)	
n	21
Age (yrs)	29.0(5.9)
Body mass (kg)	71.2(10.8)
Height (m)	1.7(0.1)
BMI (kg·m-2)	24.6(1.2)
10-km personal best (min)	43.2(4.2)

Caption: Descriptive characteristics of participants

Disclosure of Interest: None Declared

Sport

PO-0374

KINEMATICS OF BACK MOVEMENT AND LOWER LIMB POWER ARE RELATED TO THE SCRUM FORCE OF INDIVIDUAL RUGBY TIGHT FORWARD PLAYERS

Andrew C. Green [1,*] Chloe Dafkin [1] Benita Olivier [2] Sam Kerr [1] Warrick McKinon [1]

[1]School of Physiology, [2]School of Therapeutic Sciences, University of the Witwatersrand, Johannesburg, South Africa

Introduction and Objectives: Scrummaging is an essential component of rugby and was a designed to be a simple contest to restart the game after a minor transgression had occurred. The scrum contest consists of the forward packs from opposing teams involved in a physical push for the ball. An effective scrum requires the coordinative power of the team with the contribution from individuals influencing the overall outcome of the scrum. However within the modern rugby game the scrum contest has become vital to the team's success, with a winning scrum changing the course of the game and even the outcome. Research regarding the scrum is primarily aimed at injury prevention with less focus on the performance of individual scrum technique. Therefore this study aimed to identify whether individualised measurements of body anthropometry, playing experience, scrumming kinematics (technique), or lower body explosive power would predict scrumming kinetics (scrumming force production). The identification of such predictor variable may assist could assist coaches when choosing teams, or focus an individual's training in the attempt to improve performance.

Methods: The scrumming forces of twenty-eight amateur rugby forward players (experience: 9.8 ± 6.6years; mass: 103.6 ± 14.0 kg) were assessed individually using a custom instrumented scrum machine equipped with four load cells. All scrum force kinetics were measured on an outdoor rugby field. All participants were injury free at the time of measuring and all players were rugby tight forwards (inner scrum players). Lower limb power was measured using a vertical jump height, being the difference of the outstretched arm while standing and the outstretched arm at maximal point during the jump. Vertical jump power was calculated as vertical jump height multiplied by body mass.

Kinematic data was collected on a sub-sample of 21 tight forward players (experience: 8.2 ± 4.2 years; mass: 103.0 ± 12.1 kg), using an 18 camera system recording at 100Hz. Subsequent analysis was done in MatLab using custom written scripts. Flexion of the back occurring at the hips and bilateral flexion of the knees and ankles were measured. The change in angle from starting point to the point of maximal force was used.

Results: The maximal individual scrum force (269.27 ± 48.35 kg) was correlated to total body mass (r=0.45, p=0.01). Subsequent analysis of the force was standardized as the percentage force per total body mass. The force percentage was significantly correlated to the lower limb power, as measured by the vertical jump height (r=0.40, p=0.03). Separating the tight forwards into front rows and locks there was a correlation for front row player between maximal force and vertical jump power (r=0.56, p=0.02). This relationship was not present in the group of isolated locks.

A significant correlation between the change in back angle (from starting position to maximal force position) and maximal force produced was present in the combined biomechanical sample (r=0.44, p=0.04). No significant predictors were present between the right knee, left knee, right ankle, left ankle and the development of the force in the combined group of tight forwards. The isolated lock group displayed a significant correlation between the change in left knee angle and maximal force produced (r=0.80, p=0.01).

Conclusion: The study suggests that individual forces produced during scrummaging are closely related to the lower body power as determined by the vertical jump height. However lower leg power might not be a suitable test to determine the scrumagging forces in locks. Furthermore the development of the power while scrummaging can be attributed to the change in back angle and not the changing in the limb angles. However, locks when isolated, displayed a relationship between the change in left knee angle and maximal force produced. The trend for increased force values when in a more vertical position could have implications for coaches and players, regarding the limits of the laws of rugby. Furthermore by improving the strength of the lower back, surrounding musculature and lower limb power may improve scrum force development.

Disclosure of Interest: None Declared

THREATS TO INTERNAL VALIDITY FROM STUDY DESIGNS THAT REPEATEDLY ASSESS DROP JUMP TASKS

Szu-Ting Chen [1] Yuan.Mei Sun [1] Mu.San Chang [2] I.Lin Wang [3] Li.I Wang [1,*]

[1]National Dong Hwa University, Department of Physical Education and Kinesiology, [2]Tzu Chi University, Center of Physical Education, [3]National Dong Hwa University, Department of Life Science and the Institute of Biotechnology, Hualien, Taiwan, Republic of China

Introduction and Objectives: Biomechanical research often employs drop jump tasks to investigate the effect of plyometric training [5,6]. The movement characteristic of drop jump is based on a stretch-shortening cycle (SSC). This movement produces elastic energy storage and reuse and stimulates the muscle spindles, thereby increasing muscle activity [4]. The common study design of experimental tests assessing drop jump tasks involves continuous and repeated movements [6]. However, Chen et al. (2013) indicated that the counter movement jump performance increased acutely after drop jump programs [3]. Therefore, it is uncertain whether the study design involving repeatedly testing drop jump tasks interferes with internal validity. The purpose of this study was to investigate the influence of repeatedly testing drop jump tasks.

Methods: Fifteen male college students (19.47±0.72 years, 1.73±0.04 m, and 64.67±4.89 kg) from the physical education department voluntarily participated in the study. Subjects had sustained no lower extremity injuries during the six months prior to the experiment. This study was approved by the Institutional Review Board.

Kinematic and ground reaction forces data were recorded using 8 infra-red Qualisys motion capture cameras (200 Hz) and 2 force platforms (AMTI, 60 cm×90 cm) (1000 Hz). The kinematic and kinetic data were recorded using MotionMonitor analysis software. According to the Helen Hayes marker set, 21 reflective balls required for data interception were used. The reactive strength index (RSI) was calculated using the formula: *RSI=jumping height/ground contact time* [2].

The subject repeated the drop jump task five times (T_1, T_2, T_3, T_4, T_5) from a 40 cm height platform. The rest time between tests was 1 minute.

The SPSS 14.0 statistical program was used for statistical analysis. The repeated-measures one-way ANOVA was used to assess the differences between tests. The significance level was set at α=0.05. The LSD test was used as a post hoc test.

Results: The results of this study are shown in Table 1. The jump height of T4 (P=0.048) and T5 (P=0.002) were significantly greater than T1. The jumping height of T5 was significantly greater than T2 (P=0.041). There were no significantly difference (P=0.126) in ground contact time. The RSI of T_2 (P=0.037) and T_5 (P=0.037) was significantly greater than T_1 (P=0.024).

Conclusion: Drop jump tasks are often used in exercise training research. The study design typically includes repeated testing to collect the data. However, the drop jump could acutely affect lower extremity muscle strength [3].

Jumping height [7], ground contact time [1,10], and RSI are often used to evaluate the experimental results [2]. In this study, the results indicate that the repetitive drop jump tests did not reduce the interference of the ground contact time. However, the threats to internal validity based on the study design that involves repetitive testing of drop jump tasks were

observed with regard to jump height and RSI. The jump height increased from T_4, and the RSI also increased at T_2 and T_5.

Table: Table 1 The Mean (SD) of jumping height, ground contact time, and RSI during DJ of 5 tests

	T_1	T_2	T_3	T_4	T_5	post hoc test
Normalized jumping height (BH)	0.166 (0.029)	0.173(0.033)	0.173(0.035)	0.175(0.034)	0.178(0.034)	4,5>1; 5>2
Ground contact time (sec)	0.261(0.063)	0.243(0.062)	0.255(0.073)	0.259(0.077)	0.253(0.067)	-
RSI (BH/sec)	0.655(0.136)	0.747(0.228)	0.709(0.172)	0.714(0.200)	0.738(0.210)	2,5>1

References: [1] Bobbert, M.F.,et al. *Med Sci Spors Exer*, *19*, 339-346.1987.

[2] Byrne, P.J., et al. *J Strength Cond Res*, *24*, 2050-2055.2010.

[3] Chen, Z. R., et al. *J Strength Cond Res, 27*, 154-158. 2013.

[4] Flanagan, E., et al. *J Strength Cond Res*, *30*, 32-38.2008.

[5] Komi, P. V. *Exerc Sport Sci Rev*,*12*, 81-121.1984.

[6] Markovic, G. *Brit J Sports Med ,41*, 349-355. 2007.

[7] Peng, H. T. *J Strength Cond Res, 25*,*2510-2518*..2011.

[8] Taube, W., et al. *Scand Journal Med Sci Sports, 22*, 671-683.2012.

[9] Wang, L. I., et al. *Int Journal Sports Med, 35*, 522-527.2014.

[10] Walsh, M., et al. *J Strength Cond Res, 18*, 561–566.2004.

Disclosure of Interest: None Declared

KINEMATICS ANALYSIS OF TATYANA DEKTYAREVA'S HURDLE CLEARANCE TECHNIQUE

Chia-Ling Chu [1] Yi-chun LIn [1] Chun-Ju Yang [1] Wen-Tzu Tang [1,*]

[1] Coach Science Institute, National Taiwan Sport University, Taoyuan County, Taiwan, Republic of China

Introduction and Objectives: The 100 meters Hurdles is characterised by continuous alternation between cyclical (sprint) and acyclical movements (hurdle clearance) at the highest possible speed. Previous research shows the result of man 110m hurdles of a European champion, it suggests that the horizontal velocity of the hurdler between the fourth and the fifth hurdle is highly correlated with the end result in the Hurdle race. Due to the different between the physical condition of man and woman, will the different technique exist in fourth and fifth hurdle in top European woman 100m hurdles athlete. The purpose of this study is to explore the woman European champion in 100m hurdles, the 4th and 5th hurdles during the training was analysed in following phases: take-off phase, flight phase, landing phase and run between hurdles.

Methods: The woman European champion in 100m hurdles Tatyana Dektyareva was participated in this study. The first three hurdles were removed in order to develop the optimal velocity when subject reach the 4th and the 5th hurdle. Kinematic parameters were collect by 2 casio camera with 210 frame per second, the camera were synchronized and located in the area between the fourth and fifth hurdle. The film was digitized through Direct Linear Transformation method in Kwon3D motion analysis system and the center of gravity was derived with a 12-segment model (Z1-Zatsiorsky, 1983).

Results: Between 4th and 5th hurdle, the horizontal velocity of the center of gravity(COG) in the braking phase is 6.20m/s, while in the propulsion phase it increases to 8.13m/s, which has increase 23.5% and the vertical velocity is 1.23 m/s. It shows the efficiency to accelerate the velocity during take-off. The horizontal and vertical velocities define the elevation velocity of the COG, which is in this case is 8.20 m/s. The relationship between horizontal and vertical velocities shows the athlete's ability for an efficient transition from the running stride into the take-off stride. The landing phase has the largest reserve potential for improving the competition result. The result shows the horizontal velocity of the COG in the landing phase is 7.92m/s, which means it only decrease 0.21m/s during the hurdle clearance phase. Less reduction of horizontal velocity during 4th and 5th hurdle during this training shows the efficient and less energy loss during the movement.

Figure:
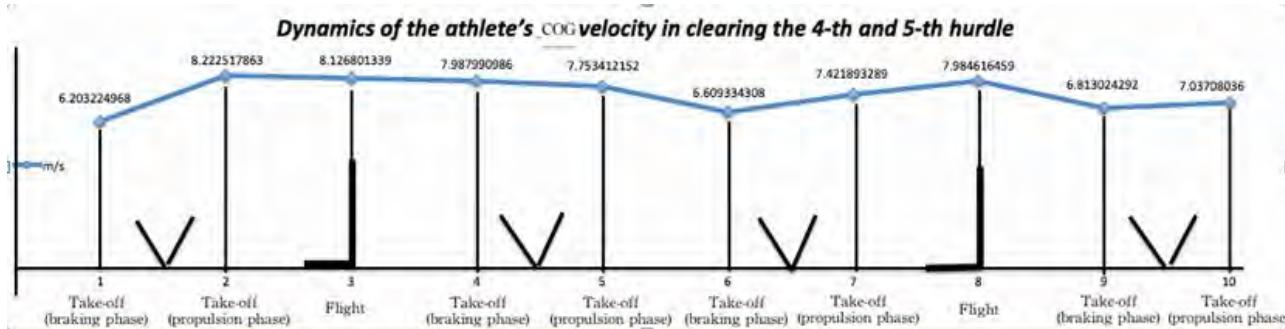
Caption: Figure 1 Dynamics of the athlete's COG velocity in clearing the 4th and 5th hurdle

Conclusion: Great energy transition during horizontal and vertical velocities at take-off phase and less velocity reduction during clearance phase was found during this study, it shows the advantage of this training method that encourage the athlete to reach the peak velocity at 4th hurdle and perform the hurdle technique.

Table: Each phases of athlete's COG velocity in Hurdle clearance

	Take-off (braking phase)	Take-off (propulsion)	Flight	Landing (braking phase)	Landing (propulsion phase)
Vx of COG	6.2m/s	8.13m/s	8m/s	7.92m/s	7.75m/s
Vy of COG	-0.2m/s	1.23m/s	1.42m/s	-1.04m/s	-0.23m/s
Vt of COG	6.2 m/s	8.2 m/s	8.1 m/s	7.9 m/s	7.7 m/s

* Vx of COG is Horizontal velocity of COG; Vy of COG is Vertical velocity of COG; Vt of COG is Velocity resultant of COG.

Caption: Table 1 Each phases of athlete's COG velocity in Hurdle clearance

References: Milan Coh（2003）. Biomechanical analysis of Colin Jackson's hurdle clearance   technique

BIOMECHANICS by IAAF 18:1; 37-45

Xu Jianguo（2007） Comparative Analysis of Chinese and Foreign Elite Women kinematic parameters hundred meters hurdler

Journal of Physical Education Institute of Shanxi Normal University Vol.22 No3 Sept.2007

SUN Ting—ring, HUANG Bei—jun, DONG Guang—xin（2011）Speed feature of world excel lent women 100meter hurdle race athletes . Journalof Sports Adult Education Vol. 27, No. 4

Disclosure of Interest: None Declared

DOES RUNNING TECHNIQUE ALTER MUSCLE ACTIVATION PATTERN IN HEALTHY RUNNERS?

Ana F. dos Santos [1,*] Theresa H. Nakagawa [1] Giovana Y. Nakashima [2] Carlos D. Maciel [2] Fábio V. Serrão [1]

[1] Department of Physical Therapy, Federal University of São Carlos, [2] Department of Electrical Engineering, University of São Paulo, São Carlos, Brazil

Introduction and Objectives: The growing number of running practitioners has been noticed all over the world. In Brazil, it is estimated a 30-fold increase in the number of runners in the last 15 years [1]. However, this practice has a potential risk for injury. It is known that most of the injuries that occur during this activity is related to the knee joint (42%) being patellofemoral pain the commonest one [2]. Recently, running with increased step rate and trunk flexion showed potential to reduce the knee joint demand and the patelofemoral joint stress [3,4]. It is important to investigate the effect of different running techniques on lower limb biomechanics in order to improve injury prevention and rehabilitation programs. In particular, it is necessary to understand the hip, knee and ankle muscle activation pattern.The purpose of this study was to compare the lower limb neuromuscular activity pattern among usual, increasing 10% step rate (10%SR) and increasing trunk flexion (TFLEX) running techniques.

Methods: Twenty healthy recreational runners (5 females, 15 males) participated in the current study. All subjects ran a minimum of 20 km/week for at least 3 months and presented a rearfoot strike pattern during running. Each subject completed a familiarization session (3 days before) when it was determined the preferred speed (9.7±1.4 km/h) and step rate (166.8±7.2 steps per min). The runners performed usual (USRUN) plus the two running techniques at a random order on a treadmill. For the 10%SR technique, they were monitored using a metronome. The TFLEX technique was verbally stimulated and visually confirmed. The electromyographic signal (EMG) of medial gastrocnemius (GASTRO), tibialis anterior (TA), vastus medialis (VM) and lateralis (VL), rectus femoris (RF), gluteus medius (GMED), biceps femoris (BF) and gluteus maximus (GMAX) were recorded at 2400 Hz, detected using 8 wireless surface EMG electrodes (Trigno™ Wireless System). The EMG signals were processed using custom MATLAB software. Raw EMG data were band-pass filtered (20-450 Hz, 4th-order Butterworth), full-wave rectified and smoothed using a 50-Hz low-pass filter (bidirectional, 6th-order Butterworth). The average of 10 stance phases of each condition from the dominant lower limb was analyzed. The mean EMG activity was normalized by the average of total gait cycle. The stance phase was defined from the minimum vertical position of the distal heel marker to the second knee extension peak. The MANOVA with repeated measures was used for analysis (alpha set at 0.05).

Results: This was the first study to compare lower limb neuromuscular activation during USRUN, 10%SR and TFLEX running techniques. The TFLEX technique showed greater differences at the average EMG curves (Fig 1 and Table 1). As expected, the 6.5º increase in trunk flexion angle resulted in greater hip extensors muscle activation during stance phase when compared to USRUN. We observed 38% increase in BF and 46% increase in GMAX activity; while GASTRO activation decreased 57%. At 10%SR technique, the VL EMG data showed 12% lower activation when compared to USRUN. Greater GMED and lower GASTRO activity during TFLEX was found when compared to 10%SR.

Previous studies have demonstrated beneficial effects of both running techniques on the knee joint [3,4]. However, each technique showed distinct biomechanics adaptation. In the current study, we showed greater activation of the proximal joints and lower demand on the distal joints during TFLEX. To the best of the authors' knowledge, this was the first study to report these results. Contrary to Chumanov et al. [5] at 10%SR, it was observed a reduction in knee extensor muscle activation during the stance phase. These results could be related to diminished knee extensor moment and consequently less patellofemoral joint stress. In addition, TFLEX, as compared to 10%SR, showed greater GMED activation, allowing greater frontal plane hip movement control potentially preventing detrimental effects on the patellofemoral joint.

Figure:
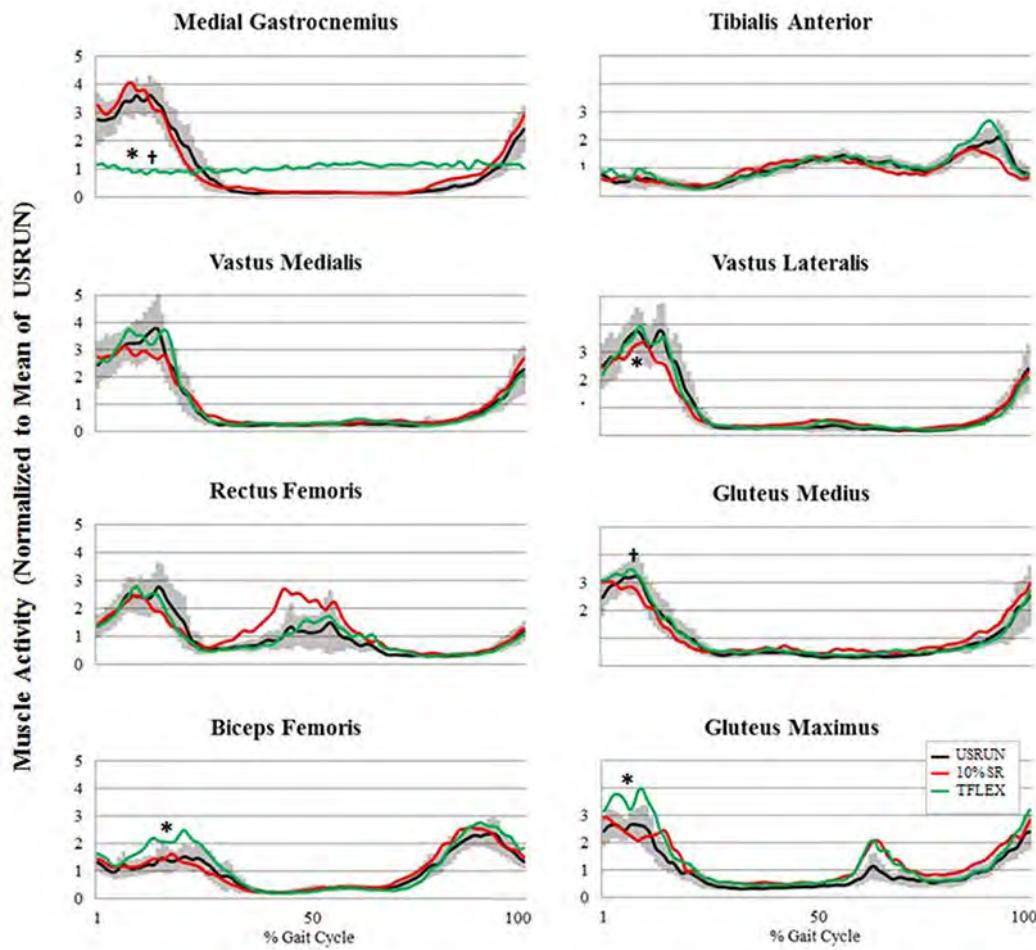
Caption: Mean muscle activities during the gait cycle. The gray shaded regions represent the USRUN EMG (mean ± 0.5 SD).

Conclusion: The 10%SR and TFLEX showed different lower limb muscular activation pattern; which could potentially reduce knee injury risk. These information may improve the physical therapists understanding of the effects of different running techniques, to better prescribe running techniques in the prevention and rehabilitation programs.

Table: Mean of muscle activity during stance phase of running.

	USRUN	10%SR	TFLEX
GASTRO	2.25	2.31	0.95*†
TA	0.41	0.43	0.54
VM	2.15	2.10	2.25
VL	2.15	1.89*	2.08
RF	1.57	1.48	1.47
GMED	1.68	1.58	1.78†
BF	1.25	1.22	1.73*
GMAX	1.48	1.66	2.09*

Caption: *Different from USRUN (p<0.01) †Different from 10%SR (p<0.01)

References: [1]Corpore Brasil."Estatística", 2013.

[2]Taunton et al., Brit J Sport Med, 36(2):95–101,2002.

[3]Lenhart et al., Med Sci Sports Exerc, 46(3):557–64,2014.

[4]Teng et al., J Orthop Sports Phys Ther, 44(10):785-92,2014.

[5]Chumanov et al., Gait Posture, 36(2):231–5,2012.

Disclosure of Interest: None Declared

Sport

PO-0379

KINEMATIC ANALYSIS OF THE SPEED MAINTENANCE PHASE OF 100 M RUNNING

Emel Cetin [1,*]Ethem Hindistan [1]Suleyman Akay [1]

[1]School of Physical Education and Sports, Akdeniz University, Antalya, Turkey

Introduction and Objectives: The speed profile is used to subdivide the 100m sprint performance into 4 phases: a start action, an acceleration phase, a phase of maximal sprint and a deceleration phase (1). Successful sprint running performance requires good starting ability, highest maximum running speed, and endurance of that speed capacity. Maximum running velocity in elite sprinters is achieved by optimal stride length (SL) and stride frequency (SF) in the distance between 30 m and 60m. Generally shorter contact time (CT) results in greater performances in sprinting; therefore, faster sprinters have shorter contact time than slower sprinters in each stride (2). Therefore, the longer speed maintenance phase will play an important role in improving the performance. The aim of the study was to evaluate further the effects of 8 week of training on the stride characteristics at speed maintenance phase of 100 m sprint running performance.

Methods: A total of fourteen male sport and physical education students (Training Group: age 19.57±1.13 years, weight 67.49±6.37 kg, height 174.86±4.34 cm; Control Group: age 21.57±1.13 years, weight 67.27±3.79 kg, height 177.86±4.34 cm) participated in this study. After completion of a 20-min warm-up, Training Group performed 12x25 m sprints at maximal intensity. Active rest was applied between sprint repetition (2.5 min) and sets (5 min). In the 5th and 6th week and in the 7th and 8th week of the training program one repetition was added at first- third and second-forth set, respectivelly. Five video cameras (Basler piA640- 210 Hz) were used to collect stride parameters recordings of the sagittal plane of between 50m-100m interval of running performance. Photocells were used to assess sprinting performance (t) and the 10 m time splits of the participants. Two-Related Samples test was used to establish if there were any significant differences between trials (pre-post). The significance level for the tests was set at $p<.05$.

Results: After 8 week sprint training, training group produced increases in running performance by 2.4 %. Working group achieved the maximum speed of running at 60m-70m interval and 50m-60m interval, pre and post training respectively. There is significant changing for stride length and stride frequency at 70m-100m interval. Compared to the pre-training at this interval, decreased stride length increased stride frequency.

Conclusion: If the 100 m sprint performance of training group is compared to the running performance for pre-post 8 week training, training group produced increases in running performance by 2.4 %. Dintiman, after 8 weeks of horizontal training, observed an improvement of 5.2% in performance for 50 m, and Suellentrop found a 2.5% improvement in 100 m performance after 6 weeks of training(3). The elite sprinters commonly achieve the maximum speed of running 50-60m interval (M.Green, D.Chambers, T. Montgomery et al.), 40-60m interval (B.Surin), or 50-70m interval (O. Thompson, K. Streete-Thompson) (4), whereas the investigated group achieved at 60-70m and 50-60m intervals, pre-post training respectively (Table 1). After 8 week training program, despite the fact that group have finished the running performance with their maximum running speed 93.72% , there were significant differences for SL and SF in last 30 m.

In this study, there is no significant improvement in RS at 60-100 m interval. However, SL showed significantly decrease 10.12% and 5.8% in this interval pre-post training, respectively. In proportion to SL, SF showed significantly increase 6.48% and 1.25 %, respectively.This indicates that the increase in performance resulted from the arrangements between SL and SF.

Table:

Training Group	50-60m	60-70m	70-80m	80-90m	90-100m
t(s) pre(13.09s) post(12.78s)	1,267 1,210	1,256 1,236	1,275 1,274	1,302 1,283	1,310 1,291
RS (ms^{-1}) pre % max RS post % max RS p	7.92±0.44 8.28±0.37 100 .018	7.98±0.41 100 8.09±0.24 97.71 .345	7.86±0.43 98.5 7.87±0.39 95.05 1.000	7.71±0.52 96.62 7.80±0.23 94.20 .611	7.66±0.50 95.9 7.76±0.34 93.72 .499
SL(m) pre post p	2.22±0.21 2.09±0.20 .310	2.27±0.20 2.40±0.14 .028	2.10±0.29 2.37±0.13 .018	2.07±0.16 2.39±0.13 .028	2.03±0.17 2.30±0.10 .018
SF(Hz) pre post p	3.47±0.46 3.80±0.29 .128	3.39±0.34 3.19±0.20 .128	3.65±0.69 3.19±0.28 .043	3.56±0.25 3.14±0.21 .018	3.61±0.33 3.23±0.16 .028

References: [1] Debaere S., Jonkers I., Delecluse C. The Contribution of Step Characteristics to Sprint Running Performance in High-Level Male and Female Athletes, Journal of Strength and Conditioning Research. 27(1)/116-124, 2013

[2] Kale M., Aşçı A., Bayrak C., Açıkada C. Relationship Among Jumping Performances and Sprint Parameters During Maximum Speed Phase in Sprinters, , Journal of Strength and Conditioning Research. 23(8)/2272-2279, 2009

[3] Paradisis, G.P. and Cooke, C.B., The Effects of Sprint Running Training on Sloping Surfaces, Journal of Strength and Conditioning Research. 20(4), 767–777, 2006

[4] Babic V., Coh M., Dizdar D. Differences in kinematic parameters of athletes of different running quality, Biol. Sport 28:115-121, 2011

Sport

PO-0380

TECHNIQUE COMPARISON OF MALE AND FEMALE HAMMER THROWERS

Suzanne Konz [1],*Iain Hunter [2]

[1]Kinesiology, Marshall University, Huntington, WV, [2]Brigham Young Unviersity, Provo, UT, United States

Introduction and Objectives: Distinct anthropometric differences occur between the sexes throwing the hammer that likely affect optimal technique. The scientific literature has focused predominately on the characteristics of male hammer throwers. No literature statistically compares the differences between the throwing technique of male and female hammer throwers. The aim of this study was to determine what the hammer throwing technique differences, if any, occur between genders.

Methods: The performances of the top 16 male and female throwers at the 2003 World Athletic Final and the top 13 male and female throwers from the 2003 USA Track and Field Nationals were examined. Video was captured using three Canon 60 Hz cameras. The best throw of each athlete was digitized and analyzed using the Peak Motus 8.2 motion analysis system.

Results: ANOVA (see Table 1.) revealed that athlete mass, athlete height, velocity at release, timing components, and centripetal force were different between sexes. The methods used to obtain greater performances also varied slightly between sexes.

Conclusion: The general movement and technique for male and female throwers is similar. However, there are certain characteristics that vary to some degree between sexes. Coaches and athletes should be aware of these differences to help athletes progress towards optimal technique between sexes.

Table:

	Men (n=14)		Female (n=15)		
Variable	Mean	SD	Mean	SD	*p* value
Athlete Mass (kg)	112.9	13	86.7	12.89	<0.001
Athlete Height (m)	1.9	0.06	1.8	0.07	<0.001
Release Vel (m/s)	29.2	1.38	27.5	1.15	0.002
Throw COM travel	1.56	0.12	1.37	0.2	0.006
Height of Swing Hip (m)					
Turn 1	0.7	0.0	0.0	0.0	0.04

	7	6	7	9	3
Time for Turn (sec)					
Turn 1	0.72	0.1	0.64	0.08	0.023
Turn Ratio					
Turn 2	1.03	0.1	1.24	0.36	0.044
Time in Phase (sec)					
Turn 1 Start of Double Support	0.39	0.08	0.31	0.07	0.018
Angle between the Shoulders and the Hips (deg)					
Turn 1 Start of Double Support	29.88	15.72	14.57	8.99	0.003

Caption: Table 1. Descriptive statistics for the sex comparison with a significance level of p = <0.05

Disclosure of Interest: None Declared

Sport

PO-0381

CHARACTERISTICS IN CENTER OF PRESSURE TRAJECTORY DURING WALKING IN SPRINTERS

Yu Kashiwagi [1,*]Tomoya Hirano [2]Noriko Hakamada [3]Kazuo Funato [2]Tadashi Wada [4]Masuhiko Mizuno [2]

[1]Graduate school of Health and Sport Science Nippon sport science university, [2]Nippon sport science university, [3]Japan institute of sports sciences, [4]Kokushikan university, Tokyo, Japan

Introduction and Objectives: Center of pressure（COP）trajectory can provide useful information in assessing the foot function and gait pattern[1]. It is not clear however, whether a sprinter can get an effective gait pattern by prolonger sprint training. The purpose of this study was to investigate the characteristic of COP trajectory during walking in sprinters. Hypothesis was considered sprint training would influence of displacement of effective COP trajectory during stance phase in walking.

Methods: Nineteen male college sprinter (SP; Age:19.9±0.9yrs, BH:174.1±5.4cm, BW:64.9±14.2kg, 100m sprint time:11.10±0.3sec) and fifteen male healthy young adults (CG; Age:20.5±2.3yrs, BH:172.6±5.8cm, BW:64.1±9.9kg) participated in this study. Subjects were asked to walk five times along the walkway at self selected walking pace. A dynamic pressure measurement system (footscan system RSscan International Belgium) was used to record the COP coordinates, velocity and progression angle. All data were recorded at measurement frequency of 500Hz and processed using scientific footscan software. Actual walking speed was measured using photo-cells set at interval of 5m in walkway. Spatio-temporal parameters were calculated from gait cycle time using high speed camera (240fps, JVC GC-P100, Tokyo, Japan). Stance phase was divided into four sub-phases; Initial contacts phase (ICP), Forefoot contact phase (FFCP), Foot flat phase (FFP), Forefoot push off phase (FFPOP). Arch index was assessed as preliminary research by Cavanagh RJ. (1987) [2] from foot pressure prints during stance phase. All statistical analysis were used by student's t-test (welch) performed on selected means to detect significant differences (effective $P < 0.05$) between SP and CG (JMP ver. 8.0 : SAS inc.).

Results: Foot arch index and spatio-temporal parameters were not different between SP and CG. In % FFP time, SP(35.3±10%) was shorter than CG(43.1±7.3%, P<0.05). On the other hand, %FFPOP time indicated longer in SP than CG (SP:51.3±10.5% vs CG:44.5±6.5%, P<0.05). Liner COP trajectory pattern of SP from heel to the second metatarsal was observed compared with CG. Thereafter COP shifted to medial side from the second metatarsal to hullx before toe-off in both SP and CG. Anterior-posterior COP velocity was larger in SP than CG during early FFP(12~33% of stance time, P<0.01, Fig.1). Larger COP velocity of FFP in SP might be considered as strategy so as to get smooth center of mass trajectory to anterior direction and also enable to get a large %FFOP in order to accelerate the body.

Figure:
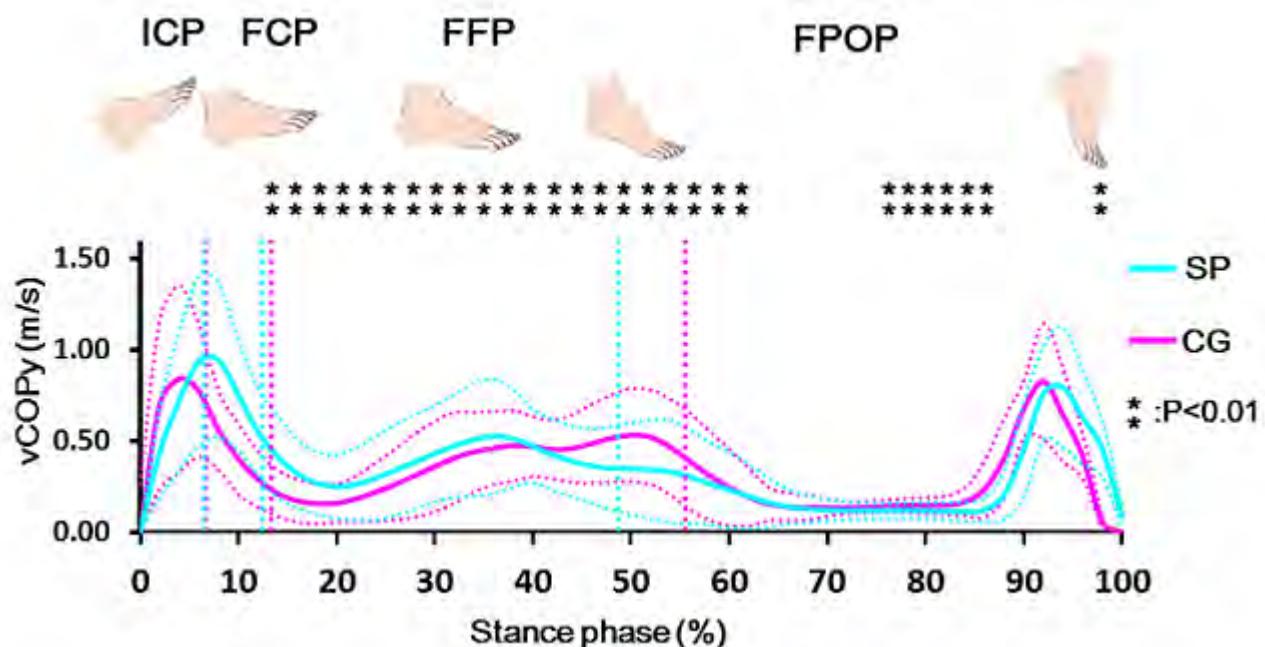
Caption: Velocity of center of pressure in anterior-posterior direction (vCOP, mean±SD) during normalized stance phase for sprinter(SP) and health young subjects(CG). Vertical dashed line divide four stance phase; ICP: Initial contacts phase, FFCP: Forefoot contact phase, FFP; Foot flat phase, FFPOP; Forefoot push off phase.

Conclusion: COP velocity in front direction during early period of Foot flat phase was larger in sprinter, as well as an effective COP trajectory pattern in Foot push off phase. These characteristics might play an important role for increasing the propulsive time transferred from hullx. This study suggests effective COP trajectory in sprinter might be results from sprint training so as to move center of mass more smoothly.

References: [1] Chiu, M.C et al., Gait and posture, 37:43-48, 2013.
[2] Cavanagh R.J., and Rodgers M.M.,. J. Biomech., 20(5):547-551, 1987.

Disclosure of Interest: None Declared

PO-0382

GENDER COMPARISON OF ANTAGONISTIC MUSCLE ACTIVITY DURING ISOKINETIC TRUNK EXTENSION

Lucie Risch [1,*] Stephan Kopinski [1] Monique Wochatz [1] Martin Wolter [1] Steffen Mueller [1] Frank Mayer [1]

[1] Sports & Health Science , University Outpatient Clinic Potsdam, Potsdam, Germany

Introduction and Objectives: It is well known that healthy males and females differ in absolute strength values. However, evidence for gender differences in muscle activity measured with surface EMG during trunk exercises show conflicting results. Females were observed recently to have higher relative agonistic trunk muscle activity during submaximal isokinetic trunk extension compared to males. If a simultaneously higher antagonistic activity for stabilization of the spine is an influencing factor for this finding is not clear. Therefore, the aim of this study was to investigate if abdominal antagonistic activity differs between healthy males and females during maximal and submaximal isokinetic trunk extension tasks.

Methods: Fifty healthy participants (25 males: 28±4 yrs, 78±8 kg, 1.82±0.06 m; 25 females: 25±3 yrs, 60±7 kg, 1.67±0.06 m) with no history of low back pain were prepared with a 6-lead bilateral surface EMG (myon RFTD-32, myon AG, Suisse) setup (M. erector spinae: L3 and Th9; M. rectus abdominis) and performed maximal and submaximal strength tests in an isokinetic trunk dynamometer (Con-Trex MJ,TP-module, Physiomed AG, Germany). Trunk motion ranged from 45° flexion to 10° extension with a movement velocity of 45°/s. After warm-up, participants completed 5 maximum voluntary contractions (MVC) in trunk extension (MVCext) and flexion (MVCflex) followed by 4 submaximal extension tests (subMVC) at 20, 40, 60, and 80% of MVCext with 5 repetitions each. Outcome measure was the root mean square (RMS) of abdominal antagonistic muscle activity during extension normalized to RMS of abdominal agonistic activity during MVCflex. Data was analysed descriptively presenting mean±SD. Mann Whitney U-test was used to test for significant differences between genders. A repeated measures ANOVA was calculated to test for an interaction effect between gender and tasks. Significance level was set at $\alpha=0.05$.

Results: Absolute extension and flexion torques were significantly higher ($p<0.001$) in males (MVCext: 317±63 Nm, MVCflex: 201±47 Nm) than in females (MVCext: 214±55 Nm, MVCflex: 126±26 Nm). Regarding abdominal antagonistic activity, females have higher activation compared to males during all tasks showing significant difference at 60% of torque production (see Tab. 1). No statistical significant interaction effect between genders was found ($p=0.78$).

Figure:

Gender	20% of MVC	40% of MVC	60% of MVC	80% of MVC	100% of MVC
Female	4.1 ± 3.6	3.7 ± 2.1	4.4 ± 2.4	5.6 ± 2.9	7.7 ± 4.0
Male	2.9 ± 1.9	2.9 ± 1.8	3.2 ± 2.0	4.2 ± 2.5	6.6 ± 4.5
P-Value	0.114	0.109	*0.047	0.076	0.177

*indicates $p<0.05$

Caption: Abdominal antagonistic activity [%, mean±SD]

Conclusion: Antagonistic activity rises with increasing torque production in both genders. Generally, antagonistic activity level relative to MVCflex is low. It is assumed that the higher antagonistic muscle activity in females might increase spinal stabilisation and may be related to the higher relative agonistic activity recently found during isokinetic extension.

Disclosure of Interest: None Declared

SCAPULOHUMERAL RHYTHM DURING ARM ELEVATION IN PATIENTS WITH ACROMIOCLAVICULAR OSTEOARTHRITIS

Catarina O. Sousa [1,*] Paula Camargo [2] Lori Michener [3] Ivana Ribeiro [2] Rodrigo Reiff [4] Tania Salvini [2]

[1]Department of Physical Therapy, Federal University of Rio Grande do Norte, Natal - RN, [2]Department of Physical Therapy, Federal University of São Carlos, São Carlos, Brazil, [3]Division of Biokinesiology and Physical Therapy, University of Southern California, Los Angeles, United States, [4]Department of Medicine, Federal University of São Carlos, São Carlos, Brazil

Introduction and Objectives: The acromioclavicular (AC) joint is a common source of shoulder pain. Cartilaginous degeneration can occur from the high axial loads transferred through the small and incongruent joint surface area during complex torsional movements during shoulder movements, leading to osteoarthritis [1]. A clinical parameter heavily affected in most shoulder disorders is the scapulohumeral rhythm (SHR) [2], which is the relationship between elevation at the glenohumeral joint and scapular upward rotation [3]. The SHR provides an important parameter to characterize shoulder function during dynamic activity [4].

Considering the lack of studies on this topic in patients with AC osteoarthritis (ACO), the purpose of this study was to describe the SHR during arm elevation (ascending and descending phases) in individuals with isolated ACO and to compare to healthy asymptomatic subjects.

Methods: The study included 49 individuals: 23 with ACO (15 men, 8 women; 42.78±11.74 years; 75.21±14.17 kg; 1.72±0.12 m); and 26 asymptomatic healthy subjects (13 men, 13 women; 45.81±8.68 years; 66.27±9.32 kg; 1.66±0.08 m). Scapular motion was collected with an electromagnetic tracking system (Flock of Birds) during elevation of the arm. The sensors were attached to the sternum, acromion of the scapula, and to a thermoplastic cuff secured to the distal humerus to track humeral motion. Anatomical coordinate systems were established for each segment by palpating and digitizing anatomical landmarks as per the International Society of Biomechanics recommended protocol [5]. The individuals completed 3 repetitions of arm elevation in the sagittal plane guided by a flat plane surface. The symptomatic shoulder was evaluated in subjects with ACO, and the shoulder for the asymptomatic healthy subjects was randomly chosen. The SHR was calculated as the ration of elevation on glenohumeral joint to upward/downward rotation on scapulothoracic joint for each trial of arm elevation with 30º of increment of humeral elevation during ascending (30º-60º, 60º-90º, 90º-120º) and descending phases (120º -90º, 90º-60º, 60º-30º), and then averaged across the three trials for data analysis.

SHR was analyzed with a separate linear mixed-model 2-way ANOVA for each phase (ascending and descending), in separate, using intervals of humeral elevation as the repeated factor and groups as the main factor. Comparisons of interest were the interactions of group by intervals of humeral elevation, or main effect (groups). The significance level of 5% was adopted.

Results: No interactions of group by intervals of humeral elevation were found for SHR in either phase of arm elevation (ascending and descending). Considering main effect factor, during ascending phase, there was difference between

groups (P= 0.01) which individuals with ACO presented lesser SHR compared to asymptomatic healthy subjects (mean difference = 0.59). During descending phase, no difference was found.

The smallest value of SHR in subjects with ACO, during ascending phase of arm elevation, must be related to greater scapular upward rotation in these subjects [6]. Scapular upward rotation is significantly increased in patients with many types of shoulder disorders [7], which may represent compensatory responses for an attempt to reduce pain during the arm elevation.

Conclusion: Individuals with ACO showed decreased SHR during the ascending phase of arm elevation compared to asymptomatic healthy subjects. These alterations may be related to an increased scapular upward rotation which may represent compensatory responses as an attempt to reduce pain in subjects with ACO. Future studies are needed, especially to verify if these alterations are associated to changes in muscle activation.

References: [1] Buttaci CJ et al. Am J Phys Med Rehabil, 83:791–7, 2004.

[2] Ludewig PM et al. J Orthop Sports PhysTher, 39: 90–104, 2009.

[3] Braman JP et al. J Shoulder Elbow Surg, 18: 960–967, 2009.

[4] Kon Y et al. J Shoulder Elbow Surg, 17:943-946, 2008.

[5] Wu G et al. J Biomech. 38:981–92, 2005.

[6] Sousa CO et al. J Electromyogr Kinesiol, 24:520–530, 2014.

[7] Kibler WB et al. J Shoulder Elbow Surg, 11:550-6, 2002.

Disclosure of Interest: None Declared

PO-0384

INTER-SESSION RELIABILITY OF SCAPULAR MUSCLE ACTIVITY DURING ISOKINETIC TESTING OF SHOULDER FLEXION AND EXTENSION IN THE SCAPULA PLANE

Monique Wochatz [1,*]Sophie Rabe [1]Martin Wolter [1]Stephan Kopinski [1]Steffen Mueller [1]Frank Mayer [1]

[1]Department Sports & Health Sciences, University Outpatient Clinic Potsdam, Potsdam, Germany

Introduction and Objectives: Overhead athletes frequently suffer from shoulder complaints. Isokinetic dynamometry is commonly used to assess muscle performance in healthy and injured populations. Additional EMG application offers the possibility to investigate neuromuscular performance in different standardized measurement conditions involving motions typical for overhead sports. Previous studies could show an association between shoulder pathologies and altered scapular muscle activity pattern. Detected differences in the scapular muscle activity level were shown to vary between 4% and 25% between healthy and injured individuals. However, data of measurement accuracy of scapular muscle EMG during isokinetic overhead motion is rare and thus limits the interpretation of detected group differences. Therefore, this study aimed to evaluate the inter-session variability of scapular muscle activity during isokinetic testing in asymptomatic individuals.

Methods: Eleven asymptomatic participants (29±2 yrs; 1.72±0.09 m; 73±15 kg) underwent isokinetic testing (Con-Trex, WS, Physiomed AG Germany) of the dominant arm twice (M1 and M2) separated by at least 5 days. Simultaneously muscle activity of the upper (UT) and lower trapezius (LT) and serratus anterior (SER) was assessed by a 3-lead surface EMG (myon RFTD-32, myon AG, Suisse). Isokinetic testing was conducted in a standing position and comprised shoulder flexion and extension in scapula plane in the following modes: concentric with 60 (CON_{60}) and 180°/s (CON_{180}) and eccentric with 60°/s (ECC). Range of motion (ROM) was set to 160° ranging from 20° to 180° of shoulder flexion. After a warm up participants executed 5 repetitions with maximum effort for each condition. EMG activity of shoulder flexion and extension quantified over the whole ROM by Root Mean Square (V, mean±SD) was averaged over the 5 repetitions and normalized to muscle activity of CON_{60} condition [%]. To evaluate the reliability test-retest variability (TRV, %), intra-class correlation coefficient (ICC, 2.1), Bias and 95% limits of agreement (LoA, Bias±1.96*SD) were calculated.

Results: Absolute EMG activity of reference condition CON_{60} ranged from 0.43 V to 0.90 V. Normalized mean muscle activity for CON_{180} and ECC of shoulder flexion ranged from 81±12% to 115±11%. During shoulder extension of CON_{180} and ECC mean muscle activity varied from 14±11% to 31±16% between LT, UT and SER. Across all conditions and muscles ICC varied between 0.37 (extension, ECC, SER) and 0.93 (extension, CON_{180}, UT) and TRV ranged from 8.6±4.6% (flexion, ECC, SER) to 30.4±27.4% (extension, CON_{180}, LT). The Bland-Altman analysis revealed a systematic error from -6.2% with LoA of 6.6 and -6.1% (flexion, CON_{180}, LT) to an error of 4.1% with LoA of 28.9 and -20.8% (extension, ECC, LT) (Table 1).

Figure:

Condition			M1 mean±SD	M2 mean±SD	ICC	TRV [%] mean±SD	Bias	LoA
Flexion	CON$_{180}$	LT	105 ± 23	111 ± 24	0.80	9.8 ± 8.5	-6.2	20.2; -32.5
		UT	109 ± 15	115 ± 11	0.57	9.6 ± 7.3	-6.0	15.6; -27.7
		SER	90 ± 12	91 ± 14	0.71	8.0 ± 5.7	-1.3	17.1; -19.6
	ECC	LT	82 ± 11	84 ± 13	0.74	9.0 ± 6.6	-1.6	15.3; -18.6
		UT	82 ± 14	81 ± 12	0.67	10.0 ± 9.3	0.9	20.6; -18.7
		SER	85 ± 20	83 ± 18	0.92	8.6 ± 4.6	2.2	16.7; -12.3
Extension	CON$_{180}$	LT	22 ± 10	20 ± 6	0.79	14.6 ± 13.0	2.2	12.2; -7.8
		UT	14 ± 11	15 ± 9	0.93	24.4 ± 16.9	-1.5	5.7; -8.7
		SER	26 ± 8	27 ± 8	0.69	21.1 ± 12.2	-1.7	9.9; -13.3
	ECC	LT	31 ± 16	26 ± 12	0.55	30.4 ± 27.4	4.1	28.9; -20.8
		UT	20 ± 7	21 ± 6	0.73	23.1 ± 21.8	-1.0	8.0; -10.1
		SER	24 ± 8	25 ± 6	0.37	21.6 ± 15.8	-1.1	13.6; -15.9

Caption: Table 1: Normalized EMG activity (% MVC CON60) of scapula muscles for M1 and M2 (mean±SD) and associated reliability measures.

Conclusion: The level of agreement of scapula muscle activity between the measurements varied across conditions and muscles from moderate to good reliability. Only SER showed high variability during shoulder extension ECC. Due to smaller scapula muscle activity levels during isokinetic shoulder extension possible group differences might be masked by the measurement variability. Concentric and eccentric isokinetic conditions during shoulder flexion seem the more feasible settings to assess differences or changes in scapular muscle activity between healthy and symptomatic athletes.

Disclosure of Interest: None Declared

TEMPLATE-MATCHING IN THE IDENTIFICATION OF ARM-HAND SKILL PERFORMANCE IN HEALTHY SUBJECTS AND STROKE PATIENTS

Ryanne Lemmens [1,*]Yvonne Janssen-Potten [2]Annick Timmermans [3]Rob Smeets [1]Henk Seelen [2]

[1]Rehabilitation Medicine, Research school CAPHRI, Maastricht University, Maastricht, [2]Adelante Centre of Experise in Rehabilitation and Audiology, Adelante Rehabilitation Centre, Hoensbroek, Netherlands, [3]BIOMED, Biomedical Research Institute, Hasselt, Belgium

Introduction and Objectives: Objectively assessing actual arm-hand skill performance (AHSP) is very important to evaluate therapy efficacy in patients with neurological disorders. Instruments to identify skills and determine both amount and quality of actual AHSP in daily life are lacking, necessitating the development of a new measure. To identify skills, pattern recognition techniques like statistical classification, neural networks, structural matching and template matching can be used. The aim of this study is to provide proof-of-principle of a method to identify activities based on template-matching, in a healthy participant and a patient with stroke.

Methods: Multiple devices, each containing a tri-axial accelerometer, tri-axial gyroscope and tri-axial magnetometer were attached to the hand, wrist, upper arm and chest of participants, i.e. four devices to the dominant arm-hand and chest of the healthy participants, and seven devices to both arms and hands and the chest of the stroke patient. Thirty healthy individuals and one patient with stroke performed the activities 'drinking', 'eating' and 'combing' 5 times in a standardized manner, i.e. with similar starting position and instruction on how to perform the skill. Signals were filtered with a 4th order zero-time lag low-pass Butterworth filter (cut off freq.: 2.5 Hz). Data analysis consisted of the following steps: 1) temporal delimitation of each of the five activity attempts, i.e. identifying the start and endpoint of each attempt recorded; 2) signal normalization in the time domain to correct for (small) variations due to differences in speed of task execution; 3) averaging signal matrices from the five attempts of each individual person to obtain an individual template, i.e. the underlying ensemble averaged signal matrix per task per individual; averaging signal matrices from the individual templates of the first 29 healthy persons included, to create a generic template, to identify this activity among the signals of the 30th person; 4) identification of dominant sub phases of templates, within a specific task, using Gaussian-based linear envelope decomposition procedures; 5) recognition of specific activity execution among various activities performed daily, i.e. searching for template occurrence among signal recordings gathered in a standardized setting, using feature extraction and pattern recognition algorithms based on 2D convolution. Templates representing a complete activity as well as templates containing sub phases of an activity were used. Cross-correlation coefficients were calculated to quantify goodness-of-fit.

Results: Performance of the activities 'drinking,' 'eating' and 'combing' were recognized with high sensitivity and high specificity in healthy participants for both the generic template and the individual template. Using the individual template, recognition occurred with high correlations (e.g. for the activity drinking a correlation of 0.93 for the template representing the complete activity and for the template containing activity sub phases mean correlations ranged between 0.89 and 0.99). Using the generic template, recognition was similar regarding sensitivity and specificity (i.e. all activity

performances were recognized) but correlations were lower (table 1). In the stroke patient performance of the activities drinking, eating and combing were unambiguously recognized using the individual template. For both the template representing the complete activity and the template containing the activity sub phases, correlations with which the activity was recognized were high (table 1). In stroke no generic template was created since only one patient was included.

Conclusion: Proof-of-concept of this method to identify a specific activity among multiple activities performed in a standardized setting was shown for both healthy participants and a stroke patient. The long-term aim is to use this method to a) identify which arm-hand skills are performed during daily life by individuals, b) determine the quantity of skill execution, i.e. amount of use, and c) determine the quality of AHSP. At the moment, as far as we know, no such instrument is available. Future research will focus on: a) optimizing the method described, and b) applying this method for more activities, in more neurological patients and in daily life situations.

Table:

		## of times an activity was:		Correlation:	
		Performed	Recognized	Complete activity	Activity sub phases
Healthy subjects	Drinking	5	5	0.79*	0.78-0.86*
	Eating	5	5	0.58*	0.69-0.80*
	Combing	5	5	0.42*	0.68-0.90*
Stroke patient	Drinking	4	4	0.99	0.81-0.99
	Eating	5	5	0.65	0.81-0.98
	Combing	4	4	0.97	0.60-0.99

*correlation based on a generic template.

Caption: Table 1: Number of performances recognized and mean cross-correlation coefficients during pattern recognition.

Disclosure of Interest: None Declared

PO-0386

RELIABILITY OF REGISTRATIONS OF DAILY LIFE ACTIVITIES MONITORED WITH MULTIPLE BODY WORN SENSORS

Ryanne Lemmens [1,*]Henk Seelen [2]Yvonne Janssen-Potten [2]Annick Timmermans [3]Marlous Schnackers [2]Richard Geers [2]Rob Smeets [1]

[1]Rehabilitation Medicine, Research School CAPHRI, Maastricht University, Maastricht, [2]Adelante Centre of Expertise in Rehabilitation and Audiology, Adelante Rehabilitation Centre, Hoensbroek, Netherlands, [3]BIOMED , Biomedical Research Institute, Hasselt, Belgium

Introduction and Objectives: Stroke patients or (children with) cerebral palsy often encounter arm-hand problems in daily life, assessment of which is important. Whereas many instruments are available to assess capacity or perceived performance, tools gauging actual skill performance are scarce (Lemmens et al., 2012). Body worn sensors quantifying specific movement patterns associated with specific activities may be used to assess actual performance. However, signal reliability during execution of activities of daily living should be determined first.

Aim of this study is to determine to what extent standardized arm-hand skill performance of both healthy adults and children can be recorded reliably using multiple body worn sensors.

Methods: Thirty healthy adults (aged > 50years, 14 women, 16 men, mean age 58.0 ± 5.1 years) and 32 healthy children, i.e. 16 aged between 6-11 years (9 girls, 7 boys, mean age 8.5 ± 1.7 year) and 16 aged between 12-18 years (8 girls, 8 boys, mean age 14.6 ± 1.5 years) performed the activities 'drinking', 'eating' and 'combing' 5 times in a standardized setting. Tasks were first performed without, and subsequently with extensive instructions on how to perform the task. Sensor devices, each containing a triaxial accelerometer, gyroscope and magnetometer were attached to the arms, hands and trunk, i.e. four devices to the dominant arm-hand and chest of the adults and seven devices to both arms and hands and the chest of the children. Signals were filtered with a 4th order zero-time lag low-pass Butterworth filter (cut off freq.: 1.28 Hz). Repetitions of each specific task were identified and intra-class correlation coefficients (ICC) for each sensor and signal type were determined as a measure of reliability, both within and between subjects. For every person, a mean ICC was calculated. Boxplots of the results are presented (Fig. 1). The ICCs were classified as very good (0.8-1.0); good (0.6-0.8); moderate (0.4-0.6); fair (0.2-0.4) and slight (<0.2).

Results: As to within-subject reliability (Fig. 1), the median ICC's were good to very good for all activities. Reliability was better in the instruction conditions than in the no-instruction conditions, especially for the skill eating. Children aged between 12-18 years showed a slightly higher reliability compared to children aged between 6-12 years.

Between-subject reliability was also good to very good for all activities performed by adults. The activity drinking performed by the children had a very good reliability, the activity combing had a good reliability whereas the activity eating had a fair to moderate reliability in the youngest children, and a good reliability in the older children. Especially for the skill eating, a large difference in reliability was seen between the instruction and no-instruction conditions. For the activities drinking and combing, reliability was comparable between younger and older children. For the skill eating, reliability was higher in the older children.

Figure:
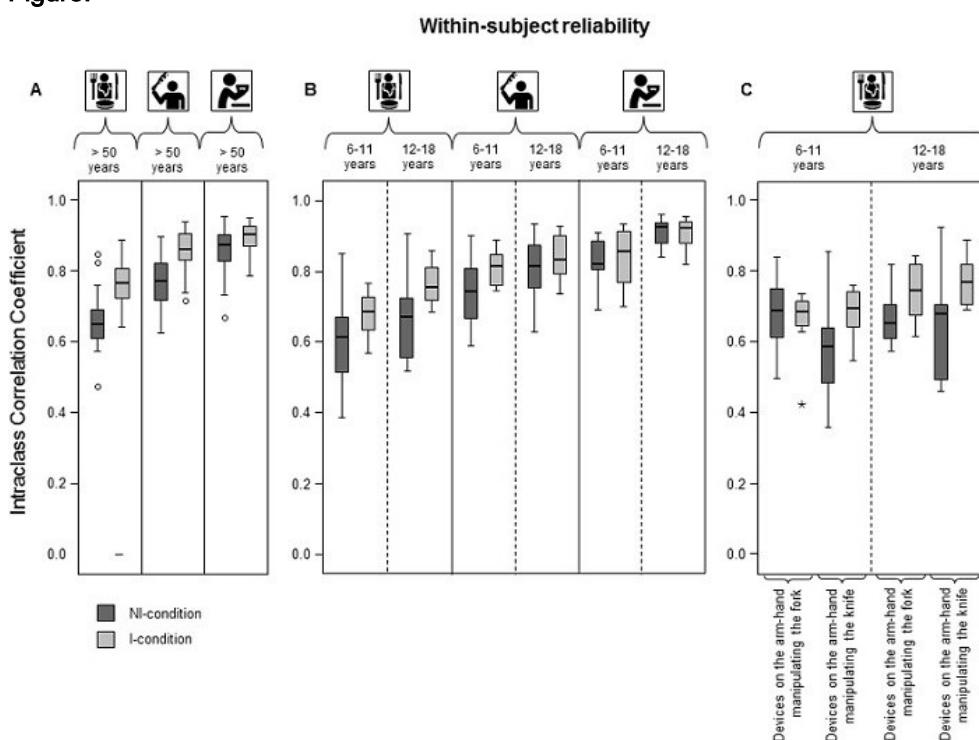
Caption: Figure 1: Within-subject reliability (ICCs) for the activities 'eating', 'combing' and 'drinking'. Dark grey bars: task performance without instruction. Light grey bars: task performance with instruction. A) performance by adults, boxplots representing the devices on the chest and arm-hand manipulating the knife, comb and cup; B) performance by children, boxplots representing the devices on the chest and arm-hand manipulating the knife, comb and cup; C) performance by children, boxplots representing the devices on each arm-hand.

Conclusion: Overall, the activities drinking, eating and combing had a good to very good within-subject reliability in both adults and children. By giving instructions about how to perform the task, the variability in execution of the task was reduced, thereby increasing reliability. The performance of the skill drinking had a higher reliability compared to the skill eating, the main reason being that drinking is a rather simple skill, which cannot be performed in many ways, whereas the skill eating consists of more sub movements and may be performed in many different ways. Between-subject reliability of the skill eating was relatively low, especially for the performance without instruction in the youngest children, the reason being that many children did not use the knife to cut the food, whereas other children had difficulties manipulating the knife. In the instruction condition, they were told how to use the knife. In conclusion, using multiple body worn sensors enable us to reliably record activities of daily life in healthy adults and children. Future research will focus on signal reliability during activities of daily life performed by *patients* and in *daily life settings*.

References: LEMMENS, R., TIMMERMANS, A., JANSSEN-POTTEN, Y., SMEETS, R. & SEELEN, H. 2012. Valid and reliable instruments for arm-hand assessment at ICF activity level in persons with hemiplegia: a systematic review. *BMC Neurology,* 12, 1-17.

Disclosure of Interest: None Declared

Upper Limb

PO-0387

BIPLANE FLUOROSCOPE MEASUREMENT OF SCAPULOHUMERAL KINEMATICS IN HEALTHY AND POST-OPERATIVE POPULATIONS

Ashley Hannon [1,*]Tom Jenkyn [2]

[1]Kinesiology, [2]Engineering, Western University, London, Canada

Introduction and Objectives: Glenohumeral kinematics in both healthy and pathologic shoulders is essential for evaluation of current clinical practices. Quantifying the motion during abduction(ABD), flexion(FF), and compound motion using a biplanar fluoroscopic technique in subjects with healthy, normal shoulders and post-surgical intervention for supraspinatus muscle repair uses a very accurate technique to describe motion in 3D, gaining insight for clinicians.

Methods: Six healthy normal subjects were performed one trial of right arm abduction(ABD) to 90˚, forward flexion(FF) to 90˚ and the compound motion of moving the right hand to the left shoulder (AAC). These were done at a self-selected pace. Two subjects diagnosed with right supraspinatus tear underwent surgical intervention to reattach the muscle. Six weeks after the surgical intervention, subjects also were recorded performing right arm ABD to 90˚, FF to 90˚ and AAC. Biplanar fluoroscopy was collected at 30 Hz on all subjects and was matched with a generic shoulder model. A radiostereometric analysis technique was employed to obtain the angles of the humerus in relation to the scapula for the motions. Data was filtered with a 4th lowpass Butterworth filter with a cutoff frequenzy of 3Hz. Data was normalized to 100% of motion and ensembled by group. Standard error was calculated to determine excursion from the mean. Descriptive statistics were determined for all three rotations of the humerus in relation to scapula, translations measuring the movement of the centre of the humeral head in relation to the origin of the scapular coordinate system at the acromial angle.

Results: Excursion values for motion of ensembled data for plane of elevation, angle of elevation and internal/external rotation grew as the range of motion increased in all trials. ABD trials had more excursion than those of FF. Rotation values for ABD and FF were similar to the values previously reported [1]. The surgical intervention group stayed within, or close to the values for the healthy, normal subjects. Variance in plane of rotation and angle of rotation were greater in ABD and FF than AAC(fig1).

Subjects in the healthy group measured ABD rotations at 90 ˚ of -5.77˚ ± 11.96˚ for plane of rotation, 31.44˚ ± 19.09˚ for angle of rotation, and -3.81˚ ± 6.18˚ for axial rotation (external). For the surgical intervention ABD rotations at 90 ˚ were -11.97˚ ± 20.02˚ for plane of rotation, 29.20˚ ± 39.68˚ for angle of rotation, and -9.81˚ ± 3.42˚ for axial rotation (external). Translations at 90 ˚ abduction were 1.74mm ±3.86mm in the x direction, 4.71mm ± 2.96mm in the y direction, and -1.96mm ± 3.88mm in the z direction for the healthy group and 3.23mm ± 4.66mm in the x direction, -9.17mm ± 3.78mm in the y direction, -5.4mm ± 6.12mm in the z direction for the post-surgical intervention group.

The FF rotations at 90 ˚ were -0.17˚ ± 4.79˚ for plane of rotation, 36.19˚ ± 18.58˚ for angle of rotation, and 0.71 ˚ ± 1.97˚ for axial rotation (internal). For the surgical intervention FF rotations at 90 ˚ were 3.55˚ ± 0.25˚ for plane of rotation, 24.26˚ ± 6.36˚ for angle of rotation, and 2.40˚ ± 0.13˚ for axial rotation (internal). Translations at 90 ˚ FF were -1.18 mm ±3.34 mm in the x direction, 1.24mm ± 2.72mm in the y direction, and -1.15mm ± 2.61mm in the z direction for the healthy group

and 0.36mm ± 1.84mm in the x direction, 0.36mm ± 1.84m in the y direction, -1.85 mm ± 3.33 mm in the z direction for the post-surgical intervention group.

Full AAC measured 1.11˚ ±5.50˚ for plane of rotation, 30.09˚ ± 9.84˚ for angle of rotation, and 3.13˚ ± 9.60˚ for axial rotation (internal). For the surgical intervention, full AAC measured 7.41˚ ± 1.21˚ for plane of rotation, 14.65˚ ± 16.33˚ for angle of rotation, and 4.57˚ ± 3.17˚ for axial rotation (external). Translations at full AAC were -1.25mm ± 2.25mm in the x direction, 5.35mm ± 2.90mm in the y direction, and 3.32mm ± 2.61mm in the z direction for the healthy group and 4.96mm ± 0.59mm, 5.82 mm ± 3.63mm, -3.00mm ± 1.37mm for the post-surgical intervention group.

Figure:
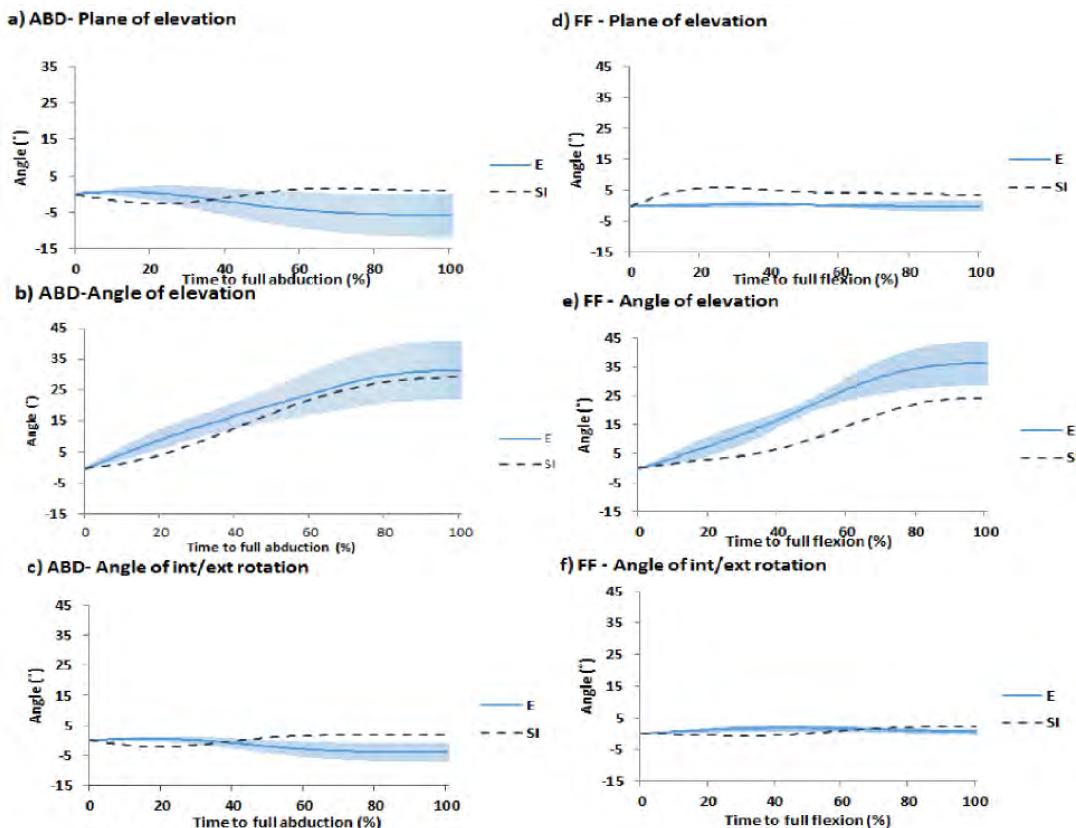
Caption: Figure 1: Rotations for ABD and FF in healthy (E) and surgical intervention (SI) groups

Conclusion: Biplanar fluoroscopy continues to be considered the gold-standard for in-vivo motion quantification. The use of a generic shoulder reduced the amount of radiations subjects were exposed to, while maintaining a high accuracy. Large excursion values illustrate that scapulohumeral motion is quite complicated due to 6 degrees of freedom where various combinations of translations and rotations could facilitate the same response. Subtle differences exist between the group with healthy shoulders and the group with surgical intervention in abduction and significant differences were calculated between groups during FF. Some of these differences may be explained through physical compensation and increased muscular synergies in the post-surgical intervention group.

References: [1] Giphard et al., J Bone Joint Surg, 95:238-245, 2013.

Disclosure of Interest: None Declared

PO-0388

EVALUATION OF FINGER INTERDEPENDENCIES DURING ACTIVITIES OF DAILY LIVING

Victor Gonzalez [1][2],[*]Jennifer Rowson [1][2]Alaster Yoxall [3]

[1]Department of Mechanical Engineering, [2]Insigneo Institute for in silico Medicine, The University of Sheffield, [3]Art and Design Research Centre, Sheffield Hallam University, Sheffield, United Kingdom

Introduction and Objectives: Dexterity assessment is important in the clinical medicine, inclusive design, and biomechanical fields. However, most movement assessment results require an understanding of biomechanics, mathematics and statistics limiting its applicability within clinical and design practice.

This article reports an experimental study that aimed to quantitatively analyse motion correlation patterns across the fingers, and examine the kinematic synergies during manipulative tasks, producing applicable and accessible data for therapy, product design, and research professionals.

Methods: Fifteen subjects performed 5 repetitions of two types of tasks: (1) activities of daily living and, (2) dexterity tests. The tasks were selected as representative of activities requiring the performance of the most commonly used grasping patterns (Table 1) [1][2]. A ten-camera opto-electronic system (Vicon, UK) measured trajectories of 26 reflective markers placed on selected hand dorsum landmarks (metacarpal base, MCP joints, proximal interphalangeal joints, distal interphalangeal joints and the nail).

Planar angular profiles for flexion–extension movements of the Metacarpophalangeal, Proximal Interphalangeal and Distal Interphalangeal joints, along with Thumb Abduction were derived from the measured markers' coordinates.

Cross-correlation coefficients were calculated for the joint angles corresponding to the selected movements for all tasks across all subjects and correlation matrices were derived from these values, representing finger movement interdependencies (Figure 1).

Results: Correlation matrices showed patterns of higher correlation (average 0.91, s.d. +/- 0.02) between joint angles for tasks requiring manipulation of small objects (Figure 1). Correlation patterns from dexterity tests confirmed this tendency across all subjects.

Higher correlation coefficients between motions were related with high proficiency in the dexterity tests for all subjects, even in those tasks requiring large object manipulations. Correlation matrices from the dexterity tests showed participants with the highest test scores had higher correlation coefficients among joint angles (Avg. 0.90, s.d. +/-0.03).

Subjects' movement correlation patterns suggest that, finger interdependency, required to proficiently complete a task, is related to the size of the object being manipulated. However, it is notable that in tasks requiring manipulation of larger objects, correlation values were lower, indicating that finger interdependencies are not necessary to accomplish all tasks proficiently.

There are convergences between new findings on kinematic synergies yielded from this study and some previous findings on hand coordination [3][4]. The current study shows a general trend of motion interdependence decreasing with anatomical distance and also a clear relationship between finger interdependency and performance of manipulative tasks. These findings are supported by what has been found from alternative methods of finger coordination quantification[3][5].

Figure:
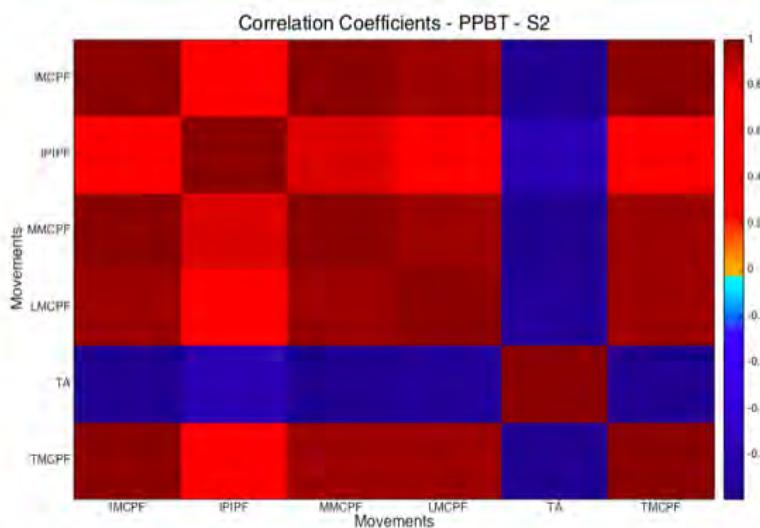
Figure 1. Correlation coefficients during completion of the Purdue Pegboard Dexterity Test for the measured movements: Index MCP Flexion (IMCPF), Index PIP Flexion (IPIPF), Middle MCP Flexion (MMCPF), Little finger MCP Flexion (LMCPF), Thumb Abduction (TA), and Thumb MCP Flexion (TMCPF)

Conclusion: The present study quantified finger interdependencies during several common manipulative tasks. Although such multi-joint acts could be carried out in seemingly an infinite number of ways, notable motion patterns do emerge as evidenced in this study. Correlation matrices allow for more applicable and accessible data, showing interdependencies patterns in a clear, observable representation. The study also rendered evidence to support the conjecture that while finger coordination is responsible for proficiency during manipulative tasks, finger interdependencies are not necessary for all types of tasks.

Table:

Task	Grasping pattern observed
Opening soft drink bottle	*Precision grip* *Cylinder grip* *Spherical grip*
Opening plastic package	*Precision grip*
Buttoning shirt	*Precision grip*
Feeding with spoon	*Lateral grip* *Precision grip*
Drinking from cup	*Cylinder grip*
Variable Dexterity Test	*Precision grip* *Cylinder grip* *Spherical grip*
Purdue Pegboard Test	*Precision grip*

Caption: Table 1. Tasks selected for the study and their required grasping patterns.

References: [1] Light et al., Arch Phys Med Rehabil, *83*(6), 776–783, 2002.

[2] Taylor et al., *Artificial Limbs*, *2*(2), 22–35, 1955.

[3] Braido et al., *Human Movement Science*, *22*(6), 661–78, 2004.

[4] Darling et al., *Journal of Biomechanics*, *27*(4), 479–91, 2004.

[5] Sancho-Bru, et al., *Proc IMechE Part H, J Engineering in Medicine*, *228*(2), 182–9, 2014.

Disclosure of Interest: None Declared

DEFINITION AND ASSESSMENT OF A MODIFIED CONSTANT SCORE THAT ACCOUNTS FOR ALTERATIONS IN SCAPULA KINEMATICS

Andrea Giovanni Cutti [1,*]Ilaria Parel [2]Andrea Pellegrini [3]Rinaldo Sacchetti [1]Paolo Paladini [4]Giuseppe Porcellini [4]Giovanni Merolla [4]

[1]Research & Development, Centro Protesi INAIL, Vigorso di Budrio, [2]"M. Simoncelli " Biomechanics Laboratory, Cervesi Hospital, Cattolica, [3]Clinica Ortopedica, Università di Parma, Parma, [4]Unit of Shoulder and Elbow Surgery, Cervesi Hospital, Cattolica, Italy

Introduction and Objectives: The Constant-Murley score (CMS) [1] is one of the most popular outcome measures for shoulder function [2,3]. It comprises 3 self-reported (pain and daily living) and 5 performance-based (shoulder mobility in elevation/rotation and strength) items, with score from 0 (worst) to 100 (best) points. During the assessment of mobility, only the humero-thoracic elevation is rated. Scapula kinematic alterations (dyskinesis) are not taken into account. This increases the risk of patients' suboptimal treatment, because an essential part of shoulder movement is neglected.

The first aim of this study was to propose a modification of CMS to account for alterations in the scapulo-humeral coordination (SHC). The new score was named Scapula-Weighted CMS (SW-CMS). The second aim was to evaluate the impact of these modifications on the scores of a group of patients after rotator cuff surgery. The ultimate goal is to understand how many patients are recovering a SHC similar to the one of the contralateral side and plan corrections in the rehabilitation approach, if needed.

Methods: We propose to weight the points for the humerus-thoracic elevation, based on the "affected-to-contralateral side difference in SHC" being greater than the typical difference in asymptomatic controls. The weighting factors W_{FE} and W_{AA} range between 0 and 1, and multiply the scores for humerus elevation in the sagittal and frontal plane, respectively (max 20 points). For a given patient, the value of W_{FE} and W_{AA} depends on the comparison of the side-to-side differences in SHC, with reference bands of asymptomatic subjects. For the motion analysis protocol ISEO [4], this set of reference prediction bands is available, separately for each scapula angle, i.e. protraction-retraction (PR-RE), medio-lateral rotation (ME-LA) and posterior-anterior tilting (P-A) [5]. In details, W_{FE} is calculated using the following rule; if the side-to-side difference during forward flexion is within the band for:

1) PR-RE vs FL-EX: $W_{FE\_PRRE}=0.3$

2) ME-LA vs FLEX: $W_{FE\_MELA}=0.3$

3) P-A vs FLEX: $W_{FE\_PA}=0.3$

4) if A, B, C are true then, $W_{FE\_BONUS}=0.1$

$W_{FE}=W_{FE\_PRRE}+W_{FE\_MELA}+W_{FE\_PA}+W_{FE\_BONUS}$

Similarly for W_{AA}, considering the elevation in the frontal plane.

The normalization of the CMS score of one side with the score of the contralateral increases the sensitivity and specificity [6]. This normalization was thus assumed for CMS and SW-CMS.

CMS and SW-CMS were applied on 32 patients (53±9 year-old, 15 males) surgically treated for rotator-cuff tear, after giving the informed consent. Each patient was assessed by a single rater at 45, 70, 90 days and > 6 months post-surgery (follow-up). Two hypotheses were then tested:

H1) CMS does not implicitly account for scapula-thoracic alterations: at each time, CMS and SW-CWS scores are significantly different;

H2) when SHC alterations are taken into account as in SW-CMS, the patients assigned a "good score" (>80 – [7]) decreases, but the "successful" patients are the 90% at 90 days.

To answer to H1 a linear mixed model with repeated measures was run in SPSS 17. The repeated measures were the *Scoring* system (fixed; CMS, SW-CMS) and the *Time* (fixed+random; 45, 70, 90, >6 months). Pairwise comparisons were calculated within *Time*, *Scoring* and their interactions. To answer to H2, at each *Time* we calculated the number of patients with a score >80 points for CMS and SW-CMS.

Results: Differences in *Scoring*, *Time*, and their interaction were statistically significant ($p < 0.40$). At each *Time*, CMS and SW-CMS were statistically different ($p<0.000$), with differences increasing from 6.5 to 10.25 points, at 45 days and follow-up, respectively. This supports the validity of H1.

Figure 1 reports the number of patients with scores >80 for CMS and SW-CMS at each time point. While both scores agree at 45 days, the difference in classification reaches a peak of 70% at 90 days: while for CMS 10/32 patients featured a "good" recovery, for SW-CMS only 3/32 exceeded 80 points. This indicates that H2 is unsupported.

Figure:

Time	CMS (absolute and %)	SW-CMS (absolute and %)	(CMS – SW-CMS)/CMS (%)
45	0 (0%)	0 (0%)	0%
70	4 (19%)	2 (9,5%)	50%
90	10 (31%)	3 (9,5%)	70%
Follow-up	28 (87,5%)	16 (50%)	43%

Caption: Figure 1. The number of patients with CMS and SW-CMS scores > 80 points.

Conclusion: Based on the results, CMS does not implicitly account for the SHC alterations. Moreover, results for H2 point out that the recovery of SHC is challenging and a minority of patients achieve this goal, especially at 90 days post-op. Therefore, improved rehabilitation programs for scapula-control should be implemented, e.g. through biofeedback.

References: [1] Constant C et al., JSES, 17:355-61, 2008.

[2] Kirkley A et al., Arthroscopy, 19: 1109-1120, 2003.

[3] Provencher MT et al., Phys Sportsmed, 42(3):120-30, 2014.

[4] Cutti AG et al., MBEC, 46(2):169-78, 2008.

[5] Cutti AG et al., J Biomech, 47(5):1035-44, 2014.

[6] Fialka C et al., Injury, 36:1159-1165, 2005.

[7] Iannotti JP et al., JSES, 5(6):449-57, 1996.

[8] Kibler WB et al., Br J Sports Med, 47:877-885, 2013.

Disclosure of Interest: None Declared

PRINCIPAL COMPONENT ANALYSIS APPLICATION ON SCAPULOTHORACIC KINEMATIC IN HEALTHY AND SHOULDER PAIN SUBJECTS

Denise M. Rossi [1,*]Renan Resende [2]Sérgio Fonseca [3]Anamaria Oliveira [1]

[1]Department of Biomechanics, Medicine and Rehabilitation of Locomotive Apparatus, Ribeirao Preto Medical School - University of São Paulo, Ribeirão Preto, [2]Department of Physiotherapy, Faculty of Biological Sciences and Health, Universidade Federal dos Vales do Jequitinhonha e Mucuri, Diamantina, [3]Department of Physiotherapy, School of Physical Education, Physiotherapy and Occupational Therapy, Universidade Federal de Minas Gerais, Belo Horizonte, Brazil

Introduction and Objectives: Appropriate scapular position and movement is fundamental to maintenance of stress and forces transmission mechanism and this knowledge is important to evaluation and intervention of shoulder clinical conditions [1,2]. There is evidence of scapular involvement in several types of shoulder pathology, but there is limited understanding of scapula role in creating or exacerbating shoulder disorders [3]. Furthermore, kinematic alterations are also present in asymptomatic persons [4]. Physical therapists are specialized in management of movement related disorders and are able to differ non-desirable movement from typical movement and kinematics methods make these observations measurable and quantifiable [5]. Variability is an inherent feature of human movement and it can provide notable information concerning the neuromuscular system function [6]. Principal Component Analysis (PCA) is a decomposition technique used to identify patterns of variation in the waveform data that are independent of each other, thus allowing comparisons of different features of the data. Although PCA has been extensively used in biomechanics, it has not been frequently applied to shoulder complex [6]. Therefore, the purpose of this study was to apply PCA on scapulothoracic kinematics data of healthy and shoulder pain subjects in order to investigate differences between groups.

Methods: This study demonstrates preliminary data of 11 participants divided into two groups. Shoulder pain group (SPG) included five participants with shoulder pain and the control group (CG) had six participants without shoulder pain. Symptomatic group included subjects with painful arc and positive impingement tests (Hawkins-Kennedy and Neer). Three-dimensional position and orientation of each subject's thorax, scapular and humerus were tracked (120 Hz sampling rate) using electromagnetic Liberty ® (Polhemus Inc) system according to ISB international recommendations. After fixing sensors and digitization of landmarks in anatomical segments, data were collected during the arm elevation and lowering in the sagittal plane. Analyses were performed in dominant member in CG and member painful in SPG. Ten complete elevation-lowering cycles were collected, but only one of the three last was considered for PCA analysis. The analysis of scapular movements relative to the thorax was made using Euler angle rotation sequence of YX'Z'' and for the humeral movements relative to the thorax was used XZ'Y''. The PCA was applied to determine the main features of the scapulothoracic kinematics in the waveform data. PCA generates principal components, which represent the patterns of variation in the original data. In addition, PCA generates scores for each original waveform on each principal component (PC), and these scores are used as dependent variables for comparisons between groups. The PCA analysis was performed to each scapular movement, inernal/external rotation, upward/downward rotation and anterior/posterior tilt,

during the arm elevation and lowering, separately. A criteria of 90% of variance explained was used to determine the number of principal components to retain for data analysis The movement cycle was normalized in 100 points between 20° and 120° of humerothoracic elevation. Student's t-Test for Independent Samples was performed to comparison between groups with α set at 0.05.

Results: The SPG group demonstrated increased scapular anterior tilt during the lowering phase when compared to the CG group ($p = 0.05$). The first PC captured 88.13% of the total variance observed in scapular tilt over time and across participants. The PC2 captured 10.52% of the total variance, but only the score of PC1 differed between groups, being lower for the SPG. Figure 1A shows that the PC1 loading vector contains coefficients of large magnitudes corresponding to scapular tilt values during the entire lowering phase. The reconstructed waveforms displayed in Figure 1B suggest that lower mean score of the SPG reflects lower magnitude of posterior tilt, i.e. increased scapular anterior tilt.

Figure:
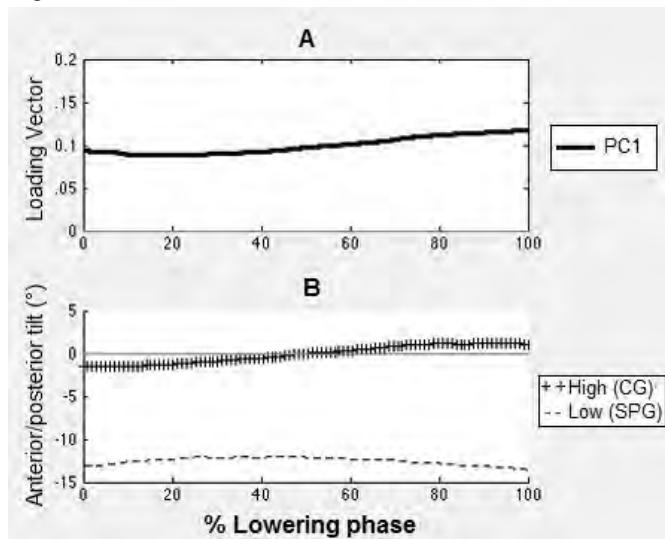
Caption: Figure 1. (A) The loading vector for PC1. (B) Scapular anterior/posterior tilt corresponding to high and low PC1 scores demonstrate the difference in magnitude during the entire lowering phase. Higher scores for control group (CG) and lower scores for shoulder pain group (SPG). Negative number indicates anterior tilt.

Conclusion: There is difference evidence in scapulothoracic kinematics waveform data between healthy and shoulder pain subjects. Despite small sample, pain seems to influence the variability pattern in order to increase scapular anterior tilt during the arm lowering.

References: [1] Levin, Biomed Sci Instrum. 33: 412-417, 1997.

[2] Roren et al., Manual Ther, 1-10, 2014.

[3] Kibler et al., Br J Sports Med, 47: 877-885.

[4] Uhl et al., J Arthrosc Relat Surg 25: 1240-1248, 2009.

[5] Spinelli et al., Manual Ther, 1-6, 2014.

[6] Jayaraman et al., Plos One, 9: e89794, 2014.

Disclosure of Interest: None Declared

Upper Limb

PO-0391

INFLUENCE OF HUMERAL POSITION AND EXTERNAL LOAD ON ELECTROMYOGRAPHICAL ACTIVITY OF TRAPEZIUS AND SERRATUS ANTERIOR MUSCLES DURING EXTERNAL SHOULDER ROTATION

Vilma Juodzbaliene [1,*] Giedre Jurgelaitiene [1] Rolandas Kesminas [1] Giedre Valiukaite [1]

[1] Applied Biology and Rehabilitation, Lithuanian Sports University, Kaunas, Lithuania

Introduction and Objectives: The position and movements of scapula is essential for appropriate humeral head position and for stable base to support motions of the shoulder in daily life and sport activities. Trapezius and serratus anterior is the most important muscles to stabilize scapula during upper extremity movements [1, 2]. Scapula dyskinesis occur 68 – 100% of shoulder injuries [3]. In a many studies scapula dyskinesis was found in patients with shoulder impingement syndrome, rotator cuff tendinopathy and tears, adhesive capsulitis, shoulder instability [4, 5, 6]. The aim of shoulder injuries rehabilitation – restore the position of scapula and movements in scapulothoracic joint. Conservative treatment consist of scapula stabilizers strengthening, therefore it is important to choose the right exercise on shoulder rehabilitation protocol [7]. External shoulder rotation at 90°of humeral abduction was suggested for scapula stabilizers strengthening [8]. It is important to know influence of different humeral position and different external load during external shoulder rotation [8]. **Goal of the study**: Evaluate influence of humeral position and external load on electromyographical activity of trapezius and serratus anterior muscles during external shoulder rotation.

Objectives of the study:

1. Evaluate electromyographical activity of upper, middle and lower parts of the trapezius and serratus anterior muscles.

2. Evaluate electromyographical activity of upper, middle and lower parts of the trapezius and serratus anterior muscles.

3. Compare electromyographical activity between upper, middle and lower parts of the trapezius and serratus muscles.

Methods: Subjects: 18 highly physically active (according IPAQ) non professional athletes took part in the study (age 20-25 years, dominant hand - right).

Criteria of subject inclusion: there is no pain in the shoulder region, have no previous shoulder injuries or surgery, full ROM, have no systemic diseases, no scapular dyskinesis, normal BMI and correct posture.

Methods: Electromyographical activity of upper, middle and lower trapezius as well as serratus anterior was registered using surface electrodes during external shoulder rotation at 0°, 45° and 90° of shoulder abduction and with different external load.

Results: External shoulder rotation produced highest electrical activity of trapezius and serratus anterior muscles at 90° of shoulder abduction and lowest at 0° of shoulder abduction ($p<0,05$). Electromyographical activity of trapezius and serratus anterior muscles was higher increasing the load on external shoulder rotation ($p<0,05$). Lower trapezius was the most active during external shoulder rotation at all shoulder loading positions. Upper trapezius and serratus anterior was least active at 0° of shoulder abduction ($p<0,05$).

Conclusion: Electromyographical activity of trapezius and serratus anterior muscles increase with greater external load and shoulder abduction from 0 to 90°.

References: [1] Neumann. Kinesiology of the musculoskeletal system: foundations for physical rehabilitation, 2 edition. Mosby, Elsevier, 2010.

[2] Struyf et al., Scand J Med Sci Sports, 21 (3): 352-358, 2011.

[3] Voight et al., J Athl Train, 35 (3): 364-372, 2000.

[4] McClure et al., Phys Ther, 86 (8): 1075-1090, 2006.

[5] Michener et al., Clin Biomech, 18 (5): 369-379, 2003.

[6] Ogston et al., & Ludewig, Am J Sports Med, 35 (8): 1361-1370, 2007.

[7] Struyf et al., Clin Rheumatol, 32 (3): 417-429, 2012.

[8] Schachter et al., J Shoulder Elbow Surg, 19: 884-890, 2010.

Disclosure of Interest: None Declared

Upper Limb

PO-0392

CAN WE NEGLECT AGE-SPECIFIC DIFFERENCES IN THE SCAPULO-HUMERAL COORDINATION WHEN EXAMINING A PATIENT?

Ilaria Parel [1] [2],*Rinaldo Sacchetti [1]Giovanni Merolla [2]Giuseppe Porcellini [2]Andrea Giovanni Cutti [1]

[1]INAIL Centro Protesi, INAIL, Vigorso di Budrio, [2]Laboratory of Biomechanics, Cervesi Hospital - AUSL della Romagna, Cattolica, Italy

Introduction and Objectives: The assessment of scapulo-thoracic motion in relation to humerus elevation, i.e. the "scapulo-humeral coordination" (SHC), plays a central role in the clinical management of patients with shoulder disorders [1]. SHC is typically evaluated by means of coordination plots, where SHC is described as a curve that correlates scapula angles variation to humerus elevation. To date, several quantitative motion analysis protocols have been developed to support in the examination of the multi-planar SHC, but, in order to use them in the clinical practice, reference values are essential. To answer this need, for the ISEO protocol [2] a set of reference prediction bands (RPB) was calculated [3], and, to date, ISEO is the only protocol that provides reference data for clinical assessment. These data were calculated separately for each scapula angle, i.e. protraction-retraction (PR-RE), medio-lateral rotation (ME-LA) and posterior-anterior tilting (P-A), during humerus elevation. RPB were computed for three age-stratified groups and differences in shape of RPB were described qualitatively. The aim of this study is to quantify the probability of misclassification when the kinematics of a patient is compared to RPB based on data of a not correspondent age-group.

Methods: One hundred eleven asymptomatic subjects (mean age ± SD: 38 ± 14) were recruited for this study after giving their informed consent. The subjects were split in 3 groups, depending on the age:

- G1, from 18 to 30 year-old, 46 subjects;
- G2, from 31 to 50 year-old, 35 subjects;
- G3, from 51 to 70 year-old 30 subjects.

The 90% coverage probability RB for humerus elevation both in the sagittal (FL-EX) and scapular (AB-AD) plane reported by Cutti et al [3] were considered. To assess the risk of misclassification of reference data from G1, a cross-comparison analysis was conducted. Kinematic data of subjects from G2 and G3 were compared to RB from G1 and cover-indexes (CI) calculated:

- CI = (total n° of subjects – n° subjects out of the band/interval) / total n° of subjects

Considering 0.87 as the minimum coverage probability resulting from comparison of group data with correspondent RB (e.g. kinematic data of subjects from G1 compared to G1-RB), the coverage probability was classified as good when CI ≥ 0.87, moderate when $0.87 > CI ≥ 0.77$, poor when $0.77 > CI ≥ 0.67$ and very poor when $CI < 0.67$. The same cross-comparison analysis was conducted also for G2 and G3.

Results: Results are summarized in Figure 1. Risk of misclassification is increased as follows:

- < 10%, green bars, for 29/72 (40%) bands (11 in FL-EX, 18 in AB-AD);
- 10%, orange bars, for 25/72 (35%) bands (15 in FL-EX, 10 in AB-AD);
- 20%, red bars, for 10/72 (14%) bands (5 in FL-EX, 5 in AB-AD);

- 30% or more, brown bars, for 7/72 (10%) bands (4 in FL-EX, 3 in AB-AD).

Figure:
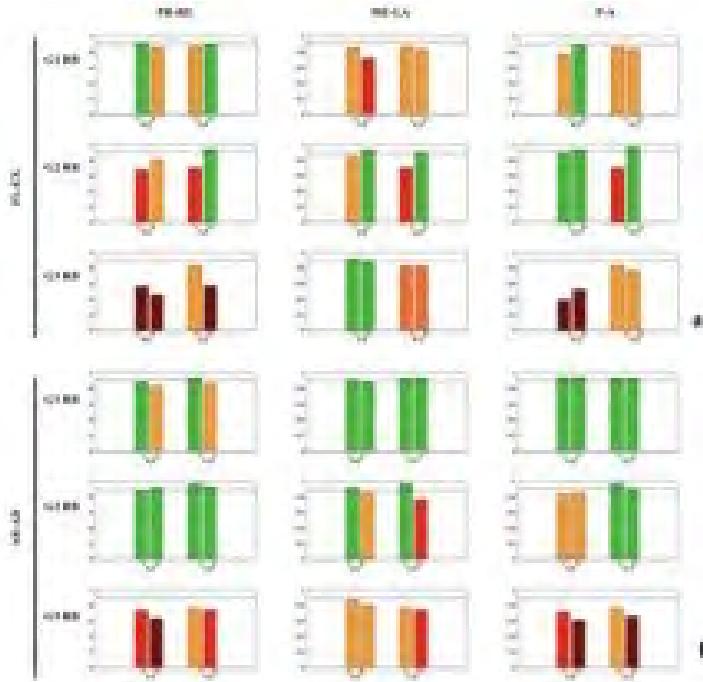
Caption: Results from cross-comparison analysis for RPB in FL-EX and AB-AD. Each row reports comparisons with respect to G1, G2 and G3 for RPB in FL-EX (a) and AB-AD (b). Each column reports results for the three scapula angles: PR-RE, ME-LA and P-A. Within each subplot, CIs from the comparison of upward (U) and downward (D) RPB with respect to "other" groups are reported. Color classification: green CI ≥ 0.87; orange 0.87 > CI ≥ 0.77; red 0.77 > CI ≥ 0.67; brown CI < 0.67.

Conclusion: Results from the analysis of the coverage probability in cross-comparison analyses highlighted that the specificity of each group should be taken into account: a general decrease of the classification-power occurs when the kinematics of a subject is compared to reference data obtained from subject belonging to other age-group. Orange, red and brown bars indicate that excessive sensitivity of the RPB can increase the risk of false-positive results, i.e. a sound kinematics is classified as altered. Otherwise, if a minimization of the risk of false-positive is sought, G1 RPB can be used to classify G2 and G3, lowering the specificity of the analysis, and increasing the risk of false-negative, i.e. an altered kinematics is classified as sound.

References: [1] Ludewig PM et al., J Bone Joint Surg Am, 39(2): 90-104, 2009

[2] Cutti AG et al, MBEC, 46:169-178, 2008

[3] Cutti AG et al, J Biomech, 47:1035-1044, 2014

Disclosure of Interest: None Declared

CORRELATION OF 3-D SCAPULAR KINEMATICS TO FUNCTION IN SUBJECTS WITH CHRONIC STROKE

Maíra Lixandrão [1,*] Paula Camargo [1] Christiane Prado-Medeiros [1] Tania Salvini [1]

[1] Departament of Physical Therapy, Universidade Federal de São Carlos, São Carlos, Brazil

Introduction and Objectives: Motor impairments following stroke may lead to scapular abnormal movements and thus can limit upper limb function. Position and control of the scapula on the thorax play a critical role in normal function of the shoulder. Scapular motions on the thorax align the glenoid fossa with the humeral head maximizing joint congruency and providing a stable base for humeral motion (Phadke et al., 2009). Therefore, an adequate scapular function can be critical for place the hand through a wide range of motion in space during activities of daily living. However, it is not known yet if there is a correlation between scapular kinematics and upper limb functionality after chronic stroke.

Methods: Fifteen individuals with chronic stroke (11 male and 4 female; 11 with dominant arm as more-affected arm; 58.14 ± 7.89 years; 24.49 ± 3.27 Kg/m²) were included in the study. Upper limb functionality was evaluated using Motor Activity Log (MAL). This instrument is a structured interview intended to examine how much and how well the subject uses their more-affected arm to accomplish 30 activities of daily living outside of the laboratory setting. The MAL is composed of quantitative and qualitative scales. Both of them are scored on six points, ranging from zero (never used) to five (the same as pre-stroke), and participants may select halfway scores. In each scale a total score corresponds to the mean of the items, calculated by the sum of the scores of all items, divided by the number of the accomplished items responded (minimum score = 0 and maximum score = 5 points). Kinematic data were collected using the Flock of Birds® electromagnetic tracking system during elevation and lowering of the more-affected arm in the scapular plane. Local coordinate systems were established for the trunk, scapula, and humerus using the digitized landmarks, following the International Society of Biomechanics recommended protocol (Wu et al., 2005). Five repetitions of the activity were recorded with subjects in the sitting position and trunk stabilized. Data analysis for scapular orientation was performed for selected angles of humerothoracic elevation (30°, 60° and 90°) and lowering (90°, 60° and 30°). Data were analyzed with the SPSS statistical package. Kolmogorov-Smirnov tests were used to check data normality. Once data do not present normal distribution a Spearman correlation test was used to identify correlations between scapular motion and MAL scores. The level of significance was considered 5%.

Results: A moderate correlation was found between MAL quantitative scale and scapular internal rotation during lowering of the arm at 60º (r =0.68, p =0.005) and 30º (r =0.60, p =0.01). MAL quantitative scale also correlated with scapular tilt during lowering of the arm at 90° (r =0.63, p =0.01). A moderate correlation was observed between MAL qualitative scale and scapular internal rotation during lowering of the arm at 90º (r =0.61, p =0.01), 60º (r =0.62, p=0.01) and 30º (r = 0.59, p =0.02). A high correlation was found between MAL quantitative scale and scapular internal rotation during lowering of the arm at 90º (r =0.72, p =0.002) and between MAL qualitative scale and scapular tilt during lowering of the arm at 90º (r =0.72, p =0.02). There was no correlation between scapular upper rotation and MAL scores (p>0.05). Scapular movements are necessary to accomplish activities like feeding, combing hair, reaching overhead and washing the

contralateral axilla (Rundquist et al., 2011). Our results showed that scapular specific movements are related to general functionality of more-affected arm in stroke patients. Scapular internal rotation during lowering of the more-affected arm at high angles seems to be more related to quantity of upper arm movements whereas scapular tilt seems to be more related to quality of upper arm movements in stroke patients.

Conclusion: More-affected upper limb functionality is correlated to scapular internal rotation and scapular tilt during lowering of the arm in scapular plane in chronic stroke subjects. Interventions addressing these scapular movements in chronic stroke patients may improve performance of activities of daily living.

References: [1] Phadke V, Camargo PR, Ludewig PM. Scapular and rotador cuff muscle activity during arm elevation: A review of normal function and alterations with shoulder impingement. Bras J of Phys Ther. 2009;13(1):1-9.

[2] Wu G, van der Helm FC, Veeger HE, et al. ISB recommendation on definitions of joint coordinate systems of various joints for the reporting of human joint motion--Part II: shoulder, elbow, wrist and hand. J Biomech. 2005;38:981-992.

[3] Rundquist PJ, Obrecht C, Woodruff L. Three-dimensional shoulder kinematics to complete activities of daily living. Am J Phys Med Rehabil. 2009;88:623-629.

Disclosure of Interest: None Declared

PO-0393-1

IN VIVO CONTACT STRESS EVALUATION IN THE TRAPEZIOMETACARPAL JOINT USING FINITE DEFORMATION BIPHASIC THEORY AND MATHEMATICAL MODELING

Benjamin Dourthe [1],[*]Priscilla D'Agostino [1] [2]Faes Kerkhof [1]Evie Vereecke [1]

[1]Development and Regeneration, KU Leuven, [2]AZ Groeninge, Kortrijk, Belgium

Introduction and Objectives: Osteoarthritis (OA) is a degenerative joint disease characterized by the loss of articular cartilage and remains a complex, disabling disease which cause is not completely understood.

Evaluating the stress distribution within the trapeziometacarpal (TMC) joint during daily activities is a clinically relevant way to investigate the biomechanical behavior of this complex articular system. Such insights will also lead to a better understanding of joint functioning and can help predict which part of the joint will be primarily affected by degenerative changes in the onset of OA. This is particularly important in establishing new prevention approaches.

The main objectives of this study are: (1) to evaluate the amount of stress occurring around the first metacarpal (MC1) and the trapezium bone during different isometric tasks, and (2) to identify which specific articular region undergoes the highest level of stress according to various loaded positions.

Methods: After permission by the medical ethical commission of the University, CT scans were obtained from 20 female volunteers (mean age: 60.8 years) using a 64 slice Discovery HD 750 CT scanner (GE Healthcare) in AZ Groeninge, Belgium. Static CT scans (slice thickness: 0.625mm, pixel size: 0.391 mm) of the hand region were taken in three different configurations: relaxed neutral, lateral key pinch and power grasp, using a radiolucent jig with embedded load cell (Brown University, USA). The applied force was recorded during a submaximal effort (80% of maximal strength) during each task. Each scan was segmented and 3D bone models were created using Mimics v. Research 17.0 x 64 (Materialise, Belgium). Four subjects showing signs of OA were excluded from the study. The total articular area of each bone was evaluated manually using 3-matic v. Research 9.0 x 64 (Materialise, Belgium). A custom-written MatLab code - based on the finite deformation biphasic theory[1] and cartilage deformation properties taken from the literature[1], [2] - was used to evaluate the contact area for each bone, as well as the contact stress distribution. The location of the most stressed area was evaluated using a quadrant division as defined by Momose et al (1999)[3].

Results: We observed no significant difference between the total articular area of MC1 and the trapezium of each subject. The trapezium, however, had a slightly smaller contact area compared to MC1. This difference was only statistically significant in the lateral pinch position ($p < 0.05$; neutral: $p = 0.05$; grasp: $p = 0.07$). The contact stress calculation revealed a similar maximal contact stress value between the neutral position and the lateral key pinch task, while this parameter was increased during the power grasp. Similar results were found by studying the average stress distribution across the joint. We observed a stress concentration around the volar beak of MC1 and the volar-ulnar aspect of the trapezium in the neutral position, as well as in the lateral key pinch position, with a few subjects showing a stress concentration around the radial aspect of the trapezium. The ulnar aspect of both MC1 and the trapezium was shown as the most constrained during power grasp with a strong consistency between subjects.

Figure:
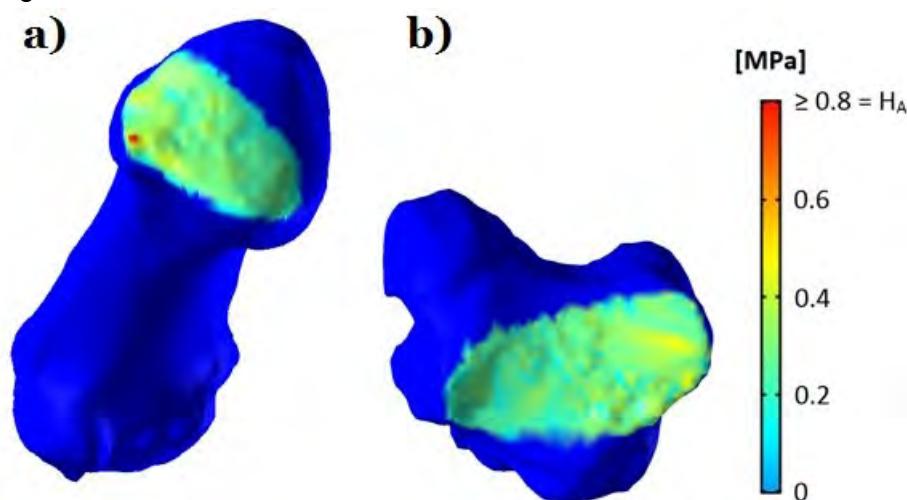
Caption: Stress distribution in the TMC joint of one subject during power grasp - a) MC1 - b) Trapezium (right hand)

Conclusion: These results suggest that for a similar load, the contact area of the trapezium appears to be smaller than for the first metacarpal, at least in the pinch position. This could show a larger stress concentration on specific aspects of the trapezium, which we assume to indicate that the trapezium is the first bone of the TMC joint to be affected by degenerative changes. However, a larger sample size is needed to further investigate this with a higher statistical power. Such insights could be of high interest in predicting which component of the TMC joint will be primarily affected by degenerative changes. Moreover, we observed a higher average stress value in the power grasp configuration compared to the neutral position and the lateral pinch task. This could highlight two interesting findings: (1) lateral key pinch does not represent a critical task to evaluate stressful configurations in the TMC joint, (2) performing a power grasp can elicit higher amounts of stress in the TMC joint, which is of interest when studying joint stability. Furthermore, the consistency of the results regarding the stress location for the different positions provides a relevant way of understanding the biomechanics of this complex joint. This study shows the importance of performing in vivo assessments of the mechanical behavior of the TMC joint by using advanced modelling techniques to provide a better understanding of this articular system in the early onset of osteoarthritis.

References: [1] Kwan et al., J. Biomech, 23: 145-155, 1990

[2] Koff et al., J Hand Surg, 28A: 597-604, 2003

[3] Momose et al., J. Hand Surg, 24A: 491-495, 1999

Disclosure of Interest: None Declared

PO-0394

COMSOL ANALYSIS OF WHEELCHAIR PUSHRIM SIX DOF LOAD CELL FOR QUANTIFYING PROPULSION EFFICIENCY BY SENSEWHEEL

Tatsuto Suzuki [1,*]Catherine Holloway [1]Andrew Symonds [2]Peter Smitham [3]Stephen Taylor [2]

[1]Civil, Environmental & Geomatic Engineering, [2]Biomedical Engineering, [3]Orthopaedic Surgery, University College London, London, United Kingdom

Introduction and Objectives: Manual wheelchair users rely on their upper extremities for self-propulsion of their wheelchair. This, over time, causes many users to suffer shoulder pain and injury, due to unconscious overuse [1]. Training in cost-efficient pushing style has the potential to alleviate pain, with resulting NHS savings. This can be assessed by measuring the 3D force acting at the pushrim.

The SenseWheel is a lightweight force-sensing handrim, comprised of three identical load cells. The load cells are interposed between the pushrim and drive wheel. The initial design SenseWheel Mk 1 measured the three orthogonal forces Fx, Fy and Fz, and axial torque Tx, applied at each load cell [2]. It has been constructed, calibrated, and used in a limited clinical trial. SenseWheel Mk1 is: 1) light weight (less than 100g), 2) able to fit s different diameter wheel or hand rim and 3) Waterproof. This paper describes the development of an improved Mk2 version of Sensewheel which uses wireless 6DOF load cells to measure Fx, Fy, Fz, Tx, Ty, and Tz. This will simplify the coupling to the wheel and handrim. Each load cell will transmit its data via Bluetooth to a master tablet/SmartPhone carried by the user or held remotely.

Methods: COMSOL was used to redesign the 6DOF load cell, using 8 quarter-bridge strain gauges equi-spaced around the inner circumference of the widest part of the load cell for good strain sensitivity and selectivity. This provided some redundancy in case of non-optimal gauge placement in the actual load cell. Each load cell is 40mm diameter at its widest, to accommodate coin cell, Bluetooth module and flexible printed circuit. The optimum orientation of the gauges was determined using COMSOL Multiphysics® with a 3D axis-symmetric finite element model generated from a 2D cross sectional model. The load cell was designed as two halves, to be screwed together after assembly, and this was modelled in COMSOL as one part. COMSOL was set to output direct strains (eX, eY, and eZ) as well as shear strains (eXY, eYZ, and eZX) in response to applied forces Fx, Fy, Fz, and torques Tx, Ty, and Tz. The strains were calculated at 5 deg intervals along the circumference of the inside wall of the load cell. These strains were then converted from the global axis of the model to the local axis at each strain gauge site using a rotation transformation matrix. The resulting strains were used to investigate both the sensitivity of each gauge to each load type, and also the selectivity of each load type. The gauge angle w.r.t. the longitudinal axis of the load cell was varied, and the strain sensitivities logged. The gauges of one semicircle of gauges were angled opposite the other semicircle to allow for separation between Fx and Mx, as previously used in an instrumented shoulder implant [3]. The correlation coefficient between force/moment pairs was then calculated to predict the optimum angle, which would give best separation between these load types. Importantly, this analysis demonstrated that the strain response, of 8 strain gauges at 45deg intervals around the circumference, to each applied load direction. is clearly distinguishable from the other load types.

Results: The peak sensitivity of the strain output by radial position, for several strain gauge angles w.r.t. the longitudinal axis, and the correlation coefficient between same axis force/moment pairs, is shown in Table 1. Figure 1 shows the strains at 5 deg increments around the circumference, for a gauge angle of 45deg, which gave a compromise between good strain sensitivity to each applied load, and adequate selectivity between load types. The designed load cells will now be manufactured, and following assembly each load cell will be calibrated to relate each strain output to each load type applied via a cross-sensitivity matrix, and measured loads are then combined to find the resultant force system on the pushrim.

Figure:
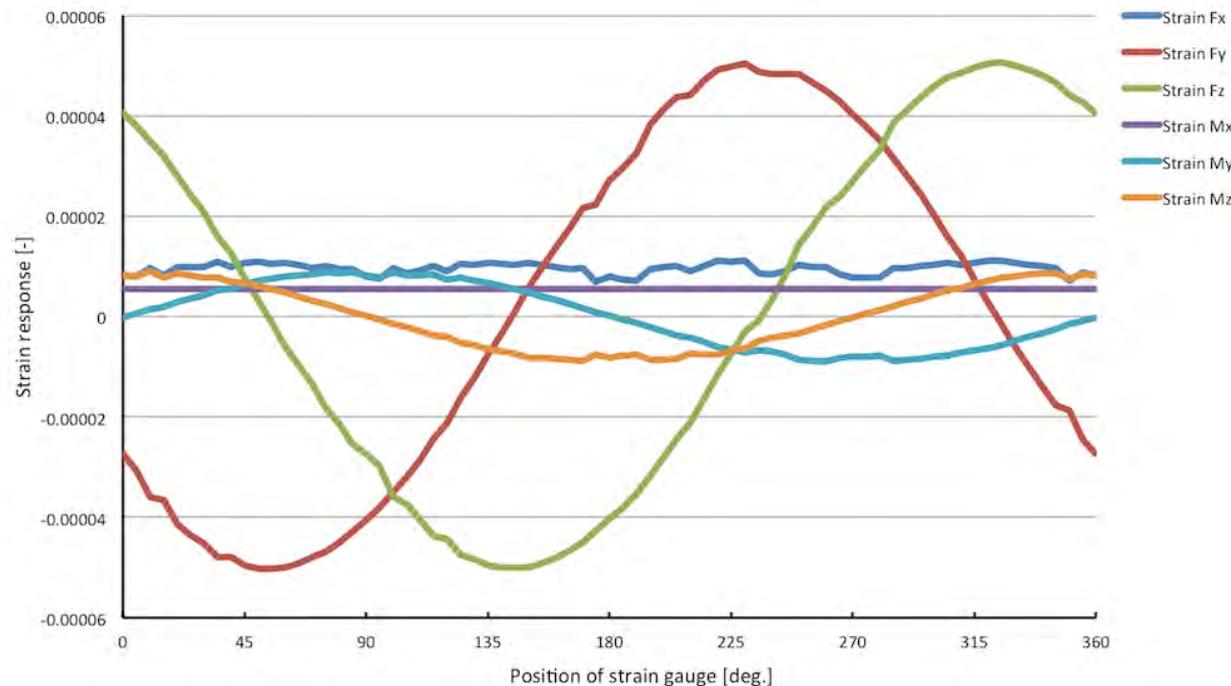
Caption: Figure 1 Strain response around circumference for six load types (DOF) (The angle of strain gauge is 45deg.)

Conclusion: The optimum angle for all gauges was found to be about 45 deg with respect to the longitudinal direction. This provided good sensitivity and separation of force components. Based on this COMSOL analysis, a wireless version of the SenseWheel will be developed, on a mobile platform. A musculoskeletal model is being developed to infer the shoulder forces, to be animated by these pushrim forces.

References: [1] Gutierrez et al. The Relationship of Shoulder Pain Intensity to Quality of Life, Physical Activity, and Community Participation in Persons With Paraplegia. J Spinal Cord Medicine, vol. 30, no3, p. 251, 2007.

[2] Tatsuto Suzuki, Catherine Holloway, Stephen JG Taylor, COMSOL Analysis to Determine Optimum Strain Gauge Locations for SENSEWHEEL, COMSOL Conference 2014 Cambridge

[3] Taylor, S., Lambert, S., Bayley, I., Blunn, G. (2008). A telemetrised glenoid prosthesis for reverse- anatomy shoulder replacement. Journal of Biomechanics, 41 S448

Disclosure of Interest: None Declared

Wheelchair

PO-0395

THE PROPER SEAT POSITION OF THE STANDING WHEELCHAIR

Jeseong Ryu [1,*]Isu Shin [1]Baekdong Cha [1]Jongman Kim [1]Soonjae Ahn [1]Jongsang Son [1]Youngho Kim [1]

[1]Biomedical Engineering, Yonsei University, Wonju, Korea, Republic Of

Introduction and Objectives: Approximately 73% of manual wheelchair users suffer from pain and injury on their upper extremities [1]. The shoulder pain and injury are the most common for manual wheelchair users. To prevent upper extremity injury, many studies have been performed for the correct seat position and effective propulsion motion. Engel et al. [2] compared three different seat positions and showed posterior seat position was the most efficient place. Van der Woude et al. [3] studied the effect of seat height on energy consumption and kinematics, and recommended the optimal elbow joint angle and seat position. Recently, in order to increase convenience for wheelchair users, a specially-designed standing wheelchair to move even in a standing posture have been developed. Since this wheelchair has separated hand rim from the wheel, an optimal design of the seat position is required.

Methods: In this study, 5 healthy male subjects (23.8±1.8 years, 71.6±5.5kg, 172.8±7.2cm) were participated (approved by the Institutional Review Board of Yonsei University (No. 1041849-201406-BM-029-01)). A prototype of the manual standing wheelchair (HANIL Hightech Co., LTD, Republic of Korea) was fixed on a brake-type wheelchair dynamometer for the measurement of torque and rotation [4]. The brake torque was set to 3 Volt (axis retarding torque 0.55Nm), and torque and RPM were sampled at 1 kHz. Nine spherical reflective markers of 6.4 mm diameter were attached on the right upper limb according to the Plug-In-Gait (PIG) model (Oxford Metrics) and a wheelchair hand rim [5], and motion kinematics was obtained at 200 Hz using the 3D motion capture system (Vicon MX system, Vicon Motion System Ltd, UK). The seat and the back supporter were moved ±6cm in both horizontal and vertical directions from the center position, thus nine different positions were tested for every subject. The subject propelled 6 times in each position at his self-selected speed, and the selection of the seat position was randomly chosen. Upper-limb joint moments and total propulsion energy were determined using the inverse dynamics and the optimization based on the minimal joint power criterion with a link-segment model [6].

Results: We assumed that the optimal seat position has the lowest total energy. As a result, a short subject showed the smallest total propulsion energy on the highest seat position, whereas tall subjects showed the largest total propulsion energy on the lowest seat position. Regardless of the subject's height, the backward seat position, however, showed the smallest total propulsion energy in the horizontal position (Table). Figure shows the optimal seat position for all subjects, using the surface fitting. As a result, the smallest total energy was shown at 1.84% backward and 2.14% upward position in proportion to the subject height from the center position.

Figure:
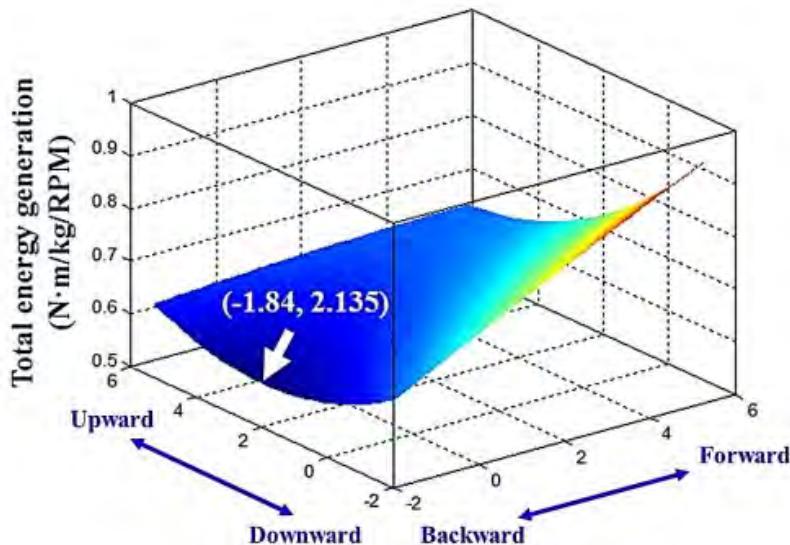
Caption: Surface fitting of the optimal seat position for all subjects

Conclusion: In this study, biomechanical analysis was performed to determine an optimal seat position for a standing wheelchair which has the separated hand rim from the wheel. Kotajarvi et al. [7] examined the effect of seat position on the hand rim biomechanics using the typical wheelchair. They measured the effective force during propulsion with the changed seat position. Results showed that tangential force output did not change with the seat position, and axial and radial forces were largest in the lowest seat position. Therefore, they concluded that the propulsion efficiency did not significantly change with the seat position. In the study, joint moments and total propulsion energy were determined with the inverse dynamics and the optimization technique. A short subject showed the smallest total propulsion energy on the highest seat position, whereas tall subjects showed the largest total propulsion energy on the lowest seat position. Total propulsion energy of all subjects was the smallest on 1.84% backward and 2.16% upward from a center seat position proportional to the height. Further study is needed to compare young people and the elderly to develop a standing wheelchair with the optimal seat position.

Table:

Subjects	Height (cm)	Vertical Position	Horizontal Position
A	160	Upward	Backward
B	175	Downward	Backward
C	176	Downward	Backward
D	176	Downward	Backward
E	176	Middle	Backward

Caption: The optimal seat position for different subjects

References:

[1] Subbarao, et al., J Spinal Cord Med, **18**:9-13, 1995.

[2] Engel, et al., Rehabilitation, **15**:217-228, 1976.

[3] Van der Woude, et al., J Rehabil Res Dev, **26**:31-50, 1989.

[4] Ryu, et al., The 5th Conference of Kor Soc Biomech, **5**:22, 2012

[5] Whang et al., J Biomech Sci Eng, **7**:349-357, 2012

[6] Whang et al., J Korean Phys Soc, **62**:648-656, 2013

[7] Kotajarvi, et al., J Rehabil Res Dev, **41**:403-414, 2004.

Disclosure of Interest: None Declared

Awards

DAVID WINTER YOUNG INVESTIGATOR AWARDS

Cardiovascular

SS-0063

SUPERCRITICAL CARBON DIOXIDE DECELLULARISATION OF PERICARDIUM: MECHANICAL AND STRUCTURAL CHARACTERISATION FOR APPLICATIONS IN CARDIOVASCULAR SURGERY

Frank R. Halfwerk [1,2,*] Jeroen Rouwkema [1] Jan Gossen [3] Bart Koopman [1] Jan Grandjean [1,2]

[1]Biomechanical Engineering, MIRA Institute for Biomedical Technology and Technical Medicine, University of Twente, [2]Thoraxcentrum Twente, Medisch Spectrum Twente Hospital, Enschede, [3]European Medical Contract Manufacturing, Nijmegen, Netherlands

Introduction and Objectives: Pericardium is used in cardiovascular surgery as a temporary graft for heart tissue recovery, reconstruction of heart valves and aortic wall, closure of pericardium and reconstruction of blood vessels (arterioplasty). However, calcification, dehiscence and formation of scar tissue occurs in the long term. These issues, in part, may be caused by decellularisation and cross-linking by glutaraldehyde, used to prevent a pro-inflammatory immune response. Current decellularisation methods are enzymatic, physical or chemical processes and result in disruption of architecture, reduction of mechanical properties and loss of surface composition. Importantly, residual chemicals inhibit beneficial properties of a cell-free scaffold.

Moreover, these treatments induce a chronic inflammation, which result in calcification and limit lifespan of the graft to 10 years. This calcification is related to host metabolism, implant structure and mechanical factors. Reoperation is often required, with high mortality, morbidities and costs.

A new method of decellularisation is supercritical carbon dioxide ($scCO_2$) processing; a mild but effective technique to remove cells and fat from tissues. This technique uses non-toxic chemicals and does not require cross-linking that interfere with degradation and a constructive remodelling process.

Thus, the aim of this study is characterisation of mechanical and structural properties of scCO2 decellularised pericardium for applications in cardiovascular surgery.

Methods: Bovine and porcine pericardia were decellularised by $scCO_2$ and compared with Peri-Guard® (bovine pericardium cross-linked by glutaraldehyde). Ultimate tensile strength (UTS), elastic modulus and suture retention strength were determined using an uniaxial tensile tester in dry and hydrated samples. Suture retention strength was measured by Prolene 4-0 interrupted sutures. Ultrastructure was visualised using Scanning Electron Microscopy.

Results: UTS of $scCO_2$ decellularised porcine and bovine pericardium was comparable to untreated pericardium, while UTS of Peri-Guard® was non-significantly higher (see Table 1). Elastic modulus was relatively high in Peri-Guard® and dry $scCO_2$ decellularised bovine pericardium, but was reduced by half in hydrated condition.

Suture retention strength was higher in dry and hydrated bovine pericardium, compared to Peri-Guard®. Three phenomena were observed: tearing, string cutting and slipping of surgical knot. Preservation of ultrastructure in $scCO_2$ decellularised porcine pericardia (Figure 1) and some deterioration of ultrastructure was observed in Peri-Guard®.

Figure:
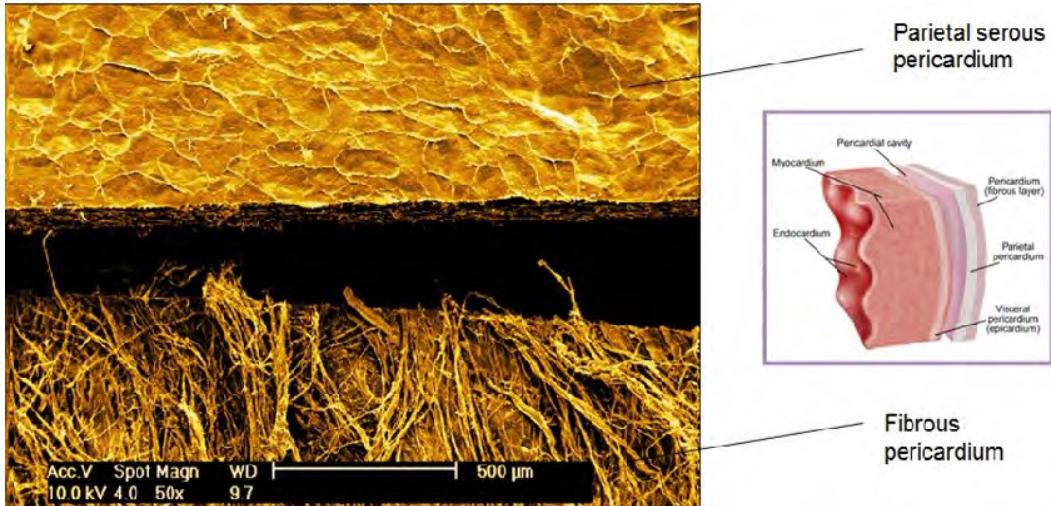
Caption: Ultrastructure of both rough and fibrous porcine pericardium decellularised by scCO2, visualised by Scanning Electron Microscopy. Inlay shows anatomic structures of pericardium. Magnification 50x.

Conclusion: Pericardium decellularised by $scCO_2$ has superior mechanical properties with preservation of ultrastructure and higher suture retention strength compared to Peri-Guard®. This makes $scCO_2$ decellularisation a promising technique and further mechanical characterisation, recellularisation capabilities and *in vitro* calcification should be investigated before use in cardiovascular surgery.

Table:

Source	Treatment	Tensile Strength (MPa)	Elastic Modulus (MPa)	Reference
Porcine	Untreated	14.4	76 ± 10	Dong, 2013
Porcine	X-100	8.0	51 ± 7	Dong, 2013
Porcine	SDS +Glutaraldehyde	7.3 ± 1.6	-	Min, 2012
Porcine	**scCO$_2$ (dry)**	**14.0 ± 4.1**	**131 ± 21**	**This study**
Human	Untreated	7.6 ± 0.96	50 ± 3	Cohn, 1987
Human	Glutaraldehyde	10 ± 3	51 ± 15	Yamashita, 2012
Bovine	Untreated	8.9 ± 0.75	53 ± 4	Cohn, 1987
Bovine	**Glutaraldehyde (Peri-Guard)**	**19.4 ± 7.3**	**91 ± 38**	**This study**
Bovine	Untreated	9 ± 3	26 ± 5	Hülsmann, 2012

Bovine	SDS +Glutaraldehyde	4.2 ± 1	5 ± 2	Hülsmann, 2012
Bovine	**scCO$_2$ (dry)**	**11.0 ± 2**	**83 ± 14**	**This study**
Bovine	**scCO$_2$ (hydrated)**	**13.4 ± 3**	**48 ± 12**	**This study**

Caption: Table 1 Mechanical properties of pericardia

References: [1] Dong et al., J Surg Res, 183: 56-67, 2013.

[2] Min et al., Korean J Thor Cardiovasc Surg, 45: 368-379, 2012.

[3] Cohn et al., Clin Mater, 2: 115-124, 1987.

[4] Yamashita et al., Ann Thorac Cardiovasc Surg, 18: 434-437, 2012.

[5] Hülsmann et al., Xenotransplantation, 19: 286-297, 2012.

Disclosure of Interest: F. Halfwerk Conflict with: Supercritical carbon dioxide decellularised pericardium was provided free of charge by EMCM in a collaborative project between the University of Twente, Medisch Spectrum Twente Hospital and EMCM with an indirect financial relationship between FH and EMCM (partial honorarium). , J. Rouwkema: None Declared, J. Gossen: None Declared, B. Koopman: None Declared, J. Grandjean: None Declared

Keywords: None

Neurological and Motor Control

AS-0085

ALTERED MUSCLE SYNERGIES DURING GAIT IN CEREBRAL PALSY ARE NOT DUE TO ALTERED KINEMATICS OR KINETICS

Katherine M. Steele[* 1], Adam Rozumalski[2, 3], Michael Schwartz[2, 3]

[1]Mechanical Engineering, University of Washington, Seattle, [2]Biomedical Engineering, University of Minnesota, Minneapolis, [3]James R. Gage Center for Gait & Motion Analysis, Gillette Children's Specialty Healthcare, St. Paul, United States

Introduction and Objectives: Walking is a complex movement, requiring the control and coordination of many muscles. For some tasks such as walking, prior research has proposed that part of how we control muscle activity is by activating muscles in weighted groups, commonly called synergies or modes [1]. Synergies are theorized to provide a simplified control strategy compared to controlling each muscle individually. Previous studies have demonstrated that only four to six synergies can describe over 90% of the variance in muscle activity during walking in unimpaired individuals [2]. Further, in individuals with stroke or cerebral palsy (CP), the number of synergies required to describe muscle activity is reduced and theorized to reflect compromised neuromuscular control and impaired function [3,4]. However, whether these changes in synergies reflect altered neural control or other factors, such as altered gait patterns, remains unclear. Biomechanics and task constraints have previously been suggested to impact synergies [5]. If synergies are mechanogenic, then individuals with CP may have altered synergies during gait just because they walk differently than unimpaired individuals.

The objective of this study was to test this theory and evaluate if altered synergies during gait in CP reflect mechanogenic or neurogenic factors. We hypothesized that, if synergies are mechanogenic, then individuals with CP who walk with more similar gait patterns (*i.e.* kinematics and kinetics) should also have more similar synergies. Since individuals with CP have been shown to have altered synergies during gait [4] and use many different gait patterns, this population provides an ideal test case to evaluate this hypothesis.

Methods: We compared the similarity of kinematics, kinetics, and synergies during gait for children with CP who had received motion analysis at a single clinical center prior to February 2013. For 1251 children, we extracted (1) joint angles, (2) joint moments, and (3) electromyography from gait analysis. Electromyography was collected from five muscles per leg and was used to calculate synergies using nonnegative matrix factorization [6]. We then compared 10,000 random pairs of limbs across all subjects to determine if limbs with more similar kinematics or kinetics had more similar synergies. For each pair of limbs, we calculated the root mean square (RMS) difference in sagittal plane joint angles and moments to compare kinematics and kinetics. To compare the similarity of synergies, we calculated two measures. First, to compare synergy structure (*i.e.,* if similar muscles were grouped together), we calculated the L2-norm of the difference in weights of the synergy that explained the most variance in EMG for each limb. Second, we calculated the difference in variance accounted for by one synergy between limbs to compare complexity of synergies (*i.e.,* an individual with more complex synergies would have a lower variance accounted for by one synergy). Linear regression was then used to compare the similarity of the 10,000 pairs of limbs and determine if individuals with more similar kinematics or kinetics also had more similar synergy structure or complexity.

Results: Similarity in joint angles or moments did not lead to greater similarity in synergies (Fig. 1). Differences in synergy weights between individuals were not associated with either differences in kinematics ($r^2 = 0.013$) or kinetics ($r^2 = 0.011$). Further, differences in synergy complexity were also not associated with differences in kinematics ($r^2 = 0.005$) or kinetics ($r^2 = 0.001$).

Figure:
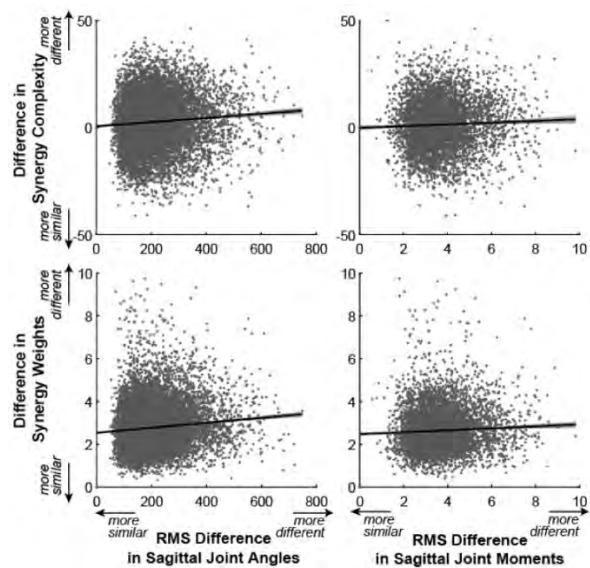
Conclusion: Altered synergies during gait among individuals with CP are not associated with altered kinematics or kinetics. These results counter our initial hypothesis that individuals with CP have altered synergies because they use different gait patterns compared to unimpaired individuals. Two individuals with CP walking with similar kinematics or kinetics can have very different synergies. Thus, synergies are not purely mechanogenic and difference in gait pattern alone cannot account for altered synergies in CP. Altered synergies in CP may reflect altered neuromuscular control strategies and provide a useful tool to quantify altered control for diagnosis or treatment planning.

Caption: Comparison of similarity of joint kinematics (degrees) and kinetics (Nm/kg) during gait and synergy complexity and structure for 10,000 random pairs of subjects with CP.

References: [1] Kiehn, Annu Rev Neurosci, 29:279-306, 2006.

[2] Neptune et al., J Biomech, 42:1282-1287, 2009.

[3] Clark et al., J Nuerophys, 103:844-57, 2010.

[4] Schwartz et al., Gait Posture, 39:S40, 2014.

[5] Kutch et al., PLoS Comp Bio, 8:e1002434, 2012.

[6] Tresch et al., J Neurophys, 95:2199-2212, 2006.

Disclosure of Interest: None Declared

Musculoskeletal

SS-0086

LARGER ISOFORMS OF TITIN ARE ASSOCIATED WITH INCREASED SARCOMERE LENGTHS AND SEVERITY OF HIP DISPLACEMENT IN CEREBRAL PALSY.

Kelly A. Larkin-Kaiser [1,*]Venus Joumaa [2]Timothy Leonard [1]Jason Howard [3]Walter Herzog [1]

[1]Kinesiology, [2]University of Calgary, Calgary, Canada, [3]Sidra Medical and Research Center, Doha, Qatar

Introduction and Objectives: Cerebral palsy (CP) is an umbrella term describing a spectrum of neurologic compromise secondary to an insult to the developing brain that can lead to musculoskeletal manifestations with growth. The resulting spastic muscle contractures and bony deformities are thought to cause subluxation/dislocation of the hip joint (hip displacement) that often leads to painful osteoarthritis (Soo, Howard, Graham et al, 2006). Previous research has suggested that spastic muscle contractures in CP patients are associated with increased sarcomere lengths for given joint configurations compared to typically developing children (Smith, Lee, Ward, Chambers, & Lieber, 2011). More recent research has suggested that the molecular spring titin may be altered in response to spasticity and contracture (Ottenheijm & Granzier, n.d.). The titin isoform shift may significantly contribute to clinical outcomes by making the overstretched sarcomeres more compliant. However, the muscular changes that occur, and their association with clinical dysfunction, are not clearly understood. Therefore, the purpose of this project was to determine whether changes in skeletal muscle titin isoforms occur in children with CP, and if these changes are associated with increased sarcomere lengths and/or clinical dysfunction.

Methods: Single gracilis muscle biopsies were obtained with consent from children with CP (spastic quadriplegia, GMFCS III-V; n=7) who underwent adductor muscle release surgery for the treatment of hip displacement. Gel electrophoresis was used to estimate the molecular weight of titin isoforms in the gracilis muscle samples. Each biopsy sample generated 10 muscle fascicles used for measurement. Sarcomere lengths were measured at 5 locations along each fascicle using laser diffraction. Radiographic measures were taken pre-operatively and used to calculate migration percentage of the head of the femur from the acetabulum. The severity of hip displacement was determined by measuring by Reimer's migration percentage (MP) from standardized anterio-posterior pelvic x-rays (Valencia, 2010).

Results: The average molecular weight of titin in the gracilis muscle tissue was 3,588 kDa (±26). Sarcomeres from a total of 70 gracilis muscle fascicles were also measured. We observed that the mean sarcomere length in the gracilis was 3.4 μm, compared to less than 3.0 μm in typically developing children. Increased hip displacement was found to be associated with heavier isoforms of titin (R^2=0.65, p<0.05), and with increased sarcomere lengths (R^2=0.80, p<0.05) (Figure 1).

Figure:
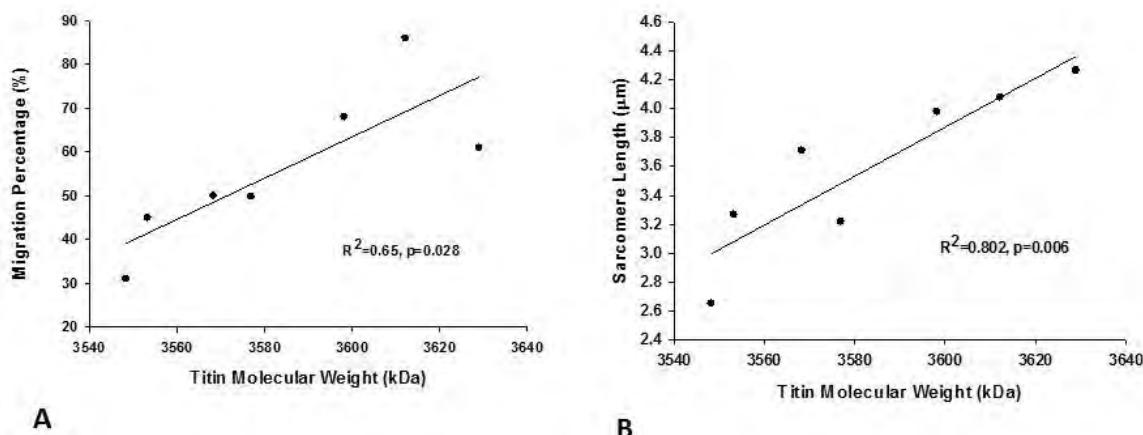
Caption: Figure 1. A) Association between titin molecular weight and migration percentage of the hip B) Association between titin molecular weight and sarcomere length

Conclusion: We observed increased sarcomere lengths in the gracilis muscle biopsies from CP patients with hip displacement. Previous research indicated sarcomere lengths of less than 3.0 µm in the musculature of typically developing children (Smith et al., 2011). Our results also suggest that larger titin isoforms are associated with these long *in situ* sarcomere lengths and with increased severity of hip displacement. It is possible that more compliant isoforms of titin and increased sarcomere lengths are expressed in spastic gracilis muscle tissue as adaptive mechanisms to reduce passive force within the muscle. We show here, for the first time, that larger titin isoforms are associated with morphological changes in children with spastic CP, and that these changes at the structural level are associated with clinical dysfunction.

References: Soo B, Howard JJ, Boyd RN, Reid SM, Lanigan A, Wolfe R, Reddihough D, Graham HK. Hip displacement in cerebral palsy. The Journal of bone and joint surgery. American volume. 2006 Jan;88(1):121-9.

Ottenheijm, C. A. C., & Granzier, H. (n.d.). Role of Titin in Skeletal Muscle Function and Disease, 105–122. doi:10.1007/978-1-4419-6366-6

Smith, L. R., Lee, K. S., Ward, S. R., Chambers, H. G., & Lieber, R. L. (2011). Hamstring contractures in children with spastic cerebral palsy result from a stiffer extracellular matrix and increased in vivo sarcomere length. *The Journal of Physiology*, *589*(Pt 10), 2625–2639. doi:10.1113/jphysiol.2010.203364

Valencia, F. G. (2010). Management of hip deformities in cerebral palsy. *The Orthopedic Clinics of North America*, *41*(4), 549–59. doi:10.1016/j.ocl.2010.07.002

Disclosure of Interest: None Declared

Keywords: None

Modelling

AS-0009

IMPLEMENTATION AND IMPORTANCE OF THE SUBJECT-SPECIFIC DISTRIBUTION OF FIXED CHARGE DENSITY OF ARTICULAR CARTILAGE IN THE KNEE

Lasse P. Räsänen [1,*] Petri Tanska [1] Mika E. Mononen [1] Pavol Szomolanyi [2] Stefan Zbyn [2] C. C. van Donkelaar [3] Siegfried Trattnig [2] Jukka S. Jurvelin [1] Miika Nieminen [4] [5] Rami K. Korhonen [1]

[1]Department of Applied Physics, University of Eastern Finland, Kuopio, Finland, [2]High Field MR Center, Department of Biomedical Imaging and Image-Guided Therapy, Medical University of Vienna, Vienna, Austria, [3]Department of Biomedical Engineering, Eindhoven University of Technology, Eindhoven, Netherlands, [4]Department of Diagnostic Radiology, University Hospital, [5]Department of Radiology, University of Oulu, Oulu, Finland

Introduction and Objectives:

Negative charges of glycosaminoglycan (GAG) side chains of proteoglycans (PGs) result in fixed charge density (FCD) of articular cartilage. FCD induces swelling of the tissue and hence plays an important role in load support of the tissue [1,2]. However, it is not known how depth-wise FCD distribution in the knee joint controls cartilage strains. Here, we implement a subject-specific FCD distribution of human knee joint cartilage, as obtained from sodium (^{23}Na) MRI, into a fibril-reinforced poroviscoelastic model with swelling properties (FRPVES). We validate the model by comparing modeled cartilage deformations to experimentally measured deformations *in vivo*, and demonstrate the importance of the subject-specific FCD distribution of knee joint cartilage under static loading.

Methods:

A 3D finite element (FE) model of an asymptomatic knee joint was constructed from manually segmented MR-images (3D-DESS at 7T (MR Centre of Excellence, Vienna, Austria), Fig. 1a,b). ^{23}Na concentration maps of the cartilage tissues were calculated from ^{23}Na MRI after applying corrections for magnetic field inhomogeneity, partial volume effect [3], biexponential T2* and monoexponential T1 to the observed signal [4,5]. The FCD maps and the depth-wise distribution of FCD were further determined for tibial cartilage by relating the obtained ^{23}Na concentrations to ^{23}Na -concentration of synovial fluid (Fig. 1a,f) [6]. For model validation purposes, the subject's knee joint was imaged under axial compression of 120 N (Fig. 1c). The experimentally loaded tibial cartilage was manually segmented and cartilage compression was determined by comparing the segmented cartilage to that obtained under no loading (Fig. 1c).

Cartilage and meniscus were modeled as FRPVES materials including FCD [7–9]. The FCD content of the tibial cartilage, determined from MRI (mean ± SD: 0.17 ± 0.09 mEq/ml), was implemented into the subject-specific model. For comparison, a model with homogeneously distributed FCD (0.17 mEq/ml, mean of the measured FCD) and a model with depth-dependent FCD distribution obtained from literature (0.1-0.2 mEq/ml, Fig. 1e) were created. The FCD distribution in the femoral cartilage (0.1-0.2 mEq/ml) and menisci (0.03 mEq/ml) were obtained from literature [10]. Ligaments were modelled by using linear spring elements [7]. The models were simulated with 120 N axial load for 780 seconds in accordance with the MRI experiment and the depth-wise axial strains in tibial cartilage of the subject-specific model were compared to those of the homogenous and literature models.

Results:

In the medial tibiofemoral contact region of the subject-specific model, the mean axial compression of tibial cartilage was 82 μm after 780 s of creep (Fig. 1d). As measured from the corresponding location of the experimentally compressed joint, the mean cartilage compression was 94 μm. Within the chosen location (Fig. 1a), strains in the model with the subject–specific FCD distribution were increased especially in the superficial tissue (up to +27%), as compared to those in the homogeneous model (Fig. 1f,g). However, strains in the subject–specific FCD model decreased up to -122% in the deep tissue with respect to those in the homogenous model (Fig. 1f,g). In the model with the FCD distribution obtained from literature, strains were in between those observed for two aforementioned models (Fig. 1f,g).

Figure:
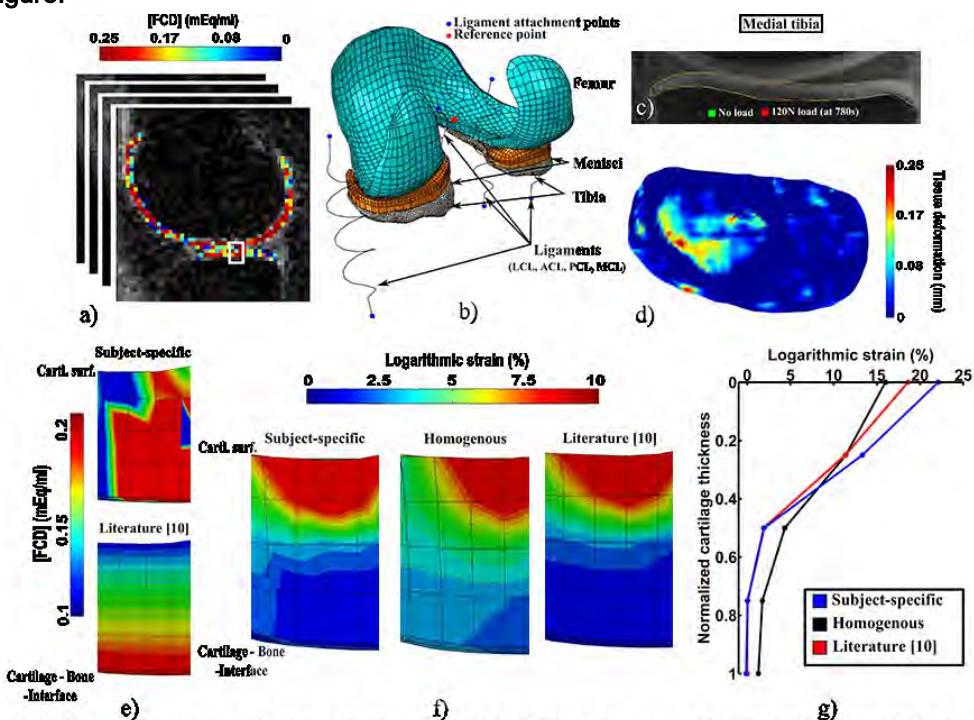
Figure 1: Workflow and results of the current study. a) A Fixed charge density (FCD)-map of tibiofemoral contact region as calculated from ^{23}Na-MRI (3D-vTE-SPGR: TR/TE$_1$ = 11/1.42 ms, resolution 1.5 x 1.5 x 2.8 mm^3). FCD was determined by relating the calculated ^{23}Na concentrations to that of synovial fluid: $FCD = [^{23}Na_f]^2 / [^{23}Na (x,y)] - [^{23}Na (x,y)]$, where $[^{23}Na_f] = 150$mM [6]. b) The meshed FE model geometry as segmented from MR images (3D-DESS: TR/TE = 7.81/2.62 ms, isotropic resolution of (0.34 mm)^3). c) The segmented and coregistered tibial tissue from imaging done during (red, 3D-DESS: TR/TE$_1$ = 8.68/2.55 ms, isotropic resolution of (0.4 mm)^3) and without static loading (green) (a slice from medial tibial cartilage compartment). d) The tibial cartilage deformation of the subject-specific model after 780 seconds of creep. e) Subject-specific (above) FCD distribution and that obtained from literature (below, $FCD = 0.11 + 0.09 \cdot h$, where h = normalized tissue depth) the models after the free swelling of the model (location highlighted in a)). f) Logarithmic axial strains in the models with patient-specific, homogenous and literature FCD distributions (corresponding location as shown in a) and e)). g) Depth-wise distribution of axial strains from f) in each model (0 = tibial cartilage surface, 1 = cartilage-bone interface).

Conclusion:

The presented model with subject-specific FCD obtained from MRI corresponded well with the experimentally measured deformations of the knee joint cartilage *in vivo*. The locally smaller FCD content in the superficial cartilage in the subject-specific model decreased the local tissue stiffness, thereby increasing strains, as compared to the model with a homogeneous FCD distribution. Correspondingly, increase in tissue stiffness in the deep tissue (due to higher amount of FCDs) decreased strains, as compared with those in the homogenous model. For the chosen location, local tissue strains

in the subject-specific model were close to those obtained from the model with the FCD distribution captured from literature.

By taking into account FCD of cartilage, more realistic estimation of tissue strains and stresses in the knee joint to mechanical loading can be obtained. The model may provide a feasible method for evaluating the effect of PG loss on tissue mechanics, as well as the onset and progression of OA in the human knee joint.

References:

[1] Mow *et al., J. Biomech.* **17,** 377–394, 1984.

[2] Korhonen *et al., J Biomech* **36,** 1373–1379, 2003.

[3] Moon *et al., J. Magn. Reson. Imaging* **38,** 1063–1072, 2013.

[4] Madelin *et al., Radiology* **268,** 481–91, 2013.

[5] Wheaton *et al., Radiology* **231,** 900–5, 2004.

[6] Shapiro *et al., Magn. Reson. Med.* **47,** 284–291, 2002.

[7] Halonen *et al., J. Biomech.* **47,** 2467–74, 2014.

[8] Tanska *et al., Comput. Math. Methods Med.* **2013,** 164146, 2013.

[9] Wilson *et al., J. Biomech.* **38,** 1195–204, 2005.

[10] Chen *et al., Osteoarthritis Cartilage*, **9**(6), 561–569, 2001.

Disclosure of Interest: None Declared

Keywords: None

Modelling

SS-0069

REAL-TIME VIRTUAL MUSCLE CONTROL FOR POWERED PROSTHESES AND EXOSKELETONS

Sandra K. Hnat [1,*]Antonie van den Bogert [1]

[1]Mechanical Engineering, Cleveland State University, Cleveland, OH, United States

Introduction and Objectives: Powered prosthetic limbs are theoretically capable of replicating able-bodied movements. These devices are typically actuated by single-joint electric motors with time-varying linear impedance control. Though substantially better than passive prostheses, able-bodied gait is usually not achieved. We hypothesize that a more muscle-like actuation system can improve performance and simplify the feedback control. Muscles are actuators with nonlinear viscoelastic properties and internal dynamics, often crossing multiple joints. It has been shown through simulation that these properties contribute substantially to the stability of walking [1]. Here we consider the possibility of actuating a powered prosthetic system with torques generated by a real-time simulation of muscle dynamics.

Real-time simulation is challenging because the ordinary differential equations (ODE) that represent muscle dynamics are highly nonlinear and have near-singularities. Consequently, fixed step ODE solvers can become unstable and variable-step solvers will be slow due to small time steps. An alternative implicit formulation and solution method has the potential to achieve accurate results with minimal computation time [2].

The purpose of this paper is to develop and test a real-time simulation of a human muscle actuation system that generates knee and ankle torques for an above knee prosthetic device. The virtual muscle system consists of six muscles, and is driven by real-time joint angle data and muscle excitation signals.

Methods: For proof of concept, we used a planar leg model with six muscles, three of which were monoarticular groups (Vasti, Soleus, Tibialis Anterior) and three were biarticular (Rectus Femoris, Hamstrings, Gastrocnemius). The inputs to the system are the joint angles (q) at the hip, knee, and ankle and the control signals (u) for the six muscles. Musculotendon length of each muscle, a required input for simulation of muscle dynamics, is computed from the three joint angles.

Muscles were represented by a Hill-type model with a contractile element (CE), series/parallel elastic elements (SEE/PEE), and a small amount of viscous damping in parallel to the contractile element. The CE has standard force-velocity and force-length properties, while PEE and SEE are modeled as nonlinear elastic. Muscle contraction dynamics was formulated as a first-order implicit differential equation (IDE). An additional first-order IDE represented the activation dynamics. The force generated by each muscle was multiplied by moment arms to obtain its contribution to the knee and ankle torques. Figure 1 is a block diagram describing the inputs and outputs of the model, in which the red box indicates the scope of this study.

Tests were performed using joint angle time histories q(t) for 30 seconds of normal walking and 1 Hz sinusoidal test signals for the muscle excitations u(t). In a prosthetic device, the former would be real-time encoder data, while the latter would be generated by a control system. Simulations were performed in Matlab with a first order Rosenbrock solver [2] using fixed time steps ranging from 0.08 to 16.0 ms. Joint torques generated by the model were compared to the result

from the smallest time step in order to determine numerical error in the simulations as a percentage of the maximum moments. Computation times were measured in all tests.

Results: Muscle forces and joint torques responded appropriately to sinusoidal muscle activations. Table 1 shows how the accuracy and speed of the simulation depended on the integrator step size. RMSE was proportional to step size, due to the first order approximation used. At 0.31 ms, the simulation was just faster than real-time and the simulation errors were well below 1%. Substantially larger time steps still resulted in acceptable accuracy. For time steps larger than 10 ms, the simulation was unstable.

Figure:
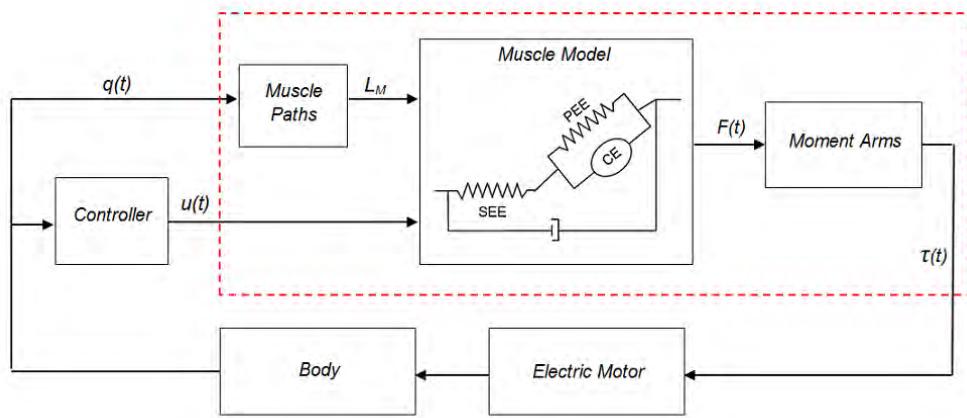
Conclusion: The tests demonstrated joint torques can be generated by a real-time simulation of muscle dynamics. Computation time was well within the requirements for real-time, even in the high-level Matlab language. The muscle dynamics and differential equation solver only require simple mathematical operations and no software libraries, making them suitable for implementation on an embedded system. We conclude that this virtual muscle actuation system can be used to drive the electric motors in a prosthesis in order to better replicate the control and dynamics of able-bodied gait.

Table:

Simulation step size (ms)	RMS error in knee moment (%)	RMS error in ankle moment (%)	Solution time (s)
0.1	0.02	0.01	57.8
0.18	0.08	0.04	32.8
0.31	0.20	0.10	18.7
0.54	0.40	0.20	10.8
0.95	0.76	0.38	6.0
1.68	1.39	0.69	3.9
2.95	2.50	1.23	2.2
5.18	4.49	2.17	1.2
9.10	8.16	3.82	0.6
16.00	15.41	6.73	0.3

Caption: Integrator step size and its effect on accuracy and speed. Error was quantified as a percentage of the maximum moments in the knee and ankle.

References: [1] Gerritsen et al., Motor Control, 2: 206-220, 1998.

[2] van den Bogert et al., Procedia IUTAM, 2: 297-316, 2011.

Disclosure of Interest: None Declared

Keywords: None

CLINICAL BIOMECHANICS AWARDS

Neurological and Motor Control

AS-0115

CORTICAL MODULATION OF ABERRANT LOWER LIMB MUSCLE SYNERGIES FOLLOWING STROKE

Andrew Q. Tan [1,*]Yasin Dhaher [2]

[1]Neuroscience, [2]Biomedical Engineering, Northwestern University, Chicago, United States

Introduction and Objectives: Growing evidence demonstrates unique synergetic signatures in the lower limb(LL) post-stroke, with a specific across-plane and across-joint representations. Observations of such neural constraints include coupled cross planar kinetic outflow[1] and altered muscle synergy structure[2]. Recent findings from our lab illustrated that additional activation of the lesioned hemisphere (L-H) upregulates the expression of these aberrant muscle synergies in the LL [3]. While the inhibitory role of the ipsilateral hemisphere in the upper limb has been widely reported, examination of the role of the contralesional hemisphere (CON-H) in modulating these synergies in the LL following stroke is lacking. Accordingly, we test the hypothesis that stimulation of L-H and CON-H motor cortices will have differential effects on the motor evoked potential (MEP) patterns of the paretic LL. We proposed a novel TMS paradigm to identify patterns of MEPs across multiple LL muscles during a task where synergistic actions have been reported.

Methods: 10 control and 12 chronic stroke participants with single hemispheric stroke were recruited. Motor evoked potentials (MEP) were elicited in 8 LL muscles using single pulse TMS. Surface electromyography (EMG) were recorded from: vastus medialis (VM), vastus lateralis (VL), rectus femoris, adductor longus (ADD), tibialis anterior (TA), medial gastrocnemius, and biceps femoris. Single pulse TMS was delivered using a Magstim 200 stimulator via a 110 mm diameter double-cone coil. The coil position was incrementally adjusted to locate the ADD hotspot over L-H motor cortex contralateral to the test limb (stroke paretic limb). Optimal coil position and intensity was mapped as the lowest stimulation intensity required to evoke ADD MEPs of 50 µV in peak-to-peak amplitude in 3 of 5 consecutive trials. The hotspot for the test limb ADD was similarly mapped for stroke contralesional hemisphere (CON-H) or control ipsilateral hemisphere to test limb. Stimulator output for the CON-H was increased in order to match contralateral (cMEP) and ipsilateral (iMEP) ADD amplitudes.

Participants were isometrically locked in the toeoff gait posture in an instrumented exoskeleton with 3 6-DOF load cells used to measure the interaction forces and moments. Participants matched isometric hip adduction torques at 40% of their maximum while receiving instantaneous visual feedback in the form of moving a circular cursor. A successful trial was considered if the participant matched the target torque within ±5% of the torque magnitude and direction and hold for a minimum of 200ms.

For each trial the TMS coil was placed over the hotspot location for either hemisphere. When the participants successfully matched the target adduction torque, the TMS device was triggered by software. Matched ADD MEPs together with nontargeted muscles were simultaneously recorded. 10-30 trials were performed for each hemisphere. An 80 ms window following the TMS pulse was searched for the MEP onset when 5 consecutive points in the EMG trace were above 3 standard deviations of the mean pre-TMS EMG activity. MEP amplitudes were measured peak-to-peak and calculated as

the difference between the background activation and the average of a 20 ms window centered at the peak MEP rectified pulse. The ratio of the mean iMEP amplitude over the mean cMEP amplitude was quantified for each muscle. A statistical value less than one indicate a reduction in iMEP amplitude relative to the cMEP amplitude following TMS of the ipsilateral hemisphere.

Results: By quantifying the CON-H / L-H MEP ratio across muscles, we characterized a significant inhibition of aberrant MEP coupling between ADD and VM (p=0.0078) and VL (p=0.047) following CON-H stimulation exclusive to the stroke group (ANOVA,p=0.028), an inhibition that was muscle dependent (ANOVA, p= 0.039). We find a significant reduction of TA MEPs in both groups following ipsilateral hemisphere stimulation (p=0.0014 stroke; p=0.015).

Figure:

Conclusion: Our results indicate that stimulation of CON-H reduced the expression of abnormal synergistic activations in individuals with stroke. Our observations seem incongruent with the notion of maladaptive motor output from CON-H post stroke suggested in the UL. Furthermore, a majority of the interhemispheric MEP onset latency differences occur below 3ms, consistent with the interpretation of ipsilateral corticospinal projections to the LL despite equivocal findings of their functionality the UL. Combined with the systemic inhibition of TA across groups, we argue that the ipsilaterally mediated MEP signature provides indirect evidence of inhibitory intracortical connectivity between abnormally synergistic muscles. This study takes an important step in exploring the relation between CON-H cortical reorganization and the modulation of abnormal LL muscle synergies post stroke.

References: [1]Tan et al., J Biomech, 2014.

[2]Cruz et al., IEEE Eng Med Bio Soc, 3956-9, 2009.

[3]Krishnan et al., Exp Neuro, 233:400-7, 2012.

Disclosure of Interest: None Declared

Keywords: None

EMERGING SCIENTIST AWARD

MUSCLE SYNERGIES AS A STRATEGY FOR COORDINATING REDUNDANT MOTOR SYSTEM

Shota Hagio

Research Fellow of the Japan Society for the Promotion of Science, Japan

Graduate School of Human and Environmental Studies, Kyoto University, Japan

To simplify a redundant degree of freedom, the concept of muscle synergies was proposed, which modularly organize a lot of muscles as the same group (Tresch et al., 1999). Although muscle synergies were calculated in a variety of movements, the neural origin remains unclear. In this lecture, I will introduce a series of our studies to clarify the underlying mechanisms of muscle synergies as neural system.

The first important question is whether the central nervous system (CNS) generates appropriate motor output through a neural circuit of muscle synergies. We demonstrated that the total activation of approximately 7 extracted muscle synergies from 15 muscles spanning knee and hip joints correlated to the target-directed variance of isometric endpoint force around a right ankle (Hagio and Kouzaki, 2015, Exp Brain Res). This result implied that the CNS indeed produces appropriate endpoint force using the neural system of muscle synergies.

Although dynamical movements involve the change of the force-generating capability of muscles due to the change of the physiological parameters, how did the CNS modulate the recruitment of muscle synergies? To clarify the question, we extracted lower-limb muscle synergies during isometric force generation with various combinations of knee and hip joint angles. Therefore, the CNS flexibly regulated the descending input to muscle synergies with merging or decomposing depending on the force generating capability of muscles (Hagio and Kouzaki, 2015, J Neurophysiol).

The flexibility of muscle synergies describing above permits a modular control of dynamical movements such as walking and running. We examined muscle synergies during a gait transition between walking and running, in which complicated control would be particularly needed to change different kinematic characteristics. As a result, regulating the activation timing of the specific muscle synergies, which dominated plantar flexor muscles, enabled a gait transition (Hagio et al., 2015, Front Hum Neurosci).

The low-dimensionality of muscle synergies is advantageous to generate movements whereas it is unclear what is a functional role of muscle synergies during motor learning. We constructed a descending neural network model including 3 intermediate layers, which were regarded as 1000 neurons in primary motor cortex, 4 spinal interneurons (muscle synergies) and 18 muscles. This model then learned the isometric force generation around a wrist. Consequently, the existence of muscle synergies demonstrated faster adaptation to a rotational perturbation than the absence of muscle synergies.

In conclusion, the flexibility and robustness of muscle synergies make a significant contribution to appropriate movement learning and production despite redundancy in motor system. Because "muscle synergy" is a fundamental topic to understand all motor control studies, a further study will be important to identify the existence of muscle synergies.

PROMISING SCIENTIST AWARD

Computer Simulation

AS-0075

TESTING MODEL-BASED CONCLUSIONS ON THE OPTIMAL CONTROL OF HUMAN MOVEMENT USING FORMAL STATISTICAL ANALYSES

Ross H. Miller [1,*]Farzad Ehtemam [1]

[1]Department of Kinesiology, University of Maryland, College Park, United States

Introduction and Objectives: Optimal control theory (OCT) has made many elegant and reasonably accurate predictions of human motor behavior. However, the traditional implementation of OCT in biomechanics [1] is extremely computationally demanding for large-scale musculoskeletal models. Consequently, most model-based OCT studies on locomotion have used a single generic model. With data from only one "subject" that does not reflect the biological variance present in even the healthy human population, the generalizability of such results is unclear.

Recent simulation methods can rapidly generate many OCT simulations in practical amounts of time [2], opening the possibility of performing "virtual" experiments with multi-subject datasets that can undergo formal statistical analysis as is standard for laboratory-based experiments, adding an important new element of validity to simulation of human movement.

Our objective was to test the hypothesis that conclusions on locomotor control from OCT are robust to healthy variation in anthropometric and muscular properties.

Methods: We used implicit direct collocation [2] to generate predictive simulations of human walking with models representing 10 subjects drawn from standard normal parameter distributions (Table 1). The basic structure of the model was the same for all 10 subjects: 12 degrees of freedom, 24 Hill-based muscles, and a model of muscle energy expenditure [3].

For each subject, walking was simulated on a temporal grid of 101 nodes/step. We first performed a data-tracking simulation that optimized the musculoskeletal states, muscle excitations, and step duration to track mean human experimental data [4] with minimum metabolic cost. The data-tracking result was used as the initial guess for predictive simulations with two different cost functions:

"Minimum Fatigue": minimize the largest muscle activation.

"Minimum Effort": minimize sum of muscle activations, each weighted by muscle mass.

Equality constraints enforced dynamic consistency, periodicity and bilateral symmetry, and Froude number 0.14. The average deviation of the knee angle from mean human experimental data in the first half of stance [4] was expressed in multiples of the experimental standard deviation (SD). Metabolic cost and average knee angle deviation was compared between cost functions using matched-pair Student's t-tests (critical $p = 0.05$).

Results: A single simulation required ~ 20 minutes in MATLAB on an iMac. The models tracked the mean human gait data to an average deviation of 0.60±0.03 SD with a metabolic cost of 3.41±0.16 J/m/kg.

The gross metabolic cost was lower for the Minimum Effort simulation (2.10±0.11 J/m/kg vs. 3.00±0.19 J/m/kg, p < 0.00001). The range in differences was 0.77-1.12 J/m/kg (Fig. 1).

The average knee angle deviation was greater for the Minimum Effort simulation (2.16±0.25 SD vs. 1.53±0.55 SD, p = 0.00084). The range in differences was 0.07-1.14 SD. Minimum Effort tended to predict a straight knee in stance, while Minimum Fatigue predicted stance phase knee flexion (Fig. 1).

Figure:

Caption: Metabolic cost (left) and knee angle accuracy (right) when using the "Minimum Fatigue" and "Minimum Effort" cost functions. Dashed lines are simulations with the different models, solid lines are means over all 10 models. The inset figures in the left panel show the average knee angle waveforms predicted by each cost function, compared to the experimental data.

Conclusion:

The qualitative consistency of predicted gaits between subjects suggests it may have been safe to draw conclusions from one subject. However, the difference in the average knee angle deviation was over 1.0 SD for three subjects and under 0.2 SD for three others. These data may suggest different conclusions if considered in isolation. Simulations with multiple model parameter sets were needed to discover the average behavior and the consistency between subjects. Simulation studies have often made modeling decisions for computational speed rather than physiological fidelity, or excluded particular analyses due to computational time rather than relevance. With rapid advances in computing power and simulation methods, the validity of these limitations is diminishing. We suggest that simulation studies whenever possible should be held to the same standards of statistical rigor applied to laboratory-based studies.

Table:

Model	Height (m)	Mass (kg)	Muscle (kg)	Speed (m/s)
1	1.66	61.0	20.9	1.10
2	1.64	57.9	19.4	1.09
3	1.72	54.6	19.4	1.12
4	1.55	55.1	17.9	1.03

www.isbglasgow.com

	1.70	69.7	23.6	1.12
5				
6	1.63	53.5	17.9	1.12
7	1.68	59.5	21.0	1.12
8	1.65	63.0	22.5	1.11
9	1.66	53.8	17.7	1.12
10	1.67	64.0	23.0	1.09
Mean	**1.66**	**59.2**	**20.3**	**1.10**
SD	**0.05**	**5.3**	**2.2**	**0.03**

Caption: Height, body mass, muscle mass, and walking speed of the 10 musculoskeletal models.

References: [1] Pandy et al., *J. Biomech. Engr.,* **114**: 450-460, 1992.

[2] Van den Bogert et al., *Proc. IUTAM,* **2**: 297-316, 2011.

[3] Minetti & Alexander, *J. Theor. Biol.,* **186**: 467-476, 1997.

[4] Miller et al., *Med. Sci. Sports Exerc.,* **46**: 572-579, 2014.

Disclosure of Interest: None Declared

Keywords: None

ISB